MMM 2022 Conference

Minneapolis, MN • October 31 - November 4, 2022 • www.magnetism.org

BOOK OF ABSTRACTS

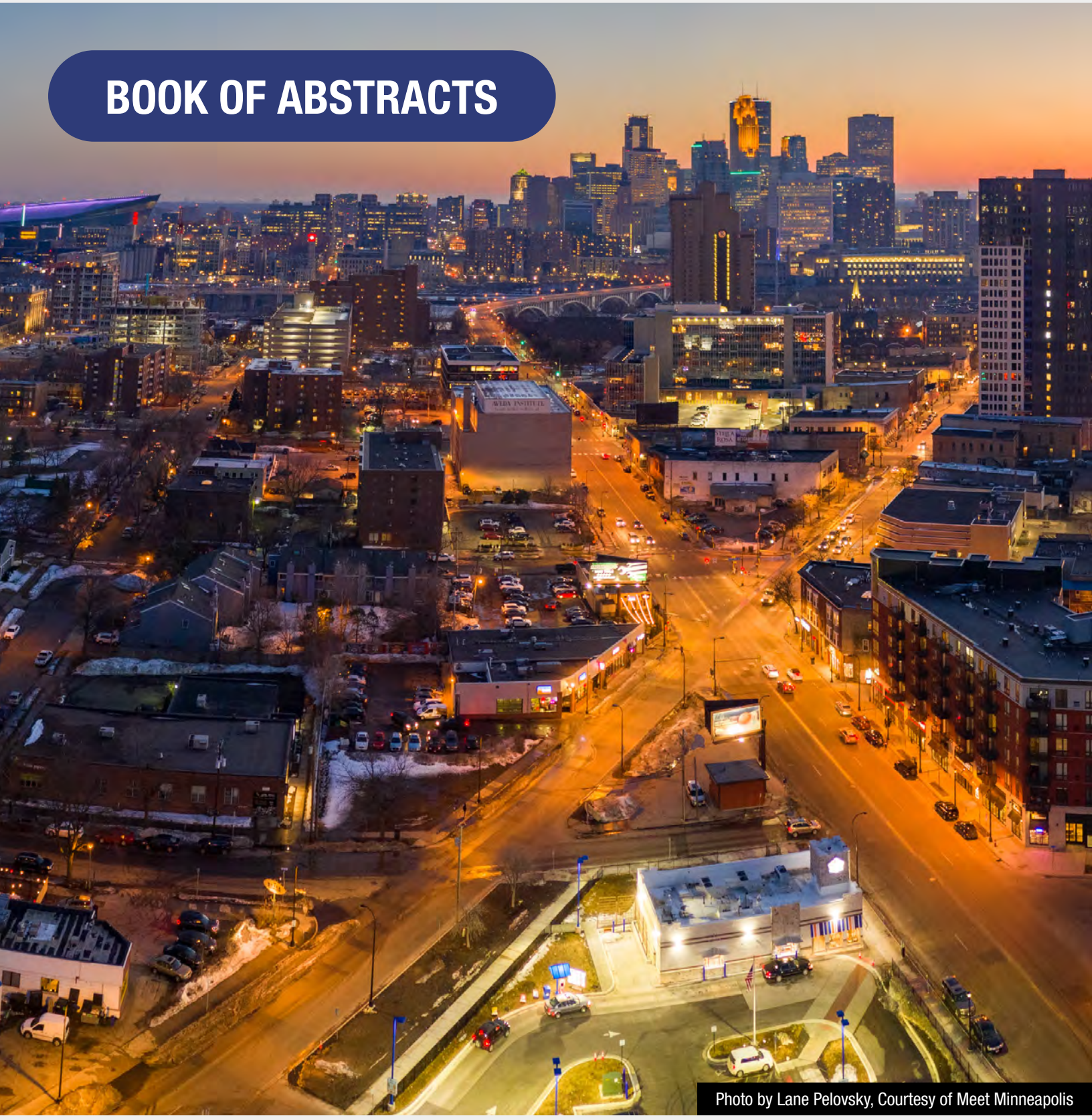

Photo by Lane Pelovsky, Courtesy of Meet Minneapolis

MMM 2022
MINNEAPOLIS, MN

Jointly sponsored by AIP Publishing LLC and the IEEE Magnetics Society

IEEE MAGNETICS

AIP Publishing

Session TU
TUTORIAL: TOWARDS 3D NANOMAGNETISM

Charudatta Phatak, Chair
Argonne National Laboratory, Lemont, IL, United States

INVITED PAPERS

TU-01. Emerging Physics in 3D Nanomagnets. *O. Fruchart*[1]
1. SPINTEC, Grenoble, France

In bulk magnetic materials, the magnetization distributions and processes are often described with effective models due to the large number of degrees of freedom involved, and the lack of knowledge of all microstructural details. Thus, reducing dimensions and dimensionality has been for decades a golden route to seek new physics and its robust understanding, such as in thin films and rather flat nanostructures. Thanks to the continuous progress of synthesis routes, characterization techniques and simulation capabilities, we now have all adequate tools to turn back to more complex objects, in the form of three-dimensional nanomagnets. Such objects combine the versatility of playing with size versus characteristic magnetic length scales, and enhanced degrees of freedom in terms of dimensionality and shape compared with flat nanostructures, opening opportunities for specific physical effects. Accordingly, in the past years the topic of 3D nanomagnets has been growing very fast. In this tutorial I will review the physics associated with these new objects, from their microscopic origin to their macroscopic manifestation. Note that many fundamental concepts had been known and often investigated theoretically in detail in the past in other contexts, yet the emergence of 3D nanomagnets in the real world revived them, allowing a finer investigation of these concepts and tuning of their practical manifestation. Most of the effects predicted and/or evidenced so far in 3D nanomagnets concern magnetization distributions and dynamics. First, I will examine the role of microscopic magnetic interactions and energies, namely magnetostatics, anisotropy and magneto-elasticity, exchange stiffness, and discuss what can be specific with these in 3D nanomagnets, influenced by the synthesis technique, curvature, dimensionality etc. Then, I will consider the scale of the entire object, two aspects specific to 3D nanomagnets. The first is the possible occurrence of volumic distribution of magnetization, giving rise to new magnetization textures: Bloch points, vortex loops; skyrmions tubes and bobbers, hopfions etc. Second is that nanomagnets come with a variety of shapes, such as cylindrical nanowires, nanotubes, bends, tores, helixes, branches and nodes, hollow structures etc, with a direct interplay with the above-mentioned magnetic objects and their dynamics. Two general physical concepts play a key role in nanomagnets. The first is topology, used in the classification of the nanomagnet shapes and magnetization textures. The second is chirality, whose importance is enhanced in 3D due to the ability of magnetization to point along all three directions, for instance in the various curling types of flux-closure configurations. Complex and sometimes competing chiral situations may arise under the interplay of curvature, real-space and magnetization chirality, and the intrinsic chirality of the LLG equation driving the precessional dynamics of magnetization. Transport in 3D nanomagnets also comes with opportunities for new physics, for instance the important role of Œrsted fields, curvature-induced symmetry breaking in spintronic effects, quantum coherence effects in circular geometries. This field is only emerging at present.

TU-02. Synthesis and Characterization of 3D Nanomagnetic Structures. *P. Fischer*[1,2] *1. LBNL, Berkeley, CA, United States; 2. UCSC, Santa Cruz, CA, United States*

An emerging research field in nanomagnetism is the scientific and technological exploration of 3-dimensional magnetic nanostructures that opens the path to exciting novel physical phenomena, originating from the increased complexity in spin textures, topology, and frustration in three dimensions. One can also anticipate a tremendous potential for novel applications with those systems in a magnetic sensor and information processing technologies in terms of improved energy efficiency, processing speed, functionalities, and miniaturization of future spintronic devices. These 3-dimensional structures, which include also 2-dimensional systems on curved surfaces are distinct from traditional bulk systems, as they harness the scientific achievements of nanomagnetism, which aimed at lowering the dimensions down to the atomic scale, but expand those now in a tailored and designed way into the third dimension [1-4]. Whereas the synthesis of 0D, 1D, and 2D nanomagnetic systems has become a mature technology, e.g., via lithography or thin film deposition techniques, e.g., molecular beam epitaxy (MBE), stepping beyond 2D magnetic systems in a tailored manner poses major challenges, particularly in terms of nanofabrication, due to the lack of standard tools for shaping and interfacing materials in 3D [5,6]. Additional, advanced characterization tools providing magnetic sensitivity to spin textures, disentangling the role of individual components in heterogeneous material at high spatial resolution, and in all three dimensions, are of large scientific interest. Advanced magnetic soft X-ray spectro-microscopies [7,8] using X-ray magnetic circular dichroism (X-MCD) as element specific, quantifiable magnetic contrast mechanism, as well as various advanced electron microscopy [9] will be key for success. This tutorial talk provides an overview of the scientific challenges and recent progress with regard to advances in synthesis approaches and state-of-the-art nanoscale characterization techniques that are prerequisite to understand, realize and control the properties, behavior, and functionalities of three-dimensional magnetic nanostructures. *Supported by U.S. DOE SC BES MSED Contr. # DE-AC02-05-CH112.*

[1] A. Fernández-Pacheco, et al. Nature Comm 8:15756 (2017) [2] P. Fischer, et al. APL Materials 8 010701 (2020) [3] R. Streubel, et al, JAP 129 210902 (2021) [4] D. Makarov and D. Sheka, Curvilinear Micromagnetism: From fundamentals to applications, Springer (2022) [5] J.D. Fowlkes, et al, ACS Appl Nano Mat 1 1028 (2018) [6] A. May et al, Comm Phys 2 13 (2019) [7] D. Sanz-Hernández, et al, ACS Nano (2020) [8] D. Donnelly et al, Nature 547 328 (2017) [9] C. Phatak et al, Curr Op in Solid State & Mat Sci 20 107 (2016)

TU-03. Novel Applications of 3D Nanomagnetism. *A. Fernández-Pacheco*[1] *1. CSIC-University of Zaragoza, Insititute of Nanoscience & Materials of Aragon, Zaragoza, Spain*

The exponential increase in number of computing devices and digital data not only poses significant challenges to The Information Technology industry, but to the future of modern society and the planet as a whole. With current computing technologies reaching their fundamental limits and their associated global energy growing to worrying levels, solutions based on denser, more efficient and better connected computing devices are required. Three dimensional nanostructures, no longer relying on purely horizontal

scaling, may play a key role in finding solutions to these challenges. In this tutorial, I will give an overview of recent advances in Three Dimensional Nanomagnetism, an emerging field devoted to the investigation and exploitation of new physical phenomena driven by 3D magnetic states [1-5]. With spin configurations and functionality not confined to a single plane anymore, but extending along the whole space, the leap to 3D brings associated great opportunities for both traditional and unconventional computing. However, moving to 3D is challenging, since the fabrication, characterization, data analysis and simulation of 3D structures is in general significantly more complicated than in standard planar systems. I will show how this new 3D paradigm starts to become possible thanks to advances in nanopatterining, chemical and physical synthesis methods, to multilayered systems with energy landscape tuned along the out-of-plane direction, to characterization techniques and computational methods devoted to probing and imaging magnetic vector fields with high sensitivity and spatial resolution. During the talk, I will review key theoretical predictions and experimental results demonstrating how the change in dimensionality results in new types of magnetic chiral interactions, new topological spin textures and defects, localized topological stray fields and unconventional spin dynamics. I will finish discussing some of the main opportunities and challenges in the field for the next few years.

[1] A. Fernández-Pacheco et al, Nature Comm. Vol. 8, p1 (2017). [2] R. Streubel et al. J. Phys. D: Appl. Phys. Vol. 49, p363001 (2016). [3] P. Fischer et al, APL Mater. Vol. 8, p010701 (2020). [4] E. Vedmedenko et al, J. Phys. D: Appl. Phys. Vol. 53, p453001 (2020). [5] D. Makarov et al, Adv. Mater. Vol. 34. p2101758 (2022).

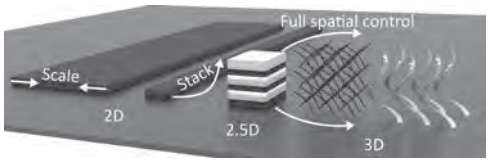

Towards 3D Nanomagnetism

Session YA
EVENING SESSION 1: MAGNETISM IN NATURE AND THE UNIVERSE

Chris Leighton, Chair
University of Minnesota, Minneapolis, MN, United States

INVITED PAPERS

YA-01. Magnetism Throughout the Universe. *B.M. Gaensler*[1,2]
1. Dunlap Institute for Astronomy and Astrophysics, University of Toronto, Toronto, ON, Canada; 2. David A. Dunlap Department of Astronomy and Astrophysics, University of Toronto, Toronto, ON, Canada

Astronomers have established that planets, stars, gas clouds, and even entire galaxies are all magnetic. Furthermore, these magnetic fields typically do not have a random, tangled, morphology, but are surprisingly organised and coherent, even on scales of millions of light years. However, the processes that create and then sustain this large scale magnetism are not yet understood, mainly because magnetic fields are not directly observable even through our most powerful telescopes. I will describe the innovative ways that astronomers have developed to make detailed measurements of
the strength and geometry of magnetic fields in distant objects throughout the Universe. These experiments have revealed extraordinary extremes of cosmic magnetism, ranging from 10-13 tesla in the depths of interstellar space, through to an incredible 1012 tesla in the cores of neutron stars. I will demonstrate some of the unique probes of cosmic evolution probed by these measurements, and will explain how in the next 5-10 years we are poised to fully open the window to the magnetic Universe.

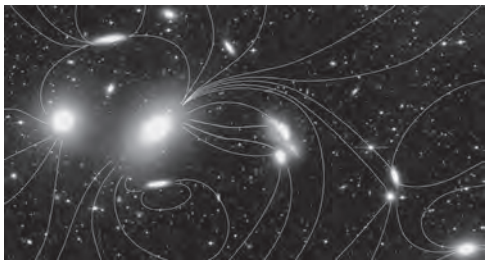

A photograph of the Virgo cluster of galaxies, with an artist's impression of one possible configuration of magnetic field lines. Credit: C. Mihos, P. Harding, J. Feldmeier, H. Morrison/Case Western Reserve University; Magnetic Field Lines: P. Huey/Science.

YA-02. Magnetism During Solar System Formation and on the Early Earth. *R. Rennan Fu*[1] *1. Department of Earth and Planetary Sciences, Harvard University, Cambridge, MA, United States*

Magnetic fields are thought to govern the dynamics of protoplanetary disks by mediating inward gas accretion and, possibly, setting up turbulent concentrations of dust to form the first planetary building blocks. A subset of these building blocks then accretes to form rocky planets, which may host a magnetic core dynamo. In the case of Earth, the crust also became partitioned into a system of mobile tectonic plates that gave rise to a biosphere. Characterizing ancient magnetic fields using rocks surviving from these early times can provide information about protoplanetary disk and dynamo physics while tracking the motion of the first continents. I will present how recent advances in paleomagnetic instrumentation based on the nitrogen vacancy color center have enabled access to complex meteorites and early Earth rocks that record magnetic fields in the protoplanetary disk and document the development of dynamos and plate tectonics on the Earth and Mars. These new techniques hold promise for challenging problems in broad areas of geomagnetism.

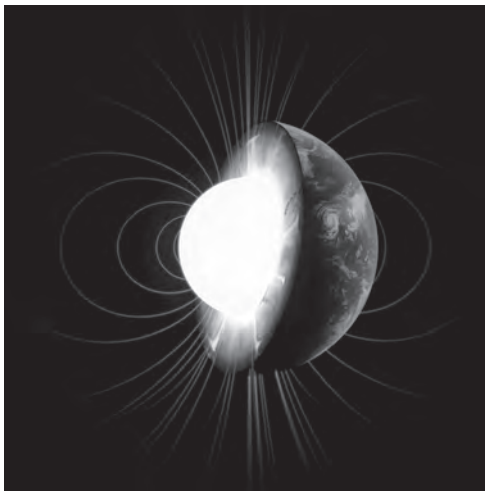

Fig. 1

Session ZA
EVENING SESSION 2: ROUNDTABLE DISCUSSION ON ADVANCED MAGNETIC MATERIALS FOR NOVEL COMPUTING PARADIGMS

Kai Liu, Chair
Georgetown University, Washington, DC, United States

INVITED PAPERS

Bio-inspired Computing Technolgies. (Invited)
D. Querlioz[1] *1. CNRS-University Paris-Saclay, Palaiseau, France*

Spin-wave Computing Technologies. (Invited)
C. Adelmann[1] *1. imec*

In-memory Computing Technologies. (Invited)
J.A. Incorvia[1] *1. University of Texas at Austin*

Session SA
2D VAN DER WAALS MAGNETS FOR PRACTICAL DEVICE APPLICATIONS

Manh-Huong Phan, Co-Chair
University of South Florida, Tampa, FL, United States
Qiming Shao, Co-Chair
The Hong-Kong University of Science and Technology, Kowloon, China

INVITED PAPERS

SA-01. Skyrmionics/Meronics in 2D Magnets for Device Engineering.
L. Balicas[1,2] 1. Physics, Florida State University, Tallahassee, FL, United States; 2. National High Magnetic Field Lab, Tallahassee, FL, United States

$Fe_{5-x}GeTe_2$ is a layered and exfoliable van der Waals (vdW) ferromagnet that displays Curie temperatures T_c ranging between 270 and 330 K, which are within a useful range for spintronic applications. Nevertheless, little is known about the interplay between topological spin textures (e.g., merons, skyrmions) and their transport properties (e.g., the topological Hall effect (THE)) which might influence the response of devices and be harvested for applications. Here, we show through a Lorentz transmission electron microscopy study in $Fe_{5-x}GeTe_2$ the coexistence of merons and anti-meron pairs with Néel skyrmions and antiskyrmions over a broad range of temperatures upon approaching a magneto-structural transition. We measured the THE associated to both types of spin textures finding that it is affected by their coexistence being measureable at room temperature and beyond [1]. Remarkably, we also observe a sizeable unconventional THE for currents and magnetic fields aligned along a planar direction, a configuration that is insensitive to the Lorentz force [2]. We attribute this to carrier interaction with magnetic field-induced chiral spin textures. Given that the Curie temperature of $Fe_{5-x}GeTe_2$ can be increased via either Ni [3] or Co [4] doping, we conclude that 2D centro-symmetric vdW magnets are ripe for the exploration of their possible applications in skyrmionics/meronics [5] and also of new hybrid spin quasiparticles as well as their possible manipulation via external stimuli such as current and light. Our results suggest that unconventional topological spin textures (that is, those distinct from merons or skyrmions) might exist in atomically thin vdW layers whose properties have yet to be unveiled.

[1] Brian W. Casas, Yue Li, Alex Moon *et al*., Room temperature unconventional topological Hall response in a van der Waals ferromagnet driven by meron-antimeron pairs (unpublished) [2] Juan Macy, Danilo Ratkovski, Purnima P. Balakrishnan *et al.*, Magnetic field-induced non-trivial electronic topology in $Fe_{3-x}GeTe_2$, Appl. Phys. Rev. 8, 041401 (2021). [3] Xiang Chen, Yu-Tsun Shao, Rui Chen *et al*., Pervasive beyond Room-Temperature Ferromagnetism in a Doped van der Waals Magnet, Phys. Rev. Lett. 128, 217203 (2022). [4] Hongrui Zhang, David Raftrey, Ying-Ting Chan *et al*., Room-temperature skyrmion lattice in a layered magnet $(Fe_{0.5}Co_{0.5})_5GeTe_2$, Sci. Adv.8, eabm7103 (2022). [5] Hamed Vakili, Jun-Wen Xu, Wei Zhou *et al.*, Skyrmionics—Computing and memory technologies based on topological excitations in magnets, J. Appl. Phys. 130, 070908 (2021).

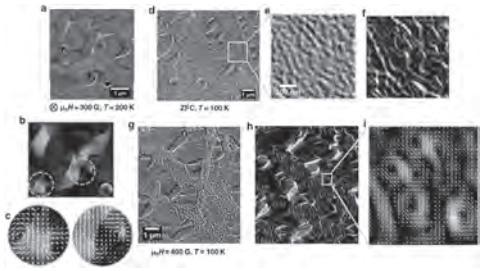

Lorentz transmission electron microscopy study of $Fe_{5-x}GeTe_2$, revealing the coexistence of merons - antimeron pairs with skyrmions - antiskyrmion pairs upon approaching its magnetostructural transition.

SA-02. Towards domain-wall devices with 2D van der Waals magnets.
E.J. Santos[1,2] 1. School of Physics and Astronomy, The University of Edinburgh, Edinburgh, United Kingdom; 2. Higgs Centre for Theoretical Physics, The University of Edinburgh, Edinburgh, United Kingdom

The family of 2D compounds has grown almost exponentially since the discovery of graphene and so too the rapid exploration of their vast range of electronic properties. Some family members include superconductors, Mott insulators with charge-density waves, semimetals with topological properties, and transition metal dichalcogenides with spin-valley coupling[1]. Among several compounds, the realization of long-range ferromagnetic order in van der Waals (vdW) layered materials has been elusive till very recently. Long searched but only now discovered 2D magnets are one of the select group of materials that retain or impart strongly spin correlated properties at the limit of atomic layer thickness. In this presentation I will discuss how different layered compounds (e.g., CrX_3 (X=F, Cl, Br, I), VI_3, $MnPS_3$, Fe_3GeTe_2, $FePS_3$, $CrGeTe_3$) can provide new playgrounds for exploration of spin correlations involving quantum-effects, topological spin-excitations and higher-order exchange interactions. I will show that this new generation of vdW magnets can help to revolutionize several technological domain wall applications from sensing to data storage, which can lead to new magnetic, magnetoelectric and magneto-optic applications in industry[2,3,4,5]. Moreover, I will discuss some challenges at the forefront of 2D vdW magnets and new opportunities to understand fundamental problems.

1. Q. Wang *et al. ACS Nano* 16, 6960 (2022). 2. D. Wahab *et al.* Adv. Mater. 33, 2004138 (2021). 3. D. Wahab *et al. Appl. Phys. Rev.* 8, 041411 (2021). 4. M. Alliati *et al. npj Comput. Mater.* 8, 3 (2022). 5. J. Macy *et al.,* Appl. Phys. Rev. 8, 041401 (2021).

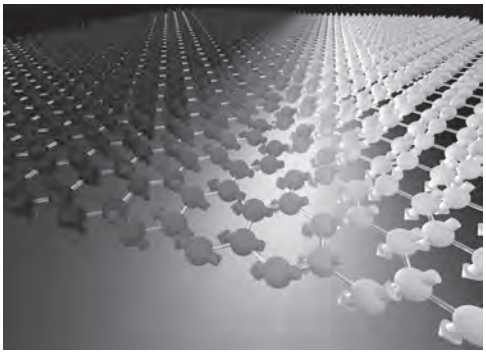

Magnetic domain wall observed in CrI_3 magnets at low temperatures and no applied magnetic fields. Dark (bright) areas correpond to spins of different orientations with the region between them changing colour accordingly to the wall configuration.

SA-03. Electrical control and spin orbit torques in van der Waals layered magnets. *H. Kurebayashi*[1], I. Verzhbitskiy[2], S. Khan[1], H. Cheng[2], J. Zhou[2], Y. Feng[2] and G. Eda[2] *1. London Centre for Nanotechnology, University College London, London, United Kingdom; 2. Department of Physics, National University of Singapore, Singapore*

Since the discovery of magnetism stabilised in a few monolayer of exfoliated van der Waals (vdW) systems [1,2], vdW magnetic materials have attracted a great deal of interest in the field of 2D materials and spintronics. These materials could potentially offer opportunities for generating novel interfacial-driven magnetism and spin transport. For example, the layered crystalline structure and vdW gap provide intrinsic electron tunnelling barrier which can be exploited as a spin-filtering barrier [3,4] to produce a large magnetoresistance. The crystalline symmetry of vdW systems is intrinsically low, which promises an exciting playground to explore novel spin-orbit torque (SOT) phenomena [5]. These intrinsic bulk properties can be further enriched by making monolayer vdW layers as well as their heterostructures, in which additional lowering of their symmetries at interfaces might produce unexplored transport effects. In this talk, we will present our recent work on electric control of magnetism (Curie temperature and magnetic anisotropy) in $Cr_2Ge_2Te_6$(CGT) [6]. The ungated electrically-insulating nature of CGT has been drastically modified by electric field, making it be a metallic conductor with the 2D carrier density of $4*10^{14}$ [cm^{-2}]. This allows us to probe the gated CGT films by magneto-transport, by which to quantify the magnetic parameters as a function of applied voltage. We found that the Curie temperature is significantly enhanced by140 K and that the easy axis of two-fold perpendicular anisotropy becomes the hard axis. The Curie temperature enhancement can be understood by the carrier-mediated double exchange mechanism. We will also discuss the allowed symmetry of spin-orbit torques (SOTs) in vdW materials, followed by our measured SOTs in the gated CGT devices.

[1] Gong et al. Nature 546 265 (2017). [2] Huang et al., Nature 546, 270 (2017). [3] Klein et al., Science 360, 1214 (2018). [4] Song et al., Science 360, 1218 (2018). [5] H. Kurebayashi et al., Nat. Rev. Phys. 4,150 (2022). [6] Verzhbitskiy et al., Nature Electron. 3, 460 (2020).

SA-04. Toward room-temperature MRAM devices with wafer-scale 2D Magnets. *T. Nie*[1] *1. School of Integrated Circuit Science and Engineering, Beihang University, Beijing, China*

To date, despite the continuous improvement of integrated circuit manufacturing technology, the scaling of device has encountered the bottlenecks of low reliability and high-power consumption, due to the quantum effect limitation. The "Moore's Law" that has lasted for nearly 50 years in the microelectronics industry will not be sustainable. The advent of two-dimensional (2D) materials may bring new opportunities to be out of current dilemmas[1]. Among them, 2D magnets exhibit a variety of fascinating electrical, optical and magnetic properties in the atomic level, which may initiate new application in information processing, magnetic memory and other technologies. However, only a few 2D ferromagnetic materials have been synthesized, and long-range ferromagnetic order was usually suppressed within a limited temperature range. The large-scale production and control of room-temperature ferromagnetism in 2D magnetic materials are the focus at current stage. Herein, wafer-scale 2D magnet of $Fe_{3+x}GeTe_2$ (FGT) was successfully achieved by MBE[2]. Combined with topological insulator of Bi_2Te_3, room-temperature ferromagnetism was demonstrated through the interface engineering effect. Based on this, SOT switching of ferromagnetism in an all-vdW heterojunction was achieved at room temperature, and the critical switching current was almost one order of magnitude lower than previous studies. Furthermore, ultrafast terahertz spin current pumped by femtosecond laser was probed by terahertz time-domain spectroscopy in such all-vdW heterostructure, which provides a potential way for ultrafast magnetization control[3]. The exploration of 2D magnet with high Curie temperature and further fabrication of novel 2D spintronic devices operating at room temperature will be an important step towards the practical application, thus promoting the extension of Moore's Law.

1. Li, M. Y.; Su, S. K.; Wong, H. S. P.; et al, How 2D semiconductors could extend Moore's law. *Nature* 2019, *567* (7747), 169-170. 2. Wang, H.; Liu, Y.; Wu, P.; et al, Above Room-Temperature Ferromagnetism in Wafer-Scale Two-Dimensional van der Waals Fe3GeTe2 Tailored by a Topological Insulator. *Acs Nano* 2020. 3. Chen, X.; Wang, H.; Liu, H.; et al, Generation and Control of Terahertz Spin Currents in Topology-Induced 2D Ferromagnetic Fe3GeTe2|Bi2Te3 Heterostructures. *Adv Mater* 2021, *34*, 2106172.

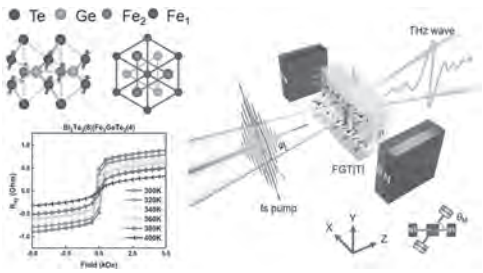

Anomalous Hall effect shows the ferromagnetism above room temperature; Illustration of terahertz emission spectrum from 2D heterostructure

SA-05. Emergent phenomena and device applications of 2D magnetic heterostructures. *G. Bian*[1] *1. Department of Physics and Astronomy, University of Missouri, Columbia, MO, United States*

In this talk, we will discuss the fabrication of ultra-thin vdWs magnet $CrTe_2$ layers and prototypical spintronic devices, which can be tuned by the electrical field, the magnetic field as well as the substrate. We will review recent experimental progress on $CrTe_2$ including (1) robust 2D ferromagnetism in $CrTe_2$ ultrathin films; (2) topological Hall effects in $CrTe_2/Bi_2Te_3$ heterostructures; and (3) giant magnetoresistance in chemically doped $CrTe_2$ compound.

(1) Xiaoqian Zhang, Qiangsheng Lu, Wenqing Liu, Wei Niu, Jiabao Sun, Jacob Cook, Mitchel Vaninger, Paul. F. Miceli, David J. Singh, Shang-Wei Lian, Tay-Rong Chang, Xiaoqing He, Jun Du, Liang He, Rong Zhang, Guang Bian, and Yongbing Xu, "Room-temperature intrinsic ferromagnetism in epitaxial CrTe2 ultrathin films", Nature Communications 12:2492 (2021) (2) Xiaoqian Zhang, Siddhesh C Ambhire, Qiangsheng Lu, Wei Niu, Jacob Cook, Jidong Samuel Jiang, Deshun Hong, Laith Alahmed, Liang He, Rong Zhang, Yongbing Xu, Steven S-L Zhang, Peng Li, and Guang Bian, "Giant Topological Hall Effect in van der Waals Heterostructures of $CrTe_2/Bi_2Te_3$," ACS Nano 15, 15710 (2021) (3) Xiaoqian Zhang, Wenqing Liu, Wei Niu, Qiangsheng Lu, Wei Wang, Ali Sarikhani, Chunhui Zhu, Jiabao Sun, Mitchel Vaninger, Paul. F. Miceli, Jianqi Li, David J. Singh,

Yew San Hor, Liang He, Rong Zhang, Guang Bian, Dapeng Yu, and Yongbing Xu, “Self-Intercalation Tunable Interlayer Exchange Coupling in a Synthetic Van der Waals Antiferromagnet,” Advanced Functional Materials, 202202977 (2022)

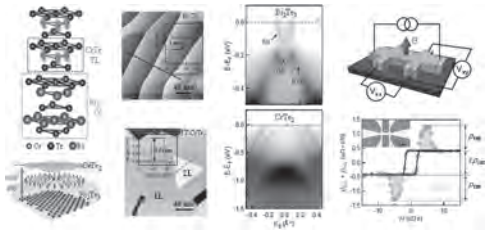

Session SB
RECENT DEVELOPMENTS IN ADVANCED MAGNETIC TUNNEL JUNCTIONS

Daniel B. Gopman, Chair
National Institute of Standards and Technology, Gaithersburg, MD, United States

INVITED PAPERS

SB-01. Magnetic tunnel junction in modern computing. *J.Z. Sun*[1]
1. IBM Research, Yorktown Heights, NY, United States

Spin-transfer-torque switchable magnetic tunnel junction is an enabling device that brought the recent technology and product offerings of spin-transfer-torque magnetic random access memory. I'll review some current understanding, with an emphasis on device and materials physics underpinning switching performance in memory technologies, and the likely requirements for future generations in related applications space[1-3]. Key considerations include switching current, speed, and data-retention trade-off, and the need to seek more efficient charge-to-spin conversion mechanisms. Finally, I will touch on some nascent applications ideas involving the magnetic tunnel junction as a compact and power-efficient CMOS backend-compatible entropy source for probabilistic computing, and the device physics related to sub-nanosecond stochastic bit-stream generation[4], with potential applications in computing schemes beyond von Neumann architecture.

1. Jonathan Z Sun, "Spin-transfer torque switched magnetic tunnel junction for memory technologies", J. Magn. Magn. Mater. https://doi.org/10.1016/j.jmmm.2022.169479 (2022). 2. Christopher Safranski, Jonathan Z. Sun, and Andrew D. Kent, "A perspective on electrical generation of spin current for magnetic random-access memories", Appl. Phys. Lett. Perspectives, Appl. Phys. Lett. 120, 160502 (2022). 3. G. Hu, G. Lauer, J. Z. Sun, P. Hashemi, C. Safranski, S. L. Brown, L. Buzi, E. R. J. Edwards, C. P. D' Emic, E. Galligan, M. G. Gottwald, O. Gunawan, H. Jung, J. Kim, K. Latzko, J. J. Nowak, P. L. Trouilloud, S. Zare, and D. C. Worledge, "2X reduction of STT-MRAM switching current using double spin-torque magnetic tunnel junction", 2021 IEEE Intl. Elect. Dev. Meeting (IEDM), 2.5.1, (2021). 4. Christopher Safranski, Jan Kaiser, Philip Trouilloud, Pouya Hashemi, Guohan Hu, and Jonathan Z. Sun, "Demonstration of nanosecond operation in stochastic magnetic tunnel junctions", Nano Letters 21, 2040 (2021).

SB-02. Energy efficient switching in magnetic tunnel junctions. *W. Wang*[1] *1. Physics, University of Arizona, Tucson, AZ, United States*

Magnetic tunnel junctions (MTJ) are the core components of magnetic random access memory (MRAM) and spin-logic devices. For memory applications, it is highly desirable to have large tunneling magnetoresistance (TMR), strong retention, low switching energy simultaneously realized in a sub-10nm MTJ. Here we present our recent study in increasing TMR and reducing switching energy in MTJ with perpendicular magnetic anisotropy (pMTJs). With a multiple-interface free layer structure, where more than one CoFeB and heavy metal layers are incorporated in the free layer of the pMTJs, TMR above 200% as well as a strong perpendicular magnetic anisotropy have been achieved. Large TMR has also been obtained in pMTJs with MgAlOx barrier, which is promising to be used with new ferromagnetic materials (particularly those with reduced damping compared to CoFeB) whose lattice doesn't match with MgO. Finally, we will present our effort in switching the pMTJs with the voltage controlled magnetic anisotropy (VCMA) effect. Though a remote doping effect of heavy elements such as Ir, energy efficient switching (as low as a few fJ) has been achieved in the pMTJs. This research is supported by NSF, DARPA and SRC.

SB-03. Strategies for Enhancing the Speed and Switching Efficiency of Three-Terminal Magnetic Tunnel Junctions. *V. Krizakova*[1]
1. Department of Materials, ETH Zurich, Zürich, Switzerland

Spin-orbit torques (SOT) provide a versatile tool to manipulate the magnetization of diverse classes of materials and devices using electric currents, leading to novel spintronic memory and computing approaches. In parallel to spin transfer torques (STT), which are presently employed in leading non-volatile memory technologies, SOT can broaden the scope of current-induced magnetic switching to applications that run close to the clock speed of the central processing unit and unconventional computing architectures [1]. SOT-switching in three-terminal magnetic tunnel junctions (MTJs) is realized by an in-plane current that flows separately from the reading path, thus reducing the read disturb errors and lifting the restrictions on switching speed. On the other hand, SOT brings new challenges related to device footprint reduction, integration-friendly field-free switching, increase of the thermal budget, and reduction of the writing current. Over a decade of development, much improvement in tackling these challenges has been made by material engineering, new device geometries, as well as designs combining SOT with other current- and voltage-induced effects. Here I will present an overview of the insights into different strategies to switch perpendicularly magnetized MTJs, gained from the combination of real-time and post-pulse electrical measurements and micromagnetic simulations [2,3]. We use devices fabricated by a CMOS-compatible process [4], and we study the magnetization reversal under different SOT current and field configurations, or during simultaneous injection of current pulses across the SOT track and the MTJ pillar [Fig. 1(a)]. Our results unravel the relative impact of the effects generated by the MTJ bias – STT, voltage control of magnetic anisotropy, and self-heating – on the switching characteristics and provide a detailed understanding of how these effects concur in the switching process [5]. Such dual-pulse switching is relevant for the optimization of SOT-MTJs as it allows for field-free operation, reduced incubation delay and dispersion of switching events [Fig. 1(b)], as well as reducing the writing energy relative to switching by SOT or STT alone on the sub-nanosecond scale. Moreover, I will show how the fieldlike SOT can be exploited to tune the efficiency and reliability of the switching. Finally, I will present device designs that allow for selectively addressing MTJs sharing the same SOT track, by the alignment of the current relative to an in-plane magnetic field. This approach can be used to create multi-bit memories with reduced footprint or efficient generation and adjustment of synaptic weights.

[1] V. Krizakova, M. Perumkunnil, S. Couet, P. Gambarella and K. Garello, J. Magn. Magn. Mater. (2022) [2] E. Grimaldi, V. Krizakova, G. Sala, *et al*., Nat. Nanotech. Vol. 15, p.111 (2020) [3] V. Krizakova, K. Garello, E. Grimaldi, G. S. Kar and P. Gambardella," Appl. Phys. Lett. Vol. 116, p.232406 (2020) [4] K. Garello, F. Yasin, H. Hody, *et al*., IEEE Symp. VLSI Technol., T194-195 (2019) [5] V. Krizakova, E. Grimaldi, K. Garello, *et al.*, Phys. Rev. Appl. Vol. 15, p.054055 (2021)

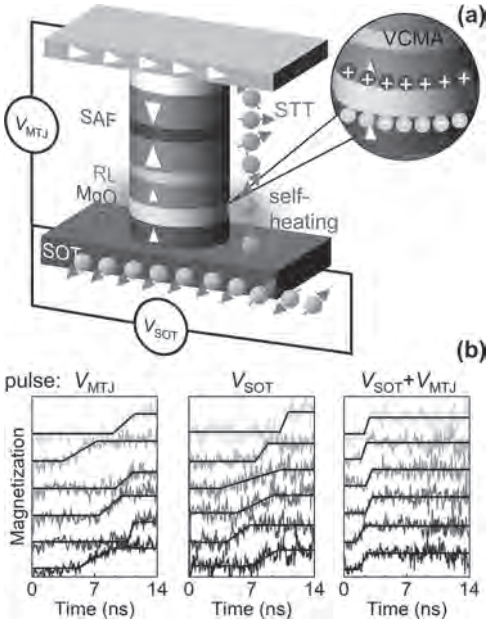

Fig. 1. (a) Schematics of a three-terminal MTJ device and the effects induced by voltage applied across the MTJ (V_{MTJ}) and on the SOT track (V_{SOT}). (b) Evolution of the magnetization in the MTJ upon application of V_{MTJ}, V_{SOT}, and their combination.

SB-04. Perpendicular Magnetic Tunnel Junctions with Crystalline Anisotropy and Energy-efficient Switching of Synthetic Antiferromagnet pMTJs by voltage-controlled exchange coupling and Spin-Orbit-Torque. *J. Wang*[1], D. Zhang[1], B.R. Zink[1], M. Bapna[2], W. Jiang[1], D. Sousa[1], Y. Liao[3], Z. Zhao[1], Y. Lv[1], P. Sahu[1], D. Lyu[1], H. Li[1], O. Benally[1], A. Naeemi[3], D.B. Gopman[4], S. Majetich[2] and T. Low[1]
1. University of Minnesota, Minneapolis, MN, United States; 2. Carnegie Mellon University, Pittsburg, PA, United States; 3. Georgia Institute of Technology, Atlanta, GA, United States; 4. NIST, Gaithersburg, MD, United States

In this talk, we first report the roadmap and development of advanced perpendicular magnetic tunnel junctions based on low-damping magnetic materials with crystalline anisotropy that can be scaled down to sub-3-nm diameter with 10 years' retention time [1]. Then, we will present the perpendicular magnetic tunnel junctions (p-MTJs) switched utilizing bipolar electric fields. Traditional voltage-controlled magnetic anisotropy only linearly lowers the energy barrier of ferromagnetic layer via electric field effect and efficiently switches p-MTJs only with a unipolar behavior. Here we propose and demonstrate a bipolar electric field effect switching of 100-nm p-MTJs through voltage-controlled exchange coupling (VCEC) [2]. The switching current density, ~1.1×10^5 A/cm^2, is one order of magnitude lower than that of the best-reported spin-transfer torque devices. Theoretical results suggest that electric field induces a ferromagnetic-antiferromagnetic exchange coupling transition and generates a field-like interlayer exchange coupling torque, which cause the bidirectional magnetization switching. We will further report our recent results to switch the p-MTJs using the interplay of SOT and VCEC, which lowers the VCEC switching current density to ~5×10^3 A/cm^2[3]. These results could eliminate the major obstacle in the development of spin memory devices beyond their embedded applications. This technology can be used directly for the future spin-orbit-torque (SOT) MRAM [3] and spin logic devices [4].

[1] D. Zhang, et al, Phys. Rev. Applied, (2018) vol. 9, 044028 [2] D. Zhang, et al, Nano Letters (2022), doi.org/10.1021/acs.nanolett.1c03395 [3] B. Zink, et al, Advanced Electronic Materials, (2022), DOI: 10.1002/aelm.202200382 [4] M. Mankalale, et al, IEEE Journal on Exploratory Solid-State Computational Devices and Circuits, 3 (2017) 27-36; 10.1109/JXCDC.2017.2690629

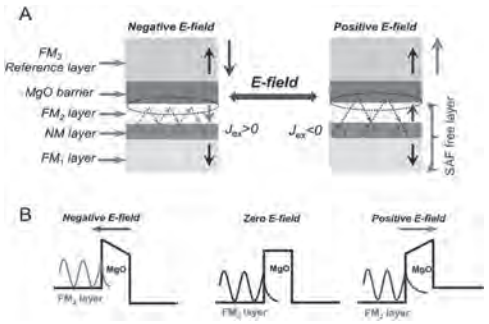

Fig. 1. (A) The IEC between FM_1 and FM_2 layers of the SAF free layer can be altered the FM-AFM exchange coupling transition under the applied E-field. (B) The VCEC originates from changes in the reflectivity of the NM/FM_2 interface influenced by the FM_2/MgO interface. The electron wave functions can penetrate the MgO tunnel barrier, modulating the reflection phases of two-electron spins (spin-up and spin-down) and the penetration length by the applied E-field, then inducing a FM-AFM exchange coupling transition.

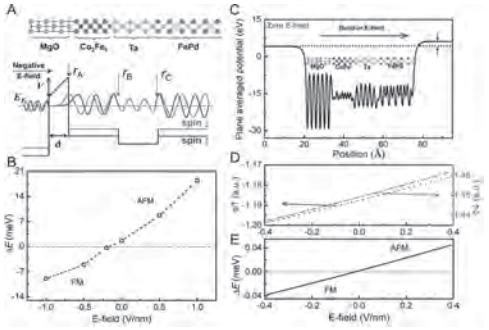

Fig.2. Voltage-controlled exchange coupling (VCEC). (A) top, Schematic of the simulation structure with a SAF stack of FePd/Ta/Co_2Fe_6 (CoFe)/MgO (top panel) which is comparable to the experimental SAF structure. (A) bottom, Schematic of the energy diagram of the SAF structure (bottom panel). (B) ΔE (IEC) vs. E-field for the FePd/Ta/CoFe/MgO SAF structure calculated by DFT. (C) An intrinsic built-in voltage potential generates the built-in E-field due to interaction at the MgO/CoFe interface, which plays a very critical role for the E-field induced AFM-FM exchange coupling transition. (D) Modified electronic density of states in the spacer layer through quantum interferences leading to a controllable transition between FM and AFM exchange couplings. (E) IEC as a function of the applied voltage.

SB-05. MTJ device physics and technologies toward deeply scaled STT-MRAM and probabilistic-computing applications. *S. Fukami*[1]
1. Tohoku University, Sendai, Japan

Magnetic tunnel junction (MTJ) serves as functional devices for various applications, e.g., magnetic field sensor, nonvolatile memory, and probabilistic computing. In this talk, the MTJ device physics and technologies for future deeply scaled nonvolatile memory and probabilistic computing will be discussed. The nonvolatile memory, so-called the magnetoresistive random access memory utilizing the spin-transfer torque-induced magnetization switching (STT-MRAM), has been commercialized recently with the MTJ size of several tens of nanometer. To apply for deeply scaled semiconductor generation in future, it is crucial to establish a technology to exhibit the high performance at ultrasmall length scale down to less than 10 nm, or X nm. We have shown that utilization of shape anisotropy [1] and magneto-static coupling [2] which become evident in X-nm regime allows the MTJs to meet the requirements for Flash-like [2] and SRAM-like [3] applications. Contrary to the nonvolatile applications, MTJ can also function as a random number generator utilizing the thermal fluctuation of magnetization.

Application of the thermally unstable stochastic MTJ for probabilistic computers was proposed [4] and a proof-of-concept was shown using eight perpendicular easy-axis MTJs with the fluctuation timescale of millisecond [5]. To realize large-scale computers that surpass classical computers for some specific complex tasks, reduction of the fluctuation timescale is indispensable. We have found that the fluctuation timescale is governed not only by the energy barrier but also by the energy landscape of magnetic anisotropy [6] and nanosecond fluctuation was observed in a sophisticatedly engineered in-plane easy-axis MTJ [7]. The work has been carried out in collaboration with H. Ohno, B. Jinnai, J. Igarashi, S. Kanai, W. A. Borders, K. Hayakawa, K. Kobayashi of Tohoku University as well as S. Datta of Purdue University and K. Y. Camsari of the UC Santa Barbara. The work is supported in part by the JST-OPERA JPMJOP1611, JST-CREST JPMJCR19K3, and JSPS KAKENHI 19H05622.

[1] K. Watanabe *et al.*, Nat. Commun. 9, 663 (2018). [2] B. Jinnai *et al.*, IEDM2020, 24.6.1 (2020). [3] B. Jinnai *et al.*, IEDM2021, 2.6.1 (2021). [4] K. Y. Camsari *et al.*, Phys. Rev. X 7, 031014 (2017). [5] W. A. Borders *et al.*, Nature 573, 390 (2019). [6] S. Kanai *et al.*, Phys. Rev. B 103, 094423 (2021). [7] K. Hayakawa *et al.*, Phys. Rev. Lett. 126, 117202 (2021).

Session SC
IMAGING MAGNETIC TEXTURES AT THE NANOSCALE

Peter Simon Rickhaus, Chair
Qnami AG, Muttenz, Switzerland

INVITED PAPERS

SC-01. Topological Defects in a multiferroic Antiferromagnet.
A. Finco[1], A. Haykal[1], S. Fusil[2], P. Kumar[1], P. Dufour[2], A. Forget[3], D. Colson[3], J. Chauleau[3], M. Viret[3], N. Jaouen[4], V. Garcia[2] and V. Jacques[1]
1. Laboratoire Charles Coulomb, Université de Montpellier and CNRS, Montpellier, France; 2. Unité Mixte de Physique, CNRS, Thales, Université Paris-Saclay, Palaiseau, France; 3. SPEC, CEA, CNRS, Université Paris-Saclay, Gif-sur-Yvette, France; 4. Synchrotron SOLEIL, Gif-sur-Yvette, France

We report on the study of the cycloidal antiferromagnetic state in bulk single crystals of the multiferroic bismuth ferrite using a combination of real-space and reciprocal magnetic imaging techniques [1]. We first discuss the origin of the magnetic stray field allowing us to image the cycloidal modulation of the antiferromagnetic state. This stray field is produced by the small uncompensated moment arising from the spin density wave which is locked to the cycloid [2]. We then use scanning NV center magnetometry to image the magnetic texture, with additional resonant X-ray diffraction measurements to obtain a larger scale insight. We observe the unexpected coexistence inside a single ferroelectric domain of magnetic domains hosting different cycloid wavevectors. We show that the direction of these wavevectors is not strictly locked to the preferred crystallographic axes as continuous rotations bridge different wavevectors. Making profit of the nanoscale spatial resolution of scanning NV-center magnetometry, we show that topological defects form at the junction between the magnetic domains. These defects are identical to those found in a broad variety of lamellar physical systems with rotational symmetries (liquid crystals, magnetic helix [3], ferromagnetic garnets, copolymers, etc.). The presence of these objects in such a multiferroic antiferromagnet offers new opportunities in terms of robustness and electrical control towards their use in spintronic devices.

[1] Finco et al, Phys. Rev. Lett. 128, 187201 (2022) [2] Ramazanoglu et al, Phys. Rev. Lett. 107, 207206 (2011) [3] Schönherr et al, Nat. Phys. 14, 465 (2018)

SC-02. Pulling Magnetic Skyrmions out of Thin Air.
G. Chen[1,2], C. Ophus[3], R. Lo Conte[4,5], A. Quintana[1], H. Kwon[6], G. Yin[1], C. Won[7], H. Ding[8], R. Wiesendanger[5], Y. Wu[9], A. Schmid[3] and K. Liu[1,2]
1. Georgetown University, Washington, DC, United States; 2. University of California, Davis, Davis, CA, United States; 3. Lawrence Berkeley National Laboratory, Berkeley, CA, United States; 4. University of California, Berkeley, Berkeley, CA, United States; 5. University of Hamburg, Hamburg, Germany; 6. Korea Institute of Science and Technology, Seoul, The Republic of Korea; 7. Kyung Hee University, Seoul, The Republic of Korea; 8. Nanjing University, Nanjing, China; 9. Fudan University, Shanghai, China

Magnetic skyrmions are topologically nontrivial spin textures with envisioned applications in energy-efficient magnetic information storage [1,2]. Toggling the presence of magnetic skyrmions via writing/deleting processes is essential for spintronics applications, which usually requires a magnetic field, current injection, electric field, laser pulse, or thermal excitation [3,4]. A key challenge is to directly image such ultrasmall spin textures in order to confirm their topological character. Using spin-polarized low-energy electron microscopy (SPLEEM), we have demonstrated a new, field-free method to write/delete magnetic skyrmions at room temperature, via hydrogen chemisorption/desorption cycles on Ni/Co/Pd/W(110) [5]. The spin structures of the written skyrmions are resolved to be hedgehog Néel-type via magnetization vector mapping using SPLEEM (Fig. 1). Supported by Monte-Carlo simulations, the skyrmion creation/annihilation is attributed to the hydrogen-induced magnetic anisotropy change on ferromagnetic surfaces. The roles of hydrogen and oxygen on magnetic anisotropy and skyrmion deletion on other magnetic surfaces are also demonstrated. In another study, we focus on the interfacial Dzyaloshinskii-Moriya interaction (DMI), which stabilizes magnetic chirality with preferred handedness. Experimentally, controlling the handedness is crucial to tune the efficiency of current-induced manipulation of spin texture. This is conventionally achieved by stacking asymmetric multilayers where the thickness of each layer is at least a few monolayers. We observed an ultrasensitive chirality switching in $(Ni/Co)_n$ multilayer induced by capping only 0.22 monolayer of Pd [6]. Using SPLEEM, we monitor the gradual evolution of domain walls from left-handed to right-handed Néel walls and quantify the DMI induced by the Pd capping layer (Fig. 2). We also observe the chiral evolution of a skyrmion during the DMI switching, where no significant topological protection is found as the skyrmion winding number varies. This corresponds to a minimum energy cost of < 1 attojoule during the skyrmion chirality switching. These results open up new opportunities for designing energy-efficient skyrmionic and magneto-ionic devices. They also illustrate the effectiveness of SPLEEM in resolving magnetization vector in chiral spin textures with high spatial resolution. This work has been supported in part by the NSF (DMR-2005108), SRC/NIST SMART Center and US DOE.

[1] R. Wiesendanger, Nat. Rev. Mater. 1, 16044 (2016). [2] A. Fert, et al. Nat. Rev. Mater. 2, 17031 (2017). [3] W. Jiang, et al. Phys. Rep. 704, 1-49 (2017). [4] X. Zhang, et al. J. Phys.: Condens. Matter 32, 143001 (2020). [5] G. Chen, *et al*. Nat. Commun. 13, 1350 (2022). [6] G. Chen, *et al. Nano Lett.,* in press; arXiv: 2206.12069.

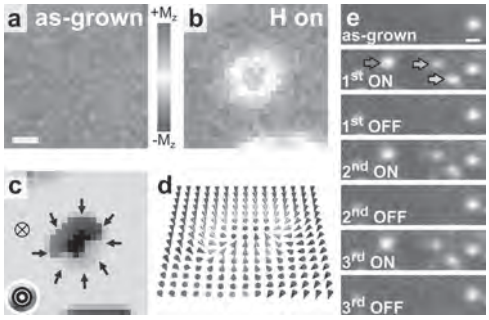

Figure 1. Hydrogen-induced reversible writing/deleting of skyrmions. (a,b) SPLEEM image of Ni/Co/Pd/W(110) on a local -M_z domain, before/after the hydrogen exposure, showing hydrogen-induced skyrmion creation. Scale bar is 100 nm. (c) Compound SPLEEM image resolving the bubble-like domain in panel b as a skyrmion. Black/light gray represent +M_z/-M_z domains (see symbols), respectively, and color wheel shows in-plane magnetization direction within domain walls (also shown by black arrows). (d) Experimentally determined arrow-array representation of panel c. (e) SPLEEM images showing reversible skyrmion writing/deleting over three hydrogen on/off cycles (indicated by the arrows), scale bar is 200 nm.

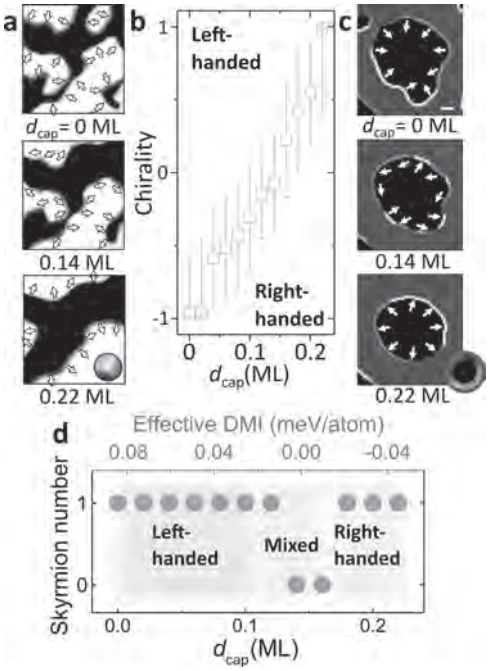

Figure 2. The chirality and skyrmion number evolution induced by sub-monolayer Pd capping layer. (a) Compound SPLEEM images of (Ni/Co)n/Pd/W(110) with various Pd capping layer thickness d_{cap}, showing a gradual chirality switching from left- to right-handedness. Black/white (or gray in panel c) represent +M_z/-M_z domains, respectively, and color wheel shows in-plane magnetization direction within domain walls (also shown by arrows). (b) The quantified chirality varies as a function of d_{cap}. (c) The compound SPLEEM images highlighting the chirality evolution of a skyrmion bubble. (d) d_{cap} / DMI-dependent skyrmion number evolution.

SC-03. Cooperative growth of macrospin and vortex chains in Artificial Spin-Vortex Ice nanomagnetic arrays. *W.R. Branford*[1], J.C. Gartside[1], K.D. Stenning[1], A. Vanstone[1], T. Dion[2], H.H. Holder[1], D.M. Arroo[3], F. Caravelli[4], M. Saccone[4] and H. Kurebayashi[5] *1. Physics, Imperial College London, London, United Kingdom; 2. Kyushu University, Kyushu, Japan; 3. Materials, Imperial Collge London, London, United Kingdom; 4. Los Alamos National Laboratory, Los Alamos, NM, United States; 5. London Centre for Nanotechnology, University College London, London, United Kingdom*

The frustrated interactions in nanomagnetic arrays can lead to the emergence of complex behaviour. Here we consider nanomagnets with dimensions on the crossover from single ferromagnetic domain (macrospin) and vortex states [1-3], in both ordered and disordered array geometries. Magnetic force microscopy reveals that there is a ratchet-like transformation of macrospins into vortices, during minor loop magnetic reversals. Simulations show that interactions with neighbouring magnets play an important role, giving cooperative growth of macrospin and vortex chains. This gradual evolution of linkages is neuromorphic in character, and interesting for both neurally-inspired computation [1] and self-assembly of magnonic circuits[3].

[1]Gartside, Jack C., et al. "Reconfigurable Training and Reservoir Computing via Spin-Wave Fingerprinting in an Artificial Spin-Vortex Ice." Nature Nanotechnology (2022) [2]Gartside, Jack C., et al. "Reconfigurable magnonic mode-hybridisation and spectral control in a bicomponent artificial spin ice." Nature Communications 12.1 (2021): 1-9. [3]Stenning, Kilian D., et al. "Magnonic bending, phase shifting and interferometry in a 2d reconfigurable nanodisk crystal." ACS nano 15.1 (2020): 674-685.

SC-04. Three-Dimensional Nanoscale Imaging of Propagating Spin Waves via Time-Resolved X-Ray Laminography. D. Girardi[1], S. Finizio[2], G. Rubini[1], S. Mayr[2], C. Donnelly[3], F. Maspero[1], S. Cuccurullo[1], J. Raabe[2], E. Albisetti[1] and *D. Petti*[1] *1. Physics, Politecnico di Milano, Milano, Italy; 2. Paul Scherrer Institut, Villigen, Switzerland; 3. Max Planck Institute for Chemical Physics of Solids, Dresden, Germany*

Spin waves are considered promising candidates for the next generation energy efficient devices for both analog and digital computing and signal processing. Despite the growing interest in harnessing the third dimension also in magnonics [1], the experimental visualization of propagating spin waves in three dimensions has been elusive, due to the harsh requirement of combining nanoscale spatial resolution in 3D, and time resolution across the GHz frequency range. In this framework, recently, the Time-Resolved Soft X-Ray Laminography (TR-SoXL) technique has been developed at the PolLux beamline of the Swiss Light Source [2]. The TR-SoXL is a synchrotron-based technique that allows to obtain the three-dimensional time-resolved reconstructions of the magnetization dynamics [3] of thin samples, with nanoscale resolution. To obtain the 3D resolution, the sample stage presents an additional rotation state, whose axis is tilted respect to the incoming x-rays. The different projections obtained at the different Laminography rotation angles are analyzed with an iterative reconstruction algorithm, which allows to recover the components of the magnetization. Here, first we reconstructed the three-dimensional static magnetization configuration of a NiFe 40/Ru 0.9/CoFeB 50 (nm) synthetic antiferromagnet (SAF) microstructure. Then, we demonstrate the time-resolved three-dimensional imaging of spin waves emitted by nanoscale spin textures (see Fig. 1), i.e. vortices and domain walls [4] stabilized at 0 field within the microstructure, and study their propagation and z-dependence in the SAF. This work opens the way to the direct visualization and study of nanoscale propagating spin waves in three-dimensions, within thin films and 3D structures. This in turn allows the design of new magnonic devices, moving from planar structures to vertically integrated magnonic devices exploiting the third dimension for novel functionalities.

[1] G. Gubbiotti, *Three-Dimensional Magnonics*. Jenny Stanford Publishing (2019) [2] S. Finizio et al., *Nano Lett.*, vol 22, pp 1971-1977 (2022). [3] C. Donnelly *et al.*, *Nat. Nanotechnol.*, vol 15, no. 5, pp. 356–360 (2020) [4] E. Albisetti *et al.*, *Adv. Mater.*, vol 32, no. 9, p. 1906439 (2020)

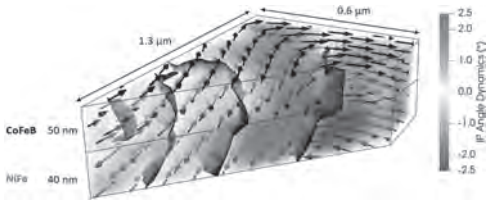

Fig. 1: Propagating spin waves emitted by a domain wall. Slice from the 3D reconstruction of the in-plane dynamic behavior of the sample magnetization. The blue/red color-code refers to the in-plane dynamic angle (θ), which is the in-plane projection of the angle of precession of the spins. Black (red) arrows correspond to the static configuration of the spins in the CoFeB (NiFe) layer. The black contours highlight the spin-wave wavefronts (θ = 0°).

SC-05. Nanoscale studies of antiferromagnetic spin-textures.

K. Wagner[1], P. Lehmann[1], O. Pylypovskyi[2], N. Hedrich[1], P. Makushko[2], B. Shields[1], T. Kosub[2], D.D. Sheka[3], D. Makarov[2] and P. Maletinsky[1]
1. Departement of Physics, University of Basel, Basel, Switzerland; 2. Institute of Ion Beam Physics and Materials Research, Helmholtz-Zentrum Dresden-Rossendorf, e.V., Dresden, Germany; 3. Taras Shevchenko National University of Kyiv, Kyiv, Ukraine

Magneto-electric antiferromagnets hold promise for future spintronic devices, as they offer magnetic field hardness, high switching speeds and both electric and magnetic control of their order parameters, owing to the magneto-electric coupling [1]. As information and functionality is encoded in the antiferromagnetic order parameter, its manipulation, read-out and nanoscale textures are paramount for device operation, as well as interesting from a fundamental point of view. For applications the surface plays a key-role as the interface often dictates the read/write functionalities and gains importance as thin film devices are targeted. Using scanning nitrogen vacancy magnetometry [2] we study a 'textbook', single crystal magneto-electric antiferromagnet Cr_2O_3 and perform nanoscale imaging of its surface magnetization, which is directly linked to its magnetic order parameter. We first confirm magneto-electric poling [3] of a homogeneous antiferromagnetic order and study the stray field polarity at the surface depending on the used field configuration. Our results are consistent with a theoretically predicted topmost disordered layer [4]. In the next step local electrodes are utilized to nucleate individual single domain walls. Manipulation of the domain wall path is demonstrated both by local laser heating, as well as the creation of an energy landscape for the domain wall position via topographic structuring [2]. Analysing the domain wall path yields further information about the boundary conditions for the order parameter at topographic edges and an estimate of the full 3D-profile of the texture based on minimizing the domain walls surface energy. A Snell like refraction of the domain wall path is found, that can be represented in an analytical approximation as a 'refractive index' for a given island dimension as demonstrated for a range of incidence angles. The demonstrated pinning and control of the domain wall position constitutes the main ingredients for logic devices based on domain walls in magneto-electric antiferromagnets and their fundamental study. Understanding the intrinsic properties and stability of the magnetic order at the direct surfaces may aid in exploring their functionality in spintronic devices that often rely on spin-scattering mechanisms at the interface.

[1] T. Jungwirth et al., Nat. Phys. Vol. 14, p.200 (2018). [2] N. Hedrich et al., Nat. Phys. Vol. 17, p.574–577 (2021) [3] B. B. Krichevtsov et al., Sov. Phys. JETP Vol. 67, p.378 (1988). [4] N. A. Spaldin, J.Exp.Theor.Phys. Vol. 132, p.493–505 (2021).

Session SD
METRICS AND MEASUREMENTS OF SPIN-ORBIT TORQUE MRAM

Shehrin Sayed, Co-Chair
TDK Headway Technologies, Inc., Milpitas, CA, United States
Jonathan Z. Sun, Co-Chair
IBM T. J. Watson Research Center, Yorktown Heights, NY, United States

INVITED PAPERS

SD-01. Spin-orbit torque switching of magnetic tunnel junctions for memory applications. *K. Garello*[1], V. Krizakova[2], V. Kateel[4,3], M. Perumkunnil[4], M. Gupta[4], G.S. Kar[4], S. Couet[4] and P. Gambardella[2]
1. Univ. Grenoble Alpes, CEA, CNRS, Grenoble INP, SPINTEC, Grenoble, France; 2. Department of Materials (D-MATL), ETH Zurich, Zurich, Switzerland; 3. Department of Electrical Engineering, KU Leuven, Leuven, Belgium; 4. imec, Leuven, Belgium

The continuous growth in the demand to store, process, and access data is one of the main drivers of spintronic research. Emerging big data and AI computing technologies require writing data in less time and storing them at a smaller scale, and consuming less energy [1]. Magnetic memories (MRAM) using spin-transfer torques have proven their place among leading non-volatile memory technologies and are currently in production for eFlash replacement applications [2]. In parallel, spin-orbit torques (SOT) have emerged and proven to be an efficient way of writing reliably magnetization at nanosecond time scale, broadening the scope of MRAM to applications that run close to the clock speed of the central processing unit, leading to novel spintronic memory and computing approaches [3], [4]. I will review across this presentation the fundamental characteristics of SOT and their use to switch perpendicularly magnetized magnetic tunnel junction (MTJ) devices. I will cover different challenges to take up SOT-MRAM from material and stack optimization to technology large-scale integration and circuit design [5]. After describing typical full-scale integration process of SOT-MRAM devices on 300mm wafers using CMOS compatible processes, I will discuss manufacturable field free methods and figures of merit for SOT-based memories. Finally, I will introduce bit-cell design considerations on scaling and performance in the perspective of circuit macro-design architectures [6], and discuss the interest to combine SOT, STT and voltage-gate (VCMA) effects to improve density and leverage performances [7]. I will conclude with opportunities to diverse SOT-MRAM application spectra, notably in the field of in-memory computing [8].

[1] G. Molas and E. Nowak, "Advances in emerging memory technologies: From data storage to artificial intelligence," *Appl. Sci.*, vol. 11, no. 23, (2021), [2] B. Dieny *et al.*, "Opportunities and challenges for spintronics in the microelectronics industry," *Nat. Electron.*, vol. 3, no. 8, pp. 446–459 (2020), [3] Q. Shao *et al.*, "Roadmap of Spin-Orbit Torques," *IEEE Trans. Magn.*, vol. 57, no. 7 (2021), [4] A. Manchon *et al.*, "Current-induced spin-orbit torques in ferromagnetic and antiferromagnetic systems," *Rev. Mod. Phys.*, vol. 91, no. 3 (2019), [5] K. Garello, F. Yasin, and G. S. Kar, "Spin-orbit torque MRAM for ultrafast embedded memories: From fundamentals to large scale technology integration," *IEEE IMW 2019*, pp. 2019–2022 (2019), [6] M. Gupta *et al.*, "High-density SOT-MRAM technology and design specifications for the embedded domain at 5nm node," *Tech. Dig. - IEDM*, vol. 2020-Decem, pp. 24.5.1-24.5.4 (2020), [7] Y. C. Wu *et al.*, "Voltage-Gate-Assisted Spin-Orbit-Torque Magnetic Random-Access Memory for High-Density and Low-Power Embedded Applications," *Phys. Rev. Appl.*, vol. 15, no. 6, pp. 1–10 (2021), [8] J. Doevenspeck *et al.*, "SOT-MRAM based Analog in-Memory Computing for DNN inference," *Dig. Tech. Pap. - Symp. VLSI Technol.*, vol. 2020-June, no. 1, pp. 2020–2021 (2020)

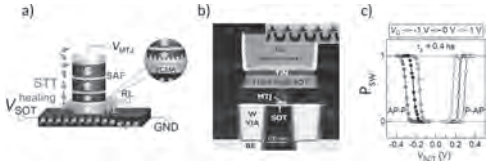

a) Illustration of a SOT-MTJ device and the different effects that can be involved (SOT, STT, VCMA, self-heat), b), Transmission electron microscopy cross section of a SOT-MTJ device, and c) Switching probability as a function of V_{SOT} and V_{MTJ}.

SD-02. Manipulating Sample Symmetry to Generate of Out-of-Plane Anti-Damping Spin-Orbit Torques. *D.C. Ralph*[1] *1. Physics, Cornell University, Ithaca, NY, United States*

Conventional spin-orbit-torque materials are constrained by symmetry to produce anti-damping torque with only one possible orientation, in the sample plane and perpendicular to the applied electric field. This orientation can drive efficient switching of magnetic layers with in-plane anisotropy, but it is much less efficient for driving switching of layers with perpendicular magnetic anisotropy that are desired for dense memory applications. For that geometry, the development of materials that can provide a significant component of out-of-plane anti-damping torque would greatly decrease the currents required for magnetic manipulation. This talk will review the progress of various strategies by which the sample symmetry can be lowered so as to provide out-of-plane anti-damping torque, including the use of spin-source materials with low crystal symmetry, ferromagnetic order, or antiferromagnetic order. It will also review metrology techniques for quantifying all components of the spin-orbit-torque vector, and how one can avoid artifacts that can interfere with such measurements.

D. MacNeill, G. M. Stiehl, et al., Nat. Physics 13, 300 (2017) T. Nan et al., Nat. Commun. 11, 4671 (2020) A. Bose et al., Nat. Electron. 5, 267 (2022)

SD-03. Two-dimensional van der Waals topological materials for SOT-MRAM. *H. Yang*[1] *1. National University of Singapore, Singapore*

The non-volatile spin-orbit torque (SOT)-MRAM is emerging as key enabling low-power technologies, which are expected to spread over large markets from embedded memories to the Internet of Things. Concurrently, the development and performances of devices based on two-dimensional (2D) heterostructures bring ultra-compact multilayers with unprecedented material-engineering capabilities. We first discuss an overview of the current developments and challenges in the field, and then outline the opportunities which can arise by implementing 2D materials into SOT-MRAM technologies (Fig. 1) [1]. We highlight the fundamental properties of atomically smooth interfaces, the reduced material intermixing, the crystal symmetries, and the proximity effects as the key drivers for possibly disruptive improvements for SOT-MRAM at advanced technology nodes. Among various spin source materials, the 2D van der Waals topological materials

such as topological insulators and Weyl semimetals, have attracted considerable attention because of their non-trivial band structures with strong spin-orbit coupling and expected giant SOT. Therefore, topological materials are regarded as promising candidates for future energy-efficient SOT device applications. However, some related physical, material, and device issues still need to be addressed. We review recent advances regarding the charge-to-spin conversion and SOT-driven magnetization switching based on the emerging 2D van der Waals materials, with an emphasis on topological insulators and Weyl semimetals, and present our perspective on practical SOT device applications using this emerging family of quantum van der Waals materials. Specifically, we show our SOT-related experimental advances that have been made in the topological material/ferromagnet heterostructures and devices, involving the giant SOT characterizations, interfacial Edelstein–Rashba effect, Dzyaloshinskii–Moriya interaction (DMI) and interfacial spin transmission. Furthermore, we highlight the highly efficient SOT-driven magnetization switching at room temperature based on 2D van der Waals heterostructures, along with the wafer-scale films prepared with industry-compatible techniques, such as molecular beam epitaxy, magnetron sputtering, and chemical vapor deposition. We anticipate that these studies will deepen the understanding of SOT on 2D van der Waals heterostructures and guide the design and applications of high-performance 2D material-based SOT devices.

[1] H. Yang *et al*., "Two-dimensional Materials Prospects for Non-volatile Spintronic Memories" Nature 606, 663-673 (2022)

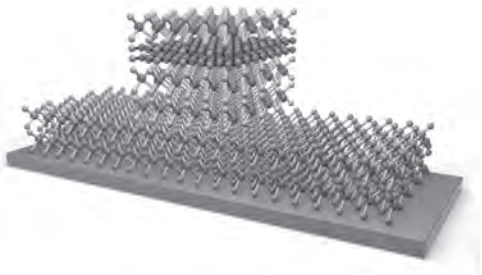

Fig. 1. 2D van der Waals material based SOT device.

SD-04. Voltage & Current Controlled Nanomagnetism For Memory and Logic. *R. Ramesh*[1] *1. Physics/ MSE, University of California, Berkeley, CA, United States*

Complex perovskite oxides exhibit a rich spectrum of functional responses, including magnetism, ferroelectricity, highly correlated electron behavior, superconductivity, etc. The basic materials physics of such materials provide the ideal playground for interdisciplinary scientific exploration with an eye towards real applications. Over the past decade the oxide community has been exploring the science of such materials as crystals and in thin film form by creating epitaxial heterostructures and nanostructures. Among the large number of materials systems, there exists a small set of materials which exhibit multiple order parameters; these are known as multiferroics, particularly, the coexistence of ferroelectricity and some form of ordered magnetism (typically antiferromagnetism). The scientific community has been able to demonstrate electric field control of both antiferromagnetism and ferromagnetism at room temperature. In parallel, there are some very intriguing new developments in SOT based manipulation of magnets. Particularly, the role of epitaxy and electronically perfect interfaces has been shown to significantly impact the spin-to-charge conversion (or vice versa). Under funding from the US. Department of Energy and the SRC-DARPA-JUMP funded ASCENT Center, current work is focused on ultralow energy (1 atto-Joule/operation) electric field manipulation of magnetism with both voltage and current, as the backbone for the next generation of ultralow power electronics. We are exploring many pathways to get to this goal. In this talk, I will describe our progress to date on this exciting possibility. The talk will conclude with a summary of where the future research is going.

SD-05. Can interfacial spin-orbit torques make magnetic devices more efficient? V.P. Amin[1], J. Zemen[2], J. Li[4], P.N. Haney[3] and *M.D. Stiles*[3] *1. Physics, Indiana University Purdue University at Indianapolis, Indianapolis, IN, United States; 2. Department of Electrotechnology, Czech Technical University in Prague, Prague, Czechia; 3. Physical Measurement Laboratory, National Institute of Standards and Technology, Gaithersburg, MD, United States; 4. DFTWorks LLC, Oakton, VA, United States*

Spin–orbit torques provide electrical control of magnetization dynamics in nanoscale heterostructures. Interfaces play a crucial role in these torques from creating the transfer of spin current to the magnetization or generating spin currents and spin accumulations. Spin-orbit torques tend to be localized to the interface because spin currents tend not to penetrate deep into ferromagnets unless the spins are aligned with the magnetization. However, describing a spin-orbit torque as interfacial generally implies that the spin-orbit coupling responsible for the torque is at the interface. That such torques might be important should not be a surprise given the importance of interfacial magnetocrystalline anisotropies and Dzyaloshinskii-Moriya interactions. Unfortunately, it can be difficult to differentiate between interfacial spin-orbit torques and those that originate away from the interfaces. There is no difference in the symmetries of the torques. In addition, changes in other properties can complicate the interpretation of thickness-dependent studies. Never-the-less, in looking to optimize spin-orbit torques, it is useful to understand the role of interfaces. In this talk, I describe the mechanisms that give rise to interfacial spin-orbit torques, discuss where they might be important, and speculate on the role they might play in the commercialization of devices based on spin-orbit torques.

V. P. Amin, P. M. Haney, and M. D. Stiles, J. of Appl. Phys. 128, 151101 (2020). V. P. Amin, J. Zemen, and M. D. Stiles, Phys. Rev. Lett. 121, 136805 (2018). V. P. Amin and M. D. Stiles, Phys. Rev. B 94, 104420 (2016). V. P. Amin and M. D. Stiles, Phys. Rev. B 94, 104419 (2016).

Session SE
EMERGING RESEARCHER SYMPOSIUM ON ARTIFICIAL SPIN ICE AND APPLICATIONS

Peter Schiffer, Co-Chair
Yale University, New Haven, CT, United States
Joseph Sklenar, Co-Chair
Wayne State University, Detroit, MI, United States

INVITED PAPERS

SE-01. Artificial spin ice: a rich platform for condensed matter magnetism. *N. Rougemaille*[1] *1. CNRS - Institut NEEL, Grenoble, France*

Artificially made, geometrically frustrated arrays of interacting magnetic nanostructures offer a remarkable playground for exploring spin ice physics experimentally [1-3]. Initially designed to capture the low-energy properties of highly frustrated magnets [4,5], artificial spin ices became in the past decade a powerful lab-on-chip platform in which to investigate cooperative magnetic phenomena and exotic states of matter. Since their introduction about fifteen years ago, the interest in artificial spin ice systems largely broadened, and the term now covers a wide range of physical phenomena and systems extending well beyond artificial ice-like magnets. Besides fundamental works, many studies were also conducted recently on the applicability of artificial spin ice geometries in magnetic architectures, in which the micromagnetic degree of freedom, spin wave excitations or topological magnetic pseudo-charges for example are envisioned as carriers for information transfer, storage and processing [6-8]. The richness of this fast evolving research field is certainly the variety of expertises and scientific backgrounds gathered within a single community, with scientists working in different, sometimes separated, areas of condensed matter magnetism, spreading from nanomagnetism and spintronics to frustrated magnetism and statistical mechanics. In this presentation, recent advances in the field will be overviewed and potential routes for future works will be discussed.

[1] C. Nisoli, R. Moessner and P. Schiffer, Rev. Mod. Phys. 85, 1473 (2013). [2] N. Rougemaille and B. Canals, Eur. Phys. J B 92, 62 (2019). [3] S. H. Skjærvø, C. H. Marrows, R. L. Stamps and L. J. Heyderman Nat. Rev. Phys. 2, 13 (2020). [4] M. Tanaka *et al.*, J. Appl. Phys. 97, 10J710 (2005); Phys. Rev. B 73, 052411 (2006). [5] R. F. Wang *et al.*, Nature 439, 303 (2006). [6] S. Gliga, E. Iacocca and O. G. Heinonen, APL Mater. 8, 040911 (2020). [7] M. T. Kaffash, S. Lendinez and M. B. Jungfleisch, Phys. Lett. A 402, 127364 (2021). [8] J. C. Gartside *et al.*, Nat. Nanotech. 17, 460 (2022).

SE-02. High-throughput Immersion Kerr Microscopy of Artificial Spin Ice: a route towards new discoveries and applications. *D. Sanz Hernandez*[1] *1. Unité Mixte de Physique, CNRS, Thales, Université Paris-Saclay, Palaiseau, France*

Artificial spin-ice systems permit the design and study of a wide family of emergent physical phenomena resulting from the combination of a very large number of interactions between simple elements. They are of great interest since the arrangement of elements, as well as their interactions, can be tuned by means of relatively simple lithography. An important challenge in the study of artificial spin-ice systems is the large number of elements involved in each system, in combination with their small physical size. Techniques such as magnetic force microscopy or X-ray microscopy are usually needed to study them. In addition, due to the dynamic and/or stochastic nature of the emerging phenomena, also a large number of states of the system need to be probed in order to have a complete physical picture of the system, or to reduce enough the uncertainty in measurements of stochasticity parameters. Finding the right balance between spatial resolution, speed and availability of experimental facilities is therefore an exciting endeavour. In this talk, we will discuss our experience with the optimization of full-field Kerr microscopy at high resolution and throughput (number of images), presenting the technique as an attractive option for the study of artificial spin-ice systems. We will present the key technical components necessary to perform this type of experiments, and, in particular, how to produce very large datasets volumes that can subsequently be employed to extract complex physical parameters via statistical analysis. See, for example, the use of automatic switch detection in Figures 1 and 2, in which 16 triangular honeycomb lattices are imaged in parallel (Figure 1) and the switching of vertical elements is automatically extracted from differential Kerr contrast (Figure 2). We will use our recent demonstration of the tunability of stochastic domain-wall decisions in honeycomb lattices using >200,000 images [1] as an example to guide the discussion. We anticipate a great interest from the artificial spin-ice community, as the size of individual elements in artificial spin-ice networks often falls within the resolution limit of the technique (≈150nm). This could open the door to exploring statistical physics and new device applications with a level of detail hardly reachable until now.

[1] Sanz-Hernández, D., Massouras, M., Reyren, N., Rougemaille, N., Schánilec, V., Bouzehouane, K., Hehn, M., Canals, B., Querlioz, D., Grollier, J. and Montaigne, F., 2021. Tunable stochasticity in an artificial spin network. *Advanced Materials*, *33*(17), p.2008135.

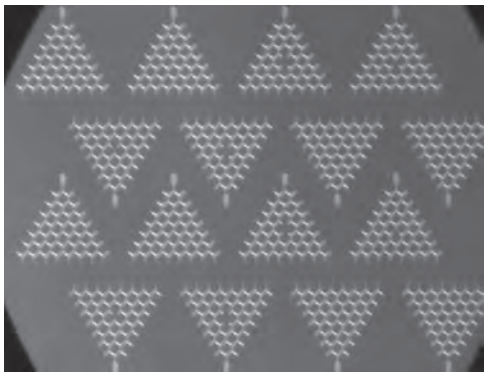

Fig. 1: Non-magnetic image of 16 triangular honeycomb ASI Galton boards. Each honeycomb lattice is formed by elements 200nm wide and 1μm long.

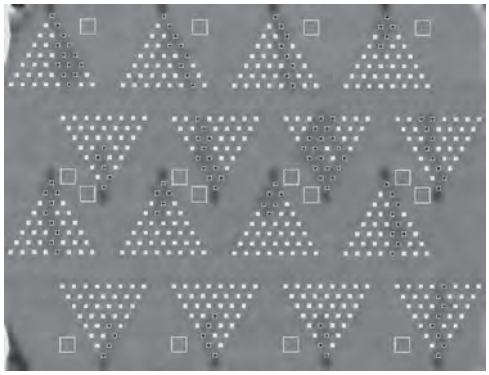

Fig. 2: Magnetic contrast obtained from Figure 1 with automatic switch extraction for vertical elements. Black squares indicate switch detection.

SE-03. Phase Transitions in Thermally Active Artificial Kagome Spin Ice. *K. Hofhuis*[1,2], S.H. Skjærvø[1,2], S. Parchenko[1,2], H. Arava[1,2], Z. Luo[1,2], A. Kleibert[3], P.M. Derlet[4] and L. Heyderman[1,2] *1. Laboratory for Mesoscopic Systems, ETH Zurich, Zurich, Switzerland; 2. Laboratory for Multiscale Materials Experiments, Paul Scherrer Institute, Villigen PSI, Switzerland; 3. Swiss Light Source, Paul Scherrer Institute, Villigen PSI, Switzerland; 4. Condensed Matter Theory Group, Paul Scherrer Institute, Villigen PSI, Switzerland*

The degree of magnetic order that can be achieved in thermally artificial kagome spin ice depends on the superparamagnetic blocking temperature of the individual nanomagnets [1] and the predicted phase transition temperature of the system [2]. The interplay between these two temperature scales dictates the observable magnetic order in experiments and in this talk, I will discuss how phase transition temperatures can be independently tuned from superparamagnetic blocking temperature. We find that by placing nanomagnetic bridges asymmetrically at the vertices of artificial kagome ice we can control the degree of frustration in the system, which allows for the independent tuning of the phase transition temperature [3]. We demonstrate that by carefully varying the widths of the bridges, we obtain various degrees of magnetic ordering and observe two magnetic phases. We then utilize the thermally active system to show that we can image the phase transition using temperature-dependent X-ray photoemission electron microscopy.

Reference: [1] K. Hofhuis, A. Hrabec, H. Arava, N. Leo, Y.L. Huang, R.V. Chopdekar, S. Parchenko, A. Kleibert, S. Koraltan, C. Abert, C. Vogler, D. Suess, P.M. Derlet, & L.J. Heyderman, Physical Review B 102, 180405(R) (2020) [2] G. Moller & R. Moessner, Physical Review B 80, 140409(R) (2009). [3] K. Hofhuis, S. H. Skjærvø, Z. Luo, S. Parchenko, A. Kleibert, P. M. Derlet, & L. J. Heyderman, Nature Physics 18, 699-705 (2022)

SE-04. How nanomagnets process information. *M. Saccone*[1,2], F. Caravelli[1], J.C. Gartside[3], K.D. Stenning[3] and W.R. Branford[3] *1. T4, Los Alamos National Laboratory, Los Alamos, NM, United States; 2. CNLS, Los Alamos National Laboratory, Los Alamos, NM, United States; 3. Blackett Laboratory, Imperial College London, London, United Kingdom*

As the era of Moore's law in transistor based computing comes to an end, it is possible that society will rely on new systems to process information [1]. Nanomagnets are an appealing candidate to supercede transistors as they may theoretically reach the Landauer limit of efficiency at room temperature [2]. Arrays of magnetic material may be patterned in nearly any 2D pattern conceivable and made of a myriad of materials to engineer a wide variety of phases, from standard ferromagnetic order to skyrmions. The interactions between domains creates Ising like behavior which naturally maps onto a variety of computing schemes, such as nanomagnetic logic [3], Hopfield networks [4], and QUBO algorithms [5]. The nonlinear field response even effectively performs the function of a reservoir in the neuromorphic computing framework of "reservoir computing" [6]. This richness of behaviors is messy and more difficult to control than CMOS systems, but offers incredible efficiency and naturally organic structure if given the appropriate problems. Artificial spin ice, nanomagnet arrays patterned to simulate the difficult to study problem of frustrated magnetism [7], has recently branched into the field of nanomagnetic computing. Here we will incorporate principles from artificial spin ice to better understand how interacting nanomagnets process information. We will also introduce a model for the mean-field dynamics of nanomagnets that illuminates how external field can drive collective behavior in such a way that the spin system's dynamics perform useful information processing. We then apply the results of this model to reservoir computing to attain a lower error signal prediction framework comprised of nanomagnets.

[1] T. Theis, and H-S. P. Wong, Computing in Science & Engineering., Vol. 19.2, p.41-50 (2017) [2] B. Lambson, D. Carlton, and J. Bokor, Physical review letters., Vol. 107.1, p.010604 (2011) [3] H. Arava, et al, Nanotechnology, Vol. 29.26, p.265205 (2018) [4] M. Saccone, et al, Nature Physics, Vol. 18.5, p.517-521 (2022) [5] A. Lucas, Frontiers in physics, Vol. 1 p.5 (2014) [6] J. Gartside, et al, Nature Nanotechnology, Vol. 17.5, p.460-469 (2022) [7] S. Skjærvø, et al, Nature Reviews Physics, Vol. 2.1, p.13-28 (2020)

SE-05. Artificial Spin System Microstate Control for Reconfigurable Magnonics & Neuromorphic Computing. *J.C. Gartside*[1], K.D. Stenning[1], A. Vanstone[1], T. Dion[3], H.H. Holder[1], F. Caravelli[2], M. Saccone[2], H. Kurebayashi[4] and W.R. Branford[1] *1. Physics, Imperial College London, London, United Kingdom; 2. Center for Nonlinear Studies and Theoretical Division, Los Alamos National Lab, Los Alamos, NM, United States; 3. Physics, Kyushu University, Fukuoka, Japan; 4. Physics, University College London, London, United Kingdom*

The vast microstate space of artificial spin ice (ASI) & related arrays is both hugely powerful for diverse processing and functionality, and highly challenging to experimentally reconfigure into more than a handful of states. In the Branford Group at Imperial College London, we work on combining an expanding suite of ASI microstate control techniques with ASI-based functional systems including reconfigurable magnonic crystals [1-4] and neuromorphic computing [4]. Microstate control techniques include direct writing via MFM-tip [5] and all-optical switching with low-power (~2.5 mW) continuous wave laser [6], and global-field preparation of classical type 1-4 ASI states [1] & bitextural vortex/macrospin domain nucleation [4]. New array architectures are presented including 3D tri-layered ASI offering substantial magnonic performance & disordered glassy spin systems, further expanding the horizons of functional ASI microstate control.

[1]Gartside, Jack C., et al. "Reconfigurable magnonic mode-hybridisation and spectral control in a bicomponent artificial spin ice." Nature Communications 12.1 (2021): 1-9. [2]Stenning, Kilian D., et al. "Magnonic bending, phase shifting and interferometry in a 2d reconfigurable nanodisk crystal." ACS nano 15.1 (2020): 674-685. [3]Dion, T., et al. "Observation and control of collective spin-wave mode hybridization in chevron arrays and in square, staircase, and brickwork artificial spin ices." Physical Review Research 4.1 (2022): 013107. [4]Gartside, Jack C., et al. "Reconfigurable Training and Reservoir Computing via Spin-Wave Fingerprinting in an Artificial Spin-Vortex Ice." Nature Nanotechnology (2022) [5]Gartside, Jack C., et al. "Realization of ground state in artificial kagome spin ice via topological defect-driven magnetic writing." Nature Nanotechnology 13.1 (2018): 53-58. [6]Stenning, Kilian D., et al. "Low power continuous-wave all-optical magnetic switching in ferromagnetic nanoarrays." arXiv preprint arXiv:2112.00697 (2021).

Session SF
COMPUTING WITH SPINTRONIC OSCILLATORS

Mark D. Stiles, Chair
National Institute of Standards and Technology, Gaithersburg, MD, United States

INVITED PAPERS

SF-01. Series of synaptic and neuronal operations in a multilayer magnetic tunnel junction network through RF-to-DC and DC-to-RF conversion. N. Leroux[1], A. Ross[1], A. De Riz[1], D. Markovic[1], D. Sanz Hernandez[1], J. Trastoy[1], P. Bortolotti[1], D. Querlioz[2], L. Martins[3], A. Jenkins[3], R. Ferreira[3], *A. Mizrahi*[1] and J. Grollier[1] *1. CNRS/Thales, Palaiseau, France; 2. CNRS, Paris Saclay University, Palaiseau, France; 3. International Iberian Nanotechnology Laboratory, Braga, Portugal*

The combination of the two key effects of spintronics, magnetization dynamics and magneto-resistive effects, allows the realization of nano-neurons and nano-synapses with high computational capabilities. However, multilayer spintronic neural networks have never been realized with these nanodevices because there is no way to connect them that can work on a large scale. I will show that it is possible to exploit the two key effects of spintronics to connect together magnetic tunnel junctions that implement both neurons and synapses of a multilayer network. The magnetic tunnel junctions perform neural operations on DC signals and output the result as RF, operate synaptic operations on RF signals and output the result as DC thus giving rise to multilayer networks based on successive, clean, and fast conversions from RF to DC and from DC to RF. I will give a proof of concept with a two-layer neural network composed of nine interconnected magnetic tunnel junctions functioning as both synapses and neurons and experimentally demonstrate its ability to solve non-linear tasks with high performance. I will show that with junctions downscaled to 20 nm, such a network would consume 10fJ per synaptic operation and 100fJ per neuronal operation, several orders of magnitude less than current software neural network implementations. Finally, I will show through physical simulations that these networks, which can process DC data, can also natively classify RF inputs, achieving state-of-the-art drone identification from their RF transmissions. This study lays the foundation for deep spintronic neural networks at the nanoscale.

SF-02. Associative Memories using Spin-Torque Oscillator Arrays. *N. Prasad*[1,2], P. Mukim[1,2], A. Madhavan[2,3] and M.D. Stiles[2] *1. Department of Chemistry and Biochemistry, University of Maryland at College Park, College Park, MD, United States; 2. Physical Measurement Laboratory, National Institute of Standards and Technology, Gaithersburg, MD, United States; 3. The Institute for Research in Electronics and Applied Physics, University of Maryland at College Park, College Park, MD, United States*

The parallels between associative learning observed in the brain and spontaneous synchronization observed in weakly coupled oscillators have led to proposals for artificial associative memories based on synchronized oscillators [1,2]. Here, we consider spin-torque oscillator arrays to form a frequency synchronized oscillator network [1]. Spin-torque oscillators are capable of frequency locking to external AC drives, provided the external drive frequencies are close to their natural frequencies [3]. Information is encoded in the coupling network while the relative phases between the frequency-synchronized oscillators encode the current state of the network. There are several possible topologies to implement the coupling networks [2] and the couplings themselves can be implemented either using magnetostatic and exchange interactions [3], or more easily though electrical circuitry. Here, we consider an all-to-all pairwise-connected feedback network, as shown in Fig. 1 with each connection representing a complex weight [4]. These complex weights consist of time-delay and scaling networks implemented using memristor-augmented CMOS circuitry. When connected in feedback, the relative phases of the oscillators stabilize into one of the states corresponding an encoded vector in the feedback network. We demonstrate storage and retrieval of twelve 16×12 images using 192 spin-torque oscillators. The pixel values of the images considered are drawn from a saturated color wheel which naturally maps to the phase of the oscillator corresponding to that pixel. A schematic of the phase evolution during a typical retrieval process is shown in Fig. 2. Starting from a corrupt state, the oscillator phases evolve in the presence of feedback so that the final image corresponds to one of the stored images that closely resembles the corrupt image. For the oscillators and circuitry considered, the image retrieval process when presented with an image with 5 % root mean square deviations from the ideal image requires approximately 5 μs and consumes roughly 130 nJ. These simulations show that for the network to function as desired, the resonant frequencies of the oscillators are required to have fractional spread lower 0.01 %.

[1] N. Prasad, P. Mukim, A. Madhavan, and M. D. Stiles. arXiv preprint arXiv:2112.03358 (2022). [2] D. E. Nikonov, G. Csaba, W. Porod, et al. IEEE J. Explor. Solid-State Comput. Devices Circuits 1, 85 (2015). [3] S. Kaka, M. R. Pufall, W. H. Rippard, et al. Nature 437, 389 (2005). [4] S. Jankowski, A. Lozowski, and J. M. Zurada. IEEE Trans. Neural Netw. 7, 6 (1996).

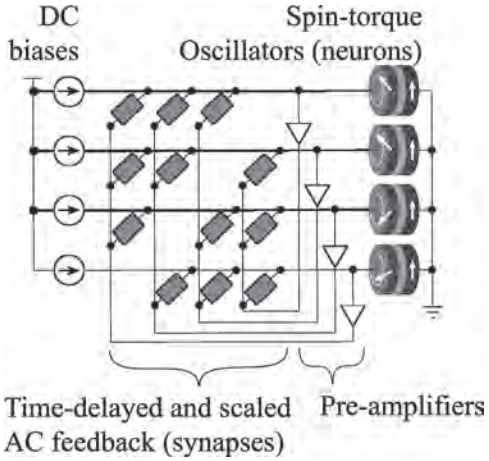

Fig. 1 Schematic of the complex-Hopfield associative memory network implemented using spin-torque oscillators.

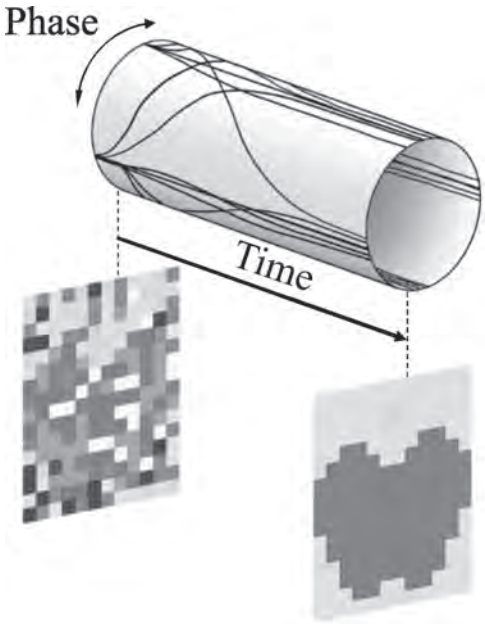

Fig. 2 Starting from an incomplete or a corrupt image representation, the oscillators evolve towards one of the images stored in the time-delayed and scaled AC feedback network. The phases of oscillators vary around the circumference and the time varies along the height of the cylinder.

SF-03. Voltage-driven Gigahertz Frequency Modulation in Spin Hall Nano-oscillators. *J. Choi*[1], J. Park[2], M. Kang[1], D. Kim[3], J. Rieh[3], K. Lee[2], K. Kim[2] and B. Park[1] *1. Department of Materials Science and Engineering, KAIST, Daejeon, The Republic of Korea; 2. Department of Physics, KAIST, Daejeon, The Republic of Korea; 3. School of Electrical Engineering, Korea University, Seoul, The Republic of Korea*

Spin Hall nano-oscillators (SHNOs) exploiting spin current-driven magnetization auto-oscillation have received much attention because of their high potential for neuromorphic applications. In particular, SHNOs provide large-scale mutual synchronization and individual control of the oscillation frequency using a gate voltage. However, the voltage-driven frequency modulation is in the megahertz range, which is not sufficient to train oscillators in response to a wide range of the input signals in the oscillatory neural network. Here, we show that the frequency of SHNO can be controlled up to 2.1 GHz by a moderate electric field of 1.25 MV/cm. The large frequency modulation is attributed to the voltage-controlled magnetic anisotropy (VCMA) in a perpendicularly magnetized Pt/$[Co/Ni]_n$/AlO_x structure. Moreover, non-volatile VCMA effect enables control of the cumulative frequency by repetitive pulses, which can mimic the potentiation and depression functions of biological synapses [1]. Our results suggest that the voltage-driven frequency modulation of SHNOs facilitates the development of energy-efficient spin-based neuromorphic devices.

[1] J.-G. Choi, *et al. Nat. Commun. accepted for publication*

SF-04. Ising Machine Based on Electrically Coupled Spin Hall Nano-Oscillators. *B.C. McGoldrick*[1], J.Z. Sun[2] and L. Liu[1] *1. Electrical Engineering and Computer Science, Massachusetts Institute of Technology, Cambridge, MA, United States; 2. IBM Thomas J. Watson Research Center, Yorktown Heights, NY, United States*

The Ising machine is an unconventional computing architecture that can be used to solve NP-hard combinatorial optimization problems more efficiently than traditional von Neumann architectures. Fast, compact oscillator networks that provide programmable connectivities among arbitrary pairs of nodes are highly desirable for the development of practical oscillator-based Ising machines. In this talk, I will discuss how an electrically coupled array of gigahertz spin Hall nano-oscillators can realize such a network *(1)*. By developing a general analytical framework that describes injection locking of spin Hall oscillators with large precession angles, I will explicitly show the mapping between the coupled oscillators' physical properties and the Ising model. I will describe how our analytical model is integrated into a versatile Verilog-A device that can emulate the coupled dynamics of spin Hall oscillator networks at the circuit level using conventional electronic components and considering phase noise and scalability. Finally, I will demonstrate how our results provide design insights and analysis tools toward the realization of a CMOS-integrated spin Hall oscillator Ising machine operating with a high degree of time, space, and energy efficiency.

1. B. C. McGoldrick, J. Z. Sun, and L. Liu, Physical Review Applied, Vol. 17 (1), p.014006 (2022). 2. J. Chou, S. Bramhavar, S. Ghosh, et. al., Scientific Reports, Vol. 9 (1), p.1 (2019).

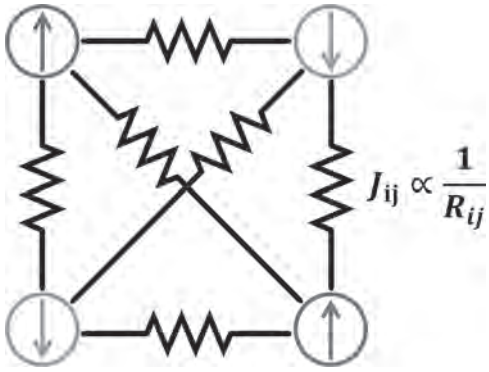

Fig. 1 Schematic of all-to-all electrically coupled network of 4 oscillators that can be mapped to the Ising model.

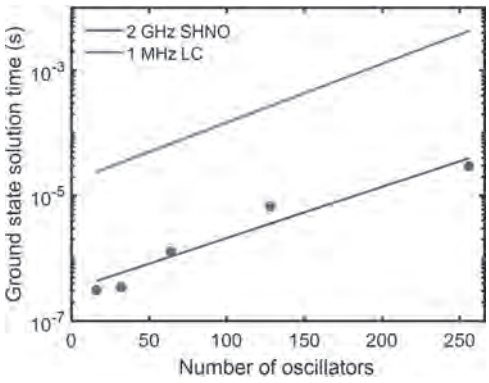

Fig. 2 Improved solution time of gigahertz spin Hall oscillator Ising machine (SHNO) compared to previously proposed LC oscillator Ising machine, reproduced from *(2)*.

SF-05. Synchronization of Spin-Hall nano-oscillators for nonconventional computing. *A.A. Awad*[1], S. Muralidhar[1], M. Zahedinejad[1], A. Houshang[1], R. Khymyn[1] and J. Åkerman[1] *1. Department of physics, Gothenburg University, Gothenburg, Sweden*

Spin Hall nano-oscillators (SHNOs) are miniaturized, ultra-broadband, microwave signal generators based on the spin Hall effect that converts a direct charge current into a transverse pure spin current, producing a spin-transfer torque into an adjacent ferromagnetic layer, which in turn excites spinwave (SW) auto-oscillations. Nano-constriction SHNOs [1] offer several advantages, thanks to their simple bilayer structure, such as significant freedom in device fabrication, material, and layout, and direct optical access to the active auto-oscillating region. SHNOs also exhibit robust frequency response [2], easy injection locking [3], and robust mutual

synchronization [4]. These properties make them ideal candidates for broadband microwave signal generation, processing, and nonconventional oscillator computing. Here we show how the controlled synchronization of SHNOs enables multiple forms of computing and demonstrations of robust mutual synchronization of two-dimensional SHNO arrays [5] (fig1.a) ranging from 2 × 2 to 8 × 8 nano-constrictions, which is observed both electrically and using micro-Brillouin light scattering microscopy (fig1.b.) Furthermore, using injection locking, we show that these SHNO arrays exposed to two independently tuned microwave frequencies exhibit the same synchronization maps (fig 1.d) as ones used for neuromorphic vowel recognition [6]. SHNOs are also potentially very appealing for oscillator network based Ising machines. Ising Machines are physical systems designed to find solutions to combinatorial optimization (CO) problems by using binary spins (Ising model). One promising approach is to use interacting non-linear oscillators that have been locked in phase to a signal at double their natural frequency. We show how phase-locked spin-Hall nano-oscillators, through the injection locking of a microwave frequency at the second harmonic, show a phase binarizations, see fig.2.(a-e), and can be used as computing units in Ising machines [7]. The core functionality required for real-world implementation of SHNOs for such potential computing applications is the individual control of the oscillators through external signal, we will show that such oscillators can be externally controlled in several ways including through optical control (fig2.f) [8]. Our demonstration of optical tuning of SHNOs might open up novel optical annealing schemes applicable to Ising machines, as well as for other computing applications. Furthermore, we discuss SHNOs readout using as well different means, which opens the way for two-dimensional synchronized SHNO networks for ultra-fast neuromorphic computing.

[1]. V. E. Demidov *et al.,* Appl. Phys. Lett. 105, 172410 (2014). [2]. A.A. Awad *et al.,* Appl. Phys.Lett 116, 232401 (2020). [3]. T. Hache *et al.,* Appl. Phys. Lett. 114,192405 (2019). [4]. A. A. Awad *et al*., Nat.Phys. 13, 292 (2017). [5]. M. Zahedinejad *et al*., Nat. Nanotechnol. 15, 47 (2020). [6]. M. Romera *et al.,* Nature 563, 230 (2018). [7]. A. Houshang *et al*., Phys. Rev. Appl. 17, 014003 (2022). [8]. S. Muralidhar *et al*., Appl. Phys. Lett. 120, 262401 (2022).

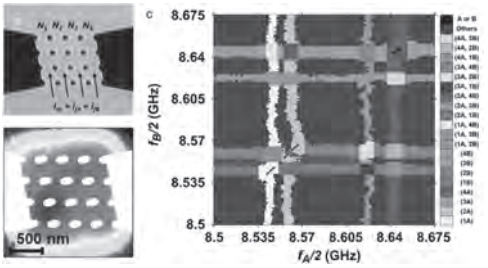

Fig. 1 (a), SEM picture of a 4 × 4 SHNO array, (b) BLS map (logarithmic scale), (c) Injection locking states of the SHNO array frequency when subjected to two independent frequency A and B.

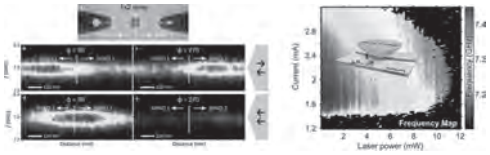

Fig. 2 (a) SEM image of the 1 × 2 SHNO array with the green arrow shows the direction of the BLS line scan. (b)–(e) Show the phase-resolved BLS of the spin-wave (SW) at two phase shifts values, indicating out-of-phase oscillations for (b),(c), and in-phase oscillations of (d),(e). (f) Current detuning of the SHNO frequency as a function of the control laser power.

Session SG
UNCONVENTIONAL SPIN-ORBIT TORQUES IN FERROMAGNETS, FERRIMAGNETS, AND ANTIFERROMAGNETS

Johan Åkerman, Chair
University of Gothenburg, Gothenburg, Sweden

INVITED PAPERS

SG-01. Quantum Sensing and Imaging of Spin Dynamics in Quantum Materials. *C. Du[1] 1. Physics, University of California, San Diego, San Diego, CA, United States*

Exploring and understanding new quantum materials with advanced properties tied to their nontrivial magnetic and electronic structures has been a central focus of modern condensed matter physics over the past decades. The success of these efforts relies simultaneously on advances in theory, material synthesis, and development of new, sensitive metrology tools to characterize the key material properties at the nanoscale. Nitrogen-vacancy (NV) centers, optically active atomic spin defects in diamond, are naturally relevant in this context due to their single-spin sensitivity, excellent quantum coherence, unprecedented spatial resolution, and remarkable functionality over a broad temperature range. Serving as a local probe of multiple degrees of freedom, NV centers are ideally posed to investigate the fundamental correlations between microscopic magnetic textures and the underlying charge, spin, and thermal transport properties of quantum materials [1-4]. In this talk, I will present our recent work on using NV centers to perform quantum sensing of emergent quantum materials. Specifically, we have utilized NV centers to visualize the exotic spin properties of topological magnetic materials, revealing the fundamental physics underlying magnetic dynamic behaviors at the nanoscale [5] [6]. Taking advantage of spin-orbit-torque in NV-magnon based hybrid systems, we also achieved electrical control of coherent spin rotations of NV spin qubits [7], promoting the role of NV centers at the forefront of quantum technologies. Our results demonstrate the unique capabilities of NV centers in accessing the local information of magnetic order and dynamics in emergent condensed matter systems and suggest new opportunities for investigating the interplay between topology, electron correlations, and magnetism in a broad range of quantum materials.

1. C. H. R. Du et al., *Science* 357, 195 (2017). 2. H. L. Wang et al., *Sci. Adv.* 8, eabg8562 (2022). 3. N. McLaughlin et al., *Nano Lett.* 21, 7277 (2021). 4. N. McLaughlin et al., *Adv. Quantum Technol.*, 4, 2000142 (2021). 5. G. Q. Yan et al, *Adv. Mater.* 34, 2200327 (2022). 6. N. McLaughlin et al., arXiv:2112.09863 (2021) 7. X. Wang et al., *npj Quantum Inf.* 6, 78 (2020).

SG-02. Tilted spin current generated by the collinear antiferromagnet RuO_2. *A. Bose[1]* and D.C. Ralph[2] *1. Institute of Physics, Johannes Gutenberg University, Mainz, Germany; 2. Dept. of Physics, Cornell University, Ithaca, NY, United States*

Symmetry plays a central role in determining the form of electrically-generated spin torques in magnetic devices. Here, we show that an unconventional out-of-plane damping-like torque can be generated in ruthenium oxide (RuO_2)/permalloy devices when the Néel vector of the collinear antiferromagnet RuO_2 is canted relative to the sample plane [1]. By measuring characteristic changes in all three components of the electric-field-induced torque vector as a function of the angle of the electric field relative to the crystal axes, we find that the RuO_2 generates a spin current with a well-defined tilted spin orientation that is approximately parallel to the Néel vector. This dependence is the signature of an antiferromagnetic spin-Hall effect predicted to arise from momentum-dependent spin splitting within the bandstructure of RuO_2, rather than from spin-orbit coupling [2]. The unconventional components are absent in the isostructural but non-magnetic rutile oxide IrO_2[3]. The out-of-plane antidamping component of the spin torque from RuO_2 is among the strongest measured in any material even with the antiferromagnetic domain structure uncontrolled, suggesting that high efficiencies are useful for switching magnetic devices with perpendicular magnetic anisotropy might be achieved by controlling the domain structure.

[1] A. Bose, N. J. Schreiber, R. Jain, et. al. Nature Electronics 5, 267 (2022). doi.org/10.1038/s41928-022-00744-8 [2] R. González-Hernández, L. Šmejkal, K. Výborný et al., Phys. Rev. Lett. 126, 127701 (2021). [3] A. Bose, J. Nelson, X. S. Zhang. et al. Effects of anisotropic strain on spin-orbit torque produced by the Dirac nodal line semimetal IrO_2. *ACS Appl. Mater. Interfaces* 12, 55411–55416 (2020).

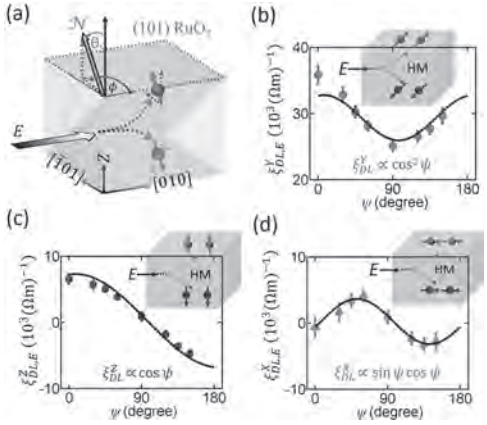

(a) Schematic representation of the tilted spin-current generated from RuO2 from the spin-split bands. Angular dependence of the generated torques in Py/(101)RuO2 bilayers originating from the y-component of the spins (a), z-component spins (b), and x-component spins (c), exhibiting angular dependence of cos2Φ, cosΦ, and sin2Φ respectively.

SG-03. Composition dependent threshold current polarity in ferrimagnetic spin Hall nano-oscillators based on GdFeCo. *L. Bainsla[1]*, A.A. Awad[1], R. Khymyn[1] and J. Åkerman[1] *1. Department of Physics, University of Gothenburg, Gothenburg, Sweden*

Due to their high spin polarization and easy manipulation, ferromagnetic materials dominate as the magnetically active element in spintronic devices but come with drawbacks such as large stray fields, limited scalability, and limited operational frequencies [1-3]. These shortcomings have recently inspired researchers to consider antiferromagnetic spintronics [4], as antiferromagnetic materials have no stray fields and possess ultrafast spin dynamics. However, antiferromagnets have no net magnetic moment, which leads to weak read-out signals and more difficult operation. Compensated ferrimagnets (FiMs) provide an alternative as they combine the properties of ferromagnets and antiferromagnets. In particular, FiMs can have near THz resonances as in antiferromagnets, while still having a net magnetic moment which can be used for strong read-out signals and frequency control, such as efficient tunable microwave signal output from FiM based nano-oscillators. Due to these unique properties, research in FiMs for spintronic applications is

intensifying [5-7]. However, to use ferrimagnets in spintronic devices such as in spin Hall nano-oscillators (SHNOs), it is important to ensure that such films retain their advantageous properties in ultrathin films and in nano devices. In the present study, ferrimagnetic GdFeCo thin films were grown using co-sputtering of Gd and $Fe_{87.5}Co_{12.5}$ on high resistance Si (100) substrates, and their magnetodynamic properties were studied using broadband ferromagnetic resonance measurements at room temperature. By tuning the stoichiometry of the GdFeCo films, a nearly compensated behavior is for the first time demonstrated in 2 nm thin film, as shown in Fig. 1. Values for the effective magnetization and effective Gilbert damping constant (α) of 0.02 Tesla and 0.0078±0.0002 are obtained for a 2 nm $Gd_{24.4}(FeCo)_{75.6}$ film [8], where α is comparable to the lowest value obtained in thick films [9]. The vertical dotted lines in Fig. 1 show literature values [6, 9-10] for the spin angular momentum (x_a) and magnetic momentum (x_m) compensation points in thick films. The composition of the films for the magnetic moment and angular momentum compensation in this work is very close to those reported in the literature. In search of high-frequency auto-oscillations in spin Hall nano-oscillators (SHNOs), constrictions with 50-300 nm widths were also prepared using GdFeCo(2-10nm)/Pt(5nm) based stacks. Brillouing Light Scattering microscopy measurements on SHNOs show auto-oscillations in the 8 GHz range, as shown in Fig. 2 [11]. Very interestingly, different Gd compositions result in different signs of the threshold current, which indicates different signs of the effective spin-orbit torque as a function of the composition.

[1] M. Romera et al*., Nature* 2018, *563*, 230. [2] M. Zahedinejad *et al*., Nat. Nanotechnol*. 15*, 47 (2020). [3] B. Dieny *et al*., Nat. Elec. 3, 446 (2020). [4] T. Jungwirth *et al*., Nat. Nanotechnol*. 11*, 231 (2016). [5] S. K. Kim *et al*., Nat. Mat. 21, 24 (2022). [6] C. Stanciu *et al*., Phys. Rev. B *73*, 220402 (2006). [7] D. Cespedes-Berrocal *et al*., Adv. Mat. 33, 2007047 (2021). [8] Lakhan Bainsla *et al*., Adv. Funct. Mater. 32, 2111693 (2022). [9] D.H. Kim *et al*., Phys. Rev. L 122, 127203 (2019). [10] Y. Hirata *et al*., Phys. Rev. B 97, 220403 (R) (2018). [11] L. Bainsla, A. A. Awad, J. Åkerman *et al*., unpublished.

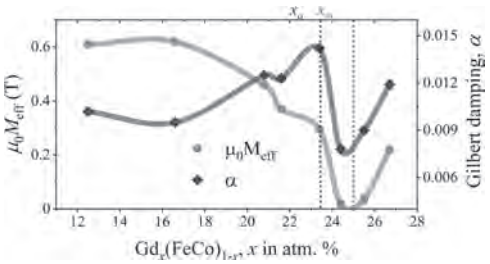

Fig. 1. Effective magnetization and effective Gilbert damping constant *vs.* composition of 2 nm $Gd_x(FeCo)_{1-x}$ films; solid symbols represent values obtained by fitting the experimental data, while solid lines are a guide to the eye.

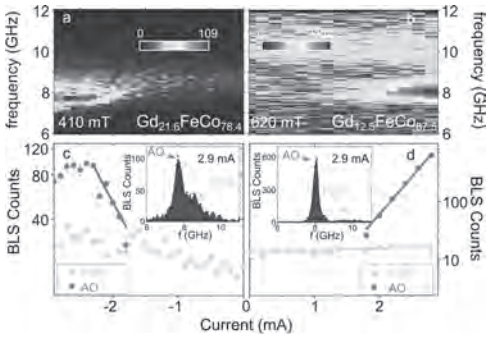

Fig. 2. (a,b) Brillouin Light Scattering Spectroscopy (BLS) vs. current of two GdFeCo based SHNOs with different Gd content, believed to operate at opposite sides of the angular momentum conpensation point (SHNO temperature > RT due to Joule heating). While thermal SWs [ferromagnetic resonace (FMR)] are seen at all currents, the Gd rich SHNO only shows auto-oscillations (AO) at negative current, and the Gd poor SHNO only shows AO at positive current. (c,d) Log plots of the BLS counts from (a,b) for the thermal spin waves SWs (green) and the AO SWs (red). While the FMR show a slight current dependence due to heating, the AO intensity shows an initially exponential increase, as expected around threshold. Insets shows the BLS spectrum profile at the highest current.

SG-04. Spin-orbit torque induced magnetization switching in single ferromagnetic layer. L. Liu[1], C. Zhou[1] and *J. Chen*[1] *1. Materials Science and Engineering, National University of Singapore, Singapore*

The combination of inversion symmetry breaking and spin-orbit coupling (SOC) give rise to spin-orbit torque (SOT), charge pumping, and chiral magnetism. In conventional SOT studies, the inversion symmetry breaking usually comes from the structure or the geometry, e.g. crystal inversion assymmety in the bulk of diluted ferromagnet with zinc-blende structure (Fig. 1a) and space inversion assymmetry in a heavy metal/ferromagnet bilayer (Fig. 1b). It was known that the SOT strength can be controlled by the magnitude of the SOC, therefore, heavy metals with large SOC has been widely used for SOT-based magnetic random-access memory (MRAM). In our study, we demonstrated that the vertical composition gradient in a single FePt layer acts as a new type of inversion symmetry breaking (Fig. 1c). The SOT efficiencies scale almost linearly with the composition gradient (G), which is defined to be the change of the Co/Pt ratio per 1 nm. We found that by changing G from 0.31 %/nm to 0.71 %, the SOT efficiency increases by 300 %. In experiments, the composition gradient can be easily controlled during sample growth. Therefore, our work provides a powerful tool to tune the SOT strength. Then we demonstrated the current-induced magnetization switching in a FePt single layer (Fig. 1e). However, this switching requires an in-plane external magnetic field to break the symmetry. For real application, it is pursued to realize magnetic field-free switching. To achieve this goal, we move our attention from $L1_0$ FePt (P4/mmm) to *fcc* $CoPt_3$. Both of them possess good perpendicular magnetic anisotropy (PMA) and hold promise in magnetic storage (media and memory). We found that the $CoPt_3$ has two structural properties, as illustrated in Fig. 2(a). One is the composition gradient along the thickness direction which can break the inversion symmetry and allows for the generation of the in-plane damping-like torque. The other is the formation of the Co platelets in the Pt-rich matrix near the substrate during growth. We can make a symmetry analysis of the Co platelet/Pt structure, and we can easily find that the mirror symmetry is broken relative to the (11-2) plane and preserved relative to the (1-10) plane. Therefore, when the current is applied along the [1-10] direction (low-symmetry axis), the lateral mirror symmetry is broken so that the out-of-plane SOT can be allowed. Then we can achieve the field-free magnetization switching (0 deg in Fig. 2c). In contrast, when the current is applied along the [11-2] direction (high-symmetry axis), the lateral mirror symmetry is preserved and there is no field-free switching (90 deg in Fig. 2c). We also found that the current-induced switching exhibit a three-fold angular

dependence on the current angle (θ_I), which is in perfect agreement with the three-fold rotational symmetry of the crystal structure in Fig. 2b. To summarize, we observed the field-assisted magnetization switching in FePt single layer by introducing a new type of inversion symmetry breaking: composition gradient. Furthermore, we demonstrated the symmetry-dependent field-free magnetization switching in the $CoPt_3$ single layer. The composition gradient along the film's normal direction gives rise to the in-plane damping-like torque while the low symmetry (3m1) property at the interface of Co platelet/Pt gives rise to the 3m torque in $CoPt_3$. The cooperation of these two effects leads to a three-fold field-free switching in the $CoPt_3$ single layer. Our result of the self-switching in $CoPt_3$ has provided one of the most simplified structures for field-free switching of perpendicular magnetization. The good endurance and high thermal stability make it a good candidate for magnetic memory devices and other spintronic applications.

[1] L. Liu, et.al., Electrical switching of perpendicular magnetization in a single ferromagnetic layer Physical Review B 101 (22), 220402 (2020). [2] L. Liu, et.al., Current-induced self-switching of perpendicular magnetization in CoPt single layer Nature Communication 13, 3539 (2022).

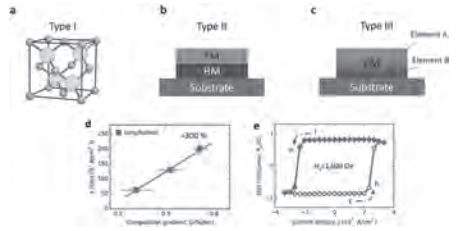

Fig 1. Three types of inversion symmetry breakings and SOT engineered by composition gradient.

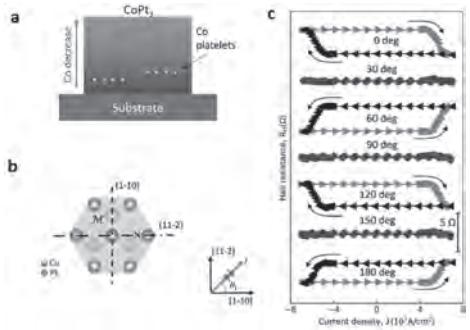

Fig 2. Symmetry-dependent field-free switching in $CoPt_3$ single layer.

SG-05. Efficient field-free spin-orbit torque switching in magnetic trilayers. J. Ryu[1], S. Kim[1], J. Kang[1], M. Kohda[2], J. Nitta[2], K. Lee[1] and *B. Park[1] 1. KAIST, Daejeon, The Republic of Korea; 2. Tohoku University, Tohoku, Japan*

Spin-orbit torque (SOT) arising from spin-orbit coupling promises efficient magnetization switching in spintronic devices. It is important for device applications that the SOT switches perpendicular magnetizations without an external magnetic field. In addition to field-free switching, reducing SOT switching current is another essential requirement for low energy consumption. In this talk, we first demonstrate spin currents and associated SOT in ferromagnet/non-magnet/ferromagnet trilayers, in which the torque on the top magnetic layer can be controlled by changing the magnetization of the bottom ferromagnetic layer. In this structure, by aligning the magnetization of the bottom magnetization parallel to the current direction, spin current can carry out-of-plane spin polarization, enabling field-free SOT switching of the top perpendicular magnetization [1]. The out-of-plane SOT is generated by spin current precession at the interface due to the interfacial spin-orbit field. Second, we show that the spin current caused by the spin anomalous Hall effect can be additionally exploited in epitaxial Co-based magnetic trilayers [2]. The large in-plane magnetic anisotropy of the epitaxial Co makes it possible to control the magnetic easy axis of the bottom magnetic layer away from the current direction. It is found that the critical current for field-free switching is reduced when the magnetization is at an angle between 30 and 45 degrees from the current direction where the spin anomalous Hall effect is non-negligible.

[1] S-h. C. Baek, et al, Nat. Mater. 17, 509 (2018) [2] J. Ryu, et al, Nat. Electron. 5, 217 (2022)

Session AOA
ELECTRONIC STRUCTURE AND CRITICAL PHENOMENA

Cheng Gong, Chair
University of Maryland, College Park, MD, United States

CONTRIBUTED PAPERS

AOA-01. Anomalous Valley Hall Effect in *A*-type Antiferromagnetic Van der Waals Heterostructures. *Y. Zhu*[1] and H. Yang[1] *1. Ningbo Institute of Materials Technology and Engineering, CAS, Ningbo, China*

Valley, as a new degree of freedom of electrons besides charge and spin, can be used to encode, transmit, store, and manipulate information [1-3]. By using various external methods, such as optical pumping, magnetic field, magnetic doping, and magnetic proximity effect, the valley polarization can be induced in materials for realizing practical valleytronic devices. Recently, ferrovalley materials, a system with intrinsic magnetic and valley characteristics, was proposed for 2*H*-VSe_2 [4]. Compared to traditional valleytronic materials, the ferrovalley materials have potential to eliminate the limitations associated with external fields in inducing valley polarization. However, to date, most of the predicted ferrovalley materials possess in-plane magnetization, which impede the appearance of valley polarization in nature. The crucial challenge is to induce large perpendicular magnetic anisotropy to achieve spontaneous valley polarization in two-dimensional ferrovalley materials. The van der Waals heterostructure, constructed by isolated atomic layer by layer in a chosen sequence, can reveal unusual properties and phenomena. Here, using first-principles calculations, we find that A-type antiferromagnetic VSe_2/CrI_3 heterostructure can realize perpendicular magnetic anisotropy and spontaneous valley polarization for realizing anomalous valley Hall effect, while the magnetic anisotropy of VSe_2 is in-plane. More interestingly, the electric-field-controlled valley states can be realized by capping a ferroelectric layer (In_2Se_3) on VSe_2/CrI_3. The half metal-to-semiconductor transition and turning off and on valley are achieved by switching the ferroelectric polarization. Our results of constructing ferrovalley/ferromagnetic and ferroelectric/ferrovalley/ferromagnetic two-dimensional van der Waals heterostrucutre to engineer electronic and valley states can be useful for developing low-dimensional spintronic and valleytronic devices.

[1] A. Rycerz, J. Tworzydlo, and C. W. J. Beenakker, Nature Physics, 3, 172 (2007). [2] D. Xiao, W. Yao, and Q. Niu, Physical Review Letters, 99, 236809 (2007). [3] F. Zhang, J. Jung, and A. H. MacDonald, Physical Review Letters, 106, 156801 (2011). [4] W. Y. Tong, S. J. Gong, and C. G. Duan, Nature Communications, 7,1 (2016).

AOA-02. Withdrawn

INVITED PAPER

AOA-03. (Magneto-)Optical properties of ferromagnetic bcc Fe: First-principles description of electron, lattice, and magnetic temperatures. *K. Kang*[1], D.G. Cahill[1] and A. Schleife[1] *1. Materials Science and Engineering, University of Illinois at Urbana-Champaign, Urbana, IL, United States*

First-principles density functional theory simulations have been popularly used to predict the optical and magneto-optical responses of magnetic materials[1]. However, the inclusion of the temperature-dependent effect is still in the infancy stage. Although it is restricted to non-magnetic materials such as silicon, perturbative approaches with harmonic approximation[2] and non-perturbative methods using *ab initio* molecular dynamics for anharmonicity[3] could effectively describe the lattice temperature effect for optical properties and electronic band structures. In this study, we expand the supercell model based on the William-Lax theory[4,5] to describe the quasiparticle temperature effect for ferromagnetic BCC Fe. Electronic temperature is depicted by the occupation number change using Fermi smearing, while the supercell with atomic and magnetic structure perturbations can allow us to mimic the lattice and magnetic temperature effects. Electron temperature up to 300 K barely affects the optical spectrum. However, a large signal generation below 1.5 eV photon energy is predicted with lattice and magnetic temperatures. This phenomenon originates from the intraband optical transitions due to the folded electronic band structure with large dipole transition matrix element changes from the perturbed structures. Furthermore, magnetic temperature induces a unique peak-redshifting behavior in the imaginary dielectric function spectrum. The redshifted peak is located around 3.0 eV, which is close to the exchange splitting of energy states. Unfolded band structure indicates that the exchange splitting is reduced due to the thermal demagnetization, resulting in the peak redshifting. Lastly, a linear magneto-optical spectrum of BCC Fe is predicted, showing a good agreement with measured spectra and following the typical temperature dependence of ferromagnetic materials. The proposed methodology be utilized to describe the paramagnetic phases at high temperatures in the future. **Illinois MRSEC NSF DMR-1720633

[1] D. Sangalli, a. Marini and A. Dbernardi, Phys. Rev. B, Vol. 86, p.125139 (2012) [2] J. Noffsigner, E. Kioupakis, C. G. Van de Walle, *et al.*, Phys. Rev. Lett, Vol. 108, p.167402 (2012) [3] M. Zacharias, M. Scheffler, C. Carbogno, Phys. Rev. B, Vol. 102, p.045126 (2020) [4] F. E. Williams, Phys. Rev. Vol. 81, p.281 (1951) [5] M. Lax, J. Chem. Phys. Vol. 20, p.1752 (1952)

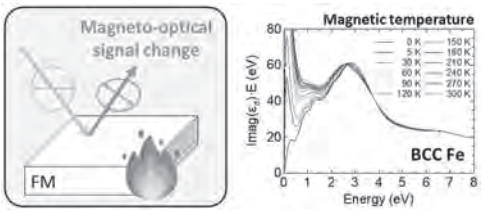

Fig. 1 (Left) A schematic plot of magneto-optical signal change with temperature change (Right) Imaginary optical conductivity spectrum of ferromagnetic BCC Fe with magnetic temperature up to 300 K

CONTRIBUTED PAPERS

AOA-04. Topological features in real and reciprocal space: a case study of metallic ferrimagnet Mn_4N. *T. Bayaraa*[1] and S. Griffin[1]
1. Lawrence Berkeley National Laboratory, Berkeley, CA, United States

Over the past few decades, many topological phenomena have been theoretically predicted in both real (e.g. skyrmions) and reciprocal space (e.g. topological insulators). In this work, we look to discover systems that host both real-space and reciprocal-space nontrivial topologies - so-called doubly topological materials. We begin with our previous finding of metastable topological phases such as a hedgehog-anti-hedgehog pairs and skyrmion tubes in antiperovskite metallic ferrimagnet Mn_4N by first-principles calculations and Monte-Carlo Simulations [1]. Such topological states were found to be stabilized by a frustration in the (long-range) magnetic exchange interactions due to its complex magnetic structure featuring three different Mn ions. Here, we show that Mn_4N has also topologically protected properties in the k-space by studying its Berry curvature and predicting its Anomalous Hall Conductivity and Anomalous Nernst Effect. Our findings show that Mn_4N is a Weyl semimetal with topological characteristics in both real and reciprocal spaces. Such interplay between magnetism and topology in both real and reciprocal spaces could open up a new door for exotic linear response effects between them.

[1] T. Bayaraa, Changsong Xu, and L. Bellaiche, Phys. Rev. Lett. 127, 217204 (2021).

AOA-05. Ab initio Crystal Field Splittings for Lanthanide Dopants in Oxide Materials for Quantum Information. *Y. Shi*[1] and M.E. Flatté[1]
1. Department of Physics and Astronomy, University of Iowa, Iowa City, IA, United States

Lanthanide dopants in oxide hosts provide excellent spin-photon interfaces for quantum technologies, including by mediating microwave to optical quantum transduction (converting a collective spin excitation to an optical excitation), and for quantum memories. The description of magnetic dipole transitions in lanthanides using model Hamiltonians principally relies on existing experimental fit parameters for terms in the Hamiltonian like the effect of the crystal field on the 4f elections. [1] Here, we deploy an ab initio extraction of crystal field parameters explored by Dadi Dai et al. [2] With ab initio, we extracted crystal field parameters in Er defects in hosts like Y2O3, and in combining the extracted crystal field parameters with the effective operator Hamiltonian approach we were able to compare the theoretical crystal field energy correction with experimental values directly and obtained a relatively good match. In further studies we're exploring a more systematic prediction of crystal field levels to pave the path for a wide search of lanthanide doped spin-photon systems. We acknowledge funding from NSF DMR-1921877.

[1] C. M. Dodson, R. Zia, Phys. Rev. B 86, 125102 (2012). [2] D. Dai, L Li, J. Ren, et al., J. Chem. Phys. 108, 3479 (1998).

AOA-06. Withdrawn

AOA-07. Optimization of electronic correlations and magnetism in $SrCo_2As_2$ via hole doping. *A. Pandey*[1] and Y. Liu[2] *1. School of Physics, University of the Witwatersrand, Johannesburg, South Africa; 2. Crystal Growth Facility, Ecole Polytechnique Federale de Lausanne, Lausanne, Switzerland*

The Co-based tetragonal compounds ACo_2As_2 (A = Ca, Sr, Ba & K) crystallize in $ThCr_2Si_2$-type structure and exhibit properties that delicately depend upon the interlayer As-As distance $d_{As\text{-}As}$ which regulates the oxidation state of Co-ions by controlling the extent of the interlayer As-As bonds. As a result, it indirectly controls the magnetic ground state of these materials. $BaCo_2As_2$, which has a large value of $d_{As\text{-}As}$ = 3.78 Å, shows a nonmagnetic ground state [1]. On the other hand, $CaCo_2As_2$ with $d_{As\text{-}As}$ = 2.73 Å exhibits an A-type collinear antiferromagnetic (AFM) ordering below its Nèel temperature [2]. $SrCo_2As_2$ with $d_{As\text{-}As}$ = 3.33 Å, intermediate to those of its Ca and Ba analogs, shows no evidence of long-range magnetic ordering but develops stripe-type AFM as well as ferromagnetic spin fluctuations [3,4]. Another recently explored compound KCo_2As_2, where the $d_{As\text{-}As}$ = 4.08 Å is largest among this series, exhibits a suppressed non-magnetic ground state [5]. These observations collectively suggest that increasing the interlayer Co-ion distance reduces the magnetic character within the ACo_2As_2 system. In this work, we explore the combined effect of the change of electron count as well as the increase in $d_{As\text{-}As}$ introduced through the partial substitution of Sr-ions with K-ions in the $Sr_{1-x}K_xCo_2As_2$ system. We report on the magnetic characteristics and electron transport properties of this hole-doped system and explore the interdependency of structural parameters, charge density and many-body interactions within the material.

[1] V. K. Anand, D. G. Quirinale, Y. Lee *et al.*, Phys. Rev. B Vol. 90, p.064517 (2014). [2] V. K. Anand, R. S. Dhaka, Y. Lee *et al.*, Phys. Rev. B Vol. 89, p.214409 (2014). [3] A. Pandey, D. G. Quirinale, W. Jayasekara *et al.*, Phys. Rev. B Vol. 88, p.014526 (2013). [4] Yu Li, Z. Yin, Z. Liu *et al.*, Phys. Rev. Lett. Vol. 122, p.117204 (2018). [5] A. Pandey, Y. Liu, S. L. Samal *et al.* arXiv:2201.10325.

AOA-08. Role of Cationic Size Mismatch to Control the Effect of A-site Disorder. *A. Khatun*[1,4], P. Aich[1,4], A. Schoekel[2], S. Panda[3], N. Mohapatra[3] and D. Topwal[1,4] *1. Physics, Institute of Physics, Bhubaneswar, India; 2. DESY Photon Science, Deutsches Elektronen - Synchrotron, Hamburg, Germany; 3. School of Basic Sciences, Indian Institute of Technology Bhubaneswar, Bhubaneswar, India; 4. Homi Bhabha National Institute, Mumbai, India*

Manganites are one of the promising materials due to their great diversity in physical properties [1-4]. These properties can be tuned by varying probability occupancy as well as ionic size of A-site cations, such as long range ordering observed in $RBaMn_2O_6$ (R=Rare earth ions) can be suppressed by cationic disorder [5-6]. We made a comparative study of structure, magnetic (M) properties and magneto-resistance (MR) in A-site ordered $NdBaMn_2O_6$ (O-NB) and A-site disordered $NdBaMn_2O_6$ (D-NB), $NdCaMn_2O_6$ (D-NC). Experimental results from T dependent synchrotron PXRD (fig.1.*a-c*) concluded that structural symmetry strongly depends on A-site cationic distribution and their ionic sizes resulting in intriguing magnetic ground states. Moreover, MR (fig.2) is considerably large in disordered systems as compared to ordered one. Refinement of PXRD data showed that the A-site cations (Nd^{3+} & Ba^{2+}) are completely ordered in O-NB. Lowering the T is accompanied with structural transition (ST) (fig.1.*a*) to lower space group. Whereas, there is no ST in disorder system, D-NB down to 120K. However, ST has been restored again in D-NC disordered system due to similar A-site cationic sizes, Nd^{3+} and Ca^{2+} ions. At the same time, M-T data show AFM ground state due to lower structural symmetry in O-NB and the ground state becomes FM in case of D-NB system due to the retainment of higher symmetric structure upto lowest T. Interestingly, AFM state has been restored in D-NC similar to that of O-NB due to presence of cationic disorder of similar sizes (fig.1.*d-f*). So, it can be argued that crystal structure and magnetic degrees of freedoms are strongly correlated with each other. Further, MR studies depict 3 times higher value of MR in both disorder compounds to that of order one (fig.2). However, behaviour of MR with H is different for D-NB and D-NC implying a different origin of this large MR in these compounds. We believe that the presence of phase separation in D-NC and AFM fluctuation in D-NB might be possible origin of their large MR with respect to O-NB system.

[1] V.N. Smolyaninova, S.E. Lofland, C. Hill, R.C. Budhani, Z. Serpil Gonen, B.W. Eichhorn, and R.L. Green, Effect of A-site cation disorder on charge ordering and ferromagnetism of $La_{0.5}Ca_{0.5-y}Ba_yMnO_3$, J. Magn. Magn. Mater.248 (2002) 348. [2] T. Nakajima, H. Kageyama,

H. Yoshizawa, K. Ohoyama, and Y. Ueda, Ground State Properties of the *A*-site Ordered Manganites, $RBaMn_2O_6$ (R = La, Pr and Nd), J. Phys. Soc. Jpn. 72 (2003) 3237. [3] J. Blasco, G. Subías, M. L. Sanjuán, J. L. García-Muñoz, F. Fauth, and J. García, Structure and phase transitions in *A*-site ordered $RBaMn_2O_6$ (R=Pr,Nd) perovskites with a polar ground state, Phys. Rev. B 103 (2021), 064105. [4] S. Yamada, H. Sagayama, K. Higuchi, T. Sasaki, K. Sugimoto, and T. Arima, Physical properties and crystal structure analysis of double-perovskite $NdBaMn_2O_6$ by using single crystals, Phys. Rev. B 95 (2017) 035101. [5] D. Akahoshi, M. Uchida, Y. Tomioka, T. Arima, Y. Matsui, and Y. Tokura, Random Potential Effect near the Bicritical Region in Perovskite Manganites as Revealed by Comparison with the Ordered Perovskite Analogs, Phys. Rev. Lett. 90 (2003) 177203. [6] T. Nakajima, H. Yoshizawa, and Y. Ueda, *A*-site Randomness Effect on Structural and Physical Properties of Ba-based Perovskite Manganites, J. Phys. Soc. Jpn. 73 (2004) 2283.

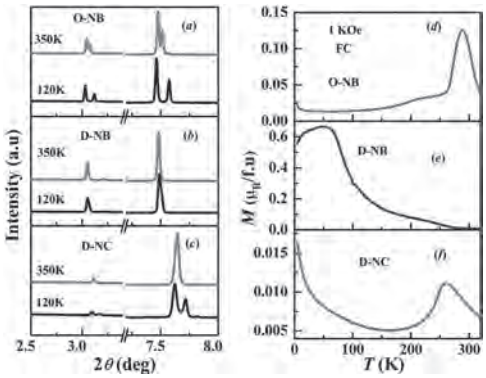

Fig.1. *T* dependent (*a*)-(*c*) XRD and (*e*)-(*f*) Magnetization.

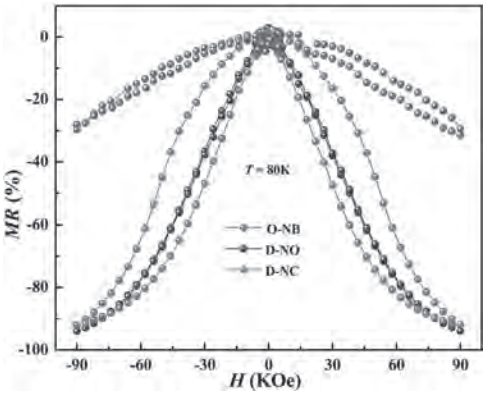

Fig.2. *MR* at 80K.

AOA-09. Magnetic Anisotropy as an Evidence of Local Magnetic Moments in Paramagnetic Phase of Cr-V Alloys. L.M. de Oliveira[1], P.N. de Souza[2], F. Yokaichiya[3], P.C. de Camargo[4] and *A.J. de Oliveira*[5]
1. Colegiado de Ciências da Natureza, Universidade Federal do Vale do São Francisco, Senhor do Bonfim, Brazil; 2. Instituto de Física, Universidade de Brasília, Brasília, Brazil; 3. Departamento de Física, Universidade Federal do Paraná, Curitiba, Brazil; 4. Instituto de Estudos Avançados e Estratégicos, Universidade Federal de São Carlos, São Carlos, Brazil; 5. Departamento de Física, Universidade Federal de São Carlos, São Carlos, Brazil

Chromium-rich Cr-V alloys exhibit three phases: Paramagnetic phase (P) above Néel temperature (T_N), a transverse polarization spin-density-wave (SDW) phase (AF_1) below T_N and above the spin-flip temperature (T_{SF}), and a longitudinal polarization SDW phase (AF_2) below T_{SF}. Varying the electron/atom ratio in the Cr alloy, one can go from incommensurate to commensurate SDW and modifies different physical properties [1]. In the paramagnetic phase, Cr exhibit a Pauli susceptibility with slight temperature dependence[1]. Otherwise, the introduction of small amounts of V in Cr not only changes T_N, but also induced a Curie-Weiss behavior (CW) that we have associated to local magnetic moments. This behavior is limited up to 0.7%V and magnetic fields of 15 kOe [2]. This behavior was also observed for different Cr alloys [3-5]. The origin of local magnetic moments has been associated with the establishment of local spin-density waves (LSDW) around V impurities [2,6]. In this work, we presented an investigation of the effects of local magnetic moments in antiferromagnetic phases in Cr-V alloys. The samples are single crystals with a concentration up to 0.7% V. Magnetization measurements as a function of temperature were performed using a VSM SQUID magnetometer MPMS3 by Quantum Design using zero field cooling (ZFC) and field cooling (FC) protocols. Figure 1 presents the magnetic susceptibility ($\chi_{DC}(T)$) as a function of temperature under a magnetic field H = 100 Oe (a) and 10 kOe (b) for single crystal of Cr-0.4 at.%V. The ZFC measurement shown in Fig 1(a) shows a jump as T_N is approached followed by a C-W behavior up to 400 K. However, below T_N χ_{DC} (T) the FC measurement exhibit a strong anisotropy, likely associated with local magnetic moments frozen in the cooling process, from the paramagnetic phase. Fig 1(b) shows that 10 kOe suppresses the CW effect above T_N, in the AF_1 phase χ_{DC} is identical for both processes ZFC and FC and in the AF_2 phase χ_{DC} becomes larger for ZFC as compared to FC. These results show that local moments around V impurities depend on magnetic history.

[1] E. Fawcett et. all. Rev. Mod. Phys. 66, 25 (1994) [2] L. M. de Oliveira, W. A. Ortiz, and A. J. A. de Oliveira, Journal of Applied Physics 93, 7154 (2003) [3] P. E. N. de Souza et. al. – J. of Physics: Cond. Matter 17, 2191 (2005) [4] B. S. Jacobs. C. J. Sheppard and A.R.E. Prinsloo – J. Magn. Magn, Mat. 546, 168856 (2022) [5] B. Muchono et. Al. – Physica B 537, 212 (2018) [6] V. V. Tugushev, Modulated and Localized Structures of the Spin-Density Wave in Itinerant Antiferromagnets in Electronics Phase Transitions, edited by W. Hanke and Yu. Kopaev Elsevier, Amsterdam, 1992.

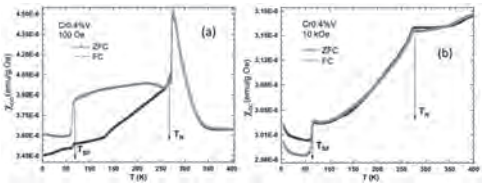

Fig. 1 - Magnetic susceptibility as a function of temperature performed to Cr-0.4 at.%V alloy. (a) H= 100 Oe and (b) H=10 kOe

AOA-10. Withdrawn

Session AOB
LOW-DIMENSIONAL SYSTEMS AND FRUSTRATED MAGNETIMS

Yaroslav Mudryk, Chair
Iowa State University, Ames, IA, United States

CONTRIBUTED PAPERS

AOB-01. Tuning exchange interactions in 1*T*-VSe_2 monolayer by alkali metal adsorption and electride substrate. *J. Jiang*[1] and W. Mi[1]
1. Department of Applied Physics, Tianjin University, Tianjin, China

The manipulation of exchange interactions in two-dimensional magnets has fundamental research value and potential applications. Based on first-principles calculations, the exchange interactions in experimental controversial ferromagnetic 1*T*-VSe_2 monolayer [1,2] are systematically studied. It is found that three shells of nearest-neighbor Heisenberg exchange interactions and higher-order interactions are crucial for an accurate description of the ferromagnetism in 1*T*-VSe_2 monolayer. Based on the understanding of tuning the magnetic interactions and the magnetic ground state in 1*T*-VSe_2 monolayer by external factors, two modulation methods, alkali metal Lithium adsorption and electride Ca_2N substrate, are proposed. In both systems, the strongly frustrated Heisenberg exchange interactions compete with higher-order exchange interactions, Dzyaloshinskii-Moriya interaction and magnetocrystalline anisotropy, leading to complex magnetic ground states, such as antiferromagnetic spin spiral, periodical antiferromagnetic cycloidal state and double row-wise antiferromagnetic states. These results highlight the effective manipulation of exchange interactions in two-dimensional magnets. This work was supported by the National Natural Science Foundation of China (51871161 and 52071233).

[1] M. Bonilla, S. Kolekar, Y. Ma, et al. Nat. Nanotechnol. 13, 289 (2018). [2] P. K. J. Wong, W. Zhang, F. Bussolotti, et al. Adv. Mater. 31, 1901185 (2019).

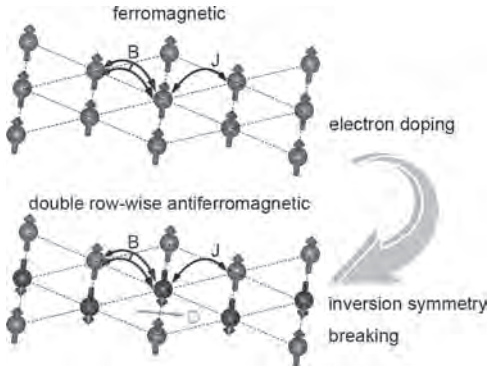

Fig. 1. Tuning exchange interactions in 1*T*-VSe_2 monolayer by electron doping mechanism.

AOB-02. Spin Dependent Electronic Structure and Magnetic Properties of Fe/Chiral Methylbenzylamine-PbI_4 Spinterfaces. *Y. Xu*[1] and W. Mi[1] *1. Department of Applied Physics, Tianjin University, Tianjin, China*

Spin selectivity depends on the magnetism of substrate and the interaction between chiral molecules and substrate[1]. Measurements of the interfaces based on chiral molecules and ferromagnet by Kelvin probe show that the length of electron spin wave function entering chiral monolayer is chirality-dependent[2]. In this work, the electronic structure and magnetic properties of *R*,*S*-methylbenzylamine-PbI_4/Fe interfaces are studied by first-principles calculations. The effects of stacking patterns and chirality on the interfaces are discussed. All four interfaces can exist at low temperature, among which the type-II is more stable. The existence of chiral organic molecules leads to the emergence of positive spatial spin polarization in the vacuum layer and the attenuation of positive spatial spin polarization in the substrate, indicating that the microstructures of interfaces will affect the spin injection efficiency. The four interfaces show negative spin polarization and perpendicular magnetic anisotropy. The effect of chiral molecules on the interfaces can be further studied by applying external electric field. This work was supported by the National Natural Science Foundation of China (51871161 and 52071233).

[1] K. Michaeli, N. Kantor-Uriel, R. Naaman and D. Waldeck, *Chem. Soc. Rev*. 45, 6478-6487 (2016) [2] Z. Huang, B. Bloom, X. Ni, Z. Georgieva, M. Marciesky, E. Vetter, F. Liu, D. Waldeck and D. Sun, *ACS Nano* 14, 10370-10375 (2020)

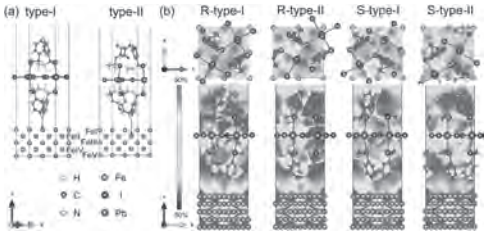

Fig. 1. (a) Two stacking patterns and (b) spatial spin polarization in [001] and [100] plane of *R*,*S*-MBA-PbI_4/Fe interfaces. The energy interval is [E_F-0.4 eV, E_F].

INVITED PAPER

AOB-03. Axial Higgs mode detected by quantum pathway interference in RTe_3. *Y. Wang*[1], I. Petrides[2], G. McNamara[1], s. Lei[6], Y. Wu[3], J. Hart[4], J. Yan[3], D. Xiao[5], J.J. Cha[4], P. Narang[2], L. Schoop[6] and K. Burch[1]
1. Physics, Boston College, Boston, MA, United States; 2. John A. Paulson School of Engineering and Applied Sciences, Harvard University, Cambridge, MA, United States; 3. Physics, University of Massachusetts Amherst, Amherst, MA, United States; 4. Materials Science, Cornell University, Ithaca, NY, United States; 5. Physics, Washington University, Seattle, WA, United States; 6. Chemistry, Princeton University, Princeton, NJ, United States

The observation of the Higgs boson solidified the standard model of particle physics. However, explanations of anomalies (e.g. dark matter) rely on further symmetry breaking 1calling for an undiscovered axial Higgs mode. In condensed matter, the Higgs was seen in magnetic, superconducting, and charge density wave(CDW) systems. Uncovering a low energy mode's vector properties is challenging, requiring going beyond typical spectroscopic or scattering techniques. Here, we discover an axial Higgs mode in the CDW system RTe3 using the interference of quantum pathways. In

RTe3 (R=La, Gd), the electronic ordering couples bands of equal or different angular momenta. As such, the Raman scattering tensor associated with the Higgs mode contains both symmetric and antisymmetric components, which can be excited via two distinct, but degenerate pathways. This leads to constructive or destructive interference of these pathways, depending on the choice of the incident and Raman scattered light polarization. The qualitative behavior of the Raman spectra is well-captured by an appropriate tight-binding model including an axial Higgs mode. The elucidation of the antisymmetric component provides direct evidence that the Higgs mode contains an axial vector representation (i.e. a pseudo-angular momentum) and hints the CDW in RTe3 is unconventional. Thus we provide a means for measuring collective modes quantum properties without resorting to extreme experimental conditions.

CONTRIBUTED PAPERS

AOB-04. Magnetic domain phase in van der Waals ferromagnet Fe_3GeTe_2 coupled to Co magnetic vortex state. *T. Wang*[1], A. Scholl[3], A. N'Diaye[3], X. Huang[2], H. Zhang[2], X. Zhang[4], C. Hwang[5], R. Ramesh[2] and Z.Q. Qiu[1] *1. Department of Physics, University of California, Berkeley, Berkeley, CA, United States; 2. Materials Science & Engineering, University of California, Berkeley, Berkeley, CA, United States; 3. Lawrence Berkeley National Laboratory, Berkeley, CA, United States; 4. King Abdullah University of Science and Technology (KAUST), Thuwal, Saudi Arabia; 5. Korea Research Institute of Standards and Science, Yuseong, The Republic of Korea*

Van der Waals ferromagnet Fe_3GeTe_2 (FGT) is known to possess spontaneous chiral stripe domains which can be transformed into topological skyrmions under certain conditions[1][2]. Using photoemission electron microscopy (PEEM), we imaged FGT magnetic domain phase under the influence of magnetic vortices. FGT flakes in contact with micron sized Co disks across a spacer layer were fabricated by dry transfer method. We find that the vortex state of the Co disk melts the FGT stripes into elongated bubble states which resemble the liquid crystal phase[3]. The FGT elongated bubbles above the Co disk region and the FGT stripes outside the Co disk region tend to be aligned parallelly to the Co local magnetization to circulate around the Co disk center. Micromagnetic simulation reproduces most of the experimental result. Our findings provide another novel spin texture phase in van der Waals magnetic materials.

1. Q. Li, et al. *Nano letters,* 18, 5974 (2018). 2. M. Yang, et al. *Science Advance,* 6, eabb5157 (2020). 3. A. Vaterlaus, et al. *Physical Review Letters*, 84, 2247 (2000).

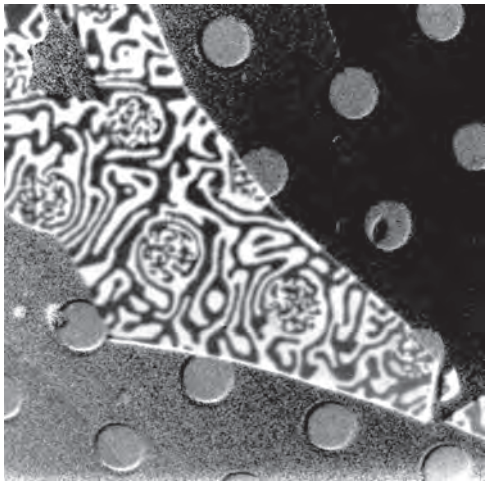

AOB-05. Evolution of anisotropic magnetic properties through helix-to-fan transition in a helical antiferromagnet $EuCo_2As_2$. *J. Kim*[1], M. Kim[1], J. Hong[1], H. Shin[1], K. Jeong[1], J. Kim[1], K. Moon[1], N. Lee[1] and Y. Choi[1] *1. Department of Physics, Yonsei university, Seoul, The Republic of Korea*

A helimagnet comprises a noncollinear spin structure formed by competing exchange interactions. Recent advances in antiferromagnet-based functionalities have broadened the scope of target materials to noncollinear antiferromagnets. However, a microscopic understanding of magnetic anisotropy associated with intricate evolution of non-collinear spin states has not been elucidated thus far. Here we have explored anisotropic magnetic aspects in a layered helimagnet of $EuCo_2As_2$ by measuring magnetic-field and angle dependences of magnetic toques. By adopting an easy-plane anisotropic spin model, we could visualize the detailed spin configurations evolving in the presence of rotating magnetic fields. This is directly related to two distinctive magnetic phases characterized by the reversal of magnetic torque variation across the helix-to-fan transition. Our advanced approach renders an in-depth understanding of anisotropic properties in the noncollinear-type antiferromagnet and a useful guidance of potential application for spin-processing functionalites.

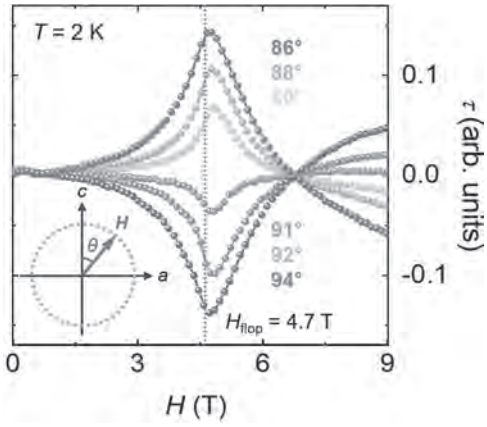

Magnetic-field dependence of the magnetic torque, τ, measured at θ = 86°, 88°, 89°, 91°, 92°, and 94° for T = 2 K

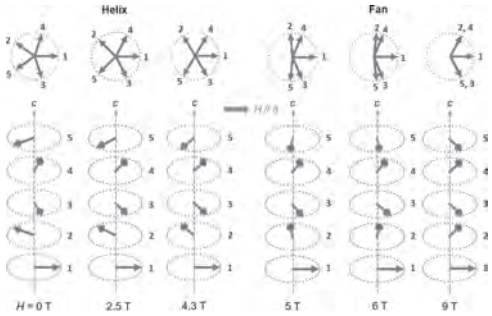

Spin states in helix and fan phases

AOB-06. Tailoring spin-dependent tunneling transport in switchable molecules based magnetic tunnel junctions. L. Jerro[1], F. Godel[1], S. Collin[1], A. Vecchiola[1], K. Bouzehouane[1], P. Yu[2], T. Mallah[2], F. Petroff[1], P. Seneor[1] and *R. Mattana*[1] *1. Unite Mixte de Physique CNRS-Thales, Palaiseau, France; 2. ICMMO, Orsay, France*

Integration of organic compounds as tunnel barrier in magnetic tunnel junctions (MTJs) is envisioned as an opportunity to engineer spintronics devices at the molecular scale. Actually, thanks to the spin-dependent hybridization at ferromagnet/molecule interfaces, spin polarization and thus tunnel magnetoresistance (TMR) can be tailored [1]. Among molecular systems, self-assembled monolayers of molecules appear as a promising tool to tailor MTJs properties. Indeed, the anchoring group, body and head of molecules can be changed to tune the coupling strength of both ferromagnetic electrodes independently. However, up to now, only basic molecules such as alkane chain have been integrated into MTJs [2-4]. These molecules could be defined as "passive" since their electronic properties cannot be switched by external stimulus. In this talk we will present molecular MTJs integrating "active" molecules from the diarylethene molecule family. These molecules can be optically switched between two stable states corresponding to an open and a closed form of its central part (figure 1). As electron delocalization, energy gap and coupling strength to the electrodes depend on the molecule state, the tunnel resistance and TMR is expected to be tuned by switching the molecule. We will first present electrical characterization (conductance and inelastic electron tunneling spectroscopy measurements) of NiFe/diarylethene/Co MTJs. This allows us to demonstrate that these photoswitchable molecules act as tunnel barrier. We will then show TMR curves obtained for molecules in both open and closed formed. Lastly, we will present the effect of the molecular switching on both tunnel resistance and TMR (figure 2). All these studies demonstrate that switchable active molecules can be successfully integrated into MTJs to build multifunctional spintronics devices electrically and/or optically controllable.

[1] C. Barraud et al., Nat. Phys. 6, 615 (2010) [2] J. R. Petta et al., Phys. Rev. Lett., 93, 136601 (2004) [3] W. Wang et al., Appl. Phys. Lett. 89, 153105 (2006) [4] M. Galbiati et al., Adv. Mater. 24, 6429 (2012)

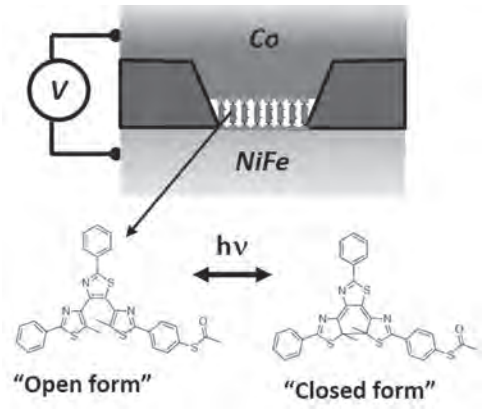

Fig. 1 Scheme of the switchable molecules based MTJs. Diarylethene molecules in both open and closed forms are also shown.

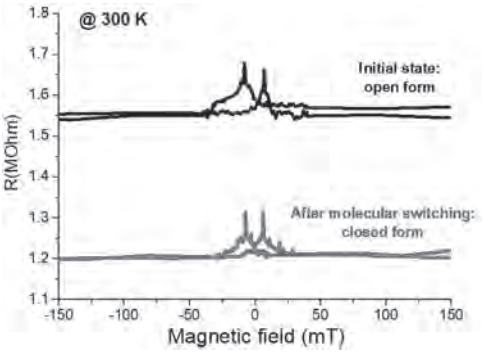

Fig. 2 TMR curves recorded at room temperature before and after molecular switching.

AOB-07. Electron Paramagnetic Resonance of Alkali Metal Atoms and Dimers on MgO. *S. Kovarik*[1], R. Robles[2], R. Schlitz[1], T.S. Seifert[1,3], N. Lorente[2,4], P. Gambardella[1] and S. Stepanow[1] *1. Department of Materials, ETH Zurich, Zurich, Switzerland; 2. Centro de Física de Materiales, San Sebastian, Spain; 3. Department of Physics, Freie Universitat Berlin, Berlin, Germany; 4. Donostia International Physics Center, San Sebastian, Spain*

Electron paramagnetic resonance (EPR) provides unique insight into the chemical structure and magnetic properties of dopants in oxide and semiconducting materials, which are of interest for applications in quantum sensing, electronics, and catalysis. EPR combined with scanning tunneling microscopy (STM) allows sub-microelectronvolt energy resolution and atomic scale spatial resolution [1], and enables coherent manipulation of the spin state of individual adsorbates [2].To implement this technique, we have installed a radio-frequency antenna into a low-temperature STM setup working at 4.5 K [3]. We use EPR–STM for probing the spin state of artificially assembled alkali metal dimers on an ultrathin MgO layer on a Ag substrate [4]. We observe a magnetic moment of 1 μ_B for Li_2, LiNa, and Na_2 indicating spin radicals with a charge state of +1e. The magnetic moment of the alkali dimers originates from an unpaired electron residing in the bonding molecular orbital. In contrast, individual alkali atoms show no magnetic moment due to the charge transfer of the valence electron to the Ag substrate. This difference between individual atoms and dimers is induced by the increase in the electron affinity when forming dimers. The alkali metal dimers represent a convenient platform for future studies of spin-spin interactions in artificially built structures thanks to the reliable atomic manipulation and simple electronic structure. Our work demonstrates the use of EPR-STM for the characterization of the electronic and magnetic state of electron donor atoms and dimers on a dielectric substrate.

[1] S. Baumann, W. Paul, T. Choi et al., Science, Vol. 350, p. 417–420 (2015). [2] K. Yang, W. Paul, S.-H. H. Phark et al., Science, Vol. 366, p. 509–512 (2019). [3] T. S. Seifert, S. Kovarik, C. Nistor et al., Phys. Rev. Res., Vol. 2, p. 013032 (2020). [4] S. Kovarik, R. Robles, R. Schlitz et al., Nano Lett., Vol. 22, p. 4176–4181 (2022).

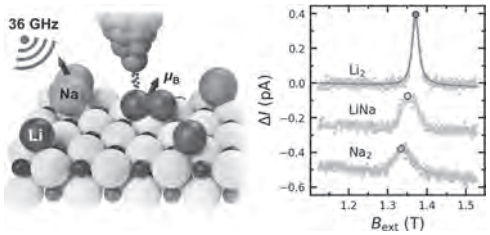

(left) Illustration of the EPR-STM measurement of individual alkali metal dimers. (right) Change of tunneling current Δ*I* induced by the radio-frequency excitation at 36 GHz as a function of the external magnetic field B_{ext}. The peak in the spectra indicates the resonant excitation of the magnetic moment. The spectra are vertically offset for clarity.

AOB-08. Critical dielectric susceptibility at a magnetic BEC quantum critical point. *D. Flavian Blasco*[1], S. Hayashida[1], Z. Yan[1], K. Povarov[1], S. Gvasaliya[1] and A. Zheludev[1] *1. ETH Zurich, Zurich, Switzerland*

We report on the latest developments on the unique physics displayed by the frustrated quantum magnet $Rb_2Cu_2Mo_3O_{12}$. Much has been argued about its magnetic and dielectric properties, including the existence of ferroelectricity driven by exotic spin-chiral order, even in the absence of long range magnetism [1,2]. However, the lack of single-crystal samples was a patent problem, hampering further understanding of the underlying relevant mechanisms. We succeeded in growing macroscopic crystalline samples of $Rb_2Cu_2Mo_3O_{12}$, which brought along a number of important breakthroughs [3,4]. Of particular interest are the results regarding the magnetic-field-tuned Bose-Einstein Condensation of magnons. The measurable magnetoelectric coupling in this material allowed to directly measure from the dielectric channel the critical susceptibility at a Bose-Einstein Condensation transition, a quantity that is usually experimentally inaccessible or even non-physical. The observed power-law behavior is in very good agreement with theoretical expectations for three-dimensional Bose-Einstein Condensation [5]. Additionally, magnetic presaturation phases are revealed in this compound, which may feature exotic order with unconventional broken symmetries.

[1] Y. Yasui, et al., J. Appl. Phys., Vol. 113, 17D910 (2013). [2] H. Ueda, et al., Phys. Rev. B, Vol.101, 140408(R) (2020). [3] S. Hayashida, et al., Phys. Rev. B, Vol. 100, 134427 (2020). [4] D. Flavián, et al., Phys. Rev. B, Vol. 101, 224408 (2020). [5] S. Hayashida, D. Flavián, et al., Phys. Rev. Research, Vol. 3, 033053 (2021).

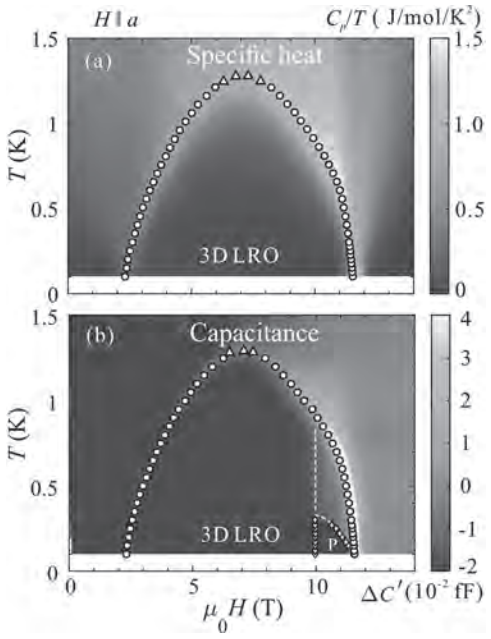

False-color plots of (a) specific heat and (b) change in capacitance in $Rb_2Cu_2Mo_3O_{12}$ single crystals. Symbols show transition points extracted from (a) specific heat data and (b) capacitance, delineating the dome of 3D long-range magnetic order. A presaturation phase (P) can be identified in the capacitance scans.

AOB-09. Direct exchange-interactions boost magnetic frustration and a large zero-point entropy in the novel $MnTa_2N_4$ diamond-lattice spinel. R. Trócoli[1], C. Frontera[1], J. Oró-Solé[1], C. Ritter[2], P. Alemany[3,4], E. Canadell[1], M. Palacín[1], A. Fuertes[1] and *J. Fontcuberta*[1] *1. ICMAB-CSIC, Bellaterra, Spain; 2. Institut Laue-Langevin, Grenoble, France; 3. Departament de Ciència de Materials i Química Física, Universitat Barcelona, Barcelona, Spain; 4. Institut de Química Teòrica i Computacional (IQTCUB), Universitat Barcelona, Barcelona, Spain*

Frustration is instrumental in the suppression of long range magnetic order. It may booster spin fluctuations that ultimately may give rise to quantum spin liquids. In geometrically frustrated systems, competing interactions may lead to a quasi-degenerate ground state and complex short-range magnetic structures. Spinels AB_2X_4, where magnetic ions exclusively occupy the tetrahedral A-sites, are examples of frustrated magnetic systems due to the presence of competing interactions among nearest-neighbors (J_{nn}) and next-nearest-neighbors (J_{nnn}) magnetic ions. Exotic phenomena such as order-by-disorder and spiral spin-liquids [1], vortex-like states [2] or kinetically inhibited-order [3] have been identified in some AB_2X_4 (X = O, S, and Se) spinel compounds. Current understanding is based on the existence of J^{in}_{nn} and J^{in}_{nnn} indirect (super) exchange interactions between the magnetic ions mediated by the bridging anions [1]. Here, we report on the synthesis and characterization [4] of new spinel nitride: $MnTa_2N_4$, where N-Ta and N-Mn hybridization are expected to modulate J^{in}_{nn} and J^{in}_{nnn} interactions. Neutrons and X-ray diffraction data confirm the spinel structure of the compound. It is found that although magnetic interactions become perceptible at temperatures as high as ≈ 80 K, a peak in the magnetic susceptibility only occurs at about 5 K, which is a signature of frustration. Magnetic order emerges at low temperature, where only a fraction (≈ 2/3) of Mn^{2+} spins order in a short-range degenerated spiral state. However, detailed analysis of structure and magnetic interactions, supported by first-principle calculations, have disclosed that the direct Mn-Mn interactions J^{d}_{nn} in magnetic spinels is much larger than commonly assumed and play a fundamental role enhancing the frustration ($f = (J^{d}_{nn} + J^{in}_{nn})/ J^{in}_{nnn})$). Interestingly, calorimetric data reveals the presence of a large zero-point magnetic entropy, which amounts about 30% of the spin entropy. This observation,

consistent with the observation of a limited magnetic order, suggest that spinel nitrides offer a new route for the research of quantum materials.

[1] D. Bergman et al. Nature Physics 3, 487 (2007) [2] S. Gao, Nature Physics 13, 157 (2017) [3] G. J. MacDougall et al. PNAS 108 15693 (2011) [4] R. Trócoli et al. Chem. Mat. Accepted for publication (2022)

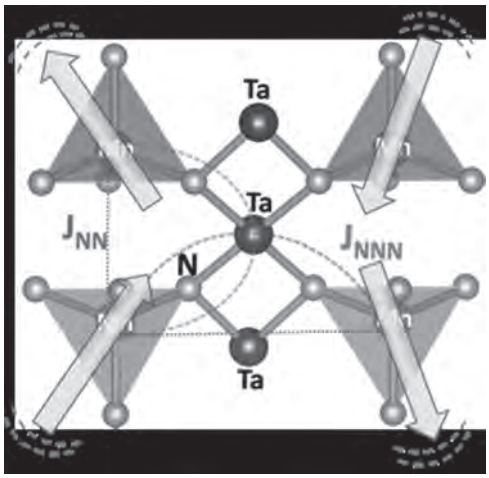

AOB-10. Energy-level-dependent magnetic characters of Ferrimagnetic TbCo film. J. Park[1], W. Kim[2], W. Won[1], J. Kang[2], S. Lee[4], B. Park[4], B. Ham[3], F. Rotermund[1] and *K. Kim*[1] *1. Physics, KAIST, Daejeon, The Republic of Korea; 2. Samsung, HwaSeong, The Republic of Korea; 3. GIST, Gwangju, The Republic of Korea; 4. Materials Science and Engineering, KAIST, Daejeon, The Republic of Korea*

Rare earth (RE)–transition metal (TM) ferrimagnet is receving of great interest [1], because the unique coupling of RE and TM moments enables the antiferromagnetic spin dynamics [2]. Since magnetic moments of RE material originates primarily from the 4*f*-electrons which locates far below the Fermi level while that of TM arises from the 3*d*-electrons near the Fermi level [3], magnetic moment configuration at different energy levels should be studied more carefully. However, such energy-level dependent approaches have largely been ignored in spintronic researches. Here we present the experimental evidences for the energy-level-dependent distinct magnetic moment configuration in ferrimagnetic TbCo alloys. Four different approaches such as Hall measurement, VSM measurement, TR-MOKE measurement, THz emission measurement, were used to study the magnetic moment at different energy levels. We found that the magnetic moments at deeper energy level are rather easily altered by the external magnetic field than those at Fermi level, suggesting that the magnetic moment responds differently depending on the energy level. Further investigation on the temperature dependence shows that the Tb moment exhibits the spin glass-like freezing possibly induced by the random anisotropy of Tb. Our results reveal the important energy-level dependent characteristics of RE-TM ferrimagnets and therefore pave the way towards a better understanding of antiferromagnetic spin dynamics in RE-TM ferrimagnets

[1] SK Kim *et al., Nat. Mater*., Vol. 21, p. 24 (2022) [2] K. -J. Kim *et al., Nat. Mater*., Vol. 16, p. 1187 (2017) [3] Khorsand, A. R et al. *Physical review letters.,* Vol. 110, p. 107205 (2013).

AOB-11. Partial lifting of Degeneracy in the J1-J2-J3 Ising Antiferromagnet on the Kagome Lattice. *J. Colbois*[1,2], B. Vanhecke[3], L. Vanderstraeten[4], A. Smerald[5], F. Verstraete[4] and F. Mila[1] *1. Institut de Physique, Ecole Polytechnique Fédérale de Lausanne, Lausanne, Switzerland; 2. CNRS / Université Paul Sabatier, Toulouse, France; 3. Faculty of Physics, University of Vienna, Vienna, Austria; 4. Department of Physics and Astronomy, University of Ghent, Ghent, Belgium; 5. Campus Alpin, KIT, Garmisch-Partenkirchen, Germany*

Motivated by dipolar-coupled artificial spin systems [1,2,3], I will present a theoretical study of the classical J1 – J2 – J3 Ising antiferromagnet on the kagome lattice [4]. We establish the ground-state phase diagram of this model for J1 > |J2|, |J3| based on exact results for the ground-state energies obtained with a method of inequalities [5] complemented by dual-worm Monte Carlo simulations [6]. When all the couplings are antiferromagnetic, the model has three macroscopically degenerate ground-state phases, and using tensor networks [7], we can calculate the entropies of these phases and of their boundaries very accurately. In two cases, the entropy appears to be a fraction of that of the triangular lattice Ising antiferromagnet, and we provide analytical arguments to support this observation. We also notice that, surprisingly enough, the dipolar ground state [1,2] is not a ground state of the truncated model, but of the model with smaller J3 interactions, an indication of a very strong competition between low-energy states in this model.

[1] I. A. Chioar, N. Rougemaille, and B. Canals, Phys. Rev. B 93, 214410 (2016). [2] J. Hamp, R. Moessner, and C. Castelnovo, Phys. Rev. B 98, 144439 (2018). [3] L. F. Cugliandolo, L. Foini, and M. Tarzia, Phys. Rev. B 101, 144413 (2020). [4] J. Colbois, B. Vanhecke, et al., arXiv:2206.11788 (2022) [5] J. Kanamori, Prog. Theor. Phys. 35, 16–35 (1966). [6] G. Rakala, K. Damle, PRE 96, 023304 (2017) [7] B. Vanhecke, J. Colbois, et al., Phys. Rev. Research 3, 013041 (2021).

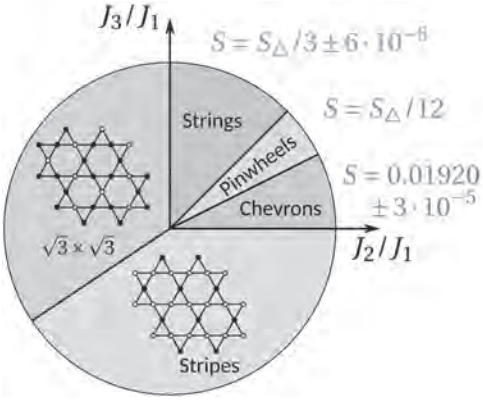

Ground-state phase diagram of the J1-J2-J3 model for J1 > J2, J3. For antiferromagnetic values of J2 and J3 we find three phases with macroscopic ground-state degeneracies.

AOB-12. Withdrawn

AOB-13. Magnetic Relaxation Dynamics of Frustrated Glassy Tetragonal Spinel $Cu_{0.2}Zn_{0.8}FeMnO_4$. *S.K. Jena*[1], T. Sarkar[2], B. Weise[3] and S. Thota[1] *1. Physics, Indian Institute of Technology Guwahati, Guwahati, India; 2. Materials Science and Engineering, Uppsala University, Uppsala, Sweden; 3. Institute for Complex Materials, Leibniz-IFW Dresden, Dresden, Germany*

Spinel oxides (AB_2O_4) are well known materials which possess two important features making them prone to exhibit unusual magnetic properties: (*i*) competing exchange interactions (J_{AB}, J_{BB}, and J_{AA}) and (*ii*) the topology of B-sublattice, particularly favorable to the development of geometrical frustration [1,2]. Among the various classes of spinels, $ZnFe_2O_4$

is a unique system where the B site cations form a network of tetrahedra sharing their corners (similar to Pyrochlore systems), giving rise to high degree of magnetic frustration. These pyrochlore like structures have great applications in magneto-electronic devices [3,4]. In the current work we focus on the magnetic relaxation dynamics and heat capacity ($C_P(T)$) studies of polycrystalline bulk $Zn(Fe_{1-x}Mn_x)_2O_4$ where the combined effects from dilute substitution of Jahn-Teller active Cu^{2+} and Mn^{3+} ions are expected to alter the exchange coupling significantly by lifting the ground state degeneracy. Our results revealed coexistence of ferrimagnetism (FiM) and spin-glass state in $Zn_{0.8}Cu_{0.2}FeMnO_4$ without signatures of standard long-range ordering, as inferred from the ac-susceptibility (χ' and χ'') and $C_P(T,H)$ studies. From the $\chi''(T)$ (loss spectrum) shown in fig. 1a, we obtain a main cusp ~ 47.2K along with two more anomalies at 8.9K and 63K. Moreover, the differential analysis ($\partial(\chi'T)/\partial T$ vs. T) yields a local minimum at 79K, referred to as the FiM Néel temperature, T_{FiM}. Frequency dispersion noticed in both $\chi'(T)$ and $\chi''(T)$ (fig. 1b) provide the signatures of spin-glass state below T_{FiM}. The empirical-scaling-laws like Vogel-Fulcher law and Power-Law ($\tau=\tau_0[(T-T_{SG})/T_{SG}]^{-z\upsilon}$) are used to determine the spin freezing temperature T_{SG}=41.8K, the critical exponent $z\upsilon$=8.9 and the relaxation time $\tau_0=1.5\times10^{-10}$s resulting in the evidence of cluster-spin-glass like state present in $Zn_{0.8}Cu_{0.2}FeMnO_4$. A detailed *dc*-field dependent static (χ_{DC}) and dynamic susceptibility studies further support the glassy characteristics of the system below T_{FiM}.

[1] S. T. Bramwell, M. J. Harris, B. C. den Hertog, M. J. P. Gingras, J. S. Gardner, D. F. McMorrow, A. R. Wildes, A. L. Cornelius, J. D. M. Champion, R. G. Melko, and T. Fennell, *Phys. Rev. Lett.* 87, 047205 (2001) [2] G. Srinivasan and M. S. Seehra, *Phys. Rev. B* 28, 1 (1983) [3] E. Maniv, R. A. Murphy, S. C. Haley, S. Doyle, C. John, A. Maniv, S. K. Ramakrishna, Y. L. Tang, P. Ercius, R. Ramesh, A. P. Reyes, J. R. Long, and J. G. Analytis, *Nat. Phys.* 17, 525 (2021) [4] W. Schiessl, W. Potzel, H. Karzel, M. Steiner, G. M. Kalvius, A. Martin, M. K. Krause, I. Halevy, J. Gal, W. Schäfer, G. Will, M. Hillberg, and R. Wäppling, *Phys. Rev. B* 53, 9143 (1996)

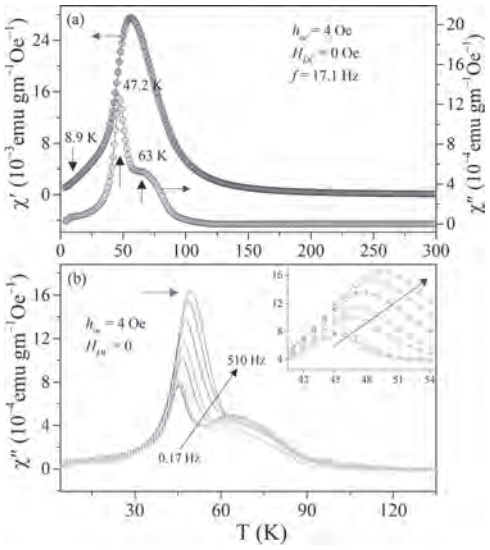

Temperature dependence of (a) real χ' (LHS) and imaginary χ'' (RHS) measured at a fixed frequency f =17.1Hz and (b) χ'' vs. T measured between f = 0.17Hz and 510Hz. Inset shows the zoomed view across the main cusp of $Zn_{0.8}Cu_{0.2}FeMnO_4$.

Session AOC
SUPERCONDUCTIVITY AND QUANTUM MATERIALS

Mahmud Khan, Chair
Miami University, Oxford, OH, United States

CONTRIBUTED PAPERS

AOC-01. Antiferromagnetic ordering and its interplay with superconductivity in Mn doped $CaKFe_4As_4$. *A. Sapkota*[1,2], J.M. Wilde[1,2], M. Xu[1,2], P.C. Canfield[1,2], S.L. Bud'ko[1,2], A. Kreyssig[4], Y. Furukawa[1,2], W. Tian[3] and Q. Ding[1] *1. Ames National Laboratory, Ames, IA, United States; 2. Iowa State University, Ames, IA, United States; 3. Oak Ridge National Laboratory, Oak Ridge, TN, United States; 4. Ruhr University, Bochum, Germany*

A phase diagram with intertwined structural, magnetic and superconducting ground states is characteristic for high-T_c iron(Fe)-based superconductors (FeSCs). Understanding the interplay of different states is key for understanding the fundamentals of unconventional superconductivity (SC) [1]. Among various structural classes within FeSCs, $AeAFe_4As_4$ (*Ae* = Alkaline Earth Metal; *A* = Alkali Metal) (1144) family [2] has some peculiar distinction in comparison to much studied 122 AFe_2As_2 family. Stoichiometric 1144 is a superconductor at ambient pressure with relatively high T_c = 35 K and has reduced crystal symmetry as compared to 122 family. On the other hand, like other FeSCs, chemical substitution does tune its physical properties and even change the ground states. For instance, partial Co or Ni-substitution at Fe site in $CaKFe_4As_4$ shifts superconducting state to coexist with exotic hedgehog-spin-vortex-crystal (hSVC) antiferromagnetic (AFM) order [3,4]. Single-crystal neutron diffraction data provided that hSVC order is non-collinear, commensurate and in-plane hSVC arrangement has simple AFM stacking along *c*-axis. Similar to 122 family, the long-range AFM order coexists and competes with SC suggesting similar interplay and pairing mechanism with s^{+-} symmetry. Because no SC was induced in Mn-doped 122 [6], the intrinsic SC in $CaKFe_4As_4$ offers possibility of studying the effects of Mn doping on SC. Despite Mn behaving like a large local magnetic impurity, it seems to have similar qualitative effects as Co or Ni doped1144 but with differences in details. Temperature-composition (T-x) phase diagram, Fig. 1, from the single-crystal study of $CaK(Fe_{1-x}Mn_x)_4As_4$ in Ref. [8] shows that increasing Mn substitution suppresses SC and stabilizes AFM order. Our NMR, Mössbauer and neutron diffraction measurements establish a non-collinear, commensurate and long-range hSVC order. Furthermore, hSVC order competes and coexists with SC indicating similar interplay. However, the previously observed suppression of magentic order below T_c is absent suggesting that magnetic pairbreaking associated with the Mn moment may be changing details of how AFM order and the SC state interact.

[1] I. I. Mazin, Nature 464, 183 (2010) [2] A. Iyo *et al.* J. Am. Chem. Soc. 138, 3410 (2016) [3] W. R. Meier *et al.* npj Quant. Mat. 3, 5 (2018) [4] A. Kreyssig *et al.* Phys. Rev. B 97, 224521 (2018) [5] R. M. Fernandes *et al.* Phys. Rev. B 93, 014511 (2016) [6] A. Thaler *et al.* Phys. Rev. B 84, 144528 (2011) [7] A. Pandey *et al.* Phys. Rev. B 84, 014405 (2011) [8] M Xu *et al.* arXiv:2204.10925 (2022)

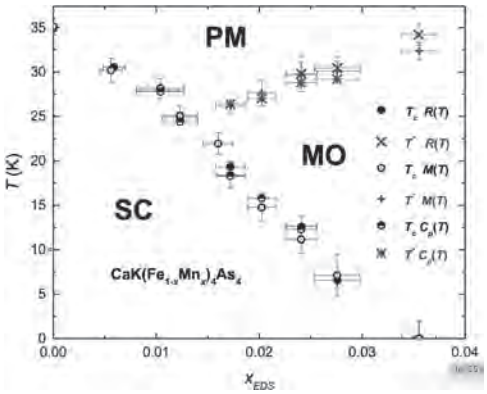

Fig. 1: T-*x* phase diagram of $CaK(Fe_{1-x}Mn_x)_4As_4$

AOC-02. Withdrawn

INVITED PAPER

AOC-03. Ferromagnetic Josephson Junctions for Cryogenic Memory. *N.O. Birge*[1] *1. Physics and Astronomy, Michigan State University, East Lansing, MI, United States*

Interest in superconducting computing is being driven by two concerns. On the one hand, large-scale computing facilities and data centers are using electrical power at an ever-increasing rate. Projections suggest that a fully superconducting computer would consume considerably less power than conventional semiconductor-based computers [1]. On the other hand, a quantum computer based on superconducting qubits would benefit from having a classical superconducting processor nearby in the cold space, to avoid a plethora of control and readout lines between room temperature and the cold space [2]. Building a large-scale memory for a superconducting computer is a challenge. One approach is to use Josephson junctions containing ferromagnetic materials as the basic memory element for such a memory [3]. In that approach, the information storage device is a Josephson junction containing a pseudo spin valve. Depending on the relative orientation of the two magnetizations in the spin valve, and with suitably chosen thicknesses of both magnetic layers, the ground-state phase difference across the junction can be either zero or π. We have demonstrated two different types of junctions that can be controllably switched between the 0-phase state and the π-phase state [4,5]. While such junctions are promising components for a scalable superconducting memory [6], much more work needs to be done to enable scaling of this approach to a large-scale memory array. Work supported by the US DOE under grant DE-FG02-06ER46341, by Northrop Grumman Corporation, and by IARPA via U.S. Army Research Office contract W911NF-14-C-0115. The views and conclusions contained herein are those of the authors and should not be interpreted as necessarily

representing the official policies or endorsements, either expressed or implied, of the ODNI, IARPA, or the U.S. Government.

[1] D.S. Holmes, A.L. Ripple, & M.A. Manheimer, IEEE Trans. Appl. Supercond. 23, 1701610 (2013). [2] E. Leonard *et al.*, Phys. Rev. Applied 11, 014009 (2019). [3] A.Y. Herr & Q.P. Herr, US Patent 8,270,209 (2012). [4] E. C. Gingrich, B. M. Niedzielski, J. A. Glick, Y. Wang, D. L. Miller, R. Loloee, W. P. Pratt Jr., and N. O. Birge, Nature Phys. 12, 564 (2016). [5] J.A. Glick, V. Aguilar, A. Gougam, B.M. Niedzielski, E.C. Gingrich, R. Loloee, W.P. Pratt, Jr., and N.O. Birge, Science Advances 4, eaat9457 (2018). [6] I. M. Dayton *et al.*, IEEE Magnetics Lett. 9, 3301905 (2018).

CONTRIBUTED PAPERS

AOC-04. Spin Pumping Long-Range Triplet Currents into Superconducting Nb Through Cr/Fe Interfaces. *A.K. Chan*[1,2], M. Cubukcu[2], X. Montiel[3], S. Komori[3], A. Vanstone[1], J. Thompson[3], G. Perkins[1], M. Blamire[3], J. Robinson[3], M. Eschrig[4], H. Kurebayashi[2] and L. Cohen[1] *1. Physics, Imperial College London, London, United Kingdom; 2. Electronic and Electrical Engineering, University College London, London, United Kingdom; 3. Materials Science and Metallurgy, University of Cambridge, Cambridge, United Kingdom; 4. Physics, University of Greifswald, Greifswald, Germany*

Understanding the conditions required to create long-range spin-polarised supercurrents, carried by triplet Cooper pairs, is a crucial aspect of superconducting spintronics. In recent years, theoretical and experimental works have shown it is possible to form long-range triplet supercurrents (LRTS) through a spatially varying magnetization at a superconducting/ferromagnetic (S/F) interface [1,2]. By including a spatially varying magnetization, singlet-to-triplet conversion can occur via the proximity effect with spin-mixing and spin-rotation processes. For example, experimental evidence of LRTS has been found in Nb/Cr/Fe/Cr/Nb Josephson junctions [3]. The Cr interdiffuses into Fe to create a spatially inhomogeneous magnetic layer. Independently, studies on spin pumping by ferromagnetic resonance (FMR) into Pt/Nb/Py/Nb/Pt stacks showed signatures of LRTS [4,5]. The presence of Pt - a strong spin-orbit-coupling layer - was necessary to observe the key signature of a broadening of the FMR linewidth. However, this empirical claim has remained contentious in the literature [6,7]. We set out to conclusively confirm the ability to spin pump LRTS into a superconductor only when the conditions are met for proximity induced triplet Cooper pairs to form. In this presentation, we discuss our results on various Nb/Cr/Fe/Cr/Nb and Nb/Fe/Nb multilayer films [8], which demonstrate in-plane uniaxial anisotropy. We study their Gilbert damping behaviour above and below the superconducting critical temperature T_c, extracted from their FMR absorption derivatives (Fig. 1). We observe key signatures of LRTS, related to the broadening of the FMR linewidth, only when certain criteria are met: when Cr is present and when the external field is applied in the films' hard axes. A triplet channel can only open when the interfacial spin layer is unsaturated. We compare the strength of the triplet channels between samples of varying anisotropy constants *K,* and discuss the implications for future experiments and the potential to exploit such uniaxial anisotropy.

[1] J. Linder and J. W. A. Robinson, *Nat. Phys.,* vol. 11, p. 307 (2015) [2] M. Eschrig, *Phys. Today*, vol. 64, p. 43 (2011) [3] J. W. A. Robinson, N. Banerjee and M. G. Blamire, *Phys. Rev. B*, vol. 89, p. 104505 (2014) [4] K-R. Jeon, C. Ciccarelli, H. Kurebayashi et al., *Phys. Rev. B*, vol. 99, p. 024507 (2019) [5] K-R. Jeon, X. Montiel, S. Komori, et al, *Phys. Rev. X*, vol. 10, p. 031020 (2020) [6] M. A. Silaev, *Phys. Rev. B*, vol. 102, p. 180502 (2020) [7] M. Muller, L. Liensberger, L. Flacke, et al., *Phys. Rev. Lett.*, vol. 126, no. 8, p. 087201 (2021) [8] A. K. Chan, M. Cubukcu, X. Montiel et al., arXiv:2202.01520 [cond-mat.supr-con] (2022)

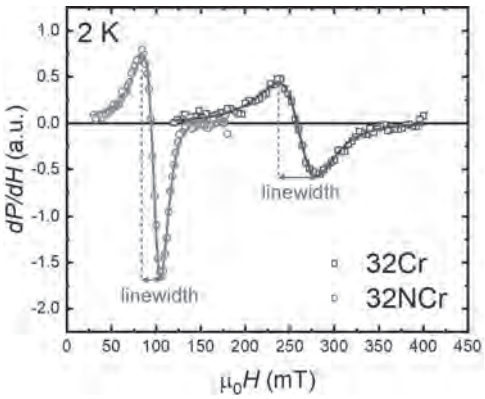

Fig.1 FMR absorption peak derivatives of a film: with Cr, 32Cr [Nb(32)/Cr(1)/Fe(6)/Cr(1)/Nb(32)]; and without Cr, 32NCr [Nb(32)/Fe(6)/Nb(32)]. Numbers in brackets are thicknesses in nm.

AOC-05. Withdrawn

AOC-06. Growth and vortex state study of Fe (Te, Se) superconducting thin films on YSZ substrates. R. Kumar[1], A. Mitra[1] and *G.D. Varma*[1] *1. Physics, Indian Institute of Technology Roorkee, Roorkee, India*

Among the Fe-based superconductors, Fe(Te, Se) superconductors are more interesting due to their simplest crystal structure and less toxic constituent elements, making them the prime candidate for investigating the mechanism of superconducting in these materials [1-4]. These superconductors show high upper critical magnetic fields ($H_{C2}(0)$) and high critical current densities even at high magnetic fields [5, 6]. In the present work, Fe(Te, Se) superconducting thin films of two different thicknesses have been deposited on (*100*) oriented yttria-stabilized zirconia (YSZ) substrates by the pulsed laser deposition technique and their structural and superconducting properties have been investigated. The XRD results reveal that the grown films are mainly (*00l*) orientated which suggests the unidirectional growth of thin films. The temperature dependent resistivity measurements show that the thin film of higher thickness has higher onset of superconducting transition of ~13.16 K compare to the lower thickness thin film. Also, the $H_{C2}(0)$ values have been calculated via Ginzburg Landau theory as well as by the Werthamer-Helfand-Hohenberg model using the magnetoresistance measurement data under the magnetic field of 0-8 T [5]. Both the models suggest that the $H_{C2}(0)$ values are high for higher thickness thin films as compare to the thin films with lower thickness. Using the $H_{C2}(0)$ values, corresponding GL coherence lengths have also been calculated. Moreover, using the magnetoresistance measurement, the thermal activation energies (TAE) of both the thin films have been estimated via the conventional as well as by the modified thermally activated flux flow (TAFF) models. From both the models, TAE have been observed high for the higher thickness thin film. Furthermore, the results for vortex phase study reveals the transition from vortex liquid region to the vortex glass region at higher temperatures for higher thickness thin film.

1. Y. Kamihara, T. Watanabe, M. Hirano, and H. Hosono, J. Am. Chem. Soc. 130, 3296 (2008). 2. F. C. Hsu, J. Y. Luo, K. W. Yeh, T. K. Chen, T. W. Huang, P. M. Wu, Y. C. Lee, Y. L. Huang, Y. Y. Chu, D. C. Yan, and M. K. Wu, Proc. Nat. Acad. Sci. U.S.A.105, 14262 (2008). 3. H. Hosono and K. Kuroki, Physica C 514, 399 (2015). 4. W. Bao, Y. Qiu, Q. Huang, M. A. Green, P. Zajdel, M. R. Fitzsimmons, M. Zhernenkov, S. Chang, M. Fang, B. Qian, E. K. Vehstedt, J. Yang, H. M. Pham, L. Spinu, and Z. Q. Mao, Phys. Rev. Lett. 102, 247001 (2009). 5. R. Kumar and G. D. Varma, Phys. Scr. 95, 045814 (2020). 6. R. Kumar and G. D. Varma, *Phys. Status Solidi B* 257, 1900552 (2019).

AOC-07. Magneto-transport phenomena of rare-earth-based kagome magnet. J.F. Casey[1], C. Hanley[1], P. Manfrinetti[2] and *A. Pathak*[1] *1. Department of Physics, State University of New York (SUNY), Buffalo, NY, United States; 2. Department of Chemistry, University of Genova, Genova, Italy*

The magnetic topological quantum materials that contain rare earth (RE) atoms are very interesting from both fundamental study and application perspectives. The physical properties of these materials are distinct from common metals and alloys and have emerged as an extraordinarily prolific ground of materials science research for high efficient electronic and quantum-phenomena-based devices. One of the examples is kagome materials which become an interesting platform to study the interplay among symmetry, magnetism, topology, and electron correlation. Our latest works in $REMn_6Sn_6$ have illustrated that this family could be fascinating to investigate various physical phenomena due to large spin-orbit coupling and strong magnetic ordering [1, 2]. However, high-quality samples are still limited, and a detailed study of magnetism and electrical transport is also lacking. Therefore, the understanding of fundamental science and thereby the design of the materials for future quantum computation applications is limited. Here we present the synthesis of various high-quality single-crystalline magnetic kagome materials and discuss their details of magnetic and electronic properties. As an example, in this presentation, we focus on the synthesis of single-crystalline $REMn_6Sn_6$ (RE = Er, Ho) materials. We also discuss the magnetic and transport phenomena at various temperatures, magnetic fields, and applied pressure.

[1] Anisotropically large anomalous and topological Hall effect in a kagome magnet G. Dhakal, F. Kabeer, A. K. Pathak, F. Kabir, N. Poudel, R. Filippone, J. Casey, A. P. Sakhya, S. Regmi, C. Sims, K. Dimitri, P. Manfrinetti, K. Gofryk, P. M. Oppeneer, and M. Neupane, Phy. Rev. B 104, L161115 (2021). [2] Unusual magnetic and transport properties with Chern gapped Dirac states in $HoMn_6Sn_6$ F. Kabir, R. Filippone G. Dhakal, Y. Lee, N. Poudel, J. Casey, A. P. Sakhya, S. Regmi, R. Smith, K. Dimitri, P. Manfrinetti, L. Ke, K. Gofryk, P. M. Oppeneer, and M. Neupane, and A. K. Pathak, Phy. Rev. Mater. 6, 064404 (2022).

AOC-08. Spin-flip-driven reversal of the angle-dependent magnetic torque in layered antiferromagnetic $Ca_{0.9}Sr_{0.1}Co_2As_2$. *J. Seo*[1], J. Kim[1], M. Kim[1], K. Jeong[1], H. Shin[1], J. Hong[1], J. Kim[1], K. Moon[1], N. Lee[1] and Y. Choi[1] *1. Physics, Yonsei University, Seoul, The Republic of Korea*

A spin–flip transition can occur in antiferromagnets under strong magnetocrystalline anisotropy, inducing a significant modification of the anisotropic magnetic properties through phase conversion. In contrast to ferromagnets, antiferromagnets have not been thoroughly examined in terms of their anisotropic characteristics. In this study, we investigate the magnetic field and temperature evolutions of the anisotropic aspects of Ising-type antiferromagnet $Ca_{0.9}Sr_{0.1}Co_2As_2$ using torque magnetometry measurements. We found that an A-type antiferromagnetic order emerges below T_N = 97 K, aligned along the magnetically easy c axis. The reversal of the angle-dependent torque across the spin–flip transition was observed, revealing the influence of the magnetocrystalline anisotropy on the anisotropic magnetic properties. Specific spin configurations associated with the magnetic torque variation in the presence of a rotating magnetic field were theoretically identified, and the experimental torque data could be fully reproduced, based on an easy-axis anisotropic spin model. Our results provide insight into fundamental and applied research on diverse antiferromagnetic compounds by opening new possibilities for distinct magnetic aspects.

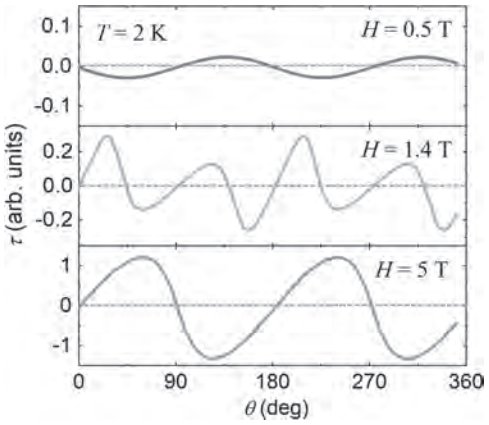

Fig. 1. Measured angle-dependent magnetic torques at 2 K.

AOC-09. Magnonic dispersion of Er_2O_3. M.E. Flatté[1] and *M. Maleki Sanukesh*[1] *1. Physics and Astronomy, University of Iowa, Iowa city, IA, United States*

Rare-earth magnets may provide useful magnetic properties for quantum technologies, including quantum transduction and quantum memories. Here we calculate the band structure of magnons in ferromagnetic Er_2O_3. Erbium, in the +3 state in this material, has 11 electrons in a 4f shell which are shielded from the surroundings by valence electrons. The localization of these 4f electrons around the ion core results in long coherence times that make Er_2O_3 a viable candidate for emerging technologies and devices such as quantum memories, single photon emitters and transduction [1]. We consider fully saturated Er_2O_3 as a ferromagnetic insulator that hosts magnons and approximate the interaction of the spins as magnetic dipole-dipole interaction. Similar models will describe other dipole-dipole interactions spins, such as ensembles of molecular spins. The Holstein-Primakoff representation is employed to quantize the Hamiltonian. Er_2O_3 has 32 erbium atoms in a non-primitive cubic unit cell. The long-range nature of magnetic dipole-dipole interaction poses a challenging issue for considering magnonic structure from dipole-dipole interactions. The dipole-dipole interaction drops as a cube power of the separation between spins, thus the strength of the coupling of the 30th nearest neighbor is 4.3% of the first nearest neighbor while the number of neighbors increases. If these long-distance neighbors are ignored the magnonic dispersion will drastically change. We will describe approaches to reach convergence in the magnon dispersion for such long-range interactions. This work was supported as part of the Center for Molecular Quantum Transduction, an Energy Frontier Research Center funded by the U.S. Department of Energy, Office of Science, Basic Energy Sciences, under Award Number DE-SC0021314.

[1] Zhong, Tian and Goldner, Philippe. “Emerging rare-earth doped material platforms for quantum nanophotonics” *Nanophotonics*, vol. 8, no. 11, 2019, pp. 2003-2015.

AOC-10. A toolbox for evaluation and optimization of proximity-induced magnetism in $MnTe/Bi_2Te_3$ heterostructures. G. Awana[1], R. Fujita[2], A. Frisk[3], P. Chen[7], Q. Yao[7], A. Caruana[4], C. Kinane[4], N. Steinke[5], S. Langridge[4], P. Olalde-Velasco[3], S. Dhesi[3], G. van der Laan[3], X. Kou[7], S. Zhang[6], T. Hesjedal[2] and *D. Backes[3] 1. Department of Physics, Loughborough University, Loughborough, United Kingdom; 2. Department of Physics, University of Oxford, Oxford, United Kingdom; 3. Diamond Light Source, Didcot, United Kingdom; 4. ISIS Neutron and Muon Source, Oxon, United Kingdom; 5. Institut Laue-Langevin, Grenoble, France; 6. School of Physical Science and Technology, ShanghaiTech University, Shanghai, China; 7. School of Information Science and Technology, ShanghaiTech University, Shanghai, China*

The introduction of magnetism in topological insulators, semiconducting materials that are non-magnetic by nature, has long been sought after in order to realize exotic quantum effects. Most prominent is the quantum anomalous Hall effect (QAHE), where electronic surface states allow the dissipationless propagation of charges through a material [1]. Additionally, these states are 100% spin-polarized and immune to external perturbations, rendering them ideal candidates for spintronic applications as well as quantum computing. The QAHE is not restricted to a particular temperature range but has so far only been observed at around 1 K in magnetically doped topological insulators [2]. Thus, the task at hand is to find new concepts to magnetize the topological insulator. Here, we investigate a new approach based on proximity induced magnetization in heterostructures, where the topological insulator Bi_2Te_3 and the topologically trivial, magnetic add-layer MnTe share an interface but are otherwise spatially separated [3]. We employ polarized neutron reflectivity, x-ray spectroscopy and magnetotransport measurements to evaluate the magnetic properties of each individual layer and the magnetic landscape at the $MnTe/Bi_2Te_3$ interface. We find the MnTe layer in a ferromagnetic instead of the anticipated antiferromagnetic state and that Mn constituents penetrate into the Bi_2Te_3 layer. Those effects go often unnoticed and can be misinterpreted as proximity induced magnetization, for which no indication can be found. Hence, we provide a robust, multitechnique approach to gain a complete picture of the magnetic structure and the toolbox to optimize the interface, thereby increasing the temperature range the QAHE can be observed in. Our work thus contributes to the transformation of magnetic topological insulators from fundamental research to practical applications.

[1] F. D. M. Haldane, Phys. Rev. Lett. 61, 2015 (1988) [2] C. Z. Chang et al., Science 340, 167 (2013) [3] G. Awana et al., Phys. Rev. Mater. 6, 053402 (2022)

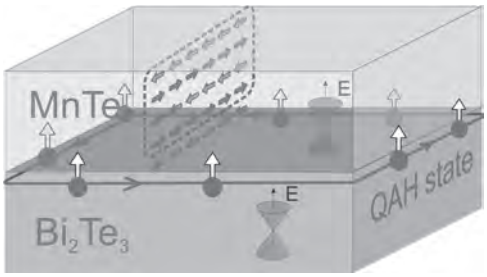

Schematic of a QAHE system based on MnTe as magnetic layer and the topological insulator Bi_2Te_3

Session APA
FUNDAMENTAL PROPERTIES AND COOPERATIVE PHENOMENA
(Poster Session)

Rajesh Chopdekar, Chair
Western Digital, San Jose, CA, United States

APA-01. Competing magnetic states in Sm_7Pd_3. *R.K. Chouhan*[2], A. Biswas[2], Y. Mudryk[2] and V. Pecharsky[2,1] *1. Department of Materials Science and Engineering, Iowa State University, Ames, IA, United States; 2. Ames National Laboratory, Ames, IA, United States*

We present results obtained within the density functional theory framework with the focus on understanding magnetic properties of Sm_7Pd_3 compound. The binary Sm_7Pd_3 compound crystallizes in the Th_7Fe_3-type structure, space group in $P6_3mc$, in which the samarium atoms occupy three independent sites two 6(c) and one 2(b), and the palladium atoms occupy a single 6(c) site. To get the correct effect of the localized Sm 4f states and account for the strong correlations between f, d and p states of constituent elements, we used the full potential linearized augmented plane wave (FP-LAPW) method as implemented in WIEN2k, along with the localized treatment of 4f states using the Hubbard U approach. Theoretically derived magnetic anisotropy confirms experimental observations, where the *c*-axis represents the easy magnetization direction. By evaluating possible magnetic states, including ferromagnetic, ferrimagnetic and partial antiferromagnetic arrangements of the magnetic moments, we find that assuming ferrimagnetic Sm_7Pd_3 leads to the best match between the calculated and experimentally observed molar magnetic moments. We also analyze and discuss how f, d, and p electrons contribute to the emergence of rather unusual magnetic phenomena observed experimentally in the magnetically hard Sm_7Pd_3 magnet. Acknowledgment: This work was performed at Ames National Laboratory and supported by the Division of Materials Science and Engineering of the Office of Basic Energy Sciences, Office of Science of the U. S. Department of Energy (DOE). Ames National Laboratory is operated for the U.S. DOE by Iowa State University of Science and Technology under Contract No. DE-AC02-07CH11358.

APA-02. Structural and Dielectric Behavior of $(Ho_{(1-x)}Nd_x)_2CoMnO_6$ (x = 0.0 – 0.2) Double Perovskite. *N. Nayak*[1] and S. Ravi[1] *1. Physics, IIT Guwahati, Guwahati, India*

Single phase polycrystalline samples of $(Ho_{(1-x)}Nd_x)_2CoMnO_6$ (x = 0.0 – 0.2) (HNCMO) double perovskite were prepared by using conventional solid state reaction route and their structural and dielectric properties were analyzed. These compounds are of monoclinic structure having space group $P2_1/n$. From the plots of XRD it is seen that the most intensed peaks are shifting towards lower Bragg angle, which reveals an increase in lattice parameters with increase in Nd doping. The grain size decreases with increase in Nd concentration which is seen from the FESEM images. The average grain size of HNCMO (x = 0.0, 0.05, 0.1, 0.2) are found to be 416μm, 347μm, 337μm, 300μm respectively. Room temperature frequency variation of real and imaginary parts of dielectric constant show a drop in their value with increase in frequency. Moreover, a dispersion in the low frequency region is observed and is attributed to the contribution of space charge polarization. At the same time, we have observed a decrease in the value of dielectric loss with Nd substitution. The frequency dependence of both real and imaginary components of impedance data show charge carriers' relaxation across grains and grain boundaries. The complex impedance data were modelled using an equivalent circuit having constant phase element and resistance. The observed impedance data deviate from the standard Debye model.

1. K. Pushpanjali Patra and S. Ravi, "Magnetic Properties and Exchange Bias Behavior in Nanocrystalline (Ho1-xSmx)2CoMnO6 (x = 0 – 0.5) Double Perovskite," *Journal of Magnetism and Magnetic Materials*, vol. 540, (2021). 2. I. N. Bhatti, I. N. Bhatti, R. N. Mahato, and M. A. H. Ahsan, "Physical properties in nano-crystalline Ho2CoMnO6," *Ceramics International*, vol. 46, no. 1, pp. 46–55, (2020). 3. Aakansha and S. Ravi, "Structural, magnetic and dielectric properties of Cr substituted yttrium iron garnets," *Journal of the American Ceramic Society*, vol. 101, no. 11, pp. 5046–5060, (2018).

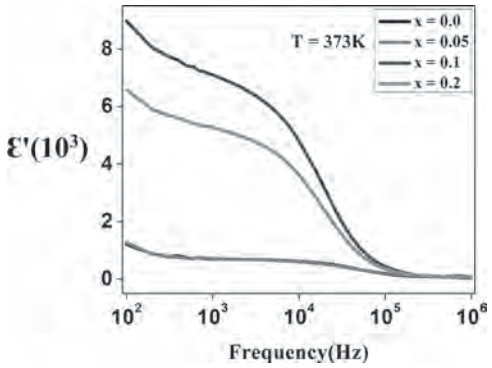

Fig.1 Variation of real part of dielectric constant with frequency at room temperature for different HNCMO samples.

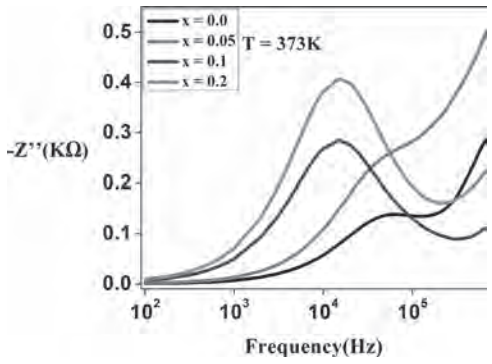

Fig.2 Variation of imaginary part of impedance with frequency at room temperature for different HNCMO samples.

APA-03. Intrinsic origin of phase transition in FeRh. M. Park[2], J. Park[1], K. Kim[1] and *M. Jung*[2] *1. Department of Physics, Korea Advanced Institute of Science and Technology, Daejeon, The Republic of Korea; 2. Department of Physics, Sogang University, Seoul, The Republic of Korea*

Phase changing materials have long been a central theme in condensed matter physics. A representative example is an iron-rhodium (FeRh) which undergoes a first-order phase transition from antiferromagnetic to ferromagnetic phase near room temperature. Along with the change of magnetic ordering, the phase transition also accompanies a significant change of electrical conductivity of about 40% [1] as well as a small expansion of the unit cell of about 1% [2]. Furthermore, the transition is modulated not only by temperature but also by magnetic field or doping [3], which makes FeRh-based materials very attractive for future applications, such as heat-mediated antiferromagnetic memory [4], magnetic refrigeration [5], and magnetic

sensors [6]. Despite the intensive researches, however, our understanding of phase transition of FeRh is still far from satisfactory. The crux of this transition is a large change in the electrical conductivity, but its origin is still under debate. Such large resistance change cannot be understood solely by the change in magnetization, i.e., magnetic scattering mechanism between antiferromagnetic and ferromagnetic spin alignments. Recently, we obtained a high-quality FeRh films with a sharp phase transition, which shows no residual magnetic moment in the antiferromagnetic phase. In this study, we investigate the fundamental electrical transport of FeRh by using terahertz time-domain-spectroscopy (THz-TDS). Based on Drude model, the extrinsic (momentum scattering time, τ) and the intrinsic (charge density/effective mass, n/m^*) contributions of electrical conductivity was quantified independently. We found that, only n/m^* changes abruptly during the phase transition, contrary to monotonic decrease of τ with increasing temperature. Therefore, our result strongly supports that the origin of the currently controversial FeRh phase transition is a change in band structure. Our work could be an important piece for the complete understanding of magnetic phase transition of FeRh.

[1] I. Sujuki *et al. J. Appl. Phys.* 109, 07C717 (2011) [2] M. Ibarra et al. Phys. Rev. B 50, 4196 (1994) [3] R. Barua et al. Appl. Phys. Lett. 103, 102407 (2013) [4] X. Marti et al. Nat. Mater. 13, 367 (2014), T. Moriyama et al. Appl. Phys. Lett. 107, 122403 (2015) [5] M. P. Annaorazov et al. J. Appl. Phys. 79, 1689 (1996), V. K. Pecharsky et al. Phys. Rev. B 64, 144406 (2001) [6] J. Van Driel et al. J. Appl. Phys. 85, 1026 (1999), V. K. Pecharsk et al. J. Magn. Magn. Mater. 321, 3541 (2009)

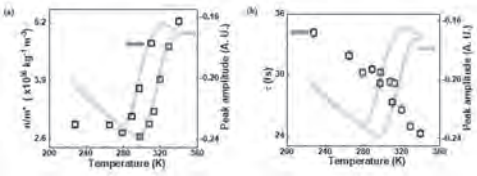

Temperature dependent negative pulse peak amplitude (grey line), compared to (a) intrinsic contribution (n/m^*) and (b) extrinsic contribution (τ) obtained by analysing complex THz conductivity based on the Drude model.

APA-04. Withdrawn

APA-05. Withdrawn

APA-06. Magnetic Phase Diagram of Antiferromagnetic Cr-Nb Alloys. *P.N. de Souza*[1], L.M. Oliveira[2], F. Yokaichiya[3], P.C. de Camargo[4] and A.J. de Oliveira[4] *1. Inst. of Physics, Universidade de Brasilia, Brasilia, Brazil; 2. Colegiado de Ciências da Natureza, Campus Senhor do Bonfim, Universidade Federal do Vale do São Francisco, Petrolina, Brazil; 3. Dept. of Physics, Federal University of Paraná, Curitiba, Brazil; 4. Dept. of Physics, Federal University of Sao Carlos, Sao Carlos, Brazil*

Chromium (Cr) is an itinerant antiferromagnet (AFM) par excellence, whose magnetic ordered state is formed by an incommensurate spin-density-wave (SDW), established by the nesting of electron and hole that comprise the Cr Fermi surface (FS). Cr and its alloys have three distinct magnetic phases, Pauli paramagnetism (P) above Neél temperature (T_N). Between T_N and T_{sf}, occurs in the transverse AFM phase, whose wave vector of the SDW is perpendicular to the spin density vector (AF_1), and below T_{sf} where the longitudinal AFM state is established, with vectors of the spin density of the SDWs are parallel to the modulation vector of the SDW (AF_2). The SF transition has been observed in several Cr alloys systems [1]. In the particular case of Cr-Nb the phase boundary between the AF1 and AF_2 has been poorly established. In this work we present the determination of the magnetic phase diagram of Cr-Nb alloys, emphasizing the spin-flip phase boundary as determined by magnetic susceptibility and electrical resistivity measurements. The samples used were polycrystalline samples of Cr-x at%Nb, with $0 \leq x \leq 3.5$, prepared by the arc-melting method, using high-purity Cr (99.9999%) and Nb (99.99%) under argon atmosphere[PC1] (99.998%). Each sample was melted several times with a mixing procedure to ensure homogeneity. The chemical composition of all samples was determined by the initial concentration of Cr and Nb, probing selected samples by Optical Emission Spectroscopy (OES). Figure 1 shows that the boundary of AF1 and P phases presents a linear dependence on Nb concentration with dT_N/dx= -71 K/at. %Nb and the antiferromagnetic order being suppressed for x = 4.4 at.%Nb. In the boundary of AF1 and AF2 phases, we found a quadratic dependence on Nb concentration and AF2 vanishes for x = 0.93 at.% Nb

[1] Fawcett, E. et al. Spin-density-waves antiferromagnetism in chromium alloys. Reviews of Modern Physics, v. 66, n. 1, p. 25-127, 1994.

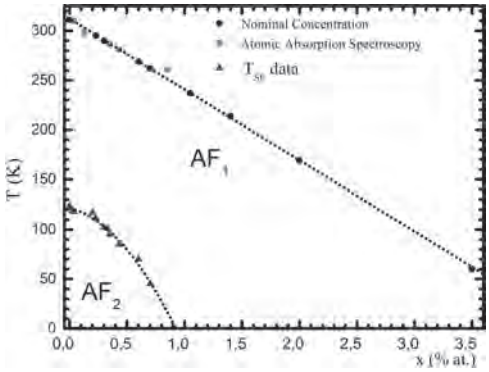

Magnetic phase diagram of CrNb alloys, showing dependence between T_N and T_{sf} vs. Nb concentration.

APA-07. Exchange Bias Effect in 6H $Ba_3Co_{0.5}Mn_{0.5}Ru_2O_9$: Effect of Magnetic Short-Range Interactions. *M.M. Kurian*[1,2] and S. Nagappan Nair[1,2] *1. Department of Physics, Indian Institute of Technology, Madras, Chennai, India; 2. Functional Oxides Research Group, Indian Institute of Technology, Madras, Chennai, India*

High pressure and high temperature synthesized 6H $Ba_3Co_{0.5}Mn_{0.5}Ru_2O_9$ (BCMRO0.5) crystalizes in $P6_3/mmc$ space group. Phase pure samples were attained at a high pressure of 8 GPa and 1100^0C. Compared to other 6H analogues, BCMRO0.5 showed broader hysteresis with coercivity 9.26 kOe at 5 K. Thermo-magnetic analysis at 100 Oe shows bifurcation between the ZFC and FC below 235 K. Below which the FC curve sharply increases and exhibits weak temperature dependence for the temperature range of 80 K - 5 K. A subtle anomaly at about 27 K in the magnetisation data is enhanced as a prominent peak in the ac susceptibility measurement. Frequency dependent shift of the ac susceptibility peak to higher temperature is noted and analysed to be driven due to short range ordering of spins below 27 K. Fairly high coercivity and non saturating isothermal magnetisation curves is a signature of system involving competing magnetic interactions. Various superexchange pathways between metal ions at the 2a and 4f crystallographic sites and direct exchange interaction between Ru ions in the 4f sites points to the possibility of coexisting FM and AFM interactions in the system. The temperature irreversibility from 235 K to lower temperatures is understood to be due to magnetic inhomogeneities extending well above the short-range ordering temperature. A maximum magnetic moment of 0.43 μ_B/F.U. is observed at 5 K for 70 kOe sweeping field. A large exchange bias of 5.828 kOe is observed at 5 K for a field cooling of 50 kOe. Exchange bias in our system is the manifestation of inhomogeneous magnetism [1]. Exchange bias training effect in BCMRO0.5 follows spin relaxation model of rotatable and frozen spins which are exchange coupled at the interface [2]. Heat capacity measurement from 2 - 300 K showed no remarkable features near the transition temperature indicating magnetic short range ordering at low temperatures. Low temperature specific heat data is well fitted by incorporating a $T^{3/2}$ term to the $C_p=\gamma T+\beta T^3$. $T^{3/2}$ term is due to spin glass contribution to heat capacity [3].

[1] J. S. Kouvel, J. Phys. Chem. Solids, 24, 795 (1963) [2] S. K. Mishra et al., Phys. Rev. Lett., 102, 177208 (2009). [3] L. Ghivelder et al., Phys. Rev., B 60, 12184 (1999)

APA-08. Antiferromagnetic Behavior in the Frustrated Intermetallic Compounds Pr_2Pd_2X (X = In, Sn). *R. Djoumessi*[1], S. Xhakaza[1], B. Sahu[1] and A. Strydom[1] *1. Physics, University of Johannesburg, Johannesburg, South Africa*

The R_2T_2X (R = rare-earth, T = transition and X = s and p block element) series of compounds are interesting owing to their fascinating structural and physical properties. In this present work, we have studied the magnetic and physical properties of Pr_2Pd_2In and its new isostructural Pr_2Pd_2Sn polycrystalline compounds. The samples were synthesized by arc-melting method and confirmed to crystallize in the Mo_2B_2Fe-type tetragonal structure with space group P4/mbm where atoms are arranged in the layered Shastry-Sutherland lattice. This structure is an intrinsically frustrated system due to the triangular arrangement of the rare-earth atoms. The dc– and ac–magnetic susceptibility, specific heat, and electrical resistivity measurements indicate an unstable antiferromagnetic transition below at T = 5 K and T = 2.5 K for Pr_2Pd_2In and Pr_2Pd_2Sn, respectively. The antiferromagnetic order is unstable in applied magnetic fields, becoming ferromagnetic beyond a field value of 1.5 T and 1.3 T for Pr_2Pd_2In and Pr_2Pd_2Sn, respectively. The field dependent magnetization shows a metamagnetic behavior in both compounds with the critical field of 1.5 T and 1.3 K at 2 K for Pr_2Pd_2In and Pr_2Pd_2Sn, respectively. The electronic specific heat coefficient values of 235 mJ/mol_{Pr} K^2 for Pr_2Pd_2In and 311 mJ/mol_{Pr} K^2 for Pr_2Pd_2Sn estimated from C_P (T) data indicated that the compounds belong to the heavy fermion family. The metallic behavior is identified from electrical resistivity of both compounds with a characteristic of electron-phonon scattering in the paramagnetic region. The variety of magnetic properties such as para-, ferro- and antiferromagnetic behavior including metamagnetic transition is observed due to the magnetic frustration from distorted triangles of Pr-atoms in Pr_2Pd_2In and Pr_2Pd_2Sn. The existence of frustrated moments due to the triangular arrangements of Pr atoms is discussed in both compounds.

APA-09. Structural and Magnetic properties of α–CoV_2O_6 and Cr doped α–CoV_2O_6. *M. Mulibana*[1], P. Mohanty[1], A.R. Prinsloo[1], C.J. Sheppard[1] and B.S. Jacobs[1] *1. Physics, University of Johannesburg, Johannesburg, South Africa*

This study investigates the structural and magnetic properties of α–CoV_2O_6 and Cr doped α–CoV_2O_6 samples synthesized through a wet chemical method [1]. X-ray diffraction (XRD) revealed that α–CoV_2O_6 form a monoclinic crystal structure [2], with lattice parameters a = 9.25 Å, b = 3.50 Å, c = 6.63 Å, β = 111.44°, and α = γ = 90°. The crystal is made of linear chains of Co^{2+} ions along the b–axis, demonstrating the one-dimensional nature of the compound [3]. Cr doping resulted in small changes in the lattice parameters and an increase of microstrain in the form of peak broadening [4], accompanied by changes in the crystallite size of the samples. Scanning electron microscopy (SEM) and transmission electron microscopy (TEM) measurements show that the particles are aggregated with nonuniform shapes and sizes, with average particle sizes of 141 ± 19 nm, 79 ± 24 nm, and 58 ± 10 nm for α–CoV_2O_6, α–$Co(V_{0.97}Cr_{0.03})_2O_6$ and α–$Co(V_{0.95}Cr_{0.05})_2O_2$ respectively. The presence of Cr in the doped samples was confirmed through energy dispersive spectroscopy (EDS). Vibrating sample magnetometry (VSM) was used to investigate the magnetic properties of the samples by measuring the temperature dependence of magnetization, M(T) at 0.1 T, 2.5 T, and 5 T, under zero-field-cooled (ZFC) and field-cooled (FC) protocols. The field dependence of magnetization, $M(\mu_0H)$ and time dependence of magnetization, M(t) were measured. M(T) curves revealed antiferromagnetic (AFM) behavior at 0.1 T with AFM to paramagnetic (PM) transitions increasing from 15 ± 0.2 K for α–CoV_2O_6 to 15.5 ± 0.2 K for α–$Co(V_{0.95}Cr_{0.05})_2O_6$. M(T) curves measured at 2.5 T reveals a ferrimagnetic (FI) like behavior with spin-glass like irreversibility between ZFC and FC. Ferrimagnetic to paramagnetic transition increase from 13 ± 0.2 K to 13.4 ± 0.2 K with increasing Cr concentration. M(T) at 5 T reveals a ferromagnetic (FM) behavior with a ferromagnetic to paramagnetic transition increasing from 14.4 ± 0.2 K to 15.1 ± 0.2 K. Field-induced metamagnetic transitions were observed in $M(\mu_0H)$ curves below 15 K for all samples with an increase of saturation magnetization with increasing Cr concentration. M(t) curves at fields between 1.5 and 5 T suggest a spin-glass-like freezing.

[1] Wang Y *et al*., *ACS Appl. Mater. Interfaces*, 8, (2016) 27291–7. [2] Shu H *et al*., *J. Magn. Magn. Mater.*, 407, (2016) 129–34. [3] He Z *et al*., *J. Am. Chem. Soc.*, 131, (2009) 7554–5. [4] Khorsand Zak A *et al*., *Solid State Sci.*, 13, (2011) 251–6.

APA-10. Superconducting Fluctuation Effect on Epitaxially Layered Films of Superconductor NbN and Half-Metallic Heusler Alloy Co_2MnSi. *I. Shigeta*[1], S. Oku[1], T. Kubota[2], S. Kimura[2], T. Seki[2], B. Shinozaki[4], S. Awaji[2], K. Takanashi[3,2] and M. Hiroi[1] *1. Kagoshima University, Kagoshima, Japan; 2. Tohoku University, Sendai, Japan; 3. Japan Atomic Energy Agency, Ibaraki, Japan; 4. Kyushu University, Fukuoka, Japan*

Heusler alloys have attracted a lot of interest as suitable materials for spintronics applications. Concerning Co-based Heusler alloy Co_2MnSi (CMS), giant magnetoresistive devices experimentally gave a high magnetoresistance ratio, indicating that CMS is half-metal [1]. Superconducting NbN is a type-II superconductor, and its superconducting transition temperature T_c and upper critical field H_{c2} are higher than other metallic superconductors [2,3]. NbN is used for superconducting Josephson devices realizing high speed and low electricity consumption [4.5]. The establishment of the fabrication process and characterization of epitaxially layered NbN/CMS films is important for the applications of novel spintronics devices combining superconductor to half-metallic material. We have fabricated epitaxially layered NbN/CMS films on a MgO(100) substrate by an ultra-high-vacuum (UHV)-compatible magnetron sputtering system. We have measured the transport properties of patterned NbN/CMS films under high magnetic fields. Figure 1 shows the temperature dependence of the excess current σ′ together with the theoretical curve which is the sum of the Aslamazov-Larkin (AL) term σ'_{AL} and the Maki-Thompson (MT) term σ'_{MT} in the superconducting fluctuation theory [6]. From the fitting analysis, the superconducting transition temperature T_c and the pair breaking parameter δ were estimated to be T_c = 10.3 K and δ = 2.5, respectively. We have further obtained the superconducting coherence length ξ_0 from high field transport measurements. Figure 2 shows the CMS thickness d_{CMS} dependence of T_c and ξ_0. T_c was decreased but ξ_0 was increased with the increase of d_{CMS}. We conclude that the superconductivity of the NbN/CMS films was suppressed, due to the superconducting proximity effect at the interface between the NbN and the CMS layers.

[1] T. Iwase, Y. Sakuraba, S. Bosu, K. Saito, S. Mitani, K. Takanashi, Appl. Phys. Express 2 (2009) 063003. [2] A. Shoji, S. Kiryu, S. Kohjiro, Appl. Phys. Lett. 60 (1992) 1624. [3] Z. Wang, A. Kawakami, Y. Uzawa, B. Komiyama, J. Appl. Phys. 79 (1996) 7837. [4] K. Senapati, M. G. Blamire, Z. H. Barber, Nat. Mater. 10 (2011) 849. [5] A. Golubov M. Y. Kupriyanov, Nat. Mater. 16, 156 (2017). [6] L. G. Aslamasov, A. I. Larkin, Phys. Lett. A 26 (1968) 238.

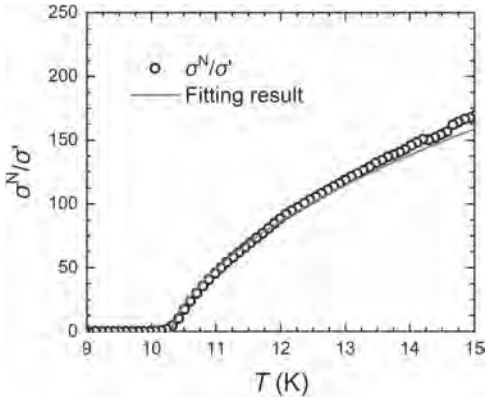

Fig. 1 The temperature dependence of the normalized excess current σ^N/σ'. The solid line is the sum of the Aslamazov-Larkin (AL) term σ'_{AL} and the Maki-Thompson (MT) term σ'_{MT} in the superconducting fluctuation theory.

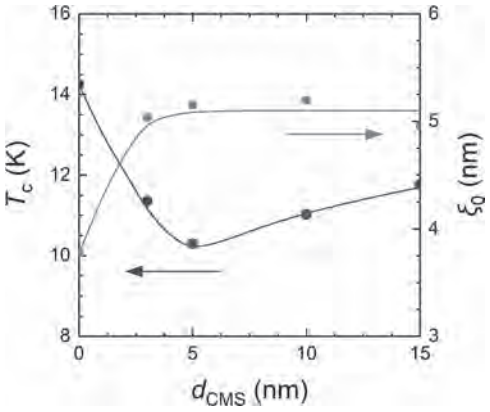

Fig. 2 The CMS thickness d_{CMS} dependence of the superconducting transition temperature T_c and the superconducting coherence length ξ_0. T_c was decreased but ξ_0 was increased with the increase of d_{CMS}.

APA-11. Superconducting properties of RE doped GdBa2Cu3O7-δ polycrystalline bulk. *K. Choi*[1], H. Lee[1], J. Choi[1], T. Lee[1], K. Kim[2], Y. Sur[2] and C. Lee[2] *1. Hyundai Motors Company, Uiwang-Si, The Republic of Korea; 2. Seoul National University, Seoul, The Republic of Korea*

REBCO-based bulk superconductors have the ability to trap larger magnetic fields than permanent magnets in cryogenic environments, which has potential for use in a variety of applications such as magnetic separation, motor/generators, and NMR/MRI. The trapped magnetic field of the bulk superconductor has a record of 17.6T at the center of two $GdBa_2Cu_3O_{7-\delta}$ (GdBCO) bulk superconductors stack at 26K and 17.24T at the center of two $YBa_2Cu_3O_{7-\delta}$ (YBCO) bulk superconductors stack at 29K. Most research on bulk superconductors has focused on single crystal growth to achieve high current density and trapped magnetic field. Single crystal bulk has high superconducting properties, but has disadvantages in terms of manufacturing time and mechanical properties. In contrast, polycrystalline bulk superconductors have low critical current density and trap low magnetic field relatively, but may be more useful in practical applications. Therefore, we have interest in how to improve the superconducting properties of polycrystalline bulk REBCO. In this study, we have investigated RE^{3+} ion doping effect on Gd^{3+} sites in GdBCO polycrystalline bulk. $(RE_x,Gd_{1-x})Ba_2Cu_3O_{7-\delta}$ (x = 0, 0.1, 0.3, 0.5) (RE = A, B, C) samples were prepared by powder metallurgy which is mixed by hand, compressed through a pelletizer and then heat treated. In these samples, the formation of superconducting phase was analyzed in these samples by X-ray diffraction(XRD), the critical temperature(T_c) and critical current density(J_c) were measured using MPMS magnetometer, and trapped magnetic field was evaluated through field cooling method. As a result, the RE^{3+} ion doped GdBCO polycrystalline bulk samples have achieved a high critical current density and trapped magnetic field, although the critical temperature is lowered.

S. Pinmangkorn, Journal of Alloys and Compounds, Vol. 881, p.160535 (2021) J H Durrell, Superconductor Science and Technology, Vol. 27, p.082001 (2014) K Huang, Superconductor Science and Tehcnology, Vol. 33, p.02LT01 (2019) M Tomita, Nature, Vol. 421, p.517 (2003) C P Bean, Review of Modern Physics, Vol. 36, p.31 (1964) A R Hmoudi, Ceramics International, Vol. 47, p.25314 (2021)

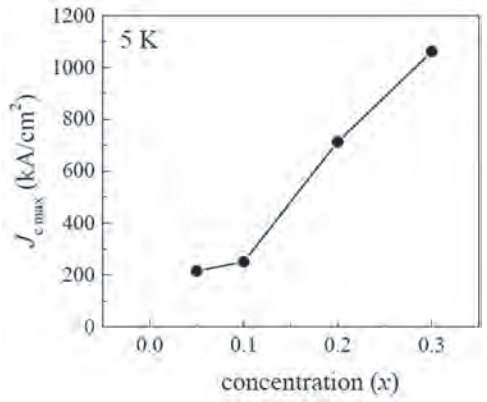

APA-12. Weak itinerant ferromagnetic behaviour in *Al* substituted $Ni_{92}Cr_8$ alloys. *D. Patra*[1], S. Vishvakarma[2], P.D. Babu[2] and S. Veeturi[1] *1. Department of Physics, Indian Institute of Technology Madras, Chennai, India; 2. UGC-DAE Consortium for Scientific Research, Mumbai, India*

Recently exotic magnetic phases have been reported on tuning the ground state by chemical pressure, mechanical pressure and/or applying an external magnetic field [1, 2]. The magnetic transitions were supressed discontinuously and continuously toward zero Kelvin at a critical concentration (x_c) and termed as quantum phase transition (QPT). Interestingly, in NiCoCr [2] and NiCr [3] systems QPT and quantum Griffiths phase (QGP) were reported near critical concentration. It is believed that strong disorder leads to observation of QGP. In this context a pertinent question is that, can we drive a system which exhibits a QPT into QGP by controlling the disorder? Therefore, in the present investigation we will attempt to control the disorder by substituting non-magnetic element like Al, Cu in NiCr system. Further investigate magnetic properties as we approach the critical concentration. For this study we have chosen $Ni_{92-x}Cr_8TM_x$ (TM: Cu, Al) alloy system. Polycrystalline samples have been synthesized by arc melting method using high purity elemental constituents under *Ar* atmosphere. Subsequently, the ingots were homogenized by annealing at 1000° C for 72 h followed by water quenching. Structural and elemental analysis suggest *fcc* crystal structure with elemental compositions close to the nominal composition. Variation of Curie temperature (T_C) as a function of concentration is shown in the Fig.1 (a) indicating role of chemical disorder when substituted with magnetic and non-magnetic elements. From temperature and field dependent magnetization data Rhodes-Wohlfarth ratio (RWR) parameter is determined to evaluate the itineracy and Takahashi-Deguchi plot is shown in Fig.1(b) along with alloys of weak itinerant character from the literature. Further detailed analysis of low temperature M-H data shows that as '*x*' approaches the x_c the spin fluctuations increase, which is the typical character to observe QPT or QGP. Results based on detailed analysis of the data will be presented.

1. A. Schroeder et al., J. Phys.: Condens. Matter 23, 094205 (2011) 2. B.C. Sales et al., njp Quant. Mater. 2, 33 (2017). 3. S.Vishvakarma and V Srinivas, J. Appl. Phys. 129, 143901 (2021).

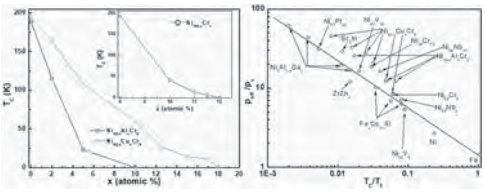

Fig. 1 (a) Curie temperature as a function of concentration (b) Generalized Rhodes-Wohlfarth plot and solid line fits to Takahashi equation.

APA-13. Quantum Hall Effect Systems of Electrons with Anisotropic Patterns. *O. Ciftja[1] 1. Physics, Prairie View A&M University, Prairie View, TX, United States*

An almost ideal two-dimensional system of electrons can now be easily created in semiconductor heterojunctions. A quantum Hall effect state of the electrons is induced via the application of a strong perpendicular magnetic under specific quantum conditions. The most robust integer and/or fractional quantum Hall states already observed show the expected characteristic magnetoresistance for such systems. However, anisotropic patterns and features in transport properties have been seen in few other peculiar cases. The origin of such anisotropic patterns may have various mechanisms or may also be due the specific details of system and material such as the isotropic or anisotropic nature of the effective mass of electrons, the nature of the host substrate parameters, the nature of the interaction potentials, as well as other subtler effects. The interplay between all these factors can lead to many outcomes. In this work we consider small quantum Hall states of electrons and study the appearance of such anisotropic patterns as a result of some form of innate anisotropy in the system.

APA-14. Spin Nematic Liquid of the S=1/2 Distorted Diamond Spin Chain in Magnetic Field. *T. Sakai[1,2] 1. University of Hyogo, Hyogo, Japan; 2. National Institute for Quantum Science and Technology, Hyogo, Japan*

The spin nematic order has attracted a lot of interest in the field of magnetism. It is a kind of multipole order of spins. The previous theoretical and numerical studies[1-3] predicted that the spin nematic order would be induced by the frustration of the ferromagnetic and antiferromagnetic exchange interactions, or the biquadratic interaction. The spin nematic order is characterized by the long-range four spin correlation and the two-magnon bound state. The previous numerical diagonalization and the finite-size scaling study had indicated that a two-magnon bound state can occur in the S=1 antiferromagnetic chain with the single-ion anisotropy under magnetic field[4].The recent analysis of the critical exponents of the spin correlation functions[5] suggested that this two-magnon bound state includes the spin nematic liquid phase, as well as the spin density wave (SDW) liquid one. The phase diagrams with respect to the anisotropy and the magnetization were obtained by the numerical diagonalization of finite size clusters. The same numerical analysis indicated that the spin nematic liquid phase appears in the magnetization process of the 1/2 spin ladder system with the anisotropic ferromagnetic rung interaction[6,7].These systems would be able to exhibit the spin nematic liquid even without the frustration or the biquadratic exchange interaction. In the present study, the S=1/2 distorted diamond spin chain is investigated using the numerical diagonalization of finite-size clusters. This system is a typical frustrated system. The recently discovered candidate material of this system, K3Cu3AlO2(SO4)4 called alumoklyuchevskite[8], includes the ferromagnetic interactions. Thus we investigated the distorted diamond chain with the ferromagnetic interactions, as well as the coupling anisotropy. As a result we found that a two-magnon bound state appears in the magnetization process. We also discus about the spin nematic liquid behaviors.

[1] A. F. Andreev and A. Grishchuk, Sov. Phys. JETP 60, 267 (1984). [2] H. H. Chen and P. M. Levy, Phys. Rev. Lett. 27, 1383 (1971). [3] T. Hikihara et al., Phys. Rev. B 78, 144404 (2008). [4] T. Sakai, Phys. Rev. B 58, 6268 (1998). [5] T. Sakai, H. Nakano, K. Okamoto and R. Furuchi, J. Phys.: Conf. Ser. 2164, 012030 (2022). [6] T. Sakai, K. Okamoto and T. Tonegawa, phys. Status solidi B 247, 583 (2010) [7] T. Sakai et al., in preparation. [8] M. Fujihara et al., Sci. Rep. 7, 16785 (2017).

APA-15. Magnetic Coupling of Divalent Metal Centers in Post Synthetic Metal Exchanged Bimetallic DUT-49 MOFs by EPR interrogations. *K. Thangavel[1,2], M. Mendt[1], B. Garai[3], V. Bon[3], S. Kaskel[3] and A. Pöppl[1] 1. Felix Bloch Institute for Solid State Physics, University of Leipzig, Leipzig, Germany; 2. School of Chemistry, Cardiff University, Cardiff, United Kingdom; 3. Department of inorganic Chemistry, Technische Universität Dresden, Dresden, Germany*

Metal-organic frameworks (MOFs) are a novel and the most prominent class of microporous materials for the applications such as gas storage and separation, catalysis, heat storage and liquid purification, owing to their unique structural diversity and tunability. [1] In the current scenario, understanding the magnetic properties of MOFs has started to be explored in the field of molecular magnetism, [2,3] and the electron paramagnetic resonance (EPR) spectroscopy is one of the inevitable tools to investigate the magnetic exchange interactions between spin centers to understand the local structure of the MOF materials [1,4,5]. Herein, EPR measurements at X- (9.4 GHz), Q- (34 GHz) and W-band (94 GHz) on paddlewheel (PW) type post-synthetic metal exchanged DUT-49(M, M): M-Zn, Mn, Cu MOFs were investigated. Temperature-dependent X-band measurements were recorded from T = 7 K to T = 170 K on DUT-49(Cu), DUT-49(Mn) and bimetallic DUT-49(CuZn) and DUT-49(CuMn) MOFs. Moreover, an EPR signal intensity of the magnetically coupled metal ion pairs in the PW units, which is proportional to the magnetic susceptibility, was extracted from the temperature-dependent X-band EPR data for all MOFs. The sign of the isotropic coupling constant ($2J$ = -239 cm^{-1}) determined via Bleaney Blowers susceptibility fit confirms the excited S= 1 state antiferromagnetic interaction above T = 60 K of DUT-49(Cu) within the paddlewheel. Also, other DUT-49(M, M) MOFs are expected to have antiferromagnetic interaction within the paddle wheel (see Table). X-band measurements at T =160 K confirm the excited spin states (S_{CuCu} = 1, S_{CuMn} = 3, and S_{MnMn} = 5) of the antiferromagnetically (AFM) coupled ions of the PW units for the DUT-49(Cu), DUT-49(CuMn) and DUT-49(Mn) MOFs, respectively. While signals observed from DUT-49(CuMn) and DUT-49(CuZn) MOFs at T = 7 K could be due to the low spin states of the coupled paramagnetic ions within the PW and corresponds to the S_{CuMn} = 2 and S_{CuZn} = 1/2 spin states, respectively.

1. M. Bracci et al., Electron Paramag Reson. 27, 1-46 (2021). 2. G.M. Espallargas et al., Chem. Soc. Rev. 47, 533-557 (2018) 3. A. E. Thorarinsdottir et al., Chem. Rev. 120, 8716-8789 (2020) 4. A. Kultaeva et al., J.Phys.Chem.C. 122, 26642-26651 (2018) 5. J. Bitzer et al., Chemistry-A European Journal, 26(25), 5667-5675 (2020)

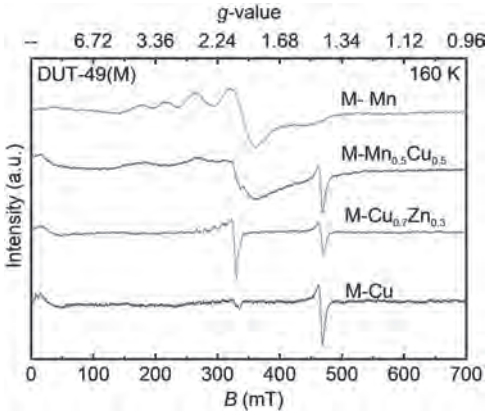

X-band EPR spectra of DUT-49(M,M) MOFs at 160 K

MOF	Spin Centers in the paddle wheel unit	S	S at 160 K (high spin state)	S at 7 K (low spin state)
DUT-49(Mn)	Mn-Mn	$S_{Mn(5/2)}$ - $S_{Mn(5/2)}$	5	0
DUT-49($Cu_{0.5}Mn_{0.5}$)	Cu-Mn	$S_{Cu(1/2)}$ - $S_{Mn(5/2)}$	3	2
		$S_{Mn(5/2)}$ - $S_{Mn(5/2)}$	5	0
		$S_{Cu(1/2)}$ - $S_{Cu(1/2)}$	1	0
DUT-49($Cu_{0.7}Zn_{0.3}$)	Cu-Zn	$S_{Cu(1/2)}$ - $S_{Zn(0)}$	1/2	1/2
		$S_{Cu(1/2)}$ - $S_{Cu(1/2)}$	1	0
DUT-49(Cu)	Cu-Cu	$S_{Cu(1/2)}$ - $S_{Cu(1/2)}$	1	0

The expected spin (S) states of DUT-49(M, M) MOFs at 7 K and 160 K temperatures

Session BOA
COMPLEX OXIDES
Daniela Petti, Chair
Politecnico di Milano, Milano, Italy

INVITED PAPER

BOA-01. Strain-Stabilized Room-Temperature Valence/Spin-State/ Metal-Insulator Transitions in Pr-Based Perovskite Cobaltites.

V. Chaturvedi[1], S. Ghosh[1], D. Gautreau[1,2], W.M. Postiglione[1], J.E. Dewey[1], P. Quarterman[3], P.P. Balakrishnan[3], B. Kirby[3], H. Zhou[4], A. Huon[5], T. Charlton[6], M.R. Fitzsimmons[6,7], C. Korostynski[1], A. Jacobson[1], L. Figari[1], J.G. Barriocanal[8], T. Birol[1], A. Mkhoyan[1] and *C. Leighton*[1]
1. Chemical Engineering and Materials Science, University of Minnesota, Minneapolis, MN, United States; 2. Physics and Astronomy, University of Minnesota, Minneapolis, MN, United States; 3. NIST Center for Neutron Research, National Institute of Standards and Technology, Gaithersburg, MD, United States; 4. Advanced Photon Source, Argonne National Laboratory, Lemont, IL, United States; 5. Thermo Fisher Scientific, Hillsboro, OR, United States; 6. Neutron Scattering Division, Oak Ridge National Lab, Oak Ridge, TN, United States; 7. Physics and Astronomy, University of Tennessee, Knoxville, TN, United States; 8. Characterization Facility, University of Minnesota, Minneapolis, MN, United States

Cobalt oxides have long been understood to display spin-state crossovers. A very different situation was recently uncovered in Pr-containing cobalt oxides, where a *first-order* spin-state/structural/metal-insulator transition occurs, driven by a remarkable Pr *valence transition*. Such valence transitions offer appealing functionality, but have thus far been confined to cryogenic temperatures in bulk materials (*e.g.*, 90 K in $Pr_{1-x}Ca_xCoO_3$). In this work we combine epitaxy with synchrotron diffraction, scanning transmission electron microscopy with electron energy loss spectroscopy, electronic and magnetic measurements, polarized neutron reflectometry, and density-functional calculations to make the first full study of strained films of the perovskite $(Pr_{1-y}Y_y)_{1-x}Ca_xCoO_{3-\delta}$. Remarkably, heteroepitaxial strain tuning enables stabilization of valence-driven spin-state/structural/metal-insulator transitions to *at least 291 K*, *i.e., around room temperature* (Fig. 1). The technological implications of this result are accompanied by fundamental prospects, as *complete strain control of the electronic ground state is demonstrated*, from ferromagnetic metal under tension to nonmagnetic insulator under compression (Fig. 2), exposing a potential novel spin-state quantum critical point [1]. Work supported by DOE through the Center for Quantum Materials.

[1] Chaturvedi *et al*., submitted (2022) (arXiv:2112.10917).

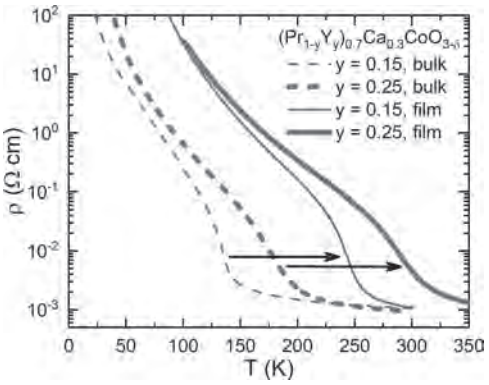

Fig. 1: Temperature-dependent resistivity of $YAlO_3(101)/(Pr_{1-y}Y_y)_{0.7}Ca_{0.3}CoO_{3-\delta}$ films (solid lines) of two compositions, compared to bulk (dashed lines). Note the large enhancements of the transition temperatures due to the ~2% compression from $YAlO_3$, reaching ~300 K at $y = 0.25$.

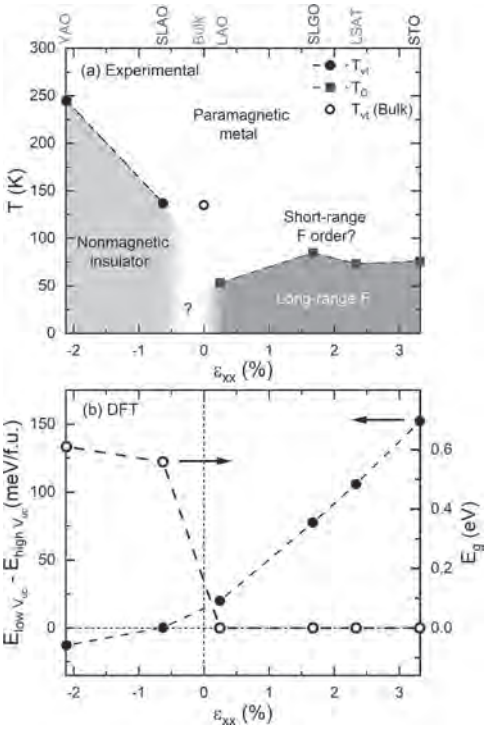

Fig. 2: (a) Strain phase diagram (temperature *vs.* in-plane strain) of $(Pr_{0.85}Y_{0.15})_{0.7}Ca_{0.3}CoO_{3-\delta}$. T_{vt} and T_C are the valence transition and Curie temperatures. Blue, green, and white denote ferromagnetic, nonmagnetic insulating, and paramagnetic metallic, respectively. Note the strong compressive stabilization of T_{vt} and the complete control of the ground state. (b) Density-functional-theory relative energies of the high-cell-volume (high-spin) and low-cell-volume (low-spin) states (left axis) and energy gap (right axis). Note the spin-state and insulator-metal transitions *vs.* strain, as in experiment.

CONTRIBUTED PAPERS

BOA-02. Phase-Coexistence *vs*. Quantum-Critical Scenarios in Strain-Tuned Epitaxial Films of Pr-Based Perovskite Cobaltites. *J.E. Dewey*[1], V. Chaturvedi[1], S. Ghosh[1], W.M. Postiglione[1], P. Quarterman[2], P.P. Balakrishnan[2], B. Kirby[2], L. Figari[1], C. Korostynski[1], A. Jacobson[1], A. Mkhoyan[1] and C. Leighton[1] *1. Chemical Engineering and Materials Science, University of Minnesota, Minneapolis, MN, United States; 2. NIST Center for Neutron Research, National Institute of Standards and Technology, Gaithersburg, MD, United States*

Pr-based cobaltites such as $Pr_{1-x}Ca_xCoO_{3-\delta}$ exhibit coupled first-order spin-state/metal-insulator/structural transitions driven by a unique Pr valence transition. Our recent work [1] used epitaxial strain to achieve complete control over the ground state in thin films of $(Pr_{1-y}Y_y)_{1-x}Ca_xCoO_{3-\delta}$, from a nonmagnetic insulator (NMI) with valence transition temperature (T_{vt}) enhanced to ~291 K under compression, to a ferromagnetic metal (FMM) with Curie temperature (T_C) up to ~80 K under tension. Here, we combine X-ray diffraction, transport, magnetometry, and polarized neutron reflectometry to map the phase behavior of compressively strained $(Pr_{1-y}Y_y)_{1-x}Ca_xCoO_{3-\delta}$ films as they strain relax. With increasing thickness on $SrLaAlO_4$ substrates (initial $\varepsilon_{xx} \approx -0.6\%$), the out-of-plane lattice parameter monotonically decreases (Fig. 1(a)), T_{vt} decreases (Fig. 1(b)), and, strikingly, T_C increases from 0 to ~40 K (Fig. 1(c)). Similar behavior occurs in strain-relaxed films on $YAlO_3$ (initial $\varepsilon_{xx} \approx -2\%$). As the NMI to FMM transition is crossed *vs*. strain, we thus find clear evidence of NMI/FMM phase coexistence (Fig. 2). This suggests a first-order phase transition, rather than a spin-state quantum critical point scenario, of broad interest in the field of magnetism. Work supported by DOE through the Center for Quantum Materials.

[1] Chaturvedi *et al*., submitted (2022) (arXiv:2112.10917).

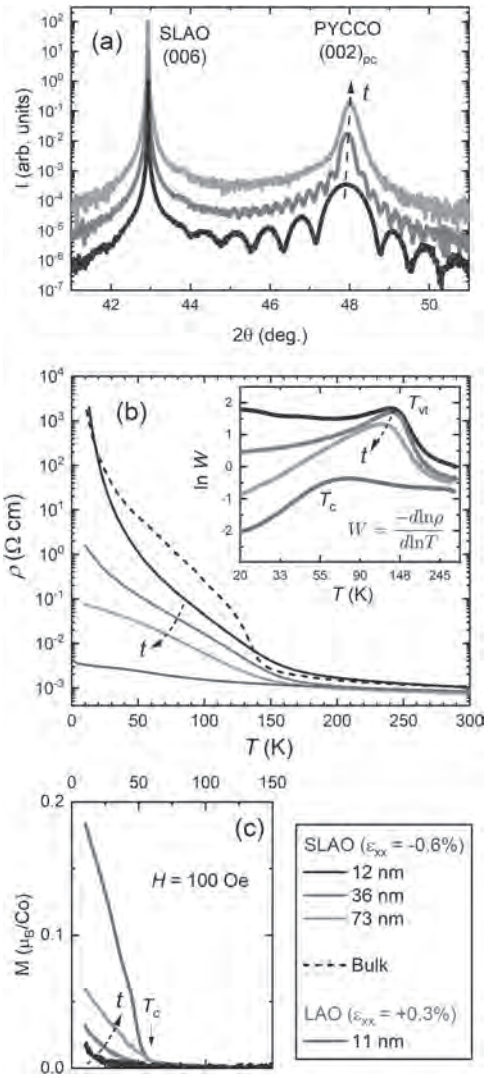

Fig. 1: (a) Specular X-ray diffraction around 002 film peaks of $(Pr_{0.85}Y_{0.15})_{0.7}Ca_{0.3}CoO_{3-\delta}$ on SLAO substrates *vs*. thickness (*t*). (b) Temperature-dependent resistivity (ρ) of $(Pr_{0.85}Y_{0.15})_{0.7}Ca_{0.3}CoO_{3-\delta}$ on SLAO (initial $\varepsilon_{xx} = -0.6\%$) and LAO (initial $\varepsilon_{xx} = 0.3\%$) at different *t*, and compared to bulk. Inset: Corresponding "Zabrodskii" plots. (c) Temperature-dependent magnetization (*M*) of $(Pr_{0.85}Y_{0.15})_{0.7}Ca_{0.3}CoO_{3-\delta}$ on SLAO and LAO at different *t*.

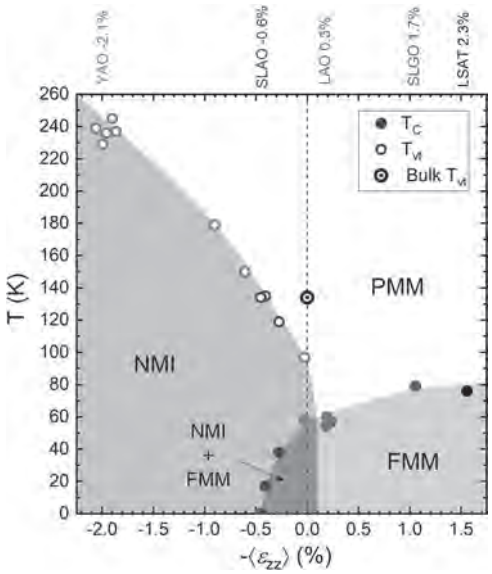

Fig. 2: Strain phase diagram (temperature *vs*. average out-of-plane strain, $\langle\varepsilon_{zz}\rangle$) of strained and strain-relaxed $(Pr_{0.85}Y_{0.15})_{0.7}Ca_{0.3}CoO_{3-\delta}$ on YAO, SLAO, LAO, SLGO, and LSAT substrates. The sign of $\langle\varepsilon_{zz}\rangle$ is inverted to arrange data by in-plane strain, ε_{xx} (indicated above substrate labels). T_{vt} and T_C are color-coded by substrate. Nonmagnetic insulator (NMI), paramagnetic metal (PMM), ferromagnetic metal (FMM), and the coexistence region, are labeled.

BOA-03. Temperature Dependence of Magnetic Anisotropy and Domain Tuning in $BaTiO_3$(111)/CoFeB Multiferroic Heterostructures.
R.G. Hunt[1], K. Franke[1], P.S. Keatley[2], P.M. Shepley[1] and T.A. Moore[1]
1. Physics and Astronomy, University of Leeds, Leeds, United Kingdom; 2. Physics and Astronomy, University of Exeter, Exeter, United Kingdom

Multiferroic hetereostructures consist of two types of ferroic materials, typically a ferroelectric and ferromagnet, linked together through interfacial interactions, often a magnetostrictive mechanism[1]. In these types of multiferroics the strain associated with the ferroelectric polarization sets a microscopic anisotropy that couples the ferroelectric domains to ferromagnetic domains[2]. These multiferroics offer interesting spin textures that can be controlled by a range of techniques which, if functionalized, could result in lower power spintronic devices. Here we use multiferroics based on $BaTiO_3$(111) substrates in which the strain has a heavy dependence on the temperature. Measurements of anisotropy are taken using a Kerr microscope in an optical cryostat. Figure 1 shows that there are three distinct regions of interest corresponding to the different crystal phases of $BaTiO_3$: tetragonal (T) at room temperature, orthorhombic (O) below 280K and rhombohedral (R) below 190K. The greatest region of anisotropy change is close to room temperature at the orthorhombic phase transition, with another significant region around the rhombohedral transition. This tunability is important when considering the domain structure. Depending on the orientation in which a magnetic field is applied[3], the magnetization can rotate in either a head-to-tail (uncharged) or head-to-head (charged) fashion. Figure 2 shows by micromagnetic simulations informed by experiments that it is possible to control domain wall width through temperature alone. Our results show that this change is heavily non-linear with temperature and show the most pronounced change in charged domain walls with a change of ~100% going from the tetragonal to rhombohedral phase. This could be exploited in a temperature activated spintronic device.

[1] - Palneedi, H., Annapureddy, V., Priya, S, *Actuators,* Vol. 5, (2016). [2] - Lahtinen, T. H. E., Franke, K. J. A., & Van Dijken, S., *Scientific Reports*, Vol. 2, (2012). [3] - Franke, K. J. A., López González, D., Hämäläinen, *Physical Review Letters*, Vol. 112, (2014).

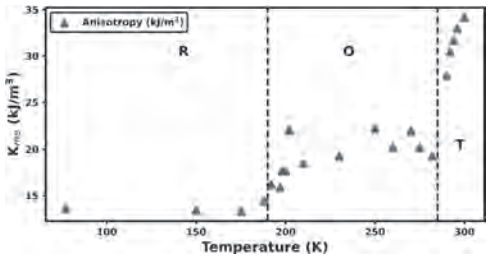

Figure 1: Temperature dependence of the microscopic uniaxial inverse magnetostrictive anisotropy. Temperatures at which the substrate goes through a crystal phase transition are marked.

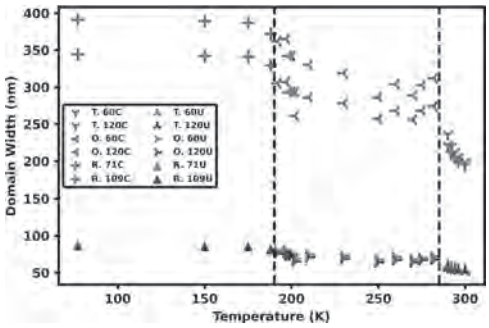

Figure 2: Micromagnetic simulation of magnetic domain wall widths using experimentally determined parameters. Markers delineate the T, O, and R phases as well as the angle between anisotropy axes and charged (C) or uncharged (U) nature.

BOA-04. Fin-geometry Multiferroic $BiFeO_3/CoFe_2O_4$ Nanocomposites formed by templated self-assembly. *T. Su*[2] and C.A. Ross[1] *1. Department of Materials Science and Engineering, Massachusetts Institute of Technology, Cambridge, MA, United States; 2. Mechanical Engineering, Massachusetts Institute of Technology, Cambridge, MA, United States*

Two-phase self-assembled epitaxial multiferroics are formed by co-deposition of $BiFeO_3$(BFO) and $CoFe_2O_3$(CFO) on a $SrTiO_3$(STO) substrate, in which the ferroelectric and ferrimagnetic phases are coupled elastically via their vertical interfaces yielding a magnetoelectric response. By templating the self-assembly, the locations of the BFO and CFO can be controlled, increasing the utility of the nanocomposite and simplifies modeling. Here, we make use of ion-matter interaction as a nucleation site to control the growth of two phases, enabling complex geometries including nano-fins and nano-dots, and extending the templating process beyond the use of 001-STO substrates. In order to counter the charging of insulating substrates (STO) during FIB patterning, a Au layer is deposited on the substrate (step2). After FIB patterning, due to ion implantation, the patterned area is expanded locally (step3, red bump) then the substrate is immersed in Au etchant and HCl, leaving patterned nanoscale trenches or dots on the surface (step4). Post annealing at 850C for 10min is used to recover the atomic flatness of the substrate surface (step5). Then a seed layer of CFO is grown on the patterned substrate(step5), followed by BFO and CFO co-deposition (step6) by pulsed laser deposition. At 700C growth temperature, the maximum diffusion length of CFO is around 200 nm defining the upper range of pattern period. The final morphology is controlled by the processing and growth parameters, including the shape, depth and width of the patterned features and the relative ratio of BFO to CFO. A conductive oxide underlayer of SRO or LSMO is used to enable mapping of the ferroelectric response. This approach was used to form fins of alternating CFO and BFO. Figure2 (top) shows the SEM morphology of the BFO/CFO composite (step 6), in which the BFO and CFO are well separated, achieving ferroelectric/ferrimagnetic nano fins with dimensions: width <100nm; length >5um. A cross-section STEM HADDF image of the nano-fins is presented in Figure 2 (bottom): the two phases are clearly defined and exhibit different heights (BFO~30 nm;CFO~15 nm).

The magnetic and ferroelectric domain patterns mapped by magnetic force microscopy and piezoresponse force microscopy will be described.

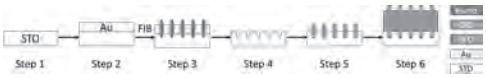

Fig. 1

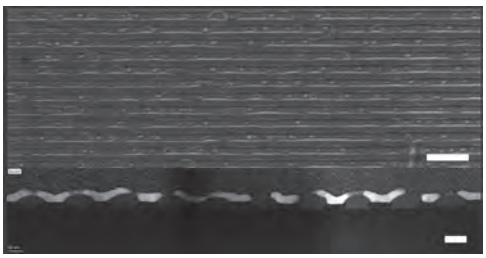

Fig. 2

BOA-05. Large Converse Magnetoelectric Effect in Strain-Engineered Multiferroic Heterostructures. L. Garten[1], *M. Staruch*[2], T.R. Mion[2], J. Wollmershauser[2], K. Bussmann[2] and P. Finkel[2] *1. Georgia Institute of Technology, Atlanta, GA, United States; 2. US Naval Research Laboratory, Washington, DC, United States*

Magnetoelectric materials present a unique opportunity for electric field-controlled magnetism. Even though strain-mediated multiferroic heterostructures have shown unprecedented increase in magnetoelectric coupling compared to single-phase materials, further improvements must be made before ultra-low power memory, logic, magnetic sensors, and wide spectrum antennas can be realized. Previously, we demonstrated strain control and converse magnetoelectric coupling in $Fe_{0.5}Co_{0.5}$/Ag multilayers on (011) $Pb(In_{1/2}Nb_{1/2})O_3$–$Pb(Mg_{1/3}Nb_{2/3})O_3$–$PbTiO_3$ piezoelectric crystals [1]. In this presentation, we will reveal how magnetoelectric coupling can be enhanced by simultaneously exploiting multiple strain engineering approaches by both applying strain during measurement, as well as growing the films with the substrates under compressive stress [2]. When both grown and measured under strain, these heterostructures exhibit an effective converse magnetoelectric coefficient in the order of 10^{-5} s m^{-1}: the highest directly measured, non-resonant value to-date. This response occurred at room temperature and at low electric fields (<2 kV cm^{-1}). This large effect is enabled by magnetization reorientation caused by changing the magnetic anisotropy with strain from the substrate and the use of multilayered magnetic materials to minimize the internal stress from deposition. Additionally, the coercive field dependence of the magnetoelectric response under strain suggests contributions from domain-mediated magnetization switching modified by voltage-induced magnetoelastic anisotropy. This work will highlight how multicomponent strain engineering enables enhanced magnetoelectric coupling in heterostructures and provides an approach to realize energy-efficient magnetoelectric applications.

[1] M. Staruch et al., Scientific Reports 6, 37429 (2016) [2] L.M. Garten et al., ACS Appl. Mater. Interfaces 14, 22, 25701-35709 (2022)

BOA-06. Enhancement of phase transition temperature beyond room temperature by formation of $Ga_{0.8}Fe_{1.2}O_3 – Y_3Fe_5O_{12}$ composite. *S. Hait*[1] and K. Mandal[1] *1. Condensed Matter and Materials Physics, Satyendra Nath Bose National Centre for Basic Sciences, Kolkata, India*

Multiferroic materials having good magnetoelectric coupling are of great interest due to their enormous applications in the field of spintronic devices [1]. Magnetoelectric (ME) gallium ferrite is an interesting material due to its room temperature (RT) piezoelectricity and near RT ferrimagnetism along with significant ME coupling (10^{-11} s/m at 4.2 K) [2]. The motive of this work is to increase the magnetic transition temperature (T_C) of the material above RT so that the material can have strong ME coupling at room temperature and can be implemented for practical applications. Several earlier reports have shown the magnetic transition temperature of $Ga_{2-x}Fe_xO_3$ increases with higher Fe contents [3]. Hence, we chose to study the properties of $Ga_{2-x}Fe_xO_3$ (GFO) only for x = 1.2. $Y_3Fe_5O_{12}$ (YIG) is another material which is RT ferromagnet with very high resistivity (resistivity ~ 10^{12} Ω.cm) [4]. In this work, by forming GFO-YIG composite with only 10% concentration of YIG, phase transition temperature is increased beyond room temperature from ~ 289 K for GFO to ~ 309 K for 0.9 GFO – 0.1 YIG as shown in Fig. 1. The remnant magnetisation is also enhanced from 0.211 emu/g to 2.82 emu/g [inset of Fig. 2] reporting a magnetisation of ~ 8.2 emu/g at 30 kOe [Fig. 2].

[1] J. F. Scott, *Nature Materials*, vol. 6, no. 4, pp. 256–257, Mar. 2007. [2] J. P. Remeika, *Journal of Applied Physics*, no. 5, 1960. [3] T. Arima *et al.*, *Physical Review B - Condensed Matter and Materials Physics*, vol. 70, no. 6, 2004. [4] W. Swee Yin, J. Hassan, W. Mohd, and D. W. Yusoff, *Solid State Science and Technology*, vol. 19, pp. 259–267, 2011.

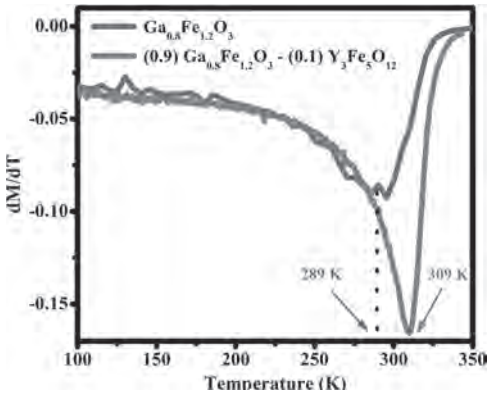

Fig. 1 dM/dT versus Temperature plot indicating the phase transition temperature (T_C)

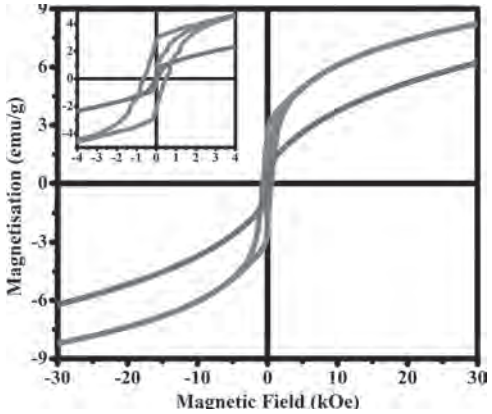

Fig. 2 Magnetic hysteresis loop obtained at room temperature. Inset of (b) shows the zoomed-out magnetic hysteresis loop of 0.9 $Ga_{0.8}Fe_{1.2}O_3$ – 0.1 $Y_3Fe_5O_{12}$ composite at a magnetic field range of 4 kOe.

BOA-07. Exchange bias effect in Ruddlesden-Popper and 6H perovskites: Role of glassy magnetic phase. M.M. Kurian[1], R.R. Das[1], V. Anusree[1] and *S. Nagappan Nair*[1] *1. Physics, Indian Institute of Technology Madras, Chennai, India*

Structural and magnetic studies on $SrLaCo_{0.5}Mn_{0.5}O_4$ (SLCMO), $SrLaFe_{0.25}Mn_{0.25}Co_{0.5}O_4$ (FMC1), $SrLaFe_{0.5}Mn_{0.25}Co_{0.25}O_4$ (FMC2), B site doped single layered Ruddlesden-Popper (RP) oxides gave insights of inhomogeneous magnetism leading to competing magnetic exchange interactions resulting in exchange bias (EB) phenomena. Doping different magnetic ions at the B-site induces site disorder and mixed valency of ions, leading to

the formation of disordered perovskite layers between the rock salt A/A'O layers. Neutron powder diffraction confirmed the absence of long-range magnetic ordering. Short range magnetic domains were again substantiated by the cluster spin glass (CG) phase identified by ac and dc magnetic studies. Below the CG transitions at 50 K, 23 K, 43 K for SLCMO, FMC1, FMC2 respectively, short range correlations with coexisting ferromagnetic (FM) and antiferromagnetic (AFM) interactions creates various boundaries between FM and AFM nanoscale domains. Giant EB values of 5.5 kOe, 2.72 kOe, 6.85 kOe is obtained at 5 K and 50 kOe cooling field for SLCMO, FMC1, FMC2 respectively. EB in these compounds is the manifestation of glassy dynamics, induced due to site disorder and multi valent states of ions [1,2]. Further we extend this competing magnetic interaction driven exchange bias behaviour to a hexagonal perovskite *6H* $Ba_3MRu_2O_9$ (M is a transition metal ion) by introducing three magnetic ions at the B-site. In the ordered *6H* structure $Ba_3MRu_2O_9$ (M = Co, Ni, Fe etc.), the Ru ions prefers the *4f* sites and the transition metal cations prefer the *2a* site [3]. *6H* $Ba_3CoFeRuO_9$ with Co, Fe and Ru at the B site in the 1:1:1 ratio was fabricated and this increased the possibility of mixed valency and as a consequence site disorder. Neutron diffraction, dc magnetic, magnetic memory and heat capacity measurements confirm the absence of long-range magnetic ordering. An EB of 2.32 kOe is obtained at 5 K and 50 Oe. The exchange bias training effect in our systems follow spin relaxation model of rotatable and frozen spins which are exchange coupled at the interface [4].

1. R. R. Das, P. Parida, A. K. Bera, T. Chatterji, B. R. K. Nanda, and P. N. Santhosh, Phys. Rev. B 98, 184417 (2018). 2. V. K. Anusree, R. R. Das, P. Neenu Lekshmi, R. Dhal, C. V. Colin, and P. N. Santhosh, Phys. Rev. B 102, 134405 (2020). 3. J. T. Rijssenbeek, Q. Huang, R. W. Erwin, H. W. Zandbergen, and R. J. Cava, J. Solid-State Chem. 146, 65 (1999). 4. S. K. Mishra, F. Radu, H. A. Dürr, and W. Eberhardt, Phys. Rev. Lett. 102, 177208 (2009).

BOA-08. Magnetism and Electron Spin Resonance (ESR) in Mo-doped $LaMnO_3$. *Y. Lee*[1] and R. Mahendiran[1] *1. Physics, National University of Singapore, Singapore*

$LaMn^{3+}O_3$ is an AFM insulator with T_N = 140 K but transforms into a FM insulator with Co^{2+} or Ni^{2+} substituted at the Mn-site in La_2CoMnO_6 and La_2NiMnO_6[1], accompanied by a change of Mn valence from 3+ to 4+. However, $LaMn_{0.96}Mo_{0.04}O_3$ is a metallic ferromagnet at low temperatures[2]. The FM Curie temperature T_C decreased only by 7 K upon 6% Mo^{6+}: d^0 substitution in $La_{0.67}Sr_{0.33}Mn_{1-x}Mo_xO_3$[3]. It was stated that Mo^{6+} doping induced Mn^{2+} (d^5) which interacted with Mn^{3+}(d^4) through Zener's double exchange giving rise to FM and metallic behavior. But, studies on Mo-doped manganites are yet rare. Here, we report the physical characterization of $LaMn_{0.94}Mo_{0.06}O_3$ prepared by solid-state route. Fig.1(a) shows the temperature dependence of magnetization (M) and inverse susceptibility (X^{-1}) measured under H = 1kOe. Fig. 1(b) shows the dc resistivity (ρ) and thermopower (S). T_c obtained from the inflection point of dM/dT is 237 K whereas the X^{-1} deviates from the Curie-Weiss behavior below 260 K. This is possibly due to Griffiths phase, i.e. nano-sizes FM clusters preformed above T_C in the PM matrix. The ρ shows an IM transition with a peak at 235 K. However, S shows a peak around 258 K, which is about 20 K above the T_C, suggesting that S is sensitive to nucleation of FM nano domains or short-range FM correlation. Fig. 1(c) shows ESR signal as a derivative microwave absorption as a function of dc magnetic field at selected temperatures near FM transition. The spectrum at 300 K is typical of ESR. While the spectrum at 300 K can be fitted to a single Lorentzian curve, the spectrum at 250 K reveals another low-intensity peak at a lower field (~1900 Oe) in addition to the ESR signal around 3200 Oe. The intensity of the ESR-signal decreases dramatically at 245 K but the intensity of the low-field peak increases. At 230 K, we do not see the ESR signal. These results indicate that the low field peak is due to FMR, but this feature start appearing above T_C confirms that FM metallic nano domains are preformed above T_C in the PM state and increase in size with lowering temperature and percolate leading to long-range FM and metallicity.

[1] G. Blasse, Ferromagnetic interactions in non-metallic perovskites, J. Phys. Chem. 26, 1969 (1965);S. Vasala and M. Karppinen, $A_2B'B''O_6$ perovskites: A review, Prog. Soild State Chem. 42, 1 (2015). [2] W. J. Lu *et al*., Induced ferromagnetism in Mo-substituted $LaMnO_3$, Phys. Rev. B, 73, 174425 (2006). [3] L. Chen *et al*., Critical behavior of Mo-doping $La_{0.67}Sr_{0.33}M_{1-x}Mo_xO_3$ perovskite, Physica B, 404,1879 (2009). R. M. thanks the Ministry of Education, Singapore for supporting this work (Grant no. R144-000-442-114)

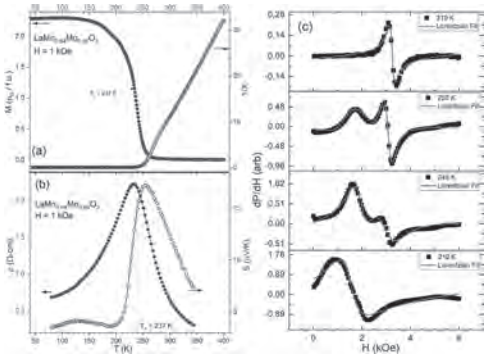

(a) T-dependence of M and X^{-1}; (b) T-dependence of ρ and S; 1(c) ESR at selected T

BOA-09. Coexistence of Magnetic Phases in $SrMnO_3$ Thin Films Revealed by Phase Shifted Angle Dependent Spin Hall Magnetoresistance. *J. van Rijn*[1], D. Wang[2], B. Sanyal[2] and T. Banerjee[1] *1. Zernike Institute for Advanced Materials, University of Groningen, Groningen, Netherlands; 2. Department of Physics and Astronomy, Ångströmlaboratoriet, Uppsala University, Uppsala, Sweden*

Magnetic insulators allow for the study of spin currents without moving electron charges in spintronics devices. Antiferromagnetic oxides are actively investigated in this context with the objective to control antiferromagnetic order, enabling ultrafast magnetization dynamics. The strongly correlated d-orbitals in manganese based antiferromagnetic perovskites invoke considerable versatility by manipulating charge, orbital and spin degrees of freedom. For our studies, we use $SrMnO_3$ that has recently gained attention due the presence of significant structure-dependent magnetic properties. Density-Functional Theory (DFT) studies show the ground state to be a G-type antiferromagnet, displaying multiferroic properties at tensile strains above approximately 1%. We find that straining $SrMnO_3$ thin films promotes an oxygen vacant phase, modifying magnetic interaction governed by the mixed Mn valency. Bulk magnetization studies show competing magnetic phases in $SrMnO_3$ thin films grown on $SrTiO_3$. This is supported by DFT calculations that incorporates oxygen vacancies, where the tilting of Mn-O-Mn bond angles over 30 degrees is found to be the origin of such varying exchange coupling. The resulting magnetic exchange parameter even indicates ferromagnetic exchange for the oxygen vacant locations. For the study of antiferromagnetic interaction in such SMO thin films, we use electronic transport schemes based on the Spin Hall effect using a Pt electrode. Such Spin Hall Magnetoresistance measurements reveal the expected antiferromagnetic nature of the material. A remarkable collection of phase shifts and negative out-of-plane angle dependent Spin Hall Magnetoresistance is observed suggestive of local anisotropic antiferromagnetic phases (Fig.1). This work brings forth a novel understanding of the local structural dependence of magnetic interactions in strained $SrMnO_3$ thin films, crucial to exploit the potential multiferroic properties in SMO.

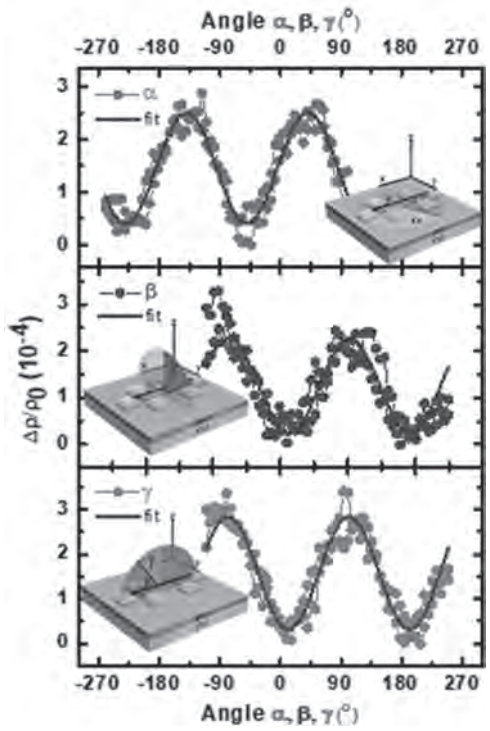

Fig. 1 Spin Hall Magnetoresistance measurements on $SrMnO_3$ films for three rotational direction at 5 K using a 7 T magnetic field. A phase shift of ~135 and 90 degree is observed for the alpha and beta/gamma directions respectively which reveals the antiferromagnetic phase.

BOA-10. Theory of absorption of the Shastry-Sutherland compound $SrCu_2(BO_3)_2$. *S. Miyahara*[1] *1. Fukuoka University, Fukuoka, Japan*

Quasi two-dimensional magnet $SrCu_2(BO_3)_2$ is a realization of the Shastry-Sutherland model, of which the ground state is rigorously described as a direct product of dimer singlet states. The magnetic proprerties of $SrCu_2(BO_3)_2$, *e.g.* spin gap excitations and magnetization plateaus, have been studied from both experimental and theoretical points of view [1]. Spin excitation spectra have been investigated by ESR and far-infrared spectroscopy and one-triplet and bound states of two triplet excitations have been observed. However, the comprehensive understanding of the mechanism and the selection rule has not yet been established. In magnetoelectric mulitferroics, there is a strong coupling between electric polarization and magnetic moment. Such a coupling induces an electro active spin wave excitation, *i.e.* electromagnon [2]. We show that such electromagnetic couplings can exist even in $SrCu_2(BO_3)_2$ and a tiplet excitation, i.e. spin gap excitation and the bound states of the two trplets can be excited by the electric components of light through the couplings. In the Shastry-Sutherland model with Dzyaloshinskii-Moriya interactions, we calculate dielectric permittivity and magnetic susceptibility by continued fraction method by using Lanczos method and clarify the mechanism and the selection rule of absorption in $SrCu_2(BO_3)_2$ comprehensively.

[1] S. Miyahara and K. Ueda, J. Phys.:Condens. Matter 15, R327 (2003).
[2] H. Katsura, A.V. Balatsky, and N. Nagaosa, Phys. Rev. Lett. 98, 027203 (2007).

BOA-11. Functional properties of Yttrium Iron Garnett thin films on graphene-coated $Gd_3Ga_5O_{12}$ for remote epitaxial transfer.
S. Leontsev[1], P. Shah[1], H.S. Kum[3,2], J. McChesney[4], F. Rodolakis[4], M. van Veenendaal[5], M. Velez[1], R. Rao[1], D. Haskel[4], J. Kim[2], A. Reed[1] and M. Page[1] *1. Air Force Research Laboratory, Dayton, OH, United States; 2. Massachusetts Institute of Technology, Cambridge, MA, United States; 3. Yonsei University, Seoul, Korea (the Democratic People's Republic of); 4. Argonne National Laboratory, Lemont, IL, United States; 5. Northern Illinois University, DeKalb, IL, United States*

Remote epitaxial growth via a graphene interlayer and subsequent mechanical exfoliation of a free-standing membrane is a recently developed technique used to transfer complex oxide thin films onto non-native substrates to form heterogeneously integrated structures for various device applications. One such oxide is Yttrium Iron Garnet (YIG), a material of choice for a wide range of magnetoelectric and spintronic devices owing to its ferromagnetism with high Curie temperature as well as high quality factor and low losses in microwave frequencies. YIG is predominantly grown on lattice matched Gadolinium Gallium Garnet (GGG) substrates, but by utilizing the remote epitaxy technique, high quality YIG films can be transferred from GGG onto another substrate such as piezoelectric Lithium Niobate (LN). Mechanical strain coupling between the layers and magnetostrictive nature of YIG would allow for the investigation of the interplay in YIG/LN structures leading to the design of novel frequency agile magneto-acoustic devices. In this study functional properties of a YIG film grown using PLD on graphene-coated GGG substrate were investigated and compared to traditional YIG on GGG. Both materials were characterized in terms of crystal structure, surface morphology, FMR and Gilbert damping, and Raman and XAS spectroscopy. It was found that YIG on graphene-coated GGG exhibits significantly higher microwave losses than standard YIG on GGG (FMR linewidth 30.9 vs 2.1 Oe at 10 GHz, and Gilbert damping coefficient 15.4×10^{-4} vs 3.4×10^{-4} respectively), which was attributed to increased concentration of Fe^{2+} cations in YIG/Graphene/GGG. While the damping is higher in these studied films compared to YIG grown directly on GGG, the resulting properties are still very favorable compared to many other competing materials which can be grown without the need for lattice matched substrates, such as metallic ferromagnets.

S. Leontsev et. al., Journal of Magnetism and Magnetic Materials, Vol. 556, p. 169440 (2022), https://doi.org/10.1016/j.jmmm.2022.169440

BOA-12. Anomalous and Topological Hall Effect in Magnetic Weyl Semimetallic Candidate $Eu_2Ir_2O_7$ (111) Epitaxial Thin Film. *M. Ghosh*[1] and P. Kumar[1] *1. Department of Physics, Indian Institute of Science, Bangalore, India*

Rare earth pyrochlore iridates $RE_2Ir_2O_7$ are predicted to be magnetic Weyl semimetallic (WSM) materials in the presence of electron correlation (U) and spin-orbit coupling (λ). Here we have studied the magnetotransport properties of epitaxial $Eu_2Ir_2O_7$ (111) thin film grown on YSZ by solid phase epitaxy technique [1]. Low-temperature longitudinal resistivity (ρ_{xx}) data shows a power-law dependence on temperature, which signifies semimetallic charge transport. By varying the film thickness, the semimetallic charge transport is tuned to realize the predicted WSM phase. The Hall resistivity (ρ_{xy}) data exhibits an anomalous Hall effect (AHE), in the temperature range of 2–25 K as shown in Fig. 1. The intrinsic AHE is explained in terms momentum space Berry curvature of the Weyl nodes. In addition to the AHE an large topological Hall effect (THE) is observed in the temperature range of 2–5 K. Due to spin chirality S_i. S_j X S_k generated by the all-in-all-out (AIAO) non-coplanar spin structure of Ir^{4+} moments, the conduction electrons acquire a real-space Berry curvature and causes a large THE [2]. Low-temperature (2–10 K) magnetoresistance (MR) data shows a non-hysteretic large negative MR, causes by reduction in scattering by the spin canting. For temperature of 15 K and above, MR shows hysteretic behavior shown in Fig. 2 up to the 90 K (metal-semimetal transition temperature). The hysteretic MR suggest magnetic field-induced domain imbalance of Ir^{4+} moments. Appearance of Hysteresis after 10 K onwards

suggests competetion between antiferromagnetic interaction and field-induced Zeeman energy. As temperature increases the Zeeman energy over comes the antiferromagnetic interaction and causes domains flipping.

1. M. Ghosh, S. G. Bhat, A. Pal, and P. S. A. Kumar, J. Phys: Condens. Matter 34, 165701 (2022). 2. Y. Taguchi, Y. Oohara, H. Yoshizawa, N. Nagaosa, and Y. Tokura, Science, 291, 2573-2576 (2001).

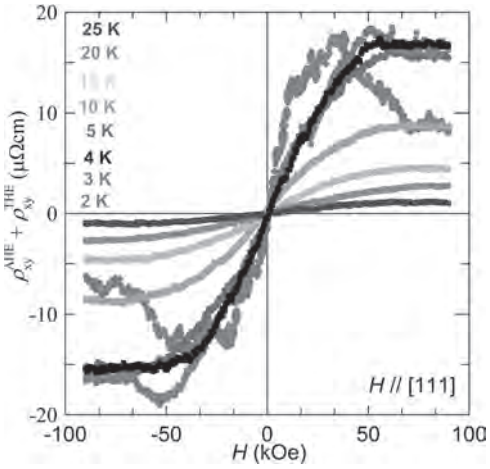

Fig. 1 Magnetic field (H) dependence of anomalous and topological Hall resistivity at various different temperature

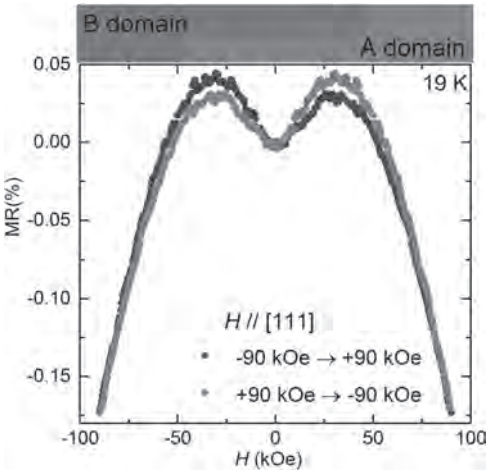

Fig. 2 Hysteretic magnetoresistance data at 19 K for applied field along [111] direction, red and blue curve corresponds to field sweep down and sweep up process

BOA-13. Room Temperature Ferroelectricity and Multiferroicity in Off-stoichiometric Canted Antiferromagnet $LuFeO_3$ Thin Films.

E. Cho[1] and C.A. Ross[1] *1. Department of Materials Science and Engineering, MIT, Cambridge, MA, United States*

Multiferroic magnetoelectric materials have drawn a lot of interest because of the ability to control the magnetic (electric) state with an electric (magnetic) field. In particular, single-phase room-temperature multiferroic materials are desired for magnetoelectric and spintronic applications such as memory devices. Recently, it was discovered that Y_{Fe} antisite defects in $YFeO_3$ (YFO) bring about a non-centrosymmetric structural distortion and induce ferroelectricity [1-3]. Here, we report room-temperature ferroelectricity in $LuFeO_3$ (LFO) and experimentally verify that the antisite defect mechanism for ferroelectricity can be generalized to other orthoferrites. Epitaxial LFO thin films with Lu/Fe ratios ranging from 0.8 to 1.2 were grown by pulsed laser deposition, with a monotonic increase in the out-of-plane lattice parameter from 3.78 Å to 3.82 Å as the film became Lu-rich (Fig. 1). Piezoresponse force microscopy (PFM) reveals that all films exhibit ferroelectricity (a Lu-rich film is shown as an example in Fig. 2), attributed to an abundance of antisite defects facilitated by smaller ionic radii difference between Lu^{3+} and Fe^{3+}. The piezoresponse increases as the film becomes more off-stoichiometric, and that of Lu-rich LFO is larger than Y-rich YFO in line with the prediction in [1] but still smaller than that of $BiFeO_3$, a well-known multiferroic material. The remnant polarization from the positive-up-negative-down (PUND) equivalent measurement of the Lu/Fe = 1.2 film was ~16 μC/cm^2 at 100 kHz; however, the leakage arising from defects and the asymmetric electrode limits the performance as a ferroelectric capacitor in the current device configuration. This work expands the candidates for room temperature multiferroicity by the antisite defect mechanism and motivates the study of magnetic rare-earth orthoferrites to explore the interaction between magnetic and electric order.

[1] S. Ning, A. Kumar and C. A. Ross, Nature Communications, Vol. 12, No. 4298 (2021) [2] A. Kumar, K. Klyukin and C. A. Ross, Advanced Functional Materials, Vol. 32, p.2107017 (2021) [3] A. Kumar, S. Ning and C. A. Ross, Advanced Electronic Materials, Vol. 8, p.2200036 (2022)

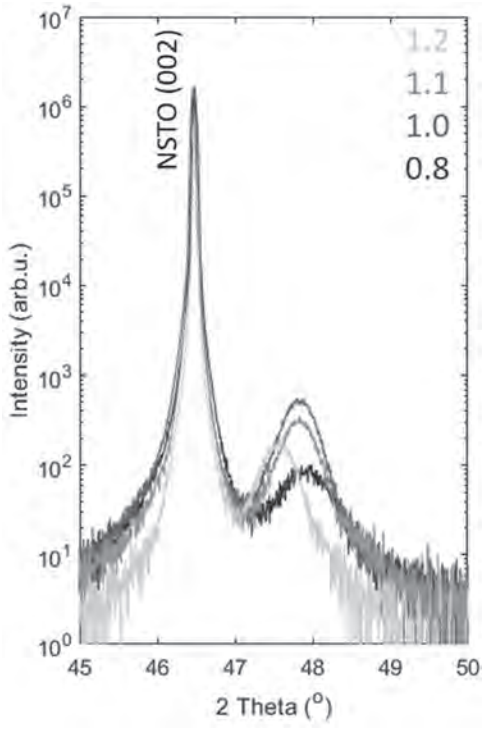

Fig. 1. X-ray diffraction peak of the LFO pseudocubic (002) reflection with different Lu/Fe ratios (represented on the top right corner).

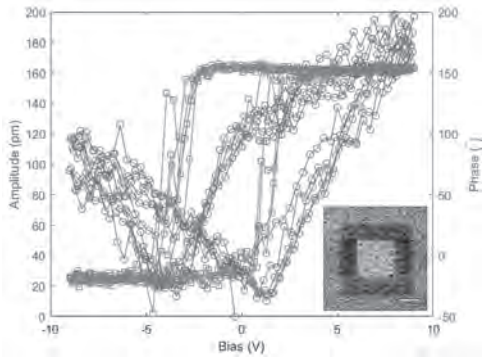

Fig. 2. Switching spectroscopy PFM hysteresis of Lu/Fe = 1.2 film grown on Nb-doped STO (NSTO) substrate. The inset is the phase contrast of the film after box-in-box writing with ±8 V.

BOA-14. Withdrawn

BOA-15. Long-range antiferromagnetic order in highly-strained (111)-oriented $LaNiO_3$ thin films. *P.P. Balakrishnan*[1], M. Kane[2], M.R. Fitzsimmons[5], T. Charlton[5], A. Suter[3], M. Holtz[4], A.J. Grutter[1] and Y. Suzuki[2] *1. NIST Center for Neutron Research, National Institute of Standards and Technology, Gaithersburg, MD, United States; 2. Stanford University, Stanford, CA, United States; 3. Swiss Muon Source, Paul Scherrer Institut, Villigen, Switzerland; 4. Colorado School of Mines, Golden, CO, United States; 5. Spallation Neutron Source, Oak Ridge National Laboratory, Oak Ridge, TN, United States*

$LaNiO_3$ (LNO) has been well studied as the only rare-earth nickelate which does not undergo a temperature-dependent magnetic or metal-insulator transition in bulk, remaining a paramagnetic metal. These phases may be accessible in (111)-oriented thin films through modification of the interfacial oxygen-octahedral connectivity. Recently, a magnetic transition has been observed in these ultrathin (111)-oriented LNO films grown on $LaAlO_3$ substrates [1]. This magnetic order has only been observed indirectly through electronic transport measurements – via the anomalous Hall effect and negative hysteretic magnetoresistance – in semiconducting or metallic films between 8 and 26 unit cells (2 to 6.5 nm) thick. In agreement with synchrotron x-ray diffraction [1], x-ray reflectometry and 4D-scanning transmission electron microscopy reveal a uniquely high strain state in the first 0.4 nm (~2 u.c.) of the film-substrate interface, exhibiting a highly expanded lattice without rotational or shear strain. These results suggest an interfacial insulating magnetic state. Using complementary techniques of polarized neutron reflectometry (PNR) and low-energy muon spectroscopy (μSR), we investigate depth-dependent magnetism in (111)-oriented LNO films. Transverse-field μSR measurements reveal that at 5 nm, the entire film magnetically orders below a temperature of 50 K, with no increase in magnetic field within the film. PNR measurements on films of multiple thicknesses find a change in scattering length density suggesting that an additional strain relaxation may occur beyond 10 nm, but observe no net magnetization in either the bulk of the films or at the strained interfaces, in agreement with bulk SQUID magnetometry. Together, these findings suggest a uniform antiferromagnetic order coexistent with a metallic state in these highly-strained LNO films.

[1] Kane, M.M., *et al. npj Quantum Mater.* 6, 44 (2021).

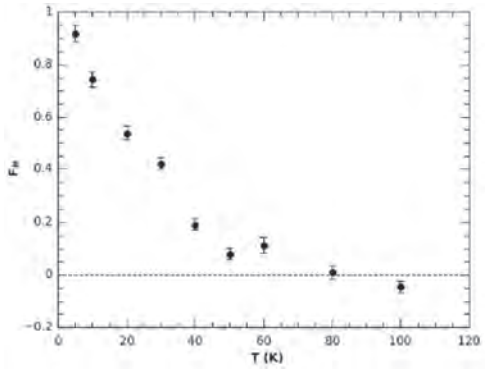

Magnetized volume fraction F_M as a function of temperature, extracted from transverse-field μSR measurements of muons implanted within a 5 nm LNO film.

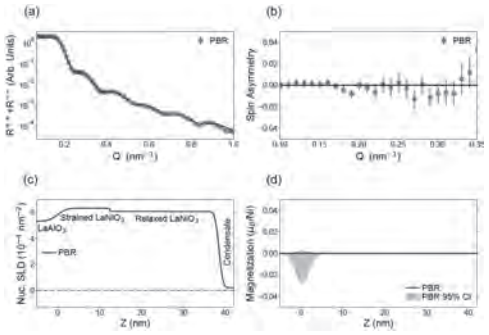

a. Polarized neutron reflectometry, b. extracted spin asymmetry, and best-fit c. nuclear and d. magnetic depth profiles of a 40 nm LNO film on LAO, with 95% confidence interval on magnetization at the LNO interface.

Session BOB
MULTIFERROIC, MAGNETOELECTRIC AND HALF-METALLIC MATERIALS

Takahide Kubota, Chair
Tohoku University, Sendai, Japan

INVITED PAPER

BOB-01. A type-II multiferroic in two dimensions. *R. Comin*[1] *1. MIT, Cambridge, MA, United States*

Multiferroic materials have garnered wide interest for their exceptional static and dynamical magnetoelectric properties [1]. In particular, type-II multiferroics exhibit an inversion-symmetry-breaking magnetic order which directly induces a ferroelectric polarization through various mechanisms, such as the spin-current or the inverse Dzyaloshinskii-Moriya effect. This intrinsic coupling between the magnetic and dipolar order parameters results in record-strength magnetoelectric effects [2]. In this context, there has been a recent surge of interest in 2D materials possessing such intrinsic multiferroic properties, enabling the integration and control of magnetoelectric effects in artificial heterostructures and nanoelectronic devices [3,4]. In this talk, I will present our recent study and realization of type-II multiferroic order in a single atomic layer of the transition metal-based van der Waals material NiI2 [5]. The multiferroic state of NiI2 is characterized by an inversion-symmetry-breaking helimagnetic order which induces a chirality-dependent electrical polarization. Using circular dichroic Raman measurements, we directly probed the magneto-chiral ground state and its electromagnon modes originating from dynamic magnetoelectric coupling. Using birefringence and second-harmonic generation measurements, we observed a highly anisotropic electronic state simultaneously breaking three-fold rotational and inversion symmetry to support polar order. The evolution of the optical signatures as a function of temperature and layer number surprisingly revealed an ordered magnetic, polar state that persists down to the ultrathin limit of monolayer NiI2 [6].

[1] Matsukura, F., Tokura, Y. and Ohno, H. Control of magnetism by electric fields. Nat. Nanotech. 10, 209 (2015). [2] Spaldin, N. A. and Ramesh, R. Advances in magnetoelectric multiferroics. Nat. Mater. 18, 203 (2019). [3] Huang, B. et al. Electrical control of 2D magnetism in bilayer CrI3. Nat. Nanotech. 13, 544 (2018). [4] Jiang, S., Li, L., Wang, Z., Mak, K. F. and Shan, J. Controlling magnetism in 2D CrI3 by electrostatic doping. Nat. Nanotech. 13, 549 (2018). [5] Kurumaji, T. et al. Magnetoelectric responses induced by domain rearrangement and spin structural change in triangular-lattice helimagnets NiI2 and CoI2. Phys. Rev. B 87, 014429 (2013). [6] Song, Q. et al. Evidence for a single-layer van der Waals multiferroic. Nature 602, 601 (2022)

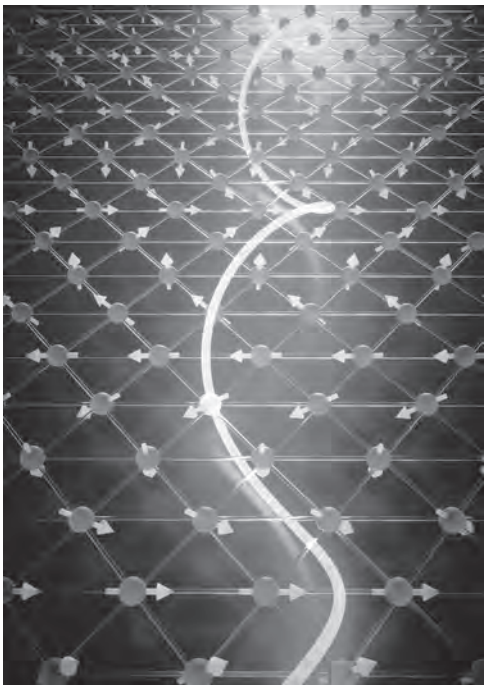

CONTRIBUTED PAPERS

BOB-02. Inducing ferroelectricity in NH_4I via doping of deuterons, bromide and potassium. *M. Zhao*[1], L. Meng[1], C. Peng[1], Y. Xu[1] and F. Yen[1] *1. Harbin Institute of Technology, Shenzhen, Shenzhen, China*

All of the polymorphs of pure ammonium iodide NH_4I have space groups that are non-polar. However, we identify that when a fraction of the hydrogen is replaced by deuterons or when small percentages of iodide are replaced by bromide or potassium, polar phases can be established. In particular, the electric polarization of the following compounds can be switched by an applied electric field: $(NH_4)_{0.67}(ND_4)_{0.33}I$ (where D is deuteron), $NH_4I_{0.91}Br_{0.09}$ and $NH_4I_{0.94}K_{0.06}$ according to pyroelectric current measurements. Magnetic susceptibility measurements indicate that the polar phases may be magnetic in origin. We explain our results by taking into account the notion that every reorienting NH_4^+ possesses a molecular magnetic moment that can couple with that of neighboring NH_4^+. The magnetic moments arise from the protons (H^+) having to orbit in concert about the central nitrogen atom when the ion reorients. In the room-temperature phases, enough orbits are available to avoid mutual resonance, but below a critical temperature, a subset of these orbits become energetically inaccessible so neighboring NH_4^+ become mutually resonant. To avoid lattice instabilities from resonant forces, the NH_4^+ become ordered to establish a spiral modulation of its magnetic moments. A replacement of a fraction of H with D or I with Br or K breaks the spatial-inversion symmetry of the modulating vector so an electric polarization emerges. Our findings provide the potential of adding an extra ferroelectric dimension to hydrogen-bonded materials.

F. Yen, Z. Zheng and Z. Si, Angewandte Chemie, 129(44), 13863-13866 (2017) L. Meng, C. He and F. Yen, The Journal of Physical Chemistry C, 124, 17255−17261 (2020)

BOB-03. Ferroelectricity Based on Orbital Resonance of Protons in CH_3NH_3Cl and CH_3NH_3Br. *L. Meng*[1], C. Peng[1], Y. Xu[1], T. Xing[1], P. Ren[1] and F. Yen[1] *1. Science, Harbin Institute of Technology, Shenzhen, Shenzhen, China*

We identify the beta and gamma phases of methylammonium chloride CH_3NH_3Cl and methylammonium bromide CH_3NH_3Br to be ferroelectric via pyroelectric current measurements. The magnetic susceptibility also exhibited pronounced discontinuities at the Curie temperatures T_C suggesting the ferroelectric phases as having magnetic origins. We explain this by considering reorienting CH_3 and NH_3 groups to possess weak orbital magnetic moments that can interact intermolecularly. In the paraelectric phase, the CH_3–CH_3 and NH_3–NH_3 magnetic interactions are weak because the number of available orbitals (modes) are large. At T_C, a subset of the orbitals becomes energetically inaccessible so orbital resonances cause the CH_3 and NH_3 to become ordered. Since the two types of magnetic moments are different in magnitude and are coupled to an electric dipole moment, a molecular-equivalent of an antisymmetric exchange interaction between the orbital magnetic moments distorts the lattice into a non-centrosymmetric fashion. This perspective may be employed to explain the plastic nature reported in many a hydrogen-bonding materials and exploited to search for more organic ferroelectrics and van der Waals crystals possessing polar ions.

BOB-04. Ferromagnetic hysteresis loop induced by electric field-effect on Pt/$CoFe_2O_4$. *L. Sakakibara*[1], Y. Katayama[1], T. Koyama[2,3], D. Chiba[2,3] and K. Ueno[1] *1. Graduate School of Arts and Sciences, University of Tokyo, Tokyo, Japan; 2. Institute of Scientific and Industrial Research (SANKEN), Osaka University, Ibaraki, Japan; 3. Center for Spintronics Research Network at Osaka, Osaka University, Toyonaka, Japan*

Pt has been considered as a system close to ferromagnetic state because Pt has a large density of states near the Fermi energy. Magnetic moment in Pt ultrathin film was reported to be induced by a magnetic proximity effect through a spinel ferrimagnet $CoFe_2O_4$(CFO) at room temperature, and a saturation value of the anomalous Hall effect (AHE), which is proportional to magnetic moment, was tuned by an electric field effect [1]. In this report, we induced a ferromagnetic hysteresis in ultrathin Pt (5.9 nm) by electric field-effect at low temperature. Both the remanence and the coercive field were tuned from zero to a finite value. A ferrimagnetic insulator CFO thin film (~ 50 nm) with T_C above 300 K were prepared on a $SrTiO_3$(STO) substrate by a pulse laser deposition. With a hall-bar shaped photoresist mask a 5.9 nm Pt film was fabricated by sputtering (Pt/CFO sample). Another Pt (5.9 nm) film was also prepared on a STO substrate as a sample for comparison (Pt/STO sample). Electric double layer transistors (EDLT) were fabricated on these samples using an ionic liquid electrolyte (DEME-TFSI) and a Pt gate electrode. Figures show a magnetic field dependence of an anomalous Hall resistivity ρ_{AH} at 2 K for the Pt/CFO (Fig. 1) and Pt/STO (Fig. 2) samples, respectively. An ordinary Hall coefficient R_H was estimated at 250 K for samples before the fabrication of the EDLT, and ρ_{AH} was estimated by $\rho_{AH} = \rho_{xy} - R_H B$. For a gate bias ($V_G$) of 0 V, both samples showed no hysteresis loop, while AHE was observed. By applying V_G = -3 V and +3 V, the Pt/CFO sample showed clear hysteresis loop, indicating ferromagnetism induced by the V_G. On the other hand, no such behavior was observed in Pt/STO. These results suggest that the ferromagnetism of Pt is induced both by the MPE from the adjacent CFO layer and tuning of Fermi level by gating. The remanence for V_G = +3 V decreased with increasing temperature, and disappeared at around 19.5 K, probably corresponding to the T_C of Pt. In the presentation, we will discuss the origin of the AHE.

[1] S. Nodo, S. Ono, and Y. Toshihiro, Appl. Phys. Exp., Vol. 13, p.063004 (2020)

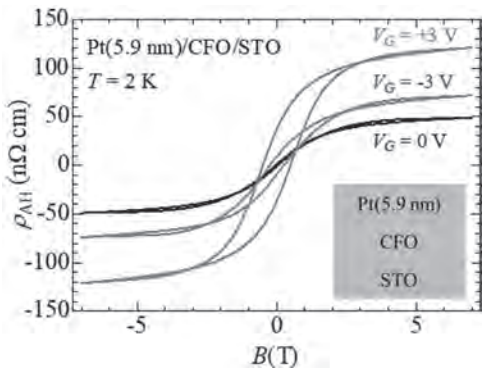

Fig. 1 Magnetic field dependence of ρ_{AH} with various V_G (= +3 V(red), 0 V(black), and -3 V(blue)) for Pt/CFO sample at 2 K.

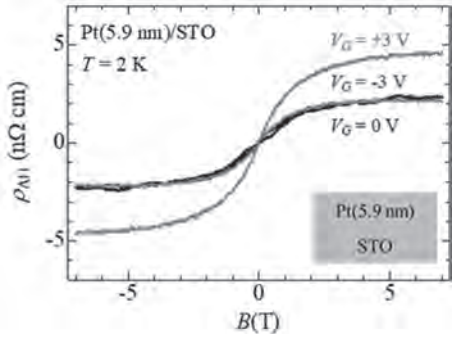

Fig. 2 Same as Fig. 1, shown for Pt/STO sample.

BOB-05. Magnetic nanoprecipitates and interfacial spin disorder in zero-field-annealed $Ni_{50}Mn_{45}In_5$ Heusler alloys as seen by magnetic small-angle neutron scattering. *M. Bersweiler*[1], P. Bender[2], I. Peral[1], E. Pratami Sinaga[1], D. Honecker[3], D. Alba Venero[3], I. Titov[1] and A. Michels[1] *1. Department of Physics and Materials Science, University of Luxembourg, Luxembourg, Luxembourg; 2. Heinz Maier-Leibnitz Zentrum, Technische Universität München, Garching, Germany; 3. ISIS Neutron and Muon Facility, Rutherford Appleton Laboratory, Chilton, United Kingdom*

In the present work, the microstructure of a zero-field-annealed off-stoichiometric $Ni_{50}Mn_{45}In_5$ Heusler alloy is investigated by magnetic small-angle neutron scattering (SANS) [1]. Thanks to its unique mesoscopic length scale sensitivity, magnetic SANS appears to be a powerful technique to disclose the structural and magnetic microstructure of magnetic materials [2] such as nanocrystalline materials [3,4]. The neutron data analysis reveals a significant spin-misalignment scattering, which is mainly related to the formation of annealing-induced ferromagnetic nanoprecipitates in an antiferromagnetic matrix. These particles represent a source of perturbation, which, due to dipolar stray fields, give rise to canted spin moments in the surroundings of the particle-matrix interface. The presence of anticorrelations in the computed magnetic correlation function reflects the spatial perturbation of the magnetization vector around the nanoprecipitates. The magnetic field dependence of the zero-crossing and the minima of the magnetic correlation function are qualitatively explained using the law of approach to ferromagnetic saturation for inhomogeneous spin states. More specifically, at remanence, the nanoprecipitates act magnetically as one superdefect with a correlation length that lies outside of the experimental *q*-range, whereas near saturation the magnetization distribution follows each individual nanoprecipitate. Analysis of the neutron data yields an estimated size of 30 nm for the spin-canted region and a value of about 75 nm for the magnetic core of the individual nanoprecipitates. The presented neutron data analysis (in Fourier and real-space) is particularly useful to study the nanoscale magnetic inhomogeneities of bulk materials at the mesoscopic length scale. Finally, it demonstrates that unpolarized magnetic SANS might be a

practicable alternative to time-consuming and low intensity polarized neutron measurements. This research was partly funded by the National Research Fund of Luxembourg (PRIDE MASSENA Grant No. 10935404 and CORE SANS4NCC Grant).

[1] M. Bersweiler, P. Bender, I. Peral, E. Pratami Sinaga, D. Honecker, D. Alba Venero, I. Titov, and A. Michels, J. Appl. Cryst. 55, in press (2022) [2] A. Michels, *Magnetic Small-Angle Neutron Scattering: A Probe for Mesoscale Magnetism Analysis* (Oxford University Press, Oxford, 2021). [3] M. Bersweiler, E. P. Sinaga, I. Peral, N. Adachi, P. Bender, N. J. Steinke, E. P. Gilbert, Y. Todaka, A. Michels, and Y. Oba, Phys. Rev. Mat. 5, 044409 (2021). [4] M. Bersweiler, M. P. Adams, I. Peral, J. Kohlbrecher, K. Suzuki, and A. Michels, IUCrJ 9, 65 (2022).

BOB-06. Withdrawn

BOB-07. Withdrawn

BOB-08. Asymmetric skew-scattering dominated anomalous Nernst effect in spin gapless semiconductors $Co_{1+x}Fe_{1-x}CrGa$. *A. Chanda*[1], D. Rani[2], J. Nag[3], A. Alam[3], K. Suresh[3], M. Phan[1] and H. Srikanth[1]
1. Physics, University of South Florida, Tampa, FL, United States;
2. Physics, Indian Institute of Technology Delhi, New Delhi, India;
3. Physics, Indian Institute of Technology Bombay, Mumbai, India

Recently, spin gapless semiconductors (SGSs) have attracted immense attention of the spintronics community due to their unconventional electronic structure; while they exhibit a finite band gap for one spin channel, the conduction and valence band edges touch for the other spin channel. [1] Because of their unique band structure, their transport properties are extremely susceptible to external stimuli, e.g., temperature and magnetic field which in combination with their high spin polarization make them potential tunable spintronic materials. Although the SGS behavior was initially predicted in diluted magnetic semiconductors (DMS), Heusler alloy-based SGS materials are more advantageous than the DMS-based SGSs because of their high Curie temperature (T_C) and sizable spin polarization.[2] The quaternary Heusler alloys $Co_{1+x}Fe_{1-x}CrGa$ with very high Curie temperature ($T_C \geq 690$ K) were found to exhibit an extraordinary SGS behavior for $x \leq 0.4$ but become completely half-metallic for $x = 0.5$. [3] Here, we have performed a comprehensive investigation of anomalous Nernst effect (ANE) in $Co_{1+x}Fe_{1-x}CrGa$ as a function of magnetic field and temperature. We found that the electron-electron elastic scattering and the weak localization effect play the dominant roles in electrical transport for all the samples at low temperatures and the contributions from these scatterings increase considerably with x for $x \leq 0.4$. On the other hand, the magnon-drag effect was found to dominate the longitudinal thermoelectric transport in all samples investigated. Our study indicates that the ANE coefficient increases gradually with x for $x \leq 0.4$ but has a drastic increase for $x = 0.5$, when the system transforms from the SGS state to the completely half-metallic state. The ANE coefficient at room temperature increases from ≈ 0.018 μV. K^{-1} for $x = 0$ to ≈ 0.063 μV. K^{-1} for $x = 0.5$, which is much higher than that for $Ni_{81}Fe_{19}$ and compressively strained $SrRuO_3$ films. Our analysis indicates that the observed ANE originates from asymmetric skew-scattering of charge carriers.

[1] X. L. Wang, Phys. Rev. Lett. 100, 156404 (2008). [2] S. Ouardi, G. H. Fecher, C. Felser, and J. Kübler, Phys. Rev. Lett. 110, 100401 (2013). [3] D. Rani, Enamullah, L. Bainsla, K. G. Suresh, and A. Alam, Phys. Rev. B 99, 104429 (2019).

BOB-09. Structural and Magnetic Properties of CoFeVGe: Experiment and Theory. *P. Kharel*[1], Z. Lehmann[1], G. Baker[1], L. Stuelke[2], S. Valloppilly[3], P. Shand[2] and P. Lukashev[2] *1. Physics, South DakotaState University, Brookings, SD, United States; 2. Physics, University of Northern Iowa, Cedar Falls, IA, United States; 3. Nebraska Center for Materials and Nanoscience, University of Nebraska, Lincoln, NE, United States*

Half-metallic Heusler alloys are of high interest to the material research community due to their potential application in spintronic devices. We have synthesized one such compound, CoFeVGe, using arc melting and high-vacuum annealing at 600°C for 48 hours. The room temperature x-ray diffraction of the sample exhibits a cubic crystal structure without secondary phases. The sample shows a single magnetic transition at its Curie temperature of 249 K, Fig. 1(a). The high field (3T) magnetization measured at 100 K is 41 emu/g. We also observed that the Curie temperature of the sample can be increased to near room temperature with slightly changing the elemental composition. The sample with composition $Co_{1.25}Fe_{0.75}VGe$ remains cubic in crystal structure, and it exhibits a Curie temperature of 294 K and saturation magnetization at 100 K of 36 emu/g. Our first principle calculations of CoFeVGe and $Co_{1.25}Fe_{0.75}VGe$ in their cubic crystal structures predict a high degree of spin polarization of 86% and 82%, respectively. Figure 1(b) shows the calculated element- and spin- resolved density of states for CoFeVGe. These results indicate that $Co_{1.25}Fe_{0.75}VGe$ has a potential for near room temperature spintronic applications. This research is supported by the *National Science Foundation* (NSF) under Grant Numbers 2003828 and 2003856 via DMR and EPSCoR.

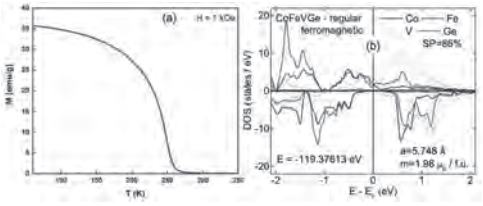

Fig.1: (a) Thermomagnetic curve, and (b) calculated element- and spin-resolved density of states of bulk CoFeVGe.

BOB-10. Low energy multiferroic magnetic domain-wall logic. *X. Li*[1], H. Singh[2], Y. Bao[1], Q. Luo[1], S. Li[1], J. Chatterjee[2], M. Goikoetxea[5], Z. Xiao[3], N. Tamura[4], R.N. Candler[3], L. You[1], J. Bokor[2] and J. Hong[1,2]
1. Huazhong university of Science and Technology, WuHan, China;
2. Department of Electrical Engineering and Computer Sciences, University of California, Berkeley, Berkeley, CA, United States;
3. University of California, Los Angeles, Los Angeles, CA, United States; 4. Lawrence Berkeley National Lab, Berkeley, CA, United States;
5. University of the Basque Country, Euskadi, Spain

Spin logic devices based on magnetic domain walls(DWs) motion provide many advantages including fast motion, high density, and non-volatility to process and store information, but at the same time rely on DW creation and annihilation using an external magnetic field limits their application indense, large-scale circuits. Meanwhile, composite multiferroic systems consisting of a piezoelectric substrate coupled with a ferromagnetic thin film offer many opportunities for the development of ultra-low power and high dense devices. Here, we proposed a method for performing all-electric logic operations and cascading using domain-wall racetracks. We demonstrate the electric field control of magnetic domains. Here, we exploits the ferroic coupling between neighboring magnetic domains induced by the electric field-controlled strain, which promotes non-collinear spin alignment, to realize DW generation (input), propagation, and pinning (output). This demonstrates the e properties of the basic building blocks for Boolean logic operation. The results show that the [100] crystallographic direction produces a tensile strain (S[100] > 0), and the [01-1] crystallographic direction produces a compressive strain (S[01-1] < 0) when an electric field is applied along the [011] direction. We propose two types of logic devices as shown in Fig. 1.

The proposed XOR/XNOR logic gate structure is shown on the left of Fig. 1a. A FM layer and two top electrodes are stacked on the (011) oriented PMN-PT substrate with a bottom electrode. If the magnetization direction of the fixed layer is opposite to the initial magnetization direction of the nanowire, a logical XOR function can be achieved, and vice versa, a logical XNOR function can be achieved. The truth table is shown in the bottom right of Figure 1a. The proposed OR/NOR logic gate structure is shown on the left of Fig. 1b. The final magnetization of the two inputs under different combinations should be like the upper right of Fig. 1b. (OR/NOR logic function). The fully voltage-controlled domain wall logic operation will pave the way for scalable all-electric magnetic logic for memory-in-logic applications.

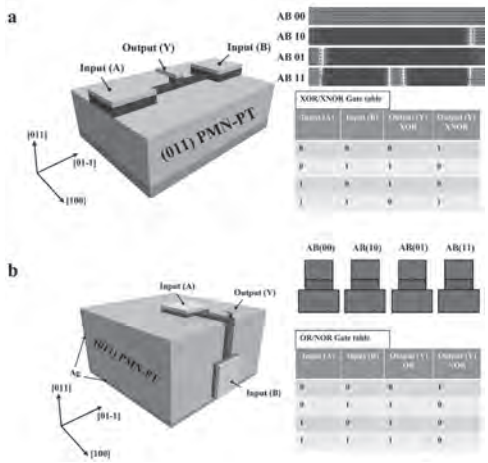

Figure 1. Implementation of spin logic function in two proposed devices.

Session BPA
MULTIFERROICS, MAGNETOELECTRICS, COMPLEX OXIDES AND HALF-METALLICS (Poster Session)

Ying-Hao Chu, Chair
National Yang Ming Chiao Tung University, Hsinchu, Taiwan

BPA-01. Effect of film thickness on the electrical transport in $Co_2FeAl_{0.5}Si_{0.5}$ thin films. *L.A. Longchar*[1], M. Rahaman[1], B.K. Hazra[1], M. Raja[2], R. Rawat[3], S. Srinath[1] and S. Kaul[1] *1. School of Physics, University of Hyderabad, Hyderabad, India; 2. Defence Metallurgical Research Laboratory, Hyderabad, India; 3. UGC-DAE Consortium for Scientific Research, Indore, India*

Thermal stability of the half-metallic band gap at the Fermi energy and high spin polarization of $Co_2FeAl_{0.5}Si_{0.5}$ (CFAS) Heusler alloys [1,2] have made these systems attractive for spintronic applications. However, a stringent requirement is a controllable growth of highly ordered CFAS Heusler alloys. Moreover, giant magnetoresistance (GMR) [3,4] and the anomalous Hall effect [5,6] crucially depend on the magnitude of electrical resistivity (ρ_{xx}) and its temperature dependence. Thus, a complete understanding of the different contributions to ρ_{xx} is needed. To investigate the effect of film thickness on the structural- and electrical- properties, CFAS thin films of thickness, *t*, in the range 12 - 75 nm, were deposited by ultrahigh vacuum dc magnetron sputtering on Si(100) substrates with SiO_2 buffer layer (300 nm), at the optimum substrate temperature of 500°C. The GIXRD patterns, shown in figure 1, reveal that *B2 structural order* grows with increasing *t* and peaks at $t = 50$ nm. The film with $t = 75$ nm showed *A2 disorder*. Irrespective of the magnitude of *t*, ρ_{xx}(T) goes through a minimum at T_{min}. An elaborate quantitative analysis [6-8] of the ρ_{xx}(T, H=0) data, taken over the temperature range 5 K to 300 K, demonstrates that the electron-diffuson (*e – d*) and weak localization (WL) effects (responsible for the *negative* temperature coefficient of resistivity (TCR) for $T < T_{min}$) compete with the electron-magnon (*e – m)* and electron-phonon *(e – p)* scattering (*positive* TCR) contributions to produce a minimum at T_{min}. Figure 2 shows the normalized resistivity ρ_{xx}(T, H=0) / ρ_{xx}(T = 300 K, H=0) (open circles) along with the optimum theoretical fits (continuous lines), go through a minimum at T_{min}. Consistent with the maximum B2 order at $t = 50$ nm, residual resistivity, ρ_{5K}, and the *e – d*, *wl*, *e - m* and *e - p* scattering contributions to ρ_{xx}(T, H=0), $\rho_{e\text{-}d}$, ρ_{wl}, $\rho_{e\text{-}m}$ and $\rho_{e\text{-}p}$, all go through a minimum at $t = 50$ nm. Regardless of *t*, the thermal renormalization of the spin-wave stiffness makes a significant contribution to $\rho_{e\text{-}m}$.

[1] G. H. Fecher and C. Felser, J. Phys. D: Appl. Phys. 40, 1582 (2007). [2] Balke et al, Appl. Phys. Lett. 90, 242503 (2007). [3] Tezuka et al., Appl. Phys. Lett. 89, 112514 (2006). [4] Tezuka et al., Appl. Phys. Lett. 94, 162504 (2009). [5] A. Valet and T. Fret, Phys. Rev. B 48, 7099 (1993). [6] Hazra et al., Phys. Rev. B 96, 184434 (2017). [7] Srinivas et al., J. Non. Cryst. Solids 248, 211 (1999). [8] Kaul et al., Phys. Rev. B 33, 4987 (1986).

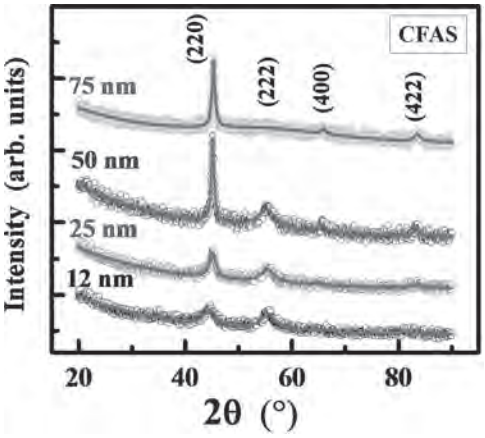

Fig. 1: Grazing incidence X-ray diffraction (GIXRD) patterns

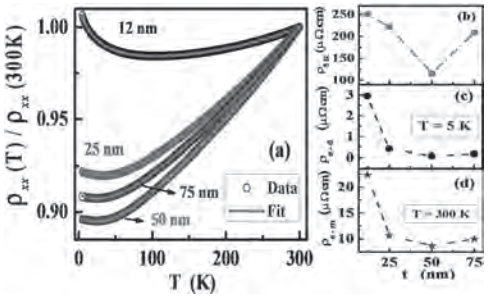

Fig. 2: (a) ρ_{xx}(T)/ρ_{xx}(300 K) (open circles) with fits (continuous lines); (b)-(d) ρ_{5K}, ρ_{e-d}, ρ_{e-m} as functions of film thickness, *t*.

BPA-02. Withdrawn

BPA-03. Investigation of Spin Gapless Semiconductor CoFeMnSi Thin Films on MgO Substrate. *J. Wang*[1], T. Nakano[1], M. Tsunoda[2] and M. Oogane[1] *1. Applied Physics, Tohoku, Sendai, Japan; 2. Electrical Engineering, Tohoku, Sendai, Japan*

The Spin-MOSFET is expected to show a high performance in integrated circuits[1]. Efficient spin injection into semiconductors from ferromagnet is important for the realization of the Spin-MOSFET. However, it is difficult to realize efficient spin injection due to the conduction mismatch problem[2]. To enhance the efficiency of spin injection, ferromagnets with high spin polarization and semiconductor like resistivity were proposed. We focused on a new class material with both these properties: Spin gapless semiconductor CoFeMnSi (CFMS). CFMS have a spin gapless structure and semiconductor behavior which have been proofed in theories and experiments[3][4]. In this study, we aim to investigate the crystal structure, magnetic and electrical properties of CMFS thin films grown on MgO substrates. A structure of CFMS (50nm)/Ta (5nm) was deposited by magnetron sputtering on MgO (100) substrates. The annealing temperature (T_a) of CFMS

layer was between 300 and 600°C. The composition of CFMS thin films was confirmed by ICP-MS (Co : Fe : Mn : Si = 25.5 : 24.2 : 26.3 : 23.9). X-ray diffraction (XRD) was performed for characterization of crystal structure. Fig. 1 shows the annealing temperature dependence of (111) peaks of CFMS thin films. The (111) peaks were obtained above T_a = 400°C, indicating that the epitaxial growth of highly ordered ($L2_1$ or Y-type) CMFS thin films was successful. Fig. 2 shows the temperature dependence of resistivity and conductivity of CFMS thin film at T_a = 500°C. Although the electrical conductivity σ_{xx} value of our sample is around 5.3×10^3 S/cm, about two orders of magnitude lower than the half metallic ferromagnetic alloy Co_2MnSi (~10^5 S/cm), non-semiconductor behaviour of resistivity was observed above 50K. Composition dependence of the CFMS thin films properties and guideline for realization of spingapless semiconductor behaviour will be presented in the conferenece. This research was conducted by participating in the GP-Spin and JST's SPRING program, Tohoku University, and supported by CSIS Organization for Advanced Studies and the CSRN.

[1] S. Datta *et al*., Appl. Phys. Lett. 56, 665 (1998). [2] G. Schmidt *et al*., Phy. Rev. B 62, R4790 (2000). [3] X. Dai *et al*., J. Appl. Phys. 105, 07E901 (2009). [4] L. Bainsla *et al*., Phy. Rev. B 91, 104408 (2015).

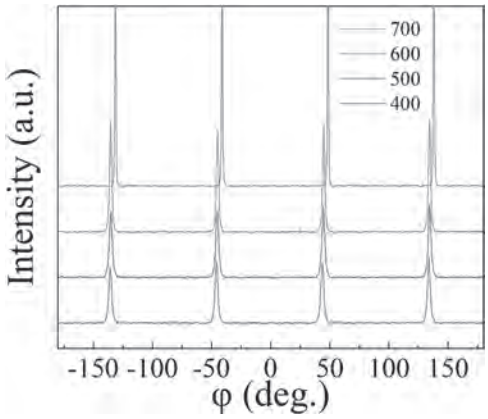

Fig. 1 Temperature dependence of XRD ϕ-scan for (111) peaks

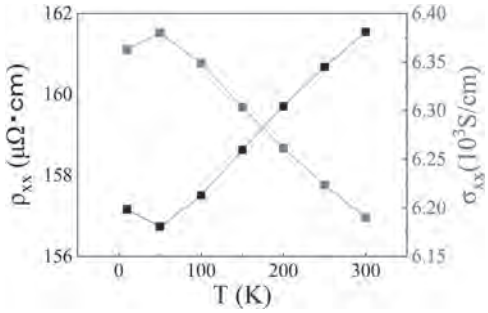

Fig. 2 Temperature dependence of resistivity and conductivity

BPA-04. Structural and Magnetic Properties of $Co_{1.5}Mo_{0.5}FeAl$ Alloy. *G. Baker*[1], J. Wysong[1], S. Valloppilly[2], P. Shand[3], P. Lukashev[3] and P. Kharel[1] *1. Physics, South Dakota State Unviersity, Brookings, SD, United States; 2. Nebraska Center for Materials and Nanoscience, University of Nebraska Lincoln, Lincoln, NE, United States; 3. Physics, University of Northern Iowa, Cedar Falls, IA, United States*

Materials showing half-metallic band structure with a high Curie temperature and moderate magnetization are attractive for spin-transport-based devices. Some Heusler compounds exhibit these features and have attracted much attention. We have synthesized one such compound, $Co_{1.5}Mo_{0.5}FeAl$, using arc melting and high vacuum annealing. The arc-melted ingot was annealed at 600 °C for 48 hours. The room temperature x-ray diffraction suggests that the sample has cubic crystal structure with A2 type disorder. The temperature dependence of magnetization measured at 1 kOe shows a very high Curie temperature of about 950 K. There is an anomaly in the M(T) curve near 750 K, Fig.1. The sample exhibits a moderate saturation magnetization of 68 emu/g at room temperature. These results show that $Co_{1.5}Mo_{0.5}FeAl$ has potential for high temperature magnetic and spintronic applications. Here, we will also discuss the electronic and magnetic properties of cubic $Co_{1.5}Mo_{0.5}FeAl$ predicted by our first principles calculations. This research is supported by the *National Science Foundation* (NSF) under Grant Numbers 2003828 and 2003856 via DMR and EPSCoR.

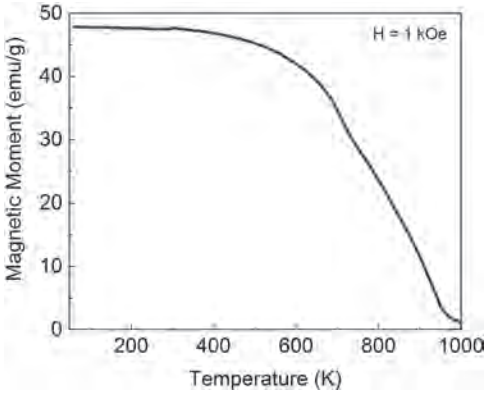

Figure 1: Thermomagnetic curve M(T) of $Co_{1.5}Mo_{0.5}FeAl$

BPA-05. Effect of substitution of 3d, 4d and 5d elements on structural, electronic, magnetic properties and XMCD spectra of Co-based Full Heusler alloys: A DFT Study. *R. Dutt*[1,2] and A. Chakrabarti[2,1] *1. Physical Sciences, Homi Bhabha National Institute, Mumbai, India; 2. Raja Ramanna Centre of Advanced Technology, Indore, India*

The promising properties of Co-based (i.e. Co_2BC) Heusler alloys (HA) such as half-metallicity, magneto-caloric effect, shape-memory effect, spin-valve like behavior, etc. make them important from technological as well as fundamental point of view.[1-5] In the present work, we have probed the role of substitution of 3d, 4d and 5d elements (i.e, with electronic configuration (EC): nd^x where n = 3-5; x = number of electrons in d level) at the B site on structural, magnetic and electronic properties of a set of Co-based full HAs using DFT based first principle calculations. We have optimized all the 30 combinations studied here in Fm-3m (A_2BC conventional HA structure) and F-43m (AABC inverse HA structure) space groups using VASP.[6] Thereafter, electronic structure (ES) calculations have been carried out using FPLAPW method as implemented in WIEN2k[7] and results obtained using PBE and mBJ exchange-correlation terms have been compared. Further, XMCD calculations have been performed using single particle approximation and Fermi-golden rule as implemented in WIEN2k[7]. It is observed that the HAs with EC: $nd^{1-6,10}$ (n = 3, 4, 5) at B site have Fm-3m as the lowest energy structure. Calculated magnetic moment of these alloys with EC: nd^{1-6} are found to be in agreement with the Slater-Pauling (SP) rule with an integer or close to integer value, except $4d^1$, $4d^6$ and $5d^6$ as shown in Figure 1. Furthermore, alloys with EC: nd^{2-6} show half-metallic or half-metallic nature. However, alloys having EC: nd^{7-9} (along with $4d^1$ and $4d^6$) at B site are found to be in F-43m space group. Further, magnetic moment of EC: nd^{7-10} show deviation from the SP rule. In order to understand the impact of nd^{1-10} electrons on the local environment of various atomic sites, detailed analyses of the XMCD spectra have been carried out on the basis of changes in the orbital projected unoccupied density of states.

1. T. Roy, *et al.,* Phys. Rev. B., 93, 184102 (2016) and references therein 2. M. Baral, *et al.,* Phys. Rev. B., 99, 205136 (2019) and references therein 3. K. Inomata, et al., J. Appl. Phys., 95, 7234 (2004) and references therein 4. R. Dutt et al., J. Phys. Condens. Matter, 33, 045402 (2020) and references therein 5. I. Galankis, *et al.,* Phys. Rev. B., 66, 134428 (2002) and references therein 6. G. Kresse *et al.*, Phys. Rev. B., 54, 11169 (1996) and references therein 7. P. Blaha, *et al.*, J. Chem. Phys. 152, 074101 (2020) and references therein

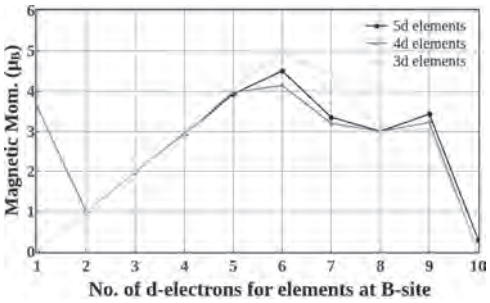

Figure 1. Shows the variation of Total magnetic moment with respect to the valence d electrons of atom at B site

BPA-06. Anomalous Hall Effect and Anisotropic Magnetoresistance Effect in $Co_2(Ti_{1-x}V_x)Si$ Heusler Alloy Single Crystal Films. *M. Liu*[1], M. Oogane[1], M. Tsunoda[1] and Y. Ando[1] *1. Tohoku University, Sendai, Japan*

Recently, Co_2TiSi Heusler alloy is theoretically predicted that is one of the ferromagnetic Weyl semimetal (WSM) candidates, and also the half-metal [1, 2, 3], which has potential for both a large anomalous Hall effect (AHE) and a large spin polarization. It is also expected that the anomalous Hall effect can be enhanced by customizing $Co_2(Ti_{1-x}V_x)Si$ due to the Fermi level shift [4, 5]. In this research, we optimized the fabrication conditions for producing $Co_2(Ti_{1-x}V_x)Si$ thin films, and investigated their AHE and anisotropic magnetoresistance (AMR) effect to discuss the electronic structure in $Co_2(Ti_{1-x}V_x)Si$. The UHV magnetron co-sputtering method was used for the preparation of thin films using Co_2TiSi and Co_2VSi targets. The structure of the sample was MgO (001) sub. / $Co_2(Ti_{1-x}V_x)Si$ (50 nm) / Ta (5 nm), and the doping amount of x was changed. We characterized the crystal structure, magnetic properties, AHE and AMR effect by XRD, SQUID, and PPMS, respectively. High quality $L2_1$ ordered single crystal films ($S_{L21} \approx 70\%$) were successfully fabricated by applying adequate annealing process. Fig. 1 shows doping value x dependence of anomalous Hall angle (AHA), measured at 10 K. AHA of $Co_2(Ti_{1-x}V_x)Si$ sample films enhanced by V doping, and the highest AHA was observed near 3% at $x = 0.31$. Fig. 2 shows measurement temperature dependence of AMR radio when the electric current flowed in the $Co_2(Ti_{1-x}V_x)Si$ [110] and [100] directions. The magnitude of AMR ratio increases with decreasing temperature for both directions, but the sign is positive for [110] and negative for [100] direction, respectively. The s-d scattering theory of AMR [6] suggests that d-orbitals of majority spin electron are split by crystal field and the density of states of ε- and γ-orbitals are well different at the Fermi level. The change of magnitude of AMR for [100] direction implies that the Fermi level tuning was realized by V doping into the Co_2TiSi Heusler alloy thin films. This research was conducted by participating in the GP-Spin and JST's SPRING program, Tohoku University, and supported by CSIS Organization for Advanced Studies and the CSRN.

[1] A. Bernevig, H. M. Weng, Z. Fang and X. Dai, J. Phys. Soc. Jpn., 87, 041001 (2018). [2] G. Q. Chang, S. Y. Xu, H. Zheng et al., Sci. Rep. 6. 38839; doi: 10.1038/srep38839 (2016). [3] J. Barth, G. H. Fecher, B. Balke et al., Phys. Rev. B 81, 064404 (2010). [4] J. Zou, Z. He, and G. Xu, Npj Computational Materials, 5(1) (2019). [5] I. Galanakis, P. H. Dederichs, and N. Papanikolaou, Phys. Rev. B 66, 174429 (2002). [6] S. Kokado and M. Tsunoda, J. Phys. Soc. Jpn. 88, 034706 (2019).

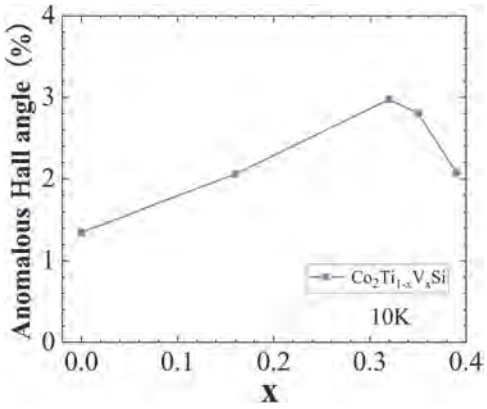

Fig. 1 Doping value x dependence of AHA

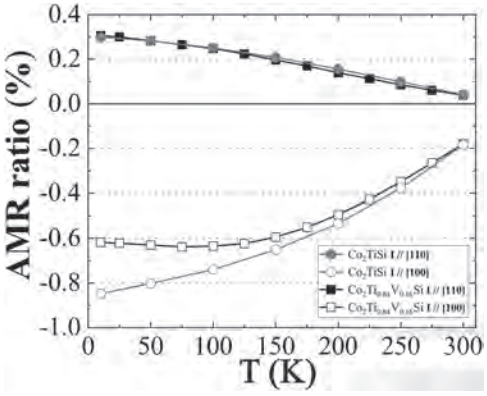

Fig. 2 Measurement temperature dependence of AMR ratio

BPA-07. Hall Coefficient of $(Cr_{100-x}Al_x)_{95}Mo_5$ Alloy System. *B. Muchono*[1,2], C.J. Sheppard[1] and A.R. Prinsloo[1] *1. Department of Physics, University of Johannesburg, Johannesburg, South Africa; 2. Department of Physics, University of Eswatini, Kwaluseni, Swaziland*

Hall coefficient (R_H) measurements have shown to be an effective method in determining the number density, $n = (qR_H)^{-1}$ and the type of majority charge carriers at the Fermi surface (FS) [1-3] of Cr and its alloys. Parts of the Fermi surface sheets that are annihilated during antiferromagnetic (AFM) ordering in Cr based alloys and have large effects on the number density resulting in an anomalous behaviour on cooling below the Néel transition temperature, T_N [4]. Previous studies on the $(Cr_{100-x}Al_x)_{95}Mo_5$ alloy system through electrical resistivity (ρ), Seebeck coefficient (S), thermal conductivity (κ), specific heat (C_p), magnetic susceptibility (χ) and neutron diffraction measurements have shown that antiferromagnetism is suppressed in the concentration range $1.4 \le x \le 4.4$ [5]. The present study was undertaken in order to extend the previous findings on this alloy system, through Hall coefficient measurements. R_H of polycrystalline $(Cr_{100-x}Al_x)_{95}Mo_5$ alloys was measured over the temperature range $2\ K \le T \le 380\ K$ in a magnetic field of 4.5 T. Anomalies in the form of an upturn were observed just below the Neel transition temperature T_N for the AFM alloys with $x \le 1.3$ and $x \ge 5.3$. In addition to these anomalies, alloys with $x = 0$, 0.5, 0.9 and 8.6 show a peculiar behaviour below T_N, in which R_H increases and then decreases depicting a hump on further cooling. Remarkably R_H for the alloy with $x = 0$ shows a sign reversal of majority charge carriers from holes to electrons on cooling below 120 K. The crossover of majority charge carriers disappears by the addition of just 0.6 at.% Al into the alloy with $x = 0$. The behaviour of alloys with $x = 0$, 0.5, 0.9 and 8.6 is explained in terms of the two band model in which both charge carriers contribute to magneto-transport properties [6]. The relative magnetic contribution to the Hall coefficient, $\Delta R_{H(2K)}/R_{H(2K)}$, indicate a suppression of antiferromagnetism in the concentration range $1.7 \le x \le 4.7$.

[1] R. Jaramillo, Y. Feng, J. Wang, and T. F. Rosenbaum, PNAS 107 (2010) 13631. [2] A. Yeh, Y.-A. Soh and J. Brooke, Nature (London) 419 (2002) 459. [3] M. Lee, A. Husmann and T. F. Rosenbaun, Phys. Rev. Lett. 92 (2004) 187201. [4] C. J. Sheppard, A. R. E. Prinsloo, H. L. Alberts, B. Muchono and A. M. Strydom, J. Alloys and Compounds 595 (2014) 164. [5] B. Muchono, C. J. Sheppard, A. M. Venter and A. R. E. Prinsloo, Physica B Condens Matter 537 (2018) 212. [6] W. R. Cox, D. J. Hayes and F. R. Brotzen, Phy. Rev. B 7 (1973) 3580.

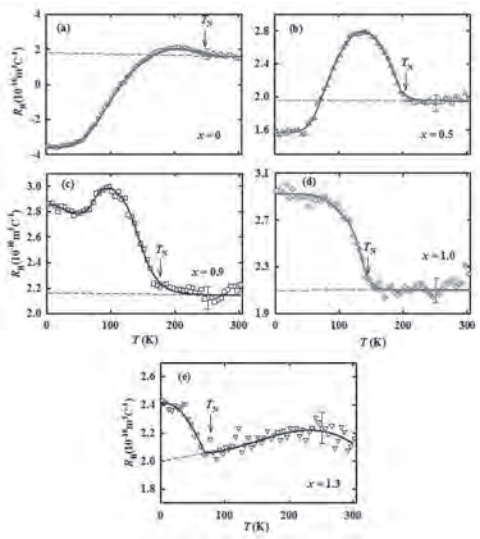

Fig. 1: The temperature dependence of the Hall coefficient, $R_H(T)$, for the ISDW $(Cr_{100-x}Al_x)_{95}Mo_5$ alloys in the range $0 \le x \le 1.3$.

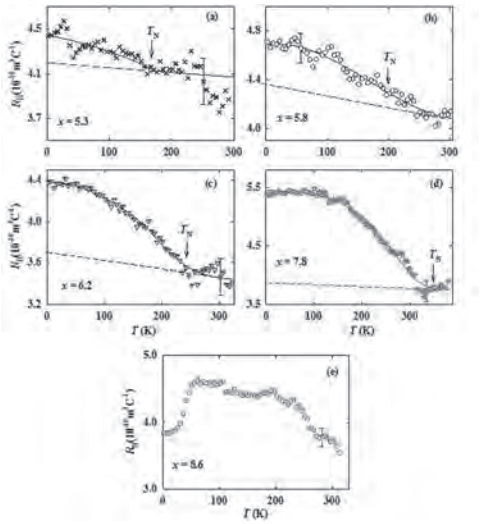

Figure 2: temperature dependence of the Hall coefficient, $R_H(T)$, for the CSDW $(Cr_{100-x}Al_x)_{95}Mo_5$ alloys in the range $4.7 \le x \le 8.6$.

BPA-08. Enhanced multiferroic properties in $Bi_{0.9}H_{0.1}FeO_3$ polycrystalline films (H = heavy rare earth elements). *T. Lin*[1], H.W. Chang[2], W. Chou[3], C. Hung[3], C. Wang[3] and D. Wei[1] *1. Institute of Manufacturing Technology and Department of Mechanical Engineering, National Taipei University of Technology, Taipei, Taiwan; 2. Physics, National Chung Cheng University, Chia-Yi, Taiwan; 3. Applied Physics, Tunghai University, Taichung, Taiwan*

In order to improve the multiferroic properties of $BiFeO_3$ (BFO), partial substitution of the A site for Bi has been reported to effective method. Last decade, two classes of dopants used include rare earth elements (R), such as Y, La, Nd, Pr, and Sm [1], and alkali earth elements, e.g. Ca, Sr, and Ba [2]. These dopants could reduce the leakage current density and improve the ferroelectric as well as magnetic properties of BFO. Although the investigations on multiferroic properties of R-doped BFO are extensive, BFO doped with heavy rare earth (H) is less discussed. To substitute H, such as Gd, Tb, Dy, Ho, and Er, for Bi in BFO is expected to improve the magnetic properties because the larger magnetic moment (7.8-10.6 μ_B) for H ions may introduce an additional magnetic interactions and ordering in BFO [3]. In this work, we adopted pulsed laser deposition (PLD) to develop $Bi_{0.9}H_{0.1}FeO_3$ (BHFO) films on glass substrates. The microstructure, ferroelectric, and magnetic properties of BHFO films are studied. BHFO films were confirmed to mainly consist of the perovskite phase. The desired multiferroic properties with the suppressed leakage is reached. The magnetic properties with the enhanced magnetization are found for BHFO films: their M_s are 18.8, 18.9, 21.3, 25.6, 18.5 emu/cm^3, for the films with H = Gd, Tb, Dy, Ho, and Er, respectively. The higher magnetic moment of H ion is, and larger M_s of the films is. The above behavior reveals magnetization of BFO films with H substitution is mainly dominated by the magnetic moment of H ion. Besides, good ferroelectric properties are also attained for BHFO films, where the largest remanent polarization ($2P_r$) of 120.1 $\mu C/cm^2$ is achieved for H = Gd, related to low leakage and high BHFO(110) texture. It might be related to the larger ionic radius for Gd than other H. Relationship between leakage mechanisms and microstructure are also discussed in those BHFO films.

[1] D. Kan et al., J. Appl. Phys. 110, 014106 (2011). [2] H.W. Chang et al., J. Alloys Compd. 683, 427 (2016). [3] N. Jeon et al., Appl. Phys. Lett. 98, 072901 (2011).

BPA-09. Ab-initio study of Chromia (Cr_2O_3): Calculation of Hubbard U parameter. *S. Sharma*[2,1], R. Mahajan[1], A. Shah[1] and A. Kashyap[1] *1. School of Basic Sciences, IIT Mandi, Mandi, India; 2. School of Physical Sciences, National Institute of Science Education and Research, Bhubaneswar, India*

We aim to investigate the magneto-electric properties of Chromia (Cr_2O_3) using the state of the art of Density functional theory methods. Chromia has solid applications in the bulk form and as thin films as shown by R Choudhary, et al., 2016 [1]. For the strong electronic correlations, it becomes important to involve the LDSA + U method. The work by R. Mahajan et al., 2021, demonstrates the Importance of intersite Hubbard interactions in the MnO_2 system [2]. While involving the Hubbard U reduce the deviations in the results to a considerable amount, the existing work in this arena has taken predefined value of the U parameter and none has attempted to find the ab-initio U values. Siqi Shi et al., has used the U value obtained from the difference in energies of Chromia in its two different configurations of filled d -orbitals [3]. Seeing the growing capabilities of the Quantum Espresso package makes us wonder if it is possible to find the Hubbard parameters from the first principle calculations. I. Timrov et al., 2018 presented the approach based on Density-functional perturbation theory for the calculation of Hubbard parameters [4]. Recently, the work by Ruchika Mahajan et al., 2022, on the MnO_2 system has shown that the Hubbard U parameter calculated through first-principle studies varies dramatically from the values mentioned in the existing literature [5]. On those lines, we have found the ab-initio Hubbard U value for Chromia and compared with the existing literature. We have studied both Anti-ferromagnetic and ferromagnetic configurations of the trigonal crystal with the R3c group symmetry as shown in Figure 1. This work is inspired by the works of R Choudhary et al., and A. Rohrbach et al., in the same direction [6], [7].

[1] R. Choudhary, P. Kumar, P. Manchanda, David J. "Interface-induced spin polarization in graphene on chromia." *IEEE Magnetics Letters* 7 (2016): 1-4. [2] R. Mahajan, Iurii Timrov, Nicola Marzari, and A. Kashyap. "Importance of intersite Hubbard interactions in β– MnO 2: A first-principles DFT+ U+ V study." *Physical Review Materials* 5, no. 10 (2021): 104402. [3] Shi, Siqi, A. L. Wysocki, "Magnetism of chromia from first-principles calculations." *Physical Review B* 79, no. 10 (2009): 104404. [4] I. Timrov, N. Marzari, and M. Cococcioni. "Hubbard parameters from density-functional perturbation theory." *Physical Review B* 98, no. 8 (2018): 085127. [5] R. Mahajan, A. Kashyap, and I. Timrov. "Electronic structure and magnetism of pristine

and Fe-doped MnO_2 from density-functional theory with extended Hubbard functionals." *arXiv preprint arXiv:2205.05977* (2022). [6] R. Choudhary, R. Skomski, and A. Kashyap. "Magnetism in Cr_2O_3 thin films: An ab initio study." *Ieee Transactions on Magnetics* 51, no. 11 (2015): 1-3. [7] Rohrbach, A., J. Hafner, and G. Kresse. "Ab initio study of the (0001) surfaces of hematite and chromia: Influence of strong electronic correlations." *Physical Review B* 70, no. 12 (2004): 125426.

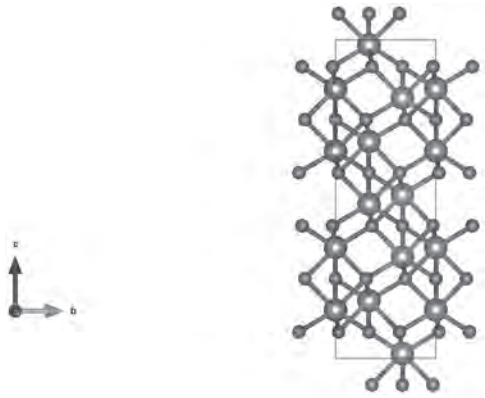

Hexagonal unit cell of Cr_2O_3. The blue (larger) atoms represent Chromium and the red (smaller) atoms are Oxygen.

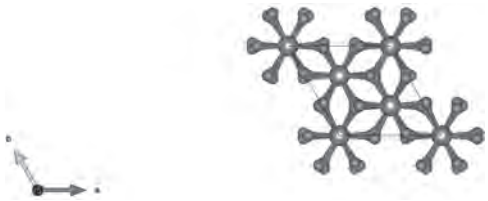

Trigonal primitive cell of Cr_2O_3

BPA-10. Tuning of Magnetic and Electrical properties of Samarium Iron Garnet by Holmium Substitution. *S. Verma*[1] and S. Ravi[1] *1. Physics, Indian Institute of Technology, Guwahati, Guwahati, India*

Holmium substituted Samarium iron garnet i.e., $Sm_{3-x}Ho_xFe_5O_{12}$ (x = 0 and 0.6) were synthesized using solid-state reaction route by sintering at 1400°C for 8 hours. Samples are found to be in single phase form as per XRD patterns and refined by Rietveld refinement technique using Ia-3d space group. The lattice constant is found to be decrease from 12.53Å to 12.43Å with Ho doping. Magnetic hysteresis loops (M-H) are measured at room temperature shows that saturation magnetization is decreases from 21.05 emu/g for x = 0 to 12.06 emu/g for x = 0.6 sample. The anisotropy constant is decreasing from 2.42×10^5 erg/cc for x = 0 to 1.7×10^5 erg/cc for x = 0.6 sample. Negative magnetization is observed for x = 0.6 sample which can be explained by using the equation i.e., $M_{net} = 3M_{Fe(d)} - [2M_{Fe(a)} + (3\text{-}x)M_{Sm} + xM_{Ho}]$, where Fe(d) and Fe(a) are the Fe atoms at tetrahedral and octahedral site respectively. The frequency dependence of real part of impedance Z' show a step like behavior which indicates the presence of dielectric relaxation in the samples. The merger of all Z' values at higher frequency is due to release of space charges. - Z'' vs. frequency is also plotted and all the plots show relaxation peaks. With the increase in temperature, the peaks are shifting towards higher frequency which suggests that the relaxation is due to thermally activated charge carriers. Keywords: Ferrimagnetic, negative magnetization, relaxation behavior.

1. Xiaobo Wu, Study on dielectric and magnetodielectric properties of $Lu_3Fe_5O_{12}$ ceramics, Applied Physics Letters 87, 042901 (2005). 2. Canglong Li, Spin reorientation, normal and inverse magnetocaloric effects in heavy rare-earth iron garnets, Ceramics International 46 (2020) 18758–18762. 3. Tingsong Zhang, Dielectric and ferroelectric properties of $Nd_3Fe_5O_{12}$, Solid State Communications 305 (2020) 113766. 4. Yu-Jhan Siao, Journal of Applied Physics 109, 07A508 (2011).

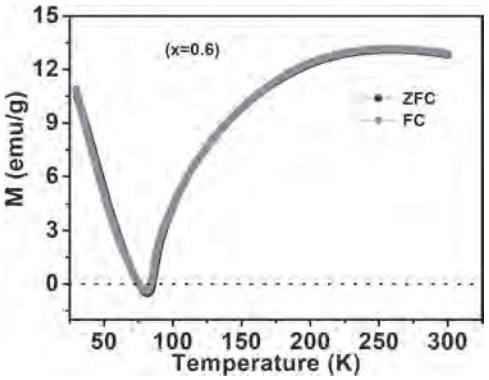

Figure 1: M-T plot for x=0.6 sample at an applied field of 500Oe.

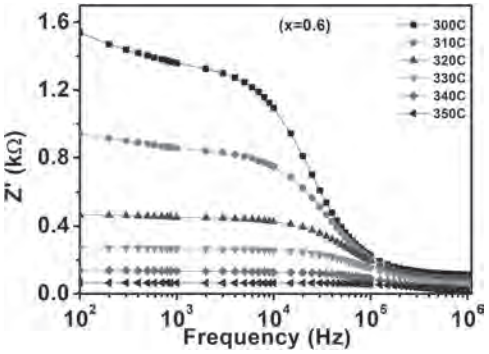

Figure 2: Frequency dependence of real part of impedance Z' at different temperatures.

BPA-11. Strain-independent Regulation of Magnetic Properties by Topotactic Phase Transformation in $LaCoO_3$ Thin Films. *Y. Fan*[1,2], Z. Yin[1], J. Wang[1], F. Hu[1], B. Li[2], A. Geng[2] and B. Shen[1] *1. Institute of Physics, Chinese Academy of Sciences, Beijing, China; 2. Beijing Technology and Business University, Beijing, China*

Transition metal oxides exhibit rich electrical and magnetic properties. The epitaxial strain plays a vital role to manipulate their magnetic ground state. In addition, Oxygen vacancies (Vo) are one of the most common point defects to play a key role in regulating the physicochemical properties of oxides.[1-4] In this context, LCO exhibits interesting phenomena in terms of the origin of magnetism. In this work, Perovskite $LaCoO_3$ (PV-LCO) films were grown at STO and LAO substrate. Then brownmillerite $LaCoO_{2.5}$ (BM-LCO) films are formed by annealing in a vacuum at 450 °C for 4h and 500 °C for 4h, respectively. The XRD spectra show that there is no impurity phase during phase transitions, indicating that the films can be fully transformed. (Fig.1a) The magnetic properties were confirmed by SQUID-VSM. The 50-nm-thick PV-LCO film on STO exhibits an obvious ferromagnetism phase. (Fig.1b-c) The tensile strain leads to a decrease of Δ_{CF} due to distortion of CoO_6 octahedron, promotes the spin state transition. [5,6] However, the same thickness coherently strain film in compression on LAO exhibits extremely weak ferromagnetism. We anticipate the reason for this is because the e_g orbitals are split into two separate energy levels due to existence of the JTD distortion, it is always accompanied by an increase of the bond distance r_{Co-O} and suppression of CoO_6 octahedral rotation and distortion. Interestingly, the BM-LCO shows no hysteresis loop. We believe the reason for this novel phenomenon is that the increase in ordered Vo leads to the expansion of the lattice, thus inhibiting the rotation and distortion of the CoO_6 octahedron and causing the generation of anti-ferromagnetic behavior. [7,8] In sum, we find that BM-LCO films in epitaxial strain and Vo ordering show no ferromagnetism. This phenomenon provided an effective way to regulate the physical properties of cobalt oxides. It would have a good application value in the fields of ion electrochemical sensors.

[1]J. H. Ngai, F. J. Walker, and C. H. Ahn, Annual Review of Materials Research 44 (1), 1 (2014). [2]A. La Spina, P. Paolicchi, and A. Kryszczynska, Nature 428 (6981), 400 (2004). [3]J. Jeong, N. Aetukuri, and T. Graf, Science 339 (6126), 1402 (2013) [4]G.E. Sterbinsky, R. Nanguneri, and J.X. Ma, Ryan, Phys. Rev. Lett. 120 197201(2018). [5]Er-Jia Guo, Ryan D. Desautels, and David Keavney, Physical Rev B 75 (14) (2007). [6]Fuchs, D. C. Pinta, and T. Schwarz, Physic Rev. B 75, 144402 (2007). [7]D. Fuchs, E. Arac, and C. Pinta, Phys. Rev. B 77, 014434, (2008). [8]Q. Zhang, A. Gao, and F. Meng, Nat Commun 12(1), 1853 (2021).

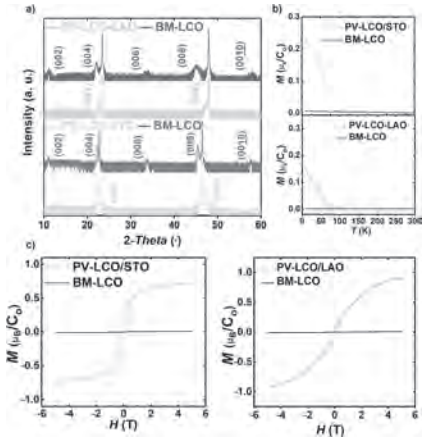

Fig.1 a) (Color online) XRD θ-2θ spectra of the 50 nm-thick LCO film on STO and LAO substrates, b) temperature-dependent magnetization *M* (T) of PV-LCO and BM-LCO at 500 Oe, c) magnetic hysteresis loops *M*(H) of PV-LCO and BM-LCO at 10 K.

BPA-12. On the synthesis and characterization of bimagnetic $CoO/NiFe_2O_4$ heterostructured nanoparticles. *M. Uddin*[1], R. Mayanovic[1] and M. Benamara[2] *1. Physics, Astronomy & Materials Science, Missouri State University, Springfield, MO, United States; 2. Materials Science & Engineering, University of Arkansas, Fayetteville, AR, United States*

Bimagnetic nanoparticles show promise for applications in energy efficient magnetic storage media and magnetic device applications. The magnetic properties, including the exchange bias of nanostructured materials can be tuned by variation of the size, composition, and morphology of the core vs overlayer of the nanoparticles (NPs). The purpose of this study is to investigate the optimal synthesis routes, structure and magnetic properties of novel $CoO/NiFe_2O_4$ heterostructured nanocrystals (HNCs). In this work, we aim to examine how the size impacts the exchange bias, coercivity and other magnetic properties of the $CoO/NiFe_2O_4$ HNCs. The nanoparticles with sizes ranging from 10 nm to 24 nm were formed by the synthesis of an antiferromagnetic (AFM) CoO core and deposition of a ferrimagnetic (FiM) $NiFe_2O_4$ overlayer. A highly crystalline magnetic phase is more likely to occur when the morphology of the core-overgrowth is present, which enhances the coupling at the AFM-FiM interface. The CoO core NPs are prepared using thermal decomposition of $Co(OH)_2$ at 600 °C for 2 hours in a pure argon atmosphere, whereas the HNCs are obtained first using thermal evaporation followed by hydrothermal synthesis. The structural and morphological characterization made using X-ray diffraction (XRD), X-ray photoelectron spectroscopy (XPS) and scanning electron microscopy (SEM) techniques verify that the HNCs are comprised of a CoO core and a $NiFe_2O_4$ overgrowth phase. Rietveld refinement of the XRD data shows that the CoO core has the rocksalt (Fd3(bar)m) crystal structure and the $NiFe_2O_4$ overgrowth has the spinel (C12/m1) crystal structure. SEM-EDS data indicates the presence and uniform distribution of Co, Ni, and Fe in the HNCs. XPS analysis of the O 1s, Co 2p, Ni 2p, and Fe 2p regions shows that both the core and overgrowth phases are well-structured. The results from PPMS magnetization measurements and high-resolution transmission electron microscopy (HR-TEM) of the $CoO/NiFe_2O_4$ HNCs will be discussed.

BPA-13. Investigations of Size-Dependent Properties of Mn-Co-NiO Based Heterostructured Nanoparticles. *F. Ishrak*[1], R. Mayanovic[1] and M. Benamara[2] *1. Physice, Astronomy, and Materials Science, Missouri State University, Springfield, MO, United States; 2. University of Arkansas, Fayetteville, AR, United States*

In this work, we investigate the synthesis, along with the structural, magnetic, and surface chemical environment properties, of novel Mn-Co-NiO-based heterostructured nanocrystals (HNCs). The objective is to develop novel, well structurally ordered inverted antiferromagnetic (AFM) NiO – ferrimagnetic (FiM) spinel phase overgrowth HNCs. Inverted HNCs are particularly promising for magnetic device applications because their magnetic properties are more easily controlled by having well-ordered AFM cores, which can result in magnetic structures having large coercivities, tunable blocking temperatures, and other enhanced magnetic effects. The synthesis of the HNCs is accomplished using a two-step process: In the first step, NiO nanoparticles are synthesized using a thermal decomposition method. Subsequently, Mn-Co overgrowth phases are grown on the NiO nanoparticles via hydrothermal nanophase epitaxy, using a fixed pH level (~5.3) of the aqueous medium. This pH level was selected based on previous work in our laboratory showing that NiO/Mn_3O_4 HNCs of constant size have optimal coercivity and exchange bias when synthesized at a pH of 5.0.[1] The crystalline structure, surface/interface chemical environment and gross morphology of the Mn-Co-NiO-based HNCs have been analyzed using X-ray diffraction (XRD), X-ray photoelectron spectroscopy (XPS) and Scanning Electron Microscopy (SEM) techniques, respectively. Analysis using these techniques shows that the HNCs are composed of a NiO core and a $CoMn_2O_4$ overgrowth phase. Rietveld refinement of XRD data shows that the NiO core has the rocksalt (*Fm-3m*) cubic crystal structure and the $CoMn_2O_4$ overgrowth has the spinel ($I4_1/amd$) crystal structure. Moreover, an increased relative amount of the $CoMn_2O_4$ overgrowth phase is deposited with decreasing NiO core particle size during the synthesis of the HNCs. Analysis of the O 1s, Ni 2p, Co 2p, and Mn 2p regions of the XPS spectra measured from our samples is consistent with well-structured core/overgrowth phases having M-OH (M: Ni, Co, Mn) bonding at their surface regions. The results from PPMS magnetization and high-resolution transmission electron microscopy (HR-TEM) characterization of the Mn-Co-NiO-based HNCs will be discussed.

[1] Shafe et al., ACS Applied Materials & Interfaces, 13, 24013–24023 (2021)

BPA-14. Exchange bias and gate-tunable magnetic anisotropy in 2D multiferroic heterostructure. *Y. Ma*[1] *1. King Abdullah University of Science and Technology, Jeddah, Saudi Arabia*

Tuning the magnetism in the electronic approach is a goal that has been pursued in the field of spintronics for a long time. However, this goal is rarely achieved on 2D materials. Here, we realized the manipulation of magnetism by developing a novel 2D multiferroic heterostructure. The exchange bias was observed in anomalous Hall effect (AHE) measurement, showing the strong coupling between ferromagnetic order and antiferromagnetic order in the heterostructure. With the application of the back gate voltage, the hysteresis field reduced, as observed from the narrowed AHE loop, suggesting the effective manipulation on magnetic anisotropy. These findings indicate a new way to manipulate magnetism in 2D systems via magneto-electric coupling.

BPA-15. Photo-Induced Paramagnetic States of Methyl Radicals Adsorbed at ZnO Nanoparticles Surface. *D. Marin*[1], A. Savoyant[1], S. Bertaina[1] and O. Margeat[2] *1. IM2NP, Marseille, France; 2. CINAM, Marseille, France*

Controlling the physical and chemical surface properties of semiconducting nanoparticles (NPs) is a key point for future nanotechnologies and information encoding, since these NPs have characteristics high surface-to-volume ratio, tunable electronic properties, photocatalytic activity and,

more rarely, specific magnetic response. As a promising candidate for future quantum applications, ZnO NPs show interesting magnetic response when submitted to violet coherent illumination (≈400nm) under 110 K. In this regime, excited paramagnetic states are observable by Electron Spin Resonance (ESR) and a blend of intrinsic ZnO and surface-related properties is observed. After irradiation by a 50 mW laser beam, an intense signal arises at *g=1.96* attributed to the ionization of zinc vacancies, thus changing from *S=0* to *S=1/2* magnetic state. Simultaneously a second and less intense signal appears, characterized by four magnetic transitions with relative intensities 1:3:3:1. The origin of this signal is proven by NMR cross-polarization and pulsed ESR to be some photo excited methyl radicals (CH_3), present at the NPs surface as a residue of the growth process. By surface functionalization, it is possible to replace the CH_3 radicals by deuterated radical CD_3, or even to suppress it entirely. These surface signals last for several hours after illumination removal. They can be reversibly suppressed and recovered by heating to room temperature, cooling back below 110 K, and illuminating. The spin dynamics of these bulk and surface photo-excited magnetic states were studied by pulse ESR. While the core defect has slower longitudinal relaxation time T_1 (spin-lattice) than the surface adsorbed CH_3 (140 μs vs 40 μs resp.), the contrary is true for the transverse relaxation time T_2 (spin-spin) which is approximately 400 ns for CH_3 and 30 ns for the core defect.

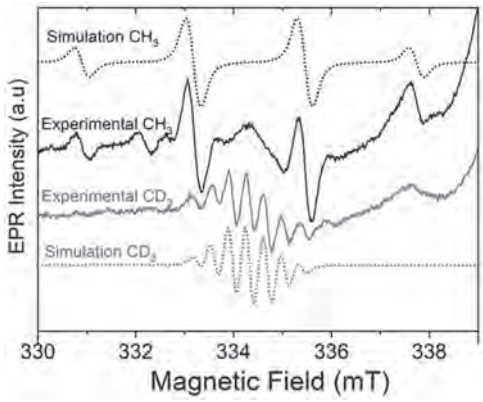

Simulated and maeasured ESR signals for CH_3 and CD_3

BPA-16. Effect of microwave instant heating on magnetic, electric, thermoelectric and microwave absorption properties of $La_{0.7}Na_{0.3}MnO_3$.
M. Marimuthu[1], L. Jiang[1], G. Chen[1], *Y. Lee*[1], A. Ghosh[1] and R. Mahendiran[1] *1. National University of Singapore, Singapore*

Stoichiometric $LaMnO_3$ has an orthorhombic crystal structure with an antiferromagnetic (T_N ~ 140 K) insulating nature[1]. The substitution of aliovalent cations (Sr^{2+} or Na^{1+}) induce holes in the partially filled *3d* shell of Mn and oxidizes the Mn^{3+} ($t_{2g}^3e_g^1$) to Mn^{4+} ($t_{2g}^3e_g^0$) and transforms the $LaMnO_3$ to ferromagnetic metal through the double exchange coupling of Mn^{4+}-O-Mn^{3+}[2]. Since the Na^{1+} (1.39 Å) has an ionic radii closer to La^{3+} (1.36 Å) this would induce a twice number of holes compared to Sr^{2+} substitution. Drastic variations in their physical properties have also been found in different synthesis methods[3,4]. Therefore, in this work, we adopted a recently emerging microwave (MW) heating to synthesise $La_{1-x}Na_xMnO_3$ (x = 0, 0.1, 0.3) from the oxide precursors. Conduction or dielectric loss heating by MW irradiation enables the fast and homogenous reaction in few minutes. We achieved 1000 °C in 10 min and dwelled the samples for 20 min. The operating MW power alone was varied from 1000 W to 1200 W and 1400 W for x = 0.3 to examine the effect of MW power on its physical properties. Temperature-dependent magnetization and resistivity of x = 0, 0.1, 0.3 with fixed MW power (1200 W) are shown in Fig. 1 (a)&(b). A broad Curie transition is observed for undoped $LaMnO_3$ with T_C of 200 K, unlike our previous report on solid-state prepared $La_{1-x}Na_xMnO_3$ where we observed T_N = 140 K for undoped $LaMnO_3$[5], and the transition becomes narrow with increased T_C as x increases. Insulating $LaMnO_3$ transforms to metallic below T_C upon Na doping. T_C is denoted in the figure by dotted vertical lines. As the MW power increases from 1000 W to 1200 W, the resistivity of x = 0.3 decreases drastically and the metal-insulator transition also becomes sharp at a temperature very close to T_C (Fig. 1(c)). The obtained microwave absorption peaks at a specific field show only a little increase with increasing the frequency of the MW signal. These findings will be correlated and discussed with the structural and morphological features acquired by microwave irradiation.

[1] T. Tokura, et al., Mater. Sci. Eng. B 31(1-2), 187–191 (1995). [2] G.H. Rao, et al., J. Phys. Condens. Matter 11, 1523 (1999). [3] Y. Regaieg, et al., Materials Letters 80, 195–198 (2012). [4] Shuai Zhang, et al., Ceramics International 46, 584–591 (2020). [5] Rajasree Das, et al., Ceramics International 47, 393–399 (2021).

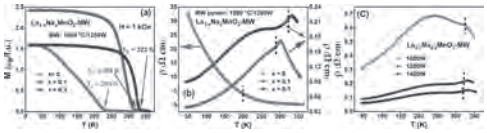

Fig. 1: Temperature-dependent (a) magnetization (b) resistivity of $La_{1-x}Na_xMnO_3$-MW (x = 0, 0.1 and 0.3), and (c) resistivity of x = 0.3 with different MW powers.

BPA-17. Magnetic Field-dependent Thermal Conductivity in $(La_{0.6}Pr_{0.4})_{0.7}Ca_{0.3}MnO_3$ Thin Films.
V. Bruchmann-Bamberg[1], K. Stroh[1], P. Henning[1], D. Steil[1] and V. Moshnyaga[1] *1. Physikalisches Institut, Georg-August-Universitaet Goettingen, Goettingen, Germany*

Transition metal oxides, like perovskite manganites $AMnO_3$, possess a strong coupling between charge, spin and lattice degrees of freedom and allow for both filling and bandwidth control of the phase transition by chemical doping via substitution at the A-site using rare earth and/or alkaline earth ions. The resulting phase diagrams reflect a complex interplay of valence states, electronic correlations, orbital ordering and magnetic interactions, all giving rise to intriguing magneto-electronic phenomena. A prominent example is the colossal magnetoresistance effect (CMR), manifesting itself in a magnetic field-induced insulator to metal transition [1]. Since thermal conductivity of a solid contains both lattice and electronic contributions, control over thermal conductivity by external magnetic fields can be achieved in CMR manganites. Here we studied $(La_{0.6}Pr_{0.4})_{0.7}Ca_{0.3}MnO_3$/MgO(100) (LPCMO/MgO) films prepared by a metalorganic aerosol deposition technique [2]. Electrical measurements of a 51 nm thick LPCMO/MgO film reveal a typical behaviour with CMR = 100%*$\Delta R(5T)/R(0T) \approx 10^4$ % in the vicinity of the FMM-PMI phase transition at $T_C \approx$ 190 K. The temperature- and magnetic field-dependent thermal conductivity was measured by means of the 3ω method [3]. We observed a significant increase of thermal conductivity κ in applied magnetic field, the so-called magnetothermal resistance MTR = 100%*$\Delta\kappa(5T)/\kappa(0T) \approx$ 30 % close to T_C, mainly caused by the electronic contribution in agreement with the Wiedemann-Franz law (Fig. 1). In addition, the slight deviation above T_C is discussed as a possible contribution of charge/orbital ordering around $T_{CO} \approx$ 210 K. Our results can be viewed as an example of active control of energy dissipation in manganite thin films. A financial support by the Deutsche Forschungsgemeinschaft (DFG) within the CRC 1073 project A02 and the DFG project 399572199 is acknowledged.

[1] Chahara, K. et al., Appl. Phys. Lett. 63, 1990 (1993) [2] Jungbauer, M. et al., Appl. Phys. Lett. 105, 251603 (2014) [3] Cahill, D., Rev. Sci. Instrum. 61, 802 (1990)

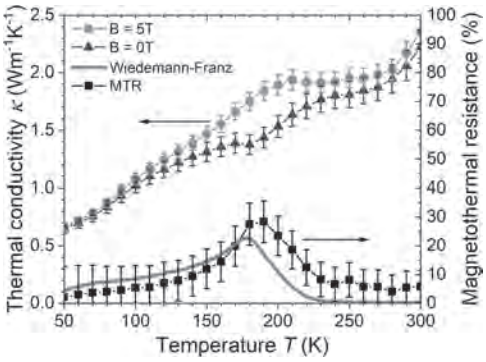

Fig. 1 Magnetic field-dependent thermal conductivity of a $(La_{0.6}Pr_{0.4})_{0.7}Ca_{0.3}MnO_3$/MgO(100) thin film

Session COA
MAGNETO-IONICS

Enric Menendez, Chair
Autonomous University of Barcelona, Cerdanyola del Vallès, Spain

CONTRIBUTED PAPERS

COA-01. Voltage Control of Skyrmions Using Solid-State Lithium-Ion Gating. *M. Ameziane*[1], R. Mansell[1] and S. van Dijken[1] *1. Applied Physics, Aalto University, Espoo, Finland*

Ionic control of magnetism has sparked interest thanks to its high magneto-electric coupling efficiency at low voltages - a property essential for next-generation low-power ICT technologies. Here we report on the creation and annihilation of skyrmions in a solid-state magneto-ionic crossbar junction using Li^+ ion gating. The structure consists of a Ta (2 nm)/Pt (4 nm)/$Co_{40}Fe_{40}B_{20}$ (0.9 nm)/Pt (0.2 nm)/LiPON (70 nm)/Pt (4 nm) stack patterned into 500 μm x 500 μm crossbar junctions (Fig. 1a). In the presence of a small magnetic field (0.7 mT), applying a positive voltage (i.e. introducing Li^+ ions into the Pt/CoFeB/Pt electrode) reduces the perpendicular magnetic anisotropy (PMA) and increases the Dyaloshinskii-Moriya interaction (DMI), leading to skyrmion nucleation. Applying a negative voltage (i.e. extracting Li+ ions from the Pt/CoFeB/Pt electrode) results in skyrmion annihilation. The observed magnetic effects are fully reversible (Fig. 1b,c,d) and persist when the bias voltage is switched off (Fig. 2a). We show that skyrmion nucleation/annihilation can be achieved by single voltage pulses with a duration of only 60 μs (Fig. 2b). Our results demonstrate a simple approach to robust voltage control of skyrmions using Li^+ ion gating, which could be utilized in spin-based nonconventional computing devices and other applications.

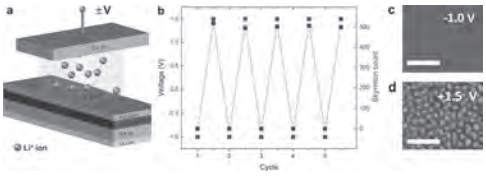

Fig.1 (a) Schematic of the crossbar structure. (b) Reversible creation and annihilation of skyrmions at positive and negative bias voltages under 0.7 mT external magnetic field. (c, d) Magneto-optical Kerr effect (MOKE) images of a crossbar junction at -1.0 V and +1.5 V. Scale bar: 5μm.

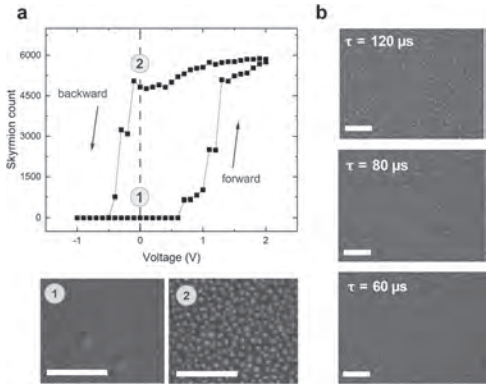

Fig. 2 (a) Skyrmion count as a function of voltage and corresponding MOKE images at zero-bias voltage. The voltage sweep direction determines the magnetic state at zero-bias voltage. (b) MOKE images of skyrmion nucleation as a function of voltage pulse duration. The pulse amplitude is +10 V. Scale bar: 10 μm.

COA-02. Withdrawn

COA-03. On-Off Ferromagnetism in Co_3O_4 by Voltage-Driven Oxygen Ion Migration. *E. Menendez*[1], S. Martins[1], J. de Rojas[1], A. Quintana[2], Z. Tan[1], J.L. Costa-Krämer[3] and J. Sort[1,4] *1. Physics, Universitat Autònoma de Barcelona, Cerdanyola del Vallès, Spain; 2. Institut de Ciència de Materials de Barcelona (ICMAB-CSIC), Cerdanyola del Vallès, Spain; 3. IMN-Instituto de Micro y Nanotecnología (CNM-CSIC), Tres Cantos (Madrid), Spain; 4. Institució Catalana de Recerca i Estudis Avançats (ICREA), Barcelona, Spain*

Voltage-driven ion transport modulation of magnetism (magneto-ionics) represents a significant breakthrough to enhance energy efficiency in magnetically-actuated devices. Particularly, voltage-driven oxygen ion motion in Co_3O_4 allows for voltage-controlled On–Off ferromagnetism, since Co_3O_4 (paramagnetic: Off) can be partially reduced to Co (ferromagnetic: On) by voltage actuation. This can be afterwards reversed by applying a voltage of the opposite polarity [1]. The way the electric field is applied has a strong impact in the room temperature magneto-ionic motion. Specifically, in electrolyte-gated 100 nm-thick paramagnetic Co_3O_4 films, the oxygen magneto-ionic motion can be sped up by an order of magnitude (from 1000 to 100 s) applying the electric field through an electrochemical capacitor configuration (*i.e.*, using, as a working electrode, an underlying conducting buffer layer beneath the Co_3O_4 film) rather than using an electric-double-layer transistor-like configuration (*i.e.*, placing the electric contact at one side of the Co_3O_4 film as a working electrode). This is due to the better uniformity and larger strength of the electric field in the capacitor design [1,2]. However, ion motion at room temperature is still too slow for applications. By reducing the Co_3O_4 film thickness down to 15 nm, sub-10 s ON-OFF ferromagnetism can be achieved in electrolyte-gated films [3].

Remarkably, cumulative magneto-ionic effects can be generated by applying voltage pulses at frequencies as high as 100 Hz, which is the frequency at which dynamic effects of biological synapses occur. Magneto-ionics in Co_3O_4 can then be used to emulate synapse functionalities, including plasticity, potentiation (magnetization increase) and depression (*i.e.*, depletion of magnetization), voltage-controlled threshold activation of ferromagnetism (*i.e.*, spike-magnitude dependence), and learning and forgetting capabilities. The former by means of spike-rate-dependent plasticity of the generated magnetization upon pulsed voltage actuation. These features demonstrate Co_3O_4 magneto-ionics can be used for the design of neuromorphic-like systems [3].

[1] A. Quintana, E. Menéndez, M. O. Liedke, M. Butterling, A. Wagner, V. Sireus, P. Torruella, S. Estradé, F. Peiró, J. Dendooven, C. Detavernier, P. D. Murray, D. A. Gilbert, K. Liu, E. Pellicer, J. Nogues and J. Sort, Voltage-controlled ON–OFF ferromagnetism at room temperature in a single metal oxide film, *ACS Nano* 12 (2018) 10291–10300 [2] J. de Rojas, A. Quintana, A. Lopeandía, J. Salguero, J. L. Costa-Krämer, L. Abad, M. O. Liedke, M. Butterling, A. Wagner, L. Henderick, J. Dendooven, C. Detavernier, J. Sort and E. Menéndez, Boosting room-temperature magneto-ionics in a non-magnetic oxide semiconductor, *Advanced Functional Materials* 30 (2020) 2003704 [3] S. Martins, J. de Rojas, Z. Tan, M. Cialone, A. Lopeandía, J. Herrero-Martín, J. L. Costa-Krämer, E. Menéndez and J. Sort, Dynamic electric-field-induced magnetic effects in cobalt oxide thin films: towards magneto-ionic synapses, *Nanoscale* 14 (2022) 842–852

COA-04. Stability of under/over oxidized magneto-ionic states in $Pt/Co_{60}Fe_{20}B_{20}/HfO_2$. *R. Pachat*[1], D. Ourdani[2], M. Syskaki[3], T. Bhatnagar-Schoeffmann[1], M. Massouras[1], S. Roy[1], A. Lamperti[4], Y. Roussigné[2], S. Ono[5], J. Langer[3], D. Ravelosona[1,6], M. Belmeguenai[2] and L. Herrera Diez[1] *1. C2N, Université Paris-Saclay, Palaiseau, France; 2. LSPM, Université Sorbonne Paris Nord, Villetaneuse, France; 3. Singulus Technologies AG, Kahl am Main, Germany; 4. IMM-CNR, Agrate Brianza, Italy; 5. Central Research Institute of Electric Power Industry, Yokosuka, Japan; 6. Spin-Ion Technologies, Palaiseau, France*

Magneto-ionics (MI) provides a nonvolatile EF modulation of magnetism through the migration of ions toward/away from the magnetic interfaces that allows for low-power spintronics devices. However, the ionic mechanism involved still needs to be explored, as key properties such as reversibility have been shown to strongly depend on the chemical composition and oxidation level of the ferromagnet (FM)/oxide interface, [1–3], and on the degree of crystallinity of the system [4]. We have recently shown that the gate-voltage driven degree of oxidation at the FM/oxide interface in Ta/$Co_{20}Fe_{60}B_{20}/HfO_2$ defines two MI regimes: (I) underoxidized to optimally oxidized, and (II) optimally oxidized to overoxidized, accompanied by a change in the magnetization easy axis from in-plane (IP) to out-of-plane (OOP) in regime I and from OOP to IP in regime II [3]. Only regime II showed reversibility, which was linked to the different binding strength of the oxygen species in regimes I and II. In this work, we present the MI behavior in $Pt/Co_{60}Fe_{20}B_{20}/HfO_2$, where also two MI regimes have been identified. In this system, both regime I and II are reversible, but the stability of the nonvolatile magnetic states was found to be significantly different in regime I and II. Magnetic states in regime I was found to be highly stable, with no significant loss of remanence in the hysteresis loops over several weeks after applying the gate voltage. In this regime, a significant variation of the Dzyaloshinskii-Moriya interaction was also observed. In contrast, the magnetic states in regime II (between OOP and IP) were found to evolve with time back to the OOP state within one day after applying the gate voltage. Interestingly, only the final overoxidized IP state is fully stable in regime II. This disparity in the stability of the MI states in regimes I and II could be attributed to differences in the gate-voltage driven chemical reactions and ionic transport, where also the composition of CoFeB may play an important role. Our results show the importance of studying the link between the ionic mechanisms and the MI state stability, in view of practical applications in spintronics.

[1]L. Herrera Diez, Y. T. Liu, M. Belmeguenai, et al., Physical Review Applied, 12, 034005 (2019), [2] A. Fassatoui, L. Ranno, S. Pizzini, et al., Physical Review Applied, 14, 064041 (2020), [3] R. Pachat, D. Ourdani, L. Herrera Diez. et al., Physical Review Applied, 15, 064055 (2021), [4] R. Pachat, D. Ourdani, L. Herrera Diez, et al., Adv. Mat. Inter., Accepted (2022)

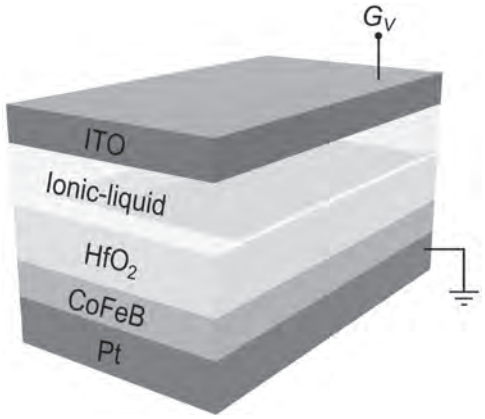

Schematic of the stack with an ionic-liquid $[EMI]^+[TFSI]^-$ gate.

COA-05. Magneto-ionic tuning of magnetic states in $Ni_{80}Fe_{20}$ nanodot arrays. *S. Honnali*[1,2], M. Kutuzau[1,3], K. Nielsch[1,2], H. Reith[1] and K. Leistner[1,3] *1. IFW Dresden, Dresden, Germany; 2. Institute of Material Science, TU Dresden, Dresden, Germany; 3. Electrochemical Sensors and Energy Storage, Institute of Chemistry, Faculty of Natural Sciences, TU Chemnitz, Chemnitz, Germany*

The advent of machine learning algorithms and point sources of data generation such as sensors and Internet of Things devices has marked the beginning of the new digital era. Large amounts of data are being generated every second which needs to stored and processed for different applications. This has led to an increase in energy consumption in all the sectors using the technology. Therefore, the use of magnetic materials which hosts topologically protected spin textures such as magnetic skyrmions and magnetic vortices are promising candidates for low power non-volatile memory devices and processing elements for reservoir computing. [1,2] To control and manipulate such magnetic spin textures, magneto-ionic approaches are currently under study. [3] Magnetic vortices in nanostructures are promising as elements for memory devices, because of its ability to store two bits of information simultaneously in its chirality and polarity. Due to its flux closure property, nanostructures with vortices have an increased areal density compared to its single bit device counterparts. [4] In this work, we report the fabrication and growth of $Ni_{80}Fe_{20}$ nanodot arrays using Talbot lithography and electrochemical deposition. Pristine samples with various thicknesses and hence different aspect ratios were grown and the magnetic ground states were probed using Vibrating Sample Magnetometry and Kerr microscope. Three different ground states were observed namely, uniform magnetization along the radial direction of the dot (in-plane single domain), uniform magnetization along the cylindrical axis (out-of-plane single domain) and magnetic vortex state. Subsequently, by using in-situ Kerr microscopy, we demonstrate voltage-induced manipulation of the magnetic state by electrolytic gating. These magneto-ionic changes occur at much lower external bias voltage (< 2 V), when compared to the strain mediated approach, which requires hundreds of volts. [5] Thereby, this magneto-ionic approach is promising for next generation memory devices along with other potential applications such as neuromorphic computing.

[1] Liu, Y., Yu, G. “MRAM gets closer to the core”, *Nat Electron* 2, 555–556 (2019) [2] D. Prychynenko et al. “Magnetic skyrmions as a Nonlinear Resistive Element: A Potential Building Block for Reservoir Computing”, Phys. Rev. Applied 9, 014034 (2018) [3] M. Nichterwitz, S. Honnali et al. “Advances in magneto-ionic materials and perspectives for their application”,

APL Materials 9, 030903 (2021) [4] V. Cambel and G. Karapetrov, "Control of vortex chirality and polarity in magnetic nanodots with broken rotational symmetry", Phys. Rev. B 84, 014424 (2011) [5] M Ghidini et al. "Voltage-driven displacement of magnetic vortex cores", 2020 *J. Phys. D: Appl. Phys*. 53 434003

INVITED PAPER

COA-06. Magneto-Ionic Switching of Superparamagnetism.
M. Gößler[1,2], S. Topolovec[2], H. Krenn[3] and R. Würschum[2] *1. Institute of Chemistry, Chemnitz University of Technology, Chemnitz, Germany; 2. Institute of Materials Physics, Graz University of Technology, Graz, Austria; 3. Institute of Physics, University of Graz, Graz, Austria*

Magneto-ionic materials are an emergent subclass of magneto-electric materials, which utilize ionic transport and electrochemical reactions for the manipulation of magnetic properties. In contrast to conventional magneto-electric approaches, the magneto-ionic one holds great promise for energy-efficient magnetic devices, as electrochemical reactions can be controlled in a narrow voltage range of only a few Volts. Hydrogen-based electrochemical reactions have the additional advantage of fast reaction kinetics and short diffusion times, which makes hydrogen magneto-ionics the fastest magneto-ionic concept to date [1]. Here, hydrogen magneto-ionics is used to control magnetism in superparamagnetic composite electrodes. Superparamagnetic particles are ideal candidates for generating large magneto-electric effects. Their giant 'hidden' magnetic moments at room temperature can be blocked into a stable magnetic state by increasing the magnetic anisotropy energy of the particles. This has been demonstrated by means of a strain-coupling to a piezoelectric substrate [2], or via electrochemical hydrogen-charging [3], which will be the subject of this talk. Our magneto-ionic setup used superparamagnetic Co clusters embedded in a nanoporous Pd matrix as composite electrode, which was prepared via electrochemical dealloying in a single fabrication step. Extensive microstructural characterization revealed polydisperse Co clusters with sizes below 2 nm, well below the superparamagnetic limit for Co. Magnetic measurements further showed a broad blocking peak, corresponding to a broad distribution of anisotropy energies in this system. Nanoporous Pd-Co composite electrodes were charged with hydrogen from an aqueous potassium hydroxide electrolyte solution, while their magnetic properties were monitored *in situ* using SQUID magnetometry. In Fig.1a the magnetization of nanoporous Pd-Co electrodes at two different potentials is depicted, which correspond to a hydrogen-charged (-1.00 V) and a hydrogen-free state (0.05 V). Both curves exhibit superparamagnetic characteristics, with a strongly increased slope upon application of a hydrogen-charging potential. Reversible variations in magnetization of up to 200% were observed during cyclic hydrogen-charging and discharging at a constant magnetic field in Fig.1b, corresponding to a complete ON- and OFF-switching of magnetization [3]. Zero field cooled magnetization curves before and after hydrogen-charging showed a strong upshift in blocking temperature, and thus directly evidenced an increasing magnetic anisotropy energy upon hydrogen-charging. To optimize the magneto-ionic effect, different Co cluster size distributions were tested and compared in terms of magneto-electric coefficients, as well as absolute magnetization changes [4]. Finally, the hydrogen magneto-ionic switching mechanism is discussed in detail, outlining remaining challenges and future prospects of this concept. Financial support by the Austrian Science Fund FWF (P30070-N36) is acknowledged. This work was performed in the framework of the inter-university cooperation of TU Graz and Uni Graz on natural sciences (NAWI Graz).

[1] A. J. Tan et al., Nat. Mater., 18, 35, (2019) [2] H. K. D. Kim et al., Nano Lett., 13, 884, (2013) [3] M.Gößler et al., Small, 15, 1904523, (2019) [4] M.Gößler et al., APL Mater., 86, 041101, (2021)

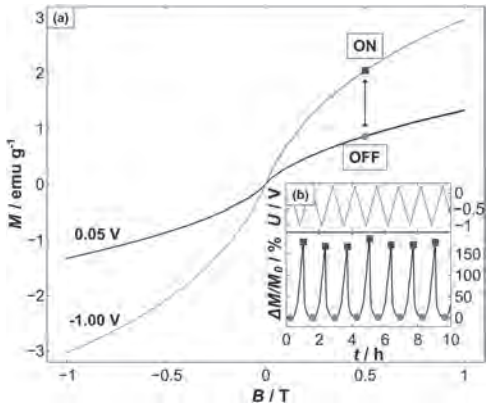

Fig.1: (a) Magnetization *M* as a function of magnetic field *B* for a nanoporous Pd-Co composite electrode in aqueous potassium hydroxide solution with different static voltages (0.05 V and -1.00 V vs. Au-reference) applied. (b) Corresponding changes in magnetization $\Delta M/M_0$ upon cyclic hydrogen-charging at 0.5 T, leading to a reversible ON- and OFF-switching of magnetism (blue/red markers).

CONTRIBUTED PAPERS

COA-07. Influence of alkaline electrolyte composition on H-based magneto-ionic effect in Ni films.
M. Kutuzau[1,2], M. Gößler[1,3], S. Topolovec[3], S. Schiemenz[2], K. Nielsch[2,4] and K. Leistner[1,2] *1. Electrochemical Sensors and Energy Storage, Chemnitz University of Technology, Chemnitz, Germany; 2. Leibniz IFW Dresden, Dresden, Germany; 3. Institute of Materials Physics, Graz University of Technology, Graz, Austria; 4. Institute of Material Science, TU Dresden, Dresden, Germany*

Hydrogen is one of the most promising species for fast magneto-ionic control in iron triad metals.[1,2] In this case, a voltage, which is applied to the magnetic metal via a solid or liquid electrolyte,[3] triggers proton reduction and subsequent hydrogen ad- and absorption. The composition of the electrolyte may have a great influence on these processes, since the absorption of hydrogen in metals is highly dependent on the pH values,[4] and moreover, additives to electrolyte can improve hydrogen permeability and diffusivity in ferromagnetic metals.[5] However, this knowledge has not been applied and tested for magneto-ionic systems yet. Thus, the optimization of electrolyte composition and the use of additives to promote hydrogen ad- or absorption may be a promising pathway to increase the efficiency of magneto-ionic systems. In this work, we study the influence of alkaline electrolyte composition on the H-based magneto-ionic effect in electrodeposited nanocrystalline Ni films. In Ni, H is expected to significantly modulate the magnetization.[6] The voltage-triggered changes in magnetic properties are analyzed by *in situ* Anomalous Hall effect and *in situ* SQUID measurements in aqueous electrolytes with different concentrations of KOH (0.5, 2 and 5 M), as well as in 0.5 M KOH with thiourea additive. H-based magneto-ionic control is clearly demonstrated by a voltage-controllable decrease and increase of saturation magnetization of the Ni films upon hydrogen absorption and desorption, respectively. We find that an increase in electrolyte pH and the addition of thiourea improves the efficiency of the H-based magneto-ionic effect. Results of in situ Raman spectroscopy indicate that the enhancement of H-absorption by thiourea relates to the formation of a $Ni(OH)_2$ layer on the Ni surface. The obtained results should stimulate further research in the field toward the use of multicomponent electrolytes and the optimization of underlying chemical and electrochemical reaction mechanisms to improve magneto-ionic efficiency. *This research was funded by the European Union's Horizon 2020 research and innovation programme under the Marie Sklodowska-Curie grant number 861145.*

1. Tan, A. J. *et al.* Magneto-ionic control of magnetism using a solid-state proton pump. *Nat. Mater.* 18, 35–41 (2019). 2. Huang, M. *et al.* Voltage control of ferrimagnetic order and voltage-assisted writing of ferrimagnetic spin textures. *Nat. Nanotechnol.* (2021) doi:10.1038/s41565-021-00940-1. 3. M. Nichterwitz, S. Honnali, M. Kutuzau, S. Guo, J. Zehner, K. Nielsch, and K. Leistner. Advances in magneto-ionic materials and perspectives for their application. *APL Materials* 9, 030903 (2021). 4. Fujimoto, N., Sawada, T., Tada, E. & Nishikata, A. Effect of pH on Hydrogen Absorption into Steel in Neutral and Alkaline Solutions. *Mater. Trans.* 58, 211–217 (2017). 5. Latanision, R. M. & Kurkela, M. Hydrogen Permeability and Diffusivity in Nickel and Ni-Base Alloys. *CORROSION* 39, 174–181 (1983). 6. León, A. *et al.* Magnetic effects of interstitial hydrogen in nickel. *Journal of Magnetism and Magnetic Materials* 421, 7–12 (2017).

COA-08. Boosting nitrogen magneto-ionics: From binary to ternary transition metal nitrides. *Z. Tan*[1], J. de Rojas[1], A. Quintana[4], J.L. Costa-Krämer[3], E. Menendez[1] and J. Sort[1,2] *1. Departament de Física, Universitat Autònoma de Barcelona, Barcelona, Spain; 2. Institució Catalana de Recerca i Estudis Avançats (ICREA), Barcelona, Spain; 3. IMN-Instituto de Micro y Nanotecnología (CNM-CSIC), Madrid, Spain; 4. Institut de Ciència de Materials de Barcelona (ICMAB-CSIC), Barcelona, Spain*

Magneto-ionics is an emerging approach to controlling the magnetic properties of materials via voltage-driven ion motion. Nitrogen-based magneto-ionics in transition metal nitride thin films (CoN & FeN) can induce reversible *ON-OFF* transitions of ferromagnetic states at faster rates and lower threshold voltages than oxygen-based magneto-ionics [1][2], attributed to the comparably smaller energy barrier for ion diffusion and the lower electronegativity of nitrogen when compared with transition metal oxide thin films. Furthermore, this effect largely relies on the strength and penetration of the induced electric field into the target material, the amount of generated ion transport pathways, and the ionic mobility inside the magnetic media. Optimizing all these factors in a simple way is a huge challenge, although highly desirable for technological applications. Here we demonstrate that introduction of suitable transition metal elements in binary nitride compounds can drastically boost magneto-ionics. More specifically, we show the multiple benefits that moderate substitution of Co by Mn brings to the magneto-ionic performance of CoN-based heterostructures. With 10% substitution of Co by Mn in the thin film composition, a transformation from nanocrystalline to amorphous-like structures, as well as from metallic to semiconducting behaviors has been observed. The former increases N ion transport channels, and the latter significantly extends the electric field effect which is normally limited to a few Å in metals. In this way, Mn incorporation leads to a 6.7-fold enhancement of the saturation magnetization (M_S) and improved toggling speeds and cyclability. In addition, Ab initio calculations reveal a lower formation energy barrier for Mn-N compared to Co-N, which allows a fundamental understanding of the crucial role of Mn addition on the voltage-driven magnetic effects. These results constitute an important step forward towards enhanced voltage control of magnetism via electric-field-driven ion motion[3].

[1] de Rojas, J. *et al*. Voltage-driven motion of nitrogen ions: a new paradigm for magneto-ionics. *Nature Communications* 11, 5871 (2020). [2] de Rojas, J. *et al*. Magneto-Ionics in Single-Layer Transition Metal Nitrides. *ACS Applied Materials & Interfaces* 13, 30826–30834 (2021). [3] Zhengwei Tan *et al*. From binary to ternary transition metal nitrides: a boost towards nitrogen magneto-ionics. *Submitted* (2021).

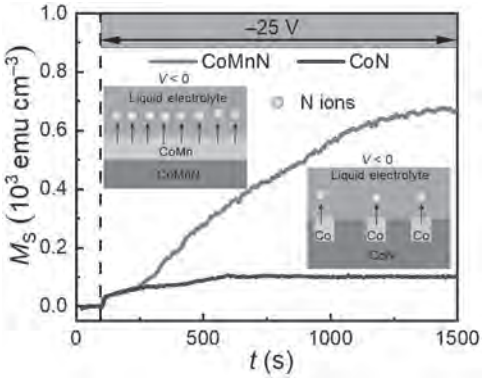

A significant enhancement of magneto-ionic effects through 10% substitution of Co by Mn in the nitride thin film composition

COA-09. Magneto-ionic and electrostatic generation of non-volatile and volatile skyrmions in MgO/Mn_2CoAl/Pd thin films using ionic liquid gating. Y. Zhang[1,2], G. Dubuis[3], C. Doyle[4], T. Butler[1,2] and *S. Granville*[1,2] *1. Robinson Research Institute, Victoria University of Wellington, Wellington, New Zealand; 2. MacDiarmid Institute for Advanced Materials and Nanotechnology, Wellington, New Zealand; 3. Measurement Standards Laboratory of New Zealand, Callaghan Innovation, Lower Hutt, New Zealand; 4. Department of Chemical and Materials Engineering, The University of Auckland, Auckland, New Zealand*

Magnetic skyrmions are topological spin textures with great potential for spintronics applications [1]. The appearance of skyrmions requires a careful balance between the magnetic anisotropy and the Dzyaloshinskii-Moriya interaction, and being able to tune these values with a voltage is an important tool for material optimisation for skyrmion devices. In this work we have explored generation of both volatile and non-volatile skyrmions in MgO/Mn_2CoAl/Pd thin films using different ionic liquid gating voltage sequences and magneto-optical Kerr effect (MOKE) microscopy. With a negative gate voltage of -2.5 V, we are able to generate *non-volatile* skyrmions ~ 1 μm diameter in films with perpendicular magnetic anisotropy K_{eff} ~ 1 x 10^4 Jm^{-3}. The same result is achieved in higher K_{eff} films by 'training' or repeatedly cycling the gate voltage, achieving a giant voltage tunability of magnetic anisotropy of 109.8 mT V^{-1}. Interestingly, *volatile* skyrmions can also be generated, by first applying a large negative 'trigger' voltage, and then skyrmions appear at a *positive* gate voltage. Using X-ray photoelectron spectroscopy, we explain the generation of skyrmions in terms of magneto-ionic and electrostatic effects [2]. Our results show the potential of ionic liquid gating for achieving large anisotropy changes to reversibly or irreversibly generate skyrmions from materials with a range of starting anisotropy values.

[1] X. Zhang, Y. Zhou, K. M. Song, T.-E. Park, J. Xia, M. Ezawa, X. Liu, W. Zhao, G. Zhao, and S. Woo, *J. Phys. Cond. Mat.* 32, 143001 (2020). [2] Y. Zhang, G. Dubuis, C. Doyle, T. Butler, and S. Granville, *Phys. Rev. Appl.* 16, 014030 (2021).

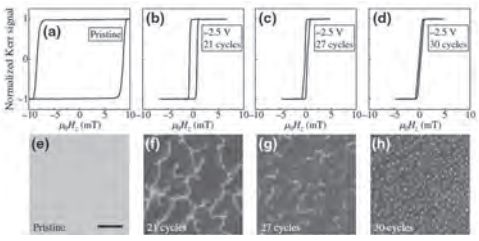

Figure: Effect of gate voltage cycling on MOKE loops (a. - d.) and magnetic domains (e. - h.)

COA-10. Non-volatile Voltage Control of Perpendicular Exchange Bias by Resistive Switching in the Co/NiO/HfO_2 Gate Device. *T. Hsin*[1], Y. Lin[1], N. Dai[1] and Y. Tseng[1] *1. National Yang Ming Chiao Tung University, Hsinchu, Taiwan*

Voltage control of exchange bias (EB) based on heterostructures is of intense research interest due to its great potential in spintronics technology [1]. A full voltage control of perpendicular EB by resistive switching (RS) at room temperature is demonstrated in a Si/SiO_2/Ta/Pt/Co/NiO/HfO_2/Ta/Pt voltage gate Hall device. We observed an EB of 40 Oe in the presitine device without applied voltage. By applying different voltages, we obtained low-resistance-state (LRS)/high-resistance-state (HRS) of the device accompanied by appearance/disappearance of EB. The coupled EB-RS was retained despite removal of applied voltage, indicating non-volatile nature of the device. The current-voltage (*I-V*) curve of the device showed unipolar RS behaviors, where the HRS/LRS was reset/set when the applied voltage exceeded 2.5/6.0 *V*. A mechanism of conductive filament (CF) is proposed to explian the voltage control of the coupled EB-RS. When the device is set in the LRS, CFs are formed in the NiO and HfO_2 layers, which break the NiO-Co exchange coupling, thus resulting in the disappearance of EB; while we reset the device in the HRS, CFs are ruptured near both Co-NiO and HfO_2-top electrode interfaces, leading to the development of EB again. The mechanism has been validated by probing the oxygen states of the prestine/set/reset devices with x-ray photoelectron spectroscopy. The materials of proposed device can be fabricated by atomic layer deposition (HfO_2) and magnetron sputtering (Co, and NiO) in which high crystallinity of the films is not required. This study therefore provides a facile approach to realize the magneto-electric devices.

[1] C. Song et al., *Progress in Materials Science,* 87, 33-82 (2017).

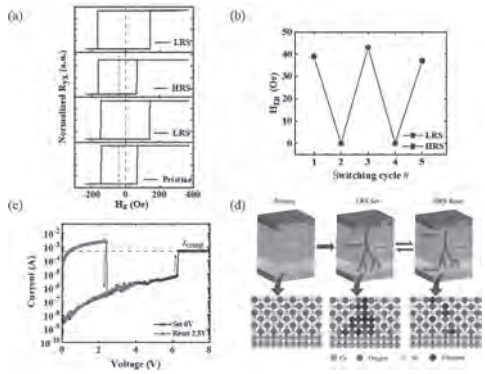

Fig. 1 (a) Hall resistance (R_{Hall}) v.s. H_z of the Ta/Pt/Co/NiO/Pt/HfO_2/Ta/Pt gate device with different reistance states. (b) LRS/HRS switching response v.s. H_{ex}. (c) *I-V* curves for resistive switching characteristics of the device. The HRS(LRS) is reset (set) when the applied voltage is above 2.5(6.0) *V*. (d) Schematic of resistive switching mechanism for the proposed device, where the prestine, forming (LRS) and breaking (HRS) of the CFs are illustrated.

COA-11. Ultimately Tunable Magnetic Materials: The Rare Earth Nitrides. *W.F. Holmes-Hewett*[1], J. Miller[1], C. Pot[1], B. Buckley[1], B. Ruck[1] and J. Trodahl[1] *1. Victoria University of Wellington, Wellington, New Zealand*

Most of the 14 rare-earth nitrides are intrinsic ferromagnetic semiconductors. Their magnetism in the 4f shell has a strong spin-orbit interaction, a contrast to the quenched orbital magnetic moments in transition-metals. The contribution of both spin and orbital moments delivers vastly contrasting magnetic properties across the series; coercive fields and magnetisations span orders of magnitude. Alloy compositional tuning allows variation of the magnetic properties i.e. S, L, J, M, which can in principle be independently selected. All promise enhanced efficacy in devices, and doping control of conduction further broadens their technical potential. Along with a brief description of the thin-film growth at the core of our programme [1], I will describe our recent progress tuning the magnetic [2] and electronic [3,4] properties of rare-earth nitride based alloys, and the application of these materials in prototype devices for cryogenic memory storage. These studies are supported by DFT computations, and a variety of laboratory-based measurements and synchrotron X-ray spectroscopies.

[1] Natali et al. Prog. Mater. Sci. 58, 1316–1360 (2013) [2] Pot et al. Appl. Phys. Lett. 119, 172406 (2021) [3] Devese et al. AIP Advances 12, 035108 (2022) [4] Holmes-Hewett, Phys. Rev. B 104, 075124 (2021)

Session COB
TOPOLOGICAL INSULATORS, DIRAC MATERIALS, 2D AND LAYERED VAN DER WAALS MATERIALS I

Marco Gobbi, Chair
CIC nanoGUNE, San Sebastian, Spain

INVITED PAPER

COB-01. Magnetic Skyrmions and Exchange Bias in van der Waals Heterostructures. *Y. Wu*[1], K. Liu[2], K. Wang[3] and J. Moodera[1]
1. Massachusetts Institute of Technology, Cambridge, MA, United States; 2. Georgetown University, Georgetown, WA, United States; 3. University of California Los Angeles, Los Angeles, CA, United States

Newly discovered long-range intrinsic magnetic orders in the 2D van der Waals (vdW) magnets provide a new platform for high-density and low-power-consumption spintronic devices. We demonstrate Dzyaloshinskii–Moriya interaction and Néel-type skyrmions are induced at an interface of a transition metal dichalcogenide with a 2D ferromagnet [1], supported by the transport measurements and Lorentz transmission electron microscopy results. By coupling Fe_3GeTe_2 to another 2D ferromagnet $Cr_2Ge_2Te_6$, we found that two groups of magnetic skyrmions can be hosted in such heterostructures, shown by magnetic force microscopy, transport measurement and micromagnetic simulations [2]. Such stacked vdW heterostructures open up new opportunities for skyrmionics heterojunctions. Furthermore, we have observed an interesting exchange bias effect in Fe_3GeTe_2 thin layers [3]. The non-antisymmetric dependence of exchange bias on field cooling is explained by considering an uncompensated antiferromagnetic interfacial layer with a noncollinear spin texture, and a weak antiferromagnetic order in the oxidized layer, at two ferromagnet/antiferromagnet interfaces.

[1]. Wu, Y., et al. "Néel-type skyrmion in WTe2/Fe3GeTe2 van der Waals heterostructure", Nat. Commun. 11, 3860 (2020). [2]. Wu. Y., et al. "A Van der Waals Interface Hosting Two Groups of Magnetic Skyrmions", Adv. Mater. 34, 2110583 (2022). [3]. Wu, Y., Wang, W., Pan, L., Wang, K. L., "Manipulating Exchange bias in a van der Waals ferromagnet", Adv. Mater. 34, 2105266(2022).

CONTRIBUTED PAPERS

COB-02. Large Dzyaloshinskii-Moriya interaction at the h-BN/ Cobalt interface. *B. El-Kerdi*[1], A. Thiaville[1], S. Rohart[1], S.K. Panigrahy[1], N. Brás[1], J. Sampaio[1] and A. Mougin[1] *1. Laboratoire de Physique des Solides, Université Paris-Saclay, CNRS, Orsay, France*

A recent theoretical paper [1] predicted a significant Dzyaloshinskii-Moriya interaction (DMI) and perpendicular magnetic anisotropy induced at the interface of hexagonal boron nitride (h-BN) and ultrathin cobalt (Co) crystals. The interfacial DMI of the Au/Co/h-BN heterostructure was investigated through the Brillouin Light Scattering technique (BLS) [2]. The Brillouin spectra consist of two peaks, Stokes (S) and anti-Stokes (AS), associated with counter-propagating spin waves, which are affected by DMI in opposite ways, and so have different frequencies [2]. The high sensitivity of the BLS technique allows detection of the small frequency differences and thus measures the DMI strength. Fig.1-a shows the BLS data obtained from Si/SiO_2/Ta/Au/Co(1 nm)/h-BN/Au at different values of wave vector k_{SW} under an external magnetic field of -962 mT. The sokes and anti-Stokes difference (f_{AS}-f_S) varies linearly with k_{SW} (Fig.1-c) following the expected relation: $f_{AS} - f_S = v_{DMI}/\pi \, .k_{SW}$ The magnon non-reciprocal velocity v_{DMI} is proportional to the DMI strength ($v_{DMI} = 2/\pi \, \gamma \, Ds / M_s \, t$) where D_S is the DMI parameter. The v_{DMI} of the Au/Co/h-BN stack is $v_{DMI} \approx 49$ m/s, as large as the one reported for the Graphene/Co/Pt interface ($v_{DMI} \approx 50$ m/s) [3]. The v_{DMI} decreases with the Co thickness confirming its interfacial nature. To check that the large DMI obtained for Au/Co/h-BN emerges from the Co/h-BN interface and not from the Au/Co interface, we have measured a reference sample composed of Au/Co (1nm)/Al and obtained $v_{DMI} \approx 14$ m/s, which is three times smaller than the Au/Co/h-BN proving that hBN induces a large DMI. A similar analysis was performed for the interfacial anisotropy, and we found that a significant anisotropy is induced by the h-BN/Co interface, as predicted [1].

[1] A. Hallal *et* al., Nano Letters 21,17, 7138-7144 (2021) [2] M. Belmeguenai *et* al., Physical Review B 91, 180405 (2015) [3] F. Ajejas *et* al., Nano Letters 9, 5364-5372 (2018)

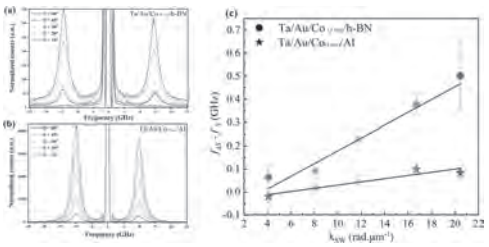

Figure 1: a,b) BLS spectra for Au/Co(1 nm)/h-BN and Au/Co(1 nm)/ Al with $\mu_0 H_{ext}$ = -962 mT and $\mu_0 H_{ext}$ = -558 mT respectively. c) S-AS frequency shift as a function of the spin-wave vector k_{SW}. The dots correspond to the experimental data and the line is a linear fit yielding the DMI strength for both stacks.

COB-03. Asymmetric Magnetic Proximity Interactions in Ferromagnet/Semiconductor van der Waals Heterostructures. *S. Crooker*[1], J. Choi[1], C. Lane[1] and J. Zhu[1] *1. Los Alamos National Lab, Los Alamos, NM, United States*

The ability of short-range proximity interactions to imbue magnetic functionality into otherwise nonmagnetic materials [1-3] has exciting prospects for devices that combine the optical and electrical properties of monolayer semiconductors with additional magnetic tuning parameters that couple directly to spin and valley pseudospin. The atomically-smooth surfaces that are nowadays routinely achieved with van der Waals (vdW) materials allow for nearly ideal interfaces between monolayer transition-metal dichalcogenide semiconductors (such as WSe_2 or MoS_2) and magnetic substrates (such as EuO or CrI_3). Magnetic proximity interactions (MPIs) between atomically-thin semiconductors and two-dimensional magnets therefore provide a means to manipulate spin and valley degrees of freedom in nonmagnetic monolayers, without the use of applied magnetic fields. In such vdW heterostructures, MPIs originate in the nanometer-scale coupling between the spin-dependent electronic wavefunctions in the two materials, and historically their overall effect is regarded as an effective magnetic field acting on the semiconductor monolayer. Here we demonstrate that this picture, while appealing, is incomplete: The effects of MPIs in vdW heterostructures can be markedly *asymmetric*, in contrast to that from an applied magnetic field [4]. Valley-resolved optical reflection spectroscopy of $MoSe_2/CrBr_3$ vdW structures reveals strikingly different energy shifts in the *K* and *K′* valleys of the $MoSe_2$, due to ferromagnetism in the $CrBr_3$ layer. Strong asymmetry

is observed at both the A- and B-exciton resonances. Density-functional calculations indicate that valley-asymmetric MPIs depend sensitively on the spin-dependent hybridization of overlapping bands, and as such are likely a general feature of such hybrid vdW structures. These studies suggest routes to selectively control *specific* spin and valley states in monolayer semiconductors.

[1] I. Zutic *et al.*, Proximitized Materials, *Materials Today,* 22, 85 (2019). [2] M. Gibertini *et al.*, Magnetic 2D materials and heterostructures, *Nat. Nanotechnol*. 14, 408–419 (2019). [3] K. F. Mak, J. Shan, D. Ralph, Probing and controlling magnetic states in 2D layered magnetic materials, *Nat. Rev. Phys.* 1, 646-661 (2019). [4] J. Choi, C. Lane, J.-X. Zhu, S. A. Crooker, Asymmetric magnetic proximity interactions in $MoSe_2/CrBr_3$ van der Waals heterostructures, arXiv:2206.09958

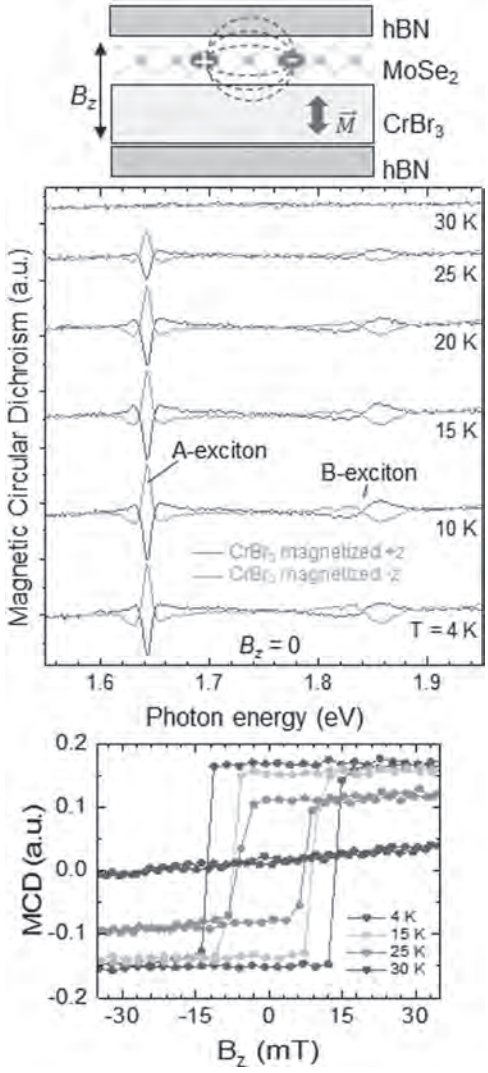

Fig. 1. The top $MoSe_2/CrBr_3$ structure. Middle MCD at B_z=0 shows strong magnetic response of the (nonmagnetic) $MoSe_2$, below T_c~28K, indicating strong MPIs. Bottom: Hysteresis of MCD.

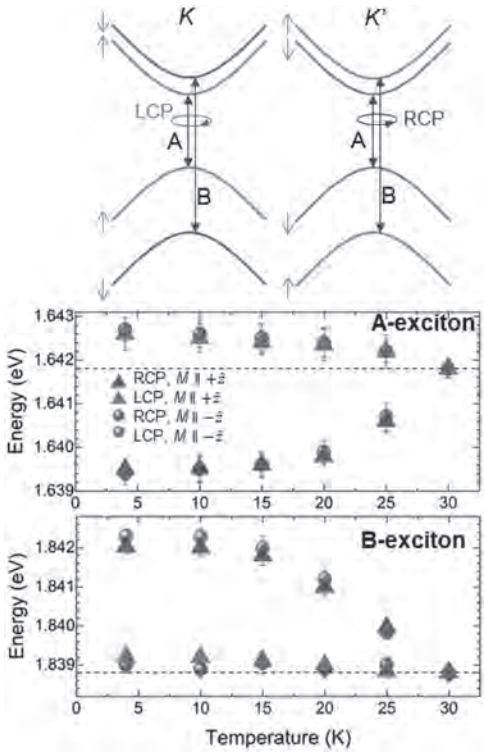

Fig. 2. Optical transitions of spin-up/down bands in *K/K′* valleys shift very *asymetrically* due to MPIs (in contrast to applied magnetic fields).

COB-04. Spin-sensitive Epitaxial In_2Se_3 Tunnel Barrier in In_2Se_3/Bi_2Se_3 Topological Van der Waals Heterostructure. *C.H. Li*[1], J. Moon[1], O. Van 't Erve[1], D. Wickramaratne[1], E. Cobas[1], M. Johannes[1] and B.T. Jonker[1] *1. Naval Research Lab, Washington, DC, United States*

Current-generated spin arising from spin-momentum locking in topological insulator (TI) surface states has been shown to switch the magnetization of an adjacent ferromagnet (FM) via spin-orbit torque (SOT) with much higher efficiency than heavy metals. However, in such FM/TI heterostructures, most of the current is shunted through the FM metal due to its lower resistance [1,2], and recent calculations have also shown that topological surface states can be significantly impacted when interfaced with a FM metal such as Ni and Co [3,4]. Hence placing an insulating layer between the TI and FM will not only prevent current shunting, therefore minimizing overall power consumption, but may also help preserve the topological surface states at the interface. Here we report the Van der Waals epitaxial growth of *b*-phase In_2Se_3 on Bi_2Se_3 by molecular beam epitaxy, and demonstrate its spin-sensitivity by the electrical detection of current-generated spin in Bi_2Se_3 surface states using an Fe/In_2Se_3 detector contact. Our density functional calculations further confirm that the linear dispersion and spin texture of the Bi_2Se_3 surface states is indeed preserved at the *b*-In_2Se_3/Bi_2Se_3 interface [5]. This demonstration of an epitaxial crystalline spin sensitive barrier that can be grown directly on Bi_2Se_3, and verification that it preserves the topological surface state, is electrically insulating and spin sensitive, is an important step towards minimizing overall power consumption in spin-orbit torque switching in TI/FM heterostructures in a fully epitaxial topological spintronic devices.

1. Wang, Y. *et al.,* Room Temperature Magnetization Switching in Topological Insulator-ferromagnet Heterostructures by Spin-orbit Torques, *Nat. Commun.* 8, 1364 (2017). 2. Mahendra, D. C. *et al.*, Room-temperature High Spin–orbit Torque due to Quantum Confinement in Sputtered $Bi_xSe_{(1-x)}$ films, *Nat. Mater.* 17, 800 (2018). 3. Zhang, J.; Velev, J. P.; Dang, X.; Tsymbal, E. Y. Band Structure and Spin Texture of Bi_2Se_3 3d Ferromagnetic Metal Interface, *Phys. Rev. B* 94, 014435 (2016). 4. Marmolejo-Tejada,

J. M. et al., Proximity Band Structure and Spin Textures on Both Sides of Topological-Insulator/Ferromagnetic-Metal Interface and Their Charge Transport Probes, *Nano Lett.* 17, 5626 (2017). 5. Li, C. H., Moon, J., van't Erve, O. M. J., Wickramaratne, D., Cobas, E. D., Johannes, M. D., Jonker, B. T., Spin-sensitive Epitaxial In_2Se_3 Tunnel Barrier in In_2Se_3/Bi_2Se_3 Topological Van der Waals Heterostructure, *under revision.*

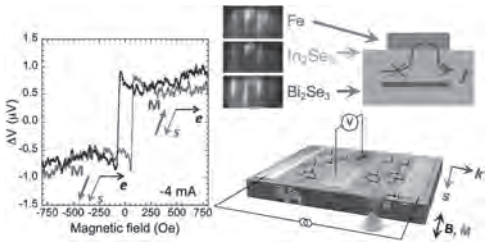

Fully epitaxial $Fe/In_2Se_3/Bi_2Se_3$ Van der Waals heterostructure grown by molecular beam epitaxy. The In_2Se_3 barrier prevents current shunting through the ferromagnetic Fe, and shows spin sensitivity in the electrical detection of current generated spins in the topological insulator Bi_2Se_3 arising from spin-momentum locking.

INVITED PAPER

COB-05. Topological Antiferromagnetic Interface in Sputtered Topological Insulator/Ferromagnet Heterostructures. N. Bhattacharjee[1], K. Mahalingam[2], A. Fedorko[1], V. Lauter[3], M. Matzelle[1], B. Singh[4], A.J. Grutter[5], A.R. Will-Cole[1], M. Page[2], R. Markiewicz[1], A. Bansil[1], J. Hart[6], A. Podpirka[7], S. Patel[8], S.H. Tolbert[8], J.J. Cha[6], D. Heiman[1] and *N. Sun*[1] *1. Northeastern University, Boston, MA, United States; 2. Air Force Research Laboratory, Hamilton, OH, United States; 3. Oak Ridge National Laboratory, Oak Ridge, TN, United States; 4. Tata Institute of Fundamental Research, Mumbai, India; 5. National Institute of Technology, Gaithersburg, MD, United States; 6. Cornell University, Ithaca, NY, United States; 7. Johns Hopkins Applied Physics Laboratory, Laurel, MD, United States; 8. University of California Los Angeles, Los Angeles, CA, United States*

Topological insulators (TIs) possess enormous spin-orbit coupling (SOC) and robust topological surface conducting states (TSS) that cannot be destroyed by disorder. [1]-[4] TIs in presence of large time-reversal symmetry breaking magnetic order can also exhibit chiral quantum anomalous (QAH) states. [5],[6] TIs of crystalline disorder varying from amorphous to *c*-axis oriented were grown using magnetron sputtering. Sputtered TI/ferromagnet (FM) heterostructure films revealed large enhancement in Gilbert damping and enhanced out-of-plane (OOP) magnetic anisotropy for *c*-axis oriented TI compared to disordered films. These effects are a signature of the TSS and a consequence of large SOC. [7],[8] The interfacial reaction of TI/FM was studied, and experiments confirmed the presence of a novel topological antiferromagnet (AFM). [9] $Bi_2Te_3/Ni_{80}Fe_{20}$ showed selective diffusion of Ni across the interface. Diffused Ni was found to react with Bi_2Te_3 and form a distinct interfacial phase due to the TSS. Magnetometry measurements at cryogenic temperatures showed the emergence of a large spontaneous exchange bias characteristic of AFM-FM interaction. Cross-section electron microscopy confirmed the presence of $NiBi_2Te_4$ in the interface, which was observed for the first time. The Neel temperature was found to be 63K which is higher than other MTI compounds, indicating a large exchange interaction in $NiBi_2Te_4$. This aligns with our theoretical findings on $NiBi_2Te_4$. TI surface reactivity was found to decrease with increasing crystalline disorder due to weakening of topological properties. [10] This was evident by reduction in loss of magnetic moments, exchange-bias field, and Neel temperature with increasing disorder. This demonstrates the persistence of topological properties, albeit weakened with disorder. Interfacial reactions of another heterostructure (molecular beam epitaxy grown Sb_2Te_3 with sputtered $Ni_{80}Fe_{20}$) were studied and showed the presence of diffused Ni across the interface accompanied by AFM phase formation due to exchange bias below 40K. These results provide new avenues to explore previously overlooked high-temperature QAH and topologically nontrivial phases at interfaces.

1. A. Bansil, H. Lin, T. Das, *Rev. Mod. Phys.* 88, 021004 (2016). 2. D. Hsieh *et al*, *Nature*, 460, 1101 (2009). 3. C. Brune *et al*, *Phys. Rev. Lett*., 106, 126803 (2011). 4. G.Schubert *et al*, *Phys. Rev. B*, 85, 201105(R), (2012). 5. C.-Z. Chang and M. Li, *J. Phys.: Condens. Matter.,* 28, 123002 (2016). 6. Y. Deng *et al*, *Science*, 367, (2020). 7. A. Baker *et al, Sci. Rep.,* 5, 7907 (2015). 8. M. Jamali *et al*, *Nano Lett.*, 15, 10 (2015). 9. N. Bhattacharjee, K. Mahalingam, A. Fedorko, V. Lauter, M. Matzelle, B. Singh, A. Grutter, A. Will-Cole, M. Page, M. McConney, R. Markiewicz, A. Bansil, D. Heiman, N.X. Sun, Topological Antiferromagnetic Van der Waals Phase in Topological Insulator/Ferromagnet Heterostructures Synthesized by a CMOS-Compatible Sputtering Technique, Adv. Mat. 34, 15, 2108790 (2022). 10. N. Bhattacharjee, K. Mahalingam, A. Fedorko, A. Will-Cole, J. Ryu, M. Page, M. McConney, H. Fang, N.X. Sun, Effects of Crystalline Disorder on Interfacial and Magnetic Properties of Sputtered Topological Insulator/Ferromagnet Heterostructures, arXiv:2205.09913v1 [cond-mat.mtrl-sci] (2022).

CONTRIBUTED PAPERS

COB-06. Ultralow power nanosecond spin orbit torque magnetization switching induced by BiSb topological insulator. *N.H. Khang*[1,2], T. Shirokura[1], F. Tuo[1], M. Takahashi[4], N. Nakatani[4], D. Kato[4], Y. Miyamoto[4] and P. Nam Hai[1,3] *1. Electrical and Electronic Engineering, Tokyo Institute of Technology, Tokyo, Japan; 2. Department of Physics, Ho Chi Minh University of Education, Ho Chi Minh, Vietnam; 3. University of Tokyo, Tokyo, Japan; 4. Science & Technology Research Labs, NHK, Tokyo, Japan*

We demonstrate spin orbit torque (SOT) magnetization switching of (Pt/Co) multilayers with large perpendicular magnetic anisotropy (PMA) by a topological insulator $Bi_{0.85}Sb_{0.15}$ layer in both thermal activation and non-thermal regime with current pulse width τ down to 1 ns. For this purpose, we deposited a stack of $Bi_{0.85}Sb_{0.15}$(10 nm)/[Pt(0.4 nm)/Co(0.4 nm)]$_2$/insulating buffer on a Si/SiO_x substrate by magnetron sputtering, as shown in Fig. 1(a). The (Pt/Co) multilayers have a large PMA with anisotropy magnetic field of 6 kOe. We then fabricated 1000 nm × 800 nm Hall bar devices for ultrafast SOT switching measurement. Figure 1 (b) shows the threshold switching current density J^{BiSb}_{th} as a function of τ at H_x = 1 kOe. The red dashed line is fitting by the thermal activation model ($\tau >> 10$ ns), which yields a zero-Kelvin $J^{BiSb}_{th0} = 2.5\times10^6$ A/cm^2. Meanwhile, the green dashed line is fitting for the non-thermal regime ($\tau < 10$ ns), which yields a larger $J^{BiSb}_{th0} = 4.1\times10^6$ A/cm^2 but still smaller than those observed in heavy metals by nearly two orders of magnitude. Figure 1(c) shows SOT switching loops at various t from 4 ns to 1 ns. From time-resolved measurement using 1 ns pulses, we observed a fast domain wall velocity of 470 m/s at a modest $J^{BiSb} = 1.6\times10^7$ A/cm^2. We then successfully demonstrated deterministic SOT switching in our device by multi pulses ($J^{BiSb} = 1.3\times10^7$ A/cm^2, τ = 3 ns) at H_x = -1 kOe and +1 kOe as shown in Fig. 2. These results demonstrate the potential of BiSb topological insulator for ultralow power and ultrafast operation of SOT-based spintronic devices [1,2].

[1] N. H. D. Khang, *et al*, Nature Mater. 17, 808 (2018). [2] N. H. D. Khang, *et al*, Appl. Phys. Lett. 120, 152401 (2022).

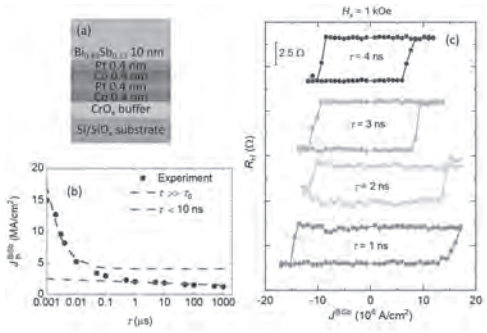

Fig. 1. (a) Schematic structure of our stack for nanosecond ultralow power SOT switching using BiSb. (b) Threshold switching current density as a function of pulse width τ at H_x = 1 kOe measured in a 1000 nm × 800 nm Hall bar device. The red dashed line is fitting by the thermal activation model (τ >> 10 ns), and the green dashed line is fitting for the non-thermal regime. (c) SOT switching loops at various τ from 4 ns to 1 ns.

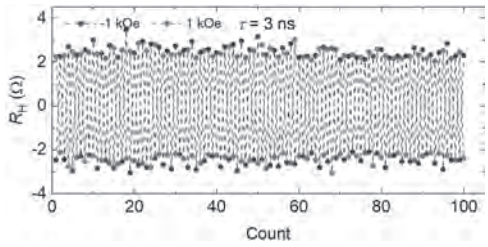

Fig. 2. Deterministic multiple switching at J^{BiSb} =1.3×10^7 A/cm^2, τ = 3 ns, and H_x = ±1 kOe.

COB-07. Gate-tunable anomalous Hall effect in a 3D topological insulator/2D magnet van der Waals heterostructure. *R. Jain*[1], V. Gupta[1], Y. Ren[2], X. Zhang[1], H. Alnaser[3], A. Vashist[3], V. Deshpande[3], D. Muller[1], D. Xiao[2], T. Sparks[3] and D.C. Ralph[1] *1. Cornell University, Ithaca, NY, United States; 2. University of Washington, Seattle, WA, United States; 3. University of Utah, Salt Lake City, UT, United States*

We demonstrate advantages of samples made by mechanical stacking of exfoliated van der Waals materials for controlling the topological surface state of a 3-dimensional topological insulator (TI) via interaction with an adjacent magnet layer [1]. We assemble bilayers with pristine interfaces using exfoliated flakes of the TI $BiSbTeSe_2$ and the magnet $Cr_2Ge_2Te_6$ (Fig. 1), thereby avoiding problems caused by interdiffusion that can affect interfaces made by top-down deposition methods. The samples exhibit an anomalous Hall effect with abrupt hysteretic switching (Fig. 2a). For the first time in samples composed of a TI and a separate ferromagnetic layer, we demonstrate that the amplitude of the anomalous Hall effect can be tuned via gate voltage with a strong peak near the Dirac point (Fig. 2b). This is the signature expected for the anomalous Hall effect due to Berry curvature associated with an exchange gap induced by interaction between the topological surface state and an out-of-plane-oriented magnet [2]. Our results demonstrate the advantages of a clean all-vdW exfoliated topological insulator-2D magnet system for manipulating topological surface states, and pave the way for improved control of topological magneto-electric effects in TI/magnet heterostructures.

[1] V Gupta, R Jain, Y Ren et al., arXiv preprint arXiv:2206.02537 (2022).
[2] D. Xiao, M. C. Chang & Q. Niu, Rev. Mod. Phys. 82, 1959 (2010).

Fig.1. Schematic of the device geometry and electrostatic gating geometry. TI and 2D magnet flakes with few-layer thickness are double-encapsulated between hBN layers on a Si/SiO_2 substrate.

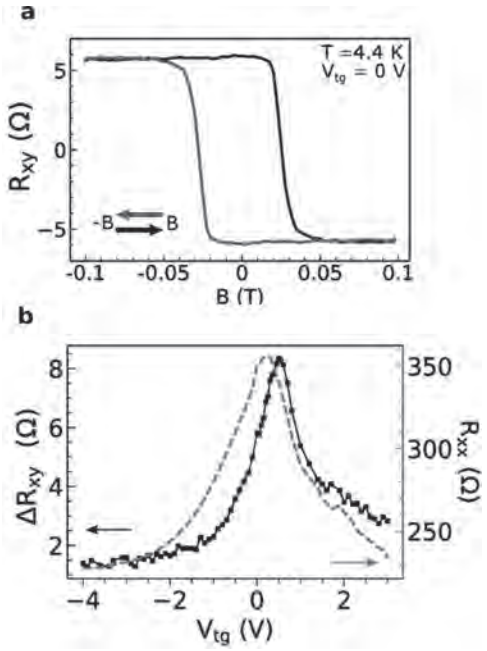

Fig.2. Anomalous Hall effect (AHE) tuned by gate voltage. (a) AHE contribution to R_{xy} at V_{tg}= 0 after subtraction of linear background. (b) (black solid line) Size of AHE signal ΔR_{xy} as a function of top-gate voltage. The trend matches closely with the observed top-gate dependence of R_{xx} (blue dashed line) measured at zero magnetic field.

COB-08. Proximity Enhanced Anomalous Hall Transport in Biphase Iron Oxide/Tungsten Disulfide Heterostructures. *C. Hung*[1], T. Diem[1], A. Chanda[1], D. Detellem[1], N. Alzahrani[1], N.A. Kapuruge[1], Y.T. Pham[1], M. Liu[2], D. Zhou[2], H. Gutierrez[1], D. Arena[1], M. Terrones[2], S. Witanachchi[1], L. Woods[1], H. Srikanth[1] and M. Phan[1] *1. Physics, University of South Florida, Tampa, FL, United States; 2. Materials Research Institute, Pennsylvania State University, Pennsylvania, PA, United States*

Interfacial properties of two-dimensional (2D) van der Waals material/magnetic material heterostructures are crucial for applications in spintronics and valleytronics. Inspired by the recent observation of room temperature ferromagnetic ordering in 2D MoS_2 induced by the ferrimagnetic yttrium iron garnet (YIG) and the antiferromagnetic exchange coupling between MoS_2 and YIG in a MoS_2 / YIG heterostructure [1], investigation into the proximity-mediated spin properties of such heterostructures has become a topic of global interest. Nonetheless, a full understanding of the magnetic proximity effect (MPE) and its temperature and magnetic field evolution in these systems is lacking. In this study, we have used biphase iron oxide (Fe_3O_4 + Fe_2O_3) as the magnetic layer and the MPE has been probed in Pt / Tungsten Disulfide / biphase iron oxide heterostructures through a comprehensive investigation of their magnetic and transport properties using magnetometry, transverse susceptibility, four-probe resistivity, and

anomalous Hall effect (AHE) measurements. Density functional theory (DFT) calculations are performed to complement the experimental findings. We find that the presence of monolayer Tungsten Disulfide flakes reduces the magnetization of biphase iron oxide and hence the total magnetization of Pt / Tungsten Disulfide / biphase iron oxide above the Verwey transition temperature of Fe_3O_4 (T_V). However, the enhanced magnetization is achieved at $T < T_V$. In the latter case, a comparative analysis of the transport properties of the Pt / Tungsten Disulfide / biphase iron oxide heterostructure and the Pt / biphase iron oxide heterostructructures from the AHE measurements reveals a ferromagnetic coupling at the Tungsten Disulfide / biphase iron oxide interface. Our study forms the foundation for understanding MPE-mediated interfacial properties and paves a new pathway for designing 2D van der Waals material/magnet heterostructures for spin-based device applications

(1) Tsai, S. P.; Yang, C. Y.; Lee, C. J.; Lu, L. S.; Liang, H. L.; Lin, J. X.; Yu, Y. H.; Chen, C. C.; Chung, T. K.; Kaun, C. C.; Hsu, H. S.; Huang, S. Y.; Chang, W. H.; He, L. C.; Lai, C. H.; Wang, K. L. Room-Temperature Ferromagnetism of Single-Layer MoS_2 Induced by Antiferromagnetic Proximity of Yttrium Iron Garnet. *Advanced Quantum Technologies* 2021, 4, 2000104. https://doi.org/10.1002/qute.202000104.

COB-09. Role of Spin-resolved Anti-bonding States Filling in Enhanced HER Performance of Monolayer WSe_2 by Transition Metals Doping. *L. Guo*[1] and W. Mi[1] *1. Department of Applied Physics, Tianjin University, Tianjin, China*

The bonding strength between adsorbates and substrate is related to the degree of anti-bonding sates filling during the adsorbates-substrate interaction, which is an important descriptor of electrochemical performance.[1,2] Based on first-principles calculations, the Gibbs free energy (ΔG_H) of transition metal doped WSe_2 (TM-WSe_2, TM=Ti, Mn, Fe, Co, Ni and Cu) are decreased, especially for the Ni-WSe_2 and Cu-WSe_2 which are -0.20 and 0.06 eV, respectively. By analyzing the partial density of states (PDOS) and integrated-crystal orbital Hamilton population (ICOHP), the decreased $ICOHP_{spin\ up}$ values of TM-WSe_2 improve the interaction of Se-H, thereby the H atom is easier to be adsorbed on the Se active site. While $ICOHP_{spin\ down}$ values of TM-WSe_2 are increased, this indicates the weak interaction of Se-H, which promotes desorption of H_2 molecule (i.e. Tafel/ Heyrovsky reaction step). Therefore, the synergistic effect of spin up and spin down anti-bonding states filling makes TM-WSe_2 possess an enhanced HER performance. This work was supported by the National Natural Science Foundation of China (22161142002).

[1] M. D. Hossain, Z. Liu, M. Zhuang, et al. Adv. Energy Mater. 9, 1803689 (2019). [2] X. Ai, X. Zou, H. Chen, et al. Angew. Chem. Int. Edit. 59, 3961-3965 (2020).

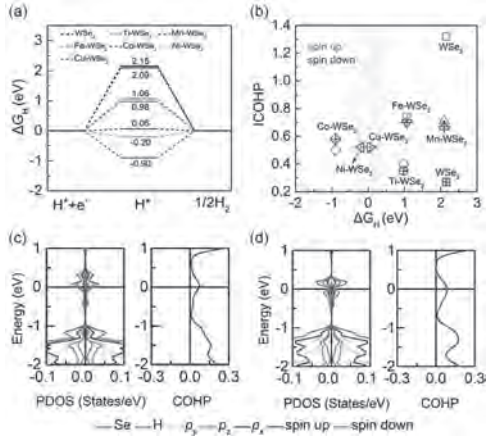

Fig. 1. (a) Gibbs free energy (ΔG_H) diagram of the Se active site in monolayer WSe_2 and TM-WSe_2 during the HER. (b) The relationship between ΔG_H and ICOHP. The PDOS and COHP of (c) Ni-WSe_2 and (d) Cu-WSe_2 with H adsorbed on Se active site.

Session COC
TOPOLOGICAL INSULATORS, DIRAC MATERIALS, 2D AND LAYERED VAN DER WAALS MATERIALS II

Shinobu Ohya, Chair
The University of Tokyo, Tokyo, Japan

INVITED PAPER

COC-01. Electrical and Optical Control of 2D Magnets. *C. Gong*[1]
1. Electrical and Computer Engineering, University of Maryland, College Park, College Park, MD, United States

The emergent two-dimensional (2D) layered magnets [1, 2] provide ideal platforms to enable the atomic-thin magneto-optical and magnetoelectric devices. Though many have envisioned that 2D magnets should allow an efficient control of magnetism by a variety of external stimuli, true breakthroughs are still lacking, with only proof-of-concept reports. There appear to be fundamental obstacles for efficient control, e.g., through electrical and optical approaches. In this talk I will analyze the challenges, and present our theoretical and experimental progress on efficient electrical and optical control of 2D magnets [3-8]. Specifically, our results show that the continuous wave laser of tens of uW/um^2 can effectively change the domain behaviors in 2D magnets, in stark contrast to the conventional adoption of intensive ultrafast laser pulses ~ 10^7 uW/um^2. We also demonstrate that the <100 mV/nm electric field can effectively change the magnetic anisotropy of 2D magnets. These efficient controls of 2D magnets potentially open up new avenues towards low-power spintronics and photonics.

1. C. Gong et al. Nature 546, 265-269 (2017). 2. C. Gong, X. Zhang. Science 363, eaav4450 (2019). 3. C. Gong, et al. Nat. Commun. 10, 2657 (2019). 4. S.-J. Gong, et al. PNAS 115, 8511 (2018). 5. E.-W. Du, et al. Nano Lett. 20, 7230 (2020). 6. Y. Gong, et al. npj 2D Materials and Applications 6, 9 (2022). 7. T. Xie, et al. under review (2022). 8. S. Liang, et al. under review (2022).

CONTRIBUTED PAPERS

COC-02. Withdrawn

COC-03. Light-mediated magnetism in van der Waals magnetic heterostructures. *V. Ortiz Jimenez*[1], Y.T. Pham[1], N.W. Mudiyanselage[1], M. Liu[2], F. Zhang[2], M. Terrones[2] and M. Phan[1] *1. Physics, University of South Florida, Tampa, FL, United States; 2. Material Science and Engineering, The Pennsylvania State University, University Park, PA, United States*

Two-dimensional van der Waals (vdW) heterostructures are at the forefront of research due to their extensive potential as a platform for spintronics and opto-spintronics applications [1]. Room-temperature ferromagnetism has been achieved in several two-dimensional (2D) magnetic materials and heterostructures [2,3]. Ferromagnetic 2D semiconductors are of particular interest since they allow for simple integration with current silicon-based electronics and their properties can be easily tuned with electric fields and optical excitations. Recently, we demonstrated light tunable magnetism in V-doped WS_2 (V-WS_2) monolayers, mediated by optically injected charge carriers [4]. A similar effect was shown in ML-VSe_2/BL-MoS_2 heterostructures in which the magnetization of VSe_2 penetrates into the non-magnetic optically active MoS_2 layer, allowing for the tunability of the magnetic properties of the heterostructure with light. The VSe_2 layer facilitates charge separation, which promotes changes in the magnetization of the MoS_2 layer, showing an enhanced light mediated magnetism effect compared to V-WS_2. We present a study of related 2D magnetic heterostructures where we compare the magneto-optical response of VSe_2/MoS_2, VSe_2/WS_2 and V-MoS_2/graphene heterostructures. We propose that, as the VSe_2 layer in the VSe_2/MoS_2 heterostructure allows for charge separation through the interface, graphene in a V-MoS_2/graphene heterostructure may play a similar role. The difference between the two systems lies in the source of the magnetism of the semiconducting layer. In the VSe_2/MoS_2 and VSe_2/WS_2 systems, the ferromagnetic VSe_2 layer is responsible for the proximity magnetism in the non-magnetic MoS_2 layer, while in V-MoS_2/graphene the semiconducting layer is magnetically doped. Moreover, V-MoS_2 shows enhanced magnetic properties when interfaced with graphene, compared to samples grown on Si/SiO_2 which may further influence the interaction between the optically injected charge carriers and the magnetic dopants. These findings show how the interactions between photogenerated charge carriers and 2D magnetic semiconductors can be tuned in carefully constructed vdW heterostructures.

[1] J.F. Sierra, J. Fabian, and R.K. Kawakami, Nature Nanotechnology., Vol. 16, p. 856-868 (2021) [2] F. Zhang, A. Sebastian, D.H. Olson, Advanced Science., Vol. 7, p. 2001174 (2020) [3] M. Bonilla, S. Kolekar, Y. Ma, Nature Nanotechnology., Vol.13, p. 289-293 (2018) [4] V. Ortiz Jiménez, Y.T.H. Pham, M. Liu, Advanced Electronic Materials., Vol. 7, p. 21000310 (2021)

COC-04. Withdrawn

COC-05. Enhanced Ferromagnetism in Artificially Stretched Quasi Two-Dimensional $Cr_2Ge_2Te_6$. *H. Idzuchi*[1,2], A.E. Llacsahuanga Allcca[3], A. Lu[4], M. Saito[1], K. Inoue[2], Y. Ikuhara[1,2], T. Nakanishi[4] and Y. Chen[3,2] *1. The University of Tokyo, Tokyo, Japan; 2. Tohoku University, Sendai, Japan; 3. Purdue University, West Lafayette, IN, United States; 4. National Institute of Advanced Industrial Science and Technology, Tsukuba, Japan*

In recent years, two-dimensional van der Waals (vdW) magnetic materials have attracted a significant attention. They serve as a model system for studying the magnetic interactions, owing to easy access to high crystallinity sample, even in quasi-two-dimensional limit. Among general ferromagnetic (FM) materials, vdW FM material typically shows a low FM transition temperature (Curie temperature, T_C), way below room temperature. This is the case for prototypical vdW FM CrI_3 and $Cr_2Ge_2Te_6$ [61 K (45K) for bulk (monolayer) CrI_3, 66 K (30K) for bulk (bilayer) $Cr_2Ge_2Te_6$]. Therefore, an effective approach to increase the T_C and understanding the mechanisms underlaying magnetism quickly arose as important issues to research. Lately, we reported that forming a $Cr_2Ge_2Te_6$/NiO heterostructure may increase the Curie temperature. However, the origin of this observation remained unclear [1]. In the present work, we reveal that a $Cr_2Ge_2Te_6$/NiO heterostructure can form a wrinkle structure causing in-plane tensile strain which cannot be accessed by conventional methods. This results in T_C being doubled compared to previous works [2]. We evaluated the strain by Raman spectroscopy and demonstrate a correlation between the Raman shift with the increase of T_C (Fig.1). Scanning transmission electron microscope

measurements indicate that the atomic distance between of Te atoms is larger near the interface with NiO (Fig.2). Further, DFT calculations show that tensile strain leads to an increase of exchange energy and magneto-anisotropy. Thus far, lattice engineering in magnetic materials has been rather limited. Our approach is effective in wide range of temperature and strain parameters to tune the electronic structure. Our method may also offer a way to engineer the effect in lateral distribution in a 2D layer, which may lead to applications such as quantum emitters, confining the potential and exhibiting moiré effect, and developing further functionalities.

[1] H. Idzuchi, A. E. Llacsahuanga Allcca, ... and Y. P. Chen, Appl. Phys. Lett. Vol. 115, p.232403 (2019). [2] in preparation.

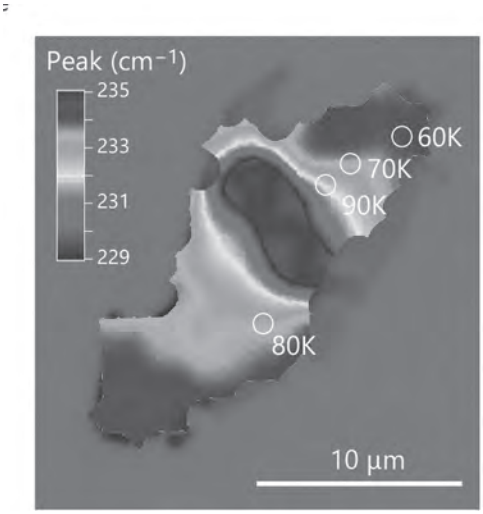

Fig. 1 Color map of Raman peak position. The Curie temperature *Tc* at four positions is also presented.

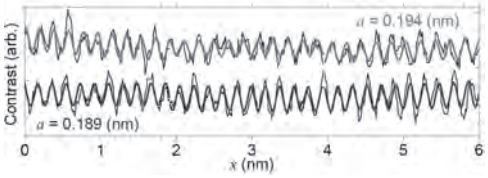

Fig. 2 Comparison of Te-Te atomic distance near (top, red line) and far from the interface (bottom, blue line), derived from oscillation of contrast in scanning transition electron microscope.

COC-06. Influence of the surface states on the nonlinear Hall effect in Weyl semimetals. *D. García Ovalle*[1], A. Pezo[1] and A. Manchon[1]
1. Aix-Marseille Université, Marseille, France

The anomalous Hall effect is an ubiquitous phenomenon in magnetic materials but it vanishes in time reversal systems. Nevertheless, Sodemann and Fu [1] suggested that a second order response in the electric field is allowed in time reversal invariant materials without inversion symmetry, as a consequence of the shift in the Fermi distribution function when the electrons go out of equilibrium. This nonlinear Hall effect is driven by the curvature dipole (BCD), which motivated several experiments [2,3] and encouraged the exploration of numerous platforms to enhance the resulting Hall current. In this context, topological materials such as Weyl semimetals (WSM) are excellent candidates to exhibit large values of nonlinear Hall effect due to monopoles of Berry curvature. In addition, the Fermi arcs that connect Weyl nodes of opposite chirality have a known impact on the anomalous Hall effect, but an extended analysis of the surface states is still missed at the level of the nonlinear Hall effect, especially in the regime when there is an important tilting of the Weyl cones. In this work [4], we reveal the contribution of the surface states to the BCD in WSM. Starting from a two-band model [5,6] and applying a slab construction method [7], we deduce that the topological nature of the surface states does not play a crucial role on the BCD. Besides, the transition between type I and type II WSM uncovers a strong impact of the Fermi pockets' projections because of a higher number of states at the surface rather than at the bulk. In contrast, after comparing to the bulk instance we notice that track states' projections does not show a profound effect on the BCD. We extend our study to the realistic case of WTe2 thin film using a Wannier-projected tight-binding representation, confirming that there is a notorious thickness dependence on the BCD subjected to the slab under consideration.

[1] I. Sodemann and L. Fu. Physical Review Letters 115, 216806 (2015). [2] K. Kang, T. Li, E. Sohn. Nature Materials 18, p. 324-328 (2019). [3] Q. Ma, S. Xu, H. Shen. Nature 565, p. 337-342 (2019). [4] D. García Ovalle, A. Pezo and A. Manchon. Arxiv 2206.08681 (2022). [5] T. Mc Cormick, I. Kimchi and N. Trivedi. Physical Review B 95, 075133 (2017). [6] C. Zeng, S. Nandy and S. Tewari. Physical Review B 103, 245119 (2021). [7] G. Manchon, S. Ghosh, C. Barreteau. Physical Review B 101, 174423 (2020).

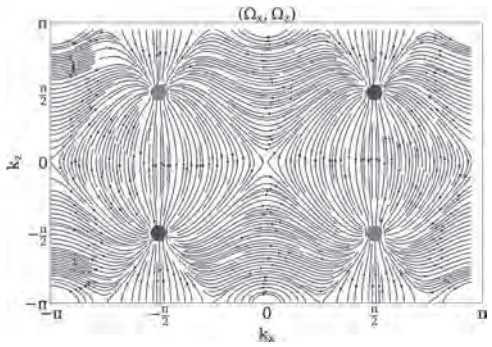

Fig. 1. Illustration of the Berry Curvature field (Ω_x,Ω_z) for the two-band model in the plane of the Weyl nodes (k_y=0). In addition, blue(red) dots represent degeneracies with positive (negative) Berry Curvature flux.

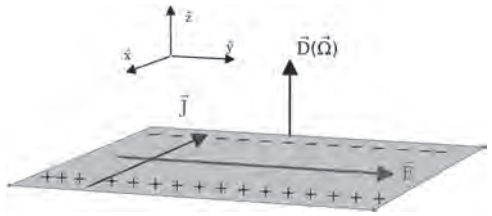

Fig. 2. Physics of the Nonlinear Hall Effect driven by the Berry Curvature Dipole.

COC-07. All-electric measurement of perpendicularly spin polarization in Weyl semimetal, WTe_2, at room temperature. *K. Ohnishi*[1], M. Aoki[1], E. Shigematsu[1], R. Ohshima[1], Y. Ando[1,2], T. Takenobu[3] and M. Shiraishi[1]
1. Electronic Science and Engineering, Kyoto Univ., Kyoto city, Japan; 2. PRESTO, JST, Honcho, Kawaguchi, Japan; 3. Applied Physics, Nagoya Univ., Nagoya, Japan

A type-II Weyl semimetal, WTe_2 is receiving great attention in spin physics because of the generation of spin polarization due to fictitious Weyl monopoles. In a previous study, in-plane spin polarization (S_y, parallel to the *b*-axis of WTe_2) originating from the Weyl node was reported by introducing an electrical method even though detection is limited at very low temperature [1]. Meanwhile, the existence of spin polarization along the *c*-axis (S_z, perpendicular to the plane) in WTe_2 was suggested by using angle-resolved photoemission spectroscopy (ARPES) [2], and S_z spin polarization can affect the spin-torque ferromagnetic resonance (ST-FMR) of adjacent ferromagnets [3]. However, the S_z spin generation using an electrical method, which is suitable for investigation of more precise origin of S_z spin polarization, has not been explored. In this study, we successfully detected the S_z spin polarization of T_d-type WTe_2 using an all-electric method that is an expansion of

the experimental technique for detecting topological surface spin polarization in BiSbTeSe [4]. Perpendicular magnetic anisotropy (PMA) electrodes made of $[Pt/Co]_{10}$ ("10" denotes a stacking number) and nonmagnetic Pt electrodes were deposited on the mechanically exfoliated WTe_2, and the out-of-plane magnetic field dependence of spin voltages was measured from 5 K to 300 K (see Fig.1). Figure 2 shows the result at 5 K and 300 K, and the hysteresis attributed to spin accumulation beneath the PMA electrode was successfully observed up to 300 K [5]. In addition, the polarity of spin voltage hysteresis was reversed by switching the electric current direction, and the hysteresis vanished when the direction of current changes to parallel to the *b*-axis of WTe_2. These evidence that the S_z spin polarization was originating from the in-plane symmetry breaking of WTe_2. Other supporting evidence and detailed discussion will be given in the presentation.

[1] P. Li *et al*., Nat. Commun. 9, 3990 (2018). [2] P.K. Das *et al.*, Nat. Commun. 7, 10847 (2016). [3] D. MacNeil *et al*., Nat. Phys. 13, 300-306 (2017). [4] Y. Ando, M. Shiraishi et al., Nano Lett. 14, 6226 (2014). [5] K. Ohnishi, Y. Ando, M. Shiraishi *et al*., under review.

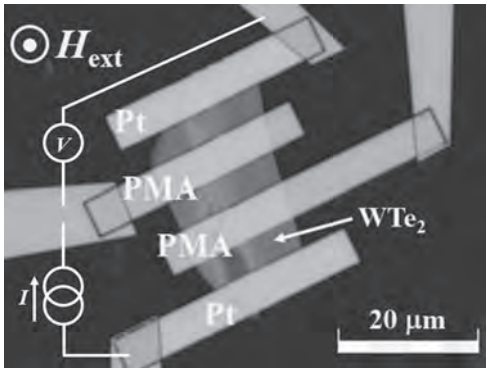

Fig. 1: Optical microscopic image of the device and measurement setup.

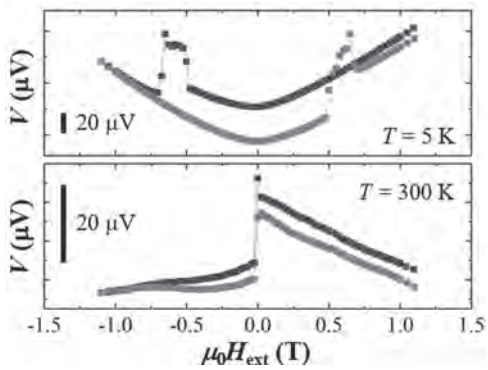

Fig. 2: Magnetic field dependence of the spin voltage at 5 K and 300 K, where the current was applied to be 1 mA. Red (blue) squares are experimental data in the upward (downward) sweeping.

COC-08. Room temperature bilinear magnetoelectric resistance in sputtered Dirac semimetal Pt_3Sn. *Y. Fan*[1], Y. Yang[1], Z. Cresswell[2], Y. Lv[1], T. Peterson[3], D. Zhang[1], J. Liu[1] and J. Wang[1] *1. Electrical Engineering, University of Minnesota, Minneapolis, MN, United States; 2. School of Chemical Engineering & Materials Science, University of Minnesota, Minneapolis, MN, United States; 3. Physics and Astronomy, University of Minnesota, Minneapolis, MN, United States*

Topological semimetal materials have become a research hotspot due to their intrinsic strong spin-orbit coupling which leads to large charge to spin conversion efficiency and novel transport behaviors. The bilinear magnetoelectric resistance (BMER), which changes linearly with both magnetic and electric field, is a strong evidence of the existence of topological states. [1,2] In this work, we have observed the BMER up to 0.1 $nm^2A^{-1}Oe^{-1}$ in sputtered Dirac semimetal Pt_3Sn single layer at room temperature. Different from the previous observations, the value of BMER in sputtered Pt_3Sn does not change when the magnetic field rotates in YZ plane [1] due to the polycrystalline nature of Pt_3Sn. The observation of BMER provides strong evidence of spin-momentum locking in the sputtered polycrystalline Dirac semimetal Pt_3Sn. By adding an adjacent CoFeB magnetic layer, the BMER value of the bilayer system can also be increased. This work broadens the material system in BMER and paves the way for high-quality topological materials growth and application.

[1] He, Pan, et al. "Bilinear magnetoelectric resistance as a probe of three-dimensional spin texture in topological surface states." Nature Physics 14.5 (2018): 495-499. [2] Zhang, Steven S-L., and Giovanni Vignale. "Theory of bilinear magneto-electric resistance from topological-insulator surface states." Spintronics XI. Vol. 10732. SPIE, 2018.

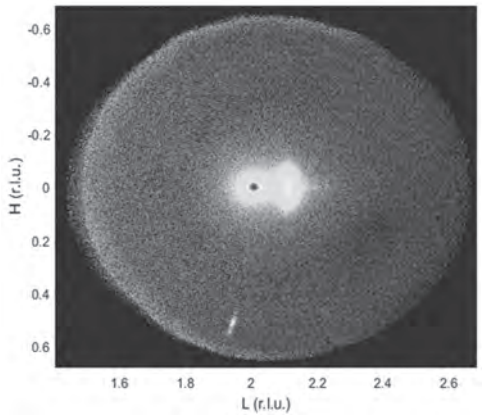

Figure 1: Reciprocal space map of a thin film of Pt3Sn on (001) single crystal MgO, with the peaks labelled as MgO (002) and Pt3Sn (002) (left and right).

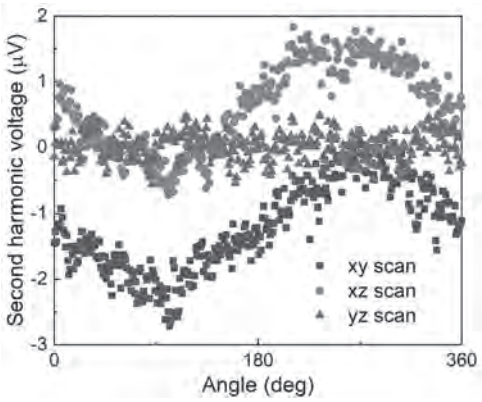

Figure 2: Angular dependence of BMER for Pt_3Sn(15nm) in XY,XZ and YZ plane.

COC-09. Layered $FeGe_2$ Films on GaAs(001) Substrates. *J. Herfort*[1], M. Terker[1], A. Trampert[1], M. Hanke[1], P. Ibanez[1] and M. Ramsteiner[1] *1. Paul-Drude-Institute for Solid State Electronics, Berlin, Germany*

Layered magnets can be seen as ideal platforms for exploring magnetism in the 2D limit [1]. To establish their potential in future technologies, the realization of high-quality magnetic layered materials exhibiting ferromagnetism (FM) and/or antiferromagnetism (AFM) close to room temperature is urgently needed. Recently, we have successfully synthesized at wafer-scale a metastable α-$FeGe_2$ layered phase using a combination of MBE and solid-phase epitaxy (SPE) down to only 4 nm in vertical trilayer stacks sandwiched between ferromagnetic Fe_3Si Heusler alloys [2]. Comprehensive X-ray diffraction (XRD) and transmission electron microscopy (TEM) revealed

the formation of the layered $FeGe_2$ allotrope (space group P4mm) which does not exist as a bulk [3]. Spin transport investigations have revealed a metallic behavior of α-$FeGe_2$ films [4]. Strikingly, the results also indicate a FM-AFM phase transition where the films are FM at low temperatures. In order to characterize α-$FeGe_2$ individually, eliminating any underlying Fe_3Si film is essential. In this study we developed a method to grow α-$FeGe_2$ films on GaAs(001) substrates, by first growing a few monolayers of crystalline Fe_3Si, and then thicker amorphous Ge in a ratio of 1:3 to obtain the right stoichiometry for $FeGe_2$. Through a detailed optimization of the solid phase epitaxy process we were able to synthesize single-crystalline, layered α-$FeGe_2$ films with very high structural and interface perfection on GaAs(001) substrates. The thickness was varied between 4 and 25 nm. In situ transmission electron microscopy experiments revealed the dynamics of the crystallization process, where the amorphous Ge first crystallizes to disordered $FeGe_2$ under the influence of Fe diffusion into the amorphous film and then it transformes into the ordered $FeGe_2$ phase. This transition starts at the Fe_3Si interface and transform the material layer by layer from bottom up. The disorder–order transition was found to proceed much slower than the crystallization. Low-temperature ferromagnetism was observed in superconducting quantum interference device as well as magnetotransport measurements for samples of various thicknesses.

[1] S. Valenzuela et al., Nat. Nanotech. 14, 1088 (2019). [2] S. Gaucher et al., Appl. Phys. Lett. 110, 102103 (2017). [3] B. Jenichen et al., Phys. Rev. Mat. 2, 051402(R) (2018). [4] D. Czubak et al., Phys. Rev. Mat. 4, 104415 (2020).

COC-10. Behavior of Bubble Lattices in Cr2Ge2Te6. *A.R. McCray*[1,2], Y. Li[1], E. Qian[3], W. Wang[4], X. Ma[4], D. Chung[1], Y. Liu[4], M.G. Kanatzidis[3], A. Petford-Long[1,5] and C. Phatak[1,5] *1. Materials Science Division, Argonne National Laboratory, Lemont, IL, United States; 2. Applied Physics Program, Northwestern University, Evanston, IL, United States; 3. Department of Chemistry, Northwestern University, Evanston, IL, United States; 4. Center for Nanoscale Materials, Argonne National Laboratory, Lemont, IL, United States; 5. Department of Materials Science and Engineering, Northwestern University, Evanston, IL, United States*

Magnetic van der Waals (vdW) materials are increasingly studied due to the discovery of ordered ferromagnetism down to monolayer thickness [1], as well as them hosting chiral and topologically protected magnetic domains [2]. $Cr_2Ge_2Te_6$ (CGT) is a particularly interesting example as a semiconducting 2D magnet which, despite its low Curie temperature at 72 K, is of potential use for its spintronic and magnetic properties. As an easily exfoliated vdW material, it can be readily incorporated into multilayer heterostructures and has additionally been proposed for interfacing with topological insulators to study the anomalous quantum Hall effect [3]. We have performed an in-situ study and directly imaged the magnetic domain structure of CGT under varied temperature and external magnetic fields using cryo-Lorentz transmission electron microscopy (LTEM). Fig. 1 shows both stripe domains and a mixed-chirality magnetic bubble lattice phase that can be created by field cooling CGT through the Curie temperature with an applied field. This is the same procedure by which magnetic skyrmion phases are generated in chiral magnets [2]. Although these bubble lattices are not topologically protected, they behave very similarly to skyrmion lattices when skyrmions are destroyed by an increasing magnetic field. Despite a lack of chiral energy terms in CGT, we have also observed topologically protected lattices containing homochiral bubbles across large regions spanning tens of microns. These are stabilized solely by dipolar forces, and the same region of film can display both mixed chirality and homochiral bubble lattices upon repeated cooling runs with identical parameters. In this work we further show how the bubble lattices of vdW CGT bear similarity to skyrmion lattices and how the chirality and alignment of these lattices are affected by strain [4].

[1] Gong, C. et al. *Nature* 546, p.265 (2017). [2] Li, Y. et al. *Jom* 74, p.2310 (2022). [3] Ji, H. et al. *J. Appl. Phys.* 114, p.114907 (2013). [4] This work was supported by the U.S. Department of Energy, Office of Science, Office of Basic Energy Science, Materials Sciences and Engineering Division.

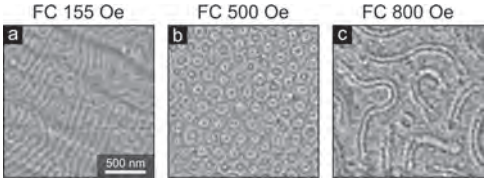

Fig. 1: LTEM images of CGT at 20 K after field cooling in an out of plan magnetic field. (a) Stripe domains are formed when field cooling in a 155 Oe field. (b) Magnetic bubble lattices are formed when cooling with field strengths between 300 Oe and 700 Oe. (c) Stripe domains are again formed when cooling in stronger fields.

COC-11. Identifying Axion Insulator by Quantized Magnetoelectric Effect in Antiferromagnetic $MnBi_2Te_4$ Tunnel Junction. *Y. Li*[1] and R. Cheng[1] *1. UC, Riverside, Riverside, CA, United States*

Intrinsic magnetic topological insulator $MnBi_2Te_4$ is believed to be an axion insulator in its antiferromagnetic ground state. However, direct identification of axion insulators remains experimentally elusive because the observed large resistance and the vanishing Hall effect, while indicating the onset of the axion field, is inadequate to distinguish the system from a trivial normal insulator. Using Green's function method, we theoretically demonstrate the quantized topological magnetoelectric current in a tunnel junction with atomically thin $MnBi_2Te_4$ sandwiched between two metalic contacts, which is a smoking-gun signal that unambiguously confirms antiferromagnetic $MnBi_2Te_4$ to be an axion insulator. Our predictions can be verified directly by experiments.

Yu-Hang Li and Ran Cheng, Identifying Axion Insulator by Quantized Magnetoelectric Effect in Antiferromagnetic $MnBi_2Te_4$ Tunnel Junction. arXiv:2111.11500

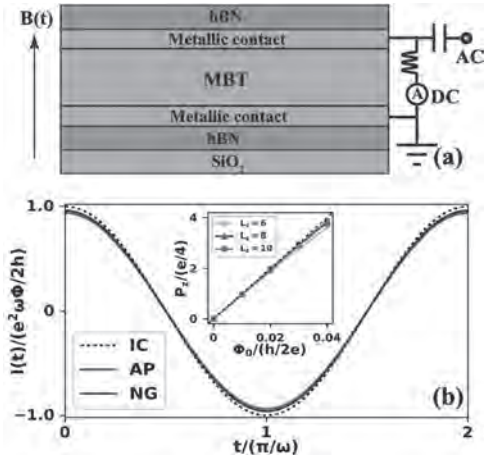

(a) Schematic of the proposed $MnBi_2Te_4$ tunnel junction to detect the dynamical topological magnetoelectric effect. The metallic leads are connected to a bias tee to separate the harmonic AC output from the DC output which is short circuited. The hexagonal boron nitride (hBN) flakes are added to avoid degradation, and the whole device is placed on a silicon dioxide substrate. (b) Output current I(t) induced by an AC magnetic field $B_z\sin(\omega t)$ calculated by the time-dependent non-equilibrium Green's function (NG) (solid blue), the adiabatic variation of the surface charge polarization (AP) (solid red), respectively. The ideal case (IC) (dotted black) for an exactly quantized axion field $\theta = \pi$ is plotted as a reference.

Session CPA
MAGNETOELECTRONIC MATERIALS AND PHENOMENA (Poster Session)

Markus Gößler, Chair
Chemnitz University of Technology, Chemnitz, Germany

CPA-01. Phase Coexistence and Strain-mediated Magnetic Anisotropy in Magnetic Weyl Semimetal Co_2MnGa Films. *N. Schulz*[1], A. Chanda[1], J.D. Gayles[1], A. Markou[2], C. Felser[2], M. Phan[1] and H. Srikanth[1] *1. Physics, University of South Florida, Tampa, FL, United States; 2. Solid State Chemistry, Max-Planck-Institute for Chemical Physics of Solids, Dresden, Germany*

Magnetic Weyl semimetals provide an opportunity to observe the coexistence of unique magnetic and electronic properties through the intrinsic time-reversal symmetry breaking. This can lead to exotic magnetic and transport properties such as large anomalous Hall and Nernst effects, chiral anomalies, etc.[1] The existence of Weyl fermions, degenerate band crossings of opposite chirality in momentum space exhibiting locally linear energy-momentum dispersion, drives these properties which has been found to exist in Co_2MnGa[2]. However, a clear understanding of the temperature evolution of the magnetization and magnetic anisotropy in Co_2MnGa is lacking. Here, the magnetic properties of an 80 nm thick magnetic Full-Heusler Weyl semimetal Co_2MnGa film are studied. The film was grown in a BESTEC UHV magnetron sputtering system on single crystal MgO(001) substrates and capped with 3 nm Si. First, the magnetic field dependent magnetization was measured for $40 \leq T \leq 300$ K in a Quantum Design Physical Property Measurement System (PPMS), utilizing the vibrating sample magnetometer (VSM) option. Two magnetic phase transitions were identified to occur around 275 K, and 200 K from the temperature dependence of the magnetization. A large thermal hysteresis was observed below 275 K between the field-cooled-cooling (FCC) and field-cooled-warming (FCW) magnetizations, varying upon applied magnetic field strength. To further explore these transitions, radio frequency tunnel diode oscillator (TDO) based transverse susceptibility (TS) measurements were performed to precisely probe the temperature evolution of the effective magnetic anisotropy (H_K^{eff}) of the system[3][4]. Measurements were performed for temperatures $40 \leq T \leq 300$ K for both in-plane (IP) and out-of-plane (OOP) configurations. Strong IP magnetic anisotropy is observed, with sharp magnetic switching at low fields. Distinct changes in H_K^{eff} were observed around the same phase transition temperatures identified in magnetometry measurements. A magnetic phase diagram is established to relate the magnetization to H_K^{eff} with respect to temperature variation. These results highlight the interplay between strain and magnetism, and the effect of phase transitions on H_K^{eff}.

[1] K. Manna, Y. Sun, L. Muechler, J. Kübler, and C. Felser, "Heusler, Weyl and Berry," *Nat. Rev. Mater.*, vol. 3, no. 8, pp. 244–256, Aug. 2018, doi: 10.1038/s41578-018-0036-5. [2] I. Belopolski *et al.*, "Discovery of topological Weyl fermion lines and drumhead surface states in a room temperature magnet," *Science (80-.).*, vol. 365, no. 6459, pp. 1278–1281, Sep. 2019, doi: 10.1126/science.aav2327. [3] A. Chanda, J. E. Shoup, N. Schulz, D. A. Arena, and H. Srikanth, "Tunable competing magnetic anisotropies and spin reconfigurations in ferrimagnetic $Fe_{100-x}Gd_x$ alloy films," *Phys. Rev. B*, vol. 104, no. 9, Sep. 2021, doi: 10.1103/PhysRevB.104.094404. [4] H. Srikanth, J. Wiggins, and H. Rees, "Radio-frequency impedance measurements using a tunnel-diode oscillator technique," *Rev. Sci. Instrum.*, vol. 70, no. 7, Jul. 1999, doi: 10.1063/1.1149892.

CPA-02. Theory of Inverse Faraday effect in massive Dirac electrons. *G. Qu*[1] and G. Tatara[1] *1. Center for Emergent Matter Science, RIKEN, Wako-Shi, Japan*

The inverse Faraday effect (IFE) [1,2,3] phenomenologically describes the static magnetization induced by the circularly polarized light. In experiments, the IFE is able to reverse the magnetization of magnets with strong laser pulse, providing an optical method of ultrafast magnetization manipulation. Recently, sensitive detection of the effective magnetic field induced by a continuous laser can be carried out electrically through the inverse spin Hall effect [4]. Here, we study inverse Faraday effect in Dirac Hamiltonian with random impurities using Keldysh formalism and diagrammatic perturbation theory in low frequency regime [5]. The mass term in Dirac Hamiltonian is essential for the IFE, where the spin magnetic moment induced by circularly polarized light is proportional to frequency of the incident light within THz regime. For massive Dirac electrons, the corrections due to the short-range impurities on spin magnetic moment vertex exhibits mixing of spin magnetic moment vertex and spin angular momentum vertex. The spin magnetic density response is divergently enhanced by the vertex corrections near the band edge.

[1] P. Pershan, Physical Review 130, 919 (1963). [2] K. Taguchi, and G. Tatara, Physical Review B 84, 174433 (2011). [3] K. Taguchi, T. Imaeda, M. Sato, and Y. Tanaka, Phys. Rev. B 93, 201202(R) (2016). [4] M. Kawaguchi, H. Hirose, Z. Chi, Y.-C. Lau, F. Freimuth, and M. Hayashi, arXiv preprint arXiv:2009.01388 (2020). [5] G. Qu, and G. Tatara. arXiv preprint arXiv:2201.10155(2022).

CPA-03. Exchange/Zeeman Competition in the Rare-Earth Nitrides and the Resulting Magnetic Compensation. *J. Miller*[1,2], B. Ruck[1,2] and J. Trodahl[2] *1. MacDiarmid Institute, Wellington, New Zealand; 2. Victoria University, Wellington, New Zealand*

The rare-earth nitrides are the only known *series* of intrinsic ferromagnetic semiconductors, with a range of magnetic behaviours stemming from the contribution of both spin and orbital *4f* moments. The similar chemistry of the rare-earths and the common structure of the nitrides simplifies their combination in superlattices and solid solutions. Recent studies of rare-earth nitride superlattices have shown enhanced superconductivity [1] and magnetic exchange spring behaviour that results from the competition between the Zeeman and Exchange interactions [2]. Yet, little has been published to date exploring the combination of these nitrides in solid-solutions. We show (with reference to magnetometry, XMCD and anomalous Hall effect measurements) that the same Exchange/Zeeman competition that leads to a complex twisted magnetic phase in superlattices manifests quite differently in solid solutions. Leading, where an orbital-dominant ferromagnet (SmN) is paired with a spin-only ferromagnet (GdN), to a composition exhibiting a net zero magnetic moment (A compensation point).

[1] E.-M. Anton, S. Granville, A. Engel et. al., Phys. Rev. B, Vol. 94, 024106 (2016) [2] E.-M. Anton, W. Holmes-Hewett, J. McNulty et. al., AIP Advances, Vol. 1, 015348 (2021)

CPA-04. Unexpected opposite dependencies of anisotropy field and strength of spin-orbit interaction on gate voltage measured in FeCoB nanomagnet. *V. Zayets*[1], I. Serdeha[2] and V. Grygoruk[2] *1. Platform Photonics Research Center, AIST, Tsukuba, Japan; 2. Educational and Scientific Institute of High Technologies, Taras Shevchenko National University of Kyiv, Kyiv, Ukraine*

VCMA effect describes the fact that in a capacitor, in which one of electrodes is made of a thin ferromagnetic metal, the magnetic properties of the ferromagnetic metal changes, when a voltage is applied to the capacitor[1]. Inside a metal the electrical field is screened by free electrons and cannot penetrate deep inside the metal. As a result, the voltage, which is applied to the capacitor dielectric (gate), may penetrate into and affect only the few uppermost atomic layers of the metal near the gate. However, the change of magnetic properties of the uppermost layer by the gate voltage affects the magnetic properties of the whole film. This can be only the case if the interfacial perpendicular magnetic anisotropy (PMA) is affected by the gate voltage [2]. The strength of PMA is characterized by the anisotropy field H_{ani} and proportional to the strength of spin-orbit interaction, demagnetization field and magnetization of nanomagnet. Fig.1 shows the measured H_{ani} and coefficient of spin-orbit interaction k_{so} in FeCoB nanomagnet under a different gate voltage. k_{so} defies the strength of the spin-orbit interaction[3]. H_{ani} decreases and k_{so} increases under an increase of gate voltage. It is unexpected because H_{ani} is linearly proportional to k_{so} [3] and should increase when k_{so} increases. It means that even though the strength of the spin-orbit interaction is affected by the gate voltage, but additionally to k_{so} there is another voltage- dependent parameter, which defines the voltage dependence of H_{ani}. The intrinsic field in nanomagnet or demagnetization field might be such a parameter. Fig.2 shows measured H_{ani} and k_{so} of different nanomagnet of different wafers. The same tendency exists in all measured nanomagnets.

[1] Y. Shiota, T. Nozaki, F. Bonell, S. Murakami, T. Shinjo, Y. Suzuki, Nat. Mater. 11 (2012) 39–43. [2] V. Zayets, T. Nozaki, H. Saito, A. Fukushima, S. Yuasa, *arXiv:1812.07077 (2018)*. [3] V. Zayets, IOA-07, MMM 2021.

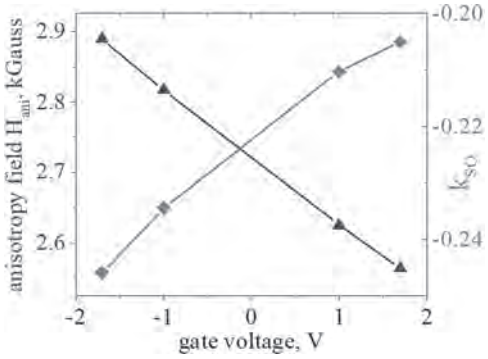

Fig.1 Measured anisotropy field H_{ani} and coefficient of the spin orbit interaction k_{so} as a function of the gate voltage in Ta(2.5 nm)/ FeB(1.1 nm)/ MgO(6 nm)/ Ta(1 nm)/ Ru(5 nm) nanomagnet.

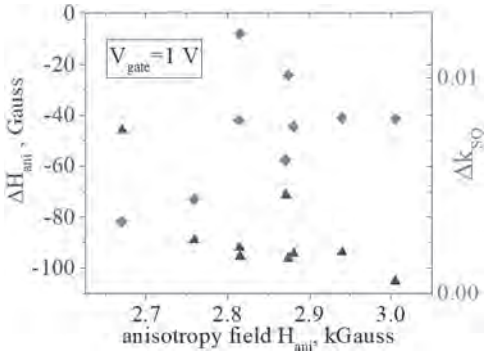

Fig.2 (a) Change of anisotropy field and coefficient of the spin orbit interaction at gate voltage of 1 V measured in different nanomagnets fabricated on the same wafer. Each dot correspond a measurement of an individual nanomagnet. The change of H_{ani} is always negative, but the change of k_{so} is always positive

CPA-05. Electric field control of magnetization reversal in FeGa/ PMN-PT. *G. Pradhan*[1], F. Celegato[1], L. Mikuličková[2], A. Magni[1], G. Barrera[1], M. Coisson[1] and P. Tiberto[1] *1. Istituto Nazionale di Ricerca Metrologica, Torino, Italy; 2. Thin film Technological Service, s.r.o., Prague, Czechia*

The recent era of information technology devices largely focusses on energy and cost efficiency [1-3]. Magnetoelectric (ME) materials possess huge potential to be used in these technologies due to its coupling between magnetization and electric-field induced strain which therefore consumes less power and significantly reduces heat losses. Research developments on device miniaturization recently performed show non-volatile and magnetic state transformation with few volts in micro and nanoscale structures [4, 5]. The application of voltage generates strain at the interface and this strain transfer to the magnetic layer from the piezoelectric layer induces change in magnetic anisotropy and domain structures [6]. In this work, magnetostrictive $Fe_{80}Ga_{20}$ thin films were deposited on (001) PMN-PT piezoelectric substrates by sputtering technique. The top and bottom electrodes were contacted to apply voltage across the stack as shown in Fig 1(a). The electric field was generated perpendicular to the sample. The magnetic field was applied in-plane of the sample and magnetic hysteresis and domain structures were recorded with MOKE microscopy. Fig 1(b) shows the hysteresis curves recorded at 0 MV/m (as-deposited), 0.06 MV/m, 0.065 MV/m and 0.08 MV/m as represented by the red, blue, green and orange curves. The domain textures recorded at near coercive field in as-deposited state and at 0.08 MV/m field is shown in fig 1(c) and 1(d), respectively. The increase in grey contrast in 1(d) represents domains along the transverse direction which clearly states the rotation of magnetic easy axis. This is further confirmed with the decrease in remanent magnetization and coercive field of the magnetic hysteresis with increase in voltage applied. The effect of change in magnetic anisotropy was found to be reversible which confirms its non-volatility. Hence, FeGa/PMN-PT system proves to be efficient for possible fabrication of magnetic nanodots to be used in memory devices.

[1] M. Gajek et al., Nature materials 6.4, 296-302 (2007) [2] H. K. D. Kim et al., Nano letters 13.3, 884-888 (2013) [3] C. Binek, B. Doudin, Journal of Physics: Condensed Matter 17.2, L39 (2004) [4] R. Lo Conte, et al. Nano letters 18.3, 1952-1961 (2018) [5] Q. Li, et al. Applied Physics Letters 110.26, 262405 (2017) [6] M.G. De Jesus, et al. Smart Materials and Structures 31.3, 035005 (2022)

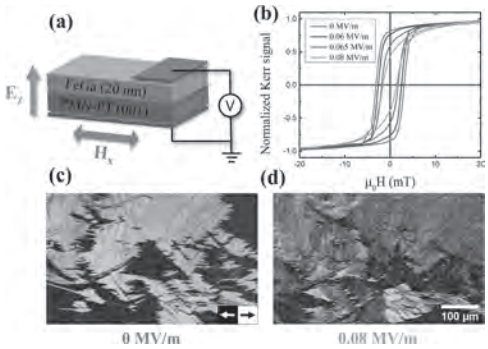

Fig. 1: (a) Schematic of voltage application setup for FeGa thin film deposited on (001) cut PMN-PT. (b) Inplane hysteresis loops for different voltages applied across the stack. (c) and (d) shows the domains recorded with MOKE at 0 MV/m and 0.08 MV/m, respectively.

CPA-06. Improving Voltage-driven ON-OFF Ferromagnetism in Cobalt Oxide via Electrolyte Engineering. *Z. Ma*[1], S. Martins[1], E. Pellicer[1], E. Menendez[1] and J. Sort[1,2] *1. Departament de Física, Universitat Autònoma de Barcelona, Barcelona, Spain; 2. Institució Catalana de Recerca i Estudis Avançats (ICREA), Barcelona, Spain*

Magneto-ionics, i.e., the modification of materials' magnetic properties by voltage-driven ion migration, offers much promise in the pursuit of voltage control of magnetism (VCM) for energy-efficient electronics. Room temperature voltage-controlled ON-OFF ferromagnetism via oxygen magneto-ionics has been shown in electrolyte-gated Co_3O_4 films[1,2], taking advantage of the formation of an electric double layer (EDL) at the interface between the films and the electrolyte, i.e., propylene carbonate (PC). Herein, by dissolving various inorganic salts such as KI, KCl and $Ca(BF_4)_2$ in anhydrous PC, we aim to increase the electric field strength in the EDL and hence enhance voltage-driven ion motion in cobalt oxide. We found that improved magneto-ionic motion is achieved when salts are added to PC. This is especially pronounced for the KI-containing electrolyte. For instance, applying -1.5V to the films in 2.5×10^{-5} M KI electrolyte not only results in a much faster magnetization variation ($\Delta M/\Delta t$), but also the maximum M value is nearly twice that for PC alone. Moreover, the threshold voltage for magneto-ionics decreases with addition of KI, from -10V for pure PC to -1.5V when small concentrations of KI exists. We further optimized the magneto-ionic properties by tuning the content of KI. From the ΔM versus biasing duration under a -1.5V (see Fig.), the ΔM firstly increases as the concentration reaches up to 2.5×10^{-4} M, then decreases with further KI addition. Remarkably, the maximum ΔM for 2.5×10^{-4} M KI electrolyte is one order of magnitude larger than that for pure PC (≈280 versus 25 emu/cm^3). Hysteresis measurements of the actuated films corroborate the effects of different KI concentration on the ON-OFF ferromagnetism in this system. XPS study confirms the reduction of cobalt oxide into Co upon voltage actuation in the electrolytes. Enhanced magneto-ionic motion gives rise to the formation of substantial metallic Co in the film electrolyte-gated in PC+2.5×10^{-4} M KI, in line with the magnetometry experiments. Our study suggests electrolyte engineering as a potential approach to achieving substantial improvements in VCM based on magneto-ionics.

References [1] A. Quintana, et. al., Voltage-Controlled ON–OFF Ferromagnetism at Room Temperature in a Single Metal Oxide Film, ACS Nano 12 (10) (2018) 10291; [2] J. de Rojas, et. al., Boosting room-temperature magneto-ionics in a non-magnetic oxide semiconductor, Advanced Functional Materials 30 (2020) 2003704

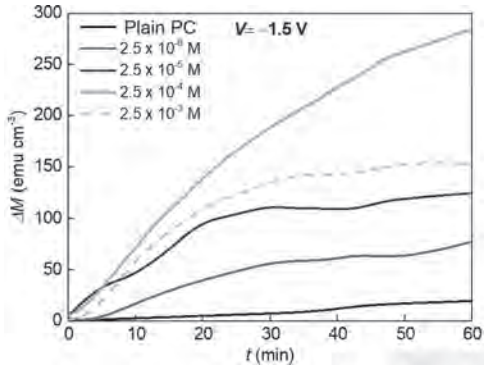

Fig. Δ*M* versus biasing time, *t*, under a -1.5V for various electrolyte-gating

CPA-07. Switching of Magnetic Anisotropy in MgO/CoFeB/W stack by Ionic Liquid Gating for Voltage Tuneable Magneto Resistive Sensor. *A. Islam*[1,2], S. Granville[1,2] and S. Acharya[1,2] *1. Robinson Research Institute, Victoria University of Wellington, Wellington, New Zealand; 2. MacDiarmid Institute for Advanced Materials and Nanotechnology, Wellington, New Zealand*

This study aims to fabricate a voltage-tuneable magneto resistive sensor with the ability to measure small magnetic field signals in three dimensions. Sensing direction in magneto resistive sensors is linked to the magnetization of reference layer. Materials like CoFe[1], CoFeB[2] and Heusler alloys[3] are good choices as reference layers due to their adjustable magnetic anisotropies. Here, using ionic liquid gating (ILG), we observed that magnetic anisotropy of reference layer CoFeB is switchable in MgO(1.5nm)/CoFeB(1.6nm)/W(0.5nm) stack. We used ionic liquid N, N-diethyl-N-methyl N-(2-methoxyethyl) ammonium bis (trifluoromethylsulfonyl) imide (DEME TFSI) (IoLiTec) for applying the gate voltage (V_G) ranging between ±3.5V. Using the magneto-optical Kerr effect, we have investigated the change of anisotropy using different gate voltages. We found that magnetic anisotropy switches from out-of-plane (virgin state) to in-plane upon the application of +3.5V, whereas removal of applied voltage +3.5V or application of -3.5V, switches magnetic anisotropy back to out-of-plane, demonstrating the switching behaviour of the stack is reversible and repeatable. Moreover, we observed that out-of-plane to in-plane anisotropy switching time is higher (~45 sec) compared to in-plane to out-of-plane switching time (~25 sec). Hence, a stack having stronger out-of-plane and switchable anisotropy is ideal to use in voltage tuneable magneto resistive sensors.

1. Parkin, S. S. P. *et al*., *Nat. Mater.,* 2004, 3, 862–867. 2. Yuasa, S. & Djayaprawira, D. D., *J. Phys. D. Appl. Phys.,* 2007, 40, 337-354. 3. Palmstrøm, C. J., *Prog. Cryst. Growth Charact. Mater.,* 2016, 62, 371–397.

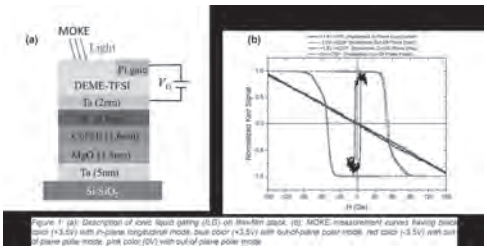

Session DOA
MAGNETORESISTANCE IN HETEROSTRUCTURES (GMR, TMR, TAMR)

William Echtenkamp, Co-Chair
University of Minnesota, Minneapolis, MN, United States
Simon Granville, Co-Chair
Victoria University of Wellington, Lower Hutt, New Zealand

INVITED PAPER

DOA-01. Brain-Inspired Computing by Chaotic Spin-Torque Oscillator. *T. Taniguchi*[1], S. Tsunegi[1], T. Yamaguchi[2], A. Kamimaki[5], N. Akashi[3], T. Kubota[4], K. Nakajima[4], H. Notsu[6], M. Kimura[6], H. Tsukahara[7], J. Grollier[8], V. Cros[8], K. Yakushiji[1], A. Fukushima[1], S. Yuasa[1] and H. Kubota[1] *1. National Institute of Advanced Industrial Science and Technology (AIST), Tsukuba, Japan; 2. RIKEN, Wako, Japan; 3. Kyoto University, Sakyo-ku, Japan; 4. The University of Tokyo, Bunkyo-ku, Japan; 5. Yokohama National University, Yokohama, Japan; 6. Kanazawa University, Kanazawa, Japan; 7. Osaka University, Osaka, Japan; 8. CNRS/Thales, Palaiseau, France*

After the report on human-voice recognition based on the algorithm of physical reservoir computing [1], the application of spin-torque oscillators (STOs) to brain-inspired computing is becoming an exciting topic in spintronics community. Physical reservoir computing aims to classify time-dependent signal by finding one-to-one correspondence between the input data and nonlinear dynamical response from physical reservoir [2]. The development of physical reservoir computing has been involved deepening our understanding on dynamical systems because their nonlinear response is the computational resource. For example, an empirically rule in the computing is that its computational capability is enhanced at the edge of chaos. However, while magnetization switching and auto-oscillation have been extensively studied, there have been very few research on excitation of chaos in nanomagnet and its application to computing. The lack of the observation of chaos in nanomagnets relates to the fact that chaos occurs in a large-dimensional phase space, while the rigid magnetic structures, such as macrospin and magnetic vortex, have only a few dynamical degrees of freedom. Recently, we have proposed theoretically that chaos can be excited in STOs by using many-body [3], nonautonomous [4], or delayed-feedback [5] systems. These methods enable us to increase the number of dynamical degrees of freedom even in the rigid magnetic structures. We provided the theoretical evidence of the existence of chaos by evaluating the Lyapunov exponent, which characterizes a timescale to observe chaos. In particular, an STO with a delayed-feedback circuit is of great interest because physical systems with feedback effects in principle have an infinite number of dynamical degrees of freedom. The tunability between chaotic and nonchaotic states by electronic means is also preferable for experimental demonstration. We showed by numerical simulation that the computational capability in physical reservoir computing is greatly enhanced when a delayed-feedback circuit is added to STOs [6]. Here, we found a periodic structure of memory function in STOs with respect to the delay time, which arises from recurrent structure of interactions among virtual neurons associated with the feedback circuit. Furthermore, we experimentally proved the existence of chaos in a vortex-type STO with a delayed-feedback circuit [7] schematically shown in Fig. 1. Here, the output power from the STO is sent to a metal line with a delay time of 250 ns and generates an oscillating magnetic field acting on the STO. The torque due to the magnetic field makes the vortex dynamics highly nonlinear. The existence of chaos in the STO was identified through the observation of multiple peaks in power spectrum density, the reproduction of the dynamical trajectory in an embedding space, and the evaluation of noise limit. Figure 2 shows examples of the reproduced trajectory for (a) small and (b) large feedback gains. A circular trajectory in Fig. 2(a) indicates a periodic oscillation in the STO, while the spread trajectory in Fig. 2(b) indicates the appearance of chaos. We also performed a function-approximation task by using the STO with the feedback circuit and found a minimization of the computational error as the dynamical state is manipulated. These results bridge magnetism, computer science, and nonlinear science and advance the development of nanoscale neural networks.

[1] J. Torrejon *et al*., Nature 547, 428 (2017). [2] K. Nakajima and I. Fischer editted, Reservoir Computing – Theory, Physical Implementations, and Applications –, Springer 2021. [3] T. Taniguchi, J. Magn. Magn. Mater. 483, 281 (2019). [4] T. Yamaguchi *et al*., Phys. Rev. B 100, 224422 (2019). [5] T. Taniguchi *et al*., Phys. Rev. B 100, 174425 (2019). See also J. Williame *et al*., Appl. Phys. Lett. 114, 232405 (2019). [6] T. Yamaguchi *et al*., Phys. Rev. Res. 2, 023389 (2020). [7] A. Kamimaki *et al*., Phys. Rev. Res. 3, 043216 (2021).

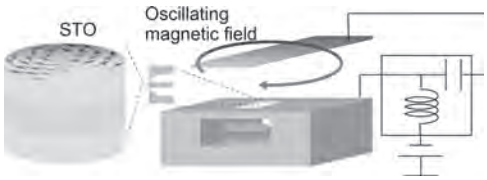

Fig. 1 Schematic illustration of a vortex-type STO with a delayed-feedback circuit. The output power from the STO is sent to the feedback metal-line and generates an oscillating magnetic field affecting the vortex dynamics.

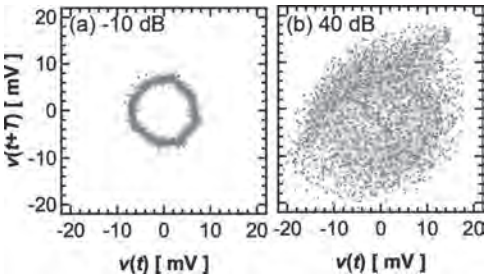

Fig. 2 The dynamical trajectory of the vortex core reproduced in an embedded space is almost circle and periodic when the feedback gain is small [-10 dB in (a)], while it becomes chaotic when the gain becomes large [40 dB in (b)].

CONTRIBUTED PAPERS

DOA-02. Large unidirectional spin Hall and Rashba–Edelstein magnetoresistance in topological insulator/magnetic insulator heterostructures. *Y. Lv*[1], J. Kally[2], T. Liu[3], P. Quarterman[4], T. Pillsbury[2], B. Kirby[4], A.J. Grutter[4], P. Sahu[5], J.A. Borchers[4], M. Wu[3], N. Samarth[2] and J. Wang[1,5] *1. Department of Electrical and Computer Engineering, University of Minnesota, Minneapolis, MN, United States; 2. Department of Physics, The Pennsylvania State University, University Park, PA, United States; 3. Department of Physics, Colorado State University, Fort Collins, CO, United States; 4. NIST Center for Neutron Research, National Institute of Standards and Technology, Gaithersburg, MD, United States; 5. School of Physics and Astronomy, University of Minnesota, Minneapolis, MN, United States*

The unidirectional spin Hall magnetoresistance (USMR) is initially discovered in ferromagnetic (FM) and normal metal (NM) structures[1] and magnetic semiconductor structures[2]. It is a phenomenon observed in bilayer structures and is related to interfacial spin generation and scattering processes at the interface. The similar unidirectional spin Hall and Rashba-Edelstein magnetoresistance (USRMR) is observed in FM-topological insulator (TI) bilayers being much larger than that in FM-NM bilayers in bilayer structures[3]. They are of particular interest due to its potential of 180-degree sensitive electrical readout of magnetization in bilayer structures for spin-orbit torque switching devices. Here, we report large unidirectional spin Hall and Rashba–Edelstein magnetoresistance in a new material family - magnetic insulator (MI)/TI $Y_3Fe_5O_{12}$ (YIG)/Bi_2Se_3 bilayers. Such heterostructures exhibit a USRMR that is about an order of magnitude larger than the highest values reported in all-metal Ta/Co bilayers[1]. The polarized neutron reflectometry (PNR) reveals a unique temperature-dependent magnetic intermediary layer at the MI-substrate interface and a proximity layer at the MI-TI interface. These PNR findings echo the magnetoresistance results in a comprehensive physics picture. Finally, we demonstrate a prototype memory device based on a MI/TI bilayer, using USRMR for electrical read out of current-induced magnetization switching aided by a small Oersted field[4].

[1] C. O. Avci, K. Garello, A. Ghosh *et al*., *Nat. Phys.*, vol. 11, no. 7, p. 570–575 (2015) [2] K. Olejník, V. Novák, J. Wunderlich et al., *Phys. Rev. B - Condens. Matter Mater. Phys.*, vol. 91, no. 18, p. 180402 (2015) [3] Y. Lv *et al.*, *Nat. Commun.*, vol. 9, no. 1, p. 111 (2018) [4] Y. Lv *et al.*, *Appl. Phys. Rev.*, vol. 9, no. 1, p. 011406, (2022)

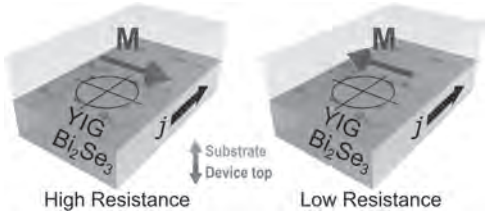

Fig. 1. Schematic illustration of USRMR in an MI/TI (YIG/Bi2Se3) bilayer[4].

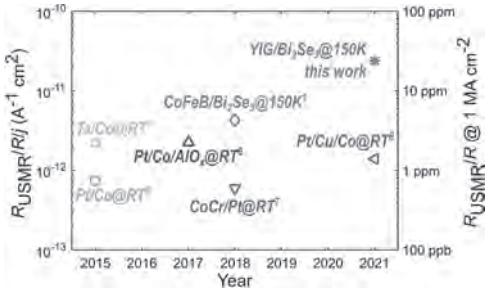

Fig. 2. Normalized USMR or USRMR in various material systems[4].

DOA-03. Controlling spin-valve effects in ferromagnet/superconductor structures via the ratio of orbital to spin moments. S. Wang[2], *K. Dumesnil*[1,2], H. Bradshaw[2], N. Stelmashenko[2] and J. Robinson[2] *1. IJL, Nancy, France; 2. Department of Metallurgy and Materials Science, University of Cambridge, Cambridge, United Kingdom*

The proximity coupling between a thin film superconductor (S) and a homogeneous ferromagnet (F) can lead to a suppression of the superconducting critical temperature (T_c) (1). This behaviour is modified when the magnetism is inhomogeneous (2,3). For example, in a superconducting spin-switch (F/S/F), the magnitude of T_c is largest for an antiparallel magnetisation-alignment of the F layers due to a net reduction of the magnetic exchange field acting on the S layer; for a S/F bilayer, T_c can be enhanced at the coercive field. Here, we investigate the superconductor proximity effect at epitaxial S/F interfaces in which the ratio of the orbital moment (Lz) to the effective spin-moment (Sz) of the F layer is systematically tuned. For this purpose, epitaxial Nb(30nm)/Ho_xGd_{1-x}(50nm)/Nb(8nm) trilayers are grown by DC-sputtering on A-plane sapphire substrates. The structural and magnetic properties of the systems are investigated by X-ray diffraction and SQUID measurements. These reveal a good crystalline quality with Nb and Ho_xGd_{1-x} layers growing along the respectively [110] and [001] directions and with mosaicities of respectively 0.1° and 0.8°. The lattice d-spacing decreases linearly with increasing the Ho content (Fig.1), revealing a good control of the sample stoichiometry. The magnetic properties are also controlled by the alloy composition: increasing the Ho content drives the stabilization of a non-collinear helical phase, over an extended T range and more robust to the application of an external magnetic field. Electronic transport measurements enable us to investigate how the Nb superconducting behaviour is influenced by the proximity with the Ho_xGd_{1-x} alloy and by its (field dependent) interface magnetic order. The results demonstrate an infinite magnetoresistance effect related to the magnetization reversal (Fig. 2), and a giant enhancement of the proximity effect for large Lz/Sz ratios, which is key for the development of superconducting spintronics devices.

(1) A. Buzdin, Rev. Mod. Phys. 77, 935-976 (2005). (2) J. Linder and J. W. A. Robinson, Nature Physics 11, 307–315 (2015). (3) G. Yang, C Ciccarelli, J.W.A. Robinson, APL Materials 9, 050701 (2021)

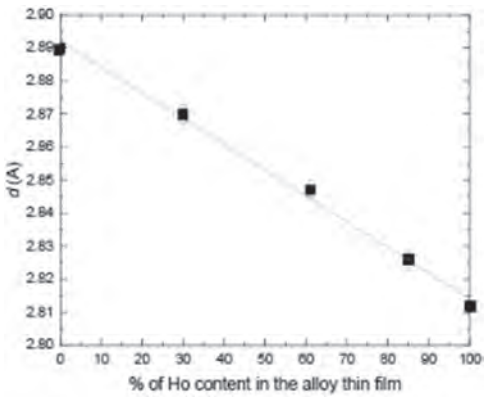

Fig. 1: d-lattice spacing as function of the Ho content (x) determined by XRD in Nb(30nm)/Ho_xGd_{1-x}(50nm)/Nb(8nm) hybrid systems

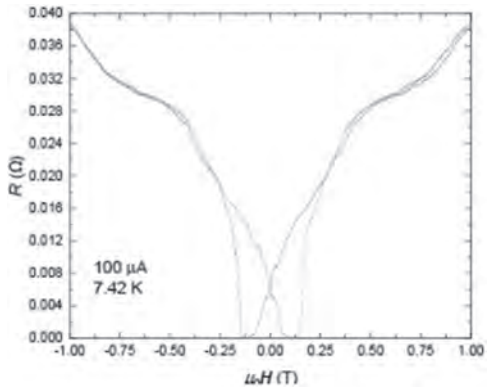

Fig. 2: magnetoresistance measured at 7.42K for a Nb/Ho/Nb trilayer

DOA-04. Giant voltage-controllable magnetoresistance switching in Ge short-channel devices with epitaxial ultra-thin Fe electrodes.
S. Tsuruoka[1], Y. Tadano[1], L.D. Ahn[1,2], M. Tanaka[1,2] and S. Ohya[1,2]
1. Department of Electrical Engineering and Information Systems, The University of Tokyo, Bunkyo-ku, Japan; 2. Center for Spintronics Research Network, Graduate School of Engineering, The University of Tokyo, Bunkyo-ku, Japan

Tunneling anisotropic magnetoresistance (TAMR) [1] is an interfacial effect between a ferromagnet and a non-magnetic material where the tunneling resistance depends on the orientation of the magnetization. Since TAMR originates from spin-orbit coupling (SOC), large TAMR is observed in materials with strong SOC such as GaMnAs [2], while observing large TAMR in weak SOC materials has been difficult [3]. In this study, we fabricated and characterized Ge-based all-epitaxial single-crystalline lateral devices with a nano-scale short channel. We have grown Fe (17 nm)/ MgO (1 nm)/ Ge:B (34 nm, B concentration: 1×10^{15} cm^{-3})/ Ge (51 nm) on an n^-Ge (001) substrate using molecular-beam-epitaxy, and then we reduced the Fe-layer thickness to less than 1 nm by Ar milling to induce a perpendicular magnetic-anisotropy (PMA) component. We have fabricated short-channel devices with a channel length of a few tens of nm by electron beam lithography and Ar milling (Fig. 1). Fig. 2 shows the perpendicular magnetic-field H dependence of the source-drain resistance R at 3 K. We observed switching between the high-resistance state and the low-resistance state at a threshold field H_{th}, where H_{th} increases with the increase in the voltage applied between the source and drain electrodes (V_{DS}). The magnetoresistance (MR) ratio, which is defined as $[R(H) - R(0)]/R(0)$, increases with increasing V_{DS}, and when V_{DS} = 9 V, the MR ratio reaches over 10000%. These results suggest that the MR switching reflects the modulation of the magnetization direction (probably of the narrower electrode) induced by electric and magnetic fields. The high and low resistance states are thought to correspond to the perpendicular and in-plane magnetization states, respectively. When V_{DS} is increased, the PMA is weakened, and larger H is needed to switch the resistance state. This work was supported by Grants-in-Aid for Scientific Research, CREST of JST, and Spintronics Research Network of Japan (Spin-RNJ).

[1] C. Gould *et al.*, Phys. Rev. Lett. Vol. 93, p. 117203 (2004). [2] C. Rüster *et al.*, Phys. Rev. Lett. Vol. 94, p. 027203 (2005). [3] J. Moser *et al.*, Phys. Rev. Lett. Vol.99, p. 056601 (2007).

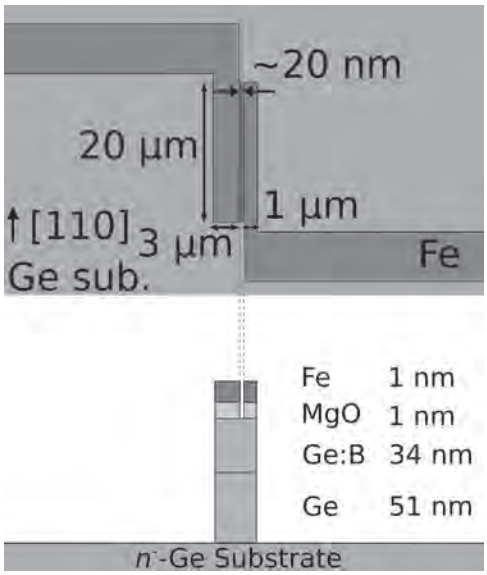

Fig. 1 Top and side views of the device.

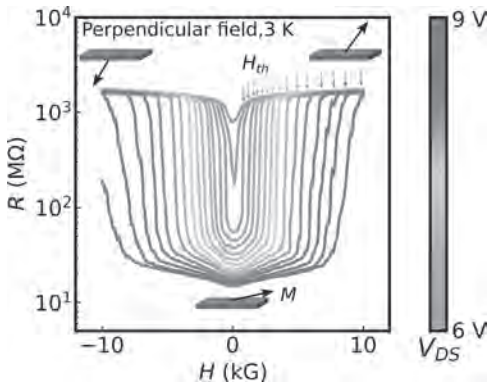

Fig. 2 Magnetic-field dependence of MR with various V_{DS} ranging from 6 V to 9 V by a 0.2 V step at 3 K, where H is applied perpendicular to the plane. The black arrows represent the direction of the magnetization M.

DOA-05. Damping constant of Co_2FeAl thin film deposited by molecular beam epitaxy and tunnel magnetoresistance effect using them.
T. Hojo[1], N. Tezuka[2], T. Nakano[1], M. Tsunoda[3,5] and M. Oogane[1,4]
1. Department of Applied Physics, Graduate School of Engineering, Tohoku University, Sendai, Japan; 2. Department of Metallurgy, Materials Science and Materials Processing, Graduate School of Engineering, Tohoku University, Sendai, Japan; 3. Department of Electronic Engineering, Graduate School of Engineering, Tohoku University, Sendai, Japan; 4. Center for Science and Innovation in Spintronics (Core Research Cluster) Organization for Advanced Studies, Tohoku University, Sendai, Japan; 5. Center for Spintronics Research Network, Tohoku University, Sendai, Japan

Magnetic Tunnel junctions (MTJs) with Co_2FeAl Heusler alloy electrode are expected to show giant TMR ratio at room temperature (RT) because of its half-metallicity. In previous work, although Co_2FeAl/MgO/CoFe-MTJ showed a TMR ratio of 330% at RT [1], it is still smaller than those for MTJs with CoFeB electrodes. In order to realize a large TMR ratio at RT, it is necessary to fabricate high-quality Heusler alloy electrodes and to control the interface at the atomic level. Therefore, I focused on molecular beam epitaxy (MBE) technique, which enables the fabrication of highly ordered Heusler alloy thin films [2] and atomic level interfacial modification [3]. In this work, we prepared epitaxial Co_2FeAl thin films by MBE technique and characterized their magnetic properties to identify the half-metallicity

of the Co_2FeAl films. In addition, TMR effect in Co_2FeAl/MgO/CoFe-MTJs fabricated by MBE were investigated. The films were deposited on MgO(001) substrate using MBE and sputtering methods. The stacking structure of the Co_2FeAl films were Cr(20)/Co_2FeAl(50)/MgO(5) (unit of nm). After the fabrication of Co_2FeAl layers, the films were annealed at T_a=200~700°C. Structural and magnetic properties were measured by XRD, VSM and FMR. The stacking structure of MTJs was Cr(20)/Co_2FeAl(30)/MgO(2.0)/CoFe(5)/IrMn(10)/Cr(5) (unit of nm). After the microfabrication, the MTJ devices were annealed at T_{MTJ}=275~425°C under 1T magnetic fields. TMR effects were measured by DC 4-probe method. The Co_2FeAl film with T_a=600°C showed high $B2$ order parameter and high magnetization. In addition, as shown in Fig.1, it showed very small damping constant α of 1.8×10^{-3}, indicating that the film has good half-metallicity. Fig.2 shows the magnetoresistance curves of the MTJs measured at RT. A relatively large TMR ratio of 125% at T_{MTJ}=400°C was observed and the TMR ratio can be improved by insertion of ultrathin Mg or Al into the Co_2FeAl/MgO interface due to suppression of the interfacial state and oxidation. This work was supported by NEDO, JSPS, GP-Spin Program and JST SPRING, Grant Number JPMJS2114.

[1] W. Wang, H. Sukegawa and K. Inomata, Appl. Phys. Lett. 95, 182502 (2009) [2] M. Oogane, A. P. McFadden and C. J. Palmstrøm, Appl. Phys. Lett. 112, 262407 (2018) [3] K. Himi, K. Takahashi and S. Mitani, Appl. Phys. Lett. 78, 1436 (2001)

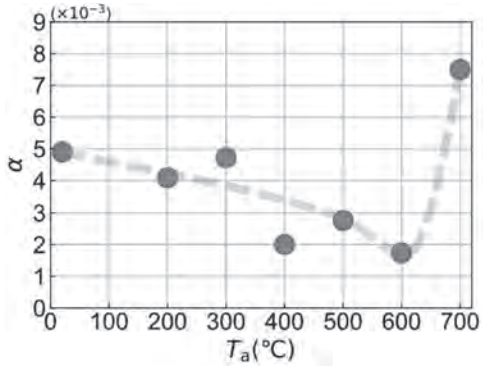

Fig.1 Annealing temperature T_a dependence of damping constant α

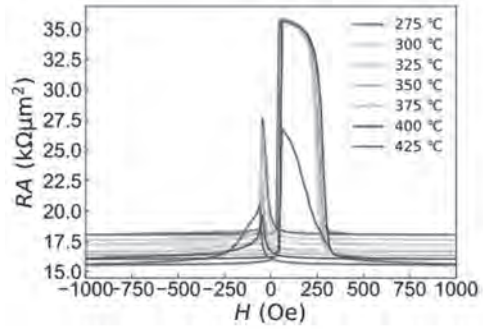

Fig.2 Magnetoresistance curve for each annealing temperature T_{MTJ}

DOA-06. Heusler Alloy Based Perpendicular Magnetic Tunnel Junctions. *S. Acharya*[1,2], A. Islam[1,2] and S. Granville[1,2] *1. Robinson Research Institute, Victoria University of Wellington, Lower Hutt, Wellington, New Zealand; 2. MacDiarmid Institute for Advanced Materials and Nanotechnology, Wellington, New Zealand*

Magnetic tunnel junctions (MTJs) are currently at the forefront of spintronics research because their large magnetoresistance (MR) and high sensitivity make them an attractive application prospect for magnetic memories and magnetic sensors [1]. MTJs with perpendicular magnetic anisotropy (PMA) are advantageous over in-plane devices due to their scalability, stronger remnant magnetization for a smaller demagnetizing field in the perpendicular direction, and higher signal-to-noise ratio due to the enhanced uniaxial orientation [1]. The perpendicular anisotropy is also essential to achieve faster magnetization switching and to minimize stray fields from a magnetoresistance junction. Heusler compounds are one of the most promising candidates for MTJ electrodes because their half-metallic states can help achieve 100 % spin polarization at room temperature, leading to an infinite magnetoresistance ratio. Furthermore, these materials have additional advantages, including high Curie temperature and long spin diffusion length [2]. Recently, our group has discovered Weyl semi-metal behaviors [3], and PMA [4] in Heusler-based Co_2MnGa ultrathin films, making it a promising material for exploring spin-polarising devices. In this work, we used Co_2MnGa electrodes to obtain perpendicularly magnetized MTJ stacks. We used thin-film sputtering and photolithography to fabricate the devices. We optimized the devices by precisely varying the thickness of each Co_2MnGa and MgO layer and annealing conditions. We used the magneto-optical Kerr effect (MOKE) microscopy for domain imaging and MR measurements of the multilayer stacks. The MTJ showed strong PMA, and we could identify two distinct magnetic steps in the field sweep curve corresponding to the switching direction of the two magnetic layers. The devices also showed high MR, demonstrating that Co_2MnGa-based perpendicular MTJs are a strong candidate for the next generation of spintronic devices.

[1] Maciel, N.; Marques, E.; Naviner, L.; Zhou, Y.; Cai, H. Magnetic Tunnel Junction Applications. *Sensors*, 2019, *20* (1), 121. https://doi.org/10.3390/s20010121. [2] Elphick, K.; Frost, W.; Samiepour, M.; Kubota, T.; Takanashi, K.; Sukegawa, H.; Mitani, S.; Hirohata, A. Heusler alloys for spintronic devices: review on recent development and future perspectives. *Sci. Technol. Adv. Mater.*, 2021, *22* (1), 235–271. https://doi.org/10.1080/14686996.2020.1812364. [3] Zhang, Y.; Yin, Y.; Dubuis, G.; Butler, T.; Medhekar, N. V.; Granville, S. Berry curvature origin of the thickness-dependent anomalous Hall effect in a ferromagnetic Weyl semi-metal. *npj Quantum Mater.*, 2021, *6* (1). https://doi.org/10.1038/s41535-021-00315-8. [4] Ludbrook, B. M.; Ruck, B. J.; Granville, S. Perpendicular magnetic anisotropy in Co 2 MnGa and its anomalous Hall effect. *Appl. Phys. Lett.*, 2017, *110* (6), 062408. https://doi.org/10.1063/1.4976078.

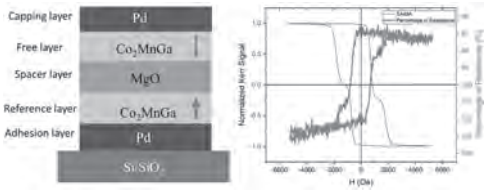

Left: Schematic of Co_2MnGa based MTJ stack. Right: magnetoresistance result of the MTJ stack.

DOA-08. Spin filtering effects at graphene/molecules interfaces. *C. Barraud*[1], L. Chen[3,1], B. Dlubak[4], A. Droghetti[2], M. Martin[4], P. Martin[3], R. Mattana[4] and P. Seneor[4] *1. Physics, Université Paris Cité, Paris, France; 2. School of Physics and CRANN, Trinity College, Dublin, Ireland; 3. Chemistry, Université Paris Cité, Paris, France; 4. Unité Mixte de Physique CNRS/Thales, Palaiseau, France*

We present a bias-controlled spin-filtering mechanism in spin-valves including a hybrid organic chain/graphene interface [1]. Wet growth conditions of oligomeric molecular chains would usually lead, during standard CMOS-compatible fabrication processes, to the quenching of spintronics properties of metallic spin sources due to oxidation. We demonstrate by X-ray photoelectron spectroscopy that the use of a protective graphene layer fully preserves the metallic character of the ferromagnetic surface and thus its capability to deliver spin polarized currents. We focus here on a small aromatic chain of controllable lengths, formed by nitrobenzene monomers and derived from the commercial 4-nitrobenzene diazonium tetrafluoroborate, covalently attached to the graphene passivated spin sources thanks to electroreduction. A unique bias dependent switch of the spin signal is then observed in complete spin valve devices, from minority to majority spin

carriers filtering. First-principles calculations are used to highlight the key role played by the spin-dependent hybridization of electronic states present at the different interfaces [2].

[1] P. Martin *et al.*, submitted (2022) [2] P. Martin *et al.*, Adv. Quant. Tech. 5, 2100166 (2022)

DOA-09. Angle-Dependent Switching in a Magnetic Tunnel Junction Containing a Synthetic Antiferromagnet. *H. Chen*[1], B. Parks[2,1], Q. Zhang[3,4], B. Fang[3], X. Zhang[3] and S. Majetich[1] *1. Physics, Carnegie Mellon University, Pittsburgh, PA, United States; 2. Intel Ronler Acres, Hillsboro, OR, United States; 3. King Abdullah University of Science and Technology, Thuwal, Saudi Arabia; 4. New York University Abu Dhabi, Abu Dhabi, United Arab Emirates*

The angle dependence of field-induced switching was investigated in magnetic tunnel junctions (MTJ) with in-plane magnetization and a pinned synthetic antiferromagnet reference layer. 60 nm x 90 nm elliptical nanopillars were patterned from a film stack of SiOx/Ta (5)/CoFeB (2.5)/MgO (1)/CoFeB (2.5)/Ru (0.85)/CoFe (2.5)/IrMn (8)/Ru (10), (units in nm). The tunnel magnetoresistance (TMR) was measured while the external field was applied at an angle θ, varying from 0° to 180° relative to the major axis of the ellipse (MAE), as shown in the inset of Fig.1. The relative angle between the free layer magnetization and the MAE, ϕ, was calculated from the TMR using an empirical cosine relation. Single sharp switches are seen when the field was applied along the MAE, but even with small deviations, reversal occurred through an intermediate state. Fig.1 shows a representative hysteresis loop measured at θ = 20°. To determine the magnetization direction at different points in the hysteresis loop, the energy landscape was modeled in terms of the effective shape anisotropy field, the external magnetic field, and the SAF stray field. Using an 8 Oe shape anisotropy effective field and the 26 Oe SAF stray field strength estimated from the loop shift, the magnetization direction as a function of the external field magnitude and direction was reconstructed. Fig.2 shows the energy diagrams of the device at the critical fields. Near 26 Oe the barrier between the two lowest energy states is low, consistent with the telegraphing observed in Fig. 1. Intentional misalignment of the SAF and shape anisotropy fields has potential for development of faster probabilistic spintronic devices [1].

1. H. Chen, et al., Appl. Phys. Lett. 120, 212401 (2022).

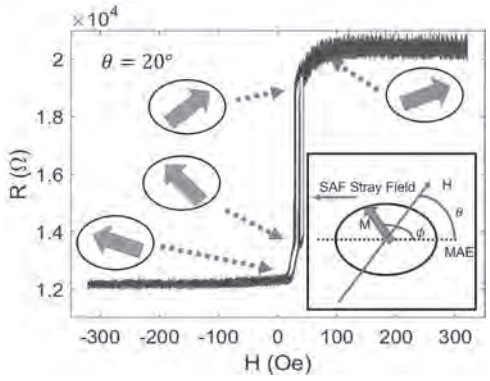

Fig.1. Hysteresis loop of a 60 nm x 90 nm elliptical dot, measured in a θ = 20° external field. Inset shows the schematic for the measurement.

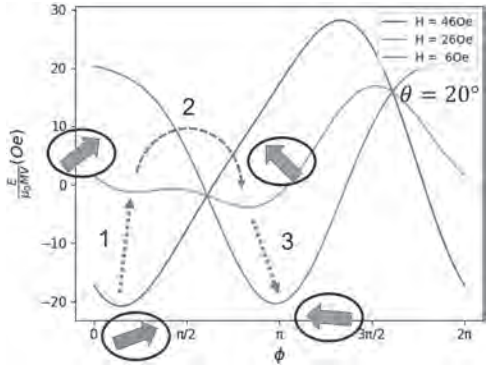

Fig.2. Energy diagram for the device at 6, 26, and 46 Oe, when the field is applied along θ = 20°

DOA-10. Quantum control of spin qubit ensembles with nanomagnets: Exchange coupling for high fidelity. *M.F. Chowdhury*[1], M. Niknam[2], M. Rajib[1], W. Misba[1], R.N. Schwartz[2], K. Wang[2], L. Bouchard[2] and J. Atulasimha[1] *1. Virginia Commonwealth University, Richmond, VA, United States; 2. University of California Los Angeles, Los Angeles, CA, United States*

Scalable implementation of fault-tolerant quantum computing [1] requires selective addressing of qubits. This is challenging when such qubits are discrete points or regions on a lattice at nanoscale dimensions as it is difficult to localize and confine a classical divergence-free field to a small volume in space. We propose a new technique for individual control of spin qubits [2,3] implemented with induced field of nanomagnets using voltage control of magnetic anisotropy (VCMA) [4]. We show that by tuning the frequency of the nanomagnet's electric field drive to the Larmor frequency of the spins confined to a nanoscale volume, and by modulating the phase of the drive, single-qubit quantum gates with fidelities approaching those for fault-tolerant quantum computing [1] can be implemented. Such single-qubit gate operations are energy efficient, requiring only tens of femto-Joules per gate operation, lossless, and purely magnetic field control (no E-field over the target volume). Furthermore, while our initial motivation for using a qubit comprising an ensemble ~10-100 spins is to improve signal to noise ratio for read out, we will investigate if exchange coupling between them can mitigate dephasing and further improve single qubit gate fidelity.

[1] Gottesman, D. Phys. Rev. A 57, 127–137 (1998). URL https://link.aps.org/doi/10. 1103/PhysRevA.57.127. [2] Cory, D. G., Fahmy, A. F. & Havel, T. F. Proc. Nat. Acad. Sci. (USA) 94, 1634–1639 (1997). URL https://www.pnas.org/content/94/5/1634. [3] Gershenfeld, N. A. & Chuang, I. L. Science 275, 350–356 (1997). URL https://science. sciencemag.org/content/275/5298/350. [4] Wang, K. L., Lee, H. & Amiri, P. K. IEEE Transactions on Nanotechnology 14, 992–997 (2015). [5] Niknam, M., Chowdhury, M.F.F., Rajib, M.M., Misba, W.A., Schwartz, R.N., Wang, K.L., Atulasimha, J. and Bouchard, L.S., 2022. arXiv preprint arXiv:2203.16720.

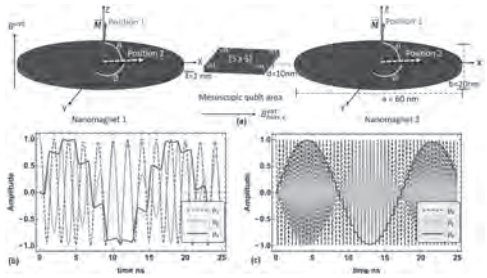

Fig. 1 (a) Schematic diagram of simulation setup in MuMax3. Nanomagnet: Ferromagnet/anti-ferromagnet interface to create exchange bias field in +x direction in the nanomagnet. Qubit: FM/Oxide interface to create PMA in the film (magnetized to point along –z) below the qubit volume that cancels part of the external magnetic bias field. Evolution of spins in the lab frame for nanomagnet induced field with 500 MHz drive (b) and 2 GHz drive (c). Average evolution of 25 spins initialized along the x, y, and z directions are projected on x, z, y axes, respectively. (Images are not to scale) Reproduced from [5]

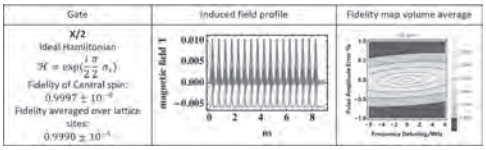

TABLE I Implementation of quantum gates using nanomagnets at 2GHz drive. Reproduced from [5]

DOA-11. Extraordinary Tunnel Electroresistance in Layer-by-Layer Engineered van der Waals Ferroelectric Tunnel Junctions. *Q. Wang*[1], T. Xie[1], Z. Song[1] and C. Gong[1] *1. University of Maryland, College Park, MD, United States*

Ferroelectric tunnel junctions (FTJs) hold remarkable potentials for electrically switchable memories, sensors, and logic devices. However, the traditional FTJs consisting of metal/oxide/metal multilayer heterostructures can only exhibit the modest tunneling electroresistance (TER, usually $<10^6$), which is fundamentally undermined by the unavoidable defect states and interface trap states. Here we constructed van der Waals (vdW) FTJs by a layered ferroelectric $CuInP_2S_6$ (CIPS) and graphene. Owing to the gigantic ferroelectric modulation of the chemical potentials in graphene by as large as ~1 eV, we demonstrated a giant TER of 10^9. While inserting just a monolayer MoS_2 between CIPS/graphene, the OFF state is further suppressed, leading to $>10^{10}$ TER. Our discovery opens a new solid-state paradigm where potential profiles can be unprecedentedly engineered in a layer-by-layer fashion, fundamentally strengthening the ability to manipulate electrons' tunneling behaviors and design advanced tunneling devices.

Session DOB
MRAM, MAGNETIC LOGIC AND RELATED DEVICES

Christopher Safranski, Co-Chair
IBM, Yorktown Heights, NY, United States
Reinoud Lavrijsen, Co-Chair
Eindhoven University of Technology, Eindhoven, Netherlands

INVITED PAPER

DOB-01. Ultrafast racetrack based on compensated Co/Gd-based synthetic ferrimagnet with all-optical switching. *R. Lavrijsen*[1], P. Li[1], T. Kools[1] and B. Koopmans[1] *1. Applied Physics, Eindhoven University of Technology, Eindhoven, Netherlands*

Spin-orbitronics and single pulse alloptical switching (AOS) of magnetization are two major successes of the fast advancing field of nanomagnetism in recent years, with high potential for enabling novel fast and energy-efficient memory and logic platforms. Fast current induced domain wall motion and single shot AOS have been individually demonstrated in different ferrimagnetic alloys. However, the stringent requirement for their composition control makes them challenging material for wafer scale production. Here, we demonstrate simultaneously fast current-induced domain wall motion and energy efficient AOS in a synthetic ferrimagnetic system based on [Co/Gd]2 multilayers. We firstly show AOS is present in its full composition range. We find current driven domain wall velocities over 2 km/s at room temperature conditions is achieved by compensating the total angular momentum through layer thickness tuning. Furthermore, analytical modelling of the current-induced domain wall motion reveals that Joule heating needs to be treated transiently to properly describe the current-induced domain wall motion for our sub-ns current pulses. Our studies establish Co/Gd based synthetic ferrimagnets to be a unique material platform for domain wall devices with access to ultrafast single pulse AOS [1].

[1] Pingzhi Li, Thomas J Kools, Bert Koopmans and Reinoud Lavrijsen. Ultrafast racetrack based on compensated Co/Gd-based synthetic ferrimagnet with all-optical switching. arXiv preprint arXiv:2204.11595, 2022.

CONTRIBUTED PAPERS

DOB-02. Picosecond Optospintronic Tunnel Junctions for Non-volatile Photonic Memories. *L. Wang*[1], W. Zhao[2], M. Heck[1] and B. Koopmans[1] *1. Eindhoven Hendrik Casimir Institute, Center for Photonic Integration, Eindhoven University of Technology, Eindhoven, Netherlands; 2. Fert Beijing Institute, MIIT Key Laboratory of Spintronics, Beihang University, Beijing, China*

Perpendicular magnetic tunnel junctions (p-MTJs) are one of the building blocks for spintronic memories, which allow fast nonvolatile data access, offering substantial potential for next-generation nonvolatile memory applications[2-3]. However, the performance of such devices is fundamentally hindered by spin-polarized-current-based schemes[2-4], with a nanosecond-spin-precession-time limitation and excessive power dissipation well over several hundred fJ per bit. [HM1]. How to overcome these physical constraints has remained a long-lasting scientific challenge for the modern spintronics community[3,4]. To address these issues, here, we report an optospintronic tunnel junction (OTJ) device using a photonic-spintronic combination. By integrating an all-optically-switchable Co/Gd bilayer[5] with a CoFeB/MgO-based p-MTJ, an all-optical "writing" of the OTJ within 10 ps is experimentally demonstrated. It also shows a reliable electrical "read-out" with a relatively high TMR of 34%, as well as promising scaling towards the nanoscale with a low energy consumption. A brief circuit-level analysis on the technology assessment aligned with other memory technologies is carried out. Moreover, the ultimate limits of this hybrid spintronic-photonic platform, regarding energy efficiency, data bandwidth, are also provided. Our proof-of-concept demonstration might pave the way towards a new category of nonvolatile integrated photonic memory devices. This development is considered highly promising towards next-generation ultrafast (picosecond) opto-MRAM technology thus further stimulating the innovation of future & emerging technologies.

[1] L. Wang, H. Cheng, P. Li., *Proceedings of the National Academy of Sciences*, *119*(24), e2204732119 (2022). [2] B. Dieny, I. L. Prejbeanu, K. Garello, *Nature Electronics*, *3*(8), 446-459 (2020). [3] Z. Guo, J. Yin, Y. Bai, Spintronics for energy-efficient computing: An overview and outlook. *Proceedings of the IEEE,* 109(8), 1398-1417 (2021) [4] A. V. Kimel, M. Li, *Nature Reviews Materials*, *4*(3), 189-200 (2019). [5] M. L. Lalieu, R. Lavrijsen, B. Koopmans, Integrating all-optical switching with spintronics. Nat. Commun. *10*(1), 1-6 (2019).

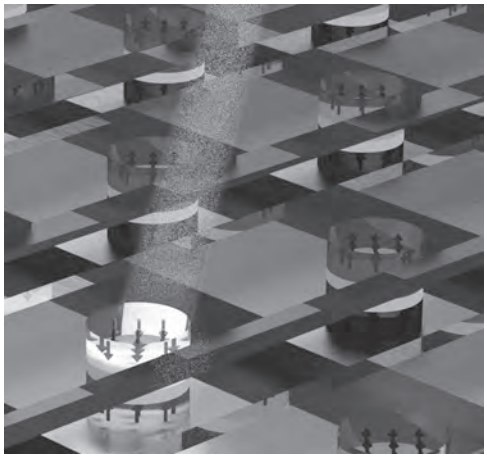

DOB-03. Fast Current Induced Domain Wall Motion in Compensated GdFeCo Nanowire. *S. Ranjbar*[1], S. Sumi[1], K. Tanabe[1] and H. Awano[1] *1. Toyota Technological Institute, Nagoya, Japan*

*E-mail: sina.ranjbar@toyota-ti.ac.jp Spintronics applications are being extensively followed for high-performance logic computing technologies and racetrack memories[1]. The principal difficulties are reaching small bits and high thermal stability and tracking them at high speed. Although there is a report that the domain wall moving speed is improved by using the angular momentum compensation of RE-TM[2], stable driving over a wide temperature range has not been achieved. We designed $Gd_x(Fe_{88}Co_{22})_{100-x}$ magnetic wires to achieve significant domain wall motion over a wide temperature range in this work. We prepared the following film stacks using rf and dc magnetron sputtering: Pt (5)/ Gd_x $(Fe_{88}Co_{22})_{100-x}$ (20)/SiN (10); the films are grown at the room temperature. The magnetic wires (3μm wide and 125 μm long) and Hall crosses were micro-fabricated by an Electron-beam lithography

(EBL) system and a lift-off method. Subsequently, we measured the domain wall velocity. We applied a single voltage pulse and then observed the DW motion using a Kerr microscope. We calculated the speed of the DW by dividing the change in position by the duration of the pulse. As a result, without applying an in-plane external magnetic field, the fastest DW velocity of 2000 m/s has been obtained as far as we know in the reports. Figure 1 shows the DW velocity of the $Gd_{24}(Fe_{88}Co_{12})_{76}$ as a function of operating temperature. DW speed obtained stable between the temperature range of R.T. $<T_{op}<70$°C for $Gd_{24}FeCo_{76}$ when pulse current of 30nsec and 3nsec is injected into the wire. As a result, a wide temperature range with a DW velocity of 1500 m/s has been obtained in $Gd_{24}(Fe_{88}Co_{12})_{76}$ for a short pulse current which is more stable than the previous reports[3]

[1] D. Bang, P. Van Thach, H. Awano, *J. Sci. Adv. Mater. Devices* 2018, *3*, 389. [2] L. Caretta, M. Mann, F. Büttner, K. Ueda, B. Pfau, C. M. Günther, P. Hessing, A. Churikova, C. Klose, M. Schneider, D. Engel, C. Marcus, D. Bono, K. Bagschik, S. Eisebitt, G. S. D. Beach, *Nat. Nanotechnol.* 2018, *13*, 1154. [3] T. Okuno, D. H. Kim, S. H. Oh, S. K. Kim, Y. Hirata, T. Nishimura, W. S. Ham, Y. Futakawa, H. Yoshikawa, A. Tsukamoto, Y. Tserkovnyak, Y. Shiota, T. Moriyama, K. J. Kim, K. J. Lee, T. Ono, *Nat. Electron.* 2019, *2*, 389.

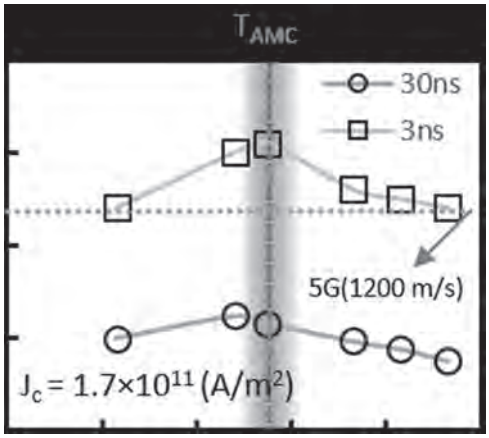

Fig. 1 Temperature dependence masuremnt for GFeCo magnetic wire.

DOB-04. Field Free Switching in Spin-Orbit Torque Memories with Spin Current Gradient. *V. Kateel*[1,2], V. Krizakova[3], M.G. Monteiro[1,2], F. Yasin[1], K. Cai[1], B. Soree[1], J. De Boeck[1], P. Gambardella[3], S. Rao[1], S. Couet[1], G. Shankar[1] and K. Garello[4] *1. IMEC, Leuven, Belgium; 2. Department of Electrical Engineering (ESAT), KU Leuven, Leuven, Belgium; 3. Department of Materials, ETH Zurich, Zurich, Switzerland; 4. Spintec, Grenoble, France*

Current-induced spin-orbit torques (SOTs) enable fast and energy-efficient writing of magnetization state in magnetic tunnel junctions (MTJs) [1,2]. For deterministic switching of perpendicularly magnetized MTJs, the inherent SOT symmetry needs to be broken; this is traditionally achieved by applying an external magnetic field along the current direction. Because the use of external fields limits the application readiness of this technology, various solutions are suggested in the literature to enable field-free switching (FFS). This is either achieved by creating a structural asymmetry, local in-plane field sources, spin current geometry or other hybrid approaches [3]. In this work, we propose and experimentally demonstrate a FFS solution in SOT-MTJs by geometrically modifying the SOT layer to create a structural asymmetry. This modification causes spatial variation of SOT charge current in the field-free structure, which creates a spin current gradient below the MTJs (Fig1.a). In contrast, the standard structure shows a uniform spin current (Fig1b). We demonstrate our FFS scheme on 60 to 100 nm diameter MTJ consisting of CoFeB/MgO/CoFeB structure and tungsten (β-W) as SOT track [2]. The field-free structures have similar MTJ properties as the standard SOT structures, with a tunnel magnetoresistance ratio of 85% and a coercive field of 66 mT. Deterministic bipolar switching is possible in the absence of a magnetic field with a current of 530 μA for field-free structures (Fig. 2a), whereas the standard structure needs a minimum of 10 mT of in-plane field (Fig.2b). We elucidate the FFS mechanism using field-dependent measurements, finite elements, and micromagnetic simulations. The presented FFS scheme is scalable, material-agnostic, and readily compatible with wafer-scale manufacturing, thus creating a pathway for developing purely current-driven SOT systems.

References [1] I.M. Miron et. al, Nature 476, 189–193 (2011) [2] K. Garello et al, IEEE 11th International Memory Workshop (IMW), 1-4, (2019). [3] Q. Shao et al, IEEE Transactions on Magnetics, 57 1-39, (2021).

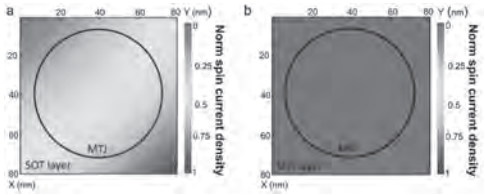

Fig. 1: Top view of the normalised spin current density in the SOT track. a) Field free structure b) standard structure.

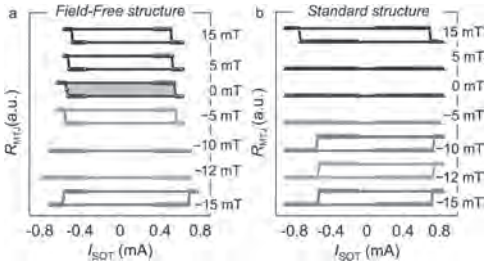

Figure 2: In-plane field dependence of the DC switching for a 60 nm MTJ device: a) Field-free structure b) Standard structure.

DOB-05. Evidence for Domain Wall Reversal in very Small Perpendicular MRAM Cells. *H. Richter*[1], G. Mihajlovic[1], N. Melendez[1], M. Grobis[1] and T. Santos[1] *1. Research, Western Digital, San Jose, CA, United States*

In recent work, the time evolution of the magnetization reversal caused by spin-transfer torque in small perpendicular MRAM cells was investigated experimentally and theoretically [1, 2]. If the magnetization reversal is incoherent, that is, it does not follow a macro-spin model, intermediate states in between magnetization up or down can be found. These states can last up to tens of ns for cell sizes of the order of 50nm, thus lengthening the reversal time. We investigated time resolved current measurements for our MRAM cells with sizes smaller than 20nm in the expectation that no longer any phenomena of this kind should be observed for very small cells that are below the "single domain limit". However, it turns out that even MRAM cells smaller than 20nm (see Fig. 1) show typical indications of domain wall pinning, *albeit* with shorter pinning times. Fig. 2 shows a clear trend that the reversal times – which have been carefully separated from the incubation times - decrease with size. The reversal times are stochastic in nature and for each size a substantial range for the reversal times exists. Even for the smallest cells, we can show that the observed features are not an artifact caused by noise. In the full paper, details of the measurements and interpretations of the data will be given.

[1] P. Bouquin et al., Phys. Rev Appl, 15, 024037 (2021) [2] I. Volvach et al., Appl. Phys. Lett. 116, 192408 (2020)

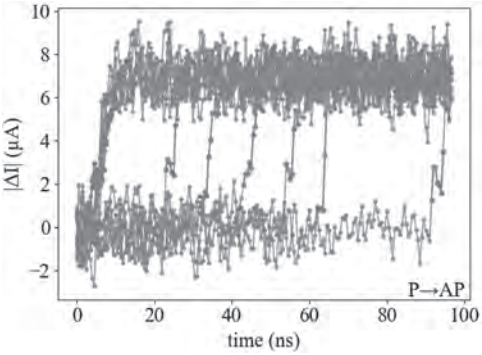

Fig. 1: Current evolution during the reversal of a 18.5nm MRAM cell. Intermediate states that last up to 3ns can be discerned with a tendency to occur at the same current level.

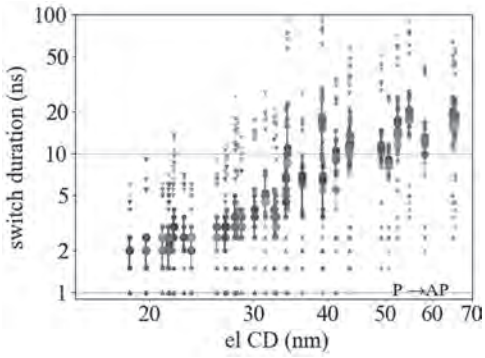

Fig. 2: Reversal times across a wide range of sizes. The big dots show the median of 200 trials each and the small triangles the shortest and longest reversal times detected.

DOB-06. Enhancing write margin of perpendicular MRAM cells using thick MgO cap layer. *G. Mihajlovic*[1], T. Santos[1], J. Li[1] and M. Grobis[1]
1. San Jose Research Center, Western Digital Corporation, San Jose, CA, United States

Implementation of spin transfer torque magneto-resistive random access memory (STT-MRAM) in memory chips requires that the write margin of the MRAM cell ΔV_{wr}, defined as the difference between breakdown voltage V_{bd} and write voltage V_{wr} for the specified endurance, write error rate and write speed, is sufficiently large in order to accommodate resistance variations arising from external chip circuitry (transistors, metal lines etc). Optimization of MRAM cell design and process as well as MRAM materials development aims at accomplishing these by either reducing V_{wr}, enhancing V_{bd}, or both [1]. In this talk we will show that ΔV_{wr} can be increased by optimizing the MgO cap layer that is already present in a perpendicular MRAM cell, whose original intended function has been to increase perpendicular magnetic anisotropy energy of the free storage layer (FL) by adding additional Fe/MgO interface, and thus improve the MRAM retention [2]. By increasing the thickness of the MgO cap layer to make its resistance-area product RA close to that of the main MgO barrier, we show that ΔV_{wr} can be increased substantially for the given write speed and endurance, without affecting thermal stability of the cell in a significant way. For example, for MRAM cells with diameters 50 - 60 nm we show that V_{wr} at 50% switching probability for 50 ns pulse width increases by about 0.28 V for thick cap (see Fig. 1(a)) while V_{bd} obtained by endurance measurements under bipolar stress at the same pulse width increases by almost 0.5 V, resulting in ΔV_{wr} improvement of approximately 0.2 V. We will discuss physical mechanisms underlying this finding and its technological importance.

[1] D. Apalkov et al., Proc. of IEEE 104, 1796 (2016). [2] G. Jan et al., APEX 5, 093008 (2012).

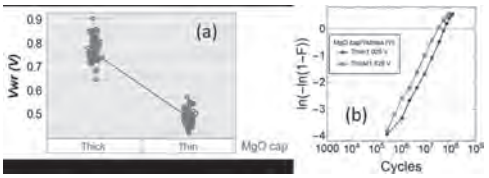

Fig. 1

DOB-07. Thermal Variation of Thermal Stability Factor and Switching Efficiency of STT-MRAM Devices. *S. Mangadahalli Siddaramu*[1], M. Hindenberg[1], M. Wagner Reetz[1], J. Müller[2] and J. Chatterjee[1]
1. Fraunhofer Institute for Photonic Microsystems, CNT, An der Bartlake 5, 01109 Dresden, Germany; 2. GlobalFoundries Fab1 LLC and Company KG, 01109 Dresden, Germany

Spin-transfer torque magnetoresistive random-access memory (STT-MRAM) is a promising non-volatile memory technology for eliminating the classical von Neumann bottleneck to build a high-speed, energy-efficient memory hierarchy.[1] One of the challenges that STT-MRAM needs to overcome, notably for automotive applications, is the robust and reliable operation in the temperature range of -40 °C to 150 °C.[2] Therefore, it is vital to investigate STT-MRAM device characteristics as a function of temperature. We investigated thermal stability factor (Δ), tunneling magnetoresistance (*TMR*) ratio, critical switching current (I_C), and the other device parameters of STT-MRAM devices from -25 °C to 150 °C. Four different device wafers (W1-4) with increasing storage layer (SL) thicknesses and three different device diameters D1, D2, and D3 (with D1<D2<D3) were studied. The temperature-dependent behavior of Δ and *TMR* ratio were analytically modeled to understand their thermal variation. Figure 1 shows the experimental values of Δ, and the fitting of its thermal variation by macrospin and domain-wall model for device D2 in W1-4. Extrapolating the thermal variation of Δ, blocking temperatures (T_b) of different types of memory cells were calculated as shown in Fig. 1. It was observed that the magnetization reversal most likely occurs by domain wall motion at lower temperatures, which changes to multinucleation of domains at larger temperatures making Δ invariable with the diameter (not shown here). Figure 2 shows the thermal variation of practical switching efficiency (κ), calculated by considering Δ at different temperatures and I_C at -25 °C. Similar to the variation of I_C (not shown here), the κ at -25 °C increases with the thickness of SL. This improvement is believed to be due to the decrease in damping constant. This temperature-dependent investigation is important to understand the retention, writing, and reading performance of STT-MRAM cells for high-temperature applications.

[1] B. Dieny, I.L. Prejbeanu, K. Garello, P. Gambardella, et al., Nat. Electron. 3, 446 (2020). [2] K. Lee, R. Chao, K. Yamane, V.B. Naik, et al., Tech. Dig. - Int. Electron Devices Meet. IEDM 2018-December, 27.1.1 (2019). [3] X. Feng and P.B. Visscher, J. Appl. Phys. 95, 7043 (2004).

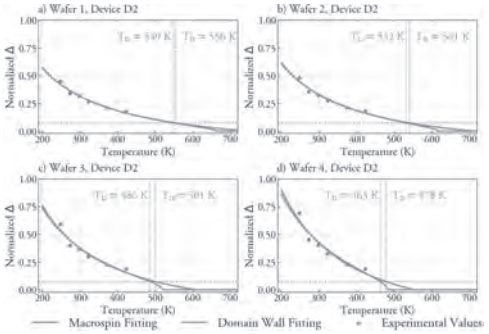

Fig. 1: Average values of Δ as a function of temperature, measured from 140 devices by switching field distribution method.[3]

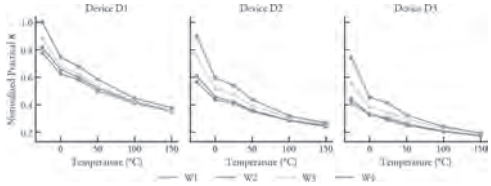

Fig. 2: Thermal variation of the practical κ, calculated using the Δ values at different temperatures and the I_C at -25 °C

DOB-08. Control of Interface Anisotropy for Spin Transfer Torque in Perpendicular Magnetic Tunnel Junctions for Cryogenic Temperature Operation. *P. Brandao Veiga*[1], A. Mora-Hernandez[1], M. Dammak[1], L.D. Buda-Prejbeanu[1], L. Prejbeanu[1], L. Vila[1], S. Auffret[1], R. Sousa[1] and B. Dieny[1] *1. IRIG-SPINTEC, Grenoble Alpes Univ., CNRS, CEA, Grenoble INP, Grenoble, France*

Quantum computation and cryogenic electronics have gained considerable importance in this last decade. Currently, a bottleneck for advancing it further is the power consumption of conventional electronic components, which is not adapted to the needs of cryogenic circuits. Perpendicular Spin-Transfer-Torque Magnetic Random Access Memory (p-STT-MRAM) has potential to comply with cryo-electronics requirements of low power. Previous works done on cryogenic temperature switching of STT-MRAM have assessed its characteristics and the Write Error Rate for different device diameters [1]. The conditions to write an STT-MRAM are promising (0.7V at 9K with 200ns pulses, corresponding to a writing energy of 11.2 pJ) [2]. However, the full integration of MRAMs into quantum processors demands a much lower operating voltage (below 0.1V). Therefore, we focused our research on engineering MTJs for low anisotropy to reduce the critical switching voltage V_C and consequentially the write energy per bit E_{bit}. Our approach consists in changing the interface of the storage layer by adding an insertion layer as in Mg+Ox/X/FeCoB/W/Y/W, where X can be wedges of Mg, FeCoB and Y is permalloy (Py). This type of device can show high thermal stability at cryogenic temperatures (i.e.4K), while having no retention at 300K. This strategy allows the reduction of the storage layer anisotropy by at least one order of magnitude. Figure 1 shows a current pulse phase diagram of a junction with Mg insertion. Upon changing the operation temperature the write current density J_C for junctions with different insertion layers is varying as reported in Figure 2. Device diameter, composition and thickness play an important role in modulating the anisotropy. Tuning these parameters it is possible to bring the switching currents close to 20μA for a 30nm diameter device at 10K (red curve), corresponding to E_{bit}=1.2pJ. This can be further improved by modulating the required current density with composition as shown in the figure 2.

[1] L. Rehm, G. Wolf, B. Kardasz, M. Pinarbasi, *and* A. D. Kent, "Sub-nanosecond spin-torque switching of perpendicular magnetic tunnel junction nanopillars at cryogenic temperatures", Appl. Phys. Lett. Vol. 115, p.182404 (2019). [2] Lili Lang, Yujie Jiang, Fei Lu, Cailu Wang, *et al*, "A low temperature functioning CoFeB/MgO-based perpendicular magnetic tunnel junction for cryogenic nonvolatile random access memory", Appl. Phys. Lett. Vol. 116, p.022409 (2020).

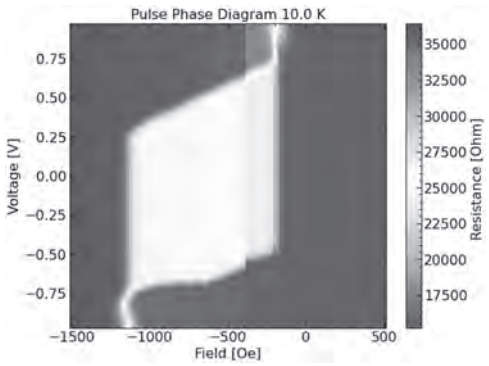

Fig. 1 Pulse phase diagram of a 30nm junction at 10K, showing switching at 0.55V with J = 2 MA/cm2 and TMR of 130%.

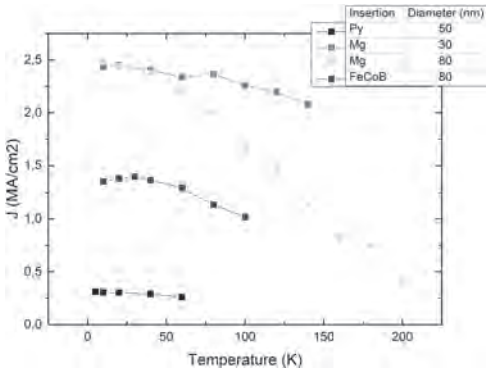

Fig. 2 Current density dependence at 100ns pulses with temperature for pMTJ with different insertion layers.

DOB-09. Reliable Sub-nanosecond MRAM with Double Spin-torque Magnetic Tunnel Junctions. *C. Safranski*[1], G. Hu[1], J.Z. Sun[1], P. Hashemi[1], S. Brown[1], L. Buzi[1], C. D'Emic[1], E. Edwards[1], E. Galligan[1], M. Gotwald[1], O. Gunawan[1], S. Karimeddiny[1], H. Jung[1], J. Kim[1], K. Latzko[1], P. Trouilloud[1] and D. Worledge[1] *1. IBM-Samsung MRAM Alliance, IBM TJ Watson Research Center, Yorktown Heights, NY, United States*

Magnetic tunnel junctions are a key component in non-volatile memory technologies such as magnetic random access memory (MRAM). Typical two-terminal MRAM write speeds have been limited to the nanosecond regime. Currently, sub-nanosecond switching has been achieved in three-terminal structures relying on spin-orbit torque switching mechanisms. However, using this mechanism increases the footprint and number of transistors needed, ultimately limiting scalability. Here, we demonstrate that it is possible to achieve reliable sub-nanosecond switching in a two-terminal design by utilizing a Double Spin Torque magnetic tunnel junction. In this design, a second reference layer is added to the standard two terminal MTJ. Using a non-magnetic spacer, we are able to do so without sacrificing magnetoresistance like in double MTJ designs. Figure 1 shows the error rates for a single device, plotted using a normal quantile scale (using the absolute value of the standard deviation from the fifty-percent switching current density), measured at -40 C, 25 C, and 85 C, for pulse widths from 225 ps to 10 ns. We demonstrate 100% successful switching for 1e6 write attempts using 225 ps wide write pulses, over the temperature range -40 C to 85 C. Further, we show reliable sub-nanosecond switching across a few hundred devices. 1e10 write-endurance testing on a handful of devices also demonstrates that reliability can be achieved as well. Lastly, we compare our Double Spin Torque magnetic tunnel junction to three-terminal spin-orbit torque MRAM. We find that with our design, a 3-10X reduction in write power consumption can be achieved.

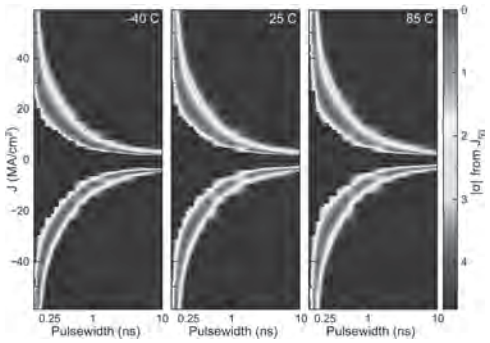

DOB-10. Switching optimization in magnetoresistive random access memories. *Z. Lin*[1], I. Volvach[1] and V. Lomakin[1] *1. University of California, San Diego, San Diego, CA, United States*

Magnetoresistive random access memories (MRAM) are envisioned to be used in many future applications. Important parameters for improving the memory switching operation are the critical current, which is desired to be reduced, and efficiency, viz. the ratio between the energy barrier and critical current, which is designed to be increased [1]. We present an approach for minimizing the critical current and increasing the efficiency by optimizing the spatial distribution of the current density. The minimization is possible because, as we show, the critical current is given by the condition of making one of the magnetization eigenstates grow in time [2]. The excitation of the eigenstates is enhanced when the spatial distributions of the eigenstates and current density overlap. Critical current can be viewed as a functional of the current density spatial distribution and the critical current can be minimized by optimizing this distribution. Fig. 1 shows the spatial distributions of the 1st, 3rd, 4th, 6th eigenstates for a magnetic tunnel junction (MTJ) with diameter of D = 80 nm (top row) and the corresponding optimized distributions (bottom row), where the stronger current density regions correspond to higher magnitude of the eigenstate spatial distributions. Practically the current density can be confined to a greater region, e.g., a circle of a radius of 10 nm-20 nm. Fig. 2 shows the size dependence of the critical current (a) and efficiency (b) with different distributions. The minimized critical current can be significantly reduced. It is evident that the critical current can increase linearly with the lateral size and the efficiency can be almost size independent.

[1] I. Volvach, J. G. Alzate and Y. Chen, *et al,* Applied Physics Letters, 116(19): 192408 (2020). [2] Z. Lin, I. Volvach, and X. Wang, *et al*, Physical Review Applied 17 (3), 034016 (2022). [3] S. Ikeda, K. Miura, and H. Yamamoto *et al*, *Nature materials* 9.9, 721-724 (2010).

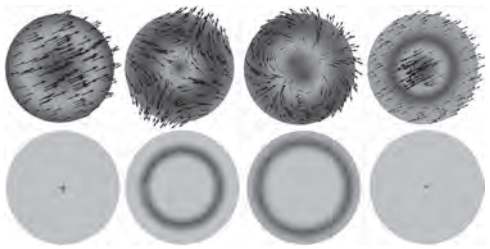

Fig. 1: Top row shows the eigenstates, where the color plot represents the spatial distribution of the magnitude, and the arrow plot represents the real part of the eigenstate. The bottom row shows the optimized current distribution for each eigenstate. The free layer has a thickness of 1nm and the material parameters are M_s=960 emu/cm³, Ku=6.11Merg/cm³, Aex=1μerg/cm, α=0.01 from CoFeB with MgO interface as free layer material [3].

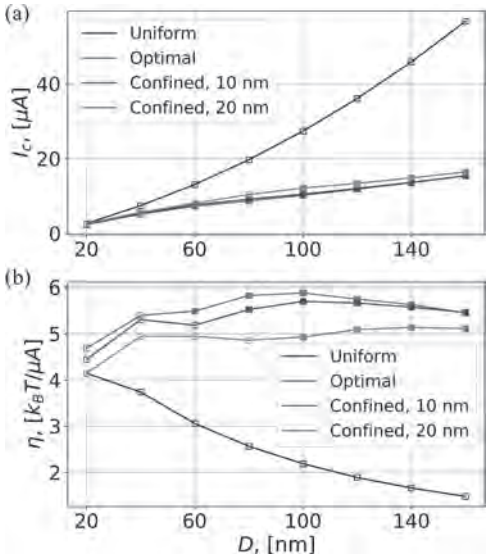

Fig. 2: The size dependence of (a) the critical current and (b) efficiency with different current density distributions.

DOB-11. Spintronic Physical Unclonable Functions in an Exchange-biased Trilayer Structure. *J. Kang*[1], S. Lee[1], T. Lee[1], M. Kang[1], J. Lee[2], S. Noh[2], H. Lee[2], J. Kwon[2], K. Kim[1] and B. Park[1] *1. Korea Advanced Institute of Science and Technology, Daejeon, The Republic of Korea; 2. R&D Division, Hyundai Motor Company, Hwaseong, The Republic of Korea*

Physically unclonable function (PUF), harnessing inherent stochastic variation of physical properties originating from the manufacturing process, is a crucial part of hardware security primitives [1]. PUF offers more robust information security than the conventional software-based ones. To date, owing to the compatibility to complementary-metal-oxide-semiconductor (CMOS) technology, silicon-based PUFs have been widely investigated [2]. However, their reliability with environmental fluctuations and susceptibility to external machine learning attacks are yet to be ascertained. Recently, graphene- or memristor-based PUFs were proposed and found out to be effective in resolving such issues [3,4]. However, their analog output inevitably involves additional circuit modules or analogue-to-digital converter, requiring significant power consumption and area overhead. Here, we demonstrate highly reliable spintronic PUFs based on field-free spin-orbit torque (SOT) switching in an IrMn/CoFeB/Ta/CoFeB structure. We show that the switching polarity of the perpendicular magnetization of the top CoFeB can be randomly distributed by manipulating the exchange bias directions of the bottom IrMn/CoFeB. Figure 1 shows stochastic field-free SOT switching polarity after the randomization process of the bottom exchange-biased layers. Ideal PUF properties are found in the spintronic PUFs: high entropy close to unity, uniqueness with an inter-Hamming distance of 0.5 and reconfigurability. Furthermore, the spintronic PUFs generate binary digital outputs, potentially eliminating the need for analog-to-digital converters and error correction codes. We observed a zero bit-error rate in 5×10^4 repetitive measurements which demonstrates the high reliability. Due to the exchange-biased bottom layers, robustness against external magnetic fields are secured. These, when integrated with magnetic random-access memory in particular, are expected to promote scalable and energy-efficient hardware information security

[1] Y. Gao, S. F. Al-Sarawi, D. Abbott, Nat. Electron., 3, 81 (2020) [2] J. L. Zhang, G. Qu, Y. Q. Lv, Q. Zhou, J. Comput. Sci. Technol., 29, 664 (2014) [3] A. Dodda, S. Subbulakshmi Radhakrishnan, S. Das, Nat. Electron., 4, 364 (2021) [4] R. A. John, N. Shah, N. Mathews, Nat. Commun., 12, 3681 (2021)

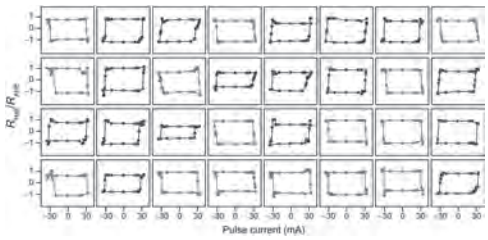

Fig. 1. Spintronic PUF based on stochastic field-free SOT switching polarity in a NiFe (1 nm)/IrMn (9 nm)/CoFeB (5 nm)/Ta (3 nm)/CoFeB (1 nm) structure. Each graph shows normalized Hall resistance as a function of current pulse.

DOB-12. Machine intelligence in new materials identification for efficient spin-orbit torque (SOT) MRAM. *S. Sayed*[1,2], H. Kleidermacher[1], G. Hashemi-Asasi[1], C. Hsu[1] and S. Salahuddin[1] *1. Electrical Engineering and Computer Sciences, University of California Berkeley, Berkeley, CA, United States; 2. TDK Headway Technologies, Milpitas, CA, United States*

There is a growing interest in materials exhibiting large spin-orbit torques (SOT) to achieve significant improvements in magnetoresistive random access memory (MRAM) technology [1]. It is well-recognized that materials with SOT ratios much greater than unity are needed to bring energy efficiency in SOT MRAM; however, only a handful of such materials have been identified using conventional theoretical and experimental methodologies. Thus, understanding the physics and materials for large SOT is a topic of ongoing research [1-2]. In this talk, I will discuss a new approach using machine intelligence to quantitatively predict new materials with large SOT ratios. I'll show that a machine can learn special concepts in materials sciences, physics, and engineering by reading the literature. Such a "well-trained" machine can identify patterns hidden within a large body of literature and quantitatively relate materials to the phenomenon of "spin-orbit torque." We use a word embedding model [3] to train a neural network with a collection of unlabeled abstract text from various scientific journals relevant to our work. The word embedding model represents words in the text corpus into high-dimensional vectors, and the relationship among these vectors exhibits knowledge in magnetism and spintronics. A correlation pattern among various vectors representing materials names and the word "spin-orbit torque" quantitatively project spin Hall conductivity and SOT factor for corresponding materials. The projected numbers for known materials agree with known experimental reports. Such quantitative agreement is non-trivial as the machine does not learn numerical values reported in the literature, but the patterns are obtained based on the context in which the words appeared in the text corpus. Surprisingly, our machine intelligence-based approach predicted 32 new materials to exhibit SOT, which have not been discussed yet in the context of SOT to our knowledge. Interestingly, 9 of these predicted materials are expected to show a SOT factor much greater than unity, with the largest expected value of 36.4. One of them quantitatively matched our independent experiment on a silicide.

[1] IEEE Trans. Magnetics 57(7), 1-39 (2021). [2] Phys. Rev. Applied 15, 054004 (2021). [3] Nature 571, 95-98 (2019).

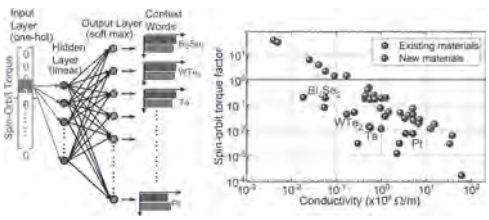

Unsupervised machine learning for SOT materials search.

DOB-13. Time-domain Computing for Boolean Logic using STT-MRAM. *R. Zhou*[1] and H. Cai[1] *1. Southeast University, Nanjing, China*

Spin transfer torque magnetic random access memory (STT-MRAM) shows great advantages for computing-in-memory (CIM) [1][2]. Time-domain (TD) in-MRAM computing can be implemented with unlimited signal accumulation and low power consumption characteristics thanks to its low precision [3]. In this paper, we propose a novel TD-CIM topology that converts bit-line (BL) voltage to time delay. Fig.1 (a) shows the structure of proposed STT-MRAM for TD-CIM. Fig.1 (b) illustrates the proposed AND/OR/Full-Adder (FA) Boolean logic circuit, with one transistor-one magnetic tunnel junction (1T-1MTJ) bit-cell. R_P/R_{AP} (parallel and anti-parallel magnetoresistance) is with data '0'/'1'. During computation mode, word-line (WL) activates two bit-cell within one row. The calculation-line (CL) generates differential V_{BL} according to the state of bit-cell. Current starved inverters (CSI) circuit is used to convert the voltage of BL to time delay [4]. The inverter chains (REF0/REF1) generate delay to represent data '0'/ '1' for FA logic, which is controlled by signal *Cin*. Time-to-Digital converter (TDC) converts CSI outputs from time domain to digital domain. The inverter chains generate reference delay for AND/OR/FA logic. CSI outputs sample the reference delay by D-flip-flop (one flip-flop for AND/OR, three flip-flops and one Multiplexer for FA). The performance is analyzed with a 28-nm CMOS process and a MTJ compact model [5]. Fig.2 (a) demonstrates the simulated 500 runs Monte-Carlo analysis of CSI outputs under different cases. Results show the successfully distinguished CSI accumulation. The power consumption of AND/OR and FA is 7.89-μW and 14.1-μW at nominal 0.9V supply (see Fig. 2(b)). Fig.2 (c) shows the computation accuracy of AND/OR/FA logic in varied tunnel magnetoresistance ratio (TMR) with different data cases. When TMR=200%, 94.2% to 100% computation accuracy can be obtained, whereas the accuracy is deteriorated when TMR equals to 125%.

[1] M. Wang et al., *Nature Communications*, vol. 9, p. 671 (2018). [2] X. Fong et al., *IEEE Trans. on Very Large Scale Integration (VLSI) Systems*, vol. 22, pp. 384–395 (2014). [3] P. -C. Wu et al., *IEEE International Solid-State Circuits Conference (ISSCC)*, pp. 1-3 (2022). [4] Q. -K. Trinh et al., *IEEE Trans. on Circuits and Systems I: Regular Papers*, vol. 65, no. 10, pp. 3338-3348 (2018). [5] Y. Wang et al., *IEEE Trans. on Electron Devices*, vol. 63, pp. 1762-1767 (2016).

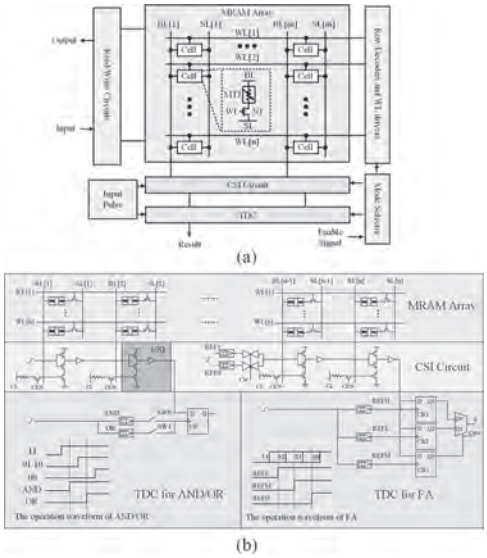

Fig. 1 (a) The proposed structure of STT-MRAM block. (b) The proposed circuit for AND/OR/FA logic.

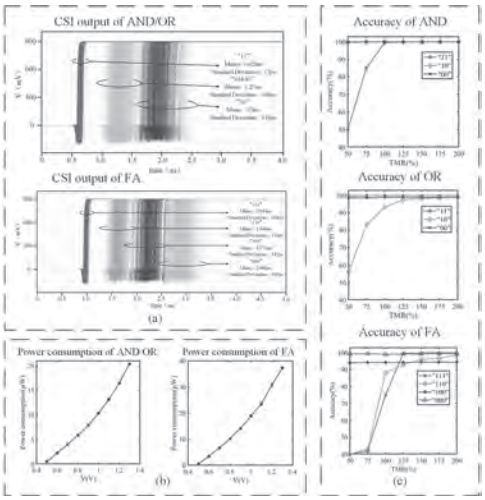

Fig. 2 (a) Monte Carlo simulation for CSI outputs of different data cases; (b) The power consumption of AND/OR/FA at different voltages; (c) The accuracy of AND/OR/FA in varied TMR.

DOB-14. Design of Domain Wall-Magnetic Tunnel Junction Analog Content Addressable Memory using Current and Projected Prototype Data. *H. Jin*[1], H. Zhu[1], K. Zhu[1], T. Leonard[1], M. Alamdar[1], D. Pan[1] and J.C. Incorvia[1] *1. Electrical and Computer Engineering, University of Texas at Austin, Austin, TX, United States*

Resource intensive computational tasks are hindered by latency issues due to the memory wall bottleneck in traditional von Neumann architectures [1]. In-memory computation (IMC) and associative memory offer a promising alternative. Among these emergent technologies is content-addressable memory (CAM). CAM allows for highly parallel comparison of an input search word to an array of storage elements in one or few clock cycles. CAM can be implemented in ternary, multi-bit, and analog operation, making it favorable in a wide range of applications, such as its use in classification tasks and search applications for memory augmented neural networks for few-shot learning and hyperdimensional computing [2]. Here, we design an analog content-addressable memory (ACAM) cell circuit using domain wall magnetic tunnel junctions (DW-MTJ). Data is stored within the ACAM cell by using DW-MTJs with distinct programmable resistance states through SOT-induced domain wall movement between multiple notches along a track under the MTJ shown in Fig. 1. The resistance states were recorded experimentally through device cycling, demonstrating 3 distinct resistance states with variability not exceeding ±1.1Ω per state over 10-15 cycles [3]. These prototype results were used to characterize the ACAM cell using simulations in Cadence, showing that we can achieve a programmable range of 80 mV for the ACAM. We then analyze the cell circuit and show that if we can achieve reasonable parameters of 5-10 resistance states at 200% TMR and 25-70 Ω×μm^2 RA, then we can achieve a larger search range and higher resolution analog/multi-bit CAM functionality, shown in Fig. 2. In addition, our ACAM circuit maintains picosecond level search latency and maintains an area consumption notably smaller than that of similar ACAM designs implementing SRAM technology and conventional TCAM architectures [4]. Given the results of both our experimentally informed and ideal simulation scenarios, we conclude that our proposed DW-MTJ ACAM is capable of reducing power consumption and search latency while also maintaining low area consumption.

[1] Wulf, W. A., McKee, S. A., *ACM SIGARCH Comput. Archit. News, vol. 23, no. 1, pp. 20–24,* (1995). [2] Kazemi, A., *et al*., "FeFET Multi-Bit Content-Addressable Memories for In-Memory Nearest Neighbor Search," in *IEEE Transactions on Computers, (2021)*. [3] Leonard, T., Liu, S., Alamdar, M., *et al.*, *arXiv:2111.11516v2[cond-mat.mes-hall],* (2021). [4] Li, C., Graves, C.E., Sheng, X. *et al.*, *Nat. Commun.* 11, 1638 (2020).

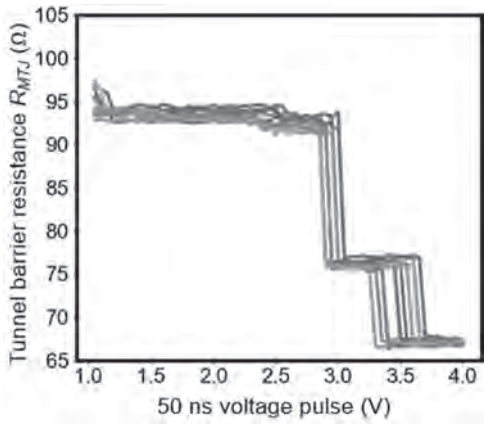

Fig. 1. Measured resistance levels for 10 cylces of trapezoidal DW-MTJ (Ref. 3).

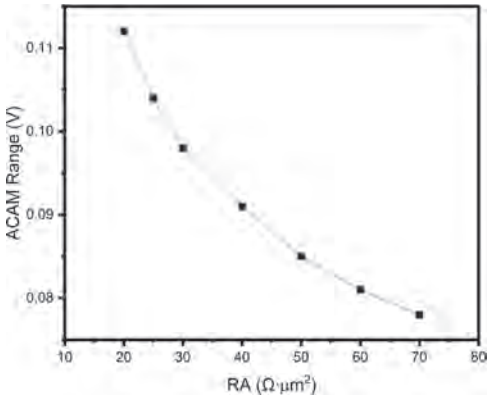

Fig. 2. Maximum ACAM bounds range vs. RA sweep.

DOB-15. Strain-Modulated Magnetic Anisotropy for Physically Secure Logic Locking. *A.J. Edwards*[1], N. Hassan[1], D. Bhattacharya[2], M.M. Shihab[1], P. Zhou[1], X. Hu[1], J. Atulasimha[3], Y. Makris[1] and J.S. Friedman[1] *1. Electrical and Computer Engineering, The University of Texas at Dallas, Richardson, TX, United States; 2. Physics, Georgetown University, Georgetown, DC, United States; 3. Mechanical and Nuclear Engineering, Virginia Commonwealth University, Richmond, VA, United States*

To prevent integrated circuit counterfeiting, logic locking secures a design with a programmable obfuscation key which activates a chip after fabrication. Successful logic locking requires that this key – stored on-chip in non-volatile memory – be secure against physical and algorithmic attacks, and it was recently demonstrated that delayering and imaging of electrical behavior can reveal an obfuscation key that is electrically stored or transported. In contrast, spintronic technologies without electrical signatures offer unique solutions for logic locking. In particular, we have proposed the first approach for physically and algorithmically secure logic locking with strain-modulated anisotropy in a nanomagnet logic (NML) system [1,2]. NML processes information magnetically through the dipole interactions of chains of nanomagnets (see Fig. 1). Through bulk crystalline strain effects, a surrounding capping layer induces perpendicular magnetic anisotropy (PMA) in the nanomagnets, causing them to prefer orientation in the plus or minus z direction. This PMA allows non-volatile storage of key bits in designated magnets. Secure NML gates are polymorphic, as an incorrect magnetization of the key magnet can cause incorrect gate functionality. NML provides physical security for the key as the capping layer is sufficiently thick to prevent magnetic imaging requiring line-of-sight or proximity to the nanomagnets (see Fig. 2a, b). Furthermore, removal of the PMA-inducing capping layer to enable imaging will return the magnetizations to stochastic

in-plane states destroying the stored key (see Fig. 2c, d). This physically and algorithmically secure logic locking is enabled by the inherent nonvolatility, polymorphism, and stochasticity of spintronic technologies, providing security capabilities unavailable in conventional electronic technologies.

[1] N. Hassan, A. J. Edwards, D. Bhattacharya, M. M. Shihab, V. Venkat, P. Zhou, X. Hu, S. Kundu, A. P. Kuruvila, K. Basu, J. Atulasimha, Y. Makris, J. S. Friedman, Secure Logic Locking with Strain-Protected Nanomagnet Logic, *Design Automation Conference*, Dec. 2021. [2] A. J. Edwards, N. Hassan, D. Bhattacharya, M. M. Shihab, P. Zhou, X. Hu, J. Atulasimha, Y. Makris, J. S. Friedman, Physically and Algorithmically Secure Logic Locking with Hybrid CMOS/Nanomagnet Logic Circuits, *Design, Automation & Test in Europe*, Mar. 2022 (invited).

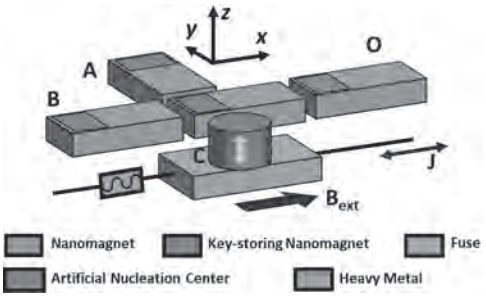

Fig. 1. Two-input (A, B) polymorphic NML majority gate with tamper-proof spin-orbit torque programming of obfuscation key magnet.

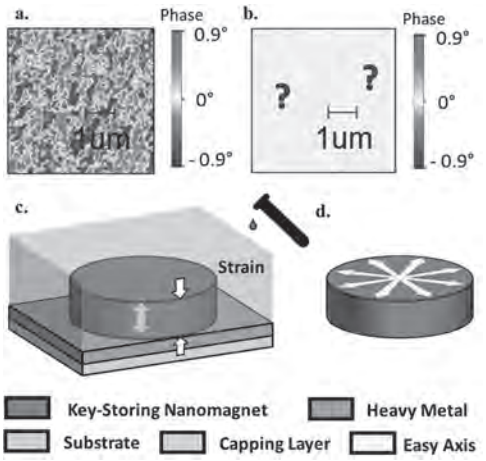

Fig. 2. a, b. Experimental demonstration that discernable magnetization domains (a.) may be protected from imaging via a 100 nm capping layer (b.) c -> d. Delayering of the PMA-inducing capping layer returns nanomagnet to an isotropic in-plane magnetization.

DOB-16. All-electrical Manipulation of Multiple Resistant States via Modifying Magnetic Anisotropy for Emulating Synaptic Memory.

T. Jin[1], F. Tan[1], H. Poh[1], S. Lee[1], S. Wu[1], G. Lim[1] and W. Lew[1] *1. Nanyang Technological University, Singapore*

Current-induced magnetization switching via spin-orbit torque (SOT) has been intensively investigated for conventional memory applications. With the emergence of multi-states devices that can be utilized in both memory and computing operations, research has pivoted to focus on all electrical-induced multiple resistant states to provide complementary hardware for unconventional computing [1]. SOT-based multi-state devices can mimic artificial synapses and neurons for unconventional computing due to their non-volatility, high scalability, and low power consumption. Artificial synapses are utilized for memory function, acting as junctions between pre-and post-neurons, these continuously being adjusted to tune the strength between two neurons. Artificial neurons integrate all the input stimuli and fire once the accumulated potential reaches a certain threshold. SOT manipulation of multiple magnetization states can be realized by controlling domain wall propagation and modulating domain wall nucleation to emulate synapses [2]. Domain wall propagation requires controllable pinning while domain nucleation can be effectively achieved by modifying the magnetic anisotropy energy. In this work, SOT-induced domain wall nucleation in Pt/Co system is demonstrated by engineering its interface to lower the anisotropy energy. A low magnetic anisotropy energy of 1.35×10^5 J/m^3 has been achieved in Pt (5 nm)/Co (1.2 nm)/HfOx (2 nm)/Ti (2 nm) structure, as obtained from the hysteresis loops shown in Fig. 1(a) and (b). Electrical and Kerr microscopy measurements were carried out to determine the multiple resistance states. Figure 2(a) shows the Hall resistance R_{xy} change with magnetic field H_{OOP}. Figure 2(b) shows the pulse current-induced multiple resistance; the insets show the domain images after sending a pulse current (I) from 6 to 9 mA. The results clearly indicate the multi-states in Pt/Co/HfOx/Ti system are driven by current, which is promising for synaptic memory-driven neuromorphic applications.

[1] Zhou, J., *et. al*., *Adv. Mater*. *33*, 2103672 (2021). [2] Jin, T., *et. al*., *J. Phys. D: Appl. Phys*, *52*, 445001 (2019).

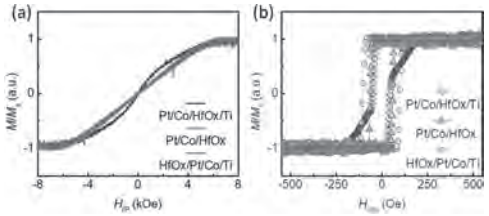

Fig. 1. Hysteresis loops along (a) in-plane (H_{IP}) and (b) out-of-plane (H_{OOP}) directions.

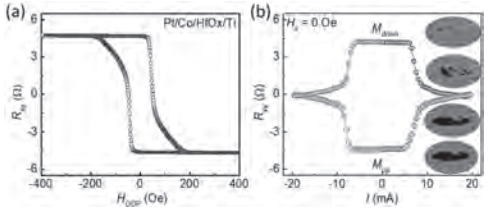

Fig. 2. Hall resistance changes with (a) H_{OOP} and (b) pulse current.

Session DOC
NEUROMORPHIC COMPUTING

Joseph S. Friedman, Chair
The University of Texas at Dallas, Richardson, TX, United States

CONTRIBUTED PAPERS

DOC-01. Binarized Neuromorphic Inference Network with STT MTJ Synapses. *P. Zhou*[1], A.J. Edwards[1], F. Mancoff[2], S. Aggarwal[2] and J.S. Friedman[1] *1. Department of Electrical and Computer Engineering, The University of Texas at Dallas, Richardson, TX, United States; 2. Everspin Technologies, Inc., Chandler, AZ, United States*

One of the primary hardware costs incurred by artificially-intelligent neural networks is due to vector-matrix multiplication (VMM), which is generally performed with floating-point binary numbers and computed exactly with cumbersome multiplication computations which scale with the number of entries in the matrix. Non-volatile analog resistive memory devices appear to naturally mimic the behavior of neurobiological synapses, and can be used to efficiently perform VMM in terms of voltage and current by taking advantage of Ohm's and Kirchhoff's laws. Most research in this area has focused on crossbars composed of memristors and phase change memory (PCM). However, these devices suffer from several major challenges, including imprecise writing, weights drifting over time, limited endurance, and compatibility challenges with modern CMOS processes. Magnetic tunnel junctions (MTJs) provide solutions to the limitations of memristors and PCM, but only exhibit binary resistance states. Importantly, it was recently proposed that stochastic MTJ switching enables analog neuromorphic behavior with MTJs [1-3]. While spintronic devices have been demonstrated for other neuromorphic functions -- e.g. spin-torque nano oscillators, domain wall MTJs, and stochastic p-bits -- a neuromorphic network has not previously been directly implemented with MTJ synapses (Fig. 1). This paper reports the experimental demonstration of a small binarized neuromorphic network with MTJ synapses for VMM (Fig. 2), greatly advancing the development of highly-efficient, robust hardware amenable to neural applications. We also simulate a large MTJ network performing MNIST handwritten digit recognition, demonstrating that MTJ crossbars can match memristor accuracy while providing increased precision, stability, and endurance.

[1] A. F. Vincent, J. Larroque, N. Locatelli, N. Ben Romdhane, O. Bichler, C. Gamrat, W. S. Zhao, J.-O. Klein, S. Galdin-Retailleau, and D. Querlioz, "Spin-transfer torque magnetic memory as a stochastic memristive synapse for neuromorphic systems," IEEE Trans Biomed Circuits Syst, vol. 9, no. 2, pp. 166–174, 2015. [2] P. Zhou, J. A. Smith, L. Deremo, S. K. Heinrich-Barna, and J. S. Friedman, "Synchronous unsupervised stdp learning with stochastic stt-mram switching," arXiv:2112.05707, 2021. [3] P. Zhou, A. J. Edwards, F. B. Mancoff, D. Houssameddine, S. Aggarwal, and J. S. Friedman, "Experimental demonstration of neuromorphic network with stt mtj synapses," arXiv:2112.04749, 2021.

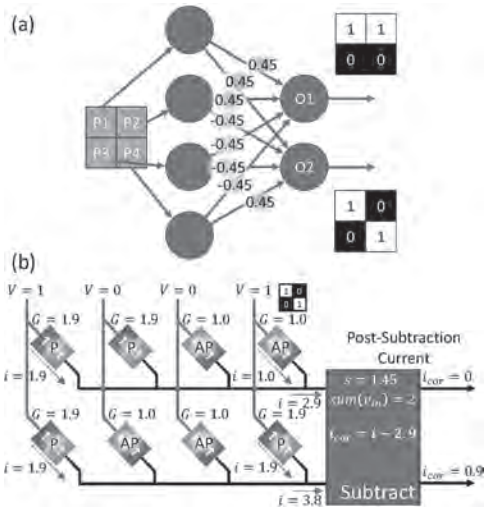

Fig. 1. (a) Image recognition using a 4x2 single layer neural network. (b) MTJ neural network after training.

Input Vector					Hamming Distance from Target		Normalized Output Current		Post-Subtraction Current		Expected VMM Output	
P1	P2	P3	P4		O1	O2	O1	O2	O1	O2	O1	O2
0	0	0	0		2	2	0.00	0.00	0.00	0.00	0	0
0	0	0	1		3	1	0.99	1.84	-0.45	0.40	-0.45	0.45
0	0	1	0		3	3	1.04	1.08	-0.40	-0.36	-0.45	-0.45
0	0	1	1		4	2	2.02	2.92	0.88	0.04	0.9	0
0	1	0	0		1	3	1.95	0.89	0.51	-0.55	0.45	-0.45
0	1	0	1		2	2	2.94	2.74	0.06	-0.14	0	0
0	1	1	0		2	4	3.00	1.95	0.12	-0.93	0	-0.9
0	1	1	1		3	3	3.97	3.80	-0.35	-0.52	-0.45	-0.45
1	0	0	0		1	1	1.87	1.98	0.43	0.54	0.45	0.45
1	0	0	1		2	0	2.84	3.81	-0.04	0.93	0	0.9
1	0	1	0		2	2	2.89	3.03	0.01	0.15	0	0
1	0	1	1		3	1	3.79	4.86	-0.53	0.54	-0.45	0.45
1	1	0	0		0	2	3.76	2.86	0.88	-0.02	0.9	0
1	1	0	1		1	1	4.74	4.75	0.42	0.43	0.45	0.45
1	1	1	0		1	3	4.63	3.87	0.31	-0.45	0.45	-0.45
1	1	1	1		2	2	5.73	5.57	-0.03	-0.19	0	0

Fig. 2. (a) Experimental setup: eight MTJs were connected by probes. (b) All possible input images were presented to the MTJ VMM network.

DOC-02. Optimized fabrication of memristor-controlled spin Hall nano-oscillators. *J. Åkerman*[1], A. Kumar[1], M. Rajabali[1], V.H. González[1], M. Zahedinejad[1] and A. Houshang[1] *1. Department of Physics, University of Gothenburg, Gothenburg, Sweden*

We recently demonstrated memristor-controlled mutual synchronization of spin Hall nano-oscillators [1]. In those devices, the gate was fabricated directly on top of the SHNO nano-constriction, without any additional

isolation against potential shorts through the nano-constriction edges. Here, we demonstrate an optimized fabrication process for electric field (voltage gate) and memristor controlled nano-constriction spin Hall nano-oscillators (SHNOs), achieving feature sizes of <30 nm with easy to handle ma-N 2401 e-beam lithography negative tone resist [2]. For the nanoscopic voltage gates, we utilize a two-step tilted ion beam etching approach and through-hole encapsulation using 30 nm HfO_x. The optimized tilted etching process reduces sidewalls by 75% compared to no tilting. Moreover, the HfO_x encapsulation avoids any sidewall shunting and improves gate breakdown. Our experimental results on W/CoFeB/MgO/SiO_2 SHNOs show significant frequency tunability (6 MHz V^{-1}) even for moderate perpendicular magnetic anisotropy. Circular patterns with diameter of 45 nm are achieved with an aspect ratio better than 0.85 for 80% of the population. The optimized fabrication process allows incorporating a large number of individual gates to interface to SHNO arrays for unconventional computing and densely packed spintronic neural networks. We also demonstrate how the gate can be placed outside of the nano-constriction region to only use the additional memristor current for SHNO control without the direct impact of the electric field-controlled perpendicular magnetic anisotropy.

[1] M. Zahedinejad et al, Nature Materials 21, 81 (2022) [2] A. Kumar et al, Nanoscale 14, 1432 (2022).

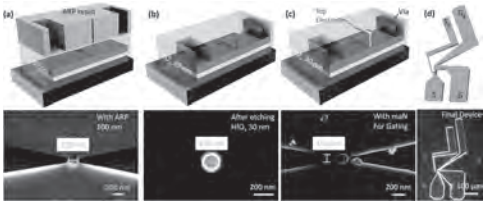

Vertical cut-through schematic and SEM images of (a) through-hole defined using 100 nm AR-P resist, (b) the hole in the 30 nm HfO_x layer after etching, and (c) gate top contacts defined using 70 nm, ma-N 2401 resist over the gate hole. The two rectangular voids on the sides are used for signal (*S*) and ground (*G*) contacts. (d) Schematic and optical image of the final gated SHNO; the ground line is shared between the gate (G_g) and the SHNO (*G*). Precise alignment of these layers with less than 5 nm shift was achieved with the EBL chip alignment method described in the text.

DOC-03. Building spintronics neuromorphic systems with Neural Ordinary Differential Equations. *X. Chen*[1*], F. Abreu Araujo[2], M. Riou[3], J. Torrejon[3], D. Ravelosona[1], W. Kang[4], W. Zhao[4], J. Grollier[3] and D. Querlioz[1] *1. Université Paris-Saclay, CNRS, Centre de Nanosciences et de Nanotechnologies, Palaiseau, France; 2. Institute of Condensed Matter and Nanosciences, Université Catholique de Louvain, Place Croix du Sud 1, Louvain-la-Neuve, Louvain-la-Neuve, Belgium; 3. Unité Mixte de Physique, CNRS, Thales, Université Paris-Saclay, Palaiseau, France; 4. Beihang University, Beijing, China*

Neuromorphic computing is a particularly exciting application of spintronics, able to exploit its rich physics to achieve low-power-consumption computation inspired by the brain. Designing neuromorphic systems requires simulating the response of spintronic devices to multiple types of inputs over long time periods. Currently, the dominant approach to predicting the complex behavior of spintronic devices is micromagnetic simulation. This technique, however, requires very long simulation times, easily reaching weeks in time-dependent experiments or in micrometer-scale devices. In this work, we take an alternative road by adopting a deep learning technique, Neural Ordinary Differential Equations (ODEs), to model spintronic devices and develop spintronic systems. We show that Neural ODEs, trained on a minimal amount of data, can predict the behavior of spintronic devices with high accuracy and an extremely efficient simulation time, compared to micromagnetic simulations. For this purpose, we re-frame the formalism of Neural Ordinary Differential Equations (ODEs) [1] to the constraints of spintronics: few measured outputs, multiple inputs and internal parameters (Fig. 1). We demonstrate with Neural ODEs an acceleration factor over 200 compared to micromagnetic simulations for a neuromorphic system -- a reservoir computer made of magnetic skyrmions (20 minutes compared to three days). We also demonstrate that this state-of-the-art deep learning technique for time series modeling can be applied to model an experimental neuromorphic experiment [2], in which spin-torque nano-oscillators are used as reservoir computers to achieve a spoken digit recognition task (Fig. 2). Neural ODEs can therefore constitute a disruptive tool for developing spintronic applications in complement to micromagnetic simulations, which are time-consuming and cannot fit experiments when noise or imperfections are present [3].

[1] R. T. Chen, Y. Rubanova, J. Bettencour, etc., Advances in neural information processing systems, pp. 6571–6583 (2018). [2] J. Torrejon, M. Riou, F. A. Araujo, etc., Nature, Vol. 547, pp. 428-431 (2017). [3] X. Chen, F. A. Araujo, M. Riou, etc., Nature Communications, Vol. 13, pp.1-12 (2022).

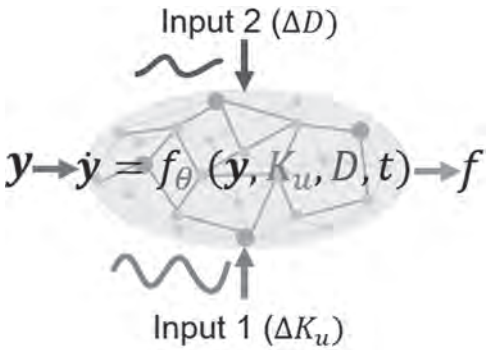

Fig.1 Sketch of a Neural ODE structure $y' = f_\theta(y, K_u, D, t)$ with ΔK_u and ΔD as external inputs into the neural network. y is a vector of system dynamics and f is defined by a neural network.

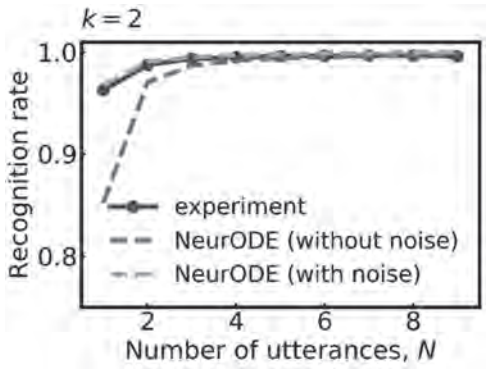

Fig.2 Performance (Neural ODE and experiment) of a spin-torque nano-oscillator based reservoir computer.

DOC-04. Stochastic Magnetic Actuated Random Transducer Devices based on Perpendicular Magnetic Tunnel Junctions. *L. Rehm*[1], C.C. Capriata[1,2], S. Misra[3], J. Smith[3], M. Pinarbasi[4], B.G. Malm[2] and A.D. Kent[1] *1. Center for Quantum Phenomena, Department of Physics, New York University, New York, NY, United States; 2. Division of Electronics and Embedded Systems, KTH Royal Institute of Technology, Stockholm, Sweden; 3. Sandia National Laboratories, Albuquerque, NM, United States; 4. Spin Memory Inc., Fremont, CA, United States*

Neuromorphic systems are of great interest for modeling and solving complex problems, offering an alternative to conventional deterministic computers[1]. They generally aim to emulate the functionality and structure of the human brain and thus require many independent true random noise signal sources. In recent years, the stochasticity of spin-transfer-torque switching of magnetic tunnel junctions (MTJs) has gained interest for such applications. Focusing on in-plane MTJs with low energy barriers, the devices investigated

thus far have fast thermally driven random fluctuations[2,3]. However, they are highly susceptible to small changes in temperature and device parameters. Here we show the room-temperature operation of medium energy barrier (Δ=39[4]) perpendicularly magnetized MTJs (pMTJs) in the ballistic switching limit (ns duration pulses) and discuss why their operation is much less sensitive to temperature and material parameters. In the ballistic limit the resulting junction state is random mainly because of the thermal distribution of the initial magnetization state. We denote this a stochastic magnetic actuated random transducer (SMART) device because the pulse activates the junction to generate a random bit stream, much like a coin flip. In fact, we analyze the stochastic nature of our SMART devices by comparing their statistics to that expected of Bernoulli trials (see Figs.1 and 2). We also test our bit stream with the NIST statistical test suite for random number generators which investigates their suitability for cryptography. We find that by whitening the bit stream with only one XOR operation, we pass all NIST tests. Our results demonstrate that medium energy barrier pMTJs are very promising candidates for true random number generation due to their easily controllable characteristics, while being robust towards environmental changes and material parameter variations.

[1]Schuman, C. D. *et al.*, arXiv:1705.06963. [2]Vodenicarevic, D. *et al.*, Physical Review Applied Vol. 8, 054045 (2017). [3]Safranski, C. *et al.*, Nano Letters Vol. 21, 2040–2045 (2021). [4]Rehm, L. *et al.*, Physical Review Applied Vol. 15, 034088 (2021).

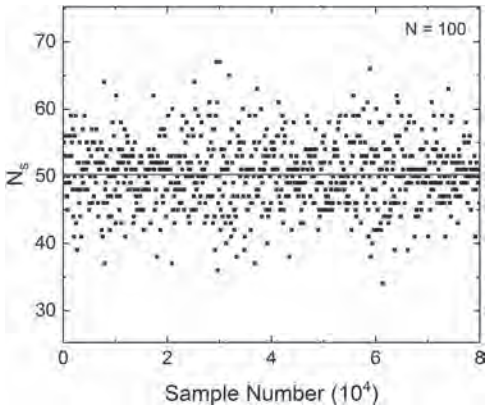

Fig.1: Number of switched events N_s in a sample size of N=100 versus the sample number of a 40nm diameter pMTJ at *T*=295K. The straight line represents the switching probability *p*=0.5027 of the whole data set.

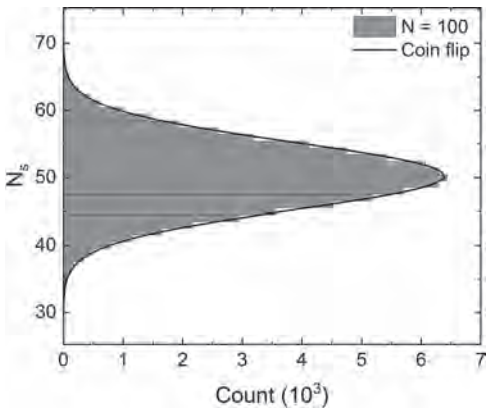

Fig.2: Histogram of N_s of the same data set. The line plot shows a normal distribution of a slightly weighted coin flip with *p*=0.5027.

DOC-05. Implementing stochastic noise using voltage-controlled magnetic tunnel junctions. *J. Kwon*[1], S. Liu[1], S.G. Cardwell[3], C.D. Schuman[2], J. Smith[3], S. Misra[3], J.B. Aimone[3] and J. Incorvia[1]
1. Electrical and Computer Engineering, University of Texas at Austin, Austin, TX, United States; 2. Electrical Engineering and Computer Science, University of Tennessee, Knoxville, TN, United States; 3. Sandia National Laboratories, Albuquerque, NM, United States

Magnetic tunnel junctions (MTJs) are a crucial component of in-memory and probability bit (p-bit) device applications.[1,2] The thermal-driven stochastic MTJ leads to generate random bit-streams that can be used for probabilistic computing. The MTJ can utilize as a *stochastic read* device, with a low-anisotropy near the superparamagnetic limit, that randomly switches magnetization at room temp.[3] Conversely, the MTJ can be employed as a *stochastic write* with a stable-anisotropy that has probabilistic switching by an applied current pulse.[4] In both, the weight of the probabilistic bit, i.e. how much time it spends in parallel (P) or antiparallel (AP) states, can be controlled using applied fields and/or DC bias voltages or currents. Here, we study an emerging way to generate stochastic bit-streams with MTJs, using voltage-controlled magnetic anisotropy (VCMA)[5] and numerical model based on LLG. The VCMA effect exerts unpredictable magnetization dynamics that has not been well explored for generating random bit-streams. For Fig.1, (a) V_b reduces the anisotropy and precessional oscillations occur as m_z orients to in-plane. When V_b is then turned off, the MTJ selects one of two stable states in either a P or AP. (b) VCMA-MTJ produces a bit-stream that shows (c) a sigmoid function. The VCMA effect controls the stable intrinsic energy state, which cannot be controlled by extrinsic inputs such as current and field. Thus, stochastic VCMA-MTJs provide the advantage of robustness to thermal energy compared to stochastic read MTJs, and the avoidance of a reset step via each state sampling, boosting speed compared to current-controlled stochastic write MTJs. We will show results on applying the VCMA-MTJ to a probabilistic circuit in comparison to the other device types in terms of bit stream speed, energy consumption, and controllability of the coinflip weight. Sandia National Laboratories is managed and operated by NTESS under DOE NNSA contract DE-NA0003525.

[1] K. Y. Camsari, B. M. Sutton and S. Datta, Appl. Phys. Rev. 6, 1 (2019). [2] W. A. Borders, A. Z. Pervaiz, S. Fukami, K. Y. Camsari, H. Ohno and S. Datta, Nature 573, 7774 (2019) [3] A. Mizrahi, T. Hirtzlin, A. Fukushima, H. Kubota, S. Yuasa, J. Grollier, et al., Nat. Commun 9, 1 (2018). [4] V. Ostwal and J. Appenzeller, IEEE Magnetic Letters 10, 4503305 (2019). [5] N. Maciel, E. Marques, L. Naviner, H. Cai and J. Yang, J of Low Power Electronics and Applications. 9, 2 (2019).

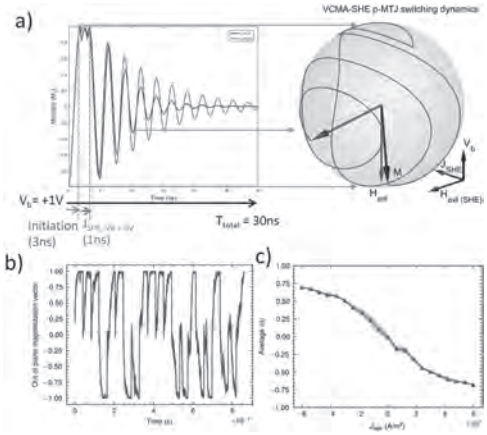

Figure 1. a) Switching dynamics of the VCMA-MTJ. Bias voltage eliminates stable states to the middle in-plane. STT or SHE can bias the switching probability. b) Bit-stream with STT-VCMA (J_{appl}). (c) Distribution of bit-streams follows a sigmoid function (time-averaged).

DOC-06. Hardware-Aware Bayesian Variational Inference Using Magnetic Tunnel Junction Noise Distributions in Artificial Synapse Arrays. *S. Liu*[1], T.P. Xiao[2], J. Kwon[1], B. Debusschere[2], S. Agarwal[2], J. Incorvia[1] and C. Bennett[2] *1. The University of Texas at Austin, Austin, TX, United States; 2. Sandia National Laboratories, Albuquerque, NM, United States*

Artificial neural networks (ANNs) are powerful tools for data intensive classification and regression, but the memory wall in von Neumann architectures prevents efficient processing [1]. Though there are many candidates for devices and architectures to realize ANNs, there are no comprehensive solutions to implement hardware Bayesian NNs (BNNs). BNNs are much less susceptible to overfitting when available data is sparse or unreliable, accomplished by representing and learning the weights of the network as distributions instead of deterministic values [2]. We propose a novel spintronic synaptic cell design that can implement tunable distributions by taking advantage of the intrinsic stochasticity of magnetic materials. The design of the cell is composed of a noise and weight encoding element respectively (see Fig. 1). The noisy element is a circular in-plane magnetic tunnel junction (MTJ) that relies on thermal activation to output a random conductance within the range of its TMR. This TMR can then be controlled through several methods such as voltage-controlled magnetic anisotropy (VCMA) [3] or magneto-ionics [4]. Combined with a weight encoding conductance element like a domain wall-magnetic tunnel junction (DW-MTJ) artificial synapse [5,6], we propose a novel cell design that can represent the distributions necessary for inference in a hardware BNN. We demonstrate device functionality through Landau-Lifshitz-Gilbert and micromagnetics [7] models, model analog Bayesian inference in CrossSim [8] for regression (see Fig. 2) and classification to detect out-of-distribution data, and compare the system's energy efficiency to CMOS implementations. These results propose a novel synapse implementation for accurate and efficient Bayesian inference, a foundational step toward hardware BNN accelerators. *SNL is managed and operated by NTESS under DOE NNSA contract DE-NA0003525.*

1. A. Sebastian, M. Le Gallo, R. Khaddam-Aljameh and E. Eleftheriou, Nature Nanotechnology., Vol. 15(7), p. 529–544 (2020) 2. T. Oess, M. P. R. Löhr, D. Schmid, M. O. Ernst and H. Neumann, Frontiers in Neurorobotics., Vol. 14, (2020) 3. Y. Shiota, S. Murakami, F. Bonell, T. Nozaki, T. Shinjo and Y. Suzuki, Applied Physics Express., Vol. 4(4), p. 043005 (2011) 4. G. Long, Q. Xue, Q. Li, Y. Shi, L. Li, L. Cheng, P. Li, J. Zhang, X. Zhang, H. Guo, J. Fu, S. Li, J.S. Moodera, and G. Miao, Advanced Electronic Materials., Vol. 7(9), p. 2100512 (2021) 5. S. Liu, T. P. Xiao, C. Cui, J. A. C. Incorvia, C. H. Bennett and M. J. Marinella, Applied Physics Letters, Vol. 118(20), p. 202405 (2021) 6. T. Leonard, S. Liu, M. Alamdar, C. Cui, O. G. Akinola, L. Xue, T. P. Xiao, J. S. Friedman, M. J. Marinella, C. H. Bennett and J. A. C. Incorvia, arXiv., 2111.11516 (2022) 7. A. Vansteenkiste, J. Leliaert, M. Dvornik, M. Helsen. F. Garcia-Sanchez and B. Vann Waeyenberge, AIP Advances., Vol. 4, p. 107133 (2014) 8. T. P. Xiao, C. H. Bennett, B. Feinberg, M. J. Marinella, and S. Agarwal. CrossSim v2.0 (2022). [Online]. Available: https://cross-sim.sandia.gov

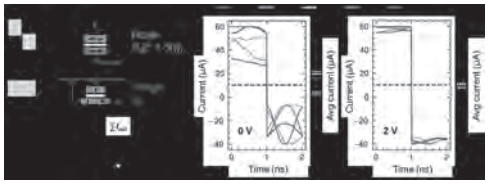

Fig. 1 a) BNN synapse cell diagram including proposed read scheme. b) Time-dependent output of synaptic cell over five runs, showing tunable noise using VCMA.

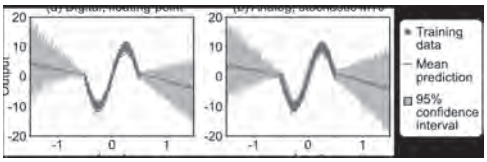

Fig.2 Performance of BNN trained to fit a sine curve, with larger uncertainty outside the trained region. (a) Digital implementation, (b) modeled performance of VCMA-based stochastic MTJ arrays.

DOC-07. Classification Using Stochastic Neural Networks Based On Domain Wall Pinning. *M.O. Ellis*[1], A. Welbourne[2], S. Kyle[2], D. Allwood[2], T. Hayward[2] and E. Vasilaki[1] *1. Department of Computer Science, University of Sheffield, Sheffield, United Kingdom; 2. Department of Materials Science, University of Sheffield, Sheffield, United Kingdom*

The non-linear properties of spintronic devices make them ideal candidates for neuromorphic computing; an approach where devices mimic the human brain to perform computing[1]. Such an approach is necessary due to the popularity of machine learning but the excessive energy costs in many deep learning applications due, in part, to the memory bottleneck[2]. However, spintronic devices are often limited by stochastic effects but in certain paradigms it can be a functional property. Here, we demonstrate how stochastic pinning of DWs at artificial defects can be tuned for application in hardware-based neural networks. We begin by demonstrating the tunability of DW pinning in Py nanowires through control of the driving field. As in Fig. 1, when DWs are propagated with fields in certain range they are pinned probabilistically which can be tuned by modulating the magnetic field strength. With the DW as a binary input these wires can be considered as stochastic synapses from which a neural network can be constructed. Based on this, we have trained a neural network model to classify handwritten digits using a stochastic learning rule. In Fig. 2, the testing accuracy is shown for both simulated wires (lines) and experimental wires (points), where to improve the classification accuracy the case where the synaptic operation has been repeated to build up an improved output. The test accuracy for increasing number of synapse repeats are shown for 2 cases; (blue squares) the network is trained with 1 repeat and (orange diamonds) trained with 128 repeats. When trained with 1 repeat, further samples during testing do not improve the accuracy. While if trained with 128 repeats, the accuracy is initially worse but improves approaching analogue neural network performance. This suggests different practical applications; if multiple repeats are allowed then the accuracy can be refined through sampling but where it is not then it is better to use a network trained with these constraints in mind.

[1] Grollier et al. Nat Electron 3, 360–370 (2020) [2] Aly et al. Proc. IEEE 107 (2019)

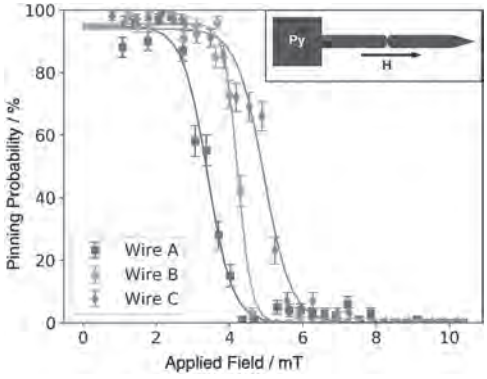

Fig. 1: Tuning of domain wall pinning probability in notched magnetic nanowire synapse with applied field.

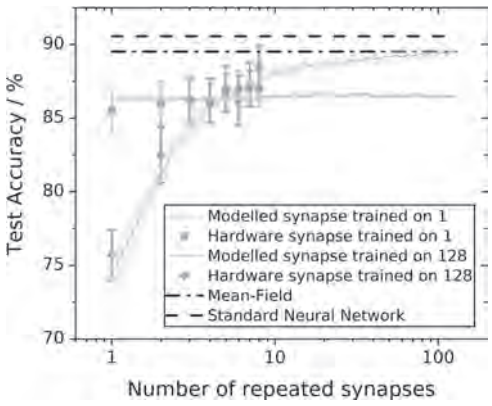

Fig. 2: Classification test accuracy on handwritten digits for simulated (lines) and hardware (points) synapses for repeated sampling.

DOC-08. Echo State Property in Vortex Spin Torque Oscillator.
Y. Imai[1], S. Tsunegi[1], K. Nakajima[2] and T. Taniguchi[1] *1. National Institute of Advanced Industrial Science and Technology (AIST), Tsukuba, Japan; 2. The University of Tokyo, Bunkyo-ku, Japan*

Physical reservoir computing [1] utilizing spin-torque oscillator (STO) [2] is an emerging topic because of its applicability to information processing with high-speed and low-power consumption. The algorithm enables the recognition of time-dependent data when one-to-one correspondence between the input data, such as human voice, and the output signal, such as magnetoresistance, is found. However, a temporal response from an STO generally depends on its initial state, which prevents learning of the correspondence between the input and output signals. Thus, the magnetization dynamics should become independent of the initial state as the input signal is injected. This property is called echo state property. It is necessary to verify the presence of echo state property in STOs, as well as its origin, to enhance the computational capability of reservoir computing by STOs. In this work, we develop a theoretical analysis on echo state property in magnetic-vortex STO through an investigation of noise-induced synchronization [3]. The noise-induced synchronization is a phenomenon where the dynamical phases of multiple STOs become independent of their initial states when random inputs are injected; see Fig. 1. The appearance of noise-induced synchronization guarantees the echo state property. Solving the Thiele equation both numerically and analytically, we found that noise-induced synchronization is efficiently achieved when the current magnitude driving the vortex oscillation is small and/or the amplitude-phase coupling is large; see Fig. 2. This is because the phase difference among STOs rapidly reaches to zero when the oscillation amplitude is small or the dependence of the frequency on the amplitude is large. We also analyze the role of thermal fluctuation and found on-off intermittency, whose frequency obeys a universal statistic in nonlinear oscillator systems [3]. This work is supported by NEDO (Grant No. JPNP16007).

[1] K. Nakajima and I. Fischer edt., Reservoir Computing – Theory, Physical Implementations, and Applications –, Springer 2021. [2] J. Torrejon *et al*., Nature (London) 547, 428 (2017). [3] Y. Imai *et al*., Phys. Rev. B 105, 224407 (2022).

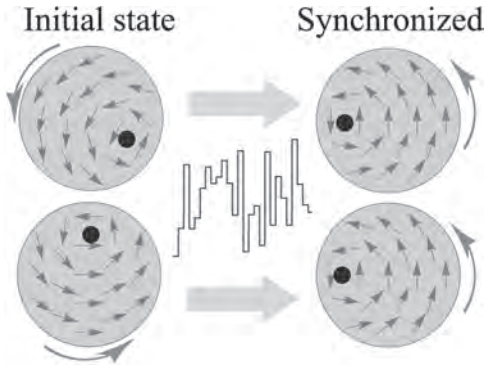

Fig.1. Schematic illustration of noise-induced synchronization. The phases of STOs become identical as random input signals are injected.

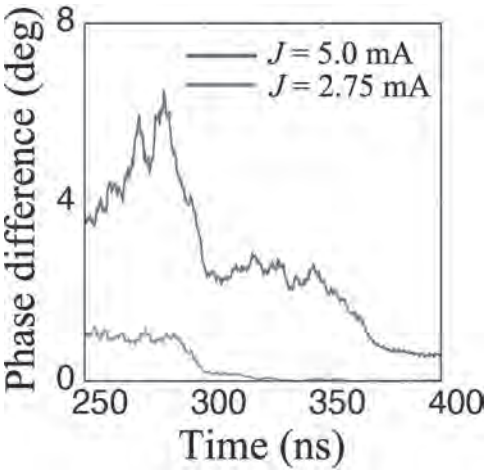

Fig. 2. Time evolutions of the phase difference between two STOs. When the current magnitude is small (large), the phase difference becomes rapidly (slowly) identical.

DOC-09. Brownian Reservoir Computing Realized Using Geometrically Confined Skyrmions.
K. Raab[1], M.A. Brems[1], G. Beneke[1], T. Dohi[1], J. Rothörl[1], F. Kammerbauer[1], J.H. Mentink[2] and M. Kläui[1] *1. Institute of Physics, Johannes Gutenberg University Mainz, Mainz, Germany; 2. Institute for Molecules and Materials, Radboud University, Nijmegen, Netherlands*

Reservoir computing (RC) has been considered as one of the key computational principles beyond von-Neumann computing. Magnetic skyrmions, topological particle-like spin textures in magnetic thin films, are particularly promising for implementing RC [1] since they respond strongly nonlinear to external stimuli and feature inherent multiscale dynamics. We propose and demonstrate experimentally a conceptually new approach to skyrmion RC that exploits the thermally activated diffusive motion of skyrmions [2]. By confining the thermal and low-energy, electrically gated skyrmion motion, together with employing spatially resolved input and readout, we find that already a single skyrmion in a confined, triangular geometry (Fig. 1) suffices to realize non-linearly separable functions, which we demonstrate for the XOR gate along with all other Boolean logic gate operations [3] (Fig. 2). Our proposed concept can be readily extended by linking multiple confined geometries and/or by including more skyrmions in the reservoir, suggesting high potential for scalable and low-energy reservoir computing.

[1] D. Prychynenko et al., "Magnetic Skyrmion as a Nonlinear Resistive Element: A Potential Building Block for Reservoir Computing", Physical Review Applied, vol. 9, iss. 1, 2018, https://doi.org/10.1103/PhysRevApplied.9.014034 [2] J. Zázvorka et al., "Thermal skyrmion diffusion used in a reshuffler device", Nature Nanotechnology, vol. 14, no. 7, 2019, https:/doi.

org/10.1038/s41565-019-0436-8 [3] K. Raab, M. A. Brems et al., "Brownian reservoir computing realized using geometrically confined skyrmions", Preprint, https://doi.org/10.48550/arXiv.2203.14720

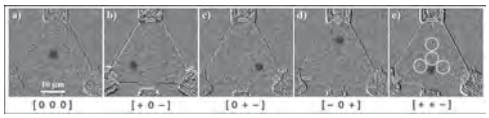

Fig. 1| Skyrmion displacement. Subtracted Kerr microscopy images of an equilateral triangular device, each with a single skyrmion (dark grey) in a) the ground state without and b)-e) with applied electrical potentials. In brackets below the input patterns of the respective state. e) shows exemplary the four regions used to mimic MTJs in our analysis.

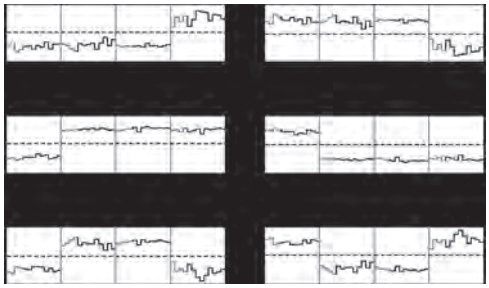

Fig. 2| Logic operations. Outputs of the linear readout optimized for different Boolean operations. For each input combination at two tips of the triangle ([0 0], [0 1], [1 0], [1 1]) the output Q of the linear readout is shown for 13 sets of local skyrmion occurrence probabilities. The light blue and black parts of the curves indicate the sets used for training and testing, respectively. The dashed horizontal line indicates a possible threshold for perceptron readout.

DOC-10. Demonstration of basic operations using skyrmions in multilayers i.e. full-electrical nucleation, motion and detection for neuromorphic devices. *T. da Câmara Santa Clara Gomes*[1], Y. Sassi[1], S. Krishnia[1], D. Sanz Hernandez[1], N. Reyren[1], M. Martin[1], P. Seneor[1], T. Bhatnagar-Schöffmann[2], D. Ravelosona[2], D. Querlioz[2], L. Herrera-Diez[2], J. Grollier[1] and V. Cros[1] *1. Unité Mixte de Physique CNRS, Palaiseau, France; 2. Centre de Nanosciences et de Nanotechnologies, CNRS, Université Paris-Saclay, Palaiseau, France*

Electrical control of magnetic skyrmions, which are particle-like topological spin textures, holds promise for emerging memory and computing applications such as racetrack memory, logic devices or neuromorphic computing [1]. Among the main advantages of magnetic skyrmions are their stability and non-volatility at room temperature, the low energy requirement for their motion, their sub-micronic size and their particle-like behavior. It has been shown, most often separately, that magnetic skyrmions can be experimentally nucleated [2-5], moved [2,5], annihilated [4] and detected electrically using anomalous Hall effect [6] in metallic multilayers. In this study, we fabricate by lithography Hall cross devices with adjustable geometry in optimized magnetic multilayers made of several repetition of [Pt(3)|Co(1.2)|Al (1)|Ta(3)|Al(3)], a system that we recently thoroughly study for optimizing both the interfacial DMI [7] and SO torques [8]. Using electrical pulses with controlled current density and duration, we show how it is possible to nucleate at room temperature a number of magnetic skyrmions proportional to the current, and move them at a few m/s velocity within micron-wide tracks. We show that skyrmions moving within a Hall cross can be detected in real time electrically through measurements of the Anomalous Hall Effect. By engineering the Hall cross device (dimensions and materials) and the electrical pulse parameters, we demonstrate that the number of detected skyrmions, *i.e.* the Hall voltage of the devices can be controlled. In complement to the transport measurements, we also show that skyrmions can be tracked in real time by magneto-optic Kerr effect microscopy. The impact of out-of-plane magnetic field on the number of skyrmions is also investigated. Moreover, we also investigate how the tuning of the magnetic anisotropy and Dzyaloshinskii-Moriya interaction of the magnetic multilayer stack using electric field manipulation can be used to influence the nucleation and motion of these magnetic skyrmions in the devices. All these basic operations using magnetic skyrmions hold promises for unconventional computing applications such as neuromorphic computing.

[1] Fert, A., Reyren, N. and Cros, V. Nat Rev Mater 2, 17031, 2017. [2] Legrand, W. et al. Nano Lett. 17, 2703, 2017. [3] Hrabec, A. et al. Nat. Commun. 8, 15765, 2017. [4] Woo, S. et al., Nat. Electron. 1, 288, 2018. [5] Woo, S. et al., Nat. Mater. 15, 501–506, 2016. [6] Maccariello, D. et al., Nat. Nanotechnol. 13, 233, 2018. [7] Ajejas, F. et al., arXiv:2109.00761 [8] Krishnia, S. et al. arXiv:2205.08486v1 Acknowledgements: this work gets supports from the Horizon2020 Framework Program of the European Commission under FET-Proactive Grant SKYTOP (824123) and by the French National Research Agency (ANR) with TOPSKY (ANR-17-CE24-0025).

DOC-11. Memristive Spin-Orbit Torque Switching in Nanocomposite CoPtCrB. *V. De Zoysa K.*[1], S. DuttaGupta[2], B. Jinnai[3], H. Ohno[1] and S. Fukami[1] *1. Lab. for Nanoelectronics and Spintronics, RIEC, Tohoku Univ., Sendai, Japan; 2. CSIS (Core Research Cluster), Tohoku Univ., Sendai, Japan; 3. WPI-AIMR, Tohoku Univ., Sendai, Japan*

Spin-orbit torques (SOTs) in heavy metal (HM)/ferromagnet (FM) have gathered much attention due to its potential for non-volatile, high-speed, and low-power spintronic devices [1-3]. While the majority of research has focused on the development of digital memories, previous studies on antiferromagnet (AFM)/FM structures showed field-free as well as analog-like (memristive) switching behavior [4,5], opening a new paradigm, the neuromorphic spintronics [6]. For applications, one needs to address a challenge that the memristive characteristics diminish with a reduction of device dimensions; for the case of PtMn/[Co/Ni] system, it totally disappears at around 200 nm [7,8]. In this study, we introduce a nanocomposite FM CoPtCrB towards SOT-based nanoscale memristors. A stack with Si sub./ Ta(4)/ Pt(4)/ CoPtCrB(7)/ Ru(1) is processed into single nanodot devices with various dot diameters (D_{dot}: 30-1000 nm) through the electron beam lithography and Ar ion milling. Memristive characteristics are studied by switching experiments with perpendicular magnetic fields or pulse currents (I_{ch}) under an in-plane external field (H_x). Fig. 1 shows the results of SOT switching at $\mu_0 H_x$ = 90 mT for D_{dot} = 400 nm. Memristive behavior is observed, in contrast to the previous work with uniform FM exhibiting much fewer intermediate states [7]. Fig. 2 shows the obtained relationship between the square root of the number of intermediate states N_{IS} and D_{dot}. D_{dot} below which devices show binary switching is around 60 nm, which is much smaller than the previous study (~ 200 nm) [7]. The present study demonstrates the potential of nanocomposite FM for nanoscale spintronic memristors. The authors thank A. Kurenkov, T. Koga, K. K. Tham, and S. Saito for their support. This work is partly supported by JST-CREST JPMJCR19K3, JSPS Kakenhi 19H05622, and RIEC Cooperative Research Projects. K. V. D. Z. acknowledges WISE program for AIE for financial support.

[1] I. M. Miron *et al*., Nature 476, 189 (2011). [2] L. Q. Liu *et al.*, Science 336, 555 (2012). [3] S. Fukami *et al.*, Nature Nanotechnol. 11, 621 (2016). [4] S. Fukami *et al.,* Nature Mater. 15, 535 (2016). [5] A. Kurenkov *et. al.*, Adv. Mater. 31, 1900636 (2019). [6] J. Grollier *et al.*, Nature Electronics 3, 360 (2020). [7] A. Kurenkov *et al*. Appl. Phys. Lett., 110, 092410 (2017). [8] G. K. Krishnaswamy *et al*. Phys. Rev. Applied 14, 044036 (2020).

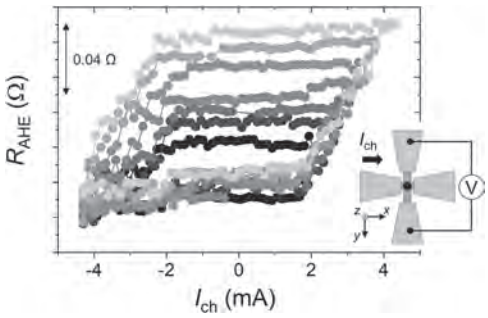

Fig. 1: SOT-induced switching in Pt/CoPtCrB heterostructure (D_{dot} = 400 nm). Inset shows a schematic representation of the device.

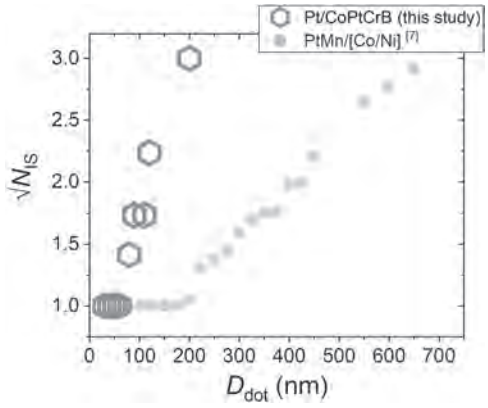

Fig. 2: Square root of the number of intermediate states N_{IS} vs dot sizes D_{dot} for the present system and its comparison with a previous study on AFM/FM structures.

DOC-12. Fully-Parallel Convolution with Chains of Spin-Diodes.
E. Plouet[1,2], D. Sanz Hernandez[1,2], P. Sethi[1,2], N. Leroux[1,2], B. Dlubak[1,2], V. Zatko[1,2], A. Mizrahi[1,2] and J. Grollier[1,2] *1. Unité Mixte de Physique CNRS Thales, Palaiseau, France; 2. Université Paris-Saclay, Palaiseau, France*

Convolutional neural networks (CNN) are state of the art algorithms for image processing. Despite a small number of synaptic weights, the CNNs remain computationally costly to train in software due to the necessity to exchange huge data flows between memory and processing units. Unconventional hardware is suited to address this limitation. In neuromorphic spintronics, it has been previously demonstrated that the spin diode effect can be used to apply a synaptic weight on a radiofrequency signal [1][2]. Here we go a step beyond, to show an experimental implementation of a convolutional layer employing chains of spin-diodes. We design a compact architecture of 3 chains with 3 spin-diodes connected in series, that performs a padded convolution with a filter of 3 pixels on 5 input pixels multiplexed in frequency in one RF signal (See Figure 1). The synaptic weights corresponding to the filter are encoded by a small frequency detuning between the inputs and the spin-diodes resonance and are controlled in parallel using currents in 3 strip lines. This architecture exploits the intrinsic weight redundancy of convolutions (all filters share the same weights) to enhance the compacity of the hardware and greatly simplify the process of updating a weight, only requiring updating a the current in one strip line. We will also present processed experimental results highlighting the scalability of the proposed architecture. An error on the performed convolution as low as 0.28% was achieved (See Figure 2). The proposed architecture enables us to both reduce the size of this hardware implementation while, at the same time, performing the convolution in one timestep contrary to previous time-multiplexed implementations. According to a previous study [3] we can achieve to decrease by one order of magnitude the energy consumption compared to current GPUs and two orders of magnitude in operating latency. This proof of concept of spintronic CNN, opens the path to spintronic neural networks that can exploit the power of convolutional layers in a fully parallel, compact, and energy efficient way.

[1] Nathan Leroux et al Phys. Rev. Applied, Vol 15, issue 3, art. 034067 (2021) [2] Nathan Leroux et al Neuromorph. Comput. Eng. 1 011001 (2021) [3] Nathan Leroux et al Neuromorph. Comput. Eng. (accepted manuscript) (2022)

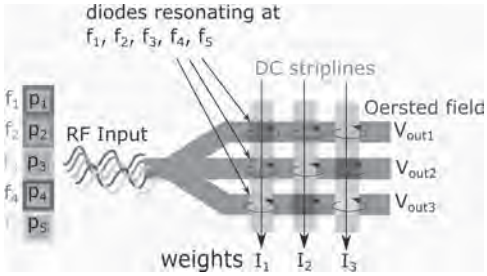

Fig. 1 : RF convolutional architecture

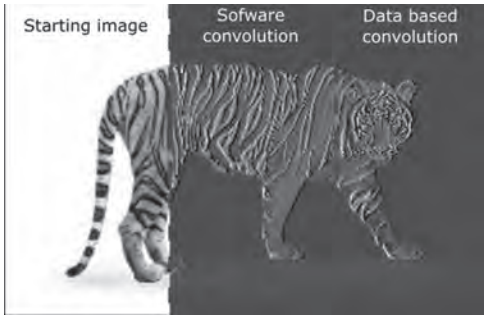

Fig. 2 Convolution based on experimental data to enhance vertical lines

DOC-13. Thermal and Edge Roughness Effects on Domain Wall Based Reservoir Computing.
R. Ababei[2], *M.O. Ellis*[1], I.T. Vidamour[2], D. Devadesan[2], D. Allwood[2], E. Vasilaki[1] and T. Hayward[2] *1. Department of Computer Science, University of Sheffield, Sheffield, United Kingdom; 2. Department of Materials Science, University of Sheffield, Sheffield, United Kingdom*

Reservoir computing (RC) is a paradigm of machine learning where a fixed system is used to transform input data such that it can be classified using a linear method. This mitigates the large energy cost of training deep neural networks by simplifying the number of trainable parameters. Many spintronic systems are suitable for this approach due to their natural nonlinearity and memory of previous inputs [1]. Recently, it has been demonstrated that a domain wall (DW) trapped between anti-notches can be used to perform reservoir computing [2]. However, the effect of thermal noise or edge roughness has not been fully explored. Here, we assess the performance of DW-based RC at finite temperature and edge roughness using a 1D collective coordinates model. Thermal noise is included as a stochastic field, while edge roughness is considered as an additional energy term that varies along the nanowire length in discrete sections. Fig 1 shows the accuracy using thermal noise at 300K for a benchmark task of classifying points belonging to a sine or square wave. With thermal noise the accuracy is reduced significantly for wires with small cross-sections (S) but wider cross-sections and larger driving fields (ΔH) can mitigate this, reaching 93% accuracy at ΔH=2.5 kA/m. Edge roughness again degrades performance but optimal input field parameters can be chosen to recover a performance of 89% with ΔH=0.5 kA/m. Finally, we discuss the performance of DWs as a reservoir when applying a spin current instead of a magnetic field with comparable performance on a speech recognition task. This work validates the potential of this device for neuromorphic computing at realistic operating conditions and shows how DW devices can be optimised for such cases by selecting suitable device parameters.

[1] Grollier et al. Nat Electron 3, 360–370 (2020) [2] Ababei et al. Sci Rep 11, 15587 (2021)

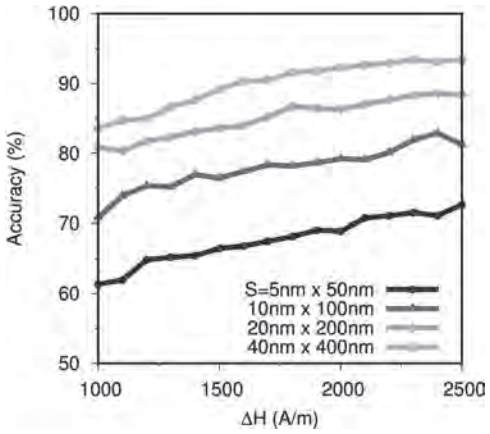

Fig 1: Classification accuracy at 300K with 100 neurons as a function of input field scaling (ΔH) for increasing wire cross-section.

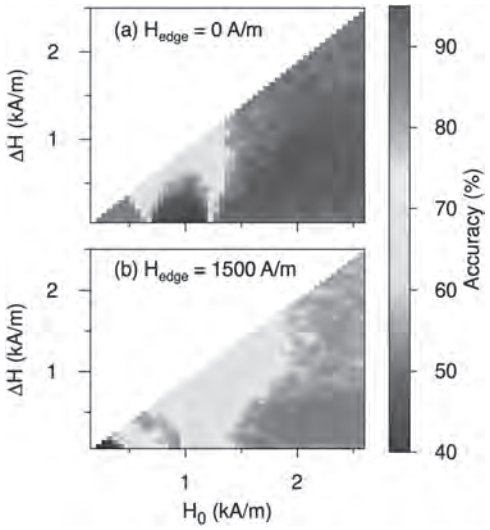

Fig. 2: Classification accuracy maps for edge roughness magnitudes of (a) 0 kA/m and (b) 1.5 kA/m over a range of input field offset and scaling parameters.

Session DPA
SPINTRONIC DEVICES FOR MEMORY AND COMPUTING
(Poster Session)

Shouzhong Peng, Co-Chair
Beihang University, Beijing, China
Luding Wang, Co-Chair
Eindhoven University of Technology, Eindhoven, Netherlands

DPA-01. Spiking dynamics with dual free layer MTJ. *L. Farcis*[1], B. Da Silva Teixeira[1], P. Talatchian[1], U. Ebels[1], S. Auffret[1], D. Salomoni[1], B. Dieny[1], L. Prejbeanu[1], A. Mizrahi[2], J. Grollier[2], R. Sousa[1] and L.D. Buda-Prejbeanu[1] *1. SPINTEC, Univ. Grenoble Alpes, CEA, CNRS, Grenoble, France; 2. Unité Mixte de Physique CNRS/Thales, Université Paris-Saclay, Palaiseau, France*

Spiking neural networks have attracted a lot of interest in the past decade as they meet the need of energy efficiency in deep neural network computing [1]. Using spikes instead of continuous signals enables low power operation, event-based computations and fast response time, which is better adapted to spatial-temporal data. Combined with unsupervised and local learning rules such as the spike-timing-dependant plasticity rule [2], SNN with magnetic tunnel junction (MTJ) based neurons provide interesting solutions for embedded technologies with better back-end-of-line compatibility [3] compared to other technologies. For the spike generation, we propose an MTJ-based neuron composed of two magnetized layers (M_1 and M_2), with low thermal stabilities, separated by an oxide tunnel barrier. Under applied current, the spin-transfer torque (STT) enables an alternating switching of both magnetic layers leading to a so-called "windmill motion" (see Fig1.a-c) previously predicted by simulation for in-plane and out-of-plane magnetized MTJs [4,5]. Here we designed, fabricated and characterized such type of structure and were able to achieve steady alternating magnetization reversal of both layers generating a characteristic spike-like resistive response. MTJ stacks of FeCoB/MgO/FeCoB, with varying FeCoB thicknesses, were deposited by magnetron sputtering and patterned into nano-pillars with diameters ranging from 50 to 200 nm. The electrical characterization of the nano-pillars reveals essential changes of the magnetization dynamics depending on the pillar diameters, layer thicknesses, voltage, applied magnetic field and temperature of the junction. As predicted by the simulation, the frequency of the oscillations and the width of the spikes evolve with the voltage amplitude and the applied field. Important similarities confirm the parameter dependence with temperature and bias voltage. Controlling the spiking rates at low voltages is a critical requirement to build an efficient spiking neural network.

Acknowledgements: This work was supported by ANR via grant SpinSpike Projet-ANR-20-CE24-0002. References [1] A. Tavanaei, M. Ghodrati and S.R. Kheradpisheh, *Neural networks*, 111, 47-63 (2019). [2] T. Iakymchuk, A. Rosado-Muñoz and J.F. Guerrero-Martínez, *EURASIP Journal on Image and Video Processing 2015,* 1-11 (2015). [3] D. Shum, D. Houssameddine and S.T. Woo, *2017 Symposium on VLSI Technology*. IEEE pp. T208-T209 (2017). [4] R. Matsumoto, S. Lequeux, and J. Grollier, *Physical Review Applied*, 11(4), 044093 (2019) [5] G. Gupta, Z. Zhu and G. Liang, *arXiv preprint arXiv*, 1611.05169 (2016).

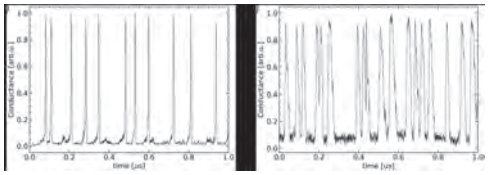

Figure 1 - (a) Simulated and (b) experimental time traces of the conductance of dual free layer MTJ under 540 mV.

DPA-02. Symmetrical Voltage-Controlled Stochasticity of Perpendicular Synthetic Antiferromagnetic Magnetic Tunnel Junctions. *Y. Lv*[1], B.R. Zink[1], D. Zhang[1] and J. Wang[1] *1. Electrical and Computer Engineering, University of Minnesota, Minneapolis, MN, United States*

For practical applications, such as random number generation (RNG)[1], and for novel computing, such as stochastic computing (SC)[2], stochastic neuromorphic computing[3], and probabilistic computing[4], the stochasticity of magnetic tunnel junctions (MTJs) serves as the physical source of stochasticity. Usually, the electrical control or tunability of the stochastic behavior is desired for robust, efficient, flexible, reconfigurable system designs and for additional functionalities. For example, the biases on an MTJ can tune the rate and mean of its stochastic fluctuation[5] to compensate for device-device variations, improve speed[6], or implement system throttling. Furthermore, the recent development of advanced MTJ involving implementing perpendicular-synthetic antiferromagnetic (p-SAF) layer structures[7], which aims at significantly improving the memory performance, also opens up new possibilities for MTJ-based stochastic signal generation. Here, we report an experimental realization of voltage-controlled spontaneous telegraphic switching. Unlike what one would expect for the voltage-controlled magnetic anisotropy (VCMA) effect, the observed telegraphic switching occurs with electrical biases of both positive and negative polarity. The nano-sized MTJ devices studied are made from a stack structure similar to that used in our previous work[8] but with thicker SAF spacer layer and lower annealing temperature to induce the stochastic behavior. Fig. 1 shows the tunneling magnetoresistance (TMR) vs. current bias. The bistability only appears around both +30 and -30 nA biases. Fig. 2 shows that under +30 and -30 nA electrical bias, the MTJ exhibits spontaneous telegraphic switching. We believe that this phenomenon is linked to the effect of both VCMA and the voltage modulation of interlayer exchange coupling[8]. The reported unique voltage-controlled stochastic behavior of p-SAF MTJ could bring new opportunities for both conventional applications and in novel computing scenarios, such as signal processing, voltage-gated RNG, device-level SC, and in neuromorphic and probabilistic computing modules.

[1] W. H. Choi *et al.*, in *Technical Digest - International Electron Devices Meeting, IEDM*, 2014, p. 12.5.1-12.5.4, (2014) [2] Y. Lv and J.-P. Wang, in *2017 IEEE International Electron Devices Meeting (IEDM)*, Dec. 2017, p. 36.2.1-36.2.4 (2017) [3] A. Sengupta, P. Panda, P. Wijesinghe *et al.*, *Sci. Rep.*, vol. 6, no. 1, p. 1–8 (2016) [4] K. Y. Camsari, B. M. Sutton, and S. Datta, *Applied Physics Reviews*, vol. 6, no. 1. (2019) [5] B. R. Zink, Y. Lv, and J. P. Wang, *IEEE Trans. Electron Devices*, vol. 66, no. 12, p. 5353–5359 (2019) [6] Y. Lv, R. P. Bloom, and J.-P. Wang, *IEEE Magn. Lett.*, vol. 10, p. 1–5 (2019) [7] D. Zhang *et al.*, *Nano Lett.*, vol. 22, no. 2, p. 622–629 (2022) [8] D. J. P. De Sousa, P. M. Haney, D. L. Zhang *et al.*, *Phys. Rev. B*, vol. 101, no. 8, p. 081404 (2020

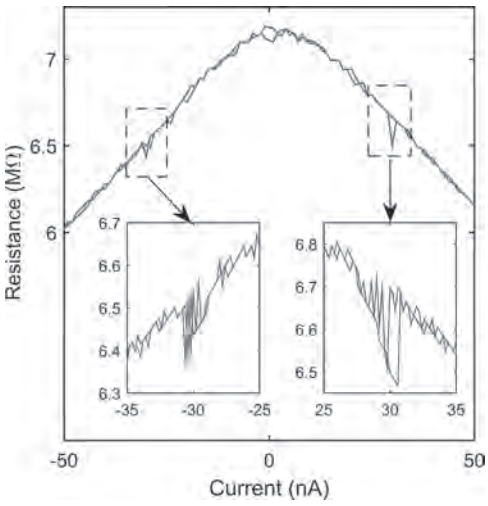

Fig. 1. Tunneling magnetoresistance (TMR) vs. current bias.

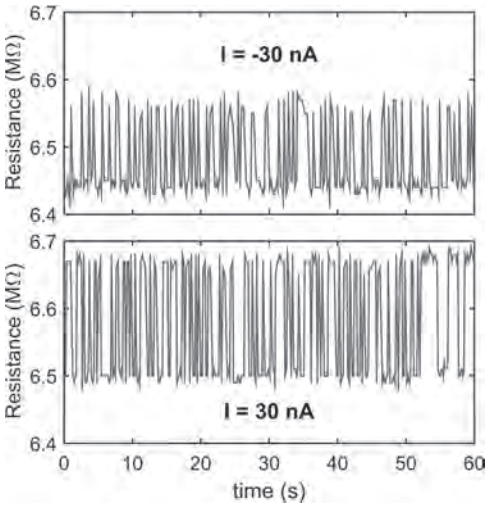

Fig. 2. TMR vs. time at bias of +30 and -30 nA.

DPA-03. Ultra-low current density switching via voltage-controlled exchange coupling assisted with spin-orbit torque. *B.R. Zink*[1], D. Zhang[1], H. Li[2], O. Benally[1], Y. Lv[1], D. Lyu[1] and J. Wang[1] *1. Electrical and Computer Engineering, University of Minnesota, Minneapolis, MN, United States; 2. Chemical Engineering and Materials Science, University of Minnesota, Minneapolis, MN, United States*

Magnetic random access memory (MRAM) is a promising candidate for beyond-CMOS memory and logic technologies and has been developed for commercial purposes in recent years [1]. The key building block of commercial MRAM is magnetic tunnel junction (MTJ), which is operated through either spin transfer torque (STT) or spin-orbit torque (SOT). STT-based MRAM benefits from higher cell density but suffers from reliability and energy-efficiency due to the current flow through the MTJ whereas SOT-based MRAM has superior reliability, endurance, and faster switching times [2]. For realizing the ultralow switching current density and ultrafast switching MRAM cell, two or more driving forces are normally employed to switch MTJs. One acts as the principal switching mechanism and the other serves to assist in switching. For example, ultrafast switching speed of ~ 0.27 ns has been reported in SOT switching of perpendicular MTJs (p-MTJs) assisted with STT and voltage-controlled magnetic anisotropy (VCMA), however, the key challenge is still large switching current densities (J_c) ~ 2.0×10^8 A/cm^2 for SOT and ~ 2.3×10^6 A/cm^2 for STT [3]. Voltage controlled exchange coupling (VCEC) occurs in perpendicular MTJs (p-MTJs) with synthetic antiferromagnetic (SAF) free layers and can realize bidirectional switching at switching current densities as low as 1 x 10^5 A/cm^2 [4]. In this work, we designed and fabricated the p-MTJ stacks with SAF free layers on bi-layered spin Hall channels (Ta/Pd). The p-MTJ stacks were patterned into 150-nm pillars, and MTJ devices are switched through combination of SOT and VCEC effects, as illustrated in Fig. 1(a). Bidirectional switching of p-MTJs were obtained with current densities as low as 3×10^3 A/cm^2 for VCEC and 6.8×10^7 A/cm^2 for SOT, as shown in Fig. 1(b), where the VCEC switching current density is two orders of magnitude lower than the reported value for VCEC-only switching [4]. Furthermore, by studying the contribution of SOT and VCEC for MTJ switching, it is found that SOT plays a crucial role for ultralow-energy VCEC bidirectional magnetization switching.

[1] J.-P. Wang et al, DAC '17: Proceedings of the 54th Annual Design Automation Conference 16, pp. 1-6 (2017). [2] Y. C. Liao *et al*, *IEEE J. Explor. Solid-State Computat*. 6, pp. 9-17 (2020). [3] E. Grimaldi *et al*, *Nat. Nanotechnol.* 15, pp. 111-117 (2020). [4] D. Zhang *et al*, *Nano Lett.*, 22, pp. 622-629 (2022).

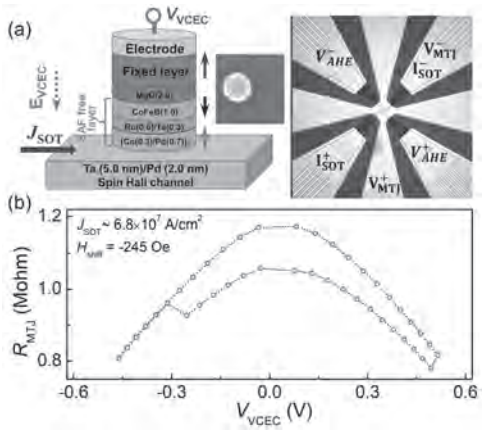

DPA-04. Simultaneous measurement of thickness, saturation magnetization and exchange parameter using propagating spinwaves. G. Riley[1,3], J.M. Shaw[1], T.J. Silva[1] and *H. Nembach*[1,2] *1. Quantum Electromagnetics Division, National Institute of Standards and Technology, Boulder, CO, United States; 2. Department of Physics, University of Colorado Boulder, Boulder, CO, United States; 3. Center for Memory and Recording Research, University of California San Diego, La Jolla, CA, United States*

The Heisenberg exchange parameter A_{ex} is a critical materials parameter for magnetic storage and logic devices. Here, we demonstrate an approach to determine A_{ex} and simultaneously the thickness t and the saturation magnetization M_s from spinwave measurements. This approach is applicable to wafer level measurements with potential for inline production monitoring [1]. Many different approaches are employed to determine A_{ex} which include the measurement of perpendicular standing spinwaves (PSSWs), the Curie temperature or Neutron scattering but not all are applicable to magnetic layers with thicknesses down to less than a few nanometers. We sputter deposited a Ta/Cu/$Co_{90}Fe_{10}$(t)/Cu/Ta sample series with t= 1.4, 3.0 and 14.0 nm. We carried out ferromagnetic resonance measurements over a broad frequency range in the perpendicular and in-plane geometry to determine the anisotropy and the spectroscopic splitting factor. We measured the spinwave frequency for a range of wavevectors with Brillouin Light scattering spectroscopy for spinwaves propagating perpendicular (Damon-Eshbach geometry) and parallel (backward volume geometry) to the applied magnetic field, see fig. 1. By simultaneously fitting the data for both geometries to the respective spinwave dispersion equation, we can extract A_{ex}, t and M_s. We determined the magnetic moment for the sample series including an additional 5 nm thick sample with SQUID magnetometry to obtain an independent measure of the magnetic dead layer. This allowed us to also extract M_s from magnetometry using the actual magnetic thickness. We fitted the temperature dependence of the magnetic moment with the Bloch $T^{3/2}$-law to

determine A_{ex}, fig.2. The magnetometry and spinwave dispersion measurement based results for A_{ex}, M_s and t are both in good agreement.

[1] G. Riley et al., Appl. Phys. Lett. 120, 112405 (2022)

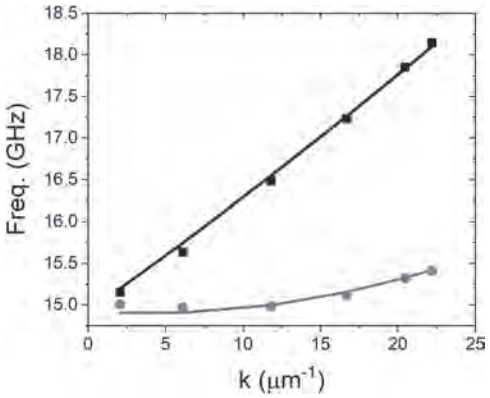

Fig.1: Spinwave dispersion for the 3 nm thick sample measured in the Damon-Eshbach (black) and backward volume (red) geometry. The lines are fits to the data with the spinwave dispersion equation.

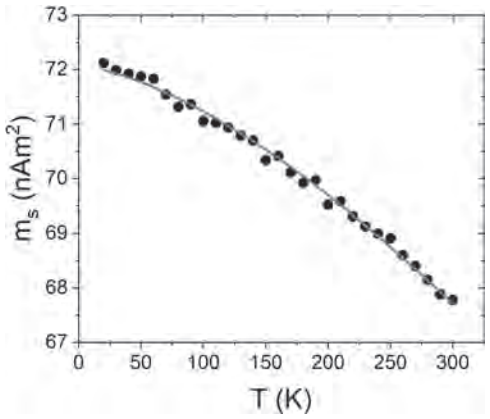

Fig. 2: Temperature dependence of the magnetic moment for the 1.4 nm thick sample measured with SQUID magnetometry. The red line is a fit with the Bloch $T^{3/2}$ law.

DPA-05. Evaluation of magnetic flux density distribution of magnetic domains recorded in racetrack memory by TMR head. *S. Kambe*[1], S. Ranjbar[1], K. Tanabe[1], S. Sumi[1] and H. Awano[1] *1. Toyota technological institute, Nagoya, Japan*

Racetrack memory is expected to be a memory device that supports the information society because of its high speed and low power consumption. Although many studies have been conducted to improve the speed of magnetic domain wall movement, few studies have been conducted from the viewpoint of Joule heat. Therefore, we have investigated the relationship between Joule heat and domain wall motion in the 2022 Joint MMM-INTERMAG.[1] In elucidating the mechanism of this current-driven domain wall motion, although the domain wall width is an essential parameter for improving the domain wall moving speed and the critical current density, the details of the domain wall width are still unknown. Generally, MFM is used for magnetic domain observation. In MFM, as shown in FIG. 1, it is possible to observe the magnetic domain shape by vibrating a thin magnetic needle up and down, but it is challenging to investigate the accurate magnetic flux density distribution. However, suppose the TMR head can be contacted with the sample and scanned. In that case, the distance between the sample and the TMR head can be kept constant to measure the accurate magnetic flux density distribution created by the magnetic recording domain. FIG. 2 shows a TMR head scan image of a magnetic domain recorded in a racetrack memory having a width of 10 μm and a length of 100 μm. The result of line scanning by enlarging this domain wall is also shown in the figure. The recording material is TbCo ferrimagnetic material, the domain wall movement is fast, and the critical current density is small [2]. Despite the small saturation magnetization due to ferrimagnetism and thin film (10 nm), the TMR head could measure a clear change in magnetic flux density within a range of ± 20 mT.

[1]Sota, K. *et al*. Relationship between pulse width and domain wall velocity in current induced domain wall motion in GdFeCo wire and the effect of joule heat on the racetrack memory, *Joint MMM-Intermag Conference,* 3628926 (2022) [2]Sina, R. *et al*. Fast Current Induced Domain Wall Motion in Compensated GdFeCo Nanowire, *Joint MMM-Intermag Conference,* 3786257 (2022)

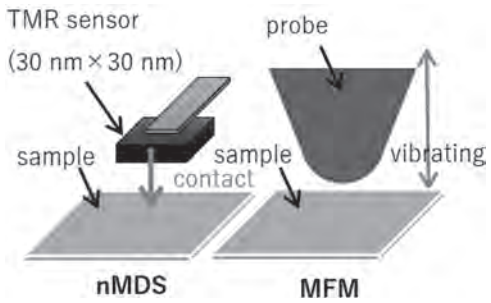

Fig. 1 Principle of magnetic domain observation for nMDS and MFM

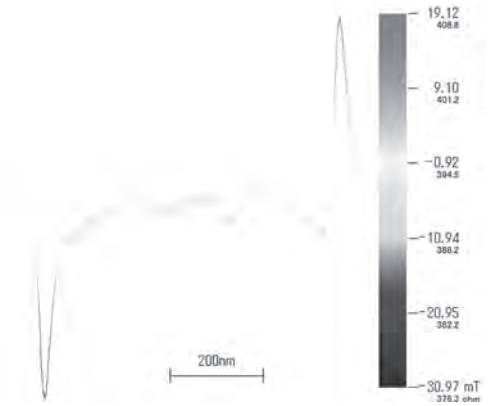

Fig. 2 TMR head scan image of a magnetic domain recorded in a racetrack memory

DPA-06. Observation of unidirectional spin Hall magnetoresistance in amorphous $PtSn_4$/CoFeB bilayers. *Y. Fan*[1], Z. Cresswell[2], S. Guo[3], D. Zhang[2], T. Peterson[2], J. Liu[1], Y. Lv[1], A. Mkhoyan[3] and J. Wang[1] *1. Electrical Engineering, University of Minnesota, Minneapolis, MN, United States; 2. Physics, University of Minnesota, Minneapolis, MN, United States; 3. Material Science, University of Minnesota, Minneapolis, MN, United States*

Unidirectional spin Hall magnetoresistance (USMR) is a magnetoresistance effect with potential applications to read two-terminal spin-orbit-torque (SOT) devices directly. In this work, we observed a large USMR value (up to $0.7*10^{-11}$ per A/cm^2, 50% larger than reported values from heavy metals) in sputtered amorphous $PtSn_4$/CoFeB bilayers. Ta/CoFeB bilayers with interfacial MgO insertion layers are deposited as control samples. The control experiments show that increasing the interfacial resistance can increase the USMR value, which is the case in $PtSn_4$/CoFeB bilayers. The observation of a large USMR value in an amorphous spin-orbit-torque material has provided an alternative pathway for USMR application in two-terminal SOT devices.

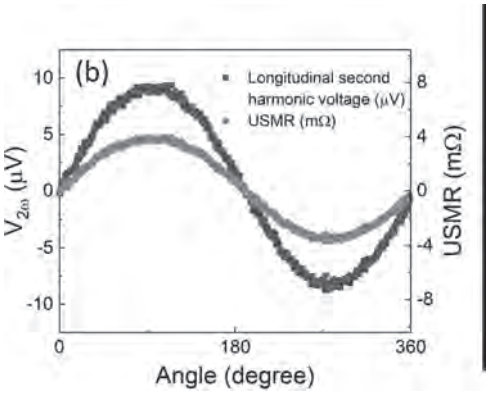

The longitudinal second harmonic angular dependent voltage (black line) and the resulting USMR (red line) under a 5T magnetic field in $PtSn_4$(5 nm)/CoFeB(7.5 nm) bilayers. The left axis is the voltage, and the right axis is the resistance change.

DPA-07. Dependence of TMR and RA on Fe insertion layer thickness in MTJs using $L1_0$-(MnCo)Al electrode and $MgAl_2O_4$ insulating layer. *R. Kikuchi*[1], M. Al-Mahdawi[2], M. Tsunoda[1] and M. Oogane[1] *1. Tohoku University, Sendai, Japan; 2. Center for Science and Innovation in Spintronics (CSIS), Sendai, Japan*

$L1_0$-ordered MnAl, a perpendicularly magnetized film material, has attracted much attention due to its high magnetic anisotropy, low saturation magnetization, and low magnetic damping for spin-transfer-torque magnetic random access memory (STT-MRAM) applications. However, in magnetic tunnel junctions (MTJs) with a single MnAl ferromagnetic layer, the TMR ratio has not been confirmed. This is due to the large lattice mismatch between MgO tunneling barrier and MnAl layer, which prevents the coherent tunneling of Δ_1 electrons [1]. In this work, we utilized Co-doped MnAl and $MgAl_2O_4$ tunneling barrier to reduce lattice mismatch and inserted a very thin Fe layer into (MnCo)Al/MgO interface to improve TMR effect. The structure of the MTJs prepared in this study is shown in Fig.1. The MTJ films were prepared using the ultrahigh vacuum magnetron sputtering method. (MnCo)Al layers with low roughness and high (001) orientation by adding 2% Co. The composition of $MgAl_2O_4$ was measured using X-ray photoelectron spectroscopy (XPS). Compositional analysis showed that the composition of $MgAl_2O_4$ was Mg : Al : O =9.2 : 18.9 : 41.5 (atom%). MTJ devices were microfabricated and characterized their TMR properties by DC 4-probe method. We succeeded in observing a TMR ratio of 8% at 300K without an insertion layer by using (MnCo)Al electrode and $MgAl_2O_4$ tunneling barrier as shown in Fig. 2(a). In addition, TMR ratio was improved to 9.4% by insertion of ultra-thin Fe layer into the (MnCo)Al/MgO interface as shown in Fig. 2(b). This translates to 18.8% in terms of magnetization parallel state. Since the *RA* product was decreased from 1.2 MΩμm^2 to 223 kΩμm^2 by insertion of Fe, coherent tunneling process was thought to be promoted by the interfacial modification. This work was supported by the Center for Advanced Spintronics Research and Development, the Center for Spintronics Cooperative Research and Education and Development, and the Center for Spintronics Cooperative Research and Education, Tohoku University.

[1] H.Saruyama, M.Oogane, Y.Ando, 2013, Jpn. J. Appl. Phys., 52, 063003

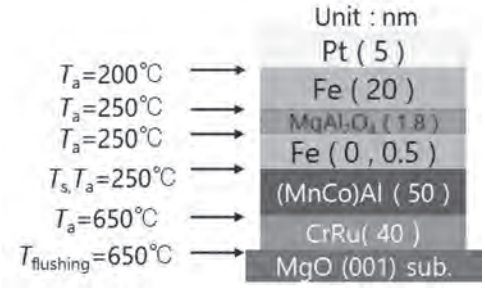

Fig. 1: Schematic illustration of a (MnCo)Al/Fe/$MgAl_2O_4$/Fe magnetic tunnel junction structure.

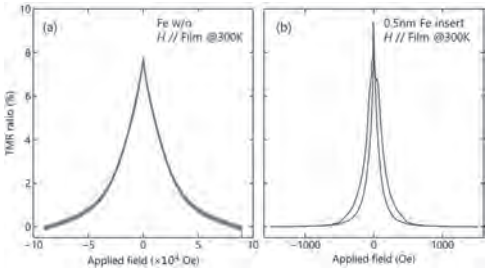

Fig.2 TMR curve for MTJ with (a)(MnCo)Al/$MgAl_2O_4$/Fe (b)(MnCo) Al/Fe/$MgAl_2O_4$/Fe structure when in-plane magnetic field is applied.

DPA-08. CoFeBX layers for MgO-based magnetic tunnel junction sensors with improved noise and detectivity. *F. Matos*[1,2], L. Martins[2], A.B. Azevedo[2], R. Macedo[1], P. Freitas[1,2] and S. Cardoso[1,2] *1. Instituto de Engenharia de Sistemas E Computadores – Microsistemas e Nanotecnologias (INESC MN), Lisbon, Portugal; 2. Instituto Superior Técnico, Lisbon, Portugal*

Magnetoresistive sensors have been enthusiastically selected for applications requiring magnetic field detection with sensors combining small footprint [1], highly linear response curves with low coercivity and low field detectivities. From the viable alternatives [2], MgO-based magnetic tunnel junctions (TMR) offer very competitive performance values, as sensitivity as large as 300 %/mT are reported [3]. The optimization of the sensor response includes using soft magnetic free layers, based on CoFeB and NiFe alloys [4]. Here we report the performance of TMR sensors including CoFeBTa and CoFeBSi soft magnetic films as free layers (FL). Magnetic tunnel junction stacks based on (Ta 5/Ru 10)$_{x3}$/Ta 5/Ru 5/MnIr 8/CoFe 2.2/Ru 0.65/CoFeB 2/MgO/CoFeB/FL2/cap (nm) [fig. 1] were grown on 200 mm wafers using a combination of ion beam and magnetron sputtering deposition from the 14 targets available in the machine. The TMR stacks were magnetically characterized by vibrating sample magnetometry and CIPT, while microfabricated devices (rectangular shaped pillars of varying areas and aspect ratios) were evaluated for transfer curve sensitivity, linear range and noise. The magneto-crystalline anisotropy, H_k, was assessed for CoFeBTa and CoFeBSi films, with values of 2.1 and 5.3 mT measured for 4 nm films integrated in the TMR stacks. Although these values are larger than for single NiFe FL (1.7 mT) [fig. 2], the global performance of the CoFeBTa/CoFeBSi-based sensors is improved, with magnetoresistance of 210 %, when comparing with 190 % (CoFeB) or 150 % (NiFe). Field sensitivities up to 80 %/mT are obtained, with similar hysteresis (H_c) as for CoFeB or NiFe stacks. The low frequency noise (1/f dominated) characteristic was evaluated for the microfabricated devices. As an example, sensors with FL2 = CoFeBTa (10 TMR elements connected in series) provided Hooge factor $\alpha_H = 2.4\text{x}10^{-10}$ μm^2 and detectivity levels of D = 4.5 nT/√Hz at 10 Hz. These values are aligned with previously reported values with similar materials [4]. Acknowledgments: FCT grant UI/BD/151461/2021

[1] M. Silva, D.C. Leitão, S. Cardoso and P. P. Freitas, IEEE Trans. Magn. 53, 7762720 (2017) [2] C. Zheng et al., IEEE Trans. Magn. 55-4, pp. 1-30

(2019) [3] TMR9001, MultiDimension Technology, Datasheet available online: http://www.dowaytech.com/en/1866.html (accessed on 24 June 2022) [4] M. Rasly et al., J. Phys. D: Appl. Phys. 54, 095002 (2021)

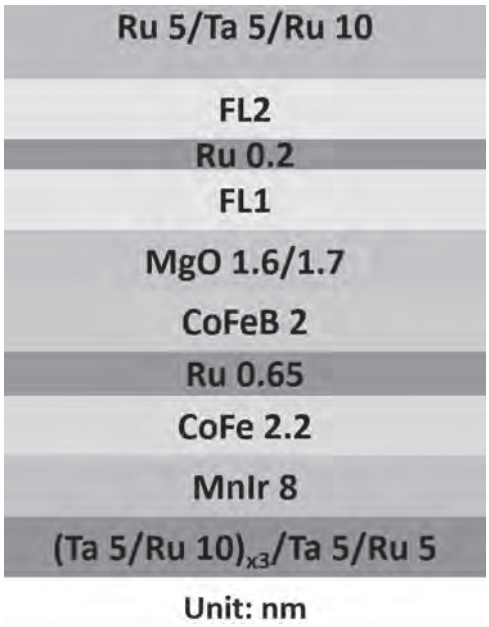

Fig. 1: Magnetic tunnel junction stack structure. FL1: $Co_{38}Fe_{42}B_{20}$, $Co_{40}Fe_{40}B_{20}$; FL2: NiFe, CoFeBTa, CoFeBSi.

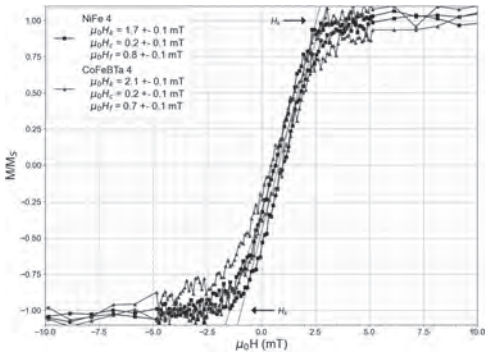

Fig. 2: Hard-axis M-H loops for 4 nm NiFe and CoFeBTa.

DPA-09. Double Barrier s-PMA MTJ-based Logic Locking in Hardware Security. *D. Divyanshu*[1], R. Kumar[1], D. Khan[1], S. Amara[1] and Y. Massoud[1] *1. Computer, Electrical and Mathematical Sciences and Engineering, King Abdullah University of Science and Technology, Thuwal, Saudi Arabia*

Spintronics-based devices offer certain key advantages like ease of fabrication with Si-substrate, non-volatile memory, low operational voltage, and non-linear device characteristics. Hardware security is a research domain that heavily relies on CMOS-based ICs, and the defense and attack mechanism is developed accordingly. In this work, we explore shape anisotropy-based PMA Double barrier MTJ based on Verilog-A behavioral model [1] to design a possible Logic locking [2] system for Hardware Security. Logic Locking is a widely used security mechanism to counter multiple threats [3]. Due to larger free layer thickness, the s-PMA DMTJ has better thermal stability even in the sub-10nm dimension. The current work focuses on Logic locking applications using this device, analyze its behavior under process variation in certain key parameters using Monte-Carlo simulations, and finally performs Eye-diagram performance analyses to test the design for high-speed digital logic applications. The results indicate that the s-PMA DMTJ has good thermal stability, smaller size (10nm dimension), robustness to device imperfections, and ability to work in high-speed digital circuits compared to other emerging MTJ structures such as STT MTJ, SOT MTJ, VG-SOT MTJ, etc. Fig. 1(a) represents the block diagram of the logic Locking block, and Fig. 1(b) represents the circuit for implementing the desired operation. We have performed electrical simulations in TSMC 40nm CMOS generic process design kit using the cadence specter simulator with W/L ratio = 3, the temperature at 300K. Fig. 2(a) and 2(c) represent some circuit performance comparisons like the Eye-diagram test for high-speed circuits, and Table 1 presents the simulation data for the same. Fig. 2(b) shows that VG-SOT MTJ [4] fails the eye-diagram test for similar applications for comparison with s-PMA DMTJ.

H. Wang *et al.,* "Modeling and Evaluation of Sub-10-nm Shape Perpendicular Magnetic Anisotropy Magnetic Tunnel Junctions," *IEEE Transactions on Electron Devices,* vol. 65, no. 12, pp. 5537-5544, Dec. 2018. H. M. Kamali, K. Z. Azar, F. Farahmandi, and M. Tehranipoor, "Advances in Logic Locking: Past, Present, and Prospects," *Cryptology ePrint Archive,* 2022. S. Bhunia, and M. Tehranipoor, "Hardware security: a hands-on learning approach," 1st Edition, 2018. K. Zhang, D. Zhang, C. Wang, L. Zeng, Y. Wang and W. Zhao, "Compact Modeling and Analysis of Voltage-Gated Spin-Orbit Torque Magnetic Tunnel Junction," IEEE Access, vol. 8, pp. 50792-50800, 2020. K. Watanabe *et al.,* "Shape anisotropy revisited in single-digit nanometer magnetic tunnel junctions," *Nature Communication*, 2018.

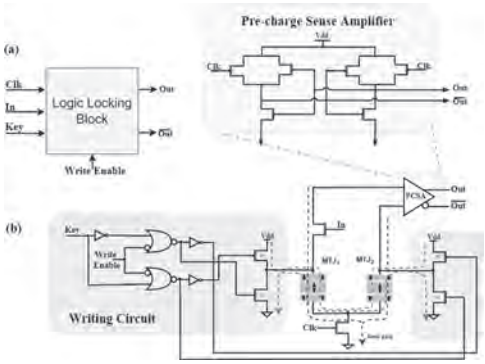

Fig. 1. (a) Logic locking block. (b) 2T MTJ s-PMA DMTJ schematic diagram for logic locking block.

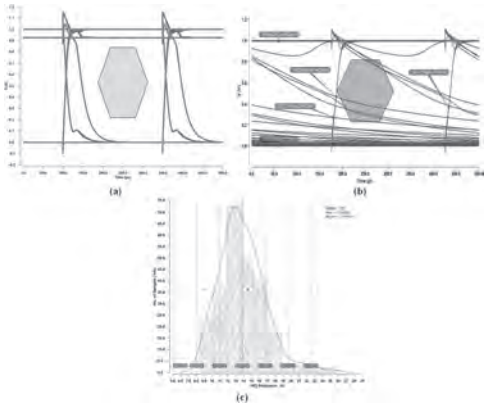

Fig. 2. (a) Eye Diagram test for s-PMA DMTJ. (b) Eye diagram test for VG-SOT MTJ. (c) 250 Times Monte-Carlo simulations result to consider the effect of Process variation.

DPA-10. Hierarchical Cache Configuration Based on Hybrid SOT- and STT-MRAM. *S. Han*[1], Q. Wang[1] and Y. Jiang[1] *1. Electrical Engineering, School of Internet of Things (IoTs), Jiangnan University, Wuxi, China*

With the rapid growth of technologies such as the Internet of Things (IoT) and artificial intelligence (AI) in recent years, giant data transmission and processing capacities of computers have faced major hurdles [1, 2].

At the moment, memory is the key bottleneck in computer processing big data processes. The CPU and the memory are distinct in the standard Von Neumann design, while frequent data exchange uses a lot of energy, resulting in the "Memory Wall" problem [3]. On-chip cache, being the crucial constituent of CPU, accounts for a pivoltal portion of the system's overall power consumption. If the power wastage of the on-chip cache could be lowered, the ultimate performance of the CPU can be strengthened. The typical SRAM-based cache is vulnerable to high static leakage power consumption, and scaling up its capacity is challenging. Magnetic random access memory (MRAM) [4], as a new non-volatile storage technology, is expected to break the limitation at the cache level [5]. In the paper, MRAM cache is used to limit static leakage power consumption. A quad-core CPU MRAM hierarchical cache system is established in the designed MRAM cache, with the high-speed Spin-Orbit-Torque (SOT)-MRAM [6] functioning as the L1 cache and the high-density Spin-Transfer-Torque(STT)-MRAM [7] serving as the L2 shared cache. A non-inclusive allocation method is adopted for the data-exchange strategy, by which the number of the write operation in the L2 STT-MRAM cache is reduced, and the energy consumption of the system is further reduced. The designed system is simulated and verified based on gem5 [8] software framework. The simulation results show that strategy of the hybrid MRAM memory is a promising candidate for high-speed and low-power on-chip cache.

[1] Y. Li, Z. Wang, R. Midya et al., Journal of Physics D: Applied Physics., vol. 51, p.503002(2018) [2] J.-M. Hung, X. Li, J. Wu et al., IEEE Transactions on Electron Devices., vol. 67, p.1444-1453(2020) [3] X. Huang, C. Liu, Y.-G. Jiang et al., Chinese Physics B., vol. 29, p.078504(2020) [4] M. Durlam, P. J. Naji, A. Omair et al., IEEE Journal of Solid-State Circuits., vol. 38, p.769-773(2003) [5] F. Oboril, R. Bishnoi, M. Ebrahimi et al., IEEE Transactions on Computer-Aided Design of Integrated Circuits and Systems., vol. 34, p.367-380(2015) [6] K. Jabeur, L. D. Buda-Prejbeanu, G. Prenat et al., International Journal of Electronics Science and Engineering., vol. 7, p.501–507(2013) [7] D. Apalkov, A. Khvalkovskiy, S. Watts et al., ACM Journal on Emerging Technologies in Computing Systems., vol. 9, p.13:1–13:35, (2013) [8] N. Binkert, B. Beckmann, G. Black et al., ACM SIGARCH computer architecture news., vol. 39, p.1-7(2011)

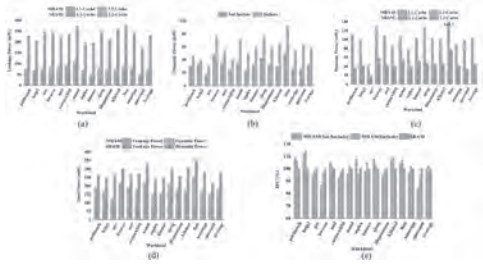

Fig.1. Cache system simulation results. (a) Comparison on the leakage power consumption. (b) Dynamic power consumption results of L2 cache within inclusion and non-inclusion policy.(c) Dynamic power consumption results between MRAM cache and SRAM cache; (d) The total power consumption results between MRAM cache architecture and SRAM architecture; (e) Performance results between MRAM cache architecture and SRAM architecture

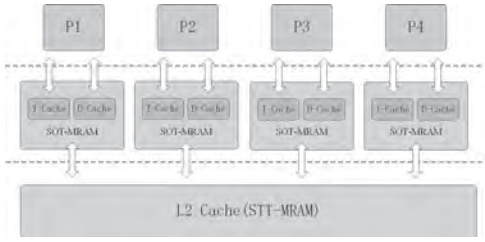

Fig.2. Structure block diagram of MRAM hierarchical cache

DPA-11. High reliability of STT-MRAM with enhanced magnetic immunity. *G. Zhang*[1] and Y. Jiang[1] *1. Department of Electrical Engineering, Jiangnan University, Wuxi, China*

Spin-transfer-torque magnetic random-access memory (STT-MRAM) is one of the promising emerging memory technologies as it offers high speed and non-volatility required for embedded applications such as SOCs, IOTs, and Microprocessors [1].However, due to the magnetic nature of the STT-MRAM, the free layer of the memory cell is sensitive to the external magnetic field and the thermal fluctuation [2]. For the practical application scenarios of STT-MRAM, the memory may be exposed to high external magnetic field for short time. In this way, high immunity is required for the STT-MRAM memory to avoid any possible data errors caused by the external magnetic field. In the paper, the memory model at array level is established to study the immunity property of STT-MRAM. By investigation on the magnetic field distribution of the memory array under different external magnetic field, the three operation modes, including standby, active read and active write modes, are simulated and analyzed. Based on the simulation results, the immunity property and the reliability of the memory array is discussed and optimized. The paper is organized as follows. Firstly, the STT-MRAM array model is established in the HFSS. The magnetic field distribution in the memory array is simulated. The influences of the key geometrical parameters on the magnetic distribution, including the thicknesses of the epoxy and the electrode layer, are investigated. Secondly, to improve the immunity property of the memory, the approach of adding high permeability magnetic shield material is proposed in the paper. Thirdly, the influence of the magnetic immunity on the data reliability of the memory is investigated. The reliability is basically all about data retention and it is determined by effective E_b [3]. And the bit error rates (BERs) of the MTJs under the states of standby, active read and active write, are also analyzed in the paper. Fig.1 The established array model of the STT-MRAM for the immunity investigation. (a) The magnetic field distribution of STT-MRAM array. (b) The magnetic distribution in single STT-MRAM cell.

[1] B. Bhushan, L. T. Guan, D. Shum et al., 2018 IEEE International Memory Workshop (IMW), p. 1-4, (2018). [2] S. Srivastava, K. Sivabalan, J. H. Kwon, et al. Applied Physics Letters, 114(17):172405. (2019). [3] T. Y. Lee, K. Yamane, L. Y. Hau, et al. 2020 IEEE International Reliability Physics Symposium (IRPS). p. 1-4 (2020).

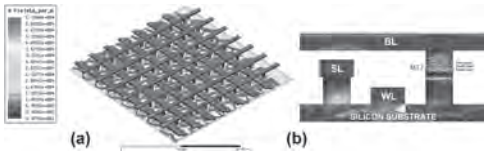

DPA-12. Novel multi-bit parallel pipeline-circuit design for STT-MRAM. *G. Zhang*[1] and Y. Jiang[1] *1. Department of Electrical Engineering, Jiangnan University, Wuxi, China*

Spin transfer torque magnetoresistive RAM (STT-MRAM) is one of the promising emerging memory technologies, with the merits of CMOS-compatibility, fast read speed, high density and non-volatile, *etc.* [1]. However, the write speed is one of the major challenges for STT-MRAM, especially in high speed applications. For a reliable writing operation, high writing current and enough duration time are required, which could decrease the life-time of the tunnel layer in the MTJ device and cause extensive power consumption. So, the writing strategy of the STT-MRAM is one of the key issues in the memory design. Several writing strategies are proposed to improve the writing reliability, lower the power consumption, as well as increase the life-time of the device. In the paper, the pipeline structure combined with the parallel shift register circuit is proposed to achieve the high write efficiency for the STT-MRAM. Figure 1 shows the block diagram of the proposed multi-bit parallel pipeline-circuit. In the designed circuit, the introduction of bit-parallel processing is essential to achieve high throughput operation [2].The parallel shift register circuit is added in the STT-MRAM to allow serial data to be transferred to the sensing circuit in parallel. Moreover,

the pipeline structure is also utilized in the peripheral circuit. Several latches operating in response to a clock signal to process the data by dividing the write operation into a plurality of stages [3]. Thus, the multi-bit parallel data can be carried out in pipelining manner, greatly increasing the average write speed and the throughput of STT-MRAM. The proposed write strategy of STT-MRAM achieves better write efficiency and high throughput, which has potential high speed application of STT-MRAM in the future. Fig.1 The block diagram of the proposed multi-bit parallel pipeline-circuit design for STT-MRAM.

[1] K. Huang, R. Zhao, N. Ning, et al., IEEE Trans. Circuits Syst., vol. 61, p. 2614-2623 (2014). [2] R. Kashima, I. Nagaoka, M. Tanaka, et al. IEEE Trans. Appl. Supercond., vol.99, p. 1-1 (2021). [3] Y. Ma, S. Miura, H. Honjo, et al., Jpn. J. Appl. Phys., vol. 59, p. SG (2020).

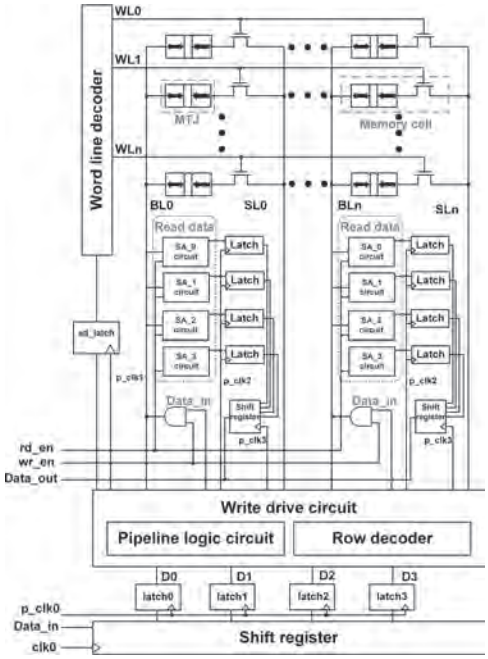

DPA-13. Binary weight network utilizing multi-functional spin-orbit torque device for image recognition. *W. Li*[1], Y. Tao[1], L. Yang[1], F. Jin[1], X. Liu[2], H. Xu[2], X. Wang[2] and K. Dong[1] *1. School of Automation, China University of Geosciences, Wuhan, China; 2. Changxin Memory Technologies, Hefei, China*

Spintronic devices driven by spin-orbit torque (SOT) have a lot of potential for future neuromorphic computing hardware platforms. Nevertheless, problems such as multistate loss, weight time-dependent variability, and output discontinuity ensue when the device size is reduced to the nanoscale, which is contradictory to the needs of traditional high-precision neural networks. In this study, we propose a high-precision all-spin neural network based on magnetization switching of a simple nanoscale multi-functional SOT device. The all-spin neural network is implemented by the Binary Weight Network, in which binary synapse is encoded by the two states formed by the device's deterministic switching and the practical neuron is realized by its stochastic switching probability. Furthermore, we use a difference derivation training algorithm for the general-purpose network in a novel way to be more compatible with the discontinuous neuron output. Using this strategy, our network recognition accuracy can reach ~81.73% on the universal CIFAR-10 dataset, paving the way for the practical hardware implementation of nanoscale SOT devices in high-precision compact neuromorphic computing.

J. Zhou, T. Zhao and J. Chen, Advanced Materials., Vol. 33, p.2103672 (2021) S. Zhang, J. Zhang and L. You, Science China Information Sciences., Vol. 65, p.1-9 (2022)

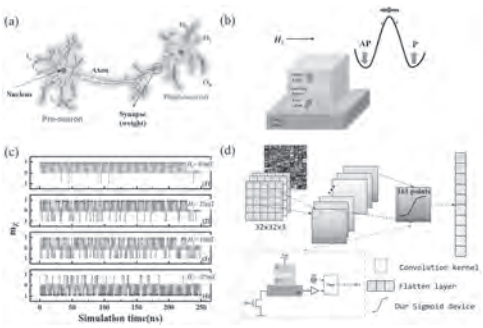

(a) Schematic illustration of a typical biological neuron. (b) Sigmoid neuron implemented by SOT-induced stochastic magnetization switching of FL. (c) Magnetization switching curves are measured at different bias external magnetic fields. (d) Schematic diagram of BWN network structure based on our SOT device. The dotted box represents the schematic diagram of the circuit that simulates a sigmoid neuron.

DPA-14. Switching of an Antiferromagnet with Neuromorphic Functionality. *J. Zubáč*[1,2], M. Surýnek[2], V. Novák[1], P. Němec[2], T. Jungwirth[1,3] and K. Olejník[1] *1. Department of Spintronics and Nanoelectronics, FZU - Institute of Physics of the Czech Academy of Sciences, Prague, Czechia; 2. Faculty of Mathematics and Physics, Charles University, Prague, Czechia; 3. School of Physics and Astronomy, University of Nottingham, Nottingham, United Kingdom*

Antiferromagnetic materials show their potential for the next generation technology due to their exceptional features: Fast terahertz magnetization dynamics, low power consumption and possible high integration density due to no cross-talk among adjacent devices are desirable for data storage and manipulation as well as for applications in unconventional computing. Among antiferromagnets, tetragonal CuMnAs proved its uniqueness for possible ultimate scaling of its magnetic textures down to the atomic level [1], analogue multilevel storage capability and the possibility of writing using a single stimulus at a broad range of timescales – from a millisecond electrical pulse to a femtosecond laser pulse [2]. These characteristics, combined with the availability of conventional electrical readout of the magnetic state, make CuMnAs an ideal testbed material for exploring novel neuromorphic functionalities. Here, we focus on the material's response to multiple optical or electrical pulses. By studying temporal correlations of two subsequent femtosecond laser pulses, we test the readiness of CuMnAs to operate at ultrashort timescales. We also demonstrate the ability to recognize the order of inequivalent pulses and investigate the multilevel character of the CuMnAs memory by applying electrical pulse sequences.

[1] F. Krizek, S. Reimers, Z. Kašpar, et al. Science advances., Vol. 8.13, p. eabn3535 (2022) [2] Z. Kašpar, M. Surýnek, J. Zubáč, et al. Nature Electronics., Vol. 4.1, p. 30-37 (2021)

DPA-15. Investigation of electronic structure of FeAlSi epitaxial films with soft magnetic property for MTJ based-sensor applications. *S. Akamatsu*[1], T. Nakano[1], M. Al-Mahdawi[1,2], M. Tsunoda[2,3], Y. Ando[1,2] and M. Oogane[1,2] *1. Department of Applied Physics, Graduate School of Engineering, Tohoku University, Sendai, Japan; 2. Center for Spintronics Research Network, Tohoku University, Sendai, Japan; 3. Department of Electronic Engineering, Graduate School of Engineering, Tohoku University, Sendai, Japan*

Ferromagnetic materials with a high tunnel magnetoresistance (TMR) and low anisotropy are required to improve the performance of magnetic tunnel junctions (MTJs) sensors. We focused on Sendust alloy ($Fe_{73.7}Al_{9.7}Si_{16.6}$) with excellent soft magnetic properties [1]. However, the electronic structure of $D0_3$-ordered FeAlSi, especially the Δ_1 band that is important to achieve a high TMR, has not been sufficiently investigated. In this study, we investigated TMR effect, tunneling conductance curves, and tunneling anisotropic

magneto-resistive (TAMR) effect in MTJs with FeAlSi epitaxial electrode to clarify the electronic structure of $D0_3$-ordered FeAlSi. The stacking structure was MgO-subs./MgO (20)/FeAlSi (30), T_a = 400 °C/MgO (2)/CoFeB (3)/Ru (0.85)/CoFe (5)/IrMn (10)/Ta (5)/Ru (10) (nm), T_a = 325 °C with 1T. The TMR and TAMR effects were investigated using DC 4-probe method and conductance curves were measured by AC lock-in technique. Fig. 1 shows the T dependence of the TMR curves. A relatively high TMR ratio of 104% (180%) was observed at room temperature (10 K), and the spin polarization of FeAlSi estimated from the TMR ratio at 10 K was 0.58 comparable to Fe [2]. Fig. 2 (a) shows the conductance curves measured at 10 K. In the parallel magnetic configuration, a peak observed near zero bias can be attributed to the tunneling through the interfacial resonant states of mixed Δ_1 and Δ_5 bands [3]. The results of TAMR measurements are shown in Fig. 2 (b). The peak around +0.1 V is due to the hybridization of the Δ_1 up-spin and the Δ_5 down-spin bands of FeAlSi as reported for MTJs with Fe electrodes [3], and this peak was observed as the broad shoulder around +0.1 V in the AP curve in Fig. 2 (a). From these results, we believe that the $D0_3$-ordered FeAlSi has a highly spin-polarized Δ_1 band at the Fermi level. This work was supported by the JSPS Grants-in-Aid for Scientific Research, the GP-Spin Program of Tohoku University, the NEDO Leading Research Project, CSIS of Tohoku University, and CIES of Tohoku University. Fig. 1. T dependence of TMR curve. Fig. 2 (a) G vs V_{Bias} for parallel (red) and anti-parallel (blue) configurations. (b) TAMR = $(G_{in\ plane}\text{-}G_{out\ of\ plane})/G_{out\ of\ plane}$ (%) vs V_{Bias}.

[1] S. Akamatsu, et al., *Appl. Phys. Lett.* 120, 242406 (2022). [2] S. Yuasa *et al.*, *Jpn. J. Appl. Phys.* 43, L588 (2004). [3] Y. Lu *et al.*, *Physical Review B* 86.18, 184420 (2012).

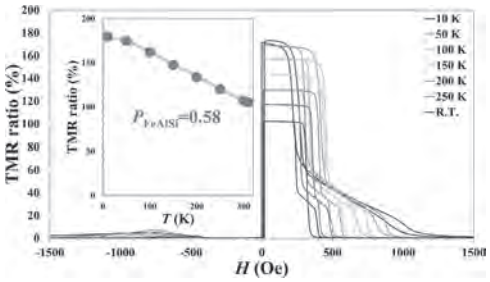

Fig. 1

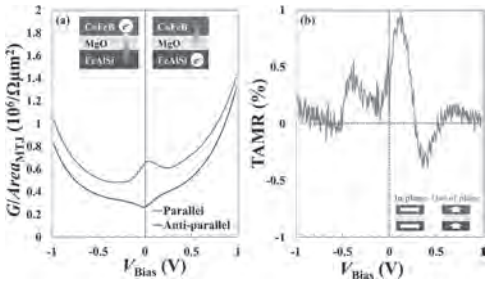

Fig. 2

Session EOA
ANTIFERROMAGNETIC SPINTRONICS I

Kab-Jin Kim, Co-Chair
Korea Advanced Institute of Science and Technology, Daejeon, The Republic of Korea
Myoung-Woo Yoo, Co-Chair
University of Illinois at Urbana-Champaign, Urbana, IL, United States

INVITED PAPER

EOA-01. Observation of the spin splitting torque and its inverse effect in an antiferromagnet. *C. Song*[1], H. Bai[1] and X. Fan[2] *1. Tsinghua University, Beijing, China; 2. Lanzhou University, Lanzhou, China*

The spin splitting torque (SST) was theoretically proposed to combine advantages of conventional spin transfer torque (STT) and spin-orbit torque (SOT) as well as enable controllable spin current [1]. This talk presents experimental evidences of SST and the inverse effect in collinear antiferromagnet RuO_2 films. First, according to spin torque ferromagnetic resonance (ST-FMR) measurements of RuO_2 films, we exhibit that spin current direction is correlated to the crystal orientation of RuO_2 and spin polarization direction is dependent on (parallel to) the Néel vector, indicating the existence of SST in RuO_2 [2]. Second, based on spin Seebeck effect and THz emission measurements, we demonstrate that inverse SST effect can convert spin current polarized along Néel vector into charge current, which manifests as Néel vector-dependent spin Seebeck voltage signals and THz emission signal [3]. These findings not only presents a new member for the spin torques besides traditional STT and SOT, but also proposes RuO_2 for both promising spin source and spin sink for spintronics.

[1] R. González-Hernández, *et al*., Phys. Rev. Lett. 126, 127701 (2021). [2] H. Bai, C. Song, *et al*. accpeted by Phys. Rev. Lett. 128, 197202 (2022). [3] H. Bai, C. Song, *et al*. In preparation.

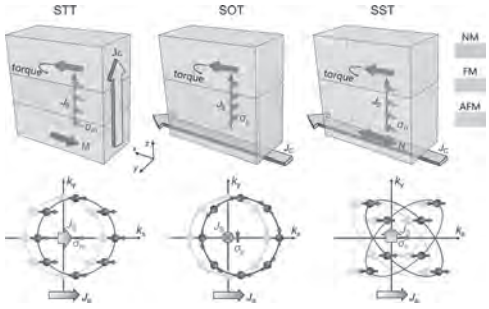

Comparison of STT, SOT, and SST.

CONTRIBUTED PAPERS

EOA-02. Withdrawn

EOA-03. Anomalous Hall effect in Pt/$(Al_{0.04}Cr_{0.96})_2O_3$ epitaxial bilayer. *I. Iino*[1], H. Sakurai[1], T. Tada[1], K. Toyoki[1,2], R. Nakatani[1,2] and Y. Shiratsuchi[1,2] *1. Department of Materials Science and Engineering, Osaka University, Suita, Japan; 2. Spintronics Research Network Division, Osaka University, Suita, Japan*

Recent spintronics revealed that the intrinsic anomalous Hall effect (AHE) emerged from an interplay between the Berry curvature and the spin-orbit coupling. Because the Berry phase theory does not require a spontaneous magnetization for AHE[1], AHE can be applied to antiferromagnetic (AFM) materials. Recently, we reported the hysteresis of AHE voltage as a function of magnetic field for the Pt/AFM-Cr_2O_3/Pt trilayer[2]. The observed AHE should not be simply interpreted because Cr_2O_3 is an insulator, and we proposed the spin chiral texture in the energy bands as an origin[3]. To address the insight of AHE, the correlation with the magnetization is helpful[1], which is difficult for Cr_2O_3 due to its AFM nature. To address this issue, the spontaneous magnetization is induced in the Cr_2O_3 thin film by Al doping[4] and investigated the correlation with AHE. Pt(2 nm)/Al-doped Cr_2O_3(200 nm) bilayer was fabricated on α-Al_2O_3(0001) substrate by a DC magnetron sputtering. Al was doped by the cosputtering with Cr in the Ar and O_2 mixed gas. Composition ratio was determined by XRF: Al/Cr = 4/96. Structural characterizations revealed that each layer grew in Pt(111)/$(Al,Cr)_2O_3$(0001). Magnetization was measured by VSM. AHE was measured using the Hall device fabricated by photolithography and Ar ion milling. Fig.1 shows the *M-H* curve and the AHE loop at 200 K for the perpendicular magnetic field. The spontaneous magnetization, ~18 emu/cc is similar to the previous report[4]. Loops show the rectangular hysteresis showing the perpendicular magnetic anisotropy. Reversal fields are similar for two loops. Temperature dependences of the remanent magnetization M_r and the remanent anomalous Hall resistivity σ_{xy} are shown in Fig.2. Although M_r monotonically decreases with increasing temperature, σ_{xy} first increase, show the maximum and decrease again. The similar temperature dependence of σ_{xy} was reported for other systems where the AHE is associated with the Berry phase. This similarity supports the Berry phase origin of AHE at the Pt/Cr_2O_3 interface.

[1] N. Nagaosa, J. Sinova, S. Onoda, *et al*., Rev. Mod. Phys. 82, 1539 (2010). [2] X. Wang, K. Toyoki, R. Nakatani, Y. Shiratsuchi, AIP Advances, 12, 035216 (2022). [3] T. Moriyama, Y. Shiratsuchi, T. Ono *et al.*, Phys. Rev. Appl. 13, 034052 (2020). [4] T. Nozaki, M. Al-Mahdawi, Y. Shiokawa, *et al*., Phys. Status Solidi RRL, 12, 180036 (2018).

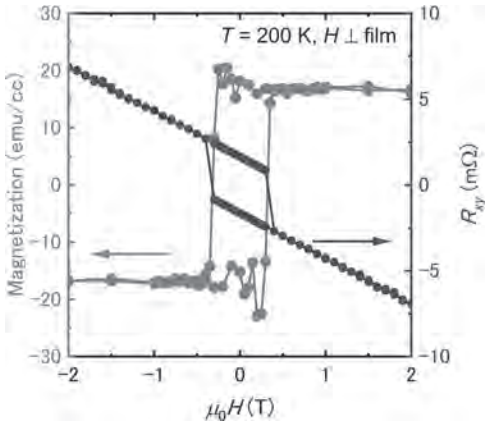

Fig. 1 *M-H* curve (left) and AHE loop (right) at 200 K. Field direction was perpendicular to the film plane.

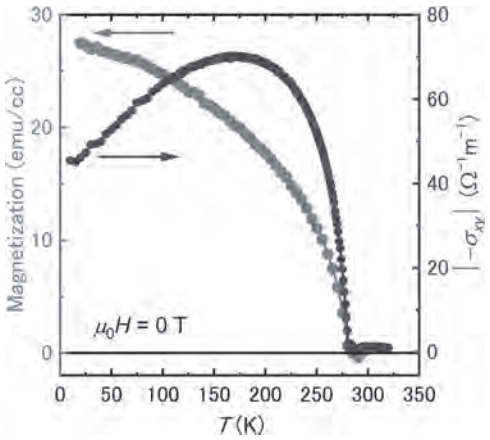

Fig. 2 Temperature dependence of remanent magnetization (left) and AHE resistivity (right).

EOA-04. Spin-Orbit Torque Switching Of Non-Collinear Antiferromagnet Mn_3NiN. *P. Madhusudan Rao*[1], B.K. Hazra[1], B. Pal[1], J. Jeon[1], J. Yoon[1] and S. Parkin[1] *1. Nanosystems for Ions, Spins and Electrons, Max Planck Institute of Microstructure Physics, Halle (Saale), Germany*

Electrical manipulation of magnetisation in Non-Collinear Antiferromagnets (NCAFM) is at the heart of future spintronic devices. So far, current-induced switching has been achieved only in the triangular AFM phase of Mn_3Sn [1]. The magnetic phase transitions in Mn_3Sn as a function of temperature changes from the triangular AFM phase to spiral and then to the spin glass phase, limiting the possibility of further investigation [2]. This limitation can be overcome in Mn_3NiN, as it has an NCAFM structure below Néel temperature, with no phase transition. This provides a platform to explore the magnetisation switching mechanism in a wide temperature range. Mn_3NiN is an fcc crystal with Mn atoms occupying the face positions of a unit cell, forming a Kagome lattice [3]. In addition to the large anomalous Hall effect, giant piezomagnetism in strained films has also been experimentally observed in this material, giving additional control over magnetism [3,4]. In this report, we demonstrate Spin-Orbit Torque (SOT) switching for different thicknesses in Mn_3NiN (001) thin films grown epitaxially on LSAT (001) substrate. The spin Hall effect in Pt overlayer provides the torque required to switch the spin states. Anomalous Hall Conductivity (AHC) measurements reveal maxima at 5 K, which decreases systematically with an increase in temperature. AHC vanishes at 230 K, consistent with previous reports [3]. We show deterministic magnetisation switching of a thick Mn_3NiN layer in the presence of an in-plane bias field (Fig. 2). SOT switching magnitude varies non-monotonically with the strength of the bias field whereas the critical current density remains independent. This observation deviates from the typical SOT switching mechanism in ferromagnets but follows the trend reported recently in Mn_3Sn [5]. We also explore the current-induced magnetisation reversal as a function of temperature to understand the role of heating. Our study provides fruitful insight into understanding the switching mechanism of Mn_3NiN.

[1] H. Tsai, T. Higo, K. Kondou, *Nature,* 580, 608–613 (2020) [2] N. H. Sung, F. Ronning, J.D. Thompson, *Applied Physics Letters*, *112*(13), 132406 (2018) [3] D. Boldrin, I. Samathrakis, J. Zemen, *Physical Review Materials*, *3*(9), 094409 (2019) [4] D. Boldrin, A. P. Mihai, B. Zou, *ACS applied materials & interfaces*, *10*(22), 18863-18868 (2018) [5] B. Pal, B.K. Hazra, B. Göbel, *Science Advances*, *8*(24), eabo5930 (2022)

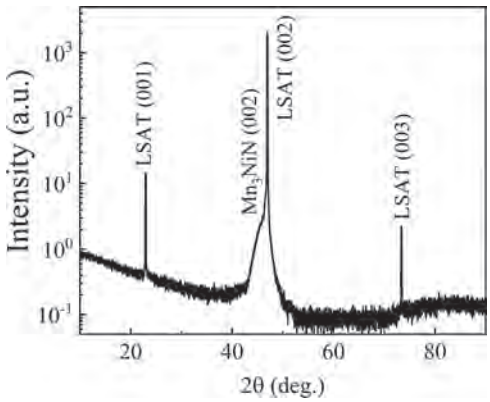

Fig. 1: Out-of-plane X-ray diffraction pattern of Mn_3NiN/Pt films on LSAT (001) substrate.

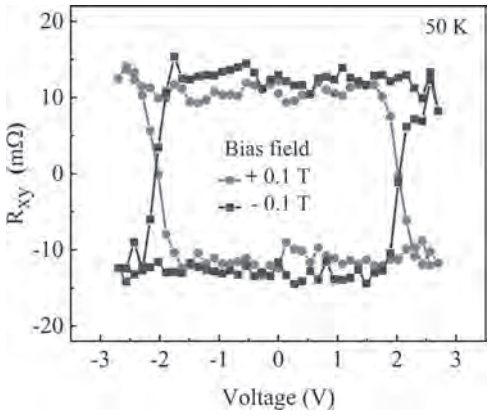

Fig. 2: SOT switching of Mn_3NiN film at 50 K, measured with an in-plane bias field of ± 0.1 T.

EOA-05. Nonlinear Hall effect in antiferromagnet/heavy-metal bilayers. *S. Shim*[1], M. Mehraeen[2], J. Sklenar[3], J. Gibbons[4], H. Saglam[5], A. Hoffmann[4], S. Zhang[2] and N. Mason[1] *1. Physics, University of Illinois at Urbana-Champaign, Urbana, IL, United States; 2. Physics, Case Western Reserve University, Cleveland, OH, United States; 3. Physics, Wayne State University, Detroit, MI, United States; 4. Materials Science and Engineering, University of Illinois at Urbana-Champaign, Urbana, IL, United States; 5. Electrical and Computer Engineering, Princeton University, Princeton, NJ, United States*

The observation of the unidirectional magnetoresistances (UMR) in spin-orbit coupled systems [1,2] has attracted a lot of interest because it can provide valuable insights into the transport properties of spin-orbit coupled systems and has potential applications in two-terminal spintronic devices. Recently, it has been demonstrated that UMR can emerge in an antiferromagnetic heterostructure when there is a spin canting in the collinear

antiferromagnet [3]. Such antiferromagnetic UMR has been attributed to the combined actions of the Rashba spin-orbit coupling at the interface and the antiferromagnetic spin canting. Here, we report a possible transverse contribution of the antiferromagnetic UMR – the nonlinear Hall effect (NLHE)- in the FeRh/Pt bilayer. We identify the NLHE signal with a field dependence similar to the antiferromagnetic UMR and different from the thermoelectric effects or nonlinear contributions of the spin-orbit torque – it undergoes a sign change with the magnetic field and its magnitude is comparable to its longitudinal counterpart [3]. Our results can motivate future studies on the emergent transport phenomena in antiferromagnets and help design novel antiferromagnetic spintronics devices.

[1] C. O. Avci et al., Nat. Phys. 11, 570-575 (2015). [2] T. Guillet et al., Phys. Rev. Lett. 124, 027201 (2020). [3] S. Shim, M. Mehraeen et al., Phys. Rev. X., in press

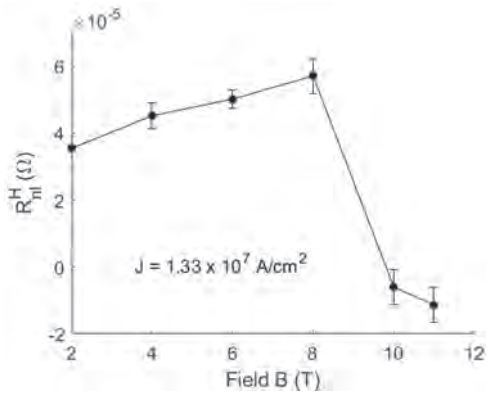

Figure 1: Field dependence of nonlinear Hall contribution R^H_{nl} in FeRh (15 nm)/Pt (5 nm), due to the anti-damping spin-orbit torque (AD-SOT), thermoelectric effect, and possibly the antiferromagnetic UMR. Sign change in nonlinear Hall contribution with respect to the field is not expected for AD-SOT or thermoelectric effect.

EOA-06. Observation of Short-Period Helical Spin Order in Nonchiral Centrosymmetric Helimagnet MnCoSi. *B. Ding*[1], Y. Yao[1], Y. Lau[1] and W. Wang[2] *1. Institute of Physics, Chinese Academy of Sciences, Beijing, China; 2. Tiangong University, Tianjing, China*

Recent development of next-generation information storage has been focused on applications exploiting the spin degree of freedom. Much attention has been given to helimagnets in which the direction of the spins spatially rotates in a plane perpendicular to their propagation vector. With application of external magnetic field, the ground state of stripes transforms into various nontrivial spin textures with unique topological numbers, such as skyrmion tubes[1], skyrmion bubbles[2], and magnetic solitons[3, 4]. In this talk, we will show that the pure helical orders with a period of approximately 3.6 nm was observed in the single crystals of meta-magnet MnCoSi[5]. To elucidate the internal 3D magnetic spiral configurations in real space, the multi-azimuth and multi-angle imaging approach of Lorentz transmission electron microscopy (LTEM) was applied, see Figure 1. The sinusoidal modulation of the line profile outlines the stripes with a period (*L)* of 3.6 nm along the [001] direction. The short-period spin order is further verified by satellite spots adjacent to the main reflections in the enlarged selected area electron diffraction (SAED) patterns. The serial-tilting characterization for the [100] thin plate confirms the stable appearance of periodic stripes along different crystallographic directions. These results strongly imply that a robust and ultrafine helical magnetic order exists in the non-chiral metallic metamagnet MnCoSi at room temperature. The discovery of nanometric spin order in MnCoSi can path a way towards interesting spintronic applications, notably the realization of a room-temperature emergent inductor.

1. M. T. Birch, D. Cortés-Ortuño, L. A. Turnbull, et al., Nat. Commun. 11 (1), 1726 (2020). 2. X. Z. Yu, Y. Onose, N. Kanazawa, et al., Nature 465 (7300), 901-904 (2010). 3. B. Roessli, J. Schefer, G. A. Petrakovskii, et al., Phys. Rev. Lett. 86 (9), 1885-1888 (2001). 4. T. Nagai, K. Kimoto, K. Inoke, et al., Phys. Rev. B 96 (10) (2017). 5. B. Ding, J. Liu, H. Li, et al., Adv. Funct. Mater. 32 (19), 2200356 (2022).

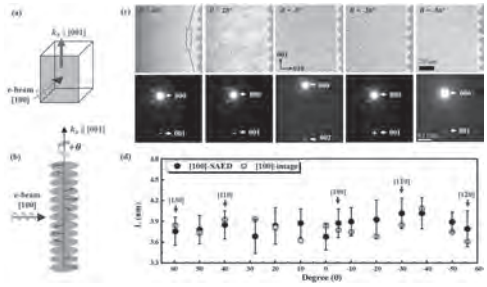

Figure 1. Angular dependence of magnetic spin textures. a) Schematic figure of the [100] specimen obtained by LTEM observation. b) The experimental setup for serial-tilting imaging in which the specimen was swayed around the screw axis (*c* axis). c) Under-focused images and corresponding SAEDs at various tilt angles. d) The measured spiral period as a function of tilted angle. The black scatters and red open circles represent the data from SAEDs and images, respectively.

INVITED PAPER

EOA-07. Long-range supercurrents through a chiral non-collinear antiferromagnet in lateral Josephson junctions. *K. Jeon*[1,3], B.K. Hazra[3], K. Cho[4,3], A. Chakraborty[3], J. Jeon[3], H. Han[3], H. Meyerheim[3], T. Kontos[2] and S. Parkin[3] *1. Physics, Chung-Ang University (CAU), Seoul, The Republic of Korea; 2. ENS, Université PSL, CNRS, Paris, France; 3. Max Planck Institute (MPI) of Microstructure Physics, Halle/Saale, Germany; 4. Korea Institute of Science and Technology (KIST), Seoul, The Republic of Korea*

The proximity-coupling of a chiral non-collinear antiferromagnet (AFM) [1,2] with a singlet superconductor allows spin-unpolarized singlet Cooper pairs to be converted into spin-polarized triplet pairs [3,4] thereby enabling non-dissipative, long-range spin correlations [3,4]. The mechanism of this conversion derives from fictitious magnetic fields that are created by a non-zero Berry phase [5] in AFMs with non-collinear atomic-scale spin arrangements [1,2]. In this invited talk, I will describe our recent achievement of long-ranged lateral Josephson supercurrents through an epitaxial thin film of the triangular chiral AFM Mn_3Ge [6]. The Josephson supercurrents in this chiral AFM decay by approximately 1–2 orders of magnitude slower than would be expected for singlet pair correlations [3,4] and their response to an external magnetic field reflects a clear spatial quantum interference. Given the long-range supercurrents present in both single- and mixed-phase Mn_3Ge, but absent in a collinear AFM IrMn, our results pave away for the topological generation of spin-polarized triplet pairs [3,4] via Berry phase engineering [5] of the chiral AFMs. If time permits, I will also present our experimental realization of spin-triplet supercurrent spin-valves (SVs) [7,8] in chiral antiferromagnetic Josephson junctions (JJs) and a direct current superconducting quantum interference device (dc SQUID), the latter of which reveals an intriguing 0-to-π phase transition [8] on top of the SV response to out-of-Kagome plane magnetic fields.

[1] Nakatsuji, S. et al. *Nature* 527, 212 (2015), [2] Nayak, A. K. et al. *Sci. Adv.* 2, e1501870 (2016), [3] Linder, J. & Robinson, J. W. A. *Nat. Phys.* 11, 307 (2015), [4] Eschrig, M. *Rep. Prog. Phys.* 78, 104501 (2015), [5] Xiao, D., Chang, M.-C. & Niu, Q. *Rev. Mod. Phys.* 82, 1959 (2010), [6] Jeon, K.-R. et al, *Nat. Mater*. 20, 1358 (2021), [7] Banerjee, N. et al. *Nat. Comm.* 5, 4771 (2014), [8] Glick, J. A. et al. *Sci. Adv.* 4, eaat9457 (2018).

CONTRIBUTED PAPERS

EOA-08. Control of Néel Vector with Spin-Orbit Torques in an Antiferromagnetic Insulator with Tilted Easy Plane. *P. Zhang*[1], C. Chou[1,2], H. Yun[3], B.C. McGoldrick[1], J.T. Hou[1], A. Mkhoyan[3] and L. Liu[1] *1. Electrical Engineering and Computer Science, Massachusetts Institute of Technology, Cambridge, MA, United States; 2. Physics, Massachusetts Institute of Technology, Cambridge, MA, United States; 3. Chemical Engineering and Materials Science, University of Minnesota, Minneapolis, MN, United States*

Electrical manipulation of spin textures inside antiferromagnets represents a new opportunity for developing spintronics with superior speed and high device density. Injecting spin currents into antiferromagnets and realizing efficient spin-orbit-torque-induced switching is however still challenging. Because of the diminishing magnetic susceptibility, the nature and the magnitude of current-induced magnetic dynamics remain poorly characterized in antiferromagnets, whereas spurious effects further complicate experimental interpretations [1-4]. In this work [5], by growing a thin film antiferromagnetic insulator, α-Fe_2O_3, along its non-basal plane orientation, we realize a configuration where an injected spin current can robustly rotate the Néel vector within the tilted easy plane, with an efficiency comparable to that of classical ferromagnets. The spin-orbit torque effect stands out among other competing mechanisms and leads to clear switching dynamics. Thanks to this new mechanism, in contrast to the usually employed orthogonal switching geometry, we achieve bipolar antiferromagnetic switching by applying positive and negative currents along the same channel, a geometry that is more practical for device applications. By enabling efficient spin-orbit torque control on the antiferromagnetic ordering, the tilted easy plane geometry introduces a new platform for quantitatively understanding switching and oscillation dynamics in antiferromagnets.

[1] P. Zhang, J. Finley, T. Safi, et al., Phys. Rev. Lett. Vol. 123, p. 247206 (2019). [2] Y. Cheng, S. Yu, M. Zhu, et al., Phys. Rev. Lett. Vol. 124, p. 027202 (2020). [3] C. C. Chiang, S. Y. Huang, D. Qu, et al., Phys. Rev. Lett. Vol. 123, p. 227203 (2019). [4] H. Meer, F. Schreiber, C. Schmitt, et al., Nano Lett. Vol. 21, p. 114 (2021). [5] P. Zhang, C.-T. Chou, H. Yun, et al., arXiv:2201.04732 (2022), accepted by Phys. Rev. Lett.

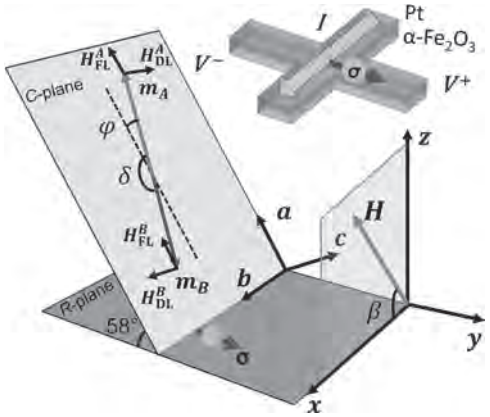

Fig. 1: 30 nm of α-Fe_2O_3 layer was epitaxially grown on an α-Al_2O_3 *R*-plane (0 1 -1 2) substrate and further covered by 5 nm of Pt, and patterned into Hall bar devices. The magnetic easy plane of α-Fe_2O_3 is the tilted *C*-plane (0001). Damping-like torque effective fields H_{DL} rotate the antiferromagnetic sublattice moments m_A and m_B constructively, while the field-like torque H_{FL} does not.

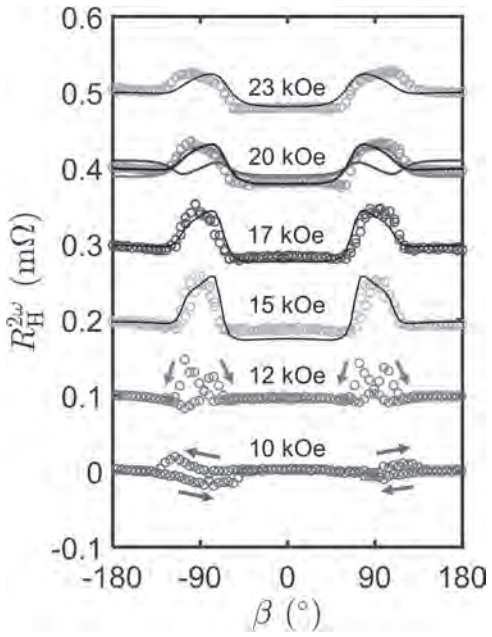

Fig. 2: The angle-dependent second-harmonic Hall resistance $R_H^{2\omega}$ as a function of β, at different external fields. The current is 4 mA (root mean square value). H_{DL} (red) and H_{FL} (blue) contributions to $R_H^{2\omega}$ at H = 20 kOe are separately plotted. H_{DL} corresponds to a damping-like torque efficiency ξ_{DL} = 0.015, comparable to the value of Pt - Ferrimagnetic Insulator bilayers.

EOA-09. Insight into the structural and magnetotransport properties of epitaxial α-Fe_2O_3/Pt(111) heterostructures. *A. Koziol-Rachwal*[1], N. Kwiatek[2], W. Skowronski[3], K. Grochot[3], J. Kanak[3], E. Madej[2], K. Freindl[2], J. Korecki[2] and N. Spiridis[2] *1. Faculty of Physics and Applied Computer Science, Krakow, Poland; 2. Jerzy Haber Institute of Catalysis and Surface Chemistry, Polish Academy of Sciences, Krakow, Poland; 3. Institute of Electronics, AGH University of Science and Technology, Krakow, Poland*

Spintronic devices based on antiferromagnets (AFMs) offer a wide range of unique properties.[1] However, the absence of a net magnetic moment in AFM materials is a challenge for electrical reading of their magnetic state, particularly when the AFM layer is insulating. Recently, the spin Hall magnetoresistance (SMR)[2] was used to probe the direction of spins in insulating AFMs in contact with a heavy metal (HM).[2] For AFMs, a 90° phase shift (so-called "negative" SMR) was observed compared to the SMR observed in ferrimagnet/HM bilayers (known as "positive" SMR) due to the orthogonal alignment of the AFM spins with respect to the external magnetic field exceeding the spin-flop field.[3] A negative SMR was presented for a Pt/α-Fe_2O_3, where hematite layers with thicknesses of a few tens of nanometers were grown by sputtering or pulsed laser deposition on Al_2O_3(0001) single crystals, followed by *in situ* room temperature deposition of thin Pt films.[4],[5] In our studies, we investigated the chemical and magnetotransport properties in the epitaxial α-Fe_2O_3/Pt structure, where hematite α-Fe_2O_3(0001) thin films with thicknesses of 6 nm and 15 nm were grown on a 7-nm thick epitaxial Pt(111) layer on MgO(111). Whereas surface-sensitive methods indicated only the hematite phase, Mössbauer spectroscopy measurements showed that the bulk-like hematite phase contributed 96% and 66% of the total spectral intensity for the thicker and thinner oxide layers, respectively. An SMR study revealed that the chemical structure determines the magnetotransport properties of the α-Fe_2O_3/Pt bilayer. We noted a sign change of the SMR from positive to negative when the thickness of the oxide was increased (Figure1). Finally, for α-Fe_2O_3(15)/Pt, we will demonstrated electrical switching (Figure2). For the as-grown sample, we registered step-like, nondecaying switching between three antiferromagnetic order states, which demonstrates the stability of the interface in our samples.[6]

[1] M. B. Jungfleisch, et al., Physics Letters A 382, 865 (2018). [2] Y. T. Chen et al., Phys. Rev. B 87, 144411 (2013). [3] J. Fischer et al., Phys. Rev. B 97, 014417 (2018). [4] J. Fischer et al., Phys. Rev. Appl. 13, 014019 (2020). [5] Y. Cheng et al., Phys. Rev. Lett. 124, 027202 (2020). [6] A. Koziol-Rachwal et al., in review.

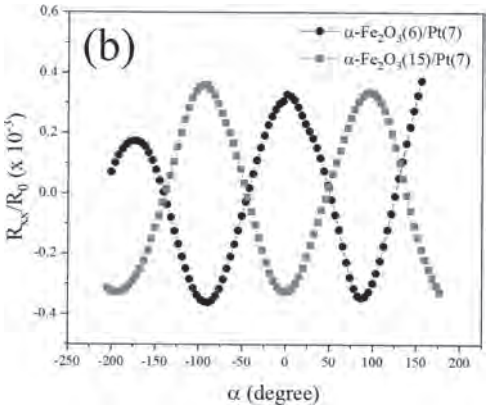

Fig. 1 **Longitudinal SMR for the α-Fe_2O_3(6)/Pt(7) (black circles) and α-Fe_2O_3 (15)/Pt(7) (red squares) bilayers.**

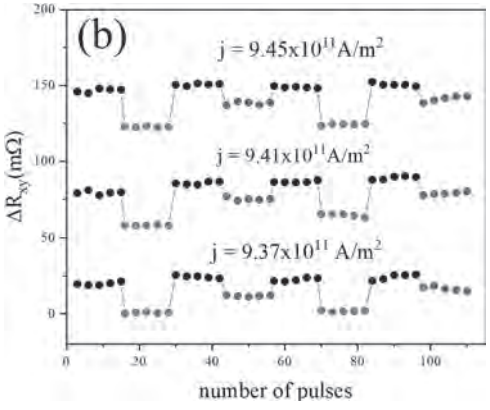

Fig. 2 **Change in the transverse resistance as a function of the number of current pulses applied along the three easy axes of hematite in α-Fe_2O_3(6)/Pt(7).**

EOA-10. Néel spin-orbit torque induced remnant switching of the Néel vector in antiferromagnetic Mn_2Au. Y. Lytvynenko[1,2], S. Reimers[1], Y.R. Niu[3], E. Golias[3], M. Kläui[1,4] and *M. Jourdan*[1] *1. Institute of Physics, Johannes Gutenberg University, Mainz, Germany; 2. Institute of Magnetism of the NAS of Ukraine and MES of Ukraine, Kyiv, Ukraine; 3. MAX IV Laboratory, Lund, Sweden; 4. Norwegian University of Science and Technology, Trondheim, Norway*

Antiferromagnets (AFMs) are strong candidates for future spintronic applications largely because of their fast dynamics and lack of stray fields. For the required switching of the Néel vector (staggered magnetization), the predicted current-induced bulk Néel spin-orbit torque (NSOT) [1] is most promising. Only two compounds with the required symmetry are known: for both CuMnAs [2,3] and Mn_2Au [4,5] experimental evidence for current-induced NSOT was shown based on a small modification of the AFM domain pattern. However, the significance of NSOT for current-induced manipulation of Neel vector orientation stays controversial because competing heating-related mechanisms result in similar effects [6-8]. Here, we investigate the effect of current pulsing with different lengths along the different crystallographic directions on the AFM domain pattern of epitaxial Mn_2Au (001) thin films. In-situ imaging of AFM domains before and after the current pulses was performed using x-ray magnetic linear dichroism photoemission electron microscopy (XMLD-PEEM). Reversible and repeated 90° Neel vector rotation of essentially the complete active area of the pattern cross structures was observed (Fig. 1). Switching was only observed for current parallel to the easy crystallographic axis resulting in a Néel vector rotation perpendicular to the pulse direction, which is consistent with the NSOT. The required current density for switching is essentially independent of the pulse length (10 μs to 1 ms) indicating that thermal activation or other thermal effects are not significant. For current pulses applied parallel to a <100> hard axis, inversion of the current pulse polarity led to a partially reversible motion of domain walls, which is consistent with the NSOT acting on them. Our results confirm the fundamental role of NSOT for current-induced Néel vector switching in Mn_2Au, providing an effective mechanism for spintronics applications.

[1] J. Zelezný H. Gao, K. Výborný *et al.*, Phys. Rev. Lett. 113, 157201 (2014). [2] P. Wadley, B. Howells, J. Zelezný *et al.*, Science 351, 587 (2016). [3] P. Wadley, S. Reimers, M. J. Grzybowski *et al.,* Nat. Nanotechnol. 13, 632 (2018). [4] S. Bodnar L. Smejkal, I. Turek *et al.*, Nat. Commun. 9, 348 (2018). [5] S. Y. Bodnar, M. Filianina, S. P. Bommanaboyena *et al.*, Phys. Rev. B 99, 140409(R) (2019). [6] T. Matalla-Wagner, J.-M. Schmalhorst, G. Reiss *et al.*, Phys. Rev. Res. 2, 033077 (2020). [7] H. Meer, O. Gomonay, C. Schmitt et al., arXiv:2205.02983v1 [cond-mat.mtrl-sci]. [8] H. Meer, F. Schreiber, C. Schmitt *et al.*, Nano Lett.21, 114-119 (2020).

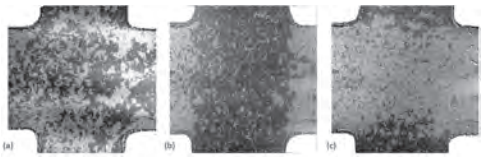

Figure 1: XMLD-PEEM images of the (a) as grown domain configuration of Mn_2Au and (b, c) after the application of a 100 ms single bipolar current pulse with j = 2.9 *10^{11} A/m^2 along perpendicular easy <110> directions.

EOA-11. Probing magnetic anisotropy and spin-reorientation transition in 3D antiferromagnet, $Ho_{0.5}Dy_{0.5}FeO_3$ │Pt using spin Hall magnetoresistance. P. Garg[1], *A.A. Wagh*[1], A. Haldar[2,1], K. Mallick[1], T. Chakraborty[1], S. Elizabeth[1] and P. Kumar[1] *1. Physics Department, Indian Institute of Science, Bengaluru, India; 2. Physics Department, University of Toronto, Toronto, ON, Canada*

Orthoferrites (*RE*FeO_3) containing rare-earth (*RE*) elements are 3D antiferromagnets (AFM) that exhibit characteristic weak ferromagnetism originating due to slight canting of the spin moments and display a rich variety of spin reorientation transitions in the magnetic field (*H*)-temperature (*T*) parameter space [1, 2]. We present spin Hall magnetoresistance (SMR) studies [3] on a *b*-plate (*ac*-plane) of crystalline $Ho_{0.5}Dy_{0.5}FeO_3$ │Pt hybrid at various *T* in the range, 11 to 300 K. In the room temperature $\Gamma_4(G_x, A_y, F_z)$ phase, the switching between two degenerate domains, $\Gamma_4(+G_x, +F_z)$ and $\Gamma_4(-G_x, -F_z)$ occurs at fields above a critical value, $H_c \approx 713$ Oe. Under $H > H_c$, the angular dependence of SMR (α-scan) in the $\Gamma_4(G_x, A_y, F_z)$ phase yielded a highly skewed curve with a sharp change (sign-reversal) along with a rotational hysteresis around *a*-axis. This hysteresis decreases with an increase in *H* (Fig.1). Notably, at $H < H_c$, the α-scan measurements on the single domain, $\Gamma_4(\pm G_x, \pm F_z)$ exhibited an anomalous sinusoidal signal of periodicity 360 deg. Low-*T* SMR curves (*H* = 2.4 kOe), showed a systematic narrowing of the hysteresis (down to 150 K) and a gradual reduction in the skewness (150 to 52 K), suggesting weakening of the anisotropy possibly due to the *T*-evolution of Fe-*RE* exchange coupling. Below 25 K, the SMR modulation showed an abrupt change around the c-axis, marking the presence of $\Gamma_2(Fx,C_y,G_z)$ phase. We have employed a simple Hamiltonian and computed SMR to examine the observed skewed SMR modulation. In summary, SMR is found to be an effective tool to probe magnetic anisotropy as well as a spin reorientation in $Ho_{0.5}Dy_{0.5}FeO_3$. Our spin-transport study highlights the potential of $Ho_{0.5}Dy_{0.5}FeO_3$ for future AFM spintronic devices.

[1] T. Yamaguchi, J. Phys. Chem. Solids, Vol. 35, p.479 (1974) [2] T. Chakraborty and S. Elizabeth, J. Magn. Magn. Mater., vol. 462, p. 78 (2018) [3] Y.-T. Chen, S. Takahashi, H. Nakayama, Phys. Rev. B, vol. 87, p. 144411 (2013)

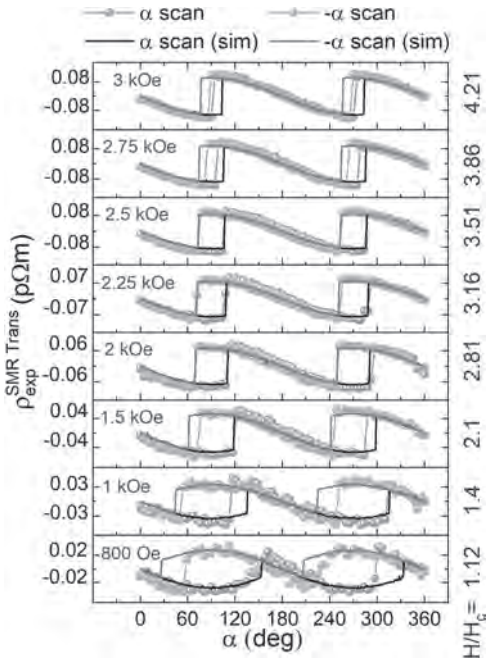

Fig.1: Experimentally measured transverse SMR (α and -α scans) curves are shown for various magnetic field values (range: 800 Oe to 3 kOe) just above a critical field (H_c = 713 Oe) and simulated SMR data at various corresponding normalized magnetic fields, denoted by H/H_c values (H/H_c = 1.12, 1.4, 2.1, 2.81, 3.16, 3.51, 3.86 and 4.21), are plotted.

EOA-12. Injection Locking of Antiferromagnetic Oscillators.

P.G. Elphick[1,2], V. Tyberkevych[1] and A.N. Slavin[1] *1. Oakland University, Rochester, MI, United States; 2. Kostal North America, Troy, MI, United States*

Spin Hall antiferromagnetic oscillators (AFMO) [1] are a promising candidate for a CMOS-compatible THz-range frequency source. The output power of a nano-scale AFMO is relatively low, and mutual synchronization of AFMOs may be used to increase the power and to reduce the generation linewidth. The first step in understanding AFMO synchronization is to investigate the injection locking of a single oscillator, i.e., synchronization to an external driving signal. Here, we numerically study the injection locking of AFMOs using the model derived in [1]. In contrast with previous studies [2, 3], we study injection locking in a wide range of AFMO frequencies and assume that the driving signal is mixed with the DC bias current, i.e., that the bias and locking spin currents have the same spin polarization, which is more suitable for practical realization. Figure 1 shows a dependence of the driven AFMO frequency f on the injected frequency f_s. Straight segment near the AFMO free-running frequency f_0 = 0.23 THz corresponds to the injection locking at the fundamental signal harmonic. The huge locking bandwidth $\Delta f_1 \approx 100$ GHz is due to strong influence of AFMO nonlinearity related to anisotropy of the antiferromagnet [1]. An additional signature of a strongly nonlinear regime is the appearance of higher-order locking bands $f=2f_s$ and $f=3f_s$. Synchronization at higher harmonics may be important in practical applications, since it allows one to synchronize THz-range AFMO by a driving signal of a lower frequency. The synchronization bandwidth Δf_1 drastically reduces with the increase of AFMO free-running frequency f_0 (Fig. 2). This effect is caused by reduction of AFMO nonlinearity and may be a serious obstacle for practical use of AFMOs in the frequency range $f > 1$ THz. Therefore, alternative methods of AFMO injection locking should be studied, such as locking to a microwave magnetic field or to a spin current with different spin polarization [2].

[1] R. Khymyn, et al., "Antiferromagnetic THz-frequency Josephson-like oscillator driven by spin current", *Sci. Rep.* 7, 43705 (2017). [2] O. Gomonay, T. Jungwirth, and J. Sinova, "Narrow-band tunable terahertz detector in antiferromagnets via staggered-field and antidamping torques", *Phys. Rev. B* 98, 104430 (2018). [3] R. Khymyn, et al., "Injection-locking of a nonlinear sub-THz antiferromagnetic spin-Hall oscillator", DE-08, Abstracts of the International Magnetics Conference INTERMAG-18, Singapore, Singapore, April 2018.

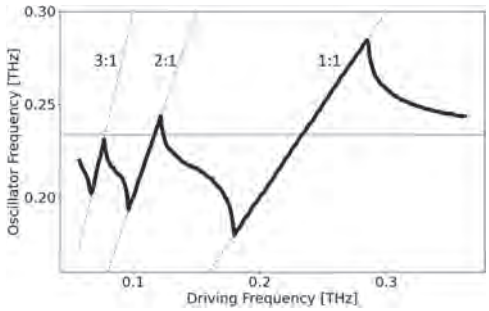

Fig.1 Driven AFMO frequency f vs the frequency of the driving signal f_s. Horizontal line at f_0 = 0.23 THz shows the AFMO free-running frequency. Straight dashed lines show exact relations $f=3f_s$, $f=2f_s$, $f=f_s$ and.

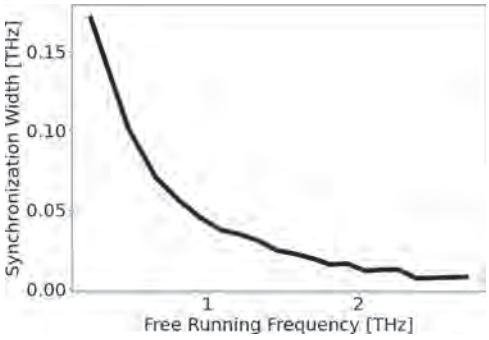

Fig.2 AFMO synchronization width vs. the oscillator's free-running frequency.

EOA-13. Out of plane spin-polarized current from Mn_3Sn/Py interface.

B.K. Hazra[1], B. Pal[1], J. Jeon[1] and S. Parkin[1] *1. NISE, Max Planck Institute of Microstructure Physics, Halle (Saale), Germany*

The spin Hall effect (SHE)[1] allows for the generation of spin currents from charge currents that are passed through the interior of metallic layers. The polarization of the spin current is typically observed to lie in the plane of the metallic layer but the quest for out-of-plane polarized[2-4] spin currents has attracted much attention as they could be used to manipulate perpendicularly magnetized film without any external magnetic field. The polarization direction of the spin current that is generated in conventional non-magnetic metals is always even under time-reversal symmetry, but it has been predicted that currents passed through non-collinear AFs, such as the Mn_3X family (X= Sn,Ir), can give rise to additional spin currents that are odd under time reversal symmetry[5]. Subsequently, a dominant odd SHE along with a small even SHE was observed in single crystals of Mn_3Sn. The odd SHE was described as a "magnetic SHE" and claimed to be related to the AF structure[6-7]. In the present study, we explore the SHE generated in epitaxial thin films of Mn_3Sn (0001) via studies of the spin torque (SOT) on epitaxial layers of ferromagnet permalloy ($Ni_{80}Fe_{20}$=Py), which are grown on top of the Mn_3Sn films. We observe robust out-of-plane (p_z) and in-plane (p_y) spin-polarized currents for various thicknesses of Mn_3Sn when a charge current is passed through the Mn_3Sn/Py device. p_z and p_y give rise to large in-plane field-like and in-plane anti-damping-like torques respectively. Both

p_z and p_y retain the same sign when large in-plane magnetic fields are applied to reverse the AF structure of the Mn_3Sn layer. By performing temperature-dependent SOT, we demonstrate that p_z is unrelated to the antiferromagnetic structure of Mn_3Sn whereas p_y strongly depends on the antiferromagnetic structure. The temperature dependence measurements further show that p_z has an extrinsic interfacial origin.

1. Sinova, J. *et al. Phys. Rev. Lett.* 92, 126603 (2004). 2. Nan, T. *et al. Nat. Commun.* 11, 4671 (2020). 3. Chen, X. *et al. Nat. Mat.* 20, 800-804 (2021). 4. You, Y. *et al. Nat. Commun.* 12, 6524 (2021). 5. Zelezny, J. et *al. Phys. Rev. Lett.* 119, 187204 (2017). 6. Kimata, M. *et al. Nature* 565, 627-630 (2019). 7. Kondou, K. *et al. Nat. Commun.* 12, 6491 (2021).

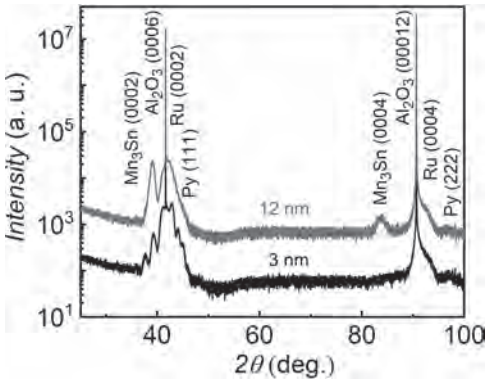

X-ray diffraction pattern of Ru/Mn_3Sn(0001)/Py structures grown on Al_2O_3(0006) substrates.

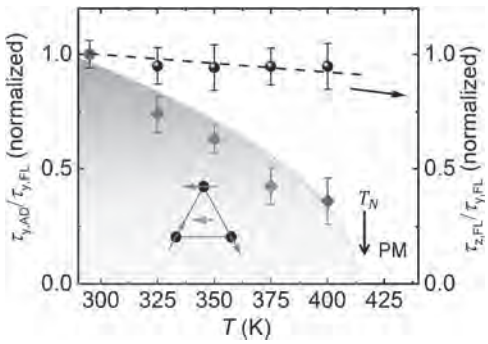

Temperature dependence of normalized torques for Mn3Sn (12 nm)/ Py (5 nm) film.

EOA-14. Symmetry driven large intrinsic magneto-optical signatures in collinear ferrimagnetic and non-collinear antiferromagnetic phases of Mn_3NiN thin films. F. Johnson[1], J. Zázvorka[2], L. Beran[2], D. Boldrin[3], L. Cohen[1], J. Zemen[4] and *M. Veis*[2] *1. Department of Physics, Imperial College London, London, United Kingdom; 2. Institute of Physics, Charles University, Prague, Czechia; 3. School of Physics and Astronomy, University of Glasgow, Glasgow, United Kingdom; 4. Faculty of Electrical Engineering, Czech Technical University in Prague, Prague, Czechia*

Antiferromagnets (AFMs) with frustrated exchange interactions between Mn ions offer unique opportunities for spintronic applications because of their chiral magnetic structures. In case of Mn_3AN (A = Ga, Sn, Ni) systems that support the G^{4g} spin arrangement in the (111) plane, the magnetic symmetry along with Weyl points in the band structure close to the Fermi energy allow for non-zero Berry phase curvature underpinning functional properties below the Néel temperature (TN), such as anomalous Hall effect [1], anomalous Nernst effect [2], and magneto-optical Kerr effect (MOKE) [3]. A long range ordered ferrimagnetic (FIM) phase was also predicted in a strained state of these materials [4]. Here, we present a systematic theoretical and experimental study of magneto-optical response of strained Mn_3NiN films on $BaTiO_3$ substrates in AFM and FIM phase (Fig. 1). The MOKE spectra showed notable evolution across TN as depicted in Fig. 2, confirming existence of a high temperature FIM phase. We employed ab-inito calculations using spin density functional theory and linear response approximation, and symmetry analysis to simulate the MOKE spectra. From the good agreement between the form of the measured and predicted MOKE spectra, we propose the AFM and FIM phases share the magnetic space group C2′/m′ and that the symmetry driven magneto-optic and magneto-transport properties are maximised at room temperature in the FIM phase due to the enhanced intrinsic Berry phase contribution. More detailed comparison between the calculations and the experiment will be discussed. A room temperature FIM phase with large optical and transport signatures, as well as sensitivity to lattice strain and magnetic field has useful prospects for high-speed spintronic applications.

[1] Chen, H., Niu, Q. & MacDonald, A. H. Anomalous Hall Effect Arising from Noncollinear Antiferromagnetism. *Physical Review Letters* 112, 017205 (2014) [2] Ikhlas, M., Tomita, T., Koretsune, T., Suzuki, M.-T., Nishio-Hamane, D., Arita, R., Otani, Y. & Nakatsuji, S. Large anomalous Nernst effect at room temperature in a chiral antiferromagnet. *Nature Physics* 13, 1085-1090 (2017). [3] Johnson, F., Zázvorka, J., Beran, L., Boldrin, D., Cohen, L. F., Zemen, J., Veis, M. Room temperature weak collinear ferrimagnet with symmetry driven, large intrinsic magneto-optic and magneto-transport signatures. *arXiv:2111.13498v2* [4] Zemen, J., Mendive-Tapia, E., Gercsi, Z., Banerjee, R., Staunton, J. B. & Sandeman, K. G. Frustrated magnetism and caloric effects in Mn-based antiperovskite nitrides: Ab initio theory. *Physical Review B* 95, 184438 (2017).

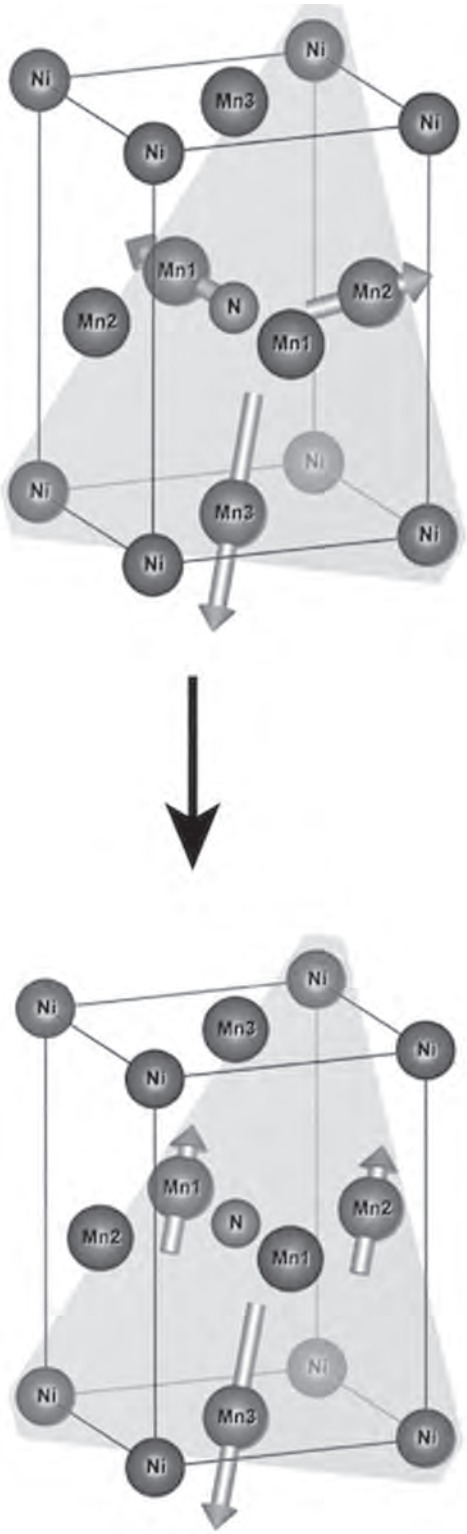

Fig. 1 Schematic picture of the unit cell of Mn_3NiN together with the Mn magnetic moment alignment across the transition from AFM to FIM phase induced by the change of temperature

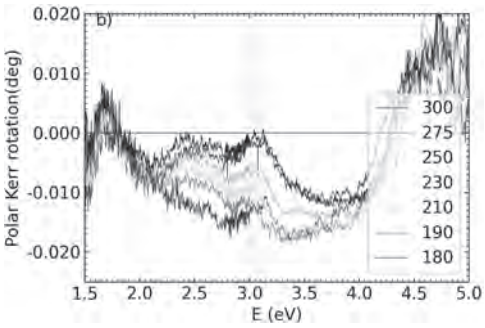

Fig. 2 Temperature evolution of experimental spectra of polar MOKE rotation.

Session EOB
ANTIFERROMAGNETIC SPINTRONICS II

Fernando Ajejas, Chair
University of California, San Diego, San Diego, CA, United States

INVITED PAPER

EOB-01. Magnetic spin Hall and related effects in noncollinear antiferromagnets. *H. Chen[1] 1. Colorado State University, Fort Collins, CO, United States*

Metallic noncollinear antiferromagnets have attracted significant attention in recent years due to their novel prospects and promises in spintronics. In this talk I will introduce several recent theoretical and experimental developments that reveal unconventional functionalities of noncollinear antiferromagnets, in particular the magnetic spin Hall effects (MSHE). Following the original proposal based on the current-induced boundary spin accumulation that changes sign under time reversal in Mn_3Sn [1], we point out that the MSHE can also lead to field-like and damping-like torques that have nontrivial dependence on the antiferromagnetic order parameter [2]. Such torques can be described in a unified manner in terms of a spin density response to electric field. Among them the field-like torque due to the MSHE has an intrinsic nature and can become large in the presence of noncollinear antiferromagnetic order. I will also talk about our recent work on a new class of indicators of the anomalous Hall effect in metallic magnets with unconventional order, named as electronic chiralization [3] and on the use of a "modern theory" of magnetic multipole moments to understand and manipulate noncollinear magnetic order. *HC acknowledges support by NSF CAREER grant DMR-1945023.

[1] M. Kimata, H. Chen, et al. Nature 565, 627 (2019). [2] K. Kondou, H. Chen, et al. Nature Communications 12, 6491 (2021). [3] H. Chen, arXiv:2202.03581

CONTRIBUTED PAPERS

EOB-02. Controlling Antiferromagnetic Domains by Current-Induced Switching and Shape Anisotropy. *H. Meer[1]*, O. Gomonay[1], F. Schreiber[1], C. Schmitt[1], R. Ramos[2,3], L. Schnitzspan[1], M. Mawass[4], F. Kronast[4], S. Valencia[4], E. Saitoh[2,5], J. Sinova[1], L. Baldrati[1] and M. Kläui[1] *1. Insitute of Physics, Johannes Gutenberg University of Mainz, Mainz, Germany; 2. WPI-Advanced Institute for Materials Research, Tohoku University, Sendai, Japan; 3. Centro de Investigación en Química Biolóxica e Materiais Moleculares (CIQUS), Departamento de Química-Física, Universidade de Santiago de Compostela, Santiago de Compostela, Spain; 4. Helmholtz-Zentrum Berlin für Materialien und Energie, Berlin, Germany; 5. Department of Applied Physics, The University of Tokyo, Tokyo, Japan*

Antiferromagnets (AFMs) could potentially replace ferromagnets (FMs) as active elements in future spintronic devices, due to the need for faster operation speeds, higher energy efficiency, and enhanced robustness against external magnetic fields [1]. However, the absence of a net magnetic moment in AFMs makes it more challenging to control the magnetic order using conventional approaches. Here, we demonstrate how the domains of NiO/Pt bilayers can be controlled by two approaches: electrical currents and AFM shape anisotropy. Previously, different mechanisms have been proposed for the current-induced magnetic switching of insulating AFM/heavy metal bilayers [2–4]. To reveal the acting mechanism, we study the switching by combining concurrent electrical readout and optical imaging with simulations of the current-induced temperature and strain gradients. Comparison of the switching in specially engineered NiO/Pt devices and different pulsing geometries, see Fig. 1, allows us to rule out dominating spin-orbit torque-based mechanisms and identify a thermomagnetoelastic mechanism that governs the switching of AFM domains, reconciling previous contradicting reports [5]. Conventional shape anisotropy in FMs leads to geometrically induced domain structures due to dipolar interactions. In AFMs without net moments, we show how shape-induced strain can be used analogously to control AFM domain structure in epitaxial NiO/Pt thin films, see Fig. 2. By varying the aspect ratio of rectangular elements, we can control of the AFM ground-state domain configuration [6]. Thus, the shape of the device and the strain from the current-induced heating do not only need to be considered in the design of AFM devices, but can potentially be used to tailor their properties, providing convenient handles to control antiferromagnetic domains.

[1] V. Baltz, A. Manchon, M. Tsoi et al., Rev. Mod. Phys. 90, 015005 (2018) [2] T. Moriyama, K. Oda, T. Ohkochi et al., Sci. Rep. 8, 14167 (2018) [3] X. Z. Chen, R. Zarzuela, J. Zhang et al., Phys. Rev. Lett. 120, 207204 (2018) [4] L. Baldrati, O. Gomonay, A. Ross et al., Phys. Rev. Lett. 123, 177201 (2019) [5] H. Meer, F. Schreiber, C. Schmitt et al., Nano Lett. 21, 114 (2021) [6] H. Meer, O. Gomonay, C. Schmitt et al., arXiv:2205.02983 (2022)

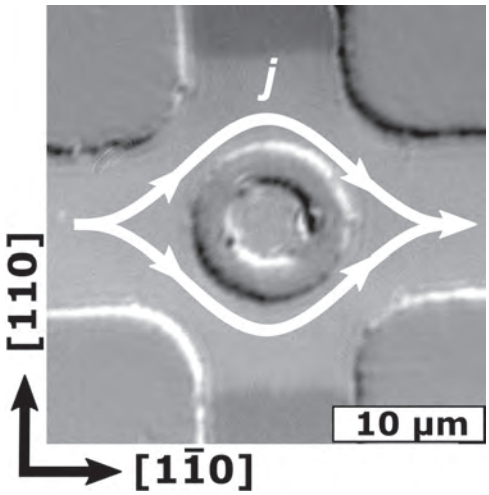

Fig. 1: Birefringence image of current-induced switching of NiO domains in an electrically isolated area. The direction of the current pulse is indicated by the white arrows.

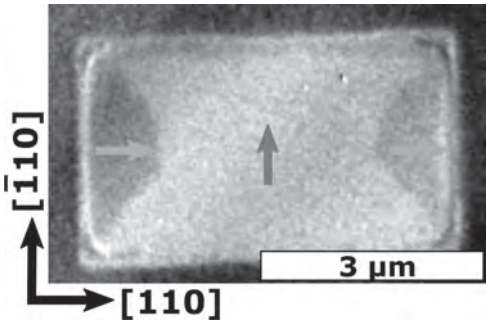

Fig. 2: XMLD-PEEM image of shape-induced NiO domains inside a rectangular element, with edges oriented along the in-plane projection of the easy axes. The in-plane component of the Néel vector in the domains is indicated by the arrows.

EOB-03. Enhancement of Thermal Stability and Switching Efficiency in SOT-MTJs with Antiferromagnetic Channel. *K. Chen*[1], Y. Chang[2], S. Yang[2], Y. Hsin[2], S. Rahaman[2], I. Wang[2], H. Lee[2], Y. Su[2], G. Chen[2], J. Wei[2], S. Sheu[2], W. Lo[2], C. Wu[4,2], C. Lai[3], D. Tang[2] and Y. Tseng[1]
1. National Yang Ming Chiao Tung University, Hsin-Chu, Taiwan; 2. Industrial Technology Research Institute, Hsinchu, Hsin-Chu, Taiwan; 3. National Tsing Hua University, Hsinchu, Taiwan; 4. National Taiwan University, Taipei, Taiwan

This work demonstrates the enhancement of thermal stability and switching efficiency by inserting an ultrathin (< 2nm) PtMn antiferromagnetic layer between CoFeB free layer and W-channel SOT system. The implementation of a baking method[1] at 200°C was necessary for such performance improvement. With the use of Cu-line, the SOT MTJs exhibited a switching time of ~ 5 ns with a tunneling magneto-resistance (TMR) > 100%. We used a switching phase diagram (SPD) method to estimate the built-in effective field per unit current (H_{eff}/current) of the MTJs, and we obtained a larger H_{eff}/current for the PtMn-inserted MTJ (4.654 Oe/mA) than that of the one without PtMn (2.076 Oe/mA). Since SPD was constructed by measuring the TMR change directly on fully-integrated MTJs, the thermal effect has been taken into account. We further discovered that the current direction determined the exchange bias direction. This reduced the unilateral switching current, and resulted in a 220% improvement in the switching efficiency with the PtMn insertion. Therefore, the trade-off between switching current density and thermal stability can be optimized in this circumstance. The heavy metal channel was then changed from W to Ta to test the thermal robustness of the proposed device. Without PtMn, we obtained a distorted R-H curve due to Ta diffusion, while it disappeared upon a 2-nm PtMn insertion. This is due to the suppression of Ta diffusion and the promotion of anisotropy energy of the free layer.

Ref [1]: L. Thomas et al., *Appl. Phys. Lett.* 106, 162402 (2015)

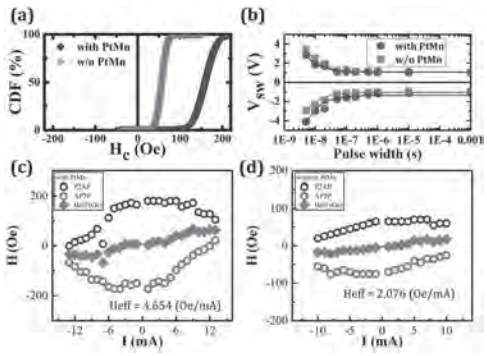

Fig.1: (a) Cumulative distribution function (CDF) output from R-H loops of the SOT-MTJs with PtMn and without PtMn, where H_c can be estimated and it statistically confirmed the enhanced thermal stability of the former. (b) Dependences of switching voltage and pulse width of the SOT-MTJs with and without PtMn, which both exhibited a switching time down to 5 ns. The switching phase diagrams of SOT-MTJs (c) with and (d) without PtMn. The effective fields per unit current (H_{eff}/current) were estimated to be 4.654 and 2.076 Oe/mA for the SOT-MTJs with and without PtMn, respectively. H_{eff}/current was obtained by averaging the H values of P→AP and AP→P switching over the current scanning region.

EOB-04. Thermal stability of non-collinear antiferromagnetic Mn_3Sn nanodot. *Y. Sato*[1,2], Y. Takeuchi[3], Y. Yamane[1,4], S. Kanai[1,6], J. Yoon[1,2], J. Ieda[5], H. Ohno[1,6] and S. Fukami[1,7] *1. Laboratory for Nanoelectronics and Spintronics, RIEC, Tohoku Univ., Sendai city, Aoba-ku, Japan; 2. Graduate School of Engineering, Tohoku Univ., Sendai city, Aoba-ku, Japan; 3. WPI-AIMR, Tohoku Univ., Sendai city, Aoba-ku, Japan; 4. FRIS, Tohoku Univ., Sendai city, Aoba-ku, Japan; 5. ASRC, JAEA, Naka, Japan; 6. CIES, Tohoku Univ., Sendai city, Aoba-ku, Japan; 7. Inamori Research Institute for Science, Kyoto City, Japan*

Antiferromagnets have unique attributes such as high-speed dynamics and small stray fields, forming a new paradigm of spintronics [1,2]. In particular, non-collinear antiferromagnets with chiral spin structures have attracted increasing attention as they exhibit various intriguing topological phenomena [3,4]. Recent studies also demonstrated current-induced reversal [5] and rotation [6] of the chiral-spin structure in thin-film systems. An important issue that has remained to be explored is the stability of antiferromagnetic spin structure against thermal fluctuation, which determines the retention time of the spin structure as well as the critical current for the electrical manipulation. Here, we fabricate non-collinear antiferromagnetic $D0_{19}$-Mn_3Sn nanodots with various diameters and measure their thermal stability factor Δ. We deposit W(2)/Ta(3)/Mn_3Sn(20)/MgO(1.3)/Ru(1) (in nm) on MgO(110) substrate by magnetron sputtering [7], followed by annealing at 500 °C for an hour. We confirm the M-plane-oriented epitaxial growth of Mn_3Sn layer by X-ray diffraction. The stack was processed into circular dot devices with a diameter D of 175-1000 nm using electron beam lithography and Ar ion milling. Figure 1 shows Hall resistance R_H as a function of the magnetic field H for different D together with the scanning electron microscopy (SEM) image. We then evaluate Δ of Mn_3Sn dot through the measurement of switching probability versus amplitude of pulse magnetic field. For the analysis, we assume a six-fold in-Kagome-plane anisotropy to model the magnetostatic energy of Mn_3Sn. Figure 2 shows D dependence of Δ. The reduction of Δ at D of less than about 300 nm is observed, indicating a single domain reversal of spin structure in this scale, consistent with a previous report on Mn_3Sn nanowire [8]. Our result offers an important insight to understand the thermal activation of antiferromagnets, allowing one to design reliable and efficient antiferromagnetic devices. This work was partly supported by JSPS Kakenhi (Nos. 19H05622 and 22K14558), Casio foundation (No. 39-11), and RIEC Cooperative Research Projects.

[1] T. Jungwirth *et al*., Nat. Nanotechnol. 11, 231 (2016). [2] V. Baltz *et al*., Rev. Mod. Phys. 90, 015005 (2018). [3] S. Nakatsuji *et al*., Nature 527, 212 (2015). [4] A. Nayak *et al*., Sci. Adv. 2, e1501870 (2016). [5] H. Tsai *et al*., Nature 580, 608 (2020). [6] Y. Takeuchi *et al*., Nat. Mater. 20, 1364 (2021). [7] J.-Y. Yoon *et al*., Appl. Phys. Express 13, 013001 (2020). [8] H. Bai *et al*., Appl. Phys. Lett. 117, 052404 (2020).

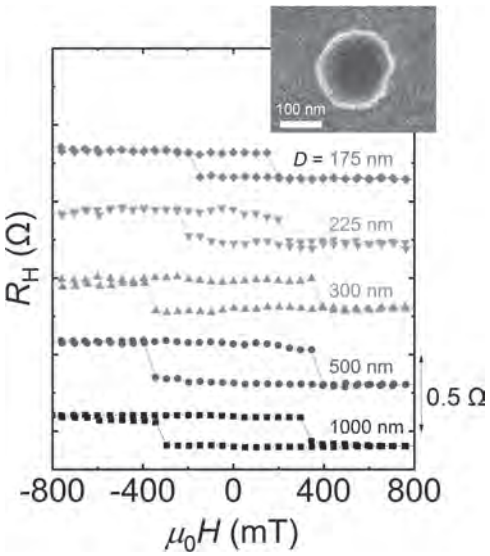

Fig.1 R_H as a function of H for different D. The inset shows SEM image of nanodot.

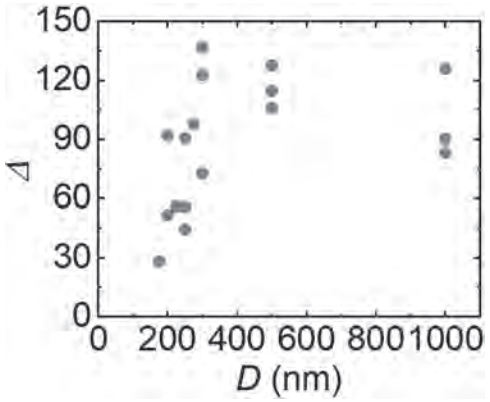

Fig.2 Δ versus D in Mn_3Sn nanodot.

EOB-05. Large antisymmetric interlayer exchange coupling enabling perpendicular magnetization switching by an in-plane magnetic field. *H. Masuda*[1,2], T. Seki[1,3], Y. Yamane[4,5], R. Modak[3], K. Uchida[3,1], J. Ieda[6], Y. Lau[1], S. Fukami[5,7] and K. Takanashi[1,6] *1. Institute for Materials Research, Tohoku University, Sendai, Japan; 2. Department of Materials Science, Graduate School of Engineering, Tohoku University, Sendai, Japan; 3. National Institute for Materials Science, Tsukuba, Japan; 4. Frontier Research Institute for Interdisciplinary Sciences, Tohoku University, Sendai, Japan; 5. Research Institute of Electrical Communication, Tohoku University, Sendai, Japan; 6. Advanced Science Research Center, Japan Atomic Energy Agency, Tokai, Japan; 7. Advanced Institute for Material Research, Tohoku University, Sendai, Japan*

Metallic superlattices such as Co/Ir/Co exhibit the symmetric interlayer exchange coupling (IEC) [1]. Recently, the antisymmetric interlayer exchange coupling (AIEC) was observed in a metallic superlattice when the in-plane spatial inversion symmetry was broken [2-5]. However, the controllability and the applicability of AIEC have not been examined yet, and the systematic experiments exploiting well-controlled in-plane structural asymmetry are indispensable. This study systematically investigated the AIEC for the wedge-shaped Pt/Co/Ir/Co/Pt to clarify the nature of AIEC. A double-wedged sample (DWS) of Ta (1)/Pt (2)/Co (t_{Co})/Ir (t_{Ir})/Co (0.5)/Pt (2)/Ta (1) (thickness in nm) was deposited on a SiO_x substrate using magnetron sputtering. The t_{Co} and t_{Ir} were continuously varied from 0.6 to 1.6 nm and from 0 to 1.5 nm, respectively. The wedge direction of the Ir layer was orthogonal to that of the wedged bottom Co layer. DWS was patterned into Hall-bar-shaped devices, and the magnetic properties were investigated by exploiting the anomalous Hall effect (AHE). The IEC in Co/Ir/Co was confirmed from the periodic change of the saturation field ($\mu_0 H_s$) against t_{Ir}. The AHE curves were largely shifted with an additional in-plane magnetic field ($\mu_0 H_{ip}$) of 50 mT (Fig. 1), indicating the existence of AIEC. The largest switching field shift ($\mu_0 \Delta H_{sw}$) was 14.8 mT at $t_{Co} \sim 0.80$ nm and $t_{Ir} \sim 0.27$ nm, which was an order of magnitude larger than the values reported previously (0.7~1.7 mT [3,5]). Similar to the t_{Ir} dependence of $\mu_0 H_s$, $\mu_0 \Delta H_{sw}$ showed the oscillatory change against t_{Ir} with a local minimum at $t_{Ir} \sim 0.87$ nm, suggesting the correlation between the symmetric IEC and the AIEC. Furthermore, we developed the extended Stoner-Wohlfarth model and proposed the tunability of the AIEC effective field by the ratio of the AIEC energy and the antiferromagnetic coupling strength. Finally, we theoretically and experimentally demonstrated the perpendicular magnetization switching solely induced by $\mu_0 H_{ip}$ for DWS. This study provides crucial information to manipulate the three-dimensional chiral magnetic structures [6].

[1] M. D. Stiles, *J. Magn. Magn. Mater.,* Vol. 200, p.322-337 (1999). [2] E. Y. Vedmedenko *et al.*, *Phys. Rev. Lett.,* Vol. 122, p.257202 (2019). [3] D.-S. Han *et al.*, *Nat. Mater.,* Vol. 18, p.703 (2019). [4] A. Fernández-Pacheco *et al.*, *Nat. Mater.,* Vol. 18, p.679 (2019). [5] K. Wang *et al.*, *Commun., Phys.* Vol. 4, p.10 (2021). [6] H. Masuda *et al.*, *Phys. Rev. Appl.,* Vol. 17, p.054036 (2022).

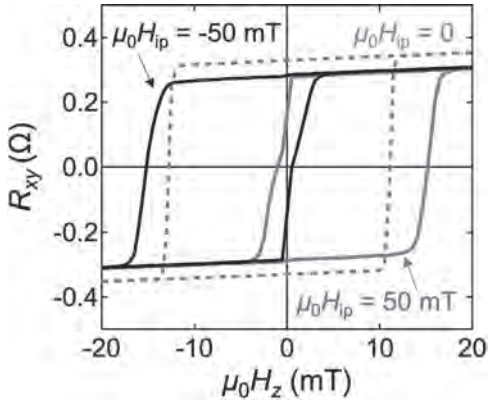

Fig. 1 AHE curves without $\mu_0 H_{ip}$ (blue) and with $\mu_0 H_{ip}$ (red and black) for DWS at $t_{Co} \sim 0.80$ nm and $t_{Ir} \sim 0.27$ nm.

EOB-06. Electrical Control of Antiferromagnetic Domain Walls in Weyl Semimetals. *Y. Semenov*[1,3] and K. Kim[1,2] *1. Department of Electrical and Computer Engineering, North Carolina State University, Raleigh, NC, United States; 2. Department of Physics, North Carolina State University, Raleigh, NC, United States; 3. V. Lashkaryov Institute of Semiconductor Physics, Kyiv, Ukraine*

The electric-field induced spin-orbit torque (SOT) in antiferromagnetic (AFM) Weyl semimetals (WSMs) is theoretically investigated. Unlike in the ferromagnetic (FM) counterparts [1], the magnetic domain walls (DWs) in the AFM WSMs appears to lack the torsion in the magnetization and thus unable to benefit from this highly efficient mechanism that originates from the axial magnetic effect. Contrarily, our calculations illustrate that the addition of the Dzyaloshinskii-Morya interaction can introduce a twist in the magnetic moment, giving rise to the non-zero axial magnetic field and net spin current in the AFM textures subjected to an electric field. The non-zero

components of the exchange fields of spin-polarized Weyl fermions are shown in Fig. 1. In the case of a Bloch DW (Fig. 1a), the direction of the driving field varies along the DW texture, significantly reducing the effect of SOT. Contrarily, the contribution of the unidirectional effective field along the Néel DW location (Fig. 1b) appears cumulative getting more efficiency. The dynamics of the DW motion is analyzed by considering the balance of energy absorption and dissipation. It reveals the need to account for the contribution of the exchange dissipation mechanism [2] beyond the Gilbert-like term to compensate the unusual superlinear rate of energy absorption by the AFM textures. The obtained DW velocity over the magnon velocity v_m vs electric field shows a significant speed-up for the Néel DW in AFM WSMs (Fig.2) compared with the FM WSM as well as those in the non-topological FMs and AFMs. The results clearly indicate the significance of the axial magnetic effect in the dynamics of spin textures in AFM WSMs.

[1] D. Kurebayashi and K. Nomura, "Theory for spin torque in Weyl semimetal with magnetic texture," Sci. Rep. 9, 5365 (2019). [2] J. H. Mentink, J. Hellsvik, D. V. Afanasiev, B. A. Ivanov, A. Kirilyuk, A. V. Kimel, O. Eriksson, M. I. Katsnelson, and Th. Rasing, "Ultrafast spin dynamics in multisublattice magnets," Phys. Rev. Lett. 108, 057202 (2012).

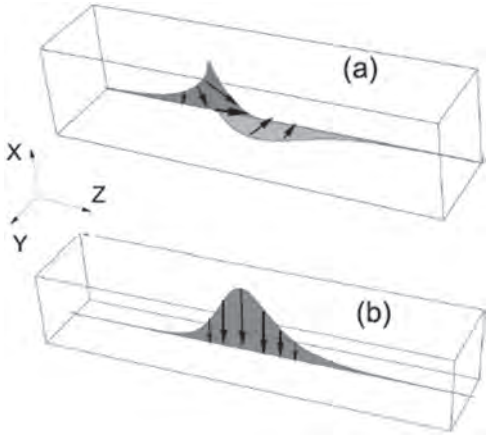

Fig.1. Configurations of the exchange fields associated with chiral anomaly in Bloch (a) and Néel (b) DWs in the AFM WSM. The lengths of arrows display the strength of the effective magnetic fields.

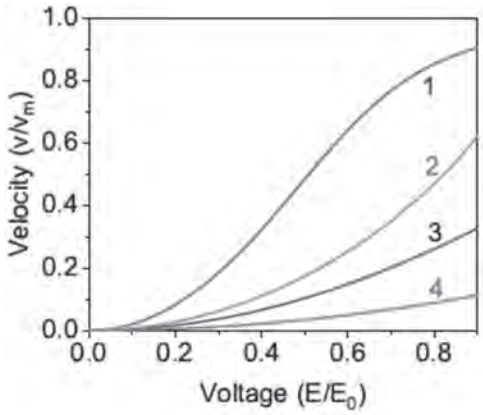

Fig.2. Stationary Néel (curves 1 and 2) and Bloch (curves 3 and 4) DWs velocity vs applied electric field E/E_0 scaled with E_0=6 kV/cm. The calculations are performed with typical WSM transport [1] and magnetic [2] parameters of AFMs under the Gilbert damping term 0.01 for curves 1 and 3 and 0.05 for curves 2 and 4.

EOB-07. Third Harmonic Characterization of Antiferromagnetic Heterostructures. *Y. Cheng*[1], E. Cogulu[2], R. Resnick[3], J. Michel[3], N.N. Statuto[2], A. Kent[2] and F. Yang[3] *1. Electrical and Computer Engineering, UCLA, Los Angeles, CA, United States; 2. Physics, New York University, New York, NY, United States; 3. Physics, The Ohio State University, Columbus, OH, United States*

Electrical switching of antiferromagnets is an exciting recent development in spintronics, which promises active antiferromagnetic devices with high speed and low energy cost. In this emerging field, there is an active debate about the mechanisms of the current-driven switching of antiferromagnets. Harmonic characterization is a powerful tool to quantify current-induced spin-orbit torques and spin Seebeck effect in heavy-metal/ferromagnet systems. However, the harmonic measurement of spin-orbit torque technique has never been verified in antiferromagnetic heterostructures. Here, we report for the first time harmonic measurements in Pt/*a*-Fe_2O_3 bilayers, which are explained by our modeling of higher-order harmonic voltages. As compared with ferromagnetic heterostructures where all current-induced effects appear in the second harmonic signals, the damping-like torque and thermally-induced magnetoelastic effect contributions in Pt/*a*-Fe_2O_3 emerge in the third harmonic voltage. Our results provide a new path to probe the current-induced magnetization dynamics in antiferromagnets, promoting the application of antiferromagnetic spintronic devices.

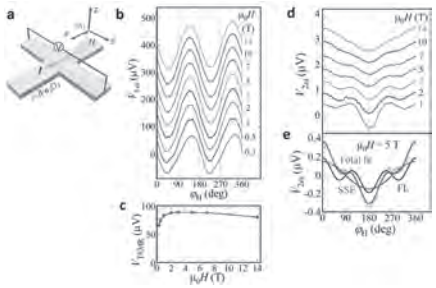

Figure 1. (a)Schematic of a Pt/*a*-Fe_2O_3 Hall cross. (b) and (d), In-plane angular dependence of first harmonic Hall voltage $V^{1\omega}$ and $V^{2\omega}$ for a Pt(5 nm)/*a*-Fe_2O_3(30 nm) bilayer at different magnetic fields from 0.3 to 14 T at 300 K. (c), Field dependence of transverse spin Hall magnetoresistance voltage V_{TSMR} extracted from (b). (e) Fitting of angular dependence of $V^{2\omega}$ at 5 T

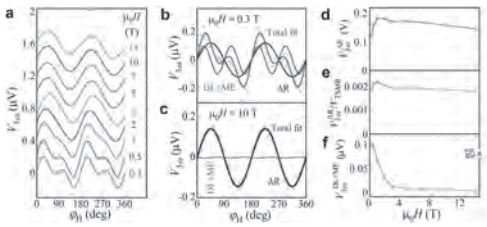

Figure 3. Third harmonic results. (a), In-plane angular dependence of third harmonic Hall voltage $V^{3\omega}$ at different magnetic fields for a Pt(5 nm)/*a*-Fe_2O_3(30 nm) bilayer at 300 K. Angular dependence of $V^{3\omega}$ at (b), 0.3 T and (c), 10 T, where the blue curve is from the change of Pt resistivity (ΔR), the green curve is from the damping-like torque (DL) and the magnetoelastic effect (ME, they have the same angular dependence), and the red curve is the total fit. Field dependencies of (d), $V^{3\omega}$(ΔR), (e), $V^{3\omega}$(ΔR) normalized by V_{TSMR}, and f, $V^{3\omega}$(DL+ME).

EOB-08. Effect of Temperature on Threshold Current Density for Current-driven Magnetization Switching in Non-collinear Antiferromagnets. *M. Yoo*[1], V.O. Lorenz[1], D.G. Cahill[1] and A. Hoffmann[1]
1. University of Illinois at Urbana-Champaign, Urbana, IL, United States

Antiferromagnets (AFs) are promising candidates for next-generation spintronic devices, because of distinct benefits, such as fast magnetization dynamics and reduced crosstalk from magnetostatic interactions [1]. Non-collinear AFs are particularly interesting for AF spintronics [2], since they exhibit a large anomalous Hall effect and magneto-optical Kerr effect, which can be used for detecting the magnetic order [3]. Furthermore, the magnetic order can be modulated electrically by spin-orbit torques [4]. A high current density, ~10^{11}-10^{12} A/m^2, is required for magnetization switching, but also increases the temperature close to the Néel temperature. However, the role of temperature in switching has not been satisfactorily explored. Here, we show the effect of temperature on the threshold current density for magnetization switching in non-collinear antiferromagnet Mn_3Sn. We fabricate Hall bar devices using polycrystalline Mn_3Sn / W multilayers on thermally-oxidized Si substrates of two different thicknesses: 300 nm- and 100 nm-thick SiO_2 layers. Different thicknesses of the oxide layer result in temperature differences between the two devices when identical electric currents are applied. The devices show similar behavior under field-driven switching as shown in anomalous Hall measurements (Fig. 1). However, in the case of current-driven switching, the devices show different threshold current densities (Fig. 2). The threshold value for the switching of the thinner-oxide-layer (100 nm) sample is ~7 x 10^{11} A/m^2, while that of the thicker-oxide (300 nm) is ~4 x 10^{11} A/m^2. The ratio of the threshold current densities is approximately √3, as we would expect for a change in oxide thickness of a factor of 3. This result shows the importance of temperature in current-driven magnetization switching in Mn_3Sn. This work is supported by the NSF through the Illinois MRSEC (DMR-1720633).

[1] T. Jungwirth, et al., Nat. Nanotech. Vol. 11, p.231 (2016) [2] T. Chen et al., Nat. Commun. Vol. 12, p.572 (2021) [3] S. Nakatsuji et al., Nature Vol. 527, p. 212 (2015) [4] H. Tsai et al., Nature Vol. 580, p.608 (2020)

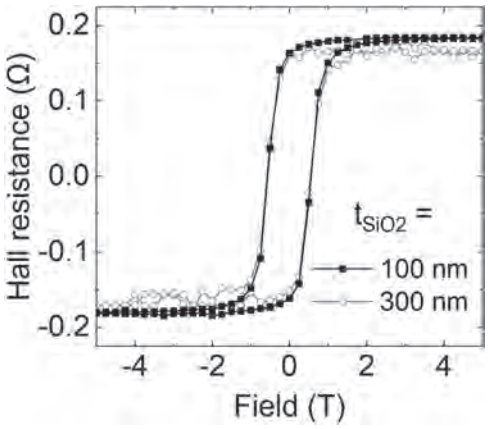

Fig. 1 Anomalous Hall resistance as a function of perpendicular magnetic field strength for different SiO_2 layer thickness, t_{SiO2}, of the sample.

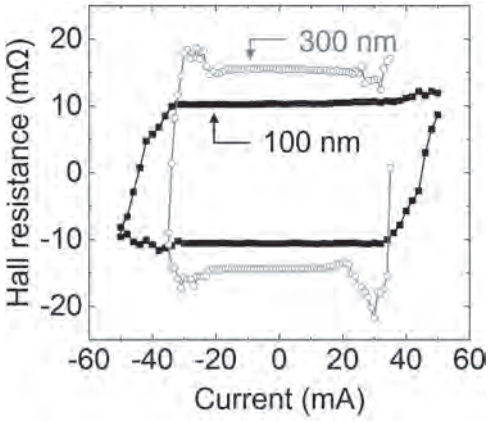

Fig. 2 Hall resistance versus write current for different t_{SiO2}.

EOB-09. Observation of Vector Spin Seebeck Effect in a Non-Collinear Antiferromagnet. *J. Xu*[1], J. He[2], J. Zhou[2], D. Qu[3], S. Huang[3] and C. Chien[1,3] *1. Johns Hopkins University, Baltimore, MD, United States; 2. University of Texas at Austin, Austin, TX, United States; 3. National Taiwan University, Taipei, Taiwan*

Spintronic phenomena to date have been established in ferromagnets (FMs) with collinear moments (e.g., Fe, Co, $Y_3Fe_5O_{12}$), where all the moments can be aligned to give a large magnetization (M). In such collinear FMs, spin injection via spin Seebeck effect (SSE) is always along the out-of-plane direction (longitudinal SSE), but not in the in-plane direction (transverse SSE). In non-collinear antiferromagnets (AFs), there are magnetic moments in directions other than that along the net magnetization M, allowing general pure spin current phenomena to be established. In this work, we report the observation of vector SSE in non-collinear AF $LuFeO_3$, where temperature gradients along both out-of-plane and in-plane direction can inject pure spin current and generate a voltage in the heavy metal via the inverse spin Hall effect. The results of longitudinal SSE (under an out-of-plane $\nabla_z T$) and the even larger transverse SSE (under an in-plane $\nabla_y T$) in $LuFeO_3$/W are shown in the Figure. By using different metal overlayers (W, Pt and Cu/W), we show that the vector SSE is a spin current effect, where the thermovoltages are due to the magnetization from the canted moments in $LuFeO_3$. We also ruled out the possibility of magnon Hall effect, spin Nernst effect and magnetic proximity effect in $LuFeO_3$. One can exploit vector SSE as a vector magnetometer for detecting very small magnetization in all directions in non-collinear AF insulators. These novel results expand the realm of spintronics and enable new device architectures for AF spintronics and reveal general pure spin current phenomena beyond those in collinear magnets. This work was supported by US NSF DMREF (1729555 and 1949701), Taiwan MOST (109-2123-M-002-002), and US DOE(DE-SC0009390).

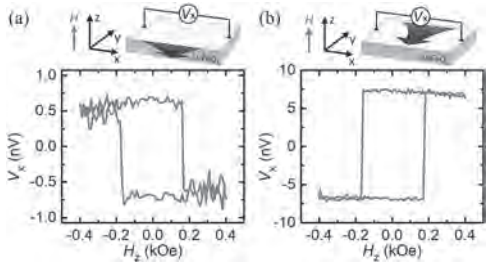

Fig. (a) Longitudinal SSE under out-of-plane $\nabla_z T$, and (b) transverse SSE under in-plane $\nabla_y T$ in $LuFeO_3$/W.

EOB-10. Ab initio comparison of spin-transport properties in ferrimagnetic tunnel junctions based on Mn_3Ga and Mn_3Al.
M.T. Stamenova[1], N. Baadji[2] and P.S. Stamenov[1] *1. Physics, Trinity College Dublin, Dublin, Ireland; 2. Physics, University of Mohamed BOUDIAF M'Sila, M'Sila, Algeria*

Among the Mn-based Heusler ferrimagnets are a number of topical materials for the emerging field of Antiferromagnetic Spintronics, combining low moments, high spin-polarisation and anisotropy. In a recent work [1], we described the long-range spatial oscillation of the spin-transfer torque (STT) in magnetic tunnel junctions (MTJs) based on tetragonal (DO_{22}) Mn_3Ga [2], present both in Fe/MgO/Mn_3Ga and in Mn_3Ga/MgO/Mn_3Ga tri-layers. Using first principles ballistic non-collinear spin transport (NEGF+SDFT) [3,4], we related the STT oscillation to the mismatch of the Fermi wavevectors of the majority and minority D_1 symmetry band in Mn_3Ga in the direction of transport. We studied the high-bias TMR effect in these stacks and found, for the symmetric MTJs, a maximum value of over 100% and a sign change below 1V, in accordance with experimental observations for similar ferrimagnetic MTJs [5]. Another Mn-based Heusler Mn_3Al has been shown to exhibit half-metallicity and almost ideally fully compensated moment in its cubic DO_3 phase [6] and proposed MTJs with GaAs have shown large theoretical TMR ratios [7]. Our ab initio geometry optimisation of Mn_3Al revealed a stable tetragonal DO_{22} solution with almost fully compensated moment (<0.002 μ_B/f.u.) and an in-plane lattice constant commensurate with MgO, which prompted a study of a familiar tri-layer. As geometrically the Mn_3Ga and Mn_3Al stacks with MgO are very similar, this could offer further insights about their Spintronic capacity. Here we compare the spin-dependent transport properties of two such junctions [3ML MgO spacer, see Fig. 1(a)]. We find that Mn_3Al is half-metallic (lacking a majority spin channel at E_F) in the direction of transport [Fig.1 (d)], which results in an enormous TMR effect [Fig.1 (c)], but also in the suppression of the long-range STT oscillation [Fig.1 (b)] and a faster decay of the STT with the barrier thickness. The STT is significant in magnitude [1] and pushes both interfacial spins in the same direction [clockwise in Fig.1 (a)]. In view of the above, aluminium-rich solid solutions of Mn_3Al-Mn_3Ga could offer enhanced low-bias TMR performance, while preserving tetragonality, at manageable growth-induced strain, in practical device stacks.

[1] M. Stamenova, P. Stamenov, F. Mahfouzi, et al., Phys. Rev. B, vol. 103, 094403 (2021). [2] K. Rode, N. Baadji, D. Betto, et al., Phys. Rev. B, vol. 87, p. 184429 (2013). [3] A. R. Rocha and S. Sanvito, Phys. Rev. B, vol. 70, p. 094406 (2004). [4] M. Stamenova, I. Rungger, S. Sanvito, et al. Phys. Rev. B, vol. 95, p. 060403(R) (2017); I. Rungger, A. Droghetti and M. Stamenova, Non-equilibrium Green's functions methods for spin transport and dynamics. In: Andreoni W., Yip S. (eds) Handbook of Materials Modeling, Springer (2018). [5] K. Borisov, D. Betto, Y.C. Lau, et al., Appl. Phys. Lett., vol. 108, p. 192407 (2016). [6] M. E. Jamer, Y. J. Wang, et al., Phys. Rev. Applied 7, 064036 (2017). [7] M. Qiu, Sh.Ye, et al. J. Phys. D: Appl. Phys. 54 115002 (2021).

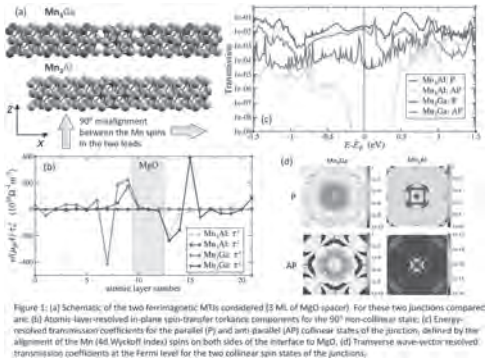

Figure 1: (a) Schematic of the two ferrimagnetic MTJs considered (3 ML of MgO spacer). For these two junctions compared are: (b) Atomic-layer-resolved in-plane spin-transfer torkance components for the 90° non-collinear state; (c) Energy-resolved transmission coefficients for the parallel (P) and anti-parallel (AP) collinear states of the junction, defined by the alignment of the Mn (4d Wyckoff index) spins on both sides of the interface to MgO. (d) Transverse wave-vector resolved transmission coefficients at the Fermi level for the two collinear spin states of the junctions.

EOB-11. Pattern Recognition Using Antiferromagnetic Artificial Spiking Neurons. *H. Bradley*[1], S. Louis[2] and V. Tyberkevych[1] *1. Physics, Oakland University, Rochester, MI, United States; 2. Electrical Engineering, Oakland University, Rochester, MI, United States*

Artificial spiking neurons may form an element base for the next generation of neuromorphic computing devices. A promising design of an ultra-fast artificial neuron is based on antiferromagnetic (AFM) spin Hall oscillators driven by a sub-threshold spin current [1]. These devices could produce ultra-short voltage spikes in response to a weak external stimulus [1]. Fixed synapses can connect these AFM neurons in simple neuromorphic circuits [2]. To create more complex neural networks, it is necessary to find learning algorithms that are compatible with AFM neurons. Here, we study the problem of AFM neural network training for pattern recognition tasks. We use reservoir computing, such that only the weights connected to the output neuron are altered during training. A supervised machine learning algorithm based on the temporal position of the spikes, called spike pattern association neuron (SPAN) [3], is used during training. Synaptic weight adjustments are governed by the difference between spikes' desired and actual temporal position. An AFM SPAN, trained to recognize a symbol made from a grid, will produce a spike at a target time when the symbol is supplied as input. SPANs, trained to recognize different symbols, are connected to the same inputs. An output layer is created to ensure that only the spike corresponding to the recognized symbol is sent to the output. This output layer consists of a clock neuron spiking at the target time and weakly fixed synapses (Fig. 1). To create an output spike, a SPAN must produce a spike at the target time along with the clock neuron (Fig. 2). Using the SPAN algorithm, we could develop a neural network with AFM artificial neurons capable of performing the pattern recognition tasks.

[1] R. Khymyn et al. Sci. Rep. 8, 15727 (2018). [2] H. Bradley and V. Tyberkevych, Q3-01, MMM, 2020. [3] A. Mohemmed, et al., Neurocomputing, vol 107, pp 3-10, 2013.

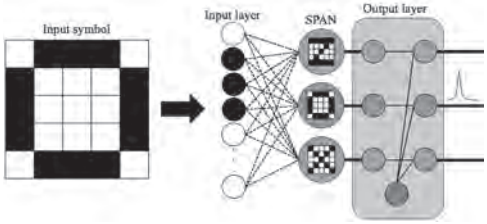

Fig. 1 Architecture of a 3 SPAN neural network. The input symbol is encoded in the spiking pattern of the input layer neurons. During training, the synaptic weights between the input layer and the SPANs are adjusted. The output layer ensures that only the spike of the recognized symbol is outputted.

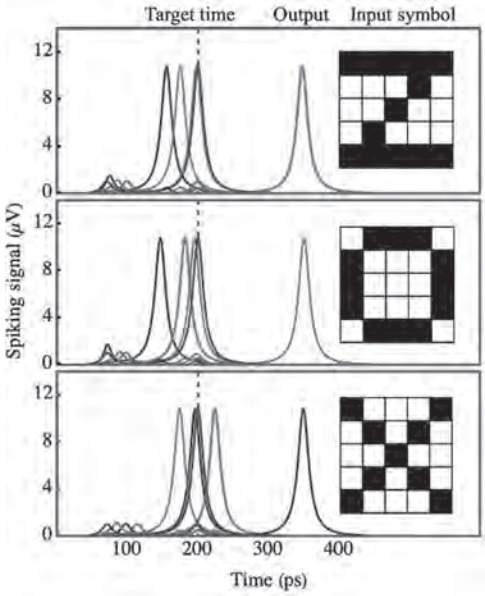

Fig. 2 A 3 SPAN neural network spike pattern for 3 different inputs. The recognized symbol's SPAN creates a spike at the target time along with the red clock neuron to create a single output spike.

EOB-12. Sign-tunable anisotropic magnetoresistance and electrically detectable dual magnetic phases in a helical antiferromagnet. *J. Hong*[1], J. Kim[1], H. Shin[1], M. Kim[1], K. Jeong[1], J. Kim[1], K. Moon[1], N. Lee[1] and Y. Choi[1] *1. Department of Physics, Yonsei University, Seoul, The Republic of Korea*

Emerging from competing exchange interactions, the helimagnetic order describes a noncollinear spin texture of antiferromagnets. Although collinear antiferromagnets act as the elemental building blocks of antiferromagnetic (AFM) spintronics, the potential of implementing spintronic functionality in noncollinear antiferromagnets has not been clarified thus far. Here, we propose an AFM helimagnet of $EuCo_2As_2$ as a novel single-phase spintronic material that exhibits a remarkable sign reversal of anisotropic magnetoresistance (AMR). The contrast in the AMR arises from two electrically distinctive magnetic phases with spin reorientation that is driven by the magnetic field prevailing in the easy-plane, which converts the AMR from positive to negative. Furthermore, based on an easy-plane anisotropic spin model, we theoretically identified various AFM memory states associated with the evolution of the spin structure under magnetic fields. The results revealed the potential of noncollinear antiferromagnets for the development of spintronic devices.

Kim et al., NPG Asia Materials, accepted (2022)

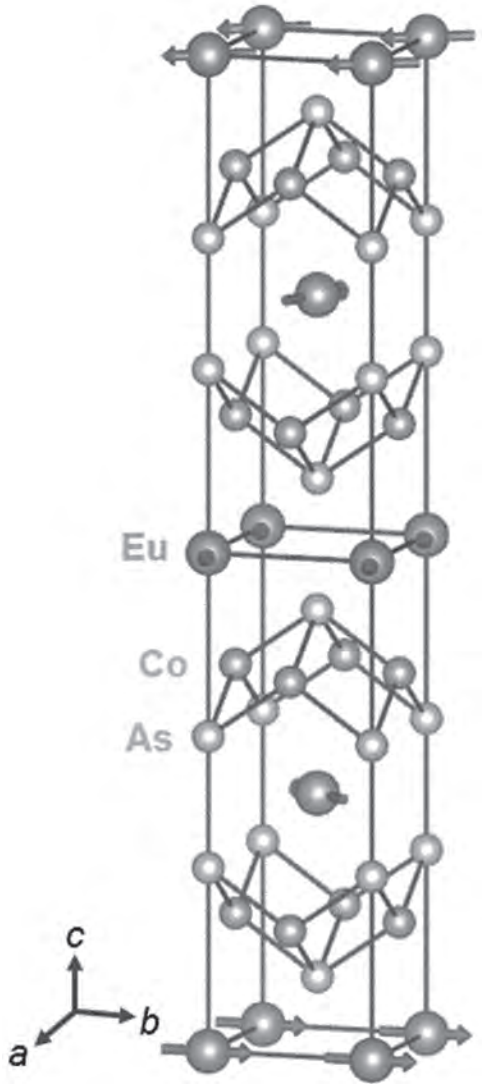

Fig. 1 Crystal and spin structures of ECA. The red, orange, and light purple spheres denote Eu, Co, and As atoms, respectively. The red arrow on each Eu atom indicates the individual spin direction. Competing exchange interactions form the helical AFM order along the *c*-axis with *k* = (0, 0, 0.79).

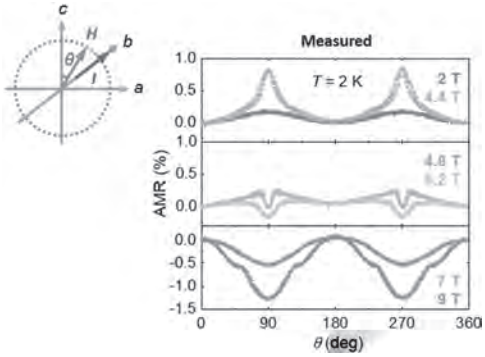

Fig. 2 Plots of the AMR (%) measured at *T* = 2 K by rotating *H* =2, 4.4, 4.8, 5.2, 7, and 9 T in the *ac* plane with the current along the *b*-axis, *I//b*. Geometry of the AMR measurement is schematically shown. θ = 0° for the *c*-axis and θ = 90° for the *a*-axis.

EOB-13. Room-temperature anomalous Hall effect and anisotropic magnetoresistance reversal in a van der Waals antiferromagnet.

H. Shin[1], M. Kim[1], J. Kim[1], J. Kim[1], J. Hong[1], K. Jeong[1], J. Seo[1], K. Moon[1], N. Lee[1] and Y. Choi[1] *1. Physics, Yonsei University, Seoul, The Republic of Korea*

Recent findings of van der Waals (vdW) antiferromagnetic crystals allow for exploring fundamentals of low dimensional spin-dependent phenomena and open opportunities for developing spin-processing functionalities. However, only a few has been known as itinerant vdW antiferromagnets that comprise an inherently low Néel temperature, limiting the feasible achievement of vdW-antiferromagnet-based spintronics. Here we achieve high-T_N itinerant antiferromagnetism with T_N = 350 K in Co-doped Fe_5GeTe_2, which reveals room-temperature large anomalous Hall conductivity and anisotropic magnetoresistance reversal driven by spin flops. Based on easy-axis anisotropic spin model, we associate the evolution of the spin structure by rotating a magnetic field with electrically measurable longitudinal and transverse resistive states. Our work offers an intrinsically magnetic platform to establish vdW-antiferromagnet-based spintroinics and more sophisticated vdW-heterostructures utilizing diverse 2D building blocks

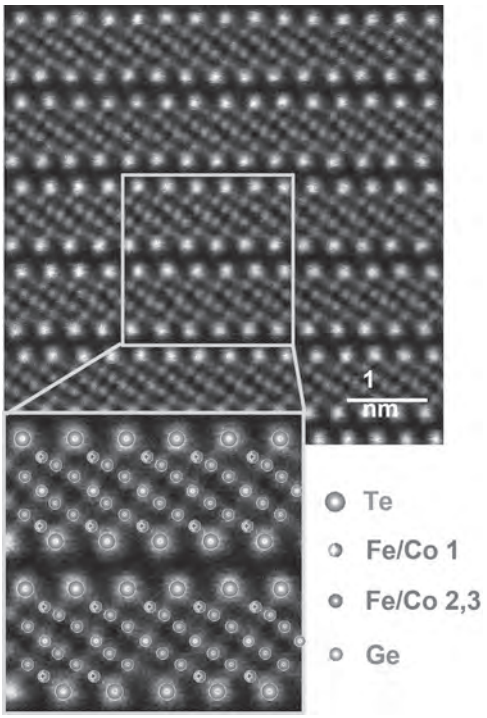

Fig. 1. Structure antiferromagnetism of $(Fe_{0.54}Co_{0.46})_5GeTe_2$ Dark-field images viewed from the [110] direction, taken using a scanning transmission electron microscpoe (STEM). the STEM image with lower magnification indicates that all the layers are regularly aligned.

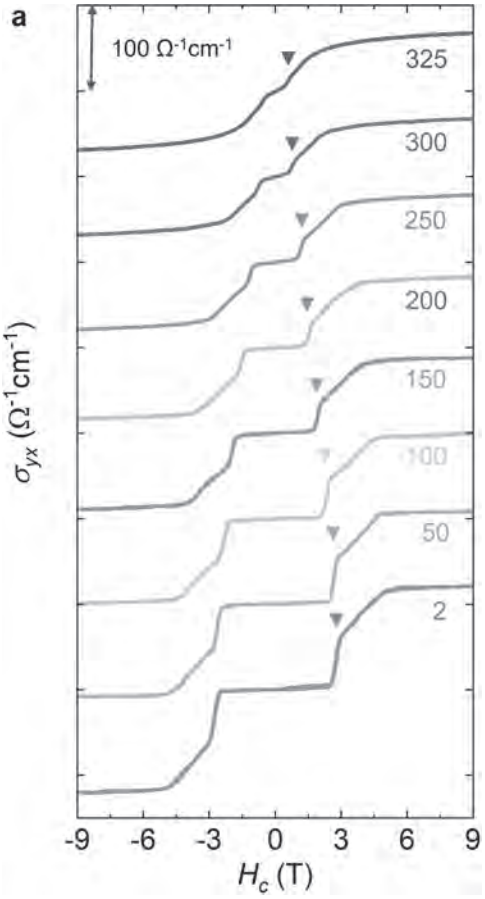

Fig. 2. Large anomalous Hall effect driven by spin-flops. The *H* dependence of anomalous Hall conductivity, σ_{yx}^{A} taken at various temperatures, *T* = 2, 50, 100, 150, 200, 250, 300, 325 K. The σ_{yx}^{A} can be scaled linearly by *M* with the relation as $S_H = \sigma_{yx}^{A}/M \sim 0.02\ V^{-1}$, independent of *T*. The σ_{yx}^{A} data are shifted vertically for clear visualization. A marked scale indicates 100 $\Omega^{-1}cm^{-1}$. Inverted triangles indicate the occurrence of H_{flop} at eact *T*.

Session EOC
SKYRMIONS I
Olivier Boulle, Chair
SPINTEC, Grenoble, France

INVITED PAPER

EOC-01. Current-driven dynamics and ratchet effect of skyrmion bubbles in a ferrimagnetic insulator. *S. Velez*[1,2], S. Ruiz-Gómez[3,4], J. Schaab[2], E. Gradauskaite[2], M.S. Wörnle[2], P. Welter[2], B.J. Jacot[2], C.L. Degen[2], M. Trassin[2], M. Fiebig[2] and P. Gambardella[2] *1. Universidad Autónoma de Madrid, Madrid, Spain; 2. ETH Zurich, Zurich, Switzerland; 3. Universidad Complutense de Madrid, Madrid, Spain; 4. Max Planck Institute for Chemical Physics of Solids, Dresden, Germany*

Magnetic skyrmions are compact chiral spin textures that exhibit a rich variety of topological phenomena and hold potential for the development of high-density memory devices and novel computing schemes driven by spin currents. In this invited talk, we will demonstrate the room-temperature interfacial stabilization and current-driven control of skyrmion bubbles in the ferrimagnetic insulator $Tm_3Fe_5O_{12}$ coupled to Pt, showing the current-induced motion of individual skyrmion bubbles [1]. The ferrimagnetic order of the crystal together with the interplay of spin–orbit torques and pinning determine the skyrmion dynamics in $Tm_3Fe_5O_{12}$ and result in a strong skyrmion Hall effect characterized by a negative deflection angle and hopping motion. Further, we will show that the velocity and depinning threshold of the skyrmion bubbles can be modified by exchange coupling $Tm_3Fe_5O_{12}$ to an in-plane magnetized $Y_3Fe_5O_{12}$ layer, which distorts the spin texture of the skyrmions and leads to directional-dependent rectification of their dynamics. This effect, which is equivalent to a magnetic ratchet, is exploited to control the skyrmion flow in a racetrack-like device.

[1] S. Vélez et al., Nature Nanotechnology (2022). https://doi.org/10.1038/s41565-022-01144-x

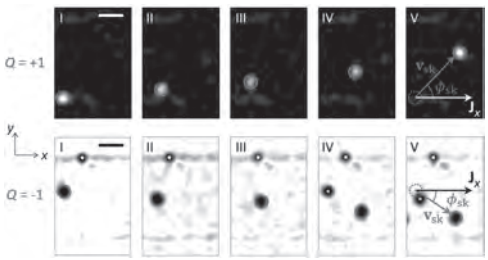

Magneto-optical Kerr effect images showing the displacement of skyrmion bubbles in $Tm_3Fe_5O_{12}$/Pt following a sequence of current pulses. The topological charge of the skyrmions (*Q*), which can be controlled by the orientation of the bubble core (bright/dark contrast), results in a transverse deflection of the skyrmions.

CONTRIBUTED PAPERS

EOC-02. Effects of Composition and Sample History on Magnetic Structures in the 2D van der Waals Magnets Fe_xGeTe_2. *K. Litzius*[1], M. Birch[1], L. Powalla[2,4], F. Schulz[1], S. Wintz[1], M. Weigand[3], K. Kern[2], M. Burghard[2] and G. Schütz[1] *1. Max-Planck-Institute for Intelligent Systems, Stuttgart, Germany; 2. Max-Planck-Institute for Solid State Research, Stuttgart, Germany; 3. Helmholtz Zentrum Berlin, Berlin, Germany; 4. École Polytechnique Fédérale de Lausanne, Lausanne, Switzerland*

Recently, the combination of 2-dimensional (2D) magnetism [1] with the field of spintronics, i.e. the manipulation of magnetic states with electric currents, has started to gain much traction in modern solid-state physics. The prospect of highly efficient low-dimensional devices, extreme ease to fabricate versatile heterostructures by stacking of separate individual layers, and the report of chiral topological magnetic solitons in 2D itinerant ferromagnets have further enhanced the field's interest in this fascinating class of materials. Requirements for technological implementation, however, are generally to understand both the history dependence of the system's magnetic textures and different potential ways to tailor the material parameters and ferromagnetic ordering temperatures [2,3] in desirable ways. In this work, we utilize real-space imaging of the magnetic texture within flakes of the van der Waals magnets Fe_xGeTe_2 to determine magnetic phase diagrams of various exfoliated films. Our findings show besides complex, history-dependent magnetization states also that changes in the composition and crystalline structure significantly alter the magnetic behavior. Most significant is the option to tune the anisotropy via small changes in the iron content and the demonstration of spatially varying chemical and magnetic areas in quenched Fe_5GeTe_2. Ultimately, the choice of material and a proper nucleation mechanism result in the stabilization of a variety of (meta-) stable magnetic configurations, including skyrmions. These findings open novel perspectives for designing van der Waal heterostructure-based devices incorporating topological spin textures.

K. S. Burch, D. Mandrus and J. G. Park, Nature., Vol. 563, p. 47–52 (2018). A. F. May et al., ACS Nano., Vol. 13, p. 4436–4442 (2019). H. Chen et al., 2D Materials., Vol. 9, p. 025017 (2022).

EOC-03. Stabilizing skyrmions deterministically for racetrack memory applications. *M. Morshed*[1], H. Vakili[2], P.V. Balachandran[3,4] and A.W. Ghosh[1,2] *1. Department of Electrical and Computer Engineering, University of Virginia, Charlottesville, VA, United States; 2. Department of Physics, University of Virginia, Charlottesville, VA, United States; 3. Department of Materials Science and Engineering, University of Virginia, Charlottesville, VA, United States; 4. Department of Mechanical and Aerospace Engineering, University of Virginia, Charlottesville, VA, United States*

Magnetic skyrmions possess intriguing features such as ultra-small size, solitonic nature, and easy mobility with small electrical currents, which make them attractive for low power, high-density memory and logic applications [1]. In a skyrmion-based racetrack, information can be encoded either by the presence and absence of skyrmions for Boolean computing or into the analog spatial coordinates of the skyrmions, which then can be translated into the timing information needed for temporal computing [2]. However,

it is essential to guarantee the positional stability of skyrmions for reliable information extraction because a randomly displaced skyrmion can alter the bit sequence and change the spatial coordinates thereby the encoded analog timings. Using micromagnetic simulations [3] for the minimum energy path (MEP), we compute the energy barriers associated with notches along a racetrack. We vary material parameters, specifically, the strength of the chiral Dzyaloshinskii-Moriya interactions (DMI), the notch geometry, and the thickness of the racetrack to get the optimal barrier height. We find a range of energy barriers up to ~ 45 k_BT for a racetrack of 5 nm thickness that can provide a year-long positional lifetime of skyrmions for long-term memory applications while requiring a moderate amount of current (~ 10^{10} A/m^2) to move the skyrmions [4]. Moreover, we derive quasi-analytical equations to estimate the energy barrier with material-dependent pre-factor constants. Currently, we are building machine learning-based surrogate models for the computationally-expensive micromagnetics simulations to accelerate the energy barrier prediction for a much broader parameter space. Our results open up possibilities to design practical skyrmion-based racetrack geometries for spintronics applications.

[1]. H. Vakili, J. Xu and W. Zhou, J. Appl. Phys., 130, 070908 (2021) [2]. H. Vakili, and M. Sakib and S. Ganguly, IEEE J. Explor. Solid-State Comput. Devices Circuits, 1 (2020) [3]. A. Vansteenkiste, J. Leliaert and M. Dvornik, AIP Adv., 4, 107133 (2014) [4]. M. Morshed, H. Vakili and A. Ghosh, Phys. Rev. Appl., 17, 064019 (2022)

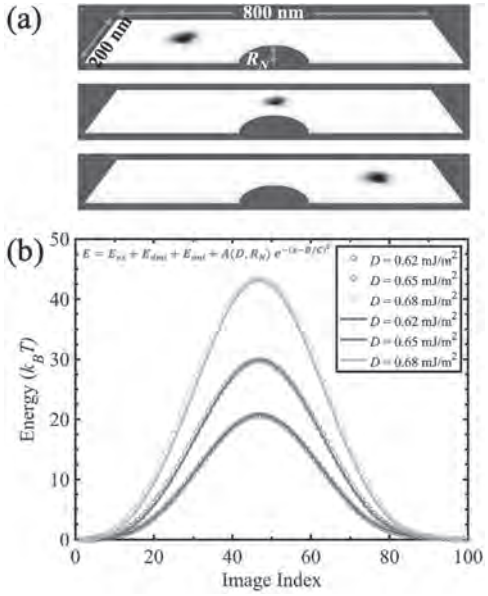

Fig. 1. (a) The simulated racetrack. (b) The energy landscape of skyrmions from simulations (scatter circles) and analytical equations (solid curves). The left valley, peak, and right valley correspond to the snapshot shown in the top, middle, and bottom panels of (a).

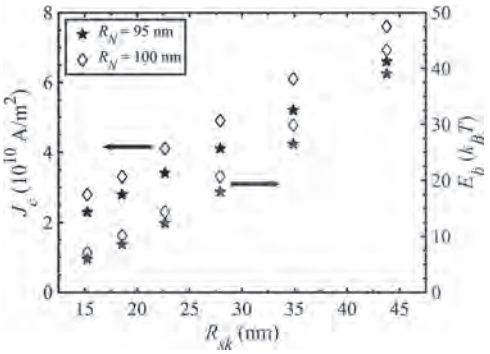

Fig. 2. The critical current J_c to unpin the skyrmion and the corresponding E_b. We find a low unpinning current with a fairly large energy barrier.

EOC-04. Spin-orbit torque engineering for efficient skyrmion motion.
Y. Sassi[1], S. Krishnia[1], D. Sanz-Hernández[1], S. Collin[1], K. Bouzehouane[1], A. Fert[1], *V. Cros*[1] and N. Reyren[1] *1. Unite Mixte de Physique CNRS, Thales, U. Paris-Saclay, Palaiseau, France*

Magnetic skyrmions are magnetic solitons in thin magnetic multilayers, which behave as particles and are topologically distinct from the uniform magnetization state. They have been identified as extremely promising for future applications (racetrack memory, neuromorphic computing, etc.), as well as of fundamental interest [1]. In fact, most of the research effort focused on material science in the last couple of years aimed at decreasing the skyrmion dimension [2] and enhance their stability. Even though the skyrmion dynamics through spin-orbit torques (SOT) have been investigated extensively [3], only a few studies specifically addressed the optimization of spin-orbit torques in skyrmion multilayers. In the present work, we investigate the SOT-induced motion of ferromagnetic skyrmions at room temperature, measured using MFM and/or MOKE microscopy in various magnetic Pt/Co/X based multilayers with X = Al, Cu, Pt or Ir. The actual amplitude of the damping-like and field-like SOT components is measured by 2nd harmonic technique (Fig.1a) [4]. Then we measure the evolution of the skyrmion velocity (Fig.1b) and skyrmion Hall angle and discuss the correlation with the measured SOT intensity. French ANR grant TOPSKY (ANR-17-CE24-0025), DARPA TEE program grant (MIPR#HR0011831554) and EU grant SKYTOP (H2020 FET Proactive 824123) are acknowledged for their financial support.

[1] A. Fert, N. Reyren, V.Cros, Nat. Rev. Mat. 2 (2017), 17031. [2] C. Moreau-Luchaire et al, Nat. Nanotech, 11 (2016), 444; S. Woo et al, Nat. Mater. 15 (2016), 501; A. Soumyanarayanan et al, Nat. Mater. 16 (2017) [3]K. Litzius et al, Nat. Phys. 13 (2017), 170; S. Woo et al, Nat. Comm. 8 (2017), 15573. [4] S. Krishnia et al., arXiv : 2205.08486.

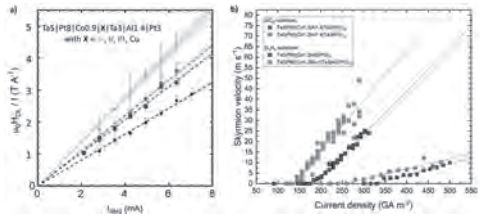

a) H_{DL} measurement for Ta|Pt|Co|X|Ta|Al|Pt with (X=Al, Ir, Ru & Cu) b) Skyrmion velocity as function of the current density for $(Pt|Co|Al|Pt)_{10}$ and $(Pt|Co|Al|Ta|Pt)_{10}$ (for two different track width). The current density is determined for the all thickness of the multilayer.

EOC-05. Skyrmion resonance induced by the spin hall effect in frustrated Fe_3Sn_2 crystal at room temperature. *N. Bernstein*[1], H. Li[2], R. Ben Shalom[1], W. Wang[2] and A. Capua[1] *1. The Hebrew University of Jerusalem, Jerusalem, Israel; 2. Chinese Academy of Sciences, Beijing, China*

Magnetic Skyrmions are attractive for high volume data storage and distribution applications. Conventionally, Dzyaloshinskii-Moriya interaction (DMI) is responsible for the Skyrmion's topological protection. Recently, frustration in ferromagnetic (FM) crystals was predicted to be also capable of providing the topological protection of the Skyrmion but without relying on the DMI and the effect was immediately discovered in Fe_3Sn_2 bulk crystals [1,2]. Interestingly, these Skyrmions survive even at room temperature and are controllable by electrical current [1] while the broken symmetry of the crystal is understood to give rise to the spin Hall effect. In this work, we study the dynamics of the Fe_3Sn_2 crystal using an optically probed ferromagnetic resonance technique. From these measurements we show that we can reconstruct the magnetic phase transition as well as distinguish between the rotational (clock-wise/counter-clock-wise) and the translational (breathing) modes. Interestingly, when current is passed through the crystal a linewidth modulation of each mode is observed in agreement to with the SHE theory. A numerical object oriented micro magnetic framework (OOMMF) of the frustrated skyrmion dynamics confirm our measurements from which we extract two different spin Hall angles relevant for each mode.

[1] Z. Hou, W. Ren, and Z. Zhang, Advanced Materials 29, 1701144 (2017). [2] J. Tang, L. Kong and H. Du, ACS Nano 14, 10986 (2020).

EOC-06. Control of the skyrmion passage by a gate electrode. *K. Hashimoto*[1], R. Ishikawa[2], M. Goto[1,3], H. Nomura[1,3] and Y. Suzuki[1,3] *1. Graduate School of Engineering Science, Osaka University, Toyonaka, Japan; 2. ULVAC Inc, Suita, Japan; 3. CSRN-Osaka, Toyonaka, Japan*

Magnetic skyrmions are recently attracting attention from the viewpoint of application to next-generation spintronics devices such as ultra-low-power Brownian computers. Skyrmions are expected to function as information carriers in those devices because of their unique features such as Brownian motion at near room temperature, small size, easy detection and easy control [1-4]. In order to realize such devices, electrical gating and amplification of the skyrmion signal are indispensable. The primary mechanism of the voltage control technique for skyrmions is the voltage-controlled-magnetic-anisotropy effect (VCMA effect) [5-6]. In the previous studies using the VCMA effect, for example, modulation of the diffusion coefficient [2] and creation/annihilation of the skyrmions [3] have been demonstrated. However, "*skyrmion gates/transistors*" have not been realized experimentally yet. Obstacles might be that the conditions creating skyrmions are easily affected by the local stress introduced from the gate fabrication. Furthermore, a non-negligible energy barrier that appears at the edge of the gate electrode, traps the skyrmions there. In this talk, we will present our attempts to realize a device in which skyrmions are *not* trapped at the edge of the gate electrode. A skyrmion film consisting of $Ta|Co_{16}Fe_{64}B_{20}|Ta|MgO|SiO_2$ was deposited on a thermally oxidized silicon substrate by the magnetron sputtering. In order to apply voltage to the magnetic layer, thin Ru gate electrodes with a thickness of 2 [nm] were deposited onto this film, and the MOKE microscope observed the motion of skyrmions. Narrow gate electrodes trapped skyrmion at the edge of the electrodes even though no voltage was applied. The wider Ru electrode enables a free passage of the skyrmions through the edge. The result is one of the fundamentals of realizing the skyrmion transistors. Acknowledgement: The authors acknowledge to Ono laboratory in Kyoto Univ. This research and development work was supported by ULVAC, Inc., JST CREST Grant number JPMJCR20C1, Japan and JSPS KAKENHI Grant Number JP20H05666.

[1] J. Zázvorka *et al*., Nat. Nanotechnol., 14, 658–661 (2019), [2] T. Nozaki *et al*., Appl. Phys. Lett., 114, 012402 (2019), [3] M. Schott *et al*., Nano Letters., 17, 3006-3012 (2017), [4] B. W. Walker *et al*., Appl. Phys. Lett., 118, 192404 (2021), [5] M. Weisheit *et al*., Science 315, 349 (2007), [6] T. Maruyama *et al*., Nature Nanotech., 4, 158 (2009), [7] Y. Jibiki *et al*., Appl. Phys. Lett., 117, 082402 (2020)

EOC-07. Walking Skyrmions. *A. Bezvershenko*[1], L. Heinen[1], M. Garst[2], A. Rosch[1], D. Mettus[3], F. Rucker[3], A. Chacon[3], A. Bauer[3], S. Muehlbauer[3] and C. Pfleiderer[3] *1. Institute for Theoretical Physics, University of Cologne, Cologne, Germany; 2. Institute of Theoretical Solid State Physics, Karlsruhe Institute of Technology, Karlsruhe, Germany; 3. Department of Physics, Technical University Munich, Munich, Germany*

Magnetic skyrmions are topologically non-trivial spin textures that attract great interest, offering a possible avenue towards novel spintronics applications. One of the reasons for it are small critical current densities needed to depin the skyrmion lattice. This poses the question about the microscopic mechanism of unpinning and its dependance on topology, electronic structure and disorder of the system. In this work, we demonstrate that upon the application of an oscillating transverse magnetic field on the MnSi skyrmion lattice the critical current density can be tuned to zero starting from the critical magnetic field amplitude. We introduce an elastic model for skyrmion strings in the presence of pinning forces and discuss its rich phase diagram (including so-called "walking" and "running" phases). Results obtained from this effective model qualitatively reproduce all of our experimental findings from the transverse susceptibility and time-resolved small angle neutron scattering (TISANE) measurements. Furthermore, we compare the unpinning processes in different systems, such as $Mn_{1-x}Fe_xSi$, where spin-transfer torques are dominated by spin-polarized charge currents and insulating material Cu_2OSeO_3 with the spin transfer torques being due to magnon currents.

EOC-08. Magnetic anisotropy dependence of entropic generation of skyrmions. *A.M. Park*[1], S. Yang[2], M. Song[1], M. You[1], T. Ju[2], C. Hwang[2] and K. Kim[1] *1. Korea Advanced Institute of Science and Technology, Daejeon, The Republic of Korea; 2. Korea Research Institute of Standards and Science, Daejeon, The Republic of Korea*

Magnetic textures in chiral magnetic material emerge from a complex energy landscape that involves multiple magnetic energy contributions. These metastable states often bear interesting twists in the spin structure, including topologically non-trivial skyrmion bubbles, which hold a unique position in applications such as racetracks or logic devices due to their high stability and controllability [1, 2]. While the generation process of the skyrmions is inevitable for the operation of skyrmion devices, the phase diagram and transition properties at the phase boundary vary widely with magnetic parameters that determine the energy landscape. In this regard, understanding the effect of tunable magnetic parameters such as perpendicular magnetic anisotropy (PMA) on the nucleation process of a magnetic skyrmion is crucial. In this work, we investigate the phase transition of chiral magnetic states in W/CoFeB/Ta/MgO multilayer using MOKE microscopy. The insertion of the Ta wedge layer between CoFeB and MgO generates a spatial gradient of PMA throughout the film. Skyrmion nucleation rates at various temperatures and anisotropy fields are measured and fitted to Arrhenius law to obtain the energy barrier and the attempt time for the skyrmion generation. We discuss the role of magnetic anisotropy in the Meyer-Neldel-type rule that indicates the entropic effects [3] in the nucleation of skyrmions in thin-film CoFeB. We present a comprehensive picture of the activation barrier between the phase transitions by directly investigating the transition time between each metastable state.

[1] A. Fert *et al., Nat. Nanotechnol.* 8, 152 (2013) [2] C. Back *et al*., *J. Phys. D: Appl. Phys.* 53 363001 (2020) [3] J. Wild *et al., Sci. Adv.* 3, e1701704 (2017)

EOC-09. Magneto-structural coupling and skyrmions lattice phase field in the lacunar spinel $GaMo_4Se_8$. *J. Alaria*[1] *1. Department of Physics & Stephenson Institute for Renewable Energy, University of Liverpool, Liverpool, United Kingdom*

The prospect of controlling topologically protected spin textures such as skyrmions lattices in high-density race-track memories offers an alternative to conventional domain wall based spintronic devices [1],[2]. A variety of skyrmion

spin structures have been observed in non-centrosymmetric compounds and understanding the phase field stability and size of the magnetic texture is of fundamental importance to control the desired functionality in the materials. The lacunar spinel family with the net formula AB_4X_8 (A = Al, Ga, Ge; B = V, Mo; X = S, Se) has gained much attention in this respect as several compounds crystallize in the non-centrosymmetric polar rhombohedral structure (R3m, C3v) at low temperature and are magnetically ordered, with skyrmion lattice observed in GaV_4S_8 [3], GaV_4Se_8 [4] and $GaMo_4S_8$ [5]. So far only polycrystalline samples of $GaMo_4Se_8$ have been studied. [6] We have performed extensive structural and magnetic characterisation on both single and poly-crystals of $GaMo_4Se_8$. Using high resolution powder neutron diffraction we confirms the phase separation below the phase transition from cubic to mixture of rhombohedral and orthorhombic phases and a significant magneto-structural coupling. Among lacunar spinels, the phenomenon of phase separation is unique to $GaMo_4Se_8$ and likely to result from the high compressive strain relaxation through the formation of the minority phase (Fig. 1a). Our small angle neutron scattering study on single crystals reveals a cycloid spin structure with a period of 15.4 nm (Fig. 1b) and upon the application of a magnetic field along the polar axis, pattern compatible with a skyrmion lattice is observed (Fig. 1c). The temperature-magnetic field phase field is established and shows that the spin texture is preserved down to the lowest temperature and under a large magnetic field of 1 T.

[1] S. S. P. Parkin, M. Hayashi, L. Thomas, Science, 2008, 320, 190. [2] A. Fert, V. Cros, J. Sampaio, Nature Nanotechnology, 2013, 8, 152. [3] I. Kezsmarki et al., Nature Materials, 2015, 14, 1116. [4] S. Bordacs et al., Scientific Reports, 2017, 7, 7584 [5] A. Butykai et al., npj Quantum Materials, 2022, 7, 26 [6] E. C. Schueller et al., Phys. Rev. Materials, 2020, 4, 064402

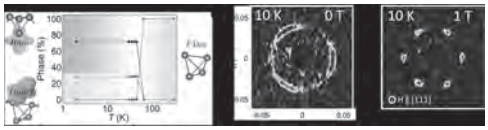

Figure 1. a) Phase composition of $GaMo_4Se_8$ refined from the powder neutron diffraction data as a function of temperature; b), c) single crystal $GaMo_4Se_8$ small angle neutron scattering patterns collected at 10K under 0 and 1 T magnetic fields along the polar direction.

EOC-10. Angular-dependent magnetoresistance and magnetic soliton lattice in $Cr_{1/3}NbS_2$. *X. Li*[1,2], B. Ding[1], H. Li[1], X. Xi[1], Y. Lau[1] and W. Wang[3] *1. Institute of Physics, Chinese Academy of Sciences, Beijing, China; 2. University of Chinese Academy of Sciences, Beijing, China; 3. Tiangong University, Tianjin, China*

$Cr_{1/3}NbS_2$, the first known magnetic soliton system, has abundant magnetic phases like chiral helimagnetic order (HM), chiral conical phase, chiral soliton lattice (CSL), tilted chiral soliton lattice and forced ferromagnetic (FM) due to the competition between Dzyaloshinskii–Moriya exchange, Heisenberg interaction, magnetocrystalline anisotropy and Zeeman energy.[1,2] These rich magnetic textures display attractive properties, such as magnetocaloric effect,[3] topological Hall effect and planar Hall effect,[4] etc. Especially, magnetic soliton, a real-space topological magnetic structure like skyrmion, owns topological protection properties and quasi-particle nature which makes $Cr_{1/3}NbS_2$ a promising platform for the spintronic devices.[5,6] Recently, we have studied the transition of various magnetic structures by magnetoresistance (MR),[7] a.c. magnetic susceptibility,[7] and Lorentz transmission electron microscopy (L-TEM). As shown in Fig. 1(a), when a magnetic field was applied along the c-axis (H ∥ c - axis) at low temperatures, we found signatures of weak antilocalization which may originate from the strong spin–orbit coupling of $Cr_{1/3}NbS_2$. When the magnetic field was applied along the ab-plane (H ∥ ab - plane), the transition from HM to CSL and FM can be detected by a.c. magnetic susceptibility (Fig. 1(b)). To better understand CSL, we adopted L-TEM measurement. As shown in Fig. 1(c) and (d), a helical period longer than theoretical calculations (~48 nm) and showing opposite chirality due to grain boundary modulation were observed in some regions on the sample. The reason for the difference in period can be the uneven content of Cr intercalation. This may provide an effective way to regulate the helical period, thus facilitating its practical application.

1. T. Miyadai, K. Kikuchi, H. Kondo, et al., J. Phys. Soc. Jpn. 52 (4), 1394-1401 (1983). 2. Y. Togawa, T. Koyama, K. Takayanagi, et al., Phys. Rev. Lett. 108 (10), 107202 (2012). 3. N. J. Ghimire, M. A. McGuire, D. S. Parker, et al., Phys. Rev. B 87 (10), 104403 (2013). 4. D. A. Mayoh, J. Bouaziz, A. E. Hall, et al., Phys. Rev. Research 4 (1), 013134 (2022). 5. Y. Togawa, T. Koyama, Y. Nishimori, et al., Phys. Rev. B 92 (22), 220412 (2015). 6. L. Wang, N. Chepiga, D. K. Ki, et al., Phys. Rev. Lett. 118 (25), 257203 (2017). 7. X. Li, Z. Li, H. Li, et al., Appl. Phys. Lett. 120 (11), 112408 (2022).

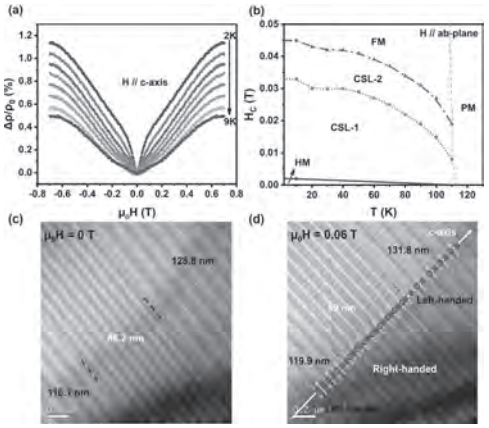

Fig. 1. (a) Out-of-plane MR as a function of H at various temperature. (b) Phase diagram of magnetic phase transition with temperature and magnetic field when in-plane fields are applied. CSL-1 refers to a state which has a larger helical array, while CSL-2 has a richer ferromagnetic array. PM is paramagnetic state. Under-focused L-TEM image at 91 K. The applied perpendicular field is 0 T (c) and 0.06 T (d).

EOC-11. Drastically enhanced thermal skyrmion diffusion in synthetic antiferromagnets. *T. Dohi*[1], M. Weißenhofer[2], N. Kerber[1], F. Kammerbauer[1], Y. Ge[1], K. Raab[1], J. Zázvorka[3], M. Syskaki[1], A. Shahee[1], M. Ruhwedel[4], T. Böttcher[4], P. Pirro[4], G. Jakob[1], U. Nowak[2] and M. Kläui[1] *1. Institut für Physik, Johannes Gutenberg-Universität Mainz, Mainz, Germany; 2. Fachbereich Physik, Universität Konstanz, Konstanz, Germany; 3. Institute of Physics, Charles University, Prague, Czechia; 4. Fachbereich Physik and Landesforschungszentrum OPTIMAS, Technische Universität Kaiserslautern, Kaiserslautern, Germany*

Magnetic skyrmions, topologically stabilized quasi-particles, have attracted major attention as their topology in real space governs intriguing electromagnetic responses [1]. In particular, the dynamics is of key importance for possible use in spintronic applications with novel functionality [2,3]. However, some of the topology-dependent features of magnetic skyrmions are recognized as an obstacle to device applications, e.g. the skyrmion Hall effect [4,5], which is a perpendicular motion component to the current flow direction. Likewise, theory predicts that the gyrotropic force originating from the finite topology gives rise to a drastic decrease in the diffusion coefficient [6–8]. While being advantageous for deterministic devices, this diffusion suppression is a key obstacle for unconventional devices that are actively making use of stochasticity [9,10]. In essence, utilizing antiferromagnetically coupled materials is the most efficient way to tailor the topology, where the effective topological charge can be easily tuned by multiple sublattices [7,11]. However, materials systems that accommodate antiferromagnetically coupled skyrmions showing diffusive dynamics have so far not been realized due to the difficulty of obtaining an extremely flat energy landscape that is indispensable to achieve diffusive dynamics. Here we demonstrate that an amorphous-like synthetic antiferromagnetic (SyAFM) system with low pinning allows for observing the thermally-activated diffusive motion

of antiferromagnetically-coupled skyrmions as shown in Fig. 1 [12]. The systematic investigation of varying the compensation ratio of magnetic moments in the SyAFM system with our analysis accounting for pinning effects allows for disentangling the influence of the topology on the diffusive motion. Our analysis reveals a more than 10 times larger diffusion coefficient for highly compensated antiferromagnetically-coupled skyrmions that is a direct consequence of the suppressed effective topological charge, which enables ultimately energy-efficient unconventional computing leveraging the enhanced stochasticity in antiferromagnetic systems [12].

[1] N. Nagaosa and Y. Tokura, Nat. Nanotechnol. 8, 899 (2013). [2] K. Everschor-Sitte *et al*., J. Appl. Phys. 124, 240901 (2018). [3] T. Dohi *et al*., Annual Review of Condensed Matter Physics 13, 73 (2022). [4] W. Jiang *et al*., Nat. Phys. 13, 162 (2017). [5] K. Litzius *et al*., Nat. Phys. 13, 170 (2017). [6] C. Schütte *et al*., Phys. Rev. B 90, 174434 (2014). [7] J. Barker and O.A. Tretiakov, Phys. Rev. Lett. 116, 147203 (2016). [8] M. Weißenhofer and U. Nowak, New J. Phys. 22, 103059 (2020). [9] J. Zázvorka *et al*., Nat. Nanotechnol. 14, 658 (2019). [10] Y. Jibiki *et al*., Appl. Phys. Lett. 117, 082402 (2020). [11] T. Dohi *et al*., Nat. Commun. 10, 5153 (2019). [12] T. Dohi *et al*., arXiv:2206.00791.

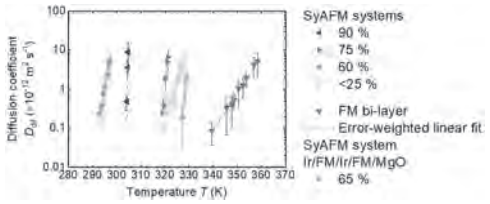

Fig. 1 Temperature dependence of the diffusion coefficient for samples with various compensation ratio.

EOC-12. Unconventional Emergent Hall Effect Phenomena and its Modification In a van der Waals Ferromagnet Fe_3GeTe_2. *R. Roy Chowdhury*[1], C. Patra[1], S. DuttaGupta[2,3], S. Fukami[3,4] and R. Singh[1]
1. Department of Physics, Indian Institute of Science Education and Research (IISERB), Bhopal, India; 2. Center for Science and Innovation in Spintronics (CSIS), Tohoku University, Japan, Sendai, Japan; 3. Research Institute of Electrical Communication (RIEC), Tohoku University, Japan, Sendai, Japan; 4. Center for Innovative Integrated Electronic Systems (CIES), Tohoku University, Japan, Sendai, Japan

Magnetism in two-dimensional (2D) van der Waals (vdW) materials has emerged as a new paradigm enunciating new condensed matter phenomena, bearing potential for application in future spintronic and quantum computing devices [1,2]. Among 2D vdW ferromagnets (FMs), metallic Fe_3GeTe_2 (FGT) is interesting owing to its high Curie temperature, uniaxial magnetic anisotropy, existence of unusual magnetic ground state. An understanding of factors responsible for unconventional magnetism and associated magnetoresistive manifestations has remained elusive. Here, we clarify the underlying physics responsible for nontrivial ground state and demonstrate tuning of emergent properties by substitution at magnetic (Fe) or nonmagnetic (Ge) sites in 2D vdW FGT. High quality single-crystalline FGT, $(Fe_{1-x}Co_x)_3GeTe_2$, $Fe_3(Ge_{1-x}As_x)Te_2$, ($0 \le x \le 1$) were grown by chemical vapor transport method. Magnetotransport measurements under $H \parallel$ c-axis result in sizeable anomalous Hall effect, arising from topological nodal lines in the band structure. Interestingly, transverse resistivity under $H \perp$ c-axis result in unconventional magnetoresistive behavior with prominent cusp-like feature (Fig. 1) [3,4]. Concomitant magneto-optical imaging indicates emergent skyrmion lattice-like structure, size varying with doping and angular magnetotransport confirms their 2D nature. Separation of magnetoresistive responses indicates dominant unconventional emergent Hall effect [3,4], tunable with magnetic or non-magnetic doping (Fig. 2), significantly larger than in other vdW, skyrmion-hosting materials [5-7]. Our results deepen understanding of emergent responses from complicated spin textures prospective for topological magnetism and non-collinear spin texture-based spintronic devices. RRC acknowledges DST for financial support (DST/INSPIRE/04/2018/001755). We thank H. Ohno for discussions. This work is partly supported by RIEC Cooperative Research Project.

[1] B. Huang *et al*., *Nature* 546, 270 (2017). [2] K. S. Burch *et al.*, Nature 563, 47 (2018). [3] R. Roy Chowdhury *et al.*, Sci. Rep. 11, 14121 (2021). [4] R. Roy Chowdhury *et al.,* Phys. Rev. Mater. 6, 014002 (2022). [5] Y. Wang *et al.*, Phys. Rev. B. 96, 134428 (pp 1-6) (2017). [6] S. Seki *et al.*, Science 336, 198-201 (2012). [7] N. Kanazawa *et al.*, Adv. Mater. 29, 1603227 (2017).

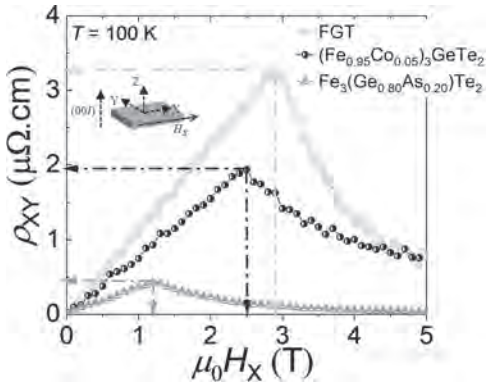

Fig. 1: Transverse resistivity (ρ_{XY}) vs. applied magnetic field ($H \perp$ c-axis). Inset shows schematic of measurement configuration.

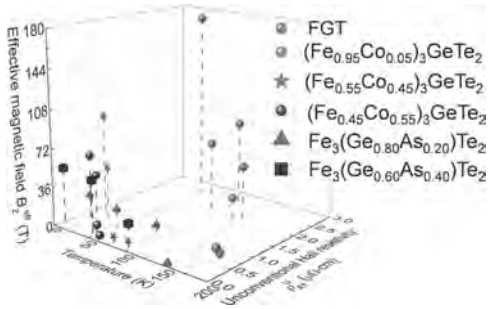

Fig. 2: 3D phase diagram of temperature (T), unconventional Hall resistivity (ρ^U_{XY}), effective emergent magnetic field (B^{eff}_Z) for FGT, $(Fe_{1-x}Co_x)_3GeTe_2$, $Fe_3(Ge_{1-x}As_x)Te_2$.

EOC-13. Skyrmion-Caloritronics: a promising Strategy to manipulate Skyrmions. *E. Raimondo*[1], E. Saugar[2], J. Barker[3], D.R. Rodrigues[4], A. Giordano[1], M. Carpentieri[4], W. Jiang[5], O. Chubykalo-Fesenko[2], R. Tomasello[4] and G. Finocchio[1] *1. University of Messina, Messina, Italy; 2. Instituto de Ciencia de Materiales de Madrid, Madrid, Spain; 3. University of Leeds, Leeds, United Kingdom; 4. Politecnico of Bari, Bari, Italy; 5. Tsinghua University, Beijing, China*

Magnetic skyrmions are "topologically protected" solitons, that have recently received increased attention due to their potential application as information carriers and for unconventional computing [1]. While the current-driven dynamics has been explored deeply, the theory of temperature gradient-induced dynamics - Skyrmion-Caloritronics [2] - is still at its early stages of development but it is particularly promising due to its low energy consumption. In this work, we study the effects of thermal gradients on skyrmion motion in different systems (single-layer FM with interfacial Dzyaloshinskii-Moriya interaction (*IDMI*), multilayer, and synthetic antiferromagnets (SAFs)) inspired by the experimental results of Ref. [2] and from a fundamental point of view. We observe that, when driven by the entropic torque, skyrmions in single layers move from the cold to the hot region with a finite skyrmion Hall angle (Fig. 1), while in multilayers they move in the opposite direction (from hot to cold region) (Fig. 2). The latter is in qualitative agreement with the experimental observations (Fig. 3a in Ref. [2]). We demonstrate that this difference is due to the distinct scaling

relations characterizing the two systems, and to the existence of a magnetostatic field gradient linked to the variation of saturation magnetization (M_S) which cannot be neglected in magnetic multilayers. The numerical results are corroborated by a generalized Thiele's equation developed for this scenario. Moreover, we show that the skyrmion Hall angle is completely suppressed in SAFs, similarly to the current-driven skyrmions [3,4]. Our results have fundamental implications in the future development of skyrmionic devices combining thermal gradients and SOTs where the proper temperature dependence of the parameters should be taken into account. See Ref. [5] for founding statement.

[1] J. Zázvorka, et al., Nat. Nanotechnol. 14, 658 (2019). [2] Z. Wang, et al., Nat. Electron. 3, 672 (2020). [3] X. Zhang, et al., Nat. Commun. 7, 10293 (2016). [4] R. Tomasello, et al., J. Phys. D. Appl. Phys. 50, 325302 (2017). [5] This work was supported by the Project No. PRIN 2020LWPKH7 funded by the Italian Ministry of University and Research, and by the PETASPIN association (www.petaspin.com). JB acknowledges support from the Royal Society through a University Research Fellowship. E.R. acknowledges the economical support of the COST Action CA 17123 (MAGNETOFON) within the STSM program. We would like to acknowledge networking support from COST Action No. CA17123 "Ultrafast opto magneto electronics for nondissipative information technology." [6] W. Li, et al., Adv. Mater. 31, 1807683 (2019).

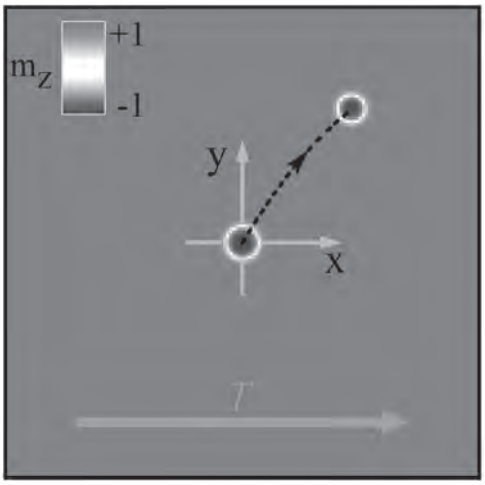

FIG. 1 Trajectory of the skyrmion induced by a linear gradient of temperature in a single FM with IDMI.

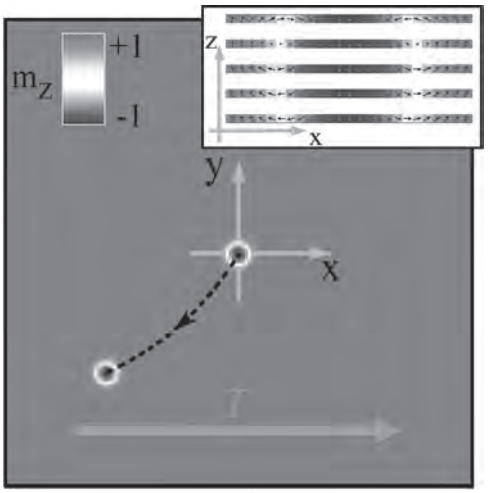

FIG. 2 Trajectory of the skyrmion induced by a linear gradient of temperature in a multilayer with 5 FM repetitions. The magnification of the skyrmion in inset shows the cross section along the multilayer thickness that highlights the existence of a hybrid skyrmion [6].

Session EOD
SKYRMIONS II
Avik W. Ghosh, Chair
University of Virginia, Charlottesville, VA, United States

INVITED PAPER

EOD-01. Skyrmionic 3D cocoons in magnetic multilayers. *M. Grelier*[1], Y. Sassi[1], C. Leveille[2], R. Battistelli[3], S. Collin[1], A. Vecchiola[1], F. Godel[1], K. Bouzehouane[1], A. Fert[1], F. Büttner[3], H. Popescu[2], N. Jaouen[2], V. Cros[1] and N. Reyren[1] *1. Unité Mixte de Physique CNRS/Thales, Université Paris-Saclay, Palaiseau, France; 2. SOLEIL Synchrotron, Saint-Aubin, France; 3. Helmholtz-Zentrum Berlin, Berlin, Germany*

Magnetic topological textures could serve as powerful tools in the development of next-generation spintronics devices, especially in terms of stability and energy consumption. Two-dimensional (2D) magnetic solitons such as chiral domain walls or skyrmions were mostly under focus for the last decade. Beyond these 2D textures, a new interest has risen for more complex quasi-particles that display variations over the thickness, *i.e.*, three-dimensional (3D) objects. Examples include different skyrmion phases [1], bobbers [2] or even hopfions [3]. In this work, we show how by engineering Pt/Co/Al based multilayers with variable Co thickness, we observe the signature of new textures, called skyrmionic cocoons [4] that are only present in a fraction of the magnetic layers. Interestingly, these cocoons can coexist with more standard 'tubular' skyrmions going through all the multilayer as evidenced by the existence of two very different contrasts in the magnetic force microscopy (MFM) images recorded at room temperature (Fig. 1a). Moreover, the field dependence of skyrmionic cocoons has also been studied with Fourier transform holography measurements (FTH) with similar observations (Fig. 1b). FTH additionally puts forward various magnetic phase transitions as well as the existence of an attractive interaction between cocoons. The presence of these novel skyrmionic textures has also been investigated by micromagnetic simulations (Fig. 1c). The relaxed states can easily be identified with the different experimental contrasts: the columnar skyrmion tubes (resp. cocoons) corresponds to the strong contrast (resp. weak contrast). Thus, this coexistence of various magnetic textures in multilayers and the discovery of a novel magnetic texture are particularly interesting as they can open new paths for three-dimensional spintronics.

[1] A.O. Mandru et al. *Nature communications* 11,1 (2020) [2] F. Zheng et al. *Nature Nanotechnology* 13, 451 (2018) [3] N. Kent et al. *Nature communications* 12, 1 (2021) [4] M. Grelier et al. *arXiv*: 2205.01172 (2022).

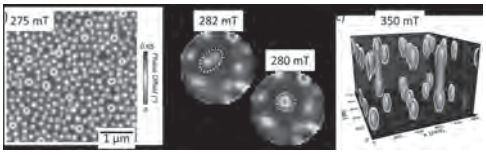

Fig. 1. Cocoons and skyrmion tubes. (a) Experimental MFM phase maps displaying two types of textures. (b) Holography images showing alignment of cocoons (Blue: up, red: down magnetization). (c) Corresponding micromagnetic simulations, evidencing the 3D nature of the cocoons and the skyrmion tubes (iso surfaces at m_z = -0.8 are displayed in red).

CONTRIBUTED PAPERS

EOD-02. Spatial control of the nucleation and dynamics of magnetic skyrmions by FIB irradiation. *S. Miki*[1,2], K. Hashimoto[1,2], R. Ishikawa[3], E. Tamura[1,2], H. Nomura[1,2], M. Goto[1,2] and Y. Suzuki[1,2] *1. Graduate School of Engineering Science, Osaka University, Toyonaka, Japan; 2. CSRN-Osaka, Osaka University, Toyonaka, Japan; 3. ULVAC, Inc., Suita, Japan*

Magnetic skyrmions are candidates for information carriers in applications for racetrack memories and Brownian computers because of their topologically protected properties. The circuits to confine the skyrmions in the 1D track with the magnetic wire or the magnetic energy wall play a key role in realizing such novel devices[1,2]. The ratchet using magnetic energy gradient is also required for improving calculation speed in ultralow-energy-consumption operation[3]. Because the focused-ion-beam (FIB) technique can vary the dose of ions locally, FIB effectively makes the circuit with the energy gradient[4]. This study aims to verify the effect of the FIB irradiation on the confinement and diffusion of the skyrmions and to structure the magnetic-energy gradient driving the skyrmions. We fabricated the stacking structure as Ta(5.9)|$Co_{16}Fe_{64}B_{20}$(1.2)|Ta(0.2)|MgO(2.2)|SiO_2(2.9) and microfabricated the surface of the sample by the FIB of the Ga^+ source. The potential condition for skyrmion creation can be controlled spatially by adjusting the dose of ions. Fig.1 shows the observations of the irradiated region indicated with the white dash line by the magneto-optical Kerr effect (MOKE) microscope. The skyrmions in the unirradiated region appear at about 333K, and in the irradiated region at about 295.5K. Fig.2(a) shows the mean squared displacement (MSD) of the skyrmions in the irradiated region. Fig.2(b) shows the temperature dependence of the diffusion coefficient before and after FIB irradiation. FIB irradiation increases the activation energy. However, the size of the diffusion coefficient after irradiation is as large as that in the sample before irradiation as far as a higher temperature is utilized. We will discuss the possibility of sputtering and of Ga^+ doping and the motion in the energy gradient. This work was supported by ULVAC, Inc., JSPS KAKENHI Grant Number JP20H05666, Japan and JST, CREST Grant Number JPMJCR20C1, Japan, and Nanotechnology Platform of MEXT, Grant Number JPMXP09 S-21-OS-0053.

[1] S. Woo, *et al*. *Nat. Mater.* 15, 501 (2016) [2] Y. Jibiki, S. Miki, *et al*. *Appl. Phys. Lett*. 117, 082402 (2020) [3] S. Miki, *et al. J. Phys. Soc. Jpn.* 90, 114703 (2021) [4] K. Fallon, *et al*. *small* 16, 1907450 (2020)

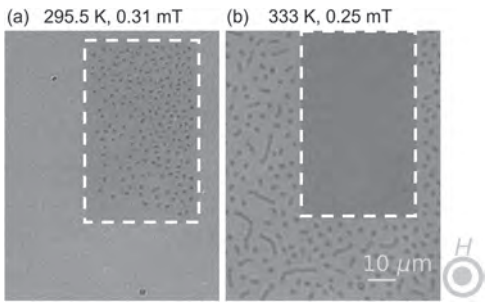

Fig.1 (a),(b) MOKE observation around the irradiated region by FIB indicated with the white dashed lines

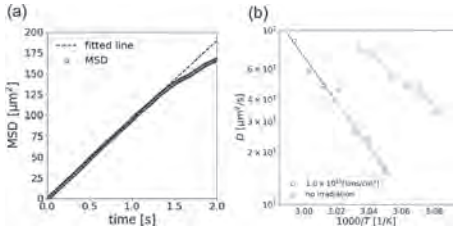

Fig.2 (a) MSD in the irradiated region. (b) the diffusion coefficient's temperature dependence.

EOD-03. Over 1 km/s Current Induced Skyrmion Motion in Synthetic Antiferromagnets without Skyrmion Hall Effect. V. Pham[1], N. Sisodia[1], j. Urrestarazu-Larrañaga[1], K. Bairagi[1], J. Pelloux-Prayer[1], L.D. Buda-Prejbeanu[1], S. Pizzini[2], G. Gaudin[1] and *O. Boulle*[1] *1. SPINTEC, Grenoble, France; 2. Institut Néel, Grenoble, France*

Skyrmions are topological spin textures which hold great promise as nanoscale bits of information in memory and logic devices [1]. The recent demonstration of room temperature skyrmions as well as their current induced motion in industry compatible sputtered thin films have lifted important roadblocks toward the realization of skyrmion based devices [2]. However, their development is impeded by a too low current induced velocity (about 100 m/s) [3] as well as the skyrmion Hall effect, namely a motion transverse to the current direction due to their topological charge which can lead to their annihilation in tracks. Antiferromagnetic (AF) skyrmions allow these limitations to be lifted owing to their vanishing magnetization and net zero topological charge, promising fast dynamics without skyrmion Hall effect. In this presentation, we address the current induced dynamics of AF skyrmions in compensated synthetic antiferromagnets (SAF). Using magnetic force microscopy, we show that skyrmions can be stabilized in Pt/Co/Ru based SAF at room temperature [4]. We show that SAF skyrmions with cancelled net topological charges can be moved by current at velocities over 1 km/s without skyrmion Hall effect. Micromagnetic simulations and analytical models using experimental parameters show that this enhanced skyrmion velocity can be explained by the compensation of the topological charges as well as an enhanced spin orbit torque in the synthetic antiferromagnet. Our results open an important path toward the realization of logic and memory devices based on the fast manipulation of AF skyrmions in tracks.

[1] A. Fert, V. Cros, and J. Sampaio, Nat. Nanotechnol. 8, 152 (2013). [2] A. Fert, N. Reyren and V. Cros, *Nat Rev Mater* 2, 17031 (2017). [3] Roméo Juge *et al.,* Phys. Rev. Appl. 12, 044007 (2019) [4] Roméo Juge *et al., arXiv:2111.11878 [cond-mat] (2021)*

EOD-04. Magnetic and Transport Properties of Chiral Antiferromagnetic $Co_{2-x}Pd_xMo_3N$ Thin Films. *B. Qiang*[1], T. Fukasawa[1], T. Hajiri[1], T. Hihara[2] and H. Asano[1] *1. Nagoya University, Nagoya, Japan; 2. Nagoya Institute of Technology, Nagoya, Japan*

Dzyaloshinskii–Moriya interaction (DMI) induced ferromagnetic (FM) skyrmions in chiral magnets have been reported last decade[1,2]. On the other hand, chiral antiferromagnet could be a great candidate to host antiferromagnetic (AFM) skyrmions, which have not been studied yet. The emergence of room-temperature FM skyrmions has been reported in the field β-Mn type $Fe_{2-x}Pd_xMo_3N$ epitaxial thin films[1]. We report Pd doping effect on magnetic and transport properties of a series of chiral antiferromagnetic filled β-Mn type $Co_{2-x}Pd_xMo_3N$ (CPMN) thin films. A series of CPMN (x = 0 ~ 1.61) thin films were fabricated on *c*-plane sapphire substrates. Figure 1(a) shows the 2θ/θ scan XRD pattern of a CPMN thin film with x = 1.01, indicating that CPMN films grown epitaxially in the (110) direction, as in case of $Fe_{2-x}Pd_xMo_3N/Al_2O_3$[1]. Figure 1(b) shows the x dependence of c_0 indicating the on-site doping of Pd. Figure 1(c) shows the *M-T* curve of a CPMN film with x = 1.01, where two anomalies are identified, which appeared in all CPMN films. The high-temperature anomaly could be related to the Néel temperature T_N, as in case of bulk Co_2Mo_3N[3]. The magnetization M_S at 200 K is 3×10^{-2} μ_B/f.u., which is 70 times smaller than that of ferromagnetic $Fe_{2-x}Pd_xMo_3N$ films[1], which suggests that the high-temperature magnetic phase is a canted antiferromagnetic (AFM) phase. The low-temperature anomaly can be ascribed to the spin reorientation, at which temperature (T_{SR}) the transition between AFM phase and spiral phase occurs as reported in chiral antiferromagnetic $K_2V_3O_8$[4]. The low-temperature spiral phase is also revealed by topological Hall effect (THE) at 4 K (Fig. 1(d)). The vanishing THE in canted AFM phase at 200 K (Fig. 1(d)) might be due to the AFM skyrmions. We will report the details of magnetic and transport properties of CPMN system.

[1] B. W. Qiang *et al*., Appl. Phys. Lett. 117, 142401 (2020). [2] R. Saha *et al*., Nat. Commun. 10, 5305 (2019). [3] W. Li et al. Phys. Rev. B 93, 060409(R) (2016). [4] M. D. Lumsden et al., Phys. Rev. Lett. 86, 159 (2001)

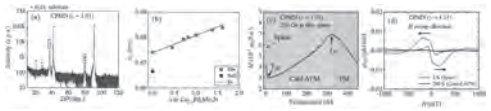

Fig.1 (a) Out of plane XRD pattern of a CPMN (x = 1.01). (b) x dependence of out of plane lattice constant c_0 with linear fitting. (c) *M-T* curve of a CPMN (x = 1.01). The magnetic field is applied perpendicular to film plane. (d) ρ_{TH} of a CPMN (x = 1.01) at 4 and 200 K, respectively. The black arrows show the sweep direction of applied magnetic field.

EOD-05. Microwave-Driven Phenomena of Magnetic Skyrmions. *M. Mochizuki*[1] *1. Department of Applied Physics, Waseda University, Shinjuku-ku, Japan*

Magnetic skyrmions (i.e., particle-like topological textures in magnets) have recently attracted significant research interest because of their potential for spintronics applications. Our theoretical studies have revealed that magnetic skyrmions in (quasi-) two-dimensional magnets driven by microwaves and thermal fluctuations exhibit interesting magnetoelectric phenomena. In this talk, I will discuss the following issues: (1) Microwave-driven translational motion of skyrmions without Hall motion [1,2]. (2) Efficient generation of a DC spin-motive force or voltage [3]. These phenomena are observed through exciting peculiar spin-wave modes of magnetic skyrmions (i.e., the counter-clockwise and clockwise rotation modes and the breathing mode [4,5]) by irradiating microwave fields under application of a magnetic field inclined from the perpendicular direction.

[1] A. Takeuchi and M. Mochizuki, Appl. Phys. Lett. 113, 072404 (2018). [2] M. Ikka, A. Takeuchi, and M. Mochizuki, Phys. Rev. B 98, 184428 (2018). [4] T. Koide, A. Takeuchi, and M. Mochizuki, Phys. Rev. B 98, 184428 (2018). [5] M. Mochizuki, Phys. Rev. Lett. 108, 017601 (2012). [6] M. Mochizuki and S. Seki, J. Phys.: Cond. Matt. 27, 503001 (2015).

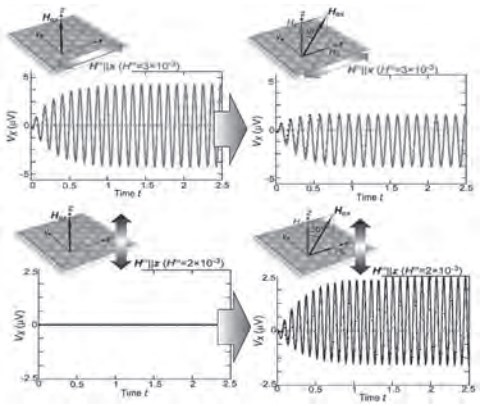

Calculated temporal profiles of spin voltage generated by exciting spin-wave modes of a skyrmion crystal via irradiating microwave fields. The oscillating spin voltage has a finite DC component when the external magnetic field is inclined from the perpendicular direction.

EOD-06. Nonlinear dynamics of bimeron in antiferromagnetic materials. *Y. Zhou*[1] *1. The Chinese University of Hong Kong (Shenzhen), Shenzhen, China*

A magnetic bimeron is a topologically nontrivial spin texture carrying an integer topological charge, which can be regarded as the counterpart of the skyrmion in easy-plane magnets. In this talk, we present an analytical model, corroborated by micromagnetics simulations, to describe the nonlinear dynamics of the current-driven bimerons in antiferromagnetic materials. The steady motion of an antiferromagnetic bimeron is analytically derived and is in good agreement with the simulation results [1]. In addition, we uncover the nonreciprocal dynamics of ferrimagnetic and antiferromagnetic bimerons in the nonlinear regime [2]. The nonreciprocal transport coefficient at the angular momentum compensation point can be more than one order of magnitude larger than the skyrmion case. The predicted nonlinear and nonreciprocal dynamics will be essential for designing innovative neuromorphic and logic devices, respectively.

[1] L. Shen, et al., Physical Review Letters, 124, 037202 (2020). [2] L. Shen, et al., Physical Review B, 105, 014422 (2022)

EOD-07. Topological Stability and Thermal Hysteretic Behavior of Metastable Néel Skyrmion Lattices in Fe_3GeTe_2. *Y. Li*[1], A.R. McCray[1,2], R. Basnet[3], K. Pandey[4], J. Hu[3,4], D. Phelan[1], W. Wang[5], X. Ma[5], A. Petford-Long[1,6] and C. Phatak[1,6] *1. Materials Science Division, Argonne National Laboratory, Lemont, IL, United States; 2. Applied Physics Program, Northwestern University, Evanston, IL, United States; 3. Department of Physics, University of Arkansas, Fayetteville, AR, United States; 4. Materials Science and Engineering Program, University of Arkansas, Fayetteville, AR, United States; 5. Center for Nanoscale Materials, Argonne National Laboratory, Lemont, IL, United States; 6. Department of Materials Science and Engineering, Northwestern University, Evanston, IL, United States*

Two-dimensional (2D) magnetic van der Waals (vdW) materials exhibit intriguing spin physics [1] and are potential candidates for spintronic devices [2] owing to their strong intrinsic spin interactions and the possibility of fabricating atomically-layered heterostructures. In particular, various nontrivial magnetic spin textures, such as Bloch- or Néel-type stripes, skyrmions, and bubbles domains, have been reported in 2D vdW materials under certain external stimuli [3-4]. It is critical to understand the magnetic domain behavior in such materials in response to external stimuli such as electric fields, magnetic fields, and temperature in order to control them by tuning the governing energy terms. Fe_3GeTe_2 is a promising magnetic vdW material as it is an itinerant ferromagnet in the 2D limit. Here we report the magnetic-field- and temperature-dependent studies of Néel skyrmion lattices in vdW Fe_3GeTe_2 by using in-situ cryo Lorentz transmission electron microscopy (LTEM). Néel skyrmions are formed in Fe_3GeTe_2 by following a field cooling protocol across the Curie temperature (~230 K). Figs 1 I and IV show the topology of the skyrmions are stable even after removing the magnetic field, and how the skyrmion sizes shrinks with increasing field. However, upon breaking the skyrmion configuration by saturating the magnetization with a large magnetic field, the sample returns to a magnetic phase with broad stripe domains rather than a uniform skyrmion phase (Figs. 1 V and VI). Furthermore, the behavior of individual skyrmions has been extensively explored. However, there is a lacking of understanding the collective behavior of Néel skyrmions. In this work, we systematically investigate the collective thermal behavior of skyrmion lattice ordering as a function of magnetic field strengths. We find a loss of lattice ordering during field cooling and a restoration of ordering after field heating, thus exhibiting a hysteretic behavior.

[1] B. Huang, G. Clark and E. Navarro-Moratalla *et al*., Nature 546 270 (2017). [2] W. Xia, L. Dai and P. Yu *et al*., Nanoscale, 9 4324 (2017). [3] B. Ding, Z. Li and G. X *et al*., Nano. Lett. 20 868 (2020). [4] Y. Li, R. Basnet and K. Pandey *et al*., JOM, 74, 2310 (2022) [5] This work was supported by the U.S. Department of Energy, Office of Science, Office of Basic Energy Science, Materials Sciences and Engineering Division.

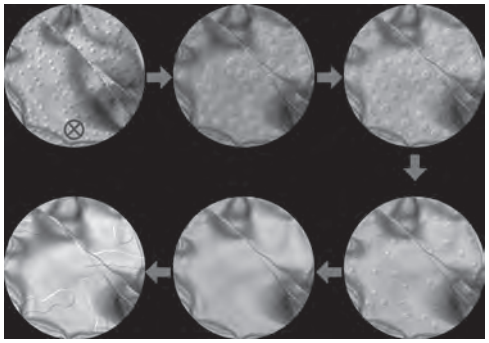

Fig. 1: LTEM images of a Fe_3GeTe_2 flake showing the response of Néel skyrmions to an in-situ perpendicular applied magnetic field at 100 K.

EOD-08. Zero-field Magnetic Skyrmions in Multilayer Films Stabilized by Interplay of Interlayer Exchange Couplings. *X. Chen*[1], T. Tai[1,2], H. Tan[1], H. Tan[1], R. Lim[1], P. Ho[1] and A. Soumyanarayanan[3,1] *1. Institute of Materials Research and Engineering, Singapore; 2. Cavendish Laboratory, University of Cambridge, Cambridge, United Kingdom; 3. Department of Physics, National University of Singapore, Singapore*

Magnetic skyrmions are promising candidates for achieving low-power, next-generation edge computing devices due to their particle-like nature, efficient coupling to electrical and spin currents and room-temperature stability in multilayer films [1]. However, in most skyrmion-hosting multilayers, the predominant magnetic textures at zero-field (ZF) are labyrinthine stripes [2]. External applied magnetic fields or geometric confinement [3] are typically used to stabilize isolated skyrmions, which limits their practicality. In this work, we design multilayers comprising three adjoining functional stacks – two repeats of skyrmion-hosting multilayers and a bias layer – coupled by two tunable interlayer exchange couplings (IECs) [4,5]. Using Lorentz transmission electron microscopy (LTEM), we demonstrate that these two IECs act as coarse and fine-tuning knobs that determine skyrmion stability and density. With micromagnetic simulations, we elucidate the unique roles played by each of the couplings and establish the advantage of a duo-IEC system in applications. This work establishes and extends the use of IEC as a means of stabilizing and shaping ZF skyrmions and paves the path to skyrmion-based devices.

[1] A. Fert, N. Reyren, and V. Cros, *Magnetic Skyrmions: Advances in Physics and Potential Applications*, Nat. Rev. Mater. 2, natrevmats201731 (2017). [2] X. Chen, M. Lin, J. F. Kong, H. R. Tan, A. K. C. Tan, S.-G.

Je, H. K. Tan, K. H. Khoo, M.-Y. Im, and A. Soumyanarayanan, *Unveiling the Emergent Traits of Chiral Spin Textures in Magnetic Multilayers*, Adv. Sci. 9, 2103978 (2022). [3] P. Ho, A. K. C. Tan, S. Goolaup, A. L. G. Oyarce, M. Raju, L. S. Huang, A. Soumyanarayanan, and C. Panagopoulos, *Geometrically Tailored Skyrmions at Zero Magnetic Field in Multilayered Nanostructures*, Phys. Rev. Appl. 11, 024064 (2019). [4] G. Chen, A. Mascaraque, A. T. N'Diaye, and A. K. Schmid, *Room Temperature Skyrmion Ground State Stabilized through Interlayer Exchange Coupling*, Appl. Phys. Lett. 106, 242404 (2015). [5] W. Legrand, D. Maccariello, F. Ajejas, S. Collin, A. Vecchiola, K. Bouzehouane, N. Reyren, V. Cros, and A. Fert, *Room-Temperature Stabilization of Antiferromagnetic Skyrmions in Synthetic Antiferromagnets*, Nat. Mater. 19, 34 (2019).

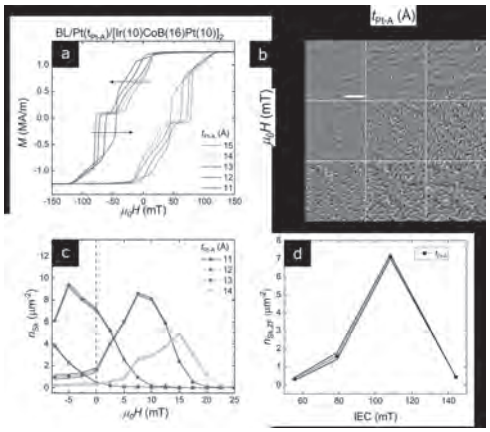

Tuning of zero-field (ZF) textures. (a) Left shift of the out-of-plane magnetic hysteresis for the combined stack $[Co(3.5)/Pt(2)]_7Co(3.5)/Pt(t_{Pt\text{-}A})[Ir(10)/CoB(16)/Pt(10)]_2$ with decreasing $t_{Pt\text{-}A}$. (b) Array of representative LTEM images (scale bar: 1 µm) illustrates the texture evolution with varying $t_{Pt\text{-}A}$ and external field $\mu_0 H$, from labyrinthine stripes to isolated skyrmions and finally to uniform magnetization. (c) The skyrmion density field evolution curve, $n_{sk}(H)$, shifts to the left and increases in peak height with decreasing $t_{Pt\text{-}A}$. (d) The ZF skyrmion density, $n_{sk,ZF}$, peaks at an IEC value of approximately 110 mT.

EOD-09. Reversal of skyrmion topological deflection across the angular compensation in GdCo ferrimagnetic thin-film. *L. Berges*[1], A. Mougin[1], J. Sampaio[1], R. Weil[1] and E. Haltz[1] *1. Physics, Laboratoire de Physique des Solides, Orsay, France*

Magnetic skyrmions are topologically non-trivial swirling magnetic textures. Their particle-like properties and defined chirality imposed by chiral interaction such as the Dzyaloshinskii-Moriya interaction, enables their efficient manipulation by spin-polarized currents. They have been well described in ferromagnetic materials [1], where they display a large sideways deflection proportional to the material's angular momentum density Ls [2], which is detrimental to most applications. Rare Earth/Transition Metal (RE/TM) ferrimagnets, such as GdCo, offer promising properties to tackle this issue. Indeed, the different nature of the two antiferromagnetically-coupled magnetic sub-lattices allows to tailor the Ls of the material by changing either its temperature or composition. In particular, it is even possible to change the sign of the net Ls across the angle compensation point which is predicted to reverse the skyrmion deflection angle. It has been shown that deflection of domains with chiral domain walls reverses when crossing the compensation temperature [3] and that skyrmion deflection is reduced near compensation temperature relative to that observed in ferromagnets [4]. We present clear evidence of the reversal of the topological deflection angle of skyrmions in GdCo across the compensation composition. We produced two thin-film samples on either side of the compensation composition, with a small out of plane anisotropy to stabilize skyrmions. The skyrmions' positions before and after current pulses, propagated by current-induced spin-orbit torques, are measured by magneto-optical imaging, and clearly show that the deflection angle in the two samples is of opposite sign. This result shows unambiguously how the skyrmion topological deflection can be tuned and suppressed in RETM ferrimagnets and paves the way towards deflectionless skyrmions at room temperature and zero magnetic field.

[1] C. H. Marrows, K. Zeissler, Appl. Phys. Lett. 119, 250502 (2021) [2] Jiang, W., Zhang, X., Yu, G. et al., Nature Phys 13, 162–169 (2017) [3] Hirata, Y., Kim, DH., Kim, S.K. et al., Nat. Nanotechnol. 14, 232–236 (2019) [4] Woo, S., Song, K.M., Zhang, X. et al., Nat Commun 9, 959 (2018)

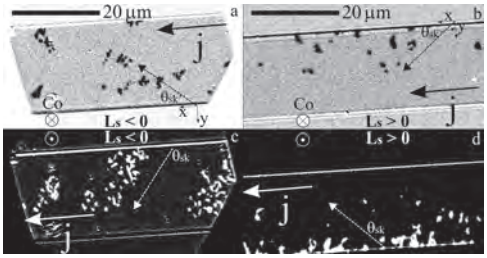

Differential MOKE images of skyrmions in a 20 µm track after a few 5 ns current pulses along j. Dashed arrow shows the propagation direction and Θsk the deflection angle. a,c shows the sample below the compensation composition (Ls<0) and b,d the sample above compensation (Ls>0). Skyrmion Co moment points down (up) in a,b (c,d).

EOD-10. High Endurance Skyrmion Control Via Vertical Current Injection with HfOx/Pt Top Electrode. *H. Jun*[1], S. Lee[1], H. Kwon[2], Y. Choi[1], J. Choi[2], T. Shim[2] and J. Park[1,2] *1. Department of Nanoscale Semiconductor Engineering, Hanyang university, Seoul, The Republic of Korea; 2. Department of Electronic Engineering, Hanyang University, Seoul, The Republic of Korea*

Recently, as an observation of the current-driven magnetic skyrmion was reported at RT, the magnetic skyrmion has received huge attention as a low power and ultra-high speed operation [1]. Since, skyrmion has high topological stability and sub-100 nm scale size, it can greatly improve the characteristics of domain-wall based racetrack memory [2], and synaptic memory [3]. In particular, skyrmion-based synaptic memory was enabled high linearity and symmetry potentiation/depression operations compared to emerging memory-based synaptic memory [3]. Stable skyrmion generation and movement are required for the operation of the skyrmion-based synaptic device. Therefore, various methods were proposed such as magnetic fields [1], voltage-controlled magnetic anisotropy [4], thermal energy [5], and vertical current injection [6]. Especially for high density of skyrmion synapses, a vertical current injection method was necessary. However, the previous study was not guarantee high endurance. Because a hard breakdown was occurred by Joule heating when current was continuously applied via breakdown filament. To solve this problem, our research team applied a set voltage (+0.9-1.2 V) to the HfOx/Pt valance change mechanism (VCM) electrode to form a stable filament against to the Joule heating. To confirm stable generation and movement of skyrmions, SiO2 sub/CoFeB/Ta/MgO/TaOx/HfOx/Pt was fabricated with 12-inch multi chamber sputter and measured by magneto-optical-Kerr-effect (MOKE) as shown in Fig.1 and Fig. 2. In our presentation, we will review in detail the perpendicular magnetic anisotropy (PMA) of the skyrmion-based synaptic memory, and improved endurance results with the MOKE observation. This research was supported by National R&D Program through the National Research Foundation of Korea(NRF) funded by Ministry of Science and ICT(2021M3F3A2A01037733)

[1] S. Woo, K. Litzius, B. Krüger, *et al. Nature Mater*., Vol. 15, p.501-506 (2016) [2] Z. Hou, Q. Zhang, G. Xu, *et al*. *Nano Letters*, Vol. 18(2), p.1274-1279 (2018) [3] K.M. Song, JS. Jeong, B. Pan, *et al. Nat Electron*., Vol. 3, p.148-155 (2020) [4] D. Bhattacharya, S.A. Razavi, H. Wu, *et al. Nat Electron*., Vol. 3, p.539-545 (2020) [5] Z. Wang, M. Guo, HA. Zhou, *et al. Nat Electron*., Vol. 3, p.672-679 (2020) [6] S. Yang, K.W. Moon, T.S Ju, et al. *Advanced Materials*, Vol. 33(45), p.2104406 (2021)

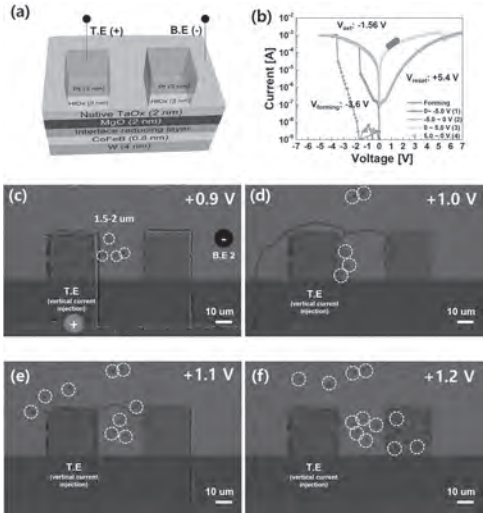

Fig. 1. I-V characteristic and skyrmion generation by vertical current injection (a) fabrication structure (b) I-V characteristic of HfOx/Pt (c) MOKE result of + 0.9 V (d) +1.0 V (e) +1.1 V (f) 1.2 V

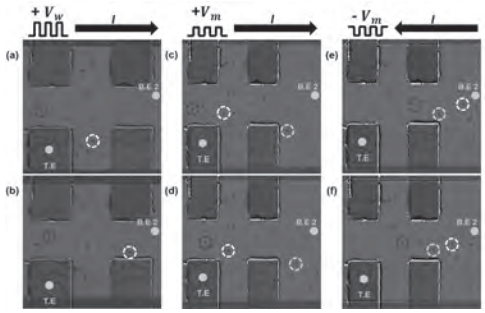

Fig. 2. Movement of skyrmion by vertical current injection. The direction of skyrmion movement was changed by current direction. (a)-(b) +0.9 V (c)-(d) +0.5 V (e)-(f) -0.5 V

EOD-11. Withdrawn

Session EOE
SPIN-ORBITRONICS I

Shinji Isogami, Co-Chair
National Institute for Materials Science, Tsukuba, Japan
Tomohiro Taniguchi, Co-Chair
National Institute of Advanced Industrial Science and Technology, Tsukuba, Japan

INVITED PAPER

EOE-01. Spin currents generation and self Spin-Orbit torque in GdFeCo ferrimagnet. *H. Damas*[1], D. Céspedes-Berrocal[1,2], J. Bello[1], D. Maccariello[5], A. Anadon[1], V. Desbuis[1], A. Arriola-Cordova[1,2], J. Alegre-Saenz[1,2], P. Tang[3], P. Vallobra[1], Y. Xu[1], S. Migot[1], J. Ghanbaja[1], S. Zhang[3], D. Lacour[1], S. Mangin[1], C. Panagopoulos[4], V. Cros[5], M. Hehn[1], S. Petit-Watelot[1], A. Fert[5] and J. Rojas-Sanchez[1] *1. Institut Jean Lamour, Université de Lorraine, CNRS, Nancy, France; 2. Universidad Nacional de Ingeneria, Rimac, Peru; 3. Departement of Physics, University of Arizona, Tucson, AZ, United States; 4. Division of Physics and Applied Physics, School of Physical and Mathematical Sciences, Nanyang Technological University, Singapore; 5. Unité Mixte de Physique, CNRS, Thalès, Palaiseau, France*

Spin currents and spin-torques generated by spin-orbit coupling (SOC) are exploited in spintronics to meet the high data demand in information technology. Nowadays, the large SOC of 5d non-magnetic heavy metals (HMs) is required to generate a pure spin current by the spin Hall effect (SHE). In turn, the pure spin current generates a spin-orbit torque (SOT) on an attached magnetic layer [1]. It is generally accepted that in magnetic materials, the spin polarization of the generated spin current is aligned with the direction of the magnetization due to the exchange interaction. The generation of such spin current is referred to as the Spin Anomalous Hall Effect (SAHE) [2]. More recent theoretical works [3,4] have shown that the latter description is incomplete for magnetic materials with large spin-orbit coupling. In this case, the spin polarization can be preserved from alignment with the magnetization, as demonstrated in ferrimagnets [5]. The total spin current is therefore the sum of SAHE-like and SHE-like spin currents [2-4] as depicted in Fig 1. The SAHE-like spin current cannot induce a torque on the magnetization because the spin polarization is aligned with the magnetization. However, the SHE-like symmetry can generate a torque if the spin current is absorbed outside the layer. We refer this torque as self-torque because the material is the source of the torque on its magnetization. In this talk, we present the study of a ferrimagnet with strong spin-orbit coupling: GdFeCo. The SAHE and SHE spin current contributions are studied by complementary Spin Torque Ferromagnetic Resonance (ST-FMR) techniques and self-torque characterization were performed by means of harmonic Hall voltage measurements. We show in GdFeCo/Cu/NiFe trilayer that the ST-FMR voltage at NiFe resonance that is sensitive to GdFeCo SHE-like symmetry does not change sign across the magnetic compensation temperature [6]. The addition of a dc current to ST-FMR experiments allows to quantify the total contribution [6,7]. Additionally, we show in GdFeCo/Cu that the effective fields associated to the self-torques are amplified in the vicinity of the magnetic compensation temperature of the ferrimagnet and reverse their sign across it [7] (see Fig 2). Finally, we present more experimental results with signatures that highlight the difference between external SOT and self-torque taking advantage of characteristics temperatures in ferrimagnets. This study paves the way for further research into the generation of spin currents in ferrimagnets and the exploitation of self-torque generated in single magnetic layer for spintronic devices. This work was supported partially from Agence Nationale de la Recherche (France) under contract N° ANR-18-CE24-0008 (MISSION), ANR-19-CE24-0016-01 (TOPTRONICS) and ANR-17-CE24-0025 (TOPSKY), from the French PIA project "Lorraine Universite d'Excellence", reference ANR-15IDEX-04-LUE. This study is partially funded by MSCA-RISE 2020-Project N°101007825 - ULTIMATE-I. D. C.-B., A.Y.A.C and H. D, acknowledge SPIN IJL team for their internship fellow 2018, 2019 and 2020, respectively. DCB also thanks "LUE Graduated" program internship 2019 from "Lorraine Université d'Excellence".

[1] A. Manchon *et al., Reviews of Modern Physics*, vol. 91, no 3, p. 035004, (2019). [2] T. Taniguchi *et al., Physical Review Applied*, vol. 3, no 4, p. 044001, (2015). [3] V. P. Amin, *et al., Physical Review B*, vol. 99, no 22, p. 220405, (2019). [4] K-W. Kim, *et al*., *Physical Review Letters*, vol. 125, no 20, p. 207205, (2020). [5] Y. Lim, *et al*., *Physical Review B,* vol. 103, no 2, p. 024443, (2021). [6] H. Damas, *et al.*, p. 2200035, *PSS RLL* (2022). [7] D. Céspedes, H. Damas, *et al., Advanced Materials*, vol. 33, no 12, p. 2007047, (2021).

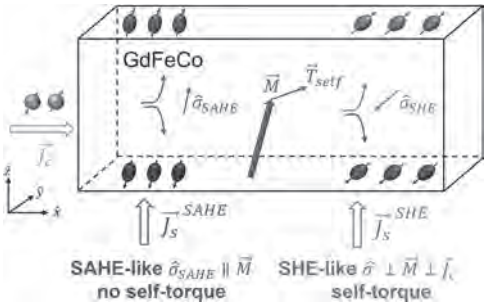

Fig.1: When a charge current J_c is injected into a magnetic material with strong spin-orbit coupling, it generates spin current of dfferent symmetries. The Spin Anomalous Hall effect spin current J_{SAHE} cannot induce a torque on the magnetization M as its spin polarization σ_{SAHE} is aligned with M. In contrast, the Spin Hall effect spin current J_{SHE}, if it is absorbed outside the layer, can induce a torque (or self-torque) T_{self} because σ_{SHE} has a component transverse to M.

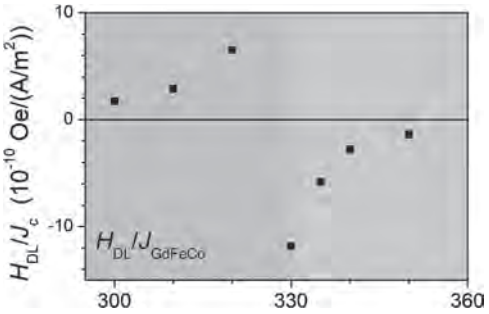

Fig.2: Temperature dependence of the damping-like effective field H_{DL} in a GdFeCo/Cu bilayer. Its sign reverses across the magnetic compensation temperature (depicted by the background change of color).

CONTRIBUTED PAPERS

EOE-02. Spin-orbit torques in Gd/CoFeB/MgO heterostructures.
J. O'Brien[1], P. Khanal[1], B. Zhou[1], A. Habiboglu[1] and W. Wang[1] *1. Physics, University of Arizona, Tucson, AZ, United States*

Spin-orbit torques (SOT) effect has been studied intensively to switch the magnetization of magnetic materials. Generally the SOT effect can arise from the bulk or interface of a single film, or a multilayered heterostructure. As the source of generating SOT effects, different materials have been explored, starting with nonmagnetic heavy metals and expanding to ferromagnets, antiferromagnets, 2D materials and topological insulators. Here we report the investigation of SOT effects in Gd/CoFeB/MgO heterostructures. Bulk Gd is ferromagnetic with a Curie temperature of about 293K. The samples were deposited on thermally oxidized Silicon wafers with the stack structure of Si/SiO2/Gd (3nm-5nm)/CoFeB (1nm)/MgO(2-3nm)/Ta (2nm). Hall bars with the dimension of 3μm x 20μm were patterned. Perpendicular magnetic anisotropy (PMA) has been obtained in these samples in the as-prepared state and after thermal annealing. Representative anomalous Hall effect (AHE) curves are shown in Figure 1. Large shift of the AHE loops were observed when this device was measured under different electric currents, with no in-plane magnetic field applied. This is an indication of an effective SOT field in the z direction generated by the charge current following in the x direction. The current density flowing through the Gd layer is estimated to be $8.7*10^6$ A/cm^2. The efficiency of the generation of the effective fields is estimated to be 30.3 Oe/10^7 Acm^{-2}, which is larger than what observed in Hf/CoFeB/MgO [1] and W/Ti/CoFeB/MgO [2] structures. We will discuss the thickness dependence and temperature dependence of the samples annealed under different conditions, with DC measurements and second-harmonic Hall measurements. This research is supported by NSF and DARPA.

[1] M. Akyol, G. Yu and J. G. Alzate, Appl. Phys. Lett. 106, 162409 (2015).
[2] A. Razavi, H. Wu and Q. Shao, Nano Lett. 20, 3703 (2020).

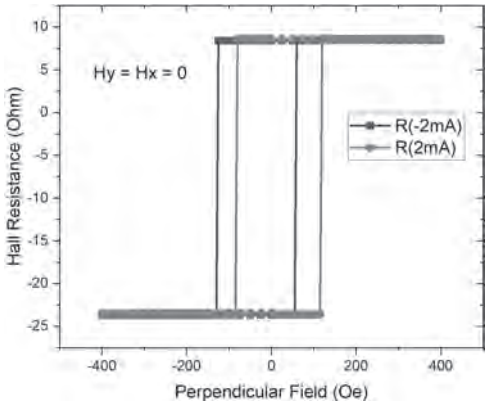

Fig. 1 AHE curves under perpendicular magnetic field are shifted based on current polarity.

EOE-03. Effect of alloying on spin-orbit torque in $Fe_{0.75}Co_{0.25}|Pt_{1-x}X_x$ bilayers.
G.G. Baez-Flores[1] and K. Belashchenko[1] *1. Physics and Astronomy, University of Nebraska - Lincoln, Lincoln, NE, United States*

Optimization of materials for efficient spin current generation and magnetization switching in ferromagnet(FM)/heavy-metal(HM) bilayers is of interest for SOT-MRAM and other applications. Experimentally, alloys of Pt with other elements have been studied as the HM source of spin current, some of which were found to increase the effective spin-Hall angle ξ_j DL and/or the dampinglike (DL) torque efficiency ξ_E DL in FM|$Pt_{1-x}X_x$ bilayers. Here we use the tight-binding LMTO implementation of the nonequilibrium Green's function (NEGF) technique [1] to calculate the DL SOT efficiencies for $Fe_{0.75}Co_{0.25}|Pt_{1-x}X_x$ bilayers with different alloying elements X, as a function of concentration. The bcc $Fe_{0.75}Co_{0.25}$ alloy is chosen for the FM layer due to its good lattice matching with fcc Pt and low Gilbert damping. The atomic potentials are obtained using the coherent potential approximation, and the torquances are then evaluated via supercell averaging over substitutional disorder. We find that the largest SOT efficiency ξ_E DL is achieved by alloying with 20% Au or 10% Rh. Using the calculated residual resistivities of the $Pt_{1-x}X_x$ alloys, we estimate the effective spin-Hall angles ξ_j DL in the alloyed systems. The results are compared with available experimental data. This work was supported by NSF grant No. DMR-1916275.

D.Pashov et al. Comput. Phys. Commun. (2020)

EOE-04. Chemical Tuning of Ferroelectricity and Rashba Spin Texture in the ternary Alloy $Sn_xGe_{1-x}Te$.
L. Nessi[1,2], F. Fagiani[1], F. Belponer[1], F. Delodovici[3], S. Cecchi[4], R. Kumar[5,6], M. Cantoni[1,2], D. Mondal[7], F. Mazzola[7], G. Vinai[7], V. Polewczyk[7], J. Fujii[7], M. Fiebig[6], A. Rubano[5], R. Calarco[8], R. Bertacco[1,2], I. Vobornik[7], S. Picozzi[3] and C. Rinaldi[1,2] *1. Politecnico di Milano, Milan, Italy; 2. Istituto di Fotonica e Nanotecnologie CNR-IFN, Consiglio Nazionale delle Ricerche, Milan, Italy; 3. Consiglio Nazionale delle Ricerche, CNR-SPIN, Chieti, Italy; 4. Paul-Drude-Institut für Festkörperelektronik, Berlin, Germany; 5. Dipartimento di Fisica "E. Pancini", Università Federico II, Naples, Italy; 6. Department of Materials, ETH Zurich, Zurich, Switzerland; 7. Istituto Officina dei Materiali (IOM)-CNR, Trieste, Italy; 8. Consiglio Nazionale delle Ricerche - Istituto per la Microelettronica e Microsistemi (CNR-IMM), Rome, Italy*

Monochalcogenides GeTe [1] and SnTe [2] are key prototypes of ferroelectric Rashba semiconductors, materials in which the ferroelectric polarization direction directly governs the Rashba spin texture chirality [3], offering an unprecedent, non-volatile and all-electric control over spin-to-charge conversion processes. In GeTe, we provided the experimental demonstration that the reversal of the ferroelectric polarization induces the reversal of the Rashba spin texture. Moreover, we demonstrated that the ferroelectric polarization in GeTe epitaxial thin films can be reliably switched by electrical gating and used to control or even reverse the spin-to-charge current conversion in such semiconductor [4]. With respect to GeTe, ferroelectric SnTe is expected to show a larger spin-to-charge conversion efficiency thanks to a predicted giant intrinsic spin Hall conductivity in 2D [5]. Unfortunately, while the Curie temperature of GeTe is about 720 K, the ferroelectric phase of SnTe does not survive room temperature, and this represents a limiting factor for practical applications. A promising route is provided by alloying the two chalcogenides in the ternary compound $Sn_xGe_{1-x}Te$, where Ge may allow for stabilization of the ferroelectric phase up to room temperature [6]. In this communication, we experimentally study the band structure and ferroelectric properties of this alloy grown in thin films by molecular beam epitaxy versus composition and temperature. The spectroscopic experiments are supported by *ab initio* calculations. The tunability of both Rashba spin-orbit coupling and ferroelectricity above room temperature on a wide range of chemical compositions is demonstrated. Further investigations exploring density functional theory calculations suggest the possibility to obtain an unprecedent coexistence of Rashba spin texture and topological features within the same ferroelectric for limited concentrations of Ge. These findings, i.e., the robustness of both Rashba effect and ferroelectricity over a wide compositional range, put the groundwork for the engineering of spin-to-charge current conversion in ferroelectric Rashba semiconductors.

[1] D. Di Sante *et al.*, Adv. Mater., 25, 509 (2013) [2] E. Plekhanov *et al.*, Phys. Rev. B, 90, 161108R (2014) [3] C. Rinaldi *et al.*, Nano Lett., 18, 2751 (2018) [4] S. Varotto *et al.*, Nat. Electron., 4, 740 (2021) [5] H. Wang *et al.*, npj Comput. Mater., 6, 7 (2020) [6] A. I. Lebedev *et al.*, Ferroelectr., 289, 189 (2004)

EOE-05. Peculiarities of measured dependencies of strength of spin-orbit interaction and anisotropy field on current density in FeCoB nanomagnet. *V. Zayets*[1], I. Serdeha[2] and V. Grygoruk[2] *1. Platform Photonics Research Center, AIST, Tsukuba, Japan; 2. Educational and Scientific Institute of High Technologies, Taras Shevchenko National University of Kyiv, Kyiv, Ukraine*

Spin accumulation, which is created by an electrical current flowing in a nanomagnet, affects the strength of spin-orbit interaction (SO) and anisotropy field H_{ani} in a nanomagnet. The reduction of Hani and SO by the current may cause a magnetization reversal. As a result, the data, which is encoded into the current, is memorized by means of two equilibrium magnetization directions of the nanomagnet. Recently, we have developed a high-precision measurement method of H_{ani} and coefficient of spin-orbit interaction k_{so} [1]. k_{so} is a numerical parameter characterizing the SO strength. Figure 1 shows kso vs. H_{ani} measured in FeCoB nanomagnets. The SO strength is larger in nanomagnet, which contains several ferromagnetic layers (shown by stars) in comparison with nanomagnets containing only one ferromagnetic layer(shown by triangles). It means that the SO strength depends on the number of interfaces. The SO strength increases with an increase of the number of FeB layers up to 5 FeB layers. Further increase of the number of FeB layers causes a decrease of k_{so} due to accumulated interface roughness. Figure 2 compares current dependency of H_{ani} for a single and multilayer nanomagnet. In the multilayer nanomagnet with a strong SO, the reduction of H_{ani} is large of about 25 % and is nearly independent of current polarity. In contrast, in the single- layer nanomagnet with a weak SO, H_{ani} changes almost linearly with the current only with a small symmetrical contribution due to heating, but the change is small of about 6%. Even such a small change of Hani is sufficient for magnetization reversal, when the conditions for the parametric resonance are met [2,3].

[1] https://www.youtube.com/watch?v=LmvYN5hG-90 [2] V. Zayets, *arXiv:2104.13008 (2021).* [3] V. Zayets, IOA-07, MMM (2021)

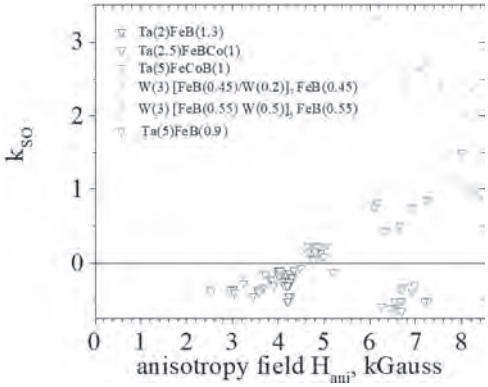

Fig.1 Coefficient of spin-orbit interaction vs. anisotropy field. Each dot corresponds to a measurement of an individual nanomagnet. Dots of the same color correspond to nanomagnets fabricated on the same wafer.

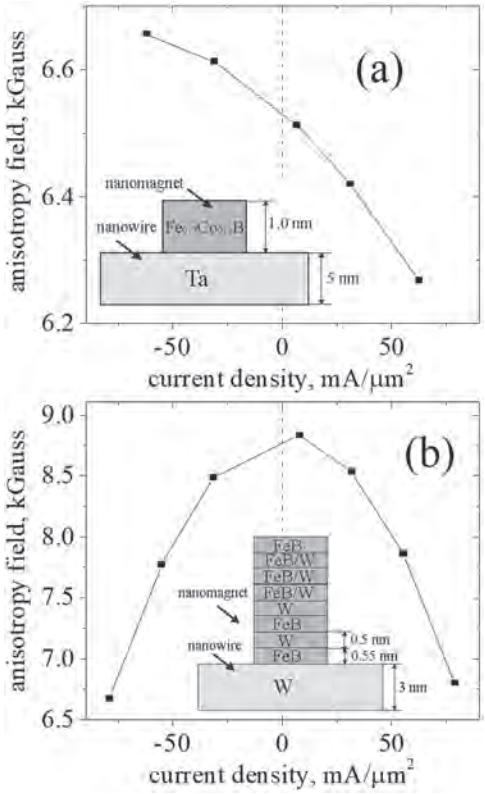

Fig.2 Anisotropy field vs.current dependence measured in nanomagnet having (a) a single ferromagnetic layer and small k_{so}=-0.63 (b) several ferromagnetic layers and large k_{so}=+1.05.

EOE-06. Spin-orbit Torques in Magnetron-Sputtered $MoTe_2$. *S. Li*[1], J. Gibbons[1] and A. Hoffmann[1] *1. University of Illinois at Urbana-Champaign, Urbana, IL, United States*

Weyl semimetals can generate large current-induced spin-orbit torques (SOT) that can manipulate the magnetization dynamics in the ferromagnetic materials, and thus play an important role in spintronic devices. Due to their concomitant reduced symmetries, Weyl semimetals are also promising for generating SOTs with novel symmetries that may be able to switch perpendicular magnetic anisotropy thin films. Recently, the T_d phase $MoTe_2$, which is Weyl semimetal, has attracted a lot of attentions in the field of spintronics, due to its theoretically predicted SOT efficiencies that are even larger than those of WTe_2 [1]. Here, we studied the effects of processing conditions on the stoichiometry and crystal structure of the magnetron-sputtered $MoTe_2$ films by using Rutherford backscattering and X-ray diffraction. Furthermore, we identified different phases of the sputtered MoTe2 thin films using Raman spectroscopy, and we have observed a stable T_d semimetal phase even at room temperature. The T_d phase is generally considered to be a low-temperature phase and only appears at temperatures below 250 K, and at room temperatures, $MoTe_2$ will be in the 1T' monoclinic phase or the 2H hexagonal phase [2]. We have also observed dimensionality-dependent phase transitions from the T_d to the 1T' phase at room temperature for sputtered $MoTe_2$ thin films as the characteristic peak for the T_d phase $MoTe_2$ gradually shifts from 264 cm^{-1} to 259 cm^{-1}(the Raman peak position for the 1T′ phase), as the thickness of the sputtered films increases (shown in Figure 1). Finally, SOT efficiencies of the $MoTe_2$ thin films were measured via spin-torque ferromagnetic resonance (ST-FMR) on $MoTe_2$/$Ni_{80}Fe_{20}$ heterostructures and we observed a large novel SOT due to the spins with out-of-plane polarization directions in both the symmetric and anti-symmetric components of the homodyne mixing voltage signals (shown in Figure 2). The efficiencies of the novel damping-like and field-like SOT are estimated to be 16% and 27%, respectively.

[1] J. Zhou, et al., *Phys. Rev. B* 99, 060408 (2019). [2] K. Zhang, et al., *Nature Comm 7*, 13552 (2016).

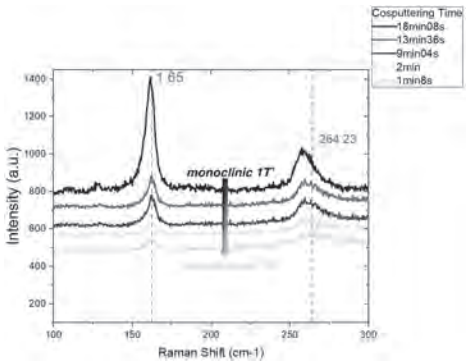

Fig.1 Raman spectroscopies on samples with different deposition times (thus different thicknesses)

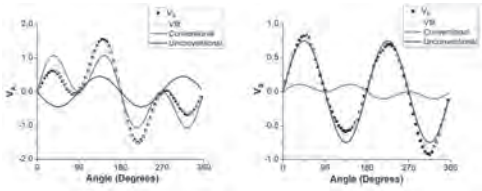

Fig.2 Antisymmetric and symmetric components as a function of the angle between the current and the applied field directions

INVITED PAPER

EOE-07. High-efficiency magnetization switching via electrical manipulation of exchange bias and magnon current. B. Fang[1], D. Zheng[1], Y. Li[1], A. Chen[1], K. Liu[2] and *X. Zhang*[1] *1. PSE, KAUST, Thuwal, Saudi Arabia; 2. Physics, Georgetown University, DC, DC, United States*

The search for efficient approaches to realize local switching of magnetic moments in spintronic devices has attracted intense interest. In particular, spin-orbit torque (SOT) that arises from materials with large spin-orbit coupling (SOC) offers a new pathway for energy-efficient and fast magnetic information storage. Recent studies on SOT-induced magnetization switching and dynamics in magnetic heterostructures have shown promise for SOT-MRAM [1-2]. We have demonstrated electrical manipulation of magnetization and exchange bias (EB) in an antiferromagnet/ferromagnet (AFM/FM) based device via SOT [3]. Perpendicular EB reversal across AFM IrMn and FM $[Co/Pt]_2$ multilayer has been shown, both in extended and confined geometries. In three-terminal perpendicular magnetic tunnel junction (MTJ) devices (Figs. 1a and 1b), we have achieved the switching of the magnetization and EB using the SOT (Fig. 1c). Both high- and low-resistances have been observed at zero magnetic field during EB switching (Fig. 1d). These findings provide a new direction in exploring the electrical control of EB in SOT magnetic random access memory (SOT-MRAM). In another study, we have demonstrated that the magnon current excited in an insulating NiO AFM layer by an electronic spin current in an all-oxide epitaxial $SrRuO_3$/NiO/$SrIrO_3$ heterostructure is effective for manipulating the perpendicular magnetization in the $SrRuO_3$ layer [4]. Fig. 2 shows the schematic of the heterostructure and TEM image of the interfaces and the current driven magnetization switching. Interestingly, the threshold current density to generate a sufficient magnon current to manipulate the magnetization was one order of magnitude smaller than that in conventional metallic systems. These results suggest a route for developing highly efficient magnon based all-oxide spintronic devices. This work has been supported by KAUST, SRC/NIST SMART center, and US-NSF.

[1] I.M. Miron, et al, Nature, 476 (2011) 189. [2] L.Q. Liu, et al, Science, 336 (2012) 555. [3]. B. Fang, et al, Advanced Functional Materials, 2022, 32, 2112406. [4]. D.X. Zheng, et al, Advanced Materials, revised and resubmitted.

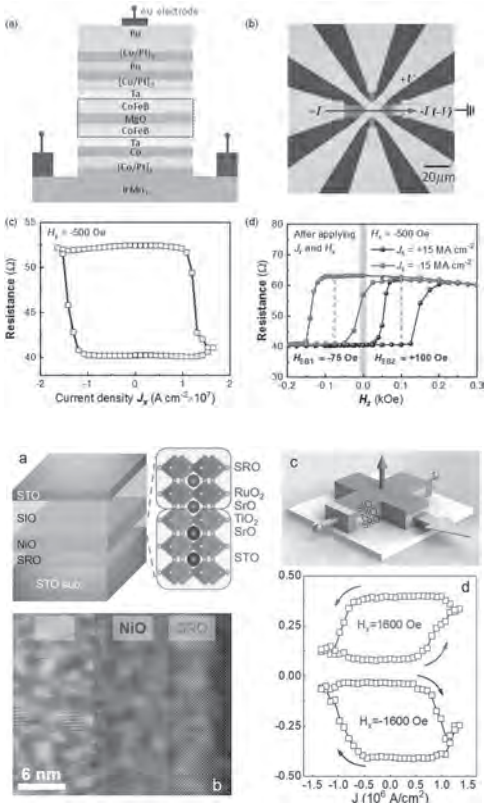

CONTRIBUTED PAPERS

EOE-08. Interfacial potential gradient modulates Dzyaloshinskii-Moriya interaction in Pt|Co|Metal multilayers. *F. Ajejas*[1,2], Y. Sassi[2], W. Legrand[2], S. Collin[2], J. Peña-Garcia[3], A. Thiaville[4], S. Pizzini[3], N. Reyren[2], V. Cros[2] and A. Fert[2] *1. Physics, University of California, San Diego, San Diego, CA, United States; 2. Unité Mixte de Physique CNRS/Thales, Palaiseau, France; 3. Institut Néel, Grenoble, France; 4. Laboratoire de Physique des Solides, Université Paris-Saclay, Orsay, France*

The actual mechanisms occurring at interfaces underlying the Dzyaloshinskii-Moriya interaction (i-DMI) remain largely an open question in nanomagnetism. In this study, we investigate the origin of the i-DMI, aiming at estimating how independent the DMI contributions of the two interfaces of a FM layer are and what their relative weight in the effective DMI amplitude is. The effective DMI is measured by the study of the asymmetric domain wall propagation in the presence of an in-plane magnetic field, in Pt|Co|*M* stacks. These measurements are completed by Brillouin light scattering (BLS) measurements. We then explore the correlation between the effective i-DMI and the properties of metal *M*, namely, its atomic number, electronegativity, and work function. A clear linear relationship is found between the i-DMI and the work function difference at the Co|*M* interface ($\Delta\Phi$) [1,2]. We define $\Delta\phi = \phi_M - \phi_{Co}$. This result is a strong evidence of the independent DMI contributions of the two interfaces for the chosen Co thickness (1 nm). These findings may guide the optimization of the magnetic properties of future spintronic devices. This work has been supported by DARPA TEE program grant (MIPR HR-0011831554), ANR grant TOPSKY (ANR-17-CE24-0025), FLAG-ERA Sograph MEM (ANR-15-GRFL-0005),

and the Horizon2020 Framework Program of the European Commission, under FET Proactive Grant Agreement No. 824123 (SKYTOP) and under Marie Sklodowska- FQ Curie Grant Agreement No. 754303 for supporting J.P.G together with the LABEX LANEF in Grenoble (ANR-10-LABX-0051). Univ. Paris-Saclay, CNRS INP, Sesame IMAGeSPIN project (nEX039175) and the LABEX NanoSaclay (ANR10 LABX0035, BLS@ PSay and SPiCY projects) are acknowledged for the BLS equipment.

[1] F. Ajejas et al., Phys. Rev. Mat., June 2022 [2] Y.-K. Park *et al*., NPG Asia Mater. 10, 995 (2018)

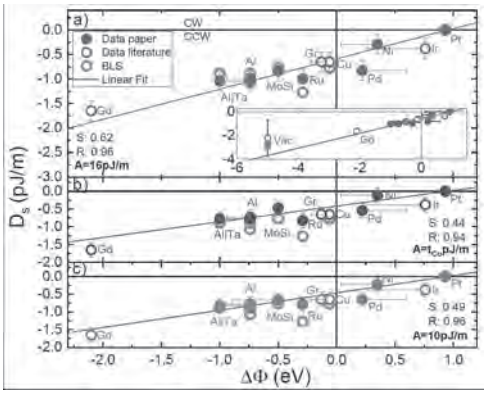

Figure 1 Dependence of the effective DMI D_s of the Co|M interfaces with work function difference between Co and M (ΔΦ). The filled circles correspond to experimental data estimated in this work by domain expansion considering in (a) A = 16 pJ/m, in (b) a linear dependence of A with Co thickness, and in (c) A = 10 pJ/m. The open circles are values reported from literature and the purple open points are values of D_s determined by BLS.

EOE-09. Blanket Film Spin-Orbit Torque Characterization via Four Probe Measurement. *H. Poh*[1], C. Ang[1], T. Jin[1], F. Tan[1], G. Lim[1] and W. Lew[1] *1. School of Physical and Mathematical Sciences, Nanyang Technological University, Singapore*

Spin-orbit torque characterization techniques generally require Hall cross that generally demands lithography resources and time. As the interest in exploring materials for improved SOT performance surges, an efficient technique to characterize SOT efficiencies with minimal processes, equipment, and time is highly desirable. Here, we demonstrate a lithography-free technique to determine the spin-orbit torque efficiency in perpendicular magnetic anisotropy ferromagnetic heterostructure. By utilizing a customized fzour-point probe in a rhombus geometry, harmonic Hall measurement was performed on a blanket films of Pt/Co/Ti structure to characterize the spin-orbit torque efficiency. Due to the non-uniform current distribution across the blanket film, a correction factor is experimentally evaluated using the ratio of the damping-like field measured on the blanket film to that of a fabricated Hall device with identical material heterostructure. Additionally, this correction factor is analytically derived and experimentally shown to be determined by the configuration of the probes and is independent of the structure material. Our measurement reveals that by performing a single calibration process for the particular set of probes, the same correction factor was validated on a second ferromagnetic heterostructure, Ti/Pt/Co/Ta hence it can be applied to other SOT films stack measurements. Our four-probe harmonic Hall technique provides an alternative and swift way for SOT investigations by eliminating multiple lithography processes necessary in conventional approaches.

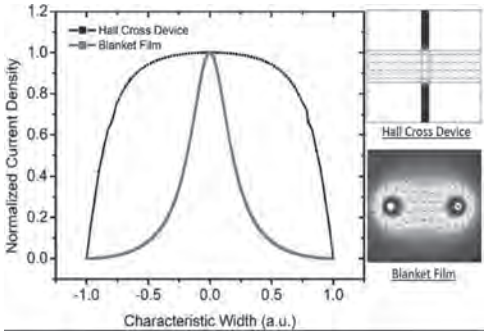

Current distribution profile of Hall cross device and continuous film.

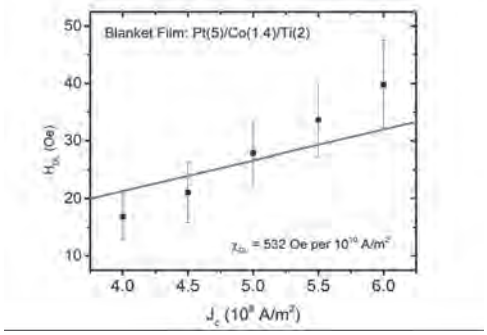

Four-probe results for damping-like field, as a function of the average current density for Pt(5)/Co(1.4)/Ti(2).

EOE-10. Power-efficient SOT properties of W-Si/CoFeB heterostructures. *S. Yoon*[1], T. Kim[1], Q.T. Nguyen[2], G.W. Kim[1], M. Lee[1], S.H. Rhim[2] and Y. Kim[1] *1. Materials Science and Engineering, Korea University, Seoul, The Republic of Korea; 2. Physics, Ulsan University, Ulsan, The Republic of Korea*

Magnetoresistive Random Access Memory (MRAM) is attracting attention as a candidate for the next-generation memory devices [1]. Among various writing mechanisms of MRAM, spin-orbit torque (SOT) exhibits advantages in rapid operation speed and power efficiency [2]. To commercialize SOT utilized MRAM, the device should use semiconductor fabrication process-friendly materials and be stable even at 450°C thermal annealing [3]. We investigated SOT properties in W-Si/CoFeB heterostructures. Using the first-principles calculation, we calculated the spin hall conductivity and phase stability while adjusting the composition of Si in the W-Si alloy. We fabricated the $W_{100-x}Si_x$/CoFeB/MgO/Ta structure and conducted post-deposition heat treatment at 300°C and 500°C for 1 h with 6 kOe magnetic field. We conducted XRD and TEM measurements and found that the lattice parameter of W-Si decreased compared with that of β-W. This result shows that Si atoms diffuse into β-W and are located at energetically stable sites. We conducted VSM measurement and confirmed that the samples exhibited perpendicular magnetic anisotropy (PMA) after 300, 500°C post-deposition heat treatment. This result implies that W-Si samples can maintain PMA property after high-temperature annealing. And we also found lower resistivity in W-Si (~135 μΩcm) at 4.0 at% samples compared with that of β-W (~ 200 μΩcm) samples [4]. We measured DLT efficiency by conducting a harmonic hall voltage measurement for the samples with PMA. The 500°C heat-treated sample with 4.0 at% shows the largest DLT efficiency and spin Hall conductivity, consistent with the theoretical calculation. To measure the magnetization switching current, the samples with PMA were used to make a 4x4 um^2 Island sample. Both 300°C and 500°C heat-treated samples show a tendency to decrease switching current density as the composition of Si increases. The switching current density of W-Si decreases by 40% compared with that of β-W samples. We calculated the power consumption

of W-Si at 4 at% using the parallel-resistor model by considering the current-shunting effect. The power consumption of W-Si is ten times lower than that of other NM materials.

[1] S. Jung et al., A crossbar array of magnetoresistive memory devices for in-memory computing, Nature 601, 211 (2022) [2] J. Ryu et al., Current-Induced Spin–Orbit Torques for Spintronic Applications, Advanced Materials 32, 1907148 (2020) [3] D. Neumaier et al., Integrating graphene into semiconductor fabrication lines, Nature Materials 18, 525 (2019) [4] Y. J. Kim et al., Microstructural evolution and electrical resistivity of nanocrystalline W thin films grown by sputtering, Materials Characterization 145, 473-478 (2018)

EOE-11. Large Voltage Controlled Magnetic Anisotropy (VCMA) Effect at metalloporphyrin decorated Graphene/Ferromagnet interface. *A. Shukla*[1], A. Erram[1], H. Mendonca[1], D. Kumar[1], R. Pandey[1], A. Chouhan[1] and A. Tulapurkar[1] *1. Electrical Engineering, Indian Institute of Technology Bombay, Mumbai, India*

Spin-Orbit Torque (SOT) based manipulation of magnetization is extremely popular among the spintronics community. The physics of SOT is Spin-Orbit Coupling (SOC) and it can have two prominent sources 1) Bulk SOC or Spin Hall Effect 2) Interfacial SOC or Rashba-Dresselhaus effect. Using graphene as heavy metal in devices has a major concern as it is having a weak SOC hence, enhancement of SOC in graphene is of contemporary interest among researchers. Two methods seem to be most prominent for enhancing SOC a) Decorating graphene with adatoms like Hydrogen or organic aromatic molecules [1]. Hydrogen silsesquioxane irradiation technique generates large SOC [2][3] and b) External electric field [4]. In this article, we are reporting an experimental study of metalloporphyrin decorated monolayer graphene/NiFe interface showing enhanced SOC and a large VCMA effect. We purchased monolayer CVD graphene from the company Graphenea and fabricated back gate Graphene Field Effect Transistor (GFET) devices to study the impact of doping. We did DC characterization of GFET before and after doping and observed that after doping Dirac point shifts towards zero. To study the interface we fabricated devices on an oxidized silicon wafer. We prepared a solution of Platinum-Porphyrin (Pt-Porphyrin) in Toluene with Molarity (M) equal to 2.47E-4 (mole/lit). We spin coat the prepared solution and dried the sample at 90°C for 5 min. We then deposited NiFe (5nm)/Al(2nm)/SiO2(2nm) stack on top of functionalized graphene. We patterned the stack in a rectangular strip of 20um X 50um using standard fabrication processes. We measured Spin Torque Ferromagnetic Resonance (ST-FMR) spectra on fabricated devices and concluded after analyzing results that if we apply back gate electric field on functionalized sample there is 1) Shifting in resonance field and 2) Modulation in linewidth, however, we did not observe any such effects in pristine graphene.

1) A., Castellanos-Gomez, A. & van Wees, B. J. Band Gap Opening of Graphene by Noncovalent π-π Interaction with Porphyrins. *Graphene* vol. 02 102–108 (2013). 2) Balakrishnan, J., Kok Wai Koon, et al. Colossal enhancement of spin-orbit coupling in weakly hydrogenated graphene. *Nat. Phys.* 9, 284–287 (2013). 3) Cao, S., Cao, C., Tian, S. & Chen, J. H. Enhancement of spin-orbit coupling and magnetic scattering in hydrogenated graphene. *Phys. Rev. B* 104, 1–6 (2021). 4) K. S. Novoselov et al. Electric Field Effect in Atomically Thin Carbon Films. 306, 666–669 (2016).

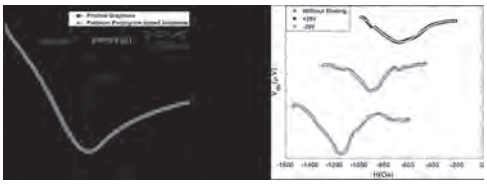

DC characterization of GFET before and after doping. Charge neutrality point shifts towards zero gate voltage upon doping with Pt-porphyrin. b) Modulation of STFMR signal w.r.t. external electric field. The resonance frequency shifts upon applying an external electric field with modulation in linewidth.

EOE-12. Rashba-like spin textures in Graphene promoted by ferromagnet-mediated Electronic-Hybridization with heavy metal. A. Gudín[1], B. Muñiz[1], I. Arnay[1], P. Olleros-Rodríguez[1], A. Anadón[1], M. Valvidares[3], G. Bihlmayer[2], R. Miranda[1], J. Camarero[1], M. Valbuena[1] and *P. Perna*[1] *1. IMDEA Nanociencia, Madrid, Spain; 2. Peter Grünberg Institut and Institut for Advanced Simulation, Forschungszentrum Jülich, Julich, Germany; 3. ALBA synchrotron, Cerdanyola del Valles, Spain*

Real world spintronics applications require the engineering of materials in which spin textures exist at room temperature, are protected from the atmosphere, and amenable to reading and writing and, if possible, integrated with a material than can sustain very long spin diffusion length over long timescale, such as graphene (Gr) [1]. Epitaxial Gr-based magnetic heterostructures have demonstrated to provide enhanced perpendicular magnetic anisotropy (PMA) and sizeable Dzyaloshinskii-Moriya interaction (DMI), both related to the interfacial Spin Orbit Coupling (SOC), which in turn allow for enhanced thermal stability and stabilization of chiral spin textures [2], enabling the realization of 2D materials spin-orbitronics. A strong PMA in Gr/Co was first discovered in structures grown onto Ir-single crystals [3] and on both Pt and Ir buffers grown onto insulating oxides [4] and related to the strong anisotropy of the angular magnetic moment [2,5]. Instead, the nature of an unexpected (since the intrinsic negligible SOC of Gr) DMI at Gr/FM interface is still under debate. Although, both theoretically [6] and experimentally works [2] pointed to a Rashba origin of such DMI, in our knowledge, no experimental evidence has been provided yet. Here, we analyze the element dependent and averaged surface/interface SOC induced magnetic properties of epitaxial Gr/FM stacks grown onto HM(Pt, Ir)/Al_2O_3(0001). In particular, by means of XAS-XMCD and spin-resolved ARPES experiments accompanied by DFT modelling, we have elucidated the nature of the induced SOC at Gr/Co interface on Ir. We have experimentally found that the interaction of the HM with the C atomic layer via hybridization with 2 ML thick FM is indeed the source of the SOC in the Gr layer. Furthermore, our studies reveal an energy splitting of in-plane spin polarized Gr π bands, consistent with an Rashba-SOC at the Gr/Co interface, which is thus either the fingerprint or the origin of the Dzyaloshinskii Moriya interaction [7]. This is then translated in a measurable induced magnetic moment in Gr. Interestingly, at larger Co thicknesses (~10 ML), neither in-plane or out-of-plane spin splitting is observed, indicating a Gr/Co interface decoupled from the Co/HM.

[1] W. Han, et al. Graphene Spintronics, Nat. Nanotech. 9, 794 (2014). [2] F. Ajejas, et al., Nano Lett. 18(9), 5364-5372 (2018). [3] H. Yang et al. Nano Lett. 16, 145 (2016). [4] F. Ajejas, et al., ACS Appl. Mater. Interfaces, 12(3), 4088-4096 (2020). [5] M. Blanco-Rey, et al. ACS Appl. Nano Mater. 4(5), 4398–4408 (2021). [6] H. Yang, et al., Nat. Mater. 17, 605 (2018) [7] B. Muñiz, A. Gudin et al. Submitted (2022), https://doi.org/10.48550/arXiv.2206.04351.

EOE-13. Evidence of unconventional spin-orbit torque in SnS/$Ni_{80}Fe_{20}$ heterostructures. *H. Bangar*[1], P. Gupta[1], S. Dewan[2], R. Mudgal[1], S. Das[3] and P.K. Muduli[1] *1. Department of Physics, Indian Institute of Technology Delhi, New Delhi, India; 2. School of Interdisciplinary Research, Indian Institute of Technology Delhi, New Delhi, India; 3. Center for Applied Research in Electronics, Indian Institute of Technology Delhi, New Delhi, India*

Recently, two-dimensional (2D) materials have emerged as a replacement for heavy metals (HM) because of their large spin-charge interconversion efficiency [1]. In this work, we explore a promising and relatively less explored 2D monochalcogenide SnS for spintronics application. Through symmetry arguments, it is proposed that SnS should exhibit unconventional spin-orbit torques (SOTs), which is very important for energy-efficient switching of magnets with perpendicular magnetic anisotropy (PMA) [1]. SnS thin films up to monolayer (ML) thickness have been grown on Si/SiO_2 substrates using pulsed laser deposition (PLD) technique at 200 °C and room temperature (RT). Two typical Raman active modes (A_g and B_{3g}) [2] can be distinguished in the acquired Raman spectra [Fig. 1]. We performed spin-torque ferromagnetic resonance (STFMR) measurements to investigate the SOTs in SnS/$Ni_{80}Fe_{20}$ system. For ST-FMR measurements, we fabricated SnS/$Ni_{80}Fe_{20}$ rectangular microstrips using the lift-off technique. For STFMR measurements, an in-plane RF current of frequency varying from 4 GHz to 8 GHz was applied to the bilayer in the presence of an external magnetic field (H). We measured the voltage (V_{mix}) across the device, which originated due to the mixing of AMR and RF current. We determine the in-plane and out-of-plane torque components by fitting the V_{mix} with a sum of symmetric and antisymmetric Lorentzian. We performed a complete angular dependence of the STFMR signal by varying the magnetization angle ϕ in the sample plane. In addition to a conventional $\sin2\phi\cos\phi$ ($V_{y,s}$) dependence, we found $\sin2\phi$ ($V_{z,s}$) dependence [Fig. 2], which is a signature of unconventional out-of-plane anti-damping like torque [3]. Thus our results suggest that SnS can be used to achieve efficient switching of magnetic devices with PMA via the strong unconventional out-of-plane anti-damping like torque.

[1] Y. Liu *et. al.,* ACS Nano 14, 9389 (2020). [2] A.N. Mehta *et. al.,* J. Microsc. 268, 276 (2017). [3] D. MacNeill, *et al.,* Nat. Phys. 13, 300 (2017).

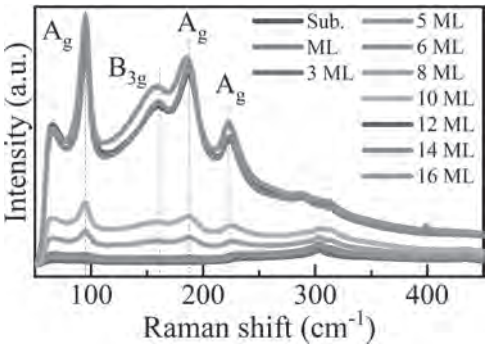

Raman spectra at various SnS thicknesses. Here ML stands for monolayer.

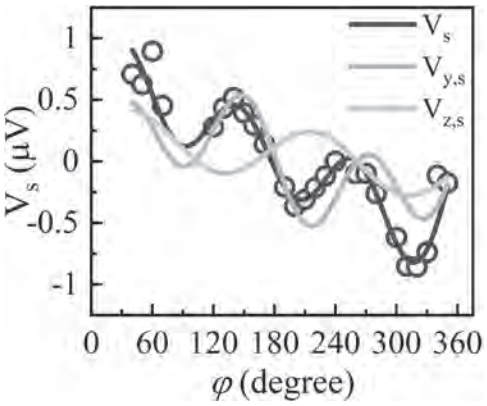

Angular dependence of symmetric ST-FMR signal for SnS (3 ML) / $Ni_{80}Fe_{20}$ (8 nm) sample at 5 GHz. Here, open circle represents the experimentally measured data while the solid lines are fit to the data. $V_{y,s}$ and $V_{z,s}$ are the components of V_s along *y* and *z*-direction, respectively.

EOE-14. Field-free switching of perpendicular magnetization by spin-orbit torques originating from an in-plane magnetized Co_2MnAl spin source. *D. Morita*[1], T. Hara[1], M. Yamanouchi[1] and T. Uemura[1] *1. Information Science and Technology, Hokkaido University, Sapporo, Japan*

Spin-orbit torques (SOTs) originating from a ferromagnetic spin source have attracted much attention for spintronics devices because they offer field-free switching of perpendicular magnetization [1]. Cobalt-based Heusler alloy Co_2MnAl (CMA) is attractive for the ferromagnetic spin source because it is theoretically predicted to be a magnetic Weyl semimetal with strong spin-orbit interaction [2]. In this work, we demonstrated SOT-induced magnetization switching for a perpendicularly magnetized CoFeB (CFB) under zero magnetic field by using an in-plane magnetized CMA spin source. We also measured modulation of coercive field by the SOTs and investigated the effective perpendicular magnetic field H_{eff} induced by them. A heterostructure consisting of, from the substrate side, MgO(10)/CMA(5)/Ti(3)/CoFeB(1.2)/MgO(3)/Ta(1) was deposited on an MgO(100) substrate (numbers in parentheses are nominal thickness in nm). Then, the stack was processed into Hall-bar devices with a 5-μm-wide channel. From measurements on transverse resistance R_{yx} reflecting the anomalous Hall effect (AHE), the CFB layer showed a clear perpendicular magnetic easy axis, whereas the CMA had an in-plane magnetic easy axis. After aligning magnetization of CMA, M_{CMA}, to parallel or antiparallel to the channel direction, we studied SOT-induced magnetization switching of CFB layer by applying current pulses I_{pulse} to the channel in the absence of magnetic field. Clear field-free switching of CFB magnetization was observed in both cases. The polarity of SOT-induced magnetization switching with respect to I_{pulse} was reversed depending on the relative direction of M_{CMA} to I_{pulse} (Fig. 1). Furthermore, we investigated H_{eff} induced by SOTs with $H_{eff} = [H_c(+I) - H_c(-I)]/2$, where $H_c(I)$ is a coercive field determined from AHE measurements, and I is a channel current. We observed sizable effective field of $\mu_0 H_{eff}$ = 1 mT at I = 3 mA. Importantly, the sign of H_{eff} was also reversed depending on the relative direction of M_{CMA} to I. These results suggest that the possible origin of the SOTs is spin-orbit precession [1].

[1] S. C. Baek *et al*., Nat. Mater., Vol. 17, p.509 (2018) [2] J. Kübler, C. Felser, EPL, Vol. 114, 47005 (2016)

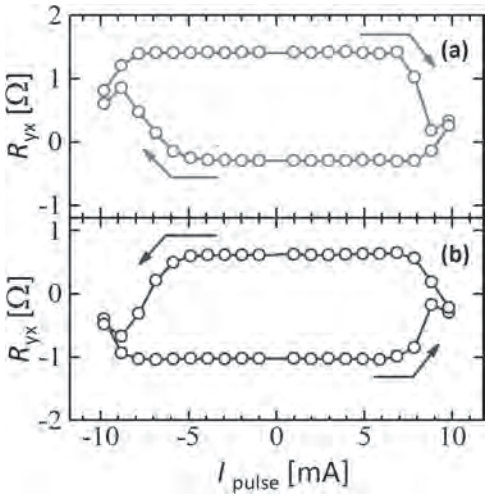

Fig.1. Current-induced field-free magnetization switching for (a) positive M_{CMA} and (b) negative M_{CMA}

Session EOF
SPIN-ORBITRONICS II
Victor Lopez Dominguez, Chair
Northwestern University, Evanston, IL, United States

INVITED PAPER

EOF-01. Field-free deterministic spin-orbit torque switching of magnetization using Weyl semimetals. *S. Singh[1] 1. Department of Physics, Carnegie Mellon University, Pittsburgh, PA, United States*

Weyl semimetals (WSMs), such as WTe_2 and $MoTe_2$, host plethora of novel phenomena that are highly relevant for quantum spintronics, namely: Dirac type dispersion, strong spin-orbit coupling (SOC), Fermi arcs, and helical spin-momentum locked surface and bulk states. WSMs provide a distinct opportunity to obtain highly efficient and unconventional charge to spin conversion owing to strong SOC, symmetry breaking, and these topology-based phenomena. On the other hand, spin-orbit torque (SOT) driven deterministic control of the magnetic state of a ferromagnet with perpendicular magnetic anisotropy is key to next generation spintronic applications including non-volatile, ultrafast, and energy efficient data storage devices. But field-free deterministic SOT switching of perpendicular magnetization remains a challenge because it requires an out-of-plane antidamping torque, which is not allowed in conventional spin source materials such as heavy metals and topological insulators due to the system's symmetry. The exploitation of low-crystal symmetries WTe_2 and $MoTe_2$ offers a unique approach to achieve SOTs with unconventional forms[1]. In this work, I will discuss our experiments to realize field-free deterministic magnetic switching of a perpendicularly polarized van der Waals magnet employing an out-of-plane anti-damping SOT generated in layered WTe_2, which is a quantum material with low-symmetry crystal structure[2]. I will also discuss our experiments aimed at achieving field-free SOT switching of semiconducting and insulating ferromagents using spin current in WSMs. Our work establishes transition metal dichalcogenides, with lower symmetry crystal structure, as an appealing spin source material for future spin-orbit torque related magnetic memory technologies.

[1]. MacNeill, D. *et al.* Control of spin–orbit torques through crystal symmetry in WTe_2/ferromagnet bilayers. *Nature Physics* 13, 300-305, (2017). [2]. Kao, I-H *et al.* Deterministic switching of a perpendicularly polarized magnet using unconventional spin–orbit torques in WTe_2. Nature Materials (2022). https://doi.org/10.1038/s41563-022-01275-5

CONTRIBUTED PAPERS

EOF-02. Enhanced spin-orbit torque in amorphous light element silicide. *C. Hsu[1*], J. Karel[2], N. Roschewsky[3], H. Kleidermacher[1], S. Sayed[1], S. Cheema[4], S. Bouma[3], F. Hellman[3,4] and S. Salahuddin[1] 1. Electrical Engineering and Computer Science, University of California Berkeley, Berkeley, CA, United States; 2. Materials Science and Engineering, Monash University, Clayton, VIC, Australia; 3. Physics, University of California Berkeley, Berkeley, CA, United States; 4. Materials Science and Engineering, University of California Berkeley, Berkeley, CA, United States*

Spin-orbit torque (SOT) has been an active field of research for the past decade owing to its potential to replace the conventional spin-transfer torque due to separate read-write current path, faster switching speed and larger material design space [1]. However, several roadblocks exist for further adoption of spin-orbit torque in memory applications including material compatibility with current silicon manufacturing platform, trade-off between conductivity and spin-torque efficiency resulting in the challenge of reducing the switching current, and the requirement of field-free switching [2]. To reduce the switching current, not only high spin-torque efficiency is important ($\xi_{SOT} > 1$) but also high conductivity is required [2]. However, the conventional scaling trend of increasing spin-torque efficiency with decreasing conductivity across different material systems [3] (or within the same alloying system [4]) prevents the further reduction of switching current via SOT. Here, we report three interesting findings in a new family of material systems - amorphous iron silicide (a-Fe_xSi_{100-x}) - for efficient generation of SOT. This work aims to address the first two roadblocks by demonstrating: 1. a large spin-torque efficiency (~ 2) in a fully amorphous non-ferromagnetic iron silicide 2. a novel scaling trend between conductivity and spin-torque efficiency which lifts the conventional trade-off and 3. a concentration dependent SOT that can be tuned by the relative energy position of the Fermi level and the reduced density of states through concentration engineering of iron and silicon. These results not only show the technological advantage of a new family of material but also serve as a new vehicle to study many spin-dependent physical phenomena.

[1] S. Salahuddin, K. Ni, and S. Datta, Nature Electronics, vol. 1, p. 442–450 (2018) [2] B. Dieny, I. L. Prejbeanu, K. Garello, *et al.*, Nature Electronics, vol. 3, p. 446–459 (2020) [3] A. Manchon, J. Zelezny, I. M. Miron, *et al.*, Reviews of Modern Physics, vol. 91, p. 035004 (2019) [4] P. Wang, A. Migliorini, S.-H. Yang, *et al.,* Advanced Materials, vol. 34, p. 2109406 (2022)

EOF-03. Harnessing the spin and orbital dynamics of iron-based 2D van der Waals ferromagnets. *T.G. Saunderson[1,2], F. Martin[1], M. Schmitt[1], A. Liedtke[1], P. Rüßmann[2,3], A. Shahee[1], H.T. Simensen[4], A. Tavabi[5], T. Denneulin[5], T. Scholz[6], D. Go[2], M. Gradhand[7,1], K. Lee[1,8], P. Mavropoulos[9], A. Kovacs[5], B. Lotsch[6], R.E. Dunin-Borkowski[5], S. Bluegel[2], A. Brataas[4], Y. Mokrousov[2,1] and M. Kläui[1,4] 1. Institute of Physics, Johannes Gutenberg University of Mainz, Mainz, Germany; 2. Peter Grünberg Institut and Institute for Advanced Simulation, Research Center Jülich, Jülich, Germany; 3. Institute of Theoretical Physics and Astrophysics, University of Würzburg, Würzburg, Germany; 4. Centre for Quantum Spintronics, Norwegian University of Science and Technology, Trondheim, Norway; 5. Ernst Ruska-Centre for Microscopy and Spectroscopy with Electrons, Research Center Jülich, Jülich, Germany; 6. Max Planck Institute for Solid State Research, Stuttgart, Germany; 7. H. H. Wills Physics Laboratory, University of Bristol, Bristol, United Kingdom; 8. Department of Semiconductor Physics, Korea University, Sejong, The Republic of Korea; 9. Department of Physics, National and Kapodistrian University of Athens, Athens, Greece*

The discovery of two-dimensional van der Waals ferromagnets [1,2] has been long anticipated since the effects of spatial dimensionality on criticality were recorded [3,4]. The potential applications of this new class of materials seem vast within the field of spintronics. Fe_3GeTe_2 has already proved highly efficient for spin-orbit torque switching [5], yet rich skyrmionic textures [6,7] and semi-metallicity [8] are also found within its roster of ever-growing phenomena. Fe_5GeTe_2, a related compound with a higher T_c [9], presents its own unique set of magnetic order that can be tuned with doping [10] and gate voltage [11]. In a recent collaboration [12] we found

spin-orbit torques within bulk Fe_3GeTe_2 due to a site preference that breaks the crystal's centrosymmetry [13]. Meanwhile, in Fe_5GeTe_2, we found skyrmionic textures present even up to room temperature [14]. To understand the origins of these effects one must delve into the underlying electronic structure to provide a comprehensive understanding of the associated spin dynamics. Using a variety of first-principles methods [12,14,15] we evaluate the exotic phenomena observed in both Fe_3GeTe_2 and Fe_5GeTe_2. In Fe_3GeTe_2 strong 'hidden' current-induced torques are harvested by each of the two-dimensional Fe_3GeTe_2 layers separately. Analysis of the electronic structure elucidates an interplay of spin and orbital degrees of freedom which have a profound impact on spin-orbit torques. A drastic difference in the behavior of the individual components of the torque results in non-trivial switching. In Fe_5GeTe_2 we use first principles methods in combination with atomistic spin-dynamics simulations to characterize the domain wall and subsequent spin textures. These distinct features from both compounds present an opportunity to tailor the spin and orbital dynamics with Fe concentration, opening a new era of van der Waals spin orbitronics.

[1] C. Gong et al., Nature 546, 265 (2017). [2] B. Huang et al., Nature 546, 270 (2017). [3] R. B. Griffiths, Physical Review 136, 437 (1964). [4] N. D. Mermin et al., Physical Review Letters 17, 1133 (1966). [5] M. Alghamdi et al., Nano Letters 19, 4400 (2019). [6] B. Ding et al., Nano Letters 20, 868 (2020). [7] H.-H. Yang et al., 2D Materials 9, 025022 (2022). [8] K. Kim et al., Nature Materials 17, 794 (2018). [9] A. F. May et al., ACS Nano 13, 4436 (2019). [10] A. F. May et al., Physical Review Materials 4, 074008 (2020). [11] C. Tan et al., Nano Letters 21, 5599 (2021). [12] F. Martin et al., arXiv:2107.09420. [13] A. Chakraborty et al., Advanced Materials 34, 2108637 (2022). [14] M. Schmitt et al., arXiv:2204.11348. [15] T. G. Saunderson at al., arXiv:2204.13052.

EOF-04. Enhancement of current to spin current conversion efficiency in synthetic antiferromagnetic layer system. *Y. Saito*[1], S. Ikeda[1,2] and T. Endoh[1,3] *1. Center for Innovative Integrated Electronic Systems, Tohoku University, Sendai, Japan; 2. Center for Science and Innovation in Spintronics, Tohoku University, Sendai, Japan; 3. Department of Electrical Engineering, Graduate School of Engineering, Tohoku University, Sendai, Japan*

Current-induced spin-orbit torque (SOT) originating from the spin-Hall effect (SHE) has attracted attention due to their potential applications for SOT-MRAM, skyrmion and domain wall devices. For their applications, heavy metal with high spin Hall angle ($|\theta_{SH}|$) and low resistivity (ρ_{xx}) is necessary for an efficient SOT operation. We have proposed Co/Pt/(Ir or Ru)/Pt/Co synthetic antiferromagnetic (AF) systems for SOT-MRAM (Fig. 1), and found that the Pt/Ir/Pt spacer layer exhibits AF interlayer exchange coupling (J_{ex}) as well as large || and low ρ_{xx} [1, 2]. In this study, we study the current-induced SOT in perpendicularly magnetized Co/Pt/Ir/Pt/Co synthetic AF system which exhibits nearly compensated magnetization. The synthetic AF structures with various Pt, Ir and Co layer thicknesses were prepared by using UHV sputtering system. The stacks were patterned into Hall bar devices and magnitude of the was evaluated from the shift of the reversal magnetic field due to the SOT current. The results were compared with those of the ferromagnetic stack systems with Co/Pt and Co/[Pt/Ir]-multilayer structures. Figures 2(a) and 2(b) show the typical current-induced SOT switching under various fixed external magnetic fields (H_y) in Sample A (Co/Pt structure) and Sample B (synthetic AF structure), respectively. The magnetizations of the two Co layers in the synthetic AF can be switched between two anti-parallel states simultaneously by SOT. The estimated values of current density () at H_y=0 mT for Samples A and B are 7.9×10^7 and 4.2×10^7 A/cm^2, respectively [3]. The magnitude of in Sample B is about half that in Sample A. The magnitudes of estimated $|\theta_{SH}|$ for Samples A and B are 7.0% and 15.6%, respectively [3], which is consistent with SOT switching behavior (Fig. 2). In this presentation, we will also show the dependence of the magnitude of SHE on the strength of J_{ex} in the synthetic AF system. This work was supported by the CIES Consortium, Spin-RNJ, RIEC, JST OPERA (JPMJOP1611), MEXT Next generation X-nics and JSPS KAKENHI (JP19H00844, JP21K18189).

[1] Y. Saito, N. Tezuka, S. Ikeda and T. Endoh, Phys. Rev. B 104,064439 (2021). [2] Y. Saito, S. Ikeda and T. Endoh, Appl. Phys. Lett. 119, 142401 (2021). [3] Y. Saito, S. Ikeda and T. Endoh, Phys. Rev. B 105, 054421 (2022).

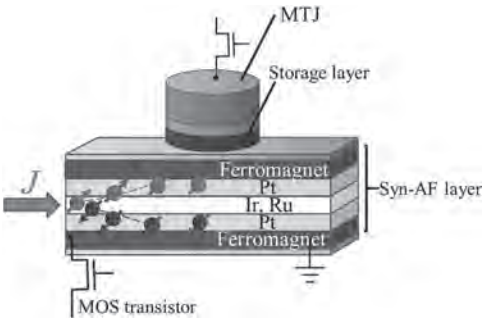

Fig. 1 Schematic diagram of our proposed memory cell with synthetic AF layer for SOT- MRAM.

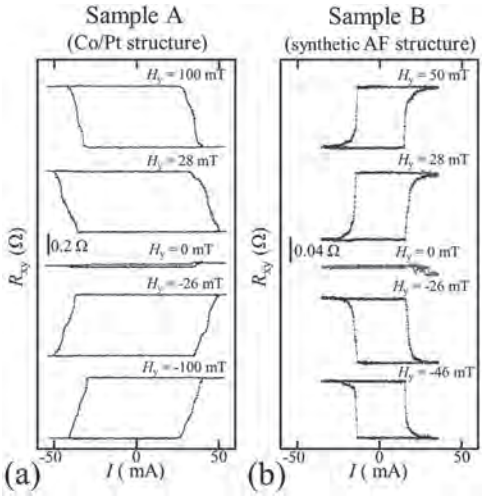

Fig. 2 SOT switching properties under various fixed external magnetic fields (H_y).

EOF-05. Detection of long-range orbital torques. *A. Bose*[1], F. Kammerbauer[1], D. Go[1,2], Y. Mokrousov[1,2], G. Jakob[1] and M. Kläui[1,3] *1. Institute of Physics, Johannes Gutenberg University Mainz, Germany, Mainz, Germany; 2. Institute for Advanced Simulation, Forschungszentrum, Peter Grünberg Institut, Jülich and JARA, 52425 Jülich, Germany, Jülich, Germany; 3. Graduate School of Excellence Materials Science, Johannes Gutenberg University, Mainz, Germany*

We report the experimental demonstration of long-range orbital torques generated by Nb and Ru and detected by spin-torque ferromagnetic resonance (ST-FMR) measurements in Nb/Ni and Ru/Ni bilayers. We identify the orbital torques from the sign-reversal and a strong enhancement in the damping-like torque observed in Nb (Ru)/Ni bilayers as compared to Nb (Ru)/FeCoB bilayers as theoretically predicted[1]. The long-range nature of orbital transport in the ferromagnet was revealed by varying the thickness of Ni in Nb (Ru)/Ni bilayers which is markedly different compared to the regular spin absorption in the ferromagnet that takes place in the first few layers confirming the recent prediction[2]. Finally, we show that the external injection of orbital current in a heavy metal such as Pt can convert the orbital current into a spin-current leading to higher switching efficiency and the enhanced spin-current generation that could both be potentially attractive for the application[3,4].

1. Go, D. & Lee, H.-W. Orbital torque: Torque generation by orbital current injection. *Phys. Rev. Res.* 2, 013177 (2020). 2. Go, D. *et al.* Long-Range

Orbital Magnetoelectric Torque in Ferromagnets. *arXiv* 2106.07928, 1–6 (2021). 3. Ding, S. *et al.* Harnessing Orbital-to-Spin Conversion of Interfacial Orbital Currents for Efficient Spin-Orbit Torques. *Phys. Rev. Lett.* 125, 177201 (2020). 4. Go, D., Jo, D., Lee, H.-W., Kläui, M. & Mokrousov, Y. Orbitronics: Orbital currents in solids. *EPL (Europhysics Lett.* 135, 37001 (2021).

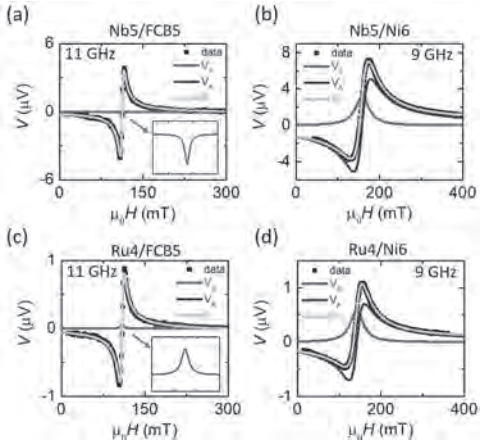

FIG. 1. ST-FMR data for Nb (Ru)/FeCoB (a,c), Nb (Ru)/Ni(b,d), Ru/Ni/Ru (e) and Nb/Ni/Nb(f) bi-layers. Sign reversal of the damping-like torque is observed in Nb (Ru)/Ni bi-layers as compared to Nb (Ru)/FeCoB samples revealing a large orbital Hall torque.

EOF-06. First-principles calculation of the 3m spin-orbit torque and simulation of its effect on magnetization dynamics in a nanodisk.
W. Fang[1], E. Schwartz[1], A.A. Kovalev[1] and K. Belashchenko[1] *1. Physics, University of Nebraska-Lincoln, Lincoln, NE, United States*

Field-free switching of perpendicular magnetization has been observed in an epitaxial $L1_1$-ordered CuPt/CoPt bilayer [1] and attributed to spin-orbit torque (SOT) arising from the crystallographic 3m point group of the interface. Using a first-principles nonequilibrium Green's function formalism [2] combined with the Andersen disorder model, we calculate the angular dependence of the SOT in a CuPt/CoPt bilayer and find that the magnitude of the 3m SOT is about 20% of the conventional dampinglike SOT. We study the magnetization dynamics in a perpendicularly magnetized circular nanodisk in the presence of the 3m SOT and Dzyaloshinskii-Moriya interaction using micromagnetic simulations and find that even a relatively small 3m torque can enable domain-wall-mediated field-free magnetization reversal. For further insight, we derive a collective-coordinate model describing the motion of a domain wall in a nanodisk. Numerical solutions and stability analysis of the equations of motion in this model are used to establish the roles of the dampinglike, fieldlike, and 3m SOT in the magnetization reversal process. Wuzhang Fang and Edward Schwartz contribute equally to this work. This work was supported by NSF through Grant No. DMR-1916275, and by the U.S. Department of Energy, Office of Science, Basic Energy Sciences under Award No. DE-SC0021019.

[1] L. Liu et al., Nat. Nanotechnol. 16, 277 (2021). [2] K. D. Belashchenko, A. A. Kovalev, and M. van Schilfgaarde, Phys. Rev. Materials 3, 011401(R) (2019); Phys. Rev. B 101, 020407(R) (2020).

EOF-07. Tunable spin orbit torques in Ferrimagnet/Ferromagnetic heterostructures.
N. Behera[1], L. Bainsla[1], A.A. Awad[1], A. Kumar[1], R. Khymyn[1] and J. Åkerman[1] *1. Department of Physics, University of Gothenburg, Gothenburg 41296, Sweden*

Spintronics utilizes the spin orbit coupling (SOC) of a heavy metal layer to generate spin currents by the spin Hall effect (SHE), which can then induce spin orbit torques (SOT) to alter the magnetization of an adjacent ferromagnet. SOT can be both fast and energy-efficient and enable technological applications in spintronic devices such as spin Hall nano-oscillators (SHNOs) [1-3], SOT based magnetic random access memory(SOT-MRAM), and spin logic devices [4,5]. However, spin currents generated by SOC also exist in magnetic materials. Recent studies evidenced very large emission of spin currents and strong SOT for magnetization switching in ferrimagnets near compensation [6,7]. In the present study nearly compensated GdFeCo, and Py, are used as spin Hall layer and ferromagnetic layer, respectively. We studied the tunable behaviour of both damping-like(DL) and field-like(FL) SOT efficiencies (θ_{DL} and θ_{FL}) with respect to a Cu insertion layer in $Gd_{26.7}(FeCo)_{73.3}$ (10 nm)/Cu(1-5 nm)/Py(3 nm) stack. We performed spin transfer torque ferromagnetic resonance (ST-FMR) measurements on microbars (6 ×12 μm^2) to determine the magneto dynamical properties such as current induced DL and FL SOT efficiencies. Figure 1 (a) and (b) show the ST-FMR spectra in the frequency range of 10-15 GHz, and the corresponding linewidth vs. frequency plot of $Gd_{26.7}(FeCo)_{73.3}$ (10 nm)/Cu(4 nm)/Py (3 nm); (c) and (d) show the Cu thickness dependent SOT efficiencies at f=8 GHz. The DL-SOT efficiency is found to be maximum, θ_{DL}~ 20%, at Cu (2 nm) followed by a decreasing trend at higher Cu thicknesses. However, FL-SOT efficiency shows a minimum, θ_{FL}~ 10%(-7%), up to Cu (2 nm) followed by ~-53%(48%) at Cu (5 nm) for +ve(-ve) direction of applied magnetic field. The larger value of θ_{FL} at higher Cu thickness will be useful for ultrafast current induced magnetization switching as seen in other ferrimagnetic systems.

1. H. Mazraati *et al.*, Low operational current spin Hall nanooscillators based on NiFe/W bilayers, Appl. Phys. Lett. 109, 242402 (2016). 2. H. Fulara *et al.*, Spin-orbit torque–driven propagating spin waves, Sci. Adv. 5, eaax8467 (2019). 3. M. Zahedinejad *et al.*, Two-dimensional mutually synchronized spin Hall nano-oscillator arrays for neuromorphic computing. Nat. Nanotechnol. 15, 47–52 (2020). 4. K. Garello *et al.*, Ultrafast magnetization switching by spin-orbit torques, Appl. Phys. Lett. 105, 212402 (2014). 5. M. Cubukcu *et al.*, Spin-orbit torque magnetization switching of a three-terminal perpendicular magnetic tunnel junction, Appl. Phys. Lett. 104, 042406 (2014). 6. D. Céspedes-Berrocal *et al*., Current-induced spin torques on single GdFeCo magnetic layers, Adv. Mater., 33, 2007047(2021). 7. R. Mishra *et al.*, Anomalous Current-Induced Spin Torques in Ferrimagnets near Compensation, Phys. Rev. Lett. 118, 167201 (2017).

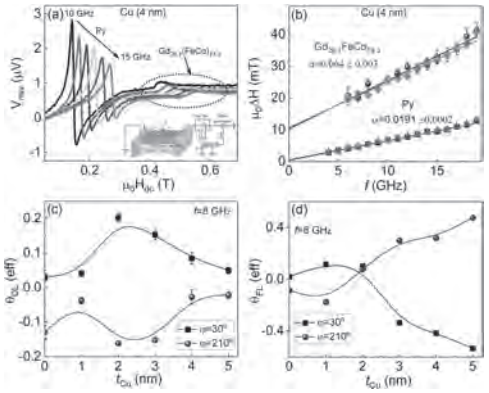

Figure 1: (a) & (b) ST-FMR spectra in the frequency range of 10-15 GHz, & corresponding linewidth vs. frequency plot of $Gd_{26.7}(FeCo)_{73.3}$ (10 nm)/Cu(4 nm)/Py (3 nm). The inset of Fig. 1(a): encircled portion highlights the peaks from $Gd_{26.7}(FeCo)_{73.3}$ and schematics of ST-FMR measurement setup. (c) & (d) Cu thickness dependent SOT efficiencies.

EOF-08. Unconventional spin-orbital torque enhanced magnetization switching by interface oxidation in CuPt/CoPt bilayer.
T. Zhao[1], L. Liu[1], C. Zhou[1] and J. Chen[1] *1. Department of Materials Science and Engineering, National University of Singapore, Singapore*

We study the current-induced spin-orbit torque (SOT) switching and out-of-plane (OOP) effective field in a CuPt/CoPt heterostructure with interface oxidation. By introducing the oxidized copper at the interface, we found

their switching abilities show remarkable improvement which is attributed to an unconventional OOP effective field. The OOP effective field is three times stronger than that without oxide treatment. Our observation identified the important role of the interface oxidation in the SOT process of CuPt/CoPt heterostructure. The spin current can trigger a torque in ferromagnetic (FM) layer to electrically manipulate the magnetization. It is promise for an Magnetoresistive random-access memory (MRAM) device due to its endurance and speed [1-3]. To efficiently manipulate the magnetism in MRAM, the key point is to increase the spin accumulation in ferromagnetism (FM). In additiona, for traditional SOT devices, the external magnetic field is required to break the symmetry. Thus, the field-free switching has attracted attention. We believe there could be a different path to enhance the field-free magnetization switching from material perspective. Previously, we studied the symmetry dependent field-free SOT switching in a CuPt/CoPt heterostructure [4]. The intrinsic broken mirror symmetry related SOT process is also reported in WTe_2 [5]. The $L1_1$ CuPt deposited on SrTiO3 (111) substrate possesses a 3-fold symmetry, as shown in figure 1. The field-free switching emerges when the current is injected along the low symmetry axes ([1-10] and the other two equivalent axes). In this work, we show the 3-fold symmetry unconventional out-of-plane torque is from the CuPt and it can be manipulated by the oxidation at the surface. Comparing to unoxidized sample, the oxidized sample approve a much larger switching ratio, since the large out-of-plane torque as the figure 2 shown. Regarding the oxidation degree of the copper is controllable by the time of oxidation treatment, thus a tuneable and efficient MRAM based on SOT induced magnetization switching is promised.

[1] K. Garello et al., 2018 IEEE Symposium on VLSI Circuits., p.81-82 (2018). [2] F. Oboril, R. Bishnoi, M. Ebrahimi and M. B. Tahoori, IEEE Transactions on Computer-Aided Design of Integrated Circuits and Systems., Vol. 34.3, p.367-380 (2015). [3] G. Prenat et al., IEEE Transactions on Multi-Scale Computing Systems., Vol. 2.1, p.49-60 (2016). [4] L. Liu et al., Nat. Nanotechnol., Vol. 16.3, p.277-282 (2021). [5] MacNeill, D., Stiehl, G., Guimaraes, M. et al., Nature Phys., Vol. 13, p.300–305 (2017).

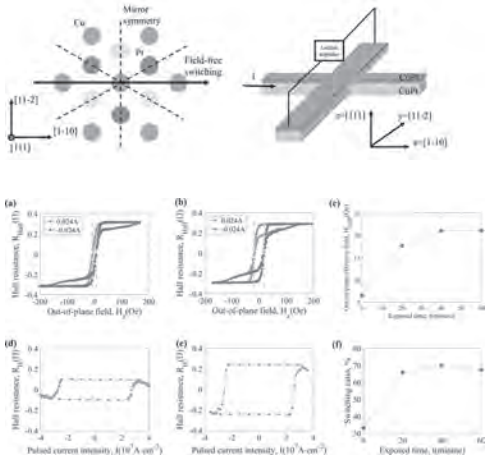

EOF-09. Spin-orbit torque switching mediated by orbital currents from CuN_x. *T. Chen*[1], Y. Hsiao[1], W. Liao[1] and C. Pai[1] *1. National Taiwan University, Taipei, Taiwan*

Current-induced spin-orbit torque (SOT) is an efficient mechanism to manipulate the magnetization in magnetic materials [1]. In principle, the sizable SOT is believed to originate from the bulk spin Hall effect (SHE) and/or the interfacial spin Rashba- Edelstein effect (SREE) in heavy metals (HMs)-based magnetic heterostructures with strong spin-orbit coupling (SOC). Strikingly, recent reports suggest that the light metals (LMs) can also generate non-negligible SOTs and these sizable charge-to-spin conversions are attributed to the orbital angular momentum (OAM) induced orbital Hall effect (OHE) and/or orbital Rashba-Edelstein effect (OREE) [2]. The OAM dominating SOT generation has been experimentally explored in various LM-based systems such as Ti, Cr, and Cu-based magnetic heterostructures [3]. In this work, we prepare the Pt/Co/CuN_x perpendicular magnetic heterostructures by reactive sputtering. By controlling the doping concentration, the overall SOT efficiency can be tuned from 6% to ~ 40%. The enhancement is attributed to combining the spin currents from Pt and the orbital currents generated by the nitrided Cu capping layer. Besides the conventional SOT characterizations, we further demonstrate the neuromorphic switching and show that the orbital currents can effectively manipulate the perpendicular magnetization. These results provide valuable information for building energy-efficient spin-orbitronic devices utilizing both the spin and the orbital effects [4].

[1] L. Liu *et al.*, Science 336, 555 (2012). [2] D. Lee *et al.*, Nature Communications 12, 6710 (2021). [3] S. Lee *et al.*, Communications Physics 4, 234 (2021). [4] T.-Y. Chen *et al.*, Physical Review Applied 17, 064005 (2022).

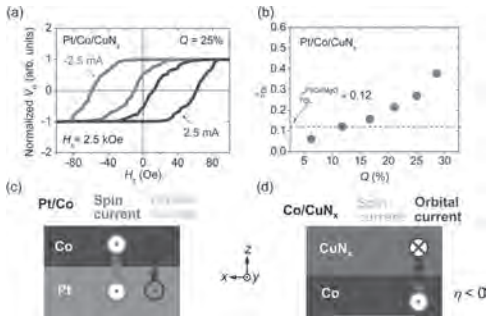

Figure 1. (a) Hysteresis loop shift measurement on a Pt/Co/CuN_x magnetic device. (b) SOT efficiency with respect to doping concentration (*Q*). Illustrations of SOT generation in (c) Pt/Co bilayer and (d) Co/CuN_x bilayer.

EOF-10. Growth, characterization and spin-orbit torque of BiSb topological insulator/MnGa perpendicular ferromagnet systems.
D. She[1,2], N. Figueiredo Prestes[1], L. Baringthon[1], S. Husain[1], L. Largeau[2], M. Morassi[2], H. Jaffres[1], N. Reyren[1], P. Le Fevre[3], J. George[1] and A. Lemaitre[2] *1. Unite Mixte de Physique CNRS, Thales, Univ. Paris Saclay, Palaiseau, France; 2. Centre de Nanosciences et Nanotechnologies (C2N), Palaiseau, France; 3. Synchrotron SOLEIL, Saint-Aubin, France*

Recently, topological insulator(TI)/ferromagnetic(FM) systems, such as Bi_2Se_3/FM [1,2], $Bi_{1-x}Sb_x$/FM [3,4] have attracted much attention with their promising properties for emerging memory technologies, such as magnetic random-access memories(MRAM). Indeed, these systems may drastically reduce the writing current using spin-orbit torque(SOT) switching. In this case SOT is generated by injecting a charge current into the TI topologically protected surface states(SS), then converted into a spin current in the FM layer. The charge current may shunt the TI SS through the metallic FMs which conductivity is often higher and may not contribute efficiently to the SOT[5]. Thus, FMs with lower conductivities are required and may help to better understand the SOT effect. Also, for applications, FMs with high Curie temperature and perpendicular magnetic anisotropy(PMA) are desirable. In this work, we focused on the molecular beam epitaxy (MBE) growth conditions of $Bi_{1-x}Sb_x$(top)/Mn_xGa_{1-x}(bottom) heterostructure on the semi-insulating GaAs(001) substrate. A high epitaxial quality was confirmed by the high-resolution scanning transmission electron microscopy (STEM) as shown in Fig.1. The $Bi_{0.85}Sb_{0.15}$ top surface states have been characterized by performing ARPES measurements. Electronic band structure with topological surface states was observed. $Mn_{0.45}Ga_{0.55}$ exhibit a PMA with a magnetization of 315 kA/m. To investigate the charge-to-spin current conversion of $Bi_{0.9}$ $Sb_{0.1}$(9 nm)/$Mn_{0.45}Ga_{0.55}$(7 nm) we first performed anomalous Hall effect (AHE) measurements at various temperatures. A large value of $\Delta R_{AHE} = 0.4\Omega$ was obtained at room temperature. We then perform second harmonic Hall voltage measurements in order to quantify the damping-like H_{DL}(Fig.2.) and field-like SOT H_{FL} by applying an ac current and in-plane external magnetic field. For this relatively large MnGa thickness (7nm), a

value of H_{DL}=2.6±1.3mT for a current density of 10^{10} A/m^2 was estimated. Part of future work will focus on controlling the growth of a thinner layer.

[1] Mellnik, A. et al. Spin-transfer torque generated by a topological insulator. *Nature* 511, 449–451 (2014) [2] Wang, Y., Zhu, D., Wu, Y. *et al.* Room temperature magnetization switching in topological insulator-ferromagnet heterostructures by spin-orbit torques. *Nat Commun* 8, 1364 (2017). [3] Fan, T., Khang, N.H.D., Nakano, S. *et al.* Ultrahigh efficient spin orbit torque magnetization switching in fully sputtered topological insulator and ferromagnet multilayers. *Sci Rep* 12, 2998 (2022) [4] Tuo Fan, Nguyen Huynh Duy Khang, Takanori Shirokura, Ho Hoang Huy, and Pham Nam Hai, Low power spin–orbit torque switching in sputtered BiSb topological insulator/perpendicularly magnetized CoPt/MgO multilayers on oxidized Si substrate, Appl. Phys. Lett. 119, 082403 (2021) [5] Liu, L. et al. Spin-torque switching with the giant spin Hall efect of tantalum. Science 336, 555–558 (2012)

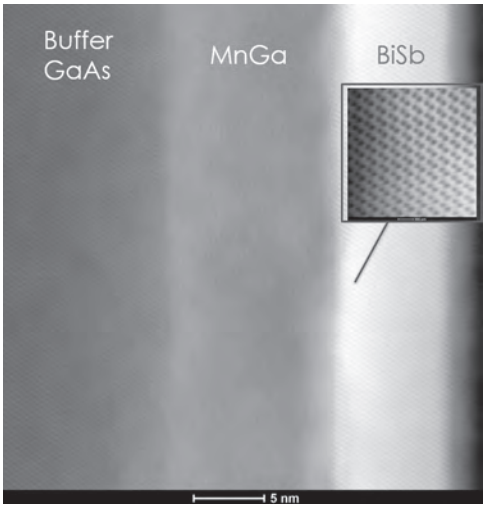

Fig. 1: STEM-HAADF cross section of $Bi_{0.9}Sb_{0.1}$(10nm)/ $Mn_{0.45}Ga_{0.55}$(10nm)

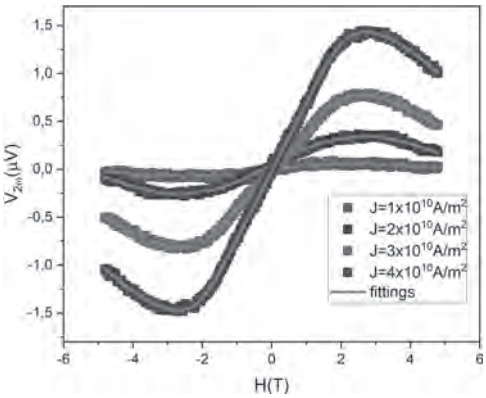

Fig. 2: Second harmonic Hall voltage vs. in-plane external magnetic field in longitudinal geometry for various current densities J

EOF-11. Intrinsic Anomalous Hall Effect and Spin Orbit Torques in Amorphous Transition Metal Silicides and Germanides.

J. Karel[1], C. Hsu[2], S. Bouma[3], C. Fuchs[3], P. Corbae[4], N. Roschewsky[2], S. Salahuddin[2] and F. Hellman[3,1] *1. Materials Science and Engineering, Monash University, Melbourne, VIC, Australia; 2. Electrical Engineering and Computer Science, University of California Berkeley, Berkeley, CA, United States; 3. Department of Physics, University of California Berkeley, Berkeley, CA, United States; 4. Materials Science and Engineering, University of California Berkeley, Berkeley, CA, United States*

Spin currents are critical to numerous low-energy electronic devices, and consequently extensive efforts have been directed towards identifying suitable materials for efficient spin current generation. However, most work has focused on crystalline materials. This talk will show that amorphous materials are promising candidates for spin current generation. Harmonic Hall measurements, electronic and magnetotransport (magnetoresistance and Hall effect) will be presented for a series of ferromagnetic amorphous transition metal thin films M_xY_{1-x} (M=Fe, Co; Y=Si, Ge; x=0.40-0.71).[1,2,3] The talk will examine the anomalous Hall effect and show, through a scaling analysis and DFT calculations, that the intrinsic mechanism is dominant in all samples studied. The anomalous Hall angle (AHA=σ_{xy}/σ_{xx}) is as large as 5%, which is substantial even for crystalline systems.[2] Finally, we will demonstrate a very large spin orbit torque efficiency (~200%) using an amorphous Fe_xSi_{1-x} / oxide / Co bilayer at room temperature.[3] We will discuss the origins of this very large SOT and show it may be driven by the non-trivial topology in the electronic structure.

[1]D.S. Bouma *et al.*, *Phys Rev B* 101 014402 (2020) [2]J. Karel *et al.*, Phys Rev Materials 4 114405 (2020) [3]C.-H. Hsu, J. Karel *et al.*, https://arxiv.org/abs/2006.07786

EOF-12. Current induced magnetization switching in (Mn-Cr)AlGe films showing perpendicular magnetization.

T. Kubota[1], S. Honda[2], Y. Sonobe[3,4], T. Kato[3] and K. Takanashi[5,1] *1. Tohoku University, Sendai, Japan; 2. Kansai University, Suita, Japan; 3. Nagoya University, Nagoya, Japan; 4. Waseda University, Tokyo, Japan; 5. Japan Atomic Energy Agency, Tokai, Japan*

An intermetallic compound, (Mn-Cr)AlGe is a material showing perpendicular magnetization in film form with (001)-texture[1]. Merits of the material are small saturation magnetization (~ 300 kA/m) and small Gilbert damping constant (α: 0.012)[1-3]. Another important feature is, in addition, these physical properties can be achieved in poly-crystalline textured film samples with a thickness range of a few nanometer[2, 3], which is attractive for practical applications. In this study, layered film samples consisting of a (Mn-Cr)AlGe | W structure were fabricated, and the current induced magnetization switching (CIMS) originating from spin-orbit torque from the W layer was investigated. Film samples were fabricated using an ultra-high vacuum magnetron sputtering machine. The stacking structure was as follows: Si,SiO_2 substrate | Ta 3 nm | W 0.3 nm | CoFeBTa 1 nm | MgO 10 nm | Mg 0.8 nm | (Mn-Cr)AlGe *t* | W 5 nm | MgO 0.8 nm | Ta 1 nm. The film composition of (Mn-Cr)AlGe was $(Mn_{0.77}Cr_{0.23})Al_{1.06}Ge_{0.94}$ (at.%). All the layers were continuously deposited at room temperature, and post-annealing was carried out using a vacuum furnace at 400 °C. The layer thicknesses (*t*) of the (Mn-Cr)AlGe were 5, 7, 10, 15 and 20 nm. From magnetization curve measurements, perpendicular magnetization showing high squareness ratio (> 0.9) was confirmed for all samples except for t = 5 nm showing no hysteresis loop. The samples were patterned into a Hall-bar shape, and the CIMS measurements were carried out at room temperature. The applied current range was ± 50 mA with a pulse width of 100 μsec and the in-plane magnetic field (H_x) of 1 kOe along the current pulse direction. Figure 1 shows a CIMS result for t = 7 nm. The polarity of the switching changes depending on the direction of H_x. Considering relatively high switching current of about 20 mA, the spin-orbit torque is relatively small from the W layer, which is possibly due to relatively poor interface quality. This work was partly supported by KAKENHI (JP20K05296) and a Cooperative Research Program (No. 21G417) of the CRDAM-IMR, Tohoku Univ.

[1] T. Kubota *et al*., Appl. Phys. Express 12, 103002 (2019) [2] T. Kubota *et al*., Appl. Phys. Lett. 118, 262404 (2021). [3] Y. Sasaki *et al*., Small 18, 2200378 (2022).

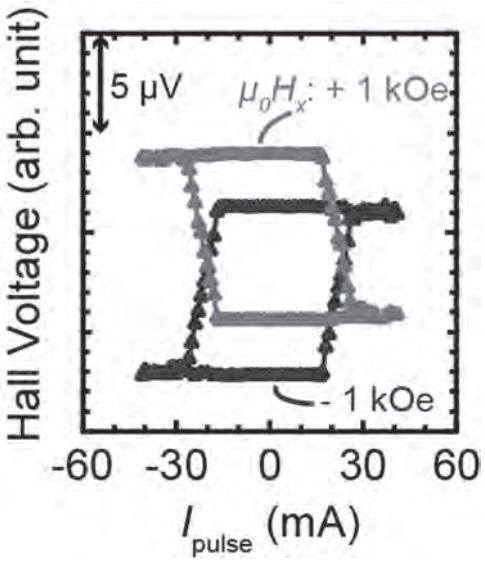

Current induced magnetization switching of a layered sample consisting of a (Mn-Cr)AlGe 7 nm|W 5 nm structure.

EOF-13. Giant spin Hall effect in a half-Heusler alloy topological semimetal with high thermal stability. *T. Shirokura*[1], F. Tuo[1], N. Huynh Duy Khang[1] and P. Nam Hai[1] *1. Tokyo Institute of Technology, Meguro, Japan*

Topological materials have great potential for ultralow power spin-orbit torque (SOT) spintronic devices thanks to their giant spin Hall effect originated from their topological surface states (TSSs). However, the giant spin Hall angle ($\theta_{SH} > 1$) is limited to a few chalcogenide-based topological insulators (TIs) with toxic elements and low melting points, making them challenging for device integration during the silicon Back-End-of-Line (BEOL) process. Here, we focus on a half-Heusler alloy topological semimetal, YPtBi, to overcome this difficulty. We synthesized YPtBi thin films by using co-sputtering method with YPt and Bi targets while changing the growth temperature. Figure 1 (a) shows the X-ray diffraction (XRD) spectra for YPtBi films grown at various temperature. YPtBi(111) peaks were clearly observed up to 600°C. Figure 1 (b) shows the Bi composition measured by X-ray fluorescence (XRF). Bi composition is stable up to 600°C. These results indicate that YPtBi crystal is stable up to 600°C which is high enough for BEOL process. To evaluate the spin Hall effect for YPtBi, we conducted the second harmonic Hall effect measurements in CoPt/YPtBi heterostructures [1]. By controlling the electric conductivity of YPtBi and spin transparency at the CoPt/YPtBi interface, we successfully realized a giant θ_{SH} up to 4.1. Figure 2 shows SOT magnetization switching by pulse currents with pulse width of 50 μs to 10 ms under an external magnetic field of 0.5 kOe applied parallel to the current. Thanks to the giant spin Hall effect originated from TSS, small threshold current of about 1×10^6 A/cm^2 was observed, which is one order magnitude smaller than that in heavy metals [2]. Our work opens the door to the next generation spin Hall materials with both giant θ_{SH} and high thermal stability [3]. Acknowledgment: this work was supported by Kioxia corporation. The authors thank Tsuyoshi Kondo of Kioxia corporation for fruitful discussion.

[1] M. Hayashi, J. Kim, M. Yamanouchi, and H. Ohno, Phys. Rev. B, Vol. 89, p.144425 (2014). [2] B. Jinnai, C. Zhang, A. Kurenkov, M. Bersweiler, H. Sato, S. Fukami, and H. Ohno, Appl. Phys. Lett. Vol. 111, p.102402 (2017). [3] T. Shirokura, T. Fan, N. H. D. Khang, T. Kondo, and P. N. Hai, Sci. Rep. Vol. 12, p.2426 (2022).

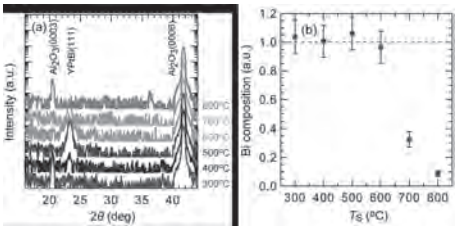

Fig. 1 (a) XRD spectra and (b) Bi composition measured by XRF in YPtBi stand-alone sample as a function on substrate temperature.

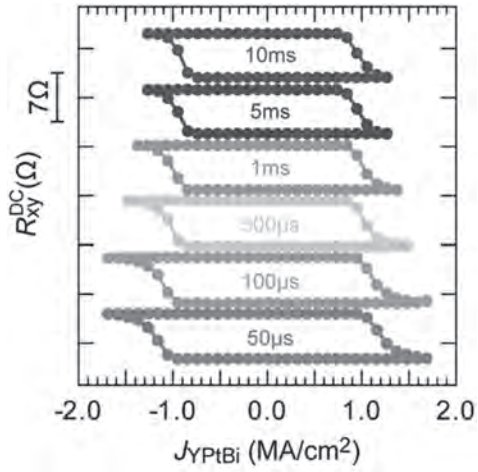

Fig. 2 Magnetization switching by pulse currents with various pulse width ranging from 50 μs to 10 ms and magnetic field of 0.5 kOe in CoPt/YPtBi heterostructure.

EOF-14. Electric field controlled quantitative magnetization switching with spin-orbit torque. *X. Li*[1], H. Singh[2], J. Chatterjee[2], M. Goikoetxea[4], Z. Xiao[3], S. Mondal[2], N. Tamura[5], R.N. Candler[3], L. You[1], J. Bokor[2] and J. Hong[1,2] *1. Huazhong University of Science and Technology, WuHan, China; 2. EECS, University of California, Berkeley, CA, United States; 3. University of California, Los Angeles, Los Angeles, CA, United States; 4. University of the Basque Country, Euskadi, Spain; 5. Lawrence Berkeley National Lab, Berkeley, CA, United States*

Multiferroics offer an energy-efficient solution to solely electrically controlled spin orbit torque (SOT) and spin transfer torque (STT) devices. Controlling magnetism also blazes a trail for us to develop further energy efficient devices in future information technologies. Here, we integrate SOT on multiferroics. We systematically study angle dependency of the SOT effect on a piezoelectric substrate to control localized in-plane strain [1] by applying out-of-plane (OOP) DC electric field across the substrate. The controlled strain makes it possible to quantitatively modulate the magnetization switching of SOT devices. We investigate such control of the switching by harmonic Hall measurement, photoemission electron microscopy (PEEM), X-ray diffraction, and magnetic force microscopy (MFM). We accomplish a quantitative electrically switchable Hall voltage in such an SOT structure without the aid of a magnetic field. As shown in Fig. 1(a), we performed the Harmonic Hall voltage measurements to determine the spin-orbit induced effective fields in HM/FM heterostructures. Under increasing magnetic field, second harmonic measurements allow us to calculate the effective field of SOT induced damping-like torque (DLT) and field-like torque (FLT) separately. The quantitative torques are shown in Fig. 1(b). Inserts show PEEM images of the device under two different circumstances: the left one with no strain and no current while the right one under substrate voltage and current. The tensile strain could reduce the SOT switching energy and control magnetization switching. MFM images of the device are shown in Fig. 1(c); from left to right are four different states. With no excitation, magnetization stayed unchanged; with strain only, partial

magnetization switched; with strain and current, the magnetization state was fully switched; while with strain and reverse current, it was fully switched to the other direction. Our experimental results pave the way to building voltage-controlled magnetization switching for low-power spintronic devices.

[1] M. Filianina, J-P. Hanke, K. Lee, D-S Han, S. Jaiswal, A. Rajan, G. Jakob, Y. Mokrousov, and M. Kläui, Phys. Rev. Lett., Vol. 124, p. 217701, 2020.

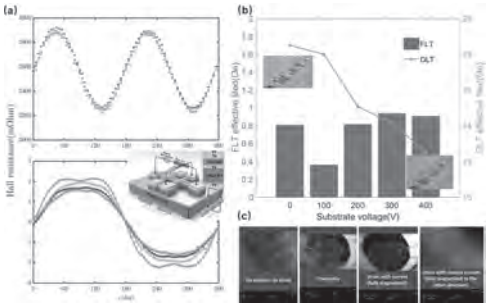

Figure 1. (a) Harmonic Hall measurement result and device structure. (b) Effective field of FLT and DLT varied with substrate voltage and PEEM images. (c) MFM micrographs of device.

Session EPA
ANTIFERROMAGNETIC SPINTRONICS III
(Poster Session)

Takeshi Seki, Chair
Tohoku University, Sendai, Japan

EPA-01. Intrinsic Unidirectional Anisotropic Magnetoresistance in Thin-Film FeRh. *E. Blake*[1], G. Newman[1], P. Sparks[1], J. Eckert[1], Y. Xiao[2], S. Patel[2] and E. Fullerton[2] *1. Physics, Harvey Mudd College, Claremont, CA, United States; 2. Center for Memory and Recording Research, University of California San Diego, La Jolla, CA, United States*

Within magnetic materials, anisotropic magnetoresistance (AMR) measures the dependence of the resistivity on the angle between the high magnetic susceptibility direction of the magnetic order and the current direction. When analyzed using spectral decomposition, the AMR of most magnetic materials is composed of even harmonics the most common of which are 2-fold (C_2) and 4-fold (C_4) arising from *s-d* scattering and crystal field effects respectively. The generation of odd harmonics in the spectral decomposition of the AMR are observed in magnetic films when the magnetic film is combined with another non-magnetic material to form a heterostructure. The observed unidirectional AMR is a result of the explicit breaking of the spatial inversion symmetry at the interface of the engineered heterostructure. Alternatively, the spatial inversion symmetry may be broken internally within the magnetic film under the application of a magnetic field leading to the observation of signatures of unidirectional AMR in the spectral decomposition without the presence of the non-magnetic material. In this work, we observe odd spectral harmonics (C_1 and C_3) associated with the presence of unidirectional AMR in 20 nm thin-films of antiferromagnetic FeRh measured at 20K, as seen in Fig. 1(A). In Fig. 1(B), the presence of the odd spectral harmonics is confirmed using a tight-binding representation of the tetragonal FeRh lattice in the antiferromagnetic phase where the transport quantities are calculated using the non-equilibrium Green's function formalism. Furthermore, we attribute the presence of the C_1 and C_3 harmonics to the magnetic moment that the Rh atoms develop when immersed in an external in-plane magnetic field. We quantify the size of the inherent unidirectional AMR component as a function of the applied magnetic field and show that the internal unidirectional AMR component is non-negligible and omnipresent in AMR measurements even in the absence of non-magnetic layers.

J. Oh, L.Humbard, V. Humbert, AIP Advances 9, 045016 (2019) T. Huong T. Nguyen, V.Nguyen, *Communications Physics* volume 4, Article number: 247 (2021)

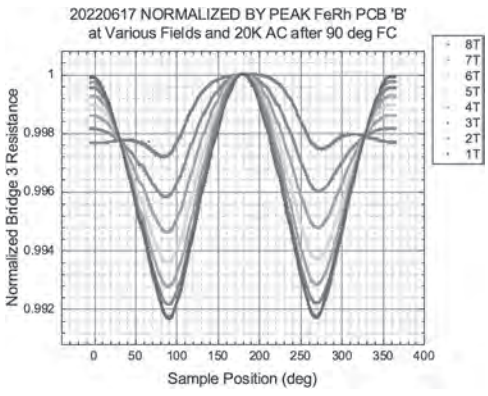

Fig.1 Experimentally measured AMR for 20 nm thick antiferromagnetic FeRh in magnetic fields ranging from 1-8 T.

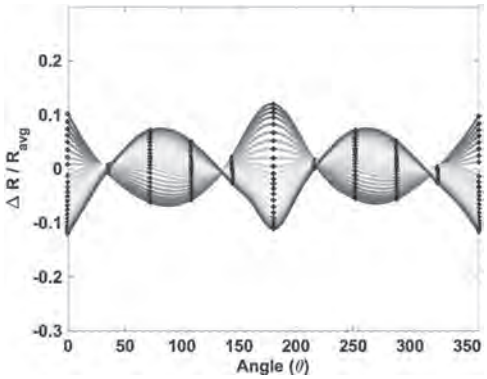

Fig.2 Theoretical AMR in FeRh calculated in a magnetic field that covers the same 1-8 T as the experiment.

EPA-02. Crystallisation Control of polycrystalline PtMn via Seed Layers. *W.J. Frost*[2], R. Carpenter[1], S. Couet[1] and G. Vallejo-Fernandez[2] *1. imec, Leuven, Belgium; 2. Department of Physics, University of York, York, United Kingdom*

Antiferromagnetic materials (AFs) are under intense study for future device applications like SOT AF spintronics and in fundamental studies, such as the origins of AF anisotropy. PtMn is a simple material with 1:1 stoichiometry in the tetragonal $L1_0$ structure which exhibits AF ordering. The growth of materials like PtMn is easily manipulated and controlled via seed layers. The enthalpy of crystallisation of the material is significantly affected by the layers interfaced with it and varying the seed layer changes any heteroepitaxy between the layers, which alters the crystallographic properties of the PtMn, including the grain size, texture and lattice constant. Subsequently the values of the anisotropy and the thermal stability can be determined [1] and optimised. Samples were deposited with seed layers of Ru, Pt and Ti, which are hexagonal, and Cu, which is fcc, as these provide a good lattice match the {111} planes of the tetragonal phase of PtMn. Additionally they all exert different strain on the lattice, ranging from compressive to tensile. The thickness of the PtMn was also varied from (5 to 15) nm. 2 nm of $Co_{60}Fe_{40}$ acts as a sensing layer to allow for magnetic measurement. Figure 1 shows the θ/2θ scans of a Pt/PtMn sample where the thickness of the PtMn is 15 nm. As deposited the sample is in a strained phase but after annealing a phase transformation to and through the fcc, paramagnetic phase begins. This contrasts strongly not only with literature values [2] but also with isolated PtMn where a phase transition is seen at 370°C. However, a small increase in coercivity from (20 to 90) Oe is observed above 400°C, although no exchange bias is induced. This indicates a mixed phase of PtMn. The neighbouring layers significantly affect the crystallization process of the PtMn as well as the thickness of the layer itself possibly playing a key role. By varying the structure we can control and enhance this phase transformation. This is extremely useful for future perspectives on device application of these materials and to study the effects on fundamental properties.

Vallejo Fernandez *et al*, *Appl. Phys. Lett.*, 91, 21 (2007). Ranjbar *et al*, *IEEE Sens. Lett.,* 4 (5), 2475-1472, (2020).

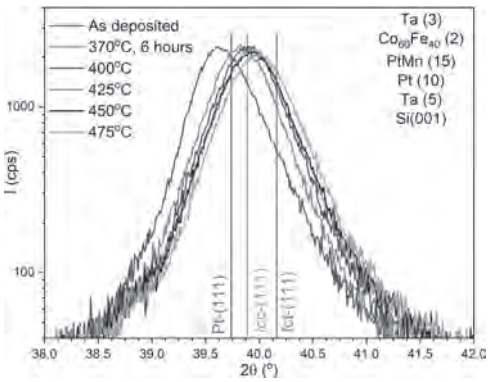

θ/2θ scans of Pt/PtMn as a function of annealing.

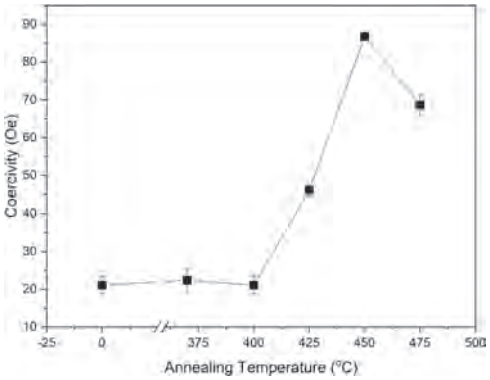

Coercivity of Pt/PtMn multilayers after annealing.

EPA-03. Investigation of spiral phase in multiferroic $YBaCuFeO_5$ | Pt heterostructure using spin Hall magnetoresistance. *K. Jha*[1], A.A. Wagh[1], S. Elizabeth[1] and P. Kumar[1] *1. Physics, Indian Institute of Science, Bangalore, Bangalore, India*

In magnetic insulator | heavy metal bilayers, electrically induced conduction electron spin current can get absorbed at the interface due to spin-transfer torque and results in a change in the resistance of the heavy metal. This phenomenon is known as spin Hall magnetoresistance (SMR) [1]. The SMR has been extensively explored in collinear magnetic materials such as ferromagnets and ferrimagnets. However recently, more exotic non-collinear magnetic materials like antiferromagnets have attracted a great deal of attention from the antiferromagnetic spintronics community. $YBaCuFeO_5$ is a uniquely interesting material because the ordering temperature of the spiral phase, T_{spiral} (~ 200 K), (below which it is magnetoelectric multiferroic in nature) can be tuned well above the room temperature by adjusting the Fe^{3+}-Cu^{2+} disorder in the material [2]. We have grown epitaxial thin films (thickness ~ 50 nm) of $YBaCuFeO_5$ on Lanthanum Aluminate ($LaAlO_3$) substrates using the pulsed laser deposition (PLD) technique. We have also deposited platinum (Pt) as a second layer (thickness ~ 5 nm) *in-situ* to get the desired quality of the heterostructure. The bilayer was characterized using the thin-film X-ray diffraction technique. A Hall bar was patterned for the SMR studies. We measured angular dependence of the SMR while rotating the magnetic field in-plane at various constant temperatures in the range:10 to 300 K. We observed negative SMR at room temperature which is a characteristic of the antiferromagnetic phase.[3] In the present study, we discuss in detail, the temperature and the field evolution of the SMR in the spiral magnetic phase. Our studies highlight prospects of tunable multiferroic material, $YBaCuFeO_5$ for future magnetoresistance-based spintronic devices.

[1] Yan-Ting Chen, Saburo Takahashi and Hiroyasu Nakayama, Phys. Rev. B, Vol. 87, p.144411 (2013) [2] Mickael Morin, Emmanuel Canevet and Adrien Raynaud, Nat. Commun., Vol. 7, p.13758 (2016) [3] Johanna Fischer, Olena Gomonay and Richard Schlitz, Phys. Rev. B, Vol. 97, p.014417 (2018)

EPA-04. Interfacial Exchange Phenomena Driven by Ferromagnetic Domains. J. Diez[1], J. Cuñado[1], P. Lapa[2], R. Solis[1], I. Arnay[1], P. Pedraz[1], P. Perna[1], A. Bollero[1], R. Miranda[1], I.K. Schuller[2] and *J. Camarero*[1] *1. IMDEA NANOCIENCIA, Madrid, Spain; 2. Department of Physics and Center for Advanced Nanoscience, University of California, San Diego, La Jolla, CA, United States*

Interfacial proximity effects in antiferromagnetic/ferromagnetic (AFM/FM) bilayers control the exchange-bias (EB) phenomena exploited in most spintronic devices, although still is lack of full understanding. Discordant results, including different exchange-bias field (HE), coercive field (HC), or blocking temperature (TB) found even in similar systems, are usually ascribed to uncontrolled parameters, namely dissimilar interfacial defects, structure, and thicknesses. Here we show experimental evidence that provides new insights on the general knowledge about EB phenomena and, surprisingly, refers to the key role of the magnetic texture of the FM layer during reversal, not considered to date [1]. Simultaneous transport and vectorial-resolved magnetic measurements performed in a V2O3/Co system during warming after different field cooling (FC) procedures exhibit a strong dependence of the EB phenomena, including reversal pathways, H_E, H_C, and T_B and their temperature dependences. Remarkably, magnetization reversal analysis reveals 35 K of variation in TB and up to a factor of two in HE. These observations can be explained within the random field model for the interfacial exchange coupling with a fixed AFM domain structure in contact with a variable (angle-dependent) FM domain structure. The results highlight the importance of the domain structure and magnetization reversal of the FM layer (not previously considered) in the EB phenomena, with potential to tailor interfacial effects in future spintronic devices. This research was partially supported by the Spanish Ministry of Economy and Competitiveness (MINECO) (grant numbers RTI2018-097895-B-C42, PCI2019-111867-2, PID2020-116181RB-C31, and CEX2020-001039-S) and by the Regional Government of Madrid (through project NANOMAGCOST-CM). JMD ackowledges support from MINECO through FPI program (BES-2017-080617). Work at UCSD supported by the Department of Energy's Office of Basic Energy Science, under grant # DE-FG02-87ER45332.

[1] J. M. Díez *et al*., *Adv. Mater. Interfaces 2022, 2200331*, DOI: 10.1002/admi.202200331

EPA-05. Tailoring compensated ferrimagnetic state in quaternary Mn-Ru-V-Ga Heusler compounds. *J. Liang*[1], W. Wang[2] and Y. Lau[1] *1. Institute of Physics, Chinese Academy of Sciences, Beijing, China; 2. Tiangong University, Tianjin, China*

Compensated ferrimagnets [1,2] with two inequivalent magnetic sublattices can exhibit finite spin polarization, anomalous Hall effect and tunneling magnetoresistance like a ferromagnet, even when the net magnetization exactly vanishes at the magnetic compensation point. This material class has attractive potential for high-density, ultrafast, and low-power spintronic applications. Cubic Mn_2Ru_xGa (MRG) is a typical example of compensated ferrimagnet with high spin polarization and high tunability of compensation temperature by freely varying the Ru content x over a broad range ($0.3 < x < 1.0$) [3]. Here, we systematically studied MRG-based polycrystalline ingots prepared by arc melting, followed by annealing at 1073 K for seven days. We surprisingly found that, in equilibrium bulk form, the cubic structure is unstable when $x < 0.75$, which substantially reduces the tunability of MRG. We concluded that previously reported Ru-deficient MRG thin films are mostly metastable. At equilibrium, MRG can never compensate below ~350 K. To overcome this limitation, we alloy MRG with a fourth element V, which helps to stabilize the cubic structure while providing less valence electron than Mn and Ru. We systematically investigate the $Mn_2Ru_{0.75}V_yGa$ quaternary system. Figure 1(a) shows the temperature dependence of magnetization $M(T)$ measured with a small applied magnetic field of 0.1 T. Adding V consistently reduces the compensation

temperature from 380 K to 260 K. For y = 0.1, the *M-H* loop at 300 K in Fig. 1(b) shows a modest increase of the coercivity (< 0.1 T) due to the vanishing net magnetization. The sign reversal of the anomalous Hall effect (AHE) shown in Fig. 2 provides another evidence that the magnetic compensation has indeed achieved near 300 K. In the talk, we will also discuss the effect of V doping on the intrinsic and extrinsic contributions of AHE.

[1] Joseph Finley and Luqiao Liu, Applied Physics Letters, 116, 110501 (2020) [2] Se Kwon Kim et al., Nature Materials, 21, 24-34 (2022) [3] H. Kurt et al., Physical Review Letters, 112, 027201 (2014)

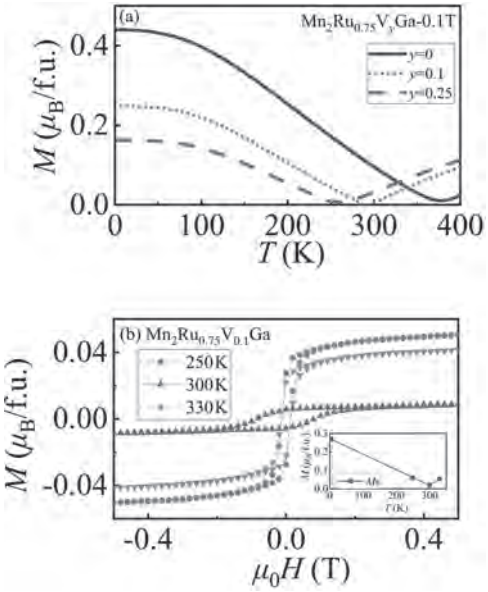

Fig. 1. (a) *M*(*T*) for $Mn_2Ru_{0.75}V_yGa$ (y=0, 0.1 and 0.25) measured in a field of 0.1T on cooling. (b) *M-H* of $Mn_2Ru_{0.75}V_{0.1}Ga$ measured at different temperatures. The inset shows the saturation magnetization at different temperatures.

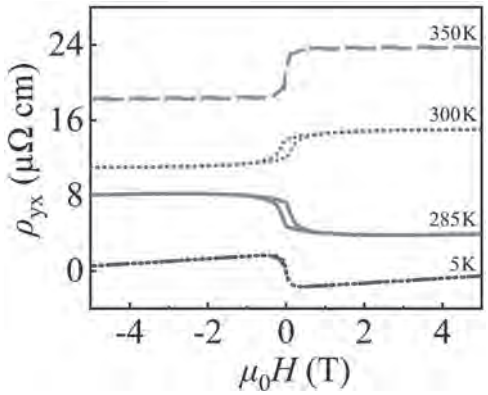

Fig. 2. ρ_{yx} for $Mn_2Ru_{0.75}V_{0.1}Ga$ measured at different temperatures.

EPA-06. XAS and XMCD Study of the Magnetic Anisotropy Transition in Co-substituted Mn_3Ga Heusler Films. *J. Kang*[1], S. Seong[1], Y. Seo[1], G. Lim[1], W. Yoo[2], M. Jung[2] and S. Han[3] *1. Physics, The Catholic University of Korea, Bucheon, The Republic of Korea; 2. Physics, Sogang University, Seoul, The Republic of Korea; 3. Physics, University of Ulsan, Ulsan, The Republic of Korea*

Some Heusler compounds were predicted to have half-metallic electronic structures [1], which are important properties in spintronics. Then Co-substituted Mn_3Ga Heusler films, which exhibit perpendicular magnetic anisotropy (PMA) and the magnetic transition from PMA to in-plane magnetic anisotropy (IMA), were considered to be potential spintronic materials [2,3]. In this work, we have investigated electronic structures of $Mn_{3-x}Co_xGa$ films by employing synchrotron radiation-excited soft X-ray absorption spectroscopy (XAS) and soft X-ray magnetic circular dichroism (XMCD). According to Co 2p XAS and XMCD, the substituted Co ions in $Mn_{3-x}Co_xGa$ consist of ferromagnetic metallic Co clusters and divalent Co ions with disordered magnetic moments. Mn 2p XAS and XMCD show that Mn ions at both the octahedral and tetrahedral sites are nearly divalent, reflecting non Jahn-Teller ions, and that the magnetic moments of Mn ions are polarized along the ordered magnetic moments of the substituted Co ions. Angle-dependent Co 2p XMCD results agree with the weak PMA-IMA magnetic anisotropy transition with increasing Co content. This work reveals that the magnetic anisotropy transition in $Mn_{3-x}Co_xGa$ is determined mainly by the ferromagnetic metallic Co clusters of the substituted Co ions. The financial funding from the NRF of Korea (Project No. 2019R1A2C1004929) is gratefully acknowledged.

[1] R. A. de Groot, et al., Phys. Rev. Lett. 50, 2024 (1983). [2] H. Kurt, et al., Phys. Rev. B 83, 020405(R) (2011). [3] Kyujoon Lee, et al., J. Alloys Compd. 858, 1582884 (2021).

EPA-07. Atomistic Control of Magnetocrystalline Anistropy in Antiferromagnets. *R.A. Lawrence*[1] and M.I. Probert[1] *1. Department of Physics, University of York, York, United Kingdom*

Magnetocystalline Anisotropy is the energetic barrier to the reorientation of spin lattices within a magnetic crystal. For exchange-bias devices, antiferromagnetic (AFM) materials are often used to 'pin' a ferromangetic layer, making evaluating the anisotropy of the AFM material key to understanding the performance of the whole device [1]. In this talk, we will discuss the use of first-principles density functional theory (DFT) simulations of the magnetocrystalline anistropy of equiatomic FCT PtMn (see figure 1) performed using the CASTEP code [2] to evaluate the total anisotropy of our example antiferromagnetic system. The use of theoretical techniques to model the anisotropy enables fine control of the structures under investigation, ensuring that any changes to the anisotropy originate in the expected changes. Furthermore, the full angular dependence of the barrier can be extracted, and we find that the phi- (azimuthal) dependence is very weak in comparison to the theta (polar) dependence, explaining why uniaxial models can provide a good approximation for these types of systems (see figure 2). Finally, we investigate further effects beyond a simple infinite bulk crystal that can be used to control the anisotropy of the system. Our simulations indicate that whilst applied biaxial compressive strain increases the anisotropy, applied tensile biaxial strain can cause the easy and hard magnetic axes of the crystal to swap, thereby providing a potential mechanism for strain control of exchange bias devices through strain engineering techniques.

[1] K O'Grady, J Sinclair, K Elphick, Journal of Applied Physics, 128(4), p040901 (2020) [2] S. J. Clark, M. D. Segall, C. J. Pickard, Zeitschrift fuer Kristallographie 220(5-6) pp. 567-570 (2005)

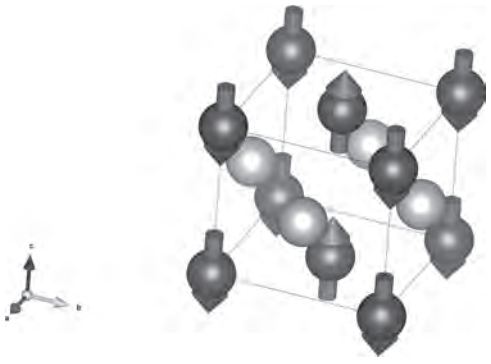

Fig. 1. The ground state geometry and magnetic structure of equiatomic FCT PtMn. Purple atoms are Mn and grey atoms are Pt.

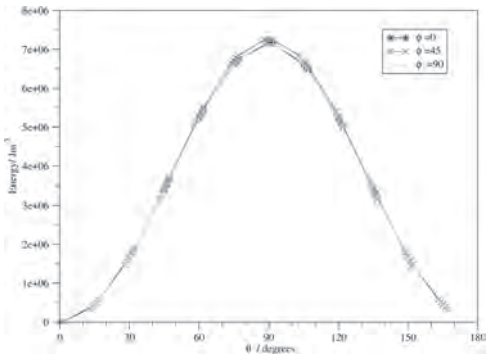

Fig. 2. Energy vs polar angle evaluated at three different azimuthal angles. Note the weak azimuthal dependence in comparison to the polar dependence of the barrier.

EPA-08. Manipulation of Exchange Bias Using Spin-Orbit Torque. *F. Ajejas*[1], A.C. Basaran[1] and I.K. Schuller[1] *1. Physics, University of California, San Diego, San Diego, CA, United States*

The development of antiferromagnetic (AFM) spintronics is an active field with great potential for improving energy consumption, reducing interference and decreasing sizes when compared to traditional spintronics. This requires the development of novel concepts and functionalities which allow control over the properties of a device containing an AFM layer. We present in this work a new device concept in which the spin configuration of an AFM insulator (FeF_2) can be modified taking advantage of spin-orbit coupling (SOC) existing in heavy metals (HM) such as W or Pt. The device consists of a trilayer: HM|AFM|FM, therefore the top FM interface can be used to monitor the changes in the AFM spin configuration. We performed Magneto-Optical Kerr effect (MOKE) to measure the FM hysteresis loops as a function of temperature (T) and applied current (I). We found that the exchange bias (E_B) and coercivity (H_c) produced at the AFM-FM top interface can be strongly modified by a current (I) passed through the HM|AFM bottom interface. This shows that an active spin-orbit torque (SOT) is produced at the HM|AFM bottom interface that reaches the AFM|FM top interface and modifies the reversal of the FM layer. Temperature-dependent control experiments using normal metals (NM) such as Au in NM|AFM|FM and without AFM in HM|FM confirm that the effect is produced by the SOT induced by the HM and is not caused by thermal heating, Oersted field or other potentially spurious effects. This research was supported by the Department of Energy's Office of Basic Energy Science, under grant # DE-FG02-87ER45332.

EPA-09. Impact of Interactions on Topological Magnonic Transport. *K. Sourounis*[1] and A. Manchon[1] *1. Theory and Numerical Simulations, CINaM, Aix-Marseille Universite, Marseille, France*

The transport of magnons in materials with topological non-trivial ground state has been investigated in various platforms (ferro- and antiferromagnets) and is characterized by anomalous mechanisms such as the thermal Hall effect and the magnon Nernst effect. Usually, these investigations are done in the framework of the Linear Spin Wave Theory and the interactions between magnons are ignored. In fact, due to the bosonic nature of magnons, such interactions can have a dramatic impact on the magnon lifetime [Chernyshev, AL et al., Phys. Rev. Lett. 117, 187203 (2016)] and band structure [Mook et al., Phys. Rev. X 11, 021061 (2021)], as recently demonstrated. In other words, these interactions are ubiquitous and can cause the alteration of the energy bands and the transport properties of the system, including damping and topological phase transitions [Y.S. Lu et al., Phys. Rev. Lett. 127, 217202 (2021)]. In this work, we investigate the influence of magnon-magnon interactions on the anomalous transport of magnons in a topologically non-trivial honeycomb antiferromagnet. Focusing on the magnon spin Nernst effect, we uncover the impact of these interactions on the magnon lifetime, band structure and anomalous transport upon increasing the temperature.

Chernyshev, AL et al., Phys. Rev. Lett. 117, 187203 (2016) Mook et al., Phys. Rev. X 11, 021061 (2021) Y.S. Lu et al., Phys. Rev. Lett. 127, 217202 (2021)

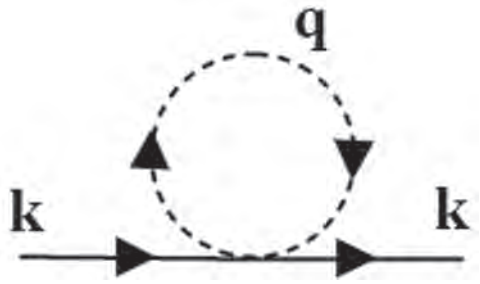

Fig. 1: Hartree diagram of a magnon interaction.

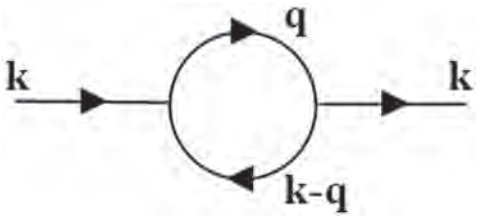

Fig. 2: Bubble diagram of a magnon interaction.

EPA-10. Nanoscale antiferromagnetic vortex states in individual NiO/Fe nanostructures. *M. Slezak*[1], P. Drozdz[1], A. Koziol-Rachwal[1], T. Mentes[2], A. Locatelli[2], D. Wilgocka-Slezak[3] and T. Slezak[1] *1. AGH University of Science and Technology, Krakow, Poland; 2. Elettra - Sincrotrone Trieste, Basovizza, Trieste, Italy; 3. Jerzy Haber Institute of Catalysis and Surface Chemistry PAS, Krakow, Poland*

Recently we reported on magnetic anisotropy in continuous CoO(111)/Fe(110) [1] and NiO(111)/Fe(110) [2, 3] bilayer films. The target of research in the present report is the magnetic domain structure of self-organized, exchange coupled NiO(111)/Fe(110) epitaxial nanostructures. The continuous, ten monolayers (ML) thick Fe(110) film was grown by molecular beam epitaxy on W(110) single crystal at room temperature and subsequently post-annealed at 800 K, leading to the formation of nanostructures with lateral dimensions of the order of several hundreds of nm and an average height ~ 6 nm. The local structure of selected as prepared as well as NiO covered nanostructures was followed using micro-low energy electron diffraction (μLEED) in low energy electron microscope (LEEM), as this approach allows to identify the structure of selected nanoscale areas on the surface. The μLEED patterns from the surface of the selected NiO-covered nanostructures indicate hexagonal NiO(111) structure on Fe(110) islands. The wide distribution of size and shape in these nanostructures and corresponding rich landscape of magnetostatic interactions in their ferromagnetic components, competing with the intrinsic magnetic surface and magnetocrystalline anisotropies, result in a variety of magnetic domain patterns. Using photoemission electron microscopy (PEEM) combined with X-ray magnetic circular and linear dichroism (XMCD and XMLD) effects we selectively probed the local, nanoscale spin orientations of both ferromagnetic and antiferromagnetic components of individual nanostructures. We directly show that antiferromagnetic NiO spins couple collinearly to and follow the local orientation of adjacent ferromagnetic Fe. In particular, ferromagnetic vortex states in Fe are one-to-one imprinted into antiferromagnetic domain patterns of NiO, as indicated by dashed arrows in exemplary XCMD- and XMLD-PEEM images shown in Fig.1. Our experimental results and micromagnetic simulations indicate the possibility for locally induced out-of-plane antiferromagnetic moments in the prototypical easy-plane NiO antiferromagnet.

[1] M. Slezak et al., JMMM 545 (2022) 168783 [2] M. Slezak et al., Phys. Rev. B 104 (2021) 134434 [3] M. Slezak et al., Nanoscale 12 (2020) 18091

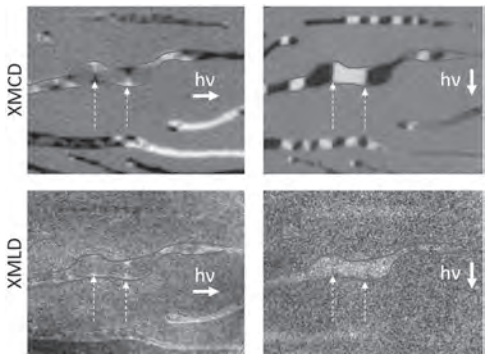

Exemplary XCMD- and XMLD-PEEM images of NiO/Fe nanostructures for two sample geometries in PEEM.

EPA-11. Current-Driven Domain Wall Motion in a Synthetic Antiferromagnet Multilayer. *C.E. Barker*[1], S. Finizio[2], E. Haltz[1], S. Mayr[2], P.M. Shepley[1], T.A. Moore[1], G. Burnell[1], J. Raabe[2] and C. Marrows[1]
1. School of Physics and Astronomy, University of Leeds, Leeds, United Kingdom; 2. Photon Science Division, Paul Scherrer Institut, Villigen, Switzerland

Synthetic antiferromagnets (SAFs) are of interest in a wide variety of spintronic applications owing to their net zero magnetisation and inherent tunability arising from control over complex stacking sequences [1]. They show very fast domain wall (DW) motion in response to spin torques [2]. Here we describe measurements of the current-driven DW motion in each of the separate magnetic sublattices of a SAF with structure Ta/[Ru/Pt/CoB/Ru/Pt/CoFeB]×5/Ru/Pt which displays both perpendicular magnetic anisotropy (PMA) and the Dzyaloshinskii-Moriya interaction (DMI). The thickness of the Ru layers is tuned to provide AF coupling between each pair of layers. The thicknesses of the alternating CoB and CoFeB layers are tuned to give net zero magnetisation (as measured by SQUID magnetometry) at a wide range of fields up to ~50 mT. The magnetic films were grown on Si_3N_4 membranes and imaged with scanning transmission x-ray microscopy (STXM). They were patterned into 2 μm wide wires with Cu leads attached to each end. The distinct chemical composition of the two sublattices means that we could use the element specificity of STXM to observe the CoFeB separately by imaging at the Fe L_3 edge, whilst contrast at the Co L_3 edge is dominated by the other sublattice of CoB layers. Inverted domain structures observed at these two edges with XMCD-STXM are shown in Fig. 1, confirm the SAF ordering of the layers. Current pulses drive domain wall motion, as shown in Fig. 2, with average velocities up to ~ 40 m/s achieved at current densities as low as 3×10^{11} A/m^2. These results demonstrate a low depinning current and fast motion compared to comparable FM multilayers we have previously studied, suggesting that domain walls in SAF heterostructures are superior to their ferromagnetic equivalents for low energy consumption racetrack technologies.

[1] R. A. Duine et al., Nature Phys. 14, 217 (2018) [2] S.-H. Yang et al., Nature Nanotech. 10, 221 (2015)

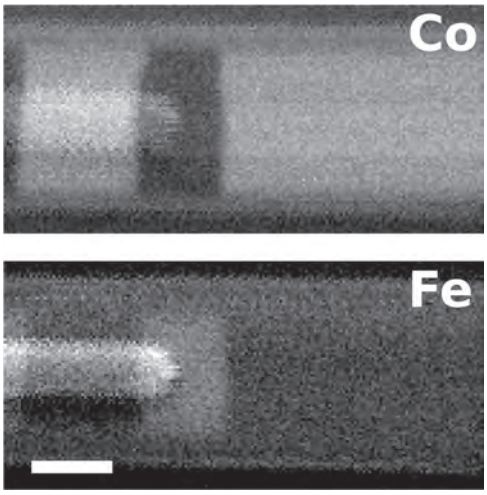

Fig. 1 STXM images acquired at zero field of a domain at the Co and Fe L_3 edges, which probe different sublattices of the SAF. A finger-shaped Cu lead is visible on the left. 1 μm scale bar.

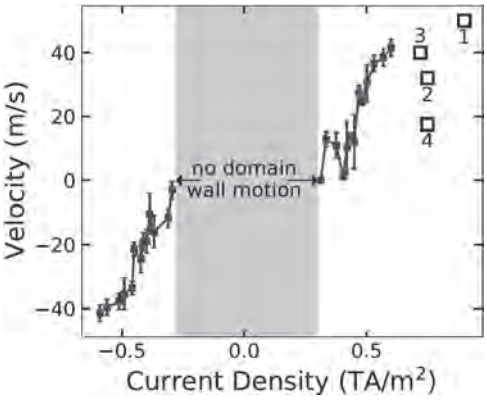

Fig. 2 DW velocity against current density measured using 5 ns current pulses. Points 1-4 relate to measurements in the literature of DW velocities in comparable FM devices.

EPA-12. Large anomalous Hall effect and anisotropic magnetoresistance in intrinsic nanoscale spin-valve-type structure of an antiferromagnet. *K. Jeong*[1], D. Oh[1], J. Kim[1], M. Kim[1], H. Shin[1], J. Hong[1], J. Kim[1], K. Moon[1], N. Lee[1] and Y. Choi[1] *1. Physics, yonsei university, Seoul, The Republic of Korea*

A spin valve is a prototype of spin-based electronic devices found on ferromagnets, in which an antiferromagnet plays a supporting role. Recent findings in antiferromagnetic spintronics show that an antiferromagnetic order in single-phase materials solely governs dynamic transport, and antiferromagnets are considered promising candidates for spintronic technology. In this work, we demonstrated antiferromagnet-based spintronic functionality on an itinerant Ising antiferromagnet of $Ca_{0.9}Sr_{0.1}Co_2As_2$ by integrating nanoscale spin-valve-type structure and investigating anisotropic magnetic properties driven by spin-flips. Multiple stacks of 1 nm thick spin-valve-like unit are intrinsically embedded in the antiferromagnetic spin structure. In the presence of a rotating magnetic field, a new type of the spin-valve-like operation was observed for anisotropic magnetoresistance and large anomalous Hall conductivity, whose effects are maximized above the spin-flip transition. In addition, a joint experimental and theoretical study provides an efficient tool to read out various spin states, which scheme can be useful for implementing extensive spintronic applications.

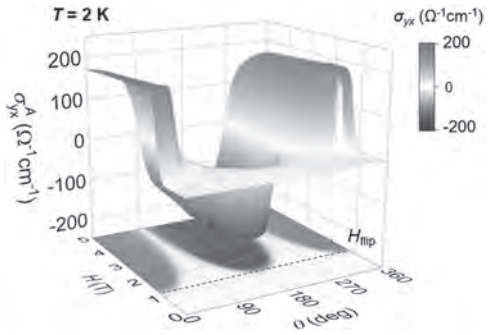

EPA-13. Magnetoresistance in Helical Antiferromagnet Eu Metal Thin Films. *N. Shrestha*[1] and J. Tang[1] *1. Physics and Astronomy, University of Wyoming, Laramie, WY, United States*

Europium (Eu) metal has a body centered cubic crystal structure which, upon a paramagnetic-to-helical magnetic transition, undergoes a body centered tetragonal distortion. The magnetic helix appears below Néel temperature (T_N) of ~90 K, and the presence of a magnetic field gives rise to conical helimagnet [1,2]. We have prepared Eu metal thin films on Si (001) substrates using Eu metal as a target by pulsed laser deposition (PLD). The transport measurement shows the helical antiferromagnetic transition at 88 K, and a thermal hysteresis reveals the first-order nature of the phase transition. We present the magnetoresistance (MR) of Eu thin films when the magnetic field (B) is applied both out-of-plane and in-plane. We found, at temperatures below T_N, the MR is positive whereas above T_N the MR is negative. We also observed the hysteretic oscillation above 30 K and below the Néel temperature. The hysteretic oscillations observed in the MR is believed to be associated with the change in the distribution of the antiferromagnetic domains in Eu caused by the interplay of the applied magnetic field and the strain in the films. This work was supported by NSF (DMR-1710512) and the USDOE (DE-SC0020074)

[1] C. E. Olsen, N. G. Nereson, and G. P. Arnold, J. Appl. Phys., 33, 1135 (1962). [2] N.G. Nereson, C. E. Olsen, and G. P. Arnold, Phys. Rev. 135, A176, (1964).

EPA-14. Tailored non-collinear magnetic structure in 111- and 110-oriented $Mn_4(N,B)$ thin films. *S. Isogami*[1], M. Ohtake[2] and Y. Takahashi[1] *1. National Institute for Materials Science, Tsukuba, Japan; 2. Yokohama National University, Yokohama, Japan*

Transition metal nitrides with ferrimagnetism have recently attracted attention because of their skyrmionic functionalities at room temperature [1,2], and the topological Hall effect (THE) was observed for Mn based transition metal nitrides such as Mn_4N thin films [3,4]. The conventional spin texture for the film is collinear with perpendicular magnetic anistoropy, which is remarkably sensitive to the growing temperature as well as substrate-induced strain [5,6]. Therefore, these characterisitcs of the Mn_4N warrants further study how the spin texture is modulated by the method of elemental doping, and it is our expectation that the turnability of spin textures of the films could allow us to realize possible skyrmionic devices that work under no external magnetic field. In this study, we investigated the THE for the sputter-deposited (111)- and (110)-oriented $Mn_4(N,B)$ films aiming the control of topological spin textures by elemental-doping of B [7]. Figures 1 shows the representative THE for the 111-oriented Mn_4N film without B at 300K. The THE component was extracted from the total AHE component, suggesting the presence of non-coplanar spin texture for the films at room temperature. Figure 2 shows the measurement temperature (T) dependence of $\rho_{xy}^{THE}/\rho_{xy}^{AHE}$ ratio for the films with and without B. The ratio increased at lower T, suggesting the stabilization of non-coplanar spin textrue at lower T. In addition, supression of THE was observed by B for all T. These results show a dilution effect in the spin frustration state with topological spin texture by B. Conversely, slight increase of THE was observed by B in the case of 110-oriented films. Therefore, B in the antiperovskite systems such as Mn_4N could acts as an efficient suppressor or booster of frustrated exchange interactions between Mn atoms.

[1] C. T. Ma, et al., APL. 119, 192406 (2021). [2] T. Bayaraa, et al., PRL. 127, 217204 (2021). [3] G. Wang, et al., APL. 113, 122403 (2018). [4] M. Meng, et al., APL. 112, 132402 (2018). [5] S. Isogami, et al., JMMM, in press (2022). [6] T. Hirose, et al., AIP Adv. 10, 025117 (2020); [7] S. Isogami, et al., JAP. 131, 073904 (2022).

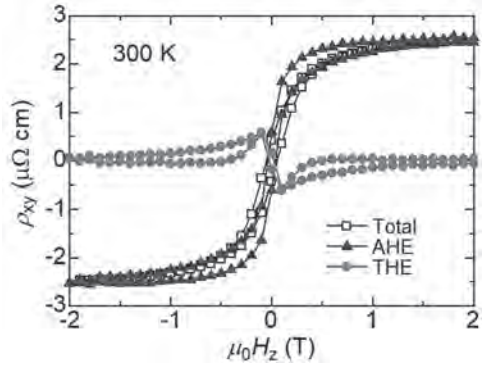

Fig. 1 Extraction of the anomalous and topological Hall resistivity from the total transverse Hall resistivity (ρ_{xy}) for the (111)-oriented Mn_4N films with B-doping measured at 300 K.

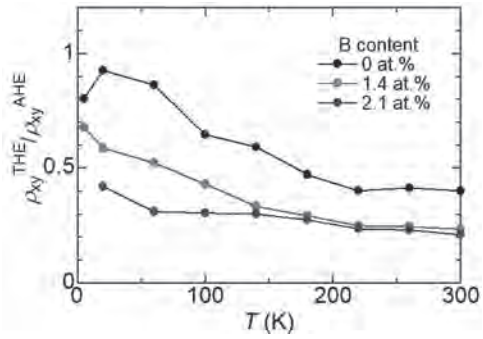

Fig. 2 Temperature (T) dependence of the topological Hall amplitude ($\rho_{xy}^{THE}/\rho_{xy}^{AHE}$ ratio) for the (111)-oriented Mn_4N films without (black) and with B-doping of 1.4 at. % (red) and 2.1 at. % (blue).

EPA-15. Characterization of laser pulse-induced quenching of resistivity of antiferromagnetic CuMnAs. *A. Farkaš*[1,2], K. Olejník[1], M. Surýnek[2], P. Němec[2], V. Novák[1] and T. Jungwirth[1] *1. FZU - Institute of Physics of the Czech Academy of Sciences, Prague, Czechia; 2. Faculty of Mathematics and Physics, Charles University, Prague, Czechia*

Antiferromagnetic materials opened up a new avenue of research with potential use in spintronic devices [1]. Compared to their ferromagnetic counterparts antiferromagnets exhibit faster dynamics, insensitivity to the external magnetic fields, and absence of stray fields promising higher integration density. Some functionalities of the antiferromagnetic spintronic devices such as readout using anisotropic magnetoresistance or reorientation of magnetic axis using current-induced spin-orbit torque [2] are directly derived from their ferromagnetic counterparts whereas other functionalities are unique to the antiferromagnets. One of these is the Quenching of the antiferromagnet into high resistivity states using electrical and optical pulses which was recently discovered in epitaxially grown thin CuMnAs films [3]. This effect is based on the change of the magnetic structure of the antiferromagnet induced by the application of high energy pulse driving the system to the vicinity of Néel temperature and its subsequent fast cooling resulting in quenching of the highly resistive disordered magnetic state. The observed changes of resistivity reach tens of percent at room temperature and even 100 percent at low temperatures and exceed by two orders of magnitude the

change of the resistivity based on anisotropic magnetoresistance induced by the reorientation of the spin axis [2]. In this contribution, we provide an overview of detailed experimental characterization of quenching of CuMnAs using a single ultrashort laser pulse for excitation. We focus on the optimization of the electrical readout response of the Hall-bar devices with regard to the size and position (Fig.1) of the laser spot, pulse length, and fluency. It provides an overview of the response for CuMnAs films with varying thickness and substrate material. Lastly, this contribution evaluates the effects of permanent damage caused by laser pulse excitation with proposed damage mitigation techniques.

[1] Jungwirth, T., Marti, X., Wadley, P. *et al.* Antiferromagnetic spintronics. *Nature Nanotech* 11, 231–241 (2016). https://doi.org/10.1038/nnano.2016.18 [2] Wadley, P. et al. Electrical switching of an antiferromagnet. Science 351, 587–590 (2016). https://doi.org/10.1126/science.aab1031 [3] Kašpar, Z., Surýnek, M., Zubáč, J. *et al.* Quenching of an antiferromagnet into high resistivity states using electrical or ultrashort optical pulses. *Nat Electron* 4, 30–37 (2021). https://doi.org/10.1038/s41928-020-00506-4

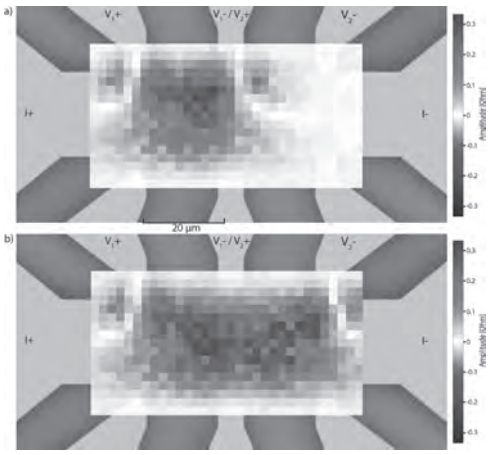

Fig. 1: Quench switching signal as function of the writing spot position on the Hall-bar device in a) single-square geometry (V1) and b) two-square geometry (V1+V2).

Session EPB
SKYRMIONS AND SPIN-ORBITRONICS (Poster Session)

Yue Li, Chair
Argonne National Laboratory, Downers Grove, IL, United States

EPB-01. Zero-field room-temperature skyrmion lattice stabilized by bias layer coupling in magnetic multilayers. *F. Ajejas*[1,2], Y. Sassi[2], W. Legrand[2], S. Collin[2], K. Bouzehouane[2], A. Vecchiola[2], A. Fert[2], N. Reyren[2] and V. Cros[2] *1. Physics, University of California, San Diego, San Diego, CA, United States; 2. Unité Mixte de Physic CNRS/Thales, Palaiseau, France*

Room-temperature skyrmions have been presented as potential candidates for encoding information bits in several types of new spintronic devices [1]. There have been many recent progresses allowing to stabilize sub-100 nm skyrmions at room temperature in crystalline ferromagnetic thick layers or in (amorphous) thin magnetic multilayers (MML) [2]. In most case, at least in extended films or large structures, the application of relatively large perpendicular field (a few 10 mT) is needed which might be unfavorable for most of the anticipated skyrmion based devices. Hence, the stabilization of zero-field isolated skyrmions or skyrmion lattices is an important step towards application. There are recent works demonstrating isolated zero-field skyrmions stabilized due to interlayer exchange in polycrystalline [3], epitaxial [4] or exchange biased [5] trilayers. Here we demonstrate a new approach showing that room-temperature zero-field skyrmion lattices can be stabilized in MML. We develop a system in which perpendicular magnetic anisotropy, chiral order and bias field strength, through a non-magnetic spacer, can be adjusted simultaneously. Typical stacking sequence is schematically presented in Figure 1 (a). The samples have been characterized first by standard magnetometry (Fig. 1b). Relying on the interlayer electronic coupling to an adjacent bias magnetic layer with strong perpendicular magnetic anisotropy (uniform configuration), we demonstrate by Magnetic Force Microscopy that the remnant wormy-stripe "as-grown" domains (Fig. 1d) can be turned into skyrmion lattice phase (Fig. 1c). The skyrmion density and size can be modified by finely tuning the thicknesses of the layers allowing the control of the parameters related in the stabilization of the lattices. ANR TOPSKY (ANR-17-CE24-0025), DARPA TEE program (MIPR#HR0011831554) and EU SKYTOP (H2020 FET Proactive 824123) are acknowledged for financial support.

[1] A. Fert, N. Reyren, V. Cros, Nat. Rev. Mat. 2, 17031 (2017) [2] C. Moreau-Luchaire *et al.*, Nat. Nanotechnol. 11, 444 (2016) [3] G. Chen *et al*., Appl. Phys. Lett. 106, 242404 (2015) [4] R. Loconte *et al*., doi : 10.1021/acs.nanolett.0c00137 [5] K. G. Rana *et al*., Phys. Rev. Applied 13, 044079 (2020)

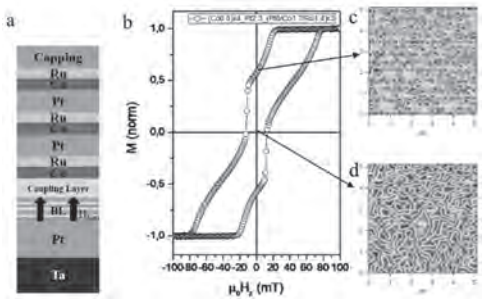

Figure 1: a) Scheme of Bias-FM MML. b) Alternating gradient force magnetometry hysteresis loops of Bias-FM MML. c) 5x5 µm magnetic force microscopy (MFM) image at remanence after the saturation presenting skyrmion lattice. d) 5x5 µm MFM image at "as-grown" state, presenting "wormy" stripe domains.

EPB-02. In-field critical behaviour of β-Mn type $Co_7Zn_7Mn_6$ skyrmion host. *P. Yadav*[1], Y. Bitla[2], A. Kumar Patra[2] and G. Basheed[1] *1. CSIR National Physical Laboratory, New Delhi, India; 2. Department of Physics, Central University of Rajasthan, Ajmer, India*

Magnetic skyrmions is a vortex like nanosized spin swirling texture with particle like property [1]. In the past decade, magnetic skyrmion has triggered great interest as component in futuristic magnetic memory devices due to its topological property, smaller size (few nm) and efficient current driven motion. The chiral cubic β-Mn type $(Co_{0.5}Zn_{0.5})_{20-x}Mn_x$ ($3 \le x \le 7$) alloys are fascinating as they allow the fine tuning of size and stability of skyrmions in wide temperature range with composition [2]. Among $(Co_{0.5}Zn_{0.5})_{20-x}Mn_x$ alloys, magnetic properties of the $Co_7Zn_7Mn_6$ alloy are of renewed interest due to the detection of two independent skyrmion phases (SkX): (i) a conventional thermodynamically stable SkX below helimagnetic to paramagnetic transition temperature ($T_C \sim 213$ K) and (ii) a disordered skyrmion phase above spin glass transition ($T_g \sim 23$ K) [3-4]. In spite of much progress made on the investigation of exotic magnetic field-temperature phase diagram of $Co_7Zn_7Mn_6$ helimagnet, the nature of its underlying magnetic interactions still remains elusive. Thus an elaborate in-field critical behavior study of skyrmion hosting polycrystalline cubic β-Mn type $Co_7Zn_7Mn_6$ chiral magnet based on magnetic isotherms measured in the vicinity of ordering temperature is presented. The critical exponents β, γ and δ for spontaneous magnetization, initial magnetic susceptibility and critical M-H isotherm, respectively are evaluated through the modified Arrott plot, Kouvel-Fisher method and critical isotherm analysis. The estimated critical exponents $\beta = 0.382(1)$, $\gamma = 1.386(2)$ and $\delta = 4.628(1)$ follow Widom equality and magnetic scaling equations of state. The values of these exponents corroborate that the critical behaviour of $Co_7Zn_7Mn_6$ system is akin to that of three-dimensional (3D) isotropic nearest-neighbour Heisenberg ferromagnet in which the attractive extended type short-range interactions between spins decay with distance r as $J(r) \sim r^{-4.94}$.

1. S. Mühlbauer, B. Binz, F. Jonietz, Science 323, 915 (2009) 2. Y. Tokunaga, X. Yu, J. White, Nat. Commun. 6 (1) 1–7 (2015) 3. K. Karube, J. S. White, D. Morikawa, Sci. Adv. 4 (9) eaar7043 (2018) 4. V. Ukleev, K. Karube, P. Derlet, npj Quant. Mater. 6 (1) 1–8 (2021)

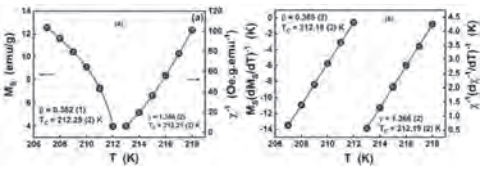

Fig.1(a): (a) The temperature dependence of spontaneous magnetization, M_S (T, 0) and the inverse initial susceptibility χ^{-1}(T), along with power law fits (solid curves). (b) The temperature dependence of M_S $(dM_S/dT)^{-1}$(T) and (d χ^{-1} /dT)$^{-1}$(T) along with linear fits (solid line).

EPB-03. Effects of self-torque in rare earth-transition metal alloy on the magnetization switching by spin-orbit torque. *P. Lee*[1], C. Huang[1], S. Mangin[2] and C. Lai[1] *1. Materials Science and Engineering, National Tsing Hua University, Hsinchu, Taiwan; 2. Institute Jean Lamour, Nancy, France*

We investigated the spin-orbit torque (SOT) switching of the single CoTb layer with or without the heavy metals (Pt and W) in different thicknesses to identify the self-torque effects generated in the CoTb layer. The generation of self-torque heavily depends on the thickness of CoTb. The SOT switching was not observed for a single CoTb layer with 3nm in thickness, suggesting self-torque may be quite weak in a very thin film. A deterministic SOT switching can be obtained for a single 9 nm CoTb layer. The amplitude of the self-torque generated in CoTb is comparable to the Pt/Co case with the same switching polarity as the Pt/Co one. When 3 nm CoTb has deposited on Pt or W underlayer, the J_c is smaller in W/CoTb than that of Pt/CoTb, which can be attributable to a high spin hall angle of W and negligible self-torque of CoTb. On the other hand, when the CoTb is increased to 9 nm, the J_c of W/CoTb is significantly increased and becomes higher than that of Pt/CoTb. The enhanced J_c of W/CoTb may result from the opposite sign of spin-orbit torque generated in W and CoTb. Since the self-torque generated in 9 nm CoTb becomes substantial, the competition of spin-orbit torque between W and CoTb occurs, leading to a high J_c. We define the switching efficiency $\eta=(2H_k^2-H_x^2)^{1/2}*M_st/J_c$ based on the macrospin model [1], in which H_k and H_x are anisotropy field and applied magnetic field along the x-direction. The variations of η with the layer structure are shown in Table 1. The addition of SOT from Pt and self-torque from CoTb leads to enhanced switching efficiency when the thickness of CoTb is increased. On the other hand, the competition of SOT from W and self-torque in TbCo of W/CoTb devices was revealed by increasing the thickness of CoTb. We further confirm this interplay by reversing the stack order, that is, CoTb/W, in which the efficiency is substantially enhanced.

1 T. Taniguchi, S. Mitani, and M. Hayashi, Physical Review B., Vol.92, 024428 (2015).

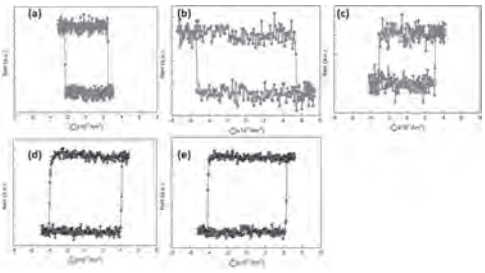

Fig.1: SOT switching curves for (a) W/CoTb 3nm (b) W/CoTb 9nm, (c) CoTb 9nm/W, (d) Pt/CoTb 3nm, and (e) Pt/CoTb 9nm.

Layer Structure	Pt/Co/AlOx	Pt/CoTb 3nm	Pt/CoTb 9nm	W/CoTb 3nm	W/CoTb 9nm	CoTb 9nm/W
SOT switching efficiency ($\times10^{-15}$emuOe/Acm^2)	1.54	2.55	5.67	4.44	3.96	6.82

Table. 1: SOT switching efficiency for various layer structures.

EPB-04. Asymmetric Pt/Co magnetic multilayers bubble expansion under in-plane and out-of-plane field. *S. Amara*[1], A. Ganguly[2], D. Khan[1], G. Das[2] and Y. Massoud[1] *1. Computer, Electrical and Mathematical Sciences and Engineering, King Abdullah University of Science and Technology, Thuwal, Saudi Arabia; 2. Khalifa University, Abu Dhabi, United Arab Emirates*

Magnetic multilayers are material systems that offer a high degree of tunability with respect to their magnetic and electronic properties. These are essential for today's spintronics and magnonics-based magnetic applications [1], [2]. The Dzyaloshinskii-Moriya interaction (DMI) [3] is one of the interesting phenomena in such multilayers that give rise to the presence of magnetic skyrmions under certain conditions even at room temperature. Pt/Co is one of the most promising classes of the multilayers that contributes to a significant DMI due to the different characters of Pt/Co and Co/Pt interfaces [4]. The performance of the films may vary depending on the substrates, deposition temperature, layer thickness, and other factors in the Pt/Co multilayers. The thermal stability can be significantly increased and the magnetic anisotropy of Pt/Co multilayers can be controlled by adding spacer layers between two Co layers [5]. In our study, we investigate magnetic bubbles in Pt/Co-based multilayer thin films. The bubbles have been expanded using an external magnetic field both in-plane and out-of-plane. In presence of the in-plane field, bubbles expand asymmetrically as observed in Fig.1(a). The in-plane field-dependent velocities of two opposite chiral domain walls are measured as shown in Fig. 1(b). The asymmetry of bubble expansion is found to be influenced by the thickness of Co which gives us information about the intrinsic chiral properties of the system. Mumax simulations are performed to understand underlying behavior. The study is important for race track memory applications.

[1]. R. E. Camley, and R. L. Stamps, "Magnetic multilayers: spin configurations, excitations, and giant magnetoresistance," *Journal of Physics: Condensed Matter,* vol. 5, no. 23, 1993. [2]. E. Y. Vedmedenko, R. K. Kawakami, D. D. Sheka, P. Gambardella, A. Kirilyukand, A. Hirohata, C. Binek, O. Chubykalo-Fesenko, S. Sanvito, and B. J. Kirby, "The 2020 magnetism roadmap," *Journal of Physics D: Applied Physics,* vol. 53, no. 45, 2020. [3]. T. Moriya, "Anisotropic Superexchange Interaction and Weak Ferromagnetism," *Phys. Rev,* 1960. [4]. A. W. J. Wells, P. M. Shepley, C. H. Marrows, and T. A. Moore, "Effect of interfacial intermixing on the Dzyaloshinskii-Moriya interaction in Pt/Co/Pt," *Phys. Rev. B,* vol. 95, 2017. [5]. S. Eimer, H. Cheng, J. Li, and X. Zhang, "Perpendicular magnetic anisotropy based spintronics devices in Pt/Co stacks under different hard and flexible substrates," *Science China. Information Sciences,* 2021.

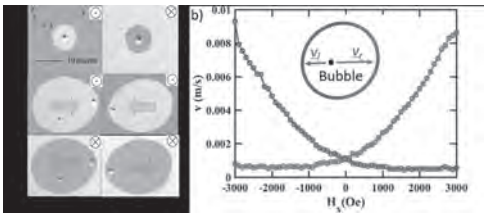

Fig. 1. (a) Bubble expansion under various field configurations, blue arrow indicates in-plane field while out of plane field indicated in the top right corner of each image. (b) Velocities of left and right domain walls as a function of in-plane field.

EPB-05. Magnetic skyrmion nucleation via current injection in confined nanowire with modified perpendicular anisotropy region.
Z. Chen[1], *G. Yu*[1], X. He[1], X. Cai[1], M. Zhu[1], Y. Qiu[1] and H. Zhou[1] *1. China Jiliang University, Hangzhou, China*

Magnetic skyrmion, as one of the topologically protected spin textures stabilized in the materials with perpendicular magnetic anisotropy (PMA) and interfacial Dzyaloshinskii-Moriya interaction (iDMI), are quite small in the nanometer size and can be driven by spin torque with lower current density, which provide a reliable technique for use in next-generation racetrack memory, logical devices, spin transfer nano-oscillator, etc. Magnetic skyrmion in the above applications are mainly based on the controllable motion of skyrmions in the confined geometrics. Furthermore, a controllable, reproducible, and realized skyrmion nucleation is another most important elements in such skyrmion-based devices. Several researchers have proposed and demonstrated skyrmion nucleation schemes, such as, patterning the magnetic structures with notches or defects, domain wall transfer or chopping to skyrmions. However, all these methods include significant structural or even geometrical modifications of the magnetic racetrack which increasing the devices design complexity. Recently works have shown that sputtering process can control magnetic properties, such as PMA and DMI, at the nanoscale. In this work, we adopted a nanoregion without PMA as a skyrmion nucleation core and demonstrate a current driven highly efficient, in-line and on-demand skyrmion nucleation schematic. Fig. 1(a) shows an illustration of skyrmion nucleation devices considered here. One key factor for realizing this is that the vanishing of the PMA and the existing of the DMI induced magnetization tilt and create a chiral perpendicular stripe domain wall at left edges. This stripe domain wall that allows spin torque to efficiently controlled and ejected from the modified region and propelled into the nanowire to form a skyrmion. As shown in Fig. 1(b), this device integrated both skyrmion nucleation and control function is more advantages in simply the devices with two terminals. This working mode could be controlled by the selective current pulse sequence with one for nucleation and another one for shifting which is important to skyrmion-based racetrack memory applications.

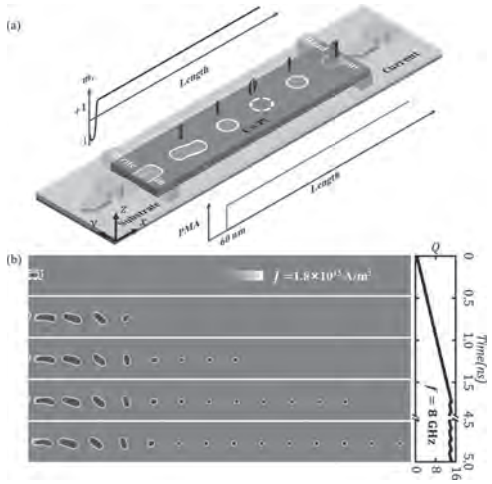

Fig. 1 (a) Schematic diagram of the devices, and (b) simulation results.

EPB-06. Magnetization-independent field-free spin-orbit torque switching in Py-based magnetic trilayer. *W. Liao*[1], T. Chen[1], T. Tsai[1], C. Huang[1], Y. Huang[1], Y. Lin[1], H. Yen[1] and C. Pai[1] *1. National Taiwan University, Taipei, Taiwan*

Realizing deterministic current-induced spin-orbit torque (SOT) switching in magnetic heterostructures having perpendicular anisotropy typically relies on symmetry breaking in the structure [1-6]. Several mechanisms have been adopted, such as wedged deposition [1], tilting the magnetization [2], and combining an antiferromagnet [3]. In addition to structural engineering, introducing an additional in-plane magnetized magnetic layer can also achieve field-free SOT switching by either interlayer exchange coupling [4], spin anomalous Hall effect [5], or the interfacial spin-orbit precession effect [6]. One of the most notable features in these magnetization dependent mechanisms is their bipolar nature, *i.e.*, the current-induced SOT switching polarity can be reversed by reversing the magnetization direction of the additional in-plane magnetic layer. In this work, we show that in some rare cases, the in-plane magnetic layer could lead to a magnetization-independent SOT switching with a unipolar nature. The heterostructure is a permalloy ($Ni_{80}Fe_{20}$, Py)-based magnetic trilayer, which is uniformly deposited by conventional magnetron sputtering. An unconventional zero-field current-induced effective field can be observed and field-free switching independent of the Py magnetization is realized in such trilayer device. Our findings suggest a new field-free SOT switching mechanism that is more related to the structural properties of the additional magnetic layer than its magnetic properties, in sharp contrast to traditional belief and previous reports.

[1] Yu G.*, et al*. Switching of perpendicular magnetization by spin-orbit torques in the absence of external magnetic fields. *Nat. Nanotechnol.* 9, 548-554 (2014). [2] You L.*, et al.* Switching of perpendicularly polarized nanomagnets with spin orbit torque without an external magnetic field by engineering a tilted anisotropy. *Proc. Natl. Acad. Sci. U.S.A.* 112, 10310 (2015). [3] Fukami S., Zhang C., DuttaGupta S., Kurenkov A., Ohno H. Magnetization switching by spin-orbit torque in an antiferromagnet-ferromagnet bilayer system. *Nat. Mater.* 15, 535-541 (2016). [4] Lau Y. C., Betto D., Rode K., Coey J. M., Stamenov P. Spin-orbit torque switching without an external field using interlayer exchange coupling. *Nat. Nanotechnol.* 11, 758-762 (2016). [5] Taniguchi T., Grollier J., Stiles M. D. Spin-transfer torques generated by the anomalous Hall effect and anisotropic magnetoresistance. *Phys. Rev. Appl.* 3, 044001 (2015). [6] Baek S. C.*, et al.* Spin currents and spin-orbit torques in ferromagnetic trilayers. *Nat. Mater.* 17, 509-513 (2018).

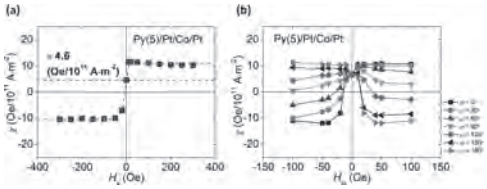

Figure 1 (a) Current-induced effective field (χ) as a function of H_x. (b) χ as a function of in-plane field (H_{in}) with different ϕ. ϕ represents the angle between applied currents and external in-plane field.

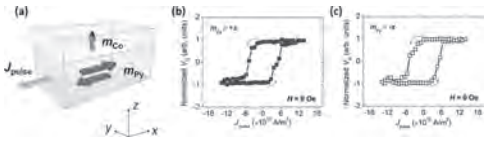

Figure 2 (a) Illustration of field-free switching with Py magnetization (m_{Py}) is initialized along ±*x*. Field-free switching results with Py magnetization parallel to (b) +*x* and (c) -*x*.

EPB-07. Rotator Gates for Six-state Boolean Spin Logic - Six state Rotation, half-Compliment, complimentary logic gates using Spin orbit Effect. *M. Isaacs*[1], A. Xu[1], V. Singh[1], H. Ketineni[1], A. Shakya[1], A. Iyer[1] and S. Manipatruni[1,2] *1. Feynman Physics Academy, Portland, OR, United States; 2. Cornell University, Ithaca, NY, United States*

Spin state of currents and magnets offers a unique ability to store, transport and process information in vector boolean states leading to extreme density of memory and logic [1]. We propose and demonstrate basic vector logic manipulation with six state magnetic and spin currents utilizing spin orbit effect in a reservoir gate. Recently investigated bulk spin orbit coupling (SOC) effects [2,3,4] hold a special solution to this complex logic problem due to the vector phenemenology of spin orbit interaction. We propose three critical gates for GF-n state logic [5, 6], known as inversion gate, and rotation gates (rotation around X axis, Y-axis and Z-axis) using the

combination of spin torque switching and spin orbit switching. 6-state memory can increase magnetic memory density of an n-bit word by 3^n, leading to extreme density of memory and logic for future AI and high-performance applications. For example, an 8-bit, 1GB MRAM can be converted into a 6.5TB MRAM with the use of six state signal manipulation. When utilised the complete informaton density of six-state logic can extend the Moore's law for many generations by improving coding [7] and information density [8,9] without needing extreme lithography and materials scaling.

[1] Manipatruni, S., et al 2018. Beyond CMOS computing with spin and polarization. *Nature Physics*, *14*(4), pp.338-343. [2] Witczak-Krempa, W., et al 2013. Correlated quantum phenomena in the strong spin-orbit regime. *arXiv preprint arXiv:1305.2193*. Vancouver [3] Everhardt, A.S., et al 2019. Tunable charge to spin conversion in strontium iridate thin films. *Physical Review Materials*, *3*(5), p.051201. [4] Zhu, L., et al 2021. Unveiling the Mechanism of Bulk Spin Orbit Torques within Chemically Disordered FePt Single Layers. *Advanced Functional Materials*, *31*(36), p.2103898. [5] Ellison, J.T., 1972. *Universal function theory and Galois logic studies*. SPERRY RAND CORP ST PAUL MN UNIVAC DEFENSE SYSTEMS DIV. AD0740849.pdf (dtic.mil) [6] Jain, S.K., Song, L. and Parhi, K.K., 1998. Efficient semisystolic architectures for finite-field arithmetic. *IEEE Transactions on Very Large Scale Integration (VLSI) Systems*, *6*(1), pp.101-113. [7] Benvenuto, C.J., 2012. Galois field in cryptography. *University of Washington*, *1*(1), pp.1-11. [8] Lloyd, S., 2000. Ultimate physical limits to computation. *Nature*, *406*(6799), pp.1047-1054. [9] Krauss, L.M. et al 2004. Universal limits on computation. *arXiv preprint astro-ph/0404510*.

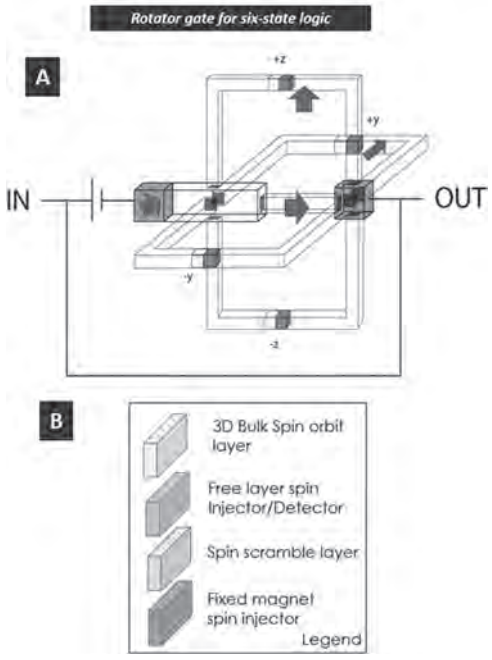

[A] Rotator gate for six state vector logic. Three rotator gates exist for rotation around X axis, Y-Axis, Z-axis [B] Material legend assumed for creating a rotator gate for siz state vector logic. Spin is injected in the X-direction with spin polarization along X, Y or Z directions producing charge voltage that is used to switch the output via a spin current.

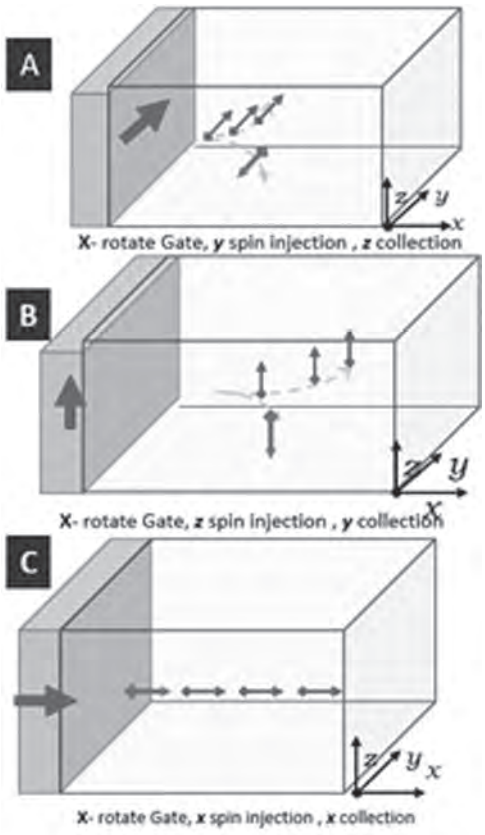

Gate-Type	Input	output
X-Rotate	+/- y	+/- z
	+/- z	-/+ y
	+/- x	+/- x
Y-Rotate	+/- z	+/- x
	+/- x	-/+ z
	+/- y	+/- y
Z-Rotate	+/- x	+/- y
	+/- y	-/+ x
	+/- z	+/-z

Operating principle for spin rotation gate (half complement gate) shown with spin injection with current vector along x direction, with [A] spin orientation along y-direction, injection current along x and collection along z [B] spin orientation along z-direction, injection along x-direction and collection along y [C] spin orientation along x-direction, injection along x-direction and collection along x direction are shown. Truth table for rotation gates for six state logic is shown in the table

EPB-08. Spin-orbit torque driven in-homogeneous spin configuration dependent energy in laterally asymmetric perpendicular magnetic anisotropy system. *S. An*[1], H. Seo[1], E. Baek[1], K. Lee[1], S. Lee[1], M. Park[1], D. Kim[1], J. Kim[1] and C. You[1] *1. DGIST, Daegu, The Republic of Korea*

Chirality is one of important research topics in the diverse field because it leads interesting phenomena.[1] Since the chirality by the inversion symmetry breaking has been observed in magnetic ordered system,[2] researches on asymmetric exchange coupling was actively investigated. [3] Here, the chirality is known as affecting to the dynamic and static

phenomena, so it can be one approach that influence on the magnetization state as well. But for understanding the role of chirality deeply, it is necessary to control the chirality as a unique variable while keeping other materials parameters. However, controlling only the chirality is limited because it is determined from the materials and structural origins in general, affecting other parameters simultaneously. Therefore, more consideration is still required for revealing the role of chirality deeply. For understanding the chirality precisely, we prepared the lateral perpendicular magnetic anisotropy (PMA) symmetry breaking system. In this system, magnetizations of each PMA react differently by the SOT, which results in in-homogeneous spin configuration (i-hSC). Here, notable point is that i-hSC can induce different system energy when it is combined with interfacial Dzyaloshinskii-Moriya interaction (DMI) as seen in Fig. 1. The effect of i-hSC can be confirmed experimentally by measuring magnetization switching because the chirality reversal also occurs simultaneously (clockwise (CW) ↔ counter-clockwise (CCW)). Here, because more (less) energy should be required for switching the stabilized (destabilized) i-hSC, opposite directional shift of hysteresis loop is shown as seen in Fig. 2. The resultant degree of shift is directly related with the system energy variation, and our experimental analysis suggests the possibility of the chirality as one method determining the magnetization state.

F. Evers, A. Aharony, N. Bar-Gill, Advanced Materials, Vol.34, p.2106629 (2022) M. Bode, M. Heide, K. von Bergmann, Nature, Vol.447, p.190-193 (2007) S.-H. Yang, R. Naaman, Y. Paltiel, Nature Reviews Physics, Vol.3, p.328-343 (2021)

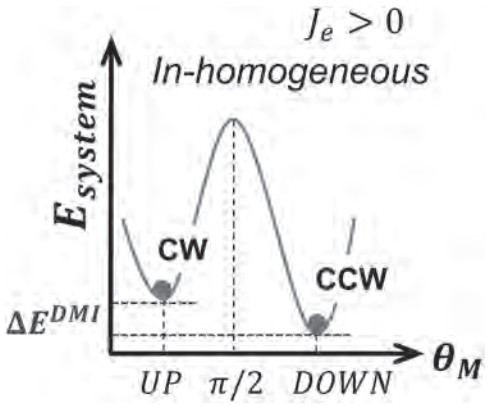

Fig. 1. Energy diagram of magnetization at homogeneous and in-homogeneous spin system. Here, current direction determines the direction of SOT, resulting in different directional i-hSC.

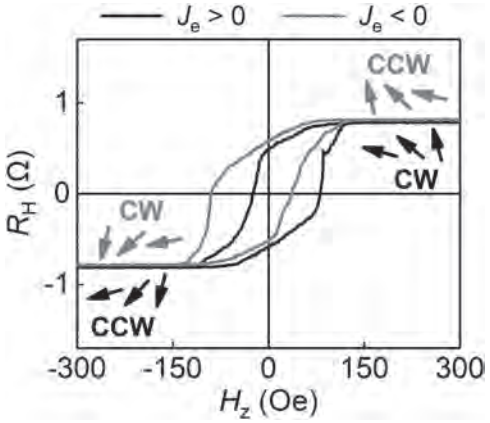

Fig. 2. Current direction dependent hysteresis loop shift with i-hSC. Each type of i-hSC is indicated as black and red arrows.

EPB-09. Logic devices based on gate-controlled skyrmion trajectory. *B. Paikaray*[1], M. Kuchibhotla[2], A. Haldar[2] and C. Murapaka[1] *1. Department of Materials Science and Metallurgical Engineering, Indian Institute of Technology Hyderabad, Sangareddy, India; 2. Department of Physics, Indian Institute of Technology Hyderabad, Sangareddy, India*

Skyrmion based logic devices are found to be promising for next-generation energy-efficient, high speed information processing technologies owing to the compact size and topologically protected spin texture of the skyrmions [1,2]. Skyrmions are nano-scale swirling spin textures with topological protection that exhibit particle-like behaviour. In this work, we exploit skyrmion for various logic operations using a Gate to locally alter the magnetic properties that control the skyrmion motion in the logic device using micromagnetic simulation. For example, we have shown the OR and AND logic operations in a single device by flowing current through a metallic gate and the resultant Oersted field (H_{Oe}) controls the skyrmion trajectory (Fig. 1(a)). The H_{Oe} generated near the *Gate* is one of the efficient ways to realize the logic operations [3]. By simply switching OFF and ON the current at the metallic gate, we can toggle between OR & AND logic operations (Fig. 1(b & c)), respectively. The binary information is denoted by the presence and absence of the skyrmion as "1" and "0", respectively. Fig. 1(d) shows the realization of the AND logic for a specific combination of skyrmion driving current density (j) and H_{Oe}. The logic functions are implemented in the device structure by virtue of several physical effects on skyrmion motion such as spin-orbit torque, skyrmion-edge repulsion, skyrmion-skyrmion topological repulsion and skyrmion Hall effect. To understand the motion of the skyrmions and stability, we estimated the Skyrmion Hall angle. The performance of the logic device is studied by varying the material and geometrical parameters. In this presentation, we would like to explain various logic operations including a majority logic device based on skyrmions with different *Gate* operation schemes and novel logic device architectures for computation. The results are interesting for next generation energy-efficient and high-density computing technologies.

[1] A. Fert, V. Cros, and J. Sampaio, Nature Nanotechnology 8, 152 (2013). [2] Luo S., Y. Long, APL Materials 9, 050901 (2021). [3] B. Paikaray, M. Kuchibhotla, A. Haldar, and C. Murapaka, ACS Applied Electronic Materials 4, 2290-2297, (2022).

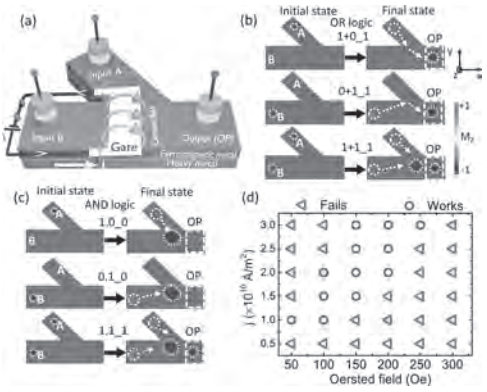

Fig. 1 (a) Schematic of the reconfigurable skyrmion based logic device with two inputs (A, B) and one output (OP). Initial and final magnetic states of logic (b) OR and (c) AND operations (d) Working window of the AND logic operation as a function of H_{Oe} and the j.

EPB-10. Observation of non-local orbital transport and sign reversal of damping-like torque in Nb/Ni and Ta/Ni bi-layers. *S. Dutta*[1] and A. Tulapurkar[1] *1. Electrical Engineering, Indian Institute of Technology Bombay, Mumbai, India*

We study the efficiencies of damping-like torque in Nb/Ni and Ta/Ni bilayers by the spin-torque ferromagnetic resonance (ST-FMR) technique[1] and compare it with Nb/$Ni_{81}Fe_{19}$(Py) and Ta/Py as a function of the thickness of ferromagnet. In both these systems, we observe that the sign of

the damping-like torque is negative for the Nb/Py and it is positive for the Nb/Ni system suggesting two competing mechanisms responsible for the torque on the magnet: (1) spin-current generated from the bulk of Nb and Ta due to spin Hall effect (SHE) producing the spin-orbit torques that are predicted to have a negative sign[1] and (2) orbital current[2,3] generated from the bulk of Nb and Ta which convert into the spin-current while entering in the ferromagnet due to the spin-orbit coupling of the ferromagnet which is predicted to produce an orbital-torque with the positive sign[4,5]. In Ta/Ni and Nb/Ni bilayers, the orbital current is dominant as Ni is predicted to be a good detector of the orbital current as compared to Py resulting in the sign reversal of the damping-like torque efficiency in Ta/Ni and Nb/Ni bilayers as compared to Ta/Py and Nb/Py samples. We further inserted a Cu spacer between the non-magnet and Ni that still shows the positive sign of the damping-like torque suggesting a generation of the orbital current from the bulk of Ta and Nb. Generation of orbital torque will open up new possibilities to manipulate the magnetization more efficiently[6].

[1] L. Liu, C.-F. Pai, Y. Li, H.W. Tseng, D.C. Ralph, and R.A. Buhrman, Science (80-.). 336, 555 (2012). [2] T. Tanaka, H. Kontani, M. Naito, T. Naito, D.S. Hirashima, K. Yamada, and J. Inoue, Phys. Rev. B 77, 165117 (2008). [3] D. Go, D. Jo, C. Kim, and H. Lee, Phys. Rev. Lett. 121, 86602 (2018). [4] D. Go, F. Freimuth, J.-P. Hanke, F. Xue, O. Gomonay, K.-J. Lee, S. Blügel, P.M. Haney, H.-W. Lee, and Y. Mokrousov, Phys. Rev. Res. 2, 033401 (2020). [5] D. Go and H.-W. Lee, Phys. Rev. Res. 2, 013177 (2020). [6] D. Go, D. Jo, H.-W. Lee, M. Kläui, and Y. Mokrousov, EPL (Europhysics Lett. 135, 37001 (2021).

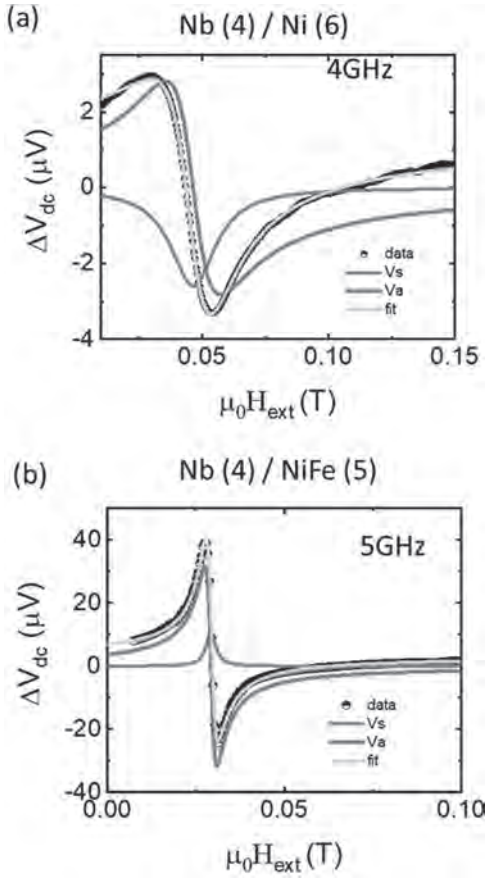

Experimentally observed ST-FMR voltage (black squares) for Nb/Ni (a), Nb/Py (b), fit by the symmetric (blue curve) and anti-symmetric Lorentzian (magenta) to quantify the in-plane damping like torque and out-of-plane field like torque efficiencies respectively.

EPB-11. Measurement of Orthogonal Spin-orbit Field Current along the [010] Crystallographic Direction in GaMnAs Film. *K. Han*[1], K. Lee[1], S. Lee[1], X. Liu[2], M. Dobrowolska[2] and J. Furdyna[2] *1. Department of Physics, Korea University, Seoul, The Republic of Korea; 2. Department of Physics, University of Notre Dame, Notre Dame, IN, United States*

We investigated orthogonal spin-orbit-induced (SOI) fields generated by a current along the [010] crystallographic direction in a ferromagnetic semiconductor GaMnAs film with 4-fold in-plane magnetic anisotropy. To perforem this study, we fabricated a Hall device aligned with the [010] direction, and carried out magnetoresistance (MR) measurements to monitor the magnetization reversal process in the film. Field scans of MR measured with opposite current polarities (Fig. 1(a)) clearly show shifts in opposite direction, indicating the presence of current-direction-dependent effective magnetic fields. The observed hysteresis shift is caused by the simultaneous presence of Dresselhaus and Rashba SOI fields that are perpendicular to each other when the current is oriented along the [010] direction. In order to quantify the two SOI fields, we performed angle-dependent MR measurements with two opposite current polarities (Fig. 1(b)). The splitting in transition angles between the two polarities increases with decreasing magnetic field. The equation relating this splitting and the applied external field was developed based on magnetic free energy that includes the effect of the two orthogonal SOI fields. Based on this formulation, we were able to obtain the magnitudes of the Rashba and Dresselhaus SOI fields from the magnetization transition angles as 0.568 and 1.632 Oe, respectively, at current density of 4.80×10^5 A/cm^2 (2mA).

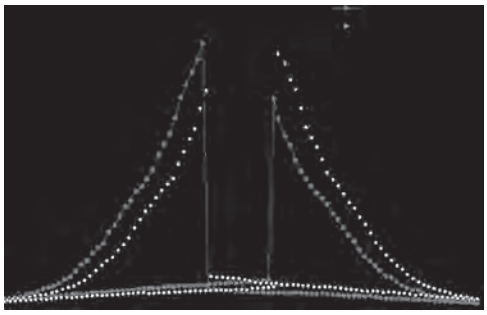

Fig. 1 Field scan (a) and angle scan (b) hysteresis measured with positive and negative currents at current density of 6.01×10^5 A/cm^2 (2.5 mA) and 4.80×10^5 A/cm^2 (2.0 mA), respectively, as magnetization reverses. Both data clearly show a hysteresis shift between two current polarities.

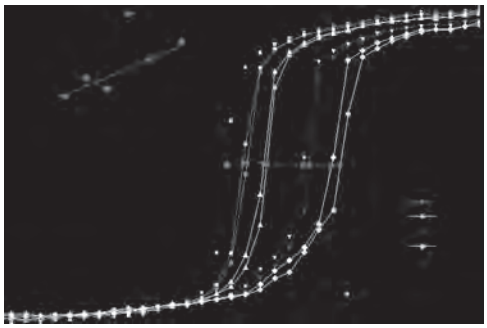

EPB-12. Stable Multi-level States Induced by Spin-orbit Torque in Composition-graded GaMnAsP Films. *K. Lee*[1], K. Han[1], S. Lee[1], X. Liu[2], M. Dobrowolska[2] and J. Furdyna[2] *1. Physics Department, Korea University, Seoul, The Republic of Korea; 2. Physics Department, University of Notre Dame, Notre Dame, IN, United States*

We have investigated spin-orbit-torque-induced magnetization switching in GaMnAsP ferromagnetic semiconductor films in which phosphorus concentration P was vertically graded from 3% to 24% over a 62.5 nm film thickness. Such continuous tuning of phosphorus induces non-uniform

strain along with additional inversion asymmetry. For spin-orbit torque (SOT) measurements, we fabricated a Hall device aligned with the [110] crystal direction, a geometry in which the Rashba and the Dresselhaus spin-orbit fields are antiparallel to each other. The SOT-induced magnetization switching was carried out by applying a current pulse with a duration of 10 ms in the presence of an in-plane bias magnetic field. The magnetization state was monitored by measuring Hall resistance (HR) with a weak direct current at 40 K. We observed very stable multi-level states in current sweeps that depended on the bias field. As an example, the amplitude of current loops was seen to clearly increase as the in-plane bias field increased from 0 Oe to 100 Oe (see Fig. 1(a)). These states were also very sensitive to angle by which the bias field deviated from the film plane, as seen in Fig. 1(b). Such multi-level states showing systematic dependence on the magnitude and angle of an in-plane bias can be used as memristor devices for neuromorphic computing.

L. Zhu, D. C. Ralph, R. A. Buhrman, Adv. Funct. Mater., Vol. 31, p.2103898 (2021)

Fig. 1. Spin-orbit-torque-induced multi-level states. The current-induced magnetization switching hysteresis shows systematic dependence on the magnitude (a) and deviation angle from the film plane (b) of the bias field.

EPB-13. Laser assisted current induced magnetization switching in a TbCo/Pt hetero-structure wire. *S. Sumi*[1], S. Ranjbar[1], K. Tanabe[1] and H. Awano[1] *1. Toyota Technological Institute, Nagoya, Japan*

A magnetic wire is one of the attractive candidates for high capacity memories and logic devices with low power consumption [1]. We reported that the wire of rare-earth transition metal (RE-TM) amorphous alloy show a current induced domain wall motion (CIDWM) with a faster wall speed of more than 1000 m/sec and a current induced magnetization switching (CIMS) with a lower current density of 5.5 MA/cm^2 [2, 3]. However, domain creation method in the wire is one of the key technologies for their applications [4, 5]. In this paper, we demonstrate a laser assisted current induced magnetization switching in TbCo/Pt hetero-structure wire. Figure 1 shows measuring setup for laser assisted current induced magnetization switching. A wire of 3 μm width is irradiated by laser spot of 1 μm diameter under applying both pulse current and external field. The film was fabricated on a thermally oxidized silicon substrate using a sputtering system. TbCo 12 nm layer was co-sputtered by Tb and Co targets and Pt layer was sputtered by Pt target as 2 nm under layer and 4 nm heavy metal layer. The film was patterned by SEM lithography with a liftoff method. CIMS was observed using a MOKE microscope. Figure 2 shows 100 nsec pulse current dependencies of magnetizing switched domain diameter with/without laser assist, where external in-plane field of 500 Oe. The inset shows microscope view of the wire. Blue line showed a CIMS threshold for without laser assist. CIMS domain diameter increased with increasing current pulse heights. Laser assisted CIMS could reduce the threshold current more than 40 % that of without a laser assisted. We demonstrated the laser assisted current induced magnetization switching of the magnetic wire. The method can reduce the current and controlled CIMS by laser. The laser assist CIMS is one of the attractive methods to create the domains in the magnetic wire. This research was supported by KAKENHI (No. 20H02185, 21K18735, 21K14202), Japan.

[1] S. S. P. Parkin et al., Science 320, 190 (2008). [2] D. Ngo et al., APEX Vol. 4, No. 9, 093002(2011). [3] K. Asari et al., AIP Advances 7, 055930 (2017). [4] S. Bandira et al., Appl. Phys. Let. Vol 99, No. 20, 202507(2011). [5] N. Roschewsky et al., Appl. Phys. Let. Vol 109, No. 11, 112403(2016).

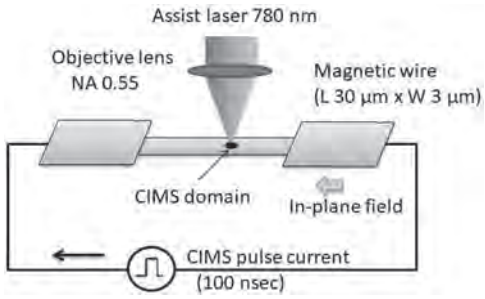

Figure 1 Measuring setup for laser assisted current induced magnetization switching (CIMS).

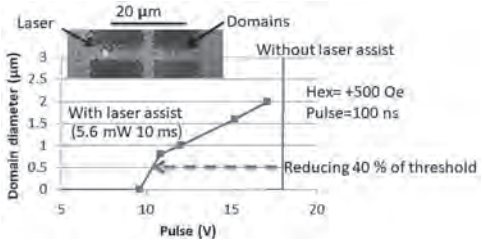

Figure 2 Current pulse dependencies of magnetizing switched domain diameter with/without laser assist.

EPB-14. Metadynamics Calculations of Skyrmion Free-Energy Landscapes. *I. Charalampidis*[1] and J. Barker[1] *1. Physics and Astronomy, University of Leeds, Leeds, United Kingdom*

Interfacial magnetic skyrmions are topological spin textures which have been proposed for use as information carriers in spintronic devices [1]. Hence, it is vital that their creation, annihilation, and motion can be accurately controlled [1]. Still, their thermal stability and interactions with lattice defects are not fully understood. Recently, many groups studied the skyrmion creation/annihilation energy paths by reconstructing associated free energy landscapes (FELs) and calculating the minimum energy paths, by combining micromagnetic simulations with an enhanced sampling technique called the nudged elastic band method (NEBM) [2]. However, micromagnetics and NEBM do not fully account for thermal effects. In addition, most computational models assume defect-free material interfaces with idealized magnetic parameters; while lattice defects alter the skyrmion dynamics and show potential to be used as pinning, destruction/creation points in future devices. To address these, we use atomic scale magnetic simulations combined with an enhanced sampling technique named metadynamics to reconstruct non-trivial FELs of certain skyrmion degrees of freedom called as collective variables (CVs) in metadynamics. Metadynamics systematically adds a potential bias on the CVs to sample states outside of the thermodynamic equilibrium and explore the whole configurational space [3,4]. Traditionally, this has been used to understand how molecules bind to surfaces. Recently, metadynamics has been used in magnetism to study simple situations such as the temperature dependence of anisotropy CVs [5]. We use it to explore how spin textures interact with defects. Thus, we demonstrate that metadynamics can be extensively used in computational magnetism to study the behaviour of spin textures by selecting appropriate CVs. Mainly, we use metadynamics to study the thermal stability of skyrmions, via studying the annihilation/creation energy barriers as a function of temperature. Additionally, we investigate how various defects modify these FELs and their associated energy barriers. Ultimately, we explore if certain defects alter the skyrmion stability, trap/repel skyrmions, disturb their motion and prevent/help their creation/annihilation.

[1] A. Fert, N. Reyren, V. Cros, Nat Rev Mater 2, 17031 (2017) [2] D. Cortés-Ortuño, W. Wang, M. Beg, et al. Sci Rep 7, 4060 (2017) [3] A. Laio, L. Parrinello, PNAS 99, 20 (2002) [4] G. Bussi, A. Laio, *Nat Rev Phys* 2, 200–212 (2020). [5] B. Nagyfalusi, L. Udvardi, L. Szunyogh, Phys. Rev. B 100, 174429 (2019)

Session FOA
SPIN DYNAMICS
Lakhan Bainsla, Chair
University of Gothenburg, Gothenburg, Sweden

CONTRIBUTED PAPERS

FOA-01. Laser-induced terahertz wave emission from Bi/Co structure.
K. Ishibashi[1,2], S. Iihama[3,2] and S. Mizukami[2,4] *1. Department of Applied Physics, Tohoku University, Sendai, Japan; 2. WPI-AIMR, Tohoku Univ., Sendai, Japan; 3. FRIS, Tohoku Univ., Sendai, Japan; 4. CSIS, Tohoku Univ., Sendai, Japan*

Bismuth (Bi) or Bi-based heterostructures has attracted much interest as candidates for spin current generator. Recently, helicity-dependent (HD) photocurrent in Bi or Bi/Cu(or Ag) thin films was reported by using pulse laser-induced terahertz (THz) emission and transport measurement[1, 2]. It is believed that spin current in Bi induced by circularly-polarized laser via photo-spin conversion effect is converted into charge current via spin-charge conversion effect. However, details of photo-spin conversion in Bi have yet to be clarified because the photo-spin and the spin-charge conversion effects are observed simultaneously, thus, one cannot distinguish two effects. Here, we studied THz emission induced by spin-current generation using the photo-spin conversion effect in Bi and the laser-induced demagnetization in an adjacent ferromagnetic Co layer in Bi/Co films to separate two spin-related conversion effects and investigate the photo-spin conversion in Bi. The samples, glass sub./Bi(t_{Bi})/Co(5)/MgO(2)/Ta(2) (thickness is in nm), were prepared by a DC/RF magnetron sputtering. Laser-induced THz emission in Bi/Co films was investigated by THz time-domain spectroscopy (THz-TDS) with 120-fs Ti: Sapphire laser[3,4]. Figure 1 and Figure 2 show the Bi thickness t_{Bi} dependence of THz peak values induced by linearly-polarized laser and HD-THz peak values, respectively. Here, HD-THz is difference between signals obtained with left- and right-circularly polarized laser. We found different t_{Bi} dependence as shown in Fig. 1 and Fig. 2, which is possibly due to the difference in spin-relaxation length of two experiments. In the presentation, we will discuss the physics behind the different THz signals obtained in two experiments and quantitative consideration of the photo-spin conversion in Bi. This work is partially supported by KAKENHI (19K15430, 21H05000). K. I. acknowledges Grant-in-Aid for JSPS Fellow (22J22178) and GP-Spin at Tohoku University. S. M. acknowledges CSRN in CSIS at Tohoku University.

[1] Y. Hirai *et al*. Phys. Rev. Appl. 14, 064015 (2020) [2] H. Hirose *et al*. Phys. Rev. B 103, 174437 (2021) [3] H. Idzuchi, *et al*., AIP Advances 11, 015321 (2021) [4] Y. Sasaki *et al*. Appl. Phys. Lett. 111, 102401 (2017)

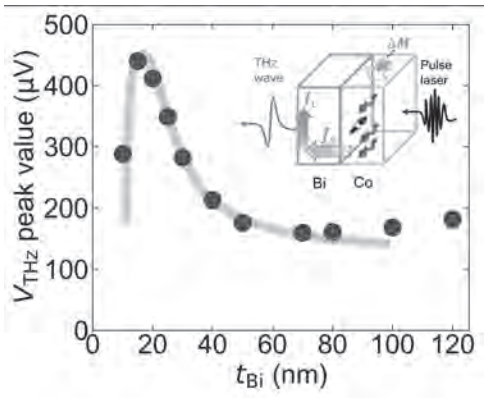

Fig. 1 Bi thickness t_{Bi} dependence of linearly-polarized laser-induced THz peak values in Bi/Co films.

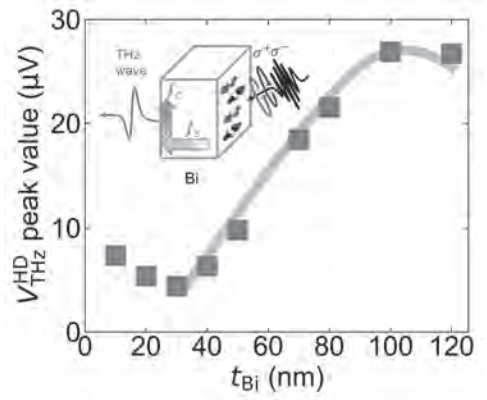

Fig. 2 t_{Bi} dependence of HD-THz peak values in Bi/Co films.

FOA-02. Spin Hall oscillators based on ferromagnetic metal/lithium aluminum ferrite bilayers with enhanced output power and quality factor.
H. Ren[4], X. Zheng[1], S. Channa[2], G. Wu[4], D.A. O'Mahoney[3], Y. Suzuki[1] and A.D. Kent[4] *1. Department of Applied Physics, Stanford University, Stanford, CA, United States; 2. Department of Physics, Stanford University, Stanford, CA, United States; 3. Department of Materials Science and Engineering, Stanford University, Stanford, CA, United States; 4. Center for Quantum Phenomena, Department of Physics, New York University, New York, NY, United States*

Spin-Hall oscillators (SHOs) are promising spintronic devices to realize dc controlled GHz frequency signals in nanoscale devices for a variety of applications[1,2], including for neuromorphic computing[3]. However, traditional SHOs have high auto-oscillation threshold currents and those based on magnetic tunnel junctions require a complex etching process. Here, we demonstrate that by combining a metallic ferromagnetic nanowire with low damping and high-quality ferromagnetic insulators, specifically epitaxial lithium aluminum ferrite thin films[4], SHO characteristics are dramatically

improved. Our magnetic bilayers SHOs are composed of Pt(5nm)/Py(5nm)/($Li_{0.5}Al_{1.0}Fe_{1.5}O_4$ (LAFO) or $Li_{0.5}Al_{0.5}Fe_2O_4$ (LFO)) (x nm) layers with varied thicknesses *x* (including x=0, i.e. just Pt/Py layers) and two different compositions of insulator. The Pt/Py layers are patterned into 400 nm wide x 400 nm long nanowires between two Au contact pads as shown in Fig. 1a. Ferromagnetic resonance (FMR) measurements of the unpatterned heterostructure and spin-torque ferromagnetic resonance (ST-FMR) of micron-scale wires show that Py and LAFO are strongly ferromagnetically coupled and thus precess coherently. In the nanowires, we observe two prominent auto-oscillation modes in all samples, which we associate with bulk and edge spin-wave modes. Increased oscillator quality factor and maximum emission power (Fig. 1b) as well as lower threshold currents are obtained in samples containing LAFO and LFO. In addition, the maximum emission power and quality factor increases with the LAFO thickness. The performance can be further enhanced by replacing LAFO with LFO which possesses higher saturation magnetization. The improved characteristics are associated with the excitation of larger spin-precession angles and volumes in LAFO and LFO samples. We further find that the presence of LAFO enhances the auto-oscillation amplitude of spin-wave edge modes, consistent with our micromagnetic modeling.

[1] V.E. Demidov, S. Urazhdin, H. Ulrichs, V. Tiberkevich, A. Slavin, D. Baither, G. Schmitz, and S.O. Demokritov, Nat. Mater. 11, 1028 (2012). [2] Z. Duan, A. Smith, L. Yang, B. Youngblood, J. Lindner, V.E. Demidov, S.O. Demokritov, and I.N. Krivorotov, Nat. Commun. 5, 1 (2014). [3] J. Grollier, D. Querlioz, K. Y. Camsari, K. Everschor-Sitte, S. Fukami, and M. D. Stiles, Nature Electronics 3, 360 (2020) [4] X.Y. Zheng, L.J. Riddiford, J.J. Wisser, S. Emori, and Y. Suzuki, Appl. Phys. Lett. 117, 1 (2020).

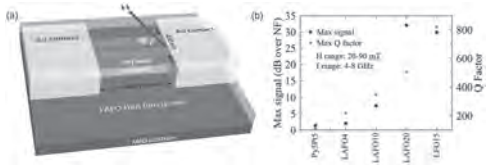

Figure 1. (a) Schematic of the nanowire sample, showing the direction of the applied field and current. (b) Maximum signal (dB over background noise level) and maximum Q factor obtained from power spectral density measurements for different samples (x indicated in nm).

FOA-03. Spin Dynamics of Ferrimagnets Jointing Ferro- and Antiferromagnets. *M. Guo*[1], H. Zhang[2] and R. Cheng[2,1] *1. Physics and Astronomy, University of California, Riverside, Riverside, CA, United States; 2. Electrical and Computer Engineering, University of California, Riverside, Riverside, CA, United States*

Ferrimagnets (FIMs) can function as high-frequency antiferromagnets while being easy to detect as ferromagnets, offering unique opportunities for ultrafast device applications. While the physical behavior of FIMs near the compensation point has been widely studied, there lacks a general understanding of FIMs that allows us to freely vary the ratio of sublattice spins between the FM and the AFM limit. Such a generic picture can not only reveal the unique features not visible near the compensation point but also unifies the spin dynamics in FIMs with that in FM and AFM materials. Here we investigate the physical properties of a two-sublattice FIM manipulated by static magnetic fields and current-induced torques. By continuously varying the ratio of sublattice spins, we clarify how the dynamical chiral modes in an FIM are intrinsically connected to their Ferro- and Antiferromagnetic counterparts, which reveals unique features not visible near the compensation point.

[1] M. Guo, H. Zhang, and R. Cheng, *Manipulating Ferrimagnets by Fields and Currents*, Phys Rev B 105, 064410 (2022). [2]C. Kim, S. Lee, H.-G. Kim, J.-H. Park, K.-W. Moon, J. Y. Park, J. M. Yuk, K.-J. Lee, B.-G. Park, S. K. Kim, K.-J. Kim, and C. Hwang, *Distinct Handedness of Spin Wave across the Compensation Temperatures of Ferrimagnets*, Nat Mater 1 (2020). [3]J. Barker and G. E. W. Bauer, *Thermal Spin Dynamics of Yttrium Iron Garnet*, Phys Rev Lett 117, 217201 (2016). [4]S. K. Kim, K.-J. Lee, and Y. Tserkovnyak, *Self-Focusing Skyrmion Racetracks in Ferrimagnets*, Phys Rev B 95, 140404 (2017).

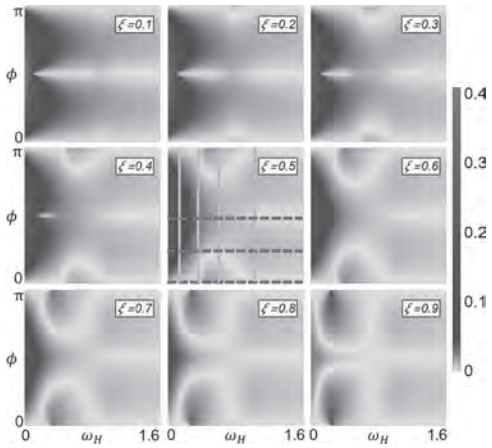

Density plot of |m⊥| as a function of the static magnetic field

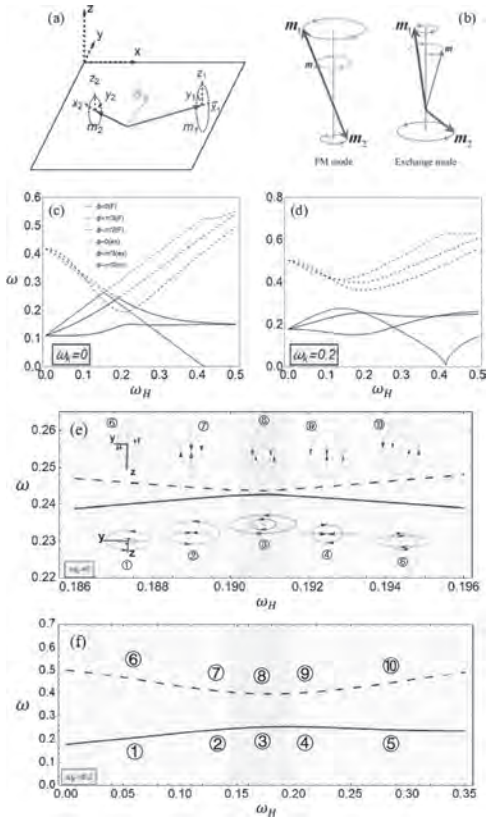

schematics of the model FIM in the presence of an in-plane magnetic field

FOA-04. Spin and vorticity transport in two-dimensional magnets with easy-plane anisotropy. *A.A. Kovalev*[1], E. Schwartz[1], M. Ali[1], H. Vakilitaleghani[1] and B. Li[1] *1. Physics and Astronomy, Department of Physics and Astronomy and Nebraska Center for Materials and Nanoscience, University of Nebraska-Lincoln, Lincoln, NE, United States*

We study the Hall response of topological defects, such as merons and antimerons, to spin currents in two-dimensional magnets with in-plane anisotropy in the vicinity of the Berezinskii-Kosterlitz-Thouless (BKT) transition [1]. We use a combination of Monte Carlo and spin dynamics

simulations to study the transition from spin superfluidity to conventional spin transport, the universal jump of the spin stiffness, and the exponential growth of the transverse vorticity current. We accompany our results by phenomenological description. We show how the spin and vorticity currents can be modulated by changes in density of free topological defects, e.g., by tuning the in-plane magnet across the BKT transition by changing the exchange interaction, magnetic anisotropy, or temperature. We further show how spin and vorticity currents can be controlled by employing connection between vorticity and spin, e.g., we demonstrate spin diode effect. This work was supported by the U.S. Department of Energy, Office of Science, Basic Energy Sciences, under Award No. DE-SC0021019.

[1] Edward Schwartz, Bo Li, and Alexey A. Kovalev, Phys. Rev. Research 4, 023236 (2022)

FOA-05. FMR-driven magnetization dynamics in epitaxial $Fe_{75}Co_{25}$ films interfaces with Bi_2Te_3. *R. Nepal*[1], V. Sharma[1], E.A. Pogue[2] and R. Budhani[1] *1. Physics, Morgan State University, Baltimore, MD, United States; 2. Chemistry, John Hopkins University, Baltimore, MD, United States*

The strong spin-orbit coupling in layered materials like Bi_2Te_3 leads to topologically protected conducting surface states, which promote interconversion of charge and spin currents. Here we report the manifestations of spin pumping across the interface of epitaxial $Fe_{75}Co_{25}$ (FeCo) ferromagnet and Bi_2Te_3 topological insulator in the linewidth of ferromagnetic resonance (FMR), driven over a frequency range of 5 to 31 GHz. The bilayers of $Fe_{75}Co_{25}/Bi_2Te_3$ were prepared by dc magnetron sputtering of $Fe_{75}Co_{25}$ and Bi_2Te_3 targets sequentially in an ultrahigh vacuum system. We first deposited 4 nm thick FeCo film on the (100) surface of $MgAl_2O_4$ (MAO) crystals at 350 ^{0}C, which resulted in epitaxial growth of the body centered cubic FeCo phase with the cubic principal axis parallel to [110] direction of MAO. This was followed by deposition of Bi_2Te_3 films of different thickness at ambient temperature. The Gilbert damping coefficient α of a FeCo single layer is found to be 7.4 x 10^{-3}. However, contrary to the common observation of enhancement in a on spin pumping, the bilayers of FeCo/Bi_2Te_3 show unremarkable changes in damping on increasing the thickness of Bi_2Te_3 layer [Fig. 1]. This behavior suggests a role of antidamping torques [1] on the magnetization of FeCo resulting from spin backflow from the interface. Acknowledgements: This research has been supported by Air Force Office of Scientific research under grant # FA9550-19-1-0082.

[1] Jiao, HuJun, and Gerrit EW Bauer. "Spin backflow and ac voltage generation by spin pumping and the inverse spin Hall effect." Physical review letters 110.21: 217602 (2013).

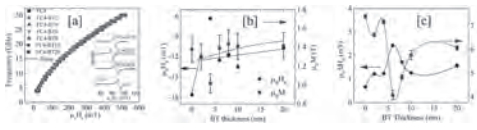

Figure 1 (a) The FMR field (μ_0H_r) plotted as a function of microwave frequency for $Fe_{75}Co_{25}/Bi_2Te_3$ bilayers of different Bi_2Te_3 layer thickness. Symbols represent the resonance field calculated from FMR lineshape analysis and solid lines are the fit to Kittel equation. Inset shows the differential FMR signal at 10 GHz with Lorentzian lineshape fitting. (b) shows the variation of in-plane anisotropic field (μ_0H_k) and effective saturation magnetization (μ_0M_{eff}) as a function of Bi_2Te_3 thickness and (c) (b) Variation of the Gilbert damping constant (α) and inhomogeneous linewidth broadening as a function of Bi_2Te_3 thickness. Dotted lines in (b) and (c) are for guide to the eyes.

FOA-06. Relating magnon propagation length to magnetic anisotropy and Gilbert damping in ferrimagnetic insulator/heavy metal heterostructures. *A. Chanda*[1], C. Holzmann[2], M. Albrecht[2], C.A. Ross[3], M. Phan[1] and H. Srikanth[1] *1. Physics, University of South Florida, Tampa, FL, United States; 2. Institute of Physics, University of Augsburg, Augsburg, Germany; 3. Department of Materials Science and Engineering, Massachusetts Institute of Technology, Cambridge, MA, United States*

Spinterfaces comprising insulating rare-earth iron garnet and heavy metal (HM) bilayers form the most appealing platform in the field of spin-based-electronics to generate, transmit, and detect pure spin currents. The discovery of the spin Seebeck effect (SSE) instigated new generation spintronic nanodevices facilitating electrical energy harvesting from renewable thermal energy, wherein a magnonic spin current is generated by applying a temperature gradient across a magnetic insulator (MI)/HM bilayer. The magnon propagation length (ξ) of a ferromagnet (FM) is one of the key factors for driving magnonic spin current across a FM/HM interface.[1] Theory predicts that is inversely proportional to the Gilbert damping (α) and the square-root of the magnetic anisotropy constant (K_{eff}).[2] However, this prediction has not been experimentally validated yet. Here we aim to address this outstanding question by employing a combined set of three distinct experiments: longitudinal SSE (LSSE), radio frequency (RF) transverse susceptibility (TS), and broadband ferromagnetic resonance (FMR) measurements performed on a $Gd_3Sc_2Ga_3O_{12}$ (GSGG)/ $Tm_3Fe_5O_{12}$ (TmIG)/ Pt film series. TmIG has been chosen because of its large negative magnetostriction coefficient that facilitates robust perpendicular magnetic anisotropy (PMA) induced by dominant magnetoelastic anisotropy.[3] Furthermore, TmIG has much higher Gilbert damping ($\alpha \sim 10^{-2}$) compared to $Y_3Fe_5O_{12}$ ($\alpha \sim 10^{-4}$). This allows for probing and magnetic anisotropy and their relative contributions to and hence LSSE. We observed a remarkable drop in the temperature dependent LSSE voltage (V_{LSSE}) in TmIG/Pt below 200 K. A temperature evolution of ξ extracted from the thickness dependent also shows a significant decrease below 200 K. This strong decrease in ξ is resulted from the strong increase in the effective anisotropy field (H^K_{eff}) and α, which are determined from the TS and FMR measurements, respectively and attributed to the presence of the single ion anisotropy and relaxation of Fe^{2+} impurities. Our study highlights the important impacts of H^K_{eff} and α on ξ and V_{LSSE} in a FM/HM system and paves a new pathway for designing highly efficient tunable spin-caloritronic nanodevices.

[1] A. Kehlberger, U. Ritzmann, D. Hinzke, E.-J. Guo, J. Cramer, G. Jakob, M. C. Onbasli, D. H. Kim, C. A. Ross, and M. B. Jungfleisch, Phys. Rev. Lett. 115, 96602 (2015). [2] U. Ritzmann, D. Hinzke, and U. Nowak, Phys. Rev. B 89, 24409 (2014). [3] S. Crossley, A. Quindeau, A. G. Swartz, E. R. Rosenberg, L. Beran, C. O. Avci, Y. Hikita, C. A. Ross, and H. Y. Hwang, Appl. Phys. Lett. 115, 172402 (2019).

FOA-07. Purely current-driven writing mechanism for domain wall-based recording devices. D. Osuna Ruiz[1], *E. Martinez*[1], Ó. Alejos[2] and V. Raposo[1] *1. Applied Physics, University of Salamanca, Salamanca, Spain; 2. Electricity and Electronics, University of Valladolid, Valladolid, Spain*

Ultrathin ferromagnetic strips, sandwiched between a heavy metal and an oxide, have been suggested as potential platforms for recording devices where the information is coded in perpendicular magnetized domains (*up* or *down*) separated domain walls (DWs). Due to the Dzyaloshinskii-Moriya interaction, such DWs depict a homochiral Néel configuration [1,2] and are displaced with high velocity (~500 m/s) by current pulses (J~1 TA/m^2) [3]. However, the writing mechanism for such DW-based devices, that is, a controlled nucleation of domains and DWs, is still challenging. Nucleation is conventionally performed by injecting an electrical current pulse along an orthogonal conducting wire [1]. However, the resulting Oersted field that nucleates a new domain also annihilates an already shifted one unless an intricate device layout is used [4]. Although some ideas have been proposed to solve this issue [5,6], a simple nucleation scheme remains elusive. Here we propose a simple geometrical design where both the nucleation and

the shifting can be purely achieved by current pulses (Fig. 1(a)). A DW is initially located in the bottom-left arm of the two symmetrical arms close to its junction with the longitudinal strip (LS), where the bits will be coded and shifted. By applying a proper voltage pulse (V_2 in Fig. 1(b)), the DW is pushed towards the LS, and split in two new DWs: one at the top-left arm and other entering in the LS. A second pulse along the same bottom-left arm (V_2) will shift the new DW along the LS. If injected along the top-left arm (V_1), another DW and domain will be nucleated whereas the former DW will be also driven along the LS. Based on this method, new domains (bits) and DWs can be simultaneously nucleated (written) and driven by alternatively applying voltage pulses between one of the two left arms and the LS of the structure. In the talk, we will show by means of realistic simulations the potential of this idea to perform the writing operation in DW-based recording devices.

[1] S. Emori et al. Nat. Mater. 12, 611 (2013). [2] K.-S. Ryu et al. Nat. Nanotechnol. 8, 527 (2013). [3] I. M. Miron et al. Nat. Mater. 10, 419 (2011). [4] O. Alejos et al. Scientific Reports, 7, 11909 (2017). [5] Z. Luo et al. Appl. Phys. Lett. 111, 162404 (2017). [6] T. Phuong Dao et al. Nano Lett. 19, 9, 5930 (2019).

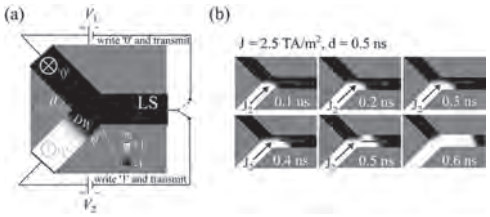

Fig.1. (a) Proposed design for simultaneously nucleating and driving DWs upon application of pulses. (b) Transient micromagnetic snapshots showing the DW dynamics for a 0.5 ns current pulse with J_2 = 2.5 TA/m².

FOA-08. Withdrawn

FOA-09. Anomalous Nernst effect in epitaxially grown $Fe_{4-x}Ni_xN$ films. *W. Yin*[1], K. Ito[1], Y. Tsubowa[2], M. Tsujikawa[2], M. Shirai[2] and K. Takanashi[1,3] *1. Institute for Materials Research, Tohoku University, Sendai, Japan; 2. Research Institute of Electrical Communication, Tohoku University, Sendai, Japan; 3. Advanced Science Research Center, Japan Atomic Energy Agency, Tokai, Japan*

The anomalous Nernst effect (ANE) generates an electric field (E_{ANE}) orthogonal to both magnetization and temperature gradient in ferromagnetic materials. In order to realize high-performance ANE-based thermoelectric power generation devices, exploring a material with a large anomalous Nernst coefficient (S_{ANE}) is essential. Fe_4N is a promising material with relatively large S_{ANE} of 2.2 μV/K [1]. In this study, $Fe_{4-x}Ni_xN$ films were fabricated and their ANEs were characterized to reveal the Ni addition effect to Fe_4N. The $Fe_{4-x}Ni_xN$ films were grown on $MgAl_2O_4$(MAO) (001) substrates at 450 °C. The structures of the samples were characterized by x-ray diffraction. The Ni/Fe ratio, x, in $Fe_{4-x}Ni_xN$ films was changed in the range of $0 \le x \le 2.8$. The samples were microfabricated into a Hall bar shape, and ANE, the Seebeck effect, and the anomalous Hall effect (AHE) were characterized [2]. The external magnetic field dependence of E_{ANE} was measured at different temperature gradient and S_{ANE} was estimated. The transverse conductivity (σ_{xy}) and the transverse thermoelectric conductivity (α_{xy}) of Fe_3NiN was calculated by the first-principles calculation [3]. The $Fe_{4-x}Ni_xN$ films were epitaxially grown on the MAO(001) substrates, but the $Fe_{4-x}Ni_xN$ phase started to decompose into FeNi at about x = 2.3. The relationship between S_{ANE}, Seebeck coefficient (S_{SE}) and x in $Fe_{4-x}Ni_xN$ is shown in Fig. 1. The S_{ANE} value decreased from 1.7 to 0.6 μV/K and the S_{SE} value increased from -2.3 to 1.2 μV/K with the increase of x. By using the experimental data, α_{xy} was calculated. The result showed that α_{xy} decreased with the increase of x and the change of α_{xy} dominated the change of S_{ANE}. In the presentation, the obtained σ_{xy} and α_{xy} values will be compared with the calculation results. This work was supported by the Grants-in-Aid for Scientific Research (S) (Grant No. JP18H05246) and (C) (Grant No. JP21K04859) from JSPS KAKENHI, Collaborative Research Center on Energy Materials, Institute for Materials Research, Tohoku University, and the Cooperative Research Project of the Research Institute of Electric Communication, Tohoku University.

[1] S. Isogami, K. Takanashi, and M. Mizuguchi, Appl. Phys. Express 10, 073005 (2017). [2] J. Wang, Y.-C. Lau, W. Zhou, T. Seki, Y. Sakuraba, T. Kubota, K. Ito, and K. Takanashi, Adv. Electron. Mater. 8, 2101380 (2022). [3] Y. Tsubowa, M. Tsujikawa, and M. Shirai, the 69th JSAP spring meeting 2022, 23a-E205-5 (2022).

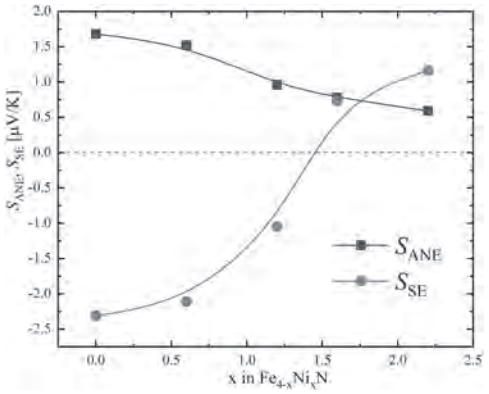

Fig. 1 The S_{ANE} and S_{SE} of $Fe_{4-x}Ni_xN$ samples as the function of Ni composition.

FOA-10. Anomalous Nernst effect in semiconductor / ferromagnetic metal multilayer. *M. Mizuguchi*[1], R. Kitaura[2], H. Sharma[3], T. Ishibe[2] and Y. Nakamura[2] *1. Nagoya University, Nagoya, Japan; 2. Osaka University, Toyonaka, Japan; 3. IMEC, Leuven, Belgium*

The anomalous Nernst effect (ANE) has recently attracted renewed attention because thermoelectric conversion efficiency based on the ANE can be higher than that based on the Seebeck effect in the case of the same dimensionless figure-of-merit[1]. It is indispensable to find the guiding principle to obtain materials with large ANE to realize a thermoelectric device based on the ANE. Thus, we have investigated the ANE in ordered alloys and nanostructures[2-4]. For the practical use of an ANE-based thermoelectric device, the reduction of thermal conductivity is also an important issue. In this paper, we propose a semiconductor / ferromagnetic metal multilayer, where the interfaces prevent heat carrier transport (thermal conductivity reduction) and are expected to enhance the ANE additionally[5]. An amorphous Si / Co multilayer film (MLF) was fabricated on an undoped Si(001) substrate. For reference, we also formed an amorphous Co film (CF) on the Si substrate. The out-of-plane thermal conductivity of the films was measured by 2w method with periodic heating. Transverse Seebeck coefficient (S_{yx}) loops as a function of the magnetic field were measured for the two films. Figure 1(a) shows a S_{yx} - H curve of the MLF. A clear hysteresis loop was observed, thus it is clarified that this signal comes from the ANE of the MLF. Figure 1(b) summarizes anomalous term in the transverse Seebeck coefficient ($(S_{yx})_{sat}$) of the MLF and the CF. Intriguingly, the MLF exhibited 3 times larger $(S_{yx})_{sat}$ than that of the CF. This result demonstrated that $(S_{yx})_{sat}$ was enhanced even in a semiconductor / ferromagnetic metal multilayer. On the other hand, the thermal conductivity of the MLF was about 30 times smaller than that of the CF, which is mainly attributed to the contribution of an amorphous Si layer with smaller thermal conductivity. These results give us a beneficial knowledge for developing an ANE-based thermoelectric material using semiconductor / metal interfaces.

[1] M. Mizuguchi and S. Nakatsuji, Sci. Tec. Adv. Mater. 20, 262 (2019). [2] M. Mizuguchi, *et al*., Appl. Phys. Express 5, 093002 (2012). [3] K. Hasegawa, M. Mizuguchi, *et al*., Appl. Phys. Lett. 106, 252405

(2015). [4] P. Sheng, M. Mizuguchi, *et al*., Appl. Phys. Lett. 116, 142403 (2020). [5] R. Kitaura, M. Mizuguchi, *et al*., Appl. Phys. Express 14, 075002 (2021).

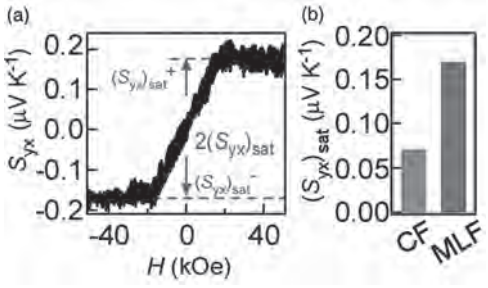

Figure 1. (a) S_{yx}-H curve of the MLF. (b) $(S_{yx})_{sat}$ of the CF and the MLF.

FOA-11. Mode transition from localized to propagating wave in perpendicular magnetic anisotropy-based spin-Hall oscillators.
M. Succar[1] and *M. Haidar*[1] *1. Physics, American University of Beirut, Beirut, Lebanon*

Spin torque oscillators (STOs) have the potential to process information without relying on the charge of the electron but rather take advantage of its intrinsic spin thanks to the spin Hall effect (SHE) [1-2] and spin-orbit effect [3]. Spin Hall nano-oscillator (SHNOs) is a prominent device as it is easy to fabricate and detect oscillations by electrical and optical means. It is now well demonstrated that the auto-oscillations can be excited efficiently where a spatial self-localization of the excited magnon is detected, due to the in-plane anisotropy, that prevents their emission into the extended magnetic films. This is accompanied by a negative nonlinearity coefficient, N, which results in a red-shift behavior [1]. To overcome the self-localization, one can design devices with sizeable perpendicular magnetic anisotropy (PMA) to compensate for the shape anisotropy and hence allow the excitation of propagating spin waves where N becomes positive that leading to a dominant blue-shift behavior [4-5]. Here we study the SHE-driven excitation in a nanowire-based SHNOs device made of CoFeB (3 nm)/Pt (5 nm) bilayers using micromagnetic simulations. We determine the nature of the excited modes whether localized or propagating as we vary the magnitude of the direct current, the strength of the PMA, and the direction of the magnetic field. Our results showed a strong mode transition from localized to propagating mode either by controlling the magnitude of the current or the strength of the PMA as shown in fig. 1. Indeed, the results demonstrate that there is a critical out-of-plane angle of the applied magnetic field for the excitation of propagating waves. This study demonstrates the role of PMA in controlling magnetization oscillation and helps in designing better devices with controlled characteristics

[1] V. E. Demidov et al., Appl. Phys. Lett. 105, 172410 (2014). [2] Z. Duan et al., Nat. Commun. 5, 5616, (2014) [3] M. Haidar et al., Nat. Commun. 10, 2362, (2019) [4] Fulara et al., Sci. Adv.;5: eaax8467, 2019 [5] M. Evelt et al.,Phys. Rev. Appl. 10, 041002 (2018).

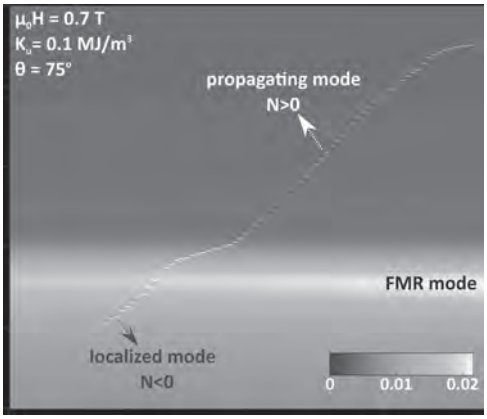

Color plot of current-induced auto-oscillation in a CFB/Pt nanowire. It shows three modes (i) localized, (ii) FMR, and (iii) propagating modes. The micromagnetic simulations are done under a magnetic field μ_0 H = 0.7 T and is applied at 75° out-of-plane. Perpendicular magnetic anisotropy of 0.1 MJ/m^3 is considered.

FOA-12. Spin Dependent Photocurrent Generation in Germanene-like Structure.
T. Nishijima[1], S. Kawa[1], Y. Ando[1], A. Ohta[2], J. Yuhara[2], M. Kurosawa[2], E. Shigematsu[1], R. Ohshima[1] and M. Shiraishi[1]
1. Department of Electronic Science and Engineering, Kyoto University, Kyoto, Japan; 2. Graduate School of Engineering, Nagoya University, Nagoya, Japan

Germanene – two dimensional materials with a honeycomb structure consisting of germanium atom is an attracting post graphene material for both fundamental and applied physics[1]. Although, a variety of attractive properties have been expected, experimental investigation has been strongly limited because germanene can be grown only on metallic layers and easily oxidized after air exposure[2]. In this study, we focus on a few layer germanene-like structure (GLS) as a first step for exploring the unique characteristics of germanene. The GLS is fabricated by segregation method of Ge atoms by thermal annealing of an epitaxial Al/Ge(111) substrate[3,4]. Using this fabrication technique, few layer GLS is grown on Al with Al_2O_3 capping layer that has a good stability against chemical reaction and acts as a blocking layer of oxidation. It is theoretically predicted that most of topological feature of germanene can appear even in the multilayer germanene as long as it keeps free standing. We investigated photogalvanic effect in the GLS. For the measurement of photogalvanic current, complicated device fabrication is not required but the result strongly reflects a spin property of the GLS. Figure 1 shows a schematic of an experimental setup for the measurement of photogalvanic current. A laser light (wavelength: 633 nm) was irradiated with in-plane angle ϕ and out-of-plane angle θ. The polarization of light is modulated by a rotatable quarter wave plate (QWP). The experiment was performed at room temperature. Figure 2 shows the photocurrent detected by lock-in technique when ϕ = 0° and θ = 60°. Horizontal axis represents the rotation angle of QWP. The photocurrent depends on both linear and circular polarity. Since circularly polarized light has finite angular momentum along in-plane direction and it is reflected onto in-plane angular momentum, the observed photocurrent is expected to be caused by the correlation between spin angular momentum and electron momentum, such as Rashba type band splitting. In the presentation, we will present further results and discussions about observed photogalvanic current from the GLS.

1 S. Cahangirov, M. Topsakal and S. Ciraci, Phys. Rev. Lett., Vol. 102, 236804 (2009) 2 M. E. Dávila, L. Xian and G. Le Lay, New J. Phys., Vol. 16, 095002 (2014) 3 K. Matsushita, A. Ohta and S. Miyazaki, Jpn. J. Appl. Phys., Vol. 61 SH1012 (2022) 4 J. Yuhara, A. Ohta, M. Kurosawa and G. Le Lay, ACS Nano, Vol. 12, 11632 (2018)

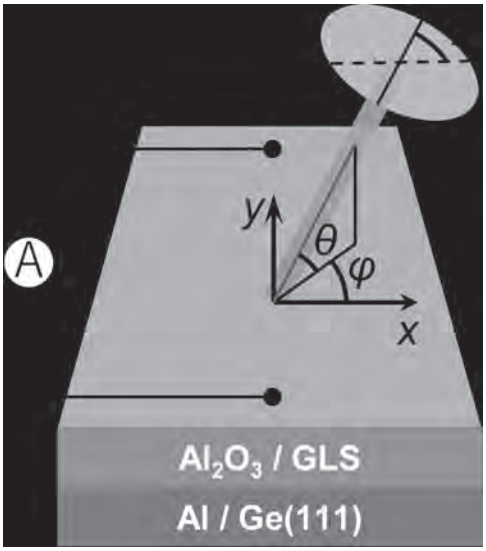

Fig.1 Experimental setup and sample structure.

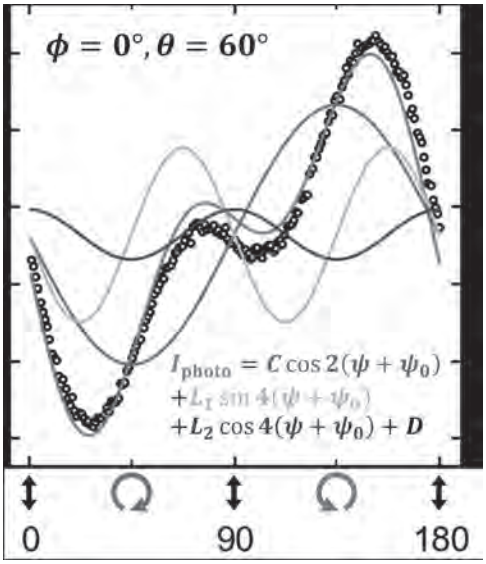

Fig.2 Polarity dependence of the photocurrent.

FOA-13. Single Molecular Magnet (SMM) Producing Photovoltaic Effect(PV) on Magnetic Tunnel Junction. *M. Savadkoohi*[1,2], D.B. Gopman[2] and P. Tyagi[1] *1. Mechanical Engineering, University of District of Columbia, DC, WA, United States; 2. Materials Science and Engineering Division, National Institute of Standard and Technology(NIST), Gaithersburg, MD, United States*

Spin based photovoltaic (PV) effect is novel research in energy harvesting area. Recently, spin-PV effect was demonstrated on magnetic tunnel junction-based molecular spintronics (MTJMSD). This prior work mainly focused on NiFe/AlOx/NiFe MTJ[1].To advance this field there is a critical need of investigating a wide range of magnetic materials. MgO insulator and CoFeB electrode-based MTJS are well established for showing high TMR ratio and heavily studied for computer memory operation. However, they have never been integrated into the molecular spintronics study. This study made effort to develop a fabrication method by which CoFeB/MgO/CoFeB MTJ could be produced in the cross-junction form to facilitate transport and electrical measurements. To do so we had to overcome numerous fabrication challenges. First, we investigated the air stability of CoFeB using reflectance study as a function of temperature. We observed that CoFeB was stable in air up to ~100C. To produce stable and low leakage current tunnel junctions we iteratively investigated the role of multiple bottom electrode fabrication factors through Taguchi Design of experiment. We produced bottom electrode in such a way that thin films have optimum tapered edge geometry and ~0.15 nm Rq roughness. To produce exposed side edges for molecule spin channel attachment we deposited MgO and top electrode through photolithorgraphically produced cavity perpendicular to the bottom electrode. To convert MTJ into MTJMSD we electrochemically bridged the SMM molecules across MgO and conducted current-voltage study before and after molecule spin channel creation. Interestingly, SMM produced current suppression at room temperature by ~200% at 300mV. Also, we observed PV effect. This MTJ produced 0.08 open circuit voltage and 5.19E-9 saturation current under 1sun(1000 mW/cm2) light intensity. To investigate the mechanism, we perform KPAFM. The difference between electrodes before and after SMM bridging was 33 and 150 mV, respectively. Higher difference in KPAFM voltage signifies a large difference in electrode resistivity. KPAFM also suggests the observed PV effect is mainly from the impacted ferromagnetic electrode region and not due to the interaction of light at molecular channels.

1- P. Tyagi and C. Riso, "Molecular spintronics devices exhibiting properties of a solar cell," Nanotechnology, vol. 30, p. 495401, 2019/09/19 2019. 2- P. Tyagi and C. Riso, "Magnetic force microscopy revealing long range molecule impact on magnetic tunnel junction based molecular spintronics devices," Organic Electronics, vol. 75, p. 105421, 2019/12/01/ 2019. 3-Heersche, H. B., De Groot, Z., Folk, J. A., Van Der Zant, H. S. J., Romeike, C., Wegewijs, M. R., ... & Cornia, A. (2006). Electron transport through single Mn 12 molecular magnets. Physical review letters, 96(20), 206801. 4- Jo MH, Grose JE, Baheti K, Deshmukh MM, Sokol JJ, Rumberger EM, Hendrickson DN, Long JR, Park H, Ralph DC. Signatures of molecular magnetism in single-molecule transport spectroscopy. Nano Lett. 2006 Sep;6(9):2014-20. doi: 10.1021/nl061212i. PMID: 16968018. 5- Bogani, L., Wernsdorfer, W. Molecular spintronics using single-molecule magnets. Nature Mater 7, 179–186 (2008). https://doi.org/10.1038/nmat2133

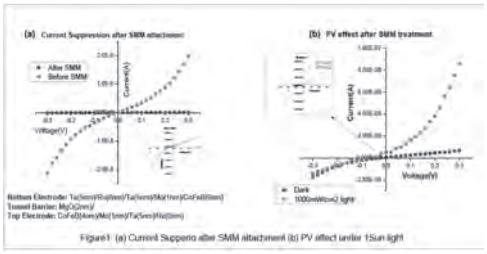

Figure1: (a) Current Suppersion after SMM attachment (b) PV effect under 1Sun light

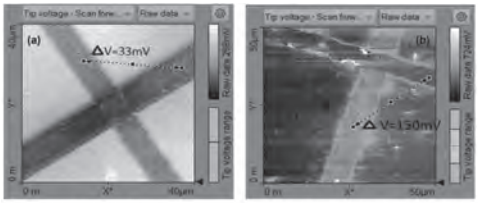

Figure2: KPFM image of MTJMSD junction (a) before molecular treatment (b) after SMM treatment

FOA-14. Theory of a Single Si Vacancy in SiC as a Quantum Sensor of Magnetic Fields. *D. Fehr*[1] and M.E. Flatté[1] *1. Department of Physics and Astronomy, University of Iowa, Iowa City, IA, United States*

Magnetometers are used for navigation, the detection of submarines and underwater debris, archaeological and geological surveys, as well as in the exploration of our solar system and even in our mobile devices [1-2]. Recently, designs of solid-state quantum magnetometers have stimulated particular interest both for their small size [3], and for their potential to operate without any optical components or applied microwave fields [4]. In this work we model Optically/Electrically Detected Magnetic Resonance (ODMR/EDMR) of the Silicon vacancy in Silicon Carbide, a budding candidate for solid-state

quantum magnetometry, using quantum master equations. The Silicon vacancy can be thought of as a S = 3/2 synthetic atom, and its spin states are sensitive to magnetic fields via the Zeeman effect. In ODMR, magnetic resonances of the Zeeman field are detected by extrema in the normalized photoluminescence signal when a transverse microwave field is applied. In EDMR, magnetic resonances of the Zeeman field are detected by extrema in the normalized current, generated when a conduction electron couples to the vacancy's spin and is allowed to recombine with a valence hole in a spin-dependent manner. In both cases, the photoluminescence/current is calculated from the steady-state density matrix populations and compared to recent experimental results [5-7]. We acknowledge support from NSF DMR-1921877.

[1] Budker, D., Romalis, M., *Nature Phys* 3, 227–234 (2007) [2] Ness, N.F., *Space Sci Rev* 11, 459–554 (1970) [3] Kraus, H., Soltamov, V., Fuchs, F. et al., *Sci Rep* 4, 5303 (2014) [4] Cochrane, C., Blacksberg, J., Anders, M. et al., *Sci Rep* 6, 37077 (2016) [5] Kraus, H., Soltamov, V., Riedel, D. et al., *Nature Phys* 10, 157–162 (2014) [6] Fischer, M., Sperlich, A., Kraus, H. et al., *Phys. Rev. Applied* 9, 054006 (2018) [7] Cochrane, C., Kraus, H., Neudeck, P. et al., *MSF* 924 988-992 (2018)

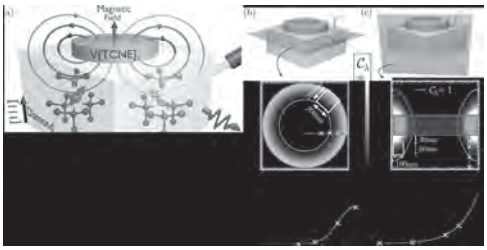

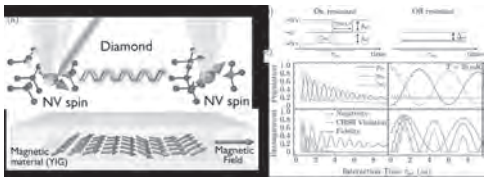

FOA-15. Magnon-mediated entanglement of solid-state spin qubits.

D.R. Candido[1], M. Fukami[2], D. Awschalom[2,3] and M.E. Flatté[1,4]
1. Department of Physics and Astronomy and Optical Science and Technology Center, University of Iowa, Iowa City, IA, United States; 2. Pritzker School of Molecular Engineering, University of Chicago, Chicago, IL, United States; 3. Center for Molecular Engineering and Materials Science Division, Argonne National Lab, Lemont, IL, United States; 4. Department of Applied Physics, Eindhoven University of Technology, Eindhoven, Netherlands

Recently, spin centers in solids (e.g., nitrogen-vacancy (NV) in diamond) have attracted significant attention due to their applications on quantum sensing and quantum information science. However, to be able to create entanglement between NVs one requires having NVs coupled to each other. Unfortunately, the bare interaction between two NV centers is week for separations > 20 nm. This creates a key challenge once NV centers cannot be optically resolvable at these distances. Therefore, providing alternative schemes to couple two NV centers over long distances became crucial to enable their use in quantum computation. To this end, magnon-mediated entanglement proposals have attracted attention due to their long-range spin-coherent propagation. Accordingly, we propose hybrid quantum systems that couple and entangle spin centers over micron length scales through the quantized spin-wave excitations (magnons) of a magnetic material[1,2]. These magnons serve as a quantum bus that transfers the information between different NV-qubits. We predict strong long-distance (>μm) NV-NV coupling via magnon modes with cooperativities exceeding unity in ferromagnetic bar, waveguide and cylindrical structures[1,2]. Moreover, we explore and compare on-resonant transduction and off-resonant virtual-magnon exchange protocols, and discuss their suitability for generating or manipulating entangled states under realistic experimental conditions[2]. Due to the absence of magnon occupation decay of the off-resonant protocol, our results show this protocol is robust at temperatures up to T ≈ 150 mK[2]. Conversely, at lower temperatures the on-resonant protocol shows a faster gate operation, and can even outperform the off-resonance protocol for small magnon damping parameters[2]. Our results will guide future experiments that aim to engineer on-chip long-distance entangling gates between spin centers mediated by magnons. This work is supported by the U.S. Department of Energy, Office of Basic Energy Sciences under Award Number DE-SC0019250 (DC and MEF), the U.S. Department of Energy, Office of Science, National Quantum Information Science Research Centers (DDA) and the Vannevar Bush Faculty Fellowship ONR N00014-17-1-3026 (MF and DDA).

[1] D R Candido, G D Fuchs, E Johnston-Halperin, M E Flatté, Mater Quantum Technol 1, 011001 (2021). [2] M Fukami, D R Candido, David D Awschalom, and M E Flatté, PRX Quantum 2, 040314 (2021).

Session FOB
SPIN HALL AND SPIN-ORBIT TORQUE I

Simranjeet Singh, Chair
Carnegie Mellon University, Pittsburgh, PA, United States

INVITED PAPER

FOB-01. Clarifying the Origin of Charge-to-Spin Conversion in Ferromagnets. *Y. Hibino*[1], T. Taniguchi[1], K. Yakushiji[1], A. Fukushima[1], H. Kubota[1] and S. Yuasa[1] *1. Research Center for Emerging Computational Technologies, National Institute of Advanced Industrial Science and Technology, Tsukuba, Japan*

Spin current is one of the key technologies for spintronics devices. Especially, generation of spin currents via electrical charge current has attracted a great deal of attentions from both fundamental physics and application point of views because it can manipulate magnetization vector of the ferromagnet [1]. This charge-to-spin conversion phenomena originate from spin-orbit coupling and has been widely studied in non-magnetic materials. Recently, the interest in spin conversion materials has extended to ferromagnetic materials (FMs). FMs can generate magnetization-dependent charge-to-spin conversion (MD-CSC), which is caused by the reduced mirror symmetry due to the presence of magnetization, and this MD-CSC can be used as a writing source for high-density MRAM (Fig. 1) [2]. However, the origin of this MD-CSC has not been calrified yet, for instance, whether the interfacial or bulk contribution is domoinant. In addition to this, a guideline for high spin conversion efficiency is highly required for realizing energy-efficient writing in MRAM devices. In this presentation, we systematically studied the charge-to-spin conversion in ferromagnetic material to clarify its origin [3]. Through precise measurement of spin conversion efficiency via spin-torque ferromagnetic resonance [4], we experimentally revealed that two different mechanisms, which originate from the bulk and at interface, contribute to the charge-to-spin conversion in ferromagnet. Next, we demonstrated a guideline to enhance the spin conversion efficiency which is to control the interface structure between Ni-Co alloy and non-magnetic spacer Cu spacer layer (Fig.2) [3]. Moreover, we show that even the sign of the MD-CSC can be tuned by changing the non-mangetic spacer material [5]. These findings would be a milestone toward realizing a high-density and energy-efficient spin-orbit torque MRAMs. This work was partly supported by Grant-in-Aid for Scientific Research (Nos. JP16J03105, JP25220604, JP15H05702, and JP19J01643) and CREST program (No. JPMJCR18T3) of JST. Part of this work was conducted at the AIST Nano-Processing Facility, supported by Nanotechnology Platform Program of the Ministry of Education, Culture, Sports, Science and Technologies (MEXT), Japan.

[1] A. Manchon et.al, Rev. Mod. Phys. 91, 035004 (2019). [2] S. C. Baek et.al, Nat. Mater. 17, 509-513 (2018). [3] Y. Hibino et al., Nat. Commun. 8, 15848 (2021). [4] Y. Hibino et.al, Phys. Rev. B 101, 174441 (2020). [5] Y. Hibino et al., APL Mater. 8, 041110 (2020).

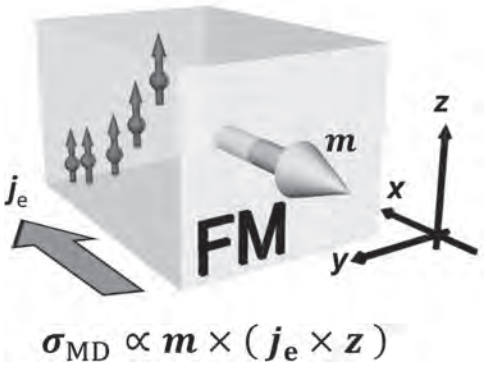

Schematic of MD-CSC in FMs. Yellow arrow and show magnetization of FM (*m*). Green in-plane arrow and red spheres with arrow represents the current direction (j_e) and spin polarization (σ_{MD}) of spin current from MD-CSC flowing along *z*-direction respectively.

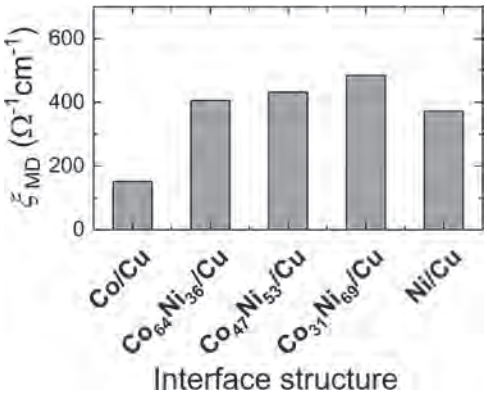

Interface structure dependence of spin conversion efficiency of MD-CSC ξ_{MD}.

CONTRIBUTED PAPERS

FOB-02. Large interfacial Rashba interaction and giant spin-orbit torque in atomically thin metallic multilayers. S. Krishnia[1], Y. Sassi[1], F. Ajejas[1], S. Collin[1], A. Fert[1], J. George[1], N. Reyren[1], H. Jaffres[1] and *V. Cros*[1] *1. Unité Mixte de Physique, CNRS, Thales, Université Paris-Saclay, 91767, Palaiseau, France, Palaiseau, France*

Spin-orbit interaction in metals and its ability to generate spin-current has been the hallmark of spintronics in the last decade. Beyond its fundamental interest as a source of spin-current, the manipulation of magnetization via transfer of the spin angular momentum has proven to be energy efficient for spin-based memory (e.g. SOT-MRAM) and also neuromorphic devices (e.g. using spin Hall nano-oscillators). Therein, charge to spin conversion is believed to be governed essentially by two main mechanisms, spin Hall effect in the bulk of heavy-metals and Rashba effect at interfaces [1], the latter being often considered negligible in all-metallic interfaces. However, in the case of atomically thin metallic layers, the underlying SOT physical

mechanisms at play have not been experimentally fully tackled. In this study, we examine the impact of the insertion of a light element interface on the nature of the SOT as well as its efficiency in terms of damping-like (H_{DL}) and field-like (H_{FL}) effective fields in ultrathin ferromagnets. Importantly, we observe unexpectedly large H_{FL}/H_{DL} ratio (~2.5) upon inserting a 1.4 nm thin Al layer in Pt|Co|Al|Pt as compared to Cu instead of Al as shown in Fig. 1. From our modeling (dotted lines in Fig.1), these experimental results strongly evidence the presence of a large interfacial Rashba effect at Co|Al interface producing giant H_{FL}. The occurrence of such enhanced torques from an interfacial origin is further validated by reducing the contribution from SHE in the bottom Pt layer as well as by demonstrating current-induced magnetization reversal at reduced current. We believe that our results are important from the application point of view as they provide a clear route for reaching ultimate spin-torque efficiency for the associated devices[2]. Acknowledgement: DARPA TEE (MIPR no. HR0011831554), the Horizon2020 Framework Program of the European Commission under FET-Proactive Grant agreement No. 824123 (SKYTOP) and the the Agence Nationale de la Recherche, France, No. ANR-17-CE24-0025 (TOPSKY).

[1] Manchon, A. *et al.,* Rev. Mod. Phys. 91, (2019). [2] Krishnia S. *et al.,* arXiv : 2205.08486.

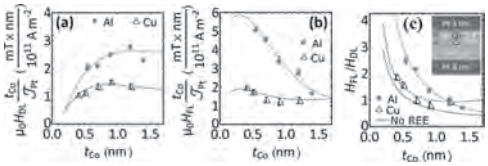

Co thickness (t_{Co}) dependence of (a) DL-SOT field and (b) FL-like SOT fields in Pt8|Co (t_{Co})|Al1.4|Pt3 (red) and Pt8|Co (t_{Co})|Cu1.4|Pt3 (blue) samples (c) $\zeta = H_{FL}/H_{DL}$ as a function of t_{Co}.

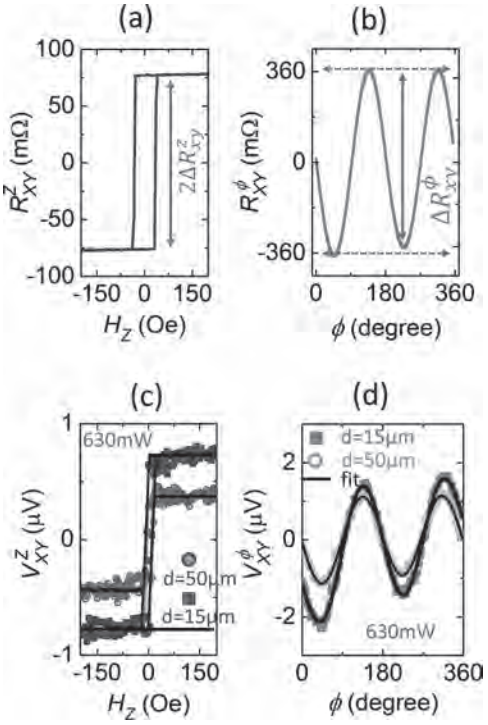

FIG.1. Results for TmIG/W. Hall resistance of TmIG/W for (a) out-of-plane magnetic-field sweep and (b) in-plane field rotation for a field magnitude of 2.7 kOe. Thermally-induced transverse voltages, (c) *Vxy z* and (d) *Vxy* ϕ, for a heater power of 630 mW and for two different heater spacings, *d* = 15 μm (closed squares) and 50 μm (open circles).

FOB-03. Origin of transverse voltages generated by thermal gradients and electric fields in ferrimagnetic-insulator/heavy-metal bilayers. *A. Bose*[1,2], R. Jain[2], J.J. Bauer[3], R. Buhrman[2], C.A. Ross[3] and D.C. Ralph[2]
1. Physics, Johannes Gutenberg University of Mainz, Mainz, Germany; 2. Physics, Cornell University, Ithaca, NY, United States; 3. Material Science, Massachusetts Institute of Technology, Cambridge, MA, United States

We compare thermal-gradient-driven transverse voltages in ferrimagnetic-insulator/heavy-metal bilayers (Tm3Fe5O12/W and Tm3Fe5O12/Pt) to corresponding electrically driven transverse resistances at and above room temperature[1]. The thermal gradient is created by an applying electric current in the lithographically patterned heater, electrically isolated from the device that is located approximately 50 μm away. We find for Tm3Fe5O12/W that the thermal and electrical effects can be explained by a common spin-current detection mechanism, the physics underlying spin Hall magnetoresistance (SMR)[2,3]. However, for Tm3Fe5O12/Pt the ratio of the electrically driven transverse voltages (planar Hall signal/anomalous Hall signal) is much larger than the ratio of corresponding thermal-gradient signals, a result which is very different from expectations for a SMR-based mechanism alone. We ascribe this difference to a proximity-induced magnetic layer at the Tm3Fe5O12/Pt interface[4]. By analyzing the ratio of electrically and thermally driven transverse voltages we find that the dominant contribution of the transverse spin-current is the intrinsic spin-Hall effect that is driven by the longitudinal electrical field either provided by the thermal gradient due to the Seebeck effect or by applying the electric current.

1. Bose, A. *et al.* Origin of transverse voltages generated by thermal gradients and electric fields in ferrimagnetic-insulator/heavy-metal bilayers. *Phys. Rev. B* 105, L100408 (2022). 2. Nakayama, H. *et al.* Spin Hall Magnetoresistance Induced by a Nonequilibrium Proximity Effect. *Phys. Rev. Lett.* 110, 206601 (2013). 3. Meyer, S. *et al.* Observation of the spin Nernst effect. *Nat. Mater.* 16, 977–981 (2017). 4. Huang, S. Y. *et al.* Transport Magnetic Proximity Effects in Platinum. *Phys. Rev. Lett.* 109, 107204 (2012).

FOB-04. Topological Insulator Spin Orbit-Torque Enhancement via Insertion Layer and Crystallinity Control of BiSb(012). *H. Poh*[1], S. Lee[1], C. Ang[1], T. Jin[1], G. Lim[1] and W. Lew[1] *1. School of Physical and Mathematical Sciences, Nanyang Technological University, Singapore*

Topological insulator with high spin orbit efficiency due to its spin-momentum locking in the Dirac surface state is a promising candidate for spintronics applications. However, the surface state is vulnerable to disruption like exchange coupling to FM. Here, we demonstrate different insertion layer (Ti, Cu, Pt) at the Co/BiSb interface to promote the topological surface state of BiSb(012). The BiSb(012) surface state is in focus based on having 3 Dirac cone at the. The insertion layers induced large spin Hall angle of up to 10.4, that were otherwise negligible without any insertion layer. We further explore the spin-orbit torque efficiency with BiSb thicknesses ranging from 10 to 100 nm. Our results show a rapidly increasing spin-orbit torque efficiency with BiSb thickness that gradually saturates above 30nm. A clear correlation between the spin-orbit torque efficiency and the crystalline size of BiSb(012) was later verified via x-ray diffractometry. Thus, confirming the crystalline orientation of BiSb(012) being the crucial factor to achieve high spin orbit efficiency [1]. Our work paves the way for the adaptation of topological insulators as the new class of spin source material for spintronics applications.

N. H. D. Khang, Y. Ueda, and P. N. Hai, *A Conductive Topological Insulator with Large Spin Hall Effect for Ultralow Power Spin–Orbit Torque Switching*, Nat. Mater. 17, 808 (2018).

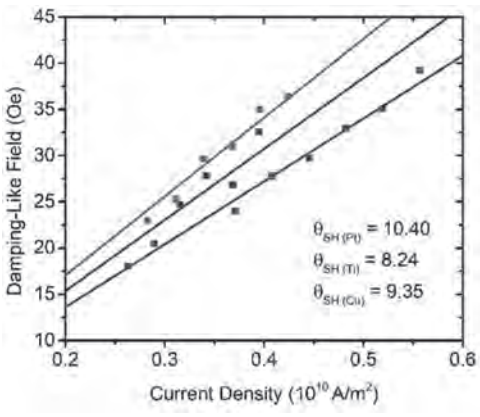

Damping-like field as a function of current density with different insertion layer.

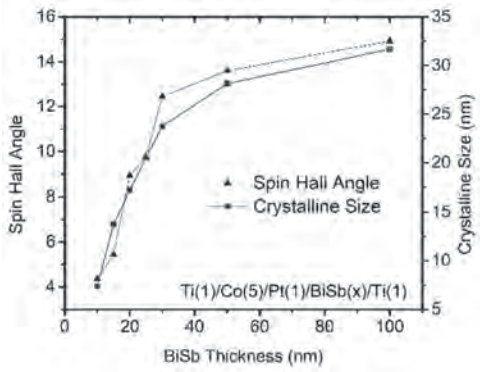

Spin Hall angle and crystalline size of Ti(1)/Co(5)/Pt(1)/BiSb(x)/Ti(1) as a function of BiSb thickness.

FOB-05. Growth-dependent Interlayer Chiral Exchange and Field-free Switching. *Y. Huang*[1], C. Huang[1], W. Liao[1], T. Chen[1] and C. Pai[1,2]
1. Department of material science and engineering, National Taiwan University, Taipei, Taiwan; 2. Center of Atomic Initiative for New Materials, National Taiwan University, Taipei, Taiwan

There are mainly two types of exchange interactions in a multiple-spins system. First being the symmetric exchange, which is directly responsible for the existence of ferromagnetism (FM) and antiferromagnetism (AFM) in which the spins collectively form either parallel or antiparallel configurations. On the other hand, the antisymmetric exchange, or the Dzyaloshinskii-Moriya interaction (DMI) [1-3] has gained significant attention lately. For the majority of cases, DMI is an intralayer effect, i.e. the nonlinear spin configurations are confined within a single magnetic layer. However, pioneering predictions [4] have recently expanded the possibility to an interlayer case, where the spins are from two distinct FM layers. We hereby demonstrate an interlayer DMI in a CoFeB/Pt/Co/Pt multilayer where CoFeB has in-plane anisotropy (IMA), while Co has perpendicular magnetic anisotropy (PMA). The wedge sputtering provides sufficient symmetry breaking for the interlayer DMI to manifest (Fig.1 (a)). A field sweep protocol involving the out of plane external field H_z sweep while applying an in-plane field H_ϕ with various ϕ orientation is used to capture the effective field experienced by the PMA layer. The resultant hysteresis loops of the Co layer are substantially shifted (Fig.1 (b)) and follow a sinusoidal form with respect to the ϕ direction (Fig.1 (d)). The importance of in-plane symmetry breaking is confirmed by comparing results with control samples without symmetry breaking (Fig.1 (c)). The reciprocal effect experienced by the IMA layer is captured by magneto-optical Kerr effect experiments (Fig.1 (d)). Moreover, it is shown that current-induced field-free switching of a PMA layer is achievable utilizing the DMI induced effective field and the switching polarity can be controlled by the interlayer DMI landscape (Fig.2).

[1] Dzyaloshinsky, A thermodynamic theory of 'weak' ferromagnetism of antiferromagnetics, J. Phys. Chem. Sol. 4, 241 (1957). [2] T. Moriya, Anisotropic Superexchange Interaction and Weak Ferromagnetism, Phys. Rev. 120, 91 (1960). [3] A. Fert and P. M. Levy, Role of Anisotropic Exchange Interactions in Determining the Properties of Spin-Glasses, Phys. Rev. Lett. 44, 1538 (1980). [4] E. Y. Vedmedenko, P. Riego, J. A. Arregi, and A. Berger, Interlayer Dzyaloshinskii-Moriya Interactions, Phys. Rev. Lett. 122, 257202 (2019).

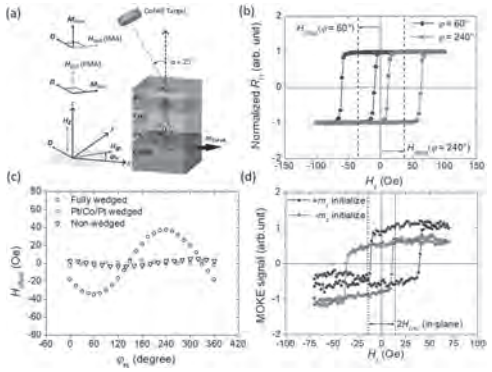

Fig.1 (a) Sketch of the magnetic multilayers, external fields, coordinate system. Interlayer DMI's manifestation on both IMA and PMA hysteresis loops presented in (b) and (d), respectively. Comparison between samples without symmetry breaking presented in (c).

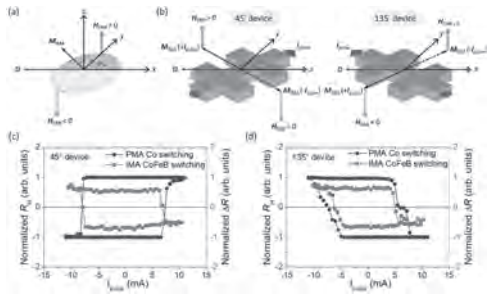

Fig.2 Interlayer DMI landscape demonstrating field free switching and the influence of the device angle on the switching polarity.

FOB-06. Spin-orbit torques in RuO_2/Co-Fe-B bilayer. *T. Nguyen*[1,2], S. DuttaGupta[1,3], Y. Saito[1], S. Fukami[3,1], D. Vu[4], H. Naganuma[2,1], S. Ikeda[2,1], T. Endoh[2,5] and Y. Endo[5,1] *1. Center for Science and Innovation in Spintronics, Tohoku University, Sendai, Japan; 2. Center for Innovative Integrated Electronic Systems, Tohoku University, Sendai, Japan; 3. Research Institute of Electrical Communication, Tohoku University, Sendai, Japan; 4. Institute of Physics, Vietnam Academy of Science and Technology, Hanoi, Vietnam; 5. Graduate School of Engineering, Tohoku University, Sendai, Japan*

Toward the applications to high-performance MRAMs [1, 2], spin-orbit torque (SOT)-induced magnetization switching has been widely investigated in various material systems. While 4*d* transition metals, such as Ru, exhibit low SOT due to the small spin-orbit coupling [3], recent works have reported the SOT generation in antiferromagnetic RuO_2 film thanks to its unique band structure [4], although the detailed understanding is still lacking. Herein, we fabricate the (100)-oriented RuO_2 film and evaluate SOT in a RuO_2/Co-Fe-B bilayer by harmonic Hall measurement. RuO_2 (4 nm)/$Co_{20}Fe_{60}B_{20}$ (1.2 nm) bilayer was fabricated on a α-Al_2O_3 (0001) substrate by DC/RF sputtering, where (100)-oriented RuO_2 film with a likely existence of a three-domain structure is expected to be grown [5]. The resistivity of the RuO_2 film was estimated as 247.4 mΩcm from the sheet resistance. A Ru

(4 nm)/$Co_{20}Fe_{60}B_{20}$ (1.2 nm) bilayer was also fabricated for comparison. The harmonic Hall measurement was performed for Hall bar devices in a rotating magnetic field [Fig. 1]. A clear second harmonic signal is observed for RuO_2/Co-Fe-B while it is negligible for Ru/Co-Fe-B, suggesting the SOT generation owing to the unique band structure of RuO_2. For RuO_2/Co-Fe-B bilayer, the effective fields with the Slonczewski-like torque (H_{SL}) and field-like torque (H_{FL}) symmetries were quantified by fitting [Fig. 2(a, b)]. Linear relation with the applied current density J [Fig. 2(c)] proves that these fields are induced by the current. These results would be important for further research on the current-induced magnetization switching using antiferromagnets. The authors acknowledge JSPS KAKENHI Grants 21K14522, 21K18189, the Core Research Cluster program, the MRAM program in CIES, Tohoku Univ. Fig. 1: The second harmonic Hall resistance vs. field direction curves for Hall bar devices of RuO_2/Co-Fe-B and Ru/Co-Fe-B. Fig. 2: Fitting of H_{SL} (a) and H_{FL} (b). J dependence of $\mu_0 H_{SL}$ and $\mu_0 H_{FL}$ (c).

[1] H. Honjo *et al.*, IEDM Technical Digest 28.5, (2019). [2] M. Natsui *et al.*, JSSC 56, 1116 (2020). [3] T. Tanaka *et al.*, Phys. Rev. B 77, 165117 (2008) [4] A. Bose *et al.*, Nature Electronics 5, 267 (2022). [5] H. Bai *et al.*, Phys. Rev. Lett. 128, 197202 (2022).

Fig. 1:

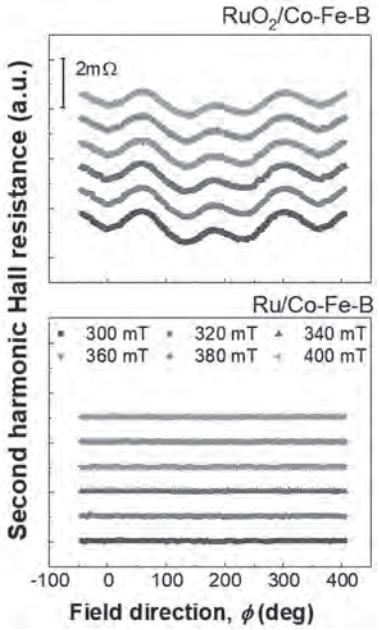

Fig. 2:

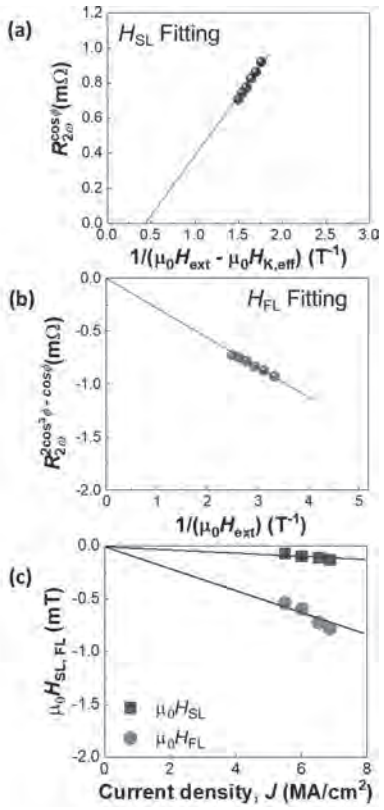

FOB-07. Enhancing Spin-Orbit Torque Efficiency via Orbital Currents. *C. Hu*[1], Y. Chiu[1], C. Tsai[1], C. Huang[1], K. Chen[1], C. Peng[1], C. Lee[2], M. Song[2], Y. Huang[2], S. Lin[2] and C. Pai[1] *1. National Taiwan University, Taipei, Taiwan; 2. Taiwan Semiconductor Manufacturing Company, Hsinchu, Taiwan*

It is of great significance in the memory industry to find a conductive spin current source (SCS) possessing a large damping-like spin-orbit torque efficiency (ξ_{DL}) higher than W, for the purpose of realizing a faster and more efficient spin-orbit torque magnetic random-access memory (SOT-MRAM). Among numerous candidates, 5d transition metal Pt is one of the more competitive spin Hall materials for efficiently generating spin-orbit torques (SOTs) in Pt/ferromagnetic layer (FM) heterostructures, due to its high spin Hall conductivity (SHC) and moderate resistivity. However, for a long while with tremendous engineering endeavors, the of Pt and Pt alloys are still limited to ξ_{DL}<0.5. In this work, we report that with proper alloying elements, particularly the 3d transition metals V and Cr with giant orbital Hall effect (OHE), the strength of the high spin Hall conductivity of Pt (σ_{SH}~6.45×10^5 (h-bar/2e) Ω^{-1} m^{-1}) is observed even in the relatively resistive regime. Especially for the Cr-doped case, an extremely high ξ_{DL}~0.9 in a perpendicular magnetized $Pt_{0.69}Cr_{0.31}$/Co device can be achieved with a moderate $Pt_{0.69}Cr_{0.31}$ resistivity of ρ_{xx}~133 μΩ cm. This sizable SOT efficiency can be attributed to the additional spin current generation from orbital-to-spin current conversion, resulting in the increasing SHC as the Cr concentration in the Pt-Cr alloy increases. Moreover, a low critical SOT-driven switching current density of is also demonstrated, and the damping constant (α) of $Pt_{0.69}Cr_{0.31}$/CoFeB structure is found to be reduced to 0.052 from the pure Pt/CoFeB case of 0.078. The overall high σ_{SH}, giant ξ_{DL}, moderate ρ_{xx}, and the reduction of α make the Pt-Cr/FM heterostructure promising for versatile extremely low power consumption SOT memory applications.

1. Miron, I.M., et al., Perpendicular switching of a single ferromagnetic layer induced by in-plane current injection. Nature, 2011. 476(7359): p. 189-U88. 2. Liu, L.Q., et al., Current-Induced Switching of Perpendicularly Magnetized Magnetic Layers Using Spin Torque from the Spin Hall Effect.

Physical Review Letters, 2012. 109(9). 3. Pai, C.F., et al., Determination of spin torque efficiencies in heterostructures with perpendicular magnetic anisotropy. Physical Review B, 2016. 93(14). 4. Liu, L.Q., et al. Spin-Torque Ferromagnetic Resonance Induced by the Spin Hall Effect. Physical Review Letter, 2011, 106, 036601. 5. Lee, Soogil, et al. "Efficient conversion of orbital Hall current to spin current for spin-orbit torque switching." Communications Physics 4.1 (2021): 1-6. 6. Hu, Chen-Yu, et al. "Toward 100% Spin–Orbit Torque Efficiency with High Spin–Orbital Hall Conductivity Pt–Cr Alloys." ACS Applied Electronic Materials 4.3 (2022): 1099-1108.

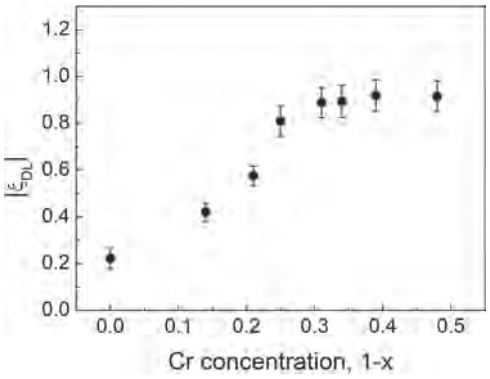

Damping-like spin-orbit torque efficiency of Pt_xCr_{1-x} alloys in Pt-Cr/Co structures.

FOB-08. Spin-orbit torque driven perpendicular magnetization switching in Re/CoFeB/MgO with high thermal stability. *A. Ranjan*[1]
1. Materials Science and Engineering, National Tsing Hua University, Hsinchu, Taiwan

Writing using spin-orbit torque (SOT) has been widely investigated in the field of magnetic random-access memory (MRAM) as it provides several advantages over Spin transfer torque (STT) based writing, including a much faster writing speed, better writing endurance, and protection to MgO from oxide breakdown due to a large current flowing across it during STT writing process, among others. Heavy metal(HM)/CoFeB/MgO is the core of this SOT-MRAM structure. The heterostructure consisting of Ta as the spin current source and CoFeB/MgO as the perpendicular magnetic anisotropy (PMA) material is the most researched structure owing to the high tunneling magneto-resistance ratio. However, Ta is difficult to be integrated into the CMOS process due to its poor thermal stability against annealing at temperatures greater than 350 °C. Currently, β-Tungsten (W) is the only heavy metal with CoFeB/MgO system, which can provide both thermal stability and spin-orbit torque switching simultaneously. Nevertheless, achieving a high resistive β phase of W is a challenging task, and the high resistivity of β-W makes the devices susceptible to Joule's heating. Here, we report another material Rhenium (Re) capable of providing thermally stable PMA up to temperature 425 °C with a perpendicular anisotropic field greater than 5000 Oe; Re possesses a spin hall angle (θ_{SH}) of 0.065 ± 0.003 and spin-orbit torque switching can be achieved with current density around 1.36×10^{11} A/m^2. Our findings pave a new avenue for the material design of perpendicular SOT-based MRAM.

G. G. An, J. B. Lee, S. M. Yang, ACTA MATERIALIA 87, 259 (2015). T. Liu, Y. Zhang, J. W. Cai, and H. Y. Pan, SCIENTIFIC REPORTS 4, 5895 (2014). B. Dieny, and M. Chshiev, REVIEWS OF MODERN PHYSICS 89, 025008 (2017). T. Liu, J. W. Cai, and L. Sun, AIP ADVANCES 2, 032151 (2012). L. Liu, C. F. Pai, Y. Li, H. W. Tseng, D. C. Ralph, and R. A. Buhrman, SCIENCE 336, 555 (2012). C. L. Yang, and C. H. Lai, SCIENTIFIC REPORTS 11, 15214 (2021). J. W. Lee, Y. W. Oh, and B. G. Park, PHYSICAL REVIEW B 96, 064405 (2017).

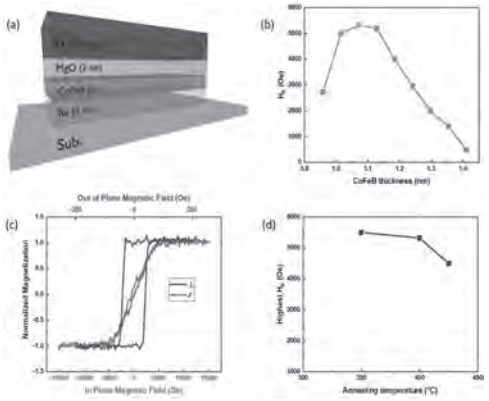

Fig. 1. Tuning Magnetic anisotropy of the sample Si/SiO_2/Re (5)/ $Co_{20}Fe_{60}B_{20}$ (t)/MgO (2)/Ta (3.5) (in nm). (a) Sample structures, and (b) H_K at different CoFeB thicknesses annealed at 400 °C, (c) In plane and out of plane MH curves for CoFeB thickness of 1.1 nm annealed at 400 °C, and, (d) Highest H_K obtained at different annealing temperatures.

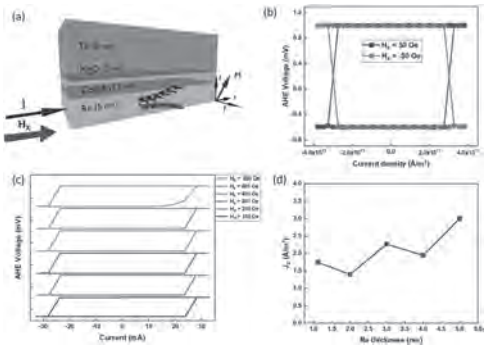

Fig. 2. SOT switching in Re(5)/CoFeB(1.1)/MgO(2)/Ta(5). (a) Current induced SOT switching using SHE and measurement set up in our structure, (b) SOT switching under $H_X = \pm 50$ Oe, and (c) SOT under different H_X, and (d) J_C for SOT switching for different Re thicknesses.

FOB-09. Spin-to-charge conversion at cryogenic temperatures in the chiral antiferromagnet Mn_3Sn interfaced with a metallic ferromagnet. *V. Sharma*[1], R. Nepal[1], H. Kaur[1] and R. Budhani[1] *1. Department of Physics, Morgan State University, Baltimore, MD, United States*

The latest findings of extremely large anomalous Hall [1] and magnetic inverse spin Hall effect [2] in chiral antiferromagnets such as Mn_3Sn have brought the study of magnetic topological states to the frontage of condensed matter research. Here we focus on the studies of spin-to-charge conversion processes in epitaxial films of Mn_3Sn interfaced with polycrystalline layer of permalloy (Py), both deposited sequentially by magnetron sputtering on (111) MgO crystals. The enhanced Gilbert damping in these bilayers, as suggested by a pronounced increase in the slope of FMR linewidth (ΔH) vs excitation frequency (f) seen in Fig. 1 above $f \geq 15$ GHz establish the presence of spin pumping at the interface. Interestingly, the FMR linewidth of these bilayers at $f \leq 15$ GHz also suggests a two-magnon scattering (TMS) contribution to damping of precessing magnetization at room temperature. The key finding of our research is the observation of two-magnon processes in the FMR driven inverse spin Hall effect (ISHE) in this chiral antiferromagnet based heterostructure down to 2.5 K (Fig. 2). The temperature dependence of ISHE spectrum has been analyzed by taking into account magnetic phase transitions in the chiral magnet and spin rectification effects in the conducting ferromagnet Py.

[1] Nakatsuji, Satoru, Naoki Kiyohara, and Tomoya Higo. "Large anomalous Hall effect in a non-collinear antiferromagnet at room temperature." Nature 527.7577 (2015): 212-215. [2] Kimata, Motoi, et al. "Magnetic and

magnetic inverse spin Hall effects in a non-collinear antiferromagnet." Nature 565.7741 (2019): 627-630.

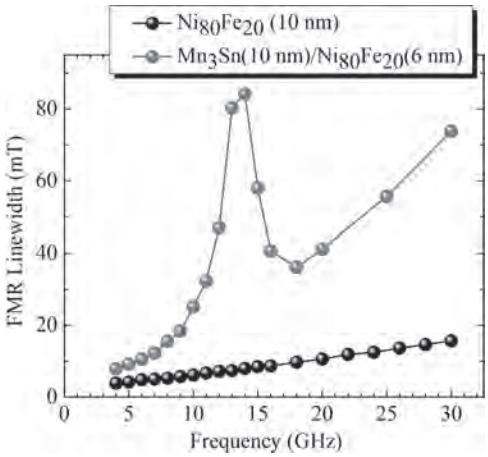

Variation of ferromagnetic resonance linewidth with frequency at room temperature for bare Py($Ni_{80}Fe_{20}$) film and Mn_3Sn/Py bilayer.

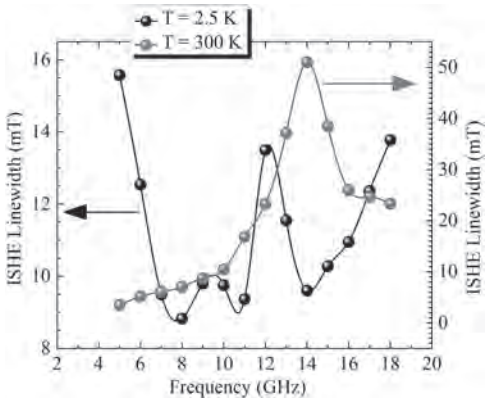

Variation of Inverse spin Hall linewidth with frequency at room temperature (300K) and 2.5 K for Mn_3Sn/Py bilayer.

FOB-10. Spin-orbit Torque Study on MBE-grown $Bi_{1-x}Sb_x$ Thin Films. *Y. Ou*[1], W. Yanez[1], Y. Huang[1], S. Ghosh[2], C. Sahin[3], M. Stanley[1], A. Richardella[1], M.E. Flatté[4], A. Mkhoyan[2] and N. Samarth[1] *1. Department of Physics, The Pennsylvania State University, State College, PA, United States; 2. Department of Chemical Engineering and Materials Science, University of Minnesota, Minneapolis, MN, United States; 3. Institute of Materials Science and Nanotechnology, Bilkent University, Ankara, Turkey; 4. Department of Physics and Astronomy, University of Iowa, Iowa City, IA, United States*

The synthesis of topological insulators (TIs) of good crystalline quality provides an attractive material platform for low power-consumption spintronic devices of relevance for non-volatile memory applications. While experimental measurements of strong spin-orbit torque (SOT) have been reported in $Bi_{1-x}Sb_x$ alloys, one of the earliest discovered TIs, key questions remain about the nature of SOT in this material system. We describe the synthesis of $Bi_{1-x}Sb_x$ thin films of good crystalline quality by molecular beam epitaxy (MBE) and the characterization of these films using *in vacuo* angle-resolved photoemission spectroscopy (ARPES) as well as *ex situ* transmission electron microscopy, x-ray diffraction, and Raman spectroscopy. ARPES measurements of samples with varying compositions allow us to track the band structure across the trivial and topological regimes. After synthesizing $Bi_{1-x}Sb_x$/Permalloy heterostructures *in vacuo* with a clean interface, we use spin-torque ferromagnetic resonance (ST-FMR) measurements at room temperature to study the SOT as a function of alloy composition. The experimentally observed behavior of charge-to-spin conversion in $Bi_{1-x}Sb_x$ is then compared to theoretical calculations of the spin Hall conductivity in this material system [Phys. Rev. Lett. 114, 107201 (2015)]. Supported by the Penn State 2DCC-MIP under NSF Grant No. DMR-2039351 and by SMART, one of seven centers of nCORE, a Semiconductor Research Corporation program, sponsored by the National Institute of Standards and Technology (NIST).

FOB-11. Large Spin Hall Effects in a Model Epitaxial $BaPb_{1-x}Bi_xO_3$ / $La_{0.7}Sr_{0.3}MnO_3$ System. *I. Harris*[1], A. Edgeton[2], X. Huang[1], R. Yalisove[1], G. Fratian[1], M. Mazur[3], L. Caretta[1], S. Susarla[4,1], C. Eom[2], D.C. Ralph[3] and R. Ramesh[1] *1. University of California, Berkeley, Berkeley, CA, United States; 2. University of Wisconsin, Madison, Madison, WI, United States; 3. Cornell University, Ithaca, NY, United States; 4. Lawrence Berkeley National Laboratory, Berkeley, CA, United States*

Spintronics is a promising field centered around next-generation devices that use electronic spin to store and manipulate information. Since there are no ohmic losses inherent in the transfer of spin – for example in magnons or pure spin currents – spintronic devices have the potential to be very energy efficient, and lots of efforts have been taken over the last few decades to apply spintronic principles to make 'beyond CMOS' devices. However, one of the major challenges in spintronics is to find material systems with efficient spin-to-charge conversion, and the lack of such model systems has kept practical, energy efficient spintronic applications from being realized. We propose a new pathway for discovering model systems with efficient spin-to-charge conversion in epitaxial oxide heterostructures. We present on one such system, $BaPb_{1-x}Bi_xO_3$ / $La_{0.7}Sr_{0.3}MnO_3$ (BPBO/LSMO), grown by pulsed laser deposition with excellent crystalline quality characterized by X-ray diffraction and TEM. Using spin-torque ferromagnetic resonance (STFMR) experiments, we measured a spin-orbit torque efficiency of 3 – over an order of magnitude greater than typical spin-orbit coupled metals. We confirm this measurement with samples grown and measured across 3 different labs, along with transverse STFMR and Second Harmonic experiments (see Fig. 1). We also find an enhancement of the spin-orbit torque efficiency for thinner layers of BPBO, indicating that the epitaxial interface plays an important role in the generation of spin-orbit torques. With a better understanding of the role of the interface in spin-orbit torque generation, and by exploring similar complex oxide systems, we hope to find a model epitaxial oxide heterostructure that can be used for energy efficient spintronic applications. We acknowledge SRC-ASCENT for funding support.

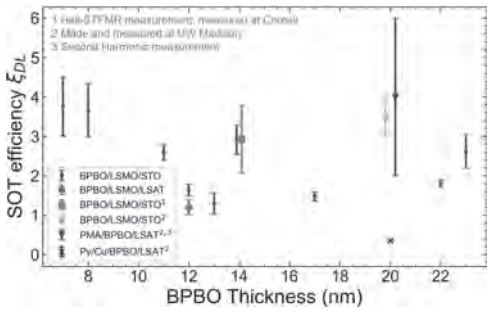

Fig. 1: Spin orbit torque (SOT) efficiency of BPBO/LSMO heterostructures across a range of BPBO thicknesses, measured by STFMR technique unless otherwise noted. A few different magnetic layers and substrates are included for comparison, confirming the high SOT efficiency of BPBO heterostructures.

FOB-12. Experimental study and first principles calculation of the spin Hall Effect in $La_{0.67}Sr_{0.33}MnO_3$. *I. Park*[1], T. Mabe[1], P. Gupta[2], A. Mishra[2], A. Swain[2], S. Bedanta[2] and V.P. Amin[1] *1. Physics, Indiana University - Purdue University, Indianapolis, Indianapolis, IN, United States; 2. School of Physical Sciences, National Institute of Science Education and Research, Jatani, India*

In spintronics, the spin Hall effect is one of the most important mechanisms to generate and manipulate the spin current in an efficient way. Recent experimental study represented in [1] shows that anti-damping and the inverse spin Hall effect are observed simultaneously in the $La_{0.67}Sr_{0.33}MnO_3$ (LSMO)/Pt heterostructure. Further, it has been observed that single layer LSMO films also exhibit significant amount of intrinsic spin Hall effect (ISHE) voltage (as seen in Fig. 1). Therefore, a series of LSMO films with varying thickness have been deposited via pulsed laser deposition technique to confirm the intrinsic ISHE in LSMO films. Polarity of measured voltage changes when we rotate our sample to 180 deg, which indicates the existence of intrinsic spin pumping in LSMO films. In order to elucidate the physical origin of experimental observations, we compute the spin Hall conductivity of LSMO using first principles calculations. First, the ground state electronic structure of LSMO is calculated using density functional theory (DFT), as implemented in Quantum Espresso package. Using Wannier90, the system was interpolated into maximally-localized Wannier functions (MLWF) basis. Then we employ the Kubo formula to compute the spin Hall conductivity tensors of LSMO to assess the generation of spin current for a given electric field.

[1]: P. Gupta, B. B. Singh, K. Roy, et al. Nanoscale., Vol. 13 p. 2714-2719 (2021)

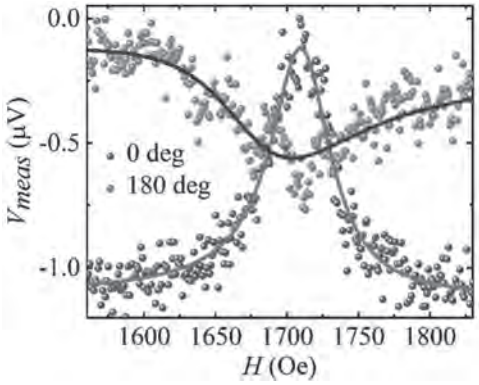

Fig. 1. V_{meas} for STO/LSMO (40 nm) sample.

Session FOC
SPIN HALL AND SPIN-ORBIT TORQUE II

Yongxi Ou, Chair
The Pennsylvania State University, State College, PA, United States

INVITED PAPER

FOC-01. Gate-Tuneable and Chirality-Dependent Charge-to-Spin Conversion in Tellurium Nanowires. *M. Gobbi*[1,2], F. Calavalle[1], M. Suárez-Rodríguez[1], B. Martín-García[1], A. Johansson[3], D.C. Vaz[1], H. Yang[1], I. Maznichenko[3], S. Ostanin[3], A. Mateo-Alonso[4,2], A. Chuvilin[1,2], I. Mertig[3], F. Casanova[1,2] and L.E. Hueso[1,2] *1. CIC nanogune BRTA, Donostia - San Sebastian, Spain; 2. Ikerbasque, Basque Foundation for Science, Bilbao, Spain; 3. Institute of Physics, Martin Luther University Halle-Wittenberg, Halle, Germany; 4. POLYMAT, University of the Basque Country UPV/EHU, Donostia - San Sebastian, Spain*

Charge-to-spin interconversion enables the electrical generation of spin currents without magnets.[1] For instance, the flow of a charge current generates a net spin polarization in materials characterized by strong spin-orbit coupling and broken inversion symmetry through the Edelstein effect. Lacking inversion and mirror symmetry, chiral materials are the ideal playground to explore the relation between structural symmetry and electronic spin transport.[2] Indeed, several studies show how chiral organic molecules act as efficient spin filters, but their poor conductivity hinders their application in field effect devices. Much less attention has been drawn on spin effects in inorganic chiral crystals, such as elemental Te, even though they offer an optimal combination of crystal structure, strong spin-orbit coupling, and good conductivity. Here, we report a chirality-dependent and gate-tuneable charge-to-spin conversion in single-crystalline Te nanowires. [3] In particular, the generation of a net spin polarization is inferred by recording a dependence of the nanowire resistance on the relative orientation of electrical current and and applied magnetic field (Figure 1). By analyzing this effect, called unidirectional magnetoresistance (UMR), we show that an electrical current along the nanowire generates a spin polarization oriented parallel to the chiral axis and pointing in opposite direction for different crystal handedness. This charge-to-spin conversion arises from the radial spin texture of the valence band of Te, which dominates the transport in the hole-doped nanowires. In addition, the charge-to-spin conversion can be tuned by electrostatic gating, leading to a modulation of the UMR amplitude by a factor of six. The all-electrical generation, control, and detection of spin polarization in chiral Te NWs opens the path to exploit chirality in spintronic devices.

[1] A. Soumyanarayanan, N. Reyren, A. Fert, and C. Panagopoulos, Nature, Vol. 539, p. 509 (2016) [2] S.-H. Yang, R. Naaman, Y. Paltiel, and S. S. P. Parkin, Nat. Rev. Phys., Vol. 3, p.328 (2021) [3] F. Calavalle, M. Suárez-Rodríguez, B. Martín-García et al., Nat. Mater., Vol. 21, p. 526 (2022)

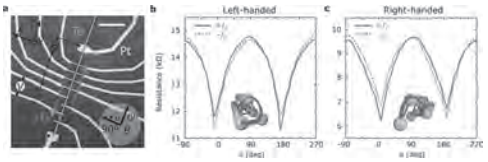

Figure 1. Chirality-dependent unidirectional magnetoresistance in Te nanowires. (a) optical image of a typical Te nanowire contacted with Pt electrodes (the scale bar corresponds to 10 μm). The current was applied in opposite direction along the chiral axis; the magnetic field was applied at an angle α between the nanowire and the applied was varied. (b,c) Angular dependence of the resistance of two Te nanowires with opposites handedness (confirmed by Transmission Electron Microscopy). Solid and dashed lines were recorded by applying the current in opposite current directions. A large difference in the resistance (up to 7%) is recorded when the magnetic field and the current are parallel and antiparallel, corresponding to α = 0 ° and 180 °, respectively. In the insets, 3D sketches of the left- and right-handed crystal structure of Te.

CONTRIBUTED PAPERS

FOC-02. Detection of spatial spin distribution in a strong Rashba channel at room temperature. *S. Kim*[1,2], W. Lee[3], K. Kim[2], K. Lee[3], G. Choi[4,5] and H. Koo[1,2] *1. KU-KIST Graduate School of Converging Science and Technology, Korea University, Seongbuk-gu, The Republic of Korea; 2. Center for Spintronics, Korea Institute of Science and Technology, Seongbuk-gu, The Republic of Korea; 3. Department of Physics, Korea Advanced Institute of Science and Technology, Yuseong-gu, The Republic of Korea; 4. Department of Energy Science, Sungkyunkwan University, Suwon, The Republic of Korea; 5. Center for Integrated Nanostructure Physics, Institute for Basic Science (IBS), Suwon, The Republic of Korea*

The charge-to-spin conversion and spin transfer from spin-orbit channel to ferromagnet (FM) layer have been a fascinating phenomena in spin transport devices. The spin current generation and modulation by spin-orbit coupling (SOC), Rashba-Edelstein effect (REE) and spin Hall effect (SHE) have been widely researched in a variety of systems. Spin-orbit torque (SOT) in a metal/ferromagnet interface has been focused due to great interests in the field of memory application. However, direct observation of these phenomena have not been rarely distinguished in an FM/semiconductor structure. In a quantum well system, spin Hall and Rashba effects have been observed via an electrical method [1] but spin distribution and spin orientation have not been spatially resolved. In this research, we directly detect the spatial spin distribution and spin-orbit torque in an InAs-based two-dimensional electron gas (2DEG). [2] The spin current, which is induced by REE and SHE at the 2DEG channel, is detected by polar- and longitudinal- magneto-optical Kerr effects (MOKEs) at room temperature. In addition to spin accumulation induced by SHE at edge of the channel, clear spin polarization by REE is distributed in entire channel area as shown in Figure 1. Furthermore, we fabricated the FM/insulator/2DEG hybrid structure for investigating REE and SOT in a 2DEG channel. We measured sizable REE-driven SOT signals in 2DEG using direct- and time-resolved MOKEs as shown in Figure 2. The detected signals agree to the behavior of field-like torque expected by

Landau-Lifshitz-Gilbert (LLG) equation. Despite a relatively thicker InAlAs and GaAlAs barrier (20 nm), spin-orbit torque from channel to FM layer is clearly observed. This clear spin transport signal with a very thick barrier in our system appears to be due to the phonon mediated transfer.

[1] W. Y. Choi, H.-j. Kim, J. Chang *et al*, *Nat. Nanotechnol.* 10, 666-670 (2015) [2] W. B. Lee, S. B. Kim, K.-W. Kim *et al*, *Phys. Rev. B* 104, 184412 (2021)

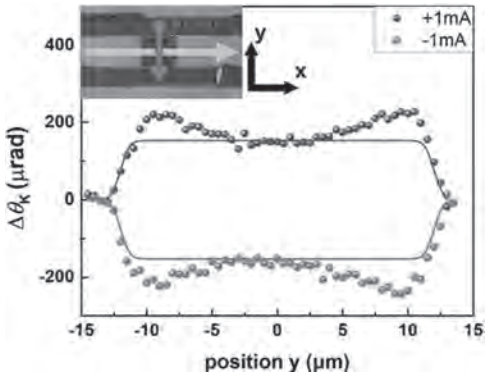

Fig 1. A spatial scanning of *y*-polarized spin accumulation driven by REE in 2DEG using MOKEs.

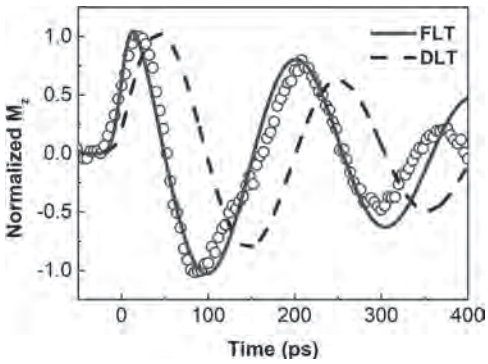

Fig 2. Transient magnetization signal in a FM/insulator/2DEG structure.

FOC-03. Anomalous Hall Effect and Exotic Torques in Non-Collinear Antiferromagnet Mn3Pt. *R. Klause*[1], S. Siddiqui[2] and A. Hoffmann[1]
1. Department of Materials Science and Engineering and Materials Research Laboratory, University of Illinois Urbana Champaign, Urbana, IL, United States; 2. Intel Corporation, Hillsboro, OR, United States

Mn_3Pt is a non-collinear antiferromagnet with an fcc crystal structure and magnetic moments on the Mn atoms that are at an angle of 120° with respect to each other. This arrangement breaks the cubic symmetry and allows for the existence of the anomalous Hall effect. Here we measure an anomalous Hall effect in Mn_3Pt thin films that is only present at temperatures below 270K. This can be explained by a transition from a collinear (above 270K) to a non-collinear (below 270K) antiferromagnetic phase, which is characterized by a sudden change in resistance of the film. Moreover, because of mirror symmetry breaking due to the magnetic structure, we expect to generate exotic spin-torques with a spin-polarization component along the out-of-plane direction, which is unlike the conventional in-plane spin polarization direction. This allows for efficient and deterministic switching of out-of-plane magnetized materials through spin-orbit torques.

FOC-04. Effect of seed layer thickness on Ta crystalline phase and spin Hall angle. K. Sriram[1], J. Pala[1], B. Paikaray[1], A. Haldar[2] and *C. Murapaka*[1] *1. Materials Science and Metallurgical Engineering, Indian Institute of Technology Hyderabad, Sangareddy, India; 2. Department of Physics, Institute of Technology Hyderabad, Sangareddy, India*

Spin-orbit coupling (SOC) plays a vital role in spin-to-charge interconversion in heavy metal (HM)-ferromagnet (FM) bilayer structures [1]. Spin pumping is an efficient method to generate pure spin current by the precessional motion of magnetization, which transfers angular momentum to HM. The efficiency of spin pumping is quantified by an interfacial parameter called spin-mixing conductance ($g_{\downarrow\uparrow}$). Electrical detection of spin current is possible via inverse spin Hall effect (ISHE) which converts spin current into charge current. The efficiency of spin-to-charge interconversion is quantified by spin Hall angle (θ_{SH}) [2]. The θ_{SH} of heavy metal highly depends on its crystalline phase and the effect of the seed layer on the phase of HMs is largely overlooked. Here, we report the effect of seed permalloy ($Ni_{80}Fe_{20}$, Py) layer thickness on the Tantalum (Ta) and Tungsten (W) crystalline phase and its θ_{SH}. We have observed a structural phase transition in Ta as a function of seed layer thickness (t_{Py}) affecting the θ_{SH} of the Ta layer. Due to strain at the interface between crystalline Py and Ta, Ta exhibits a mixed-phase (α+β) on the seed permalloy layer when $t_{Py} > 12$ nm. However, Ta nucleates as α-Ta on Py with $t_{Py} < 8$ nm, Py does not exhibit prominent crystalline nature. The phase transition of Ta is primarily attributed to strain at the Py/Ta interface which is not observed in both Py(t_{Py})/W(10) and $Co_{40}Fe_{40}B_{20}$ (t_{CFB})/Ta(18) bilayer structure. Ferromagnetic resonance (FMR) based spin pumping shows that effective damping is enhanced for all samples. The maximum $g_{\downarrow\uparrow}$ of 10.1×10^{18} m^{-2} is observed for Si/Py(20)/Ta(18) and the minimum value of 7.9×10^{18} m^{-2} for Si/Py(8)/Ta(18) which corresponds to (α+β)-phase of Ta and α-phase of Ta, respectively. The estimated θ_{SH} for (α+β)-Ta is 0.15 ± 0.009, which is higher than α-Ta. The combined effect of symmetry breaking and low longitudinal resistance are the primary reason for the high $g_{\downarrow\uparrow}$ and θ_{SH}. Our systematic study provides an insight into Ta phase transition via seed layer thickness and gives an alternative route for tuning [3].

[1] A. Brataas, Y. V. Nazarov, and G. E. W. Bauer, Finite-Element Theory of Transport in Ferromagnet–Normal Metal Systems, Phys. Rev. Lett. 84, 2481 (2000). [2] Y. Tserkovnyak, A. Brataas, and G. E. W. Bauer, Nonlocal Magnetization Dynamics in Ferromagnetic Heterostructures, Rev. Mod. Phys. 77, 1375 (2005). [3] K. Sriram, A. Haldar, and C. Murapaka, Effect of Seed Layer Thickness on the Ta Crystalline Phase and Spin Hall Angle, Nanoscale 13, 19985 (2021).

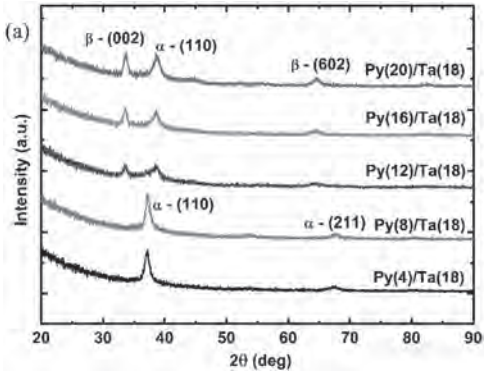

(a) Ta(18) phase transition from α-Ta to (α+β)-Ta as function of Py thickness (t_{Py}).

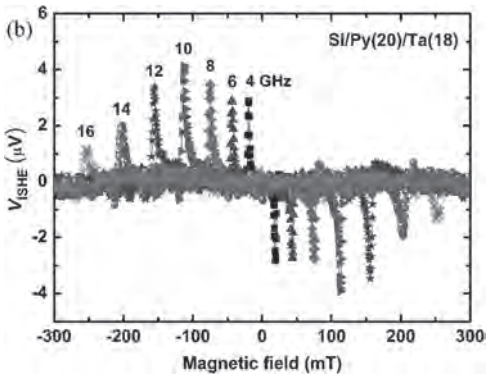

(b) Inverse spin Hall voltage drop for Py(20)/(α+β)-Ta(18).

FOC-05. High-throughput study of spin and orbital transport in magnetic materials. *Y. Yahagi*[1,2] and J. Zelezny[3] *1. Applied Physics, Tohoku University, Sendai, Japan; 2. NEC-AIST Quantum Technology Cooperative Research Laboratory, NEC Corporation, Tsukuba, Japan; 3. Institute of Physics, Czech Academy of Science, Prague, Czechia*

We study the spin Hall effect (SHE) and the orbital Hall effect (OHE) in magnetic materials using automatic high-throughput calculation scheme. The SHE is a phenomenon in which an applied electric field induces a spin current. This effect plays a key role in various spintronics devices. Although the SHE has been researched mainly in nonmagnetic materials, SHE in magnetic materials has gained a considerable attention recently as they can exhibit a large SHE[1]. The OHE, a phenomenon in which electric field generates a flow of orbital angular momentum, has also been attracting attention as a new driving mechanism of devices [2]. For future application, exploring materials with large SHE or OHE is demanded. In this study, we perform a systematic evaluation of the spin Hall conductivity (SHC) and the orbital Hall conductivity (OHC) of select materials from MAGNDATA[3], a database of magnetic materials. We target collinear materials both ferromagnets and antiferromagnets, and evaluate their intrinsic contributions of SHC and OHC based on Kubo-formula. Figure 1 shows the results of SHC and OHC of 84 materials. The OHCs in most materials are nearly ten times larger than the SHCs. Interestingly, the Mn3Pt has a colossal OHC reaching about 14000 (hbar/e)S/cm, which is higher than either OHC of Mn (~10000) and Pt (~2000) [4], suggesting the importance of the material structure. Further analysis of both theoretical aspect and data science will be presented at the conference.

[1] C. Qin, et al., Phys. Rev. B 96, 134418 (2017); Y. Zhang et al., New J. Phys. 20, 7 (2018). [2] H. Kontani, et al., J. Phys. Soc. Jpn., 76, 103702 (2007). [3] S.V. Gallego et al., J. Appl. Crystallogr. 49, 1750 (2016). [4] D. Jo, D. Go, and H-W. Lee, Phys. Rev. B 98, 214405 (2018).

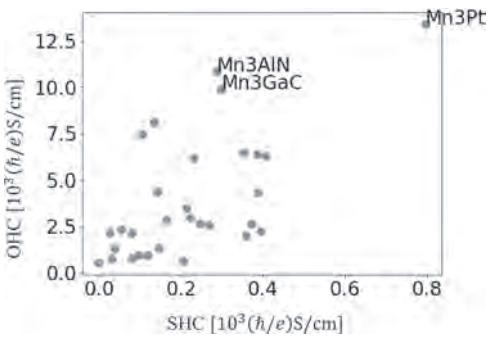

Figure 1: Calculation results of the spin Hall conductivity (SHC) and the orbital Hall conductivity (OHC).

FOC-06. Tuning Spin-Orbit Torque Efficiencies of Pt via Sub-monolayer Insertions of Cr and Cu. *W. Janssens*[1,2], G. Talmelli[2], K. Cai[2], R. Carpenter[2], J. De Boeck[1,2], G.S. Kar[2] and S. Couet[2] *1. Department of Electrical Engineering, KU Leuven, Leuven, Belgium; 2. imec, Leuven, Belgium*

One of the biggest challenges to date to achieve fast and energy-efficient spin-orbit torque magnetic random-access memories (SOT-MRAM) is significantly decreasing its switching current. This can be realised by increasing the damping-like SOT (DL-SOT) efficiency in spin current source/ferromagnet heterostructures [1]. Among the different systems, a promising candidate for this heterostructure is Pt/Co. It yields good perpendicular magnetic anisotropy (PMA), moderate resistivities and its DL-SOT efficiency can be significantly increased by alloying Pt with other heavy metals like Cu [2] and Cr [3]. In this study we propose a different approach where 0.2nm Cu and Cr are inserted in a 5nm Pt matrix. A number of insertions up to 8 is considered to increase the resistivity (Fig.1) theoretically via interfacial scattering as in [4]. From X-ray diffraction (XRD), transmission electron microscopy (TEM) and energy-dispersive X-ray spectroscopy (EDS), textured PtCr- and PtCu-alloys are observed. Specifically, f.c.c. crystals are obtained for all Cr contents and Cu below 12%, while above 12% hexagonal crystalline structure. The alloying behaviour is in contrast with the hypothesis that the resistivity increase is governed by interfacial scattering and can thus be attributed solely to a decrease of Pt content in the alloy. 1 nm of in-situ sputtered Co is used as magnetic layer and shows PMA for all structures with a 50-60% reduction of coercivity with increasing Cr or Cu insertions (in-set Fig.2). A 20% loss of magnetic moment is observed after one insertion but no further reduction is obtained for more (Fig.2). Using 2nd harmonic voltage technique on Hall bars, a two times improvement of the DL-SOT efficiency is observed compared to the Pt reference. Additionally, annealing up to 400°C is examined for this study in the same layers both from structural (alloy evolution) and magnetic (loss of PMA due to diffusion) point of view. In the full work, an in-depth comparison between the two systems will be presented considering structural, chemical, electrical and magnetic properties. W. J. acknowledges funding by The Research Foundation Flanders (FWO) – grant number 1S34022N.

[1] Garello K., et al. (2019). *2019 IEEE 11th International Memory Workshop : IMW 2019 : 12-15 May 2019, Monterey, California, USA.* [2] Hu, C. Y., Pai, C. F. (2020). Benchmarking of Spin–Orbit Torque Switching Efficiency in Pt Alloys. *Advanced Quantum Technologies*, *3*(8). [3] Chuang, T. C., Pai, C. F., & Huang, S. Y. (2019). Cr-induced Perpendicular Magnetic Anisotropy and Field-Free Spin-Orbit-Torque Switching. *Physical Review Applied*, *11*(6). [4] Zhu, L., Ralph, D. C., & Buhrman, R. A. (2021). Maximizing spin-orbit torque generated by the spin Hall effect of Pt. *Applied Physics Reviews, 8(3), 031308*.

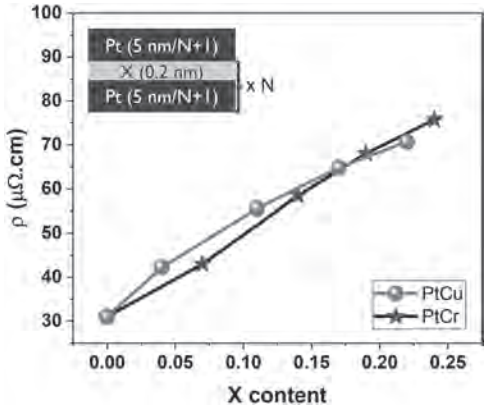

Fig.1 Resistivity trend

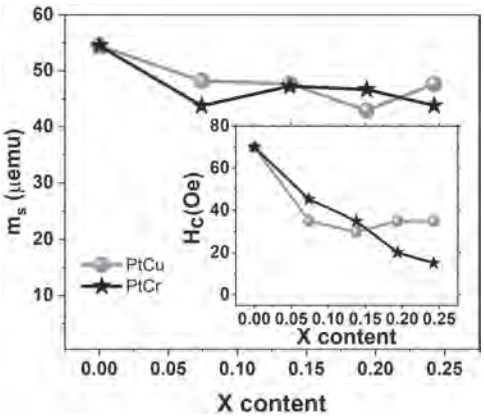

Fig. 2 Magnetic properties

FOC-07. Anatomy of Type-*x* Spin-Orbit Torque Switching: Simulations and Experiments. *Y. Liu*[1], C. Huang[1], Y. Huang[1], K. Chen[1], C. Tsai[1], Y. Li[1], T. Chang[1], C. Cheng[1] and C. Pai[1,2] *1. Department of Material Science and Engineering, National Taiwan University, Taipei, Taiwan; 2. Center of Atomic Initiative for New Materials, National Taiwan University, Taipei, Taiwan*

Current-induced type-*x* spin-orbit-torque (SOT) switching configuration describes the orthogonal relationship between the magnetic easy-axis (EA) of ferromagnetic (FM) layer and the injected spin polarization σ from heavy metal (HM) layer, which has potential to eclipse the conventional type-*y* scenario (EA‖σ) at short pulse regime [1,2]. In this study, we systematically investigate type-*x* SOT switching properties in HM/FM heterostructures. First, through macrospin simulations, we demonstrate that deterministic type-*x* switching can be realized by applying an assisting *z*-direction external field (H_z) or by introducing a canted EA. From current pulsed width (t_{pulse}) dependent simulations, we observe that the critical switching current (I_{sw}) of type-*x* is indeed smaller than that of type-*y* in the sub-ns regime [Fig. 1(a)]. By further considering a positive field-like SOT (FLT) in the simulated system, type-*x* switching mode results in a lower I_{sw} than that of type-*y* when t_{pulse} < 10 ns [Fig. 1(b)], suggesting the advantage of employing the type-*x* design with material system having sizable FLTs. Accordingly, we choose W/CoFeB bilayer structure, which has a sizable FLT, to experimentally observe type-*x* SOT switching in micron-sized devices. By utilizing current-sensed differential planar Hall signal [3], the field-free type-*x* switching is observed for both positively and negatively *y*-canted devices [Fig.2 (a) and (b)], with opposite switching polarities. A *z*-direction internal field originated from the canted EA in concert with the damping-like SOT is observed by analyzing H_z-assisted switching phase diagram. Under the zero-field condition, as canting angle (ϕ_{EA}) increases, the switching dynamics evolves from a pro-type-*x* scenario to a pro-type-*y* scenario [Fig.2 (c) and (d)]. Our systematic work therefore verifies the advantage of canted EA for field-free type-*x* SOT applications, which can be informative for designing more efficient next generation SOT-MRAMs.

[1] S. Fukami, T. Anekawa, C. Zhang, and H. Ohno, A spin-orbit torque switching scheme with collinear magnetic easy axis and current configuration, Nat. Nanotechnol. 11, 621 (2016). [2] S. Fukami, T. Anekawa, A. Ohkawara, Z. Chaoliang, and H. Ohno, A sub-ns three-terminal spin-orbit torque induced switching device, IEEE Symposium on VLSI Technology, 61 (2016). [3] G. Mihajlović, O. Mosendz, L. Wan, N. Smith, Y. Choi, Y. Wang, and J. A. Katine, Pt thickness dependence of spin Hall effect switching of in-plane magnetized CoFeB free layers studied by differential planar Hall effect, Appl. Phys. Lett. 109, 192404 (2016).

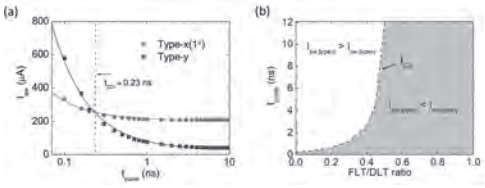

Fig.1 Macrospin simulations (a) t_{pulse} dependence of I_{sw} and (b) I_{sw} phase diagram for type-*x* and type-*y* schemes.

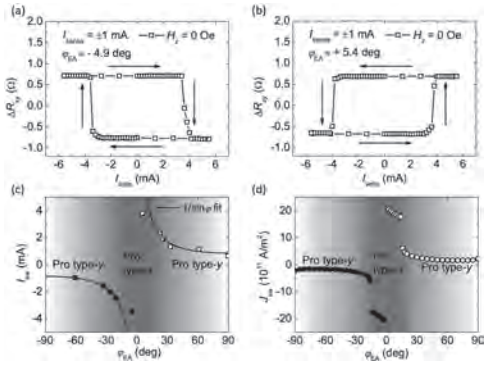

Fig.2 The field-free SOT switching results for (a) ϕ_{EA} = -4.9° and (b) ϕ_{EA} = +5.4°. Switching phase diagram through (c) experiments and (d) simulations.

FOC-08. Efficient generation of spin currents by the orbital Hall effect in Cu and Al. *A. Rothschild*[1], N. Am-Shalom[1], N. Bernstein[1], M. Meron[1], T. David[1], E. Frohlich[1], B. Assouline[1], J. Xiao[2], B. Yan[2] and A. Capua[1] *1. The Hebrew University of Jerusalem, Jerusalem, Israel; 2. Weizmann Institute of Science, Rehovot, Israel*

Spin currents are the primary building block of spintronics technology. The spin Hall effect (SHE) has proven to be a well-established method for generating spin currents. The SHE relies widely on heavy metals due to their large spin-orbit coupling (SOC). However, the large SOC [1-2] is also responsible for a high Gilbert damping. The orbital counterpart of the SHE is the orbital Hall effect (OHE). In the OHE an orbital current is generated without relying on SOC [3-5], and thus is expected to overcome the penalty of the high losses associated with heavy metals. In this work we demonstrate the ability to polarize spins using pure Cu and Al in agreement with the OHE theory [6]. To that end an ultra-thin layer of SOC is used to convert the orbital current to a useful spin current. Furthermore, our results show that Cu and Al are capable of generating spin currents more efficiently as compared to the SHE of Pt while benefiting from lower Gilbert damping. Our results open a new avenue for atomically engineered spin-based devices.

[1] J. E. Hirsch, Physical Review Letters 83, 1834 (1999). [2] S. Murakami, N. Nagaosa, and S.-C. Zhang, Science 301, 1348 (2003). [3] S. Zhang and Z. Yang, Physical Review Letters 94, 066602 (2005). [4] B. A. Bernevig, T. L. Hughes, and S.-C. Zhang, Physical Review Letters 95, 066601 (2005). [5] T. Tanaka, H. Kontani, M. Naito, Physical Review B 77, 165117 (2008). [6] D. Jo, D. Go, and H.-W. Lee, Physical Review B 98, 214405 (2018).

FOC-09. Spurious symmetric voltage signals on the spin torque ferromagnetic resonance measurement induced by oxide substrates. *G. Ji*[1], Y. Chai[1], D. Jiang[1], H. Chen[2], D. Yi[2] and T. Nan[1] *1. School of Integrated Circuits and Beijing National Research Center for Information Science and Technology, Tsinghua University, Beijing, China; 2. Material Science and Technology, Tsinghua University, Beijing, China*

Recently, transition metal oxide thin films with strong bulk or interfacial spin-orbit coupling have demonstrated to exhibit exceptionally large spin Hall angle, which can potentially enable energy-efficient spin-orbit torque

devices. To characterize the spin Hall efficiency, spin-torque ferromagnetic resonance (ST-FMR) or spin pumping measurements that operate at microwave frequencies have been widely used in oxide epitaxial thin films on various oxide substrates. At high frequency, the dielectric loss of those oxide substrates could significantly influence the resonance spin torque signals. However it has not been well considered when evaluating the spin Hall efficiency. Here we report that some insulating oxide substrates could generate significant spurious symmetric voltage signals on ST-FMR measurements, leading to serious overestimation of spin-Hall angle. We investigate the spurious signals in five widely used insulating oxide substrates $SrTiO_3$, $KTiO_3$, $DySrO_3$, LSAT, and Al_2O_3 by performing ST-FMR measurements in oxide substrate/ferromagnetic bars. We find that all the devices present considerable resonance voltage signals even with the absence of spin source layer, see Fig.1. Among which, STO, KTO, DSO show significant symmetric voltage signals, while Al_2O_3 presents S/A smaller than other oxides due to its large A signal. In contrast, the low frequency second harmonic Hall measurements give no signals for all the devices, indicating that the extra resonance signals on ST-FMR are not originated from spin Hall effect. Our work reveals significant influence of oxide insulator substrates on ST-FMR measurement that should be taken into account on study of spin Hall angle.

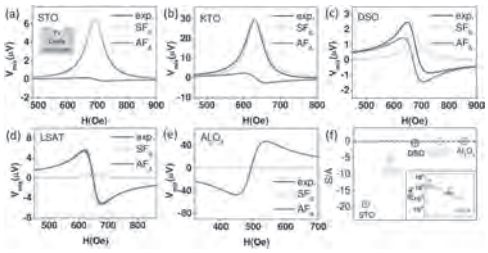

Fig. 1 ST-FMR spectra of oxides/Py devices. The oxides utilized are (a) STO, (b)KTO, (c)DSO, (d)LSAT and (e)Al_2O_3, repectively. The dark grey solid line is experimental data; cyan solid line, the symmetric Lorentzian fitting; and the magenta solid line, antisymmetric Lorentzian fitting. All the tests were conducted at $f = 6$ GHz, $\phi = 45°$ and room temperature. Compare of S/A value for all the oxides/Py devices are present on (e). The grey dash line illustrates the reference when S/A equals to zero. The inset is |S/A| shown in logarithmic scale.

FOC-10. Synchronization of Spin-Torque Nano-Oscillators. *F. Ai*[1,2] and V. Lomakin[1,2] *1. University of California, San Diego, La Jolla, CA, United States; 2. Center for Memory and Recording Research, La Jolla, CA, United States*

Spin-transfer nano-oscillators (STNO) can generate a microwave voltage output based on a DC input current. However, a single oscillator generates a relatively small amount of power. To address this issue, a solution is to have an array of STNOs and synchronize them, thus leading to much greater generated power. Achieving synchronization in a large array of oscillators can be challenging due to the complexity of interactions. Here, we proposed a structure that can allow synchronization in a large array of STNO by means of spin waves in a thin magnetic film. The structure is based on a honeycomb configuration, which has low-damping hexagonal regions with high-damping embedded triangle regions (Fig. 1). STNOs are placed at each narrow neck of the pattern. The spin waves generated by the STNO propagate within the low-damping region, whereas they are damped in the high-damping regions. The narrow neck width is smaller than the spin wave wavelength, so that the spin waves do not pass there. Thus, each STNO only has nearest-neighbor interactions (Fig. 2). By limiting the range of interaction, synchronization in a large array of STNOs is possible. Furthermore, the coupled oscillations can be tuned by either changing the STNO driving current or using extra current on the high damping region to reduce the effective damping constant to allow more connections among adjacent STNOs within a certain region.

Fig 1. Illustration of the model. The green regions are of low damping allowing for the spin wave propagation. The colored triangular regions have higher damping to absorb spin wave. STNOs are shown as the small dots.

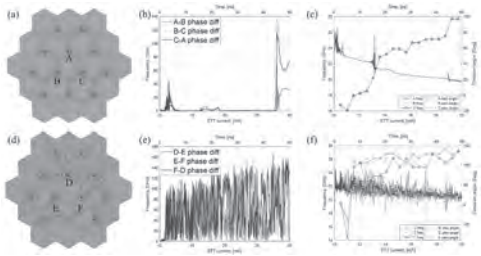

Fig 2. Synchronization of 12 oscillators under different STT currents. (a) the spin wave interference pattern with high-damping regions present. (b) time dependence of the phase differences between oscillators A, B, and C with the linearly increasing current. The stable phase difference indicates synchronization. (c) time dependence of the frequency and elevation angle. (d-f) present the same results as in (a-c) but for the case with no high-damping regions. Here, no synchronization is achieved.

FOC-11. Interfacial and bulk spin-Hall contributions to field-like spin-orbit torque generated by Iridium. *S. Dutta*[1], A. Bose[2], A. Tulapurkar[1], R. Buhrman[3] and D.C. Ralph[4] *1. Electrical Engineering, Indian Institute of Technology Bombay, Mumbai, India; 2. Physics, Institute of Physics, Johannes Gutenberg University of Mainz, Mainz, Germany; 3. Applied & Engineering Physics, Cornell University, Ithaca, NY, United States; 4. Physics, Cornell University, Ithaca, NY, United States*

We present measurements of spin-orbit torques (SOTs) generated by Ir as a function of film thickness in sputtered Ir/CoFeB and Ir/Co samples[1] via spin-torque ferromagnetic resonance (ST-FMR)[2] and second harmonic Hall[3] techniques. We find that Ir provides a damping-like component of spin-orbit torque with a maximum spin-torque conductivity (and a maximum spin-torque efficiency of $\xi_{DL} = 0.042 \pm 0.005$, which is sufficient to drive switching in an 0.8 nm film of CoFeB with perpendicular magnetic anisotropy. We also observe a surprisingly large field-like spin-orbit torque (FLT). Measurements as a function of Ir thickness indicate a substantial contribution to the FLT from an interface mechanism so that in the ultrathin limit there is a non-zero FLT with a maximum torque conductivity(. When the Ir film thickness becomes comparable to or greater than it's spin diffusion length, 1.6 ± 0.3 nm, there is also a smaller bulk contribution to the field-like torque.

1. Dutta, S., Bose, A., Tulapurkar, A. A., Buhrman, R. A. & Ralph, D. C. Interfacial and bulk spin Hall contributions to fieldlike spin-orbit torque generated by iridium. *Phys. Rev. B* 103, 184416 (2021). 2. Liu, L., Moriyama, T., Ralph, D. C. & Buhrman, R. A. Spin-Torque Ferromagnetic Resonance Induced by the Spin Hall Effect. *Phys. Rev. Lett.* 106, 036601 (2011). 3. Hayashi, M., Kim, J., Yamanouchi, M. & Ohno, H. Quantitative characterization of the spin-orbit torque using harmonic Hall voltage measurements. *Phys. Rev. B* 89, 144425 (2014).

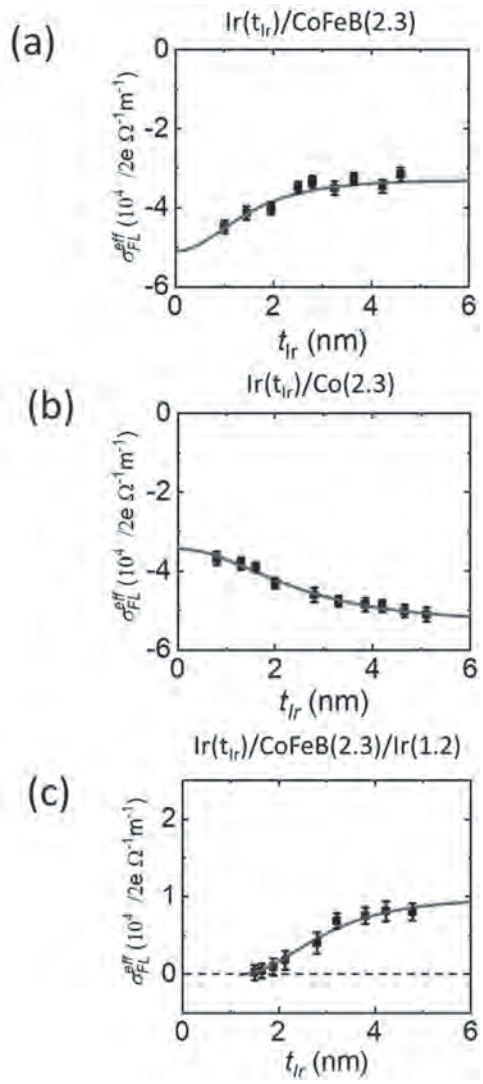

Effective field-like spin-torque conductivity as a function of Ir thickness for (a) Ir/CoFeB(2.3), (b) Ir/Co(2.3), (c) Ir/CoFeB(2.3)/Ir(1.2).

FOC-12. Helium Ion Microscopy for Deterministic Multi-level SOT switching. J. Kurian[1], *A. Joseph*[1], G. Hlawacek[2], S.C. Hertel[1], C. Fowley[2], P. Dunne[1], G. Atcheson[3], M. Venkatesan[3], J.M. Coey[3] and B. Doudin[1]
1. IPCMS UMR 7504, Université de Strasbourg, CNRS, Strasbourg, France; 2. Institute of Ion Beam Physics and Materials Research, Helmholtz-Zentrum Dresden - Rossendorf, Dresden, Germany; 3. AMBER and School of Physics, Trinity College, Dublin, Ireland

Spin Orbit Torque (SOT) induced multilevel magnetization switching shows potential applications in the field of high-density data storage[1] and neuromorphic computing[2]. However, the difficulty to locally pattern magnetic bits with a well-defined set of several different controlled SOT switching current values limits the practical applicability of this technology. We investigate the current induced switching properties of Pt/Co/W heterostructures with perpendicular magnetic anisotropy (PMA) by patterning into Hall bars and performing focused He^+ beam assisted mask-less irradiation. The critical current required to switch the magnetic state depends on the saturation magnetization and magnetic anisotropy, which are interface dependent and can be tuned by the He^+ irradiation dose [3]. By means of partial irradiation of the Hall junction with several different doses, we design a device whose intermediate multi-domains states can be deterministically accessed using an electric current, resulting in a SOT induced multi-level switching. We do the *in-situ* monitoring of the Hall voltage under ion irradiation of different exposed areas (Fig. 1a) which not only allow us to determine the critical dose but also confirms the Hall bar's spatial sensitivity towards partial junction irradiation. By irradiating the Hall cross distinct areas with two different doses, we achieve a 4-level switching. To better understand the sample behavior and to optimize parameters, in operando magneto-optical Kerr effect (MOKE) imaging is used during SOT measurements. A thorough investigation of irradiation dose and pattern design make possible up to 8-level switching as shown in Fig. 1b. We demonstrate a promising and practical approach for improved data storage and high-performance computation in SOT-based spintronic devices which opens the door to preferential current driven magnetisation switching of predetermined areas of the sample, defined down the nm resolution of ion beam microscopy.

[1] K.-F. Huang, D.-S. Wang, M.-H. Tsai, H.-H. Lin, and C.-H. Lai, "Initialization-Free Multilevel States Driven by Spin–Orbit Torque Switching," *Adv. Mater.*, vol. 29, no. 8, p. 1601575, 2017, doi: https://doi.org/10.1002/adma.201601575. [2] Y. Cao, A. Rushforth, Y. Sheng, H. Zheng, and K. Wang, "Tuning a Binary Ferromagnet into a Multistate Synapse with Spin–Orbit-Torque-Induced Plasticity," *Adv. Funct. Mater.*, vol. 29, no. 25, p. 1808104, 2019, doi: 10.1002/adfm.201808104. [3] C. Chappert *et al.*, "Planar Patterned Magnetic Media Obtained by Ion Irradiation," *Science*, vol. 280, no. 5371, pp. 1919–1922, Jun. 1998, doi: 10.1126/science.280.5371.1919.

Figure 1(a) Evolution of in-situ anomalous Hall resistance with irradiation for different exposed area of Hall cross. (b) MOKE acquired SOT induced magnetization switching curve of 8-level switching device under a bias field of 125 mT.

Session FOD
SPIN TRANSPORT

Bhaskaran Muralidharan, Co-Chair
Indian Institute of Technology, Bombay, India
Yuki Hibino, Co-Chair
National Institute of Advanced Industrial Science and Technology, Tsukuba, Japan

INVITED PAPER

FOD-01. Giant Spin-valve Effect in Oxide-based Lateral Nano-scale Channel Devices. *T. Endo*[1], S. Tsuruoka[1], S. Kaneta-Takada[1], L. Anh[1,2], S. Ohya[1,2] and M. Tanaka[1,2] *1. Department of Electrical Engineering and Information Systems, The University of Tokyo, Bunkyo, Japan; 2. Center for Spintronics Research Network, The University of Tokyo, Bunkyo, Japan*

Spin MOSFET [1] is one of the devices proposed as post-Moore devices since it accommodates transistor and non-volatile memory functions within a single device structure. So far, vertical- and lateral-type spin-MOSFET structures have been studied. In the vertical type spin-MOSFET, high magnetoresistance (MR) was achieved, but the transistor capability was not at all satisfactory [2], indicating the difficulty of modulating the electrical current in a non-magnetic channel layer between two ferromagnetic (FM) electrodes by applying a gate voltage. Adopting the lateral structure will overcome this difficulty, but previous works on this type reported small MR ratios (~1 %), owing to the small spin polarization of the FM electrodes, e.g., Fe, or a long channel length (~ μm). In this work, we use emerging properties of perovskite oxides and nano-fabrication technology to solve these problems. We introduced the half-metallic perovskite oxide [3], $La_{2/3}Sr_{1/3}MnO_3$ (LSMO), as the FM material and fabricated spin-valve devices with a very short (~30 nm) channel (Fig. 1). In this device, we see an extremely high MR ratio of 115 %, the highest value ever reported for lateral spin-valve structures, and confirmed that it maintains a high MR ratio of ~50 % when the bias voltage is as high as 100 mV (Fig. 2). These results highlight the potential of oxide nanostructures for spintronics three-terminal devices. This work was partly supported by Grants-in-Aid Scientific Research, the CREST program of JST, and the Spintronics Research Network of Japan.

[1] S. Sugahara and M. Tanaka, Appl. Phys. Lett., Vol. 84, p.2307 (2004) [2] T. Kanaki, *et al.*, Appl. Phys. Lett., Vol. 107, p.242401 (2015) [3] J. H. Park *et al.*, Nature Vol. 392, p.794 (1998)

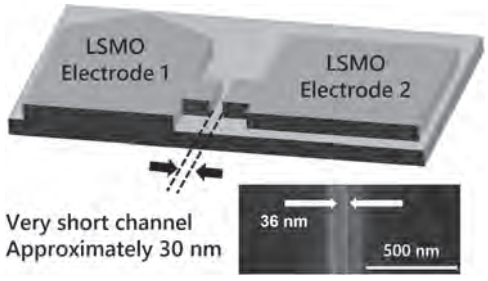

Fig. 1 Schematic illustration of the lateral spin-valve device, with two LSMO FM electrodes separated by a ~30 nm length channel. The inset shows the scanning electron microscopy (SEM) image of the device.

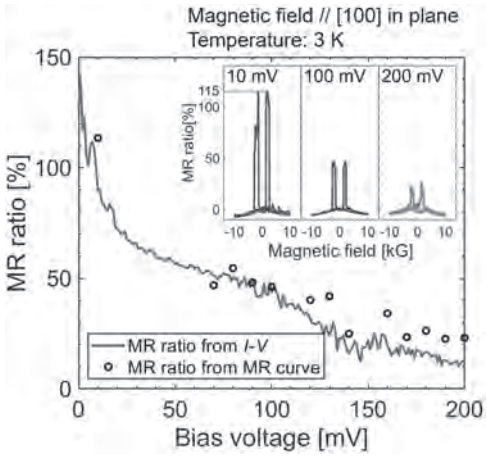

Fig. 2 Bias-voltage dependence of the MR ratio measured at 3 K. The solid line was obtained using the *I-V* data in the parallel and antiparallel magnetization states. The dots represent the MR ratio obtained from the MR curve at each bias voltage. The inset shows the MR curves at bias voltages of 10 mV, 100 mV, and 200 mV. Extremely large spin-valve signal (MR ratio: 115 %) is observed at 10 mV. The MR ratios of the spin-valve signals at 100 mV and 200 mV are 46 % and 23 %, respectively.

CONTRIBUTED PAPERS

FOD-02. Long-distance spin transport in strained SiGe. *T. Naito*[1], M. Yamada[2,3], Y. Wagatsuma[4], K. Sawano[4] and K. Hamaya[3,5] *1. Graduate School of Engineering Science, Osaka University, Toyonaka, Japan; 2. PRESTO, JST, Kawaguchi, Japan; 3. Center for Spintronics Research Network, Osaka University, Toyonaka, Japan; 4. Advanced Research Laboratories, Tokyo City University, Setagaya, Japan; 5. Institute for Open and Transdisciplinary Research Initiatives, Osaka University, Suita, Japan*

Recent studies revealed that spin diffusion length (λ_s) and spin lifetime (τ_s) of electrons in Ge are governed by spin-flip scattering among conduction band valleys (intervalley spin-flip scattering) [1]. To reduce the intervalley spin-flip scattering frequency, Tang *et al*. have theoretically predicted that lifting the degenerate four valleys through a lattice strain is effective [2]. In this study, we experimentally study the effect of strain on spin transport in strained $Si_{0.1}Ge_{0.9}$, which exhibits a Ge-like electronic band structure. A strained *n*-$Si_{0.1}Ge_{0.9}$ spin transport layer (~70 nm) with a carrier concentration (*n*) of ~1×10^{18} cm^{-3} was grown on Ge/Si(111) substrates by molecular beam epitaxy (MBE), where the in-plane tensile strain of ~0.66% was confirmed by reciprocal space map. Then, we fabricated lateral spin-valve (LSV) devices with a Co-based Heusler alloy spin injector/detector [3,4]. A representative four-terminal nonlocal spin signal ($|\Delta R_{NL}|$) at room temperature is shown in the inset of Fig. 1. Figure 1 shows contact distance (*d*)-dependent $|\Delta R_{NL}|$ at room temperature for LSV devices with the

strained n-$Si_{0.1}Ge_{0.9}$ and an n-Ge. The dashed lines are fits to the data using $|\Delta R_{NL}| \propto \exp(-d/\lambda_s)$ and the estimated value of λ_s for the strained n-$Si_{0.1}Ge_{0.9}$ (n-Ge) is estimated to be ~0.93 μm (~0.50 μm). Notably, an approximately twofold increase in λ_s is attributed to the enhanced electron mobility and spin lifetime, induced by lifting the valley degeneracy and by obtaining relatively low carrier concentration [5]. We also demonstrate long-distance spin-drift transport under the electric field (E) and clearly observe pronounced Hanle oscillations with d = 7 μm at T = 50 K in a three-terminal measurement with a drift current of I_D = -0.5 mA, as shown in Fig. 2.

[1] K. Hamaya *et al*., J. Phys. D: Appl. Phys., Vol. 51, p.393001 (2018) [2] J. -M. Tang *et al*., Phys. Rev. B, Vol. 85, p.045202 (2012) [3] M. Yamada *et al*., NPG Asia Mater., Vol. 12, p.47 (2020) [4] K. Kudo *et al*., Appl. Phys. Lett., Vol. 118, p.162404 (2021) [5] T. Naito *et al*., Phys. Rev. Applied (accepted)

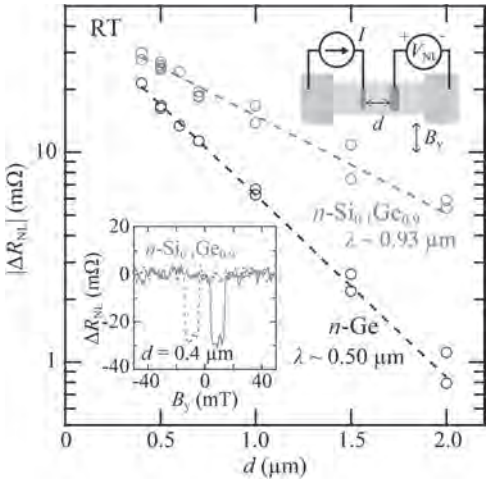

Fig. 1. Contact distance (d)-dependence of $|\Delta R_{NL}|$ at room temperature for the strained n-$Si_{0.1}Ge_{0.9}$ and the n-Ge. The insets show a four-terminal nonlocal measurement setup (right) and a representative spin signal (left).

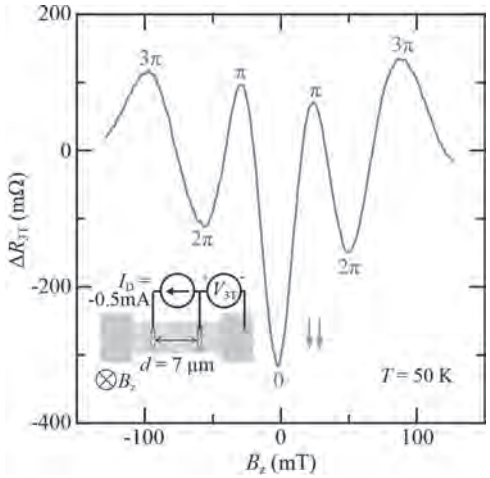

Fig. 2. Hanle precession signal in a parallel magnetization state at d = 7 μm, at I_D = -0.5 mA, and at T = 50 K. Inset shows a three-terminal setup for spin-drift transport measurements.

FOD-03. Spin Transport in Mg-based Nonlocal Spin Valves.

J. Ramberger[1], B. Kaiser[1], J.E. Dewey[1] and C. Leighton[1] *1. Department of Chemical Engineering and Materials Science, University of Minnesota - Twin Cities, Minneapolis, MN, United States*

Substantial gaps remain in the understanding of spin transport in low-Z nonmagnetic (N) metals, despite their use in spintronic technology. While Elliot-Yafet spin relaxation is known to prevail in such metals, the β_i constants that relate spin relaxation times to momentum relaxation times are only known for certain defect types (i), primarily in simple metals like Cu [1] and Al [2]. Other low-Z metals with potentially long spin diffusion lengths have been barely explored [3], and their β_i remain unknown. In this work we thus explore spin transport in Mg, using nonlocal spin valves (NLSVs). Mg-based NLSVs were deposited by UHV evaporation on Si/SiN_x using Al and Ti seed layers. As shown by specular wide-angle X-ray diffraction (Fig. 1(a)) and (0002) pole figures (Fig. 1(b)), strong out-of-plane (0001) texture arises, while in-plane texture (Fig. 1(c)) is negligible. Significantly, the (0001) texture of HCP Mg is significantly stronger with HCP Ti *vs*. FCC Al seeds (right and left of Figs. 1(b,c)). These Mg films exhibit the lowest residual resistivities (0.99 μΩ cm) and highest residual resistivity ratios (>6) reported for polycrystalline Mg films and nanowires. In NLSVs, the low-temperature spin diffusion length, β_{phonon}, and β_{defect} reach 550 nm, 28000, and 5300 in $Ni_{80}Fe_{20}$/Al(5 nm)/Mg(100 nm) NLSVs, compared to 370 nm, 16000, and 1200 in $Ni_{80}Fe_{20}$/Ti(4 nm)/Mg(100 nm) NLSVs (Fig. 2). We hypothesize that these improvements in spin transport parameters in the Al-seed case arise due to weaker (0001) texture. Specifically, recent spin-hot-spot-based [4] theoretical predictions for HCP Mg predict 2200% higher β for spins injected along the Mg c-axis vs. in the basal plane [5]; our results may constitute the first experimental evidence for this highly anisotropic spin relaxation. This work was supported by the NSF.

[1] J. D. Watts, L. O'Brien, J. S. Jeong et al., Phys. Rev. Mater., Vol. 3, p.124409 (2019). [2] J. D. Watts, J. T. Batley, N. A. Rabideau et al., Phys. Rev. Lett., Vol. 128, p.207201 (2022). [3] H. Idzuchi, Y. Fukuma, L. Wang et al., Appl. Phys. Exp., Vol. 3, p.049202 (2010). [4] J. Fabian and S. Das Sarma, Phys. Rev. Lett., Vol. 81, p.5624 (1998). [5] B. Zimmermann, P. Mavropoulos, N. Long et al., Phys. Rev. B, Vol. 93, p.144403 (2016)

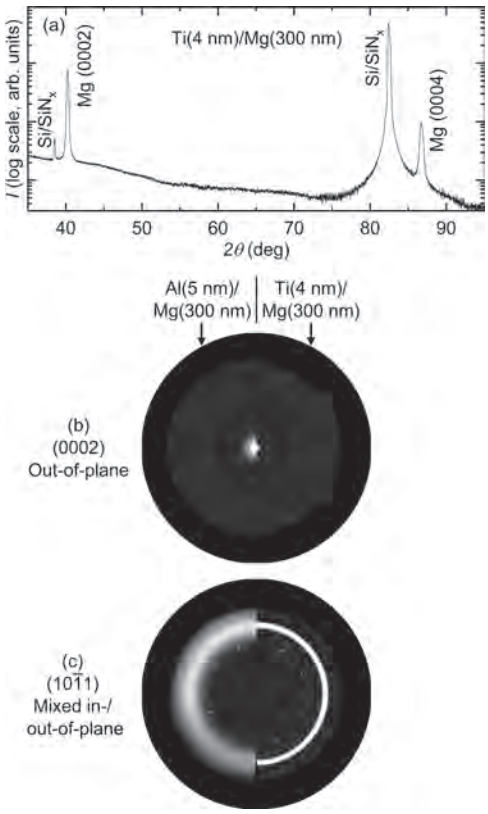

Fig. 1: (a) Integrated 2D XRD intensity versus scattering angle *2θ* for a Ti(4 nm)/Mg(300 nm) film. (b-c) (0002) and (10-11) pole figures projected onto the substrate normal for Al(5 nm)/Mg(300 nm) (left) and Ti(4 nm)/Mg(300 nm) (right).

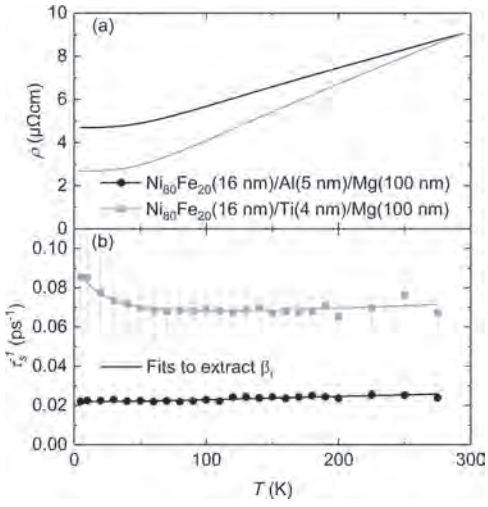

Fig. 2: Representative resistivities (a) and spin relaxation rates (b) vs. temperature for $Ni_{80}Fe_{20}$/ Mg(100 nm) NLSVs with Al and Ti seed layers.

FOD-04. Room temperature spin signals improved by low-temperature annealing in Co_2MnSi/Fe/Ge lateral spin-valve devices. *M. Yamada*[1,2], K. Sumi[3], T. Naito[3], K. Sawano[4] and K. Hamaya[2,5] *1. PRESTO, JST, Kawaguchi, Japan; 2. Center for Spintronics Research Network, Osaka University, Toyonaka, Japan; 3. Graduate School of Engineering Science, Osaka University, Toyonaka, Japan; 4. Advanced Research Laboratories, Tokyo City University, Setagaya, Japan; 5. Institute for Open and Transdisciplinary Research Initiatives, Osaka University, Suita, Japan*

When the thermal annealing processes were conducted for spintronic device structures consisting of ferromagnet/semiconductor heterojunctions, electrical spin injection/detection efficiencies could drastically decrease owing to the interfacial outdiffusion of an element in semiconductors into the ferromagnetic electrodes [1]. Recently, we demonstrated $L2_1$ ordered Co_2MnSi/Fe/Ge heterostructures to suppress the outdiffusion, resulting in an achievement of high MR ratio of ~ 0.1% at room temperature even in lateral spin valve (LSV) devices [2]. Here, we investigate the detailed annealing temperature dependence of nonlocal spin signals (ΔR_{NL}) at room temperature for Co_2MnSi/Fe/Ge LSV devices. To explore the annealing effect on the spin signal, we fabricated LSV devices with 8-nm-thick Co_2MnSi (CMS)/0.7-nm-thick Fe/*n*-Ge Schottky-tunnel contacts. As a reference, a $Co_2FeAl_{0.5}Si_{0.5}$ (CFAS)/0.7-nm-thick Fe/*n*-Ge LSV device was also fabricated [3]. Then, the devices were annealed from 100 to 300°C in N_2 atmosphere. The normalized $|\Delta R_{NL}|$ at room temperature is plotted as a function of the annealing temperature (T_{anneal}) in Fig. 1. While the normalized $|\Delta R_{NL}|$ for the CFAS/Fe/Ge LSV device monotonically decreases with increasing T_{anneal}, the normalized $|\Delta R_{NL}|$ for the CMS/Fe/Ge LSV device is enhanced up to approximately twice values at T_{anneal} = 240°C, as shown in the inset of Fig. 1. These results indicate that the $L2_1$ ordered CMS ferromagnetic contacts are useful for semiconductor-based spintronics devices with thermal annealing fabrication processes less than ~250°C. This work was supported by JSPS KAKENHI (Nos.19H05616, 19H02175, 21H05000, and 21K18719), JST PRESTO (No. JPMJPR20BA), and Spin-RNJ.

[1] B. Kuerbanjiang *et al.*, Phys. Rev. B vol. 98, p.115304 (2018) [2] K. Kudo *et al.*, Appl. Phys. Lett. vol. 118, p.162404 (2021) [3] M. Yamada *et al.*, NPG Asia Mater. vol. 12, p.47 (2020)

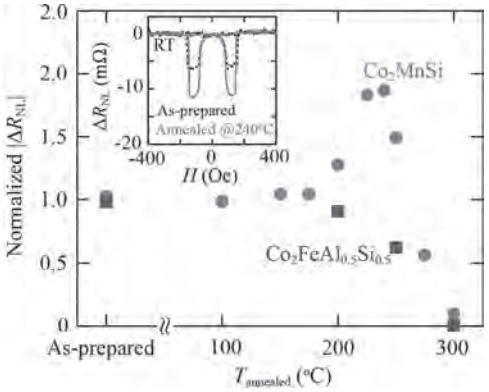

Fig. 1 Annealing temperature dependence of normalized nonlocal spin signal ($|\Delta R_{NL}|$) at room temperature for LSV devices with Co_2MnSi/Fe/Ge (red) and $Co_2FeAl_{0.5}Si_{0.5}$/Fe/Ge (bule) Schottky-tunnel contacts. The inset shows ΔR_{NL} for the Co_2MnSi/Fe/Ge LSV device with and without annealing at 240°C.

FOD-05. Epitaxial growth of Sn-doped Mn_4N films and their magneto-transport properties at room temperature. *T. Yasuda*[1], T. Komori[1], T. Hirose[1], T. Horiuchi[1], K. Toko[1] and T. Suemasu[1] *1. Univ. of Tsukuba, Tsukuba, Japan*

Ferrimagnetic Mn_4N (Fig. 1) is a promising candidate for various spintronics devices thanks to their small magnetization (M_s ~ 100 kA/m) and clear perpendicular magnetic anisotropy (K_u = 0.1 MJ/m)[1]. Ni-[2,3] and

Co-doped[4] Mn_4N films have magnetic compensation (MC) points. Using Ni-doped Mn_4N films at the vicinity of the MC composition, our group demonstrated ultrafast domain wall motion (v_{DW} = 3,000 m/s[5]) driven only by spin-transfer torque at RT thanks to the compensation. Additionally, In-doped Mn_4N[6] films show ferromagnetism. In this work, we focus on Sn-doped Mn_4N ($Mn_{4-x}Sn_xN$) film. Although the MC in $Mn_{4-x}Sn_xN$ bulks was reported at low temperature[7], no studies have been reported on MC of $Mn_{4-x}Sn_xN$ films. Therefore, we fabricated $Mn_{4-x}Sn_xN$ epitaxial films and evaluated their properties. 25-nm-thick $Mn_{4-x}Sn_xN$ epitaxial films (x = 0.0–1.0) were grown on the MgO(001) substrates by plasma-assisted molecular beam epitaxy. Both the longitudinal and transverse resistivities (ρ_{xx} & ρ_{xy}) were measured with van der Pauw method at RT. The ordinary Hall coefficient (R_H) was calculated from the slope of the ρ_{xy}-$\mu_0 H$ loops at high field regime. The anomalous Hall resistivities ρ_{AH} were derived by excluding the component of ordinary Hall effect from ρ_{xy}. Fig. 2 shows the ordinary Hall coefficient (R_H) and the anomalous Hall angle (θ_{AH} (= ρ_{AH}/ρ_{xx})) of $Mn_{4-x}Sn_xN$ films as a function of Sn composition, x. x_{cc} is the composition where the sign of R_H reversed. It suggests that the dominant career-type changed from electrons ($R_H < 0$) to holes ($R_H > 0$) with increasing x. Moreover, the sign reversal of θ_{AH} was observed twice at the composition except x_{cc}, indicating it was not caused by change in the career-type. Although similar results were also obtained in Ni-[2], Co-[4] and In-[6] doped Mn_4N, this was the first report that the multiple sign reversals of θ_{AH} were confirmed in Mn_4N-based compounds. The origin seems to be the change of magnetic structures such as MC and ferrimagnetic-to-ferromagnetic transition.

[1] T. Hirose *et al.*, AIP Adv. 10, 025117 (2020). [2] T. Komori *et al.*, J. Appl. Phys. 125, 213902 (2019). [3] T. Komori *et al.*, J. Appl. Phys. 127, 043903 (2020). [4] H. Mitarai *et al.*, Phys. Rev. Mater. 4, 094401 (2020). [5] S. Ghosh *et al.*, Nano Lett. 21, 2580 (2021). [6] T. Yasuda *et al.*, J. Phys. D. Appl. Phys. 55, 115003 (2022). [7] M. Mekata, J. Phys. Soc. Japan 17, 796 (1962).

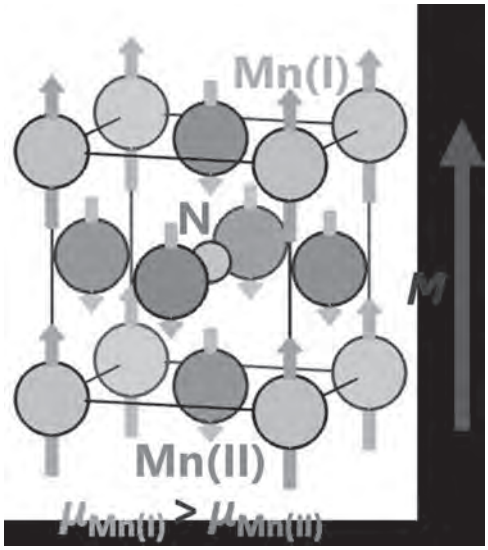

Fig. 1 The structure of antiperovskite ferrimagnetic Mn_4N.

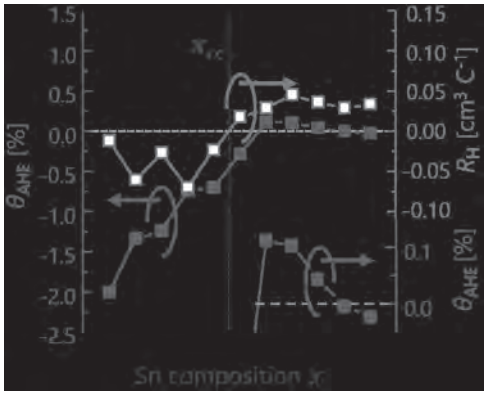

Fig. 2 Ordinary Hall coefficients R_H and anomalous Hall angles θ_{AH} of $Mn_{4-x}Sn_xN$ films. (inset: the enlarged part of θ_{AH} for $x \geq 0.6$.)

FOD-06. Underlying Mechanism of the Driving Force for Generating Spin Currents Thermally in a Ferrimagnetic Insulator Due to a Temperature Gradient. *M. Imamura*[1], H. Asada[2], Y. Kano[1], R. Matsuda[1], D. Tashima[1] and J. Kitagawa[1] *1. Fukuoka Institute of Technology, Fukuoka, Japan; 2. Yamaguchi University, Ube, Japan*

Spin precession and spin wave propagation with ferromagnetic resonance (FMR) rely essentially on the following points: a) the external field H_{ex} is applied in order to set the precession axis of spins in the direction of H_{ex}, b) the generated spin wave propagates in the direction perpendicular to the H_{ex}, and c) the generation of spin waves owes its origin to the ferromagnetic spin exchange interaction acting between neighboring spins. Although in the case of the spin thermoelectric (STE) generation the precession of local 3*d*-electron spins in Fe^{3+} is thermally excited and its excitation is irrelevant to the resonance phenomenon,[1] the three points noted above on FMR are considered to be important also for generating spin currents thermally in a ferrimagnetic insulator (FMI) due to the temperature gradient ∇T. Ref. 2 noted that the driving force for generating spin currents is due to the nonequilibrium dynamics of magnons in the FMI driven by ∇T.[2] Based on our studies on STE generation[1,3,4], we consider that the spin exchange interaction plays a major role as the driving force for the generation of spin currents in an FMI. The process in Fig. 1 shows the role of the ferromagnetic spin exchange interaction for generating spin currents in the FMI due to ∇T. We regard the ferromagnetic spin exchange interaction as the cause of the driving force for generating spin currents. Fig. 2 illustrates the generation of spin currents in YIG or Bi-substituted YIG by ∇T in the longitudinal spin Seebeck effect (LSSE). Each spin makes the spin precession of different magnitude due to ∇T, because each position of the spins is different in temperature. The precession of each spin then reaches a steady state, settling down to a uniform-mode-like state at t_n from the initial state at t_0 due to the exchange force working between spins. This idea well explains the generation of STE voltage for all the H_{ex} and ∇T arrangements that have been reported in experiments so far.

[1]M. Imamura, H. Asada and R. Nishimura, IEEE Trans. Magn., Vol. 58, p.4500111 (2022) [2]K. Uchida, H. Adachi and T. Kikkawa, Proc. IEEE, Vol. 104, p.1946 (2016) [3]M. Imamura, H. Asada and R. Nishimura, AIP Advances, Vol. 11, p.035143 (2021) [4]M. Imamura, H. Asada and R. Nishimura, J. Magn. Magn. Mater., Vol. 550, p.169081 (2022)

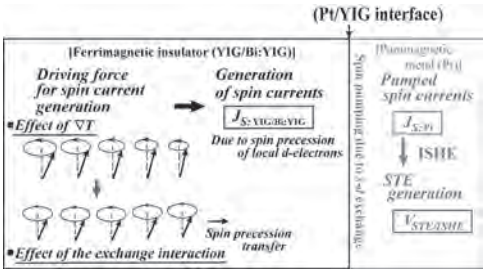

Fig. 1. Schematic illustration of the generation of spin currents in YIG or Bi-substituted YIG by means of ∇T.

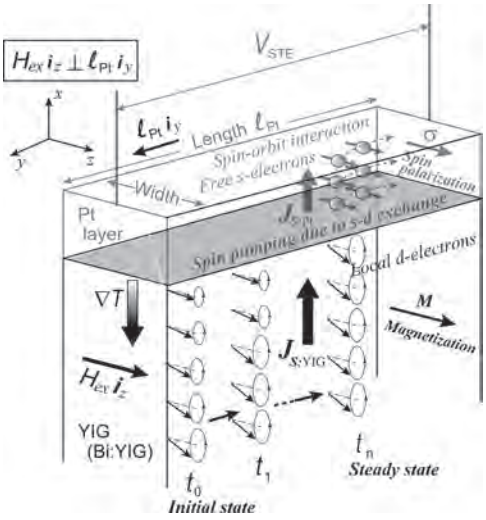

Fig. 2. Schematic illustration of the generation of spin currents in the LSSE in YIG or Bi:YIG by ∇T.

FOD-07. Enhanced Spin Signal in Metallic Non-Local Spin Valves with Highly-Spin-Polarized $Co_{1-x}Fe_x$ Injectors/Detectors. *B. Kaiser*[1], J.D. Watts[1,2], J. Ramberger[1], J.E. Dewey[1] and C. Leighton[1] *1. Chemical Engineering and Material Science, University of Minnesota - Twin Cities, Minneapolis, MN, United States; 2. Physics and Astronomy, University of Minnesota - Twin Cities, Minneapolis, MN, United States*

Magnetic-tunnel-junction-based hard disk drive read-heads have been highly successful. They face pressing current challenges, however, due to high resistance-area product, which leads to impedance-mismatch-driven signal-to-noise issues as scaling continues [1]. Alternative all-metal spintronic devices are thus of high interest, including spin accumulation sensors based on non-local spin valves (NLSVs) [2]. Due to low output signals in such devices, and also for fundamental research, it is highly desired to improve the spin signal in metallic NLSVs. As this spin signal is essentially proportional to the square of the current spin polarization, α [3], we have explored integration of high-spin-polarization $Co_{1-x}Fe_x$ alloy ferromagnetic injectors/detectors into NLSVs. $Co_{1-x}Fe_x$ alloys are known to display a peak in α at $x \approx 0.25$ and have been employed in other spintronic devices [4,5]. Otherwise identical Al-based NLSVs were fabricated with either conventional Co or $Co_{75}Fe_{25}$ ferromagnetic injectors/detectors *via* single-shot ultrahigh vacuum evaporation into electron-beam-lithographic masks (Fig 1, inset). X-ray and spectroscopic characterization indicates site-disordered BCC $Co_{75}Fe_{25}$ films. Comparing $Co_{75}Fe_{25}$ and Co, the non-local spin signal (ΔR_{NL}) increases by factors of 3 and 4, respectively, at 275 and 5 K (Fig. 1), confirming significant enhancement. Full analysis of the temperature and injector/detector separation dependence reveal α values of ~60%, with a strikingly weak temperature dependence (Fig. 2). We thus establish a facile route to ~2-fold enhancement of spin polarization over conventional ferromagnets used in NLSVs (Fig. 2), thereby inducing ~4-fold enhancement in spin signal, of interest for both applied and fundamental purposes. This work is supported by the NSF and the Advanced Storage Research Consortium.

[1] T. Nakatani, Z. Gao, and K. Hono, MRS Bull., Vol. 43, p. 106 (2018) [2] H. Takagishi, K. Yamada, and H. Iwasaki, IEEE Trans. Mag., Vol. 46, p. 2086 (2010) [3] S. Takahashi, and S. Maekawa, PRB, Vol. 67(5), p. 052409 (2003) [4] D. J. Monsma, and S. S. P. Parkin. Appl. Phys. Lett., Vol. 77(5), p. 720 (2000) [5] S. V. Karthik, T. M. Nakatani, A. Rajanikanth, J. Appl. Phys., Vol. 105(7), p. 07C916 (2009)

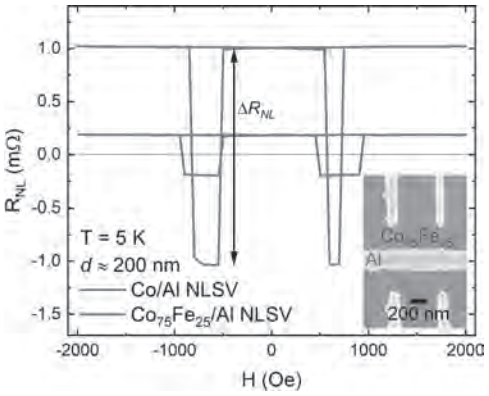

Fig. 1: 5-K background-subtracted non-local resistance (R_{NL}) *vs.* applied field H (at 200 nm separation) for Al-based NLSVs with Co (blue) and $Co_{75}Fe_{25}$ (red) ferromagnets. Inset: Scanning electron micrograph of an NLSV.

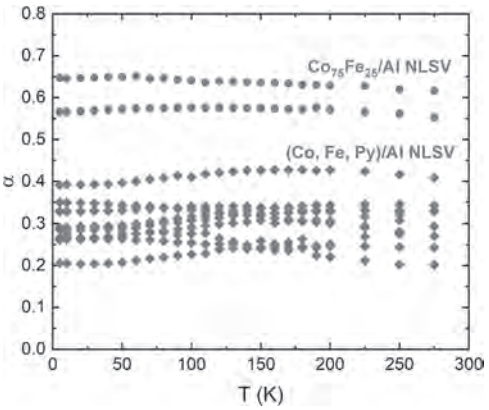

Fig. 2: Temperature (T) dependence of the current spin polarization (a) for Al-based NLSVs with $Co_{75}Fe_{25}$ ferromagnets (red) or Co, Fe, or Py ferromagnets (blue).

FOD-08. Highly tunable spin Hall magnetoresistance in room-temperature magnetoelectric multiferroic, $Sr_3Co_2Fe_{24}O_{41}$|Pt hybrids. A.A. Wagh[1], *P. Garg*[1], K. Mallick[1], S. Elizabeth[1] and P. Kumar[1] *1. Physics, Indian Institute of Science, Bangalore, Bangalore, India*

We present spin transport studies on a low-field, room-temperature magnetoelectric multiferroic polycrystalline $Sr_3Co_2Fe_{24}O_{41}$|Pt heterostructure wherein a highly tunable transverse conical magnetic phase is responsible for static and dynamic magnetoelectric coupling [1, 2]. We measured angular dependence of spin Hall magnetoresistance (SMR) at constant magnetic fields (H) in the range of 50 to 100 kOe. Application of field below the critical value ($H_{c1} \approx 2.5$ kOe), yielded negative SMR and the H-evolution of normalized SMR ($\Delta R/R_0 \times 100$ %) exhibited a negative gradient. Further, an increase in the H resulted in the positive slope of $\Delta R/R_0 \times 100$ % Vs. H and later at higher H around 14 kOe, a crossover from negative to positive SMR was observed. We employed a simple model for estimating the equilibrium magnetic configuration and computed the SMR modulation at various values of H. We argue that the tilting of the cone is dominant and in turn responsible for the observed nature of SMR

below 2.5 kOe (Fig.1) while, the closing of the cone-angle is pronounced at higher fields causing a reversal in sign of the SMR from negative to positive (Fig.2). Importantly, SMR experiments revealed that a change in the helicity with a reversal of the magnetic field has no influence on the observed SMR. Longitudinal spin Seebeck effect (LSSE) signal was measured to be ≈ 500 nV at 280 K, under application of thermal gradient, ΔT = 23 K and field, 60 kOe. The observed LSSE signal, originating from pure magnon spin current, showed a similar *H*-dependent behavior as that of the magnetization of $Sr_3Co_2Fe_{24}O_{41}$. Our detailed spin transport studies on polycrystalline $Sr_3Co_2Fe_{24}O_{41}$|Pt heterostructure demonstrate high tunability of the amplitude and the sign of the SMR, highlighting its potential for novel spintronic devices such as SMR-based spin valves [3] and voltage-controlled spin transport devices.

[1] Y. Kitagawa, Y. Hiraoka, T. Honda, Nat. Mater., Vol. 9, p. 797 (2010) [2] H. Ueda, Y. Tanaka, Y. Wakabayash, Phys. Rev. B, Vol. 100, p. 094444 (2019) [3] Y.-T. Chen, S. Takahashi, H. Nakayama, Phys. Rev. B, Vol. 87, p. 144411 (2013)

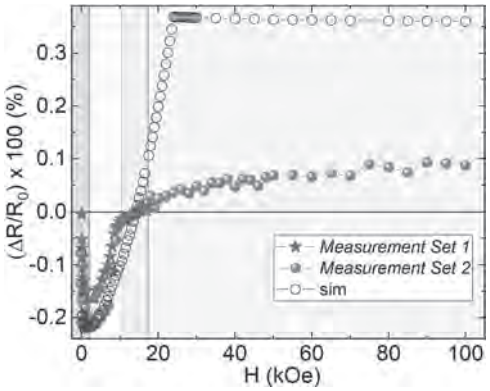

Fig.1: Normalized simulated SMR amplitude, $\Delta R/R_0 \times 100$ % plotted as a function of *H*, and compared with experimental data (*Measurement Set 1* and *Measurement Set 2*).

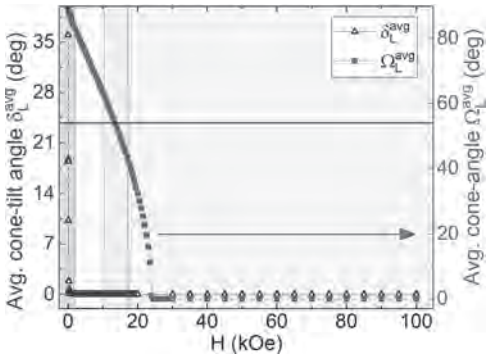

Fig.2: Simulated *H*-evolution of average cone-tilt angle and average cone-angle for $\mu_{L1,2}$.

FOD-09. Electron and Spin Transport in an Ultrathin Al Film for Use as a Nonlocal Spin Valve. *Y. Liu*[1] and R.H. Victora[1,2] *1. School of Physics and Astronomy, University of Minnesota, Minneapolis, MN, United States; 2. Department of Electrical and Computer Engineering, University of Minnesota, Minneapolis, MN, United States*

Our work predicts the effect of scattering, associated with surface and bulk defects, on electronic and spin relaxation in aluminum-based ultrathin films using the Landauer-Buttiker formalism. Our results can potentially facilitate the realization of magnetic recording read heads based on nonlocal spin valves with smaller shield-shield spacing. Poor device performance has been previously observed in these films, in particular for thickness of metallic channels smaller than 10nm [1]: this is probably caused by the combination of spin-orbit coupling with various extrinsic defects. In this work, the contributions from surface roughness, grain boundary scattering, vacancies and surface reconstruction to momentum and spin relaxation are investigated using the recursive Green's function technique that reduces computational complexity by the square of the number of layers. [2]. Resistivity and spin diffusion length are determined assuming that both the leads and the metallic channel are made of Al with 3.6nm thickness at T=0K and embedded in vacuum. Our calculations demonstrate that, for thin sputtered films, momentum relaxation is dominated by point vacancy scattering and that surface reconstruction and point vacancies are the dominant contribution to spin relaxation: our results yield reasonable spin diffusion length and Elliott-Yafet constant as shown in Fig.1 and Fig.2. It is also found that Matthiessen's rule and the Elliott-Yafet prediction of β are violated in the presence of surface periodicity. However, when including both random surface corrugations and increasing vacancy concentration, the Elliott-Yafet predictions and Matthiessen's rule are recovered as the symmetry breaking length scale becomes commensurate with the concentration of random defects.

[1] S. Rakheja, S. Chang and A. Naeemi, *IEEE Trans.Electron Device*, Vol.60, NO.11(2013). [2] M.L Sancho, J.L Sancho and J. Rubio, *J.Phys*. F 14, 1205(1984).

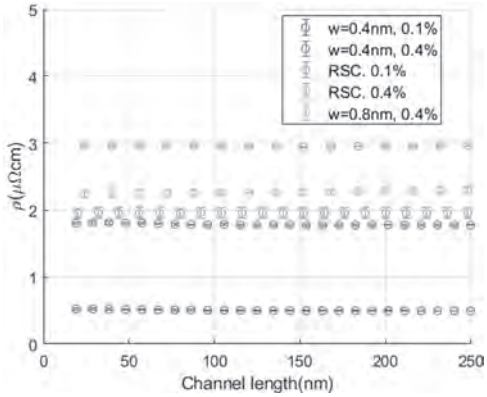

Fig1. Resistivity of 3.6nm thick film versus channel length in the presence of periodic surface corrugation/ random surface corrugation (RSC) with varying point vacancy concentrations, where w denotes the period of repetitive indentation on the surface.

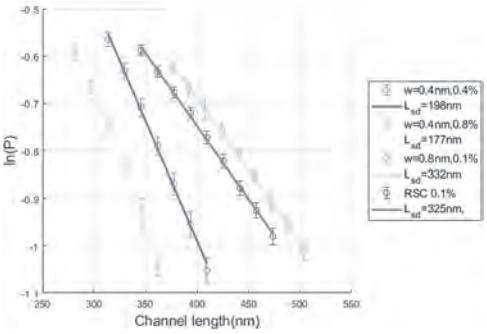

Fig2. Extraction of spin diffusion length for a 3.6nm thick Al-films at T=0K under the same conditions as above. P is the spin polarization. SOC=0.0018Ry. L_{sd} varies between ~200nm and ~350nm.

FOD-10. Electrical detection of magnetization of a layered semiconducting ferromagnet using WTe_2. *I. Kao*[1], S. Yuan[1], J. Katoch[1] and S. Singh[1] *1. Department of Physics, Carnegie Mellon University, Pittsburgh, PA, United States*

Spin-orbit torque (SOT) switching devices fabricated by combining van der Waals (vdW) based semiconducting ferromagnets (FMs) and Weyl semimetal (WSMs) are appealing because of electric field-controlled magnetism and unconventional charge to spin conversion, which can be exploited for

modular memory and logic devices. For instance, the vdW based FM semiconductors, such as $Cr_2Ge_2Te_6$ (CGT), offer us the opportunity to study SOT devices where electric field-controlled magnetism can be used for enhanced device functionalities[1]. Also, we have recently shown that field-free deterministic switching of perpendicular magnet can be obtained by utilizing the unconventional spin orbit torque in WTe_2[2]. In SOT switching devices, the electrical readout of the semiconducting FM layer is essential for device functionality. Electrical detection of magnetization in conventional insulating/ semiconducting ferromagnet (FM) is routinely achieved by utilizing the spin hall effect generated by the adjacent heavy metal layer[3]. The electrical readout of magnetization in 2D semiconducting FM has been demonstrated by coupling $Cr_2Ge_2Te_6$ with heavy metals[4] and topological insulators[5]. However, few reports have shown electrical detection in a vdW based semimetal/FM-semiconductor heterostructures. As shown in Fig. 1, our initial measurements have demonstrated electrical detection of magnetization in $Cr_2Ge_2Te_6$ by measuring the anomalous Hall resistance in WTe_2/ CGT bilayers. On the same device, the resistance of individual CGT is more than 100 times higher than the resistance of the bilayer structure as plotted in Fig. 2, therefore most of the current is flowing through the WTe_2 layer. We will present detailed measurements, which are required to understand the observed anomalous Hall effect induced at the interface in WTe_2/CGT bilayer systems.

1. I. A. Verzhbitskiy, H. Kurebayashi and H. Cheng, Nat. Electron., Vol. 3, p.460 (2020). 2. IH. Kao, R. Muzzio and H. Zhang, Nat. Mater. (2022). 3. A. S. Ahmed, A. J. Lee and N. Bagués, Nano Lett., Vol. 19(8), p.5683 (2019). 4. V. Gupta, T. M. Cham and G. M. Stiehl, Nano Lett., Vol. 20(10), p.7482 (2020). 5. V. Gupta, R. Jain and Y. Ren, arXiv:2206.02537 (2022).

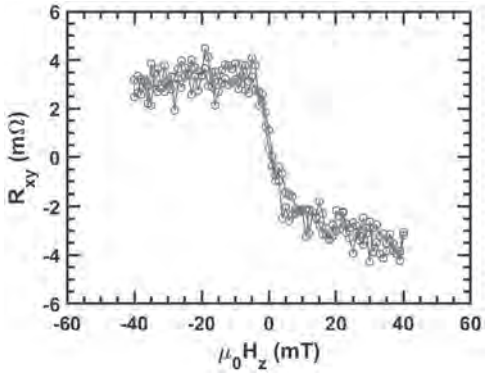

Fig. 1. The anomalous Hall resisitance observed in CGT/ WTe_2 bilayer at 8.4 K.

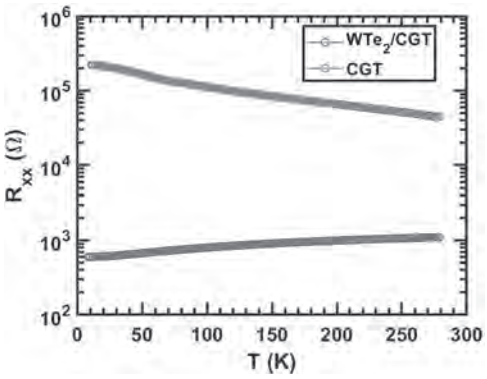

Fig. 2. The temperature dependence of longitudinal resistance of the WTe_2/ CGT bilayer and the CGT layer.

FOD-11. Non-local measurement as a probe of the spin Hall effect in topological insulators. *G.M. Stephen*[1], A. Hanbicki[1], J. DeMell[1], P. Taylor[2], O. Vail[2], J. Robinson[4], T. Schumann[3], S. Stemmer[3] and A. Friedman[1] *1. Laboratory for Physical Sciences, College Park, MD, United States; 2. Army Research Lab, Adelphi, MD, United States; 3. University of California Santa Barbara, Santa Barbara, CA, United States; 4. Naval Research Lab, Washington D.C., DC, United States*

Topological materials (TIs) are promising candidates for novel computing device designs. In particular they have great potential for spintronic devices where utilization of electron spin rather than charge would allow for lower power and higher performance computing in next generation architectures. Efficient conversion between spin and charge signals is crucial to spintronic technology. TIs provide highly efficient spin-to-charge conversion as a result of their unique topological properties. One way to electrically quantify conversion efficiency is with the spin Hall effect (SHE). Here we present SHE measurements of the topological insulator $Bi_2Te_{2.5}Se_{0.5}$ and topological Dirac semimetal Cd_3As_2. Because of the topological nature of these materials, we can measure the SHE without the use of ferromagnetic injectors or detectors. Using the non-local resistance. Furthermore, the ferromagnet-free measurement allows for quick diagnostics of the spin properties without the need to fabricate multilevel devices.

Session FPA
SPIN CURRENT AND DYNAMICS (Poster Session)

Lucas Caretta, Chair
Brown University, Providence, RI, United States

FPA-01. Giant spin Hall effect and spin-orbit torques from 5*d* transition metal - aluminum alloys for energy efficient synthetic antiferromagnetic racetrack memories. *P. Wang*[1] and S. Parkin[1] *1. NISE, Max Planck Institute for Microstructure Physics, Halle, Germany*

The energy efficient manipulation of chiral spin textures via spin-orbit torques is critical to the development of advanced magnetic Racetrack Memories. Here, we demonstrate giant charge to spin conversion ratios via the spin Hall effect in the family of 5d transition metal-Al alloy thin films that exhibit a $L1_0$- like structure. We demonstrate giant spin Hall angles that exceed 1 in alloys that have very high resistivities that are a result of disorder potential scattering. We show a systematic variation of the spin Hall angle and resistivity with the filling of the 5d band. Using Ir_xAl_{100-x} alloys we generate giant spin-orbit torques that can move chiral domain walls in synthetic antiferromagnetic (SAF) racetracks several times more efficiently than using conventional heavy-metal elements. A particular feature of these racetracks, that are formed from ultra-thin layers of Co and Ni with a $L1_0$ RuAl layer as an antiferromagnetic coupling layer, is that they are oriented along the [001] crystal direction rather than [111] as in prior-art SAF racetracks [1]. This makes the integration of MgO (100) tunnel barrier based magnetic tunnel junction reading devices highly practical. These novel materials provide a route for the multifunctional use of racetrack memories that are compatible with complementary metal-oxide semiconductor technologies.

Peng, Wang, Stuart S.P. Parkin. *Advanced Materials* 2109406, (2022).

FPA-02. Enhanced charge-to-spin efficiency for modified tungsten-based-SOT channel. *S. Lu*[1], X. Ma[1], J. Yin[1], X. Ning[1], H. Zhang[1], X. Shang[2], T. Xu[2], H. Sun[2], C. Zhang[2], B. Man[2], S. Li[2], D. Li[2], S. Lyu[2], W. Chen[2], G. Wang[2], W. Zhao[1], K. Cao[1] and H. Liu[2] *1. Fert Beijing Institute, School of Integrated Science and Engineering, Truth Memory Tech, Beijing, China; 2. Truth Memory Tech, Beijing, China*

Currently, the commercialization of SOT-MRAM is hampered by high switching current density due to relatively low switching efficiency. One of the key parameters determines the switching efficiency is the spin hall angle (SHA, θ_{SH}). The maximum θ_{SH} of commonly used materials in foundries are: Ta (~-0.12), Pt (~0.1), and β-W (~-0.3) [1-3]. Even though there are promising SOT channel materials, like topological insulators (TI), showing high $\theta_{SH} > 1$, the resistivity is several orders higher than above mentioned normal heavy metals (HM). Meanwhile, TI is hard for manufacturing as it consists of materials not friendly to be used in silicon-based fabs. Then, it is important to pursue high θ_{SH} for HM for the SOT-MRAM. The purpose of our study is to re-visit at the θ_{SH} of modified tungsten-based SOT channels. We demonstrated relatively high θ_{SH} up to -0.44 and low resistivity ~130 μΩcm in the nitrogen-doped W buffer (WN) /W interlayer/ferromagnetic hybrid system measured by spin-torque ferromagnetic resonance (ST-FMR). The θ_{SH} of the sample with WN/W SOT channel was nearly twice as large as 5nm β-W and 5nm β-WN (Fig. 1). The magnetic tunnel junctions (MTJ) with three kinds of SOT channels were also fabricated in order to check the device performance. Fig. 2 shows the typical R-J curves of MTJ devices by DC measurements. The switching current density of MTJs with the 3WN/2W SOT channel is 16.6 MA/cm^2, which is 36.4% and 26.2% smaller than 26.1 MA/cm^2 and 22.5 MA/cm^2 respectively in the devices with 3.5W and 3.5WN SOT channels. The Damping like torques $\Xi_{DL} = T_{int}\theta_{SH}$ estimated from the switching current density is 0.28 for the system with 3WN/2W SOT channel, which is close to 2 times of that for the sample with 3.5W. The results from MTJ devices are consistent with values obtained from ST-FMR. Our promising results give potential solutions to the low switching efficiency issue for the W-based SOT-MTJ devices.

[1] Luqiao Liu, R. A. Buhrman, et al. Spin-torque switching with the giant spin hall effect of tantalum, Science 336 (6081) (2012) 555–558 [2] Minh-Hai Nguyen, R. A. Buhrman, et al. Spin torque study of the spin hall conductivity and spin diffusion length in platinum thin films with varying resistivity, Phys. Rev. Lett. 116 (2016) 126601 [3] Chi-Feng Pai, R. A. Buhrman, et al. Spin transfer torque devices utilizing the giant spin Hall effect of tungsten, Appl. Phys. Lett. 101 (2012) 122404

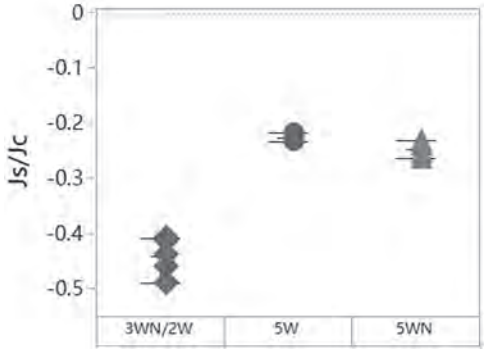

The SHA of samples with 3WN/2W (red diamonds), 5W(blue circles), and 5WN (green triangles) channels.

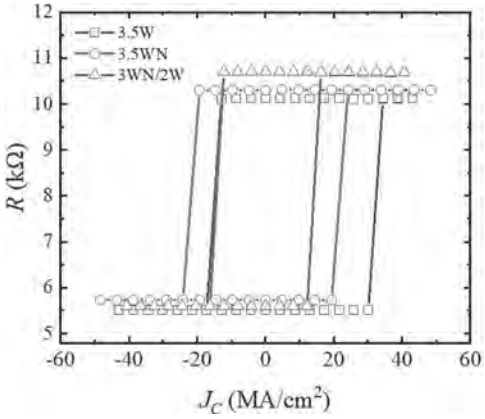

The typical R-J curves of MTJ devices with three kinds of SOT channels, i.e., 3.5W (black squares), 3.5WN (red circles), and 3WN/2W (blue triangles).

FPA-03. Anomalous inverse spin Hall effect in perpendicular magnetized Co/Pd multilayers. *M. Yang*[1], B. Miao[1], J. Cheng[1], K. He[1], X. Yang[1], Y. Zeng[1], Z. Wang[1], L. Sun[1], X. Wang[2,3], A. Azevedo[4], S. Bedanta[5] and H. Ding[1] *1. Department of Physics, Nanjing University, Nanjing, China; 2. Physics Department, The Hongkong University of Science and Technology, Kowloon, Hong Kong; 3. PHKUST Shenzhen Research Institute, Shenzhen, China; 4. Departamento de Física, Universidade Federal de Pernambuco, Recife, Brazil; 5. Laboratory for Nanomagnetism and Magnetic Materials (LNMM), National Institute of Science Education and Research (NISER), Jatni, India*

The spin Hall effect (SHE) and the inverse spin Hall effect (ISHE) have been widely utilized to interconvert the charge and spin current. In them, the charge current, spin current and spin polarization are orthogonal to each other [1]. Based on the general tensor requirement of the spin-charge conversion, additional possibilities can be introduced when the order parameter, the magnetization of a ferromagnet, is involved [2]. We herein report the spin-charge conversion in perpendicular magnetized Ti(3 nm)/Co(0.6 nm)/Pd(2 nm)/[Co(0.4 nm)/Pd(2 nm)]$_4$ multilayers, simplified as Co/Pd multilayers, with the spin pumping measurements. We unambiguously observed the anomalous inverse spin Hall effect (AISHE) in Co/Pd multilayers, where the charge current is collinear with the spin polarization. And both the sign and magnitude of AISHE can be linearly regulated by the out-of-plane magnetization of Co/Pd multilayers. Further, the observed amplitude ratio of AISHE/ISHE in spin pumping measurements is independent of the applied microwave frequency, indicating that it is a material specific parameter.

[1] J. E. Hirsch, Phys. Rev. Lett. 83, 1834 (1999). [2] X. R. Wang, Commun. Phys. 4, 55 (2021).

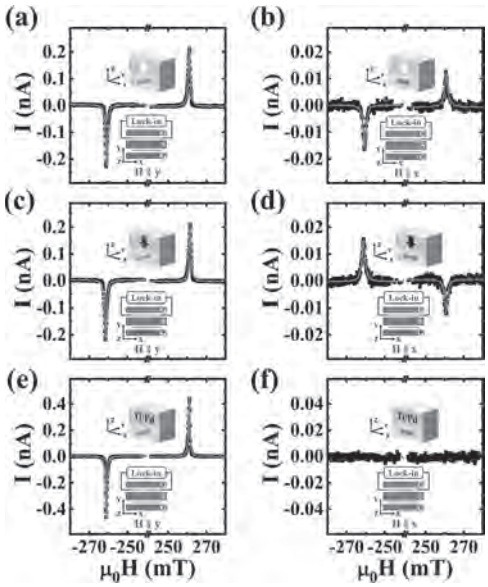

FIG. 1. (a-d) are measurements of spin pumping current of Co/Pd multilayers at 9 GHz. (a) and (b) are when the magnetization of Co/Pd multilayers is along the +*z* direction and the magnetic field is applied along the *y*-direction and *x*-direction, respectively. (c) and (d) are the similar measurements, however, the magnetization of Co/Pd multilayers is along the –*z* direction. (e) and (f) are the measurements of spin pumping current of Ti/Pd at 9 GHz when the magnetic field is applied along the *y*-direction and *x*-direction, respectively.

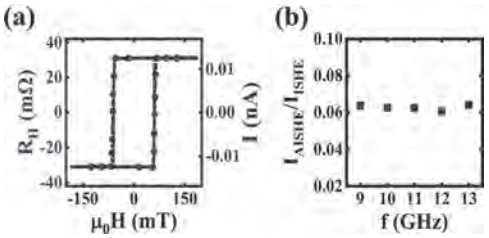

FIG. 2. (a) Comparison of the hysteresis loops measured by anomalous Hall effect (Brown) and AISHE (blue) for Co/Pd multilayers. (b) The frequency dependent ratio of the amplitudes of AISHE signal to ISHE signal.

FPA-04. A coherent picture on the pure spin transport between Ag/Bi and ferromagnets. *J. Cheng*[1], B. Miao[1], Z. Liu[2], M. Yang[1], K. He[1], Y. Zeng[1], H. Niu[1], X. Yang[1], Z. Wang[1], X. Hong[1], s. Fu[1], L. Sun[1], Y. Liu[2], Y. Wu[3], Z. Yuan[2] and H. Ding[1] *1. Physics, Nanjing University, Nanjing, China; 2. Center for Advanced Quantum Studies and Department of Physics, Beijing Normal University, Beijing, China; 3. Physics, Fudan University, Shanghai, China*

Inverse Rashba-Edelstein effect (IREE) [1] refers to the spin-to-charge conversion at the interface/surface with strong spin-orbit coupling and broken symmetry. Ag/Bi related system is a prototype system for studying the IREE and has been hotly discussed but with a long-term controversy [2-5]. In a joint effort of both experiments and first-principles calculations, we reconcile almost all the published experimental data in literatures with controversial conclusions and provide a coherent picture on the pure spin transport between Ag/Bi and ferromagnets. We demonstrate a strong IREE at the interface between Ag/Bi with a ferromagnetic metal (FM) but not with a ferromagnetic insulator. This is in sharp contrast with the previously claimed IREE at Ag/Bi interface or inverse spin Hall effect dominated spin transport. In addition, a more than one order of magnitude modulation of IREE signal is realized for different Ag/Bi-FM interfaces, casting strong tunability and a new direction for searching efficient spintronics materials.

[1] V. M. Edelstein, Solid State Commun. Vol. 73, p. 233 (1990). [2] J. C. R. Sánchez, L. Vila, and A. Fert, Nat. Commun. Vol. 4, p. 2944 (2013). [3] M. Matsushima, Y. Ando, and M. Shiraishi, Appl. Phys. Lett. Vol. 110, p. 072404 (2017). [4] D. Yue, W. W. Lin, and C. L. Chien, Phys. Rev. Lett. Vol. 121, p. 037201 (2018). [5] J. H. Shen, Z. Feng, and X. F. Jin, Phys. Rev. Lett. Vol. 126, p. 197201 (2021).

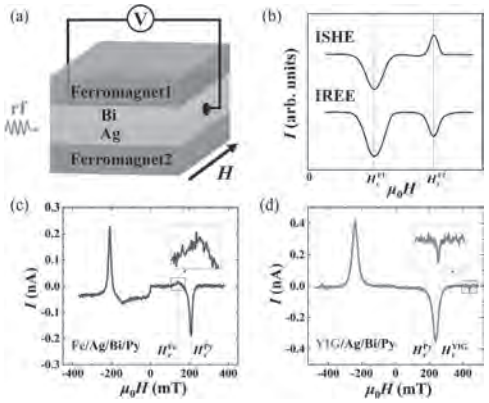

Fig. 1 (a) Schematic illustration of spin pumping measurement for Ag/Bi bilayer sandwiched by two different ferromagnets. Under their different resonance conditions, the spin current can be injected into Ag/Bi from either side. (b) Spin currents injected from opposite directions result in the same (opposite) sign of charge currents in the IREE (ISHE) mechanism, with "double-peak" ("peak-and-dip") feature. Spin pumping signals at the frequency of 14 GHz for (c) Fe(10)/Ag(5)/Bi(6)/Py(10), and (d) YIG/Ag(5)/Bi(6)/Py(10), respectively.

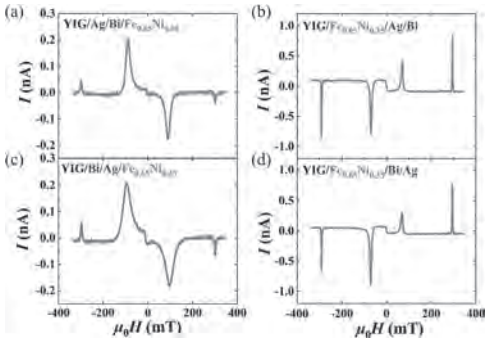

Fig. 2 Spin pumping signals for (a) YIG/Ag(5)/Bi(6)/$Fe_{0.65}Ni_{0.35}$(10), (b) YIG/$Fe_{0.65}Ni_{0.35}$(7)/Ag(5)/Bi(6), (c) YIG/Bi(6)/Ag(5)/$Fe_{0.65}Ni_{0.35}$(10) and (d) YIG/$Fe_{0.65}Ni_{0.35}$(7)/Bi(6)/Ag(5). Note: $\theta_{SH} \approx 0$ for $Fe_{0.65}Ni_{0.35}$.

FPA-05. Magnetic field dependence of mV class spin motive force due to domain wall motion in GdFeCo magnetic wire. *M. Oikawa*[1], S. Kambe[1], S. Sumi[1], K. Tanabe[1] and H. Awano[1] *1. Toyota Technological Institute, Nagoya, Japan*

Spin transfer torque[1] is an important phenomenon in order to develop of non-volatile magnetic memory. Using this spin transfer torque principle, it was predicted[2] and experimentally confirmed[3] that a voltage could be generated in the magnetic nanostructure. This effect is called spin motive force and is expected for next-generation power sources. It is not clear how the Faraday electromotive force[4] can be separated from the spin motive force, and there are few studies reported and the spin motive force in μV class. It is very small. In the previous 15th Joint MMM-Intermag Conference, we fabricated $Gd_{21}(Fe_{75}Co_{25})_{79}$ magnetic wire and succeeded in generating a spin motive force by domain wall motion. From the previous result, we prepared a sample with reduced resistance, that is, increased film thickness in order to increase power, and conducted an experiment. We prepared the following film stacks using rf and dc magnetron sputtering: Gd_{21} $(Fe_{75}Co_{25})_{79}$ (40)/SiN (10), the films are grown at room temperature. The magnetic wires (3 μm wide and 100 μm long) and Hall crosses were micro-fabricated by an Electron-beam lithography (EBL) system and a lift-off method. Next, we prepared a sample with injection of domain wall and a sample without injection of domain wall. A magnetic field was applied to the sample, and the generated voltage was observed by an oscilloscope through a 10x amplifier. Spin motive force is determined by subtracting the induced electromotive force generated in the sample without injection of domain wall. Figure 1 shows the magnetic field dependence of the spin motive force by subtracting the induced electromotive force. Thus, the instantaneous maximum output of the 3 μm x 100 μm GdFeCo element was about 0.1 μW to understand the meaning of value, we compared it with various energy harvesting techniques[6]. The results are shown in Fig. 2. Our results were found to be comparable to the output of solar cells with the same area. This is financially supported by KAKENHI 21K18735,20H02184.

[1] J. C. Sloczewski, J. Magn. Magn. Mater. 159, L1 (1996). [2] S. E. Barnes and S. Maekawa, Phys. Rev. Lett. 98, 246601 (2007). [3] S. A. Yang et al., Phys. Rev. Lett. 102, 067201 (2009). [4] M. Hayashi et al., Appl. Phys. Express 3, 113004 (2010). [5] M. Oikawa et al., 15th Joint MMM-Intermag Conference GDP-11 (2022). [6] https://xtech.nikkei.com/atcl/nxt/mag/ne/18/00001/00171/

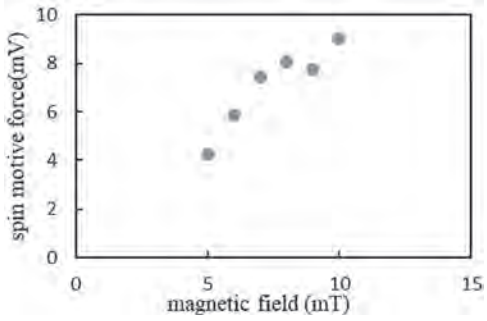

Magnetic field dependence of spin motive force.

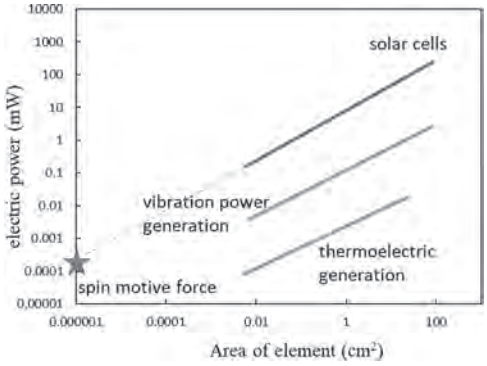

Comparison with energy harvesting technologies.

FPA-06. Absence of cross-sublattice spin pumping and spin torques in collinear antiferromagnets: symmetry and microscopic theory. *J. Tang*[1] and R. Cheng[2,1] *1. Department of Physics and Astronomy, University of California, Riverside, Riverside, CA, United States; 2. Department of Electrical and Computer Engineering, University of California, Riverside, Riverside, CA, United States*

Spin pumping is one of the most common ways to generate the desired spin current in experiment. With much shorter timescales than in ferromagnets (FM), antiferromagnetic (AFM) spin dynamics can offer much more attractive properties for potential applications in ultrafast spintronics devices. In recent years, although the AFM sub-terahertz spin pumping has been sucessfully observed, there is still some debate over the existence of cross-sublattice spin pumping in AFM. Here, we start from the most general form of AFM spin pumping and phenomenologically derive its Onsager reciprocal effect--current induced torque. By symmetry analysis we argue that the off-diagonal elements of spin-mixing conductance in net magnetization *m* and Neel vector *n* basis must vanish for a collinear AFM. The anti-damping like torques and cross-sublattice torques are shown to be proportional to the symmetric and asymmetric parts of the diagonal spin-mixing conductance respectively. For a conclusive evidence, we explicitly derive a more general form of spin-mixing conductance by scattering matrix method. For a insulating compensated AFM interface, the asymmetric parts of the diagonal spin-mixing conductance vanishes, manifesting the absence of cross-sublattice torques and spin pumping in collinear AFM.

[1] Ran Cheng, Jiang Xiao, Qian Niu, and Arne Brataas. Phys. Rev. Lett.113,057601 (2014). [2] Akashdeep Kamra and Wolfgang Belzig.Phys. Rev. Lett.119,197201 (2017). [3] Roberto E. Troncoso, Mike A. Lund, Arne Brataas, and Akashdeep Kamra. Phys. Rev.B 103, 144422 (2021). [4] Kjetil M. D. Hals Yaroslav Tserkovnyak and Arne Brataas. Phys. Rev. Lett.106, 107206 (2011).

FPA-07. High Frequency Spin Torque Oscillation in Orthogonal Magnetization Disks with Strong Biquadratic Magnetic Coupling.
L. Chuhan[1], Y. Kurokawa[1], N. Hashimoto[1], T. Tanaka[1] and H. Yuasa[1]
1. Kyushu University, Fukuoka, Japan

We numerically studied the spin transfer torque oscillation (STO) in a magnetic orthogonal configuration by introducing a strong biquadratic magnetic coupling [1]. The advantage of the orthogonal configuration is the high efficiency of spin transfer torque leading the high STO frequency, but it is difficult to maintain the STO in a wide range of electric current. By introducing a biquadratic magnetic coupling into the orthogonal structure, it became possible to expand the electric current region realizing the stable STO, resulting that a high STO frequency. In this report, we systematically compared STO properties between the orthogonal magnetization disks with and without the biquadratic magnetic coupling, that is, B_{12}=0.0 and -0.6. In our model, the orthogonal configuration is FePt 2 nm/spacer 2 nm/$Co_{90}Fe_{10}$, or $Ni_{80}Fe_{20}$, or Ni 2 nm. The time-domain magnetization precessions of the top layer Ni under current density J=0.5×10^7 A/cm^2, 3.0×10^7 A/cm^2, and 6.0×10^7 A/cm^2 are shown in Fig.1 (a), (b) and (c). Only B_{12} was changed and A_{12} is set 0 for simplicity. In the case of the biquadratic magnetic coupling B_{12}=0.0, the STO was observed only when J=0.5×10^7 A/cm^2. Compared to this, in the case of B_{12}=-0.6, the STO can be obtained in the wide range of J. This means that by introducing biquadratic magnetic coupling, we can expand the electric current region realizing the stable STO and increase the frequency. In Fig. 2, we show the STO frequency and the intensity as a function of the current density. First, even when the top layer is changed from Ni, to $Ni_{80}Fe_{20}$, or $Co_{90}Fe_{10}$, the current density region realizing the stable STO is widened by introducing the biquadratic magnetic coupling. In addition, we increased STO frequency and the intensity, meaning the stable STO.

[1] C. Liu, et al. IEEE Trans. Mag., 58 (2022) 172504.

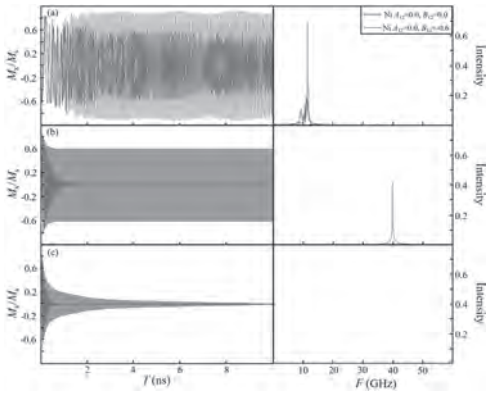

Fig.1. Time-domain magnetization precessions M_x/M_s and FFT profiles of the top layer Ni. The current densities are 0.5×10^7 A/cm^2 (a), 3.0×10^7 A/cm^2 (b), and 6.0×10^7 A/cm^2 (c).

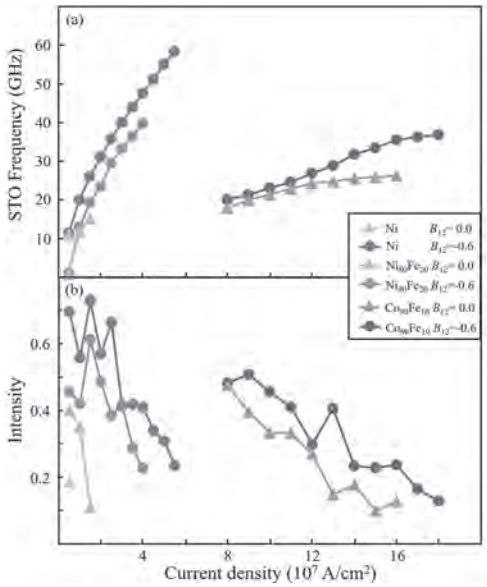

Fig.2. Current density dependences of frequency (a) and intensity (b) for Ni, $Ni_{80}Fe_{20}$ and $Co_{90}Fe_{10}$ top layers in the orthogonal configurations.

FPA-08. Novel Phase Formation and Magnetism at the $Sb_2Te_3/Ni_{80}Fe_{20}$ Interface.
A.R. Will-Cole[1], J. Hart[2], A. Podpirka[3], M. Matzelle[4], N. Bhattacharjee[1], S. Patel[5], S.H. Tolbert[5], A. Bansil[4], J.J. Cha[2], D. Heiman[4] and N. Sun[1] *1. Electrical Engineering, Northeastern University, Boston, MA, United States; 2. Materials Science and Engineering, Cornell University, Ithaca, NY, United States; 3. Johns Hopkins Applied Physics Laboratory, Laurel, MD, United States; 4. Physics, Northeastern University, Boston, MA, United States; 5. Chemistry, University of California Los Angeles, Los Angeles, CA, United States*

Bilayer topological insulator/ferromagnet heterostructures are promising for spintronic memory applications due to their low switching energy and therefore power efficiency.[1] Topological insulators have been grown with molecular beam epitaxy (oriented, epitaxial films)[2,3] and RF magnetron sputtering (amorphous to crystalline oriented films)[4-6], etc., and have demonstrated large spin-to-charge conversion efficiencies. However, the reactivity of topological insulators with ferromagnetic films is often overlooked in the spin-orbit-torque literature, even though there are reports that it is energetically favorable for topological insulators to react with metals and form interfacial layers.[7-11] Previously, we have investigated the interface of Bi_2Te_3/$Ni_{80}Fe_{20}$ and discovered that a novel topological antiferromagnetic phase, $NiBi_2Te_4$, formed at the bilayer interface due to selective Ni diffusion, which is possibly catalyzed by the topological surface states.[12] In our current work, we have grown Sb_2Te_3 molecular beam epitaxy to ensure a highly ordered and epitaxial film, and deposited Ni80Fe20 films on the MBE grown Sb_2Te_3. The $Sb_2Te_3/Ni_{80}Fe_{20}$ heterostructures were examined with temperature-dependent magnetometry, high-angle annular dark-field scanning transmission electron microscopy, and theoretical calculations. We found this interface to be highly complex with multiple phase formations, including a novel antiferromagnetic phase evident by the presence of a large exchange bias at cryogenic temperatures with a Neel temperature of 40K. Despite the complex nature of the $Sb_2Te_3/Ni_{80}Fe_{20}$ interface, a significant enhancement of the Gilbert damping and reduction of effective in-plane magnetization were observed, indicating a strong spin pumping in this heterostructure – Sb_2Te_3 is a spin sink due to its large spin-orbit-coupling.[13] This work highlights the role of interfacial chemistry and new interfacial phase formation in topological insulator/ferromagnet heterostructures, and how the interfacial phase formation may affect the spin pumping and other behaviors of these magnetic/topological insulator thin-film heterostructures.

1.Y. Cao et al, *iScience*, 23, 101614, (2020). 2.S. Hsuan Su et al, *ACS Appl. Electron. Mater.*, 3, 2988-2994, (2021). 3.N.H.D. Kang et al, *Nat. Mater.,* 17, 808-813, (2018). 4.M. DC et al, *Nat. Mater.,*17, 800-807, (2018). 5.W. Jie Wang et al, *Sci. Rep.*, 6, 25291, (2015). 6.T. Fan et al, *Sci. Rep.*, 12, 2998, (2022). 7.C.D Spataru et al, *Phys. Rev. B.,* 90, 085115 (2014). 8.W. Ye et al, *arX*iv*, (2015).* 9.L.A. Walsh et al., *J. Phys. Chem. C*, 121, 23551 (2017). 10.S.J. Chang et al., *RSC Adv*., 8, 7785–7791, (2018). 11.G. Li and C. Felser, *Appl. Phys. Lett.,* 116, 070501, (2020). 12.N. Bhattacharjee et al., *Adv. Mater.*, 2108790, (2022). 13.A.A. Baker et al., *Sci. Rep.,* 5, 7907 (2015).

FPA-09. Withdrawn

FPA-10. Enhanced spin pumping in CoFeB/Ta/Ni heterostructure by temperature induced Ni → NiO interface. *P. Kumar*[1,2], V. Sharma[2], R. Kumar[2], M.K. Khanna[3] and B.K. Kuanr[2] *1. Department of Electronic Science, University of Delhi, South Campus, New Delhi, India; 2. Special Centre for Nanoscience, Jawaharlal Nehru University, New Delhi, India; 3. Ramjas College, University of Delhi, New Delhi, India*

The spintronics functionality of CoFeB thin film can be evident by its potential use in magnetic tunnel junction and has applications in memory devices (MRAM) [1]. In this investigation, CoFeB (4:4:2) thin films have been utilized in combination with Ta, and Ni→NiO layer to probe the dominance of favourable interface for efficient spin transport. The fabricated heterostructure has the form of Si/SiO_2/CoFeB(20nm)/Ta(4nm)/Ni(20nm) via sputtering and in-situ oxygen annealed at different temperature for the controlled transformation of Ni to NiO. The ferromagnetic resonance (FMR) spectra revealed two distinct resonances for the two ferromagnetic (FM) layers with a gradual change of Ni peak which signifies the effect of annealing temperature (T_{ann}) on the heterostructure. Fig. (1) shows significant decrement in the effective magnetization (M_{eff}) from 5.7 kOe for pristine Ni (unannealed) to 2.2 kOe for Ni→NiO layer (T_{ann} =450°C). In contrast CoFeB layer magnetization remain nearly unchanged as shown in the Fig.1(a) due to the presence of protective Ta layer. The interface quality and FMR induced spin pumping can be characterized by measuring effective spin mixing conductance ($g_{eff}^{\uparrow\downarrow}$) using the relation [2]: $g_{eff}^{\uparrow\downarrow} = [(M_{eff}t_{CFB})/(g\mu_B)] (\alpha_{CFB/Ta} - \alpha_{CFB})$ The term $g_{eff}^{\uparrow\downarrow}$ quantify the transfer of spin angular momentum across the FM/NM interface. α_{CFB} is the intrinsic Gilbert damping of CoFeB layer, and $\alpha_{CFB/Ta}$ represents the Gilbert damping of the fabricated CoFeB/Ta interface, whereas t_{CFB} denotes the thickness of CoFeB layer. Fig.1(b) shows the Gilbert damping (α) obtained from the LLG equation. Fig. 2 shows the change in $g_{eff}^{\uparrow\downarrow}$ of the trilayer heterostructure with annealing temperature. $g_{eff}^{\uparrow\downarrow}$ remains constant up to 350°C and then increased sharply by 260% for the sample annealed at 450° C. This large enhancement in $g_{eff}^{\uparrow\downarrow}$ suggest a significant increment in the spin movement by spin pumping from CoFeB to Ta layer due to the evolution of antiferromagnetic (AFM) NiO layer upon annealing. The enhancement of spin pumping induced by engineered AFM NiO spin reservoir favouring the flow of spins from the CoFeB which can be a novel spintronic functionality.

[1] H. Yang *et al.*, "Two-dimensional materials prospects for non-volatile spintronic memories," *Nature*, vol. 606, no. 7915, pp. 663–673, 2022, doi: 10.1038/s41586-022-04768-0. [2] H. L. Wang, C. H. Du, Y. Pu, R. Adur, P. C. Hammel, and F. Y. Yang, "Scaling of spin Hall angle in 3d, 4d, and 5d metals from Y 3 Fe 5 O 12/metal spin pumping," *Phys. Rev. Lett.*, vol. 112, no. 19, p. 197201, 2014.

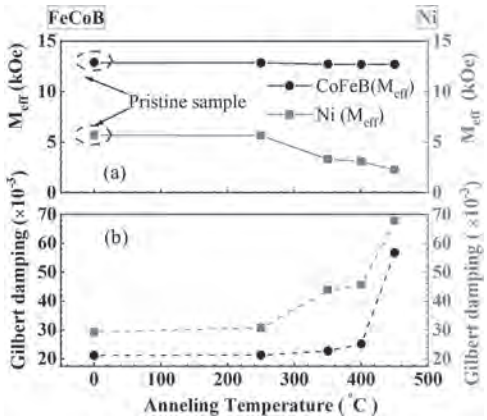

(a) M_{eff} and (b) α versus annealing temperature

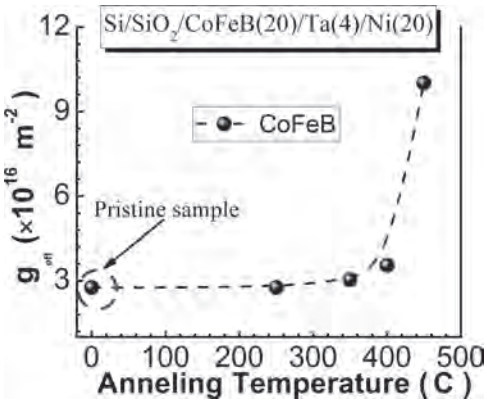

Shows $g_{eff}^{\uparrow\uparrow}$ vs T_{ann}

FPA-11. Local spin Seebeck effect on polycrystalline YIG/thermally evaporated chromium bilayers. *S. Bleser*[1], R. Greening[1], X. Fan[1] and B. Zink[1] *1. University of Denver, Denver, CO, United States*

Continued efforts toward both fundamental knowledge and application of spintronics rely on improved materials for converting spin to charge and vice-versa. We recently demonstrated that the longitudinal spin Seebeck effect (LSSE) [1] shows large spin-charge conversion and large spin Seebeck voltages of thermally-evaporated chromium thin films relative to sputtered platinum at room temperature. However, determining the exact nature and control of thermal gradients in LSSE experiments is imperative, especially at the interface [2,3]. In this work, we adopt the Hall bar geometry and current-driven heating [4,5] for LSSE experiments in a vacuum cryostat for better manipulation of thermal gradients. In figure 1, we show the LSSE signal for a 10 nm thin film of chromium (Cr) and 10 nm sputtered platinum (Pt) thin film both grown on a polycrystalline yttrium iron garnet (YIG) substrate under the same experimental conditions using Peltier devices to establish a thermal gradient external to the sample. Figure 2 shows the local LSSE signal for a 10 nm Cr and 25 nm Pt Hall bar utilizing a local heating method via Joule heating in a controlled vacuum cryostat environment. The high resistance of the evaporated Cr leads to very large local LSSE voltages, indicating this easily prepared film holds promise for probing thermally generated spin current phenomena in a range of magnetic insulators.

[1] Bleser, Greening, Roos, *et al*. J. Appl. Phys. 131, 113904 (2022). [2] Sola, A., Bougiatioti, P., Kuepferling, M. *et al. Sci Rep* 7, 46752 (2017). [3] A. Sola *et al*. *IEEE Transactions on Instrumentation and Measurement*, vol. 68, no. 6, pp. 1765-1773, June 2019. [4] W.X. Wang, S. H. Wang, L. K. Zou, *et al*. Appl. Phys. Lett. 105, 182403 (2014). [5] Michael Schreier, *et al*. Appl. Phys. Lett. 103, 242404 (2013).

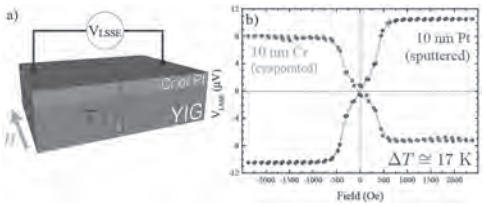

FIG 1: a) Schematic of standard LSSE, where (Cr, Pt)/YIG samples were subjected to a thermal gradient in the z-direction and a transverse magnetic field which resulted in comparable LSSE voltages using both Pt and Cr metal films. b) Longitudinal spin Seebeck voltage plotted against magnetic field for a 10 nm Cr (green) sample and a 10 nm Pt (blue) sample at a temperature difference of 17 K.

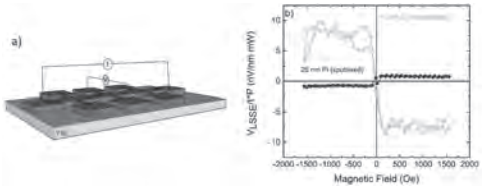

FIG 2: a) Schematic of local LSSE, where (Cr, Pt)/YIG Hall bar samples were subjected to an applied current density to establish a -z-directed thermal gradient via Joule heating and a transverse magnetic field which resulted in an observable voltages across the samples via LSSE. b) LSSE voltage normalized by thickness and heating power plotted against magnetic field for a 10 nm Cr (green) sample is much larger than for a 25 nm Pt (blue) sample.

FPA-12. Study of Cobalt-Based Spin Gapless Semiconducting Heusler Alloy Thin Film. *S. Nadeem*[1], S. Amara[1], D. Khan[1], S. Chaudhary[2] and Y. Massoud[1] *1. Computer, Electrical and Mathematical Sciences and Engineering, King Abdullah University of Science and Technology, Thuwal, Saudi Arabia; 2. Department of Physics, Indian Institute of Technology, Dehli, India*

Spintronics is a prime candidate for information storage and logic devices due to its significant advantages over traditional CMOS technology, such as low-power consumption, non-volatility, and high endurance. Recently, spin-gapless semiconductors (SGSs) have been introduced for modern spintronics-based applications and are promising candidates for designing quantum computing, data storage, coding, and decoding. In SGSs, spin-polarized charge carriers or spin current are the primary functions of these magnetic materials [1]. SGS materials such as CoFeMnSi Heusler Alloy offer high spin polarization (64%), high Curie temperature (620 K), and low damping constant (0.0046) are all intriguing properties that can be used in room-temperature spintronic device applications [2]. SGS has unique features such as almost temperature-independent carrier concentration, and quantum linear magnetoresistance in a low-temperature range [3]. In this abstract, the effect of changing the sputtering power from 30W to 50W and 90W on an RF sputtered thin film of CoFeMnSi (CFMS) Heusler alloy with a nominal thickness of 30 nm with temperature-dependent electrical and magneto-transport properties has been studied. Fig. 1(a) shows Hall resistivity as a function of applied magnetic field for CFMS 90W (30nm) thin-film recorded at 10K, 50K, 100K, 200K, 250K, and 300K. Fig. 1(b) demonstrates the SGS behavior of the material in nearly temperature-independent carriers' concentrations with the same order up to 300K. Fig. 1(c) depicts magnetoresistance (MR) curves of 90W (30nm) CFMS thin film within the temperature range of 10K to 200K. The MR curves exhibit a linear field-dependent trend. In this temperature range, the observed MR is negative. The peak presence at zero magnetic fields signifies the localization and as we increase the field, the path contributing to localization is go out of the phase.

[1]. D. Rani, L, Bainsla, A. Alam, and K. G. Suresh, "Spin-gapless semiconductors: Fundamental and applied aspects", *Journal of Applied Physics,* vol. 128, no. 22, 2020. [2]. L. Bainsla, A. I. Mallick, M. Raja, A. K. Nigam, B. Varaprasad, Y. Takahashi, A. Alam, K. G. Suresh, and K. Hono "Spin gapless semiconducting behavior in equiatomic quaternary CoFeMnSi Heusler alloy", *Physical Review B*, vol. 91, 2015. [3]. X. L. Wang, "Proposal for a new class of materials: spin gapless semiconductors", Physical review letters, vol. 100, 2008.

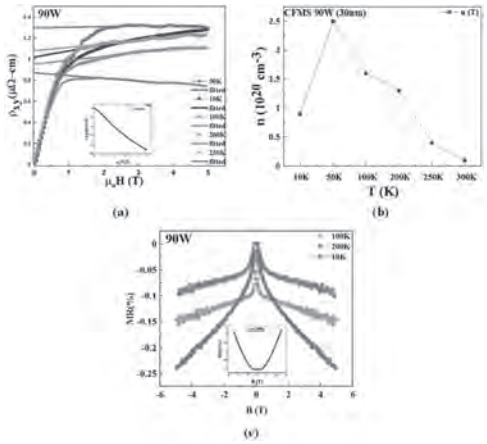

Fig. 1. (a) Hall resistivity data with applied magnetic field for CFMS 90W (30nm) thin-film recorded at 10K, 50K, 100K, 200K, 250K, and 300K. (b) Nearly temperature-independent carriers' concentrations with the same order up to 300K. (c) Linear magnetoresistance at a low-temperature range of 90W (30nm) CFMS thin-film recorded at 10K, 100K, and 200K.

FPA-13. Large spin current generation from the Rashba surface at Ti/Pt interface. *S. Dutta*[1] and A. Tulapurkar[1] *1. Electrical Engineering, Indian Institute of Technology Bombay, Mumbai, India*

We report a large spin-current generation from the interface of the Ti/Pt bilayer. By doing the spin-torque ferromagnetic resonance (ST-FMR)[1] in Ti(5)/Pt(1.5)/Py(5)/Pt(1.5) heterostructure, we observe a large enhancement of the damping-like torque that cannot be explained by the spin Hall effect (SHE) of Pt due to the cancellation of the spin-current generated from the symmetrically placed Pt layers on either side of the ferromagnet. We observe that the sign of damping-like torque generated in Ti/Pt/Py/Ti heterostructure is opposite as compared to Pt/Py bilayers which rule out the possibility of the conversion of orbital-current generated by Ti into the spin-current using the spin-orbit coupling of Pt[2–5]. This effect is reproduced for different thicknesses of Py (4 -8 nm). We confirm that this effect disappears when Pt is substituted by Cu. All these pieces of evidence together suggest a possible formation of the Rashba surface at the Ti/Pt interface due to their work function difference (approximately 1.3 eV). This could be a way to boost up the generated spin-current by exploiting the interfacial Rashba-Edelstein effect and bulk spin hall effect together for practical applications.

[1] L. Liu, T. Moriyama, D.C. Ralph, and R.A. Buhrman, Phys. Rev. Lett. 106, 1 (2011). [2] D. Go, F. Freimuth, J.P. Hanke, F. Xue, O. Gomonay, K.J. Lee, S. Blügel, P.M. Haney, H.W. Lee, and Y. Mokrousov, Phys. Rev. Res. 2, 1 (2020). [3] Y. Choi, D. Jo, K. Ko, D. Go, and H. Lee, ArXiv:2109.14847v1 1 (2021). [4] S. Lee, M.G. Kang, D. Go, D. Kim, J.H. Kang, T. Lee, G.H. Lee, J. Kang, N.J. Lee, Y. Mokrousov, S. Kim, K.J. Kim, K.J. Lee, and B.G. Park, Commun. Phys. 4, 3 (2021). [5] S. Ding, A. Ross, D. Go, L. Baldrati, Z. Ren, F. Freimuth, S. Becker, F. Kammerbauer, J. Yang, G. Jakob, Y. Mokrousov, and M. Kläui, Phys. Rev. Lett. 125, (2020).

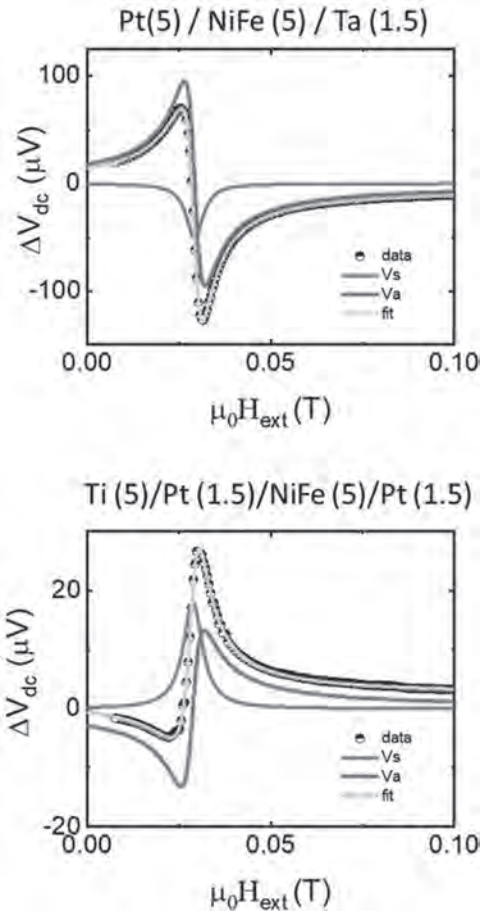

ST-FMR voltage signal (black squares) for (a) Pt(5)/NiFe(5) and (b) Ti(5)/Pt(1.5)/NiFe(5)/Pt(1.5) sample, fit by the symmetric (blue curve) and anti-symmetric Lorentzian (magenta) to quantify the in-plane damping like torque and out-of plane field like torque efficiencies respectively.

FPA-14. Study of Spin Orbit Torque in $PtSe_2$/NiFe/Pt Heterostructure.

R. Mudgal[1], A. Jakhar[2], P. Gupta[1], H. Bangar[1], N. Chowdhury[1], S. Das[2] and P.K. Muduli[1] *1. Department of Physics, Indian Institute of Technology Delhi, Delhi, India; 2. Centre for Applied Research in Electronics, Indian Institute of Technology Delhi, Delhi, India*

Transition metal dichalcogenides (TMDs) are potential materials for exerting efficient spin-orbit torque (SOT) on the adjacent ferromagnetic (FM) layer due to their high spin-orbit coupling (SOC) and broken inversion symmetry at the interface [1]. An unconventional SOT is recently observed in WTe_2/NiFe heterostructures due to low symmetry in WTe_2 [2]. $PtSe_2$ is one of the TMDs having high SOC [3]. In this work, we measured the effective spin Hall efficiency (SHE) in $PtSe_2$/NiFe/Pt heterostructure using spin-torque ferromagnetic resonance (STFMR). $PtSe_2$ was synthesized by salinization of a sputtered Pt (3 nm) film. The growth of $PtSe_2$ was confirmed using Raman measurements, which shows two peaks at 176 cm^{-1} (E_g) and 206 cm^{-1} (A_{1g}). Subsequently, a 6 nm thick NiFe (Py) layer followed by Pt (3 nm) capping layer was deposited on $PtSe_2$ using magnetron sputtering. For STFMR measurements, RF current of frequency varying from 3 GHz to 7 GHz was applied to the device in the presence of an external magnetic field (H). The mixing voltage (V_{mix}) across the device was measured and the symmetric & anti-symmetric components (V_S, V_A) of V_{mix}, linewidth (ΔH), and resonance field (H_r) were extracted (Fig.1) from the fitting of STFMR spectra. Effective SHE was calculated using the ratio of V_S and V_A and found to be increased 33% for $PtSe_2$/Py/Pt compared to reference (Py/Pt). This change in SHE is due to the presence of $PtSe_2$, which was further confirmed by making a stack with Pt/Py/Pt structure. STFMR signal of all three stacks has been compared in Fig. 1 (a). No clear signal was observed for Pt/Py/Pt which confirms the presence of SOT due to $PtSe_2$. Damping parameter was extracted by the fitting of linewidth (ΔH) vs. frequency (f) curve (Fig. 2) and was found to be enhanced by 131% in the case of $PtSe_2$/Py/Pt compared to its reference Py/Pt. Large enhancement in damping parameter indicates large spin pumping into $PtSe_2$. These results indicate the suitability of using $PtSe_2$ as a potential material for spin-orbit torque.

[1] Q. Shao et al., Nano Letter 16, 7514-7520 (2016) [2] D. MacNeill et. al., Nature Physics, 13, 300-305 (2017) [3] Marcin Kurpas and Jaroslav Fabian, Physical Review B, 103, 125409 (2017)

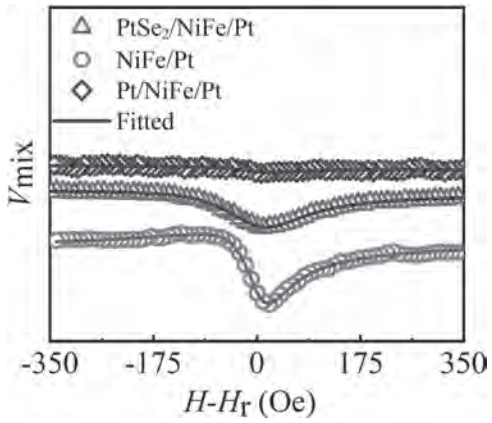

Fig. 1. Measured STFMR signal at 5 GHz for $PtSe_2$/Py/Pt, Py/Pt and Pt/Py/Pt. The solid lines represent fits.

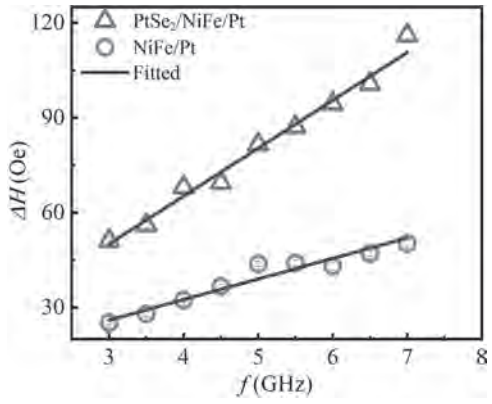

Fig. 2. Linewidth Vs. Frequency plot for $PtSe_2$/Py/Pt and Py/Pt. Solid lines represent fits

FPA-15. High Frequency (5 GHz – 40 GHz) Microwave Resonant Absorption and Inverse Spin Hall Effect in Py/Pt Thin Film stacking.
S. Sahu[1] and G. Basheed[1] *1. CSIR-National Physical Laboratory, New Delhi, India*

Microwave resonant (FMR) and Inverse Spin Hall effect (ISHE) in ferromagnetic materials have attracted high interest due to its significant contribution in spintronic devices [1]. Co-planar waveguide ferromagnetic resonance (CPW-FMR) technique is versatile tool to study the spin dynamics and its related parameters- saturation magnetization (M_s), spin mixing conductance ($g^{\uparrow\downarrow}$), anisotropy field ($H_{k)}$, geomagnetic ration (γ), Gilbert damping (α) and role of inhomogeneity (ΔH_0) in magnetic thin films. In the present study, high frequency (5 GHz - 40 GHz) dependent FMR and FMR induced spin current (ISHE) measurement has been performed on DC magnetron sputtered $Ni_{80}Fe_{20}$ (10 nm) and $Ni_{80}Fe_{20}$ (10 nm) /Pt (5 nm) thin film stacking via CPW - FMR set up. RT field swept microwave absorption spectra of $Ni_{80}Fe_{20}$ thin films fig. 1(a) and FMR induced voltage spectra (ISHE) fig.1 (b) of thin films were recorded. The spin dynamics parameters such as α, (ΔH_0), ($g^{\uparrow\downarrow}$) are 7.61 x 10^{-3}, 4.12 Oe and ~ 1.04 x 10^{20} m^{-2} respectively extracted via line shape analysis as shown in inset of fig.1(a). Other parameters- M_{eff}, γ, H_k are deduced from the above detailed CPW- FMR studies using Kittle fit eq. [2] in f vs Hres curve as shown in inset of fig.1(a) are ~ 1.047 T, 1.61 x 10^{11} $s^{-1}T^{-1}$, 88.38 Oe respectively. The ability to pump the spins from Py layer to Pt layer interface has induced by one order from ~ 10^{19} m^{-2} to 10^{20} m^{-2} in our studies as compare to previous reported literatures [3-4], which is attributed to the highly homogeneity and low magnetic interfacial anisotropy present in Py/Pt thin film stacking. Frequency dependent induced voltage (V_{ISHE}) is symmetric in nature inactive of the detection of pure spin current and magnitude is higher (V_{ISHE}^{2GHz} ~ 120 μV) which is in corroboration with damping and spin mixing conductance of Py/Pt thin film. The ISHE results are in agreement with the literature [5-6]. The thickness dependent study is under progress for the tuneable detection of pure spin current.

1.I. Zutic, J. Fabian, and S. D. Sarma, *Reviews of modern physics*, *76*(2), 323 (2004). 2.C. Kittel, *Physical Review*, *71*(4), 270. (1947). 3.O. Mosendz et al, *Physical Review B*, *82*(21), 214403 (2010). 4.S. Mizukami, *Journal of magnetism and magnetic materials*, *226*, 1640-1642 (2001) 5.R. Iguchi e al, *Japanese journal of applied physics*, *51*(10R), 103004 (2012). 6.S. Martín-Rio, *Journal of Magnetism and Magnetic Materials*, *500*, 166319 (2020).

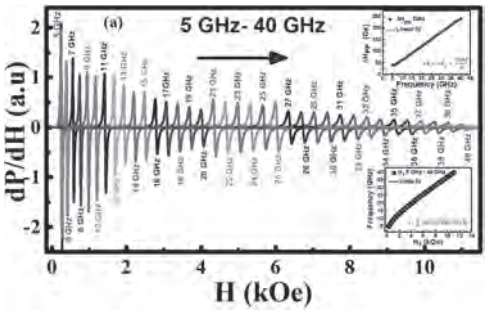

Fig.1 :(a) FMR spectra in freq. range 5- 40 GHz. The inset shows Hres and ΔHpp as function of freq.

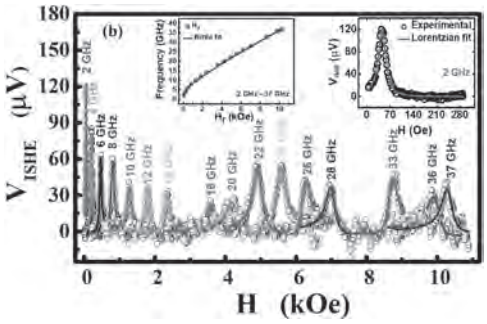

Fig.1:(b) V_{ISHE} vs freq. with fit. The inset show H_{res} vs freq. and ISHE spectra at 2 GHz.

FPA-16. Characteristics of Magnon-phonon Coupling in Magnetic Insulator based on Boltzmann equation.
C. Chen[1], Y. Li[1] and J. Zhang[1] *1. Tongji University, Shanghai, China*

The spin Seebeck effect (SSE) is a means of producing pure spin currents through temperature gradients. In the study of the magnon transport efficiency excited by the spin Seebeck effect as a function of the magnetic field strength, anomalous transport phenomenon of magnons was discovered [1]. Due to anomalous transport phenomena and magnons and optical and acoustic phonon dispersion relations are obviously interrelated. Therefore, the magnon-phonon interaction has become an important factor affecting magnon transport properties. In this paper, we try to use Boltzmann method to solve the coupling characters of magnon and phonon. In the magnon Boltzmann equation, we introduce the "reverse diffusion" effect [2] to study the transport efficiency of magnons recently discovered in experiments Inhibition due to increased magnetic field strength. In describing magnon-phonon interactions, the spatial dependence of the magnetic field in the Zeeman interaction, which is mainly studied in this paper, leads to magnon-phonon coupling, which directly depends on the spatial gradient of the built-in magnetic field strength [3]. Among them, the interaction of magnons and phonons is manifested as the expansion of a non-uniform magnetic field with small displacements of atomic vibrations. From this, the scattering term generated by the phonon scattering by the magnon can be obtained, and the scattering term is brought into the Boltzmann equation to obtain the final form to describe the transport properties of magnons. Based on this equation, this paper serially studies the regulation mode of phonon and magnon scattering mechanism and its influence on magnon transport, and then studies the physical mechanism of anomalous transport in magnon transport at low temperature.

[1] Kikkawa T, Shen K, Flebus B, et al. Magnon polarons in the spin Seebeck effect[J]. Physical review letters, 2016, 117(20): 207203. [2] Liu T, Wang W, Zhang J. Collective induced antidiffusion effect and general magnon Boltzmann transport theory[J]. Physical Review B, 2019, 99(21): 214407. [3] Vidal-Silva N, Aguilera E, A Roldán-Molina, et al. Magnon Polarons induced by a magnetic field gradient[J]. Physical review. B, Condensed matter, 2020.

$$v_k \frac{\partial n_k}{\partial r} - v_k \left(-\frac{\partial N_k^0}{\partial \varepsilon_k}\right)\left[\frac{\varepsilon_k}{T_m}(-\nabla T_m) + g\mu_B\left(\nabla H_{loc} + H_{loc}\frac{\nabla \overline{n_k}}{N_k^0}\right)\right] = -\frac{n_k - \overline{n_k}}{\tau_m} - \frac{n_k - N_k^0}{\tau_{th}} - \frac{n_k - f_{k\lambda}}{\tau_{mp}}$$

Session GOA
MAGNETIZATION DYNAMICS I

Vijaysankar Kalappattil, Chair
Colorado State University, Fort Collins, CO, United States

INVITED PAPER

GOA-01. Polarized phonons carry the missing angular momentum in femtosecond demagnetization. *U. Nowak*[1], M. Evers[1], H. Lange[1], S. Tauchert[2], M. Volkov[1] and P. Baum[2] *1. Department of Physics, University of Konstanz, Konstanz, Germany; 2. Deparment of Physics, LMU, Garching, Germany*

The transfer and control of angular momentum is a key aspect for spintronic applications. When a thin nickel film is subjected to ultrashort laser pulses, it can lose its magnetic order almost completely within merely femtosecond times. This phenomenon, which can also be observed in many other materials, offers opportunities for rapid information processing or ultrafast spintronics at frequencies approaching those of light. Consequently, ultrafast demagnetization is central to modern material research, but a crucial question has remained elusive: If a material loses its magnetization within only femtoseconds, where is the missing angular momentum on such short time scales? Here we use molecular dynamics simulations to investigate the role of phonons during ultrafast demagnetization in nickel. For this purpose, we transfer angular momentum corresponding to the observed amount of demagnetization into the lattice and calculate the resulting changes in the diffraction pattern. Our results are in line with ultrafast electron diffraction measurements which show an almost instantaneous, long- lasting, non-equilibrium population of anisotropic high-frequency phonons that appear as quickly as the magnetic order is lost. The anisotropy plane is perpendicular to the direction of the initial magnetization and the atomic oscillation amplitude is 2 pm. Theory and experiment indicate a rotational lattice motion on atomic dimensions after the excitation with the laser pulse that takes up the missing angular momentum [1] before the onset of a macroscopic Einstein-de Haas rotation [2]. Acknowledgements This research was supported by the German Research Foundation (DFG) via SFB 1432.

[1] S. R. Tauchert et al. Nature 602, 73–77 (2022). [2] C. Dornes et al. Nature 565, 209-212 (2019).

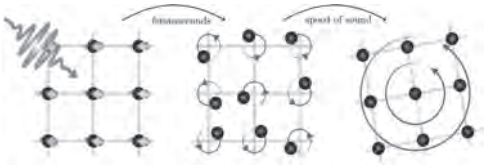

CONTRIBUTED PAPERS

GOA-02. Element specific ultrafast magnetization dynamics of strained NFO films using ultra short XUV pulses. *S. Saha*[1,2], R. Knut[1], R.S. Malik[1], K. Jatkar[1], R. Stefanuik[1], J. Soderstrom[1], V. Kapaklis[1], C. Luo[3], F. Radu[3] and D. Arena[4] *1. Uppsala University, Uppsala, Sweden; 2. Ashoka University, Sonepat, India; 3. Helmholtz-Zentrum Berlin für Materialien und Energie, Berlin, Germany; 4. University of South Florida, Tampa, FL, United States*

$NiFe_2O_4$ (NFO) [1], is an insulating ferrimagnet with an inverse spinel structure and already has gained a considerable attention of scientific community due to its potential applications in spintronic devices. For NFO thin films, a coherent strain can be introduced by growing them on different substrates: $ZnGa_2O_4$ (ZGO) and $MgAl_2O_4$ (MAO) with lattice mismatch of 0.06% and 3.1% respectively. This strain greatly affects physical properties such as magnetic damping, where damping for the NFO film grown on ZGO is considerably smaller than the damping of the NFO film grown on MAO film [2]. Magnetic damping should also affect ultrafast processes such as the demagnetization and remagnetization time of the system. Koopmans *et al.* [3] showed that the demagnetization time is inversely proportional to the effective Gilbert damping. In this work we explore the underlying mechanisms ultrafast demagnetization processes of strained NFO films by using table-top high harmonic generation (HHG) in the extreme ultraviolet (XUV) regime [4], which enables element-specific tracking of spin dynamics. To understand the HHG asymmetry spectra, we compare the discrete HHG spectra to the reflectivity spectra acquired using a continuous synchrotron-based source. The comparison shows good agreement, thereby facilitating assignment of HHG asymmetry features. Time-resolved HHG scans indicate that the demagnetization amplitude is larger for NFO on the MAO substrate while NFO films on both substrates exhibit the similar demagnetization and remagnetization times. In contrast to damping of spin motion at longer timescales, which is highly sensitive to issues such as defect density, the similarity in the magnetization dynamics in the first few ps following a demagnetization pulse reveals the local nature of the ultrafast dynamics. The results display the utility of M-edge spectroscopy for studying spin dynamics in insulating oxide films, which is highly relevant for spintronics based on ferrimagnetic insulators.

[1] R. Knut et al., J. Phys.: Condens. Matter 33, 225801(2021) [2] A. V. Singh et al., Advanced Materials 29, 1701222 (2017). [3] B. Koopmans et al., Physical Review Letters 85, 844 (2000). [4] S. Jana et al., Phys. Rev. Research 2, 013180 (2020).

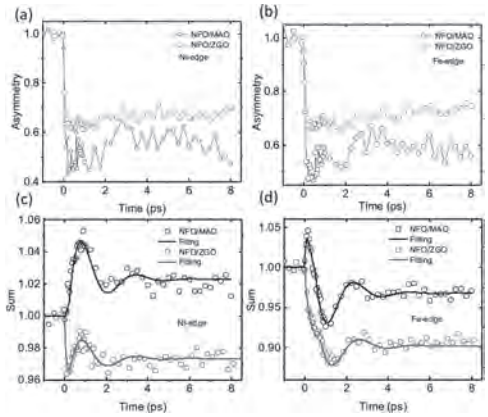

Fig. 1: (a), (b)The asymmetry and (c), (d) the total reflectivity as a function of time delay for Ni and Fe-edge. In (c) and (d) Solid lines correspond to the calculation done using three temperature model.

GOA-03. Withdrawn

GOA-04. Nonlinear evolution of nanoscale magnetic domains following ultrafast laser excitation. *R. Jangid*[1], N.Z. Hagström[2], M. Madhavi[1], J.M. Shaw[5], J. Brock[4,8], M. Pancaldi[3], F. Capotondi[3], E. Pedersoli[3], H. Nembach[5], S. Bonetti[2,6], E. Fullerton[4], M.W. Keller[5], R. Kukreja[1], E. Iacocca[7] and T.J. Silva[5] *1. Department of Materials Science and Engineering, University of California Davis, Davis, CA, United States; 2. Department of Physics, Stockholm University, Stockholm, Sweden; 3. Elettra-Sincrotrone Trieste S.C.p.A., Trieste, Italy; 4. Center for Memory and Recording Research, University of California San Diego, La Jolla, CA, United States; 5. Quantum Electromagnetics Division, National Institute of Standards and Technology, Boulder, CO, United States; 6. Department of Molecular Sciences and Nanosystems, Ca' Foscari University of Venice, Venezia, Italy; 7. Center for Magnetism and Magnetic Materials, University of Colorado Colorado Springs, Colorado Springs, CO, United States; 8. Paul Scherrer Institute, Villigen, Swaziland*

In recent years, optical manipulation of magnetization at ultrafast timescales has gained significant interest due to its potential applications in energy-efficient high speed magnetic storage and memory devices. [1] However, most of the studies have focused on magnetization switching of uniformly magnetized samples. Recently, ultrafast demagnetization studies of textured magnetic materials have been reported which show additional demagnetization pathways not observed in homogeneously magnetized systems [2–5]. However, systematic studies of textured magnetic materials which can access both nanometer lengthscales and femtosecond timescales are lacking. We utilized time-resolved small-angle x-ray scattering at free electron laser at FERMI, Italy to measure the ultrafast response of mixed domain state in CoFe/NiCu multilayers. A novel 2D fitting routine was employed to disentangle the isotropic and anisotropic scattering components due to presence of both labyrinth and stripe domains in the mixed state [6]. Magnetization quench showed linear dependence with pump fluence in agreement with the literature. On the other hand, nonlinear behavior was observed for both isotropic and anisotropic scattering peak position and width indicating changes in the domain structure. Below a fluence threshold (~ 7 mJ/cm^2), negligible changes were observed in peak position and width which are related to domain periodicity and correlation length, respectively. Above this fluence threshold, peak position and width for isotropic scattering increased drastically. The anisotropic scattering showed similar nonlinear behavior albeit a smaller magnitude of the response. Another striking observation was that the quench time for peak position and the peak width was found to be twice as slow as the quench time for magnetization amplitude. Our findings indicate that a critical amount of magnetization quench is required to initiate ultrafast changes in the domain structure. Furthermore, labyrinth domains show a stronger effect compared to the stripe domains. Our studies reveal a clear dependence on the domain structure highlighting the role of nanoscale morphology on the ultrafast magnetization dynamics.

[1] S. Jeppson and R. Kukreja, APL Mater. 9, 100702 (2021). [2] B. Pfau, S. Schaffert, L. Müller, C. Gutt, et al., Nature Communications 3, 1100 (2012). [3] B. Vodungbo, J. Gautier, G. Lambert, et al., Nature Communications 3, 999 (2012). [4] M. Hennes, A. Merhe, X. Liu, et al., Phys. Rev. B 102, 174437 (2020). [5] D. Zusin, E. Iacocca, L. L. Guyader, et al., arXiv:2001.11719v4 (2020). [6] N. Z. Hagström, R. Jangid, Meera, et al., arXiv:2112.09587v1 (2021).

GOA-05. Withdrawn

GOA-06. All Optical Switching of Antiferromagnetic Domains. *H. Meer*[1], S. Wust[2], C. Schmitt[1], P. Herrgen[2], F. Fuhrmann[1], B. Bednarz[1], A. Rajan[1], R. Ramos[6,7], M. Foerster[3], M. Niño[3], F. Kronast[4], A. Kleibert[5], E. Saitoh[6,8], B. Stadtmüller[1,2], M. Aeschlimann[2] and M. Kläui[1] *1. Institute of Physics, Johannes Gutenberg-University Mainz, Mainz, Germany; 2. Department of Physics and Research Center OPTIMAS, Universität Kaiserslautern, Mainz, Germany; 3. ALBA Synchrotron Light Facility, Barcelona, Spain; 4. Helmholtz-Zentrum Berlin für Materialien und Energie, Berlin, Germany; 5. Swiss Light Source, Paul Scherrer Institut, Villingen, Switzerland; 6. WPI-Advanced Institute for Materials Research, Tohoku University, Sendai, Japan; 7. Departamento de Química-Física, Universidade de Santiago de Compostela, Centro de Investigación en Química Biolóxica e Materiais Moleculares (CIQUS), Santiago de Compostela, Spain; 8. Department of Applied Physics, The University of Tokyo, Tokyo, Japan*

Antiferromagnetic materials (AFMs) are ideal candidates for fast, and energy-efficient spintronic devices. AFMs possess two or more antiferromagnetically coupled magnetic sublattices, with a vanishing net magnetization. The absence of magnetic stray fields enables a higher bit packing density of AFMs compared to ferro(i) magnetic materials (FMs) and enhanced robustness against interfering external magnetic fields. Another key advantage of AFMs is the potential for ultrafast applications, due to their intrinsic dynamics with resonance frequencies in the THz regime [1]. In ferri- and ferromagnetic material systems, fs laser-induced all-optical switching (AOS) has been intensively studied [2,3]. Thermally induced switching has been observed in ferrimagnetic GdFeCo alloys [2] and all-optical helicity-dependent switching (AO-HDS) based on the inverse Faraday effect has been observed in a wide range of ferri- and ferromagnetic materials [4]. Recently, helicity-dependent switching of the antiferromagnetic order in easy plane antiferromagnets has been theoretically proposed [5]. Here, we have used XMLD-PEEM to investigate antiferromagnetic domains after the irradiation with laser-light. We studied the effect of several fluences on the antiferromagnetic order and observe a laser-induced switching of the antiferromagnetic domains. By studying the optically induced switching for different laser-polarizations, we uncover the underlying mechanism and lay the foundation for using AOS in antiferromagnets.

[1] V. Baltz, A. Manchon, M. Tsoi et al., Rev. Mod. Phys. 90, 015005 (2018) [2] C. D. Stanciu, F. Hansteen, A. V. Kimel et al., Phys. Rev. Lett. 99, 047601 (2007) [3] M. S. El Hadri, M. Hehn, G. Malinowski, and S. Mangin, J. Phys. D. Appl. Phys. 50, 133002 (2017) [4] S. Mangin, M. Gottwald, C.-H. Lambert, et al., Nat. Mater. 13, 286 (2014) [5] T. Dannegger, M. Berritta, K. Carva, et al., Phys. Rev. B 104, L060413 (2021)

GOA-07. Robust toggle switching in Tb-based multilayers by a single-shot laser pulse. *Y. Peng*[1], D. Salomoni[2], G. Malinowski[1], L.D. Buda-Prejbeanu[2], R. Sousa[2], L. Prejbeanu[2], J. Hohlfeld[1], M. Verges[1], S. Mangin[1] and M. Hehn[1] *1. Institut Jean Lamour, UMR CNRS 7198, Université de Lorraine, Nancy, France; 2. Spintec, Université Grenoble Alpes, CNRS, CEA, Grenoble INP, IRIG-SPINTEC, Grenoble, France*

Since the first all-optical switching experiments carried on GdFeCo ferrimagnet [1-2], the all-optical switching represents an ultrafast and easy method to manipulate magnetization without any applied field. Single pulse helicity independent all-optical switching (HI-AOS) has been demonstrated in ferrimagnetic GdFeCo alloy, Gd/FM bilayers where FM is a ferromagnet, and recently in a ferrimagnetic Heusler alloy and Tb/Co multilayer-based electrode [2-5]. In this work, we demonstrate that robust toggle HI-AOS has been observed in ferrimagnetic Tb based multilayers (Fig.1a). The properties of single pulse HI-AOS in Tb-based multilayers mainly differ in two ways compared to GdFeCo alloys. First, the shape of the state diagram of Tb-based multilayers in which the toggle switching can be observed at a pulse duration of 10 ps is completely different from that of GdFeCo alloy [6] (Fig.1d). The threshold switching fluence (F_{switch}) is independent of the laser pulse duration of at least up to 10 ps (Fig. 1b). Moreover, the multi-domain fluence (F_{multi}), above which a multidomain state is observed in the center of the spot, increases slightly for pulse durations below 3 ps and then remains constant for longer pulse durations. This indicates that the mechanisms responsible for the Tb-based multilayers switching differ from those of Gd-based alloys. Second, the observed equilibrium state after the first laser pulse excitation shows a complex structure with rings of opposite magnetization directions when the fluence increases. This ring structure was observed in all Tb-based multilayer films we have studied so far. The number and the size of the rings depend on the sample composition (thickness of the Tb and transition metal layers) as well as on the annealing condition. Acknowledgments: UFO, COMRAD

[1] C. D. Stanciu, F. Hansteen, A. V. Kimel, Phys. Rev. Lett. 99, 047601, 2007. [2] T. A. Ostler, J. Barker, R. F. L. Evans, Nat. Commun. 3, 666, 2012. [3] M. Beens, M. L. M. Lalieu, A. J. M. Deenen, Phys. Rev. B 100, 220409(R), 2019. [4] L. Avilés-Félix, A. Olivier, G. Li, C. S. Davies, Sci. Rep. 10, 5211, 2020. [5] C. Banerjee, N. Teichert, K. Siewierska, Nat. Commun., 11, 4444, 2020. [6] J. Wei, B. Zhang, M. Hehn, Phys. Rev. Applied 15, 054065, 2021.

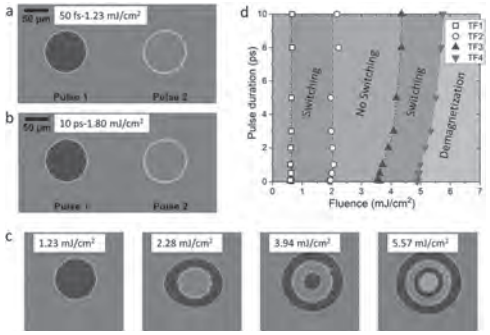

Fig 1: a-b: Background subtracted images after each single shot with pulse duration of a: 50 fs and b: 10 ps; c: State diagram obtained by plotting threshold fluences as a function of the pulse duration in; (d) Switching images after first single shot with 50 fs of different laser fluences. All the results shown here are obtained in $[Tb/Fe]_4$ multilayers.

GOA-08. Generation of Large Spin Current Burst during Magnetic Phase Transition of FeRh. T. Lee[1], M. Park[2], S. Kim[1], M. Jung[2] and *K. Kim*[1] *1. Physics, Korea Advanced Institute of Science and Technology, Daejeon, The Republic of Korea; 2. Physics, Sogang University, Seoul, The Republic of Korea*

Spin current generation lies at the heart of modern spintronics. Pure spin current can be generated via spin pumping, wherein the magnetization precession of ferromagnet produces a spin current into a neighboring non-magnetic layer.[1] So far, the spin pumping has mainly been used as a tool for quantifying magnetic parameters, including the spin Hall angle, spin diffusion length, spin mixing conductance, etc.,[2-4] because the efficiency of spin current generation is not large enough for use in spintronic applications, such as current-induced magnetization switching.[5] In this study, we propose a novel method to generate a large spin current via spin pumping. We utilize a FeRh which undergoes a magnetic phase transition from an antiferromagnet (AFM) to ferromagnet (FM) around 370 K.[6] The magnetic phase transition of FeRh from AFM to FM accompanies the change of total angular momentum from zero to finite. The change of angular momentum generates a spin current into a neighboring non-magnetic layer, and is converted to the charge current through the inverse spin Hall effect (ISHE). We find that the ISHE voltage is generated exclusively during the phase transition. Furthermore, the measured signal is found to depend on the sign of spin Hall angle and the direction of magnetization of FeRh, confirming that the observed signal indeed originates from the phase transition-induced spin pumping and ISHE. The generated spin current density is at least 3 orders of magnitude higher than those in previous spin pumping reports,[7,8] and is comparable to that generated by the spin Hall effect.[5] Our work provides a novel way to generate spin current, which could be utilized in potential spintronics applications.

[1] Y. Tserkovnyak, *et al. Phys. Rev. B* Vol. 66, p.224403 (2002). [2] O. Mosendz, *et al. Phys. Rev. B* Vol. 82, p.214403 (2010), [3] W. Zhang, *et al. Appl. Phys. Lett.* Vol. 103, p.242414 (2013) [4] E. Saitoh, *et. al. Appl. Phys. Lett.* Vol. 88, p.182509 (2006). [5] L. Liu, *et. al. Science* Vol. 336, 6081, p.555-558 (2012). [6] S. Maat, *et al. Phys. Rev. B* Vol. 72, p.214432 (2005). [7] H. L. Wang, *et al. Phys. Rev. Lett.* Vol. 112, p.197201 (2014) [8] Y. Wang, *et al. Nat. Commun.* Vol. 11, p.275 (2020).

GOA-09. Symmetry-dependent ultrafast manipulation of nanoscale magnetic domains. *N. Zhou Hagström*[1], R. Jangid[2], M. Madhavi[2], D. Turenne[3], J. Brock[4], E.S. Lamb[5], B. Stoychev[5], J. Schlappa[6], N. Gerasimova[6], B. Van Kuiken[6], R. Gort[6], L. Mercadier[6], L. Le Guyader[6], A. Samartsev[6], A. Scherz[6], G. Mercurio[6], H.A. Dürr[3], A.H. Reid[7], M. Arora[8], H. Nembach[8,9], J.M. Shaw[8], E. Jal[10], E. Fullerton[4], M.W. Keller[8], R. Kukreja[2], S. Bonetti[1,11], T.J. Silva[8] and E. Iacocca[13,12] *1. Department of Physics, Stockholm University, Stockholm, Sweden; 2. Materials Science and Engineering, University of California, Davis, Davis, CA, United States; 3. Department of Physics and Astronomy, Uppsala University, Uppsala, Sweden; 4. Center for Memory and Recording Research, University of California, San Diego, La Jolla, CA, United States; 5. Department of Physics, University of California, San Diego, La Jolla, CA, United States; 6. European XFEL GmbH, Schenefeld, Germany; 7. Linac Coherent Light Source, SLAC National Accelerator Laboratory, Menlo Park, CA, United States; 8. National Institute of Standards and Technology, Boulder, CO, United States; 9. Department of Physics, University of Colorado, Boulder, Boulder, CO, United States; 10. LCPMR, Sorbonne Université, Paris, Finland; 11. Department of Molecular Sciences and Nanosystems, Ca' Foscari University of Venice, Venice, Italy; 12. Department of Mathematics, Physics and Electrical Engineering, Northumbria University, Newcastle upon Tyne, United Kingdom; 13. Center for Magnetism and Magnetic Materials, University of Colorado, Colorado Springs, Colorado Springs, CO, United States*

The quest towards controlling magnetism at the femtosecond timescales is driven by the demand for energy efficient and fast magnetic storage devices [1]. Many studies have focused on switching the magnetization in different

materials. However, it has also been recognized that the spatial evolution of the magnetization plays a role in both switching [2] and stabilization of non-trivial textures [3]. Here, we study the ultrafast response of magnetic multilayers with different domain pattern symmetries [5]. Utilizing time-resolved small-angle, resonant X-ray scattering at the European XFEL and an accurate 2D fitting routine, we find a symmetry-dependent behavior of the ultrafast response. We study a unique sample that exhibits regions with both labyrinth and stripe domain characteristics to varying degree, see Figure 1(a-b). By isolating the isotropic and anisotropic components of the scattering by our fitting method, we find that only the labyrinth domains exhibit an ultrafast shift in the isotropic diffraction peak position, see Figure 1(c). Our results do not only confirm the results of previous studies [4], our findings also reveal the unpredicted dependence of the ultrafast spin dynamics on the spatial configuration of magnetic domains and invites further investigation on far-from-equilibrium spin transport.

[1] A. Kirilyuk, A. V. Kimel, and Th. Rasing, Rev. Mod. Phys. 82, 2731-2784 (2010) [2] E. Iacocca *et al.*, Nature Communications 10, 1756 (2019) [3] F. Büttner *et al.*, Nature Materials 20, 30-37 (2021) [4] B. Pfau *et al.*, Nature Communications 3, 1110 (2012); B. Vodungbo *et al.*, Nature Communications 3, 999 (2012), D. Zusin et al, arXiv:2001.11719; M. Hennes *et al.*, Phys. Rev. B 102, 174437 (2020) [5] N. Zhou Hagström et al., arXiv:2112.09587

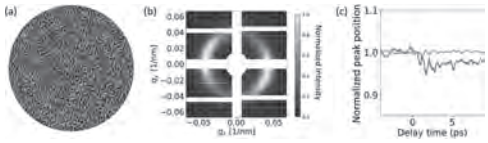

(a) MFM image of mixed domain pattern with labyrinth and stripe characteristics. (b) Representative X-ray scattering intensity of mixed state. (c) Simultaneous ultrafast change in the isotropic (blue) and anisotropic (orange) peak position.

GOA-10. Determination of sub-ps lattice dynamics in FeRh thin films. *M. Grimes*[1,2], H. Ueda[2], D. Ozerov[2], F. Pressacco[4], S. Parchenko[5], A. Apseros[2,3], M. Scholz[4], Y. Kubota[6], T. Togashi[6,7], Y. Tanaka[6], L. Heyderman[2,3], T. Thomson[1] and V. Scagnoli[2,3] *1. University of Manchester, Manchester, United Kingdom; 2. Paul Scherrer Institut, Villigen, Switzerland; 3. ETH Zurich, Zurich, Switzerland; 4. DESY, Hamburg, Germany; 5. European XFEL, Hamburg, Germany; 6. RIKEN, Hyogo, Japan; 7. JASRI, Hyogo, Japan*

FeRh is an archetypal system for the investigation of ultrafast behaviour in coupled transitions due to its meta-magnetic phase transition occurring around 380 K [1]. In this coupled phase transition, the electronic structure transforms lowering the resistivity by ≈ 33%, the lattice expands isotropically with a volumetric expansion of ≈ 1%, and the magnetic order changes from a G-type antiferromagnet (AF) to a ferromagnet (FM) [1], [2]. Previous x-ray diffraction (XRD) studies have indicated that the lattice expands with first-order dynamics within 10-30 ps [3], with long-range AF order throughout the transition [4]. The sub-ps capabilities of the SACLA free-electron laser allowed for investigation of the ultrafast behaviour of the FeRh lattice upon laser excitation. This shows new dynamics at high fluences which were compared to the quasi-static behaviour of the Bragg peaks as measured using heated XRD. We describe the lattice temperature (see Fig. 1a) and expansion as a function of pump-probe delay. We have observed a perturbation to the expected dynamics above fluences of 5 mJ cm^{-2} where the lattice initially contracts before finally expanding as predicted. We demonstrate that a model (see Fig. 1b) using a transient lattice state [5] can explain the observed behaviour. Our model suggests that the transient state is paramagnetic, reached by a subset of the phonon bands which are preferentially coupled to the electronic system [6]. A complete description of the FeRh structural dynamics requires consideration of coupling strength variation across the phonon frequencies.

[1] J. S. Kouvel and C. C. Hartelius, J. Appl. Phys., 33, 1343, (1962). [2] J. S. Kouvel, J. Appl. Phys., 37, 1257–1258, (1966). [3] S. O. Mariager, F. Pressacco, G. Ingold, et al., Phys. Rev. Lett., 108, 087201, (2012). [4] M. Grimes, N. Gurung, H. Ueda, et al., AIP Adv., 12, 035048, (2022). [5] B. Mansart, M. J. G. Cottet, G. F. Mancini, et al., Phys. Rev. B, 88, 054507, (2013). [6] M. Grimes, H. Ueda, D. Ozerov, et al., Sci. Rep., 12, 8584 (2022)

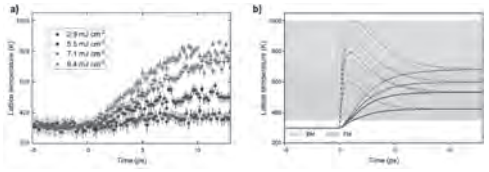

Figure 1 - a) Lattice temperature as a function of pump-probe delay based on the intensity of the transient XRD peaks. b) Predicted evolution of the lattice temperature using a transient lattice state model of electron-phonon coupling. Reproduced from Grimes et al. [6]

INVITED PAPER

GOA-11. Asynchronous switching of rare-earth and transition-metal sublattices in ferrimagnetic alloys induced by spin-orbit torques. *G. Sala*[1], C. Lambert[1], S. Finizio[2], V. Raposo[3], V. Krizakova[1], G. Krishnaswamy[1], M. Weigand[4], J. Raabe[2], M. Rossel[5], E. Martinez[3] and P. Gambardella[1] *1. ETH Zurich, Zürich, Switzerland; 2. Paul Scherrer Institut, Villigen, Switzerland; 3. University of Salamanca, Salamanca, Spain; 4. Max Planck Institute for Intelligent Systems, Stuttgart, Germany; 5. Electron Microscopy Center, EMPA, Dübendorf, Switzerland*

Rare-earth transition-metal (RE-TM) ferrimagnetic alloys have attracted considerable attention in the pursuit of magnetic materials with fast dynamics and efficient control. In particular, the discovery of all-optical switching raised strong interest in the intriguing and unexpected dynamics excited by an ultrafast laser excitation [1-2]. During a laser pulse, the antiferromagnetically-coupled RE and TM sublattices reverse their direction by forming a transient ferromagnetic state on the timescale of a few ps. This non-equilibrium configuration results from the combination of the rapid and strong demagnetization induced by the laser in combination with the conservation of angular momentum. In addition to optical means, current-induced spin-orbit torques (SOTs) can also trigger and manipulate the dynamics of RE-TM ferrimagnets [3-4]. Recent works have shown that SOTs are enhanced at the magnetization compensation point [5], where the RE and TM magnetizations balance each other. However, the current-induced dynamics are fastest at the compensation point of the angular momentum, where domain walls reach record speeds of several km/s [6-7]. This rapidity, which is inaccessible in ferromagnets, makes ferrimagnets attractive and promising for data storage technologies. At the same time, the easier excitation and detection of the dynamics of ferrimagnets as compared to antiferromagnets provides a fertile ground to explore the behavior of antiferromagnetically-coupled systems. Yet, in contrast to all-optical switching, the response of the individual RE and TM sublattices to SOTs has remained unexplored so far. Here we present the first time-, space, and element-resolved study of the ferrimagnetic dynamics triggered by SOTs [8]. We investigate the magnetization switching induced by ns and sub-ns-long electric pulses in GdFeCo and TbCo by combining scanning transmission X-ray microscopy and X-ray magnetic circular dichroism (XMCD), which allow for a temporal resolution of ~70 ps, a spatial resolution of ~30 nm, and sublattice sensitivity. We discover a variety of dynamics characterized by a variable degree of coupling between the RE and TM sublattices. While being antiferromagnetically coupled in equilibrium, the two sublattices can evolve asynchronously in time and inhomogeneously in space during and after the electric pulses. This difference takes the form of a delay between domain walls in the two sublattices or, in the extreme case, of a transient ferromagnetic state as long as 2 ns. This configuration is reminiscent of the temporary ferromagnetic alignment caused by intense laser pulses, but occurs on a much longer

timescale. Micromagnetic simulations and electron microscopy measurements identify the origin of the asynchronous dynamics with the combination of two factors: i) the weakness of the antiferromagnetic exchange interaction between the RE and TM sublattices and its dependence on the atomic structure of the alloys; ii) the preferential interaction of SOTs with the TM sublattice. Our study answers fundamental open questions on the action of SOTs on the RE and TM sublattices and their dynamics, and provides a novel and unique insight into the behavior of antiferromagnetically-coupled systems.

[1] C. D. Stanciu, F. Hansteen, A. Kimel et al., Physical Review Letters, Vol. 99, p. 047601 (2007) [2] I. Radu, K. Vahaplar, C. Stamm et al., Nature, Vol. 472, p. 205–208 (2011) [3] A. Manchon, J. Zelezny, I. Miron et al., Reviews of Modern Physics, Vol. 91, p. 035004 (2019) [4] G. Sala, V. Krizakova, E. Grimaldi et al., Nature Communications, Vol. 12, p. 656 (2021) [5] R. Mishra, J. Yu, X. Qiu et al., Physical Review Letters, Vol. 118, p. 167201 (2017) [6] L. Caretta, M. Mann, F. Büttner et al., Nature Nanotechnology, Vol. 13, p. 1154–1160 (2018) [7] K. Cai, Z. Zhu, L- Lee et al., Nature Electronics, Vol. 3, p. 37–42 (2020) [8] G. Sala, C.-H. Lambert, S. Finizio et al., Nature Materials, Vol. 21, p. 640–646 (2022)

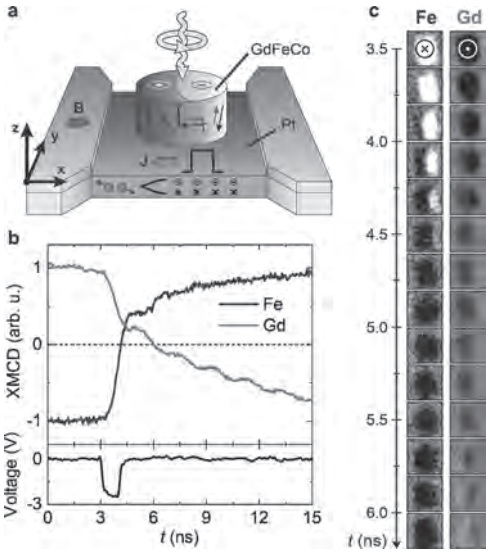

Fig. 1. Time-, space-, and element-resolved current-induced switching of GdFeCo. (a), Schematic of the sample layout, which consists of a ferrimagnetic GdFeCo dot on a Pt current line. The current pulse J induces the switching of the RE and TM magnetizations by SOTs. A magnetic field B is applied collinear to the current to achieve deterministic switching. (b), Time-dependence of the XMCD signal at the Fe L_3 and Gd M_5 edges (top panel) measured while applying bipolar electric pulses with 1 ns duration and 2.5 V amplitude (bottom panel). (c), Snapshots of the dynamics in (b). The vertical axis defines the timing (in ns) of the frames, which have a dimension of 1.2 x 1.2 μm^2.

Session GOB
MAGNETIZATION DYNAMICS II

Ezio Iacocca, Chair
University of Colorado Colorado Springs, Colorado Springs, CO, United States

CONTRIBUTED PAPERS

GOB-01. Magnonic interferometer's leaky-mode influence on spin-wave beam reflection. *K. Sobucki*[1], W. Smigaj[2], P. Graczyk[3], M. Krawczyk[1] and P. Gruszecki[1] *1. Faculty of Physics, Adam Mickiewicz University, Poznan, Poland; 2. Met Office, Exeter, United Kingdom; 3. Institute of Molecular Physics, Polish Academy of Sciences, Poznan, Poland*

Wood's anomaly is a phenomenon discovered in 1902 [1], manifesting as a decrease of the reflected waves amplitude due to the excitation of a surface mode that is still investigated in photonics [2]. Another curious effect observed in the reflection of obliquely incident waves is the Goos-Hanchen effect (GHE) [3,4], which causes a spatial shift of the reflected waves. One of the configurations suitable for observing both phenomena for spin waves (SWs) is the Gires-Tournois interferometer (GTI) proposed in Ref. [5,6], made of a magnetic stripe placed above the edge of a magnetic layer. We use micromagnetic simulations to study the reflection of an oblique incident SW beam at such a GTI. We identified the resonance conditions required to efficiently excite SW modes in the GTI by the incident SW beam, which give rise to magnonic Wood's anomaly in our system. The amplitude of these modes is confined in the stripe and emits SWs back to the layer; therefore, these modes can be classified as 'leaky-modes'. The consequence of the leaky-mode is the creation of multiple spatially shifted SW beams in the layer parallel to one another. Furthermore, the excitation of the leaky-modes is accompanied by a significant GHE for the primary reflected beam with values spanning between -175 nm and 225 nm with respect to the non-resonant case. In Fig. 1a and 1b we show the distributions of SW intensity for the case with the resonant excitation of a leaky-mode and without the excitation, respectively. In Fig. 1b multiple reflected SW beams are evident. Our findings contribute to understanding and utilizing the interaction of propagating SWs in thin films with the localized leaky-modes. Additionally, an incident beam's excitation of modes in GTI provides a platform for investigations of SWs inelastic scattering on interferometer's modes. We acknowledge the funding from the Polish National Science Centre project No. UMO-2019/33/B/ST5/02013.

[1] RW. Wood, Lond. Edinb. Dublin philos. mag. j. sci. 4, 396 (1902). [2] E. Galiffi, YT. Wang, Z. Lim, Phys. Rev. Lett. 125, 127403 (2020). [3] F. Goos, H. Hänchen, Annalen der Physik 436, 333 (1947). [4] P. Gruszecki, J. Romero-Vivas, Yu. S. Dadoenkova, Appl. Phys. Lett. 105, 242406 (2014). [5] K. Sobucki, W. Smigaj, J. Rychly, Sci. Rep. 11, 4428 (2021). [6] K. Sobucki, P. Gruszecki, J. Rychly, IEEE Trans. Magn, 58.2, 1-5, (2021)

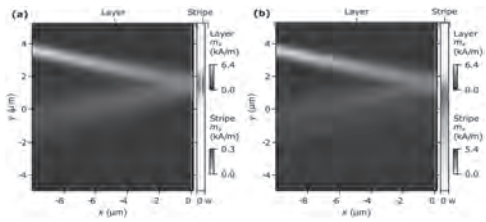

Figure 1: The distribution of SW amplitude in the layer (left panels) and in the stripe (right panels) placed above the film in the systems, (a) with M_S = 350 kA/m and (b) M_S = 550 kA/m, without and with excited leaky-mode, respectively.

GOB-02. Spectroscopy and mlcroscopy of propagating spin-waves in a synthetic anti-ferromagnet by Brillouin Light Scattering. *J. Adam*[1], F. Millo[1], S. Ngom[1], A. Mouhoub[1], J. Kim[1], C. Chappert[1], A. Solignac[2] and T. Devolder[1] *1. Université Paris-Saclay/CNRS, Palaiseau, France; 2. SPEC / CEA/ CNRS /Université Paris-Saclay, Gif-sur-Yvette, France*

Spin-waves in synthetic antiferromagnets (SAF) present two branches due to the sizeable magnetic coupling between the two magnetic layers. These two modes – acoustical and optical - of spin-waves can be excited and present strong different non-reciprocities opening new opportunities in controlling the transfer of energy [1]. Here we study propagating spin-waves in a symmetric SAF made of CoFeB (17 nm) and Ruthenium (0.7 nm) layers patterned in 5 μm wide stripe. Spin-waves are excited by an r.f. magnetic field emitted by a single wire antenna – Fig. 1-b. We report on their measurement using micro-focused Brillouin Light Scattering using a 532 nm wavelength LASER focused on the sample with a lateral size of about 350 nm in diameter. Localised spectroscopy allows to identify both acoustical and optical spin-waves with an increased sensitivity to the acoustical mode since the magnetization dynamics in both CoFeB layers are excited '*in phase*' with a constructive contribution to the optical signal - Fig. 1a. These spectra evidences a complex structure of the acoustical mode composed of a main band with parallel modes at both higher and lower frequencies than the main mode. In order to gain more details about theses modes, we performed BLS intensity mapping at fixed static magnetic field and r.f. pumping magnetic field. For excitation frequencies matching the main mode, we could observe uniform like propagating spin-waves – see Fig. 1c right panel – while for the other modes, the modes are strongly non uniform with nodes in the width – see Fig. 1c left and central panels – as well as of directional spin-wave beams propagating not along the magnetic stripe – see Fig. 1c central panel. We calculated numerical dispersion relations and used micromagnetic simulations to explain these behaviours which cannot be accounted for by simple demagnetizing contributions but by the large non-reciprocities of the dispersion relations in SAF.

[1] R.A Gallardo *et.al.* Physical Review B 104, 174417 (2021)

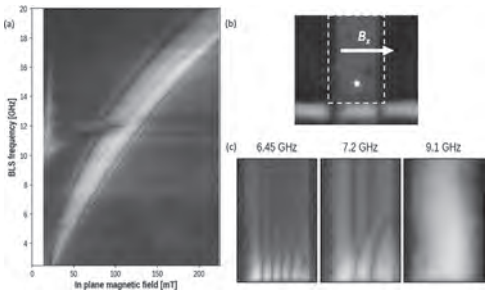

Fig. 1. (a) BLS intensity as a function of the applied magnetic field applied transversely to the SAF stripe at the laser spot position represented in the optical imaging (b). (c) BLS intensity maps recorded for two different r.f. excitation frequencies under a transverse magnetic field of 75 mT.

GOB-03. Electrical Detection of Short-Wavelength Nonreciprocal Magnons in Magnetic Thin Film Device. *Y. Li*[1], T. Lo[2], J. Qian[2], Z. Jiang[2], J. Pearson[1], R. Divan[3], A. Schleife[2], W. Pfaff[4], J. Zuo[2], U. Welp[1], W. Kwok[1], A. Hoffmann[2] and V. Novosad[1] *1. Materials Science Division, Argonne National Laboratory, Lemont, IL, United States; 2. Materials Science Engineering, University of Illinois at Urbana Champaign, Urbana, IL, United States; 3. Center for Nanoscale Materials, Argonne National Laboratory, Lemont, IL, United States; 4. Department of Physics, University of Illinois at Urbana Champaign, Urbana, IL, United States*

Nonreciprocal magnon propagation has recently become a highly potential approach for developing miniaturized and chip-embedded microwave isolation components for advanced information processing. Because magnons have the capability to reach ultra-small wavelength down to nanometer scale at microwave frequency excitations, they can be utilized to build coherent microwave components and transducers with highly suppressed lateral dimensions for circuit integration. In addition, the spatial symmetry in magnetic excitations can be broken due to the unique precession chirality of magnetizations, which leads to their nonreciprocal propagation in space. Although nonreciprocal magnon transducers have been well studied in macroscopic scales, high performance of magnon isolation in magnetic thin-film devices is still demanding for practical applications. In this work, we experimentally realized broad-band nonreciprocal magnon propagation in a 100-nm yttrium iron garnet (YIG) thin film transducer at both room temperature and cryogenic temperature. With nanofabrication of nanoscale (down to 200 nm) microwave antennas on fabricated YIG thin film (100 nm) device (Fig. 1), we successfully demonstrate short-wavelength spin wave propagation and transduction with high group velocity and nanosecond time delays. In addition, we achieve strongly nonreciprocal magnon transduction with isolation of more than 25 dB, which is due to the nonreciprocal excitations of surface spin waves at top or bottom surface of YIG thin film with different excitation efficiencies. Furthermore, we obtain a high signal-to-noise ratio for the magnon transduction, thanks to the optimal design and fabrication of the transducer waveguide for minimizing spurious microwave transduction. Our result provide a realistic platform for chip-embedded microwave isolator for quantum information processing such as qubit noise reduction and entanglement purification. The architecture is also highly desired for device miniaturization in order to curb decoherence with shorter transduction distance.

Work at Argonne and UIUC was supported by the U.S. DOE, Office of Science, Basic Energy Sciences, Materials Sciences and Engineering Division under contract No. DE-SC0022060. Use of the Center for Nanoscale Materials (CNM), an Office of Science user facility, was supported by the U.S. Department of Energy, Office of Science, Office of Basic Energy Sciences, under Contract no. DE-AC02-06CH11357. U.W., W.-K.K. and V.N. acknowledge support by the U.S. DOE, Office of Science, Basic Energy Sciences, Materials Sciences and Engineering Division.

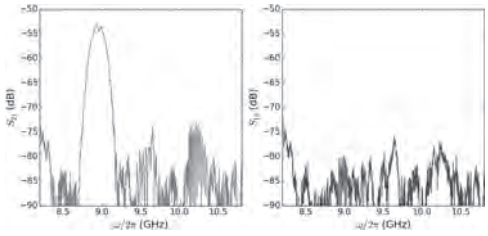

Nonreciprocal magnon propagation for the YIG transducer

GOB-04. Magnetoelectric transducers for spin wave. *F. Ciubotaru*[1], D. Narducci[1,2], M. Geilen[3], F. Vanderveken[1,2], B. Heinz[3], G. Talmelli[1], B. Hillebrands[3], J. De Boeck[1], P. Pirro[3] and C. Adelmann[1] *1. imec, Leuven, Belgium; 2. KU Leuven, Leuven, Belgium; 3. Technische Universität Kaiserslautern, Kaiserslautern, Germany*

Spin waves in magnetic waveguides with sub-μm wavelengths have been proposed as data carriers in future information processing systems. Conventionally, spin waves are excited using inductive antennas, however with low efficiency and poor scaling behavior, as they depend on currents. Spin-transfer and spin-orbit torques depend on current density with better scaling behavior, but the overall efficiency is still too low for practical device applications. By contrast, magnetoelectric transducers promise to generate spin waves or switch magnets with much better energy efficiency. Magnetoelectric transducers couple magnetic and mechanical degrees of freedom via (inverse) magnetostriction. When the mechanical stress is generated by piezoelectric effects, voltage signals can be used to control of the anisotropy of a nanomagnet or to generate spin waves in a magnetic waveguide. In this work we report on the fabrication, characterization, and modeling of CMOS-compatible magnetoelectric transducers based on piezoelectric PZT pillars of different geometries from μm to sub-100 nm feature sizes. The piezo elements are mechanically coupled to a magnetostrictive CoFeB waveguide for spin waves propagation (Fig. 1(a)). Brillouin light scattering (BLS) microscopy reveals the generation of both propagating phonons and spin waves. The phonon spectra strongly depend on the geometry and size of the pillar due to quantization effects. The emission of spin waves depends on the magnetization direction with respect to the waveguide, a direction of 45° being more favorable for excitation (Fig. 1(b)). The mechanical response is studied using COMSOL Multiphysics whereas micromagnetic MuMax code was used to analyze the magnetic behavior. Both elastic waves (phonons) and spin waves have been studied in terms of dispersion relations and amplitude distributions for various device configurations. The magnetoelastic fields were estimated as well (Fig. 2).

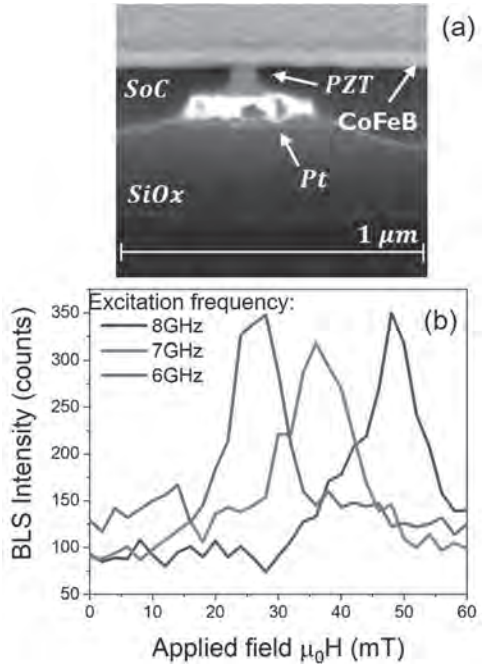

Fig. 1: (a) Cros-section of a magnetoelectric transducer for spin waves. (b) Spin-wave spectra recorded by BLS on top of an ME transducer as a function of the excitation frequency and bias applied magnetic field.

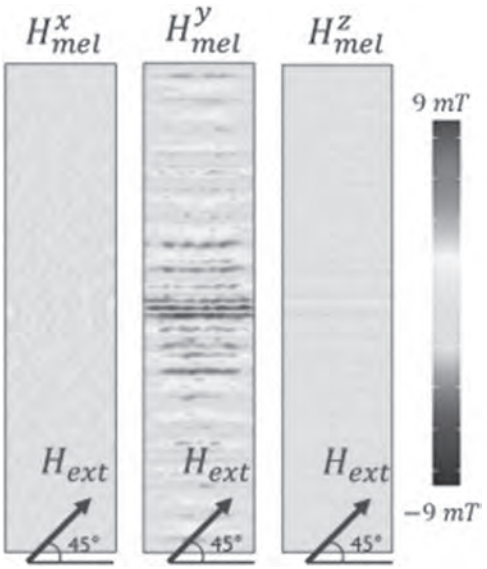

Fig. 2: Magnetoelastic field estimated from the strain distribution simulated in COMSOL

GOB-05. Measuring a Population of Spin Waves from the Electrical Noise of an Inductively Coupled Antenna. *T. Devolder*[1], S. Ngom[1], A. Mouhoub[1], J. Létang[1], J. Kim[1], P. Crozat[1], J. Adam[1], A. Solignac[2] and C. Chappert[1] *1. Université Paris-Saclay, CNRS, Centre de Nanosciences et de Nanotechnologies, Palaiseau, France; 2. SPEC, CEA, CNRS, Université Paris-Saclay, Gif-sur-Yvette, France*

Spin waves (SW) possess specific properties that make them well-suited for microwave applications. Very often these applications rely on magnetic bodies where large populations of coherently pumped spin waves share a common space with their less coherent biproducts and with the thermal populations of spin waves. It is thus of interest to develop experimental techniques able of measuring spin waves in broad frequency intervals with a large dynamic range, ideally from the floor of the thermal population of spin waves up to the regime of large amplitudes of magnetization precession. We have studied how a population of spin waves can be characterized from the analysis of the electrical microwave noise delivered by an inductive antenna placed in its vicinity [1]. The measurements are conducted on a synthetic antiferromagnetic thin stripe covered by a micron-sized antenna that feeds a spectrum analyzer after amplification. The antenna noise contains two contributions. (i) The population of incoherent spin waves generates a fluctuating field that is sensed by the antenna: this is the "magnon noise." (ii) The antenna noise also contains the contribution of the electronic fluctuations: the Johnson-Nyquist noise. The latter depends on all impedances within the measurement circuit, which includes the antenna self-inductance. As a result, the electronic noise contains information about the magnetic susceptibility of the stripe, though it does not inform on the absolute amplitude of the magnetic fluctuations. For micrometer-sized systems at thermal equilibrium, the electronic noise dominates and can account for the measured entire noise (see Figure 1) ; in this case the pure magnon noise cannot be determined. If in contrast the spin wave bath is not at thermal equilibrium with the measurement circuit, and if the spin wave population can be changed then one could measure a mode-resolved effective magnon temperature provided specific precautions are implemented.

[1] T. Devolder et al., Phys. Rev. B 105, 214404 (2022)

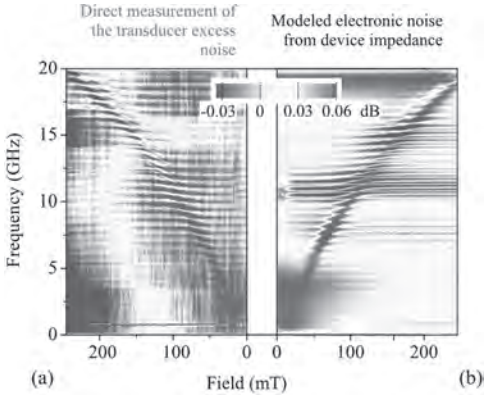

Figure 1. (a) Field dependence of the experimental excess noise. (b) predicted excess Johnson-Nyquist noise of the antenna calculated from the measured field dependence of the antenna impedance.

GOB-06. Inelastic spin-scattering of confined magnons in magnetic interfaces by electrons. *J.A. do Nascimento*[1] and V. Lazarov[1] *1. Physics, University of York, York, United Kingdom*

The ability to probe magnons on an nm scale is of importance for the further development of spin-based devices. Neutron and light beams have been used extensively to study magnons, however, the need of studying spin excitations on small scale requires sub-nm probes. Advances in electron beam monochromators in scanning transmission electron microscopy (STEM) have opened possibilities of using electron beams for studying magnons with sub-nm resolution. Collecting signals of scattered electrons via electron energy loss spectroscopy (EELS) by phonons has been already demonstrated, and a number of experiments are ongoing to demonstrate the detection of magnons by EELS. Even though the magnon's interaction with the electrons is 3 or 4 orders of magnitude weaker, it has been shown experimentally that magnetic ordering can be detected by Brag reflections of electrons in TEM. Recent theoretical prediction of EELS signal from thermal magnons in bulk specimens was also reported. This confirms that STEM/EELS can be used for measuring magnons in confined geometries including interfaces and surfaces. In our work, we calculate the dynamics of magnons in finite systems using the second quantisation of the Heisenberg Hamiltonian for thin film and interfaces, as well as hetero-structure between FM and AFM layers, including surface and interface anisotropies. Realspace snap-shots of spin configurations were used as an input for multislice inelastic electron scattering calculations. These calculations provide momentum resolved energy dependence of the inelastic scattering, which is directly correlated to the local EELS signal. We also calculate the spin scattering function (SSF) to calculate magnon dispersion for considered heterostructures. Based on the SSF, magnon band structure and density of states are obtained from which the strength of the electron-magnon interaction has been estimated. Experiments are ongoing to confirm the predictions of this work.

[1] Ondrej L. Krivanek, Tracy C. Lovejoy, *et. al.,* Nature, Vol.514, p.209-212, (2014) [2] J. C. Loudon. Phys. Rev. Lett., Vol.109,p.267204 (2012) [3] Keenan Lyon, Anders Bergman, Paul Zeiger *et. al.,* Phys. Rev. B, Vol.104, p.214418 (2021)

GOB-07. Withdrawn

GOB-08. Control of the spin-wave spectra by magnetic field orientation and magnitude in crescent-shape ferromagnetic nanorods. *H. Reshetniak*[1], N.B. Lesniewski[1], U. Makartsou[1], M. Golebiewski[1], M. Moalic[1], P. Gruszecki[1] and M. Krawczyk[1] *1. Faculty of Physics, Adam Mickiewicz University, Institute of Spintronics and Quantum Information, Poznan, Poland*

Spintronic devices operating on spin waves (SW) can be more efficient than oxide semiconductors due to their high frequencies and low energy cost. Therefore, SW based technology may prove to be more powerful than CMOS devices due to its intrinsic characteristics [1]. Magnetic field is the primary stimuli controlling magnetism and SW dynamics. Thus, the study of the influence of the magnetic field on ferromagnetic nanostructures with different geometries is critical for modern technologies, especially for the development of 3D-magnonic circuits, where the geometric constraints generate a strong relationship between the fields of demagnetization, exchange and bias. Recently, it has been experimentally demonstrated that the 3D network formed from the crescent-shape nanorods (CSN) is promising for development of 3D ferromagnetic systems for various applications [2]. As yet, CSN-s have not been investigated for their effect on SW spectra and manipulations in relation to magnitude and magnetic field orientation. Untypical results make our analysis relevant for future investigations and applications. In particular, we show that there are edge localized and bulk SW modes. The edge modes decouple when the external magnetic field rotates, Fig. 1. Thus, the two edges of the CSN behave as two distinct channels for SW guiding, whose frequency can be controlled by the magnetic field magnitude and orientation. Interestingly, both the polar and azimuthal rotations of the field significantly affect the ferromagnetic resonance spectra. It alters the number of most intense lines in the spectra and their frequency range. When additional magnetic layer is added to the CSN, the magnetostatic coupling between the elements leads to additional modes splitting, Fig. 2. Thus, the CSN-s can support 3D magnonic circuits at nanoscale, which operate at wide range of frequencies, offer multimode operation, and promise nonreciprocal effects. The research has received founding from the NCN Poland, project no 2020/39/I/ST3/02413.

[1] A. V. Chumak et al., Advances in Magnetics Roadmap on Spin-Wave Computing, IEEE Trans. Magn. 58, 1 (2022). [2] A. May, et al., Realisation of a frustrated 3D magnetic nanowire lattice. Commun. Phys. 2, 13 (2019).

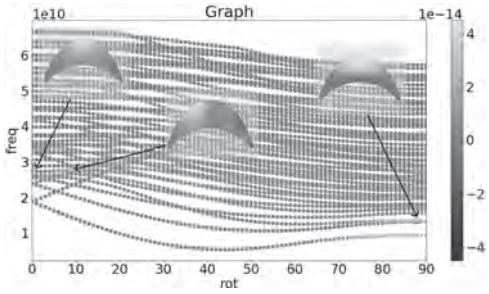

Fig. 1 Scatter plot for the single crescent-shaped nanorod, showing the frequency as a function of a polar angle. Colorbar shows magnetization modes intensity.

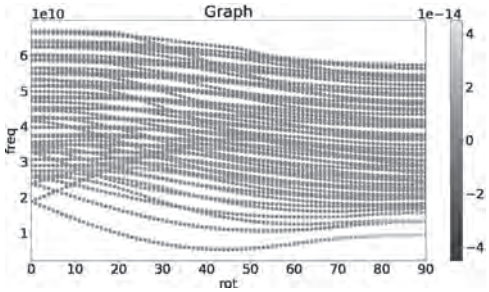

Fig. 2 The same as in Fig. 1, but multi-layered nanorod.

GOB-09. Excitation of short-wavelength propagating spin waves in thin YIG film waveguides. *S. Louis*[1], C. Liu[2], J. Xu[3], C. Trevillian[4], V. Kalappattil[2], D.B. Gopman[5], D. Jin[3], J.M. Shaw[6], H. Nembach[7], V. Tyberkevych[4], X. Zhang[3], A.N. Slavin[4] and M. Wu[2] *1. Electrical and Computer Engineering, Oakland University, Rochester, MI, United States; 2. Physics, Colorado State University, Fort Collins, CO, United States; 3. Consortium for Advanced Science and Engineering, University of Chicago, Chicago, IL, United States; 4. Physics, Oakland University, Rochester, MI, United States; 5. Materials Science Engineering Division, National Institute of Standards and Technology, Gaithersburg, MD, United States; 6. Nanoscale Spin Dynamics Group, National Institute of Standards and Technology, Boulder, CO, United States; 7. Spin Electronics Group, National Institute of Standards and Technology, Boulder, CO, United States*

Recent progress in nano-structuring of magnetic materials created a necessity to excite short-wavelength spin waves (SW) [1-3]. Short-wavelength exchange-dominated spin waves, the dispersion of which is mainly determined by the exchange interaction, have a relatively large group velocity which is beneficial for magnon-based microwave signal processing and computing applications. In this experimental work, we report the excitation of spin waves with a wavelength of 2 μm by simple strip-line or meander-shaped transduces with a sub-micrometer in-plane width. The experimental set-up was fabricated as follows. First, an yttrium iron garnet (YIG) film of the thickness of 200 nm was grown, and then patterned into several waveguides with a width of 25 μm. The fabricated YIG waveguides were found to have a Gilbert damping rate of 0.0001. Then, 32 pairs of Au transducers (either coplanar waveguides or a meander waveguides) were deposited onto the YIG waveguide. The separation between each pair of transducers was varied from 50 to 500 μm. Figure 1 shows time resolved characterization for 3 devices, with the transmitting and receiving transducers separated by 80, 170, and 200 μm. In each case, a 30 ns excitation pulse with a carrier frequency of 2.6 GHz, was submitted to the input transducer at the time t = 0. This pulse travels as electromagnetic radiation immediately to the receiver, and, also excites a SW packet which, after a delay, arrives at the same receiving transducer. The delay of SW pulses measured for a particular transducer separation allowed us to determine the SW group velocity (1.7 μm /ns), and, also, to find the wavelength (2.0 μm) of the excited SW. The measured value of the SW group velocity agrees well with the theoretical expectations for the experimental YIG waveguide. Thus, we were able to prove experimentally that transducers of a simple geometry are capable of exciting SWs having the wavelength of 2.0 μm (at which they start to be influenced by the inhomogeneous exchange interaction), and propagating for more than 100 wavelengths in a sub-micron YIG film waveguide.

[1] Lake, S. R., Divinskiy, B., Schmidt, G., Demokritov, S. O., & Demidov, V. E. (2021). Efficient geometrical control of spin waves in microscopic YIG waveguides. *Applied Physics Letters*, *119*(18), 182401. [2] Lake, S. R., Divinskiy, B., Schmidt, G., Demokritov, S. O., & Demidov, V. E. (2022). Interplay between nonlinear spectral shift and nonlinear damping of spin waves in ultrathin yttrium iron garnet waveguides. *Physical Review Applied*, *17*(3), 034010. [3] Böttcher, T., Ruhwedel, M., Levchenko, K. O., Wang, Q., Chumak, H. L., Popov, M. A., ... & Pirro, P. (2022). Fast long-wavelength exchange spin waves in partially compensated Ga: YIG. *Applied Physics Letters*, *120*(10), 102401.

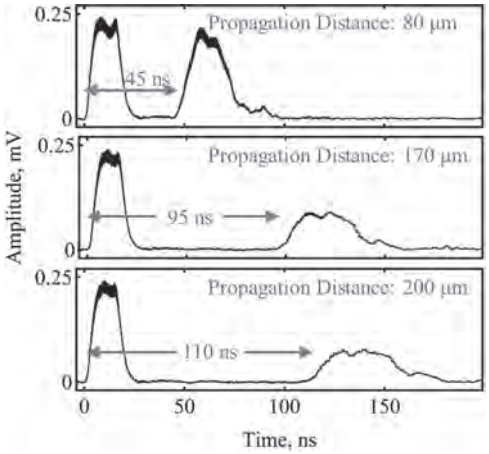

Figure 1: Time resolve characterization for 3 devices, with propagation lengths as labeled. Data was collected with a field of ~100 Oe.

GOB-10. Tunable Magnonic Chern Bands and Chiral Spin Currents in Magnetic Multilayers. *Z. Hu*[1], L. Fu[2] and L. Liu[1] *1. Department of Electrical Engineering and Computer Science, Massachusetts Institute of Technology, Cambridge, MA, United States; 2. Department of Physics, Massachusetts Institute of Technology, Cambridge, MA, United States*

Realization of novel topological phases in magnonic band structures represents a new opportunity for the development of low-dissipation magnonics [1-5]. The previous proposals require materials with either special crystal symmetries [2-3] or artificially modulated structures that demand advanced nanofabrication techniques [4-5], both of which bring in difficulties for experimental realization. In this work, we theoretically study the magnonic band structure of antiparallelly aligned magnetic multilayers (Fig. 1), and reveal their field-tunable topological phases [1]. We show that the long-range dipolar interaction between propagating magnons is chiral in nature, whose strength depends on the wave vector direction and therefore breaks time-reversal symmetry. Consequently, the dipolar interaction plays a role like spin-orbit coupling in electronic systems and generates bulk bands with non-zero Chern integers and ultra-localized magnonic surface states that carry chiral spin currents (Fig. 1). Through an external magnetic field, the topological phases can be switched, which therefore provides a tunable for transferring spin angular momenta in this synthetic antiparallelly aligned heterostructure. Besides analytical study, we also carry out micromagnetic simulations on the simplest multilayer system – YIG/Py bilayers using MuMax3 [6]. The magnonic band structure with a degeneration point only in one half of the reciprocal space and the unidirectional propagation of spin waves (Fig. 2) both validate our analytical results. Our study provides an easy-to-implement system for realizing topologically protected magnonic surface states and low-dissipation spin transport in a tunable manner, which is expected to benefit various areas of modern spintronics and magnonics.

[1] Z. Hu, L. Fu and L. Liu, Phys. Rev. Lett., Vol.128, p.217201 (2022) [2] L. Zhang, J. Ren, J.-S. Wang and B. Li, Phys. Rev. B, Vol.87, p.144101 (2013) [3] S. K. Kim, H. Ochoa, R. Zarzuela and Y. Tserkovnyak, Phys. Rev. Lett., Vol.117, p.227201 (2016) [4] R. Shindou, R. Matsumoto, S. Murakami and J.-i. Ohe, Phys. Rev. B, Vol.87, p.174427 (2013) [5] Y.-M. Li, J. Xiao and K. Chang, Nano Lett., Vol.18, p.3032 (2018) [6] A. Vansteenkiste, J. Leliaert, M. Dvornik, M. Helsen, F. Garcia-Sanchez and B. Van Waeyenberge, AIP Adv., Vol.4, p.107133 (2014)

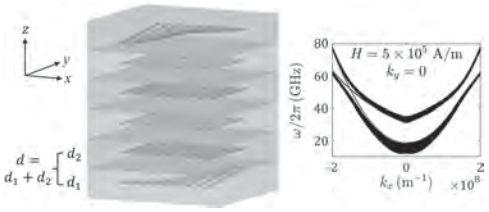

Left: antiparallelly aligned magnetic multilayers with chiral surface spin currents. Right: magnonic band structure in the topological non-trivial phase, where the black lines correspond to bulk states, and the red (blue) line corresponds to the surface state localized in the bottom (top) layer.

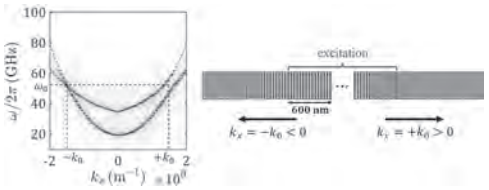

Left: simulated magnonic band structure for YIG/Py bilayers with theoretical fitting. Right: unidirectional propagation of spin waves at the degeneration point.

GOB-11. Spin Wave Diffraction in Curvilinear Antennas.
V. Vlaminck[1,2], L. Temdie[1,2], V. Castel[1,2], M. Jungfleisch[3], M. Grassi[4], H. Majjad[5], R. Bernard[5], D. Stoeffler[5], Y. Henry[5] and M. Bailleul[5] *1. Microwave Dept., IMT Atlantique, Brest, France; 2. Lab-STICC, UMR 6285 CNRS, Brest, France; 3. Dept. of Physics and Astronomy, University of Delaware, Newark, DE, United States; 4. Uppsala University, Uppsala, Sweden; 5. IPCMS - UMR 7504 CNRS, Strasbourg, France*

The direct interference of short wavelength spin waves in continuous layers is bringing new opportunities for efficient signal processing [1-2]. Several pionneer works established the possibility to shape the propagation of spin waves in ferromagnetic thin films using concepts borrowed from optics [3-5]. Along these ideas, we demonstrated that the focused emission of spin waves beams in ferromagnetic thin films from constricted coplanar waveguide follows directly the near-field interference pattern of the constriction geometry [6]. In this communication, we investigate the interference patterns of spin waves excited by curvilinear shaped antennas, which produce either a concentrating or a diffusing effect. Namely, we focused our study on two different types of demonstrators: (i) a spin wave "concentrator" as shown in Fig. 1, and (ii) the equivalent of a "Young double-slit" experiment for spin waves shown in Fig. 2. Firstly, we will present a near-field interference model that can be readily implemented for all spin wave modes and any arbitrary shape of antenna [7]. We show the validity and efficiency of our approach by comparing the near-field diffraction patterns obtained with our model and the corresponding MuMax3 micromagnetic simulations for a wide scope of geometries. Secondly, we present series of propagating spin wave spectroscopy done on 30nm YIG films and a 20nm $Ni_{80}Fe_{20}$ film magnetized out-of-plane, allowing for a discrete mapping of the spin wave intensity with a spatial resolution of about 1μm. We show that the transmission signals S_{21} measured at different locations follow very closely the simulated interference patterns for all the demonstrators, thus paving the way for future prototypes of magnon interferometric devices. This work was supported by the French ANR project "*MagFunc"*, and the Département du Finistère through the project "*SOSMAG"*.

[1] J. Chen, Nano Letters, 21 (14), 6237–6244 (2021) [2] A. Papp, Nat. Comm. 12, 6422 (2021) [3] J. Stigloher, et al., Phys. Rev. Lett. 117, 037204 (2016) [4] P. Gruszecki, et al., Phys. Rev. B 95, 014421 (2017) [5] H. S. Körner, et al., Phys. Rev. B 96, 100401 (2017) [6] N. Loayza, et al, Phys. Rev. B 98, 144430 (2018) [7] V. Vlaminck, et al., hal-02310439, CLN (2019)

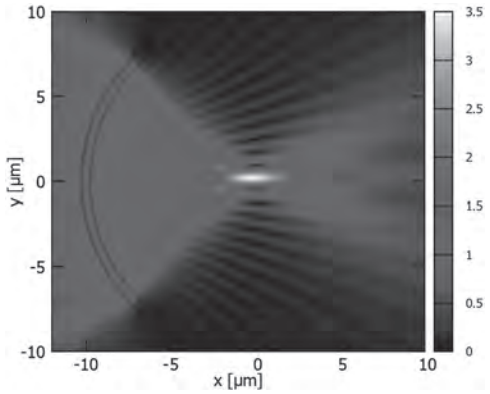

Near-field diffraction simulation of a spin wave concentrator device on a 30nm YIG film at a 492mT out-of-plane field.

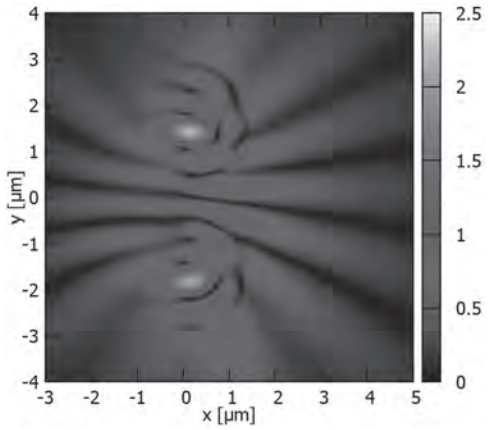

Near-field diffraction simulation of a spin wave Young double-slit device on a 20nm Py film at a 1.15T out-of-plane field.

GOB-12. Low-Loss Nanoscopic Spin-Wave Guiding in Continuous YIG Films. H. Qin[1], R. Holländer[1], L. Flajšman[1] and *S. van Dijken*[1]
1. Department of Applied Physics, Aalto University, Espoo, Finland

Magnonics based on the transfer of angular momentum in the form of spin waves provides a promising technology for wave-based information processing [1] and neuromorphic computing [2]. A key challenge in realizing a viable spin-wave technology is the connection of multiple computational units into integrated magnonic circuits, which requires a scalable materials platform for low-loss spin-wave transport. Conventionally, magnonic waveguides are fabricated by patterning ferromagnetic metal or YIG films into narrow conduits. The spin-wave decay length in fully patterned nanoscopic waveguides is typically limited to a few mm. Here, we introduce a new spin-wave waveguiding structure consisting of a continuous YIG film and ferromagnetic metal nanostripes patterned on top [3]. In this hybrid structure, dipolar coupling between the two magnetic materials defines nanoscopic spin-wave transporting channels within the YIG film, along which spin waves propagate with low loss. We demonstrate spin-wave decay lengths of ~20 mm in 160-nm-wide waveguides at small magnetic bias fields. Moreover, we show that spin waves are efficiently guided through magnetically induced bends in the continuous YIG film (Fig. 1). The combination of low-loss scalable transport and efficient redirection of spin waves in our hybrid waveguiding structures provides a new strategy for the implementation of low-loss magnonic devices and integrated circuits without YIG nanopatterning.

[1] A. Mahmoud et al., Introduction to Spin Wave Computing. J. Appl. Phys. 128, 161101 (2020) [2] A. V. Chumak et al., Advances in Magnetics Roadmap on Spin-Wave Computing. IEEE Trans. Magn. 58, 0800172 (2022) [3] H. Qin, R. B. Holländer, L. Flajšman, and S. van Dijken, Low-Loss Nanoscopic Spin-Wave Guiding in Continuous Yttrium Iron Garnet Films. Nano Lett. (2022), published online at https://pubs.acs.org/doi/10.1021/acs.nanolett.2c01238

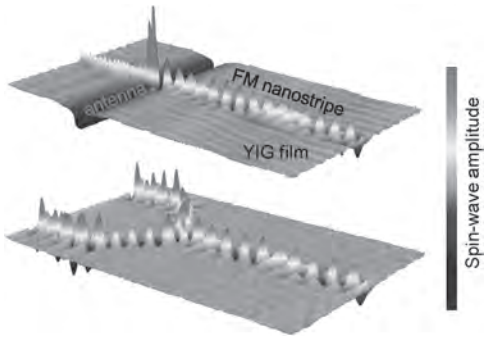

Fig. 1: Long-distance spin-wave transport along straight and Y-shaped nanoscopic waveguides made of a continuous YIG film and ferromagnetic metal nanostripes patterned on top.

Session GOC
MAGNETIZATION DYNAMICS III

Steven Louis, Chair
Oakland University, Rochester, MI, United States

CONTRIBUTED PAPERS

GOC-01. Analog quantum control of magnonic cat states on-a-chip by a superconducting qubit. *M. Kounalakis*[1], G. Bauer[2,1] and Y. Blanter[1]
1. Kavli Institute of Nanoscience, Delft University of Technology, Delft, Netherlands; 2. WPI-AIMR, Tohoku University, Sendai, Japan

We propose to directly and quantum-coherently couple a superconducting transmon qubit to magnons — the quanta of the collective spin excitations, in a nearby magnetic particle. The magnet's stray field couples to the qubit via a superconducting interference device (SQUID) leading to strong and tunable interactions. More specifically, we predict a resonant magnon-qubit exchange coupling, similar to the one studied in 3D cavity setups [1], and a novel magnon-qubit nonlinear interaction that is similar to the radiation-pressure coupling in optomechanics [2]. We show that the latter can be resonantly enhanced by dynamically driving the flux in the SQUID, and demonstrate a quantum control scheme to generate magnon-qubit entanglement and magnonic Schrödinger cat states with high fidelity. Our results [3] enrich the quantum control toolbox in magnonic devices and open new possibilities for constructing quantum magnonic networks on a chip.

[1] Y. Tabuchi, S. Ishino, A. Noguchi, T. Ishikawa, R. Yamazaki, K. Usami, and Y. Nakamura, Science Vol. 349, p. 405 (2015). [2] M. Aspelmeyer, T. J. Kippenberg, and F. Marquardt, Rev. Mod. Phys. Vol. 86, p. 1391 (2014). [3] M. Kounalakis, G. E. W. Bauer, Y. M. Blanter, arXiv:2203.11893 (2022).

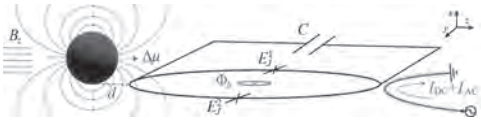

Fig. 1. Proposed circuit architecture.

GOC-02. Travelling Photons-Mediated Coherent and Dissipative Couplings in Long-distance Cavity Magnonics. *Y. Yang*[1], P. Fong[3], H. Lau[3], W. Lu[2] and C. Hu[1] *1. Physics, University of Manitoba, Winnipeg, MB, Canada; 2. Shanghai Institute of Technical Physics, Chinese Academy of Sciences, Shanghai, China; 3. Physics, Simon Fraser University, Burnaby, BC, Canada*

Engineering coupling between systems is essential for many phenomena of quantum physics and technology, especially in long distance without field overlap. We construct a long-distance cavity magnonic system to realize indirect coupling mediated by travelling photons. A high-quality dielectric resonator (cavity photon mode) and an Yttrium Iron Garnet sphere (YIG, magnon mode) are placed along the transmission line with a longitudinal distance of over 1 metre to avoid direct coupling. By tuning the longitudinal distance given by phase and the YIG sphere's transverse position, we realized indirect coupling in transmission: in the reciprocal case with the YIG sphere in the center of the transmission line, we have coherent and dissipative couplings at the longitudinal phase $\Phi=(2n+1)\pi$ and $\Phi=(2n+2)\pi$; while in the nonreciprocal case with the YIG sphere on the side of the transmission line, we have coherent and dissipative couplings for the left- and right-going travelling photons at the longitudinal phase $\Phi=(2n+0.5)\pi$ and $\Phi=(2n+1.5)\pi$. The coupled-mode theory modified by a higher-order coupling term is adopted to explain our results and enhances our understanding of long-distance coupling and nonreciprocity. Our illustration of switching long-distance coherent and dissipative couplings, gives access to designing nonreciprocal links and constructing advanced remote-control strategies among spatially separated systems to build networks.

[1] Karg, Thomas M., et al. "Light-mediated strong coupling between a mechanical oscillator and atomic spins 1 meter apart." *Science* 369.6500 (2020): 174-179. [2] Röhlsberger, Ralf, et al. "Collective Lamb shift in single-photon superradiance." *Science* 328.5983 (2010): 1248-1251.

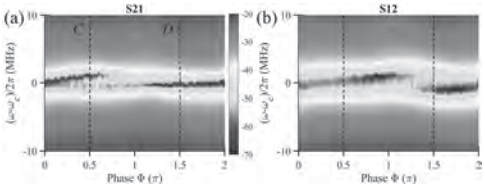

The measured nonreciprocal transmission amplitudes are plotted as a function of phase Φ when the cavity and magnon modes are on-resonant $\omega_c=\omega_m$. (a) |S21| reaches maximum mode splitting in position C at $\Phi=(2n+0.5)\pi$ and minimum splitting in position D at $\Phi=(2n+1.5)\pi$, as indicated by the black dashed line. (b) |S12| show reversed effect.

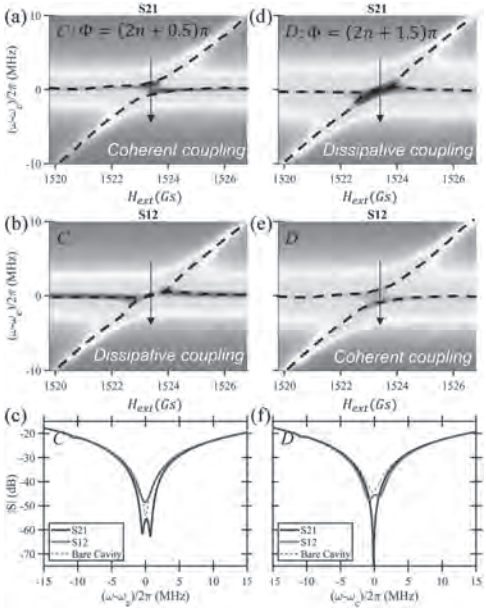

The measured transmission amplitudes at fixed phase Φ when changing the magnon frequency ω_m. In position C at $\Phi=(2n+0.5)\pi$, (a) $|S_{21}|$ shows coherent coupling with energy level repulsion and (b) $|S_{12}|$ shows dissipative coupling with energy level attraction, the on-resonant cuts indicated by the black arrow are shown in (c). In position D at $\Phi=(2n+1.5)\pi$ the coupling effects are reversed for (d) $|S_{21}|$, (e) $|S_{12}|$ and (f) on-resonant cuts.

GOC-03. Hybridizing antiferromagnetic magnons with spin pumping and exchange fields. *M.M. Subedi*[1], Y. Xiong[2], M.T. Hossain[3], P. Meisenheimer[4], J. Heron[4], M. Jungfleisch[3], W. Zhang[2] and J. Sklenar[1] *1. Wayne State University, Detroit, MI, United States; 2. Oakland University, Rochester, MI, United States; 3. University of Delaware, Newark, DE, United States; 4. University of Michigan, Ann Arbor, MI, United States*

Researchers are attracted to antiferromagnets due to their high frequency dynamical properties with a possibility of developing terahertz frequency range spintronics devices. We use magnetic multilayer heterostructures consisting of successive ferromagnetic layers separated by a non-magnetic metal of suitable thickness to have an antiferromagnetic coupling. These structures are called synthetic antiferromagnets (S-AFM). We use permalloy as a ferromagnetic material and ruthenium as a non-magnetic metal to prepare tetralayer synthetic antiferromagnets. We theoretically predict and experimentally verify the existence of two types of magnon-magnon couplings for antiferromagnetic magnons localized on surface and interior layers of tetralayer synthetic antiferromagnet. Macrospin modeling and micromagnetic simulations are used to show that the dynamic part of Ruderman–Kittel–Kasuya–Yosida (RKKY) interaction is responsible for the self-hybridization of acoustic and optical magnons localized on surface and interior layers due to an accompanying field-like torque. Likewise, surface optical magnons hybridize with interior acoustic magnons by spin pumping, which creates antidamping torque on neighboring ferromagnetic layer. It is reflected in the double-gap in magnon spectrum, that is, an additional magnon-magnon interaction is observed. Thus, interlayer spin pumping is a magnon-magnon interaction control mechanism in in S-AFMs that can be used to help develop energy efficient and high-speed spintronics devices. Research at University of Michigan was supported from NSF CAREER grant DMR-1847847. Work at Oakland University was funded by NSF under award number ECCS-1941426, and that at University of Delaware was supported from NSF grant DMR-2011824.

[1] J. Sklenar and W. Zhang, Phys.Rev.Appl.15, 044008(2021) [2] Y. Li et al., Phys.Rev.Lett.123, 107701(2019) [3] Y. Shiota et al., Phys.Rev. Lett.125, 017203(2020) [4] R. Duine et al., Nat.Phys.14, 217(2018) [5] A. Sud et al., Phys.Rev.B 102, 100403(2020)

GOC-04. Withdrawn

GOC-05. Complex Dynamics In Mutually Coupled Spin Torque Vortex Oscillators. *K. Ho*[1], S. Wittrock[1,2], S. Perna[3], C. Serpico[3], P. Bortolotti[1], R. Lebrun[1] and V. Cros[1] *1. Unité Mixte de Physique CNRS, Thales, Université Paris-Saclay, Palaiseau, France; 2. Max Born Institute For Nonlinear Optics & Short Pulse Spectroscopy, Berlin, Germany; 3. Department of Electrical Engineering and ICT, University of Naples Federico II, Naples, Italy*

Spin torque nano-oscillators are spintronic devices in which radiofrequency magnetization oscillations can be generated through spin-transfer effects. Due to their nonlinearity, these devices display interesting properties such as frequency stability and high tunability, opening up possibilities from wireless telecommunication to neuromorphic computing [1]. In this study, we will focus on vortex-based spin-torque nano-oscillators (STVO) and study the response of mutually coupled STVOs. To couple them, we use the RF current emitted by one STVO, which is first amplified and then sent through the antenna located above the second STVO and vice versa. The resulting external RF field hence mediates the coupling between the two STVOs. Using this approach, beyond the expected improvement of their RF properties, i.e., power emission and spectral purity [2], we have recently shown that strong coupling can lead to new phenomena beyond synchronization, such as amplitude death, mode branching, and non-trivial states associated with exceptional points (EPs) [3]. EPs, defined as singularities of non-Hermitian problems, can indeed emerge from such systems. Combining experimental results (Fig.1) and theoretical modeling (Fig.2), we succeed in demonstrating that the presence of mode branching (see Fig.1) can be connected to the coalescence of the system complex eigenvalues, i.e., the existence of an EP, in a specific current range. The next step is to investigate, both in frequency and time domain, how these EPs' existence is sensitive to the individual properties of each STVO and the path used to approach this EP state [4]. We believe that this study opens spintronic devices to the field of non-Hermitian Hamiltonian physics, already observed in several variable loss/gain systems in photonics and electronics [5]. By proving the engineering of EPs for high sensitivity mode control, the objective will be to show the potential of this technique in sensor-type systems.

[1] N. Locatelli, V. Cros, and J. Grollier, Nature Materials, 13, 1, 11 (2016) [2] R. Lebrun, et al., Nat. Comm. 8, 15825 (2017) [3] S. Wittrock, et al., arXiv:2108.04804 (2021) [4] C. Dembowski et al., Phys. Rev. Lett. 86, 787 (2001) [5] Z. Liu, et al., arXiv:2009.07713 (2020)

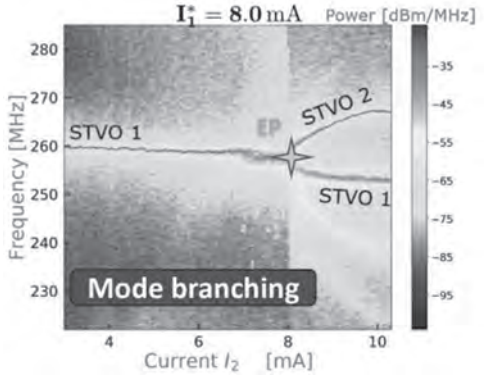

Fig.1 Frequency spectra of the coupled STVOs versus STVO2 current $I_{DC,2}$ and fixed $I_{DC,1}$. An EP is observed at $(I^*_1,I_2) = (8,8)$ mA.

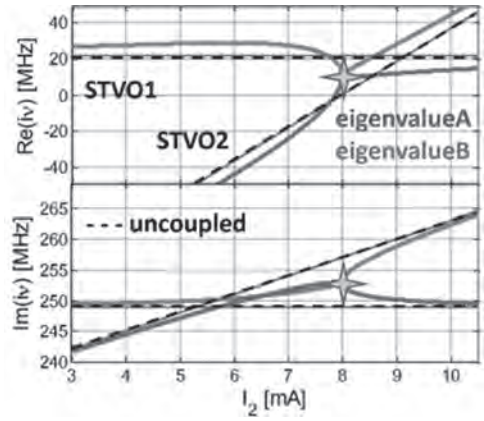

Fig.2 Corresponding complex eigenvalues versus STVO2 current $I_{DC,2}$. Eigenvalues are in dashed (uncoupled) and solid (coupled) lines.

GOC-06. Computational Capability of Physical Reservoir Computing in Spin Torque Oscillator with Two Free Layers. *T. Yamaguchi*[1], S. Tsunegi[2] and T. Taniguchi[2] *1. Center for Emergent Matter Science (CEMS), Riken, Wako, Saitama, Japan; 2. Research Center for Emerging Computing Technologies, National Institute of Advanced Industrial Science and Technology (AIST), Tsukuba, Japan*

Applying spintronics devices to neuromorphic computing have recently gained much attention. For example, a speech recognition task using a spin-torque oscillator (STO) and based on the algorithm of physical reservoir computing was experimentally demonstrated [1]. In this experiment, the nonlinear magnetization dynamics in STO is used as a computational resource, where the modulation of the dynamics due to the injection of human voice, converted to electric voltage, is used to recognize the input

data. Therefore, it is essential to investigate the relationship between the physical properties reflected in the magnetization dynamics and the computational capability of physical reservoir computing. It has been widely believed that the computational capability of physical reservoir computing is enhanced at the edges of chaos because complex dynamics near the chaos is useful to distinguish several kinds of input data. However, the physical reservoir computing in previous works has been performed in the dynamical state far away from chaos. Therefore, the computational capability of STO near the edge of chaos is still unclear. In this work, we investigated the relationship between the dynamical properties of STO and the computational capability in reservoir computing. We consider two kinds of STO, where the one is a conventional STO consisting of a pinned (P) and free (F) layer, while the other, P/F/F, includes two free layers; see Fig. 1. This is because, in principle, the former cannot show chaos while the latter has a possibility to show chaotic dynamics, and therefore, the comparison between them is useful to study the role of the chaos on the computational capability. We evaluate the short-term memory capacity [2] as a figure of merit and the Lyapunov exponent [3] to distinguish the dynamical state. It was found that the short-term memory capacity in P/F/F STO is greatly enhanced near the edge of chaos (see Fig. 2) and becomes much larger than the maximum value of the capacity in the conventional P/F STO.

[1] J. Torrejon *et al*., Nature 547, 428 (2017). [2] K. Fujii and K. Nakajima, Phys. Rev. Applied 8, 024030 (2017). [3] S. H. Strogatz, Nonlinear Dynamics and Chaos: With Applications to Physics, Biology, Chemistry, and Engineering (Westview Press, Boulder, CO, 2001).

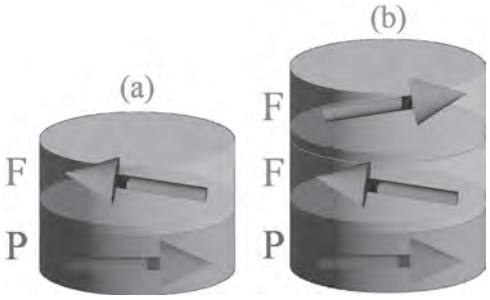

Fig.1 Conceptual picture of (a) P/F and (b) P/F/F.

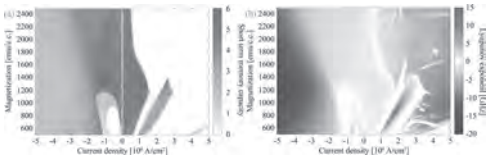

Fig.2 (a) Short-term memory capacity and (b) Lyapunov exponent in P/F/F combination.

GOC-07. Withdrawn

GOC-08. Spin Cavitronics System: from Strong to Ultra-Strong Coupling. *G. Bourcin*[1], V. Castel[1] and V. Vlaminck[1] *1. IMT Atlantique, Brest, France*

Over the last decade, quantum systems offering new computational and sensing capabilities have emerged [1]. One of these promising hybrid systems involves the interaction between photons and magnons. This interaction is quantitatively known by the strength coupling g and furthermore by its ratio with the cavity frequency g/ω. It exists three different domains of this ratio: the Strong Coupling (SC) for $g/\omega < 0.1$; the Ultra-Strong Coupling (USC) for $0.1 < g/\omega < 1$; and the Deep-Strong Coupling (DSC) for $g/\omega > 1$. One of the objectives of this last decade is to achieve the USC, and to approach the DSC [2]. A few experimental works already exist on the USC regime [3] and it is still complicated to understand the different Hamiltonian approximations used to fit experimental data [2]. Here, we present a tuneable hybrid system which makes possible experimental observation of a coupling regime from strong to ultra-strong at room temperature (RT). The hybrid system presented here is made of a double re-entrant cavity and a commercial single crystal of YIG (see Fig. 1). It is possible to tune the ratio g/ω with decreasing the gap between the top of pillars and cavity which will decrease ω without changing g. We optimized two different cavities considering two YIG shapes (sphere and slab). These two cavities work in the USC regime, from the SC/USC limit to $g/\omega = 0.6$. One of these measures is presented in Fig. 2 where is shown the S_{21} parameter according to a sweep on RF frequencies and the static H-field. With the use of Finite Element Modelling, we were able to follow the coupling strength from the SC to the USC domains and were in a good agreement with measurements. We observed that the standard Hamiltonians (Dicke and Hopfield) do not describe our system. With modifying the Dicke model with adding a frequency shift ω_Δ on the FMR, we were able to fit measures and simulations. It should be noted that this added term is proportional to g^2/ω. We demonstrated the capability of a 3D magnonic cavity to work in the USC regime and its tuneability with playing with the gap. To reach the DSC, it will be interesting to work on other cavity shapes to have a bigger ratio g/ω.

[1] D. Lachance-Quirion, Y. Tabuchi, A. Gloppe, Appl. Phys. Exp., vol. 12, p. 070101 (2019) [2] I.A. Golovchanskiy, N.N. Abramov, V.S. Stolyarov, Phys. Rev. Applied., vol. 16, p. 034029 (2021) [3] A.F. Kockum, A. Miranowicz, S. De Liberato, Nat. Rev. Phys., vol. 1, p. 19-40 (2019)

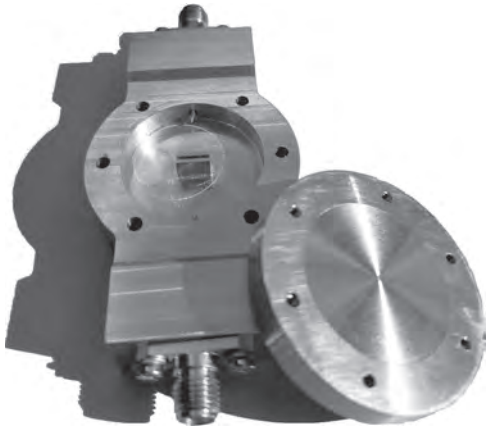

Fig. 1: ***Machined cavity***

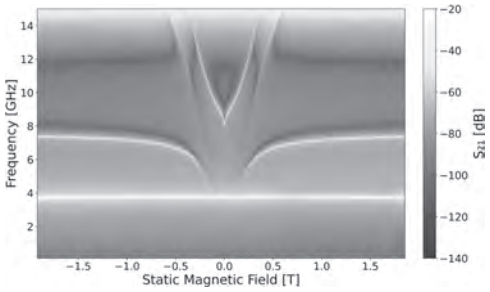

Fig. 2: ***Spectral transmission S_{21}***

GOC-09. Bistability in Dissipatively Coupled Cavity Magnonics.
H. Pan[1,2], Y. Yang[2], Z. An[1] and C. Hu[2] *1. Department of Physics, Fudan University, Shanghai, China; 2. Department of Physics and Astronomy, University of Manitoba, Winnipeg, MB, Canada*

Dissipative coupling of resonators arising from their cooperative dampings to a common reservoir induces intriguingly new physics such as energy level attraction. In this study, we report the nonlinear properties in a dissipatively coupled cavity magnonic system. A magnetic material YIG (yttrium iron garnet) is placed at the magnetic field node of a Fabry-Perot-like microwave cavity such that the magnons and cavity photons are dissipatively coupled. Under high power excitation, a nonlinear effect is observed in the transmission spectra, showing bistable behaviors. The observed bistabilities are manifested as clockwise, counterclockwise, and butterfly-like hysteresis loops with different frequency detuning. The experimental results are well explained as a Duffing oscillator dissipatively coupled with a harmonic one and the required trigger condition for bistability could be determined quantitatively by the coupled oscillator model. Our results demonstrate that the magnon damping has been suppressed by the dissipative interaction, which thereby reduces the threshold for conventional magnon Kerr bistability. This work sheds light upon potential applications in developing low power nonlinearity devices, enhanced anharmonicity sensors and for exploring the non-Hermitian physics of cavity magnonics in the nonlinear regime.

[1] H. Pan, Y. Yang and Z.H. An, arXiv:2206.01231 (2022) [2] P. Hyde, B. M. Yao, Y. S. Gui, Phys. Rev. B 98, 174423 (2018)

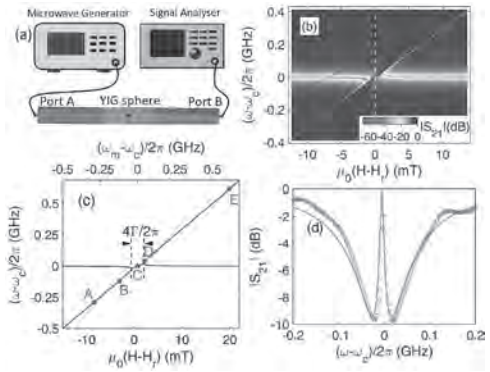

FIG. 1. (a) Illustration of the experimental setup, where a YIG sphere is imbedded in an assembly cavity. (b) Transmission coeffcient mapping of the hybridized cavity-magnon system. (c) Dispersion relation of hybridized cavity and magnon mode, where points A and E indicate off-resonance, and point C indicates on-resonance, and points B and D indicate intermediate frequencies. (d) The fixed field cut of transmission coeffcient mapping at the coupling condition.

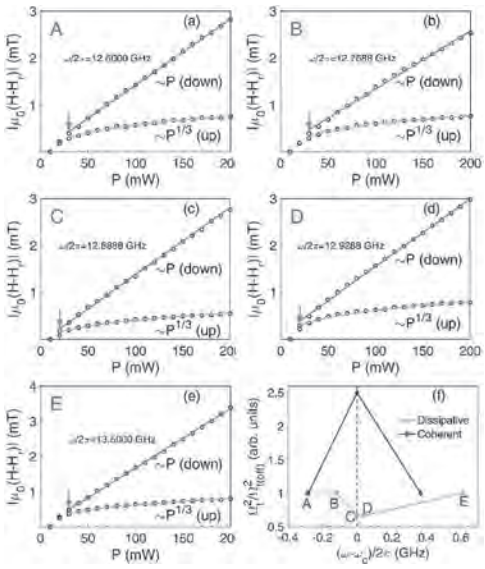

FIG. 2 The jump position of field foldover hysteresis versus P at cavity frequencies (a) A, (b) B, (c) C, (d) D, (e) E. Purple (blue) circle symbols are experimental results of forward (backward) H field sweeping. The yellow and cyan solid curves are fitted. (f) The threshold for coherent and dissipative coupling system when off- and on-resonance. The threshold for coherent coupling is from Ref. [2].

GOC-10. Measurement Scheme for Single Magnon Decoherence.
C. Trevillian[1] and V. Tyberkevych[1] *1. Physics, Oakland University, Rochester, MI, United States*

Recent advances in quantum magnonics [1-3], e.g., strong magnon-photon coupling [2] and single magnon sources [3], enable study of fundamental magnon properties. It is interesting to use these effects to answer fundamental questions of single magnon decoherence (SMD) mechanisms, understanding of which is necessary to use finite magnon number states. Here, we propose a simple measurement scheme for SMD. It is based on entangling a magnon and a qubit (with a much longer lifetime) with resonant frequencies ω_m and ω_q, respectively, and coupling rate κ. When the detuning $\Delta\omega=\omega_m-\omega_q$ is large ($|\Delta\omega| \gg \kappa$), the magnon and qubit states evolve independently. A magnetic field pulse can temporary couple ($|\Delta\omega| \ll \kappa$) the system, thereby entangling or unentangling it. The scheme (Fig. 1) is a temporal-domain Mach-Zehnder interferometer and works as follows. Initially, the qubit is excited, and the system is unentangled. A magnetic pulse entangles the system and then it evolves freely for some time τ before another "unentangling" pulse is applied. When τ is comparable to the magnon lifetime, the final qubit population $P(\tau)$ depends on the SMD mechanisms. Using the Lindblad quantum master equation [4], we numerically simulated the proposed scheme (Fig. 2). We included two possible SMD mechanisms, namely, damping (Fig. 2a) and dephasing (Fig. 2b) with decoherence rates Γ and Γ', respectively. The fast oscillations in Fig. 2 are caused by usual quantum interference, while decay of the interference pattern is due to SMD. Note, that the two mechanisms lead to different dependences of $P(\tau)$; in particular, dephasing alone does not change the average qubit population. We derived analytical expressions that determine both rates Γ and Γ' from the measurements of $P(\tau)$, even when both processes are present simultaneously (Fig. 2c). In summary, we proposed a simple measurement scheme for SMD, which can be realized using currently available technology and which can be used to study fundamental questions of quasi-particle decoherence at a single quantum level.

[1] D. D. Awschalom *et al.*, *IEEE Trans. Quantum Eng.* 2, 5500836 (2021). [2] P. G. Baity *et al.*, *Appl. Phys. Lett.* 119, 033502 (2021). [3] A. V. Chumak *et al.*, *IEEE Trans. Magn.* 58, 6, 0800172 (2022). [4] H.-P. Breuer and F. Petruccione, *Oxford University Press* (2002).

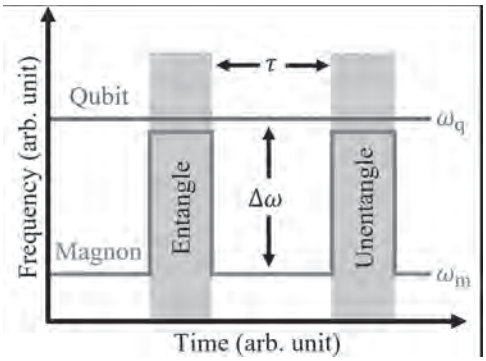

Fig. 1 Proposed SMD measurement scheme.

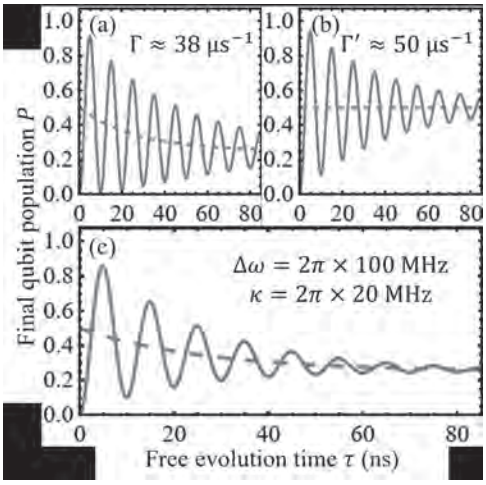

Fig. 2 Numerical simulation of SMD measurement scheme. (a): damping Γ≈38 μs^{-1}. (b): dephasing Γ′≈50 μs^{-1}. (c): mixture of (a) and (b). Dashed lines: average *P*.

GOC-11. Imaging of biologically grown magnetic nanostructures by X-ray microscopy. *T. Feggeler*[1], R. Meckenstock[2], D. Spoddig[2], B. Zingsem[2,3], J. Lill[2], D. Günzing[2], S. Wintz[4], M. Weigand[5], H. Wende[2], M. Farle[2], M. Winklhofer[6], K. Ollefs[2] and H. Ohldag[1,7] *1. Advanced Light Source, Lawrence Berkeley National Laboratory, Berkeley, CA, United States; 2. Faculty of Physics, University of Duisburg-Essen, Duisburg, Germany; 3. Ernst Ruska Center, Research Center Juelich, Juelich, Germany; 4. MPI Stuttgart, Stuttgart, Germany; 5. Helmholtz Center Berlin, Berlin, Germany; 6. School of Mathematics and Science, University of Oldenburg, Oldenburg, Germany; 7. Department of Material Sciences and Engineering, Stanford University, Stanford, CA, United States*

Biologically grown magnetic nanoparticles caught high interest due to their formation of single domain magnetite or greigite nanoparticles inside intracellular membrane organelles by biomineralization [1]. Such nanoparticle chains are promising candidates for magnonic computing due to the DNA tailorability of the particle arrangement, which allows to design and control the magnonic dispersion of such a particle ensemble [2, 3]. Here we present element-specific and spatially resolved measurements of the magnonic response of Fe3O4 nanoparticle (single particle edge length of 40 to 50 nm) chains grown inside of magnetotactic bacteria Magnetospirillum Magnetotacticum [4] by Time Resolved Scanning Transmission X- ray Microscopy (TR-STXM) [5]. TR-STXM allows the ps sampling of magnetic dynamic excitations with spatial resolution below 50 nm [5]. Using TR-STXM we reveal localized, amplitude and phase-resolved non-uniform and uniform magnonic excitations in different nanoparticle arrangements at room temperature and dynamic excitations ranging from 4 to 7 GHz [6]. Lawrence Berkeley National Laboratory is acknowledged for funding through LDRD Award: Development of a Continuous Photon Counting Scheme for Time Resolved Studies. We thank the Deutsche Forschungsgemeinschaft (DFG, German Research Foundation) – Project No. OL513/1-1, 321560838 and Project-ID 405553726 TRR 270 for financial funding.

1. Faivre, D. and D. Schüler, Magnetotactic Bacteria and Magnetosomes. Chemical Reviews, 2008. 108(11): p. 4875-4898. 2. Barman, A., et al., The 2021 Magnonics Roadmap. J Phys Condens Matter, 2021. 3. Zingsem, B., et al., Biologically encoded magnonics. Nature Communications, 2019. 10: p. 4345. 4. Maratea, D. and R. Blakemore, Aquaspirillum magnetotacticum sp. nov., a Magnetic Spirillum. International Journal of Systematic Bacteriology, 1981. 31(4): p. 452-455. 5. Bonetti, S., et al., Microwave soft x-ray microscopy for nanoscale magnetization dynamics in the 5–10 GHz frequency range. Review of Scientific Instruments, 2015. 86(9): p. 093703-1-093703-9. 6. Feggeler, T., et al., Spatially resolved GHz magnetization dynamics of a magnetite nano-particle chain inside a magnetotactic bacterium. Physical Review Research, 2021. 3(3).

GOC-12. Dynamic properties of magnetic nanoparticles in highly ordered arrangements: distance and frequency-dependent properties. *N. Neugebauer*[1,2], Y. Wang[3], P. Marburger[1,2], T. Hache[4,5], A. Fabian[6,2], M. Czerner[6,2], D. Hofmann[1,2], H. Schultheiss[4,7], M. Elm[1,2], X. Ye[3], C. Heiliger[6,2] and P. Klar[1,2] *1. Institute of Experimental Physics I, Justus Liebig University, Giessen, Germany; 2. Center for Materials Research (LaMa), Justus Liebig University, Giessen, Germany; 3. Department of Chemistry, Indiana University, Bloomington, IN, United States; 4. Institute of Ion Beam Physics and Materials Research, Helmholtz-Center Dresden-Rossendorf, Dresden, Germany; 5. Institute for Physics, Technische University Chemnitz, Chemnitz, Germany; 6. Institute for Theoretical Physics, Justus Liebig University, Giessen, Germany; 7. Institute for Physics, Technische Universität Dresden, Dresden, Germany*

Nowadays, magnetic nanoparticles may be arranged into highly ordered, crystal-like structures, so-called mesocrystals. Compared to their bulk counterpart, the characteristics of mesocrystals are not only determined by the specific material employed, but also by the shape of its nanoscale constituents, their ordering on the meso- and on the macroscale and the resulting mutual interactions between them. We use ferromagnetic resonance (FMR) experiments and Brillouin light scattering (BLS) microscopy in combination with micromagnetic simulations to investigate and characterize dipolar interactions between magnetic nanoparticles (MNPs) within such mesocrystals. The MNPs investigated in this work consist of iron oxide (magnetite - Fe_3O_4) and are coated with non-magnetic polymers, forming highly ordered hexagonal monolayer crystals as shown in fig. 1 a. The magnetic response of the regularly arranged hexagonal mesocrystals can be tuned in a controlled way by varying the thickness of the non-magnetic polymer coating of the MNPs and thus the lattice constant of the mesocrystal. The spectral features reveal that the dipolar coupling strength between the MNPs decreases as the spacing between MNPs increases, as shown in fig. 2 a. Structuring the monolayer by employing electron beam lithography, well-defined, circularly shaped MNP assemblies can be fabricated as shown in fig. 1 b. Performing BLS experiments a main signal accompanied by a satellite signal can be observed, showing distinct dependencies on the externally applied field. 2D-BLS-mapping of the circular assembly reveals the associated active areas within the assembly for the two resonances. The experimental findings of the FMR and BLS experiments are fully corroborated by micromagnetic simulations.

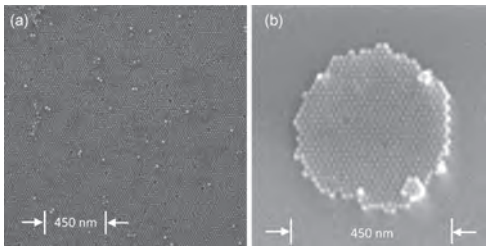

(a) Self-assembled, hexagonally arranged MNP monolayer. (b) Using electron beam lithography, well-defined MNP assemblies can be fabricated from monolayers as shown in (a).

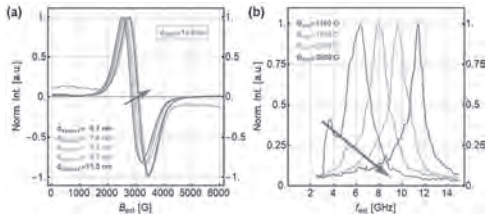

(a) In FMR experiments on MNP monolayers (see fig. 1 (a)) of different spacing between the MNPs, but constant MNP size. (b) Investigations of structured MNP assemblies as shown in fig. 1 (b) by BLS reveal two signals, both showing distinct dependencies on the externally applied field.

GOC-13. Hybrid Spin-Orbit Torque and Spin-transfer Torque Switching in Coupled Free Layer Systems. *V. Kateel*[1,2], M.G. Monteiro[1,2], F. Yasin[1], J. De Boeck[1,2], B. Soree[1], S. Rao[1] and S. Couet[1] *1. IMEC, Leuven, Belgium; 2. Department of Electrical Engineering (ESAT), KU Leuven, Leuven, Belgium*

Spin-orbit torque-based magnetoresistive random-access memory (SOT-MRAM) with perpendicularly magnetised ferromagnet is promising for memory and in-memory computing applications owing to its non-volatility, high endurance, and fast switching. The commercialisation of SOT-MRAM faces bottlenecks with high switching current, thermal stability degradation with scaling and the requirement of in-plane field (B_{ip}) to achieve deterministic switching. Utilising a synthetic antiferromagnet (SAF) in the free layer (FL) of magnetic tunnel junction has been demonstrated to overcome the former two challenges [1]. However, in this configuration, a higher magnitude of symmetry breaking in-plane field is required to overcome the exchange field and Dzyaloshinskii–Moriya interaction field [2]. To further lower the switching current and enable switching in the absence of an in-plane field, we propose the hybrid SOT switching with the assistance of spin-transfer torque (fig 1a) for SAF-coupled FL with platinum SOT layer. Our results show deterministic switching for 80 nm-sized MTJs in the absence of an in-plane field with the assistance of STT current (Fig. 1b). Furthermore, hybrid SOT+STT switching enables fast switching down to 300 ps with a lower switching current than pure SOT switching (which needs the presence of an in-plane field). Finally, the switching energy with this hybrid scheme is 20% lower than pure SOT-driven switching at 1 ns. To understand the role of SOT and STT pulses in the reversal process [3], we introduce a delay between the pulses. The early onset of SOT pulse improves the switching efficiency (Fig. 2), indicating that SOT initiates the switching process. However, the role of the STT pulse requires further investigation. In this talk, we will elucidate the reversal mechanisms in synthetic coupled FL systems and the role of both spin-torque sources with micromagnetic simulations and experiments. These insights will also enable the development of energy-efficient SOT MRAM devices.

[1] S. Couet *et al*., "BEOL compatible high retention perpendicular SOT-MRAM device for SRAM replacement and machine learning," *2021 Symposium on VLSI Technology*, 2021, pp. 1-2. [2] Chen, R. *et al.* Reducing Dzyaloshinskii-Moriya interaction and field-free spin-orbit torque switching in synthetic antiferromagnets. *Nat Commun* 12, 3113 (2021). [3] W. Cai *et al*., "Sub-ns Field-Free Switching in Perpendicular Magnetic Tunnel Junctions by the Interplay of Spin Transfer and Orbit Torques," in *IEEE Electron Device Letters*, vol. 42, no. 5, pp. 704-707, May 2021.

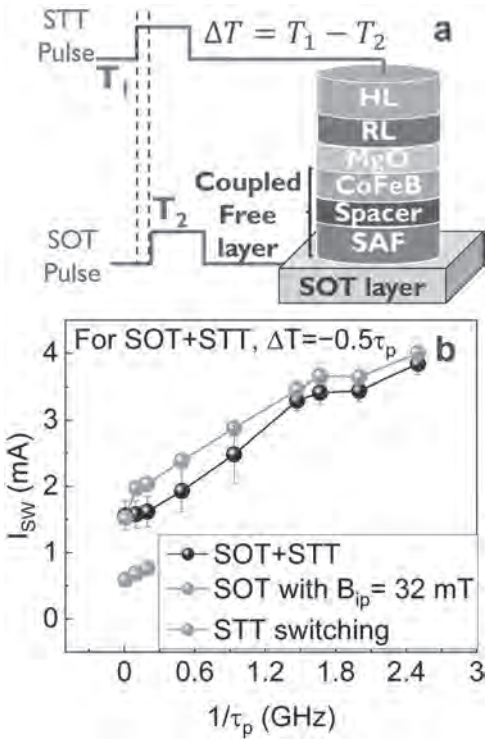

Fig. 1: a) Schematic of SOT and STT current on the MTJ stack. b) Switching with a sub-ns pulse

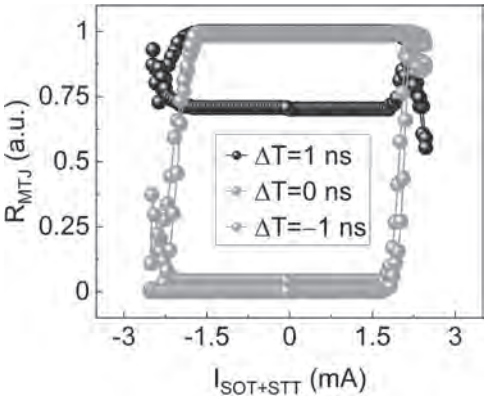

Fig. 2: Impact of delay between the SOT and STT pulse on switching for 2 ns pulse.

GOC-14. Damping in STT-MRAM Free Layers at Elevated Temperatures. *A. Whitney*[1], C. Liu[1], T. Santos[2], R. Chopdekar[2], M. Carey[2], G. Street[1], V. Kalappattil[1] and M. Wu[1] *1. Department of Physics, Colorado State University, Fort Collins, CO, United States; 2. Western Digital Research Center, Western Digital Corporation, San Jose, CA, United States*

In spin-transfer torque (STT) magnetic random-access memory (MRAM), both the switching current and the switching time critically depend on the damping of the free layer. It is known that magnetic damping varies with temperature (*T*); because STT-MRAM cells operate above room temperature, there is an urgent need to clarify damping properties in MRAM free layers at elevated temperatures. This presentation reports on measurements of damping in an ultrathin free layer at elevated temperatures. The sample consists of three CoFeB layers separated by two W layers, with a total thickness of only 1.38 nm [1]. It shows perpendicular magnetic anisotropy and square-like hysteresis loops at room temperature. The Gilbert damping constant (α) was determined through frequency-dependent ferromagnetic resonance (FMR) measurements using a high-*T* FMR technique [2,3]. The data show that the free layer exhibits a damping of $\alpha = (3.45 \pm 0.03) \times 10^{-3}$ at room temperature. This value is very close to the intrinsic damping in Fe, thereby demonstrating the high quality of the free layer. As *T* increases from 300 K to 520 K, α increases monotonically and reaches $(7.9 \pm 1.2) \times 10^{-3}$ at 520 K. Such damping enhancement indicates that the damping in the free layer originates primarily from spin-flip magnon-electron scattering over the *T* range concerned here. Further, the FMR data also show that as *T* increases from 300 K to 520 K, the effective anisotropy field H_a - $4\pi M_S$ (H_a – anisotropy field, $4\pi M_S$ – saturation induction) drops from 2200 Oe to 200 Oe, and the inhomogeneity broadening of the FMR linewidth decreases from 135 Oe to 40 Oe. The significant decrease in H_a - $4\pi M_S$ results mostly from the decrease of H_a with *T* because the decrease of $4\pi M_S$ over 300-520 K is relatively small. The large decrease in the inhomogeneity line broadening indicates that the line broadening in the free layer is mostly due to the spatial inhomogeneity in H_a.

[1] T. Santos, G. Mihajlović, and N. Smith, J. Appl. Phys., 128, 113904 (2020) [2] D. Richardson, S. Katz, J. Wang, Physical Review Applied, 10, 054046 (2018) [3] D. Richardson, K. Srinivasan, A. Kalitsov, Physical Review Applied, 11, 044016 (2019)

GOC-15. Harmonic Hall Analysis of Current-Induced Torques in Fe_2O_3/Pt Heterostructure. *H. Zhang*[1] and R. Cheng[1] *1. University of California, Riverside, Riverside, CA, United States*

Harmonic Hall analysis is a powerful technique to quantify current-induced torques, but so far it remains an open question in antiferromagnets. We formulate an analytical theory of the first and second harmonic responses of an antiferromagnet/heavy metal (HM) heterostructure driven by current-induced torques and other concomitant effects, which is substantially different from its ferromagnetic counterpart and can well be confirmed by numerical simulations. By rotating a magnetic field of variable strength in three orthogonal planes, we can unambiguously distinguish the contributions from the field-like torque, the damping-like torque, and the thermal effects through analyzing the second harmonic signals. As a case study, we apply our theory to a Fe_2O_3/Pt heterostructure studied in a recent experiment. To quantify the relative strength of the field-like torque over the damping-like torque, we further compute the interfacial spin mixing conductance in the Fe_2O_3/Pt and find that the imaginary part of the spin mixing conductance can be unexpectedly larger than the real part, which is different from what one normally expects in ferromagnet/HM heterostructures. Our theory of harmonic Hall analysis provides direct and general guidance to current and future experiments, and the indicative finding about spin mixing conductance may inspire further studies of antiferromagnet/HM heterostructures.

[1] H. Zhang, and R. Cheng, J. Magn. Magn. Mater., Vol. 556, p. 169362 (2022). [2] E. Cogulu, H. Zhang, N. N. Statuto, Y. Cheng, F. Yang, R. Cheng, and A. D. Kent, Phys. Rev. Lett., Vol. 128, p. 247204 (2022).

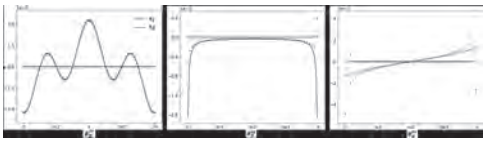

The second harmonic component of voltage in Fe_2O_3/Pt. (a), (b) and (c) correspond to rotating magnetic field in the xy, xz and yz plane, respectively. In all figures, τ_F and τ_D correspond to the contribution from field-like torque and damping-like torque, respectively.

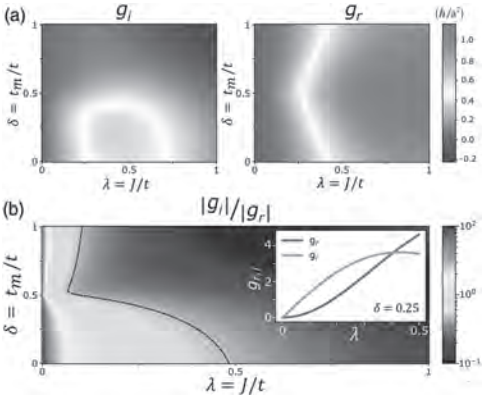

(a) The imaginary (left) and real (right) parts of the spin mixing conductance ($g = g_r + i\, g_i$) of an AFM-HM interface. The scale is indicated by the shared color bar on the right, where a is the lattice constant. (b) Ratio of $|g_i|$ to $|g_r|$. The dashed line shows $|g_i| = |g_r|$. The color bar scale is logarithmic in this case. The inset shows a line cut of gr and gi vs λ at δ=0.25.

Session GOD
MAGNETIZATION DYNAMICS IV

Dmytro A. Bozhko, Chair
University of Colorado Colorado Springs, Colorado Springs, CO, United States

INVITED PAPER

GOD-01. Quantifying Spin-Mixed States in Ferromagnets. *J.M. Shaw*[1]
1. NIST, Boulder, CO, United States

I will provide an overview on our work to experimentally quantify and verify the presence of spin-mixed states in ferromagnetic 3d transition metals via the precise measurement of the orbital moment. [1] While central to phenomena such as Elliot-Yafet scattering, quantification of the spin-mixing parameter $\langle b^2 \rangle$ has hitherto been confined to theoretical calculations. We demonstrate that this information is also available by experimental means. Comparison of ferromagnetic resonance (FMR) spectroscopy with x-ray magnetic circular dichroism (XMCD) results show that Kittel's original derivation [2] of the spectroscopic g-factor requires modification, to include second order terms in spin-mixing of valence band states. Such modification can have a large effect on the measured value of the spectroscopic g-factor in these materials. Not only does it explain discrepancies between XMCD and FMR, but provides the means to quantify $\langle b^2 \rangle$. Our results are supported by ab-initio relativistic electronic structure theory, which show good agreement between the measured and predicted values of $\langle b^2 \rangle$.

[1] J. M. Shaw, R. Knut, A. Armstrong, S. Bhandary, Y. Kvashnin, D. Thonig, E. K. Delczeg-Czirjak, O. Karis, T. J. Silva, E. Weschke, H. T. Nembach, O. Eriksson, and D. A. Arena, Phys. Rev. Lett. 127, 207201 (2021). [2] C. Kittel, Phys. Rev. 76, 743 (1949).

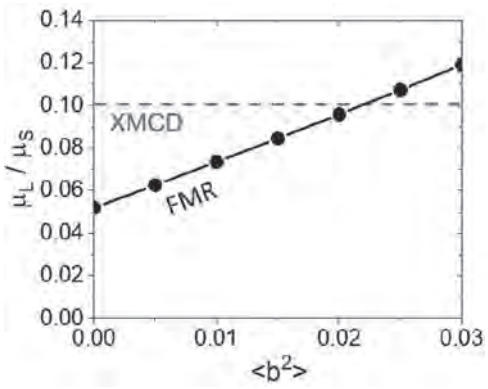

Figure 1: Experimental values of `/s obtained from XMCD and FMR for a 10 nm thick $Ni_{80}Fe_{20}$ sample. The value obtained from XMCD is indicated as the horizontal dashed line. In the case of FMR (solid line), μ_L / μ_S is calculated from the experimentally determined g-factor and application of the modified equation for the g-factor for various values of b^2. The value of $b^2 = 0.02$ for this material can be graphically determined by the intersection of the two lines.

CONTRIBUTED PAPERS

GOD-02. Precessional dynamics of geometrically scaled magnetostatic spin waves in two-dimensional magnonic fractals. J. Zhou[1,2], M.K. Zelent[3], Z. Luo[1,2], V. Scagnoli[1,2], M. Krawczyk[3], L. Heyderman[1,2] and *S. Saha*[2,4] *1. Laboratory for Multiscale Materials Experiments, Paul Scherrer Institute, Villigen, Switzerland; 2. Laboratory for Mesoscopic Systems, Department of Materials, ETH Zurich, Zurich, Switzerland; 3. Faculty of Physics, Adam Mickiewicz University, Poznan, Poland; 4. Department of Physics, Ashoka University, Sonipat, India*

Spin-wave band structures can be engineered by varying the crystal geometries and this is important to facilitate the realization of many functional magnonic devices [1], such as band stop filters and magnonic transistors. Recently, we have shown [2] the magnetostatic mode formation in an artificial magnetic structure, going beyond the crystal geometry to a fractal structure, where the mode formation is related to the geometric scaling of the fractal structure. Fractals [3] are composed of self-similar structures across different length scales, which look similar under different magnifications. This property is commonly referred to as dilation symmetry. Snowflakes, Romanesco broccoli, and coastlines are popular examples of fractals observed in nature. We have determined the evolution of the magnetostatic spin-wave modes from a simple geometric structure toward a Sierpinski carpet and Sierpinski triangle by imaging the precessional dynamics using time resolved scanning Kerr microscope as shown in Fig. 1. The experimentally observed evolution of the precessional motion could be linked to the progression in the geometric structures that results in a modification of the demagnetizing field. Furthermore, we have found sets of modes at the ferromagnetic resonance frequency that form a scaled spatial distribution following the geometric scaling. Based on this, we have determined the two conditions for such mode formation to occur. One condition is that the associated magnetic boundaries must scale accordingly, and the other condition is that the region where the mode occurs must not coincide with the regions for the edge modes. This established relationship between the fractal geometry and the mode formation in magnetic fractals provides guiding principles for their use in magnonics applications.

Reference: M. Krawczyk and D. Grundler, J. Phys.: Condens. Matter 26, 123202 (2014). J. Zhou, M. Zelent, Z. Luo, V. Scagnoli, M. Krawczyk, L. J. Heyderman, S. Saha, Phys. Rev. B 105, 174415 (2022) C. Swoboda, M. Martens, and G. Meier, Phys. Rev. B 91, 064416 (2015).

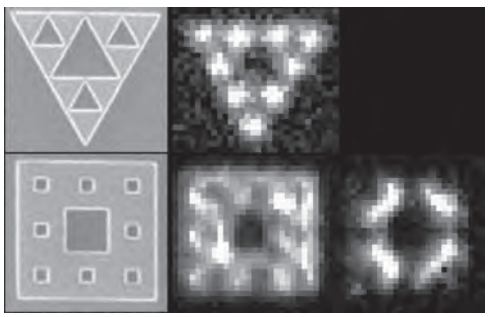

Fig. 1: SEM and scanning Kerr images of (a) Sierpinski triangles (b) Sierpinski squares with iteration number 3.

GOD-03. Reversal of nanostructured ferromagnets by magnon pulses in underlying yttrium iron garnet. *A. Mucchietto*[1], K. Baumgaertl[1] and D. Grundler[1,2] *1. Institute of Materials, EPFL, Lausanne, Switzerland; 2. Institute of Electrical and Micro Engineering, EPFL, Lausanne, Switzerland*

Magnon-induced switching of nanomagnets is one of the key milestones to realize magnon-based in-memory computing. Spin waves (magnons) have been reported to move domain walls [1] and induce the reversal of $Ni_{81}Fe_{19}$ (Py) nanostripes (NSs) fabricated on YIG [2]. We report the observation of magnon-induced reversal of bistable nanomagnets by time-resolved Brillouin light scattering microscopy. We used Py nanostripes separated from YIG via an intermediate insulating layer (Fig. 1). Thereby, we suppressed the interlayer exchange interaction between Py and YIG. A coplanar waveguide (CPW) was fabricated on top of an array of Py NSs. The device performed as a grating coupler [3]. Short-wave magnons were emitted into YIG which then propagated underneath remotely positioned nanostripes. We saturated the device at +80 mT and then decreased the field to -24 mT. We measured the thermal magnon spectrum of the unswitched Py NSs before magnon emission. After magnon excitation we observed characteristic modifications in the magnon spectrum (Fig. 2). Beyond a critical power level, peak A and peak B vanished and a new peak B' appeared. These specific modifications indicated the reversal of the nanomagnets and occurred for both the pulsed and continuous wave magnon excitation. Our experimental data suggest that dipolar coupling is sufficient to achieve magnon-induced switching. We report experiments performed in the linear and non-linear regime of magnon excitation. The latter experiments are important for the realization of recurrent neural networks based on ferromagnet/ferrimagnet hybrid structures as proposed in Ref. [4]. Our results suggest that the storage of magnon signals in reversed magnetic bits become possible thus paving the way towards magnon-based in-memory computing platforms. We acknowledge the financial support from SNSF via Grant No. 197360.

[1] J. Han, P. Zhang, J.T. Hou, Science, Vol. 366, 1121-1125 (2019) [2] K. Baumgaertl, D. Grundler, submitted [3] H. Yu, G. Duerr, R. Huber, Nature Communications, Vol. 4, 2702 (2013) [4] Á. Papp, W. Porod, G. Csaba, Nature Communications, Vol. 12, 6422 (2021)

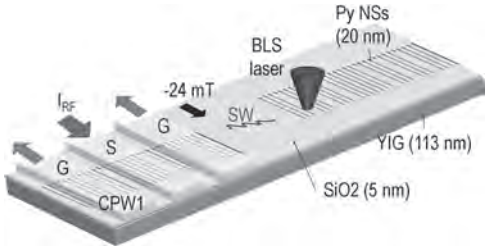

Sketch of the device. An oscillating current is injected in the CPW to excite magnons which propagate in the bare YIG until reaching separately positioned Py nanostripes. Each material thickness is indicated between parenthesis.

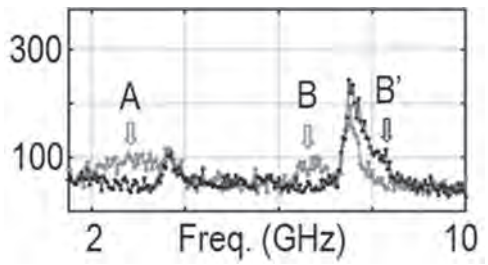

BLS thermal magnon spectra on Py stripes before (magenta) and after (black) magnon excitation at -24 mT.

GOD-04. Anomalous angular dependence of ferromagnetic resonance linewidths in perpendicular Bi:YIG films with ultralow damping. *W. Peria*[1,2], B. Khurana[3], T. Fakhrul[3], C.A. Ross[3] and P.A. Crowell[1] *1. Physics, University of Minnesota, Minneapolis, MN, United States; 2. National High Magnetic Field Laboratory, Los Alamos National Laboratory, Los Alamos, NM, United States; 3. Materials Science, Massachusetts Institute of Technology, Cambridge, MA, United States*

Bismuth-substituted yttrium iron garnets (Bi:YIG) have attracted recent interest due to the possibility of having coexisting perpendicular magnetic anisotropy (PMA) and ultralow Gilbert damping (~10^{-4}) [1–3]. The existence of ultralow damping, however, has so far been accompanied by the presence of substantial inhomogeneous broadening (~10–100 Oe). The relevant parameter for applications is the total ferromagnetic resonance (FMR) linewidth, and so it is of interest to minimize the inhomogeneous broadening as well as the damping. Here we demonstrate the presence of both ultralow damping ($\leq 5 \times 10^{-4}$) and low inhomogeneous broadening ($\approx$ 10 Oe) in a series of epitaxial PLD-grown Bi:YIG/GSGG(111) films. However, achieving these low linewidths requires the magnetization to be approximately parallel to the [100] crystallographic direction (roughly 55 degrees relative to the film normal), as seen in the figure. It is extremely unusual to observe a minimum linewidth for intermediate angles—typically a sharp maximum is observed where the angle of the magnetization is most sensitive to changes in the angle of the applied field [4]. We show that for a film grown on a GGG(100) substrate, the perpendicular FMR linewidth at 20 GHz ($\approx$ 30 Oe) is much smaller than for the films grown on (111) substrates ($\geq$ 60 Oe). Furthermore, the minimum in the linewidth as a function of angle is not nearly as sharp and occurs at approximately 35 degrees relative to the film normal. For applications, it is crucial for the FMR linewidth to be small for perpendicular magnetization. We discuss potential causes for the anomalous angular dependence of the FMR linewidth and how to minimize it for perpendicular magnetization. This work was supported by SMART, a center funded by nCORE, a Semiconductor Research Corporation program sponsored by NIST.

[1] Soumah *et al.,* Nat. Comm. 9, 3355 (2018). [2] Lin *et al.,* JMMM 496, 165886 (2020). [3] Caretta *et al.,* Science 370, 1438 (2020). [4] Woltersdorf and Heinrich, Phys. Rev. B 69, 184417 (2004).

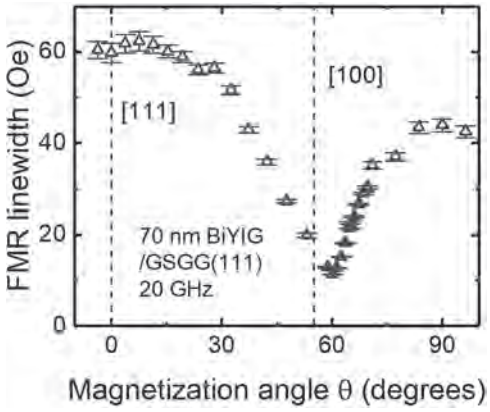

Full-width-at-half-maximum FMR linewidth as a function of magnetization angle θ relative to the film normal for a 70 nm Bi:YIG/GSGG(111) film. Angles corresponding to [111] and [100] crystallographic directions are indicated.

GOD-05. Generation of Magnons with Nanoscale Wavelengths using Voltage Controlled Parametric Resonance. *A. Deka*[1,2], B. Rana[3,4], K. Miura[5], H. Takahashi[5], Y. Otani[3,6] and Y. Fukuma[2,3] *1. Electrical and Computer Engineering, Purdue University, Lafayette, IN, United States; 2. Kyushu Institute of Technology, Iizuka, Japan; 3. RIKEN, Tokyo, Japan; 4. ISQI, Faculty of Physics, Adam Mickiewicz University, Poznan, Poland; 5. Hitachi R&D, Kokubunji, Japan; 6. ISSP, University of Tokyo, Tokyo, Japan*

Inspired by the success of FETs in electronics, voltage controlled magnetic anisotropy (VCMA) induced magnetization dynamics has emerged as an important integrant in low-power spintronic devices. In this talk, I will discuss our recent demonstration of VCMA induced parametric resonance excitation for generating magnons with exchange-interaction wavelengths [1]. Earlier, we had shown that the growth-induced magnetocrystalline anisotropy can be used for giving rise to a direction-specific magnon scattering [2]. This was shown using epitaxy dependent anisotropic damping in (111), (110) and (100) YIG/GGG thin films. However, metallic ferromagnets grown on Si have a better compatibility with CMOS processes. Therefore, we choose CoFeB/MgO junctions, that have emerged to be technologically relevant owing to its high perpendicular magnetic anisotropy, low damping, and high TMR ratios. Following an introduction to our earlier work on YIG, I will focus on the excitation of VCMA induced magnetization dynamics for in-plane magnetized CoFeB/MgO junctions (Fig. 1a), a long-standing limitation of VCMA. This is done using VCMA of interfacial in-plane anisotropy [1], that is induced by magnetic annealing [3]. At high powers, VCMA induced parametric resonance is observed (Fig. 1b). The wavelengths of corresponding magnons are estimated to be tuned down to the exchange-interaction length scales using magnetic field, power and frequency of excitation (Fig. 1c). Power dependent parametric pumping amplitudes reveal unique trends at different dynamical excitation regimes (Fig. 1d). The crucial role of excitation frequency in distinguishing VCMA induced magnetization dynamics will be discussed. Finally in Fig 1(e-f), using angular dependent measurements, we prove the presence of electric-field torque from VCMA in both linear and non-linear magnetization dynamics [1].

[1] A. Deka *et al.*, *Phys. Rev. Research* 4, 023139 (2022). [2] R.M.*, A. Deka* *et al.*, *Appl. Phys. Lett.* 119, 162403 (2021). (*Equal first author) [3] A. Deka *et al., Phys. Rev. B* 101 (17), 174405 (2020).

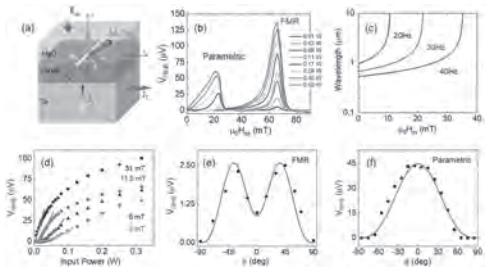

Fig. 1 (a) Illustration of VCMA excitation. (b) Power dependent inverse spin Hall effect voltage V_{ISHE}. (c) Calculated frequency and magnetic field H_{ex} dependence on wavength of magnons. (d) Power dependence of V_{ISHE} at different wavelengths. In-plane angle dependence of V_{ISHE} amplitudes at (e) uniform and (f) parametric resonances. Lines are fits to equations in Ref. 1.

GOD-06. Dynamics of 3D topological spin textures. *D.W. Raftrey*[1,2] and P. Fischer[1,2] *1. Physics, University of California Santa Cruz, Santa Cruz, CA, United States; 2. Material Science, Lawrence Berkeley National Laboratory, Berkeley, CA, United States*

The push into three dimensions in nanomagnetic systems is a growing theme in basic nanomagnetism research and potential spintronics devices. In two dimensions, magnetic Skyrmions are an established platform to explore the physics of real-space topological spin textures. In three dimensions, the analogous spin texture is the recently observed magnetic Hopfion [1]. A Hopfion is a toroidal spin texture equivalent to a Skyrmion string twisted and closed into a torus (fig. 1). 3D magnetic systems are also predicted to host additional novel spin textures including Skyrmion tubes, chiral bobbers, and torons. These 3D spin textures, which have so far only been observed statically, now hold promise for dynamical studies. Investigating transitions between these novel 3D spin textures under applied magnetic fields or currents is within reach with experimental studies with time-resolved x-ray microscopy and scattering techniques. (fig. 2). I will present numerical calculations investigating how the dynamics of Hopfions and related 3D spin textures couple to their topology [2]. This work has implications for experimental design and 3D spintronic device engineering. This work was funded by the US DOE, Office of Science, Basic Energy Sciences under Contract No. DE-AC02-05-CH11231.

[1] N. Kent *et al.*, "Creation and observation of Hopfions in magnetic multilayer systems," *Nature Communications*, vol. 12, no. 1, p. 1562, 2021, doi: 10.1038/s41467-021-21846-5. [2] D. Raftrey and P. Fischer, "Field-Driven Dynamics of Magnetic Hopfions," *Physical Review Letters*, vol. 127, no. 25, p. 257201, Dec. 2021, doi: 10.1103/PhysRevLett.127.257201.

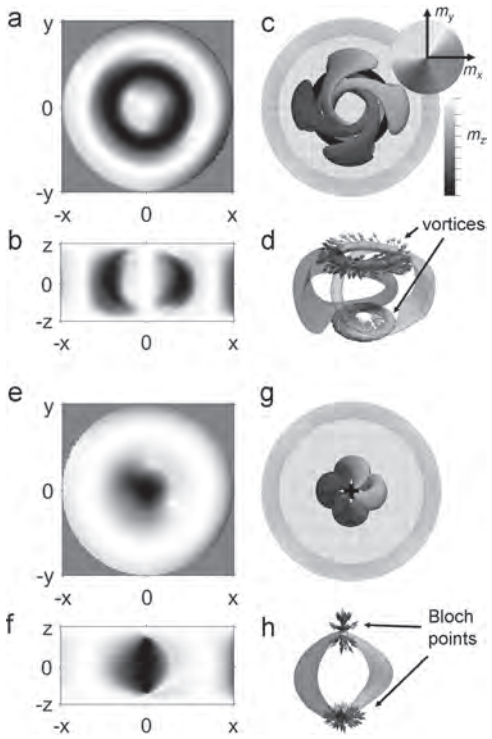

(a) Magnetization color map of a Hopfion at the z=0 plane. (b) Magnetization color map of Hopfion at the y=0 plane. (c) Hopfion spin textures with linked magnetization isosurfaces. The Hopf invariant or linking number, Q, is the number of times the isosurfaces are linked. (d) Detail of Hopfion vortex rings. (e) Magnetization color map of a toron at the z=0 plane. (f) Magnetization color map of toron at the y=0 plane. (g) Toron spin textures with unlinked isosurfaces. A toron has Q=0. (h) Detail of toron Bloch points (monopole antimonopole pair).

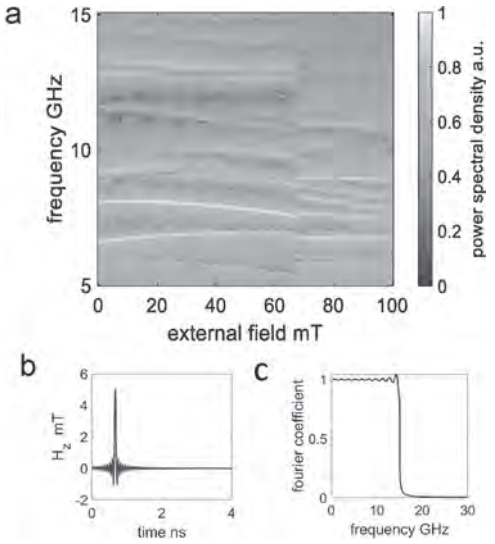

(a) Power Spectral Density response of a Hopfion to a field pulse under static applied external field. (b) Magnetic excitation pulse applied in the x direction in the time domain. Pulsed field is the cardinal sign or sinc function. (c) Fourier transform of the excitation pulse in the frequency domain. The sinc function creates a square wave with equal sampling frequency up to a maximum frequency of 15 GHz.

GOD-07. Parametrically excited modes in YIG microdisks: identification and nonlinear interactions. *T. Srivastava*[1], I. Ngouagnia Yemeli[1], G. de Loubens[1], H. Merbouche[2], S. Demokritov[2], V. Demidov[2], M. d'Aquino[3], C. Serpico[3], J. Kim[4], G. Csaba[5], O. Klein[6], N. Beaulieu[7], J. Ben Youssef[7], M. Muñoz[8], I. Boventer[9], V. Cros[9], P. Bortolotti[9] and A. Anane[9] *1. SPEC, CEA, CNRS, Université Paris-Saclay, Gif sur Yvette, France; 2. Institute for Applied Physics, University of Muenster, Muenster, Germany; 3. Department of Electrical Engineering and ICT, University of Naples Federico II, Naples, Italy; 4. Centre de Nanosciences et de Nanotechnologies, CNRS, Université Paris-Saclay, Palaiseau, France; 5. Pázmány Péter Catholic University, Faculty of Information Technology and Bionics, Budapest, Hungary; 6. Spintec, CEA, CNRS, Université Grenoble-Alpes, Grenoble, France; 7. LabSTICC, CNRS, Université de Bretagne Occidentale, Brest, France; 8. Instituto de Tecnologías Físicas y de la Información (CSIC), Madrid, Spain; 9. Unité Mixte de Physique, CNRS, Thales, Université Paris-Saclay, Palaiseau, France*

Spin-wave (SW) dynamics exhibit a variety of nonlinear phenomena ranging from parametric instabilities to chaos. In confined structures, SW modes are quantized in wave-vector and energy, which limits the possible nonlinear processes due to conservation laws but also opens opportunities to understand and control them in more detail [1–3]. In this work, we use magnetic resonance force microscopy (MRFM) and micro-focused Brillouin light scattering (BLS) to probe parametric SWs in microdisks patterned from a 50 nm thick YIG film, excited by a pumping field parallel to the in-plane bias magnetic field. As expected and shown in Fig. 1, the parametrically excited SWs are quantized [4,5]. Comparing experimental data to computed eigen-frequencies [6], we demonstrate that all eigen-modes are accessible through parametric excitation, as shown in Fig. 2. Next, to study the nonlinear interactions between the SW eigenmodes, we simultaneously excite two of them by parametric pumping. Time-resolved BLS allows for evidence of two main scenarios: indirect mode interaction and nonlinear phase locking of the modes. Two-tone MRFM spectroscopy demonstrates that each mode is coupled to all other modes, and shows that nonlinear interactions are complex, with enhanced or suppressed peaks, and the appearance of additional peaks in the spectrum. Micromagnetic simulations and a computational approach based on normal modes [7] provide some insight into these nonlinear processes.

[1] Y. Li et al., Phys. Rev. X 9, 041036 (2019) [2] K. Schultheiss et al., Phys. Rev. Lett. 122, 097202 (2019) [3] M. Mohseni et al., Phys. Rev. Lett. 126, 097202 (2021) [4] H. Ulrichs et al., Phys. Rev. B 84, 094401 (2011) [5] F. Guo et al., Phys. Rev. B 89, 104422 (2014) [6] M. d'Aquino et al., J. Comput. Phys. 228, 6130 (2009) [7] S. Perna et al., J. Magn. Magn. Mater. 546, 168683 (2022)

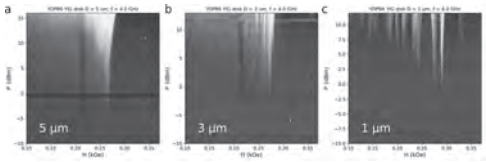

Fig 1. Intensity map of the parametrically excited modes in the field-power coordinates, measured by MRFM on disks with diameters 5 µm (a), 3 µm (b), and 1 µm (c). The parallel pumping field has the frequency f = 4 GHz

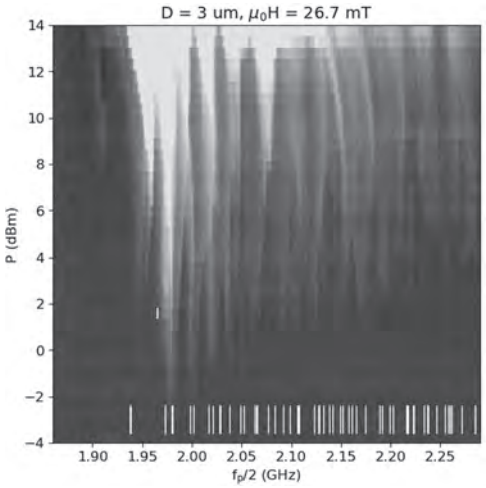

Fig 2. Intensity map of the parametrically excited modes in the frequency-power coordinates, measured by MRFM on a 3 µm disk at 26.7 mT. The white ticks at the bottom indicate the simulated eigen-frequencies for the same configuration.

GOD-08. Spin Wave Induced Domain Wall Motion in BiYIG. *M. Gross*[1], Y. Fan[1], T. Fakhrul[1], L. Liu[1] and C.A. Ross[1] *1. Massachusetts Institute of Technology, Cambridge, MA, United States*

Spin waves can travel up to macroscopic distances in low-damping materials and can impart angular momentum to domain walls [1] via spin transfer torque, which drives the domain wall in the opposite direction compared to the travelling spin wave. Spin-wave-driven domain wall motion has been demonstrated in thin films of magnetic metals [2]; however, it has yet to be studied in ferrimagnetic insulators. Here the interactions between spin waves and domain walls are explored in bismuth-substituted yttrium iron garnet (BiYIG). 17nm of BiYIG is grown on a GSGG substrate via pulsed laser deposition. The films have perpendicular magnetic anisotropy due to magnetoelastic effects, magnetization of 140 kA/m, coercivity of ~10 Oe, a zero-field resonance frequency of 4.1 GHz based on ferromagnetic resonance (FMR) measurements and Gilbert damping factor of 0.001. Films are etched to form racetrack devices of width 5 µm with pairs of gold metal antennas patterned on top spaced 5 – 30 µm apart. Domain walls are introduced by field cycling and are commonly pinned under the antennas. Transmissivity measurements between the two antennas show that power is most effectively coupled to spin waves in the BiYIG from the metal antennas for excitation frequencies around the FMR frequency. A domain wall placed between the two antennas attenuates the transmission at this frequency (Figure 1). Spin waves also translate domain walls between the antennas using pulses as small as 1 ns and frequencies around the resonant frequency. As the pulse

width narrows, the range of frequencies that interacts domain walls also narrows. Figure 2 shows an example of a domain wall that propagated 15 μm after applying a 1 ns pulse at 4.35 GHz to one antenna. No other frequency moves the domain wall with a 1 ns pulse, but 4.25-4.45 GHz can move a domain wall with a 2 ns pulse. Similarly, a 3 ns pulse translates domain walls at frequencies of 3.75-4.65 GHz. This high-speed modulation of domain walls is significant for future spintronic devices.

[1] P. Yan, X. S. Wang, and X. R. Wang, "All-magnonic spin-transfer torque and domain wall propagation," *Phys. Rev. Lett.*, vol. 107, no. 17, 2011, doi: 10.1103/PhysRevLett.107.177207. [2] J. Han, P. Zhang, J. T. Hou, S. A. Siddiqui, and L. Liu, "Mutual control of coherent spin waves and magnetic domain walls in a magnonic device," *Science (80-.).*, vol. 366, no. 6469, 2019, doi: 10.1126/science.aau2610.

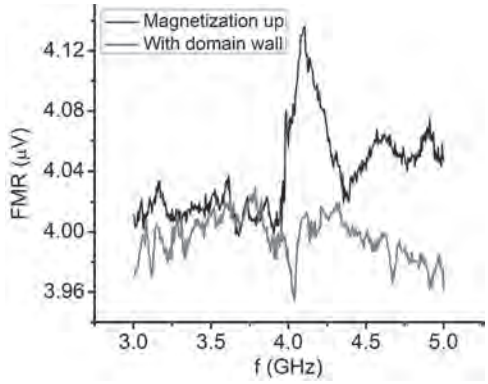

FMR voltage measurements showing domain wall attenuating spin waves around resonance.

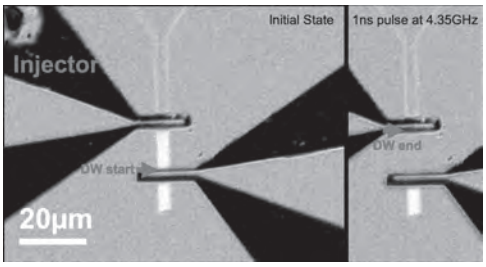

Before and after domain wall motion from 1ns pulse width spin wave.

GOD-09. Amplification of the Gyrotropic Mode Power via Interaction with a Hot Magnon Gas. *P. Artemchuk*[1], V. Tyberkevych[1] and A.N. Slavin[1] *1. Physics, Oakland University, Rochester, MI, United States*

A rapidly cooling hot magnon gas demonstrates non-trivial thermodynamic behavior [1]. Thus, the chemical potential of the gas increases, which may lead to formation of a Bose-Einstein condensate (BEC) [1, 2]. Studies of the interaction between the rapidly cooling magnon gas and nonlinear bullet mode [3] or propagating spin waves [4] indicate possibility of a coherent magnon transfer from the gas to other types of magnonic excitations. Here, we theoretically investigate interaction of a hot magnon gas with a gyrotropic vortex mode (GVM). Frequency of a GVM lies below the spectrum of propagating spin waves and, thus, this problem is an example of interaction of a magnon gas with an isolated mode. Using analytical methods, we show that four-magnon scattering leads to an additional contribution to GVM damping $\Delta\Gamma \propto (hf_0 - \mu)$, where f_0 is the GVM frequency and μ is the chemical potential of the magnon gas. If the gas's chemical potential μ increases above the GVM frequency, $\Delta\Gamma$ becomes negative, which should lead to amplification of the GVM. To check these predictions, we performed numerical simulations using the model developed in [1] with additional isolated mode. Fig. 1 shows an example of the time evolution of the GVM power when a heating pulse is applied to the sample. After the heating pulse is off, the magnon gas undergoes rapid cooling and the GVM power increases. When the cooling process ends ($t \approx 250$ ns) the chemical potential of the gas drops to zero and the GVM continues to decay with the same rate as before. The GVM amplification gain (Fig. 2) strongly depends on the maximum chemical potential acquired by the magnon gas during the cooling process. Partial compensation of GVM damping starts at $\mu_0 \approx hf_0$ but significant amplification is achieved when the gas is driven close to the point of BEC formation ($\mu_0/h \approx 5.3$ GHz) and population of low-energy magnon states substantially increases.

[1] M. Schneider, T. Brächer, D. Breitbach, et al., *Nature Nanotech.* 15, 457 (2020). [2] M. Schneider, D. Breitbach, R.O. Serha, et al., *Phys. Rev. Lett.* 127, 237203 (2021) [3] M. Schneider, D. Breitbach, R.O. Serha, et al., *Phys. Rev. B* 104, L140405 (2021). [4] M. Schneider, D. Breitbach, B. Lägel, et al., E4-12, 65th Annual Conference on Magnetism and Magnetic Materials, November 2020.

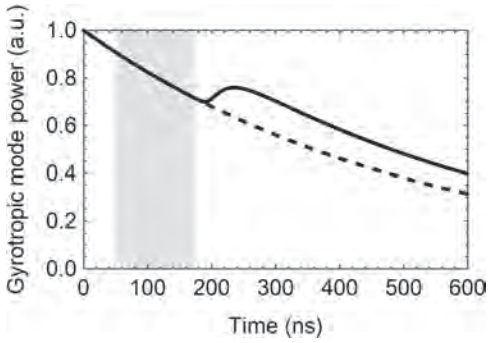

Fig. 1. Normalized gyrotropic mode power vs time with (solid line) and without (dashed line) interaction with a hot magnon gas. Shaded area shows the duration of the heating pulse.

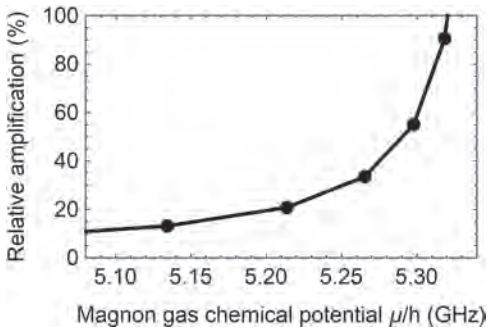

Fig. 2. Relative amplification of a gyrotropic mode power depending on the maximum chemical potential of the hot magnon gas interacting with it.

GOD-10. Scattering Reversals and Higher-Order Interactions in Three-Magnon Scattering of Ferromagnetic Resonance. *A. Hamill*[1], T. Qu[2], R.H. Victora[2] and P.A. Crowell[1] *1. School of Physics and Astronomy, University of Minnesota, Minneapolis, MN, United States; 2. Department of Electrical and Computer Engineering, University of Minnesota, Minneapolis, MN, United States*

The FMR magnon population (hereafter defined as the FMR amplitude c_0) can become unstable when driven by microwave power P_a greater than a threshold power P_S, such that it undergoes three-magnon splitting to two magnons $c_{\pm k}$ of half the frequency and equal and opposite wavevectors [1]. We employ time-resolved homodyning spectroscopy to examine this instability over five orders of magnitude in microwave power P_a. We observe an additional threshold power P_{osc}, above which the splitting induces oscillations in c_0 [2]. At high powers, we find that these oscillations induce 180° phase shifts in FMR. Our model predicts these phase shifts and that, similarly, the half-frequency magnons undergo 90° phase shifts. Notably, we find that these phase shifts correspond to reversals in the three-magnon scattering

direction between splitting and confluence (see Fig. 1a,b). The scattering direction is found to be determined by $|\Psi_0|$, the absolute phase between FMR and its three-magnon scattering term. These reversals generate pronounced oscillations of the FMR amplitude after turning off the microwave excitation (see Fig. 1b,d). We also observe broadening in the frequency spectra of the oscillations (see Fig. 2a,b). From our micromagnetic simulations, we find that this corresponds to higher-order scattering processes that vary with FMR frequency (see Fig. 2c,d). These findings shed light on the relationship between three-magnon splitting and confluence, the role of phase dynamics in magnon scattering, and the higher-order magnon scattering processes at high microwave powers.

[1] H. Suhl, J. Phys. Chem. Solids, Vol. 1, pp. 209-227 (1957) [2] T. Qu†, A. Hamill†, R. H. Victora, and P. A. Crowell, arXiv:2204.11969 (2022)
The Minnesota Supercomputing Institute (MSI) provided resources that contributed to the research results reported within this abstract. The authors acknowledge support by SMART, a center funded by nCORE, a SRC program sponsored by NIST. The authors also acknowledge support by DARPA under Grant W911NF-17-1-0100, MINT at Minnesota, and the NSF XSEDE through Allocation No. TG-ECS200001.

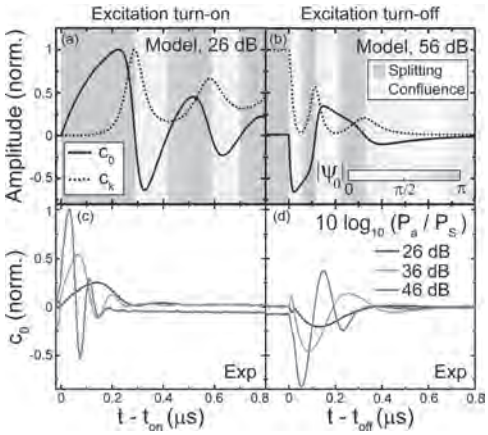

Fig. 1. (a,b) Numerical solutions of the magnon amplitudes c_0 and c_k during and after microwave excitation. Color-coding corresponds to $|\Psi_0|$. (c,d) Corresponding experimental data of c_0, showing the power dependence of the oscillations and scattering reversals. Data is normalized to the turn-on peak at 46 dB.

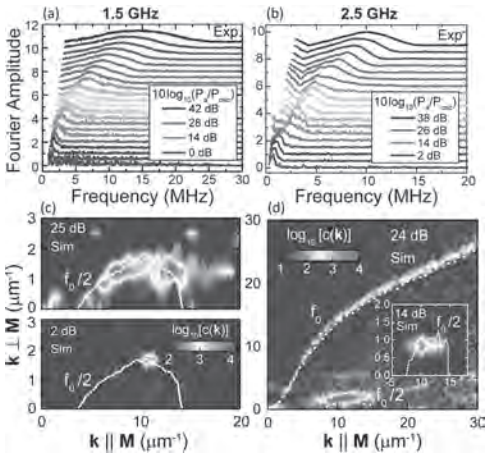

Fig. 2. (a,b) Measured frequency spectra of the oscillations, at various powers P_a relative to P_{osc}, for FMR frequencies of 1.5 GHz (left column) and 2.5 GHz (right column). (c,d) the corresponding simulated magnon amplitudes at powers below and above the onset of broadening, showing the different higher-order scattering processes at 1.5 GHz and 2.5 GHz.

GOD-11. Withdrawn

GOD-12. Withdrawn

Session GOE
MAGNETIZATION DYNAMICS V

Jose Angel Fernandez-Roldan, Co-Chair
Helmholtz Zentrum Dresden-Rossendorf, Dresden, Germany
Raghav Sharma, Co-Chair
National University of Singapore, Singapore

CONTRIBUTED PAPERS

GOE-01. Electrical Evidence and Modeling of the Giant Non-Reciprocity of Spin-Waves In Synthetic Antiferromagnets. *F. Millo*[1], A. Mouhoub[1], J. Kim[1], J. Adam[1], C. Chappert[1], S. Ngom[1], A. Solignac[2] and T. Devolder[1] *1. Université Paris-Saclay, CNRS, Centre de Nanosciences et de Nanotechnologies, Palaiseau, France; 2. SPEC, CEA, CNRS, Université Paris-Saclay, Gif-sur-Yvette, France*

Non-reciprocal (NR) microwave components providing a unidirectional flow of energy are essential for signal processing. Spin waves (SWs) possess attractive characteristics that make them commonly harnessed to design NR components. However these components are presently mainly ferrite-based and bulky; more compact and integrable systems are desirable. Synthetic antiferromagnet (SAF) films with strong dipole-dipole interactions have been proposed [1] as a versatile platform on which strongly NR behaviors could be obtained at micron-scale physical dimensions in the frequency range of their eigen excitations. We have studied the NR behavior of SWs in Co40Fe40B20 (17 nm) /Ru (0.7 nm)/CoFeB (17 nm) SAFs using inductive propagative spin wave spectroscopy, analytical modeling and numerical micromagnetics using the mumax3 softtware. The films were patterned in 20 micron-wide stripes used as SW conduits. Two inductive antenna separated by a variable distance [2-8 microns, Fig. 1(a)] are used to generate and collect the spin waves by means of a 2-port vector network analyzer. We determine the forward and backward transmission parameters for variable applied fields and variable field-to-wavevector orientations. When the SAF is in the scissors state, all directions show substantial frequency and amplitude non-reciprocities (Fig. 1), except when the wavevector is perpendicular to the applied field, where only NR amplitude is observed. We model this behavior by computing the dispersion relation of the acoustical and optical spin waves of the SAF and their sensitivity to the radio frequency (RF) fields of the antenna, as well the inductive transduction back to the electrical domain. We will show how the dispersion relations and the symmetries of the susceptibility tensor can be used to design optimally NR transmission parameters.

[1] Mio Ishibashi et al., Science Advances, 6, eaaz6931 (2020).

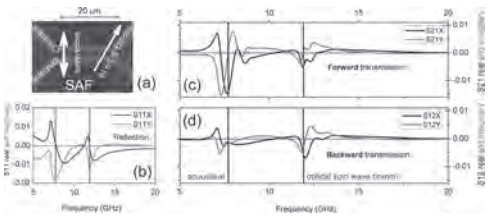

Fig. 1: (a) Device and geometrical conventions; (b) Reflection parameter of antenna 1, used to identify the frequencies of the acoustical and optical modes at k=0 (blue lines). (c) and (d) forward and backward transmission parameters.

GOE-02. Interparticle magnetic correlations and dynamics of fluctuations in assemblies of Fe_3O_4 nanoparticles. *K. Chesnel*[1], J. Rackham[1], D. Griner[1], C. Hawk[1], R. Harrison[1] and A.H. Reid[2] *1. Physics, Brigham Young University, Provo, UT, United States; 2. SIMES, SLAC, Stanford, CA, United States*

Magnetic nanoparticles (NPs) provide an ideal support for developing a wide range of nanotechnologies and biomedical applications, such as drug-delivery, gene delivery, hyperthermia, or contrast agents for MRI.[1] Magnetite (Fe_3O_4) NPs are good candidates for these applications due to their non-toxicity and long-life in the bloodstream. To optimize these applications, it is crucial to well control the magnetic response of individual NP when manipulating a collection of them via a magnetic field. In particular, it is useful to identify any interparticle magnetic correlations that may cause the magnetic response to deviate from superparamagnetism, induce superferromagnetism and magnetic hysteresis, and affect the dynamics of fluctuations. To that end, we have studied the magnetic response of 5 – 100 nm Fe_3O_4 NPs and its dependence on NP size, using magnetometry [2] and spin muon resonance [3]. However, this information remains macroscopic or spatially averaged. Here we show how nanoscale spatial information on inter-particle magnetic correlations can be obtained via x-ray resonant magnetic scattering (XRMS) [4] as illustrated in Figure 1. By tuning the energy of the x-rays to resonant edges of Fe and comparing opposite polarization helicities, we have extracted information about the local inter-particle magnetic orders within NP assemblies of various sizes.[5] We fitted the XRMS data using a model based on chains of NPs.[6] The data fitting shows ferromagnetic ordering when an external magnetic field is applied, and the emergence of antiferromagnetic ordering, competing with magnetic randomness, when the field is brought back near the coercive point (zero net magnetization). We studied how these correlations depend on particle size and found an enhancement of magnetic couplings and antiferromagnetic orders for bigger particles. [7] Additionally we will show preliminary studies of the dynamics of magnetic fluctuations via x-ray photon correlation spectroscopy (XPCS).

1. Frey *et al.*, Chem. Soc. Rev. 2009, 38, 2532-2542 (2009) 2. Klomp *et al.*, IEEE Trans. Mag. 56, 2300109 (2020) 3. Frandsen et al., Phys. Rev. Matter 5, 054411 (2021) 4. Kortright *et al.*, *Phys. Rev. B* 71, 012402 (2005) 5. Chesnel *et al.*, *Magnetochemistry* 4, 42-58 (2018) 6. Rackham *et al.*, *AIP Advances* 9, 035033 (2019) 7. Rackham *et al.*, *to be submitted* (2022)

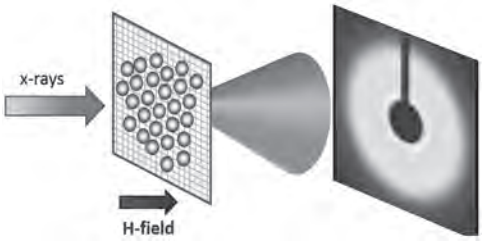

Figure 1: Layout of the x-ray resonant magnetic scattering (XRMS) measurement of a nanoparticle assembly.

GOE-03. Ferromagnetic Resonance in FePt Thin Films at Elevated Temperatures. *C. Liu*[1], K. Srinivasan[2], A. Ajan[2], E. McCollum[1], A. Kalitsov[2], V. Kalappattil[1] and M. Wu[1] *1. Colorado State University, Fort Collins, CO, United States; 2. Western Digital, San Jose, CA, United States*

Understanding of damping processes in ferromagnetic thin films at elevated temperatures has significant implications for heat-assisted magnetic recording, spin-transfer torque memory, and magnetic sensors operating at high temperatures. Through cavity-based high-temperature ferromagnetic resonance (FMR) measurements, this work examined the FMR linewidth and damping properties of continuous cubic FePt thin films at elevated temperatures. The data show that the FMR linewidth and the Gilbert damping constant both increase monotonically when temperature is increased from room temperature toward the Curie temperature. This temperature dependence is opposite to that observed previously in FePt thin films that are granular, rather than continuous, and have $L1_0$ structure, rather than cubic structure; in those films, the FMR linewidth decreases monotonically with an increase in temperature [1]. These opposite results originate from the difference in the crystalline structure and microstructure of the films. In the previous work, the granular $L1_0$-order FePt films hold dense material imperfection and thereby may host strong two-magnon scattering (TMS); the TMS-produced damping decreases with an increase in temperature, giving rise to reduced FMR linewidths at high temperatures. In the current work, the continuous cubic FePt films have much less imperfection and thereby host weak TMS, and the dominant damping mechanism is spin-flip magnon-electron scattering (SF-MES). The SF-MES process becomes stronger with an increase in temperature, giving rise to larger linewidth and higher damping at high temperatures. This work and the previous work together demonstrate that for a given thin-film material, the temperature dependence of the FMR linewidth critically relies on the structural properties of the film. They also indicate that one can engineer damping in magnetic thin films through the control of the structural properties of the films.

[1] D. Richardson, S. Katz, J. Wang, Y. K. Takahashi, K. Srinivasan, A. Kalitsov, K. Hono, A. Ajan and M. Wu, Phys. Rev. Appl., Vol. 10, p.054046 (2018).

GOE-04. Compensation of anisotropy in spin-Hall systems for realizing neuromorphic applications. *P. Sethi*[1], D. Sanz Hernandez[1], F. Ajejas[1], S. Krishnia[1], Y. Sassi[1], V. Cros[1], D. Markovic[1] and J. Grollier[1] *1. Unité Mixte de Physique CNRS/Thales, Université Paris-Saclay, 91767 Palaiseau, France, Palaiseau, France*

Spintronic nano-oscillators can provide energy efficient solution to realize neuromorphic applications. They have been shown to emulate biological neurons and perform machine learning tasks with an accuracy similar to that of state-of-the-art neural networks [1]. Moreover, they can serve as synapses when operated as a spin diode [2]. In this context, systems with compensated anisotropy could offer key advantages. For instance, an easy plane geometry achieved by compensating the anisotropy can produce spikes as an output, a phenomenon, recently demonstrated via micromagnetic simulations for a spin Hall nano-oscillator (SHNO) geometry [3]. Moreover, an SHNO with a compensated or near zero effective magnetization would require low operating current and exhibit extremely low phase noise, making it suitable to realize large chain of synchronized neurons [4]. A synapse or a spin diode with a compensated anisotropy would also resonate at a relatively fixed frequency, which is an essential requirement for frequency multiplexing and transmitting data from the SHNO based neurons. This motivates us to study spin Hall systems with compensated anisotropy. Here, Pt/CoFeB based thin films are used as the spin Hall system. The anisotropy has been tuned by varying the thickness of the magnetic layer. The thin films have been fabricated into micro-strip waveguides and nano-constrictions to study the magnetization dynamics in these systems which emulate the behaviour of an SHNO. Spin-torque ferromagnetic resonance (ST-FMR) technique is employed to evaluate the effective magnetization of the fabricated devices. The measurements indicate the fabricated devices achieve compensation when the starting thin films have perpendicular anisotropy, implying the effects of post-fabrication anisotropy reduction and shape anisotropy. Different nano-constriction geometries have been studied to evaluate the effect of shape on the compensation point. We also demonstrate frequency tunability of the nano-synapses and thereby its weights by anisotropy modification. We then propose a non-volatile method to control the synaptic weights via electric fields which would enable realization of compact and energy efficient neuromorphic chips.

[1] J. Torrejon et al., "Neuromorphic computing with nanoscale spintronic oscillators", *Nature* 547, 428 (2017). [2] N. Leroux et al., "Radio-Frequency Multiply-and-Accumulate Operations with Spintronic Synapses", *Phys. Rev. Appl*. 15, 034067 (2021). [3] D. Markovic et al., "Easy-plane spin Hall nano-oscillators as spiking neurons for neuromorphic computing", *Phys. Rev. B* 105, 014411 (2022). [4] A.A. Awad et al., "Long-range mutual synchronization of spin Hall nano-oscillators", *Nat. Phys*. 13, 292 (2017).

GOE-05. Withdrawn

GOE-06. Spin-Orbit Torque Induced Ultrafast Magnetization Switching in a Ferromagnet. *D. Polley*[1,2], A. Pattabi[2], A. Rastogi[2], K. Jhuria[1], E. Diaz[3], A. Lemaitre[4], M. Hehn[3], J. Gorchon[3] and J. Bokor[1,2] *1. Material Science Division, Lawrence Berkeley National Laboratory, Berkeley, CA, United States; 2. Department of Electrical Engineering and Computer Sciences, University of California, Berkeley, Berkeley, CA, United States; 3. Université de Lorraine, Nancy, France; 4. Université Paris Sud, Palaiseau, France*

Spin-orbit-torque (SOT) based magnetic devices[1] have gained considerable attention due to their non-volatility, speed, and energy efficiency. SOT-induced magnetization switching studies are limited by the rise-time and duration of available pulsed current sources[2,3]. Recently, ultrafast SOT switching has been demonstrated using ~ps current pulses[4], obtained from an optically excited photoconductive (Auston) switch[4,5], although the switching dynamics have not yet been reported. Here, we report the ultrafast magnetization dynamics measured via the time-resolved polar magneto-optical Kerr effect (MOKE)[5] in a ferromagnet (inset of Fig. 1), using the ultrafast SOT effect due to a ~ 9 ps long current pulse generated from an Auston switch. The ~ps current pulse, without any in-plane magnetic field, introduces a demagnetization of ~30% and softens the magnet at an ultrafast timescale. In the presence of a 1600 Oe symmetry-breaking in-plane field, SOT tries to rotate the magnetic moments away from the saturation state, for a negative current pulse (blue line in Fig. 1), which when combined with the ultrafast demagnetization, shows a reduced initial demagnetization coupled with SOT-oscillations at longer timescales. However, for positive current, it induces a coherent rotation of the softened magnetic moments toward the negative saturation. Magnetization crosses zero in ~65 ps and switches fully after about ~200 ps (red line in Fig. 1). Sub-ns current pulse-induced SOT dynamics are governed by domain-wall propagation with an additional incubation delay due to domain nucleation[6-8]. The absence of any incubation delay combined with the fast-switching time leads us to believe that the switching is probably governed by the coherent rotation of the softened magnetic moment due to ultrafast heating by the ~ps current pulse excitation. A micromagnetic simulation coupled with 2-temperature ultrafast heating qualitatively agrees well with the observed dynamics (dotted lines in Fig. 1). Our work sheds significant insights on the mechanism of picosecond SOT-induced magnetization dynamics.

1. D. Polley, A. Pattabi, J. Chatterjee, et al., Appl. Phys. Lett. 120, 140501 (2022). 2. I.M. Miron, K. Garello, G. Gaudin, et al., Nature 476, 189 (2011). 3. K. Garello, C.O. Avci, I.M. Miron, et al., Appl. Phys. Lett. 105, 212402 (2014). 4. K. Jhuria, J. Hohlfeld, A. Pattabi, et al., Nat. Electron. 3, 680 (2020). 5. Y. Yang, R.B. Wilson, J. Gorchon, et al., Sci. Adv. 3, e1603117 (2017). 6. E. Grimaldi, V. Krizakova, G. Sala, et al., Nat. Nanotechnol. 15, 111 (2020). 7. V. Krizakova, K. Garello, E. Grimaldi, et al., Appl. Phys. Lett. 116, 232406 (2020). 8. G. Sala, V. Krizakova, E. Grimaldi, et al., Nat. Commun. 12, 656 (2021).

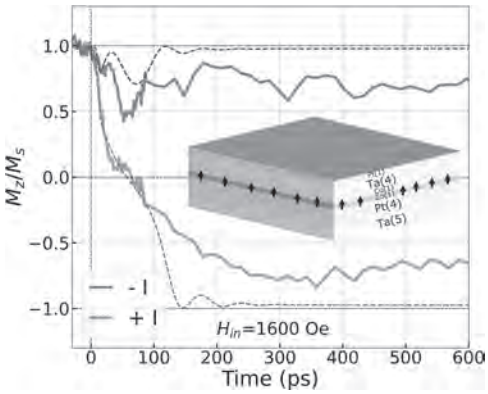

Fig. 1. Ultrafast magnetization dynamics with positive and negative ~ps current pulse direction. The theoretical analysis is shown in dotted lines.

GOE-07. Investigation of Sub-Nanosecond Fluctuations on Amorphous FeGe Near a Magnetic Phase Transition. *R. Tumbleson*[1,2], N. Burdet[3], E. Holingworth[4], A. Singh[2], A. Us Saleheen[2], M. McCarter[2], D.W. Raftrey[1,2], V. Esposito[3], A. Tadesse[3], S.A. Morley[2], D.A. O'Mahoney[4], F. Decker[3], A.H. Reid[3], G. Dakovski[3], S. Kevan[2], P. Fischer[2], F. Hellman[4], J. Turner[3] and S. Roy[2] *1. UC Santa Cruz, Santa Cruz, CA, United States; 2. Lawrence Berkeley National Laboratory, Berkeley, CA, United States; 3. SLAC, Menlo Park, CA, United States; 4. UC Berkeley, Berkeley, CA, United States*

Competition between the symmetric and antisymmetric exchange interactions can give rise to non-trivial magnetic spin textures that are both physically interesting and technologically promising. Here, I present results from a recent experiment conducted at LCLS that probed the magnetic fluctuations of an amorphous FeGe film. In this experiment, the magnetic phase transition between a helical and a paramagnetic state was investigated by means of X-ray photon fluctuation spectroscopy. By analyzing the statistical distribution of photon arrival events, sub-nanosecond timescales could be probed. This work provides both insight into the stabilization of magnetic spin textures as well as a template for future sub-nanosecond experiments that are now available due to X-ray Free Electron Lasers.

GOE-08. Field-free spin-orbit torque switching of synthetic antiferromagnet through interlayer Dzyaloshinskii-Moriya interaction. *Z. Wang*[1,2], A. Fert[1,3], B. Koopmans[2] and W. Zhao[1] *1. Beihang University, Beijing, China; 2. Applied Physics, Eindhoven University of Technology, Eindhoven, Netherlands; 3. University of Paris-Saclay, Palaiseau, France*

In the post-Moore era, spintronic is one of the key technologies to break the bottleneck of high energy consumption of electronic devices[1]. However, as the process node moves on, conventional ferromagnet-based spintronic devices meet the superparamagnetic size limit. Under such circumstance, perpendicular synthetic antiferromagnets with high scalability and readability, strong immunity to external field and ultrafast dynamics, become a competitive choice for the next generation spintronics memory and logic devices[2]. Here, we propose a strategy to energy efficiently operate their magnetic order by spin orbit torque (SOT) under zero external field through the introduction of interlayer Dzyaloshinskii–Moriya interaction (DMI)[3,4]. By macro-spin simulation, we show that the speed of field-free switching increases with the in-plane mirror asymmetry of injected spins. We experimentally observe the existence of interlayer DMI in our SAF sample by an azimuthal angular dependent anomalous Hall measurement. Field-free switching is accomplished in such a sample and the strength of the effective switching field demonstrates its origin from interlayer DMI. Compared with previous field-free switching solutions, the performance of SOT device is well preserved. Our work pave the way for a wide range of potential high performance SOT devices[5].

1 Z. Guo, J. Yin, Y. Bai et al., Proceedings of the IEEE., vol.109, p.8, (2021) 2 R. A. Duine, K. J. Lee, S. S. P. Parkin, M. D. Stiles, Nature Physics., Vol.14, p.217–219 (2018). 3 D. Han, K Lee, J Hanke et.al., Nature Materials., Vol.18, p.703–708 (2019) 4 A. Fernández-Pacheco, et al., Nature Materials., Vol.18, p.679–684 (2019). 5 Z. Wang, P. LI, Y. Yao et al., https://arxiv.org/abs/2205.04740, (2022)

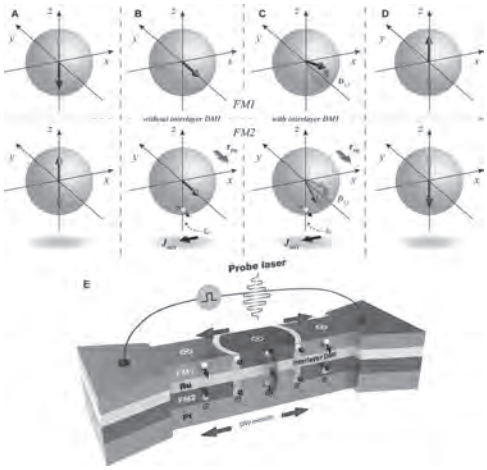

Schematic illustration of SAF field-free SOT switching through interlayer DMI. (A-D) Spin textures' evolution with time during the application of a SOT current pulse along -x. (E) A sketch of the experimental setup where the switching mechanism under a domain nucleation and propagation regime is indicated. The probe laser is used to detect the MOKE signal in our experiment.

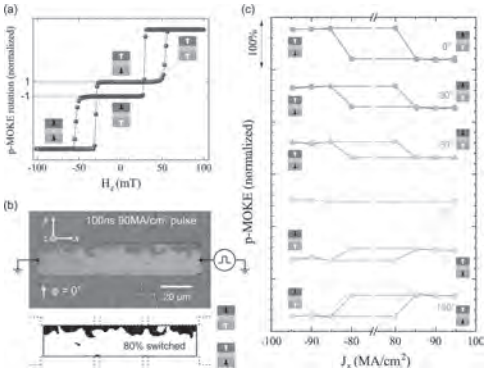

Field-free SOT switching detected by optical Kerr measurement. (A) Normalized p-MOKE signal of the studied film. (B) Kerr image after the application of a current pulse. The switching area is counted from the composite image below. (C) Summarization of current induced switching behavior as a function of azimuthal direction.

GOE-09. Spin Dynamics, Loop Formation, and Cooperative Reversal in Artificial Quasicrystals with Tailored Exchange Coupling.
V.S. Bhat[1], S. Watanabe[2], F. Kronast[3], K. Baumgaertl[2] and D. Grundler[2,4]
1. International Research Centre MagTop, Institute of Physics, Polish Academy of Sciences, Warsaw, Poland; 2. Laboratory of Nanoscale Magnetic Materials and Magnonics, Institute of Materials (IMX), Ecole Polytechnique Federale de Lausanne (EPFL), Lausanne, Switzerland; 3. Helmholtz-Zentrum Berlin fur Materialien und Energie, Berlin, Germany; 4. Institute of Electrical and Micro Engineering (IEM), Ecole Polytechnique Federale de Lausanne (EPFL), Lausanne, Switzerland

Aperiodicity and un-conventional rotational symmetries allow quasicrystalline structures to exhibit unprecedented physical and functional properties [1-4]. We report broadband spin-wave spectroscopy and X-ray photoemission electron microscopy on different quasicrystal lattices consisting of ferromagnetic $Ni_{81}Fe_{19}$ nanobars arranged on aperiodic Penrose and Ammann tilings with different exchange and dipolar interactions. The width w of nanobars, their thickness, and inner vertex spacing were kept at 120 nm, 25 nm, and 810 nm, respectively. We varied the lengths D of nanobars from sample to sample between 810 nm and 408 nm. We imaged the magnetic states of partially reversed quasicrystals and analyzed their configurations in terms of the charge model, geometrical frustration, and the formation of flux-closure loops. Only the exchange-coupled lattices are found to show aperiodicity-specific collective phenomena and non-stochastic switching. Both exchange and dipolarly coupled quasicrystals show magnonic excitations with narrow linewidths in minor loop measurements. Thereby reconfigurable functionalities in spintronics and magnonics become realistic. Acknowledgment: The research was supported by the Swiss National Science Foundation via Grant No. 163016. We thank HZB for the allocation of synchrotron radiation beamtime. V.S. Bhat acknowledges support from the foundation for Polish Science through the IRA Programme financed by EU within SG OP Programme and National Science Center, Poland, via grant number UMO-2020/38/E/ST3/00578.

[1] Shechtman, D., Blech, I., Gratias, D. & Cahn, J. W. *Phys. Rev. Lett.* 53, 1951 (1984). [2] Goldman, A. I. *et al.* . *Nat. Mater.* 12, 714–718 (2013). [3] Penrose R. *The Mathematical Intelligencer* 2, 32 (1979). [4] Bhat, V. S. *et al. Phys. Rev. Lett.* 332, 111, 077201 (2013).

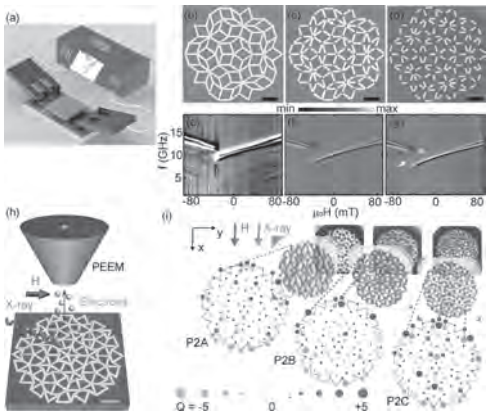

FIG. 1. (a) Sketch of broadband spin wave spectroscopy. SEM images showing 3rd generation (b) connected [P3A] (c) partially disconnected [P3B] (d) disconnected nanobars [P3C] on Penrose P3 lattices. Gray-scale spin wave spectra obtained on 8th generation (e) P3A, (f) P3B, and (g) P3C samples. (h) Sketch of the XPEEM imaging experiment performed on ferromagnetic quasicrystals. (i) (Back row) PEEM topography, XPEEM, and analyzed images of nanobars arranged on Penrose P2 lattices P2A (left), P2B (center), and P2C (right).

GOE-10. Micromagnetics simulations of transient nonlinear spin wave processes under parametric excitation. *M. Massouras*[1] and J. Kim[1]
1. Centre for Nanoscience and Nanotechnology (C2N), CNRS, Université Paris-Saclay, Palaiseau, France

Spin waves are elementary excitations in magnetic materials and their nonlinear dynamics has provided a rich subject of research over the past few decades. A particularly interesting aspect concerns parametric excitation, whereby the dynamics is driven by time-dependent fields along the longitudinal direction of the magnetization and spatially nonuniform modes can be populated by using the appropriate driving frequencies. Here, we examined using micromagnetic simulations with the MuMax3 code [1] the transient dynamics associated with parametric excitation in a YIG disk at finite temperatures. We first examine the thermal spectrum of eigen-excitations by integrating the stochastic dynamics over several microseconds, from which we determine the mode frequencies and profiles. We then focus on the parametric excitation of a subset of these modes, an example of which is given in the figure for an excitation frequency of f_0 = 5.8 GHz, corresponding to a mode at $f_0/2$ = 2.9 GHz. The power spectrum in the vicinity of this modes exhibits satellite peaks around the primary excitation, whose spatial profiles are shown. By using these profiles, we can determine the time dependence of the populations. In this example, we find that it takes over 100 ns for the primary mode population, which then saturates after about 200 ns. After this, we can observe the onset of secondary modes, followed by tertiary modes of lower intensity, with an oscillatory behavior in the intensity that suggests a periodic transfer of energy between modes. Our simulations allows us to gain insight into the initial transient magnon growth processes involved with parametric excitation, which might find some use in novel computational schemes. This work has supported by the Horizon2020 Framework Programme of the European Commission under contract number 899646 (k-Net).

[1] A. Vansteenkiste et al, AIP Advances, vol. 4, 107133 (2014).

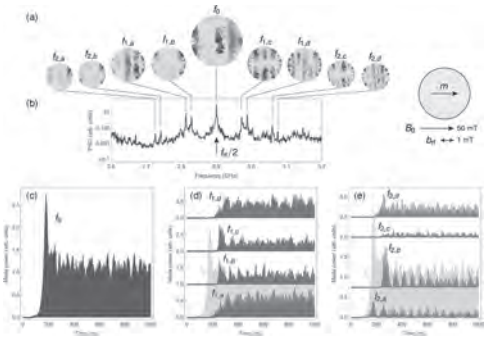

(a) Profiles of the primary (f_0), secondary ($f_{1,\alpha}$), and tertiary ($f_{2,\alpha}$) modes by parallel pumping at 5.8 GHz. (b) Power spectral density of the magnetization fluctuations in the frequency range of interest, with the corresponding modes indicated. The geometry is shown on the inset on the right. (c,d,e) Mode power as a function of time for the (c) primary and (d,e) secondary modes.

GOE-11. Single-Layer Vertically Graded Fe-Ni Films with Low Damping. *R.E. Maizel*[1], S. Wu[1], P.P. Balakrishnan[2], A.J. Grutter[2], C. Kinane[3], A. Caruana[3], P. Nakarmi[4], B. Nepal[4], D.A. Smith[1], J.L. Jones[1], W.C. Thomas[1], T. Mewes[4] and S. Emori[1] *1. Physics, Virginia Polytechnic Institute, Blacksburg, VA, United States; 2. Center for Neutron Research, National Institute of Standards and Technology, Gaithersburg, MD, United States; 3. ISIS-Neutron and Muon Source, STFC Rutherford Appleton Laboratory, Didcot, United Kingdom; 4. Physics and Astronomy, University of Alabama, Tuscaloosa, AL, United States*

Energy-efficient spintronic memories and oscillators require a large spin-orbit torque (SOT) and low effective damping for exciting magnetic precession. Conventional SOT-driven bilayers, consisting of a heavy metal and

an ultrathin ferromagnet (e.g., ~1 nm), suffer from high damping due to interfacial spin pumping and scattering. Recently, SOTs have been reported in thicker (~10 nm) single-layer ferromagnetic films with vertical compositional gradients [1-3]. We hypothesize that thick vertically graded ferromagnets can also enable low damping, potentially coexisting with substantial SOTs. Here, we examine the impact of intentional compositional gradients on damping and SOTs, specifically in graded films consisting of two ferromagnetic elements: Fe with low intrinsic damping [4] and Ni with sizable spin-orbit coupling [5]. We grew 10-nm-thick graded and homogeneous Fe-Ni films by continuously tuning the sputtering powers on Fe and Ni sources [Fig. 1(a-c)]. The targeted vertical compositional and magnetic gradients are confirmed and quantified by polarized neutron reflectometry. In-plane broadband ferromagnetic resonance (FMR) [Fig. 1(d)] points to low *effective* damping parameters of ≈0.0045 for the graded films, comparable to ≈0.0038 for the homogenous film. Out-of-plane FMR [Fig. 1(e)] reveals *intrinsic* damping parameters of ≈0.0032 for both the graded and homogenous Fe-Ni films. These FMR results indicate that low damping is maintained despite the steep, intentional vertical inhomogeneity. From spin-torque FMR measurements on a graded sample, we detect a modest (at most ≈2%) linear change in the FMR linewidth with a DC current density of 1×10^{11} A/m^2 [Fig. 2], suggesting a small damping-like SOT. Our findings constitute a step toward understanding and engineering low-damping single-layer ferromagnetic films for SOT-driven applications.

[1] Liu, L., Yu, J., Gonzalez-Hernandez, R., Phys Rev. B., Vol. 101, p. 220402 (2020) [2] Tang, M., Shen, K., Xu, S., Advanced Materials, Vol. 32, p. 2002607 (2020) [3] Zhu, L., Ralph, D. C., & Buhrman, R. A. Advanced Functional Materials p. 2103898 (2021) [4] Wu, S., Smith, D.A., Nakarmi, P., et. al., Phys Rev. B., Vol, 105, p. 174408 (2022) [5] Du, C., Wang, H., Yang, F., et. al., Phys Rev. B., Vol. 90, p. 140407 (2014)

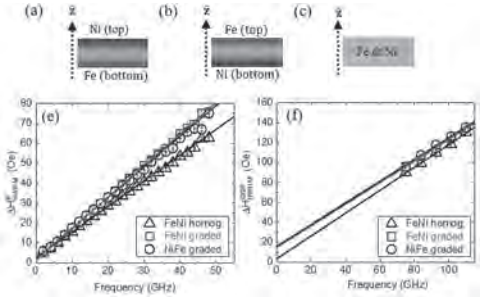

Fig. 1: (a,b) Schematics of (a) FeNi graded, (b) NiFe graded, and (c) FeNi homogeneous films. (d,e) Frequency dependence of (d) in-plane and (e) out-of-plane FMR linewidth for homogeneous and graded Fe-Ni films.

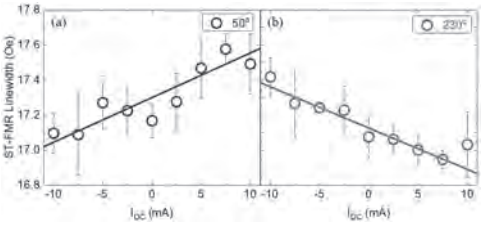

Fig. 2: DC bias current dependence of spin-torque FMR linewidth for 10-μm-wide graded NiFe strip at 7 GHz, magnetized at in-plane angle (a) 50° and (b) 230°.

GOE-12. Ultra-fast spin waves with few mm-long decay length in canted antiferromagnet Hematite (α-Fe_2O_3). *M. Hamdi*[1], F. Posva[1] and D. Grundler[1,2] *1. Institute of Materials, Laboratory of Nanoscale Magnetic Materials and Magnonics, École Polytechnique Fédérale de Lausanne (EPFL), CH-1015 Lausanne, Switzerland; 2. Institute of Electrical and Micro Engineering, Laboratory of Nanoscale Magnetic Materials and Magnonics, École Polytechnique Fédérale de Lausanne (EPFL), CH-1015 Lausanne, Switzerland*

Low magnetic damping and high group velocity of magnons are two crucial parameters for functional magnonic devices with low-power computation. The first one determines losses and the latter is responsible for the processing speed. These two combined determine the decay length of the magnon, which is of fundamental importance for realistic magnonic devices. We report the two parameters for a bulk Hematite crystal. We determine the magnetic damping by means of VNA-FMR technique (Fig. 1) to be 1.1×10^{-5}. This value is almost 3 times smaller than that of bulk YIG (3×10^{-5}) [1], which has been appreciated to be the lowest damping material for magnonics applications at room temperature so far. We measure the magnon dispersion by means of wave vector (k)-resolved inelastic Brillouin Light scattering (Fig. 2a). Fitting the BLS peak maxima with the Fink formula [2], we obtain the dispersion relation of magnons (Fig. 2b) and obtain their group velocity (Fig. 2c). For the k-values of up to 2.5 rad/μm (accessible by nano-scale coplanar waveguides (CPWs)), we observe a group velocity of 10 km/s. Using the damping and group velocity values, we obtain a magnon decay length of 6.3 mm for magnons with wave number 2.5 rad/μm, which is one orders of magnitude larger than that of YIG. Our results open a new pathway for more efficient magnonic devices using Hematite instead of YIG. The work is supported by SNSF via grant 177550.

[1] M. C. Onbasli, A. Kehlberger, D. H. Kim, *et. al.*, APL Mater., Vol. 2, p. 106102 (2014) [2] H. J. Fink, Phys. Rev., Vol. 133, p. A1322 (1964)

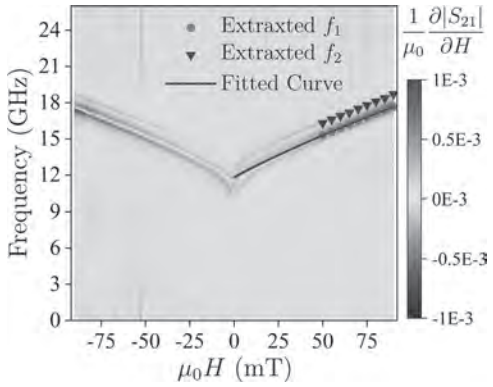

Figure 1. Color-coded neighbor subtracted VNA-FMR spectra for a Hematite crystal obtained using a CPW in flip-chip configuration. The static magnetic field is applied in the A-Plane and perpendicular to the C-axis of the crystal. The rf-magnetic field of the CPW is parallel to C-axis.

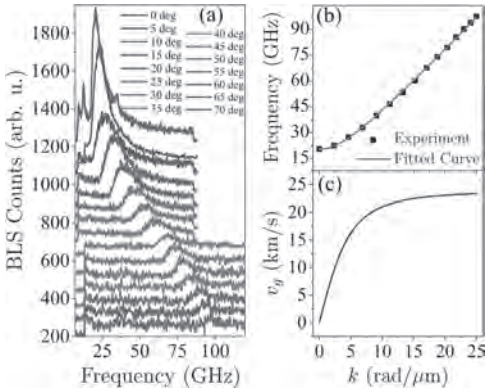

Figure 2. (a) BLS spectra measured on a Hematite crystal with the same applied field direction as in Fig. 1 measured by a green laser (532 nm) in back reflection geometry. Legends indicate the angle of the incident beam with respect to the normal of the sample, which is the A-axis of the crystal. (b) Dispersion relation obtained by considering the peak maximum in (a) and the corresponding *k*-value to the angles in legends of (a). (c) The magnon group velocity determined by the derivative of the magnon dispersion shown in (b).

GOE-13. Study on magnetization dynamics modulated by spin-orbit-torque using rectifying planar Hall effect. *A. Yamaguchi*[1], Y. Utsumi[1], N. Matsumoto[2], W. Yoshikawa[2] and Y. Fujii[2] *1. University of Hyogo, Kamigori, Japan; 2. KRI, Kyoto, Japan*

The modulation of magnetization dynamics has attracted much attention for not only fundamental research but also application such as data processing and oscillators. It has been discovered that magnetization dynamics can be induced by spin transfer toque (STT) and spin-orbit-torque (SOT). The STT is exerted on the magnetization due to the spin angular momentum transfer, and the SOT occurs at the bilayer comprising a ferromagnetic metal (FM)/nonmagnetic heavy metal (HM).[1] In this study, using the rectifying planar Hall effect (PHE), we investigate the SOT-induced magnetization dynamics in the multilayer consisting of HM/FM/Antiferromagnetic layer (AFM)/FM. Samples were pattered as the Hall bar device on a SiO_2/Si substrate were fabricated via microfabrication technique based on the lift-off method using magnetron sputtering process and electron beam lithography, as shown in Fig. 1. We fabricated the following system comprising 25-nm-thick $N_{81}Fe_{19}$/3-nm-thick NiO/5-nm-thick $Ni_{81}Fe_{19}$/Pt electrode on the substrate. An external magnetic field was applied at an angle θ from the one axis of the cross-type electrode, which was fixed parallel along to rf + dc electric current, as shown in Fig. 1. To measure the device, a ground-signal-ground (GSG)-type microwave probe was connected to the electrode. Using a home-made automatic rotating magnetic field application system, we evaluate the simultaneous magnetoresistance and PHE properties as a function of θ. Figures 2(a) shows a typical rectifying PHE voltage spectrum obtained at θ = 15°. The magnetic field angle dependences of these rectifying voltages are found to be in good agreement with the analytical prediction curves of cos2θcosθ. [2] Figure 2(b) displays the resonance frequency as a function of dc current, I_{dc}. The resonance frequency is linearly decreased with increasing I_{dc}. Full width at Half Maximum (FWHM) is also linearly modulated by the application of I_{dc}. These results indicate that the magnetization dynamics can be modulated by the spin current in the multilayer structure.

[1] X. Qiu, K. Narayanapillai, Y. Wu, P. Deorani, D. –H. Yang, W. –S. Noh, J. H. Park, K. –J. Lee, H. –W. Lee, and H. Yang, *Nat. Nanotechnol*. 10, 333 (2015). [2] A. Yamaguchi, A. Hirohata, B. Stadler, *Nanomagnetic Materials: Fabrication, Characterization and application*, Elsevier, 2021.

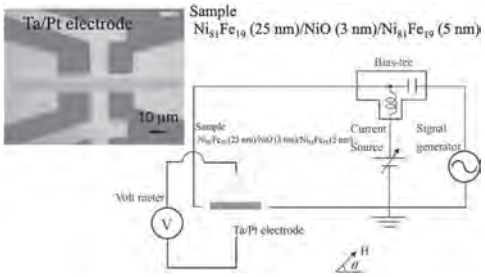

Figure 1 Schematic circuit of measurement and optical micrograph of system.

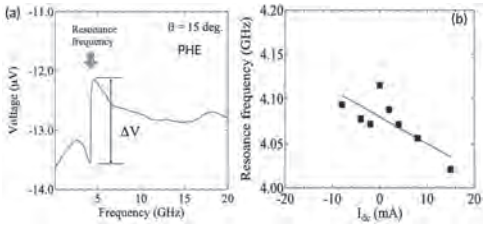

Figure 2(a) Typical rectifying PHE spectrum obtained at θ=15°. (b) dc current dependence of resonance frequency.

INVITED PAPER

GOE-14. Freezing and thawing magnetic droplet solitons. *M. Ahlberg*[1], S. Chung[2], S. Jiang[3], A. Frisk[1], M. Khademi[4], R. Khymyn[1], A.A. Awad[1], Q. Le[1], H. Mazraati[5], M. Mohseni[4], M. Weigand[6], I. Bykova[6], F. Groß[6], E. Goering[6], G. Schütz[6], J. Gräfe[6] and J. Åkerman[1] *1. University of Gothenburg, Gothenburg, Sweden; 2. Korea National University of Education, Cheongju, The Republic of Korea; 3. Northwestern Polytechnical University, Xi'an, China; 4. Shahid Beheshti University, Tehran, The Islamic Republic of Iran; 5. KTH Royal Institute of Technology, Stockholm, Sweden; 6. Max Planck Institute for Intelligent Systems, Stuttgart, Germany*

We use nanocontact spin-torque oscillators (STNOs) to explore the applied field and current dependence of magnetic droplets. These dissipative solitons are found in magnetic layers with perpendicular anisotropy, and they are inherently dynamic and characterized by a core of reversed spins surrounded by a precessing perimeter [1, 2, 3, 4]. The precession frequency lies between the ferromagnetic and Zeeman resonances, but the droplet is also prone to drift which gives additional dynamics [5, 6]. Orthogonal pseudo-spin-valves are usually used in experiments to harvest a strong magnetoresistive dynamic signal [2, 3, 5, 6], but here we use an all-perpendicular layout to study the otherwise inaccessible low field region. Electrical measurements reveal that the droplet transforms, freezes, into a static bubble at low fields. Figure 1 illustrates the electrical characteristics of the different states. The resistance is similar for the droplet and the bubble (Fig. 1a), but the difference in noise level is striking (Fig. 1b) and demonstrates the bubble's static nature. Once formed, the bubble is stable without a sustaining current. Furthermore, the droplet-to-bubble transition is fully reversible, and the bubble can thaw back to a droplet at sufficient high field and current. The findings are corroborated by X-ray microscopy, which images the magnetic states during the freezing. Experimental data together with simulations identify pinning as the main mechanism behind the bubble stability.

[1] Hoefer et al., *Theory for a dissipative droplet soliton excited by a spin torque nanocontact* Phys. Rev. B 82, 054432 (2010) [2] Mohseni et al., *Spin Torque–Generated Magnetic Droplet Solitons* Science 339, 1295 (2013) [3] Chung et al., *Spin transfer torque generated magnetic droplet solitons (invited)* J. Appl. Phys 115, 172612 (2014) [4] Chung et al., *Direct Observation of Zhang-Li Torque Expansion of Magnetic Droplet Solitons* Phys.

Rev. Lett. 120, 217204 (2018) [5] Xiao et al., *Parametric autoexcitation of magnetic droplet soliton perimeter modes* Phys. Rev. B 95, 024106 (2017) [6] Chung et al, *Magnetic droplet nucleation boundary in orthogonal spin-torque nano-oscillators* Nature Com. 7, 11209 (2016)

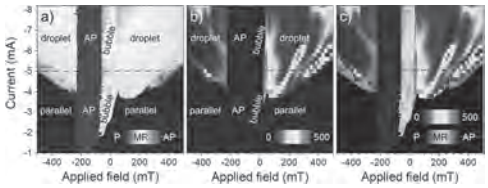

Figure 1: Phase diagrams based on the resistance and the microwave noise. (a) STNO resistance and (b) integrated (0–0.5 GHz) microwave noise level as a function of field and current. (c) shows the noise level in (b) overlaid on the resistance in (a) displayed using a gray scale highlighting intermediate resistance levels indicative of droplets/bubbles. The parallel (P) and antiparallel (AP) states are easily discernible in the MR-map (a) as dark blue and dark red, while both the droplet and the bubble are characterized by intermediate resistance in green–yellow. The stark difference between the droplet and the bubble is revealed in the noise spectrum (b), where the stability of the bubble is manifested. Note however that the light-blue flanges in (a) correspond to a different droplet regime not captured in the microwave signal presented in (b).

Session GPA
MAGNETIZATION DYNAMICS VI
(Poster Session)

Joseph Sklenar, Co-Chair
Wayne State University, Detroit, MI, United States
Shuyuan Shi, Co-Chair
Beihang University, Beijing, China

GPA-01. Variation of Gilbert damping constant via interface induced magnetic anisotropy in LSMO/PMN-PT heterostructures. A. Das[1], *M. Mrinalini*[1], T. Usami[2], S. Pati[2], T. Taniyama[2] and V. Gorige[1] *1. School of Physics, University of Hyderabad, Hyderabad 500046, India; 2. Department of Physics, Nagoya University, Furo-cho, Chikusa-ku, Japan*

The field of magnonics is emerging at blistering pace due to its promising room-temperature applications in logic-based devices at low-power consumption. In view of this, the exploration of suitable ferromagnetic (FM) $La_{0.67}Sr_{0.33}MnO_3$ (LSMO) and ferroelectric (FE) $Pb(Mg_{0.33}Nb_{0.67})O_3$-$PbTiO_3$ (PMN-PT) magnetoelectric (ME) heterostructures is of prime interest due to their intimate interface contact [1]. In the present work, a 50-nm-thick LSMO was grown on PMN-PT(001) and PMN-PT(111) single crystals by using pulsed laser deposition. The epitaxial nature of LSMO is confirmed by x-ray diffraction data. The static and dynamic magnetic response of LSMO/PMN-PT is studied by performing magnetization (*M*) and ferromagnetic resonance (FMR) measurements. Due to strong ME coupling at the interface, the LSMO/PMN-PT(001) shows four-fold symmetry of magnetic anisotropy (MA) whereas LSMO/PMN-PT(111) shows isotropic behaviour (see Fig. 1). The observation can be interpreted on the basis of coupling between the resultant polarisations of PMN-PT and the net *M* vector of LSMO [2]. To know the effect of ME-induced MA on the magneto-dynamic response of LSMO, FMR measurements were carried. The FMR data are fitted with the Kittel's equation and obtained the Gilbert damping constant (α), which is a key parameter for spin-wave (SW) dynamics, is in the order of 10^{-2}. As the LSMO/PMN-PT(001) is anisotropic in nature, α is found to be smaller along the hard axis than the easy direction. On the other hand, the LSMO/PMN-PT(111) is isotropic in nature, so that the α remains same in all directions. In order to explore the electric (*E*-) field effect on the spin dynamics, FMR data are collected for the LSMO/PMN-PT poled (E = ±10 kV/cm) samples, where a significant reduction in α values is seen. From these combined results, we conclude that α depends strongly on MA of the films other than its surface roughness, defects, etc. [3]. Although more investigations are required, this particular work hints that it becomes possible to realize *E*-field controlled SWs in FM/FEs to develop futuristic magnonic devices.

[1] D. Pesquera, E. Khestanova, M. Ghidini, S. Zhang, A. P. Rooney, F. Maccherozzi, P. Riego, S. Farokhipoor, J. Kim, X. Moya, M. E. Vickers, N. A. Stelmashenko, S. J. Haigh, S. S. Dhesi, and N. D. Mathur, *Nat. Commun*. 11, 3190 (2020). [2] G. Venkataiah, Y. Shirahata, M. Itoh, and T. Taniyama, *Appl. Phys. Lett.* 99, 102506 (2011). [3] K. Yamada, K. Kogiso, Y. Shiota, M. Yamamoto, A. Yamaguchi, T. Moriyama, T. Ono, and M. Shima, *J. Magn. Magn. Mater*. 513, 167253 (2020).

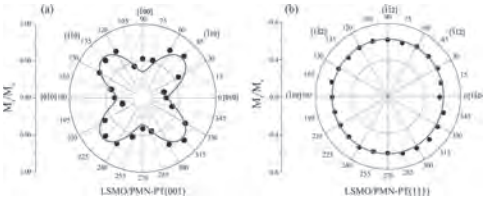

Fig.1. The polar plots of normalized remanent magnetization (M_r/M_s) of (a) LSMO/PMN-PT(001) and (b) LSMO/PMN-PT(111) heterostructures.

GPA-02. Spin Waves in Unsaturated Single-Layered Ferromagnetic Nanorings with Interfacial Dyzaloshinski-Moriya Interactions. *B. Hussain*[1] and M.G. Cottam[1] *1. Physics and Astronomy, University of Western Ontario, London, ON, Canada*

A distinctive feature of ferromagnetic nanorings, where the thickness is small compared with the inner and outer radii, is the existence of two states of magnetic ordering [1], depending typically on the interplay of the applied magnetic field with the exchange and dipole-dipole interactions. These states are the low-field vortex state and the higher-field bidomain or onion state. In recent work [2] we analyzed the spin waves (SWs) in nanorings using a microscopic, or Hamiltonian-based, formalism to calculate the discrete frequencies and spatially-dependent intensities of the quantized SWs. The formalism is applicable to both the vortex and onion states, as well as to the field-induced switching. Here we report on the novel SW results obtained when the antisymmetric Dyzaloshinski-Moriya (DM) interactions are taken into account. Although these interactions may typically be rather small, it has emerged in recent years that they can be greatly enhanced when a thin ferromagnetic layer is interfaced with certain heavy metals as a substrate material [3]. Numerical applications including interfacial DM interactions are made here to permalloy nanorings with realistic magnetic parameter values and sizes (outer diameters ranging up to 200 nm), generalizing the methodology in [2]. In Figs. 1 and 2 we show some results obtained for the lowest SW frequencies with and without the inclusion of interfacial DM interactions, respectively. It is found in our model that the transition field value between vortex and onion states is shifted by the inclusion of DM interactions. Significantly, the SW frequencies are also modified with the effects being largest in the onion state close to the transition field.

[1] C. A. F. Vaz et al., J. Phys. Condens. Matter, Vol. 19, p.255207 (2007) [2] B. Hussain and M. G. Cottam, J. Phys. D, Vol. 54, p.165002 (2021) [3] J.-H. Moon et al., Phys. Rev. B, Vol. 88, p.184404 (2013)

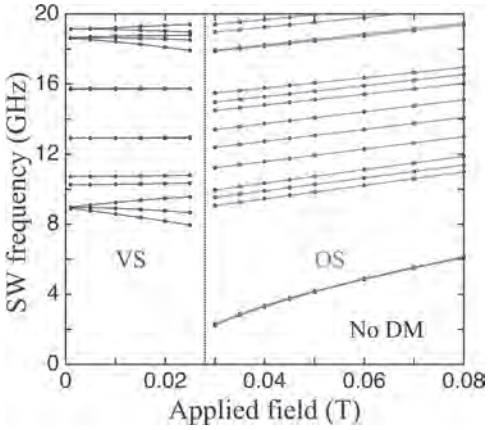

Fig. 1. SW frequencies plotted versus the applied magnetic field for a single-layered permalloy nanoring with outer radius 60 nm, inner radius 24 nm, and thickness 4 nm, for the case when DM interactions are absent. The dotted vertical line represents the transition field between the low-field vortex state (VS) and the higher-field onion state (OS).

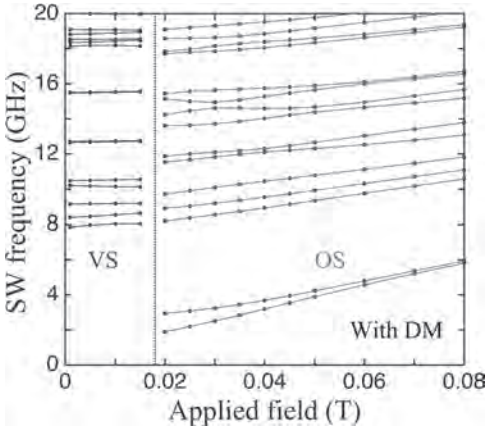

Fig. 2. The same as in Fig. 1, but with the effects of interfacial DM interactions now included. The transition field and the SW frequencies are seen to be modified.

GPA-03. Probing magnon-phonon non-equilibrium in thulium iron garnets by optical reflectometry. G. Lee[1], T. Lee[1], P.C. Van[2], D. Kim[1], M. Seo[1], Y. Jo[3], J. Jeong[2] and *K. Kim[1] 1. Physics, Korea Adavanced Institute of Science and Technology, Daejeon, The Republic of Korea; 2. Material Science and Engineering, Chungnam National University, Daejeon, The Republic of Korea; 3. Division of Scientific Instrumentation, Korea Basic Science Institute, Daejeon, The Republic of Korea*

Understanding the interaction between magnons and phonons is the key for magnonic applications. In this work, we develop an optical reflectometry to investigate the population of magnons and phonons. Unlike the Brillouin light scattering (BLS) spectroscopy [1, 2], where the sophisticated tandem Fabry-Perot interferometer and single frequency laser with sharp line width are necessary, we use a simple laser-based reflectometry to measure the Kerr rotation and reflectance which are sensitive to the magnon and phonon, respectively. Using this optical technique, we study the spatial distribution of magnons and phonons in a thulium iron garnet (TmIG) under the temperature gradient generated by current induced Joule heating. Both the magnon and phonon populations are decaying exponentially as a function of distance from the electrical heating line. We find that the characteristic decay length of the population of magnons and phonons are different, indicating the non-equilibrium between magnons and phonons in TmIG. Moreover, the characteristic length of magnon population decreases as increasing the heating power or decreasing the magnetic field, while that of phonon population is almost constant. The different characteristic length of magnon and phonon population is attributed to the enhanced non-linear magnon scattering processes at high magnon population regime. Our work revealing the magnon-phonon non-equilibrium in TmIG will motivate the magnonic researches where the role of the magnon-phonon interaction is crucial [3].

[1] M. Agrawal., *et al.*, *Phys. Rev. Lett*. 111, 107204 (2013). [2] K. An., *et al.*, *Phys. Rev. Lett*. 117, 107202 (2016). [3] G.-H. Lee., *et al.*, *Appl. Phys. Lett*. 119, 152406 (2021).

GPA-04. Characterization of long-distance spin transport in antiferromagnetic NiO. *I. Sugiura*[1], Y. Kobayashi[1], Y. Shiota[1,2], T. Ono[1,2] and T. Moriyama[1,3] *1. Institute for Chemical Research, Kyoto University, Uji, Japan; 2. Center for Spintronics Research Network, Kyoto University, Uji, Japan; 3. PRESTO, Japan Science and Technology Agency, Kawaguchi, Japan*

Long-distance transmission of spin angular momentum in antiferromagnetic insulators has attracted much attention [1]. In our previous study, we investigated the spin transmission in NiO by the enhancement of the damping constant due to the spin pumping effect in NiO t_{NiO} nm/FeNi multilayer films. The results imply that the spin transmission length could be much greater than 100 nm [2]. In order to accurately determine the transmission length, the structure used in those measurements requires the NiO thickness t_{NiO} >> 100 nm because the pumped spin current diffuses in the film thickness direction. However, depositing such a thick NiO layer while maintaining the film quality is not practical. In this study, we devise a structure having the spin transmission in the lateral direction of the NiO layer as shown in Fig. 1 and characterize the damping constant enhancement with respect to the lateral length l_{NiO}. Multilayers of NiO 10 nm/FeNi 5 nm/Au 5 nm were fabricated on a single crystalline MgO substrate by magnetron sputtering. The epitaxial growth of the NiO was confirmed by the RHEED images. We performed the homodyne ferromagnetic resonance measurements for various l_{NiO}. From the l_{NiO} dependence of the damping constant obtained from the measurements, we attempted to derive the in-plane spin transmission length in the NiO.

[1] R. Lebrun *et al*., *Nature* 561, 222 (2018) [2] T. Ikebuchi *et al., Appl. Phys. Exp.* 14, 123001 (2021)

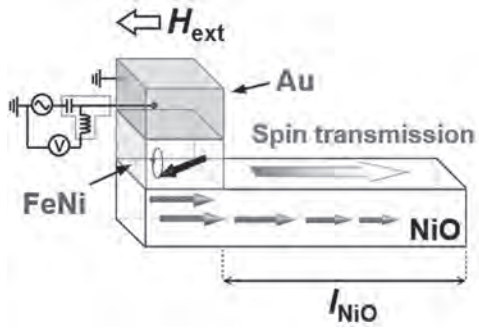

Fig. 1 Schematic illustration of the lateral device and measurement configuration

GPA-05. Magnetic Field Detection Using Spin Torque Nano-Oscillator Combined with Magnetic Flux Concentrators. *D. Tonini*[1], K. Wu[1,2], R. Saha[1] and J. Wang[1] *1. Department of Electrical and Computer Engineering, University of Minnesota, Minneapolis, MN, United States; 2. Department of Electrical and Computer Engineering, Texas Tech University, Lubbock, TX, United States*

In this work, we report the design of a spin torque nano-oscillator (STNO) combined with magnetic flux concentrators (MFCs) to improve the sensitivity of detecting magnetic fields, where the STNO consists of two out-of-plane (OP) ferromagnetic layers separated by a MgO insulating layer (see Fig. 1(a)) and the MFCs placed next to STNO are permalloy. We

carried out micromagnetic simulations on the spin-transfer torque (STT) induced magnetic dynamics in the free layer of STNO. Based on the Landau-Lifshitz-Gilbert (LLG) equation with STT term, the time evolved magnetization precession of the free layer is plotted in Fig. 1(b). First, we show that the ferromagnetic resonance frequency (FMR) of the free layer magnetization precession can be tuned by the charge current density and external magnetic fields. In addition, the FMR as a function of external magnetic field strength is also studied on STNO with and without MFCs, see Fig. 1(c). We observed a general suppression of the resonance frequency due to the damping effect of the magnetization induced by MFCs placed at different distances to the STNO (see Fig. 1(d)). The FMR shift of the STNO free layer magnetization as function of external magnetic field is summarized in Fig 1. (e). By placing MFCs next to STNO, the lowest detectable magnetic field strength is enhanced from 10 μT to 10 nT. It is concluded that MFCs improve the sensitivity of STNO to external fields due to the distortion caused by the magnetization damping. The results presented in this work could inspire the optimal design of STNO and MFC-based ultra-low magnetic field sensors.

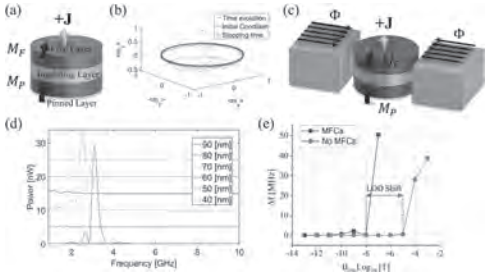

Fig. 1. (a) Schematic view of STNO with a diameter of 80 nm. Charge current is defined as +J and applied in the positive direction. (b) Evolution of the free layer magnetization resonating in-plane from the initial condition $<m_{x,y,z}> = (0, 0, 1)$. (c) Schematic view of MFCs placed next to STNO. (d) The distance between MFCs and STNO affects the resonance frequency. J=5e10 A/m². (e) FMR shift of the magnetization induced by an external magnetic field for an STNO with and without MFCs, where LOD stands for limit of detection. J=5e10 A/m², MFCs are placed at 70 nm to the STNO.

GPA-06. Ultra-thin high-quality magnetic insulator films. B. Elkhoury[1], *M. Haidar*[1] and S. Isber[1] *1. Physics, American University of Beirut, Beirut, Lebanon*

Due to fundamental limitations, the miniaturization of CMOS devices becomes very difficult, and alternative concepts that allow for higher storage density at low power are required [1]. Spin waves, the elementary low-energy excitations in magnetic systems, exist in the high-frequency regime and are considered a potential technology that can complement the CMOS devices. However, the common magnetic materials, such as Nickel, iron, cobalt, and their alloys used in devices are not ideal for spin-wave propagation due to their high magnetic losses, which translated into shorter propagation lengths. The solution lies in using materials with ultralow damping, such as yttrium iron garnet (YIG) [2-4]. Typically, YIG films are prepared by liquid phase epitaxy (LPE) with a thickness range of tens of microns which is not ideal for applications. In this study, we prepared ultra-thin YIG films with a thickness down to 30 nm by the pulsed laser deposition technique. We study the static and dynamic properties of the YIG films using a broadband ferromagnetic resonance (FMR) technique where we investigate the effect of the laser energy and the oxygen pressure on the saturation magnetization and the Gilbert damping in these films. We find that high-quality films are achieved at high laser energy and under high oxygen pressure. We report ultra-low damping ($\alpha = 2x\ 10^{-4}$) and M_s =0.2 T which approaches the recorded values of the bulk YIG films.

[1] V. V. Kruglyak et al., *J. Phys. D: Appl. Phys.* 43, 264001 (2010). [2] Y. Kajiwara et al., *Nature* 464, 262 (2010). [3] Y. Sun et al., *Phys. Rev. Lett.* 111, 106601 (2013). [4] M. Haidar et al., J. Appl. Phys. 117. 17D119, (2015).

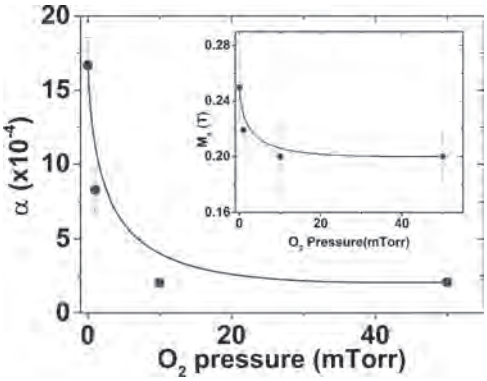

Variation of the Gilbert damping and the saturation magnetization (inset) as a function of the oxygen pressure for 30 nm yig films.

GPA-07. Magnon-drag observed via field-dependent measurements of thermopower in low-damping ferromagnetic alloy $Co_{25}Fe_{75}$. *M.R. Natale*[1], D. Wesenberg[1], E. Edwards[2], H. Nembach[2,3], J.M. Shaw[2] and B. Zink[1] *1. Physics and Astronomy, University of Denver, Denver, CO, United States; 2. Quantum Electromagnetics Division, National Institute of Standards and Technology, Boulder, CO, United States; 3. JILA, University of Colorado Boulder, Boulder, CO, United States*

Recent experimental and theoretical work has focused new interest on how magnons can influence the transport properties of metallic ferromagnets (FM). Here we demonstrate the influence the Gilbert damping parameter, α_{GD}, has on both the electron and magnon populations available for transport in two distinctly different Co_xFe_{1-x} alloys. The absolute Seebeck coefficient, α_{abs}, is measured for each of the films [1], and we compare to our calculated total thermopower, α_{tot}. To calculate the electronic and magnonic components, we employ a semi-classical approach; the classical free-electron model estimates the diffusive thermopower component, α_{Mott} [2], while we compute the relativistic magnon-drag component, α_{md}, based on the spin transfer mechanism [3,4]. From these results, we obtain quantitatively comparable measured Seebeck coefficients for both alloys, subsequently showing α_{md} dominates the low-damping sample, while the alloy with normal damping follows α_{Mott} well over our temperature regime. We further present anisotropic magnetoresistance (AMR) [5] and magnetothermopower (MTP) [6] measurements over the temperature range of interest from 125 to 250 K, where we previously reported a significant non-electronic thermal conductivity [7]. AMR measurements align with expected FM metal behavior, while MTP shows a field-dependence as $H \parallel \nabla T$ in the low-damping FM metal. We estimate the magnitude of this behavior using the relationship between $\alpha(H,\perp)$ and the inverse resistance, R^{-1}, and calculated the expected $\alpha(H,\parallel)$ [6]. This argues for an additional field-direction dependent contribution to thermopower, which could be a novel form of magnon-drag.

1. S. J. Mason, A. Hojem, and D. J. Wesenberg, *Journ. of Appl. Phys.* 127 (2020). 2. M. Jonson and D. Mahan, *Phys. Rev. B* 21 (1980). 3. M. E. Lucassen, C. H. Wong, and R. A. Duine, *Appl. Phys. Let.* 99 (2011). 4. B. Flebus, R. A. Duine, and Y. Tserkovnyak, *EPL* 115 (2016). 5. J. Shi, S. S. Parkin, and L. Xing, *Journ. Of Mag. and Mag. Mater*. 125, (1993). 6. A. D. Avery, M. R. Pufall, and B. L. Zink, *Phys. Rev. B – Cond. Mat. and Mater. Phys*. 86,(2012). 7. M. R. Natale, D. J. Wesenberg, and E. R. Edwards, *Phys. Rev. Mater.* 5, (2021). 8. M. R. Natale, D. J. Wesenberg, and E. R. Edwards, *in preparation*

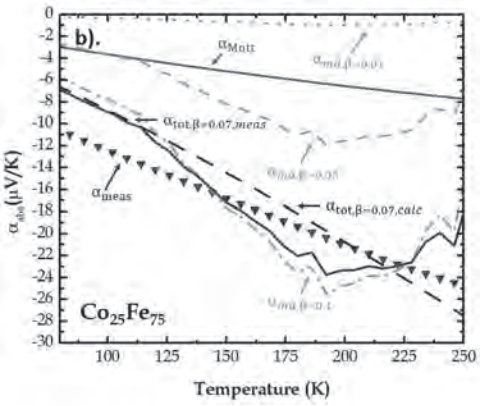

Fig. 1: Temperature dependence of absolute thermopower for $Co_{25}Fe_{75}$ alloy. Calculated diffusive, α_{Mott}, (green), magnon-drag, α_{md}, (orange), and total thermopower, α_{tot}, (marron) overlayed with experimental measurements, α_{meas}, from 125-250K.

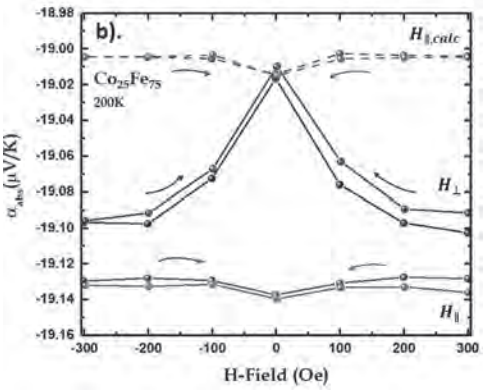

Fig. 2: MTP measurement for $Co_{25}Fe_{75}$ at 200K. $\alpha_{abs}(H)$ is measured in-plane for $H_{ext} \perp \nabla T$ and $H_{ext} \parallel \nabla T$. Curved arrows indicate the field sweep direction and are color coordinated to distinguish between field-orientation. Dotted lines are expected values.

GPA-08. Electrical detection of antiferromagnetic resonance modes by using 154 GHz gyrotron irradiation. *S. Funada*[1], T. Moriyama[1,2], K. Hayashi[3], T. Sano[3], K. Sugi[1], Y. Ishikawa[3], Y. Fujii[3], S. Mitsudo[3], M. Kimata[4], Y. Shiota[1,2] and T. Ono[1,2] *1. Institute for Chemical Research, Kyoto University, Uji, Japan; 2. Center for Spintronics Research Network, Kyoto University, Uji, Japan; 3. Research Center for Development of Far-Infrared Region, University of Fukui, Fukui, Japan; 4. Institute for Materials Research, Tohoku University, Sendai, Japan*

THz magnetization dynamics is a key property of antiferromagnets that could harness the THz forefront and spintronics. Recent advancements in THz measurement techniques have realized some of the key experiments on antiferromagnetic resonance [1,2]. However, the measurement principles used in those studies, such as the magneto-optical effect and resonant absorption, rely on the volume of the materials. Therefore, the same principle can hardly be applied for characterizing the dynamics of antiferromagnetic thin films which is a central interest when considering any antiferromagnetic integration devices. One of the solutions could be the DC voltage detection of the magnetic resonance resulting from a nonlinear coupling of a time-dependent induction current and a time-dependent magnetoresistance change associating with the magnetization dynamics [3]. Since both the magnetoresistance and the induction current are irrespective to the volume of the material, it is in principle possible to detect the dynamics in thin films. The only concern for this method is that it generally requires a sizable irradiation power of > mWatt, which is to be resolved by the gyrotron irradiation [4] that is introduced in this study. Test samples were made of ferrimagnetic $Gd_{1-x}Co_x$ films (20 nm) covered by Ta (3 nm) deposited on a Si substrate by magnetron sputtering. They were shaped into a 1.5 mm x 5 mm piece with electric leads connected on the longitudinal ends for measuring DC voltage. The sample is then placed at the end of a hollow waveguide carrying 154 GHz continuous electromagnetic wave with a nominal power of about 500 mW fed from the gyrotron apparatus. DC voltage measurements were carried out with sweeping external magnetic field. Figure 1 shows DC voltage measurements for $Gd_{0.39}Co_{0.61}$ film at various temperature. We observed a clear DC voltage peak (marked by the asterisk) and the peak shifts with varying the temperature, which are consistent with the temperature-dependent antiferromagnetic resonance modes of GdCo [5]. As the gyrotron frequency is scalable up to THz [4], our demonstration can be an important milestone toward the THz measurements for antiferromagnetic thin films.

[1] T. Moriyama, K. Hayashi and K. Yamada *et al.,* Phys. Rev. B, Vol. 101, p.060402 (2020). [2] T. Satoh, S.-J. Cho and R. Iida *et al.,* Phys. Rev. Lett., Vol. 105, p.077402 (2010). [3] W. G. Egan and H. J. Juretschke, J. Appl. Phys., Vol. 34, p.1477 (1963). [4] T. Idehara and S. P. Sabchevski, J. Infrared, Milli, Terahertz Waves, Vol. 38, p.62 (2017). [5] C.D. Stanciu, A. V. Kimel and F. Hansteen *et al.*, Phys. Rev. B Vol. 73, p.220402 (2006).

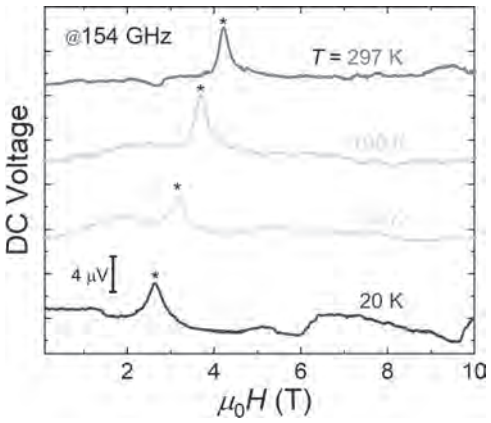

Fig. 1 DC voltage vs magnetic field.

GPA-09. Transient retrograde motion of spin wave-driven skyrmions in multilayer wave guides. *L. Huang*[1], G. Burnell[1] and C. Marrows[1] *1. University of Leeds, Leeds, United Kingdom*

Skyrmions are of great interest in spintronic devices because their small size and the high-speed motion when driven by a current or a spin-wave (SW). Skyrmion motion along a narrow track is important for racetrack-type spintronic devices, since a skyrmion moving along the propagation direction of an injected electrical or SW current (forward) is the means by which data are moving[1]. To design the devices, knowing how to adjust the skyrmion motion becomes important. We carried out simulations of SW driven skyrmion motion using OOMMF [2], with fixed parameters D = 1.5 mJ/m^2, M_S = 1004 kA/m, A = 3.6 pJ/m, and K_u = 1 MJ/m^3. We found that for tracks narrower than 50 nm the skyrmion always moves forwards. For wider tracks, the skyrmion will initially move both backward and close to the track edge, before moving forward at longer times once the track edge is reached, as shown in Fig 1. We attribute this to an additional repulsive force on the skyrmion from the track edge. For samples with Gilbert damping constant $\alpha > 0.06$, the skyrmion will move forward without retrograde motion. The Thiele equation is a widely-used way to analyse skyrmion motion. The SW driving force on a skyrmion is usually the SW scattering force [3], but the strength of the scattering and the energy change associated with changes in skyrmion size owing to absorbed SWs are hard to extract from magnetization data. Thus, we use the SW transmission T and reflection coefficients R to make an estimate of the forces involved. We can obtain T from the ratio of the SW amplitude downstream of the skyrmion and without skyrmion at same position. Similarly, we obtain R from the difference between magnetization data upstream of the skyrmion and without skyrmion. As an example, we consider the data from a simulation with track width w = 100 nm

and $\alpha = 0.03$. By Analysing *T* and *R*, the decrease in T after ~30 ns, shown in Fig.2, will reduce the effort that leads to the skyrmion moving backward. Meanwhile the increasing force from the sample edge also helps the skyrmion overcome the Spin-Ttansfer Torque between transmitted SW and skyrmion[4], allowing it to move forwards.

1. Sampaio, J., Cros, V. et al. *Nature Nanotech* 8, 839–844 (2013) 2. Donahue, M., Porter D. et al, *National Institute of Standards and Technology*(1999) 3. Zhang, X. *et al New J. Phys.* 19, 065001 (2017) 4. Yan, X., S. Wang et al. *Phys. Rev. Lett.* 107, 177207 (2011)

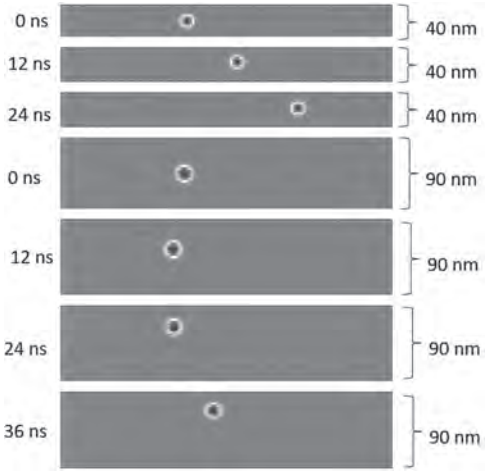

The snapshots of w = 40 nm, 90 nm tracks

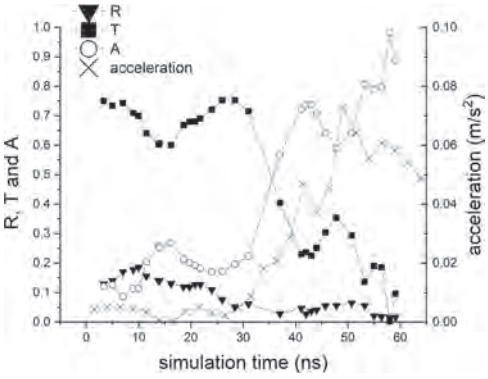

Time-dependent SW T, R, A and skyrmion acceleration data

GPA-10. Asymmetric Control of Spin Wave Propagation Behavior Using Vortex Chirality. *X. Zhang*[1], X. Yang[2], X. Ma[1,2], J. Shim[2,3], C. Song[4], H. Yu[5] and H. Piao[1,2] *1. China Three Gorges University, Yichang, China; 2. Yanbian University, Yanji, China; 3. POSTECH, Pohang, The Republic of Korea; 4. Tsinghua University, Beijing, China; 5. Beihang University, Beijing, China*

Spin waves (SWs) asymmetric propagation is receiving more and more attention because it can be developed in information and communication technology and can also be modulated asymmetrically[1,2]. In particular, SW asymmetric modulation based on spin texture has the advantages of reconfiguration and flexibility[3]. By design, it can meet the requirements of integration, miniaturization and low power consumption of devices. In our work, an asymmetric propagation behavior of SW in a cross-shaped ferromagnetic nanostructure with chiral magnetic vortex was investigated by means of micromagnetic simulations. We have found that the interaction between spin wave and chiral vortex leads to asymmetric propagation behavior of spin wave on nanostructures which is mainly controlled by the chiral vortex core gyromotion behavior dependent on the vortex core polarity, as shown in Fig1(a)-(d). And this behavior results in the intrinsic lower-frequency gyromotion of the vortex core (VC) with a higher-frequency-mode rotation, as shown in Fig1(e). It's very beneficial to the development and design of future magnonic logic devices based on chiral magnetic vortex.

[1] A. V. Chumak, P. Kabos, M. Wu, et al. IEEE T. Magn. 58(6), 0800172 (2022). [2] L. Sheng, J. Chen, H. Yu, Materials China 40(12), 939 (2021). [3] H.-K. Park, J.-H. Lee, J. Yang, and S.-K. Kim, J. Appl. Phys. 127, 183906 (2020).

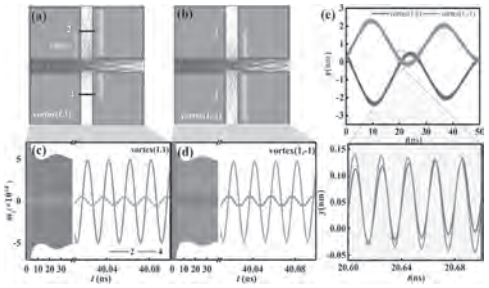

Fig.1 (a)-(d) Snapshots of SW distribution and mz-t curves for vortex (1,1) and vortex (1,-1). (e) The VC y-axis position changing with time.

GPA-11. Magnetocrystalline anisotropy energy and Gilbert damping of two-dimensional half-metallic RhX_2 (X = I, Br, Cl) ferromagnets: Density functional theory study. *S. Bhardwaj*[1], B.K. Kuanr[1] and R. Ghosh[2] *1. Special Centre for Nanonscience, Jawaharlal Nehru University, New Delhi, India, New Delhi, India; 2. Electronics and Communications Engineering, IIIT Delhi, India, New Delhi, India*

Two-dimensional (2D) intrinsic half-metallic ferromagnets (HMFs) are potential candidates for ultrathin spintronic device applications [1]. The understanding of magnetocrystalline anisotropy energy (E_{MCA}) and Gilbert damping (α) is required to determine their use in practical applications. In particular, the thermal stability and critical current of magnetization switching of spin-transfer-torque magnetic random-access memories highly depend on E_{MCA} and α [2]. Therefore, using density functional theory, we study the monolayer Rhodium dihalides family, RhX_2, where X= I, Br, Cl. First, we find that RhX_2 prefer 1T phase (octahedral symmetry) than the other possible 1H phase (trigonal prismatic symmetry). The ferromagnetic ordering is energetically favourable in RhX_2 monolayers. The Curie temperature of RhI_2, $RhBr_2$ and $RhCl_2$ crystals calculated using spin-wave theory (& Ising model) [3,4] is 182 (304) K, 92 (189) K and 17 (45) K respectively. We then calculate the spin-polarized electronic band structure which reveals wide intrinsic half-metallic gap (> 1.1 eV) in the down spin bands of RhX_2 monolayers. It results in 100% spin-polarization about the Fermi level and should prevent the spin-current leakage in nanoscale devices. The inclusion of spin-orbit coupling (SOC) does not affect the band's profile much and the half-metallic character remains intact. Moreover, the metallic nature arises mainly from the hybridization of Rh 4d-orbitals and X p-orbitals which are present on the Fermi level. The E_{MCA} and α which originate from SOC control the spin dynamics. We use force theorem [5] for E_{MCA} calculation and the results show substantial in-plane magnetic anisotropy in RhI_2 (-2.3 mJ/m^2) and $RhBr_2$ (-0.57 mJ/m^2) whereas small perpendicular anisotropy in $RhCl_2$ (0.04 mJ/m^2) [6]. To calculate α we employ Kambersky's torque-torque correlation model [7] and it comes out relatively low (2.1×10^{-2} to 4.0×10^{-3}). This work highlights the importance of 2D RhX_2 HMFs in fabrication of future spintronic devices.

[1] T. Song, X. Cai and M. W. Y. Tu, Science 360, 1214 (2018). [2] S. Ikeda, K. Miura and H. Yamamoto, Nat. Mater. 9, 721 (2010). [3] J. L. Lado and J. Fernández-Rossier, 2D Mater. 4, 035002 (2017). [4] J. M. Dixon, J. A. Tuszynski and E. J. Carpenter, Physica A 349, 487 (2005). [5] D. Li, C. Barreteau, M. R. Castell and F. Silly, Phys. Rev. B 90, 205409 (2014). [6] Ram Krishna Ghosh, Ashna Jose and Geetu Kumari, Phys. Rev. B 103, 054409 (2021). [7] K. Gilmore, Y. U. Idzerda and M. D. Stiles, Phys. Rev. Lett. 99, 027204 (2007).

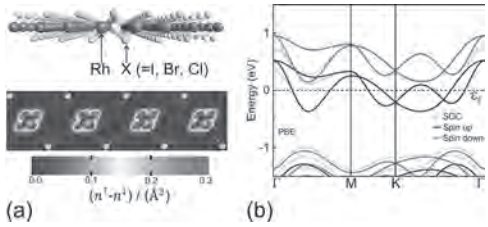

Fig.1 a) Side view of 1T-RhX_2 monolayer and difference between spin charge densities about Rh and I atoms, b) Electronic band structure of RhI_2.

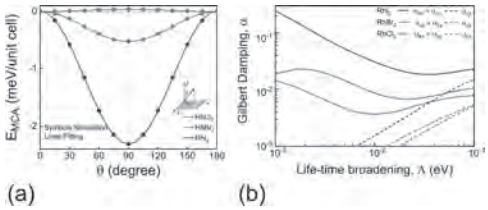

Fig.2 a) E_{MCA} vs. θ, b) Gilbert damping tensors vs. life-time broadening.

GPA-12. Dipole-Exchange Spin Waves in 2D van der Waals Ferromagnetic Films and Stripes. *B. Hussain*[1] and M.G. Cottam[1] *1. University of Western Ontario, London, ON, Canada*

The recent discovery of van der Waals magnets has heralded exciting new possibilities in two-dimensional (2D) magnetism. These materials can be fabricated as monolayers, often with the magnetic ions lying on a 2D honeycomb lattice (see [1] for a review). Here we present a spin-wave (SW) theory that includes dynamic effects of the long-range dipole-dipole interactions for monolayers of van der Waals ferromagnets. The dipolar interactions provide an additional interaction in these materials, along with Ising and Heisenberg exchange interaction and single-ion anisotropies in previous SW calculations (see e.g. [2]) that typically stabilize the 2D magnetic ordering. Analytical results for the linearized SW energies are obtained for ferromagnets in two different geometries: complete films and finite-width stripes (or ribbons). In both cases it is found that the inclusion of the dipole-dipole interactions leads to a shift and sometimes a splitting of the SW modes in the van der Waals structure. In the latter case, with the edges assumed to be along the zigzag lattice directions, the dipole-dipole interactions are found to play a role (as well as perturbations in the edge exchange) in modifying the localized edge spin waves. A numerical example of the dispersion relations for the discrete SWs for a stripe sample of ferromagnetic CrI_3 is given in Fig.1. The stripe width is expressed in terms of the number N of lines of Cr atoms in the honeycomb structure (with interpenetrating A and B sublattices). Here the results are characterized by a wave-vector component k_y along the stripe length. Our formalism also enables the bulk-like and localized edge SW amplitudes (including phase) to be calculated, and an example is given in Fig. 2.

[1] M. Blei et al., App. Phys. Revs., Vol. 8, p.021301 (2021) [2] V. Mkhitaryan and L. Ke, Phys. Rev. B, Vol. 104, p.064435 (2021)

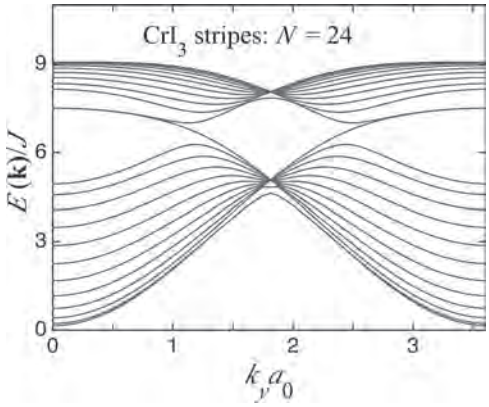

Fig. 1. Dispersion relations for discrete SW modes in a CrI_3 monolayer stripe with 24 lines of Cr atoms. The ratio of SW energies E(k) to the nearest-neighbor exchange parameter J is plotted versus longitudinal wave-vector component $k_y a_0$ (with a_0 the separation between Cr atoms).

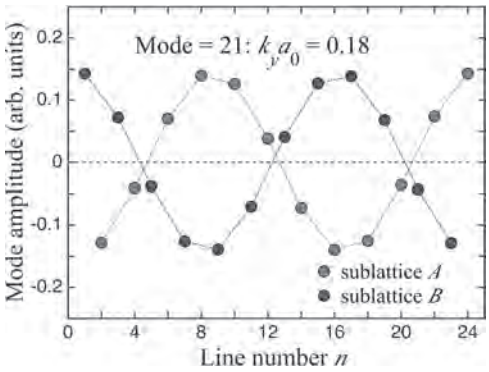

Fig. 2. Complex amplitude (including phase) for bulk-like standing SW mode 21 for the stripe in Fig. 1 when $k_y a_0 = 0.18$. The amplitudes on sublattice A (odd n) and sublattice B (even n) rows are shown separately.

GPA-13. Photo-induced FMM-like Phase in Underdoped Manganite Thin Films. *K. Stroh*[1], T. Titze[1], C. Seick[1], M. Schumacher[1], S. Mathias[1], D. Steil[1] and V. Moshnyaga[1] *1. Physikalisches Institut, Georg-August-Universitaet Goettingen, Goettingen, Germany*

The ground state of perovskite manganites, like $La_{1-x}Sr_xMnO_3$ (LSMO), is well-known to be tuneable by chemical doping. Their complex phase diagrams specify doping levels and temperatures, where two equilibrium phases exist in close proximity. For example, lightly doped LSMO with $x \sim 0.1 - 0.15$ and $T>T_C$ lies close to the phase boundary at $x = 0.175$ between paramagnetic-insulating (PMI) and ferromagnetic-metallic (FMM) ground states [1]. A similar situation is found for self-doped $La_yMnO_{3+\delta}$ (LMO) with $y \sim 0.9$ [2]. Ultrashort laser pulses can be used to optically dope such systems by exciting electrons from Mn^{3+} to Mn^{4+} ions [3], establishing a double exchange interaction essential for the FMM state in mixed-valence manganites. Consequently, the above mentioned LMO and LSMO with a PMI ground state could be promising candidates to observe photo-induced phase transitions. Thin films of La-deficient LMO and underdoped LSMO have been grown epitaxially on $SrTiO_3$(100) substrates by a metalorganic aerosol deposition technique. Optimally doped LSMO ($x \sim 0.33$), possessing an FMM ground state and being far away from any chemical phase boundaries, has been studied for comparison. We performed femtosecond time-resolved magneto-optical Kerr effect (MOKE) and pump-probe reflectivity (PPR) measurements for various temperatures, pump fluences, and magnetic fields on timescales up to a nanosecond. PPR data of the underdoped manganite films measured 5 - 40 K above their $T_C \sim 160$ K in a PMI state, show a characteristic zero-crossing within ps after laser excitation and a further increase of ΔR/R for up to a few hundred ps, resembling the positive ΔR/R signal observed in the FMM state of optimally doped LSMO. In the same

temperature range, an unexpected MOKE signal appears on the timescale of the laser pulse, indicating a spin ordering which decays on a ps to ns timescale. In summary, our experiments suggest that it is possible to photoexcite underdoped manganites into a transient FMM-like state above their static T_C on a sub-ps timescale by laser excitation. We acknowledge financial support by the German Research Foundation DFG via Project 399572199 and within the CRC 1073 (subprojects A02 and A06).

[1] J. Hemberger et al., Physical Review B, Vol. 66, 094410 (2002) [2] A. Gupta et al., Applied Physics Letters, Vol. 67, 34940 (1995) [3] M. Matsubara et al., Physical Review Letters, Vol. 99, 207401 (2007)

GPA-14. Withdrawn

GPA-15. Field-free switching model of Spin-Orbit Torque (SOT-MTJ) device with thermal effect based on voltage-controlled magnetic anisotropy (VCMA). *S. Li*[1] and Y. Jiang[1] *1. Department of Electrical Engineering, Jiangnan University, Wu Xi, China*

Electrically driven magnetization switch utilizing voltage-controlled magnetic anisotropy (VCMA) have attracted much attention in the new generation memory, especially for spin-orbit torque (SOT)-based magnetic random access memory (MRAM) [1,2]. For the traditional SOT switching, an additional magnetic field is needed to break the inversion symmetry, which makes the circuit difficult to implement [3]. Combining the SOT with the VCMA effect can realize the certain switching in SOT-MRAM with lower critical switching current [4]. With the development of the SOT-MRAM, device model is urgently needed for the device characterization. However, the published models are facing limitations as the size shrinks down to nanometer. Also, the effect of the elevated temperature caused by repeated operation on the device is non-negligible [5]. Therefore, an effective model is needed to represent the switching dynamic of the device concerning the influence of the nanoscale and the thermal effect. In the paper, a compact model of three-terminal VCMA assisted SOT switching is established. The influence of the VCMA effect on the field-free SOT switching is considered by numerically solving the LLG equations. Furthermore, a 3D model of the VCMA+SOT device is established by finite element method to demonstrate the thermoelectric behavior. Considering the influence of the thermal effect generated in the working state on the switching characteristics, the electro-thermal behavior is integrated into the compact model to show the influence of the temperature on the switching behavior, highlighting the importance of the thermal effect for the realistic modelling of SOT switching. Additionally, considering the influence of thermal effect, the switching error rate of the device under different working voltage conditions is evaluated. Finally, a novel voltage pulse scheme is proposed, which can effectively shorten the inversion time and improve the reliability of the device. The established model provides strategies and guidelines for next-generation memory design and application.

[1] W. Kang, Y. Ran and Y. G. Zhang et al., IEEE Trans. Nanotechnol., Vol. 16, p. 387 (2017). [2] S. Sharmin, A. Jaiswal, and K. Roy, IEEE Trans. Electron Devices, vol. 63, p. 3493 (2016). [3] A. Manchon, I. M. Miron and T. Jungwirth et al., Rev. Mod. Phys., vol. 91, p. 035004 (2019). [4] S. Shreya and B. K. Kaushik, IEEE Trans. Electron Devices, vol. 67, p. 90 (2019). [5] J. J. Kan, C. Park and C. Ching et al., IEEE Trans. Electron Devices, vol. 64, p. 3639 (2017).

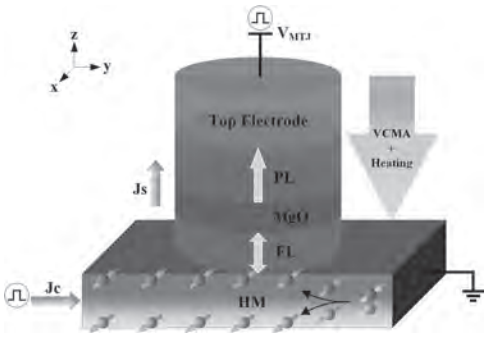

Fig.1 Schematics of the three-terminal device allowing for field-free SOT switching with an illustration of the influences of VCMA and thermal effects.

GPA-16. Effects of Permalloy-Cobalt Cosputtering in a Nanowire Structure on Magnetic Fluctuation and Auto-Oscillation. B. Kim[1], *S. Yoon*[2], S. Han[3] and B. Cho[1] *1. School of Materials Science and Engineering, Gwangju Institute of Science and Technology, Gwangju, The Republic of Korea; 2. Nano Photonics Group, Korea Institute of Industrial Technology, Gwangju, The Republic of Korea; 3. Division of Navigation Science, Mokpo National Maritime University, Mokpo, The Republic of Korea*

Spin torque nano oscillator(STNO) and spin Hall nano oscillator(SHNO) are the promising devices to generate spin wave with thermal stability and low power consumption.[1,2] But the spin wave has in nature the low power density for device applications. Thus, various spin wave excitation methods have been studied, such as synchronization of auto-oscillation via multiple SHNO array[4-7] and utilizing high spin Hall angle in a heavy metal.[8] Here, we designed a permalloy (Py) ferromagnetic layer in a rectangular bar type for spin wave excitation by auto oscillation and investigated the effects of a transition metal (Co) alloying on the excitation efficiency. The magnetic fluctuation in bar type layers of $Py_{1-x}Co_x$ (x = 0, 0.11, 0.21, 0.29, and 0.40), fabricated by Py-Co cosputtering, is estimated from micro-Brillouin light scattering (μ-BLS) spectroscopy data, as shown in Fig. 1. And the threshold current for auto oscillation in the bar layers is estimated from the current dependence of integral intensity of the spectra. It is found that Py-Co cosputtering reduces the threshold current for auto oscillation, e.g., 27.3% for $Py_{1-x}Co_x$ (x = 0.21), compared with that of Py layer. It is conjectured that the cosputtering enhances the spin Hall transparency while it causes almost no change in the effective Gilbert damping constant in the layer. Details will be discussed in the poster presentation and conference proceeding paper.

[1] J. Wunderlich, B. Kaestner, and T. Jungwirth, Phys Rev Lett 94, 047204 (2005). [2] J. Torrejon *et al.*, Nature 547, 428 (2017). [3] A. Slavin and V. Tiberkevich, IEEE Transactions on Magnetics 45, 1875 (2009). [4] Y. Ou, D. C. Ralph, and R. A. Buhrman, Phys Rev Lett 120, 097203 (2018). [5] Y. Yin *et al.*, Physical Review B 92 (2015). [6] M. A. W. Schoen, D. Thonig, and J. M. Shaw, Nature Physics 12, 839 (2016). [7] Y. Fu *et al.*, IEEE Transactions on Magnetics 45, 4004 (2009). [8] H. Mazraati *et al.*, Applied Physics Letters 109 (2016).

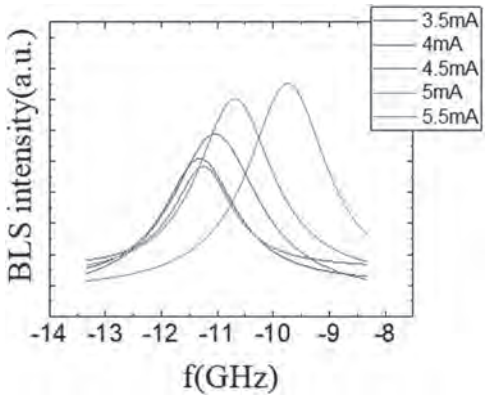

Figure 1. Brillouin light scattering (BLS) intensity spectra of $Py_{1-x}Co_x$ (x = 0.21) (Py = permalloy) nanowires with various applied DC currents of 3.5, 4.0, 4.5, 5.0 and 5.5 mA.

GPA-17. High Wave Vector Non-reciprocal spin Wave Beams.

L. Temdie[1,2], *V. Vlaminck*[1,2], G. Pradan[3], J. Solano[3], H. Majjad[3], Y. Henry[3] and M. Bailleul[3] *1. MicroWave Dept., IMT Atlantique, Brest, France; 2. UMR 6285 CNRS, Lab-STICC, Brest, France; 3. IPCMS - UMR 7504 CNRS, Strasbourg, France*

Non-reciprocal microwave components such as circulators, isolators, and phase shifters are indispensable tools in both today's communication systems and future quantum computers [1-2]. However, these components rely almost entirely on field-based bulky ferrimagnet, which tend to be relatively large, off-chip, and costly to assemble. In this context, different fields of research are investigating solutions to miniaturize these non-reciprocal devices compatible with integrated circuit technology. Among them, the field of magnonic plays a key role in this search benefiting from a wide range of non-reciprocal properties in the propagation of spin waves [3]. Recently, unidirectional transmission of spin waves was achieved by taking advantage of the chiral coupling between the uniform resonance of Co nanowires and exchange spin waves in a thin YIG film [4, 5]. Here, we further miniaturized this method and demonstrate the possibility of shaping non-reciprocal spin wave beams in a continuous thin YIG film. We performed spin wave spectroscopy on a series of devices made of arrays of Co bars of dimensions: L=10μm in length, w=200 nm in width, 40nm in thickness, and laterally spaced by a=400nm (see Fig. 1). The transmission spectra done with the external field applied along the length of the Co bars show perfect non-reciprocity for several peaks located around the resonance frequency of the Co bars, e.g. 8.4 to 10.4 GHz range as shown in Fig. 2. These peaks correspond to integer values of the lateral spacing between Co bars, e.g. $k_n=n\pi/a$ ranging up to 80rad/μm. Additional non-reciprocal peaks occurring at lower frequencies ranging between 2 and 6 GHz correspond to the satellite peaks of the antenna directly coupled to the YIG film. Surprisingly, some of the peaks display a reversed non-reciprocity. Finally, we make use of this multitude of transmission peaks to characterize the k-dependence of the relaxation time and the group velocity of dipole-exchange spin waves.

[1] W. Palmer, et al., IEEE Micr. Magazine 20, 36 (2019) [2] M. Devoret, et al., *Superconducting circuits for quantum information,* Science 339, 1169 (2013) [3] J. Chen, et al., J. Phys. D. Appl. Phys. 55, 123001 (2022) [4] H. Wang, et al., Nano Res. 14, 2133–2138 (2021) [5] J. Chen, et al., Phys. Rev. B 100, 104427 (2019)

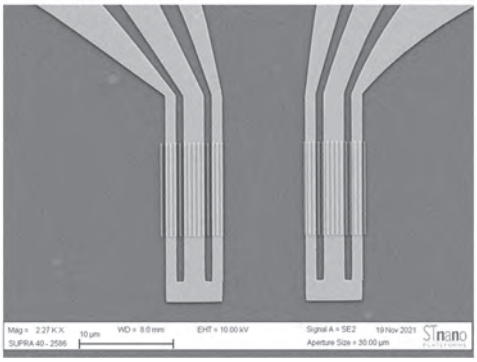

SEM image of Co nanowires with length L=10μm, width w=200nm, and period a=400nm lithographed on a 50nm YIG film with thickness, and located under 2 μm wavelength Au coplanar waveguides (CPW)

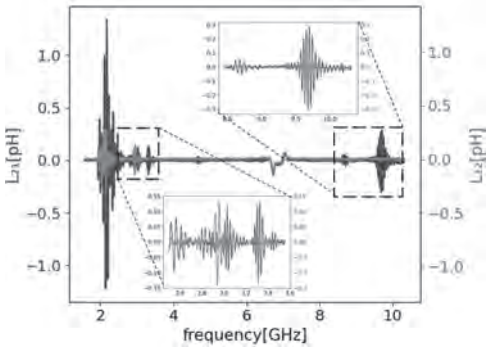

Transmission spectrum ΔL_{21} (blue) and ΔL_{12} (red) at 24mT applied field.

GPA-18. Theory of confined magnons in 3D heterostructures.

J.A. do Nascimento[1] and V. Lazarov[1] *1. Physics, University of York, York, United Kingdom*

Understanding magnons in confined geometry that relates to experimental devices is rather challenging, since device heterostructures, e.g. Spin Seebeck devices, are a combination of both ferromagnetic (FM) and antiferromagnetic (AFM) layers [1]. The size of the layers can range from hundreds to several atomic layers, hence discontinuities on a short length scale where a change of magnetic properties is abrupt, in presence of magnetic anisotropies, bring an extra challenge in determining the magnon dynamics, dispersion as well as prorogation in such structures. In this work, we extend the method, used in [2] where the spin-scattering function was calculated for 1D finite chains, to 3D systems. In particular, we show how to modify this approach to calculate the dynamics of magnon modes in finite systems using second quantisation of the Heisenberg Hamiltonian for thin film and interfaces, as well as hetero-structure between FM and AFM layers, taking into account surface and interface anisotropies and exchange parameters. The effect of such changes in the parameters of the system leads to the appearance of confined states at the surfaces and interfaces of the heterostructures, Fig. 1. We study the effect that such confined states have on the spin-scattering function, which can be regarded as a proxy for neutron-scattering.

[1] Lin, W., et. al. Physical Review Letters, Vol.116, p.186601 (2016) [2] Bearisto, B., Phys. Rev. B, Vol.104, p.134415 (2021) [3] Pajda, M., Phys. Rev. B, Vol.64, p.174402 (2001)

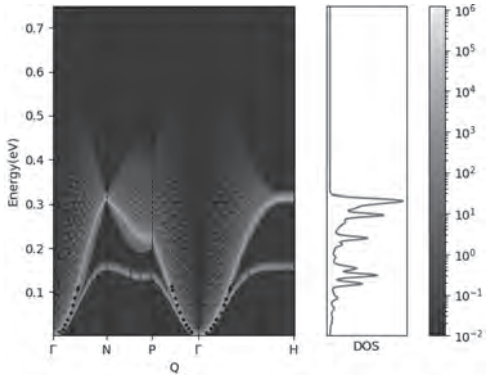

Spin scattering function for Fe BCC, exchange parameters are taken from [3] and experimental points (solid black dots) were reproduced from the same paper. We can see a clear resonance matching the bulk dispersion, as well as a line that corresponds to localized surface states.

Session HOA
MAGNETIC IMAGING AND MAGNETIZATION DYNAMICS

Andrew Kunz, Chair
Marquette University, Milwaukee, WI, United States

CONTRIBUTED PAPERS

HOA-01. Direct Imaging of Decision-Making in Nanomagnetic Galton Boards. *H. Arava*[1], D. Sanz Hernandez[2], F. Montaigne[3], J. Grollier[2] and A. Petford-Long[1] *1. Materials Science Division, Argonne National Laboratory, Chicago, IL, United States; 2. Unité Mixte de Physique CNRS-Thales, Palaiseau, France; 3. Université de Lorraine, Nancy, France*

In a classical Galton board, a series of metal pegs are positioned at locations that mimic the geometry of a Pascal's triangle. Metal balls dropped from the top of such a board will undergo a series of decision-making events, travel to either left or right of each peg, before dropping off into separate bins at the bottom. A nanomagnetic realization of such a Galton Board is made of interconnected bars of permalloy arranged onto a honeycomb lattice. Unlike the classical Galton board, in a nanomagnetic Galton board, a domain wall is injected from the top of the board and the reversal is field driven to the bottom. Recently [1], in an experimental realization of the nanomagnetic Galton Board it was found that the domain wall reversal is inherently stochastic, thus an excellent way to realize a random number generator. Additionally, the robust nature of the stochasticity in the nanomagnetic Galton boards may find use in nanomagnet based artificial neural networks and other unconventional computing solutions. Even though the stochastic nature of nanomagnetic Galton boards is rigorously established, the exact nature of domain wall reversal leading to the observed stochasticity is not fully understood. Here, I will present a direct imaging of domain wall reversal in nanomagnetic Galton boards using Lorentz Transmission Electron Microscope (LTEM). LTEM enables us to directly image local changes to the magnetic microstructure during a decision-making process. We experimentally identify that decision making in a nanomagnetic Galton board relies on three key factors (1) topology of the injected domain wall, (2) size of the vertices, and (3) local disorder in the patterned samples. Beyond the nanomagnetic Galton board, our results will broadly aid in the understanding of domain wall reversals in other nanomagnetic networks with built in bifurcations such as Y shaped junctions, and artificial spin ices.

[1] D. Sanz-Hernández et al., Advanced Materials 33, 2008135 (2021).

HOA-02. Coherent Correlation Imaging: Resolving fluctuating states of matter. *C. Klose*[1], F. Büttner[2,3], W. Hu[4], C. Mazzoli[4], K. Litzius[3], R. Battistelli[2], I. Lemesh[3], J.M. Bartell[3], M. Huang[3], C.M. Günther[5], M. Schneider[1], A. Barbour[4], S.B. Wilkins[4], G. Beach[3], S. Eisebitt[6,7] and B. Pfau[1] *1. B2: Imaging and Coherent X-rays, Max Born Institute for Nonlinear Optics and Short Pulse Spectroscopy, Berlin, Germany; 2. Helmholtz-Zentrum für Materialien und Energie GmbH, Berlin, Germany; 3. Department of Materials Science and Engineering, Massachusetts Institute of Technology, Cambridge, MA, United States; 4. National Synchrotron Light Source II, Brookhaven National Laboratory, Upton, NY, United States; 5. Technische Universität Berlin, Zentraleinrichtung Elektronenmikroskopie (ZELMI), Berlin, Germany; 6. Max Born Institute for Nonlinear Optics and Short Pulse Spectroscopy, Berlin, Germany; 7. Technische Universität Berlin, Institut für Optik und Atomare Physik, Berlin, Germany*

Fluctuations are ubiquitous in nanometer-scale systems, spanning orders of magnitude in space and time. Real-space access to fluctuating states is impeded by a dilemma between spatial and temporal resolution. Averaging over an extended period of time (or repetitions) is key for the majority of high-resolution imaging experiments, especially in weak contrast systems. If, by lack of better knowledge, averaging is indiscriminate, it leads to a loss of temporal resolution and to motion-blurred images. We present coherent correlation imaging (CCI) – a high-resolution, full-field imaging technique that realizes multi-shot, time-resolved imaging of stochastic processes. The key of CCI is the classification of camera frames that correspond to the same physical state (Fig. 1) even at low photon count, where imaging is not possible. CCI combines a correlation-based similarity metric with powerful classification algorithm developed for genome research [1] realizing informed, non-sequential signal averaging while maintaining single frame temporal resolution. We apply CCI to study previously inaccessible magnetic fluctuations in a highly degenerate magnetic stripe domain state. Our material is a Co-based chiral ferromagnetic multilayer with magnetic pinning low enough to exhibit stochastically recurring dynamics that resemble thermally-induced Barkhausen jumps near room temperature. CCI reconstructs sharp, high-contrast images of all domain states by phase retrieval [2] and, unlike previous approaches, also tracks the time when these states occur. The spatiotemporal imaging reveals an intrinsic transition network between the states and unprecedented details of the magnetic pinning landscape (Fig. 2).

[1] G. Sherlock, et. al., Current Opinion in Immunology 12, 201-205 (2000)
[2] Flewett, S. et al., Optics Express 20, 29210–29216, 2012

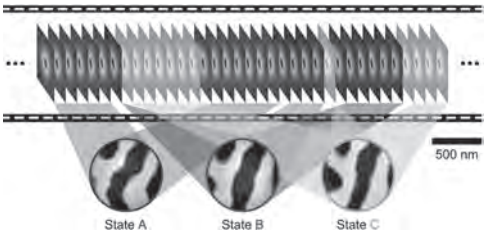

Principle of time-resolved coherent correlation imaging. Top: Sequence of camera frames showing Fourier-space coherent scattering patterns. Coherent correlation imaging classifies scattering frames by their underlying domain state, as indicated by the colors. Bottom: Real-space images reconstructed from an informed average of same-state frames.

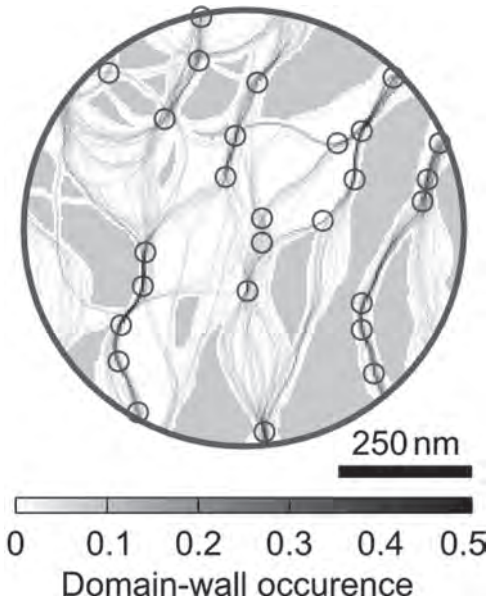

Map of attractive (blue dots) and repulsive (red areas) pinning sites. The background shows the position of the domain walls and their relative occurrence observed in the experiment.

HOA-03. Surface Acoustic Waves Effect on Domain Wall Motion.
J. Shuai[1], L. Lopez-Diaz[2], J.E. Cunningham[3] and T.A. Moore[1] *1. School of Physics and Astronomy, University of Leeds, Leeds, United Kingdom; 2. Department of Applied Physics, Universidad de Salamanca, Salamanca, Spain; 3. School of Electronic and Electrical Engineering, University of Leeds, Leeds, United Kingdom*

Domain walls (DWs) in thin films with perpendicular magnetic anisotropy (PMA) are promising information carriers for the next generation of data storage and logic operation devices.[1,2] However, controlling DW motion efficiently remains unsolved. Here, we experimentally demonstrated an enhanced DW velocity in a PMA film using both standing and travelling surface acoustic waves (SAWs). Two interdigitated transducers (Fig.1a), centre frequency 47.93 MHz (Fig. 1b), were patterned on opposite side of a Ta(5)/Pt(2.5)/Co(0.5)/Ta(5) film (thicknesses in nm). The film was dc magnetron sputtered onto a lithium niobate substrate. Kerr microscopy was used to measure the DW velocity by measuring the DW displacement due to a pulsed field. Results showed that DW velocity increased from 7±1 to 34±1 μm/s with an increasing magnetic field from 10.9 to 14.8 Oe without SAWs (Fig.1c). A significant DW velocity increase can be observed in the presence of the standing SAW (Fig.1c) with applied SAW power from 15.5 to 20.5 dBm. An up to 24-fold DW velocity increase (870±10 μm/s at 14.8 Oe) can be found in the presence of standing SAWs at 20.5 dBm compared to that without SAW at the same field. A less significant DW increase (372±6 μm/s at 14.8 Oe) can also be observed with the application of travelling SAWs (Fig.1d). SAWs locally and periodically lower and raise the anisotropy of the thin film due to the magnetoelastic coupling effect, temporarily assisting the DW to overcome pinning energy barriers during its motion.[3,4] This process is possibly an accumulative effect, which can explain the velocity difference between results for the travelling and standing SAW. This study demonstrates the potential for SAWs to efficiently manipulate magnetic DWs.

[1] Marathe et al. Vacuum, 14, 329, (2017) [2] Li et al., J. Appl. Phys, 115, 17E307 (2014) [3] Shepley Sci. Rep. 5, 7921 (2015) [4] Shuai et al. Appl. Phys. Lett. 120, 252402 (2022)

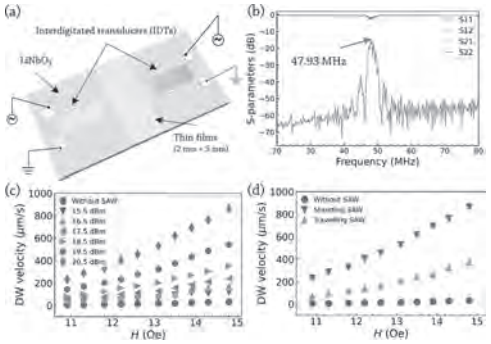

Fig. 1 (a) Experimental set-up; (b) S-parameters of the SAW device; (c) Domain wall velocity against the applied field with standing SAWs (various applied SAW power) and without SAW. (d) Domain wall velocity against the applied field without SAW and with standing/travelling SAWs (applied SAW power of 20.5 dBm).

HOA-04. Effect of nonuniform perpendicular anisotropy in ferromagnetic resonance spectra in magnetic nanorings and nanodisks.
E. Saavedra[1], A. Riveros[2] and *J.L. Palma*[2,3] *1. Physics Department, Universidad de Santiago de Chile, Santiago, Chile; 2. Engineering School, Universidad Central de Chile, Santiago, Chile; 3. CEDENNA, Center for the Development of Nanoscience and Nanotechnology, Santiago, Chile*

A study of the effect of a nonuniform perpendicular magnetic anisotropy on the magnetic configurations and on the ferromagnetic resonance (FMR) spectra in two systems was performed by micromagnetic simulations, by applying a short magnetic pulse [1-3]. First system corresponds to magnetic nanorings of different widening with radial distribution of the perpendicular magnetic anisotropy (RPMA) [1]. Both the resonant frequencies and the number of peaks depend on the lower energy magnetization configuration [4] (figure 1) which in turn is a function of anisotropy gradient. Also, we compare the diagram between nanorings with and without RPMA showing that the effects of the RPMA are relevant even for the narrowest ring of 10 nm wide [1]. The second system corresponds to nanodisks with radial distribution but with the center of the distributed anisotropy displaced from the center of the nanodisk (figure 2). This break on the symmetry of the RPMA with respect to the disk center, allows several new magnetic configurations such as skyrmionium-like magnetic states and therefore the resonance spectra of FMR have several new modes and peaks compared to non-breaking symmetry of RPMA. The results show that by controlling the RPMA strength K of the anisotropy gradient, and its symmetry, several new resonance modes and magnetic configurations can be obtained for instance, vortex, meron and knot states in nanorings and skyrmionum in nanodisks. Authors acknowledge DICYT Grant 042131EM, PAI77190042, Fondecyt 1201491 and Basal AFB 180001.

[1] Saavedra, E. et al. Effect of nonuniform perpendicular anisotropy in ferromagnetic resonance spectra in magnetic nanorings. Sci. Rep. 11, 14230 (2021). [2] McMichael, R.D. and Stiles, M.D. Magnetic normal modes of nanoelements. J. Appl. Phys. 97, 10J901 (2005). [3] Baker, A. et al. Proposal of a micromagnetic standard problem for ferromagnetic resonance simulations. J. Magn. Magn. Mater. 421, 428 (2017). [4] Castro, M.A. et al. New magnetic states in nanorings created by anisotropy gradients. J. Magn. Magn. Mater. 484, 55–60 (2019).

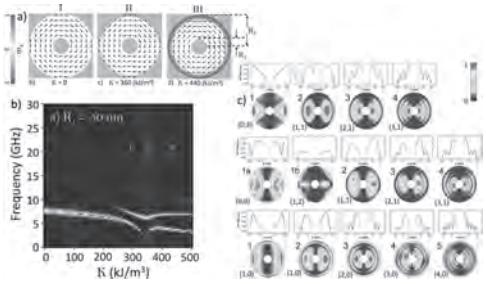

Figure 1: a) Minimal energy configurations as a function of the RPMA strength K: I, II, and III correspond to vortex, knot and meron states respectively. b) Imaginary component of the dynamic susceptibility for R1 = 50 nm c) Spatial distribution of the amplitude for vortex (K =300 kJ/m³), knot (K = 350 kJ/m³) and meron (K = 450 kJ/m³), respectively.

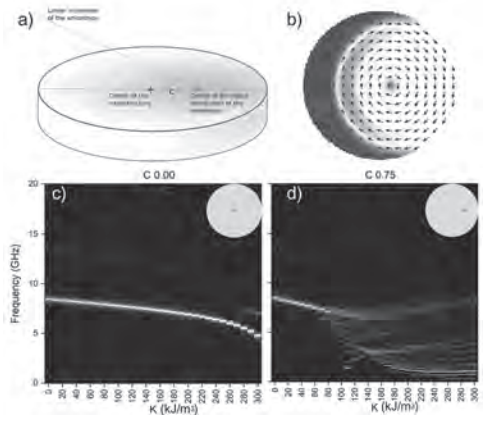

Figure 2: a) Scheme of a nanodisk with RPMA, c is the ratio between the deviation of the RPMA center and the disk radius. b) Skyrmionum-like state when c = 0.75 and K = 200 (kJ/m³) (direction of magnetization colormap: blue enter to the plane, red out of plane, white in plane). c) Imaginary component of the dynamic susceptibility when c) c = 0 and d) 0,75.

HOA-05. Exploring multiple strain geometries in PMN-PT/Ta/CoFeB/MgO magneto-electric devices. *S. Roy*[1], A. Solignac[2], T. Bhatnagar-Schöffmann[1], E. Monteblanco[3], R. Pachat[1], A. Harouri[1], R. Juge[3], T. Maroutian[1], D. Ravelosona[1,3], G. Agnus[1] and L. Herrera Diez[1] *1. Centre de Nanosciences et de Nanotechnologies, CNRS, Université Paris-Saclay, Palaiseau, France; 2. SPEC, CEA Saclay, CNRS, Université Paris-Saclay, Gif sur Yvette, France; 3. C2N, Spin-Ion Technologies, Palaiseau, France*

Strain-induced modification of magnetic properties in hybrid piezoelectric/ferromagnetic heterostructures is being intensively investigated due to its potential for low-power spintronics applications based on magnetic domain wall (DW) motion ([1], [2]). In this study, we present PMN-PT(011)/Ta/CoFeB/MgO-based devices where both out-of-plane and in-plane strain configurations have been exploited to control DW dynamics. In PMN-PT (011), the application of a gate voltage along the out-of-plane (OOP) direction of the sample leads to a non-volatile polarisation state which can be reverted back to the un-poled state by annealing at temperatures above the Curie temperature ([3]), which was confirmed in our system by piezoresponse force microscopy. In this configuration, we observe a non-volatile increase in the coercivity in 10μm wires in the poled state of about 90% with respect to the unpoled state. This response can be linked not only to a strain-control of magnetic anisotropy but also to a strain-controlled change in the homogeneity of the magnetic landscape. The multiple polarisation directions of the domains in the un-poled state of the PMN-PT can translate into a wider anisotropy distribution in the magnetic system, compared to the poled state. This can significantly affect DW nucleation/depinning fields, which opens the door to using strain to control magnetic disorder. We also combine this non-volatile effect with local, volatile, in-plane control of DW dynamics, dominated by strain-induced changes in magnetic anisotropy. In conclusion, we present a multifunctional strain-controlled device where both disorder and anisotropy can be manipulated. We show that multiple strain configurations in piezoelectric/ferromagnetic hybrid structures can open new opportunities for the electrical manipulation of DW dynamics.

[1] Na Lei, Thibaut Devolder, Guillaume Agnus, et al., Nature Communications, 4, 1-4 (2013) [2] P. M. Shepley, A. W. Rushforth, M. Wang, et al., Scientific Reports, 5, 1-5 (2015) [3] V.S. Kathavate, B. Praveen Kumar, I. Singh, et al., Ceramics International, 46, 12876-12883 (2020)

HOA-06. Stress-Engineered Microwave Generation induced by Phonon-Magnon-Photon Coupling in Patterned Arrays of Nanowires. *A. Samanta*[1,2] and S. Roy[1,2] *1. Micropower Devices and Nanomagnetics Group, Tyndall National Institute, Cork, Ireland; 2. Department of Physics, University College Cork, Cork, Ireland*

The emergence of the Internet of Things (IoT) devices, one of the crucial building blocks of modern technologies, shows of late a remarkable interest in the field of microwave-based technologies, e.g., RF energy harvesting, radars, miniaturized antennas, ultra-low field magnetic sensors etc. [1-5]. The voltage-controlled microwave oscillators typically consume a large amount of power to produce microwave frequencies with moderate frequency stabilities. The conventional batteries cannot be used for powering such power-hungry IoT devices and prohibitory cost for replacement in wireless sensor nodes (WSN), particularly in inaccessible locations and their sustainability due to the overall pollution they are likely to produce. Hence, researchers are looking to invent state-of-the-art microwave oscillators [5] for such cutting-edge applications. In this work, we report the domain wall movement in the patterned array of rectangular magnetostrictive nanomagnets/piezoelectric heterostructures caused by surface acoustic waves (SAW) for microwave generation. A surface acoustic wave launched on the substrate produces periodic strain within the patterned nanomagnets, which, in turn, stimulates the magnetization precession of the nanomagnets resulting in different magneto-dynamical resonance modes in the array of nanomagnets with a rich spin wave (SW) texture. The generated SWs (magnons) further interact with the EM wave radiation (photons) at the SAW frequency [6]; this phonon-magnon-photon coupling generates a 0.56 GHz microwave frequency with a 13.9 MHz linewidth and Q-factor of 40. The generated non-volatile spin textures of the nanowires are also useful in energy-efficient logic and low-power computing applications [7].

Acknowledgement: Both, AS and SR gratefully acknowledge the financial support for this work from the "EU-H-2020" project, "EnABLES-JRA", Project ID: 730957. References: [1] T. Nan, H. Lin, Y. Gao, Nature Communications 8, 296 (2017). [2] J.-S. Kim, M.-A. Mawass, A. Bisig, Nat. Commun. 5, 3429 (2014). [3] T. Ono and Y. Nakatani, Appl. Phys. Express 1, 61301 (2008). [4] R. Sbiaa, M. Al Bahri, and S. N. Piramanayagam, J. Magn. Magn. Mater. 456, 324 (2018). [5] S. Bhatti and S. N. Piramanayagam, Phys. Status Solidi – Rapid Res. Lett. 13, 1800479 (2019). [6] R. Fabiha, J. Lundquist, S. Majumder, Advanced Science 9, 2104644 (2022). [7] V. Sampath, N. D'Souza, D. Bhattacharya, Nano Letters 16, 5681 (2016).

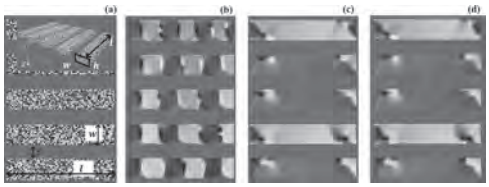

(a)Initial magnetization configuration of NWs; l, w, are length, width of each NWs along the x, y directions, respectively, and s is the spacing between the NWs in xy plane.(b)The multidomain state with transverse stress.(c)The multidomain structures in (b) vanished upon launching of SAW.(d)Final spin structure after completion simulation, retaining the domain structure in (c).

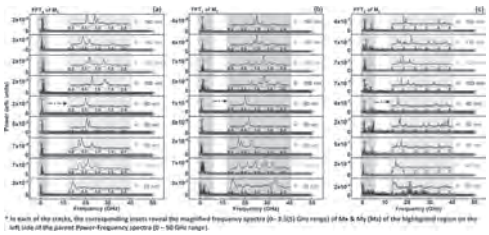

Power distribution as a function of spacing between the neighbouring NWs along x, y, z directions in (a), (b), (c), respectively.

HOA-07. Computational Validation of Method for Decomposition of Mechanical Stress Effect on Magnetic Property of Silicon Steel Sheet. H. Shimizu[1], Y. Marumo[1], Y. Mishima[1] and *T. Matsuo*[1] *1. Kyoto University, Kyoto, Japan*

Experimental and computational studies on the stress-dependent magnetic property of silicon steel are on-going. A physical magnetization model, an energy-based multiscale magnetization model called multi-domain particle model (MDPM) [1], was developed, which successfully predicted the stress-dependent properties of silicon steel without using measured stress-dependent data. To avoid measurement under arbitrary combination of stress and magnetization directions, several stress models have been developed. This study examines two of them by comparing with the MDPM. One is the equivalent stress (ES) theory [2] and the other is the stress decomposition (SD) method [3]. The latter assumes that the stress effect can be decomposed into its principal directions. A rotational single sheet tester applied a compressive stress to a non-oriented silicon steel sheet in the rolling direction (RD, ϕ=0). A magnetic field was applied along ϕ = 0 or π/4. Fig. 1 shows the measured stress dependence of hysteresis loss w_x in the RD when the amplitude of B_x is 0.5, 0.7 and 1.0 T, where B_y has only a small effect on the stress dependence of w_x. It supports the assumption of stress decomposition. BH loops under the excitation angle of π/4 were simulated using the MDPM, where the directions of stress and applied magnetic field are denoted by ϕ_σ and ϕ_H. Fig. 2 shows BH loops as below: [reference, blue lines] ϕ_H=π/4 and ϕ_σ=0 with σ = –40, –80 MPa, [ES theory, green lines] ϕ_H=ϕ_σ=π/4 with σ = –10, –20 MPa based on the ES theory, [SD, brown lines] synthesized loops of ϕ_H=ϕ_σ=0 with σ = –40, –80 MPa and ϕ_H=ϕ_σ=π/2 with σ = 0, and [modified SD, red lines] synthesized loops of ϕ_H=ϕ_σ=0 with σ = –40, –80 MPa and ϕ_H=ϕ_σ=π/2 with σ = +40, +80 MPa. The ES theory roughly predicts the stress dependent loops along ϕ = π/4, but fails to predict decomposed loops along ϕ = 0, π/2. The SD fails to reconstruct loops along ϕ=π/2 because a compressive stress along ϕ=0 acts as a tensile stress along ϕ=π/2. The modified SD roughly predicts the stress dependent loops in all the directions by giving tensile stresses along ϕ=π/2.

[1] T. Matsuo, Y. Takahashi, K. Fujiwara, *J. Magn. Magn. Mater.*, vol. 499, 166303, 2020. [2] M. Rekik, L. Daniel, O. Hubert, *IEEE Trans. Magn.*, vol. 50, 2001604, 2014. [3] M. Nakano, et. al, *IEEJ Trans. Ind. Appl.*, vol. 129, pp. 1060–1067, 2009.

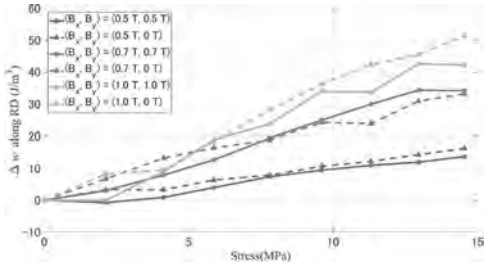

Comparison of measured loss increase Δw_x with ϕ_H = 0, π/4 and ϕ_σ = 0.

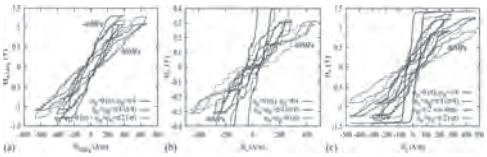

Simulated BH loops along (a) ϕ = π/4, (b) ϕ = 0, and (c) ϕ = π/2.

HOA-08. Revealing nanoscale disorder in W/CoFeB/MgO ultra-thin films with domain wall motion. *J.W. van der Jagt*[1,2], V. Jeudy[3], A. Thiaville[3], M. Sall[1], N. Vernier[4,5], L. Herrera Diez[4], M. Belmeguenai[6], Y. Roussigné[6], S.M. Chérif[6], M. Fattouhi[7], L. Lopez-Diaz[7], A. Lamperti[8], R. Juge[1] and D. Ravelosona[1,4] *1. Spin-Ion Technologies, Palaiseau, France; 2. Université Paris-Saclay, Gif-sur-Yvette, France; 3. Laboratoire de Pysique des Solides, Orsay, France; 4. Centre de Nanosciences et de Nanotechnologies, Palaiseau, France; 5. Universite Paris-Saclay, CNRS, ENS Paris-Saclay, CentraleSupelec, LuMIn, Gif-sur-Yvette, France; 6. Laboratoire des Sciences des Procédés et des Matériaux, Villetaneuse, France; 7. Applied Physics, Universidad de Salamanca, Salamanca, Spain; 8. Unit of Agrate Brianza, CNR-IMM, Agrate Brianza, Italy*

Spintronic devices based on domain wall (DW) motion offer exciting perspectives for non-volatile memory and logic applications. One of the main issues to overcome is DW pinning at intrinsic material defects. Pinning leads to thermally activated creep and depinning regimes [1], reducing the efficiency of DW motion. In our work [2], we study DW motion in differently crystallized W/CoFeB/MgO thin films, which are archetype materials for spintronic devices. We use different crystallization techniques based on annealing and He^+ irradiation [3, 4] to fabricate samples with similar micromagnetic properties. This offers a unique opportunity to selectively analyze the effects of disorder on DW dynamics without the influence of changes in magnetic properties. Fig. 1 shows that the DW velocity in the creep, depinning, and flow regimes varies significantly between the samples. With an analytical model [5] for the creep and depinning regimes to extract nanoscale pinning parameters, we reveal important variations in the disorder landscape. We observe a strong variation of the pinning energy barrier k_BT_d, pinning correlation length ξ and pinning site density b. Furthermore, in Fig. 2, we show that the DW roughness varies significantly, with the irradiated samples exhibiting much smoother DWs, indicating a greater material homogeneity. Using micromagnetic simulations to study the DW velocity in the flow regime, we show that the variations in pinning length scales can be linked to variations in crystallite grain size through the velocity plateau (see inset Fig. 1) [6]. Our results indicate that controlling the microscopic properties is a prerequisite for controlling DW motion in polycrystalline materials and that DW motion is an excellent tool to characterize disorder.

[1] V. Jeudy, A. Mougin, S. Bustingorry et al., *Phys. Rev. Lett.* 117, 057201 (2016) [2] J.W. van der Jagt, V. Jeudy, A. Thiaville et al., *submitted* (2022) [3] T. Devolder, I. Barisic, S. Eimer et al., *J. of Appl. Phys.* 113, 203912 (2013) [4] D. Ravelosona, US patent US2016/0005537 A1 (2016) [5] P. Géhanne, S. Rohart, A. Thiaville et al., *Phys. Rev. Res.* 2, 043134 (2020) [6] M. Voto, Luis Lopez-Diaz and Luis Torres, *J. Phys. D: Appl. Phys.* 49, 185001 (2016)

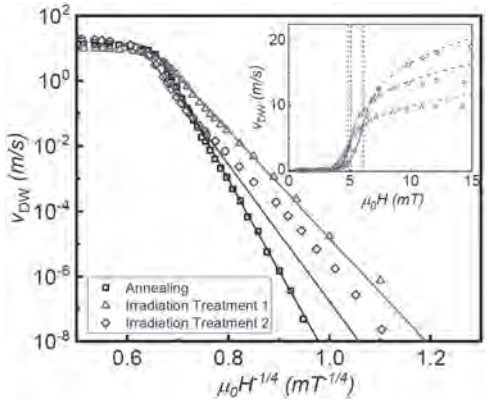

Fig. 1 DW velocity as a function of the OOP magnetic field strength. The solid and dashed lines are fits in the creep and depinning regimes. The inset shows the depinning transition. The dotted vertical lines denote the depinning fields H_{dep}.

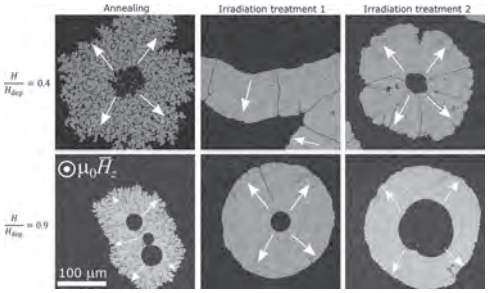

Fig. 2 Differential Kerr microscopy images showing DW expansion at zero magnetic field after an OOP field pulse at two different values of H/H_{dep}, with H_{dep} the depinning field. The white arrows denote the direction of expansion of the DW.

HOA-09. Role of the thermal magnetization fluctuation in depinning of domain wall from constraints on the ferromagnetic nanowire. *S. Ahn*[1,2] *1. Center for Semiconductor Technology Convergence, Pohang University of Science and Technology (POSTECH), Pohang 37673, Gyeongbuk, The Republic of Korea; 2. Department of Electrical Engineering, Pohang University of Science and Technology (POSTECH), Pohang 37673, Gyeongbuk, The Republic of Korea*

It is important to understand physically how to reliably control the domain wall (DW), because the promising applications such as solid-state spintronic memories utilizing DW displacements along ferromagnetic nanowires (NWs) [1] are directly connected to the reproducibility of repeatable DW motion. As those are based on operations at room temperature, extensive studies on how the thermal effect on DW depinning can be controlled by various geometrical and methodological considerations should be required for enhancing controllabilty of the DW motion. In the previous study, we have found that their depinning fields from artificial constraints (notches) on ferromagnetic NWs can be experimentally oscillated under a magnetic field H_T transverse to the nanowire [2]. Interestingly, this study is focused on the thermal fluctuation of the 2D magnetization (M) vector, $\underline{m}(\underline{r},t)=m_x(\underline{r},t)\underline{x}+m_y(\underline{r},t)\underline{y}$ [3]. Figure 1(a) shows noise spectra in magnetization components at specific frequencies under H_T. Figure 1(b) depicts schematics of thermal M fluctuation at each frequency corresponding to Fig. 1(a), which means the red region indicates the highest magnetization fluctuation at each mode. It is clearly seen that the specific modes of thermal M fluctuations in the DWs exist and the trend of tilting-angle difference between magnetizations at mode 4 of Fig. 2(a) is consistent with that of depinning field from notches as shown in Fig. 2(b). This depinning behavior is related to the thermal M fluctuation in the DWs pinned at the notches, as confirmed by a micromagnetic simulation.

[1] S. Parkin and S. –H. Yang, Nature Nanotech. 10, 195 (2015). [2] S.-M. Ahn *et al*., J. Nanosci. Nanotechnol. 11, 6472 (2011). [3] N. Smith, J. Appl. Phys. 90, 5768 (2001).

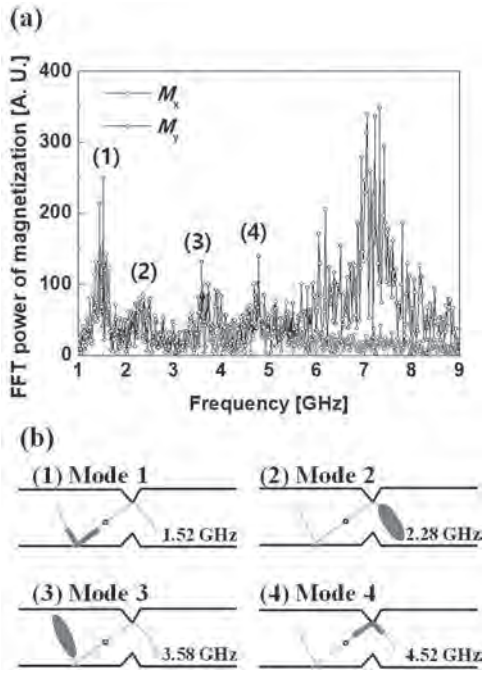

Fig. 1 (a) Noise spectra in magnetization components (m_x and m_y). (b) Schematic maps of thermal M fluctuations at specific frequencies, (1) 1.52 GHz, (2) 2.28 GHz, (3) 3.58 GHz, and (4) 4.52 GHz.

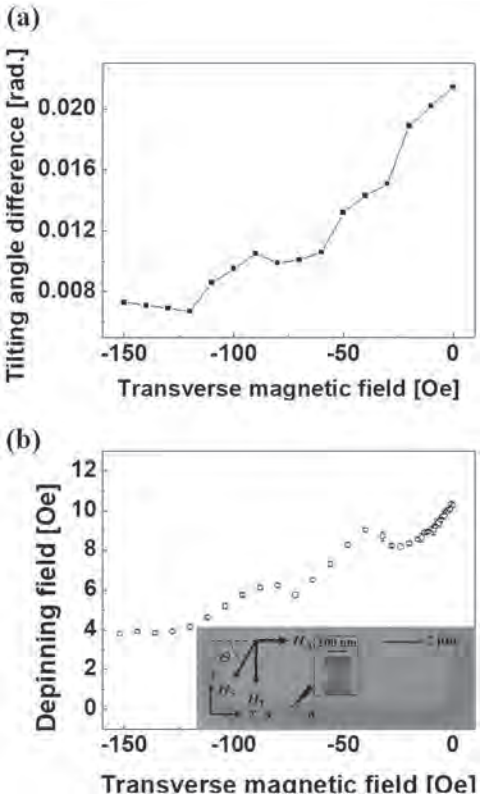

Fig. 2 (a) Tilting-angle difference for the depinning field with respect to H_T (simulation). (b) The depinning field as a function of H_T. Inset : High resolution image of U-shaped 350-nm-wide Permalloy nanowire structure with double notches.

HOA-10. Oersted-Field Driven Domain-Wall Motion in Core-Shell Nanotubes. M. Scheuerlein[1], M. Jaber[2], A. Masseboeuf[2], W. Ensinger[1], S. Finizio[3] and *O. Fruchart[2] 1. Technical University Darmstadt, Darmstadt, Germany; 2. SPINTEC, Grenoble, France; 3. Paul Scherrer Institut, Villigen, Switzerland*

Magnetic nanowires have been investigated for decades as a prototypical one-dimensional situation for micromagnetics and domain-wall motion [1]. More recently magnetic nanotubes have been considered, with the inner versus outer diameter as an extra degree of freedom. Nanotubes offer even more elaborate situations if core-shell structures are considered, *e.g.*, opening the field to spintronic effects, which require interfaces between different materials. Here, we consider nanotubes of diameter 580nm made of a ferromagnetic shell, with a material chosen to favor azimuthal magnetization, here CoNiB [2], and a metallic core, fabricated by several steps of electroless deposition in porous polycarbonate membranes. Each layer is a few tens of nanometers thick. The membranes are dissolved, tubes are dispersed on a highly-resistive Si wafer and single objects are contacted electrically by laser lithography. Magnetic imaging is performed under static conditions using XMCD combined with STXM. We evidence than nanosecond pulses of current enable the motion of domain walls separating domains with opposite azimuthal circulation. The direction of motion is opposite between consecutive walls, consistent with the OErsted field as a driving force. We report domain-wall speed above 100m/s with current density around 10^{11} A/m^2, translating in a magnetic field around 10mT. This prooves the concept of using nanotubes as a platform for the application of sub-ns pulses of magnetic field with strength potentially 100mT or more, which is out of reach of flat stripline geometries, and explore new physics of domain-wall motion under very strong stimulus.

[1] M. Stano, O. Fruchart, Magnetic nanowires and nanotubes, in Handbook of magnetic materials, 27, E. Brück Ed. Elservier (2018) [2] M. Stano, S. Schaefer, A. Wartelle, M. Rioult, R. Belkhou, A. Sala, T. O. Mentes, A. Locatelli, L. Cagnon, B. Trapp, S. Bochmann, S. Martin, E. Gautier, J.-C. Toussaint, W. Ensinger, O. Fruchart, Flux-closure domains in high aspect ratio electroless-deposited CoNiB nanotubes, SciPost Physics, 5 (4), 038 (2018)

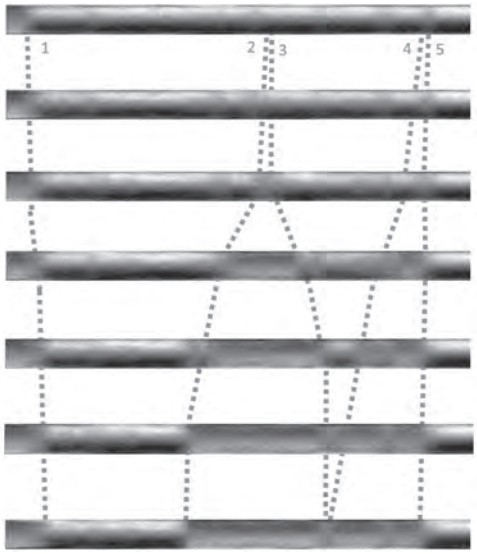

Following OErsted-field driven domain-wall motion (labeled 1 to 5) between ns pulses of electric current in a 560nm core-shell nanotubes. Some domain walls remain pinned after a few pulsed under the strength of current used here.

HOA-11. Analysis of magneto-transport properties in $Mn_{4-x}Au_xN$ epitaxial films and their magnetic structures by x-ray magnetic circular dichroism. *T. Horiuchi*[2], T. Komori[2], T. Hirose[2], T. Yasuda[2], K. Amemiya[1], K. Toko[2] and T. Suemasu[2] *1. KEK-IMSS, Tsukuba, Japan; 2. Univ. of Tsukuba, Tsukuba, Japan*

Antiperovskite ferrimagnetic Mn_4N film is a candidate for the domain wall (DW) motion devices. It possesses perpendicular magnetic anisotropy and small spontaneous magnetization (M_S ~ 80 kA/m). Due to these properties, we achieved a high DW velocity (v_{DW} ~ 900 m/s) with a current density $j = 1.3\times10^{12}$ A/m^2 only by spin transfer torque at RT[1]. Besides, magnetic compensation (MC) composition in $Mn_{4-x}Ni_xN$ was found by x-ray absorption spectroscopy (XAS) and x-ray magnetic circular dichroism (XMCD) measurements[2]. Using microstrips of $Mn_{4-x}Ni_xN$ at the vicinity of MC, we achieved v_{DW} ~ 3,000 m/s at $j = 1.2\times 10^{12}$ A/m^2 [3]. Now, we have focused on $Mn_{4-x}Au_xN$ epitaxial films as another candidate because a previous research reported the sign reversal of AHE at 155 K in Au-doped Mn_4N films fabricated onto MgO(001)[4]. In this work, we succeeded in the epitaxial growth of $Mn_{4-x}Au_xN$ films on $SrTiO_3$(001) and observed the sign reversal of AHE at RT. We prepared 23-nm-thick $Mn_{4-x}Au_xN$ (x = 0.0, 0.1 and 0.2) films onto $SrTiO_3$(001) substrates by molecular beam epitaxy. Hall effect measurements were conducted with physical properties measurement system. XAS and XMCD measurements were performed at the twin APPLE-II undulator beamline BL-16A of KEK-PF in Japan. The magnetic fields of ± 5T and circularly polarized x-rays were applied at an incident angle of 54.7° (magic angle)[5] from the sample normal. Figure 1 shows the transverse resistivity ρ_{xy} of $Mn_{4-x}Au_xN$ epitaxial films. The sign of AHE was reversed between x = 0.1 and 0.2. Figure 2 shows XAS and XMCD spectra of Mn-$L_{2,3}$ absorption edges. No significant difference was observed in the XAS spectra. In the XMCD spectra, the peak β of $Mn_{3.8}Au_{0.2}N$ appeared in the opposite direction

to that of $Mn_{3.9}Au_{0.1}N$. We consider that the sharp peak α originates mainly from isolated Mn atoms at corner (I) sites, whereas more-itinerant Mn atoms at face-centered (II) sites contribute to the broad peak β[6]. Thus, we conclude that the magnetic moment of Mn (II) changed its direction and became parallel to that of Mn (I), and the sign reversal of AHE was ascribed to this change.

[1] T. Gushi *et al.*, Nano Lett. 19, 8716 (2019). [2] T. Komori *et al.*, J. Appl. Phys. 127, 043903 (2020). [3] S. Ghosh *et al.*, Nano Lett. 21, 2580 (2021). [4] D. Li *et al.*, Mater. Res. Bull. 122, 110646 (2020). [5] T. Koide *et al.*, Phys. Rev. Lett. 87, 257201 (2001). [6] K. Ito *et al.*, Phys. Rev. B 101, 1 (2020).

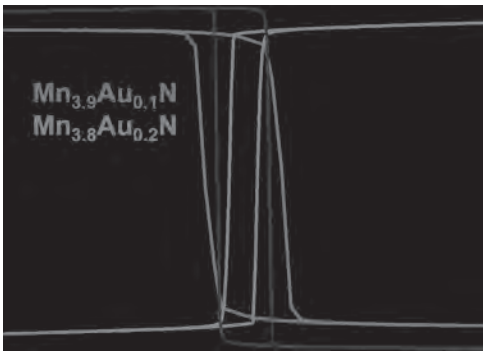

ρ_{xy} of $Mn_{4-x}Au_xN$ epitaxial films at RT

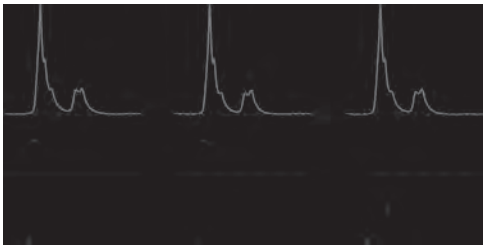

XAS and XMCD spectra in $Mn_{4-x}Au_xN$ epitaxial films at Mn-$L_{2,3}$ edges

HOA-12. All-Optical Switchable Racetrack based on Compensated Co/Gd quad-layers. *P. Li*[1], T. Kools[1], B. Koopmans[1] and R. Lavrijsen[1]
1. Applied Physics, Eindhoven University of Technology, Eindhoven, Netherlands

Co/Gd based synthetic ferrimagnets have received considerable attention owing to the coexistence of both pronounced spin-orbitronic effects and all-optical switching (AOS), allowing for novel, hybrid devices [1,2]. Previous studies [3,4] have shown that spin-orbit torque (SOT) driven domain wall motion in these 3d-4f ferrimagnets system is most efficient at angular momentum compensation. Following this notion, in this study, we explore the stack engineering of Co/Gd based synthetic ferrimagnets to achieve high SOT-driven domain wall motion at room temperature. Here, we experimentally demonstrate that magnetization compensation can be achieved and tuned by varying layer thicknesses in Co/Gd(x)/Co/Gd quad-layer systems (see inset of Fig. 1), which shows AOS in the full range of Gd thickness[5]. Fig. 1 (a) shows the coercivity and polar magneto-optical Kerr effect (MOKE)-signal in such a quad-layer system where the middle Gd layer is wedged. The sign change of the MOKE signal and divergence of the coercivity indicate a compensated system. The CIDWM velocity as a function of Gd thickness of this stack has been investigated, after structuring a series of domain wall conduits from another wedge sample grown in the same batch. In Fig. 1 (b) it can be observed that for low to moderate current densities the optimum in velocity can be found at compensation. As the current density is increased the optimum in velocity is found to shift towards larger Gd thicknesses, likely due to the difference in the temperature dependence of the magnetization in Co and Gd leading to a shift in the compensation thickness due to Joule heating during the applied current pulses. We further conducted further numerical modeling of the domain wall motion considering the Joule heating effect, a reasonable agreement was found [5]. Our study shows a significant improvement of the room temperature domain wall velocity in synthetic ferrimagnetic systems through stack engineering.

[1] Lalieu, M.L.M., *et al*. *Physical Review B* 96.22 (2017): 220411. [2] van Hees, Youri LW, *et al*. *Nature communications* 11.1 (2020): 1-7. [3] Caretta, L. *et al*. *Nature Nanotechnology* 13.12(2018): 1748-3395 [4] Blaesing, R. *et al*. *Nature Communications* 9.1(2018): 2041-1732 [5] Li *et al*. arXiv:2204.11595

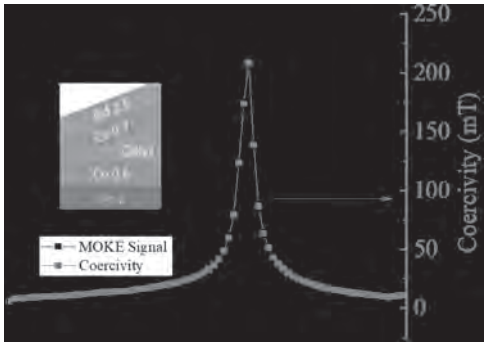

Fig. 1 Coercivity, polar MOKE signal (a) and current-driven domain wall velocity (b) as a function of Gd thickness in our multilayer system. The dashed vertical line in (b) indicates the Gd thickness for angular momentum compensation.

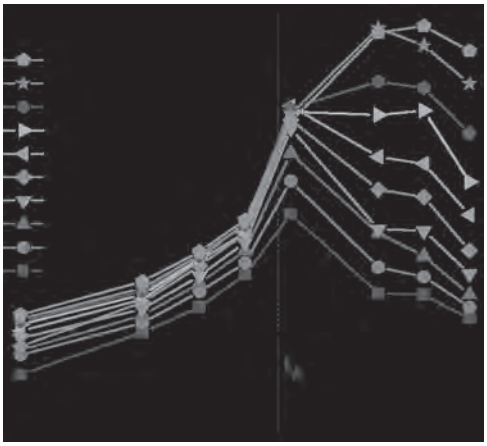

Fig. 2

HOA-13. Tuning domain wall edge pinning in microwires with He^+ irradiation. *J.W. van der Jagt*[1,2], M. Massouras[3], D. Mailly[3], E. Monteblanco[1], L. Herrera Diez[3], R. Juge[1] and D. Ravelosona[1,3]
1. Spin-Ion Technologies, Palaiseau, France; 2. Université Paris-Saclay, Gif-sur-Yvette, France; 3. Centre de Nanosciences et de Nanotechnologies, Palaiseau, France

Spintronic devices based on domain wall (DW) motion offer exciting new opportunities for non-volatile data storage, neuromorphic, and logic applications. However, extrinsic edge defects induced by standard nanofabrication processes can introduce DW edge pinning [1], significantly reducing the efficiency of DW motion-based devices. Edge pinning causes the DW in the wire to slow down at the edges, increasing its tensile energy, reducing its velocity and increasing its random behavior [2]. In this work, we address this problem by irradiating the edges of W-CoFeB-MgO micro-wires, with

widths between 5 μm and 40 μm, using a He^+ ion beam. He^+ irradiation is a powerful tool to engineer magnetic materials at the atomic scale enabling the precise control of magnetic properties [3] and the disorder of our material [4]. We show that the edge pinning can be tuned or even quenched depending on the irradiation fluence, resulting in a significant increase in the DW velocity in the narrower wires. To shed light on modulating the magnetic properties of magnetic wires, we first studied the effect of He^+ irradiation on the overall magnetic properties of W-CoFeB-MgO layers for different fluences. Then, different configurations of edge irradiation were used to modulate the edge magnetic properties. Fig. 1 shows two images of a DW moving through a 40-μm-wide wire. In Fig.1a, the edges are untreated and the DW has a positive curvature, *i.e.* the DW is slowed down by edge disorder. In Fig.1b, the edges are irradiated within the green rectangles. Before entering the irradiation zone, the DW still has positive curvature, but in the irradiated zone the curvature has become flat. This release in the tensile strength indicates a significant reduction in edge pinning due to local He^+ irradiation. Our results show that He^+ irradiation is a versatile tool, not only to post process magnetic properties in materials but also reduced extrinsic pinning due to nanofabrication process.

[1] Herrera Diez, V. Jeudy, G. Durin *et al.*, *Phys. Rev. B* 98, 054417 (2018) [2] Herrera Diez, F. Ummelen, V. Jeudy *et al.*, *Appl. Phys. Lett.* 117, 062406 (2020) [3] J. Fassbender, D. Ravelosona and Y. Samson, *J. Appl. Phys.* 37, R179 (2004) [4] J.W. van der Jagt, V. Jeudy, A. Thiaville *et al.*, *submitted* (2022)

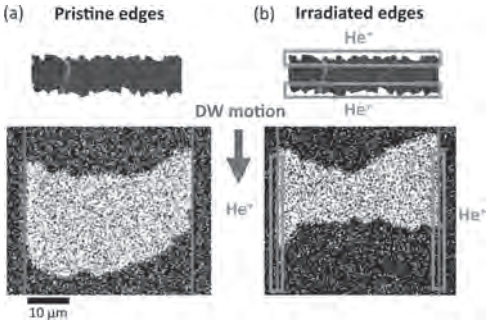

Differential Kerr microscopy images of a DW traveling through (a) a pristine wire, and (b) a wire with irradiated edges. The red vertical lines indicate the wire. The green rectangles denote the area irradiated with 10^{17} He^+ ions.

HOA-14. Emergence of sizeable interfacial Dzyaloshinskii-Moriya interaction at Cobalt/Fullerene spinterface. *E. Pandey*[1], B. Ojha[1] and S. Bedanta[1] *1. Physical Sciences, National Institute of Science Education and Research, Bhubaneswar, Khordha, India*

Interfacial Dzyaloshinskii-Moriya interaction (iDMI) originating at heavy metal(HM)\ferromagnet(FM) interface plays a crucial role in stabilizing chiral spin textures in magnetic multilayers [1]. Apart from HM, recently, a significant iDMI found to be originated from a FM\Graphene interface, owing to an enhanced Rashba spin-orbit coupling (SOC) of graphene [2]. Similarly, a curvature enhanced SOC has already been reported for other carbon (C) allotropes, namely, fullerene (C_{60}) and carbon-nanotubes (CNT) [3]. Thus, emergence of a sizeable iDMI can also be expected from the interface of C-allotrope\FM system. In this context, we have elucidated the magnetization reversal, domain wall (DW) dynamics and iDMI strength in Pd(4.0nm)/Co(0.5nm)/C_{60}(t_{C60})/Pd(2.0nm) system, where t_{C60}*= 0, 0.8 and 1.6nm*. DW velocity measured in the creep region revealed a two order higher DW velocity for the samples with 1.6nm thick C_{60}, due to lower depinning field and modified PMA in comparison to the sample without C_{60}. Further, DMI strength has been measured by the assymmetric domain expansion method using MOKE microscopy. A systematic increase in iDMI from -0.07 to -0.46 mJ/m^2 has been observed with increasing t_{C60} which turned the Bloch wall into left handed chiral Neel wall. Upon preparing a control sample we found that a finite iDMI has been originating from the Co/fullerene interface ($D_{Co/C60}$ ~ -0.10 mJ/m^2), which makes C based materials a promising candidate for chiral DW based device applications.

1. A. Fert, N. Reyren, and V., Nature Reviews Materials 2, 17031 (2017). 2. F. Ajejas, A. Gudin, R. Guerrero *et al.*, Nano letters 18, 5364 (2018). 3. D. Huertas-Hernando, F. Guinea, and A. Brataas, Physical Review B 74, 155426 (2006)

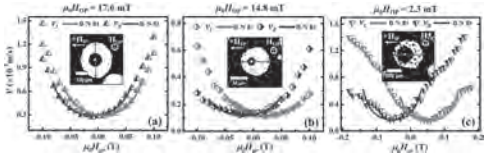

The pink and blue symbols represents the DW velocities along the left and right sides of the domains and plotted with the in-plane field $\mu_0 H_{IP}$, at a constant driving field $\mu_0 H_{OP}$, for samples with t_{C60} = 0, 0.8 and 1.6 nm in (a), (b) and (c) respectively. The solid lines represent the B-N fit of the curves by the modified creep law. The inset in each figure shows the direction of domain elongation w.r.t. the IP field ($\mu_0 H_{IP}$) direction. Scale bar for domains is shown in each figure separately.

HOA-15. Influence of Laser Cutting on Magnetic Domain Structure of Non-oriented Steel. C. Zhang[1] and *Y. Zhang*[1] *1. School of Electrical Engineering, Hebei University of Technology, Tianjin, China*

Facing on the global energy crisis, the power efficiency of electrical equipment has been paid more and more attention. Non-oriented electrical steel is chosen as the main core material of rotating motor due to its slightly magnetic anisotropy. As a new processing method, laser cutting is widely used in the processing of electrical steel due to its advantages of non-contact, high cutting speed and efficiency [1-4]. However, the stresses generated during the processing of electrical steel sheets largely affect the magnetic properties of the edge positions of motor core, resulting in a significant increase in core loss. Meanwhile, the macroscopic magnetic properties of ferromagnetic materials originate from the dynamic evolvement of magnetic domain structure. Thus, it is of great significance to study the variations of domain structure and grain size near the edge of silicon steel sheet after laser cutting[5-8]. In this paper, the various samples were manufactured by laser cutting, which micro-structure and magnetic domains were observed by magneto-optical Kerr microscope. Then, the nonlinear magnetic-mechanical properties after laser cutting was simulated by finite element model of non-oriented steel, including the distribution and variation of temperature and stress fields. It is concluded that the residual stress introduced by temperature after laser cutting is the primary cause of magnetic deterioration of non-oriented electrical steel. In mesoscopic, the residual stress results in the uneven pinning effect, which hinders the movement of magnetic domain walls and the rotation of magnetic moment. Moreover, the average width of the domain of the samples increases by two times and the moving velocity of the domain wall increases leading to the increase of hysteresis loss and abnormal loss. The effect of laser cutting on grain morphology near the cutting edge is relatively small, while the hardness near the cutting edge hardly changes. Therefore the experimental and theoretical method in the paper proved to be effective and intuitive for the mass engineering process of silicon steel in power electrical industry.

[1]Herzog D, Jaeschke P, Meier O, et al. Investigations on the thermal effect caused by laser cutting with respect to static strength of CFRP[J]. International Journal of Machine Tools & Manufacture, 2008,48(12-13):1464-1473. [2]Riveiro A, Quintero F, del Val, et al. Laser cutting of aluminum alloy Al-2024-T3[J]. Procedia Manufacturing, 2017,13:396-401. [3]Araujo E G, Schneider J, Verbeken K, et al. Dimensional effects on magnetic

properties of Fe–Si steels due to laser and mechanical cutting[J]. IEEE Transactions on Magnetics, 2010, 46(2): 213-216. [4]B.S. Yilbas, Akhtar S, Karatas C. Laser circular cutting of Kevlar sheets: Analysis of thermal stress filed and assessment of cutting geometry[J]. Optics & Laser Technology, 2017, 96:180-189. [5]Fu C H, Sealy M B, Guo Y B, et al. Finite element simulation and experimental validation of pulsed laser cutting of nitinol[J]. Journal of Manufacturing Processes, 2015,19. [6]Yilbas B S, Arif A F. Laser cutting of steel and thermal stress development[J]. Optics and Laser Technology, 2010,43(4). [7]Gbordzoe S, Yarmolenko S, Kanakaraj S, et al. Effects of laser cutting on the structural and mechanical properties of carbon nanotube assemblages[J]. Materials Science and Engineering, 2017,223:143-152. [8]Loisos G and Moses A J. Effect of mechanical and Nd:Y AG laser cutting on magnetic flux distribution near the cut edge of non-oriented steels[J]. Journal of Materials Processing Technology, 2005,161(1-2):151–155.

Session HOB
MAGNETIZATION DYNAMICS AND MICROMAGNETICS
Gabriel David Chaves-O'Flynn, Chair
Polska Akademia Nauk Instytut Fizyki Molekularnej, Poznan, Poland

CONTRIBUTED PAPERS

HOB-01. Field-free CoFeB/Ta/CoFeB SOT Devices Achieved by Modulating Spacer Thickness:Simulation and Experiment. *Y. Lin*[1], C. Cheng[1], W. Chan[2], Y. Huang[1], Y. Lin[2], Y. Huang[1], M. Chen[3], S. Chang[3], G. Chen[2] and Y. Tseng[1] *1. National Yang Ming Chiao Tung University, Hsinchu, Taiwan; 2. National Chung Cheng University, Hsinchu, Taiwan; 3. Powerchip Semiconductor Manufacturing Corporation, Hsinchu, Taiwan*

We demonstrate field-free spin–orbit torque (SOT) switching in a perpendicular CoFeB/Ta/CoFeB tri-layer device through manipulation of inter-layer exchange coupling. This finding is based on experimental and simulation results. In the Ta thickness range of 0.5~3 nm, the device exhibited a clear Ruderman–Kittel–Kasuya–Yosida (RKKY) oscillation where the anisotropy can be modulated. This resulted in a tilted magnetic moment and thus created a tunable SOT switching window. We found that the SOT switching current density (J_c) also appeared to vary with the Ta thickness (t_{Ta}). By cross-tuning the anisotropy and J_c with Ta spacer thickness, field-free SOT can be enabled in this tri-layer system. With microspin simulation we show that, when the out-of-plane spin polarization from the pinned layer generated a torque that broke the symmetry of the free layer, precession could be enabled along the x-y plane. This made it possible to achieve perpendicular magnetization switching without an external magnetic field by overcoming the damping torque. Through simulations we also confirm that the Neel orange peel effect became non-negligible due to interface roughness and coupling effect in the presence of perpendicular anisotropy. Fortunately, the Neel field induced by the Neel orange peel effect was found to favor the zero-field reversal.

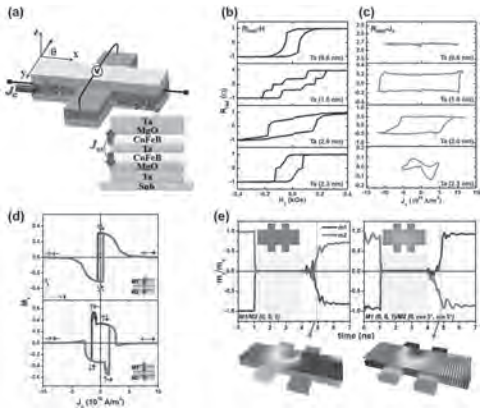

Fig.1 (a) Schematic illustration of the Ta/MgO(1)/CoFeB(1.2)/Ta(1.0)/CoFeB(1.2)/MgO(1)/Ta (thickness in nanometer) Hall bar device and corresponding measurement configuration. (b) Hall resistance (R_{Hall}) v.s. perpendicular magnetic field (H_z) for the proposed device with varying t_{Ta}. (c) Current-induced magnetic switching with varying t_{Ta}. (d) Upper figure: macro-simulated M_z v.s. J_c with M1 tilting from +Z to +Y by 20 deg. but M2 lying perfectly along +Z direction; lower figure: simulated M_z v.s. J_c with M1 lying along + Z direction but M2 tilting from + Z to + Y by 20 deg. (e) micro-simulated switching of the proposed device; left: both M1 and M2 with (001) alignment; right: M1 with (001) but M2 with (0, cos5°, sin5°) alignment. Snapshots of the magnetization reversal configurations corresponding to the two switching conditions, which were taken at ~4.9 ns (marked by vertical dashed lines).

HOB-02. Energetics of the Spin-Flop and Spin-Flip Transitions in Antiferromagnets. M. Hu[1], M.A. Hoefer[1] and *M.J. Donahue*[2] *1. University of Colorado Boulder, Boulder, CO, United States; 2. NIST, Gaithersburg, MD, United States*

Antiferromagnets (AFM) exhibit a host of properties which make them attractive materials for applications. Although they are robust against perturbation by external magnetic fields, magnetic phases do manifest in bipartite AFMs depending on the applied field and the material properties. The phases are surprisingly complex even in the small particle limit where the individual lattices are uniformly magnetized. While previous work [1,2,3,4,5] has examined similar systems and determined some of the equilibrium states, this work comprehensively identifies all critical energy points (local minima, local maxima, saddle points) under the macrospin model [6] where the energy is composed of an applied field (h_0) aligned with a uniaxial anisotropy (h_k) mediated by a spatially homogeneous AFM exchange (h_e). Both easy axis (h_k>0) and easy plane (h_k<0) cases are considered. In this analysis eleven candidate magnetization configurations are identified as critical energy states. Six of these are shown to be local energy minima (metastable) for some range of material and field parameters, illustrated in the Fig. 1 phase diagram. Note the bi- and tristable regions in this diagram that can support hysteretic behavior. The lowest energy (ground) states, representing long-term stable phases in the presence of thermal effects, are presented in Fig. 2. Saddle points identified by this analysis determine the energy barrier between local minima and can be used to estimate the time scale for thermally activated switching. The transition between phases driven by changing h_0 is also studied, including in particular the well-known spin-flip and spin-flop behaviors [7]. Consideration of energy levels in this analysis shows that of the eleven candidate phases alluded to above, the five which are never local energy minima also do not occur during adiabatic phase transitions.

1) F. B. Anderson and H. B. Callen, *Phys. Rev.,* 136, p. A1068 (1964). 2) N. Yamashita, *J. Phys. Soc. Jpn.,* 32, p. 610 (1972). 3) A. N. Bogdanov and U. K. Rößler, *Appl. Phys. Lett.,* 89, p. 163109 (2006). 4) A.-V. Plamadă, D. Cimpoesu and A. Stancu, *Appl. Phys. Lett.,* 96, p. 122505 (2010). 5) H.-F. Li, *npj Comput. Mater.*, 2, p. 16032 (2016). 6) V. Baltz, A. Manchon, M. Tsoi, *Rev. Mod. Phys.*, 90, p. 015005 (2018). 7) N. Ntallis and K.G. Efthimiadis, *Comput. Mater. Sci.*, 97, p. 42 (2015).

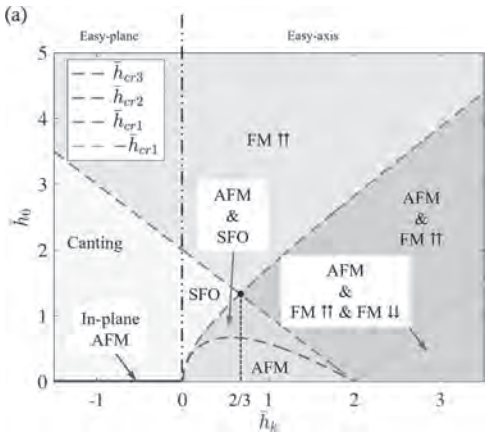

Fig. 1: Phase diagram for energetically stable (local energy minima) configurations in an AFM. SFO (spin-flopped) is an easy-axis canted phase. All parameters and fields are scaled by h_e, denoted by a bar on top.

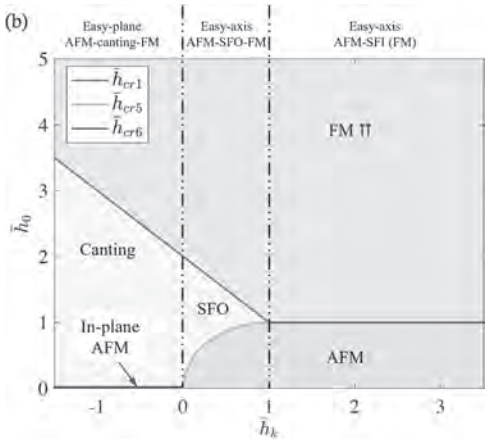

Fig. 2: Phase diagram for energetically preferred configurations (global energy minima). All parameters and fields are scaled by h_e, denoted by a bar on top.

HOB-03. Micromagnetic Modelling of Multi Coupled Free Layers for Magnetic Tunnel Junction Devices. *M.G. Monteiro*[1,2], V. Kateel[1,2], K. Fan[1,2], J. De Boeck[1,2], K. Cai[1], S. Rao[1], S. Couet[1] and G.S. Kar[1]
1. IMEC, Leuven, Belgium; 2. Department of Electric Engineering (ESAT), KU Leuven, Leuven, Belgium

Magnetic Tunnel Junctions (MTJ) are one of the major building blocks of spintronics, used in random access memory designs due to non-volatility, endurance and fast switching. Regardless of the choice of writing scheme, e.g Spin-Transfer Torque (STT)[1] or Spin-Orbit Torque (SOT)[2], we need to tailor the intrinsic properties of the switchable magnet (the *Free Layer*) in order to ensure a high retention time of the magnetization state, representing a trade off with respect to the switching energy, i.e the more retention, the more energy required to operate the device. To overcome the dilemma and enable MTJs with high retention and low writing energy, a *Hybrid Free Layer* (HFL) concept has been previously proposed by integrating a Synthetic Antiferromagnet (SAF) stack into the widely used CoFeB/MgO Free Layer stack[3]. This HFL has two intrinsic interlayer couplings tailored by a SAF and SFM (synthetic ferromagnet) spacers (Fig. 1). The SAF spacer reduces the stray field and gives an exchange coupling torque from the motion of either layer II or III, leading to faster overall motion of the stack. The SFM spacer allows for flexibility in the choice of SAF design, as it couples the layer I directly to layer II, but also decouples the crystallization of the Tunneling Barrier interface from layer II, preventing lattice mismatching effects and bad electronic band conditions in a wide range of materials[4]. This work explores this design focusing on compensation of ground states (where the stack adds up to no field). We demonstrate by micromagnetics that adding a SFM to a SAF stack impacts the energy and layer trajectories in non-trivial ways. For instance, in Fig. 2 the hysteresis loop of HFL stacks with both compensated equilibrium states and *Top Major* (layers I, II generate field) show that even at compensation point we have *degeneracy* of states, i.e regions of external field where both low/high energy states are stable. This contrasts with SAF only stacks where outside of compensation a behavior towards saturation is observed (Fig.2 Right). Different switching speeds can also be found by tailoring the coupling strengths.

[1] S. Sakhare et al., *2018 IEEE IEDM;* [2] S. Couet *et al*., *2021 Symposium on VLSI Technology*, 2021, pp. 1-2. [3] E. Raymenants et al., *Nature Electronics, volume 4, pgs 392–398* (2021). [4] Liu, E. et al., *IEEE Trans. Magn. 53, 1–5* (2017).

Fig.1 HFL design with top MTJ.

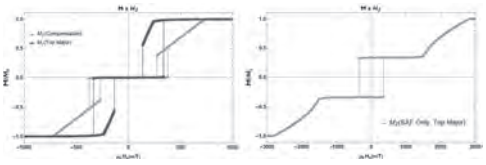

Fig. 2 HFL (left) and SAF (right) hysteresis loops.

HOB-04. Bloch points in helimagnetic nanostrips. *M. Lang*[1,2], M. Beg[1,3], O. Hovorka[1] and H. Fangohr[1,2] *1. Faculty of Engineering and Physical Sciences, University of Southampton, Southampton, United Kingdom; 2. Max Planck Institute for the Structure and Dynamics of Matter, Hamburg, Germany; 3. Department of Earth Science and Engineering, Imperial College London, London, United Kingdom*

Complex magnetic materials hosting topologically non-trivial particle-like objects such as skyrmions are intensely researched and could fundamentally change the way we store and process data. One important class of materials are helimagnetic materials with Dzyaloshinskii-Moriya interaction. Recently, it was demonstrated that nanodisks consisting of two layers with opposite chirality can host a single stable Bloch point of two different types [1]. The Bloch point represents an interesting topological excitation in a helimagnetic system, which expands the set of well-known magnetic states such as domain walls, vortices, and skyrmions. In this work [2], we use micromagnetic simulations [3, 4] to show that FeGe nanostrips consisting of two layers with opposite chirality can host multiple coexisting Bloch points. We demonstrate that the two different Bloch-point types (Fig. 1) can

be geometrically arranged in any arbitrary order, and these magnetization configurations are meta-stable (within certain constraints on the strip width and length). We can determine an optimal spacing between Bloch points within a line of Bloch points (corresponding to a distance over which a Bloch point extends). This allows us to predict strip geometries suitable for an arbitrary number of Bloch points, which we verify for an example 80-Bloch-point configuration (Fig. 2).

[1] M. Beg et al., Scientific Reports, Vol. 9, p. 7959 (2019). [2] M. Lang et al. arXiv:2203.13689 (2022). [3] M. Beg, M. Lang and H. Fangohr, IEEE Transactions on Magnetics, Vol. 58, p. 7300205 (2022) [4] M. Beg, R. A. Pepper and H. Fangohr, AIP Advances, Vol. 7, p. 56025 (2017)

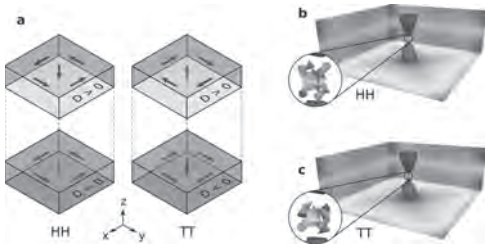

Fig. 1 (a) The Bloch-point configuration originates from vortices with identical circularity, but opposite polarisation, which are stabilised through the DMI of the material, which fixes the core orientation relative to circularity through the left- or right-handed chirality. (b, c) Simulation results for the two different Bloch-point types.

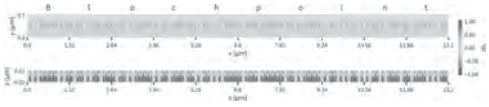

Fig. 2 ASCII encoding of the string "Blochpoint" using 80 Bloch points. The two cross sections show an xy plane in the top layer and an xz plane at the Bloch-point position. The strip length is chosen according to the predicted value for a nostrip with width w = 100 nm.

HOB-05. Withdrawn

HOB-06. Geometry-driven dynamics of magnetic topological solitons.
K. Yershov[1,2] *1. IFW Dresden, Dresden, Germany; 2. Bogolyubov Institute for Theoretical Physics, Kyiv, Ukraine*

Here, we present the effect of the spontaneous drift of magnetic topological solitons (domain walls and skyrmions) in curved wires and films under the action of the curvature gradients without any external stimuli. For the case of 1D magnetic systems [1,2,3], the strength of curvature-induced driving is defined by the gradient of the curvature. At the same time, for the case of skyrmions [4], the strength of the curvature-induced driving is determined by the type of Dzyaloshinskii--Moriya interaction, while the trajectory is determined by the type of magnetic ordering. Using a collective variable approach we derive effective equations of motion for the domain walls and skyrmions. (i) It is shown that a local bend of a nanowire is a source of pinning potential for a domain wall. Eigenfrequency of the domain wall free oscillations at the pinning potential and the effective friction are determined as functions of the curvature. (ii) We show that for the case of Neel skyrmion the driving force is linear with respect to the gradient of the curvature, while for Bloch skyrmion the driving is proportional to the product of mean curvature and its gradient. During the motion along the surface, skyrmion experiences deformation which depends on the skyrmion type. All analytical predictions are confirmed by numerical simulations.

1. Kostiantyn V. Yershov, Volodymyr P. Kravchuk, Denis D. Sheka, and Yuri Gaididei, Phys. Rev. B 92, 104412 (2015) 2. Kostiantyn V. Yershov, Volodymyr P. Kravchuk, Denis D. Sheka, Oleksandr V. Pylypovskyi, Denys Makarov, and Yuri Gaididei, Phys. Rev. B 98, 060409(R) (2022) 3. Kostiantyn V. Yershov, Phys. Rev. B 105, 064407 (2022) 4. Kostiantyn V. Yershov, Attila Kákay, and Volodymyr P. Kravchuk, Phys. Rev. B 105, 054425 (2022)

HOB-07. Micromagnetics and Current-Induced Domain-Wall Dynamics in Chemically-Modulated Nanowires.
L. Alvaro-Gomez[1,2], S. Ruiz-Gómez[3], C. Fernández González[2,4], M. Schöbitz[1,5], N. Mille[6], D. Tiwari[1], M. Foerster[7], L. Aballe[7], R. Belkhou[6], J. Toussaint[8], C. Thirion[8], A. Masseboeuf[1], D. Gusakova[1], L. Pérez[2,4] and *O. Fruchart*[1]
1. SPINTEC, Grenoble, France; 2. IMDEA Nanociencia, Madrid, Spain; 3. Max Planck Institute for Chemical Physics of Solids, Dresden, Germany; 4. Dpto. de Fisica de Materiales, Universidad Complutense de Madrid, Madrid, Spain; 5. Univ. Erlangen-Nürnberg, Erlangen, Germany; 6. Synchrotron SOLEIL, Gif-sur-Yvette, France; 7. ALBA Synchrotron Light Facility, Barcelona, Spain; 8. Institut Néel, Grenoble, France

Cylindrical magnetic nanowires are a textbook platform to explore various magnetization phenomena. For instance, they host a unique type of magnetic domain wall (DW) known as the Bloch-point wall (BPW), whose topology is expected to enable ultrafast DW motion [1]. We recently provided the first experiment evidence for BPW motion under oure STT (no field assistance) with velocities above 600 m/s[2]. Here, we propose a more elaborate nanowire system comprising long Permalloy segment separated by specific short modulations of composition ($Fe_{80}Ni_{20}$). Besides, the heat management during the electric pulse was improved by packaging in an insulating overlayer. We used several types of x-ray magnetic microscopies to access the three-dimensional magnetization textures, all based on XMCD: PEEM in shadow mode: PEEM, TXM, STXM and ptychography at ALBA and SOLEIL synchrotrons. Magnetic images reveal curling of magnetization around the wire axis at the chemical modulations, which results from the occurence of magnetic charges at the interface between materials, due to magnetization mismatch. We analyzed quantitatively the experiments, and provide both analytical modeling and numerical simulations providing a comprehensive overview of the phenomenon. We evidence the deterministic switching of BPW and modulation switching driven by the Œrsted field, above a certain current density [3]. We also witnessed different current-induced events: transformation from BPW to TVW and viceversa, DW expulsion out of the modulation, DW coming to the modulation, and DW motion between modulations (Fig. 1). The direction of motion was 80% of the events along STT. DW velocities obtained exceeds theoretical limits, opening new aspects to clarify.

[1] R. Hertel, *J. Phys. Condens. Matter* 28, 483002 (2016). [2] M. Schöbitz, et al., *Phys. Rev. Lett.* 123, 217201 (2019). [3] L. Alvaro-Gomez et al., arXiv 2205.06705

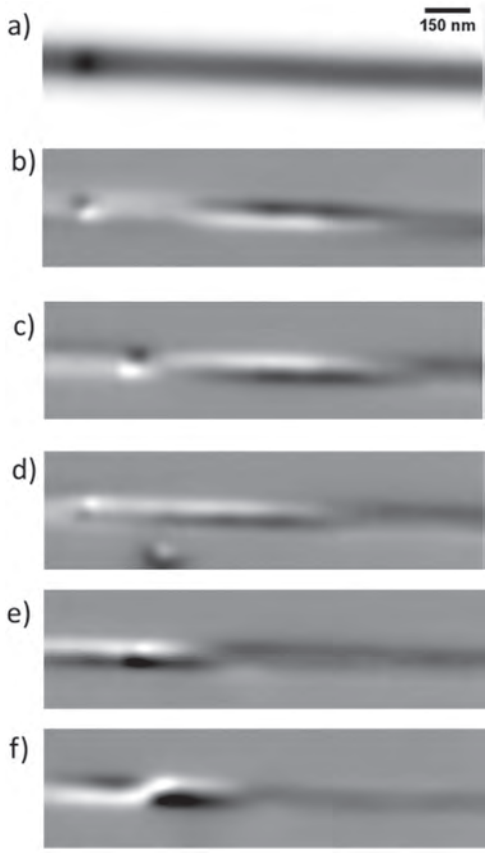

a) Ptychographic XAS reconstructed image at the Fe L3 edge of a 110 nm diameter permalloy nanowire with a $Fe_{80}Ni_{20}$ chemical modulation of 20 nm length. b) XMCD image of a). c) d) e) f) XMCD images show DW dynamics under consecutive 1 ns electric pulses of amplitudes (0.46, 1.18, 3.20, 3.20) x 10^{12} A/m^2 respectively.

HOB-08. Reconfigurable domain wall pinning in synthetic antiferromagnets. T. Lee[1], S. Jeong[2], S. Kim[2] and *K. Kim[1] 1. Physics, Korea Advanced Institute of Science and Technology, Daejeon, The Republic of Korea; 2. Physics, Ulsan University, Ulsan, The Republic of Korea*

Magnetic domain wall (DW) motion has been received much attention owing to its potential for applications in next-generation computing devices, such as memory [1], logic [2], and neuromorphic devices [3]. In such devices, it is essential to manipulate the domain wall position in a controllable way. The extrinsic pinning sites such as 'notch' have conventionally been used for the reliable positioning of DW. However, such extrinsic pinnings are not relevant in device applications because the extrinsic treatments cause the damage to the sample. Furthermore, the pinning position is not reconfigurable because the extrinsic treatments change the properties of sample permanently. In this study, we present a novel method to control the DW position in a damage-free and reconfigurable way. We utilize the interdomain wall interaction in synthetic antiferromagnets (SAF). The SAF is composed of two magnetic layers separated by non-magnetic spacer. In this system, domain wall at the bottom layer ('bottom-DW') feels the dipolar field from the DW at the top layer ('top-DW'). As the dipolar field produces the repulsive force to the DW, the bottom-DW can be effectively pinned by the top-DW. Therefore, the top-DW can act as an effective pinning site for the bottom-DW motion. We demonstrated this idea experimentally that the bottom-DW can be pinned by top-DW for both the field- and current-driven DW motion. Furthermore, we found that the position of pinning site can be freely changed by changing the position of top-DW. Our work demonstrates the damage-free and reconfigurable pinning site for the DW motion, which could provide a novel functionality for DW-motion-based spintronics applications.

[1] S. Parkin, *et al. Science* Vol. 320, 5873, p.190 (2008). [2] Z. Luo, *et al. Nature* Vol. 579, p.214 (2020). [3] T. Jin, *et al. J. Phys. D: Appl. Phys.* Vol. 52, 44, p.445001 (2019).

HOB-09. Coupled Néel-Brown magnetization dynamics of magnetic nanoparticles for thermal and magnetic particle imaging. *T.Q. Bui*[1], A.J. Biacchi[1], K.N. Quelhas[1], F.M. Abel[1], M. Henn[1], E. De Lima Correa[1], W.L. Tew[1], A.R. Hight Walker[1], C. Dennis[1], M.J. Donahue[1], P.N. Haney[1] and S.I. Woods[1] *1. National Institute of Standards and Technology, Gaithersburg, MD, United States*

The prospect of thermal imaging and control in magnetic particle imaging (MPI) is an important advancement for non-invasive medical diagnostics and therapeutics. Current MPI systems focus mainly on imaging from measurement of nanoparticle concentrations. Accurate derivation of temperature relies on detailed understanding of magnetization dynamics in the presence of AC drive fields and variable temperature [1]. It is well established that MPI performance is critically impacted by nanoparticle relaxation dynamics [2]. The dynamic response of magnetic nanoparticles in magnetic fields depends strongly on the particles' magnetic and structural properties, inter-particle interactions, and the local environment. We report an arbitrary-wave magnetic particle spectrometer for characterizing dynamics over the 200 K to 350 K temperature range. These measurements can separately identify features of Brownian and Néel relaxation and quantify the timescales and amplitudes associated with these processes. Here, we discuss measurements of magnetization dynamics using AC susceptibility and pulsed excitation for ferrite and cobalt-doped ferrite nanoparticles ranging in diameter from 7 nm to 70 nm. For example, Fig. 1 show the imaginary component, χ'', peak frequency for two different sizes of ferrite nanoparticles [3]. Fig. 2 shows the time domain measurement of 7 nm cobalt-doped ferrite under pulsed excitation in which both field-on and field-free relaxation are observed and quantified. Frequency and time domain measurements for cobalt-doped ferrites show the presence of both Néel and Brownian dynamics, and the temperature dependence reveals their intrinsic coupling. To resolve this coupling, we used stochastic Monte Carlo methods to simulate the field and temperature dependence of magnetization dynamics. This knowledge will eventually inform strategies for design of magnetic nanoparticles with properties targeted for accurate and sensitive thermal imaging using MPI.

[1] Thinh Q. Bui, Weston L. Tew, Solomon I. Woods. "AC magnetometry with active stabilization and harmonic suppression for magnetic nanoparticle spectroscopy and thermometry." *J. Appl. Phys*. 128, 224901 (2020). [2] Zhi Wei Tay, Daniel W Hensley, Erika C Vreeland, Bo Zheng, Steven M Conolly. "The Relaxation Wall: Experimental Limits to Improving MPI Spatial Resolution by Increasing Nanoparticle Core size." *Biomed Phys. Eng. Express*, 3 (3), 035003 (2017) [3] Thinh Q. Bui, Adam J. Biacchi, Cindi L. Dennis, Weston L. Tew, Angela R. Hight Walker, Solomon I. Woods. "Advanced characterization of magnetization dynamics in iron oxide magnetic nanoparticle tracers." *Applied Physics Letters*, 120, 012407 (2022).

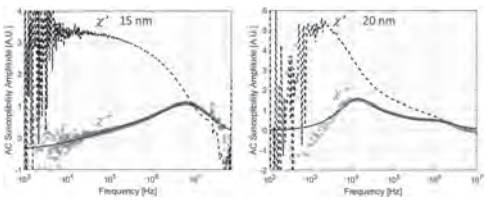

Fig. 1: ACS spectrum of 15 and 20 nm ferrites. The real (χ') imaginary (χ'') parts, and fits (blue) using a semi-empirical analytical model.

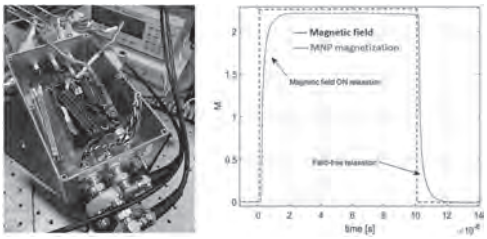

Fig. 2: Magnetic field (~ 5 mT) with 20 ns rise time (blue). Magnetization step-response of 7 nm cobalt-doped ferrite (red).

HOB-10. Magnetic Coupling in asymmetric $Co_{65}Fe_{35}$/Ru Heterostructures. *U. Karki*[1], B. Nepal[1], G.J. Mankey[1] and T. Mewes[1]
1. Physics and Astronomy, The University of Alabama, Tuscaloosa, AL, United States

We investigated the bilinear and biquadratic exchange coupling strengths in sputtered $Co_{65}Fe_{35}$(10 nm)/Ru(t_{ru})/$Co_{65}Fe_{35}$(5 nm) structures, where the ruthenium thickness t_{ru} varies from 0.30 nm to 1 nm in 0.05 nm step size. We used broadband ferromagnetic resonance (FMR) and vibrating sample magnetometer (VSM) techniques for the quasi-static and dynamic magnetic characterization of the samples. The change from ferromagnetic and antiferromagnetic coupling is clearly seen in the hysteresis loops. Using a Stoner-Wohlfarth model, we fit hysteresis loops and determine the bilinear and biquadratic exchange coupling constants J_1 and J_2 respectively. However, this analysis is limited to samples with thicknesses of ruthenium spacer layer that result in antiferromagnetic coupling. Similar to B. Khodadadi et. al [1], we also observed a systematic frequency dependence of the field separation between the acoustic and optic modes when studying the dynamic response of the heterostructures. This is caused by the difference of the effective magnetization M_{eff} of the two layers of $Co_{65}Fe_{35}$. Broadband FMR characterization enables extraction of the coupling constants for both ferromagnetically and antiferromagnetically coupled structures.

[1] B. Khodadadi, J. B. Mohammadi, J. Jones, Physical Review Applied., 8, 014024 (2017)

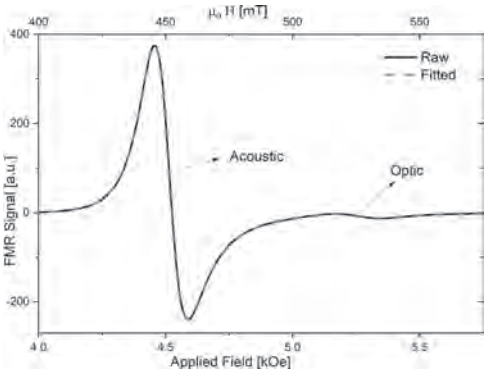

Fig.1 : Raw and fitted FMR spectra at 30 GHz microwave frequency showing the acoustic and optic mode of trilayer $Co_{65}Fe_{35}$(10 nm)/Ru (0.60 nm)/$Co_{65}Fe_{35}$(5 nm)

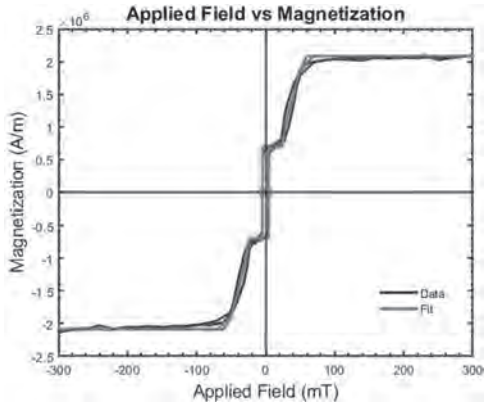

Fig. 2 : Hysteresis curve with fit using Stoner-Wolfarth model of trilayer $Co_{65}Fe_{35}$(10 nm)/Ru (0.60 nm)/$Co_{65}Fe_{35}$(5 nm)

HOB-11. Domain Walls Dynamics in Randomized Dzyaloshinskii-Moriya Interaction Mediated Amorphous Fe-Ge Thin Films. *A. Singh*[1], E. Holingworth[2], S.A. Morley[3], X. Chen[1,4], A.U. Saleheen[3], R. Tumbleson[1,5], M. McCarter[3], P. Fischer[1,5], F. Hellman[2], S. Kevan[3] and S. Roy[3,1] *1. Materials Sciences Division, Lawrence Berkeley National Laboratory, Berkeley, CA, United States; 2. Department of Physics, University of California, Berkeley, CA, United States; 3. Advanced Light Source, Lawrence Berkeley National Laboratory, Berkeley, CA, United States; 4. NSLS2, Brookhaven National Laboratory, Upton, NY, United States; 5. Department of Physics, University of California, Santa Cruz, CA, United States*

Amorphous magnetic systems provide a unique platform to study dynamics of exotic spin-textures which are fundamentally intriguing and potentially promising for spintronics. A key question to address is how symmetric and anti-symmetric exchange coupling between atomic spins modulate the length scale of fluctuations near critical phase transition points [1, 2]. Amorphous Fe-Ge thin films is a prototype system whereby controlling the Fe concentration one can tune the magnitude and randomness of the symmetric Heisenberg exchange and anti-symmetric Dzyaloshinskii-Moriya interaction (DMI) respectively [3, 4]. In this work we performed soft x-ray photon correlation spectroscopy (XPCS) measurements to probe the nanoscale magnetic fluctuations of stripe domains in amorphous Fe_xGe_{1-x} thin films for x=0.51, 0.52 and 0.53 [5, 6]. At lower temperatures all the domains remain static but with increase in temperature few domains of certain length scales start showing higher fluctuations indicative of intermittent behavior. As temperature reaches the phase transition, domains of all length scales fluctuate collectively with increased magnitude showing the scale invariance nature at critical points. For similar reduced temperature, we observed dramatically activated fluctuations for Fe = 0.51 concentration. Such enhanced fluctuations away from the critical temperature could be driven by the proximity from a critical point that is quantum in origin [7]. The higher instability of the stripe domains with lowering in Fe concentration also corroborate the increased resistivity trend previously observed in those systems [3].

1]. J. Wild, T. N. G. Meier, S. Pöllath, Science Advances., 3, e1701704 (2017) 2]. L. Shen, M. Seaberg, E. Blackburn, MRS Advances., 6, 221, (2021) 3]. D. S. Bouma, Z. Chen, B. Zhang, Phys. Rev. B., 101, 014402 (2020) 4]. R. Streubel, D. S. Bouma, F. Bruni, Advanced Materials., 33, 2004830 (2021) 5].S. K. Sinha, Z. Jiang, and L. B. Lurio, Advanced Materials., 26, 7764 (2014) 6]. M. Holt, M. Sutton, P. Zschack, Physical Review Letters., 98, 065501 (2007). 7]. Y. Feng, J. Wang, R. Jaramillo, Proceedings of the National Academy of Sciences., 109, 7224, (2012)

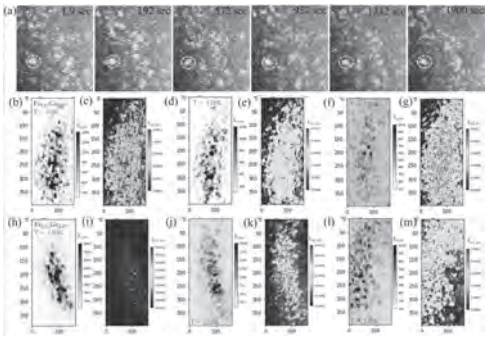

Figure 1. (a) Magnified images of the speckle pattern evolution at 210K for Fe = 0.52 from 1.9 sec to 1900 sec. Light blue and red color dotted circles showing a static and a dynamic portion respectively of the speckle pattern. Mean intensity (gray colormap) and temporal heterogeneity (jet colormap) of (b, d, f & c, e, g) $Fe_{0.51}Ge_{0.49}$ and (h, j, l & i, k, m) $Fe_{0.53}Ge_{0.47}$ at different temperatures. With increase in temperature more speckles fluctuate with higher amplitude. Red boxes in (b, h) maps the mean intensity with (c, i) fluctuation heterogeneity for same Q_r positions.

HOB-12. Magnetic Switching and Stoner-Wohlfarth Model of 2D Single Domain Magnets. *E. Ibrahim*[1] and S. Zhang[1] *1. Physics, University of Arizona, Tucson, AZ, United States*

Due to the strong spin fluctuation in two dimensions, the magnitude of the magnetization is highly dependent on both the exchange interaction and the magnetic anisotropy at any finite temperature and the existence of an energy gap is essential for the long-range order, which is known as the Wigner and Mermin theorem. As a result, the process of magnetic switching for the 2D magnets is completely different from the process we know for the 3D case. We show here several fundamentally different hysteresis properties between 2D and 3D magnets. The magnetization switching diagram known as the asteroid figure in the conventional Stoner-Wohlfarth model becomes highly temperature-dependent and asymmetric with respect to the transverse and longitudinal magnetic fields. Also, we show the difference in the magnetic switching dynamics between both cases. Our results provide new insights for 2D magnetic materials-based spintronics applications.

HOB-13. Current-induced magnetic octupole domain-wall dynamics. *M. Wu*[1,2], T. Chen[3], T. Nomoto[4], H. Isshiki[1], Y. Nakatani[5], T. Higo[6], T. Tomita[6], K. Kondou[2], R. Arita[4], S. Nakatsuji[6] and Y. Otani[1,2] *1. ISSP, The University of Tokyo, Kashiwa, Japan; 2. CEMS, RIKEN, Wako, Japan; 3. School of Physics, Southeast University, Nanjing, China; 4. Research Center for Advanced Science and Technology, The University of Tokyo, Hongo, Japan; 5. Department of Computer Science, University of Electro-Communications, Meguro-ku, Japan; 6. Department of Physics, The University of Tokyo, Hongo, Japan*

A magnetic domain wall is a topological soliton that extensively exists in magnetic materials. The electrical control of the magnetic domain walls is an essential technique for nonvolatile memory devices using magnetic bits. Past decades have witnessed well electrically controllable domain-wall applications, including nonvolatile memories and logic devices. Fast domain-wall velocities exceeding a few hundred meters per second are available in ferromagnets, ferrimagnets, and synthetic antiferromagnets. However, the required current density is as high as ~10^{12} A m^{-2} causing inevitable energy loss. On the other hand, AFMs with intrinsic terahertz spin dynamics have drawn considerable attention from the condensed matter physics community, which may provide a new perspective for the domain-wall study. In addition, the nature of the zero-stray field is favorable for miniaturization and high-density integration. Nevertheless, manipulating and detecting antiferromagnetic domain walls are challenging due to the poor magnetoelectric responses. The recent progress happened in both collinear[1] and noncollinear AFMs[2,3]. Notably, in noncollinear AFMs Mn_3X (X = Sn[2], Ge[3]), the magnetic octupole domain (MOD)[4] are both electrically[2,3] and optically[5,6] detectable; in addition, electrically manipulable[7] via spin-orbit torques using spin Hall materials. Our previous study[8] revealed the possibility of electrically nucleating, displacing, and detecting a MOD wall (MODW) using a wedged Mn_3Sn Hall device. However, we could not identify the detailed structure, sizeable velocity, and current-induced mechanism for MODW motion through the anomalous Hall detection. This work demonstrates the optical detection of the current-induced MODW dynamics in a microfabricated Mn_3Ge strip under a significantly small current density without a magnetic field. Moreover, our theoretical calculation reveals the novel spin-torque mechanism accounting for the MODW motion in noncollinear AFMs. Our results open a new route to developing a responsible mechanism for domain-wall-based antiferromagnetic spintronic devices. This work was partially supported by JST-CREST(No. JPMJCR18T3) and JST-Mirai (JPMJMI20A1).

[1] Wadley, P. *et al. Science.* 351, 587–590 (2016). [2] Nakatsuji, S., Kiyohara, N. & Higo, T. *Nature* 527, 212–215 (2015). [3] Kiyohara, N., Tomita, T. & Nakatsuji, S. *Phys. Rev. Appl.* 5, 064009 (2016). [4] Liu, J. & Balents, L. *Phys. Rev. Lett.* 119, 087202 (2017). [5] Higo, T. *et al. Nat. Photonics* 12, 73–78 (2018). [6] Wu, M. *et al. Appl. Phys. Lett.* 116, 132408 (2020). [7] Tsai, H. *et al. Nature* 580, 608–613 (2020). [8] Sugimoto, S. *et al. Commun. Phys.* 3, 1–9 (2020).

Session HOC
NEW APPROACHES IN COMPUTATIONAL MAGNETISM
Michael Joseph Donahue, Chair
National Institute of Standards and Technology, Gaithersburg, MD, United States

INVITED PAPER

HOC-01. Generative deep learning for permanent magnet microstructures. A. Kovacs[1,2], A. Kornell[1,2], Q. Ali[1,2], J. Fischbacher[1,2], M. Gusenbauer[1,2], H. Oezelt[1,2], M. Yano[3], N. Sakuma[3], A. Kinoshita[3], T. Shoji[3], A. Kato[3] and *T. Schrefl*[1,2] *1. Christian Doppler Laboratory for Magnet design through physics informed machine learning, Wiener Neustadt, Austria; 2. Department for Integrated Sensor Systems, University for Continuing Education Krems, Wiener Neustadt, Austria; 3. Advanced Materials Engineering Div., Toyota Motor Corporation, Mishuku Susono, Japan*

Traditionally, imaging, magnetic measurements, and micromagnetic simulations have been applied to understand the impact of microstructure on the magnetic properties. Here, we apply a data-driven approach to map the microstructure of a nano-crystalline permanent magnet to its demagnetization curve. We represent the demagnetization curve by a few discrete anchor points and train a neural network regressor to predict these points from the granular structure. Once the model is trained, hysteresis properties can be estimated without the need of time-consuming simulation. To reduce the required number of micromagnetic simulations, we combine unsupervised and supervised learning. In a first step, we learn low-dimensional representations of the grain structures. This can be done in an unsupervised fashion. In a second step, we learn the mapping from a low-dimensional latent code that represents a grain structure to anchor points of the demagnetization curve. Through the dimensionality reduction step, we can reduce the number of trainable parameters in the neural network for prediction of the hysteresis properties. Therefore, less training data is needed. Fig. 1 compares the predictions the demagnetization curve for previously unseen granular structures with the ground truth. The mean absolute errors are $0.015M_s$ (magnetization) and $0.02H_A$ (anisotropy field) for the remanence and coercivitiy. For dimensionality reduction, we apply a variational autoencoder. It maps a 2D image of the grain structure to a latent code. Hereby we achieve a compression rate of 98 percent. Variational autoencoders are generative models which can generate new samples within the input space which differ from the original training set. Like face morphing, we generate new magnets by linear interpolation between two points in the latent space. Fig. 2 shows the generation of new magnet microstructures through morphing. The financial support by the Austrian Federal Ministry for Digital and Economic Affairs, and the Christian Doppler Research Association is gratefully acknowledged.

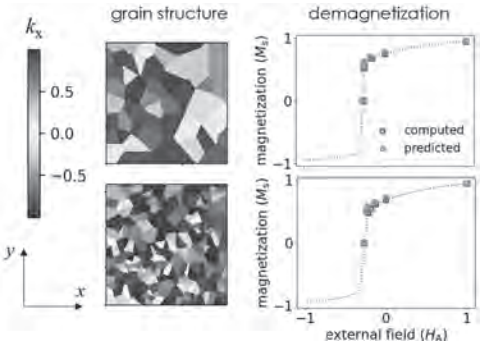

Fig. 1. Predictions of demagnetization properties from the granular structure.

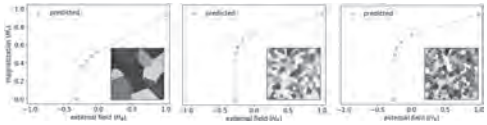

Fig. 2. The structure in the center was generated by morphing from the two other structures shown.

CONTRIBUTED PAPERS

HOC-02. Transformer Neural Networks for Predicting Magnetization Dynamics. *S. Pollok*[1], S.T. Kotewitz[1], N.M. Lassen[1] and R. Bjørk[1] *1. Department of Energy Conversion and Storage, Technical University of Denmark, 2800 Kgs. Lyngby, Denmark*

For modern applications, e.g., magnetic storage devices [1], we need to describe magnetic effects inside material on a nanometer length scale. Using a continuum approach, the micromagnetic formalism [2] allows exactly for this. Within this formalism, a material is modeled with local magnetization vectors m, resolving magnetic structures, e.g., domain walls. Existing simulation frameworks, e.g., MagTense [3], are validated by solving standardized benchmarks, e.g., μMAG Standard Problem #4 [4]. In this work, we present a data-driven approach for predicting magnetization dynamics, and validate it on exactly this standard problem. We create a large dataset of magnetization dynamics using MagTense [3], and by optimizing the parameters of a neural network, we are able to generalize dynamics across the physical setup, and subsequently, to ask for solutions of the whole parameter space. We use convolutional neural networks to embed m into a low-dimensional latent space. Here, time evolution is then performed with the recent Transformer [5] architecture, which allows for overcoming memory constraints and computational limitations of numerical approaches. As shown in Fig. 1, we embed the external magnetic field H_{ext}, the exchange interaction constant A_{exch}, and the anisotropy constant K along with the local magnetization vectors (m_x, m_y, m_z) into latent space. From the obtained 128-dimensional vector, we can then reconstruct the global sample magnetization M with a mean error of 5 mT per time step, as depicted in Fig. 2. Previously, Kovacs et al. [6] have similarly modeled magnetization dynamics in latent space. In contrast to that approach, we are able to represent a spatially varying external magnetic field of increased range, and to include crystal anisotropy and exchange interaction into our model.

[1] S. Tehrani *et al.*, Proceedings of the IEEE, Vol. 91, no. 5, pp. 703–714 (2003). [2] W. F. Brown Jr., Journal of Applied Physics, Vol. 30, no. 4, pp. S62–S69 (1959). [3] R. Bjørk *et al.*, Journal of Magnetism and Magnetic Materials, Vol. 535, p. 168057 (2021). [4] B. McMichael *et al.*, μMAG Standard Problem #4. URL: https://www.ctcms.nist.gov/~rdm/mumag.org.html (2000). [5] A. Vaswani *et al.*, Advances in Neural Information Processing Systems, Vol. 30 (2017). [6] A. Kovacs *et al.*, Journal of Magnetism and Magnetic Materials, Vol. 491, p. 165548 (2019).

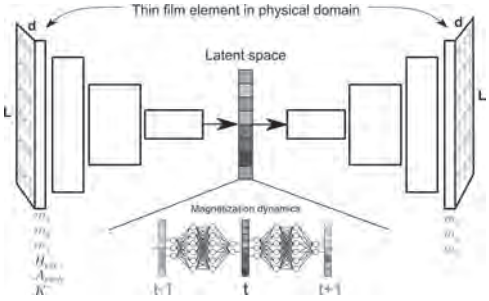

Fig. 1: Deep learning architecture for modeling magnetization dynamics. Using a Transformer [5], the low-dimensional embedding of all contributions is integrated in time before it is mapped back to the original physical domain.

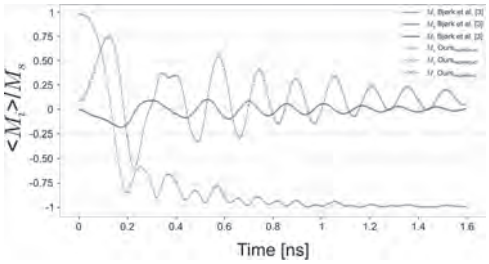

Fig. 2: Reconstruction of the normalized global sample magnetization M from latent space. The reconstructed spatial components M_x, M_y, and M_z are compared to the published solution of Bjørk et al. [3].

HOC-03. Artificial Neural Networks for the Analysis of Ferromagnetic Resonance Spectra. D.W. Slay[1] and *M. Charilaou*[1] *1. Physics, University of Louisiana at Lafayette, Lafayette, LA, United States*

Magnetic nanoparticles and nanostructures are important elements in a wide range of applications, and the key properties that determine their performance is the saturation magnetization and the magnetic anisotropy, which in turn determine the internal anisotropy fields. Quantifying these internal anisotropy fields is key for understanding nanomagnetic phenomena and for developing novel materials for applications. Ferromagnetic Resonance spectroscopy (FMR) is a powerful technique for quantifying internal anisotropy fields. The interpretation of FMR spectra, however, requires the use of an appropriate model and forward calculations; no inverse methods are available to extract internal fields from FMR spectra. We will present the use of artificial neural networks for spectral recognition, i.e., to identify the internal magnetic anisotropy fields from the FMR spectrum, as illustrated in the figure. We have trained two different types of networks, a convolutional neural network and a multi-layer perceptron, by feeding the networks with FMR spectra that were pre-computed based on a Stoner-Wohlfarth-type model [1] and labeled with the corresponding anisotropy fields. We tested the trained networks with unseen FMR spectra and found that they successfully predict the correct anisotropy fields with a precision of a few militesla. Surprisingly, the neural networks performed well for data that was beyond their training range [2]. These results demonstrate the potential benefit of using artificial neural networks for accelerated high-throughput analysis of magnetic materials and nanostructures.

[1] M. Charilaou: Ferromagnetic resonance of biogenic nanoparticle chains. J. Appl. Phys. 122, 063903 (2017) [2] D. Slay and M. Charilaou: Spectral Recognition of Magnetic Nanoparticles with Artificial Neural Networks. arXiv 2022 (DOI: 10.48550/arXiv.2206.00166)

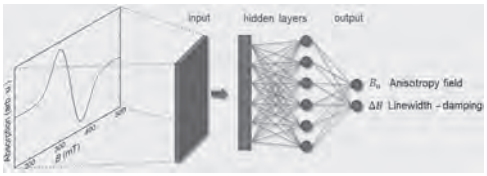

Figure 1

HOC-04. Finite Element Solver for Harmonic Linearized Landau-Lifshitz-Gilbert Equation. *Z. Lin*[1] and V. Lomakin[1] *1. University of California, San Diego, San Diego, CA, United States*

We present a numerical formulation for a linearized Landau-Lifshitz-Gilbert equation (LLGE) based on the finite element method (FEM) for the study of the magnetization dynamics in nanomagnetic structures under weak time-harmonic (given frequency) excitations. The linearized LLGE is obtained by assuming small magnetization deviations around the equilibrium state. Assuming an excitation by an AC field or current at a given frequency, the linearized LLGE is manipulated into a harmonic linearized LLGE for complex magnetization deviation amplitude, which is transverse to the equilibrium state. The resulting linear system of equations is solved by an iterative linear solver. A preconditioner is constructed based on the exchange stiffness matrix and incomplete LU decomposition, which significantly improved the convergence of the linear iterations. The formulation was implemented as a module of the FastMag micromagnetic simulator where all the fields and operators are computed as outlined in [1]. The validity, effectiveness, speed, and scalability of the linear solver are demonstrated by numerical simulations in Figs. 1 and 2. Figure 1 shows the magnetization states obtained by using the introduced harmonic LLGE solver and the full time-domain LLGE solver. The figure shows the magnetization state snapshots at different times. The results show good agreement, but the harmonic LLGE solver is much faster and allows handling complex frequencies, which may be important for understanding the solution behavior. Figure 2 shows the number of linear iterations as a function of the structure size for using different types of the ILU preconditioners. Using the preconditioners significantly reduces the number of iterations and the computational time.

[1] R. Chang, S. Li, M. Lubarda *et al*. Journal of Applied Physics, 109(7): 07D358 (2011).

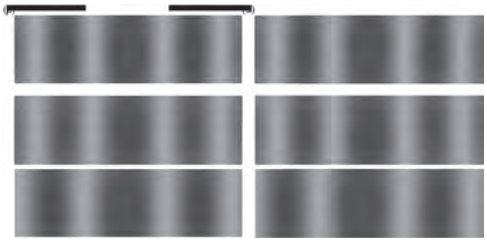

Fig. 1 Magnetization snapshot at t=17.4, 42.8, and 58.9 ns from top to bottom obtained via (a) harmonic linearized LLG solver and (b) non-linear time domain LLGE for a 5×30×100 nm stripe with an excitation field in the middle at 20 GHz frequency and 50 Oe magnitude in the y-direction. The mesh edge length is 2 nm. The material parameters are M_s = 800 emu/cm^3, A_{ex} = 10^{-6} erg/cm, α = 0.01.

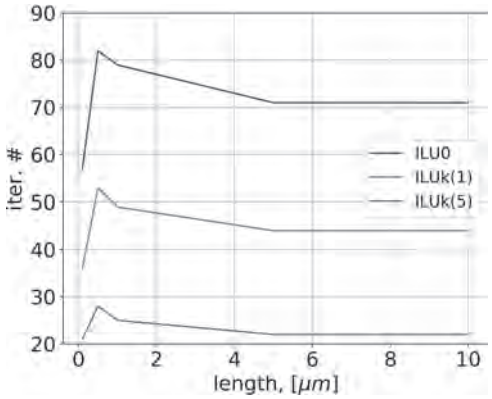

Fig. 2 The linear solver iteration number versus the stripe length with different preconditioners.

HOC-05. Reduced Order Model for Large Multigrain Systems. *H. Oezelt*[1,2], M. Gusenbauer[1,2], A. Kornell[1,2], J. Fischbacher[1,2], Q. Ali[1,2], L. Breth[2], M. Yano[3], N. Sakuma[3], A. Kinoshita[3], T. Shoji[3], A. Kato[3] and T. Schrefl[1,2] *1. Christian Doppler Laboratory for Magnet design through physics informed machine learning, Wr. Neustadt, Austria; 2. Department for Integrated Sensor Systems, Danube University Krems, Wr. Neustadt, Austria; 3. Advanced Materials Engineering Div., Toyota Motor Corporation, Mishuku Susono, Japan*

Micromagnetic simulations are a viable tool for optimizing magnetic behavior of permanent magnets. The used finite element mesh must be fine enough to represent domain walls, hence the size of the simulated magnet is limited to a few micrometers. Due to grain sizes up to a few micrometers, only a small number of interacting grains can be simulated within reasonable time. In this work we developed a reduced order model that allows the simulation of large multigrain systems with thousands of grains in a few hours. The magnetic configuration is represented by one magnetic moment per grain. Previous research suggests that magnetization reversal of a grain starts near its edges. Therefore, determining the critical field for these regions is sufficient to reverse the entire grain. As a fast method to approximate the magnetic state of a grain we use the embedded Stoner-Wohlfarth (SW) model[1,2]. This approach adapts the original SW method for small ferromagnetic particles to additionally account for long-range interactions of uniformly magnetized grains. We define evaluation points at a distance d L_{ex} from the grain surfaces, with L_{ex} being the exchange length (Fig. 1). The total field acting on an evaluation point is the sum of the applied field, the magnetostatic interaction field H_{demag} and the exchange field $H_{exch}=1/l^2M$. The interaction field H_{demag} is computed by analytical formulas for polyhedral geometries[3], employing hierarchical matrices as implemented with *h2tools*[4], to reduce storage and CPU time. In our model the two free parameters d and l, for the interaction field and the exchange field respectively, were tuned for single cubic grains with different grain sizes and anisotropic easy axis by using a Bayesian optimizer. The calculated coercive fields of the reduced order model with optimized free parameters are in excellent agreement with the full micromagnetic results (Fig. 2). The financial support by the Austrian Federal Ministry for Digital and Economic Affairs, and the Christian Doppler Research Association is gratefully acknowledged.

[1] J. Fischbacher, A. Kovacs, et al., Scripta Materialia, 154, 253–258 (2018) [2] R. Wood, IEEE Transactions on Magnetics, 45(1), 100–103 (2009) [3] D. Guptasarma, B. Singh, GEOPHYSICS, 64(1), 70–74 (1999) [4] A. Mikhalev, I. Oseledets, Numerical Linear Algebra with Applications, 23(2), 230–248 (2016)

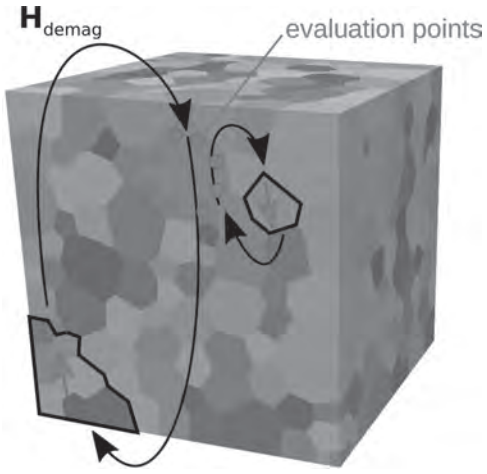

Fig. 1 Evaluation points for Embedded Stoner-Wohlfarth model.

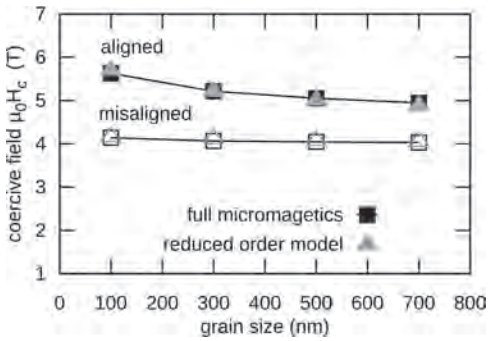

Fig. 2 Excellent agreement of tuned reduced order model with full micromagnetic simulations.

HOC-06. Simulation of Soft Magnetic Composites with Periodic Strayfield Calculation. *A. Ducevic*[1], F. Bruckner[1], C. Abert[1] and D. Suess[1] *1. Functional Materials, University of Vienna, Vienna, Austria*

Soft magnetic composites(SMCs) consist of ferromagnetic particles, in the micrometer-range which are embedded in an electrically insulating material, in order to reduce the eddy-currents in the high-frequency regime. We want to utilize numerical simulations in order to optimize such materials in terms of power-loss and permeability. The problem one faces is that the samples have macroscopic sizes, however if one would want to resolve these materials on the micro-scale, it would limit the total simulation size to a few micrometers. Introducing a truncated geometry or cut-off would also not solve this problem as demagnetization effects would come into play for any finite sized sample. However due to the torus-like shape of the sample, the magnetic flux closure reduces the strayfield to zero. To overcome these issues we developed and implemented our own method for calculating the micromagnetic strayfield with periodic boundary conditions(PBCs)[1]. PBCs allow us to simulate an infinite sample and therefore avoid the demagnetization effects. A complete magnetic simulation framework including PBCs will be presented with which the spatially- and time-resolved magnetization response to an external field is simulated. The model will be validated among other things by reproducing experimental setups that have successfully reduced the power-loss of SMCs. Suetsuna et al.[2] have shown that the power-loss reduces by roughly half when the sample is exposed to a magnetic field during annealing, because an aligned anisotropy direction is induced. This was replicated in the simulation and as can be seen in figure 1 the simulated power-loss P_m decreases by half when an aligned anisotropy is applied, without altering the relative permeability mu_r.

[1] Bruckner, Florian, et al. "Strayfield calculation for micromagnetic simulations using true periodic boundary conditions." Scientific Reports 11.1 (2021): 1-8. [2] Suetsuna, Tomohiro, et al. "Soft magnetic composite containing magnetic flakes with in-plane uniaxial magnetic anisotropy." Journal of Magnetism and Magnetic Materials 473 (2019): 416-421.

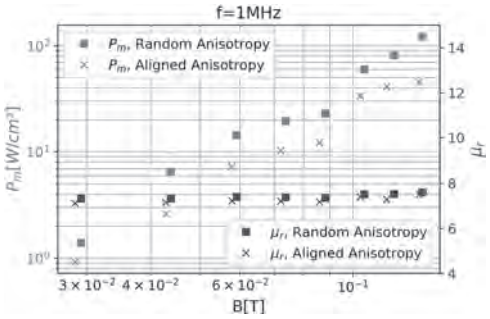

Fig. 1 Powerloss P_m and permeability mu_r were calculated from hysteresis simulations utilizing the SMC model with aligned and random anisotropy.

HOC-07. Accurate finite-difference micromagnetics of magnets including RKKY interaction - analytical solution and comparison to standard micromagnetic codes. *D. Suess*[1], S. Koraltan[1], F. Bruckner[1] and C. Abert[1] *1. University of Vienna, Vienna, Austria*

Within this talk we show the importance of accurate implementations of the RKKY interactions for antiferromagnetically coupled ferromagnetic layers with thicknesses exceeding the exchange length. In order to evaluate the performance of different implementations of RKKY interaction, we develop a benchmark problem by deriving the analytical formula for the saturation field of two infinitely thick magnetic layers that are antiparallelly coupled (Fig. 1). Without external field, the magnetization in the layers is parallel to the easy axis (y-direction) in the +y and -y direction. When a field in the x-direction is applied, a partial domain wall is formed (Fig. 1). We find that there exists a critical field that fully saturates the structure in the x-direction which is given by, $H_{x,crit} = 2\ K_1/J_s\ [1+J_{rkky}^2/(AK_1)]$, where J_{rkky} is the RKKY coupling strength, K_1 the anisotropy constant and A exchange constant [1]. This benchmark problem shows that state-of-the-art implementations in commonly used finite-difference codes lead to errors of the saturation field that amount to more than 20% for mesh sizes of 2 nm which is well below the exchange length of the material. In order to improve the accuracy, we develop higher order cell based (see Fig. 2 - paper, cell O1 and O2) and nodal based finite-difference codes (see Fig. 2 - paper, node) that significantly reduce the error compared to state-of-the-art implementations (see Fig. 2 - mumax) [2]. For the second order cell based and first order nodal based finite element approach, the error of the saturation field is reduced by about a factor of 10 (2% error) for the same mesh size of 2 nm.

[1] D. Suess, S. Koraltan, F. Slanovc, F. Bruckner, C. Abert, "Accurate finite-difference micromagnetics of magnets including RKKY interaction -- analytical solution and comparison to standard micromagnetic codes", https://arxiv.org/abs/2206.11063 [2] Vansteenkiste, Arne, and Ben Van de Wiele. "MuMax: A new high-performance micromagnetic simulation tool." *Journal of Magnetism and Magnetic Materials* 323.21 (2011): 2585-2591.

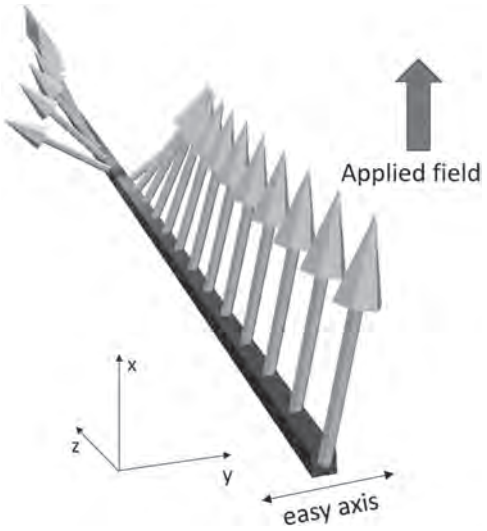

Fig. 1: Analytic benchmark problem of two infinitely extended layers, that are antiferromagentically coupled via J_{rkky}.

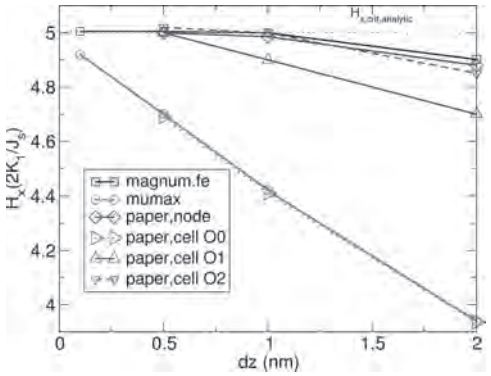

Fig. 2: Convergence towards the analytic solution of H_x =5 x 2 K_1/J_s for different micromagnetic codes as function of discretization length dz. It is shown that standard finite difference codes (e.g. mumax) that uses zero order methods for the RKKY interaction show significant errors. The developed method (paper, cell O2) shows significantly better convergence.

HOC-08. An improved Preisach distribution function identification method considering reversible magnetization effect. L. Chen[1], *L. Cui*[1], T. Ben[1], L. Jing[2] and Q. Liu[2] *1. College of Electrical Engineering and New Energy, China Three Gorges University, Yichang, China; 2. Hubei Provincial Research Center on Microgrid Engineering Technology, China Three Gorges University, Yichang, China*

I Introduction Accurate calculation of the hysteresis characteristics of magnetic materials is of great significance for the optimal design of electrical equipment. In previous studies, the Preisach model based on the centered cycle method is widely used for the simulation of hysteresis characteristics as this method uses data that can be easily obtained [1]. However, the existing centered cycle method model cannot correctly consider the influence of reversible magnetization and leads to a large error when calculating the small major hysteresis loops [2]. In this paper, an improved centered cycle method for identifying the Preisach distribution function (PDF) considering the reversible magnetization is proposed, which can improve the accuracy of predicting the symmetrical minor loops. II Method and Discussion As shown in Figure 1, an improved PDF identification method considering the reversible magnetization is proposed, which is consistent with the principle of the magnetization process. The reversible relative permeability is obtained by derivation at the reversal points of the centered cycles with different

measured magnetic flux densities and obtained parametric equation, which is integrated to obtain the reversible magnetization. Four centered cycles of different magnetic flux densities are used to discretize the Preisach plane, and the values of the PDF are calculated through the modified magnetic flux densities. The irreversible magnetization is obtained by accumulating the values of the PDF. The final output value is obtained by superposing the irreversible magnetization and the reversible magnetization. The simulation results of grain-oriented silicon steel based on B30P105 are shown in Fig. 2, and the expected accuracy can be achieved. III Conclusion In this paper, a modified Preisach model with centered cycle method under the magnetization principle is developed. Obtained results show that the accuracy of the simulated symmetrical minor loops can be improved.

[1] Bernard Y, Mendes E, Ren Z. Determination of the distribution function of Preisach's model using centred cycles[J]. COMPEL: The International Journal for Computation and Mathematics in Electrical and Electronic Engineering, 2000. [2] Peng D, Sima W, Ming Y, et al. An Improved Centered Cycle Method for Identifying the Preisach Distribution Function[J]. IEEE Transactions on Magnetics, 2018, PP(11):1-5.

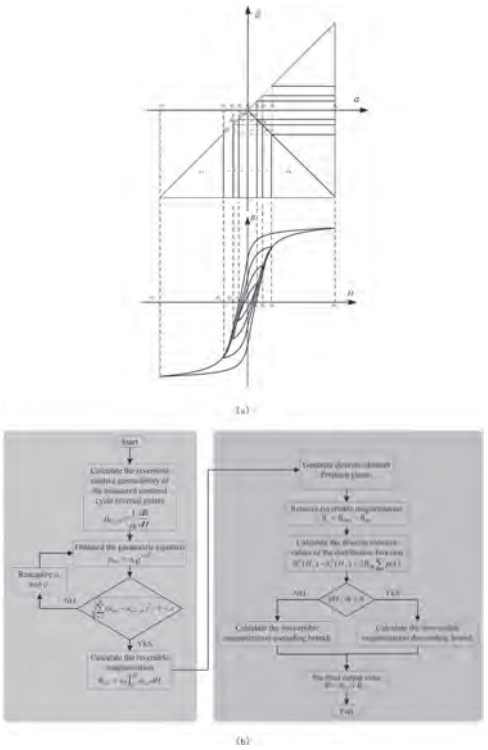

Fig.1. (a) Discretized Preisach Plane. (b) Numerical discrete calculation process of improved Preisach Model.

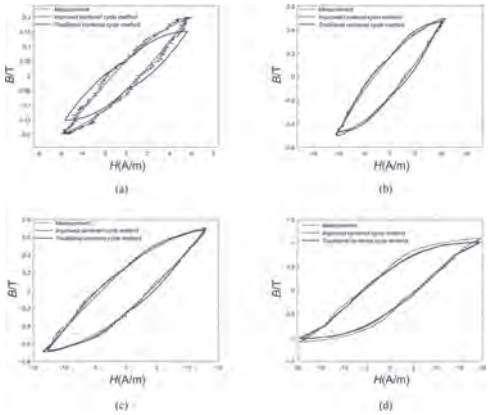

Fig.2. Comparison of simulation results of B30P105 silicon steel. (a) B_p=0.2T. (b) B_p=0.5T. (c) B_p=0.7T. (d) B_p=1.1T.

HOC-09. mag2exp: Simulating experimental techniques from computational micromagnetics. *S. Holt*[1], M. Lang[1,2], J. Loudon[3], T. Hicken[4,5], S. Pathak[1,2], D. Cortés-Ortuño[1,6], M. Beg[1,7] and H. Fangohr[1,2]
1. University of Southampton, Southampton, United Kingdom; 2. Max Planck Institute for the Structure and Dynamics of Matter, Hamburg, Germany; 3. University of Cambridge, Cambridge, United Kingdom; 4. Royal Holloway, Egham, United Kingdom; 5. Durham University, Durham, United Kingdom; 6. Utrecht University, Utrecht, Netherlands; 7. Imperial College London, London, United Kingdom

The number of experimental techniques, and their capability to measure and image magnetic behavior, is constantly increasing. Analogously, the ability to computationally study magnetic systems using techniques such as micromagnetics or Monte Carlo is also growing. However, it is often not trivial to combine experimental and computational results such that one can predict the results of experimental techniques directly from computational magnetization structures. We have produced the Python software package *mag2exp* [1], which integrates with the micromagnetic simulation environment *Ubermag* [2, 3], and enables realistic virtual experiments to be easily and quickly performed on magnetic structures using a range of experimental techniques. These techniques include Lorentz transmission electron microscopy, magnetic force microscopy, x-ray holography, small angle neutron scattering, torque magnetometry, along with other useful experimental capabilities. The *mag2exp* software is compatible with Jupyter Notebook allowing for the visualization of data and documentation of the entire simulation workflow, thus making the research more reproducible and re-usable [4]. This package aims to help bridge some of the gap between computational simulations and experiments, leading to the potential for simulations to inform real world experiments and *vice versa*. Here, we show how the *mag2exp* package can be used to study the magnetic behaviors for the system under investigation by converting a digital magnetization field to an experimental result. We also present the results of using the experimental techniques included in *mag2exp* on complex magnetization structures created using micromagnetic simulations such as magnetic skyrmions, vortices, and other solitons. This work was financially supported by the EPSRC Program grant on Skyrmionics (EP/N032128/1).

[1] S. J. R. Holt, *et al.*, https://github.com/ubermag/mag2exp [2] M. Beg, *et al.*, IEEE Trans. Magn. 58, 2 (2022) [3] https://ubermag.github.io/ [4] M. Beg, *et al*., Comput. Sci. Eng., 23, 2 (2021)

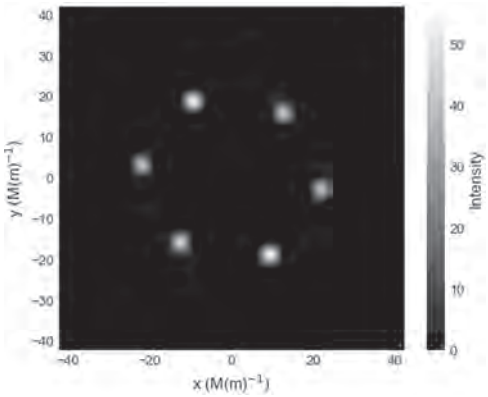

Small angle neutron scattering pattern generated by *mag2exp* of a micromagnetic skyrmion lattice.

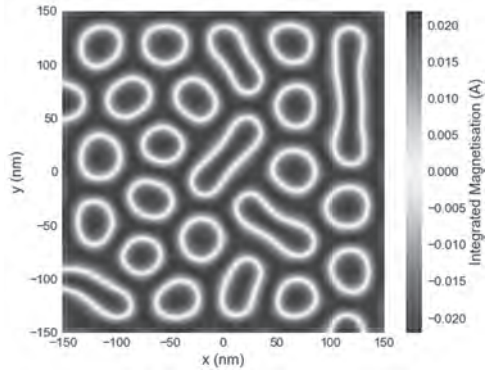

X-ray holography image generated by *mag2exp* of a mixed magnetization state.

HOC-10. Modeling Magnetic Domain Wall Motion with Neural Ordinary Differential Equations. *N. Hassan*[1], F. Garcia-Sanchez[2], D. Querlioz[3] and J.S. Friedman[1] *1. Electrical and Computer Engineering, University of Texas at Dallas, Dallas, TX, United States; 2. Departamento de Física Aplicada, Universidad de Salamanca, Salamanca, Spain; 3. Centre de Nanosciences et de Nanotechnologies, Université Paris-Saclay, Palaiseau, France*

The domain wall (DW) magnetic tunnel junction (MTJ) is a promising component of next-generation neuromorphic, in-memory, and logical computing hardware due to features including non-volatility, multiple analog resistive states, low power, and ultrafast read-write operation [1-3]. Predicting the DW motion along a magnetic track involves complicated and time-consuming micromagnetic simulations, which greatly impede the development of computing systems designed with interconnected DW-MTJ devices [4]. The neural ordinary differential equations (ODE) is a recently conceptualized deep learning framework that can predict the behavior of dynamic systems [5]. In this approach, the ODE that defines the time derivative of the system output is expressed as a deep neural network; when provided with initial conditions, an ODE solver determines the system response at future times. Chen *et al*. [6] extended this approach by expressing hidden variables that are difficult to probe with higher-order derivatives of the output, which are then replaced with mathematically equivalent time-delayed versions. External inputs can be applied to the network in a similar time-delayed fashion. In this work, DW motion by spin-transfer torque excitation is modeled utilizing the neural ODE framework. Temporal DW position data along a magnetic track excited by a set of random sinusoidal current inputs are generated by mumax3 [7] and are used to train a neural ODE in a supervised fashion through backpropagation. For a different set of random sinusoidal current inputs, the DW position forecasted by the trained network matches with the results generated by mumax3 with very high accuracy (Fig. 2) while reducing the simulation time by a factor greater than 200x, thereby opening the path to efficiently design integrated systems interconnecting a large number of DWMTJs.

[1] M. Alamdar, T. Leonard, C. Cui *et al.*, *Appl. Phys. Lett.*, vol. 118, no. 11, p. 112401 (2021). [2] N. Hassan, X. Hu, L. Jiang-Wei *et al.*, *Jour. Appl. Phys.*, vol. 124, no. 15, p. 152127 (2018). [3] W. H. Brigner, N. Hassan, L. Jiang-Wei *et al.*, *IEEE Trans. Electron Devices*, vol. 66, no. 11, pp. 4970-4975 (2019). [4] X. Hu, A. Timm, W. H. Brigner *et al.*, *IEEE Trans. Electron Devices*, vol. 66, no. 6, pp. 2817-2821 (2019). [5] R. T. Q. Chen, Y. Rubanova, J. Bettencourt*et al.*, *Proceedings of NeurIPS*, 31 (2018). [6] X. Chen, F. A. Araujo, M. Riou *et al*, *Nat. Comm.*, vol. 12, no. 1016 (2022). [7] A. Vansteenkiste, J. Leliaert, M. Dvornik *et al.*, *AIP Advances*, vol. 4, no. 10, p. 107133 (2014).

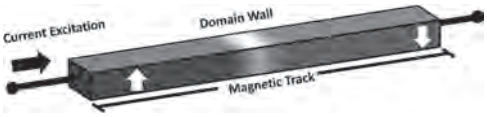

Up (blue) and down (red) polarized magnetic domains along a track separated by a DW (yellow). Current inputs control the position of the DW by applying spin-transfer torque.

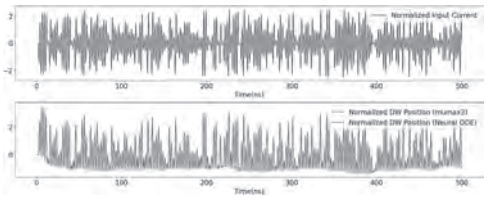

DW position forecasted by a trained neural ODE in comparison with mumax3 simulation.

HOC-11. Proper modeling of material interfaces in numerical micromagnetics. *C. Abert*[1], P. Heistracher[1], F. Bruckner[1], T. Schrefl[2] and D. Suess[1] *1. University of Vienna, Vienna, Austria; 2. Danube University Krems, Krems, Austria*

Micromagnetic energy contributions depending on spatial derivatives of the magnetization, like the exchange energy, introduce boundary conditions to the micromagnetic model. The implications of these boundary conditions and their proper implementation in numerical codes have been widely discussed in various publications, e.g. [1,2]. Less focus has been put on material interfaces where dicontinuities in material parameters such as the exchange constant introduce well defined jump conditions for the derivatives of the magnetization. An accurate numerical description of the boundary and jump conditions is crucial for the exact calculation of magnetic properties such domain-wall pinning on internal interfaces. The implementation of these jump conditions in standard finite-difference micromagnetics is somewhat cumbersome, since the sample points of the finite-difference scheme are usually chosen to lie in the center of each simulation cell. However, material interfaces are naturally chosen to coincide with the boundaries of simulation cells, see Fig. 1. In order to properly handle this mismatch, we propose to introduce virtual ghost nodes which account for the jump conditions and whose values are used in the stencils of the respective energy contributions. In this talk we introduce a benchmark problem for the domain-wall pinning at a material interface with changes in saturation magnetization, exchange constant and anisotropy along with an analytical solution for the depinning field. We demonstrate the importance of a proper interface handling in finite-difference micromagnetics. Moreover, we extend our considerations to phase transitions in the antisymmetric exchange interaction as introduced by the Dzyaloshinskii–Moriya interaction (DMI).

[1] M. Fähnle, A. Slavin, and R. Hertel. “Role of the sample boundaries in the problem of dissipative magnetization dynamics.” Journal of magnetism and magnetic materials 360 (2014): 126-130. [2] D. Cortés-Ortuño, et al. “Proposal for a micromagnetic standard problem for materials with

Dzyaloshinskii–Moriya interaction." New Journal of Physics 20.11 (2018): 113015. [3] P. Heistracher, C. Abert, et al. "Proposal for a micromagnetic standard problem: domain wall pinning at phase boundaries." Journal of Magnetism and Magnetic Materials 548 (2022): 168875.

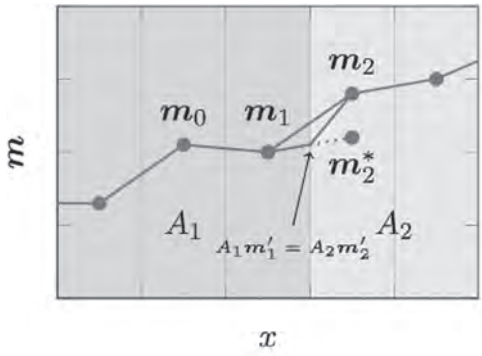

Fig. 1 Illustration of material interface as modeled in finite-difference micromagnetics. The sample points are located at the cell centers. The jump condition is considered by introducing a virtual ghost node.

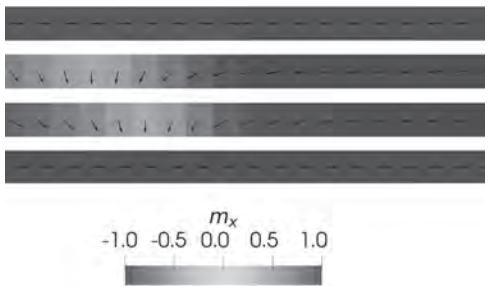

Fig. 2 Domain-wall pinning at material interface. Proposed benchmark problem for the correct handling of material interfaces in micromagnetics.

HOC-12. Modeling magnetic correlations in magnetite nanoparticle assemblies using x-ray magnetic scattering data. *J. Rackham*[1], K. Chesnel[1] and M. Transtrum[1] *1. Physics, Brigham Young University, Provo, UT, United States*

Magnetic nanoparticles are used in nanotechnologies and biomedical applications, such as drug targeting, MRI, bio-separation. Magnetite (Fe_3O_4) nanoparticles stand to be effective in these roles due to the non-toxic nature of magnetite and its ease of manufacture [1-4]. To this end, a greater understanding of the magnetic behavior of the individual magnetite nanoparticles is needed when a collection of them is used. This research seeks to discover the local magnetic ordering of ensembles of magnetite nanoparticles (see Fig.1a) occurring at various stages of the magnetization process at temperatures above and below their blocking temperature for various particle sizes [5]. We use x-ray circular dichroism (XMCD) [6] and x-ray resonant magnetic scattering (XRMS) [7] (see Fig.1b), which provides information about the spatial magnetic orders in the material. Here we discuss the modeling of the XRMS data (Fig.1c,d) using a one-dimensional chain of nanoparticles in real space [8 (see Fig.1e), on one hand, as well an empirical Gaussian packet model in q-space, on the other hand. We find that at low temperature and near the coercive point, inter-particle magnetic correlations emerge, including a combination of ferromagnetic and antiferromagnetic alignments of the nanospins.

[1] Frey N.A.; Peng S.; Cheng K.; Sun S. Chem. Soc. Rev. 38, 2532-2542 (2009) [2] S. Mornet et al., J. Mater. Chem. 14, 2161 (2004) [3] E. Duguet et al., Nanomedicine 1(2), 157 (2006) [4] J. H. Gau et al., Acc. Chem. Res. 42(8),1097 (2009) [5] K. Chesnel et al, Journal of Physics: Conference Series, Volume 521 (2014) [6] Y. P. Cai et al, J. Appl. Phys. 115 (17), 17B537 (2014) [7] K. Chesnel, et al., Magnetochemistry 4 (4), 42 (2018) [8] J. Rackham et al, AIP Advances 9, 035033 (2019)

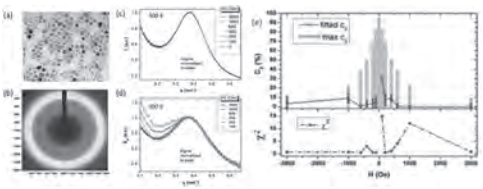

Fig. 1: Left. (a) TEM image of the Fe_3O_4 NP assembly, (b) 2D XRMS pattern, (c) 1D integrated charge scattering signal, (d) associated magnetic ratio signal, (e) Top: fitted antiferromagnetic coverage (c2) including error bars at 95% confidence intervals for range of magnetic fields. The blue bars indicate the possible range for c2. Bottom: Fitting residual.

HOC-13. Simulation on time-dependent voltage distribution regarding van der Waals tunneling gap. *K. Kim*[1,2], H. Kwon[2], T. Park[2], S. Kim[1] and K. Kim[2] *1. Physics, University of Ulsan, Ulsan, The Republic of Korea; 2. Center for spintronics, Korea Institute of Science and Technology, Seoul, The Republic of Korea*

Since the discovery of graphene, a great number of studies have demonstrated exotic phenomena based on electrical properties of two-dimensional (2D) materials. Although 2D material systems particularly have a van der Waals (vdW) gap, it has been mostly neglected to understand experimentally observed longitudinal and Hall conductivities, usually denoted by σ_{xx} and σ_{xy}, respectively. To include phenomena related to vertical transport related to the vdW gaps, we develop a simulation tool on time-dependent voltage distribution, which can reproduce real situations in vdW-based devices. For that, we firstly propose a simulation model to account for not only the conventional fixed resistivity, but also a variable resistivity depending on interlayer voltage differences. We finally visualize the current distribution as a function of time under different voltage bias with our simulation. The developed simulation based on the resistance model can provide a good template to understand the dynamics on electrical properties of 2D-based systems.

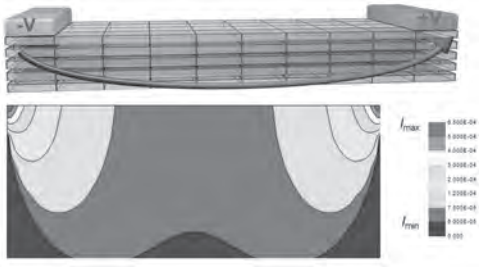

Figure 1. The schematic image of the simulation and current density distribution obtained by the simulation.

HOC-14. Classification of Coexisting Defects from Magnetic Flux Leakage Data Using Deep Learning Method. *G. Piao*[1], J. Ling[2] and J. Li[1] *1. Department of Electrical and Computer Engineering, Michigan State University, East Lansing, MI, United States; 2. School of Engineering, The University of British Columbia, Kelowna, BC, Canada*

Ferromagnetic materials are widely used in infrastructures, such as steam generators and storage tanks. During their service time, ferromagnetic materials are subject to deterioration and defects are prone to generate which could damage infrastructures and cause catastrophic accidents. Magnetic flux leakage (MFL) is one of the widely used nondestructive evaluation methods to detect and characterize defects in ferromagnetic materials to ensure infrastructure safety and reliability. However, over the ages,

extensive research work has been carried out on the modeling, classification, and characterization of a single defect, while the scenario of coexisting defects is ignored. In the practical field, the coexistence of surface and subsurface defects within a certain area can cause much earlier than expected deterioration or even penetration of ferromagnetic materials, the result of which is more damaging. Here, we propose a convolutional neural network (CNN) based deep learning method to differentiate between single defect and coexisting defects scenarios. First, finite-element-method simulation models are developed to investigate the effect of coexisting defects on the measured MFL image data, as shown in Fig. 1. The models with different defect parameters are calculated to generate 354 MFL images for the training and testing of our deep learning method. The architecture of CNN is shown in Fig. 2. The convolution and max-pooling layers are designed to extract deep features from the input MFL image. The pattern with convolution and max-pooling layers is repeated five times to obtain the feature maps with deeper depth and smaller size. With the flatten layer, the feature maps are converted into a 1-D vector, which is fed to the fully connected layers. The output calculated by the softmax function indicates the classification result. Finally, the classification result of our method is around 92.78% and higher than other traditional classification methods, which is promising and can be a good classification tool for the coexisting defects scenario. Acknowledgment The authors would like to acknowledge the support of the IEEE Magnetics Society.

[1] X. Peng, U. Anyaoha, Z. Liu, IEEE Transactions on Magnetics, Vol. 56, no. 6, p. 1-15 (2020) [2] G. Piao, J. Guo, T. Hu, NDT & E International, Vol. 103, p. 26-38 (2019) [3] D. A. G. Trevino, S. M. Dutta, F. H. Ghorbel, IEEE Transactions on Magnetics, Vol. 52, no. 12, pp. 1-7 (2016) [4] S. Lu, J. Feng, H. Zhang, IEEE Transactions on Industrial Informatics, Vol. 15, no. 1, p. 213-224 (2019) [5] M. Augustyniak, Z. Usarek, Journal of Nondestructive Evaluation, Vol. 35, no. 3, p. 1-15 (2016) [6] M. R. Kandroodi, B. N. Araabi, M. M. Bassiri, IEEE Transactions on Magnetics, Vol. 53, no. 3, p. 1-10 (2017) [7] Z. D. Wang, Y. Gu, Y. S. Wang, Journal of Magnetism and Magnetic Materials, Vol. 324, no. 4, p. 382-388 (2012) [8] J. Liu, M. Fu, F. Liu, IEEE Transactions on Instrumentation and Measurement, Vol. 67, no. 1, p. 12-23 (2018)

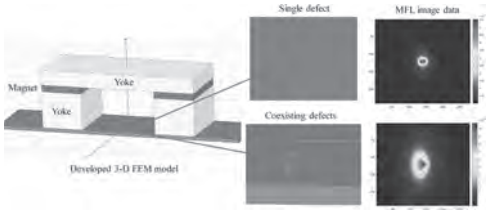

Fig. 1. Simulation models and MFL images

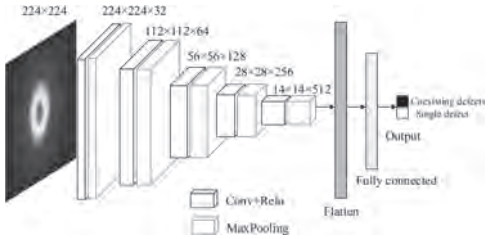

Fig. 2. Architecture of developed CNN

INVITED PAPER

HOC-15. Forecasting the Outcome of Spintronic Experiments with Neural Ordinary Differential Equations. *D. Querlioz*[1] *1. Univ. Paris-Saclay, CNRS, Palaiseau, France*

Reaching the full potential of spintronics requires modeling to predict the results of spintronic experiments, optimize structures, and design systems. Currently, the gold standard for modeling spintronic structures is micromagnetic simulations. Unfortunately, these simulations can be extremely slow and struggle with modeling accurately the imperfections and noise inherent to experimental devices. In this work, we introduce an alternative approach: design models for spintronic devices by letting an artificial intelligence automatically generate a model based on examples of the device behavior. For this, we make use of the recently-proposed formalism of Neural Ordinary Differential Equations (Neural ODE) [1], which we adapt to the specificities of spintronics [2]. An appropriately-trained Neural ODE can simulate a skyrmion-based device 200 times faster than micromagnetic simulations while being highly accurate, even in complex situations and for multiple values of materials parameters (magnetic anisotropy, DMI). We also train a Neural ODE based on five milliseconds of experimental measurements of vortex-based spin-transfer nano oscillators. The Neural ODE could then predict weeks of experimental measurements. We show how to adapt the Neural ODE, an originally deterministic formalism, to incorporate noise and show that the predictions of the Neural ODE match the experiments very precisely. All these results highlight the potential of Neural Ordinary Differential Equations for developing spintronic applications.

[1] R. T. Chen, Y. Rubanova, J. Bettencourt, and D. K. Duvenaud, “Neural Ordinary Differential Equations”, *Advances in Neural Information Processing Systems*, 6571–6583 (2018). [2] X. Chen, F. A. Araujo, M. Riou, J. Torrejon, D. Ravelosona, W. Kang, W. Zhao, J. Grollier, D. Querlioz, “Forecasting the outcome of spintronic experiments with Neural Ordinary Differential Equations”, Nature Communications 13, 1016 (2022).

Session HOD
SKYRMIONS: CHARACTERIZATION, DYNAMICS AND CONTROL

Kab-Jin Kim, Co-Chair
Korea Advanced Institute of Science and Technology, Daejeon, The Republic of Korea
Thomas Brian Winkler, Co-Chair
JGU Mainz, Mainz, Germany

CONTRIBUTED PAPERS

HOD-01. Nonlinear dynamics of skyrmion and bimeron in the presence of deformation. *Q. Shao*[1,2], Z. Chen[2], X. Wang[1], L. Shen[3] and Y. Zhou[3] *1. ECE, The Hong Kong University of Science and Technology, Hong Kong, Hong Kong; 2. Physics, The Hong Kong University of Science and Technology, Hong Kong, Hong Kong; 3. The Chinese University of Hong Kong, Shenzhen, Shenzhen, China*

In this big data era, information explosion demands a high-density, fast, robust, and non-volatile storage memory technology. We here focus on the dynamics of skyrmion and bimeron (an in-plane analog of a magnetic skyrmion), which are promising solutions for future storage devices [1]. For high-speed applications, high-drive currents are needed. In this regime, their dynamics are complicated and nonlinear and are not well understood [2]. We present an analytical model describing the nonlinear dynamics of the current-driven skyrmion in the presence of skyrmion deformation (Fig. 1). This model can precisely predict the deformation and moving velocity of the current-driven skyrmion, facilitating the discovery of new phenomena [3]. As an example, we find the nonreciprocal motion of skyrmion in the presence of an in-plane magnetic field, which can help build a skyrmion diode [4]. In addition to skyrmions, we uncover the nonreciprocal dynamics of ferrimagnetic bimerons in the nonlinear regime [4]. The nonreciprocal transport coefficient at the angular momentum compensation point can be more than one order of magnitude larger than the skyrmion case (Fig. 2). The predicted nonlinear and nonreciprocal dynamics will be essential for designing neuromorphic and logic devices, respectively.

[1] Q. Shao, et al., Nat Electron 2, 182-186 (2019) [2] Q. Shao, Nat Electron 3, 16-17 (2020) [3] Z. Chen, et al., Phys Rev Applied 17, L011002 (2022) [4] L. Shen, et al., Phys Rev B 105, 014422 (2022)

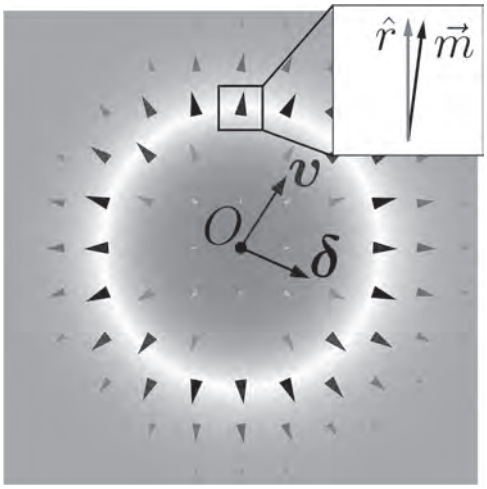

Figure 1. Imbalance of radial and tangential forces-induced spin canting in the presence of current-generated spin-orbit torques.

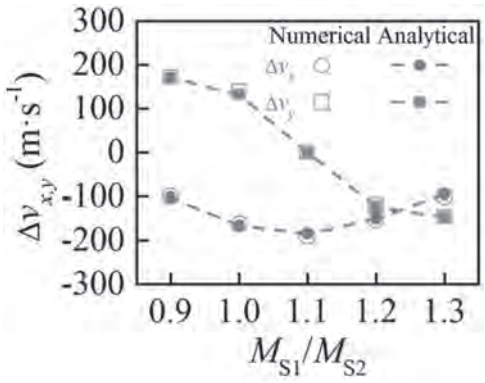

Figure 2. Longitudinal (v_x) and transverse (v_y) velocities as a function of sublattice magnetization ratio. Note that the ratio of sublattice gyromagnetic ratio is 1.1.

HOD-02. Elliptical Ferromagnetic Skyrmions. *K. Takahashi*[1], T. Naruse[1] and K. Kondo[1] *1. RIES, Hokkaido Univ., Sapporo, Japan*

Magnetic skyrmions are vortex-like spin textures. They are topologically protected from external perturbation and can be driven with extremely low currents. Therefore, they have been paid much attention and they are expected to be applied to the spintronic devices such as the magnetic memories and the logic devices. They can be discovered in so-called chiral magnets which are lacking in the inversion symmetry. The one of the characteristics of the chiral magnets is non-vanishing Dzyaloshinskii-Moriya interaction (DMI). The DMI, which tilts the neighboring spins, is an essential interaction to stabilize the magnetic skyrmions. The characteristics of the DMI are determined by the symmetry of the system. The Neel-type skyrmions are generally observed in C_{nv} symmetric thin film materials. Recently, the elliptical skyrmions have been observed and they are stabilized in the C_{2v} symmetric systems. This is because the different values of the DMI constants of the *x*-axis and *y*-axis can be allowed in the C_{2v} symmetric systems. The elliptical skyrmions have several advantages in comparison with circular skyrmions when applied to the spintronic devices. For example, the skyrmion Hall angles of the elliptical skyrmions can be controlled by changing the shapes of them [1]. In this study, we investigate both the dynamics and the phase diagram of elliptical ferromagnetic skyrmions. We consider Co thin films on W as ferromagnetic materials [2]. We drive the elliptical skyrmions by applying the spin current in the *x*-direction. Figures 1 and 2 show the dependences of the velocity ($|v|$) and the skyrmion Hall angle (θ_{SkHE}) on the elliptical ration (b/a), respectively. Here, a (b) is the length of major (minor) axis of the elliptical skyrmions. We find that $|v|$ increases with the decreasing the value of b/a and θ_{SkHE} decreases with the decreasing the value of b/a Therefore, the elongated skyrmions along the current direction are useful in comparison with the circular skyrmions when applied to the spintronic devices. At the conference, we are going to show the phase diagrams and discuss the regions where the elliptical skyrmions appear.

J. Xia, X. Zhang, M. Ezawa, Q. Shao, X. Liu, and Y. Zhou, Appl. Phys. Lett., Vol. 116, p.022407 (2020) L. Camosi, J. PeñaGarcia, and J. Vogel *et al*, New J. Phys., Vol. 23, p.013020 (2021)

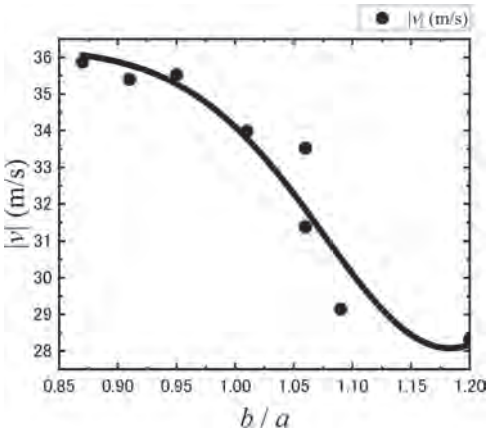

Fig. 1 The dependence of $|v|$ on b/a.

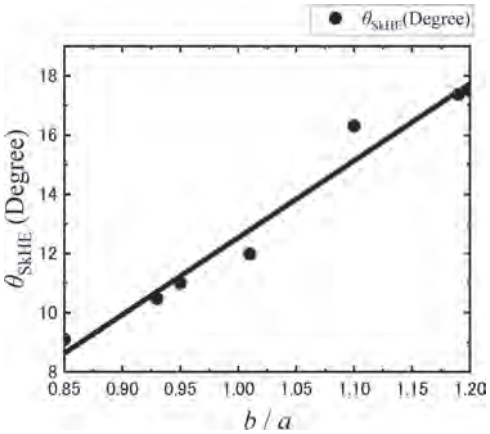

Fig. 2 The dependence of θ_{SkHE} on b/a.

HOD-03. Magnetic bubbles in low-damping ultra-thin garnets with perpendicular magnetic anisotropy. *D. Gouéré*[1], Y. Sassi[1], K. Bouzehouane[1], C. Carrétéro[1], P. Bortolotti[1], V. Cros[1], N. Reyren[1] and A. Anane[1] *1. Unité Mixte CNRS / THALES /Univ. Paris-Saclay, Palaiseau, France*

Topological magnetic textures have been the focus of a large investigation effort in the recent years. This effort has been fuelled by the discovery of magnetic Skyrmions at room temperature in magnetic multilayers [1]. In this study, we rely on a new class of materials exhibiting low-magnetic losses: nanometers-thick insulating Iron garnets. This material family has been extensively used in the 1970's for the development of bubble memories, yet using very thick garnet films in the range of a few micrometers, in which the stabilized bubbles had typically micron-size diameters [2]. However, it is only very recently that ultra-thin Bi doped garnet films with perpendicular magnetic anisotropy (PMA), suitable for magnonics have been shown to have a Gilbert damping in the range of few 10^{-4} [3] and current induced domain wall motion with speed exceeding 4000 m/s [4]. In this work, we have prepared ultra-thin $Bi_1Y_2Fe_5O_{12}$ (Bi-YIG) films, about 20 nm thick, grown using pulsed laser deposition. The growth conditions have been optimized to tune the out-of-plane easy axis and reach a vanishing effective magnetization through a combination of magneto-elastic and growth induced anisotropies that compensate the dipolar one. Kerr magneto-optical investigation has been lead to image those films and evidenced a long-range coherence of the bubbles auto-organization that forms a dense lattice. To further characterize the properties of these bubbles, we have used scanning NV microscopy. We find that their average diameter is about 200 nm (Fig.1), that is, to our knowledge, the smallest bubble size ever observed in garnets. Our findings open prospect for spin-orbitronic devices that take advantage of the nanoscale bubble size together with the very low Gilbert damping. *Financial supports from ANR under the grant ANR-17-CE24-0025 (TOPSKY) and ANR-20-CE24-001 (MARIN). and as part of the "Investissements d'Avenir" program (Labex NanoSaclay, reference: ANR-10-LABX-0035 "SPiCY" and by the Ile-de-France region SESAME (IMAGESPIN project No. EX039175). We acknowledge financial support from the Horizon 2020 Framework Programme of the European Commission under FET-Open Grant No. 899646 (k-NET)*

[1] A. Fert *et al.*, Nat. Rev. Mat. 2, 17031 (2017) [2] P. Hansen *et al.*, IEEE Trans. Magn. 20, 1099–1104 (1984) [3] L. Soumah *et al.*, Nat. Commun. 9, 1 (2018) [4] L. Caretta *et al.*, Science 370, 6523 (2020)

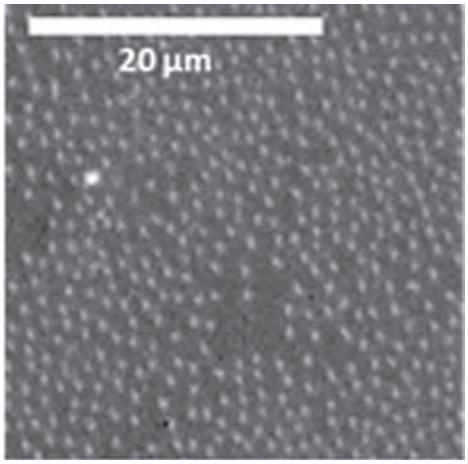

Figure 1

HOD-04. Annealing a skyrmion lattice with spin wave excitations. T. Srivastava[1], G. de Loubens[2] and *J. Kim*[2] *1. Centre for Nanoscience and Nanotechnology (C2N), CNRS, Université Paris-Saclay, Palaiseau, France; 2. SPEC, CEA, CNRS, Université Paris-Saclay, Gif-sur-Yvette, France*

Skyrmion lattices are present in many different chiral magnetic systems and their existence derives from a number of competing interactions. In a recent work [1], we showed that Pt/FeCoB/Al_2O_3 multilayers can host skyrmion lattices over a range of applied perpendicular fields. A particular feature of this material system is the presence of a "high-frequency" mode (HFM) under transverse field pumping, in the range of 12-18 GHz, which involves the coherent precession of the skyrmion cores and results in the generation of spin waves that flow into the uniform background region between skyrmions. Here, we discuss the results of micromagnetics simulations with the MuMax3 code [2] where we examine the role of spin wave interactions with the skyrmion cores. As the applied field increases and skyrmions begin to annihilate, leaving vacancies in the hexagonal lattice, the excitation of the HFM can serve to "anneal" the lattice, resulting in a glassy state as shown in the Figure. The spin wave interactions are found to provide a dynamical repulsive force between the skyrmion cores, which result in a more homogeneous arrangement in terms of density, but at the expense of crystalline order. These results also shed new light on how dynamical excitations can influence phase transitions associated with the melting of skyrmion lattices [3].

[1] T. Srivastava et al, arXiv:2111.11797 (2021). [2] A. Vansteenkiste et al, AIP Advances, vol. 4, 107133 (2014). [3] P. Huang et al, Nat. Nanotechnol., vol. 15, 761 (2020).

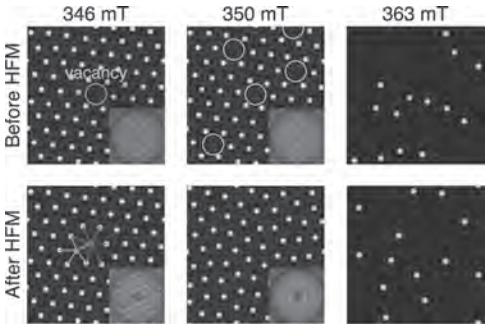

Simulated MFM images of skyrmion lattices under different applied fields, before and after the excitation of a high-frequency mode (HFM) that generates spin waves. The insets show discrete Fourier transforms of the spatial order.

HOD-05. Analysis of the stochastic process of skyrmion with transfer entropy. *H. Mori*[1], M. Goto[1,2], R. Ishikawa[3], S. Miki[1], H. Nomura[1,2] and Y. Suzuki[1,2] *1. Graduate school of Engineering Science, Osaka University, Toyonaka, Japan; 2. CSRN-Osaka, Osaka University, Toyonaka, Japan; 3. ULVAC, Inc., Suita, Japan*

Recently, there has been extensive research on computational devices that utilize the randomness or probabilistic properties in systems, such as Brownian computing and probabilistic-bits devices. In these systems, the stochastic process is essential clarifying information propagation. One of the systems in which stochastic behavior can be observed in solids at ambient temperature is skyrmion. Skyrmion has a topologically stable spin structure and can be expected to convey information through a repulsive interaction between skyrmions. However, the stochastic process in such a system has not been thoroughly investigated. Here, we focus on transfer entropy (TE) [1] and conditional Shannon entropy (CSE) [2], which are calculated from probabilities. This study evaluates TE from the Brownian motion of two skyrmions confined in a cell and surveys the stochastic process in this system. Our sample structure is SiO_2 substrate/Ta/$Co_{16}Fe_{64}B_{20}$/Ta/MgO/SiO_2. In such a sample, skyrmions are confined in the square region, patterned by additional deposition of a square of SiO_2 [3]. Fig. 1 shows two skyrmions confined in a square cell, as observed by MOKE microscopy. The pink line depicts the trajectory of Skyrmion A. We evaluated CSE and TE by using the trajectories as binary time-series data. Fig. 2 shows the result of TE over time. Red dots indicate the difference in CSE $H(b_n|a_{n-j},b_{n-j})$-$H(b_n|a_{n-j},b_{n-j},a_{n-j-1},b_{n-j-1})$. a_{n-j} (b_{n-j}) represents stchastic variables for the position of Skyrmion A (B) at step *n-j*. *n* and *j* represent discrete time. Blue (Orange) dots indicate the difference in TE calculated from two uncorrelated skyrmions (two random number sequences), which means an analysis error. In the Markov system, the results indicated by red dots should have the same values as the analysis error. However, the analysis results show different values, showing that the stochastic process in the skyrmion system is non-Markov. Also, we found that the attenuation of CSE differed for each nature of the information. This research was supported by JST, CREST Grant Number JPMJCR20C1, Japan and JSPS KAKENHI Grant Number JP20H05666.

[1] T. Schreiber, *Phys. Rev. Lett.* 85, 461 (2000) [2] C. E. Shannon, *The Bell System technical journal* 27, 379 (1948) [3] Y. Jibiki *et al., Appl. Phys. Lett.* 117, 082402 (2020)

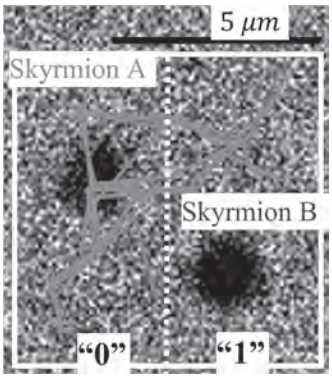

Fig. 1, The trajectory of Skyrmion A.

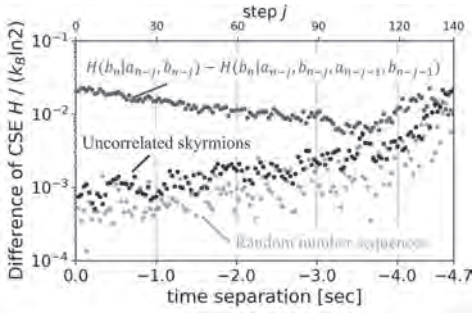

Fig. 2, The difference of CSE calculated from Skyrmion A and B.

HOD-06. Hysteretic resonances of chiral spin textures in multilayer films. *S. Thyagarajan*[1], J. Huang[1], X. Chen[2], H. Tan[2], A. Ghosh[2], J. Zhou[2], H. Tan[2] and A. Soumyanarayanan[1,2] *1. Physics, National University of Singapore, Singapore; 2. Institute of Materials Research and Engineering (IMRE), Agency for Science, Technology and Research (ASTAR), Singapore*

Microwave resonances of ultrathin magnetic films are actively investigated for myriad applications in microwave computing and information processing. Of particular interest of late are chiral spin textures such as magnetic skyrmions, whose topological spin structures are expected to additionally host localized resonances. The localized resonance modes of skyrmions in bulk crystals, arising from the gyration and dynamics of spin configurations at low temperatures, have been extensively characterized[1]. Meanwhile, the character, extent, and tunability of the resonance modes of Neel spin textures in technologically relevant chiral multilayers remain largely unexplored. Here, we report a detailed investigation of the microwave resonance phenomenology of Co/Pt based chiral multilayers hosting dense Neel textures. Figure 1 shows the microwave spectra recorded in transmission mode with magnetic field applied above saturation (polarized) and driven to the unpolarized region through zero field, as well as corresponding Lorentz transmission electron microscopy (L-TEM) images acquired at selected fields following the similar sweep protocol. The microwave spectra show distinct resonances on the polarized and unpolarized sides of the chiral multilayer, thereby exhibiting a clear hysteretic character. By combining, the spectroscopic measurements with L-TEM imaging, and micromagnetic simulations on a tunable skyrmion platform, we establish the localized, confined, and extended modes of the resonances, and their hysteretic behavior with varying field. In particular, we find strong correlations between the hysteretic character of microwave resonances and the formation mechanism of the chiral spin textures as established by thermodynamic and microscopic techniques[2,3]. Finally, the hysteretic resonances exhibited remarkable tunability with material parameters determining chiral domain stability, and field history, offering an intriguing approach to engineering magnonic bands for myriad applications.

[1] Schwarze, T., et al., Nat. Mater. 14, 478-483 (2015). [2] Chen Xiaoye, et al., Phys. Rev. Appl. 17, 044039 (2022). [3] Chen Xiaoye, et al., Adv. Sci. 9, 2103978 (2022).

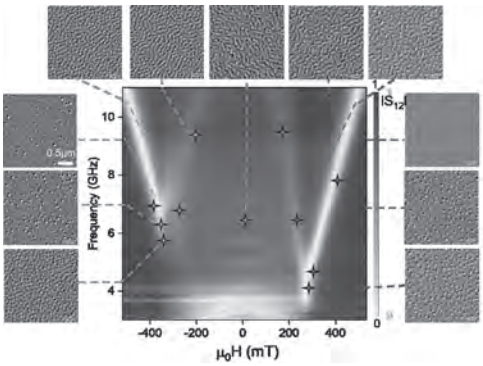

Fig 1: Microwave resonances of chiral multilayer Ir/Fe/Co/Pt. Color plot of normalized S_{12} as a function of magnetic field and frequency, and corresponding LTEM images recorded at selected fields following the similar FMR field protocol.

HOD-07. Theoretical Consideration of Logic Gates Based on Skyrmions in Antiferromagnets. *T. Naruse*[1] and K. Kondo[1] *1. RIES, Hokkaido Univ., Sapporo, Hokkaido, Japan*

Magnetic skyrmions are topological structures in magnetic materials such as ferromagnets (FMs) and antiferromagnets (AFMs). They are expected to become promising candidates of the logic gates in the next generation. Among them, the skyrmions in the FMs have been studied extensively. However, there exists main obstacle such as the skyrmion Hall effect when making the logic gates using skyrmions in the FMs. Recently, the skyrmions in the AFMs have been proposed in order to overcome the main obstacle. Moreover, the skyrmions in the AFMs move much faster than the skyrmions in the FMs. Therefore, it is very beneficial to make the logic gates based on the skyrmions in the AFMs. However, the logic gates based on the skyrmions in the AFMs have not been well studied. In this study, we propose the logic gates based on the skyrmions in the AFMs. We assume $KMnF_3$ thin films on Pt as the AFMs [1-3]. Figures 1 and 2 show the micromagnetic simulation results of the logic AND gate for the input combinations (1, 0) and (1, 1), respectively. The black circles represent the input and the output positions of the logic gate. The black arrows represent the elapse of time. The existence or the non-existence of a skyrmion represents one bit of "1" or "0", respectively. As shown in Figs. 1 and 2, we can obtain the outputs 0 and 1 for input combinations (1, 0) and (1, 1), respectively. Similarly, we can obtain the outputs 0 for the input combinations (0, 0), (0,1). It is found that the antiferromagnetic systems in Figs. 1 and 2 act as the logic AND gates. Therefore, we have been able to realize the logic AND gate using the skyrmions in the AFMs. In our presentation, we are going to discuss the micromagnetic simulation results of not only "the logic AND gate" but also both "the logic OR gate" and "the logic NOT gate". Moreover, we are going to discuss how to transfer the output of one logic gate to the input of another logic gate. We consider that this study would be useful for making the logic gates using the skyrmions in the AFMs.

J. Barker and O. A. Tretiakov, *Phys. Rev. Appl* 116, 147203 (2016). N. Bindal, C. A. C. Ian, W. S. Lew, and B. K. Kaushik, *Nanotechnol*. 32, 215204 (2021). X. Zhang, Y. Zhou, and M. Ezawa, *Sci. Rep.* 6, 24795 (2016).

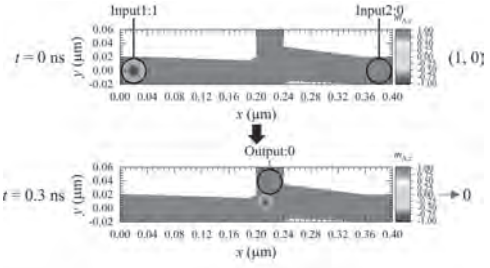

Fig. 1 The micromagnetic simulation results of the logic AND gate for the input combination (1, 0).

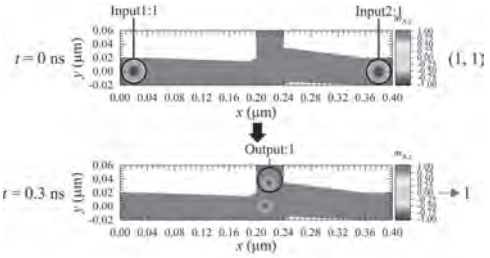

Fig. 2 The micromagnetic simulation results of the logic AND gate for the input combination (1, 1).

HOD-08. Three-dimensional Skyrmion Confinement Through Thickness Modulation. *S. Pathak*[1,2], M. Lang[2,3], S. Holt[2], H. Fangohr[2,3] and R. Hertel[1] *1. IPCMS, University of Strasbourg, Strasbourg, France; 2. Faculty of Engineering and Physical Sciences, University of Southampton, Southampton, United Kingdom; 3. Max Planck Institute for the Structure and Dynamics of Matter, Hamburg, Germany*

Magnetic skyrmions are a topic of extensive research due to their unique magnetic properties and spintronic applications. The primary way to achieve skyrmion dynamics is through electric currents, via STT effects [1]. The current can displace a skyrmion, but it usually also imparts an unwanted perpendicular velocity component known as skyrmion Hall effect (SkHE) [2]. Finding a way to counter SkHE has recently become a topic of intense research [3, 4]. In this work, we show that geometric variations can be used to achieve confinement of skyrmions in both static and dynamic cases. We have analyzed skyrmions in FeGe structures using finite-element and finite-difference micromagnetic simulations. For the static case, we find that by locally lowering the film thickness in dot-shaped regions (Fig. 1), skyrmions can be "captured" at geometrically defined sites [5]. In this way, skyrmions can be stabilized at positions such as square lattices, which otherwise do not occur in usual non-centrosymmetric ferromagnets. For the dynamic case, we consider a novel "H"-shaped racetrack geometry (Fig. 2). In the presence of a current along the track length, the simulations confirm that the barrier counters the SkHE while allowing skyrmion propagation along the geometrically defined path. We further analyze its trajectories and velocities as a function of current density and compare the numerical results with Thiele's equation [6]. Our study confirms that the numerically obtained skyrmion velocities are in accordance with Thiele's equation. In summary, we present a way to confine three-dimensional skyrmions by exploiting the dependence of skyrmion energy on the film thickness. This can prove valuable in the study of exotic configurations such as a rectangular skyrmion lattice. It may also prove relevant to countering the SkHE in skyrmion-based racetrack devices. This work was financially supported by initiative of excellence IDEX-Unistra (ANR-10-IDEX-0002-02) and the EPSRC Program grant on Skyrmionics (EP/N032128/1).

[1] J. Sampaio *et al*., *Nat. Nanotechnol.*, 8, 839 (2013). [2] I. Purnama *et al.*, *Sci. Rep.*, 5, 10620 (2015). [3] W. Legrand *et al.*, *Nat. Mater.*, 19, 34 (2020). [4] B. Göbel *et al*., *Phys. Rev. B*, 99, 020405 (2019). [5] S. A. Pathak & R. Hertel, *Magnetochemistry*, 7, 26 (2021). [6] J. Iwasaki *et al.*, *Nat. Nanotechnol.*, 8, 742 (2013).

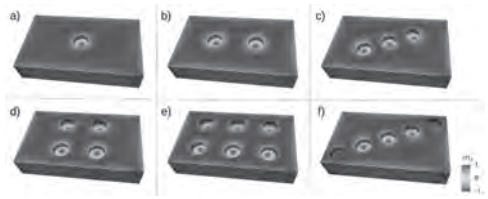

Fig. 1 Geometrically constrained skyrmions in FeGe platelets with circular pockets.

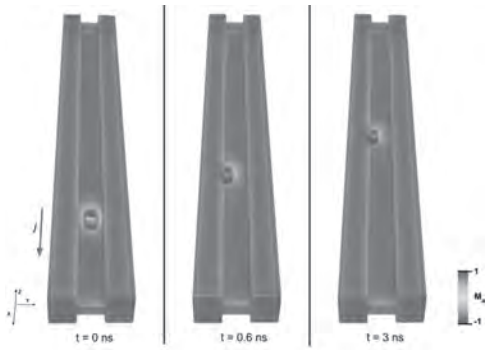

Fig. 2 Snapshots of the skyrmion dynamics in an H-shaped racetrack geometry.

HOD-09. Controlled skyrmion creation from a Domain wall pair for logic gate applications. *H. Perumal*[1], S. S K[1], B. Priyanka[1] and J. Sinha[1] *1. Department of Physics and Nanotechnology, SRM Institute of Science and Technology, Chennai, India*

The ability to manipulate the topological spin textures, such as magnetic skyrmions, is one of the crucial requirements in advance spintronics research. Recently, attempts have been made to understand the mechanism of Domain wall (DW) pair to skyrmion conversion in a specially designed nanotrack which may be useful in memory and logic operation [1,2]. Here, using micromagnetic simulation, we investigate the role of geometry in controlling the DW to skyrmion conversion in a three-channel narrow nanotrack adjoined to a wide nanotrack. Dimension of the nanotrack is as follows; length – 800 nm, thickness – 1 nm, width of narrow nanochannel - 20 nm, width of wider nanochannel - 200 nm, with spacing between the three narrow channels (lower -1, middle – 2, and upper – 3) varied symmetrically and asymmetrically from 10 - 30 nm in step of 10 nm. The simulations are performed using a python interfaced OOMMF known as Ubermag, where a Zhang-Li torque evolver in the Landau-Lifshitz-Gilbert equation is incorporated to understand the magnetization dynamics under the influence of spin current [3]. In figure 1, by keeping the separation between narrow channels 1 and 2 as well as 2 and 3 fixed as 10 nm, Gilbert damping $\alpha = 0.3$ and non-adiabatic torque parameters $\beta = 0.3$, conversion of DWs to two skyrmions are shown [4]. Interestingly, we note that while the steady state velocity for both the skyrmions are same, the time scale involved in DW to skyrmion for individual skyrmion varies resulting in difference in the x-position. By increasing the separation between channel 2 and 3 to 30 nm and keeping all other parameters fixed, formation of a skyrmion and a meron is observed in figure 2. We envision that such difference in the observation of topological spin texture by changing the separation between the narrow nanochannels will be useful for implementing futuristic skyrmion-based logic gate devices.

[1] A. Fert, V. Cross, J. Sampaio Nature Nanotech., Vol. 8, p. 152, (2013). [2] Y. Zhou, M. Ezawa, Nat. Commun., Vol. 5, p. 4652, (2014). [3] M. Beg, M. Lang, H. Fangohr., IEEE Trans. Magn. Vol. 58, p. 1-5 (2021) [4] P. Hari Prasanth, Syamlal S K, B. Priyanka, J. Sinha, Manuscript under preparation.

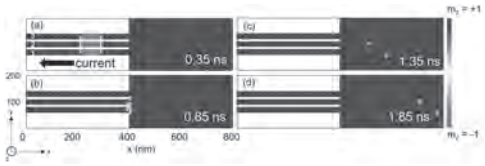

Fig 1: Snapshot of DW to skyrmion conversion from the three symmetrically separated narrow nano-channels for $\alpha = \beta = 0.3$ and separation - 10 nm.

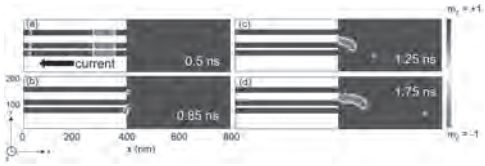

Fig 2: From asymmetrically separated narrow nano-channels (separation between 1 and 2 - 10 nm and between 2 and 3 - 30 nm) and for $\alpha = \beta = 0.3$ conversion of DWs into a skyrmion and a meron.

HOD-10. Analyzing collective thermal Skyrmion Dynamics by coarse graining. *T.B. Winkler*[1], J. Rothörl[1], M.A. Brems[1], K. Raab[1], H. Fangohr[2,3] and M. Kläui[1] *1. Institute of Physics, Johannes Gutenberg university, Mainz, Germany; 2. Scientific Support Unit for Computational Science, Max Planck Institute for the Structure and Dynamics of Matter, Hamburg, Germany; 3. Computational Modelling Group, Faculty of Engineering and Physical Sciences, Hamshire, United Kingdom*

Magnetic skyrmions [1] are magnetic quasi-particles with interesting properties for possible future applications in efficient low-power neuromorphic computing concepts. Thermally excited skyrmions in confined geometries, as necessary for device applications, have been shown to arrange based on commensurability effects [2]. Here, we investigate the enhanced dynamics and altered equilibrium state of a system in which the intrinsic skyrmion-skyrmion and skyrmion-boundary interaction compete with spin-orbit torques (SOTs) due applied currents [3]. In particular, we employ particle-based simulations to study four skyrmions in a triangular confinement, while injecting spin-polarized currents between two corners of the structure [4]. To analyze the observed positions of the skyrmion ensemble, we coarse-grain the skyrmion states in the system. In the context of neuromorphic computing, such coarse-graining may be key to identify the most suitable positions for potential readouts as well as to understand the collective skyrmion dynamics in systems with competing interactions at different scales.

[1] K. Everschor-Sitte et al., *Journal of Applied Physics* 124, 240901 (2018) [2] C. Song et al., *Adv. Funct. Mater.* 31, 2010739 (2021) [3] K. Raab et al., arxiv:2204.14720 (2022) [4] T. Winkler et al., in preparation (2022)

HOD-11. Withdrawn

HOD-12. Current-induced Bifurcation of a Three-dimensional Topological Skyrmion String. *J. Xia*[1], X. Zhang[1], O. Tretiakov[2], H.T. Diep[3], J. Yang[4], G. Zhao[5], M. Ezawa[6], Y. Zhou[7] and X. Liu[1] *1. Shinshu University, Nagano, Japan; 2. The University of New South Wales, Sydney, NSW, Australia; 3. CY Cergy Paris Université, Cergy, France; 4. Peking University, Beijing, China; 5. Sichuan Normal University, Chengdu, China; 6. The University of Tokyo, Tokyo, Japan; 7. The Chinese University of Hong Kong, Shenzhen, Guangdong, China*

Nanoscale topological spin textures in magnetic materials are promising building blocks for future information storage and computing applications [1-4]. The manipulation and control of two-dimensional and three-dimensional

(3D) topological spin textures are prerequisite for the realization of spintronic devices based on topological spin textures [3, 4]. The manipulation of 3D topological objects is also of fundamental interest in many branches of physics. In this work, we show by spin dynamics simulations that the bifurcation of a 3D skyrmion string in a layered frustrated system could be induced by the damping-like spin-orbit torque [5]. The bifurcation of a skyrmion string happens when the skyrmion string carries a minimal topological charge of $Q = 2$. We demonstrate that three types of bifurcations could be realized by applying different current injection geometries, which lead to the transformation from I-shaped skyrmion strings to Y-, X-, and O-shaped ones. Besides, different branches of a bifurcated skyrmion string may merge into an isolated skyrmion string spontaneously. The mechanism of bifurcation should be universal to any skyrmion strings with $Q \geq 2$ in the layered frustrated system and could offer a general approach to manipulate 3D string-like topological objects for spintronic functions.

[1] A. N. Bogdanov and D. A. Yablonskii, Sov. Phys. JETP 68, 101 (1989). [2] N. Nagaosa and Y. Tokura, Nat. Nanotechnol. 8, 899 (2013). [3] B. Göbel, I. Mertig, and O. A. Tretiakov, Phys. Rep. 895, 1 (2021). [4] X. Zhang *et al.*, J. Phys.: Condens. Matter 32, 143001 (2020). [5] J. Xia *et al.*, Phys. Rev. B 105, 214402 (2022).

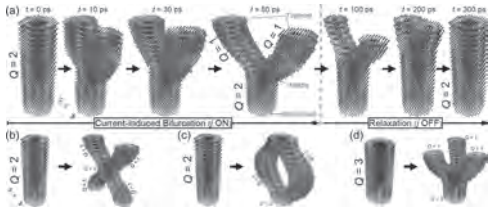

Fig. 1. (a) Current-induced bifurcation of an I-shaped skyrmion string to a Y-shaped skyrmion string. Bifurcation of an I-shaped skyrmion string to an X-shaped (b), O-shaped (c), or trident-like (d) skyrmion string is also possible.

HOD-13. Magnetization dynamics of skyrmion tubes and Bloch points in exchange-spring heterostructures. *M. Charilaou*[1] *1. Physics, University of Louisiana at Lafayette, Lafayette, LA, United States*

When the size of ferromagnetic particles is comparable to their exchange length, magnetization reversal is bound by topological constraints. Topologically non-trivial magnetization textures, such as skyrmions, chiral bobbers, and Bloch points, are promising candidates as information carriers in nanomagnetic devices. Importantly, the motion of these nanoscopic textures induces emergent electrodynamics, and due to the high velocity of Bloch points and their small size, emergent electric fields with substantial magnitude are predicted [1,2]. In this computational work [3], it is shown that exchange-spring-type heterostructures, where soft ferromagnets with azimuthal symmetry are exchange-coupled to a ferromagnetic layer with perpendicular magnetic anisotropy, can be used for the creation and control of skyrmion tubes and Bloch points during magnetization reversal of the soft ferromagnet upon the application of an external field. Once the external field is removed, the exchange coupling to the hard ferromagnet restores the system to its original configuration, making the process fully reversible and repeatable, and the duration of the magnetization processes and the motion of the Bloch points can be tuned by adjusting the size of the ferromagnet. The rapid motion, both with and without an external field, of the Bloch points, which move at instantaneous speeds of ~1000 m/s, induces an emergent electric field with a magnitude of the order of megavolts per meter. Hence, these numerical predictions suggest that exchange-spring heterostructures could be used to generate picosecond electromagnetic pulses.

[1] M. Charilaou, H.-B. Braun, J. F. Löffler, Phys. Rev. Lett 121, 097202 (2018) [2] Y. Li, L. Pierobon, M. Charilaou, H.-B. Braun, N. R. Walet, J. F. Löffler, J. J. Miles, C. Moutafis, Phys. Rev. Research 2, 033006 (2020) [3] M. Charilaou, APL Mater. (Accepted for publication, 2022)

HOD-14. The Role of Disclinations in the Thermal Stability of Magnetization Textures in Confined Helimagnetic Nanostructures. *G.D. Chaves-O'Flynn*[1], D.L. Stein[2] and P. Kuswik[1] *1. Institute of Molecular Physics, Polish Academy of Sciences, Poznan, Poland; 2. Department of Physics and Courant Institute of Mathematical Sciences, New York University, New York, NY, United States*

We discuss thermally activated switching between micromagnetic states in nanodisks with perpendicular anisotropy and a large strength of the interfacial Dzyaloshinskii-Moriya interaction, D. For large D, the magnetization on infinite planes acquires a cycloidal configuration in the ground state. However, Isolated singularities that are analogous to disclinations of cholerestic phases [1] are topologically protected and prevent the system from reaching the cycloidal phase (for examples see Fig. 1). In confined geometries, a rich variety of possible configurations with complex magnetization textures that are also energy minima of the energy landscape [2] has been observed. We argue that characterizing these different states as arrangements of disclinations is an effective way for understanding them. We support this statement on results of String Method [3] calculations done using OOMMF to examine the energy landscape of nanodisks (Fig. 2). We found that the transition states correspond to motion of individual merons across the device's edge (first maximum in Fig. 2), and to merging of disclinations inside the structure (2nd, 3rd and 4th maxima in Fig. 2). An additional advantage of emphasizing the importance of these magnetic singularities is the possibility of adopting them for collective coordinate descriptions which can be treated using low-dimensional stochastic methods to study their dynamics in the presence of thermal noise.

[1] Phys. Rev. B 99, 214408 (2019) [2] The Philosophical Magazine. 22:178, 739-749 [3] J. Chem. Phys. 126, 164103 (2007) *This research was supported in part by the National Science Centre Poland under OPUS funding Grant No. 2019/33/B/ST5/02013 (GDC, PK) and U.S. National Science Foundation Grant DMR 1610416 (DLS).*

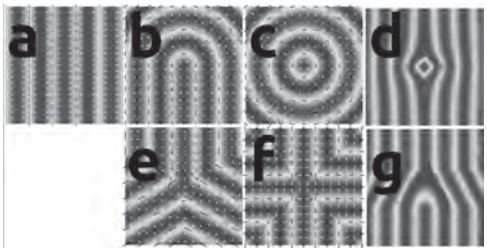

Examples of disclinations on the cycloidal phase of a ferromagnet with large DMI. (a) cycloidal phase without singularities. Disclinations occur when the *helical axis* rotates by a multiple of π. (b,c,e,f) Examples of disclinations, respectively their values are: (π,2π,-π,-2π). (d) a skyrmion shown as a 2π disclination embedded in a cycloidal background, (g) a meron shown as a π disclination embedded in a cycloidad background.

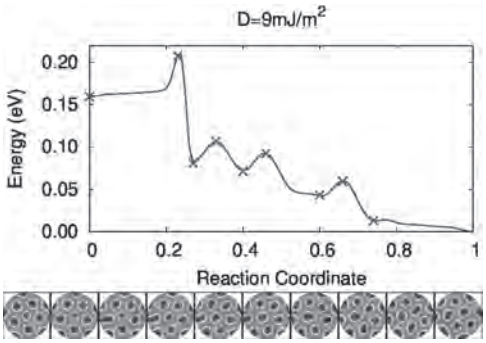

Results of String Method calculations on nanodisks with high DMi for thermally activated switching between two different micromagnetic configurations. The highest maxima occurs when a meron reaches the in-plane edge. The other maxima are the result of -π disclinations merging briefly into a +2π disclination resulting on re-acommodation of adjacent skyrmionic domains.

HOD-15. Image-recognition-assisted Characterization of Disordered Skyrmion States in Chiral Magnetic Thin-film Simulations.

C. Rudderham[2], A. Zelenskiy[2], M. Plumer[1,2] and T. Monchesky[2] *1. Physics and Physical Oceanography, Memorial University of Newfoundland, St. John's, NL, Canada; 2. Physics and Atmospheric Science, Dalhousie University, Halifax, NS, Canada*

We perform micromagnetic simulations wherein randomly magnetized thin-film samples of B20 chiral compounds are allowed to relax in a uniform in-plane external magnetic field, resulting in systems containing a large number of localized magnetic textures. Using numerical analysis techniques based on image recognition, we are able to extract detailed statistical information about the shape, size and locations of these localized states, and to explore how the corresponding distributions depend on the usual control parameters - namely the sample film thickness and the strength of the applied field. This approach allows us to quantify the nucleation probabilities of the various different skyrmionic textures that can arise, as well as to extract descriptions of the average ordering of these localized states. It is found that the average density distributions of the in-plane skyrmion states obtained upon relaxation are qualitatively similar to those obtained in circle-packing problems, and that these distributions can depend sensitively on both the sample thickness and the strength of the applied field. Interestingly, there are sample thicknesses for which the observed layering is relatively independent of the applied field strength, and others for which the layering depends sensitively on the field strength. To assist with the interpretation of the layering observed in these disordered systems, we also generate a phase diagram for perfectly ordered states against which our results are compared. This work represents a novel method for determining the control parameter combinations most likely to produce specific localized states and/or orderings thereof, which may assist with the identification of promising new experimental approaches.

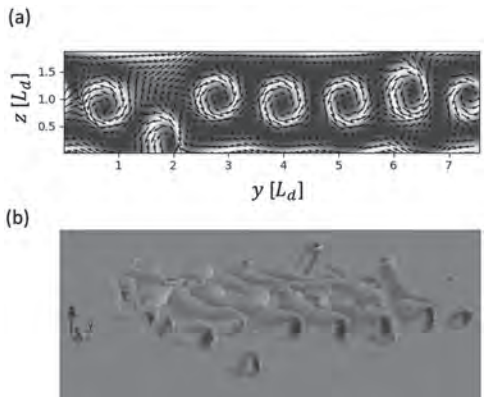

FIG. 1. (a) Representative cross-section of a texture obtained after relaxing a randomly magnetized thin-film (d = 26.3 nm) in an in-plane magnetic field (h=0.588). (b) 3D representation of the aforementioned magnetic texture. Only the regions within which the normalized magnetization vectors satisfy m_x < -0.50 are rendered.

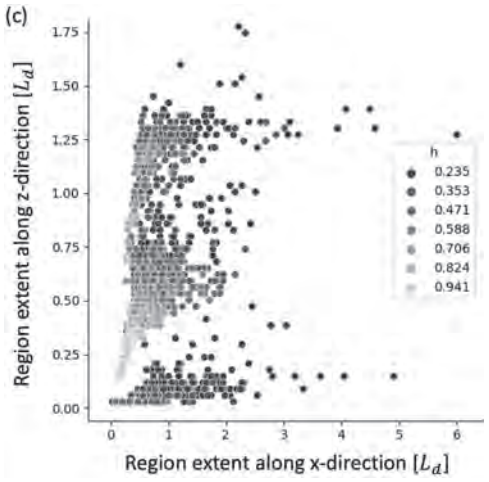

Fig. 2. Distribution of sizes for all regions identified (using the criteria described in the caption for Fig. 1) across all simulations of 26.3 nm thick films.

Session HPA
MAGNETIZATION DYNAMICS AND MICROMAGNETICS
(Poster Session)

Stefan Pollok, Co-Chair
Danmarks Tekniske Universitet, Kgs. Lyngby, Denmark
Alexander Kovacs, Co-Chair
Danube University Krems, Wiener Neustadt, Austria

HPA-01. Electronic Heat Bath Simulations for Ultra-fast Spin Dynamics. *J. Ross*[1], R. Chantrell[1] and R. Evans[1] *1. Physics, University of York, York, United Kingdom*

Magnetic modelling for ultrafast simulations at the atomistic and micromagnetic scale make common use of Langevin Dynamics to model the effect of thermal fluctuations on the procession of the magnetic moment. Such a model is simple to add to any finite-temperature simulation: a Gaussian distribution scaled against a collection of material dependent parameters are included in the effective field term in the LLG spin Hamiltonian, and at picosecond timescales is uncorrelated in space or time [1]. In general, however, the thermal fluctuations in a material are correlated through collective occupation of electron, phonon, and magnon modes in the system. Analytical solutions for these relationships under conditions of non-equilibrium require simple materials or drastic approximations, conditions ill-suited to ultrafast ferri and antiferromagnetic materials. We present an improved thermostat for ultrafast atomistic scale magnetic simulations using a computationally determined conduction band environment based on semi-classical electron-electron and electron-phonon scattering events [2][3]. Currently, our environment simulates charge and heat transport in metals on ultra-fast time scales during severe non-equilibrium caused from applied electric fields or laser-heating pulses. The electron-electron and electron-phonon relationship is parametrized into the relaxation time approximation using constants derived from experimental data [3][4]. Our environment successfully reproduces the popular *two-temperature model* (TTM) used to simulate laser-heating of experimental samples (fig. 1), and currently reproduces the phenomena of effective Joule heating from applied external fields and super-diffusive electron transport. The current work lays the foundation for the inclusion of electron spin into the conduction band environment, offering the ability to include correlated spin effects not possible in Langevin Dynamics. *Figure 1. Simulated electron and lattice temperatures (solid) following laser exposure compared to the standard TTM (dash). The varying colours and dynamics are a result of varying the electron-electron scattering constant.*

[1]. R F L Evans *et al* 2014 *J. Phys.: Condens. Matter* 26 103202 [2]. M van Kampen *et al* 2005 *J. Phys.: Condens. Matter* 17 6823 [3]. W Miao *et al* 2019 *Phys. Rev. B* 99, 205433 [4]. L Jiang *et al* 2005 *ASME. J. Heat Transfer* 127(10): 1167

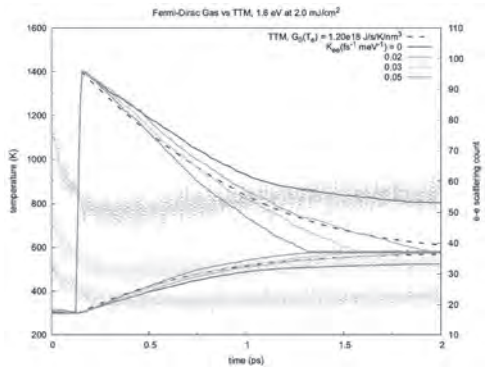

HPA-02. Simulation of Magnetic Hysteresis in Cobalt-Based Metal Amorphous Nanocomposites. *K.S. Cole-Piepke*[1], P. Nakarmi[1], A. Koenig[2], T. Mewes[1], G. Thompson[2], R. Noebe[3] and A. Leary[3] *1. Department of Physics and Astronomy, The University of Alabama, Tuscaloosa, AL, United States; 2. Department of Metallurgical and Materials Engineering, The University of Alabama, Tuscaloosa, AL, United States; 3. Materials and Structures Division, NASA Glenn Research Center, Cleveland, OH, United States*

We report on the development of a process to simulate magnetic hysteresis curves in metal amorphous nanocomposites (MANCs). The methodology utilizes a Voronoi tessellation method [1] to simulate random crystal growth in a material. In our simulations we include grain boundary regions that serve as the amorphous matrix of the material, while the grains represent the crystallites. The individual crystallites and the matrix can be assigned different material parameters depending on the desired magnetic behavior (Fig. 1). Utilizing experimental results obtained from Srivastava *et al.* [2] as a baseline for the crystallite properties, we simulate the hysteresis of a MANC using varying values for the saturation magnetization and exchange of the matrix to determine the effects of the matrix on the coercivity (Fig. 2). We perform these calculations for crystallites ranging from 3.9nm to 14.1nm in size and a crystallite to matrix ratio of approximately 11%. We find that with a weakly to non-magnetic matrix, coercivity values are significantly influenced by the size of the magnetic crystallites. However, as the saturation magnetization and/or the exchange coupling of the soft magnetic matrix increases, the crystallite size has less of an influence on the overall coercivity. Acknowledgments: Funding support has been provided through NASA grant CAN80NSSC18M0023.

[1] T. Suzudo and H. Kaburaki, Physics Letters A, Vol. 373, p.4484 (2009)
[2] A. Srivastava, K. Cole, A. Wadsworth et al., Journal of Magnetism and Magnetic Materials, Vol. 500, p.166307 (2020)

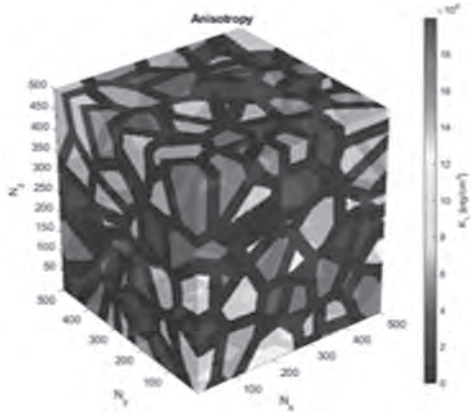

Fig. 1: A volume containing approximately 200 grains simulated using the Voronoi tessellation method, showing regions of high anisotropy (crystallites) and zero anisotropy (amorphous matrix). N_x, N_y, and N_z correspond to the number of computation cells used to generate the tessellation.

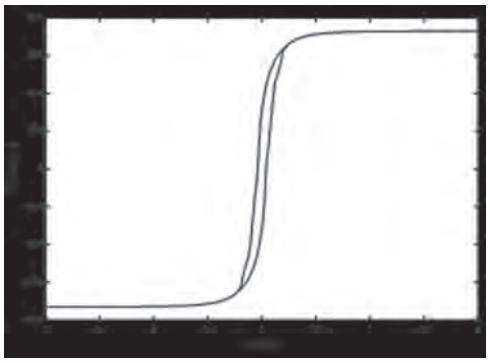

Fig. 2: A simulated hysteresis curve for a tessellation with an average crystallite size of 6.56[nm], assuming a completely non-magnetic matrix.

HPA-03. Theoretical Investigation of Tunable Ferrimagnetic Spin-Chain Oscillation Based on Atomistic Spin Model Simulation. *B. Cai*[1], X. Zhang[2], Z. Zhu[2] and G. Liang[1] *1. Department of Electrical and Computer Engineering, National University of Singapore, Singapore; 2. School of Information Science and Technology, ShanghaiTech University, Shanghai, China*

Ferrimagnets (FiMs) persist in ultra-fast dynamics similar to antiferromagnets but are as easy to be electrically manipulated as ferromagnets, leading to a promising approach for achieving ultrafast devices with feasible tunability. Furthermore, spin-chain is of fundamental importance in condensed-matter physics, revealing unique properties such as quantum phase transition, edge effect, etc.[1] Although the dynamics of FiM have been widely described by a two sublattices macro-spin model[2], it hardly captures the sophisticated physical properties in multi-spin systems such as spin chains. Hence, we developed an atomistic spin model to investigate the spin dynamics in the FiM spin chain deployed by current-induced spin-transfer torque(STT). Our simulation results showed that in the finite FiM spin chain, first, the oscillation started from opposite-spin spatial region, defined as "oscillation core (OC)". Next, the oscillation spatial region would expand and finally only some specific spins formed stable oscillation (Fig.1). To further understand this phenomenon, we first introduce one OC into the spin chain. When excited by STT, the exchange mode can be further classified into non-flipped exchange mode (region I), critical exchange mode (region II), and flipped exchange mode (region III). In region I and III, the frequency increased linearly with different slops as the current density increased, yet in region II, the frequency slightly decreased, indicating the competition among exchange field (H_{ex}), uniaxial anisotropy, and STT (Fig.2a). Next, when two OCs interacted, we find that smaller distance gives lager frequency, which is attributed to different H_{ex}. Hence, proper choice of distance allows us to tune the H_{ex}, achieving large-angle precession with THz frequency(Fig.2b). In summary, our work offers a novel understanding of FiM oscillation and proposes a strategy to construct energy-efficient spintronic oscillators with THz frequency. (This work at the National University of Singapore is supported by MOE-2019-T2-2-215 and FRC-A-8000194-01-00)

[1] H. Brune, Science., Vol. 312, p.1005-1006 (2006) [2] M. Guo, H. Zhang and R. Cheng, Phys. Rev. B., Vol. 105, p.064410 (2022)

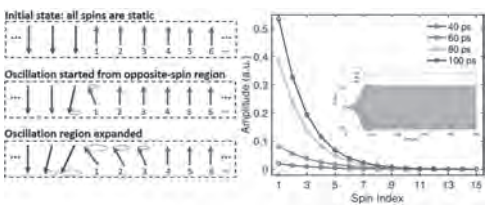

Fig.1 Schematic of FiM spin chain oscillation behavior evolved with time.

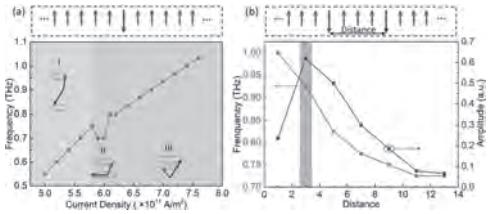

Fig.2 Numerical results of the oscillation in the FiM spin chain with (a) one OC and (b) two OCs.

HPA-04. Withdrawn

HPA-05. Co Layer-Resolved Measurement of Dzyaloshinskii-Moriya Interaction at Pt/Co Single Interface. *J. Yu*[1], S. Lee[1], M. Kim[1] and S. Choe[1] *1. Physics and Astronomy, Seoul National University, Seoul, The Republic of Korea*

Dzyaloshinskii-Moriya interaction (DMI) that occurs in structural inversion asymmetric systems stabilizes chiral domain-walls (DWs) which is a key issue to achieve high performance spintronic applications such as memory and data storage devices with high speed and high durability [1-4]. It is therefore important to analyze the strength of DMI and thus, there have been numerous efforts devoted to quantifying the DMI both theoretically and experimentally [4-6]. Unfortunately, the inconsistency between theory and experiment inevitably occurs because the theory predicts the strength of DMI based on single interface, however, the experiments must be implemented based on at least, double interface because of Ex-Situ nature [2-6]. Here, we first, measure the strength of DMI at Pt/Co single interface in In-Situ nature. To measure the strength of DMI at single interface, we set up In-Situ Magneto-Optical-Kerr-Effect (MOKE) microscopy with UHV magnetron sputtering chamber. Then, we quantified the strength of DMI with respect to Co layer thickness. Fig.1 clearly shows the plot of H_{DMI} with respect to t_{Co} based on Je's method [5].

[1] S. S. P. Parkin, M. Hayashi, and L. Thomas, Science 320 (5873), 190-194. (2008). [2] I. E. Dzialoshinskii, Sov. Phys. JETP 5, 1259 (1957). [3] T. Moriya, Phys. Rev. 120, 91 (1960). [4] A. Fert, V. Cros, and J. Sampaio, Nat. Nanotechnol. 8, 152 (2013). [5] S.-G. Je, K.-J. Lee, and S.-B. Choe, Phys. Rev. B 88, 214401 (2013). [6] J. Cho, B. Koopmans, and C.-Y. You, Nat. Commun. 6, 7635 (2015).

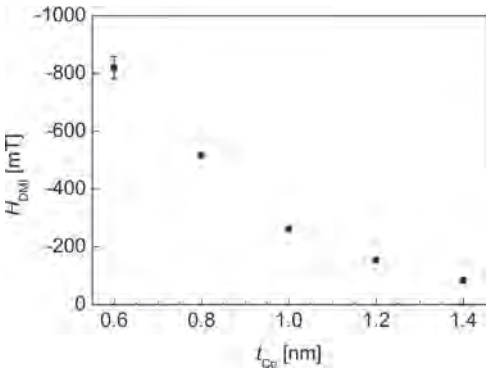

Fig. 1 The plot of H_{DMI} with respect to t_{Co}.

HPA-06. Torsion and curvature induced effects in magnetic twisted nanotubes. *M.M. Salazar Carona*[1] and J.A. Otalora Arias[1] *1. Physics, Universidad Católica del Norte, Antofagasta, Chile*

Recently, researchers developed 3d magnetization models for magnetic shells with curvature and torsion [1]. For example, in a thin nanotube, the curvature induced a magnetostatic anisotropy [2]. Also, in the case of the

nanocylinder, the curvature induces dipole-dipole interaction [3]. However, in these tubular systems, torsion has not been explored yet. Here we propose to study a nanocylinder with torsion that we call the twisted nanotube. In Figure 1, we present the system. It has an internal radius *r,* an external radius *R*, infinite length *L*, an elliptical transversal area, curvature κ and torsion τ. Figure 1. The magnetization vector in terms of the base vectors (e_1 e_2, e_3). The parametrization of a 2D tubular surface γ, embedded in a 3D space defines these vectors. For the twisted nanotube, we compute the dipolar interaction by implementing the model for the energy of the nanocylinder [3]. Furthermore, the torsion is introduced by defining the reference frame for the magnetization, as is suggested in a recent approach developed for magnetic shells [1]. Hence, the magnetization base vectors are derived in terms of the surface curvilinear parametrization, as presented in Figure 1. With this methodology, we show that in the twisted nanotube, there are volumetric charges because of the torsion of the system. In equation *(1)*, we present the expression for the volumetric charges, where the term Γ_d is the contribution of the torsion. Also, the developed model shows that the torsion does not induce surface charges. With this work, we expect to contribute to future developments of spintronic technology, for example, supporting a theoretical model for a magnonic transducer, like the one developed for the nanocylinder [4]. $\nabla \bullet M = M \sin\Theta \; (\sin p/\rho - \partial_z\Theta + \Gamma_d)$ *(1)*

[1] Gaididei, Yuri, Volodymyr P. Kravchuk, and Denis D. Sheka, "Curvature effects in thin magnetic shells," Physical review letters vol. 112, no. 25, pp. 257203, 2014. [2] Landeros, Pedro, and Álvaro S. Núñez, "Domain wall motion on magnetic nanotubes," Journal of Applied Physics vol. 108, no. 3, pp. 033917, 2010. [3] Otálora, J. A., et al, "Breaking of chiral symmetry in vortex domain wall propagation in ferromagnetic nanotubes," Journal of magnetism and magnetic materials vol. 341, pp. 86-92, 2013. [4] Salazar-Cardona, Monica M., et al, "Nonreciprocity of spin waves in magnetic nanotubes with helical equilibrium magnetization," Applied Physics Letters vol. 118, no. 26, pp. 262411, 2021.

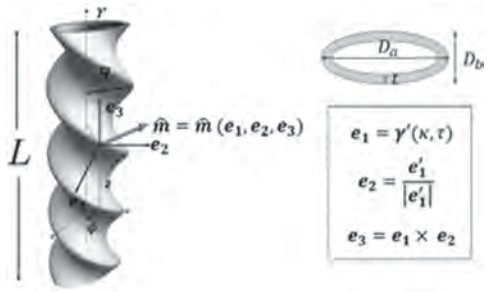

Figure 1. The magnetization vector in terms of the base vectors (e_1 e_2, e_3). The parametrization of a 2D tubular surface γ, embedded in a 3D space defines these vectors.

HPA-07. Withdrawn

HPA-08. Withdrawn

HPA-09. Investigation on simple numerical modeling of anomalous eddy current loss in steel sheet using multiple boundary conditions.
Y. Gao[1], T. Ohira[1], Y. Gotoh[1], W. Guan[2], X. Zhao[3] and K. Muramatsu[4]
1. Oita University, Oita, Japan; 2. Wuhan Unviversity, Wuhan, China; 3. North China Electric Power University, Baoding, China; 4. Saga University, Saga, Japan

I.Introduction Understanding of excess loss in electrical steel sheets, which is the difference between the measured iron loss and the sum of static hysteresis loss and classical eddy current loss [1], is difficult as it is related to non-repeatable dynamic domain wall motion inside the steel [2], whereas it is normally agreed upon that the anomalous eddy current loss, which is due to the micro eddy current generated by domain wall motion, is one main source of the excess loss for grain-oriented steel sheets [3]. One famous model coping with the anomalous eddy current loss is the Pry and Bean domain model [4] and we have established a numerical domain model based on it [5]. However, this model cannot model the skin effect of the flux density and it cannot represent the nonlinear *BH* curve of the steel sheets. In this paper, a simple numerical method using multiple boundary conditions is proposed to calculate the micro eddy currents and the classical eddy currents simultaneously while considering the nonlinear *B-H* constitutive relation of steel sheets. II.Analysis model and Conditions The domain pattern of grain-oriented steel sheet is considered as a simple periodic one as shown in Fig. 1. Half of one periodic region is chosen as the analyzed model. Micro eddy currents are generated around the domain walls when the domain wall moves. In the proposed analysis, the overall alternating magnetization to induce the classical eddy currents is imposed by using one Dirichlet boundary condition. And the local magnetization change due to domain wall motion is imposed by using another Dirichlet boundary condition to induce the micro eddy currents. III.Analysis Results The calculated flux and eddy current distributions are shown in Fig. 2. The skin effect of flux density can be observed in the flux distribution. To show the micro eddy currents clearly, the eddy current calculated by using the proposed method is subtracted with the classical one, and the obtained micro eddy currents are shown in Fig. 2 (b)(ii). We can see that micro eddy current around the domain walls are generated.

References [1] G. Bertotti, "Hysteresis in Magnetism: For physicists, Materials scientists, and Engineers", Academic Press, San Diego, (1998). [2] A. J. Moses, "Energy efficient electrical steels: magnetic performance prediction and optimization", *Scripta Materialia*, vol. 67 no. 6, pp. 560–565, 2012. [3] J. E. L. Bishop, "Enhanced eddy current loss due to domain displacement", *Journal of Magnetism and Magnetic Materials*, vol. 49, no. 3, pp. 241-249, 1985. [4] R. H. Pry and C. P. Bean, "Calculation of the energy loss in magnetic sheet materials using a domain model," *Journal of Applied Physics*, vol. 29, no. 3, pp. 532-533, 1958. [5] Y. Gao, Y. Matsuo, and K. Muramatsu, "Investigation on simple numeric modeling of anomalous eddy current loss in steel plate using modified conductivity," *IEEE Trans. on Magn.*, vol. 48, no. 2, pp, 635-638, 2012.

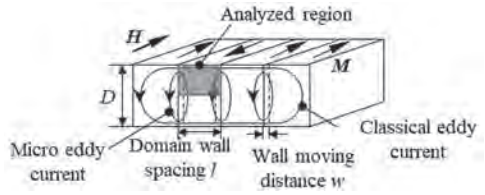

Fig. 1. Analysis model (*D*: sheet thickness).

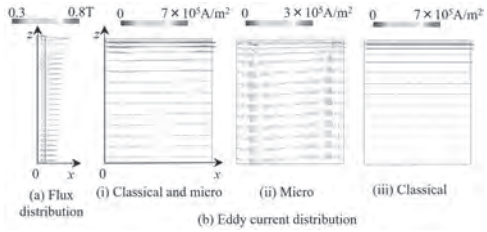

Fig. 2. Flux and eddy current distributions.

HPA-10. The Study of the Three-dimensional Vector Hysteresis Model based on the SAE model and Play operator.
Y. Ma[1], Y. Li[1], R. Chen[1], S. Yue[1] and H. Sun[1] *1. Hebei University of Technology, Tianjin, China*

The hysteresis modeling of ferromagnetic materials in electrical equipment is one of the basic theoretical studies in the field of electrical engineering. In this paper, a three-dimensional vector hysteresis model is proposed based on Stacked Auto-Encoder (SAE) model and hysteresis operator space theory. Multiple 3D vector Play hysteresis operators are used to construct

an hysteresis operator space to create the high-dimensional operator data. By the operator space, the nonlinear hysteresis relationship in the hysteresis data is transformed into a nonlinear mapping between the operator data and the output of the model. And the SAE model is used to characterize this nonlinear mapping. In the training of the SAE model, training set is composed of operator data and magnetic field strength data. The structure of the vector hysteresis model is determined by taking the output of the operator space as the input of the SAE model. The simulation results show that the model can effectively describe the nonlinear characteristics and anisotropic of the Soft Magnetic Composite under 3D vector excitation. In addition, this model has certain generalization ability.

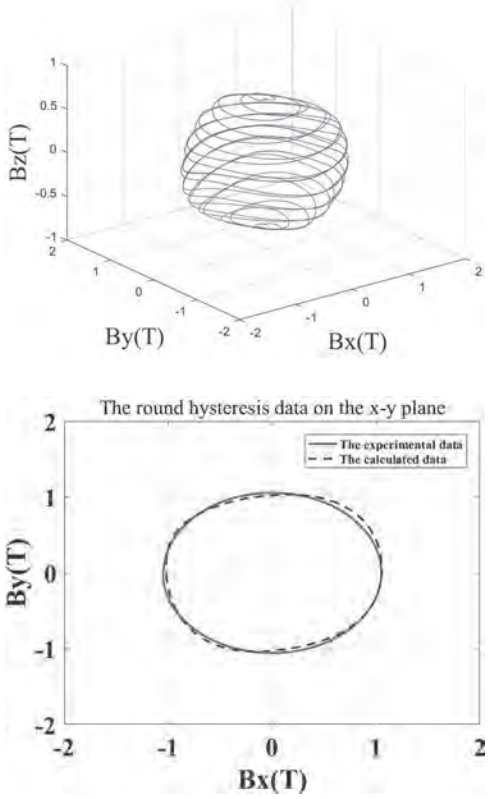

HPA-11. Effects of Mixed Coordination Numbers in Artificial Spin Ice Systems. *A. Kunz*[1] and L.J. Ruffolo[1] *1. Physics, Marquette University, Milwaukee, WI, United States*

Artificial spin ice is a two-dimensional metamaterial consisting of patterned magnetic nanoislands arranged on lattices to mimic naturally occurring systems. Two commonly investigated geometries are based on the rectangular (square) lattice with a coordination number of four (four magnets interact at each vertex) and the Kagome lattice with a coordination number of three which exhibits a high degree of frustration. Studies on decimated lattices, which give rise to mixed coordination numbers, demonstrate changes to the so-called ice-rule which can be tracked via the topological at each vertex [1,2]. In this work we present the results on a pair of structures built with regular rhombuses giving rise to mixed coordination numbers: the dice lattice with 3 – 6 coordination and a Penrose tiling with all integer coordination numbers between three and seven as shown in Fig. 1. We have carried out a combination of Metropolis Monte Carlo and LLG micromagnetic simulations to understand the energetics and dynamical processes in these systems of mixed coordination with large and small coupling (controlled by changing the rhombus edge length). The dice lattice is well-behaved with a defined ground state and anti-ferromagnetic coupling; alternating lines of charge are readily observed in Fig. 1(a). However, the Penrose tiling due to its quasi-periodicity, reliance on two different rhombuses to fill space (Fig. 2), and rich offering of coordination numbers exhibits more complicated dynamics. While at low temperature the majority of the vertices follow the ice rule the variable structure and mixed coordination numbers lead to the system exhibiting ice-rule fragility, where local energetics oppose the ice rule. This is an effect not observed in mono-coordinated spin ice lattices.

A. Libál, et al., Nature Communications, Vol 9, 4146 (2018). N. Greenberg and A. Kunz, AIP Advances 8, 055711 (2018).

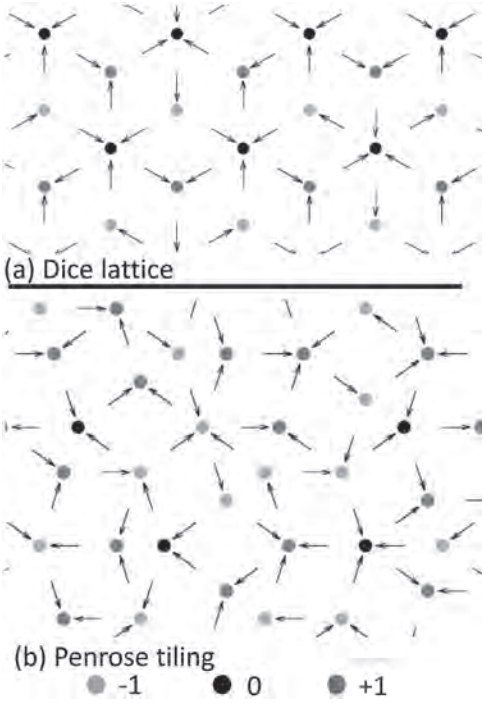

Fig. 1 (a) In the strongly coupled regime shown the ice rule is obeyed with alternating spins and highly ordered topologic charges. (b) A region of the Penrose tiling where the ice rules are obeyed yet the topologic charges are not ordered due the varying coordination numbers.

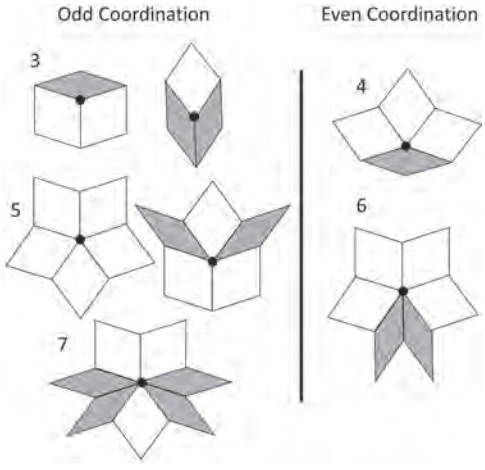

Fig. 2 Vertices for each of the even and odd coordination numbers in the Penrose tiling. Coordination of 3 and 5 have two non-degenerate orientations changing the local energetics.

HPA-12. Generalized Auto-oscillator Model for Arbitrary Artificial spin ices. *G. Alatteili*[1] and E. Iacocca[1] *1. Physics and Energy Science, University of Colorado Colorado Springs, Colorado Springs, CO, United States*

Artificial spin ices are ensembles of geometrically structured, interacting magnetic nano-elements that exhibit frustration as a result of their design [1]. Due to their periodicity, they are considered magnonic crystals [2]. The magnon dispersion relation in artificial spin ices has been explored for a square configuration so far[3], and collective magnons have been quantitatively defined for a charge ice [4]. So far, analytical approaches have been limited for square ice only[5]. Here, we present a semi-analytical model to compute the magnon dispersion of arbitrary artificial spin ice geometries. The foundation of our model is Holstein-Primakoff transformation [6] to account for the relative orientation of nanoislands and the magnetization vector within a general reference frame. We validate the use of the general reference frame by computing Kittel's equation, as shown in Figure 1. Panel (a) shows the simple field dependence of the perpendicularly magnetized film, including the geometry and rotational frame in Cartesian coordinates. Panel (b) shows the angular dependence of the Kittel equation for an applied field of constant magnitude. The model is currently being completed to include non-local dipole fields that will give rise to the magnonic band structure. Because of the independence to the coordinate system, this model will be applicable to arbitrary artificial spin ice geometries, even in three dimensions.

[1] S. H. Skjærvø *et al.*, Nat. Rev. Phys. 2, 13 – 28 (2020) [2] S. Gliga, E. Iacocca, and O. G. Heinonen, APL Materials 8, 040911 (2020) [3] M. B. Jungfleisch *et al.*, Phys. Rev. B 93, 100401 (2016) [4] E. Iacocca, S. Gliga, and O. G. Heinonen, Phys. Rev. Appl. 13, 044047 (2020) [5] E. Iacocca et al., Phys. Rev. B 93, 134420 (2016); T. D. Lasnier and G. M. Wysin, Phys. Rev. B 101, 224428 (2020) [6] A. Slavin and V. Tiberkevich, IEEE Trans. Magn. 45, 1875 – 1918 (2008)

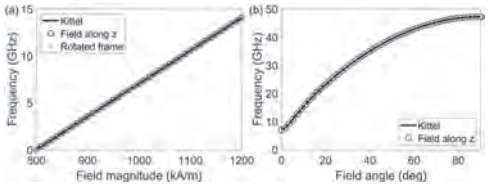

Figure 1: (a) Ferromagnetic resonance of a perpendicularly magnetized thin film. The solid black line is Kittel's equation. The blue circles are obtained from our model with a field in the z direction, normal to the plane. The yellow asterisks are obtained by rotating both the equilibrium magnetization and the external field by 33 deg and 233 deg for the polar and azimuth angles, respectively. (b) Ferromagnetic resonance as a function of the polar angle with an applied field of $\mu_0 H = 1$ T.

HPA-13. Study of temperature influences on the vortex chirality probability in asymmetric disk array. *K. Lai*[1], C. Chen[1], D. Shiu[1] and L. Horng[1] *1. Physics, National Changhua University of Education, Changhua, Taiwan*

We using Mumax3 to simulate a 5×5 asymmetric disk array. By changing the temperature, we explored the variety of energy during the evolution of the vortex and the probability of the vortex chirality. We also controled disc spacing to adjustment the magnitude of stray field. The material we used amorphous permalloy, simulation parameters were saturation magnetization 8.6×10^5 A/M, exchange length 13×10^{-12} J/m, damping constant 0.01, cell size 5x5x5 nm^3, and temperatures changed from 0K to 300K. Geometric parameters were disk diameter 1000 nm, thickness 40 nm, asymmetric ratio 0.3, and disc spacing 200, 500 and 800 nm. In the previous research, vortex chirality seems to be related to a rise in total energy. When increase temperature will also increase the total energy in our simulation. We analyze the total energy, demagnetization energy and exchange energy separately then we finded the exchange energy increases significantly with temperature. It can be speculated that changes in temperature make the magnetic moments less parallel to each other, resulting in a significant increase in exchange energy and increase in the probability of CW vortices.

Arne Vansteenkiste, Jonathan Leliaert, Mykola Dvornik, et al. *AIP Advances, 4*, 107133(2014) Mi-Young Im, Ki-Suk Lee, Andreas Vogel, et al. NATURE COMMUNICATIONS, 5:5620(2014) Dustin A. Gilbert, Brian B. Maranville, Andrew L. Balk, et al. NATURE COMMUNICATIONS 6 8462 (2015) Mi-Young Im, Peter Fischer, Hee-Sung Han, et al. NPG Asia Materials 9 (2017)

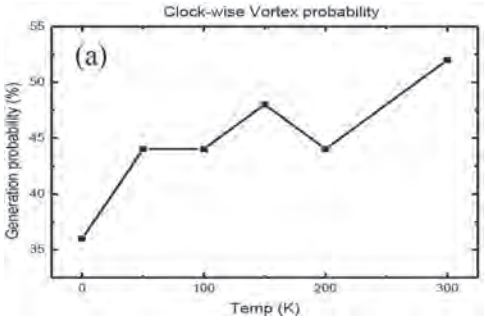

Fig1. Clock-wise vortex probability.

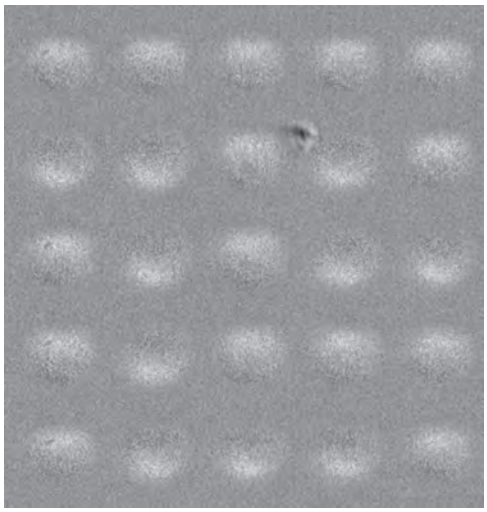

Fig2. MOKE image of disk array.

HPA-14. Reliable control of magnetic vortex chirality in asymmetrically optimized magnetic nanodisk. *H. Zhang*[1], H. Yu[1], X. Zhang[1], X. Yang[2], J. Shim[2,3], X. Ma[2,1] and H. Piao[2,1] *1. Hubei Engineering Research Center of Weak Magnetic-Field Detection, China Three Gorges University, Yichang, China; 2. College of Science, Yanbian University, Yanji, China; 3. POSTECH, Department of Physics and Center for Attosecond Science and Technology, Pohang, The Republic of Korea*

Magnetic vortex have attracted extensive attention in the field of information storage because of their topological spin structures with chiral bistable states[1,2]. If the vortex core polarity and vortex circulation sense can be precisely controlled simultaneously in a nanodisk, which will be more beneficial to realize the multi-bit ultrahigh density storage[3,4]. In this paper, a reliable control scheme for magnetic vortex chirality is proposed by optimizing the structure of Pac-Man-like nanodisk, as shown in Fig1(a)-(b). The results show that the polarity and circulation of the vortex can be precisely controlled simultaneously by simply changing the direction of the global magnetic field, and even the chiral states of the vortex can be determined by simply detecting the stray field distribution on the surface of the nanodisk, as shown in Fig1(c). The optimized Pac-Man-like nanodisk can provide a simplified experimental method for the control and detection of magnetic

vortex chirality, which will be beneficial to the realization of multi-bit magnetic storage or magnetic logic technology in the future.

[1]H.-S. Han, S. Lee, D.-H. Jung, et al. Appl. Phys. Lett. 117(4), 042401(2020). [2]K. A. Zvezdin, E. G. Ekomasov. Phys. Met. Metallogr. 123(3), 201(2022). [3]J. A. Fernandez-Roldan, R. P. del Real, C. Bran, et al. Phys. Rev. B. 102(2), 024421 (2020). [4]D. Yu, J. Kang, J. Berakdar, C. Jia, NPG Asia Mater. 12(1), 1(2020).

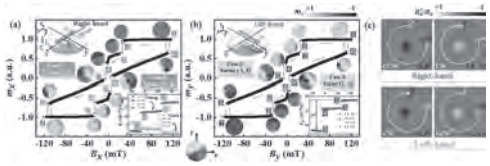

Fig. 1. (a) and (b) show that the four chiral states of vortex can be precisely controlled. (c) It is shown that the vortex chirality can be determined by the distribution of the stray field on the surface of the nanodisk.

HPA-15. Micromagnetic investigation of the influence of magnetoelastic anisotropy on magnetisation processes in rapidly quenched magnetostrictive amorphous nanowires. *C. Rotarescu*[1], J. Pinto de Queiros Fradet[2], O. Chubykalo-Fesenko[2], H. Chiriac[1], N. Lupu[1] and T. Óvári[1]
1. National Institute of Research and Development for Technical Physics, Iasi, Romania; 2. Instituto de Ciencia de Materiales, CSIC, Madrid, Spain

Amorphous glass-coated $Fe_{77.5}Si_{7.5}B_{15}$ nanowires with the diameters well below 1 μm are excellent candidates for novel applications in miniaturised devices, such as micro and nanosensors. Experimentally, all the investigated samples are magnetically bistable, being characterized by rectangular hysteresis loops [1]. Here, the dependence of the coercivity values on the diameters of the nanowires have been analyzed and interpreted by micromagnetic simulations in order to understand the interplay between magneto-elastic and shape anisotropies in cylindrical amorphous nanowires prepared by rapid quenching from the melt. In this study, we are modelling the hysteresis loops of the amorphous nanowires in the quasi-static regime [2] in which the magnetization process is fully controlled by the domain nucleation. The most important feature is the inclusion of the magnetoelastic anisotropy term that originates in the specific production process of these amorphous nanowires. Following the known distribution of magnetoelastic anisotropy, it has been assumed to vary from axial to radial direction as the distance from the nanowire center increases. In order to understand mechanism that controls the magnetization switching process and to reveal the relation between the main anisotropy terms we analyze the magnetization reversal modes and the role of different energy terms. Fig. 1 shows a family of simulated hysteresis loops considering that the sample diameter varies in the range 20-200 nm (a), and the dependence of the switching field on the nanowire diameter (b). The obtained results show that coercivity decreases with the nanowire thickness and reveal the importance of three factors: dimensions, geometry, and composition in order to design cylindrical amorphous nanowires for the future applications. Acknowledgement: Work supported by the Executive Unit for Financing Higher Education, Research, Development and Innovation (UEFISCDI) under the project PN-III-P4-ID-PCE-2020-1856 (contract no. PCE 1/2021).

References: [1] C. Rotarescu, H. Chiriac, N. Lupu, T.-A. Óvári, AIP Advances 9 (2019) 105316. [2] A. Vasteenkiste, J. Leliaert, M. Dvornik, et al., AIP Advances 4 (2014) 107133.

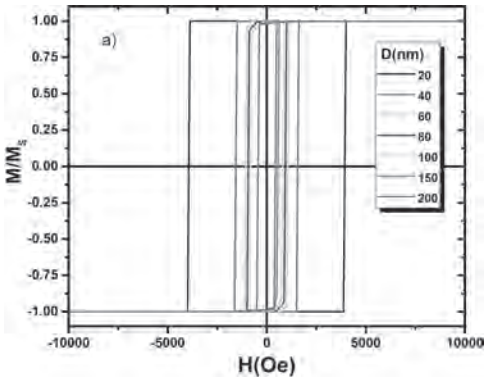

Fig. 1: a) Simulated hysteresis loops for different diameters;

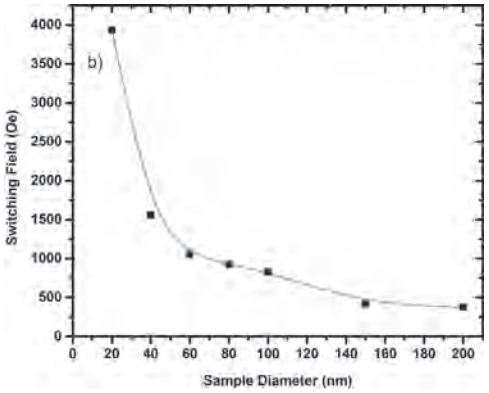

Fig. 1: b) Switching field dependence on the sample diameter.

HPA-16. Withdrawn

HPA-17. Design and research of the New Hybrid excited consequent pole Brushless Doubly Fed Machine. T. Ren[1,2], *X. Wu*[1], X. Zhang[2], C. Kan[1], X. Li[1] and W. Zhuo[2] *1. Hefei University of Technology, Hefei, China; 2. Anhui CRRC Ruida Electric Co., Ltd., Hefei, China*

Permanent magnet machines have many advantages such as high efficiency, high power density and so on, it have been widely used in the fields of aerospace, wind power generation and electric vehicles. However, permanent magnet machines have the disadvantage that the air-gap magnetic field is difficult to be adjusted. To effectively solve this problem, many scholars have proposed a hybrid excitation machine, in which the electrically excited magnetic potential plays an auxiliary role in adjusting the air-gap magnetic field [1]. The hybrid pole permanent magnet machine was proposed[2], which has a simple structure and high electric excitation efficiency. It has a permanent magnet and ferromagnetic pole structure on the rotor, but it has brush structure. A new hybrid excited consequent pole brushless Doubly Fed Machine (HE-CPBDFM) is proposed in this paper, and the performance of the machine is studied. Fig.1 gives the structure of the HE-CPBDFM. There are two sets of windings on the stator of the machine, a power winding with 3 pole pairs and a control winding with 1 pole pair;the number of permanent magnets on the rotor is the same as the number of poles of the control winding, and the polarity is the same, and the mechanical angle of the ferromagnetic pole with a smaller circumference between the two permanent magnets is 60°. The direction of the magnetic field synthesized by the control winding is facing the axis of the ferromagnetic pole, and the air gap magnetic field is adjusted by changing the magnitude of the excitation of the control winding. Keeping the external 220Ω load on the power winding side unchanged, the relationship curves between the power winding output voltage and the control winding excitation current under different excitation are shown in Fig.2. From Fig.2, it can be seen that the power winding output

voltage increases with the increase of excitation current, and when the excitation current increases to 4A, the voltage growth rate slows down with the increase of machine saturation.

[1] Ullah S, McDonald S P, Martin R, et al. "A permanent magnet assist, segmented rotor, switched reluctance drive for fault tolerant aerospace applications,". IEEE Trans. on Ind. Appl., vol. 55, no. 1, pp. 298-305, Jan./Feb.2018. [2] Q. Zhang, S.R. Huang, G. D. Xie. "Design and experimental verification of hybrid excitation machine with isolated magnetic paths,". IEEE Trans. Energy Conversion, vol. 25, no. 4, pp. 993-1000, Dec.2010. [3] Ayub M, Jawad G, Kwon B. "Consequent-pole hybrid excitation brushless wound field synchronous machine with fractional slot concentrated winding,". IEEE Trans. Magn., DOI: 10.1109/TMAG.2018.2890509,2019.

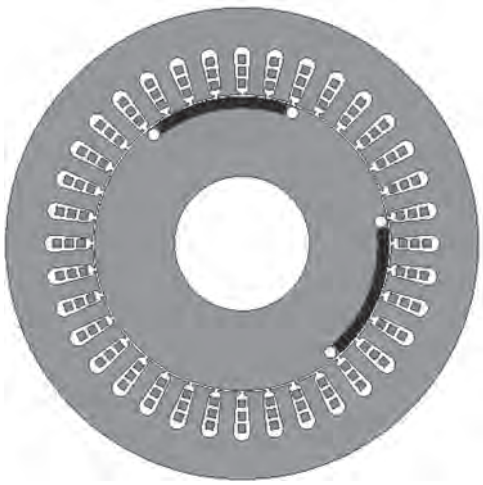

Fig.1. Machine structure diagram

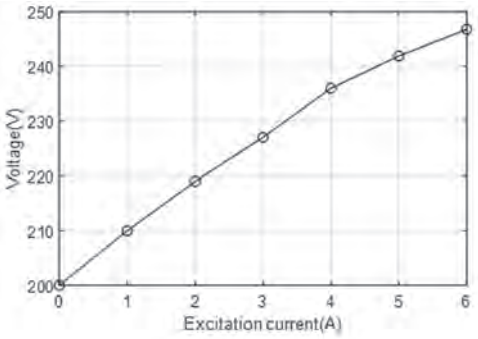

Fig.2. The relationship between the output voltage of the power winding and the excitation current of the control winding under different excitations

HPA-18. Construction of High-performance Nanocomposites Based on Shape Anisotropy of Soft Phase. *Y. Teng*[1], Y. Li[1], M. Yue[1], W. Liu[1] and D. Zhang[1] *1. Faculty of Materials and Manufacturing, Beijing University of Technology, Beijing, China*

Nanocomposite permanent magnets have attracted extensive attention because their theoretical magnetic energy product is more than twice that of $Nd_2Fe_{14}B$-based magnet. Moreover, the nanograins also inspire the advantages of high corrosion resistance, low eddy current loss and high mechanical properties. Micromagnetic simulation method can provide theoretical guidance and reference model for the research and development of magnetic materials. In this paper, the effects of the shape anisotropy of soft phase on the magnetic properties of the $Nd_2Fe_{14}B/Fe_{65}Co_{35}$ nanocomposites were simulated and analyzed. The model of square prism soft phase ($Fe_{65}Co_{35}$, d_s = 10 nm) wrapped by hard grains ($Nd_2Fe_{14}B$, d_h = 5 nm) is established (Fig. 1a). accordingly, when the aspect ratio (I) of the soft phase varying from 1 to 5, the soft phase content (v) in the model increases from 12.5 *vol*. % to 20.8 *vol*. %. The saturation magnetization ($4\pi M_s$), remanence ($4\pi M_r$) and maximum magnetic energy product [$(BH)_m$] of the nanocomposites increase continuously, with the increase of I. When $I \leq 2.5$, $4\pi M_s$, $4\pi M_r$ and $(BH)_m$ increased rapidly, while the increase rate is slow as $I > 2.5$. When $I = 5$, $(BH)_m$ reaches 79 MGOe. However, the coercivity of nanocomposites first decreased rapidly ($I < 3$) and then increased slightly ($I \geq 3$), as I increased. However, the nucleation field during the demagnetization of the nanocomposites remains basically unchanged ($I \leq 2$), with the increase of I, and then gradually increases, as shown in Fig. 1b. When $I = 5$, the coercivity is close to the nucleation field, and a nearly square hysteresis loop can be obtained. In addition, the evolution of magnetization configuration of the nanocomposites was observed in detail, and the mechanism of shape anisotropy of soft phase on the enhancement of nucleation field was discussed in detail. Our simulation results show that using the shape anisotropy of soft phase can obtain excellent magnetic coupling effect, which is an effective way to achieve high performance of nanocomposite magnets.

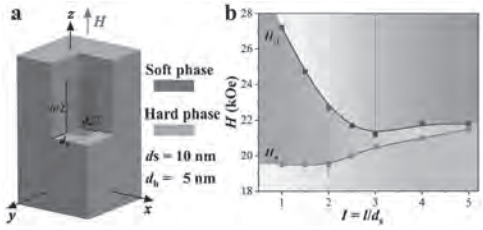

HPA-19. Magnetization reversal dynamics of a triangular-shaped magnetic fractals. *R. Mehta*[1] and S. Saha[1] *1. Department of Physics, Ashoka University, Sonipat, India*

Fractals are composed of self-similar structures across different length scales, which look similar under different magnifications. They possess a non-integer dimension with a self-similarity and scale invariance, which is commonly referred to as the Hausdorff dimension or fractal dimension. Romanesque cauliflower, fern, frost, and snowflakes are popular examples of naturally observed fractals. The concept of fractals namely, Sierpinski square and triangles are also implemented in magnetic systems to study the modification of spinwave dynamics [1, 2]. It is also important to study their magnetization reversal process for their further use in spintronics. Here we have investigated the magnetization reversal process of a Sierpinski triangle which is a nonperiodic but ordered fractal structure. To understand the magnetization reversal process of Sierpinski triangles with the increase of the iteration level of the fractal structure are studied using a micromagnetic simulator namely object oriented micromagnetic framework (OOMMF) [3]. The magnetic parameters used for the simulation are taken from Ref. [1]. The hysteresis loop (M-H curve) is calculated for a structure going from simple geometric structures toward a Sierpinski triangle. TRI-0 is an equilateral triangle with the side length of 3 μm. To generate TRI-1, an equilateral triangle is removed from the center of TRI-0. To further generate, TRI-2 and TRI-3 an iteration process with a scaling factor of ½ is used. Due to the structurization, the coercivity and saturation magnetization are increased significantly with the increase of the iteration number as shown in Fig. 1(a). The simulated magnetization images during the reversal for Tri-0 and Tri-4 are shown in Fig. 1 (b) and (c) for three different magnetic fields. The interesting thing to note is that magnetization reversal occurs by the creation of a vortex. The observations have a great impact on their applications in spintronic and magnonic devices.

1. J. Zhou, M. Zelent, Z. Luo, V. Scagnoli, M. Krawczyk, L. J. Heyderman, S. Saha, Phys. Rev. B105, 174415 (2022) 2. C. Swoboda, M. Martens, and G. Meier, Phys. Rev. B 91, 064416 (2015). 3. M. Donahue and D. G. Porter, "OOMMF User's guide, Version 1.0," NIST Interagency Report No. 6376 _National Institute of Standard and Technology, Gaithersburg, MD, 1999_, URL: http://math.nist.gov/oommf.

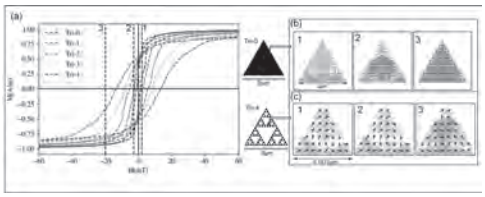

Fig. 1 (a) Simulated hysteresis loops for different samples. Simulated magnetization images at various applied magnetic field values marked by '1', '2' and '3' for (b) Tri-0 (c) Tri-4 [a single triangle is taken from the whole structure]

HPA-20. Effect of Dzyaloshinskii-Moriya Interactions on Magnetization Reversal in Perpendicularly Magnetized Nanodots of Different Shape. *S. S K*[1], B. Priyanka[1], H. Perumal[1] and J. Sinha[1] *1. Department of Physics and Nanotechnology, SRM Institute of Science and Technology, Kattankulathur, Chennai, India*

Analysis of magnetization reversal in ferromagnetic nanodots of different shapes with dimension in the range of 100 nm in the presence of Dzyaloshinskii-Moriya Interaction (DMI) is extremely important for technological application [1]. Though a few studies have explored the effect of DMI on the magnetization reversal mechanism in nanostructures, to disentangle the influence of shape and DMI requires further systematic studies [2-4]. Here, we investigate the effect of DMI (D) and in-plane bias field (H) on magnetization reversal in perpendicularly magnetized isolated square, circular, and triangular nanodot using the micromagnetic simulation Mumax^3 [5]. The side length/diameter of the nanodot is chosen as 128 nm and the thickness as 1 nm and the material parameters of Co is selected. Our results indicate that the coercive field monotonically decreases as the strength of D increases and loop becomes asymmetric in the presence of both D and H in all three shapes. Interestingly, for $D = 0$ and $H \neq 0$, nucleation of the reverse domain occurs at the central region of the nanodot (Figs. 1(a-c)), and in case of $D \neq 0$ and $H \neq 0$ chiral nucleation occurs at the far edge (Figs. 1(d-f)). Due to lateral asymmetry of the triangular nanodot, the total energy value is smaller for the triangular nanodots (for -100 mT < H < +100 mT, and -1 mJ/m^2 < D < + 1 mJ/m^2) thereby making it preferred for energy efficient magnetization reversal as compared to other two shapes. However, at sufficiently higher value of the magnitude of H (> 200 mT) and D (> 1 mJ/m^2), due to the laterally symmetric sides of the square the energy barrier for the magnetization reversal reduces drastically (cf. Fig.1(f)). These findings indicate that the effect of D and H in lowering the energy barrier for the magnetization reversal is intricately related to the symmetry associated with the shape of the nanodots.

[1] F. Hellman, A. Hoffmann, Y. Tserkovnyak *et al*., Rev. Mod. Phys., Vol.89, p.025006 (2017) [2] S. Pizzini, J. Vogel, S. Rohart *et al*., Phys. Rev. Lett., Vol.113, p.047203 (2014) [3] D.-S. Han, N.-H. Kim, J.-S. Kim *et al*., Nano Lett., Vol.16, p.4438 (2016) [4] Syamlal S K, Hari Prasanth Perumal, and Jaivardhan Sinha., Mater. Lett., Vol.303, p.130492 (2021) [5] A. Vansteenkiste, J. Leliaert, M. Dvornik *et al*., AIP Adv., Vol.4, p.107133 (2014)

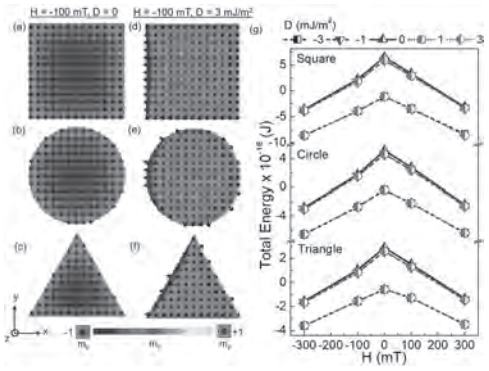

Figure 1: Snapshot of the spin configuration for square, circular and triangular nanodot during down to up (D-U) switching at H = -100 mT and D = 0 (a-c), H = -100 mT and D = 3 mJ/m^2 (d-f). (g) Variation of total energy as a function of in-plane bias field for square, circular, and triangular nanodots at different value of D is plotted during D-U switching.

HPA-21. Magnetization in Iron-based compounds: A Machine Learning Model Analysis. *Y. Khatri*[1], A. Shah[1] and A. Kashyap[1] *1. IIT Mandi, Mandi, India*

The availability of large databases like materials project [1], Aflow consortium [2], NOMAD [3], OQMD [4] etc., has made it possible to apply machine learning (ML) in the materials science domain to get good predictions for various materials properties like Curie temperature [5], formation energy [6], etc. Here, we have used Materials project database to gather a data of 11545 iron-based compounds using the MAPI [7] and the pymatgen package [8]. This data consists of total magnetization, crystal structure and formation energy etc for all the compounds. As a first step, we transformed the data for ML modeling by using the orbital-field matrix (OFM) representation by Pham et al. [6]. In OFM, the structure of the compounds is turned into a 32*32 matrix corresponding to 1024 features, known as descriptor. With this data, we used various ML algorithms and chose to work with random forest as it provides the best results for our dataset with a 5-fold cross-validation. In order to understand the model, we used SHAP (SHapley Additive exPlanations) analysis, which is a game-theoretic approach to explain the output of any machine learning model. It gives us the most dominating features in the model. Based on the SHAP values for various datasets, the features which are dominating the overall magnetization results along with the corresponding description of the features as per the OFM descriptor are presented in Fig. 1. For example, in some oxides listed in Fig. 2, one can see that only features 173, 421, 429 are dominant as per the SHAP values. However, this is not a universally true picture for the whole dataset. Therefore, we further need to process the dataset based on the fact that not all features contribute equally in all types of materials. It is concluded that the simple ML techniques used on large dataset may give misleading results if the ML model is not improved after understanding the data we are dealing in the material science domain.

[1] A. Jain, P. Ong, G. Hautier, S.P. Ong, W. Chen, W.D. Richards, S. Dacek, S. Cholia, D. Gunter, D. Skinner, G. Ceder, K.A. Persson, Cite as APL Mater 1 (2013) 11002. [2] S. Curtarolo, W. Setyawan, S. Wang, J. Xue, K. Yang, R.H. Taylor, L.J. Nelson, G.L.W. Hart, S. Sanvito, M. Buongiorno-Nardelli, N. Mingo, O. Levy, Comput. Mater. Sci. 58 (2012) 227–235. [3] C. Draxl, M. Scheffler, J. Phys. Mater 2 (2019) 36001. [4] J.E. Saal, S. Kirklin, M. Aykol, B. Meredig, C. Wolverton, JOM 65 (2013) 1501. [5] T. Long, N.M. Fortunato, Y. Zhang, O. Gutfleisch, H. Zhang, Mater. Res. Lett. 9:4 (2021) 169–174. [6] T. Lam Pham *et.al.* Sci. Technol. Adv. Mater. 18 (2017) 756–765. [7] S.P. Ong, S. Cholia, A. Jain, M. Brafman, D. Gunter, G. Ceder, K.A. Persson, Comput. Mater. Sci. 97 (2015) 209–215. [8] S.P. Ong, W.D. Richards, A. Jain, G. Hautier, M. Kocher, S. Cholia, D. Gunter, V.L. Chevrier, K.A. Persson, G. Ceder, Comput. Mater. Sci. 68 (2013) 314–319.

Feature	33	1	165	429	421	173	36	37	45	177
Interactions of orbitals	s^2-s^2	s^1-s^2	p^6-p^6	d^9-d^9	d^8-p^4	p^4-d^6	s^2-p^3	s^2-p^4	s^2-d^9	p^6-d^{10}

Fig. 1- Dominating features and corresponding orbital interaction.

Full formula	Magnetization (μ_B)	Available features with interactions
$Eu_2Fe_2O_6$	22.54008	429 ($3d^9$ - $3d^9$), 421 ($3d^8$ - $2p^5$) and 173 ($2p^5$ - $3d^8$)
Mn_3FeO_6	48.99825	421 ($3d^8$ - $2p^5$) and 173 ($2p^5$ - $3d^8$)
Fe_3O_4	14	429 ($3d^9$ - $3d^9$), 421 ($3d^8$ - $2p^5$) and 173 ($2p^5$ - $3d^8$)
$MnFeO_3$	9.006555	421 ($3d^8$ - $2p^5$) and 173 ($2p^5$ - $3d^8$)
$MnFe_2O_4$	13.00266	429 (d^9-d^9), 421 ($3d^8$ - $2p^5$) and 173 ($2p^4$ - $3d^8$)

Fig. 2- Few compounds with magnetization values and valence band configuration.

Session HPB
SKYRMIONS AND DOMAIN WALLS
(Poster Session)

Jackson Ross, Co-Chair
University of York, York, United Kingdom
Harald Oezelt, Co-Chair
Danube University Krems, Wiener Neustadt, Austria

HPB-01. Voltage-controlled domain wall-based nanodevices for artificial neurons in a strain-mediated multiferroic heterostructure. X. He[1], *G. Yu*[1], Z. Chen[1], X. Cai[1], M. Zhu[1], Y. Qiu[1] and H. Zhou[1] *1. China Jiliang University, Hangzhou, China*

Recently, artificial intelligence (AI) has received widespread attention, and artificial neural networks (ANN) are the foundation of AI, while artificial neurons are the basic information processing units of ANN. Spintronic devices mimicking the function of biological neurons are considered as one of the very promising candidates for the implementation of ANN in the future. In this work, we propose to realize the leaky integrate-and-fire (LIF) properties of artificial neurons through the voltage-controlled strain gradients and current induced spin-transfer torque co-driven the motion of domain wall (DW). In addition, the proposed device can be threshold-tuned in various ways, such as strain gradient, current density, and pulse width, etc. In particular, this structure can also break the limitation of ANN learning and recognition ability by the inherent activation function. By modulating the strain gradient applied on the nanowire, the relevant nonlinear activation function can be configured, thereby improving the learning performance of ANN. As shown in Fig. 1(a), the proposed device model consists of ferromagnetic/heavy metal (FM/HM) nanowire deposited on a piezoelectric substrate. By modulating the magnitude of the electrode voltage below the piezoelectric substrate, the voltage-controlled strain gradient applied to the nanowire will be changed, and finally affects the motion of DW. The corresponding magnetoconductance (TMG) can be read by the magnetic tunnel junction (MTJ). Fig. 1(b) shows the artificial neuron with the LIF function. The DW motion dynamics depend on the competition between the gradient magnetoelastic energy of the nanowire and the current driving force. The DW undergoes a total of five cycle current pulses, which finally reaches the threshold TMG of 0.63 and is detected by the MTJ. Next, the DW "fires" a signal output, and resets to the initial state. The above simulation results reveal the great potential of magnetic DW-based electric field modulation of artificial neurons for applications of next-generation artificial intelligence devices.

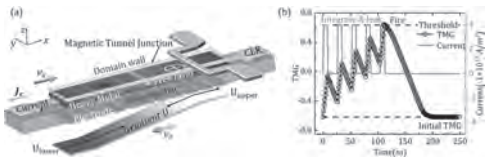

Fig. 1 (a) Schematic diagram of voltage-controlled DW-based nanodevices. (b) LIF behaviors.

HPB-02. Precise Trajectory Control of Skyrmion Motion by Surface Acoustic Waves. *J. Shuai*[1], L. Lopez-Diaz[2], J.E. Cunningham[3] and T.A. Moore[1] *1. School of Physics and Astronomy, University of Leeds, Leeds, United Kingdom; 2. Department of Applied Physics, Universidad de Salamanca, Salamanca, Spain; 3. School of Electronic and Electrical Engineering, University of Leeds, Leeds, United Kingdom*

Skyrmions (Sks) are topologically protected chiral spin structures showing great potential for the next generation of data storing and processing devices.[1] However, controlling such chiral spin textures efficiently and precisely remains unsolved. Here, we demonstrate precise trajectory control of Sk motion by surface acoustic waves using micromagnetic simulations (Mumax3).[2] The computational region dimension was 400×100×1 nm^3. The velocity, wavelength and amplitude of the SAW were 4000 m/s, 200 nm and 0.03, respectively. The Sk was initialised at different positions along the track. Results showed that with the application of the standing SAW, the Sk did not move if its initial position was at nodes of the standing SAW. Whereas starting from an anti-node, the Sk did move towards the closest node of the standing SAW (Fig.1a). The highest velocity occurs between the nodes and anti-nodes of the standing SAW, where the strain gradient is the highest, indicating that the strain gradient is the origin of the SAW-driven Sk motion.[3] The Sk moves continuously in the presence of the travelling SAW regardless of its initial position with a higher velocity (2.3 m/s) than that of the standing SAW-induced (average of 0.3 m/s) Sk motion (Fig.1b). This is due to the travelling SAWs providing a constant driving force to the skyrmion. The skyrmion also moves in the vertical direction owing to its chirality (Fig.1c). Horizontal travelling SAWs together with vertical standing SAWs were then applied to the Sk (Fig.1d), which can drive Sk motion and pin the Sk in the desired trajectory, respectively. Results showed that in the presence of both SAWs, the Sk moved along the centre of the nano-track with very limited vertical motion (Fig.1d to f). This study indicates the possibility of energy-efficient and precise control of skyrmion motion.

[1] Parkin et al. Science, 320(5873), 190-194 (2008) [2] Vansteenkiste et al. AIP Advances 4, 107133 (2014) [3] Nepal et al. Appl. Phys. Lett. 112, 112404 (2018)

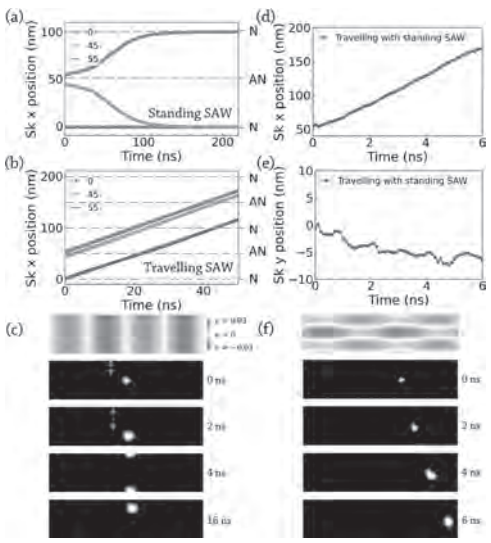

Fig. 1 Skyrmion motion in the horizontal direction with standing (a) and travelling (b) SAW. (c) Spatial strain profile at 0 ns, skyrmion position at 0 to 16 ns, respectively. Skyrmion motion in horizontal (d) and vertical (e) direction with horizontal travelling SAW and vertical standing SAW. (f) Spatial strain profile at 0 ns, skyrmion position at 0 to 6 ns, respectively.

HPB-03. Reconfigurable Skyrmion Logic Gates with Circular Track.
L. Yang[1,2], W. Li[1,2], Y. Tao[1,2], K. Dong[1,2] and H. Li[3] *1. School of Automation, China University of Geosciences, Hubei, China; 2. Hubei key Laboratory of Advanced Control and Intelligent Automation for Complex Systems, Hubei, China; 3. Beijing Superstring Academy of Memory Technology, Beijing, China*

Magnetic skyrmion, with its nanoscale and topological features, can be employed as an information storage medium and logic function device in next-generation spintronic systems, attracting a lot of interest. Among all skyrmion logic devices, reconfigurable skyrmion logic devices have attracted much attention because they can efficiently perform different operations with the least number of devices to create different logical functions or operations. In 2018, Luo et al.[1] proposed reconfigurable skyrmion logic gates by adding voltage control terminals to H-type nanotracks. This paper proposes a voltage-controlled reconfigurable skyrmion circular orbit logic gate in Fig1(f). The complete logic family is implemented based on our skyrmion logic gates, in which the trajectories of skyrmion are manipulated by various effects including skyrmion-edge repulsions and the voltage control of magnetic anisotropy (VCMA) effect. Fig.1(a) represents the unique orbital model, Fig.1(b)-(d) show the anisotropic energy regulated by the VCMA effect, and Fig. 1(e) shows the logic function realized by the potential energy well distribution that we studied before[2]. The above logic functions can be integrated into a single skyrmion device, reconfigured by controlling the terminal voltage, and reused by the circular track structure. The corresponding skyrmion state and motion trajectories are shown in Fig.2. Because of the scheme, every logic judgment necessitates the generation and destruction of the skyrmion, increasing the logic device's energy consumption. Furthermore, the current drive in this system will create Joule heat, which will have an impact on skyrmion stability.

[1] S. Luo, M. Song and X. Li, *Nano Letters.*, vol. 18, pp. 1180-1184 (2018).
[2] L. Yang, F. Jin and W. Mo, *IEEE Transactions on Magnetics.*, vol. 58, pp. 1-5 (2022).

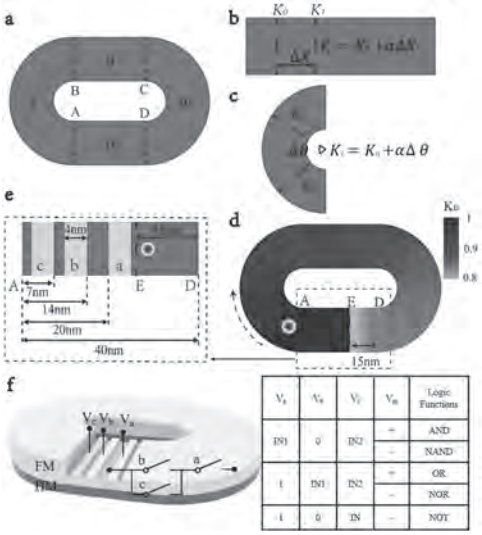

Fig.1 (a) Geometric dimensions of the circular track. (b) and (c) Voltage-controlled magnetic anisotropy gradient by using wedge structure. (d) Magnetic anisotropic energy distribution in skyrmion multiplexing. (e) The arrangement of potential wells to realize logical functions. (f) Structure of a reconfigurable skyrmion logic gate with the circular track.

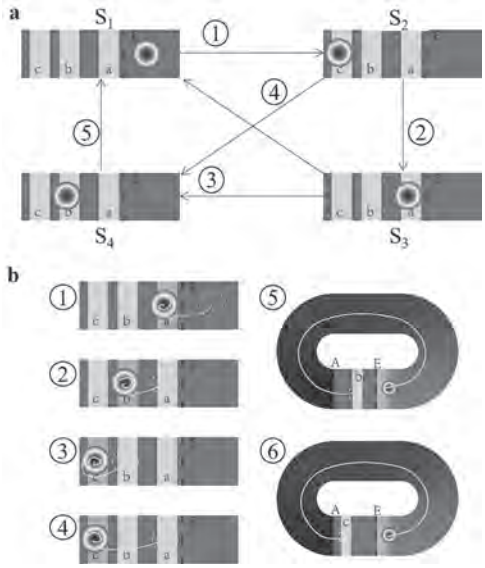

Fig.2 (a) State and conversion process of skyrmion on the device. (b) The trajectories of skyrmion on the device.

HPB-04. Improvement of Domain Wall Velocity and Reduction of Current Density by Laser Annealing to the TbCo Wires.
Y. Miyose[1], S. Ranjbar[1], S. Sumi[1], K. Tanabe[1] and H. Awano[1] *1. Toyota Technological Institute, Nagoya, Japan*

In recent years, Racetrack memory[1] has been actively studied as a candidate of the future magnetic memory. Many papers on magnetic wire memories using ferromagnetic materials with large magnetization have been reported. Recently, it has been found that this current density can be reduced by using a ferrimagnetic material with small magnetization. However, the current density reduction of current-induced domain wall (DW) motion and improvement of the DW velocity remain as big issues for practical use. In this study, laser annealing (laser irradiation) effect on the ferrimagnetic wire is investigated to reduce further the current density. A magnetic wire of 1 μm width and 70 μm in length is prepared by using electron beam lithography and magnetron sputtering. The sample structure is Pt (5 nm) / $Tb_{27}Co_{73}$ (6 nm) / SiN (10 nm) on a Si substrate with a thermal oxide film (350 nm). It is placed in the field of view of polarizing microscope with an objective lens NA of 0.5, and a blue laser is irradiated to the TbCo wire through the objective lens. The spot size is approximately 1 μm in diameter which is almost same as the wire width. Laser annealing is scanned along the TbCo wire and the speed is 7 μm/s. Laser annealing can slightly change the DW energy of the TbCo wire. Fig. 1 shows DW velocity versus current density when the DW in the magnetic TbCo wire is driven by applying 3 ns pulse currents to the wire. Black squares and red circles are the symbols before and after laser annealing with the laser power of 3.1 mW. As shown in this figure, It was found that by laser annealing to the TbCo wire, the current density required for driving the DW was reduced by 20 %, and the DW velocity was doubled. Fig. 2 shows the mobility of the domain wall before and after laser annealing. Mobility is DW velocity divided by current density. After laser annealing, mobility is about 1.8 times higher than before. These may be due to the slight decrease in the DW energy caused by laser annealing. This work is partially supported by Grant-in-Aid for Scientific Research (20H02185 and 21K18735).

[1] S. S. P. Parkin, M. Hayashi and L. Thomas, Science, Vol. 320, p.190-194 (2008). [2] K. S. Ryu, L. Thomas and S.H. Yang, Nat. Nanotechnol., Vol. 8, p.527-533 (2013). [3] S. H. Yang, K. S. Ryu and S. Parkin, Nat. Nanotechnol., Vol. 10, p.221-226 (2015).

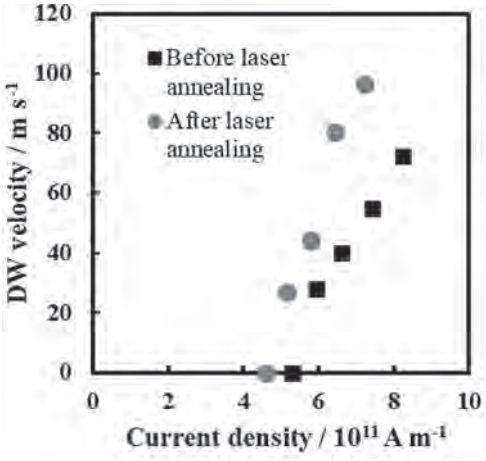

DW velocity versus current density in TbCo wire.

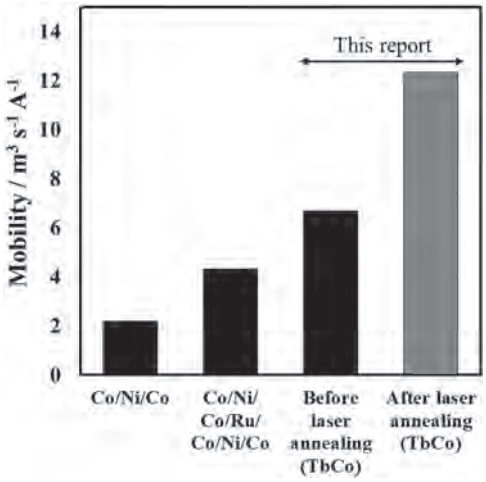

Comparison of the DW mobility before and after laser annealing with other reports[2][3].

HPB-05. Withdrawn

HPB-06. Annealing Process of Co-Fe-B based Multilayers showing Skyrmion Brownian Motion. *M. Goto*[1,2], R. Ishikawa[3], H. Nomura[1,2] and Y. Suzuki[1,2] *1. Osaka University, Toyonaka, Japan; 2. CSRN-Osaka, Toyonaka, Japan; 3. ULVAC Inc., Suita, Japan*

Magnetic skyrmions are topologically protected spin textures that have been attracting attention because of its diverse physical phenomena and possibilities of applications. Recently, various investigation regarding the Brownian motion of skyrmions have been reported [1-3]. However, because skyrmion Brownian motion is sensitive to the change in magnetic properties, the change in the magnetic potential and vanishing skyrmions have often been observed due to the change in magnetic properties of Co-Fe-B based multilayers during microfabrication and observation processes. The possible origin of the change is atom migration such as boron diffusion in Co-Fe-B [4] or oxidation of capping. Although the annealing vanishes such the change, the typical annealing process takes approximately 1 hour in vacuum. In this study, we annealed the Co-Fe-B based multilayers for 3 min in air to shorten the time of annealing process and to avoid the change in magnetic properties. The multilayer structure is Ta (5.9) | $Co_{16}Fe_{64}B_{20}$ (1.22) | Ta(0.27) | MgO (1.6) | SiO_2 (2.9) on thermally oxidized silicon substrates. The multilayer was post-annealed in air and vacuum at various temperature. Figure 1 shows the perpendicular magnetic field dependence of normalized magneto-optical Kerr effect (MOKE) signal with various annealing processes; as deposited, 200 °C for 3 min in air, and 200 °C°C for 1 hour in vacuum. The annealing in vacuum (air) suppresses (enhances) the perpendicular anisotropy. We observed the change of magnetic domains by annealing in air and temporal variation. Figure 2 shows the MOKE microscope images of domains. While the annealing less than 200 °C induces the temporal change, 250 °C annealing suppresses it. In 250 °C annealed sample, the skyrmion Brownian motion is observed at room temperature. This research was supported by the Toyota-Riken Scholar, ULVAC Inc., JSPS KAKENHI Grant Number JP20H05666, and JST CREST Grant Number JPMJCR20C1.

[1] J. Zázvorka *et al.*, Nat. Nanotechnol. 14, 658 (2019), [2] Y. Jibiki *et al.*, Appl. Phys. Lett. 117, 082402 (2020), [3] R. Ishikawa *et al.*, Appl. Phys. Lett. 119, 072402 (2021), [4] T. Miyajima *et al.*, Appl. Phys. Lett. 94, 122501 (2009)

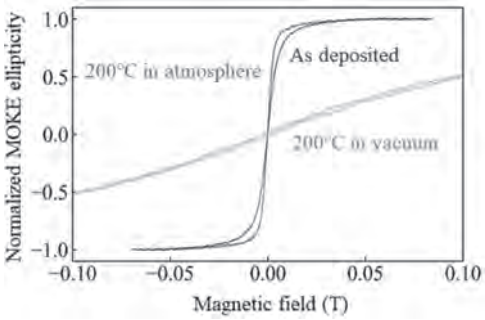

Normalized MOKE ellipticity of the multilayers with different annealing processes.

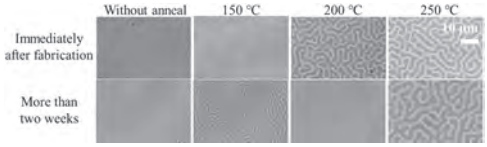

MOKE microscope images of magnetic domains. Column shows the annealing temperature dependence. Row shows temporal variation.

HPB-07. Deformation Induced Skyrmion Rotation and Locomotion. *D. Foiles*[1] and A. Hoffmann[1] *1. Materials Science and Engineering, University of Illinois Urbana-Champaign, Urbana, IL, United States*

Skyrmions are topological spin textures with quasiparticle-like properties that may make them useful in advanced computing architectures. In this work, we studied the dynamics of magnetic skyrmions using micromagnetic simulations. We observe novel rotational and orbital motion of skyrmions when a time-varying out-of-plane magnetic field is applied to skyrmions in confined systems and excites their breathing modes. This phenomenon can be explained by the asymmetric redistribution of topological charge as skyrmions expand and contract in a confined environment. An example of this behavior can be seen below. As skyrmions expand from application of an out-of-plane field, they begin moving around the center of the system. Decreasing the magnetic field causes the skyrmions to shrink but maintain their individual rotation. Increasing the magnetic field again causes the cycle to repeat. This motion illustrates how the topological properties and the spontaneous emergence of chirality in skyrmions can result in unexpected complex behavior. Furthermore, it may have practical relevance to applications of skyrmions to neuromorphic and reservoir computing, where information may be encoded in the positions of different skyrmions. Previous groups have also observed skyrmion rotation, but have explained this with the presence of a thermal gradient.[1] Our work demonstrates a similar rotation but without having to introduce disorder into the system, possibly making the system more realizable in a practical setting. This material is based upon work supported by the National Science Foundation under Grant No. 1922758.

1. Mochizuki, M. *et al. Nature Materials.* Vol 13., p. 241–246 (2014).

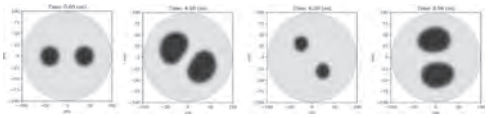

Fig. 1: Snapshots of different magnetic configurations of two skyrmions in a confined disc structure upon excitation with time varying out-of-plane fields.

HPB-08. Tuning domain wall chirality of Pt/Co/Pt based Perpendicularly Magnetized systems with Au insertion. *S. Maji*[1], S. Kayal[1], A. Mukhopadhyay[1] and P. Kumar[1] *1. Physics, Indian Institute of Science Bangalore, Bengaluru, India*

Perpendicular magnetic anisotropy (PMA) systems that involve HM/FM/HM tri-layer structure have immense scope for constructing high speed memory devices [1,2]. Broken inversion symmetry at HM/FM interface introduces interfacial Dzyaloshinskii- Moriya interaction (iDMI) which stabilizes chiral Neel wall that can be manipulated with spin polarized current. The current induced deterministic switching of PMA systems also realized with [3] or without [4,5] application of bias magnetic field. Several methods have been introduced to estimate the iDMI of HM/FM/HM as well as HM/FM/metal-oxide thin films in last few years. In this work, we have used field induced domain wall motion (FIDWM) to estimate iDMI strength, D_{eff} of sputter deposited Ta (3.5 nm)/Pt (3 nm)/Co (0.4 nm)/Au (x nm)/Pt (1 nm) thin films where x = 0, 0.3, 0.5 and 0.7 nm. The domain wall velocity (DMV) of a nucleated bubble domain was estimated applying pulsed H_z in presence of H_x. The asymmetric expansion of bubble domain reveals the chirality of domain wall of the samples. Ta/Pt/Co/Pt systems has Neel walls with right-handed chirality whereas the chirality reverses with introduction of ultrathin Au layer as shown in Fig. 1. The iDMI can be manifested as an effective in-plane magnetic field (H_{DMI}) in PMA system. The H_x dependence of the DMV has a minimum at $H_x = H_{DMI}$. iDMI strength calculated using the formula described by Je *et. al* [6] and displayed in Fig. 2. The D_{eff} of symmetric Ta/Pt/Co/Pt system have very small negative value which can be attributed to the difference of roughness of bottom Pt/Co and top Co/Pt interface. D_{eff} increases as the asymmetry around Co layer was introduced with insertion of Au layer. The maximum Deff was observed for the sample with highest degree of asymmetry (Au thickness = 0.7 nm). The D_{eff} also becomes positive when Au is introduced at top Co/Pt interface. The Pt/Co and Au/Co interface has opposite polarity of iDMI [7]. These two interfaces of Ta/Pt/Co/Au/Pt effectively reverse the iDMI sign.

1. S. S. Parkin, M. Hayashi, and L. Thomas, Science 320, 190–194 (2008) 2. A. Fert, V. Cros, and J. Sampaio, Nature nanotechnology 8, 152–156 (2013) 3. C. Onur Avci, K. Garello, and P. Gambardella, Applied Physics Letters 100, 212404 (2012) 4. V. M. P, K. R. Ganesh, and P. S. A. Kumar, Phys. Rev. B 96, 104412 (2017) 5. S. Guddeti, A. K. Gopi, and P. S. Anil Kumar, IEEE Transactions on Magnetics 54, 1–5 (2018) 6. S. G. Je, K. J. Lee, and S. B. Choe, Physical Review B 88, 214401 (2013) 7. H. Yang, A. Fert, and M. Chshiev, Phys. Rev. Lett. 115, 267210 (2015)

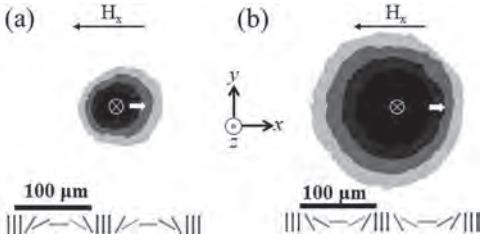

Asymmetric expansion of bubble domain at an in-plane magnetic field, H_x = 30 mT of (a) Au (t = 0 nm) and (b) Au (t = 0.3 nm)

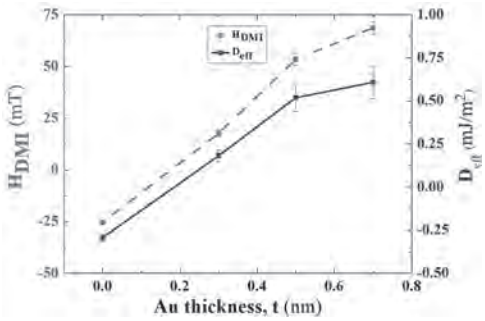

Effective in-plane field of iDMI, H_{DMI} and iDMI strength, D_{eff} as a function of Au layer thickness

Session IOA
MAGNETIC RECORDING I
Simon Greaves, Chair
Tohoku University, Sendai, Japan

CONTRIBUTED PAPER

IOA-01. Pt-Transition Metal Synthetic Ferrimagnets for All Optical Switching. *J.N. Scott*[1], M. Dabrowski[2], W. Hendren[1], A. Frisk[3], D. Burn[3], D. Newman[2], C. Sait[2], P.S. Keatley[2], A. N'Diaye[4], T. Hesjedal[5], G. van der Laan[3], R. Hicken[2] and R. Bowman[1] *1. Queen's University Belfast, Belfast, United Kingdom; 2. University of Exeter, Exeter, United Kingdom; 3. Diamond Light Source, Didcot, United Kingdom; 4. Advanced Light Source, Berkeley, CA, United States; 5. University of Oxford, Oxford, United Kingdom*

Synthetic ferrimagnets (SFi) two ferromagnetic (FM) layers with different magnetic moments, exchange-coupled via the RKKY interaction across a non-magnetic spacer layer, are of particular interest as a feasible media for all optical magnetic switching (AOS) [1]. Design of the magnetic properties of these SFi structures requires knowledge and control of the magnetisation, M(T), and anisotropy, K(T), of each FM layer, and the strength of the exchange coupling between them, $J_{ij}(T)$. We have shown it is possible to engineer the magnetic properties of series of compensating Ni_3Pt/Ir/Co SFi and Ni/Pt multilayer based SFi, fabricated by magnetron sputtering and exhibiting perpendicular magnetic anisotropy. The tuneability of these structures (through variation of the Ni_3Pt deposition temperature and the thickness of each layer) provides an ideal system with which to investigate the effect of M(T), K(T) and $J_{ij}(T)$ on reversal mechanisms within SFis, with the added benefit of distinct magnetic species allowing element and layer specific characterisation. Pump/probe experiments reveal that it is possible to switch these SFis by application of multiple laser pulses [2]. However, single shot AOS likely requires stronger antiferromagnetic exchange coupling and/or anisotropies than can be achieved in the Ni, Pt, Ir and Co system [3]. Here we look to present initial results on FePt based SFi. Enhanced anisotropies will open a new parameter space with which to further explore the underlying mechanisms behind all optical switching, whilst utilising a material palette already relevant to existing technologies.

[1] S. Mangin et al, Nature Materials 13, 286 (2014) [2] M Dabrowski et al, Nano Lett. 2021, 21, 21, 9210–9216 [3] R. F. L. Evans et al, Appl. Phys. Lett. 104, 082410 (2014)

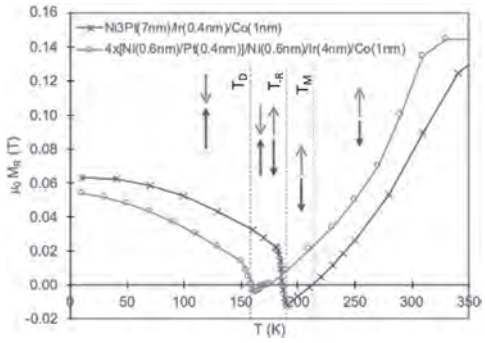

Remanent magnetisation (M_R) versus temperature of a Ni_3Pt based SFi with arrows denoting the layer alignment, Co (green) and Ni_3Pt (red), with the positions of the magnetisation compensation point, T_M, and T_{-R}, the onset temperature of negative M_R, marked. A mixed domain state occurs between T_D and T_{-R}. The multilayer sample shows the same temperature dependent behaviour.

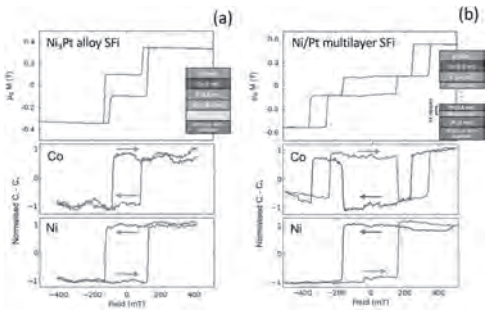

Squid (top) and element specific XMCD hysteresis loops measured at 100K (arrows depict the field sweep direction) of (a) Ta(5nm)/ Ni_3Pt(8.5nm)/Ir(0.5nm)/Co(1nm)/Ir(3nm) and (b) Pt(5nm)/4x-[Ni(0.6nm)/Pt(0.4)]/Ni(0.6nm)/Ir(0.4nm)/Co(0.9nm)/Ir(3nm) SFi.

INVITED PAPER

IOA-02. Energy efficient single pulse switching of magnetic nanodisks using surface lattice resonances. *M. Verges*[1], S. Perumbilavil[2], J. Hohlfeld[1], F. Freire-Fernandez[3], Y. LeGuen[1,2], N. Kuznetsov[2], G. Malinowski[1], F. Montaigne[1], D. Lacour[1], M. Hehn[1], S. van Dijken[2] and S. Mangin[1] *1. Institut Jean Lamour, UMR CNRS 7198, Université de Lorraine, Nancy, France; 2. Department of Applied Physics, Aalto University School of Science, Aalto, Finland; 3. Department of Materials Science and Engineering and Department of Chemistry, Northwestern University, Evanston, IL, United States*

Plasmonic surface lattice resonances, visible in periodic arrays of nanodisks, arise from radiative coupling between the localized surface plasmon resonance[1-3] of individual particles and diffracted orders[4]. Here, we study the impact of these optical modes on the magneto-optical properties[5,6] and energy absorption efficiency[7] of $[Co/Gd/Pt]_N$ nanodisks by measuring the response of different arrays to optical excitations as function of the light

wavelength, the disk diameter, and the array period. We demonstrate that surface lattice resonances allow All-Optical single pulse switching[8,9] of the nanodisks using much less energy than for the thin film, with an energy absorption enhanced by more than 400 %. Besides, these optical modes increase the magneto-optical Faraday effect by more than 2000 %. The influence of the disk diameter and array period on the amplitude, width and position of the resonances is in qualitative agreement with theoretical calculations and opens the way to design magnetic metasurfaces for all-optical magnetic recording.

[1] Liu, T.-M., *et al.* Nanoscale Confinement of All-Optical Magnetic switching in TbFeCo – Competition with Nanoscale Heterogeneity. Nanoletters, 15:6862 – 6868, 2015. [2] Savoini, M., *et al.* Highly efficient all-optical switching of magnetization in GdFeCo microstructures by interference-enhanced absorption of light. Physical Review B, 86:140404, 2012. [3] Cheng, F., *et al.* All-Optical Manipulation of Magnetization in Ferromagnetic Thin Films Enhanced by Plasmonic Resonances. Nanoletters. 20:6437 – 6443, 2020. [4] Kataja, M., *et al.* Surface lattice resonances and magneto-optical response in magnetic nanoparticle arrays. Nature Communications, 6:1 – 8, 2015. [5] Freire-Fernández, F., *et al.* Surface-plasmon-polariton driven narrow-linewidth magneto-optics in Ni nanodisk arrays. Nanophotonics, 9:113 – 121, 2019. [6] Freire-Fernández, F., *et al.* Magnetoplasmonic properties of perpendicularly magnetized $[Co/Pt]_N$ nanodots. Physical Review B, 101:054416, 2020. [7] Kataja, M., *et al.* Plasmon-induced demagnetization and magnetic switching in nickel nanoparticle arrays. Applied Physics Letters, 112:072406, 2018. [8] Radu, I., *et al.* Transient ferromagnetic-like state mediating ultrafast reversal of antiferromagnetically coupled spins. Nature, 472:205 – 208, 2011. [9] Lalieu, M. L. M., *et al.* Deterministic all-optical switching of synthetic ferrimagnets using single femtoseccond laser pulses. Physical Review B, 96:220411, 2017.

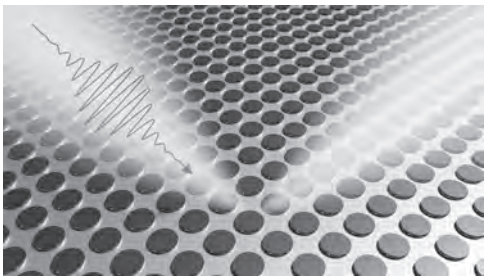

Fig. 1. Magnetic $[Co/Gd/Pt]_N$ metasurface.

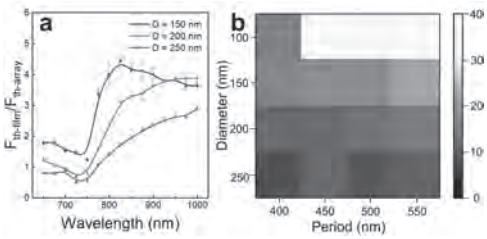

Fig. 2. a) Ratio of the All-Optical switching threshold fluence measured on the film and metasurfaces with P = 500 nm and different array diameters. b) Average Faraday readout-sensitivity among 6 samples, defined as the ratio of the Faraday angle of $[Co/Gd/Pt]_N$ metasurfaces on resonance and in the continuous $[Co/Gd/Pt]_N$ films at the same wavelength, scaled with the packing density.

CONTRIBUTED PAPERS

IOA-03. All optical writing and current-driven shifting of bits in ferrimagnetic strips: a micromagnetic study. V. Raposo[1] and *E. Martinez[1] 1. Fisica Aplicada, Universidad de Salamanca, Salamanca, Spain*

Ferrimagnetic (FiM) alloys as GdFeCo, formed by rare-earth (RE:Gd) and transition-metal (TM:FeCo) sublattices antiferromagnetically coupled, constitute the most promising platform to develop the next generation for ultrafast spintronics devices. These alloys combine the advantages of ferromagnetic and antiferromagnetic materials, and their properties can be easily manipulated by tunning the relative composition of the RE and TM. For instance, except at the magnetization compensation point, they present a finite magnetization which can be detected with the same techniques as done in ferromagnets. At the same time, FiM are almost insensitive to external magnetic fields and their negligible magnetostatic interaction makes them ideal candidates to store information with high density. They have recently raised strong interest owing to their ultrafast magneto-optical switching properties [1], and the possibility to drive series of domain-walls (DWs) with high speed under current pulses due to spin-orbit torques (SOTs) [2]. We have developed an advanced micromagnetic model (mM) to explore both the local all-optical switching (AOS) under ultrashort laser pulses with duration of a few fs, and the subsequent domain and DW dynamics by injection of current pulses along a heavy metal (HM) underneath the FiM. The scheme is shown in Fig. 1(a). Starting with a uniform state where both sublattices are anti-parallel aligned along the z-axis, a laser pulse is applied. A proper selection of the fluence and duration of the laser pulse [3] results in a reversed domain flanked by two homochiral DWs, which are subsequently driven along the FiM strip upon injection of the current pulses along the HM [4]. Fig 1(b)-(c) shows an example of the laser-induced writing and current-driven shifting of a sequence magnetic domains (bits). In the talk, we will describe the details of the mM and how it can be used to infer the potential of these FiM/HM stacks to develop DW-based memory devices.

[1] See for instance T. A. Ostler *et al*. Nat. Commun. 3, 1666 (2012). [2] L. Caretta *et al*. Nature Nanotechnology. 13, 1154 (2018). [3] V. Raposo *et al*. Phys. Rev. B 105, 104432 (2022). [4] E. Martinez *at al*. J. Magn. Magn. Mater. 491, 165545 (2019).

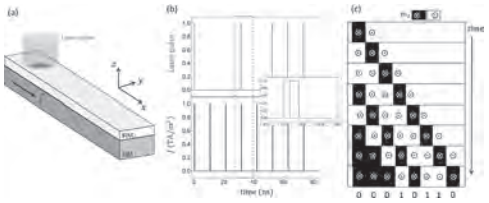

Fig.1. (a) Scheme of the HM/FiM stack with the laser. (b) Temporal sequence of laser (top) and current (bottom) pulses to write a 01101000 bit sequence. (c) Snapshots of the resulting bit sequence.

IOA-04. Field-free all optical switching in Tb/Co multilayer magnetic tunnel junction. *D. Salomoni*[1], Y. Peng[2], L. Farcis[1], S. Auffret[1], M. Hehn[2], G. Malinowski[2], S. Mangin[2], B. Dieny[1], L.D. Buda-Prejbeanu[1], R. Sousa[1] and L. Prejbeanu[1] *1. SPINTEC, CEA/ CNRS/ UGA, Grenoble, France; 2. Institut Jean Lamour, UMR CNRS 7198, Université de Lorraine, Nancy, France*

Magnetic random access memories (MRAM) store information on magnetization direction instead of electric charge. All optical switching (AOS) of a magnetic tunnel junction provides an efficient way to enable writing at speeds orders of magnitude faster than electrical alternatives based on spin torque methods, allowing for write operations at THz frequencies. The [Tb/Co] multilayer is particularly interesting, since its large perpendicular magnetic anisotropy would allow data retention at small sizes and could be

integrated into a magnetic tunnel junction [1-2]. This work reports magnetization reversal driven by femtosecond light pulses on a [Tb/Co] based perpendicular magnetic tunnel junction patterned to sub-100nm lateral dimensions. This optical switchable electrode was integrated into an MgO based MTJ having synthetic anti-ferrimagnet reference layer element, where the AOS magnetization direction can be read directly from the resistance state of the junction. The optically switchable electrodes are $[Tb/Co]_{x5}$ multilayers coupled to a 1.4nm FeCoB layer through a 0.2nm W insertion layer. Patterned AOS-MTJ nanopillars fabricated with diameters down to 80 nm showed TMR ratios up to 74% and a resistance area product of 112 $\Omega\ \mu m^2$. Figure 1) shows the hysteresis loop for a $[Tb\ 0.6nm/\ Co\ 1.4nm]_{x5}$ multilayer. It was possible to observe a toggle switching between low and high resistance states, corresponding to parallel and anti-parallel alignment of the two electrodes, after each 50 fs long laser pulse applied on the device. A systematic study on the switching probability will be compared to existing results of AOS experiments on continuous films. There it was possible to demonstrate that reliable and robust toggle switching can be achieved for specific Tb and Co thickness in the range of 0.6-0.9 nm of Tb and 1.3-1.5 nm of Co. The magnetization reversal is reliable after a 150.000 pulse sequence. Single shot AOS is achievable using laser pulse durations from 50 fs up to 10 ps and fluences 3-6.5 mJ/cm^2. These results pave the way towards an AOS ultra-fast and energy-efficient memory.

[1] A. Olivier et al., Nanotechnology 31, 425302 (2020). [2] L. Avilés-Félix et al., Scientific Reports 10, 1 (2020).

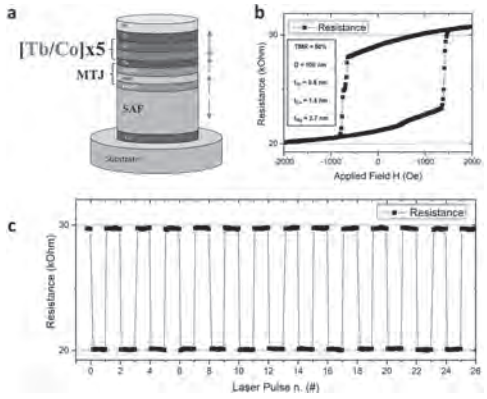

Figure 1 a) AOS-MTJ stack illustration b) R-H loop in perpendicular field c) AOS field-free toggle switching between P and AP states.

IOA-05. Efficiency Enhanced Magnetic Resonance Switching of Single Domain Particle with Uniaxial Anisotropy. *J. Zhu[1] 1. Data Storage Systems Center, Carnegie Mellon University, Pittsburgh, PA, United States*

As microwave-assisted magnetic recording (MAMR) is being employed in commercial hard disk drives, technology challenges remain [1][2]. A key one of them is the need for relatively strong ac field amplitude. Here, we present a novel scheme to substantially enhance the efficiency of the ac field. For a single domain magnetic particle of uniaxial anisotropy, the anisotropy energy is $E_{an}=K\sin^2\theta$ where θ is the angle between the magnetic moment of the particle and the easy axis and K is the anisotropy energy density. The effective magnetic field due to this anisotropy is $H_{an}=H_k\cos\Theta$ where $H_k = 2K/M_s$. Since the anisotropy field is a cosine function of the magnetization angle, the resonance frequency varies during a magnetization reversal. Hence, if the applied ac field frequency can match this resonance frequency variation during a magnetization reversal, the efficiency of the ac field should be significantly enhanced. Figure 1 shows the calculation for a single domain particle of Hk=30kOe. A magnetic field with a 2° angle w.r.t. the easy axis and duration of 1ns is applied opposite to the initial magnetization The ac field is a rotating perpendicular to the easy axis with a during of 1ns. The ac field frequency is either a constant (black), linearly decreases to zero, or follows the function of $\omega_0\cos(0.86t/\tau)$ where $\tau=1ns$. The horizontal axis is the initial ac field frequency. The ac field amplitude is set as1% of the anisotropy field at 300 Oe. In the case of the cosine-varying frequency ac field, the switching field reduction is more than 75% H_k at 6kOe. The substantially enhanced switching field reduction shows the efficiency gain by having ac field frequency following the resonance frequency reduction during the magnetization reversal. Figure 2 shows the switching field of a particle of H_k=25kOe and the ac field frequency is the cosine-varying case. When the ac field amplitude exceeds 350 Oe, the switching can be achieved without the reversal field applied.

[1] J.-G. Zhu, X. Zhu, and Y. Tang, "Microwave assisted magnetic recording," IEEE Trans. Magn., vol. 44, no. 1, pp. 125–131, Jan. 2008. [2] Akihiko Takeo, et al, "Extended Concept of MAMR and its Performance and Reliability," Paper C1, TMRC 2020, August 2020.

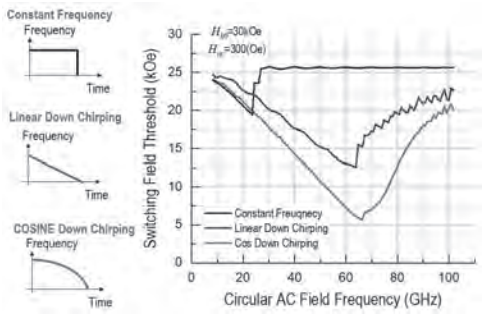

Fig. 1. Switching field vs the initial frequency of ac fields with the frequency being constant (black), linearly decreasing (blue), or cosine-varying (red).

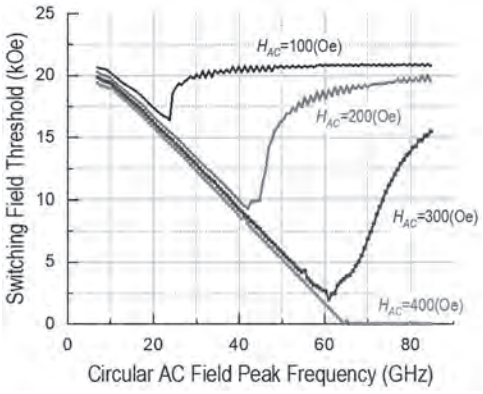

Fig. 2. Switching field vs initial ac field frequency for a cosine-varying frequency rotating ac field.

IOA-06. Plasmonic Near Field Transducer of Nanocomposite with Distributed Feedback. *T. Du[1,2], D.E. Laughlin[1,2], J. Bain[1,3], W. Zhang[1,3] and J. Zhu[1,3] 1. Data Storage Systems Center, Carnegie Mellon University, Pittsburgh, PA, United States; 2. Dept. of Materials Science and Engineering, Carnegie Mellon University, Pittsburgh, PA, United States; 3. Dept. of Electrical and Computer Engineering, Carnegie Mellon University, Pittsburgh, PA, United States*

A near field transducer (NFT) is a key component for heat-assisted magnetic recording (HAMR). The lollipop design and its variations have had success in HAMR recording systems employed in hard disk drives [1][2]. The designed mode resonance, or mode beating, results in excellent coupling between optical light and the excitation of plasmonic current in the NFT. However, the resonant plasmonic oscillation also yields substantial heating, bringing reliability challenges. In addition, such a resonant design can make the plasmonic excitation of media grains highly dependent on the spacing between the NFT recording peg and the grains in the media. In this paper, we present a design analysis for a novel NFT using a nanocomposite structure to create distributed optical feedback (DFB) for maintaining plasmonic

resonance. Figure 1 shows a schematic view of the design. The NFT is made of an array of Au rectangular rods, each separated by a constant gap, *G*, of nanometer dimension and the Au rods are embedded in a dielectric material. The insert in the figure shows the 2D COMSOL simulation results of the optical field intensity at the peg end of the NFT with W=660nm and G=5nm. For this structure, the optimal free-space optical wavelength λ=710nm. The 2μm long DFB Au nanocomposite has an optical coupling efficiency of 30% with very little field intensity decay at the peg end. Figure 2 shows the calculated electric field intensity in the dielectric gap before the last rod as a function of the width of the Au rods for different gap spacing. In conclusion, the DFB Au nanocomposite NFT design enables enhanced material stability, hence, enhancing the NFT reliability. Plasmonic excitation of medium grains by the NFT has also been modeled and the analysis of its sensitivity to the spacing between the NFT and medium grain will be presented.

[1] W.A. Challener, et al, Nature Photonics, 3 (4), 220-224 (2009). [2] K. Shimazawa, W. Xu, K. Fujil, US11,315,591B1, Headway Technologies, (2022)

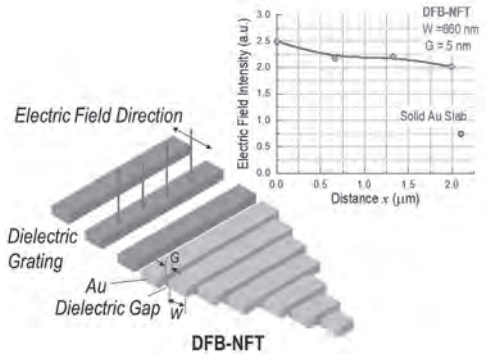

Fig.1 Schematic view of the distributed feedback Au nanocomposite NFT design. The insert shows the simulation results of optical field intensity inside the dielectric gaps along the 2μm long NFT. The optical wavelength is optimal at λ=710 nm.

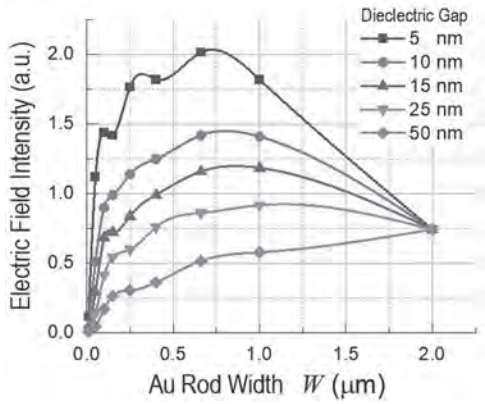

Fig.2. Optimization of the DFB Au nanocomposite NFT for Different Au rod width and dielectric gap. The electric field is measured at the end of 2μm long NFT.

IOA-07. Giant inverse spin Hall effect in BiSb topological insulator for SOT reader. *H. Ho*[1], J. Sasaki[1], N. Huynh Duy Khang[1], P. Nam Hai[1], Q. Le[2], B. York[2], C. Hwang[2], X. Liu[2], M. Gribelyuk[2], X. Xu[2], S. Le[2], M. Ho[2] and H. Takano[2] *1. Tokyo Institute of Technology, Tokyo, Japan; 2. Western Digital Inc., San Jose, CA, United States*

Scaling TMR reader down to sub 20 nm for magnetic storage technology beyond 4 Tb/in^2 is challenging, due to its complex film stack and increasing noise at smaller size. Recently, a spin-orbit torque (SOT) reader based on the inverse spin Hall effect was proposed as an alternative candidate [1]. The SOT reader consists of a SOT layer and a ferromagnetic layer (FM). A spin-polarized current is injected from the FM layer to the SOT layer, which generates an output voltage via the inverse spin Hall effect. However, the output voltage and signal-to-noise ratio (SNR) of SOT reader using traditional heavy metals are insufficient due to the relatively small spin Hall angle (SHA) and low sheet resistance [2]. Hence, a SOT material with large SHA is essential to generate a large output and sufficient SNR. The topological insulator (TI) BiSb emerges as potential candidate for SOT reader thanks to its giant SHA [3] and larger sheet resistance. In this work, we demonstrate a proof-of-concept for a BiSb-based SOT reader with large output voltage and SNR. Figure 1 shows the schematic structure of our device. The SOT reader is a 20 μm × 20 μm pillar of CoFe (5 nm)/MgO (2 nm)/BiSb (10 nm) on top of a 20 nm-thick Ta/Pt bottom current electrode deposited on an oxidized silicon substrate. Then, a top current electrode was deposited on top of the pillar. A perpendicular bias current was applied to the pillar, and the output voltage of the inverse spin Hall effect was read out during sweeping an in-plane magnetic field. Figure 2(a) shows a representative data at J_{app} = 6.25 kA/cm^2 for the inverse spin Hall resistance $R_{ISHE} = V_{ISHE}/I_{app}$ of the reader. Figure 2(b) shows the characteristics of the reader. The output is as large as 15 mV, which is 3 orders of magnitude larger than that of Pt-based devices [2]. We project a giant inverse spin Hall angle of 24 for this device, which demonstrates the potential of BiSb for SOT reader application.

[1] P. A. V. Heijden, Q. Le, K. S. Ho, US patent US9947347B1 (2016). [2] V. T. Pham, I. Groen, S. Manipatruni, Nat. Elec. 3, 309 (2020). [3] N. H. D. Khang, Y. Ueda, and P. N. Hai, Nat. Mater. 17, 808 (2018).

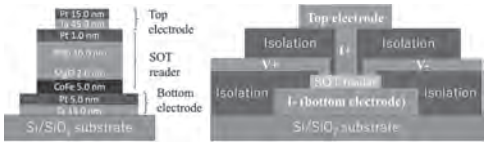

Schematic device structure of our BiSb-based SOT reader.

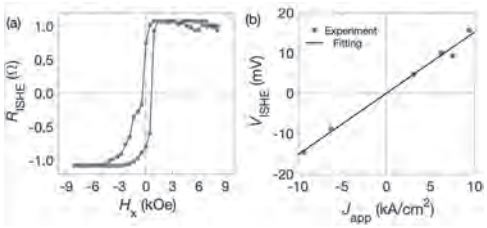

(a) Inverse spin Hall resistance at J_{app} = 6.25 kA/cm^2. (b) Output voltage at various applied current density.

IOA-08. Magnetic Read Head Design using a Lateral Spin Valve. *R. Hao*[1] and R. Victora[1] *1. Electrical and Computer Engineering, University of Minnesota, Minneapolis, MN, United States*

We propose a magnetic read head design based on a lateral spin valve (LSV) structure as shown in Fig. 1(a). We have the same spin injection structure as the LSV read head design in [1], but a different spin detection design and measurement mechanism. For spin detection, we place an MTJ (FM2/tunnel barrier/reference layer) below the Al channel for tunneling magnetoresistance (TMR) signal readout [2], and apply an additional voltage across the right part. The direct contact of FM2 and Al enables large numbers of spin-polarized electrons from the Al channel to enter FM2 and change its magnetization effectively, thereby enhancing signal-to-noise ratio (SNR) as shot noise becomes less important. The applied voltage (1) also drives electrons from FM2 across the tunnel barrier to improve signal readout through the MTJ; (2) suppresses reverse spin diffusion from the reference layer into FM2, thus further reducing shot noise in the detector. We have also performed micromagnetic simulation for our read head design with thermal magnetic noise following a Gaussian distribution. Simulation results indicate that large dimensions for FM1 but small dimensions for FM2, large saturation magnetization for FM1 (M_{S1}) but small one for FM2 (M_{S2}), small

damping constants for both, large interfacial spin polarizations, small biasing field, and a large media field, all favor SNR optimization. Fig. 1(b) is an SNR calculation of magnetization under a sinusoidal media field of 1-GHz frequency at room temperature. $m_{z1} = M_{z1} / M_{S1}$ and $m_{z2} = M_{z2} / M_{S2}$ are normalized magnetizations in the z direction of FM1 and FM2, respectively. The injection current density in FM1 is $J_q = 1 \times 10^8$ A/cm^2. M_{S1} is set to be 2000 emu/cm^3. It shows that small M_{S2} can give SNR of FM2 above 20 dB.

[1] M. Yamada, D. Sato, N. Yoshida, *et al*., in *IEEE Transactions on Magnetics*, Vol. 49, no. 2, p. 713-717, (2013), doi: 10.1109/TMAG.2012.2226871. [2] T. Valet and A. Fert, *Phys. Rev. B*, Vol. 48, no. 10, p. 7099-7113, (1993), doi: 10.1103/PhysRevB.48.7099.

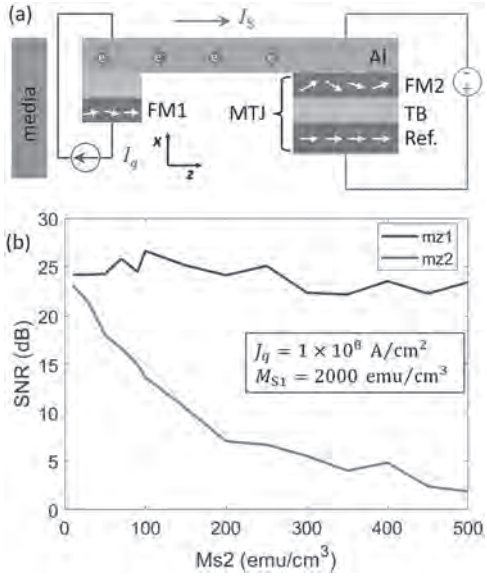

Fig. 1. (a) Our magnetic read head design based on lateral spin valve. The left part is for spin injection and the right part for spin detection. The right part has a magnetic tunnel junction (MTJ) adjacent to the Al channel. FM1 and FM2 are ferromagnets. TB is the nonmagnetic tunnel barrier. Ref. is a ferromagnetic reference layer with pinned magnetization direction. (b) Micromagnetic simulation result of signal-to-noise ratio (SNR).

IOA-09. Optimized mitigation of asymmetric oscillation noise in magnetic readers. *A. Stankiewicz*[1] and M. Samiepour[2] *1. Recording Head Group, Seagate Technology, Bloomingtom, MN, United States; 2. Recording Head Group, Seagate Technology, Londonderry, United Kingdom*

It has been shown both numerically [1] and experimentally [2] that randomly simulated asymmetric oscillations can produce significant noise at frequencies much lower than the resonance frequency f_0. Their low frequency spectrum often resembles 1/f noise. In particular, this mechanism of low frequency noise (LFN) generation may compromise the signal-to-noise ratio (SNR) of magnetic readers. This effect can be mitigated by finding the correlation between LFN and the amplitude fluctuations of asymmetric oscillations, extracted from the envelope of band-pass filtered resonance signals [3]. These filter parameters are critical for process efficiency, but in the patent [3] they were selected arbitrarily for demonstration purposes. Here we present systematic optimization of the method's parameters for maximum SNR improvement, using a bi-harmonic oscillator model [1]. Waveforms with $f_0 = 5$GHz were simulated, and we considered LFN bandwidth (*LFN_BW*) of 1 GHz (Fig. 1) and 2 GHz (Fig. 2). For pure asymmetric oscillations, SNR Gain grows monotonically with bandwidth of resonance filtration *FiltBand*, but tend to saturate at ~5x the full width at half maximum ($FWHM \sim 0.5$ GHz $<< f_0$) for $LFN\_BW = 1$ GHz. However, as we add moderate white noise (representing Johnson and shot noise), the optimal *LFN_BW* tends to become much lower, with SNR Gain saturating at *FiltBand* ~3x *FWHM*, and then slowly decreasing. These observations allow to predict optimal filtering parameters for maximum SNR Gains. We also tried several types of band-pass filters, finding a simple Butterworth to be as good as more sophisticated filters. The findings from the simple numerical model were also be applied for experimental noise waveforms in real magnetic readers, showing noise reduction efficiency similar to modeled waveforms.

1. T. Pipathanapoompron, A. Stankiewicz, K. Subramanian, A. Grier, and A. Kaewrawang, "Modeling of Magnetic Thermal Noise in Stable Magnetic Sensors," *Journal of Applied Physics*, vol. 127, p. 073 902, 2020. 2. T. Pipathanapoompron, A. Stankiewicz, J.Wang, K. Subramanian, and A. Kaewrawang, "Magnetic reader testing for asymmetric oscillation noise," *Journal of Magnetism and Magnetic Materials*, vol. 514, p. 167 064, 2020. 3. A. Stankiewicz, S. Stokes, and K. Subramanian, "Mitigation of noise generated by random excitation of asymmetric oscillation modes," US Patent, vol. 10,615,887, 2020.

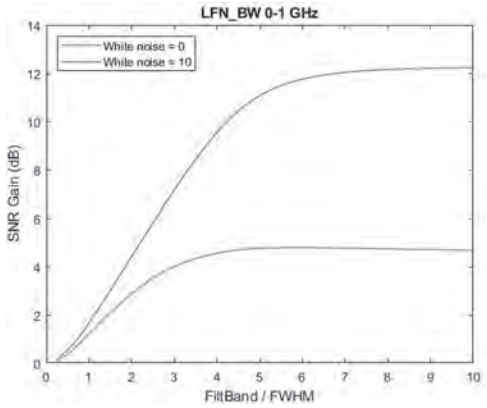

Figure 1

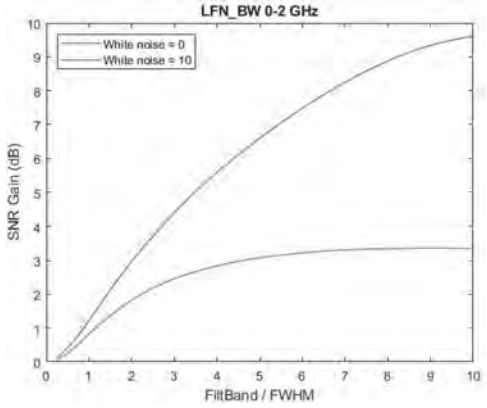

Figure 2

IOA-10. High Symbol De-Bruijn Code as an Absolute Pattern for Rotary Magnetic Encoders of Arbitrary Size. *K. Peng*[1], H. Hsiao[1] and J. Chang[1] *1. Power Mechanical Engineering, National Tsing Hua University, Hsinchu, Taiwan*

The work presented in this research is aimed at development of a novel absolute encoding method using De-Bruijn sequence with Hall-effect sensors to enable coding pattern of rotary encoders not limited to axial direction or to a specific disc size. This coding pattern resolves problem of repeated coding at the junction of a rotary encoder through creation of mathematical models and permutations of different sizes of sub-array. Based on the De-Bruijn sequence theory, the length of sub-array controls the number of Hall-effect sensing elements represented by *n* as illustrated in Figure 1, of which elements are linearly arranged on the sensing head. The proposed firmware of the measuring presets specific gates for the sensing elements with various limitations to distinguish certain codes on the pattern without misjudgment

when external magnetic field changes. Through calibrated experiments, it was found and validated that when the sequence was constituted by a string of codes with high symbol, which is denoted as *k*, the gate value could determine the correctness of the absolute position. When the measurement system structure operates at a constant moving speed, the output data from the A, B, C and D sensing elements as shown in Figure 2 can be discriminated synchronously. The results obtained in this research demonstrate two things. Firstly, the absolute position can be identified by lookup table corresponding to the specific code with 1 mm resolution. Secondly, the De-Bruijn code can be regarded as a circular code to avoid misjudgments that commonly observed with traditional methods.

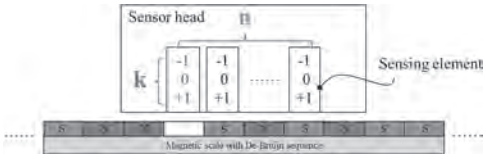

Schematic of a measuring system consisting of a sensor head and a magnetic medium with a De-Bruijn code pattern.

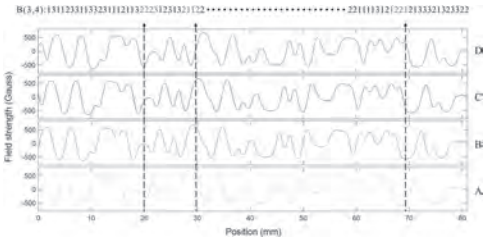

Experimental results with four channels of the analog signal. The symbol detected in each channel can be treated as a subsequence.

Session IOB
MAGNETIC RECORDING II
Chris Rea, Chair
Seagate Technology, Edina, MN, United States

CONTRIBUTED PAPERS

IOB-01. Withdrawn

IOB-02. Machine learning assisted micromagnetic approximation for FePt HAMR media. *A. Bolyachkin*[1], E. Dengina[1,2], H. Sepehri-Amin[1,2], Y. Takahashi[1] and K. Hono[1,2] *1. National Institute for Materials Science, Tsukuba, Japan; 2. University of Tsukuba, Tsukuba, Japan*

The areal recording density of hard disk drives has a potential to reach 4 Tb/in^2 with the heat-assisted magnetic recording (HAMR) technology [1]. So far, the best candidate for HAMR media is FePt nanogranular thin films with the $L1_0$ ordered structure. To improve the recording density and reduce the jitter noise, the bimodal grain size distribution and nanostructural defects, that are unavoidable in actual FePt films, must be suppressed. Grains with {111} twinning variants, [200] misoriented grains, and disordered grains with negligible magnetic anisotropy constants ($K = 0$) can be listed among the detrimental defects. Evaluation of their volume fractions, V_{111}, V_{200} and $V_{K=0}$ respectively, is of a vital interest. A new micromagnetic characterization of FePt nanogranular media is proposed in this work [2]. We developed a method of constructing finite element models of FePt granular media based on high-resolution transmission electron microscopy (TEM) images taken from top and side views of the films (Fig. 1). Using the TEM image based model, an accurate micromagnetic approximation of the out-of-plane hysteresis loops was achieved for MgO(6 nm)/FePt-BN(1 nm)/FePt-(C,SiO_2) (7 nm) thin films as shown in Fig. 2. It yielded parameters of uniaxial magnetic anisotropy (mean magnetic anisotropy constant K, its standard deviation, distortion of easy magnetization axes) and the volume fractions of the defects. Evaluated V_{111} and V_{200} were in excellent agreement with those determined by synchrotron XRD. After such an experimental validation, we collected a dataset of demagnetization curves by micromagnetic simulations upon different parameters of magnetic anisotropy and volume fractions of defects, then a neural network was trained to predict these parameters and use them as an initial set for the micromagnetic approximation that speeded up the approach significantly [3]. Thus, the developed TEM image based micromagnetic simulations assisted by machine learning can boost optimization of FePt HAMR media linking its nanostructural features to magnetic properties.

[1] K. Hono et al., MRS Bull. 43 (2018) 93. [2] A. Bolyachkin et al., Acta Mater. 227 (2022) 117744. [3] E. Dengina et al., Scripta Mater. 218 (2022) 114797.

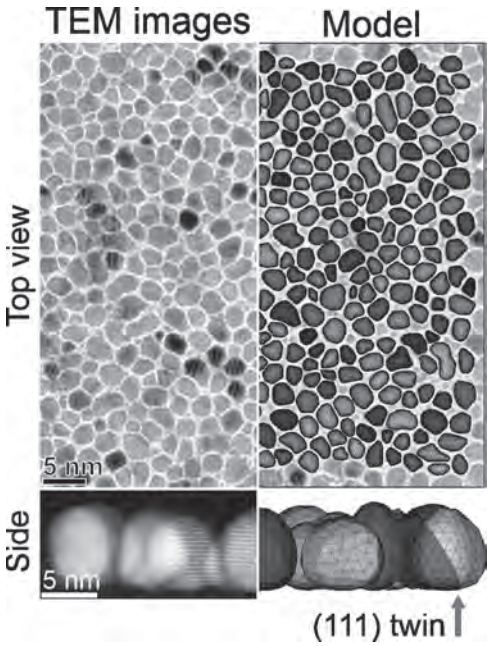

Fig. 1. Finite element model of FePt granular media constructed based on TEM images.

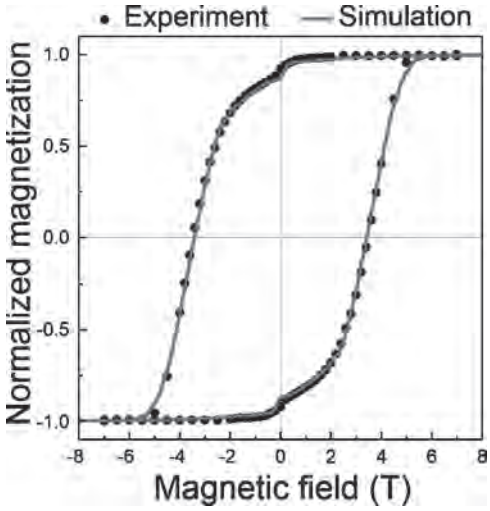

Fig. 2. Micromagnetic approximation of an experimental out-of-plane hysteresis loop.

IOB-03. RF-Biased sputtering induced formation of hexagonal boron nitride (h-BN) grain boundaries in $L1_0$ FePt-BN granular thin films. *C. Xu*[1], B. Varapasad[1], D.E. Laughlin[2] and J. Zhu[1] *1. Department of Electrical and Computer Engineering, Carnegie Mellon University, Pittsburgh, PA, United States; 2. Department of Materials Science and Engineering, Carnegie Mellon Univeristy, Pittsburgh, PA, United States*

Sputtering technique has been the choice for fabricating $L1_0$ FePt granular thin-film media for heat-assisted magnetic recording (HAMR). A variety of amorphous grain boundary materials have been studied extensively [1,2]. Among them, SiOx has been shown to facilitate columnar growth of FePt grains; however, its limitation on deposition temperature prevents high ordering. Amorphous carbon can yield high-temperature-enduring microstructure, however, with a limitation on grain height leveling to an aspect ratio ~1. Amorphous BN was also reported to affect the ordering of FePt [3]. In this paper, we report a study for creating a granular FePt-$L1_0$ film with crystalline BN grain boundaries that facilitate small grains with high aspect ratios and high ordering. By applying RF substrate bias with a substrate temperature of 700 °C, a microstructure of columnar FePt grains separated and wrapped around by hexagonal boron nitride(h-BN) layers is produced, as shown in Fig. 1(a). The spacing of the lattice fringes in grain boundaries is ~0.34 nm, close to that of h-BN basal planes (0.331 nm). The electron energy loss spectrum (EELS) shows the π* peak at 191.8 eV in the B-K edge, confirming the formation of turbostratic h-BN. Fig.1(e) shows columnar grains with an aspect ratio of ~1.85. A similar nanostructure was observed in FePt-Carbon film deposited with RF substrate bias, in which the graphite phase was likely formed in grain boundary regions. The covalent binding within the honeycomb structured nanosheets imparts the grain boundary materials high stability at high temperatures. This study provides an extendibility of FePt-based granular media to utilize partial crystalline grain boundary materials to improve microstructure. It also presents more understanding of why carbon and BN can maintain good grain isolation at quite high temperatures.

[1] A. Perumal, Y.K. Takahashi, K. Hono, $L1_0$ FePt-C Nanogranular Perpendicular Anisotropy Films with Narrow Size Distribution, 1 (2008) 101301. https://doi.org/10.1143/apex.1.101301. [2] C. Xu, B. Zhou, T. Du, B.S.D.C.S. Varaprasad, D.E. Laughlin, J.-G. Zhu, Understanding the growth of high-aspect-ratio grains in granular $L1_0$-FePt thin-film magnetic media, APL Materials. 10 (2022). https://doi.org/10.1063/5.0089009. [3] B.H. Li, C. Feng, X. Gao, J. Teng, G.H. Yu, X. Xing, Z.Y. Liu, Magnetic properties and microstructure of FePt/BN nanocomposite films with perpendicular magnetic anisotropy, Applied Physics Letters. 91 (2007). https://doi.org/10.1063/1.2798584.

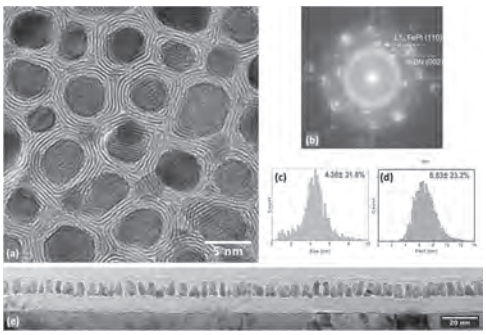

Fig.1 (a) Plane-view HRTEM of FePt-hBN film, (b) FFT shows a ring pattern of h-BN (002), corresponding to a d-spacing of 0.33~ 0.35 nm; (c) and (d) grain size and center-to-center pitch distance distributions; (e) cross-sectional TEM image of the 8-nm-thick FePt-hBN film grown on MgO seed layer. An order parameter of 0.84 was achieved with substrate temperature around 700 °C.

IOB-04. Reactive Molecular Dynamics Modeling of Plasma Etching of $L1_0$-FePt Magnetic Media. *J. Zhu*[1] and J. Wang[1] *1. Electrical and Computer Engineering, University of Minnesota, Minneapolis, MN, United States*

Patterned FePt media solutions, such as Bit-Patterned Media (BPM) and Embedded Hardmask Patterning (EMP), have been proposed as alternative methods to improve Heat-Assisted Magnetic Recording areal density. Understanding etching mechanism of FePt material is important to warrent the low damage to the magnetic properties caused by micro-fabrication process. In this research, Reactive Molecular Dynamics (MD) modeling is carried out to study methanol (MeOH) plasma etch on $L1_0$-FePt media. The atomistic-level etch simulation process is divided into two sequential MD simulation steps: the radical-based reactive treatment step, followed by the ion-based physical etch step. Carbon-monoxide (CO) and H_2 molecules are identified as the main etch precursors in methanol plasma interacting with substrate. Reactive interaction between CO/H_2 radicals and Fe/Pt atoms is studied using bond-order ReaxFF force field with atomic charge calculation. Bond energy calculation shows the positively charged Fe and Pt and the negatively charged C atoms in CO molecules can form ionic carbonyl bonds that are shown more stable than Fe-Pt metallic bonds. As the result, it is found that the number of Fe(CO) and Pt(CO) carbonyl bonds are dominated among the new bonds produced after the reactive-treatment process. In the following physical etch step simulated with Ar or He ion bombardment, in comparison with FePt surface without CO/H_2 treatment, the sputter yield of FePt can significantly improve by 2-4X on the samples with the CO/H_2-treatment step.

[1] H. Wang, H. Zhao, P. Quarterman, and J.-P. Wang, Appl. Phys. Lett., vol. 102, no. 5, p. 052406, 2013 [2] Patent: US10,347,467B2, J.-P. Wang, P. Quarterman and J. Zhu [3] LAMMPS - A flexible simulation tool for particle-based materials modeling at the atomic, meso, and continuum scales, Comp. Phys. Comm. (accepted 09/2021), DOI:10.1016/j.cpc.2021.108171 [4] J. Zhu, P. Quarterman, J.-P. Wang, AIP Advances 2017, 7 (5), 056507. https://doi.org/10.1063/1.4977223

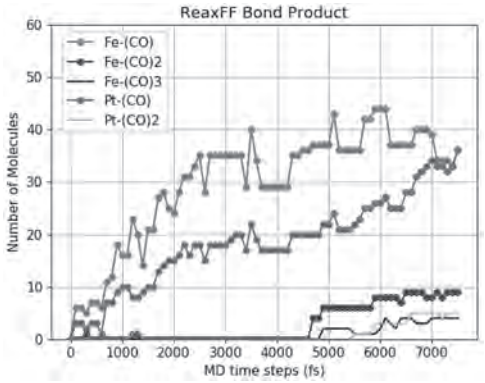

Figure 1. Number and types of carbonyl bonds created on FePt surface after CO/H_2 exposure

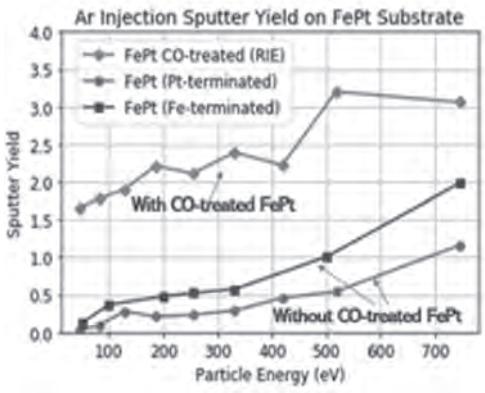

Figure 2. FePt sputter yield (with Ar ions) comparison on CO/H_2-treated and non-treated surface

IOB-05. FePt-BN Granular HAMR Media with High Grain Aspect Ratio and High $L1_0$ Ordering on Corning Lotus™ NXT Glass.
V. Bollapragada[2], C. Xu[2], M. Huang[3], D.E. Laughlin[1] and J. Zhu[2]
1. Department of Materials Science and Engineering, Carnegie Mellon University, Pittsburgh, PA, United States; 2. Department of Electrical and Computer Engineering, Carnegie Mellon University, Pittsburgh, PA, United States; 3. Corning Research and Development Corporation, Corning, NY, United States

The key to realizing high area recording density capability (ADC) for heat assisted magnetic recording (HAMR) is to achieve small grain size (and pitch) in the granular $L1_0$ FePt media with a sufficiently high grain aspect ratio [1]. Media such as FePt-C, FePt-SiO_x, and FePt-TaO_x, or multilayers made of a combination of them, appear not able to reach the desired goal because of their failure to achieve either high grain aspect ratio, small grain size, or high $L1_0$ ordering, respectively [2, 3]. In this study, using the co-sputtering technique, we demonstrate the fabrication of FePt-BN granular media with much reduced FePt grain size and high grain aspect ratio. In particular, an underlayer stack of Ta(5nm)/Cr(50)/MgO(9) is first deposited on Corning Lotus™ NXT glass followed by co-sputtering of FePt and BN at an elevated substrate temperature along. A RF bias is applied to the substrate during the FePt-BN deposition with a short and optimized delay. Figure 1C shows the order parameter as a function of substrate temperature for the FePt-BN granular film media, calculated from XRD measurements. The volumetric concentration of BN is at 38%. Figure 1A on the left of the figure shows a cross-section TEM micrograph of the FePt-BN layer formed at a substrate temperature of 725 °C. Figure 1B shows a cross-section TEM picture of FePt-BN/FePt-SiO_x multilayer granular film with temperature and composition graded over the grain height for producing tall grains [4] for comparison. The grain size of single layer FePt-BN film (Figure1 A) is around 4 nm with an aspect ratio of 2 while the grain size of the FePt-BN/FePt-SiO_x multilayer film is around 7nm and grain height 11nm. The small grain size with a relatively high grain aspect ratio in the single layer FePt-BN film is promising for enabling high area recording density capability.

[1]Y. Kubota et al., "Heat-Assisted Magnetic Recording's Extensibility to High Linear and Areal Density," IEEE Transactions on Magnetics, vol. 54, no. 11, Nov. 2018. [2] A. Perumal, Y.K. Takahashi, K. Hono, "L10 FePt-C Nanogranular Perpendicular Anisotropy Films with Narrow Size Distribution", Appl. Phys. Express 1 101301 (2008). [3] B. S. D. C. S. Varaprasad, M Chen, YK Takahashi, K Hono "L1-Ordered FePt-Based Perpendicular Magnetic Recording Media for Heat-Assisted Magnetic Recording" IEEE transactions on magnetics 49 (2), 718-722 (2013) [4] C. Xu, B. Zhou, T. Du, B.S.D.C.S. Varaprasad, D.E. Laughlin, J.-G. Zhu, Understanding the growth of high-aspect-ratio grains in granular L10-FePt thin-film magnetic media, APL Materials. 10 (2022).

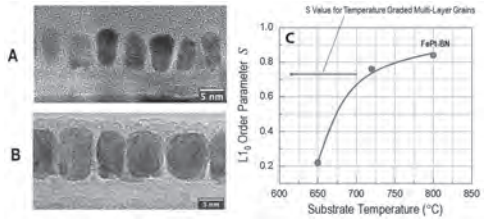

Figure 1 (A) Out of plane micrographs of FePt-BN (8 nm) (B) Out of plane micrographs of FePt-BN/FePt-SiO 2 (11 nm) and (C) Order parameter Vs set temperature of FePt-BN sample

IOB-06. A Rate-7/8 Modulation Code for Double-Track Reading Scheme in BPMR Systems.
C. Buajong[2], S. Koonkarnkhai[1], P. Kovintavewat[1] and C. Warisarn[2] *1. Nakhon Pathom Rajabhat University, Nakhon Pathom, Thailand; 2. College of Advanced Manufacturing Innovation, King Mongkut's Institute of Technology Ladkrabang, Bangkok, Thailand*

To increase an areal density (AD) of magnetic recording technology, bit-patterned media recording (BPMR) is one of the promising candidates for the next generation of hard disk drive [1]. To achieve a high AD, the track pitch and bit length must be greatly reduced. Because the reader's sensitivity response has a wider coverage area than the width of a written track, the inter-track interference will be unavoidable [2,3]. To improve the performance of a double-track reading (DTR) scheme in a staggered BPMR system as shown in Fig. 1; therefore, we propose a rate-7/8 two-dimensional (2-D) modulation code, which guarantees that the BPMR readback signal will not be corrupted by severe interference. To do so, we first analyze the peak amplitude of all possible $2^8 = 256$ data patterns in a matrix form of 2×4 bits, which are arranged as a staggered array BPMR, where the peak amplitude of each data pattern is obtained by the 2-D convolution between its magnetization and the readhead sensitivity response as shown in Fig. 1. Consequently, we found that when the 2×4 data pattern contains many 1's and -1's, the readback signal amplitude will be degraded which easily causes an error in the data recovery process. Therefore, this condition is utilized as a criterion for codeword designing to avoid such destructive data patterns. The encoding process easily operates based on a look-up table, while the Euclidean distance concept is applied in the decoding process. We evaluate the performance of 1) the proposed DTR system with a rate-7/8 2-D modulation code, 2) the DTR system without coding [4], and 3) the conventional system which uses one reader. The user density (UD) is defined as UD = AD×R, where R is a code rate. We define SNR = $10\log_{10}(1/\sigma^2)$ in dB, where σ is a standard deviation of AWGN. As depicted in Fig. 2, it is clear that at BER = 10^{-5} the proposed coded system at UD = 2.6 Tb/in^2 performs better than the uncoded system of about 1.0 dB and is superior to the conventional system.

[1] Y. Shiroishi et al., IEEE Trans. Magn., vol. 45, no. 10, pp. 3816-3822, Oct. 2009. [2] S. Nabavi and B. V. K. V. Kumar, in Proc. of ICC, pp. 6249–6254, Jun. 2007. [3] H. Muraoka and S. J. Greaves, IEEE Trans. Magn., vol 51, no.11, pp. 3002404, Nov. 2015. [4] C. Buajong and C. Warisarn, in Proc. of iEECON 2017, pp. 457-460, Mar. 2017

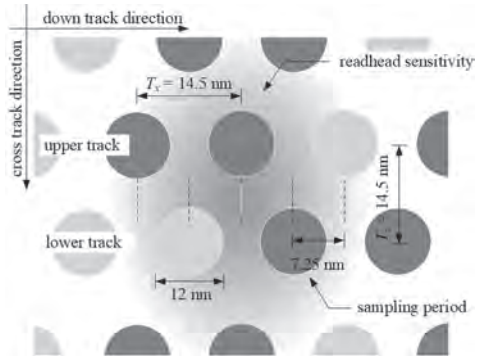

Fig. 1. Configuration of the proposed DTR systems at AD = 3.0 Tb/in² under the readhead sensitivity response that is positioned between the desired upper and lower tracks.

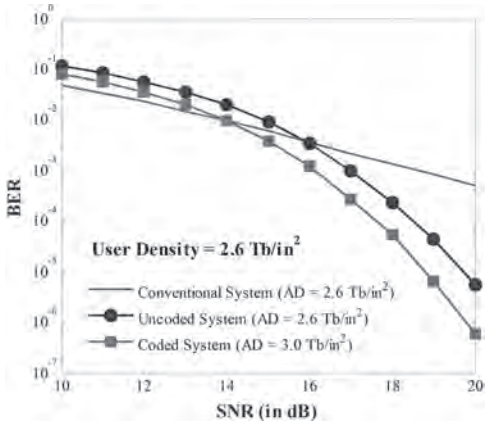

Fig. 2. Performance comparison of various systems at UD = 2.6 Tb/in².

IOB-07. Double-Layer Magnetic Recording with Multilayer Perceptron Decoder for Single-Reader/Two-Track Reading in BPMR Systems. *N. Rueangnetr*[1], S. Koonkarnkhai[2], P. Kovintavewat[2] and C. Warisarn[1] *1. College of Advanced Manufacturing Innovation, King Mongkut's Institute of Technology Ladkrabang, Bangkok, Thailand; 2. Nakhon Pathom Rajabhat University, Nakhon Pathom, Thailand*

The distance between islands must be reduced to increase an areal density (AD) in bit-patterned media recording (BPMR) [1]-[2], which means both inter-symbol interference (ISI) and inter-track interference (ITI) effects are avoidably increased. Therefore, BPMR system performance is effortlessly degraded [3]. In prior work [4], constrained code working with a multilayer perceptron (MLP) decoder in a staggered-array BPMR system was proposed. However, to get more improvement in the overall system performance of the magnetic recording system, we propose to apply the three-dimensional (3-D) magnetic recording that has double recording layers [5] with the constrained code performing with the MLP decoder. Here, a double recording layer medium is designed as a staggered pattern as shown in Fig. 1. Each layer is arranged as a regular array. Both of them are then arranged in a staggered pattern. The proposed double recording layer not only avoids the significant signal degradation from inter-layer interference (ILI) but also mitigates ISI and ITI effects. An input sequence, $u_k \in \{\pm 1\}$, is encoded by LDPC code and the rate-3/5 constrained encoder to obtain two encoded data sequences, $[x_{k,0}, x_{k,1}]$ as shown in Fig. 2. The odd, $x_{k,0}$, and even, $x_{k,1}$, data sequences are recorded in the upper and lower layers, respectively. A single reader is always positioned between two desirable tracks to retrieve the readback signal, which is then oversampled at time $t = kT_x/2$ to obtain a data sequence, r_k, where T_x is a bit period. The 1-D equalizer and 1-D modified-soft output Viterbi algorithm (m-SOVA) are used to equalize and determine a log-likelihood ratio (LLR), λ_k, respectively. Then, it is decoded and produced the improved LLR values, respectively, with the rate-3/5 decoder and LLR estimator based on MLP, λ''_k. Finally, the estimated user bit, $\hat{u}_k$, is produced using an LDPC decoder. Simulation results indicate that, at the same user density (UD), the proposed system (AD = 5 Tb/in²) provides BER performance over the previous system [4].

Y. Shiroishi et al., IEEE Trans. Magn., vol. 45, pp. 3816-3822 (2009) R. L. White, R. M. H. New, and R. F. W. Pease, IEEE Trans. Magn., pp. 990-995 (1997) P. W. Nutter et al., IEEE Trans. Magn., vol. 41, pp. 3214-3216 (2005) N. Rueangnetr et al., 19th ECTI-CON 2022, pp. 1-4 (2022) Y. Nakamura et al., IEEE Trans. Magn., vol. 58, pp. 1-5 (2022)

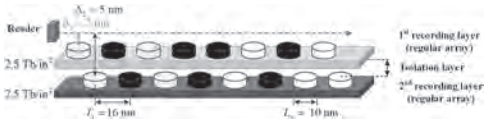

Fig. 1. Cross-section of head-media geometry for double recording layer medium.

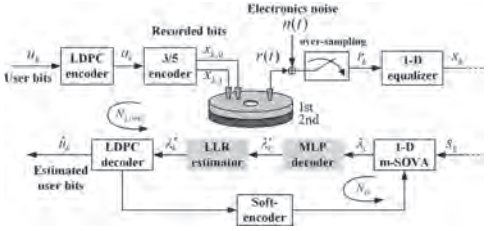

Fig. 2. A code BPMR channel model with the rate-3/5 constrained code.

IOB-08. A Study of Bit Island Spacing Optimization of Staggered Patterned Media-based SRTR Scheme in BPMR Systems. *M. Mattayakan*[1], S. Koonkarnkhai[2], P. Kovintavewat[2] and C. Warisarn[1] *1. King Mongkut's Institute of Technology Ladkrabang, Bangkok, Thailand; 2. Nakhon Pathom Rajabhat University, Nakhon Pathom, Thailand*

Many promising recording technologies have been introduced for hard disk drives to increase an areal density (AD), this paper considers the bit-patterned magnetic recording (BPMR) technology because it can achieve AD beyond 4 Tb/in² [1]. To increase an AD in BPMR, which unavoidably leads to a problem of two-dimensional (2D) interference. To combat this difficulty, several techniques have been proposed based on modulation codes [2] and iterative processing [3]. Additionally, the BPMR system performance can be further enhanced by the proper island placement [4]. In this paper, we propose to optimize the bit-length (T_x) and track pitch (T_z) of BPMR under a single reader/two-track reading (SRTR) technique, which leads to getting greatly improved BER performance. Here, we arrange the island in a staggered pattern. The single reader was then employed to read both desired data tracks simultaneously. The signal waveforms from the upper and lower tracks, and the readback signal, that correspond to the data bits stored in the staggered medium through our proposed system are illustrated in Fig. 1. Here, we then investigate five cases under an iterative partial response maximum likelihood (PRML) system as follows: Case 1: T_x = 13.0 nm and T_z = 16.2 nm, Case 2: T_x = 14.0 nm and T_z = 15.0 nm, Case 3: T_x = 14.5 nm and T_z = 14.5 nm, Case 4: T_x = 15.0 nm and T_z = 14.0 nm, and Case 5: T_x = 16.2 nm and T_z = 13.0 nm, to obtain AD of 3 Tb/in². Its data samples that were obtained from the over-sampling technique will then be processed through iterative PRML detection. Simulation results indicate that a system that has a larger bit-length distance, T_x, (Case 5) can provide the highest system performance when compared to other cases as shown in Fig. 2. In addition, the proposed system that encountered media noise still provides the highest system performance. It means that choosing proper T_x and T_z spacing can increase the efficiency of the staggered SRTR BPMR system.

[1] M. Mehrmohammadi et al., IOPscience, pp. 1-8 (2010) [2] C. Warisarn, A. Arrayangkool, and P. Kovintavewat, IEICE Trans. Electronics, vol. E98-C, pp. 528-533 (2015) [3] M. Tuchler, R. Koetter, and A. C. Singer,

IEEE Trans. Commun., vol. 50, pp. 754-767 (2002) [4] S. Jeong, J. Kim, and J. Lee, Trans. Magn. vol. 54, pp. 1-4 (2018)

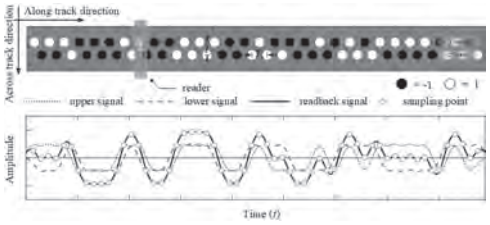

Fig. 1. Position of a single reader between two desired tracks over the staggered island pattern and its readback signal.

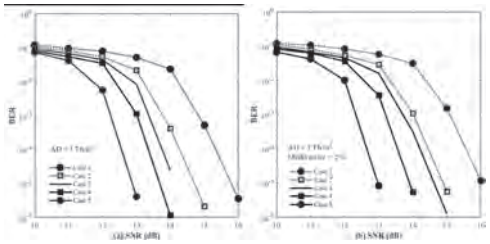

Fig. 2. BER performances of different cases of SRTR BPMR system (a) without and (b) with 5% media noises.

IOB-09. Dependence of User Density on System and Media Parameters for Shingled Heat Assisted Magnetic Recording (HAMR). *K. Hosen*[1] and R.H. Victora[1] *1. Department of Electrical and Computer Engineering, University of Minnesota, Minneapolis, MN, United States*

We predict how design aspects of the HAMR system such as media properties, thermal profile, and the geometry of the magneto-resistive (MR) reader affect user density through micromagnetic simulation [1]. It is found that maximum user density is achievable by optimizing the track pitch. Fig 1. shows dependence on track pitch for a small grain pitch, fly height, and thermal spot size: Fig 2. shows corresponding data for large values. User density increases when the value of shield-to-shield spacing (SSS) of the reader is reduced owing to improved resolution, even though SNR often decreases [2]. Moreover, the impact of the shield-to-shield spacing is much stronger in case of small grain size compared to larger grain size because the limit to resolution becomes the transition broadening induced by the grain pitch. It is also evident that higher full width at half maximum (FWHM) of the temperature profile reduces user density owing mostly to increased track pitch, but also owing to increased erase after write. Transition curvature in combination with shingled recording is predicted to yield asymmetric transitions with respect to the track center [3]. Therefore, to adequately match the curvature of these asymmetrical curved transitions, we employed a rotated read head rotation: a single rotated head ($\theta_{opt} = 35^0$) results in a 9% improvement in user density over a single non-rotated head at 5.8 nm grain pitch, 15 nm reader width, 30 nm FWHM, 16 nm SSS, and 15 nm track pitch. Finally, we also demonstrate that media T_c variation impacts density more severely at high densities, but anisotropy field variation is the more significant effect at lower densities.

[1] R. H. Victora and P.-W. Huang, *IEEE Trans. Magn.*, vol. 49, no. 2, pp. 751–757, (2013) [2] Z. Liu, Y. Jiao, and R. H. Victora, *Appl. Phys. Lett.*, vol. 108, no. 23, p. 232402, (2016) [3] W.-H. Hsu and R. H. Victora, *Appl. Phys. Lett.*, vol. 118, no. 7, p. 72406, (2021)

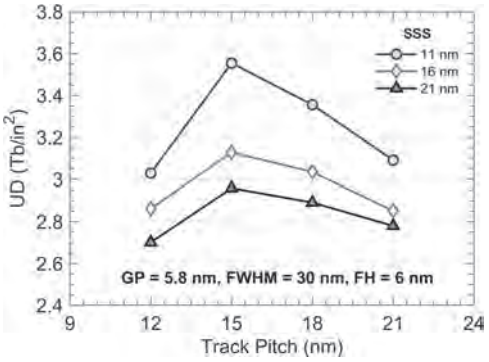

Fig. 1. User density as a function of track pitch for different shield-to-shield spacing (SSS) of ECC (FePt) media for optimal bit length = 9nm and reader width =15nm.

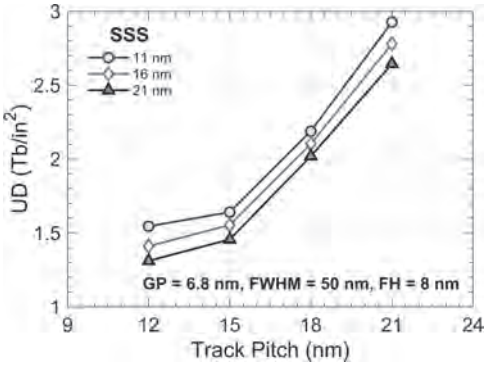

Fig. 2. User density profile as a function of track pitch for different shield-to-shield spacing (SSS) of ECC (FePt) media for optimal bit length = 9nm and reader width =15nm.

IOB-10. Effectiveness of a Pulsed Laser in Heat Assisted Magnetic Recording. *Y. Chen*[1] and R.H. Victora[1] *1. University of Minnesota, Minneapolis, MN, United States*

Recently, much effort has been directed towards increasing the areal density of Heat-Assisted Magnetic Recording (HAMR) [1-2]. Here, we use our HAMR recording simulation [3] that employs renormalized media parameters to examine the potential use of a pulsed laser instead of a continuous laser. By carefully tuning parameters such as peak temperature, decay rate and inter-granular exchange, the pulsed laser is shown to have better recording performance. It also produces less average heat in the media and thus improves near field transducer lifetime. We employ the thermal profile of the discontinuous laser described in our previous work [4]. Optimization yields a peak temperature of around 950K and a time constant for heat dissipation of about 0.5 nS. This is fortunate because 0.5 nS also appears to be the experimental value of time constant for at least some media stacks. Inter-granular exchange of 10% is found to be optimal for both the continuous and pulsed laser configurations. Our results show that the optimized pulsed laser reduces Adjacent Track Erasure (ATE) relative to the continuous laser. For example, Fig. 1 shows that the pulsed laser system shows a lower decay rate with write number than the continuous laser. This could be understood from Fig. 2, where the averaged thermal activation is calculated. Here, the pulsed laser has a narrower distribution along the cross-track direction, which means the signals written on track 1 are less affected by the signals written on the adjacent track. We believe that the effectiveness of our pulsed laser approach relies on properly synchronizing the pulse with the magnetic field change: 0.1 nS delay works best. This allows the gradient at the edge of the writing bubble to almost double when transitions are initiated.

[1] McDaniel, Terry W. Journal of Physics: Condensed Matter 17.7 (2005): R315. [2] Weller, Dieter, et al. IEEE transactions on magnetics 50.1 (2013):

1-8. [3] Victora, R. H., and Pin-Wei Huang, IEEE Transactions on Magnetics 49.2 (2013): 751-757. [4] Natekar, Niranjan A., and R. H. Victora, IEEE Transactions on Magnetics 57.3 (2020): 1-11.

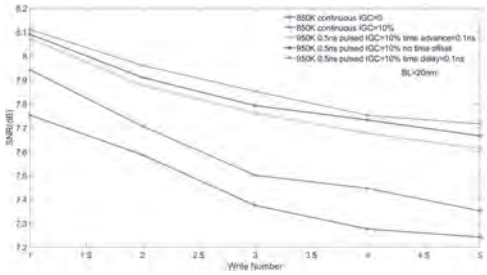

Fig1. SNR variation of pulsed laser and continuous laser for different IGC for ECC media. Write Number is the number of times the adjacent track is overwritten. ECC media is made up of 3nm superparamagnetic writing layer and 6nm FePt storage layer. Bit length is 20 nm and velocity is 20 m/sec.

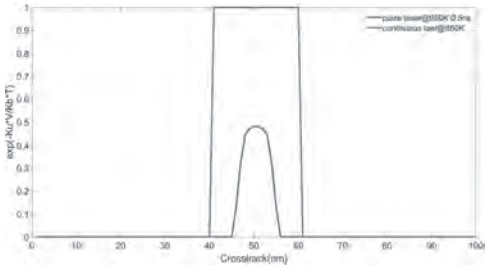

Fig2. Averaged thermal activation of pulsed laser and continuous laser along cross-track direction.

IOB-11. Skew Angle Estimation and Alleviation Based Multi-Layer Perceptron in V-Shaped Read-Head Array BPMR Systems. *K. Fatika*[1], S. Koonkarnkhai[2], P. Kovintavewat[2] and C. Warisarn[1] *1. College of Advanced Manufacturing Innovation, King Mongkut's Institute of Technology Ladkrabang, Bangkok, Thailand; 2. Nakhon Pathom Rajabhat University, Nakhon Pathom, Thailand*

Attaining high areal density (AD) in bit-patterned magnetic recording (BPMR) technology means reducing its bit period and track pitch [1,2]. When the readers move from the initial to other zones of the disk, a skew angle (SA) takes place, leading to a degradation of the system performance [3]. Therefore, controlling SA properly is necessary. Prior works introduced SA detection along with the suppression [4] and the study of SA in a read-head array [5]. To the best of our knowledge, this is the first proposed scheme of combining a multi-layer perceptron (MLP) with a V-shaped read-head array to estimate and alleviate SA in BPMR. We propose SA estimation and alleviation schemes in BPMR by combining the V-shaped read-head array, as shown in Fig. 1, with MLP. The V-shaped read-head array is investigated in three zones of the disk, i.e., inner, middle, and outer zones, which are notated as ID, MD, and OD, respectively. The initial positions of all three readers in the middle zone are fixed at 5, -5, and 5 degrees for upper, middle, and lower readers, respectively. The sensitivity functions of these readers are shown in Fig. 2, in which their changes as they move from one zone to another are also illustrated. Note that when the sensitivity changes, the channel coefficient, and their readback signals will also change. Therefore, the SA estimation process can utilize readback signals that are produced from the array reader as the input of an MLP-based SA estimator. The next process is attenuating the SA effect in the system by designing an appropriate 2-D equalizer for each SA level in the mentioned zones of the disk, based on a minimum mean-square error approach, before sending an equalized sequence to the Viterbi detector. We found that five levels of estimated SA to signal-to-noise (SNR) values, by using a V-shaped read-head array in BPMR, can estimate nearly 100% of the SA value equal to 0 degree, while the positive and negative SA values also gain high percentages. Furthermore, the accuracy percentage of our proposed scheme is independent to SNR.

[1] Y. Shiroishi et al., IEEE Trans. Magn., vol. 45, no. 10, pp. 3816-3822, 2009. [2] H. J. Richter et al., IEEE Trans. Magn., vol. 42, no. 10, pp. 2255–2260, 2006. [3] M. R. Elidrissi, K. Sann Chan, S. Greaves, et al., Journal of Applied Physics, 115(17), 2014. [4] S. Koonkarnkhai, C. Warisarn, and P. Kovintavewat, AIP Advances 11, 015229, 2021. [5] E. Hwang, T. Oenning, G. Matthew, et al., IEEE Trans. Magn., vol. 51, no. 4, 2015.

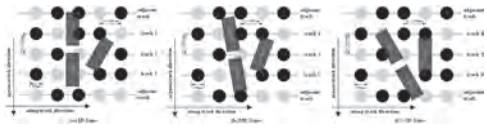

Fig. 1. V-shaped read-head array in various zones.

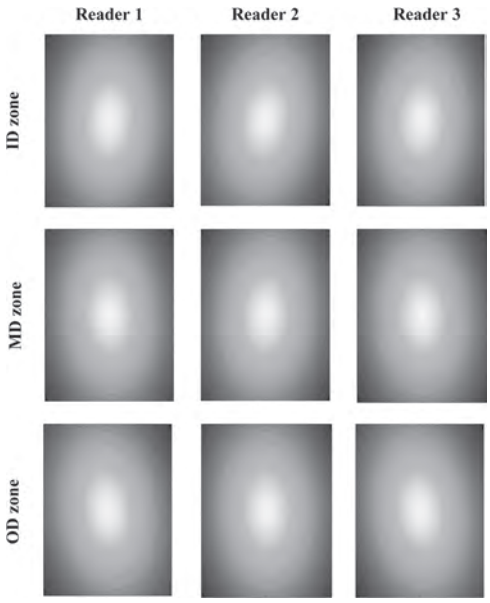

Fig. 2. Reader sensitivity functions in various zones.

IOB-12. Trajectory Sampling Method for Reaction Rate Computation in Micromagnetic Simulations. *X. Wang*[1], J. Duan[1] and V. Lomakin[1] *1. ECE, UCSD, La Jolla, CA, United States*

Trajectory sampling methods can provide important information about thermally-driven statistical properties of micromagnetic systems. Transition state theory (TST) describes reaction rates based on the reaction coordinate in energy phase space [1] but has limitations. Transition path sampling (TPS) [2] and later transition interface sampling (TIS) [3] methods were developed assuming that the system is at a stable state and reaction rate does not change over time. Based on TIS, forward flux sampling (FFS) method was presented by replacing the Monte Carlo trajectory sampling method used in TIS by a direct Langevin simulation that is only forward in time, which eliminates reversable symmetry limitation [4, 5]. Here, a modification of the FFS method, referred to as trajectory sampling method (TW-FFS) is introduced. In FFS simulation, the computation stage is divided into the initial reaction rate computation stage and the following ratio computation stages. For the initial reaction rate computation stage, original method presented in FFS suffers from the parameter tuning problems, which may significantly affect the accuracy, stability, and efficiency of the FFS algorithm. The presented approach combines the above two stages together in a time-weighted manner leading a more stable, accurate and efficient algorithm behavior in micromagnetic simulations. From Fig. 1, TW-FFS gives a much better tolerance in terms of the choice of the initial flux interface as well as provides significantly more accurate results.

[1] Eyring H 1935 The activated complex in chemical reactions J.Chem. Phys. 3 107–15 [2] Dellago C, Bolhuis P G, Csajka F S and Chandler D 1998, Transition path sampling and the calculation of rate constants J. Chem. Phys. 108 1964–77 [3] van Erp T S, Moroni D and Bolhuis P G 2003 A novel path sampling method for the calculation of rate constants J. Chem. Phys. 118 7762 [4] Allen R, Valeriani C and Wolde P, Forward flux sampling for rare event simulations, J. Phys.: Condens. Matter 21 (2009) 463102 [5] Vogler, C., Bruckner, F., Suess, D., & Dellago, C. (2015). Calculating thermal stability and attempt frequency of advanced recording structures without free parameters. Journal of Applied Physics, 117(16). https://doi.org/10.1063/1.4918902

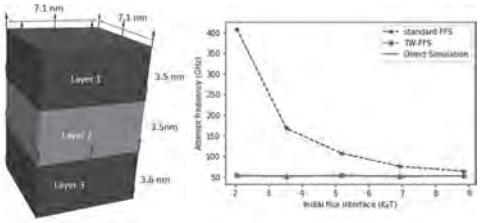

Fig1: (a) Target grain structure comprised of a three-layer stack with the following material parameters: bulk exchange constant: 1e-6 erg/cm, saturation magnetization: {562, 525, 625} emu/cm3, uniaxial anisotropy: {224800, 315000, 562500} erg/cm3, interface exchange coupling: 0.1 erg/cm2. (b) Attempt frequency for different methods as a function of the initial flux interface energy difference with respect to the equilibrium state (λ). The energy barrier here was 9 kBT to allow comparisons with the direct stochastic simulations and the number of the FFS interfaces was {5,4,3,2,1} for each node with increasing λ, respectively.

Session IPA
MAGNETIC RECORDING III
(Poster Session)

Dafine Ravelosona, Chair
Universite Paris Saclay, Palaiseau, France

IPA-01. Small amount of grains with *c*-axis parallel to film plane and high saturation magnetization for FePt granular films with nitride grain boundary material for heat assisted magnetic recording media.

K. Tham[1], R. Kushibiki[1] and S. Saito[2] *1. Tanaka Kikinzoku Kogyo, Tsukuba, Japan; 2. Electronic Engineering, Tohoku University, Sendai, Japan*

The $L1_0$ type FePt phase is attracting attention as the heat assisted magnetic recording medium material due to its high uniaxial crystalline magnetic anisotropy energy of 5×10^7 erg/cm^3 at room temperature. To achieve this, the research of FePt granular thin films added with various grain boundary materials (GBMs), such as C[1,2], SiO_2[3], TiO_2[4], MgO[5], Ta_2O_5[6], B_2O_3[7] have been widely conducted. Based on our previous report, FePt granular films with oxides GBMs consist higher content of in-plane (001) texture component compared to that of carbon GBM[8]. To address the issue with oxide GBM, we have carried out the experiment to replace oxides with nitrides as the GBMs. In this paper, we will report the evaluation result of nanostructure and magnetic properties of the granular films. Fig. 1 shows dependence of saturation magnetization (M_s) of FePt granular films with various GBMs on melting point (T_m) of the GBMs. An inset shows layered structure of the samples. At the same T_m, M_s of FePt-nitride shows higher values of around 50 emu/cm^3 than that of FePt-oxide. Furthermore, FePt-nitride shows similar tendency with that of FePt-oxide granular films, where M_s varies almost linearly against T_m. This suggests that M_s in FePt-nitride granular films is determined by the degree of separation between FePt magnetic grains and non-magnetic GBMs. Fig. 2 shows in-plane XRD profiles for FePt-nitride granular films with various GBMs. For the comparison with the typical FePt-oxide granular films, the profiles of FePt-SiO_2 and FePt-TiO_2 granular films are also shown in the figure. In the profiles, mainly, the (110), (200), and (220) diffractions from $L1_0$-FePt phase can be observed, which indicates that FePt grains have *c*-plane sheet texture. Concerning other diffractions, the integral intensities of (001) diffraction for FePt-nitride granular films are smaller compared to those of with oxide can be observed which reveals that the ratio of FePt grains with their *c*-axes parallel to normal to the film plane is reduced by using nitride GBM.

(1) J. S. Chen et al., *Appl. Phys. Lett.*, 91, 132506 (2007). (2) A. Perumal et al., *J. Appl. Phys.*, 105, 07B732 (2009). (3) E. Yang et al., *J. Appl. Phys.*, 104, 023904 (2008). (4) Y. F. Ding et al., *Appl. Phys. Lett*., 93, 032506 (2008). (5) Y. Peng et al., *J. Appl. Phys*., 99, 08F907 (2006). (6) B. C. Lim et al., *J. Appl. Phys.*, 105, 07A730 (2009). (7) T. Saito et al., *Jpn. J. Appl. Phys*., 59, 045501 (2020). (8) K. K. Tham et al., 2021 IEEE INTERMAG, 1-5 (2021), doi: 10.1109/INTERMAG42984.2021.9580144.

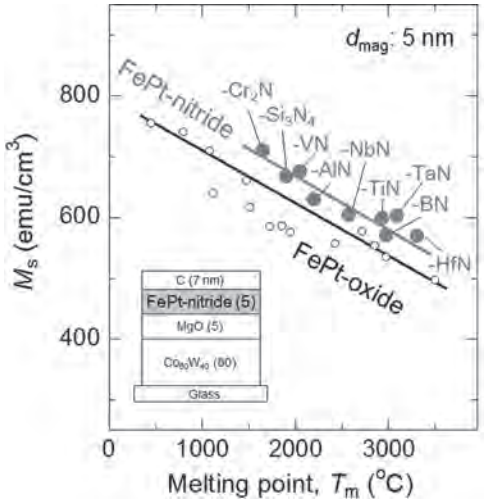

Fig. 1 Dependence of M_s of FePt granular films with various GBMs on T_m of the GBMs. An inset shows layered structure of the samples.

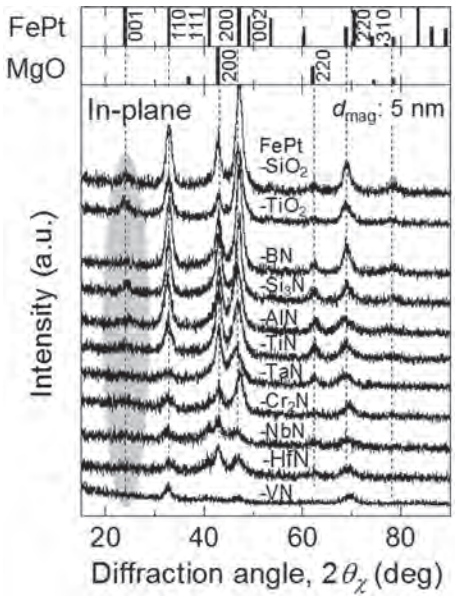

Fig. 2 In-plane XRD profiles for FePt-nitride granular films.

IPA-02. Combination dependence of printing characteristics in double magnet master media for energy-assisted magnetic recording.

T. Komine[1] *1. Graduate School of Science and Engineering, Ibaraki University, Ibaraki 316-8511, Japan*

Energy-assisted magnetic recording (EAMR) is thought to solve the trilemma by improving writability and enhancing areal recording density [1, 2]. On the other hand, servo signal writing time, which takes a few days per one drive on manufacturing process, is one of serious problems for high areal recording

density in hard disks. Magnetic printing is a strong candidate for servo track writing with extremely high speed and low cost. A new master structure, herein called double magnet master (DMM) medium, was recently proposed for magnetic printing to improve printing characteristics onto EAMR media [3, 4]. However, the detailed combination of double magnets to further improve printing characteristics, has not been clarified yet. In this study, the micromagnetic simulation has been carried out in order to reveal an appropriate combination of magnets in DMM. The conventional single magnet master media were proposed by our previous reports [5, 6]. The magnetic pattern in the conventional master media is a soft single magnet (SSM) of FeCo or a single hard magnet (HSM) of CoPt. Thus, the DMM can be expected to utilize two kinds of magnet combinations such as soft-hard double magnet (SDM) and (semi-) hard-hard double magnet (HDM). The recording field distribution and the printed magnetization were calculated by utilizing micromagnetic simulation [3]. The recording media consists of hexagonal grain with diameter of 4.6 nm and has the coercivity of 10kOe. The magnetizations printed by 4 kinds of master were shown in Fig. 1. The printed magnetic pattern is L/S with the same pattern width of 10nm corresponding to the bit length. The upper panels of each magnetization distribution of Fig. 1 schematically shows 4 kinds of combinations of magnets. SDM and HDM can clearly print the L/S pattern better than SSM and HSM. Moreover, the SDM has better printing characteristics than that of HDM. The SDM has the FeCo pattern with large magnetization to enhance the recording field, which is larger than that of CoPt in HDM during the application of printing field more than about 8kOe. Therefore, the SDM master is more adequate for magnetic printing onto EAMR media.

[1] M. H. Kryder et al., "Heat assisted magnetic recording", *Proc. IEEE*, vol. 96, no. 11, pp. 1810-1835 (2008). [2] J.-G. Zhu, X. Zhu and Y. Tang, "Microwave assisted magnetic recording", *IEEE Trans. Magn.*, vol. 44, no. 1, pp. 125-131 (2008). [3] T. Komine, "Master structure dependence of double magnet master on performance of magnetic printing onto energy-assisted magnetic recording media", *IEEE Trans. Magn.* (2022) Early access. DOI: 10.1109/TMAG.2022.3147910 [4] T. Komine, "Double magnet master media for magnetic printing onto energy-assisted magnetic recording media", *IEEE Trans. Magn.* Vol. 58, 3200105 (2021). [5] T. Komine, T. Murata, Y. Sakaguchi and R. Sugita, " Feasibility of perpendicular magnetic printing at 1Tb/in^2 ", *IEEE Trans. Magn.*, vol. 44, no. 11, pp. 3416-3418 (2008). [6] N. Sheeda, M. Nakazawa, H. Konishi, T. Komine and R. Sugita, "Perpendicular anisotropy master medium in magnetic printing for writing high-density servo signal", *IEEE Trans. Magn.*, vol. 45, no. 10, pp. 3676-3678 (2009).

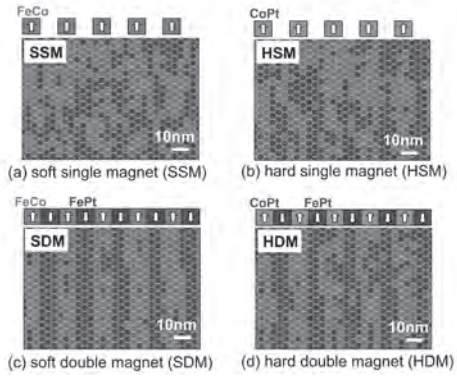

Fig.1 Magnetization distribution of printed by 4 kinds of master media.

IPA-03. Evaluation of blocking temperature and its distribution for $L1_0$ typed FePt granular films. *D. Isurugi*[1], T. Saito[1], S. Kaneko[1], K. Tham[2], T. Ogawa[1] and S. Saito[1] *1. Tohoku University, Sendai, Japan; 2. Tanaka Kikinzoku Kogyo K. K., Tsukuba, Japan*

The $L1_0$ typed FePt granular film with moderate Curie temperature (T_C) is a promising candidate as a next-generation technology material for HAMR [1]. In HAMR, since laser heat was utilized for decreasing switching field (H_{sw}) during recording, controlling the temperature dependence of H_{sw} and its distribution is required. The temperature where $H_{sw} = 0$ without and with taking into account of thermal fluctuation are T_C and blocking temperature (T_B), respectively. Therefore, T_B/T_C and $\Delta T_B/T_C$ show thermal fluctuation indexes. In this presentation we propose a method to evaluate T_B and its distribution by measuring thermal hysteresis of remanent magnetization (M_r) for FePt granular films. Fig. 1 shows a schematic diagram of T_B evaluation method and its distribution. First, the magnetization of all the magnetic grains in a granular film is aligned in the same direction. As the temperature rises, the number of blocking grains increases, and the magnetization of those grains is frozen in the opposite direction due to dipole field from the surrounding grains. Here the M_r during temperature rise and fall are defined as M_r^{for} and M_r^{back}, the percentage of blocking grains is expressed as $(M_r^{for} - M_r^{back}) / 2M_r^{for}$, and its temperature dependence corresponds to the cumulative distribution of thermally demagnetized grains. The derivative of the cumulative distribution curve gives the frequency distribution of blocking grains, which corresponds to the T_B distribution. Fig. 2 shows the ratio of the average value of T_B (T_B^{ave}) to T_C (T_B^{ave}/T_C) versus ΔT_B for FePt granular films with various GBMs, where the minimum and maximum values of the T_B variance are defined as T_B^{min} and T_B^{max}, respectively, and $\Delta T_B = T_B^{max} - T_B^{min}$. For each temperature, ΔT_B varied from 86.4 to 182.7 K, depending on the GBM, and showed negative correlation with T_B^{ave}/T_C with the present measurement time condition (τ) of thermal hysteresis of 60 s. Based on this result, the ΔT_B at $\tau = 2 \times 10^{-7}$ s, which corresponds to the recording time of HDD, was calculated to be ΔT_B = 18.8- 53.9 K ($\Delta T_B/T_C = 4.49\times 10^{-2}$- 7.32×10^{-2}).

[1] D. Weller et al., *Phys. Status Solidi A*, 210, 1245 (2013).

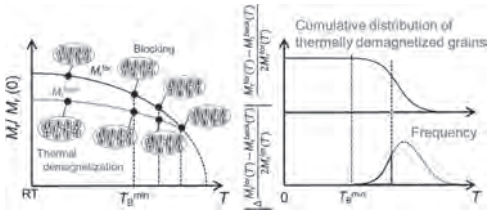

Fig. 1 Evaluation method of blocking temperature.

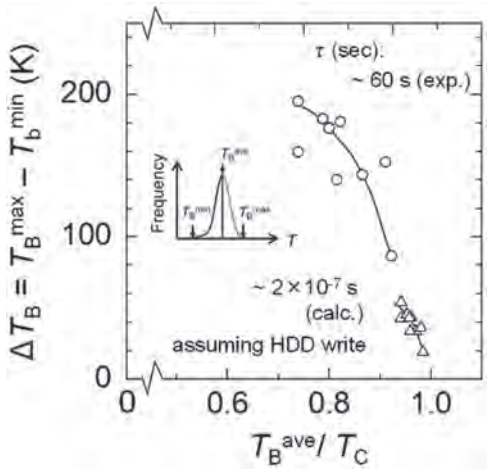

Fig. 2 T_B^{ave}/T_C versus ΔT_B for FePt granular films with various GBM.

IPA-04. Numerical analysis of magnetization switching assisted by AC voltage-controlled magnetic anisotropy effect. *X. Ya*[1], K. Kawakami[1] and T. Tanaka[1] *1. Kyushu University, Fukuoka, Japan*

Voltage-controlled magnetic anisotropy (VCMA) effect in ferromagnetic ultrathin films is an emerging technology that enables energy-efficient magnetization switching [1,2]. Besides, microwave assisted magnetization switching (MAS) technology has also attracted interests as an energy assisted magnetization switching method [3]. On the other hand, microwave voltage applied to a VCMA gate on an ultrathin ferromagnetic nanowire results

the parametric excitation of magnetization precession and propagating spin wave [4]. In this study, we numerically demonstrated AC voltage-induced magnetization switching, which showed magnetization switching was well assisted. Fig. 1(a) shows the schematic illustrations for the ferromagnetic nanodot covered by a dielectric layer. DC bias magnetic field (H_b) was applied at θ with respect to the anisotropy axis. The voltage-induced modulation of the anisotropy was numerically modeled by the local sinusoidal $\Delta H_{k\text{-change}}$ with the amplitude of $0.1H_k$. The dependence of the precession amplitude on the excitation frequency f_{exc} when H_b close to the switching field at various incident angles is plotted in Fig. 1(b). Two resonance peaks are observed, which represent the ferromagnetic resonance ($f_{exc} = f_{precession}$) and the parametric resonance ($f_{exc} = 2f_{precession}$). The parametric resonance presents a typical spectrum that the precession amplitude abruptly increases with frequency. Fig. 1(c) presents the dependence of switching fields on the excitation frequency as a parameter of the field incident angle. When the field applied non-parallel to the anisotropy axis, the switching field shows two local minima, which are due to the resonances in Fig. 1(b). The comparison of the switching fields among the 3 different switching methods is shown at Fig. 2. The switching field with AC voltage-induced method is 35% smaller than magnetic field only, demonstrated that the AC voltage-induced method assist magnetization switching well.

[1] T. Yamamoto, et al., *Phys. Rev. Appl.*, Vol. 13, p.014045 (2020). [2] J. Liu, et al., *J. Magn. Magn. Mater.*, Vol. 513, p.167105 (2020). [3] J. Zhu, et al., *IEEE Trans. Magn.*, Vol. 44-1, p.125-130 (2008). [4] R. Verba, et al., *Sci. Rep.*, Vol. 6, p.25018 (2016).

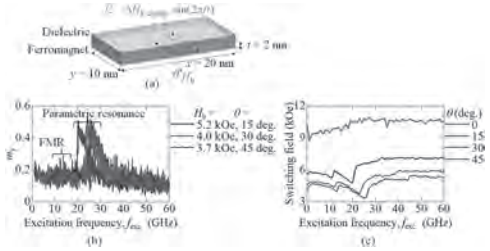

Fig. 1 (a) The schematic illustrations for the ferromagnetic nanodot covered by dielectric layer. Dependence of the precession amplitude (b) and the switching field (c) on the excitation frequency.

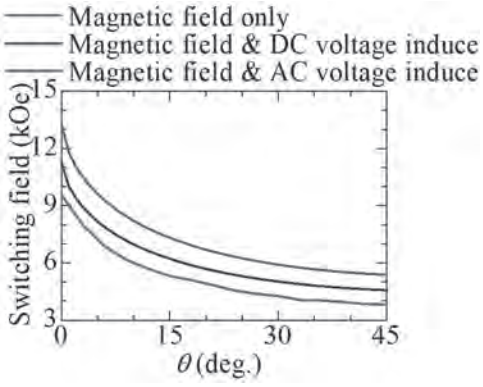

Fig. 2 Comparison of the switching field among 3 different methods.

IPA-05. Magneto-optical observation of magnetic domain formation and drive in magnetic nanowire memory with topological insulator BiSb.

M. Takahashi[1], N. Nakatani[1], D. Kato[1], K. Ogura[1], Y. Iguchi[1], P. Nam Hai[2,3] and Y. Miyamoto[1,3] *1. NHK STRL, 1-10-11 Kinuta, Setagaya-ku, Japan; 2. Tokyo Institute of Technology, 2-12-1 Ookayama, Meguro-ku, Japan; 3. JST-CREST, 7 Goban-cho, Chiyoda-ku, Japan*

Our research is focused on a magnetic nanowire (NW) memory that utilizes current-driven domain wall motion for the storage of future spatial 3D-imaging TV [1]. We have reported that both ultrafast magnetization reversals and reduction of the drive current of magnetic domains can be achieved in BiSb-attached NWs, because BiSb shows strong spin-orbit torque [2,3] and also studied the fundamental operation of magnetic NW memory consisted of BiSb/[Co/Tb] layers. In the photolithography for NW patterning, NW materials were exposed to heat up to 150 °C for several times, the perpendicular magnetic anisotropy (PMA) in Co/Tb was degraded or lost due to the diffusion of Sb. Therefore, Pt/Ta underlayer was inserted to stabilize the PMA in Co/Tb film, result in the thermal tolerance. Fig. 1 shows an optical microscopy image of the prototype memory with four magnetic NWs and a writer. The magnetic NWs, consisted of BiSb(10)/$[Co(0.3)/Tb(0.55)]_3$/Pt(3)/Ta(3) (units in nm), were deposited on surface-oxidized silicon substrates by ion beam sputtering. The periodic notches at 6 μm intervals and by 7 %-reduction in the width direction were installed into the NWs. When we applied write current of 1.9×10^7 A/cm^2 and drive pulses of 3.6×10^6 A/cm^2 simultaneously, primary magnetic domains were formed in the first interval region at the right of the writer as shown in Fig. 2(a). Next, after the drive pulses of 5.0×10^6 A/cm^2 applied only to the second magnetic NW, the domain was driven independently to the next interval while keeping its length as shown in Fig. 2(b). It means that magnetic domain length was successfully controlled by the periodic notches through the magnetic domain formation and drive. Here, the drive pulse current was reduced to approximately 1/7 of that of the NW without BiSb stacking. These results indicate that BiSb is a promising material for reducing the power consumption of the magnetic NW memory operation.

[1] M. Okuda *et al*., *IEEE Trans. Magn.,* vol. 52, 3401204 (2016) [2] N.H.D. Khang *et al.*, *Sci. Rep.*, vol. 10, 12185 (2020) [3] N.H.D. Khang *et al., Appl. Phys. Lett.*, vol. 120, 152401 (2022)

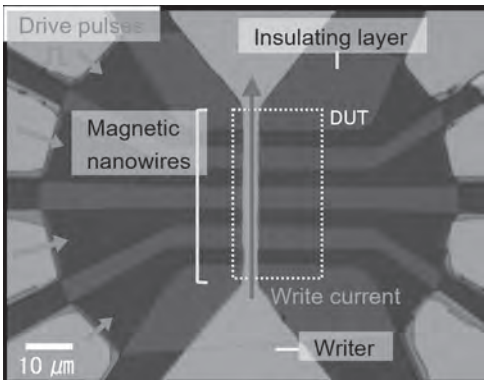

Microscopy image of magnetic NW device.

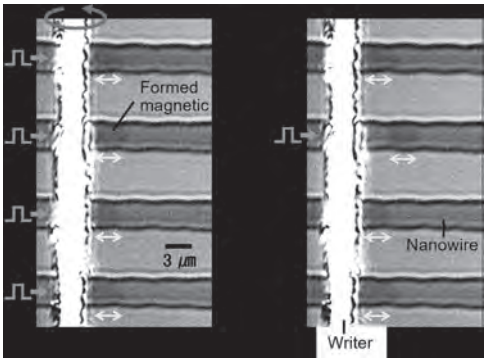

Magneto-optical Kerr effect microscopy image for (a) formed primary magnetic domains in the first interval of notches and (b) driven domain to the next interval in the second NW.

IPA-06. Approximation of microwave assisted magnetization switching field applied with incident angle. *K. Kawakami*[1], N. Narita[2], X. Ya[1] and T. Tanaka[1] *1. Kyushu University, Fukuoka, Japan; 2. Toshiba Corporation, Kawasaki, Japan*

Microwave-assisted magnetic recording (MAMR) [1] has attracted much attention as one of the recording techniques for the ultra-high-density recording. Theoretical analysis of microwave-assisted magnetization switching (MAS) was studied in the case when DC field was applied parallel to the anisotropy direction [2, 3], which indicated that the effect of microwave assistance was explained by the equivalent magnetic field applied along anisotropy axis given by $\omega/\gamma H_k$. However, the analysis of MAS is quite complex when DC field is applied non-parallel to the anisotropy axis. This study proposes an approximated estimation method when DC field is applied non-parallel to the anisotropy axis. Fig. 1 shows the schematic drawing of the normalized equivalent field, $\omega/\gamma H_k$ due to magnetization dynamics. Normalized DC field (h_{DC}) is applied at θ with respect to the anisotropy axis. Circular polarized normalized field (h_{AC}) is applied in the x-y plane. Here, the angle of the precession axis ϕ is approximated by the average of ϕ_1 and ϕ_2 which stand for the angles between the anisotropy axis and the magnetization directions at the maximum m_x and the minimum m_x, respectively. The direction of the equivalent field is defined to be anti-parallel to the precession axis in this study. In our previous study, we confirmed the in-plane and z components of the normalized effective fields were approximated by Eqs. (1). These equations well explained micromagnetic calculation and the resultant switching fields (h_{SW}) well agreed with the asteroid curve Eq. (2). $h_{xy} = h_{DC}\sin\theta - \omega/\gamma H_k \sin\phi + h_{AC}$, $h_{xy} = h_{DC}\cos\theta - \omega/\gamma H_k \cos\phi$ Eqs. (1) $h_{xy}^{2/3} + h_z^{2/3} = 1$ Eq. (2) Hence, h_{SW} is given by ϕ. ϕ_1 and ϕ_2 are obtained from the equilibrium condition ($\partial E/\partial\phi_{1,2} = 0$) of the magnetic energy defined by Zeeman and anisotropy energy. Fig. 2 compares the approximation and micromagnetic calculation for various θ when h_{AC} is 0.05. h_{SW} are plotted as a function of the microwave frequency lower than critical frequency. The error between the approximation and micromagnetic simulation is less than 2% which is quite small.

[1] Jian-Gang Zhu, et al., IEEE Trans. Magn., Vol. 44, pp.125-131 (2008). [2] G. Bertotti, et al., Phys. Rev. Lett., Vol. 86-4, pp. 724-727 (2001). [3] S. Okamoto, et al., J. Appl. Phys., Vol. 107, 123914 (2010).

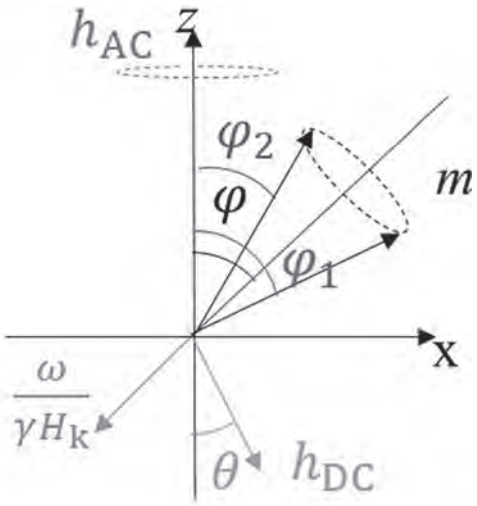

Fig. 1 Schematic illustrations for the equivalent field.

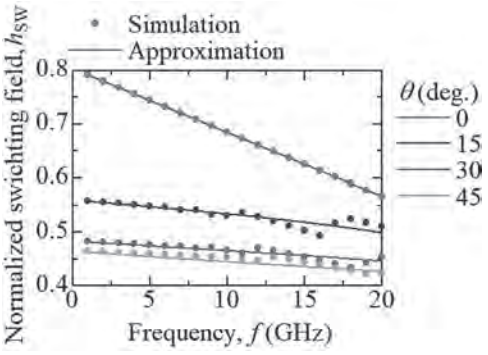

Fig. 2 Comparison between approximation and micromagnetic simulations.

IPA-07. Writing domains in nanowires using a spin torque oscillator. *S. Greaves*[1] and Y. Sonobe[2] *1. RIEC, Tohoku University, Sendai, Japan; 2. Research Organization for Nano & Life Innovation, Waseda University, Tokyo, Japan*

Magnetic nanowires can be used to store information, encoded by the presence or absence of domains and domain walls [1]. Typically, writing of domains is carried out using the Oersted field from a write line orthogonal to the nanowire. However, if the nanowire has high uniaxial anisotropy writing of domains can require a high current density. Another way to reverse the magnetisation is to use a spin torque oscillator (STO) [2]. The magnetisation of the field generating layer (FGL) of a STO can rotate at high frequencies and magnetisation reversal of patterned elements and nanowires can occur near the ferromagnetic resonance frequency [3]. The field from the FGL can switch media with much higher anisotropy than an Oersted field of similar strength. The STO driving current can also be much smaller than the DC current needed to generate a similar Oersted field. In this work we show using simulations that STOs can be used to write domains in nanowires. A schematic of the model is shown in fig. 1. The nanowires consisted of hard and soft layers to reduce the resonance frequency. The FGL was above and to the side of the nanowire and not in contact with it. The STO oscillation frequency was varied and, for the parameters listed in fig. 1, magnetisation reversal occurred when the oscillation frequency was around 9 GHz. Fig. 2 shows an example of writing multiple domains in a nanowire with perpendicular anisotropy; a constant current flowed in the nanowire to push the domains to the left as they were written. The STO polarity was reversed at 3 ns intervals to write “up” and “down” domains. The somewhat irregular domain sizes evident in fig. 2 meant that when domain walls were written at shorter intervals, e.g. 2 ns, there were instances where two domain walls would collide and be annihilated some time after being written. Tuning of the nanowire properties, e.g. the exchange coupling strengths in the hard and soft layers, can be used to control the spacing between domain walls and limit the drift velocity.

[1] S.S.P. Parkin et al., Science 320, p190, (2008). [2] D. Houssameddine et al., Nature Materials 6, p447, (2007). [3] S.J.Greaves et al., AIP Advances 9, 125332, (2019).

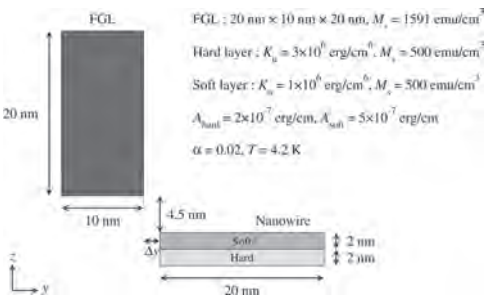

Fig. 1 Dimensions and properties of the nanowire and FGL

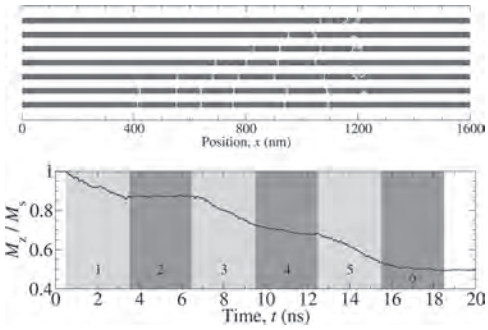

Fig. 2 Writing of six domains in a nanowire. Top: images of domains after each write pulse (the STO is at x = 1200 nm). Bottom: nanowire magnetisation vs. time

IPA-08. Optimization of Two-Dimensional Generalized Partial Response Target Using Multi-Layer Perceptron for Bit Patterned Media Recording Systems. *T.A. Nguyen*[1] and J. Lee[1] *1. Soongsil University, Seoul, The Republic of Korea*

In bit patterned media recording (BPMR), the areal density is increased by reducing the distance between the magnetic islands. Thus, the BPMR faces a two-dimensional (2D) interference problem. To solve the 2D interference, the output of the BPMR channel is passed through the equalizer to convert it into the desired signal, which has the known coefficient interference. However, mapping between the output of the BPMR channel and the desired signal is a nonlinear problem. Therefore, the nonlinear equalizer based on neural network structure is proposed in [1]. However, because the training process is too complicated, the equalizer based on the neural network is used to estimate the 1D generalized partial response (GPR) target. To improve the equalizer based on the neural network, we introduce the neural network equalizer and method to train the neural network equalizer with a 2D GPR target. In the proposed model (Fig. 1), firstly, we use the method in [2] to estimate the parameters of the serial target (step 0). These target coefficients are kept to create the desired signal $d[j,k]$ as the label for the training process of the neural network. To train the neural network, we use the received signal $y[j,k]$ as the input and the signal $d[j,k]$ as the label (step 1). Next, we re-train the target's coefficients by using the trained neural network to create the $y[j,k]$ as the label and the modulated signal $a[j,k]$ as the input (step 2). Finally, the neural network is re-trained using the target coefficients from step 2 and remaking step 1 (step 3). Therefore, the GPR target is optimized by the nonlinear equalizer of the multi-layer perceptron (MLP). The results from the simulations (Fig. 2) show that our proposed model improves the bit error ratio (BER) performance compared to the previous studies [1] and [2] after re-training the neural network at step 3.

[1] J. Shen and N. Nangare, "Nonlinear Equalization for TDMR Channels Using Neural Networks," *2020 54th Annual Conference on Information Sciences and Systems (CISS)*, 2020, pp. 1-6. [2] T. A. Nguyen and J. Lee, "Effective Generalized Partial Response Target and Serial Detector for Two-Dimensional Bit-Patterned Media Recording Channel Including Track Mis-Registration," *Appl. Sci.*, 2020.

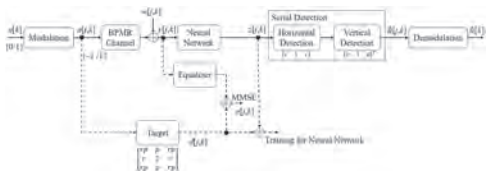

Fig.1. Diagram of the proposed model.

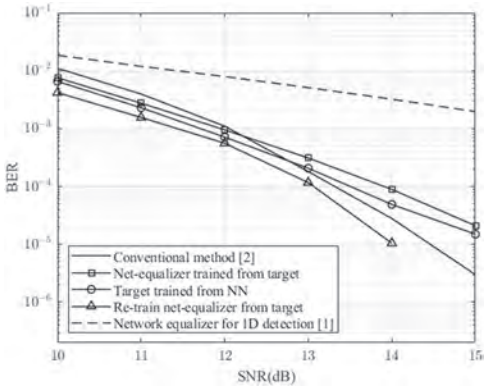

Fig. 2. BER performance of the proposed model.

Session JOA
AMORPHOUS AND NANOCRYSTALLINE SOFT MAGNETS I

Manuel Vázquez, Co-Chair
Instituto de Ciencia de Materiales de Madrid, Madrid, Spain
Charudatta Phatak, Co-Chair
Argonne National Laboratory, Lemont, IL, United States

CONTRIBUTED PAPERS

JOA-01. Magnetization process evaluation and tensile stress effect in direct magnetostriction measurement of amorphous microwires.
M. Vázquez[1] and J. Moya[2] *1. Institute of Materials Science of Madrid, CSIC, Madrid, Spain; 2. INTECIN UBA-CONICET, Universidad Católica de Salta, Salta, Argentina*

Under a longitudinal applied magnetic field, microwires increase/decrease length depending on the magnetostriction sign, where the magnetostrictive elongation is due to magnetization rotational processes as well known in classical magnetism. In amorphous alloys, magnetostriction is usually evaluated making use of inverse magnetoelastic effects (e.g., SAMR method) that sometimes is not fully reliable (e.g., for positive magnetostriction) [1]. This study in magnetostrictive and non-magnetostrictive amorphous microwires introduces two original aspects: i) Direct magnetostrictive elongation measurements as a function of applied field and tensile stress; and ii) Re-interpretation of the magnetization mechanism by comparing magnetostrictive elongation and magnetization curve. A home-made setup with suitable induction/pickup coils, a mechanical system to apply stress and a high-accuracy LVDT position sensor has been used to measure magnetization, M, and magnetostrictive elongation, $\delta l/l$,[2] in two amorphous microwire families: i) In-water-quenched (~145 μm diameter) highly magnetostrictive FeSiB, and vanishing positive/negative magnetostriction (CoFe)SiB microwires; and ii) Glass-coated FeSiBC microwire (20 μm diameter). The figures show high-sensitivity (down to $\delta l/l=10^{-8}$) representative data of $\delta l/l$ vs. M/M_{max} and H where the applied stress increases/reduces the elongation for negative/positive magnetostriction. Quantitative information on the rotational magnetization for low/high field regions is obtained: note in Fig. 1 the different elongation slopes for low (domain wall) and high (rotational) magnetization processes. It is also noticeable the magnetostrictive effect in Fig. 2 inset during domain wall motion in the tiny wire due to a helical magnetization component. This method to properly quantify the magnetostrictive elongation allows for a new magnetization/magnetostrictive analysis as required in mechanical sensor devices.

[1] C. Gómez-Polo and M. Vazquez, J. Magn. Magn. Mater. 118, 86 (1993); K. Chichay et al., J. Appl. Phys. 116, 173904 (2014). [2] J. Moya et al., J. Magn. Magn. Mater. 476, 248 (2019).

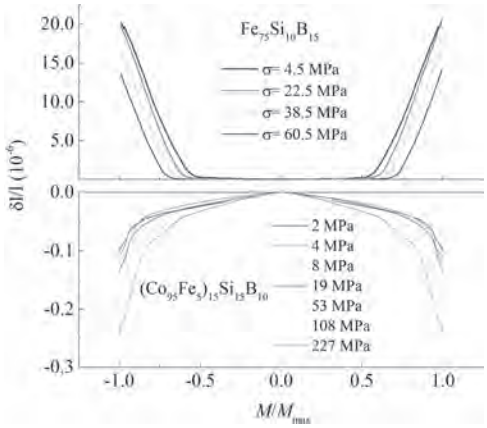

Fig.1 Magnetostrictive elongation ($\delta l/l$) vs. Magnetization (M/M_{max}) for a range of applied stresses (σ) in water quenched microwires.

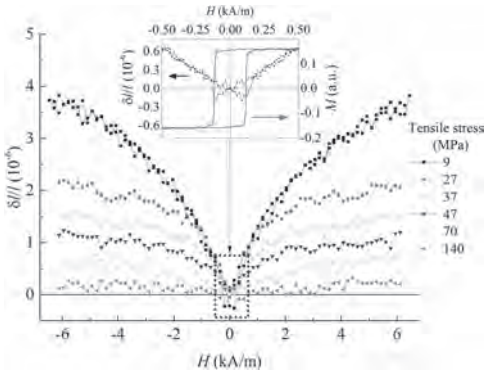

Fig. 2 Magnetostrictive elongation (dl/l) vs. applied Field (H) in FeSiB glass-coated microwire. The inset shows the low-field magnetization and elongation loops.

JOA-02. Optimizing Laser Additive Manufacturing for Fe-based Amorphous Magnetostrictive Materials.
M.G. Ozden[1] and N. Morley[1] *1. Material Science and Engineering, University of Sheffield, Sheffield, United Kingdom*

The process parameters optimization in laser powder bed fusion (LPBF) technique have been studied extensively by using the volumetric energy input ($E=P/(v.t.h)$) equation, which includes the major build parameters; laser power (P), scan speed (v), layer thickness (t) and hatch spacing (h) [1-3]. Even though utilizing laser energy density to predict final properties of a specified materials is a good way to start, only considering this is not enough [4]. Researchers have generally focused on the effect of laser power and scan speed on the final properties [5-8]. This study indicates how major process parameters influence the physical and magnetic

properties of LPBF-processed Fe-based amorphous/nanocrystalline composites (($Fe_{87.38}Si_{6.85}B_{2.54}Cr_{2.46}C_{0.77}$ (mass%)). The figure illustrates the magnetization (*M*)-magnetic field (*H*) loops corresponding sample microstructures fabricated by using same *E* (=60 J/mm^3) and *v* (=1000 mm/s) and varying *P*, *h* and *t* (left corner). It is obvious that despite being printed with same energy density, changing *h* and *t* (Sample 1 and 2) or changing *P* and *h* (Sample 2, 3 and 4) led to the quite different results. It was found that bulk density improves as *P* increases, *v*, *t* and *h* decreases, i.e., high *E* is necessary, however, greater than 80 J/mm^3 (due to the keyhole effect) and less than 45 J/mm^3 (because of the insufficient energy input to the powder bed) causes either failing parts or large and high number of pores. Owing to the laser scanning nature, the microstructure evolves as molten pool (MP) and heat affected zones (HAZ) due to the high thermal gradient occurred between laser tracks [9]. MP form around the scans, having Fe_2B nanograins mainly, whereas HAZ generally contains α-Fe(Si) and Fe_3Si nanocrystalline clusters. The sizes and quantities of those nanocrystallites determine the magnetic properties. With same *E* (60 J/mm^3), *v* (1000 mm/s) and *t* (50 μm), only changing *P* and *h* caused samples to have different saturation magnetization; 206 emu/gr (*P*: 90 W and *h*: 30 μm) and 150 emu/gr (*P*: 150 W and *h*: 50 μm) (Figure).

[1] H. Gong, K. Rafi and H. Gu, *Materials and Design,* Vol. 86, p. 545-554 (2015). [2] S. Liu, H. Li and C. Qin, *Materials and Design,* Vol. 191, ID: 108642 (2020). [3] H. Gong, K. Rafi and H. Gu, *Additive Manufacturing,* Vol. 1, p. 87-98 (2014). [4] K. Prashanth, S. Scudino and T. Maity, *Materials Research Letters,* Vol. 5, p. 386-390 (2017). [5] S. Alleg, R. Drablia and N. Fenineche, *Journal of Superconductivity and Novel Magnetism,* Vol. 31, p. 3565-3577 (2018). [6] H. Jung, S. Choi and K. Prashanth, *Materials and Design,* Vol. 86, p. 703-708 (2015). [7] Y. Nam, B. Koo and M. Chang, *Materials Letters,* Vol. 261, ID: 127068 (2020). [8] D. Ouyang, W. Xing and N. Li, *Additive Manufacturing,* Vol. 23, p. 246-252 (2018). [9] C. Zhang, D. Ouyang and S. Pauly, *Material Science and Engineering R,* Vol. 145, ID: 100625 (2021).

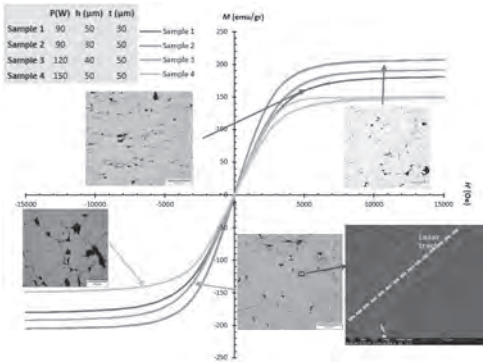

Figure: *M-H* loops and micrographs of the samples LPBF-processed with same *E* (=60 J/mm^3) and *v* (=1000 mm/s).

JOA-03. Design and in-situ Fabrication of Nano-crystalline Fe-Si-B-Co-Nb-Cu-Cr Ultra-thin Ribbons with Excellent Soft-magnetic Properties. *H. Baghbaderani*[1], A. Masood[1], R. Sai[1], C. Ó Mathúna[1,2], P. Stamenov[1,3] and P. McCloskey[1] *1. Tyndall National Institute, Cork, Ireland; 2. University College Cork, Cork, Ireland; 3. Trinity College Dublin, Dublin, Ireland*

Commercial melt-spun ribbons are typically available in the range of 17–30 μm thickness which limits their high-frequency application due to high eddy current loss. In addition, the ribbons can be annealed for nanocrystallisation to optimise their power loss behaviour [1]. However, possible oxidation during annealing and the brittle nature of as-annealed ribbons, makes core fabrication difficult. It is possible, however, to straightforwardly design an alloy composition with moderate Amorphisation Ability (AMA) to in-situ fabricate ultra-thin [2] nano-crystallised ribbons [3], using a high-speed melt spinner. By changing the percentages of mainly Si, B and Nb, three alloy compositions with various Amorphisation Ability (AMA) have been designed, based on different liquidus temperatures calculated using CALPHAD, enthalpies of mixing, and atomic mismatch factors. Ultra-thin ribbons of the designed alloys have been synthesised by a high-speed melt spinner, to obtain the advantages of improved material performance and lower costs over commercial ribbons. The melt-spun ultra-thin ribbons (*t*~5 μm) of Alloys 1 and 2 exhibit nanocrystalline structure owing to their moderate AMA, whereas Alloy 3 with a higher AMA is amorphous (Fig. 1). Interestingly, in-situ nanocrystallised alloys show lower H_c and higher H_k compared to the amorphous alloy (Fig. 2) which makes them perfect candidates for high-frequency applications as they will show lower hysteresis loss (due to low H_c) and lower anomalous loss (less domain wall motion due to high H_k). Additionally, owing to low eddy current loss in ultra-thin ribbons, almost one-fifth of the best available commercially, the total loss is expected to be very low. The lower H_c of nanocrystallised alloys can be attributed to the cancellation of the magnetostriction of the amorphous matrix by the formed nanocrystals. Additionally, the high H_k of such alloys can be owing to the pinned domain walls by the nanocrystals. We have found a cutting-edge methodology to in-situ fabrication of nano-crystallised ultra-thin ribbons which are ideal for minaturised and efficient high-frequency magnetic cores.

[1] G. Herzer, J. Magn. Magn. Mater. 133, 248 (1994). [2] A. Masood, H.A. Baghbaderani, V. Ström, P. Stamenov, P. McCloskey, C. Mathúna, and S. Kulkarni, J. Magn. Magn. Mater. 483, 54 (2019). [3] K.L. Alvarez, H. Ahmadian Baghbaderani, J.M. Martín, N. Burgos, P. McCloskey, J. González, and A. Masood, J. Non. Cryst. Solids 574, (2021).

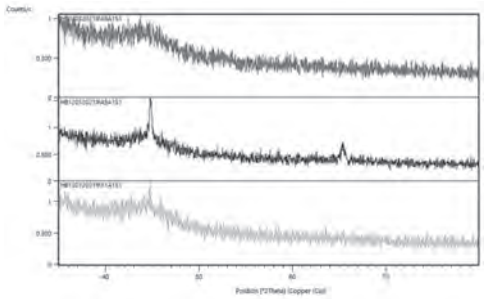

Figure 1. XRD patterns of melt-spun alloys.

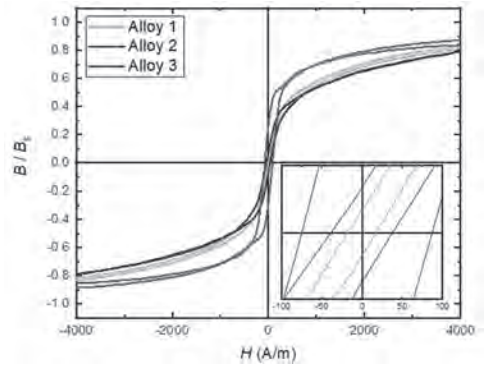

Figure 2. B-H loops of three alloys.

JOA-04. Development of Novel FeCo based Amorphous FeCoBPSiCr Alloy with High B_s of 1.71T and High Corrosion Resistance. *A. Hasegawa*[1], Y. Kajiura[1], M. Hosono[1], K. Yoshidome[1] and H. Matsumoto[1] *1. Materials Research Center, TDK Corporation, Narita, Japan*

The magnetic properties and the corrosion resistance were investigated in $(Fe_{1-\alpha}Co_\alpha)_{83}B_xP_ySi_z$ and $(Fe_{1-\alpha}Co_\alpha)_{82}B_xP_ySi_zCr_1$ amorphous alloy ribbons. $(Fe_{1-\alpha}Co_\alpha)_{83}B_{11}P_4Si_2$ (α=0-0.6), $(Fe_{1-\alpha}Co_\alpha)_{82}B_{11}P_4Si_2Cr_1$ (α=0-0.3) and $(Fe_{0.7}Co_{0.3})_{86-x}B_{11}P_xSi_2Cr_1$ (x=3-5) alloy metallic ribbons were prepared by

a single-roller melt-spinning method. The B_s increased until the ratio of Co to Fe in FeCoBPSi(Cr) alloy increase to 20%, then decreased B_s. On the other hand, the corrosion resistance improved with Co ratio increase. $(Fe_{0.8}Co_{0.2})_{83}B_{11}P_4Si_2$ exhibited high B_s of 1.78 T and the corrosion resistance of the alloy showed high corrosion potential of -607 mV and low corrosion current density 29 μA/cm^2 compared with conventional $Fe_{79}B_{13.5}Si_{5.5}C_2$ alloy. In addition, $(Fe_{0.7}Co_{0.3})_{82}B_{11}P_4Si_2Cr_1$ alloy with Cr addition for the purpose of increasing the corrosion resistance exhibited high B_s of 1.71 T with equivalent corrosion resistance compared with conventional $Fe_{73}B_{11}Si_{11}C_3Cr_2$ alloy. The corrosion potential and corrosion current density of $(Fe_{0.7}Co_{0.3})_{82}B_{11}P_4Si_2Cr_1$ were -509mV and 18 μA/cm^2, respectively. In other word, the FeCoBPSiCr amorphous alloys are compatible high B_s and high corrosion resistance. Furthermore, the $(Fe_{1-\alpha}Co_\alpha)_{82}B_{11}P_4Si_2Cr_1$ alloys was indicated high amorphous forming ability because of observed a single amorphous phase in metallic ribbons with thickness of 60 μm over. In addition, $(Fe_{0.7}Co_{0.3})_{86-x}B_{11}P_xSi_2Cr_1$ alloys (x=3-5) indicated to improve amorphous stability with increasing P content by observed glass transition point, T_g meaning high amorphous forming ability in $(Fe_{0.7}Co_{0.3})_{81}B_{11}P_5Si_2Cr_1$ alloy. Therefore, we concluded that the novel FeCoBPSiCr amorphous alloys with high B_s, high corrosion resistance and high amorphous forming ability have the possibility of the powderization

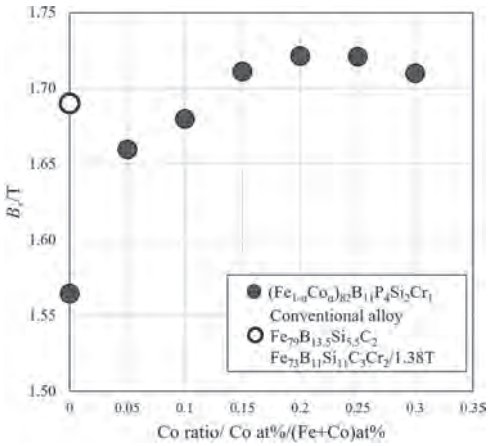

Fig.1 Dependence of B_s on Co ratio in $(Fe_{1-x}Co_x)_{82}B_{11}P_4Si_2Cr_1$ alloys

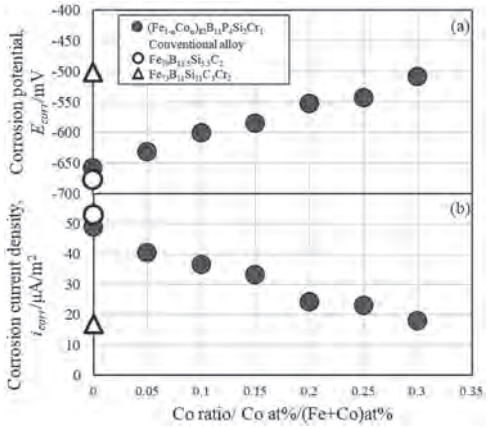

Fig.2 Effect of Co ratio on (a) corrosion potential and (b) corrosion current density in $(Fe_{1-x}Co_x)_{82}B_{11}P_4Si_2Cr_1$ alloys

JOA-05. Effect of grain size on the core loss of nanocrystalline $Fe_{86}B_{13}Cu_1$ prepared by ultra-rapid annealing. *H. Huang*[1], R. Parsons[1], H. Tsukahara[2,5], M. Yano[3], T. Shoji[3], A. Kato[3,4], K. Ono[2,5] and K. Suzuki[1]
1. Department of Materials Science and Engineering, Monash University, Clayton, VIC, Australia; 2. Institute of Materials Structure Science, High Energy Accelerator Research Organization, KEK, Tsukuba, Japan; 3. Toyota Motor Corporation, Susono, Japan; 4. National Institute for Materials Science, Sengen, Japan; 5. Department of Applied Physics, Graduate School Engineering, Osaka University, Suita, Japan

Ultra-rapid annealing (URA) is an effective method to induce nanocrystallization in Fe-B based melt-spun amorphous precursors. The grain size after nano-crystallization depends on the heating rate employed for URA and thus, samples with a range of mean grain sizes can be prepared without altering the chemical composition. Such nanocrystalline samples are ideal for investigating the effect of mean grain size (D) on the core loss. In this study, we prepared a series of nanocrystalline $Fe_{86}B_{13}Cu_1$ samples with grain sizes of 14.5, 21.7, 31.9 and 40.6 nm by varying heating rate between 10 and 10^4 K s^{-1}. The core loss was measured on an Epstein frame in a frequency range between 10 Hz and 30 kHz. The measured core loss was separated into 3 parts, *i.e.* the hysteresis loss (P_h), classical eddy current loss (P_c) and the residual part, often referred to as the anomalous loss (P_a). Figure 1(a) shows an example of the relationship between P_a and the product of frequency (f) and the maximum polarization (J_m). The anomalous loss at J_m between 0.6 and 1.0 T is described universally by a simple power dependence with an exponent of about 1.4 over a wide frequency range between 10 Hz to 30 kHz. The grain size dependence of the coercivity (H_c) and the loss per cycle is shown in Fig. 1(b). H_c follows roughly a D^3 dependence, suggesting that the samples contain large induced anisotropies. The hysteresis loss per cycle (P_h/f) reflects this steep D dependence while the anomalous loss at low frequencies appears almost independent of the grain size. Thus, the grain size effect on the total loss at low frequencies is attributable to the change in the hysteresis loss which reflects the static coercivity. However, the anomalous loss at 30 kHz shows a clear increase with an increase in D, indicating that the anomalous loss also becomes influential to the grain size dependence of the total core loss at high frequencies.

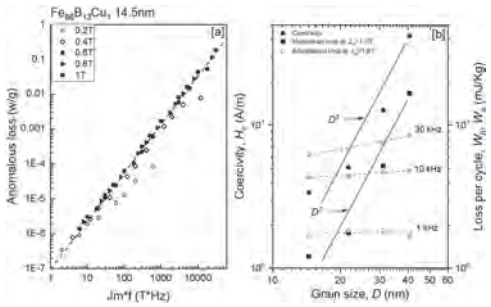

Fig. 1. (a) Anomalous loss versus J_m*f for a mean grain size (D) = 14.5 nm, and (b) changes in the coercivity and core loss per cycle as a function of D for nanocrystalline $Fe_{86}B_{13}Cu_1$.

JOA-06. Controlling Devitrification in Amorphous FeSiB Using Static Magnetic Fields. *X. Zhang*[1], E. Rinko[2,3], I. Anderson[2,3], M. Vázquez[4] and L. Lewis[1,5] *1. Mechanical and Industrial Engineering, Northeastern University, Boston, MA, United States; 2. Materials Science and Engineering, Iowa State University, Ames, IA, United States; 3. Ames Laboratory, Ames, IA, United States; 4. Instituto de Ciencia de Materiales de Madrid (CSIC), Madrid, Spain; 5. Chemical Engineering, Northeastern University, Boston, MA, United States*

Modern electric machines with improved efficiency and performance require ferromagnetic materials with optimized structures and properties; these aspects often rely on the control of phase transformations that are sensitive to processing variables such as temperature and magnetic field. Apart from exhibiting technological significance as soft ferromagnets, FeSiB amorphous

alloys also serve as good testbeds for fundamental research on phase transformations due to their uniform starting state. Here, we demonstrate that application of a mild, static magnetic field during thermal treatment promotes devitrification of amorphous FeSiB alloys, impacting the resulting structural and magnetic features. Calorimetric, structural, and magnetic data confirm the formation of ferromagnetic Fe(Si) crystallites during devitrification (at 400 – 500 °C) of two different forms of $Fe_{79}Si_{11}B_{10}$ metallic glass: water-quenched microwires and melt-spun ribbons. Both samples were annealed at a temperature T_{ann} immediately below the devitrification onset temperature T_{onset} ($T_{ann}/T_{onset} \sim 0.98$) with or without a 0.5 T magnetic field, applied along sample length, provided by a permanent magnet setup[1]. While all annealed samples contain $D0_3$-type Fe(Si) crystallites, field annealing produces an enhanced {110} surface texture, up to ~40% reduced grain size, a larger density of crystallites, and smaller values of residual stress (by up to 25%), as compared to the zero-field treatment. Further, field annealing incurs a three-fold reduction in magnetic susceptibility along sample length while donating a two-fold increase in susceptibility across sample length, in addition to a 20% decrease in coercivity that is independent of field direction (Fig.1). These results suggest that annealing with engineering-approachable magnetic fields can achieve controlled microstructure and stress profile of alloys, resulting in modified magnetic anisotropy and response. Acknowledgments: This work was supported by IEEE MagSoc Educational Seed Funding and was performed at Northeastern University.

[1] N. Maât, I. McDonald, R. Barua, et al., Acta Materialia, 196, 776-789 (2020).

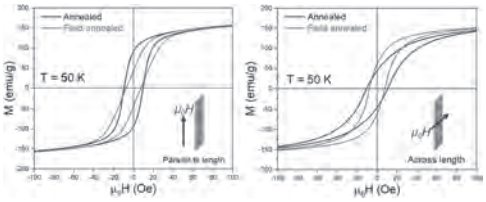

Fig.1. M-H curves were measured along sample length (left) and across sample length (right) for $Fe_{79}Si_{11}B_{10}$ ribbon in zero-field annealed and field annealed states.

JOA-07. Fabrication and soft magnetic properties of FeSiB-based flakes with insulating surface layer. *R. Das*[1], L. Ye[1], H. Baghbaderani[1], P. McCloskey[1] and R. Sai[1] *1. Microsystems Centre, Tyndall National Institute, Cork, Ireland*

Soft magnetic material with high magnetic flux density (*B*), high permeability (μ), and high resistivity (ρ) is the key for miniaturized high frequency (>10 MHz) passive devices. The popularity of ferrites wane beyond 10 MHz owing to their prohibitively large magnetic losses (P_m), similarly, the spherical ferromagnetic alloys are too lossy due to eddy current losses (P_e). Of late, composites of electrically insulated magnetic particles attracted much attention. However, the trade-offs between μ, ρ, P_m and P_e, etc. demand judicious design of materials to stem eddy-current losses and skin effect by optimizing the thickness and properties of the insulation layer surrounding the magnetic body [1,2]. Here we demonstrate magnetically-aligned FeSiB-based soft magnetic flakes (SMFs; 63-106 μm, *t*:2-5 μm) coated with optimally thick (~10 nm) SiO_2 as the potential magnetic core for power inductors operating beyond 10 MHz. The SMFs with such a high aspect ratio was fabricated by combination of mechanical ball milling of ribbons and then electrically insulted by an optimized sol-gel procedure in presence of silane coupling agent (APTES). Milling helped to reduce ribbon thickness below its skin depth to eliminated P_e at high frequencies. The effect of milling (duration, RPM, BPR) and coating conditions on the properties of the SMFs were thoroughly investigated. An optimally-tiny fraction of the milled flakes is allowed to become nanocrystalline (Fig. 1c) that augments B and μ without incurring losses. XPS and magnetization measurement results indicate that the thin but robust insulation layer is preserved through the post-annealing process which is necessary for removal of stress. B-H loop shows post-processing, coercivity is reduced significantly (from ~57 to ~6 Oe), but magnetic flux remains same.

[1] T. Suzukia, P. Sharmaa, A. Makino, J. Magn. Magn. Mater. 491 (2019) 165641 [2] F. Luo, X. Fana, Z. Luoa, W. Hua, J. Wangd, Z. Wu, G. Li, Y. Li and X. Liu, J. Magn. Magn. Mater. 498 (2020) 166084

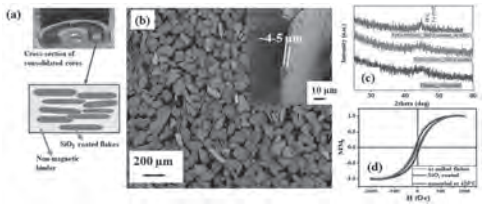

Fig 1: (a) Schematic representation of the SMFs core. (b) SEM image of the FeSiB-based as-milled flakes. (c) XRD patterns and (d) hysteresis loops of the as-milled and of SiO_2 coated flakes (~63-106 μm) before and after annealing at 425°C in an inert atmosphere.

JOA-08. Substantial Thinning of Melt-Spun Ribbons by an Optimised and High-Yield Ball-Milling Process. *L. Ye*[1], R. Das[1], H. Baghbaderani[1], P. McCloskey[1] and R. Sai[1] *1. MNS, Tyndall National Institute, Cork, Ireland*

Ferromagnetic FeSi-based alloy ribbons are ubiquitous for high-frequency inductor core due to their high flux density and high permeability. However, these ribbons are prone to eddy current losses at MHz frequencies, necessitating thinning and fragmenting the ribbon into smaller flakes. In this regard, ball milling is the best choice[1,2]. Despite several advancement of this technique over the years, little attention has been given to milling yield, which is an important factor for large-scale production. Here we report an optimized ball-mill processing recipe to enhance the yield significantly while achieving superior material characteristics. We report fabrication of magnetic flake particles from ribbons using ball milling. The starting material is $Fe_{83.21}Cu_{1.22}Nb_{5.44}Si_{8.69}B_{1.44}$ as-quenched ribbon with a thickness of 19 μm. The ribbons were annealed at 350 and 450 °C, cut into small pieces and milled in ethanol for 10 hours. The produced powders are then separated into size ranges of 0-40, 40-63, 63-106, and >106 μm by mechanical sieving. We were able to substantially reduce the ribbon thickness from 19 μm to 2-4 μm (Figure 1). Reducing the annealing temperature from 450 to 350 °C increases yield in 40-63 μm size range by a factor of 3, while doubling the batch amount from 10 to 20 g increases the yield by a factor of 10. Therefore, by optimizing annealing temperature and batch size, we achieved a yield of 17%, a significantly high number considering the flake dimensions. This makes it more efficient to produce thinned magnetic flake powders. The produced powder can then be used for the fabrication of soft magnetic cores for high frequency power conversion applications. We also did BH loop on the as-quenched ribbons, ball milled powders. We observed an increase in coercively after ball milling from 139 A/m to 1352 A/m. This can be reduced to 341 A/m by performing post-mill annealing. Our study provides the framework for efficient fabrication of ultra-thin flakes in a desired size range using ball milling.

[1] J. Konieczny, C. Techniques, Structure and properties of the powder obtained from the amorphous ribbon, 18 (2006) 143–146. [2] J. Bednarčík, E. Burkel, K. Saksl, P. Kollár, S. Roth, Mechanically induced crystallization of an amorphous CoFeZrB alloy, J. Appl. Phys. 100 (2006) 1–6.

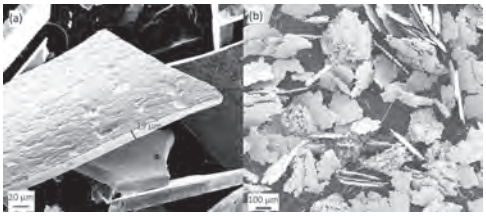

Figure 1 (a) As-quenched ribbons and (b) Thinned and sieved flakes with thickness of 2- 4 µm.

JOA-09. Metal Amorphous Nanocomposite (MANC) $(Fe_xNi_yCo_{100-x-y})_{80}B_{14}Nb_4Si_2$ Magnetic Properties. *K. Schneider*[1], Y. Krimer[2], S. Simizu[2], M. De Boer[1] and M. McHenry[2] *1. Mechanical Engineering, Carnegie Mellon University, Pittsburgh, PA, United States; 2. Materials Science and Engineering, Carnegie Mellon University, Pittsburgh, PA, United States*

Metal Amorphous Nanocomposites (MANCs) are a class of high-frequency soft magnetic materials that exhibit low magnetic hysteresis and high saturation flux density. MANCs are formed as long, thin ribbons, a shape factor which coupled with their high electrical resistivity minimizes eddy current losses. This, along with their 1 GPa strength, makes them attractive candidates for high-speed, high-power density electric motors[1], [2]. Promising soft magnetic properties have been reported[3], [4] in an $(Fe_{70}Ni_{30})_{80}B_{14}Nb_4Si_2$ MANC alloy, namely low coercivity (H_c=2.42 A/m) and high saturation induction (B_s=1.3 T). This composition, however, has a magnetostriction coefficient of $\lambda_s \sim 15$ ppm, which leads to additional switching losses through magnetoelastic coupling influencing loop shape[4] and acoustic loss. Thus, it is of interest to reduce λ_s and increase Curie temperature (T_c) and saturation induction in new alloys. In effort to improve properties, 15 new compositions derived from an $(Fe_{70}Ni_{30})_{80}B_{14}Nb_4Si_2$ parent alloy were produced by planar flow casting by partial substitution of Co for Fe and/or Ni. Crystallization temperatures were measured by differential scanning calorimetry (DSC) and annealing recipes were designed based on these results. Vibrating sample magnetometry magnetization, M(T), and magnetostriction measurements were employed to catalog the composition dependence of properties. Promising compositions were identified, yielding low-temperature B_s>1.5 T and T_c>400°C, with reduced λ_s. These results will be presented with a discussion of their significance for future state-of-the-art high-frequency power magnetic devices.

[1] S. Simizu, P. R. Ohodnicki, and M. E. McHenry, *IEEE Trans. Magn.*, vol. 54, no. 5, pp. 1–5 (2018) [2] S. Simizu *et al.*, *2021 IEEE Energy Convers. Congr. Expo. ECCE 2021 - Proc.*, pp. 3866–3872 (2021) [3] N. Aronhime, V. DeGeorge, V. Keylin, P. Ohodnicki, and M. E. McHenry, *Jom*, vol. 69, no. 11, pp. 2164–2170 (2017) [4] K. Byerly, Y. Krimer, C. Phatak, E. Theisen, and M. E. McHenry, *J. Mater. Res. (*2021)

JOA-10. Properties Optimization for Manufacturing of Metal Amorphous Nanocomposite (MANC) Axial Motors. *M. McHenry*[2], K. Schneider[1], Y. Krimer[2], J. Egbu[2], S. Simizu[2], M. De Boer[1], S. Bhattacharya[3] and E. Theisen[4] *1. Mechanical Engineering, Carnegie Mellon University, Pittsburgh, PA, United States; 2. Materials Science & Engineering, Carnegie Mellon University, Pittsburgh, PA, United States; 3. Electrical & Computer Engineering, North Carolina State University, Raleigh-Durham, NC, United States; 4. R&D, Metglas, Conway, SC, United States*

Metal amorphous nanocomposites (MANC) are high-performance soft magnetic materials (SMMs) studied for manufacturing efficient magnetic tape wound core (TWC) components used in high-speed motor (HSM) applications. MANCs comprise soft magnetic nanocrystals embedded in a continuous, highly resistive amorphous matrix, providing low eddy current losses. MANC TWC's enhanced performance derives from their low core loss, which enables magnetic switching at 1-100 kHz. We have reported new (Fe70Ni30)85Nb0.5B14.5Si0 (B_s = 1.5 T) and (Fe70Ni30)80Nb4B14Si2 ($W_{1T,400Hz}$=0.51 W/Kg, H_c=2.42 A/m, μ_r>35000) MANCs with excellent magnetic properties and attractive core losses and alloying additions to further optimize magnetic properties. For use in high speed axial motors, TWCs must possess mechanical properties sufficient to allow: (1) core winding and/or strain annealing; (2) manufacturing of rotor laminates and slots, and most importantly (3) stresses required for spinning at high rotational speeds. Additionally, the impact of residual stresses on magneto-mechanical (magnetostrictive) coupling derived losses must be mitigated. Here I will relate lessons learned in manufacturing of MANC rotors. These include (1) the mechanical properties (strength, Weibull Modulus, and Young's Modulus) of MANC ribbons; (2) epoxy wetting to MANC ribbons; (3) the role of vacuum impregnation bonding of epoxies for rotor mechanical integrity and (4) failure mechanisms of MANC/epoxy laminates. These will identify paths to defining factors of safety (FOS) required for efficient HSMs designed for powers of 34 kW with future electric vehicle (EV) applications on the horizon.

JOA-11. Effect of temperature on magnetic properties and magnetoimpedance effect in Fe-rich microwires. *P. Corte-Leon*[1,2], I. Skorvanek[3], F. Andrejka[3], V. Zhukova[1,2], J. Blanco[2], M. Ipatov[1,2] and A. Zhukov[1,2] *1. Polymers and Advanced Materials: Physics, Chemistry and Technology, UPV/EHU, San Sebastian, Spain; 2. Applied Physics I, UPV/EHU, San Sebastian, Spain; 3. Slovak Academy of Science, Kosice, Slovakia*

Recently, multifunctional composite materials with magnetic wire inclusions for non-destructive and non-contact stress and temperature monitoring have been proposed [1]. Therefore, studies of temperature dependence of the Giant magnetoimpedance, GMI, effect become essentially relevant. There are only very few studies on temperature dependence of GMI and most of them were performed in thick amorphous wires without glass coating and in very limited temperature range [2,3,4]. Although usually the highest GMI effect is observed in Co-rich magnetic wires, GMI effect of Fe-rich glass-coated microwires can be substantially improved by stress-annealing induced magnetic anisotropy [5]. GMI effect and magnetic properties under temperature influence of as-prepared and stress annealed (annealing temperature T_{ann}= 325 °C, stress applied during the annealing σ= 190MPa) thin amorphous $Fe_{75}B_9Si_{12}C_4$ glass-coated microwires produced by the Taylor Ulitovsky technique are analyzed. Remarkable change in the hysteresis loops and GMI effect is observed for both samples upon heating. For as-prepared FeBSiC microwire a beneficial influence of temperature on the GMI ratio is observed and hysteresis loops change of character from almost rectangular shape to inclined one (Fig.1). On the other hand, although GMI ratio improvement after stress-annealing decreases with the temperature increasing (Fig.2), temperature dependence can be tuned by the stress annealing conditions. Additionally, almost complete reversibility of the changes induced by the temperature is observed. Temperature dependence of the hysteresis loops and GMI effect of studied microwires is explained considering the heating effect on the internal stresses relaxation, the modification of the thermal expansion coefficients of the metallic nucleus and the glass coating and in terms of the Hopkinson effect.

[1] A. Allue et al., *Compos. Part A Appl. Sci. and Manuf.*, Vol. 120, p.12 (2019). [2] J. Nabias, A. Asfour and J. Yonnet, *IEEE Trans. Magn.,* Vol. 53(4), p.4001005 (2017). [3] J.D. Santos, R. Varga, B. Hernando and A. Zhukov, *J. Magn. Magn. Mater.* 321, p.3875 (2009). [4] M. Kurniawan et al., *J. Electron. Mater.,* Vol. 43, p.4576 (2014). [5] V. Zhukova et al., *Scr. Mater.*, Vol. 142, p.10 (2018).

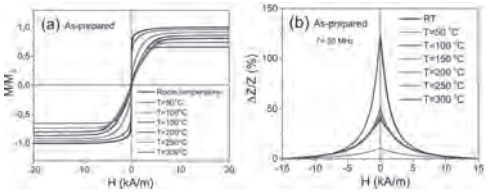

Fig.1. Hysteresis loops (a) and GMI ratio at *f*= 50 MHz (b) of as-prepared sample, measured at different temperature.

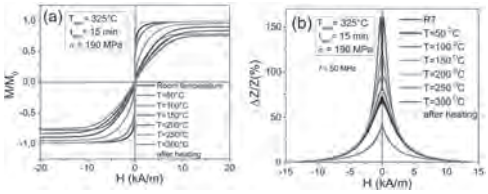

Fig.2. Hysteresis loops (a) and GMI ratio at *f*= 50 MHz (b) of stress annealed sample at 325 °C during 15 min (applied stress σ= 190 MPa), measured at different temperature.

JOA-12. Magnetic properties and giant magnetoimpedance effect in multilayered microwires. R. Lopez Antón[1], J. Andrés González[1], J. González Sanz[1], A. Garcia-Gomez[2], V. Zhukova[2], M. Ipatov[2], P. Corte-Leon[2] and *A. Zhukov*[2,3] *1. Instituto Regional de Investigación Científica Aplicada (IRICA) and Department of Applied Physics, University of Castilla-La Mancha, Ciudad Real, Spain; 2. Dept. Polymers and Advanced Mater., Dept. Appl. Phys. and EHU Quantum Center, Univercity of Basque Country, UPV/EHU, San Sebastian, Spain; 3. IKERBASQUE, Basque Foundation for Science, Bilbao, Spain*

Studies of Giant Magnetoimpedance (GMI) effect have attracted considerable attention considering various technological applications [1,2]. Up to now, most attention has been paid to the achievement of the highest GMI as well as to tailoring of the magnetic field dependence of GMI effect through the modification of the magnetic anisotropy of the magnetic materials. Generally, the magnetic anisotropy of amorphous materials can be controlled by the magnetostriction coefficient (that to great extend is linked to the chemical composition of material) or by special thermal treatment (including magnetic field or stress-annealing) [2,3]. Most of studies of GMI effect are performed in different families of magnetic wires [1-3]. Recently, a new approach allowing to tune the magnetic anisotropy of magnetic wires by depositing of magnetic and non-magnetic layers onto the glass-coating [4]. Accordingly, the purpose of this paper is to study the GMI effect in amorphous Co-rich microwires with Co- layers deposited onto glass-coating. Studies of magnetic properties and GMI effect of as-prepared amorphous $Fe_{3.6}Co_{69.2}Ni_1B_{12.5}Si_{11}Mo_{1.5}C_{1.2}$ and of the same microwires with deposited Co-layer microwires reveals that both samples present soft magnetic properties and high GMI effect. Low field hysteresis loops of both samples are rather similar, while the contribution of Co-layer is observed in hysteresis loop measured at higher magnetic field (see Figs 1a,b). Such character of hysteresis loop is similar to those observed in microwires with mixed amorphous- crystalline structure [5]. However, the GMI ratio, ΔZ/Z and magnetic field, *H*, dependences of GMI effect are affected by the Co-layer (see Fig.2). In particularly, higher GMI ratio and sharper peaks on ΔZ/Z (H) dependencies. We discussed observed experimental dependences considering both change of the internal stresses originated by the Co-layer as well as the magnetostatic interaction between the amorphous ferromagnetic nucleus and deposited Co Layer.

[1] T. Uchiyama, K. Mohri, and Sh. Nakayama, IEEE Trans. Magn., 47, No 10 (2011) pp. 3070-3073 [2] F. Qin, H.-X. Peng, Prog.Mater. Sci, 58 (2013) 183–259 [3] A. Zhukov, et.al. J. Alloys Compound 814 (2020) 152225, [4] K.R. Pirota, M. Hernandez-Velez, D. Navas, A. Zhukov and M. Vázquez, Adv. Funct. Mater. 14 No 3 (2004) 266-268. [5] V. Zhukova, et.al., Chemosensors, 9 (2021) 100, doi: https://doi.org/10.3390/ chemosensors9050100

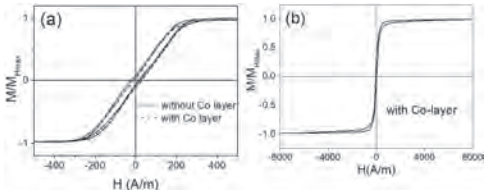

Fig.1 Low field (a) and high field hysteresis loops of studied microwires

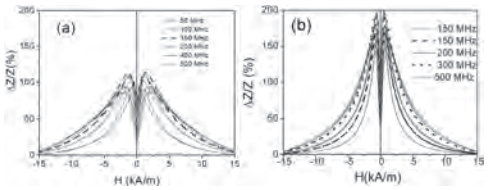

Fig.2. ΔZ/Z (H) dependencies of microwire without Co-layer (a) and with Co-layer deposited onto glass-coating (b)

JOA-13. Electronic structure and magnetization of epitaxial Fe_4N thin films probed using hard X-ray photoemission. *S. Seema*[1], M. Gupta[2], A. Gupta[3], A. Hloskovsky[4] and M. Müller[1] *1. Fachbereich Physik, Universität Konstanz, Konstanz, Germany; 2. UGC-DAE Consortium for Scientific Research, Indore, India; 3. Physics Department, University of Petroleum and Energy Studies, Dehradun, India; 4. Deutsches Elektronen-Synchrotron DESY, Hamburg, Germany*

Tetra iron nitride (Fe_4N) is an interesting compound belonging to the family of transition metal nitrides and its excellent electrical and magnetic properties make it a material of choice for futuristic spintronic and storage devices [1]. Therefore, the magnetization in Fe_4N films is investigated for decades using conventional magnetic characterizations such as SQUID-VSM, PNR, XMCD, etc.[1,2]. Recent advancements in synchrotron science allow polarization selection of incident x-rays enabling the utilization of another emerging method called hard x-ray photoemission spectroscopy- magnetic circular dichroism (HAXPES-MCD) for magnetization measurements using polarization selection [3]. In the present work, we carried out polarization-dependent HAXPES in a thin-film sample of Fe_4N. Epitaxial Fe_4N thin film (26 nm) samples have been deposited using dcMS technique on $SrTiO_3$ (100) at 523 K. The phase purity and epitaxy of the film have been confirmed using x-ray diffraction (XRD) and reflection high energy electron diffraction (RHEED) scans as shown in Fig. 1. We carried out our HAXPES-MCD scans at P22, PETRA III Desy, Hamburg, Germany [3]. Fe *2p* spectra measured in Fe_4N films in the remnant state using oppositely polarized light are shown in fig. 2. Subtle differences could be seen in terms of intensity and peak shifts. Along with this, the obtained asymmetry value = $(Is^+ - Is^-) / (Is^+ + Is^-)$ is about 19%, suggesting that the magnetic moment is localized at the Fe atoms, corresponding to corner sites the in Fe_4N lattice. Additionally, we also observed a non-zero MCD signal at a shoulder at nearly 3 eV from the $2p_{3/2}$ peak (marked by an arrow in fig. 2). A qualitative analysis of the electronic structure and magnetization of Fe_4N films derived from the very first HAXPES experiments will be discussed and presented in this work.

[1]. G. Scheunert, et al. *Applied Physics Reviews*, 3, 011301, 2016. [2]. B. Yang et al. *Physical Review Applied* 9.5 (2018): 054019. [3]. C. Schlueter, et al. *Synchrotron Radiation News* 31.4 (2018): 29-35.

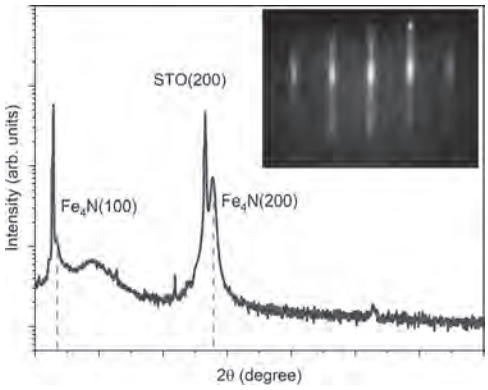

XRD and RHEED scans of Fe_4N film.

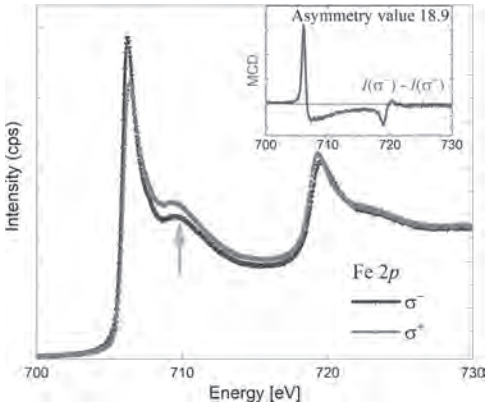

Magnetic dichroism in Fe 2*p* photoemission spectra in Fe_4N film.

JOA-14. In-situ Magnetic Domain Behavior of Annealed Fe-Ni-based Soft Magnetic Alloys. *C. Phatak*[1], V. Brajuskovic[1], A. Talaat[2], J. Egbu[3], K. Byerly[3], M. McHenry[3] and P. Ohodnicki[2] *1. Argonne National Laboratory, Lemont, IL, United States; 2. University of Pittsburgh, Pittsburgh, PA, United States; 3. Carnegie Mellon University, Pittsburgh, PA, United States*

FeNi-based nanocomposites are ideal candidates for high frequency SMMs due to crucial properties such as high resistivity due to amorphous matrix, low hysteresis losses due to averaging of random magnetic anisotropies, and improved mechanical properties relative to Fe-based nanocomposite alloys[1,2]. Recent review has shown that rapid thermal annealing techniques provides suitable control of the microstructure while maintaining high saturation magnetization[3,4]. To further understand the structure-property relationship of these nanocomposites, we have used in-situ Lorentz transmission electron microscopy (LTEM) to correlate microstructure and magnetic domain structure of such alloys at a high spatial resolution [4]. In this work, we report on the characterization of FeNi nanocomposites with reduced glass former content ((Fe70Ni30)85Nb0.5B14.5)) that have undergone two distinct thermal protocols: (1) conventional annealing (CA) with heating/cooling rate of the order of 5 C/min and (2) flash annealing (FA) with heating/cooling rates of the order of 400 C/sec. The former case shows formation of both FCC and BCC FeNi nanocrystallites which are relatively coarse and exhibit a large coercivity due to domain wall pinning (~625A/m), while the latter only shows formation of FCC nanocrystallites which are substantially refined in grain size and display lower coercivity (~17A/m). In-situ LTEM to apply in-plane magnetic field to study the magnetization reversal in these two alloys as shown in Fig. 1. The magnetic domain walls show high tortuosity in the CA sample along with various pinning sites at large grains. We will present a detailed analysis of the domain wall motion and pinning behavior observed in these alloys and correlate it with the local microstructure, and specifically the observed grain size which plays a critical role in domain wall pinning as is expected from the random anisotropy model. The results provide further insights towards understanding the role of average grain size and pinning sites for future development these nanocomposites alloys.

[1] M.A. Willard and M. Daniil: Nanocrystalline soft magnetic alloys two decades of progress. In Handbook of Magnetic Materials, Vol. 21 (Elsevier B.V., Amsterdam, 2013). [2] A. Leary, et. al., *J. Mater. Research*, 31, 3089 (2016). [3] A. Talaat, D.W. Greve, M.V. Suraj, P.R. Ohodnicki, J. Alloys Compd. 854 (2021) 156480. [4] A. Talaat, J. Egbu, C. Phatak, K. Byerly, M.E. McHenry, P.R. Ohodnicki, Materials Research Bulletin, Volume 152, 2022, 111839, ISSN 0025-5408, https://doi.org/10.1016/j.materresbull.2022.111839. [5] C. Phatak, A. K. Petford-Long, and M. De Graef, Curr. Opin. Solid State Mater. Sci. 20, 107 (2016). [6] This work was supported by U.S. Department of Energy (DOE), Office of Science, Basic Energy Sciences, Materials Sciences and Engineering Division.

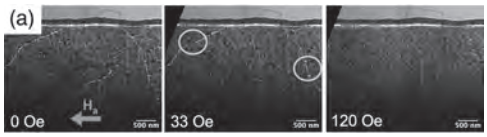

Fig. 1. A series of LTEM images of the CA sample under applied in-situ magnetic field showing the pinning of magnetic domains at sites identified by orange circles.

JOA-15. Study on Deterioration of Iron Loss of Amorphous Alloy by Wire Electrical Discharge Machining. *B. Tian*[1], J. Wang[1], D. Ma[1], Y. Ma[1] and R. Pei[1] *1. Department of Electric Engineering, Shenyang University of Technology, Shenyang, China*

Amorphous alloys have excellent low loss characteristics and are suitable for high-performance motor cores [1]. Due to the limitation of the thickness of extremely thin soft magnetic materials, stamping is not suitable for processing. At present, the most commonly used processing method is EDM [2], but this method will generate high temperature at the edge of the material, thereby changing the internal structure of the edge of the material, making iron loss worsens. In this paper, a ring-like experiment method was used to explore the effect of EDM on the deterioration of iron loss. The first part of the paper analyzes the research situation of the scholars on the deterioration of the iron loss at the edge of the soft magnetic material core; The second part introduces the basic principles and specific methods of the ring-like experiment(The sample and principle are shown in Fig. 1), and explores the relationship between the ratio of the area affected by cutting to the total area and the deterioration of iron loss. Taking 0.05mm ultra-thin silicon steel as a control(Some experimental results are shown in Fig. 2), comparing the degree of iron loss deterioration of the two materials, and analyzing the iron loss deterioration law of ultra-thin soft magnetic materials; The third part analyzes the metallographic diagram of the material, observing the crystallization of amorphous alloys at the edge after EDM cutting and the behavior of 0.05mm ultra-thin silicon steel grains, and explains the reasons for the difference in the degree of deterioration of the two materials from a microscopic point of view; Finally, summarize the relevant conclusions. To sum up, this paper compares the iron loss deterioration of amorphous alloys and other ultra-thin soft magnetic materials, and explores the iron loss deterioration law of amorphous alloys with different proportions of the area affected by cutting from the perspective of experimental data and microstructure. In the follow-up work, according to this law, the exact value of the iron loss deterioration at the cutting edge of the material is deduced to provide guidance for the application of amorphous alloys.

[1] Li T, Zhang Y, Liang Y, et al. Multiphysics Analysis of an Axial-Flux In-Wheel Motor With an Amorphous Alloy Stator[J]. IEEE Access, 2020, 8:1-1. [2] Chai F, Li Z, Chen L, et al. Effect of Cutting and Slot Opening on Amorphous Alloy Core for High-Speed Switched Reluctance Motor[J]. IEEE Transactions on Magnetics, 2020, PP(99):1-1.

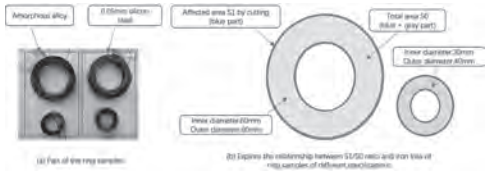

Fig. 1 Test ring samples and principle

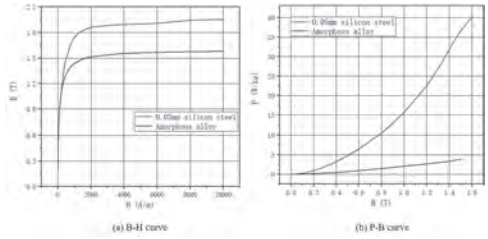

Fig. 2 Part of the experimental data

Session JOB
FERRITES, GARNETS AND MAGNETO-DIELECTRIC MATERIALS I
Ramanathan Mahendiran, Chair
National University of Singapore, Singapore

INVITED PAPER

JOB-01. Observation of the angular momentum compensation of ferrimagnetic material. *M. Imai*[2], H. Chudo[2], M. Matsuo[1,2], S. Maekawa[2,3] and E. Saitoh[2,4] *1. Kavli Institute for Theoretical Sciences, University of Chinese Academy of Sciences, Beijing, China; 2. Advanced Science Research Center, Japan Atomic Energy Agency, Tokai, Japan; 3. Riken Center for Emergent Matter Science, Wako, Japan; 4. Department of Applied Physics, The University of Tokyo, Bunkyo, Japan*

Ferrimagnets contains multiple types of magnetic ions; their magnetic moments align in opposite direction. In some ferrimagnets, the net angular momentum becomes zero at the angular momentum compensation temperature T_A. We demonstrated the observation of T_A by using the Barnett effect [1, 2]. The Barnett effect is a phenomenon in which a matter is magnetized by mechanical rotation Ω[1], resulting from angular momentum J of electrons in material aligning with the rotation axis through the spin-rotation coupling ($-J\cdot\Omega$). The Barnett effect does not apply when the net angular momentum $\langle J_{net}\rangle = 0$, which is the definition of the angular momentum compensation. We have constructed the temperature variable apparatus for measuring the Barnett effect at low temperatures, and determined T_A of the ferrimagnetic insulator $Ho_3Fe_5O_{12}$. Fig. 1 shows a schematic illustration of our experimental setup [1]. The sample packed in a capsule was floated by bearing air and rotated by blowing driving air on the impeller. The magnetization induced by mechanical rotation was detected with a fluxgate magnetic sensor through the stray magnetic field from the sample. To realize the measurement under low temperatures, the system was placed into a cryostat and the rotor was driven by nitrogen gas cooled through a heat exchanger. We observed the temperature dependence of the Barnett effect for $Ho_3Fe_5O_{12}$, and determined T_A to be 240 K [1]. With the focus on magnetic dynamics at T_A, a microscopic method was required to investigate the spin dynamics at T_A. We propose an NMR method to explore the spin dynamics at T_A. In ferro(ferri) magnets, the NMR signal is enhanced via hyperfine interactions. Particularly, the NMR signal from nuclei in domain walls is strongly enhanced due to the magnetic domain wall motion (Fig. 2). We show that ^{57}Fe-NMR measurements can be used to explore domain wall dynamics near T_A in $Ho_3Fe_5O_{12}$. We found that the NMR signal shows a maximum at T_A in the multi-domain state. We provide a simple model for describing this NMR signal enhancement caused by enhancement of domain-wall mobility at T_A. This enhancement of the signal enables us to determine T_A by the NMR measurement [4].

[1] M. Imai, Y. Ogata, H. Chudo *et al*., Appl. Phys. Lett., vol. 113, p. 052402 (2018). [2] M. Imai, H. Chudo, M. Ono, *et al*., Appl. Phys. Lett., Vol. 114, p. 162402 (2019). [3] S. J. Barnett, Phys. Rev., Vol. 6, p. 239 (1915)., S. J. Barnett, Rev. Mod. Phys., Vol. 7, p. 129 (1935). [4] M. Imai, H. Chudo, *et al*., Phys, Rev. B, Vol. 102, p. 014407 (2020).

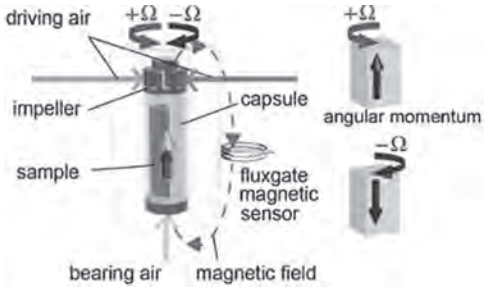

Fig. 1 The apparatus for the Barnett effect measurement using an air-driven rotor system.

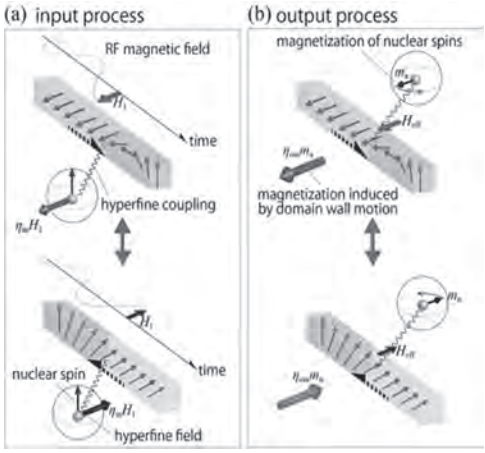

Fig. 2 Schematic illustration of enhancement of the NMR signal in a domain wall.

CONTRIBUTED PAPERS

JOB-02. CMOS-compatible growth and investigation of room-temperature ferromagnetism in nanocrystalline zinc oxide-based dilute magnetic semiconductors. *N. Joshi*[1], J. Narayan[1] and R. Narayan[1] *1. Materials Science and Engineering, North Carolina State University, Raleigh, NC, United States*

Dilute magnetic semiconductors (DMS) have been studied widely for elucidating spin-transport mechanism as well as realizing potential magneto-optic and spintronic devices [1,2]. Doped ZnO is a popular DMS owing to its semiconducting, optical, and piezoelectric properties, with Co being the most popular dopant due to its high T_c [3]. The observation of room-temperature ferromagnetism (rt-FM) in bulk transition metal (tM)-doped ZnO is widely debated, with contending reports that claim [4] a mechanism for ferromagnetism or attribute [3] the observed results to paramagnetism. Despite such ambiguity, many researchers reported rt-FM even in nano-ZnO and used it to fabricate novel devices [2]. However, the synthesis of tM-doped ZnO below 200 °C has not been reported, making this class of technologically important materials CMOS-incompatible. In the present

work, we report rt-FM observed in nano $Co_xZn_{1-x}O$ (x= 0.01, 0.02, 0.05, 0.1) and show the in situ growth of ZnO nanostructures can be explored to alter and tune magnetocrystalline anisotropy. As such, the impact of inter-particle interaction on the magnetic properties of the aggregates is studied. We demonstrate a single-step, low-temperature, microwave-assisted solution synthesis to obtain Co:ZnO with varied Co-concentrations, making it CMOS-compatible and enabling the practical use of DMS. The as-synthesized samples indicate the formation of single-phase wurtzite ZnO without any impurity phase. The dc magnetic characterization of the as-prepared samples was performed at various temperatures and fields. The M-H curves of Co:ZnO samples measured at 300 K (Fig. 1) reveal substantial hysteresis (>30 Oe), a clear indication of rt-FM. Temperature-dependent magnetization and hysteresis measured at various low temperatures indicated the presence of free electron spins as well as clusters. The decreasing moment observed with increasing Co-doping when the dilution is high (<0.05) is indicative of the competition between free-spins and clusters. This finding reveals the magnetic behavior of ZnO-based DMS nanostructures as prominent spin sources for spintronics.

[1] Ohno, H., 1998. Making nonmagnetic semiconductors ferromagnetic. *Science*, *281*(5379), pp.951-956. [2] Pan, F., Song, C., Liu, X.J., Yang, Y.C. and Zeng, F., 2008. Ferromagnetism and possible application in spintronics of transition-metal-doped ZnO films. *Materials Science and Engineering: R: Reports*, *62*(1), pp.1-35. [3] Lawes, G., Risbud, A.S., Ramirez, A.P. and Seshadri, R., 2005. Absence of ferromagnetism in Co and Mn substituted polycrystalline ZnO. *Physical Review B*, *71*(4), p.045201. [4] Sharma, P., Gupta, A., Rao, K.V., Owens, F.J., Sharma, R., Ahuja, R., Guillen, J.M., Johansson, B. and Gehring, G.A., 2003. Ferromagnetism above room temperature in bulk and transparent thin films of Mn-doped ZnO. *Nature Materials*, *2*(10), pp.673-677.

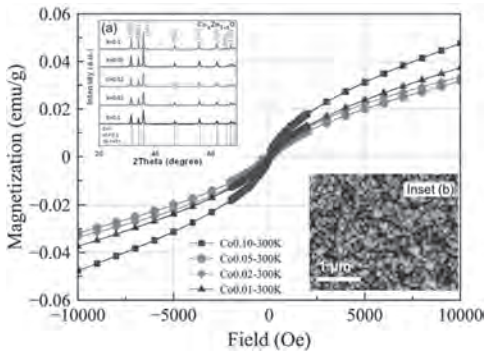

Fig. 1 M-H curves for Co:ZnO with varied Co-concentration; Inset shows XRD patterns and SEM image of the samples.

JOB-03. Anisotropy Landscape Analysis in (110) Rare-earth Iron Garnet Films. *Y. Song*[1], A. Kaczmarek[1], G. Beach[1] and C.A. Ross[1] *1. Materials Science and Engineering, Massachusetts Institute of Technology, Cambridge, MA, United States*

Rare-earth iron garnets, a ferrimagnetic insulator, have received attention for their many properties including small damping and tunable magnetization and angular momentum compensation temperatures. Most research efforts have been focused on garnet thin films grown on the (111) plane because of their perpendicular magnetic anisotropy (PMA), and the in-plane anisotropy, however neglected, can be important for our understanding of the switching behavior and the energetics of magnetic textures. In-plane anisotropy can be conveniently explored in garnet thin films on (110) planes. Here we combine a theoretical and experimental analysis of the anisotropy landscape for Europium iron garnet (EuIG) epitaxially grown on (110) Gadolinium Gallium garnet (GGG) using pulsed laser deposition. The angular dependence of anisotropy is calculated by combining the individual contributions including magnetocrystalline anisotropy, magnetoelastic anisotropy, shape anisotropy and growth-induced anisotropy, which may contribute for non-ideal stoichiometry. This predicts an easy axis out of plane along [110], with hard and intermediate axes in plane along [001] and [1-10] respectively. The anisotropy landscape is probed with vibrating sample magnetometry (VSM) and spin-Hall magnetoresistance (SMR) measurements. The SMR result is simulated and fitted to a Stoner-Wohlfarth model. The experimental measurements yield the expected hard and easy axes but the model requires additional multi-domain consideration to capture the hysteresis behavior when the external field is swept along the intermediate in-plane axis. Understanding the in-plane anisotropy effect, especially the unexpected hysteresis in in-plane direction for a PMA film could have help with the interpretation of the switching behavior.

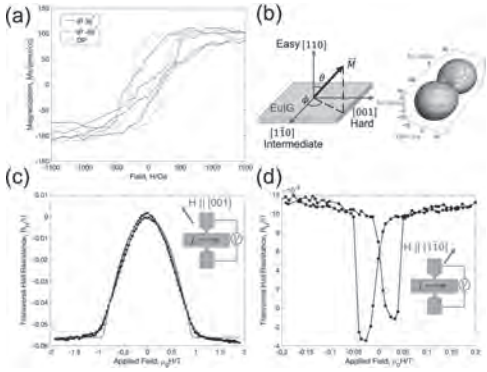

Fig. 1 (a) VSM measurement along the in-plane easy (IP 35, [1-10]), in-plane hard (-55, [001]) and out-of-plane (OP, [110]) axes. (b) Left: Principal anisotropy axis definition in EuIG and setup for Stoner Wohlfarth simulation. Right: 3D polar plot for anisotropy landscape in EuIG. (c) SMR measurement for field swept along the hard anisotropy axis, with fit (red). (d) SMR measurement for field swept along the intermediate anisotropy axis.

JOB-04. Combinatorial measurement of FMR in YIG-based magnetic garnet dots. *Y. Omori*[1], H. Someya[1] and M. Ishida[1] *1. NEC Corporation, Tokyo, Japan*

Magnetic garnets (MG) such as Yttrium Iron Garnet (YIG: $Y_3Fe_5O_{12}$) are recently attractive type of magnetic materials. Especially the low gilbert damping and strong magneto-optic effects are the important features for the magnetic devices [1]. There are many interesting physics and applications in MG. For instance, it is pointed that YIG dots have potential to be used for probabilistic bit operation [2]. On the other hand, it is still challenging to optimize the condition such as the kind of elements, composition ratio, and the shape in the many possible candidates. In this study, to accelerate the optimization of these conditions, we performed combinatorial approach for the magnetic garnets. First, we established the sputtering growth process to prepare well crystalline YIG thin films on GGG (111) substrates. We measured the Ferromagnetic Resonance (FMR) of the film whose peak-to-peak linewidth was 0.2mT at 9.5GHz. Based on this sputtering technique, we performed combinatorial magnetron sputtering to obtain widely different composition ratio in a single substrate. We patterned the film to dot shape. Finally, by using Vector Network Analyzer and auto-prober system, we measured the FMR properties of the hundreds dots in a short time. The effect of the doped elements and the shape will be discussed at the presentation. This work was supported by JST-CREST (JPMJCR20C1).

[1] Y Yang, et al., “Recent advances in development of magnetic garnet thin films for application in spintronics and photonics”, Journal of alloys and Compounds 860 158235 (2021). [2] T. Makiuchi, et al., “Parametron on magnetic dot: Stable and stochastic operation”, Appl. Phys. Lett. 118, 022402 (2021).

JOB-05. The Role of Co^{2+} Cation Addition in Enhancing the AC Heat Induction Power of $(Co_xMn_{1-x})Fe_2O_4$ Superparamagnetic Nanoparticles. *J. Wang*[1], H. Kim[1], S. Ota[2], C. You[3], Y. Takemura[4] and S. Bae[1] *1. Electrical Engineering, University of South Carolina, Columbia, SC, United States; 2. Shizuoka University, Hamamatsu, Japan; 3. Daegu Gyeongbuk Institute of Science & Technology, Daegu, The Republic of Korea; 4. Yokohama National University, Yokohama, Japan*

Enormous research activities to develop advanced superparamagnetic iron oxide nanoparticles (SPIONPs) enabling to generate higher AC heat induction temperature (T_{AC}) or specific loss power (SLP) at the biologically safe and physiologically tolerable range of AC magnetic field (H_{AC}) ($H_{AC,safe} < 1.8 \times 10^9$ A m^{-1} s^{-1}, $f_{appl} < 120$ kHz, $H_{appl} < 190$ Oe (12.5 A m^{-1})) have been intensively made in the past two decades for magnetic hyperthermia application [1-3]. According to the reports made so far, a high magnetic softness (or high magnetic moment m) and a high initial susceptibility (χ_0) at the DC magnetic field were revealed to be critical parameters in enhancing the T_{AC} (SLP) due to the correspondingly enhanced Néel relaxation time constant (τ_N), which is the same as the effective relaxation time constant (τ_{eff}), $\tau_N \approx \tau_{eff}$, in solid-state SPIONPs. However, $MnFe_2O_4$ SPIONPs with high magnetic moment usually show low T_{AC} (SLP) compared to magnetically semi-hard $CoFe_2O_4$ SPIONPs with a relatively low m [4,5]. In this work, our research efforts primarily focused on exploring the physical and chemical reasons why $MnFe_2O_4$ SPIONPs with high DC magnetic softness show an extremely low T_{AC} (SLP) by systematically investigating the physical role of magnetically semi-hard Co^{2+} cation addition in enhancing T_{AC} (SLP) of solid $(Co_xMn_{1-x})Fe_2O_4$ SPIONPs. According to the experimentally and theoretically analyzed results, it was clearly demonstrated that the enhancement of magnetic anisotropy (K_u)-dependent AC magnetic softness including the Néel relaxation time constant τ_N ($\approx \tau_{eff}$), and its dependent out-of-phase susceptibility (χ'') are the most dominant parameters to enhance the T_{AC} (SLP). This clarified result strongly suggests that the development of new design and synthesis methods enabling to significantly enhance the K_u by improving the crystalline, shape, stress (magnetoelastic), thermally-induced, and exchange anisotropies is the most critical to enhance the T_{AC} (SLP) of SPIONPs at the $H_{AC,safe}$ (particularly at the lower f_{appl} < 120 kHz) for clinically safe magnetic nanoparticle hyperthermia.

[1] Joshi *et al*, J. Phys. Chem. C, 113, 17761-17767 (2009) [2] Lee *et al*, Nat. Nanotechnol., 6, 418-422 (2011) [3] Sathya *et al*, Chem. Mater., 28 1769-1780 (2016) [4] Mameli *et al*, Nanoscale, 8 10124-10137 (2016) [5] Albino *et al*, J. Phys. Chem. C, 123, 6148-6157 (2019)

JOB-06. Synthesis of magnetic nanoparticles studied by synchrotron X-ray spectroscopy. *J. Kuciakowski*[1,2], A. Kmita[2], K. Pitala[1,2], S. Lafuerza-Bielsa[3], M. Gajewska[2], J. Zukrowski[2], D. Koziej[4] and M. Sikora[2] *1. Faculty of Physics and Applied Computer Science, AGH University of Science and Technology, Krakow, Poland; 2. Academic Centre for Materials and Nanotechnology, AGH University of Science and Technology, Krakow, Poland; 3. European Synchrotron Radiation Facility, Grenoble, France; 4. Institute for Nanostructures and Solid States Physics, Center for Hybrid Nanostructures, University of Hamburg, Hamburg, Germany*

Nanoparticles (NPs) exhibit strong divergence from bulk form and variety of effects emerging in nano scale, for what remain promising research area. Our goal was to characterize growing NPs in *in-situ* experiment during synthesis. Research on NPs is challenging due to size/shape distribution, interactions within sample and with environment etc., especially using solutions of magnetic NPs, what limits characterization methods. We have used X-ray Magnetic Circular Dichroism in Resonant Inelastic X-ray Scattering (RIXS-MCD), high resolution synchrotron technique, which allows measurements for very low concentrations, is element selective and ensures high selectivity towards growing NPs, without contribution of a container/channel/tube, reaction byproducts and carrier liquid. Spectra are background free and pre-edge features display strong MCD in order of several percent of pre-peak intensity [1-3]. Magnetite and cobalt ferrite NPs were synthesized and examined *ex-situ* via Mossbauer spectroscopy, TEM imaging, SAXS, VSM. Syntheses were measured on-the-fly using 1s2p RIXS-MCD separately on both iron and cobalt edges, continuously, over few sufficiently slow reactions. Well-defined pre-edge features provide information on local environment and site distribution of selected Fe or Co ions, edge of farther interactions with neighbors and valence, whereas MCD is used to determine net magnetic moment of probed element (fig. 1). Multivariate Curve Resolution optimized by Alternating Least Squares algorithm (MCR-ALS) was employed to determine reaction dynamics. Linked *ex-situ* and *in-situ* experiments results allowed to model development of the structure and magnetism in growing NPs. Ferromagnetic cobalt ferrite NPs with open hysteresis loop and superparamagnetic iron oxide NPs with very distinctive magnetic behavior for similar structure and size were compared. Performed analysis shows that iron oxide NPs with size lower than 5 nm lacks strong moments coupling and superparamagnetic response (fig. 2).

1. A. Juhin, A. Lopez-Ortega, M. Sikora, et al., Nanoscale, Vol. 6, 11911 (2014). 2. N. Daffé, M. Sikora, M. Rovezzi, et al., Advanced Materials Interfaces, Vol. 4, 1700599 (2017). 3. J. Kuciakowski, A. Kmita, M. Sikora et al., Nanoscale, 12, 16420 (2020).

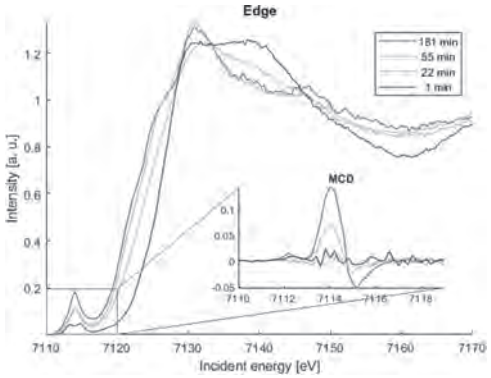

Figure 1. Spectra obtained during synthesis of magnetite nanoparticles.

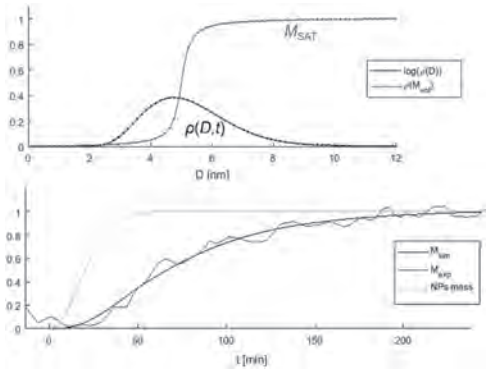

Figure 2. Saturation magnetization as a function of particle diameter (top) and comparison of simulated and experimental magnetization of particles (bottom).

JOB-07. Development of a Hafnium-Iron-Cobalt Ternary Alloy for Use in Thin Film Multiferroic Systems. *M. Staruch*[1], T.R. Mion[1], K. Bussmann[1], O. Van 't Erve[1], H. Ryou[1], S.B. Quadri[1] and P. Finkel[1] *1. Material Science and Technology, US Naval Research Laboratory, Washington, DC, United States*

The structurally coupled interaction between a piezoelectric and ferromagnetic magnetostrictive material can be exploited to develop magnetoelectric systems which have potential to rival current technologies with reduced power consumption and size. In a magnetoelectric multiferroic system the bilateral control of the magnetic and piezoelectric response is dictated by the material properties, where a soft magnetic material with large magnetostriction facilitates the large voltage-induced strain in the piezo/ferroelectric

layer. Thin film deposition techniques utilized for device fabrication often complicate the optimization of the interaction between layers due to inherent stresses occurring during deposition which are often deleterious to the magnetoelectric functionality. While incorporation of metalloid substitutions, such as in $(Fe_{0.5}Co_{0.5})_{1-x}C_x$, and $(Fe_{0.5}Co_{0.5})_{1-x}B_x$ are able to reduce the inherent coercive field and retain a high magnetostrictive and piezomagnetic properties the as-deposited stress states are rarely discussed [1,2]. To this end we have studied the incorporation of Hafnium in to an $Fe_{50}Co_{50}$ matrix with a focus on correlation between the film stress and magnetic properties. In these sputter-deposited thin films we find a relationship among the magnetic and stress properties as a function of doping percentage. With increasing Hf composition the system exhibits a minimum coercive field occurring at a crossover from a compressive to tensile stress state. Scanning electron microscopy (SEM) and X-ray diffraction (XRD) of the $(Fe_{0.5}Co_{0.5})_{1-x}Hf_x$ system reveal the magnetic softening is also correlated to emergence of an amorphous phase with reduced grain size for these sputter-deposited films. This ternary alloy presents an additional avenue for optimization of artificial magnetoelectric systems and has applications for multiple types of microelectromechanical devices.

[1] J. Wang, Phys. Rev. Applied 12, 034011 (2019) [2] J. Lou, Appl. Phys. Lett. 91, 182504 (2007)

JOB-08. Correlation between orbital degree of freedom, lattice-striction and magneto-dielectric coupling in ferrimagnetic $Mn_{1.5}Cr_{1.5}O_4$. *H. Chou*[1,2], G. Dwivedi[1], S. Kumawat[1,3], C. Wang[4] and D. Kakarla[1] *1. Department of Physics, and Center of Crystal Research, National Sun Yat-sen University, Kaohsiung, Taiwan; 2. Department of Applied Physics, National University of Kaohsiung, Kaohsiung, Taiwan; 3. International Ph.D. Program for Science (IPPS), National Sun Yat-sen University, Kaohsiung, Taiwan; 4. National Synchrotron Radiation Research Center, Hsinchu, Taiwan*

This report confirms the occurrence of dielectric anomaly observed in cubic $Mn_{1.5}Cr_{1.5}O_4$ around ferrimagnetic ordering temperature (T_N) is linked with magneto-dielectric coupling in the system. The temperature-dependent neutron diffraction results show a rapid decay in structural parameters (lattice-striction (DL/L) and transition metal–oxygen (TM-O) bond length) around T_N. We confirmed that these changes in structural parameters at T_N are not related to structural transition but the consequences of orbital-ordering of Mn^{3+}. The rapid decay in transition metal–oxygen bond length under internal magnetism of the system shows that magnetism could certainly manipulate the electric dipole moment and hence the dielectric constant of the system. Magneto-striction acts as a link between magnetic and dielectric properties.

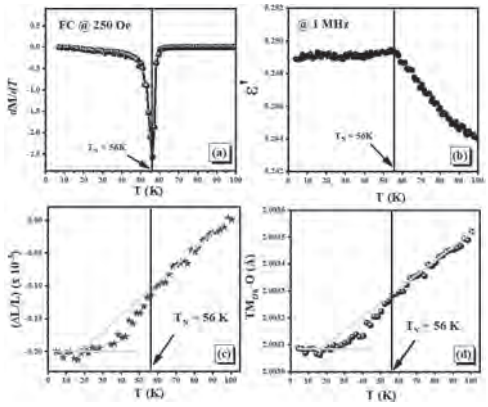

Figure: (a) Variation of first-order derivative of magnetization (dM/dT) measured with Field-cooled condition at applied field 250Oe, (b) dielectric constant at 1MHz frequency, (c) lattice-striction (DL/L), and (d) Transition metal-oxygen bond length as a function of temperature for $Mn_{1.5}Cr_{1.5}O_4$ are shown.

JOB-09. Emerging Magneto-Dielectric Materials for 5G Antenna Miniaturization: 18H Hexaferrites. *Q. Li*[1], Y. Chen[2] and V.G. Harris[3] *1. School of Materials and Energy, University of Electronic Science and Technology of China, Chengdu, China; 2. Innovation Center, Rogers Corporation, Burlington, MA, United States; 3. Department of Electrical and Computer Engineering, Northeastern University, Boston, MA, United States*

High-performance magneto-dielectrics with high permeability and permittivity, low magnetic and dielectric losses, and high cutoff frequency are promising candidate materials for next-generation communication applications, owing to their significant advantages for antenna miniaturization and bandwidth enhancement. Due to limited resonant frequencies and large natural resonance linewidths, conventional microwave ferrites and their composites, which are usually used over the frequency range from several hundred MHz to several GHz, do not meet the requirements for 5G communications.[1-3] A unique type of hexaferrites named Mg-Zn 18H hexaferrite, whose crystal structure can be interpreted as the structure of Y-type hexaferrites with intercalation of a three-layered hexagonal barium titanate block into the middle of the T-block as shown in Fig. 1a, has been synthesized, and its microwave properties have been comprehensively investigated for the first time.[4] The Mg-Zn 18H hexaferrite shows an extremely low damping coefficient of 0.1-0.2, indicating concentrated magnetic loss within a narrow frequency band and a narrow ferrimagnetic resonance linewidth of 486-660 Oe. Owing to this remarkably low damping coefficient, the Mg-Zn 18H hexaferrite possesses an excellent magnetic loss tangent as low as 0.06 and a small dielectric loss tangent less than 0.006 over 2-4 GHz, representing superior magneto-dielectric performance among the reported microwave ferrites for the S band applications as shown in Fig. 1b. Moreover, excellent thermal stability for the damping coefficient is observed to be 0.0004 K^{-1} over the temperature variation of most practical applications. When employed as the substrate of a 3.6-GHz patch antenna, the Mg-Zn 18H hexaferrite shows a miniaturization factor of ~5 and significant bandwidth improvement of ~50-110% over conventional dielectrics. These results imply the great technological potential and commercial value of the 18H hexaferrites for 5G communications.

[1]V. G. Harris, IEEE Trans. Mag. 48, 1075 (2012). [2]V. G. Harris, A. Geiler, Y. Chen, S. Yoon, M. Wu, A. Yang, Z. Chen, P. He, P. V. Parimi, X. Zuo, C. E. Patton, M. Abe, O. Acher, and C. Vittoria, J. Magn. Magn. Mater. 321, 2035 (2009). [3]Q. Li, Y. Chen, C. Yu, K. Qian, V. G. Harris, J. Am. Ceram. Soc. 103, 5076 (2020). [4]Q. Li, Y. Chen, C. Yu, L, Young, J. Spector, and V. G. Harris, Acta Mater. 231, 117854 (2022).

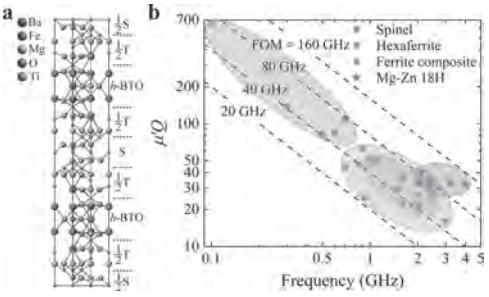

(a) Schematic illustration of the Mg 18H hexaferrite unit cell with the stacking subunit blocks denoted. (b) Performance of magneto-dielectric materials for microwave applications. The figure of merit (FOM) are indicated by the dashed lines.

JOB-10. Withdrawn

JOB-11. Role of Composition and Oxygen in Ferrimagnetic Gd_xCo_{1-x} Alloys for Microwave/mm-Wave Non-Reciprocal Devices.
K. Srinivasan[1], Y. Chen[2], L. Cestarollo[2] and A. El-Ghazaly[1] *1. Electrical and Computer Engineering, Cornell University, Ithaca, NY, United States; 2. Materials Science and Engineering, Cornell University, Ithaca, NY, United States*

Tunable perpendicular magnetic anisotropy (PMA) in thin film magnetic devices provides an isotropic in-plane permeability, necessary for integrated microwave and mm-wave devices and an opportunity to break inversion symmetry that allows implementations of non-reciprocal devices like circulators and isolators. In ferrimagnetic alloys like Gd_xCo_{1-x}, this is usually achieved by changing the composition such that the magnetic properties lie on either side of the composition-dependent magnetic compensation at room temperature, as shown in Fig. 1. Different compositions achieved in this work by changing the sputtering power of the Gd target show that magnetic compensation window lies between x = 28-32, and the effective anisotropy diverges about the compensation point. One less explored pathway is the incorporation of oxygen, which until now has been ruled out as a detriment to the ferrimagnetic properties [1]. Here, we show that preferential oxygenation of Gd_xCo_{1-x} through a reactive sputtering process, such that the cation (Gd and Co) to oxygen anion ratio is 1:1, increases the effective anisotropy energy density by two orders of magnitude compared to the corresponding alloys without oxygen. X-ray photoelectron spectroscopy reveals that strong PMA with an optimal oxygen flow results in a Co-deficient stoichiometry of $Gd_{21}Co_{28}O_{51}$, which suggests that strong ferrimagnetic order likely arises from a superexchange-like coupling between Gd and Co via the nonmagnetic O [2]. This can produce a spontaneous magnetization in the out-of-plane direction due to weaker exchange interactions within the alloy in a heavy-metal/ferrimagnet heterostructure for PMA. Even greater anisotropy fields on the order of 11 kOe are achieved in a super-lattice with 10 repetitions of the Gd_xCo_{1-x} heterostructure unit-cell, which corresponds to an operating frequency of 30 GHz. Therefore, not only does oxygenation increase PMA and provide tunable anisotropy to amorphous Gd-Co films, but the oxygen incorporation itself also increases the resistivity of the film, making it even more suitable for that frequency range.

[1] K. Ueda, A. J. Tan, and G. S. D. Beach, *AIP Advances*, vol. 8, no. 12, p. 125204, Dec. 2018. [2] R. J. Gambino and J. J. Cuomo, *Journal of Vacuum Science and Technology*, vol. 15, no. 2, pp. 296–301, Mar. 1978.

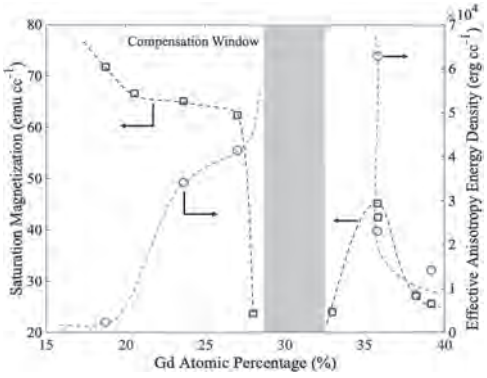

Fig. 1. Saturation Magnetization and Effective Anisotropy Energy Density for varying Gd_xCo_{1-x} compositions for x = 18-39.

JOB-12. Investigation of Soft Magnetic Material Cores in Transcranial Magnetic Stimulation Coils and the Effect of Changing Core Shapes on the Induced Electrical Field in Small Animals.
M. Tashli[1], G. Weistroffer[2], M. Baron[3,4] and R.L. Hadimani[1,5] *1. Mechanical and Nuclear Engineering, Virginia Commonwealth University, Richmond, VA, United States; 2. Biomedical Engineering, Virginia Commonwealth University, Richmond, VA, United States; 3. Neurology, Virginia Commonwealth University, Richmond, VA, United States; 4. Hunter Holmes McGuire VA Medical Center, McGuire Research Institute, Richmond, VA, United States; 5. Dept. of Psychiatry, Harvard Medical School, Boston, MA, United States*

Transcranial magnetic stimulation (TMS) is a safe, effective and non-invasive treatment for several psychiatric and neurological disorders. TMS is FDA approved treatment for depression and obsessive-compulsive disorders [1]–[3]. Lately, there has been a research surge in utilizing this novel technology in treating other neurological and psychiatric ailments. The application of TMS on other several neurological disorders requires the magnetic flux density and electrical field to be focal and targeted to a small region in the brain [4]. Multiple coil designs have been introduced in the literature to improve the focality of TMS coils, whereas, slight few numbers of these designs have adapted soft magnetic materials as coil cores to focus the magnetic flux. In this study, several soft magnetic materials will be investigated as TMS coil cores both in Finite Element Simulations and experimentally on rat head model. Finite element analysis of the rat head model will be done using Sim4life while investigating variations associated with changing the coil core material. In addition to investigate the effect of adding a V- shape tip to the core with 2 different angels 60 and 120 degrees [5]. Materials proposed for the analysis in this study include but not limited to Iron Cobalt Vanadium alloy (FeCoV), AISI 1010 Carbon Steel and Manganese Zinc ferrites (MnZn). Magnetic Properties of these materials will be characterized using Physical Property Measurement System (PPMS) to ensure using accurate magnetic properties in our simulations. Simulation results are presented below in (Fig. 2), indicating significant E-Field distribution variation when introducing a ferromagnetic core in TMS coil, concentrating the E-Field to the targeted region in rat head model without stimulating adjacent regions. It was observed that the relative permeability of the core material affects the focality of the stimulation significantly. Acknowledgment: Authors acknowledge Commonwealth Cyber Initiative Central Virginia Node Grant # FP00010500.

[1] M. S. George *et al. Arch. Gen. Psychiatry*, vol. 67, no. 5, pp. 507–516, May 2010 [2] D. W. Dodick, C. T. Schembri, M. Helmuth, and S. K. Aurora *Headache J. Head Face Pain*, vol. 50, no. 7, pp. 1153–1163, Jul. 2010 [3] O. of the Commissioner, *FDA*, Mar. 24, 2020. [4] J. Selvaraj, P. Rastogi, N. Prabhu Gaunkar, R. L. Hadimani, and M. Mina *IEEE Trans. Magn.*, vol. 54, no. 11, pp. 1–5, Nov. 2018 [5] I. C. Carmona, D. Kumbhare, M. S. Baron, and R. L. Hadimani, *AIP Adv.*, vol. 11, no. 2, p. 025210, Feb. 2021

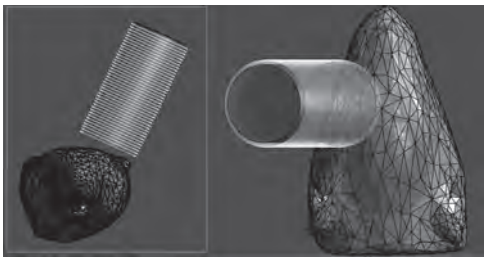

Figure 1: TMS coil postion on rat head model.

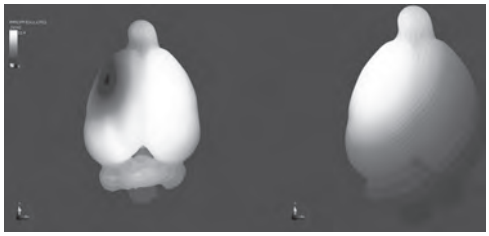

Figure 2: E-Field distribution simulation results. Left: E-Field distribution without ferromagnetic core. Right: E-Field distribution including a ferromagnetic core.

Session JOC
SOFT MAGNETIC CRYSTALLINE ALLOYS I

Victorino Franco, Chair
University of Seville, Seville, Spain

CONTRIBUTED PAPERS

JOC-01. Withdrawn

JOC-02. Application of electroplated Ni-Fe thick film to magnetostrictive material in vibration power generator. *S. Aketa*[1], E. Ishikawa[1], Y. Nakamura[1], M. Ohtake[1], T. Kawai[1] and M. Futamoto[1]
1. Faculty of Engineering, Yokohama National University, Yokohama, Japan

Magnetostrictive vibration power generation has attracted much attention as one of important energy harvesting technologies. Cantilever beam is a key component which influences the power generation property and it is generally prepared by forming a magnetostrictive plate of 25-500 μm thickness on a thicker base plate, where neutral plane exists in the base plate and either tensile or compressive stress is occurred in the magnetostrictive plate. Recently, magnetic materials with low magnetic anisotropies (K_{mag}) and moderately-large magnetostriction coefficients (λ_s) such as Fe-B alloy[1-3] have been used as magnetostrictive materials as well as those with large λ_s and moderately-low K_{mag} such as Fe-Ga alloy.[4-6] Ni-Fe alloy is a typical soft magnetic material and shows moderately-large λ_s (-43 - +32 ppm) by adjusting the composition.[7,8] In the present study, Ni-Fe alloy is tried to be used as a magnetostrictive material in vibration power generator. Ni-Fe films of about 40 μm thickness are prepared on Cu planets of 50 mm length, 10 mm width, and 300 μm thickness by electroplating. The effect of film composition on the power generation property is investigated. Figure 1 shows the measurement system of vibration power generation. The cantilever is vibrated by an actuator. The acceleration is fixed at 1.0 G and the frequency is adjusted to be the resonance frequency of each beam (about 115 Hz). The bias magnetic field is applied along the longitudinal direction of beam by Helmholtz coils and the strength is varied up to 100 Oe (= 7.96 kA/m). The output voltage is picked up by using a coil with 8000 turns. The structural, magnetic, and magnetostrictive properties are measured by XRD, VSM, and cantilever method, respectively. Figure 2(a) shows the example of output voltage waveform, which is measured by using an $Ni_{36}Fe_{64}$ (at. %) film. A high peak voltage of 0.8 V is successfully obtained. Figures 2(b) and (c) show the compositional dependences of maximum peak voltage and bias magnetic field required for obtaining the maximum value. The power generation property is strongly influenced not only by the λ_s but also by the K_{mag} of Ni-Fe film, which will be explained in detail at the conference.

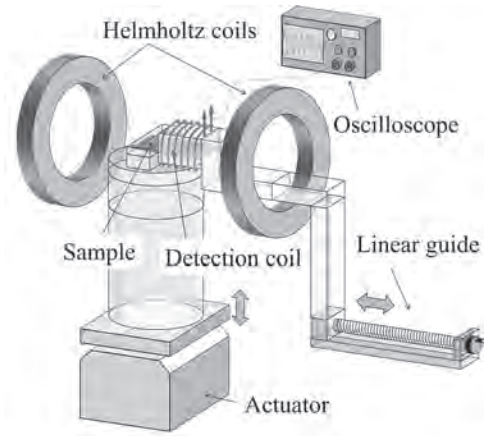

Fig. 1 Measurement system of vibration power generation.

1) M. Zucca, O. Bottauscio, C. Beatrice, A. Hadadian, F. Fiorillo, and L. Martino, *IEEE Trans. Magn.*, 50, 8002104 (2014). 2) F. Osanai, S. Hashi, and K. Ishiyama, *31st IEEJ National Convention*, 2-129, Hokkaido, Japan (2019). 3) E. Ishikawa, T. Kawai, M. Ohtake, and M. Futamoto, *46th Annual Conference of the Magnetics Society of Japan*, Nagano, Japan (2022). 4) T. Ueno, *AIP Adv.*, 9, 035018 (2019). 5) J. H. Yoo and A. B. Flatau, *J Intell Mater Syst Struct*, 23, 648 (2012). 6) S. Palumbo, P. Rasilo, and M. Zucca, *J. Magn. Magn. Mater.*, 469, 354 (2019). 7) R. M. Bozorth and J. G. Walker, *Phys. Rev.*, 89, 624 (1953). 8) R. M. Bozorth, *Ferromagnetism*, p. 669 (Wiley, Van Nostrand, New York, 1964).

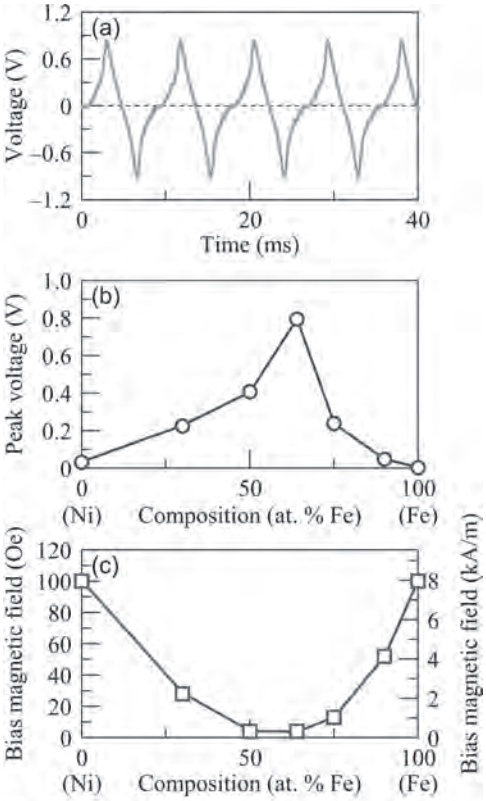

Fig. 2 (a) Output voltage waveform obtained by using an $Ni_{36}Fe_{64}$ thick film. [(b), (c)] Compositional dependences of (b) maximum peak voltage and (c) bias magnetic field required for obtaining the maximum value.

JOC-03. $CoFeMn_{0.5}Al_x$: High magnetization CoFe based soft alloys with reduced Co content. R. Rowan-Robinson[1], Z. Leong[1] and *N. Morley*[1] *1. University of Sheffield, Sheffield, United Kingdom*

The high cost of CoFe alloys has prevented their widespread use regardless of their promising properties: high magnetisation, high Curie temperature, as soft magnetic materials for high temperature applications. Our research has shown that the additional of AlMn can be used to create CoFeMnAl alloys, which have reduced Co content but similar saturation magnetisation as CoFe alloys, therefore providing a more economical alternative to pure CoFe soft magnets. The research studied how the addition of Al to $CoFeMn_{0.5}$ changed the alloy phases and hence the magnetic properties. The $CoFeMn_{0.5}Al_x$ alloys ($0 < x < 0.75$) were fabricated using arc-melting, and characterised using X-ray diffraction (phases present), scanning electron microscope (composition) and SQUID magnetometry (magnetic properties as a function of magnetic field and temperature). It was found that for Al content of $x < 0.2$, there existed mixed FCC and BCC phases, while with further addition of Al, the BCC phase was stabilised (Figure 1a.). This lead to an increase in the saturation magnetisation and a decrease in the coercive field (Figure 1b). The alloy $CoFeMn_{0.5}Al_{0.25}$ was determined to have a competitive saturation magnetisation compared to CoFe, but with the reduction of Co concentration in the alloy should also be cheaper to produce.

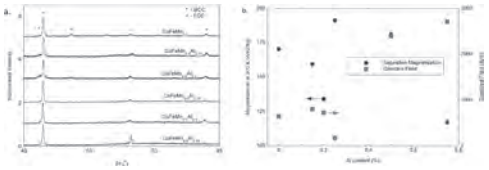

Figure 1a. XRD of the $CoFeMn_{0.5}Al_x$ alloys. 1b Saturation magnetisation and coercive field as a function of Al concentration.

JOC-04. Systematic investigation of FeAlSi epitaxial films with excellent soft magnetic property. *S. Akamatsu*[1], T. Nakano[1], M. Tsunoda[2,3], Y. Ando[1,2] and M. Oogane[1,2] *1. Department of Applied Physics, Graduate School of Engineering, Tohoku University, Sendai, Japan; 2. Center for Spintronics Research Network, Tohoku University, Sendai, Japan; 3. Department of Electronic Engineering, Graduate School of Engineering, Tohoku University, Sendai, Japan*

Sendust alloys ($Fe_{73.7}Al_{9.7}Si_{16.6}$) [1] have high Δ_1-band spin polarization and low magneto-crystalline anisotropy, and thus have great potential for use in the free layer of tunnel magnetoresistance (TMR) sensors [2]. The purpose of this study is to control the composition and atomic ordering of FeAlSi films for achieving excellent soft magnetic properties, and to clarify the mechanism of soft magnetic properties. The stacking structure was MgO subs./MgO (20 nm)/FeAlSi (30 nm)/MgO (1.5 nm)/Ta (1 nm). FeAlSi films with various compositions were deposited and annealed at T_a = 300-600 °C after deposition. The magnetic domain of the samples were measured by magneto-optical Kerr effect (MOKE) microscopy. Figure 1 shows the experimental and simulated results for K_1 at the film compositions where $K_1 \sim 0$ was obtained. The results for the bulk are also shown. The simulated results, which use K_1 of each ordered phase [3, 4] and degree of $D0_3$ order (S_{D03}), show the same trend as the experimental results, with the $K_1 \sim 0$ point shifting towards an Al-rich composition as the atomic order decreases. It was found that FeAlSi films with excellent soft magnetic properties can be obtained by controlling the volume ratio of $D0_3$-Fe_3Al that is the unique phase with negative K_1 in the ordered phases of FeAlSi films. Figure 2 shows the MOKE results for the $Fe_{73.7}Al_{9.7}Si_{16.6}$ film annealed at T_a = 450 °C. The MOKE image shows a separation into easy axis-like areas ($K_1 < 0$) and hard axis-like areas ($K_1 > 0$). As a result of the phase separation, an overall $K_1 \sim 0$ is realized. The separation into different K_1 areas suggests that the composition and atomic ordering are not uniform in whole area of the FeAlSi films. This study indicates that the FeAlSi film is a promising material to significantly improve the performance of TMR sensors. This work was supported by JSPS Grants-in-Aid for Scientific Research, Tohoku University GP-Spin Program, NEDO Leading Research Project, Tohoku University CSIS, and Tohoku University CIES. Fig. 1. Experimental (plotted points) and simulation (solid lines) results of K_1 dependence on Al concentration. Fig. 2 The comparison of MOKE and VSM results for the $Fe_{73.7}Al_{9.7}Si_{16.6}$ film annealed at T_a = 450 °C.

[1] H. Masumoto, T. Yamamoto, J. Jpn. Inst. Met. Vol. 1, p. 127 (1937) [2] S. Akamatsu, M. Oogane *et al.*, AIP Adv. Vol. 11, p. 045027 (2021) [3] M. Takahashi *et al.*, J. Jpn. Inst. Met. Vol. 10, p. 221 (1986) [4] T. Kamimori *et al.*, J. Magn. Magn. Mater. Vol. 54, p. 927 (1986)

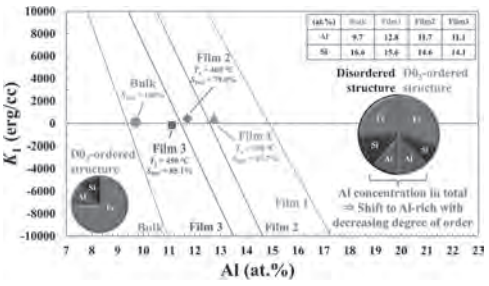

Figure 1

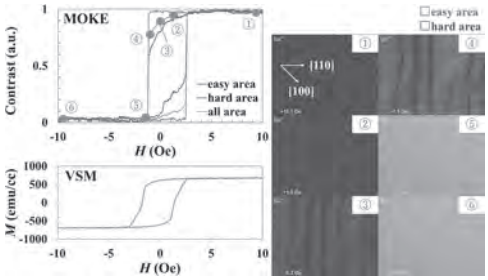

Figure 2

JOC-05. The processability and physical properties of boron alloyed melt-spun Fe-6.5%Si ribbons. *G. Ouyang*[1], M.J. Kramer[1], I. Anderson[1] and J. Cui[1] *1. Ames Laboratory of USDOE, AMES, IA, United States*

Energy-efficient and high-energy density soft magnetic material (SMM) is one of the key enablers for high efficiency electric motors for electric vehicles and other critical technologies. The need for increased motor speed for increased power density requires novel SMMs that can keep the eddy current (iron) losses low even at high frequencies. Amorphous and nanocrystalline SMMs can have low iron losses but are brittle and lack sufficient magnetic saturation. Among the crystalline SMMs, Fe-6.5%Si (wt.%) is a promising candidate due to its low raw materials cost and increased electrical resistivity. Its iron loss is much lower than the widely used low (3.2%) silicon steel, especially at higher frequencies. However, the increased Si content can lead to chemical ordering-related embrittlement, limiting thin sheet production by cold rolling. Rapid solidification by melt spinning is suitable for Fe-6.5%Si ribbon production, but there is a limitation on the width and surface quality of the ribbon due to its high melting point. Boron alloying can change the melting point and interfacial energy, improving the melt characteristics. In this work, B-alloying from 0.1 at% to 10 at% into Fe-6.5%Si and its effect on processing, magnetic properties, and mechanical properties were studied. Minor boron alloying was shown to significantly change the melt-wheel wetting and increase the quench characteristics with minimum impact on the magnetic saturation.

JOC-06. Magnetostriction Property Modeling of Silicon Steel Considering Stress-induced and Magnetocrystalline Anisotropy. T. Ben[1,2], *Y. Kong*[1], L. Chen[1] and F. Chen[1] *1. College of Electrical Engineering and New Energy, China Three Gorges University, Yichang, China; 2. State Key Laboratory of Reliability and Intelligence of Electrical Equipment and the Province-Ministry Joint Key Laboratory of EFEAR, Hebei University of Technology, Tianjin, China*

I Introduction To obtain the magnetic properties of silicon steel in different directions, it is necessary to establish a magnetostrictive model related to the anisotropy of silicon steel. Studies on the magnetostrictive model based on the magnetic domain deflection can simulate the hysteresis magnetization of silicon steel in different magnetization directions [1, 2]. But it did not consider the effect of stress. This paper proposed a hysteresis anisotropy-dependent magnetostriction model based on the free energy of silicon steel, which can consider stress-induced and magnetocrystalline anisotropy. II Method and Discussion Firstly, the two-dimensional free energy model of silicon steel, which includes magnetic field energy, magnetic crystal anisotropy energy and stress anisotropic energy, is incorporated into the anhysteretic magnetization parameter M_{an}, which is coupled with the Jiles-Atherton model, as shown in Fig.1. Based on the two-dimensional free energy model and thermodynamic principle, the hysteresis anisotropy-dependent magnetostriction model of silicon steel is proposed. Then, to obtain the magnetic field and deformation parameters related to stress-induced and magnetocrystalline anisotropy, the magnetostrictive deformation curves of silicon steel at different magnetization directions are measured. Finally, based on the measured parameters of the proposed model, magnetostrictive loops with the magnetic field under varying magnetization directions are simulated. By comparing the measurement results with the simulation results, the effectiveness and accuracy of the proposed model are verified, as shown in Fig.2. III Conclusion In this paper, a hysteresis anisotropy-dependent magnetostriction model of silicon steel is proposed. The measured and simulated results show that the magnetostrictive strain decreases with the stress increases in a certain range. The magnetostrictive strain will be larger and anisotropy will be more obvious with the increase of magnetization direction under the same stress.

[1] A.P.S. Baghel, B. Sai Ram, K. Chwastek, et al. Hysteresis modelling of GO laminations for arbitrary in-plane directions taking into account the dynamics of orthogonal domain walls[J]. Journal of Magnetism and Magnetic Materials, 2016, 418:14-20. [2] S. Mbengue, N. Buiron, and V. Lanfranchi. Macroscopic modeling of anisotropic magnetostriction and magnetization in soft ferromagnetic materials[J]. Journal of Magnetism and Magnetic Materials, 2016, 404:74-78.

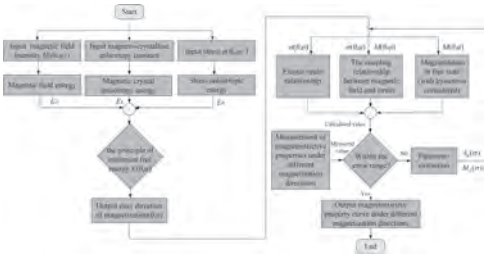

Fig.1 Flow chart of modeling magnetostriction property considering anisotropy

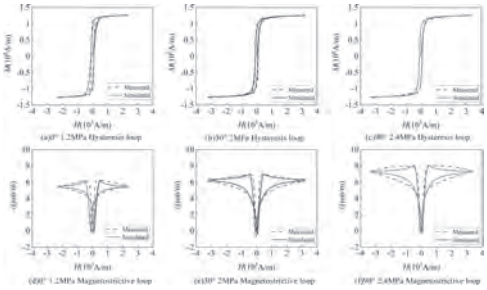

Fig.2 The hysteresis loops and magnetostrictive loops under different stress when the magnetization directions are 0°, 30° and 90°

JOC-07. Development of Dual Phase Soft Magnetic Laminate for Advanced Electric Machines. *S. Huang*[1], M. Zou[2], W. Zhang[1], V. Rallabandi[3], S. Buresh[1], J. Zierer[1], L. Dial[1] and F. Johnson[4] *1. GE Research, Niskayuna, NY, United States; 2. Lab Magnetics, San Jose, CA, United States; 3. Oak Ridge National Lab, Oak Ridge, TN, United States; 4. Niron Magnetics, Inc., Minneapolis, MN, United States*

The development of dual phase soft magnetic laminate for advanced electric machines at General Electric is summarized, including alloy development, properties, manufacturing trials, prototype experience, potential applications, and future material development. Dual phase soft magnetic laminates provide the flexibility to tune magnetic/non-magnetic state at the desired locations, using solution nitriding treatment with protective mask/coating. This enabling material technology benefits electric machine performance by reducing flux leakage in the laminates. It also decouples electromagnetic and mechanical design, which opens up the design space for advanced electric machines. Magnetic and mechanical properties of dual phase laminates were compared to commercial FeSi and FeCo soft magnetic laminates. Driven by the market needs for high power density and high-speed electric machines, a synchronous reluctance (SynRel) machine without permanent magnets and an interior permanent magnet machine using dual phase soft magnetic laminates were assessed in machine electromagnetic performance as well as rotor stress analysis by finite element simulation. Successful prototype

build and testing further retired manufacturing risks and advanced the technology maturity level. Future material development with higher mechanical strength, higher saturation magnetization, higher permeability, and lower loss are highly desired for ground and air transportation electrification.

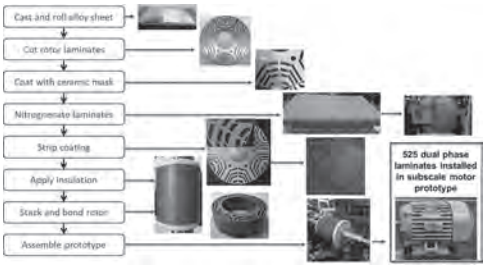

Figure 1. Dual phase laminate processing route for motor prototype.

JOC-08. Fabrication and Feasibility Study of Motor Laminations with Radially Varying Coercivity via Transverse Induction Annealing. *T. Paplham*[1], M. Ghosh[1] and P. Ohodnicki[1,2] *1. Mechanical Engineering and Materials Science, University of Pittsburgh, Pittsburgh, PA, United States; 2. Electrical and Computer Engineering, University of Pittsburgh, Pittsburgh, PA, United States*

The share of electric vehicles (EVs) on the road has seen a dramatic upward trend in the last decade as maximum range per charge has increased and the necessary infrastructure has grown to increase competitiveness with conventional gasoline-powered vehicles. However, maximal efficiency, achieved by minimizing the losses experienced by the motor stator and rotor, is limited by a tradeoff between low coercivity and high mechanical strength, which is necessary to withstand the significant torques experienced during operation [1–3]. Radiofrequency (RF) transverse induction annealing (T-IA) is suggested as a novel pathway for imposing a continuous spatial variation in microstructure of bulk crystalline soft magnetic alloys [4,5]. Via local control of grain size, magnetic and mechanical properties may be separately prioritized as functions of position, enabling fabrication of optimized motor laminations with reduced losses while still possessing requisite mechanical strength. Here we demonstrate through FEA modeling the dependence of achievable temperature profile on lamination and coil geometry, and we confirm feasibility of spatially optimized microstructure through experiments. We find that certain combinations of coil/lamination geometry may allow for simultaneous stamping of spatially optimized laminations, due to enhanced heating and higher temperature distributions in the region of the laminations where the magnetic flux density is greatest. We also present a basic feasibility modeling study examining performance of a motor containing motor laminations with radial variation in coercivity to motivate future work in this area.

[1] T. Sourmail, Prog. Mater. Sci., Vol 50, p.816–880 (2005) [2] P. Ramesh and N.C. Lenin, IEEE Trans. Magn., Vol. 55, 0900121 (2019) [3] T. Sourmail, Scr. Mater., Vol. 51, p.589–591 (2004) [4] A. Talaat, D.W. Greve, and S. Tan, Adv. Energy Mater., Vol. 2022, 2200208 (2022) [5] A. Talaat, D.W. Greve, and M. V. Suraj, J. Alloys Compd., Vol. 854, 156480 (2021)

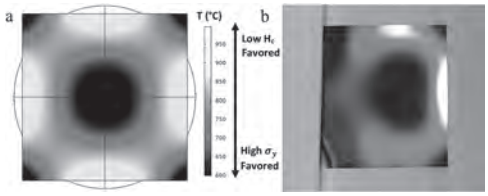

Fig. 1: (a) Schematic of temperature/property profile achievable with a cylindrical coil as simulated in COMSOL Multiphysics (b) Experimental temperature profile observed with a cylindrical coil and square Hiperco lamination.

JOC-09. Magnetization of microwave synthesized $La_{0.7}Sr_{0.3}MnO_3$: Impacts of microwave power and dwelling time. M. Marimuthu[1], Y.H. Lee[1] and *R. Mahendiran*[1] *1. Physics, National University of Singapore, Singapore*

The ferromagnetic metallic $La_{0.7}Sr_{0.3}MnO_3$ (LSM30) is a technologically important oxide because of its colossal magnetoresistance property and its application in magnetic tunnel junction devices[1]. Synthesis of LSM30 by solid-state reaction in a conventional electrical furnace takes 5 to 7 days but a few studies indicate that is possible to synthesize single-phase LSM30 or close compositions within 30 to 45 min by irradiating a stoichiometric mixture of precursors by microwave (MW) in a domestic MW oven operating at 2.45 GHz [2-3]. The exact mechanism of MW heating is not fully understood yet although it is generally accepted that one or more of the precursors absorb MW energy and frictional force to electrical dipole reorientation results in rapid heating which accelerate chemical reactions [4]. There is a lack of systematic investigation on how synthesis parameters affect the magnetic and electrical properties of LSM30. We report the impact of dwelling time (during of MW irradiation at a fixed temperature) and microwave power on the magnetic properties of LSM30. We fixed the temperature of calcination to 1000°C and varied (i) dwelling time from 5 min to 30 min at a constant MW power (1600 W) and (ii) varied microwave power (1000 W to 1600 W) with a constant dwelling time (20 min). The samples were characterized by X-ray diffraction, electron microscopy, magnetization and broadband magnetic resonance. Magnetization data are summarized in Fig. 1(a)-(d). When dwelling time is less than 10 min, the ferromagnetic transition is broad in temperature. Ferromagnetic Curie temperature (T_C) initially increases with dwelling time up to 10 min and becomes independent at higher dwelling time. With a fixed dwelling time of 20 min also, the T_C initially increases with MW power and becomes independent above 1400 W. The value of magnetization increases with both the dwelling time and the microwave power. We will discuss the observed results in relation to nucleation of magnetic domains, crystallinity, and grain size. R. M acknowledges the Ministry of Education, Singapore for supporting this work (Grant no. R144-000-442-114).

[1] Qi Liu et al, ACS Appl. Mater. Interfaces, 14, 13883 (2022). [2] K. E. Gibbons et al., Chem Comm. 159 (2000). [3] S. N. Kale et al. Mater. Lett. 62, 191 (2008); R. Ran et al. Catalysis Today, 126, 394 (2007); J. Moradi et al. J. Solid State Chem 215, 1 (2014). [4] J. P. Sibbert et al., Appl. Phys. Rev. 6, 041314 (2019); J. P-Gonjal. R. Schmidt and E. Moran, Inorganics, 3, 101 (2015).

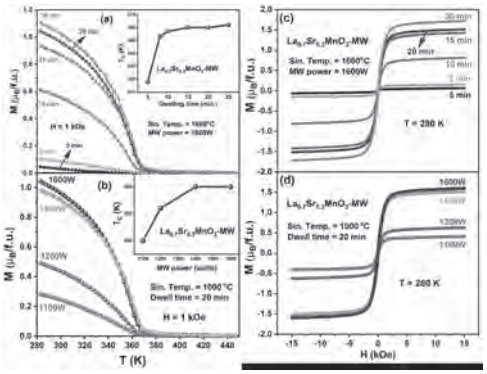

Figure 1

JOC-10. Sharp Goss Texture and Magnetostriction in Primary Cold Rolled Fe-Ga Thin Sheets by Composite Precipitates. *Z. He*[1], Z. Xinya[1], Y. Sha[2], X. Zhu[1] and F. Li[1] *1. School of Materials Science and Engineering, Shenyang University of Technology, Shenyang, China; 2. Key Laboratory for Anisotropy and Texture of Materials (Ministry of Education), Northeastern University, Shenyang, China*

Fe-Ga alloy is an advanced magnetostrictive material for actuators and sensors in terms of combining excellent mechanical and magnetostrictive properties. It is desirable to produce η(<100>//RD) textured Fe-Ga sheets due to the magnetostriction anisotropy with the largest coefficient along <100> direction and the serious eddy current loss in high-frequency use[1,2]. Current methods of promoting η texture in Fe-Ga alloy mainly include: (I) Micron-sized NbC particles were added to inhibit the normal grain growth, while the abnormal grain growth (AGG) of Goss ({110}<001>) texture was induced by surface energy effect from H_2S atmosphere[3-5]. (II) Micron-sized NbC particles were precipitated, and AGG of Goss texture was induced by the surface energy effect under sulfur atmosphere[6,7]. (III) Nanometer-sized sulfides were dispersedly precipitated during rolling, and AGG of Goss texture was produced by the degrading pinning effect of inhibitor[8-10]. However, two-stage cold rolling and intermediate annealing processes are indispensable to regulating microstructure and texture in Fe-Ga alloy sheets. Distinct from the current methods in Fe-Ga alloy, a primary cold rolling method with a large reduction ratio was used in the grain-oriented silicon steel to produce sharp Goss texture with a lower deviation angle[11,12]. The nanometer-sized inhibitors are precipitated at hot rolling and normalization to induce secondary recrystallization of Goss grains. In this paper, sharp Goss texture is successfully produced in Fe-Ga alloy sheet by primary cold rolling with a reduction ratio of ~85%. The nanometer-sized composite inhibitor was precipitated during rolling and annealing to induce secondary recrystallization of Goss texture. Nanometer-sized sulfides and NbC are dispersedly precipitated during hot rolling and normalization as inhibitors for secondary recrystallization. Fine grains textured by strong {111}<112> distributed through sheet thickness in primarily annealed sheets, which can provide a favorable environment for secondary recrystallization. Centimeter-sized Goss grains and large magnetostriction coefficient are obtained in Fe-Ga alloy by conventional primary cold rolling and annealing methods without surface energy effect.

[1]S.-M. Na and A. B. Flatau, Scripta Mater. Vol. 66, p. 307-310 (2012). [2]J. H. Li, Q. L. Qi, C. Yuan, X. Q. Bao and X. X. Gao, Mater. Trans. Vol. 57, p. 2083-2088 (2016). [3]S. M. Na and A. B. Flatau, J. Mater. Sci. Vol. 49, p. 7697-7706 (2014). [4]S. M. Na, K. M. Atwater and A. B. Flatau, Scripta Mater. Vol. 100, p. 1-4 (2015). [5]S. M. Na and A. B. Flatau, AIP Adv. Vol. 7, p. 056406 (2017). [6]C. Yuan, J. H. Li, W. L. Zhang, X. G. Bao and X. X. Gao, J. Magn. Magn. Mater. Vol. 374, p. 459-462 (2015). [7]C. Yuan, J. H. Li, W. L. Zhang, X. Q. Bao and X. X. Gao, J. Magn. Magn. Mater. Vol. 391, p. 145-150 (2015). [8]Z. H. He, H. B. Hao, Y. H. Sha, W. L. Li, F. Zhang and L. Zuo, J. Magn. Magn. Mater. Vol. 478, p. 109-115 (2019). [9]F. Lei, Y. Sha, Z. He, F. Zhang and L. Zuo, Materials. Vol. 14, p. 3818 (2021). [10]Z. H. He, H. J. Du, Y. H. Sha, W. L. Li, S. H. Chen, X. F. Zhu, F. ZHang, L. J. Chen and L. Zuo, IEEE Trans. Magn. Vol., p. (2022). [11]Z. S. Xia, Y. L. Kang and Q. L. Wang, J. Magn. Magn. Mater. Vol. 320, p. 3229-3233 (2008). [12]S. Mishra and V. Kumar, Mater. Sci. Eng. B. Vol. 32, p. 177-184 (1995).

Session JPA
AMORPHOUS AND NANOCRYSTALLINE SOFT MAGNETS II (Poster Session)

Cristina Bran, Chair
Instituto de Ciencia de Materiales de Madrid, Madrid, Spain

JPA-01. Composition and Oxidation Mechanism Optimization of FeNi-based Amorphous and Nanocomposite Alloys. *J. Egbu*[1], J. Baltrus[3], S. Calderon[1], A. Talaat[2], P. Ohodnicki[2] and M. McHenry[1]
1. Materials Science & Engineering, Carnegie Mellon University, Pittsburgh, PA, United States; 2. Mechanical Engineering and Materials Science, University of Pittsburgh, Pittsburgh, PA, United States; 3. National Energy Technology Laboratory, Pittsburgh, PA, United States

Metal amorphous nanocomposites (MANCs) are high-performance for high-speed motor (HSM) applications. A key technical metric for evaluating SMM's performance in HSM is low magnetic core loss in an AC field. MANCs comprise high induction nanocrystals embedded in a highly resistive continuous amorphous matrix, providing low core losses. Here, we report on two newly developed FeNi-based MANCs, (Fe70Ni30)85Nb0.5B14.5Si0 (B_s = 1.5 T) [1] and (Fe70Ni30)80Nb4B14Si2 ($W_{1T,400Hz}$=0.51 W/Kg, H_c=2.42 A/m, μ_r>35000) [2] with excellent magnetic properties and core losses. Both alloys exhibited improved soft magnetic properties by a rapid annealing process with (Fe70Ni30)85Nb0.5B14.5Si0 showing the most significant improvement. [3] Here, a systematic study, including rapid (RA) and conventional annealing (CA), was performed to identify the oxidation mechanism and role of Si in the growth of the passivating surface oxide [4,5] on MANCs that contributes to lower losses in tape wound cores. The top surface in the as-cast MANC alloy was rich in Fe-oxides as seen in Fig. 1. After heat treatment, the average thickness of the Fe-oxides layer increased significantly in CA and RA (Fe70Ni30)85Nb0.5B14.5Si0 to ~20 nm at 450 °C (Fig. 2) and up to 200 nm at 550 °C (CA samples only) compared to only ~5 nm at 450 °C and ~10 nm at 550 °C in CA (Fe70Ni30)80Nb4B14Si2 alloys. We show a sub-surface passivating Si oxide layer to form in heat-treated (Fe70Ni30)80Nb4B14Si2 alloy retarding Fe-oxide layer growth compared to alloys without Si. In addition, Nb oxide appears in the surface oxide layer of heat-treated (Fe70Ni30)80Nb4B14Si2, but not observed in Nb deficient (Fe70Ni30)85Nb0.5B14.5Si0 (Fig. 2). Finally, we establish an oxidation model for the growth of surface oxides in these FeNi-based MANCs. Bulk resistivity was measured in as-cast (Fe70Ni30)80Nb4B14Si2 alloys to be 157 ± 3 μΩ-cm and 119 ± 1 μΩ-cm for (Fe70Ni30)85Nb0.5B14.5Si0. Temperature-dependent bulk resistivity in both alloys is presented to compliment the oxidation mechanism established herein. The reported results will assist in manufacturing tape wound magnetic cores for HSM used in electric vehicle applications.

1. Y. Krimer, A. Barberis, and M. E. McHenry, J. Mater. Res. 2021 368 36, 1666 (2021). 2. K. Byerly, Y. Krimer, C. Phatak, E. Theisen, and M. E. McHenry, J. Mater. Res. 2021 3614 36, 2843 (2021). 3. A. Talaat, J. Egbu, C. Phatak, K. Byerly, M. E. McHenry, and P. R. Ohodnicki, Mater. Res. Bull. 152, 111839 (2022). 4. J. Egbu, P. R. Ohodnicki, Jr, J. P. Baltrus, A. Talaat, R. F. Wright, and M. E. McHenry, J. Alloys Compd. 912, 165155 (2022). 5. P. Ohodnicki, J. Egbu, Y. Yu, J. Baltrus, N. Aronhime, Y. Krimer, P. Anand, K. Byerly, and M. E. McHenry, J. Alloys Compd. 834, 155038 (2020).

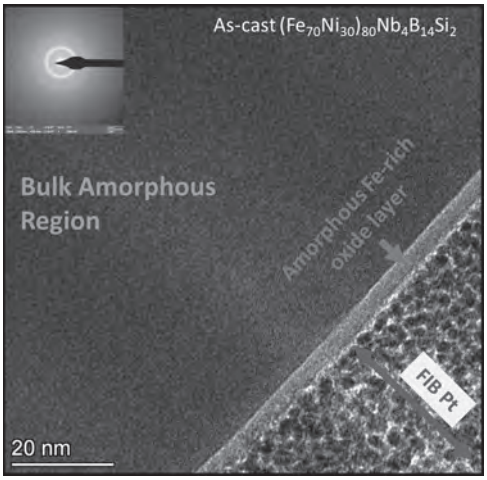

Fig. 1 TEM Image of as cast FeNi80

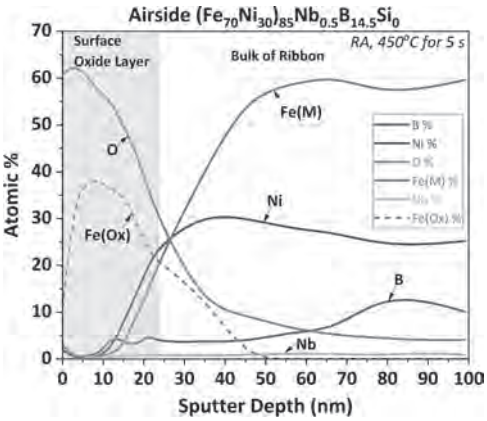

Fig. 2 XPS depth profile of FeNi85 alloy

JPA-02. Withdrawn

JPA-03. Effect of Applied Stresses on Magnetic Properties of Co and Fe-rich Glass-coated Microwires. *A. Garcia-Gomez*[1,2], P. Corte-Leon[1,2], M. Ipatov[1,2], V. Zhukova[1,2] and A. Zhukov[1,2] *1. Advanced Polymers and Materials: Physics, Chemistry and Technology, UPV/EHU, Donostia-San Sebastián, Spain; 2. Departament of Applied Physics, EIG, Universidad País Vasco, UPV/EHU, Donostia-San Sebastián, Spain*

In the last years, the railway industry has been one of the leading sectors in the research of alternatives to reduce the costs associated with maintenance. The components of railway tracks suffer huge amounts of pressure that could compromise railway safety and must be revised, repaired and renew frequently according to strict criteria. In the case of the sleeper, the maximum stress allowed by the different authorities is in the order of ~100 MPa [1] before substitution. Currently, the main testing procedures

are based on visual inspection or in situ measurements, making maintenance procedures economically inefficient. With the development of industry 4.0, researchers have been studying the fabrication of smart-sleepers capable of monitoring the sleeper structural stress in real-time [2]. Current technology makes extensive use of expensive optical fiber based instruments [2,3]. Thus, making it difficult to extend its use to big extensions of railway lines. Magnetic microwires fabricated by the Taylor-Ulitovsky technique appear in this context as an alternative for smart-sleeper technology. The microwires obtained using this technique are characterized by their small cross section (d =0 .5-40 μm), environment insulation thanks to the glass-coating and high sensitivity to external stimuli [4]. These properties, along with their cheap fabrication costs has motivated the study of this microwires for structural measurements in concrete structures similar to concrete sleepers [5]. In this work we show the possibility of glass coated magnetic microwires of working as railway monitorization devices. This is done by measuring the effect of longitudinal stress on the hysteresis loops of several Co- and Fe-rich microwires with different compositions. By analyzing the hysteresis loops, as shown in Fig 1 and Fig 2, we are able to obtain a calibration function that relates the coercitive field, H_c, with the applied stress over a wide applied stresses range.

[1] Parvez A., Foster, S. J., *Engineering Structures*, Vol 141, p 241-250, (2017). [2] Jing G. *et al.*, *Construction and Building Materials,* Vol 271, 121533*,* (2021). [3] Butler *et al*., *Structural Health Monitoring*, Vol 17(3), p 635-653, (2018). [4] Corte-Leon P. *et al*, *Journal of Alloys and Compounds*, Vol *789*, p 201-208. (2019) [5] Olivera, J., *et al* (2019. *Sensors,* Vol 19(21), 4685 (2019)

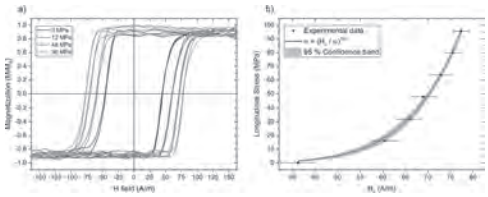

Figure 1: Response of wire $Fe_{4.39}$ $Co_{65.12}$ $Si_{6.79}$ $Cr_{8.88}$ $Mo_{0.15}$ to stress a) Hysteresis loop evolution. b) Microwire calibration function.

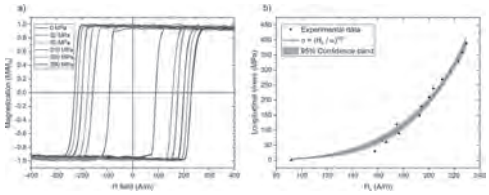

Figure 2: Response of wire $Fe_{66.99}$ $Si_{6.45}$ $Nb_{5.79}$ $Ni_{1.13}$ upon to stress a) Hysteresis loop evolution. b) Microwire calibration function.

JPA-04. Current Annealing Dependence of Magnetic Properties of Thick Fe-rich Glass-coated Microwires with Different Lengths.
A. Gonzalez Villegas[1,2], P. Corte-Leon[1,2], V. Zhukova[1,2], A. Garcia-Gomez[1,2], M. Ipatov[1,2], J. Blanco[2] and A. Zhukov[1,2] *1. Advanced Polymers and Materials: Physics, Chemistry and Technology, Universidad del Pais Vasco, San Sebastian, Spain; 2. Department of Applied Physics, EIG, Universidad del Pais Vasco, San Sebastian, Spain*

Amorphous ferromagnetic glass-coated microwires are known for their excellent magnetic properties, such as magnetic softness, ultrafast magnetization switching and the giant magnetoimpedance (GMI) effect. Said properties, as well as the hysteresis loop shape and domain structure of as-prepared microwires are strongly affected by the magnetostriction constant [1]. However, these properties are prone to change after submitting the microwires to different annealing processes and/or external stimulus, and are dependent on the sample's geometry [1,2]. The combination and manipulation of these parameters are widely studied to adapt magnetic microwires to new technological applications. Fe-rich microwires commonly exhibit bistable magnetic behaviour and poor GMI values. Past experiments on thin Fe microwires have shown an enhancement on their GMI effect after current annealing of samples, with hints to a change in their magnetic domain structure [3]. However, while thin microwires are promising materials for development of microsensors, thicker ones are suitable for different applications, such as stress monitoring and tuneable composite materials. Thus, a study of Fe-rich, thick microwires is carried out. A $Fe_{71.8}B_{13.27}Si_{11.02}Nb_{2.99}Ni_{0.92}$ glass-coated microwire was produced, with metallic nucleus and total diameters d=47.9μm and D=63.2μm (ρ=d/D≈0.8). While short (12cm, same lenght as the pick-up coil used for measurement) samples show regular squared hysteresis loops, common for Fe microwires, asymmetric hysteresis loops are observed in 24cm long samples (Figure 1.a). Current annealing results in coercivity, H_c, increasing in both samples, being most noticeable for the long one (Figure 1.b). On the other hand, GMI measurement yields an unexpected result, as, while its current annealing results in a proportionally smaller GMI ratio, ΔZ/Z, enhancement than that obtained on thin ones, the as-prepared microwire shows much higher ΔZ/Z -values and a double peak structure, usually denoting a different domain structure (Figure 2).

[1]: V. Zhukova, M. Churyukanova, A. Talaat, et al. *Effect of stress-induced anisotropy on high frequency magnetoimpedance effect of Fe and Co-rich glass-coated microwires*. J. Alloys Compound, Vol. 735, p.1818-1825 (2018). https://doi.org/10.1016/j.jallcom.2017.11.235 [2]: V. Zhukova, J.J. del Val, L. Gonzalez-Legarreta, et al. *Optimization of Soft Magnetic Properties in Nanocrystalline Fe-Rich Glass-Coated Microwires*. JOM, Vol. 67, p.2108–2116 (2015). https://doi.org/10.1007/s11837-015-1546-x [3]: A. Gonzalez, M. Ipatov, P. Corte-Leon, et al. *Effect of Joule heating on GMI and magnetic properties of Fe-rich glass-coated microwires*, AIP Advances, Vol. 12, p.035021 (2022). https://doi.org/10.1063/9.0000290

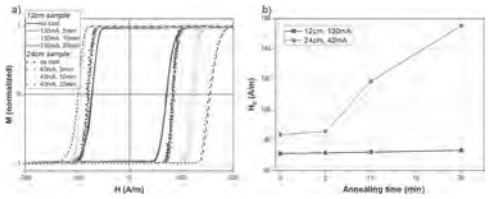

Fig.1: a) hysteresis loops of annealed samples and b) coercive field dependence on annealing times.

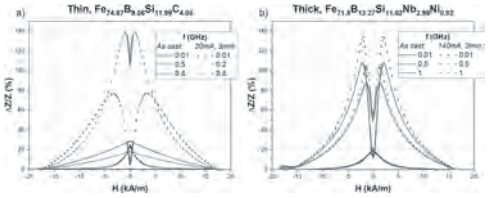

Fig.2: GMI ratios of as-prepared and annealed a) thin and b) thick microwires.

JPA-05. Controlled Domain Wall Interactions in Nearly Zero Magnetostrictive Amorphous Submicronic Wires.
S. Corodeanu[1], C. Hlenschi[1], C. Rotarescu[1], H. Chiriac[1], N. Lupu[1] and *T.A. Ovari*[1] *1. National Institute of R&D for Technical Physics, Iasi, Romania*

Rapidly solidified submicronic amorphous glass-coated wires have been extensively investigated recently due to their unique combination of reduced diameters (100 to 900 nm), very long sample length (10^{-2} to 10^{3} m), and bistable magnetic behavior, suitable for both sensing and magnetic logic applications [1]. Here we report on the interaction between domain walls that propagate inside amorphous $(Co_{0.94}Fe_{0.06})_{72.5}Si_{12.5}B_{15}$ glass-coated submicronic wires with nearly zero magnetostriction ($\lambda = -1 \times 10^{-7}$). The experimental set-up relies on six pick-up coils (C2 through C7) distributed evenly along the wire and two nucleation coils (C1 and C8) placed at its ends, the entire system being in a long magnetizing solenoid. If there is no signal in the nucleation coils, the sample magnetization reverses from one end (C1) to the other (C8), with only one propagating domain wall being detected successively by the pick-up coils: C2 → C3 → C4 → C5 → C6 → C7.

By applying synchronized rectangular nucleation signals in C1 and C8, magnetization reversal starts at both wire ends. Through the signal amplitudes, we adjusted the time interval between the generation of the two domain walls moving towards each other, and, in this way, the location on the wire axis where the two domain walls would collide. The collision results in a double amplitude peak within one of the pick-up coils, as compared to the peak that corresponds to a single domain wall passing through such a coil. By keeping the nucleation signal constant in C1 at 0.5 mA and varying the signal in C8 between 0.1 and 0.9 mA, one can relocate the domain wall interaction point in any pick-up coil. Fig. 1 shows the displacement of the collision point for an amorphous sample with 750 nm in diameter. The results show that the interaction of domain walls in such small diameter cylindrical amorphous wires is fully controllable, which is vital for magnetic logic applications. Work supported by the Romanian Executive Unit for Financing Higher Education, Research, Development and Innovation (UEFISCDI) through project PN-III-P4-ID-PCE-2020-1856 MaDWallS (contract PCE1/2021).

[1] S. Corodeanu, C. Hlenschi, C. Rotarescu, H. Chiriac, N. Lupu, T.-A. Óvári, J. Alloy. Compd., Vol. 905, 164260 (2022).

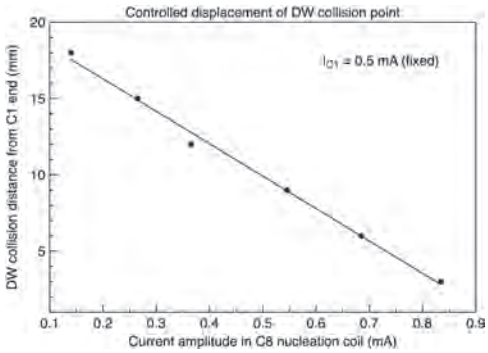

Fig. 1. Displacement of domain walls interaction point for an amorphous submicronic wire with 750 nm in diameter.

JPA-06. Time-resolved MOKE Visualization of the Domain Wall in Microwire Combined with Induction Measurements. *L. Fecova*[1], R. Varga[2] and K. Richter[2] *1. Institute of Physics, P. J. Safarik University, Kosice, Slovakia; 2. CPM-TIP, P. J. Safarik University, Kosice, Slovakia*

One of the most significant features of thin microwires (app. 30 microns in diameter) is their peculiar domain wall (DW) dynamics that has a high application potential [1]. Fast DWs in microwires have been in focus of intensive studies [2, 3]. Yet, the DW shape in motion and the DW interaction with pinning centres is still an open question. Surface DW shape can be effectively mapped by the recently developed setup based on the magneto-optical Kerr effect (MOKE) [4, 5]. However, the method does not provide an insight into the internal spin structure of the domain wall. Here, we present the enhanced MOKE setup that implements the induction system as well. Two opposite magnetic fields stabilize a DW by creating an effective one-dimensional potential well. The periodic motion of the potential well is precisely synchronized with the MOKE imaging. The pick-up coil placed below the LASER spot (Fig.1) is used to examine the internal spin dynamics of the DW in motion. A direct correlation between the surface DW deformation and the internal spin dynamics is performed (Fig.2). Our results show that the potential well gradient is a critical parameter that determines the DW position and reproducibility of its motion. The DW experiences a jerky motion for low values of the gradient, while a smooth DW propagation is observed at higher gradients. Furthermore, the length of the internal spin structure is almost five times larger (1.5 cm) than the surface length of the DW (2.9 mm). The strong disproportion implies that the DW does not have a simple tilted planar shape as concluded in previous works [4, 5]. Moreover, we found out that higher gradients of the potential well shrink the internal spin structure of the DW, while the surface shape seems to be unaffected. This means that the DW in microwires has an internal structure independent on the surface shape. Our findings reveal the complexity of the DW in microwires.

[1] V. Zhukova, et al., Nanomaterials, Vol. 10 (12), p. 2407 (2020). [2] J. Horniaková et al., Journal of Magnetism and Magnetic Materials, Vol. 529, p. 167846 (2021). [3] K. Chichay et al., Journal of Alloys and Compounds, Vol. 835, p. 154843 (2020). [4] O. Vahovsky, R. Varga and K. Richter, Journal of Magnetism and Magnetic Materials, Vol. 483, p. 266 (2021). [5] O. Vahovsky et al., Journal of Magnetism and Magnetic Materials, Vol. 537, p. 168168 (2021).

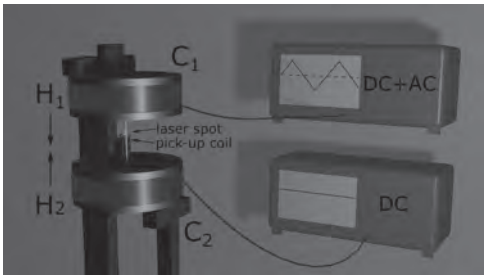

Fig. 1 Schematic illustration of the experimental setup. Coils C_1 and C_2 generate opposite magnetic fields H_1 and H_2. A sample is placed inside the pick-up coil.

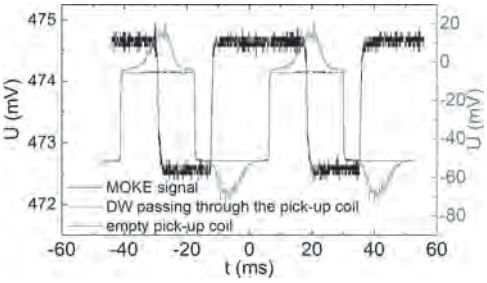

Fig. 2 The voltage as measured by oscilloscope for empty pick-up coil (blue) and for coil with microwire (red). The MOKE signal (black) is detected by a photodetector.

JPA-07. Studies of FMR in amorphous glass–coated microwires. *V. Zhukova*[1,2], P. Corte-Leon[1,2], C. Garcia[3], J. Gonzalez[1,2] and A. Zhukov[1,2] *1. Polymers and Advanced Materials: Physics, Chemistry and Technology, UPV/EHU, San Sebastian, Spain; 2. Applied Physics I, UPV/EHU, San Sebastian, Spain; 3. Physics, UTFSM, Valparaíso, Chile*

Studies of amorphous magnetic wires have become a traditional topic of applied magnetism owing to excellent magnetic properties and the development of prospective applications [1,2]. Taylor-Ulitovsky fabrication technique provides the broadest microwires diameters range together with improved corrosion, mechanical properties and biocompatibility related to the presence of the glass-coating [2,3]. However, the latter is a source of additional magnetoelastic anisotropy, K_{me}, which is one of the most important factors determining the magnetic properties of the amorphous materials. One effective method for evaluation of magnetic anisotropy in magnetic wires is the ferromagnetic resonance, FMR [2]. Additionally, FMR allows the evaluation of several material properties as saturation magnetization, g-factor, damping parameter, etc. [2,4]. We report experimental results of FMR and magnetic properties of various Fe and Co-based glass-coated microwires. We observed that the coercivity, H_c, of Co-Fe-rich microwires depends on the chemical composition: the highest H_c is observed for the microwire with highest Fe content. Such dependence must be attributed to Fe content influence on the magnetostriction coefficient, λ_s [3]. FMR spectra presents considerable dependence on resonance field, H_r, frequency, f (Fig.1) and K_{me} [4]. In all studied microwires H_r increases with f. H_r is also affected by the microwire diameter: the FMR spectra for microwires with similar chemical composition, but diameter almost an order of magnitude different are shown

in Fig.2. On the other hand, even for the same λ_s (mostly determined by the chemical composition), K_{me} is affected by the value of the internal stresses, σ_i that it is mostly determined by the ratio ρ, between metallic nucleus diameter, *d*, and total microwire diameter, *D* [3,4]. Therefore, the difference observed in FMR spectra must be attributed not only to different *d*, but also to the difference in σ_i. Additionally, in thin enough microwires the interface layer between the glass-coating and metallic nucleus can affect the FMR behavior [3].

[1] M. Knobel, M. Vázquez, L. Kraus, Giant Magnetoimpedance, in Handbook of Magnetic Materials, Elsevier, Vol. 15, p497 (2003). [2] K. Mohri, et al., *IEEE Trans. Magn.,* Mag-26, p.1789 (1990). [3] A. Zhukov et al., *J. Alloys Compd*., Vol. 814, p. 152225 (2020), doi:10.1016/j.jallcom.2019.1522250925-8388. [4] L. Kraus, Ferromagnetic resonance in individual wires: From micro- to nanowires, in Magnetic Nano- and Microwires (ed. M. Vázquez), Elsevier, ch. 15 (2015).

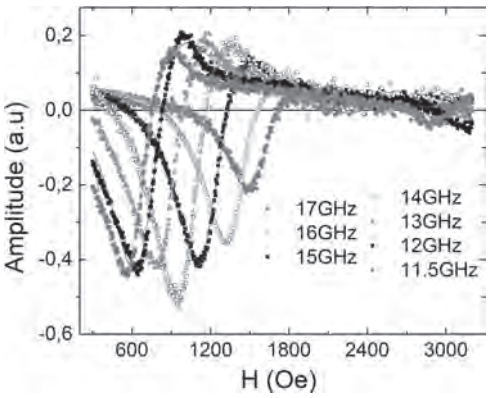

Fig.1. FMR spectra of $Fe_{79}B_8Si_{10}C_3$ microwire (*d*=19.2 μm).

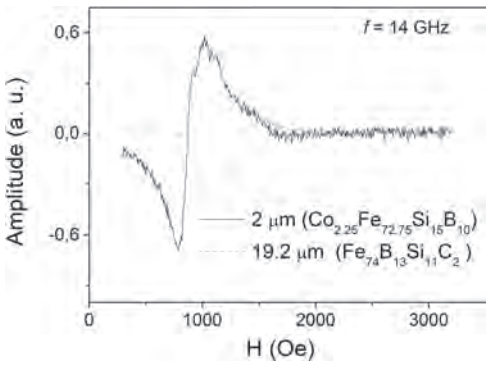

Fig.2. FMR spectra of $Fe_{74}B_{13}Si_{11}C_2$ (*d*=19.2 μm) and $Co_{2.25}Fe_{72.75}Si_{15}B_{10}$ (*d*=2 μm) microwires.

JPA-08. Strip domains influenced high frequency permeabiltiy spectra in CoZrTaB thin films. *G. Wei*[1], D. Lordan[1], A. Masood[1] and P. McCloskey[1] *1. Tyndall National Institure, Cork, Ireland*

A series of different thicknesses of amorphous magnetic CoZrTaB films were deposited on Si-substate. Strip domain structures induced secondary peak show up in high frequency imaginary permeability spectra when thicknesses increased to above 100 nm. In order to verify this, biased in-plane magnetic fields was applied during high frequency permeability measurement to eliminate strip domain structure, and at the same time the secondary peak was observed to disappear. Furthermore, OOMMF simulations were done to study strip domain induced high frequency imaginary permeability spectra. As strip domain became wider, the blue shift of the secondary peak shows up in consistent with measurement results.

1-Z. Tang, H. Ni, and B. Lu. Journal of Magnetism and Magnetic Materials, Vol. 426, P.444 (2017) 2-S. Ha, J. Yoon, and S. Lee, Journal of Applied Physics, Vol. 105, P.07D544-1 (2009). 3- V, Gehanno, R. Hoffmann, and Y. Samson, The European Physical Journal B, Vol. 10, P. 457 (1999).

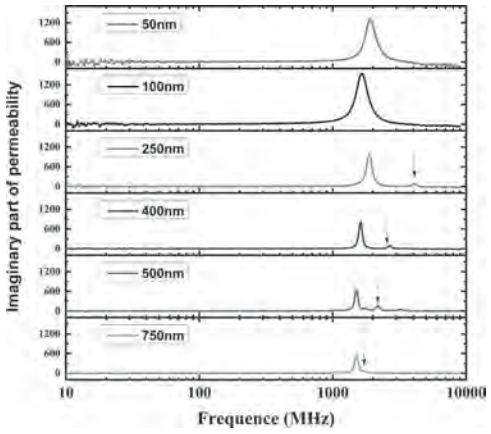

Fig.1

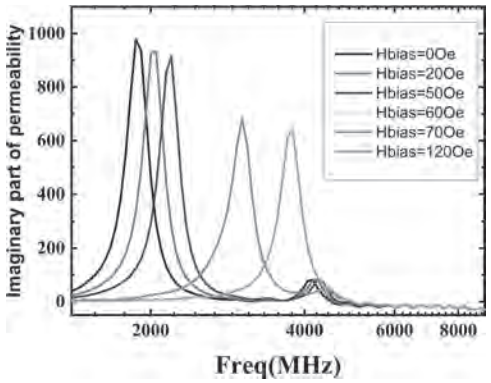

Fig.2

JPA-09. Temperature dependent intrinsic Gilbert damping in magnetostrictive FeCoSiB thin film. *W. Hu*[1], M. Huang[1] and F. Bai[1] *1. University of Electronic Science and Technology of China, Chengdu, China*

The magnetostrictive effect can be used in advanced magnetic field sensors, magnetoelectric antennas, non-reciprocal microwave devices and spin wave logic devices. Among the primary considerations in the design of these devices is Gilbert damping. However, a full understanding of the mechanisms which cause damping of magnetization dynamics in ferromagnets remains elusive. Of particular interest is whether magnetoelastic coupling contributes to the Gilbert damping in highly magnetostrictive films. There is no clear answer yet. Most studies have focused on yttrium iron garnet (YIG) film, which is weakly magnetostrictive. Recently, some researchers[1] reported a large anisotropy of the Gilbert damping in highly magnetrostrictive FeGa films, and the measured in-plane damping factors is one order of magnitude higher than the out-of-plane one. The result was attributed to the enhanced magnetoelastic contribution to the Gilbert damping, which is mitigated for perpendicular-to-plane fields. Amorphous FeCoSiB is a well-known soft magnetic material with excellent magnetostrictive properties. Here, we have prepared FeCoSiB(58nm)/Ti(5nm) film on Si substrate, and performed vector network analyzer ferromagnetic resonance (VNA-FMR) measurements using a coplanar waveguide from 10 to 300 K. The temperature-dependent in-plane Gilbert damping factor of the film is extracted and shown in Fig. 1. A very low Gilbert damping factor $\alpha_{Gilbert}$ of about 0.004 is observed at 300K. With the decrease of temperature, $\alpha_{Gilbert}$ firstly increases and then decreases, and reaches a peak value at ~40 K. The similar trend is

also reported in the permalloy film with a TaN capping layer, and can be explained as bulk Gilbert damping and surface/interface damping. The bulk Gilbert damping is conductivitylike and comes from intraband scattering. However, the magnetoelastic damping α_{me} contributed by magnetostriction and viscosity is not observed.

[1] Peria W K, Wang X, Yu H, et al. Magnetoelastic Gilbert damping in magnetostrictive $Fe_{0.7}Ga_{0.3}$ thin films[J]. Physical Review B, 2021, 103(22): L220403.

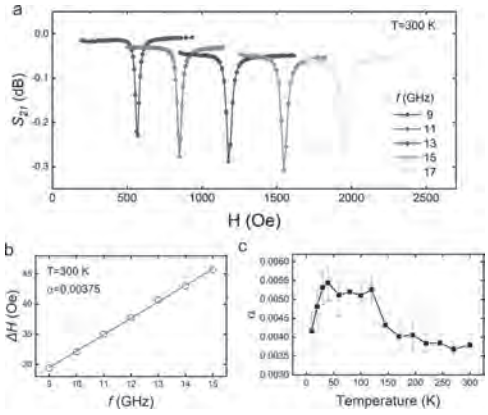

Fig. 1 Measurement of Gilbert damping in FeCoSiB(58nm)/Ti(5nm) thin films. (a) VNA-FMR spectra at 9, 11, 13, 15 and 17 GHz at 300 K, after background subtraction. (b) frequency dependent in-plane FMR linewidths. (c) temperature dependent Gilbert damping factor.

JPA-10. Synthesis of Amorphous and Nanocrystalline Powders by a Three Jet Gas-Liquid Technique. F. Borza[1], I. Murgulescu[1], M. Grigoras[1], H. Chiriac[1] and *N. Lupu*[1] *1. National Institute of Research and Development for Technical Physics, Iasi, Romania*

The nanocrystalline powders offer opportunities for the design of soft magnetic materials with improved magnetic properties (high saturation magnetization, high permeability, low magnetostriction) to be used for high frequency applications magnetic cores [1-4]. The aim of the work is to develop $Fe_{73.5}Cu_1Nb_3Si_{13.5}B_9$ powders with a high percentage of particles having the size in the range where nanocrystalline state is directly achieved, by using a new three-jet gas atomization technique (consisting in the use two jets of Ar gas and one jet of water), directed in such a configuration so that the molten alloy jet to be successively fragmented in droplets by the gas jets and further broken intro droplets and cooled by the liquid jet. Powders with the diameter size in the ranges 0-20 μm, 20-32 μm, 32-63 μm, and 63-100 μm have been prepared. Scanning Electron Microscopy (SEM), X-ray diffraction (XRD), thermomagnetic, and magnetic measurements have been performed to assess the structural and magnetic differences of powders between the groups of samples after sieving. The SEM images revealed the formation of particles with almost spherical shape. The X-Ray diffraction patterns show that in the range 0-32 μm the structure of particles is a mixture of amorphous and nanocrystalline phases, approx. 50 % of particles being in amorphous state, which is a quite high percentage. The magnetic measurements, performed using the Vibrating Sample Magnetometer technique (VSM) show that the Curie temperature increases from 350°C to 520°C and the saturation magnetization is between 130 to 145 emu/g. The coercive field, Hc, takes a very low value of 4 Oe for as-cast powders with the smallest diameter range, the value decreasing to down to under 2 Oe after annealing. These properties combined with good thermal stability, low cost price, the possibility to develop components with reduced dimensions/masses, make the amorphous and nanocrystalline alloys competitive and economic solutions in electronics, telecommunications, sensors, etc. Work supported by the Romanian Ministry of Research, Innovation and Digitalization under NUCLEU Program – contract no. 33N/2019, project PN 19 28 01 01.

[1] T. Suzuki, P. Sharma, and L. Jiang, IEEE Trans. Magn., Vol. 54, 2801705 (2018) [2] L. Chang, L. Xie, and M. Liu, J. Magn. Magn. Mater., Vol. 452, p. 442 (2018) [3] K.L. Alvarez, J.M. Martín, and M. Ipatov, J. Alloys Compd., Vol. 735, p. 2646 (2018) [4] K. L. Alvarez, H.A. Baghbaderani, and J.M. Martín, J. Magn. Magn. Mater., Vol. 501, 166457, (2020)

JPA-11. Magnetic Relaxation and Magnetic Resonance Effect of Mg-Zn Ferrite Nanoparticles. S. Hamada[1], A. Usui[2], K. Ohara[1], K. Nakazawa[3], N. Kataoka[1] and *Y. Ichiyanagi*[1] *1. Physics, Yokohama National University, Yokohama, Japan; 2. Medicine, Tohoku University, Sendai, Japan; 3. Yokohama National University, Yokohama, Japan*

In recent years, magnetic nanoparticles have attracted attention and been actively discussed for biomedical applications. Mg-Zn ferrite nanoparticles embedded in amorphous SiO_2 were synthesized using the wet chemical method, and their magnetic properties and transverse relaxation for application as a medium for magnetic resonance imaging (MRI) were examined. We previously found that these Mg-Zn ferrite nanoparticles exhibited significant hyperthermia effect for human breast cancer cells [1]. Namely, if this material shows function as a contrast agent for MRI, it is expected to be useful for both diagnosis and treatment as theranostics [2]. Image contrast in MRI is caused by the difference in MR signal due to the magnetic moment of the protons, which are hydrogen nuclei. That contrast depends on the proton density, T_1 relaxation time, and T_2 relaxation time. In this study, magnetic relaxation phenomena were analyzed by magnetization measurements and AC magnetic susceptibilities. The AC magnetic susceptibilities for various particle sizes of the $Mg_{0.8}Zn_{0.2}Fe_2O_4$ nanoparticles were measured in the range of 150–350 K under an AC magnetic field of 1 Oe, 100 Hz. The temperature corresponding to the peak of χ'' shifted to higher values as the particle size increased. Relaxation phenomena were evaluated using Cole-Cole plot analysis, and these samples were found to follow the Debye single-relaxation phenomenon. Spin-echo magnetic resonance measurements for $Mg_{0.8}Zn_{0.2}Fe_2O_4$ nanoparticles with particle sizes between 8 and 20 nm were performed using a 0.3-T MRI system. The particles exhibited a significant T_2 shortening effect compared with that of agarose as a background control. All particles exhibited effective relaxivity, *R2*, which was five times higher than that of the intrinsic core of conventional iron oxide agents of ferucarbotrans. The results show that Mg-Zn ferrite nanoparticles embedded in amorphous SiO_2 have the potential for theranostics applications.

[1] Hamada, S., Aoki, K., Kodama, K., Nashimoto, and Ichiyanagi, Y., 2022. AC magnetic susceptibility and heat dissipation of Zn-doped Mg-ferrite nanoparticles. J. Magn. Magn. Mater. 559 p.169539. [2] S.S. Kelkar, T.M. Reineke, 2011. Theranostics: Combining imaging and therapy, Bioconjug. Chem. 22 (10) Pp.1879–1903.

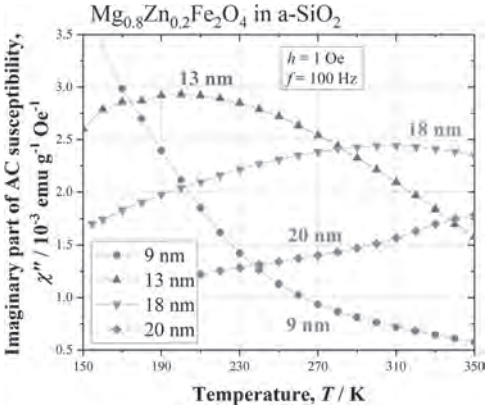

Fig1. Imaginary parts of the AC magnetic susceptibilities of $Mg_{0.8}Zn_{0.2}Fe_2O_4$ for various particle sizes.

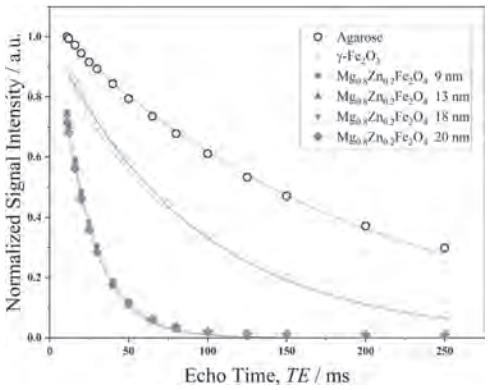

Fig.2 T_2 relaxation curves of $Mg_{0.8}Zn_{0.2}Fe_2O_4$ nanoparticles nanoparticles. Iron oxides and agarose samples are shown for comparison.

JPA-12. Core Loss Measurement and Analysis for Soft Magnetic Materials Under Complex Non-Sinusoidal Excitations. Y. Li[1], *S. Mu*[1], C. Zhang[1] and M. Yang[1] *1. Hebei University of Technology, Tianjin, China*

Along the advances of wide-bandgap power devices, the electrical equipment is developing toward higher switching frequencies and more complex switching modes in recent years [1]. Accurate prediction of the core loss of magnetic components has been a challenge for electrical equipment as the excitation varies depending on the operating mode of switched-mode power supplies [2]. However, few studies provide systems with variable-characteristic-parameters excitations [3]. It is not clear how the core loss of soft magnetic materials was affected by the characteristic parameters of complex non-sinusoidal excitations. Therefore, this paper presents the results of an extensive core loss study performed on nanocrystalline alloy (FT-3KL), amorphous alloy (1K101) and ultra-thin oriented silicon steel (GT-50). Firstly, an automatic experimental setup for core loss measurement of soft magnetic materials fed by a SiC MOSFET full-bridge inverter is built, as shown in Fig 1. This setup can provide real-time voltage waveforms adjustment, data visualization and automatic post-processing, which makes the measurement more rapid and accurate. Then, the effect of characteristic parameters of square waveforms, rectangular waveforms contained zero-voltage, pulse-width-modulation (PWM) waveforms and sinusoidal-pulse-width-modulation (SPWM) waveforms on core loss are analyzed comparatively. For square and rectangular excitations, the core loss shows regular distributions with duty cycles and phase shift ratios. For SPWM excitations, the effect of the modulation ratios on the core loss is greater than that of the carrier ratios. Meanwhile, the SPWM excitation with bipolar modulation will produce greater loss than that with unipolar modulation. The results are partly shown in Fig 2. In addition, the regular distributions will be interfered by the severe switching oscillations from the inverter, which makes the prediction of core loss more complicated. This paper can provide reference for the performance optimization of high-frequency electrical equipment.

[1] J. Wang, N. Rasekh and X. Yuan, IEEE Transactions on Industry Applications., vol. 57, p.650-663 (2021) [2] E. Stenglein and T. Dürbaum, IEEE Transactions on Magnetics., vol. 57, p.1-10 (2021) [3] I. Sirotić, M. Kovačić and S. Stipetić, IEEE Transactions on Industry Applications., vol. 57, p.4796-4804 (2021)

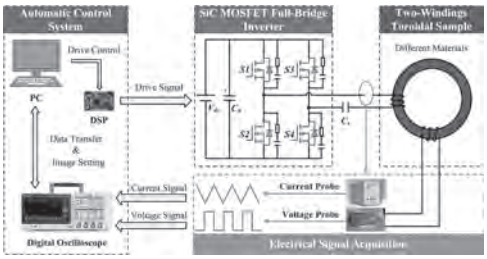

Fig 1: Schematic diagram of the experimental setup for core loss measurement.

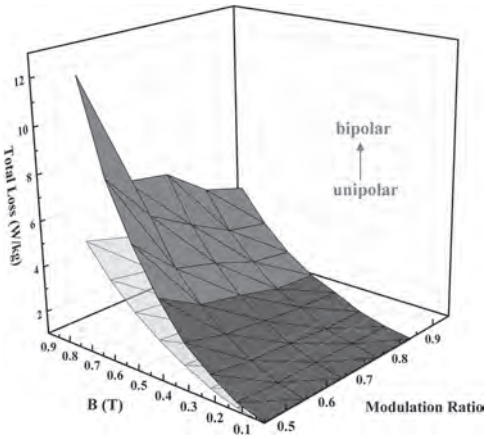

Fig 2: Core loss of FT-3KL under SPWM excitations with variable modulation ratios.

JPA-13. Magnetic property measurement and analysis of high-frequency transformer core material under non-sinusoidal excitation considering temperature effect. Y. Li[1], *C. Jin*[1], M. Yang[1], C. Zhang[1] and S. Mu[1] *1. College of Electrical Engineering, Hebei University of Technology, Tianjin, China*

High-frequency transformer operates under high temperature and non-sinusoidal excitation. The magnetic properties and loss of soft magnetic materials under these conditions are complicated, which are quite different from those under normal temperature and sinusoidal excitation[1-2]. At present, most of the relevant researches separate the temperature dependence of magnetic properties from non-sinusoidal excitation, which not sufficient to characterize the magnetic properties of soft magnetic materials[3-4]. This paper carried out magnetic property measurement and analysis under various temperatures (25~120°C) of high-frequency magnetic materials ferrite (N87) and nanocrystalline (FT-3KL) with multi-frequency (1~20kHz), different non-sinusoidal waveform excitation (square and rectangular wave), and multiple excitation states (Duty ratio 0.1~0.9). As shown in Fig.1(a), the temperature dependence of ferrite is significant, and its loss is less affected by the excitation state, while nanocrystalline is more sensitive to the excitation waveform. As shown in fig.1(b), the loss of nanocrystalline appears to be a minimal when the duty ratio is 0.5 and exhibits a symmetrical distribution. As shown in Fig.2, Based on experimental data, we consider the effect of temperature in the modeling of loss prediction and improve the model which based on the Steinmetz formula. By comparing the measured results and the predicted values, the accuracy of the new loss model is within 15%, which is greatly improved compared to other existing loss models under the influence of temperature. This work can provide a theoretical basis for the micro-magnetization mechanism of magnetic materials under complex operating conditions. The complete analysis of the magnetic properties and new loss model of the above materials will be shown in the full-text version.

[1] J. Chen, D. Wang and Y. Jiang, IEEE Transactions on Magnetics, vol. 54, no. 11, pp. 1-7, Nov. 2018 [2] S. Li, B. Sarlioglu and S. Jurkovic, IEEE Transactions on Industry Applications, vol. 53, no. 5, pp. 4923-4933,

Sept.-Oct. 2017 [3] Shaoshen Xue et al., IET Science, Measurement & Technology, 2016, 10(8) : 846-854. [4] S. Barg, K. Ammous and H. Mejbri, IEEE Transactions on Power Electronics, vol. 32, no. 3, pp. 2146-2154, March 2017

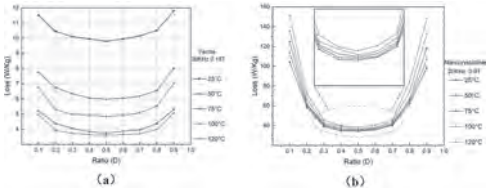

Fig. 1 (a) Duty ratio and loss curve of N87 excited by 20KHz square wave, B=0.15T (b) Duty ratio and loss curve of FT-3Kl excited by 20KHz square wave, B=0.9T

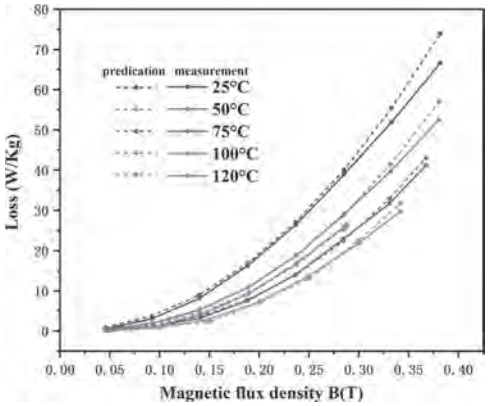

Fig. 2 Comparison of N87 loss prediction and measurement results

JPA-14. Loss Analysis of Magnetized Annealed Amorphous Alloy Applied to Stator Teeth. *J. Wang*[1], B. Tian[1], H. Hu[1] and R. Pei[1]
1. Department of Electric Engineering, Shenyang University of Technology, Shenyang, China

With the development of high-speed motors, how to reduce the iron loss of the motor has become the focus of attention in academia and industry. Amorphous alloys have been gradually applied to high-speed motors due to their high frequency and low iron loss characteristics. However, due to their low saturation flux density, As a result, the motor torque is greatly limited. When the amorphous alloy is formed, a large internal stress is generated in the material due to the rapid temperature change[1]. Usually, annealing treatment is required to eliminate the influence of internal stress on magnetic properties. During the annealing treatment of amorphous transformer cores, a magnetic field is usually applied in the direction of the magnetic circuit to improve the state of the magnetic domain, increase the saturation magnetic flux density in this direction and reduce the iron loss[2]. However, the magnetic field annealing technology has not been applied to the field of motors. In this paper, the amorphous material processed by this process is made into the shape of stator teeth, and the stator yoke is spliced with non-magnetic field annealing to form a complete stator core, as shown in Figure 1. Show. Since the magnetic field of the tooth is a pulsed magnetic field, this technology can effectively reduce the iron loss of this part and increase the motor torque to a certain extent. In order to reduce the difficulty of motor processing and the loss caused by many splicing positions, the motor structure is further optimized. As shown in Figure 2, the motor stator is composed of four parts with the same structure, and the teeth of each part are approximately parallel to the magnetization direction. However, due to the fact that the magnetic field of the yoke part is not always consistent with the direction of the magnetic field treatment in the actual motor operation, the iron loss of the stator yoke part of this structure is slightly larger than that of the stator structure without magnetic field treatment. The structure of the ratio realizes the optimal distribution of iron loss and performance improvement.

[1]Sato, T., & Todaka, T. (2018). Effect of magnetic annealing on magnetic characteristic of amorphous wound core. IEEE Transactions on Magnetics, 54(11), 1-4. [2]Gao Jie, He Chengxu, Song Wenle, Yang Fuyao, Liu Yang. Effects of Longitudinal Magnetic Annealing Treatment and Tensile Stress on Magnetization Characteristics and Loss of 1K101 Amorphous Alloy Ribbon [J]. Metal Heat Treatment, 2022,47(03):39-43.

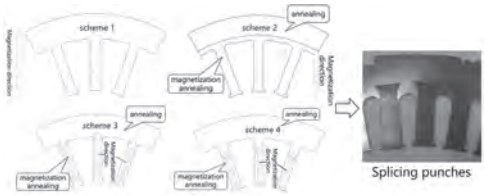

Fig.1 Four splicing schemes and stator punching

Fig.2 Magnetic properties test samples of amorphous alloys

JPA-15. A Study on Reducing Cogging Torque of 3-D Printing Axial Flux Motor using Fe-4.5Si-based Material. *M. Hong*[1], H. Pyo[1], D. Nam[1] and W. Kim[1] *1. Gachon University, Seongnam-Si, The Republic of Korea*

To produce the core of an axial flux motor, an amorphous steel sheet can be rolled, or a core shape can be manufactured by compressing a soft magnetic powder material. However, in the case of Amorphous steel sheet, as it is rolled up, so mass productivity is low. when using a powder material, since the use of a mold is essential, the degree of freedom of shape due to the manufacturing cost of the mold is very small. With the recent development of 3-D printing technology, Fe-4.5Si-based magnetic powder material manufacturing technology has been developed, making it possible to freely manufacture soft magnetic materials with 3-D printing. This has a better degree of freedom in shape production compared to the conventional Amorphous steel sheet or powder material. Fig. 1 shows a 3D-printed teeth made of FE-4.5SI magnetic powder material. Axial flux motors, which have higher output density than radial flux motors, are increasingly being adopted in fields requiring high output performance. However, designing to reduce cogging torque, which causes vibration and noise, is difficult. In general, as a method for reducing the cogging torque of an axial magnetic flux motor, a method of rotating the magnet at a certain angle about the center of the magnet is mainly used. However, in the case of the method of rotating the center of the magnet to the axis, the use of magnets is reduced compared to the existing model. In this paper, 3-D printing is used to design a shape that gives a skew to the stator teeth, and compared to the existing magnet skew, the amount of magnet used is maintained and the cogging torque is reduced. In addition, in order to compensate for the reduction of Back-EMF due to skew, an axial motor advantageous for unidirectional rotation was manufactured by applying an asymmetric air gap of the teeth. Fig. 2 shows asymmetric air gap of the teeth. Compared to the existing magnet skew, it was confirmed that the Back-EMF increased by 6%, the cogging torque was reduced by 6%, and the thd was reduced by 4%. The optimal model was selected by comparing the performance under load. The validity of the proposed model was verified using the finite element method.

H. Pyo, J. W. Jeong, J. Yu, S. G. Lee and W. Kim, “Design of 3D-Printed Hybrid Axial-Flux Motor Using 3D-Printed SMC Core,” in IEEE Transactions on Applied Superconductivity, vol. 30, no. 4, p.1-4, (2020) H. -J. Pyo, J. W. Jeong, J. Yu, D. -W. Nam, S. -H. Yang and W. -H. Kim, “Eddy Current Loss Reduction in 3D-Printed Axial Flux Motor Using 3D-Printed SMC

Core," 2020 IEEE Energy Conversion Congress and Exposition (ECCE), p. 1121-1125 (2020) J. H. Choi, J. H. Kim, D. H. Kim and Y. S. Baek, "Design and Parametric Analysis of Axial Flux PM Motors With Minimized Cogging Torque," in IEEE Transactions on Magnetics, vol. 45, p.6 (2009)

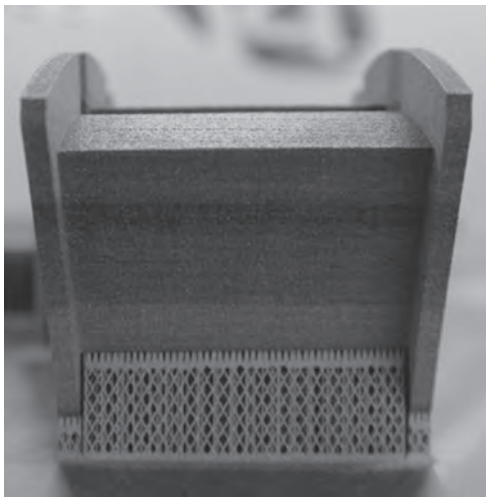

Fig. 1

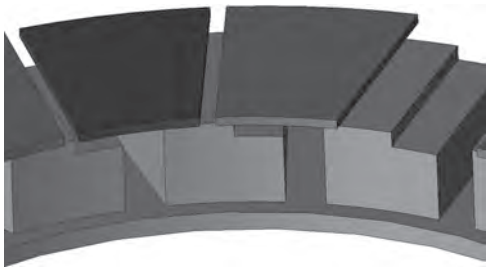

Fig. 2

Session JPB
FERRITES, GARNETS AND MAGNETO-DIELECTRIC MATERIALS II (Poster Session)

Chuanpu Liu, Chair
Colorado State University, Fort Collins, CO, United States

JPB-01. Low- and High-field Spin-Hall Anomalous Hall Effect in Pt/TbIG with Epitaxial YAG Insert Layer. *P. Li*[1], J. Liang[1], S. Ng[1] and C. Leung[1] *1. Department of Applied Physics, The Hong Kong Polytechnic University, Hong Kong, China*

We studied the spin-Hall magnetotransport across an epitaxial and nonmagnetic $Y_3Al_5O_{12}$ (YAG) insertion layer in the Pt/$Tb_3Fe_5O_{12}$ (TbIG) system. YAG (t_{YAG} nm) /TbIG (30 nm) bilayers were grown on $Ga_3Gd_5O_{12}$ (GGG) (111) substrates by pulsed laser deposition, before 5 nm of Pt was sputtered on the sample and patterned into Hall bars. t_{YAG} dependences of anomalous Hall resistance (R_{AHE}, with linear background contribution subtracted) were measured. At low t_{YAG} values, a hysteretic R_{AHE} loop is observed at low fields but with reducing effect with rising t_{YAG}. At high fields R_{AHE} behaviour is present, with magnitudes comparable with Pt/TbIG sample. The temperature dependence of low- and high-field R_{AHE} were investigated, with the goal of identifying the origin of such discrepancies and further guidance for interfacial design of spintronics devices.

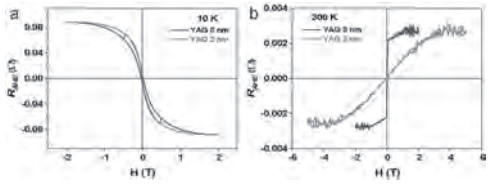

Fig. 1. Field dependence of R_{AHE} of Pt/YAG/TbIG samples at 10 K (a) and 300 K (b).

JPB-02. Magnetic domains of iron garnet film calculated by micromagnetic simulation. *T. Goto*[1], T. Koguchi[1,2], M. Inoue[1], K. Ishiyama[1] and P. Lim[2] *1. Research Institute of Electrical Communication, Tohoku University, Sendai, Japan; 2. Toyohashi University of Technology, Toyohashi, Japan*

Magnetics domains have been used in many magnetooptical applications, like magnetooptical disks and magnetooptical three-dimensional displays. Recently, we demonstrated a magnetooptical Q-switched laser [1,2] using an iron garnet film showing magnetic domains (MDs). The power of its output pulse was kilowatt, and the device size was three digits smaller than previous reports, Hence, this device is promising, but the mechanism of the output is not clear. To know how the MDs work, micromagnetic simulation (MMS) is a good tool. However, the size of the MD in the iron garnet film is more than 1 mm, larger than other works using MMS. Thus, the size of a simulation model, the number of cells, and the calculation time are significantly large. Hence, the calculation has been challenging, and there are no reports. In this study, we used large-scale parallel computing and calculated the MDs in iron garnet film. For the calculation, MMS software EXAMAG version 2.2.4 was used. The parallel computer comprising 128 cores with 960 GB memory was used. The model size was 20×20×2 μm, which is sufficiently larger than the MD size. The cell size was 80×80×80 nm. The total number of cells in this model was 4.770×10^6. The magnetic parameters were set so that the MDs appeared. The saturation magnetization was 40 mT, and the exchange coupling constant was 7 pJ/m. The anisotropic magnetic field was 2.5×10^5 A/m. The energy minimization method was used for obtaining the MDs. The calculation took about 30 minutes, and the inset of Fig. 1 shows the obtained maze pattern of MDs. The width of the MD was ~3 μm, and the length of the domain wall was ~0.3 μm. A magnetic field of 50 mT was applied perpendicular to the film, and the magnetization was calculated. Fig. 1 shows the obtained hysteresis loop. The MDs disappeared at the field of 20 mT, and the direction of magnetization was rotated in a plane. This behavior is qualitatively close to the experimental results. These calculation results are important for obtaining the dynamic magnetooptical response of MDs and further development of magnetooptical devices.

[1] T. Goto, *Opt. Express*, 24, 17635 (2016). [2] R. Morimoto, Sci. Rep., 7, 15398(2017).

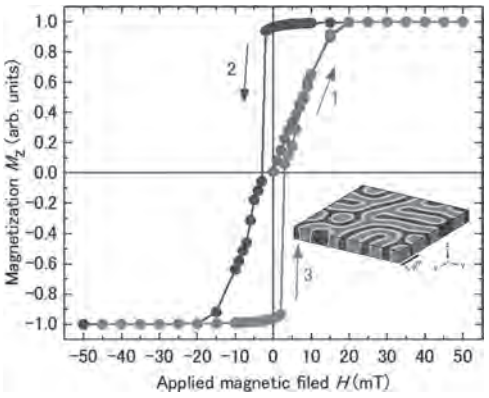

Fig. 1 Calculated hysteresis loop of iron garnet film showing magnetic domains.

JPB-03. Field Dependent Magneto-Optical Spectra of Ferrimagnetic Garnets to Identify Magnetic Contributions. *M. Vančík*[1], T. Fakhrul[2], K. Hayashi[2], J. Zázvorka[1], C.A. Ross[2] and M. Veis[1] *1. Faculty of Mathematics and Physics, Charles University, Prague, Czechia; 2. Department of Materials Science and Engineering, Massachusetts Institute of Technology, Cambridge, MA, United States*

Ferrimagnetic rare earth iron garnets ($X_3Fe_5O_{12}$, where X denotes a rare earth element) are promising materials for various applications, such as magneto-optical (MO) isolators, spintronic and spin wave devices. The three types of cation sites (dodecahedral, octahedral and tetrahedral) can be occupied by a wide range of ions resulting in a large variation of the physical properties of the garnet. This can be utilized to tailor its MO response or magnetic properties. To determine the contribution of each sublattice to the MO response and therefore to characterize sublattice magnetism, an analysis of spectrally dependent MO hysteresis loops can be used [1]. For this purpose, we measured field dependent polar MO Kerr effect (MOKE) spectra in the range from 1.4 eV to 4.5 eV of various ferrimagnetic garnet thin films, such as terbium iron garnet (TbIG) or yttrium iron garnet (YIG), prepared by pulsed laser deposition on GGG substrates. This allowed us to extract MOKE hysteresis loops with very high spectral resolution. The resulting hysteresis loops exhibited spectrally dependent shapes and were modelled as a sum of two hysteresis loops, shown for 300 nm thick epitaxial TbIG in Fig. 1. Moreover, their contributions to the MOKE spectra were separated as shown in Fig. 2. These results suggest that rather than sublattice contributions this analysis led to the identification of components with two different magnetic anisotropies within this particular film. The TbIG has a

strain-induced perpendicular magnetic anisotropy when grown on GGG. This anisotropy, however, may not be retained for thicker samples [2] due to strain relaxation leading to an evolution of magnetic anisotropy across the layer. These results can be compared with those on YIG films, where the spectral response of the octahedral and tetrahedral Fe sublattices can be separated. This work demonstrates field dependent MOKE spectra as an effective tool to separate not only sublattice contributions but also an evolution of magnetic anisotropy across the film.

[1] M Deb, E Popova, A Fouchet and N Keller, J. Phys. D: Appl. Phys. 45 455001 (2012) [2] V. H. Oritz, M. Aldosary, J. Li, et al. APL Materials 6, 121113 (2018)

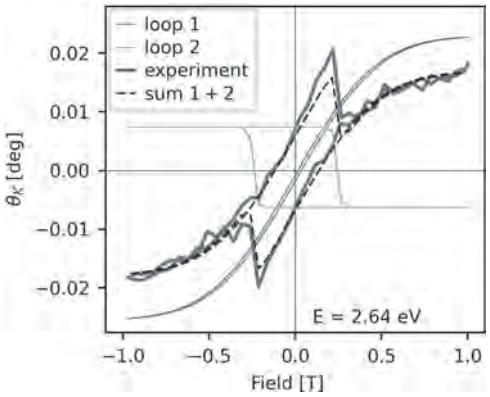

Fig. 1 Separation of MOKE hysteresis loop of 300 nm thick TbIG film on GGG

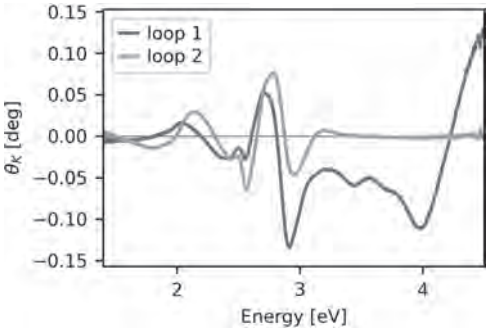

Fig. 2 Individual loop contributions to the MOKE spectra of 300 nm TbIG on GGG

JPB-04. Two-step annealing and diffusion-driven exfoliation of cerium-doped terbium iron garnet on silicon substrates. *P. Liu*[1] and K. Srinivasan[2,3] *1. Chemical Engineering and Materials Science, University of Minnesota, Minneapolis, MN, United States; 2. Electrical and Computer Engineering, University of Minnesota, Minneapolis, MN, United States; 3. Electrical and Computer Engineering, Cornell University, Ithaca, NY, United States*

Thin-film rare-earth iron garnets are very promising non-reciprocal materials for isolators or circulators in photonic devices due to large Faraday rotation and low optical absorption. However, integration of these garnets as thin films in photonic systems faces some challenges, including reduced magneto-optical properties due to poor crystallinity in as-deposited films and limited acceptable annealing of semiconductor devices. To solve these problems, cerium-doped terbium iron garnet (CeTbIG) thin films have been deposited on silicon wafers in this work by sputtering followed by various two-step annealing. During deposition, the Ce content was controlled using the bias voltage of the Ce-target for reproducible CeTbIG. A systematic study of annealing was conducted, involving a first low temperature anneal and a second crystallization treatment to determine when exfoliation will occur. Specifically, a 400°C anneal for 3 minutes followed by a set of high-temperature treatments (950°C for 30 seconds then 900°C for 5 minutes) shows excellent crystallinity without the formation of any undesired phases. This is an improvement compared to traditional single-temperature anneals. Also, the high-temperature sequence caused vacancy diffusion, leading to the formation of a gap just inside the CeTbIG thin film at the substrate interface. This gap enables easy exfoliation. By analysis of diffusivities of iron and rare-earth cations from strain rate-stress data, it was determined that the diffusion mechanism may be related to Nabarro-Herring (lattice diffusion) model. The saturation magnetization and Faraday rotation of the exfoliated CeTbIG film were measured and found comparable to those of the CeTbIG film on the silicon substrate. By applying the two-step annealing an optimized CeTbIG exfoliated films were obtained.

1. T. Fakhrul, S. Tazlaru, B. Khurana, L. Beran, J. Bauer, M. Vančík, A. Marchese, E. Tsotsos, M. Kučera, Y. Zhang, M. Veis, and Caroline A. Ross, "High Figure of Merit Magneto-Optical Ce- and Bi-Substituted Terbium Iron Garnet Films Integrated on Si'', Adv. Optical Mater. 2021, 9, 2100512 2. K. Srinivasan, A. Schwarz, J. C. Myers, N. C. A. Seaton, and Bethanie J. H. Stadler, "Diffusion-Driven Exfoliation of Magneto-Optical Garnet Nanosheets: Implications for Low Thermal Budget Integration in Si Photonics", ACS Appl. Nano Mater. 2021, 4, 11, 11888–11894

JPB-05. Design of Magnetization Yoke to Reduce the Number of Double Spoke Type PMSM Magnetization using I-Core. *D. Nam*[1] and W. Kim[1] *1. Gachon University, SeongNam-si, The Republic of Korea*

This paper conducted a study on the reduction of the number of split Magnetization and the prevention of irreversible demagnetization using the I-Core of a double spoke type motor. Recently, as interest in spoke-type motors using ferrite permanent magnets has increased, the need for research on magnetization and irreversible demagnetization in double spoke-type rotor shapes has emerged. However, in the existing spoke-type rotor shape, the magnet was deeply embedded in the rotor, making it difficult to magnetization. As it is important to use permanent magnets excluding rare earths in the future, the use of spoke-type motors becomes important, and design to consider magnetization and prevent irreversible demagnetization accordingly is important. Therefore, this paper proposed a magnetization yoke shape design in consideration of magnetization and irreversible demagnetization on using I-Core of Double Spoke type PMSM to solve this problem. Currently, the price of rare earth materials is soaring to the highest level due to the rapid increase in demand for rare earth materials worldwide. Against this background, permanent magnet motors (PMSM) using existing rare earths are increasing in manufacturing costs and the electric motor used to solve this problem is a spoke type permanent magnet synchronous motor (PMSM) using a ferrite permanent magnet. However, the general spoke type PMSM does not have much difference in inductance between the d-axis and the q-axis, so the use of the reluctance torque is small. However, this shape is a conventional magnetization model, and there is a disadvantage that it does not become a magnet when magnetization proceeds. Since there is an increase in the number of magnetization and inconvenience in a irreversible demagnetization during division and magnetization, a magnetization yoke shape is proposed to solve this problem. This study investigated the method for reducing the number of magnetization in the existing split magnetization method using I-Core of Double spoke type PMSM and the magnetization yoke shape to prevent irreversible demagnetization.

H. S. Seol, T. C. Jeong, H. W. Jun, J. Lee, D. W. Kang, "Design of 3-Times Magnetizer and Rotor of Spoke-Type PMSM Considering Post-Assembly Magnetization", IEEE Transactions on Magnetics, vol. 53, no 11, pp. 1-5, (2017) H. W. Kim, K. T. Kim, Y. S. Jo, and J. Hur,"Optimization methods of torque density for developing theneodymium free spoke-type BLDC motor," IEEE Trans.Magn., vol. 49, no. 5, pp. 2173–2176, (2013) D. -W. Nam, K. -B. Lee, and W. -H. Kim, "A study onCore Skew considering manufacturability of double-layerspoke-type PMSM," Energies 2021, 14, 610, (2021) S. I. Kim, S. Park, T. Park, J. Cho, W. Kim, and S. Lim,"Investigation and Experimental Verification of a NovelSpoke-Type Ferrite-Magnet Motor for Electric-VehicleTraction Drive Applications", IEEE Trans. Ind. Electron., vol.61, no. 10, pp. 5763-5770, (2014)

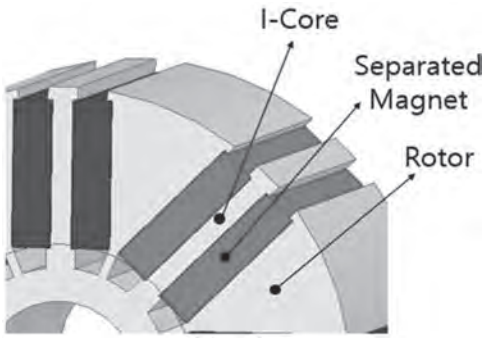

Fig. 1 It is a rotor shape using I-Core.

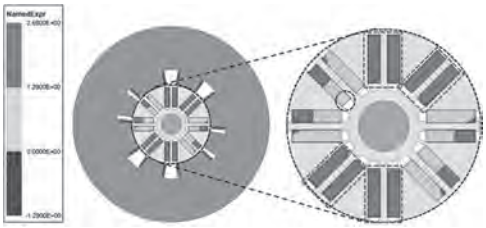

Fig. 2 It is the magnetization result of a double spoke type rotor.

JPB-06. Annealing, low temperature superparamagnetic contributions and exchange bias in samarium substituted zinc ferrite nanoparticles.
S. Ali[1] and M. Zulqarnain[2] *1. School of Physical Sciences, University of the Punjab, Lahore, Pakistan; 2. Physics, The University of Lahore, Lahore, Pakistan*

Co-precipitation method has been employed to synthesize samarium substituted zinc spinel ferrite ($ZnSm_{0.5}Fe_{1.5}O_4$) nanoparticles (NPs). The ferrites samples have been annealed at temperature 400°C, 500°C, 600°C and 700°C followed by the investigation of structural, morphological, magnetic and optical trends against the heat treatment. Cubic spinel sructure has been found [Fig. 1] with increase in average crystallite size (9-16 nm) with the increase in annealing temperature owing to Ostwald ripening process [1]. Morphology found to be agglomerated comprising of bigger grains of few hundred nanometers. Magnetic properties of $ZnSm_{0.5}Fe_{1.5}O_4$ NPs have been investigated through Vibrating Sample Magnetometer (VSM) at lower temperatures up to 5 K. At lower temperatures the overall magnetic behavior of the sample increased significantly and the values of coercivity (H_c = 11-1591 Oe) and saturation magnetization (M_s = 0.027-0.08 emu/g) are found to be increased with decrease of temperature as shown in figure 2 (a,b). Exchange bias phenomenon has been observed with considerably improved values (up to 556 Oe) at lower temperatures [Fig. 2(b)]. At such a cool environment, reduced thermal fluctuations and the very small fine NPs in blocking state play important role in tuning the basic magnetic parameters [2,3]. Through UV-Visible spectroscopy, optical behavior of $ZnSm_{0.5}Fe_{1.5}O_4$ nanoparticles manifested strong absorption in the visible region ranging 452-492 nm. Energy band gap (E_g) of as prepared and all the annealed samples have been calculated through Tauc plot showing a decreasing trend with increase in annealing temperature. The minimum value E_g = 1.54 eV has been found in our study unlike the previously reported one i. e E_g = 1.95 eV. This decrease in E_g is attributed to the possible redistribution of octahedral and tetrahedral sites owing to the smaller Δ_t as compared to Δ_o [4,5].

[1] M. Zulqarnain, S. S. Ali, Uzma Hira, J. F. Feng, M. I. Khan, M. Rizwan, K. Javed, Ghulam Farid, M. S. Hasan, Journal of Alloys and Compounds 894 (2021) 162431 [2] J. Y. Chen, N. Ahmad, D. W. Shi, W. P. Zhou, X. F. Han, J. Appl. Phys. 110 (2011) 073912 [3] S. S. Ali, W. J. Li, K. Javed, M. Irfan, Fazal-e-Aleem, G. J. Zhai, X. F. Han, J. Alloys Compd. 722 (2017) 83-87 [4] D. Sharma and N. Khare, Appl. Phys. Lett., 105 (2014) 032404 [5] B. Zhou, Y. W. Zhang, Y. J. Yu, C. S. Liao, and C. H. Yan, Phys. Rev. B. 68 (2003) 024426

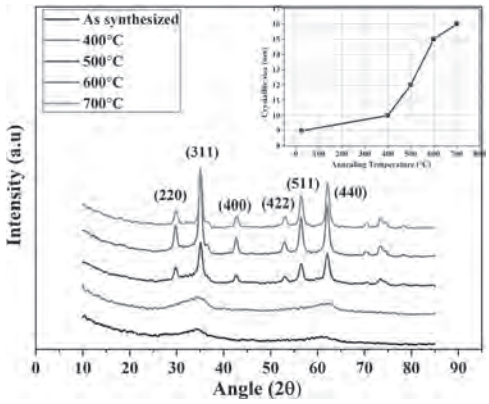

Fig. 1 XRD patterns of $ZnSm_{0.5}Fe_{1.5}O_4$ nanoparticles annealed at different temperatures. Inset shows the gradual change in average crystallite size at the cost of heat treatment.

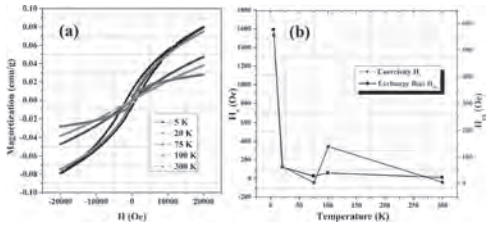

Fig. 2 (a) M-H hysteresis loops of $ZnSm_{0.5}Fe_{1.5}O_4$ nanoparticles at lower temperatures up to 5 K. (b) Temperature dependent variation in coercivity (H_c) and exchange bias (H_{ex}).

JPB-07. Magnetic and spin resonance studies of $Ni_xFe_{3-x}O_4$ ($0 \le x \le 0.7$) magnetic nano particles.
K. Prajapati[1], M. Khan[1] and G. Basheed[1]
1. BND, CSIR, New Delhi, India

In this study, we observe the effect of doping Nickel in Fe_3O_4 lattice coated with oleic acid. Fe_3O_4 particles agglomerate and lost their nanoparticle regime hence the addition of Nickel decreases the magnet moment slightly to get a good monodisperse particle and better stability in the nano region (10-12nm). In the present study, Ni Doped Fe_3O_4 MNPs were synthesized through the coprecipitation method and the single-phase has been confirmed via XRD, and coating is confirmed by FTIR. The magnetic variation is explained as Ni^{2+} ions ($3\mu_B$) have a lesser magnetic moment than Fe^{2+} ($4\mu_B$) and Fe^{3+} ($5\mu_B$) ions. As a result, $M = M_B - M_A$ gives the net magnetization. The saturation magnetization of the bulk magnetite (Fe_3O_4) is found to be lower i.e. (0.5 emu/g for x=0.7) as compared to the Ms value for the synthesized Fe_3O_4 nanoparticles (3 emu/g). Due to the presence of vacancy at the octahedral site of Fe/Ni, the magnetization value of x=0.1 decreases abnormally (fig.1). The suppression of saturation magnetization (Ms) as the concentration of Ni^{2+} ions rises might be because of the reduced magnetic field contribution by Ni^{2+} ions compared to Fe^{2+} and Fe^{3+} ions as shown in insert fig.1. To investigate the spin dynamics in $Ni_xFe_{3-x}O_4$ electron paramagnetic resonance (EPR) measurements have been performed as shown in the power adsorption derivatives (PAD) (fig 2). The resonance field (H_{res}) also lies in the range from 3.25 kOe to 3.75 kOe while increasing the Ni concentration of $Ni_xFe_{3-x}O_4$ ($0 \le x \le 0.7$) nanoparticles in corroboration with field-dependent magnetic behavior where Ni suppresses the moment and resulted in the random orientation of the spins. The decrease in peak-to-peak line width (ΔH_{PP}) is attributed to the weak magnetic interactions (super-exchange) between Ni-O-Fe with the increase in doping Ni concentration from x = 0.1 to x = 0.7. The detailed structural and electron paramagnetic resonance measurements on oleic acid-coated $Ni_xFe_{3-x}O_4$ ($0 \le x \le 0.7$) provide a tunable spin dynamic and improve the saturation magnetization, which is a key parameter for spintronics, magneto-optoelectronics, EMI shielding, and supercapacitor applications.

1. K. Usadel Phys. Rev. B. 73 (2006). 2. E. De Biasi, E. Lima, C.A. Ramos, A. Butera, R.D. Zysler, J. Magn. Magn. Mater. 326 (2013) 138–146. 3. A. Sukhov, K.D. Usadel, U. Nowak, J. Magn. Magn. Mater. 320 (2008) 31–35. 4. C.A. Ramos, E. De Biasi, R.D. Zysler, E. Vassallo Brigneti, M. Vázquez, J. Magn. Magn. Mater. 316 (2007) e63–e66.

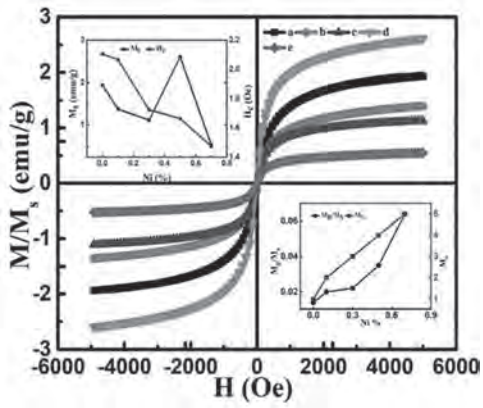

Figure 1

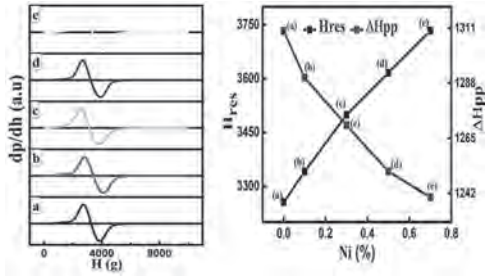

Figure 2

JPB-08. The Role of Stoichiometry in $Mn_{1-x}Zn_x$ Ferrite Microwave Absorbers. *A.S. Padgett*[1] *1. High Voltage Science and Experiment, Sandia National Laboratories, Albuquerque, NM, United States*

As 5G technology moves higher into the microwave frequency regime, the risk of coupling EM energy into susceptible electronic circuits grows. Minimizing this interference is driving the need for compact, lightweight broadband absorbers to protect sensitive and high precision electronics. Manganese zinc ferrite ($Mn_{1-x}Zn_xFe_2O_4$) microparticles have previously been demonstrated to be magnetically lossy up to 10 GHz, the desired frequency regime, and have the potential to meet the energy density and attenuation performance needs [1, 2]. However, optimizing the shielding effectiveness requires improved understanding of $Mn_{1-x}Zn_x$ stoichiometry and the dominant dielectric and magnetic absorption mechanisms for each stoichiometry. This presentation discusses results, up to 20 GHz, from experimentally investigating the shielding effectiveness and quality factor attenuation of $Mn_{1-x}Zn_xFe_2O_4$ with a mean particle size of 30 microns, loaded to 50 volume percent in epoxy, and variation in x values from 0 to 1 in intervals of 0.1. Complex permeability and permittivity measurements were conducted to identify the absorption mechanism. An increase in absorption was observed in $Mn_{1-x}Zn_xFe_2O_4$ for x=0.3 and 0.4 compared with other stoichiometries. A likely explanation of the observed increase is provided [3].

[1] T. Tsutaoka, Journal of Applied Physics 93, 2789 (2003); https://doi.org/10.1063/1.1542651 [2] R. Dosoudil, M. Usakova, J. Franek, J. Slama and A. Gruskova, "Particle Size and Concentration Effect on Permeability and EM-Wave Absorption Properties of Hybrid Ferrite Polymer Composites," in *IEEE Transactions on Magnetics*, vol. 46, no. 2, pp. 436-439, Feb. 2010, doi: 10.1109/TMAG.2009.2033347. [3] This work was supported by the Laboratory Directed Research and Development program at Sandia National Laboratories, a multimission laboratory managed and operated by National Technology and Engineering Solutions of Sandia LLC, a wholly owned subsidiary of Honeywell International Inc. for the U.S. Department of Energy?s National Nuclear Security Administration under contract DE-NA0003525.

JPB-09. Study of crystallite size on magnetic properties of nanocrystalline $FeCo_2O_4$. *D. Verma*[1], A. Verma[1], T. Maitra[1] and G.D. Varma[1] *1. Physics, Indian Institute of Technology Roorkee, Roorkee, India*

In the present work, the effect of crystallite size on the magnetic properties of nanocrystalline $FeCo_2O_4$, synthesized by co-precipitation technique, has been studied. The as synthesized sample has been annealed at 500, 900 & 1000 to vary the crystallite size. The XRD results confirm the presence of single cubic phase in all the annealed samples and increase in the crystallite size with the increasing annealing temperature. FESEM images show the spherical morphology of prepared nanoparticles which become irregular in shape as temperature increases and particle size also increases with increasing annealing temperature. XPS analysis confirms the mixed oxidation states of Fe with Fe^{+2} and Fe^{+3}, Co with Co^{+2} and Co^{+3}. The temperature dependence magnetization (M-T curves) and field dependence magnetization (M-H curves) at different temperatures have been measured using Quantum design MPMS3 SQUID magnetometer. The low temperature M-H curves show the presence of metamagnetic phase transition in the samples annealed at 900 °C and 1000 °C. This possibly occurs due to the co-existence of ferromagnetic and antiferromagnetic phases in the synthesized samples. The coexistence of AFM and FM phases may be attributed to spin canting/surface spin disorder in nanocrystalline magnetic nanoparticles. Furthermore, the samples annealed at higher temperature show strong ferromagnetism, higher saturation magnetization, higher coercivity and remanence. Moreover, the M-H curves, measured below 100 K, of the samples annealed at 500 °C and 900 °C show jumps in the magnetization value at certain magnetic fields (see Fig. 1). The detail correlation between structural and observed magnetic properties will be described and discussed in this paper.

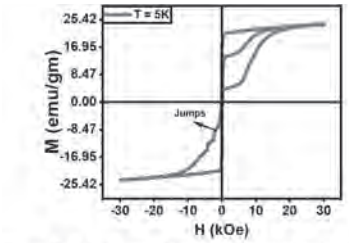

Fig. 1: The M-H curve of the sample annealed at 900 °C, measured at 5 K, showing jumps in the magnetization (marked by arrow).

JPB-10. Magnetic Hyperthermia of AFe_2O_4 (A=Fe, Mn, Co) Nanoparticles Prepared by Co-precipitation Method. A. Chandel[1], *Y. Kaur*[1] and B. Chudasama[1,2] *1. School of Physics and Material Science, Thapar Institute of Engineering and Technology, Patiala, India; 2. TIET-VT Center of Excellence in Emerging Materials, Thapar Institute of Engineering and Technology, Patiala, India*

With 10 million deaths in 2020 cancer remains one of the most challenging diseases in contemporary medicine. Chemotherapy, surgery, and radiation therapy are commonly used to treat cancer. These treatments severely harm healthy tissues and succeed rarely in advance stages of disease. Recent studies indicate that magnetic hyperthermia, which involves targeted delivery of magnetic nanoparticles to tumor cells followed by localised remote heating of cancer tissues could revolutionise clinical practice in the treatment of cancer, either as standalone intervention or adjunct to radiotherapy and chemotherapy. Water dispersible magnetic nanoparticles (MNPs) of ferrites (AFe_2O_4; A=Fe, Mn, Co) are the promising candidates for magnetic hyperthermia due to their high chemical stability, biocompatibility, moderate magnetization and high specific absorption rates (SAR). In this article, we have evaluated magnetic hyperthermia efficiency of water based magnetic fluids of AFe_2O_4 nanoparticles. AFe_2O_4 nanoparticles were

synthesized by chemical co-precipitation method. Nanoparticles were coated with a bilayer of oleic acid and dispersed in water. MNPs concentrations in magnetic fluids were 70 mg/mL for Fe_3O_4, 200 mg/mL for $MnFe_2O_4$ and 60 mg/mL for $CoFe_2O_4$. Structural and magnetic properties of MNPs were investigated by X-Ray diffraction (XRD) and vibrating sample magnetometer (VSM), respectively. XRD study revealed that AFe_2O_4 NPs exhibits cubic inverse spinel structure. Fe_3O_4 (M_s = 48 emu/g, M_r = 2.60 emu/g, H_c = 49 Oe), $MnFe_2O_4$ (M_s = 40 emu/g, M_r = 2.60 emu/g, H_c = 35 Oe) and $CoFe_2O_4$ (44 emu/g, M_r = 10.10 emu/g, H_c =440 Oe) NPs exhibits soft ferromagnetic behaviour. Magnetic hyperthermia measurements were performed as a function of magnetic field strength (2-10 mT) and field frequency (162-935.6 kHz) for 10 minutes. MNPs exhibits highest SAR values for 10 mT field strength at 935.6 kHz. Amongst the tested MNPs, Fe_3O_4 has the highest SAR value (27.35 W/g), followed by $MnFe_2O_4$ (1.91 W/g) and $CoFe_2O_4$ (0.94 W/g). Considering this, it is concluded that amongst the inverse spinel ferrite nanostructures AFe_2O_4 (A=Fe, Mn, Co), Fe_3O_4 nanoparticles are most suitable for magnetic fluid hyperthermia applications.

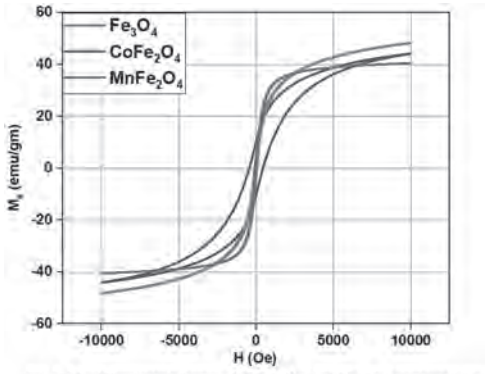

Fig 1. M – H hysteresis loops of AB_2O_4 (A = Fe, Mn, Co) nanoparticles

JPB-11. Structural, Magnetic and Magnetocaloric study of Cr doped Gd_3Fe_{5-x} Cr_xO_{12}, ($0.0 \le x \le 0.3$). *J. Sultana[1] 1. Physics, The University of Texas at Arlington, Arlington, TX, United States*

The rare-earth iron garnets $R_3Fe_5O_{12}$ are important magnetic materials due to their ferrimagnetic property above room temperature. Some of them are potential candidate materials in magnetic refrigeration, which works on the magnetocaloric effect (MCE). Researchers have focused on improving the magnetic entropy change along with these garnet's relative cooling power (RCP), primarily via doping strategies. This study reports the structural, magnetic, and magnetocaloric effect in Cr-doped Gd_3Fe_{5-x} Cr_xO_{12} garnet. The powder samples with a composition of $Gd_{3-x}RE_xFe_5O_{12}$ (x=0.0,0.1,0.2,0.25 and 0.3) were prepared via facile autocombustion method followed by an annealing process. The phase and structural properties obtained by using x-ray diffraction show samples are single-phase with cubic *Ia3d*symmetry. The lattice parameter and cell volume decreased upon Cr^{3+} substitution because of the preferential occupation of smaller Cr^{3+} (0.615A) ions at the octahedral site of Fe^{3+} (0.645A) ions. All Cr^{3+} doped samples showed paramagnetic behavior at RT and ferromagnetic behavior at 6 K. The isothermal magnetic entropy changes, $-\Delta S_M$, was derived from the magnetic isotherms in a field up to 5T. The maximum magnetic entropy change, increased with Cr^{3+} substitution. The Cr^{3+} doped $Gd_3Fe_{4.75}Cr_{0.25}O_{12}$ sample exhibit a maximum value of (3.87 J $kg^{-1}K^{-1}$) which is ~ 1.8% higher than $Gd_3Fe_5O_{12}$ (3.8 J $kg^{-1}K^{-1}$) sample. While the maximum relative cooling power value of 412 J kg^{-1} was measured for the x = 0.25 sample, which is ~ 6 % higher than $Gd_3Fe_5O_{12}$ (389 J kg^{-1}) sample. These values are relatively high and comparable to some noticeable magnetocaloric materials. The observed magnetic changes are ascribed to altered Fe-O-Fe bond angle and bond distances. Thus, based on these results, our samples are promising materials for magnetic refrigeration technology. Authors: J. Sultana, Dr. J. Mohapatra, Dr. S. R. Mishra.

JPB-12. Structural, Magnetic, and Magnetocaloric Study of Rare Earth-doped $Pr_{0.6-x}RE_xCa_{0.4}MnO_3$ (x=0.1; RE = Nd, Sm, Eu, and Y) Manganite Nanoparticles Synthesized via Autocombustion Method. *J. Sultana[1] 1. Physics, University of Arkansas, Fayetteville, AR, United States*

Perovskite manganites having the general formula, R_{1-x} A $_xMnO_3$ (where R is a rare-earth ion and A an alkaline-earth ion) have been considered as potential candidates for magnetic refrigeration based on MCE because of the large magnetic entropy change at moderate fields. Also their extraordinary chemical stability and tunable phase transitions are also added advantages to choose manganites for magnetic refrigeration applications. The study reports the structural, magnetic, and magnetocaloric effect in rare-earth-doped Perovskite manganite $Pr_{0.6-x}RE_xCa_{0.4}MnO_3$(x=0.1; RE=Nd, Sm, Eu,Y), PRECMO. The powder samples were prepared by a facile autocombution method followed by annealing at 1100 C for 12 hours. Structural characterization was done through XRD, SEM, and FTIR analysis. XRD pattern reveals that all the PRECMO samples crystallize in the perovskite phase with an orthorhombic structure (space group Pnma). The lattice parameter of the powder samples was calculated from the XRD pattern refinement, which showed a decrease in lattice parameter and volume upon rare-earth substitution in Nd<Sm<Eu<Y order. This systemic change in the lattice volume is the result of the lanthanide contraction of RE ionic radii. FTIR spectra identify the characteristic Mn–O bond stretching vibration mode near 60cm^{-1} which shifts toward high wavenumbers due to distortion of the MnO6 octahedron with RE substitution. Field-cooled (FC) and zero-field cooled (ZFC) magnetization were measured at 100 Oe. The magnetic phase transition temperature for all RE^{3+} doped manganite lies below 100 K. Isothermal magnetization curves were investigated in the temperature range of 5-300 K in fields up to 8T. All RE^{3+} doped samples showed paramagnetic behavior at RT and ferromagnetic behavior at 5K. Nd-doped PRECMO showed maximum magnetization of 65 emu/g, followed by Eu,Y, and Sm. The purpose of this work is to investigate the magnetocaloric effect for low-temperature magnetic refrigeration applications. The magnetic isotherms are being investigated to derive the compound's maximum entropy change and relative cooling power. Authors: J. Sultana, Dr. J. Hu, Dr. S. R. Mishra.

JPB-13. Structural, Magnetic, and Magnetocaloric effect in Al-doped $HoCrO_3$. *J. Sultana[1] 1. Physics, Buffalo State College, Buffalo, NY, United States*

Rare-earth chromites ($RCrO_3$) are an important sub-class of functional materials with interesting magnetic and magnetocaloric properties. These materials are a promising candidate for magnetic refrigeration applications as the Ho^{3+} ion owns a large magnetic moment of ~ 10.61$_{\mu B}$. This study reports synthesis and magnetocaloric effect in rare-earth and aluminum-doped polycrystalline $HoCrO_3$, $Ho_{0.67}Tm_{0.33}CrO_3$, and $Ho_{0.67}Gd_{0.33}CrO_3$ orthochromites. The samples were synthesized via the facile sol-gel autocombustion method. The pure orthorhombic phases with space group Pnma have been confirmed by X-ray diffraction. The lattice parameter of the samples was calculated from the XRD pattern refinement. The lattice parameters and volume decreased with the Al^{3+} substitution as the ionic radius of Al^{3+} (0.535 A) is smaller than Cr^{3+} (0.615A). In addition, the FTIR spectroscopy confirmed the formation of the Ho–O bond, and Cr–O, and Cr–Cr bonds in all samples. Raman's study confirmed the stretching vibration mode of CrO_6 octahedra near 580 cm^{-1}. The magnetic measurement of compounds showed that the samples exhibit a transition below 20 K. Enhanced magnetization and increased magnetic entropy change, () from 6.50 J $kg^{-1}K^{-1}$ ($HoCrO_3$) to 8.25 $Jkg^{-1}K^{-1}$ ($HoCr_{0.5}Al_{0.5}O_3$) was observed in the field up to 5T. A variation in maximum entropy changes and relative cooling power is observed to be dependent on Al^{3+} substitution in the studied chromites which are related to changes in Cr^{3+}-Cr^{3+} exchange coupling resulting from changes in the Cr1-O1-Cr1 bond angle and Cr1-O1 bond lengths respectively. To our knowledge, Al^{3+} doped $HoCrO_3$ has not been reported in the literature. The studied Al^{3+} doped chromites have potential low-temperature magnetic refrigeration application. Authors: J. Sultana, Dr. A. K. Pathak, Dr. S. R. Mishra

JPB-14. Effect of Oxidation on the Microwave Absorption Properties of Rare-earth Intermetallics $La_2Fe_4Co_{10}B$. *K. Li*[1,2], Z. Liu[1], Y. Wang[1], P. Zhang[1], W. Yang[1], J. Han[1], S. Liu[1], C. Wang[1] and J. Yang[1] *1. State Key Laboratory for Mesoscopic Physics, Beijing, China; 2. Beijing Key Laboratory for Magnetoelectric Materials and Devices, Beijing, China*

Microwave absorbers are increasingly being used to enhance shielding performance at higher frequencies. Great effort has been made to develop materials with superior reflection loss (RL), thin thickness, wide bandwidth, and low density to improve their efficiency in electromagnetic microwave absorption. However, for the magnetic absorbing materials, the higher complex permittivity makes the impedance matching effect poorer, and it is hard to obtain a better microwave absorption. In this work, the rare-earth intermetallics $La_2Fe_4Co_{10}B$ fine powders with planar magnetocrystalline anisotropy and high magnetization were prepared using the hydrogenation desorption (HD) technique. By annealing the obtained magnetic powders at different temperatures in the air to slowly form an oxide layer on their surfaces, its complex permittivity can be significantly reduced without changing its complex permeability, and its microwave absorption can be dramatically enhanced. For the $La_2Fe_4Co_{10}B$/paraffin composite, the real part of the complex permittivity at 10 GHz can be reduced from 18.0 to 8.4, with a decreasing range of 53.3%. The reflection loss (RL) is -25.4 dB at 1.6 mm with an effective absorption bandwidth of 6.2 GHz. As an efficient and lightweight absorber, $La_2Fe_4Co_{10}B$/paraffin composite has potential application value in constructing new microwave absorber.

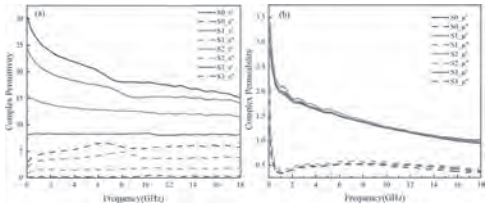

Fig.1. Frequency dependence of electromagnetic parameters of $La_2Fe_4Co_{10}B$/paraffin composites with different annealing temperatures: (a) the complex permittivity; (c) the complex permeability.

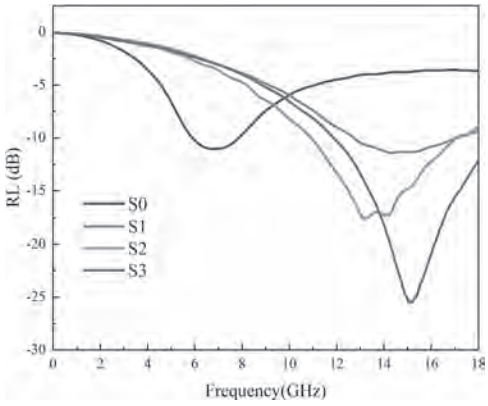

Fig.2. The RL curves with the broadest effective absorption bandwidth of $La_2Fe_4Co_{10}B$/paraffin composites with different annealing temperatures.

JPB-15. Withdrawn

Session JPC
SOFT MAGNETIC CRYSTALLINE ALLOYS II
(Poster Session)

Nicola Morley, Chair
University of Sheffield, Sheffield, United Kingdom

JPC-01. First-order-reversal curve study of inhomogeneous microstructures in high-strain-rate deformed steels. *S. Kobayashi*[1], A. Odeshi[2] and J. Szpunar[2] *1. Iwate university, Morioka, Japan; 2. University of Saskatchewan, Saskatoon, SK, Canada*

Investigations and quality improvement of structural steels with high resistance to impact loading, used for automobile parts, are critically important because of minimizing passenger's injuries during a crash. Extensive microstructural investigations revealed that high-strain-rate deformation under impact loading leads to the formation of hard and narrow adiabatic shear band in a soft matrix [1]. The formation of such inhomogeneous microstructure results from excessive thermal softening and thermo-viscous instability, leading to strain localization. Despite the recent growing understanding of the formation mechanism, effects on physical properties were not understood because of few reports available. Here, we report results of measurements of magnetic first-order-reversal curves (FORCs) for high-strain rate deformed steels for the possible application to non-destructive evaluation (NDE) of inhomogeneous microstructural changes. FORCs are one kind of asymmetrical minor loops and provide useful information on interaction field (Hu) and coercivity (Hc) distribution, which can not be obtained from conventional major hysteresis loop. Cylindrical samples of high-tensile AISI4340 steels were subjected to high-strain-rate deformation using a split Hopkinson pressure bar. We prepared samples with different strain rates up to 4500 s^{-1}. FORCs were measured at room temperature using a SQUID magnetometer. Figure 1(a) and 1(b) show FORC diagrams after high-strain rate deformation with a strain rate of 1800 and 4500 s^{-1}, respectively. In addition to a large FORC distribution peak which extends along Hu direction (peak 1), we found that a small additional peak appears at Hc~400 Oe (peak 2 in Fig.1), whose position gradually shifts toward a higher Hc with increasing strain rate. This indicates that a small fraction of magnetically hard regions (i.e. adiabatic shear bands) are formed in a soft matrix and the regions become magnetically harder at higher strain rate. These observations clearly demonstrate that FORCs can be a useful technique of investigating inhomogeneous microstructures under impact loading.

[1] A. G. Odeshi, M. N. Basim, et al., J. Mater. Proc. Tech. vol.169 (2005) 150. [2] B.C. Dodrill, J. Lindemuth, C. Radu, H. Reichard, MRS Bulletin vol.40 (2015) 903.

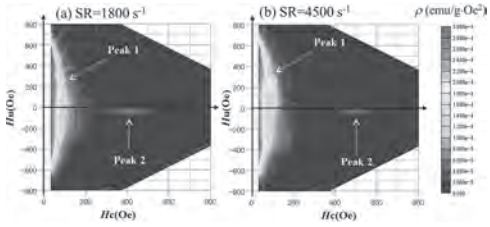

Fig. 1 FORC diagram after high-strain rate deformation with a strain rate (SR) of (a) 1800 and (b) 4500 s^{-1}.

JPC-02. Magnetic properties of Fe-Ni films deposited on a non-conductive substrate using an electroless plating method. *R. Shiokawa*[1], Y. Hidaka[1], A. Yamashita[1], T. Yanai[1], M. Nakano[1] and H. Fukunaga[1] *1. Nagasaki University, Nagasaki, Japan*

In recent years, the driving frequency of electric equipment has increased, and we need to reduce eddy current loss to apply typical metallic soft magnetic materials into high-frequency driving equipment. As a practical method to reduce the loss is a reduction in the thickness, we recently reported a fabrication process of Fe-Ni thin films (< 10 μm) using an electroless plating method [1]. Although many reports for electroless deposited Fe-Ni films, as well as ours, employed conductive substrates [2-3], the conductive substrates are not suitable since eddy current also flows in the substrates. We, therefore, focused on the polyimide (PI) used as a non-conductive substrate and investigated a fabrication process of Fe-Ni films using the PI substrate. Since the PI does not have catalytic activity for the deposition of Fe-Ni films, we investigated a chemical metallization process of PI [4]. First, we immersed the PI sheet in a KOH solution and then in an $AgNO_3$ one. By these immersions, the PI sheet obtains catalytic activity. The details of our electroless plating process are described in Ref. [1]. To obtain suitable conditions for the metallization of the PI surface, we investigated the effect of immersion time in KOH and $AgNO_3$ on the film thickness. Figure 1 shows the thickness as a function of the immersion time in each solution. The thickness slightly increased with increasing the immersion time in $AgNO_3$, and we observed the correlation between thickness and the immersion time in KOH, implying that the immersion time in KOH is more important than that for $AgNO_3$. Figure 2 shows the coercivity of the films as a function of thickness. We changed the thickness by adjusting the DMAB concentration or the deposition time. In our experimental conditions, the coercivity increased with increasing the thickness due to an increase in the roughness, and the value of coercivity was almost the same as previously reported ones (H_c =30-96 A/m) using conductive substrates [1-3.5]. We, therefore, concluded that the Fe-Ni films with low coercivity could be obtained by the optical metallization of the PI surface.

[1] T. Yanai *et al.*, *AIP Advances*, Vol.10 ,#015047 (2020) [2] R. Anthony *et al*., *Applied Surface Science*, Vol.357, pp.385-390 (2015) [3] M. Takai *et al*., *IEICTE Trans. Electron*., Vol.E78-C, pp. 1530-1535 (1995) [4] G. Stéphane *et al.*, *Applied surface science,* Vol.307, pp.716-723 (2014) [5] T. Yokoshima *et al*., *Journal of Electroanalytical Chemistry*, Vol.491, pp.197-202 (2000)

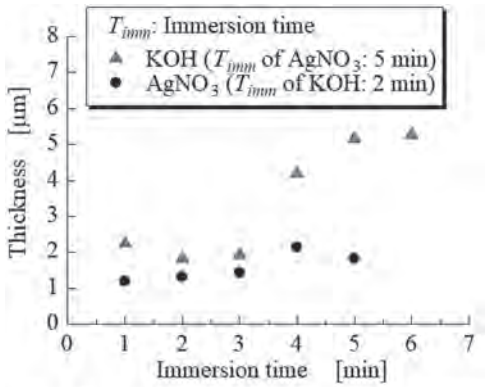

Fig.1 Thickness as a function of the immersion time.

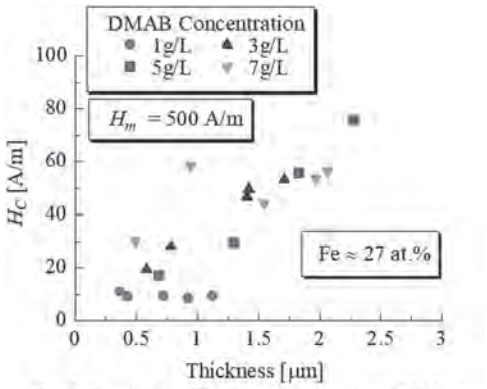

Fig.2 Coercivity of the films as a function of thickness.

JPC-03. Soft magnetic bilayer thin ribbons prepared using an electroplating method. *Y. Yamaguchi*[1], Y. Hayashida[1], A. Yamashita[1], T. Yanai[1], M. Nakano[1] and H. Fukunaga[1] *1. Nagasaki University, Nagasaki, Japan*

In recent years, metallic soft magnetic materials, which can be used at high frequency, have been strongly required due to the development of power electronics techniques. When driving the metallic materials at a high frequency, we need to reduce the thickness or control the magnetization process (the anisotropy) to reduce eddy current loss. In the present study, we focused on an electroplating method to prepare thin ribbons and a bilayer structure to control the direction of anisotropy using the magnet elastic effect. To construct a bilayer structure, we firstly electroplated 8 μm-thick Fe_6Ni_{94} films on a stainless substrate and then electroplated 8 μm-thick $Fe_{56}Ni_{44}$ films. The plating bath and conditions were almost the same as ref [1]. Figure 1 shows a schematic representation of the electroplating, and we prepared 140 mm-long bilayer films. After electroplating, the bilayer film was peeled off from the substrate. The ribbon (peeled film) formed into a toroidal core (D = 10 mm). Figure 2 shows the hysteresis loop of the core, and the difference between the loops is the inside layer. The blue and red loops are for the inside layer of Fe_6Ni_{94} and $Fe_{56}Ni_{44}$, respectively. An obvious difference was observed between the two loops. It is well-known that the magnetostriction constant of Fe-Ni alloys depends on the composition. The sing of magnetostriction constant for Ni-rich phase such as Fe_6Ni_{94} is negative, whereas Fe-rich one such as $Fe_{56}Ni_{44}$ is positive. When the ribbon formed a toroidal shape, bending stress is induced in the ribbon. The stress of the outer side and the inner one is tension and compression, respectively. In the case of the inside layer of $Fe_{56}Ni_{44}$, the directions of the induced anisotropy are perpendicular to the ribbon axis for both phases, indicating that the easy axis is perpendicular to the ribbon axis. Consequently, the permeability and the hysteresis loss decrease. As the perpendicular anisotropy is effective in reducing the eddy current loss, we found that thin bilayer ribbons, which consist of two phases with positive and negative magnetostriction, are an attractive structure for high-frequency applications.

[1]T. Yanai, J. Kaji, K. Koda, K. Takashima, M. Nakano, H. Fukunaga, "Magnetic Properties of Exchange-Coupled Fe-Ni/$Fe_{22}Ni_{78}$ Double-Layered Thick Films", *IEEE Transactions on Magnetics*, 54 (2018) #2002503.

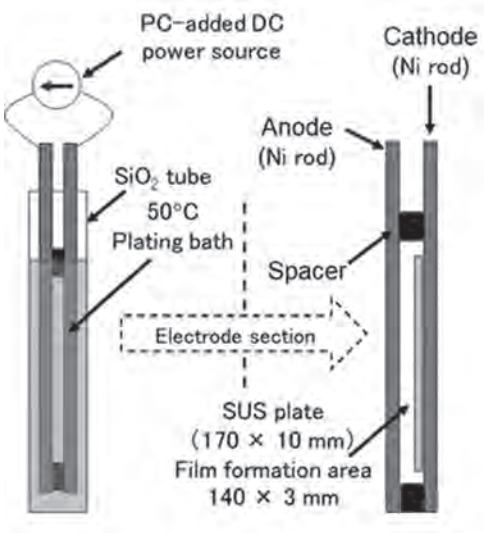

Fig.1 schematic representation of the electroplating.

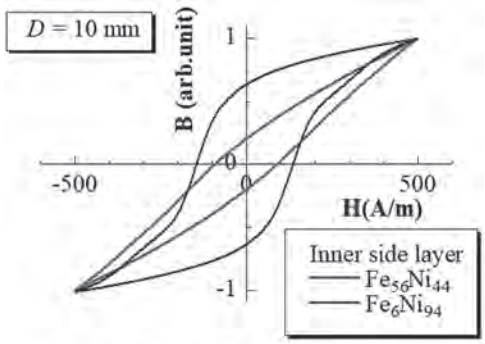

Fig.2 B-H loops of a toroidal core prepared from the $Fe_6Ni_{94}/Fe_{56}Ni_{44}$ bilayer ribbon.

JPC-04. Tunable magnetocrystalline anisotropy and high-frequency magnetic properties of $Y_2(Co_{1-x}Fe_x)_{17}$ and their composites. *P. Zhang*[1,2], Y. Wang[1,2], C. Yun[1,2], W. Yang[1,2], C. Wang[1,2] and J. Yang[1,2] *1. State Key Laboratory for Mesoscopic Physics, School of Physics, Peking University, Beijing, China; 2. Beijing Key Laboratory for Magnetoelectric Materials and Devices, Beijing, China*

Rare-earth transition-metal (R-T) intermetallic compounds are emerging as competitive candidates for novel microwave absorption materials (MAMs) since they show high magnetization and tunable easy magnetization directions (EMDs). In this work, $Y_2(Co_{1-x}Fe_x)_{17}$ ($0 \le x \le 0.3$) compounds with the Th_2Ni_{17} hexagonal structure were prepared with the purpose of tuning the EMDs. As x increases, the EMDs of the $Y_2(Co_{1-x}Fe_x)_{17}$ compounds change from the ab-plane ($0 \le x < 0.0329$) to the cone ($0.0329 \le x \le 0.038$) and then to the c-axis direction ($0.038 < x \le 0.3$). Furthermore, it was found that the extremely high cutoff frequency of the uniaxial anisotropy materials gives them considerably potential for microwave absorption applications above 10 GHz, despite their relatively low initial permeability compared to the planar anisotropic materials. By studying the high-frequency properties of $Y_2(Co_{1-x}Fe_x)_{17}$/paraffin composites, it is noted that uniaxial anisotropy compounds with x=0.1 and x=0.3 can possess higher permeability above 10 GHz as compared to both planar anisotropy and conical anisotropy

compounds (x<0.1) due to their high cutoff frequencies arising from large magnetocrystalline anisotropy fields. This can improve the impedance matching and thus lead to a better microwave absorption performance in the range of 10 to 40 GHz for materials with uniaxial anisotropy. Among all the compositions, the $Y_2(Co_{0.9}Fe_{0.1})_{17}$/paraffin composite exhibits a minimum reflection loss (*RL*) of -50 dB at 6 GHz with a thickness of 2.5 mm and a wide qualified bandwidth (*QB*, *RL*<-10 dB) of 9.6 GHz at a center frequency of 30.3 GHz with a thickness of 0.6 mm, thus making it a promising candidate for MAMs above 10 GHz.

R.S. Perkins, H. Nagel, The magnetocrystalline anisotropy of Y2(Co1-xFex)17, Phys. B+C. 80 (1975) 143–152. J.M. Silveyra, E. Ferrara, D.L. Huber, T.C. Monson, Soft magnetic materials for a sustainable and electrified world, Science. 362 (2018). E.A. Périgo, B. Weidenfeller, P. Kollár, J. Füzer, Past, present, and future of soft magnetic composites, Appl. Phys. Rev. 5 (2018) 031301. J. Yang, W. Yang, F. Li, Y. Yang, Research and development of high-performance new microwave absorbers based on rare earth transition metal compounds: A review, J. Magn. Magn. Mater. 497 (2020) 165961.

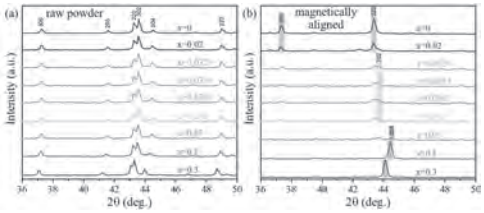

Fig. 1. X-ray diffraction patterns of (a) $Y_2(Co_{1-x}Fe_x)_{17}$ (0≤x≤0.3) raw powders and (b) magnetically aligned $Y_2(Co_{1-x}Fe_x)_{17}$ (0≤x≤0.3) powders indicating the changing of the EMD with x.

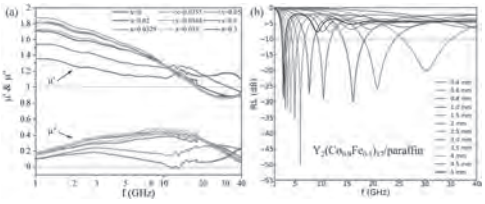

Fig. 2. Frequency dependences of (a) complex permeability of $Y_2(Co_{1-x}Fe_x)_{17}$/paraffin composites (0≤x≤0.3) and (b) reflection loss of the $Y_2(Co_{0.9}Fe_{0.1})_{17}$/paraffin composite at various thicknesses.

JPC-05. The microwave absorption properties of several soft magnetic materials in frequency up to 40GHz. *Y. Wang*[1,2], P. Zhang[1], Z. Liu[1], K. Li[1], W. Yang[1], J. Han[1], S. Liu[1], C. Wang[1] and J. Yang[1] *1. State Key Laboratory for Mesoscopic Physics, Beijing, China; 2. Beijing Key Laboratory for Magnetoelectric Materials and Devices, Beijing, China*

With the development of the 5G applications, micrometer and millimeter microwaves have been full filling the space around people. They not only interfere with tons of electronic devices but damage human health as well. To combat these problems, there is an urgent need for microwave absorption materials. However, most of the research on microwave absorption materials stays within the 2~18GHz frequency range, while the 5G millimeter microwave's frequency can reach up to 24GHz or higher. Thus, more studies of microwave absorption properties in a higher frequency band are necessary. In this work, we report the microwave absorption properties of several soft magnetic composites in frequency up to 40GHz. Common materials such as iron, $Y_2Fe_{16}Si$, $Ce_2Fe_{17}N_{3-\delta}$, $La_2Fe_4Co_{10}B$ micron powders which experience excellent microwave absorption properties in 2~18GHz are included. Within 2~40GHz, the reflection loss(RL) of iron/paraffin, $Y_2Fe_{16}Si$/paraffin, $Ce_2Fe_{17}N_{3-\delta}$/paraffin and $La_2Fe_4Co_{10}B$ /paraffin composites could reach -46.2dB, -71.4dB, -49.1dB, and -49.0dB, respectively. And their effective absorption bandwidth(RL<-10dB) could reach 16.9GHz, 8.53GHz, 10.08GHz, and 7.4GHz, respectively. Though the measurements are extended to 40GHz, the RL of most of these materials could not maintain a low level at 40GHz, which is restricted by the cutoff frequencies of the materials. The measured data shows that these soft magnetic composites are good candidates for high-frequency microwave absorption materials, while exploring magnetic materials with further higher cutoff frequencies may result in a better performance.

Hu, Q. W., Qiao, G. Y., Yang, W. Y. et al., J. Phys. D: Appl. Phys., Vol. 53, p.115001 (2020) Qiao, G. Y., Yang, W. Y., Lai, Y. F. et al., Mater. Res. Express., Vol. 6, p.016103 (2019) Zuo, W. L., Qiao, L., Chi, X. et al., J. Alloys Compd., Vol. 509, p.6359-6363 (2011)

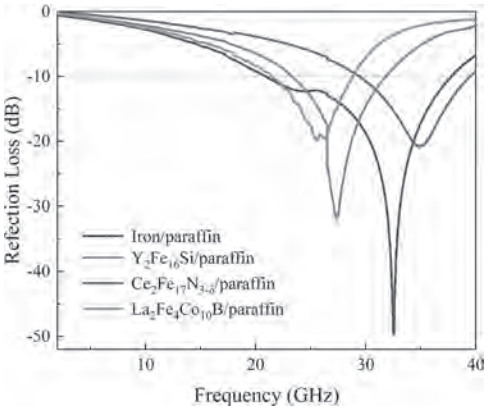

Fig.1 The RL curves with the broadest effective absorption bandwidth of different composites.

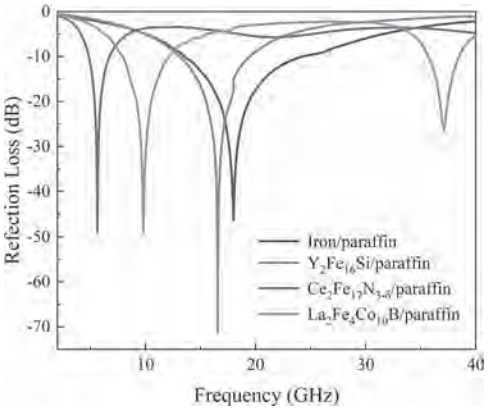

Fig.2 The RL curves with the minimum RL of different composites.

JPC-06. Effect of Si/Al addition on magnetic properties of Fe-Co alloy. *T. Sato*[1] and H. Takabayashi[1] *1. Research and Development Laboratory, Daido Steel Co., Ltd., Nagoya, Japan*

Introduction Motor-driven systems are estimated to use over 40% of all global electricity consumption, giving rise to over 6 Gt of CO_2 emissions [1]. To reduce the impact, motors should have higher efficiency. Electrical steels, Fe-Si which have low iron losses are commonly used as soft magnetic materials for motors but higher B_s materials have been desired for higher power density motors. It is well known that Fe-Co alloys have the highest B_s among bulk, stable materials. In fact, Permendur, 49Fe-49Co-2V (mass %) is already used in some high-performance motors, since it has a good soft magnetic properties. However, the drawbacks of Permendur are poor workability owing to the existence of a the brittle B2 phase (ordered phase). In this study, we first conducted neutron diffraction measurements on the Fe-Co alloys with different Co contents to check the existence of the B2 phase in these alloys. And then, the effect of Si/Al addition on magnetic properties of 82Fe-18Co alloy was investigated in order to improve the soft magnetic properties. Experimental Procedures Four samples with different Co contents (49Fe-49Co-2V, 73Fe-27Co, 82Fe-18Co, and 95Fe-5Co) were prepared through melting, casting, forging and annealing processes. The

neutron diffraction study was conducted with iMATERIA spectrometer at the Materials and Life Sciences Facility at the J-PARC (Japan Proton Accelerator Research Complex). For the study of Si/Al addition, 0.2 mm-thick sheets with the addition of Si/Al in the range of 0~1.75 mass% were prepared by melting, casting process, followed by forging, annealing, hot and cold rolling processes. Magnetic properties were measured with a BH-tracer. Results The result showed that 49Fe-49Co-2V and 73Fe-27Co alloys contained the B2 phase. On the other hand, 82Fe-18Co and the 95Fe-5Co did not contain B2, which suggests that these two alloys will likely to have good workability. Therefore, we chose 82Fe-18Co alloy for the investigation of Si/Al addition. Fig. 1 shows the soft magnetic properties of 82Fe-18Co with and without Si/Al addition. It was found that the small addition of Si/Al reduced the iron loss while maintaining high B_s.

[1] Paul Waide & Conrad U. Brunner et al., IEA Energy Efficiency Series, Working Paper, 2011.

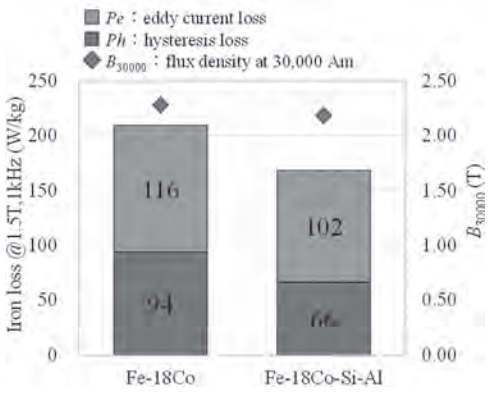

Fig. 1 Effect of Si and Al addition on the soft magnetic properties of Fe-18Co alloy

JPC-07. Study on the Loss Characteristics of Silicon Steel with Different Si Content Considering the Effect of Temperature. *D. Ma*[1], B. Tian[1] and R. Pei[1] *1. Department of Electric Engineering, Shenyang University of Technology, Shenyang, China*

Motor cores usually operate at high temperatures, and the temperature affects their magnetic properties. It has been shown that the iron loss of 3.5% silicon steel decreases with the increase of temperature, and a model of iron loss considering the effect of temperature is proposed[1-2], but this model is not applicable to high silicon steel. It is reported that the iron loss of 6.5% silicon steel increases with the temperature[3]. Therefore, the study on the evolution of the temperature-dependent iron loss of silicon steel with different Si contents is particularly important, and there are few studies in this area. In the second part of this paper, the magnetic properties of silicon steels with different Si contents (2.5%, 3.5%, 4.5%, 5.5%, 6.5%) were tested at variable temperatures (-70°C-200°C) using a self-built multi-physical field coupling test system and non-standard ring sample test method, as shown in Fig 1. Some of the experimental results are shown in Fig 2, which reveal variation of iron loss law of silicon steel with different Si content under the effect of temperature, and explain the reason of this phenomenon from the internal microstructure of the material. The third part of this paper uses the above experimental data to reconstruct the loss model for a 6.5% silicon steel. The correlation analysis of temperature effects on eddy current losses and hysteresis losses of high silicon steel is carried out respectively, and the temperature-dependent loss coefficients are added to the corresponding mathematical model. The fourth part of this paper compares the experimental test data of high silicon steel loss, the calculated data of traditional loss model and the calculated data of this loss model to analyze their error accuracy, and finally verifies that for the loss calculation of high silicon steel, the proposed iron loss model is more accurate than the traditional calculation model. Finally, this study will be of greater guidance for the design of subsequent high-silicon steel motors.

[1] J. Q. Chen, D. Wang, and S. W. Cheng,"Modeling of temperature effects on magnetic property of non-oriented silicon steel lamination," vol.51, no.11, Nov. 1, 2015. [2] N. Takahashi, M. Morishita, D. Miyagi, "Examination of magnetic properties of magnetic materials at high temperature using a ring specimen,",vol. 46, no. 2, pp. 548–551, Feb.2010. [3] Ou, J, Liu, Y, Breining, P, Experimental Characterization and Feasibility Study on High Mechanical Strength Electrical Steels for High-Speed Motors Application. 57(1), 284-293.

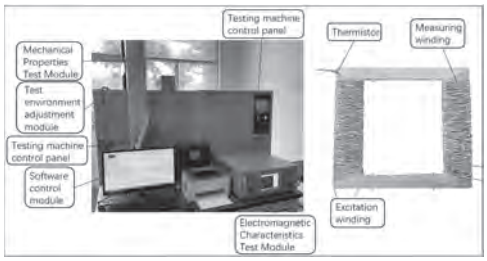

Fig.1 Multiphysics coupled magnetic performance testing system and test sample

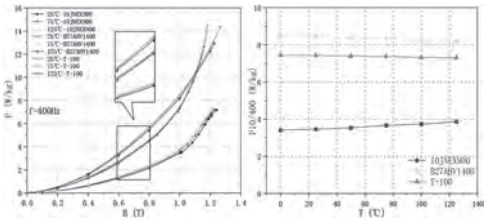

Fig.2 (left) Iron loss curves at different temperatures. (right) Variation of iron loss with temperature

JPC-08. Measurement of magnetic properties of grain-oriented electrical steel under bending stress in a wide frequency range. L. Chen[1], *D. Yan*[1], T. Ben[1], L. Jing[2] and Q. Liu[2] *1. China Three Gorges University, Yichang, China; 2. Hubei Provincial Research Center on Microgrid Engineering Technology, Yichang, China*

I Introduction Studying the magnetic properties of the Grain-Oriented(GO) electrical steel under different stresses in a wide frequency range is of great significance for improving the energy conversion efficiency of the motors or transformers. Residual bending stress can cause deterioration of the magnetic properties of the motor and lead to an increase in core losses[1]. However, only the effect of bending stress on the magnetic properties of GO electrical steel sheets at 50 Hz has been studied so far, and the magnetic properties at higher frequencies magnetization under bending stress is still unclear[2]. Aiming at this problem, the magnetic properties of GO electrical steel sheet under different bending stress up to 1kHz is investigated by developing a measuring system under different curvature loading mechanisms. II Method and Discussion For investigating the magnetic properties of the GO steel sheet under different bending stress, the single sheet specimen to be measured were bended into different radius of curvatures as shown in Fig.1. Because of the deterioration of the magnetic characteristics caused by the bend of the sample, it is very difficult to maintain the sinusoidal waveform for standardized testing in the measurement process. A robust digital control algorithm in the frequency domain with a normalized dual-loop control loops is proposed. Fig.2 shows the some measuring results of GO steel B27R090. It can be found that with the increase of bending stress, the loss increases significantly and the higher the frequency, the greater the influence of bending stress is found. III Conclusion The magnetic properties of electrical steel under different bending stress over a wide frequency range are measured by the proposed measuring system with a normalized frequency domain dual-loop feedback control algorithm in this paper. Obtained results show that the bending stress of electrical steel sheet has a great influence on the iron loss, and the influence becomes more obvious with the increase of frequency.

[1] T. Wang et al. Fabrication and Experimental Analysis of an Axially Laminated Flux-Switching Permanent-Magnet Machine [J]. IEEE Transactions on Industrial Electronics, vol. 64, no. 2, pp. 1081-1091, Feb. 2017.
[2] H. Hagihara, Y. Takahashi, K. Fujiwara, Y. Ishihara and T. Masuda. Magnetic Properties Evaluation of Grain-Oriented Electrical Steel Sheets Under Bending Stress [J]. IEEE Transactions on Magnetics, vol. 50, no. 4, pp. 1-4, April 2014, Art no. 2002104.

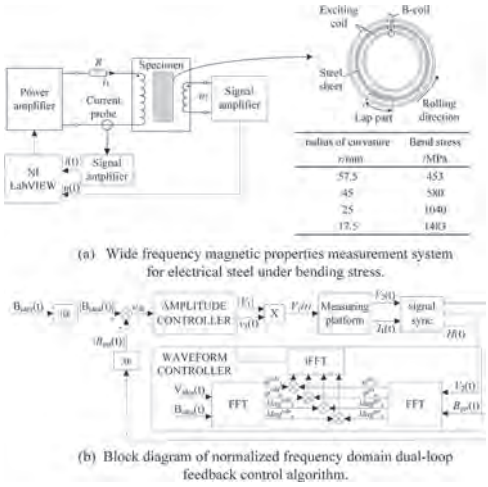

Fig.1. Magnetic properties measurement system for electrical steel under bending stress and dual-loop control algorithm used.

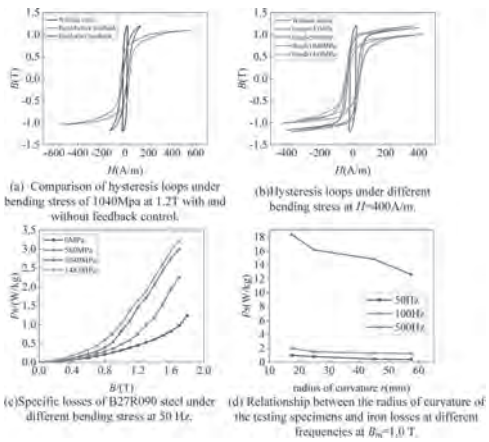

Fig.2. Measurement results of electrical steel at different bending stresses.

JPC-09. Accurate calculation of global hysteresis properties of grain-oriented silicon steel based on an improved J-A model with variable parameters. L. Chen[1], *X. Wen*[1], T. Ben[1], L. Jing[2] and Q. Liu[2]
1. College of Electrical Engineering and New Energy, China Three Gorges University, Yichang, China; 2. Hubei Provincial Research Center on Microgrid Engineering Technology, China Three Gorges University, Yichang, China

I Introduction Accurate calculation of hysteresis properties of magnetic materials is of great significance for the optimal design of electromagnetic devices. At the state of the art, the J-A model is widely used in the FEM procedures as it is easy to implement. However, the existing J-A models relying on the parameters identified by the static limiting hysteresis loops can only ensure the accurate calculation of grain-oriented (GO) silicon steel sheets at high magnetic densities, which have relatively poor calculation accuracy at low magnetic densities[1]. Aiming at this problem, this paper proposes an improved J-A model, which can accurately and quickly calculate the global hysteresis loops of GO silicon steel sheets with only a small amount of data. II Method and Discussion As shown in Fig. 1, an improved anisotropic J-A model suitable for GO silicon steel sheets is proposed introducing the some variable parameters. To solve the problem of low calculation accuracy when the magnetized state of the material is far from saturation, a damping factor R is introduced to correct the irreversible changing susceptibility of the J-A model. Meanwhile, the pinning coefficient k and domain flexing coefficient c of the J-A model are assumed that should be changed with the magnetic flux density B. It can be seen from Fig.2 (a, b, c) that the parameters k, c, and R have a good functioning relationship with the magnetic flux density B, so the parameters under the remaining magnetic flux densities can be quickly obtained. The velocity-controlled particle swarm (VCPSO) algorithm is used to identify various parameters[2]. The calculation results are shown in Fig 2 (d), which are in good agreement with the experimental data. III Conclusion This paper presents an improved anisotropic J-A model by introducing a damping factor R and considering the parameter R, k and c are as a function of magnetic flux densities. Obtained results show that the proposed model can accurately and quickly simulate the global hysteresis characteristic of GO silicon steel sheets.

[1] Podbereznaya I, Pavlenko A. Accounting for dynamic losses in the Jiles-Atherton model of magnetic hysteresis - ScienceDirect[J]. Journal of Magnetism and Magnetic Materials, 2020, 513. [2] Chen L, Yi Q, Tong B, et al. Parameter identification of Preisach model based on velocity-controlled particle swarm optimization method[J]. AIP Advances, 2021, 11(1):015022.

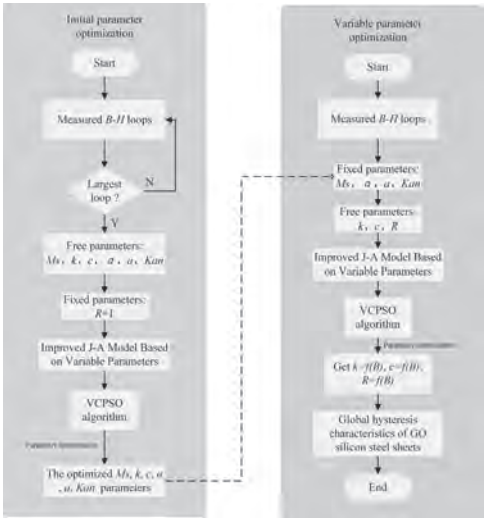

Fig.1. Improved J-A Model Calculation Process

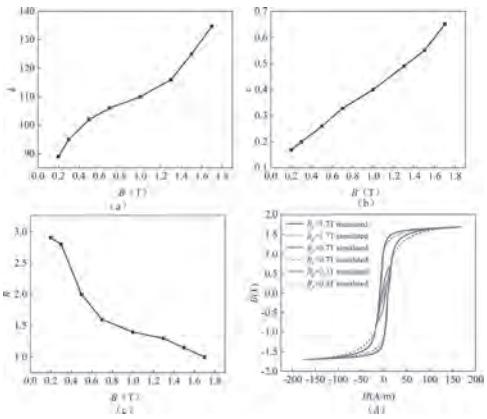

Fig.2. (a) Parameter *k=f(B)*. (b) Parameter *c=f(B)*. (c) Parameter *R=f(B)*. (d) The simulation curve is compared with the measured data.

JPC-10. A Study on the Supporter Removal Shape of Axial Flux Motor Using 3D Printing Processible Materials. H. Pyo[1], Y. Lee[1], I. Yang[2] and *W. Kim[1] 1. Electrical Engineering, Gachon University, Seongnam-Si, The Republic of Korea; 2. Electrical Engineering, Hanyang University, Seoul, The Republic of Korea*

The demand for Axial Flux Permanent Magnet Synchronous Motor(AFPMSM) is increasing in the motor market. It has the advantage of having higher performance compared to the existing Radial Flux Motor Permanent Magnet Synchronous Motor (RFPMSM). However, there is a disadvantage of making the shape of AFPMSM through the existing electrical steel sheet. Therefore, in the case of the existing AFPMSM, it was a structure made by compressing Soft Magnetic Composite(SMC) into a frame. However, it is possible to manufacture AFPMSM through 3D printing technology using the Fe-Si material proposed in this paper. There is a problem when manufacturing AFPMSM with 3D printing process through 3D-printed material. When manufacturing AFPMSM through 3D printing, support structure through a supporter is required. The structure of AFPMSM, the stator is formed with teeth structure and shoe structure so that magnetic flux flows well along the iron core. Basically, the structure of the teeth and the shoe is 90 degrees. Figure 1 shows the stator structure of AFPMSM with dual rotor structure. Shown in Figure 1, it could be seen that the structure of the stator teeth and the stator shoe has a 90degree angle. Therefore, in this paper, support is provided as shown in Figure 1. The reason for placing the supporter as shown in Figure 1 is the area of the stator shoe that generates torque in the motor. Therefore, a constant tolerance is very important because the magnetic flux generated by the stator shoe and the rotor permanent magnet generates torque in the air gap. Figure 2 shows a picture of the 3D printing process using 3D-printable materials. When manufacturing AFPMSM using 3D printing process, there is an advantage in small quantity production of multiple types rather than the existing mass production method of small types. When manufacturing AFPMSM through existing electrical steel sheet or SMC core, it is difficult to make an actual precise shape. Therefore, a comparative analysis was conducted with the actual SMC core process through finite element analysis. As a result, it was confirmed that the performance increased by 5.8%.

[1] N. A. Rahim, H. W. Ping, and M. Tadjuddin, "Design of axial flux permanent magnet brushless DC motor for direct drive of electric vehicle," *2007 IEEE Power Eng. Soc. Gen. Meet. PES*, 99. 1-6, 2007. [2] F. Caricchi, F. G. Capponi, F. Crescimbini, and L. Solero, "Experimental Study on reducing cogging torque and no-load power loss in axial-flux permanent-magnet machines with slotted winding," *IEEE Trans. Ind. Appl.*, vol.40, no. 4, pp. 1066-1075, 2004.

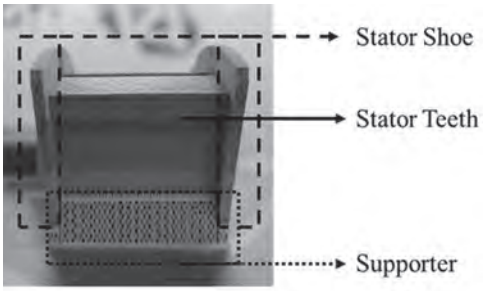

Fig. 1 Structure of the stator teeth and the shoe with supporter

Fig. 2 3D printing process using 3D-printable materials

JPC-11. Analysis of the Stator Magnetic Properties of an Aerospace Axial Flux Motor Considering the Thermal Stress of Material Lamination. *J. Li[1]*, D. Li[1], S. Xu[1] and R. Pei[1] *1. Department of Electric Engineering, Shenyang University of Technology, Shenyang, China*

Axial flux motors for aviation systems operate at high altitudes, and the initial operating temperature of the motor is low, but due to the thin air, the motor temperature rise is high and the stator material temperature variation range is large[1], especially the segmented stator is close to the motor winding coil, and the thermal stress has a non-negligible effect on its material[2]. The segmented stator laminated magnetic energy model has been extensively studied in past researches, and no research has been proposed to consider the magnetic energy model of the laminated structure under the thermal stress of the material. When the temperature changes, the segmented stator is not completely free to expand and contract due to the external constraints and the mutual constraints between the internal parts, thus generating thermal stresses [3]. Previous studies have shown that the temperature itself affects the magnetic properties of the material. In this paper, we intend to analyze the magnetic properties of the material by means of a coupled material multi-physics field testbed, and to divide the temperature-induced effects into the effects of temperature on the inherent properties of the material itself and the effects of thermal stresses induced by temperature changes on grain-oriented silicon steel, and to separate them equivalently. In this paper, a comparative analysis of the stator with different thicknesses of grain-oriented silicon steel is carried out, and the deformation of different stator materials under thermal stress is calculated by finite elements. Finally, the thermal stress effect percentage is tested experimentally. It is found that the use of thinner oriented silicon steel material will greatly reduce the effect of thermal stress on its magnetic properties.

[1] Paredes J A, Saito C, Abarca M, et al. Study of effects of high-altitude environments on multicopter and fixed-wing UAVs' energy consumption and flight time[C]//2017 13th IEEE Conference on Automation Science and Engineering (CASE). IEEE, 2017: 1645-1650. [2] Wu Y, Ming T, Li X, et al. Numerical simulations on the temperature gradient and thermal stress of a thermoelectric power generator[J]. Energy conversion and management, 2014, 88: 915-927. [3] Yong L, Liang W, Qian W, et al. Calculation of deformation and material stress of a rotary voice coil motor used in aerospace[J]. Journal of Computational and Theoretical Nanoscience, 2015, 12(11): 4499-4505.

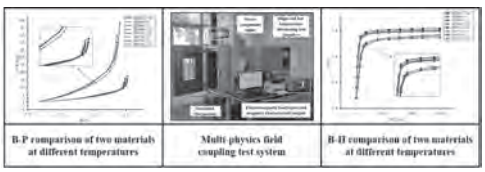

Fig. 1 Multi-physics field testing of two materials

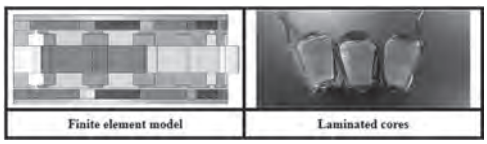

Fig. 2 Simulation and physical model

Session KOA
HARD MAGNETIC MATERIALS I: RARE EARTH-BASED COMPOUNDS

Thomas Schrefl, Chair
Danube University Krems, Wiener Neustadt, Austria

INVITED PAPERS

KOA-01. Formation of $ThMn_{12}$-type Phase and Conditions for High Coercivity in $(Sm,Zr)(Fe,Co,Ti)_{12}$ Alloys. *A. Gabay*[1], C. Han[1], B. Lejeune[2], K. Jinn[2], C. Ni[1], L. Lewis[2] and G.C. Hadjipanayis[1,2]
1. University of Delaware, Newark, DE, United States; 2. Northeastern University, Boston, MA, United States

Due to their excellent intrinsic magnetic properties, the $Sm_{1-x}Zr_x(Fe,Co)_{12-y}Ti_y$ compounds ($0.5 \le y < 1$), isostructural to the $ThMn_{12}$ compound have been predicted to lead to new iron-based permanent magnets that require a lower concentration of rare earth elements than Nd-Fe-B and exhibit superior performance at elevated temperatures [1]. However, obtaining a high coercivity H_c in these compounds proved to be difficult. For $y < 1$, the highest H_c values reported to date are 13.2 kOe for epitaxially grown thin films [2] and 12.6 kOe for monocrystalline powders prepared through reduction diffusion of mechanically activated elemental oxides [3]. Determining the conditions and mechanisms for the development of high H_c in such powders may provide the foundation for the future development of new types of rare-earth-lean magnets, thus reducing the current need for the critical elements. In this work, the formation and growth of the monocrystalline particles were studied for reduction diffusion experiments performed with excess of the calcium reducing agent varying from 15% to 65%. To capture the earliest stages of the reduction process, the mechanically activated precursors were placed in a furnace preheated to 1200 °C for time intervals starting from 8 s. With a larger amount of excess Ca, the intended alloy composition could be attained almost instantaneously, followed by a prompt formation of the magnetically hard 1:12 phase (Fig. 1, squares). However, it was found that the 1:12 phase formed in a samarium-depleted environment, due to a smaller amount of excess Ca, provided the highest values of H_c (Figs. 1–2), reaching the record value of 16.3 kOe. Microscopic examination has linked the development of the higher H_c to the faceted morphology and crystallinity of the particles. The work was supported by the U.S. Department of Energy, Office of Basic Energy Sciences under Award Number DE SC0022168.

[1] T. Kuno, S. Suzuki, K. Urushibata, K. Kobayashi, N. Sakuma, M. Yano, A. Kato, A. Manabe, AIP Adv. 6 (2016) 025221; P. Tozman, H. Sepehri-Amin, Y.K. Takahashi, S. Hirosawa, K. Hono, Acta Mater. 153 (2018) 354. [2] A. Bolyachkin, H. Sepehri-Amin, M. Kambayashi, Y. Mori, T. Ohkubo, Y.K. Takahashi, T. Shima, K. Hono, Acta Mater. 227 (2022) 117716. [3] A.M. Gabay, G.C. Hadjipanayis, Scr. Mater. 196 (2021) 113760; A.M. Gabay, Chaoya Han, Chaoying Ni, G.C. Hadjipanayis, J. Magn. Magn. Mater. 541 (2022) 168550.

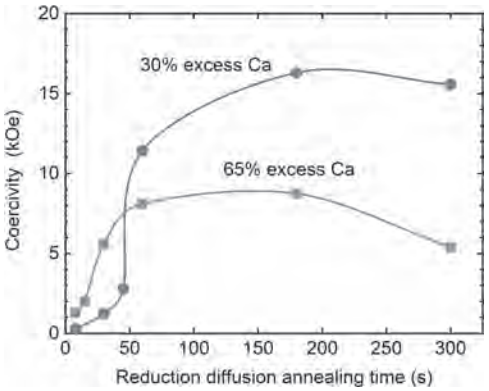

Fig. 1. Evolution of room-temperature coercivity with nominal annealing time for alloys prepared with two different excesses of the reducing agent.

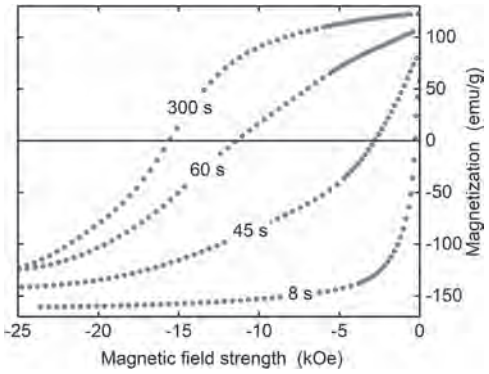

Fig. 2. Selected demagnetization curves of magnetic-field-oriented powders prepared with 30% excess Ca with the nominal reduction diffusion annealing time indicated.

KOA-02. Development of rare-earth lean $SmFe_{12}$-based permanent magnets. *H. Sepehri-Amin*[1], J. Zhang[1], X. Tang[1], A. Srinithi[1], P. Tozman[1], A. Bolyachkin[1], T. Ohkubo[1] and K. Hono[1] *1. NIMS, Tsukuba, Japan*

Research interest in rare-earth lean $SmFe_{12}$-based compounds has been revived due to their excellent intrinsic hard magnetic properties making them potential for new permanent magnet materials that are not dependent on scarce elements such as Dy [1,2]. In order to realize these materials for practical applications, the main challenge is development of anisotropic $SmFe_{12}$-based sintered magnet with a large coercivity and high remanent magnetization. We carried out machine-learning on a dataset extracted from literature on $Sm(Fe,X)_{12}$-based alloys to understand the most influential parameters for coercivity. It was found addition of V to the alloy composition is the most influential to coercivity [3]. The prediction from machine learning was experimentally validated by developing $SmFe_{11}Ti$ and $SmFe_{10}TiV$ melt-spun ribbons where coercivity increased from 0.5 T to 1.1

T upon addition of V. Detailed microstructure characterizations revealed enhanced coercivity is originated from formation of Sm-rich intergranular phase enveloping $SmFe_{12}$-based grains. The formation of Sm-rich intergranular phase acts as pinning cites against magnetic domain wall propagation resulting in an enhanced coercivity in the V-containing magnet. Motivated by this study, we have developed anisotropic $Sm(Fe,Ti,V)_{12}$-based sintered magnet via conventional powder processing including the development of jet-milled powders, preparation of green compact, and liquid sintering process [4,5]. The sintered magnets showed coercivity of $\mu_0 H_c$=0.6-1.0 T and remanent magnetization of $\mu_0 M_r$ = 0.6-0.8 T depending on Ti content (Fig. 1). Detailed multi-scale microstructure characterizations showed the origin of realizing a coercivity of above 0.6 T is the formation of Sm-rich intergranular phase [4,5]. However, {101} twins were also observed in the microstructure of the magnets as shown in Fig. 2 (a). The origin of the twins is induced stress in the powders during the jet-milling process. MOKE observations showed that the magnetization reversal can start from twinned grains which can be detrimental for coercivity (Fig. 2). However, micromagnetic simulations showed that the existence of intergranular phase isolating individual grains can overcome the detrimental effect of twins to coercivity by preventing the propagation of reversed domains to the neighboring grains and hence resulting in a large coercivity. Based on our detailed microstructure investigations and micromagnetic simulations, we will discuss how an optimum microstructure can be realized in the anisotropic $SmFe_{12}$-based magnets which results in a large $\mu_0 H_c$ and $\mu_0 M_r$.

[1] K. Ohashi, Y. Tawara, R. Osugi, M. Shimao, J. Appl. Phys. 64 (1988) 5714-5716. [2] P. Tozman, H. Sepehri-Amin, Y.K. Takahashi, S. Hirosawa, K. Hono, Acta Mater. 153 (2018) 354. [3] Xin Tang, J Li, AK Srinithi, H Sepehri-Amin, T Ohkubo, K Hono, Scripta Mater. 200 (2021) 113925. [4] J.S. Zhang, Xin Tang, H. Sepehri-Amin, A.K. Srinithi, T. Ohkubo, K. Hono, Acta Mater. 217 (2021) 117161. [5] J.S. Zhang, Xin Tang, A. Bolyachkin, A.K. Srinithi, T. Ohkubo, H. Sepehri-Amin, K. Hono, Submitted.

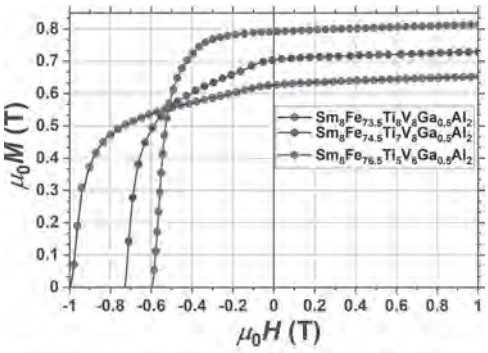

Figure 1: Demagnetization curves of sintered magnets $Sm_8Fe_{73.5+x}Ti_{8-x}V_8Ga_{0.5}Al_2$ (x=0-3) at.%.

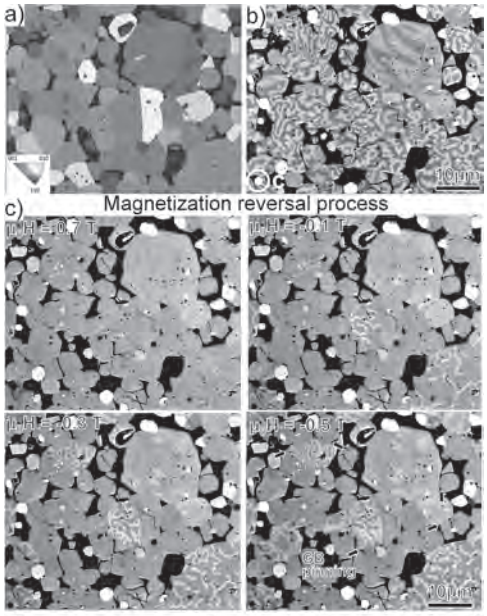

Figure 2: Inverse pole figure (IPF) map of 1:12 grains of sintered magnet with $\mu_0 H_c$ = 0.6 T. MOKE image in (b) thermally demagnetized state and (c) showing magnetization reversal process of the magnet.

CONTRIBUTED PAPERS

KOA-03. First-Principles Investigation of the Compositional Dependence of Exchange Interactions in $RETM_{12}$ Magnets.

C.E. Patrick[1], J.B. Staunton[2], A. Gabay[3], G.C. Hadjipanayis[4,3] and L. Lewis[4,5] *1. Department of Materials, University of Oxford, Oxford, United Kingdom; 2. Department of Physics, University of Warwick, Coventry, United Kingdom; 3. Department of Physics and Astronomy, University of Delaware, Newark, DE, United States; 4. Department of Chemical Engineering, Northeastern University, Boston, MA, United States; 5. Department of Mechanical and Industrial Engineering, Northeastern University, Boston, MA, United States*

$RETM_{12}$ magnets continue to attract attention as candidate rare-earth-lean permanent magnets, thanks to their reduced reliance on critical elements compared to Nd-Fe-B. Stabilizing $REFe_{12}$ magnets requires substituting some of the iron with other transition metals like Ti [1], which in turn affects their magnetic properties. This effect has been studied for many years, for instance in bcc Fe as reported at the 1958 MMM conference [2]. There, Arrott and Noakes showed that rather than diluting and weakening the exchange interactions, a small amount of Ti actually raised the Curie temperature T_C. This was explained in terms of the Ti atoms modifying the structure, lengthening Fe-Fe bonds and strengthening the exchange. In the intervening years diverse behavior has been observed across many materials, understood to originate from competition between atomistic and electronic structural effects [3]. Here we report first-principles calculations of T_C for the canonical Ti-doped REFe12 magnet, using the density-functional theory-based formulation of the disordered local moment picture [4]. The calculations have the useful feature of being able to isolate, control and assess different factors which may affect T_C, e.g. modifications to the crystal structure or the precise location of dopants. Fig. 1 shows how T_C depends on whether the Ti atoms are substituted on the 8i, 8f or 8j sublattices (Fig. 2). By calculating the inter-sublattice exchange coupling constants, we have quantified the magnetic interactions at different atomic sites, allowing us to rationalize this behavior. The data also show how the simplest treatment of Ti doping (ignoring structural relaxations) is unable to reproduce

the experimentally-measured behavior of T_C, which hardly varies with Ti content [5]. We also present calculations of the magnetization and anisotropy field across a range of temperatures using the methodology developed in Ref. [6]. Research performed in part under the auspices of the U.S. Department of Energy, Office of Science and the UK Royal Society Research Grant RGS\R1\201151.

[1] P. Tozman, H. Sepehri-Amin and K. Hono, Scripta Mat., Vol. 194, p.113686 (2021) [2] A. Arrott and J. E. Noakes, J. Appl. Phys., Vol. 30, p.S97 (1959) [3] B.-P. Hu and J. M. D. Coey, J. Less-Common Met., Vol. 142, p.295 (1988) [4] B. Gyorffy et al., J. Phys. F: Met. Phys., Vol. 15, p.1337 (1985) [5] B.-P. Hu, H.-S. Li and J. M. D. Coey, J. Appl. Phys., Vol. 67, p.4838 (1990) [6] C. E. Patrick and J. B. Staunton, Phys. Rev. Mater., Vol. 3, p.101401(R) (2019)

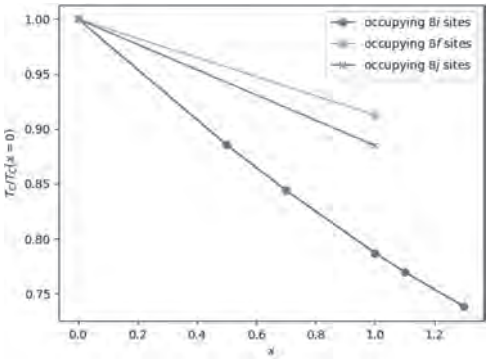

Fig.1 Calculated T_C dependence on concentration and location of Ti dopants in $YFe_{12-x}Ti_x$

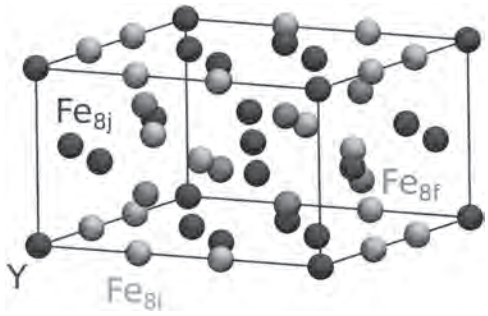

Fig.2 $REFe_{12}$ crystal structure, labeling different Fe sites

KOA-04. Enhancing stability and magnetism of $ThMn_{12}$-type cerium-iron intermetallics by site substitution[1]. C. Bhandari[1] and *D. Paudyal*[1]
1. Ames Lab, Ames, IA, United States

By performing the first-principles electronic structure calculations, we investigate the lattice stability and the intrinsic magnetic properties of Ti- or Zr-substituted Ce-based 1:12 materials. The formation energies indicate that all the compositions can form in the bulk structure except $CeFe_{12}$. We compute the phonon dispersions for Ti/Zr-substituted rare-earth-based (Ce 1:12) intermetallic compounds. We find no soft-mode frequencies that indicate all compositions are dynamically stable. The mixed valency of Ce is confirmed by examining the electronic structure in different approximations, e.g., with Ce(4*f*) as core- and valence- electrons, including the on-site electron-correlation effect. The computed Ce(4*f*) charges suggest that the valence state fluctuates between Ce^{3+} and Ce^{4+} depending upon the substituted element as well as the nitrogens. Interestingly, the net magnetic moment is predicted larger in Zr substitution than in Ti substitution, which is attributed to a more delocalized nature of Zr(4*d*) orbitals. The interstitial nitrogens improve the net magnetic moment for all consistent with experiments. The on-site electron correlation is crucial for the MCA due to the mixed-valence character of Ce. The predicted values of K_1 show all compositions uniaxial along the crystalline c-direction. Specifically, the value of K_1 is the largest for $CeZrFe_{11}$ caused by the polarization of Ce(4*f*) charge along the c-axis and stronger SOC (Figure 1), which would be interesting to examine experimentally. This work is supported by the CMI, an Energy Innovation Hub funded by the USDOE, Office of EERE, AMO.

1. C. Bhandari and D. Paudyal, Phys. Rev. Research 4, 023012 (2022)

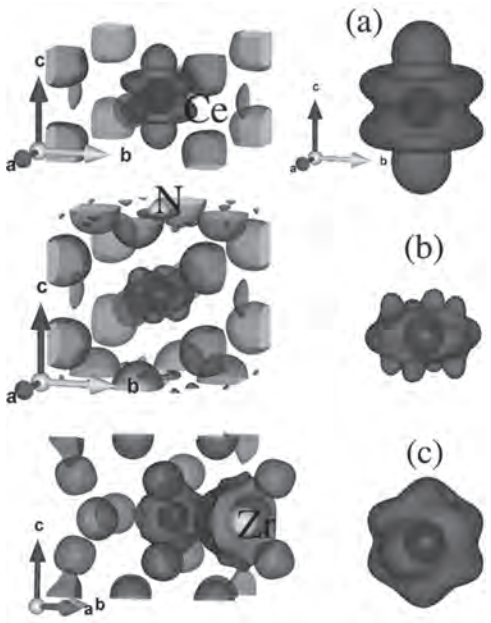

Figure 1. Electron spin density contours of Ce and nearby atoms (left) and enlarged view of Ce-only (right) in (a) $CeFe_{12}$, (b) $CeFe_{12}N$, and (c) $CeZrFe_{11}$.

KOA-05. Investigation of the effect of V on the intrinsic and extrinsic magnetic properties of $Sm(Fe,V)_{12}$ by model thin film. *P. Tozman*[1], H. Sepehri-Amin[1], T. Abe[1], A. Bolyachkin[1], T. Fukazawa[2], T. Miyake[2], S. Hirosawa[1], K. Hono[1] and Y. Takahashi[1] *1. National Institute for Materials Science, Tsukuba, Japan; 2. National Institute of Advanced Industrial Science and Technology, Tsukuba, Japan*

The demand to reduce the global CO_2 emissions induce the rapid growth of green energy industries thus the demand for high-performance Nd-Fe-B-based magnets which are used in traction motors operating at 100-200°C. For promoting the balanced use of rare earth elements other than Nd, Dy, and Tb, $SmFe_{12}$-based compounds, which have the highest Fe content among the 4f-3d compounds, receive revived interest as a potential candidate owing to their superior intrinsic magnetic properties [1,2]. Their phase stability in the bulk state can be established by substituting Fe atoms in $SmFe_{12-x}M_x$ with phase stabilizing elements, M such as Ti and V with the expense of magnetization. In this work, we synthesized $Sm_xFe_{bal}V_y$ for $5.7 \le x \le 15$ and $0 \le y \le 30$ by using an ultrahigh vacuum co-sputtering system and performed DFT and CALPHAD analyses to understand the effect of V on the magnetic properties and microstructure for paving a way for $SmFe_{12}$-based magnet development. The crystal structure, microstructure, and magnetic characterization were carried out by XRD, TEM/EDS, and PPMS, up to 14 T. We found that V helps to stabilize the 1:12 phase in $Sm_{7.7}Fe_{92.3-y}V_y$ for $0 \le y \le 10.8$ by decreasing the lattice parameters *c* and the *c*/*a* ratio and a single 1:12 phase is obtained [3]. Interestingly, unlike Ti, Curie temperature (T_c) and anisotropy field ($\mu_0 H_a$) do not show a decreasing trend with increasing V so $\mu_0 H_a$ is kept between 10-12 T at 300 K [4]. Additionally, V enhances T_c in $Sm_{7.7}Fe_{92.3-y}V_y$ from 533 K for $y=0$ to 660K for $y=7.7$ in good accordance with DFT calculations (Fig.1). Tuning V further and Sm towards off stoichiometry induces the formation of the secondary phases in which the V-rich amorphous intergranular phase is found to be beneficial for coercivity. $Sm_8Fe_{72}V_{20}$ exhibits a good

squareness ratio M_r/M_s=0.96 with sufficiently large coercivity $\mu_0 H_c$ = 0.9 T due to the formation of this V-rich along with some Sm-rich intergranular phase. The calculated Sm-Fe-V phase diagram shows that this is achieved due to the coexistence of 1:12 with two types of liquid phases (V-rich and Sm-rich) which is the first time observed experimentally.

[1] K. Ohashi, Y. Tawara, R. Osugi, M. Shimao, J. Appl. Phys. 64 (1988) 5714-5716. [2] P. Tozman, H. Sepehri-Amin, K. Hono, Scr. Mater. 194 (2021) 113686. [3] A. Makurenkova, D. Ogawa, P. Tozman, S. Okamoto, S. Nikitin, S. Hirosawa, K. Hono and Y. K. Takahashi, J. Alloys Compd. 861 (2021) 158477. [4] P. Tozman, T. Fukazawa, D. Ogawa, H. Sepehri-Amin, A. Bolyachkin, T. Miyake, S. Hirosawa, K. Hono and Y. K. Takahashi, Acta Mater. 232 (2022) 117928.

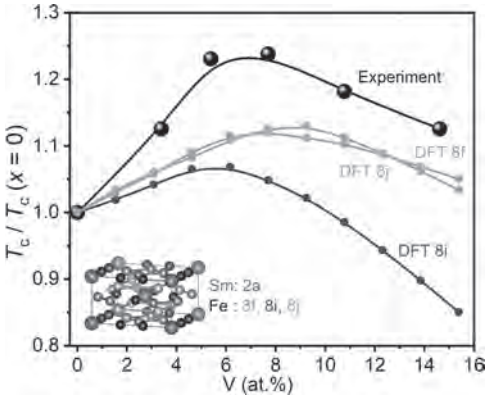

Figure 1. The trend on Tc with V in $Sm(Fe,V)_{12}$.

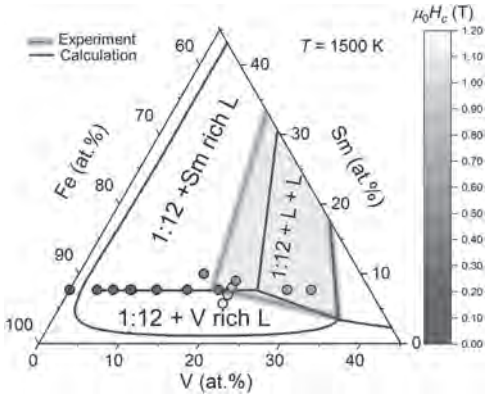

Figure 2. Calculated and constructed Sm-Fe-V phase at 1500 K

KOA-06. From chemical composition and temperature to micromagnetic anisotropy and vice-versa. *A. Kovacs*[1,2], A. Kornell[1,2], Q. Ali[1,2], J. Fischbacher[1,2], M. Gusenbauer[1,2], H. Oezelt[1,2], M. Yano[3], N. Sakuma[3], A. Kinoshita[3], T. Shoji[3], A. Kato[3] and T. Schrefl[1,2]
1. Christian Doppler Laboratory for Magnet design through physics informed machine learning, Viktor Kaplan-Straße 2E, 2700 Wiener Neustadt, Austria; 2. Department for Integrated Sensor Systems, Danube University Krems, Viktor Kaplan-Straße 2E, 2700 Wiener Neustadt, Austria; 3. Advanced Materials Engineering Div., Toyota Motor Corporation, 1200, Mishuku Susono, Shizuoka 410-1193, Japan

We present a framework capable of mapping compositions of $(NdLaCePr)_2Fe_{14}B$ system and temperature to intrinsic magnetic properties. An experimental database is augmented with data from ab initio simulations which include exchange integrals and Curie temperature. The presented work exclusively uses the well-established Partial Least Squares (PLS) regression [1] which has similarities to Principal Component Regression to detect outliers and to map chemical concentrations to the magnetocrystalline anisotropy constants and/or the spontaneous magnetizations. We show how many latent space dimensions are necessary to sufficiently predict the intrinsic properties. We will highlight the application of nested cross-validation in contrast to other error estimation strategies such as cross-validation with hyper-parameter optimization or leverage corrected errors. A first simple PLS regression based on experimental data only is prone to outliers. If the training data is augmented with the ab-initio data, which includes the magnetization at zero temperature, outliers can be stabilized. Overall, the fusion of experimental and ab-initio data improves the prediction accuracy by 10 percent for the anisotropy constant. Figure 1 shows the prediction of the anisotropy constant and the spontaneous magnetization at 433 K for $(Nd_{1-x}La_x)_2Fe_{14}B$. The trained model at hand, can be called inversely as well. In that case questions like, which chemical composites will provide certain intrinsic material properties given constraints in the chemical composition space such as using only Nd and La for the rare-earth. The financial support by the Austrian Federal Ministry for Digital and Economic Affairs and the Christian Doppler Research Association is gratefully acknowledged. Ab initio data are provided by the National Institute of Advanced Industrial Science and Technology and the Institute for Solid State Physics, the University of Tokyo under “Program for Promoting Researches on the Supercomputer Fugaku”.

[1] S. Wold, M. Sjöström, and L. Eriksson, “PLS-regression: a basic tool of chemometrics,” *Chemometrics and Intelligent Laboratory Systems*, vol. 58, no. 2, pp. 109–130, Oct. 2001. doi: https://doi.org/10/cv6jxq

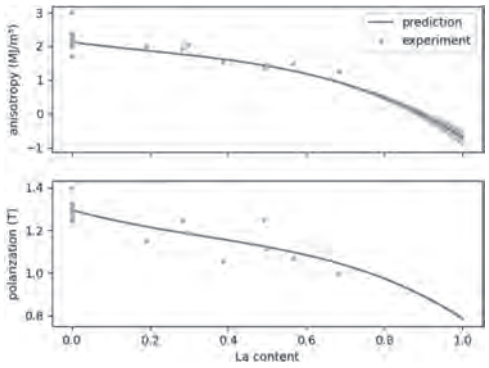

Figure 1. Predicted magnetocrystalline anisotropy constant and magnetic polarization as function of the La content in $(NdLa)_2Fe_{14}B$ at 433 K. The shaded area gives the 95% confidence interval.

KOA-07. Interplay between magnetism and band topology in Kagome magnets RMn_6Sn_6. Y. Lee[1], R. Skomski[2], X. Wang[3], P. Orth[1,4], A. Pathak[5], B. Harmon[1,4], R. McQueeney[1,4], I. Mazin[6] and *L. Ke*[1] *1. Ames Laboratory, Ames, IA, United States; 2. University of Nebraska, Lincoln, NE, United States; 3. Sophyics Technology, McLean, VA, United States; 4. Iowa State University, Ames, IA, United States; 5. SUNY Buffalo State, Buffalo, NY, United States; 6. George Mason University, Fairfax, VA, United States*

Kagome-lattice magnets RMn_6Sn_6 recently emerged as a new platform to exploit the interplay between magnetism and topological electronic states [1]. Some of the most exciting features of this family are the dramatic dependence of the easy magnetization direction on the rare-earth specie, despite other magnetic and electronic properties being essentially unchanged, and the Kagome geometry of the Mn planes that in principle can generate flat bands and Dirac points; gapping of the Dirac points by spin-orbit coupling has been suggested recently to be responsible for the observed anomalous Hall response in the member $TbMn_6Sn_6$. In this work [2], we address both issues with density functional calculations and are able to explain, with full quantitative agreement, the evolution of magnetic anisotropy, including a complete reversal upon adding an f-electron with zero magnetic orbital quantum number when going from Ho to Er. We also show the microscopic origin of this computational result using a simple and physically transparent analytical model. We analyze in detail the topological properties of

Mn-dominated bands and demonstrate how they emerge from the multiorbital planar Kagome model. We further show that, despite this fact, most of the topological features at the Brillouin zone corner K are strongly 3D, and therefore cannot explain the observed quasi-2D AHE, while those few that show a quasi-2D dispersion are too far removed from the Fermi level. We conclude that, contrary to previous claims, Kagome-derived topological band features bear little relevance to transport in RMn$_6$Sn$_6$, albeit they may possibly be brought to focus by electron or hole doping.

[1] J.-X. Yin, S. S. Zhang, H. Li, K. Jiang, G. Chang, B. Zhang, B. Lian, C. Xiang, I. Belopolski, H. Zheng, T. A. Cochran, S.-Y. Xu, G. Bian, K. Liu, T.-R. Chang, H. Lin, Z.-Y. Lu, Z. Wang, S. Jia, W. Wang, and M. Z. Hasan, Giant and anisotropic many-body spin-orbit tunability in a strongly correlated kagome magnet, Nature 562, 91 (2018) [2] Y. Lee, R. Skomski, X. Wang, P. P. Orth, A. K. Pathak, B. N. Harmon, R. J. McQueeney, I. I. Mazin, and L. Ke, Interplay between magnetism and band topology in Kagome magnets RMn6Sn6, arXiv 2201, 11265 (2022), https://arxiv.org/abs/2201.11265

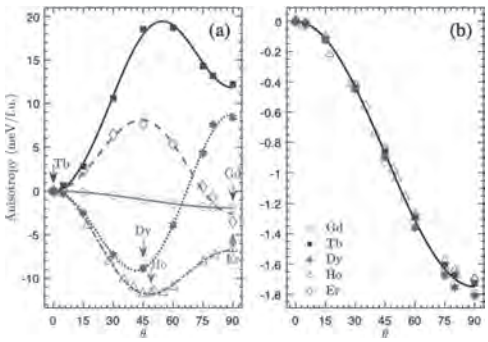

Fig. 1 Variation of magnetic energy (in meV/f.u.) as a function of spin-axis rotation in RMn$_6$Sn$_6$, with R = Gd, Tb, Dy, Ho, and Er, calculated (a) with and (b) without R-4f contributions. θ is the angle between the spin direction and the out-of-plane direction. The experimental easy directions for each compound are denoted by arrows in panel (a). The lines are just guides for the eye.

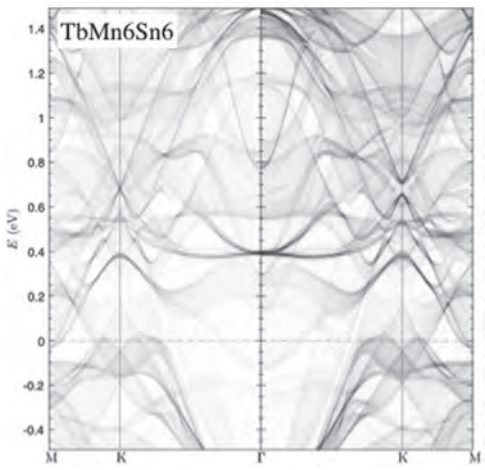

Fig. 2 Band structures projected on surface BZ calculated without (blue) and with (red) SOC in TbMn$_6$Sn$_6$. The k-dependent DOS are integrated along k_z and are calculated in DFT.

KOA-08. Novel Quasi-trivalent Dual-main-phase Ce Magnets with High Performance Driven by Magnetic Anisotropy Energy Gap.

Q. Sun[1,2], M. Zhu[1,2] and W. Li[1] *1. Division of Functional Materials, Central Iron and Steel Research Institute, Beijing, China; 2. School of Materials Science and Engineering, Northeastern University, Shenyang, China*

The application of Nd-Fe-B magnet with substitution of Nd by cheap and abundant Ce elements is seriously limited due to the intrinsically inferior magnetic properties of Ce-Fe-B [1-3]. Recently, dual-main-phase (DMP) sintered magnet was successfully developed [4], which allowed special distribution of heterogeneous main phases (Ce-rich and Nd-rich R2Fe14B main phases), contributing remarkably to balance the utilization of high-abundance rare earths and the performance. This work demonstrated a novel design of quasi-trivalent DMP Ce magnets using the strategy of two main phases with giant magnetic anisotropy energy gap (MAEG). The maximum energy product of DMP Ce magnet with 40% weight percentage of Ce over total rare earth is optimized to be 40.57 MGOe, as shown in Fig. 1, which is the energy-product record. The superior magnetic properties are closely corelated to the average valence of Ce. The average valence of Ce in the DMP magnets was quasi-trivalent, proved by XPS spectroscopy, as shown in Fig. 2, which was lower than that in the single-main-phase magnets. Furthermore, with an isostructural heterogenous configuration in the DMP magnets could manipulate electron migration and induce magnetic Ce3+ in the main phase, thereby improving the remanence. It was possible to control the Ce valence for the design of high-performance Ce magnets using main phases with diversity of MAEG. This would undoubtedly provide ideas for researching and developing new rare earth materials with a synergistic composition and structure. Compared with Nd-Fe-B magnets, the new quasi-trivalent DMP Ce magnets would save 30-40% Nd and remarkably reduce the production cost of magnets with much higher Ce content.

[1] J. F. Herbst, Rev. Mod. Phys. 63, 819 (1991). [2] D. Li, Y. Bogatin, J. Appl. Phys. 69, 5515 (1991). [3] S. X. Zhou, Y. G. Wang, R. Høier, J. Appl. Phys. 75, 6268, (1994). [4] M.G. Zhu, W. Li, Y.K. Fang, et al. J. Appl. Phys. 109, 07A706 (2011).

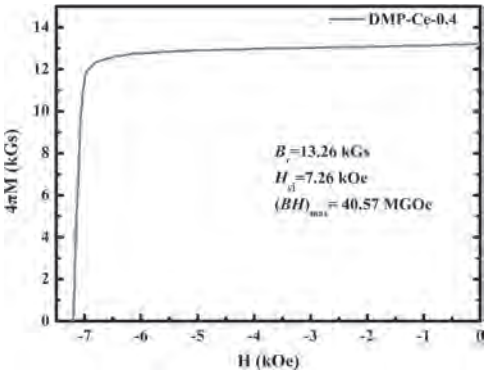

Fig. 1 Demagnetization curve of the DMP-Ce-0.4 magnet at room temperatures. The energy-product record of 40.57 MGOe is reported for DMP-Ce-0.4 magnet.

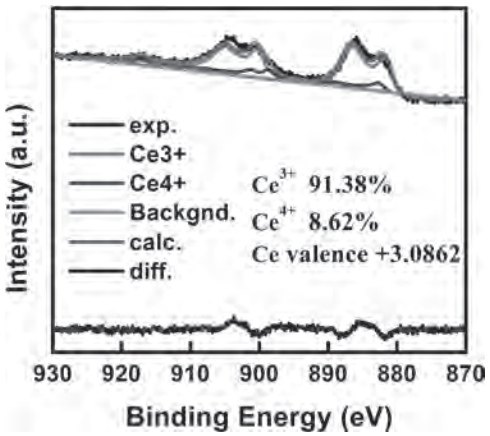

Fig. 2 Semi-quantitative fitting of the Ce 3d core-level spectra for the DMP-Ce-0.4 magnet using the ordinary least squares approach, where the standard XPS spectra of Ce3+ and Ce4+ were sourced from the Avantage software database.

KOA-09. Discovery of a new high-T_c ferromagnet in Fe-rich Ce – Fe – Zr alloys. *M. Nazmunnahar*[1], O. Palasyuk[1,2] and A. Palasyuk[1] *1. The Critical Materials Institute, Ames Laboratory (USDOE), Ames, Iowa, United States, IA, United States; 2. Department of Materials Science and Engineering, Iowa State University, Ames, Iowa, United States, IA, United States*

Ce – Fe ferromagnetic phases are very economical, considering abundance and low cost of both, Ce, and Fe. They represent an alternative material for RE-permanent magnets containing critical, thus expensive, RE like Nd, Sm and Dy, as well as nearly critical Co [1,2]. Introducing Fe instead of Co is advantageous both, from the material cost prospective, as well as from the standpoint of generally higher saturation magnetizations, because of higher magnetic moment of Fe. However, there is no Ce – Fe permanent magnet yet known. One reason is the lack of Ce – Fe compounds; another is that the existing Ce – Fe binaries do not exhibit ferromagnetism above the room temperature. We have discovered a new ferromagnetic compound, rhombohedral (Ce,Zr)Fe_3 phase ($PuNi_3$-type, *R*-3*m*). In contrast to all known Ce – Fe binary compounds, which are not ferromagnetic at room temperature, the new phase is strongly ferromagnetic with Curie point 550 K (see Figure below). The saturation magnetization of the system at room temperature reaches 9.3 kG at 3T external field. These are intrinsic indicators of practical 20 – 25 MGOe permanent magnet. The material contains no critical elements and allows utilization of abundant domestic Ce (50 % of MP ore). All the above factors place it well along the target to win industry adoption for substitutes of the rare earth magnets.

[1] K. Strnat, G. Hoffer, J. Olson, W. Ostertag, and J. J. Becker, A Family of New Cobalt-Base Permanent Magnet Materials, J. Appl. Phys. 38 (1967) 1001. [2] Galler, S. Ener, F. Maccari, I. Dirba, K. P. Skokov, O. Gutfleisch, S. Biermann, and L. V. Pourovskii, intrinsically weak magnetic anisotropy of cerium in potential hard-magnetic intermetallics, arXiv:2006.01792.

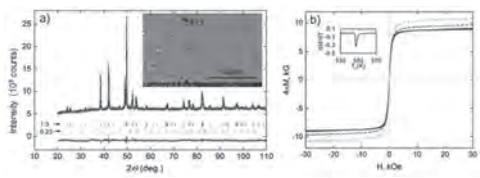

Fig: a) Rietveld refinement of the X-ray powder pattern of the heat-treated (Ce,Zr)Fe_3 confirming the hexagonal $PuNi_3$-type crystal structure (Inset: SEM backscattered electrons image of the same sample showing > 90% single-phase material at Ce:Zr ~ 2/3, b) M/H curves of heat-treated samples along the 75 at.% Fe (Inset: Curie point at 550 K of the Ce:Zr ~ 2/3 sample)

KOA-10. Coercivity enhancement of PrCu diffused Dy-free-NdFeB sintered magnets. *W. Tang*[1], G. Ouyang[1], J. Wang[1], M.J. Kramer[1,2], J. Cui[1,2] and I. Anderson[1,2] *1. Ames National Laboratory, Ames, IA, United States; 2. Materials Science & Engineering, Iowa State University, Ames, IA, United States*

Efficient high power density electric drive motors require permanent magnets with high energy product, good thermal stability, and less critical materials. $Nd_2Fe_{14}B$-based sintered magnets are one of the primary candidates for these applications. However, Nd-Fe-B based magnets without heavy rare earth elements (HREE) have poor magnetic properties above 150°C, target operating temperature for most electric vehicles (EV). HREE, such as, Dy, have been added to the magnets to enhance the coercivity and improve their performance at elevated temperatures. The operating temperature of the magnets depends on the amount of Dy added. For the magnet to be operable at 200 °C, the amount of Dy required could exceed 10 wt.%. Unfortunately, Dy is a critical element. Therefore, the development of Dy-lean or free Nd-Fe-B magnets capable of high temperature operation becomes a great interest to the EV industry. It is well accepted that the coercivity of these magnets is controlled by the nucleation of reversal domains at locally low-anisotropy surfaces of the individual 2:14:1 grains. The coercivity is sensitive to grain boundary structure, grain boundary chemistry, and grain size. Engineering microstructure techniques to develop Dy-lean or free Nd-Fe-B magnets include grain boundary diffusion by doping with a low melting point metal or rare earth oxide (REO), and grain size reduction. In this work, PrCu eutectic alloy powder is added as a sintering aid, blending with magnet feedstock powder. The PrCu alloy forms at a grain boundary phase after the magnet was sintered. The effect of PrCu on magnetic properties of Dy-free NdFeB sintered magnets was systematically studied by varying the sintering conditions. Sintering temperature can be significantly lowered with assistance of PrCu liquid phase, which is beneficial to reduce grain growth and thus enhance the coercivity. With increasing PrCu from 0, 5, 7.5 to 10 wt.%, as shown in Fig 1, the magnets obtained Hc of 14.6, 16.6, 18.6, and 18.8 kOe, and $(BH)_{max}$ of 37.8, 39.5, 35.0 and 28.4 MGOe, respectively. The microstructure and PrCu roles in the magnets will be analysed and discussed.

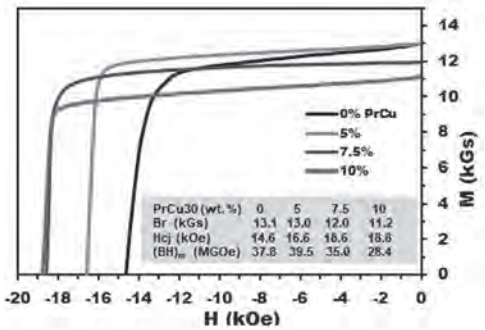

Fig. 1 Demagnetization curves of the magnets with different addition of PrCu

KOA-11. Phase stability and coercivity in $La_2Fe_{14}B$ magnet. *X. Liu*[1] and C.I. Nlebedim[1] *1. Ames Laboratory, Ames, IA, United States*

Resource-rich and cost-effective $La_2Fe_{14}B$ based alloy has the potential to be a gap permanent magnet and has been intensively investigated [1-3]. However, $La_2Fe_{14}B$ (2:14:1) is a metastable phase and decomposes into La, α-Fe and $LaFe_4B_4$ phases below 1067 K [3], which promotes the formation of structural defects and/or impurity phases. In this work, we investigated the effect of the structural defects and impurity phases on coercivity in $La_2Fe_{14}B$ magnet using micromagnetic simulation. For an ideal $La_2Fe_{14}B$ particle (a cube with an edge length of 256 nm) without any structural defects and soft magnetic secondary phases, the computed coercivity (8.5 kOe) is reduced to about 40% of its magnetic anisotropy field (H_a = 20 kOe), due to the local demagnetization field (Fig.1). Further, the coercivity sharply reduces to 3.2

kOe upon the formation of a thin layer (2 nm) of α-Fe in the surface of the $La_2Fe_{14}B$ cube particle (Fig.1). Our first-principles density functional (DFT) calculations indicate that a partial replacement of La by other rare-earth (R) elements can enhance the structural stability of 2:14:1, besides an improvement of the magnetocrystalline anisotropy. The gains in formation energy are -0.75, -0.10 and -0.33 eV per formula unit in $(La_{0.5}R_{0.5})_2Fe_{14}B$ with R = Ce, Pr, and Nd, respectively. Stabilizing the 2:14:1 structure is one of the main challenges for developing La_2Fe_{14} B-based magnet, which can be achieved via the partial substitution of La by other rare earth elements such as Ce, Pr, and Nd. This work is supported by the Critical Materials Institute (CMI), an Energy Innovation Hub funded by the U.S. Department of Energy (DOE), Office of Energy Efficiency and Renewable Energy, Advanced Manufacturing Office. Ames Laboratory is operated for the U.S. Department of Energy by Iowa State University of Science and Technology under Contract No. DE-AC02-07CH11358.

1 G.C. Hadjipanayis, Y.F. Tao, K. Gudimetta, Formation of Fe14La2B phase in as-cast and melt-spun samples, Appl. Phys. Lett. 1985 (1985) 757-758. 2 Jin, J., Wang, Z., Bai, G., Peng, B., Liu, Y., Yan, M. Microstructure and magnetic properties of core-shell Nd-La-Fe-B sintered magnets, (2018) J. Alloys Compd., 749, pp. 580-585 3 Li, X., Lu, Z., Yao, Q., Wei, Q., Wang, J., Du, Y., Li, L., Long, Q., Zhou, H., Rao, G. Thermal stability of high-temperature compound La2Fe14B and magnetic properties of Nd-La-Fe-B alloys (2021) J. Alloys Compd., 859, art. no. 157780

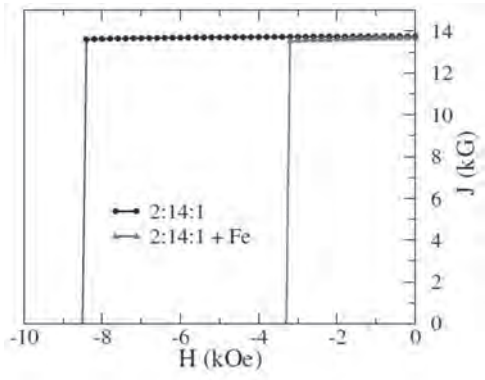

Figure 1 Calculated demagnetization curve (J-H) of a La2Fe14B particle (256nm) without any structural defects (black) and that of the La2Fe14B particle with a thin layer (2 nm) of α-Fe on the surface.

KOA-12. Near net shape fabrication of anisotropic Nd-Fe-B magnet using hot roll method. *C. Pan*[1], G. Ouyang[2], W. Tang[2] and J. Cui[1,2]
1. Iowa State University, Ames, IA, United States; 2. Ames Laboratory, U.S. DOE, Ames, IA, United States

Nd-Fe-B based magnet is the more powerful than any other magnets at room temperature. It plays a dominant role in energy efficiency and renewable energy applications due to its high energy density. However, making Nd-Fe-B magnets, especially into small sizes, can be challenging and costly. The part failure rate can be high during machining due to its brittleness. The reproducibility can be poor due to the variance in composition and microstructure inherent to the currently available fabrication methods. And the manufacturing cost is high due to the limited productivity of the batch based processes. Moreover, Nd-Fe-B needs heavy rare earth elements to be functional at higher temperature. These HRE are critical materials. One approach to bypass this HRE criticality issue is to utilize the grain size effect on coercivity, e.g., nanograin size magnet can perform the same as the micron-grain size magnet with 4-6% of Dy. However, making nanograin magnet requires a two-steps process: hot-press for densification and hot-deformation for texture. It is an inherently expensive process. Here, we report a novel Nd-Fe-B fabrication method that is continuous and near-net-shape. The process starts with loading Nd-Fe-B powders into a metal tube, packing the powder to 60% dense, then hot-rolling the powders into full density. We showed that hot rolling at 800°C with 70% thickness reduction can result in nearly full density (93%) anisotropic magnet with high energy product (31.6 MGOe). This novel method allows cost-effective production of near-net-shape Nd-Fe-B magnetic with good and consistent magnetic properties. Moreover, the method allows the making of continuous strip magnet that can be curved to match motor radius, making it possible to maximize the magnetic flux density on rotor circumference, thereby increase motor powder density.

KOA-13. Development of low-temperature reduction-diffusion process using new reductant of Li-Ca eutectic melt. *J. Kim*[1], S. Okada[1] and K. Takagi[1] *1. Magnetic Powder Metallurgy Research Center, National Institute of Advanced Industrial Science and Technology (AIST), Nagoya, Japan*

Metastable Sm-Fe magnets such as $ThMn_{12}$-type $Sm(Fe_xCo_{1-x})_{12}$[1] and $TbCu_7$-type $(Sm,Zr)(Fe,Co)_{10}N_x$[2] have superior magnetic properties to surpass Nd-Fe-B magnet, which is the currently best magnet in commercial magnets. What is emphasized is these metastable phases are synthesized at lower temperature below 973 K. Recently, Okada et al. produced single crystalline $TbCu_7$-type Sm-Fe powder, which can be an anisotropic magnet, at 873 K by developing a low-temperature reduction-diffusion (LTRD) process using LiCl molten salt.[3, 4] Molten salt has a role of a solvent for Ca to enable the RD reaction at lower temperature than the melting point of Ca. Since the melting point of LiCl is about 873 K, the RD reaction may not occur at below this temperature. Li is considered as a new idea to lower the melting point of Ca, because Li-Ca alloy has very low eutectic point (503 K) and has potential to cause RD reaction at very low temperature. In this study, Sm-Fe binary phases at the unexplored low synthesis temperature was investigated by developing a new LTRD process using Li-Ca eutectic melt to investigate whether metastable phase is synthesized or not. Li-Ca eutectic melt was prepared from Ca and Li granules (1:1 molar ratio) in iron crucible by heating at 673K with stirring under Ar. After cooling to room temperature, Fe and Sm_2O_3 powders were put into this crucible and mixed at 573 K with stirring. The LTRD reaction was subjected at 873 K for 10 h under Ar. The products were washed by water and interstitial hydrogen atoms in Sm-Fe phases were removed by annealing in vac. at 473 K for 3 h. Fig. 1 shows XRD patterns of the obtained powder synthesized by the developed LTRD process in this study. $TbCu_7$-type Sm-Fe phase was successfully synthesized. From this result, it is clarified that the RD reaction was possible at lower temperature than melting point of Ca and there is no problem in synthesizing Sm-Fe phase because Li did not form any compound even if the Li-Ca melt is used. The LTRD process at lower temperatures than 873 K will be presented later.

[1] Y. Hirayama, Y.K. Takahashi, S. Hirosawa, K. Hono, Scripta Materialia, Vol. 138 p. 62-65 (2017) [2] S. Sakurada, A. Tsutai, T. Hirai, Y. Yanagida, M. Sahashi, S. Abe, T. Kaneko, Journal of Applied Physics, Vol.79 p. 4611-4613 (1996) [3] S. Okada, K. Takagi, Journal of Rare Earths, (2021), https://doi.org/10.1016/j.jre.2021.1005.017 [4] J. Kim, S. Okada, K. Takagi, AIP Advances Vol. 12, p. 035306 (2022)

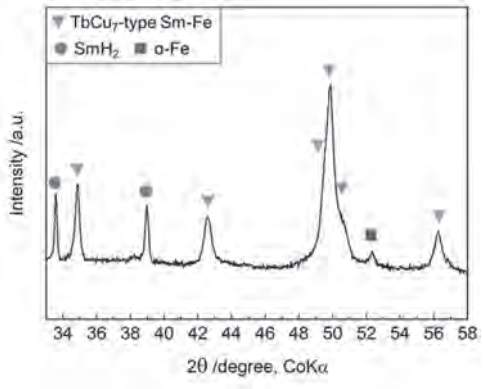

Fig. 1 XRD patterns of the obtained powders synthesized by a new LTRD process using Li-Ca melt at 873 K for 10 h.

KOA-14. Mechanically robust high magnetic-performance Sm-Co sintered magnets through microstructure engineering. *B. Cui*[1], X. Liu[1], C.I. Nlebedim[1] and J. Cui[1] *1. Critical Materials Institute, Ames Laboratory, Ames, IA, United States*

Samarium-cobalt (Sm-Co) sintered magnets have high magnetic energy densities, great resistance to demagnetization and corrosion, and excellent thermal stability in a wide temperature range (–50 °C to 550 °C). However, the utilization of these magnets is restricted by their brittleness. Based on micromechanical and the Zener pinning model, Sm-Co sintered magnets with improved mechanical properties have been designed and fabricated via microstructure engineering. A small amount of fine Sm_2O_3 particulates (0–3 wt%) has been incorporated into $Sm_2(CoFeCuZr)_{17}$ sintered magnets to refine the grain size by up to approximately 50% (from 45 to 22 μm) and narrow the grain size distribution. Doping with 3 wt% Sm_2O_3 increased the flexural strength by 62% while maintaining magnetic performance. Both grain-refined unimodal microstructure and heterogeneous laminated coarse/fine grain microstructure were formed by strategically designed assemblies of Sm_2O_3-added Sm-Co powder feedstock mixtures. The technology is compatible with existing magnet manufacturing processes. Numerical micromechanics simulation indicates that the fracture is dominated by intragranular mode. The mechanical strength is mainly enhanced by the additive-induced grain refinement, while the small amount of Sm_2O_3 addition has little direct effect on mechanical properties. These magnets will be more cost-effective, efficient, and robust for various functional applications.

Session KOB
HARD MAGNETIC MATERIALS IV: RARE-EARTH FREE HARD MAGNETIC MATERIALS

Brian Lejeune, Chair
Northeastern University, Boston, MA, United States

CONTRIBUTED PAPERS

KOB-01. Integrated *ab initio* computational modelling of magnetic anisotropy and $L1_0$ order in non-critical transition metal magnets.
J.B. Staunton[1], B.J. Wieder[2], G. Fiete[2] and L. Lewis[3,4] *1. Physics, University of Warwick, Coventry, United Kingdom; 2. Physics, Northeastern University, Boston, MA, United States; 3. Mechanical and Industrial Engineering, Northeastern University, Boston, MA, United States; 4. Chemical Engineering, Northeastern University, Boston, MA, United States*

While CoPt and FePt magnets have high magnetic anisotropy (MAE) when chemically ordered into $L1_0$ structures, their components' high criticality calls for a search for more sustainable systems. *Ab initio* modelling confirms the pivotal role of the tetragonal order for this useful permanent magnetic property [1]. $L1_0$-FeNi, found in meteoritic, tetrataenite samples, also has significant uniaxial anisotropy [2,3]. We report integrated modelling of ternary FeNi-based alloys of both the propensity for $L1_0$ order and the MAE. We study $Fe_{50}Ni_{40}X_{10}$ alloys (X = Pt, Pd, Al, Ti, Mo, Nb, Ta, W). Crucially, to guide material design, our modelling accounts for the physics that the same electrons which produce the MAE also glue the atoms into their places in the crystal structure. There are 3 steps: 1. The MAE is calculated for an ideal (prescribed) ferromagnetic (FM) $L1_0$ ordered material (top figure) - alternating Fe and $Ni_{80}X_{20}$ layers. These values, per formula unit (FU), are shown in the 5th column (col) of the table. 2. The atomic, short-range order (ASRO) in a high temperature, paramagnetic (PM), f.c.c. solid solution, $Fe_{50}Ni_{40}X_{10}$ is calculated [4] to learn whether $L1_0$ order forms readily (col 2) and to determine the compositions of the alternating layers (col 3) if it does (lower figure). 3. The MAE of the ensuing $L1_0$ alloys are calculated (col 4). FM $L1_0$ Fe-$Ni_{80}Pt_{20}$ has a large MAE of 0.39 meV/FU but Fe-$Ni_{80}Al_{20}$'s value of 0.23meV/FU is significant and twice that of $L1_0$-FeNi. The chemical ordering, however, supported by the electrons of the materials, does not lead to these desired atomic arrangements and only the Pt, Pd, Al-doped alloys adopt any $L1_0$ order with sharply reduced MAEs (col 4). Comparison of the ASRO in PM and FM $Fe_{50}Ni_{50}$ solid solutions shows a way to circumvent this issue and explain the $L1_0$-order in meteoritic FeNi samples. Spin-polarized electronic structure is paramount to establish $L1_0$ order - PM $Fe_{50}Ni_{50}$ has no propensity whatsoever to adopt this order in sharp contrast to the alloy in a FM state which is predicted to order into the $L1_0$ structure below 670K [5]. [Research performed in part under the auspices of the U.S. Department of Energy, Office of Science under Award Number DE SC0022168.]

[1] J. B. Staunton et al., https://doi.org/10.1103/PhysRevB.74.144411 [2] R. S. Clarke and E. R. D. Scott, *American Mineralogist* 65, no. 7-8 (1980): 624-630. [3] N. Maat et al. *Acta Materialia*. 2020 Sep 1;196:776 [4] C. D. Woodgate and J. B. Staunton, https://doi.org/10.1103/PhysRevB.105.115124 [5] V. Crisan et al., https://doi.org/10.1103/PhysRevB.66.014416

Alloy	$L1_0$?	Fe/Ni/X (layer1) Fe/Ni/X (layer 2)	MAE (meV/FU)	MAE (meV/FU) $L1_0$ $Ni_{0.8}X_{0.2}$-Fe
$Fe_{50}Ni_{50}$	No	-	-	0.127
$Fe_{50}Ni_{50}$	Yes FM	1.00/ 0.00/ 0.00 0.00/ 1.00/ 0.00	0.127	0.127
$Fe_{50}Pt_{50}$	Yes	1.00/ 0.00/ 0.00 0.00/ 1.00/ 0.00	2.74	2.74
$Fe_{50}Ni_{40}Pt_{10}$	Yes	0.41/ 0.39/ 0.20 0.59/ 0.41/ 0.00	0.195	0.387
$Fe_{50}Ni_{40}Pd_{10}$	Yes	0.47/ 0.33/ 0.20 0.53/ 0.47/ 0.00	0.013	0.127
$Fe_{50}Ni_{30}Al_{10}$	Yes	0.51/ 0.29/ 0.20 0.49/ 0.51/ 0.00	0.016	0.226
$Fe_{50}Ni_{40}Ti_{10}$	No	-	-	0.141
$Fe_{50}Ni_{40}Mo_{10}$	No	-	-	0.184
$Fe_{50}Ni_{40}Nb_{10}$	No	-	-	0.187
$Fe_{50}Ni_{40}Ta_{10}$	No	-	-	0.212
$Fe_{50}Ni_{40}W_{10}$	No	-	-	0.102

Figure 1

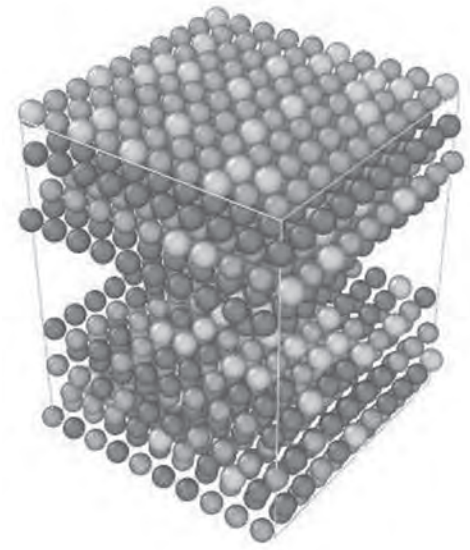

Figure 2

KOB-02. Magnetic-Field-Driven Chemical Ordering in $L1_0$ Ferromagnetic Compounds.
B. Lejeune[1], X. Zhang[2], J.B. Staunton[3] and L. Lewis[1,2] *1. Chemical Engineering, Northeastern University, Boston, MA, United States; 2. Mechanical and Industrial Engineering, Northeastern University, Boston, MA, United States; 3. Physics, University of Warwick, Coventry, United Kingdom*

Expanding the portfolio of advanced permanent magnets will relieve supply pressure on current rare-earth-based materials. To this end, the rare-earth-free ferromagnetic compound $L1_0$ FeNi (*aka* tetrataenite) demonstrates promise [1] as a "gap" magnet [2], with appreciable magnetocrystalline anisotropy derived from the chemical order of Fe and Ni; however, the highly sluggish ordering kinetics present a formidable synthesis challenge. To this end, the application of energetic drivers for chemical ordering has been investigated

in the analogous but more accessible model system MnAl, which undergoes a similar chemical ordering phase transformation as does FeNi. Melt-spun ribbons comprised of kinetically retained, chemically disordered ε-MnAl were subjected to a mild passive magnetic field during annealing at temperatures both above and below the Curie temperature of the $L1_0$ τ-MnAl phase (378 °C) for up to 1 hour to achieve partially ordered states. The resultant structural, magnetic, and calorimetric features were assessed and compared with those obtained from zero-field annealing. A significant increase in the τ-MnAl phase fraction is observed in the magnetic field-annealed sample relative to that present in the zero-field-annealed sample under the same heat-treatment conditions. Microstructural and crystallographic features of these samples are correlated with the applied field configuration to understand its impact on diffusion and chemical ordering. This work confirms that magnetic field annealing facilitates formation of $L1_0$ τ-MnAl phase in the MnAl system. Acknowledgments: This work was supported in part by the U.S. Department of Energy, Office of Basic Energy Sciences under Award Number DE SC0022168.

[1] L.H. Lewis *et al.*, J. Phys. Condens. Matter 26, 1 (2014). [2] J.M.D. Coey, Scr. Mater. 67, 524 (2012).

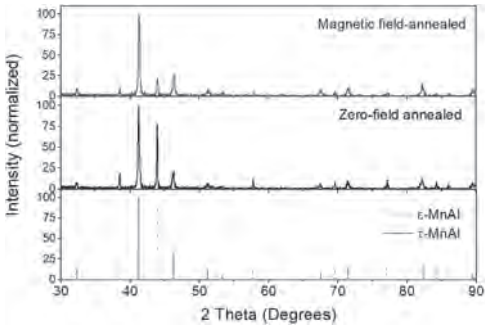

Fig. 1. XRD data of MnAl samples heat-treated with and without magnetic field. The field-annealed sample shows a significantly greater fraction of chemically ordered τ-MnAl relative to the zero-field annealed sample.

KOB-03. Nanotwins assisted nitridation in FeNi nanopowders synthesized by induction thermal plasma. *J. Wang*[1], Y. Hirayama[1], Z. Liu[2], K. Suzuki[1], W. Yamaguchi[1], K. Park[1], K. Takagi[1], H. Kura[3], E. Watanabe[3] and K. Ozaki[1] *1. Magnetic Powder Metallurgy Research Center, National Institute of Advanced Industrial Science and Technology (AIST), Nagoya, Japan; 2. Innovative Functional Materials Research Institute, National Institute of Advanced Industrial Science and Technology (AIST), Nagoya, Japan; 3. Advanced Research and Innovation Center, DENSO CORPORATION, Nagoya, Japan*

$L1_0$ ordered FeNi alloy is considered as a promising candidate for rare-earth-free and environment-friendly permanent magnet. Highly ordered single-phase $L1_0$ FeNi is challenging to synthesize due to its low chemical order-disorder transition temperature. Recently, a nonequilibrium synthetic route utilizing a nitrogen topotactic reaction was considered as a valid approach although the detailed phase transformation mechanism is missing. [1] In this work, we investigated the formation mechanism of the tetragonal FeNiN precursor phase during the nitridation of FeNi nanopowders. [2] A low oxygen induction thermal plasma system was applied to synthesize the FeNi nanopowders (NPs). The processed FeNi NPs were annealed under a hydrogen gas flow at 1 L/min for 2 h at 400 °C. Then, the NPs were nitrided at 350 °C under ammonia with gas flowing at 2 L/min for 16 h. The detailed microstructure analysis was performed with an atomic resolution analytical electron microscope JEM ARM200F. High-resolution TEM observation reveals intensive nanotwins in the nitrided FeNi NPs which results in a distorted lattice Interestingly Fe segregates at the TBs was confirmed with EDS mapping. Thus, the nanotwins region may provide preferential nucleation sites for the FeNiN product phase in the Fe_2Ni_2N parent matrix Furthermore, detailed microstructure characterization shown in Fig.1 revealed that the growth of the FeNiN product phase followed a massive transformation with high index irrational orientation relationships and ledgewise growth motion characteristics detected at the FeNiN/Fe_2Ni_2N migrating interface. Based on the results, we delineated a potential formation route of the FeNiN precursor phase in the FeNi NPs during nitridation. *Acknowledgment* This work was partially supported by the project Development of Magnetic Material Technology for High Efficiency Motors which was commissioned by Japan's New Energy and Industrial Technology Development Organization (NEDO).

1) G oto, S. *et al.* Synthesis of single-phase $L1_0$ FeNi magnet powder by nitrogen insertion and topotactic extraction. *Sci Rep* 7, 13216, doi:10.1038/s41598 017 135622 (2017). 2) Wang, J., Hirayama, Y., Liu, Z. *et al.* Massive transformation in FeNi nanopowders with nanotwin assisted nitridation. *Sci Rep* 12, 3679, doi.org/10.1038/s41598-022-07479-8 (2022).

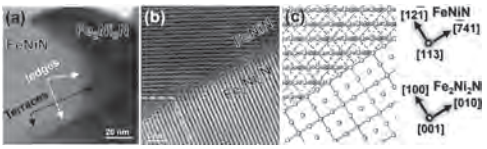

Fig. 1. ABF-STEM images of nitrided FeNi NPs with terraces/ledges demonstrating the ledgewise growth motion of the FeNiN/Fe_2Ni_2N interface (a & b). (c) schematizes the representative high-index orientation relationship present in (b).[2]

KOB-04. Phase Stabilization and Coercivity Enhancement in Multi-principal Element FeCoNiMnCu Thin Films. *W. Beeson*[1], H. Zhang[2,3], A. Davydov[2], G. Yin[1] and K. Liu[1] *1. Department of Physics, Georgetown University, Washington, DC, United States; 2. Materials Science and Engineering Division, National Institute of Standards and Technology, Gaithersburg, MD, United States; 3. Theiss Research, Inc., La Jolla, CA, United States*

The vast multi-principal element alloy (MPEA) composition space is promising for discovery of new material phases with unique combinations of properties.[1] We have explored the potential to achieve high magnetic anisotropy materials in MPEA FeCoNiMnCu thin films. Thin films of FeCoNiMnCu sputtered on thermally oxidized Si/SiO_2 substrate at room temperature exhibit soft magnetic properties with a coercivity on the order of 10 Oe. After post-deposition rapid thermal annealing (RTA), the films exhibit a single face-centered cubic (FCC) phase from grazing incidence X-ray diffraction (GIXRD), as shown in Fig. 1, as well as a continuous surface morphology measured by atomic force microscopy. Magnetometry measurements reveal a coercivity of 400 Oe, a nearly 40-fold increase compared to as-grown samples. First-order reversal curve (FORC) analysis[2] of the RTA sample reveals a distinct feature in the high coercivity regime of the FORC distribution, as shown in Fig. 2, indicating the presence of a single magnetic phase with much enhanced coercivity. Additionally, we have explored inclusion of Pt to facilitate uniaxial structure and enhance magnetic anisotropy. We find that RTA of the FeCoNiMnCuPt films induces ordering into an $L1_0$ intermetallic phase. A significant enhancement of coercivity to over 2 kOe after RTA has been observed, compared to 5 Oe before RTA, along with the development of an out-of-plane magnetic easy-axis, reflecting the formation of a high anisotropy $L1_0$ phase. These results demonstrate the potential in achieving high magnetic anisotropy materials using the multi-principal element approach. This work has been supported by the NSF (ECCS-2151809).

1. J.W. Yeh, S.K. Chen, S.Y. Chang et al., *Adv. Eng. Mater.*, 6, 299-303, (2004). 2. D.A. Gilbert, J.W. Liao, K. Liu et al., *APL Mater.*, 2, 086106, (2014).

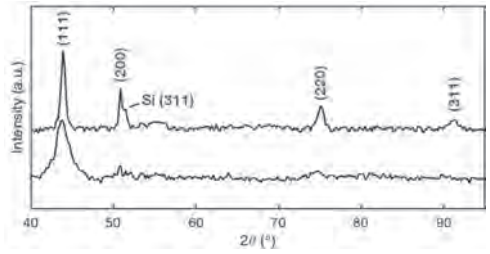

Fig. 1. Grazing-incidence XRD for FeCoNiMnCu films (bottom) as-grown and (top) after RTA.

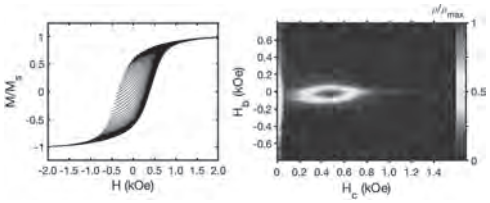

Fig. 2. (left) Family of first-order reversal curves (FORC) and (right) FORC distribution of an FeCoNiMnCu film after RTA.

KOB-05. Simulation of Thermal Decomposition of γ′-Fe_4N using Molecular Dynamics Method. *J. Zhu*[1] and J. Wang[1] *1. Electrical and Computer Engineering, University of Minnesota, Minneapolis, MN, United States*

α″-$Fe_{16}N_2$ is a promising environmentally-friendly rare-earth-free permanent magnet material with ultra-high saturation magnetization. Recent research has demonstrated experimentally through a thermally quenching treatment using γ′ phase Fe_4N as a precursor to synthesize α″-$Fe_{16}N_2$ in bulk format. In this research, we investigated γ′-Fe_4N thin film thermal decomposition process and potential localized phase transition from *fcc* phase to *bct* phase using Molecular Dynamics (MD) simulation method. As nitrogen concentration is much higher in γ′-Fe_4N (5.9 wt.%) than that in α′-Fe_8N or α″-$Fe_{16}N_2$ (3 wt.%), Nitrogen "depletion" process must have to occur during the thermal decomposition to form possible lower-Nitrogen content *bct* Fe-N solid solution. A localized "Nitrogen-rich" grain boundary lattice defect model is designed to induce Nitrogen bond forming through the recombination of nitrogen pair atoms, and therefore significantly improves local reduction of Nitrogen content in the α′-Fe_4N lattice sample during thermal treatment. Modified Embedded Atom Method (MEAM) interatomic potential of Fe-N system is applied. Bond forming/breaking and local Nitrogen displacement analysis (MSD) are also performed in the thermostat-controlled heating/quenching simulation process. We use virtual XRD method and formation energy calculation to assess and detect the new material phases on the thermally-treated and energy minimized lattice sample.

[1] Jian-Ping Wang, "Environment-friendly bulk $Fe_{16}N_2$ permanent magnet: Review and Prospective", Journal of Magnetism and Magnetic Materials, 497(2020) 165962 [2] J. Zhu, G, Guo and J.-P. Wang, "Study of γ′-F_4N Annealing Process Through Molecular Dynamics Modeling", TMS 2022 151st Annual Meeting, The Minerals, Metals & Materials Series, Page 109-117, https://doi.org/10.1007/978-3-030-92381-5_11 [3] M.H. Wetzel, M.R. Schwarz, A. Leineweber, High-pressure high-temperature study of the pressure induced decomposition of the iron nitride γ′-Fe4N, Journal of Alloys and Compounds, Volume 801, 2019, Pages 438-448

KOB-06. Withdrawn

KOB-07. Processing and characterization of melt-spun Nd-Fe-B ribbons for the preparation of hot deformation magnets. *S. Singh*[1,2], A. Diraviam[2], R. Sarkar[2], A. Haldar[1] and M. Muthuvel[2] *1. Physics, Indian Institute of Technology Hyderabad, Hyderabad, India; 2. Defence metallurgical Research Laboratory, Hyderabad, India*

Nd-Fe-B magnets are widely used in electric vehicles (EVs), wind turbines, and electronic devices in civilian and defence sectors due to their high magnetic performance. Alternate to the sintering route, the hot-deformation route does not require heavy rare elements (HRE) such as Dy and Tb and is a promising route to produce Nd-Fe-B magnets at low cost [1]. Hot deformed magnets are produced through melt spinning and hot pressing/deformation techniques [2]. Nd-Fe-B powder prepared from the melt-spun ribbon is used as precursors and hence optimization of melt spinning parameters is important to obtain desirable grain size and hard magnetic properties [3]. Hence a study was undertaken to prepare Nd-Fe-B melt-spun ribbons to tailor the microstructure and hard magnetic properties. Melt spun ribbons with a nominal composition of $Nd_{13.6}Fe_{73.6}Co_{6.6}Ga_{0.6}B_{5.6}$ alloy were prepared at various wheel speeds from 17 to 25 m/s. While the structure of the ribbons was obtained using X-Ray diffraction, the microstructure was obtained by transmission electron microscope (TEM). The magnetic properties and thermomagnetic properties were obtained using a vibrating sample magnetometer (VSM). XRD analysis showed $Nd_2Fe_{14}B$ phase with strong (00l) texture in all ribbons and texture fades away at higher wheel speeds. Thermal stability studied by calorimetry showed that the $Nd_2Fe_{14}B$ phase was stable up to 500°C, beyond which precipitation of the α-Fe phase takes place. TEM analysis (Fig.1) showed that the $Nd_2Fe_{14}B$ phase was distributed uniformly throughout the sample with a grain size of 50-150 nm. The average grain size was found to decrease with an increase in the wheel speed. The remanence (B_r) and coercivity (H_c) values were found to increase with the increase in wheel speed up to 23 m/s and beyond which it starts decreasing gradually (Fig.2). Ribbons with the highest magnetic properties having a B_r value of 6.6 kG and H_c value of 12.3 kOe were obtained at 23 m/s and may be best suited for the fabrication of hot deformed Nd-Fe-B magnets.

[1] N.J. Yu, M.X. Pan, P.Y. Zhang, and H.L. Ge, J. Magn. 18, 235 (2013). [2] K. Hioki, Sci. Technol. Adv. Mater. 22, 72 (2021). [3] C. Rong and B. Shen, Chinese Phys. B 27, 117502 (2018).

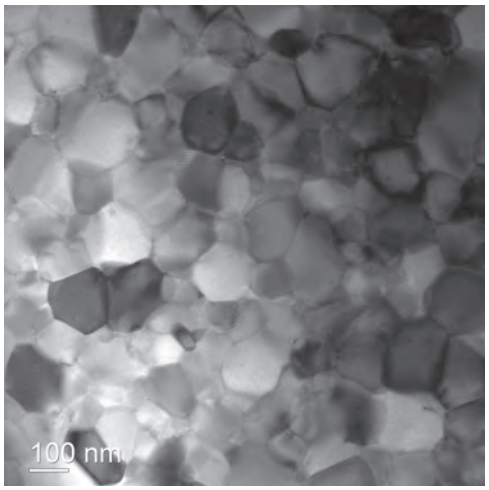

Fig.1: TEM image showing the microstructure of Nd-Fe-B ribbon prepared at a wheel speed of 23 m/s

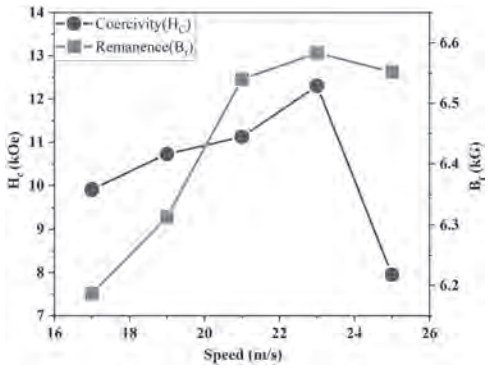

Fig.2: Magnetic properties (B_r and H_c) of Nd-Fe-B ribbon prepared at different wheel speeds

Session KOC
HARD MAGNETIC MATERIALS VI: NANOSTRUCTURED, COMPOSITE AND OTHER HARD MAGNETIC MATERIALS (INCLUDING INTERMETALLIC ALLOYS AND L10 ALLOYS)

Chuanpu Liu, Chair
Colorado State University, Fort Collins, CO, United States

CONTRIBUTED PAPERS

KOC-01. Challenges and Opportunities for Manufacturing Novel Magnets. *C.I. Nlebedim*[1] *1. Critical Materials Institute, Ames Laboratory, Ames, IA, United States*

The recent global trend to transition to a cleaner society by transforming various sectors of the economy, particularly the transportation and energy sectors, has strongly underscored the importance of permanent magnets to the modern society. However, Nd-Fe-B magnets widely used in many applications is regarded as subject to supply disruption relative to the demand for applications. Hence, rare earth (RE) lean and RE-free permanent magnets have attracted more research attentions. High performance permanent magnets need suitable intrinsic magnetic properties and proper microstructure for extrinsic properties development. Many potential RE-lean and RE-free magnetic compounds show good intrinsic magnetic properties, including high magnetization, large or moderate magnetic anisotropy, and high Curie temperature, all of which can potentially be exploited for the development of novel permanent magnets. Based on Stoner-Wolfforth (SW) model, the ideal microstructure magnet has a single domain-sized grain and is isolated by a non-magnetic grain boundary phase. However, many potential permanent magnet compositions such as $RE(Fe,M)_{12}$, $RE(Fe,M)_7$, Ce-Co-Cu-Fe, (Fe,Co)-X (X=B, C and N), $Sm_2Fe_{17}N_x$, MnAl, Fe-Ni, etc., are metastable phases. Hence processing them result in the formation of local structural defects or the second soft magnetic phase, or decomposition at high temperature. The low phase stability brings a big challenge to achieving SW-type microstructure to gain high coercivity using traditional thermo-mechanical processing synthesis methods. This talk presents the correlation between thermodynamics and microstructure evolution and its effect on coercivity. We will discuss the strategy for the composition and microstructure design and the development of novel synthesis routes to maximize the coercivity and mitigate the challenge of the metastable behavior of the magnetic phases. This work is supported by the Critical Materials Institute, an Energy Innovation Hub funded by the U.S. DOE, Office of Energy Efficiency and Renewable Energy, Advanced Manufacturing Office. Ames Laboratory is operated for the U.S. Department of Energy by Iowa State University of Science and Technology under Contract No. DE-AC02-07CH11358

KOC-02. *Ab initio*-based Thermodynamic Modeling for Sustainable Hard Magnetic Materials. *H.I. Sözen*[1,2], T. Klüner[2] and T. Hickel[1,3]
1. Max-Planck-Institut für Eisenforschung GmbH, Düsseldorf, Germany; 2. Carl von Ossietzky University, Oldenburg, Germany; 3. BAM Federal Institute for Materials Research and Testing, Berlin, Germany

The resource criticality of rare-earth (RE) elements on the global market has triggered significant research into more resource-efficient alternative hard-magnetic materials[1]. The utilization of the RE-lean $ThMn_{12}$ materials system in combination with the abundant RE element Ce is a promising strategy. One of the main challenges for the Ce-based hard-magnetic materials is the formation of detrimental Laves phases next to the $ThMn_{12}$-type compound $CeFe_{11}Ti$[2]. In this contribution, we present an *ab initio-based* approach to modify the stability of these phases in the Ce-Fe-Ti system by additions of 3*d* and 4*d*-elements. We start with Cu and Ga substitutions and employ state-of-the-art approaches for vibrational, electronic, and magnetic entropy contributions[3,4] to calculate the Helmholtz free energy $F(T,V)$ for all relevant phases. The results are used to provide two fundamental methodological insights. One of them is our new modeling concept of partial decomposition, which considers the enrichment of the added solutes in phases that would at the considered temperature not be stable in a full decomposition. In the case of Cu, this effect suppresses the formation of $CeFe_{11}Ti$, whereas in the case of Ga this ensures the presence of a small phase fraction of $CeFe_{11}Ti$. The second conclusion is the dominant impact of 0 K formation enthalpies on the solute-enhances phase stability compared to finite temperature entropy terms. Based on this a screening approach, considering the substitution of all 3*d* and 4*d*-elements, is developed. We show that substituted elements with more than a half-filled 3*d*-shell or with less than a half-filled 4*d*-shell mainly reduce the formation temperature of the 1:12 phase. According to these thermodynamic considerations, especially Zn and Tc turn out to be promising substitution candidates. Therefore, more detailed finite temperature *ab initio* evaluations of the free energies have been performed for these elements. The difference between the screening determination of the critical temperature and a fully temperature-dependent determination of free energies is within the error bar of the other approximations. This demonstrates the robustness and efficiency of our developed screening approach.

[1] O. Gutfleisch, et al.: Magnetic materials and devices for the 21st century: Stronger, lighter, and more energy efficient. Advanced Materials, 23, (2011) 821. [2] H. I. Sözen, et al.: *Ab initio* phase stabilities of Ce-based hard magnetic materials and comparison with experimental phase diagrams. Physical Review Materials, 3 (2019) 084407. [3] H. I. Sözen, et al.: Impact of magnetism on the phase stability modeling for rare-earth based hard magnetic materials. CALPHAD: Computer Coupling of Phase Diagrams and Thermochemistry, 68 (2020) 101731. [4] H. I. Sözen, et al.: *Ab initio* phase stabilities of rare-earth lean Nd-based hard magnets. Journal of Magnetism and Magnetic Materials, 559 (2022) 169529.

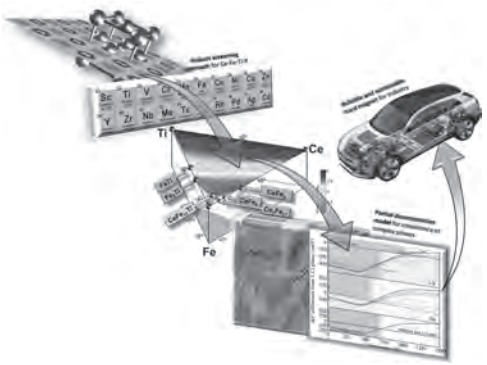

Figure 1

KOC-03. Coercivity limits in nanoscale ferromagnets: Brown's paradox revisited. J. Mohapatra[1], X. Meiying[1], J. Elkins[1] and *J. Liu*[1]
1. Department of Physics, The University of Texas at Arlington, Arlington, TX, United States

Brown's theorem on coercivity of ferromagnetic materials has predicted that the coercivity level is substantially higher than in practice for all the materials studied in experiments in the past seven decades, which is known as Brown's paradox. In this work, a coercivity close to that predicted by Brown's theorem is obtained.[1,2] It is found that the aspect ratio and diameter of the nanocrystals have a strong effect on the coercivity. When the nanocrystals have an increased aspect ratio, the coercivity is significantly higher than the magnetocrystalline anisotropy field of hcp Co crystal. An analysis based on the current experimental results and related literature[3,4] reveals a coercivity ceiling in consideration of geometrical dimensions and effective magnetic anisotropy. In addition, this study provides a quantitative correlation between the structure and coercivity, paving the way for future materials design of advanced permanent magnets.

[1] J. Mohapatra, M. Xing, J. Elkins, J. Beatty, and J. P. Liu, Adv. Funct. Mater. 31, 2010157 (2021). [2] J. Mohapatra, J. Fischbacher, M. Gusenbauer, M. Y. Xing, J. Elkins, T. Schrefl, and J. Ping Liu, Phys. Rev. B (2022), DOI: 10.1103/PhysRevB.00.004400. [3] J. Fischbacher, A. Kovacs, M. Gusenbauer, H. Oezelt, L. Exl, S. Bance, and T. Schrefl, J. Phys. D: Appl. Phys. 51, 193002 (2018). [4] H. Li, Q. Wu, M. Yue, Y. Peng, Y. Li, J. Liang, D. Wang, and J. Zhang, J. Magn. Magn. Mater. 481, 104 (2019).

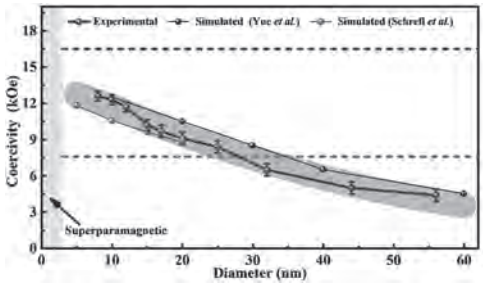

Figure 1: Diameter dependence of coercivity in Co NWs. The lower and upper dashed lines represent the magnetocrystalline anisotropy field and the effective magnetic anisotropy field (sum of the magnetocrystalline anisotropy and the shape anisotropy fields), respectively.

KOC-04. Tuning Magnetocrystalline Anisotropy of LTP-MnBi*. *M. Choi*[1], Y. Hong[1], H. Won[1], C. Yeo[2], N. Shah[2], J. Lee[3], T. Lee[3] and T. Lim[3] *1. Electrical and Computer Engineering, The University of Alabama, Tuscaloosa, AL, United States; 2. Mechanical Engineering, Texas Tech University, Lubbock, TX, United States; 3. Institute of Fundamental and Advanced Technology (IFAT), Hyundai Motor Company, Uiwang-si, The Republic of Korea*

Spin orientation of LTP-MnBi can be controlled by partially substituting Bi of hexagonal LTP-MnBi with either the third alloying element or temperature. The spin reorientation occurs at about 90 K from *ab*-plane (0 - 90 K) to *c*-axis (T > 90 K) of LTP MnBi [1]. Sakuma et al. have performed first-principles calculations on Sn-doped Mn ($Bi_{1-x}Sn_x$) and found that magnetocrystalline anisotropy constant (K_u) increases to about 3 MJ/m^3 (x = 0.1) from -0.5 MJ/m^3 (x = 0.0) at 0 K and then remains unchanged up to x = 0.3 [2]. However, Stutius et al. reported -0.15 MJ/m^3 (x = 0.0) of the measured K_u at 4.3 K [3]. Therefore, Sakuma's calculated K_u (x = 0.0) does not agree with the experimental K_u in [3]. This may be attributed to 300 K lattice constants in [2] used in the calculation. Sakuma did not relax the MnBi formula unit to obtain lattice constants at the ground state. In this study, we have performed first-principles calculations on $Mn_{0.5}Bi_{0.5}$, $Mn_{0.5}Bi_{0.25}Sn_{0.25}$ (substitutional doping: SD), and $(Mn_{0.5}Bi_{0.5})_{66.7}Sn_{33.3}$ (interstitial doping: ID) in Fig. 1 and used the relaxed lattice constants. Both *a* and *c* decrease from 4.287 and 6.118 Å to 3.954 and 5.456 Å, respectively, when Sn substitutes for Bi of LTP-MnBi. However, the *a* of ID increases to 4.611 Å, while the *c* decreases to 5.683 Å. Figure 2 shows density of states for MnBi-Sn. The net magnetic moment is 7.224 μ_B/*f.u.* for LTP-MnBi, 5.034 μ_B/*f.u.* for SD, and 6.609 μ_B/*f.u* for ID. The K_u is changed from in-plane (-0.202 MJ/m^3) to out-of-plane (1.711 MJ/m^3) by substitutionally doping Sn and maintains in-plane with interstitially doping Sn-MnBi (-0.043 MJ/m^3). Our results agree with experimental one [3], but Sakuma's. The Curie temperature decreases from 716 K for LTP-MnBi to 445 K for SD and 285 K for ID. * This work was supported in part by the National Science Foundation (NSF) under Grant No. 2137275.

[1] Michael A. McGuire, Huibo Cao, Bryan C. Chakoumakos, and Brian C. Sales, *Phys. Rev.* B 90, 174425 (2014). [2] Akimasa Sakuma, Yuki Manabe, and Yohei Kota, *Journal of the Physical Society of Japan* 82, 073704 (2013). [3] W.E. Stutius, T. Chen, and T.R. Sandin, AIP Conf. Proc. 18, 1222 (1974)

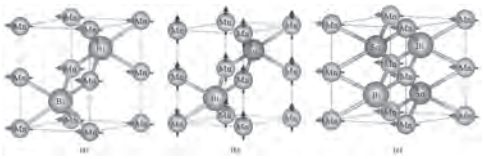

Figure 1. Magnetic structure for (a) LTP-MnBi (in-plane), (b) substitutionally (out-of-plane), and (c) interstitially (in-plane) Sn-doped MnBi.

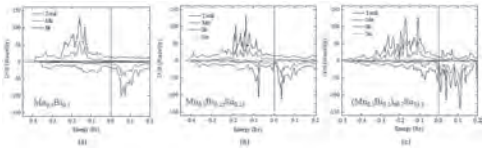

Figure 2. Density of states for (a) LTP-MnBi ($Mn_{0.5}Bi_{0.5}$), (b) substitutionally Sn-doped MnBi ($Mn_{0.5}Bi_{0.25}Sn_{0.25}$), and (c) interstitially Sn-doped MnBi ($(Mn_{0.5}Bi_{0.5})_{66.7}Sn_{33.3}$).

KOC-05. Bulk Rare Earth Free MnBi-based Permanent Magnets by Severe Plastic Deformation. *L. Weissitsch*[1], S. Wurster[1], H. Krenn[2], R. Pippan[1] and A. Bachmaier[1] *1. Erich Schmid Institute of Materials Science of the Austrian Academy of Sciences, Leoben, Austria; 2. Institute of Physics, University of Graz, Graz, Austria*

High-performance permanent magnets (PMs) consists of materials containing a significant amount of rare-earth elements (REE). Such elements are already recognized as critical materials by international institutes and supply shortages will be a crucial problem for the global economic and social development. In addition, the public awareness in green technologies, i.e., wind power plants and electric mobility, fosters the growing demand for PMs. Facing these problems, this study focusses on the reduction of REE usage by utilization of the REE-free intermetallic α-MnBi phase, which exhibits exceptional hard magnetic properties. In case the α-MnBi phase is exchange coupled with a soft magnetic phase, generating so called 'spring magnets', the magnetic performance of these composites competes with nowadays PMs. However, the production of the α-MnBi phase is a challenging task. Strongly differing melting temperatures, crystal structures and a segregation of Mn upon solidification are impeding a direct phase formation from the liquid phase. High-pressure torsion (HPT), a method of severe plastic deformation, allows to overcome current processing limitations. The resulting disc shaped samples exhibit dimensions of several mm to cm, whereas the microstructure simultaneously features grain sizes in the range between several micrometres to tens of nanometres. HPT further enables the formation of a textured nanocomposite allowing to process anisotropic spring magnets. Herein, we present the successful generation of the α-MnBi phase by HPT-deformation, compare and report on different processing steps utilized for this phase formation. HPT-deformed powder blends of Mn and Bi are subjected to magnetic field assisted thermal treatments in vacuum and the α-MnBi phase formation is monitored by in-situ synchrotron X-ray diffraction and SQUID magnetometry. Furthermore, FeCo powder is added

to induce exchange coupling with the ultimate goal to form anisotropic, REE-free MnBi-based magnets. This project has received funding from the European Research Council (ERC) under the European Union's Horizon 2020 research and innovation programme (grant agreement No 101069203).

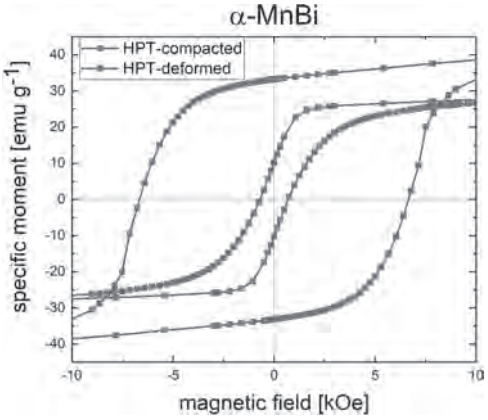

Figure 1: Beneficial magnetic properties for HPT-deformed materials

KOC-06. Effects of Uniaxial Compressive Stress on Textured Grain Growth in Powder-based Alnico Magnet Alloys with an Engineered Microstructure. *I. Anderson*[1,2], E. Rinko[2], N. Argibay[1] and M.J. Kramer[1,2]
1. Ames National Laboratory (USDOE), Ames, IA, United States;
2. Materials Science and Engineering, Iowa State University, Ames, IA, United States

Alnico, a family of rare earth-free permanent magnet alloys, now has demonstrated abnormal grain growth (AGG) behavior upon de-binding and sintering in vacuum at high temperatures (up to 1240C), even in a Co-lean alnico, previously reluctant to undergo AGG. We obtained AGG behavior within Co-lean alnico by engineering a bi-modal starting powder size distribution that utilized the concept of particle-assisted AGG (PA-AGG), where particles (average 500 nm diameter) came from residual prior particle boundary oxides and the bimodal powder sizes formed the starting grain size difference demanded by PA-AGG theory [1]. While the ability to promote AGG behavior is desirable to achieve a large-grained microstructure as a starting condition for magnetic annealing, superior magnetic properties result when grains also exhibit a <001> texture. Current supply/price pressure on Co resources motivates the exploration of this beneficial texture development within Co-lean alnico. Previous success for texturing several full-Co alnico samples was achieved by imposing a uniaxial compressive stress (by dead weighting) at sintering temperatures [2], but not for Co-lean alnico alloys. Fortunately, our new successful promotion of AGG behavior in Co-lean alnico is ripe for further compressive stress loading experiments to assert a preferred texture on the fully sintered microstructure. In this follow-on study, we vacuum sintered (1190C, 4h) bi-modal Co-lean alnico powder into a partially developed AGG condition (90% dense) that preserved the grain growth "momentum" conditions (from PA-AGG theory). These samples were subsequently exposed to a compressive stress (279 kPa) at high temperatures (1240C, 20h) in attempt to impose PA-AGG of certain grains to grow with a crystallographic direction close to the <001>. We will report SEM results on final grain size and resulting texture development in these new alnico samples, along with initial magnetic property levels after standard magnetic annealing and draw cycles. Funded by USDOE-OTT-TCF with EERE-VTO support and by KC-NSC through Ames Lab contract no. DE-AC02-07CH11358.

[1] A. Rollett, G. Rohrer, J. Humphreys, *Recrystallization and Related Annealing Phenomena*, 3rd edition, Elsevier (2017). [2] I. E. Anderson, et al., *AIP Advances* 7, 056209 (2017)

KOC-07. Magnetic Behavior and Chaining of Strontium Ferrite-Nylon Composite Above the Melting Temperature. *T. Ahmed*[1], C. Selsor[2], J. Tate[3] and W. Geerts[4] *1. Materials Science, Engineering, and Commercialization, Texas State University, San Marcos, TX, United States; 2. Aerospace Engineering, Texas A&M University, College Station, TX, United States; 3. Mechanical and Manufacturing Engineering, Texas State University, San Marcos, TX, United States; 4. Department of Physics, Texas State University, San Marcos, TX, United States*

Magnetic Field Assisted Additive Manufacturing (MFAAM), or 3D printing in a magnetic field, is a new manufacturing method that will allow for the realization of new materials and devices whose magnetic anisotropy axis varies as a function of position. Applications of hard magnetic MFAAM materials include Halbach cylinders for use in energy-efficient electromotors and generators and high-performance permanent magnets for use in portable MRI equipment. To better understand the MFAAM process here we study the effect of a magnetic field on the orientation and distribution of Sr-ferrite particles in a molten PA-12 matrix. VSM measurements are made on fused deposition modeling filaments of different packing fraction (4-70 wt%) made using a twin-screw extruder. To induce an easy axis, the samples are field annealed at 230 °C in 22000 Oe. 5 mm long cylindrical-shaped filament wrapped in Teflon tape are loaded in a Pyrex glass tube and secured with high-temperature silicone glue. The rotation of the sample's magnetic moment upon application of a field perpendicular to the easy axis is monitored through biaxial VSM using a MicroSense EZ9. The observed transients depend on the temperature of the composite, the applied alignment field, but also on the initial field anneal procedure that is used to induce that easy axis. Longer field anneals result in larger time constants and seems to induce a hurdle that prevents complete alignment at low temperatures and/or for small fields (Fig. 1a). So, the molten composite is a non-Newtonian fluid that can support a yielding stress. SEM microscopy images taken on samples annealed for 3 minutes (Fig. 1b) show strong chaining with little PA-12 left between individual Sr-ferrite particles suggesting that direct particle-to-particle interaction is the reason for the observed non-zero yielding stress. Torque Magnetometry measurements show that magnetic anisotropy depends on the field annealing process through induced shape anisotropy contributions originating from agglomerates.

This abstract work was supported in part by NSF through a DMR-MRI grant under award 1726970.

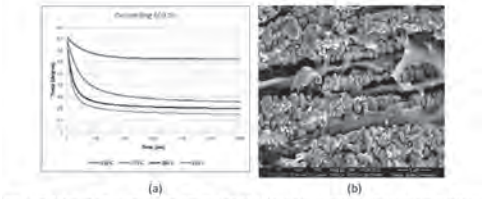

Fig.1: (a) Magnetic transient upon application of a 500 Oe field perpendicular to the easy axis for 40 wt% composite (left); (b) SEM image of field annealed 40 wt% composite.

KOC-08. Magnetic and Structural Properties of Spark Plasma Sintered Strontium and Barium Hexaferrites. *A. Sassi*[1], A. Pasko[1] and F. Mazaleyrat[1] *1. SATIE, ENS Paris-Saclay, 91190 Gif-sur-Yvette, France*

M-type hexaferrites show advantages due to their low cost of production, the abundance of their raw materials that do not belong neither to the rare earths nor to the strategic materials and their magnetic properties that allow them to be used in a variety of domains. Lanthanum (a rare earth element) and Cobalt (a strategic metal) are being used in La-Co substitued hexaferrites to improve the magnetic properties of permanent magnets [1]. To end the dependance on rare earths and strategic elements, nanostructured powders of ferrites are used for their neatly improved higher coercivity [2]. In this work, nanopowders of Sr and Ba hexaferrites have been synthesized using a wet chemistry route, then have been calcined at temperatures ranging from 800°C to 1050°C (with a step of 50°C) for 2 hours. The obtained powders were then Spark Plasma Sintered (SPS) at 800°C for 5 min to make 8mm-diameter

pellets. XRD analyses and magnetic measurements were made on the powders and on the sintered pellets. Results showed that single phase ($BaFe_{12}O_{19}$ and $SrFe_{12}O_{19}$) powders and sintered pellets with a nanometric graine size can be obtained with a calcination at 800°C for 2h. Powders had a saturation magnetization (Ms) of 62 to 64 A m^2/kg for BaFM and 65 to 68 A m^2/kg for SrFM, and the sintered pellets had a saturation magnetization of 64 A m^2/kg for BaFM and 67 A m^2/kg for SrFM), this means that SPS has a limited effect on the saturation magnetization. Coercivity, on the other hand, showed a different behavior (Fig. 1), it depended on calcination temperature for both, powders and sintered pellets, with a maximum value of 0.57 T for BaFM for and 0.58 T for SrFM for powders and 0.51 T for BaFM and 0.53 T for SrFM for sintered pellets. The drop in coercivity values in the sintered pellets is due to the increase in grain size. This study showed the value of conducting more investigation on the effect of Spark Plasma Sintering on Sr hexaferrite which is widely used in industry for the production permanent magnets but relatively less investigated in the nanostructured form compared to Br hexaferrites.

[1] F. Kools, A. Morel, R. Grössinger, J. M. Le Breton, P. Tenaud, J. Magn. Magn. Mat., Vol. 242-245, p. 1270-1276 (2002) [2] F. Mazaleyrat, A. Pasko, A. Bartok, M. Lobue, Journal of Applied Physics., Vol. 109, 07A708 (2011)

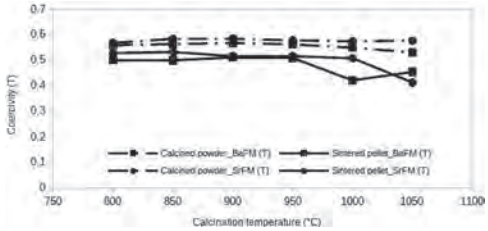

Fig. 1. Effect of calcination temperature on coercivity

KOC-09. Influence of Low Sintering Temperature of Substituted M-type Barium Hexaferrite on its Static and High Frequency Electromagnetic Properties. *K. Rana*[1,3], M. Tomar[1] and A. Thakur[2,3]
1. Physics, Delhi University, Delhi, India; 2. Physics, Amity University, Gurugram, India; 3. Innovative Science Research Society, Shimla, India

Cobalt substituted M-type barium hexaferrite with nominal composition $BaCo_xFe_{12-x}O_{19}$ ($0.0 \leq x \leq 1.0$) in the steps of 0.2 were prepared via chemical co-precipitation method. Thermal analysis was performed on pure BaM sample before undergoing thermal treatments to extract the beneficial information about their crystallization point. From TGA/DTA analysis it was confirmed that 900°C was an ideal sintering temperature for the pure BaM ferrite sample. On that basis all the six samples were sintered at same temperature. XRD confirmed the formation of M phase in all the samples where as the morphology of all the samples were investigated by using FESEM technique. Magnetic parameters like saturation magnetization (M_s), coericivity (H_c) and squareness ratio (SQR) were examined by using VSM. The value of M_s was found to decrease from 65.74 emu/g to 54.30 emu/g at very initial stage (x=0.2) due to the small amount of dopant but after that with increase in the dopant content, M_s value found to increase upto x=0.8 and reached to 65.39 emu/g. Moderate M_s value with higher coericivity of 3784 Oe was obtained for x=0.8. On the other hand, the variation of complex permittivity and complex permeability with composition was investigated over the X-band frequency range (8.2GHz-12.4GHz). Excellent and sustainable values of real permittivity (10.66) and tangent loss $Tan\delta_\mu$ (at x=0.021) at x=0.8 makes this composition suitable for high frequency application as well as electromagnetic shielding.

S. Kumar, S. Supriya and R. Pandey, Journal of Magnetism and Magnetic Materials., 458, 30-38(2018). R.S. Meena, S. Bhattachrya and R. Chatterjee, Materials Science and Engineering B., 171, 133-138(2010). R.C.Pullar, Progress in Material Science., 57, 1191 (2012). Y. Jing, L. Jia and Y. Zheng, RSC Advances., 9, 33388-33394 (2019). S. K. Godara, R. K. Dhaka and N. Kaur, Results in Physics., 22, 103903 (2021) K.S. Moon, E. S. Lin and Y. M. Kang, Journal of Alloys and Compound., 771, 350-355 (2019).

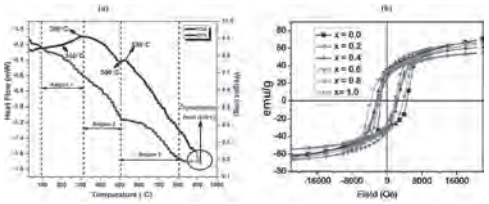

Fig. 1 TGA-DTA of pure BaM and M-H loops of cobalt substituted BaM.

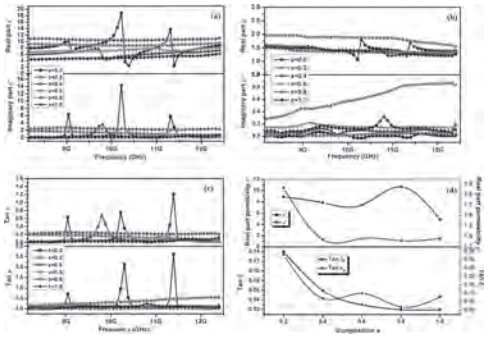

Fig. 2 Electromagnetic study of cobalt substituted BaM hexaferrites sintered at 900°C in X band.

KOC-10. $(Fe,Co)_2(P,Si)$ rare-earth free permanent magnets. *F. Guillou*[1], B. Lingling-Bao[1], H. Yibole[1], W. Hanggai[2], N. van Dijk[2] and E. Brück[2] *1. Inner Mongolia Normal University, Hohhot, China; 2. FAME Group, Department of Radiation Science & Technology, Delft University of Technology, Delft, Netherlands*

Rare-earth magnets exhibit unchallenged hard-magnetic properties, yet looking for alternatives based on inexpensive elements of non-critical supply remains of the highest interest. From this point of view, Fe_2P-related materials made of widely available elements are advantageous. However, while the binary parent Fe_2P presents a large magnetocrystalline anisotropy, its Curie temperature ($T_C \approx 214$ K) is too low for potential permanent magnet applications. Very recently, polycrystalline studies in quaternary $(Fe,Co)_2(P,Si)$ compounds have suggested the possibility to increase the Curie temperature much above room temperature while preserving the hexagonal crystal structure and a large magnetocrystalline anisotropy. Yet an accurate determination of the magnetic anisotropy using single crystal was missing. In addition, the possibility to induce coercivity remained to be demonstrated [1]. Here, we report the growth and characterization of $(Fe,Co)_2(P,Si)$ single crystals. Large magnetocrystalline anisotropy, high Curie temperatures and an appreciable saturation magnetization are achieved in such crystals. A comparison between $(Fe,Co)_2P$ and $(Fe,Co)_2(P,Si)$ single crystals highlights that Si substitution reduces the low-temperature magnetocrystalline anisotropy, but strongly enhances T_C, making quaternary compounds more promising for applications. Submicron-sized particles of $Fe_{1.75}Co_{0.20}P_{0.75}Si_{0.25}$ were prepared by ball-milling approach and demonstrated that permanent magnetic properties can be achieved in $(Fe,Co)_2(P,Si)$ quaternary compounds [2]. In addition, in order to establish the range where the desired hexagonal Fe_2P-type structure is observed and for which compositions the permanent magnetic properties can be optimized, the structural and magnetic phase diagrams of polycrystalline $Fe_{1.93-x}Co_xP_{1-y}Si_y$ were explored over a large composition range. A competition between three different crystal structures is observed upon chemical substitutions. Simultaneous Co for Fe and Si for P substitutions are found to increase the range where the hexagonal structure is observed in comparison to ternary compounds [3].

[1] F. Guillou et al., J. Alloy. Compd. 800 (2019) 403–411. [2] H. Yibole et al., Acta Materialia 221 (2021) 117388. [3] L.L. Bao et al., J. Alloy. Compd. 903 (2022) 163770.

Session KPA
HARD MAGNETIC MATERIALS II: RARE EARTH-BASED COMPOUNDS (Poster Session)

Enric Menendez, Chair
Autonomous University of Barcelona, Cerdanyola del Vallès, Spain

KPA-01. Effect of laser power on structural and magnetic properties of anisotropic Nd-Fe-B film magnets prepared by PLD method.
A. Yamashita[1], S. Hanada[1], T. Yanai[1], M. Nakano[1] and H. Fukunaga[1]
1. Nagasaki University, Nagasaki, Japan

Anisotropic rare-earth thick-film magnets have various applications such as MEMS (Micro Electro Mechanical Systems) devices and miniaturized electronic devices[1][2]. We have already fabricated anisotropic rare-earth film magnets by the substrate heating[3][4]. In the substrate heating process, increasing the deposition time might cause the grain size of Nd-Fe-B to increase. Our approach to anisotropic Nd-Fe-B thick-film magnets is to make them by increasing laser beam power for high deposition rate. This contribution reports the effect of laser power on several properties of anisotropic Nd-Fe-B film magnets using PLD method. A rotated Nd-Fe-B target was ablated using an Nd-YAG pulse laser. The laser beam power was set at 2-4 W. During deposition, a Ta substrate was heated by Joule heating utilizing electric current through the substrate. J-H loops were measured with a vibrating sample magnetometer (VSM). The perpendicular loops were corrected by using the demagnetization factor of 0.8. Figure 1 shows J-H loops of the Nd-Fe-B films deposited at each laser power. The films had the easy direction of magnetization in the plane of the perpendicular. The residual magnetic polarization ratio is defined by J_{rper} / J_{rin} , where J_{rper} and J_{rin} are the residual magnetic polarization values out-of-plane and in-plane direction, respectively. J_{rper} / J_{rin} ratio suggests that the decreasing laser power puts the easy direction of magnetization out-of-plane of the film. Figure 2 shows X-ray diffraction patterns of samples deposited by 2 W and 4 W. The peak intensities corresponding to the c-axis prepared by laser beam power at 2 W were stronger than those for 4 W. As the relative intensity ratio of (006) / (105) increase with the decreasing laser beam power {4 W : 0.8, 2 W : 1.3}, the increase in intensity ratio is consistent with the increase in the J_{rper} / J_{rin} value. Although it was difficult to prepare anisotropy Nd-Fe-B films with high deposition rate, we found that the crystalline texture for the Nd-Fe-B film magnets depends on the laser power.

[1] P. Mcguiness, D. Jezeršek, S. Kobe, J. Magn. Magn. Mater., vol. 305, no. 1, pp. 177–181 (2006). [2] R. Fujiwara, T. Shinshi, and M. Uehara, Int. J. Automot. Technol., vol. 7, no. 2, pp. 148–155 (2013). [3] M. Nakano, S. Tsutsumi, T. Yanai, J. Appl. Phys., vol. 105, Issue 7, pp. 07A739-07A742 (2009). [4] Y. Furukawa, H. Koga, T. Yanai, IEEE Magn. Lett., vol. 8, #5502104 (2017).

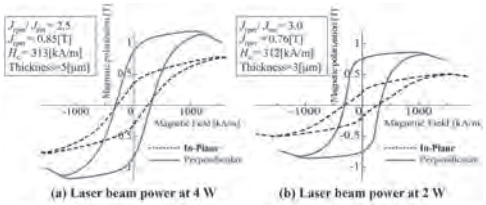

Figure 1 : In-plane and out-of-plane J-H loops of Nd-Fe-B film magnets deposited at (a)4 W and (b)2 W.

Figure 1 : In-plane and out-of-plane J-H loops of Nd-Fe-B film magnets deposited at (a)4 W and (b)2 W.

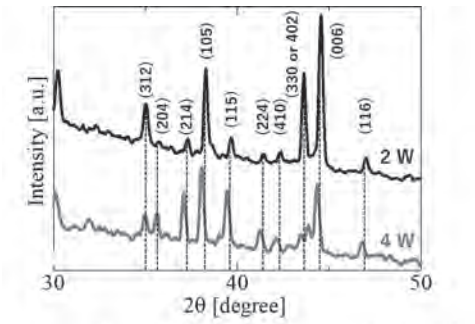

Figure 2 : X-ray diffraction patterns obtained for different laser beam powers.

Figure 2 : X-ray diffraction patterns obtained for different laser beam powers.

KPA-02. Investigation on crystallization process in isotropic rare-earth rich (Nd or Pr) -Fe-B films. *I. Fukuda*[1], K. Higuchi[1], A. Yamashita[1], T. Yanai[1], M. Nakano[1] and H. Fukunaga[1] *1. Nagasaki University, Nagasaki, Japan*

A lot of researchers have reported anisotropic (Nd or Pr) -Fe-B films prepared by a sputtering method [1]. In the experiment, the condition of annealing processes has been deeply investigated for obtaining excellent magnetic properties. We have demonstrated a miniaturized motor including PLD (Pulsed Laser Deposition)-fabricated isotropic (Nd or Pr) -Fe-B films with rare-earth rich composition compared to stoichiometric one [2]. Due to amorphous structure after the laser deposition, post-annealing is required to form the 2-14-1 phase to obtain isotropic hard magnetic films. Although a detailed investigation on the crystallization process is required to enhance isotropic magnetic properties, unfortunately there are not many reports on isotropic (Nd or Pr)-Fe-B films. In the study, we focused on the different phenomena through a post-annealing between isotropic rare-earth rich Nd-Fe-B and Pr-Fe-B films. Figure 1 shows coercivity of (Nd or Pr)-Fe-B films with rare earth content of 15.5 - 18.5 at. % as a function of annealing temperature in a resistance heating furnace. While the coercivity value of Nd-Fe-B films did not change up to 650 °C, the value of Pr-Fe-B films enhanced between 600 and 650 °C. Moreover, figure 2 shows the results of pulse (flash) annealing using an infrared furnace after the deposition of rare earth-rich (Nd or Pr)-Fe-B films. Although two films were annealed at the same annealing time of 1.7 s, the shoulder of a J-H loop (dotted line) for only a Pr-Fe-B film was open. X-ray diffraction patterns indicate that the 2-14-1 phase formed in the Pr-Fe-B film. In contrast, we observed that the Nd-Fe-B film had amorphous structure. Assuming that the crystallization temperatures of $Pr_2Fe_{14}B$ and $Nd_2Fe_{14}B$ phases are the same, the phenomenon is due to the difference in diffusion transfer of each rare earth atom during the annealing process. We consider the correlation between the diffusion transfer and the melting points (Nd: 1024 °C, Pr: 930 °C) of each element.

[1] N. M. Dempsey et.al., Appl. Phys. Lett. Vol. A90, 092509(2007). [2] M. Nakano et.al., IEEE Trans. Magn. Vol. 56, 7516303(2020).

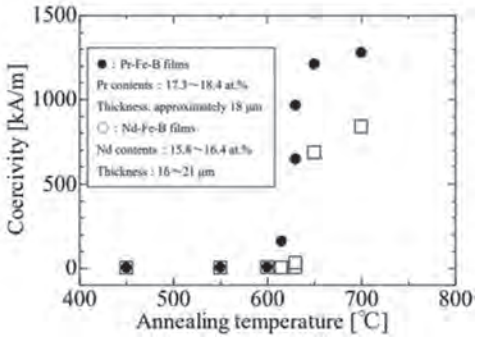

Fig. 1 Coercivity values of isotropic Pr-Fe-B and Nd-Fe-B films as a function of annealing temperature. (resistance heating furnace)

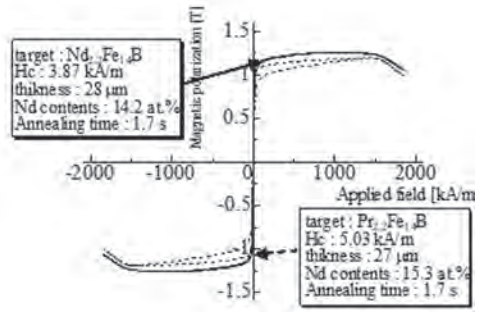

Fig. 2 J-H loops of Pr-Fe-B(dotted line) and Nd-Fe-B(solid line) films annealed at 1.7 s. (infrared furnace)

KPA-03. Preparation of Nd-Fe-B film magnets with Nb additive using vacuum arc deposition. *K. Otsuka*[1], A. Yamashita[1], T. Yanai[1], M. Nakano[1], T. Shinshi[2] and H. Fukunaga[1] *1. Nagasaki University, Nagasaki, Japan; 2. Tokyo Institute of Technology, Yokohama, Japan*

Although Nd-Fe-B thick-films with the thickness above 10 microns have been prepared by a sputtering and a PLD (Pulsed Laser Deposition) to develop the miniaturization of devices including a magnet [1][2], it is generally said that the sputtering is not suitable for a thick-film process due to the limitation of deposition rate and the PLD has difficulty in achieving the both of large deposition area together with high deposition rate. In the case of PLD-made Nd-Fe-B films, the area has been fixed at 5 mm square. Recently, we proposed a vacuum arc deposition with a rotational substrate system to obtain an isotropic Nd-Fe-B film magnet with a 20 mm square under a deposition rate above 10 μm/h. Furthermore, compositional and thickness distribution could be reduced to ±0.4 % and ±16 %, respectively. We, however, found that the squareness of a J-H loop and $(BH)_{max}$ drastically deteriorated at the edge of the sample. This contribution reports improvement of the deterioration by taking advantage of Nb additive to achieve target values of magnetic properties (H_{cb} > 420 kA/m, Br > 0.78 T, $(BH)_{max}$> 62 kJ/m^3) applied to a miniaturized device. Figure 1 shows the relationship between coercivity (H_{cb}) and squareness of post-annealed Nd-Fe-B films after the vacuum arc deposition. Each symbol shows the properties of 5 mm square films cut from different area in a 20 mm square (Black circle, Black triangle: within 10 mm square from the center) and the edges (White circle, White triangle : outside of Black circle, Black triangle). Usage of Nb additive enabled us to improve the squareness and suppress the dependence of deposition position. Moreover, Scherr's equation using X-ray diffraction patterns reveled that the distribution of grain size due to the different deposition positions could be reduced by using Nb additive. It was also clarified that the target values except H_{cb} could be achieved.

[1] N. M. Dempsey et.al., Appl. Phys. Lett. Vol. A90, 092509(2007). [2] M. Nakano *et al., IEEE Trans. Mag.* vol.56, 7516303(2020).

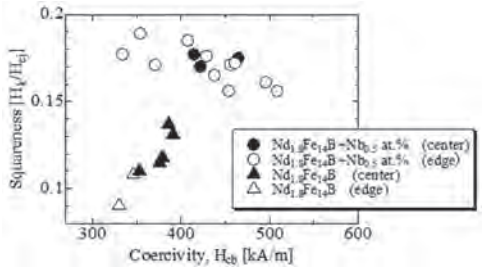

Fig. 1 Relationship between coercivity and squareness of post-annealed films deposited on different positions.

KPA-04. Improvement in magnetic properties of Nd-Fe-B/glass two-layered films on Si substrates. *K. Higuchi*[1], I. Fukuda[1], A. Yamashita[1], T. Yanai[1], M. Nakano[1], T. Shinshi[2] and H. Fukunaga[1] *1. Nagasaki University, Nagasaki, Japan; 2. Tokyo Institute of Technology, Yokohama, Japan*

Sputtering-made Nd-Fe-B films with the thickness of 20 microns on Si substrates are expected to apply magnetic materials to MEMS (Micro Electro Mechanical Systems) as future devices of a miniaturized sensor and actuator [1]. On the other hand, we have fabricated isotropic Nd-Fe-B thick-film magnets thicker than 100 microns on Si substrates by a PLD (Pulsed Laser Deposition) method [2]. In addition, micro-magnetization of the thick-films could be achieved by taking advantage of a glass buffer layer [3]. Investigation on an optimum condition to enhance magnetic properties of Nd-Fe-B/glass two-layered films, however, has not been completed, since there are many parameters of the fabrication process such as Nd contents, annealing conditions and thicknesses ratio of each film. In the study, annealing time in a pulse-annealing process after the deposition was optimized at 4.0 s through systematic investigation under Nd contents range from 14 to 16 at.%. Moreover, effect of the thickness ratio of a glass film and an isotropic Nd-Fe-B film on magnetic properties was examined. Figure 1 shows coercivity as a function of the ratio. Here, each thickness varied from 15 to 60 microns for Nd-Fe-B films and 12 to 114 microns for glass films, respectively. It was found that the ratio less than 2 enabled us to increase coercivity up to 500 kA/m. The detail mechanism of the phenomenon is under investigation. In addition, J-H loops of Nd-Fe-B/glass two-layered films on Si substrates were compared as seen in Fig. 2. The red loop and dotted loop are corresponding to an obtained film showed in Fig. 1 and a micro-magnetized film reported in the reference [3], respectively. Enhancement of $(BH)_{max}$ could be achieved through the above-mentioned optimization.

[1] R Fujiwara et al., Int. J. Autom. Technol. Vol. 7, 148(2013). [2] M. Nakano et al., IEEE Trans. Magn. Vol. 51, 2102604 (2015). [3] D. Han et al., IEEE Magn. Letters, Vol. 11, 8103804 (2020).

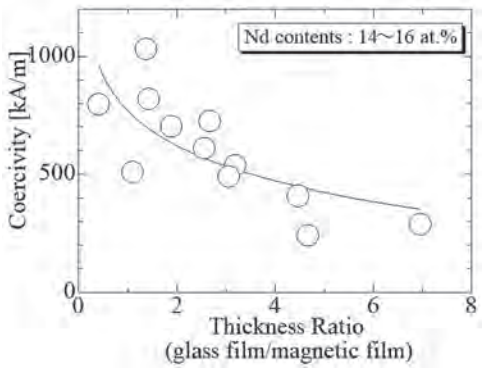

Fig.1 Coercivity of samples as a function of thickness ratio

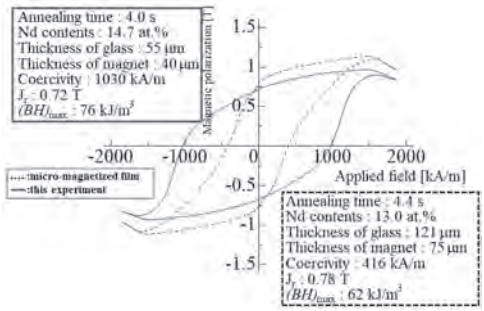

Fig.2 Comparison of J-H loops of two Nd-Fe-B-glass samples

KPA-05. Coercivity enhancement of hot-deformed NdFeB magnets by in-situ two-end-diffusion with $R_{70}Cu_{30}$ alloy powders (R = NdPr and Ce). *Y. Wong*[1], W. Huang[1], H.W. Chang[1] and W. Chang[1] *1. Physics, National Chung Cheng University, Chiayi, Taiwan*

NdFeB magnet prepared by hot deformation (HD) exhibits anisotropic nano-structure, and therefore higher coercivity than that of the traditional sintered magnet with micrometer-scale structure. However, the magnetic anisotropy field of $Nd_2Fe_{14}B$ phase drastically decreases with increasing temperature, thus inhibiting the applications at higher temperature [1-2]. To enhance the coercivity, grain boundary diffusion and doping heavy rare earth (HRE) containing alloys have been reported to significantly increase $_iH_c$ of the HD magnet effectively. Nevertheless, the above methods have the disadvantages of the large reduction of B_r and $(BH)_{max}$ and much complex process for the former. In this work, we hereby present a simple process, called in-situ two-end diffusion (TED), to overcome the above disadvantage. At first, 1 wt.% $(Nd_{0.75}Pr_{0.25})_{70}Cu_{30}$ (NdPrCu) alloy powders are placed upon and underneath the commercial MQU-F powders each in the mold, and the fully bulk magnets are prepared by hot pressing followed with hot deformation, followed with proper heat treatment to the HD magnets. Coercivity is increased from 15.1 kOe to 18.7 kOe for the magnet TED with NdPrCu, which is larger than 17.6 kOe for the magnet doped with 2 wt.% NdPrCu alloy traditionally. Besides, the magnet TED with NdPrCu exhibits good (00L) texture and therefore could support high $(BH)_{max}$ of 43.0 MGOe. In addition, comparison on the magnetic properties of HD NdFeB magnets by traditional doping and TED with low-melting and low-cost $Ce_{70}Cu_{30}$ (CeCu) is also studied. Similarly, the magnet TED with CeCu exhibit much higher magnetic properties of B_r = 12.8 kG, $_iH_c$ = 18.0 kOe and $(BH)_{max}$ = 40.7 MGOe than traditional doping with CeCu (B_r = 11.7 kG, $_iH_c$ = 16.4 kOe and $(BH)_{max}$ = 34.2 MGOe). For TED process, low-melting CeCu can infiltrate into the center of the magnet, and most Ce distribute at grain boundary. The distribution of Ce and Cu at grain boundary can reduce the magnetization of grain boundary phase, strengthen the decoupling effect between grains and contribute to the coercivity enhancement. This work demonstrates TED with low-melting HRE-free alloys is a simple method to effectively enhance coercivity and keep high B_r and $(BH)_{max}$ for HD NdFeB magnets.

[1] S. Hirosawa et al., J. Appl. Phys. 59 (1986) 873. [2] X. D. Xu et al., Scr. Mater. 160 (2019) 9-14.

KPA-06. High-coercivity HRE-free NdFeB sintered magnets developed by doping $Ce_{85}Al_{15}$ and grain boundary diffusion with $Pr_{70}Cu_{15}Al_{15}$. *Y. Wong*[1], H.W. Chang[1], Y. Lee[1], W. Chang[1], C. Chiu[2] and C. Mo[3] *1. Physics, National Chung Cheng University, ChiaYi, Taiwan; 2. New Materials Research & Development Department, China Steel Corp., Kaohsiung, Taiwan; 3. R&D Department, Himag Magnetic Corporation, Pingtung, Taiwan*

NdFeB magnets are widely applied in various fields, such as renewable energy system, communication system, and so on. The applications of NdFeB magnets at 120 °C require the magnets at least to reach the magnetic level of SH grade, where the coercivity is larger than 20 kOe. However, traditional NdFeB sintered magnets with magnetic level of SH are usually containing with considerable amount of high-cost heavy rare earth (HRE), such as Dy or Tb. How to reach high coercivity larger than 20 kOe without using HRE is a challenge for the NdFeB magnets containing abundant Ce. In this study, high coercivity of 21.4 kOe can be reached for the HRE-free NdFeB magnet doped with $Ce_{85}Al_{15}$ (CeAl) alloy and grain boundary diffusion (GBD) with $Pr_{70}Cu_{15}Al_{15}$ (PrCuAl) alloy powders, where Ce/RE ratio is about 15 % within the magnet. The magnetic properties attained in this work are comparable to HRE-free sintered NdFeB magnets GBD with $Pr_{70}Cu_{10}Al_{20}$ ($_iH_c$ of 21.4 kOe) [1] and those made by doping with Dy-containing alloy ($_iH_c$ of 17.4 kOe) [2]. For the as-sintered CeAl-doped magnet, the network-like distribution of Ce at grain boundary is observed, strengthening decoupling effect between adjacent 2:14:1 grains, and therefore contributing to coercivity enhancement. After GBD treatment, the formation of $Pr_2Fe_{14}B$ shell around grains can increase the local magnetic anisotropy filed and therefore enhance the coercivity, even though part of Ce entering into 2:14:1 grain may lead to the reduction of magnetization and magnetic anisotropy field of 2:14:1 phase. This study provides a cost-effective way to obtain high coercivity for HRE-free NdFeB sintered magnet via doping $Ce_{85}Al_{15}$ and GBD with $Pr_{70}Cu_{15}Al_{15}$.

[1] H. Zeng et al., J. Magn. Magn. Mater. 471, 97 (2019). [2] T. Zhou et al., J. Alloy Compds. 856, 158191 (2021).

KPA-07. Effect of rotation rate on the recovery of Nd-Fe-B sludge via rotation-reduction diffusion method. *L. Cong*[1], H. Xu[1], Q. Lu[1] and M. Yue[1] *1. Beijing university of technology, Beijing, China*

In recent years, the in-situ regeneration method of recovering the sintered Nd-Fe-B sludge via calcium reduction diffusion has attracted wide attention [1]. But one of the problems of this method is the low regeneration capacity, which is only at the level of a few grams to a dozen of grams [2]. In this study, a new process of batch recycling of sludge was developed by introducing rotary diffusion technology. The reduction diffusion reaction was carried out in a dynamic process, which promoted the flow of molten calcium as well as the effective mixing of the reactants, and finally realized the batch regeneration of the Nd-Fe-B sludge by an order of magnitude. This paper mainly focused on the effects of the rotation rate, a key factor affecting the performance and microstructure of regenerated magnetic powder. Single-phase $Nd_2Fe_{14}B$ regenerated magnetic powders can be obtained by using different rotation rates [Fig. 1(a)]. The maximum saturation magnetization (M_{3T}) of the regenerated $Nd_2Fe_{14}B$ magnetic powder is 138.22 emu/ g at 10 rpm, which is 11.6 % higher than that of the purged sludge [Fig. 1(b)]. The regenerated magnetic powders obtained at this rate exhibit obvious anisotropy. After orientation, the value of $I_{(006)}/I_{(105)}$ reaches 3.29 [Fig. 1(c)]. The particle size distribution of the regenerated $Nd_2Fe_{14}B$ magnetic powder obtained at the rotation rate of 10 rpm is uniform and normal, with an average grain size of 4.12 μm [Fig. 1(d)]. In addition, the particles have good dispersion, which is not only conducive to their orientation in the magnetic field, but also to the removal of by-products during the washing process, reducing the residual Ca and O. In summary, the rotation-reduction diffusion process can realize the large-scale recovery of the Nd-Fe-B sludge, and the appropriate rotation rate of 10 rpm is beneficial to the high-performance regeneration.

[1] S.K. Haider, J.Y. Lee and D. Kim. ACS Sustainable Chem. Eng., Vol. 8, p.8156-8163 (2020). [2] H.B. Xu, F. Wang and Q.M. Lu. J. Magn. Magn. Mater., Vol. 543, p.168606 (2022).

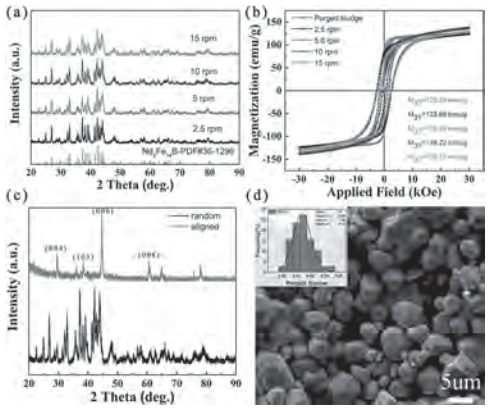

Fig. 1 (a) XRD patterns and (b) Hysteresis loops of regenerated $Nd_2Fe_{14}B$ magnetic particles prepared at different rotation rates; (c) XRD results before and after orientation and (d) the morphology (the inset is the particle size distribution) at a rotation rate of 10 rpm.

KPA-08. Effect of Sm substitution on the structural and magnetic properties of $Nd_2Fe_{14}B$. *Z. Lin*[1], G. Qiao[1], L. Qiao[2], W. Yang[1] and J. Yang[1,3] *1. School of Physics, Peking University, Beijing, China; 2. Institute of Applied Magnetics, Lanzhou University, Lanzhou, China; 3. Beijing Key Laboratory for Magnetoelectric Materials and Devices, Beijing, China*

Since Sm possesses opposite first-order Stevens factors in contrast to Nd, Sm-doped $Nd_2Fe_{14}B$ can modulate Snoek limit to achieve high-frequency applications. Due to the strong *J*-mixing effect and complex structure, the magnetic mechanism of (Nd, Sm)$_2$Fe$_{14}$B homologous compounds is still obscure. In this work, X-ray diffraction, ^{57}Fe Mössbauer spectroscopy and magnetic measurement were used to determine the structural and magnetic properties of $(Nd_{1-x}Sm_x)_2Fe_{14}B$ ($0 < x < 0.5$, and $x = 1$). With the x increasing from 0 to 0.5, the decrease in average quadrupole interaction shows Sm concentration has affected the lattice stability of the 2:14:1 phase, implying a decrease of uniaxial magneto-crystalline. An abnormal increase of average isomer shift in $x = 0.3$ is mainly originated from the mobility of the electron between the 4c and $8j_1$ site, and then in turn decreases the *s* valence charge density at nucleus sites. The saturation magnetization and hyperfine field increase with the increasing x from 0 to 0.1 attributed to the chemical bonding effect of 4e, $8j_2$ sites, and it decreases with the increasing x from 0.1 to 0.5 caused by the magnetic dilution of Sm and the appearance of RE_2O_3/$RE_{1.1}Fe_4B_4$. Due to fewer paramagnetic phases, the $x = 1$ show higher saturation magnetization than that of the $x = 0.5$. These results reveal the microscopic mechanisms for the structural and magnetic properties of Sm-substitution $Nd_2Fe_{14}B$, providing a perspective on developing low-cost magnetic materials with tunable anisotropy.

[1] G.Y. Qiao, Q. Hu, P. Zhang, W. Yang, Z. Liu, S. Liu, C. Wang, J. Yang, The effect of samarium substitution on magnetic properties and microwave absorption of the rare earth-iron-boron compounds and composites, J. Alloys Compd. 825 (2020) 154179. [2] Z.C. Lin, L. Zha, F. Wang, Z. Liu, R. Wu, J. Yang, M. Xue, W. Yang, G. Tian, X. Ma, L. Qiao, A. Franz, Q. An, W. Liu, C. Wang, J. Yang, Effect of Ce substitution on the structural and magnetic properties of $Nd_2Fe_{14}B$, Acta Mater. 200 (2020) 502-509. [3] O. Crisan, J.M.L. Breton, M. Nogu s, F. Machizaud, G. Filoti, Magnetism and phase structure of crystallized Sm Fe B melt spun ribbons, J. Phys.: Condens. Matter 14 (2002) 12599-12609.

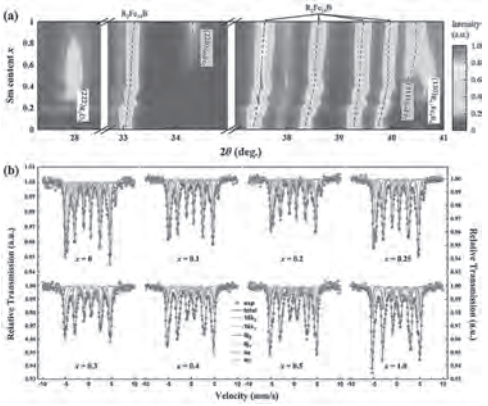

Fig. 1. (a) Contour map of X-ray diffraction patterns of $(Nd_{1-x}Sm_x)_2Fe_{14}B$ at room temperature. (b) ^{57}Fe Mössbauer spectra for $(Nd_{1-x}Sm_x)_2Fe_{14}B$ at room temperature.

KPA-09. Suppression of the formation of soft magnetic phase for Sm(Fe-Co) thin films by introducing Sm seed layer. *Y. Mori*[1], S. Nakatsuka[1], M. Kambayashi[1], S. Hatanaka[1], K. Hirayama[1], M. Doi[1] and T. Shima[1] *1. Tohoku-Gakuin Univ., Tagajo, Japan*

$Sm(Fe_{0.8}Co_{0.2})_{12}$ thin films with the $ThMn_{12}$ type crystal structure are expected as a new high-performance permanent magnet material because they possess excellent magnetic properties such as high saturation magnetization $\mu_0 M_s$ of 1.78 T, anisotropy field $\mu_0 H_A$ of 12 T and Curie temperature T_C of 879 K [1]. Recently, it has been clarified that a coercive force $\mu_0 H_c$ as high as 1.2 T can be successfully obtained in the Sm(Fe-Co) thin films with B addition. It is considered that this is mainly due to the formation of RFe_{12} grains with columnar structure separated by the B-rich amorphous grain boundary phase [2]. In addition, $\mu_0 H_c$ was further increased by the diffusion of Si into the grain boundary phase in the Sm(Fe-Co)-B thin films. Then, it is predicted that $\mu_0 H_c$ will be further increased by reducing the soft magnetic phase existing at the vicinity of the initial interface between V under layer and Sm(Fe-Co)-B main layer [3]. In this study, a Sm seed layer was inserted between the V under layer and the Sm(Fe-Co) layer to suppress the initial growth of soft magnetic phase such as α-Fe and α-(Fe-Co), and the crystal structure and magnetic properties were investigated in detail. The samples were prepared by using the ultra-high vacuum magnetron sputtering system. First of all, a V buffer layer of 20 nm was deposited onto the MgO (100) single crystal substrate at substrate temperature T_s of 673 K. Then, the thickness t_{Sm} of the Sm seed layer was changed from 0 to 5 nm and while that of Sm(Fe-Co)-B layer was fixed at 100 nm. Finally, a V cover layer of 10 nm was deposited. The B composition was changed up to 5 at.%. It was confirmed that the introduction of the Sm seed layer into Sm(Fe-Co) layer clearly decreases the intensity of the peaks obtained from α-(Fe-Co) and increases the intensity of the (002) and (004) peaks in the RFe_{12} phase. In addition, improvement of remanent magnetization ratio while maintaining $\mu_0 H_c$ above 1.0 T was confirmed. It was thought that the Sm seed layer plays an important role to suppress the formation of α-(Fe-Co) phase and to improve the orientation of the 1:12 phase. The detailed results will be discussed at the conference.

[1] Y. Hirayama, Y. K. Takahashi, S. Hirosawa and K. Hono, *Scr. Mater.*, 138 (2017) 62-65. [2] Sepehri-Amin, Y. Tamazawa, M. Kambayashi, G. Saito, Y. K. Takahashi, D. Ogawa, T. Ohkubo, S. Hirosawa, M. Doi, T. Shima, K. Hono, *Scr. Mater.*, 194 (2020) 337-342. [3] A. Boyachkin, H. Sepehri-Amin, M. Kambayashi, Y. Mori, T. Ohkubo, Y. K. Takahashi, T. Shima, K. Hono, *Acta. Mater.*, 227 (2022) 117716.

KPA-10. Effect of Hydrogen Pressure and Temperature on Hydrogen Absorption Behavior of Sm(CoFeCuZr)$_z$ Strip-Casting Flake. *J. Yang*[1,2], D. Zhang[1], Y. Li[1], C. Meng[1], J. Jia[1], W. Liu[1] and M. Yue[1] *1. Faculty of Materials and Manufacturing, Beijing University of Technology, Beijing, China; 2. School of Mechanical Engineering, Anyang Institute of Technology, Anyang, China*

Nowdays, Nd-Fe-B magnetic powder is usually prepared by the strip casting (SC), hydrogen decrepitation (HD) and jet milling (JM), so as to obtain high performance. However, due to the harsh hydrogen absorption conditions of Sm-Co alloy, the HD is rarely used for its powder preparation, and there is no research on the hydrogenation behavior of SC flake. Therefore, it is urgent to introduce a new powder preparation process for mass production. In this study, the hydrogen absorption behavior of Sm(CoFeCuZr)$_z$ SC flake was systematically investigated. The SC flake with nominal composition of $Sm(Co_{0.065}Fe_{0.28}Cu_{0.05}Zr_{0.02})_{7.6}$ was prepared by a single-roller SC technology. The SC flake composes of the free surface, wheel surface and cross section. The cross section consists of I-columnar grains region, III-fine grains region, and II-mixed region of fine grains and columnar grains [Fig1. (a-b)]. The weight of each sample involved in hydrogen absorption is 1.8 kg. The hydrogen absorption curves show that: when the hydrogen pressure is higher than 4.5MPa, the SC flake can break into powders by absorbing hydrogen at 20 °C. When the temperature increases to 50 °C, even if the hydrogenthe pressure reduces to 4 MPa, the SC flake can still absorb hydrogen and break. Increasing the hydrogen pressure can promote the particle refinement to a certain extent. However, increasing the temperature can obviously accelerate the HD process, but if the temperature is higher, the particle size will be coarse. The powders with small particle size, uniform distribution and full of cracks can be obtained under 50 °C-6 MPa [Fig2. (b)], which is conducive to the subsequent preparation of fine powder. The particles size distribution of the powder after JM are uniform [Fig2. (c-d)]. In conclusion, the hydrogen pressure and temperature are the key factors for HD process. The SC, HD and JM can be used as a new powder preparation process, which is expected to prepare high-performance Sm(CoFeCuZr)$_z$ magnets in the future.

[1] A. Eldosouky, I. Škulj, J. Sustain. Metall., vol. 4, p. 516–527(2018). [2] A. Kianvash, I.R. Harris, J. Mater. Sci., vol. 20, p. 682–688(1985).

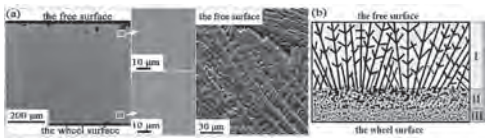

Fig. 1. (a) Back-Scaterred Electron of the flake, (b) Microstructure model

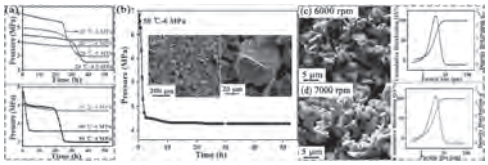

Fig. 2. (a) Hydrogen absorption curves, (b) Hydrogen absorption curve under 50 °C-6 MPa, (c-d) Powder micrograph and particle size distribution after JM

KPA-11. Effect of casting-alloy methods on magnetic properties of Sm(CoFeCuZr)$_z$ magnet. *C. Meng*[1], J. Jia[1], D. Zhang[1], J. Yang[1,2], Y. Teng[1], Y. Li[1], W. Liu[1] and M. Yue[1] *1. Faculty of Materials and Manufacturing, Key Laboratory of Advanced Functional Materials, Ministry of Education of China, Beijing University of Technology, Beijing, China; 2. School of Mechanical Engineering, Anyang Institute of Technology, Anyang, China*

The 2:17 type SmCo permanent magnets are well known for their excellent magnetic properties, good thermal stability and strong corrosion resistance, which are widely used in high temperature applications [1-2]. There are few reports on the preparation of SmCo magnet using strip-casting alloys. In this paper, the effect of casting-alloy methods on the microstructure and magnetic properties of Sm(CoFeCuZr)$_z$ magnets was investigated. The magnetic properties of the PM magnet prepared by mechanical crushing and ball milling are better than those of the SC magnet, especially the orientation. In detail, the magnetic properties of PM magnet are B_r=11.63kG, H_{cj}=25.65kOe, $(BH)_{max}$=30.97MGOe, while the magnetic properties of the SC magnet are B_r=11.45kG, H_{cj}=24.00kOe, $(BH)_{max}$=30.03MGOe, respectively. Both random magnets mainly consist of 1:5 and 2:17R phases [Fig. 1(a)]. After oriented, the intensity ratio of (006) and (104) peaks is used to characterize the orientation degree [3], $I_{(006)}/I_{(104)}$=24.33 in the PM magnet, while this value is 18.23 in the SC magnet. This means that PM magnet has better orientation degree. The EBSD results confirm above result. Meanwhile, there are a few grains with poor orientation in the inverse pole figure [Fig. 1(b)] of the SC magnet, and such grains will reduce the orientation. Figure 1(c) shows the (0001) pole figure (PF) and inverse pole figure (IPF) of normal direction, from which we can see the MRD values in PF and IPF of PM magnet are both higher than those of SC magnet. The BSE photographs of the different alloy cross-sections show that the PM alloy consists of columnar grains region, equiaxed grains region [Fig. 2a], while the SC alloy consists mainly of columnar grains region and fine grains region. Due to the existence of fine grains region in the SC[Fig. 2b], it is difficult to obtain all single grain in the subsequent ball-milling process. So the SC magnet has worse orientation than the PM magnet.

[1] J.F. Liu, Y. Ding, G. C. Hadjipanayis, J. Appl. Phys., vol.85, p. 2800–2804 (1999). [2] Wei Sun, Minggang Zhu, Yikun Fang,. J. Magn. Magn. Mater., vol.378, p. 214-216(2015). [3] Q. J. Zheng, S. Xia, A. Dozier., Mater. Sci. & Tech., vol. 22, p. 1476-1482(2006).

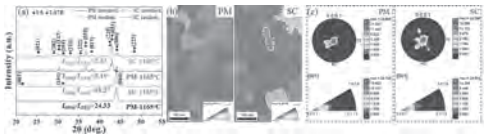

Fig. 1 (a)The XRD patterns of random and oriented magnets, (b) inverse pole figure of magnets, (c)the (0001) pole figure and inverse pole figure of normal direction

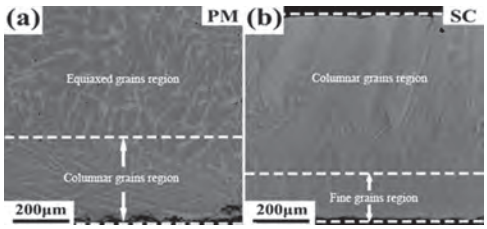

Fig. 2 The Cross-sectional BSE of (a) plate ingot alloys and (b) strip-casting alloys.

KPA-12. Partitioning of alloying elements in Sm-Co-Fe-Cu-Zr magnet during the heat treatment. *X. Liu*[1], B. Cui[1] and C.I. Nlebedim[1] *1. Ames Laboratory, Ames, IA, United States*

Sm_2Co_{17}-type sintered magnets have high magnetic performance and excellent thermal stability, originating from their unique cellular structure mainly composed of $SmCo_5$-type (1:5), and Sm_2Co_{17}-type (2:17) magnetic phases. They also contain $SmCo_3$-type (1:3) minor phase and the chemical element partitioning between 1:5, 1:3, and 2:17, generated during the aging heat-treatment process [1,2]. In this work, the thermodynamical origin of the micro-segregation of the chemical elements between different phases, its relationship with the formation of the cellular structure and its effect on coercivity have been theoretically studied. Our DFT total energy calculations indicate that the substitution energy (E_{sub}) of Co replaced by Fe in 1:5 and 2:17 are positive (0.08 eV/Fe) and negative (-0.04eV/Fe), respectively. On the other hand, E_{sub} for the Co substituted by Cu are negative and positive for 1:5 (-0.23 eV/Cu) and 2:17 (0.1 eV/Cu), respectively. This energy difference

drives the Cu and Fe atoms to occupy the 1:5 and 2:17 lattice sites, respectively. Zr atom prefers to occupy the Sm site in the solid solution precursor ($TbCu_7$-type structure) and partially replaces the Sm atoms in the 1:3-type phase during aging heat treatment. In addition, Cu atoms prefer to enter the 2c site in 1:5 while Fe atoms tend to occupy the 6c site in 2:17, derived from the substitution energy difference at the different crystallographic sites. The preferential site substitution of Co by Cu and Fe results in an anisotropic lattice expansion of the 1:5 and 2:17 structures, respectively. This anisotropic lattice expansion changes the lattice mismatch at the interface between 1:5 and 2:17 and affects micro-elastic energy, which determines the morphology of the 1:5 and 2:17 phases in the cellular structure. Proper control of the chemical composition and aging heat treatment conditions can enable modification of the atomic diffusion rate and the micro-elastic energy at the interface between the 1:5 and the 2:17 phases, hence determining the size and morphology of the cellular structure and resultant coercivity in Sm-Co-Fe-Co-Zr magnet.

[1] Mishra R K, Thomas G, Yoneyama T, Fukuno A, and Ojima T, 1981, J. Appl. Phys. 52 2517 [2] Fidler J, Schrefl T, Hoefinge S and Hajduga M, 2004, J. Phys.: Condens. Matter 16 S455

KPA-13. Effects of zirconium and titanium additions on magnetic properties of $Sm(Fe,Co)_{10}$ melt-spun ribbons. *T. Saito[1] 1. Chiba Institute of Technology, Narashino, Japan*

It is known that Sm-Fe-N alloys possesses a high saturation magnetization with a large anisotropy field and a high Curie temperature [1]. There have been made many fundamental investigations on the Sm-Fe-N alloys [2-5]. Sm-Fe-N alloys have been prepared in powder form by the nitrogenation of Sm-Fe alloy powders.It would be desirable if the magnetic properties of the Sm-Fe alloy could be increased without the need for nitrogenation. In this study, we investigated the possibility of improving the magnetic properties of the $Sm(Fe,Co)_{10}$ alloy by the addition of zirconium and titanium. The structures and magnetic properties of $Sm(Fe,Co)_{10}$ melt-spun ribbons with added Zr and Ti are discussed. $(Sm_{1-x}Zr_x)(Fe_{0.7}Co_{0.3})_{10-y}Ti_y$ (x=0–0.4, y=0–0.5) alloy ingots were prepared by induction melting under an argon atmosphere. The molten alloy ingots were then ejected through an orifice with argon onto a copper wheel rotating at a surface velocity of 40 ms^{-1}. The melt-spun ribbons obtained this process were annealed under an argon atmosphere at 773–1173 K for 1 h. The specimens were examined by an X-ray diffraction (XRD) and vibrating sample magnetometer (VSM). Regardless of the Zr and Ti content, these ribbons showed low coercivity of less than 1 kOe. The coercivity of the $(Sm_{1-x}Zr_x)(Fe_{0.7}Co_{0.3})_{10-y}Ti_y$ (x=0–0.4, y=0–0.5) melt-spun ribbons increased as the annealing temperature and the amounts of Zr and Ti increased. It was found that the optimally annealed $(Sm_{0.6}Zr_{0.4})(Fe_{0.7}Co_{0.3})_{9.5}Ti_{0.5}$ melt-spun ribbon exhibited the highest coercivity of 4.35 kOe.

[1] J. M. D. Coey and H. Sun, J. Magn. Magn. Mater. 87, L251 (1990). [2] K. Schnitzke et al, Appl. Phys. Lett. 57, 2853 (1990). [3] J. P. Liu et al., J. Less-Common Met. 170,109 (1991). [4] S. Miraglia et al., J. Less-Common Met. 171, 51 (1991). [5]T. Iriyama et al., IEEE Trans. Magn. 28, 2326 (1992).

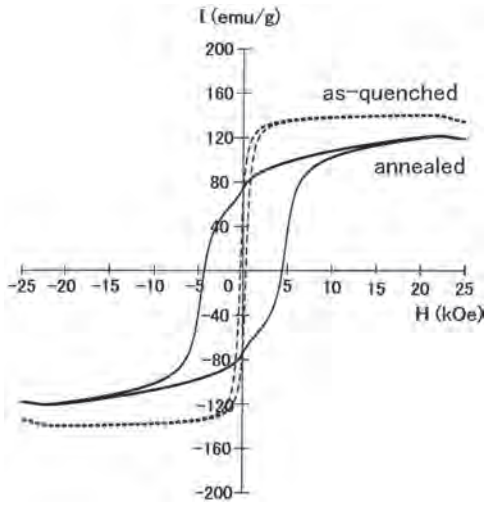

Fig.1 Hystersis loops of the $(Sm_{0.6}Zr_{0.4})(Fe_{0.7}Co_{0.3})_{9.5}Ti_{0.5}$ melt-spun ribbons.

KPA-14. Study of the Anisotropic $Sm_2Fe_{17}N_3$ Powders with High Performance. *D. Liang[1]*, W. Yang[1], X. Wang[2], Q. Xu[1], J. Han[1], S. Liu[1], C. Wang[1], H. Du[1], Z. Luo[1] and J. Yang[1] *1. School of Physics, Peking University, Beijing, China; 2. Ningxia Magvalley Novel Materials Co., Yinchuan, China*

$Sm_2Fe_{17}N_3$ was regarded as a prospective candidate for high-performance permanent magnets, since it possessed intrinsic magnetic properties that were superior or comparable to those of $Nd_2Fe_{14}B$. Unlike that used in Nd-Fe-B magnets, liquid phase sintering was not available for the production of Sm-Fe-N dense magnets. Therefore, the fabrication of high-performance anisotropic $Sm_2Fe_{17}N_3$ powders was the first step and the key to producing Sm-Fe-N sintered and bonded magnets. In this work, the strip casting technique was first used to prepare the Sm_2Fe_{17} parent alloys. Next, the $Sm_2Fe_{17}N_3$ powders were synthesized using a gas-solid reaction of Sm_2Fe_{17} powders with N_2. Then, the anisotropic $Sm_2Fe_{17}N_3$ powders with different particle sizes were prepared by surfactant-assisted grinding method in gasoline solvent. The addition of surfactant effectively decreased particle size, and the gasoline solvent prevented $Sm_2Fe_{17}N_3$ powders from severe oxidation during the grinding process. It was found that the coercivity ($_iH_c$) of ground increases with decreasing the average particle size (D_m), while the saturation magnetization (M_s) decreased with the reduction of D_m. The maximum value of $_iH_c$ of 17.5 kOe was obtained at the D_m =1.3 um. Ground powders with D_m of 3.1 um show a maximum energy product ($(BH)_{max}$) of 35 MGOe and a remanence ratio (M_r/M_s) over 95%. The temperature dependency of magnetic properties for ground powder from 10 K to 373 K (100 °C) was also characterized. The $Sm_2Fe_{17}N_3$ powder can exhibited a very high iH_c of 36.1 kOe at 10 K. Above 300 K, $Sm_2Fe_{17}N_3$ powders mixed with epoxy resin showed a low remanence temperature coefficient of $\alpha_{(RT\text{-}100\ ^\circ C)}$ =-0.022% $°C^{-1}$.

[1] J.M.D. Coey, P. Stamenov, S.B. Porter, et al. Sm-Fe-N revisited; remanence enhancement in melt-spun Nitroquench material, Journal of Magnetism and Magnetic Materials, 480 (2019) 186-192. [2] T. Horikawa, M. Yamazaki, M. Matsuura, et al. Recent progress in the development of high-performance bonded magnets using rare earth–Fe compounds, Science and Technology of Advanced Materials, 22 (2021) 729-747. [3] X.B. Ma, Y.C. Yang, J.B. Yang, et al. Anisotropic Sm–Fe–N particles prepared by surfactant-assisted grinding method, Journal of Alloys and Compounds, 612 (2014) 110-113.

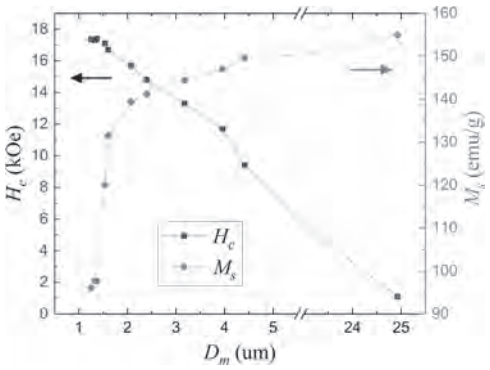

Figure 1 Dependence of coercivity iH_c and saturation magnetization M_s on average particle size D_m for ground $Sm_2Fe_{17}N_3$ powders

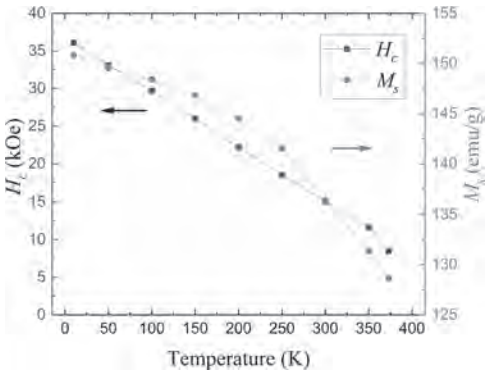

Figure 2 Temperature dependence of coercivity $_iH_c$ and saturation magnetization M_s for ground $Sm_2Fe_{17}N_3$

KPA-15. Understanding the magnetism of multicomponent rare earth intermetallic compound $Tb_{0.33}Ho_{0.33}Er_{0.33}Ni$. *A.P. Mohapatra*[1], A. Chelvane[2], A.V. Morozkin[3], S. Ramaprabhu[1] and R. Nirmala[1] *1. Department of Physics, Indian Institute of Technology Madras, Chennai, India; 2. Defence Metallurgical Research Laboratory, Hyderabad, India; 3. Department of Chemistry, Moscow Lomonosov State University, Moscow, Russian Federation*

Equiatomic rare earth intermetallic compounds RNi (R = heavy rare earth such as Gd, Tb, Dy, Ho and Er) exhibit excellent magnetocaloric effect near their ferromagnetic ordering temperature and alloying the rare earth site has been found to be an efficient method to tailor the magnetic transition temperature and the associated magnetic entropy change [1]. In the present work, three rare earth elements Tb, Ho and Er in equimolar concentration occupy the rare earth site in RNi compound. Polycrystalline $Tb_{0.33}Ho_{0.33}Er_{0.33}Ni$ has been prepared by arc-melting under argon atmosphere and characterized by powder X-ray diffraction and magnetization measurements. Multicomponent $Tb_{0.33}Ho_{0.33}Er_{0.33}Ni$ compound has FeB-type orthorhombic crystal structure (space group *Pnma*, No.62) at room temperature. The sample orders ferromagnetically at ~59 K (T_C) [Fig. 1a]. Paramagnetic susceptibility is Curie-Weiss like [Inset in Fig. 1a]. It should be recalled that the compounds with individual rare-earths viz. TbNi, HoNi and ErNi order ferromagnetically at about 67 K, 36 K and 11 K respectively. Magnetization has been measured at 5 K as a function of magnetic field up to 70 kOe. Magnetization saturates in applied magnetic field [Fig. 1b] and the saturation magnetization value is about 9.9 μ_B/f.u. A minor hysteresis with a coercive field of ~930 Oe is observed. By measuring isothermal magnetization data around T_C, magnetocaloric effect is estimated. A moderate isothermal magnetic entropy change has been obtained near T_C that is of the same order as in the end member RNi compounds. Understanding magnetic properties of such multicomponent rare earth intermetallic compounds should pave a way to comprehend the complex magnetism of rare earth high-entropy alloys.

1. X. Q. Zheng, B. Zhang, H. Wu, F. X. Hu, Q. Z. Huang and B. G. Shen, J. Appl. Phys. 120 (2016) 163907

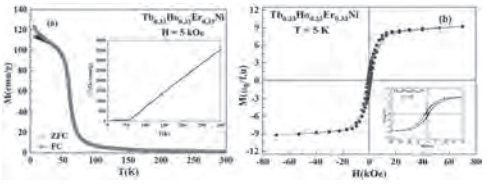

Fig. 1. (a) Magnetization vs temperature and (b) magnetization vs field of $Tb_{0.33}Ho_{0.33}Er_{0.33}Ni$ compound.

KPA-16. Development of rare-earth thick-film magnets applied to ultra-small stepping motors. *K. Kouno*[1], A. Yamashita[1], T. Yanai[1], M. Nakano[1] and H. Fukunaga[1] *1. Nagasaki Univercity, Nagasaki, Japan*

We have fabricated isotropic Pr-Fe-B thick-film magnets with the thickness of 0.25 mm on a stainless shaft using a PLD (Pulsed Laser Deposition) method and applied them to an ultra-stepping motors with the diameter of less than 3 mm by taking advantage of $Pr_2Fe_{14}B$ phase with a large anisotropic magnetic field at room temperature [1]. In this study, we focused on the fact that the linear expansion coefficient of Nd element (9.6×10^{-6} 1/K) is closer to that of stainless steel($10\sim11\times10^{-6}$ 1/K) than that of Pr element (6.7×10^{-6} 1/K). Moreover, evaluation on the temperature dependence of magnetic properties and observation in the mechanical characteristic of Nd-Fe-B thick-film magnets on a stainless substrate (shaft) were carried out. Figure 1 shows the temperature dependence of the energy product at the operating point of (Nd or Pr)-Fe-B thick-film magnets fabricated on stainless substrates. At 125 °C, the energy product of a Nd-Fe-B thick-film exceeds those of a Pr-Fe-B one and a Nd-Fe-B bond magnet. The result is considered to be attributed to the different temperature dependence of each anisotropic magnetic field for $Pr_2Fe_{14}B$ and $Nd_2Fe_{14}B$ phases. We also observed the mechanical characteristic of the both films on a stainless substrate and shaft. Several as-deposited Pr-Fe-B film magnets with the Pr contents exceeding 15 at % on the substrate showed exfoliation phenomenon. On the other hand, as-deposited and annealed Nd-Fe-B films (Nd contents : 14 ~ 18 at. %) on the substrate didn't show mechanical destruction. Although almost all the films showed good adhesion on the stainless shafts as displayed in Fig. 2, one Pr-Fe-B thick-film magnet had a slight crack at the boundary of the shaft and the film. Consequently, enhancement in coercivity of Nd-Fe-B thick-film using an additive at room temperature is a promising method to propose an alternative material of a previously reported Pr-Fe-B thick-film.

[1] M. Nakano et.al., IEEE Trans. Magn. Vol. 56, 7516303(2020).

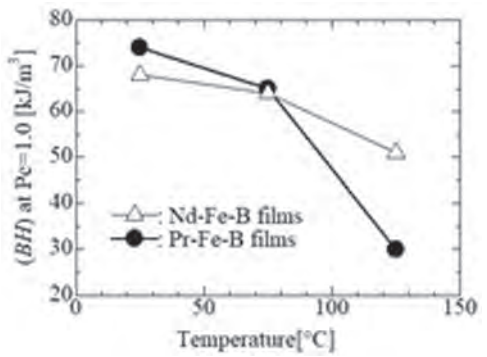

Fig 1 Energy product (Pc =1.0) of (Nd or Pr)-Fe-B thick film magnets as a function of operating temperature.

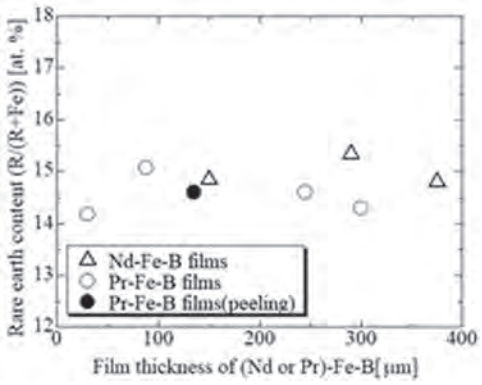

Fig. 2 Exfoliation phenomenon of as-deposited (Nd or Pr)-Fe-B thick-films on stainless shafts.

Session KPB
HARD MAGNETIC MATERIALS III: RARE EARTH-BASED COMPOUNDS (Poster Session)

Zheng Ma, Chair
Universitat Autònoma de Barcelona, Barcelona, Spain

KPB-01. Withdrawn

KPB-02. A Study on Weight Reduction through Slotless SPMSM in High-Speed Operation. *S. Lee*[1], S. Song[2], D. Kim[2], J. Min[1] and W. Kim[1]
1. Electrical Engineering, Gachon Universiy, Gyeonggi-do, The Republic of Korea; 2. Electrical Engineering, Hanyang University, Seoul, The Republic of Korea

1. Introduction The Slotless Surface Mounted Permanent Magnet Synchronous Motor (SPMSM) is expected to be a great advantage in terms of weight saving because it has no slots (stator teeth) compared to the slotted surface mounted permanent magnet synchronous motor. In this paper, the performance comparison of slotless surface mounted synchronous motors was analyzed through Finite Elements Analysis (FEA) and Mechanical Stiffness Analysis, and the study was conducted to take advantage of various applications through weight reduction. 2. Comparison of Weight between the Conventional model and the slotless model In case of weight, the conventional model was 1,816g and the improved model was 1,539g, which could be reduced by about 15%. The weight was compared to the total weight including the stator, rotor, and coil weights. In the stator, compared to the conventional model (1,467g), the improved model (976g) was able to reduce the weight significantly because the slot was removed. It could be seen that the increase was observed by designing considering However, as a result, it was confirmed that the total weight of the improved model was reduced compared to the conventional model by significantly reducing the weight in the stator due to the change of the topology. 3. Conclusion In this paper, the existing model of the surface-attached permanent magnet synchronous motor (SPMSM) was designed as a slotless model during high-speed operation of 15kW class, and weight reduction was conducted through Finite Element Analysis (FEA) and Mechanical Stiffness Analysis. Because the existing model had a long stator tooth length and took up a lot of area, I thought that it would be possible to bring many advantages through topology change to slotless without the stator tooth, so the study was conducted.

[1] T. Han, Y. Wang and J. -X. Shen, "Analysis and Experiment Method of Influence of Retaining Sleeve Structures and Materials on Rotor Eddy Current Loss in High-Speed PM Motors," in IEEE Transactions on Industry Applications, vol. 56, p. 4889-4895 (2020) [2] H. W. Yang, H. W. Kim, Y. Y. Koh, Y. J. Kim, S. Y. Jeong, Size design through loss analysis of high-speed permanent magnet synchronous motors. Proceedings of the Korean Electrical Society Conference, p.1117-1118 (2021)

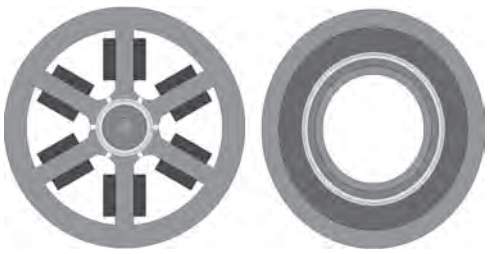

Fig 1. Motor shape of the Conventional model (left) and slotless model (right)

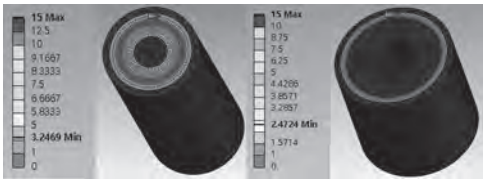

Fig 2. Results of mechanical stiffness analysis of the Conventional model (left) and slotless model (right)

KPB-03. A Study on the Optimization Characteristics of High-Speed Permanent Magnet Synchronous Motor Driveable in a Cryogenic Environment. *D. Kim*[1], D. Kim[2], M. Jeong[1], S. Lee[1] and W. Kim[1]
1. Gachon University, Seongnam, The Republic of Korea; 2. Hanyang University, Seoul, The Republic of Korea

I. Introduction This paper analyzes the magnetic characteristics of permanent magnets based on the performance of the existing submerged LNG pump induction motor driven in a cryogenic environment and designs a permanent magnet synchronous motor that can maximize efficiency in a cryogenic environment. Torque and efficiency analysis during rated operation was performed through loss separation of the existing 15 kW induction motor and stator current density test. Although copper loss ratio is the highest among the total losses of existing induction motors, it has the advantage of high current density due to excellent cooling performance according to the characteristics of the cryogenic environment. By replacing the existing induction motor with a permanent magnet synchronous motor, the loss can be reduced compared with the induction motor, and high-speeding and miniaturization can be achieved. II. Rotor and stator design considering high speed operation In the case of interior permanent magnet models, the THD for no-load phase voltage is higher than that of surface permanent magnet models, and the higher the number of poles, the higher the torque ripple. When considering high-speed driving, it should be designed in a way that reduces THD and torque ripple. For the stator, models of 6 slots, 12 slots, and 24 slots were compared due to size fluctuations for optimal efficiency. In the case of 24 slots, they showed the highest performance in terms of torque ripple, THD reduction, and efficiency. However, the 12slot model is only 0.1% different in efficiency from the 24slot model, but it is the best condition considering the production by reducing the use of permanent magnets by 12%. III. Conclusion The final model through FEM was derived by replacing the existing submerged LNG pump induction motor with a permanent magnet synchronous motor. By reducing and accelerating the volume by 33.4%, the efficiency increased by 1.2%, and the power density increased. In addition, irreversible demagnetization did not occur when the permanent magnet demagnetization phenomenon was conducted under extreme conditions.

[1] Sung-Yoel Cho, Hui-Min Kim, Dong-Sok Kim, Gwan-Soo Park.(2010). A study on the temperature characteristic analysis of a stator core for cryogenic motor design., KIEE Conference, 888-889. [2] X. Lv, D. Sun and L. Sun, "Design and Performance Analysis of High-Speed Cryogenic Permanent Magnet Synchronous Motor," 2019 22nd International Conference on Electrical Machines and Systems (ICEMS), 2019, pp. 1-6, doi: 10.1109/ICEMS.2019.8922560.

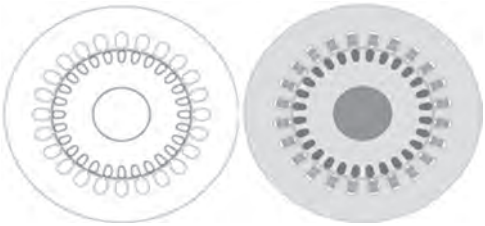

Fig 1. 15kW 6,000rpm Convetional Induction Motor

Fig 2. SPMSM 2P12S

KPB-04. Design of Noiseless Motor through Application of New Materials and High-speed Operation. *D. Kim*[1], D. Nam[2], J. Min[2], J. Lee[1] and W. Kim[2] *1. Hanyang University, Seoul, The Republic of Korea; 2. Gachon University, Seongnam, The Republic of Korea*

Recently, as the demand for high-speed motors increases for miniaturization and high-outputting of products, noise from the motor during high-speed operation has become a new issue[1-4]. Research on motor noise reduction is being actively conducted, and in particular, research to reduce electromagnetic noise of motors through reduction of cogging torque and THD is mainly conducted. However, there is a limit to reducing electromagnetic noise, and measures to reduce mechanical noise generated from bearings should also be considered. In this paper, we propose a noiseless motor design through new materials and high-speed operation. Design an ultra-high-speed surface-attached permanent magnet synchronous motor (SPMSM) that operates at 20 kHz or higher, which is outside the human audible frequency, as shown in Fig.1. Stator tapering and rotor pole ratio optimal design were carried out to reduce harmonics, and harmonic components affecting noise were analyzed. In addition, a permanent magnet for high-speed operation was developed to reduce permanent magnet eddy current loss caused by harmonics during high-speed operation. Permanent magnets for high-speed operation were manufactured through meso-scale structure manufacturing as shown in Fig. 2, and crystal grains were controlled through external magnetic field and post-heat treatment process. In order to remove mechanical noise other than electromagnetic noise, a porous thin-film sound-absorbing material was developed, and mechanical noise was minimized by applying it to the motor housing and bearings.

[1] L. Zhao et al., "A Highly Efficient 200 000 RPM Permanent Magnet Motor System," in IEEE Transactions on Magnetics, vol. 43, no. 6, pp. 2528-2530, June 2007 [2] O. Bottauscio, F. Casaro, M. Chiampi, S. Giors, C. Maccarrone and M. Zucca, "High-Speed Drag-Cup Induction Motors for Turbo-Molecular Pump Applications," in IEEE Transactions on Magnetics, vol. 42, no. 10, pp. 3449-3451, Oct. 2006 [3] Z. Kolondzovski, A. Arkkio, J. Larjola and P. Sallinen, "Power Limits of High-Speed Permanent-Magnet Electrical Machines for Compressor Applications," in IEEE Transactions on Energy Conversion, vol. 26, no. 1, pp. 73-82, March 2011 [4] S. -W. Song, I. -J. Yang, S. -H. Lee, D. -H. Kim, K. S. Kim and W. -H. Kim, "A Study on New High-Speed Motor That Has Stator Decreased in Weight and Core-loss," in IEEE Transactions on Magnetics, vol. 57, no. 2, pp. 1-5, Feb. 2021

Fig. 1 SPMSM shape operating outside the audible frequency

Fig. 2 Manufacture of one-dimensional meso-scale structure permanent magnet

KPB-05. Distinguishing Method of Local Demagnetization and Short-circuit Fault of Six-phase Interior Permanent-magnet Machine based on Voltage in Synchronous Frame. *Z. Yuan*[1], M. Wang[1], J. Bai[1], W. Liu[1] and P. Zheng[1] *1. Harbin Institute of Technology, Harbin, China*

The multi-phase interior permanent-magnet machines are widely used in the application with high power density and high reliability requirements such as aerospace and electrical vehicles due to the reluctance torque utilization and phase redundancy [1]. Part of the permanent magnet material will work at lower magnetization states irreversibly when the machines work in serious overcurrent, vibration or high temperature environment, causing local permanent magnet fault in the machines [2]. Most of current research on fault diagnosis focuses on a single fault based on the analysis of signal characteristics [3,4,5], but the validity is not evaluated adequately when other fault types are considered. Research in this paper is conducted to distinguish the local demagnetization and short-circuit faults, which accounts for a high proportion in faults of machines [6]. The model of EMF generated by one pole is established first. Meanwhile, the short-circuit current model and the voltage disturbance in healthy phases owing to the mutual inductances between short phase and healthy phases are analyzed. The harmonic spectrums of the voltage in natural frame and synchronous frame are investigated and it's shown that the $12k/p^{th}$ and 2^{nd} harmonics of voltages in synchronous frame are salient features of local demagnetization and short-circuit current fault respectively by comparing different severities and locations of faults, in which k=1,2, … and p is the number of pole pairs. To solve the problem of the amplitude calculation residual between integer and non-integer harmonics, a diagnosis method based on the mean and the variance of the dataset containing the Fourier coefficients of $12/7^{th}$ and 2^{nd} harmonics at different initial sampling points is proposed. The values of mean and variance are close to zero in normal condition, but that in two faults condition shows discriminative characteristics. The method is easy to integrate into the

controller due to the low computational complexity. The reliability of the distinguishing method is also evaluated.

[1] F. Barrero and M. J. Duran, *IEEE Trans. Ind. Electron.*, Vol. 63, p.449-458 (2016) [2] S. Hamidizadeh, N. Alatawneh and R. R. Chromik, *IEEE Trans. Magn.*, Vol. 52, p.1-4 (2016) [3] H. Chen, C. Gao and J. Si, *IEEE Trans. Instrum. Meas.*, Vol. 71, p.1-12, (2022) [4] X. Song, J. Zhao and J. Song, *IEEE Trans. Power Electron.*, Vol. 35, p.7816-7825 (2020) [5] R. Hu, J. Wang and A. R. Mills, *IEEE Trans. Ind. Electron.*, Vol. 68, p.59-69 (2021) [6] B. Sen and J. Wang, *IEEE Trans. Ind. Electron.*, Vol. 63, p.3148-3157 (2016)

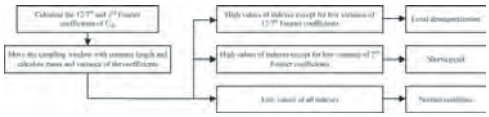

Fig. 1. Distinguishing method flow diagram of local demagnetization and short-circuit fault

Indexes		Local Demagnetization	Short-circuit	Normal condition
Mean	12/7th	7.47	196	3.13×10-2
	2nd	11.4	176	8.01×10-2
Variance	12/7th	3.14×10-4	160	2.80×10-4
	2nd	10.6	4.94×10-2	1.60×10-3
Ratio of variance to mean	12/7th	4.21×10-5	0.813	8.92×10-3
	2nd	0.930	2.81×10-4	2.00×10-2

Fig. 2. Table of comparison on mean and variance values in two types of fault conditions

KPB-06. A study on the application of consequent poles to the STM model to reduce weight and use of magnets. S. Song[1], S. Lee[2], J. Lee[1] and *W. Kim*[2] *1. Department of Electrical Engineering, Hanyang University, Seoul, The Republic of Korea; 2. Department of Electrical Engineering, Gachon University, Seong-Nam, The Republic of Korea*

For high performance and high efficiency, rare earth magnets have been widely used in recent motors. Rare earth is very unstable as a future industry due to limited resources and monopoly of some countries. For this reason, as the price of rare earth magnets and overall materials has increased recently, the issues of cost reduction and weight reduction are increasing. In this paper, iron usage and weight were reduced by changing the existing EPS motor to the STM model [1]. However, the STM model showed low performance compared to the amount of magnet used because large leakage occurred in the lips. To compensate for these shortcomings and to reduce the amount of magnet used, consequent poles were applied. When Consequent pole is applied, the usage of rare earth magnet is greatly reduced. Therefore, the weight and price are greatly reduced. In general, the consequent pole reduces the use of magnets by half, so the performance is also reduced by half. However, in the STM model, the magnetic flux leakage from the lips is greatly reduced by removing the poles. Therefore, the performance is reduced by about 35%, not by half. Therefore, even though the use of magnets has been reduced by half, by applying STM as a consequent pole rather than a general consequent pole with the same performance, many advantages such as weight reduction and reduced use of magnets can be brought. The application of this motor is EPS. For EPS, cogging torque is the most important performance factor. However, when the Consequent pole is applied, only the N pole or the S pole exists and the rest is made of iron, so a lot of cogging torque and torque ripple occurs. In this paper, after applying the consequent pole to the STM model, various methods are applied to reduce the cogging torque. Finally, it can be seen that the weight and magnet usage are reduced with the same performance, and the cogging torque is similarly generated.

[1] S. -W. Song, I. -J. Yang, S. -H. Lee, D. -H. Kim, K. S. Kim and W. -H. Kim, "A Study on New High-Speed Motor That Has Stator Decreased in Weight and Coreloss," in *IEEE Transactions on Magnetics*, vol. 57, no. 2, pp. 1-5, Feb. 2021, Art no. 8201105, doi: 10.1109/TMAG.2020.3012482.

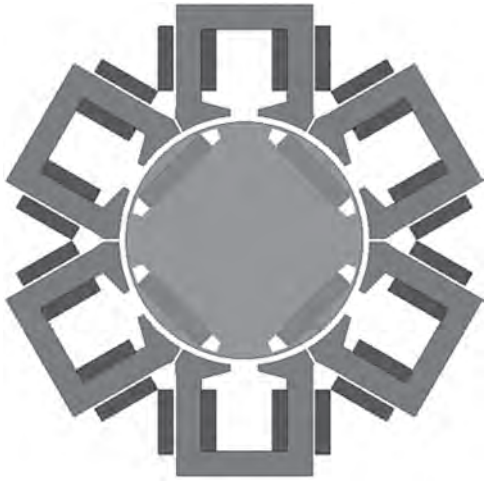

Fig. 1 Consequent pole applied to STM structure

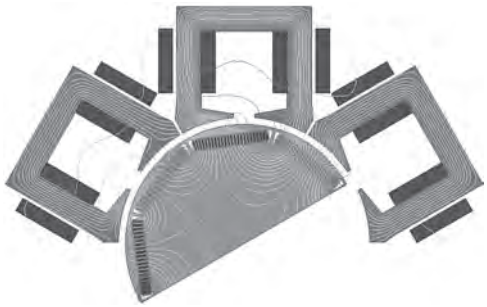

Fig. 2 STM structure magnetic flux line

KPB-07. A Study on the Combination of the Number of Poles and the Number of Slots in the Integral Magnetic Bearing for Uniform Rotor Control and the Number of Bearing Phases. *M. Hong*[1], I. Yang[2], S. Song[2], D. Jung[3] and W. Kim[1] *1. Gachon University, Seongnam-Si, The Republic of Korea; 2. Hanyang University, Seoul-Si, The Republic of Korea; 3. Halla University, Won-Ju-Si, The Republic of Korea*

In this paper, the formulas for the number of stator pole slots and the number of bearing phases to eliminate the structurally generated force asymmetry between the bearing phases for the linear position control of the rotor of the integral magnetic bearing is presented. In the case of the existing magnetic bearing motor, as the rotor rotates, there is an advantage in that loss and noise due to friction do not occur. The reduction in losses and noise is a huge advantage in high-speed rotating motors. However, since it is a structure in which the rotor is controlled from the outside of the motor, it has a disadvantage in that the size increases. The Halva array has a structure in which magnets having different magnetization directions are arranged to increase the magnetic flux density on one side and decrease the magnetic flux density on the other side. By applying the halva arrangement, an All-In-One Motor can be designed that secures the space inside the rotor as a space to insert the magnetic bearing. Fig. 1 shows an integral magnetic bearing. In the case of the All-In-One Motor, since the bearing exists inside the rotor, the bearing magnetic flux that controls the rotor position is affected by the magnetic field of the permanent magnet and the rotating magnetic field of the stator. In this case, there is a combination of the number of pole slots and the number of bearings that causes asymmetry of the force between the bearing phases in a specific combination of the number of pole slots. Fig. 2 shows the force waveforms of the X-axis bearing and the Y-axis bearing according to the rotation angle of the 6-pole 9-slot. In order to eliminate the asymmetry of the force between the bearing phases, the angle between the phases of the bearing should be determined with a difference of 360 degE between the phases, and it should be determined as the number of intersections of the prime factor of the pole pair and the prime factor of the equivalent number of

coils. The formula was verified by comparing and analyzing the force waveforms for each bearing phase of 4-phase, 6-pole, 9-slot, and 16-pole, 24-slot bearings. The validity of the proposed model was verified using the finite element method.

W. Zhang, Y. Ruan, S. Ji, X. Sun and H. Zhu, "Variable stiffness coefficient analysis and control system study for radial AC hybrid magnetic bearing," *Proceedings of the 30th Chinese Control Conference*, pp. 3494-3499 (2011)
R. Chen, H. Li and J. Tian, "The relationship between the number of poles and the bearing capacity of radial magnetic bearing," Chinese Automation Congress (CAC), pp. 5553-5557 (2017)

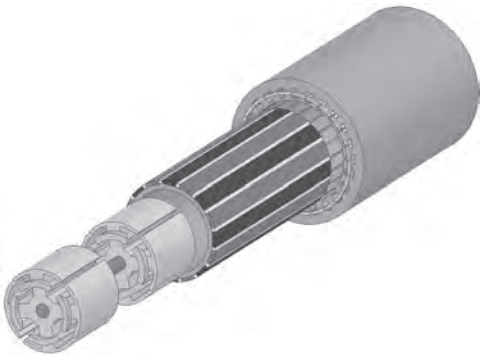

Fig. 1

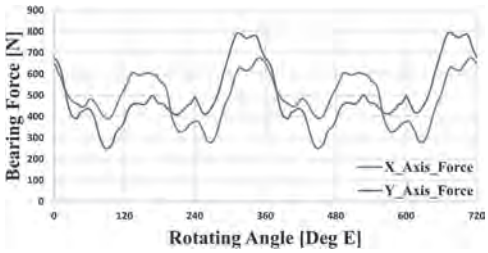

Fig. 2

KPB-08. Semi-physical Demagnetization Model for the Temperature Dependency of Permanent Magnets in Electrical Machines. *A. Kern*[1], N. Leuning[1] and K. Hameyer[1] *1. Institute of Electrical Machines, RWTH Aachen University, Aachen, Germany*

Motivation Losses during the operation of electrical machines heat up permanent magnets (PMs) which in turn leads to a deterioration of their demagnetization behavior. Moreover, the relation between the magnetic flux density B and the field strength H may become nonlinear. Existing material models either lack of accuracy, do not involve all boundary constraints or are parameterized with a higher number of variables [1-4]. The use of temperature coefficients for the remanence B_r and coercivity H_c is insufficient for modeling the demagnetization behavior $B(H)$ as it does not contain any information about the location of the knee point [5]. This paper presents a novel semi-physical material model for PMs with a reduced number, physically based and independent variables, which enables a transition between a description of linear and nonlinear demagnetization behavior. Parametrization For the modeling of the demagnetization behavior the function $B(H)=\mu_0\mu_{PM}(H+H_{cB})+a_1 tanh(a_2(H+H_{cB}))$ in relation to the Takács model is used [6-7]. The recoil permeability μ_{PM} is the physically related parameter that is determined by the fraction of the remanence to the coercivity. The free parameters are the amplitude parameter a_1 and the shape parameter a_2, that are obtained by least-square curve fitting. Based on the parameter identification, a_1 is recalculated such that $B(0)=B_r$ is fulfilled. In the transition to a nonlinear course the amplitude parameter is $a_1 \neq 0$ and the shape parameter adjusts according to the curvature in the characteristic knee point. Results Figure 1 shows modeled and measured temperature dependent demagnetization curves for a sample PM. Figure 2 illustrates the temperature course of the recoil permeability and the amplitude parameter. The demagnetization behavior at any desired temperature can be obtained by interpolation of the parameters. Conclusion and Outlook The proposed model is capable to describe linear and nonlinear demagnetization courses with low residuals and fulfills physical boundary constraints by parametrization. In future work, the proposed model is used in order to study and quantify relations between the macroscopic temperature behavior of PMs and their intrinsic material properties.

[1] J. Chen, D. Wang, S. Cheng, Y. Jiang, X. Teng, Z. Chen, Y. Shen, F. Birnkammer and D. Gerling, "A Hysteresis Model Based on Linear Curves for NdFeB Permanent Magnet Considering Temperature Effects," in IEEE Transactions on Magnetics, vol. 54, no. 3, pp. 1-5, 2018. [2] S. Ruoho, E. Dlala and A. Arkkio, "Comparison of Demagnetization Models for Finite-Element Analysis of Permanent-Magnet Synchronous Machines," in IEEE Transactions on Magnetics, vol. 43, no. 11, pp. 3964-3968, 2007. [3] S. Hamidizadeh, N. Alatawneh, R. R. Chromik and D. A. Lowther, "Comparison of Different Demagnetization Models of Permanent Magnet in Machines for Electric Vehicle Application," in IEEE Transactions on Magnetics, vol. 52, no. 5, pp. 1-4, 2016. [4] N. Leuning, S. Elfgen, B. Groschup, G. Bavendiek, S. Steentjes and K. Hameyer, "Advanced Soft- and Hard-Magnetic Material Models for the Numerical Simulation of Electrical Machines," in IEEE Transactions on Magnetics, vol. 54, no. 11, pp. 1-8, 2018. [5] P. Zhou, D. Lin, Y. Xiao, N. Lambert and M. A. Rahman, "Temperature-Dependent Demagnetization Model of Permanent Magnets for Finite Element Analysis," in IEEE Transactions on Magnetics, vol. 48, no. 2, pp. 1031-1034, 2012. [6] J. Takács, "The T(x) model for the description of hysteresis", Wiley-VCH, 2003. [7] G. Bavendiek, F. Müller, J. Sabirov and K. Hameyer, "Magnetization dependent demagnetization characteristic of rare-earth permanent magnets", in Archives of electrical engineering, vol. 68, no. 1, pp. 33-45, 2019. Acknowledgment The measurement equipment was partly funded by the Otto-Junker Stiftung.

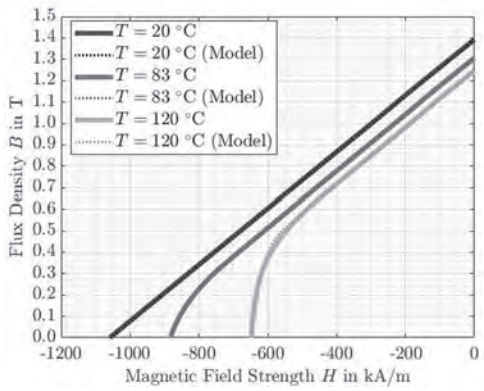

Fig.1

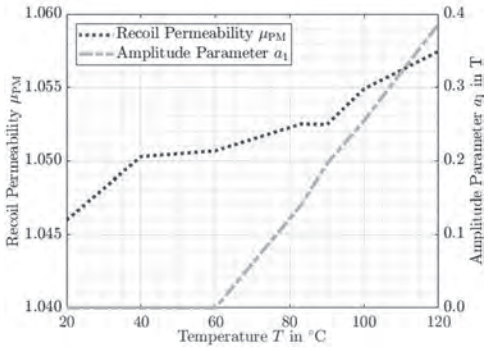

Fig.2

KPB-09. A Study on Shape Design to Improve Power of 200W Axial Flux Motor for Cooperative Robot. J. Min[1], D. Nam[1], H. Pyo[1], N. Kang[1] and *W. Kim*[1] *1. Electrical Engineering, Gachon University, Seongnam, The Republic of Korea*

Cooperative robots are intended to collaborate with humans, and their necessity is increasing to improve work efficiency. The motor used for the joint of the cooperative robot must have an ultra-thin structure to satisfy light weight, high torque, and limited axial length. In this paper, a shape improvement design of a permanent magnet type motor for robot joints with an ultra-thin structure is proposed to increase the payload of cooperative robots. The shape dimensions of the conventional radial flux motor were changed to an axial flux type motor, and the performance was analyzed for various shapes [1], [2]. In the shape of an axial flux motor with a very short axial length, the factors that significantly affect the power density are the saturation of the core and the selection of the number of turns [3]. As shown in Fig. 1, the axial length of the magnet and the width between the magnets were selected as design variables. And the tooth width was selected as a design variable, and the number of turns according to the slot area and the tendency of tooth magnetic flux density were analyzed. The most optimal model was obtained through finite element analysis, and it was confirmed that the rated torque at the same current density increased by about 24% from 0.689Nm to 0.851Nm. In the structure of single rotor, the volume of stator back yoke must be secured due to core saturation, but in the case of NS type among dual rotor structures, the stator yoke can be removed to increase the slot area to increase the number of turns. However, it should be analyzed to secure space for dual rotors in the limited axial length. As a result of performing the design with the same process as the previous structure, the torque ripple increased from 2% to 5% due to stator shoe saturation, but the average torque increased by about 5%. Due to the thin yoke thickness in the slot type axial flux motor, it is not easy to generate high power in an ultra-thin structure. Therefore, in this paper, a new slotless type shape is proposed. Fig. 2 shows the shape of the slotless type that can remove the tooth and yoke structure of the stator.

[1] W. Zhao, T. A. Lipo and B. -I. Kwon, "Comparative Study on Novel Dual Stator Radial Flux and Axial Flux Permanent Magnet Motors With Ferrite Magnets for Traction Application," in *IEEE Transactions on Magnetics*, Vol. 50, no. 11, p. 1-4 (2014) [2] M. Fasil, N. Mijatovic, B. B. Jensen and J. Holboll, "Finite-Element Model-Based Design Synthesis of Axial Flux PMBLDC Motors," in *IEEE Transactions on Applied Superconductivity*, Vol. 26, no. 4, p. 1-5 (2016) [3] H. Pyo, J. W. Jeong, J. Yu, S. G. Lee and W. Kim, "Design of 3D-Printed Hybrid Axial-Flux Motor Using 3D-Printed SMC Core," in *IEEE Transactions on Applied Superconductivity*, Vol. 30, no. 4, p. 1-4 (2020)

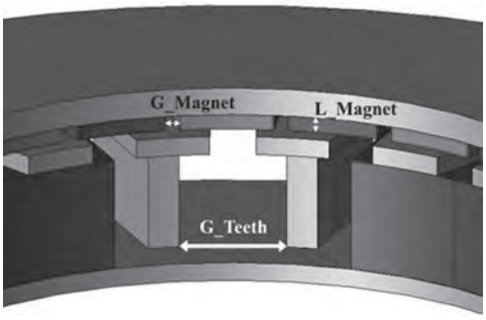

Fig. 1. Axial flux motor design variables

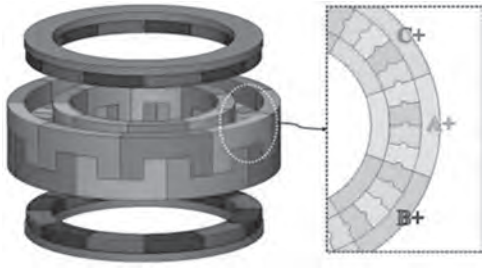

Fig. 2. Proposed shape of slotless type axial flux motor

Session KPC
HARD MAGNETIC MATERIALS V: RARE-EARTH FREE HARD MAGNETIC MATERIALS (Poster Session)

Julius de Rojas, Chair
University of Durham, Durham, United Kingdom

KPC-01. Maximum Energy Product of Exchange-coupled $Sm(FeCo)_{12}$/α-Fe Nanocomposite Particle. *R. Uda*[1], K. Koike[2], N. Inaba[3], H. Kato[2], M. Itakura[4], S. Okubo[5], H. Ohta[5] and H. Tsuchiura[6] *1. Graduate School of Science and Engineering, Yamagata University, Yonezawa, Japan; 2. Applied Mathematics and Physics, Yamagata University, Yonezawa, Japan; 3. Informatics and Electronics, Yamagata University, Yonezawa, Japan; 4. Interdisciplinary Graduate School of Engineering Sciences, Kyushu University, Kasuga, Japan; 5. Molecular Photoscience Research Center, Kobe University, Kobe, Japan; 6. Applied Physics, Tohoku University, Sendai, Japan*

The use of Nd-Fe-B magnets with $Nd_2Fe_{14}B$, which are used in high performance motors, is increasing. However, it is predicted that inexpensive Nd will become unavailable in near future, and there is a need to reduce the amount of Nd used and develop new magnets [1]. Exchange-coupled nanocomposite magnets consisting of magnetic hard and soft nanoparticles, NPs have been proposed as candidate [2]. The $Sm(Fe_{0.8}Co_{0.2})_{12}$ with $ThMn_{12}$ structure has higher saturation magnetization, M_s, and uniaxial magnetocrystalline anisotropy, K_u than $Nd_2Fe_{14}B$ and is expected to be a magnetic hard phase in the Fe-based system without Nd [3]. We investigate the effect of the direction of the α-Fe coating surface and the volume fraction of α-Fe, V_{Fe} on the demagnetization process and the maximum energy product, $(BH)_{max}$ of exchange-coupled $Sm(Fe_{0.8}Co_{0.2})_{12}$ /α-Fe nanocomposite NPs using LLG simulations [4]. $Sm(Fe_{0.8}Co_{0.2})_{12}$ NPs is as reference model #1. The nanocomposite NPs of $Sm(Fe_{0.8}Co_{0.2})_{12}$ coated with α-Fe on top/bottom, and both sides are model #2 and #3. For both # 2 and #3, α-Fe layer thickness is 1 nm ≤ t_{Fe} ≤ 7 nm. The size of NPs are $x = y = 50$ nm and $z = 100$ nm. The magnetic properties of $Sm(Fe_{0.8}Co_{0.2})_{12}$ and α-Fe were taken from references [3, 5-7]. The cell volume is 1 nm^3. External field, H_{ex} is applied parallel to *c*-axis of $Sm(Fe_{0.8}Co_{0.2})_{12}$ along to *z*-axis of NPs. Fig. 1 shows V_{Fe} dependence of $(BH)_{max}$ for #2 and #3. The $(BH)_{max}$ of #1 was 630 kJ/m^3, while the $(BH)_{max}$ of #2 and #3 with optimized t_{Fe} were larger, 636 kJ/m^3 for #2 with V_{Fe} = 4 % (t_{Fe} = 2 nm) and 657 kJ/m^3 for #3 with V_{Fe} = 12 % (t_{Fe} = 3 nm). Fig. 2 shows distribution of demagnetizing field, H_d at H_{ex} = 0 T for #2 and #3. The H_d acting on top/bottom surfaces of NPs was larger for #2, which was coated on top/bottom surfaces with α-Fe, which is larger than M_s of $Sm(Fe_{0.8}Co_{0.2})_{12}$, than for #3, which was coated on sides with α-Fe. Therefore, remanence and $(BH)_{max}$ of #3 are larger than those of #2. From the above discussion, it is clear that side coating of magnetic soft phase is effective in increasing $(BH)_{max}$ of $Sm(FeCo)_{12}$/α-Fe NPs.

[1] S. Hirosawa, M. Nishino and S. Miyashita, Adv. Nat. Sci: Nanosci. Nanotechnol., 8, (2017) 013002. [2] R. Skomski and J. M. D. Coey, *Phys. Rev*. B, 48, (1993) 15812. [3] Y. Hirayama *et al*., *Scripta Mater*., 138, (2017) 62–65. [4] M. J. Donahue and D. G. Porter, "OOMMF User's Guide, Version 1.0," NISTIR 6376, National Institute of Standards and Technology, Gaithersburg, MD (Sept 1999). ; M. J. Donahue, D. G. Porter (2021), "OOMMF: Object Oriented MicroMagnetic Framework," https://nanohub.org/resources/oommf. (DOI: 10.21981/8RRA-5656). [5] Felix Jimenez-Villacorta and Laura H. Lewis, Chapter 7 "Advanced Permanent Magnetic Materials" Nanomagnetism, edited by J. Gonzalez (OCP Publishing Group) (2014). [6] D. Ogawa, T. Yoshioka *et al*., *J. Magn. Magn. Mater*., 497, (2020) 165965. [7] T. Fukazawa, H. Akai *et al*., *J. Magn. Magn. Mater*., 469, (2019) 296-301.

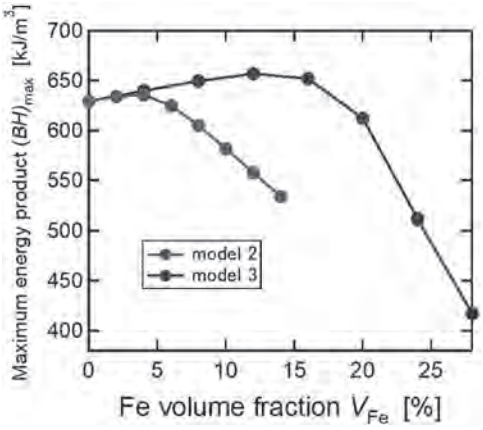

Fig. 1 V_{Fe} dependence of $(BH)_{max}$ for #2 and #3.

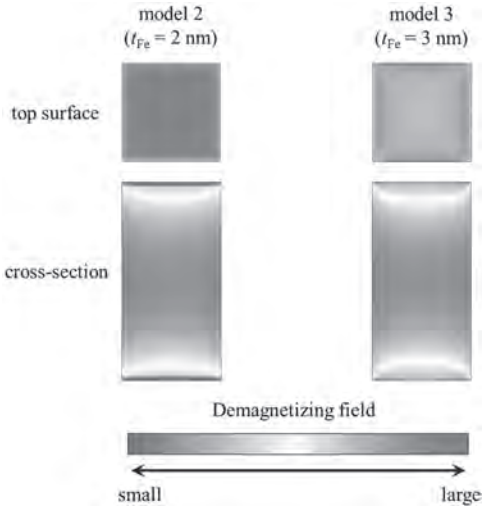

Fig. 2 H_d distribution on the top surface and the cross-section of NPs for #2 and #3 at H_{ex} = 0 T.

KPC-02. Analysis of the Magnetic Hardening Mechanism in Hot-deformed Nano-heterostructure $SmCo_5$ Permanent Magnet. *Y. Teng*[1], Y. Li[1], W. Liu[1], M. Yue[1] and D. Zhang[1] *1. Faculty of Materials and Manufacturing, Beijing University of Technology, Beijing, China*

Due to its large H_a and high T_c, SmCo magnets have an irreplaceable status in high temperature applications. The nanocrystalline hot-deformed $SmCo_5$ magnets were expected to obtain strong magnetic properties, and also good mechanical properties and corrosion resistance due to small grain size. The $SmCo_5$ compound has low structural symmetry and does not contain rich rare-earth grain boundary phases, so it is difficult to deform and obtain texture. Our previous study[1] found that the deformation and texture formation of $SmCo_5$ magnet can be promoted by constructing Sm-rich nanophases. In this study, the anisotropic heterostructure $SmCo_5$ magnet was prepared,

and the magnetic hardening mechanism of the magnet was analyzed. Compared with the magnet deformed at low temperature[1], the M_r and $(BH)_{max}$ of the magnet deformed at high temperature and large height reduction have been greatly improved, reaching 8.18 kG and 15.81 MGOe respectively. However, the high deformation temperature reduces the coercivity (9.63 kOe) of the magnet. The XRD and EBSD results confirm that good c-axis texture with an average misorientation angle of 27.3° was achieved. The high deformation temperature and the formation of c-axis texture lead to the merging growth of adjacent grains in the magnet, resulting in the final average grain size reaching 2.7 μm. TEM results show that a lot of Sm-rich nanophases are distributed in $SmCo_5$ matrix (see Fig.1(a)). The coercivity mechanism is analyzed through the initial magnetization curve and its first derivative (see Fig.1(b)). At the low applied field (H<5 kOe), the magnetization increases rapidly with the increase of the applied field, indicating that the coercivity mechanism of the magnet is mainly nucleation mechanism. However, from the corresponding first derivative curve, it can be found that there are two pinning peaks at H=1.07 and 2.46 kOe, which may be due to the pinning at grain boundaries and second phase grains on the motion of domain walls. Two pinning processes of grain boundary and grain boundary containing Sm-rich nanophases were further confirmed by LTEM.

[1] X.C. Xu, Y.Q. Li and Z.H. Ma, Scripta Materialia, 178, 34 (2020).

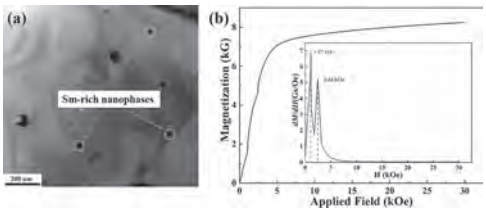

Fig.1 BF TEM image (a) and initial magnetization curve and corresponding first derivative (b) of the magnet

KPC-03. Bonded Magnets Development using Hydrogen Decrepitation. *H.G. Parmar*[1], X. Liu[1], M. Paranthaman[2] and C.I. Nlebedim[1] *1. Critical Materials Institute, Ames Laboratory, Ames, IA, United States; 2. Critical Materials Institute, Oak Ridge National Laboratory, Oak Ridge, TN, United States*

We will present our results on the possibility of deriving high performance magnet powder for bonded magnets production via hydrogen decrepitation (HD) and heat treatment. Applications of permanent magnets (PMs) in the energy conversion industry and in electric vehicles have attracted enormous recent interest. The flexibility of bonded magnets manufacturing allows for high degree of magnet shape customization. They are manufactured by blending rare earth magnet powder with thermoset or thermo-plastic polymers. The magnetic properties of bonded magnets, such as maximum energy product, depend on the loading of the starting powders. By developing an approach for producing bonded magnets via HD, we will enable future opportunity to recycle end-of-life sintered magnets into high performance bonded magnets. In this work, HD of N52 sintered magnets were performed at 1bar, 1.5bar, 2bar and 4bar pressure. The resultant powder due to the absorption of the hydrogen gas and pulverization of the material shows soft magnetic characteristics. The HD powder was characterized by DSC to find the degassing temperature. Fig.1 shows the DSC curve of 4 bar pressure produced HD powder. The peak at T_1=151°C attribute to removal of H_2 from $Nd_2Fe_{14}B$ phase, T_2=175°C conversion of Nd trihydride to Nd dihydride and the Peak at T_3=655°C correspond to formation of Nd rich phase at grain boundary after degassing from NdH_2 [1]. Hence, we carried out degassing in vacuum furnace at 800°C for 2h. The degassed samples show hard magnetic properties (Fig.2) however, final powder product magnetic property does not vary with pressure in HD process. Therefore, we selected the powder treated at 4bar, which shows 30 MGOe maximum energy product for bonded magnets development. The bonded magnets were developed by compression molding of a mixture of 60 vol% of magnetic powder and 30 vol% Nylon 12 at 180 °C for 5 min, followed by ambient cooling. Throughout the process, 3kPa pressure was applied to achieve maximum density. The bonded magnets had a density of 4.1 g/cc. Magnetic field alignment was performed on the bonded magnets at 180 °C under 0.8 T field to obtain 13MGOe maximum energy product.

M.Zakotnik, E.Devlin, I.R.Harris, A.J.Williams, Journal of Alloys and Compounds, 450, 525-531, 2008

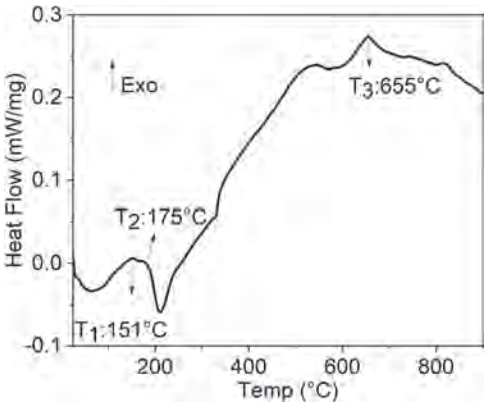

Fig. 1 DSC of HD powder

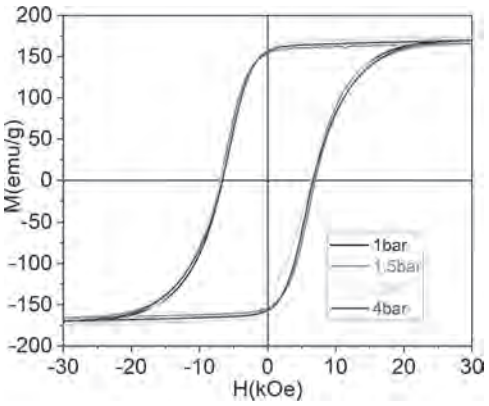

Fig. 2 MH loop of annealed powder

KPC-04. Production of Nd-Fe-B bulk nanocomposite magnets by hot deformation. *T. Saito*[1] and D. Hamane[2] *1. Chiba Institute of Technology, Narashino, Japan; 2. The University of Tokyo, Kashiwa, Japan*

There has been a great deal of interest in nanocomposite R-Fe-B magnets due to their high remanence magnetization and maximum energy products [1]. The nanocomposite magnets are currently produced by the annealing of either melt-spun ribbons or mechanically alloyed powders [1,2]. One of the most promising techniques for obtaining bulk nanocomposite R-Fe-B magnets is the spark plasma sintering (SPS) method [3]. It has been reported in recent years that the addition of Nd-Cu alloy powder increases the magnetic anisotropy and coercivity of Nd-Fe-B hot-deformed magnets [4]. Thus, we examined the effects of Nd-Cu alloy powder addition on the microstructures and magnetic properties of Nd-Fe-B nanocomposite magnets by the hot deformation. Small amounts of $Nd_4Fe_{77.5}B_{18.5}$ alloy ingots were melt-spun in an argon atmosphere. The amorphous melt-spun ribbons were comminuted into powders and then consolidated into bulk materials at 723 K by the SPS method. Hot deformation of the hot-pressed magnets was performed in a vacuum at 923 K under a pressure of ~200 MPa. The structures and magnetic properties of the hot-deformed Nd-Fe-B nanocomposite magnets were examined by x-ray diffraction (XRD), a transmission electron microscope (TEM), and a vibrating sample magnetometer (VSM). The bulk material consolidated at 723K was identified as amorphous and showed a low coercivity. Hot deformation of the amorphous bulk materials resulted in the formation of $Nd_2Fe_{14}B$ and Fe_3B phases. Figure 1 shows the hysteresis loops of the $Nd_4Fe_{77.5}B_{18.5}$ bulk nanocomposite magnets hot-deformed at 923

K. It was found that the coercivity of the $Nd_4Fe_{77.5}B_{18.5}$ bulk nanocomposite magnets increased with the Nd-Cu addition.

[1] R. Coehoorn, D. B. de Mooij, J. P. Duchateau, and K. H. J. Buschow, J. Phys. 49, C8-669 (1988). [2] J. Jakubowicz, A. Szlaferek, and M. Jurczyk, J. Alloys and Compounds 283, 307 (1999). [3] M. Tokita, J. Soc. Powder Technol. Jpn. 30, 790 (1993). [4] H.Sepehri-Amin, et al. Scripta Mater., 68, 167 (2013).

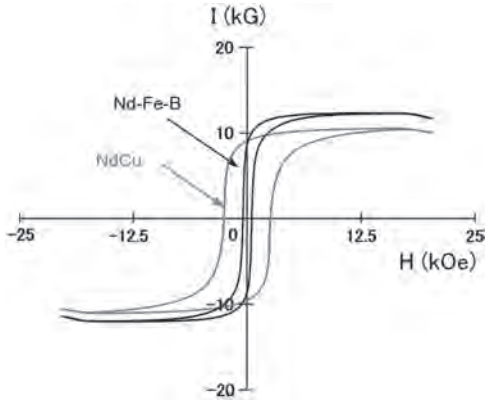

Fig.1 hysteresis loops of the $Nd_4Fe_{77.5}B_{18.5}$ bulk nanocomposite magnets with and without Nd-Cu addition.

KPC-05. Constituent contribution to the magnetocrystalline anisotropy in $Mn(Al_{1-x}Ga_x)$. *X. Liu*[1], D. Ryan[1] and Z. Altounian[1] *1. Physics, McGill University, Montreal, QC, Canada*

While tetragonal MnAl with the $L1_0$-type structure (P4/mmm #123) is metastable, it displays good intrinsic hard magnetic properties such as large magnetization (M_s=110 emu/g), high magnetocrystalline anisotropy field (H_A=40 kOe), and moderate Curie temperature (T_c=600 K),[1] which make it highly attractive as a sustainable rare-earth free permanent magnet. However, the metastable behavior of the MnAl $L1_0$-phase promotes the formation of structural defects that degrade its intrinsic magnetic properties such as the local magnetocrystalline anisotropy (MCA). In this work, we study the effects of a partial replacement of Al by Ga on the stability of the $L1_0$-phase, and both the magnetization and the MCA using a first-principles density functional calculation. We find that increasing the Ga content, enhances the phase stability while the total magnetic moment per formula unit (f.u.) remains almost unchanged. The site-, atomic- and spin-resolved MCA has been estimated by evaluating the spin-orbit coupling energy using a second-order perturbation approximation. Structural distortion, chemical effects and different spin components in $Mn(Al_{1-x}Ga_x)$ all contribute to the MCA. The site- and atomic-resolved MCA calculations show that the MCA energy (MAE) mainly comes from the Mn atoms. With increasing Ga content, the MAE at both Mn and Al(Ga) sites increases and the total MAE increases from 0.2 meV/f.u. for x=0 to 0.34 meV/f.u for x=1 (Fig. 1). However, the structural distortion induced by the partial replacement of Al by Ga reduces the MCA. The spin-resolved MCA and band structure calculations indicate that the microscopic origin of high MCA is mainly associated with the spin flipping behavior near the Fermi level, induced by the spin-orbit coupling. The derived effective magnetic anisotropy field increases from 37 kOe (x=0) to 46 kOe (x=1), in agreement with experiments. Doping with Ga improves the stability of the $L1_0$ structure and enhances the magnetic anisotropy field, which facilitates the development of high coercivity Mn-Al based permanent magnets.

1 L Pareti, F. Bolzoni, F. Leccabue, A.E. Ermakov, J. Appl. Phys. 59, 3824 (1986)

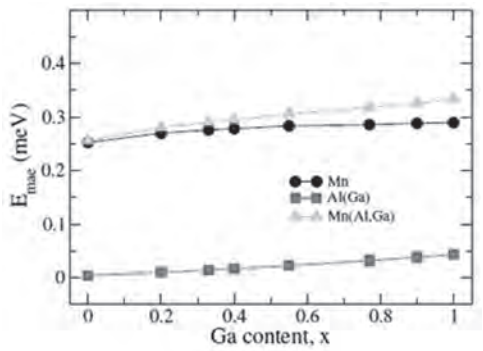

Fig. 1 Dependence of MAE on Ga content, x, in $Mn(Al_{1-x}Ga_x)$.

KPC-06. Controlling Chemical Ordering in $L1_0$-type Permanent Magnet Compounds. *X. Zhang*[1], B. Lejeune[2] and L. Lewis[1,2] *1. Mechanical and Industrial Engineering, Northeastern University, Boston, MA, United States; 2. Chemical Engineering, Northeastern University, Boston, MA, United States*

A high degree of chemical ordering in ferromagnetic $L1_0$-type compounds donates substantial magnetocrystalline anisotropy, making these materials good candidates for next-generation permanent magnets. While it remains highly challenging to obtain the "holy grail" $L1_0$ FeNi compound (*aka* tetrataenite), the analogous proxy system of MnAl provides a good testbed for investigating and identifying factors that control chemical ordering in relevant ferromagnetic systems. To this end, a study of chemical disorder–order transformation in MnAl reveals the consequence of dispersions of chemically ordered nuclei on the ordering kinetics. Structural, magnetic, and calorimetric data confirm attainment of $L1_0$-ordered τ-MnAl upon heating the disordered ε-MnAl phase that is metastably retained in two different forms: rapidly solidified from a molten precursor and water-quenched from a solid precursor. Both sample types consist of nominally phase-pure (> 99 wt.%) disordered ε-phase and a small trace (< 1 wt.%) of chemically ordered τ-phase. Calorimetric data indicate that chemical ordering in the rapidly solidified sample occurs 40 degrees lower than that of the water-quenched one (Fig.1). Analysis of calorimetric data using the Johnson-Mehl-Avrami approach reveals that ordering in the rapidly solidified sample develops from a large density of pre-existing nuclei, presumably with the $L1_0$ structure, while ordering in the water-quenched sample proceeds with a nucleation step that does not heavily rely on pre-existing nuclei. These differences in chemical ordering behavior are attributed to the different number density and varied distribution of quenched-in τ phase nuclei that may be subtly controlled by specific quenching conditions. The results of this work provide insights into controlling phase stabilities and chemical ordering kinetics in other relevant ferromagnetic systems of applied interest as permanent magnets. Acknowledgments: This work was supported by the U.S. Department of Energy, Office of Basic Energy Sciences under Award Number DE SC0022168 and performed at Northeastern University.

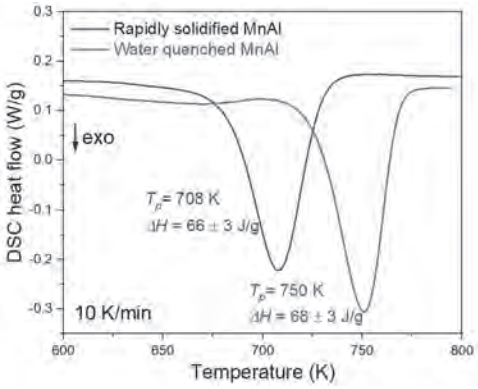

Fig.1. Calorimetric response of rapidly solidified and water-quenched MnAl.

KPC-07. Magnetic ordering in $CeCrGe_3$: magnetization and hyperfine interactions measurements. *B.S. Corrêa*[1], W. Ferrira[1], A.A. Miranda-Filho[1], B. Bosch-Santos[1,2], E. Correa[1,2], G.A. Cabrera-Pasca[3,4] and A.W. Carbonari[1] *1. Instituto de Pesquisas Energéticas e Nucleares - IPEN, São Paulo, Brazil; 2. Material Measurement Laboratory, National Institute of Standards and Technology-NIST, Gaithersburg, MD, United States; 3. Programa de Pós-graduação em Ciência e engenharia de Materiais-PPGCEM, Ananindeua, Brazil; 4. Universidade Federal do Pará, Campus de Abaetetuba, Abaetetuba, Brazil*

Magnetic transitions in the intermetallic compounds $RECrGe_3$ (RE = rare-earth) are intriguing because, despite the presence of RE elements, they are governed by magnetic interactions involving Cr-moments [1-3] and crystallize in the perovskite structure, which is typically found in oxides. The magnetic ordering temperatures of polycrystalline $CeCrGe_3$ were investigated in this study using perturbed angular correlation (PAC) and magnetization measurements. Polycrystalline samples were prepared by arc melting method and, in order, to homogenize and remove the impurity phases, the melted samples were sealed in an evacuated quartz tube and annealed at 900 °C for three weeks. The structural characterization by x-ray diffraction (see Fig. 1), shows that the samples exhibit the hexagonal perovskite structure type (space group $P6_3/mmc$), as previously reported by Das et al [2]. Carrier-free ^{111}In nuclei were introduced into the sample by thermal diffusion at 800 °C for 12 hours, in a sealed quartz tube under a low He atmosphere. PAC measurements were performed in the temperature range from 20 K to 1073 K, the results indicate that this compound have thermic structural stability and exhibit antiferromagnetic followed by a ferromagnetic ordering of Cr-moments when temperature decreases from a range from 70 K to 65 K. Magnetization results shows a ferromagnetic transition of 68 K.

[1] H. Bie, O. Ya. Zelinska, A. V. Tkachuk, A. Mar, *Chem. Mater.,* vol. 135, p.4613 (2007) [2] D. Das, T. Gruner, H. Pfau, U. B. Paramanik, U. Burkhardt, C. Geibel, and Z. Hossain, *J. Phys.: Condens. Matter.,* vol. 26, p.106001 (2014) [3] K. Rana, H. Kotegawa, R.R. Ullah, J.S. Harvey, S.L. Bud'ko, P.C. Canfield, Y. Furukawa, *Physical Review B*, vol. 99(21), p.214417 (2019)

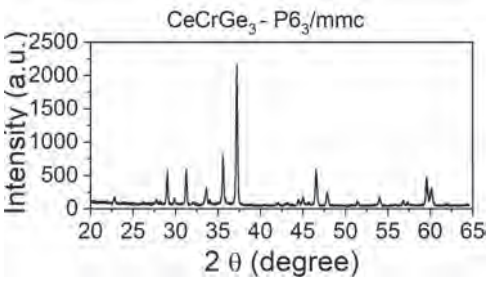

Fig. 1

KPC-08. Effect of Hubbard *U* on Calculations of Magnetic Properties of α″–$Fe_{16}N_2$. *P. Stoeckl*[1], P.W. Swatek[2] and J. Wang[2] *1. Physics, University of Minnesota, Minneapolis, MN, United States; 2. Electrical and Computer Engineering, University of Minnesota, Minneapolis, MN, United States*

The ordered iron nitride phase α″–$Fe_{16}N_2$ has long been a candidate giant saturation magnetization material, but first-principles electronic-structure calculations have struggled to reproduce recent observations of high magnetic moment, while calculations of magnetocrystalline anisotropy (MCA) vary significantly. Within the framework of density-functional theory (DFT), a common extension to the usual generalized-gradient approximation (GGA) exchange-correlation (XC) functional is the inclusion of Hubbard parameters *U* (*J*) as GGA+*U*. A number of previous papers have applied this method to $Fe_{16}N_2$, each with their own choice of Hubbard parameters. The plane-wave DFT code Quantum ESPRESSO was employed to more comprehensively study the effect of the value of Hubbard parameters *U*, *J* on the system, particularly with respect to its magnetic properties. Various approaches for setting *U*, *J* were compared, including self- consistent calculations via the linear-response method.

P. Stoeckl, P. Swatek, & J.-P. Wang, AIP Advances 11(1), 015039 (2021).

KPC-09. Structural and magnetic characterizations of La^{3+} and Li^{1+} co-substituted M-type strontium hexaferrite. C. Kim[2] and *S. Yoon*[1] *1. Department of Physics, Gunsan National University, Gunsan, The Republic of Korea; 2. Department of Physics, Kookmin University, Seoul, The Republic of Korea*

Effects of La^{3+} and Li^{1+} co-substitution on structural and magnetic properties of M-type strontium hexaferrite have been studied by using crystallographic and magnetic measurements. Stoichiometric $Sr_{1-x}La_xFe_{12-x/2}Li_{x/2}O_{19}$ (x=0, 0.25, 0.4, 0.5, and 0.6) samples have been prepared by the conventional ceramic method using La_2O_3, $SrCO_3$, Fe_2O_3, and Li_2CO_3 powders with repeated sinterings at 1250 °C for 24 hours. XRD patterns showed that when $x > 0.6$, $LaFeO_3$, $SrFeO_{3-\delta}$, and other spinel ferrite coexisted along with the M-type hexaferrite. Lattice parameters deduced from the GSAS refinement shows that both *a* and *c* decrease with increasing *x*, but the change in *c* is more outstanding (Table 1). Variations of the saturation magnetization *M*s and the coercivity *H*c with *x* was obtained from room temperature VSM measurement as in Table 1. Whereas the *M*s decreases slightly with *x*, the *H*c increases with the La^{3+} - Li^{1+} co-substitution throughout the doping range examined. Effective magnetic anisotropy constants *K* are calculated as well from the hysteresis curves using the law of approach to saturation method. *K* shows slight decrease with increasing *x* as listed in Table 1. XPS scan shows the Li 1s peak at ~56 eV (Fig. 1(a)). Apparently, monovalent Li^{1+} is non-magnetic. In view of the facts that Li^{1+} in the lithium ferrite ($LiFe_5O_8$) preferentially occupies the octahedral site and that the M-type hexaferrite has the spinel S-block in its structure, the decreasing trend of *M*s with x strongly suggests that Li^{+1} ions preferentially replace Fe^{3+} ions either at 12k or 2a sites (rather than the $4f_2$ site in R-block). Non-magnetic substitution at those sites is known to give rise to negative contribution to *M*s. Finally, Mössbauer spectra show gradual decrease in 2a intensity, in support of the octahedral 2a site preference of Li^{1+} in M-type hexaferrite (Fig. 1(b)).

Table 1.

x	a (Å)	c (Å)	Ms (emu/g)	Hc (Oe)	K (J/m3)
0	5.8838	23.0575	58.6	1520	3.82×10^5
0.25	5.8828	23.0160	58.7	740	3.09×10^5
0.4	5.8825	23.0137	55.9	1080	3.06×10^5
0.5	5.8820	22.9748	55.6	2110	3.01×10^5
0.6	5.8735	22.9651	54.4	1160	2.95×10^5

Table 1. Various structural and magnetic parameters for $Sr_{1-x}La_xFe_{12-x/2}Li_{x/2}O_{19}$ (x=0, 0.25, 0.4, 0.5, and 0.6)

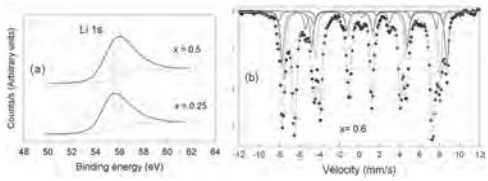

Figure 1. (a) A comparison of Li 1s XPS scan for $Sr_{1-x}La_xFe_{12-x/2}Li_{x/2}O_{19}$ (x=0.25 and 0.5) and (b) ^{57}Fe Mössbauer spectrum for $Sr_{0.4}La_{0.6}Fe_{11.7}Li_{0.3}O_{19}$ taken at room temperature.

Session KPD
HARD MAGNETIC MATERIALS VII: NANOSTRUCTURED, COMPOSITE AND OTHER HARD MAGNETIC MATERIALS (INCLUDING INTERMETALLIC ALLOYS AND L10 ALLOYS)
(Poster Session)

Xin Tang, Chair
NIMS, Tsukuba, Japan

KPD-01. Study on preparation, structure and magnetic properties of high purity Mn_4C. *F. Wang*[1], S. Fan[1], Z. Lin[1], H. Du[1], J. Han[1], W. Yang[1], S. Liu[1], C. Wang[1], Q. Xu[1], Y. Yang[1] and J. Yang[1] *1. Peking University, Beijing, China*

The magnetization of Mn_4C with face centered cubic structure increases with the increase of temperature within a certain temperature range, which means that Mn_4C may be applied to the field requiring high working temperature of magnetic materials through further research and development. Unfortunately, Mn_4C is a metastable phase [1-3], so it is difficult to synthesize high-purity Mn_4C. High-purity Mn_4C powders was prepared by melt spinning, grinding and magnetic separation in this paper. It is found that high cooling rate is beneficial to obtain high-purity Mn_4C material. Moreover, compared with argon gas as the grinding medium, grinding Mn_4C melt-spun strips in alcohol solution is not only conducive to refining the size of the ground particles, but also conducive to improving the dispersion of the particles. Therefore, Mn_4C powders with higher purity can be obtained after magnetic separation (see Fig. 1). The magnetization of Mn_4C powders remained unchanged with the increase of temperature in the range of 2 K -50 K, but increased with the increase of temperature in the range of 50 K to 300 K (see Fig. 2). This may be because there is a spin glass state in Mn_4C powders. At low temperature, the spins are frozen, but the frozen spins are gradually thawed with the increase of temperature. Further investigation is in progress. Crystal and magnetic structure of Mn_4C powders was investigated by variable temperature neutron diffraction technique. The magnetization change of Mn_4C with temperature should be mainly due to its own magnetic phase transition, and is closely related to the antiparallel arrangement of the magnetic moments of Mn atoms at the symmetrical crystal positions 1a and 3c in the Mn_4C lattice. The total magnetic moment of crystal cells increases with the increase of temperature.

1. Si, PZ, Qian, HD, Ge, HL, et al. Applied physics letters, 2018, 112(19):192407. 2. Park , J, Qian, HD, Si, PZ, et al. Journal of magnetism and magnetic materials, 2021, 527:167765. 3. Tagawa, Y and Motizuki, K. Journal of physics-condensed matter, 1991, 3(12): 1753-1761

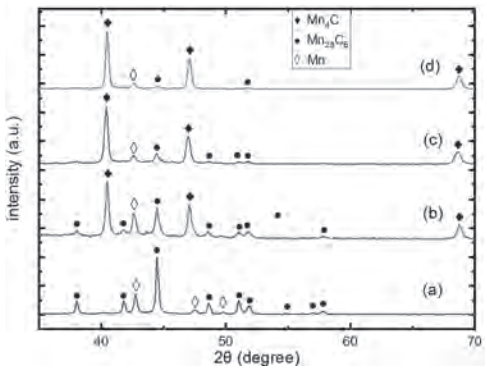

Fig.1 XRD patterns of Mn_4C obtained by (a) arc melting, (b) Suction casting, (c) melt spinning technology (50m/s), and (d) grinding and magnetic separation of the same strips as (c) in alcohol solution. (a) (b) and (c) are both heat treated and ground and magnetically separated in argon.

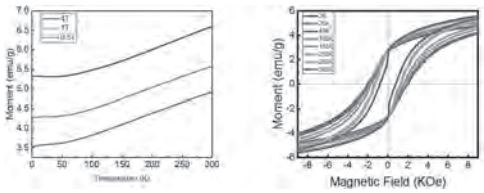

Fig.2 (a) Variation of magnetization of Mn_4C powder with temperature under different magnetic field; (b) Hysteresis loops of Mn_4C powders at 2K-300K

KPD-02. Preparation and orientation control of FeMnS thin films with high saturation magnetization. *R. Hikichi*[1], T. Shima[1] and M. Doi[1] *1. Tohoku Gakuin University, Tagajo, Japan*

Nd-Fe-B sintered magnets possess superior magnetic properties among permanent magnets. Because of this, it is used in a wide range of applications such as speakers, sensors, and motors for hybrid and electric vehicles. However, rare earth (RE) elements, especially heavy rare earth elements such as Tb and Dy are expensive and unevenly distributed. Then, RE-free or less permanent magnet is strongly required. One of the candidate material is Mn-based alloys. Among them, MnGa, MnAl and MnS alloys are expected to become the next generation permanent magnets because of their high magnetocrystalline anisotropy. It has been theoretically reported that MnS compounds possess a high magnetic moment as high as 5 [1]. In addition to that, Mn and S are abundant in the earth's crust, making them inexpensive as a material cost. However, there have been few detailed reports on the crystal structure and magnetic properties of MnS alloys. In this study, the crystal structure and magnetic properties of Fe-doped Fe-Mn-S thin films were investigated in detail, focusing on MnS, which is predicted to have a high magnetic moment. The samples were prepared by using an ultra-high vacuum magnetron sputtering system. A Cr buffer layer of 20 nm was grown on a thermally oxidized Si substrate at room temperature (R.T.). $[Mn\ (t_{Mn})\ /\ (FeS_2)\ (t_{FeS})]_n$ multilayer was deposited at a substrate temperature T_s of 648 ~ 848 K. The total film thickness was fixed at 50 nm. The thicknesses of Mn and FeS layer were t_{Mn} = 0 ~ 12.5 nm and t_{FeS} = 1.875 ~ 50 nm, respectively. The repetition number n was changed from 1 to 20. Then, the samples were annealed at 648 ~ 848 K. Finally, a Cr cover layer of 30 nm was deposited. The peak from α - MnS (200) was clearly observed for Mn/ (FeS_2) thin films and it was confirmed that MnS compound was obtained by alternating lamination. The value of magnetization was increased from 297 to 419 emu/cm^3 with increasing Mn content from 0 to 28.5 at.%. It is confirmed that the formation of the MnS phase increases the saturation magnetization. This results suggests further improvement of magnetic properties.

J. Phys. Soc. Jpn., 25, 82-88, (1968).

KPD-03. Understanding of the Phase Evolution with Temperature in Pure SrM, BaM and CaM. *R. Liu*[1,2], X. Yu[3], L. Wang[2], Z. Xu[2], T. Zhao[3], F. Hu[3] and B. Shen[1] *1. School of Rare Earths, University of Science and Technology of China, Hefei, China; 2. Ganjiang Innovation Academy-,Chinese Academy of Sciences, Ganzhou, China; 3. State Key Laboratory of Magnetism, Institute of Physics,Chinese Academy of Sciences, Beijing, China*

Structural changes and evolution taking place in ferrites with increasing processing temperature are crucial from their performance point of view. Three M-type hexaferrites were prepared using solid-state reaction at 650-1250 °C: $SrFe_{12}O_{19}$ (SrM), $BaFe_{12}O_{19}$ (BaM), and $CaFe_{12}O_{19}$ (CaM). The evolution of phases was studied with X-ray powder diffraction and thermogravimetry investigation. The structural studies reveal that the formation M-type phase begins at 820, 850, and 1200 °C, respectively, and different mid-phases of $SrFe_{3-x}$, $BaFe_2O_4$, and $CaFe_2O_4$ were formed. The structural studies in all cases were successfully refined using the $P6_3/mmc$ (No.194) space group but Ca^{2+} shrank the hexaferrite crystal lattice. Their magnetic properties were studied with respect to their composition and microstructure by scanning electron microscopy (SEM). The different phase evolution leading to the different magnetic properties of M-type hexaferrite were discussed in the present work.

T (°C)	SrM Phase Evolution	BaM Phase Evolution	CaM Phase Evolution
550	$SrCO_3$+α-Fe_2O_3	$BaCO_3$+α-Fe_2O_3	$CaCO_3$+α-Fe_2O_3
650	$SrCO_3$+α-Fe_2O_3	$BaCO_3$+α-Fe_2O_3+$BaFe_2O_4$	$CaCO_3$+α-Fe_2O_3
750	$SrCO_3$+α-Fe_2O_3+$SrFe_xO_{3-x}$	α-Fe_2O_3+$BaFe_2O_4$	$CaCO_3$+α-Fe_2O_3
850	SrM+α-Fe_2O_3+$SrFe_xO_{3-x}$	BaM+α-Fe_2O_3+$BaFe_2O_4$	$CaFe_2O_4$+α-Fe_2O_3
950	SrM+α-Fe_2O_3+$SrFe_xO_{3-x}$	BaM+α-Fe_2O_3	$CaFe_2O_4$+α-Fe_2O_3
1050	SrM+α-Fe_2O_3	BaM+α-Fe_2O_3	$CaFe_2O_4$+α-Fe_2O_3
1150	SrM+α-Fe_2O_3	BaM+α-Fe_2O_3	CaM+$CaFe_2O_4$+α-Fe_2O_3
1250	SrM	BaM	CaM+α-Fe_2O_3

Table 1 The phase evolution with the temperature of SrM, BaM and CaM

KPD-04. Development of Mn based Permanent Magnet Material for Electric Motor. *H. Lee*[1], T. Lee[1], J. Kim[2] and M. Kang[2] *1. R&D Division, Hyundai Motor, Uiwang-Si, The Republic of Korea; 2. Department of Materials Science and Chemical Engineering, Hanyang University, AnSan-Si, The Republic of Korea*

Permanent magnets are an essential material in many electrification technologies, such as electric vehicles and Air mobility. So, Many efforts have paid for enhanced magnetic flux density and robust high temperature for electrification technologies application. As a representative example, efforts are being made to reduce the negative temperature coefficient coercive force and use less rare earth by developing NdFeB magnet. Among the rare-earth-free magnets candidates, MnBi alloy have been regarded as one of the most attractive candidates with promising magnetic properties and the positive temperature coefficient coercivity. The theoretical (BH) max value at room temperature of the LTP MnBi is about 17 MGOe and can reach a high real value of 6.5 MGOe at 400 K. This magnetic performance of the LTP MnBi is can be replace NdFeB magnets in high-temperature magnet applications. This study has been developed based on Density functional theory(DFT) calculation and experimental. First, thermodynamic calculations were used for MnBi lattice modeling to select substitutable elements for Mn and Bi lattice sites, and then DFT calculations were used to predict magnetic moments. The MnBi-X alloy candidate material selected through prediction was manufactured using the melt spinning method. A vibratory sample magnetometer (VSM) was used to evaluate the magnetic properties and a trial and error method was used to finally optimize the MnBi alloy composition. MnBi-Sb magnetic powder has a comparative advantage over ferrite magnets and has the same performance as rare earth bonded magnets. (magnetic flux density 4kG, coercive force 9kOe and coercive force coefficient 0.68~0.91%/K)

1. Yang-Ki Hong, AIP Advances., 3, 052137 (2013) 2. S. Kavita, Journal of Magnetism and Magnetic Materials., Vol. 377, P. 485(2014) 3. C. Curcio, Physics Procedia., Vol. 75, P. 1230 (2015) 4. Sumin Kim, Journal of Alloys and Compounds., vol 708, p1245 (2017) 5. A.M. Gabay, Journal of Alloys and Compounds., vol. 792, p.77 (2019) 6. Truong Xuan Nguyen, Physica B., vol. 552, p.190, (2018)

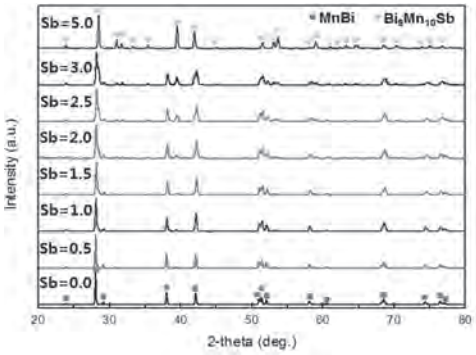

Fig. 1 *X-Ray Diffraction* (*XRD*) data of the Mn-Bi-Sb alloys.

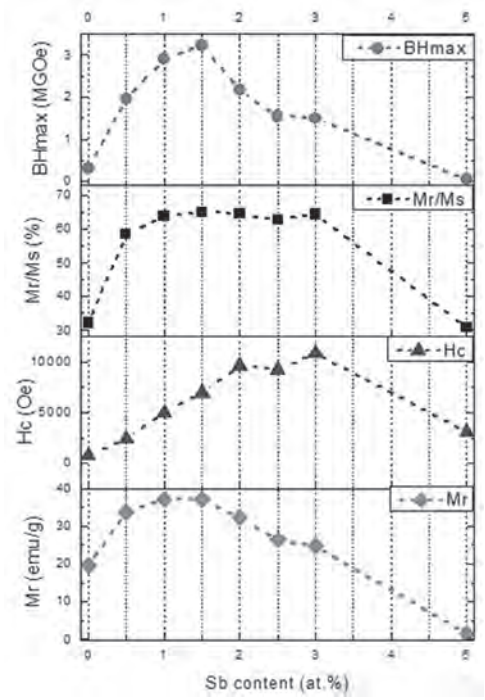

Fig. 2 Analysis of M-H curve in Mn-Bi-Sb alloys.

KPD-05. Withdrawn

KPD-06. Withdrawn

KPD-07. A Study on the Shape of Polar Anisotropic Magnetizing Yoke to Reduce Dead Zone of Ring Magnet. J. Min[1], D. Nam[1], H. Pyo[1], *S. Lee*[1] and W. Kim[1] *1. Department of Electrical Engineering, Gachon University, Seongnam, The Republic of Korea*

Recently, safety window motor has been used to prevent an accident of being caught in vehicle window. This uses the principle that ferrite ring bonded magnet is attached to the bottom of the rotor and the hall sensor detects the magnetic flux to detect the position. The magnetic flux between the N

and S poles of the magnet is very weak, so a dead zone occurs in which the Hall sensor cannot detect the magnetic flux. It is important that this dead zone is small for precise position control. In this study, the shape of polar anisotropic magnetizing yoke with a magnetic flux concentration structure is proposed to reduce the range of the dead zone. The shape of the conventional model and proposed model is shown in Fig. 1. In the case proposed model, by changing the non-magnetic inner pin of the conventional model to a magnetic material, the magnetic flux generated from the magnetizing yoke can penetrate deeply into the ring magnet. And, by inserting a core for concentrating magnetic flux in the magnetizing yoke, the ring magnet can be magnetized by utilizing a higher magnetic flux density compared to the conventional model. Finite element analysis was performed to select the final model that can maximize the magnetic flux at 12.5 degrees, where the dead zone starts. The inner teeth thickness and outer teeth thickness were used as the design parameter. The design parameters of inner and outer teeth thickness were set range of 0mm to 12mm. Through the analysis, the model with an inner teeth thickness of 11mm and an outer teeth thickness of 0mm can concentrate the magnetic flux the most, so it is obtained as a final model. A comparison of the magnitude of the magnetic flux density is shown in Fig. 1. Fig. 2 is a waveform of the air gap magnetic flux density of the proposed model and the conventional model. The proposed model has 23% increase in air gap flux density compared to the conventional model. As a result, dead zone decreased by about 22%. The prototype of the final model was manufactured, and the validity of the analysis result was verified.

S. Wang, D. Peng and Z. Wu, "Embedded Position Detection for Permanent Magnet Synchronous Motor With Built-In Magnets," in *IEEE Sensors Journal*, Vol. 19, p. 9818-9825 (2019) Y. N. Zhilichev and D. Miller, "Hysteresis model and magnetization of a radially anisotropic magnet ring," in *IEEE Transactions on Magnetics*, Vol. 39, p. 2968-2970 (2003) H. Seol, T. Jeong, H. Jun, J. Lee and D. Kang, "Design of 3-Times Magnetizer and Rotor of Spoke-Type PMSM Considering Post-Assembly Magnetization," in *IEEE Transactions on Magnetics*, Vol. 53, p. 1-5 (2017)

Fig. 1. Magnetic flux density distribution of conventional model and proposed model

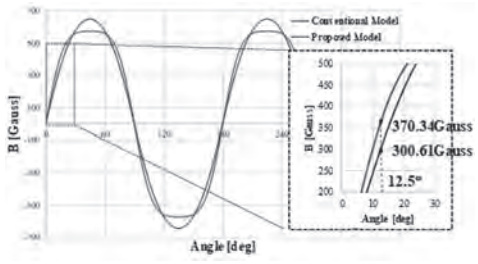

Fig. 2. Magnetic flux density waveform comparison of conventional model and proposed model

KPD-08. Spoke-type Permanent Magnet Synchronous Generator Design for Wind Power Generator Considering Magnetization and Cogging Torque. D. Kim[1], *S. Song*[1], H. Pyo[2], J. Lee[1] and W. Kim[2]
1. Hanyang University, Seoul, The Republic of Korea; 2. Gachon University, Seoungnam, The Republic of Korea

Nowadays, in wind power generator systems, the use of a permanent magnet synchronous generator with high output density is increasing[1-7]. Among them, the magnetization performance of the spoke-type Permanent Magnet Synchronous Generator (PMSG) is low compared to that of the other types of permanent magnet synchronous generators owing to its structural characteristics. Magnetization performance is critical because it is directly related to demagnetization and mass productivity of permanent magnets, and it can cause a reduction in the load performance when non-magnetization occurs owing to low magnetization performance. In addition, an important parameter in the wind turbine is the starting performance, which is affected by the cogging torque of the permanent magnet synchronous generator. This is because lower the cogging torque of the generator, lower is the torque required for starting. Also, the cogging torque affects not only the vibration and noise of the wind turbine, but also the torque ripple. Therefore, in this study, we propose a spoke-type PMSG rotor shape design that considers magnetization and cogging torque. First, the magnetization principle and factors affecting the magnetization performance were analyzed. Based on this, a model with improved magnetization performance was designed as shown in the Fig.1, and in the case of the proposed model, it can be confirmed that the magnetization is well done to the inside of the permanent magnet. In addition, to reduce cogging torque, the advantages and disadvantages of tapering and skew, the existing cogging torque reduction methods, were compared. Afterwards, considering the performance and manufacturability, the cogging torque reduction was confirmed by designing the rotor barrier asymmetrically as shown in the Fig.2, and the performance was compared with the conventional spoke type. Finally, the performance of the proposed model was analyzed through Finite Element Analysis(FEA), and design feasibility was verified by manufacturing and testing prototypes.

[1] K. Ko, S. Jang, J. Park, H. Cho and D. You, "Electromagnetic Performance Analysis of Wind Power Generator With Outer Permanent Magnet Rotor Based on Turbine Characteristics Variation Over Nominal Wind Speed," in IEEE Transactions on Magnetics, vol. 47, no. 10, pp. 3292-3295, Oct. 2011. [2] Y. Gu, Y. Huang, Q. Wu, C. Li, H. Zhao and Y. Zhan, "Isolation and Protection of the Motor-Generator Pair System for Fault Ride-Through of Renewable Energy Generation Systems," in IEEE Access, vol. 8, pp. 13251-13258, 2020. [3] Y. Fang, K. Jia, Z. Yang, Y. Li and T. Bi, "Impact of Inverter-Interfaced Renewable Energy Generators on Distance Protection and an Improved Scheme," in IEEE Transactions on Industrial Electronics, vol. 66, no. 9, pp. 7078-7088, Sept. 2019. [4] M. Hassan Zamani, G. Hossein Riahy and M. Abedi, "Rotor-Speed Stability Improvement of Dual Stator-Winding Induction Generator-Based Wind Farms By Control-Windings Voltage Oriented Control," in IEEE Transactions on Power Electronics, vol. 31, no. 8, pp. 5538-5546, Aug. 2016. [5] X. Yang, D. Patterson and J. Hudgins, "Permanent magnet generator design and control for large wind turbines," 2012 IEEE Power Electronics and Machines in Wind Applications, 2012, pp. 1-5. [6] Yicheng Chen, Pragasen Pillay and A. Khan, "PM wind generator comparison of different topologies," Conference Record of the 2004 IEEE Industry Applications Conference, 2004. 39th IAS Annual Meeting., 2004, pp. 1405-1412 vol.3 [7] Wang Fengxiang, Hou Qingming, Bo Jianlong and Pan Jian, "Study on control system of low speed PM generator direct driven by wind turbine," 2005 International Conference on Electrical Machines and Systems, 2005, pp. 1009-1012 Vol. 2.

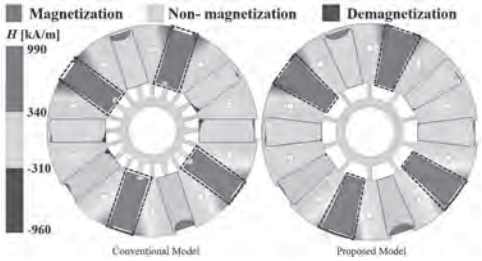

Fig. 1 Comparison of magnetization analysis results

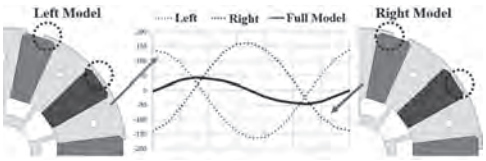

Fig. 2 Comparison of no-load cogging torque of the conventional and proposed models

KPD-09. A Study on Performance Improvement by Reducing Axial Force of Double-layer Spoke-type PMSM with Core Skew Structure. *D. Nam*[1], D. Kim[2], I. Yang[2] and W. Kim[1] *1. Gachon University, Seong-Nam, The Republic of Korea; 2. Hanyang University, Seong-Nam, The Republic of Korea*

Double-Layer Spoke type PMSM can concentrate magnetic flux using a ferrite permanent magnet instead of a rare earth type permanent magnet similar to an conventional spoke type motor. In addition, the conventional spoke type permanent magnet motor did not utilize the reluctance torque properly because the d-axis and q-axis magnetoresistance were not large, but the Double-Layer Spoke type PMSM divides each permanent magnet into two. By inserting an iron core to reduce the q-axis magnetoresistance, the difference with the d-axis magnetoresistance is increased, and a high reluctance torque can be used. However, as the magnetoresistance difference between the d-axis and the q-axis increases, factors, such as cogging torque and torque ripple, increase, which adversely affects the operation of the motor. This will soon cause performance degradation, such as vibration, noise, and poor position and speed control. In order to compensate for this, in general, the method of applying a skew structure is most widely used, but it is also difficult to manufacture and sometimes increases the torque ripple, so it is not a good solution. Therefore, in [1], a study was conducted to improve manufacturability by applying core skew and to reduce cogging torque and torque ripple. In this paper, it was confirmed that the cogging torque, torque ripple in the high-speed operation area, and no-load THD were significantly reduced. However, it was confirmed that this core skew also increases the torque ripple in the low-speed operation area. There are many factors that affect the torque ripple, but as shown in Fig. 1, it can be confirmed that the axial force has some effect on the torque ripple. In addition, the axial force continuously transmits a mechanical load to the bearing connected to the motor, causing vibration and noise, and shortening the life of the motor. Since the target model of this paper uses sensorless control, the torque ripple that affects the back electromotive force used for detection must be reduced. In this paper, a symmetrical core skew shape is proposed to reduce axial force. The model specifications are shown in Fig. 2.

[1] D. -W. Nam, K. -B. Lee, and W. -H. Kim, "A study on core skew considering manufacturability of double-layer spoke-type PMSM," *Energies 2021,* 14, 610, Jan. 2021.

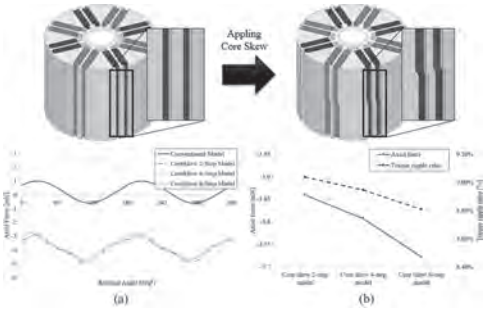

Fig.1 Existing Core Skew Model Diagram and Axial Force of Core Skew Model

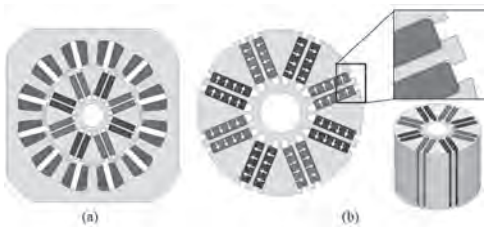

Fig.2 Conventional Model

KPD-10. Design for minimizing irreversible demagnetization based on the back EMF contribution of a Dy-free magnet. *S. Song*[1], H. Pyo[2], D. Nam[2], J. Lee[1] and W. Kim[2] *1. Department of Electrical Engineering, Hanyang University, Seoul, The Republic of Korea; 2. Department of Electrical Engineering, Gachon University, Seongnam, The Republic of Korea*

In this paper, a process for minimizing irreversible demagnetization by using permanent magnets completely devoid of rare earth, maintaining equivalent performance, and compensating for low coercive force is proposed. The design process for irreversible demagnetization minimization is illustrated in Fig. 1. For the given process, several rotor parameters are changed to determine its shape initially. In other words, after determining the rotor shape (bar type, V-shaped type, or spoke type), the performance and irreversible demagnetization ratio are analyzed. If the target performance is not met or the irreversible demagnetization ratio is not reduced, the rotor shape must be redesigned. If the target performance is satisfied, the back EMF(electromotive force) contribution of the magnet is analyzed. The analysis is performed using the flux linkage equation, which does not change with time. This is because the back EMF of the magnet changes depending on the rotor position when it changes with time. After analyzing the back EMF according to the position of the magnet, a design is carried out to shift the region where irreversible demagnetization occurs. That is, the position where irreversible demagnetization occurs is shifted to the side where the back EMF contribution of the magnet is low. This is because even if irreversible demagnetization occurs in the same range, the irreversible demagnetization ratio is reduced. Next, the barriers and bridges are redesigned. If the target performance is satisfied, the process continues. However, if it is not satisfied or the irreversible demagnetization ratio is not reduced, the barrier and bridge should be redesigned. Then, an air hole is inserted into the pole piece in front of the region where irreversible demagnetization occurs. By inserting an air hole, the irreversible demagnetization area is reduced, and it is moved to a part with a low contribution to the back EMF. The following process was performed to reduce irreversible demagnetization

[1] T. H. Kim, H. W. Lee, and S. S. Kwak, "The internal fault analysis of brushless DC motors based on the winding function theory," IEEE Trans. Magn., vol. 45, no. 5, pp. 2090-2096, May 2009.

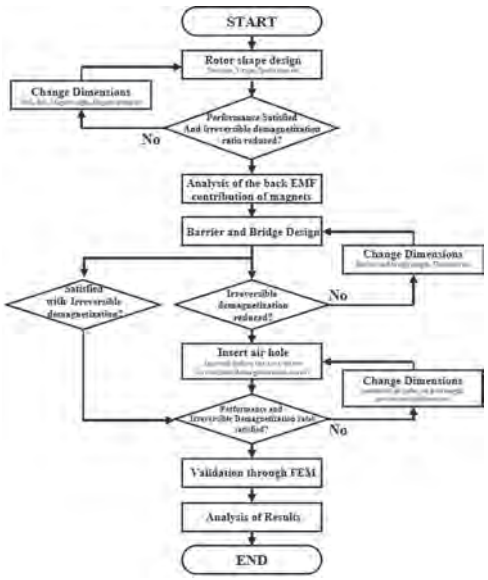

Fig. 1 Rotor design to minimize irreversible demagnetization.

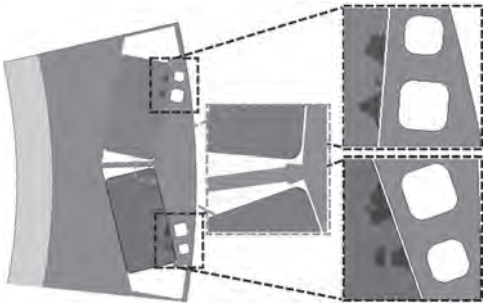

Fig. 2 Irreversible demagnetization area of final model

KPD-11. A Study on Improving Post-assembly Magnetization Performance of Spoke-type Permanent Magnet Synchronous Motor.

M. Jeong[1], S. Song[1], H. Pyo[1], D. Kim[1] and W. Kim[1] *1. Gachon University, Seongnam-si, The Republic of Korea*

In the process of manufacturing a permanent magnet motor, magnetization of a permanent magnet is essential. Permanent magnet magnetization methods include single product magnetization and post-assembly magnetization. single product magnetization is a method of magnetizing individual or multiple magnets, and since a magnetizing magnetic field is directly applied to the magnet, complete magnetization is possible. However the single product magnetization method is not suitable for mass production. And the problems of single product magnetization described above, a method of magnetizing after assembling a permanent magnet to a rotor is widely used. The post-assembly magnetization method is a method of applying a magnetized magnetic field after inserting an unmagnetized magnet into the rotor. Since an unmagnetized magnet is inserted into the rotor before magnetization, there are no difficulties and tolerances in assembly due to attraction force. Therefore, many magnetization companies currently use the magnetization method after assembly. However, the above method is difficult to apply to all permanent magnet motors. For example, Spoke-type PMSM, the permanent magnets are arranged in the radial direction in the rotor, so the magnetic field is divided in half and flows during magnetization. That is, only half of the magnetizing magnetic field is applied to the permanent magnet, so the magnetization performance is greatly degraded. Also, during magnetization, the magnetic flux does not reach the permanent magnet located inside the rotor due to magnetic saturation of the pole piece of the rotor. Spoke types are motors that are in the spotlight as motors that use non-rare earth to generate high magnetic energy. However, because of a fact that it is not fully magnetized during magnetization, there are restrictions on its use, so research is needed to solve this. Therefore, in this paper, a study was conducted on magnetization method to improve the magnetization performance of the spoke type motor.

[1] H. Seol, T. Jeong, H. Jun, J. Lee and D. Kang, "Design of 3-Times Magnetizer and Rotor of Spoke-Type PMSM Considering Post-Assembly Magnetization," in IEEE Transactions on Magnetics, vol. 53, no. 11, pp. 1-5, Nov. 2017 [2] S. G. Lee, J. Bae and W. Kim, "Design Process of Spoke-Type Permanent Magnet Synchronous Motor Considering Magnetization Performance," in *IEEE Transactions on Applied Superconductivity*, vol. 30, no. 4, pp. 1-6, June 2020 [3] S. G. Lee, J. Bae and W. -H. Kim, "A Study on the Maximum Flux Linkage and the Goodness Factor for the Spoke-Type PMSM," in IEEE Transactions on Applied Superconductivity, vol. 28, no. 3, pp. 1-5, April 2018

Session LOA
THIN FILMS AND PATTERNED STRUCTURES

Franca Albertini, Chair
Institute of Materials for Electronics and Magnetism, National Research Council, Parma, Italy

CONTRIBUTED PAPERS

LOA-01. Direct Observation of Magnetic Ordering in Artificial Rhombus Spin Ice. *T.R. Cote*[1,2], C. Phatak[1,2] and A. Petford-Long[1,2] *1. Materials Science Division, Argonne National Laboratory, Lemont, IL, United States; 2. Materials Science & Engineering, Northwestern University, Evanston, IL, United States*

Artificial spin ice ices (ASIs) are two-dimensional arrays of Ising-like nanomagnets that exhibit magnetic frustration, giving rise to emergent phenomena and novel magnetic states[1,2]. Current efforts have studied the behavior of disordered ASI systems[3,4], and recently have shown spin glass behavior. Here we report a systematic approach to studying disordered ASIs generated from rhombus tilings. Each rhombus ASI (R-ASI) is constructed using unique combinations of only five vertex motifs, allowing great tunability of magnetic frustration. We studied five geometries, ranging from periodic to random (Figure 1a), of cobalt R-ASIs fabricated using electron beam-induced deposition. The magnetization states of the ASI arrays were obtained by imaging with Lorentz transmission electron microscopy (LTEM) and reconstructing the projected magnetic induction map. Two states were investigated: the as-grown state and a rotationally demagnetized state. Phase reconstruction showed extended ferromagnetic ordering in chains of nearest neighbor islands (Figure 1b). This ordering occurred across all R-ASIs, but the underlying geometry and additional competing interactions altered the domain behavior. To understand the energy landscape of the R-ASI, micromagnetic simulations were used to estimate the energies of the unique magnetic configurations for each vertex motif. This allowed a quantitative comparison of the energy of magnetization states at the local scale between vertices and at the global scale between ASI geometries. We observed a reduced effectiveness of demagnetization in lowering the energy of the random R-ASI compared to periodic geometries. Progressively disordered geometries introduce further vertex frustration where not all vertices can enter their lowest energy configuration. However, we observe that specific vertices and vertex-pairs form trap states in the energetic landscape, mediating higher energy excitations.

[1] A Farhan, A Scholl, and S van Dijken *et al*., Nature Communications, 7. 12635 (2016). [2] M Morrison, T Nelson, and C Nisoli, New Journal of Physics, 15. 045009 (2013). [3] M Saccone, A Scholl, and A Farhan, *et al*., Physical Review B, 99. 224403 (2019). [4] M Saccone, F Caravelli, and A Farhan, *et al*., Nature Physics, 18. 517-521 (2022). [5] This work was supported by the U.S. Department of Energy, Office of Science, Office of Basic Energy Science, Materials Sciences and Engineering Division.

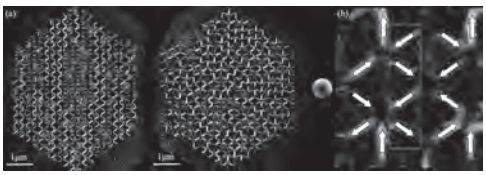

Fig. 1: (a) Reconstructed magnetic induction maps of the demagnetized state for a (left) periodic and (right) random Co R-ASI. (b) Magnified region of the random geometry showing an extended chain of ferromagnetically coupled islands observed in each ASI geometry.

LOA-02. Study of field-orientation dependent logic for bi-material L-shape patterned structures. *R. An*[1,2], C.H. Leow[1,2], B. Myint[1,2] and V. Ng[1,2] *1. Information Storage Materials Laboratory, National University of Singapore, Singapore; 2. Department of Electrical and Computer Engineering, National University of Singapore, Singapore*

Achieving Boolean logic via shape anisotropy is not a foreign concept and the usage of fringe field-based interactions between single-domain nanomagnets has been explored [1-2]. However, bi-material ASI systems to fulfil two-input Boolean logic has not been reported. We are motivated to explore field-orientation-dependent logic-based reversal on bi-material structures. Co and Py nano-trapezoids orientated at 90° were fabricated via self-aligned stepwise nanosphere lithography [3] forming L-shape structures. Field-orientation dependent magnetization reversal studies were conducted via MFM by applying magnetic field at different angles and values. Fig.1(a) shows the AFM image while Fig.1(b-e) show the remnant magnetic domain images after applying a saturation field of 3 kOe at various field angles. Different configurations of Co (red) and Py (blue) can be defined as logic 0 or 1, as shown in Fig.2(a). The configurations can be divided into four stable and repeatable states ‘00’, ‘10’, ‘11’, ‘01’ which agree well with MFM in Fig.1(b-c) respectively. All the conceivable states vs various orientations are shown in Fig.2(b). The one-in-one-out configuration, which can be attained when the structures are magnetized along the geometrical easy axis for each component, was found to be the most stable [4]. By setting this as logic 0 and others as logic 1, each L-shape can be considered as a two-input XOR gate. Under various external field values and orientation, the magnetic switching behavior of bi-material L-shape structures will be explored by MFM and compared to OOMMF [5] simulation results. Our preliminary simulations show that the bi-material system exhibits three stable states which can be set as logic 0 and 1 whereas the pure material system only produced two stable states which can only be set as logic 0. We will explore how the bi-material system can be exploited to fulfil other logic functions.

[1] Kurtz S, Varga E, Siddiq M J, et al. Journal of Physics: Condensed Matter, 2011, 23(5): 053202. [2] F. S. Ma, V. L. Zhang, Z. K. Wang, et al. Journal of Applied Physics 108, 053909 (2010). [3] B. Myint, D. Yap and V. Ng, Nano Express, vol. 1, no. 2, p. 020029, 2020. [4] Schiffer P, Nisoli C. Applied Physics Letters, 2021, 118(11): 110501. [5] M. J. Donahue and D. G. Porter, OOMMF User’s Guide, Version 1.0 Interagency Report NISTIR 6376 (1999).

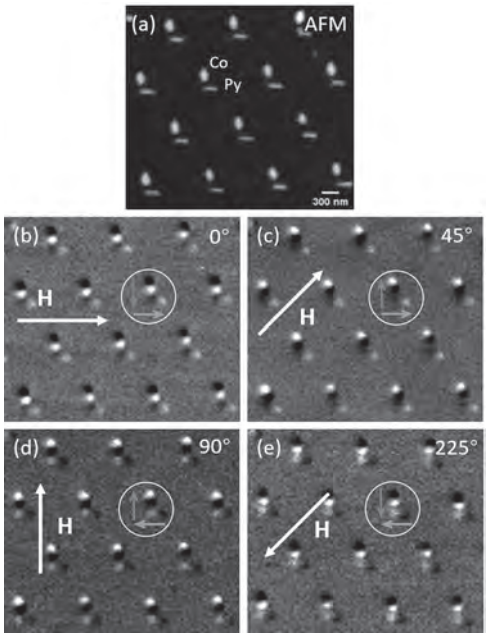

Fig.1(a)AFM image;(b-e)Remnant MFM magnetic domain images of Co-Py L-shape at 3 kOe for different field-angles:(b)0°;(c)45°; (d)90°;(e)225°

(a)

	Permalloy (Py)		Cobalt (Co)	
Direction	→	←	↓	↑
States	0	1	0	1

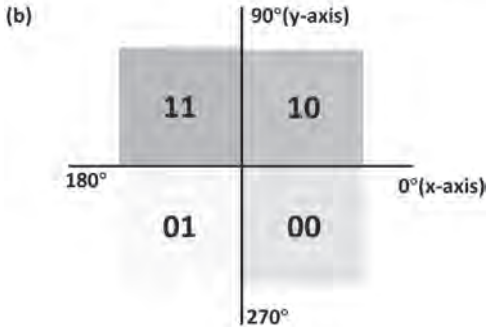

Fig.2(a) Definition of logic states;(b) Conceivable states based on field-angles

LOA-03. Effects of thermal fluctuations within and among the magnetic textures in artificial spin ice. *S. Slöetjes*[1], B. Skovdal[1], M. Pohlit[1], H. Stopfel[1], B. Hjörvarsson[1] and V. Kapaklis[1] *1. Department of Physics and Astronomy, Uppsala University, Uppsala, Sweden*

Artificial spin ice lattices consist of extended arrays of dipole coupled nanomagnets. This relatively simple system has seen a striking amount of applications, such as mimicking spin frustration, reconfigurable magnonic crystals, and in the last years it displayed potential for novel forms of computation. We have recently investigated the effects of the internal texture of these nanomagnets, specifically the thermal behavior, and found the excitation of magnons, and additional fluctuations at the ends of the nanomagnet. These effects offer a different view of the effect of temperature on the magnetism than the traditional flipping of the Ising spin. Here, we present measurements using AC susceptibility and temperature dependent MOKE of artificial spin ice structures, which indicate the presence of these additional texture fluctuations. It is shown that, even though they exist on a different length scale than the binary switch of the internal magnetization, both types of fluctuations can be tuned through the interaction strength of the mesospins. In addition, we present a detailed simulation study that shows the effects of coupling of these texture fluctuations across a gap, both in a double magnet configuration and an ASI vertex, and capture these fluctuations in energy landscapes. We determine the energy barriers, eigenmodes, and curvatures of the energy landscapes at the metastable minima and relate them to the attempt frequencies of the system. These investigations of the internal texture could lead to a rethinking of the artificial spin ice lattice, in which case the internal textures could be used to mimic magnetic effects on different length scales.

[1] Slöetjes, S. D., Hjörvarsson, B., Kapaklis, V., Appl. Phys. Lett. 118, 142407 (2021); [2] Skovdal, B. E., Slöetjes, S. D., Pohlit, M., Stopfel, H., Kapaklis, V., & Hjörvarsson, B. (2022). *arXiv:2205.00938*. [3] Slöetjes, S. D., Hjörvarsson, B., Kapaklis, V., *manuscript in preparation*

LOA-04. Development of Dy μ-disks for coherent imaging of helimagnetic domains. I. de Moraes[1], G. Beutier[2], L. Badie[3], D. Wermeille[4] and *K. Dumesnil*[3] *1. CEA, Grenoble, France; 2. SIMAP, Grenoble, France; 3. IJL, Nancy, France; 4. ESRF, Grenoble, France*

Non-collinear antiferromagnetic orders are of strong interest in the fields of spintronic, topological magnetism and multiferroicity [1]. However, the magnetic imaging of these materials is particularly challenging due to their zero net magnetization. The main goal of this work is to achieve the fully vectorial reconstruction of a non-collinear magnetic order, by the combination of Resonant X-ray Magnetic Scattering (RXMS) [2] and Coherent Diffraction Imaging (CDI) [3]. Dy epitaxial films exhibiting an antiferromagnetic helical phase and strong X-ray magnetic scattering at the Dy L_3 edge [4] are interesting candidates. The micro-patterning of Dy nanofilms (top-down approach) is required to synthetize model micro-objects and to efficiently implement this technique. We present the results of the microfabrication process and the full structural and magnetic characterization of the Dy μ-disks. The high crystalline quality of the Dy(0001) epitaxial films is maintained after the optical lithography and Ion Beam Etching. X-ray diffraction (Fig.1) indicates moderate decrease in the coherence length (10%) and increase in mosaïcity (17%) in 2mm diameter disks compared with continuous films. A fcc phase however tends to form, most likely due to hydrogenation during the patterning process. SQUID measurements and Resonant X-Ray Magnetic Scattering (BM28-ESRF) confirm the occurrence of the helical phase in the Dy μ-disks, with similar Néel and Curie temperatures as in continuous films. (002-t) magnetic satellites reveal that helical turn angles in the patterned samples do not differ significantly from those observed in epitaxial films [5] (Fig. 2). The role of the buffer layer (Nb or Nb/Y) on the crystal quality and the presence of crystalline defects is also carefully investigated, since structural speckles in CDI have to be avoided for measurements and proper analysis of the magnetic contributions.

[1] S.-W. Cheong, M. Fiebig, W. Wu, L. Chapon, V. Kiryukhin, Seeing is believing: visualization of antiferromagnetic domains, Npj Quantum Mater. 5 (2020) 3. https://doi.org/10.1038/s41535-019-0204-x. [2] L. Paolasini, F. de Bergevin, Magnetic and resonant X-ray scattering investigations of strongly correlated electron systems, Cr Phys. 9 (2008) 550–569. https://doi.org/10.1016/j.crhy.2007.06.005.. [3] J. Miao, T. Ishikawa, I.K. Robinson, M.M. Murnane, Science. 348 (2015) 530–535. https://doi.org/10.1126/science.aaa1394 [4] K. Dumesnil, C. Dufour, Ph. Mangin, G. Marchal, Magnetostrictive model for the determination of the energy diagram of dysprosium epitaxial films, Phys Rev B. 53 (1996) 11218–11221. https://doi.org/10.1103/physrevb.53.11218. [5] K. Dumesnil, A. Stunault, Ph. Mangin, C. Vettier, D. Wermeille, N. Bernhoeft, S. Langridge, C. Dufour, G. Marchal, Resonant magnetic x-ray studies of magnetic ordering in dysprosium layers, Phys Rev B. 58 (1998) 3172–3179. https://doi.org/10.1103/physrevb.58.3172.

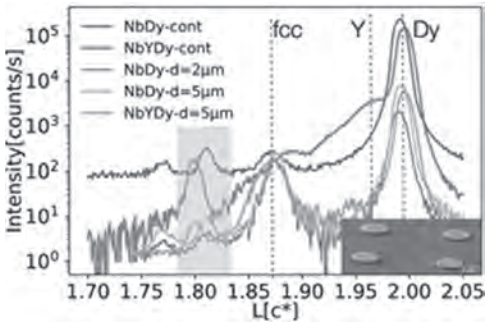

Fig.1: RXMS (0 0 L) scans at the Dy L_3 edge measured for Nb/Dy (green), Nb/Y/Dy (orange) and their respective μ-disks at 130 K. Grey region indicates the magnetic satellites. Insert: SEM tilted view of Dy μ-disks

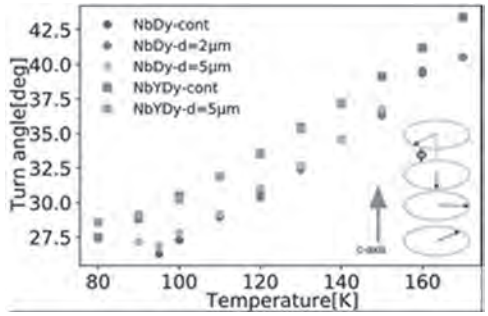

Fig. 2: Turn angle of the Dy helical phase as function of temperature (same samples as in Fig.1).

LOA-05. Imaging thermally-induced Ising-vortex transformations in $La_{0.7}Sr_{0.3}MnO_3$-based artificial spin ices. *D.Y. Sasaki*[1], M. Feng[1], I. Nihal[1], S.T. Retterer[2], A. Scholl[3], R. Chopdekar[3] and Y. Takamura[1]
1. Materials Science and Engineering, University of California, Davis, Davis, CA, United States; 2. Center for Nanophase Materials Sciences, Oak Ridge National Laboratory, Oak Ridge, TN, United States; 3. Advanced Light Source, Lawrence Berkeley National Laboratory, Berkeley, CA, United States

Artificial spin ices (ASIs) are arrays of Ising-like magnetic nanoislands that are of interest for investigating fundamental physics as well as designing information processing devices. Recent efforts have pushed ASIs beyond the Ising model by using systems capable of possessing both Ising and complex spin textures (CSTs) such as vortices, which alters the nature of dipolar coupling and gives rise to exotic physics in existing ASI lattices [1-3]. CST-Ising studies in metal-based ASIs have primarily focused on field-dependent properties, as temperature-dependent experiments present challenges for metal-based systems. However, we have found that ASIs fabricated from the epitaxial complex oxide La0.7Sr0.3MnO3 (LSMO) can facilitate studies of CST-Ising formations in thermally active ASIs. CST-Ising formations in thermalized LSMO ASIs occurs through a careful balance of inter- and intra-island energetics enabled by the LSMO magnetic parameters [1]. Using x-ray photoemission electron microscopy (XPEEM) to perform magnetic domain imaging, we studied the thermal evolution of ex situ magnetized LSMO-based brickwork ASIs using a series of short (~5 min) annealing steps at 350 K (near LSMO bulk Tc ~ 370 K). We observed that the spin texture evolution can be tuned through the ASI lattice parameter, a. While ASIs with a = 600 nm formed only Ising states and experienced a few spin flips (~1 % of nanoislands) between annealing steps, ~20% of initially Ising nanoislands transformed into CSTs after the first annealing step for ASIs with a = 638 nm. Furthermore, we observed that thermal fluctuations in nanoisland domain states can occur through several different routes including Ising spin flips and transformations in magnetization topology (i.e., Ising-to-CST, CST-to-Ising, and CST-to-CST states). These results suggest the potential to introduce exotic kinetics in existing ASI lattices and would provide further insights into designing magnetically-reconfigurable computing architectures.

[1] D. Y. Sasaki et al., Phys. Rev. Appl., in press (2022) [2] J. C. Gartside et al., Nat. Nanotechnol., 17, 460-469 (2022) [3] A. Talaparta et al., Phys. Rev. Appl., 13, 014034 (2020)

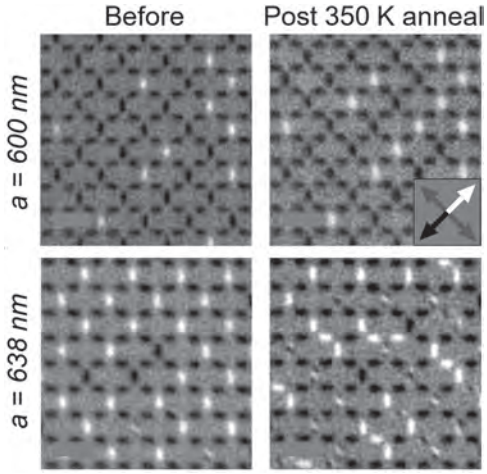

Fig. 1: XPEEM magnetic contrast images of LSMO-based ASIs before and after a 5 minute anneal. Magnetization direction is indicated on the inset. CSTs appear as double and triple domains with alternating dark/bright contrast. Scale bars are 1 μm.

LOA-06. Structural and Magnetic Properties of Pt/Co/Mn Multilayers. *M. Lonsky*[1,2], M. Yoo[1], Y. Huang[1], J. Qian[1], J. Zuo[1] and A. Hoffmann[1]
1. Department of Materials Science and Engineering, University of Illinois at Urbana-Champaign, Urbana, IL, United States; 2. Department of Physics, Goethe-University Frankfurt, Frankfurt, Germany

Magnetic multilayers constitute a rich class of material systems with a number of precisely tunable parameters (e.g., layer thickness and repeat number) that determine both their magnetic and electronic properties [1]. We present a comprehensive characterization of structural and magnetic properties of the novel system Pt/Co/Mn, which extends the group of Pt/Co/*X* (*X* = metal) multilayers that have been investigated thus far. The structural properties of the sputter-deposited Pt/Co/Mn stacks were determined from X-ray reflectometry and scanning transmission electron microscopy experiments. Subsequently, we performed magnetometry measurements in order to study hysteresis loops as a function of varying layer thickness values. We demonstrate that an increasing Co layer thickness changes the magnetic anisotropy from out of plane to in plane, whereas the deposition of thicker Mn layers leads to a decrease in the saturation magnetization, see Fig. 1. Temperature-dependent magnetometry measurements reinforce the hypothesis of antiferromagnetic coupling at the Co/Mn interfaces being responsible for the observed Mn thickness dependence of the magnetization reversal. Moreover, magneto-optical imaging experiments indicate systematic changes in magnetic domain patterns as a function of the Co and Mn layer thickness and suggest the existence of bubblelike domains—potentially even magnetic skyrmions—in the case of sufficiently thick Mn layers, which are expected to contribute to a sizable Dzyaloshinskii-Moriya interaction in the multilayer stacks. We identify Pt/Co/Mn as a highly complex multilayer system with strong potential for further fundamental studies and possible applications [2]. This work is supported by the Deutsche Forschungsgemeinschaft (DFG) through the research fellowship LO 2584/1-1, the NSF through I-MRSEC Grant No. DMR-1720633 and US DOE, Office of Science, MSED under Contract No. DE-SC002260.

[1] I. K. Schuller *et al.*, J. Magn. Magn. Mater. 200, 571 (1999) [2] M. Lonsky *et al.*, Phys. Rev. Materials 6, 054413 (2022)

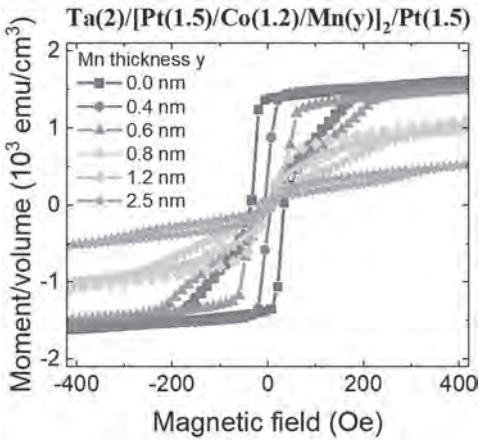

Fig. 1. Hysteresis loops of $[Pt/Co/Mn]_2$ samples at room temperature for varying Mn layer thickness values. Antiferromagnetic coupling introduced by Mn leads to a reduced magnetic moment.

LOA-07. Tunable in-plane chirality via Interlayer DMI interactions in Synthetic Anti-Ferromagnets. *M.A. Cascales Sandoval*[1], A. Hierro-Rodríguez[2,1], C. Donnelly[3], S. Ruiz Gómez[3,4], M. Niño[4], M. Foerster[4], D. McGrouther[1], E.Y. Vedmedenko[5], C. Leveille[6], N. Jaouen[6], S. Flewett[7] and A. Fernández-Pacheco[8,1] *1. University of Glasgow, Glasgow, United Kingdom; 2. Universidad de Oviedo, Oviedo, Spain; 3. Max Planck Institute for Chemical Physics of Solids, Dresden, Germany; 4. ALBA Synchrotron, Cerdanyola del Vallés, Spain; 5. Institute of Applied Physics, University of Hamburg, Hamburg, Germany; 6. SOLEIL Synchrotron, Gif-Sur-Yvette, France; 7. Pontificia Universidad Católica de Chile, Santiago, Chile; 8. Instituto de Nanociencia y Materiales de Aragón CSIC, Zaragoza, Spain*

Interlayer DMI (IL-DMI) has been recently predicted and observed in multilayer thin film heterostructures[1-3], coupling two neighboring magnetic films via a non-magnetic interlayer in a chiral fashion. IL-DMI could be utilized to obtain complex chiral magnetic states in one layer, controlled by the magnetic configuration of a neighboring layer, of great interest to spintronic applications. Previous work using magnetometry techniques indicates the existence of non-zero IL-DMI in Synthetic Antiferromagnetic (SAF) bilayers with highly asymmetric properties; one layer close to the spin reorientation transition, and the other fully out-of-plane. In these systems, IL-DMI is manifested as a chiral exchange bias under in-plane magnetic fields. In this contribution, we further investigate these systems via a combination of X-ray magnetic scattering and imaging techniques, revealing the presence of periodic chiral magnetic structures. In particular, X-ray Magnetic Circular Dichroism Photo Electron Emission Microscopy (XMCD-PEEM) measurements evidence the formation of ring-like structures of sizes after applying a field cycling protocol (Fig. 1). In order to understand more in detail the magnetic configuration of these textures, we reconstruct the spatially resolved magnetization vector by combining different relative sample-beam XMCD projections, yielding the presence of 360 degree domain walls separating the outer and inner domains. During the presentation, we will discuss in detail the role that IL-DMI and other magnetic interactions play in the formation and shape of these rings.

[1] E.Vedmedenko, P. Riego and J. Ander, Phys. Rev. Lett. 122, 257202 (2019) [2] A. Fernández-Pacheco, E. Vedmedenko and F. Ummelen, Nature Materials, 18, 679-684 (2019) [3] H. Dong-Soo, K. Lee and J.P. Hanke, Nature Materials, 18, 703-708 (2019)

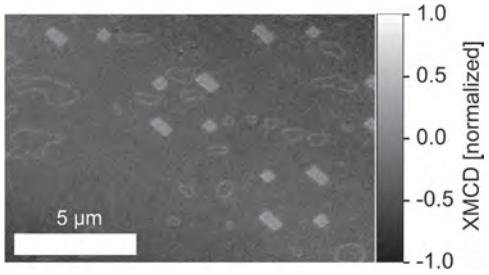

Fig. 1: XMCD-PEEM image showing ring structures. Square structures consist of Pt deposits serving as reference non-magnetic marks.

LOA-08. Strong Bulk Spin-orbit Torque Effect Enabled by Microstructural Disordering. *Y. Huang*[1], H. Chen[1], J. Lin[2], Y. Huang[2] and Y. Tseng[1] *1. National Yang Ming Chiao Tung University, Hsin-Chu, Taiwan; 2. National Synchrotron Radiation Research Center, Hsin-Chu, Taiwan*

Self-spin-orbit torque (SOT) that arises from within the ferromagnetic layer itself, such as FePt [1] and CoPt [2] systems, offers new design possibilities for the SOT devices. Unlike FePt's self-SOT that relies on chemical ordering and apparent global symmetry breaking, CoPt was found to possess rather robust self-SOT with A1-disorder phase. This kind of bulk-SOT which does not rely on the apparent symmetry-breaking attracted our attention. A question arises as to whether the bulk-SOT generated by the structural disorder is comparable to that generated by apparent symmetry-breaking such as composition gradient and interface cutting? This study investigates the microstructural ordering effects on the CoPt's self-SOT phenomena using orientation-resolved synchrotron x-ray diffraction. Three samples, (i)Ta/CoPt (20nm)/Ta (denoted as baseline-CuPt); (ii) Ta/$[Co(0.5nm)/Pt(0.5nm)]_{20}$/Ta (denoted as superlattice-CoPt); (iii) Ta/Cu(2nm)/CoPt(20nm)/Cu(2nm)/Ta (denoted as Cu-CoPt), were investigated. All three samples were determined to possess the A1 phase with close ρ_{xx} (≈ 55 μΩ●cm) under the Hall device structure. The baseline-sample possessed a (111)-textured A1-phase microstructure, and it yielded a damping-like torque efficiency ε_{DT}=0.174±0.037. This value is close to that reported in the representative literature of CoPt self-SOT [2]. A similar microstructure, while with an enhanced ε_{DT}=0.636±0.0333, was obtained in the superlattice sample due to the multi-interface symmetry-breaking effects. However, we found that the microstructure appeared to contain randomly-oriented grains in the Cu-CoPt sample, and this resulted in ε_{DT}=0.502±0.089. The results imply that the short-range symmetry-breaking could contribute to the SOT in a level close to that achieved by the apparent symmetry-breaking.

[1] M. Tang, K. Shen, S. Xu, H. Yang, S. Hu, W. Lü, C. Li, M. Li, Z. Yuan, S.J. Pennycook, K. Xia, A. Manchon, S. Zhou, and X. Qiu, Advanced Materials 32, 2002607 (2020). [2] L. Zhu, X.S. Zhang, D.A. Muller, D.C. Ralph, and R.A. Buhrman, Advanced Functional Materials 30, 2005201 (2020).

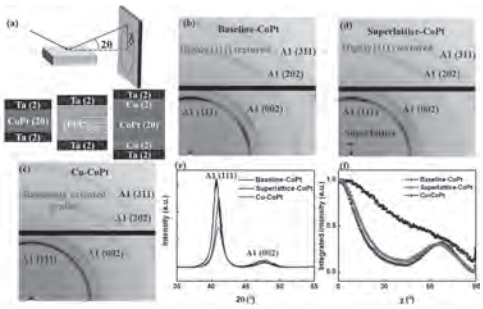

Figure 1. (a) Schematic illustration of 2D-XRD setup and film stackings of the three investigated samples. (b), (c) and (d) show the integrated 2D Laue diffraction patterns taken along the out-of-plane film direction of the baseline-CoPt, superlattice CoPt and Cu-CoPt samples, respectively. (e) converted θ-2θ scan converted from the 2D diffraction patterns; (f) χ scans specifically converted from the (111) diffraction rim.

LOA-09. The impact of the Fe layer thickness on the interlayer exchange coupling in $[Fe/MgO]_N$ (100) superlattices. *A.L. Ravensburg*[1], G.K. Pálsson[1], V. Ukleev[2], J. Stahn[3], B. Hjörvarsson[1], A. Vorobiev[4] and V. Kapaklis[1] *1. Physics and Astronomy, Uppsala University, Uppsala, Sweden; 2. Spin and Topology in Quantum Materials, Helmholtz-Zentrum Berlin for Materials and Energy, Berlin, Germany; 3. Paul Scherrer Institut, Villigen, Switzerland; 4. Institut Laue-Langevin, Grenoble, France*

We report on how the interlayer exchange coupling in Fe/MgO superlattices changes with Fe layer thickness. It has been shown previously that the thickness of the MgO spacer layer and the number of bilayer repetitions influence the coupling strength and magnetic order across the superlattice layers [1,2], with the influence of the Fe layer thickness not been investigated so far. Distinct plateaus for the magnetization in the hysteresis loops, attributed to layer-by-layer switching, are observed for applied fields along the Fe magnetic easy axis, but also for the first time for applied fields along the Fe magnetic hard axis, attributed to the improved crystal quality of the samples in this study. Using a combination of longitudinal magneto-optical Kerr effect measurements and polarized neutron reflectometry, the direction of magnetization in each Fe layer at different applied magnetic fields as well as the switching order for different Fe layer thicknesses are investigated. The results show that an increase in Fe layer thickness between 14 and 23 Å for 8 and 10 bilayer repetitions increases the coupling strength in Fe/MgO superlattices. This study completes the picture on the investigation on the influences on the coupling strength within these superlattices, which is important for possible applications of Fe/MgO superlattices in devices exploiting the discrete magnetic states.

[1] R. Moubah, F. Magnus, T. Warnatz et al., Physical Review Applied 5 (2016) [2] T. Warnatz, F. Magnus, N. Strandqvist et al., scientific reports 11 (2021)

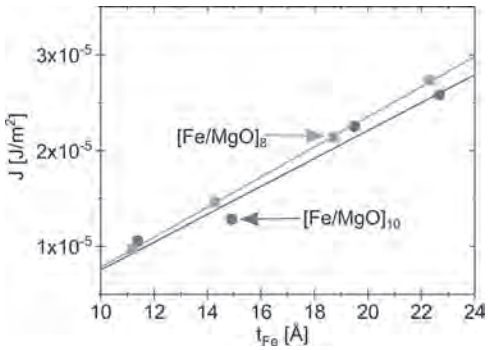

Fig. 1 Calculated coupling strength J plotted over Fe layer thickness t_{Fe} for 8 and 10 bilayer repetitions. The MgO layer thickness was kept constant at t_{MgO} = 17 Å.

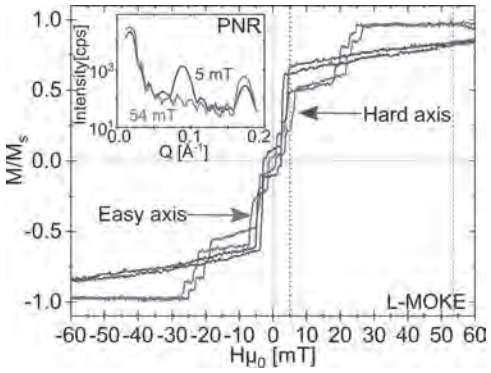

Fig. 2 Hysteresis loops measured on a $[Fe/MgO]_{10}$ superlattice within a longitudinal magneto-optical Kerr effect (L-MOKE) setup at applied magnetic fields along the Fe magnetic easy and hard axes. Polarized neutron reflectometry (PNR) measurements at 5 and 54 mT applied field along the easy axis (marked as vertical lines in the plot) are shown in the inset. The sample has Fe and MgO layer thicknesses of 20 and 17 Å, respectively.

LOA-10. Frequency Tunability with Field-Angle in Hybrid-Anisotropy $[CoPd]_8$-Pd-NiFe Magnetic Multilayers. *J. Leon*[1], D. Bangay[1], N.A. Johansson[1], H.J. Waring[1] and T. Thomson[1] *1. Computer Science, University of Manchester, Manchester, United Kingdom*

Hybrid anisotropy heterostructures consist of two exchange coupled magnetic layers with in-plane and out-of-plane magnetic anisotropy where the exchange coupling is controlled by a non-magnetic spacer layer [1,2], Fig.1. Previous studies have investigated the quasi-static magnetic properties of these structures using magnetometry and polarised neutron reflectivity (PNR) to determine the magnitude and extent of the coupling in these layer [3]. In this work we extend the study of hybrid anisotropy thin films to include the dynamic properties of these structures. We undertake angle dependent FMR measurements using VNA-FMR where the angle of the applied magnetic field can be varied whilst keeping the waveguide in a fixed position. The experimental details of our measurement are identical to those report in [4] except that we replace the Picoprobe waveguide with a NanOsc Coplanar Waveguide v4. Our results demonstrate that the angle dependence of the resonance frequency depends on the degree of coupling between the two magnetic layers. In systems with significant exchange coupling (e.g.: Pd spacer thickness of 1.2 & 2 nm) we observe a dominant 'acoustic' mode which shows a maximum frequency for an applied field angle of approximately 40° to the sample plane, Fig.2. The increase in frequency is ~25% for an applied field of 6 kOe. To further understand this effect, we have conducted micro-magnetic simulations using MuMax3 [5] which are able to reproduce the key features of the experimental results which will be presented in the full paper for spacer thicknesses of 0, 1.2, 2, 4, 6 and 100 nm). This shows that the angle of the applied field may be used to tune the resonance response of these materials over a significant frequency range.

[1] T. N. Anh Nguyen, Y. Fang, V. Fallahi, et al., Appl. Phys. Lett. 98, 172502 (2011) [2] C. Morrison, J. J. Miles, T. N. Anh Nguyen, et al., J. Appl. Phys. 117, 17B526 (2015) [3] W. Griggs, et al., Phys. Rev. Materials 6, 024403 (2022) [4] H. J. Waring, et al., Phys. Rev. Applied 13, 034035 (2020) [5] Arne Vansteenkiste, Jonathan Leliaert, Mykola Dvornik, et al., AIP Advances 4, 107133 (2014)

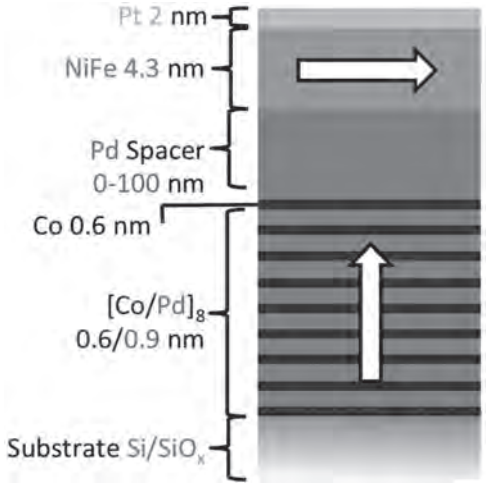

Fig.1: Schematic diagram of the $[CoPd]_8$-Pd-NiFe multilayer structure used in this study. Samples with Pd spacer between 0-100 nm were investigated

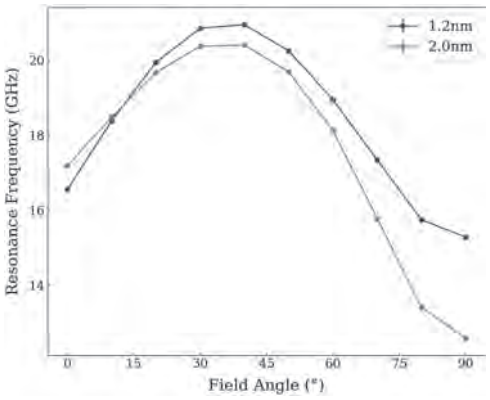

Fig.2: Plot showing the angular dependence of FMR frequency for the acoustic mode in strongly coupled samples (for an applied field of 6 kOe). Here 0 deg. is the in-plane direction and the solid lines are a guide to the eye.

LOA-11. Investigation of van der Waals $Fe_5GeTe_2/NiPS_3$ ferromagnet/antiferromagnet heterostructure. *T. Wang*[1], Q. Li[2], M. Yang[3], A. N'Diaye[4], C. Klewe[4], X. Huang[5], H. Zhang[5], P. Shafer[4], X. Zhang[6], C. Hwang[7], R. Ramesh[5] and Z.Q. Qiu[1] *1. Physics, University of California Berkeley, Berkeley, CA, United States; 2. University of Science and Technology of China, Hefei, China; 3. Anhui University, Hefei, China; 4. Lawrence Berkeley National Laboratory, Berkeley, CA, United States; 5. Materials Science & Engineering, University of California Berkeley, Berkeley, CA, United States; 6. King Abdullah University of Science and Technology, Thuwal, Saudi Arabia; 7. Korea Institute of Science and Technology, Seoul, The Republic of Korea*

Van der Waals $Fe_5GeTe_2/NiPS_3$ heterostructures were prepared by dry transfer method on top of a tiny x-ray window so that we can apply x-ray magnetic circular dichroism (XMCD) to measure the hysteresis loops of the sample. Compared to freestanding Fe_5GeTe_2, the coercivity of $Fe_5GeTe_2/NiPS_3$ measured at the Fe L3 edge is gradually enhanced as temperature decreases below the $NiPS_3$ Néel temperature, showing the existence of ferromagnet/antiferromagnet (FM/AFM) coupling between Fe_5GeTe_2 and $NiPS_3$. However, no noticeable exchange bias was detected in the $Fe_5GeTe_2/NiPS_3$ heterostructure. We find that the Fe_5GeTe_2 hysteresis loop becomes less square below the $NiPS_3$ Néel temperature with a noticeable slope near the coercivity field. Variable mechanisms will be discussed as compared to FM/AFM systems of conventional materials.

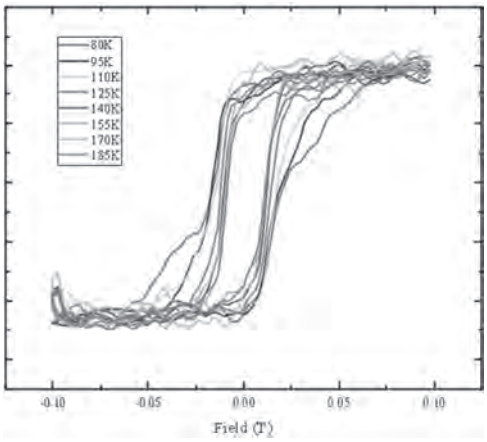

Fig. 11

LOA-12. Introduction of nitride underlayer and caplayer for preparation of $Mn_4N(001)$ single-crystal thin film with perpendicular magnetic anisotropy. *K. Imamura*[1], M. Ohtake[1], S. Isogami[2], M. Futamoto[1], T. Kawai[1], F. Kirino[3] and N. Inaba[4] *1. Faculty of Engineering, Yokohama National University, Yokohama, Japan; 2. Research Center for Magnetic and Spintronic Materials, National Institute for Materials Science (NIMS), Tsukuba, Japan; 3. Graduate School of Fine Arts, Tokyo University of the Arts, Tokyo, Japan; 4. Graduate School of Science and Engineering, Yamagata University, Yonezawa, Japan*

$Mn_4N(001)$ films with anti-perovskite structure slightly deformed along the *c*-axis (*c*/*a* = 0.99) show perpendicular magnetic anisotropy (PMA)[1-5] in addition to low M_s[6]. Therefore, Mn_4N films have attracted much attention to spintronics applications. Oxide single-crystal substrates such as MgO, $SrTiO_3$ etc. have been used to promote the epitaxial growth of Mn_4N films. However, Mn is known to be easily oxidized and there is a possibility that MnO is formed at the film/substrate interface, which will influence the spin transport properties. Therefore, it is desirable to employ a nitride underlayer with high chemical stability. In the present study, introduction of vanadium nitride (VN, NaCl-type structure) underlayer and caplayer is proposed for the preparation of $Mn_4N(001)$ film. A UHV sputtering system with *in-situ* RHEED facility is employed for film preparation. A V-N underlayer is grown on an MgO(001) substrate at 600 °C. Then, a Mn-N film and a V-N caplayer are sequentially formed on the underlayer at 200 °C. Finally, the sample is annealed at 600 °C. The resulting film structure is investigated by AFM, XPS, XRR and XRD. The magnetic property is measured by AHE. Fig. 1(a) shows the RHEED patterns of a V-N underlayer, a Mn-N film, and a V-N caplayer. (001) surface with NaCl-type structure is observed for the underlayer and the caplayer, whereas that with anti-perovskite structure is recognized for the Mn-N film. A fully epitaxial film of $VN/Mn_4N/VN$ is successfully obtained. The orientation relationship is determined as shown in Fig. 1(b). Formation of chemically sharp and flat interfaces is confirmed by XPS and XRR (not shown here). A flat surface is realized as shown in Fig. 1(c). Fig. 2 shows the XRD patterns. (001) out-of-plane and (100) in-plane superlattice reflections are clearly recognized. The *c*/*a* value is estimated to be 0.99. The Mn_4N lattice is apparently deformed due to accommodation of the lattice misfits with respect to underlayer and caplayer. The Mn_4N film shows strong PMA, which reflect the lattice deformation (not shown here). The present study has shown that introduction of VN underlayer and caplayer is effective in preparation of Mn_4N film with chemically sharp interface and with strong PMA.

1) K. Kabara and M. Tsunoda, *J. Appl. Phys.*, 117, 17B512 (2015). 2) Y. Yasutomi, K. Ito, T. Sanai, K. Toko, and T. Suemasu, *J. Appl. Phys.*, 115, 17A935 (2014). 3) T. Hirose, T. Komori, T. Gushi, A. Anzai, K. Toko, and T. Suemasu, *AIP Adv.*, 10, 025117 (2020). 4) A. Foley, J. Corbett, A. Khan, A. L. Richard, D. C. Ingram, A. R. Smith, L. Zhao, J. C. Gallagher, and F.

Yang, *J. Magn. Magn. Mater.*, 439, 236 (2017). 5) S. Isogami, K. Masuda, and Yoshio Miura, *Phys. Rev. Mater.*, 4, 014406 (2020). 6) S. Nakagawa and M. Naoe, *J. Appl. Phys.*, 75, 6568 (1994).

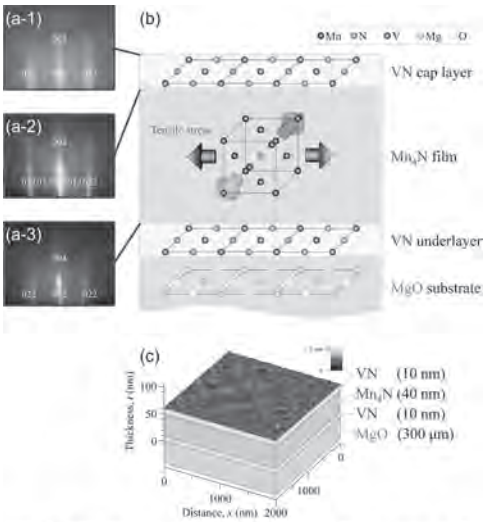

FIG. 1 RHEED patterns observed for (a-1) a V-N under-layer, (a-2) a Mn-N film, and (a-3) a V-N caplayer. (b) Crystallographic orientation relationship of a VN/Mn_4N/VN film grown on MgO(001) substrate. (c) Surface morphology observed by AFM and the cross-sectional schematic diagram of film.

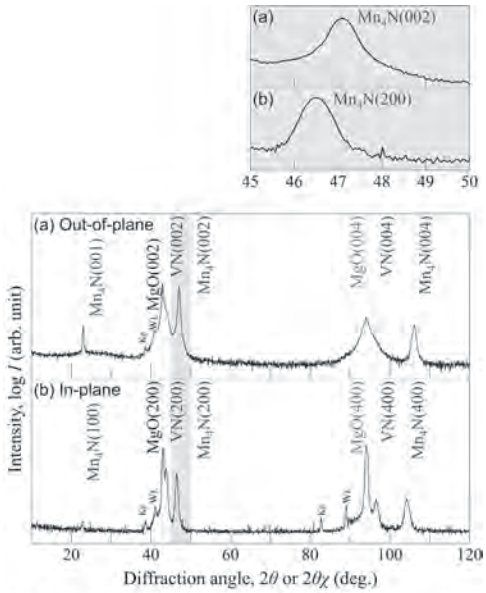

FIG. 2 (a) Out-of-plane and (b) in-plane XRD patterns measured for a VN/Mn_4N/VN film grown on MgO(001) substrate.

LOA-13. Study of Amorphous CoFeB Film Interfaced with Heavy Metals using Magnetic Circular Dichroism in Hard X-Ray Photoemission. *A. Hloskovsky*[1], C. Schlueter[1], M. Singh[2], K. Sarathlal[2], M. Gupta[3], V. Reddy[3] and A. Gupta[2] *1. Photon Science, Deutsches Elektronen-Synchrotron DESY, Hamburg, Germany; 2. Physics Department, University of Petroleum and Energy Studies, Dehradun, India; 3. UGC-DAE Consortium for Scientific Research, Indore, India*

Heterostructures consisting of HM/CoFeB/HM (HM=Heavy Metal) are important for the development of low power spintronics, thanks to the phenomena like Interfacial Dzyaloshinskii–Moriya Interaction, Spin Hall effect etc. The HM interface layers can significantly affect the magnetic properties as well as thermal stability of the CoFeB layer [1]. Further, local structure around Co atoms can differ significantly from that around Fe atom [2]. In the present work, magnetic circular dichroism in hard x-ray photoemission (MCD-HAXPES) has been used to elucidate the possible difference in the electronic structure of Fe and Co atoms and the effect of interfacing HM layer on the same. Multilayers: Si(substrate)/HM 20nm/ $Co_{40}Fe_{43}B_{17}$ 10nm/ HM 3nm/ Al 3nm (HM=Mo, W) were deposited using magnetron sputtering. CoFeB layer is amorphous in nature. MCD-HAXPES measurements were done at beamline P22 of PETRA III [3], Hamburg, using 6 keV X-rays, falling at a grazing angle of 2^0. The helicity of the photons was changed using the in-vacuum phase retarder based on a 400 μm thick diamond single crystal with (100) orientation. Measurements were done in the remnant state of the films with the easy axis along the propagation direction of x rays. For Mo_CoFeB sample, the polarization-dependent spectra for the Fe and Co 2p core levels are shown in Fig. 1. The maximum asymmetry is found to be 39% for Fe and 23.6% for Co. Splitting of the main $2p_{3/2}$ line is found to be 430 meV and 130 meV for Fe and Co atoms respectively. In the sample W_CoFeB, the splitting of $2p_{3/2}$ line is 310 meV and 90 meV for Fe and Co respectively, which is significantly lower, suggesting that the magnetic moments of both Fe and Co are lower in the sample W_CoFeB as compared to Mo_CoFeB. Co spectrum has an additional weak shoulder at 4 eV from the main $2p_{3/2}$ line. This may be an indication of a correlation-induced satellite of majority spin nature in Co. Detailed analysis of the results in terms of the electronic and magnetic structure of Fe and Co atoms, and dependence of the same on the interfacing heavy metal layers, will be presented.

[1] J. Dwivedi et al., J. Magn. Magn. Mater. 466 311 (2018). [2] K Pussi et al., J. Phys.: Condens. Matter 33 395801 (2021). [3] C. Schlueter et al., 13th International Conference on Synchrotron Radiation Instrumentation, SRI2018, Taipei, Taiwan, AIP conference proceedings 2054(1), 040010 (2019).

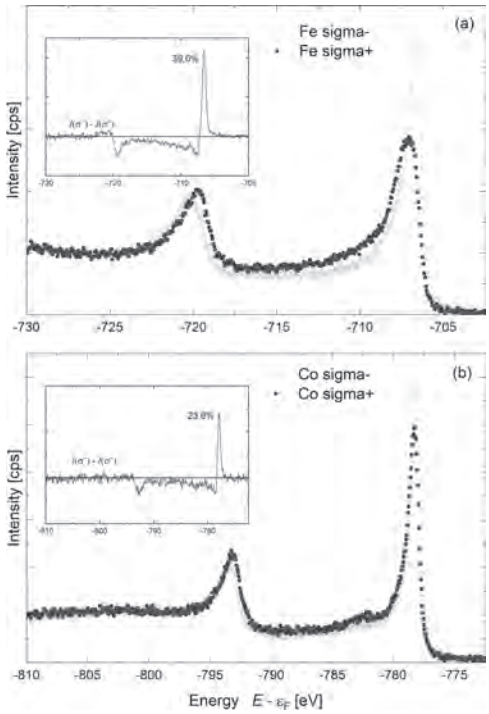

Fig. 1. Polarization-dependent core-level spectra for the Fe and Co 2p excitations. Insets show the dichroism in the HAXPES spectra.

LOA-14. Fabrication of 3 nm Width Dielectric Segregant Lines for Radially Ordered Grain Pattern Media Recording. X. Yang[1], *S. Xiao*[1], J. Wu[1], Y. Hsu[1], Z. Yu[1], D. Staaks[1], P. Steiner[1], K. Lee[1] and T.Y. Chang[1]
1. Seagate Media Research, Fremont, CA, United States

Grain Pattern Media Recording (GPMR) technology is proposed as a candidate to replace Bit Pattern Media (BPM). GPMR media fabrication process shows great promise to resolve the technical and manufacturing issues associated with conventional BPM. Rather than a highly aggressive subtractive process with thick masking layers to pattern magnetic bits, GPMR employs a bottom-up new approach where thin (2nm) and narrow (3nm) radial line pattern is fabricated on top of the interlayer, then FePt granular alloy is deposited using conventional sputter deposition. This Line pattern acts as nucleation constraints to force the newly deposited FePt grains to grow on the interlayer along the radial direction to ensure alignment of grain edges. Fig. 1 shows a illustration of the GPMR magnetic configuration and radial lines. To ensure grains only grow on the interlayer and no grains grow on top of segregant lines, the segregant lines needs to be controlled to be less than ~3 nm. We proposed to use simple sidewall patterning approach which combines nano-imprint lithography with dry plasma etch technique to create < 3 nm width dielectric segregant lines for fabricating GPMR media. Two sidewall processes with different mandrel materials have been developed to successfully fabricate < 3 nm SiO2 lines on MTO surfaces on the disks. The segreant line width is determined by the deposition thickness of SiO2, whereas the segregant line height of 1-3 nm is determined by the CF4 etch process. Fig. 2A shows the sidewall process flow and the top-down SEM image with inserted TEM cross sectional image of 2.8 nm linewidth radial segregant SiO2 line patterns on MTO (pitch= 32 nm). Fig. 2B shows that TEM image of 2 nm FePt grains was deposited on 3 nm SiO2 lines on MTO at 650C (pitch= 160 nm). This is the first successful experimental demonstration of phase segregation of ordered FePt granular media using this newly invented bottoms up approach to form patterned media.

[1] T. R. Albrecht et al., in IEEE Transactions on Magnetics, vol. 51, no. 5, pp. 1-42, May 2015, TMAG.2015 [2] D. S. Kuo et al., 2016 International Conference of Asian Union of Magnetics Societies (ICAUMS), 2016, pp. 1-1, 2016.

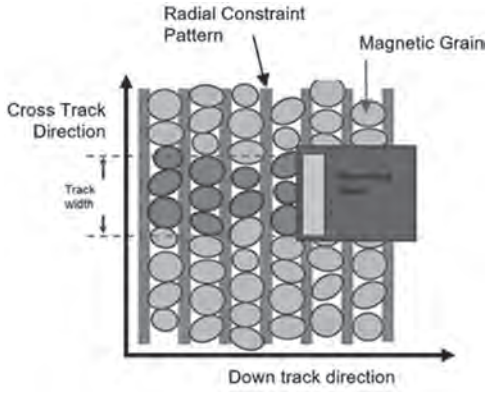

Fig. 1 The proposed design with single-grain-row-per-line pitch design for GPMR media

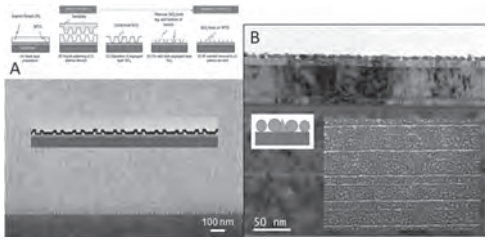

Fig. 2(a) The sidewall process and SEM image of 2.8 nm linewidth SiO2 lines on MTO (pitch= 32 nm). Fig. 2(b) shows 2 nm FePt grains deposited on 3 nm SiO2 lines

Session LOB
THIN FILMS AND SURFACE EFFECTS

Paola Tiberto, Co-Chair
INRIM, Torino, Italy
Joao Paulo Sinnecker, Co-Chair
Centro Brasileiro de Pesquisas Físicas, Rio de Janeiro, Brazil

CONTRIBUTED PAPERS

LOB-01. Interface Degradation in Magnetic Multilayer Stacks Characterised by X-Ray Reflectometry and Polarised Neutron Reflectometry. *B.W. Wilson*[1], Y. Khaydukov[2], J. Scott[1], W. Hendren[1], A. Vorobiev[3], A. Dobrynin[4] and R. Bowman[1] *1. School of Mathematics and Physics, Queen's University Belfast, Belfast, United Kingdom; 2. Max Planck Institute for Solid State Research, Stuttgart, Germany; 3. Departent of Physics and Astronomy, Uppsala University, Uppsala, Sweden; 4. Seagate Technology, Derry, United Kingdom*

Magnetic dead layers (MDLs) can be formed at the interface of ferromagnetic (FM) and non-magnetic thin films as a result of interfacial diffusion typically during the fabrication process [1][2], causing degradation of magnetic layers' properties, such as the magnetic moment and exchange coupling. For patterned films it also poses thermal stability problems due to a decrease in the magnetic anisotropy energy, leading to a reduction in thermal activation energies [3]. X-Ray reflectometry (XRR) has been used in conjunction with polarised neutron reflectometry (PNR) to investigate the formation of magnetic dead layers in $Co_{70}Fe_{30}$ thin films with Ta interfaces in addition to sample degradation over time. The rate at which the Ta diffuses into the $Co_{70}Fe_{30}$ layer differs between the top and bottom interfaces resulting in MDLs of different thicknesses, 3.04Å and 1.87Å respectively as indicated in figure 1(b). It is clear that the formation of magnetic dead layers has resulted in a loss of magnetisation in the thin $Co_{70}Fe_{30}$ layer. This is of particular technological importance for spintronic devices in which the magnetic properties at the interfaces are crucial. Ta has been known to provide very good adhesion between the substrate and the soft FM layer. It is also widely used as a passivation layer to prevent oxidisation in air [4]. Our results show that this is not the case, with Ta unsuitable as a seed due to the formation of MDLs and not viable as a capping layer due to oxygen passivation over time as shown by XRR in figure 2.

[1] T. L. Monchesky and J. Unguris, Phys. Rev. B 74, 24130 (2006). [2] K. Oguz *et al.*, J. Appl. Phys. 103, 07B526 (2008). [3] M. Tokaç *et al.*, AIP Advances 7, 115022 (2017). [4] H. S. Jung *et al.*, J. Appl. Phys., Vol. 93, No. 10, (2003).

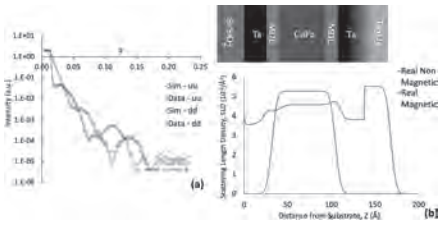

Fig. 1. (a) PNR measurements, raw data shown as points while the fitted simulated data is indicated by a solid line. (b) Depth profiles of nuclear and magnetic scattering length density (SLD) for the sample structure in the schematic above. MDLs have been introduced in the interfaces between the top and bottom interfaces of the CoFe layer.

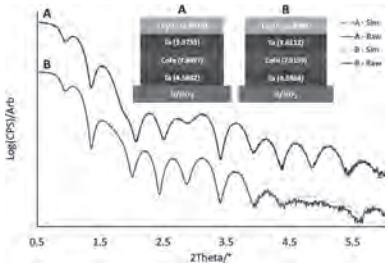

Fig. 2. XRR curves for the sample structure denoted in the inset above. Sample A was measured as soon as deposited whilst sample B was measured 15 months later which has clearly degraded over time as seen on the fringes and as well as the differences in thickness of the sample.

LOB-02. Fabrication of $Co_{25}Fe_{75}$/Hf multilayer thin films to decrease the magnetic damping coefficient. *S.C. Mills*[1] and M. Staruch[1] *1. Materials Science and Technology, U.S. Naval Research Laboratory, Washington, DC, United States*

In magnonic and spintronic devices, a low magnitude magnetic damping is desired for efficient operation via the long-range propagation of spin waves [1]. However, thin magnetic ferrite films (low damping but insulating) may not suffice if a charge current is needed [2]. Thin films of the conducting binary alloy of cobalt and iron ($Co_{25}Fe_{75}$) have exhibited low damping (~10^{-3}) [3]. To further decrease the damping of this system, a multilayer film consisting of ten 10 nm layers of $Co_{25}Fe_{75}$ alternated with 2 nm layers of hafnium (Hf) is proposed. This structure would decrease the damping by preventing eddy current losses and decrease coercivity and magnetic saturation via smaller crystallite sizes [4,5]. These single and multilayer films were deposited via sputtering, with thicknesses (t) of 10, 50, and 100 nm. The ferromagnetic resonance (FMR) of the films showed as the t increases, at a constant frequency (17 GHz shown), the FMR field decreases and linewidth increases, but the 100 nm multilayered film maintains the linewidth and FMR field of the 10 nm film (Fig. 1). The linewidth and FMR for each film (at 14-17 GHz) in addition to the saturation magnetization were used to calculate the damping parameter (α) of each film. This showed that as t increases up to 100 nm, the damping increases from ~$1x10^{-2}$ (10 and 50 nm) to ~$8x10^{-2}$ (100 nm) (Fig. 2). The damping of the multilayered film (~$5x10^{-3}$) is below that of the 10 nm film, an order of magnitude improvement. This work shows that increasing t for single layered $Co_{25}Fe_{75}$ decreases FMR field, increases linewidth, and increases damping. The multilayer structure shows the ability to tune the FMR and damping. This provides avenues for other heterostructures, including the use of an insulating interlayer or other magnetic materials.

[1] H. Glowinski, F. Lisiecki, P. Kuswik, *J. Alloys Compd.*, 785, 891-896 (2019). [2] E. Edwards, H. Nembach, and J. Shaw, *Phys. Rev. Appl.*, 11, 054036 (2019). [3] R. Weber, D. Han, I. Boventer, *J. Phys. D: Appl. Phys.*, 52, 325001 (2019) [4] S. Balaji and M. Kostylev, *J. Appl. Phys.*, 121,

123906 (2017). [5] L. Garten, M. Staruch, K. Bussmann, *ACS Appl. Mater. Interfaces*, 14, 25701-25709 (2022).

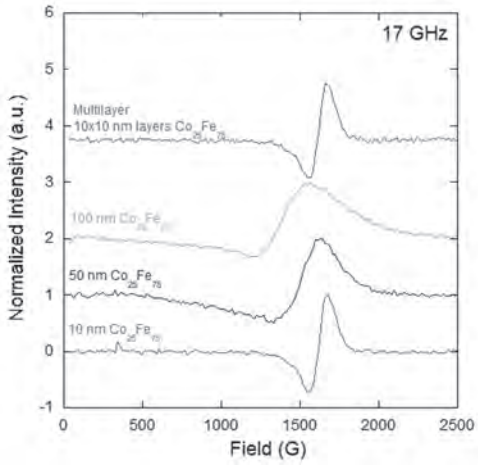

Fig. 1. FMR measurements of the CoFe films at 17 GHz, showing a decrease in FMR field and increase in linewidth as thickness increases, and the multilayer sample returns to the FMR and linewidth of the 10 nm film.

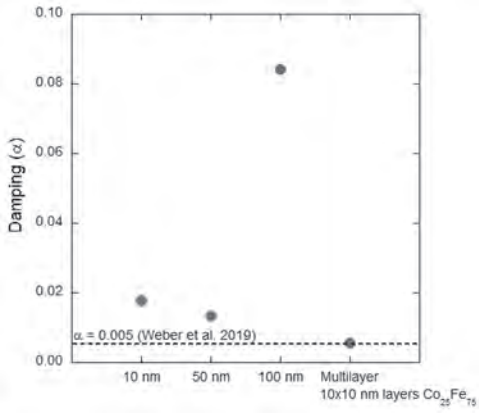

Fig. 2. Calculated damping parameters of the CoFe films, showing that the multilayered film damping (0.0055) is comparable to a typical low damping value of CoFe (0.005) [3].

LOB-03. Tailoring Perpendicular Magnetic Anisotropy of Cobalt-Iron alloy (CoFeB) Using Ion Irradiation. *A. Mahendra*[1,2], P. Murmu[2,3], S. Acharya[1,3], A. Islam[1,3], P. Gupta[2,3], S. Granville[1,3] and J. Kennedy[2,3]
1. Robinson Research Institute, Victoria University of Wellington, Wellington, New Zealand; 2. National Isotope Centre, GNS Science, Lower Hutt, New Zealand; 3. The MacDiarmid Institute for Advanced Materials and Nanotechnology, Wellington, New Zealand

Magnetic Tunnel Junctions (MTJs) are multi-layered devices that use tunnel magnetoresistance (TMR) to detect changes in magnetic field. [1]. MTJs with specific characteristics are relatively complex to fabricate due to the high dependence of their magnetic properties, especially perpendicular magnetic anisotropy (PMA), on individual film thicknesses and interfaces. Post-growth modification tools, such as ion irradiation [2], are perfect when the properties of such structures are to be modified. Ion irradiation is a versatile tool that causes structural changes in the material's lattice by forming point defects, that in turn cause changes in the magnetic properties, which can be controlled by tuning the fluence, energy, and ion current density of the ion beam [3]. In this study, we use 30 keV argon and neon ions to modify the magnetic properties of a MTJ half stack [Sub-SiO_2/ Ta (5)/ MgO (1.5)/ $Co_{40}Fe_{40}B_{20}$ (1.6)/ W (0.5)/ Ta (2)] by irradiating with fluences between 1×10^{13} ions/cm^2 and $1x10^{15}$ ions/cm^2. The low fluence ion irradiation ($<10^{14}$ ions/cm^2) changed the anisotropy of magnetic layers from out-of-plane to in-plane, and even achieve a canted anisotropy. The calculated displacement per atom (DPA) in CoFeB using the TRIM [4] simulation tool ranges between 0.13 and 32.75 for fluences 1×10^{13} ats/cm^2 and $1x10^{15}$ ions/cm^2. We found that an irradiation of even 10^{13} ions/cm^2 fluence may cause a reduction in effective anisotropy by around 53%. We envisage that low fluence irradiation ($<10^{14}$ ions/cm^2) limits significant intermixing of layers which avoids the formation of a dead layer in the stack and degradation of TMR performance. These findings are important for fabricating better magnetic sensors with lower signal-to-noise ratios, MRAMs with voltage tunability, tuning properties of spin-orbit-torque based devices, etc. Detailed experimental results obtained from Magneto Optical Kerr Effect Spectroscopy (MOKE) and superconducting quantum interference device (SQUID) supported by DYN-TRIM simulations will be presented in the conference.

[1] C. Zheng, K. Zhu, S.C. de Freitas, J.Y. Chang, J.E. Davies, P. Eames, P.P. Freitas, O. Kazakova, C.G. Kim, C.W. Leung, S.H. Liou, A. Ognev, S.N. Piramanayagam, P. Ripka, A. Samardak, K.H. Shin, S.Y. Tong, M.J. Tung, S.X. Wang, S. Xue, X. Yin, P.W.T. Pong, Magnetoresistive Sensor Development Roadmap (Non-Recording Applications), IEEE Transactions on Magnetics. 55 (2019) 1–30. [2] J. V. Kennedy, W.J. Trompetter, P.P. Murmu, J. Leveneur, P. Gupta, H. Fiedler, F. Fang, J. Futter, C. Purcell, Evolution of Rutherford's ion beam science to applied research activities at GNS Science, J R Soc N Z. (2021) 1–18. [3] A. Mahendra, P. Gupta, S. Granville, J. Kennedy, Tailoring of magnetic anisotropy by ion irradiation for magnetic tunnel junction sensors, Journal of Alloys and Compounds. 910 (2022) 164902. [4] J.F. Ziegler, M.D. Ziegler, J.P. Biersack, SRIM - The stopping and range of ions in matter (2010), Nuclear Instruments and Methods in Physics Research, Section B: Beam Interactions with Materials and Atoms. 268 (2010) 1818–1823.

LOB-04. Modifying the Magnetic Properties of Polycrystalline Co Thin Films by a Molecular Interface. *M. Benini*[1], G. Allodi[2], G. Varvaro[3], A. Surpi[1], R.K. Rakshit[1], K. Lin[4], L. Gnoli[1], A. Riminucci[1], M. Singh[1], S. Sanna[5], I. Bergenti[1] and V. Dediu[1] *1. CNR-ISMN, Bologna, Italy; 2. Dipartimento di Scienze Matematiche, Fisiche e Informatiche, University of Parma, Parma, Italy; 3. Institute of Structure of Matter, Consiglio Nazionale delle Ricerche, Rome, Italy; 4. Department of Materials Science and Engineering, NCHU, Taichung, Taiwan; 5. Department of Physics and Astronomy, University of Bologna, Bologna, Italy*

The formation of hybrid *p-d* bonds at a 3d-ferromagnet/molecule interfaces has proven effective in modifying the effective spin-orbit coupling, density of states and other fundamental parameters of the ferromagnetic (FM) layer [1-4]. We report on novel results related to extraordinary modification of the magnetic parameters in polycrystalline Co thin films (5 and 7 nm) interfaced with C_{60} or Gaq_3 molecular layers. A drastic, molecule-dependent enhancement of the in plane coercive fields is observed with respect to both Al-capped and bare cobalt samples, taken as reference (see Fig. 1). The effect is present even at room temperature featuring a significant enhancement by factor of 2, while it grows enormously when decreasing temperature, showing qualitatively different trends and reaching a one order of magnitude increase already at 150 K. In addition to this, Co interfaced with both molecules undergoes a reduction of the in-plane uniaxial anisotropy, observed for the reference Co/Al systems. This is accompanied by an increase in the surface anisotropy term, leading to higher saturation field along the out-of-plane direction, with respect to the reference Co/Al systems. In-plane ^{59}Co Zero-Field NMR [5] characterization of Co(7nm)-based bilayers confirms the magnetic hardening of the FM layer when interfaced with C_{60} or Gaq_3, showing that the maximum of the FNR signal is moved to higher power of the applied rf field, regardless of the resonance frequency (see Fig. 2). The analysis of the ^{59}Co FNR spectra shows that the FM layer is modified by this interfacial hybridization on characteristic lengths of several nm and that the surface Co atoms undergo a reconstruction of their magnetic environment. These results, obtained on polycrystalline samples, reveal conceptually new

physics going beyond the current understanding, established on epitaxial cases and localized hybridization effects.

[1] M. Cinchetti, V. A. Dediu, L. Hueso, Nat. Mater., Vol. 16, p.507 (2017) [2] K. V. Raman, A. M. Kamerbeek, Arup Mukherjee *et al*., Nature, Vol. 493, p.509 (2013) [3] K. Bairagi, A. Bellec, V. Repain *et al.*, Phys. Rev. Lett., Vol. 114, p.5 (2015) [4] T. Moorsom, M. Wheeler, Taukeer Mohd Khan *et al*., Phys Rev. B, Vol. 90, p.6 (2014) [5] C. Meny, P. Panissod, Annual Reports on NMR spectroscopy, Vol.103 p.47 (2021)

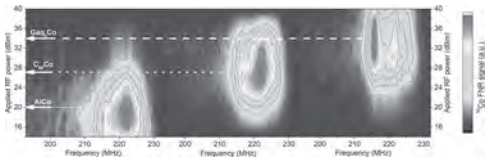

Fig. 1 2D colormaps showing the ^{59}Co FNR spin-echo intensity versus applied rf field frequency and applied rf field power of Co/Al (left), Co/C_{60} (center) and Co/Gaq_3 (right).

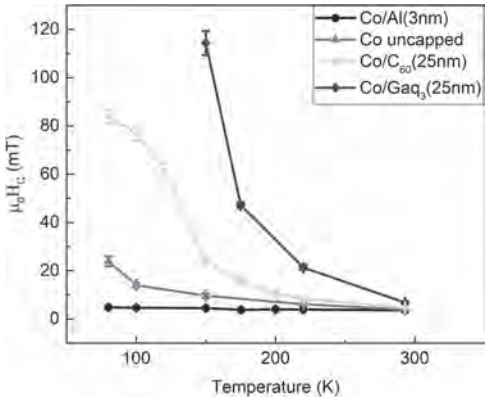

Fig. 2 Temperature dependence of the coercive fields for Co/Molecule bilayers and reference Co/Al and bare Co samples.

LOB-05. Magnetostrictive properties of flat Fe-Co epitaxial films grown on VN(001) single-crystal underlayers. *Y. Nakamura*[1], M. Ohtake[1], T. Kawai[1], M. Futamoto[1], F. Kirino[2] and N. Inaba[3] *1. Faculty of Engineering, Yokohama National University, Yokohama, Japan; 2. Gradute School of Fine Arts, Tokyo University of the Arts, Tokyo, Japan; 3. Graduate School of Science and Engineering, Yamagata University, Yonezawa, Japan*

Fe-Co alloys have attracted much attention as one of magnetostrictive materials for applications like actuators, sensors, and vibration energy harvesting devices. It is reported that Fe-Co poly-crystal films prepared by annealing at high temperatures show large magnetostriction values of 150×10^{-6} – $+250\times10^{-6}$.[1)] The enhancement of magnetostriction is interpreted to be due to strain of bcc-*A*2 lattice caused by inclusion of bcc-*B*2 or fcc-*A*1 nanocrystals.[2)] In our previous studies,[3,4)] Fe-Co single-crystal films were prepared on MgO(001) substrates at 300 °C by varying the Co content from 0 to 70 at. %. The magnetostriction coefficients, (λ_{100}, λ_{111}), increased from ($+40\times10^{-6}$, -40×10^{-6}) to ($+270\times10^{-6}$, $+80\times10^{-6}$) with increasing the Co content from 0 to 50 at. %, respectively. A higher substrate temperature may enhance the magnetostriction, but it also causes the surface roughness. To improve the surface flatness, it is useful to employ VN underlayer material whose surface energy is larger than that of Fe-Co alloy. In the present study, $Fe_{100-x}Co_x$ (x = 0–100 at. %) films are prepared on VN(001) single-crystal underlayers at 600 °C by UHV sputtering. The magnetostrictive properties of flat Fe-Co films prepared at a high substrate temperature are investigated. Fig. 1 compares the AFM images observed for $Fe_{50}Co_{50}$ films with and without VN underlayers prepared on MgO(001) substrates at 600 °C. Flat film surface is realized by introducing a VN underlayer. Fig. 2(a) shows the magnetostrictive properties of $Fe_{50}Co_{50}$ film formed on VN underlayer. The (λ_{100}, λ_{111}) are estimated to be ($+300\times10^{-6}$, $+140\times10^{-6}$), which are higher than that observed for $Fe_{50}Co_{50}$ film formed on MgO(001) substrate at 300 °C, as shown in Fig. 2(b). The XRD result (not shown here) shows that *B*2 ordered phase is mixed with *A*2 disordered phase for the $Fe_{50}Co_{50}$ film formed at 600 °C. *B*2 ordering may have increased the λ_{100} and the λ_{111}. The influence of film composition on the magnetostrictive property will also be presented at the conference.

1) D. Hunter, W. Osborn, K. Wang, N. Kazantseva, J. Hattrick-Simpers, R. Suchoski, R. Takahashi, M. L. Young, A. Mehta, L. A. Bendersky, S. E. Lofland, M. Wuttig, and I. Takeuchi, *Nat. Commun.*, 2, 518 (2011). 2) Y. Han, H. Wang, T. Zhang, Y. He, J.M.D. Coey, and C. Jiang, *J. Alloys Compd.*, 699, 200 (2017). 3) K. Serizawa, M. Ohtake, T. Kawai, M. Futamoto, F. Kirino, and N. Inaba, *J. Magn. Soc. Jpn.*, 43, 50 (2019). 4) S. Noro, M. Ohtake, T. Kawai, M. Futamoto, F. Kirino, and N. Inaba, *AIP Adv.,* 12, 035144 (2022).

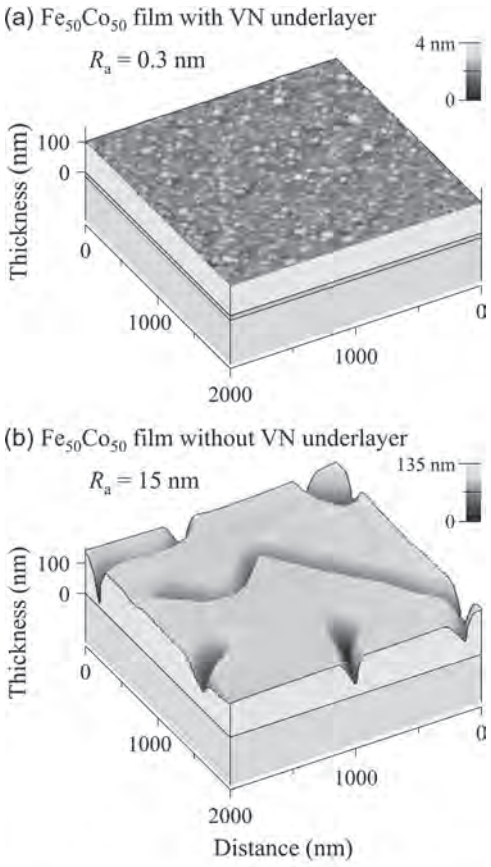

Fig. 1 AFM images observed for $Fe_{50}Co_{50}$ films (a) with and (b) without VN undelayer formed on MgO(001) substrates at 600 ºC.

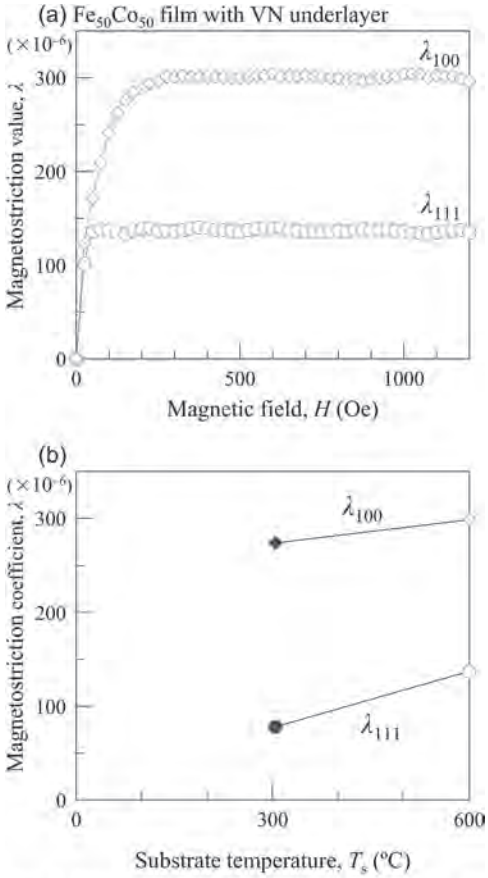

Fig. 2 (a) Magnetic field dependences of λ_{100} and λ_{111} measured for an $Fe_{50}Co_{50}$ film with VN underlayer formed at 600 °C. (b) Substrate temperature dependences of λ_{100} and λ_{111} measured for $Fe_{50}Co_{50}$ film. The values of the film formed at 300 °C are cited from our previous paper. [3)]

LOB-06. In-depth structural and magnetic study of Ni/NiO epitaxial thin films on various single crystalline substrates grown using pulsed laser deposition. *M. Iqbal*[1] and K. Ghosh[1] *1. Physics, Astronomy and Materials Science, Missouri State University, Springfield, MO, United States*

The crystallographic orientation plays the foremost significant role in the modern magnetic heterostructure devices, especially in the arena of spintronics device. In terms of magnetic property, domain orientation is solely dependent on the structural homogeneity. This research work deals with the development of epitaxial thin films of Ni/NiO on various single-crystalline substrates including sapphire (0006) and $LiNbO_3$ (104). Pulsed laser deposition (PLD) technique was used at 650°C in constant oxygen pressure of 0.01 mbar to deposit films on reported substrates. Phase mixture of Ni (ferromagnetic)/NiO (antiferromagnetic) in the thin films was achieved via hydrogen reduction annealing at 600°C for 30 minutes which induced point defects by incorporating oxygen vacancies into the as-deposited pure NiO crystal structure. Two major structural characterizations— X-ray diffraction and Scanning electron microscopy were done to find out the desired phases and surface morphology. X-ray diffraction shows preferential growth of NiO on both sapphire and lithium niobate along the (111) plane (XRD peak at 37.25° on sapphire, 37.28° on $LiNbO_3$), sharp peaks of Ni at 44.4° and 50.3° on sapphire and lithium niobate substrates indicate that a handful amount of NiO converted to Ni phase. Additionally, Rietveld refinement using Diffrac plus Topas shows 99.7% and 99.6% Ni phase presence after doing the reduction annealing of NiO thin films on sapphire and lithium niobate substrates accordingly. Moreover, single crystalline domains with two different crystallographic orientations (due to having twin phase) were noticed at 60° apart via phi scan and pole figure techniques. Scanning electron microscopy images with Energy dispersive spectroscopy shows the surface homogeneity with atomic percentages of Ni in both annealed thin films. Temperature and field dependent magnetization data collected using SQUID magnetometer show ferromagnetism and antiferromagnetism in pure Ni and NiO films, respectively. Spin canting has been observed in the phase mixture, holding a potential wide range magnetic exchange coupled phenomena.

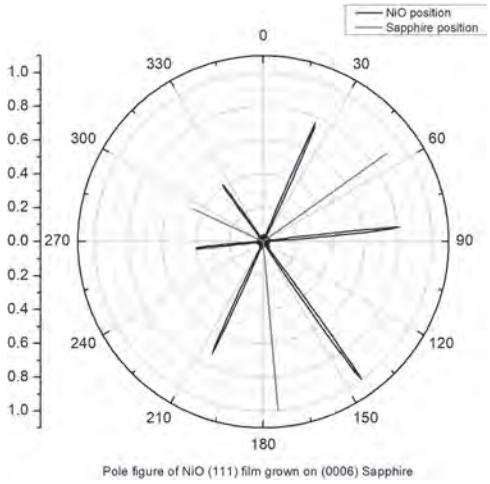

Fig. 1: Pole figure of NiO (111) film grown on Sapphire (0006)

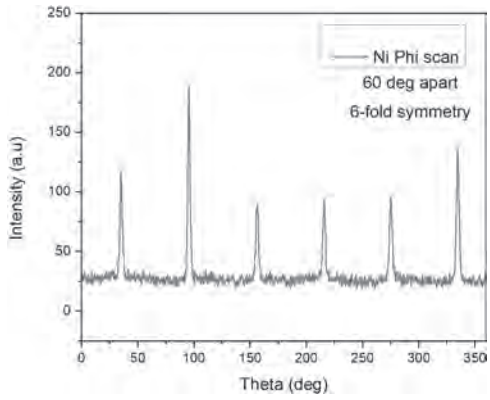

Fig.2 : Phi Scan of Ni (111) film grown on Sapphire (0006)

LOB-07. Perpendicular Magnetic Anisotropy of Ferrimagnetic Mn_4N Thin Film Improved by the Pd Buffer Layer. *Y. Zhang*[1] and S. Granville[1] *1. Victoria University of Wellington, Wellington, New Zealand*

Ferrimagnets composed of two or multi antiferromagnetically coupled magnetic sublattices have attracted much attention recently due to the easily controlled and detected net magnetization and a fast magnetic dynamic behavior [1]. Especially, ferrimagnetic thin films with perpendicular magnetic anisotropy (PMA) show great potential for high-density spintronics devices [2]. Currently, most of work focus on the rare earth-transition metal ferrimagnetic alloys, such as GdFeCo and TbCo. However, the magnetization of these materials is sensitive to the temperature and composition [3]. The antiperovskite Mn4N compound is a rare-earth-free ferrimagnet showing a PMA, high thermal stability, high spin polarization and low saturation magnetization which make it promising for practical

spintronics devices [4]. For the crystalline structure of Mn_4N compound, Mn atoms occupy the corners (Mn_A) and face-centers (Mn_B) of the cubic unit cell, respectively, while N atom is located at the body center, as shown in Fig. 1(a). The magnetic moment of Mn_A and Mn_B are antiferromagnetically coupled with a high Curie temperature, 740 K. PMA in Mn_4N thin films had been observed by epitaxially depositing it on the MgO substrate. However, the large lattice mismatch between Mn_4N and MgO, −6%, induces a misfit dislocation of Mn_4N resulting in a poor PMA. In this work, by inserting a thin Pd buffer layer with a very close lattice constant of Mn_4N, we prepared the stacks MgO(substrate)/Pd(t = 0, 2 and 8 nm)/Mn_4N(80 nm)/Ta(3 nm). We systematically studied the effect of Pd buffer layer on the crystalline structure and magnetization of Mn_4N thin films. With inserting a Pd buffer layer, a good quality of crystalline structure can be formed which significantly improves the PMA, as shown in Fig. 1(b).

[1] S. K. Kim *et al.*, Nat. Mater. 21, 24–34 (2022) [2] B. Dieny and M. Chshiev, Rev. Mod. Phys. 89, 025008 (2017) [3] H. Bai *et al.*, Adv. Electron. Mater. 8, 2100772 (2022) [4] Z. Zhang and W. Mi, J. Phys. D: Appl. Phys. 55 013001 (2022)

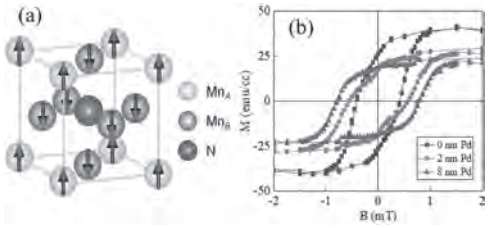

Fig. 1: (a) Crystalline structure of Mn_4N. (b) Pd thickness dependence of magnetization of Mn_4N under an external out-of-plane magnetic field.

LOB-08. Determining Quantitatively the Induced Magnetic Moment in Graphene by Polarised Neutron Reflectivity and X-ray Magnetic Circular Dichroism. *R. Aboljadayel*[1,2], C. Kinane[3], C.A. Vaz[4], D.M. Love[2], R. Weatherup[5], P. Braeuninger-Weimer[5], M. Martin[5], A. Ionescu[2], A. Caruana[3], T. Charlton[3], J. Llandro[2], P.M. Monteiro[2], C.H. Barnes[2], S. Langridge[3] and S. Hofmann[5] *1. School of Physics and Astronomy, University of Leeds, Leeds, United Kingdom; 2. Cavendish Laboratory, physics department, University of Cambridge, Cambridge, United Kingdom; 3. STFC Rutherford Appleton Laboratory, ISIS Neutron and Muon Source Facility, Harwell, United Kingdom; 4. Swiss Light Source, Paul Scherrer Institut, Villigen PSI, Switzerland; 5. Department of Engineering, University of Cambridge, Cambridge, United Kingdom*

Graphene has unique electronic properties which make it a promising material for next-generation electronics. It has high electron mobility at room temperature and a long spin-diffusion length. The latter is due to its weak intrinsic hyperfine interactions and small spin-orbit coupling. Therefore manipulating spins directly in a layer of pristine graphene is not easy. However, this can be overcome by an induced proximity effect using an exchange-coupled interface between the graphene and a ferromagnetic layer. Several studies predicted that the conduction band of graphene will spin split at the interface with a ferromagnetic substrate [1-4]. We report the magnitude of the induced magnetic moment in graphene as a result of the proximity effect in the vicinity of a Ni layer using polarised neutron reflectivity (PNR) and X-ray magnetic circular dichroism (XMCD). The Ni film was grown by sputtering upon which the graphene was grown by chemical vapour deposition. The growth parameters were tuned to produce epitaxial and rotated graphene domains (Fig. 1). The XMCD results at the C *K*-edge confirm the presence of magnetic polarisation in rotated graphene. Intensive quantitative analysis of the PNR fits, ascertained based on Bayesian analysis, indicate that at 10 K 0.53 and 0.38 μ_B/C atom is induced in rotated and epitaxial graphene grown on Ni(111), respectively. These values are three times higher than those predicted in other studies [4,5]. Two possible mechanisms were elaborated for the observed induced magnetic moment [4,6,7]. To clarify the origin of the measured moment, further PNR measurements were carried out on graphene grown on a non-magnetic substrate (Ni_9Mo_1) [8]. We will present the different models used to fit the data and discuss the challenges of fitting the PNR of a 2D material which is within the resolution limit of the technique. We will also show the results of other techniques used to characterise the samples.

[1] H. Haugen et al., Phys. Rev. B 77, 115406 (2008). [2] Q. Zhang et al., Appl. Phys. Lett. 98, 032106 (2011). [3] H.X. Yang et al., Phys. Rev. Lett. 110, 046603 (2013). [4] M. Weser, Y. Rehder *et al.*, Appl. Phys. Lett. 96, 012504 (2010). [5] H. -Ch. Mertins et al., Phys. Rev. B 98, 064408 (2018). [6] V. Karpan, P. Khomyakov *et al.*, Phys. Rev. B 78, 195419 (2008). [7] F. Ma'Mari, T. Moorsom *et al.,* Nature 524, 69 (2015). [8] R. O. M. Aboljadayel et al., arXiv:2101.09946v2 (2022).

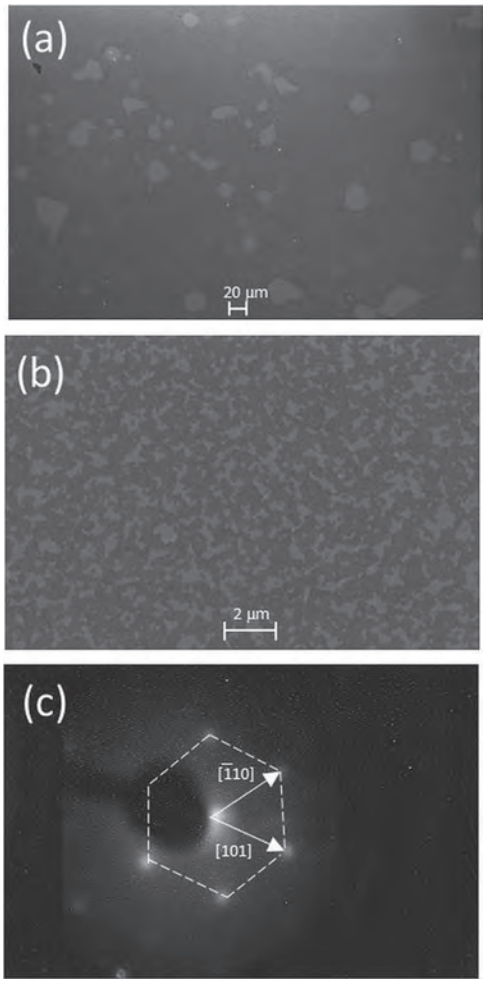

SEM images at 1 kV showing the graphene domains for (a) epitaxial graphene/Ni and (b) rotated graphene/Ni and (c) The LEED diffraction pattern of epitaxial graphene on a Ni(111) substrate at 300 eV. The red circle in (b) highlights a single graphene domain with a diameter of ~ 0.25 µm.

LOB-09. The Effect of Cap Materials and Cooling Time on the Magnetic Properties of Ferrimagnetic $(FeCo)_{(1-y)}Gd_y$ Thin Films. *N. Alzahrani*[1,2], D. Khan[1] and D. Arena[1] *1. Physics, University of South Florida, Tampa, FL, United States; 2. Physics, University of Jeddah, Jeddah, Saudi Arabia*

Ferrimagnetic thin films comprised of transition metals such as Fe and Co alloyed with rare earth materials such as Gd can exhibit an intriguing phenomenon termed magnetic compensation, where the differing temperature profiles of the magnetization of the transition metals (Fe & Co) and

the lanthanide species (Gd) lead to near-complete cancelation of the net magnetic moment. However, in FeGd thin films with varying thickness, a thickness-dependent nanoscale phase segregation has been shown to greatly affect magnetic compensation and other magnetic properties [1,2]. Unintended heating of the sample during deposition may be a reason for the variation in magnetic properties. Here, 100 nm FeCoGd thin films with the same nominal composition ($[FeCo]_{71}Gd_{29}$, with a Fe:Co ratio of 9:1) were grown via DC magnetron sputtering from elemental targets and subsequently cooled in ultrahigh purity Ar or vacuum environments before depositing a 5 nm capping layer (cap = Ta or Al). The waiting time before deposition of the cap varied from two to ten minutes, allowing the FeCoGd film to cool before deposition of the cap layer. The hysteresis loops and M vs. T curves were measured with vibrating sample magnetometry (VSM) and magneto-optical Kerr effect (MOKE). Large differences in the M vs. T curves and hysteresis loops are observed as a function of wait time and cap material, and the reversal of the MOKE loops allows us to track the magnetic compensation. The differing capping treatments lead to considerable variation in the magnetic properties, such as shifts of the magnetic compensation temperature of over 150 K. We will discuss these modifications and related effects related to capping with light (Al) and heavier (Ta) elements.

1. E. Kirk, C. Bull, S. Finizio, H. Sepehri-Amin, S. Wintz, A. K. Suszka, N. S. Bingham, P. Warnicke, K. Hono, P. W. Nutter, J. Raabe, G. Hrkac, T. Thomson, and L. J. Heyderman, Phys. Rev. Mater. 4, 074403 (2020). 2. A. Chanda, J. E. Shoup, N. Schulz, D. A. Arena, and H. Srikanth, Phys. Rev. B 104, 094404 (2021).

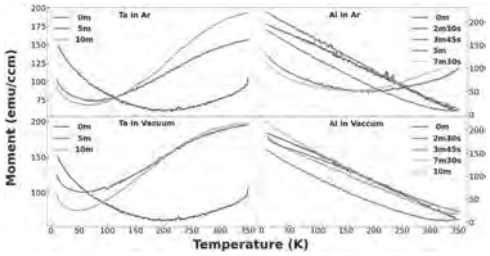

Fig.1 Magnetization as a function of temperature curves for FeCoGd capped with Al or Ta with variable cooling time in ultrahigh purity Ar or in vacuum environments.

LOB-10. Towards Optimised Tunable NiFe Multilayers for High-Frequency Applications. *M.R. McMaster*[1], W. Hendren[1], J. Scott[1] and R. Bowman[1] *1. Mathematics and Physics, Queen's University Belfast, Belfast, United Kingdom*

Control of the electromagnetic properties of synthetic magnetic structures at gigahertz frequencies is advantageous for the simulation and design of components for high-frequency applications, such as shielding materials in magnetic recording. In such applications, it is desirable to have a high saturation magnetization, low coercivity, high permeability, and near-zero magnetostriction. A typical material is Ni_xFe_{100-x}, where x ~ 80 provides near-zero magnetostriction but relatively low magnetization. Multilayer structures such as $Ni_{80}Fe_{20}/Ni_{20}Fe_{80}$ may benefit some static properties such as magnetization while retaining low magnetostriction [1] and therefore will extend the parameter space. We present a systematic study of the ferromagnetic resonance (FMR) of sputter-deposited thin-film NiFe bilayers of the form $Ni_xFe_{100-x}/Ni_yFe_{100-y}$ using VNA-FMR [2], vibrating sample magnetometry and x-ray diffraction, with the purpose of investigating the relation between dynamic magnetic and microstructure properties of such structures. Of particular interest are layer combinations involving both fcc and bcc crystal structures since studies on single films of Ni_xFe_{100-x} have shown dramatically increased damping of the FMR when Ni content is reduced across the transition from fcc to bcc near x ~ 40, figure 1. A result that was not to be expected from the single-layer studies was that the FMR response of certain bilayers was strong even when the bcc NiFe layer was the dominant layer in the structure, figure 2. The possibility of incorporating the best properties of both layers in this way has significance for achieving an optimized material design.

[1] C.B. Hill. "Manipulation and Magnetostriction of NiFe Films for Advanced Reader Shielding Application", PhD Thesis, Queen's University Belfast (2013) [2] Y. Ding, T. J. Klemmer and T. M. Crawford, J. Appl. Phys. Vol. 96, p.2969 (2004)

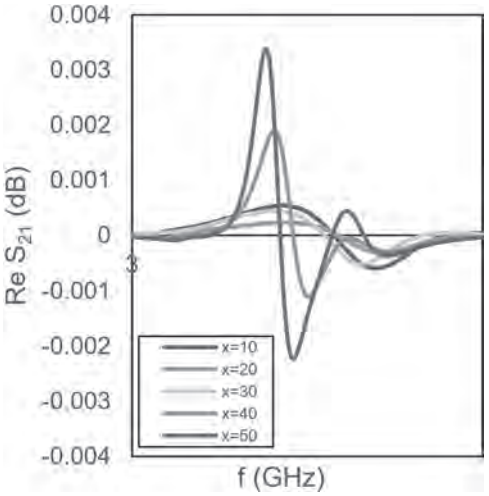

Fig. 1: FMR spectra of 100nm Ni_xFe_{100-x} single layer thin films with x varying from 10 to 50 across the fcc/bcc phase transition boundary. Note that all measurements were performed at an applied field H=253Oe.

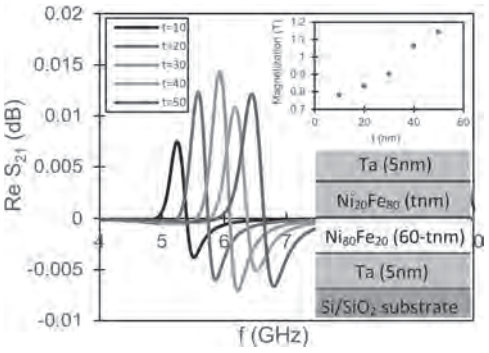

Fig. 2: FMR spectra of $Ni_{80}Fe_{20}$(60-t nm) / $Ni_{20}Fe_{80}$(t nm) thin films with varying bcc layer thickness, t. Note that all measurements were performed at an applied field of 253Oe. Magnetization trend and structure schematic is inset.

LOB-11. Quantification of Micromagnetic Parameters in Ultrathin Asymmetrically Sandwiched Magnetic Thin Films. *O.M. Volkov*[1], I.A. Yastremsky[2], O. Pylypovskyi[1], F. Kronast[3], C. Abert[4], E. Oliveros Mata[1], P. Makushko[1], M. Mawass[3], V.P. Kravchuk[5], D.D. Sheka[2], B.A. Ivanov[2,6], J. Fassbender[1] and D. Makarov[1] *1. Institute of Ion Beam Physics and Materials Research, Helmholtz-Zentrum Dresden-Rossendorf, Dresden, Germany; 2. Faculty of Radio Physics, Electronics and Computer Systems, Taras Shevchenko National University of Kyiv, Kyiv, Ukraine; 3. Helmholtz-Zentrum Berlin, Berlin, Germany; 4. Faculty of Physics, University of Vienna, Vienna, Germany; 5. Karlsruher Institut für Technologie (KIT), Karlsruhe, Germany; 6. Institute of Magnetism, National Academy of Sciences and Ministry of Education and Science, Kyiv, Ukraine*

Ultrathin asymmetrically sandwiched ferromagnetic films support fast moving chiral domain walls (DWs) and skyrmions [1,2]. This paves the way to the realization of prospective racetrack memory concept, the performance of which is determined by the static and dynamic micromagnetic

parameters [3]. The necessity of having strong Dzyaloshinskii-Moriya interactions (DMI) and perpendicular magnetic anisotropy requires the utilization of ultrathin (~1 nm) layers, which compromize structural quality and substantially enhance the damping for non-collinear magnetic textures. Here, we present the experimental and theoretical analysis of ultrathin Co films with asymmetric interfaces //CrO_x/Co/Pt and estimation of their micromagnetic parameters based on the analysis of the temperature dependence of magnetization as well as imaging of the DW morphology in stripes. We show that in the frame of magnon thermodynamics the best fit to the magnetometry data up to room temperature is obtained within a quasi-2D model, accounting for the lowest transversal magnons [4]. The developed approach provides access to the exchange constant in asymmetric stacks, which is found to be about 1 order of magnitude smaller compared to the bulk Co. The experimentally observed tilt of magnetic DWs in stripes in statics can be explained based on two models: (I) A unidirectional tilt could appear in equilibrium as a result of the competition between the DMI and additional in-plane easy-axis anisotropy, which breaks the symmetry of the magnetic texture and introduce tilts [5]. (II) A static DW tilt could appear due to the spatial variation of magnetic parameters, which introduce pinning centers for moving tilted DWs driven by magnetic field and can fix them at remanence [6]. We found that the second model is in line with the experimental observations and allows to determine self-consistently the DW damping parameter and DMI constant for the particular layer stack. The DW damping is found to be about 0.1 and explained by the enhanced longitudinal relaxation mechanism. The latter is shown to be much stronger than the standard transversal relaxation and can be even stronger than the spin pumping contribution for the case of ultrathin magnetic films [7].

[1] N. Nagaosa and Y. Tokura, "Topological properties and dynamics of magnetic skyrmions", Nat. Nanotechnol. 8, 899 (2013). [2] A. Fert, N. Reyren, and V. Cros, "Magnetic skyrmions: advances in physics and potential applications", Nat. Rev. Mater. 2, 17031 (2017). [3] C. Garg, S.-H. Yang, T. Phung, A. Pushp and S. S. P. Parkin, "Dramatic influence of curvature of nanowire on chiral domain wall velocity", Sci. Adv. 3, e1602804 (2017). [4] I. A. Yastremsky, O. M. Volkov, M. Kopte, T. Kosub, S. Stienen, K. Lenz, J. Lindner, J. Fassbender, B. A. Ivanov and D. Makarov, "Thermodynamics and Exchange Stiffness of Asymmetrically Sandwiched Ultrathin Ferromagnetic Films with Perpendicular Anisotropy", Phys. Rev. Appl. 12, 064038 (2019). [5] O. V. Pylypovskyi, V. P. Kravchuk, O. M. Volkov, J. Fassbender, D. D. Sheka and D. Makarov, "Unidirectional tilt of domain walls in equilibrium in biaxial stripes with Dzyaloshinskii–Moriya interaction", J. Phys. D: Appl. Phys. 53, 395003 (2020). [6] O. M. Volkov, F. Kronast, C. Abert, E. Se. Oliveros Mata, T. Kosub, P. Makushko, D. Erb, O. V. Pylypovskyi, M.-A. Mawass, D. Sheka, S. Zhou, J. Fassbender and D. Makarov, "Domain-Wall Damping in Ultrathin Nanostripes with Dzyaloshinskii-Moriya Interaction", Phys. Rev. Appl. 15, 034038 (2021). [7] I. A. Yastremsky, J. Fassbender, B. A. Ivanov, and D. Makarov, "Enhanced Longitudinal Relaxation of Magnetic Solitons in Ultrathin Films", Phys. Rev. Appl. 17, L061002 (2022).

LOB-12. Growth-Induced Order in Anisotropic Mixed Rare-Earth Iron Garnet Thin Films. *A. Kaczmarek*[1], Y. Song[1], E.R. Rosenberg[1], G. Beach[1] and C.A. Ross[1] *1. Materials Science and Engineering, Massachusetts Institute of Technology, Cambridge, MA, United States*

Films with perpendicular magnetic anisotropy (PMA) enable high data packing density and are useful for many spintronic phenomena. In rare-earth iron garnets (REIGs), PMA typically originates from magnetoelastic anisotropy either as a result of lattice mismatch with a single crystal garnet substrate or from thermal mismatch upon annealing[1]. However, PMA derived from magnetoelastic anisotropy requires specific combinations of strain and magnetostriction coefficients, so there is interest in finding new ways to control PMA. We draw inspiration from 1960s-era growth-induced PMA demonstrated for garnets synthesized by liquid phase epitaxy (LPE), which has recently been revisited for pulsed laser deposited (PLD) films of (Y,Tm) garnet[2,3]. In this study we show that PMA can be obtained from a dominant growth-induced anisotropy (GIA) in europium thulium iron garnet ($Eu_xTm_{3-x}Fe_5O_{12}$) grown by PLD. By varying the Eu:Tm ratio, the lattice parameter of each garnet was changed, resulting in films under compression or tension on gadolinium gallium garnet. Vibrating sample magnetometry indicates that PMA is present even in films with near-zero strain, where magnetostriction cannot yield PMA. We quantified GIA and other contributions to anisotropy in the films with spin Hall magnetoresistance measurements (Fig. 1). GIA peaks for x = 1.5 at 70 kJ/m^3, a magnitude five times greater than predictions based on data from LPE bulk crystals. To determine if GIA arises from the site preference model, which describes ordering of rare-earth ions on energetically inequivalent lattice sites during growth, we look to electron dispersive spectroscopy scanning transmission electron microscopy (EDS STEM) of films with large GIA (Fig. 2). This work shows that precise engineering of composition and structure in these films creates new methods for control of thin film properties for spintronic applications and confirms the origins of GIA in mixed REIGs.

1. Rosenberg, E. R. *et al.* Magnetism and spin transport in rare-earth-rich epitaxial terbium and europium iron garnet films. *Phys. Rev. Mater.* 2, 094405 (2018). 2. Rosenberg, E. R. *et al.* Magnetic Properties and Growth-Induced Anisotropy in Yttrium Thulium Iron Garnet Thin Films. *Adv. Electron. Mater.* n/a, 2100452. 3. Eschenfelder, A. H. *Magnetic Bubble Technology*. (Springer-Verlag, 1980).

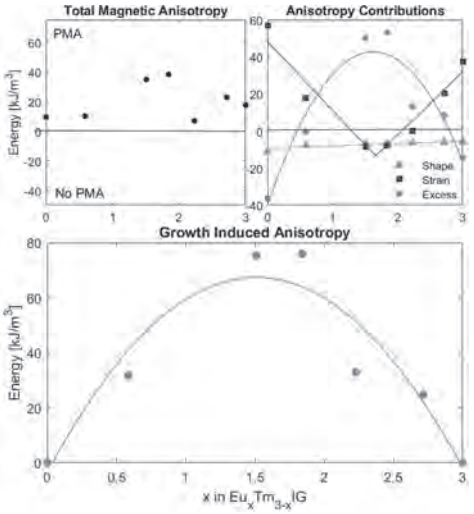

Fig. 1. Contributions to magnetic anisotropy from shape and strain anisotropy reveal excess energy attributed to GIA in the mixed REIG.

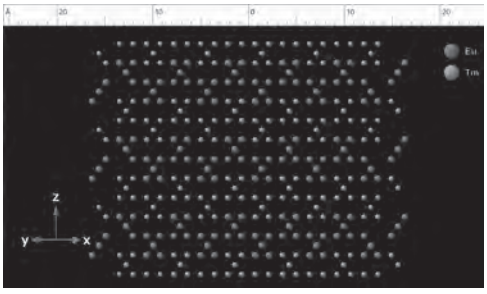

Fig. 2. Model of [110] view EDS STEM shows preferential ordering on dodecahedral sites within the garnet crystal structure with 1:1 Eu:Tm ratio during [111] growth.

LOB-13. High-coercive PrFeB Films with Strong Perpendicular Magnetic Anisotropy. *J. Soler Morala*[1], C. Navio[1], G. Gkouzia[4], P. Pedraz[1], L. Zha[2,3], J. Yang[2,3], L. Alff[4] and A. Bollero[1] *1. IMDEA Nanociencia, Madrid, Spain; 2. Beijing Key Laboratory for Magnetoelectric Materials and Devices, Beijing, China; 3. State Key Laboratory for Mesoscopic Physics, Peking University, Beijing, China; 4. Materials science, Technische Universität Darmstadt, Darmstadt, Germany*

Rare-earth transition metal thin films hold great potential for implementation in devices at the micro and nanoscale [1-3]. While $Nd_2Fe_{14}B$ and $Pr_2Fe_{14}B$ share almost the same intrinsic magnetic properties (M_s, K_u…), $Nd_2Fe_{14}B$ has a limited use for low temperature applications (i.e. aerospace) due to the spin reorientation that occurs at 135 K [4]. This limitation can be overcome using $Pr_2Fe_{14}B$, whose magnetization direction remains along the c-axis until 4.2 K [4]. The understanding and optimization of these systems is of great importance when attempting their integration in novel miniaturized devices [5]. In this study, high coercivity PrFeB thin films of 100 nm have been fabricated by magnetron sputtering. The effect on the substrate temperature (T_s) in the structure and morphology and its resulting impact on the magnetic properties has been evaluated. Our research stablishes the optimum T_s to be 600°C where a highly textured growth of $Pr_2Fe_{14}B$ is achieved according to the X-Ray Diffraction (XRD) analysis (Fig. 1a). $Pr_2Fe_{14}B$ crystalline phase is accompanied by a Pr-rich phase that can be identified in all the XRD patterns. The role that these Pr-rich areas play in the magnetism of these systems has also been thoroughly studied by Energy Dispersive X-Ray Spectroscopy (EDX) (Fig. 1c). Regardless of T_s, all films present strong perpendicular magnetic anisotropy (Fig.2c,d) which is in good accordance with the c-axis oriented preferential growth. Out of plane coercivities up to 14 kOe have been obtained at RT. Atomic and Magnetic Force Microscopy (AFM and MFM, respectively) have also been used to determine influence of T_s on the roughness and magnetic domains (Fig 2a,b).

References: [1] X. Liu, T. Okumoto, M. Matsumoto, A. Morisako. *J. Appl. Phys.* 97, 10K301 (2005). [2] T.-S. Chin, *J. Magn. Magn. Matter*. 209, 75-79 (2000). [3] A. Bollero, V. Neu, V. Baltz *et al.*, *Nanoscale*, 12, 1155-1163 (2020). [4] TT. B. Lan, G.C. Hermosa and A.C. Sun, *J. Phys. Chem. Solid*. 144, 109506 (2020). [5] H2020 FET-OPEN project "UWIPOM2": https://cordis.europa.eu/project/id/857654. Acknowledgements: Authors acknowledge financial support from EU through the H2020 FET Open UWIPOM2 project (Ref. 857654). J. S-M. acknowledges financial support from Comunidad de Madrid (PEJD-2019-PRE/IND-17045).

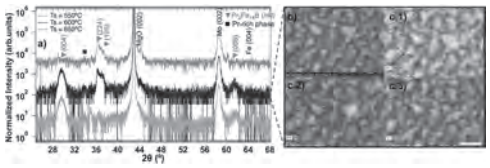

Fig. 1. a) XRD pattern of PrFeB thin films grown at different Ts, b) Scanning electron microscopy (SEM) image of a PrFeB film grown at 600ºC, c) EDX mapping of a PrFeB film with a Ts = 600ºC showing the distribution of Pr and Fe (c.1) Prdistribution (c.2) Fe distribution (c.3). The scale bar is 800 nm in all cases.

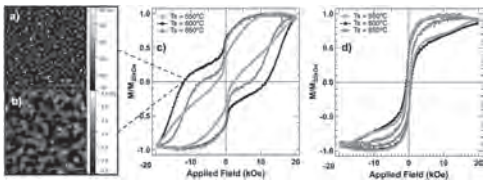

Fig. 2. a) AFM and b) MFM image of a PrFeB film grown at 600ºC, c) Out of plane and d) In Plane room temperature hysteresis loops with a maximum applied field of 20 kOe for PrFeB thin films grown at different Ts.

LOB-14. Chirality-induced asymmetric magnetization reversal in perpendicularly exchange biased micro stripes. *S. Akhundzada*[1], P. Kuswik[3], M. Kowacz[3], C. Janzen[1], T. Mewes[2], A. Ehresmann[1] and M. Vogel[1] *1. Institute of Physics and Center for Interdisciplinary Nanostructure Science and Technology (CINSaT), University of Kassel, Kassel, Germany; 2. Department of Physics and Astronomy, University of Alabama, Tuscaloosa, AL, United States; 3. Institute of Molecular Physics, Polish Academy of Sciences, Poznan, Poland*

Hybrid magnetic layer systems consisting of a heavy metal, an ultrathin ferromagnet (F), and an antiferromagnet (AF) are interesting material systems that potentially exhibit both the interface-driven exchange bias (EB) effect and the asymmetric exchange interaction, known as Dzyaloshinskii-Moriya interaction (DMI) [1]. The DMI is essential for stabilizing chiral spin-structures like skyrmions, which are promising candidates for magnetic memory technologies [2]. Due to the DMI and the resulting Néel domain walls with chirality set by DMI, tilted magnetic moments are present at the domain edges [3]. Experimentally, this effect has been observed as asymmetric domain propagation while applying in-plane and perpendicular magnetic fields simultaneously [4]. While the DMI and EB can be modified independently from each other [5], only few studies so far have focused on the interplay between chiral DMI and the unidirectional EB anisotropy, affecting the magnetic domain texture and the resulting magnetization reversal. We report on a systematic study of the magnetization reversal in perpendicularly exchange biased Ti/Au/Co/NiO/Au micro stripes by high-resolution Kerr microscopy. Thereby, the magnetization reversal process is observed to be asymmetric with respect to the two branches of the hysteresis loop. We are able to quantify this as an asymmetry of the nucleation density formed in the two field branches as a function of the structure width. Additionally, a local asymmetry in the domain nucleation and domain wall movement within each stripe is observed. This phenomenon is investigated by field-cooling and the application of additional in-plane magnetic fields during the magnetization reversal. Additionally, XMCD/XMLD-PEEM experiments were performed to reveal the corresponding domain patterns in the F and AF. The results pave the way in the understanding of the interplay between chiral DMI and the unidirectional EB anisotropy in micro- and nanostructures.

[1] F. Hellman *et al.*, "Interface-induced phenomena in magnetism," *Rev. Mod. Phys.*, vol. 89, no. 2, pp. 1–79, 2017, doi: 10.1103/RevModPhys.89.025006. [2] A. Manchon *et al.*, "Current-induced spin-orbit torques in ferromagnetic and antiferromagnetic systems," *Rev. Mod. Phys.*, vol. 91, no. 3, 2019, doi: 10.1103/RevModPhys.91.035004. [3] S. Rohart and A. Thiaville, "Skyrmion confinement in ultrathin film nanostructures in the presence of Dzyaloshinskii-Moriya interaction," *Phys. Rev. B - Condens. Matter Mater. Phys.*, vol. 88, no. 18, pp. 1–8, 2013, doi: 10.1103/PhysRevB.88.184422. [4] P. Kuswik *et al.*, "Asymmetric domain wall propagation caused by interfacial Dzyaloshinskii-Moriya interaction in exchange biased Au/Co/NiO layered system," *Phys. Rev. B*, vol. 97, no. 2, pp. 1–7, 2018, doi: 10.1103/PhysRevB.97.024404. [5] P. Kuswik, M. Matczak, M. Kowacz, F. Lisiecki, and F. Stobiecki, "Determination of the Dzyaloshinskii-Moriya interaction in exchange biased Au/Co/NiO systems," *J. Magn. Magn. Mater.*, vol. 472, no. April 2018, pp. 29–33, 2019, doi: 10.1016/j.jmmm.2018.10.002.

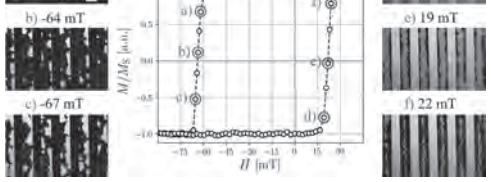

Fig. 1: Asymmetric nucleation in 10 µm wide Ti/Au/Co/NiO/Au stripes. The Kerr images show that for the decreasing field branch a)-c) the domains are formed preferentially at one edge, smaller ones are formed equally at both edges for the increasing field branch d)-f).

Session LPA
STRUCTURED MATERIALS
(Poster Session)

Yu Shiratsuchi, Chair
Osaka University, Osaka, Japan

LPA-01. Withdrawn

LPA-02. Doping Dependent Coercive Field in the Reduced Dimensional System $La_{1-x}Sr_xMnO_3$ ($0.04 \le x \le 0.5$). *T.M. Pekarek*[1], K. Taylor[1], C.T. Bryant[1], R. Marquez Tavera[1], J. Payne[1], D. Brown[1] and M.P. Warusawithana[1]
1. Physics, University of N. Florida, Jacksonville, FL, United States

We have investigated the electronic and magnetic ground state of a series of $La_{1-x}Sr_xMnO_3$ thin films as a function of doping for $0.04 \le x \le 0.5$. The films were grown by molecular-beam epitaxy, epitaxially strained to (001) oriented strontium titanate substrates. We find that the ground state of these crystalline thin films is, in general, consistent with that observed in both bulk and thin film samples synthesized under a multitude of techniques. Our systematic study also reveals subtle features in the temperature dependent electronic transport and magnetization measurements that may correspond to Jahn-Teller type distortions in the lattice as a function of doping and temperature. The doping dependent coercive field in this series of samples was investigated. We find the coercive field increases from the minimum value of $H_c = 0.0080$ T at 5 K for $x = 0.33$ as the doping is changed in either direction from $x = 0.33$. At 5 K, the coercive field increases to $H_c = 0.0283$ T for $x = 0.20$ and increases to $H_c = 0.0450$ T for $x = 0.50$. The temperature dependent coercive field was also studied for individual doping concentrations. For the $x = 0.50$ sample, we observe a dramatic cusp in the coercive field at 100 K that is better defined than the more subtle features observed in both magnetization and resistivity data at this temperature. The authors acknowledge support from the UNF Office of Undergraduate Research. T.M.P. acknowledges support from the UNF Terry Presidential Professorship and the National Science Foundation (NSF) Grant Nos. DMR-16-26332 and DMR-14-29428. M.P.W. acknowledges support from the UNF Scholarship Grant.

LPA-03. Element-specific magnetocrystalline anisotropy of Sm-Co thin films. *G. Gkouzia*[1], D. Günzing[2], R. Xie[1], T. Wessels[2,3], M. Major[1], A. N'Diaye[4], H. Zhang[1], H. Wende[2], K. Ollefs[2] and L. Alff[1] *1. Materials Science, Technical University of Darmstadt, Darmstadt, Germany; 2. Faculty of Physics and Center for Nanointegration (CENIDE), University of Duisburg-Essen, Duisburg, Germany; 3. Ernst Ruska-Centre for Microscopy and Spectroscopy with Electrons and Peter Gruenberg Institute, Juelich, Germany; 4. Lawrence Berkeley National Laboratory, Berkeley, CA, United States*

Rare earth/transition metal permanent magnets have gained significant interest due to their outstanding performance, which has made them key materials for many applications. The most well-known compounds $Nd_2Fe_{14}B$, $SmCo_5$, and Sm_2Co_{17} combine a large energy density, high Curie temperature, and a large magnetocrystalline anisotropy (MCA). Besides, $SmCo_5$ exhibits the highest known uniaxial MCA[1]. Due to their importance, a detailed understanding of their hysteresis behavior has come into the focus of research[2]. Since the extrinsic magnetic properties of magnetic materials depend on their complex defect and nanostructure, we follow the strategy to disentangle intrinsic and extrinsic properties as well as the effect of specific defects by investigating $SmCo_5$ and Sm_2Co_{17} phases in thin film model systems grown by molecular beam epitaxy (MBE). The Sm-Co system, when grown as thin films in a certain parameter range, undergoes a phase decomposition into a nanocomposite of $SmCo_5$ and Sm_2Co_{17} phases. Due to the structural similarity of the two phases, it is challenging to discriminate their phase contributions. Extended X-ray absorption fine structure (EXAFS) analysis combined with transmission electron microscopy (TEM) allows the unambiguous quantification of the nano-domain phase decomposition in the thin films[3]. In this work, we have studied the behavior of the magnetic anisotropy of Co and Sm using - for the first time, to our knowledge - angle-dependent X-ray magnetic circular dichroism (XMCD) at Sm $M_{4,5}$ and Co $L_{2,3}$ edges in 1.9 Tesla external applied field. $SmCo_5$ and Sm_2Co_{17} thin films have been grown onto Al_2O_3 substrates and pre-characterized by X-ray diffraction (XRD) and superconducting quantum interface device (SQUID). XMCD and X-ray absorption spectroscopy (XAS) gave access to element-specific information and have been complemented by detailed atomistic spin dynamics (ASD) calculations. Element-specific hysteresis curves demonstrate strong coupling between Sm and Co, however, the spectroscopy indicates different saturation behavior. The XMCD spectra for the Sm $M_{4,5}$ edges show surprisingly only a minor angle dependence. Using ASD simulations, we estimate the exchange field at the Sm site to be of the order of -200 T.

[1] K. J. Strnat & R. M. W. Strnat, J. Magn. Magn. Mater. 100, 36 (1991). [2] O. Gutfleisch *et al.*, Adv. Mater. 23, 821 (2011). [3] S. Sharma *et al.*, ACS Appl. Mater. Interfaces 13, 32415 (2021).

LPA-04. Magnetic, optical and magneto-optical properties of strain-free $La_{2/3}Sr_{1/3}MnO_3$ thin films on Si substrates with $Ca_2Nb_3O_{10}$ nanosheet seed layer. *T. Maleček*[1], T. Maroutian[2], G. Agnus[2], L. Horák[1], A. Melzer[1], P. Lecoeur[2] and M. Veis[1] *1. Faculty of Mathematics and Physics, Charles University, Prague, Czechia; 2. Centre for Nanoscience and Nanotechnology (C2N), Palaiseau, France*

Hole doped $La_{2/3}Sr_{1/3}MnO_3$ (LSMO) is an auspicious candidate for spintronic applications due to its high spin polarization [1] and colossal magnetoresistance [2]. However, the growth of LSMO thin films on silicon, and other substrates important for applications, is extremely challenging due to their structural incompatibility and high reactivity with oxygen. Here, we demonstrate the possibility to grow strain-free LSMO thin films on silicon substrates with magnetic, magneto-optical and optical properties comparable to epitaxial layers grown on $SrTiO_3$ (STO). This growth was achieved using a two-dimensional $Ca_2Nb_3O_{10}$ nanosheet (NS) seed layer which induces epitaxial stabilization of LSMO. The 20 and 40 nm thick films of LSMO were grown by pulsed laser deposition with identical conditions for both the silicon and STO substrates. X-ray diffraction characterization of the samples confirmed strained epitaxial LSMO layers on STO and relaxed fibre textured films with unified out-of-plane orientation on Si with NS seed layer. Magnetization measurements, shown in Fig. 1, revealed smaller saturation magnetization for samples grown on Si. This might be attributed to the textured nature of the samples. However, these samples exhibit a higher Curie temperature by more than 10 K, which is the result of strain relaxation. For a closer insight into the electronic structure of the material a combination of spectroscopic ellipsometry and magneto-optical spectroscopy experiments were performed. The results allowed to derive the full permittivity tensor of the material in the spectral range from 1.5 to 5 eV. The spectral dependence of the off-diagonal element of the permittivity tensor, shown in Fig. 2, revealed striking similarity between the LSMO samples grown on STO and Si. Three electronic transitions around 1.9, 2.9, and 3.5 eV were identified in the spectra, suggesting the main contribution to the optical response arises from Mn states [3].

[1] M. Bowen, M. Bibes, A. Barthélémy, et al., Appl. Phys. Lett., Vol. 82, p.233–235 (2003) [2] A.P. Ramirez, J. Phys.: Condens. Matter, Vol. 9, p.8171–8199 (1997) [3] M. Zahradník, T. Maroutian, M. Zelený, et al., Phys. Rev. B, Vol. 99, p.195138 (2019)

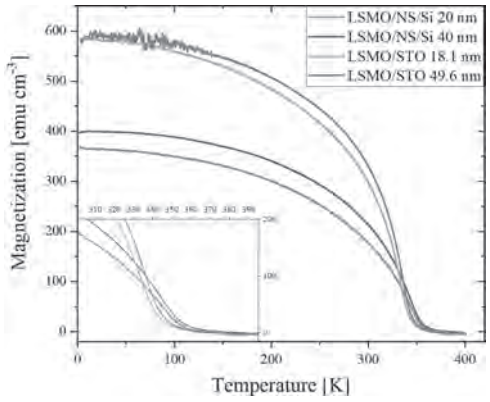

Fig. 1: Temperature dependent magnetization of LSMO samples on STO and Si in saturation.

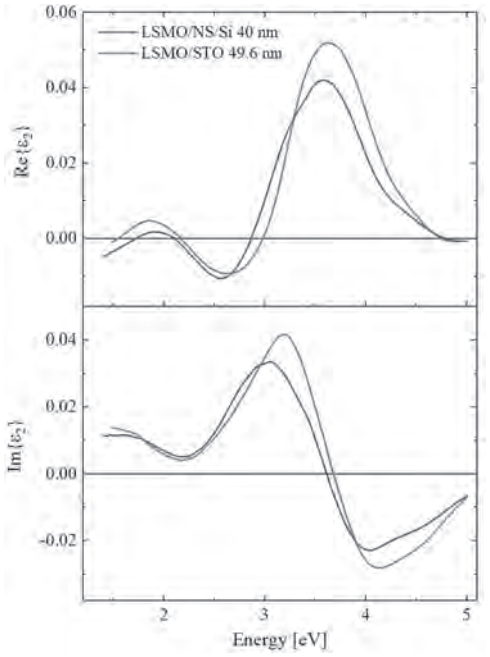

Fig. 2: Spectral dependence of the off-diagonal element of the permittivity tensor of LSMO samples on Si and STO.

LPA-05. Strong Perpendicular Magnetic Anisotropy in Co/Pt and Co/Pd Synthetic Antiferromagnets. *M. Caseiro*[1,2], R. Macedo[1], P. Araujo[1,2], S. Cardoso[1,2], M. Erkovan[1] and P. Freitas[1,2] *1. INESC MN, Lisbon, Portugal; 2. Instituto Superior Técnico, Lisbon, Portugal*

Perpendicular magnetic tunnel junctions (p-MTJs) have shown great potential in spintronics applications such as STT-MRAM [1] and magnetic sensors [2] due to having enhanced thermal stability and lower switching currents, while also offering compatibility with industrial semiconductor processing [3,4]. They usually rely on the perpendicular synthetic antiferromagnetic (p-SAF) structures often based on Co/Pt and Co/Pd multilayers, which exhibit large perpendicular magnetic anisotropy (PMA) energy and high exchange interlayer energy (IEC), as large as 2.6 erg/cm^2 [5]. This work explores the RKKY interaction in Co/Pt-and Co/Pd-based p-SAF systems using an Ir spacer. The multilayer films were deposited in a 6 target Nordiko 2000 magnetron sputtering system (deposition base pressure 5.5x10^{-8} Torr) with the following structures: a) Ta 2.5/Pt 3/[Co t_1/Pt 0.2]$_{n1}$/Co t_1/Ir 0.32/[Co t_2/Pt 0.2]$_{n2}$/Ta 2.5 and b) Ta 2.5/Pd 3/[Co t_1/Pd 0.22]$_{n1}$/Co t_1/Ir 0.32/[Co t_2/Pd 0.22]$_{n2}$/Co t_2/Ta 2.5 (thicknesses in nm) with varying thicknesses t_1 and t_2, and number of multilayers n_1 and n_2. The magnetic properties and interlayer couplings were obtained at RT via vibrating sample magnetometry (VSM) under out-of-plane magnetic fields. Figure 1 shows representative M(H) loops of the Co/Pt-based systems. The multilayer number has direct impact in the exchange coupling fields where the interlayer exchange energy, calculated through, is -2.01 erg/cm^2. The corresponding Co/Pd-based p-SAFs (Figure 2) showed a dramatically lower IEC of -0.71 erg/cm^2, which is comparable with in-plane SAFs. Thermal stability and dependency on size for patterned devices will be investigated. The authors acknowledge the Q-HADAR Project-20123419-AWD, funded by DARPA, in cooperation with Purdue University. The authors also wish to acknowledge the Fundação para a Ciência e a Tecnologia for funding of the Research Unit INESC MN (UID/05367/2020) through plurianual BASE and PROGRAMATICO financing, the PhD research grant of P. Araújo (PD/BD/150391/2019).

[1] K. Elphick, et al., Applied Physics Letters 109 (5) (2016) 052402 [2] P. P. Freitas, et al., Journal of Physics: Condensed Matter 19 (16) (2007) 165221 [3] Heinonen, et al., J. Appl. Phys. 108, 014305 (2010) [4] Chun, K. C. et al., IEEE J. Solid-State Circuits 48, 598–610 (2013) [5] Yakushiji, et al., Applied Physics Letters 110 (9) (2017)

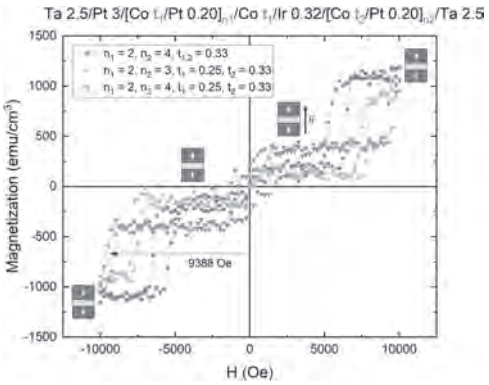

Fig.1 - M(H) loops obtained with [Co/Pt] multilayers (in nm).

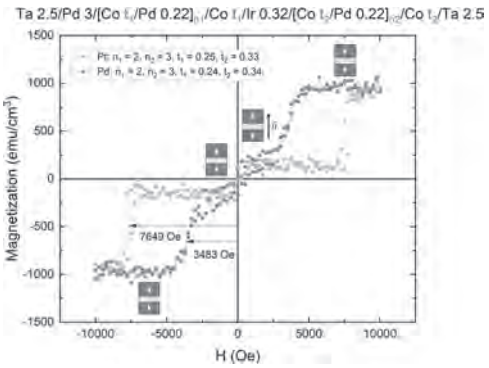

Fig.2 - M(H) loops obtained with [Co/Pd] multilayers (in nm).

LPA-06. Fabrication of β-Mn type CoZnMn(001) film on MgO single crystal substrate. *D. Oshima*[1], R. Mitsuhashi[1], N. Ikarashi[2], T. Kato[2] and M. Nagao[2] *1. Electronics, Nagoya University, Nagoya, Japan; 2. Institute of Materials and Systems for Sustainability, Nagoya University, Nagoya, Japan*

β-Mn type CoZnMn is one of chiral magnets and is reported to host Bloch skyrmions above room temperature [1]. CoZnMn epitaxial thin films are attractive for the device application, however, there is no report on the fabrication of the epitaxial film, although polycrystalline CoZnMn films were reported in the previous study [2]. Here, we report CoZnMn epitaxial

films grown on MgO(001) single crystal substrates. [Co-Zn(10 – t nm)/Mn(t nm)]$_{15}$ multilayers were prepared by rf magnetron sputtering of Co-Zn composite target and Mn target. The multilayers were grown on 10 nm-thick W buffer layer. The total thickness of the multilayers was kept constant at 150 nm, and the Mn composition was controlled by varying the Mn layer thickness t. The composition of Co-Zn layer was estimated to be Co/Zn = 0.8 by energy dispersive x-ray spectroscopy. 10 nm-thick W capping layer was deposited on the multilayers. After the deposition, the multilayers were annealed at 300 °C in vacuum to obtain the CoZnMn alloy. Crystal structure was characterized by x-ray diffraction. Figure 1(a) shows a reciprocal space mapping of the sample for t = 2 nm in the plane parallel to MgO(130), where Q_y and Q_z are parallel to MgO[310] and MgO[001], respectively. In the figure, β-Mn type CoZnMn 103, 104 and 204 diffraction spots were observed, indicating the epitaxial growth of β-Mn type CoZnMn film with (001) orientation. Figure 1(b) shows ϕ scan profile for β-Mn type CoZnMn 103 diffractions. 8 peaks were observed in the in-plane scanning even though β-Mn type CoZnMn has 4-fold symmetry, which means the existence of twinned crystal grains with CoZnMn[100]//MgO[310] and CoZnMn[100]//MgO[3 -1 0] in the film. Although there exists twin crystals in the film, β-Mn CoZnMn (001) film was successfully fabricated on a MgO single crystal substrate.

[1] Y. Tokunaga et.al., Nat. Comm. 6, 7638 (2015). [2] Ishikawa et.al., The 66th JSAP Spring Meeting, 9p-PB1-15 (2019).

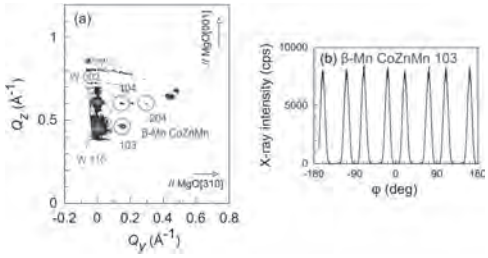

Fig. 1 (a) Reciprocal space mapping of the CoZnMn film in the plane parallel to MgO(130). (b) ϕ scan for β-Mn type CoZnMn 103 diffractions.

LPA-07. Withdrawn

LPA-08. Inhomogeneous strain induced new interfacial phase of $La_{0.7}Sr_{0.3}MnO_3$ thin film. S.P. Pati[1], T. Usami[1], S. Komori[1] and *T. Taniyama[1] 1. Department of Physics, Nagoya University, Nagoya, Japan*

Oxide-electronics comprising interfaces between transition-metal-oxides (TMOs) is an open playground, where the interfacial properties can be controlled by polar discontinuities, band bending, epitaxial strain etc [1]. In this work, we report on the emergence of an additional distinct interfacial phase of $La_{0.7}Sr_{0.3}MnO_3$(LSMO) due to growth induced inhomogeneous strain. 100-nm-thick LSMO layers were epitaxially grown on $SrTiO_3$(001) (STO) and $[Pb(Mg_{0.3}Nb_{0.7})O_3]_{0.7}$-$[PbTiO_3]_{0.3}$(001) (PMN-PT) substrates by pulsed laser deposition [2]. X-ray diffraction results indicate that the lattice mismatch is large in case of LSMO/PMN-PT that can lead to a sudden relaxation of strain, while a small lattice mismatch at the interface of LSMO/STO results in inhomogeneous relaxation of strain. Due to the inhomogeneous strain, an additional structural and magnetic phase, so called quasi two-dimensional electronic states (strained phase) of LSMO, is evolved at the interface with STO which is absent in LSMO/PMN-PT. For example, LSMO/PMN-PT possesses a single magnetic phase transition at the Curie temperature (T_C) ≈355K, whereas LSMO/STO exhibits two different T_C at 310 and 355 K, corresponding to the strained and relaxed phases, respectively. We also find a double dispersion relation in the ferromagnetic resonance (FMR) spectrum of LSMO/STO, in contrast to a single dispersion for LSMO/PMN-PT [3]; the weaker and stronger dispersions are assigned to the strained region and the relaxed phases, respectively. Effective saturation magnetization (M_{eff}) is estimated to be 428 and 176 kA/m for the strained and relaxed phases, respectively. Similarly, effective Gilbert damping constant (α_{eff}) is found to be larger in case of strained phase (α_{eff}≈0.02) than the relaxed phase (α_{eff}≈0.01). These clear evidences of the additional interfacial phase indicate that the lattice mismatch induced strain plays an important role in the formation of new interfacial magnetic phases. This work was supported in part by JST CREST Grant No. JPMJCR18J1, JSPS KAKENHI Grants Number 21H04614, JSPS Bilateral Joint Research Projects Grant No. JPJSBP120197716, and the Asahi Glass Foundation.

[1] J. Mannhart et al., *Science* 327, 1670 (2010). [2] S. P. Pati et al., *J. Phys. D* 53, 054003 (2020). [3] Y. Zhao et al., *ACS Appl. Mater. Interfaces* 13, 59511, (2021).

LPA-09. Growth temperature-controlled Gilbert damping and anisotropies in PLD grown epitaxial Co_2FeSi Heusler alloy thin film. *V. Sharma[2]*, P. Kumar[2], V. Sharma[1] and B.K. Kuanr[2] *1. Department of Physics, Morgan State University, Baltimore, MD, United States; 2. Special Centre for Nanoscience, Jawaharlal Nehru University, New Delhi, India*

The utilization of spin rather than charge as a functional aspect in the electronic devices will result in an energy-efficient, thermally stable, and ultrafast operation. Cobalt-based Heusler alloy Co_2FeSi (CFS) offers excellent possibilities due to its high curie temperature, large spin polarization, and low Gilbert damping [1]. The small value of Gilbert damping (α) makes the alloy fascinating for STT-MRAM devices where a low α causes a low value of switching current [2]. In the present investigation we are dealing with the effect of growth temperature on the chemical, structural and magnetic properties of the Pulsed Laser Deposition (PLD) grown single-crystal CFS film of thickness 50 nm on a lattice-matched (001) MgO substrate. The XRD data suggest that Co site atomic ordering and overall film crystallinity improved with temperature, resulting in a minimal value of Gilbert damping obtained from ferromagnetic resonance (FMR) experiment (performed in a broadband FMR system) in the film grown at 600^0 C as shown in Fig 1. (a-b). The azimuthal angular variation of FMR data shown in Fig 1. (c) gives a four-fold butterfly-like anisotropy pattern that confirms the single-crystal CFS film epitaxially grown on the MgO substrate. Two in-plane anisotropies, namely cubic (four-fold) and uniaxial, were determined for these samples. These two anisotropies, which appear due to cubic crystalline symmetry and magnetoelastic interaction in a strained film, are the critical parameters and play a centric role in the fabrication of energy-efficient Spin-Transfer Torque (STT) based memory and processing devices.

[1] I. Galanakis, P. H. Dederichs, and N. Papanikolaou, "Slater-Pauling behavior and origin of the half-metallicity of the full-Heusler alloys," *Phys. Rev. B*, vol. 66, no. 17, p. 174429, 2002. [2] J. Manschot, A. Brataas, and G. E. W. Bauer, "Reducing the critical switching current in nanoscale spin valves," *Appl. Phys. Lett.*, vol. 85, no. 15, pp. 3250–3252, 2004.

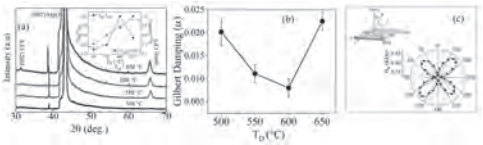

(a) XRD pattern of PLD deposited CFS/MgO film with different deposition temperature (T_D), inset shows the ratio of integrated intensity peak of (002) and (004) with T_D. (b) Gilbert damping obtained from FMR linewidth vs frequency data with T_D. (c) Azimuthal angle (ϕ) vs resonance field (H_r) for CFS film deposited at 600^0C.

LPA-10. Control of grain orientation spread and inhomogeneous broadening in $L1_0$ -phase FePd thin films with low damping and high perpendicular magnetic anisotropy. *J.E. Shoup*[1,3], J.A. Borchers[2], J. Wang[4], D. Arena[1] and D.B. Gopman[3] *1. University of South Florida, Tampa, FL, United States; 2. NIST Center for Neutron Research, National Institute of Standards and Technology, Gaithersburg, MD, United States; 3. Materials Science and Engineering Division, National Institute of Standards and Technology, Gaithersburg, MD, United States; 4. Department of Electrical and Computer Engineering, University of Minnesota, Minneapolis, MN, United States*

Future embedded and standalone magnetic random access memory (MRAM) solutions require materials possessing bulk magnetocrystalline anisotropy at sub-10 nm feature sizes. FePd in its $L1_0$-ordered phase delivers MJ/m^3 bulk anisotropy energy density (K_u) [1], large interlayer exchange coupling through Ru [2], Gilbert damping (α) below 0.008 [3] and robust compatibility across a range of Pt-group buffer layers [4]. Transitioning FePd films into mature spintronic applications requires a higher level of process control realize highly uniform microstructural, magnetic and magnetotransport properties. We demonstrate control of the orientation distribution of the c-axis in highly (001)-oriented $L1_0$ FePd. Using direct current magnetron sputtering on (001)-cut, polished MgO substrates, we explore an N_2 substrate anneal, variation in the individual thicknesses of the Cr/Pt underlayer and post-anneal modules between layers. Each sample had an 8-nm-thick FePd layer grown at 350 °C and post-annealed at 500 °C, leading to a high degree of $L1_0$ ordering, with K_u ranging between 0.8 MJ/m^3 and 1.1 MJ/m^3 and α ranging from 0.0067 to 0.0133. Despite the relatively narrow spread in these key parameters, we observed a wide range of inhomogeneous linewidth broadening ($\mu_0\Delta H_0$) from ferromagnetic resonance measurements, ranging from below 0.01 T to nearly 0.2 T (Fig. 1(a)). Variation in $\mu_0\Delta H_0$ correlates with the FePd grain orientation distribution, as measured by x-ray diffraction rocking curve scans of the (002) Bragg peak (Fig. 1(b)). Our process controls enable varying the full-width-half-maximum (FWHM) of the (002) peak from 14 degrees down to nearly 2 degrees, leading to narrowing of the local anisotropy distribution and reduction in the $\mu_0\Delta H_0$ (Fig. 1(b) inset). These process improvements will deliver the large-scale uniformity needed to implement FePd-based MRAM solutions.

[1] M. Futamoto *et al*., AIP Advances 6, 085302 (2016) [2] D.-L. Zhang *et al*., Phys. Rev. Appl. 9, 044028 (2018) [3] D.-L. Zhang *et al.,* Appl. Phys. Lett. 117, 082405 (2020) [4] X. Wang *et al.,* AIP Advances 11, 025106 (2021)

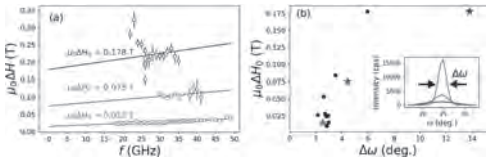

Figure 1: (a) FMR Linewidth versus frequency for three samples with inhomogeneous line broadening of 0.178 T (blue), 0.075 T (green) and 0.015 T (red). (b) Inhomogeneous line broadening versus FWHM of FePd(002) (Δω), with (inset) exemplary FePd(002) rocking curve scans of the red, blue and green star samples highlighted with colored markers in (a)

LPA-11. Modification and control of magnetic properties of multilayer systems via buffer layer. *J. Zázvorka*[1], C. Verbeno[1], L. Nowak[1] and M. Veis[1] *1. Faculty of Mathematics and Physics, Institute of Physics, Charles University, Prague, Czechia*

Magnetic multilayer systems are of interest due to their application potential, e.g. magnetic tunnel junctions, skyrmion racetracks[1-2], as their magnetic properties can be controlled by external parameters, such as thicknesses of individual layers or interface modifications. Tuning of magnetic properties (e.g. saturation magnetization, coercive field) is needed to produce multilayers with specific parameters required by different applications[3]. The interfaces between individual layers influence magnetic anisotropy[4] of the system and their modification can be used to prepare the multilayers with desired coercive field. This can be done by varying the thickness and surface roughness of a special buffer layer grown below the magnetic multilayer. We present a systematic study of $Au_x/Pt_{5nm}/Co_{0.7nm}/Au_{5nm}$ model system prepared by magnetron sputtering on Si substrate. The thickness of Au buffer layer varies from 0 to 20 nm. The surface morphology of Au_x/Pt_{5nm} was studied by AFM. Surface roughness of the Au_x/Pt stack strongly depends on the Au layer thickness (Fig.1) due to its island-like growth (Volmer-Weber mode)[5]. When the nominal Au thickness increases, the islands grow in larger lateral size, resulting in a higher overall roughness. This effect can be utilized to modify the Pt/Co interface via the sputtering process. Comparing magnetometry (Fig.2) with AFM measurements confirms this conclusion. A gradual increase of coercive field without a change in saturation magnetization, attributed to additional anisotropy produced by the increased Au layer roughness is observed. Using this mechanism, the coercivity of the system can be tuned in relatively large range. To investigate whether the effect is not connected to specific material of the buffer layer, we investigate the use of a Cu instead of Au with similar conclusions. The impact of the additional anisotropy induced by the buffer layer on the multilayer magnetic properties is further investigated using a ferrimagnetic system $Si/Au_x/Pt_{5nm}/[Co_{0.7nm}/Tb_y]_{\times 6}/Au_{5nm}$, where the changes in the buffer layer result in compensation temperature shifts.

1. Raymenants, E., et al., Nanoscale domain wall devices with magnetic tunnel junction read and write. Nature Electronics, 2021. 4(6): p. 392-398. 2. Everschor-Sitte, K., et al., Perspective: Magnetic skyrmions—Overview of recent progress in an active research field. Journal of Applied Physics, 2018. 124(24). 3. Mallik, S., Mallick, S., and Bedanta, S., Effect of the growth conditions on the anisotropy, domain structures and the relaxation in Co thin films. Journal of Magnetism and Magnetic Materials, 2017. 428: p. 50-58. 4. Maziewski, A., et al., Tailoring of magnetism in Pt/Co/Pt ultrathin films by ion irradiation. Physical Review B, 2012. 85(5). 5. Guimarães, A.P., Principles of Nanomagnetism. 2009, New York - USA: Springer.

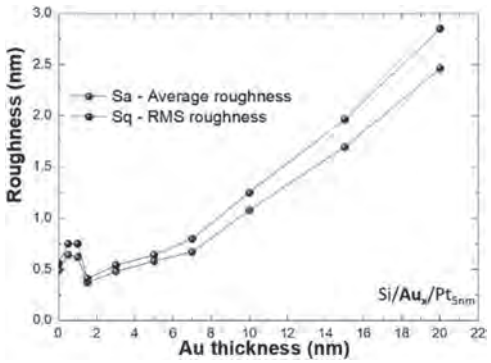

Au_x/Pt_{5nm} surface roughness as a function of Au thickness.

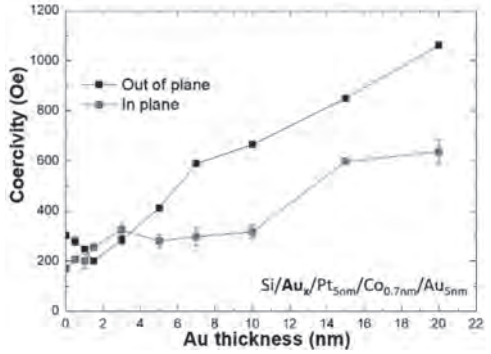

The effect of Au layer thickness on the magnetic coercivity.

LPA-12. Antiferromagnetically coupled CoFe/MgO/CoFe Thin Films.
S. Ahn[1,2] 1. Center for Semiconductor Technology Convergence, University of Science and Technology (POSTECH), Pohang, Gyeongbuk, The Republic of Korea; 2. Department of Electrical Engineering, University of Science and Technology (POSTECH), Pohang, Gyeongbuk, The Republic of Korea

Exchange coupling in as-deposited and annealed magnetic trilayers $Co_{80}Fe_{20}$ (CoFe)/MgO/$Co_{80}Fe_{20}$ (CoFe) for MgO thickness spanning 0.45 to 4.5 nm has been studied. Unlike relevant existing results and theories, antiferromagnetic exchange coupling behavior was observed in annealed CoFe/MgO/CoFe with 2.7-nm MgO insulating barrier. Figure 1 shows in-plane minor hysteresis loops of the as-deposited and annealed CoFe/MgO/CoFe trilayer for MgO thickness spanning 1.8 to 4.5 nm, respectively. Interestingly, the shift of the hysteresis loop toward positive or negative field depends on the temperature. For the temperature range of 25 to 500 deg. C, the hysteresis loop is shifted to the negative and to the positive field for 600 deg. C as shown in Fig. 2(a) [1]. Figure 2(b) a transition from antiferromagnetic to nearly paramagnetic response to applied magnetic field was found around 520 deg. C—conceptually called as Neel temperature. Based on grazing incidence x-ray diffraction study, formation of CoO and $CoFe_2O_4$ were found at annealed CoFe/MgO interfaces [2], which indicates they act as antiferromagnetic sources giving rise to the exchange-coupled antiferromagnetic/ferromagnetic interface and then antiferromagnetic coupling across the magnetic trilayer [3].

[1] T. Ambrose et al., Phys. Rev. B 56, 83 (1997). [2] S. Grytsyuk et al., Eur. Phys. J. B. 85, 254. (2012). [3] J. Spray et al., J. Phys. D: Appl. Phys. 39, 4536 (2006).

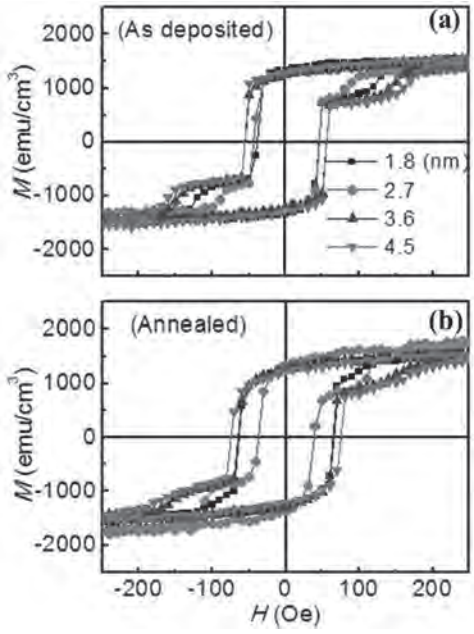

Fig. 1 Magnetic hystereis loops of (a) as-deposited and (b) annealed CoFe/MgO/CoFe films for MgO thickness spanning 1.8 to 4.5 nm.

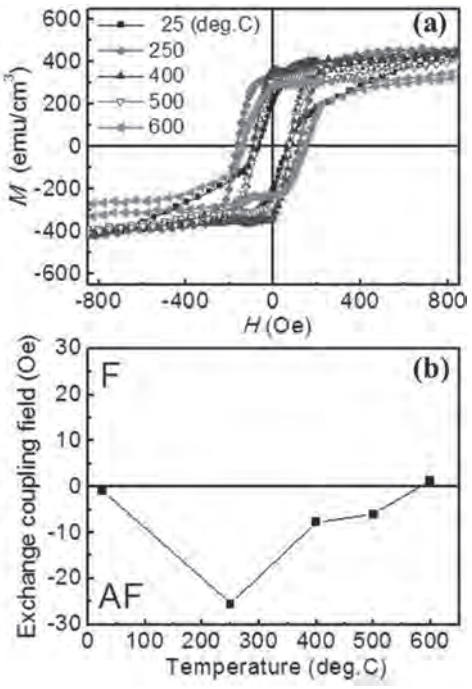

Fig. 2 (a) Temperature dependence of magnetic hysteresis loops of 4-nm CoFe/2.7-nm MgO/8-nm CoFe film annealed at 250 deg. C for 1 hour at the rotation angle 75 deg. (b) exchange coupling field of the same film as mentioned in (a).

LPA-13. Surface effects and spatial distribution of magnetic properties in a Kagomé artificial spin ice.
B.M. Cecchi[1], R. Lourenço[2], J.G. Fernandez[4], M. Velo[1], L. Soares[1], N. Cruz[1], J. Marqués Marchán[3], M. Vázquez[3], A. Asenjo[3], M. Knobel[1], D.N. Otero[3], W. Macedo[2], V.M. Prida[4] and *K.R. Pirota[1] 1. Condensed Matter Physics, UNICAMP, Campinas, Brazil; 2. CDTN, Belo Horizonte, Brazil; 3. ICMM (CSIC), Madrid, Spain; 4. Universidad de Oviedo, Oviedo, Spain*

Artificial spin ices (ASI) are arrays of nanoscale magnets, usually arranged in frustrated geometries. Among the ASI, the kagome geometry (AKSI) has been extensively studied and considered to explore a wide range of interesting Physics phenomena, including mimicking bulk spin ice materials, and acting as a metamaterial for applications in magnonics [1]. The goal of this work is to study the global and local spatial dependence of the coercivity of a Permalloy AKSI (20 nm thick elliptical magnetic islands). The magnetization curves were acquired by magneto-optic Kerr effect measurements with the laser spot adjusted for the required purpose (either global or local). The angular dependence of coercivity exhibits a periodic behavior with a period of 60°, which reflects the symmetry of the underlying honeycomb pattern. The coercivity values vary from ~120 Oe to ~145 Oe, resulting in a peak-to-peak amplitude of ~25 Oe. The minima (maxima) occur when the applied field is perpendicular (parallel) to the magnet's long axis. This result agrees with the fact that the long axis direction being an easy axis of a single nanomagnet. A 20 nm permalloy continuous thin film with similar lateral dimensions as the AKSI lattice shows a nearly constant coercivity around only a few Oe. This indicates that the higher magnitude of the AKSI coercivity is due to the thin film patterning. On the other hand, it is well known that small systems with long range order interactions exhibit pronounced size effects, intuitively understood from the fact that long range interactions are limited by the sample size [2]. By controlling the position of the laser spot to 2 um nominal diameter it was possible to scan the whole sample and determine a spatial map of the coercivity, where each point of the map corresponds to a distinct subregion of the lattice. The results clearly show that the magnetisation reversal properties are locally affected depending on how close to the edge the hysteresis loop is measured. A continuous decrease of the coercive

fields close to the array edges reveals that surface effects are present in AKSI and, in principle, could be explained in the light of translation symmetry breaking in systems with long range order interactions.

[1] S. Skjærvø, H. Christopher and R. Stamps, Nature Reviews, Vol. 2, p. 13 (2020). [2] K. Binder and P. C. Hohenberg, Phys. Rev. B, Vol. 6, p. 3461 (1972).

LPA-14. Mechanical magnetostriction effect of Permalloy dots depending on aspect ratio and bending direction. N. Kim[1] and *S. Yoon*[1] *1. Korea Institute of Industrial Technology, Gwangju, The Republic of Korea*

Flexible electronics has been widely studied for the future applications, such as flexible display, wearable health care device and electronic skin for robots [1-2]. In particular, the stress effect on the thin film is a key element to develop magnetic sensors and actuators. Permalloy is well known material for the flexible applications due to its very low magnetostriction under the stress [3]. In this study, we have measured the mechanical magnetostriction effect on the Permalloy thin film and dot array patterns, where the aspect ratio (length/width) varied 0.5, 1.0, and 2.0, as shown in Figure 1. The width of the dot array was fixed as 10 μm. The stress anisotropy field was measured using ferromagnetic resonance (FMR) method and calculated by Kittel model. The FMR signals depending on the aspect ratio of the dot array are shown in Figure 2, where the excitation microwave frequency was 6 GHz. The stress anisotropy field was significantly affected by the bending repetition and the curved direction with the shape of the dot arrays. The details of the experimental and results will be discussed.

[1] A. Nathan, A. Ahnood, M.T. Cole, S. Lee, Y. Suzuki, P. Hiralal, F. Bonaccorso, T. Hasan, L. Garcia-Gancedo, A. Dyadyusha, S. Haque, P. Andrew, S. Hofmann, J. Moultrie, D. Chu, A.J. Flewitt, A.C. Ferrari, M.J. Kelly, J. Robertson, G.A.J. Amaratunga, and W.I. Milne, Proc. IEEE 100, 1486 (2012). [2] R. Dahiya, N. Yogeswaran, F. Liu, L. Manjakkal, E. Burdet, V. Hayward, and H. Jörntell, Proc. IEEE 107, 2016 (2019). [3] R. Bonin, M. Schneider, T. Silva, and J. Nibarger, J. Appl. Phys. - J APPL PHYS 98, (2005).

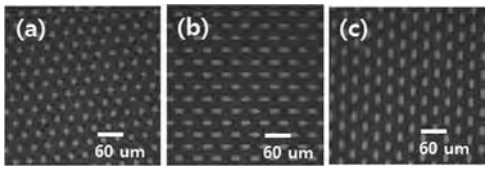

Figure 1. Permalloy dot arrays, where the aspect ratio varied 0.5 (a), 1.0 (b), and 2.0 (c).

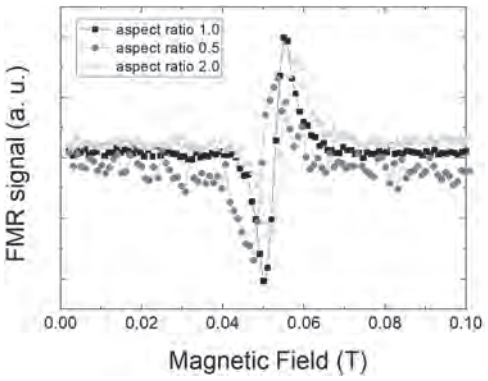

Figure 2. Ferromagnetic resonance signals depending on the aspect ratio of the dot arrays.

Session MOA
NANOCOMPOSITE MAGNETIC MATERIALS

Johan van Lierop, Co-Chair
University of Manitoba, Winnipeg, MB, Canada
Amal El-Ghazaly, Co-Chair
Cornell University, Ithaca, NY, United States

INVITED PAPER

MOA-01. Nucleation and Motion of Domain Walls in Cylindrical Nanowires. *C. Bran*[1], J. Fernandez-Roldan[1,2], E. Saugar[1], R. P. del Real[1], A. Asenjo[1], M. Vázquez[1] and O. Chubykalo-Fesenko[1] *1. Instituto de Ciencia de Materiales de Madrid (ICMM - CSIC), Madrid, Spain; 2. Helmholtz-Zentrum Dresden-Rossendorf e. V. (HZDR), Dresden, Germany*

One of the most promising magnetic systems studied in the last years are the 3D nanostructures with curved geometry where novel and interesting magnetization textures and dynamics are involved [1-2]. One of these nanostructures, cylindrical nanowires, present multiple topologically non-trivial magnetization structures such as Bloch-point domain walls, faster and more stable as compared to those in planar nanowires, vortices, and skyrmion tubes [2-3]. This talk presents different ways to manipulate the magnetization configuration and the domain wall dynamics in cylindrical nanowires. The control and stabilization of domains and domain walls have been achieved in multi-segmented structures [4] by alternating the magnetic anisotropy or by imprinting notches along the nanostructures length. The domain wall dynamics, under the influence of magnetic field or current pulses, was investigated by XMCD-PEEM and micromagnetic simulations. The results indicate that large current densities induce domain wall nucleation while smaller currents move domain walls preferably against the current direction but also along it. The pinning of domain walls has been observed not only at geometrical constrictions but also induced by the Oersted field which creates chiral domain walls.

[1] R. Streubel et al, J. Phys. D: Appl. Phys. 2012, 49, 363001. [2] A. Fernández-Pacheco et al., Nat Commun 2017, 8, 15756. [3] J.A. Fernandez-Roldan et al., Nanoscale 2018, 10, 5923. [4] C. Bran et al., ACS Nano 2020, 14, 12819–12827.

CONTRIBUTED PAPERS

MOA-02. Induced exchange bias in a single layer FeRh thin film by a single step Fe^+ ion irradiation. C. Cress[2], O. Van't Erve[1], J. Prestigiacomo[1], S. LaGasse[2], A. Glavic[3], V. Lauter[4] and *S.P. Bennett*[1] *1. Materials Science and Technology Division, The US Naval Research Laboratory, Washington, DC, United States; 2. Electronics Science and Technology Division, The US Naval Research Laboratory, Washington, DC, United States; 3. Paul Scherrer Institute, Villigen, Switzerland; 4. Neutron Sciences Directorate, Oak Ridge National Laboratory, Oak Ridge, TN, United States*

Modern spintronics relies heavily on the exchange bias effect to pin the orientation of magnetic layers in magnetic logic and memory. Current implementation of exchange bias in spintronic devices requires the deposition and patterning of dedicated layers of antiferromagnetic and ferromagnetic materials with pristine interfaces.[1]–[3] Here we reveal an interfacial exchange bias introduced by a single step low energy irradiation step in a single layer FeRh thin film.[4], [5] The highly localize irradiation created using the heavy Fe^+ ions spatially induces the FeRh's metamagnetic transition, converting the layer from antiferromagnetic to ferromagnetic ordering by the introduction of atomic scale disorder in a thin layer. We directly scrutinize this exchange bias effect in magnetic depth profiles obtained by polarized neutron reflectivity which clearly show a pinned ferromagnetic layer adjacent to the disordered layer created by low energy Fe+ ions.[6] The close proximity and sharp interface of disorder to the antiferromagnetic bulk of the film creates a perfect environment for the robust magnetization pinning required by modern spintronics. These discoveries reveal new physics of the irradiation induced controllability of the metamagnetic transition in FeRh thin films, and bring to light a new single step method to implement exchange bias into an antiferromagnetic layer, opening the door to low cost high speed antiferromagnetic spintronics using metamagnetic transitions.

[1] P. K. Manna and S. M. Yusuf, "Two interface effects: Exchange bias and magnetic proximity," *Physics Reports*, vol. 535, no. 2, pp. 61–99, (2014) [2] A. Rai *et al.*, "Unidirectional and uniaxial anisotropies in the MnN/CoFeB exchange bias system," *Journal of Magnetism and Magnetic Materials*, vol. 485, pp. 374–380, (2019) [3] X. F. Zhou *et al.*, "Exchange Bias in Antiferromagnetic Mn_3Sn Monolayer Films," *Phys. Rev. Applied*, vol. 14, no. 5, p. 054037, (2020) [4] C. D. Cress *et al.*, "Direct-Write of Nanoscale Domains with Tunable Metamagnetic Order in FeRh Thin Films," *ACS Applied Materials and Interfaces*, vol. 13, no. 1, (2021) [5] S. P. Bennett *et al.*, "Magnetic order multilayering in FeRh thin films by the He-ion irradiation," *Materials Research Letters*, (2018) [6] S. P. Bennett *et al.*, "N+ Irradiation and Substrate-Induced Variability in the Metamagnetic Phase Transition of FeRh Films," *Coatings*, vol. 11, no. 6, Art. no. 6, (2021)

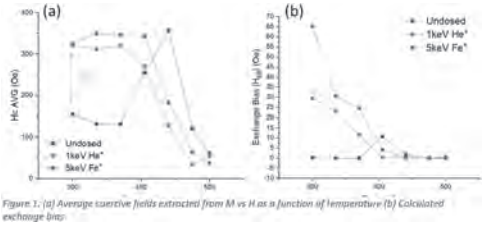

Figure 1. (a) Average coercive fields extracted from M vs H as a function of temperature (b) Calculated exchange bias

MOA-03. NiFe/FeMn based exchange bias system for bias-field-free magnonic medium. *B. Panigrahi*[1], M. Muthuvel[3], C. Murapaka[2] and A. Haldar[1] *1. Department of Physics, Indian Institute of Technology Hyderabad, Sangareddy, India; 2. Department of Materials Science and Metallurgical Engineering, Indian Institute of Technology Hyderabad, Sangareddy, India; 3. Advanced Magnetic Group, Defence Metallurgical Research Laboratory Hyderabad, Sangareddy, India*

A magnonic medium that supports magnonic modes or magnetic oscillations without any external bias magnetic field is of great importance for spin wave-based spintronic or magnonic technologies [1,2]. Usually, a large external bias is used in magnonic devices, and it hinders the on-chip integration of magnonic devices [3]. Here, a well-known exchange bias (EB) system is shown to offer excellent opportunities for a new class of bias-field-free magnonic medium. The EB systems are fabricated from sputtered deposited Ta(15nm)/$Ni_{80}Fe_{20}$(12nm)/$Fe_{50}Mn_{50}$(t = 4, 8, 12, 16 and 20 nm) layers, henceforth abbreviated as *FeMn*(*t*) samples. Note that a *Ta* seed layer is used to facilitate the (111) *FeMn* growth and no magnetic field was

applied during deposition. Magnetization reversal mechanisms are investigated via magneto-optical Kerr effect (MOKE) hysteresis loops as shown in Fig. 1. A significant exchange-bias shift (H_{EB}) in the hysteresis loops can be observed while the maximum shift is recorded to be ~58 Oe for *FeMn*(8) sample. The negative/positive H_{EB} is found as there was no field applied during the growth. To probe the magnonic modes at remanence, ferromagnetic resonance (FMR) spectra are recorded by using a lock-in-based broadband FMR technique. Shown in Fig. 2 are the magnonic modes of the EB samples near the exchange bias field range. Resonant modes are found to have similar EB shifts as observed in the magnetic hysteresis loops. The results show that the EB samples support magnetic oscillations below 3 GHz at remanence thereby offering a route for a bias-field-free magnonic waveguide. In addition, one can achieve tunable resonant modes of the sample by applying a small external field. For example, the resonant mode of the *FeMn*(20) sample is found to vary ~1 GHz for a mere 50 Oe field that can be realized by a current-induced Oersted field for device applications. In this presentation, a detailed report on the magnonic modes and their field angle dependence will be discussed by correlating the results with corresponding magnetic hysteresis behavior, interface quality, and thickness.

[1] A. Chumak et. al., IEEE Trans. Magn. 58, 0800172 (2022) [2] A. Haldar and A. O. Adeyeye, Appl. Phys. Lett. 119, 060501 (2021). [3] A. Chumak, V. Vasyuchka, A. Serga, and B. Hillebrands, *Nature Phys* 11, 453–461 (2015).

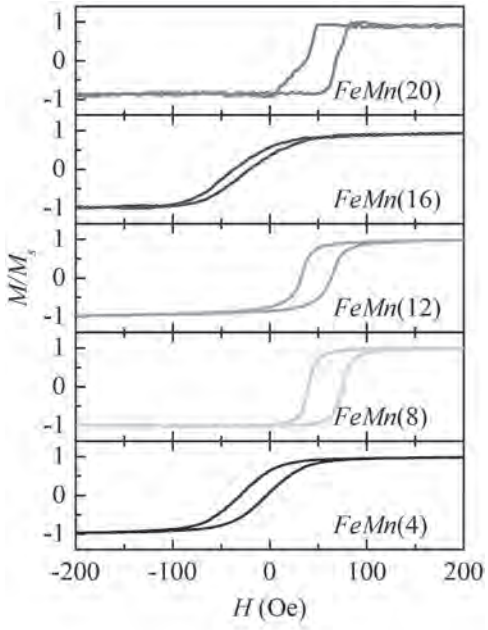

Fig. 1

MOKE hysteresis loops with varying *FeMn* thickness

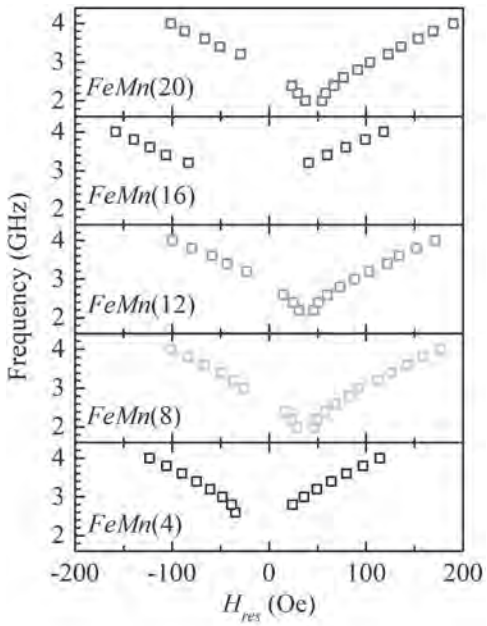

Fig. 2

Excitation frequency *vs.* H_{res} plots for all the EB samples with varying *FeMn* thickness

MOA-04. Role of Mn Interfacial Layers on Ir/Mn Exchange Bias Systems. *W.J. Frost*[1], J. Gompertz[1], R. Carpenter[3,2], S. Hassan[3], M.W. Ormston[3], K. O'Grady[1] and G. Vallejo-Fernandez[1] *1. Department of Physics, University of York, York, United Kingdom; 2. imec, Leuven, Belgium; 3. Seagate Technology, Londonderry, United Kingdom*

IrMn-alloys are the best antiferromagnetic (AF) materials known. Applications range from the established hard disc drive industry to emergent technologies in AF spintronics. Interfaces are well known to significantly affect performance and IrMn alloys are no exception, where the termination layer can significantly influence the exchange bias phenomena. The ready diffusion of Mn between layers results in the formation of mixed layers at the interface. The phase diagram of CoMn is complicated and forms a range of magnetic orders including F, AF and superparamagnetic [1]. In this work interfacial layers Mn of varying thickness were added between the IrMn and CoFe layers. The stack consisted of Si(001)//Ta (2)/ Ru (2)/ IrMn (10)/Mn (*d*)/CoFe (5)/Ru (5) (thicknesses in nm) where *d* was varied from (0.05 to 0.6). The thickness *d* varies from less than one atom thick and by no means ensures a uniform, continuous layer will be formed. Figure 1 shows the dependence of the exchange bias on the thickness of the interfacial Mn. A peak in the value of the loop shift H_{ex} is observed as the value of *d* decreases to 0.05 nm with a reduction in H_{ex} from (-1260 ± 10) Oe to (1160 ± 10) Oe when the Mn is not present. The increase in H_{ex} we attribute to the development of clusters of CoMn alloys at the interface with mixed magnetic ordering possibly forming a spin-glass-like matrix composed of weakly coupled spin clusters. Figure 2 shows the median blocking temperature which behaves in the opposite way showing that this is clearly a compositional effect resulting from the ready diffusion of manganese into the stack. This implies that a thicker Mn interlayer increases either the volume of the AF grains by mixing with the IrMn or that it increases the anisotropy of the material magnetically, by modifying the exchange interactions. Previous work has shown that annealing these structures does not remove the effect thus it cannot be due to an isolated Mn layer. Since it is believed that such Mn layers are incorporated in almost all read heads, understanding the role of such layers is of critical importance.

A. Z. Men'shikov, *et al*, *Sov. Phys. JETP*, 62, 734 (1985) M. Tsunoda *et al*, *Phys. Status Solidi B*, 244, 4470 (2007)

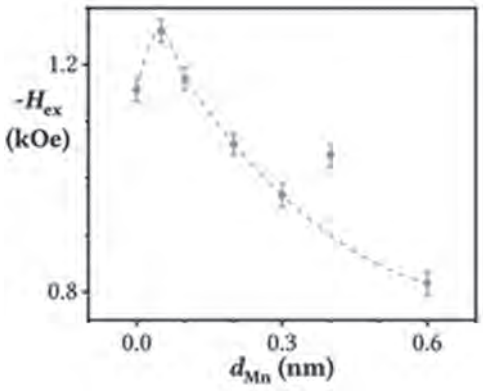

The exchange bias of films with interfacial Mn layers.

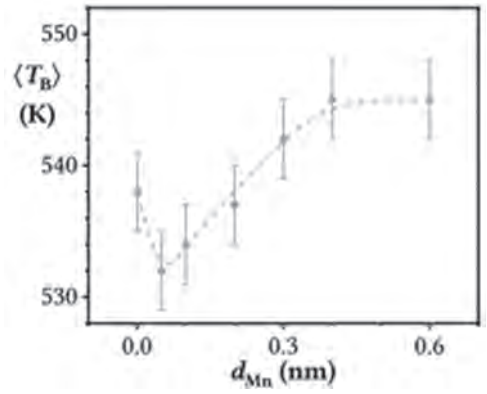

The median blocking temperature of films with interfacial Mn layers.

MOA-05. The effect of x-ray illumination on magnetic domain memory in [Co/Pd] / IrMn multilayers. *C.S. Walker*[1], M. Parkes[2], T. Anderson[1], D. Keavney[3], E. Fullerton[4] and K. Chesnel[1] *1. Physics, Brigham Young University, Provo, UT, United States; 2. Auburn University, Auburn, AL, United States; 3. Advanced Photon Source, Lemont, IL, United States; 4. Center for Memory and Recording research, UCSD, San Diego, CA, United States*

We are studying the effect that illumination by coherent resonant x-rays may have on magnetic domain memory (MDM) in a [Co/Pd] / IrMn multilayers [1-3]. MDM is the ability of the magnetic domains to retrieve their exact same domain topology upon field cycling. In the case of [Co/Pd] / IrMn multilayers, MDM is induced by exchange couplings between the Co/Pd ferromagnetic layer and the IrMn antiferromagnetic layer. We found that under high dose of x-ray illumination, the material may lose its existing MDM. To investigate this potential effect, we have used both x-ray resonant magnetic scattering (XRMS) along with magneto-transport measurements [4,5] to track the exchange bias while the sample is illuminated with x-rays, as illustrated in Figure 1. Magneto-transport is here used to measure the hysteresis loop of the multilayered material and observe exchange bias. A loss of exchange bias would indicate that the x-rays illumination dose may alter the strength of the exchange couplings and ultimately the amount of MDM. Knowing if a loss of exchange bias has occurred requires collecting magneto-transport data as well as XRMS data and correlating the observed changes under various dose of x-ray illumination. The data has been collected at different angles, different configurations, and different temperatures. These configurations consist of Hall effect measurements as well as magnetoresistance measurements. Also, data was collected using various sets of electrical contacts: a set of inner contacts around the x-ray transmission window and as set of outer contacts for reference. The outer contacts were located at a distance of ~1 cm whereas the spacing between inner contacts was ~100 microns. These measurements have been carried at BYU in order to better understand the shape of the data observed in-situ at the APS

[1] K. Chesnel, A. Safsten, M. Rytting, and E.E. Fullerton, Nature Communications 7, (2016). [2] K. Chesnel, B. Wilcken, M. Rytting, S.D. Kevan, and E.E. Fullerton, New Journal of Physics 15, 023016(2013). [3] K. Chesnel, J. Nelson, B. Wilcken, and S.D. Kevan, Journal of Synchrotron Radiation 19, 293 (2012). [4] C. Hurd, *Hall Effect in Metals and Alloys* (Springer, 2012). [5] L.J. van der Pauw, A Method of Measuring Specific Resistivity and Hall Effect of Discs of Arbitrary Shape (1958).

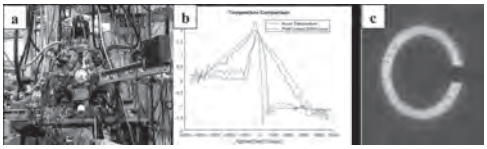

a) Instrumental setup used for our x-ray resonant magnetic scattering (XRMS) experiment at the APS, showing the vacuum scattering chamber and the octupolar magnet. b) Magneto-transport measurement carried on [Co/Pd] / IrMn multilayers at room temperature and at 25 K, well below the blocking temperature. c) XRMS speckle pattern measured at the Co L_3 edge on the [Co/Pd] / IrMn film,.

MOA-06. Analysis of the Magnetic Interactions in FeNi Nanowire Arrays through FORC and Angular Coercivity Measurements. *A.J. Campos-Hernandez*[1], E.M. Palmero[1] and A. Bollero[1] *1. Permanent Magnets and Applications Group, IMDEA Nanociencia, Madrid, Spain*

Arrays of magnetic nanowires (NWs) are an attractive platform with tremendous potential for developing novel magnetic applications, e.g., next-generation information technologies or sensors [1]. The synthesis of NWs by electrochemistry shows multiple degrees of freedom allowing for tailoring the composition, crystallographic structure and, consequently, magnetic properties [2,3]. Herein, FeNi NWs were grown by electrodeposition into anodized aluminum oxide (AAO) membranes (Fig. 1a). The broad range of electrolytes and voltages used, allowed us to study the anomalous FeNi co-deposition by a compositional analysis, being explained within a modified Bocris-Drazic-Despic (BDD) model [4]. X-ray diffraction patterns showed a change from *bcc* crystallographic structure for Fe-rich NWs to *fcc* structure at mid and low Fe content, with biphasic *bcc-fcc* phase for equiatomic NWs. Tuning the synthesis conditions led to FeNi NWs with a range of magnetic hardness, observing an increase in coercivity (from 0.2 kOe to 1 kOe) for a decreased Fe content (Fig. 1b). Coercivity angular measurements showed that the magnetization reversal is dominated by transverse domain wall reversal and indicated a decrease in magnetostatic interactions among NWs as the source of the coercivity rise. First-order reversal curves (FORCs) highlighted the limited role of the magnetic interactions in the arrays, except for $Fe_{0.80}Ni_{0.20}$ NWs which showed a FORC diagram for magnetically interacting NWs (Fig. 1c). This study shows how the magnetic properties of the NWs can be tailored through an optimized control of the synthesis conditions and adapted to the requirements of the final application. *Fig. 1: (a) SEM image of NWs grown inside the AAO template, (b) Hysteresis loops for FeNi NWs with different compositions, and (c) FORC diagram for $Fe_{0.80}Ni_{0.20}$ NWs.* Acknowledgements Authors acknowledge support from EU M-ERA.NET and MICINN through *COSMAG* (PCI2020-112143) and *NEXUS* (PID2020-11521RB-C21). A.J.C.-H. and E.M.P. acknowledge support from "La Caixa" Foundation (ID 100010434) through the Doctoral INPhINIT Incoming program (LCF/BQ/DI20/1178002) and AEI (JdC-I program, IJC2020-043011-I/MCIN/AEI/10.13039/501100011033) and EU by NextGenerationEU/PRTR, respectively.

[1] Fischer, P. et al., APL Mater., Vol. 8, p. 010701 (2020) [2] Palmero, E.M. et al., Nano Res., Vol. 12, p. 1547–1553 (2019) [3] Palmero, E.M. et al., Nanotechnology, Vol. 27, p. 435705 (2016) [4] Dragos, O. et al., J. Electrochem. Soc., Vol. 163, p. 83–94 (2015)

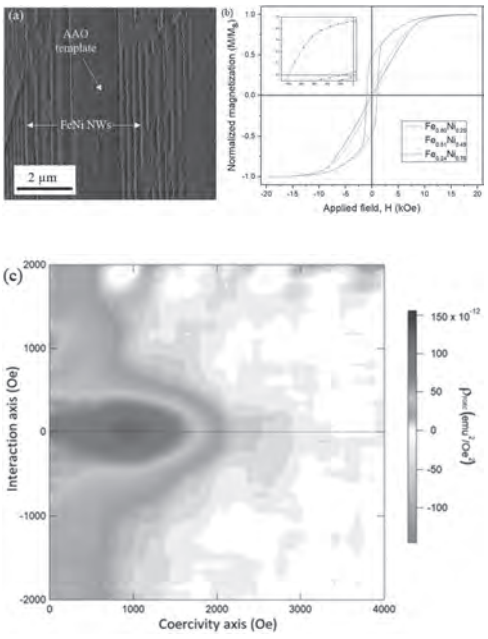

MOA-07. Magnetization Reversal in Cylindrical NiFe Nanowires. *V. Brajuskovic*[1], A.R. McCray[1,2], Y. Zhang[3] and C. Phatak[1] *1. Materials Science Division, Argonne National Laboratory, Lemont, IL, United States; 2. Applied Physics Program, Northwestern University, Evanston, IL, United States; 3. Applied Materials Division, Argonne National Laboratory, Lemont, IL, United States*

Curved magnetic structures often exhibit unique magnetic behavior both as a result of their curvilinear boundary conditions as well as curvature-induced energy effects, such as the curvature-induced Dzyaloshinskii-Moriya (DM) interaction and curvature induced anisotropy. These structures are also of considerable interest for technological applications. For example, magnetic systems have been proposed for a number of wearable devices, such as wearable magnetoreceptors [1] or wearable touchless sensors [2], and the development of such devices requires an understanding of the effects of curvature in magnetic systems. Such effects are best studied in 3D structures, where the curvature can have a significant spatial extent. Nanowires are relatively simple 3D curved structures capable of exhibiting unique magnetization configurations, especially during magnetization reversal [3], and are well suited for applications requiring integration with electrical contacts. Here we have simulated the magnetization reversal in cylindrical NiFe nanowires and supported the results of these simulations with *in situ* Lorentz TEM images. We found that the reversal of these nanowires falls into two different regimes, depending on the diameter of the nanowire. For nanowires with a diameter less than or equal to 100 nm, magnetization reversal occurred via coherent rotation of the spins. For nanowires with a diameter greater than or equal to 150 nm, reversal occurred through a winding of the magnetization at the edges that eventually resulted in a double-helix configuration at the zero-field state, shown in Figure 1. The reversal completed through the gradual unwinding of the double helix state. In both regimes, domain wall propagation was not observed to occur during reversal.

[1] G. S. C. Bermúdez, D. D. Karnaushenko, D. Karnaushenko, A. Lebanov, L. Bischoff, M. Kaltenbrunner, J. Fassbender, O. G. Schmidt, and D. Makarov, *Sci. Adv.* 4, eaao2623 (2018). [2] J. Ge, X. Wang, M. Drack, O. Volkov, M. Liang, G. S. C. Bermúdez, R. Illing, C. Wang, S. Zhou, J. Fassbender, M. Kaltenbrunner, and D. Makraov, *Nat. Comm.* 10, 4405 (2019). [3] S. M. Reddy, J. J. Park, S. M. Na, M. M. Maqableh, A. B. Flatau, and B. J. H. Stadler, *Adv. Funct. Mater.* 21, 4677-4683 (2011).

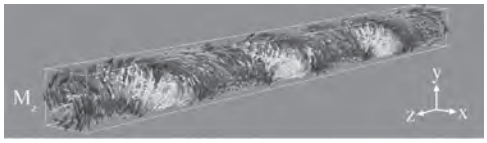

Figure 1—The double helix configuration at the zero-field state of the magnetization reversal of a 150 nm diameter NiFe wire.

MOA-08. Controlling Spin Stability in Three-Dimensional Bi-material Nanostructures. *C.H. Leow*[1,2], B. Myint[1,2] and V. Ng[1,2] *1. Information Storage Materials Laboratory, National University of Singapore, Singapore; 2. Department of Electrical and Computer Engineering, National University of Singapore, Singapore*

2D bi-material artificial spin ice systems have been well studied [1-4] but restricting spins to 2D limits functionality. Extending into 3D provides an extra degree of freedom, but the underlying physics need deeper understanding. We show how spin stability can be controlled via introduction of mixed materials and overlap layer (OL) in 3D nanostructures (NS), with potential applications in computation and memory [5]. Self-aligned hexagonally arranged Py and Co NS were fabricated via stepwise nanosphere lithography [6] via a two-step deposition at different orientation. A mixture of Co NS, Py NS and 3D overlapped Co/Py NS (OLNS) comprising of a Co parallelogram on top of a Co/Py base layer is formed (Fig 1a&b). Magnetization reversal studies were done via MFM. Fig 1c-f show remanant domain configurations at different field values. After +3 kOe saturation (Fig 1c), most Py NS (circled) reversed at -300 Oe (Fig 1d). At -700 Oe (Fig 1e), a Co NS reversed (circled) while OLNS exhibited stable transition states (arrows). OOMMF [7] simulations showed a Néel wall (circled) in Fig 2a but none in Fig 2b for NS without OL. Shape anisotropy causes spins in the OL to lie along the geometrical easy axis. Vertical spins of the Néel wall also connect spins in the base layer and OL via strong exchange coupling, causing in-plane spins to remain unperturbed over large fields. The in-plane spins were seen in Fig 2a to also pin nearby spins in the base layer outside the OL in the same direction (light blue), resulting in the stable transition state in Fig 1e. In contrast, reversal begins at the constituent NS' corners without any OL, as seen in Fig 2b (circled). The tunability of spin stability via OL's shape and area, material and size will be further discussed via experiments and simulations. These interesting static observations in 3D show promise for new dynamic spin wave propagation behavior in 3D. This study aims to extend well-established static and dynamic magnetic behavior of 2D structures into 3D.

[1] A. Rodríguez, L. Heyderman, F. Nolting, *Appl. Phys. Lett.*, vol. 89, p. 142508 (2006) [2] S. Choudhury, S. Saha, R. Mandal, *ACS Appl. Mater. Interfaces*, vol. 8, p. 18339 – 18346 (2016) [3] A. O. Adeyeye, S. Jain, and Y. Ren, *IEEE Trans. Magn.*, vol. 47, p. 1639 – 1643 (2011) [4] S. Choudhury, S. Pan, S. Barman, *J. Magn. Magn. Mater*., vol. 490, p. 165484 (2019) [5] S. Sahoo, A. May, A. van Den Berg, *Nano Letters*, vol. 21, no. 11, p. 4629-4635 (2021) [6] B. Myint, D. Yap and V. Ng, *Nano Express*, vol. 1, p. 020029 (2020) [7] M. Donahue and D. Porter, OOMMF User's Guide, Version 1.0 Interagency Report NISTIR 6376 (1999)

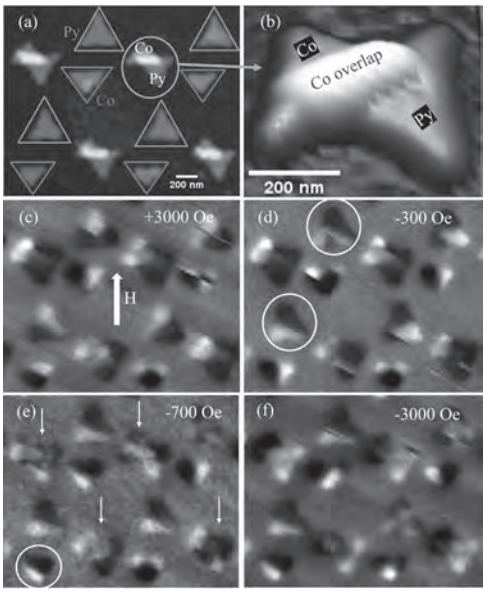

Fig.1: (a-b) AFM of bi-material NS, (c-f) remanent MFM magnetic domain images at different field values. Blue and red triangles represent Py and Co NS respectively.

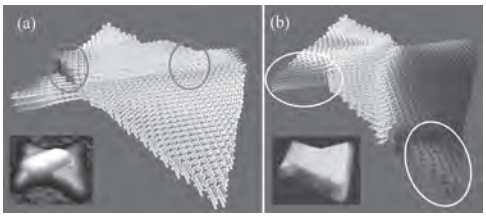

Fig.2: Simulated bi-material NS at -200 Oe a) with and b) without OL

MOA-09. Size-dependent Magnetization Reversal Characteristics of Synthetic Antiferromagnetic Nanoplatelets. *J. Li*[1], W. Sijtsma[1], B. Koopmans[1] and R. Lavrijsen[1] *1. Applied Physics, Eindhoven University of Technology, Eindhoven, Netherlands*

The synthetic antiferromagnetic (SAF) nanoplatelets (NPs) with perpendicular magnetic anisotropy (PMA) are of particular interest for torque-related applications due to their large anisotropy [1]. However, previous research indicates that the coercivity (H_c) increases significantly for small structures with PMA due to thermally activated-magnetization reversal [2]. As the size of NPs drops, larger field is required, and its distribution increases, to activate the NPs which is undesirable for applications. This raises a question of how the magnetization reversal characteristics of the SAF-PMA system scale with size. In this work, we study the magnetization reversal process of PMA-SAF systems of different sizes and materials (CoB/Pt and CoFeB/Pt). The basic thin-film stack is shown in the insert of Fig 1. PMA-SAF nanoplatelets with different sizes are fabricated through electron beam lithography (EBL) and measured using polar magneto-optic Kerr effect (MOKE) magnetometry. One example of the fabricated nanoplatelets is shown in Fig 1. An increase of H_c and its distribution (indicated by the error bar in Fig 2.) is observed with decreasing size as shown in Fig 2. An overall smaller H_c is observed in CoFeB/Pt system compared to CoB/Pt system which can be attributed to the decrease of anisotropy and the different defect-nucleation distribution of the materials. A model based on a local anisotropy distribution and thermal activation is established to simulate the data [3]. The model can accurately predict the H_c behavior, giving further insights into how the size, materials, and anisotropy affect the underlying reversal process. In this talk, we present the size-depended magnetization reversal process of SAF NPs, discuss the physics based on the simulation, and propose the methods to control the switching distribution. This will pave the way to tune the activating magnetic field of PMA-SAF NPs for applications.

Mansell, R., et al. Scientific reports 7.1 (2017): 1-7. Li, J., et al. Under review (2022). Thomson, T., et al. Physical review letters 96.25 (2006): 257204.

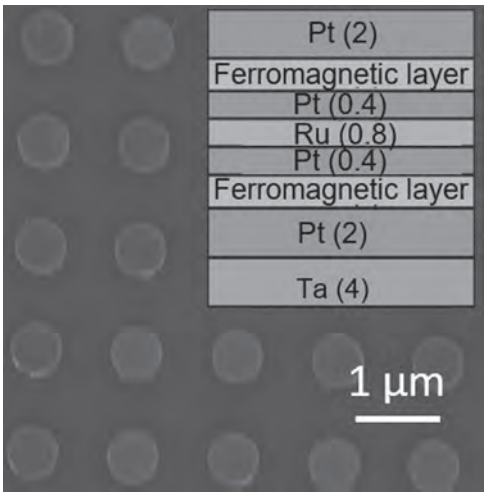

SEM image of 600 nm diameter PMA-SAF nanoplatelets fabricated through EBL. The insert shows the schematic of the basic thin-film stack of the SAF NPs. The thickness between parentheses is in nanometer.

Coercivity (H_c) as a function of the diameter of NPs. The error bar indicate the distribution of the H_c.

MOA-10. Formation of magnetic nanowire arrays by cooperative lateral growth. *F. Chen*[1], Z. Yang[1], J. Li[1], F. Jia[1], F. Wang[1], D. Zhao[1], R. Peng[1] and M. Wang[1,2] *1. Nanjing University, Nanjing, China; 2. American Physical Society, New York, NY, United States*

Fabrication of nanostructures can be categorized into top-down and bottom-up approaches. The top-down approach uses various kinds of lithography, which has unprecedented accuracy and controllability, yet requires sophisticated equipment and expensive operating costs. On the other hand, the bottom-up approaches are cost-efficient and do not rely on sophisticated facilities. However, it is determined by self-organization, which lacks strict repeatability and spatial homogeneity over a long distance. Here, we report an unprecedented electrochemical growth of ordered metallic nanowire arrays from an ultrathin electrolyte layer, which is achieved by solidifying the electrolyte solution below the freezing temperature. We apply the electric voltage pulses across two straight, parallel electrodes. The thickness of the electrodeposit is instantaneously tunable by the applied electric pulses, leading to parallel ridges on webbed film without using any template.

An array of metallic nanowires with desired separation and width determined by the applied pulses is formed on the substrate with arbitrary surface patterns by etching away the webbed film thereafter. Unlike conventional nanowires growing along their longitudinal axial direction, here the whole nanowire simultaneously develops in the direction perpendicular to the wire axis. Besides, the nanowires can be fabricated on a surface with any topography, including silicon grating with a high–aspect ratio surface pattern. This work[1] demonstrates a previously unrecognized fabrication strategy that bridges the gap of top-down lithography and bottom-up self-organization in making ordered metallic nanowire arrays over a large area with low cost.

[1]. F. Chen, Z. Yang, J.-N. Li, F. Jia, F. Wang, D. Zhao, R.-W. Peng, M. Wang, Science Advances., Vol 8, p. eabk0180 (2022)

MOA-11. Modulating Oxygen Octahedra Tiltings in ε-Fe_2O_3 Nanoparticles using Transition-metal Doping. *R. Nickel*[1*], M.M. Shepit[1], C. Sun[2], D. Motta Meira[2] and J. van Lierop[1] *1. Physics & Astronomy, University of Manitoba, Winnipeg, MB, Canada; 2. Argonne National Laboratory, Argonne, IL, United States*

ε-Fe_2O_3 is the least common and understood iron oxide polymorph, isomorphic to $GaFeO_3$ and κ-Al_2O_3. Initial reports of ε-Fe_2O_3 date back to the 1930s; however, synthesis of phase pure samples only became achieved in the late 1990s when a silica matrix was used to stabilize the intermediate ε phase between metastable γ-Fe_2O_3 and thermodynamically stable α-Fe_2O_3.[1,2] ε-Fe_2O_3 has attracted significant interest recently for its unique properties, including a huge coercivity at room temperature, millimeter wave ferromagnetic resonance and magnetoelectric coupling.[3] Applications exploiting ε-Fe_2O_3's properties are an expanding field of research so understanding the electronic interactions underlying this unique ferrimagnetic multiferroic material is critical. This research examines transition metal-doped ε-Fe_2O_3 nanoparticles to identify the electronic configurations of the different ion sites and how they impact the overall multiferroic properties. Silica-free 25 nm ε-$(M_xFe_{1-x})_2O_3$ (M=Cr, Mn, Co, Ni, Cu, Zn; x=0.005-0.12) were prepared. X-ray diffraction reveal the samples have the expected orthorhombic structure (Fig. 1) while EDS and ICP-OES measurements confirm successful doping. Temperature dependent susceptibility and hysteresis measurements show the characteristic spin reorientation transition (SR) at 150 K, where the system transforms from an incommensurate state to a high-coercivity canted antiferromagnet. While this SR is preserved in all samples, the type and concentration of dopant ion does alter the magnetism (see Fig. 2) Notably, Mn and Cu dopants increase the coercivity to >2 T. ^{57}Fe Mössbauer spectroscopy and extended x-ray absorption fine structure analysis correlate changes in the local and electronic structure to the observed magnetic behaviour. Overall, small electronic changes induced by the dopant ions impact the orbital molecule behaviour that controls the magnetic properties.

[1] S. Sakurai et al. Advanced Functional Materials, Vol. 17, p.2278–2282 (2007) [2] M. Popovici et al. Chemistry of materials, Vol. 16, p.5542–5548 (2004) [3] J. Tucek et al. Chemistry of Materials, Vol. 22 p.6483–6505 (2010)

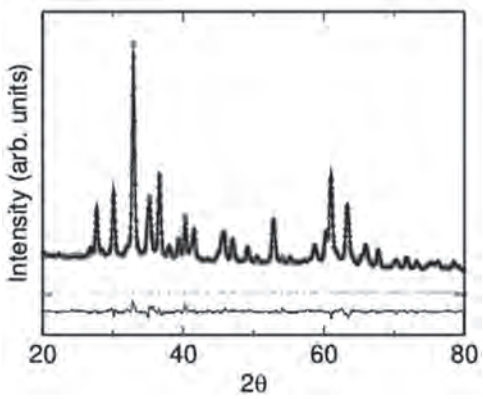

Fig. 1: XRD pattern of ε-$(Mn_{0.04}Fe_{0.96})_2O_3$.

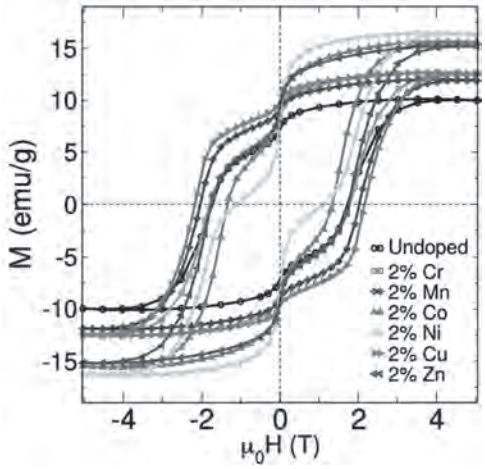

Fig. 2: Hysteresis loops of ε-$(M_{0.02}Fe_{0.98})_2O_3$ (M=Cr, Mn, Co, Ni, Cu, Zn) at 300 K.

MOA-12. Exploring Magnetic Nanochain Anisotropy for Flexible Composite Micro-Actuators. *Y. Chen*[1*] and A. El-Ghazaly[2] *1. Materials Science and Engineering, Cornell University, Ithaca, NY, United States; 2. Electrical and Computer Engineering, Cornell University, Ithaca, NY, United States*

Anisotropic assemblies of magnetic nanoparticles (NPs) are highly powerful for designing micro-actuators in various applications, from robotics to biomedicine. Despite great potential, the challenge remains of how to controllably fabricate them at the micro scale due to two limitations: i) the lack of high-remanence nanoscale magnetic materials, which would dictate the resolution and displacement of the actuator; and ii) the lack of robust method for the large-scale synthesis of such materials. In this work, iron cobalt (Fe-Co) magnetic nanochains are prepared with a novel strategy, where the nanochains are formed from dipole-dipole alignment of individual Fe-Co NPs in the absence of an external magnetic field. As opposed to the widely studied field-guided assembly, our spontaneous assembly reported here enables high-throughput fabrication of anisotropic Fe-Co chains. Experiments and simulations show that dipolar magnetism plays a key role in the resulting structures of the Fe-Co chains, whose morphology, width, and length can be tuned by varying the amounts of precursors and fluid rotating speed during the synthesis. The randomly-oriented Fe-Co chains show a remanent magnetization of 28 emu/g, increasing by a factor of 2 compared to the Fe-Co NPs with equal side lengths. Furthermore, this higher remanence in the nanochains is experimentally shown to be advantageous in the development of magnetic soft actuators with a much larger mechanical deformation response to an externally applied field. To demonstrate this point, anisotropic magnetic elastomer composites were fabricated and their

mechanical deformation behavior tested in both bending and twisting actuation modes. Both cases showed, very large, visible deformations in low magnetic fields (< 200 Oe). Thus, by developing high-remanence magnetic chains with enhanced yields, composite materials can be made to maximize their effectiveness as micro-actuators or as other device technologies.

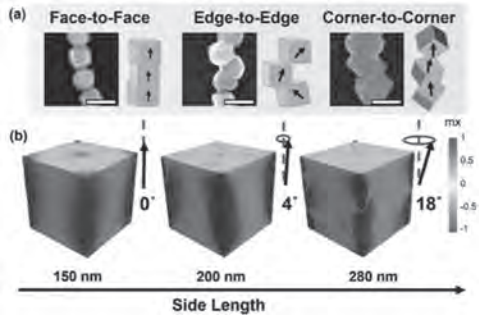

(a) SEM images of various self-assembly modes (scale bars = 200 nm). (b) Simulated magnetization vectors of cubes with respective sizes.

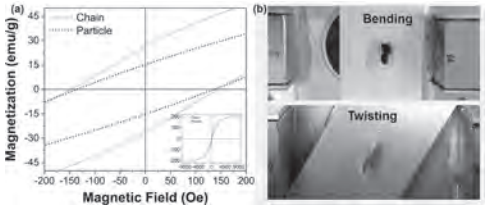

(a) Room temperature zoom in hysteresis of randomly-oriented Fe-Co NPs and nanochains. (b) Photos of the actuator bending and twisting.

MOA-13. Domain Wall Automotion for Three-Dimensional Magnetic Interconnectivity. L. Skoric[1], C. Donnelly[2], A. Hierro-Rodríguez[4], M.A. Cascales Sandoval[3], S. Ruiz-Gómez[2], M. Foerster[5], M. Niño[5], R. Belkhou[6], C. Abert[7], D. Suess[7] and *A. Fernández-Pacheco*[8] *1. University of Cambridge, Cambridge, United Kingdom; 2. Max Planck Institute for Chemical Physics of Solids, Dresden, Germany; 3. University of Glasgow, Glasgow, United Kingdom; 4. University of Oviedo, Oviedo, Spain; 5. ALBA synchrotron, Barcelona, Spain; 6. SOLEIL Synchrotron, Paris, France; 7. University of Vienna, Vienna, Austria; 8. CSIC-University of Zaragoza, Zaragoza, Spain*

The automotion of spin textures, where geometrical gradients are exploited to propagate localized magnetic states without the need of external stimuli, is a promising phenomenon for fast, low-power transmission of magnetic information, as previously demonstrated in planar nanowire systems [1]. Here, we show that automotion is an attractive mechanism in 3D nanowire circuits for the vertical interconnectivity of functional magnetic planes, alternative to the standard current-based spintronic effects normally employed to move spin textures. To showcase this new approach, we have prototyped 3D spiral nanowires by a combination of 3D-printing Focused Electron Beam Induced Deposition and physical vapor deposition methods [2, 3]. The magnetic devices (Fig. 1) are made of Permalloy and are 3 μm tall, 150 nm wide, presenting curvature gradients of 0.09 μm^{-2}. Due to the high directionality of the physical deposition process, they have average thickness gradients of -5.3nm/μm; this very large thickness gradient results to be the dominating mechanism responsible for 3D domain wall automotion, as micromagnetic simulations indicate. We have directly imaged the automotion of domain walls in the 3D spirals using "shadow" X-ray photoelectron microscopy [4]. In these experiments, we nucleate a pair of domain walls at different locations within the spirals using external magnetic fields, and directly observe the evolution of the system as the field is reduced until reaching zero value (Fig. 2). The experiments show the successful automotion of the walls along the 3D interconnectors, and its competition with the intrinsic pinning present in the devices at localized regions. This work thus proposes and successfully demonstrates the automotion of spin textures as a viable effect to create 3D interconnected magnetic devices [5].

[1] K. Richter et al, Phys. Rev. Applied 5, 024007 (2016). [2] L. Skoric et al, Nano Lett. 20, 184 (2020). [3] D. Sanz-Hernández et al, ACS Nano 11, 11066 (2017). [4] Kimling et al, Phys. Rev. B 84, 174406 (2011). [5] Skoric et al, ACS Nano (2022), doi.org/10.1021/acsnano.1c10345

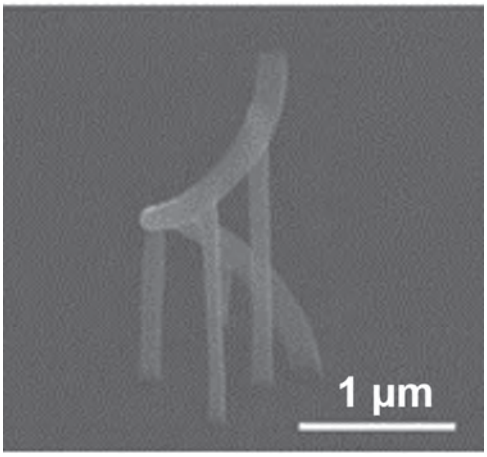

SEM image of a 3D nanowire spiral at 45º tilt.

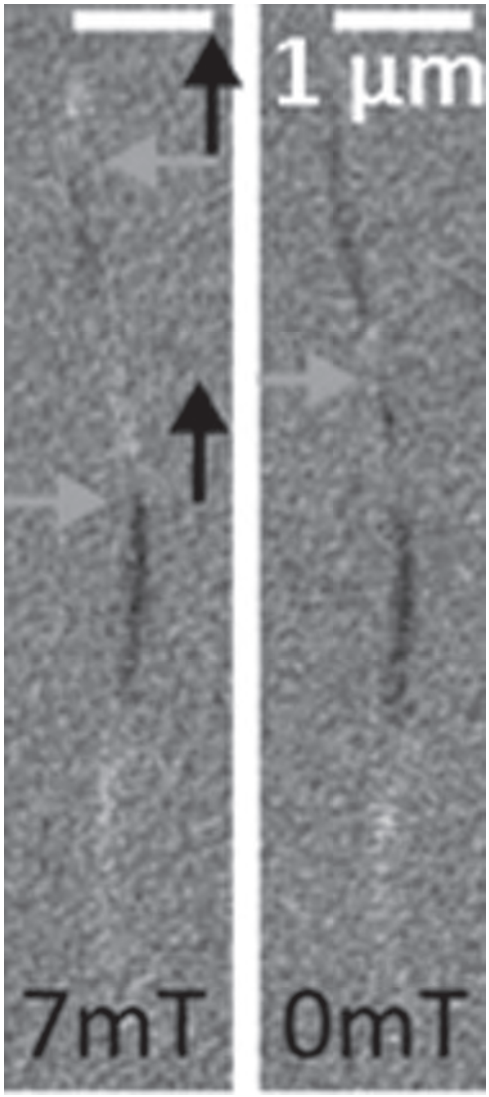

"Shadow-PEEM" images of a spiral at two magnetic field values, showing the automotion of a pair of domain walls (marked with arrows).

MOA-14. Local and Nonlocal Curvature-induced Chiral Effects in Nanomagnetism. *O.M. Volkov*[1], O. Pylypovskyi[1], A. Kakay[1], V.P. Kravchuk[2], D.D. Sheka[3], J. Fassbender[1] and D. Makarov[1] *1. Institute of Ion Beam Physics and Materials Research, Helmholtz-Zentrum Dresden-Rossendorf, Dresden, Germany; 2. Karlsruher Institut für Technologie (KIT), Karlsruher, Germany; 3. Faculty of Radio Physics, Electronics and Computer Systems, Taras Shevchenko National University of Kyiv, Kyiv, Ukraine*

The interplay between geometry and topology of the order parameter is crucial properties in soft and condensed matter physics, including cell membranes [1], nematic crystals [2,3], superfluids [4], semiconductors [5], ferromagnets [6] and superconductors [7]. Until recently, in the case of magentism, the influence of the geometry on the magnetization vector fields was addressed primarily by the design of the sample boundaries, aiming to tailor anisotropy of the samples. With the development of novel fabrication techniques allowing to realize complex 3D architectures, not only boundary effects, but also local curvatures can be addressed rigorously for the case of ferromagnets and antiferromagnets. It is shown that curvature governs the appearance of geometry-induced chiral and anisotropic responses [6-8]. Here we provide experimental confirmations of the existence of local and non-local curvature-induced chiral interactions of the exchange and magnetostatic origin in conventional soft ferromagnetic materials. Namely, we will present the experimental validation of the appearance of exchange-driven Dzyaloshinskii-Moriya interaction interaction (DMI, local effect) for the case of conventional achiral yet geometrically curved magnetic materials [9,10]. This curvature induced DMI is predicted to stabilize skyrmions [11] and skyrmionium states [12]. Furthermore, we will address the impact of nonlocal magnetostatic interaction on the properties of curvilinear ferromagnets, which enables the stabilization of topological magnetic textures [13,14], realization of high-speed magnetic racetracks [15] and curvature-induced asymmetric spin-wave dispersions in nanotubes [16]. Furthermore, symmetry analysis demonstrates the possibility to generate a fundamentally new chiral symmetry breaking effect, which is essentially nonlocal [13]. Thus, geometric curvature of thin films and nanowires is envisioned as a toolbox to create artificial chiral nanostructures from achiral magnetic materials.

[1] H. T. McMahon and J. L. Gallop "Membrane curvature and mechanisms of dynamic cell membrane remodelling", Nature 438, 590 (2005). [2] T. Lopez-Leon, V. Koning, K. B. S. Devaiah, V. Vitelli and A. Fernandez-Nieves, "Frustrated nematic order in spherical geometries", Nature Physics 7, 391 (2011). [3] G. Napoli, O. V. Pylypovskyi, D. D. Sheka and L. Vergori, "Nematic shells: new insights in topology- and curvature-induced effects", Soft Matter 17, 10322-10333 (2021). [4] H. Kuratsuji, "Stochastic theory of quantum vortex on a sphere", Phys. Rev. E 85, 031150 (2012). [5] C. Ortix, Phys, "Quantum mechanics of a spin-orbit coupled electron constrained to a space curve", Phys. Rev. B 91, 245412 (2015). [6] D. D. Sheka, O. V. Pylypovskyi, O. M. Volkov, K. V. Yershov, V. P. Kravchuk and D. Makarov, "Fundamentals of Curvilinear Ferromagnetism: Statics and Dynamics of Geometrically Curved Wires and Narrow Ribbons", Small 18, 2105219 (2022). [7] D. Makarov, O. M. Volkov, A. Kakay, O. V. Pylypovskyi, B. Budinská and O. V. Dobrovolskiy, "New Dimension in Magnetism and Superconductivity: 3D and Curvilinear Nanoarchitectures", Adv. Mater. 34, 2101758 (2022). [8] Y. Gaididei, V. P. Kravchuk and D. D. Sheka, "Curvature Effects in Thin Magnetic Shells", Phys. Rev. Lett. 112, 257203 (2014). [9] O. M. Volkov, D. D. Sheka, Y. Gaididei, V. P. Kravchuk, U. K. Rößler, J. Fassbender and D. Makarov, "Mesoscale Dzyaloshinskii-Moriya interaction: geometrical tailoring of the magnetochirality", Sci. Rep. 8, 866 (2018). [10] O. M. Volkov, A. Kákay, F. Kronast, I. Mönch, M.-A. Mawass, J. Fassbender and D. Makarov, "Experimental observation of exchange-driven chiral effects in curvilinear magnetism", Phys. Rev. Lett. 123, 077201 (2019). [11] V. P. Kravchuk, D. D. Sheka, A. Kákay, O. M. Volkov, U. K. Rößler, J. van den Brink, D. Makarov and Y. Gaididei, "Multiplet of Skyrmion States on a Curvilinear Defect: Reconfigurable Skyrmion Lattices", Phys. Rev. Lett. 120, 067201 (2018). [12] O. V. Pylypovskyi, D. Makarov, V. P. Kravchuk, Y. Gaididei, A. Saxena and D. D. Sheka, "Chiral Skyrmion and Skyrmionium States Engineered by the Gradient of Curvature", Phys. Rev. Appl. 10, 064057 (2018). [13] D. D. Sheka, O. V. Pylypovskyi, P. Landeros, Y. Gaididei, A. Kákay and D. Makarov, "Nonlocal chiral symmetry breaking in curvilinear magnetic shells", Commun. Phys. 3, 128 (2020). [14] C. Donnelly, A. Hierro-Rodriguez, C. Abert, K. Witte, L. Skoric, D. Sanz-Hernández, S. Finizio, F. Meng, S. McVitie, J. Raabe, D. Suess, R. Cowburn and A. Fernández-Pacheco, "Complex free-space magnetic field textures induced by three-dimensional magnetic nanostructures", Nat. Nanotech. 17, 136–142 (2022). [15] M. Yan, A. Kákay, S. Gliga and R. Hertel, "Beating the Walker limit with massless domain walls in cylindrical nanowires", Phys. Rev. Lett. 104, 057201 (2010). [16] J. A. Otálora, M. Yan, H. Schultheiss, R. Hertel and A. Kákay, "Curvature-induced asymmetric spin-wave dispersion", Phys. Rev. Lett. 117, 227203 (2016).

Session MPA
NANOPARTICLES, EXCHANGE BIAS AND 3D STRUCTURES (Poster Session)

Charudatta Phatak, Chair
Argonne National Laboratory, Lemont, IL, United States

MPA-01. Effect of thermal cycling on exchange bias in NiFe/IrMn bilayers. *A.D. Talantsev*[1], M. Bakhmetiev[1] and R. Morgunov[1] *1. Magnetic and Spin Logic Devices, Institute of Problems of Chemical Physics, Moscow, Russian Federation*

Magnetization reversal in NiFe/IrMn exchange-biased thin films was investigated under thermal cycling in an external magnetic field, applied opposite to the direction of the exchange bias field. Thermal hysteresis of magnetization accompanied by changes in magnetization polarity was observed in the applied field close to the exchange bias value. This effect appears when thermally induced variations of the exchange bias exceed the corresponding variations in coercivity. The amplitude of magnetization reversal in NiFe/IrMn structures exceeds ~100 times the corresponding amplitude in spin-crossover molecular compounds. The observed bistability of the magnetic state, revealed by thermal hysteresis, gradually disappears with an increase in the number of cooling–heating thermal cycles, that indicates an irreversible quenching of the interfacial magnetization configuration. This effect paves the way for the creation of a new class of switching devices with thermally assisted bistability in the ferromagnetic state. The work was supported by AAAA-A19-119092390079-8 government task of Institute of Problems of Chemical Physics.

MPA-02. Effect of ion-irradiation and thermal annealing on Exchange bias and the training effect in FeCo/NiO bilayers. *R. Gupta*[1], S. K[1], A. Lakhani[2], V. Reddy[2], F. Singh[3] and A. Gupta[4] *1. School of Instrumentation, Devi Ahilya Vishwavidyalaya, Indore, India; 2. UGC DAE CSR, Indore, India; 3. Inter University Accelerator Center, New Delhi, India; 4. Physics, University of Petroleum and Energy Studies, Dehradun, India*

After thermal annealing and ion-irradiation, we have studied the behavior of the FeCo/NiO film's magnetization reversal. It exhibits exchange bias at room temperature. Magnetization experiments are conducted in the temperature range of 80 K–300 K after the NiO antiferromagnetic layer has been field-cooled down to below its Neel temperature. Kerr microscopy was used for measurements. The exchange bias of the as-deposited film does not change as a function of the number of loops, and the hysteresis curve at 80 K is not asymmetric for the first and second magnetization reversals. In the temperature range of 80 K to 300 K, $3X10^{13}$ ions/cm^2 of 100 MeV Au-ions had no discernible impact on the behavior of the magnetization. The training behavior of the FeCo/NiO system is unaffected by the H_{EB} value decreasing at an ion-fluence of $5X10^{13}$ Au ions/cm^2. After thermal annealing at 673 K, H_{EB} has grown in value. When thermal annealing is used, the training effect is entirely distinct from that of ion-beam irradiated films and as-deposited films. Technologically speaking, the FeCo/NiO system develops into a magnetically stable system at room temperature. It might be a competitor for infinite field sweeping-insensitive spin-valves. Low ion-fluence materials maintain their magnetic properties, making them good candidates for fabrication. In this case, ion-irradiation was employed to create the materials.

MPA-03. Understanding magnetization reversal mechanisms and exchange interactions in nanostructured cobalt ferrites using first order reversal curves (FORC). *S.V. Mullurkara*[1], R. Egli[2], B.C. Dodrill[3], S. Tan[4,5] and P. Ohodnicki[1,5] *1. MEMS, University of Pittsburgh, Pittsburgh, PA, United States; 2. Zentralanstalt für Meteorologie und Geodynamik (ZAMG), Vienna, Austria; 3. Lake Shore Cryotronics, Westerville, OH, United States; 4. Petersen Institute of Nano Science and Engineering, Univesity of Pittsburgh, Pittsburgh, PA, United States; 5. Department of Electrical and Computer Engineering, University of Pittsburgh, Pittsburgh, PA, United States*

Cubic spinel ferrites are a class of oxides represented by the chemical formula AB_2O_4 with A and B being divalent and trivalent cations occupying octahedral and tetrahedral voids. Magnetization arises from superexchange interactions between cations via the oxygen anion. Among these, cobalt ferrites have been shown to undergo spinodal decomposition to form periodic microstructures at the nm length scale. The resultant changes in magnetic properties have been shown to be dependent on the periodicity and degree of decomposition. Complex nanostructured microstructures with concomitant spatial variations of intrinsic magnetic properties and magnetic interactions can yield wasp-waisted major hysteresis loops indicative of multiple magnetization reversal events[1]. Detailed analysis requires advanced magnetometry techniques, in order to disentangle reversible, irreversible, and viscous magnetization processes and their dependence on previous magnetic history. In this work, cobalt ferrite samples have been synthesized using standard powder processing techniques. Different degrees of decomposition have been achieved by varying the annealing time within the coherent spinodal range. TEM has been used to determine periodicity, degree of decomposition, lattice mismatch and the associated coherency strains between the decomposed phases. Magnetization processes occurring in these materials have been investigated through vibrating sample magnetometry using major M-H loops and temperature-dependent magnetization. These measurements have been complemented with non-saturating high-resolution first order reversal curve (FORC) diagrams obtained with different pre-conditioning fields, in order to explore magnetic states inaccessible to the major loops. Various switching events corresponding to the features observed in the FORC diagrams have been identified and correlated with microstructural observations. Finally, a better insight into the nature of the switching events has been obtained with Rayleigh loop measurements along selected FORCs.

1. M. V. Suraj, A. Talaat, B. C. Dodrill, Y. Wang, J. K. Lee, and P. R. Ohodnicki Jr., AIP Advances 12, 035031 (2022)

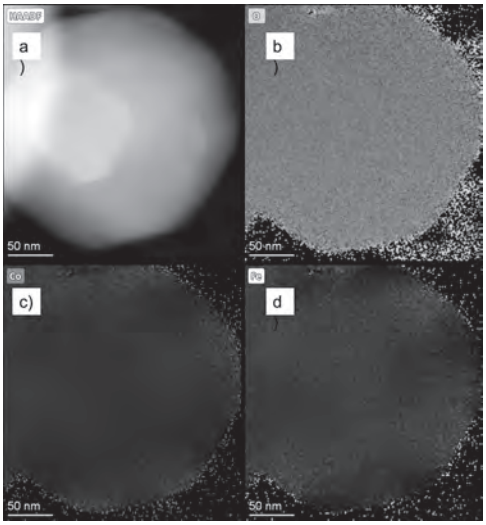

HDAAF image (a) combined with EDS mapping (b,c & d) of a spinodally decomposed Co-Ferrite particle

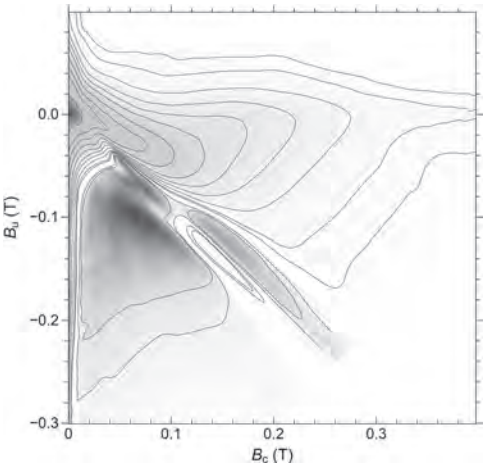

High resolution FORC plot of spinodally decomposed Cobalt ferrite annealed for 120 hrs at 700C

MPA-04. Underlying mechanism for exchange bias in single molecule magnetic junctions. *Y. Tang*[1], B. Huang[1] and Y. Chuang[1] *1. Physics, National Central University, Taoyuan, Taiwan*

When two materials are brought into close proximity, the magnetic proximity effects, including the exchange anisotropy, exchange bias (EB), and coercivity, are among the most fascinating and active materials research areas today. Among them, the interlayer exchange coupling (IEC) plays a crucial role to manipulate the magnetic hysteresis loop in a variety of solid-state magnetic heterostructures. Such IEC can be understood by the equilibrium field-like spin torque (FLST) of magnetic tunnel junctions (MTJs) in noncollinear magnetic configuration. Recently, electrical and spin switches across a single organic molecule connecting ferromagnetic electrodes are also burgeoning fields for possible applications in the so-called molecular spintronics. The ability to calculate the noncollinear spin torque effect and spin dynamics of magnetic heterostructures is difficult but important to include the complex structural, electronic, and magnetic properties at spinterfaces for nanoscale spintronics devices. In this study, the molecular scale magnetic proximity effect is proposed in single-molecule magnetic junctions (SMMJs) consisting of an amine-ended 1,4-benzenediamine (BDA) molecule coupled to two ferromagnetic Co electrodes. The magnetotransport calculation is carried out using the generalized Landau-Lifshitz-Gilbert (LLG) equation combined with density functional theory (DFT) and our self-developed JunPy calculated spin-torque effect. We first demonstrate that the equilibrium FLST plays a crucial role in the strain-controlled exchange bias with current-controlled magnetic coercivity in single-molecule magnetic junctions [1]. In consideration of the resonant tunnelling and the multi-reflection processes at interfaces, our DFT+JunPy+LLG calculation results [2,3] illustrate the underlying mechanism in an important aspect, namely, molecular scale exchange bias effect, via the modulation of angular dependence of equilibrium FLST in amine-ended SMMJs with complex contact deformation and interfacial bonding during breaking junction techniques. This work is supported by the Ministry of Science and Technology (108-2628-M-008-004-MY3).

[1] Y. -H. Tang and B. -H. Huang, Phys. Rev. Research 3, 033264 (2021) [2] K. -R. Chiang and Y. -H. Tang, ACS Omega 6, 19386 (2021) [3] Y. -H. Tang, Y. -C. Chuang, and B. -H. Huang, submitted to Front. Phys. : Charge, Heat and Spin Transport Through Molecular Nanostructures

MPA-05. Tunable Magnetism and Exchange Bias effect in Multiphase Iron oxide Nanocubes. *S.B. Attanayake*[1], A. Chanda[1], R. Das[2], M. Phan[1] and H. Srikanth[1] *1. Physics, University of South Florida, Tampa, FL, United States; 2. SEAM Research Centre, South East Technological University, Waterford, Ireland*

Iron oxide-based magnetic nanoparticles offer ample possibilities for a wide range of biomedical applications such as magnetic resonance imaging, hyperthermia treatment, targeted drug delivery, etc. [1] Understanding the complex magnetic textures in the microscopic dimensions by tailoring the size and morphology of these multifunctional structures is of utmost importance for controlled and optimized applications. The coexistence of multiple phases in these nanostructures provides an additional degree of freedom to tune their functionalities. Despite extensive investigations on the magnetic properties of core-shell iron oxide nanostructures with different shapes, sizes and morphologies, limited studies are available on the influence of phase coexistence on iron oxide nanocubes. Here we report on a comprehensive investigation of magnetic properties of multiphase iron oxide nanocubes with different sizes ranging between 10-43 nm synthesized using a chemical decomposition technique.[2] The exposure to air resulted in an α-Fe_2O_3 shell layer on the surface of the nanocubes, with the core formed of a possible composite mixture of Fe_3O_4 and FeO phases. Magnetometry indicative of the Morin (α-Fe_2O_3) and Verwey (Fe_3O_4) transitions at ~250 K and ~120 K, respectively identify the two phases, while FeO, the third phase is identified through XRD and Raman spectra. The smaller nanocubes up to average size 24 nm showed the exchange bias (EB) effect below 250 K with 15 nm showing the strongest. The EB effect is attributed to the strong interfacial coupling between the ferrimagnetic (FiM) Fe_3O_4 phase and antiferromagnetic (AFM) FeO phase. The Fe_3O_4/α-Fe_2O_3 (FiM/AFM) interfaces are found not to contribute to the EB effect. [3] Our results have enabled us to view the basis of the EB effect in multi-phase iron oxide nanosystems and could open up possibilities to design tunable exchange-coupled nanomaterials with desirable magnetic properties for biomedical and spintronic applications.

[1] C. S. S. R. Kumar and F. Mohammad, Adv. Drug Deliv. Rev. 63, 789 (2011). [2] H. Khurshid, S. Chandra, W. Li, M. H. Phan, G. C. Hadjipanayis, P. Mukherjee, and H. Srikanth, *Journal of Applied Physics*, Vol. 113 (2013). [3] S. B. Attanayake, A. Chanda, R. Das, M. H. Phan, and H. Srikanth, AIP Adv. 12, 035136 (2022).

MPA-06. Modifying the Exchange Interactions of (Cu, Ni, and Fe) Doped Co_3O_4 Nanoplates via Ligand Holes. *M.M. Shepit*[1], J. van Lierop[1] and R. Nickel[1] *1. Physics and Astronomy, University of Manitoba, Winnipeg, MB, Canada*

Co_3O_4 is a transition metal oxide with atypical exchange interactions that propagate through nonmagnetic ions giving rise to weak antiferromagnetism[1]. Thus, small changes to the exchange pathways can lead to large changes in the observed magnetism. Cu, Ni, and Fe-doped Co_3O_4 nanoplates were synthesized (Fig. 1) to investigate the differences in magnetic response

as a result of the new exchange interactions, including contributions from the surface and core[2]. Through the addition of other transition metal ions we disrupt the intrinsic exchange interactions and investigate the effect on the electronic and magnetic structures. The electronic structure of doped materials can be altered to form ligand holes in the oxygen band. Instead of the holes residing on the metal ion – creating a mixed valence structure of 2+ and 3+, the holes occupy the oxygen band creating a ligand hole[3,4]. This manifests in interesting ways such as modifying the exchange interactions through delocalization of the electrons. The addition of dopants into the A (tetrahedral) site leads to a change in the number of unpaired spins, decreasing the strength of the extended exchange interactions responsible for the antiferromagnetic order. Occupation of the B (octahedral) site leads to stronger ferromagnetic interactions. By replacing the Co^{3+} ions which have no magnetic moment with Cu, Ni, or Fe ions, we introduce unpaired spins into the B site. Fe-doped Co_3O_4 shows the strongest exchange interactions. For example, 25% atm. Fe shows the largest magnetic saturation at room-temperature compared to similar dopings of Ni, and Cu (Fig. 2). The strong magnetic response is a result of Fe^{3+} occupying the B site interacting with Co^{2+} on the A site. Interestingly, both Cu and Ni occupy the B site with a 2+ oxidation state (replacing Co^{3+}) which disrupts the charge balance of the system. This forces Cu and Ni to appropriate electrons from the surrounding oxygen ions. This behaviour can modify the existing exchange interactions, similar to what happens in the high temperature superconducting cuprates.

[1] - W.L. Roth, J Phys. Chem. Solids, Vol. 25, 1, p.1-10 (1964). [2] - M. Shepit, V.K. Paidi, C.A. Roberts, et al., Sci Rep., Vol. 10, 20990 (2020). [3] - M. Shepit, V.K. Paidi, C.A. Roberts, et al., Phys. Rev. B, Vol. 103, 024448 (2021). [4] - G. Sawatsky, R. Green, Quantum Materials: Experiment and Theory, Autumn School on Correlated Electrons (Jülich), (2016).

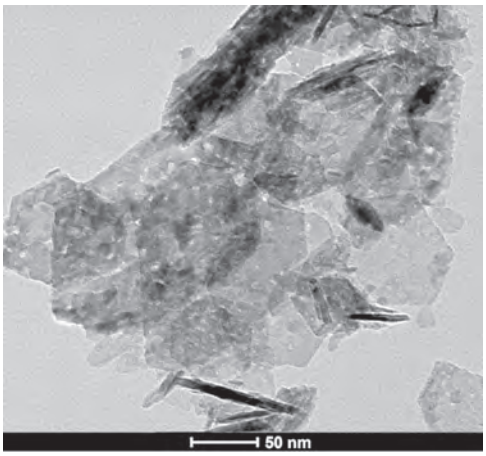

Fig. 1 TEM image of 10% Ni-doped Co_3O_4.

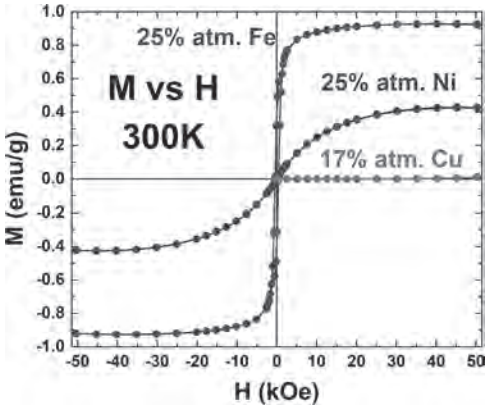

Fig. 2 Magnetometry measurements at 300 K for the single-phase 17% atm. Cu, 25% atm. Fe, and 25% atm. Ni-doped Co_3O_4.

MPA-07. Withdrawn

MPA-08. Exchange Bias Properties of Cr Doped $Ni_2Mn_{1.4-x}Cr_xGa_{0.6}$ Heusler Alloys. B.L. Reese[1], *K.M. Stillwell*[1], R. Chapai[1] and M. Khan[1]
1. Physics, Miami University, Oxford, OH, United States

Although materials exhibiting exchange bias (EB) phenomena have found use in many modern technologies[1], [2], much of their underlying physics remain highly debated. For bulk alloys, EB cannot be understood within the context of interfacial antiferromagnetic (AFM) / ferromagnetic (FM) interactions[3]. Rather, for certain Mn-rich Heusler alloys, EB is better understood within the context of many different exotic magnetic interactions[4], [5]. For the Mn-Ni-Ga system, excess Mn can fill free Ni / Ga lattice sites leading to competing FM / AFM type interactions[6]. Competition is believed to govern EB effect in these systems. Considering the common valence structure and smaller radius of Cr atoms, it is interesting to study the effect of Mn-Cr swapping. The smaller Cr atoms should reduce nearest neighbor bond radii and promote AFM behavior. Here we report on a set of $Ni_2Mn_{1.4-x}Cr_xGa_{0.6}$ ($0.00 \leq x \leq 0.40$) compounds fabricated via standard arc-casting and annealing procedures. At dilute Cr content, $x \leq 0.10$, AFM interactions in the system were enhanced. This behavior resulted in enhanced EB properties of the system. The $x = 0.10$ sample exhibited maximum EB fields of $H_{EB} \sim 723$ Oe and $H_{EB} \sim 300$ Oe for ZFC / FCC conditions respectively. For higher Cr content, the FM response of the system was enhanced, and a secondary precipitate was observed as the bulk of the samples began to reject new Cr atoms. The observed EB phenomena of samples containing Cr content in excess of $x = 0.25$ was suppressed significantly. Relevant structural, compositional, and magnetic data will be presented for the $Ni_2Mn_{1.4-x}Cr_xGa_{0.6}$ system.

[1] M. Bibes, J. Villegas and A. Barthelemy, Adv. Phys., Vol. 60, p.5-84 (2011) [2] C. Tsang, R. Fontana and T. Lin, IEEE Trans. Magn., Vol. 30, p.3801-3806 (1994) [3] J. Nogués and I. Schuller, J. Magn. Magn. Mater., Vol. 192, p.203-232 (1999) [4] M. Khan and A. Albagami, J. All. Comp., Vol. 727, p.100-106 (2017) [5] Y. Zhang, J. Li, and F. Tian, Intermetallics, Vol. 107, p.10-14 (2019) [6] P. Lazpita, J. M. Barandiaran and J. Feuchtwanger, J. Phys.: Conf. Ser., Vol. 325, p.012016 (2011)

MPA-09. Coexistence of Negative Magnetization and Sign Reversal of both Spontaneous and Conventional Exchange Bias in Double Perovskite Y_2FeCrO_6 Nanoparticles. *K. Patra*[1] and S. Ravi[1] *1. Department of Physics, Indian Institute of Technology Guwahati, Guwahati, India*

Here we have opted gel combustion route to prepare single phase nanoparticles of Y_2FeCrO_6 sample and reported its structural and magnetic behavior. According to the room temperature XRD and Raman spectra, the sample is formed in monoclinic phase with $P2_1/n$ space group. The average particle size as per the microstructural image is 67 nm. Magnetization versus temperature (M-T) study revealed that the Neel temperature, T_N is 327 K, which is much greater than the previous findings. Super-exchange interactions in Cr^{3+}- O – Cr^{3+}, Fe^{3+}- O – Fe^{3+} and Fe^{3+}- O – Cr^{3+} networks are thought to be responsible for the AFM transition. In addition, we have introduced a novel magnetic property such as magnetization reversal (MR) with a high compensation temperature (T_{comp}), as well as sign reversal in both spontaneous and conventional exchange bias fields. It exhibits MR with $T_{comp} = 192$ K (at 100 Oe) and a spin reorientation with T_{SR} at around 30 K. A zero field cooled maximum spontaneous exchange bias (SEB) field of - 431 Oe is observed at 55 K. However, after field cooling the sample at 0.5 T, the maximum value of the exchange bias field (CEB) at 5 K is found as 2.1 kOe. The SEB shows a sign reversal across T_{SR} and the field cooled exchange bias reverses its sign across T_{comp} respectively. A typical thermal hysteresis and loop width of magnetic hysteresis versus field curve confirms a first order phase transition and multi magnetic phase in the material. Bipolar switching of magnetization has been demonstrated at 50 K. The competition between single ion anisotropy and Dzyaloshinsky-Moriya interaction is responsible for the above behaviours.

[1] S. Vasala and M. Karppinen, Progress in Solid State Chemistry. 43, 1-36 (2015). [2] Y. Su, J. Zhang, Z. Feng, L. Li, B. Li, Y. Zhou, Z. Chen, S. Cao, J. Appl. Phys. 108, 013905 (2010). [3] J.H. Lee, Y.K. Jeong, J.H. Park, M. Oak, H.M. Jang, J.Y. Son, J.F. Scott, Phys. Rev. Lett. 107, 117201 (2011).

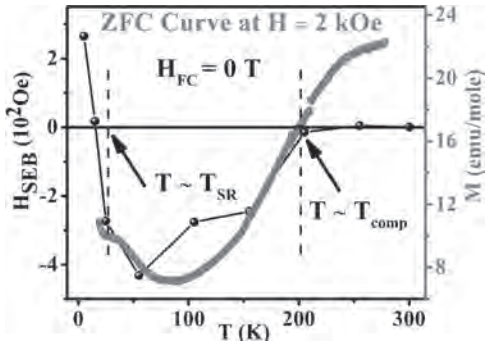

Fig.1 Temperature variation of H_{SEB} (Left side scale) and ZFC magnetization (right-side scale).

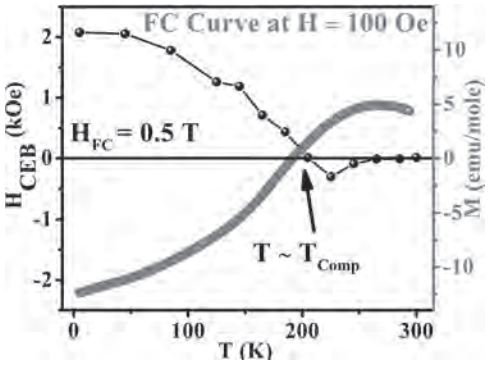

Fig.2 Temperature variation of H_{CEB} (Left side scale) and FC magnetization (right-side scale).

MPA-10. Exchange bias effects in Co/CoO coupled with molecular layers. *L. Gnoli*[1], M. Benini[1], A. Riminucci[1], M. Singh[1], R.K. Rakshit[1], V. Dediu[1] and I. Bergenti[1] *1. CNR-ISMN, Bologna, Italy*

The distinctive features of Exchange bias (EB) at the FM/AFM interface are the shift of the FM hysteresis loop and the modification of its coercivity. The ratio between the interface coupling energy and the anisotropy energy of the AFM determines the coupling regime and the magnetization reversal mechanism. In this work, we were able to tune the EB effect acting on the spin configuration of the AFM layer by the insertion of a molecular layer on top of the FM/AFM interface. We deposited polycrystalline thin films of Co, ranging from 5 to 10 nm in thickness, and we formed a bilayer with a single interface between Co and CoO by exposing the sample to a controlled oxygen atmosphere (10^2L), generating an oxide layer of 2 nm. On the top of CoO, a thick molecular layer (25nm) was deposited. We focus on Gaq3(Gallium-quinoline) and C60 (buckminsterfullerene) as molecular layers as they have been proven to hybridize with magnetic layers modifying their magnetic properties [1,2]. Temperature dependence of Co hysteresis loops of the samples were acquired after cooling down to 50 K in different magnetic fields after appropriate training. The results have been compared with Co/CoO samples without additional layers. The presence of the molecular layer determines a different hardening of the Co layer: C60 shows a visible increase of coercive field of Co for CoO. Additionally the two molecular layers show different field cooling dependency of the coercive field. [3] We interpret our data considering the hybridization with molecular layer as source of AFM magnetic defects[4]. These defects decrease the anisotropy locally and lead to an overall reduction of the AF energy. This reduction of the AF energy gives rise to a local energy minimum for certain defect positions relative to the interface. The domain walls can be pinned at such positions and contribute to the increase of coercivity. This work is supported by European Union's Horizon 2020 Research and Innovation programme under grant agreement No 964396 FET-Open SINFONIA (Selectively activated INFOrmation technology by hybrid Organic Interfaces).

[1] I. Bergenti and V. Dediu, V, Nanomaterials science 2019 1, 149. [2] M. Cinchetti, V. Dediu, L.E. Hueso, Nat. Mater., 2017, 16, 507 [3] L.Del Bianco et al. Phys. Rev. B 70.5 2004: 052401. [4] R.E. Camley et al., J. Vac Sci. & Tec. A 1999, 17, 1335.

MPA-11. Magnetization Switching of Single 120 nm Diameter Synthetic Antiferromagnetic Nanoplatelets with Perpendicular Magnetic Anisotropy. *J. Li*[1], S. Adhikari[2], Y. Wang[2], L. Ruijs[1], P. Spaeth[2], B. Koopmans[1], M. Orrit[2] and R. Lavrijsen[1] *1. Applied Physics, Eindhoven University of Technology, Eindhoven, Netherlands; 2. Huygens-Kamerlingh Onnes Laboratory, Leiden University, Leiden, Netherlands*

Synthetic antiferromagnetic nanoplatelets (NPs) with perpendicular magnetic anisotropy (PMA) are promising candidates for nano-torque-related applications [1]. To manipulate the NPs, a good understanding of the homogeneity in magnetic and structural properties is required. Most techniques measure these properties based on ensemble techniques [2], however, an efficient and easy magnetic characterization technique on single particle level, down to the nanometer range, is currently lacking. Here, we present a characterization method based on photothermal magnetic circular dichroism (PT MCD), which measures the differential absorption of left and right circularly polarized light of an individual magnetic nanoparticle due to the polar Kerr effect [3]. In this way the hysteresis loop on a single 120 nm diameter SAF NP is obtained (see Fig 1b). When compared to SQUID (of ~10^6 particles) as shown in Fig. 1c, the loop exhibits comparable behavior i.e., the antiferromagnetic state at zero applied field and a sharp magnetization switch at a large field. We notice that the values of the switching fields (B_L and B_H as schematically represented in Fig. 1b) are different from the SQUID measurement, which is due to the increased temperature of the NP during the PT MCD measurement. The statistics of the switching fields by PT MCD are shown in Fig 1d where a difference in the distribution is observed for the B_H and B_L switch, which we attribute to a change in the dominant magnetic reversal mechanism of the NPs [4]. Our results will pave the way to a deeper understanding of torque based applications using PMA-SAF NPs and introduce the PT MCD method to the magnetic-nanoparticle community [5].

[1] Mansell, R., *et al*. Scientific reports 7.1 (2017): 1-7. [2] Wasielewski, M. R., *et al*. Nature Reviews Chemistry 4.9 (2020): 490-504. [3] Spaeth, Patrick, *et al*. Nano letters 22.9 (2022): 3645-3650. [4] Thomson, T., *et al*. Physical review letters 96.25 (2006): 257204. [5] Adhikari, S, Li, J., *et al*. In-Preparation (2022)

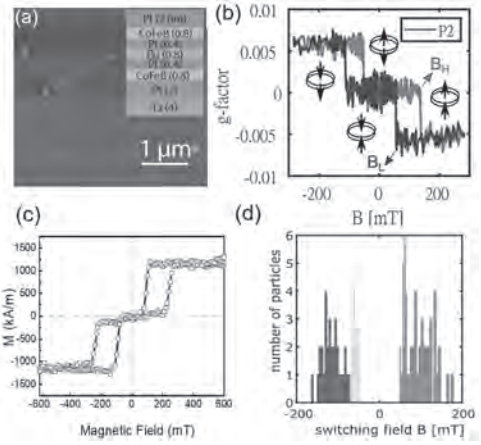

Fig 1. (a) SEM image of NPs used in the work. The insert shows the thin film stack. (b). Hysteresis loop on a single NP measured by PT MCD with the field applied along the out-of-plan direction. (Inset) Schematic representation of orientations of the two CoFeB layers. B_H and B_L are indicated by the arrows. (c). Hysteresis loop of the unreleased NPs measured by SQUID. (d) Histograms of the switching fields of 32 NPs measured by PT MCD. Blue: negative B_H; cyan: negative B_L; red: positive B_H; magenta: positive B_L.

MPA-12. Magnetic nanowires rotation in suspension under the influence of magnetic field. *R. Kolisnyk*[1], A. Harpel[1], P. Liu[1], Y. Chen[1] and B. Stadler[1] *1. University of Minnesota Twin Cities, Minneapolis, MN, United States*

Nanomotors —such as drug delivery vehicles or self-assembled structures requires efficient manipulation of nanoparticle motion. Magnetic field manipulation provides a contactless and sensitive solution to the issue. Here, magnetic nanowires (MNWs) of various lengths and radii were fabricated via electrochemical deposition into nanoporous templates. As a working electrode one side of templates was sputtered with a Cu film. Suspensions were created by removing the MNWs from the template firstly by etching away the Cu film, and then dissolving the template in NaOH. The MNWs were then rinsed several times with deionized water, then redispersed using ultrasonic agitation and placed into the liquid to be studied. A rotating external magnetic field can apply a magnetic torque to balance the drag torque, caused by liquid, and rotate the MNWs in sync with the field. Magnetic torque arises when the magnetic field is not parallel to the nanowires. In addition, nanowire size has large effect on their rotation speed - a longer MNW will experience slower acceleration and larger drag, while a MNW with larger diameter rotates faster. At low frequency rotations of the magnetic field, the nanowires rotate synchronously with the applied field. When the frictional torque exceeds the magnetic torque, the MNW no longer synchronizes with the rotating external field. When the driving field frequency is very high the nanowire will keeps oscillating around its position. By exploring MNW diameters from 20-200nm and lengths from 1-5μm and rotation frequencies from 60-200rpm in liquids from aqueous to viscous (including cryopreservation agents for the new field of nanowarming organs and tissues), a phase diagram of MNW control has been created.

MPA-13. Influence of fiber structure on thermoelectric effect of magnetic electrospinning nanofibers. *H. Huang*[1] *1. National Applied Research Laboratories, Hsinchu, Taiwan*

This study aims to measure the thermoelectric effect of magnetic electrospinning nanofibers. In the experiment, nanofibers with different thicknesses and orientations was fabricated by electrospinning, and a 120-nm-thick Permalloy was deposited on the electrospinning nanofibers by thermal evaporation. Figure 1(a) shows the thermoelectric voltage curves of magnetic electrospinning nanofibers with different diameters. The data reveals the high temperature differences between the two ends of the electrospinning sheet cause the large thermoelectric voltage. The smaller the diameter of magnetic electrospinning nanofibers, the larger the thermoelectric voltage. Figure 1(b) shows the thermoelectric voltage curves of electrospinning nanofibers with a diameter of 220 nm, and the orientation is parallel or perpendicular to the temperature difference. The figure exhibits thermoelectric voltage in the perpendicular direction is larger than that in the parallel direction. The preliminary results show that the thermoelectric effect of magnetic electrospinning nanofibers can be enhanced by adjusting the fiber diameters and orientations.

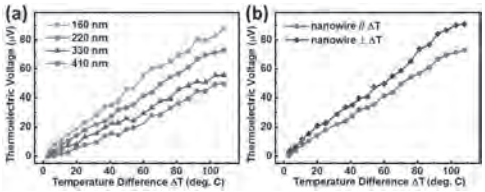

Fig 1 (a) the thermoelectric voltage curves of magnetic electrospinning nanofibers with (a) different diameters and (b) orientations. The diameter is 220 nm in (b). The orientation is parallel or perpendicular to the temperature difference.

MPA-14. Magnetic vortex mobility for hollow Fe_3O_4 submicron particles studied by a hysteresis scaling technique. *S. Kobayashi*[1], T. Kiseleva[2], D. Sangaa[3], N. Jargalan[3] and E. Uyanga[3] *1. Iwate University, Morioka, Japan; 2. Moscow M.V. Lomonosov State University, Moscow, Russian Federation; 3. Mongolian Academy of Sciences, Ulaanbaatar, Mongolia*

Magnetic iron oxide nanoparticles have been extensively studied in the biomedical field due to their diverse application such as magnetic hyperthermia, targeted drug delivery. Recently, larger magnetic particles with a vortex ground state has been recognized as useful biomedical materials, because of high saturation magnetization and wider tunability of a particle size from sub-100 nm to submicrometer scale. The vortex particles showed a high heating efficiency, which is comparable to that of superparamagnetic nanoparticles and is enhanced with the number of vortices [1,2]. However, spin reorientation process under alternating fields, for submicron particles in particular, has not been fully understood, though the understanding is of crucial importance for the improvement of the biomedical performance. Here, we report results of magnetic hysteresis scaling for hollow Fe_3O_4 spherical submicron particles with a vortex structure [3,4]. A scaling coefficient is deduced from the power law scaling and examined to elucidate the relation with particle morphology. We examined hollow Fe_3O_4 spherical particles with varying 400-700 nm diameter [4]. A set of symmetrical minor loops were measured with increasing field amplitude step-by-step up to 2 kOe. Fig. 1 shows a typical example of a hysteresis scaling at $T = 300$ K for various particle sizes. The relation between hysteresis loss and remanence of minor loops follows a power law with an exponent of ~1.5 in a limited field range (< ~ 500 Oe), where a vortex state is stabilized. Such exponent was universally obtained for other particle size and in a wide temperature range of 10-300 K. As shown in the inset, the scaling coefficient monotonically decreases with increasing inner/outer diameter ratio and temperature, indicating a decrease of domain wall pinning strength [5] and an increasing vortex mobility under alternating fields. The results demonstrate that the scaling coefficient is an useful physical parameter for evaluating a vortex mobility in a ferromagnetic particle.

[1] N. A. Usov, et al., Sci. Rep. 8, 1224 (2018). [2] D. W. Wong, et al., Nanoscale Res. Lett. 14, 376 (2019). [3] N. Hirano, et al., Appl. Phys. Lett. 119, 132401 (2021). [4] M. Chiba et al., J. Magn. Magn. Mater. 512, 167012 (2020). [5] S. Kobayashi et al., J. Appl. Phys. 107, 023908 (2010).

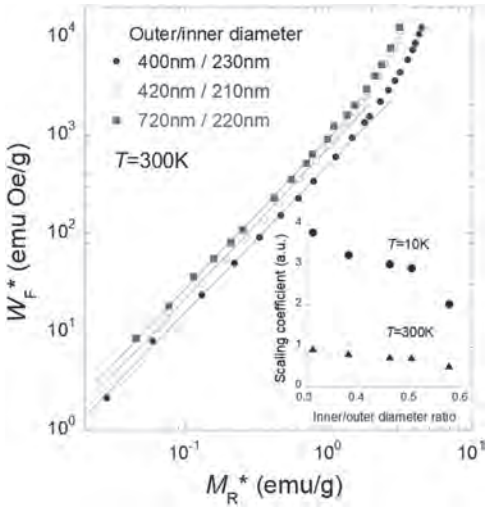

Relation between hysteresis loss W_F^* and remanence M_R^* at T=300K for various hollow particles. The inset shows a coefficient as a function of inner/outer diameter ratio at T = 10 and 300 K.

MPA-15. Withdrawn

Session NOA
MAGNETO-ELASTIC AND -OPTICAL PHENOMENA

Michelle E Jamer, Chair
United States Naval Academy, Annapolis, MD, United States

INVITED PAPER

NOA-01. NiMn-based Heusler thin films: an amazing class of ferromagnetic shape memory alloys. *F. Albertini*[1], M. Takhsha Ghahfarokhi[1], F. Casoli[1], L. Nasi[1], S. Fabbrici[1], R. Cabassi[1], J. Arregi[3], V. Uhlir[3], F. Maccari[2], S. Ener[2], O. Gutfleisch[2], P. Tiberto[4], F. Celegato[4] and G. Barrera[4] *1. IMEM-CNR, Parma, Italy; 2. Technical University of Darmstadt, Darmstadt, Germany; 3. CEITEC BUT -Brno University of Technology, Brno, Czechia; 4. INRIM, Torino, Italy*

Metamagnetic Heusler compounds display a first order structural transformation associated with large changes of magnetization and/or magnetic order. Their properties can be tuned by suitable changes in composition making them a versatile class of multifunctional materials, thanks to the strong interplay between thermal, mechanical and magnetic degrees of freedom [1]. In addition, their hierarchically interrelated twin-with-twin microstructure, in the low temperature martensitic phase, and the strong spin-lattice coupling allow to control their magnetic and multifunctional properties from the atomic to the micro-scale by tuning growth conditions and applying external fields [2, 3]. In my talk I will report on our recent results on nano/microscale materials obtained by different fabrication methods (e.g. epitaxial thin films, patterned and free-standing structures) [3-6]. Thin films and micro/nanostructures are of particular interest not only for the realization of new-concept devices, but also for providing insights into the magnetostructural coupling at the different length scales. The talk will focus on microstructure engineering and microstructure related effects on the martensitic transformation, also in view of the possible exploitation of this class of materials in energy related and smart applications. In particular, by an accurate magnetic and structural investigation at different length-scales, I will demonstrate how growth temperature and simple post-growth treatments, i.e. post-annealing at low T, magnetic field cooling and mechanical stress, are suitable to manipulate the twin variant configuration in epitaxial thin films. X-type variants with out-of-plane magnetic easy axis or Y-type variants with in-plane magnetic easy-axis can be selected, as well as their geometrical distribution, in films with mixed X/Y-type microstructure [3]. Taking advantage from the possibility to manipulate microstructure we have studied the role of specific martensitic configurations on the martensitic transition path. By advanced magnetic force microscopy imaging in a wide temperature (260–350 K) and magnetic field range (up to 14 T) we have directly observed the nucleation and the self-accommodation of the martensitic twinning configurations under zero-field, isofield and isothermal conditions. We have found that between the two possible twinning configurations, the Y-type, which nucleates first, shows a significantly smaller thermal hysteresis as well as a sharper phase transition with respect to X-type microstructure, for all the three investigated conditions [4]. The effects of lateral size, shape and geometry on the properties of patterned epitaxially grown Ni-Mn-Ga films will also be discussed. In particular, I will present the characterization of arrays of microstructures, obtained by means of different lithographic techniques, with lateral sizes down to 200 nm range and having different shapes and orientations with respect to the substrate edges [5]. The last part of my talk will be devoted to free-standing nanostructures in view of their possible exploitation as micro/nano actuators exploiting microstructure-controlled actuation mechanisms by the combined application of temperature and magnetic field [6].

[1] M. Acet, L. Mañosa, A. Planes, Handbook of Magnetic Materials (Ed: K. H. J. Buschow), Elsevier, Amsterdam 2011, pp. 231–289 [2] P. Ranzieri et al., Adv. Mater. 2015, vol. 27, p. 4760 [3] M. Takhsha Ghahfarokhi et al. Acta Mater. vol. 187, p. 135–145 (2020) [4] M. Takhsha Ghahfarokhi et al. Acta Mater. vol. 23, 117356 (2021) [5] M. Takhsha Ghahfarokhi, et al. Appl. Mater. Today vol. 23, p. 101058 (2021). [6] M. Campanini et al., Small, vol. 14, p. 1803027 (2018)

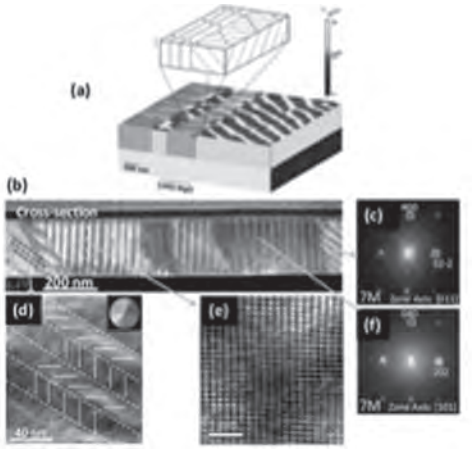

Figure 1 (a) Schematic representation of the twinning and magnetic configuration of Ni-Mn-Ga epitaxial films on (001) MgO: 3D slice of X- and Y-type twins including the direction of the easy magnetization axes. The resultant MFM signal is shown on the surface; (b) cross-section HAADF-STEM image and (c, f) corresponding FFT plots; (d) magnetic induction color map by electron holography for X- type twin variants in cross section; (e) HRTEM image of the marked twin boundary in Y-type microstructure.

CONTRIBUTED PAPERS

NOA-02. Additive manufacturing of Ni-Mn-Sn Heusler alloy - From powder to bulk. *F. Scheibel*[1], C. Lauhoff[2], P. Krooß[2], S. Riegg[1], L. Schäfer[1], K. Opelt[1,3], D. Koch[1], H. Gutte[4], N. Sommer[5], S. Böhm[5], T. Niendorf[2] and O. Gutfleisch[1] *1. Institute of Materials Sience, Technical University of Darmstadt, Darmstadt, Germany; 2. Institute of Materials Engineering, University of Kassel, Kassel, Germany; 3. Material Cycles and Resource Strategies IWKS, Fraunhofer, Hanau, Germany; 4. Institute for Iron and Steel Technology, TU Bergakademie Freiberg, Freiberg, Germany; 5. Institute for Production Technologies and Logistics, University of Kassel, Kassel, Germany*

Ni-Mn-Sn Heusler alloys are known for their large caloric effects during the first-order phase transition (FOMST), allowing the possible utilization for caloric refrigeration [1]. Using a multiple stimuli cycle (magnetic field and compression stress) can here even enhance the cyclic performance of the material [2]. Ni-Mn-Sn shows attractive magnetocaloric properties, but the alloy is brittle and the polycrystalline material is suffering from premature failure. One possibility to enhance the mechanical stability is

grain boundary engineering utilizing additive manufacturing (AM). This was already demonstrated for Co-Ni-Ga shape memory Heusler alloy. It was possible to process a textured alloy with excellent superelastic properties by Direct Energy Deposition (DED) [3,4]. Our goal is to transfer this knowledge about the process from Co-Ni-Ga to Ni-Mn-Sn. For a detailed study the relevant AM processing parameters several kilograms of powder with spherical particle shape are required. In this work, the material properties for the whole AM process from raw material to powder by gas atomization to AM by DED are presented (Fig. 1). For all steps, the functional properties of Ni-Mn-Sn such as magnetization, Curie temperature, FOMST, composition and crystal structure were determined. We also determined the functional properties as a function of particle size distribution ranges: 150-75, 75-63, 63-50, 50-20, and < 20 μm. In contrast to powder synthesis by milling, gas atomization does not apply mechanical force on the particles, thus, it is not inducing defects from the production. This allows the size effect on FOMST to be studied independently of an else to be regarded grinding time. It was found that the FOMST is very sharp for smaller particles, while a lower thermal hysteresis is observed for larger particles (Fig. 2). The work is supported by the ERC Adv. Grant "CoolInnov", and the CRC/TRR 270 "HoMMage" (DFG).

[1] T. Gottschall, K.P. Skokov, M. Fries, A. Taubel, I. Radulov, F. Scheibel, D. Benke, S. Riegg, O. Gutfleisch, Making a Cool Choice: The Materials Library of Magnetic Refrigeration, Adv. Energy Mater. 9 (2019) 1901322. [2] T. Gottschall, A. Gràcia-Condal, M. Fries, A. Taubel, L. Pfeuffer, L. Mañosa, A. Planes, K.P. Skokov, O. Gutfleisch, A multicaloric cooling cycle that exploits thermal hysteresis, Nature Mater. 17 (2018) 929–934. [3] C. Lauhoff, N. Sommer, M. Vollmer, G. Mienert, P. Krooß, S. Böhm, T. Niendorf, Excellent superelasticity in a Co-Ni-Ga high-temperature shape memory alloy processed by directed energy deposition, Materials Research Letters. 8 (2020) 314–320. [4] F. Scheibel, C. Lauhoff, S. Riegg, P. Krooß, E. Bruder, E. Adabifiroozjaei, L. Molina-Luna, S. Böhm, Y. I Chumlyakov, T. Niendorf, O. Gutfleisch, On the impact of additive manufacturing processes on the microstructure and magnetic properties of Co-Ni-Ga shape memory Heusler alloys, Adv. Eng. Mater. (2022), 2200069

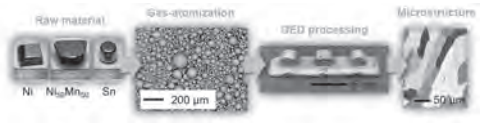

Fig.1: Processing path from raw material to additive manufactured Ni-Mn-Sn

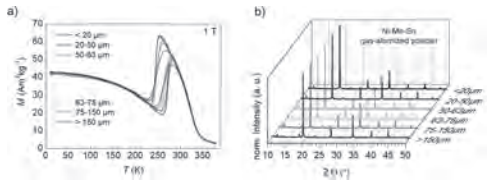

Fig. 2: a) *M*(*T*) and b) x-ray diffraction for different particle size fractions

NOA-03. Magnetoelectric coupling and switching in nanoscale devices.

C. Adelmann[1], A. Guerenneur[1,2], F. Luciano[1,2], P. Van Dorpe[1,2], S. De Gendt[1,2] and F. Ciubotaru[1] *1. Imec, Leuven, Belgium; 2. KU Leuven, Leuven, Belgium*

Nanoscale magnetoelectric devices have recently seen a renaissance due to their multiple applications as transducers between electrical signals and magnetic excitations. When device dimensions are scaled down, one expects much increased magnetoelectric coupling coefficients, which could enable new spintronic applications in both memory and logic domains. A key challenge is the switching of nanomagnets using voltage signals at ultralow power. Previously, nanomagnet switching on piezoelectric substrates has already been shown using high voltages. To develop such structures further towards low-voltage memory, logic circuits, or sensors applications [1], their dimensions should be reduced. Here, we demonstrate by anisotropic magnetoresistance (AMR) [2] large magnetoelectric coupling in sub-μm Ni stripes on top of a piezoelectric PZT layer. Applying a voltage between two gate electrodes generates strain and consequently a magnetoelastic (ME) field in the magnetostrictive Ni. The ME field can be extracted from the magnetisation angle using AMR for a given applied voltage. The analysis in Fig. 1 finds a ME field in Ni as large as 35 Oe/V. The magnitude of the effect agrees with combined finite element and micromagnetic simulations of the magnetoelectric response. Further device miniaturization as well as material optimization can increase the effect even further. When the aspect ratio of the magnetostrictive element is reduced, the induced magnetoelastic field can rotate the magnetization upon application of a voltage. Figure 2 demonstrates a >60° rotation of the magnetization, as deduced from AMR, by voltage application. We will discuss effects of the device geometry and possible optimization routes.

[1] K. Roy et al., J. Appl. Phys., Vol. 112, p. 023914 (2012). [2] V. Iurchuk et al., Phys. Proc., Vol. 75, p. 956 (2015).

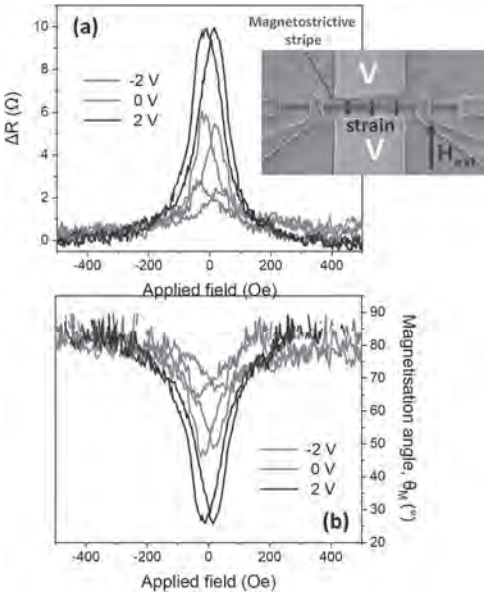

Fig. 1: (a) AMR loops for 800 nm wide Ni stripe at different gate voltages under transversally applied field. (b) Magnetization angle in the stripe deduced from AMR.

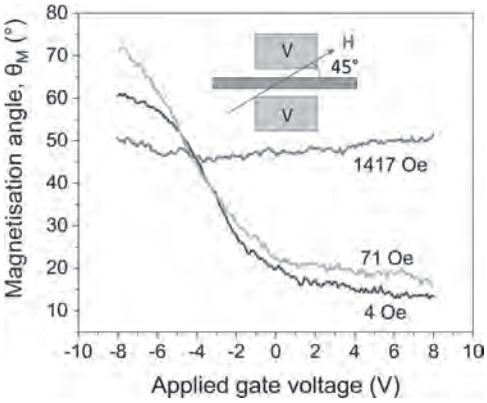

Fig. 2: Magnetization angle *vs.* gate voltage in a 800 nm wide and 10 μm long Ni stripe with an electrode gap of 750 nm at different magnetic bias fields oriented at 45°. At low fields, the magnetoelastic field induced by the applied bias rotates the magnetization.

NOA-04. Power transfer in magnetoelectric resonators.
F. Vanderveken[1,2], B. Soree[1,2], F. Ciubotaru[1] and *C. Adelmann*[1] *1. Imec, Leuven, Belgium; 2. KULeuven, Leuven, Belgium*

Hybrid magnonic-electric computing architectures are promising for ultra-low power data processing [1,2]. To realize these computing systems, scalable magnetoelectric transducers are required that efficiently convert signals between the electric and magnetic domain. Several transducer types have been proposed of which voltage-based concepts are expected to have the best scaling characteristics [3]. A promising voltage-based transducer type consists of a piezoelectric/magnetostrictive bilayer [4]. When a voltage is applied to this transducer, dynamic strain is induced in the bilayer via the piezoelectric effect. This dynamic strain then interacts with the magnetization via the magnetostrictive effect and a coupling between the electric and magnetic domain is obtained. Although this transducer type is very promising, its fundamental understanding as well as energy efficiency estimates are currently lacking. In this work, we develop a theoretical model of the displacement and magnetization dynamics in a resonator consisting of a piezoelectric/magnetostrictive bilayer. The model considers both elastic as well as magnetic resonances and captures the magnetoelastic effect via an effective stiffness. Via this approach, both the elastic and magnetic power flow inside the device can be determined. A comprehensive analysis was conducted of the dimensional as well as material parameter influence on the elastic and magnetic power dissipation (see Fig. 1). Furthermore, the power calculation also results in magnetic transducer efficiency estimates. The results show that magnetic excitation efficiencies up to 90% can be achieved for nanometer thick magnetostrictive layers (Fig. 2). Finally, a figure of merit is determined which allows to select the optimal piezoelectric-magnetostrictive material combination.

1. A. Khitun and K. L. Wang, J. Appl. Phys. 110, 034306 (2011). 2. B. Dieny, I. L. Prejbeanu, K. Garello, P. Gambardella, P. Freitas, R. Lehndorff, W. Raberg, U. Ebels, S. O. Demokritov, J. Akerman, et al., Nature Electron, 3 (2020). 3. F. Vanderveken, V. Tyberkevych, G. Talmelli, B. Soree, F. Ciubotaru, and C. Adelmann, Sci. Rep. 12, 3796 (2022). 4. A. Khitun, D. E. Nikonov, and K. L. Wang, J. Appl. Phys. 106, 123909 (2009).

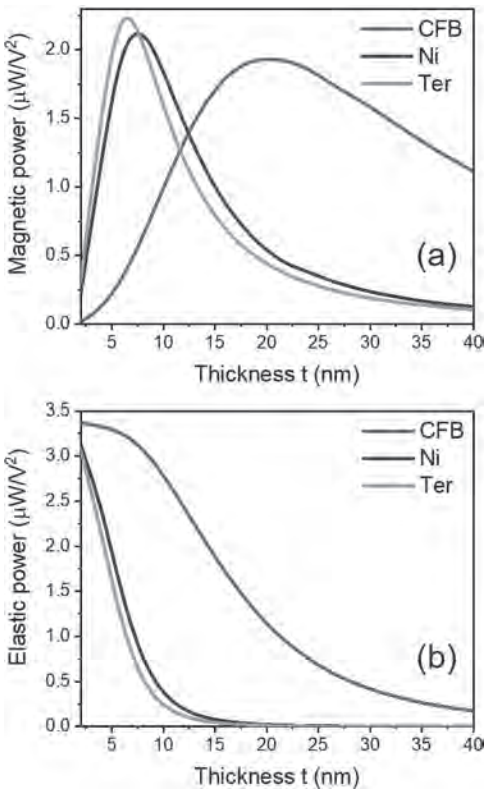

Fig. 1 (a) Magnetic power and (b) elastic power as a function of magnetostrictive layer thickness t using CoFeB (CFB), Ni, and Terfenol-D (Ter) material parameters.

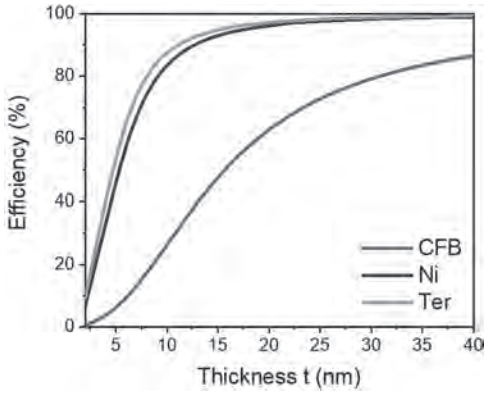

Fig. 2 Magnetic transduction efficiency as a function of magnetostrictive layer thickness t using CoFeB (CFB), Ni, and Terfenol-D (Ter) material parameters.

NOA-05. Relationship between bias magnetic field and output voltage in magnetostrictive vibration power generator.
E. Ishikawa[1], M. Ohtake[1], T. Kawai[1] and M. Futamoto[1] *1. Faculty of Engineering, Yokohama National University, Kanagawa, Yokohama, Japan*

Magnetostrictive vibration power generation has attracted much attention as one of energy harvesting technologies.[1-3)] The device generally consists of a cantilever beam including magnetostrictive material, a permanent magnet to apply a bias magnetic field to the beam, and a coil to detect the variation of magnetic flux in the beam. In order to enhance the rotation of magnetization in inverse magnetostrictive effect, the strength of bias magnetic field is required to be controlled. However, there are few studies on the influence of bias magnetic field,[4)] since it is not easy to vary the strength and the direction of magnetic field in devices using permanent magnets. In

the present study, bias magnetic field is applied by using Helmholtz coils to reveal the mechanism of magnetization behavior. The effects of direction and strength of magnetic field on the power generation property are investigated. A cantilever beam is prepared by combining a Cu plate of 0.3 mm thickness and an Fe-B-Si amorphous ribbon of 25 μm thickness, as shown in Fig. 1. The beam is vibrated at the resonance frequency of 105 Hz and with the acceleration of 1.0 G. The bias magnetic field is applied along the length or width direction and the strength is varied from 0 to 100 Oe (= 7.96 kA/m). The output voltage is picked up by using a coil of 8000 turns. Figure 2 shows the dependences of output voltage (V_{out}) on the magnetic fields applied along the length (H_{length}) and the width (H_{width}) directions. The V_{out} increases to 376 and to 260 mV with increasing the H_{length} to 10 Oe and with increasing the H_{width} to 38 Oe, respectively. As the H_{length} and the H_{width} further increase, the V_{out} decreases. A higher maximum V_{out} of 376 mV is achieved when the magnetic field is applied along the length direction. On the contrary, higher V_{out} of 200-250 mV are obtained at high magnetic fields of 30-100 Oe when the magnetic field is applied along the width direction. These results can be explained by considering the magnetization behavior associated with shape magnetic anisotropy energy, magneto-elastic energy, and bias magnetic field, as shown in the upper parts of Figs. 2(a) and (b), which will be explained in detail at the conference.

1) T. Ueno, *J. Appl. Phys.,* 117, 17A740 (2015). 2) S. Inoue, T. Okada, S. Fujieda, F. Osanai, S. Hashi, K. Ishiyama, S. Suzuki, S. Seino, T. Nakagawa, and T.A. Yamamoto, *AIP. Adv.*, 11, 035021 (2021). 3) L. Wang and F. G. Yuan, *Smart Mater. Struct., 17, 045009 (2008).* 4) Z. Yang, R. Ono.dera, T. Tayama, Z. Yang, R. Onodera, T. Tayama, M. Watanabe, and F. Narita, *Appl. Phys. Lett.*, 115, 243504 (2019).

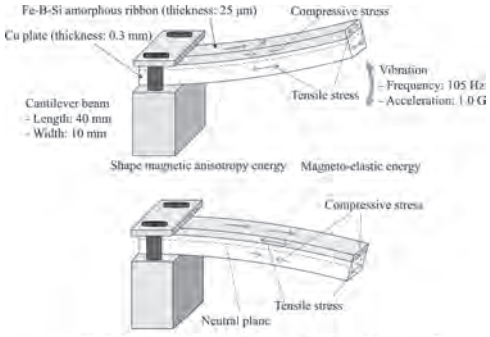

Fig. 1. Schematic diagram of cantilever beam used in the present study.

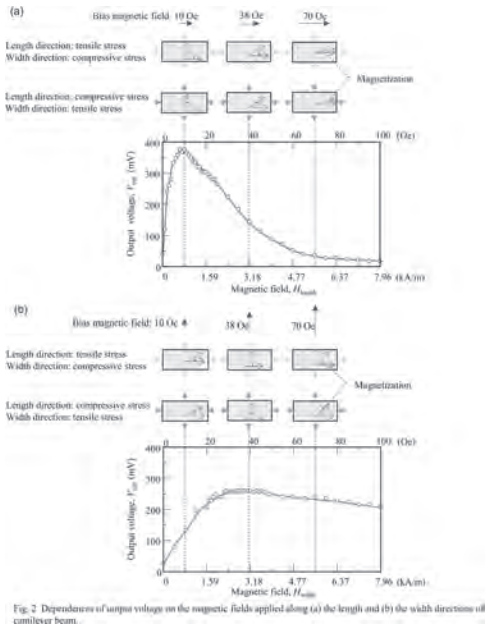

Fig. 2. Dependences of output voltage on the magnetic fields applied along (a) the length and (b) the width directions of cantilever beam.

NOA-06. Heterogeneously Integrated Magneto-Acoustic Resonators.

V.J. Gokhale[1], B.P. Downey[1], S. Mack[1], D.S. Katzer[1], J.A. Roussos[1], D.J. Meyer[1], A. Jander[2] and *P. Dhagat[2] 1. US Naval Research Laboratory, Washington, DC, United States; 2. School of Electrical Engineering and Computer Science, Oregon State University, Corvallis, OR, United States*

Magneto-acoustic devices, integrating ferri- and ferro-magnetic materials with surface and bulk acoustic wave transducers, are of interest for nonlinear signal processing applications such as frequency selective and tunable filtering, signal correlation and isolation [1-3]. Typically, the devices are fabricated by sputter depositing the piezoelectric material needed for acoustic transduction onto the magnetic substrate. Lack of epitaxy as well as thermal budget constraints in the sputtering processes, however, restrict the combinations of piezoelectric and magnetic materials possible for these devices. In this work, we present an alternate fabrication approach based on heterogeneous integration whereby the acoustic transducer is grown on an epitaxially suitable substrate and subsequently transferred to the desired magnetic material [4], allowing for device design and performance to be optimized unhindered by process limitations. A magnetoelastic high overtone bulk acoustic resonator (ME-HBAR) is implemented as an example device, as shown in Fig. 1. A GaN acoustic transducer with a top Al electrode is grown on epitaxially compatible 4H-SiC and released for transfer onto a Cu/YIG substrate by etching a sacrificial NbN layer. Cu serves as the bottom electrode of the acoustic transducer and an acoustic matching layer. The frequency response of the ME-HBAR is measured as a function of magnetic field vector. Two representative responses corresponding to zero field and B_x = 56 mT (in-plane component) and B_z = 180 mT (normal component) are shown in Fig. 2. Around 2.75 GHz, the resonant acoustic modes are strongly attenuated and shifted in frequency due to hybridizing with spin wave modes of similar frequency and wavelength to form coupled magneto-elastic waves [5]. Sufficiently far from the crossover region (not shown), the frequency shift is attributed to the ΔE effect, which together with the lossy hybridization region may be used to realize tunable bandpass and notch filters respectively.

1. X. Liang, C. Dong, H. Chen, et al., Sensors, Vol. 20 p. 1532 (2020) 2. Y Li, C. Zhao, W. Zhang, et al., APL Materials, Vol. 9, art. 060902 (2021) 3. M. Frommberger, Ch. Zanke, A. Ludwig, et al., Microelectronic Engineering, Vol. 67, p. 588 (2003) 4. B. Downey, A. Xie, S. Mack, et al., IEEE 2020 Device Research Conference, p. 1 (2020) 5. C. Kittel, Phys. Rev., Vol. 110, p. 836 (1958)

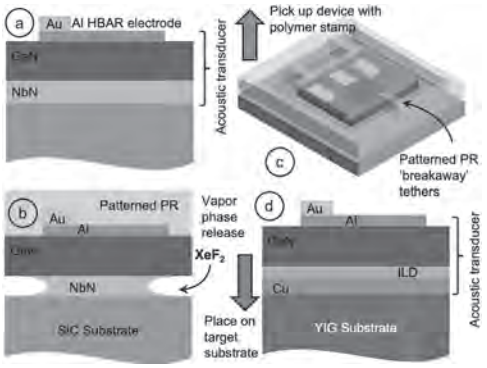

Fig. 1. A magnetoelastic HBAR fabricated by transfer printing a GaN acoustic transducer, grown epitaxially on 4H-SiC, onto a Cu/YIG substrate.

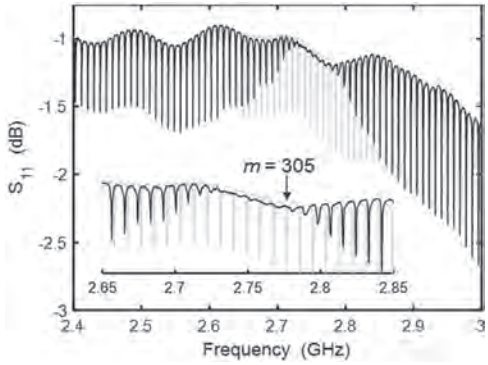

Fig. 2. Acoustic resonances at zero field (green) and at B_x = 56 mT, B_z = 180 mT (black).

NOA-07. Nonlinear adaptive wave mixing and Bose-Einstein condensation in magnetoacoustic iron borate. *D.A. Bas*[1,2], V. Safonov[1], D. Berman[3], Y.V. Rostovtsev[4], J.A. Roberts[4], M.E. McConney[1] and M. Page[1] *1. Materials and Manufacturing, AFRL, WPAFB, OH, United States; 2. Azimuth Corp., WPAFB, OH, United States; 3. Department of Materials Science and Engineering, University of North Texas, Denton, TX, United States; 4. Department of Physics, University of North Texas, Denton, TX, United States*

Iron borate ($FeBO_3$) is a canted antiferromagnet featuring a highly nonlinear magnetoacoustic wave system. Nonlinear wave dynamics appear in countless physical fields, from quantum and neuromorphic computing, to laser physics, to climate dynamics. Studying these dynamics in a tabletop system can lead to greater understanding and control. To demonstrate this [1], we pump single-crystal iron borate with microwave radiation while modifying a static magnetic field, coupling the radiation to the magnetism of the system. Noisy pumping self-organizes to produce coherent waves, much like in the pumping of lasers or weather systems such as cyclones. Frequency mixing produces radiation at satellites near the pump frequency, for which many signals can coexist, a phenomenon which can be harnessed in logic devices for spin wave computing. When a modest threshold pump intensity is reached, quasiparticles accumulate at the bottom of the spectrum, organizing in a macroscopic quantum ground state. These oscillations form a Bose-Einstein condensate: A manifestation of quantum physics in a readily achievable tabletop system. Iron borate remains antiferromagnetic until 348 K, so no cooling is required for these studies. The relative proximity to phase transition means that the system fluctuates significantly, making the ease of achieving clear results even more remarkable. Up to 12 coexisting signals and their satellites were observed at once, and the linewidth of the BEC was measured to be less than 10 Hz, giving it an impressive Q factor of 10^8. These results exemplify the clear, reproducible physics that can be observed in this elegant system.

[1] Safonov, Vladimir L., *et al*. *IEEE Access* 9 (2021): 80847-80853.

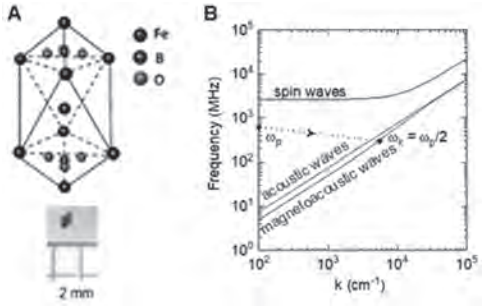

A: Rhombohedral lattice of iron borate and sample photograph. B: Spectra of spin waves, acoustic waves, and their hybrid magnetoacoustic waves. The dashed line shows parametric pumping at a frequency ω_p which populates the magnetoacoustic branch.

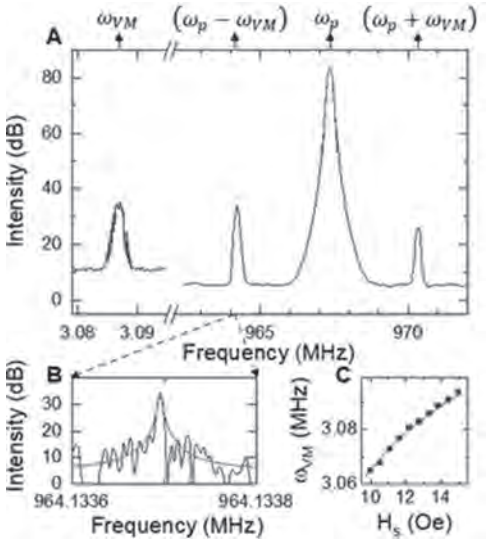

A: Appearance of vibration mode (VM) representing BEC of magnetoacoustic quasiparticles at ~3 MHz, along with the satellites produced via frequency mixing near the ~1 GHz pump. B: Satellites have a Q factor on the order of 10^8. C: Field dependence of the peak position agrees with theory.

NOA-08. Soft Magnetic Elastomer Composites Enabling Magnetic Actuation and Field Sensing Based on Fiber-Optic Interferometry. *Z. Li*[1], S. Warnarathna Jayasuriya[1], F. Iacoviello[1], C. Joanna M[1], P. Prokopovich[2], I. Parkin[1], A. Desjardins[1] and S. Noimark[1] *1. University College London, London, United Kingdom; 2. Cardiff University, London, United Kingdom*

Soft magnetic elastomers (ME) are a class of smart materials consisting of magnetic particles dispersed within soft elastomer networks. Their excellent magnetic and mechanical properties enable fast, untethered and reversible responses to external magnetic induction[1]. Magnetic field sensors have rather broad applicability in many biomedical applications such as biological activity monitoring or medical devices navigation. Fiber-optic magnetic field sensors are promising alternatives to their electrical counterparts due to their small size, low cost, no field-induced heating, intrinsic material safety and immunity to electromagnetic (EM) interference.[2] Nevertheless, their development is largely limited by the low sensitivity and reliability due to poor integration of magnetic materials with the optical fiber, and the complexity of the sensor design. In this work, we proposed a compact design for a fiber-optic magnetic sensor based on highly responsive ME composites, which enables real-time measurement of small changes in magnetic fields using interferometric interrogation scheme. Dip-coating method was introduced to directly deposit uniform ME composite films on the end of a single mode

fiber and create a interferometric structure for sensing of mechanical deformations induced by external magnetic field (Fig1 and 2). ME composites of different compositions and magnetic sensors with various coating structures were developed and further optimized. A fiber-optic interferometric sensing system was established for magnetic actuation and sensing performance evaluation. The proposed sensor exhibited excellent sensing performance enabling measurement of magnetic fields in millitesla level. These highly sensitive, miniature sensors are cost-effective, simple in design, immune to EM interference and are well-suited to a wide range of biomedical applications. Further studies will entail simultaneous measurement of magnetic field and gradient.

1. Bira, N., Dhagat, P. & Davidson, J. R. *Front. Robot. AI* 7, 1–9 (2020). 2. Peng, J. *et al. Sensors* 19, 2860 (2019).

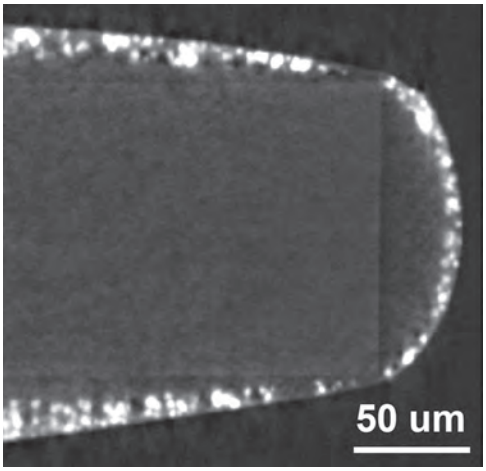

Figure 1. Micro-CT image of fiber-optic magnetic sensor probe fabricated via multi-layer dip-coating method on the cleaved end of a single mode fiber (dia. 125um)

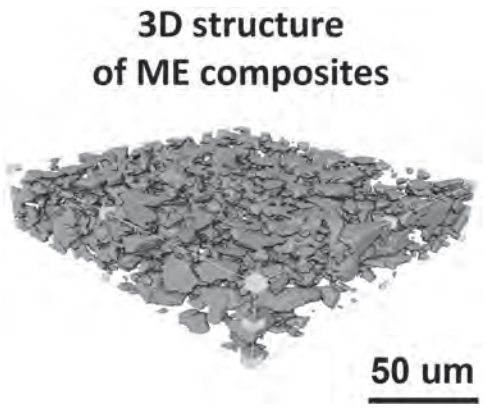

Figure 2. Micro-CT Simulated 3D structure of ME composites (wt. 60%)

NOA-09. 3D-printed Magnetic Elastomers: Parameters to Achieve Large and Complex Magnetoaction. *B. Nelson-Cheeseman*[1], J.M. Ennis[1], J. Lu[1], W.M. Howell[1], S.J. Ziemann[1] and T. Höft[2] *1. Mechanical Engineering, University of St. Thomas, Saint Paul, MN, United States; 2. Mathematics, University of St. Thomas, Saint Paul, MN, United States*

Magnetic elastomers are of interest for soft robotics where remote contactless activation is desired. These smart materials are made of magnetic particulate embedded in an elastomeric matrix and respond to applied magnetic fields (H) with mechanical deformation (magnetoaction). Anisotropy leads to increased magnetoactive performance. The 3D-printing technique, Fused Deposition Modeling (FDM), can be used to create anisotropy in magnetic elastomers. FDM creates sub-structures by extruding 1D lines of molten material ("infill") in 2D patterns that build up to a 3D part. This infill pattern is customizable allowing one to tune the properties of the part. We study how parameters on multiple length-scales influence magnetoaction in FDM-printed magnetic elastomers. Specifically, we study how FDM *infill percentage* and *infill orientation* influences magnetoaction. We also report on filament and extrudate studies (where filament is the FDM stock material and extrudate is what exits the FDM nozzle), involving *magnetic annealing* and multiple *soft vs. hard magnetic particulates*. A custom setup measures magnetoaction, where the sample is suspended vertically with transverse H applied. Magnetoaction is quantified as the angle of sample deflection for a given H. Digital images are captured and overlayed for angle quantization. Magnetic, mechanical and structure (SEM) studies investigate the origins of the magnetoactive differences. The greatest magnetoaction is found when combining low infill percentages and infill oriented perpendicular to H. These effects arise from maximizing anisotropy and limiting infill cross-linking. Magnetic annealing of the stock filament increased magnetoaction, and this increase was maintained in the extrudate after extrusion through the FDM nozzle. This result allows for more accessibility to FDM-printing of high performance magnetic elastomers. Finally, the soft magnets (Fe & Fe_3O_4) gave the greatest magnetoaction and—when magnetically annealed—magnetoaction at lower H, while the magnetically annealed hard magnet (SrFerrite) allowed for complex multi-dimensional magnetoaction. These results highlight key parameters that lead to enhanced magnetoactive performance in 3D-printed magnetic elastomers.

INVITED PAPER

NOA-10. Reprogrammable Liquid-metal/NdFeB/Silicone Composite Magnetic Elastomer. *R. Zhao*[3,1], H. Dai[1,2], G. Zhou[4,1], H. Yao[5,2] and B. Zhang[6] *1. Quanzhou Institute of Equipment Manufacturing of Haixi Institutes, Chinese Academy of Sciences, Jinjiang, China; 2. Fujian Institute of Research on the Structure of Matter, Chinses Academy of Sciences, Fuzhou, China; 3. Zhongyuan-Petersburg Aviation College, Zhongyuan University of Technology, Zhengzhou, China; 4. Guangdong Technion-Israel Institute of Technology, Guangzhou, China; 5. University of Chinese Academy of Sciences, Beijing, China; 6. School of Energy and Intelligent Engineering, Henan University of Animal Husbandry and Economy, Zhengzhou, China*

Hard-magnetic soft materials has a lot of application scenarios in the field of soft robots and flexible sensors. But, due to the coupling of magnetization process and manufacturing process, the functions of these devices can not be changed. Therefore, the technique of repeatedly program magnetic anisotropy on magnetic elastomer is of great significance for changing the functions of magnetic soft robot and sensor. This paper presented a reprogrammable mangetic elastomer based on Liquid-metal/NdFeB/Silicone composites. The NdFeB particles wrapped in gallium can be re-orientated by thermal-ssisted magnetic programming(Figs.1a-1c). Thus, the magnetization profile can be reconfigurated on the elastomer(Fig.1d). X-ray diffraction (XRD) analysis shows the phase composition of gallium, Silicone and $Nd_2Fe_{14}B$ (Fig.2a). The elstomer's magnetic properties are tested by the comprehensive physical property measurement system (PPMS). The moment-temperature (M-T) curve shows the material's moment jumps at 303 K(the melt point of gallium)(Fig.2b). And the moment-magnetic field (M-H) curves indicate that the elastomer exhibit hard and soft magnetic properties respectively (Fig.2c), when the temperatureis lower (293 K) or higher (313 K) than the phase-transition temperature of gallium. A hexagon-shape robot was manufactured and then programmed to two modals of grasping and walking respectively(Figs.2d and 2e). The experimental results verify the reprogrammability of the proposed composite elastomer. The elastomer is expected to be used to manufacture multi-modal magnetic soft robot.

1. H. Chung, A. M. Parsons, L. Zheng. Magnetically Controlled Soft Robotics Utilizing Elastomers and Gels in Actuation: A Review. Advanced Intelligent Systems, 2020, 2000186. 2. Y. Yan, Z. Hu, Z. Yang, etc. Soft magnetic

skin for super-resolution tactile sensing with force self-decoupling. Science Robotics, 2021, 6, eabc8801. 3. L. Cao, D. Yu, Z. Xia, etc. Ferromagnetic Liquid Metal Plasticine with Transformed Shape and Reconfigurable Polarity. Advanced Materials, 2020, 2000827. 4. R. Zhao, H. Dai, H. Yao. Liquid-Metal Magnetic Soft Robot with Reprogrammable Magnetization and Stiffness. IEEE Robotics Automation and Letters, 2022, 7(2): 4535-4541.

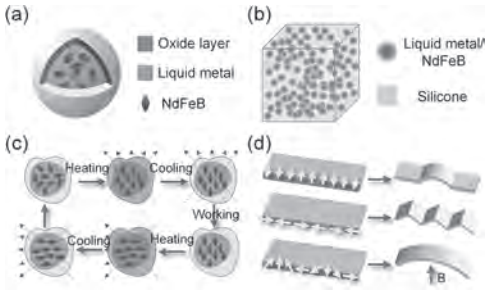

Fig.1 Principle of magnetic elastomer: (a) gallium/NdFeB composites, (b)Liquid-metal/NdFeB/Silicone composite elastomer, (c) Repeatable magnetic programming, and (d) Magnetic responses based on different magnetization profiles.

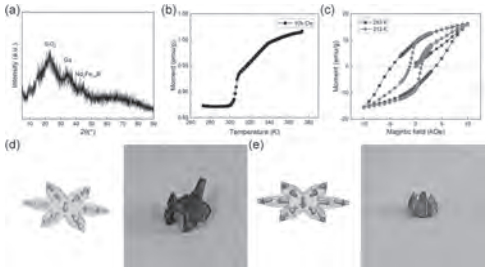

Fig.2 Properties and applications of the elastomer: (a) XRD,(b) M-T curve, (c) M-H curve, (d) waking action and (e) graspinig action.

CONTRIBUTED PAPERS

NOA-11. Magnetically Sensitive Electronic Skins for Supervised Folding of Origami Actuators. *E. Oliveros Mata*[1], P. Makushko[1], M. Ha[2], G. Cañón Bermúdez[1], J. Liu[3], B.A. Evans[4], J.B. Tracy[3] and D. Makarov[1]
1. Helmholtz-Zentrum Dresden-Rossendorf, Dresden, Germany; 2. Gwangju Institute of Science and Technology, Gwangju, The Republic of Korea; 3. North Carolina State University, Raleigh, NC, United States; 4. Elon University, Elon, NC, United States

Soft actuators are required to deform, fold, or unfold in order to interact with their surroundings.[1] One strategy to achieve the movement of mechanically soft systems is the use of magnetic fields for untethered actuation. Flexible magnetic composites have been demonstrated as functional grippers, rollers, and walkers upon applied external magnetic fields.[2] Being controlled with electromagnetic coils, magnetic actuators can profit from high-speed actuation to quickly respond to their environment.[3] The development of an appropriate sensory tracking system for soft actuators is a research topic with open challenges. Light, conformal, and mechanically imperceptible sensing systems are to be developed to be compatible with soft actuators. In this work, we present flexible magnetosensitive electronic skin which relies on thin-film magnetic field sensors to enable onboard folding control of origami-like soft actuators. The flexible electronic skin consists of thin film giant magnetoresistive GMR and Hall effect sensors that are used to measure the magnetization state of the actuator, the applied magnetic fields, and the completeness of the bending process. The resulting intelligent material is mechanically designed to fold even when the flexible magnetic skin is attached to the soft actuator.[4] The magnetic origami actuators are made of thin DiAPLEX foils, a shape memory polymer, with embedded NdFeB particles. Such composite can be used to achieve magnetically induced motion using magnetic fields and a directed light source to increase locally the temperature. We experimentally found the best thickness (60 μm) and concentration (40 NdFeB wt%) parameters to achieve magnetic folds. [4] The integration of magnetic soft actuators with e-skins allowed the self-guided assembly of the origami foils. We showed two case studies showing that this approach is useful for assembling boxes and boat-like origami shapes. This integration process was monitored, followed, and controlled by the output of the laminated sensors. [4]

[1] A. Miriyev, K. Stack, H. Lipson, et al. *Nat. Commun.,* Vol. 8, p.596 (2017) [2] S. Wu, W. Hu, Q. Ze, et al. *Multifunct. Mater.* Vol. 3, p.042003 (2020) [3] X. Wang, G. Mao, G. Jin, et al. *Commun. Matter.* Vol. 1, p.67 (2020) [4] M. Ha, G.S. Cañón Bermúdez, J.A.-C- Liu, et al. *Adv. Mater.* Vol. 33, p.2008751 (2021)

NOA-12. Magneto-Optical Properties of Cobalt-Glass Nanocomposites. *G. El Haber*[1,2], F. Goutaland[1], D. Luneau[2], D. Jamon[1], J. Chatelon[1], J. Michalon[1] and F. Royer[1] *1. Univ Lyon, UJM-Saint-Etienne, CNRS, Institute of Optics Graduate School, Laboratoire Hubert Curien UMR CNRS 5516, St-Etienne, France; 2. Laboratoire des Multimatériaux et Interfaces (LMI), Université Claude Bernard Lyon, Villeurbanne Cedex, France*

Nanocomposites (NCs) are multicomponent materials in which a nanoscale reinforcement is added to a host matrix to combine their different properties. In this work, we investigate the magneto-optical (MO) properties of an NC made of Soda Lime Glass (SLG), which is a transparent, nonmagnetic, and cheap matrix doped by nanostructures of Cobalt (Co), a magnetic material. Among various MO effects, the Faraday Effect (FE) describes the polarization modifications of a linearly polarized light when it travels through a magnetized material. This effect manifests itself as two angles (θ, ε) depicting the polarization rotation and the ellipticity of the emerging light. The Co-SLG NC was formed in two successive steps: a Co layer was deposited on the glass surface, then diffused into the glass using the thermal poling technique [1]. The FE effect was measured at different wavelengths (λ), while the applied magnetic field (H) varied between -800 and +800 mT. Such FE-H curves describe the magnetic properties of the material under consideration. “Fig. 1-2” shows the θ-H curves measured at λ=700 nm, for the Co layer “Fig. 1”, as well as for Co-SLG NC “Fig. 2”. The Co layer exhibits a hysteresis loop, which is characteristic of ferromagnetic materials (FM). After thermal poling, the curve is linear, which indicates that the diffusion of the Co layer within the glass matrix changes drastically its magnetic behavior, most likely due to the oxidation of the Co ions since the SLG matrix is oxygen-rich. “Fig. 3” presents the spectral behavior of this FE effect for the cobalt layer (saturation value of θ as a function of λ) and the NC (slope of θ-H curve as a function of λ). Two main bands are observed in the case of the NC, centered at around 700 nm and 1400 nm, whereas no bands are observed for the Co layer. These two bands are assigned to MO dipolar transitions of Co^{2+} ions in the tetrahedral sites of the Co_3O_4 structure [2]. If this NC is irradiated with a continuous wave laser, Co_3O_4 can be transformed reversibly to CoO [1]. Since Co_3O_4 and CoO have different magnetic and MO behaviors, such NCs may lead to a promising photomagnetic feature that can be used in data storage applications or optical MO switching.

[1] R. Faraj, F. Goutaland, N. Ollier, Physica Status Solidi B., Vol. 257, p.2000155 (2020) [2] W. F. J. Fontijn, P. J. van der Zaag, L. F. Feiner, R. Metselaar, M. A. C. Devillers, Journal of Applied Physics, Vol. 85, p.5100-5105 (1999)

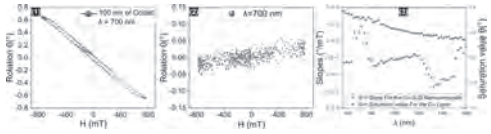

Fig. 1-3

NOA-13. Magneto-Optical Figure-of-Merit Dependence on Size and Tb^{3+} Doping of Fe_3O_4 Nanoparticles in Polymer Films. *T. Ba Tis*[1], J. Bartos[2], M. Nie[2], S. Huang[2] and W. Park[2,1] *1. Materials Science & Engineering program, University of Colorado Boulder, Boulder, CO, United States; 2. Department of Electrical, Computer & Energy Engineering, University of Colorado Boulder, Boulder, CO, United States*

Recently, there has been a growing interest in developing and using magneto-optical polymer nanocomposites (MO-PNCs) as efficient Faraday rotators [1,2]. A common strategy to improve the Verdet constant, V, of MO-PNCs is by increasing the nanoparticle (NP) loading [3]. However, since the absorption coefficient, α, also increases with the loading, the figure-of-merit, FOM = V/α, remains unchanged. In this work, we first showed that the FOM in Fe_3O_4-based MO-PNCs is independent of NP loading in the absence of aggregation and decreases when NPs aggregate. Secondly, we demonstrated that the FOM is strongly sensitive to the NP size and composition via doping with terbium ions (Tb^{3+}). In the loading study, we used a polymerizable ligand to fabricate poly (methyl methacrylate) films containing 8 nm Fe_3O_4 NPs with high optical quality [4]. When the NP loading was increased from 3.5 to 12.8 wt%, the Verdet constant of the films improved from 4500 to 13500 °/Tm whereas the FOM remained constant at 2.9 °/T. This result confirms our expectation that increasing the loading does not enhance the overall MO performance. When the NP diameter was increased from 8 to 17 nm, we observed a 7-fold enhancement in the FOM from 2.9 to 23.1 °/T (Fig. 1) which can be attributed to the NPs reaching the critical size (~20 nm) at which their magnetic domains become stable against thermal fluctuations [5]. For larger sizes, however, the Verdet constants saturated while FOMs declined due to increased aggregation. The FOM was further improved to ~70 °/T by doping with the highly MO-active Tb^{3+} ions (Fig. 2) [6]. The drop in FOM at high Tb^{3+} doping is likely due to the increased lattice distortions and failure to incorporate the dopants inside the NPs [7]. At the optimal doping and size, the Verdet constant of 4wt% loaded MO-PNC film is 5.6×10^5 °/Tm which is among the highest reported in the literature, especially for moderately loaded films [1]. The MO-PNCs reported in this work are promising candidates for compact room-temperature optical magnetometers that can be used for sensing and medical imaging.

[1] K. Carothers et al., Chem. Mater., vol. 34, p.2531–2544, (2022) [2] N. Pavlopoulos et al., J. Mater. Chem. C, vol. 8, p.5417–5425, (2020) [3] K. Carothers et al., Chem. Mater., vol. 33, p.5010–5020, (2021) [4] Y. Jin et al., J. Mater. Chem. C, vol. 4, p.3654–3660, (2016) [5] A. Muxworthy et al., J. R. Soc. Interface, vol. 6, p.1207, (2009) [6] K. Miyamoto et al., J. Am. Chem. Soc., vol. 131, p.6328–6329, (2009) [7] K. Rice et al., Appl. Phys. Lett., vol. 106, p.062409, (2015)

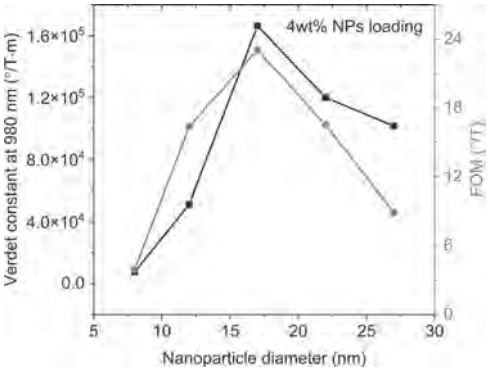

Fig. 1 Verdet constant and FOM dependence on Fe_3O_4 NPs size.

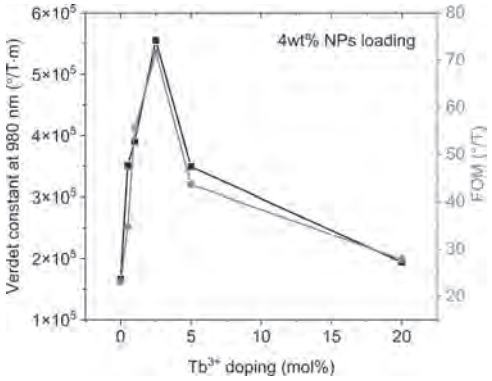

Fig. 2 Verdet constant and FOM dependence on Tb^{3+} doping of 17 nm Fe_3O_4 NPs.

Session NOB
MAGNETOCALORIC MATERIALS I

Brittany Nelson-Cheeseman, Chair
University of St. Thomas, Saint Paul, MN, United States

CONTRIBUTED PAPERS

NOB-01. Fabrication and characterisation of compositionally graded La(Fe,Si)$_{13}$ films. E. Fontana[1], T. Devillers[1] and *N. Dempsey*[1] *1. Inistitut NEEL CNRS, Grenoble, France*

La(Fe, Si)$_{13}$ has been widely studied for use in magnetic refrigeration. This alloy family exhibits a large magnetocaloric effect (MCE) due to a magne-to-volume effect that occurs during the transition from the paramagnetic to the ferromagnetic states. Adjusting the Si-content, it is possible to modify the crystal structure (cubic <-> tetragonal), magnetisation, Curie temperature (Tc) and the MCE [1,2]. Furthermore, the Tc can be increased to above room temperature by doping (e.g. Co) and hydrogenation [2] or it can be reduced by application of isostatic pressure [1,3]. While literature reports focus on bulk materials, we recently reported on the fabrication of thick films of La(Fe, Si)$_{13}$ [4]. Synthesize in film form opens new possibilities for material studies and for eventual integration into micro-systems. Here we will report on compositionally graded La-Fe-Si films. The films were deposited onto stationary Si substrates of diameter 100 mm, by co-sputtering of three targets. Films of nominal thickness 1 - 5 μm were deposited at room temperature and annealed ex-situ (900°C / 5 min). EDX analysis was used to measure the composition spread of as-deposited films and annealed samples from certain regions were characterized by optical and scanning electron microscopy, XRD and VSM-SQUID. We will show how the structural and magnetic properties and fracture behavior vary as a function of composition, thickness and cooling rate. The variation in Tc with lattice parameter of the cubic 1:13 phase of select samples is plotted in figure 1. The difference in the slope compared with literature results for bulk samples is attributed to the influence of substrate mediated strain. A Tc of 286 K, which is 27 K higher than the maximum value reported for bulk ternary La(Fe, Si)$_{13}$ [2], was measured on the thinnest sample studied. We will finish up by discussing future prospects for the high throughput characterization of compositionally graded films of materials of interest for magnetic refrigeration and power generation.

[1] B. G. Shen, et al., Adv. Mater. 21 (2009) 454 [2] K. Niitsu et al, J. Alloys Compd. 578 (2013) 220227 [3] L. Jia et al., Appl. Phys. Lett. 92 (2008) 101904 [4] N. H. Dung, et al, J. Appl. Phys. 127 (2020) 215103

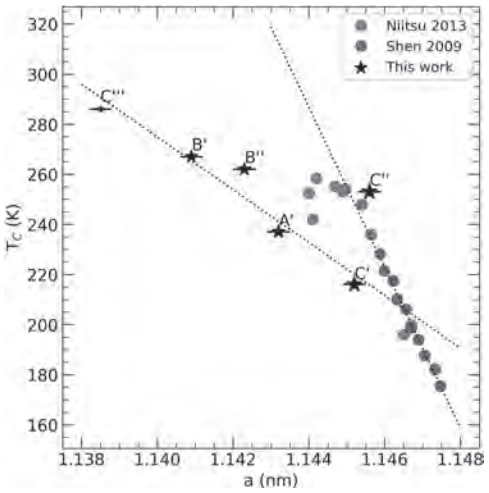

Fig. 1: Tc vs lattice parameter of La(Fe, Si)$_{13}$ films (letters identify the overall film composition, the superscript the thickness and cooling rate) compared to bulk data [1,2].

NOB-02. Machine learning assisted optimization towards high-performance La(Fe,Si)$_{13}$-based magnetocaloric materials. *A. Srinithi*[1,2], A. Bolyachkin[2], X. Tang[2], S. Dieb[2], H. Sepehri-Amin[1,2] and K. Hono[1,2] *1. University of Tsukuba, Tsukuba, Japan; 2. National Institute for Materials Science, Tsukuba, Japan*

La(Fe,Si)$_{13}$-based (1:13) compounds exhibit giant magnetocaloric effect and are promising candidates for room temperature as well as cryogenic magnetic refrigeration [1,2]. The magnetic refrigeration materials require a comprehensive evaluation of their properties such as transition temperature (T_{tr}), entropy change (ΔS_m), adiabatic temperature change (ΔT_{ad}), thermal hysteresis (ΔT_{hys}), relative cooling power (RCP), thermal conductivity and mechanical stability [3]. Extensive studies on tuning these properties have been carried out for the 1:13 system by varying the chemical compositions and processing conditions. However, an excellent combination of properties has not been achieved yet, hindering any practical application [4]. In this work, we employed machine learning (ML) to address the optimization problem in the 1:13 system. A dataset containing over 1000 samples in total was collected using data mining across 200 articles. Several machine learning models were trained to predict T_{tr}, ΔS_m, RCP and T_{hys} as targets and compared using the root mean squared error (RMSE) metric. We found that random forest (RF) and gradient boosting (GB) regressors outperformed other models such as decision tree and k-NN regressors. The achieved performance of the former model is demonstrated in Fig. 1 for the case of predicting T_{tr}. The relative feature importance extracted from the trained RF model in Fig. 2 shows the important parameters for tuning the T_{tr}, while the corresponding Pearson correlation co-efficients (PCC) shows how these parameters influence the T_{tr}. Similarly, the critical parameters were found out for the other target properties and used for further optimization study. The compositional optimization of the 1:13 system was performed by means

of the differential evolution technique with a multi-objective target toward the best combination of the magnetocaloric properties.

1. A. Fujita et al., Phys. Rev. B, 67 (2003) 104416. 2. S. Fujieda et al., Appl. Phys. Lett., 89 (2006) 062504. 3. V. Franco et al., Annual Review of Materials Research, 42 (2012) 305-342. 4. V. Paul-Boncour et al., Magnetochemistry, 7 (2021) 13.

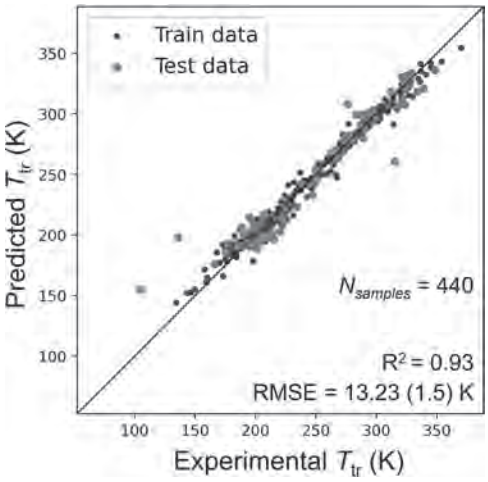

Fig. 1: Experimental transition temperatures (T_{tr}) of 1:13 samples vs. predicted ones by random forest.

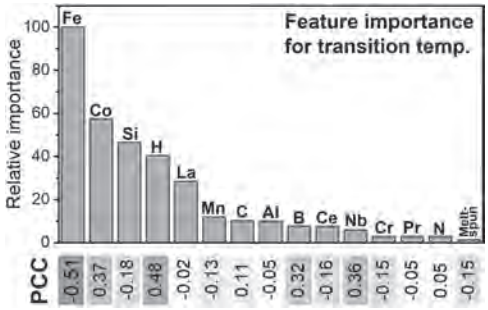

Fig. 2: Relative importance of features such as atomic concentrations of Fe, Co, Si, H and other elements on tuning T_{tr}, and corresponding Pearson correlation co-efficients (PCC).

NOB-03. Tailoring mechanical properties and magnetocaloric effect in $LaFe_{11.8}Si_{1.2-z}X_zH_y$ (X = Al, Ga, In). *A. Pathak*[1], Y. Mudryk[2], O. Dolotko[2] and V. Pecharsky[2,3] *1. Department of Physics, State University of New York (SUNY), Buffalo State, Buffalo, NY, United States; 2. The Ames Laboratory, U. S. Department of Energy, Iowa State University, Ames, IA, United States; 3. Department of Materials Science and Engineering, Iowa State University, Ames, IA, United States*

The ability of certain magnetic materials to change their entropy and/or temperature with the application and removal of a magnetic field (magnetocaloric effect, MCE) is a physical phenomenon that could lead to the realization of clean, energy-efficient heat pumping systems. We report a series of $LaFe_{11.8}Si_{1.1}X_{0.1}$ compounds, where X = Al, Ga, and In, added in small concentrations, substantially reduce brittleness intrinsic to unsubstituted $La(Fe_{1-x}Si_x)_{13}$, while preserving or enhancing their giant MCEs [1]. Room temperature powder X-ray diffraction confirms formation of $LaFe_{11.8}Si_{1.1}X_{0.1}$ adopting the $NaZn_{13}$-type structure as major phases, with ~10 to 15% of αFe impurity. Surprisingly, relatively large amounts of αFe do not deteriorate the magnetic field-induced entropy change (ΔS), yet the resultant alloys have much improved mechanical stability. The corresponding maximum ΔS are -18, -17, and -13 J kg^{-1} K^{-1} for X = In, Al, and Ga, respectively, in ΔH = 2 T in the vicinities of their respective Curie temperatures. The Curie temperatures of $LaFe_{11.8}Si_{1.1}X_{0.1}$ materials can be increased to room temperature and above by hydrogenation, preserving the giant MCE. For example, a fully hydrogenated $LaFe_{11.8}Si_{1.1}In_{0.1}H_{2.3}$ exhibits maximum ΔS close to -16 J kg^{-1} K^{-1} at T~344 K and ΔH =2 T. This work was supported by the Division of Materials Science and Engineering of the Office of Basic Energy Sciences of the U.S. DOE. Ames Laboratory is operated for the U.S. Department of Energy (DOE) by Iowa State University under Contract No. DE-AC02-07CH11358. AKP acknowledges the finanacial support from faculty startup fund from the Dean's Office, School of Arts and Sciences, SUNY Buffalo State.

[1] Arjun K Pathak, Yaroslav Mudryk, Oleksandr Dolotko, Vitalij K Pecharsky, US Patent # US 11,289,248 B2, publication date March 29 (2022).

NOB-04. Synthesis and magnetic properties of $LaFe_{13-x-y}M_xSi_yN_3$ nitrides. A. Thayer[1], I. Hlova[1], *Y. Mudryk*[1], X. Liu[1] and V. Pecharsky[1,2] *1. Ames Laboratory of US DOE, Iowa State University, Ames, IA, United States; 2. Department of Materials Science and Engineering, Iowa State University, Ames, IA, United States*

$LaFe_{13-x-y}M_xSi_yN_3$ compounds (M = Mn) were synthesized by flowing ammonia over intermetallic precursors at 623 K for 4 hours. The nitrides were characterized by room temperature powder X-ray diffraction, magnetic thermogravimetry (mTGA), differential scanning calorimetry (DSC), and magnetization measurements. The nitrides derived from Si-poor (y ≤ 3) cubic intermetallics retain the $NaZn_{13}$-type crystal structure and the lattice parameters, *a*, of the synthesized trinitrides increase by ~3 % compared to the precursors. The nitrogenation increases ferromagnetic ordering temperature by approximately 200 K when compared with the corresponding nitrogen-free $NaZn_{13}$-type phases, but unlike those of the latter, T_Cs of the nitrides are independent of the Fe/Si ratio. Partial substitution of Fe with Mn lowers T_C of the trinitride similarly to the non-nitrogenated precursors. The magnetic ordering transitions in the nitrides are broad, resulting in rather weak magnetocaloric effects peaking at -2.0 J/Kg K for a 0 to 5 T magnetic field change. The nitrides are stable below 750 K, but they begin to lose nitrogen above this temperature, fully decomposing above 1050 K. Ames Laboratory is operated for the U.S. Department of Energy (DOE) by Iowa State University under Contract No. DE-AC02-07CH11358. This work was supported by the Division of Materials Science and Engineering of the Office of Basic Energy Sciences of the U.S. DOE.

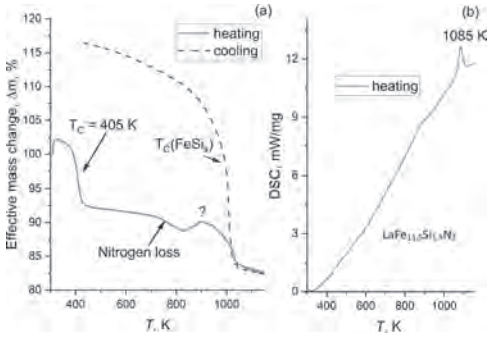

Figure 1. Results of the (a) mTGA and (b) DSC measurements of the $LaFe_{11.5}Si_{1.5}N_3$ compound.

NOB-05. Impact of F and S doping on $(Mn,Fe)_2(P,Si)$ giant magnetocaloric materials. *F. Zhang*[1], I. Batashev[1], Q. Shen[1], Z. Wu[1], R. Smith[2], G. de Wijs[3], N. van Dijk[1] and E. Brück[1] *1. TUDelft, Delft, Netherlands; 2. The ISIS Facility, Didcot, United Kingdom; 3. Radboud University, Nijmegen, Netherlands*

The quarternary $(Mn,Fe)_2(P,Si)$-based materials with a giant magnetocaloric effect (GMCE) at the ferromagnetic transition T_C are promising bulk materials for solid-state magnetic refrigeration [1-3]. In the present study we demonstrate that doping with the light elements fluorine and sulfur can be used to adjust T_C near room temperature and tune the magnetocaloric properties. For F doping the first-order magnetic transition (FOMT) of $Mn_{0.60}Fe_{1.30}P_{0.64}Si_{0.36}F_x$ (x = 0.00, 0.01, 0.02, 0.03) is enhanced, which is explained by an enhanced magnetoelastic coupling. The magnetic entropy change $|\Delta S_m|$ at a field change ($\Delta\mu_0 H$) of 2 T markedly improved by 30% from 14.2 $Jkg^{-1}K^{-1}$ (x = 0.00) at 335 K to 20.2 $Jkg^{-1}K^{-1}$ (x= 0.03) at 297 K. For the F doped material the value of $|\Delta S_m|$ for $\Delta\mu_0 H$ = 1 T reaches 11.6 $Jkg^{-1}K^{-1}$ at 294 K, which is consistent with the calorimetric data (12.4 $Jkg^{-1}K^{-1}$). Neutron diffraction experiments reveal enhanced magnetic moments by F doping in agreement with the prediction of DFT calculation. For S doping in $Mn_{0.60}Fe_{1.25}P_{0.66-y}Si_{0.34}S_y$ (y = 0.00, 0.01, 0.02, 0.03, 0.04) three impurity phases have been found from microstructural analysis, which reduce the stability of the FOMT in the main phase and decrease T_C, e.g. the $|\Delta S_m|$ reduces from 7.9(12.6) $Jkg^{-1}K^{-1}$ (332 K) for the undoped sample to 3.4(6.2) $Jkg^{-1}K^{-1}$ (313 K) for the maximum doped sample for $\Delta\mu_0 H$ = 1(2) T. Neutron diffraction experiments combined with first-principles theoretical calculation, distinguish the occupation of F/S dopants and the tuning mechanism for light element doping, corresponding to subtle structural changes and a strengthening of the covalent bonding between metal and metalloid atoms. It is found that the light elements F and S can effectively regulate the magnetocaloric properties and provide fundamental understanding of $(Mn,Fe)_2(P,Si)$-based intermetallic compounds.

[1] O. Tegus, E. Brück, K.H.J. Buschow, F.R. de Boer, *Nature*. 415, 150-152 (2002). [2] F. Guillou, G. Porcari, H. Yibole, N. van Dijk, E. Brück, *Adv Mater*. 26, 2671-2675 (2014). [3] T. Gottschall, K.P. Skokov, M. Fries, A. Taubel, I. Radulov, F. Scheibel, D. Benke, S. Riegg, O. Gutfleisch, *Adv Energy Mater*. 9, 1901322 (2019).

NOB-06. Study of the magnetostructural transition in critical-element free $Mn_{1-x}Ni_{1-x}Fe_{2x}Si_{0.95}Al_{0.05}$. *B. Eggert*[1], K. Wang[2], S. Jafarzadeh[2], C.R. Bahl[2], B.C. Hauback[1] and C. Frommen[1] *1. Hydrogen technology, Institute for Energy Technology, Kjeller, Norway; 2. DTU Energy, DTU, Copenhagen, Denmark*

Magnetocaloric materials are researched as promising alternatives to conventional gas compression technologies for heat conversion. Within the known magnetocaloric materials, the MM′X system is promising as it features a strong first order magnetostructural transition (MST) enabled by partial substitution of M, M′ and X sites, where M and M′ are transition metals and X is a p-block element in orthorhombic/hexagonal structures[1]. Commonly used intermetallics (MnNiGe, MnCoGe [2,3]) employ Ge and Co, which are critical for their applications in electronics, and cathode materials for batteries, respectively. In the present study, Fe and Al substitutions inside a MnNiSi-based intermetallic induce a MST without critical or expensive elements. All alloys have been synthesized by arc melting, and heat treated followed by quenching. By convenient substitution, the studied $Mn_{1-x}Ni_{1-x}Fe_{2x}Si_{0.95}Al_{0.05}$ alloys exhibit Curie temperatures around room-temperature, which were captured by Vibrating Sample Magnetometry (VSM) as well as In-field differential scanning calorimetry (DSC) [4]. The VSM magnetization over temperature data in the $Mn_{0.69}Ni_{0.69}Fe_{0.62}Si_{0.95}Al_{0.05}$ sample with applied field $\mu_0 H$ = 1 T shown in Fig. 1 displays an abrupt variation of magnetization with temperature, where the derivatives of magnetization exhibit a minimum between 279 and 290 K during cooling and heating, respectively. From the VSM measurements, what can be thought of as a single-phase transition due to a single derivative minimum can be elucidated with the use of a 1K/min heating/cooling rate in the DSC. In fact, this MST is a convolution of different transitions all close to one another, as shown during the cooling protocol in Fig. 2 from in-field DSC data with 1 T applied field. The main article will investigate the cause of such distribution of transitions and its effect on the isothermal entropy change during heating and cooling transformations, as evaluated by a concurrent VSM and DSC study.

[1] W. Bazela, A. Szytula, J. Todorovic, A. Zieba, Crystal and magnetic structure of the $NiMnGe_{1-n}Sin$ System, Phys. Status Solidi. 64 (1981) 367–378. https://doi.org/10.1002/pssa.2210640140. [2] A. Taubel, T. Gottschall, M. Fries, T. Faske, K.P. Skokov, O. Gutfleisch, Influence of magnetic field, chemical pressure and hydrostatic pressure on the structural and magnetocaloric properties of the Mn-Ni-Ge system, J. Phys. D. Appl. Phys. 50 (2017). https://doi.org/10.1088/1361-6463/aa8e89. [3] S.K. Pal, C. Frommen, S. Kumar, B.C. Hauback, H. Fjellvåg, G. Helgesen, Enhancing giant magnetocaloric effect near room temperature by inducing magnetostructural coupling in Cu-doped MnCoGe, Mater. Des. 195 (2020) 109036. https://doi.org/10.1016/j.matdes.2020.109036. [4] K.K. Nielsen, H.N. Bez, L. Von Moos, R. Bjørk, D. Eriksen, C.R.H. Bahl, Direct measurements of the magnetic entropy change, Rev. Sci. Instrum. 86 (2015). https://doi.org/10.1063/1.4932308.

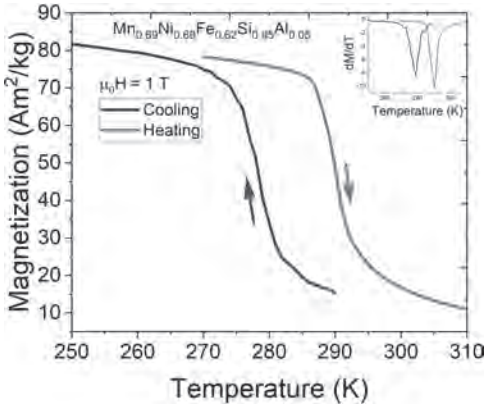

Magnetization as a function of temperature during heating and cooling for an ingot of $Mn_{0.69}Ni_{0.69}Fe_{0.62}Si_{0.95}Al_{0.05}$ with a 1 T applied field.

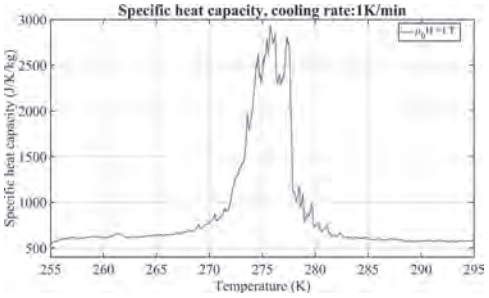

Cooling transformation in $Mn_{0.69}Ni_{0.69}Fe_{0.62}Si_{0.95}Al_{0.05}$ as measured by In-field DSC with 1 T applied field.

NOB-07. The effects of Cu substitution on magnetocaloric effects of the $HoCo_{1-x}Cu_xSi$ ($0 \le x \le 0.4$) phases. B. Liu[1], G. Zeng[1], *J. Chen*[2] and W. Cui[1] *1. Northeastern University, Shenyang, China; 2. Aerospace Information Research Institute, CAS, Beijing, China*

There are many investigations of chemical substitutions in RTX system, such as $TmNi_{1-x}Cu_xAl$ system, which is iso-structure alloying [1]. However, few studies carry out hetero-structural alloying in RTX system. In our recent work, we found that the entropy change (ΔS_M) also can be enhanced by hetero-structural alloying [2]. By hetero-structural alloying ferromagnetic (FM) TiNiSi-type orthorhombic HoCoSi with antiferromagnetic (AFM) Ni_2In-type hexagonal HoCuSi, the magnetic and structural evolutions have been observed in $HoCo_{1-x}Cu_xSi$ ($0 \le x \le 0.4$) alloys. With increased Cu substitution for Co, the phase transition is changed from ferromagnetic for

$x \leq 0.3$ to antiferromagnetic for $x = 0.4$. For $\Delta\mu_0 H$ of 0-5 T, the maximum magnetic entropy changes are 10.1 J/kgK, 8.6 J/kgK, 7.6 J/kgK, 10.0 J/kgK and 13.6 J/kgK in $HoCo_{1-x}Cu_xSi$ ($x = 0$, 0.1, 0.2, 0.3 and 0.4) alloys. It is obvious that the maximum magnetic entropy changes are decreased for $x \leq 0.2$, which is caused by magnetic moment dilution effects that reduced the saturation magnetization. However, the maximum magnetic entropy changes are increased for $0.3 \leq x \leq 0.4$. With increasing the substitution amount ($0.3 \leq x \leq 0.4$), $HoCo_{1-x}Cu_xSi$ system undergoes AFM - Paramagnetic (PM) transition at the critical component. And the field-induced metamagnetic transition is the first-order phase transition nature at low temperature, which leads to the enhancement of ΔS_M.

[1] Z.Y. Xu, Z.G. Zhang, R.L. Gao, W.J. Gong, A.L. Lin, Rare Met. (6) 1-5 (2016). [2] G. Yao, S. Sun, J. Yang, H. Wu, Q. Wang, J. Zhu, W. Cui, Scr. Mater. 194 113649 (2021).

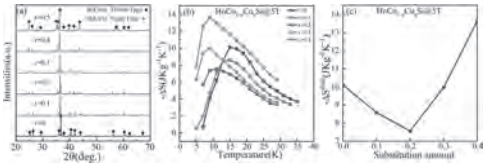

Fig. 1 (a) the XRD patterns and (b) magnetic entropy changes under the field change 7 T of $HoCo_{1-x}Cu_xSi$ ($x \leq 0.4$) alloys. (c) the maximum magnetic entropy changes as a function of the content of Cu.

NOB-08. Magnetocaloric effect in melt-spun $Ni_{45}Co_5Mn_{36.7}In_{13.3-x}Ge_x$ (x=0 and 3) ribbons. *M. Norouzi-Inallu*[1,2], A. Ghotbi Varzaneh[2], P. Kameli[2], D. Salazar[3], K. Ullakko[1] and V. Chernenko[3,4] *1. Material Physics Laboratory, Lappeenranta-Lahti University of Technology LUT, Lappeenranta, Finland; 2. Department of Physics, Isfahan University of Technology, Isfahan, The Islamic Republic of Iran; 3. Basque Center for Materials, Applications and Nanostructures and University of Basque Country, Leioa, Spain; 4. Ikerbasque, Basque Foundation for Science, Bilbao, Spain*

In the present work, the effect of Ge substitution instead of In on structural, martensitic transformation (MT), and magnetocaloric effect (MCE) exhibited by $Ni_{45}Co_5Mn_{36.7}In_{13.3}$ metamagnetic shape memory alloys (MetaMSMAs) has been studied as promising candidates for magnetic cooling. The compound should have a high surface/volume (S/V) ratio to enhance the efficiency of magnetic cooling and heat exchange rate. Hence, ribbon samples were prepared by melt-spinning to maximize the S/V ratio and characterized by recording X-ray diffraction at different constant temperatures across MT besides calorimetry. The ribbons show narrow thermal hysteresis moderately dependent on Ge-doping and adjustable MT temperatures close to ambient temperature. The inverse and conventional MCEs were analyzed by calculating the magnetic entropy (ΔS_M) using thermomagnetization curves up to 5 T and the Maxwell relationships. It is found that the Ge-doped ribbons showed values of |27| J/kgK for inverse MCE as well as |1,5| J/kgK for conventional, which is a significant value compared to the literature. These results can motivate further study and development of MCE in $Ni_{45}Co_5Mn_{36.7}In_{10.3}Ge_3$ MetaMSMAs, which can have potential applications for magnetic refrigeration systems as ribbon shapes.

1. P. Álvarez-Alonso, C. O. Aguilar-Ortiz, J. P. Camarillo, D. Salazar, H. Flores-Zúñiga and, V. A. Chernenko, Applied Physics Letters, 109(21), p.212402 (2016) 2. C. O. Aguilar-Ortiz, D. Soto-Parra, P. Álvarez-Alonso, P. Lázpita, D. Salazar, P.O. Castillo-Villa, H. Flores-Zúñiga, and V. A. Chernenko, Acta Materialia, 107, pp.9-16 (2016) 3. A. G. Varzaneh, P. Kameli, I. A. Sarsari, M. G. Zavareh, C. S. Mejía, T. Amiri, Y. Skourski, J. L. Luo, T. H. Etsell, and V. A. Chernenko, Physical Review B, 101(13), p.134403 (2020) 4. M. N. Inallu, P. Kameli, I. A. Sarsari, A. G. Varzaneh, D. Salazar, I. Orue, and V. A. Chernenko, Journal of Physics D: Applied Physics, 52(23), p.235001, (2019) 5. A. Wójcik, W. Maziarz, M. J. Szczerba, M. Sikora, A. Zywczak, C. O. Aguilar-Ortiz, P. Álvarez-Alonso, E. Villa, H. Flores-Zúñiga, E. Cesari, and J. Dutkiewicz, Journal of Alloys and Compounds, 721, pp.172-181 (2017) 6. Z. Ghazinezhad, P. Kameli, A. G. Varzaneh, I. A. Sarsari, M. Norouzi-Inallu, T. Amiri, D. Salazar, B. Rodríguez-Crespo, D. Vashaee, T. H. Etsell, and V. A. Chernenko, Journal of Physics D: Applied Physics, 55(25), p.255001 (2022) 7. H. Zhang, X. Zhang, M. Qian, L. Yin, L. Wei, D. Xing, J. Sun, and L. Geng, Applied Physics Letters, 116(6), p.063904 (2020) 8. M. Norouzi-Inallu, P. Kameli, A. G. Varzaneh, I. A. Sarsari, M. A. Eskandari, I. Orue, B. Rodríguez-Crespo, and V. A. Chernenko, Journal of Physics: Condensed Matter, 34(22), p.225803 (2022)

NOB-09. Magnetocaloric effect close to room temperature in R_6TX_2 intermetallics (R = Gd, Tb, Dy; T = Fe, Mn, Co, Ni; X=Sb, Te). A. Oleaga[1], A. Herrero[1], *I.R. Aseguinolaza*[1], A.V. Garshev[2], V.O. Yapaskurt[3] and A.V. Morozkin[2] *1. Applied Physics, University of the Basque Country, Bilbao, Spain; 2. Chemistry Department, Moscow State University, Moscow, Russian Federation; 3. Faculty of Geology, Moscow State University, Moscow, Russian Federation*

R_6TX_2 family has interesting magnetic and magnetocaloric properties in different temperature ranges, depending on the particular composition. The combination of different rare earths, transition metals and p-block elements allows to tune these properties to a desired temperature and to improve them. We show in this work how this can be done close to room temperature (RT) based on the previous experience with this family [1, 2]. Nine different combinations have been studied: $Gd_3Tb_3FeSbTe$, $Tb_2Dy_4FeSb_2$, $Gd_2Dy_4Fe_{0.75}Mn_{0.25}Sb_2$, $Gd_2Tb_4Fe_{0.75}Mn_{0.25}SbTe$, $Tb_2Dy_4Fe_{0.75}Mn_{0.25}Sb_2$, $Tb_6Fe_{0.75}Mn_{0.25}SbTe$, $Tb_6Co_{0.75}Mn_{0.25}SbTe$, $Tb_6Ni_{0.75}Mn_{0.25}SbTe$, and $Tb_6Ni_{0.5}Mn_{0.5}SbTe$. All these intermetallics present a paramagnetic to ferromagnetic transition (PM-FM) between 185 K and RT followed, as temperature decreases, by a spin-reorientation one. Therefore, the lower temperature magnetocaloric effect helps sustaining the magnetocaloric parameters of the higher temperature one (see Fig. 1). The critical behavior of the PM-FM transitions has been studied obtaining the magnetic critical exponents β,γ, δ , which suggest long-range order interactions, though in many cases there is an unconventional critical behavior (see Fig. 2). The magnetocaloric scaling laws have been checked reinforcing the obtained critical exponents, and the universal curves for the magnetocaloric effect have also been found for all cases. The role of the different ions in the properties is discussed.

[1] A. Herrero, A. Oleaga, I. R. Aseguinolaza, A.J. Garcia-Adeva, E. Apiñaniz, A.V. Garshev, V.O. Yapaskurt, A.V. Morozkin, Journal of Alloys & Compounds 890, 161849 (2021) [2] A. Oleaga, A. Herrero, A Salazar, A.V. Garshev, V.O. Yapaskurt, A.V. Morozkin, Journal of Alloys & Compounds 843, 155937 (2020)

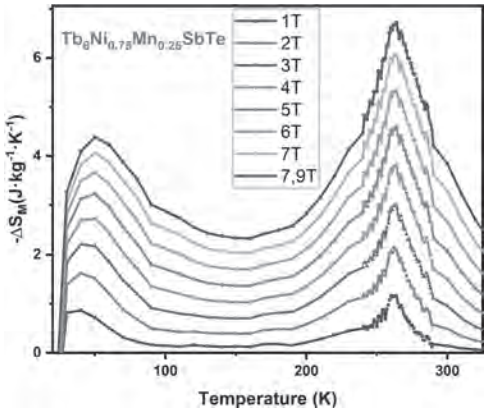

Fig. 1: Magnetocaloric effect for $Tb_6Ni_{0.75}Mn_{0.25}SbTe$

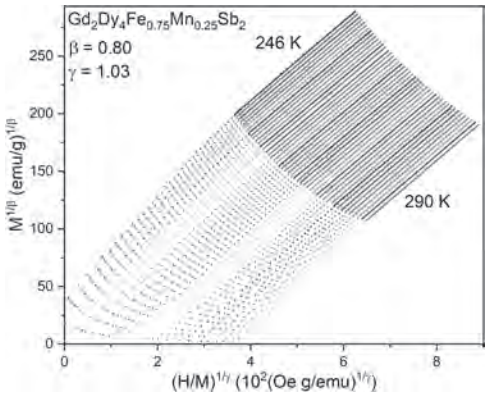

Fig. 2: Modified Arrott Plot for $Gd_2Dy_4Fe_{0.75}Mn_{0.25}Sb_2$

NOB-10. Chemically controllable magnetic transition temperature and magneto-caloric properties in MnZnSb based compounds. *J. Alaria*[1]
1. Department of Physics & Stephenson Institute for Renewable Energy, University of Liverpool, Liverpool, United Kingdom

A viable compound for magnetic refrigeration at ambient temperature must present a large change in magnetic entropy, with minimum hysteresis and should be composed of earth abundant and non-toxic elements. [1] Recently a computational proxy was developed to identify new magnetocaloric materials whereby first principle structure relaxation is carried out with and without spin polarization to ascertain the degree of magnetic deformation. [2] By applying this method to ferromagnets in the PbFCl family we found magnetic deformation of around 2% which is similar to other magnetocaloric compounds. We therefore have focussed our experimental study on MnZnSb, which is reported to be an itinerant ferromagnet with a second order phase transition and Curie temperature about room temperature. [3] Detailed magnetization measurements were carried out and Arrott analysis (Fig 1. a)) yields a Curie temperature of 304K, with the system being described as one universality class across all order parameters and identified as '2-dimensional long-range.' We find a reasonably large magnetic entropy change of 4.5 $Jkg^{-1}K^{-1}$ with a relative cooling power of 153 Jkg^{-1}. Temperature dependant powder neutron diffraction was used to investigate the origin of the significant magnetic entropy change around the magnetic transition which is attributed to the release of crystallographic strain through the magnetic transition. We identify the *c/a* parameter as an accurate crystallographic proxy to control the magnetic transition (Fig. 1 b)). Using this concept, chemical substitution on the square-net allows to experimentally tune the Curie temperature over a broad temperature span between 252-322 K (Fig. 1 c)). A predictive machine learning model for the c/a parameter is developed to guide future exploratory synthesis.

[1] T. Gottschall, K. P. Skokov, M. Fries, A. Taubel, I. Radulov, F. Scheibel, D. Benke, S. Riegg, O. Gutfleisch, Adv. Energy Mater., 2019, 9, 901322. [2] J. D. Bocarsly, E. E. Levin, C. A. C. Garcia, K. Schwennicke, S. D. Wilson, R. Seshadri, Chem. Mater., 2017, 29, 1613. [3] N. Y. Pankratov, V. I. Mitsiuk, V. M. Ryzhkovskii, S. A. Nikitin, J. Magn. Magn. Mater., 2019, 470, 46.

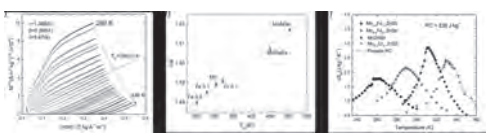

Figure 1: a) Arrott-Noakes plot for the isothermal magnetization of MnZnSb. b) Variation of the *c/a* for ferromagnets with the PbFCl structure. c) Magnetic entropy changes between 0 – 5 T as function of temperature for various composition based on MnZnSb. The grey line outlines the combined isothermal for the four different compositions.

NOB-11. Tailoring thermal hysteresis and microstructure of Ni-Mn-based Heusler alloys for multicaloric cooling applications. *A. Taubel*[1], F. Scheibel[1], L. Pfeuffer[1], N. Shayanfar[1], B. Beckmann[1], T. Gottschall[2], K.P. Skokov[1] and O. Gutfleisch[1] *1. Materials Science, Technical University Darmstadt, Darmstadt, Germany; 2. Dresden High Magnetic Field Laboratory (HLD-EMFL), Helmholtz-Zentrum Dresden-Rossendorf, Dresden, Germany*

Refrigeration based on the magnetocaloric effect (MCE) attracts a lot of attention since it can be more energy efficient and environmentally friendly than current vapor compression technology. The concept uses a solid-state magnetic material that heats up and cools down cyclically when exposed to a changing magnetic field. The development of multicaloric materials using more than one transformation-inducing stimulus opens up further possibilities to enhance the efficiency of a multicaloric cycle. One approach is to use magnetic field and uniaxial pressure alternatingly to trigger the cyclic phase transition in a multicaloric material [1,2]. In this work, we present a novel multi-stimuli cooling concept including potential material systems and methods to tailor their functional and mechanical properties. The main objective is adopting the properties for a classical MC cycle towards the extended needs of the multi-stimuli cycle using intrinsic and extrinsic means. We investigated for Ni-Co-Mn-In and Ni-Co-Mn-Ti Heusler alloys the influence of different microstructures from chemical variation and different processing routes on the magnetocaloric and elastocaloric performance [3,4]. We found that preferential grain orientation in [001] direction along the compression direction is beneficial for the stress-induced transformation [3], whereas introducing secondary phases enhances the long-term stability under cyclic stress application while maintaining the caloric performance [5]. For single phase Ni-Co-Mn-Ti, we tailor the phase transition by optimizing the heat treatment and varying the stoichiometry. By this, we can achieve large isothermal entropy changes of up to 40 $Jkg^{-1}K^{-1}$ in 2 T [4]. In combination with very good mechanical strength, this makes Ni-Co-Mn-Ti alloys a suitable candidate for the multi-stimuli cooling cycle. We acknowledge funding by ERC (Adv. Grant "Cool Innov", GrantNo. 743116) and by DFG (CRC "HoMMage", Project-ID 405553726 –TRR 270)

[1] T. Gottschall et al., Nature Mat. 17, 929–934 (2018) [2] Patent 10 2016 110 385.3, 6. June 2016; Cooling device and a refrigeration process. German patent application [3] L. Pfeuffer et al., Acta Materialia 217 1175157 (2021) [4] A. Taubel and B. Beckmann et al., Acta Mater. 201, 425-434 (2020) [5] L. Pfeuffer et al., Acta Materialia 221, 117390 (2021)

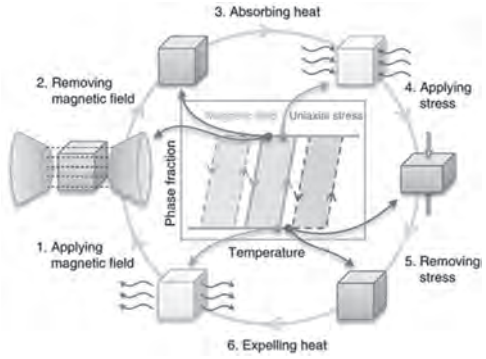

Schematic of the six-step multi-stimuli cycle, which makes use of a large thermal hysteresis [1] (© patented [2])

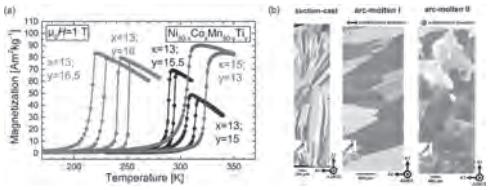

Tailoring the phase transition of Ni-Co-Mn-Ti by varying the stoichiometry (a) [3] and analyzing grain orientations for different processing routes (b) [2]

NOB-12. Tuning in the vast high-entropy alloy space for competitive magnetocaloric properties. *J. Law*[1], Á. Díaz-García[1], L.M. Moreno-Ramírez[1] and V. Franco[1] *1. Dept. Condensed Matter Physics, University of Seville, Seville, Spain*

High-entropy alloys (HEAs), instead of employing one or two main constituents like in traditional alloy development, adopt a different design concept where it combines a blend of multi-principal elements in large concentrations. This design idea enables them with large values of configurational entropy of mixing and a vast compositional space which offers a huge window of exploration opportunities. Magnetocaloric HEAs have been limited to low-temperature range or showing sub-par performance till recent extensions to the first-generation equiatomic HEA design approach have been devised [1, 2]. The magnetocaloric performance of equiatomic magnetocaloric HEAs heavily depends on the choice of element selection and thus the likelihood of relying on the rare-earth (RE) elements due to their intrinsic large magnetic moments. Extending beyond the equiatomic point towards non-equiatomic in the HEA region combined with directed search strategies, overcomes the above-mentioned limitations of magnetocaloric HEAs: the low temperature limit is improved (48 % increase as displayed in Fig 1) and ≥ 5-fold performance enhancement (Fig 2) [3-5]. In this talk, we will show the various design strategies of magnetocaloric HEAs and how to tackle the vast HEA space to tune for the desired magnetocaloric properties. Work supported by Grant PID2019-105720RB-I00 funded by MCIN/ AEI/ 10.13039/501100011033. Additional support Consejería de Economía, Conocimiento, Empresas y Universidad de la Junta de Andalucía (grant P18-RT-746), US Air Force Office of Scientific Research (FA8655-21-1-7044) and Sevilla University under VI PPIT-US program.

[1] J. Y. Law, V. Franco, "Designing Magnetocaloric High-Entropy Alloys", Submitted to Journal of Materials Research (2022). [2] J. Y. Law, V. Franco, "Pushing the limits of magnetocaloric high entropy alloys", APL Materials 9, 080702 (2021). [3] Á. Díaz-García, J.Y. Law, L.M. Moreno-Ramírez, and V. Franco, To be published (2022). [4] J.Y. Law, Á. Díaz-García, L.M. Moreno-Ramírez, and V. Franco, Acta Materialia 212, 116931 (2021). [5] J.Y. Law, L.M. Moreno-Ramírez, Á. Díaz-García, A. Martín-Cid, S. Kobayashi, S. Kawaguchi, T. Nakamura, and V. Franco, Journal of Alloys and Compounds 855, 157424 (2021).

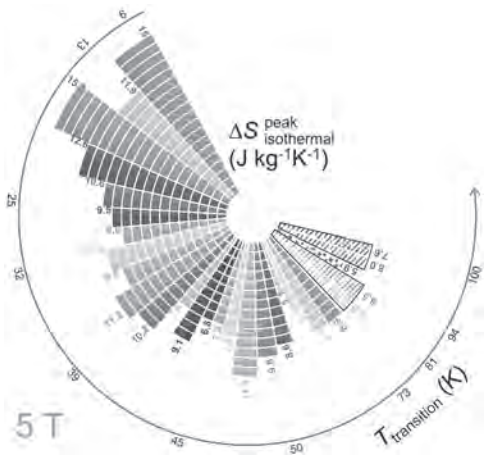

Fig 1. Magnetocaloric performance of equiatomic (solid-filled) and non-equiatomic RE-containing HEAs (outline and pattern filled). The latter overcomes the typical low temperature limit faced in amorphous RE-containing HEAs.

Fig 2. Non-equiatomic RE-free HEAs (outlined hollow regions) surpass the sub-par performance of equiatomic RE-free HEAs.

Session NOC
MAGNETOCALORIC MATERIALS II

Nora Dempsey, Chair
Insttitut NEEL CNRS, Grenoble, France

CONTRIBUTED PAPERS

NOC-01. Direct measurement of multicaloric effects under magnetic fields and uniaxial stress in FeRh. L. Pfeuffer[1], N. Shayanfar[1], T. Gottschall[2], *F. Scheibel*[1], A. Taubel[1], A. Aubert[1], K.P. Skokov[1] and O. Gutfleisch[1] *1. Technical University of Darmstadt, Darmstadt, Germany; 2. Dresden High Magnetic Field Laboratory, Dresden, Germany*

The world's rising temperature and prosperity come along with an urgent need for more sustainable and energy-efficient cooling solutions. A promising alternative to currently utilized gas compression technology is magnetic cooling which is based on the magnetocaloric effect. While particularly large magnetocaloric effects in moderate external fields are obtained near first-order phase transformations, their intrinsic thermal hysteresis limits reversibility during cyclic operation and is therefore a major bottleneck for the technological breakthrough of magnetic cooling. In order to tackle this issue, we have developed a novel multicaloric cooling concept which even makes use of hysteresis (see Figure 1) [1]. In this case the magnetic material is transformed from a low- to a high-magnetization state by magnetic field application. As the thermal hysteresis hinders the back transformation upon magnetic field removal the material is trapped in the high-magnetization state. For that purpose, uniaxial stress is applied in the next step ensuring the back transformation to the initial low-magnetization state. In comparison with conventional magnetic cooling, this so-called "exploiting-hysteresis cycle" allows to achieve higher cyclic effects and substantially reduce the required amount of permanent magnets [2]. Suitable materials for the "exploiting hysteresis cycle" need to show an inverse magnetocaloric and a conventional elastocaloric effect or the vice versa combination in vicinity of the first-order phase transition. In this work, we present a novel multicaloric testbed which allows the direct measurement of the multicaloric material performance in an "exploiting-hysteresis cycle". Using this purpose-built device we study the multicaloric performance of FeRh under different magnetic fields and uniaxial loads. We demonstrate that in FeRh a cyclic multicaloric effect of about 2.5 K can be achieved (see Figure 2) whereas its magnetocaloric counterpart in similar fields is negligibly small. We acknowledge the ERC "CoolInnov" and the CRC/TRR 270 "HoMMage" for funding this work.

[1] T. Gottschall et al., Nature Mat. 17, 929–934 (2018) [2] L. Pfeuffer et al., Acta Mater. 117157 (2021)

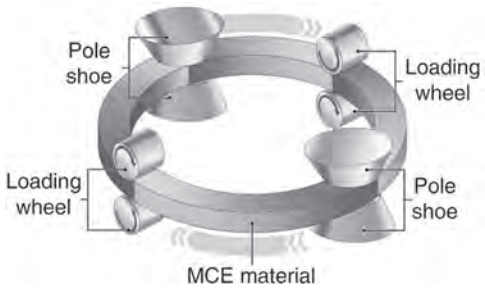

Schematic of multicaloric "exploiting-hysteresis cycle [1]

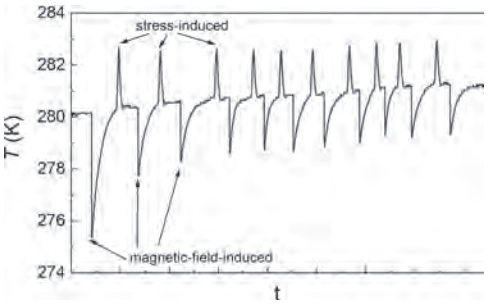

Temperature-time profile in a multicaloric exploiting-hysteresis cycle of FeRh

NOC-02. Heat Capacity and Giant Magnetocaloric Effect of a MnFe(P,Si,B) Compound investigated by semi-adiabatic and Peltier Cell Calorimetry Techniques. *H. Yibole*[1], J. Xu[1], S. Suye[1], B. Narsu[1], F. Guillou[1], R. Hamane[2] and V. Hardy[2] *1. Inner Mongolia Normal University, Hohhot, China; 2. Normandie University, ENSICAEN, UNICAEN, CNRS, CRISMAT, Caen, France*

Heat capacity is a basic physical quantity most important for studying magnetocaloric materials. Not only it reflects how much heat can be stored in the material, but it also allows to quantify the two main performance parameters: the isothermal entropy change ΔS and the adiabatic temperature change ΔT_{ad}. On top of that, being sensitive to structural, electronic and magnetic degrees of freedom, heat capacity also provides fundamental insights. In Fe_2P materials, at the exception of the binary parent, heat capacity studies were so far limited to indirect determinations of the magnetocaloric effect. Here, we will present an extensive heat capacity study of a prototypical MnFe(P,Si,B) compound. Semi-adiabatic relaxation calorimetry, commercial heat flow and home-made Peltier cells differential scanning calorimeters were used to record the heat capacity both around first-order ferromagnetic transition and at low temperatures. This systematic investigation fills several knowledge gaps on the promising MnFe(P,Si,B) magnetocaloric materials. First, we will describe the development of a Peltier cell differential scanning calorimeter designed "as an option" for commonplace commercial cryostat equipped with high magnetic field. This system can be used to measure *directly* the isothermal entropy change ΔS induced by a magnetic field and it even allows targeting the cyclic (reversible) effect due to successive magnetization/demagnetization. In $MnFe_{0.95}P_{0.585}Si_{0.34}B_{0.075}$, an exceptionally large cyclic entropy change at intermediate field (ΔS_{cyclic} = 13.2 J kg^{-1} K^{-1} for $\mu_0\Delta H$ = 1 T) is observed. Then, the heat capacity is analyzed over a broad temperature range to provide an estimate of several important parameters, such as the electronic density of states ($N(E_F)\approx$ 7.2 states eV^{-1}f.u.$^{-1}$) or an estimate of the Debye temperature $\theta_D \approx$ 455 K. Different methods (non-magnetic reference, Debye function, phonons calculations) were used to model the lattice contribution to the heat capacity. Our study highlights the difficulty to disentangle lattice, electronic and magnetic contributions in Fe_2P-type materials. It nonetheless reveals that the magnetic entropy plus latent heat is considerably larger in MnFe(P,Si,B) than in the parent Fe_2P.

NOC-03. Influence of Metamagnetic transition on Magnetocaloric and Magnetoresistance properties of $Tb_2Co_3Ge_5$. *U. Remya*[1], A. Kumar[1], S. Sakthivel[1], A. Dzubinska[2], M. Reiffers[3,4] and R. Nagalakshmi[1]
1. Physics, National Institute of Technology, Trichy, Trichy, India; 2. CPM-TIP, University Pavol Jozef Safarik, Kosice, Slovakia; 3. Faculty of Humanities and Natural Sciences, Presov University, Presov, Slovakia; 4. Institute of Experimental Physics, SAS, Kosice, Slovakia

Investigations on rare-earth intermetallics are at the forefront as they exhibit novel physical phenomena and can be used for spintronics, magnetic refrigeration, and memory applications. $R_2T_3X_5$ series (R-rare-earth element, T-Transition element, and X-*p*-block element) is one of these well-studied systems with novel physical phenomena[1,2], whose application perspectives must be further explored. Hence, in this work, magnetic, magnetoresistance(MR), and magnetocaloric(MCE) properties of $Tb_2Co_3Ge_5$ from the same series have been investigated to gain a better understanding of its physical features and potential applications[3]. The compound has been prepared by arc-melting technique followed by 15 days of annealing at 1023K. The compound crystallizes in $Lu_2Co_3Si_5$ structure (SG - *I12/c1*) and exhibits successive antiferromagnetic transitions at T=31.5 K, 19.4 K, and 11 K, respectively. The antiferromagnetic character is confirmed by the modified Curie-Wiess behavior in the inverse magnetic susceptibility (B=10 kOe) with Curie-Weiss temperature (θ_P)= -8.2 K. Further studies of heat capacity and electrical resistivity show that the crystal electric field effect has an effect and that, at low temperatures, there is a magnon gap of 17.6 K, which is a sign of the complex antiferromagnetic ground state. As the magnetic field(B) increases, the antiferromagnetic ground state shows a metamagnetic transition around the critical magnetic field, B_c=40 kOe, which has an impact on both MR and MCE. As shown in Fig.1, the MR properties reveal a crossover from positive to negative around B_c, due to the presence of metamagnetic transition. At higher fields, B=90 kOe, the negative MR reaches a maximum of 51% at 12 K. Similarly, variation of B above B_c alters the inverse MCE to conventional type with enhancement in MCE properties (See Fig.2). The crossover in the MR and MCE is more suitable for the magnetic refrigeration application[4] as it can switch between cooling and heating cycles as B varies. Acknowledgments: ITMS: 313011D232 ERDF; and also by VEGA1/0705/20, 1/0404/21.

[1] Y. Singh, S. Ramakrishnan, Physical Review B., 69, 174423 (2004). [2] N.H. Sung, C.J. Roh, and K.S. Kim, Physical Review B., 86, 224507 (2012). [3] R. U.D., A. K., and S. S., Journal of Alloys and Compound., 889,161536 (2021). [4] H. Zhang, Y.J. Sun, and L.H. Yang, Journal of Applied Physics., 115, 063901 (2014).

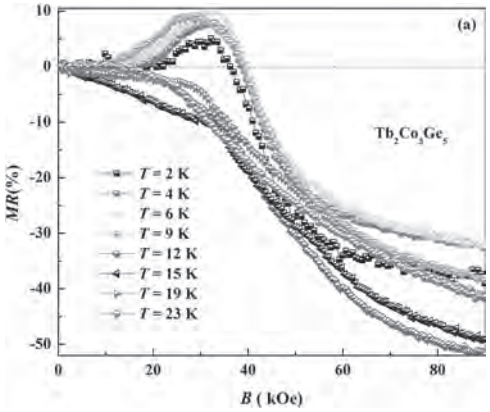

Fig. 1 Variation of MR with the applied magnetic field.

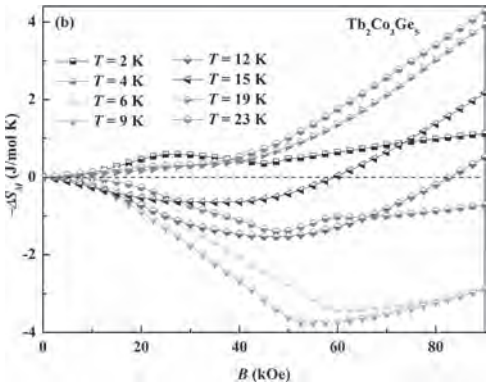

Fig. 2 Magnetic field dependence of MCE property

NOC-04. Enhancing the hysteresis of phase transformation in $Fe_{48}Mn_{24}Ga_{28}$ Heusler alloy via asymmetric thermomagnetic coupling. *W. Li*[1], Y. Zhang[2], L. Song[1], D. Huang[1], X. Xi[1], W. Wang[3], G. Wu[1] and Y. Lau[1] *1. Institute of Physics, Chinese Academy of Sciences, Beijing, China; 2. School of Civil Engineering, Guangzhou University, Guangzhou, China; 3. Tiangong University, Tianjin, China*

According to Clausius–Clapeyron relation $\Delta T/\Delta H = \Delta M/\Delta S$, a large field-induced transition temperature modulation ΔT can be expected for a phase transformation involving substantial change of the saturation magnetization ΔM [1]. Fig. 1(a) describes a strategy for obtaining large ΔM by exploiting the transition between a ferromagnetic martensite and a paramagnetic austenite [2]. The Curie temperature of the austenite T^A_C is far below the martensitic and reverse martensitic transition temperatures, denoted as T_M and T_A, respectively. Applying a magnetic field stabilizes the ferromagnetic phase, giving rise to increased T_M and T_A, without changing the thermal hysteresis T_M - T_A. We next consider a particular case where $T_M < T^A_C < T_A$ (Fig. 1(b)). Since $T_M < T^A_C$, the martensitic transition now involves two ferromagnetic phases with much smaller ΔM. In contrast, the ΔM of the reverse martensitic transition is unaffected. Such an asymmetric thermomagnetic coupling controlled by the position of T^A_C provides a unique opportunity to tune the thermal hysteresis by external field. As a proof of concept, off-stoichiometric $Fe_{48}Mn_{24}Ga_{28}$ Heulser alloy with $T^A_C \sim 180$ K satisfying the above conditions was chosen. The ingots were prepared by arc melting followed by annealing at 1273 K and then quenched in cold water. We used differential scanning calorimetry (DSC), thermomagnetic (M-T) curves, isothermal magnetization (M-H) loops and M-T minor loops [3] to characterize the dissimilar magnetic field effects on the martensitic and the reverse phase transformations. Figure 1(c) shows the experimental M-T curves with applied fields up to 8 T. T_M clearly shows weaker field dependence than T_A, leading to large field-controlled tunability of the thermal hysteresis. In the talk, we will also discuss the role of interface friction and magnetic entropy change in the phase transformation of this alloy.

[1] C. Jiang, G. Feng, and H. Xu, Appl. Phys. Lett. 80, 1619-1621 (2002). [2] W. Zhu, et al., Appl. Phys. Lett. 95, 222512 (2009). [3] W.-H. Wang, et al., Phys. Rev. B 65, 012416 (2001).

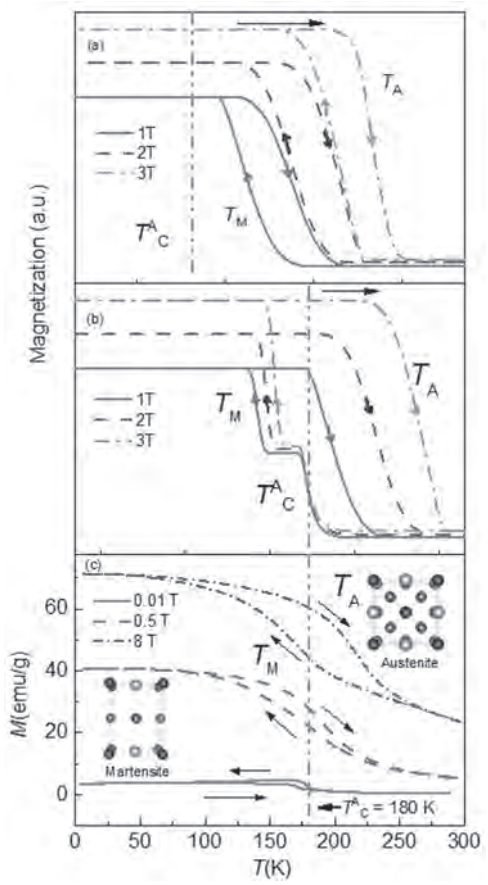

Figure 1: (a-b) Schematics of isofield *M-T* curves for Curie temperature of austenite T^A_C being (a) well below the martensitic transition temperature T_M and (b) between T_M and the reverse martensitic transition temperature T_A. (c) Experimental *M-T* curves of $Fe_{48}Mn_{24}Ga_{28}$, showing enhancement of thermal hysteresis by applying an external field.

NOC-05. Preparation and magnetic properties of Co_2-based Heusler alloy glass-coated microwires with high Curie temperature. M. Salaheldeen[1,2], V. Zhukova[1], A. Garcia-Gomez[1], P. Corte-Leon[1], M. Ipatov[1] and *A. Zhukov*[1,3] *1. Dept. Polymers and Advanced Mater., Dept. Appl. Phys. and EHU Quantum Center, Univ. of Basque Country, UPV/EHU, San Sebastian, Spain; 2. Physics Department, Faculty of Science, Sohag University, Sohag, Egypt; 3. IKERBASQUE, Basque Foundation for Science, Bilbao, Spain*

Co_2-based full-Heusler compounds are among the most promising materials due to their exotic transport properties, high thermal stability, high Curie temperatures ($T_c \approx 1100$ K) for the bulk sample, high magnetic moment (~ 6 μ_B/f.u.), low Gilbert damping constant ($\alpha = 0.004$) and large anomalous Hall effect linked with their band structure [1-3]. The Taylor-Ulitovsky technique, known since 60-s and allows fast (up to a few hundred meters per minute) preparation quite long (up to few kilometers) and thin (typically 0.5 to 40 μm in diameter) metallic wires coated by flexible and insulating glass coating [4]. In addition, the existence of thin, flexible, insulating, and highly transparent glass coating, enhanced mechanical properties and fast and inexpensive fabrication method, glass coating can be useful for biomedical applications due to its biocompatibility [5]. We report on preparation and magnetic properties of Co_2FeSi Heusler alloy glass-covered microwires with a metallic nucleus diameter of about 4,4 μm and total sample diameter of about 17,6 μm. From the X-ray diffraction, XRD, analysis of the as-prepared Co_2FeSi, it was shown that the structure consists of a mixture of nanocrystalline and amorphous phases. An increase in the average grain size, D_g, from 17.8 to 31.6 nm and content of nanocrystalline phase, C from 52 % to 97 % upon annealing at 873 K (1 h) is obtained from XRD analysis. Estimated from temperature dependence of magnetic moment T_c is between 1040 K and 1059 K. As illustrated in Fig. 1, the Co_2-based Heusler glass-coated microwires present strong dependence of the magnetization and the structural properties on the annealing conditions. For annealing temperatures between 873 K and 973 K magnetic phase transition has been observed, as evidenced by sharp drop of the magnetic moment when we applied 50 Oe and 200 Oe external magnetic fields during FC and FH and change in hysteresis loops (see Fig.1).

[1] K. Manna, Y. Sun, L. Muechler, J. Kübler, and C. Felser, "Heusler, Weyl and Berry," *Nat. Rev. Mater.,* vol. 3, no. 8 (2018) 244–256, doi: 10.1038/s41578-018-0036-5. [2] P. Li *et al.*, "Giant room temperature anomalous Hall effect and tunable topology in a ferromagnetic topological semimetal Co2MnAl," *Nat. Commun.* vol. 11, no. 1 (2020) pp. 1–8, doi: 10.1038/s41467-020-17174-9. [3] I. Belopolski *et al.*, "Discovery of topological Weyl fermion lines and drumhead surface states in a room temperature magnet," *Science,* vol. 365, no. 6459 (2019) 1278–1281, doi: 10.1126/SCIENCE.AAV2327/SUPPL_FILE/AAV2327_BELOPOLSKI_SM.PDF. [4] C. Garcia, V. Zhukova, S. Shevyrtalov, M. Ipatov, P. Corte-Leon, and A. Zhukov, "Tuning of magnetic properties in Ni-Mn-Ga Heusler-type glass-coated microwires by annealing," *J. Alloys Compd.*, vol. 838 (2020) p. 155481, 2020, doi: 10.1016/J.JALLCOM.2020.155481. [5] O. Mitxelena-Iribarren *et al.*, "Glass-coated ferromagnetic microwire-induced magnetic hyperthermia for in vitro cancer cell treatment," *Mater. Sci. Eng. C*, vol. 106,(2020) 110261, doi: 10.1016/J.MSEC.2019.110261.

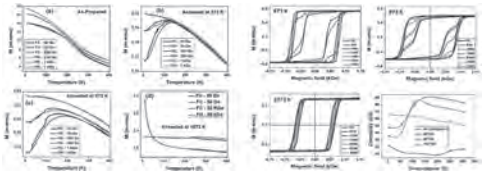

Figure 1. Temperature dependence of magnetization (Left) and hysteresis loops and coercivity behavior with T (K) (Right) for as-prepared and annealed at different temperatures Co_2-based Heusler alloy glass-covered microwires.

NOC-06. Magnetic ordering in Eu_2In, a compound exhibiting a non-hysteretic giant magnetocaloric effect. D. Ryan[3], Y. Mudryk[1], A. Pathak[2], P. Manfrinetti[4], C. Ritter[5], D. Paudyal[1], V. Pecharsky[1] and *A. Provino*[4] *1. Ameslab, Ames, IA, United States; 2. Physics, Buffalo State, Buffalo, NY, United States; 3. Physics, McGill University, Montreal, QC, Canada; 4. Chemistry, University of Genova, Genova, Italy; 5. ILL, Grenoble, France*

Eu_2In crystallises in the orthorhombic Co_2Si-type structure (Pnma #62) with In atoms on one *4c* site and the Eu atoms split between two other *4c* sites. Eu_2In has a nearly ideal first-order magnetostructrural transition (FOMT) at 55K with less than 0.1K hysteresis, a large entropy change and an adiabatic temperature change of 5.0K in a field of 2T [1]. The anhysteretic nature of the FOMT is likely due to there being no change in cell symmetry and relatively small changes in the lattice parameters ($\Delta V/V \approx 0.1\%$). Here we present powder neutron diffraction (Fig.1) and ^{151}Eu Mössbauer spectroscopy data (Fig.2) used to investigate the nature of the magnetic order established below the FOMT at 55K. Both datasets show an abrupt loss of magnetic order on warming through 55K, and neutron diffraction confirms the small isostructural volume expansion associated with the FOMT. Analysis of the diffraction data taken at 2.5K shows that the order is ferromagnetic, with the europium moments on both Eu(*4c*) sites oriented parallel to the *a*-axis. The ^{151}Eu Mössbauer spectrum at 5K shows two equal area components, consistent with europium occupying two equal multiplicity crystallographic sites. However they have quite different hyperfine fields (B_{hf}) of 27T and 17T, suggesting that the europium moments on the two *4c* sites are not the same size. This was confirmed by neutron diffraction where moments of $6.8\mu_B$ and $6.5\mu_B$ were found. Electronic structure calculations with appropriate

electron-electron correlations and spin orbit coupling show that the different moments and hyperfine fields observed on the two inequivalent Eu sites is due to the dissimilar exchange between 4f and 5d states. The calculations further show that spin orbit coupling contributes to the easy a-axis.

[1] F. Guillou, A.K. Pathak, D. Paudyal, Y. Mudryk, F. Wilhelm, A. Rogalev, and V.K. Pecharsky, Non-hysteretic first-order phase transition with large latent heat and giant low-field magnetocaloric effect, *Nature Comm.* 9 (2018) 2925.

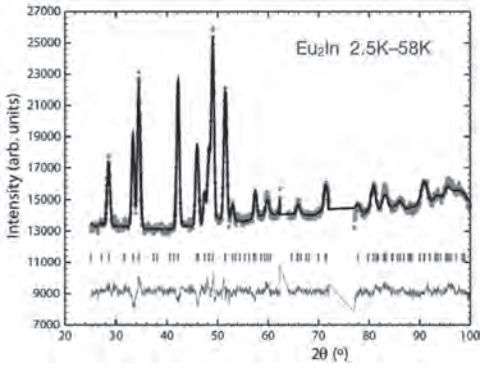

Fig.1 Magnetic-only diffraction pattern for Eu_2In showing a large number of strong reflections. The pattern was formed by subtracting a paramagnetic (58K) pattern from the 2.3K pattern.

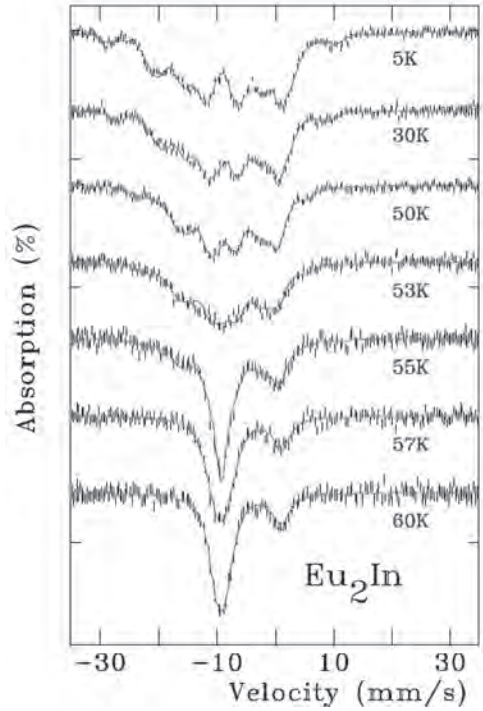

Fig.2 ^{151}Eu Mössbauer spectra of Eu_2In showing the evolution of the magnetic order with temperature. The feature near 0 mm/s is due to a non-magnetic Eu^{3+} impurity formed during the mounting of this air-sensitive material.

NOC-07. Strong spin-orbital coupling-induced unusual magnetic and magnetocaloric features in $YbVO_3$ single crystals. *M. Balli*[2,3], S. Mansouri[1], S. Ait Jmal[2], P. Fournier[3] and S. Jandl[3] *1. Centre Énergie, Matériaux et Télécommunications, Institut National de la Recherche Scientifique, Varennes, QC, Canada; 2. AMEEC Team, LERMA, International University of Rabat, Rabat, Morocco; 3. Institut Quantique, Université de Sherbrooke, Sherbrooke, QC, Canada*

In this paper, we mainly focus on the magnetic and magnetocaloric properties of $YbVO_3$ single crystals. As shown in Fig.1 (a, b) the grown crystals unveil several phase transitions close to 104 K, 65 K and 20 K. The observed 104 K feature originates from the occurrence of a C-type antiferromagnetic ordering of V^{3+} magnetic moments while that close to 65 K corresponds to the transformation of the established C-type spin ordering (SO) into a G-type antiferromagnetic ordering which is associated with a change in the orbital ordering (OO) from G-type to C-type. The phase transition taking place close to 20 K is more probably attributed to the ordering of Yb^{3+} magnetic moments. On the other hand, the below 65 K ordering state constituted of G-type SO/C-type OO remains very stable even under sufficiently high magnetic fields as reported in Fig.1-b. This underlines the weakness of f-d exchange couplings in the $YbVO_3$ vanadate being in contrast with other RVO_3 orthovanadates containing smaller rare earth elements such as $DyVO_3$ compound [1]. Additionally, we particularly demonstrate that the complex electronic and magnetic structures of $YbVO_3$ result in interesting levels of thermal effects over a wide temperature range including a giant negative magnetocaloric effect close to 60 K. In fact, the maximum entropy change is found (Fig. 1-c) to be almost 12 J/kg K in the magnetic field change of 7 T applied along the c axis and the ab-plane at 64.25 K and 65.5 K, respectively. More interestingly, the strong magnetic anisotropy shown by the V^{3+} sublattice (Fig. 1-a) results in a large rotating magnetocaloric effect (RMCE) at relatively high temperatures (Fig.1-d). This would open the avenue for the design of efficient magnetic refrigerators with simplified designs [2]. Our findings are discussed in the frame of DFT calculations.

[1] S. Miyasaka, T. Yasue, J. Fujioka, Y. Yamasaki, Y. Okimoto, R. Kumai, T. Arima and Y. Tokura, Phys. Rev. Lett. 99, 217201 (2007). [2] M. Balli, S. Jandl, P. Fournier, M. M. Gospodinov, Appl. Phys. Lett. 104, 232402 (2014).

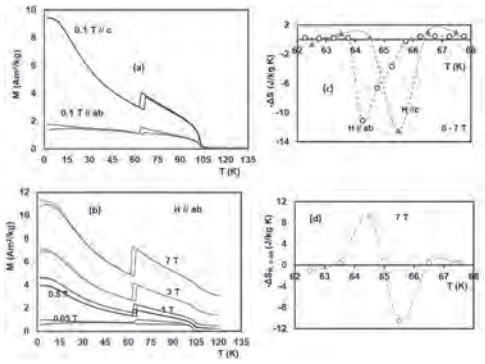

(a, b) Thermomagnetic curves of YbVO3 single crystal along the c axis and the ab plane. (c) Isothermal entropy changes as function of temperature in the magnetic field change of 7 T applied along the c axis and the ab plane. (d) Entropy change resulting from the rotation of YbVO3 single crystals between the c axis and the ab plane in a constant magnetic field of 7 T initially parallel to the c axis.

NOC-08. Temperature First Order Reversal Curves (TFORC) measurement optimization and thermal loop reconstruction. Á. Díaz-García[1], L.M. Moreno-Ramírez[1] and *V. Franco*[1] *1. Condensed Matter Physics, University of Seville, Seville, Spain*

Temperature First Order Reversal Curve (TFORC) distributions, the temperature counterpart of the conventional magnetic field FORC, enables the characterization of the thermal hysteresis associated to first-order phase

transitions in magnetocaloric materials [1]. This technique boosts features of the thermal hysteresis loops that are not easily observed by just exploring the major loop, such as effects of inhomogeneities, asymmetries or slowdown in the transformation [1-4]. One disadvantage of the TFORC technique is the long measurement time as the thermal inertia as well as the thermal dynamic effects need to be minimized. In this work, we explore the influence of different experimental factors on TFORC distributions of magnetocaloric materials looking for measurement time optimization: optimization of the number of minor loops measured, optimal temperature sweeping rates and smoothing algorithms. It is shown that the reconstructed hysteresis loops from the TFORC distributions can be used as an internal test to evaluate the significance of the distributions obtained by different conditions. As an example, Figure 1 shows the effect of the Pike's smoothing algorithm [5] on the reconstructed major thermal loops and how this smoothing, even though making the distributions more aesthetic, have a deleterious effect on their usefulness for predicting the thermomagnetic behavior of the samples. Work funded by Grant PID2019-105720RB-I00 funded by MCIN/AEI/10.13039/501100011033; Consejería de Economía, Conocimiento, Empresas y Universidad de la Junta de Andalucía (P18-RT-746); US Air Force Office of Scientific Research (FA8655-21-1-7044) and Sevilla University under VI PPIT-US program. LMMR acknowledges a postdoctoral fellowship from Junta de Andalucía and European Social Fund (ESF).

[1] V. Franco et al. IEEE Magnetics Letters, 2016, 7, 6602904. [2] A. S. Komlev et al. Journal of Alloys and Compounds, 2021, 874,159924. [3] L.M. Moreno-Ramírez et al. Metals, 2020, 10, 1039. [4] Á. Díaz-García et al. Journal of Alloys and Compounds, 2021, 867, 159184. [5] R. Pike et al. Journal of Applied Physics, 1999, 85, 6660.

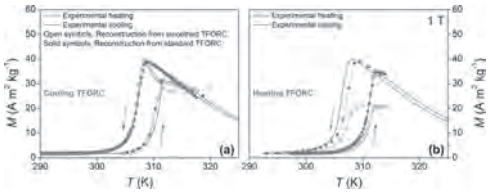

Fig. 1. Reconstructed magnetization loops of a Ni-Mn-In Heusler alloy from the integration of cooling (a) and heating (b) TFORC distributions for 1 T, respectively.

NOC-09. Rotating Magnetocaloric Effect in Low Dimensional Molecular Compounds. *P. Konieczny*[1], D. Czernia[1] and R. Pelka[1] *1. The Henryk Niewodniczanski Institute of Nuclear Physics Polish Academy of Sciences, Krakow, Poland*

Low dimensional molecular magnets are considered to be one of the best materials for cryogenic magnetocaloric effect (MCE) [1,2]. The magnitudes of magnetic entropy change for the most efficient molecular materials are comparable to that of the famous gadolinium gallium garnet ($Gd_3Ga_5O_{12}$). Although much research effort is focused on searching high efficient compounds for conventional MCE, a new type of magnetocaloric effect, namely rotating magnetocaloric effect (RMCE), has been introduced. In RMCE, the applied magnetic field is constant and the aligned material (often in single crystal form) with significant magnetic anisotropy is being rotated. Cooling with rotation has several advantages compared to the conventional MCE cooling setups: high efficiency (high frequency cooling cycles), simple construction and low power consumption (possibility of using permanent magnets). In our research we have investigated the RMCE in 2D compounds (based on Mn^{II}-Nb^{IV} [3] and Cu^{II}-W^{V} [4] ions) and clusters (based on Tb^{III} and Dy^{III} [5]). We have noticed that the inverse magnetocaloric effect can be used to enhance RMCE (in our case up to 51 % for the 2D compounds). In the case of the Tb cluster, with large uniaxial anisotropy, the magnetic entropy change for conventional and rotating MCE is comparable, showing significant values ($\Delta S_{max} \approx 4$ J K^{-1} kg^{-1}) at 2.0 K in low field ($\mu_0 H \approx 1.2$ T), which can be achieved with permanent magnets.

[1] P. Konieczny, W. Sas, D. Czernia, A. Pacanowska, M. Fitta, R. Pelka, Magnetic cooling: a molecular perspective *Dalt. Trans*. (under review) [2] M. Fitta, R. Pelka, P. Konieczny and M. Balanda, Multifunctional molecular magnets: Magnetocaloric effect in octacyanometallates *Cryst*. 9 (2019) 9 [3] P. Konieczny, L. Michalski, R. Podgajny, S. Chorazy, R. Pelka, D. Czernia, S. Buda, J. Mlynarski, B. Sieklucka, T. Wasiutynski, Self-Enhancement of Rotating Magnetocaloric Effect in Anisotropic Two-Dimensional (2D) Cyanido-Bridged Mn^{II}-Nb^{IV} Molecular Ferrimagnet *Inorg. Chem*., 56 (2017) 2777-2783. [4] P. Konieczny, R. Pelka, D. Czernia, R. Podgajny, Rotating Magnetocaloric Effect in an Anisotropic Two-Dimensional $Cu^{II}[W^{V}(CN)_8]_3^-$ Molecular Magnet with Topological Phase Transition: Experiment and Theory *Inorg. Chem*., 56 (2017) 11971-11980. [5] P. Konieczny, D. Czernia, K. Takashi, Rotating Magnetocaloric Effect in Highly Anisotropic Tb^{III} and Dy^{III} clusters *J. Alloys Compd*. (submitted) Acknowledgements The present research was financed by National Science Centre (Poland) grant SONATA No. (2018/31/D/ST8/02118)

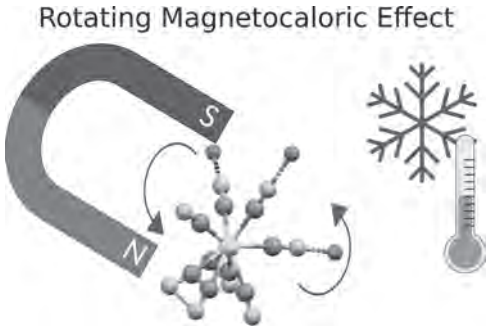

Fig. 1. The idea of rotating magnetocaloric effect.

NOC-10. Influence of Powder Feedstock Characteristics and Process Parameters on Extrusion-based 3D Printing of Magnetocaloric Structures. *V. Sharma*[1], M. Dey[2], S. Gupta[2], R.L. Hadimani[1,3], H. Zhao[1] and R. Barua[1] *1. Mechanical and Nuclear University, Virginia Commonwealth University, Richmond, VA, United States; 2. Department of Mechanical Engineering, University of North Dakota, Grand Forks, ND, United States; 3. Department of Biomedical Engineering, Virginia Commonwealth University, Richmond, VA, United States*

Magnetic refrigeration is a sustainable, energy-efficient alternative to the conventional vapor-compression cooling technology. A key challenge in manufacturing magnetocaloric devices is that lack of fabrication methods for shaping the brittle caloric alloys into thin-walled channeled regenerator structures with optimized heat transfer properties, and gradient transformation temperature, while preserving the functional response of the materials system, Fig 1.[1] To this end, we have recently developed a novel extrusion-based additive manufacturing (AM) method to 3D print spatially designed porous magnetocaloric structures with channel dimensions in the range 150-800 μm, Fig 2.[1] Building on this proof-of-concept demonstration, research efforts pertaining to AM process development using three precursor magnetocaloric powders will be presented - (1) $La_{0.6}Ca_{0.4}MnO_3$ nanoparticles (dia~10 nm) prepared by Pechiniuidelines for minimizing porosity and lack-of-fusion defects in the 3D printed magnetocaloric parts.

[1] Sharma, Vaibhav, et al. "Room-temperature Polymer-assisted Additive Manufacturing of Microchanneled Magnetocaloric Structures." *Journal of Alloys and Compounds* (2022): 165891. [2] Tsui, Melissa HM, et al. "Enhanced near room temperature magnetocaloric effect in La 0.6 Ca 0.4 MnO 3 for magnetic refrigeration application." *RSC Advances* 7.74 (2017): 46589-46593. 3 Dey, Maharshi, et al. "Synthesis of nanolayered ternary borides powders (MAB phases) by sustainable molten salt shielded synthesis/sintering (MS3) process." *Journal of Materials Science* 57.4 (2022): 2436-2454.

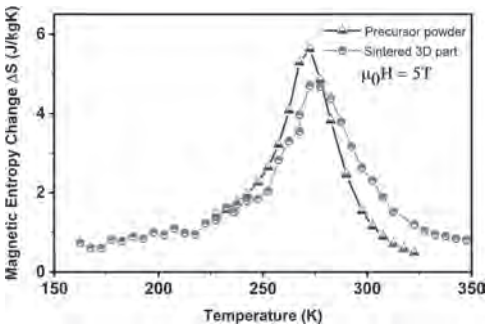

Fig 1. Magnetic entropy change curves of $La_{0.6}Ca_{0.4}MnO_3$ powders and corresponding 3D printed structure.

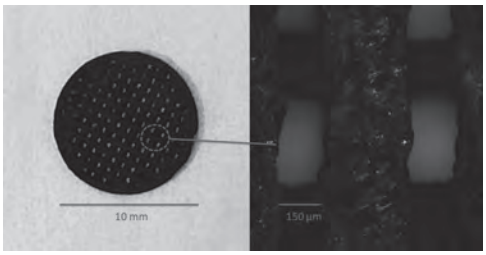

Fig 2. Channeled magnetocaloric part with ~150 µm spatial resolution.

NOC-11. Magnetic and Magnetocaloric Properties of Iron Nanoparticles Embedded Titanium Nitride Thin Film Matrix.

K. Sarkar[1], M. Roy[1], J. Som[1] and D. Kumar[1] *1. Mechanical Engineering, North Carolina A&T State University, Greensboro, NC, United States*

The magnetic refrigeration, based on the magnetocaloric effect(MCE), is an efficient and environment-friendly solid-state cooling technology [1]. Rare earth free nanoparticles and heterostructure systems can be used as an alternative to traditional bulk magnetocaloric materials(MCMs) due to control over the entropy change across the magnetic phase transition that can be maneuvered by varying particle size [2]. The present study is focused on the MCE properties of Fe nanoparticles embedded in titanium nitride thin film grown on sapphire substrates using pulsed laser deposition. To study the effect of thermal hysteresis, M-T measurements were carried out in three different modes: zero-field cooled(ZFC), field cooled warming (FCW), and field cooled cooling (FCC). As seen in Fig.1, there is no separation between FCC and FCW curves, but there is a pronounced bifurcation between ZFC and FCW curves at 0.025T, 0.05T, and 0.1T. The absence of any separation between FCW and FCC curves suggests a negligible thermal hysteresis loss above blocking temperature. Quantitative information about the isothermal entropy change (ΔS) and the MCE in the Fe-TiN heterostructure system has been obtained by applying Maxwell relation to the magnetization versus temperature data at various fields. The Fe-TiN system shows a sizable isothermal entropy change (ΔS) over a broad range of temperatures (T_B<T<300 K) as seen in Fig.2. With the dynamic magnetic hysteresis absent above the blocking temperature, the negative ΔS as high as 4.18×10^3 J/Km^3 is obtained for 3T at 300 K. The refrigeration capacity(RC) at various applied fields have also been evaluated with the realization of a maximum value of 7.4×10^5 J/m^3 at 3 T. With a combination of a broad range of usable ΔS and easy accessibility, the Fe-TiN material system can give us insight for the fabrication and design of novel MCMs with improved refrigeration efficiency needed for next-generation solid-state cooling.

[1] V.K. Pecharsky, K.A. Gschneidner Jr, Journal of magnetism and magnetic materials, Vol. 200, p. 44-56 (1999). [2] P. Poddar, J. Gass, D. Rebar, Journal of magnetism and magnetic materials, Vol. 307, p. 227-231 (2006)

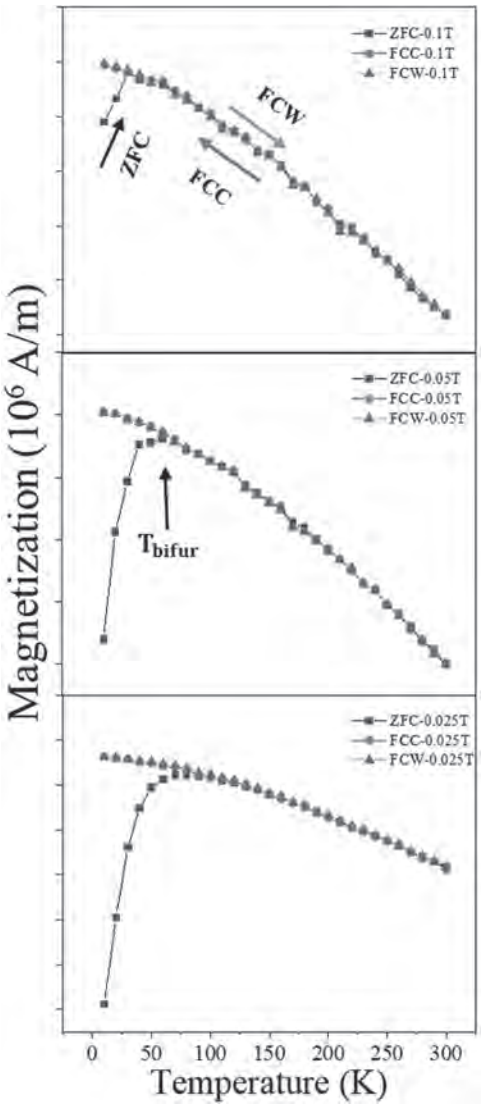

Fig. 1. Zero field cooled magnetization, field cooled cooling and field cooled warming as a function of temperature at a field range of 0.025 T, 0.5T and 0.1 T.

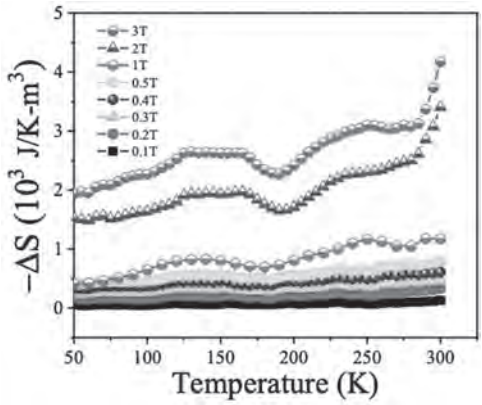

Fig. 2. Temperature dependence of the magnetic entropy change ΔS obtained under various fields from 0.1 to 3 T.

NOC-12. Magnetic phase transitions and magnetocaloric effect in $DyCrTiO_5$ nanoparticles. *B. Bharati*[1,2], P. Mohanty[2], A.R. Prinsloo[2] and C.J. Sheppard[2] *1. Spectrum Analytical Facility, Faculty of Science, UNIVERSITY OF JOHANNESBURG, Johannesburg, South Africa; 2. Department of Physics, UNIVERSITY OF JOHANNESBURG, Johannesburg, South Africa*

Rare-earth (*R*) compounds of the form $RCrTiO_5$, crystallizing in an orthorhombic structure with space group *Pbam*, belongs to the multiferroic family that are currently of interest as these can find applications in spintronic and memory devices. Recently, there were limited reports on the $RCrTiO_5$ materials in their bulk form [1-4]. Das *et al*. [1] investigated the magnetic ground state of the $DyCrTiO_5$ in a bulk sample through dc magnetization and showed the ferromagnetic nature of the material, as well as spin reorientation at low temperatures because of the interaction between Dy^{3+} and Cr^{3+}. However, there are currently limited reports in the literature on $DyCrTiO_5$ in its nano form, probing dimensionality effects [5]. Therefore, the present work highlights the magnetic transitions of the $DyCrTiO_5$ nanoparticles and their magnetocaloric behavior. The nanoparticles were synthesized through a cost-effective sol-gel technique and subsequently calcined at 800 C. The orthorhombic structure of the material with lattice parameters, *a*, *b*, *c* of 7.3158(7), 8.6431(9), 5.8390(8) Å, respectively, is established from the x-ray diffraction (XRD) pattern. The particle size obtained from transmission electron microscopy (TEM) is 43 ± 2 nm. The Néel temperature has obtained from the magnetization as a function of temperature ($M(T)$) measurement, as T_N = 146 ± 1 K (Fig. 1). In addition, spin reorientation is observed at a temperature, T_{SR} = 51 ± 1 K (Fig. 1). A loop appeared in field-cool-cooling (FCC) and field-cool-warming (FCW) $M(T)$ curves at low temperatures, not previously observed for the sample in bulk form, indicating a ferromagnetic-antiferromagnetic (FM-AFM) transition [5]. The FM nature, with exchange bias effect, is further confirmed for the sample from field-dependent magnetization measurements. Additionally, a change in isothermal magnetic entropy ($-\Delta S_m$) of 6.6 ± 0.3 $J.kg^{-1}.K^{-1}$ is found at a 6 T difference in the field. The observed magnetic behavior of $DyCrTiO_5$ nanoparticles is discussed in terms of the competing interactions of Cr^{3+} and Dy^{3+}, respectively.

[1] M. Das, S. Roy and K. Mahalingan, J. Phys.: Condens. Matter. Vol. 32, p.035802 (2020). [2] M. Das, S. Roy and N. Khan, Phys. Rev. B Vol. 98, p.104420 (2018). [3] T. Basu, D.T. Adroja and F. Kolb, Phys. Rev. B Vol. 96, p.184431 (2017). [4] J. Hwang, E.S. Choi and H.D. Zhou, Phys. Rev. B Vol. 85, p.024415 (2012). [5] B. Bharati, P. Mohanty, C.J. Sheppard, J. Magn. Magn. Mater. 546, p. 168862 (2022).

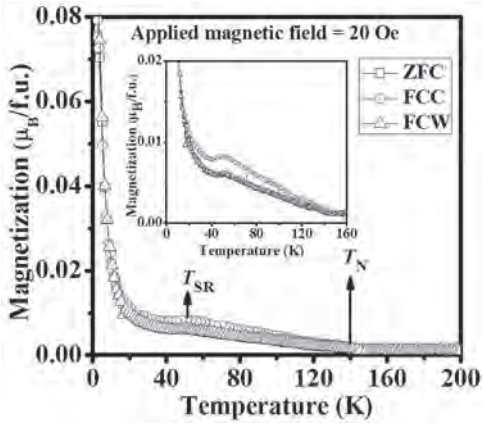

Fig. 1. $M(T)$ data for $DyCrTiO_5$ nanoparticles. Inset shows the zoomed view.

NOC-13. AC and DC Magnetic Softness Enhanced Dual-doped γ-Fe_2O_3 Nanoparticles for Highly Efficient Cancer Theranostics. *J. Wang*[1], J. Kim[1], K.W. Kang[2], S.H. Paek[2], Y. Takemura[3] and S. Bae[1] *1. Electrical Engineering, University of South Carolina, Columbia, NC, United States; 2. Seoul National University College of Medicine, Seoul, Korea (the Democratic People's Republic of); 3. Yokohama National University, Yokohama, Japan*

"Theranostics" by magnetic nanofluid hyperthermia (MNFH) combined with T_2-weighted MR contrast imaging (MRI) using superparamagnetic nanoparticles (SPNPs) has been drawn a huge attraction in nanomedicine [1,2]. However, insufficient AC heating power at the biologically safe range of AC magnetic field (H_{AC}) (H_{appl} < 190 Oe, f_{appl} < 120 kHz) and unsatisfactorily low r_2-relaxivity keep SPNPs challenging for cancer theranostics agent applications [3,4]. In this work, innovatively designed and developed AC and DC magnetic softness enhanced dual-doped ($Ni_{0.6}Zn_{0.4}$)-γFe_2O_3 (MSEγ-IO) SPNPs with significantly enhanced both intrinsic loss power (ILP, ~ 4.0 nH m^2 kg^{-1}) at the H_{appl}×f_{appl} =1.23×10^9 A m^{-1} s^{-1} and r_2-relaxivity (r_2 = 660.4 mM^{-1} s^{-1}) are reported. The significantly enhanced ILP, and r_2-relaxivity of dual-doped MSEγ-IO SPNPs were primarily attributed to the distinctly enhanced AC magnetic softness directly related to the H_{AC} absorption and f_{appl} resonance efficiency, and the DC magnetic softness dominantly controlled by the occupation and spatial distribution of Ni^{2+} in O_h vacancies sites, and Zn^{2+} cations in T_d sites of γ-Fe_2O_3, respectively. The biocompatibility and bioavailability experimentally evaluated by *in-vitro* and *in-vivo* studies demonstrated that the dual-doped MSEγ-IO SPNPs can be a promising candidate for highly efficient cancer theranostics agent for future nanomedicine.

[1] Hyom et al, Adv. Mater., 21, 2133-2148 (2009) [2] Yoo et al, ACC Chem. Res., 44, 863-874 (2011) [3] Jang et al, Adv. Mater., 30, 1-8 (2018) [4] Martinez *et al*, Adv. Funct. Mater., 22, 3737-3744 (2012)

Session NPA
MAGNETO-ELASTIC, -OPTICAL AND OTHER PHENOMENA (Poster Session)

Radhika Barua, Chair
Virginia Commonwealth University, Richmond, VA, United States

NPA-01. Magnetoactive Properties of 3D Printed Magnetic Elastomer Structures: Effects of Infill Orientation and Infill Percentage. *J.M. Ennis*[1], H.G. Thatcher[1], T.M. Calascione[2,1], J. Lu[1], N.A. Fischer[1], S.J. Ziemann[1], T. Höft[1] and B. Nelson-Cheeseman[1] *1. The University of St. Thomas, St. Paul, MN, United States; 2. The University of Colorado Boulder, Boulder, CO, United States*

Magnetic elastomers are flexible smart materials that can be manipulated by magnetic fields to achieve reversible mechanical deformation. These highly configurable materials are instrumental in transforming biomedical applications such as artificial muscles, dampeners, and other vibration absorbers. Magnetic elastomer structures must be customizable to satisfy these complex applications leading to the use of fused filament fabrication (FFF) in creating them. FFF is a 3D printing process where material is extruded in 1D lines (infill) to build 2D planes layer-by-layer, resulting in a 3D structure. This research used magnetoactive testing to investigate how varying the internal infill structure affected the mechanical response of the structures within an applied magnetic field. Different infill percentages and infill orientations were tested to account for different mechanical stiffnesses and internal geometries. The elastomers were made by adding 40wt% magnetite (Fe_3O_4) to a thermoplastic polyurethane (TPU) matrix. Each sample was magnetoactively tested with three different transverse magnetic field orientations (Front, Back and Top). The samples were placed between two electromagnets, and the angle of deflection was recorded as a function of applied field. Maximum angles of deflection for the testing setup were reached when both lower infill percentages, translating to less material in the cross-section of the sample, and lower infill orientations, creating much less crosslinking between infill lines, were used. Transverse fields applied parallel to the print plane (Front, Back sample orientations) demonstrated the most magnetoaction due to less crosslinking constraining the bending stiffness. The anisotropy of the infill structure likely also contributed to the large response from certain samples. It was concluded that for this fixed base material, it is more important to 3D print structures with lower stiffnesses than more net magnetic particulate in achieving the most magnetoaction. According to this data, 3D printed magnetite-TPU structures are viable for creating components easily stimulated by a magnetic field unlocking many possibilities for the creation of useful technological components.

NPA-02. Complex Magnetoactuation of 3D-Printed Hard Magnetic Elastomers: Effects of Infill Orientation and Percentage. *W.M. Howell*[1], J.M. Ennis[1], D.P. Fagan[1], J. Schewe[1], T. Höft[2] and B. Nelson-Cheeseman[1] *1. Mechanical Engineering, University of St. Thomas, St. Paul, MN, United States; 2. Mathematics, University of St. Thomas, St. Paul, MN, United States*

Magnetic elastomers are composite smart materials made up of a flexible polymer and magnetic particulate which mechanically actuate in response to an applied magnetic field (H). They allow for a highly configurable and untethered actuator. To enhance configurability, 3D-Printing allows for great control of the objects meso and macro structure, both in terms of shape geometry and property anisotropy. Specifically, Fused Filament Fabrication (FFF) is a process by which material is extruded in lines (infill) to gradually build up an object through layer-by-layer extrusion. In this study, we explore how multiple FFF structural parameters (infill orientation and infill percentage, and sample orientation relative to H) affect the magnetoactive response of printed Strontium Ferrite (SrF) magnetic elastomer structures. Magnetic elastomers with hard magnetic particulate have the unique advantage of performing more complex actuation, such as rolling, twisting and folding. SrF is an excellent hard magnet candidate given its lower price and greater accessibility compared to NdFeB. Magnetoactive properties are measured by a custom setup where each printed sample beam is suspended and optically tracked for a transverse H up to 0.4 T. For each sample, multiple orientations relative to H are studied. A custom program overlays the digital images for increasing H in order to quantify the magnetoactive deformation that results. The magnetoactive responses exhibited by the various sample types highlight clear design goals for tailoring large and complex magnetoactive actuation modes. In addition to the traditional transverse bending seen from typical (soft) magnetic elastomers, we also observe complex twisting and torquing of the beams in multiple dimensions based upon the printed structure and the sample orientation relative to H. These effects are greatest for the orientations and structures that maximize magnetic anisotropy and minimize the infill crosslinking. This work demonstrates the clear potential to tailor complex magnetoactive responses from FFF-printed hard magnetic elastomers, opening the door to highly complex actuators that can be readily and accessibly designed and created.

NPA-03. Impact of 3D Printing Extrusion on Magnetically Annealed High Performance Hard/Soft Magnetic Elastomers. *J. Lu*[1], N.A. Fischer[1], S.J. Ziemann[1], J.M. Ennis[1], T. Höft[2] and B. Nelson-Cheeseman[1] *1. Mechanical Engineering, University of St. Thomas, St. Paul, MN, United States; 2. Mathematics, University of St. Thomas, St. Paul, MN, United States*

Magnetic elastomers can mechanically deform under a magnetic field. Hard magnetic elastomers can perform more complex motions, but soft magnetic elastomers have a greater magnetoaction. 3D printing, such as Fused Deposition Modeling (FDM), can enhance the magnetoactive properties of magnetic elastomers by creating anisotropy. 3D printing filaments are the stock material for FDM. Recent work has shown that magnetic annealing of magnetic filaments during extrusion creates greater magnetoaction in the filaments. This research studies whether this enhanced performance from magnetically annealed filaments remains once they are extruded through the 3D printing nozzle. The composite samples were made of polyurethane and varying amounts of soft and hard magnetic particulate (carbonyl iron (Fe) and strontium ferrite (SrF)). The composites were extruded into 1.75 mm diameter filaments. Magnetically annealed filaments traveled through a uniform axial magnetic field. Final samples were extruded through a 0.8 mm FDM nozzle into extrudates. The magnetoactive properties were measured by a custom setup, whereby extrudates were hung between electromagnets. Images of samples were captured, overlaid, and analyzed at seven field strengths. The enhanced magnetoactive performance of magnetically annealed filaments was present in the final extrudates, indicating that the magnetic annealing effects were preserved. The higher performance magnetic annealing effects were (1) magnetoaction at lower applied fields for the Fe-containing samples and (2) non-zero magnetoaction in the highest SrF samples. Quantitatively, the least magnetoactive deflection was seen in the highest SrF samples. Mechanical tensile testing data showed that the stiffness of the composite variant increased with a higher percentage of SrF. Magnetically, the samples with more SrF content had lower saturation magnetization (Ms) and higher coercive field (Hc). The high stiffness and magnetic properties contribute to

the limited magnetoaction. This approach to magnetic annealing of magnetic elastomers can be used to 3D print accurate and complex components for high-performance soft robotic applications.

NPA-04. Multifunctional bipolar resistive switching characteristics in AlN/FSMA/SS based ME heterostructure for flexible ReRAM application. *P. Kumar*[1] and D. Kaur[1] *1. Physics, Indian Institute of Technology, Roorkee, Roorkee, India*

Resistive random access memory (ReRAM) has been a promising future candidate for various applications such as nonvolatile data storage and neuromorphic devices. Moreover, multifunctional flexible electronics is the ongoing demand for fabricating wearable data storage and communication devices. The magnetoelectric (ME) heterostructure consisting of piezoelectric (AlN) and ferromagnetic magnetic shape memory alloy (FSMA (Ni-Mn-In)) was fabricated over stainless steel (SS) substrate for resistive random access memory application. The Cu/AlN/FSMA/SS metal-insulator-metal (MIM) based memory cell displays bipolar resistive switching (RS) behavior. The formation of Cu metallic filament at a particular SET voltage leads the memory cell in a low resistance state (LRS) from its pristine high resistance state (HRS). The LRS and HRS are explained well by Ohmic and space charge limited conduction (SCLC) mechanisms, respectively. The fabricated memory cell displays excellent endurance (~5000 cycles) and data retention (~10^4 seconds) capability with high OFF/ON ratio of ~ 1.2×10^3. Furthermore, the multifunctionality of the ME heterostructure-based RAM was investigated by tuning the SET voltage with ambiance temperature and external magnetic field remotely. A significant change in the SET voltage could be ascribed to the temperature and magnetic field-induced strain transferred to the AlN piezoelectric layer from magnetostrictive FSMA (Ni-Mn-In) bottom electrode. The residual Lorentz force explains the remotely controlled LRS and HRS in transverse magnetic field for multi-bit data storage applications. Moreover, the RS characteristics remain stable even after 800 bending cycles as well as with bending angle (0 to 180°). Hence, the present ME heterostructure integrated with flexible SS substrate can be a better choice for highly flexible, low-cost and multifunctional futuristic RAM application.

[1] C. Gu and J.S. Lee, ACS Nano 10, 5413 (2016). [2] Y. Park and J.S. Lee, ACS Appl. Mater. Interfaces 9, 6207 (2017). [3] N.A. Spaldin and R. Ramesh, Nat. Mater. 18, 203 (2019). [4] P. Kumar and D. Kaur, Nanotechnology 32, (2021). [5] A. Kumar, S. Pawar, S. Sharma, and D. Kaur, Appl. Phys. Lett. 112, (2018).

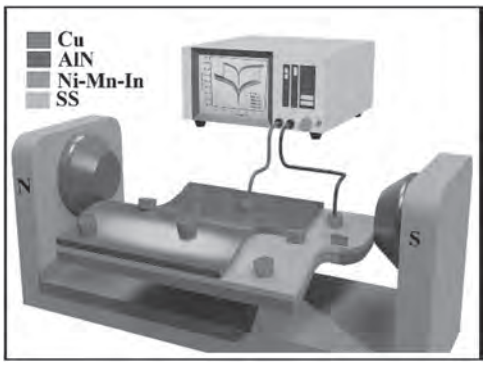

Fig 1. Schematic of complete measurement system using SCS 4200 and electromagnets.

NPA-05. Phase transition, electrical transport and magnetic entropy change of $LaFe_{2-y}Co_ySi$ alloys prepared by suction casting. *N. Kramer*[1], C. Kubiak[1], J.F. Casey[1], C. Hanley[1] and A. Pathak[1] *1. Department of Physics, State University of New York (SUNY), Buffalo State, Buffalo, NY, United States*

Considering the natural abundance of the constituting elements and first-order phase transition (FOPT), $LaFe_{13-x}Si_x$-derived compounds have been extensively studied for magnetocaloric effect, a phenomenon that causes the cooling or heating of material when placed in an external magnetic field [1]. They are, however, extremely brittle and mechanically friable, showing rather low thermal conductivities and measurable irreversibility, which thus far could not be eliminated completely. Recently, Pathak et al. [2] reported the first-time discovery of a two-phase, naturally formed at the $LaFe_2Si$ stoichiometry rather than $LaFe_{13-x}Si_x$ compound. $LaFe_2Si$ exhibits strongly responsive behaviors without the degradation in properties that can be exploited in weak magnetic fields. However, the phase transition happens rather at low temperatures and the saturation moment is low. We are working on this material to further enhance the phase transition temperature and also to improve the magnetic and mechanical properties of the alloy. In this presentation, we will present the synthesis and characterization of $LaFe_{2-y}Co_ySi$. We prepared $LaFe_{2-y}Co_ySi$ by making the first pre-alloy of FeCoSi and then added Co and melted several times. The alloys were further homogenized by the vacuum suction casting technique, which prepared a 4 to 5 cm long rod with a 6mm diameter of sample. The ferromagnetic to paramagnetic transition temperature increases from 199K for x = 0 to 273K for x = 0.3 and the full width at the half-maximum value of magnetic entropy changes increases significantly with Co doping. We discuss the phase transition, electrical transport, magnetic and magnetocaloric properties of $LaFe_{2-y}Co_ySi$ compounds.

[1] S. Fujieda, A. Fujita, K. Fukamichi, Y. Yamazaki, and Y. Iijima, Appl. Phys. Lett. 79, 653 (2001) [2] A. K. Pathak, Y. Mudryk, N.A. Zarkevich, D.H. Ryan, D.D. Johnson, V.K. Pecharsky, Acta Materialia 215, 117083 (2021)

NPA-06. Directional growth effect on magneto-mechanical properties of $Fe_{81}Al_{19}$ alloy. H.W. Chang[2], S. Jen[1], Y. Liao[2], *Y. Wong*[2], C. Chiu[3] and W. Chang[2] *1. Institute of Physics, Academia Sinica, Taipei, Taiwan; 2. Department of Physics, National Chung Cheng University, Chia-Yi, Taiwan; 3. New Materials Research & Development Dept., China Steel Corp, Kaohsiung, Taiwan*

Materials with large magnetostriction (λ_s) have attracted much attention due to their potential applications in acoustic sensors, actuators, and magneto-mechanical devices. Low-cost Alfenol Fe-Al alloys has attracted much attention due to moderate λ_s at much lower saturation magnetic field, low magnetic hysteresis, better mechanical properties, including Young's modulus (E) and ductility, and good manufacturability and workability. The enhanced λ_s with Al substitution is attributed to both the increase of magnetoelastic coupling and the shear elastic softening. To obtain high magnetostriction alloys, texture control is needed. The traditional casting causes inhomogeneous heat flow during solidification and therefore, leads to the difficulties on texture control. To meet the above challenge, the directional solidification (DS) technique is adopted in this work, because less report on binary Fe-Al alloys prepared by DS is available, especially for magneto-mechanical properties. Therefore, directional growth effect on magneto-mechanical properties of $Fe_{81}Al_{19}$ alloy is studied. The ideal model of heat flux for directional solidification (DS) technique is proposed, and the tuned A/L (the ratio of cross-sectional area and length for the ingot) and ΔT (temperature difference) are adopted to increase heat flux (q). The experimental result shows that the increase of q effectively promotes the degree of (011)[100] Goss texture and therefore helps to form an oriented stripe domain structure. Large λ_{100} of 93.8 ppm attained for this optimized $Fe_{81}Al_{19}$ alloy prepared by DS method is very close to that of the $Fe_{81}Al_{19}$ single crystal (95.0 ppm). Besides, remarkable magneto-mechanical properties could be attained for DS-prepared $Fe_{81}Al_{19}$ alloy, such as high $\Delta E_s/E_0$ of ~10% and attractive $\Delta E/E_0$ of 8.2 % at small H = 0.25 kOe as well

as large change in damping capacity (ζ) of 6.0 %. The above remarkable magneto-mechanical properties, low cost of $Fe_{81}Al_{19}$, and simple process of DS favor for applications. This work proposes an ideal model to emphasize the importance of heat flux in DS. Most importantly, the experimental result suggests a cost-effective method to attain remarkable magneto-mechanical properties for $Fe_{81}Al_{19}$ alloy.

none

NPA-07. Growth of iron/tungsten disulfide heterostructure films with controlled interface and magnetic properties. *N.W. Mudiyanselage*[1], D. Detellem[1], V. Ortiz Jimenez[1], S. Abdallah[1], A. Hornsey[1], Y.T. Pham[1], N. Alzahrani[1,2], D. Arena[1], H. Srikanth[1], S. Witanachchi[1] and M. Phan[1] *1. University of South Florida, Tampa, FL, United States; 2. University of Jeddah, Jeddah, Saudi Arabia*

The ability to harness excellent magnetic and optical properties within a heterostructure film composed of a magnetic material and a transition metal dichalcogenide (TMD) semiconductor paves a new pathway for the development of multifunctional sensing devices, information storage technology, etc[1]. Atomically thin tungsten disulfide (WS_2) (thickness ≤ 5 nm) has been widely explored as a promising candidate for applications in optoelectronics, spintronics, and valleytronics. The valleytronic property of WS_2 can be enhanced when interfacing it with another magnetic material such as iron (Fe), due to the magnetic proximity effect[2]. However, the growth of this 2D-TMD with controllable thickness, using chemical vapor deposition (CVD), and transferring it onto another substrate (Fe) via a commonly used wet transfer process have remained a challenging task. To overcome this, we employ a combination of pulsed laser deposition (PLD) and sputtering (SP) techniques to grow Fe/WS_2 heterostructure films with a controlled interface and desirable magnetic/optical properties. A 5nm thick WS_2 film was first grown on MgO substrate using PLD, and a 5nm thick Fe film was then deposited on WS_2/MgO using SP. A 2nm thick Ta layer was sputtered on the Fe surface to protect the film from oxidization. X-ray diffraction, Raman and Photoluminescence spectroscopy, and atomic force microscopy confirmed the structure of the heterostructure and the quality of the Fe/WS_2 interface. Vibrating sample magnetometry, magneto-optical Kerr effect (MOKE), and magnetic force microscopy indicated that the excellent magnetic properties of Fe are preserved in the Ta/Fe/WS_2/MgO heterostructure relative to the Ta/Fe/MgO reference film. MOKE showed a sharp, square magnetic hysteresis loop of Ta/Fe/WS_2/MgO with a coercive field (H_c ~ 25 Oe) similar to that of the reference film, Ta/Fe/MgO (H_c ~ 23 Oe). The combined excellent magnetic and optical properties make the Ta/Fe/WS_2/MgO heterostructure a promising candidate for a wide range of applications in spintronics, valleytronics, and opto-spincaloritronics[3]. Our study provides a new, efficient method for the growth of novel 2D van der Waals TMD-based heterostructures with controlled interface properties.

1. J.F. Sierra, J. Fabian, R.K. Kawakami, et al., Nature Nanotechnology 16, 856 (2021) 2. T. Norden, C. Zhao, P. Zhang, et al., Nature Communications 10, 4163 (2019) 3. M.H. Phan, M.T. Trinh, T. Eggers, et al., Applied Physics Letters 119, 250501 (2021)

NPA-08. Influences of Thickness to Magnetooptical Effect of Polycrystalline Cerium Substituted Yttrium Iron Garnet Film Prepared by Ion Beam Sputtering. *Y. Yoshihara*[1,2], P. Lim[2], C.A. Ross[3], K. Ishiyama[1], M. Inoue[1] and T. Goto[1] *1. Research Institute of Electrical Communication, Tohoku University, Sendai, Japan; 2. Toyohashi University of Technology, Toyohashi, Japan; 3. Massachusetts Institute of Technology, Cambridge, MA, United States*

Cerium substituted yttrium iron garnet (Ce:YIG) film is widely studied because of its large Faraday rotation (FR) and low optical absorption in the near infrared region[1)]. Polycrystalline Ce:YIG films can be fabricated on non-garnet substrates and has been used in magnetooptical isolators and magnetophotonic crystals. Increasing thickness is needed to obtain large FR, hence, evaluating the thickness dependence of magnetooptical properties is important. In this study, we prepared ten polycrystalline Ce:YIG films with various thicknesses from 51 nm to 2056 nm and measured their crystalline, surface, optical, electronic, magnetic, and magnetooptical properties. Ce:YIG films deposited on synthetic fused silica substrates were prepared using radio-frequency ion beam sputtering (RF-IBS) at 200°C substrate temperature. Annealing was performed in a glass chamber to crystallize the films at 800°C and 2 Pa pressure for 20 minutes. Crystallinity was measured by grazing incidence x-ray diffraction, showing polycrystalline garnet structure without other phases. The surface roughness increased with increasing film thickness. Film cracking was observed for >515 nm thick samples, caused by the difference in thermal expansion between film and substrate which results in tensile film stress. An amorphous layer of 5 nm thickness between film and substrate was observed by transmission electron microscopy which increased the optical absorption of thinner films. The film properties varied non-monotonically with thickness, with optimum magnetooptical response peaking just below the onset of cracking. We calculated the magnetooptical figure of merit (FOM), defined as FR divided by absorption. As shown in Figure 1, the FR of the 338 nm thick sample is a function of wavelength and is characteristic of a hard-axis loop for field applied perpendicular to the film. The calculated FOM was 127 °/dB at a wavelength of 1550 nm, about three times larger than previous reports, making this material useful in magnetooptical devices.

1) T. Goto et al., Journal of Applied Physics, 113, 17A939, (2013).

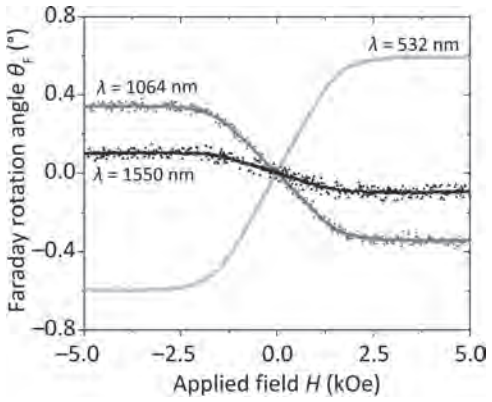

Faraday rotation angle loops of the 338 nm thick Ce:YIG film at the wavelength λ of 532, 1064, and 1550 nm.

NPA-09. The effect of substitution on the structural and magnetic properties of Fe_3Ga_4. *S. Harrington*[1], O. Bishop[2,3], V. Sharma[2], D. Heiman[4,5], B. Wilfong[1], R. Barua[2] and M.E. Jamer[1] *1. Physics, United States Naval Academy, Annapolis, MD, United States; 2. Mechanical & Nuclear Engineering Department, Virginia Commonwealth University, Richmond, VA, United States; 3. Commonwealth Center for Advanced Manufacturing, Petersburg, VA, United States; 4. Physics, Northeastern University, Boston, MA, United States; 5. Plasma Science and Fusion Center, Massachusetts Institute of Technology, Cambridge, MA, United States*

Materials with metallic antiferromagnetic (AFM) behavior at room temperature have been a focus of recent research due to the unique interplay of electron spin and charge. These materials are especially important in AFM spintronic devices, if they are metallic, for the next generation of devices. A material of interest is intermetallic Fe_3Ga_4, which displays a complex magnetic phase evolution with respect to temperature and magnetic field. The ground state of Fe_3Ga_4 is ferromagnetic (FM), which transitions to an intermediate AFM phase at T_1 ~ 68 K that exists over a wide temperature range, and transitions to a high-temperature FM phase at T_2 ~ 360 K.[1] The intermediate helical spin spiral AFM phase exists at room-temperature, is metallic, and exhibits complex metamagnetic evolution that is integral to its exotic properties. The multiple magnetic transitions isare from a unique competition of states with the AFM being the ground state and any added temperature or magnetic field causes the spins to align ferromagnetically. [2] In this work, we have systematically studied the effects of dopants on the parent compound's Fe3Ga4 properties with respect to the magnetic

transitions. $Fe_{3-x}Y_xGa_4$ [(Y = Ti, V, Cr, Mn,Fe,Co,Ni), x = 0.01-0.6)] and $Fe_3Ga_{4-x}Al_x$ (x = 0.1-4) were synthesized via arc melting and subsequent annealing forming the parent's monoclinic-type lattice confirmed via synchrotron diffraction. The magnetic properties of the doped compounds indicate that doping within 2-5% (depending on dopant) starts to suppress the range of the AFM state - leading to T_2 transitions close to room temperature.[3] Fig. 1 (upper) illustrates the effect of V-doping, where the magnetic transition shifts closer to room temperature, and eventaualy T_1 is fully suppressed with higher doping. Fig. 1 (lower) demonstrates that the AFM phase is fully supressed with applied field. Similar relationships are revealed with various dopants, and the optimized composition for each is determined for tuning the transition temperature of T_2. Overall, this work determines the effects of charge and orbital radius on the parent compound leading to valuable insight on the competition of states and the stabilization of the magnetic transitions.

[1] B. Wilfong, V. Sharma, J. Naphy, *et al*, Journal of Alloys and Compounds, Vol. 894, 162421 (2022). [2] B. Wilfong, A. Fedorko, D. Baigutlin, *et a*l, Journal of Alloys and Compounds, Vol. 917, 165532 (2022). [3] B. Wilfong, V. Sharma, O. Bishop, *et al*, Journal of Magnetism and Magnetic Materials, submitted Apr. 2022.

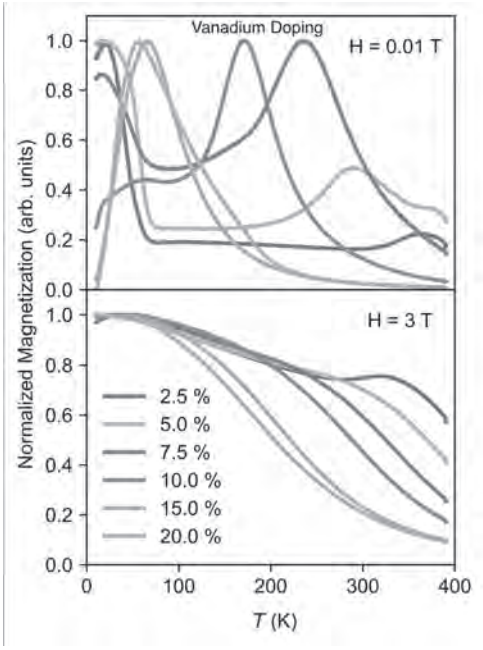

Fig. 1

NPA-10. Ferromagnetic resonance in magnetoelastic NiFeCu/FeCoSiB bilayers near spin reorientation transition. *M. Huang*[1], W. Hu[1], Y. Liu[1] and F. Bai[1] *1. University of Electronic Science and Technology of China, Chengdu, China*

Anisotropic magnetoelastic thin films have a significant modification of the acoustic properties near spin reorientation transition (SRT)[1]. These high sensitivity and nonlinearity of the magnetic system have great potential applications in ultrasonic diagnosis and imaging, magnetic sensor and microactuation[2]. In this work, we have prepared FeCoSiB (20 nm)/NiFeCu (10-80 nm) bilayers with induced uniaxial anisotropy on Si substrate by magnetron sputtering, and investigated the magnetization dynamics using a low field ferromagnetic resonance (FMR) technique. As shown in Figure 1, the imaginary permeability spectra gradually split from single to double peaks and then to a single peak, when an opposing magnetic field is applied along the easy axis. Fig. 2 shows the variation of the resonance frequencies with the external magnetic field from -150 to 150 Oe. Although the frequency of the single resonance peak satisfies the linear relation of modified Kittel formula[3,4], the splitting of resonance peaks was not captured in previous work to the best of our knowledge. Independent on the NiFeCu thickness, this splitting always occurs at certain magnetic field near the coercivity, thus, may be attributed to spin reorientation transition (SRT)[5]. In the SRT region, the intensity of the low frequency peak decreases with the increase of the reverse magnetic field, while the intensity of the high frequency peak increases continuously, indicating that the Zeeman interaction compensates the anisotropy. Moreover, the field range of SRT region is related to the thickness of bilayer, the effective magnetization, the exchange coupling constant and the magnetoelastic constants. It is found that the FeCoSiB (20 nm)/NiFeCu (30 nm) bilayer has the maximum SRT magnetic field range, where the NiFeCu layer is expected to be near the SRT thickness. These results provide insights into the design of novel straintronic devices and the understanding of magnetization dynamics of ferromagnetic bilayers.

[1] V.I. Ozhogin, V.L. Preobrazhenskii, Journal of Magnetism and Magnetic Materials, Vol. 100, p.544–571(1991). [2] Nicolas Tiercelin, Vladimir Preobrazhensky, Olivier BouMatar et al. Proc. SPIE 10357, Spintronics X, p.103571T (2017) [3] Yunpeng Chen, Xin Fan, Yang Zhou et al., Adv. Mater, Vol. 27, p.1351–1355 (2015) [4] Wenfeng Wang, Guozhi Chai and Desheng Xue, J. Phys. D: Appl. Phys. Vol. 50, p.365003 (2015) [5]J. Choi, J. Wu, C. Won et al., Phys. Rev. Lett. Vol. 98, p.207205 (2007)

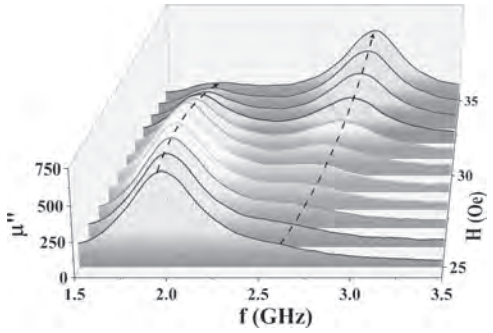

Fig. 1 The imaginary permeability spectra of FeCoSiB (20 nm)/NiFeCu (30 nm) bilayer in the SRT region.

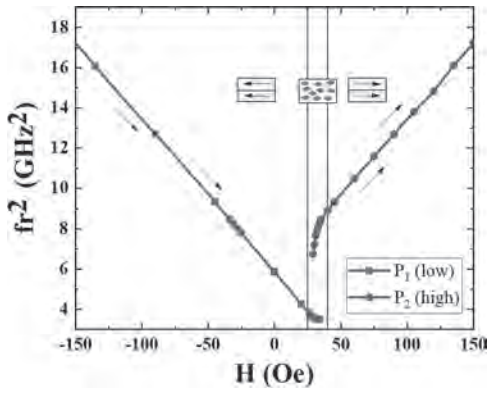

Fig. 2 The variation of the frequencies of two resonance peaks with the external magnetic field along the easy axis.

Session NPB
MAGNETOCALORIC MATERIALS III
(Poster Session)

Arjun Pathak, Chair
State University of New York, Buffalo State, Buffalo, NY, United States

NPB-01. The change of atomic environments caused by Co doping in $La(Fe_{1-x}Co_x)_{11.4}Si_{1.6}$ magnetocaloric materials. *B. Wang*[1], H. Zhou[1], F. Hu[1] and B. Shen[1] *1. Institute of Physics, Chinese Academy of Sciences, Beijing, China*

Solid-state refrigeration based on magnetocaloric effect (MCE) has been regarded as an attractive alternative to the conventional gas compression technique. $La(Fe,Si)_{13}$ materials exhibit giant MCE and negative thermal expansion (NTE), which are regarded as one of the most likely materials to be used in room temperature magnetic refrigeration. Our recent study proved that hydrostatic pressure in $La(Fe_{0.92}Co_{0.08})_{11.9}Si_{1.1}$ sharpens the magnetoelastic transition and enlarges the volume change during the transition, through alerting the intra-icosahedron Fe-Fe bonds (B1, B2, B3) rather than the inter-icosahedral bonds (B4, B5) in the $NaZn_{13}$-type structure, thus MCE and barocaloric effect get enhanced. However, Co doping in $La(Fe_{1-x}Co_x)_{11.4}Si_{1.6}$ induces the decrease of MCE, where the intrinsic mechanism remains unknown. In order to clarify the essence from atom level, we studied the doping-dependent variation of Fe-Fe bonds by Co in $La(Fe_{1-x}Co_x)_{11.4}Si_{1.6}$ (x=0, 0.06) by variable temperature XRD and Retveld refinements. Unlike hydrostatic pressure, due to Co doping, the five Fe-Fe bonds have different elongations in the temperature range 150~300K covering phase transition (Fig.2). This demonstrates the increase in exchange distance and enhancement of the exchange interaction, which is consistent with a large increase in the Curie temperature (Fig.1a). Compared to $LaFe_{11.4}Si_{1.6}$ with negative volume change ΔV/V (-1.30%) during FM-PM transition, $La(Fe_{0.94}Co_{0.06})_{11.4}Si_{1.6}$ shows a decreased ΔV/V (-0.96%) by 26.2% in magnitude and the phase transition becomes slower (Fig.1b). Similar study on doping at La sites is under way. Examining the variation of atom local environments can provide insight for understanding the intrinsic origin of magnetocaloric properties, which is helpful for optimizing magnetocaloric materials.

[1] Shen B., Sun J., Hu F., et al. *Adv. Mater.*, 21, 4545 (2009). [2] Hu F., Shen B., Sun J., et al. *Appl. Phys. Lett.*, 78, 3675 (2001). [3] Fujita A., Fujieda S., Fukamichi K. *Phys. Rev. B*., 65, 014410 (2001). [4] Wang G., Wang F., Di N., et al. *J. Magn. Magn. Mater.,* 303, 84 (2006). [5] Gschneidner K. A., Mudryk Y., Pecharsky V. K. *Scr. Mater.,* 67, 572 (2012). [6] Hao J., Hu F., Wang J., et al. *Chem*. *Mater*., 32, 1807 (2020).

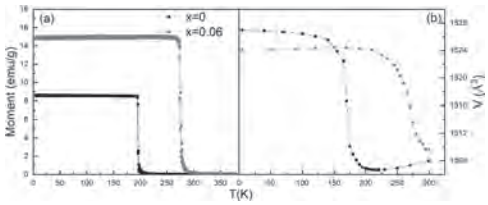

Fig.1 (a) M-T curves under 0.01T and (b) lattice volume as a function of temperature for $La(Fe_{1-x}Co_x)_{11.4}Si_{1.6}$.

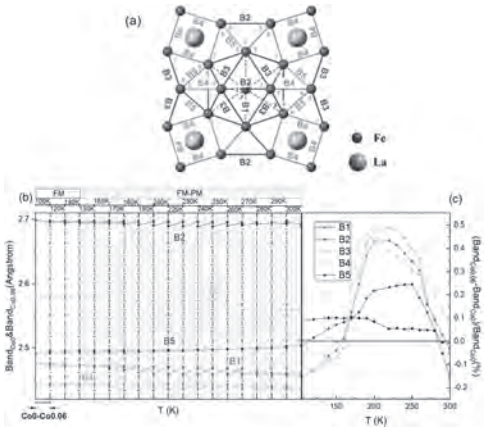

Fig. 2 (a) Schematic view of Fe-Fe bonds in $LaFe_{13}$ with $NaZn_{13}$-type structure, (b) the compared Fe-Fe bonds for $La(Fe_{1-x}Co_x)_{11.4}Si_{1.6}$ with and without 6 at.% Co doping at different temperatures covering phase transition temperature, (c) the change ratio of Fe-Fe bonds caused by 6 at.% Co doping.

NPB-02. The effect of acid treatment on the magnetic and magnetocaloric properties of Al-rich $Al_{0.85+x}Si_{0.15}Fe_2B_2$. *K.M. Stillwell*[1], B. Birch[1], N. Kramer[3], B. Reese[1], A. Pathak[2] and M. Khan[1] *1. Physics, Miami University, Oxford, OH, United States; 2. Ames National Laboratory, Ames, IA, United States; 3. SUNY Buffalo State College, Buffalo, NY, United States*

Owing to the relative abundance of its constituent elements and large MCE observed near room temperature, the $AlFe_2B_2$ system has attracted much attention recently [1]. As an alternative to current rare earth materials, $AlFe_2B_2$ promises the realization of cleaner, energy efficient refrigeration technologies based on phenomena associated with MCE [2]. Additionally, excess Al is believed to generate phase impurities which can change the observed MCE properties of this system [3]. By dissolving certain impurities in acid, a significant enhancement of the MCE properties of this system have been observed [4]. Considering this behavior, we have studied the effect of acid treatment on the magnetic, magnetocaloric, and transport properties of $Al_{0.85+x}Si_{0.15}Fe_2B_2$ (x = 0.2, 0.4). The goal was to explore the possibility of enhancing the MCE properties of the materials by adding excess aluminum and subjecting them to acid treatment after annealing. The samples were prepared by arc melting followed by drop-casting. The drop-casted samples were annealed followed by acid treatment. The alloys were characterized by x-ray diffraction, scanning electron microscopy, dc magnetization, and electrical resistivity measurements. The second order ferromagnetic phase transitions were observed near room temperature (~298 K – 315 K) and peak magnetic entropy changes (-ΔSM) of more than 4 J/kg K were observed for a field change of 5 T. The details of phase purity, microstructure, magnetic, and transport properties of the acid treated and the drop casted annealed materials will be presented.

[1] A. Loudaini, M. Aggour, L. Bahmad, O. Mounkachi, Magnetic properties, magnetocaloric effect and cooling performance of AlFe2B2 compound: Ab initio, Monte Carlo and numerical modeling study, Materials Science and Engineering: B, 264 (2021). [2] Xiaoyan Tan, Ping Chai, Corey M.

Thompson, Michael Shatruk, Magnetocaloric Effect in AlFe2B2: Toward Magnetic Refrigerants from Earth-Abundant Elements, Journal of the American Chemical Society, 135 Iss. 25 9553-9557 (2013). [3] Tahir Ali, M. N. Khan, E. Ahmed, Asad Ali, Phase analysis of AlFe2B2 by synchrotron X-ray diffraction, magnetic and Mossbauer studies, Progress in Natural Science: Materials International, 27 251-256 (2017). [4] J.W. Lee, M.S. Song, B.K. Cho, Chunghee Nam, Magnetic properties of pure AlFe2B2 formed through annealing followed by acid-treatment, Curr Appl Phys., 19 933-937 (2019).

NPB-03. Magnetocaloric properties of Co-doped $Mn_{0.5}Fe_{0.5}Ni_{1-x}Co_xSi_{0.94}Al_{0.06}$ intermetallic alloys. *S. Bhattacharjee*[1], N. Kramer[2], M. Khan[1] and A. Pathak[2] *1. Physics, Miami University, Oxford, OH, United States; 2. Physics, State University of New York, Buffalo, NY, United States*

Magnetic refrigeration is an environmentally friendly cooling technology, which is believed to be significantly more efficient than the currently employed gas-compression-based cooling technologies. The commercialization of this technology is crucially dependent on the discovery of materials that exhibit large magnetocaloric effects and can be easily fabricated using cheap, non-toxic, and readily available elements. The intermetallic $Mn_{1-x}Fe_{x-\delta}Ni_{\delta}Si_{1-y}Al_y$ compounds are known to exhibit large magnetocaloric effects at the relatively low magnetic field (H = 2T or lower) and tunable phase transition [1, 2]. These materials have gained much interest in recent years due to the fact that the constituent elements are cheap and readily available. However, selected drawbacks including large thermal hysteresis and mechanical instability make these materials unsuitable for application. More research efforts are required to eliminate these drawbacks so that the application potential for these materials can be realized. Therefore, we have synthesized the substitution of Ni with Co in $Mn_{0.5}Fe_{0.5}Ni_{1-x}Co_xSi_{0.94}Al_{0.06}$ ($0.025 \le x \le 0.075$) alloys by arc melting followed by a rapidly quenched vacuum suction casting technique and study the magnetic and magnetocaloric properties of the system, which has not been reported yet. X-ray diffraction and scanning electron microscopy (SEM) data indicated that the samples exhibited a single-phase. Peak magnetic entropy changes of ($-\Delta S_M$) of as-cast alloy with x =0.025 is found to be 12 and 31 J kg-1K-1 for ΔH = 2 and 5 T, respectively around 225 K. The observed large MCEs are due to the first order magneto-structural phase transition exhibited by the materials from low-temperature ferromagnetic orthorhombic phase to high-temperature paramagnetic hexagonal phase. In this presentation, we present details of phase purity, microstructure, and magnetic properties of as-prepared and heat-treated alloys with $0.025 \le x \le 0.075$

[1] A. Biswas, A.K. Pathak, N.A. Zarkevich, X. Liu, Y. Mudryk, V. Balema, D.D. Johnson, and V.K. Pecharsky, Acta Mater. 180, 341 (2019). [2] M Khan, RC Das, J Casey, BL Reese, B Akintunde, AK Pathak, AIP Advances 12, 035227 (2022).

NPB-04. Magnetostructural transition and magnetocaloric effect in thermally annealed $Mn_{0.5}Fe_{0.5}NiSi_{1-x}Al_x$ melt-spun ribbons (x= 0.055 and 0.060). *M.d. Arreguin Hernandez*[2,1], A. Dzubinska[2], M. Reiffers[3], J. Sanchez[1,4], C.F. Sanchez Valdés[5] and R. Varga[2] *1. Materiales, Instituto Potosino de Investigacion Cientifica y Tecnologica, San Luis Potosi, Mexico; 2. CPM-TIP, UPJS, Kosice, Slovakia; 3. Faculty of Humanities and Natural Sciences, University of Presov, Presov, Slovakia; 4. Departamento de Fisica, Universidad de Oviedo, Oviedo, Spain; 5. Div. Multidisciplinaria, UACJ, Ciudad Juarez, Mexico*

The giant magnetocaloric (MC) effect measured in $Mn_{0.5}Fe_{0.5}NiSi_{1-x}Al_x$ alloys (0.05 £ x £ 0.07) for a low magnetic field change ($|\Delta S_M|^{max}$ ~16-24 $Jkg^{-1}K^{-1}$ at 2 T) [1], and the fact that they are based on cheap and abundant elements motivated the interest on their study. The effect is linked to their first-order martensitic-like magnetostructural transformation (MST) from a high-temperature hexagonal Ni_2In-type paramagnetic (PM) phase to a low-temperature orthorhombic TiNiSi-type ferromagnetic (FM) phase which is tunable over wide temperature range by changing the Al content [1,2]. As melt spinning is a rapid solidification technique able to produce alloy ribbon samples with a high chemical homogeneity and may result very appropriate to fabricate these five-elements alloys, we produced $Mn_{0.5}Fe_{0.5}NiSi_{1-x}Al_x$ melt-spun ribbons with x=0.055 and 0.060 that were thermally annealed at 1123 K for 4 h; their MST and MC characteristics were studied. RT XRD pattens show that samples are nearly single phase with a major Ni_2In-type phase coexisting with a minor amount of the TiNiSi-type one. DSC, $M(T)^{5mT}$ and $M(T)^{2T}$ curves, shown in Fig. 1, denote the occurrence of the MST with a large thermal hysteresis (~ 32 K), the substantial effect of Al-content on the tuning of the MST temperature without a significant change in the magnetization change across the MST which led to similar $\frac{1}{2}DS_M(T)\frac{1}{2}^{max}$ values (as Fig. 2 shows). The results are discussed and compared with previous data reported in literature for bulk alloys.

[1] A. Biswas et al., Acta Mater. 180, 341–348 (2019). [2] C.L. Zhang et al., Appl. Phys. Lett. 105, 242403 (2014).

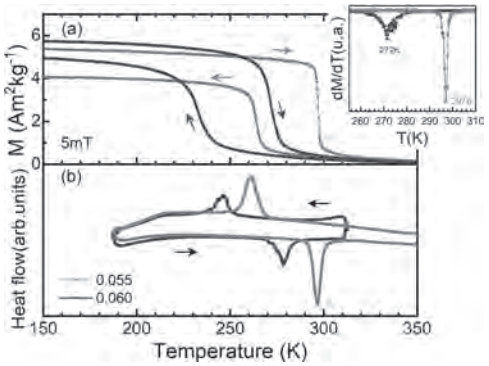

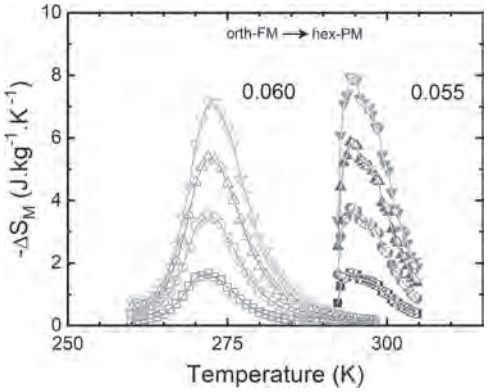

NPB-05. Magnetocaloric properties and exchange bias in arc melted Mn_5Sn_3 alloy. *L. Bachhraj*[1], P. Babu[2] and G. Basheed[1] *1. CSIR-National Physical Laboratory, New Delhi, India; 2. UGC-DAE Consortium for Scientific Research, Mumbai Centre, BARC Campus, Mumbai, India*

Magnetic refrigeration (MR), exploiting the adiabatic demagnetization phenomena, is preferable over conventional cooling technology due to its high efficiency with environment friendly method [1-3]. Owing to this, the earth-abundant Mn-based alloys, i.e. Mn_5Sn_3, crystallizes in Ni_2In type hexagonal structure (space group $P6_3/mmc$), occupies two non-equivalently sites with opposite spin alignment: Mn_I at 2a site with a moment of 0.8 μ_B and Mn_{II} at 2(d) site with a moment of 3.8 μ_B and Sn atom occupies 2c site. The temperature and field-dependent dc magnetization measurements have been carried out to study the MCE and exchange bias in Mn_5Sn_3 alloy. The M (T) curve at 100 Oe shows ordering temperature at T_c ~ 227 K and spin glass (SG) transition at T_g ~ 110 K [Fig. 1a]. The origin of SG is due to geometrical frustration, that comes from vacancy and disordering present at Mn_{2d} site. Furthermore, the M (H) hysteresis loop at 5 K reveals the typical soft ferromagnetic behaviour, saturation magnetisation (M_S) of 62 emu/g [Fig.1(b)], where MH loop slightly shifted towards a negative field direction,

indicating the presence of exchange bias phenomena with exchange bias field (H_{EB}) 5.67 mT at 50 K. Apart from this, Isothermal magnetic entropy change ($\Delta S_M(T)$) is (calculated Using Maxwell equation) 2.16 J/Kg-K at 5 T [Fig. 2], also $\Delta S_M(T)$ evolve with applied magnetic field as - $\Delta S_M(T) = aH^n$, where n is local exponent, power law fit gives n = 0.649 (1) [Inset of Fig 2(a)]. From Inset fig. 2(b), It is quite apparent that all the normalized entropy curves with various ΔH values collapse into a single curve, confirming second-order magnetic phase transition. The relative cooling power (RCP) value is obtained as 242 J/kg for a field change of 5 T which is significantly larger than the earlier reported Mn_5Sn_3 study [4]. Hence, with negligible thermal/magnetic hysteresis and reasonable RCP, the Mn_5Sn_3 is prominent candidate for MR devices.

1. V. Franco, J. Bluez, J. Ipus, J. Law, L. Moreno - Ramz, A. Conde, Prog. Mater. Sci. 93, (2018) 112–232. 2. V. K. Pecharsky, K. A. Gschneidner Jr, J. Magn. Magn. Mater. 200 (1), (1999) 44–56. 3. V. Franco, J. Blazquez, B. Ingale, A. Conde, Annu. Rev. Mater. Res. 42, (2012) 305–342. 4. Jian Huang, Jie Xiang, Ce Zhi, Xuezhen Wang, Xueling Hou, Adv. Mat. Res. 299-300 (2011) 520-524.

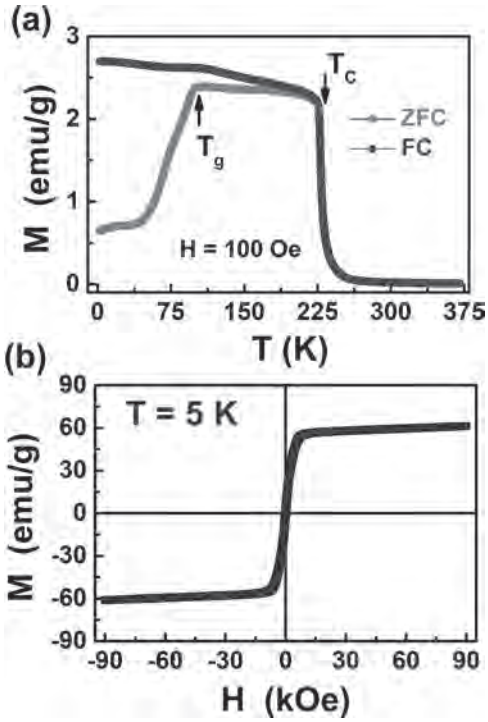

(a) MT curve of Mn_5Sn_3 alloy under 100 Oe applied magnetic field, (b) MH loop measured at 5 K upto 9 T.

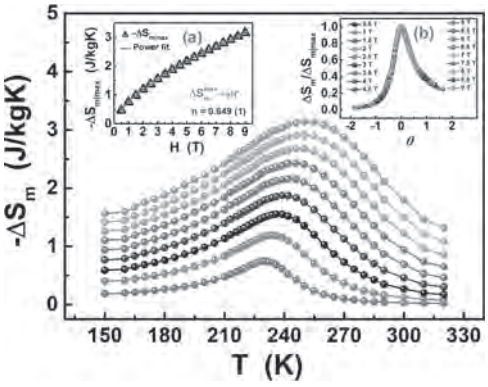

The temperature dependence of $-\Delta S_m$ in the field range of 1 T – 9 T (ΔH = 1 T), Inset (a): Power-law behaviour of $-\Delta S_{m|max,}$ (b): Normalized $-\Delta S_m$ as a function of the rescaled temperature (θ)

NPB-06. Large reversible magnetocaloric effects in $Pr_{2-x}Nd_xIn$.

A. Biswas[1], R.K. Chouhan[1], A. Thayer[1,2], *Y. Mudryk*[1], O. Dolotko[1] and V. Pecharsky[1,2] *1. Ames National Laboratory, Ames, IA, United States; 2. Department of Materials Science and Engineering, Iowa State University, Ames, IA, United States*

Over the last few decades, interest in discovery of materials that exhibit large magnetocaloric effects below room temperature and can support energy-efficient magnetocaloric liquefaction of various gases is on the rise. Here we report a series of rare-earth based $Pr_{2-x}Nd_xIn$ compounds, where Curie temperatures are tunable by adjusting x_{Nd} between 57 and 110 K. Every member of the family exhibits a sharp magnetic transition between the paramagnetic and ferromagnetic states. These transitions give rise to magnetic field-induced entropy changes comparable to or larger than those reported in any other known material in the same temperature range, making $Pr_{2-x}Nd_x$ In compounds suitable for liquefaction of technologically important gases including oxygen, nitrogen, and natural gas. The magnetic transitions in these intermetallics do not show any detectable thermomagnetic hysteresis which is advantageous from the application point of view. While the transition temperature increases with x_{Nd}, the maximum entropy change is slightly reduced from 15 J/ Kg K at 57 K when x_{Nd} = 0 to 13 J/Kg K at 110 K when x_{Nd} = 2, all quoted values are for the magnetic field changing between 0 and 2 T. Notably, the thermodynamic nature of phase transitions for the end-members of the series is different. In case of Pr_2In, the transition is first-order magnetoelastic, as evidenced by symmetry-invariant discontinuous changes in cell volume occurring in concert with the ferromagnetic ordering/disordering transitions.[1,2] Conversely, the phase transition in Nd_2In is rather unconventional, being intermediate between a typical first-order and a typical second-order kind. Density functional theory calculations, providing insights into the electronic structure of the end members and expounding differences in their physical behaviors, will be also discussed. Acknowledgement: This work was performed at Ames National Laboratory (AMES) and was supported by the Division of Materials Science and Engineering of the Office of Basic Energy Sciences of the U.S. Department of Energy (DOE). AMES is operated for the U.S DOE by Iowa State University under Contract No. DE-AC02-07CH11358.

1. A. Biswas, R. K. Chouhan, O. Dolotko, A. Thayer, S. Lapidus, Y. Mudryk, V. K. Pecharsky, ECS J. Solid State Sci. Technol. 11, 043005 (2022). 2. A. Biswas, N. A. Zarkevich, A. K. Pathak, O. Dolotko, I. Z. Hlova, Y. Mudryk, D. D. Johnson, V. K. Pecharsky, Phys. Rev. B 101, 224402 (2020).

NPB-07. Effect of X-Ray Irradiation on Magnetocaloric Material, $(MnNiSi)_{1-x}Fe_2Ge_x$.

J.J. Nunez[1], V. Sharma[1], J. Rojas[1], R. Barua[1] and R.L. Hadimani[1,2] *1. Mechanical & Nuclear Engineering, Virginia Commonwealth University, Richmond, VA, United States; 2. Psychiatry, Harvard University, Boston, MA, United States*

Magnetic refrigeration based on magnetocaloric effect at room temperature is generally considered a potential substitution for classical vapor compression systems due to its high efficiency and environmental friendliness. $(MnNiSi)_{1-x}(Fe_2Ge)_x$ materials are attractive multicaloric materials that change their magnetic properties with the application of magnetic field, pressure, and temperature [1],[2]. The effects of electron and proton irradiation techniques in magnetocaloric materials have been reported in peer-reviewed articles therefore, this study investigated the effects of X-ray irradiation on $(MnNiSi)_{1-x}(Fe_2Ge)_x$. Polycrystalline $(MnNiSi)_{1-x}(Fe_2Ge)_x$ samples were prepared by arc-melting the constituent elements of purity better than 99.9% in an ultrahigh argon atmosphere to ensure sample homogeneity[2]. The procedure utilized X-RAD 225XL Precision X-Ray. The study evidences an observable effect in the $(MnNiSi)_{1-x}Fe_2Ge_x$, x = 0.34 composition when exposed to an absorbed X-ray dosage of ~120Gy/min for 5 hours. A Quantum Design PPMS was used to measure the magnetization (M) of the $(MnNiSi)_{1-x}(Fe_2Ge)_x$ with applied magnetic fields from -3T to 3T. Fig.1(a) shows the M-T data from 200K to 350K with T_c ~ 292K before treatment and 286K after treatment (cooling curve). There was also a significant change in the magnetization ~47.4% from 2.72 emu/g to 4.01 emu/g at an applied magnetic field=100Oe. Fig.1(b) presents the M-H (magnetization vs.

magnetic field) loops from 300K to 345K as it exhibited irradiation-induced hysteresis in comparison to the pristine sample. Fig.2(a) exhibits an observable change of 10Oe in the magnetic coercivity at 200K after treatment. Fig.2(b) presents the hysteresis graphs for the samples at 200K and shows a saturation magnetization decrease but yielded an increase in magnetization from H=0Oe-4500Oe for the treated sample. These presented results would provide base guidelines for factors affecting the performance of magnetocaloric materials in extreme environments.

[1] Zhang, C. L., et al. "Magnetostructural Transition and Magnetocaloric Effect in MnNiSi-Fe_2Ge System." *Applied Physics Letters*, vol. 107, no. 21, 2015, p. 212403., https://doi.org/10.1063/1.4936610. [2] D. Clifford, V. Sharma, K. Deepak, R. V. Ramanujan, and R. Barua, "Multicaloric Effects in (MnNiSi)1−x(Fe_2Ge) x Alloys," in *IEEE Transactions on Magnetics*, vol. 57, no. 2, pp. 1-5, Feb. 2021, Art no. 2500405, doi: 10.1109/TMAG.2020.3025002.

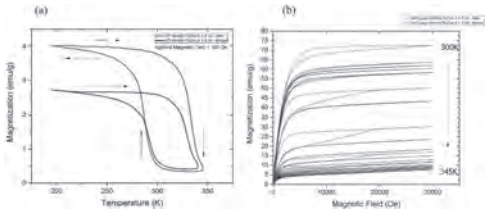

Fig.1 (a)MT Data from temperature range 200K-350K at 100Oe. (b)MH Loops 300K–345K exhibiting irradiation-induced hysteresis.

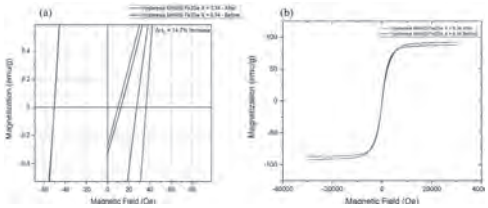

Fig.2 (a) Coercivity Data at 200K with an increase of 14.7% after treatment. (b) Hysteresis data from -3T to 3T at 200K.

NPB-08. Near-room temperature magnetocaloric effect in $Mn_{4.9}Cu_{0.1}Ge_3$ compound. *S. Sakthivel*[1], A. Kumar[1], U. Remya[1], S. Athul[1], A. Dzubinska[2], M. Reiffers[3] and R. Nagalakshmi[1] *1. Intermetallics and NLO Laboratory, Physics, National Institute of Technology Tiruchirappalli, Tiruchirappalli, India; 2. Center for Progressive Materials-Technology and Innovation Park, University Pavol Jozef Šafárik, Kosice, Slovakia; 3. Faculty of Humanities and Natural Sciences, Presov University, Presov, Slovakia*

Magnetic refrigeration based on magnetocaloric effect is an effective technology to curb greehouse gas emission. It is crucial to choose a viable magentocaloric material with reversible room temperature magnetocaloric effect. Mn_5Ge_3 based compounds are the perfect fit to this class. They are rare-earth free and exhibits a magnetic entropy change () of 9.3 J/kg K and relative cooling power () of 400 J/kg in = 5 T around 296 K[1]. Here, the magnetic interaction between and among the Mn atoms in *4d* and *6g* sites dictates the magnetocaloric effect which can be manipulated *via* tuning the Mn-Mn distance[2]. A best method to do so is doping and in this work, a non-magnetic element Cu is doped in place of Mn as a new attempt. $Mn_{4.9}Cu_{0.1}Ge_3$ polycrystalline compound, synthesized by arc melting method, has crystallized in Mn_5Si_3-type D8 hexagonal crystal structre (*SG: P6₃/mcm*). The thermomagnetic measurements reveal a paramagnetic to ferromagnetic transition at 288.7 K, and shifts to higher value as the applied magnetic field is increased (*Fig. 1*). Arrott plot constructed from field-dependent magnetization demonstrates second order nature of the magnetic transition. In a magnetic filed change of 5 T, $Mn_{4.9}Cu_{0.1}Ge_3$ compound shows = 6.03 J/kg K and RCP = 360.7 J/kg at 292 K (*Fig. 2*). The wide temperature working span has deemed its RCP closer to the parent compound and also it is comparable with other compounds in this class. The near-room temperature, second order magnetocaloric effect are valuable properties for a magnetic refrigerant and this makes $Mn_{4.9}Cu_{0.1}Ge_3$ compound a remarkable magnetocaloric material.

Acknowledgement: *This work is the implementation of following projects and awards: DST-INSPIRE award (No. DST/INSPIRE/03/2018/000691), University Science Park TECHNICOM for Innovation Applications Supported by Knowledge Technology, ITMS: 26220220182, VEGA 1/0404/21 and VEGA 1/0705/20.*

[1] T. Tolinski and K. Synoradzki, Intermetallics 47, 1 (2014). [2] Q. Zhang, J. Du, Y. B. Li, N. K. Sun, W. B. Cui, D. Li, and Z. D. Zhang, J. Appl. Phys. 101, 123911 (2007). [3] S. S, A. K, R. U D, A. Dzubinska, M. Reiffers, and N. R, Intermetallics 132 (2021). [4] K. H. Kang, Y. Oh, J. H. Kim, E. J. Kim, H.-S. Kim, and C. S. Yoon, J. Alloys Compd. 681, 541 (2016). [5] K. H. Kang, J. H. Kim, Y. Oh, E. J. Kim, and C. S. Yoon, J. Alloys Compd. 696, 931 (2017).

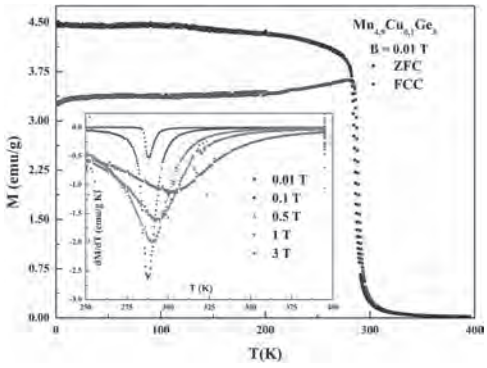

Temperature dependent zero field cooled and field cooled curves in B = 0.01 T. Inset: *dM/dT* vs *T* graph demonstrating shift in transition temperature in various magnetic fields

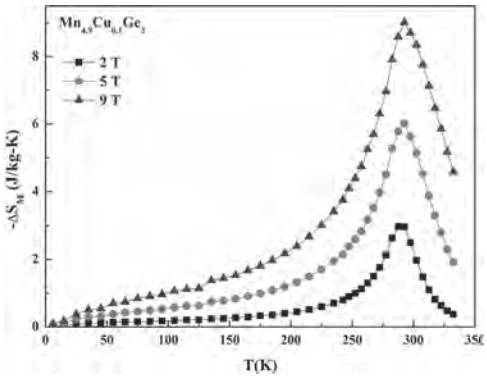

Magnetocaloric effect in $Mn_{4.9}Cu_{0.1}Ge_3$ compound

NPB-09. Structural, magnetic and magnetocaloric characterization of Ni_2MnSn microwires prepared by Taylor-Ulitovsky technique. *M.d. Arreguin Hernandez*[1,2], M. Varga[1,3], M. Hennel[1,3], T. Ryba[4], J. Sanchez[2,5] and R. Varga[3,4] *1. Inst. Phys., Fac. Sci., UPJS, Kosice, Slovakia; 2. Materiales, IPICYT, San Luis Potosí, Mexico; 3. CPM-TIP, UPJS, Kosice, Slovakia; 4. RVmagnetic, Kosice, Slovakia; 5. Departamento de Fisica, Universidad de Oviedo, Oviedo, Spain*

In this work, we addressed the fabrication of Ni_2MnSn glass-coated microwires (mws) by using the Taylor-Ulitovky technique, as well as their structural, magnetic and magnetocaloric (MC) characterization. Apart from the physical characteristics of the material itself, wire-shaped MC materials bring additional features of interest from the viewpoint of refrigeration applications such as an easier magnetization saturation along wire length, and a large surface-to-volume ratio [1]. The former may lead to reach a given MC effect value at a lower magnetic field change $m_0\Delta H$, whereas the latter allows a high heat-transfer rate with the exchange fluid. Microwires were prepared from a bulk arc-melted ingot of nominal composition Ni_2MnSn

produced from highly pure elements (≥ 99.9 %). Their average metallic core diameter was 86 μm (as the inset of Fig. 1(a) shows). Their characteristic XRD pattern, shown in Fig. 1(a), was indexed based on a single-phase austenite with the $L2_1$ structure (space group Fm-3m; a= 5.98 Å). The foreground graph in Fig. 1(b) shows that the $M(T)$ curves measured upon heating and cooling cycles under magnetic fields m_0H of 10 mT, 50 mT, and 1 T almost overlap; austenite shows a Curie temperature of 350 K. The thermal dependencies of the magnetic entropy change $-\Delta S_M(T)$ for different $m_0\Delta H$ values are shown at the inset of the figure; the curves are broad reaching a $|\Delta S_M|^{max}$ value of 2.3 $Jkg^{-1}K^{-1}$ at 3.0 T. The results are compared with those previously reported for bulk and melt-spun ribbons of the same composition [2,3].

[1] J. Alam et al., J. Magn. Magn. Mater. 513, 167074 (2020). [2] M. Nazmunnahar et al., J. Magn. Magn. Mater. 386, 98–101 (2015). [3] T. Krenke et al., Phys. Rev. B 72, 014412 (2005).

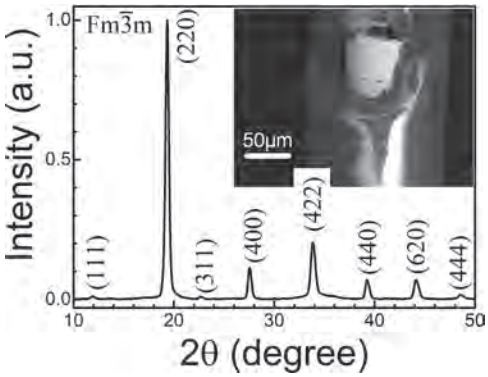

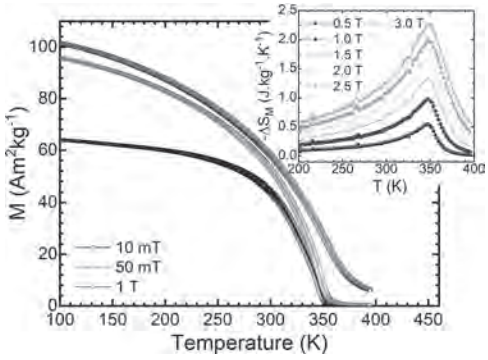

NPB-10. Investigation Of Structural And Magnetic Properties Of Nanocrystalline $Pr_{0.57}Bi_{0.1}Ca_{0.33}MnO_3$. *G. Singh*[1], A. Gaur[1] and R.N. Mahato[1] *1. School Of Physical Sciences, JNU, New Delhi, India*

Perovskite manganite oxide shows that various future technologies (eg. spintronics, magnetic sensors, infrared detectors, magnetic storage media, colossal magneto-resistance application, thermo-electric applications, and magnetic refrigerants) are greatly relying on these materials [1]. Double exchange (DE) interaction and super-exchange (SE) interaction play a vital role in the above-given properties [2]. We have investigated the structural and magnetic properties of nanocrystalline powder $Pr_{0.57}Bi_{0.1}Ca_{0.33}MnO_3$ (PBCMO) synthesized by the sol-gel technique. PBCMO is very interesting shows various magnetic transition as compare to $La_{0.57}Bi_{0.1}Ca_{0.33}MnO_3$ which shows only one magnetic transition [3]. The Rietveld analysis of the X-ray diffraction (XRD) pattern reveals that the compound crystallizes in a single orthorhombic phase with the Pbnm space group. The Crystallite size was calculated using the Scherrer formula and it is found to be ~27 nm. Scanning electron microscope (SEM) images confirm the homogeneity of the sample and the average particle size from SEM image using particle size distribution with Lorentz fit was found to be 110 nm. This has revealed that each particle consists of several crystallites. Temperature dependence Magnetization measurements under the external magnetic field of 500 Oe, in Fig.1, have shown that the sample exhibits magnetic transition at temperature ~ 44 K from ferromagnetic (FM) to paramagnetic (PM) phase with increasing temperature. Moreover, we have observed three small bumps near temperatures 75 K, 158 K, and 222 K that may suggest us simultaneous occurrence of the FM phase and antiferromagnetic phase [4]. Field-dependent magnetization for nanocrystalline PBCMO has exhibited ferromagnetism (FM) at low temperature (5 K) and the linear hysteresis loop corresponds to the paramagnetic region at room temperature as shown in Fig.2.

1) Dipak Mazumdar, Kalipada Das and I. Das, J. Appli. Phys. 127, 093902-1 (2020) 2) A. Pal, A. Rao and D. Kekuda, Journal of Magnetism and Magnetic Materials. 512. 167011. 10.1016/j.jmmm.2020.167011. 3) Arpit Gaur, Meenakshi, Vipin Nagpal and Priyanka Bisht, Solid State Communications. 340. 114504. 10.1016/j.ssc.2021.114504. 4) J.R. Sun, J. Gao and Y. Fei, PHYSICAL REVIEW B 67, 144414 (2003)

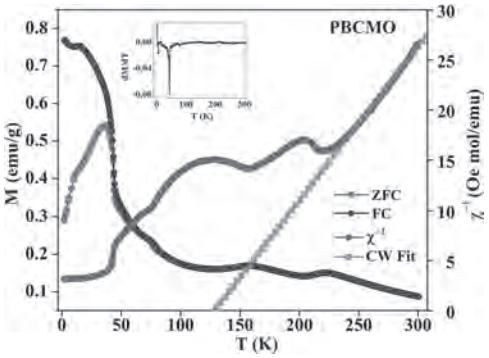

Fig.1 Temperature dependence of FC and ZFC magnetizations for nanocrystalline $Pr_{0.57}Bi_{0.1}Ca_{0.33}MnO_3$ sample at applied field of 500 Oe. Inset shows the derivative of M (T) curve (dM/dT versus T plot).

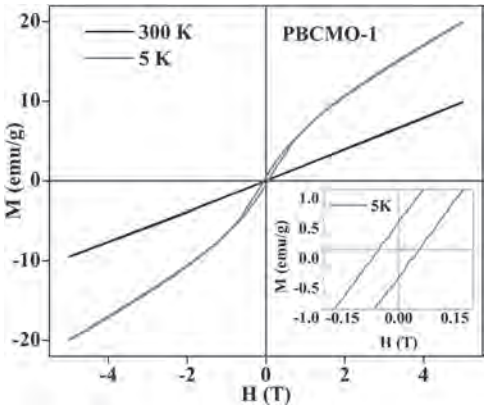

Fig.2 Magnetisation (M) versus applied magnetic field (H) plot at 5 K and 300 K temperature. Inset shows the magnified view of M versus H plot at 5 K.

NPB-11. Withdrawn

NPB-12. Magnetocaloric properties in $Pr_{1-x}Sr_xMnO_3$(x=0.48 and 0.52): Study using Landau and Maxwell Model. A.K. Saw[1], J.J. Nunez[2], *R.L. Hadimani*[2] and V. Dayal[1] *1. Department of Physics, Maharaja Institute of Technology Mysore, Mandya, India; 2. Department of Mechanical and Nuclear Engineering, Virginia Commonwealth University, Richmond, VA, United States*

The magnetocaloric effect (MCE) is a common phenomenon in magnetic materials, and the essence of which is a thermal effect caused by the change of magnetic moment order under an adiabatic condition. A wide range of materials showing the first-order (FO)/second-order (SO) magnetic phase

transitions (PT) exhibiting large/moderate magnetic entropy change (ΔS_M) has been reported [1-4]. Among the magnetic materials, the perovskite manganites which shows FOPT/SOPT below room temperature (RT) finds importance in cryogenic technology for laboratory purpose and space technology and have been an interest for the researcher to study the MCE effect in the vicinity of magnetic PT [5-6]. In this paper, we present magnetic and MCE properties in $Pr_{0.52}Sr_{0.48}MnO_3$ (PSMO48) and $Pr_{0.52}Sr_{0.48}MnO_3$ (PSMO52) perovskite manganite. PSMO48 show a paramagnetic to ferromagnetic, a SOPT at Tc (Curie temperature)=258 K, while PSMO52 undergoes SOPT at T_c=224 K followed by a charge disordered ferromagnetic to A-type antiferromagnetic at T_N (Neel temperature)~ 139 K. PSMO52 shows irreversibility during the cooling and heating cycle in temperature-dependent magnetisation measurement, a signature of first-order phase transition at low temperature. Furthermore, ΔS_M has been calculated using the magnetic field (H)-dependent magnetisation (M) isotherms data using the Maxwell model. PSMO48 shows a trivial ΔS_M value ~ 4.7 J/kg K at H=8T (around T_c). PSMO52 showed a giant ΔS_M value of ~ 3.7 J/kg K (around T_c) and 4.2 J/kg K (around T_N) at H=8T. The simulation of ΔS_M carried out using the phenomenological Landau free energy Model shows good agreement with the experimental results as shown in Fig 1. The magnetotransport study of the samples shows a significant magnetoresistance in the vicinity of PT. Acknowledgement: This work is supported by UGC-DAE CSR, Indore, India (CSR-IC/CRS-89/2014-2018) granted to VD. AKS (Project fellow II) acknowledges UGC DAE CSR and MRF-MITM for fellowship.

Refernces: 1. E. Warburg, annalen der physik 249, 141 (1881). 2. V. Franco, J. S. Blázquez, B. Ingale, and A. Conde, Annu. Rev. Mater. Res. 42, 305 (2012). 3. R Rawat and I Das, J. of Phys: Condens Matt. 12 L57 (2001). 4. Ravi L. Hadimani, Joao H. B. Silva, Andre M. Pereira, Devo L. Schlagel, Thomas A. Lograsso, Yang Ren, Xiaoyi Zhang, David C. Jiles, and Joao P. Araújo Appl. Phys. Lett. 106, 032402 (2015) 5. A. Jerbi, A. Krichene, N. Chniba-Boudjada, and W. Boujelben, Phys. B Condens. Matter, 477, 75–82 (2015). 6. Ajay Kumar Saw, Ganesha Channagoudra, Shivakumar Hunagund, Ravi L Hadimani, Vijaylakshmi Dayal, Materials Research Express, 7, 016105 (2020)

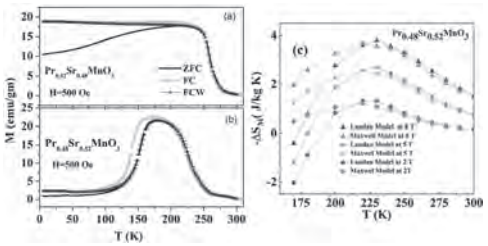

Temperature dependence of magnetization (M) in ZFC, FCC and FCW mode at H =0.05 T (a) for $Pr_{0.52}Sr_{0.48}MnO_3$ (b) $Pr_{0.48}Sr_{0.52}MnO_3$ (c) Comparison of ΔS_M at 2T, 5T and 8T, calculated using numerical integration of Maxwell relation and Landau model for $Pr_{0.52}Sr_{0.48}MnO_3$.

NPB-13. "Study of magnetotransport and Magnetocaloric properties of Calcium (Ca) doped $La_{0.97-x}Ca_xHo_{0.03}MnO_3$ composite system".

M. Azim[1], J. Mohapatra[2] and S. Mishra[1] *1. Physics and Material Science, University of Memphis, Memphis, TN, United States; 2. Physics, University of Texas, Arlington, Arlington, TX, United States*

Magnetic refrigeration technology, which works on the magnetocaloric effect (MCE) of magnetic materials, has attracted the interest of numerous research groups over traditional gas refrigeration. It has several advantages, including being highly energy-efficient, environmentally friendly, and cost-effective. The major effort is directed in improving the magnetic entropy change along with the relative cooling power (RCP) of rare earth double perovskite oxide magnetocaloric materials. This study reports the magnetotransport and magnetocaloric properties of different concentration of alkaline earth metal such as Ca doped $La_{0.97-x}Ca_xHo_{0.03}MnO_3$ (x = 0.3, 0.33 and 0.37) composites which were synthesized via the facile autocombustion technique. The second-order phase transition temperature may be supposed to appear at the temperature-dependent field-cooled magnetization curve near room temperature. These compounds with individual ferromagnetic phase transition temperatures vary from 100 K to 130 K that consequently exhibits the spin glass nature behavior. Moreover, spin glass cluster may turn into spin glass state which greatly decreases the resistance by developing new magnetic order to promote the transport of electrons. Furthermore, ferromagnetic ordering can be observed in these composites due to the existence of double exchange mechanism from both Mn^{3+} and Mn^{4+} ions that develops the electronic holes in Mn–O bands, which is favored by the doped Ca^{2+} ion. In addition, increasing the doping concentration of Calcium may increase the Curie temperature, T_c that tend to decrease the change in magnetic entropy, $-\Delta S_m$. The fundamental key of this work is to demonstrate the potentiality of enhancing the magnetotransport and magnetocaloric effect in the framework via spin coupling transfer of Calcium doped rare earth perovskite compounds.

1. The effect of holmium doping on the magnetic and transport properties of La0.7−xHoxSr0.3MnO3 (0 6 x 6 0.4) *P Raychaudhuri, T K Nath, P Sinha, C Mitra, A K Nigam, S K Dhar and R Pinto* 2. Enhanced metal–insulator transition and magnetoresistance in melt-processed La 0.67 Ca 0.33 MnO 3 and Ho-doped manganites *A K Pradhan, B K Roul, Y Feng, Y Wu, S Mohanty, D R Sahu, and P Dutta* 3. Study of structural, magnetic, and magnetocaloric properties of Ho1−xCaxMnO3 *K P Shinde, E J Lee, M Manawan, A H Lee, S Y Park, Y Jo, B K Koo and J S. Park* 4. Effect of sintering process on the magnetotransport properties of Ho-doped La0.67Ca0.33MnO3 *D R Sahua, A K Pradhanb P K Mishrac, D Beherad P Dattae and B K Roul*

NPB-14. Concentration-dependent Oscillation of Specific Loss Power in Magnetic Nanofluid Hyperthermia.

J. Wang[1], J. Kim[1], H. Kim[1] and S. Bae[1] *1. Electrical Engineering, University of South Carolina, Columbia, SC, United States*

Magnetic nanofluid hyperthermia (MNFH) using colloidal superparamagnetic nanoparticles (SPNPs) has attracted considerable attentions as a potential treatment modality in cancer clinics due to its clinical efficacies including deep tissue penetration of AC magnetic heat induction power (specific loss power (SLP)) and prominently low side effect [1,2]. Accordingly, plenty of research activities were conducted to design and develop high-performance SPNPs with sufficient SLP for destroying tumors by cancer apoptosis or necrosis [3,4]. However, magnetic dipole coupling between the colloidal SPNPs depending on the concentration was regarded as a critical role in characterizing SLP in MNFH. Although the concentration-dependent SLP change behavior has been intensively investigated, the physical mechanism is still poorly understood, and some contradictory results have been recently reported [5,6]. In this work, interparticle distance ($d_{c\text{-}c}$)-dependent magnetic dipole coupling energy induced in nanofluids and their physical contribution to the SLP change behavior were investigated and analyzed by measuring the intrinsic/extrinsic magnetic parameters of nanofluids as a function of concentration. We first found and reported that the SLP of SPNP MNFH agent shows strong concentration-dependent oscillation behavior. According to the experimentally and theoretically analyzed results, the energy competition among the magnetic dipole interaction energy (E_{dip}), magnetic potential energy (E_p), and exchange energy (E_{ex}), was revealed as the main physical reason for the oscillation behavior shown in Fig. 1. The empirically demonstrated new finding and physically established model on the concentration-dependent SLP oscillation behavior is expected to provide biomedically crucial information in determining the critical dose of an agent for clinically safe and highly efficient MNFH in cancer clinics.

[1] Jordan *et al*, J. Magn. Magn. Mater., 201, 413-419 (1999) [2] Jang *et al*, Adv. Mater., 30, 1704362 (2018) [3] Sharifi *et al*, J. Magn. Magn., Mater. 324, 903–915 (2012) [4] Jeun *et al*, Appl. Phys. Lett., 96, 74319 (2010) [5] Haase *et al*, Phys. Rev. B 85, 2-6 (2012) [6] Martinez *et al*, Adv. Funct. Mater., 22, 3737-3744 (2012)

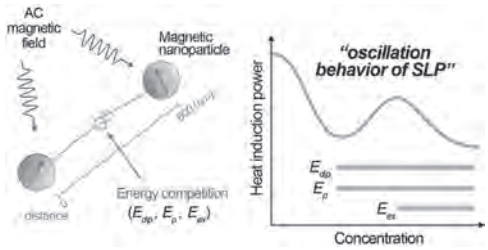

Fig. 1. A physical model describing concentration-dependent oscillation behavior of SLP caused by the energy competition among the magnetic dipole interaction energy (E_{dip}), magnetic potential energy (E_p), and exchange energy (E_{ex}).

NPB-15. Heatrapy 2.0: a two-dimensional upgrade for computing dynamic heat transfer processes in Python involving non conventional phenomena. *D. Silva*[1] *1. IFIMUP – Institute of Physics for Advanced Materials, Nanotechnology and Photonics, Faculty of Science of the Porto University, Porto, Portugal*

Modeling and computing heat transfer phenomena involving the magnetocaloric effect is of paramount importance for designing new heat management systems. The heatrapy python package has been used to compute heat transfer phenomena in magnetic refrigerators and heat pumps for the past 5 years [1-3]. It uses the finite difference method to solve the unidimensional heat conduction equation. So far, the package was downloaded over 50,000 times by the pip package manager [4]. A considerable share of devices can be modeled in one dimension. However, there are others where this is not sufficient. In those systems, at least two-dimensional approaches are required. Moreover, devices only relying on heat conduction require more complex heat transfer mechanisms, beyond the magnetocaloric effect, so that they can show functional behaviours, such as thermal phenomena involving phase transitions. To account for these issues, the heatrapy python package was upgraded aiming to add three new major features. The first is the extension to two-dimensional models. The second is to allow the live visualization of the computation. The third feature is to allow the incorporation of phase change transitions. Figure 1 shows an example for the computation of a magnetized structure made of aluminium and gadolinium. The detailed implementation is described, as well as minor updates.

[1] D. J. Silva et al., SoftwareX, 7, 373 (2018). http://dx.doi.org/10.1016/j.softx.2018.09.007 [2] K. Klinar et al., iScience, 25, 103779 (2022). https://doi.org/10.1016/j.isci.2022.103779 [3] D. J. Silva et al., International Journal of Energy Research, 45, 18498 (2021). http://dx.doi.org/10.1002/er.7023 [4] https://github.com/djsilva99/heatrapy

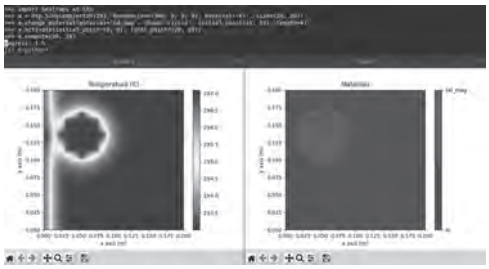

Fig. 1: Progress of the computation of 100 s after creating a single 2D thermal object and changing the thermal properties of one different shaped region to gadolinium. The figure is a screen shoot when the progress was at 3%

Session OOA
MAGNETIC SENSORS AND DEVICES I

Nicoleta Lupu, Co-Chair
National Institute of R&D for Technical Physics, Iasi, Romania
Carmine Stefano Clemente, Co-Chair
University of Sannio, Benevento, Italy

INVITED PAPER

OOA-01. Non-Reciprocity and Non-linearity in Engineered Magneto-Acoustic Devices. D.A. Bas[1], R. Verba[2], P. Shah[1], S. Leontsev[1], A. Matyushov[3], M. Newburger[1], N. Sun[3], V. Tyberkevych[4], A.N. Slavin[4] and *M. Page[1] 1. Air Force Research Laboratory, WPAFB, OH, United States; 2. Institute of Magnetism, Kyiv, Ukraine; 3. Department of Electrical and Computer Engineering, Northeastern University, Boston, MA, United States; 4. Department of Physics, Oakland University, Rochester, MI, United States*

Nonreciprocity, the property of merit for a variety of RF components such as isolators and circulators, is typically difficult to achieve with the magnitude required for applications. Many systems which demonstrate non-reciprocity are not suitable for scaling to the size, weight, and power required for applications, or do not exhibit a sufficient intensity of the effect for applications relevance. One such physical system which generally does not exhibit non-reciprocity is that of acoustic waves. Acoustic waves are an important medium for information transport, but they are inherently symmetric in time. By achieving non-reciprocity in an acoustic system, the decades of industrial research in this relatively mature field can be leveraged for new applications. To this end, I will discuss discoveries of non-reciprocity and non-linearity in surface acoustic waves interacting with magnetic materials. Giant Nonreciprocity of 48.4 dB (ratio of 1:100,000) is achieved in the transmission of surface acoustic waves on a lithium niobate substrate coated with ferromagnet/insulator/ferromagnet (FeGaB/Al2O3/FeGaB) multilayer structure.[1] This same structure has now also demonstrated very large phase shifts due to a similar interaction, and the nature of the magnetic ordering and coupling to the acoustic system will be discussed. Nonlinearity will also be discussed and is demonstrated using focused interdigitated transistors employing curved fingers, in contrast to the straight fingers typically used. These transducers are engineered to concentrate acoustic energy towards a small region in the center of the device allowing driven magnetic precession much higher than was previously possible. Enhanced acoustic absorption and modeling of the response will be shown. Finally a variety of characterization of such devices, including Brillouin Light scattering, MOKE, and NV center magnetometry will be presented. These devices promise functionality which outperforms current state of the art high frequency devices in a novel acoustic wave system that facilitates unprecedented size, weight, and power reduction.

[1] P. Shah, et al, Sci. Adv. 6, eabc5648 (2020).

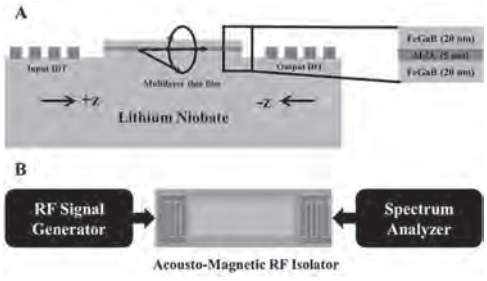

Fig. 1. Schematic of device design and experimental setup for measurement. (A) Schematic cross-section representation of the magnetoelastic isolator device. The geometry of the device is similar to the standard ADFMR device. The multilayer thin film stack in this study is FeGaB/Al_2O_3/FeGaB thin film. (B) Schematic top view representation of the isolator device including measurement setup. [1]

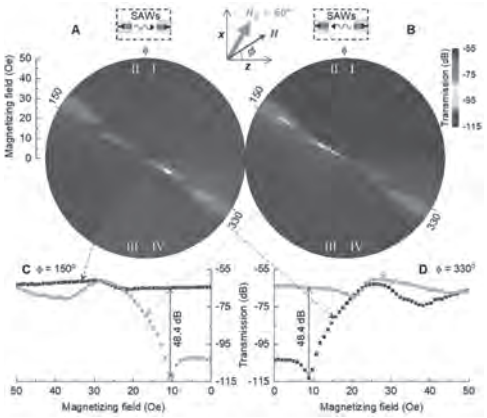

Fig. 2. Nonreciprocal SAW transmission in FeGaB/Al_2O_3/FeGaB multilayer stack with growth field at 60°. ADFMR plot with 1435-MHz SAWs traveling in (A) +z-direction (forward) and (B) -z-direction (reverse). Absorption (blue on color scale) occurs at ADFMR resonance, which we observe in directions perpendicular to the growth field. (C) Field sweeps at 150° for forward (blue) and reverse (orange) SAW propagation. (D) Field sweeps at 330° for forward (blue) and reverse (orange) SAW propagation. The difference between forward and reverse sweeps at a common static field condition is the isolation.[1]

CONTRIBUTED PAPERS

OOA-02. Low Power High Precision MI Sensor Driven by Low-Frequency Wiegand Pulse. *R. Yao*[1,2], Y. Takemura[2] and T. Uchiyama[1]
1. Graduate School of Engineering, Nagoya University, Nagoya, Japan; 2. Division of Electrical and Computer Engineering, Yokohama National University, Yokohama, Japan

We present a magneto-impedance (MI) sensor having a low power consumption of 2.44 μW per pulse and driven by Wiegand pulses at 10 Hz. The oscillator circuit conventionally used for a MI sensor is replaced by a Wiegand sensor to generate a pulse voltage. The MI sensor exhibited a good output linearity of 0.04 mV/μ_0T for detecting magnetic field in the range of ±150 μT when Wiegand pulses of amplitude 1 V were supplied. This method reduces the power consumption of MI sensor down to μT level, enabling its use as battery-less sensors and Internet of Things (IoT) devices in Intelligent Transport Systems (ITS) and bio-sensing fields [1, 2]. The Wiegand sensor consisted of a twisted FeCoV wire (Wiegand wire) and a 3000-turn pick-up coil. The length and diameter of the wire were 11 mm and 0.25 mm, respectively. A 10 Hz AC magnetic field of 5 mT/μ_0 was applied to the Wiegand sensor. A fast magnetization reversal of the wire induced a pulse voltage [3]. Alternating Wiegand pulses of 12 V (±2 V) and 20 μs width were induced in the pick-up coil. The impedance of an amorphous wire changes sensitively with the external magnetic field with an applied AC current. This is called the MI effect [4]. The pulse parameters affecting the MI effect have been explored. For pulse frequency below 500 kHz, the rise time and the excitation current control the MI effect. The MI effect driven by pulses with rise times in microseconds is too small to be observed and is greatly affected by fluctuations in the voltage. A fast rise time pulse shaping circuit was designed to shape the Wiegand pulse with a fixed amplitude and a rise time less than 100 ns, as shown in Fig. 1. The shaping IC input voltage V_{CC} can be adjusted and supplied by a coin cell. The low power consumption was achieved under the conditions of the 100 ns rise time and 0.3 mA excitation current. The characteristic of the output voltage of the MI sensor E_w with respect to the applied magnetic field H_{ex} is shown in Fig. 2. A DC power supply using the Wiegand pulses was designed [5], which could make the MI sensor completely battery-less.

1) T. Uchiyama, J. Ma, Journal of Magnetism and Magnetic Materials, Vol.514, 2020, 167148 2) Y. Takemura, N. Fujinaga, A. Takebuchi, etc., IEEE Trans. Magn., 53, 4002706, 2017. 3) J. R. Wiegand and M. Velinsky, U.S. Patent 3,820,090, (25 June 1974). 4) K. Mohri, T. Uchiyama, L.P Shen, etc., Journal of Magnetism and Magnetic Materials, Vol.249, p.351-356, 5) Sun, X.; Iijima, H.; Saggini, etc. *Energies* 2021, *14*, 5373.

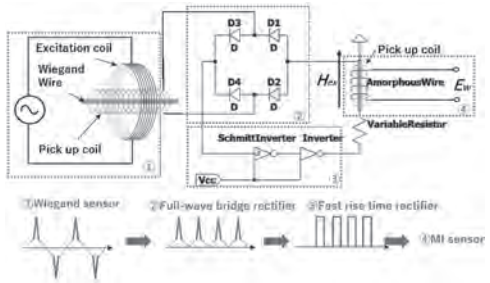

MI sensor driven by fast rise-time pulses originated from Wiegand pulses.

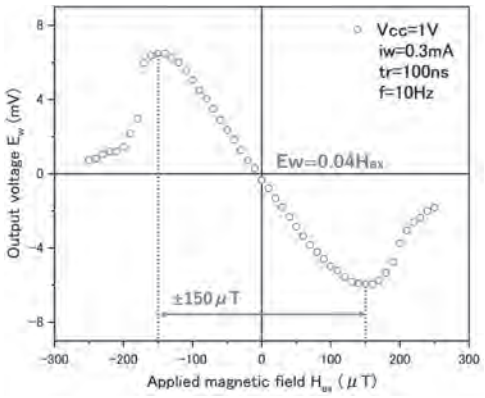

***E_w-H_{ex}* characteristics of the MI sensor driven by Wiegand pulses (V_{CC} =1V).**

OOA-03. Monolithic 3D (IP_OoP) MTJ sensor for low footprint and compact size sensor applications. *M. Kandzija*[2,1], P. Freitas[2,1], R. Macedo[2], S. Cardoso[2,1] and M. Erkovan[2,1] *1. Instituto Superior Técnico, Lisbon, Portugal; 2. INESC MN, Lisbon, Portugal*

Depending on the application magnetic sensors are required to sense magnetic field in one, two or three directions. Increasing the number of spatial components to all three directions can largely improve the sensor's precision, as well as its potential applications. We demonstrated [1] 2D magnetometer based on in-plane magnetic tunnel junctions (MTJ), enabling x and y detection in a Wheatstone Bridge configuration, in a unique chip (using 4 MTJ stack depositions, microfabricated in a single step, without annealing). The challenge of z-sensitive sensors is the significantly different MTJ stacks required for in-plane (IP) out-of-plane (OoP) detection, and the optimization of their respective sensitivities and cross field immunities. Here, we present three-dimensional magnetic sensor based on combined in-plane and out-of-plane MTJs. To achieve sensing in three directions we use MgO-based IP-MTJs for detection of *x* and *y* components (IrMn antiferromagnetic pinning layer, NiFe free layer and shape anisotropy for *x, y* sensitive axis) and OoP-MTJ for detection of *z* component (perpendicular synthetic anti-ferromagnetic Pt/Co multilayers as a pinned layer, FeCoB as a free layer). There are two main issues to overcome in combined IP and OoP MTJ structures. The first one is the additional level of complexity in the microfabrication process due to the difference in stacks materials and overall thicknesses and the second is the annealing conditions. In this presentation we demonstrate IP and OoP MTJ sensors microfabricated simultaneously in the same wafer, and also annealed under the same conditions. This has a strong impact on the 3D sensor integration costs, and offers ideal alignment tolerances (only limited by the lithography tools resolution). The 3D sensor footprint is ~1x1 mm2, which is remarkably small, as shown in Figure 1. Figure 2 shows the sensor transfer curves R(H), with TMR of 64% and 75%, and sensitivities of 234 mV/T and 83 mV/T, respectively for IP and OoP sensors. Moreover we will address cross-field immunity for the IP and OoP sensors, for optimum performance.

[1] P. Ribeiro, A. Silva, and S. F. Cardoso, (2020). IEEE Magnetics Letters., Vol. 11, p.1-5 (2020)

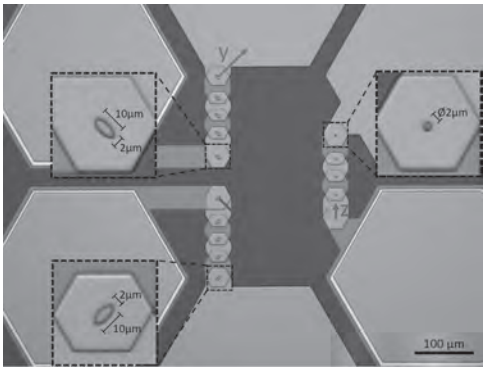

Fig.1. Microfabricated sensor with array of five pillars in series.

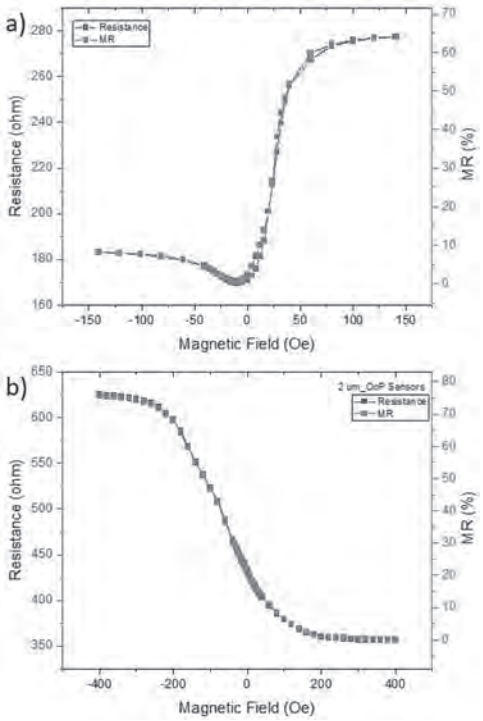

Fig 2. Transfer curves of (a) in-plane MTJ, (b) out-of-plane MTJ.

OOA-04. Evaluation of Coplanar Line Type Thin Film Magnetic Field Sensor with Narrow Slits. *M. Sakamoto*[1], R. Suzuki[1], T. Ishihara[1], J. Honda[1] and S. Yabukami[1] *1. Tohoku University, Sendai, Japan*

In our previous work, we developed the highly sensitive thin film sensor and indicated the successful measurement of Magnetocardiogram signals without the magnetic shielding [1]. But the sensitivity was poor around the ferromagnetic resonance frequency (in GHz bands) since the sensor had the severe reflection loss because of the impedance mismatching [2]. In this research, we have improved the impedance matching of the sensor by employing the slits in the magnetic thin-film and evaluated the appropriate slit width. As shown in Fig. 1, the proposed sensor composes of CoNbZr, SrTiO, and Cu/Cr films. The CoNbZr film was annealed in rotating and static magnetic fields to induce transverse magnetic anisotropy. Several sensors having 6, 10, 26, 36, and 50 mm slit widths were fabricated and evaluated from the phase and the amplitude of the transmission coefficient (S_{21}) measured by the network analyzer (Advantest Corp., R3767CG). In the measurement, the DC magnetic field of 0-20 Oe was applied to the longitudinal direction of the coplanar by a Helmholtz coil. The amplitude of S_{21} was improved about five times larger by employing the narrow slits. Although the changes of the amplitude and the phase by the magnetic field were small as the narrow slit, the maximum amplitude of S_{21} became large. Fig. 2 shows the sensor sensitivity versus the slit width. The sensitivity of the sensor was evaluated by assuming it to be proportional to the product of the phase and the amplitude gradients as the magnetic field and the carrier signal strength [3]. The appropriate slit width was around 10 mm for the coplanar line type thin film magnetic field sensor and the sensitivity will enhance more than 10 times higher than the sensor without slits [1]. However, it is expected that the sensor can get higher sensitivity by using amplitude modulation.

[1] S. Yabukami et al, J. *Magn. Soc. Jpn.*, Vol. 38, pp. 25-28 (2014) [2] T. Ishihara et al, *Journal of Magnetic of Japan*, vol. 6 (2022) [3] N. Horikoshi et al, *Journal of Magnetic of Japan*, vol. 29, pp. 472 (2005)

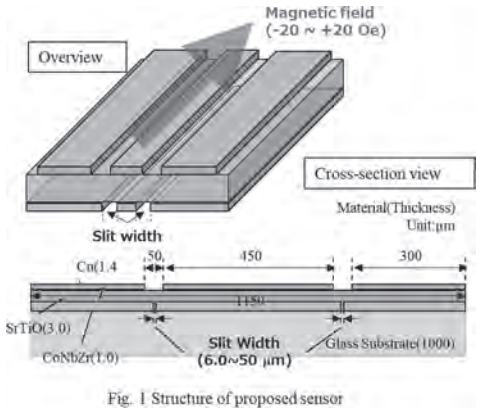

Fig. 1 Structure of proposed sensor

Fig. 1 Structure of proposed sensor

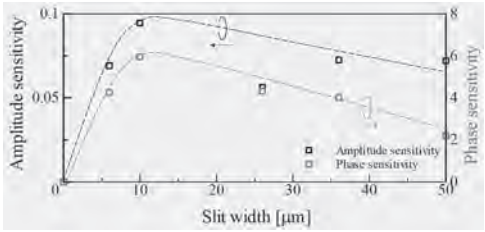

Fig. 2 Amplituden and phase sensitivities of sensor

OOA-05. Grain Structure Influence on Synchronized Two-Dimensional Spin-Hall Nano-Oscillator. *C.C. Capriata*[1] and B.G. Malm[1] *1. Division of Electronics and Embedded Systems, KTH Royal Institute of Technology, Stockholm, Sweden*

Two-dimensional synchronized arrays of Nanoconstriction Spin-Hall nano-oscillators (NC-SHNO) [1] have several promising features like higher power, better stability, and applications in neuromorphic computing [2-3]. For all these applications, the synchronization of the oscillator array is crucial. Oscillators are synchronized with the neighboring ones via dipolar and exchange coupling. In a recent study [4], NC-SHNO arrays were simulated under an injection locked condition and a one-dimensional array was investigated in [5]. Our previous study [6] demonstrated how local variations of the exchange coupling can induce multiple oscillation modes in single devices and cause variability in the oscillation frequency. In this study, the aim is to expand the modeling to free-running 2x2 and 4x4 synchronized arrays using the MuMax3 [7] micromagnetic simulator. Here, we illustrate results from the 2x2 array with 100 nm pitch and 50 nm width (Fig.1 inset). The exchange coupling is reduced to 15 % at a line in between the columns or rows. The presence of grains is equivalent to the coexistence of multiple lines and it is an expansion towards a real thin film representation. In this case, the exchange is randomly reduced to 10-30 % and assigned to each grain. Modifying the exchange coupling inside the array results in a minor shift of the synchronized frequency at low and medium currents while the array is much more disturbed at high currents, Fig.1. The phase and power analysis, Fig.2, shows that the shape of the oscillating volume is disturbed

by the presence of grains. At high current (3 mA), the excited mode becomes propagating while at lower currents it is localized and well phase synchronized. In general, disturbed oscillators can be synchronized column-wise or diagonally, the extreme case is only one device of the array delivering output power. Similar results have been found for the 2x2 array with 200 nm pitch and 120 nm width, highlighting that the phase synchronization is not always guaranteed or can be broken by local variations in the exchange coupling strength in some operating conditions.

[1]: V. E. Demidov, et al. "Nanoconstriction-based spin-Hall nano-oscillator", Appl. Phys. Lett. 105, 172410 (2014) [2]: A. Smith, et al. "Dimensional crossover in spin Hall oscillators", Phys. Rev. B 102, 054422 – Published 17 August 2020. [3]: M. Zahedinejad, et al. "Two-dimensional mutually synchronized spin Hall nano-oscillator arrays for neuromorphic computing", Nat. Nanotechnol. 15, 47–52 (2020). [4]: A. Houshang, et al. "Phase-Binarized Spin Hall Nano-Oscillator Arrays: Towards Spin Hall Ising Machines", Phys. Rev. Applied 17, 014003 – Published 3 January 2022. [5]: T. Kendziorczyk, at al. "Mutual synchronization of nanoconstriction-based spin Hall nano-oscillators through evanescent and propagating spin waves", Phys. Rev. B 93, 134413 – Published 11 April 2016. [6]: C. C. M. Capriata, et al. "Impact of Random Grain Structure on Spin-Hall Nano-Oscillator Modal Stability", IEEE Electron Device Letters, vol. 43, no. 2, pp. 312-315, Feb. 2022. [7]: J. Leliaert, et al. "Adaptively time stepping the stochastic Landau-Lifshitz-Gilbert equation at nonzero temperature: Implementation and validation in MuMax3", AIP Advances 7, 125010 (2017).

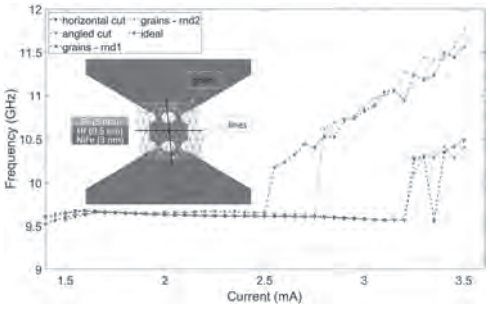

Frequency stability of 2x2 NC-SHNO array under different conditions.

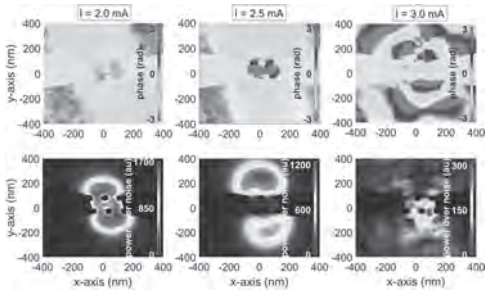

Phase and power plots at different operating conditions.

OOA-06. Investigation of signal and noise in symmetric response GMR under AC modulation. *Y. Higashi*[1], A. Kikitsu[1], Y. Kurosaki[1] and S. Shirotori[1] *1. Toshiba Corporation, Kawasaki, Japan*

High-sensitive Magneto-resistance (MR) sensors, for which it is easy to integrate to system, have attracted much attention to inspect Li ion battery and semiconductor circuit [1]. To improve the detectivity, it is effective to adopt an AC modulation system [2]. In the previous work, we have reported the origin of unique noise in symmetric response GMR under AC modulation [3]. Skirt noise, which is important to detectivity at low frequency, are caused by magnetic 1/f noise and the SNR strongly depends on modulation condition. In this paper, we investigated the dependence of signal and noise characteristics under AC modulation for enhancing the SNR. When the symmetric response GMR transfer curve, (R(H)), is modeled by Eq.(3) and magnetic field H consists of measurement field (H_m),AC and DC field for modulation (H_{ac} and H_b) and noise field (H_n) which is dependent to frequency, the output signal (S) and the noise (N) of GMR can be expressed as follows: $H=H_m*e^{-j\omega mt}+H_{ac}*e^{-j\omega act}+H_b+H_n$ (1) $H_n=\int H_n(f)df$ (2) $R(H)=a_4H^4+a_3H^3+a_2H^2+a_1H$ (3) $S=2H_mH_{ac}\{6a_4+(H_b+a_3/4a_4)^2+a_2-(a_3/4a_4)^2\}$ (4) $N=2H_n(f)H_{ac}\{6a_4+(H_b+a_3/4a_4)^2+a_2-(a_3/4a_4)^2\}$ (5) Figure1 shows the signal, noise and SNR as a function H_b. The dash line in Fig.1 represents the predicted signal (blue line) and noise (red line), which is obtained by Eq. (4) and (5) respectively. Each parameter (a_4~a_1) obtained from fitting transfer curve under modulation using Eq.(3). The signal is good agreement in the predicted signal, whereas below -36 A/m noise is reduced compared with the predicted noise. As a result, the maximum SNR is at -76 A/m. This result indicates adding H_b may reduce magnetic domain fluctuations. By optimizing the AC modulation conditions, we successfully realized a symmetric response GMR with 12pT/√Hz at 10Hz (Fig.2). This work was supported by the Cabinet Office (CAO), Crossministerial Strategic Innovation Promotion Program (SIP), "An intelligent knowledge processing infrastructure, integrating physical and virtual domains" (funding agency: NEDO).

[1] K. Kimura et al.: *J. Inst. Electr. Eng. Jpn*., vol. 135, no. 7, pp. 437–440, 2015. [2] W.Tian,et al., *IEEE Trans. Magn.,* vol. 52, Issure:2, Feb. 2016, Art. no. 4000306. [3] Y. Higashi et. al., Intermag 2022 IOC-12

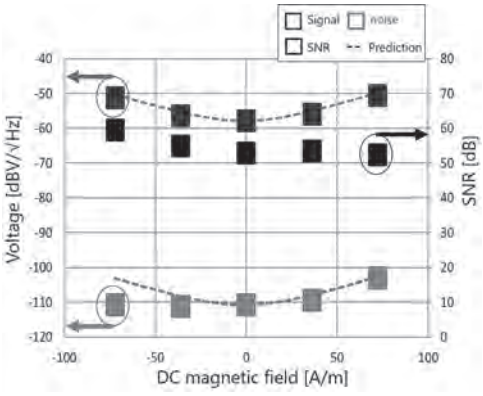

Fig.1 DC magnetic field dependance of signal, noise and SNR.

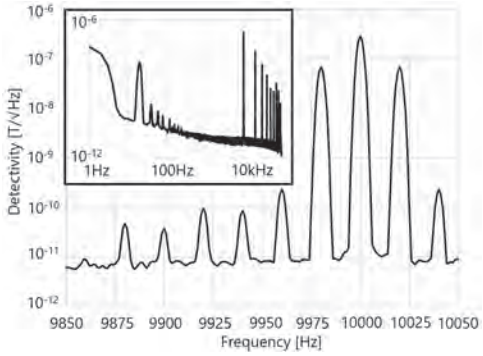

Fig.2 The noise equivalent magnetic field power spectral density. Measurement field is 111nT at 20Hz and modulation frequency is 10kHz.

OOA-07. Sensitivity Distribution Function of an AC Field Modulation GMR Sensor with Magnetic Field Concentrators. *A. Kikitsu*[1], Y. Higashi[1], Y. Kurosaki[1], S. Shirotori[1], T. Nagatsuka[2], K. Suzuki[2] and Y. Terui[2] *1. Toshiba Corp., Kawasaki, Japan; 2. Toshiba Nanoanalysis Corp., Yokohama, Japan*

INTRODUCTION A high-sensitive Giant Magneto-Resistance (GMR) sensor using an AC field modulation has been developed [1]. It was applied to a magnetic field microscope and imaged a magnetic field from a 150

μm Cu wire [2]. Employing large magnetic field concentrators (MFCs) is effective to increase the sensitivity but it accompanied by the degradation of the spatial resolution. In this study, the spatial resolution of the GMR sensor with MFCs was investigated by calculating the sensitivity distribution function (SDF). Comparison with the experimental results and optimized MFC designs are discussed. RESULTS AND DISCUSSION Magnetic field microscope system including a GMR sensor unit was the same as in the previous study [2]. Objective sample was a 150 μm Cu wire flowing an AC current. The sensor unit was faced to the sample and was scanned. The spacing was 1 mm. Figure 1 shows the magnetic field images by two sensor units with different MFC size. The double image was observed for a sensor with large MFCs. It was due to the large distance between two GMR elements. SDF was calculated according to the reciprocal theory using a finite element method. GMR elements were assumed as bar magnets magnetized along the short axis (sensing) direction. Magnetic properties of NiFe were used for MFCs. SFD is a magnetic field from the GMR elements along the sensing direction. Figure 2 shows a contour of the SFD in the x-z plane for the sensor with large MFCs (z: sample-sensor direction, x-y plane: sensor plane). The sensitivity shows two peaks at the sample-sensor distance of 1 mm and its FWHM is about 3/4 of the sensor unit length. This result corresponds to the experimental result shown in Fig.2. The analysis found that sharing the central MFCs was effective to reduce the spatial resolution with a small degradation of the sensitivity. This work was supported by the Cabinet Office (CAO), Cross-ministerial Strategic Innovation Promotion Program (SIP), "Intelligent Processing Infrastructure of Cyber and Physical Systems" (funding agency: NEDO).

[1] S. Shirotori et. al.: IEEE Trans. Magn., 57, 4000305 (2021) [2] A. Kikitsu et.al.: Joint MMM-Intermag 2022, IOF-07 (2022)

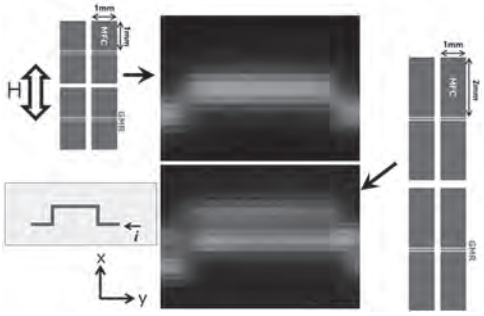

Fig.1 Magnetic field images observed by two types of the GMR sensor units.

Fig.2 SDF of the sensor with 2-mm MFC. Broken line indicates the sample-sensor distance of 1 mm.

OOA-08. Offset-free magnetic sensing principle and the role of the spin-orbit torque coefficients. *J.M. Salazar-Mejía*[1], S. Koraltan[1], C. Abert[1], F. Slanovc[1], P. Flauger[1], M. Agrawal[2], A. Satz[3], C. Schmitt[4], G. Jakob[4], M. Kläui[4], H. Brückl[5] and D. Suess[1] *1. Physics of Functional Materials, University of Vienna, Wien, Austria; 2. Infineon Technologies AG, Neubiberg, Germany; 3. Infineon Technologies Austria, Villach, Austria; 4. Institute of Physics, Johannes Gutenberg-University Mainz, Mainz, Germany; 5. Department für Integrierte Sensorsysteme, Universität für Weiterbildung Krems, Wiener Neustadt, Austria*

Nowdays magnetic field sensors rely on magnetoresistive effects (Suess, 2018). Commonly, such sensors are used in a Wheatstone bridge configuration, which in practice leads to a zero field offset due to fabrication tolerances and different temperature drifts. We propose a robust differential resistivity measurement on a single device with perpendicular anisotropy, which is situated on top of a heavy metal (HM). By applying charge current through the HM, spin-orbit torques (SOT) are induced on the magnetization. For currents under the switching threshold, the magnetization experiences small deviations from its initial out-of-plane state. From $+J$ and $-J$ currents, the induced SOT acts equally in opposite directions. When an external magnetic field is present, the SOT symmetry is broken and a distinct deflection occurs, see Fig.1 a. Consequently, by measuring the magnetization m_z component for both currents a transfer curve with zero-offset can be achieved, as illustrated in Fig.1 b. By macrospin simulations, we observe that intrinsic material parameters, such as the field-like and damping-like SOT coefficients play a key role on the magnetization dynamics (Abert, 2019). Thus, their accurate determination is crucial for correct simulation of the sensor performance. An analytical solution for the magnetization is used to predict the sensing output (Daoqian, 2020). To determine the SOT coefficients, a harmonic voltage analysis is performed. Finally, with an adequate set of parameters, micromagnetic simulations are performed using the LLG eqn., in parallel with experimental measurements, to design a sensor with zero-offset for industrial applications.

D. Suess, Bachleitner-Hofmann A., Satz A., et al. Nature Electronics Vol. 1, p. 362 (2018) C. Abert. European Phys. Journal B Vol. 92, p. 120 (2019) Z. Daoqian, C. Weishan. Phys. Rev. A Vol. 13, 044078 (2020)

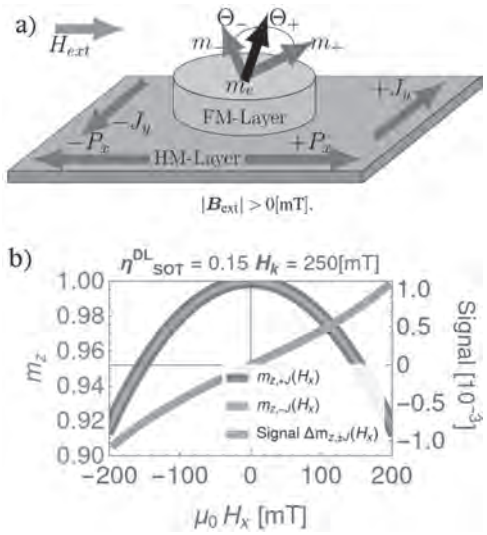

(a): Schematic of the sensor geometry. (b): Analytic solution of the sensor signal

OOA-09. Improved Permanent Magnet Geometry to Read Soft Magnetic Barcodes Using Magnetoresistive Sensors. *S. Abrunhosa*[1,2], I. Gibb[3], R. Macedo[1], E. Williams[3], P. Freitas[1,2] and S. Cardoso[1,2] *1. INESC MN, Lisbon, Portugal; 2. Instituto Superior Técnico, Universidade de Lisboa, Lisbon, Portugal; 3. MagVision Ltd., Frome, United Kingdom*

The possibility of burying soft magnetic barcodes under several layers of non-transparent material is opening new applications for magnetic reading heads, namely for secure labelling and recyclable packaging. Additionally, this technology is cheap and easily accessible in the form of laserjet toners. Prior work has demonstrated an implementation of a portable reading head that can read such barcodes through at least 1 mm of paper [1], which would ideally be extended to 2 mm. This scanning device uses a tunnel magnetoresistive (TMR) sensor, which is ideal to detect the small magnetic fields (few μT for typical reading distances) [2,3], and a disc-shaped permanent magnet to maximize the barcode signal during reading. However, the simultaneous use of TMR sensors and magnets requires careful optimization of the geometry and placement of the magnet. The field created to bias the barcode can also be detected by the sensor, lowering its sensitivity and preventing accurate reading. For typical TMR curves, the linear range limit along the sensitive direction (x axis) occurs for a magnetic flux density of 5 mT, a parameter that was used as a boundary for optimization. The usage of an axially symmetric magnet creates a region at sensor level where B_x is smallest. On the other hand, it must also create a magnetic flux density normal to the surface of the barcode (z axis) higher than its saturation (125 mT) when at a distance from the sensor higher than 2 mm. Based on these boundaries, we simulated the magnetic flux density created by diverse commercially available magnet geometries (N45 grade) at sensor and barcode levels using finite elements modelling (Figure 1). It is shown that the shape in use does not satisfy both criteria, but two others do while remaining small enough to be used in a portable device (diameter < 10 mm). We have also acquired scans with several shapes to obtain an experimental comparison of the different geometries.

[1] S. Abrunhosa et al., IEEE Transactions on Magnetics, accepted manuscript (2022) [2] A. Hirohata et al. Journal of Magnetism and Magnetic Materials, 509, p.166711 (2020) [3] S. Cardoso et al. Microsystem technologies, 20(4-5), pp.793-802 (2014)

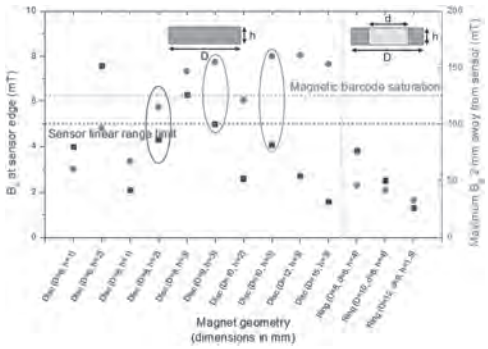

Fig. 1 – Comparison of the magnetic field components produced by different magnet geometries when the barcode is placed 2 mm away from the sensor. The geometry currently in use is highlighted in blue and the two new promising ones in green.

OOA-10. Thin Film Microstrip Line Type Probe with Slits and Permeability Measurement of Thick Magnetic Material. *S. Yabukami*[1], M. Sakamoto[1], J. Honda[1], Y. Watanabe[1] and K. Okita[1] *1. Graduate School of Biomedical Engineering, Tohoku University, Sendai, Japan*

The need to measure high-frequency magnetic permeability has increased due to the 5th generation mobile communication system. We developed a microstrip line-type probe and demonstrated comprehensive bandwidth permeability measurement up to 67 GHz [1]. For the permeability measurement of the thick magnetic sample, the demagnetizing effect caused the measurement error and the shift of the ferromagnetic resonance (FMR) [2-3]. In this study, a microstrip conductor with slits has been developed to enhance the current uniformity and reduce the demagnetizing effect in the thick magnetic material, as shown in Fig. 1 (a). This in-plane excitation decreased the demagnetizing effect. Fig. 1(b) shows the photograph of the microstrip line type probe with slits. The probe consists of a microstrip conductor (1.3 mm in total width) on a glass substrate and a ground plane. The 15 μm wide copper conductors (2 μm in thickness) and 15 μm wide gap were fabricated by lift-off process and rf sputtering. Also, the SMA connectors were connected with both input and output terminals. First, S_{21} is calibrated by applying a strong DC field (2 T) in the vertical direction of the high-frequency field to saturate the sample. Secondly, S_{21} is measured without a strong DC field. The complex permeability was optimized by the complex impedance and FEM analysis [2]. Fig. 2 shows the relative permeability of the NiZn ferrite sheet (3 mm x 1 mm, 100 μm thick). Measured permeability agreed well with the value of the Nicolson-Ross-Weir method [4]. The measurement point was 201 from 0.1 GHz to 20 GHz. 96% of the whole real part was within ±15%, and 92% of the entire imaginary part was within ±15%. We have demonstrated that this microstrip line type probe with slits can accurately evaluate thick magnetic material because the uniform current inside the microstrip conductor prevents the measurement error caused by the demagnetizing effect.

[1]S. Yabukami et. al., *IEEE Transactions on Magnetics*, Vol. 57, No. 2, 6100405 (2021). [2]S. Yabukami et al., *IEEE Transactions on Magnetics*, vol. 58, No. 2, 6100305 (2022). [3]K. Takagi et. al., *Journal of Magnetic of Japan*, vol. 46 (2022, in press). [4]A. M. Nicolson et. al., *Transactions on Instrumentation and Measurement*, vol. 19, no. 4, pp. 377-382 (1970).

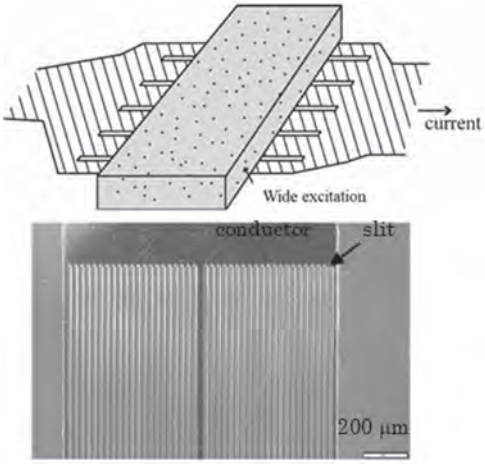

Fig. 1 Microstrip line type probe. (a) Schematic view of a microstrip conductor with slits and a thick magnetic sample. (b)Fabricated microstrip line type probe with narrow slits.

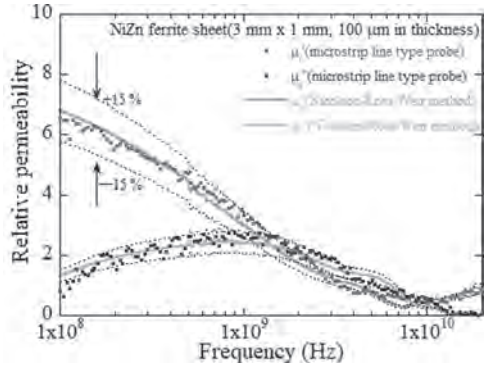

Fig. 2 Measured complex permeabilities of NiZn ferrite sheet (3mm x 1mm, 100 μm in thickness).

OOA-11. Development of a Magnetic Sensor Using Co:MgO Antidots.
Y. Ding[1], D.C. Lloyd[1] and *A. Hirohata*[1] *1. University of York, York, United Kingdom*

Current magnetic sensors have been used to detect position, angle, rotation and magnetic fields, based on three key types of technologies: Hall, anisotropic and giant magnetoresistance effects [1]. Hall sensors are made by patterning Silicon into a cross-bar, where sensitivity can be increased by replacing Si with compound semiconductors such as InAs and GaAs. However, these sensors suffer from large temperature dependence of their output in a finite magnetic field and have limitations in their working temperature range (between -40 and 120°C) as well as their detectable field range (between 10^{-2} and 10^{2} T). We have demonstrated a linear response in magnetisation under a small magnetic field (up to +/-50 mT) in an antidot structure consisting of ferromagnetic Fe nanoparticles dispersed in insulating MgO matrix [2]. In this study, we have adopted this system to replace ferromagnetic Fe dots with Co and have measured magnetisation dynamics. We co-deposited Co and MgO at the ratio of 2:1 by electron-beam evaporation on MgO(001) and (011) substrates in ultrahigh vacuum molecular beam epitaxy. The total film thickness was 30 nm. The films were *ex-situ* annealed at 400°C for up to 3 hours under vacuum. All the samples show very strong magnetic anisotropy, which is different from the Fe:MgO films previously reported [2]. The MgO[010] direction is found to be the easy axis, while the MgO[100] is the hard axis. The squareness is estimated to be 0.936 for the as-deposited film, improving up to 0.939 for the 3-h annealed film. Along the hard axis, the magnetisation curve shows almost linear response within ± 750 Oe, which is broader than that for the Fe:MgO films (± 500 Oe) [2]. This may indicate the Co nanoparticles dispersed in the MgO matrix are crystallised in fcc. with the epitaxial relationship of Co(001)[010]//MgO(001)[010] [3]. We will also report the results on the Co:MgO films grown on MgO(011) and discuss the steps towards the sensor applications.

[1] M. A. Khan *et al.*, *Eng. Res. Exp.* 3, 022005 (2021). [2] M. Rummey *et al.*, *IEEE Trans. Magn.* 48, 4010 (2012). [3] M. Hashimoto *et al.*, *J. Cryst. Growth* 166, 792 (1996).

OOA-12. Detecting Magnetic Fields with Printed Magnetoresistive Sensors on Rigid and Flexible Substrates.
E. Oliveros Mata[1], C. Voigt[2], X. Rui[1], M. Ha[3], G. Cañón Bermúdez[1], T. Kosub[1], I. Moench[1], Y. Zabila[1], R. Illing[1], Y. Wang[1], N. Valdez-Garduño[4], M. Fritsch[2], S. Mosch[2], M. Kusnezoff[2], J. Fassbender[1] and D. Makarov[1] *1. Helmholtz-Zentrum Dresden Rossendorf, Dresden, Germany; 2. Fraunhofer-Institut für Keramische Technologien und Systeme, Dresden, Germany; 3. Gwangju Institute of Science and Technology, Gwangju, The Republic of Korea; 4. Centro de Nanocencias y Nanotecnología, Ensenada, Mexico*

The development of functional printable materials enables the production of electronic components in unconventional materials and different form factors[1]. Here, we show magnetically sensitive inks/pastes based on magnetoresistive powder that can be printed via stencil, dispenser, or screen printing. We employ bismuth microparticles[2] as well as [Co/Cu], [Py/Cu],[3] and permalloy [4] flakes showing giant, anisotropic, or non-saturating large magnetoresistance, respectively. We demonstrate that magnetic field sensors based on various types of magnetoresistive flakes can be printed onto rigid, flexible, and deformable substrates. We employed block-copolymers and elastic binders to enable mechanical resilience of these sensors: they can withstand bending down to 16 µm, 100% of stretching, and bending for hundreds of cycles without losing functionality.[3] Additionally, by automatizing the dispenser printing process of bismuth-based pastes, we demonstrate the production of fully printed magnetic field sensors. The use of a micro-optically optimized high-power diode laser array provided a versatile approach for selective sintering of sensors over flexible foils in areas exceeding several square centimeters. In this work we experimentally confirm that such sensors retain their non-saturating magnetoresistive performance (MR = 146%) in high field conditions, allowing operation above 5 T. [2] Our printed magnetic field sensors can be used to create interfaces that are responsive to magnetic fields through remote human input. Being flexible, they can be laminated on the skin, or stuck onto any object, from a desk to a house wall. We demonstrate the capabilities of printed magnetic field sensors to work as an interface to navigate through digital maps, as input panels for smart home applications, and as interactive wallpapers.

[1] A. Kamyshny, S. Magdassi. *Chem. Soc. Rev.* Vol. 48, p.1712 (2019) [2] E.S. Oliveros-Mata, G.S. Cañón Bermúdez, M. Ha, et al. *Appl. Phys. A* Vol. 127, p.280 (2021) [3] M. Ha, G.S. Cañón Bermúdez, T. Kosub, et al. *Adv. Mater.* Vol. 33, p.2005521 (2021) [4] E.S. Oliveros-Mata, C. Voigt, G.S. Cañón Bermúdez, et al. *Adv. Mater. Technol.* p.2200227 (2022)

OOA-13. Optimization of MnIr growth for high temperature magnetic sensor operation.
P. Araujo[1,2], R. Macedo[1], S. Cardoso[1,2], D. Leitao[1] and P. Freitas[1,2] *1. Instituto de Engenharia de Sistemas E Computadores – Microsistemas e Nanotecnologias (INESC MN), Lisboa, Portugal; 2. Instituto Superior Técnico, Universidade de Lisboa, Lisboa, Portugal*

Magnetoresistive sensors provide many advantages for precise magnetic field detection while offering low power consumption and a small footprint [1]. In key industrial and automotive applications, it is also required to sustain temperatures that may reach ~200 °C [2]. Under these conditions, degradation of the pinning field strength can occur, affecting the magnetic reference of the sensor. Routes to enhance the thermal stability of the sensors include tuning the deposition conditions or material engineering of the thin film device [3, 4]. This work focus on developing a magnetic reference system able to sustain high temperatures. We have combined ion beam deposition (IBD) and magnetron sputtering to grow exchange biased bilayers and MgO magnetic tunnel junctions (MTJ). We took advantage of IBD growth for buffer layers based on Ru, Ta, and CuN. This was combined with magnetron sputtering of the magnetic layers, at different deposition pressures and deposition gas flux [fig 1A]. A clear dependence of exchange bias on temperature on such parameters is observed allowing us to tune the thermal stability and infer the temperature operation range in MTJ sensors. The blocking temperature (T_b) and its distribution were addressed for all samples showing that T_b can improve by 40 °C with optimized deposition conditions. The T_b value further improved using CuN/Ta multilayers as seed [fig 1B]. In MTJs, the width of the antiferromagnetic plateau – evaluated by (H_0^{+-}) [fig 2A] - is a critical operation parameter as it defines the field range on which the sensor has a magnetic reference. The dependence of Hex(T) and H0(T) will be discussed [fig 2B]. For optimized reference layers, plateaus of ~500 Oe are still present up to 300 °C supporting the suitability for high temperatures environments. These results support our approach based on the major role played by buffers and growth conditions. Acknowledgements: UID/0537/2020, PD/BD/150391/2019

[1] C. Zheng et al., *IEEE Transactions on Magnetics*, vol. 55, no. 4, pp. 1-30 (2019) [2] J. Iwata-Harms et al., *Scientific Reports*, vol. 8, no. 1 (2018) [3] H. Lv et al., *Journal of Magnetism and Magnetic Materials*, vol. 477, pp. 68-73 (2019) [4] X. Tang et al., *Journal of Magnetism and Magnetic Materials*, vol. 429, pp. 65-68 (2017)

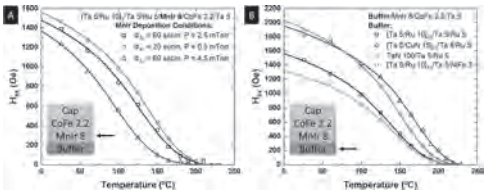

Fig. 1: Exchange bias field as a function of temperature, Hex(T), for [A] different deposition conditions of MnIr and [B] different buffer layers.

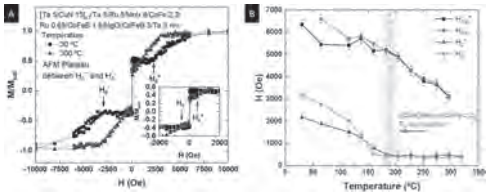

Fig. 2: Selected MTJ: [A] M(H,T) loops and [B] characteristic fields as a function of temperature.

Session OOB
MAGNETIC SENSORS AND DEVICES II
Atsufumi Hirohata, Chair
University of York, York, United Kingdom

INVITED PAPER

OOB-01. Surface Acoustic Wave based Resonant Magnetic Field Sensors with Ferromagnetic Layer as the Acoustic Waveguide.
C. Zhang[1] and T. Nan[1] *1. School of Integrated Circuits and Beijing National Research Center for Information Science and Technology (BNRist), Tsinghua University, Beijing 100084, China, Beijing, China*

Recently, resonant magnetic field sensors based on surface or bulk acoustic waves showed great potential in the detection of weak and low frequency magnetic field that can be useful for bio-magnetic applications. Their sensing mechanism can be understood as the ΔE effect (in ferromagnetic layer) induced resonance frequency shift in the mechanical resonant body. As a result, the design of the resonance mode and the acoustic wave propagation can greatly influence the sensitivity of the resonant magnetic field sensors. Here, we demonstrate ultra-sensitive Love wave mode surface acoustic wave magnetic sensors that utilize the sensing layer, a ferromagnetic metal, as the acoustic waveguide. The devices consist of a bulk $LiNbO_3$ single crystal as piezoelectric substrate, a thin SiO_2 as insulating layer, and a FeGaB film as the sensing and waveguide layer. By optimizing device structure, the maximum frequency shift of ~5.1 MHz was obtained at the magnetic anisotropy field with the acoustic resonance frequency of about 418 MHz at zero external magnetic field, which corresponds to a relatively high magnetic field sensitivity of ~0.9 MHz/mT. We also get a phase noise of -61 dBc/Hz@1 Hz which can lead to a low limit of detection. These results show the significant magnetic field sensitivity enhancement in resonant magnetic field sensors by the design of acoustic wave propagation.

[1] A. Kittmann, P. Durdaut and S. Zabel, Scientific Reports, 8(1), 278 (2018) [2] X. Liu, B. Tong and J. Ou-Yang, Applied Physics Letters, 113(8), 082402 (2018)

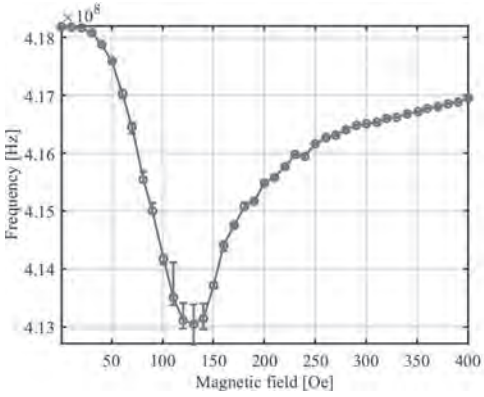

Fig. 1. Frequency shifts of the sensor versus an external magnetic field along the hard axis.

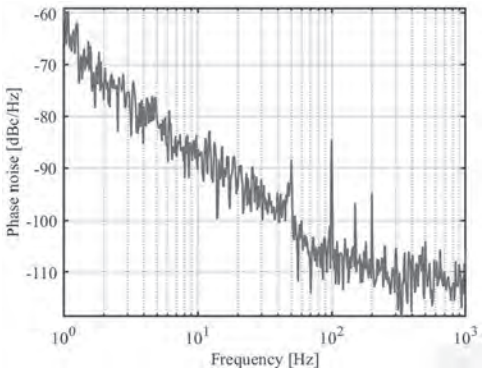

Fig. 2. Phase noise of the sensor versus offset frequency.

CONTRIBUTED PAPERS

OOB-02. Integration of hard magnetic layer in MEMS process.
S. Cuccurullo[1], G. Pavese[1], A. Plaza[1], O. Koplak[1], F. Maspero[2] and R. Bertacco[1] *1. Physics, Politecnico di Milano, Milano, Italy; 2. DICA, Politecnico di Milano, Milano, Italy*

Permanents magnets, or hard ferromagnets, provide a "free" source of magnetic field, with no need of external power. Considering the integration with microsystems, permanent micromagnets are critical components for the fabrication of microscale motors, generators, switches, pumps, acoustic speakers and energy harvester. Even though the understanding of magnetism and magnetic materials has led to advancements in their magnetic properties [1], the application of permanent magnets in microsystems is still limited. The reasons for that are: i) the methods for magnet fabrication at the macroscale (casting and powder processing) are fundamentally different to thin-film microfabrication approaches (physical vapor deposition, chemical vapor deposition, electrochemical deposition); ii) even if microfabrication approaches are exploited, difficulties remain in depositing thick magnetic films (> 1 μm) and issues due to process compatibility [2]. In this work, we present a process to integrate MEMS (MicroElectroMechanical Systems) and thick permanent magnets. We have designed test structures (Fig. 1) and optimized a process to fabricate the devices. The optimizations concern: i) deposition of a micron-thick layer of a magnetic material; ii) thermal treatment to enhance the magnetic characteristics of the material; iii) patterning technique employed to obtain micromagnets; iv) introduction of a passivation layer to protect the material from the subsequent process steps. An image of the final fabricated device is shown in Fig.2. Examples of application of said process to devices for energy harvesting and magnetic sensing will be discussed.

M. Sagawa, S. Fujimura, N. Togawa, Journal of Applied Physics, Vol. 55, p. 2083 (1984) D. P. Arnold, N. Wang, Journal of microelectromechanical systems, Vol. 18, p.1255 (2009)

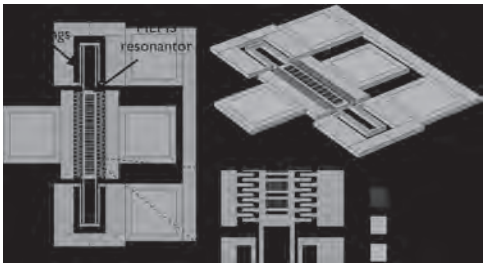

Fig. 1: 3D image of the test device.

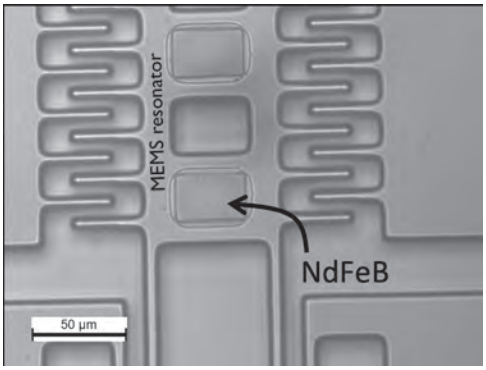

Fig. 2: Image at the optical microscope of the fabricated device.

OOB-03. Superparamagnetic ferrite film based RF inductors: on-chip integration and enhanced performance. *S. Arackal*[1], R. Kahmei[1], N. Bhat[1], S.A. Shivashankar[1] and R. Sai[1,2] *1. Centre for Nano Science and Engineering, Indian Institute of Science, Bengaluru, India; 2. Tyndall National Institute, Cork, Ireland*

The era of 5G and IOT demands on-chip RF inductors being operated beyond 10 GHz – inciting a demand of CMOS integrable and low-lossy magnetic-core with resonance behavior well above the said operating frequency. Our previous work demonstrated a significant enhancement of inductance (13%) for C-band inductors with spinel ferrite thin films core deposited by a CMOS-compatible microwave-assisted solvothermal (MAS) process. However, the efficacy of Zn-ferrite and MnZn-ferrite so deposited is limited due to their low permeability and lower resonance frequency, respectively[1,2]. Nanocrystalline Ni-based ferrites are deemed to be a better choice. But, the difficulty in integrating a thicker (>1 μm) Ni-ferrite film on-chip seems unachievable owing to the chemical nature of the supported Ni-precursors that can be used in MAS process. In this paper, we report an optimized MAS process recipe for Ni-ferrite (NF) and NiZn-ferrite (NZF) films with thickness >2 μm. Furthermore, we developed a wet etching process to pattern the deposited ferrite layers on silicon. We also report a thorough pan-wafer analysis of inductance enhancement comprising 11 inductors. The structure and composition of the films were characterized by XRD, SEM, EDS, and Raman spectroscopy. Detailed magnetic measurements (both DC and high-frequency) suggest that both deposited films are superparamagnetic and show superparamagnetic resonance frequency as high as 25 GHz[3]. The performance of NF and NZF film cores is investigated using on-chip inductors with self-resonating frequencies in the S, C, and X bands. To facilitate proper measurements, we further optimized a wet etch recipe to pattern the ferrite film to expose the contact pads (Fig. 1b). Inductors that are integrated with NF and NZF cores show an increase in inductance of about 35% and a Q-factor of about 17% (Fig. 2) – more than 2-fold increase compaired to previous reports.

[1] R. Sai, S.D. Kulkarni, M. Yamaguchi, N. Bhat, and S.A. Shivashankar, IEEE Magn. Lett. 8, 1 (2017). [2] R. Sai, R.D. Ralandinliu Kahmei, S.A. Shivashankar, and M. Yamaguchi, IEEE Trans. Magn. 55, 1 (2019). [3] S. Arackal et al., Manuscript under review

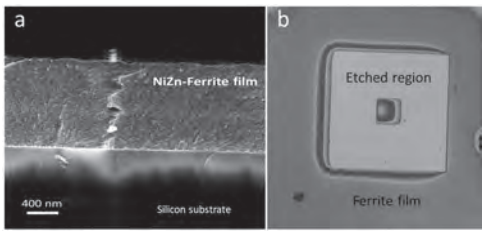

Fig. 1 (a) Cross-sectional SEM of NZF on silicon. (b) Etched ferrite film using the optimized recipe.

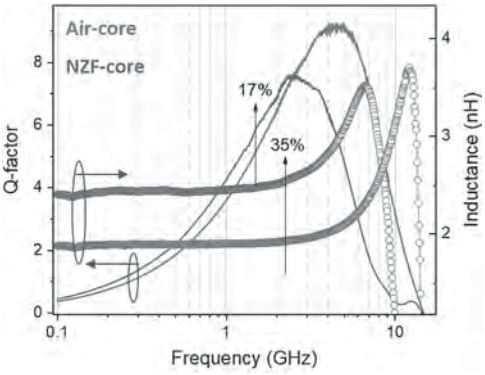

Fig. 2: Inductance and Q-factor improvement for NZF-core RF inductor.

OOB-04. Self-resonant frequency of inductors for quantification of magnetic nanoparticles. *J.L. Marqués*[1], M. Salvador[1], J.C. García-Martínez[1], P. Fernández-Miaja[2], A. García[3] and M. Rivas[1] *1. Physics, Universidad de Oviedo, Oviedo, Spain; 2. Electrical Engineering, Universidad de Oviedo, Gijón, Spain; 3. Electricity and Electronics, UPV, Bilbao, Spain*

The usage of antibody selective biding for the detection of biomolecules provides a fast and low-cost testing platform. The most common type of antibody selective biding bio-detection tags the bio-molecule of interest with a visual marker. An example of this type of bio-detection is the lateral flow immunoassays like the pregnancy or rapid COVID tests [1]. These visual nanotags are a valid solution for binary detection in high concentrated samples. To have a quantifiable and high sensitivity bio-sensing we use magnetic nanoparticles. The measurements of this type of magnetic nanotags require expensive laboratory equipment. A novel method using the self-resonant frequency (SRF) of inductors allows high sensitivity with low-cost and portable systems. Using the equivalent impedance calculation [2] and the Lichtenecker's mixing formulas [3] we extracted an analytic simplification to describe the relation between masses of nanomaterial in the sensing area to variations of the SRF of the inductor. The model correlates variations of the refraction index of the nanotag making the technique able to quantify not only magnetic nanotags but other types of nanomaterials like gold or latex. The mathematical model and its simplifications are tested against electromagnetic simulations and experimental measurements. These verifications demonstrate the validity of the model, the value of magnetic nanoparticles as nanotags for precise quantification, and the advantages of the SRF measuring method for low-cost, high-sensitivity systems.

1] Moyano, A. et al., 2020. Magnetic Lateral Flow Immunoassays. *Diagnostics.* [2] Qin Yu. et al., 2002. RF Equivalent Circuit Modeling of Ferrite-Core Inductors and Characterization of Core Materials. [3] A.V. Goncharenko. et al., 1999. Lichtenecker's equation: applicability and limitations.

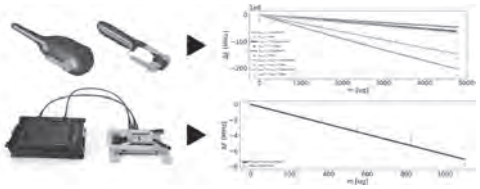

OOB-05. Method for Measuring Magnetic Susceptibility of Magnetic Nanoparticles up to Millimeter-Wave Frequency Range. *Y. Pu*[1], Y. Watanabe[3], L. Ton That[2], T. Murayama[3], K. Okita[3] and S. Yabukami[1] *1. School of Enginneering, Tohoku University, Sendai, Japan; 2. Graduate School of Enginneering, Tohoku University, Sendai, Japan; 3. Graduate School of Biomedical Engineering, Tohoku University, Sendai, Japan*

Susceptibility measurement of magnetic nanoparticles (MNPs) in radio frequency (RF) has been widely studied. However, most of the studies only examined frequencies up to 20 GHz [1]. In addtion, applying two axial DC fields to increase resonance in specific frequency range and magnetic susceptibility has hardly been done before, since applying a single static DC field is more common [2-3]. The MNPs can be used for magnetic hyperthermia and biological substances detection [4-6]. In this study, we proposed a novel method for measuring magnetic susceptibility by a broadband microstrip line type probe up to 67 GHz [7]. Fig. 1 shows the basic principle of the experimental setup. The microtube with MNPs (SVM-025-5H, 200 nmf, about 300 ml) was put on the microstrip line type probe, which is connected with a network analyzer (N5227A) to generate a magnetic field in a range of 10 MHz to 67 GHz. The MNPs were put between two electromagnets connected with power supplies to generate a changeable DC field up to 1000 Oe and another orthogonal about 35 Oe DC field. When the two orthogonal DC fields are around equal, the magnetic susceptibility of MNPs should maximize because of the magnetic switching theory [8], which results in enhancing the signal to noise ratio. By applying the bias magnetic field, we measured the transmission coefficient, S_{21}, of the microstrip line type probe and obtained magnetic susceptibility [7]. Fig. 2 shows the magnetic susceptibility when the DC field ranges from 0 Oe to 1000 Oe. In the DC field around 0 Oe, the magnetic susceptibility was very low because the MNPs were relaxed. However, in the DC field of 25 Oe-75 Oe, we observed clear magnetic resonances in 20 - 40 GHz. The resonance frequency increased as the DC field increased. In this case, both fixed and changeable DC fields are around 35 Oe, which means the magnetic susceptibility is biggest at this condition and the orthogonal DC field enhance the signal to noise ratio to detect magnetic nanoparticle. The clear magnetic resonance of MNPs has hardly been observed in this broad bandwidth up to 67 GHz before.

[1] B. K. Kuanr, V. Veerakumar and K. Lingam, *Journal of Applied Physics*, Vol. 105 (2009). [2] M. Jadav, S. P. Bhatnagar, *IEEE Transactions on Magnetics*, Vol. 56, p. 1-8 (2020). [3] P. C. Fannin, I. Malaescu and C. N. Marin, *The European Physical Journal E*, Vol. 27, p. 145-148 (2008). [4] A. Shikano, L. Tonthat, *Transaction of the Magnetics Society of Japan Special Issues*, Vol. 6, p. 100-104 (2022). [5] S. Yabukami, T. Murayama and S. Takahashi, *IEEE Transactions on Magnetics*, Vol. 58, 6100305 (2022, in press). [6] T. Yoneyama, A. Kuwahata and T. Murayama, *IEEE Transactions on Magnetics*, Vol. 58 (2022, in press). [7] S. Yabukami, C. Iwasaki and K. Nozawa, *IEEE Transactions on Magnetics*, Vol. 58, No. 2, p. 1-5 (2022). [8] S. Iida, Y. Sakurai and S. Iwasaki, *Magnetic Thin Film Engineering*, p. 143 (1977).

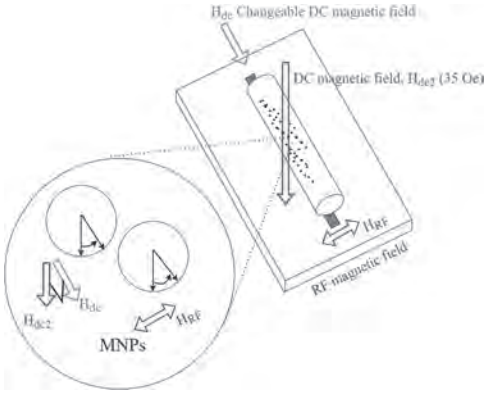

Fig. 1 Basic principle of the experimental setup.

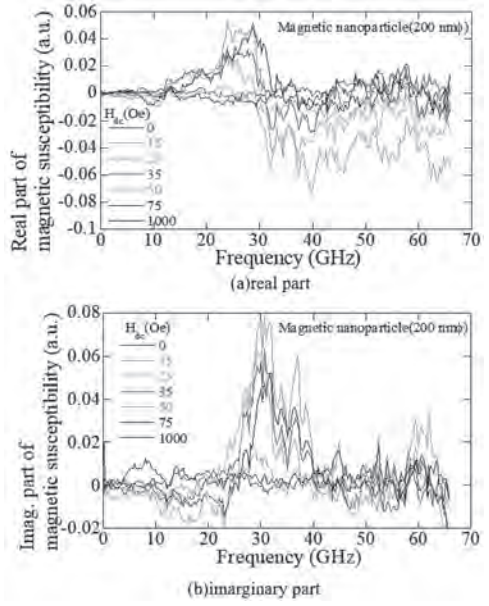

Fig. 2 Magnetic susceptibility of the magnetic nanoparticle (200 nmf).

OOB-06. Creep-induced Magnetic Anisotropy of Nanocrystalline Wire as a Core of Fluxgate Sensor. *D. Hrakova*[1] and P. Ripka[1] *1. Faculty of Electrical Engineering, Czech Technical University in Prague, Prague, Czechia*

One of the most important parts of a fluxgate sensor is the magnetic core. This work is dedicated to the study of fluxgate sensors based on the nanocrystalline wire as a core and comparing them to the performance of amorphous wire with chemical composition $(Co_{94}Fe_6)_{75}Si_{15}B_{10}$ [1]. Both wires were manufactured by the Institute of Technical Physics, Iasi, Romania. Compared to the previous studies on nanocrystalline materials, we demonstrate that proper processing of nanocrystalline alloys can bring sensors with properties comparable to the traditionally used amorphous alloys, but with better stability at elevated temperatures. The amorphous $Fe_{73,5}Si_{13,5}B_9Cu_1Nb_3$ master alloy wires 0.5m in length, and 0.12 mm in diameter were annealed by DC pulse to achieve the nanocrystalline structure. Contrary to other researchers we found problems with surface oxidation in air, so our annealing was performed in Argon. During the annealing and cooling, we applied mechanical stress to achieve transverse anisotropy. The character of changing H_c varies depending on tension as shown in Fig.1. Higher tension increases anisotropy and reduces the longitudinal permeability (Fig. 2). Best results were shown by wires annealed under tension 9 g and 13 g with the current in the range 485 mA up to 510 mA. In these cases, coercivity was in the range of 7 A/m up to 17 A/m at 1 kHz. Annealed wires were used as

a core for fluxgate sensors of the Förster and Vacquier types and with ring core. As an example, Förster type sensor with amorphous (H_c = 20 A/m) wire as a core had max. sensitivity of 0.88 V/mT and min. the noise of 164pT/√Hz at 1 Hz. By using nanocrystalline wire with Hc = 17A/m we achieved lower sensitivity (0.7 V/mT) but lower noise (111 pT/√Hz). The nanocrystalline core with lower H_c (9 A/m) had higher sensitivity (1.1 V/mT) but higher noise (204 pT/√Hz) compared to the amorphous core. And the core with Hc = 13A/m had almost the same results as the amorphous wire. This study was supported by the Grant Agency of the Czech Republic within the Nano-fluxgate project (GACR GA20-27150S).

[1] P. Ripka, D. Hrakova, "Multiwire Parallel Fluxgate Sensors", IEEE Transactions on Magnetics. 2022, 58(2), 1-5. ISSN 0018-9464. DOI 10.1109/TMAG.2021.3093017 [2] Y.-F. Li, M. Vazquez, D.-X. Chen, "Circular magnetization process of nanocrystalline wires as deduced from impedance measurements", Journal of Applied Physics 97, 124311 (2005)

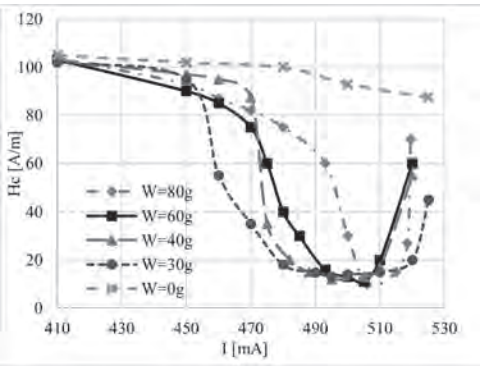

Fig. 1 – Tension dependence, 1kHz, 10V

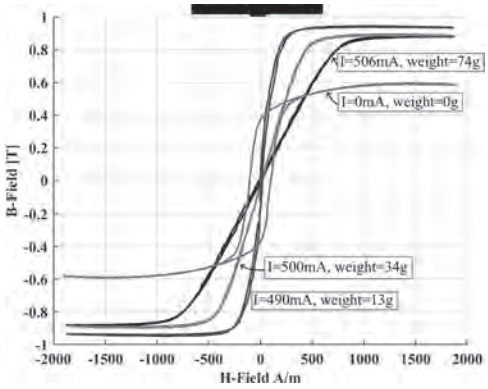

Fig. 2 – BH loop of the core, 1kHz, 10V

OOB-07. Multiple-wire orthogonal fluxgate with cross-spectrum noise suppression. *M. Butta*[1], M. Dressler[1] and M. Janosek[1] *1. Faculty of Electrical Engineering, Czech Technical University in Prague, Prague, Czechia*

Traditionally orthogonal fluxgates have been based on multiple amorphous magnetic wires [1] to achieve larger sensitivity compared to a sensor based on a single wire. Typically the pick-up coil surrounds all the wires and collects the total flux from all them. In this work we tried a different approach: we used single coils with smaller diameter (1.8 mm) wound on each magnetic wire instead of a large coil (7 mm) surrounding all wires. The first step was to compare the noise achieved with the small coils around the single wires to the noise obtained with the traditional large coil used for multiple wires. Contrary to common believe [2], we found out that the noise level was similar both with the large and the small coil. This shows that we can make use of the multiple small coils each wound around each wire (instead of using a single coils around all the wires) without increasing the noise. This paves the way to new methods of extracting the signal from the fluxgate: in this work we reduced the noise by using two magnetic wires in series (sharing the same excitation current, 50 mA dc over 50 mA ac at 42 kHz) and we demodulated the output voltages of the two small pick-up coils around the single wires with two synchronous demodulators. Then we calculated the cross-spectrum of the signals from the two wires. The main idea is that both wires will be exposed to the same magnetic field, thus the signal will be strongly correlated, whereas the noise will be generally uncorrelated. By taking the the cross-spectrum we keep only the correlated part (measured field) and we suppress the noise. We found that even if the wires are very close (3.8 mm apart) unexpectedly the coherence of the noise was below 10% for frequency above 3 Hz. This allowed us to decrease the noise floor from 750 to 300 fT/√Hz in the cross-spectrum (Fig.1), with a noise reduction ratio of more than 2, which cannot be achieved by a single coil wound around both wires even if the noise were totally uncorrelated. Moreover, such noise reduction is achieved without increasing the size of the sensor.

[1] K. Goleman and I. Sasada, "A Triaxial Orthogonal Fluxgate Magnetometer Made of a Single Magnetic Wire With Three U-Shaped Branches," in IEEE Transactions on Magnetics, vol. 43, no. 6, pp. 2379-2381, June 2007 [2] D. Scouten, "Sensor noise in low-level flux-gate magnetometers," in *IEEE Transactions on Magnetics*, vol. 8, no. 2, pp. 223-231, June 1972

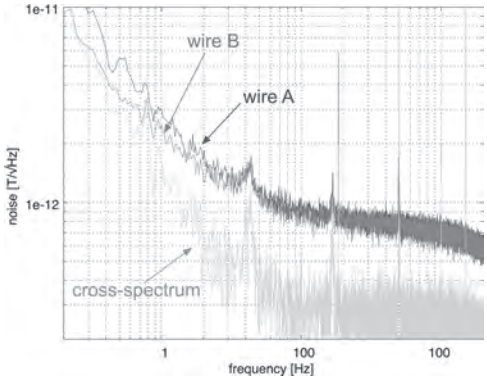

Fig. 1 Power spectral density of the noise of the voltage demodulated from the two pick-up coils wound around the two single wires and their cross spectrum.

OOB-08. Skin-conformal magnetoreceptors for human-machine interaction. *P. Makushko*[1,2], E. Oliveros Mata[1], G. Cañón Bermúdez[1], M. Hassan[3,4], S. Laureti[3], C. Rinaldi[5], F. Fagiani[5], G. Barucca[4], Y. Zabila[1], J. Fassbender[1], I. Vladymyrskyi[2], M. Albrecht[6], G. Varvaro[3], X. Rui[1] and D. Makarov[1] *1. Institute of Ion Beam Physics and Materials Research, Helmholtz-Zentrum Dresden-Rossendorf e.V., Dresden, Germany; 2. Paton Institute of material Science and Electric Welding, National Technical University of Ukraine "Igor Sikorsky Kyiv Polytechnic Institute", Kyiv, Ukraine; 3. Istituto di Struttura della Materia, Consiglio Nazionale delle Ricerche, Roma, Italy; 4. Dipartimento SIMAU, Università Politecnica delle Marche, Ancona, Italy; 5. Department of Physics, Politecnico di Milano, Milano, Italy; 6. Institute of Physics, University of Augsburg, Augsburg, Germany*

Artificial magnetoception, i.e., electronically expanding human perception to detect magnetic fields, is a new and yet unexplored route for interacting with our surroundings. This technology relies on thin, soft, and flexible magnetic field sensors, dubbed magnetosensitive electronic skins (e-skins) [1]. These devices enable reliable and obstacle insensitive proximity, orientation and motion tracking features [2, 3] as well as bimodal touchless-tactile interaction [4]. Although, basic interactive functionality has been demonstrated, the current on-skin magnetoreceptors are not yet employed as advanced spintronics-enabled switches and logic elements for skin compliant electronics. The major limitation remains primarily due to the use of in-plane magnetized layer stacks. The predominant in-plane sensitivity prevents these devices from becoming intuitive switches or logic elements for

interactive flexible electronics, as the natural actuation axis of switches is out-of-plane. Here, we will introduce current technologies towards realization of skin-conformal magnetoelectronics for touchless and tactile interactivity in virtual and augmented reality. The focus will be put on the fabrication of on-skin spin valve switches with out-of-plane sensitivity to magnetic fields [5]. The device is realized on a flexible foil relying on Co/Pd multilayers with perpendicular magnetic anisotropy and synthetic antiferromagnet as a reference layer. Owing to the intrinsic tunability, these interactive elements can provide fundamental logic functionality represented by momentary and permanent (latching) switches and reliably discriminate the useful signals from the magnetic noise. The flexible device retain its performance upon bending down to 3.5 mm bending radii withstand more than 600 bending cycles. We showcase the performance of our device as on-skin touchless human-machine interfaces, which allows interactivity with a virtual environment, based on external magnetic fields. We envision that this technology platform will pave the way towards magnetoreceptive human-machine interfaces or virtual- and augmented reality applications, which are intuitive to use, energy efficient, and insensitive to external magnetic disturbances.

[1] G. S. C. Bermúdez, & D. Makarov, Advanced Functional Materials 31, 2007788 (2021). [2] M. Melzer, M. Kaltenbrunner, D. Makarov, D. Karnaushenko, D. Karnaushenko, T. Sekitani, T. Someya, and O. G. Schmidt, Nature Communications 6, 6080 (2015). [3] G. S. C. Bermúdez, H. Fuchs, L. Bischoff, J. Fassbender, and D. Makarov, Nature Electronics 1, 589 (2018). [4] J. Ge, X. Wang, M. Drack, O. Volkov, M. Liang, G. S. C. Bermúdez, R. Illing, C. Wang, S. Zhou, J. Fassbender, M. Kaltenbrunner, D. Makarov, Nature Communications 10, 4405 (2019). [5] P. Makushko, E. S. O. Mata, G. S. C. Bermúdez, M. Hassan, S. Laureti, C. Rinaldi, F. Fagiani, G. Barucca, N. Schmidt, Y. Zabila, T. Kosub, R. Illing, O. Volkov, I. Vladymyrskyi, J. Fassbender, M. Albrecht, G. Varvaro, and D. Makarov, Advanced Functional Materials 31, 2101089 (2021).

OOB-09. Development of an Auto-Oriented Circulator Based on Hexaferrite Materials in the 5G Frequency Band. *R. Mansour*[1], Z. Riah[1], S. Clevers[2], V. Nachbaur[2], M. Jean[2] and S. Jouen[2] *1. IRSEEM, ESIGELEC, Rouen, France; 2. GPM, Université de Rouen, Rouen, France*

Ferrite-based junction circulators [1,2] are microwave devices made of at least three ports that have been widely used in emission/reception applications ensuring an isolation between the incoming and outgoing signals. They are especially useful in single antenna applications where signals are being transmitted and received simultaneously. Conventional circulators are based on a ferrite disk, magnetized to saturation, placed under the central conductor ensuring electromagnetic waves to propagate in a non-reciprocal manner. The external magnetic field allowing this saturation is provided by a permanent magnet positioned right above of the central conductor. Due to the size, weight, cost of these systems and the fact that high frequency applications are recently the main concern, the miniaturization of the circulator is inevitable. This can be achieved using self-biased hexagonal ferrite materials [3,4] which eliminates the use of a permanent magnet. These self-polarized materials, suitable for high frequency applications, are pellets made out of hexaferrite powder pressed and sintered. During pressing, the orientation of the particles should be achieved in the remanence state using an external magnetic field. In order to avoid the application of a magnetic field during pressing, and thus to minimize the cost of manufacturing circulators, we propose to design and manufacture circulators based on hexaferrite particles in the form of platelets. It has been shown that this platelet shape, as shown in Fig. 1, induces a self-alignment of the crystals with the particles orienting themselves spontaneously, therefore dropping the application of an external magnetic field in any way. This material will be then characterized using a coaxial cell capable of determining its dielectric and magnetic properties such as the permittivity and the permeability [5]. The values obtained will then be used in the simulation of a coplanar circulator [6,7], that operates in the 5G band especially around 28 GHz, using HFSS simulator.

1. H. Bosma, *IEEE Transactions on Microwave Theory and Techniques*, Vol 12(1), p. 61-72 (1964). 2. Y. S. Wu and F. J. Rosenbaum. *IEEE Transactions on Microwave Theory and Techniques* Vol 22(10), p. 849-856 (1974). 3. N. Zeina, H. How, C. Vittoria, In *1992 IEEE International Magnetics Conference (INTERMAG)*, pp. 458-458 (1992). 4. N. Noutehou, C. Patris, D. Névo, Circulateur planaire ultra-compact en bande Q." In *JNM* (2019). 5. F. Costa, M. Borgese, M. Degiorgi, In *Electronics*, Vol 6(4), p. 95 (2017). 6. O. Zahwe,H. Harb and H. Nasrallah, *Int. Arab J. Inf. Technol.*, Vol 16(3A), p.600-608 (2019). 7. R. El Bouslemti,F. Salah-Belkhodja and Y. H. A. Fekhar, *Revue Méditerranéenne des Télécommunications*, Vol 4(1) (2014).

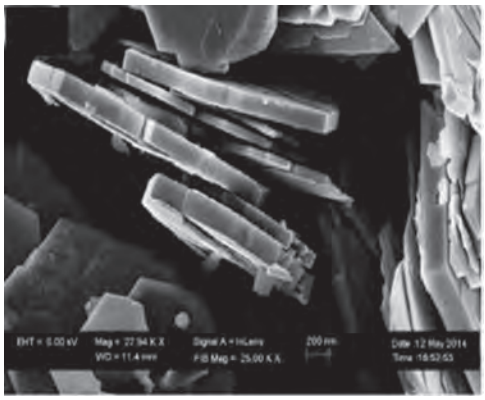

Fig.1. Hexaferrite particles in the form of platelets after moderate pressing of the powder.

OOB-10. Ferromagnetic shape memory alloy-based SAW resonator towards magnetic field sensor application. P. Kumar[1] and *D. Kaur*[1] *1. Physics, Indian Institute of Technology, Roorkee, Roorkee, India*

Surface acoustic wave (SAW) devices have been of significant interest in the modern electronics industry for wide applications such as radio frequency (RF) components in high-frequency devices, resonators, filters and sensors. The small size and remote operation of SAW devices make them robust for their use in extreme environmental conditions. In the present study, a novel highly magnetostrictive ferromagnetic shape memory alloy (FSMA) interdigital transducers (IDTs) have been fabricated over AlN piezoelectric layer in the surface acoustic wave (SAW) resonator. The influence of an external magnetic field on the fabricated SAW device has been investigated in terms of device parameters such as resonance frequency (f_R), frequency shift and electro-mechanical coupling coefficient (K^2). A resonance frequency of ~ 2.258 GHz was observed at 0 Oe and a frequency shift ~ 89 MHz occurs at 1350 Oe. The present device shows high tunability ~ 3.9 %. It could be ascribed to the strain-induced giant delta E-effect in the highly magnetostrictive Ni-Mn-In layer at room temperature. The experimental results have been fitted with a modified Butterworth-Van Dyke (mBVD) circuit model to extract the equivalent circuit parameters in the absence and presence of the magnetic field. A maximum electromechanical coupling coefficient was calculated to be ~ 0.58, which decreases to 0.35 with the magnetic field. The fabricated SAW resonator displays a high sensitivity of ~ 0.66 Hz/nT. Such magnetostrictive FSMA IDTs based tunable SAW resonator could be a potential candidate for room temperature remote magnetic field sensors and multifunctional MEMS devices.

[1] J. G. Rodríguez-Madrid et al., IEEE Electron Device Lett., vol. 33, no. 4, pp. 495–497, 2012. [2] V. Schell et al., Appl. Phys. Lett., vol. 116, no. 7, Feb. 2020. [3] S. Pawar et al., IEEE Electron Device Lett., vol. 41, no. 2, pp. 280–283, 2020. [4] X. Liu et al., Appl. Phys. Lett., vol. 114, no. 6, 2019.

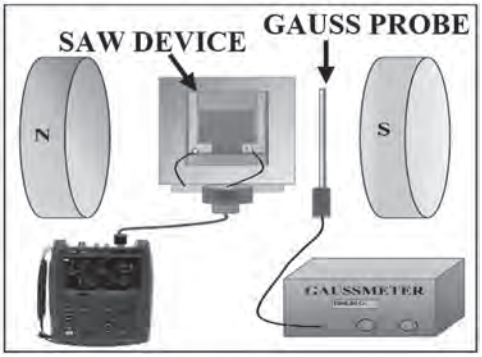

Fig. 1 Schematic of measurement setup to characterize the SAW resonator with VNA.

Session OPA
MAGNETIC SENSORS AND DEVICES III
(Poster Session)

Diana Leitao, Chair
Eindhoven University of Technology, Eindhoven, Netherlands

OPA-01. Electrical compact modelling of GMR devices for neuromorphically inspired sensors. A. Ghilas[1], C. Reig[1], M. Cubells-Beltran[1], F. Pardo[2], J.A. Boluda[2], F. Vegara[2], S. Abrunhosa[3] and *S. Cardoso*[3] *1. Electronic Engineering, University of Valencia, Burjassot, Spain; 2. Computer Science, University of Valencia, Burjassot, Spain; 3. INESC-MN, Lisbon, Portugal*

Due to their inherent characteristics regarding sensitivity and flexible design, Giant Magnetoresistance (GMR) based sensors are the preferred option for the measurement of low magnetic fields within small volumes (electronic compass, bio-magnetism, non-destructive testing…) [1]. In addition, GMR devices have demonstrated their compatibility with different standard technologies (such as CMOS) and other emerging ones (such as microfluidics) [2], so broadening their fields of application. For example, GMR sensors have been successfully used as currents sensors in integrated circuits and also as bio-detectors for different specimens in Lab-on-chip systems. More recently, GMR elements have been proposed as basic detectors in neuromorphicaly approached magnetic field imaging sensors, for potential applications in biotechnology and testing. The design and optimization of this kind of system demand electrical models which are compatible with conventional microelectronics design tools [3]. In this sense, partial solutions have been proposed, providing static, noise and thermal models, mainly for discrete components applications in electrical current sensing [4]. In this work, the development of a compact dynamic electrical model for GMR sensors is described. The Verilog-A high-level description language has been considered in order to provide a useful model for being used in conventional CMOS design tools, such as Cadence Virtuoso. The model includes the proper blocks for alternate current and transient analysis, which are mandatory by the high speed related to the design of neuromorphicaly approached imaging sensors. Functional parameters were obtained from specifically designed sensors including single resistors, voltage dividers and full bridges (see Fig. 1). The schematic of the model for the single resistor sensor is depicted in Fig. 1. Fig. 2 displays preliminary impedance results comparing experimental measurements with model-predicted behaviour for a frequency sweep in the range of interest. Fig. 2 also includes transient modelling for the voltage divider topology.

[1] C. Reig, S. Cardoso, S. Mukhopadhyay, "Giant Magnetoresistance (GMR) Sensors - From Basis to State-of-the-Art Applications" *Springer*, 2013, doi: 10.1007/978-3-642-37172-1 [2] M.D. Cubells, C. Reig, J. Madrenas *et. al*. "Integration of GMR Sensors with Different Technologies", *Sensors*, (2016) 16(6) 939, doi: 10.3390/s16060939. [3] N. G. Hadjigeorgiou and P. P. Sotiriadis, "Parasitic Capacitances, Inductive Coupling, and High-Frequency Behavior of AMR Sensors," *IEEE Sensors J.* 20 (2020) 2339–2347, doi: 10.1109/JSEN.2019.2953351. [4] E.-M. Stetco, Ovidiu A. Pop, M. Gabor *et al.* "PSpice Model for a Current Sensor Based on Spin-Valve Magnetoresistive Microstructure", IEEE 8th Electronics System Integration Technol. Conf. (ESTC) (2020), doi:10.1109/ESTC48849.2020.9229833

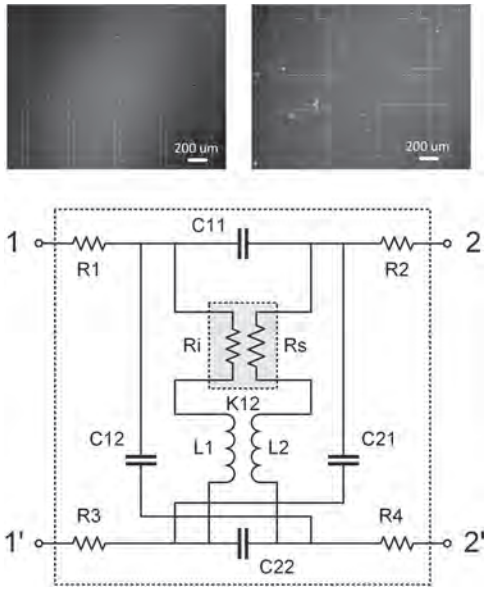

Fig. 1. Micrograph of the developed sensors. Electrical model for the elemental case.

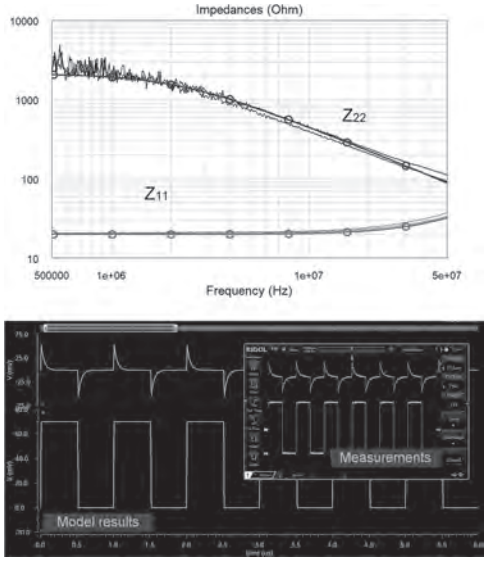

Fig. 2. Input impedance vs. frequency. Transient response (1 MHz)

OPA-02. MTJ-based Marine Sensor for Jellyfish Cassiopea Response to the Environmental Change. *S. Amara*[1], G. Izhar[1], D. Khan[1] and Y. Massoud[1] *1. Computer, Electrical and Mathematical Sciences and Engineering, King Abdullah University of Science and Technology, Thuwal, Saudi Arabia*

Understanding the behavior of free-living marine organisms is pivotal for many conservation efforts (REF) and examining how to change, such as overfishing and climate variability, affect marine ecosystems [1]. For this, many researchers have turned to animal-attached tag technology [2] where study animals carry archival "smart" tags that record a suite of parameters to quantify particular aspects of their behavioral ecology or physiology. It was demonstrated that the Pelagic jellyfish blooms are increasing worldwide as a potential response to climate change. The results shown in [3] suggest an enhanced growth of the jellyfish in response to global warming, whereas low temperatures may set the limits for successful invasion of the jellyfish into colder water bodies. Therefore, we are developing an underwater reliable wireless marine monitoring system composed of a flexible magnet (NdFeB-PDMS) and an MTJ-based sensor as shown in Fig. 1 in order to count the number of the jellyfish contractions under different environmental conditions. The fabrication process of the NdFeB-PDMS composite magnet involves minimal complexity, has lower cost, and is highly versatile with respect to the shape of the magnets [4] which play the role of a monitor of any jellyfish movement that would be detected by our MTJ-based sensor over time as can be seen in Fig 2. The composite magnet is coated with Paralyne C to protect the composite from degradation, make the remanent magnetization constant, and provide resistance against corrosion and biofouling, flexibility, and biocompatibility. The results show the suitability of the composite magnets for marine applications. Our results provide a framework for understanding the physiological tolerance of Cassiopea under possible future climate changes, which can be better interpreted by statistical coming studies using a wireless marine monitoring system based on our MTJ sensors.

S. M. Maxwell, E. L. Hazen, S. J. Bograd, B. S. Halpern, G. A. Breed, B. Nickel, N. M. Teutschel, Nat. Commun. 2013, 4 2688. Y. Ropert-Coudert, R. P. Wilson, Front. Ecol. Environ. 2005, 3437. S. M. Aljbour, M. Zimmer, and A. Kunzmann. "Cellular respiration, oxygen consumption, and trade-offs of the jellyfish Cassiopea sp. in response to temperature change." Journal of Sea Research 128 (2017): 92-97. Kaidarova, M. A. Khan, S. Amara, N. R. Geraldi, M. A. Karimi, A Shamim, R. P. Wilson, C.M. Duarte, and J. Kosel, "Tunable, flexible composite magnets for marine monitoring applications." Advanced Engineering Materials 20.9 (2018): 1800229.

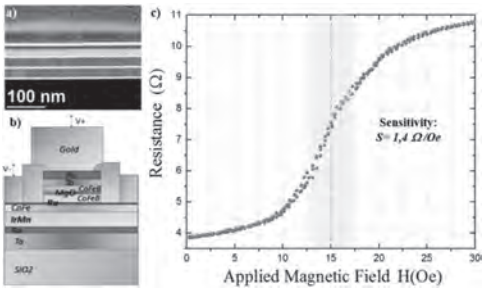

Fig. 1. (a) TEM image of the MTJ-based sensor stack. (b) MTJ sensor structure. (c) MTJ sensor hysteresis loop with implemented sensor on the jellyfish.

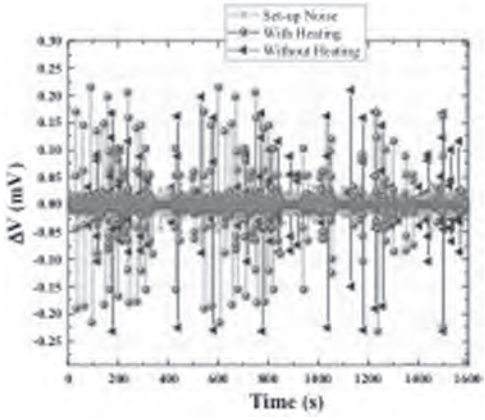

Fig. 2. Example of recorded movement of jellyfish over time under two different environmental conditions.

OPA-03. Magnetic elliptical array biosensor based on ferromagnetic resonance signal. *H. Huang*[1] *1. National Applied Research Laboratories, Hsinchu, Taiwan*

Ferromagnetic resonance signals of magnetic elliptical arrays were used as a biological detection. Magnetic elliptical arrays with a long axis of 26 μm and a short axis of 6.5 μm was fabricated by photo lithography technology and metal deposition process. The material of the magnetic structure is Permalloy with the thickness is of 90 nm, and the sample size is 5 mm^2. Figure 1 is the ferromagnetic resonance curves of magnetic elliptical arrays. It can be observed that the resonance signals of the elliptical arrays become larger as the external magnetic field become larger. The magnetic field were applied along the long or short axis of the ellipse, resulting in different resonant signal curves. The ferromagnetic resonance signals applied along the long axis are larger than that along the short axis. When Fe_3O_4 nanoparticles with a diameter of 20 nm were added to the elliptical array, the ferromagnetic resonance of the elliptical arrays vary. Whether the magnetic field was applied along the long or short axis of the ellipse, the ferromagnetic resonance signals would be reduced.

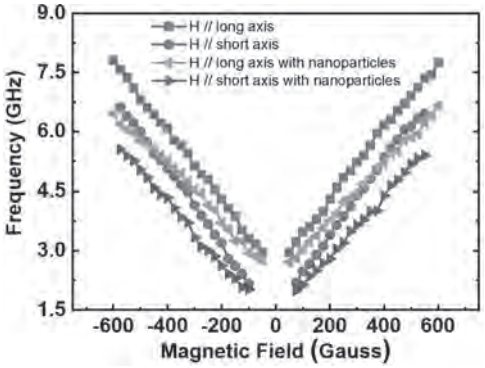

Fig 1. The ferromagnetic resonance curves of the magnetic elliptical array before and after adding the magnetic nanoparticles. The magnetic field is applied along the long and short axes of the ellipse.

OPA-04. Novel Sensing Technique for Non-Destructive Composites Monitoring. *V. Zhukova*[1], P. Corte-Leon[1], A. Allue[2], K. Gondra[2], M. Ipatov[1], J. Blanco[3], J. Gonzalez[4] and A. Zhukov[1,5] *1. Dept. Polymers and Adv. Mater., Dept. App. Phys. and EHU Quantum Center, University of Basque Country, UPV/EHU, San Sebastian, Spain; 2. Gaiker Technological Centre, Zamudio, Spain; 3. Dept. App. Phys. and EHU Quantum Center, University of Basque Country, UPV/EHU, San Sebastian, Spain; 4. Dept. Polymers and Adv. Mater. and EHU Quantum Center, University of Basque Country, UPV/EHU, San Sebastian, Spain; 5. IKERBASQUE, Basque Foundation for Science, Bilbao, Spain*

The real time non-destructive monitoring of stresses and temperature is one of the most demanded solutions in the field of sensor technologies. One of the most prospective technologies addressing this problem is a novel sensing technique for non-destructive monitoring utilizing ferromagnetic wire inclusions presenting the high frequency magnetoimpedance, MI, effect quite sensitive to tensile stress and magnetic field [1]. One of the advantages of this technology is that proposed free space microwave spectroscopy allows remote monitoring of external stimuli, like stress, magnetic field or temperature. The glass-coated microwires with typical diameters from 1 to 50 μm can provide new functionalities such as improved mechanical and corrosive properties, adherence with polymeric matrices and biocompatibility [2]. In the present paper a novel sensing technique for direct non-destructive and non-contact monitoring of the composite polymerization utilizing ferromagnetic glass-coated microwire inclusions with magnetic properties sensitive to tensile stress and temperature is described. We provide in-situ studies of the evolution of the hysteresis loop of arrays consisting of Co- rich ($Fe_{3.8}Co_{65.4}Ni_1B_{13.8}Si_{13}Mo_{1.35}C_{1.65}$) microwires during the composites matrix polymerization. We observed remarkable change of the hysteresis loops upon matrix polymerization: remarkable coercivity change and transformation of linear hysteresis loop into rectangular in the arrays with Co-rich microwires placed inside the matrix (see Fig.1a). Using the free space technique we observed considerable variation of the Transmission parameter of the microwires array in the range of 4-7 GHz upon the matrix polymerization (see Fig.1b). Observed dependencies are discussed considering heating during the matrix polymerization measured using a standard thermocouple (Fig.1c) and the matrix shrinkage and their influence on magnetic properties and MI effect of glass-coated microwires.

1. D. Mahnovskiy, L. Panina. C. García, A. Zhukov and J. González, *Phys. Rev.*, *B* 74, (2006) 064205-1-11 2. M. Churyukanova, S. Kaloshkin, E. Shuvaeva, A. Stepashkin, M. Zhdanova, A. Aronin, O. Aksenov, P. Arakelov, V. Zhukova, A. Zhukov, *J. Alloys Compd. 748 (2018)* 199.

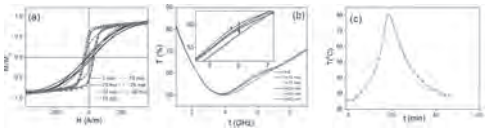

Fig. 1. Effect of the matrix polymerization on hysteresis loops of the array containing the $Fe_{3.8}Co_{65.4}Ni_1B_{13.8}Si_{13}Mo_{1.35}C_{1.65}$ microwires (a) and on the Transmission, T, parameter measured using free-space system (b) and on heating (c) during the composite solidification.

OPA-05. Indirect Observation of Circumferential Domain Magnetization Reversal of Amorphous Wires Using Orthogonal Fluxgate Effect. *M. Dressler*[1], M. Butta[1] and M. Janosek[1] *1. Department of Measurement, Czech Technical University in Prague - Faculty of Electrical Engineering, Prague, Czechia*

Magnetic microwire fluxgates are used in fundamental mode with a large DC bias to achieve lower noise and with the DC bias polarity flipping as an offset drift compensation as reported in [1], [2]. The circumferential magnetization reversal process of microwire surface domains is often observed on different wire sections using MOKE. A method of circ. BH loop measurement from the inductive component on wire termination was also described in [3], but it provides the measurement only for the whole length of the wire. We take an advantage of sensitivity sign change after the DC bias polarity is flipped. We operate the magnetic microwire as in a normal fluxgate magnetometer with AC excitation and longitudinal pickup coils. The DC bias is not set to a constant, but rather to a triangular wave with amplitude required to flip the circumferential domains and thus the sensitivity sign. Secondly, the sensor needs to be exposed to an axial field to obtain any output signal. The domain reversal is observed through its effect on sensitivity sign, more precisely through output signal amplitude and phase change. We adopted the multi-section coil design with simultaneous sampling and demodulation in digital domain. We used eight 1cm coil sections covering the whole length of the microwire. This allowed us to indirectly measure the shape of the circumferential BH loops of different portions of the microwire along its axis. While the output can be used to easily distinguish as-cast and annealed wire, the results are of individual sections differs slightly as shown in Fig. 1, depending on the excitation parameters and external field value. We consider this approach advantageous in terms of the practical measurement system simplification for observation of slow magnetic domain behaviour simultaneously using a fluxgate and a MOKE microscopy. The high frequency excitation leads to a larger pickup coil sensitivity and is averaged out during camera exposure time in the latter case.

[1] I. Sasada, J. Appl. Phys., Vol. 91, no. 10, pp. 7789-7791, (2002) [2] M. Butta and I. Coroli, IEEE Transactions on Magnetics, Vol. 53, no. 4, pp. 1-6, (2017) [3] P. Ripka, M. Butta, et al., Sensors and Actuators A: Physical, Vol.145-146, pp. 23-28, (2008)

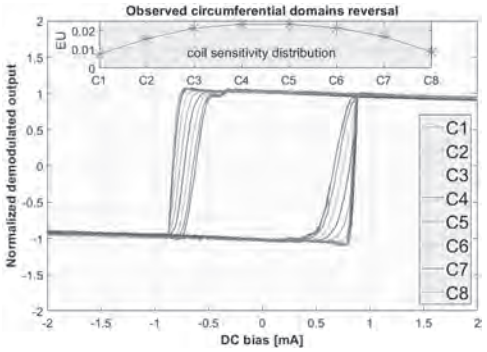

Fig. 1 An example of observed sensitivity sign change using multiple coils along the length of annealed Unitika microwire. Axial field of 36 μT and amplitude of 73kHz AC excitation was equal to 4.5 mA. Triangular waveform of DC bias was set to 4mApp and 500 mHz.

OPA-06. Spin Hall magnetic field sensors for vehicles using the Wheatstone bridge. *J. Kwon*[1], S. Noh[1], J. Lee[1], H. Lee[1], S. Jang[2,3], B. Min[2] and D. Han[2] *1. Materials Research and Engineering Center, Hyundai Motor Company, Uiwang-si, The Republic of Korea; 2. Center for Spintronics, Korea Institute of Science and Technology (KIST), Seoul, The Republic of Korea; 3. School of Electrical Engineering, Korea University, Seoul, The Republic of Korea*

The spin-orbit torques (SOTs) from the spin Hall effect (SHE) are of interest due to their potential applications to ultra-fast, high-dense, energy-efficient non-volatile memory and logic devices [1]. Recently, there have been attempts to exploit the SHE-related phenomena in magnetic sensors [2] for distance, angular position, and rotation detections with high sensitivity and operational range. Here, we propose magnetic sensors for vehicles using a 2nd-harmonic Hall voltage and magnetization switching by the SOTs. As a proof-of-concept, we employ magnetic thin films of $[Pt/Hf]_n$/Pt/Co/Ta/MgO/TaO_x with a perpendicular magnetization at a remanent state. The Pt/Hf multilayers and Ta provide the SOTs with the opposite sign of spin Hall angles, resulting in large spin-orbit fields in the Co layer. The 2nd-harmonic Hall voltage is measured in the Wheatstone bridge structures at AC currents, of which current density is ~ 10^7 A/cm^2. We found that the Wheatstone bridge allows an improved signal-to-noise ratio (SNR) and a 0.16 mV/T of field sensitivity in the -0.4 ~ 0.4 T range, which is a factor of 5 larger than that of the Hall bar structure. (Fig. 1) Moreover, we demonstrate

magnetic rotation sensors using magnetization switching by SOTs. The permanent magnets with alternative magnetic poles on the motor shaft produce magnetic stray field components parallel to the current applied to the device, which allows the inversion symmetry breaking in magnetization switching and leads to a deterministic switching of the perpendicular magnetization. (Fig. 2) In the rotating motor, the magnetization switching occurs repetitively as the stray field on the ferromagnetic thin films changes its sign, generating a periodic square pulse train in the output signal. The position of the rotor can be detected from the time gaps between the square pulses. These results may be applicable to speed and angle position sensors in vehicles with higher energy efficiency and a more straightforward manufacturing process than commercial magnetoresistive (MR) sensors.

[1] I. M. Miron G. Gaudin, S. Auffret, Nature, Vol. 9, p. 230 (2010) [2] Y. Xu, Y. Yang, M. Zhang, Adv. Mater. Technol., Vol. 3, no. 1800073 (2018)

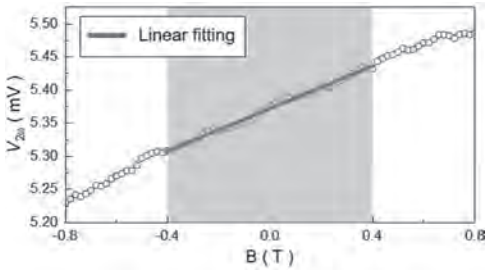

Fig. 1. The 2nd-harmonic output voltage in the spin Hall magnetic field sensor with the Wheatstone bridge.

Fig. 2. Schematics for application of spin Hall magnetic field sensor to a rotor.

OPA-07. Tailorable force sensor based on stress-magneto-impedance effect in amorphous wires. S. Corodeanu[1], C. Hlenschi[1], H. Chiriac[1], *N. Lupu*[1] and T.A. Ovari[1] *1. National Institute of Research and Development for Technical Physics, Iasi, Romania*

The amorphous magnetic wires are widely used as magnetic or magneto-mechanical sensors due to their very soft magnetic properties and high sensitivity to stress. [1-4]. A new design of a high sensitivity sensor with high capability to measure applied forces or load is proposed by this paper. The sensor consists in four pieces of high permeability $Co_{68.18}Fe_{4.32}Si_{12.5}B_{15}$ amorphous magnetic wire, 120 μm in diameter, 20 mm in length, glued prestressed on a pcb board having 0.3 mm in thickness, 7 mm in width and 30 mm in length (Figure 1). The ends of each wire is soldered on the PCB to form a Wheatstone bridge circuit. The opposite arms of the bridge are placed on the same side of the pcb to increase the bridge unbalance when stressed. Also, all wires forming the bridge arms are parallel and close one to another to minimize the effect of the surrounding magnetic field. By using different PCB support for the bridge, it is possible to tailor the sensitivity and force measuring range. A special designed electronic device was built to power the bridge using a high frequency sinusoidal signal and to extract and amplify the unbalanced voltage of the bridge. The dependence of the output voltage/gain versus applied force, for a signal excitation frequency of 1 MHz, is shown is showin figure 2. The sensor shows linear behavior between ± 0.15N and sensitivity of 43.7 mV/N, without gain, in the linear region. Financial support by the NUCLEU Program (PN 19 28 01 01) is gratefully acknowledged.

1. M. Vázquez, Physica B, vol. 299, pp. 302–313, 2001. 2. A. Zhukov, J. Mag. Mag. Mater., vol. 242–245, pp. 216–223, 2002. 3. S. Corodeanu, H. Chiriac, T.-A. Óvári, N. Lupu, AIP Advances, vol. 7(5) no. 056621, 2017. 4. C. Hlenschi, S. Corodeanu, N. Lupu, H. Chiriac, IEEE Sensors Journal, vol. 19(16). pp. 6644-6649, 2019

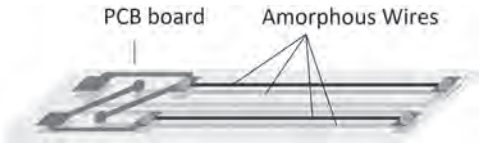

Figure 1. Force sensor design.

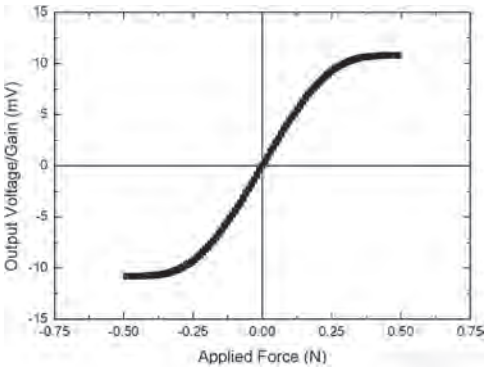

Figure 2. Sensor response to external applied force.

OPA-08. Multifunctional Phase Change Composites for Passive Thermal Management and Electromagnetic Shielding of High-Frequency Devices. *W. Salter*[1], J. Lundquist[1], W. Lohr[2], O. Fitchorova[3,4], V.G. Harris[3,4], E. Topsakal[1], R.L. Hadimani[5] and R. Barua[5] *1. Electrical Engineering, Virginia Commonwealth University, Richmond, VA, United States; 2. Biomedical Engineering, Virginia Commonwealth University, Richmond, VA, United States; 3. KRI at Northeastern University, LLC, Burlington, MA, United States; 4. Electrical Engineering, Northeastern University, Boston, MA, United States; 5. Mechanical & Nuclear Engineering, Virginia Commonwealth University, Richmond, VA, United States*

With the rapid advancement in electronics systems, there is a high demand for components that achieve size, weight, power, and cost reductions (SWaP+C). This need for greater miniaturization has contributed to a dramatic increase in heat generation within these systems, resulting in compromised performance, sacrificed reliability, and reduced device lifecycle.[1] In addition, with ever-increasing spectral congestion and since electronic products incorporate faster components operating at higher frequencies than ever before, electromagnetic interference is becoming challenging to mitigate, posing a major concern for human health and the environment.[2] It is therefore highly critical to develop high-performance material systems that can concurrently mitigate the detrimental effects of thermal and EM radiation while maintaining the highly desired SWaP+C configurations. To this effect, we have developed an innovative synthesis strategy involving melt blending, vacuum impregnation, and magnetic-field assisted spin coating to fabricate flexible multicomposite films comprising of FeSi particles (~30-50 μm) and graphene nanoflakes (200-300 nm) confined in a shape-stabilized phase change material (PCM) matrix. In this multifunctional material, the PCM enables efficient heat absorption via the phase change process, the graphene flakes enhance the thermal conductivity to facilitate heat dissipation, and the FeSi particles enhance electromagnetic absorption in the X and Ku bands due to their high magnetization and magnetic anisotropy. With the synergistic effect of graphene and FeSi, the resulting composite displays a thermal conductivity of 0.60-0.75 W/mK, latent heat of 110-120 J/g at 70 °C, and excellent EM shielding effectiveness

(SE) in the range of 10-60 dB depending on thickness in the range 200 μm to 2 mm (an example is shown in Fig 1). Processing-structure-property correlations of the multifunctional films will be discussed in the context of their percolation threshold. Research supported by the Commonwealth Cyber Initiative (Grants HV-2Q22-003 and HV-4Q21-002).

[1] Moore, Arden L., and Li Shi. "Emerging challenges and materials for thermal management of electronics." *Materials today* 17.4 (2014): 163-174. [2] Bilal, Muhammad, et al. "Miniaturized and flexible FSS-based EM shields for conformal applications." *IEEE Transactions on Electromagnetic Compatibility* 62.5 (2020): 1703-1710.

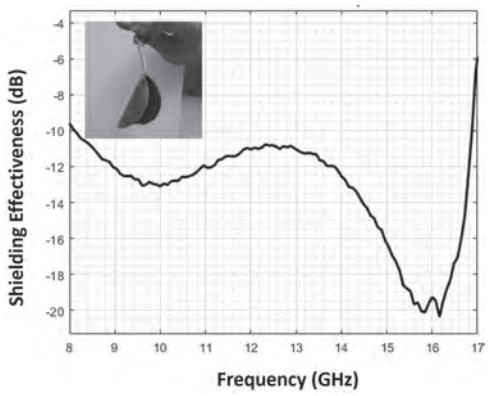

Fig 1. Shielding Effectiveness of a PCM composite film of 1 mm thickness (2.5 wt % graphene, 20 wt% FeSi). Inset shows the flexibility of the conformal film.

OPA-09. Periodic THz Absorber Design for Sensor Applications.
A. Eroglu[1] and B. Chowdhury[1] *1. ECE, North Carolina A&T State University, Greensboro, NC, United States*

THz devices have been a focus for researchers due to their applications in several areas including sensing, imaging, radiation detection, and biomedicine [1-3]. A compact THz detector development was initiated when first perfect metamaterial absorber was designed in 2008 [4]. Landy et al. designed an absorber with an improved electrically coupled ring resonator that achieved 95% absorption at 1.13 THz in 2009 [5]. Semiconductor multilayer metamaterial structure increases design flexibility and enhances performance of the structure against temperature, light intensity, applied voltage and external magnetic fields [6-8]. In this paper, periodic THz absorber for sensor applications has been designed, simulated and implemented. THz absorber unit cell based on semiconductor metamaterial has been developed and analyzed. Semiconductor metamaterial absorber unit cell has multilayers including Glass substrate, InSb semiconductor layer, MgF2 buffer layer, InSb Resonator ring, buffer layer, and a mask. The sample is modeled using Drude and Debey models to include the frequency dependency of the permittivity for accuracy. 10x10 periodic structure is formed and then simulated using the concept of Floquet ports with 3D EM simulator. The performance of the absorber is investigated for various conditions including absorption, transmission and reflection versus frequency, and wavelength. It has been shown that semiconductor metamaterial absorbers have better tuning characteristics while they have fabrication complexity. The simulated results showing the performance of the unit cell absorber in Fig. 1a against frequency are illustrated in Fig. 1b. The results in Fig. 1b show that the proposed absorber provides absorbance of 0.98 and refection of 0.018 at 0.3THz. 10x10 periodic structure is then formed as shown in Fig. 2a and simulated using 3D EM simulator. The results shown in Fig. 2b verify that the absorption at 0.3THz was 0.91 as expected.

[1] J. F. Federici, B. Schulkin, F. Huang, D. Gary, R. Barat, F. Oliveira, and D. Zimdars, "THz imaging and sensing for security applications—explosives, weapons and drugs," Semiconductor Science and Technology 20, S266 (2005). [2] Z. D. Taylor, R. S. Singh, D. B. Bennett, P. Tewari, C. P. Kealey, N. Bajwa, M. O. Culjat, A. Stojadinovic, H. Lee, and J. Hubschman, "THz medical imaging: in vivo hydration sensing," Terahertz Science and Technology, IEEE Transactions on 1, 201-219 (2011). [3] S. Komiyama, "Single-photon detectors in the terahertz range," Selected Topics in Quantum Electronics, IEEE Journal of 17, 54-66 (2011). [4] N.I. Landy, S. Sajuyigbe, J.J Mock, D.R. Smith, W.J. Padilla, "Perfect metamaterial absorber," Phys. Rev. Lett. 2008, 100. [5] N.I., Landy,C.M., Bingham, T. Tyler, N. Jokerst, D.R. Smith, W.J. Padilla, "Design, theory, and measurement of a polarization-insensitive absorber for terahertz imaging," Phys. Rev. B 2009, 79. [6] H. Tao, N. I. Landy, C. M. Bingham, X. Zhang, R. D. Averitt, and W. J. J. O. e. Padilla, "A metamaterial absorber for the terahertz regime: design, fabrication and characterization," vol. 16, no. 10, pp. 7181-7188, 2008. [7] Y. Cheng, Y. Nie, R. J. O. Gong, and L. Technology, "A polarization-insensitive and omnidirectional broadband terahertz metamaterial absorber based on coplanar multi-squares films," vol. 48, pp. 415-421, 2013. [8] H.-T. Chen, W. J. Padilla, M. J. Cich, A. K. Azad, R. D. Averitt, and A. J. J. N. p. Taylor, "A metamaterial solid-state terahertz phase modulator," vol. 3, no. 3, p. 148, 2009.

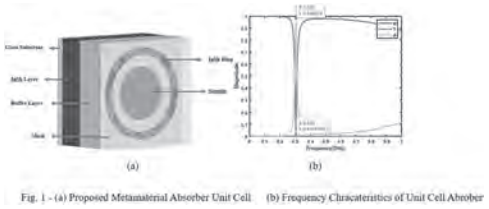

Fig. 1 - (a) Proposed Metamaterial Absorber Unit Cell (b) Frequency Chracateristics of Unit Cell Abrober

Fig. 1 - (a) Proposed Metamaterial Absorber Unit Cell (b) Frequency Chracateristics of Unit Cell Abrober

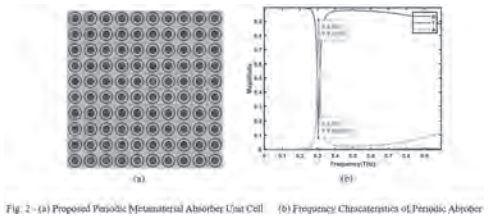

Fig. 2 - (a) Proposed Periodic Metamaterial Absorber Unit Cell (b) Frequency Chracateristics of Periodic Abrober

Fig. 2 - (a) Proposed Periodic Metamaterial Absorber Unit Cell (b) Frequency Chracateristics of Periodic Abrober

OPA-10. Magnetic tunnel junctions for positioning systems with down to 100 nm resolution. *A. Talantsev*[1], E. Paz[1], A. Araujo[1], M. Majeed[2], P. Pedrosa[2] and R. Ferreira[1] *1. Spintronics, Internatinal Iberian Nanotechnology Laboratory, Braga, Portugal; 2. DTX Colab, University of Minho, Guimaraes, Portugal*

Positioning systems with high resolution are in a high demand for robotics, operating in a wide scales of positioning ranges from tens of meters in heavy machine industry, down to few nanometers in high-precision electronics. A promising approach for a robust positioning at nanoscale is integration of magnetic field sensors into the positioning electronics and detection of magnetized objects by their induced magnetic fields. In this work, we introduce an approach for magnetic-based positioning, in which the displacement of a magnetized micro-object is detected by magnetic field sensor, as a variation of magnetic field, associated with this displacement. For the purpose to have higher resolution in positioning, magnetic sensor was composed of an array of magnetic tunnel junctions, having magnetoresistance of ~ 170 percent, whereas the geometry of the magnetized object was optimized to have a higher gradient of magnetic field along the positioning direction. The magnet-sensor configuration was optimized as follows: i) magnetization direction in the magnetized object, as well as the displacement direction were varied in respect to field sensing direction of the MTJ sensor, to achieve high linearity of the sensor signal variations with the displacements of the object, ii) the shape of the magnetized object was optimized to improve sensitivity of the MTJ sensor array to positioning displacements of this object, iii) the distance between the MTJ sensor array and the magnetized object was optimized to have largest dynamic range of MTJ output voltage variations,

without oversaturating the sensor, iv) the lateral and transversal dimensions of the MTJ sensor array were optimized to improve sensitivity to gradient of magnetic field, induced by the micromagnet. With the optimized configuration the positioning sensitivity of the sensor platform was tested with a micromagnet, placed on a nano-positioning piezo-stage, operating in a closed-loop feedback mode with 10 nm step resolution. The tests in open environment demonstrate robust operation of the magnetic tunnel junction sensor-based platform as a positioning sensor for displacements of magnetized objects with a resolution down to 100 nm.

The work is supported by the project NeWeSt - New generation of cyberphysical Weighing Systems, with the reference POCI-01-0247-FEDER-069716, co-funded by COMPETE 2020 - Operational Programme for Competitiveness and Internationalisation under the PORTUGAL 2020 Partnership Agreement, through the European Regional Development Fund (ERDF).

OPA-11. Withdrawn

OPA-12. High-performance MTJ-based Sensors for Monitoring of Atmospheric Pollution. *S. Amara*[1], A. Aljedaibi[1], D. Khan[1] and Y. Massoud[1]
1. Computer, Electrical and Mathematical Sciences and Engineering, King Abdullah University of Science and Technology, Thuwal, Saudi Arabia

Airborne particulate matter (PM) have been significantly increasing over the past two decades carrying significant health risks such as premature death, damage to the lungs, heart tissue, and even cancer. PM2.5 is the main concern as it has the most harmful health effects while being more difficult to detect [1]. Moreover, these magnetic nanoparticles are readily absorbed into the bloodstream causing neurodegenerative diseases such as Alzheimer's and cancerous tumors [2]. Therefore, it is essential to monitor the magnetic portion of PM and its adverse effects on health [3], [4]. This work focuses on developing, modeling, and simulation of a new kind of magnetic sensor that can count and localize these magnetic nanoparticles. Additionally, we have fabricated a novel low-noise and high-precision readout circuit for tunneling magnetoresistive (TMR) array to evaluate the bio-magnetic measurement platform's suitability for detecting weak bio-magnetic fields. The proposed sensors could help to prevent these nanoparticles from the polluted environment and undoubtedly reduce their adverse risks to humans. The modeled magnetic system consists of a TMR sensor array, a conducting line, and the detected magnetite nanoparticles as shown in Fig. 1(a). The localization and quantization of these Fe3O4 nanoparticles (characterized in Fig. 1(b)) can be achieved by analyzing total output voltages from the TMR sensor array. The Fe_3O_4 magnetite is injected inside the small closed chamber and they are exerting an external magnetic field that is aligned or opposed to the pinning field, which results in shifting the MTJ curve as seen in Fig. 1(c). After applying a current in the conducting line and creating an external field, the magnetite gets polarized and approaches the MTJ sensors. This technique can detect 50-200 nm magnetic particles compared to existing commercial monitoring solutions that are limited to 1-3μm particles.

[1]. C. I. Davidson, R. F. Phalen, and P. A. Solomon, "Airborne particulate matter and human health: a review," *Aerosol Sci. Technol.,* vol. 39, no. 8, pp. 737–749, 2005. [2]. B. A. Maher *et al.,* "Magnetite pollution nanoparticles in the human brain," *Proc. Natl. Acad. Sci.,* vol. 113, no. 39, pp. 10797–10801, 2016. [3]. Eve McGlynn *et al.,* "The Future of Neuroscience: Flexible and Wireless Implantable Neural Electronics," *Adv. Sci.* vol. 8, 2021. [4]. L. Occhipinti, and P. Oluwasanya, "Particulate Matter Monitoring: Past, Present, and Future," *International Journal of Earth & Environmental Sciences,* vol. 2, 2017.

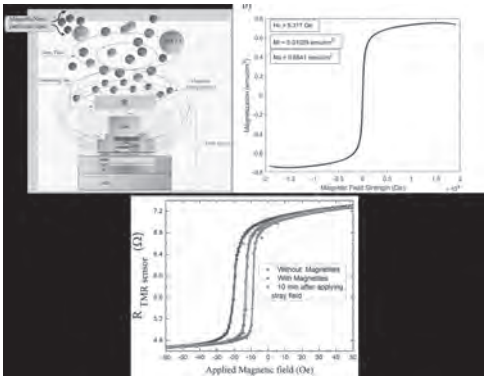

Fig. 1. (a) Magnetic sensing method showing PM particles above Sensor. (b) Hysteresis plots of Fe3O4 nanoparticles. (c) Hysteresis change of TMR sensors before and after injecting Magnetic nanoparticles on the container.

OPA-13. On-chip Quantitative Cell sorting based on High Performance Magnetic Tunnel Junction. *A. Aljedaibi*[1], S. Amara[1] and Y. Massoud[1]
1. CEMSE, KAUST, Thuwal, Saudi Arabia

Early cancer detection greatly enhances the prognosis and allows for higher treatment success. Cancer metastasis, which occurs in later stages, is believed to cause more than 90% of cancer-related deaths [1]. In earlier cancer stages, circulating tumor cells (CTCs) may be detected in the blood of cancer patients, which can correlate with patient survival rate. Accurate, non-invasive separation of these cells allows for early detection of cancer and aids in increasing therapeutic efficacy [2]. This work provides an integrated on-chip quantitative cell sorting platform that separates and counts magnetically labeled cells through a microfluidic channel. First, an immunomagnetic assay is utilized to label CTCs with highly selective magnetic nanoparticles. Then, magnetically labeled cells are separated and guided through the microfluidic channel by electromagnetics and ferromagnetic strips [3]. After cell separation, magnetically labeled biomarkers are detected by the magnetic tunnel junction (MTJ) sensor that measures stray fields surrounding the labeled CTCs, generating an electrical signal for each passing particle. Additionally, biomarkers with different sizes, such as CTCs and protein-based cancer biomarkers, can be detected and quantified as they move through the microfluidic channel at different speeds, yielding distinct peaks at the MTJ output [3][4]. This work demonstrates a highly selective platform that actively sorts magnetically labeled biomarkers by combining magnetophoresis-based cell sorting and MTJ-based flow cytometry allowing for highly sensitive quantitative on-chip cell sorting.

[1] Hoshino, K., Huang, Y.-Y., Lane, N., Huebschman, M., Uhr, J. W., Frenkel, E. P., & Zhang, X. (2011). Microchip-based immunomagnetic detection of circulating tumor cells. *Lab on a Chip*, *11*(20), 3449. https://doi.org/10.1039/c1lc20270g [2] Liang, W., Liu, J., Yang, X., Zhang, Q., Yang, W., Zhang, H., & Liu, L. (2020). Microfluidic-based cancer cell separation using active and passive mechanisms. *Microfluidics and Nanofluidics*, *24*(4). https://doi.org/10.1007/s10404-020-2331-x [3] Hejazian, M., Li, W., & Nguyen, N.-T. (2015). Lab on a chip for continuous-flow magnetic cell separation. *Lab on a Chip*, *15*(4), 959–970. https://doi.org/10.1039/c4lc01422g [4] Amara, S., Bu, R., Alawein, M., Alsharif, N., Khan, M. A., Wen, Y., Zhang, X., Kosel, J., & Fariborzi, H. (2018). Highly-sensitive magnetic tunnel junction based flow cytometer. *2018 IEEE International Symposium on Medical Measurements and Applications (MeMeA)*. https://doi.org/10.1109/memea.2018.8438652

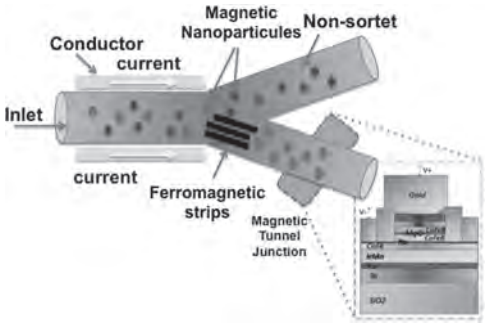

Magnetic Tunnel Junction based sorting cytometer image.

OPA-14. An Integrated and Highly-Sensitive Magnetic Tunnel Junction based Cytometer. A. Aljedaibi[1], *S. Amara*[1] and Y. Massoud[1]
1. CEMSE, KAUST, Thuwal, Saudi Arabia

Flow cytometry is a powerful technique that enables cell quantification and analysis. As a result, it has become an essential instrument in biomedical research and clinical testing for disease diagnosis or treatment monitoring. However, the current technique is large and expensive, driving research into smaller, cheaper, and more efficient flow cytometers [1]. One approach to tackle this problem can be with the application of spintronic sensors such as giant magnetoresistance sensors for cell quantification [1][2]. In this work, we report a highly sensitive flow cytometer based on magnetic tunnel junction (MTJ) technology. After external labeling of cells with magnetized beads placed above the MTJ sensor to measure stray magnetic field surrounding the beads. When labeled cells pass through the sensitive area, a signal peak will be generated at the output of the MTJ sensor [3]. Alternatively, magnetic flow cytometers can evaluate the efficacy of certain cancer immunotherapies where cancer cell membranes coat magnetic nanoparticles to activate a specific natural killer (KT) cell response [4]. One of the cytometer applications is Live/dead cancer cells discrimination. This cytometer can detect the presence of these magnetic nanoparticles to ensure proper activation of KT cells and thorough removal of the modified magnetic particles. This result demonstrates a novel MTJ-based, highly sensitive flow cytometer design for quantifying magnetically labeled cells and cancer therapy involving magnetic nanoparticles. Using our suggested device, we can distinguish and separate between cancer cells and prove Live/dead cancer cells discrimination.

[1] Soares, R., Martins, V. C., Macedo, R., Cardoso, F. A., Martins, S. A., Caetano, D. M., Fonseca, P. H., Silvério, V., Cardoso, S., & Freitas, P. P. (2019). Go with the flow: Advances and trends in magnetic flow cytometry. *Analytical and Bioanalytical Chemistry*, *411*(9), 1839–1862. https://doi.org/10.1007/s00216-019-01593-9 [2] Kokkinis, G., Cardoso, S., Keplinger, F., & Giouroudi, I. (2017). Microfluidic platform with integrated GMR sensors for quantification of cancer cells. *Sensors and Actuators B: Chemical*, *241*, 438–445. https://doi.org/10.1016/j.snb.2016.09.189 [3] Amara, S., Bu, R., Alawein, M., Alsharif, N., Khan, M. A., Wen, Y., Zhang, X., Kosel, J., & Fariborzi, H. (2018). Highly-sensitive magnetic tunnel junction based flow cytometer. *2018 IEEE International Symposium on Medical Measurements and Applications (MeMeA)*. https://doi.org/10.1109/memea.2018.8438652 [4] Wu, D., Shou, X., Zhang, Y., Li, Z., Wu, G., Wu, D., Wu, J., Shi, S., & Wang, S. (2021). Cell membrane-encapsulated magnetic nanoparticles for Enhancing Natural Killer Cell-mediated cancer immunotherapy. *Nanomedicine: Nanotechnology, Biology and Medicine*, *32*, 102333. https://doi.org/10.1016/j.nano.2020.102333

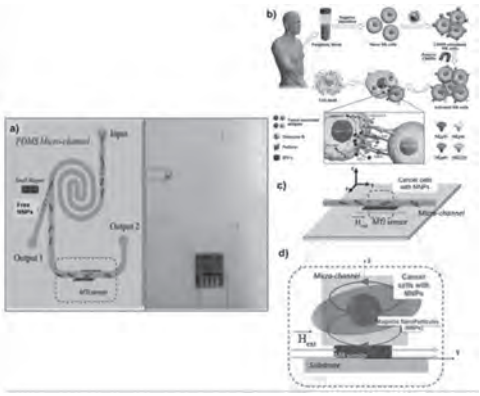

Fig 1: a) PDMS spiral curvilinear micro-channel used to isolate free nanoparticules which are trapped by the magnet. b) Schematic depicting the synthesis of cancer cell membrane-coated nanoparticles (CMNPs) and their functions to stimulate NK cells for elevated tumor-killing responses (ref4). c) Labelled cancer cells going through the TMR sensor. d) schematic of the cancer cell labelling.

Session OPB
MOTORS, ACTUATORS AND RELATED (Poster Session)

Mattia Butta, Chair
Czech Technical University in Prague, Praha, Czechia

OPB-01. Analysis and Design of Watch Speaker to Enhance Mid-frequency Sound Pressure Level with Magnetic Circuit Size Expansion. *J. Park*[1], Z. Jiang[1] and S. Hwang[1] *1. Mechanical engineering, Pusan national university, Busan, The Republic of Korea*

With the rapid development of smartphone technology, wearable devices have developed significantly simultaneously. Smartwatches, typical wearable smart devices, will help users check the notifications and phone calls from smartphones and provide various functions to detect healthy conditions, such as oxygen blood level, and heart rate. Nowadays, the size of the smartwatch's display has increased, as shown in fig.1 (a), causing the size expansion of the microspeaker, which is called a watch speaker. Watch speakers are mainly used for exercise beep or message alert that requires immediate feedback. It needs to make a stimulating sound to the human ear. The human auditory system is most sensitive to frequencies between 2,000 and 5,000 Hz [1]. Thus, it is necessary to improve the mid-frequencies sound pressure level of the watch speaker. This study proposes some new designs of watch speakers with 20% improvement of magnetic size in three directions (Length, width, and height). Electromagnetic-mechanical-acoustic coupling analysis method [2] is used to obtain the sound pressure level (SPL) result of the watch speaker. The prototype of the watch speaker and its exploded view is shown in Fig.1 (b). The B&K equipment has been employed to do the experimental verification for the prototype. The measurement method and simulation result matches well, as shown in Fig.1 (c). Three directions of magnetic size expanding ways are shown in Fig.2 (a). Each direction has 4 types expanding size, there are total 12 cases are analyzed by using finite element method. According to analysis results, width increase design direction Prms_rate, multiplied by effective area and force factor divided by moving mass, is the most significant increase compared to other ways, as shown in Fig.2 (b). The SPL comparison between the prototype and 20% improvement of magnetic size in three directions are shown in Fig.2 (c). As a result, Width_20, which is the best way to improve mid-range SPL, has a 2.52 dB improvement on average of mid-frequency SPL compared to the prototype.

1. Stanley A. Gelfand, Essential of Audiology., p87(2011) 2. Park, KH, Jiang ZX, and Hwang, SM. Design and analysis of a Novel Microspeaker with Enhanced Low-Frequency SPL and Size Reduction. Applied Sciences., Vol.10(24), p.8902 (2020 Dec 13)

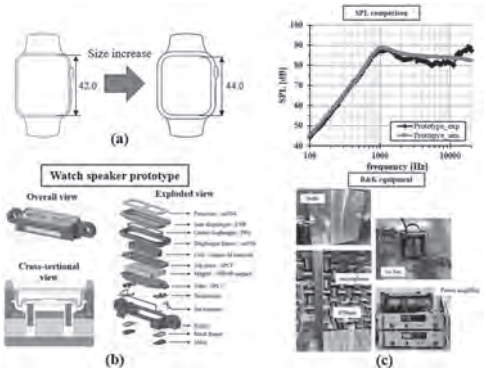

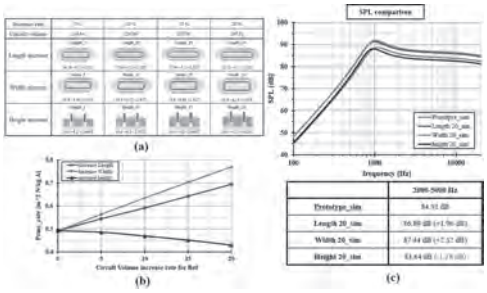

OPB-02. Electromagnetic Alternators with Composite Amorphous Alloy Housing for Improving Characteristics. *C. Hsu*[1] *1. Mechanical Engineering, Asia Eastern University of Science and Technology, Banqiao District, Taiwan*

The AC two-pole generator proposed in this study has two forms, one is a non-cover (NC) naked motor, and the other is an iron-based amorphous alloy material as the outer casing of the generator (No Cover, NC). Cover with amorphous slice) for coating. Due to the change of magnetic pole and space magnetic field, different permanent magnet motors have magnetic material shell and no shell structure, as shown in Figure 1. Magnetic field distribution In the demagnetization area, the power and magnetic field changes are tested by order wave analysis and the surface magnetic flux density tester of amorphous materials. The order wave measurement results of different shell shapes can show the magnetic flux density node in the magnetized direction of the demagnetization area. cover. In the experimental measurement of the surface of the amorphous shell, the magnetic flux at the inner and outer center points is about 1.2-2.4 (mT), which is relatively strong, while the magnetic flux distribution at the four corners is about 0.6-1.0 (mT), which is relatively weak. The experimental goal is to set the effect of demagnetization on the electromagnetic parameters, and it is concluded that the permanent magnet salient pole motor has better generator power characteristics in the cladding demagnetization and the magnetic flux distribution of the amorphous shell. In addition, the experiment is also carried out and a local flame is proposed. The annealing process method is used as the coating of the generator and the measurement of the magnetic properties. The experimental verification is that the magnetic flux density of the material surface at the local center point of the high temperature is close to the Curie temperature. The above, but the order wave and power performance of the generator of the flame partial annealing process are poor, as shown in Figure 2.

[1] D. Y. Kim, J. K. Nam, and G. H. Jang, "Reduction of magnetically induced vibration of a spoke-type IPM motor using magnetomechanical coupled analysis and optimization," IEEE Trans. Magn., vol. 49, no. 9, pp. 5097–5105, Sep. 2013. [2] K. Yamazaki and Y. Kato, "Iron loss analysis of interior permanent magnet synchronous motors by considering mechanical stress and deformation of stators and rotors," IEEE Trans. Magn., vol. 50, no. 2, pp. 909–912, Feb. 2014. [3] C. A. Hernandez-Aramburo, T. C. Green, and A. C. Smith, "Estimating rotational iron losses in an induction machine," IEEE Trans. Magn., vol. 39, no. 6, pp. 3527–3533, Nov. 2003.

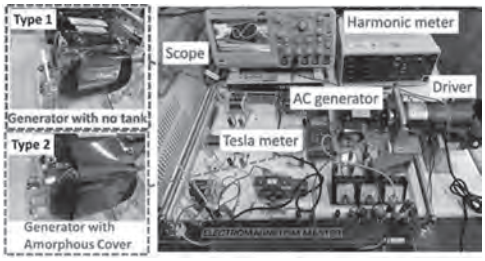

Fig. 1 Structure and experimental structure of the amorphous alloy material covered (uncovered) by the alternator shell

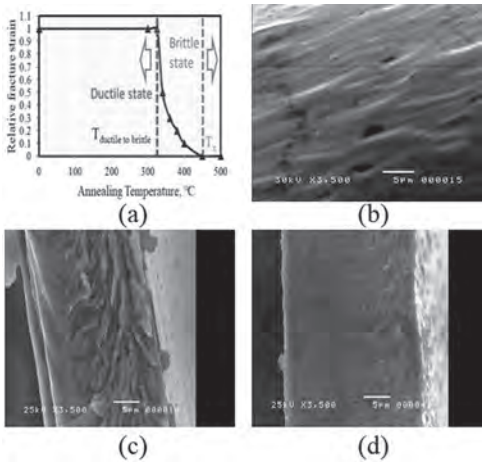

Figure 2 Microstructure measurement of three amorphous material samples: (a) ductility and brittleness temperature range measurement after material annealing, (b) 350°C, (c) 390°C, (f) 450°C

OPB-03. Microwave Absorption Performance of CoTi-doped M-type Hexagonal Ferrite in the Millimeter-wave Spectrum. *H. Won*[1], Y. Hong[1], M. Choi[1], H. Garcia[2], H. Xin[2], H. Jung[3] and K. Lee[3] *1. Department of Electrical and Computer Engineering, The University of Alabama, Tuscaloosa, AL, United States; 2. Department of Electrical and Computer Engineering, The University of Arizona, Tucson, AZ, United States; 3. Semiconductor Materials R&D/Advanced Materials, LG Chemistry Ltd, Seoul, The Republic of Korea*

Due to the lack of bandwidth and potential allocation in microwave spectrum (3-30 GHz), many electronic industries shift their attention to millimeter-wave (mmWave) spectrum (30-300 GHz). Along with this trend, radiated EMI (electromagnetic interference) cause problems like noise within and outside an electronic device. To suppress EMI, materials that absorb radiated EM waves in the mmWave spectrum are in great demand [1, 2]. Recently, Dong *et al.* reported M-type hexaferrite, $BaCo_xTi_xFe_{12-2x}O_{19}$ (x = 0.3, 0.4, and 0.5), that absorbs EM signal between 30-40 GHz [1]. The effects of water content required in the wet milling process have not been reported. In this study, we investigated the effects of processing water content on the microwave absorption performance of $BaCo_{0.3}Ti_{0.3}Fe_{11.4}O_{19}$. $BaCo_{0.3}Ti_{0.3}Fe_{11.4}O_{19}$ was prepared by the conventional solid-state process [1]. The precursors, $BaCO_3$, TiO_2, Co_2O_3, and Fe_2O_3, were mixed in the stoichiometric ratio to make 2g of $BaCo_{0.3}Ti_{0.3}Fe_{11.4}O_{19}$ and wet milled with high energy ball with x mL of deionized water (x = 0.2, 0.3, 0.4, 0.5) for 2 h. Then, the mixed powder was calcined at 1315 °C for 2 h and sintered at 1310 °C for 2 h in air. Fig. 1 shows the intrinsic coercivity (H_{ci}) was and saturation magnetization (M_s) of $BaCo_{0.3}Ti_{0.3}Fe_{11.4}O_{19}$ with different processing water contents. The H_{ci} decreases from 246 to 175 Oe as the x increases from 0.2 to 0.5 mL, while the M_s increases from 64.6 to 66 emu/cc. The reflection (S_{11}) and transmission (S_{21}) coefficients with different processing water contents are present in Fig. 2. Both S_{11} and S_{21} decrease as x increases from 0.2 to 0.5 mL. The higher the water content, the higher the absorption and transmission losses. However, it is noted that the S_{11} is not below -10 dB (90% absorption). This is due to the thin sample thickness (1.3 mm) We will present the microwave absorption performance of thicker samples in the mmWave spectrum. This work was supported in part by the National Science Foundation IUCRC under Grant No. 2137275.

[1] C. Dong, X. Wang, and P. Zhou, *Journal of Magnetism and Magnetic Materials*, 354, 340 (2014). [2] H. Won, Y. Hong, and M. Choi, *Journal of Magnetism and Magnetic Materials*, 560, 169523 (2022).

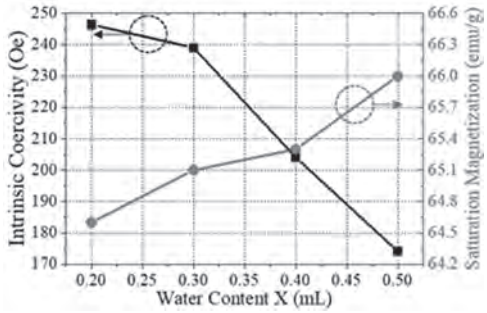

Intrinsic coercivity and saturation magnetization of $BaCo_{0.3}Ti_{0.3}Fe_{11.4}O_{19}$ with various water content.

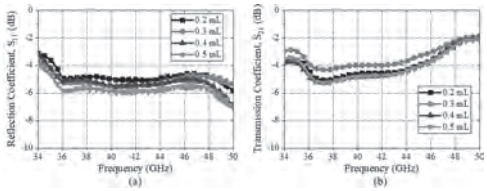

(a) Reflection and (b) transmission coefficient of $BaCo_{0.3}Ti_{0.3}Fe_{11.4}O_{19}$ with various water content.

OPB-04. A New Approach to Identify the Motor Vibration and Noise Dependent on Harmonic and FFT Transform. *C. Hsu*[1] *1. Mechanical Engineering, Asia Eastern University of Science and Technology, New Taipei City, Taiwan*

1. Study Objective The vibration measurement is mainly used natural frequency and resonance frequency to predict the magnetic device operation status. These categories are the value of the predicted frequency. There are applicable the smart device induced as the motor, transformer, robot integration platform [1]. This common feature is focused the electric motor device where is made by the electromagnetic silicon steel sheet. This study is used the magnetostrictive variation induced by the electromagnetic silicon steel sheet through the exciting power of the current and magnetic field which is to accelerate the vibration and noise variation. It is caused by the excitation of the core and coil. It can intercept the required characteristic signal, analyze the performance of dynamic magnetostrictive of ESS under DC bias and its complex dynamic anisotropy. The motors running under high-frequency conditions cause noise and vibration due to the interaction between magnetomotive forces (MMF) is concerned. 2. Experiment Results and Discussion Regarding to the vibration frequency prediction as a multi-type classification problem, it uses the neural network features of deep learning to combine the input signal, as shown in Figure 1. That is classified into different categories. To use an optimized method with feedforward convolutional neural network, it can predict the frequency and analyze the AC and DC vibration frequency of the power motor and the non-fixed periodicity of the mechanical robot arm belong to different spectrum models. The sound pressure level is related to the sound intensity level (SIL). The conversion of voltage signal, current signal, and time domain and frequency domain FFT. As shown in Figure 2, to predict the vibration and sound module by using artificial intelligence method, it is verified the operating system through by measurement, numerical analysis and optimal calculation of NN method to identify the vibration and noise of the motor.

[1] Eshaan Ghosh, Aida Mollaeian, Seog Kim, Jimi Tjong, Narayan C. Kar, DNN-Based Predictive Magnetic Flux Reference for Harmonic Compensation Control in Magnetically Unbalanced Induction Motor, IEEE Transactions on Magnetics, Volume: 53, Issue: 11, 2017.

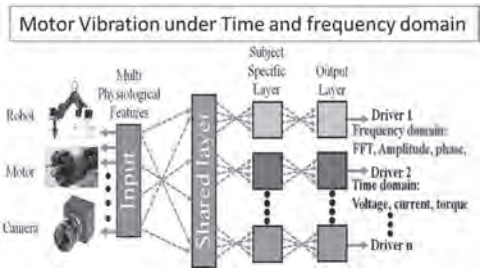

Figure 1 Motor vibration and noise recognition by NN method.

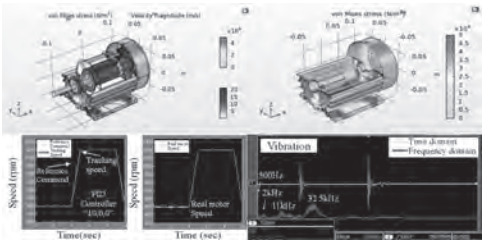

Figure 2 Motor Vibration and Noise: (a)-(b) FEA stress, (c) time domain and (d) frequency domain.

OPB-05. Optimal Design of High-Speed Permanent Magnet Synchronous Machine Based on NSGA-II Considering Mechanical Characteristics. *S. Jo*[1], W. Kim[3], Y. Lee[1], T. Bang[2], H. Lee[1], J. Lee[1] and J. Choi[1]
1. Electrical Engineering, Chungnam National University, Daejeon, The Republic of Korea; 2. Hyundai Mobis R&D Center, Yongin, The Republic of Korea; 3. Hyundai elevator R&D Center, Chungju, The Republic of Korea

Because the rotor of high-speed permanent magnet synchronous machines (PMSMs) rotate at high speeds, a retaining sleeve is used to support the magnet and prevent mechanical problems. In addition, from an electromagnetic perspective, the sleeve acts as an air gap; thus, the thinner the sleeve, the higher the output of the device. Hence, the high-speed PMSM should be designed considering mechanical and electromagnetic properties. [1-3] Based on the equivalence of each part of the machine, intuitive analysis results can be derived via modeling using the analytical method of a PMSM. This method is suitable for an optimal design that requires many design points because it enables rapid characteristic analysis. Fig. 1(a), and (b) show electromagnetic and mechanical modeling using the analytical method, and Fig. 1(c), and (d) compare the analytical method and FEM. Similar results validate the analytical method. Non-Governing Sort-Based Genetic Algorithm (NSGA-II) repeatedly selects, crosses, and mutates within the designated variables range based on the optimization objective to find the optimal point. [4] This study selected an optimal model with efficiency and power density as objective functions. Further, current density, magnetic flux saturation, PM, sleeve, and contact stress were chosen as limiting conditions based on the characteristics derived via the analytical method. Fig. 2(a) shows the optimization result for the proposed method and the Pareto front. Fig. 2(b) compares the shapes of the initial and optimal models, and changes in the PM, sleeve, and stator are shown. Fig. 2(c) shows the experimental configuration of the fabricated optimal model. Fig. 2(d) shows the analysis results of the initial/optimal model and experimental results of the optimal model. The stress acting on the PM and sleeve satisfies the safety requirements while the efficiency is maintained, and the output density is improved.

[1] D. Gerada, A. Mebarki, and N. L. Brown, "High-Speed Electrical Machines: Technologies, Trends, and Developments," in IEEE Transactions on Industrial Electronics, vol. 61, no. 6, pp. 2946-2959, June 2014.

[2] G. Du, N. Huang, and Y. Zhao, "Comprehensive Sensitivity Analysis and Multiphysics Optimization of the Rotor for a High Speed Permanent Magnet Machine," in IEEE Transactions on Energy Conversion, vol. 36, no. 1, pp. 358-367, March 2021. [3] H. -W. Jun, J. Lee and H. -W. Lee, "Study on the Optimal Rotor Retaining Sleeve Structure for the Reduction of Eddy-Current Loss in High-Speed SPMSM," in IEEE Transactions on Magnetics, vol. 51, no. 3, pp. 1-4, March 2015. [4] Y. Hua, H. Zhu and M. Gao, "Multi-objective Optimization Design of Permanent Magnet Assisted Bearingless Synchronous Reluctance Motor Using NSGA-II," in IEEE Transactions on Industrial Electronics, vol. 68, no. 11, pp. 10477-10487, Nov. 2021

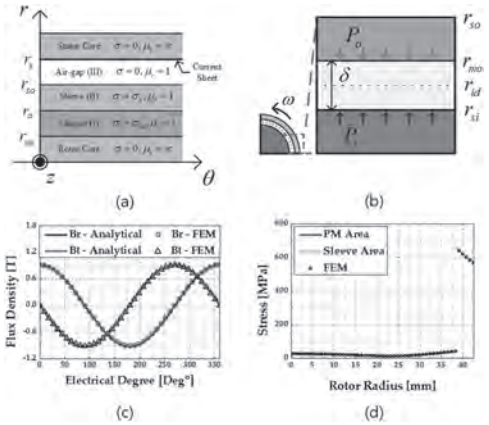

Fig 1. (a) Analytical modeling, (b) comparison between results of FEM and analytical methods, (c) flow chart

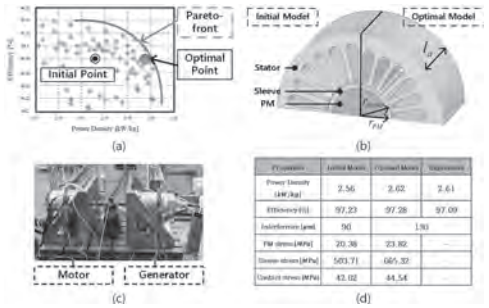

Fig 2. (a) Pareto front through NSGA-II, (b) comparison of the two models' shapes, (c) manufactured model, (d) results of initial and optimal models and the experiment

OPB-06. Prediction of Abnormal Noise and Harmonic of Electromagnetic Motor on Electric Vehicle. *C. Hsu*[1] *1. Mechanical Engineering, Asia Eastern University of Science and Technology, New Taipei City, Taiwan*

This paper proposes the transmission and identification of energy sensing signals for IoT smart vehicles. The article proposes two research structures, including deep learning to detect abnormal sound signals of vehicle motors. The Internet of Things technology to collect vehicle sensing signals upload to the cloud system. A new approach of tunable FOPID (fractional-order proportional-integral-derivative) fuzzy controller for reduction of power losses on electric vehicle, which saving energy included as the AC generator, supercapacitors and Li-ion battery charging device etc., is proposed as shown in Figure 1. The energy consumption for power inverter, AC generator, transformer and supercapacitors battery was calculated. A modified switching pulse width-modulation (PWM) inverter, which a generator with signal AC/DC inverter FOPID controller is performed. A deep learning neural network method to solve motor unformal signal is proposed. Long short term memory (LSTM) have a higher accuracy of intercepting motor noise than conventional machine learning methods. Additionally, the disadvantage of deep learning algorithms is that they require large datasets to ensure an efficient performance. In this study, a combination of CNN and LSTM is proposed

to prevent failure cause by the motor anomalous noise. This is applied to the CNN for noise image feature material. In addition, the LSTM is combined with the actual noise measurement spectrum data between 40 Hz – 20 kHz to analyze the noise of the motor. The CNN-LSTM can be effectively analyzed substantial anomalous motor noises. This approach yields a reduction in the switching losses and an improvement in the converting efficiency evidenced by the numerical data, as shown in Figure 2. Finally, experimental results also show that FOPID with fuzzy controller in saving energy can improve power loss, compared with that of conventional PID controller around 35%.

[1]Chang-Hung Hsu, et. al. " Effect of magnetostriction on the core loss, noise, and vibration of fluxgate sensor composed of amorphous materials," IEEE Transactions on Magnetic, vol. 49, no. 7, pp. 3862-3865, 2013. [2] Chang-Hung Hsu, et. al. "Effects of magnetostriction and magnetic reluctances on magnetic properties of distribution transformers," Journal of Applied Physics, vol. 115, no. 17, pp. 17E718-1-3, 2014.

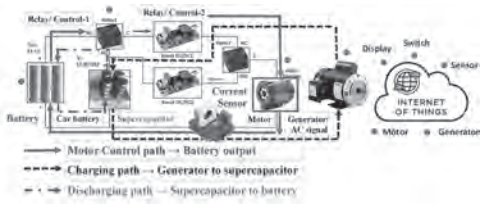

Figure 1 Electric vehicle charging and discharging system with IoT and Cloud system.

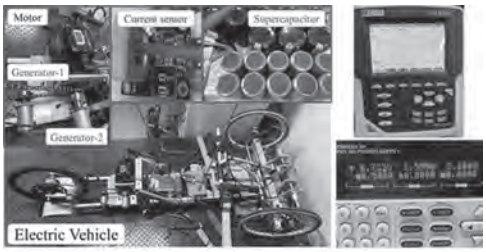

Figure 2 Electric vehicle changing and discharging experiment environment with supercapacitors, magnetic current sensor and measured equipment, respectively.

OPB-07. Withdrawn

OPB-08. A Novel Fault-Tolerant Multi-Tooth Field Modulated Machine with Hybrid Excitation. *Z. Jin*[1], X. Zhu[1], S. Ding[1] and X. Wang[1]
1. Nanjing Normal University, Nanjing, China

I. Introduction Hybrid-excited (HE) machine and fault-tolerant (FT) machine have attracted wide attention due to their several advantages, such as easy adjustment of air-gap magnetic field, high power density and high efficiency in wide speed range of HE machine, and reliability of FT machine [1]-[2]. Nowadays, multi-tooth field modulated (MTFM) machines have become a research hotspot thanks to their capability of sufficiently utilizing harmonics to promote the average output torque [3]. In this paper, to apply the advantages of HE machine and FT machine to MTFM machine, a novel hybrid-excited fault-tolerant multi-tooth field modulated (HEFT-MTFM) machine is proposed. The topology of proposed machine is shown in Fig. 1. To have lower demagnetization risk, parallel-hybrid-excited structure is adopted in the machine. II. Electromagnetic Performance The electromagnetic performances of HEFT-MTFM machine are presented in Fig. 2. It can be seen that regulating the magnitude of air-gap field by excitation windings can change the magnitudes of flux linkage, back-EMF and electromagnetic torque, and keep flux linkage and back-EMF good sinusoidal and also keep the magnitude of cogging torque and torque ripple small. In terms of the fault-tolerant capability, It can be observed from Fig. 2 (e) that the self-inductance of HEFT-MTFM machine is larger than that of traditional fault-tolerant field modulated machine by same motor size. Overall, the proposed HEFT-MTFM machine exhibit good flux regulation capability, sinusoidal flux linkage and back-EMF, small cogging torque and torque ripple, short-circuit current restrained capability due to high self-inductance and magnetically isolated capability due to low mutual-inductance. The operation principle, machine optimization and more detailed performances including the loss of PMs and operation efficiency will be further discussed in the full paper.

[1] E. F. Farahani, M. A. J. Kondelaji and M. Mirsalim, "An innovative hybrid-excited multi-tooth switched reluctance motor for torque enhancement," *IEEE Trans. Ind. Electron.*, vol. 68, no. 2, pp. 982-992, Feb. 2021. [2] Y. Wang and Z. Deng, "A multi-tooth fault-tolerant flux-switching permanent-magnet machine with twisted-rotor, " *IEEE Trans. Magn.*, vol. 48, no. 10, pp. 2674-2684, Oct. 2012. [3] L. Cao, K. T. Chau, C. H. Lee, and W. H. Lam, "Design and analysis of a new parallel-hybrid-excited machine with harmonic-shift structure," *IEEE Trans. Ind. Electron*., vol. 67, no. 3, pp. 1759-1770, Mar. 2020.

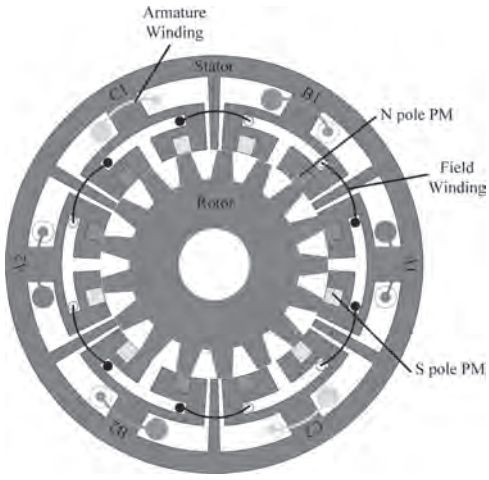

Fig. 1. Topologies of HEFT-MTFM machine.

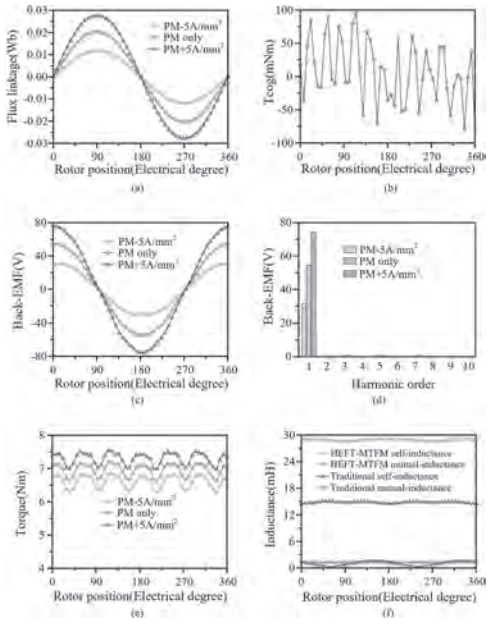

Fig. 2. Electromagnetic performances of HEFT-MTFM machine. (a) Flux linkage. (b) Cogging torque. (c) Back-EMF. (d) Harmonics of back-EMF. (e) Electromagnetic torque. (f) Inductance.

OPB-09. Comparative Analysis of Three Novel Fault-Tolerant Multi-Tooth Flux-Switching Permanent-Magnet Machine. *Z. Jin*[1], X. Zhu[1], S. Ding[1] and L. Liu[1] *1. Nanjing Normal University, Nanjing, China*

I. Introduction Flux-switching permanent-magnet (FSPM) machine has been received much attention due to its advantages of high torque density and easy heat management, etc. [1]. In order to enhance the torque/power capability, FSPM machine with multi-tooth structure (MFSPM) has been proposed [2]. However, not only high power density but also high reliability and good fault-tolerance capability are required for PM machine and hence three novel fault-tolerant MFSPM (FT-MFSPM) machines are proposed in this paper based on the MFSPM machine in [2]. The topologies of proposed machines are shown in Fig. 1. To increase the torque density, a new outer rotor FT-MFSPM (Model I) shown in Fig. 1 (a) is proposed based on [2]. To further increase the output torque, a middle PM is added in each dummy slot (Model II) as shown in Fig. 1 (b). Employing more PMs is an effective method to improve the toque without consuming the operating energy and thus the dual PM modulated FT-MFSPM machine (Model III) is proposed and shown in Fig. 1 (c). II. Performance comparisons The electromagnetic performances of three FT-MFSPM machines are presented in Fig. 2. It can be seen that though Model III exhibits the highest value of flux linkage, back-EMF and electromagnetic torque, it also exhibits the highest value of cogging torque and torque ripple and the most distorted back-EMF. In terms of the fault-tolerant capability, it can be observed from Fig. 2 (e) that the self-inductance of Model I and Model II is almost the same, which is higher than that of Model III. Overall, Model II is superior to Model I and Model III since Model II has greater output torque and smaller torque ripple than Model I with a few increase of PMs and has greater short-circuit current restrained capability due to higher self-inductance and smaller torque ripple with less PMs. The machine optimization and more detailed comparisons including the losses and efficiency will be further discussed in the full paper.

[1] X. Zhu, W. Hua, Z. Wu, H. Zhang and M. Cheng, "A analytical approach for cogging torque reduction in flux-switching permanent magnet machines based on magnetomotive force-permeance model," *IEEE Trans. Ind. Electron.*, vol. 65, no. 3, pp. 1965-1979, Mar. 2018. [2] G. Zhao and W. Hua, "Comparative study between a novel multi-tooth and a v-shaped flux-switching permanent magnet machines," *IEEE Trans. Magn.*, vol. 55, no. 7, pp. 1-8, July. 2019.

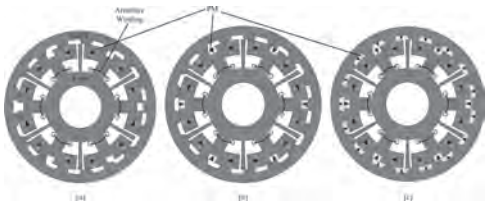

Fig. 1. Structures of FT-MFSPM machines. (a) Model I. (b) Model II. (c) Model III.

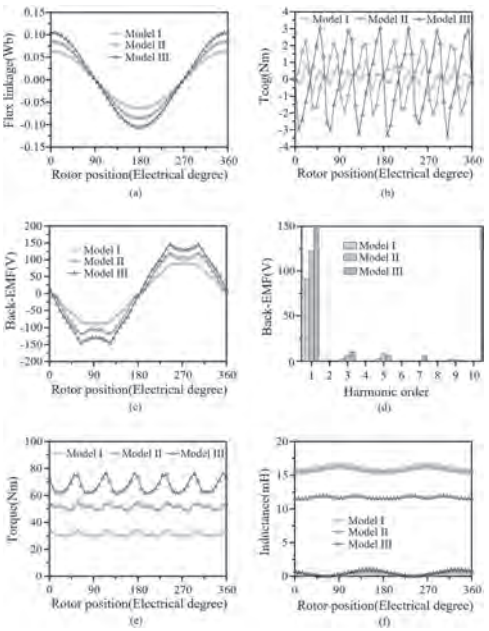

Fig. 2. Electromagnetic performances of FT-MFSPM machines. (a) Flux linkage. (b) Cogging torque. (c) Back-EMF. (d) Harmonics of back-EMF. (e) Electromagnetic torque. (f) Inductance.

OPB-10. Torque Analysis of a Permanent Magnet Synchronous Motor using Flux Densities in Air Gap. *S. Lee*[1], C. Kim[1], Y. Choo[1], G. Yun[1] and C. Lee[1] *1. Electrical Engineering, Pusan National University, Busan, The Republic of Korea*

Permanent magnet synchronous motors (PMSMs) having high power density and high efficiency are rigorously researched in various premium applications. Among PMSMs, many studies have been conducted on interior permanent magnet synchronous motors (IPMSMs) to improve torque ripple [1-3], but its accurate estimation is not straightforward. Therefore, a six-pole nine-slot IPMSM is adopted as a base model due to its popularity in academia and industries. Other two pole/slot combinations (8p/12s, 10p/15s) having the same winding factor of 0.866 are additionally selected to investigate mainly the influence of a pole/slot combination on torque performance. Air gap force is separated into its radial and tangential components, and the tangential force density (F_t) is determined by two magnetic flux densities in air gap [4]. Due to proportional relation between F_t and the torque [4], torque performance is easily identified by analyzing. In case of maximum and minimum torque at the instant of t_{max} and t_{min}, respectively, the distribution of F_t along air gap is illustrated in Fig. 1 to analyze torque ripple. The biggest gap between $F_t(\theta_m, \omega t_{max})$and $F_t(\theta_m, \omega t_{min})$ as indicated in red and blue, respectively, occurs around the right side of a stator pole surface as shaded in yellow in case of anticlockwise rotation. Since F_t is proportional to the product of B_r and B_t [4], magnetic flux densities in air gap have to be examined to analyze the variation of F_t. The moment of maximum torque is given in Fig. 2, and it is noted that the change of B_t in increasing a pole number is much greater than that of B_r. Compared to B_t of 6p/9s, in particular, that of 10p/15s is significantly reduced by 46% around the right side of a stator pole, and hence, torque ripple is improved in the 10p/15s combination. In conclusion, in varying pole and slot numbers, the impact of B_t is dominant on torque ripple. Especially, the change of B_r and B_t with respect to a pole/slot combination will be meticulously analyzed and explained in terms of its reason and relationship with torque ripple.

[1] Qian Chen *et al*., IEEE Transaction on Industrial Electronics., Vol.65, p.8520-8531 (2018) [2] Shushu Zhu, Weifang Chen *et al*., IEEE Transactions on Magnetics., Vol.54, p.1-5 (2018) [3] Jang-Young Choi, Yu-Seop Park, and Seok-Myeong Jang, IEEE Transactions on Magnetics., Vol.48, p.987-990 (2012) [4] J. F. Gieras, Permanent magnet motor technology: design and applications, CRC press (2018)

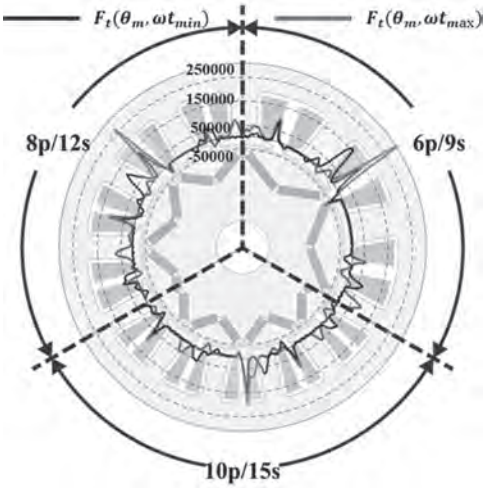

FIg. 1. Distribution of tangential force density in case of maximum and minimum torque

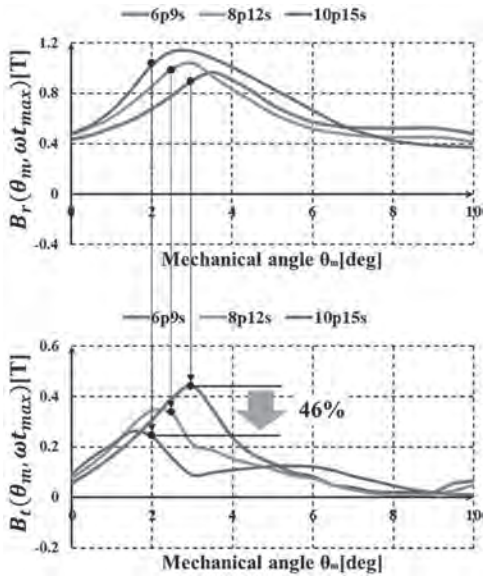

Fig. 2. Distribution of B_r and B_t in case of maximum torque

OPB-11. Vibration Analysis of a Permanent Magnet Synchronous Motor by a Pole/Slot Combination. *G. Yun*[1], Y. Choo[1], C. Kim[1], S. Lee[1], D. Hong[2] and C. Lee[1] *1. Electrical Engineering, Pusan National University, Busan, The Republic of Korea; 2. Electric Motor Research Center, Korea Electrotechnology Research Institute, Changwon, The Republic of Korea*

The increase of power density in permanent magnet synchronous motors(PMSMs) has been getting more crucial these days, and there are two methods to improve the power of a PMSM. One is the increase of magnetic loading(ML) by changing the grade and/or size of permanent magnets [1]. The other is the change of electric loading(EL) by modifying winding design and/or current [2]. ML and EL leading to magnetic flux density in air gap affect electromagnetic and mechanical performance at the same time. Thus, Balance between ML and EL should be examined in terms of efficiency and vibration. In this paper, a sixteen-pole eighteen-slot PMSM for a vertical articulated robot is chosen as a reference model [3], and other two pole/slot combinations (20p/18s, 20p/24s) are together compared in terms of electrical and mechanical performance. In the electric motor, electromagnetic vibration is generated by air gap radial force(P_r) whose density is determined by radial and tangential magnetic flux densities. At a given instant of time, the flux densities are spatially distributed along air gap with respect to mechanical angle, and their spatial distribution changes by spinning the rotor. P_r distributed in a three-dimensional manner is decomposed into harmonics as Fig.1. In the case of 16p18s, the 16th radial force is dominant on the x-axis of a temporal harmonic order. Regarding the y-axis of a spatial harmonic order, the 2nd and 16th are important. The vibration displacement is calculated by the harmonics of P_r as Fig.2. At the frequency of 533.3Hz, the RMS of vibration acceleration of the 16th temporal order on the x-axis is 1.14m/s^2, and the 2nd and 16th spatial harmonics have the portion of 83% and 9%, respectively, in vibration acceleration. The influence of ML and EL on the radial force density of the 2nd and 16th spatial harmonics is significantly different each other. In conclusion, balance between magnetic and electric loading has to be examined in terms of efficiency and vibration. Especially, trade-off between efficiency and vibration will be meticulously analyzed and explained during the increase of power in PMSMs.

[1] Hyeon-Jin Park, Myung-Seop Lim, and Chung-Seong Lee, IEEE Access 7., p.137207-137216 (2019) [2] J. W. Chin, K. S. Cha, M, R, Park, IEEE Transactions on Energy Conversion., Vol. 36, p.883-894 (2020) [3] Do-Kwan Hong, Wook Hwang, Ji-Young Lee, IEEE Transactions on Magnetics., Vol. 54, p.1-4 (2017)

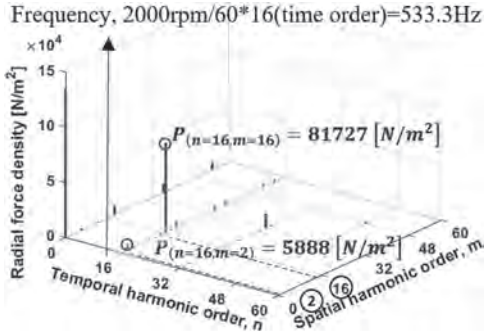

Spatial and temporal harmonics of radial force density in 16p18s

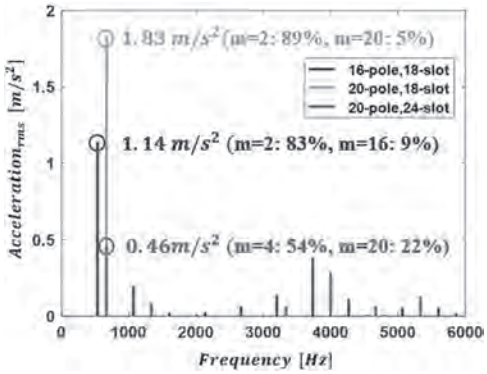

Vibration acceleration in three motors

OPB-12. Withdrawn

OPB-13. Analysis and Measurements of Influence of Current Harmonics on Vibration of High-Speed Motors with Rare-Earth Permanent Magnets. *J. Woo*[1], H. Lee[1], S. Kim[1], J. Lee[1], K. Kim[2] and J. Choi[1] *1. Electrical Engineering, Chungnam National University, Yuseong-gu, The Republic of Korea; 2. In-wheel system development cell, Hyundai mobis, Giheung, The Republic of Korea*

Recently, high-speed permanent magnet motors have been used in various fields by applying rare-earth permanent magnets. Because they rotate at high speeds, the effects of noise, vibration, and harshness (NVH) should be analyzed for mechanical stability. Based on many studies, electromagnetic-exciting sources affecting NVH are classified into cogging torque, torque

ripple, electromagnetic force density distribution (MPF), and unbalanced electromagnetic force [1-2]. Therefore, an analysis reflecting the complex excitation source is required in designing a stable high-speed motor [3]. In this study, after analyzing the effect of carrier harmonics generated in the pulse-width modulation control method on the electromagnetic-exciting source through dynamic simulations, the unbalanced electromagnetic force was derived. Finally, the effect on the mechanical aspects was analyzed. Fig. 1(a) shows the 3D structure of the proposed model, and Fig. 1(b) shows the experimental set. Fig. 1(c) and (d) show the variations in the current and magneto-motive force (MMF) waveforms, respectively, according to carrier harmonics through dynamic simulation. Fig. 2(a) shows the UMF of the armature reaction, and Fig. 2(b) shows the harmonics of the torque. The NVH analysis results based on these effects are shown in Fig. 2(c) and (d). Fig. 2(c) shows the NVH when a sinusoidal current is applied, and Fig. 2(b) shows the NVH when the inverter generates a harmonic current. Based on the analysis results, it was confirmed that the higher the vibration order of the frequency related to the unbalanced electromagnetic force, the more significant its influence on the vibration and noise. These results indicate that vibration and noise analyses considering the inverter are essential in the design and performance analysis of high-speed motors. Detailed comparative analysis and experimental results will be presented in the complete paper.

[1] P. Beccue, J. Neely, S. Pekarek, and D. Stutts,"Measurement and control of torque ripple-induced frametorsional vibration in a surface mount permanent magnetmachine,"IEEETrans. Power Electron., vol. 20, no. 1, pp. 182–191, Jan. 2005. [2] H. Yang and Y. Chen, "Influence of radial force harmonicswith low mode number on electromagnetic vibration ofPMSM,"IEEETrans. Energy Convers., vol. 29, no. 1, pp. 38–45, Mar. [3] Tae-chul Jeong, "Current Harmonics Loss Analysis of 150-kW Traction Interior Permanent Magnet Synchronous Motor Through Co-Analysis of d-q Axis Current Control and Finite Element Method", IEEE Transactions on magnetics, Vol. 49, No. 5, 2343, 2013

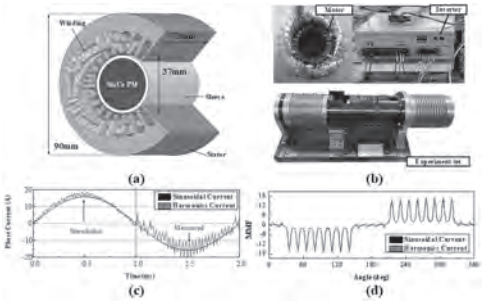

(a) 3D structure of high-speed motor, (b) experimental system, and (c) variations in current waveform and (d) MMF waveform according to carrier harmonics

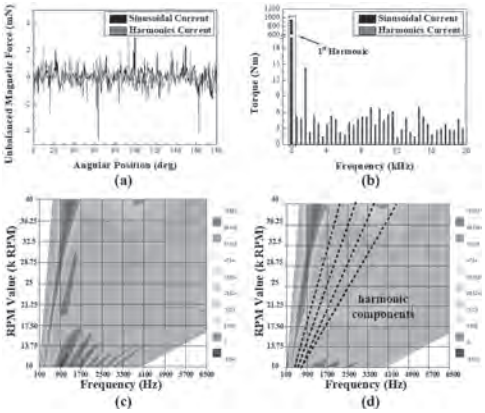

Comparison of (a) UMF and (b) harmonics of the torque, analysis results for NVH according to (c) sinusoidal current and (d) harmonics current.

OPB-14. The Influence of Structural Parameters and Layout Form of Silicon Sheet on The Spectrum Characteristics of Magnetic Field in Propulsion Motor. *X. Liang*[1], W. Li[1], J. Gao[1], M. Wang[1] and P. Zheng[1]
1. School of Electrical Engineering and Automation, Harbin Institute of Technology, Harbin, China

Recently, the synchronous reluctance motor (SRM) with uneven arrangement of silicon sheet has been paid to more attention in high-power propulsion.[1] Because SRM contains complex structure and too many parameters, the parameter scanning method is usually adopted by finite element analysis (FEA). However, when the arrangement of silicon sheet and the structure of motor change, the previous simulations cannot provide effective reference. So, the slow and time-consuming parameter scanning needs to be used again. In order to improve the designing efficiency, the influence of structural parameters and layout form of silicon sheet on the spectrum characteristics of propulsion motor's electromagnetic field is researched. When the law between the magnetic field distribution and the structure of SRM is clear, the design scheme only needs to be verified in a small parameter range. Therefore, the high-efficiency design of motor using silicon sheet can be realized. In ideal situation, the q-axis magnetic field is weakened without effecting the d-axis by using the combination of low- and high- permeability materials, high-performance SRM is realized. To achieve this effect, the analysis method based on the spectrum characteristics of motor structure is adopted to avoid repeated parameter scanning, as shown in Fig. 1. Based on prototype that can reflect different combinations of high- and low- permeability materials, the d- and q- axis magnetic field of SRM is calculated by FEA. The relationship between the spectrum characteristics of the magnetic field and the spatial distribution of silicon sheet in SRM is obtained, as shown in Fig. 2. With the change of position, width and proportion of low permeability materials, the spectrum characteristics of d- and q- axis magnetic field are different, and the variation rules of harmonics of different orders are also different. The specific spatial distribution of silicon sheet can be obtained according to the specific design requirements. Referencing to the analysis results, the parameters of SPM can be quickly confirmed in small range.

[1]. Tawfiq, K.B., et al., Performance Improvement of Synchronous Reluctance Machines—A Review Research. IEEE Transactions on Magnetics, vol.57, p. 1-11(2021).

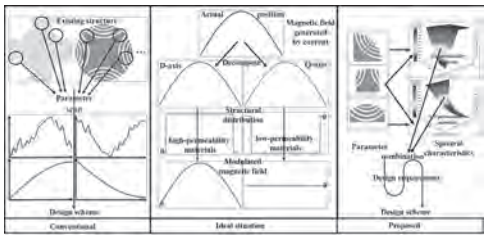

Fig. 1. Comparison of different design and analysis process

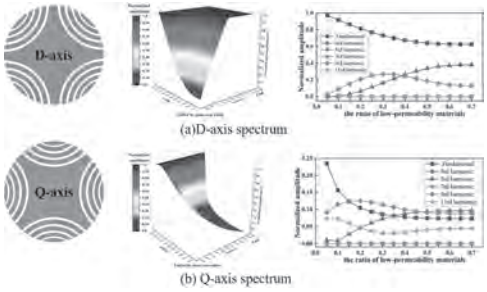

Fig. 2. Spectrum characteristics of different structural parameters

Session PPA
MAGNETICS FOR POWER ELECTRONICS AND CONTROL
(Poster Session)

Yongjian Li, Chair
Hebei University of Technology, Tianjin, China

PPA-01. Development of a Novel Radial - Axial Flux Permanent Magnet Claw Pole Machine with SMC Cores and Ferrite Magnets. *C. Liu*[1], F. Yang[1] and Y. Wang[1] *1. Hebei University of Technology, Tianjin, China*

Soft magnetic composite (SMC) material is a relative new soft magnetic material, which has many advantages over traditional silicon sheets, however it has many disadvantages as well. For the better utilization of SMC material in developing electrical machines, some design guidelines should be followed, e.g., 3D magnetic flux path, high frequency operation, and permanent magnet excitation [1]. There are many electrical machines with SMC cores had been developed in the past decades. Based on global ring winding and 3D magnetic flux path, permanent magnet claw pole machine (PMCPM) has shown its high torque ability compared with other electrical machines [2]. For the most PMCPM, three same single phase PMCPM modules are required with shifting 120 degrees electrically each other to form three phase operation, and each one phase module has its own PM rotor thus the PM utilization is very low [3]. In this paper, for improving the PM rotor utilization a novel axial radial flux permanent magnet claw pole machine ARPMCPM is proposed and designed where there stators share one PM rotor. For the performance prediction, 3D finite element method (FEM) is used. Fig. 1 shows the main magnetic structure of the ARPMCPM. As shown, one radial flux claw pole stator and two axial flux claw pole stators are required, the global ring winding is adopted, and spoke PM configuration is adopted for the PM rotor. To form three phase operation, these three claw pole stators are shifted 120 degrees electrically to each other and the winding section area needs to be designed reasonably. Fig. 2 shows no load magnetic field distribution, parameters and main performance of ARPMCPM based on 3D FEM. Fig. 2(b) shows the no load PM flux linkage of winding A, B and C. As shown, A phase PM flux linkage higher than the other PM flux linkages as winding A is located on the radial flux claw pole stator. Fig. 2(c) shows the induced voltages. Fig. 2(d) shows the torque waveform under the current density of 6 A/mm^2. Fig. 2(e) and (f) are the core loss and efficiency map. More details and design methods for the ARPMCPM will be presented in the full submission.

[1] C. Liu, J. Zhu, Y. Wang, G. Lei and Y. Guo, "Design Considerations of PM Transverse Flux Machines With Soft Magnetic Composite Cores," in IEEE Transactions on Applied Superconductivity, vol. 26, no. 4, pp. 1-5, June 2016, Art no. 5203505, doi: 10.1109/TASC.2016.2531982 [2] C. Liu, J. Zhu, Y. Wang, Y. Guo and G. Lei, "Comparison of Claw-Pole Machines With Different Rotor Structures," in IEEE Transactions on Magnetics, vol. 51, no. 11, pp. 1-4, Nov. 2015, Art no. 8110904, doi: 10.1109/TMAG.2015.2443022. [3] C. Liu et al., "Performance Evaluation of an Axial Flux Claw Pole Machine With Soft Magnetic Composite Cores," in IEEE Transactions on Applied Superconductivity, vol. 28, no. 3, pp. 1-5, April 2018, Art no. 5202105, doi: 10.1109/TASC.2017.2777927.

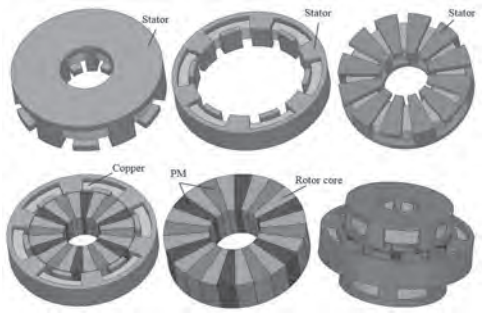

Fig. 1 Main magnetic structure of the ARPMCPM

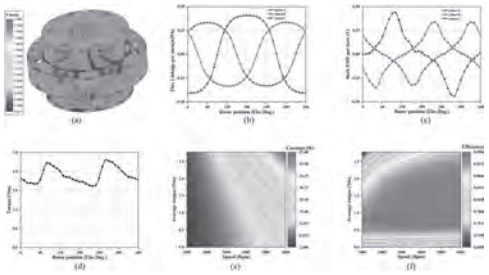

Fig. 2 Performance analysis of ARPMCPM

PPA-02. Study on magnetic stability of low corrective force permanent magnet in memory machine under inverter open-circuit fault. *X. Zhao*[1], H. Lin[1], W. Liu[1] and X. Zeng[1] *1. Southeast University, Nanjing, China*

I. Introduction Variable flux memory machines (VFMMs) can adjust the air-gap magnetic field by changing the magnetization state (MS) of the low corrective force (LCF) permanent magnet (PM)[1]. LCF PM is easily demagnetized by the magnetomotive force (MMF) of the armature currents. As a traction machine forelectric vehicles, the VFMMs need to be connected with an inverter. However, the open-circuit (OC) fault of the inverter will change the armature current, which will affect the magnetic stability of LCF PM. Moreover, the inverter working principle determines that its IGBT needs to be frequently switched, which increases the probability of the OC fault. It is worth noting that most research focuses on the VFMM topology innovation [2-3]. The research on the effect of the OC fault on LCF PM demagnetization has not been found. II. Model The inverter OC fault is realized by the field-circuit coupling method, as shown in Fig. 1. Moreover, the VFMM employs a 27-slot and 4-pole structure, and high corrective force (HCF) and LCF PMs form a series magnetic circuit. III. Research Results The preliminary results are shown in Fig. (2). In Fig.2 (a), the positive half-wave of the A-phase current will become 0 after the fault. The DC component appears in the 3-phase currents, which makes them unbalanced and the phase angle changed. In region II, the phase angle difference between the B- and C-phases is π. As shown in Fig2 (b), with the increase of the B- and C-phase currents, the total MMF of region II will exceed that of normal operation. Hence, the LCF PM working point is significantly decreased after the fault load currents are applied, which indicates that LCF PM is demagnetized, as shown in Fig. 2 (c). Besides, affected by the fault currents and

LCF PM demagnetization, compared with the torque and torque ripple in normal, the torque is reduced by 29.5% and the torque ripple is increased by 7.8 times in fault. From the above analysis, it can be seen that the influence of the OC fault on the VFMM performance is significant, and further study is necessary. This will be shown in the full paper.

[1] V. Ostovic, "Memory motors—A new class of controllable flux PM machines for a true wide speed operation, " *Proc. 36th IAS Annu. Meeting IEEE Ind. Appl. Conf.*, Chicago, USA, Sep./Oct. 2001, vol. 4, pp. 2577–2584. [2] H. Hua, Z. Q. Zhu, A. Pride, R. P. Deodhar and T. Sasaki, "A Novel Variable Flux Memory Machine With Series Hybrid Magnets," *IEEE Trans. Ind. Appl*, vol. 53, no. 5, pp. 4396-4405, Sept.-Oct. 2017. [3] R. Tsunata, M. Takemoto, S. Ogasawara and K. Orikawa, "Variable flux memory motor employing double layer delta-type pm arrangement and large flux barrier for traction applications," *IEEE Trans. Ind. Appl.,* vol. 57, no. 4, pp. 3545-3561, July-Aug. 2021.

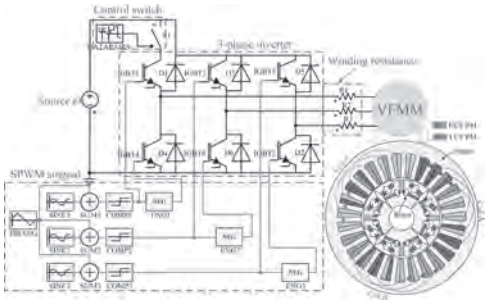

Fig. 1. Field-circuit coupling model.

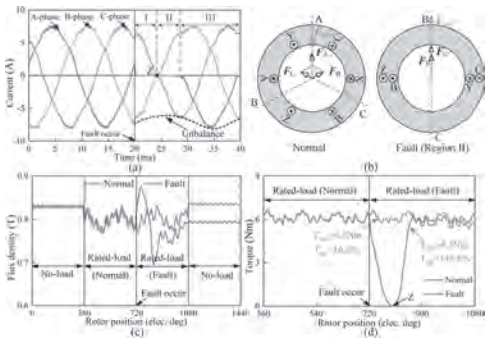

Fig. 2. Preliminary results. (a) Current. (b) Synthetic MMF. (c) LCF PM working point. (d) Torque.

PPA-03. Electromagnetic Analysis and Experimental Study of Permanent Magnet Synchronous Machine considering Axial Leakage Flux using Subdomain Method. *K. Shin*[1], J. Lee[1], H. Cho[2], J. Choi[2] and S. Sung[3] *1. Chonnam National University, Yeosu, The Republic of Korea; 2. Chungnam National University, Daejeon, The Republic of Korea; 3. Korea Research Institute of Ships and Ocean Engineering, Daejeon, The Republic of Korea*

Permanent magnet synchronous machine (PMSM) has been widely used in various applications such as industries, home appliances, and electric propulsion systems due to the technological progress for producing permanent magnets with high energy density and power electronics [1], [2]. Since the 2D analysis cannot consider the axial leakage magnetic flux, it is difficult to accurately predict the machine performance under the rated condition. To overcome these problems, the axial leakage magnetic flux can be considered through a 3D analysis. Therefore, in this study, the electromagnetic analysis of PMSM considering axial leakage is proposed using a 2D subdomain method as shown in Fig. 1. In the design phase, 2D subdomain method not only provides insights into the relationship between design variables and performances but can also consider end effects by applying permeability to slot and slot opening regions [3], [4]. The magnetic field and the electromagnetic performance obtained using the proposed analytical method were compared with those obtained using the finite element (FE) analysis, and experimental measurement. To measure the operating characteristics, a back-to-back system with a prototype and load generator is constructed as shown in Fig. 2. Under the rated conditions, the conventional 2D FE analysis includes high torque and a wide operating range, and the proposed analytical method and experimental results show similar operating performances. Therefore, the proposed analytical method can predict an accurate characteristic analysis by considering the axial leakage flux in the initial design stage. The analytical approach, analysis, and experimental results will be presented in more detail in the full paper.

[1] E. Sulaiman, T. Kosaka, and N. Matsui, IEEE Trans. Magn., Vol. 47, pp. 4453–4456, (2011). [2] J. Jung, H. Park, J. Hong, and B. Lee, IEEE Trans. Magn., Vol. 53, (2017). [3] K.-H. Shin, H. I. Park, H.-W. Cho, and J.-Y. Choi, IEEE Trans. Magn., Vol. 53, (2017). [4] T. Lubin, S. Mezani, and A. Rezzoug, IEEE Trans. Magn., Vol. 48, pp. 2080–2091, (2012).

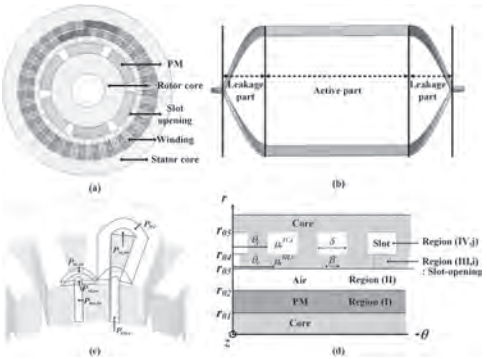

Fig. 1. Structure of PMSM: (a) analysis model, (b) winding with active and leakage part, (c) stator with permeances and (d) simplified analytical model.

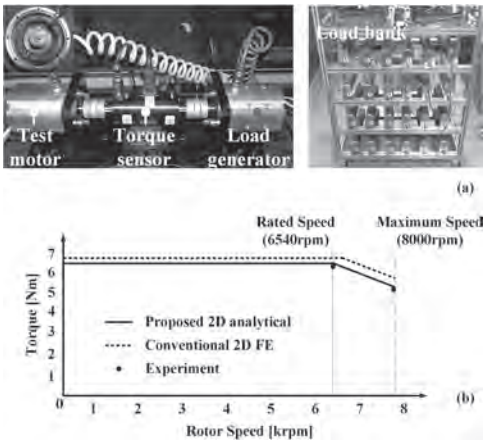

Fig. 2. (a) Experimental setup and (b) torque-speed curve obtained by 2D FE analysis, analytical and experimental results.

PPA-04. Characteristic Analysis and Experimental Study for Accurate Prediction of Electromagnetic Losses in High-Speed Permanent Magnet Synchronous Motors. *K. Shin*[1], J. Lee[1], H. Cho[2], J. Choi[2], S. Lee[3] and M. Koo[3] *1. Power System Engineering, Chonam National University, Yeosu, The Republic of Korea; 2. Chungnam National University, Daejeon, The Republic of Korea; 3. Korea Institute of Industrial Technology, Gwangju, The Republic of Korea*

High-speed permanent magnet synchronous motors (HPMSMs) are developed in direct-drive applications such as centrifugal compressors and vacuum pumps because of the advantages of compact size and high efficiency [1]. However, due to the small size, it has a high loss density and a limited

heat dissipation surface, which causes difficulties in cooling [2]. Therefore, the accurate prediction of electromagnetic losses is very important in the design stage of HPMSM. In this study, electromagnetic analysis considering pulse width modulation (PWM) inverter and effective three-dimensional (3D) electromagnetic structure is proposed for predicting accurate electromagnetic losses of HPMSM. Fig. 1 shows the 3D structure and side view of the HPMSM and the evaluation system of the prototype. To accurately predict the applied current, it is necessary to derive the back EMF constant, resistance, and inductance using the 3D finite element method (FEM). Using the dynamic model based on the derived machine constants, it is possible to predict the applied PWM current similar to the experimental results as shown in Figs. 2(a) and (b). As shown in Fig.2(c), mechanical losses according to speed can be calculated by subtracting the core losses calculated from FEM from the measured no-load losses. Using the proposed effective 3D model, accurate electromagnetic losses such as AC and DC copper losses, core loss, and rotor loss can be predicted. Considering mechanical losses, the error between the proposed electromagnetic loss analysis and the experiment is within 3% according to the operating condition as shown in Fig. 2 (d). The analysis, discussions, and measurements of HPMSM will be explained in more detail in the full paper.

[1] D. Gerada, A. Mebarki, and A. Boglietti, *IEEE Trans. Ind. Electron.*, Vol. 61, pp. 2946–2959 (2014). [2] D.-K. Hong, B.-C. Woo, and D.-H. Koo, *IEEE Trans. Magn.*, Vol. 48, pp. 871–874, (2012).

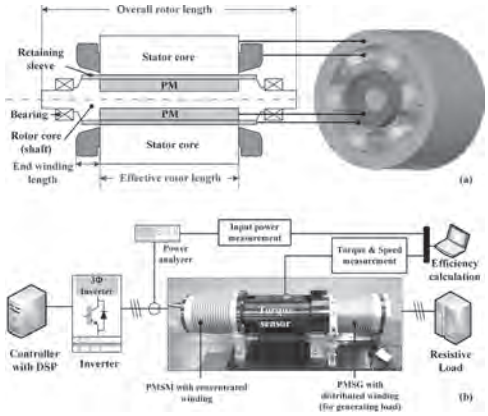

Fig. 1. (a) Structure of HPMSM with concentrated winding and (b) performance evaluation system.

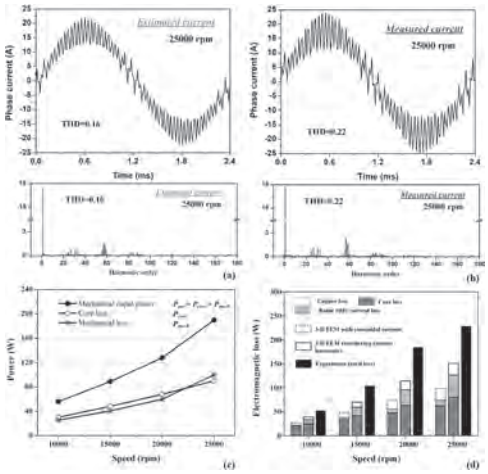

Fig. 2. Comparison with analysis and experimental results: (a) estimated, (b) measured phase current, (c) measured mechanical loss, and (d) electromagnetic losses.

PPA-05. Optimization of Detent Force in Linear Oscillatory Generator with Assisted Permanent Magnet and Stacking Effect for Stirling Engines Using Analytical Method. *K. Shin*[1], J. Lee[1], H. Cho[2], J. Choi[2], S. Lee[3] and M. Koo[3] *1. Chonnam National University, Yeosu, The Republic of Korea; 2. Chungnam National University, Daejeon, The Republic of Korea; 3. Korea Institute of Industrial Technology, Gwangju, The Republic of Korea*

A single-phase linear oscillatory generator (LOG) is widely used in direct-drive systems such as the Stirling engine system due to its advantages such as high transmission efficiency and simple structure as shown in Fig. 1 [1], [2]. However, one of their drawbacks is the generation of detent force caused by the attraction between the permanent magnet (PM) and the iron core. A large detent force causes thrust ripples and noise, which results in poor positioning accuracy [3]. Therefore, the prediction of the detent force is an important factor to be considered in the design of the LOG with PM mover. To solve these problems, this study proposes an electromagnetic analysis using an analytical method to optimize the detent force by applying spring PM to the PM mover [1]. This paper derives analytical solutions in terms of magnetic vector potential based on the subdomain model as shown in Figs 1 (b) and (c). From the analytical solution, the electromagnetic force is derived using the Maxwell stress tensor. The validity of the proposed method is verified through comparison with the results of finite element (FE) analysis as shown in Figs. 2 (a) and (b). Fig. 2 (c) shows the analysis result of the detent force according to the width of the spring PM at a minimum position of the stroke. Therefore, positive values of the detent force are generated to use restoring force. Fig. 2 (d) shows the comparison between the detent force with and without spring PM. It is observed that the direction of the detent force changes in the spring PM model and the force is hardly generated in the stroke region. The analytical technique, analysis results, discussions, and measurements of the LOG will be presented in more detail in the full paper.

[1] J.-M. Kim, J.-Y. Choi, K.-S. Lee, and S.-H. Lee, AIP Adv., Vol. 7, Art. no. 056667 (2017). [2] J. Sjölund, M. Leijon, S. Eriksson, AIP Adv., Vol. 10, Art. no. 035312 (2020). [3] K. H. Shin, K. H. Kim, K. Hong, J. Y. Choi, IEEE Trans. Magn., Vol. 53, Art. no. 810450 (2017).

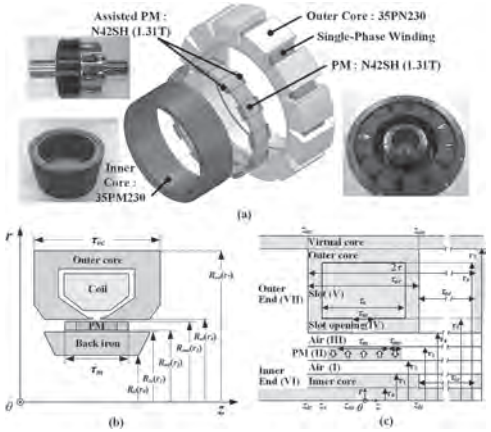

Fig. 1. Structure of single-phase PM LOG: (a) prototype, (b) analysis, and (c) analytical model.

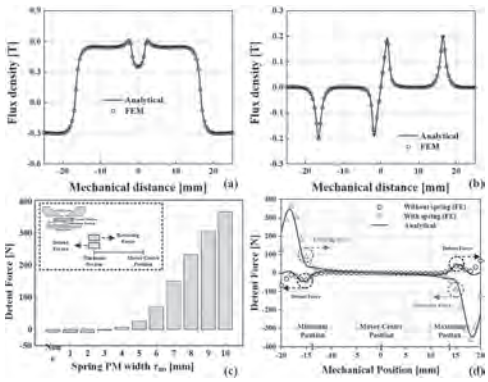

Fig. 2. Comparison between analytical and FE results: (a) radial flux density, (b) tangential flux density, (c) detent force according to the width of spring PM, and (d) detent force with and without spring PM.

PPA-06. Analysis and comparison of permanent magnet synchronous motor according to rotor type under same design specification. *W. Jung*[1], H. Lee[1], Y. Lee[1] and J. Choi[1] *1. Chunnam National University, Daejeon, The Republic of Korea*

The surface-mounted permanent magnet synchronous motor (SPMSM) is an electric motor that has a simple magnetic circuit design, fast responsiveness, linear torque-current, speed-voltage characteristics, and has advantages with respect to its constant speed operation.[1] SPMSMs use only magnetic torque, but interior PMSMs (IPMSMs) have high power density because they can use reluctance torque.[2] In addition, when flux weakening control is used, it has the advantage of a wide operating range compared to SPMSM.[4] This paper addresses the comparative analysis of characteristics of SPMSM and bar-type IPMSM. Characteristic analyses were performed by setting the same stator shape as the same pole /slot combination of 6 poles / 27 slots, rated speed, number of turns, winding specifications, voltage limit, and magnet usage. Next, the no-load back electromotive force (back-EMF), cogging torque, and loss characteristics were compared, and a characteristic analysis of each model was performed while satisfying the design specification. Fig. 1 depicts the experimental setup and manufactured models. The analysis model was selected as 6 pole 27 slots. No-load and load tests are performed using a back-to-back system.[3] Fig. 2(a) and (b) shows results of the back-EMF and cogging torque of an SPMSM with experimental results. It can be confirmed that the results of the analysis and experimental results are in good agreement, and the reliability of the analysis results is guaranteed. Fig. 2(c) and (d) indicate the loss characteristics according to the rotor type. Fig. 2(c) shows the comparison result of the core loss of SPMSM and IPMSM, and Fig. 2(d) shows the eddy current loss of SPMSM and IPMSM. SPMSM is about 8.5% superior to IPMSM in terms of the core loss, and it can be seen that the eddy current loss is greater than that of IPMSM. More detailed data and discussion will be presented in the subsequent full paper.

[1] John R. Hull and Larry R. Turner, "Magnetomechanics of Internal-Dipole, Halbach-Array Motor/Generators" IEEE Trans. Magn., vol. 36. no. 4, 2004-2011, July, 2000. [2] S. B. Bhat, "design and Analysis of Ferrite Based Permanent Magnet Motor for Electric Assist Bicycle," IEEE ICEMS, 2014 [3] Yoshio Tomigashi, "Reducing Cogging Torque of Interior Permanent Magnet Synchronous Motor for Electric Bicycles," IEEE European Conference on Power Electronics and Applications, 2005 [4] Kyung-Hun Shin, "Characteristic Analysis of Interior Permanent-Magnet Synchronous Machine With Fractional-Slot Concentrated Winding Considering Nonlinear Magnetic Saturation," IEEE Trans. Appl. Supercond., vol. 26, no. 4, 2016

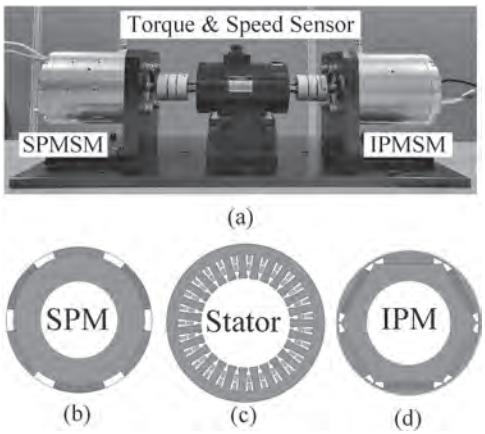

Fig. 1. (a) Experimental setup, (b) rotor of SPMSM, (c) stator, and (d) rotor of IPMSM.

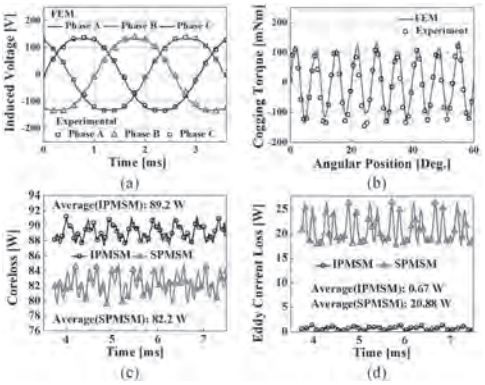

Fig. 2. Results of characteristic analysis: (a) no-load Back-EMF of SPMSM, (b) cogging torque of SPMSM, (c) core loss, and (d) eddy current loss.

PPA-07. A Study on the Prediction of Electromagnetic and NVH Characteristics of Permanent Magnet Synchronous Machine according to the different Pole/Slot Combination. *Y. Lee*[2], T. Bang[1], H. Lee[2], K. Shin[3], J. Choi[2] and S. Jo[2] *1. HYUNDAI MOBIS, Gyeonggi-do, The Republic of Korea; 2. Electrical engineering, Chungnam National university, Daejeon, The Republic of Korea; 3. Power System Engineering, Chonnam National university, Yeosu-si, The Republic of Korea*

Permanent magnet synchronous motor (PMSM) is widely used in the industry owing to its various advantages, such as high-speed operation, high efficiency, and compact design. Additionally, research on the integration of each component is becoming a trend for miniaturization of the system, and it is important to minimize interference caused by unnecessary vibration and noise between each system element. However, as PMSMs use energy-dense permanent magnets, they have the disadvantages of noise and vibration due to the interaction between the stator and rotor magnets [1]-[3]. Moreover, PMSMs require independent inverters for driving, and the noises and vibrations have a significant impact on the overall performance of the system. The vibration and noise of the motor cause problems, such as eccentricity, bearing defects, and poor PMSM alignment. Therefore, it is important to determine the source of electromagnetic vibration that affects vibration and noise [4]-[7]. Thus, in this study, to analyze the influence of each source, we derived the pole/slot combination, which is the dominant model for each electromagnetic vibration source. The derived pole/slot combinations were the 8-pole/9-slot and 8-pole/12-slot. Electromagnetic and structural acoustic analyses were conducted through finite element analysis. Then, vibration and noise characteristics were analyzed using electromagnetic force data generated through the electromagnetic analysis results of two different pole/slot combinations. The prototype model used for the electromagnetic vibration/

noise analysis and experiment is shown in Fig. 1. Fig. 2. shows the 8-pole/9-slot model vibration–acoustic experiment results and electromagnetic and structural–acoustic analysis results. Based on the analysis result, we can predict the frequency property of electromagnetic noise/vibration source. Detailed analysis and measurement results are discussed in the full paper.

[1] Z. Q. Zhu, "Influence of Design Parameters on Cogging Torque in Permanent Magnet Machines", IEEE Trans. Energy Convers., vol. 15, no. 5, pp. 407-412, Dec. 2000. [2] L. J. Wu, Z. Q. Zhu, J. T. Chen and Z. P. Xia, "An Analytical Model of Unbalanced Magnetic Force in Fractional-slot Surface-Mounted Permanent Magnet Machines," IEEE Trans. Magn., vol. 46, no. 7, pp. 2686-2700, Jul. 2010. [3] S. Q. A. Shah, T. A. Lipo, and B. I. Kwon, "Modeling of Novel Permanent Magnet Pole Shape SPM Motor for Reducing Torque Pulsation", IEEE Trans. Magn., vol. 48, no. 11, pp. 4626-4629, Oct. 2012. [4] J. A. Güemes, "Comparative Study of PMSM with Integer-slot and Fractional-slot Windings", ICEMS 2010, Oct. 2010. [5] S. Zhu, "Fractional Slot Concentrated Winding PM Synchronous Motors for Transport Electrification Applications," Dissertation, University of Nottingham, 2020. [6] Y. X. Li and Z. Q. Zhu, "Cogging Torque and Unbalanced Magnetic Force Prediction in PM Machines With Axial-Varying Eccentricity by Superposition Method," IEEE Trans. Magn., vol. 53, no. 11, pp. 1-4, Nov. 2017. [7] Y. Wang, Z. Q. Zhu, J. Feng, S. Guo, Y. Li, and Yu Wang, "Investigation of Unbalanced Magnetic Force in Fractional-Slot Permanent Magnet Machines Having an Odd Number of Stator Slots," IEEE Trans. Energy Convers., vol. 35, no. 4, pp. 1954-1963, May 2020.

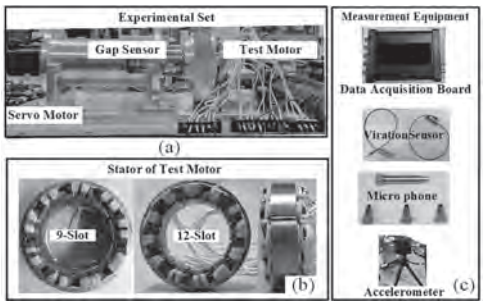

Fig. 1 Experimental equipment and manufactured motor: (a) experimental setup, (b) manufactured motor, and (c) experimental equipment.

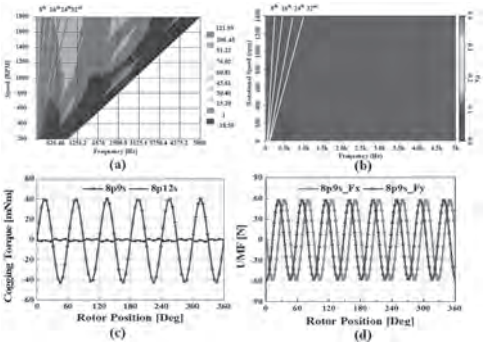

Fig. 2 Experiment results and analysis results: (a) 8p9s analysis result, (b) 8p9s experiment result, (c) cogging torque, and (d) unbalanced magnetic force.

PPA-08. Design and Analysis of a New Field-modulated Permanent Magnet Machine with an Improved PM Rotor. F. Bian[1], *M. Li*[1], C. Ke[1] and J. Su[1] *1. Zhong Yuan University of Technology, Zhengzhou, China*

I.Introduction Nowadays, the field-modulated permanent magnet (FMPM) machines have attracted significant attention in direct-drive applications. However, the rare-earth PMs have fluctuation price and unstable supply. Thus, the rare earth reduction of FMPM machine is extensively regarded as a candidate for electric vehicles [1]. It is investigated that the rotor consequent-pole PM (R-CPM) machine exhibits higher torque capability than the stator CPM machine because of the fact that various rotor permeance harmonics are more involved in torque generation [2]. Based on the study, this paper designs and analyzes a new FMPM machine with one airgap, which adopts the half Halbach array PMs embedded in the rotor slot and possesses the merit of high PM utilization ratio. II.Topology and Operation Principle As shown in Fig. 1, the proposed FMPM machine consists of rare earth PMs and windings, which are located in the rotor and stator respectively. Compared to the existing FMPM machine, the key difference is that half Halbach array PMs are employed in rotor slot. The rotor teeth, which provide a mechanical support and better effect of heat dissipation for PMs, build the routes for the fields of PM and armature winding. III. Results Fig. 2(a) presents the no-load phase back-EMFs of the existing and proposed FMPM machines under the same speed. It can be observed that the maximum back-EMF obtained by the proposed HEFM machine is similar to the existing machine that excited by both rare earth PMs and ferrite PMs. Fig. 2(b) shows that the torque densities with the same rated armature current of 5Arms. It is found that the torque density of the proposed machine is similar to the superposition of torque produced by the machines with rare earth PMs and ferrite PMs, while the PM volume is only 66% of the existing one. It proves the effectiveness of the improved rotor structure.

[1] C. Gong and F. Deng. Design and optimization of a high-torque-density low-torque-ripple vernier machine using ferrite magnets for direct-drive applications. *IEEE Transactions on Industrial Electronics*, vol. 69, no. 6, pp. 5421-5431, June 2022. [2] Y. Li, H. Yang and H. Lin. Comparative study of torque production mechanisms in stator and rotor consequent-pole permanent magnet machines. *IEEE Transactions on Transportation Electrification*, vol. 7, no. 4, pp. 2694-2704, Dec. 2021.

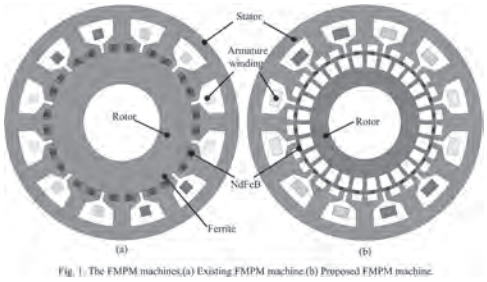

Fig. 1. The FMPM machines.(a) Existing FMPM machine.(b) Proposed FMPM machine.

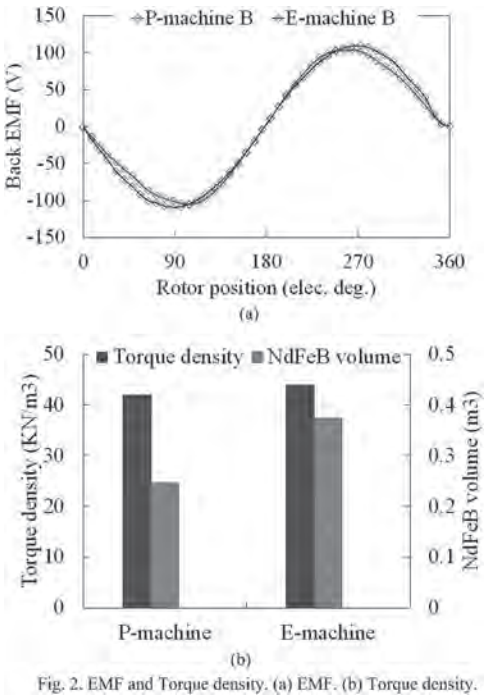

Fig. 2. EMF and Torque density. (a) EMF. (b) Torque density.

PPA-09. Multi-Objective Optimal design of Surface-mounted permanent magnet synchronous motor using analytical method and Particle swarm optimization algorithm. *S. Kim*[1], J. Woo[1], W. Kim[2], K. Shin[3] and J. Choi[1] *1. electrical engineering, Chungnam National University, Daejeon, The Republic of Korea; 2. Hyundai Elevator, Chungju, The Republic of Korea; 3. Power System Engineering, Chonnam National University, Yeosu, The Republic of Korea*

Permanent magnet synchronous motors (PMSMs) are used in various applications, such as propulsion systems, owing to their light weight and high efficiency. Commonly used optimal design methods for PMSMs are based on surrogate models or methods repeatedly designed by a designer. Thus, determining whether a model derived through these approaches is the optimal model is difficult, and selecting a design point without empirical data is challenging. Although an optimal design method of a PMSM using a probabilistic algorithm has been recently proposed to solve this problem [1] [2], applying this method to the efficiency- and power density-based optimization process is difficult considering only the copper loss. In this paper, an optimal design method using an analytical method and a probabilistic algorithm is proposed. The analytical method derives the iron and eddy current losses, and the optimal design point is selected using the probabilistic algorithm. This method is then applied to a surface-mounted permanent magnet synchronous motor (SPMSM) design process [3][4], as indicated in the flowchart in Fig. 1 (a), and the results are compared with the finite element method results. The magnetic field of the rotor is selected by optimizing rotor parameters through the particle swarm optimization algorithm. Fig. 1 (a) shows the design framework for designing the electric field of the stator according to the magnetic field of the selected rotor. Figs. 1(b) and (c) illustrate the Pareto front derived from 200 design candidates through 40,000 iterations using the random search method. A design point with high efficiency and power density is selected as the optimal design point. Fig. 2(a) depicts the initial model of the manufactured SPMSM, and Fig. 2(b) illustrates a comparison of dimensions between the initial and optimal models. Fig. 2(c) compares the objective function values of the initial and optimal models.

[1] C.H Kim, J.W Kim, Y.J Kim and S.Y Jung "Particle Swarm Optimization with Multiple Regression for Optimal Design of Interior Permanent Magnet Synchronous Motor", ICEMS, p.1-2, DEC 2019 [2] C. Ma, L. Qu, "Multiobjective Optimization of Switched Reluctance Motors Based on Design of Experiments and Particle Swarm Optimization", IEEE Trans. Magn., VOL. 30, NO. 3, p.2-4, SEP 2015 [3] J.H Lee, J.W Kim, J.Y Song, D.W Kim, Y.J Kim, and S.Y Jung, "Distance-Based Intelligent Particle Swarm Optimization for Optimal Design of Permanent Magnet Synchronous Machine", IEEE Trans. Magn., VOL. 53, NO. 6, p.3-5, June 2017 [4] J.H Lee, J.Y Song, D.W Kim, J.W Kim and Y.J Kim, "Particle Swarm Optimization Algorithm with Intelligent Particle Number Control for Optimal Design of Electric Machines", IEEE Trans. Ind. Electron., VOL. 65, NO. 2, p.4-6, Feb 2018

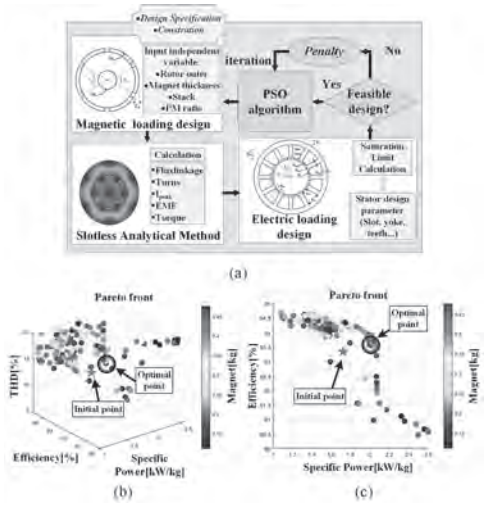

Fig. 1. (a) Proposed method flow chart (b) 3D Pareto Front of Power Density, Efficiency, Magnet Consumption and THD (c) Top view of 3D Pareto Front

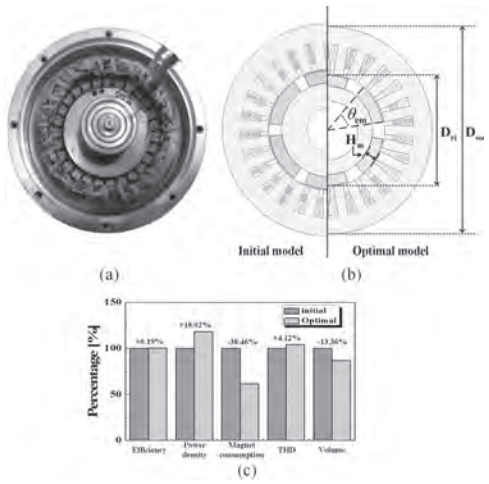

Fig. 2. (a) Manufactured initial model (b) Initial & Optimal model design (c) Comparison of objective function results between the initial model & the optimal model

PPA-10. Magnetic field and Torque Analysis of Coaxial Magnetic Gear Using Semi-Analytical Method. *H. Lee*[1], J. Lee[1], K. Shin[2] and J. Choi[1] *1. Chungnam National University, Daejeon, The Republic of Korea; 2. Chonnam National University, Yeosu, The Republic of Korea*

Magnetic gears have advantages such as noise and vibration reduction, friction loss removal, and self-protection in case of overload [1][2]. A coaxial magnetic gear modulates the magnetic field from the inner and outer rotors through multiple modulation poles to produce a gear ratio between the two rotors [3][4]. Methods for analyzing and designing coaxial magnetic gears include the analytical method and finite-element method (FEM). The FEM considers the nonlinear characteristics of materials and more accurately interprets complex shapes. However, the interpretation takes a long time. On the contrary, the analytical method has a shorter analysis time than the FEM and is advantageous in understanding the change in characteristics of design variables [5]. The difficulty in applying the analytical method to a magnetic gear is in consideration of the modulation pole, and it is essential to consider the modulation pole region to predict the force transmitted from the primary to the secondary. Therefore, in this study, the analysis model was simplified to apply the analytical method, and the magnetic field and torque characteristics analysis in each analysis area were performed through several assumptions and appropriate boundary conditions. The analysis result was

compared with the finite-element analysis result, and the validity of the presented analysis method was verified. Fig. 1 shows the prototype model of the coaxial magnetic gear. The analysis model has six, 32, and 19 modulation poles. Fig. 2 shows the simplified model for applying the analytical method and presents the analysis results. Figs. 2(b)–(d) depict the pull-out torque and magnetic flux densities at the inner and outer air gaps. The analysis results obtained through the analytical method agree well with the FEM. More-detailed results and discussion are presented in the full paper, as well as the desired effects.

[1] K. Davey, T. Hutson, L. McDonald and G. Hutson, "The design and construction of cycloidal magnetic gears", Proc. IEEE Int. Electr. Mach. Drives Conf. (IEMDC), pp. 1-6, May 2017. [2] B. Praslicka, M. C. Gardner, M. Johnson and H. A. Toliyat, "Review and analysis of coaxial magnetic gear pole pair count selection effects", IEEE J. Emerg. Sel. Topics Power Electron., Jan. 2021. [3] M. C. Tsai and C. C. Huang, "Development of a variable-inertia device with a magnetic planetary gearbox", IEEE/ASME Trans. Mechatronics, vol. 16, no. 6, pp. 1120-1128, Dec. 2011. [4] K. Atallah, S. D. Calverley and D. Howe, "Design analysis and realisation of a high-performance magnetic gear", IEE Proc.—Elect. Power Appl., vol. 151, no. 2, pp. 135-143, 2004. [5] T. Lubin, S. Mezani and A. Rezzoug, "Analytical computation of the magnetic field distribution in a magnetic gear", IEEE Trans. Magn., vol. 46, no. 7, pp. 2611-2621, Jul. 2010.

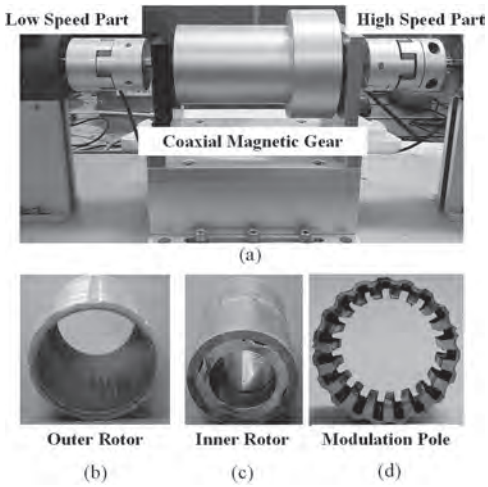

Fig. 1. (a) Coaxial magnetic gear, (b) outer rotor, (c) inner rotor, and (d) modulation pole.

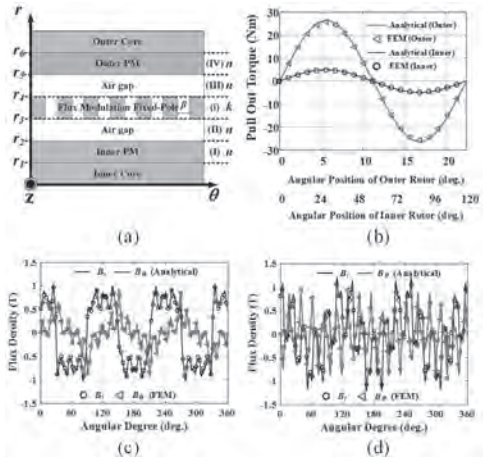

Fig. 2. (a) Simplified analytical model, (b) pull-out torque, (c) magnetic field distribution at inner air gap, and (d) magnetic field distribution at outer air gap.

PPA-11. A New Magnetic-Field Modulated Machine with Compound-structure Magnets of Spoke PMs and Halbach PMs. F. Bian[1], *C. Ke*[1], J. Su[1] and M. Li[1] *1. Zhong Yuan University of Technology, Zhengzhou, China*

I.Introduction The magnetic-field-modulated permanent magnet (MFMPM) machines have attracted wide attention in hybrid electric vehicles. In order to improve the torque density, many MFMPM machines employ two or three portions of PMs and two air gaps [1]. However, the structures with two air gaps increase the complexity and maintenance difficulty. To solve above problems, alternative flux barriers and alternative flux bridges are introduced in the MFMPM machines with one air-gap [2]. In order to improve the utilizations of rotor space and torque density per unit volume, this paper proposes a new MFMPM Machine with compound-structure PMs, in which both the spoke and Halbach array PMs are set in the rotor. II.Topology and Operation Principle Fig. 1 shows the configuration of the proposed MFMPM machine with the compound-structure Magnets. The stator contains flux-modulation tooth and slots which are filled with single layer concentrated winding. The rotor is formed by the spoke PMs, Halbach array PMs and alternative flux bridges. The proposed MFMPM machine can be identified as the combination of the spoke MFMPM machine and Halbach array MFMPM machine. Both the MFMPM machines work on the principle of field modulation effect. Besides, Halbach array PMs are inserted between the flux bridge and spoke rare-earth PMs to reduce the flux leakage, resulting in improving the utilizations of spoke PMs field. III.Results Fig. 2(a) shows that the back EMF waves of proposed MFMPM machine. It can be seen that the proposed MFMPM machine can achieves 172 V which is almost equal to the sum of the back-EMFs of spoke MFMPM machine and Halbach array MFMPM machine. The waveforms of torque can be obtained, as shown in Fig. 2(b). It reveals that the torque of proposed machine can achieve 25N.m while the torques of the spoke MFMPM machine and Halbach array MFMPM machine are 19N.m and 7.3N.m respectively. It validates that proposed compound-structure machine can realize the superposition of spoke PMs and Halbach array PMs.

[1] G. Liu, P. Zheng, J. Bai, et al. Investigation of a dual-winding dual-flux-concentrated magnetic-field-modulated brushless compound-structure machine. *IEEE Transactions on Magnetics*, vol. 58, no. 2, pp. 1-5, Feb. 2022, Art no. 8100505. [2] Y. Zhang, D. Li, P. Yan, et al. A high torque density claw-pole permanent-magnets vernier machine. *IEEE Journal of Emerging and Selected Topics in Power Electronics*, vol. 10, no. 2, pp. 1756-1765, April 2022.

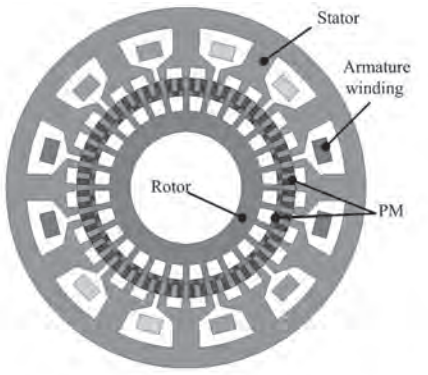

Fig. 1. The configuration of proposed compound-structure machine.

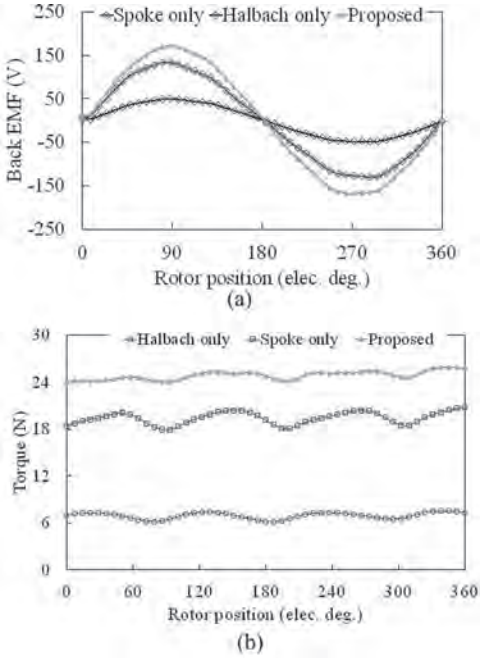

Fig. 2. EMF and Torque. (a) EMF. (b) Torque.

PPA-12. Thermal Analysis and Experimental Verification of Permanent Magnet Synchronous Motor by Combining Lumped-Parameter Thermal Networks with Analytical Method. *M. Nguyen*[1], H. Lee[1], Y. Lee[1] and J. Choi[1] *1. Chungnam National University, Daejeon, The Republic of Korea*

In general, three aspects of an entire electrical machine design task should be analyzed: electromagnetic, mechanical, and thermal. However, in practice, designers tend to focus on the electromagnetic aspect and deal superficially with mechanical analysis and thermal analysis. It is necessary to perform mechanical and thermal analysis in applications for high-speed and high-power machines. The thermal analysis can be done using two approaches: the method using lumped-parameter thermal networks (LPTNs) also known as "thermal equivalent circuits," and the analytical method. The LPTN is a simple model that makes it possible to obtain quickly. However, defining one or two main heat-transfer paths is necessary first, so the final result is not highly accurate. The analytical method based on complex differential equations and boundary conditions provides more reliable results. In this study, a comprehensive thermal analysis model was developed and applied to an 8/12 permanent magnet synchronous motor prototype. Fig. 1 shows the manufactured model and experimental setup. Fig. 2 illustrates an LPTN model according to the front view and side view in Figs. 2(a) and (b), respectively. Fig. 2(c) shows the simplified circuit in the winding, and Fig. 2(d) shows the temperature results for some positions. The detailed work and experiment results will be presented in the full paper.

1. A. Boglietti, A. Cavagnino, D. Staton, M. Shanel, M. Mueller and C. Mejuto, "Evolution and Modern Approaches for Thermal Analysis of Electrical Machines," in IEEE Transactions on Industrial Electronics, vol. 56, no. 3, pp. 871-882, March 2009 2. G. J. Li, J. Ojeda, E. Hoang, M. Lecrivain and M. Gabsi, "Comparative Studies Between Classical and Mutually Coupled Switched Reluctance Motors Using Thermal-Electromagnetic Analysis for Driving Cycles," in IEEE Transactions on Magnetics, vol. 47, no. 4, pp. 839-847, April 2011 3. D. Staton, A. Boglietti and A. Cavagnino, "Solving the more difficult aspects of electric motor thermal analysis in small and medium size industrial induction motors," in IEEE Transactions on Energy Conversion, vol. 20, no. 3, pp. 620-628, Sept. 2005

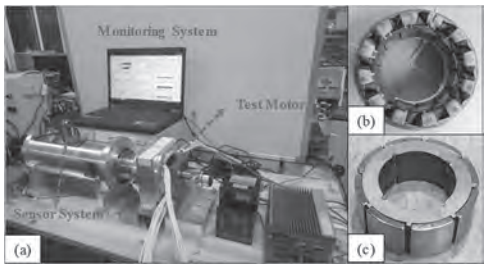

Fig. 1. (a) Experimental setup, (b) stator, and (c) rotor.

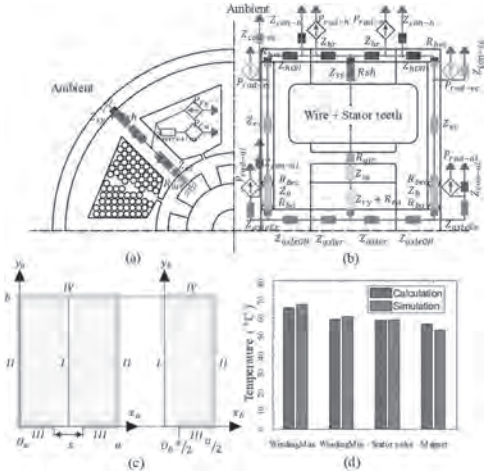

Fig. 2. (a) front view of a thermal equivalent circuit for the entire machine, (b) side view of a thermal equivalent circuit for the entire machine, (c) simplified winding model, and (d) heat increase.

PPA-13. Fault Operation Analysis Of A Novel Dual-Three-Phase Dual-Rotor Flux-Switching Permanent Magnet Machine. *Z. Chang*[1], G. Zhao[1], Z. Li[1], Y. Zhou[1] and X. Jiang[1] *1. Nanjing Normal University, Nanjing, China*

I.Introduction Double mechanical port permanent-magnet (DMP-PM) motor is one of the research highlights in motor field in recent years[1], [2]. As shown in Fig. 1, this motor called NS-DRFSPM machine. In this paper, the performances of NS-DRFSPM machine under several fault operation conditions are compared and analyzed. The simultaneous operation of two groups of armature windings and the first group of permanent magnets is called state I, namely S1;The simultaneous operation of two groups of armature windings and the second group of permanent magnets is called state II, namely S2;The first group of armature windings and two groups of permanent magnets operate at the same time, which is called state III, namely S3;The second group of armature windings and two groups of permanent magnets operate at the same time, which is called state IV, namely S4. II.Performance comparisons A series of comparisons of electromagnetic performance of several fault operation states are conducted by finite element analysis (FEA). Fig.2(a) compares the no-load phase back-EMF per turn waveforms of four fault operation states of the NS-DRFSPM machine at 1500r/min based on FEA. It can be seen that the back-EMF amplitude of the third operating state of the motor is the smallest, and the second is the largest. Fig.2(b) shows the flux linkage waveforms of four fault operation states of the NS-DRFSPM machine. The cogging torque waveforms of four fault operation states of NS-DRFSPM machine shown in Fig.2(c). The cogging torque waveforms of state III and state IV are almost the same, and the torque ripple is the smallest. Fig.2(d) present the electromagnetic torque of the NS-DRFSPM machine under i_d=0 control with current densities J_{sa}=5A/mm^2. The best performance of average torque and torque ripple of the NS-DRFSPM machine is state II(6.9Nm,42.1%). III.Conclusion The other performance, such as the FFT results analysis and simultaneous fault operation of single armature winding and magnet, will be shown in the full paper.

[1]J. Bai, P. Zheng, C. Tong, Z. Song, and Q. Zhao,"Characteristic Analysis and Verification of the Magnetic-Field-Modulated Brushless Double-Rotor Machine," *IEEE Trans. Ind. Electron.*, vol. 62, no. 7, pp. 4023–4033, Jul. 2015. [2]X. Zhu, L. Chen, L. Quan, Y. Sun, W. Hua, and Z. Wang,"A new magnetic-planetary-geared permanent-magnet brushless machine for hybrid electric vehicle,"*IEEE Trans. Magn*., vol. 48, no. 11, pp. 4642–4645, Nov. 2012.

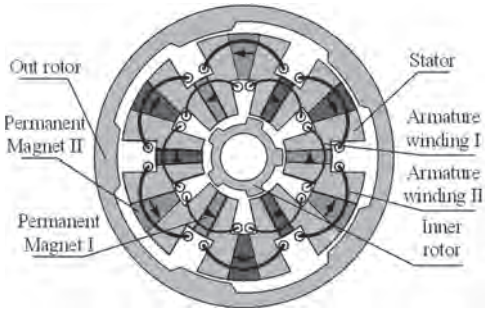

Fig. 1 Topology of NS- DRFSPM machine.

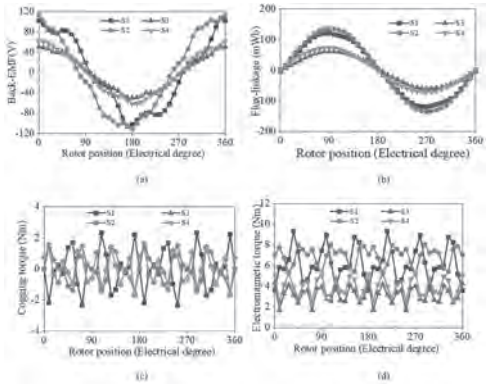

Fig. 2 Performance comparisons.(a) Phase back-EMF per turn waveforms.(b)Flux-linkage waveforms.(c)Cogging torque waveforms.(d) Electromagnetic torque waveforms.

PPA-14. Design and analysis of a novel asymmetric-stator-pole hybrid excited flux reversal machine. H. Yang[1], *H. Huang*[1], Y. Liu[1], H. Lin[1] and Z. Zhu[2] *1. Electrical Engineering, Southeast University, Nanjing, China; 2. The University of Sheffield, Sheffield, United Kingdom*

I. INTRODUCTION The flux reversal permanent magnet machine (FRPM) is a typical stator permanent magnet (PM) synchronous machine. In addition to the inherent advantages of traditional PM machine such as high torque density/efficiency, and operational reliability, it also has the advantages of simple rotor structure, strong robustness and suitability for AC brushless operation.[1]-[4] In order to expand its range of speed regulation, this paper proposes a new type of asymmetric-stator-pole hybrid excited flux reversal (ASP-HEFR) machine by introducing the design concept of "asymmetric stator consequent pole" and installing DC field windings on the non-PM excitation teeth. II. TOPOLOGY AND OPTIMIZATION OF THE NOVEL ASP-HEFR MACHINE The optimal model of this novel ASP-HEFR machine is shown in Fig 1(a). The conventional HEPM machine can be divided into series or parallel relationship according to the magnetic circuit relationship between permanent magnet and electric excitation, so that the electric excitation flux can increase or decrease the permanent magnet flux equivalently, which based on the "variable harmonics" theory. COMPARISON OF TWO NOVEL ASP-HEFR MACHINES This paper compare and analyze the electromagnetic characteristics of the two different ASP-HEFR machines with 12/17- and 12/16-stator slot/rotor tooth under the condition of the same overall size. Summarize the electromagnetic performance differences between the odd-number and even-number tooth structures. Fig. 1(b) and (c) show the Magnetic dense cloud and magnetic field distribution of 12/16- and 12/17-stator slot/rotor tooth machines respectively. EXPERIMENTAL VERIFICATION The test results of the open-circuit back-EMF of the prototype of the proposed 12/17-stator slot/rotor tooth ASP-HEFR machine at different magnetization states are shown in Fig. 2. It can be observed that the experiments agree well with the FE-predicted results, which confirms the proposed 12/17-stator slot/rotor tooth machine has higher torque and better flux adjusting capability.

[1]Z. Q. Zhu. "Permanent magnet machines for traction applications," *John Wiley & Sons, Ltd*, 2014. [2]Z. Q. Zhu, Y. S. Chen and D. Howe, "Online optimal flux-weakening control of permanent-magnet brushless AC drives," *IEEE Trans. Ind. Appl.*, vol. 36, no. 6, pp. 1661-1668, Nov.-Dec. 2000. [3] R. P. Deodhar, S. Andersson, I. Boldea and T. J. E. Miller, "The flux-reversal machine: a new brushless doubly-salient permanent-magnet machine," *IEEE Trans. Ind. Appl.*, vol. 33, no. 3, pp. 786-793, Jan. 1997. [4]H. Yang, H. Lin, Z. Q. Zhu, S. Lyu and Y. Liu, "Design and Analysis of Novel Asymmetric-Stator-Pole Flux Reversal PM Machine," *IEEE Trans. Ind. Electron.*, vol. 67, no. 1, pp. 101-114, Jan. 2020.

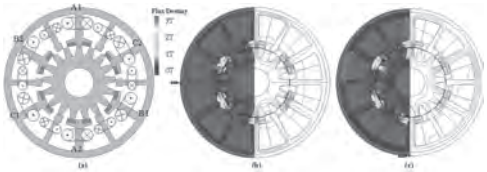

Fig.1 (a) Machine topologies. (b) 12/16-stator slot/rotor tooth ASP-HEFR. (c) 12/17-stator slot/rotor tooth ASP-HEFR.

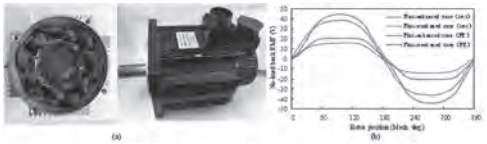

Fig. 2 Test results of back-EMF waveforms. (a) Prototype. (b) Back-EMFs (1000rpm)

PPA-15. A Novel Variable Flux Memory Machine with Weak Saliency Ratio. *X. Zeng*[1], H. Lin[1] and X. Zhao[1] *1. Southeast University, Nanjing, China*

For efficient magnetization and demagnetization, low coercive force (LCF) permanent magnets (PM) are typically placed on the *d*-axis magnetic circuit in the variable flux memory motor (VFMM), resulting in a large difference between the *d*-axis inductance (L_d) and the *q*-axis inductance (L_q) [1-2]. Therefore, the VFMM tends to obtain a high salient ratio. To achieve maximum torque per ampere (MTPA) operation, the high salient ratio VFMM will distribute more armature current on the *d*-axis, which will reduce the stator flux linkage, resulting in a narrow air gap flux regulation range. In this paper, the *q*-axis magnetic barrier is introduced into the VFMM to reduce the difference between L_d and L_q and realize a weak salient ratio, so that the MTPA trajectory will be shifted to the high flux linkage region. Therefore, high torque density and wide air gap flux regulation range can be obtained simultaneously. Fig. 1 shows the configuration of the novel VFMM with a weak saliency ratio, where flux barriers are introduced into the *q*-axis magnetic circuit. Fig. 2 (a) shows the air-gap flux density waveforms of the proposed machine under flux-enhanced state and flux-weakened state. Fig. 2(b) illustrates the variation of L_d and L_q with the current angle. As the current angle increases, the rotor saturation is weakened due to the decrease of *q*-axis current, resulting in a decrease in *q*-axis reluctance and an increase in *d*-axis reluctance. Fig. 2(c) depicts the variation of different torque components versus the current angle. It can be seen that the reluctance torque makes a small contribution to the total torque at 20° and the weak salient ratio is verified by the low reluctance torque. Fig. 2(d) shows the torques under two magnetization states (MSs) are 5.60Nm and 3.56Nm respectively. Fig. 2(e) and (f) show the combined efficiency maps and MSs maps of the proposed machine. It is clear that the proposed machine obtains a wide high-efficiency region and the high-efficiency region is shifted to the

high-speed region. Besides, the high proportion of flux-weakened status in the MS map indicates that the machine can make use of the variable flux characteristics of LCF PMs.

[1] W. Liu, H. Yang, H. Lin, S. Lyu and Y. Zhong, "A Novel Variable Flux Memory Machine with Separated Series-Parallel PM Structure," in *IEEE Transactions on Industrial Electronics*, doi: 10.1109/TIE.2022.3174293.
[2] G. Qiao, M. Wang, F. Liu, Y. Liu, and P. Zheng, "Analysis of novel hybrid-PM variable-flux PMSMs with series-parallel magnetic circuits," *IEEE Trans. Magn.*, vol. 57, no. 2, pp. 1–6, Feb. 2021.

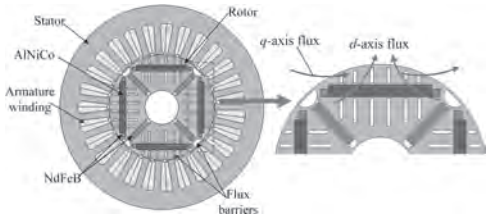

Fig. 1 Topology

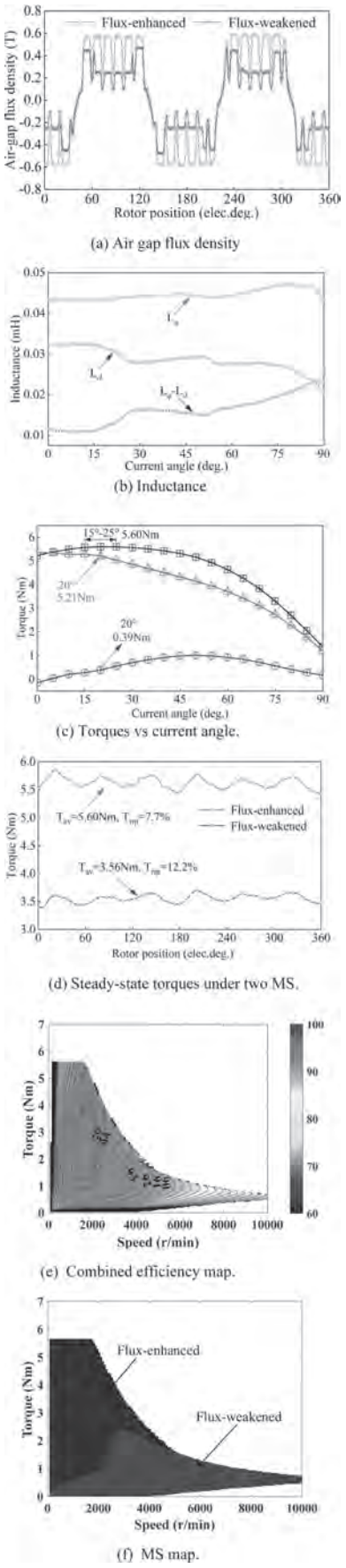

Fig. 2 Electromagnetic performances

Session PPB
SHIELDING, LEVITATION AND PROPULSION
(Poster Session)

Jang-Young Choi, Chair
Chungnam National University, Daejeon, The Republic of Korea

PPB-01. Three-dimensional Analytical Modeling of Coreless Linear Induction Maglev Motor with Uneven Air Gap Conditions. *W. Qin*[1]
1. EE, Beijing Jiaotong University, Beijing, China

The Coreless Linear Induction Maglev Motor (CLIMM) used in ultra-high speed maglev, which may lead to an uneven air-gap between its primary and secondary[1-2], is proposed and investigated. The analytical model is set up in 3D cartesian coordinates to calculate the magnetic field and electromagnetic performance. Firstly, the basic structure and principle of the proposed motor is introduced as shown in Fig.1. Then, the 3D magnetic field distribution function and its Fourier series of the primary based on integral approach is proposed. Based on second order vector potential (SOVP), a 3D analytic model of the motor was proposed in the paper, thus, we can get the expression of the lift force, thrust force and powerlosses. The calculations of magnetic field in the air gap, forces and powerlosses were conducted by finite element method and analytical method, respectively, the outcome proves that the analytical model in this paper is correct and practical shown as in Fig.2 and Fig.3. Finally, a small scale prototype is manufactured, and experiments are carried out to verify the predicted results shown as in Fig.1.

[1]Qin Wei, Fan Yu, Xu Hongze*, et al.* A Linear Induction Maglev Motor with HTS Traveling Magnetic Electromagnetic Halbach Array[J], Transactions of China Electrotechnical Society, 2018,33 (23):5427-5434 [2] W. Qin, Y. Ma, G. Lv, F. Wang, and J. Zhao, "New Levitation Scheme With Traveling Magnetic Electromagnetic Halbach Array for EDS Maglev System," *IEEE Transactions on Magnetics, 2022,58(2)*:1-6.

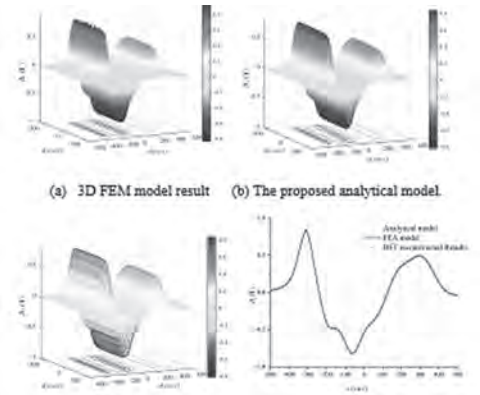

(a) 3D FEM model result (b) The proposed analytical model.

(c) Topology of CLIMM. (d) 2D DFT reconstructed results

Fig.2 The Bz with g=40 mm with primary rotates 5 degrees around the x axis at t=0

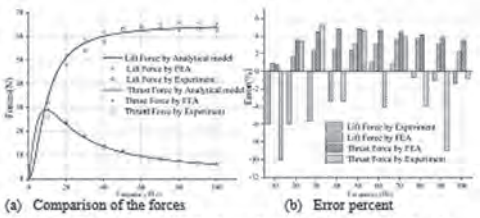

(a) Comparison of the forces (b) Error percent

Fig. 3. Comparison of the forces between FEA, Analytical and experiment results

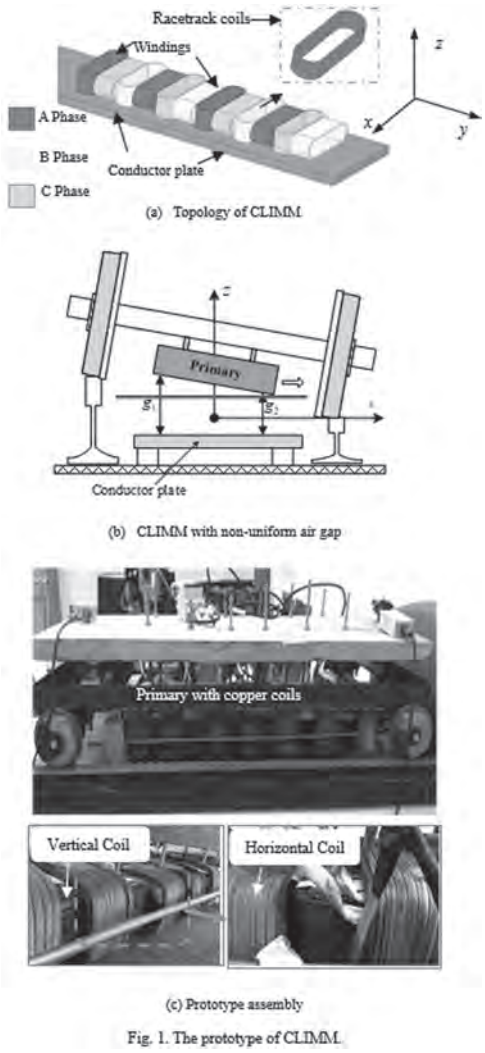

(a) Topology of CLIMM

(b) CLIMM with non-uniform air gap

(c) Prototype assembly

Fig. 1. The prototype of CLIMM.

PPB-02. Design and Analysis of Reduced Rare-Earth Magnet Surface Permanent Magnet Motor using Sandwich Magnets. *A.P. Singh*[1], X. Liu[1] and C.I. Nlebedim[1] *1. Critical Material Institute, Ames Laboratory, AMES, IA, United States*

Surface Permanent magnet (SPM) motors are generally used in small traction applications due to high power density, simple designing and easy manufacturing processes. SPM motors dominates the market particularly for small permanent magnet motors. However, the major concern with the SPM motors is their higher demagnetization risks due to close exposure of PM to the stator windings [1]. In order to avoid demagnetization risks, such motors use the critical rare-earth permanent magnets (REPMs) which are prone to supply disruption and critical availability, hence poses a long-time sustainability challenge [2]. Many attempts have been made [3-4], for

reduction of critical REPMs in permanent magnet motors. However, most of these attempts focus on the interior permanent magnet motors but rarely on SPM motors. This work proposes a reduced rare-earth sandwich surface permanent magnet (SSPM) motor, which uses cost-effective and abundant ferrite permanent magnets (FPM, $(BH)_{max}$=3 MGOe) between two high-energy product rare-earth PM (Nd-Fe-B, $(BH)_{max}$ =33 MGOe) layers. The main idea of such a magnet structure is that the REPM drives the FPM to operate at higher flux density which reduces demagnetization susceptibilities of the FPM without degrading torque capability of the motor. Equivalent magnetic circuit (EMC) approach is applied to investigate the SSPM motor and the approach can also be applied to represent a sandwiched multiple type magnet structure with an equivalent single magnet. The performance of sandwich-type magnets is carried out on a small traction motor (1.75 kW, 640 rpm motor) [5]. The output torque and demagnetization performance of the motor with different magnets are given in Table-I and Fig.1. The present work offers a way to reduce the consumption of critical REPM materials in PM motors without significant performance degradation. This research was supported by the Critical Materials Institute, an Energy Innovation Hub funded by the U.S. Department of Energy, Office of Energy Efficiency and Renewable Energy, Advanced Manufacturing Office.

[1] A. M. El-Refaie. T. M. Jahns, and D. W. Novotny, *IEEE Trans. Magn.*, vol. 21, pp. 34-43, 2006. [2] R. T. Nguyen, D. D. Imholte, A. C. Matthews, and W. D. Swank, *Waste Management*, vol. 83, Pp. 209-217, 2019, [3] W. Wu, X. Zhu, L. Quan, Y. Du, Z. Xiang and X. Zhu, *IEEE Transactions on Applied Superconductivity*, vol. 28, pp. 1-6, 2018. [4] Y. Chen, T. Cai, X. Zhu, D. Fan and Q. Wang, *IEEE Transactions on Applied Superconductivity*, vol. 30, pp. 1-6, 2020. [5] N. Y. Braiwish, F. J. Anayi, A. A. Fahmy and E. E. Eldukhri, *49th International Universities Power Engineering Conference (UPEC-2014)*, pp. 1-5, 2014.

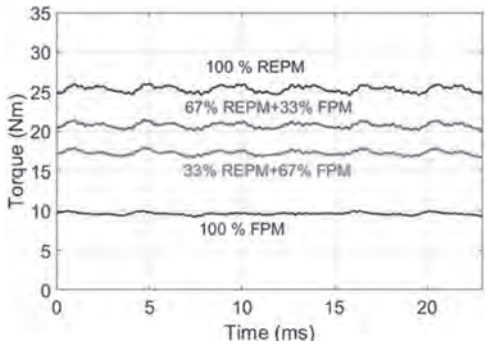

Fig. 1 O/p torque with different sandwich magnets in a 1.75 kW, 640 rpm SSPM motor

Table-I O/p Torque and demagnetization values of SSPM motor with different magnets

Model	Torque (Nm)	Demagnetization (T)
100% REPM (Model-I)	25	-0.9
67% REPM+33%FPM (Model-II)	21	-0.54
33% REPM+67% FPM (Model-III)	17	-0.31
100% FPM (Model-IV)	10	0.01

Table 1. O/p Torque and demagnetization values of SSPM motor with different magnets

PPB-03. Shape Design Optimization of Interior Permanent Magnet Synchronous Machine with Hybrid GO and NGO Silicon Sheet Cores.

C. Liu[1], X. Huang[1] and Y. Wang[1] *1. Hebei University of Technology, Tianjin, China*

Compared with non-grain-oriented silicon sheet (NGO), the grain-oriented silicon sheet (GO) has superior magnetic characteristic along its rolling direction, but bad characteristic along other directions. GO silicon sheet is a popular material used in transformers [1]. For electrical machines, it can be only used to design the stator teeth [2]. While, reasonable design and optimization of joint part between the GO silicon sheets and NGO silicon sheets is very important, otherwise the main performance of electrical machine with hybrid GO - NGO cores will be reduced. In the pasts, optimizing main dimensions is a main mainstream however shape optimization of the joint part was neglected. In this paper, the shape design optimization method is adopted for obtaining the best joint shape between the GO and NGO silicon sheets based on an 12 slot 8 pole (12s8p) interior permanent magnet machine (IPMSM) as shown in Fig. 1(a). For achieving better machine performance, the magnetic barrier shape are optimized as well. Specifically, the GO silicon sheets are used for building the stator teeth, and the others are made by NGO silicon sheets. By using finite element method (FEM), the main performance of the IPMSM with different GO silicon sheets can be obtained. Piecewise linear interpolation method is used to establish the GO silicon sheets and rotor barrier shape, as shown in Fig. 1(b) and (c). Fig. 1(d) shows the obtained new rotor barrier shape after optimization. For benchmark comparison the optimized traditional IPMSM with 12s8p and IPMSM with 48s8p with NGO silicon sheets are adopted. Fig 2 shows the performance comparison of 12s8p IPMSM using NGO (NGO-IPMSM (12 Slot)), 12s8p IPMSM using GO teeth (GO-IPMSM (12 Slot)), 12s8p IPMSM using GO teeth and new magnetic flux barriers (GO-B-IPMSM (12 Slot)), and 48s8p IPMSM using NGO (NGO-IPMSM (48 Slot)). More results will be presented in the final submission.

[1] S. Magdaleno-Adame, T. D. Kefalas, A. Fakhravar and J. C. Olivares-Galvan, "Comparative Study of Grain Oriented and Non–Oriented Electrical Steels in Magnetic Shunts of Power Transformers," 2018 IEEE International Autumn Meeting on Power, Electronics and Computing (ROPEC), 2018, pp. 1-7. [2] Y. Tsuchiya and K. Akatsu, "A Study of the Switched Reluctance Motor using Grain-Oriented Electrical Steel Sheets," 2020 IEEE Energy Conversion Congress and Exposition (ECCE), 2020, pp. 3623-3628.

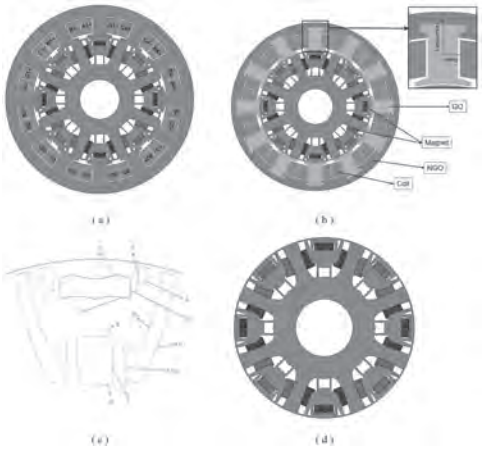

Fig. 1 (a) NGO-IPMSM(12 Slot), (b) GO-IPMSM(12 Slot), (c) magnetic flux barriers shape, (d) optimized shape.

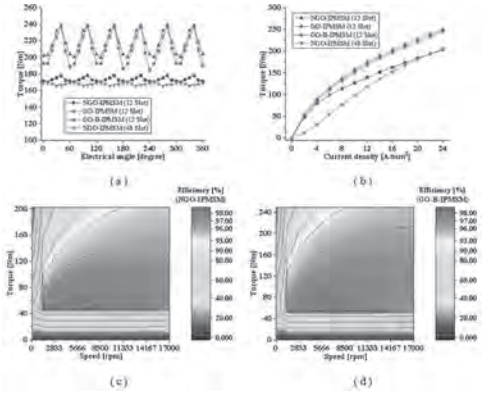

Fig. 2. (a) torque waveform, (b) torque ability, (c) efficiency map of NGO-IPMSM(12 Slot), (d) efficiency map of GO-B-IPMSM(12 Slot).

PPB-04. Characteristic Analysis of a Permanent Magnet Synchronous Generator Considering Overhang and Bolting Structure Based on Analytical Method. *J. Hong*[1], H. Lee[1], H. Shin[1], K. Shin[2] and J. Choi[1]
1. Chungnam National University, Daejeon, The Republic of Korea;
2. Chonnam National University, Yeosu, The Republic of Korea

Bolting or sleeve are applied to permanent magnet synchronous generators (PMSGs) to prevent shattering permanent magnet (PM)-generated defects[1],[2]. Of these, bolting is more useful than a sleeve during manufacturing. However, as the magnetic flux is reduced due to the material characteristics of the bolting, overhang structure is often used for PM machines to compensate for the flux reduction[2]. Therefore, the axial length of the rotor must be considered during the overhang structure-based 3D analysis[2]. However, the analysis of a 3D model with diverse and complex design variables is time-intensive[2]. In this study, we analyzed a PMSG considering the bolting and overhang structure based on an analytical method. Preferably, the initial design process must consider several variables, and the analysis time of a PMSG with a complex structure must be reduced[2]. Characteristic analyses using a semi-3D method have been employed previously. However, there is a limit to the variation of 2D design variables to ensure that they are not saturated when considering a 3D shape. Therefore, we propose analytical methods using electromagnetic transfer relations[3]. It was used to analytical method considering the operating point of the PM calculated through magnetic energy analyses of the overhang and 3D models [2]–[4]. These were applied to the region of PMs with the overhang[1],[2]. Performance analysis of the separated overhang and bolting regions was conducted based on the superposition principle[1],[2]. A circuit parameter was derived based on the predicted results and applied to the equivalent circuit of the generator[2]. The performance results were compared with the 3D model and experimental results. Figs. 1(a)–(c) and 2(a) illustrate the manufactured and analysis models, respectively. Fig. 2(b) depicts the variation in the operating point of the PM. Figs. 2(c) and (d) illustrate the results obtained from the comparison of 3D, analytical, and experiment models. The results appear to be in near agreement.

[1] K.H Shin, J.Y. Choi, "Electromagnetic Analysis of Permanent Magnet Synchronous Generator Considering Permanent Magnet Bolting" KOSMEE, pp. 154-154, 2018. [2] J.S. Hong, K.H. Shin, J.Y. Choi., "Semi-3D Analysis of a Permanent Magnet Synchronous Generator Considering Bolting and Overhang Structure." *Energies* 15, no. 12: 4374.2022. [3] S. Jang, M. Koo, J. Choi, "Characteristic Analysis of Permanent Magnet Synchronous Machines Under Different Construction Conditions of Rotor Magnetic Circuits by Using Electromagnetic Transfer Relations," in IEEE Transactions on Magnetics, vol. 47, no. 10, pp. 3665-3668, Oct. 2011. [4] J. Song, J. H. Lee, S. Jung, "Computational Method of Effective Remanence Flux Density to Consider PM Overhang Effect for Spoke-Type PM Motor With 2-D Analysis Using Magnetic Energy," in IEEE Transactions on Magnetics, vol. 52, no. 3, pp. 1-4, March 2016.

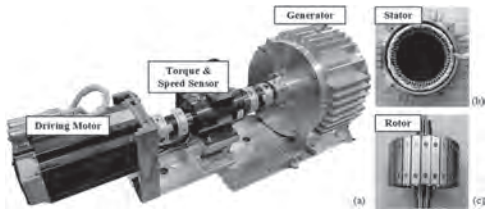

Fig. 1 Manufactured model: (a) experimental set, (b) stator, (c) rotor

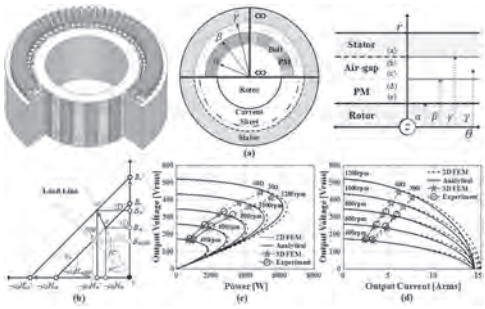

Fig. 2 (a) Analysis model, (b) demagnetization curve, and load power characteristic curve: (c) power-voltage curve, (d) current-voltage curve.

PPB-05. Research on Improvement of Torque and Loss Characteristics for an In-Wheel Permanent Magnet Motor Considering Featured-Airgap-Harmonic. *J. Ren*[1] and Z. Xiang[1] *1. School of Electrical and Information Engineering, Jiangsu University, Zhenjiang, China*

In-wheel motor technology is committed to provide a better travel for electric vehicles (EVs), which leads the way to innovation for a new generation of EVs. Quite excitingly, the in-wheel motor generates power directly in vehicle wheel. It means that improved power performance and operation efficiency can be achieved potentially for the EVs with in-wheel drive. Generally, the motor torque guarantees general drive requirements, while the loss determines operation efficiency. It is noted that, during the design process of motor, there is relatively complex association between the two performances. Hence, how to obtain a capability of excellent low-speed large-torque and low loss characteristic is the essential entry point for the study of in-wheel motor [1],[2]. In this paper, the research on improvement of torque and loss characteristics is presented for a spoke-type in-wheel PM (SIW-PM) motor. In the perspective of flux modulation, a concept of featured airgap harmonic is introduced into the motor design. By purposely designing the featured harmonic, a well tradeoff is realized between the torque and loss of SIW-PM motor. Fig. 1 shows the topology of the motor. Fig. 2 shows an analysis of the amplitude of main harmonics, the torque contribution of harmonics, and the rotor magnetic density, in which the 5th harmonic produces positive loss and negative torque. Reducing the amplitude of the fifth harmonic can effectively reduce rotor loss and improve the output torque. As is shown in Fig. 3, sensitivity analysis is used to find the parameters with high sensitivity to 5th flux density harmonic amplitude [3]. Fig. 4 shows Pareto front of harmonic amplitude generated by parameter optimization, in which optimal sample is selected as optimization results. Fig. 5 shows the rotor core loss distribution before and after optimization. The comparison of torque and rotor loss before and after optimization is given, as shown in Fig. 6 and Fig. 7. The results show that the rotor core loss is reduced and the output torque is increased by suppressing the amplitude of the 5th harmonic. More detailed analysis and experimental verification will be presented in the full paper.

[1] Z. Q. Zhu and J. T. Chen, *IEEE Trans. Magn.*, vol. 46, no. 6, pp. 1447-1453, Jun. 2010. [2] X. Zhou, X. Zhu and W. Wu, *IEEE Transactions on Industrial Electronics.*, vol. 68, no. 8, pp. 6516-6526, Aug. 2021. [3] G. Lei, C. Liu, and J. Zhu, *IEEE Transactions on Energy Conversion.*, vol. 30, no. 4, pp. 1574-1584, Dec. 2015.

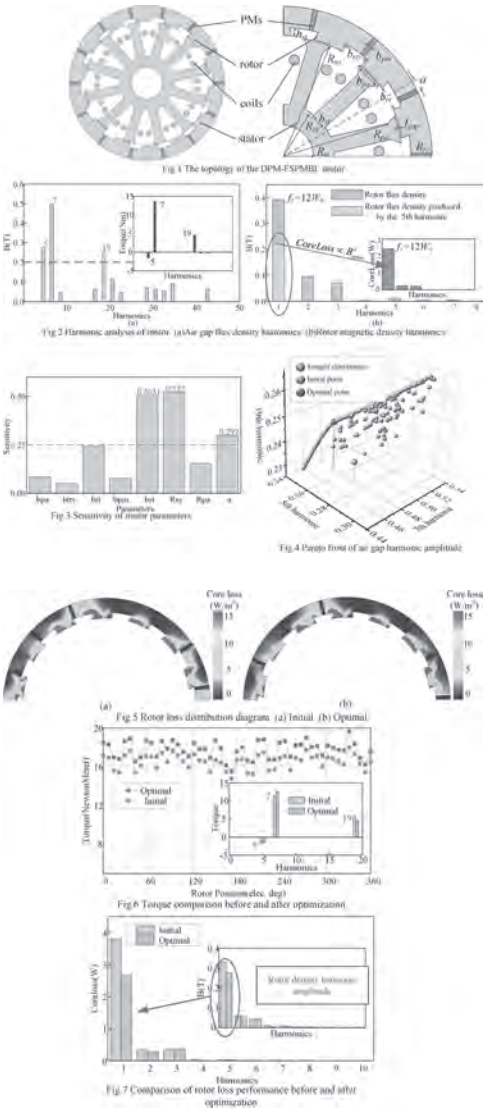

PPB-06. EMI Materials Design for High Shielding Effectiveness using AI (Machine Learning). *M. Choi*[1], Y. Hong[1], H. Won[1], H. Jung[2] and K. Lee[2] *1. Electrical and Computer Engineering, The University of Alabama, Tuscaloosa, AL, United States; 2. Semiconductor Materials R&D/ Advanced Materials, LG Chemistry, Seoul, The Republic of Korea*

Electromagnetic interference (EMI) causes various serious problems such as data loss, misinterpretation of data, and cross-talk between electronic devices. Thus, the materials with high shielding effectiveness (SE) have been quested to attenuate or reflect EM waves. Various materials and compositions and synthetic methods have been investigated, optimized, and adapted to achieve the desired SE (> 30 dB) [1-4]. These approaches can provide the optimal SE of the material of interest but are costly due to a long period of optimization and expensive characterization of investigated materials. To reduce EMI materials development time and effort, we propose Artificial Intelligence (AI)-based modeling, predicting the SE of materials. We used MATLAB to create random input parameters, Simulink to calculate SE, and Classification Learner to determine data reliability. We take the following nine input parameters to estimate SE of FINEMET (Fe-Si-Nb-Cu-B-Cr-Mn-Ni-Co), MnZn-ferrite, and NiZn-ferrite: incoming electric field, transmission (TC) and reflection (RC) coefficients, thickness, frequency, and real and imaginary parts of permeability (μ_r) and permittivity (ε_r). Fig. 1 shows the Simulink block diagram for calculating SE. First, we sampled 200 random TC and RC of the materials and then calculate the SEs with seven fixed input parameters. Among calculated SEs (Fig. 2e), the reliable SEs (Fig. 2f) are determined using AI. Our preliminary results show that the reliability was 19.5%, meaning that 39 of 200 samples are reliable. The estimated SE was compared with the experimental SE [1] to assess the accuracy of the developed AI modeling. The estimated and experimental maximum SEs are 31.87 dB and 30.61 dB, respectively, as shown in Fig. 2 (d,f,g). Accordingly, the effectiveness of our proposed method is validated. We will present how to predict the SE of EMI materials in detail. *This work was supported in part by the National Science Foundation (NSF) IUCRC under Grant No. 2137275.

[1] Anatoly B. Rinkevich, Dmitry V Perov, and Yuriy I Ryabkov, *Materials*, 14, 3499 (2021). [2] Isa ARAZ, *Turkish Journal of Electrical Engineering & Computer Sciences*, 26, 2996 (2018). [3] Jing Li, yao-Jiang Zhang, Aleksandr Gafarov, Soumya De, Marina Y. Koledintseva, Joel Marchand, David Hess, Todd Durant, Eric Nickerson, James L. Drewniak, and Jun Fan, *2012 IEEE International Symposium on Electromagnetic Compatibility*, 646, (2012). [4] Jae Man Song, Dong Il Kim, and Kyeung Jin O, *Journal of the Korea Electromagnetic Engineering Society* 6, 71, (2006).

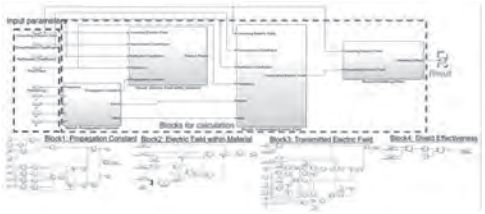

Fig.1. Block diagram for SE calculation.

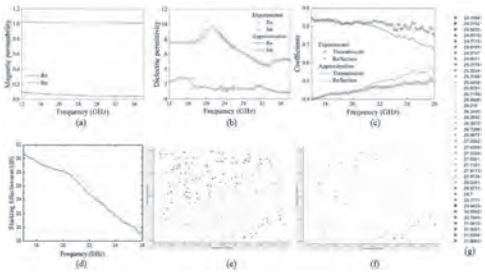

Fig.2. (a) μ' and μ'' of μ_r, (b) ε' and ε'' of ε_r, and (c) TC and RC [1], (d) calculated SE from (a,b,c), (e) SE of 200 samples before training, and (f) SE of reliable 39 samples from (g) data after training.

PPB-07. A Selective Magnetic Field Generation Method for the Manipulation of Two-Dimensional Magnetic Microrobots Using a Triad of Electromagnetic Coils. *D. Lee*[1], Y. Lee[1] and S. Jeon[1] *1. Mechanical and Automotive Engineering, Kongju National University, Cheonan, The Republic of Korea*

Magnetic microrobots actuated by a magnetic navigation system (MNS) have gained importance as a versatile device with minimally invasive and wireless manipulation abilities in various biomedical applications [1, 2]. Generally, MNSs are composed of multiple numbers of coils and massive turns of wires to generate a sufficiently strong magnetic field to manipulate the microrobots' mechanical motions. In our previous research, we proposed a geometrically compact and magnetically efficient MNS composed of a triad of electromagnetic coils (TEC), as shown in Fig. 1 [3, 4]. In the TEC, there are only three control variables (three coil currents) for manipulating two-dimensional (2D) microrobots. In this research, we investigated a new magnetic field generation method to improve the TEC's magnetic efficiency in generating 2D microrobot motions. Based on the physical property of a magnetic coil that acts as a pulling magnet for a microrobot, we established a process and several equations by which one can maneuver the 2D microrobot motions via the selective control of only two coil currents of the TEC. We also employed a closed-loop controller for the method so that the microrobot can move along a programmed pathway actuated by the TEC. We then

constructed an experimental setup to demonstrate and validate the controlled motions of the microrobot using the proposed method. The experimental results shown in Fig. 2 state that the combination of only two coils of the TEC can also generate relatively complex 2D motions of a microrobot. This research can contribute to developing an optimal MNS and strategy that can be used to manipulate 2D magnetic microrobots for various biomedical and biological applications, including minimally invasive surgery, targeted drug and cargo delivery, microfluidic control, etc.

[1] L. Wang, Z. Meng, Y. Chen and Y. Zheng, "Engineering magnetic micro/nanorobots for versatile biomedical applications.," *Advanced Intelligent Systems.,* vol. 3, no. 9, pp. 2000267, 2021. [2] T. Xu, J. Yu, X. Yan, H. S. Choi and L. Zhang, "Magnetic actuation based motion control for microrobots: An overview.," *Micromachines.,* vol. 6, no. 9, pp. 1346-1364, 2015. [3] H. Lee and S. Jeon, "Two-dimensional manipulation of a magnetic robot using a triad of electromagnetic coils.," *AIP Advances.,* vol. 10, no. 1, pp. 015003, 2020. [4] H. Lee, D. Lee, and S. Jeon, "A two-dimensional manipulation method for a magnetic microrobot with a large region of interest using a triad of electromagnetic coils.," *Micromachines.,* vol. 13, no. 3, pp. 416, 2022.

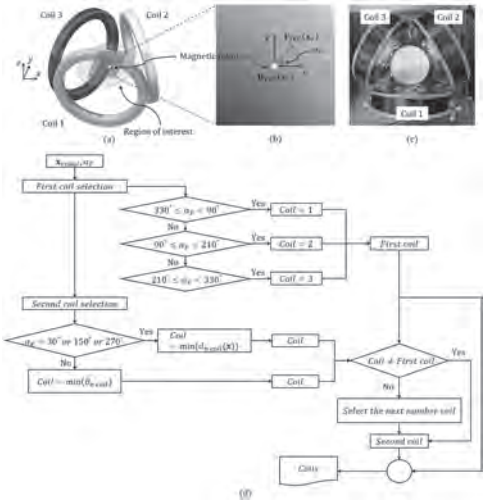

Fig. 1 Schematic views of the (a) TEC and the (b) 2D magnetic robot. (c) Experimental TEC. (d) The process of the selective magnetic field generation method using the TEC.

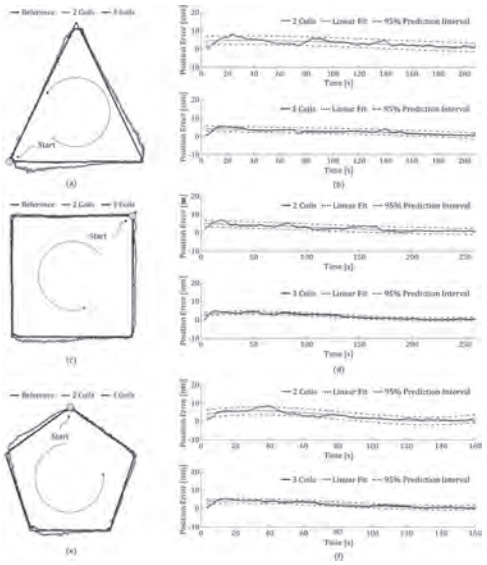

Fig. 2 Closed-loop motions of a microrobot and its position error along (a), (b) triangle-, (c), (d) square-, and (e), (f) pentagon-shaped programmed pathways actuated by the conventional (3 coils) and proposed (2 coils) methods using the TEC.

PPB-08. Research on High-efficiency Region of Interior Permanent Magnet Synchronous Motor with Variable Magnetic Field Effect.

X. Yu[1] and Z. Xiang[1] *1. School of Electrical and Information Engineering, Jiangsu University, Zhenjiang, China*

Recently, interior permanent magnet motors have been widely employed in various commercial electric vehicles. To expand the cruising range of EVs, the analysis and improvement of efficiency for the IPM motors have attracted increasing attention [1]. For the IPM motors, a large current is often required to weaken the PM magnetic field to increase the speed range, which inevitably increases the copper and iron losses of the motor, resulting in a decrease in efficiency under high speed [2]. Consequently, it is necessary and full of challenges to research and expands the high-efficiency region of the IPM motor, especially at high speed. In this paper, by introducing the new magnetic field variable effect into an interior PM motor, the variable magnetic field can be obtained under different operation conditions, which not only helps to reduce the copper and core losses under different operation conditions but also widens high-efficiency region.[3] Fig 1 shows the topology of the proposed VMF motor and the structure of the corresponding variable magnetic field. To explore the performance advantage of the proposed VMF motor, three operation points are selected to investigated, which can be classified into two operation conditions, as shown in Fig. 2. By the purposeful design of variable magnetic field structure, the increased efficiency of high-speed operation point and the expanded high-efficiency region can be realized. Fig 3 shows the comparison of the performance of the VMF and IPM motor, including no-load flux density and back-EMF. Fig 4 shows the flux density distributions of the VMF motor under different operation condition. Furthermore, the loss distributions of the IPM and VMF motor under different conditions are shown in Fig 5. As can be seen from the Table I and Fig6, the efficiency of the motor has been improved and broadened, especially at point C, the efficiency has increased to 96.5%. Consequently, it is noted that the efficiency of the VMF motor is improved and the high-efficiency region is widened, which verifies the effectiveness of the VMF motor design proposed in this paper. More detailed analysis and experimental verification will be presented in the full paper.

[1] W. Jiang, S. Feng and Z. Zhang, *IEEE Transactions on Magnetics.*, vol. 54, no. 11, pp. 1-5, Nov. 2018, Art no. 8108005. [2] H. Hua and Z. Q. Zhu, *IEEE Trans. Energy Convers*, vol. 32, no. 2, pp. 495-504, June 2017. [3] A. Athavale, T. Fukushige and T. Kato, *IEEE Trans. Ind. Appl.*, vol. 52, no. 1, pp. 234-241, Jan.-Feb. 2016.

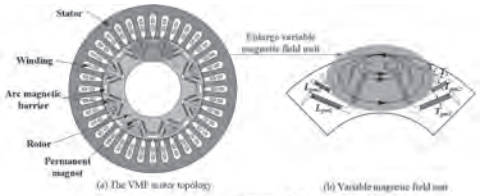

(a) The VMF motor topology (b) Variable magnetic field unit

Fig.1. Topology and variable magnetic field unit of VMF motor

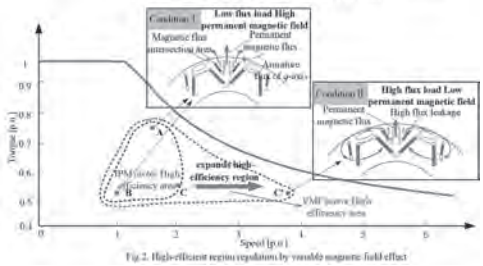

Fig.2. High-efficient region regulation by variable magnetic field effect

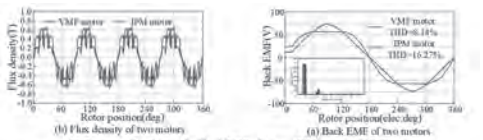

(b) Flux density of two motors (a) Back EMF of two motors

Fig.3. Air-gap flux density And back EMF between IPM motor and VMF motor

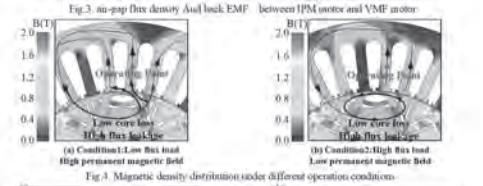

(a) Condition1:Low flux load High permanent magnetic field (b) Condition2:High flux load Low permanent magnetic field

Fig.4. Magnetic density distribution under different operation conditions

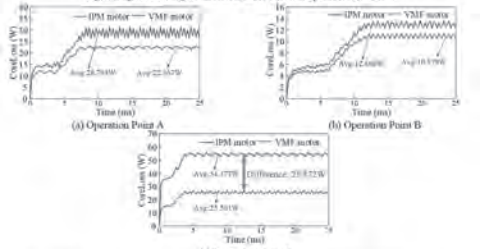

(a) Operation Point A (b) Operation Point B

(c) Operation Point C

Fig.5. Iron loss distribution of IPM motor and VMF motor under different operation conditions

Table I. Current loss and efficiency distribution of Normal PM motor and VMF motor

Operating Point	Motor Type	Current(A)	CopperLoss(W)	CoreLoss(W)	Efficiency
A	IPM	12.7	121.4	28.7	96.1%
	VMF	12.9	124.8	22.4	96.0%
B	IPM	4.7	16.4	12.9	96.2%
	VMF	4.8	17.4	10.9	96.3%
C	IPM	11.3	96.8	54.1	93.7%
	VMF	9.2	63.7	28.9	96.5%

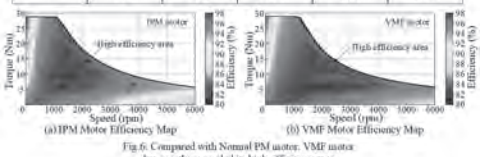

(a) IPM Motor Efficiency Map (b) VMF Motor Efficiency Map

Fig.6. Compared with Normal PM motor, VMF motor has greatly expanded its high-efficiency area

PPB-09. Design and Analysis of a V-Shaped Leakage-Flux-Controllable PM Machine with Improved Torque Performances. *X. Cai*[1] and X. Zhu[1] *1. School of Electrical and Information Engineering, Jiangsu University, Zhenjiang, China*

Permanent magnet (PM) motors have been widely applicable for electric vehicles due to their excellent power density and efficiency. Yet, due to the relatively constant airgap magnetic field, the motor always suffers from a limited speed range. So, the achievement of a wide speed range is one of the hot research orientations for PM motors. In recent years, a type of leakage-flux-controllable (LFC) motor has attracted some interest and attention of researchers, where the magnetic bridge and flux barrier are purposely designed in PM rotor for forming the controllable leakage flux[1]. Based on this, the LFC-PM motor possesses the potential advantages of speed regulation[2]. It is noted that to realize the condition of no leakage flux in motor drive process, a relatively strong armature field is usually required to be applied at this time, and, correspondingly, the magnetic saturation comes with that. It means that the torque capability of LFC PM motor is worthy of attention and full of challenge, especially on the drive requirements of low-speed large torque. In this study, a V-typed leakage-flux-controllable PM (VFLC-PM) motor with multiple functional magnetic flux barrier units is proposed, which can provide relatively high output torque and a wide speed range. The motor topology and magnetic barrier structure analysis are shown in Fig. 1. The magnetic field distributions under different operating conditions are shown in Fig. 2. At no load, the flux leakage barrier guides parts of PM flux into the flux leakage path and reduces the air gap effective flux. As the armature current increases, the flux focusing barrier guides the PM flux to pass through the air gap rather than flux leakage path, and the main flux is enhanced. And then, a response surface method is adopted to optimize the key parameters related to the magnetic flux barrier units in Fig. 3. After optimization, the torque performances of the motor are significantly improved both at different operating conditions as shown in Fig. 4. Finally, the torque characteristics of the motor are verified through experiments in Fig. 5. The experimental results are in good agreement with the simulation results, which verifies the effectiveness of the motor design.

[1] T. Kato, T. Matsuura and K. Sasaki, *Proc. IEEE Energy Convers. Congr. Expo.*, 2017, pp. 5803–5810. [2] X. Zhou, X. Zhu and W. Wu, *IEEE Trans. Ind. Electron.*, vol. 68, no. 8, pp. 6516–6526, Aug. 2021.

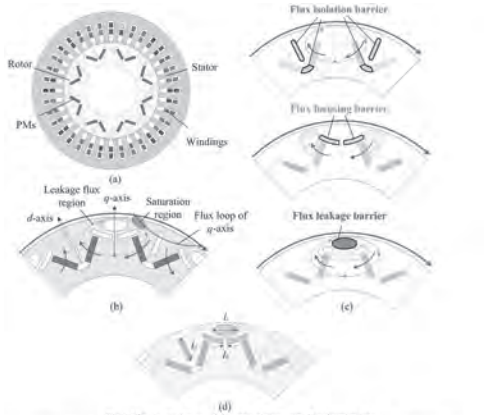

(a) (b) (c) (d)

Fig.1 Motor topology and functional magnetic flux barrier units.
(a)Motor topology (b) Operating principle (c) Functional magnetic flux barrier units design (d) Design variables

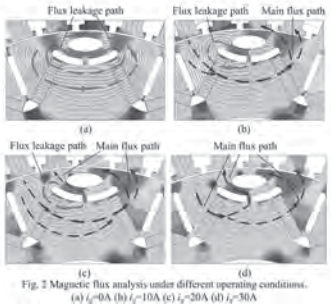

(a) (b) (c) (d)

Fig. 2 Magnetic flux analysis under different operating conditions.
(a) i_d=0A (b) i_d=10A (c) i_d=20A (d) i_d=30A

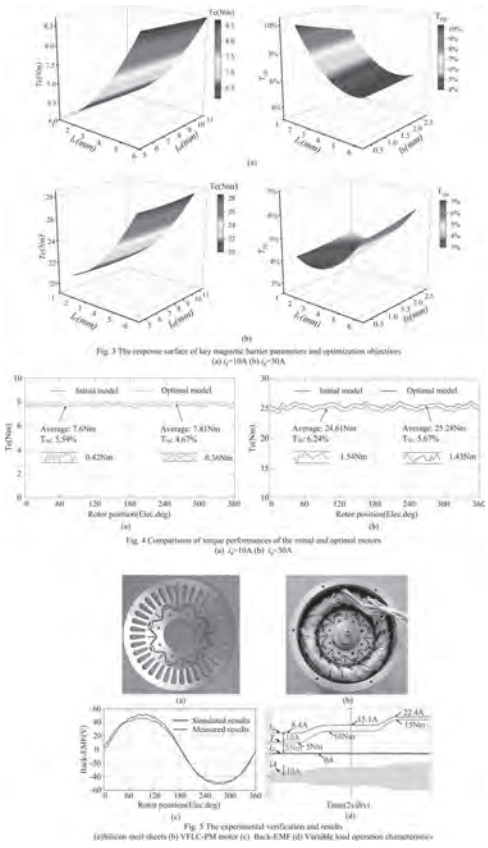

PPB-10. Low Vibration Design of Variable Leakage Flux Permanent Magnet Motor Considering Multiple Working Conditions. *T. Liu*[1] and L. Quan[1] *1. School of Electrical and Information Engineering, Jiangsu University, Zhenjiang, China*

In recent years, variable leakage flux permanent magnet (VLF-PM) motors, which can realize different operation conditions, have attracted increasing attention [1]. In this kind of motors, by the purposeful design of flux barriers and PMs, design requirements of different operation conditions can be satisfied [2]. It is noted that, under different working conditions, different flux density distribution often leads to significant changes in radial electromagnetic force distribution and characteristics of vibration noise [3]. Thus, it is necessary to design and analyze the characteristic of vibration noise of VLF-PM motor under multiple working conditions. In this paper, the characteristics of electromagnetic vibration of VLF-PM motor under different working conditions are researched. And, an low vibration design method is proposed for VLF-PM motors, considering multiple working conditions. Fig. 1 shows the proposed VLF-PM motor and operation principle under different operation conditions. Fig. 2 presents the characteristics of electromagnetic vibration of the VLF-PM motor in different working regions. According to the operation principle, two typical working points are selected for analysis. The sensitivity of design parameters to the desired optimization objective are depicted in Fig. 3, and the selected sensitive parameters are marked. The characteristics of sensitive design parameters are illustrated in Fig. 4. The basic electromagnetic performances under two working points are shown in Fig. 5. It can be seen that under the two working conditions, the output torque of the two motors is almost the same, and the torque ripple of the optimal motor is obviously reduced. Fig. 6 shows the vibration characteristics of VLF-PM motor. Due to the lower amplitudes of low-order radial force density, especially, 4th, the vibration and noise characteristics of the optimal VLF-PM motor is preferred under the two working points, which verifies the effectiveness of the low vibration design of the VLF-PM motor proposed in this paper. More detailed analysis and experimental verification will be presented in the full paper.

[1] H. Hu, Z. Xiang and X. Zhu, *IEEE Transactions on Magnetics*, vol. 58, no. 2, pp. 1-6, Feb. 2022, Art no. 8102606. [2] X. Zhou, X. Zhu and W. Wu, *IEEE Transactions on Industrial Electronics*, vol. 68, no. 8, pp. 6516-6526, Aug. 2021. [3] M. S. Islam, R. Islam and T. Sebastian, *IEEE Transactions on Industry Applications*, vol. 50, no. 5, pp. 3214-3222, Sept.-Oct. 2014.

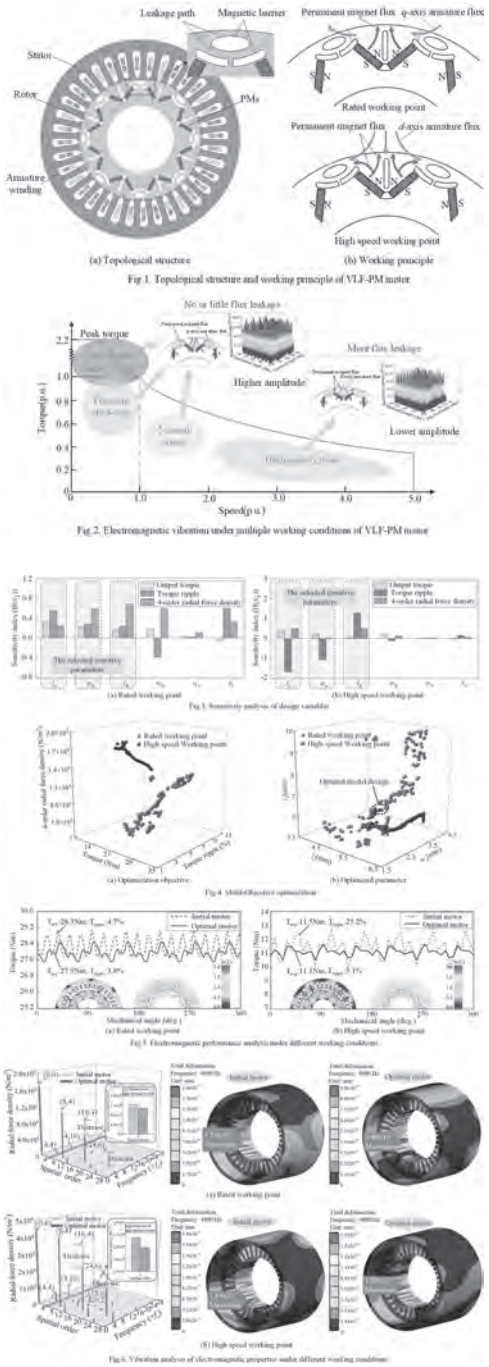

PPB-11. Airgap-Harmonic-Oriented Partitioned Design Method of PMV Motor with Improved Torque Performances. *Z. Wu*[1] and D. Fan[1] *1. School of Electrical and Information Engineering, Jiangsu University, Zhenjiang, China*

Due to the advantage of high torque at low speed, permanent magnet vernier (PMV) motor has become an excellent candidate for low-speed direct-drive applications [1], such as electric vehicles. With the increasing critical demand for electric vehicle drives, multiple design requirements have also

been proposed for performance of electric vehicle drive motors, including output torque and torque ripple [2]. Recently, many researchers have contributed to improving torque performances of PMV, mainly by the design of permanent magnet and stator teeth [3][4]. Yet, it is noted that, current literature on improving motor performances would either increase output torque or reduce torque ripple, while the comprehensive improvement of torque performances can hardly be achieved. Thus, in this paper, an airgap-harmonic-orientated partitioned design method is newly proposed for PMV motors. In the proposed design method, considering the effect of different harmonics on torque performance, the torque designed region of rotor is artfully divided into torque enhanced region and ripple reduced region. And, by the purposeful design of these two regions, output torque is increased while torque ripple is reduced effectively. Fig. 1 shows the configurations of proposed and initial PMV motors. The airgap-harmonic-orientated partitioned design principle is presented in Fig. 2, providing theoretical guidance for motor torque performance improvement. Fig. 3 shows the magnetic field and flux distributions of proposed motor. Meanwhile, based on partition design principle, the airgap flux density waveforms, and the main airgap harmonic variations related to output torque and torque ripple are presented in Fig. 4 and Fig. 5 respectively. It can be seen from Fig. 6 that, by the reasonable design of torque enhanced region and ripple reduced region, output torque of motor is significantly increased by 82.6% while torque ripple is reduced by 61.1% efficiently as expected. Thus, by the proposed airgap-harmonic-orientated partition design method, improved output torque and reduced torque ripple can be realized effectively. The detailed theoretical analysis and simulation results will be presented in the full paper.

[1] Y. Ma and W. Fu, *IEEE Trans. Magn*, vol. 57, no. 6, pp. 1-5, June 2021. [2] B. Lee, Z. Zhu and L. Huang, *IEEE Trans. Ind. Appl*, vol. 55, no. 3, pp. 2510-2518, May-June 2019. [3] X. Zhu, M. Jiang and Z. Xiang, *IEEE Trans. Ind. Electron*, vol. 67, no. 7, pp. 5337-5348, July 2020. [4] L. Fang, D. Li and X. Ren, *IEEE Trans. Ind. Electron,* vol. 69, no. 6, pp. 6058-6068, June 2022.

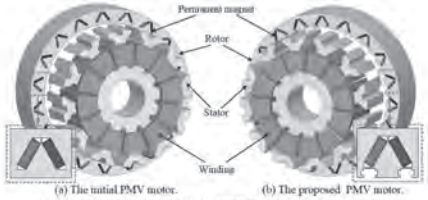

(a) The initial PMV motor. (b) The proposed PMV motor.
Fig. 1. Topologies of the initial PMV motor and the proposed PMV motor.

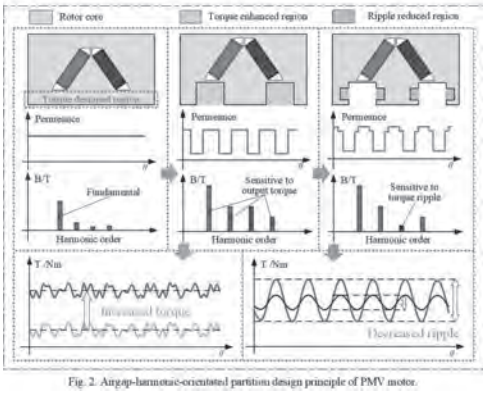

Fig. 2. Airgap-harmonic-orientated partition design principle of PMV motor.

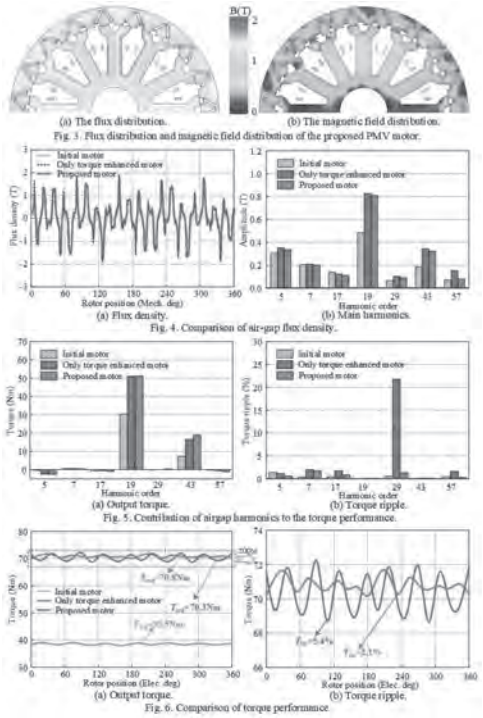

Fig. 3. Flux distribution and magnetic field distribution of the proposed PMV motor.
Fig. 4. Comparison of air-gap flux density.
Fig. 5. Contribution of airgap harmonics to the torque performance.
Fig. 6. Comparison of torque performance.

PPB-12. Multi-Level Robust Optimization Design of Double-Stator Vernier Permanent Magnet Motor. *C. Yang*[1] and L. Quan[1] *1. School of Electrical and Information Engineering, Jiangsu University, Zhenjiang, China*

Recently, flux modulated permanent magnet motors have aroused considerable attention, due to the merits of relatively high output torque at low speed. To further improve motor torque output capability, double stator vernier permanent magnet (DS-VPM) motors have attracted increasing attention [1]. However, due to the relatively complicated relationship among airgap flux harmonic, motor structure and performances, the difficulty and time burden of the optimization design of DSVPM motor is increased significantly [2]. Besides, during actual motor manufacturing process, there exists many unavoidable design uncertainties, which would result in motor performance degradation [3]. Thus, it has been a hot but challenging issue on how to realize high-efficiency optimization design of DS-VPM motor consider parameter fluctuation. In this paper, an airgap-harmonic-based multi-level robust optimization design method is proposed for DS-VPM motor. By the proposed optimization method, motor performances can be improved comprehensively considering parameter fluctuation. The structure of the investigated DS-VPM motor is shown in Fig. 1 (a), and corresponding design parameters of DS-VPM motor are presented in Fig. 1 (b). The flowchart of the proposed airgap-harmonic-based multi-level robust optimization method is presented in Fig. 2. Firstly, the detailed relationship among design parameters, design parameters, and motor performances are investigated, as shown in Fig. 3 and Fig. 4. Then, based on multi-objective genetic algorithm and response surface method, deterministic optimal design of DS-VPM motor is determined. Furthermore, robust optimization method is utilized to achieve the robust optimal motor deign. Electromagnetic performances of the optimal DS-VPM motor are presented in Fig. 5 and Fig. 6, while the normal distribution of the initial and final motor performances is presented in Fig. 7. Consequently, it is noted that that not only motor performances are improved effectively, but the fluctuations of the motor performances are reduced significantly which verifies the effectiveness of the proposed robust multi-level optimization method. More simulation and experimental results will be presented in the full paper.

[1] W. Zhao, T. A. Lipo and B. -I. Kwon, *IEEE Trans. Magn*, vol. 51, no. 11, pp. 1-4, Nov 2015. [2] X. Zhu, M. Jiang and Z. Xiang, *IEEE Trans. Ind.*

Electron, vol. 67, no. 7, pp. 5337-5348, July 2020. [3] M.-M. Koo, J.-Y. Choi and K. Hong, *IEEE Trans. Magn*, vol. 51, no.11, pp. 1-4, Nov 2015.

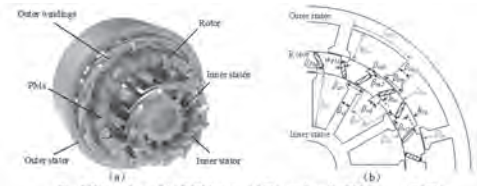

Fig. 1 The topology of the DSPM motor. (a) The topology the DSPM motor. (b) The geometric parameter model of the DSPM motor

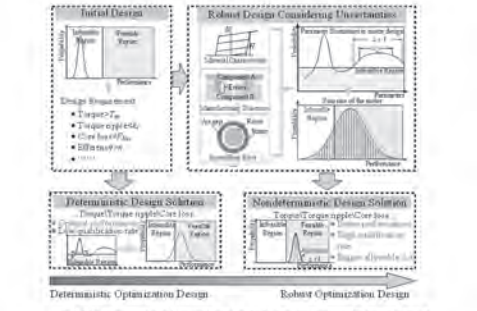

Fig. 2 The proposed airgap-harmonic-based multi-level robust optimization design approach

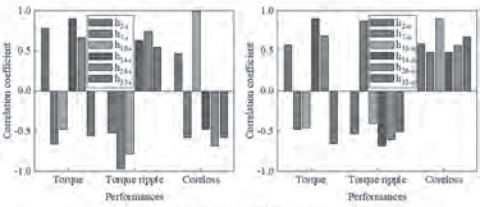

Fig. 3 The correlation of airgap harmonics to the motor performances

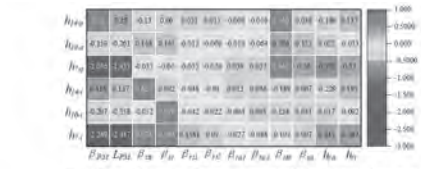

Fig. 4 The sensitivity value of motor parameters to the leading airgap harmonics

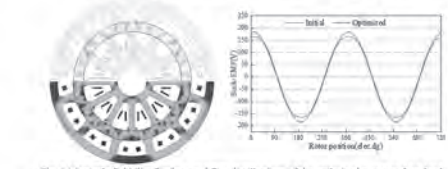

Fig. 5 Magnetic field distributions and flux distributions of the optimized motor and no-load back-EMF waveforms

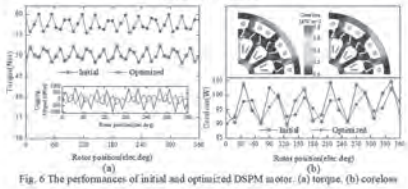

Fig. 6 The performances of initial and optimized DSPM motor. (a) torque. (b) coreless

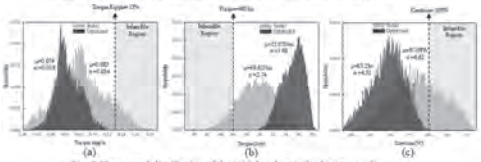

Fig. 7 The normal distribution of the initial and optimized motor performances (a) torque ripple. (b) torque. (c) coreless.

PPB-13. Optimization Design and Analysis of an In-Wheel PM Motor Based on Common-Node Magneto-Thermal Bidirectional Coupling Network Model. *Z. Yang*[1] and X. Zhu[1] *1. School of Electrical and Information Engineering, Jiangsu University, Zhenjiang, China*

In-wheel motor is regarded as the most promising drive system of next generation electric vehicles in merit of high transmission efficiency, flexible control and compact structure [1]. Since the in-wheel motor often operates under different conditions and possesses multiple external heat sources, electromagnetism-thermal analysis is essential during the motor design stage [2]. Generally, the current electromagnetism-thermal analysis is based on finite element analysis (FEA), the large time-consumptions of this method brings challenges to the design of this kind of motor [3]. Therefore, a rapid design method of in-wheel motor based on a common-node magneto-thermal bidirectional coupling network (CMTBCN) model is proposed in this paper. In the CMTBCN model, some nodes of the motor are used as common nodes of the equivalent magnetic network (EMN) model and the equivalent thermal network (ETN) model to avoid repeated modeling. Then the effect of temperature on the coercivity and permeability of permanent magnets is considered in EMN, the losses calculated by EMN at initial temperature are used as the heat sources of ETN to calculate the new temperature. The temperature of each component of the motor and the electromagnetic performance under different working conditions can be obtained more accurately by using the bidirectional coupling method. Finally, an in-wheel motor is designed and optimized based on CMTBCN model. Fig. 1 (a) shows the 3D structure and parametric model of the in-wheel motor. Fig. 1 (b) shows the proposed common-node magneto-thermal bidirectional coupling network model. Fig. 2 (a) compared the airgap flux density and its harmonic analysis obtained by CMTBCN and FEA. Fig. 2 (b) compared the A-phase no-load flux linkage and back-EMF obtained by CMTBCN and FEA at -20 and 100 degrees Celsius. Fig. 2 (c) shows the static temperature distribution of the in-wheel motor under the rated load obtained by FEA. Fig. 2 (d) shows the prototype of stator and rotor of the proposed in-wheel motor. More detailed analysis and experimental verification will be presented in the full paper.

[1] P. Liang, F. Chai and Y. Yu, *IEEE Transactions on Industrial Electronics*, vol. 66, no. 2, pp. 1162-1171, Feb. 2019. [2] X. Chen and G. Li, 2020 13th International Conference on Intelligent Computation Technology and Automation (ICICTA), 2020, pp. 683-686. [3] X. Li, F. Shen and S. Yu, *IEEE Transactions on Industrial Electronics*, vol. 68, no. 8, pp. 6560-6573, Aug. 2021.

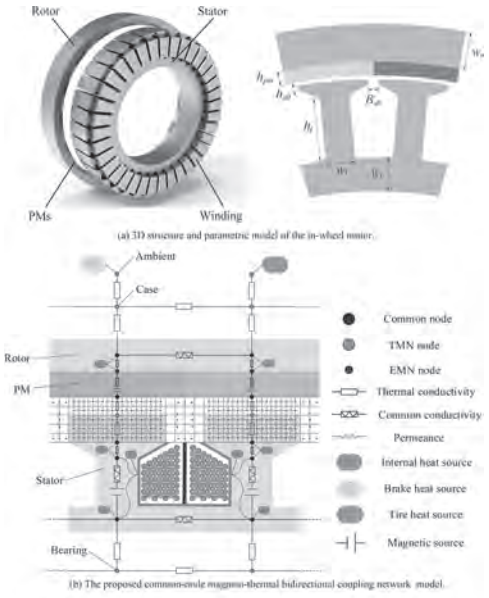

Fig. 1. 3D structure and parametric model of the in-wheel motor and the proposed common-node magneto-thermal bidirectional coupling network model.

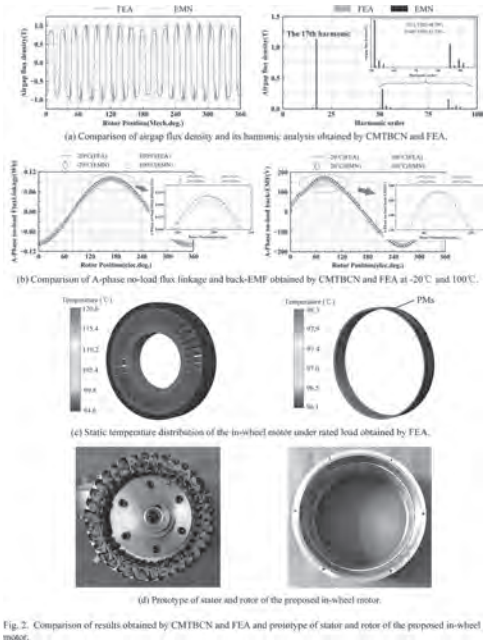

(a) Comparison of airgap flux density and its harmonic analysis obtained by CMTBCN and FEA.

(b) Comparison of A-phase no-load flux linkage and back-EMF obtained by CMTBCN and FEA at -20℃ and 100℃.

(c) Static temperature distribution of the in-wheel motor under rated load obtained by FEA.

(d) Prototype of stator and rotor of the proposed in-wheel motor.

Fig. 2. Comparison of results obtained by CMTBCN and FEA and prototype of stator and rotor of the proposed in-wheel motor.

PPB-14. Research on Vibration Characteristic of a V-shaped PM In-Wheel Motor Considering Radial Electromagnetic Force Modulation Effect. *J. Bai*[1] and X. Zhu[1] *1. School of Electrical and Information Engineering, Jiangsu University, Zhenjiang, China*

In-wheel motors have been considered as one of the core technologies for the future developments of electric vehicles (EVs), where the outstanding feature is that the drive motor is directly connected to the vehicle wheel [1]. It indicates that, to the EVs, the short transmission chain and high transmission efficiency can be achieved potentially by adopting the in-wheel motor [2]. Yet, the direct-drive with in-wheel motor gaining advantages of power transmission, while it also makes the motor straightly faced with the complex drive environment, such as the diverse operation conditions and road conditions. It means that, to the in-wheel motor, the problems of vibration and noise are more prominent and worthy of concern. This is essential for realizing the high reliability and desirable comfort of EVs. Therefore, how to effectively suppress the vibrations and reduce noise is becoming a hot research field and full of challenge. Then, a new perspective of radial electromagnetic force (REF) modulation is proposed for studying the vibration characteristic of a V-shaped PM in-wheel (VPM-IW) motor in this paper. By purposely considering the modulation effect of REF into motor design, the electromagnetic vibration of VPM-IW motor is suppressed effectively. Firstly, Fig.1(a) shows that the VPM-IW motor with the pole-slot combination of 40-pole/24-slot is selected as the design example. Fig.1(b) shows the deformation on the motor caused by the different orders of REF. And Fig. 1(c) shows the principle of REF modulation. Then, Fig. 2(a)-Fig. 2(d) show the relationship between radial flux density (RFD) and REF. It can be seen that, the dominant spatial order of REF, such as 4^{th}, is generated by $4k^{th}$ RFD harmonics. Hence, 4^{th} REF can be suppressed by reducing $4k^{th}$ RFD harmonics. Next, the multi-objective genetic algorithm (MOGA) is adopted considering the force modulation effect. Fig. 2(g) to Fig. 2(n) show the comparison of performances. Fig. 2(m) and Fig. 2(n) show that the optimal structure realizes the reduction of vibration and noise and the highest vibration peak appears around 4979 Hz, which is frequency of 4^{th} mode. The more detailed theoretical analysis and research results will be provided in the full paper.

[1]W. N. Fu and S. L. Ho, *IEEE Transactions on Magnetics*, vol. 46, no. 1, pp. 127-134, Jan. 2010. [2] S. Zuo, F. Lin and X. Wu, *IEEE Transactions on Industrial Electronics*, vol. 62, no. 10, pp. 6204-6212, Oct. 2015.

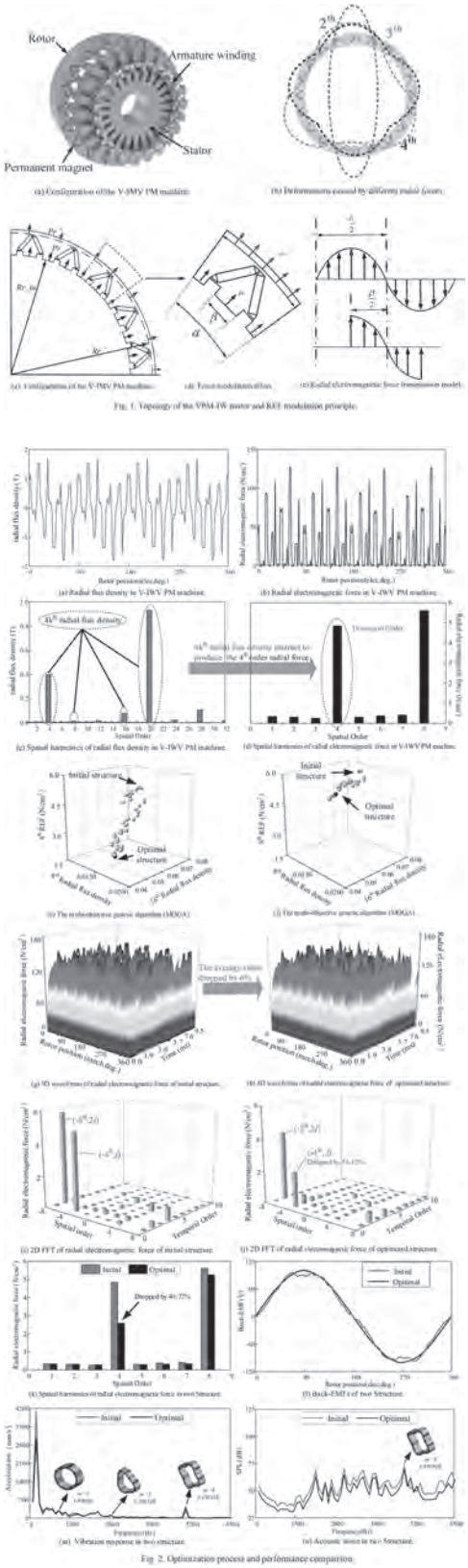

Fig. 1. Topology of the VPM-IW motor and REF modulation principle.

Fig. 2. Optimization process and performance comparison.

PPB-15. A Novel Magnetic Field Calculation Method for Propulsion Motor with Uneven Arrangement of Silicon Sheet. *X. Liang*[1], M. Wang[1], P. Zheng[1], J. Gao[1] and W. Li[1] *1. School of Electrical Engineering and Automation, Harbin Institute of Technology, Harbin, China*

Propulsion Motor which can utilize reluctance torque with power electronics is considered as a promising candidate for high-power propulsion. When the motor is operating under load, magnetic field is modulated by silicon sheet arranged unevenly. The alternating placement of high- and low-permeability materials to achieve energy conversion is studied by lumped parameter method such as L_d and L_q [1]. The electromagnetic field inside the motor cannot be comprehensively analyzed, and the distribution of q-axis magnetic field is ignored for simplification. However, the high-efficiency conversion of energy depends on the interaction of specific magnetic fields and currents. So, it is necessary to study the theoretical relationship between the structure parameters and d- and q- axis magnetic field distribution. Considering the distribution of high- and low-permeability materials and excitation sources, a novel method to calculate the distribution of the magnetic field is proposed. In the proposed, the magnetic field generated by the current is projected on the d- and q- axis, respectively. In the d-axis flux path, considering cogging structure, the magnetic field is calculated by the improved winding function method. The effect of rotor materials in q-axis is derived and calculated based on the actual flux path and variation of permeance with curvature. The total power is obtained by subtracting the power calculated from the current and magnetic field projected on two directions, as shown in Fig. 1. The theoretical prototype is the motor widely used for high-power propulsion, considering the structure layers, proportions, spatial distribution and other factors of its high- and low-permeability materials. Supposing the current angle on load is 45°, the calculated and simulated results of the distribution of magnetic field are shown in Fig. 2. The errors of d-axis, q-axis and magnetic field located 45°-axis are 0.37%, 6.8%, 2.69% in fundamental amplitude, respectively. By adopting the proposed method, the material structural parameters of high-performance motor for high-power propulsion can be quickly obtained.

[1] Zheng, S., et al., Comparative Analysis and Multi-Objective Optimization of Hybrid Permanent Magnet Motors Considering Different Saliency Characteristics. IEEE Transactions on Applied Superconductivity, vol31, p. 1-5(2021).

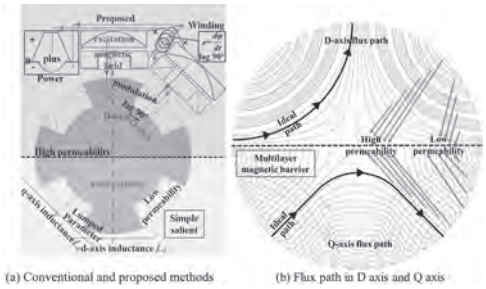

Fig. 1. Analysis model

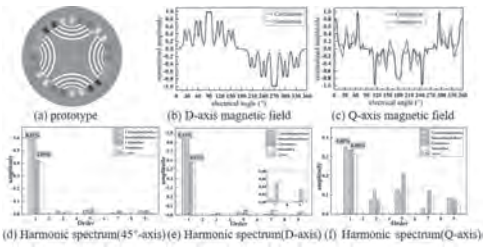

Fig. 2. Comparison of calculation and simulation

Session PPC
TRANSFORMERS AND INDUCTORS
(Poster Session)

Xiaojun Zhao, Chair
North China Electric Power University, Baoding, China

PPC-01. Iron loss evaluation method for SiFe sheet material under PWM inverter excitation. *H. Matsumori*[1], T. Yamaguchi[1], T. Kosaka[1], T. Shimizu[2] and N. Matsui[1] *1. Electrical and Mechanical Engineering, Nagoya Institute of Technology, Nagoya, Japan; 2. Tokyo Metropolitan University, Tokyo, Japan*

This paper presents an iron loss evaluation method for SiFe sheet material under high-frequency current ripple due to PWM inverter switching. The PWM inverter switching makes dynamic minor loops on the BH plane, which cause iron loss [1-3]. Furthermore, in magnetic material with wide major loops, such as SiFe sheet material, an iron loss of one dynamic minor loop is different by flux density Bias B_0 difference even if the same magnetic field bias H_0, as shown in Fig. 1. In this case, the previous paper reported an iron loss calculation error [4] because conventional iron loss calculation method, such as Steinmetz equation, iGSE, i2GSE, and Loss map method, does not consider the iron loss of the flux density Bias B_0 characteristic [4-9]. Therefore, the authors modified the previously developed iron loss measurement system [10] to collect for the iron loss of the flux density Bias B_0 characteristic. Then, the measured iron loss data for the flux density Bias B_0 characteristics are added to the conventional loss map (i.e., our iron loss datasheet for SiFe materials expressed by flux density ripple DB, excitation frequency, and magnetic field bias H_0). Finally, the iron loss of SiFe sheet material is evaluated by the conventional loss map method and the proposed method, which use an improved loss map. The iron loss calculation result for PWM inverter excitation is shown in Fig. 2. Compared to the conventional calculation method, the calculation error of iron loss due to the difference in the flux density Bias Bo is reduced. In this case, the measured iron loss value is 10.68W, the proposed method is 11.48W, and the conventional method is 11.82W. The calculation error is reduced from 10.7% to 7.5%. The final paper will explain the detail of the iron loss measurement system for the flux density Bias B_0 characteristic and iron loss calculation method for SiFe sheet material. Also, the iron loss calculation results for other operating conditions are inserted. The proposed method has better calculation accuracy in all conditions than the conventional method.

[1] L. Chang, T. M. Jahns and R. Blissenbach, "Characterization and Modeling of Soft Magnetic Materials for Improved Estimation of PWM-Induced Iron Loss," *2018 IEEE Energy Conversion Congress and Exposition (ECCE)*, Portland, OR, USA, 2018, pp. 5371-5378. doi: 10.1109/ECCE.2018.8557438 [2] M. Kawabe, T. Nomiyama, A. Shiozaki, H. Kaihara, N. Takahashi and M. Nakano, "Behavior of Minor Loop and Iron Loss Under Constant Voltage Type PWM Inverter Excitation," in *IEEE Transactions on Magnetics*, vol. 48, no. 11, pp. 3458-3461, Nov. 2012. doi: 10.1109/TMAG.2012.2198199 [3] A. Boglietti, A. Cavagnino, D. M. Ionel, M. Popescu, D. A. Staton and S. Vaschetto, "A General Model to Predict the Iron Losses in PWM Inverter-Fed Induction Motors," in *IEEE Transactions on Industry Applications*, vol. 46, no. 5, pp. 1882-1890, Sept.-Oct. 2010. doi: 10.1109/TIA.2010.2057393 [4]H. Matsumori, T. Shimizu, T. Kosaka and N. Matsui, "Iron loss calculation under PWM inverter switching for SiFe steel materials," 2019 IEEE Energy Conversion Congress and Exposition (ECCE), 2019, pp. 2315-2320, doi: 10.1109/ECCE.2019.8912818. [5] H. Matsumori, T. Shimizu, X. Wang and F. Blaabjerg, "A Practical Core Loss Model for Filter Inductors of Power Electronic Converters," in *IEEE Journal of Emerging and Selected Topics in Power Electronics*, vol. 6, no. 1, pp. 29-39, March 2018. doi: 10.1109/JESTPE.2017.2761127 [6] Z. Gmyrek, A. Boglietti and A. Cavagnino, "Iron Loss Prediction With PWM Supply Using Low- and High-Frequency Measurements: Analysis and Results Comparison," in *IEEE Transactions on Industrial Electronics*, vol. 55, no. 4, pp. 1722-1728, April 2008. doi: 10.1109/TIE.2008.917067 [7]K. Venkatachalam, C. R. Sullivan, T. Abdallah and H. Tacca, "Accurate prediction of ferrite core loss with nonsinusoidal waveforms using only Steinmetz parameters", Proc. IEEE Workshop Comput. Power Electron., pp. 36-41, 2002. [8] J. Muhlethaler, J. Biela, J. W. Kolar and A. Ecklebe, "Core Losses Under the DC Bias Condition Based on Steinmetz Parameters," in *IEEE Transactions on Power Electronics*, vol. 27, no. 2, pp. 953-963, Feb. 2012. doi: 10.1109/TPEL.2011.2160971 [9]H. Matsumori, T. Shimizu, K. Takano and H. Ishii, "Evaluation of Iron Loss of AC Filter Inductor Used in Three-Phase PWM Inverters Based on an Iron Loss Analyzer," in IEEE Transactions on Power Electronics, vol. 31, no. 4, pp. 3080-3095, April 2016, doi: 10.1109/TPEL.2015.2453055. [10]Hiroaki Matsumori, Toshihisa Shimizu, Takashi Kosaka, Nobuyuki Matsui, High-speed Core Loss Base Data Collection for Core Loss Calculation Under Power Electronics Converter Excitation, IEEJ Journal of Industry Applications, 2021, Volume 10, Issue 1, Pages 84-90, 2021, doi:10.1541/ieejjia.20006557

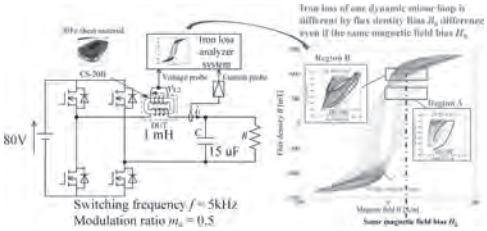

Fig. 1 Overview of iron loss characteristics under PWM inverter excitation using Si-Fe sheet material.

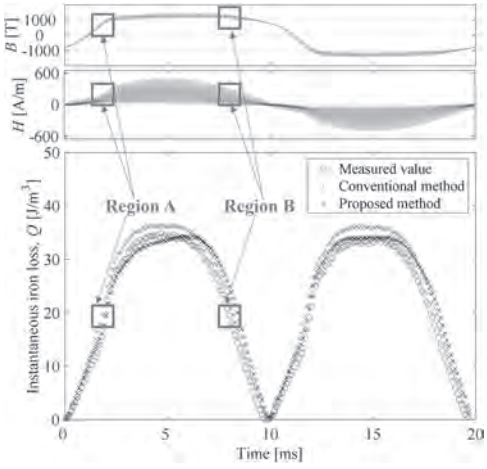

Fig. 2 Comparison of the iron loss evaluation result.

PPC-02. Analysis and Design of Constant Current and Constant Voltage Outputs of Integrated Coil Wireless EV Charging System.
L. Chen[1], *F. Wu*[1], T. Ben[1], C. Zhang[1], L. Jing[1] and Q. Liu[1] *1. Hubei Provincial Research Center on Microgrid Engineering Technology, China Three Gorges University, Yichang, China*

I Introduction Typically, EVs adopt lithium-ion batteries as power supply. Therefore, constant current (CC) mode and constant voltage (CV) mode can be implemented for battery charging applications. At present, various control strategies have been proposed. However, these methods require complex control strategies and additional components, often lead to increased switching losses[1] and frequency bifurcation[2], and are difficult to achieve with zero phase angle input (ZPA). In this paper, a switchable hybrid compensation structure is designed to achieve load-independent output current and load-independent output voltage under ZPA conditions by switching the receiver-side compensation structure without additional devices and complex control methods. II Method and Discussion A hybrid topology using different compensations in the receiver side, i.e., *LC-LC* compensation and *LC-LCCL* compensation is developed. Meanwhile, the compensation coil is integrated into the receiving coil, the magnetic field is enhanced without any reactive power flow between the compensation and receiving coils, which can effectively improve the power transmission distance, efficiency, and capacity. At a fixed frequency, no complicated control methods are required, and constant voltage and constant current can be achieved under ZPA conditions. Besides, by optimizing the integrated coil and designing compensation parameters, the system can still maintain good CC-CV output characteristics when misalignment happens. III Conclusion According to the experimental results, the wireless charging system can operate within 100mm misalignment in X-axis when the maximum fluctuations of the charging current I_B in CC mode and the charging voltage V_B in CV mode are less than 7% which is consistent well with the theoretical analysis. Besides, the wireless charging system can achieve the maximum efficiency at 93.43% with a 15-cm air gap when delivering 1442 W to the load.

[1] Z. Li, C. Zhu, J. Jiang, K. Song, and G. Wei, "A 3 kW wireless power transfer system for sightseeing car supercapacitor charge," IEEE Trans. Power Electron., vol. 32, no. 5, pp. 3301–3316, May. 2017. [2] C. W. Wang, G. A. Covic, and O. H. Stielau, "Power transfer capability and bifurcation phenomena of loosely coupled inductive power transfer systems," IEEE Trans. Ind. Electron., vol. 51, no. 1, pp. 148–157, Feb. 2004

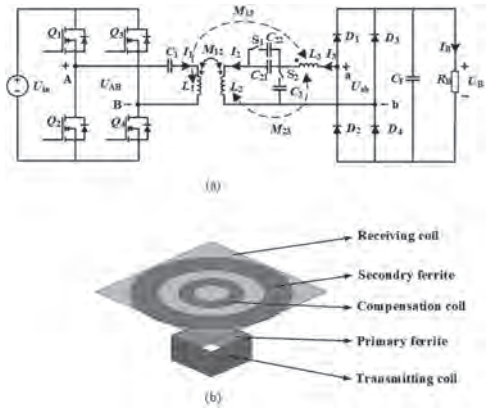

Fig.1. (a) The switchable hybrid structure.(b) The integrated coil structure.

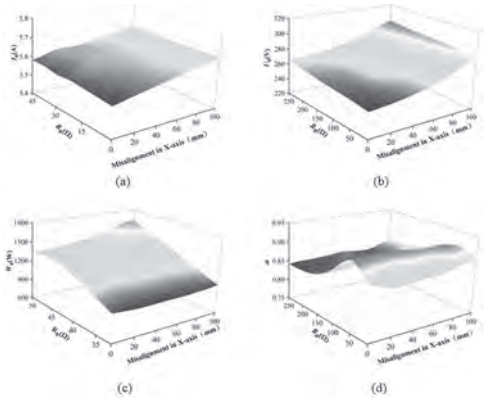

Fig.2. (a) The variation of I_B in CC mode. (b) variation of V_B in CV mode. (c) the variation of W_B. (d) the variation of η versus R_B and misalignment in X-axis.

PPC-03. Design of lower vibration combined with magnetic equivalent circuit.
T. Ben[1,2], M. Fang[1], L. Chen[1] and P. Zhang[1] *1. College of Electrical Engineering and New Energy, China Three Gorges University, Yichang, China; 2. State Key Laboratory of Reliability and Intelligence of Electrical Equipment and the Province-Ministry Joint Key Laboratory of EFEAR, Hebei University of Technology, Tianjin, China*

Vibration noise will threaten the reliable operation of the reactor and causes great noise pollution. The global topology optimization algorithms used in vibration reduction of gapped-iron reactors will achieve the optimal performance under certain constraints. The inductance value should remain constant before and after optimization. Although Finite Element Analysis (FEA) can accurately predict inductance [1], the amount of computation required for FEA is large. Another method is to use the magnetic equivalent circuit (MEC) model which has the advantages of fast calculation speed and acceptable accuracy. The traditional MEC model can not accurately calculate the flux density of the core at the air gap[2], leading to a large error in the calculation of inductance. In this paper, a reactor optimization model(iMEC) combined with a magnetic equivalent circuit is proposed. Firstly, since the flux is relatively divergent near the core and air gap partition, the air gap reluctance is segmented and equivalent, as shown in Figure 1(b), and are connected in parallel to obtain, and are connected in parallel to obtain, is connected in series with and then in parallel with, as shown in Figure 1(c), and Kirchhoff is used to voltage law to establish a system of lattice equations, and the nonlinear algebraic system of equations has been solved using Newton–Raphson algorithms. Secondly, the inductance value is used as the constraint, and the electromagnetic force is used as the objective function, combined with the genetic algorithm to realize the optimal design of the reactor. Finally, compared with the simulation, the inductance value is consistent and the vibration displacement is reduced by 10%, and the results are shown in Figure 2. In this paper, an optimization model of reactor incorporating magnetic equivalent circuit is proposed. The results show that the model improves the calculation accuracy of the inductor and reduces the vibration.

[1] Najafi A, Iskender I. Comparison of core loss and magnetic flux distribution in amorphous and silicon steel core transformers[J]. Electrical Engineering, 2017, 100(2):1-7. [2] Qian J, Chen X, Chen H, et al. Magnetic Field Analysis of Lorentz Motors Using a Novel Segmented Magnetic Equivalent Circuit Method[J]. Sensors, 2013, 13(2):1664-1678.

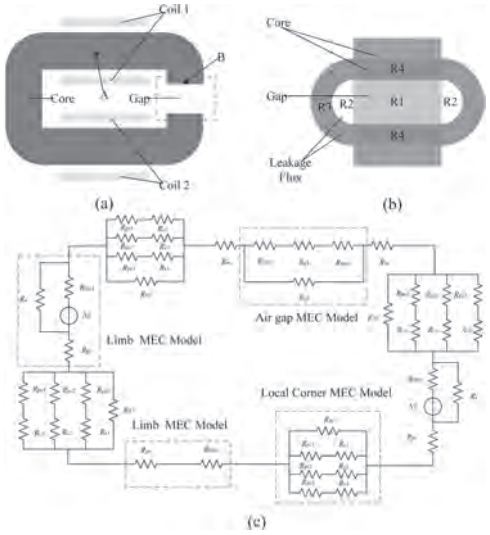

Fig.1. (a) Reactor structure drawing. (b) Air gap magnetic field distribution. (c) The iMEC of inductor.

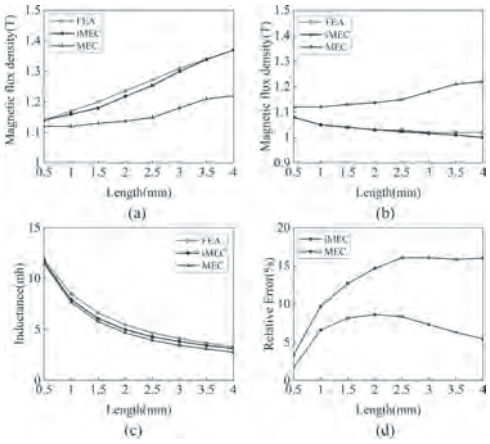

Fig.2. (a) Flux density at point A. (b) Flux density at point B. (c) The inductance curve with the length. (d) The relative error of inductance.

PPC-04. A Model Order Reduction of Hysteretic Eddy-current Fields in Electric Machines Using Cauer Ladder Network Method. *M. Tobita*[1] and T. Matsuo[1] *1. Graduate School of Engineering, Kyoto University, Kyoto, Japan*

Numerical analyses should include the computation of magnetic hysteresis to estimate the performance of electric machines accurately. However, the finite element method (FEM) requires significant time to simulate the hysteretic field because a hysteretic function modeled by, e.g., the Preisach model or the play model [1] must be called for each element and time step. The model order reduction (MOR) methods can effectively reduce the computation time of the FEM. This study aims to establish a new hysteretic MOR method for electric machines. Specifically, we incorporate the hysteretic characteristics to the Cauer ladder network (CLN) method [2], a spatial mode decomposition technique showing superior convergence. It retains physical interpretation, i.e., the inductances and resistances of the ladder network are directly computed from the decomposed modes. Therefore the nonlinear magnetic characteristics can be directly incorporated [3]. The hysteresis effect is incorporated in the first inductor shown in Fig. 1. The magnetic fluxes flowing through the inductors are used as state variables. A semi-implicit time-marching scheme is developed to reflect hysteretic properties without nonlinear iterations. Static I-ϕ loops are used to identify the scalar play model representing the first inductor. Those loops are obtained by FE magnetostatic analysis, where the hysteretic behavior is calculated by the vector play model [1]. The reversible component is used to represent the second or later inductors, considering the characteristics of the minor loop [4]. The resistances of the CLN are prepared as functions of the first stage magnetic flux with anhysteretic approximation. 3. Numerical analysis An iron-cored inductor was analyzed, where a PWM voltage input was applied to the coil. Fig. 2 shows the locus of total current I_1 and the first stage magnetic flux ϕ_1 obtained by the proposed CLN method (solid red line), which agreed with the transient FEM result (solid black line) better than the conventional equivalent circuit (dotted red line).

[1] R. Mitsuoka et al., IEEE Trans. Magn., vol. 49, no. 5, pp. 1689–1692 (2013). [2] A. Kameari et al., IEEE Trans. Magn., vol. 54, no. 3, 7201804 (2017). [3] H. Eskandari and T. Matsuo, IEEE Trans. Magn., vol. 56, no. 2, 7505904 (2020). [4] Y. Shindo, T. Miyazaki and T. Matsuo, IEEE Trans. Magn., vol. 52, no. 3, 6300504, (2016).

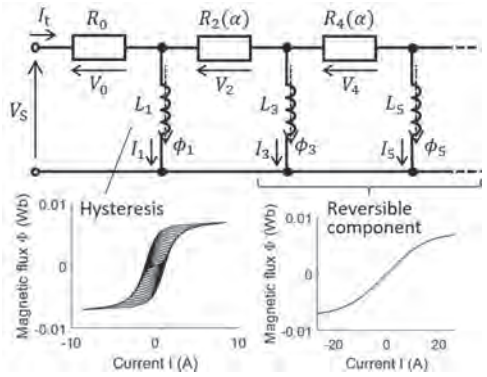

Fig. 1 The Cauer ladder network (CLN) incorporating hysteresis in the first stage.

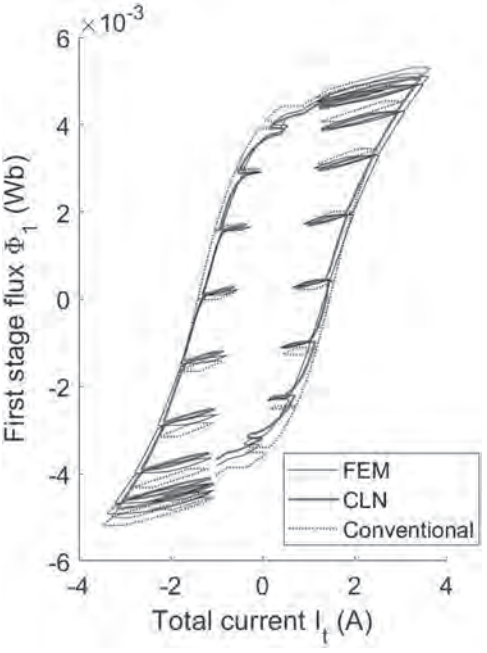

Fig. 2 Numerical results with PWM input.

PPC-05. Optimal Design of Low Noise Medium-High Frequency Transformer Considering the Influence of Excitation Waveform. Y. Li[1], *Z. Yang*[1], P. Guo[1] and C. Zhang[1] *1. Hebei University of Technology, Tianjin, China*

With the increase of the operating frequency of the transformer and the increase of the complexity of the operating condition, the vibration and noise problem of the transformer becomes more complicated [1-3]. Therefore, it is

very important to study the transformer vibration and noise under complex working conditions to improve the reliability of the transformer. In order to further reduce the vibration and noise of the transformer, the source of the vibration and noise of the medium-high frequency transformer is analyzed. The effects of waveform parameters on vibration and noise under sinusoidal excitation and rectangular wave excitation are analyzed. Considering the mechanical anisotropy of ferromagnetic materials and the parameters of excitation waveform, a coupling model of electromagnetic field-mechanical vibration-sound field of medium and high frequency transformers is established. Taking the minimum vibration noise as the goal, considering the excitation waveform parameters, the transformer core structure is optimized. A prototype of the transformer was made to verify the effectiveness of the design. Fig. 1 and Fig. 2 show the deformation caused by the Maxwell force and the magnetostrictive force, the main vibration sources of the transformer core. The Maxwell force causes both sides of the core to compress inward and is mostly distributed in the inner corners of the transformer core where the magnetic flux density is highest. The core extends in the direction of the magnetic flux due to the magnetostrictive force. Additionally, it is clear from the research that the deformation caused by the magnetostrictive force is 15,000 times that of the Maxwell force.

[1]Rossi M, Besnerais J L. Vibration Reduction of Inductors Under Magnetostrictive and Maxwell Forces Excitation[J]. IEEE Transactions on Magnetics, 2015, 51(12):1-6. [2]Zhang P, Li L, Cheng Z, et al. Study on Vibration of Iron Core of Transformer and Reactor Based on Maxwell Stress and Anisotropic Magnetostriction[J]. IEEE Transactions on Magnetices, 2019, 55(2):1-5. [3]KY Yoo, BK Lee, DH Kim. Investigation of Vibration and Acoustic Noise Emission of Powder Core Inductors[J]. IEEE Transactions on Power Electronics, 2018, 34(4):3633-3645.

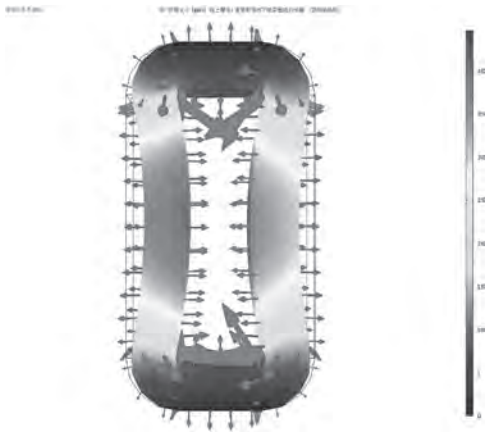

Fig. 1. Medium-high frequency transformer core deformation of ultra-thin oriented silicon steel (GT-100) caused by maxwell force (*B* = 1.2T, *f* = 1kHz)

Fig. 2. Medium-high frequency transformer core deformation of ultra-thin oriented silicon steel (GT-100) caused by magnetostrictive force (*B* = 1.2T, *f* = 1kHz)

PPC-06. Extremely Low Frequency Multi-Directional Electromagnetic Wave Energy Harvester Based on Special Double Pendulum Structure.
Y. Li[1], J. Qiu[1], T. Lan[1] and H. Song[1] *1. Chongqing University, Chongqing, China*

In the marine environment, energy supply for distributed sensors is one of the main difficulties facing Internet of Things technology. Up to now, a variety of energy harvesters have been created to convert wave kinetic energy into electrical energy through electromagnetic induction, piezoelectric effects and other principles. At present, although some wave energy harvesters can collect wave energy and provide power for some low-power products, the overall output response frequency is greater than 1Hz[1], which is higher than the most common wave frequency of 0.25Hz-1.0Hz. Some experts with extensive achievements in energy harvesters are committed to the research of low-frequency and broadband, however, the output voltage of the designed wave energy harvester is too small[2], meantime the overall structure is extremely complex[3]. In addition, scholars have not explored the multi-directional energy harvesting enough, and the existing studies are mostly based on the spherical friction structure[4], but spherical shapes can lead to lower energy density or material utilization. In this paper, an electromagnetic wave energy harvester with a special double pendulum structure (as shown in Fig.1) has been proposed, the energy harvester can also capture vibrational energy in multiple directions, responding to minimum frequencies of less than 0.25Hz and to currents with velocities of approximately 0.4m/s. This energy harvester can charge a 220μF capacitor to about 32V in 50s with a peak power of 120mW under vibration conditions with a vertical height of 50 cm and a frequency of 1.0Hz, and can charge the capacitor to about 16V in 50s at a horizontal speed of 0.72m/s (as shown in Fig.2). The results show that the wave energy harvester designed in this paper can respond to multi-directional vibrations, and the response frequency is lower and wider, which is more favorable for wave energy harvesting.

[1] H. Liang, G. Hao and O. Z. Olszewski, International Journal of Mechanical Sciences., Vol. 219, 107130 (2022) [2] M. Li, X. Jing, Energy Conversion and Management., Vol. 244, 114466 (2021) [3] Z. Li, X. Jiang and P. Yin, Applied Energy., Vol. 302, 117569 (2021) [4] Q. Gao, Y. Xu and X. Yu, ACS Nano., Vol. 16, p.6781-6788 (2022)

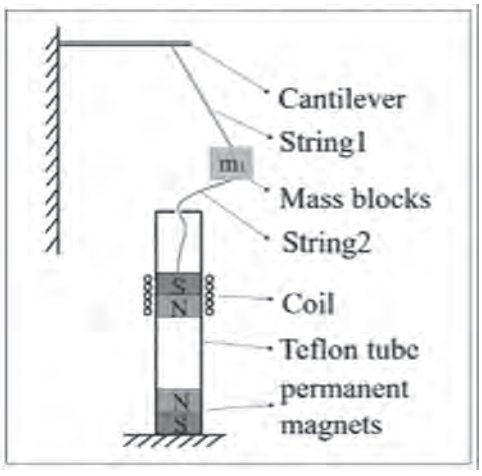

Fig.1: Three-dimensional model of the energy harvester

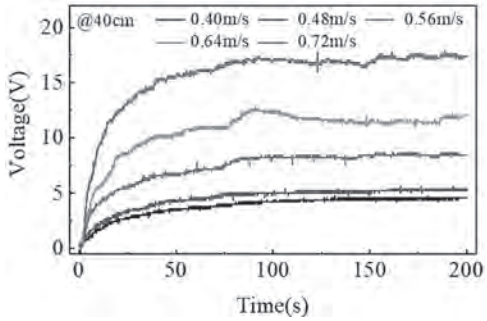

Fig. 2 220μF capacitor charged by energy harvester at horizontal movement speeds of 40cm and movement speeds of 0.40m/s, 0.48m/s, 0.56m/s, 0.64m/s, 0.72m/s

PPC-07. A Study on Stator Shape to Reduce Cogging Torque and Torque Ripple of Double-Layer Spoke Type PMSM. D. Nam[1], S. Song[2], N. Jo[1] and *W. Kim*[1] *1. Electrical Engineering, Gachon University, Seong-Nam, The Republic of Korea; 2. Electrical Engineering, Hanyang University, Seong-Nam, The Republic of Korea*

The general interior permanent magnet synchronous motor (IPMSM) uses NdFeB magnets to take advantage of the high airgap magnetic flux density. However, it had an adverse impact on cost of the motor because there are fluctuation of the cost from limited sources of heavy rare earth. Therefore, for stable supply of permanent magnets, a lot of development of a spoke type permanent magnet synchronous motor (PMSM), which is a structure capable of concentrating magnetic flux by using a ferrite magnet having a low magnetic flux density, has been conducting. The spoke type PMSM concentrates the magnetic flux density and can replace the NdFeB magnet used in the extant PMSM with a ferrite magnet. However, in general spoke type PMSM, the portion of reluctance torque is low because the difference in inductance between the d-axis and the q-axis is not large. In order to further utilize this reluctance torque, a double-layer spoke type shape that can maximize the difference in inductance between the d-axis and the q-axis can be used to bigger reluctance torque to improve motor performance [1]. However, increasing the reluctance torque increases cogging torque, torque ripple, and total harmonic distortion (THD), which in turn leads to vibration and noise problems. Therefore, the double-layer spoke type PMSM needs a design that can reduce cogging torque and THD. As a representative method, it can be solved by applying skew to the rotor, but the conventional method of applying skew is not a good method in terms of productivity because it is difficult to manufacture because it divides the stages of the permanent magnet. Therefore, in this paper, the skew is not applied to the rotor and the asymmetrical design of the shoe is carried out in the stator. Then, we propose a new stator shape that can apply a Skew-like effect by cross-stacking stators with an asymmetric design. Design the stator by dividing it into Stack No. 1 and Stack No. 2, respectively. And stack No.2 is symmetrical with Stack No.1, and design is proceeded by applying each stack by half of the stacking length.

[1] S. I. Kim, S. Park, T. Park, J. Cho, W. Kim, and S. Lim, "Investigation and experimental verification of a novel spoke-type ferrite-magnet motor for electric-vehicle traction drive applications," *IEEE Transactions on Industrial Electronics*, vol. 61, no. 10, pp. 5763–5770, Oct. 2014

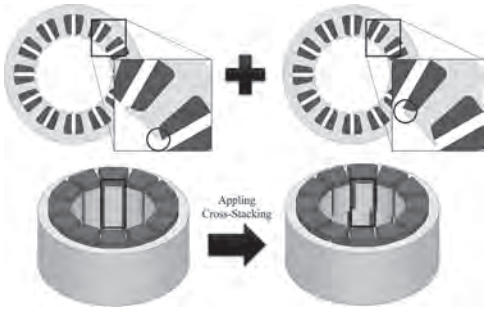

Fig.1. Suggestion diagram of the stator shape with the same effect as skew

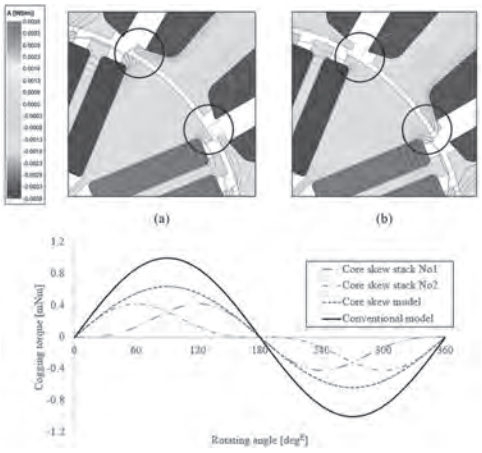

Fig.2. Principle of the skew effect

PPC-08. Study on Vibration and Noise Reduction of Anodic Saturable Reactor. C. Zhang[1], *T. Chen*[1], Y. Li[1], Q. Yang[1], Y. Dou[1] and S. Song[1] *1. School of Electrical Engineering, Hebei University of Technology, Tianjin, China*

Anodic saturable reactor (ASR) plays an indispensable role in protecting the thyristor and the EHV DC converter valve [1]. In order to improve magnetic saturation intensity and prevent over-voltage and over-current in power grid, anodic saturable reactor core type-wound of ultra-thin silicon steel is opened with a narrow air gap. The presence of air gap can cause intense vibration during magnetization. Besides, the magneto-strictive properties of ultra-thin silicon steel can also aggravate vibration and acoustic noise of anodic saturable reactor [2-4]. It not only causes mechanical failure, but also reduce service life of equipment and pollute the surrounding environment [5]. So, it is of great significance to study the vibration and noise characteristics of anodic saturable reactor and find effective ways of vibration and noise reduction for reducing the occurrence of power accidents, prolonging the service life of equipment and improving the environment. In this paper, the core of anodic saturable reactor is taken as the research object. The vibration testing platform as shown in Fig.1 is built and the vibration and noise characteristics of anodic saturable reactor core are measured under sinusoidal excitation. The vibration intensity of core is acquired by acceleration sensor at different magnetic induction intensity levels. The anisotropic material model is established, which include Young's modulus, Poisson's ratio and shear modulus, etc. The anodic saturable reactor core was simulated in magnetic-structure coupling field, as shown in Fig.2. The simulation results are in good agreement with the experimental results, which proved the accuracy of anisotropic material model. Two ways of vibration and noise reduction for anodic saturable reactor are designed and simulated by finite element software based on the model. The results show that the two ways proposed in this paper can effectively reduce the vibration intensity of anodic saturable reactor.

[1] Safonov, E, and N. Lozinova. Materials Science and Engineering. Vol. 643. No. 1. IOP Publishing (2019). [2] X. G. Yao, T. P. P. Phway and A.

J. Moses, et al. IEEE Transactions on Magnetics, vol. 44, no. 11, pp. 4111-4114 (2008). [3] P. N. Zhang, L. Li. International Journal of Electrical Power & Energy Systems, vol. 123 (2020). [4] S Peng, B Juergen. IEEE Transactions on Power Electronics, vol. 32, no. 10, pp. 7916-7931 (2016). [5] P. N. Zhang, L. Li and Juanjuan Z, et al. International Journal of Electromagnetics and Mechanics, vol. 58, no. 2, pp. 261-273 (2018).

Fig.1. Vibration testing platform for anodic saturable reactor core

Fig.2. The distribution of magnetic induction intensity and volume force density vector in the core of anodic saturable reactor.

PPC-09. Analysis of flux barrier effect of LCF PM in series hybrid magnet variable flux memory machine. H. Yang[1], *Y. Huang*[1], H. Zheng[1], H. Lin[1] and Z. Zhu[2] *1. Southeast University, Nanjing, China; 2. The University of Sheffield, Sheffield, United Kingdom*

Variable flux memory machines (VFMM) using low coercive force (LCF) permanent magnets (PM) have been extensively investigated [1]-[5]. Normally, the series hybrid magnet topology equipped with both PM with high coercive force (HCF) and LCF PMs to achieve high torque density and extended constant power speed range simultaneously, and two kinds of PMs are magnetically connected in series to avoid unintentional demagnetization in LCF magnets. Nevertheless, the role LCF PM acts in the series magnetic circuit and its potential effect on the air-gap flux density remain unclear. In this paper, the flux barrier effect of LCF PM on series VFMM is revealed and investigated, and an approach to preventing the air-gap flux density drop is presented. The conventional series hybrid magnet VFMM and interior permanent magnet (IPM) machine sharing identical usage of HCF PMs are shown in Fig.1. In Fig.1(e), the back-EMF amplitude of the series VFMM is lower than that of the IPM machine. This is mainly due to the fact that the air-gap flux enhancement by the magnetomotive force of the LCF PM cannot compete with the weakening effect by the magnetic reluctance of LCF PM. As a result, the flux barrier effect of the LCF PMs is identified, which further leads to a reduction of the torque density. The topology of VFMM with dual-layer PMs is shown in Fig.1(c). The separation of the PMs weakens the barrier effect on the HCF PM and the bypass flux path reduces the equivalent reluctance in the magnetic circuit. It can be observed in Fig.1 (d) that the air-gap flux density and flux variable range are improved. That is to say, the magnetic flux barrier effect of LCF PM is reduced with the proposed dual-layer PM design. The test results of the open-circuit back-EMF of the dual-layer series hybrid magnet VFMM prototype are shown in Fig.2. The experiments agree well with the FE-predicted results. The detailed analysis, suppression methods of the flux barrier effect, and the detailed test results, will be given in the full paper.

[1] V. Ostovic, "Memory motors," *IEEE Ind. Appl. Mag*., vol. 9, no. 1, pp. 52-61, Jan./Feb. 2003. [2] K. Sakai, K. Yuki, Y. Hashiba, N. Takahashi and K. Yasui, "Principle of the variable-magnetic-force memory motor," in *Proc. Inter. Conf. Elec. Mach. System. (ICEMS)*, 2009, pp. 1-6. [3] N. Limsuwan, T. Kato, K. Akatsu and R. D. Lorenz, "Design and evaluation of a variable-flux flux-intensifying interior permanent-magnet machine," *IEEE Trans. Ind. Appl.*, vol. 50, no. 2, pp. 1015-1024, Mar./Apr. 2014. [4] H. Hua, Z. Q. Zhu, A. Pride, R. Deodhar and T. Sasaki, "A novel variable flux memory machine with series hybrid magnets," in *Proc. 2016 IEEE Energy Conversion Congress and Exposition (ECCE)*, 2016, pp. 1-8. [5] H. Yang, H. Zheng, H. Lin, Z. Q. Zhu and S. Lyu, "A novel variable flux dual-layer hybrid magnet memory machine with bypass airspace barriers," in *Proc. 2019 IEEE International Electric Machines & Drives Conference (IEMDC)*, 2019, pp. 2259-2264.

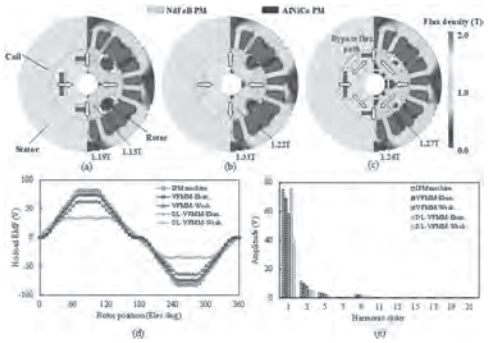

Fig.1 Machine topology (a) Conventional hybrid magnet VFMM. (b) IPM machine. (c) Dual-layer hybrid magnet VFMM. (d) Waveforms of back EMF. (e) Spectrum.

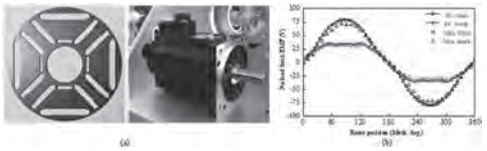

Fig. 2 Test results of back-EMF. (a) Prototype. (b) Back-EMFs (1500rpm)

PPC-10. Withdrawn

PPC-11. Inter-Turn Fault Early Diagnosis of Dual Three-Phase PM Machine Using Multi-Orthogonal Spaces. *Z. Yuan*[1], W. Liu[1], Y. Sui[1], M. Wang[1] and P. Zheng[1] *1. Harbin Institute of Technology, Harbin, China*

Compared with the three-phase permanent-magnet (PM) machines, the multi-phase machines have advantages in applications with high reliability command due to the fault tolerant ability [1]. The inter-turn fault is one of the frequent faults in machine systems, usually causing severe heating in winding and even demagnetization on PMs [2]. Research on current and voltage signals, high-frequency impedance and search coils voltage contribute to the identification of the inter-turn fault [3]-[6]. But in the early stage of the inter-turn fault, the short-circuit current and the fault signatures vary with the severity of short-circuit fault, which causes difficulty on accurate fault diagnosis. In this paper, an inter-turn fault early diagnosis method of dual three-phase PM machine is proposed, utilizing the feature of more control dimensions in dual three-phase PM machine due to the existence of multi-orthogonal spaces, and therefore has ability to evaluate various fault levels in early fault stage. The fault characteristics are analyzed base on a 24-solt/14-pole dual three-phase interior PM machine, and the short-circuit currents are analyzed in different additional resistances, which correspond to different fault stages. The equivalence models of flux and voltage are analyzed for the inter-turn fault in single strand and between different strands in one set of coils, and the equivalence circuit is deduced, which is shown in Fig.1. The extra voltage harmonics in orthogonal fundamental space, 3rd and 5th harmonic spaces are investigated in fault condition. Considering the significant 3rd harmonic of back electromotive force in the investigated machine, different harmonic characteristics due to the 3rd harmonic of short-circuit current are also analyzed. Parts of results of the harmonics amplitude in multi-orthogonal spaces under different loads and fault conditions through finite element method, which are shown in Fig. 2. The response speed of the diagnosis method based on the fault indexes in multi-orthogonal spaces is also evaluated.

[1] F. Barrero, M. J. Duran, IEEE Trans. Ind. Electron., Vol. 63, p.449-458 (2016) [2] A. Gandhi, T. Corrigan and L. Parsa, IEEE Trans. Ind. Electron., Vol. 58, p.1564-1575 (2011) [3] Y. Zhang, G. Liu and W. Zhao et al, IEEE Trans. Transp. Electrific., Vol. 7, p.104-113 (2021) [4] B. Wang, J. Wang, and A. Griffo et al, IEEE Trans. Ind. Electron., Vol. 65, p.7279-7289 (2018) [5] R. Hu, J. Wang and A. R. Mills et al, IEEE Trans. Power Electron., Vol. 36, p.785-794 (2021) [6] K. Kim, S. Lee and J. Hur, IEEE Trans. Magn., Vol. 50, p.885-888 (2014)

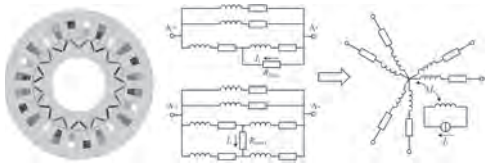

Fig. 1. Machine topology, inter-turn short-circuit model and its equivalent model

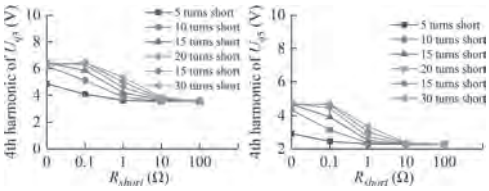

Fig. 2. Harmonic characteristics in multi-orthogonal spaces under different conditions

PPC-12. Study on the characteristics of power transmission side of leaky magnetic field canceling coil for contactless power transfer while running. *M. Yokosawa*[1], H. Kojima[1], F. Sato[1], S. Miyahara[1], H. Matsuki[2], K. Iada[3] and S. Sasaki[4] *1. Tohoku-gakuin University, Tagajo, Japan; 2. Tohoku University, Sendai, Japan; 3. NITTOKUCo. Ltd., Fukushima, Japan; 4. HikaridenshiCo. Ltd., Osaki, Japan*

1, Background In recent years, AGVs have been attracting attention from the perspectives of improving work efficiency and reducing labor costs; the advantages of AGVs are improved work efficiency and reduced labor costs, but because they are powered by storage batteries, they do not operate indefinitely. Therefore, to maximize the potential of AGVs, we propose an in-transit non-contact power supply system. In this system, a power receiving coil attached to the AGV passes close to a power transmitter to supply power contactless while the vehicle is in motion. To realize this system, it is necessary to pay attention to the stability of the power supply and the reduction of the magnetic field leakage to the surroundings. Therefore, in this study, a coil shape that satisfies these two requirements ware investigated. 2, Simulation and Results In this study, a leakage field canceling coil based on an 8-shaped coil, which has the effect of reducing leakage magnetic fields, was examined as a coil for supplying power during running. The cancellation coil has a double 8-shape structure, in which the 8-shaped coil is doubled by making connections so that adjacent wires are in phase with each other at both ends of the 8-shaped coil. Based on the results of the power supply to the 8-shaped coil measured in advance, the current value of the cancellation coil and the width of the cancellation coil were varied, and the point where the leakage magnetic field is the smallest was examined. The simulation results are shown in Figure 2. From Figure 2, it was confirmed that there is a point at which the leakage magnetic field is minimized depending on the width of each cancel coil and that the narrower the coil width, the higher the required current value. The final paper presents the details of the simulation and the results of the actual measurements based on the simulation. While the abstract discusses the transmitter and receiver sections, the final paper focuses only on the transmitter section and describes the characteristics of only the transmitter and cancel coil sections.

[1]Takuma.Abe, Shohei.Oba, Fumihiro.Sato, “Contactless power supply feeding system with a leakage magnetic flux reduction for EV driving”, IEEJ Transactions on Fundamentals and Materials, Vol.140, No.4 pp.193-200,(2019) [2]Y. Ota, T. Takura, F. Sato, “Relationship between Leakage Magnetic Field Reduction and Coil Shape for Wireless Power Transfer”, J. Magn. Soc. Jpn., 38, pp. 11-14, (2014) [3]AOKI Syuta, and other : “Reduction of Leakage Electromagnetic Field from Feeding Coil for Contactless Charging System for Moving Electric Vehicles”, IEICE technical report 115(82), 43-48, (2015)

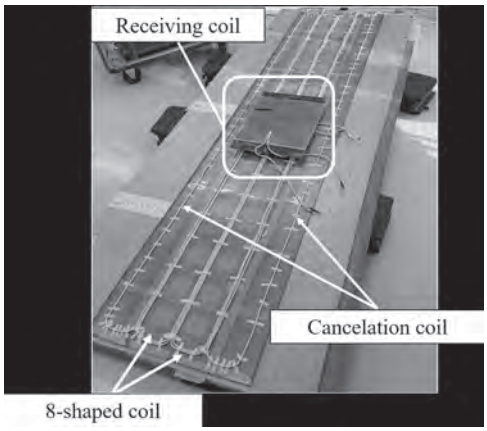

Fig.1 Actual cancellation coils created

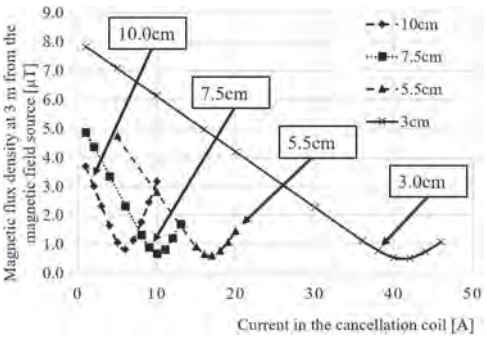

Fig.2 Magnetic field leakage for each cancellation coil width

PPC-13. The Influence of Electromagnetic Noise of Volume Magnetostriction Anisotropy on Power Transformers. *C. Hsu*[1] *1. Mechanical Engineering, Asia Eastern University of Science and Technology, New Taipei City, Taiwan*

This paper presents the effects of magnetostriction of core loss and sound level on the design of power transformers and the results of analysis via the particle swarm optimization (PSO) method. The core losses and the magnetostrictive forces in the ferromagnetic cores of transformers of various capacities, ranging from 15 MVA to 120 MVA, were found to be significantly different from each other, as shown in Figure 1. Further, core loss was approximately proportional to capacity and core volume. However, the sound level performance was not linear because of the squareness ratio (). This study utilized three types of soft core material: 30ZH105, 27ZH100 (Japan), and 27PH100 (Korea). The hysteresis loop and magnetostriction were measured for various magnetic parameters. It was found that extremely high does not directly affect core loss. Whenwith respect to the sound level is high, the experimental and design values are almost the same. The PSO method simulation results for transformers with several capacities, with respect to sound level and core loss performance, were analyzed and compared with experimental values, as shown in Figure 2.

[1] L. Bernard, et. al., “Effect of stress on switched reluctance motors: A magnetoelastic finite-element approach based on multiscale constitutive laws,” *IEEE Trans. on Magnetics*, vol. 47, no. 9, pp. 2171–2178, 2011. [2] Chang-Hung Hsu, et. al., “Reduction of vibration and sound-level for a single-phase power transformer with large capacity,” *IEEE Trans. on Magnetics*, vol. 51, no. 11, pp. 8403204-1-4, 2015.

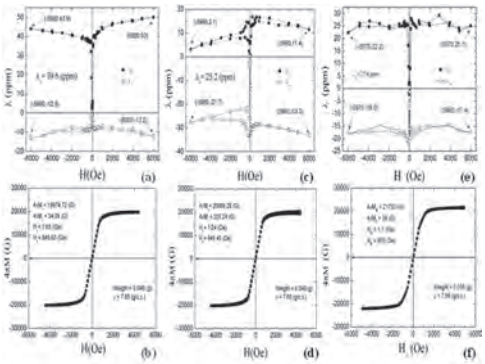

Figure 1 Magnetism properties of soft silicon material: (a)-(b) 27PH100, λ(ppm)/B-H, (c)-(d) 27ZH100, λ(ppm)/B-H, (e)-(f) 30ZH105, λ(ppm)/B-H.

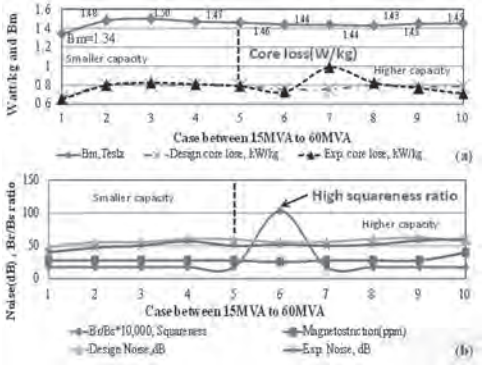

Figure 2 Serval capacity magnetic property between 15MVA to 60MVA: (a) core loss, and (b) noise level.

Session QOA
BIOMEDICAL APPLICATION OF MAGNETIC NANOPARTICLES
Frank M Abel, Chair
National Institute of Standards and Technology, Gaithersburg, MD, United States

CONTRIBUTED PAPERS

QOA-01. Exceptionally Large Magnetism in Gd Implanted MoS_2 Due to Both Radiation Damage and Gd^{3+} Ions. M. Zhang[1], W. Cheng[1], M. Ying[1] and *G.A. Gehring[2] 1. Key Laboratory of Beam Technology of Ministry of Education, College of Nuclear Science and Technology, Key Laboratory of Beam Technology of Ministry of Education, College of Nuclear Science and Technology, Beijing Normal University, Beijing 100875, China; 2. Physics and Astronomy, University of Sheffield, Sheffield, United Kingdom*

There has been much interest in the layered material MoS_2 Waals interactions because some of the intrinsic defects are magnetic, including a vacancy on an S site and Mo on an S site[1]. After implantation with Gd ions XRD, XSP, Raman scattering indicated the presence of S vacancies and conductive behaviour at room temperature [2]. We report on detailed investigation of a film deposited with Gd implantation, 1×10^{15} ions/cm^3, over a temperature range $5<T<300$K in fields up to 70kOe in order to clarify the contribution of the native defects produced as a result of radiation damage and that from the Gd ions. Below 80K hysteresis loops were analysed in terms of two components, Curie behaviour from small independent clusters and larger clusters that saturated in 70kOe as shown in raw data in Fig 1 and the saturating part in Fig 2. respectively. In all cases the magnetisation per Gd ion vastly exceeded the ~7m_B expected for Gd^{3+}. The fall in the saturated part of the magnetisation, 2,700 m_B/Gd at 5K to 40 m_B/Gd at 150K, was also apparent in the paramagnetic part where the Curie constant dropped from 18,000 m_B/Gd at 40K to 1,200 m_B/Gd at 150K. This indicated that the moments arising from isolated the native defects are unstable at high temperature. Very different behaviour was seen between 150K and 300K where the saturation magnetisation remained constant at 40 m_B/Gd. Moreover the magnetisation per Gd fell only slightly as the implantation dose of Gd was raised to 5×10^{15} ions/cm^3, leading to a magnetisation of ~340emu/cm^3 in a 40nm layer with a coercive field of 400Oe. This behaviour has not been seen with other rare earth ions [3] and indicates a specially strong interaction between the Gd ions and the native defects such that some native defects are enabled to retain their moments at 300K and provide exchange between the Gd ions.

HK Komsa and A. V. Krasheninnikov Phys Rev B 91, 125304 (2015) M. Zhang, M. Ying et al X. Ding, X. Cui *Adv. Quantum Technol.* 2000093 (2020)

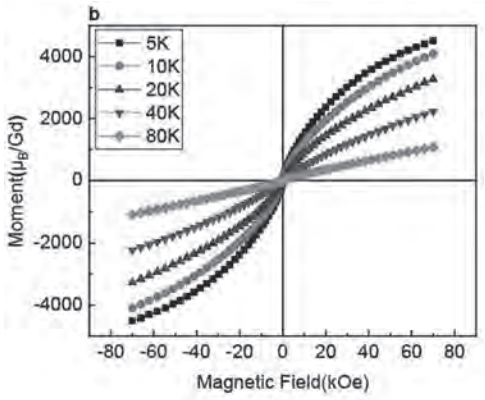

Fig 1 Raw hysteresis loops

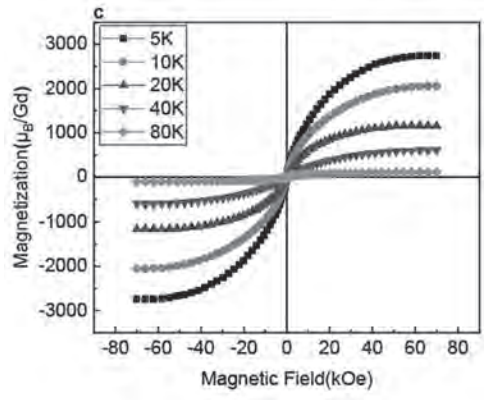

Fig 2 Loops with the linear part subtracted

QOA-02. Effect of the distribution of anisotropy constants on the magnetic properties of iron oxide nanoparticles. D.M. Clarke[1], C. Marquina[2,3], D.C. Lloyd[4] and *G. Vallejo-Fernandez[1] 1. Physics, University of York, York, United Kingdom; 2. Fisica de la Materia Condensada, Universidad de Zaragoza, Zaragoza, Spain; 3. INMA, CSIC, Zaragoza, Spain; 4. Electronic Engineering, University of York, York, United Kingdom*

Lately, magnetic nanoparticles have gathered significant interest due to their promising applications in medical diagnostics/therapeutics. Of particular interest are iron oxide nanoparticles. The magnetic properties of such particles are controlled by their volume with many reports taking into account the distribution of particle sizes. However, the energy barrier to reversal is also controlled by the magnetic anisotropy constant of the material, K. In most reports, a constant value of K is assumed. This is mainly due to the fact that measuring the distribution of anisotropy constants in a given system is significantly more complicated and time consuming than measuring the distribution of particle sizes. However, there are certain cases, e.g. magnetic

nanoparticles with shape anisotropy, in which assuming a uniform value of K is an unrealistic assumption. In this work the distribution of shape anisotropy constants in two colloids of iron oxide nanoparticles has been measured from the distribution of particle elongations within each system [1]. The results are in good agreement with the values calculated from the temperature decay of remanence shown in Figure 1, $1.29x10^5$ erg/cc and $0.36x10^5$ erg/cc, respectively. For a fluid with a saturation magnetisation of 420 emu/cc and an average particle elongation of ~1.3, the distribution of energy barriers is controlled by both the distribution of particle sizes and elongations. This is highlighted by the quality of the fit in Figure 1 (dashed red line) where both the measured distributions of particle volumes and shapes were taken into account. If a single value of K is assumed the agreement is very poor (solid red line). For a 320 emu/cc fluid and a wide distribution of particle sizes, the energy barrier to reversal is controlled by the distribution of particle volumes alone as indicated by the quality of the fit in Figure 1 (solid blue line) where only the distribution of particle volumes was taken into account.

[1] D.M. Clarke, C. Marquina, D.C. Lloyd and G. Vallejo Fernandez, J. Magn. Magn. Mater. Vol. 559, p.169543 (2022).

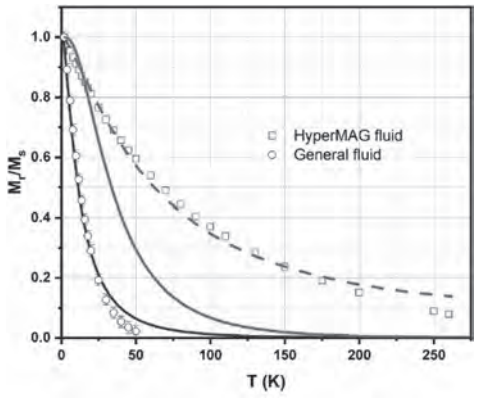

Fig. 1. Temperature decay of remanence for the samples studied in this work. The solid line for the general/HyperMAG® fluid assumes a uniform value of K while the dashed red line corresponds to the fit for the HyperMAG® fluid assuming a non-uniform value of K.

INVITED PAPER

QOA-03. Nanoflowers vs Nanobiots: Inorganic vs biological agents for cancer theragnosis applications. *E.M. Jefremovas*[1], L. Gandarias[2], L. Marcano[3,4], A. García-Prieto[5], I. Orue[6], A. Muela[2], M. Fernández-Gubieda[4], L. Fernández Barquín[1] and J. Alonso Masa[1] *1. Depto. Ciencias de la Tierra y Física de la Materia Condensada, Universidad de Cantabria, Santander, Spain; 2. Depto. Inmunología, Microbiología y Parasitología, Universidad del País Vasco, Leioa, Spain; 3. Helmholtz–Zentrum Berlin für Materialien und Energie, Berlin, Germany; 4. Depto. Electricidad y Electrónica, Universidad del País Vasco, Leioa, Spain; 5. Depto. Física Aplicada, Universidad del País Vasco, Bilbao, Spain; 6. SGIker Medidas Magnéticas, Universidad del País Vasco, Leioa, Spain*

Fe-oxides have been extensively studied during the history of Magnetism. Their ubiquity in Nature enabled humans to access them easily from a very early stage, becoming rapidily captivated by their magnetic properties. In the last half century, the blooming of the nanoscience has encumbrated iron oxide nanoparticle ensembles (IONPs) as exceptional candidates for biomedical applications, owing to their ideal magnetic properties and high biocompatibility. Among all, maghemite (γ-Fe_2O_3) and magnetite (Fe_3O_4) IONPs have become the best exponents of this trend, attracting the vast majority of efforts and works from the scientific community [1]. In this sense, hierarchichal maghemite nanostructures, such as those arranged into flowers (nanoflowers, NF), have showcased exceptional properties for cancer treatment through magnetic hyperthermia [2]. Moreover, Fe-oxide based nanoensembles also constitute a phenomenal playground for investigating the setting of spin textures that may arise as a consequence of geometric arrangments. This has been shown, for instance, in the case of magnetite/maghemite nanorings, that have revealed to host vortex-like states [3]. On the other hand, magnetite nanoparticles are also exceptional for magnetic hyperthermia purposes, even better than γ-Fe_2O_3 [4]. However, pure Fe_3O_4 nanoparticles are hard to be found, due to the inherent tendency of Fe_3O_4 to oxidise towards γ-Fe_2O_3 phase. In this sense, many of the so-called *magnetite* nanoparticles actually consist of an (uncontrolled) mixture of γ-Fe_2O_3 and Fe_3O_4 phases. To this respect, nature offers a solution to obtain high quality and stable Fe_3O_4 nanoparticles. Magnetotactic bacteria, aquateous motile microorganism, synthesize chains of magnetosomes, which are magnetite based magnetic crystals surrounded by a lipics bilayer that acts as a natural barrier against oxidation. The magnetic hyperthermia performance of these magnetosomes has been compared with that of commercial maghemite NFs of the same size (around 40 nm), obtaining a heating efficiency up to 2.5 times higher for magnetosomes compared to NFs [5]. Although the production of magnetosomes at a scale comparable to that of commercial nanoparticles is still to be achieved, the allocation of magnetite IONPs within the bacterial body (biocompatible, motile, orientable) offers new exciting possibilities for their use as anticancer agents. One of the main problems in the use of IONPs for cancer treatment is their very low targeting and delivery efficiency when injected in the blood stream [6]. In this sense, magnetotactic bacteria can be externally traced and guided, with no chances for undesired nanoparticle leaks. In addition, due to their anaerobic characteristics, these organic nano-bio-robots (nanobiots) tend to selectively migrate towards hypoxic regions of tumors, showcasing a much better targeting capacity than inorganic IONPs [7]. The assets of magnetotactic bacteria do not stop at this point, as we have also managed to tune their magnetic properties and enhance their biomedical capabilities by a doping process. In this way, we have grown bacteria in the presence of Tb and Gd salts, and they have successfully incorporated Tb^{3+} and Gd^{3+} ions into the magnetosome structure [8]. This has altered their magnetic properties, modifying their magnetocrystalline and uniaxial anisotropy, and, what is even more fascinating, has endowed these nanobiots with luminescent (Tb^{3+}) and MRI contrast (Gd^{3+}) properties, paving the way to use them as dual-agent for cancer diagnosis and treatment. Taking all this into account, it can be foreseen that we are just at the dawn of a new revolution concerning the use of magnetic nanoparticles, in general, and IONPs, in particular, for biomedical applications. The combination of organic motile entities with inorganic high quality nanoparticles will help overcoming some of the main limitations existing for the clinical translation of these nanoparticles.

[1] Q. A. Pankhurst et al. J. of Phys. D: Appl Phys 42.22 (2009); W. Wu et al. Science and Technology of advanced materials (2015) [2] P. Hugounenq et al. J. of Phys. Chem. C 116.29 (2012); P. Bender et al. J. Phys Chem C 122.5 (2018) [3] G. R. Lewis et al. Nano letters 20.10 (2020); Jia, Chun-Jiang, et al. J. of the American Chemical Society 130.50 (2008) [4] I. Castellanos-Rubio et al. Nanoscale 11.35 (2019) [5] E. M. Jefremovas et al. IEEE Acces 9 (2021) [6] S. Wilhelm et al. Nat. Rev. Mat. 1.5 (2016) [7] M. L. Fdez-Gubieda et al. J. of Appl Phys 128.7 (2020) [8] E. M. Jefremovas et al. Nanoscale Advances (2022)

CONTRIBUTED PAPERS

QOA-04. Synthesis and antigen-antibody reaction of ultrasmall FeCo nanoparticles. *L. Ton That*[1], T. Murayama[2], N. Kobayashi[3], S. Yabukami[1,2], W. Ikeda-Ohtsubo[4] and K. Arai[3] *1. Graduate School of Engineering, Tohoku University, Sendai, Japan; 2. Graduate School of Biomedical Engineering, Tohoku University, Sendai, Japan; 3. Research Institute for Electromagnetic Materials, Denjiken, Tomiya, Japan; 4. Graduate School of Agricultural Science, Tohoku University, Sendai, Japan*

Antibody-conjugated magnetic nanoparticles (MNPs) have attracted considerable attention in bioseparation and clinical diagnostics assays. By utilizing the magnetic response of MNPs-antibody-antigen aggregates, we developed a rapid detection system for oral bacteria for point-of-care testing[1-2]. To improve its sensitivity for smaller antigens, we also synthesized MNPs of 4 nm and proposed a novel method for adsorbing antibodies directly on their surface without coating any proteins[3]. Although the smaller MNPs have a greater surface-to-volume ratio to interact with bacteria or viruses, their magnetization decreases with decreasing their size. Therefore, to enhance their magnetic moment without increasing their size, this study examines FeCo MNPs for bacteria or virus detection. The FeCo MNPs were prepared by dissolving the fabricated FeCo-BaF films in water since Ba-F in the matrix was deliquescent. The FeCo-BaF thin films composed of crystal phase of BaF_2 matrix and FeCo alloy MNPs (Fe:Co:Ba:F=14:11:21:54 at.%) were fabricated using an RF sputtering tool[4]. Our experiment showed that the FeCo MNPs well dispersed in water could not be collected by a magnet. As such, we used ultracentrifugal separation at 110,000 rpm for 90 mins to collect them as well as the antibody (abcam ab53891)-conjugated FeCo MNPs, and the antigen (*Candida albicans*)-antibody FeCo MNPs. Fig. 1(a) shows the magnetization curve of FeCo-BaF film and the TEM image of FeCo MNPs. Considering that the magnetization of the film is caused by the FeCo alloy MNPs, the magnetization of ~5 nm FeCo MNPs at 1.4 T could be estimated at approximately 13 kG. Fig. 1(b) shows the number of *C. albicans* counted from the micrographs of the aggregates of FeCo MNPs and *C. albicans*. The number of bacteria bound to FeCo MNPs increased significantly by adding sonication treatment to the FeCo-BaF film before bounding them to antibodies. The success of antigen-antibody reaction of ultra-small MNPs improves detection sensitivity as well as offers potential detection for smaller biomolecules. Acknowledge: This research is supported by the Ministry of Internal Affairs and Communications in Japan (JPJ000254), the Comprehensive Growth Program for Accelerator Sciences and the Joint Development Research 2022-ACCL-1 at High Energy Accelerator Research Organization (KEK), JST A-STEP Grant Number JPMJTM22AB, Japan, and Japan Society for the Promotion of Science KAKENHI Grant Numbers 20K20210.

1) L. Tonthat *et al.*, AIP Advances, 9 (12), 125325 (2019); 2) S. Yabukami *et al.*, IEEE Trans. Magn., 58, (2022) (in press); 3) T. Yoneyama *et al.*, IEEE Trans. Magn., 58, (2022) (in press); 4) N. Kobayashi *et al.*, Electron Comm Jpn., 104 (2), e12308 (2021)

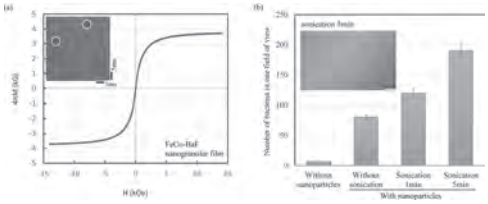

Fig. 1. (a) Magnetization curve of FeCo-BaF thin film at 300K and TEM image and (b) the number of *C. albicans* counted from the micrographs of MNPs-*C. albicans* aggregates.

QOA-05. Structural, Magnetic, and Self-Heating Study of Eu-doped Magnetite Nanoparticles towards the Application of Magnetic Hyperthermia. *K. Hazarika*[1] and J.P. Borah[1] *1. Physics, NIT Nagaland, Dimapur, India*

Magnetic hyperthermia has a specific limitation in treating localized and relatively accessible malignant tumors regardless of its promising therapeutic regime. In this work, Eu doped Fe_3O_4 magnetic nanoparticles (MNPs) were prepared via coprecipitation root and confirmed the structural conformation and phase purity by XRD, FTIR, TEM, and SEM analysis. TGA analysis was carried out for thermal stabilization and to verify the formation of a stable phase. The occupancy of Eu ions at the octahedral sites and cationic distribution can be calculated from the Rietveld refinement analysis. The relaxation mechanism, dipolar- dipolar interactions among the particles, and randomly directed magnetic anisotropy axes were examined by ESR spectroscopy. Furthermore, the magnetic results enumerate that increasing Eu doping concentration leads to an increase in saturation magnetization with enhancing effective anisotropy constant and a decrease in coercivity and retentivity. The self-heating properties of the doped nanoparticles were characterized by measuring a specific absorption rate (SAR). These findings are a milestone on the road near the controlled magnetic hyperthermia application with negligible side effects.

1. Slimani, Y. *et al.* Impact of Sm3+ and Er3+ Cations on the Structural, Optical, and Magnetic Traits of Spinel Cobalt Ferrite Nanoparticles: Comparison Investigation. *ACS Omega* 7, 6292–6301 (2022). 2. Ghosh, M. P. & Mukherjee, S. Emergence of large exchange anisotropy in Pr doped nanocrystalline spinel ferrites. *Mater. Chem. Phys.* 261, 124208 (2021). 3. Jagadeesha Angadi, V. *et al.* Magnetic properties of larger ionic radii samarium and gadalonium doped manganese zinc ferrite nanoparticles prepared by solution combustion method. *J. Magn. Magn. Mater.* 529, 167899 (2021). 4. Kahmann, T., Rösch, E. L., Enpuku, K., Yoshida, T. & Ludwig, F. Determination of the effective anisotropy constant of magnetic nanoparticles – Comparison between two approaches. *J. Magn. Magn. Mater.* 519, 167402 (2021). 5. Alotaibi, I. *et al.* Synthesis, characterization and heating efficiency of Gd-doped maghemite (γ-Fe2O3) nanoparticles for hyperthermia application. *Phys. B Condens. Matter* 625, 2–10 (2022). 6. Fopase, R., Saxena, V., Seal, P., Borah, J. P. & Pandey, L. M. Yttrium iron garnet for hyperthermia applications: Synthesis, characterization and in-vitro analysis. *Mater. Sci. Eng. C* 116, 111163 (2020).

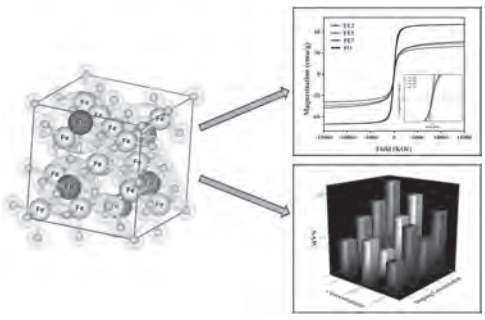

Fig. 1

QOA-06. Enhanced magnetic hyperthermia in $CoFe_2O_4$ nanorods. J. Mohapatra[1], J. George[1], A. Arellano[1] and *J. Liu*[1] *1. Department of Physics, The University of Texas at Arlington, Arlington, Arlington, TX, United States*

Localized heat induction using magnetic nanoparticles under an alternating magnetic field (AMF) is an emerging technology applied in cancer treatment, thermally activated drug release, and remote activation of cell functions. The intrinsic and extrinsic magnetic parameters influencing the heating efficiency of magnetic nanoparticles should be effectively engineered to enhance the induction heating efficiency of magnetic nanoparticles. In this work, an efficient magnetic hyperthermia agent with a high

specific absorption rate (SAR) value is obtained. Monodispersed $CoFe_2O_4$ nanorods of length (25- 250 nm) and diameter (10-28 nm) are synthesized via a thermolysis technique using oleylamine as a multifunctionalizing agent (surfactant, solvent and reducing agent). $CoFe_2O_4$ nanorods of 70 nm length encapsulated with citric acid show a very high SAR value of 860 W/g for an AMF of 625 Oe. The improved heating effects of nanorods are related to shape-induced predominant changes in magnetic properties. As nanorod length increases, coercive loss increases, resulting in more excellent heating effects. When the length of nanorods increased above 70 nm, the coercivity increased above the applied AMF, which led to a decreased ac hysteresis loop area and a rapid decrease in the SAR values. Our findings open new avenues for manipulating the magnetic properties of magnetic nanoparticles and establishing a qualitative relationship between effective magnetic anisotropy and heating efficiency.

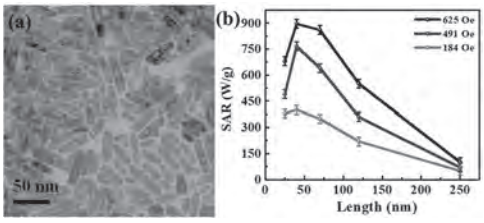

Figure 1

QOA-07. Ultra-short pulse magnetic fields on effective magnetic hyperthermia for cancer therapy. *A. Kuwahata*[1], Y. Adachi[1] and S. Yabukami[1] *1. Tohoku University, Sendai, Japan*

For cancer therapy with magnetic hyperthermia by using magnetic nanoparticles (MNPs) [1, 2], alternating magnetic fields (AMF) H_{AC}, typically sinusoidal wave, can deliver the magnetic energy into the deeper location in the body. In this study, we proposed a highly effective heat generation method for the MNPs by the application of an ultra-short pulse. We numerically evaluated the heating power with a variety of parameters, such as pulse width, field amplitude, and frequency [3]. Figure 1 shows effective magnetic hyperthermia with the ultra-short pulse magnetic field (Fig.1 (a)). The hysteresis curve and magnetization dynamics clearly indicate larger energy dissipation (Figs. 1 (b) and (c)). Figure 2 shows the energy dissipation and efficiency [4, 5] on the two-dimensional parameter space of field strength and duty ratio. Hysteresis loss and the input energy increases increasing with field strength and duty ratio (Figs. 2(a) and (b)) and there is a large efficiency power condition (Fig.2 (c)). To evaluate the effective heat generation and practical temperature increment, a larger imaginary part of magnetic susceptibility ($\chi'' > 30$) and specific loss power (SLP > 10^5 W/kg) are required (Figs. 2 (d) and (e)). In addition, larger intrinsic loss power (100 nHm^2/kg) is achieved (Fig. 2 (f)). Finally, we found the optimal condition of applied AMF (duty ratio = 1.2% and H_{AC} = 16 kA/m) considering the practical uses. The results indicate that magnetic harmonics signals with a higher frequency range significantly enhance the heat generation of MNPs. We explore further studies of the development of an effective pulse generator for clinical applications and evaluation of the heating effect in animal experiments.

[1] D. Kouzoudis *et al.*, *frontiers in Materials* 8, 638019 (2021) [2] A. Shikano *et al.*, *T. Magn. Soc. Jpn. (Special Issues)* 6, 100-104 (2022) [3] H. Mamiya *et al.*, *PLOS ONE* 10, 1371 (2015) [4] R. E Rosensweig, *J. Magn. Magn. Mater*. 252, 370 (2002) [5] T. Yamaminami *et al.*, *frontier in Materials* 8, 638019 (2021)

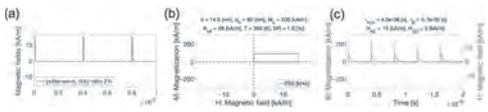

Fig. 1 Effective heating with ultra-short pulse field: (a) applied magnetic field, (b) hysteresis loss, and (c) magnetization characteristics in time scale.

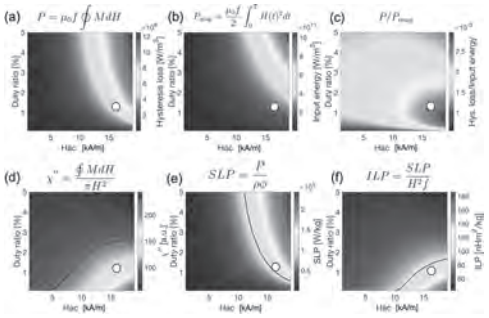

Fig. 2 Optimization of applied magnetic field on two-dimensional parameter spaces of field strength and duty ratio; (a) hysteresis loss [W/m^3], (b) input magnetic energy [W/m^3], (c) power ratio of hysteresis loss to input energy, (d) imaginary part of magnetic susceptibility, (e) specific loss power [W/kg], and (f) intrinsic loss power [nHm^2/kg].

QOA-08. Development of gold-coated magnetic nanoparticles as a theranostic agent for magnetic hyperthermia and micro-CT imaging applications. *L. Ton That*[1], M. Kimura[2], T. Ogawa[1], N. Kitamura[2], Y. Kobayashi[3], K. Gonda[2] and S. Yabukami[1] *1. Graduate School of Engineering, Tohoku University, Sendai, Japan; 2. Graduate School of Medicine, Tohoku University, Sendai, Japan; 3. Graduate School of Science and Engineering, Ibaraki University, Mito, Japan*

Gold-coated magnetic core-shell nanoparticles (NPs) have attracted much interest due to their potential applications in cancer therapy through the combination of target drug delivery, diagnostic imaging, and magnetic hyperthermia. We previously developed a simple magnetic hyperthermia system[1], and synthesized iron oxide magnetic NPs[2] and gold NPs[3] with a size of sub-10 nanometer. This study aims to develop gold-coated Fe_3O_4 (Fe_3O_4@Au) NPs as a theranostic agent for magnetic hyperthermia and micro-CT imaging applications. The Fe_3O_4 NPs were synthesized via thermal decomposition method that reduced iron (III) oleate using 1,2-hexadecanediol in the mixture of oleylamine and oleic acid as capping agents, and the gold was then deposited onto the surface of Fe_3O_4 NPs by reducing gold acetate using 1,2-hexadecanediol in the mixture of oleylamine and oleic acid at 190°C. The synthesized NPs were then characterized by TEM, XRD, EDS, DLS, magnetization curve measurement, magnetic hyperthermia, and CT value evaluations. In Fig. 1(a), Fe_3O_4 NPs after coating with Au appeared much darker than Fe_3O_4 due to the generation of contrast depending on the atonic number of atoms composing the NPs. The average sizes of Fe_3O_4 and Fe_3O_4@Au NPs were 5.2 nm and 6.1 nm, and the average thickness of Au coating was 0.45 nm. In Fig. 1(b), the magnetization of Fe_3O_4@Au NPs (9.7 emu/g-Fe_3O_4) at 300K was much smaller than that of Fe_3O_4 (52.4 emu/g-Fe_3O_4). This decrease is considered to be due to a decrease in magnetic moment coupling as a result of the increased interparticle spacing of magnetic core by gold shell and organic capping agents. In Fig. 1(c), the heating efficiency of Fe_3O_4@Au in water was sufficient to treat the tumor at 43-45°C, and their CT value (851 HU) was much higher than that of Fe_3O_4 (158 HU). The obtained results indicate the synthesized Fe_3O_4@Au NPs are a potential theranostic agent for the combination of magnetic hyperthermia and micro-CT imaging applications. Acknowledge: This research is supported by the Ministry of Internal Affairs and Communications in Japan (JPJ000254), the Comprehensive Growth Program for Accelerator Sciences and the Joint Development Research 2022-ACCL-1 at High Energy Accelerator Research Organization (KEK), JST A-STEP Grant Number JPMJTM22AB, Japan, and Japan Society for the Promotion of Science KAKENHI Grant Numbers 20K20210.

1) A. Shikano *et al.*, Trans. Magn. Soc. Jpn., 6(1), 100-104, (2022) 2) L. Tonthat *et al.*, IEEE Trans. Magn., 54 (7), 5400506, (2018) 3) T. Inose *et al.*, Colloids Surf. B: Biointerfaces, 203, 111732, (2021)

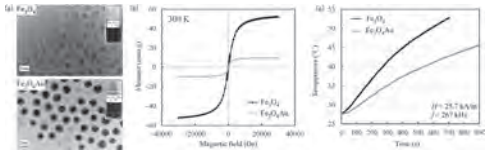

Fig. 1 (a) TEM images and photographs of Fe_3O_4 and Fe_3O_4@Au NPs in hexane, (b) their magnetization curves for dried NPs at 300K, and (c) their temperature rise in water (sample volume: 0.5 ml, concentration: 36.6 mg/ml) under *H*=25.7 kA/m and *f*=267 kHz.

QOA-09. Porous metal-organic framework as magnetothermally-triggered on-demand release carriers by iron oxide nanoparticles confinement. *X. Ge*[1] and S. Ma[1] *1. Chemistry, University of North Texas, Denton, TX, United States*

To improve the heating efficiency of iron oxide nanoparticles (IONPs) for the application of magnetothermally-triggered drug release, one key factor could be the intimate contact between IONPs and the drug carriers. Metal-organic frameworks (MOFs) could offer inherent condition for the spatial confinement and segregation of incorporated IONPs due to their well-defined pore structures together with multiple binding sites. Although some IONPs/MOF composites have been explored in drug delivery systems, the construction of such composites for optimizing heating efficiency remains challenging as it requires preservation of the MOF morphology, retention of the MOF porosity, and segregation of the incorporated IONPs and graft thermal-responsive nanocap simultaneously remains challenging. Herein, we have demonstrated a strategy for overcoming this challenge, spatially distributing IONPs within a MOF matrix with intimate contact between IONPs and MOF matrix created to prevent the aggregation of incorporated IONPs and also facilitate heat transfer, thus achieving a higher specific absorption rate value, which is about 12 times greater than pristine IONPs. It can be furtherly covalently attached with a thermal nanocap on the exterior surface of MOF to construct an alternating magnetic field (AMF)-responsive nanocomposite. On-demand drug release from MOF pores can be activated by AMF. The drug-loaded IONPs/MOF composites with a thermal nanocap successfully demonstrate *in vitro* treatment by combining controlled drug release and hyperthermia. The IONPs/MOF composites with negligible cytotoxicity and high transverse relaxivity (r_2) value show promising potential for T_2-magnetic resonance (MR) imaging due to completely confining incorporated IONPs within the MOF matrix. This finding opens up a new avenue for magnetothermally-triggered drug release, magnetic hyperthermia therapy, and MR imaging.

QOA-10. Wireless temperature monitoring by using magnetic nanoparticles for clinical trials on magnetic hyperthermia treatment. *A. Kuwahata*[1], R. Hirota[1], A. Sukhbaatar[1], T. Kodama[1] and S. Yabukami[1] *1. Tohoku University, Sendai, Japan*

Magnetic hyperthermia with magnetic nanoparticles (MNPs) has been introduced to selective treatment of tumor [1,2] and the MNPs also has demonstrated diagnosis [3, 4]. For non-invasive treatment, a therapeutic system with a temperature monitoring that can avoid overheating in normal tissues is of vital importance. We have developed a temperature monitoring/control system with an optical fiber temperature probe in vivo [2]. However, the optical fiber involves an invasive measurement due to the contact with the body. In this study, we have developed a wireless temperature monitoring system by utilizing the combination of magnetic harmonic signals of the MNPs for clinical trials. Figure 1 shows the developed wireless monitoring system with Resovist® (a clinically approved MNP). Under the application of alternating magnetic fields, the detected harmonics were analyzed to extract only temperature-dependent signals. Figure 2 shows the measured temperature of Resovist® phantom. We achieved an accurate measurement with an error of 0.18°C (Fig. 2(a)). For practical use on breast/oral cancer, a detectable distance of 10 mm is required. We measured the accurate temperature at a 10 mm distance (Fig. 2(b)). To demonstrate the feasibility toward clinical trials, we investigated the dependency on the detectable distance and the amount of Resovist®. The error is less than 0.5°C in a 10 mm distance (Fig. 2(c)). Resovist® travels to the whole body from the injection site via the lymphatic system, resulting in a decrement of the amount at the injection site. Our system can measure the correct temperature regardless of Resovist® amount (Fig. 2(d)). The results indicate that our system can apply to clinical trials. We will pursue further study of a temperature monitoring system under magnetic hyperthermia treatment.

[1] D. Kouzoudis *et al.*, *frontiers in Materials* 8, 638019 (2021) [2] A. Shikano *et al.*, *T. Magn. Soc. Jpn. (Special Issues)* 6, 100-104 (2022). [3] M. Sekino *et al.*, *Scientific Reports* 8, 1195 (2018) [4] K. Taruno *et al.*, *J. Surg. Oncol.* 120, 1391 (2019)

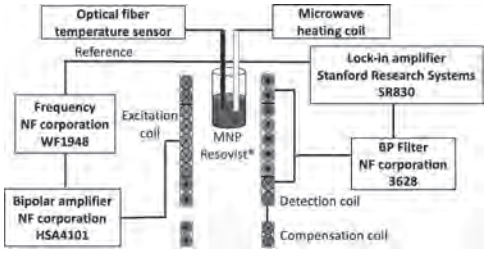

Fig. 1 Wireless temperature monitoring system by using magnetic nanoparticles and magnetic harmonic signals.

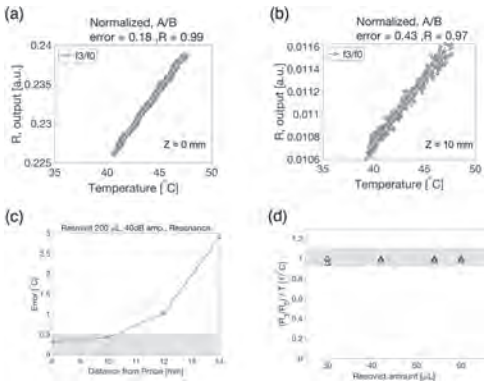

Fig. 2 Wireless temperature monitoring by using magnetic nanoparticles. (a) Accurate absolute temperature monitoring with the error of 0.18°C. (b) Accurate temperature monitoring for far location of 10 mm, (c) dependency on distance from probe, and (d) accurate temperature monitoring regardless of Resovist® amount.

QOA-11. Thermosensitivity Through Exchange Coupling in Ferrimagnetic/Antiferromagnetic Nano-Objects for Spatially Resolved Thermometry. *F.M. Abel*[1], E. De Lima Correa[1], A.J. Biacchi[1], T.Q. Bui[1], S.I. Woods[1], A.R. Hight Walker[1] and C. Dennis[1] *1. National Institute of Standards and Technology, Gaithersburg, MD, United States*

Advances in temperature metrology are crucial for the development of numerous technologies ranging from biomedicine to microelectronics.[1,2] Temperature measurement requires a physical property that changes rapidly with temperature in the desired measurement range. This is a major limiting factor in the development of thermometry using magnetic nano-objects (MNOs) as most do not exhibit a strong temperature-dependent magnetization (thermosensitivity) near room temperature (200 K to 400 K). Here we have developed an approach to improve the thermosensitivity of 10 nm iron oxide (ferrite) by growing cobalt oxide (CoO) on the surface of the particles. The resulting interface exchange coupling between the ferrimagnetic (FiM) ferrite and antiferromagnetic (AFM) CoO, along with Co diffusion into the ferrite changes the temperature-dependent magnetization. Three different morphologies have been synthesized: one ferrite/CoO MNO exhibits a

particle-like, nanoflower morphology, the other two have cluster-like morphologies. The structure and morphologies were confirmed by X-ray diffraction, Raman spectroscopy, and electron microscopy. Figure 1 shows the liquid DC magnetization vs. temperature for the ferrite and ferrite/CoO MNOs. In addition, liquid DC magnetization vs. applied magnetic field measurements at 100 K confirm the presence of exchange bias between the CoO and the ferrite. A strong measurable AC response at room temperature was measured with magnetic particle spectroscopy (MPS), Figure 2. Our results show the viability of these MNOs as temperature sensors.

1. C. D. S. Brites, P. P. Lima, N. J. O. Silva, et al., Nanoscale., Vol. 4, p. 4799 (2012) 2. T. Q. Bui, W. L. Tew, S. I. Woods, J. Appl. Phys., Vol. 128, p. 224901 (2020)

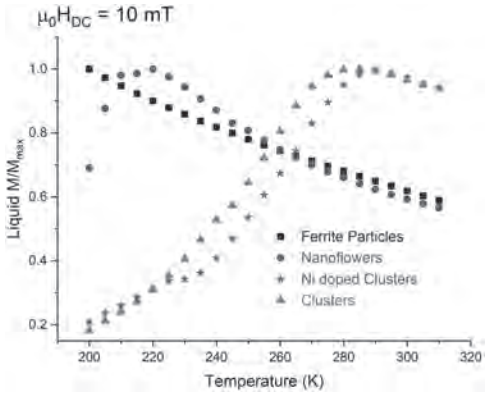

Fig. 1 DC magnetization vs. temperature normalized by the maximum magnetization in the range of 200 K to 310K of 10 nm ferrite particles, ferrite/CoO nanoflowers, ferrite/CoO clusters, and Ni doped ferrite/CoO clusters in hexanes.

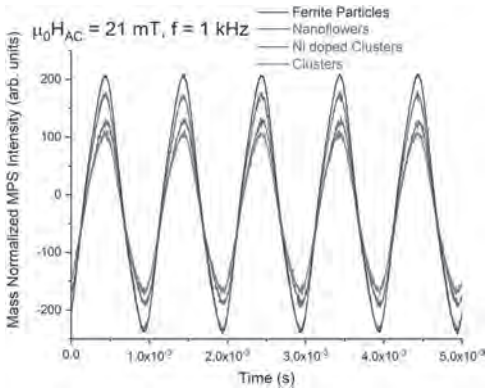

Fig. 2 Room temperature MPS of 10 nm ferrite particles, ferrite/CoO nanoflowers, ferrite/CoO clusters, and Ni doped ferrite/CoO clusters in hexanes.

QOA-12. Neural Network Approach for Event Classification in a Magnetic Micro Flowmeter. *B. Martin*[1,2], D.M. Caetano[1,2], R. Afonso[1,2], A.R. Soares[1,2], V. Silverio[1,2] and S. Cardoso[1,2] *1. INESC MN, Lisbon, Portugal; 2. Instituto Superior Tecnico, Lisbon, Portugal*

Organ-on-chip devices gained increased attention in the past years, resulting in an increasing number of applications [1,2]. Many of these systems require a minimally invasive flow rate measurement. One application benefitting from precision flow rate assessment is cell growth in microchambers regarding the control of several processes, e.g., provision of nutrients and oxygen, and removal of metabolites and other toxins; exertion of mechanical forces by means of the fluid flow; or optimization of cellular function by flow rate regulation [3]. Thus, in these processes the flow rate is a critical parameter that must be precisely measured and adjusted. We describe an integrated precision flowmeter based on magnetoresistive (MR) biosensors [4,5] as well as detection of 2.8μm magnetic particles (MP) using time-of-flight to estimate flow rates from 0.24 to 5.96μL/min. The device (fig. 1) comprises GMR sensors (2μm width; 0.62Ω/Oe sensitivity), located at the bottom of a microfluidic channel (10μm height; 100μm width), that detect the MP's magnetic field. The system's output is a bipolar Gaussian monocycle. By having two sensors spaced by a known distance (74μm), one can estimate the time a single MP takes to travel between two sensors and calculate the particle's velocity with v=Δy/Δt. We propose the use of a patented neural networks-based algorithm (NNA) to evaluate the signal output and detect the target pulses reliably (fig. 2) [6]. To correlate the MP's velocity with the fluid's flow rate it is necessary to perform a statistical study regarding particle speed according to height (smaller than 10μm) and distribution [7] as well as concentration (from 10 to 1000MP/μL). We describe the optimization of the NNA and particle concentration to automatically obtain particle speed distributions and consequently an accurate flow rate measurement. Acknowledgments: FCT for funding the Research Unit INESC MN (UID/05367/2020) through plurianual BASE and PROGRAMATICO financing; projects Moore4Medical (ECSEL/0007/2019) and (MAG-ID H2020/870017).

[1] A. E. Danku, E.-H. Dulf and C. Braicu, Frontiers in Bioengineering and Biotechnology, vol. 10 (2022) [2] C. M. Leung, P. de Haan and K. Ronaldson-Bouchard, Nature Reviews Methods Primers, vol. 2, p. 33(2022) [3] L. Kim, Y.-C. Toh, J. Voldman and H. Yu, Lab on a Chip, vol. 7, p. 681 (2007) [4] J. Loureiro, R. Ferreira and S. Cardoso, Applied Physics Letters, vol. 95, p. 034104 (2009) [5] A. R. Soares, R. Afonso and V. C. Martins, Biosensors and Bioelectronics: X, vol. 11, p. 100149 (2022) [6] D. Caetano, J. Fernandes and T. Kuntz, Portugal Patent PT116 012A, Dec 18, 2019. [7] M. Abbas, P. Magaud and Y. Gao, Physics of Fluids, vol. 26, p. 123301 (2014)

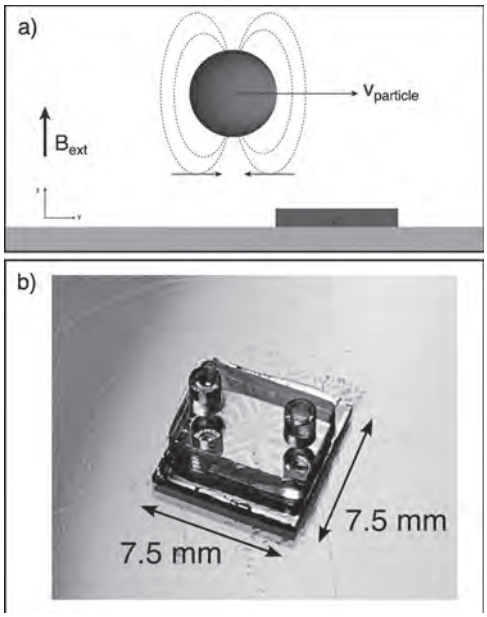

Fig. 1. a) Schematic of magnetized MP flowing above a sensor. b, c) Fabricated biochip.

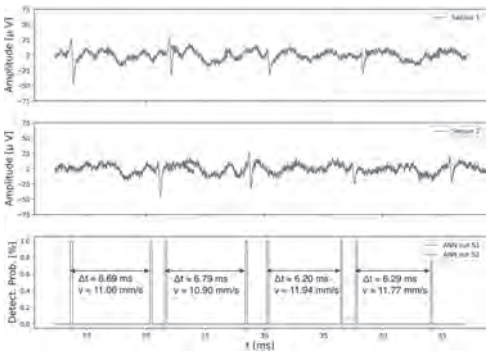

Fig. 2. Output of two sensors, time between detection events, and resulting particle velocity.

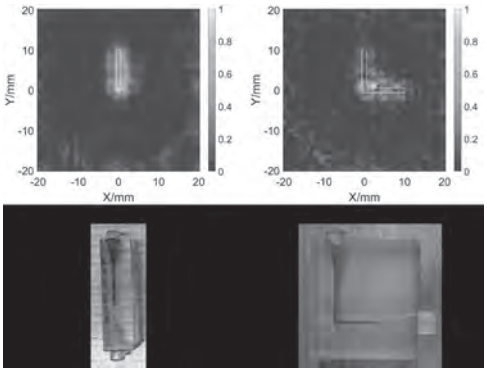

Fig. 1 Reconstructed image of a rod phantom and elbow rod phantom

QOA-13. Two-Dimensional Imaging Using a Single Sided Field Free Line Magnetic Particle Imaging Scanner. *C. McDonough*[1] and A. Tonyushkin[1] *1. Physics, Oakland University, Rochester, MI, United States*

Magnetic Particle Imaging (MPI) is a novel medical imaging modality that is in a preclinical stage [1]. MPI scanners use rf magnetic fields to excite and measure oscillations in superparamagnetic iron oxide nanoparticles (SPIO) so that the signal is proportional to SPIO's concentration. Applying a gradient magnetic field allows an MPI scanner to spatially localize the signal. Our group has designed a single sided field-free line (FFL) scanner, which has all hardware on a single side of the device providing an open imaging volume, useful for imaging larger subjects such as humans. Compared to a field-free point scanner [2], our device promises higher sensitivity and robust image reconstruction. In the past, we demonstrated 1D imaging capabilities by implementing electronic scanning of field-free line (FFL) across a simple rod phantom [3] and simulated 2D image reconstruction with backprojection technique [4]. In this work we demonstrate the 2D imaging capability of our prototype scanner by imaging phantoms, which include a single rod and two rods in orthogonal orientation, i.e. "elbow". Each rod has a diameter of 1.2 mm and a length of 10 mm and filled with undiluted SynomagD SPIO. To excite the SPIO in our samples we applied an rf magnetic field created by a low noise sinusoidal current source at 25 kHz producing a magnetic field of 1.5 mT at the surface of the scanner. For image encoding the FFL is created and dynamically scanned across the sample by two programmed DC power supplies providing a gradient of 0.58 T/m. The signal is recorded at 0.5 mm step over 4 cm interval of a rotated sample at diffrent discrete angles. The resulted backprojection reconstruction images are shown in the Fig.1. The final images were also deconvoluted with the experimentally obtained point spread function providing a spatial resolution of 4 mm. At this relatively low field gradient this is a reasonable result and in the future we will incorporate higher field gradient and dynamic trajectory correction to improve the uniformity of the image. This work is a significant first step towards human MPI imaging that can be potentially used for diagnostics and biopsy of cancer.

[1] B. Gleich, and J. Weizenecker, Nature., Vol. 435, p.1214-1217 (2005) [2] T. F. Sattel, T. Knopp, and S. Biederer, Journal of Physics D: Applied Physics, Vol. 42, p.022001 (2009) [3] C. McDonough, D. Newey, and A. Tonyushkin, IEEE Transactions on Magnetics, 1d imaging of a superparamagnetic iron oxide nanoparticle distribution by a single-sided ffl magnetic particle imaging scanner [4] C. Chinchilla, C. McDonough, and A. Tonyushkin, International journal on magnetic particle imaging, Vol. 7, p.2104001 (2021)

QOA-14. Sub-pT oscillatory magnetometric system using magnetoresistive sensor array for a low-field magnetic particle imaging. *S. Trisnanto*[1], T. Kasajima[2], T. Akushichi[2] and Y. Takemura[1] *1. Yokohama National University, Yokohama, Japan; 2. TDK Corporation, Tokyo, Japan*

Magnetic particle imaging (MPI) is a technique to visualize magnetic nanoparticles with high spatial and temporal resolutions based on nonlinear magnetization response.[1] One of major challenges toward clinical MPI system is how to implement low ac excitation fields. For brain MPI particularly,[2] a 24 kHz excitation field intensity with amplitude over 3.5 mT may induce peripheral nerve stimulation on human head.[3] However, low-field MPI scenario degrades spatial resolution since the detected signal has no harmonic components but high contamination from the excitation fields. Previously, we applied 1 MHz excitation field to elevate signal-to-noise ratio of receive coil.[4] To further decontaminate magnetization signal spectrally, we used magnetoresistive (MR) sensor to transform monotone signal into harmonic-rich one and reconstructed phantom image from odd harmonic components.[5] Extensively, MR sensor can be used to map quasistatic stray field of magnetic nanoparticles.[6] Here, we will report the use of a 6×6 channels array of TDK Nivio xMR sensors to detect sub-pT magnetic signal and obtain its spatial distribution. While each sensor is operated at 5 V, signal processing circuit rises its sensitivity to 20 mV/ pT at 10 kHz with 0.25 pT noise level. We used a 40-turns coil with 1 mm diameter and 5 mm length to represent magnetic moment. The distance between MR sensor and the coil (d_x) was 250 mm [Fig. 1(a)]. From Fig. 1(b), MR sensor recognizes magnetic signal from mini coil fed with a 10 kHz ac current. Magnetic field detected by the sensor (H_d) is linear with coil input current (i). Furthermore, we simultaneously recorded the signals from 36 sensor channels to map at 200 Hz. We set d_x=50 mm to obtain high contrast showing coil position relative to the array. From Fig. 2, the change in field polarity is observable from frames (i), (ii), (iii), and (iv) with channel c16 as reference. This result highlights usability of MR sensor array for low-field MPI system.

1. B. Gleich and J. Weizenecker, Nature, 435, 1214 (2005). 2. M. Graeser, F. Thieben and T. Knopp, Nat. Commun., 10, 1936 (2019). 3. A. A. Ozaslan, M. Utkur and E. U. Saritas, Int. J. Mag. Part. Imag., 8, 2203028 (2022). 4. S. B. Trisnanto and Y. Takemura, Phys. Rev. Appl., 14, 064065 (2020). 5. S. B. Trisnanto, T. Kasajima and Y. Takemura, Appl. Phys. Express, 14, 095001 (2021). 6. S. B. Trisnanto, T. Kasajima and Y. Takemura, J. Appl. Phys. 131, 224902 (2022).

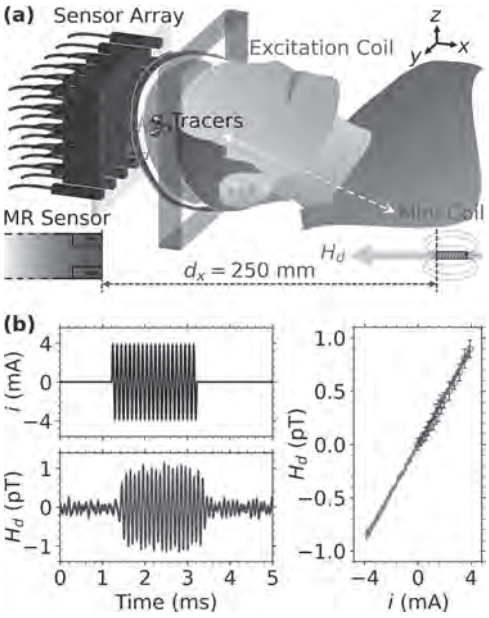

Fig.1 (a) Oscillatory magnetometric system using MR sensor array and (b) output linearity of single MR sensor below 1 pT at 10 kHz.

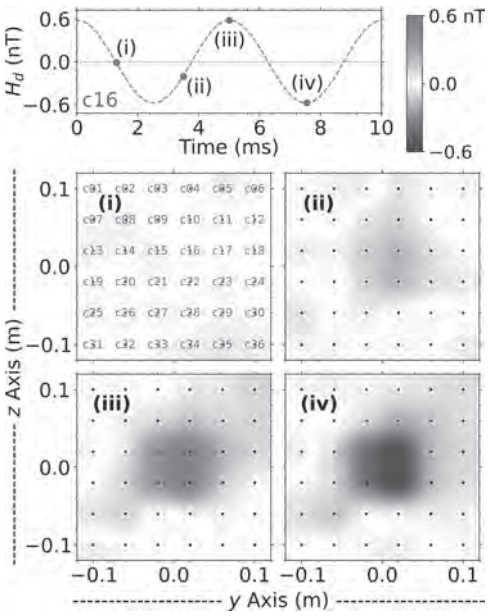

Fig.2 Magnetic field of mini coil mapped at 50 mm apart from a 6×6 channels MR sensor array. Coil input current was 30 mA at 200 Hz.

QOA-15. Rapid Virus Detection using Magnetic Second Harmonics of Superparamagnetic Iron Oxide Nanoparticles. *R. Hirota*[1], T. Murayama[1], R. Katsumi[2], T. Kawawaki[3], S. Yabukami[1,4], R. Igarashi[5], Y. Negishi[3], M. Kusakabe[6,7], M. Sekino[8], T. Yatsui[2] and A. Kuwahata[1]
1. Graduate School of Engineering, Tohoku University, Aoba-ku, Sendai, Japan; 2. Graduate School of Engineering, Toyohashi University of Technology, Tempaku-cho, Toyohashi, Japan; 3. Department of Applied Chemistry, Faculty of Science, Tokyo University of Science, Kagurazaka, Shinjuku-ku, Japan; 4. Faculty of Engineering, Tohoku Gakuin University, Chuo, Tagajo, Japan; 5. Institute for Quantum Life Science, National Institutes for Quantum and Radiological Science and Technology, Anagawa Inage-ku, Japan; 6. Research Center for Food Safety, Graduate School of Agricultural and Life Sciences, The University of Tokyo, Tokyo, Japan; 7. Matrix Cell Research Institute Inc., Ibaraki, Japan; 8. Graduate School of Engineering, The University of Tokyo, Hongo, Bunkyo-ku, Japan

There has been a need for rapid screening of people infected virus including with COVID-19 or influenza. Virus detection methods using magnetic harmonics of magnetic nanoparticles (MNPs) with superparamagnetism has been reported [1, 2]. In this study, we report the detection of influenza virus based on magnetic second harmonic signals [3], and the detection sensitivity was 100 pg/mL. Figure 1 shows the developed system for virus detection. The excitation coil generated AC magnetic fields of amplitude of 6.6 mT with 1 kHz and the detection coil detect the second harmonic signals of MNPs under DC magnetic field of 6.6 mT. The measurement of the magnetization response of MNPs completed in one minute. The samples contained MNPs (Nanomag-D, average diameter 20 nm, 5 mg/mL, 9.24×10^{12} particles) coated with protein-A, with which antibodies (Nucleoprotein InA245). Antigens (Influenza A virus) bound to the antibodies by antigen-antibody reaction. Figure 2 shows the relation between the second harmonic signal normalized by the fundamental signal R_2/R_0 and the third harmonic signal normalized by the fundamental signal R_3/R_0 with five different antigen concentrations (0, 10^3, 10^5, 10^7, 10^9 antigens). R_2/R_0 was about 2.3 times larger than R_3/R_0. This result indicates that the detection of viruses using the second harmonic signal has a larger detectable range of the number of antigens. In addition, the value of R_2/R_0 significantly reduce at 10^4 antigens (Fig. 2(a)). This result indicate that we can detect 10^4 antigens (100 pg/mL). In the future, we aim to achieve detection sensitivity of the PCR method (1 pg/mL) by investigating the optimal detection coil shape, excitation frequency, and concentration of MNPs for virus detection.

[1] K. Wu *et al*., *ACS Appl. Mater. Interfaces* 12 (12), 13686-13697 (2020). [2] V. K. Chugh *et al*., *J. Phys. Chem. C*. 125, 17221-17231 (2021). [3] R. Hirota *et al.*, *IEEJ TEEE* (2022).

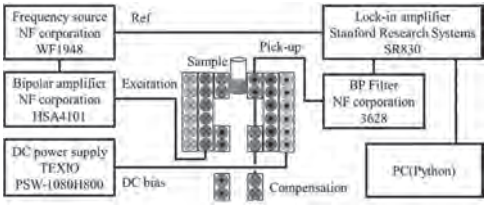

Fig.1 A virus detection system using the second harmonics of MNPs.

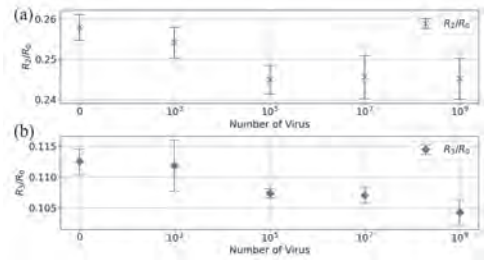

Fig.2 Amount of virus dependence of (a) the second, and (b) the third harmonic signals normalized by fundamental signal.

QOA-16. Field induced structural transitions in the para-magnetic enzyme Urease. *T. Moorsom*[1], M. Chauhan[2], A. Scott[1] and A. Jha[1]
1. University of Leeds, Leeds, United Kingdom; 2. University of York, York, United Kingdom

Jack Bean Urease is a unique metal dependent enzyme which plays an important role in hydrolysis of urea to ammonia. [1] Controlling the hydrolysis of urea can inhibit the growth of *H. Pylori* bacteria in the stomach, which is a class 1 carcinogen associated with the formation of peptic ulcers and gastric cancer. [2] Urea hydrolysis involves the binding of the molecule to a nickel ion in one of six active sites in the urease enzyme. Each active site contains two nickel ions bridged by a hydroxide ion. [3] Due to the presence of magnetic ions in this enzyme and their critical role in the hydrolysis reaction, there have been several attempts to perform magnetic characterization on crystalline Jack Bean Urease (JBU) which have determined that binding of urea to the active site is accompanied by a change in paramagnetic susceptibility due to the different role of high and low spin Ni sites in the reaction. [4] In this work, we have observed a hysteretic phase transition which, to our knowledge, has never before been observed in this enzyme. Samples of crystalline JBU were cooled in zero field to 10 K, then warmed in an applied field of 50 mT, revealing a blocking-like transition at 62 K. Using Raman Spectroscopy, we have identified that vibrational modes associated with the Histidine ligands, which are bonded to the Ni active site, become Raman active in the presence of a magnetic field. Based on this, and with the assistance of Density Functional Theory simulations of the active site, we hypothesize that the magnetic field changes the bond length of the Ni hydroxide complex, in a manner analogous to the spin crossover mechanism in i.e Nickel porphyrins, [5] resulting in structural distortions of the active site which are visible as a phase transition at low temperatures. We intend to further model this behavior using advanced DFT methods and x-ray diffraction in order to determine whether magnetic fields alone may have an inhibitory effect on Urease hydrolysis.

[1] H L T Mobley, Helicobacter pylori: Physiology and Genetics, Chapter 16, pg 179 – 188, ASM Press, 2001. [2] H L T Mobley et al, Microbiol Rev, 59, 451-480, 1995. [3] A Balasubramanian et al, Jour Mol Bio, 400, 3, 2010. [4] M G Finnega et al, J Am Chem Soc, 113, 10, 1991. [5] S Thies et al, Chem Eur J, 16, 10074-10083, 2010.

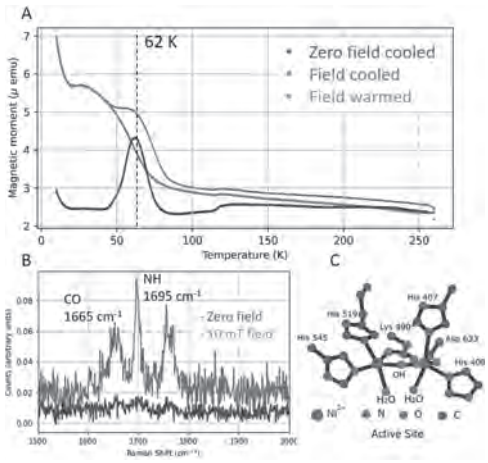

Figure 1: A. Moment v Temperature for JBU, showing the phase transition at 62 K during the warming cycle. B. Raman spectroscopy with and without applied field. C. Diagram of the active site, showing the Ni ion pair.

Session QOB
MAGNETIC STIMULATION IN BIOLOGY, MAGNETIC FLUIDS AND ACTUATORS

Ahmed El-Gendy, Chair
The University of Texas at El Paso, El Paso, TX, United States

INVITED PAPER

QOB-01. Beyond conventional neurostimulation: effects of TMS-like magnetic fields on cells and nanomaterials and their potential applications in oncology and regenerative medicine. B. Heng[1], B. Gunasegaran[1], R. Zeng[1], M. Villanueva[1], S. Ahn[1], S. Clement[2] and *A. Guller*[1] *1. Macquarie Medical School, Macquarie University, Sydney, NSW, Australia; 2. School of Biomedical Engineering, The University of Sydney, Sydney, NSW, Australia*

Transcranial magnetic stimulation (TMS) [1] is a non-invasive pain-free medical technology clinically approved for treatment of drug-resistant depression [2, 3]. TMS uses pulsed magnetic fields to induce eddy currents [4] in the brain. The biological mechanism of rTMS effects is tought to be mostly relying on the long-lasting changes of the neuronal excitability and the brain functional plasticity, respoectively [5]. However, the effects of TMS-like fields on non-neuronal cells and artificial systems are almost unknown. The aim of this study was to explore the potential of repetitive magnetic stimulation (RMS) performed by TMS devices in oncology, controllable drug release and regenerative medicine applications. Using a standard TMS device "Magstim Rapid^2", we examined effects of >30 experimental regimes of RMS on viability and phenotype of various tumour (glioblastoma, pancreatic, liver, colorectal [6] and breast cancers) and immune cells (microglia and macrophages). We also tested the effect of RMS on drug release from polymer nanoparticles and reactive oxygen species generation (ROSG) in cancer and immune cells. Finally, we examined the combined effects of RMS and drugs targeting tissue growth. RMS selectively modulated viability and functional polarisation of microglia and macrophages in a frequency/intensity-dependent manner and affected the proliferation/viability of cancer cells (cancer type, frequency- and pulse number-dependent up- and downregulation). RMS induced triggering of drug release from nanoparticles, enhancement of ROSG and additive drug effects. Our pioneering findings demonstrate the potential of TMS technology repurposing for immunomodulation, cancer treatment, and drugs and nanomedicines treatment. We thank Sydney Vital (for seed grant) and Medilink Australia (for providing the "Magstim"). The authors gratefully acknowledge the support of the Macquarie University FMHHS Laboratory Operations Team. A.G. is thankful for support of her work by the Macquarie University Research Fellowship.

1. A. T. Barker, R. Jalinous, and I. L. Freeston, "Non-invasive magnetic stimulation of human motor cortex," *Lancet,* vol. 1, no. 8437, pp. 1106-7, May 11 1985, doi: 10.1016/s0140-6736(85)92413-4. 2. A. T. Barker, I. L. Freeston, R. Jalinous, and J. A. Jarratt, "Magnetic stimulation of the human brain and peripheral nervous system: an introduction and the results of an initial clinical evaluation," *Neurosurgery,* vol. 20, no. 1, pp. 100-9, Jan 1987, doi: 10.1097/00006123-198701000-00024. 3. P. M. Rossini *et al.*, "Non-invasive electrical and magnetic stimulation of the brain, spinal cord, roots and peripheral nerves: Basic principles and procedures for routine clinical and research application. An updated report from an I.F.C.N. Committee," *Clinical neurophysiology : official journal of the International Federation of Clinical Neurophysiology,* vol. 126, no. 6, pp. 1071-1107, Jun 2015, doi: 10.1016/j.clinph.2015.02.001. 4. M. Hallett, "Transcranial magnetic stimulation and the human brain," *Nature,* vol. 406, no. 6792, pp. 147-50, Jul 13 2000, doi: 10.1038/35018000. 5. J. P. Lefaucheur *et al.*, "Evidence-based guidelines on the therapeutic use of repetitive transcranial magnetic stimulation (rTMS)," (in English), *Clinical neurophysiology : official journal of the International Federation of Clinical Neurophysiology,* vol. 125, no. 11, pp. 2150-2206, Nov 2014, doi: 10.1016/j.clinph.2014.05.021. 6. B. Heng, S. B. Ahn and A. Guller, "TMS-like Magnetic Fields Modulate Metabolic Activity of Hepatic and Colorectal Cancer Cells." *IEEE Transactions on Magnetics*: 1-1, doi: 10.1109/tmag.2022.3147219.

CONTRIBUTED PAPERS

QOB-02. Prediction of Stimulation Strength of Transcranial Magnetic Stimulation in the Brain with Deep Convolutional Neural Network based Encoder-Decoder Network. *M. Alam*[1], M. Tashli[1], J. Gong[2], C.J. Lewis[3], C.L. Peterson[3], H. Eldardiry[2], R.L. Hadimani[1,3] and J. Atulasimha[1,4] *1. Mechanical and Nuclear Engineering, Virginia Commonwealth University, Richmond, VA, United States; 2. Computer Science, Virginia Tech, Blacksburg, VA, United States; 3. Biomedical Engineering, Virginia Commonwealth University, Richmond, VA, United States; 4. Electrical and Computer Engineering, Virginia Commonwealth University, Richmond, VA, United States*

Transcranial magnetic stimulation (TMS) is a non-invasive, effective, and safe neuromodulation technique used to diagnose and treat neurological disorders [1]-[2]. A key challenge involved with TMS is to determine stimulation strength in critical regions of the brain accurately. The induced electric field is affected by complexity and heterogeneity of the brain and numerical computation methods like finite element analysis (FEA) can be used to estimate electric field distribution. However, these methods need exceedingly high computational resources and are time-consuming [3]-[6]. The purpose of this study was to develop and test a machine learning algorithm that can efficiently predict stimulation strength based on neuroanatomy. Head models were developed from magnetic resonance images of eleven recruited subjects using SimNIBS pipeline [7]-[8]. We used Sim4Life, an FEA software to compute induced electric fields due to simulated TMS; the induced electric fields served as training data. A deep convolutional neural network (DCNN) inspired encoder-decoder network (Fig 1) was developed to predict induced electric fields from T1-weighted and T2-weighted magnetic resonance imaging (MRI) based anatomical slices. Three representative cases of electric fields predicted by the DCNN algorithm, along with the corresponding reference electric fields are shown in Fig 2. For the trained network, the training data and the testing data peak signal to noise ratios are 32.83dB and 28.01dB respectively. The key contribution of this study is the ability to predict the induced electric fields in real-time as well as accurately and efficiently predicting TMS strength in the targeted brain regions saving both time and computational resources. Acknowledgment: This work was supported by VCU CERSE. Further funding was provided by the CCI CVN (Proposal ID #: FP00010500).

[1] D. J. Stultz, S. Osburn, T. Burns, S. Pawlowska-Wajswol, and R. Walton, Transcranial magnetic stimulation (TMS) safety with respect to seizures: A literature review, Neuropsychiatric disease and treatment, vol. 16, p. 2989 (2020). [2] M. Kobayashi, and A. Pascual-Leone, 2003. Transcranial magnetic stimulation in neurology, The Lancet Neurology, vol. 2, no. 3, p. 145-156 (2003). [3] E. G. Lee, W. Duffy, R. L. Hadimani, M. Waris, W. Siddiqui, F. Islam, M. Rajamani, R. Nathan, and D. C. Jiles, Investigational effect of brain-scalp distance on the efficacy of transcranial magnetic

stimulation treatment in depression, IEEE Transactions on Magnetics, vol. 52, no. 7, p. 1–4 (2016). [4] L. J. Crowther, R. L. Hadimani, A. G. Kanthasamy, and D. C. Jiles, Transcranial magnetic stimulation of mouse brain using high-resolution anatomical models, Journal of Applied Physics, vol. 115, no. 17, p. 17B303 (2014). [5] F. Syeda, H. Magsood, E. G. Lee, A. A. El-Gendy, D. C. Jiles, R. L. Hadimani, Effect of anatomical variability in brain on transcranial magnetic stimulation treatment, AIP Advances, vol. 7, no. 5, p. 056711 (2017). [6] F. Syeda, K. Holloway, A. A. El-Gendy, and R. L. Hadimani, Computational analysis of transcranial magnetic stimulation in the presence of deep brain stimulation probes, AIP Advances, vol. 7, no. 5, p. 056709 (2017). [7] N. Mittal, C. Lewis, Y. Cho, C. L. Peterson, and R. L. Hadimani, Effect of fiber tracts and depolarized brain volume on resting Motor thresholds during transcranial magnetic stimulation, IEEE Transactions on Magnetics (2022). [8] N. Mittal, B. Thakkar, C. B. Hodges, C. Lewis, Y. Cho, R. L. Hadimani, and C. L. Peterson, Effect of neuroanatomy on corticomotor excitability during and after transcranial magnetic stimulation and intermittent theta burst stimulation, Human Brain Mapping (2022).

Figure 1: DCNN inspired encoder-decoder network architecture used for predicting electric fields from MRI based anatomical slices.

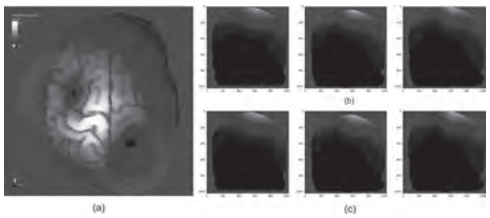

Figure 2: (a) Observed induced electric field (with TMS coil position) after TMS is applied to the primary motor cortex. (b) Reference electric fields. (c) Corresponding electric fields predicted with the trained network.

QOB-03. Core – Shell Magnetoelectric Nanoparticles as Wireless, Nanoscale Alternatives to Electrodes for Direct Neural Stimulation.
E. Zhang[1], M. Abdel-Mottaleb[2], Y. Akin[1], B. Navarrete[1], M. Alberteris[1], I. Smith[2], B. Yildirim[1], V. Andre[2], M. Shotbolt[2], P. Liang[3] and S. Khizroev[1]
1. Electrical and Computer Engineering, University of Miami, Coral Gables, FL, United States; 2. Biomedical Engineering, University of Miami, Coral Gables, FL, United States; 3. Cellular Nanomed, Irvine, CA, United States

Directly controlling firing in the brain via electrical stimulation has typically been in the domain of macro-scale, wired devices. This approach is a vital treatment pathway for Parkinson's, essential tremor, epilepsy, depression, and other neurological diseases[1]. As used in methods such as Deep Brain Stimulation (DBS), it provides a highly responsive way to modulate neuronal firing rates with a large degree of control. Despite the efficacy of DBS, it suffers from several known drawbacks, which stem from the requirement that stimulation electrodes be implanted in the brain. In addition to carrying the surgical risks of infection, stroke, and brain hemorrhage, the inflammatory response to the wires can degrade their performance over time[1]. Other attempts to stimulate neurons without relying on wires have faced issues from requiring gene modification[2], slow response times[2], or difficulty with spatial resolution[3]. Magnetoelectric nanoparticles (MENPs) offer a way to target specific regions of the brain with magnetic fields that do not otherwise interact with the body. These nanoscale approaches could target neurons by moving through the blood brain barrier, eliminating the need for extensive surgery. In this work, we demonstrate the ability to wirelessly modify the inherent firing frequency of neurons in vitro and in vivo in a controllable, rapid, and reversible manner using MENPs. These core-shell nanoparticles convert long range magnetic fields that can safely pass through tissue to short range electric fields that locally activate neurons, giving direct control over firing activity. This technology opens a possible approach to replacing Deep Brain Stimulation with nanoscale wireless devices, and a way forward to building a brain-machine interface.

1. Bronstein, J. M., Tagliati, M., Alterman, R. L., Lozano, A. M., Volkmann, J., Stefani, A., Horak, F. B., Okun, M. S., Foote, K. D., Krack, P., Pahwa, R., Henderson, J. M., Hariz, M. I., Bakay, R. A., Rezai, A., Marks, W. J., Moro, E., Vitek, J. L., Weaver, F. M., ... DeLong, M. R. (2011). Deep Brain Stimulation for Parkinson Disease. Archives of Neurology, 68(2). https://doi.org/10.1001/archneurol.2010.260 2. Chen, R., Romero, G., Christiansen, M. G., Mohr, A., & Anikeeva, P. (2015). Wireless magnetothermal deep brain stimulation. Science, 347(6229), 1477–1480. https://doi.org/10.1126/science.1261821 3. Mahoney, J. J., Hanlon, C. A., Marshalek, P. J., Rezai, A. R., & Krinke, L. (2020). Transcranial magnetic stimulation, deep brain stimulation, and other forms of neuromodulation for substance use disorders: Review of modalities and implications for treatment. Journal of the Neurological Sciences, 418, 117149. https://doi.org/10.1016/j.jns.2020.117149

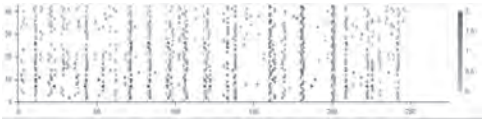

Fig. 1 Spike train plots of neurons stimulated by MENPs. First 5 vertical lines represent magnetic field based stimulation while last 3 vertical lines denote electrical stimulation.

QOB-04. Position Control Method of a Robotically Assisted Magnetic Navigation System to Improve the Pushability of a Magnetic Catheter by Maximizing Magnetic Force.
D. Lee[1], E. Jung[1], J. Kwon[1] and G. Jang[1]
1. Hanyang University, Seoul, The Republic of Korea

Magnetic catheter (MC) controlled by a magnetic navigation system (MNS) and a feeding device have been developed to overcome the steerability and the pushability of conventional catheters.[1,2] External magnetic field (EMF) produced from the MNS generates magnetic torque at the magnets in the MC to remotely steer the MC's distal end while the feeding device pushes the proximal end of the MC to move the MC forward.[3,4] Sometimes, it does not work effectively when buckling of a flexible catheter occurs in complex blood vessels. We propose a position control method (PCM) of the Robotically Assisted MAgnetic Navigation (RAMAN) system to improve the pushability of the MC by maximizing magnetic force (MF). Fig 1(a). shows the developed RAMAN system in which the 7-axis stage robot can move the 8 electromagnets (EMs) and the workspace surrounded by them. Fig 1(b). shows the MF in the region of interest (ROI) which is 80% of the workspace. The PCM takes advantage of the fact that the MF increases as the magnet moves close to the EM. When the MF generated at the MC is not sufficient, the PCM compares the MF of each vertex in the ROI and controls the 7-axis stage robot to move the ROI in such a way that the MC is located close to one of the EMs to generate maximum MF. Fig 2. shows calculated maximum MF at the center of the ROI and at the point selected by the PCM where an axially magnetized ring magnet (OD: 2 mm, ID: 1 mm, Length: 10 mm) of NdFeB 52 is located along θ and Φ directions. It shows that the PCM generates larger MF in any directions and 5 times larger MF on average than the maximum MF generated at the center. We performed a navigation experiment of the MC along the aorta to the right coronary artery in a cardiac vascular phantom model. We observed a buckling of the MC, and the maximum MF of 2.61 mN at the center did not overcome the buckling. We applied the PCM which generated the MF of 20.1 mN to release the buckling of the MC. The PCM may contribute to controlling of the MC for robotic endovascular intervention.

[1]B. J. Nelson, I. K. Kaliakatsos, and J. J. Abbott, Annual Review of Biomedical Engineering., Vol. 12, 55 (2010). [2]N. Kim, S. Lee, W. Lee, and G. Jang, AIP Advances, Vol. 8, 056708 (2018). [3]J. Nam, W. Lee, E. Jung, and G. Jang, IEEE Transactions on Industrial Electronics, Vol. 65, 5673 (2018).. [4]E. Jung, W. Lee, N. Kim, J. Kim, J. Park, and G. Jang, AIP Advances, Vol 9, 125230 (2019).

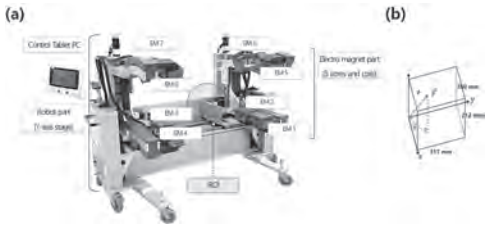

Fig. 1. (a) RAMAN system. (b) The direction of the MF in the ROI.

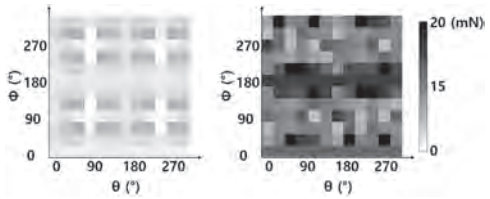

Fig. 2. Maximum MF at the center of the ROI and at the point selected by the PCM according to the direction of the MF.

QOB-05. Resonant Control Method to Suppress the Self and Mutual Inductances of a 3-phase Magnetic Navigation System for Fast Drilling Motion of Micro Helical Robots. *J. Kwon*[1], J. Sa[1], D. Lee[1] and G. Jang[1]
1. Hanyang University, Seoul, The Republic of Korea

Micro helical robots actuated by an external magnetic field have been investigated for a possible application to treat occlusive vascular disease. It requires a high-speed rotating magnetic field (RMF) which generates fast drilling motion of the micro helical robot to tunnel the clogged lesions in blood vessels.[1-3] The RMF is generated by the magnetic navigation systems (MNSs) composed of multiple coils or electromagnets. However, as the frequency increases, the impedance from the inductance of the coils decreases the current and the magnetic field. To overcome this problem, prior researchers utilized a resonance by including additional capacitance to their MNS.[2,3] The electromagnets with magnetic cores generate a large magnetic field.[4] Unlike the MNS with coils only, the MNS with electromagnets has significant mutual-inductance due to the magnetic flux linkages between electromagnets, but any resonance method suppressing the self and mutual inductances of the electromagnets of the MNS has not been reported. We propose a method to suppress both the self and mutual-inductance effect of the 3-phase MNS with multiple electromagnets. First, we set the imaginary part and the real parts except the resistance in the voltage equation to be zero to express the resonance. After solving the real part of the voltage equation and the actuation matrix equation which relates applied current with flux density together, we can determine 3-phase currents and corresponding phases at resonance. The capacitance at resonance can be determined by solving the imaginary part in the voltage equation. Fig. 1 shows the 3-phase MNS developed for the experiments and Fig. 2 shows the calculated and measured 3-phase currents and RMF with the application of the proposed method to generate a magnetic flux density of 10 mT. It shows that the calculated current matches well with the measured one within 5 % discrepancy. The proposed method in this research can contribute to improving the tunneling performance of micro helical robots by generating a high-speed RMF even in the MNS with the electromagnets.

[1]Q. Wang, X. Du, and L. Zhang, "Real-time ultrasound Doppler tracking and autonomous navigation of a miniature helical robot for accelerating thrombolysis in dynamic blood flow," *ACS Nano,* vol. 16, no. 1 (2022). [2]K. T. Nguyen, B. Kang and J. Park, "High-frequency and High-powered electromagnetic actuation system utilizing Two-stage resonant effects," *IEEE/ASME Transactions on Mechatronics*, vol. 25, no. 5 (2020). [3]J. Nam, W. Lee, and G. Jang, "Magnetic navigation system utilizing resonant effect to enhance magnetic field applied to magnetic robots," *IEEE Transactions on Industrial Electronics*, vol. 64, no. 6 (2017). [4]J. Nam, W. Lee, E. Jung, and G. Jang, "Magnetic navigation system utilizing a closed magnetic circuit to maximize magnetic field and a mapping method to precisely control magnetic field in real time," *IEEE Transactions on Industrial Electronics*, vol. 65, no. 7 (2018).

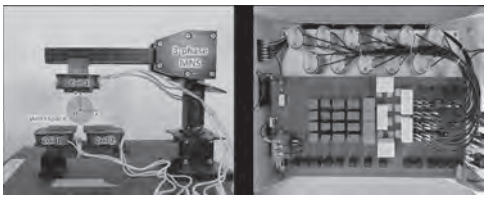

FIG. 1. (a) The 3-phase MNS. (b) The capacitor module.

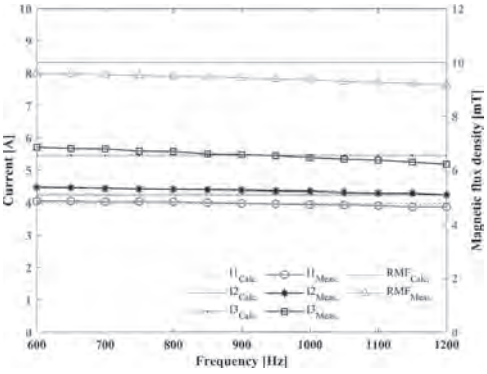

FIG. 2. The calculated and measured 3-phase currents and RMF.

QOB-06. Sawtooth Head Helical Magnetic Robots to Improve Drilling Performance for Robotic Endovascular Intervention. *J. Sa*[1], J. Kwon[1] and G. Jang[1] *1. Hanyang University, Seoul, The Republic of Korea*

Helical magnetic robots driven by an external magnetic field have been extensively studied for a possible robotic endovascular intervention to treat occlusive vascular disease. As shown in Fig. 1(a), most of previous researchers have utilized Cone-shaped head Helical Magnetic Robots (CHMRs) with helical blades for thrombus drilling.[1,2] Helical blades in a cone-shaped head of the CHMR generate additional propulsive force and allow the CHMR to move fast. However, in actual vascular conditions, the CHMR may damage the vessel or lose tracking by swimming too fast in the vessel. Also, the CHMR may be stuck in the thrombus, or the drilling performance may be significantly reduced after the cone-shape head enters the thrombus. We propose a Sawtooth head Helical Magnetic Robot (SHMR) as shown in Fig. 1(b) to improve the drilling performance. The helical blades in the body of the SHMR generates the propulsive force and the sawtooth head of the SHMR actually grinds the thrombus to reduce the possibility of the SHMR getting stuck in the thrombus. As shown in Fig. 2(a), the velocity of the SHMR according to pitch was investigated in the glass tube with a diameter of 5 mm filled with 40 % glycerol under the application of a rotating magnetic field of 1 mT. The SHMR with the pitch of a 10 mm has the greatest propulsive force. Furthermore, the drilling performance of the SHMR and the CHMR with the pitch of 10 mm were investigated in in vitro experiments of a 10 mm pseudo-blood clot and the magnetic field density of 5 mT and a rotating frequency of 155 Hz. The concentration ratio of agar was controlled to express different stiffness.[3] Fig. 2(b) shows that the SHMR has faster thrombus removal rate than the CHMR in three cases of different pseudo-blood clot, and that the SHMR is effective in drilling stiff thrombus. It may contribute to designing a magnetic robot for treating occlusive vascular disease.

[1] S. Lee, S. Lee and H. Choi, Scientific reports, vol. 8, p. 3691 (2018). [2] H. Lee and S. Jeon, AIP Advances, vol. 11, p. 025236 (2021). [3]Z. Yang, L. Yang and L. Zhang, IEEE/ASME Transactions on Mechatronics, to be published, doi: 10.1109/TMECH.2021.3121267 (2021).

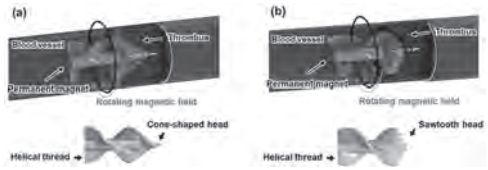

Fig.1 Structure of (a) the CHMR and (b) the SHMR.

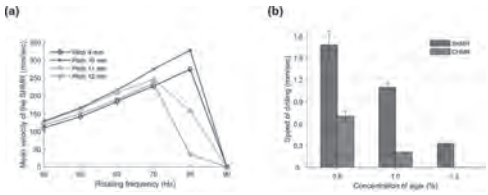

Fig.2 (a) Mean velocity of the SHMR(diameter: 4 mm, body length: 6 mm) with different pitches in a glass tube filled with 40 % glycerol. (b) Drilling speed of the SHMR and CHMR for pseudo-blood clot (10 mm) made of different concentration ratio of agar

QOB-07. On Locomotion of Magnetized Spherical Solids in Soft Media. *D.F. Volchonok*[1], J. Tur[1] and G. Friedman[1] *1. Electrical and Computer Engineering, Drexel University, Philadelphia, PA, United States*

Most research on remotely driven magnetic micro-robots focuses on their manipulation within fluids [1]. Actuating their motion in soft media and living tissue raises challenges along with new opportunities for minimally invasive medicine. In contrast to fluids, moving solids in soft media irreversibly rearranges the material, leading to highly non-linear and history dependent reaction forces. The present work demonstrates that this behavior enables solutions of certain long-standing problems. One problem stems from using magnetic field gradients to generate forces which limits their range particularly for sub-millimeter size magnetic robots. Locomotion by the transfer of energy via a time varying uniform magnetic field provides an alternative. In fluids where locomotion effectively occurs through swimming at low Reynolds numbers, this strategy can be costly, requiring more complex shapes (e.g. a screw [2]) and control over a non-reciprocal motion gait [3]. In tissues, such complex shapes have difficulties in changing their trajectory direction over short distances. The novel finding in this work is that soft media enables locomotion of simple solids, such as a pair of spheres (see Fig. 1), without requiring them to execute a complex motion gait. Using an external uniform magnetic field to change the relative orientations of the magnetic moments, the disconnected spherical solids of slightly different diameters can locomote as one in a soft medium via ratchet-like movements that are completely reciprocal. Such a configuration also allows the pair to change the direction of locomotion quickly. A demonstration is carried out in this work via development of a theoretical model and its numerical simulation, although some experimental observations support these findings.

[1] J. J. Abbott *et al.*, "How should microrobots swim?," *The international journal of Robotics Research,* vol. 28, no. 11-12, pp. 1434-1447, 2009. [2] T. W. Fountain, P. V. Kailat, and J. J. Abbott, "Wireless control of magnetic helical microrobots using a rotating-permanent-magnet manipulator," in *2010 IEEE International Conference on Robotics and Automation*, 2010: IEEE, pp. 576-581. [3] E. Lauga, "Life around the scallop theorem," *Soft Matter,* vol. 7, no. 7, pp. 3060-3065, 2011.

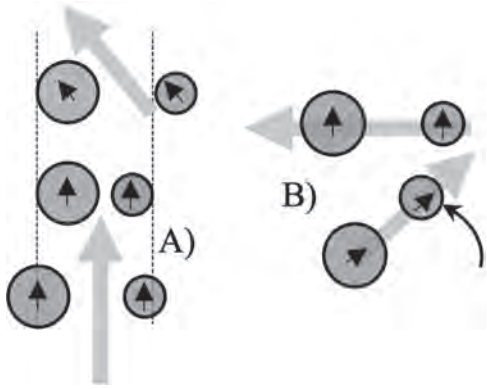

Fig. 1. A) Illustration of ratchet-like motion of magnetized spheres: in the first stoke large sphere sticks and smaller one slips. In the return stroke, both bots slip. B) Illustration of a bot trajectories during direction change.

QOB-08. Development of Magnetorheological Fluids within 3D Printed Elastomeric Cellular Structures with an Accumulator. *J. Park*[1], Y. Choi[1], A. Flatau[1] and N.M. Wereley[1] *1. University of Maryland, College park, MD, United States*

Magnetorheological fluids (MRFs) consist of micron-sized magnetic particles dispersed in a carrier fluid for which rheological properties can be tuned reversibly with magnetic field.[1] If an MRF is contained in a cellular elastomeric encapsulant (CEE), its mechanical properties, such as stiffness and damping, can be controlled via magnetic field. Such tunability can be exploited for adaptive vibration control or energy absorption systems. A magnetorheological damper often uses an accumulator to modulate pressure injected by external forces applied to the damper.[2] An accumulator is implemented into the cellular encapsulant to enable essentially incompressible fluid to enter the accumulator and to allow compression of the cellular material to take place, and also enables a mechanical bulge stiffness to the design. Here, MRF was prepared with silicon oil (40% vol. fraction). Thermoplastic polyurethane (TPU) was 3-D printed as the CEE system. (Fig. 1 a). The MRF was injected into the TPU-CEE, followed by the printing of a sealing layer. The wall adjacent to the sealing layer had a circular opening and a TPU membrane was bonded to its perimeter so that the pressurized MRF could flow through the opening and be accumulated in the resulting pocket. An external magnetic field (0 and 7 kG) was applied along the sample longitudinal axis at the time of uniaxial dynamic testing with 5% pre-strain. The TPU-CEE samples were characterized via force-displacement tests at 1 Hz under strain amplitudes. The MR effect on the dynamic stiffness is defined as the ratio of the dynamic stiffness under the maximum magnetic field to the dynamic stiffness in the absence of a magnetic field. Dynamic stiffness in the presence as opposed to the absence of magnetic field was 264%. (Fig.2a) The area of the force-displacement curve of the system with an accumulator is about 41% greater than one without an accumulator. The accumulator enhanced the increase in damping (Fig. 2b). The increase in damping capacity generally increased as strain amplitude increased.

1. Ashtiani M, Hashemabadi SH, Ghaffari A. A review on the magnetorheological fluid preparation and stabilization. *Journal of Magnetism and Magnetic Materials*. 374, 716. (2015) 2. Yu, Jianqiang & Dong, Xiaomin & Wang, Xuhong & Pan, Chengwang & Zhou, Yaqin. Asymmetric Dynamic Model of Temperature-Dependent Magnetorheological Damper and Application for Semi-active System. *Frontiers in Materials*. 6. 227. (2019)

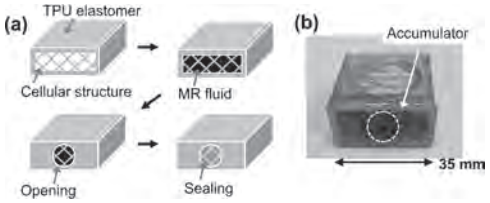

FIg. 1 (a) Schematic diagram of a TPU-CEE fabrication (b) Image of TPU-CEE device.

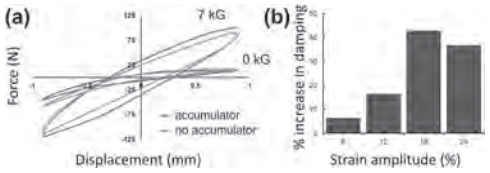

Fig.2 (a) Force-displacement curves of TPU-CEE samples (b) % increase in damping with strain amplitudes.

QOB-09. Sedimentation of Magnetorheological Fluids Measured Using a Automated Vertical Axis Inductance Monitoring System. R. Ma[2] and *N.M. Wereley*[1] *1. Aerospace Engineering, University of Maryland, College Park, MD, United States; 2. Jiangsu Normal University, Xuzhou City, China*

Magnetorheological fluids (MRFs) can change their viscosity in response to applied magnetic field. Magnetorheological energy absorbers (MREAs) are being investigated for adaptive shock isolation because MREAs can adjust their stroking load to severity of impact when magnetic field is used to control MRF viscosity. Employing MRFs in MREAs requires a highly stable suspension to maintain a uniform concentration, because MREAs would be used only in the event of an impact or crash event, that is, rarely. Suspension stability of MRFs can be studied using an automated vertical axis inductance monitoring system (AVAIMS), where an inductance sensor is translated vertically along a column of MRF to measure particle concentration as a function of column height and time [1,2]. The AVAIMS allows for tracking discontinuities in density or shocks including: the mud-line (boundary between the topmost supernatant (clear fluid) zone and the original concentration zone), the gel-line (boundary between the original concentration zone below mud-line and variable concentration zone), and the cake-line (boundary between the variable concentration zone and the sediment zone at the bottom of the column). MRF sedimentation can be evaluated comprehensively analyzing these boundaries. The AVAIMS developed here (Fig. 1) seeks to improve sedimentation zone boundary localization using an optimized inductance sensor to measure concentration gradient as a function of time. The inductance sensor design, material selection, and geometry were optimized and permalloy and plastic were used advantageously to improve sensor sensitivity. The calibration curve of the sensor was obtained by measuring samples with different particle volume fractions. The sensor design was validated by examining a uniformly mixed MRF column for seven consecutive days after preparation of an MRF with an Fe solids loading of 20 vol%. These tests show that the AVAIMS developed here was able to better localize sedimentation zone boundaries using concentration gradient profile method (Fig. 2).

J. Chambers, and N.M. Wereley (2016). "Vertical Axis Inductance Monitoring System to Measure Stratification in a Column of Magnetorheological Fluid." *IEEE Trans. on Magnetics*. 53(1):4600205. M. Wen, J. Chambers, S.G. Sherman, and N.M. Wereley (2019). "Monitoring sedimentation of magnetorheological fluids using a vertical axis monitoring system with a low aspect ratio sensor coil." *Smart Materials and Structures*. 28(2):025039.

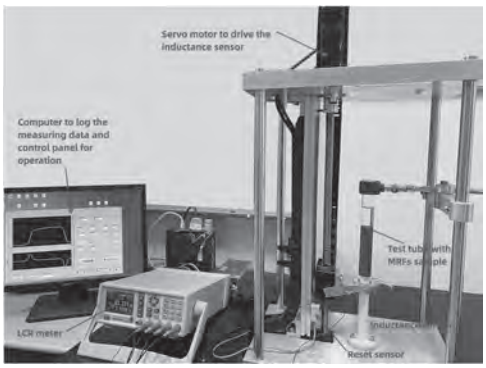

Fig. 1 AVAIMS used to measure particle concentration in an MRF column

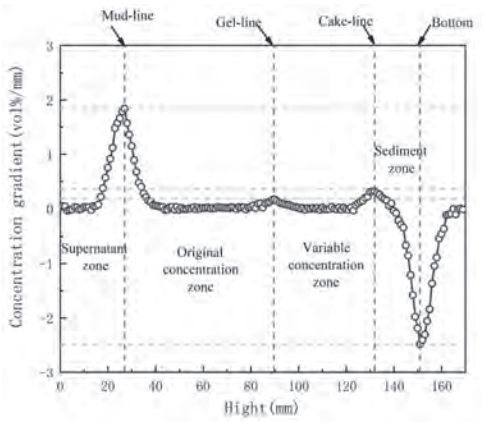

Fig. 2 Identified sedimentation zone boundaries for 20 vol% MRF

QOB-10. Rod mangle rotation patterns for magnetic field generation. *C.R. Fernandes*[1], J. Ventura[1] and D. Silva[1] *1. IFIMUP, Institute of physics for advanced materials, nanotechnology and photonics, Faculty of Science of the Porto University, Porto, Portugal*

The use of time-varying magnetic field sources is indispensable in numerous applications, such as magnetic resonance imaging, sensors, motors, actuators, magnetometers or magnetic refrigerators. Halbach cylinders have been used as an alternative to electromagnets, since they have no losses by the Joule effect. However, rod mangle systems are cheap and promising alternatives to the currently used Halbach cylinders [1-3]. The use of rotation patterns has potential for application in several innovative áreas [4]. In this work, we modeled rod mangle structures with different number of rods, aiming to control the magnitude, direction and homogeneity of the magnetic field. Figure 1 (a) shows the modeled system for 3 rods. After determining the configuration with the maximum magnetic flux density at the center of each system, it was possible to generate a homogeneous magnetic field. The homogeneity increases with the number of rods and for a large number of rods, the rod mangle structure begins to resemble an ideal Halbach. We also analyzed two different rotation patterns to generate a decreasing magnetic field over time. For the first pattern only the direction of the magnetic field of the odd configurations remained constant. For the second rotation pattern, after the magnetic field is reduced to zero, it starts to increase in the opposite direction and then decreases to zero again. If we rotate all rods counterclockwise, the magnetic field will rotate clockwise, keeping the magnitude fairly constant. Finally, we validated the results experimentally with structures of 3 and 4 rods (Fig 1 (b)).

[1] J. M. D. Coey, Permanent magnet applications, Journal of Magnetism and Magnetic Materials 248 (3) (2002) 441–456. [2] O. Cugat, P. Hansson, J. M. D.Coey, Permanent magnet variable flux sources, IEEE Transactions on Magnetics 30 (6) (1994) 4602–4604. [3] F. Hiptmair, Z. Major,

R. Haßlacher, S. Hild, Design and application of permanent magnet flux sources for mechanical testing of magnetoactive elastomers at variable field directions, Review of Scientific Instruments 86 (8) (2015) 085107. [4] H. Sakuma, T. Nakagawara, Optimization of rotation patterns of a mangle-type magnetic field source using covariance matrix adaptation evolution strategy, Journal of Magnetism and Magnetic Materials 527 (2021) 167752.

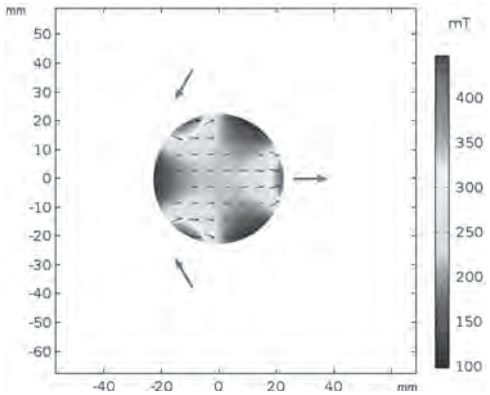

Fig. 1 (a) Magnetic flux density maps for 3 rod mangle structure.

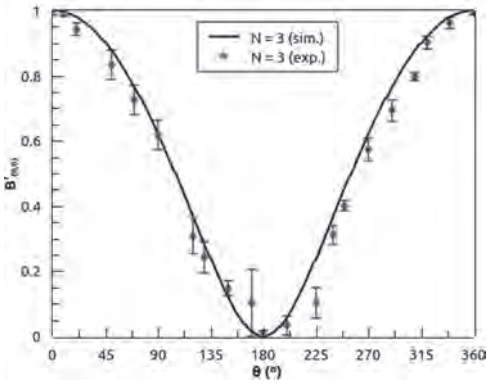

Fig. 2 (b) Experimental validation with the normalized results for the rotation of one rod.

Session QPA
APPLICATIONS OF MAGNETIC NANOPARTICLES IN BIOMEDICINE (Poster Session)

Eduardo De Lima Correa, Chair
National Institute of Standards and Technology, Gaithersburg, MD, United States

QPA-01. Estimating transcranial magnetic stimulus resolution using magnetic flux density. *T. Torii*[1,2], K. Tanabe[2], I. Toda[2], H. Sakamoto[3], A. Sato[1,2] and M. Iwahashi[3] *1. Department of Human Information Engineering, Tokai University, Kumamoto, Japan; 2. Department of Medical Care and Welfare Engineering, Tokai University, Kumamoto, Japan; 3. Department of Clinical Engineering, Komatsu University, Ishikawa, Japan*

Transcranial magnetic stimulation (TMS) is a noninvasive method of modulating cortical brain activity via electric currents induced by magnetic fields. Although TMS is often used to treat neurological disorders and analyze brain function, details regarding the distribution of magnetic energy after magnetic stimulation is unclear. Thus, the aim of the current study was to examine and characterize the energy distribution after delivering TMS to the cortex. To assess magnetic energy, we measured the magnetic flux density using a device comprising a probe and a simple electronic circuit (e.g., an integrator and a buffer amplifier). The primary probe consisted of a sensor coil, twisted pair line, and lead-out cable, while a second, similarly constructed probe without a sensor coil was used to measure background noise. Magnetic induction was initiated using a Rapid 2 stimulator with a figure-8 flat coil. TMS was applied to a human brain model using 10 consecutive pulses (pulse width = 320 μs, strength = 75%), and the distance from the scalp to the model cerebral cortex was assumed to be 15 mm. Magnetic flux density was measured at a depth of 15 mm directly below the magnetic stimulus coil, within a range of 40 mm on either side of a line that passed through the center of the long axis of the stimulation coil (the center line). Results showed that the highest magnetic flux density was found in the target region on the center line (approximately 240 mT at average), and TMS resolution was approximately 6 mm. Because average background noise was approximately 60 mT, magnetic flux density for the target cortex was estimated at 180 mT. Additionally, we found that magnetic flux density decreased steadily with distance on the center line (±5 mm: 178 mT ($p < 0.001$), ±20 mm: 120 mT ($p < 0.001$), ±40 mm: 0 mT ($p < 0.001$)). These results indicate that a simple magnetic flux density-measuring device can estimate the magnetic flux density within the cortex. These findings will be useful for setting appropriate stimulus intensities for TMS.

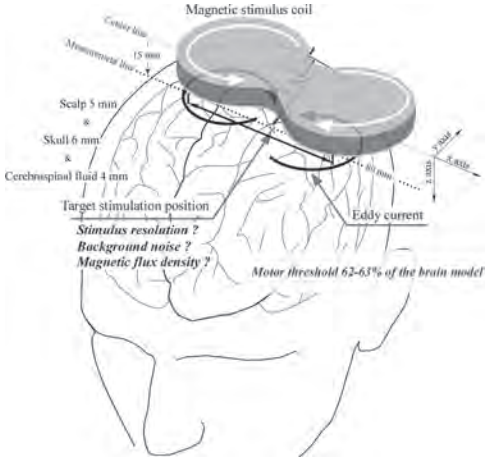

Fig. 1 Transcranial magnetic stimulation and human brain model.

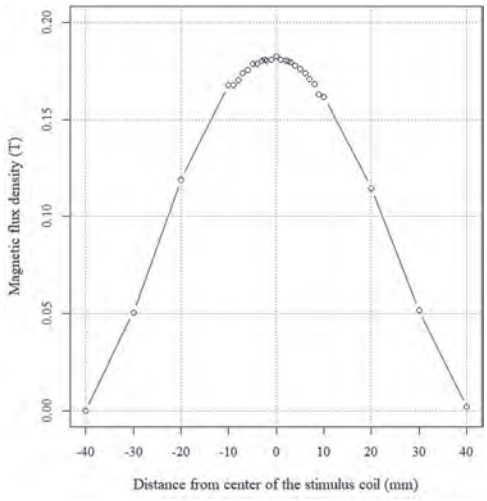

Fig. 2 After noise removal, magnetic flux density decreased with distance from the stimulus coil's center.

QPA-02. Relationship Between Resting Motor Threshold and Neuroanatomy in Mild to Moderate Traumatic Brain Injury Patients during Transcranial Magnetic Stimulation. *C.J. Lewis*[1], L.M. Franke[7,5], G.T. Gitchel[5,1], R.A. Perera[6], K.L. Holloway[4,5], W.C. Walker[7,5] and R.L. Hadimani[2,3] *1. Biomedical Engineering, Virginia Commonwealth University, Richmond, VA, United States; 2. Mechanical and Nuclear Engineering, Virginia Commonwealth University, Richmond, VA, United States; 3. Psychiatry, Harvard Medical School, Boston, MA, United States; 4. Neurosurgery, Virginia Commonwealth University, Richmond, VA, United States; 5. Hunter Holmes McGuire Verterans Affaris Medical Center, Richmond, VA, United States; 6. Biostatistics, Virginia Commonwealth University, Richmond, VA, United States; 7. Physical Medicine and Rehabilitation, Virginia Commonwealth University, Richmond, VA, United States*

Introduction: Transcranial Magnetic Stimulation (TMS) is a neuromodulation technique currently FDA approved to treat depression, migraine and obsessive-compulsive disorder (OCD). TMS outcomes are known to vary based on individual neuroanatomy, tractography derived structural connectivity, and functional connectivity which is not well understood [1,2]. There is a disconnection between what is measured empirically in resting motor threshold (RMT)/treatment outcomes, and computer simulated induced electric fields (E-Field) values based on Magnetic Resonance Imaging (MRI) derived head models. In this study, we aim to gain an understanding and explanation of this variability and offer an improvement by taking region of interest (ROI) specific gray matter (GMV) and white matter volume (WMV) over a previously published relationship between the brain scalp distance (BSD) and E-Field in the Transcranial Magnetic Stimulation (TMS). Experimental Details: Twenty-six mild-to-moderate traumatic brain injury (mTBI) patients were recruited as described in our previous publication [3]. Participants underwent MRI scans followed by guided repetitive TMS using a NextStim NBS4 figure-of-eight double coil. RMTs were taken as a percentage of the maximum stimulator output (%MSO). T1 weighted

MRI images went through SimNIBS pipeline (v3.2.6) to create anatomically accurate head models for each patient. Head models were imported into Meshmixer (v3.5) where BSD and individual segment volume were taken from the precentral gyrus (knob) as described in [4]. Results: Preliminary analysis indicates a weak but negative correlation between both GMV ($R^2 = 0.0307$, $p = 0.392$) and WMV ($R^2 = 0.0388$, $p = 0.335$) versus RMT. And a stronger positive correlation between BSD ($R^2 = 0.29$, $p = 0.0046$) and RMT. Conclusion: Segmented ROI brain volume didn't improve the correlation between RMT and 3D brain-scalp volume compared to RMT and 1D brain-scalp distance. Further investigations into E-Field and correlating empirically collected patient outcomes will enable better TMS dosages as a percentage of patient specific RMT for TMS procedures.

[1] T. Herbsman, L. Forster, C. Molnar, et al., Human Brain Mapping., 30(7), 2044-2055 (2009). Motor threshold in transcranial magnetic stimulation: the impact of white matter fiber orientation and skull-to-cortex distance. [2] N. Mittal, B. Thakkar, C. B. Hodges, C. Lewis, Y. Cho, R. L. Hadimani, & C. L. Peterson, Human Brain Mapping, 1-16 (2022). Effect of neuroanatomy on corticomotor excitability during and after transcranial magnetic stimulation and intermittent theta burst stimulation. [3] L. M. Franke, G. T. Gitchel, R. A. Perera, R. L. Hadimani, K. L. Holloway & W. C. Walker, Brain Injurty, 36:5, p. 683-692, (2022) Randomized trial of rTMS in traumatic brain injury: improved subjective neurobehavioral symptoms and increases in EEG delta activity. [4] T. A. Yousry, U. D. Schmid, H. Alkadhi, D. Schmidt, A. Peraud, A. Buettner, P. Winkler, Brain, Vol. 120, p.141-157 (1997) Localization of the motor hand area to a knob on the precentral gyrus. A new landmark.

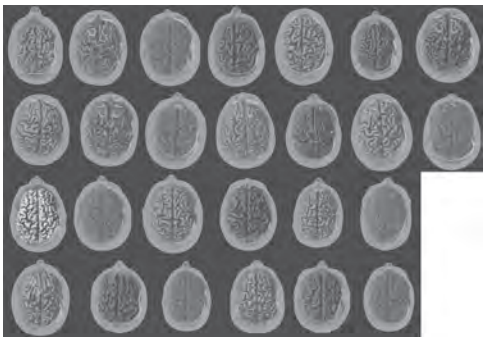

Fig 1. Head Models from 26 mTBI Patients Imported to Meshmixer.

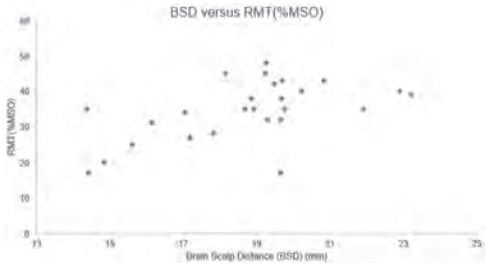

Fig 2. Brain Scalp Distance vs Resting Motor Threshold (%MSO)

QPA-03. Development of Novel Transcranial Magnetic Stimulation Technique Using High-frequency Modulation for Treatment of Parkinson's Disease. *I.C. Carmona-Tortolero*[1], D. Kumbhare[2,4], G. Weistroffer[2,3] and M. Baron[2,5] *1. Dept. of Mechanical and Nuclear Engineering, VIrginia Commonwealth University, Richmond, VA, United States; 2. McGuire Research Institute, Hunter Holmes McGuire VA Medical Center, Richmond, VA, United States; 3. Dept. of Biomedical Engineering, Virginia Commonwealth University, Richmond, VA, United States; 4. Dept. of Neurosurgery, Louisiana State University Health Science, Shreveport, Shreveport, LA, United States; 5. Dept. of Neurology, Virginia Commonwealth University, Richmond, VA, United States*

Lowering the power requirements of transcranial magnetic stimulation (TMS) would allow reducing the size and form factor of the stimulating coils, increasing the focality and penetration depth during the stimulation. Commercial TMS equipment typically uses frequencies from 1 to 5 kHz, while the coil currents vary from 1 to 5 kA. According to the Maxwell-Faraday equation, a large –dB/dt is required in the coil to induce an E-field above a stimulation threshold around 100 V/m at the target (Fig 1). Therefore, the development of technologies able to obtain similar E-field strength with lower currents is required. This work shows the design, construction, and tests of a novel high-frequency TM stimulator. For the first time to our knowledge, we have used analog modulations (AM/DSB-SC) over a carrier of 25 kHz to obtain a –dB/dt 10 times larger than the commercial stimulators. This permitted the reduction of the TMS currents in the same ratio, with a stimulation tone of 1.5 kHz over the carrier. The modulation shifts the stimulating energy out of the TMS band and audible range, leading to soundless operation compared to the uncomfortable clicking sound in current TMS equipment. Our results demonstrated: a reduction of currents to reach the referential E-field threshold of 100 V/m; a decrease of power dissipation in coils with possibility of unrestricted repetitive TMS (rTMS); a reduction in the coil sizes with increased focality and penetration depth; and hardware requirement reduction. Experimental work with rodents is in progress to demonstrate that, although the modulated signal will not stimulate neurons directly at such high frequency (due to the low-frequency response of the cell membrane), the demodulated version of it, obtained within the brain tissue with the superposition of a non-modulated carrier, can effectively recover the low-frequency envelope, stimulate neurons and induce motor evoked potentials (MEPs) (Fig. 1 and 2).

[1] N. Grossman *et al.*, "Noninvasive Deep Brain Stimulation via Temporally Interfering Electric Fields," *Cell*, vol. 169, no. 6, pp. 1029-1041. e16, 2017, doi: 10.1016/j.cell.2017.05.024. [2] C. Wang *et al.*, "Magnetically Induced Temporal Interference for Focal and Deep-Brain Stimulation," *Front. Hum. Neurosci. | www.frontiersin.org*, vol. 15, p. 693207, 2021, doi: 10.3389/fnhum.2021.693207. [3] G. Zarubin, C. Gundlach, V. Nikulin, A. Villringer, and M. Bogdan, "Transient Amplitude Modulation of Alpha-Band Oscillations by Short-Time Intermittent Closed-Loop tACS," *Front. Hum. Neurosci.*, vol. 14, p. 366, Sep. 2020, doi: 10.3389/FNHUM.2020.00366/BIBTEX. [4] L. J. Gomez, S. M. Goetz, and A. V Peterchev, "Design of transcranial magnetic stimulation coils with optimal trade-off between depth, focality, and energy," *J. Neural Eng*, vol. 15, pp. 46033–46047, 2018, doi: 10.1088/1741-2552/aac967.

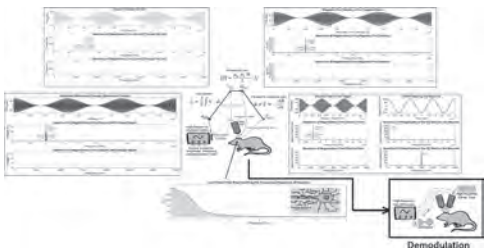

Fig. 1 Signal diagram of the modulated TMS pulses and demodulation process.

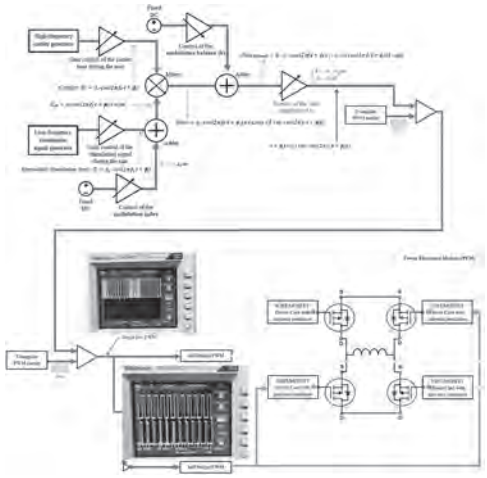

Fig. 2 – Generation of the modulated TMS pulses over AM/DBS-SC with PWM.

QPA-04. Temporal Interference for Increased Focality of Transcranial Magnetic Stimulation. *J. Boldrey*[1], Z. Higgs[1] and D. Jiles[1] *1. Electrical and Computer Engineering, Iowa State University, Ames, IA, United States*

Transcranial Magnetic Stimulation (TMS) coils are usually specialized for use in either deep brain or focal stimulation. One of the challenges in the development of TMS therapy is the ability to deliver a focused magnetic field to the desires target in the brain. In the process of delivering a sufficiently strong H field to the target, surrounding areas of the brain can be stimulated unnecessarily. A new technique is used here whereby deep and focal stimulation can be achieved using temporal interference (TI). TI is a method that allows for control of steerability, focality, and depth of penetration. TI uses the frequency difference of two independent electric fields [1]. The TI stimulation frequencies in at 10kHz and is filtered by the brain's inherent lowpass [2] behavior [3]. The frequency difference between the two induced electric fields results in an envelope which allows improved focality of stimulation. By using a coil assembly as shown in Figure 1, and using TI, the focality of the peak induced electric can be increased with respect to the surrounding area as shown inf Figure 2.. This focal point can also be steered along the centerline between the two coils. Our current work involves using Sim4Life software on 50 unique head models derived from magnetic resonance imaging (MRI) scans. We are investigating the focality of the induced electric field using our coil design with TI signals. The results will be compared with the commonly used figure-of-eight TMS coil and the novel design Quadruple Butterfly Coil (QBC) [4].

[1] M. Zaeimbashi, A. Khalifa, C. Dong, Y. Wei, S. Cash, and N. Sun, "Magnetic Temporal Interference For Noninvasive, High-resolution, and Localized Deep Brain Stimulation: Concept Validation," 2020. [2] B. Hutcheon and Y. Yarom, "Resonance, oscillation and the intrinsic frequency preferences of neurons," Trends in Neurosciences, vol. 23, no. 5, pp. 216–222, 2000. [3] M. M. Sorkhabi, K. Wendt, and T. Denison, "Temporally Interfering TMS: Focal and Dynamic Stimulation Location," 2020 42nd Annual International Conference of the IEEE Engineering in Medicine & Biology Society (EMBC), 2020. [4] P. Rastogi, "Novel coil designs for different neurological disorders in transcranial magnetic stimulation," PhD Thesis, Iowa State University, Ames, IA, USA, 2019. Available: https://lib.dr.iastate.edu/etd/17547 Brain Mapping, vol. 29, no. 1, pp. 82–96, 2007.

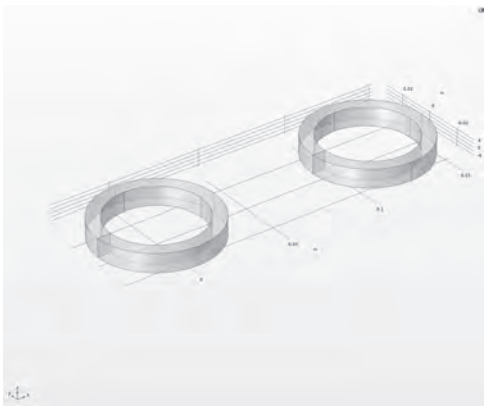

Figure 1. Temporal Interference TMS coil design.

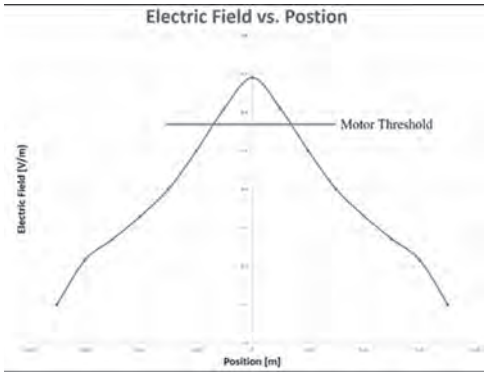

Figure 2. Electric Field at 1 kHz frequency with a 100 Hz envelope.

QPA-05. Transient phosphene perceptions caused by changes in DC magnetic field: Qualities of its simplicity and reproducibility. *H. Nakagawa*[1] and S. Ueno[2] *1. Tokyo Denki University, Tokyo, Japan; 2. Kyushu University, Fukuoka, Japan*

Our previous reports using extremely low frequency (ELF) magnetic stimuli provided new findings concerning the duration of complementary colors after the stimuli [1]–[6]. These findings are expected to bring about important knowledge for the development of support machines for the handicapped with lost visual functions. As a new attempt, we considered examining magnetic effects of phosphenes like blindsight induced by changes in the DC fields as part of therapeutic eyesight exercises. We prepared a prototype of a DC power source equipped with a changeover-switch for switching the direction of electric current through the coil. This system mainly consists of a main switch (Nikkai, S-301), a diode bridge (Vishay, GBPC2508), a toggle switch (Nikkai, S-822), and four electrolytic condensers (Nippon Chemi-Con, 250V, 220uF). Magnetic stimuli were carried out in a place about 30 mm from the center of each subject's left eyeball. Phosphene perceptions were generated by changes in the DC field, the moment the power switch was simply turned on or off. The thresholds of the phosphene in the turning-on and -off moments in darkness were both approximately 14.5 mT in each, on average. On the other hand, the results obtained with reversing the direction of the DC field for the phosphene could be regarded as significant compared to the experiment described above. The threshold in reversing directions of the magnetic fields of up to 60 mT at the tip of the coil varied widely depending on the phosphene appearance. Particularly, there were a few distinct patterns that appeared in each subject's visual field. We strongly suggest that the use of momentary phosphenes like blindsight induced by changes in a DC field is an excellent candidate for a clinical test for lost visual functions, because of the qualities of its simplicity and reproducibility. In addition, it is perfectly painless.

1) H. Nakagawa and S. Ueno, IEEE Trans. Magn. 50, 5000904 (2014). 2) H. Nakagawa and S. Ueno, IEEE Trans. Magn. 50, 5000804 (2014). 3) H.

Nakagawa and S. Ueno, J. Appl. Phys. 117, 17B315 (2015). 4) H. Nakagawa and S. Ueno, IEEE Trans. Magn., 51, 5000604 (2015). 5) H. Nakagawa and S. Ueno, IEEE Trans. Magn. 53, 5000604 (2017). 6) H. Nakagawa and S. Ueno, AIP Advances 9, 035216 (2019).

QPA-06. *In vivo* Micromagnetic Stimulation of the Rat Sciatic Nerve.

R. Saha[2], Z. Sanger[1], R. Bloom[2], O. Benally[2], K. Wu[2], D. Tonini[2], W. Low[3], S. Keirstead[4,5], T. Netoff[1] and J. Wang[2] *1. Biomedical Engineering, University of Minnesota, Twin Cities, Minneapolis, MN, United States; 2. Electrical & Computer Engineering, University of Minnesota, Twin Cities, Minneapolis, MN, United States; 3. Neurosurgery, University of Minnesota, Twin Cities, Minneapolis, MN, United States; 4. Stem Cell Institute, University of Minnesota, Twin Cities, Minneapolis, MN, United States; 5. Integrative Biology and Physiology, University of Minnesota, Twin Cities, Minneapolis, MN, United States*

In this *in vivo* study, we have used Magnetic Pen or MagPen (see Fig. 1(a)) to stimulate the rat sciatic nerve which led to the report of the dosage response curve for micromagnetic stimulation (μMS). As reported earlier [1], the MagPen prototype consists of sub-mm size microcoil (μcoil) at its tip (see Fig. 1(b)). When driven by alternating current, this μcoil generates a time-varying magnetic field, which induces an electric field on any conductor (here, the sciatic nerve) according to Faraday's Law of electromagnetic induction. This induced electric field activates the nerve. This work reports how the directionality of the magnetic μcoil plays a direct role in activating nerves directly observed in hind limb muscle twitches. These limb twitches have been quantitatively characterized using electromyography (EMG) recordings. Furthermore, we have studied how on varying the amplitude and frequency of the micromagnetic stimuli, alters hind limb muscle movements. Thereby, a dosage response curve for μMS was generated. The highlight of this dosage response curve is that, at higher frequencies, significantly smaller amplitudes of MagPen stimuli can trigger limb twitches. This frequency-dependent nerve activation can be explained directly from Faraday's Law as the magnitude of the induced electric field used in neuromodulation is proportional to frequency. In our previous work of *in vitro* μMS of rat hippocampal slices [1], we explained the frequency-dependent, low-power activation of μMS through numerical simulations. This work further corroborates the same concept through experiments. Implantable μMS is a novel neuromodulation technique which is still in its infancy and aims to address the potential drawbacks of electrical implants in terms of MRI compatibility and biofouling. Since the induced electric fields from these magnetic μcoils are not in galvanic contact with the nerve, μMS offers flexibility in applying waveforms to drive these magnetic implants (see Fig. 1(c)). Fig 1. (a) Different directionalities of the MagPen prototype. Only Type V can activate the sciatic nerve. (b) Size of the sub-mm size μcoil implant compared to a rice grain. (c) The waveform that activated the nerve.

[1] Saha R., Faramarji S *et al.* (2022) Strength-frequency curve for micromagnetic neurostimulation (μMS) through EPSPs and numerical modeling. *J. Neural Eng. 19 016018.*

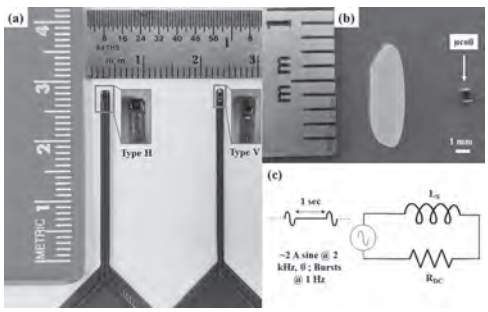

Figure 1

QPA-07. Effect of pulsed magnetic field in murine T lymphoma EL4 cells.

B. Lee[1], J. Jung[1], S. Kim[1] and H. Lee[1] *1. Sangji University, Wonju, The Republic of Korea*

Maintenance of homoeostasis in human body is a very important indicator in all cell activities. Persistent acid-base imbalance leads to diseases such as metabolic and respiratory acidosis or alkalosis. When exposed to a disease, various immune cells are activated due to the inflammatory response, and particularly T cells play a role in inducing apoptosis of mutated cells such as tumor cells. When the activity of T cells is very low, infection by external invasion is easy, and on the contrary, excessive activation lead to chronic inflammation caused by autoimmune diseases. Many clinical studies related to pulsed magnetic field (PMF) demonstrated its efficacy in reducing pain, improving blood circulation, as well as blood's acid-base balance.[1-2] Therefore, our study has tried to investigate the influence of PMF on the regulation of acid-base homeostasis in EL4 cells, which are T cells formed through lymphoma generated by inducing 9,10-dimethyl-1,2-benzanthrance to C57BL mice. In addition, we tried to explain the role of PMF on immune cell activity by measuring the level of pro-inflammatory cytokines such as TNF-α and INF-γ in culture supernatants. EL4 cells were cultured in a DMEM medium supplemented with 10% FBS and 1% penicillin at a concentration of 5.5×10^4 cells/ml in an incubator at 37 °C and 5% CO_2 condition. Our PMF stimulator has the maximum intensity of 4700G at a transition time of 222 μs with pulse intervals of 1Hz. The homoeostasis in pH was improved as the intensity of PMF increases.(Fig.1) Cell viability decreased by 32% after PMF stimulus of 4700G. It was observed that the concentration of TNF-α and INF-γ, a cytokine related to inflammation, also decreased as the strength of PMF increased. These results suggest that PMF stimulus improves the anti-inflammatory effect, therefore, it is thought to affect the immune system of the human body by balancing the activation and suppression of immune cells. For clinical use, our study might suggest non-invasive PMF can be developed as a medical devices modulating immune system, although it is necessary to optimize the PMF conditions such as pulse shape, duration, or repetition rate.

[1] N. M. Shupak, F. S. Prato & A. W. Thomas, Neurosci. Lett. Vol. 363, p.157–162(2004). [2] S. Bang & H. Lee, AIP Advances, 11(1), 015242(2021).

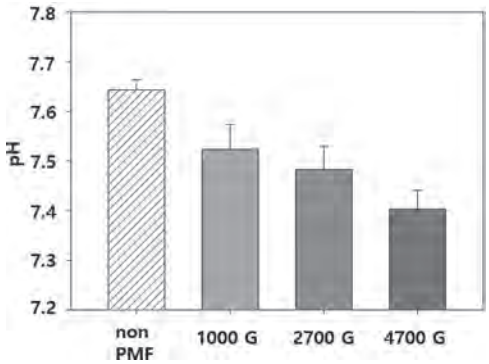

Fig. 1 The change of pH vs. PMF strength

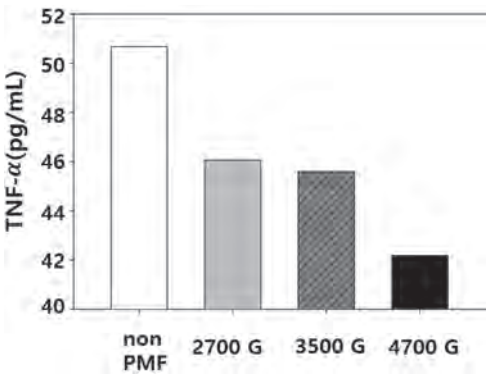

Fig. 2 Change in TNF-α level vs. PMF strength

QPA-08. Cancer cell destruction by magneto-mechanical actuation of nanowires compared with nano/micromagnetic particles. H. Chiriac[1], A.E. Minuti[1,2] and *N. Lupu*[1] *1. National Institute of Research and Development for Technical Phisics, Iasi, Romania; 2. Faculty of Physics, Alexandru Ioan Cuza University, Iasi, Romania*

The use of magnetic nanoparticles for cancer cell destruction is widely known due to their applications such as magnetic hyperthermia and magneto mechanical actuation (MMA). Previously, we presented our results regarding a new type of magnetic particles (MPs), i.e. Fe-Cr-Nb-B MPs, prepared by wet milling of superferromagnetic precursor glassy ribbons, designed for cancer treatment by MMA [1]. These MPs have an important shape anisotropy and a large saturation magnetization, which generates an improved torque in a rotating magnetic field, producing important damages on the cellular viability of cancer cells. Inspired by these findings, we tested the possibility of using magnetic nanowires (NWs) that have a higher shape anisotropy. Furthermore, the Fe-Co alloy that we propose has high saturation magnetization values. We prepared $Fe_{64.5}Co_{35.5}$ NWs with lengths of 4 microns by electrolytic deposition in alumina membranes with a pore diameter of 200 nm. The Fe-Cr-Nb-B MPs and Fe-Co nanowires were tested on human osteosarcoma cells (HOS) using various concentrations of particles and found that both are biocompatible *in vitro*. Subsequently, we studied the effect of MMA in a rotating 80 Oe magnetic field and frequency of 2 Hz on the viability of HOS. We used MPs and NW with different concentrations, and exposure time of 30 minutes, applied 24 hours after the introduction of the MPs and NWs into cell culture media. The results indicated that with a concentration of 1 mg/ml of MPs and 0.1 mg/ml of NWs, respectively, the cell viability decreased to about 6-7%. The concentration of NWs needed to induce cancer cell death is 10 times lower than the one needed for MPs. It is worth mentioning that although NWs are more efficient when using low quantities, due to their higher magnetization and anisotropy, the magnetic nanoparticles are better internalized and metabolized by cells. Therefore, MPs can be better targeted in tissues harder to reach than NWs. The latter are also harder to control, being more suitable for superficially-developed cancer tissues. Supported by (UEFISCDI) Contract no. PCE20/2021 (PN-III-P4-ID-PCE-2020-2381).

1. H. Chiriac et al. Sci. Rep., 8.11538 (2018)

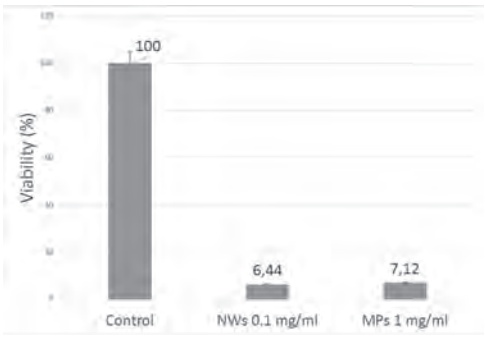

Fig. 1. Cell viability of HOS after magneto mechanical actuation

QPA-09. Thermo-responsive copolymer coated magnetic liposomes for hyperthermia therapy and controlled drug delivery. *S.A. Shah*[1] *1. Forman Christian College (University) Lahore, Lahore, Pakistan*

This study is about multifunctional magnetic nanoparticles and liposomes surface-modified with bilayer oleic acid, and coated with a thermo-responsive copolymer poly(N-isopropylacrylamide-co-acrylamide) by emulsion polymerization, for controlled drug delivery and magnetic hyperthermia applications. Nanoparticles were loaded with anticancer drug doxorubicin into the copolymer chains at 25C. Composite nanoparticles (hydrated) of average diameter 45 nm were of core-shell structure having magnetic core of about 18 nm and shell was composed of organic compounds and water. Magnetic core was superparamagnetic lacking coercive force and remanance due to the pseudo-single domain nanostructure. Lower critical solution temperature (LCST) of the thermo-responsive copolymer was observed to be around 39C. Below this temperature, copolymer was hydrophilic, hydrated and swelled. But above LCST, copolymer became hydrophobic, dehydrated and shrank in volume. UV visible spectrophotometer was used to investigate the drug loading and releasing profile at different temperatures as well as under magnetic heating. There was almost absence of drug release at around 37C (normal body temperature). Drug was released at temperatures above LCST, which is significant for controlled drug delivery. Magnetic heat-generation was studied by exposing the magnetic fluid to alternating magnetic field of 7.2 kA m-1 having frequency 70 kHz. A simple magnetic capturing system (simulating a blood vessel) was used to analyze the capturing of magnetic nanoparticles under various applied fields for drug targeting purpose.

[1] S.A. Shah, M.U. Hashmi, S. Alam, A. Shamim, Mater. Sci. Eng. C 3 (2011) 1010. [2] S.A. Shah, M.U. Hashmi, S. Alam, A. Shamim, J. Magn. Magn. Mater. 322 (2010) 375. [3] S.A. Shah, M.U. Hashmi, S. Alam, A. Shamim, Appl. Phys. A : Mater. Sci. Process 100 (2010) 273e280.

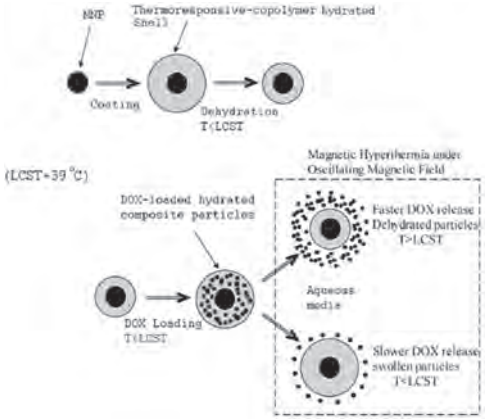

Fig. 1. Schematic overview of the processes involved in this study.

QPA-10. Magneto- luminescent ferrite-lanthanide complex core-shell nanocomposite as efficient bioimaging and cancer therapy platform.
R. Meena[1], A. Chauhan[2], A. Das[1] and B.K. Kuanr[1] *1. Special Centre for Nanoscience, Jawaharlal Nehru University, New Delhi, India; 2. Institute of Nanoscience and Technology, Mohali, India*

Cancer has been major health problem for world since long time. Superparamagnetic nanoparticles are very useful in magnetic hyperthermia due to its heating efficiency under magnetic field. We have designed novel magneto luminescent nanocomposites of $EuMnFe_2O_4$ for radio-frequency hyperthermia therapy [1]. An oxidative hydrolysis synthesis route was followed for $EuMnFe_2O_4$ magnetic nanocomposites [2]. For luminescence property outer shell of manganese ferrite was coated with europium chelate which is further coated by silica coating. Colloidal stability of this nanocomposites is good in solvent so due to this high SAR value of 312 W/gm (at 0.5 mg/ml) and corresponding intrinsic loss power (ILP) value of 4.01 nHm^2kg^{-1} was achieved. The synthesized nanocomposites depict good colloidal stability and low cytotoxicity *in vitro*. *In vitro* cytotoxicity studies (MTT assay) on C6 cell line depicts approximately 70% cell viability at 200 μg/ml of $EuMnFe_2O_4$ nanocomposites, a comparable concentration for clinical use by FDA standard. We also demonstrate the magnetic hyperthermia on C6 cell line and cell death (Figure 1) has been observed at 44 °C for 30 minutes under alternating magnetic field (AMF) exposure [3]. In this nanocomposites coating of europium chelate is very useful for bioimaging purpose as shown in Figure 2 by confocal microscopy. It is further verified by magnetic resonance imaging (MRI) [4]. For clinical trial purpose magnetic hyperthermia should be minimal side effects on patient so that we could achieve better cure for cancer. In this way these kind of developed nanocomposites have potential in the efficient treatment of cancer at clinical level.

[1] Bettaieb, A.; K, P.; A, D. Hyperthermia: Cancer Treatment and Beyond. In Cancer Treatment - Conventional and Innovative Approaches; Rangel, L., Ed.; InTech, 2013. [2] Hui, C.; Shen, C.; Yang, T.; Bao, L.; Tian, J.; Ding, H.; Li, C.; Gao, H.-J. Large-Scale Fe_3O_4 Nanoparticles Soluble in Water Synthesized by a Facile Method. J. Phys. Chem. C 2008, 112, 11336–11339. [3] Mohapatra, J.; Xing, M.; Liu, J. P. Inductive Thermal Effect of Ferrite Magnetic Nanoparticles. Materials 2019, 12, 3208. [4] Reisch, A.; Klymchenko, A. S. Fluorescent Polymer Nanoparticles Based on Dyes: Seeking Brighter Tools for Bioimaging. Small 2016, 12, 1968–1992.

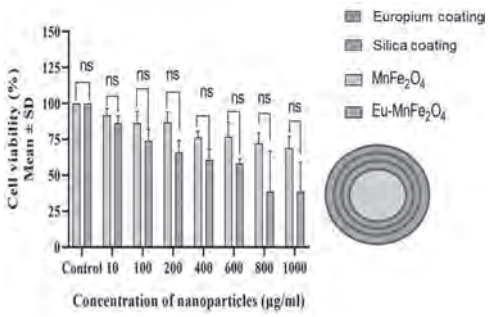

Fig. 1 Cytotoxicity assay (MTT assay) of $EuMnFe_2O_4$

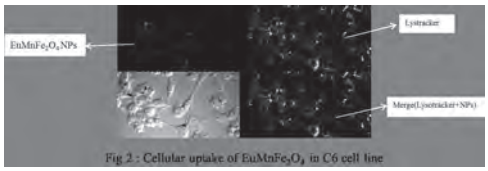

Fig. 2 Cellular uptake of $EuMnFe_2O_4$ in C6 cell line

QPA-11. Biocompatible Superparamagnetic $NiFe_2O_4$ Nanoparticles for Magnetic Hyperthermia Treatment using a ZVS Circuit. *T. Moriwaki*[1], K. Ohara[2], K. Nakazawa[1], T. Sakamoto[2], K. Nii[2], M. Abe[3] and Y. Ichiyanagi[2]
1. Natural Environment, Yokohama National University, Yokohama, Japan; 2. Physics, Yokohama National University, Yokohama, Japan; 3. Graduate School of Eng. Sci., Osaka University, Toyonaka, Japan

Nanosized magnetic materials form a single domain and, as a result, magnetic nanoparticles (MNPs) usually lose their ferromagnetic properties. However, superparamagnetic NPs can generate sufficient heat to kill cancer cells under a weak magnetic field. In this study, $NiFe_2O_4$ NPs with particle sizes of 3–17 nm were prepared for application in magnetic hyperthermia treatment (MHT), and their biocompatibility was improved by modification with polyethylene glycol (PEG). PEG is hydrophilic and is often used in the medical field. Direct current (DC) magnetization measurements showed that all the samples exhibited no hysteresis or superparamagnetic behavior at 300 K. The temperature dependence of the alternating current (AC) magnetic susceptibilities revealed that the peak temperature of the imaginary part of AC magnetic susceptibilities (χ'') varied significantly with particle size, and the 17 nm sample had a peak at approximately 310 K. It is known that χ'' contributes significantly to heat generation owing to magnetic relaxation losses. The temperature increase of the samples under an AC magnetic field (f = 15 kHz, h = 150 Oe) was measured. The sample with 17 nm particles showed a significant heating effect compared to the other samples, reaching over 42.5 °C, which is sufficient to suppress cancer cells. Human breast cancer cells (MDA-MB-231) were cultured on a petri dish, and PEG-coated $NiFe_2O_4$ NPs were added. The sample was heated using an AC magnetic field. Approximately 30% of cancer cells were successfully killed, and the magnetic hyperthermia effect was confirmed (Fig.1). To evaluate the toxicity of PEG-coated magnetic NPs toward cancer cells, cell viability was observed for 24 h after the particles were dispersed in the culture dishes. PEG-coated $NiFe_2O_4$ NPs successfully improved biocompatibility. Thus, $NiFe_2O_4$ NPs are expected to be useful agents for MHT. By using a zero-voltage switching (ZVS) circuit and generating an AC magnetic field from a DC power source, a temperature rise two to eight times higher than that using conventional coils was achieved (Fig.2).

P. Das, M. Colombo, D. Prosperi, Coll. Surf. B 174, 42 (2019)

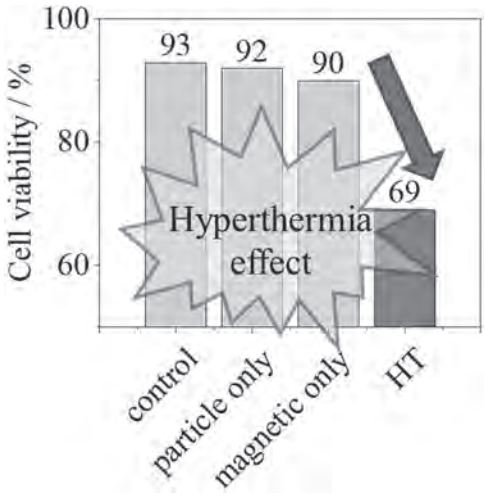

Fig. 1. Cell viability of human breast cancer cells (MDA-MB-231).

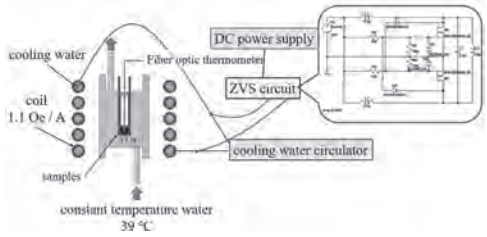

Fig. 2. Tempature rise measurement system using ZVS circuit.

QPA-12. Proposal of a Transmitting and Receiving Coil Configuration Focusing on Contactless Power Supply to Biometric Information Acquisition Devices for Small Experimental Animals. *T. Omori*[1], F. Sato[1], F. Yoshiki[2] and S. Sasaki[2] *1. Tohoku-gakuin university, Tagajo, Japan; 2. Hikaridenshi Co., Ltd., Osaki, Japan*

In the field of drug discovery and medical technology development, investigation of actions and side effects using experimental animals is essential. The details of that investigation are recording changes in the biometric information of experimental animals that occur during the course of the experiment, and this information is used to discuss the effects of the drug or technology on the animals. There are a wide variety of devices used to acquire biometric information, but in recent years, the most commonly employed devices are those implanted in the body. This is because they can accurately and continuously acquire biometric information such as body temperature, heart rate, activity level, and blood pressure. However, there are also issues related to the power supply to the device. Currently, the mainstream method is to supply power from a battery embedded with the biometric information acquisition device. Although this method can provide a stable power supply wirelessly, it has the disadvantage of not having sufficient capacity for experiments. As a result, it is difficult to meet the greatest requirement in experimental animal experiments, which is to monitor biometric information in real time. To solve this problem, a system is constructed in which power is constantly supplied to the biometric acquisition device by electromagnetic induction between the receiving coil inside the body of the experimental animal and the transmitting coil placed under the floor of the rearing cage. The most important part of the system construction is the power transmission coils that generate a special magnetic field uniformly. Fig. 1 shows the appearance of the biometric device to be constructed, and Fig. 2 shows that the magnetic flux density at the bottom of the power transmission coil is uniform within the range of the breeding cage.

K. Furiya, T. Takura, F. Sato, H. Matsuki, T. Sato, and T. Yanada, JMSJ., Vol.2, pp165-168(2010) K. Furiya, T. Takura, F. Sato, H. Matsuki, T. Sato, JMSJ., Vol.3, pp333-336(2009) F. Sato, H. Kotake, T. Takura, T. Sato, H. Matsuki, and S. Yanada, JMSJ., Vol.35, pp404-407(2011)

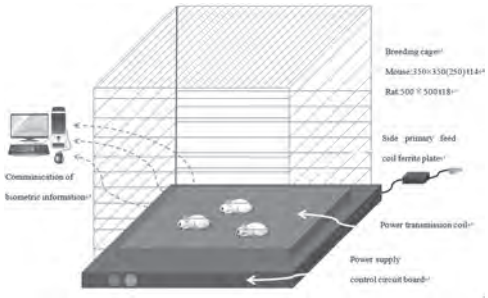

Fig.1 Biometric information acquisition device

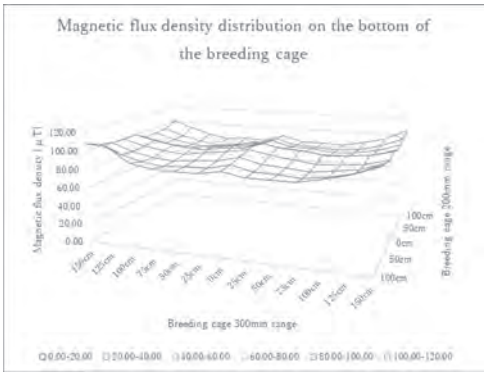

Fig.2 Magnetic flux density distribution on the bottom of the breeding cage

QPA-13. Development of Colloidal Magnetic Nano-objects with Strong Liquid-Phase AC Field Response for Remote 3D Thermometry and Sensing. *A.J. Biacchi*[1], T.Q. Bui[1], F.M. Abel[1], E. De Lima Correa[1], C.A. Richter[1], C. Dennis[1], S.I. Woods[1] and A.R. Hight Walker[1] *1. National Institute of Standards and Technology (NIST), Gaithersburg, MD, United States*

Colloidal magnetic nano-objects (MNOs) are an important class of nanomaterials being investigated for use in a host of therapeutic and diagnostic modalities. These applications exploit the very soft magnetic behavior found in certain materials, often ferrites, when they are confined to tens of nanometers in diameter or less. Such nanoscale magnets may produce a strong collective response to applied alternating current (AC) magnetic fields, while simultaneously remaining dispersed in liquid media. Recently, remote magnetic imaging of temperature has been identified as a potential diagnostic application of colloidal MNOs. The technique, which is a variation of magnetic particle imaging, is based on the temperature-dependent response of MNOs to an applied AC magnetic field. However, significant challenges remain in the development of this metrology, including a need to finely engineer the MNOs to increase both their magnetic thermosensitivity and magnitude of AC signal. Here, we report on our development of MNOs designed with a robust liquid-phase response to applied AC magnetic fields, specifically for solution-phase thermometry and sensing. A series of colloidal nanocrystals based on ferrites were synthesized *via* solution routes in a variety of sizes (Fig. 1) and compositions. These MNOs were then investigated using solid- and liquid-phase AC and DC field magnetometry measurements (Fig 2.). The results were cross-correlated with detailed structural characterization, including advanced electron microscopy, to develop a set of structure-property relationships. Finally, we tune these parameters to optimize a robust thermosensitive AC magnetic signal and conduct spatial imaging of MNO magnetic response. Collectively, these studies illuminate the complex behavior of MNOs under AC driving fields, reveal extensive correlations between nanoscale size/composition and liquid-phase magnetic response, and provide guidelines for the design of MNOs used in magnetic thermal imaging and other remote sensing applications.

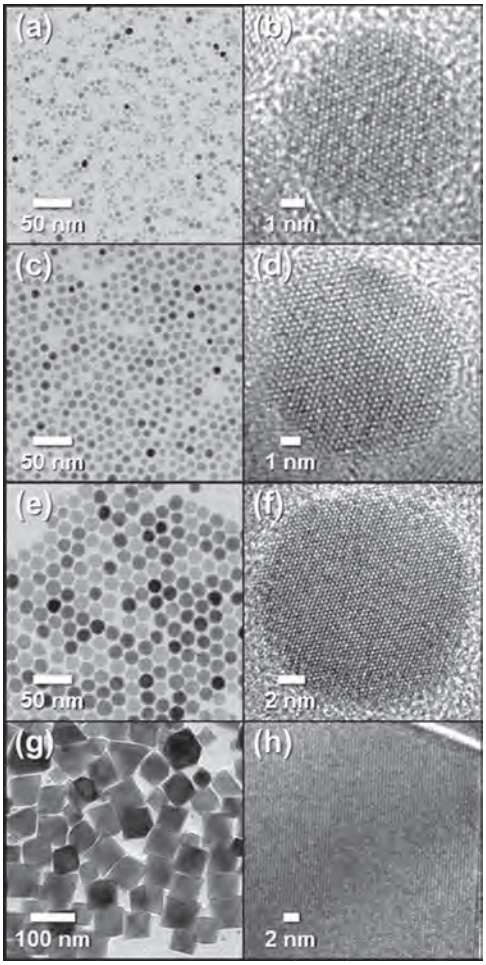

Fig. 1: TEM micrographs of crystalline ferrite nano-objects synthesized in high yield with distinct size regimes (7, 10, 18, 80 nm).

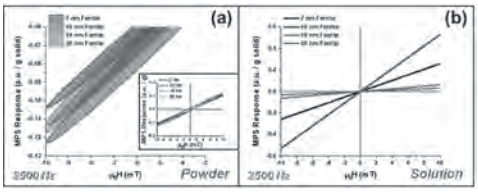

Fig. 2: AC magnetic response comparison of MNO (a) powders and (b) solutions.

QPA-14. Mixed Brownian alignment and Néel rotations in superparamagnetic iron oxide nanoparticle suspensions driven by an AC field. *S.A. Shah*[1] and K.M. Krishnan[2] *1. Forman Christian College (University) Lahore, Lahore, Pakistan; 2. University of Washington, Seattle, WA, United States*

Superparamagnetic iron oxide nanoparticles with highly nonlinear magnetic behavior are attractive for biomedical applications like magnetic particle imaging and magnetic fluid hyperthermia. Such particles display interesting magnetic properties in alternating magnetic fields and here we document experiments that show differences between the magnetization dynamics of certain particles in frozen and melted states. This effect goes beyond the small temperature difference (ΔT~20C) and we show the dynamics to be a mixture of Brownian alignment of the particles and Néel rotation of their moments occurring in liquid particle suspensions. These phenomena can be modeled in a stochastic differential equation approach by postulating log-normal distributions and partial Brownian alignment of an effective anisotropy axis. We emphasize that precise particle-specific characterization through experiments and nonlinear simulations is necessary to predict dynamics in solution and optimize their behavior for emerging biomedical applications including magnetic particle imaging.

[1] K. M. Krishnan, Biomedical nanomagnetics: A spin through possibilities in imaging, diagnostics, and therapy, IEEE Trans. Magn. 46, 2523 (2010). [2] B. Gleich and J. Weizenecker, Tomographic imaging using the nonlinear response of magnetic particles, Nature (London) 435, 1214 (2005). [3] S. A. Shah, R. M. Ferguson, and K. M. Krishnan, Slew rate dependence of tracer magnetization response in magnetic particle imaging, J. Appl. Phys. 116, 163910 (2014). [4] R. Ferguson, A. Khandhar, E. Saritas, L. Croft, P. Goodwill, A. Halkola, J. Borgert, J. Rahmer, S. Conolly, and K. Krishnan, Magnetic particle imaging with tailored iron oxide nanoparticle tracers, IEEE Trans. Med. Imaging 34, 1077 (2015). [5] M. Visscher, S. Waanders, H. J. G. Krooshoop, and B. ten. Haken, Selective detection ofmagnetic nanoparticles in biomedical applications using differential magnetometry, J. Magn. Magn. Mater. 365, 31 (2014).

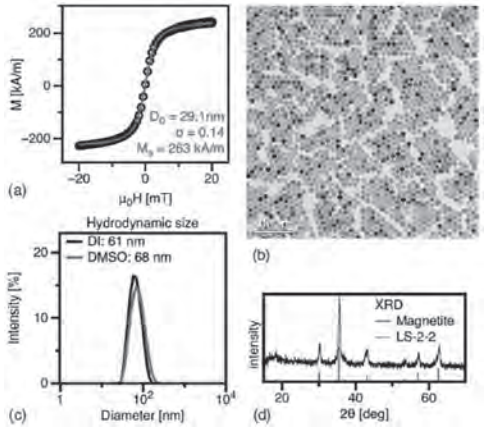

Fig. 1. SPIOs were characterized by complementary methods to obtain magnetic, size, and structural information: (a) VSM curve, (b) TEM image of nanoparticles showing monodisperse size distribution, (c) DLS plot, and (d) x-ray diffraction plot.

QPA-15. Frequency Domain Studies on Single- and Multi-core Magnetic Nanoparticles in Volumetric Magnetic Particle Spectroscopy (MPS). *V.K. Chugh*[1], K. Wu[1,2], V.D. Krishna[3], M.C. Cheeran[3] and J. Wang[1] *1. Department of Electrical and Computer Engineering, University of Minnesota, Minneapolis, MN, United States; 2. Department of Electrical and Computer Engineering, Texas Tech University, Lubbock, TX, United States; 3. Department of Veterinary Population Medicine, University of Minnesota, St. Paul, MN, United States*

The appropriate choice of magnetic tracers presents an interesting question for the field of bioassays utilizing magnetic particle spectroscopy (MPS). Nowadays, there are two widely used MPS methodologies, namely, the surface-based MPS[1,2] and volumetric MPS[3–5]. Where the surface-based MPS relies upon Néel relaxation of the MNPs to provide a quantifiable result of analyte presence and multi-core MNPs are used for such tests. Whereas the volumetric MPS monitors the harmonic spectral change of MNPs, which is due to the analyte-induced clustering and therefore relies on the Brownian relaxation of magnetic tracers. Both single- and multi-core MNPs have been reported for volumetric MPS assays. Herein, using a volumetric MPS system, we systematically study the harmonic spectral change of single- and multi-core MNPs with reference to their unbound states, over a range of excitation fields. Specifically, two types of streptavidin-coated magnetic tracers are compared: 30 nm single-core MNPs – SHS30, and 50 nm multi-core MNP – SuperMag50. Two samples are prepared respectively for each type of MNP tracer. The first sample containing MNPs evenly suspended in PBS buffer is used as a reference MPS spectral signal level, i.e., the unbound state. The second sample contains MNPs mixed with an excess number

of biotinylated antibodies and hence clusters are presented, i.e., the bound state. The MPS spectral changes over a wide frequency range relative to the unbound state are plotted in Fig.1. The results indicate that multi-core MNPs are most suitable for the surface-based MPS methodologies utilizing dual-excitation frequencies. For volumetric MPS methodology, single-core MNPs are the favorable choice for dual-excitation frequency MPS, whereas multi-core MNPs are the preferred choice for single-excitation frequency MPS.

[1] J. Pietschmann, N. Voepel, L. Voß, S. Rasche, M. Schubert, M. Kleines, H.-J. Krause, T.M. Shaw, H. Spiegel, and F. Schroeper, Front. Microbiol. 12, 841 (2021). [2] A.V. Orlov, J.A. Malkerov, D.O. Novichikhin, S.L. Znoyko, and P.I. Nikitin, Food Chem. 383, 132427 (2022). [3] K. Wu, V.K. Chugh, V. D. Krishna, A. di Girolamo, Y.A. Wang, R. Saha, S. Liang, M.C.-J. Cheeran, and J.-P. Wang, ACS Appl. Mater. Interfaces 13, 44136 (2021). [4] J. Zhong, E.L. Rösch, T. Viereck, M. Schilling, and F. Ludwig, ACS Sens. 6, 976 (2021). [5] X. Zhang, D.B. Reeves, I.M. Perreard, W.C. Kett, K.E. Griswold, B. Gimi, and J.B. Weaver, Biosens. Bioelectron. 50, 441 (2013).

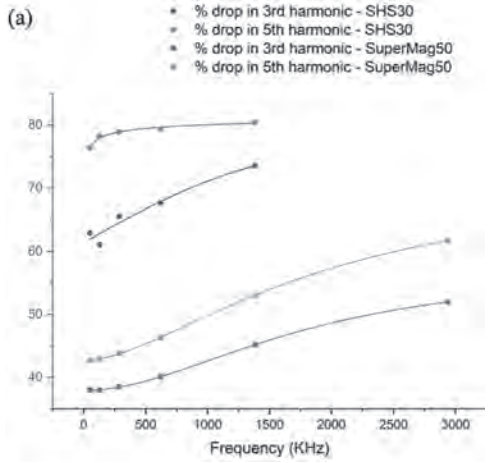

Fig.1: MPS spectral change in the 3rd and 5th harmonic signals with respect to excitation frequencies are presented for SHS30 and SuperMag50 MNPs for (a) single-frequency and (b) dual-frequency MPS systems. MPS spectral change is calculated as the drop in harmonic spectra for clustered MNPs with respect to MNPs suspended in PBS.

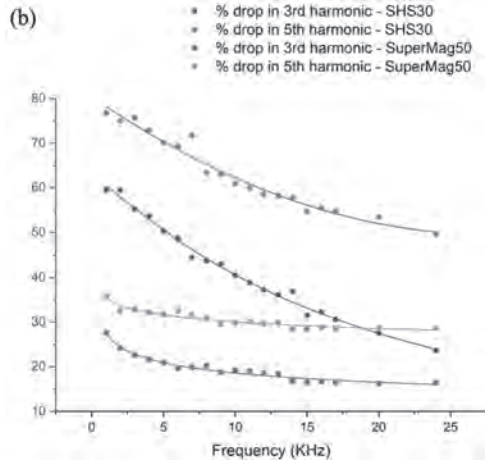

Figure 1(b) dual-frequency MPS systems. MPS spectral change is calculated as the drop in harmonic spectra for clustered MNPs with respect to MNPs suspended in PBS.

QPA-16. Portable Magnetoresistive Device for the Simultaneous Detection of Dengue RNA and Anti-dengue Antibodies. *D. Albuquerque*[1,2], V.C. Martins[1], E. Fernandes[3], D.M. Caetano[1], L. Zé-Zé[4,5], M. Alves[4] and S. Cardoso[1,2] *1. INESC MN - Instituto de Engenharia de Sistemas E Computadores – Microsistemas e Nanotecnologias, Lisboa, Portugal; 2. IST - Instituto Superior Técnico, Lisboa, Portugal; 3. INL - International Nanotechnology Laboratory, Braga, Portugal; 4. INSA-CEVDI - National Institute of Health Doutor Ricardo Jorge, Centre for Vectors and Infectious Diseases Research, Águas de Moura, Portugal; 5. BioISI - Biosystems and Integrative Sciences Institute, Lisboa, Portugal*

This work describes the use of magnetoresistive (MR) sensors coupled with a portable platform for the detection of dengue virus (DENV), a mosquito-borne infection endemic to low- and middle-income countries, affecting 100-400 million people each year[1]. Nowadays, diagnosis relies on molecular or serological tests. Still, these tests remain discrete (RNA vs. antibodies), and tend to be complex and/or expensive, requiring expert staff and fully equipped laboratories. As such, this work aims to combine both assays in a single analysis by simultaneously detecting DENV RNA and anti-DENV antibodies using a portable platform[2,3]. A spin-valve based biochip was designed and functionalized with specific DNA oligo probes and secondary antibodies (Fig1A)[4]. Extracted RNA and serum samples were provided by INSA-CEVDI and used as targets in molecular and serological assays, respectively. In both assays, streptavidin coated 250 nm magnetic nanoparticles were used for biolabeling. The measurement output is represented by a voltage drop (dV/V) proportional to the number of captured target molecules (Fig1B). However, to increase the dynamic range of the assays, the percentage difference of dV/V signals obtained using different immobilization strategies/probes, was taken as the final output signal. Using the MR-platform, individual tests were carried out for the detection of DENV RNA and anti-dengue human antibodies. The RNA target was detected down to a few hundreds of pM (Fig2A). For the serological response, a calibration curve with an LOD of 1.38 nM was achieved. Infected patients' serum was also tested for anti-DENV antibodies, obtaining a sensitivity of 100% and a specificity of 92%(Fig2B). Finally, simultaneous detection of antibodies and RNA was successfully achieved on the same chip, showing no differences to the individual assays. To increase the multiplexing capability of the assay, a biochip with 144 sensors and multi-level contact layers was developed and is under testing using DENV as a model disease. This chip design will allow the simultaneous discrimination of various viruses endemic in the same regions.

[1] Who.int. 2022. *Dengue and severe dengue*. [online] Available at: <https://www.who.int/news-room/fact-sheets/detail/dengue-and-severe-dengue> [Accessed 14 June 2022]. [2] J. Germano *et al.*, Sensors 9, 4119 (2009). [3] V. C. Martins *et al.*, Biosensors and Bioelectronics 24, 2690 (2009). [4] D. C. Albuquerque *et al.*, Biosensors and Bioelectronics 210, 114302 (2022).

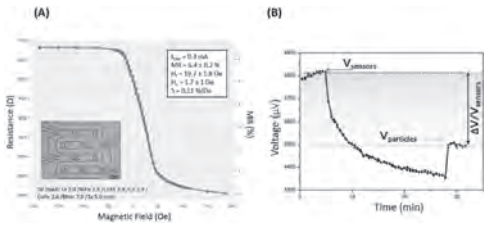

Fig1: Example of sensor (A) transfer curve and (B) output signal.

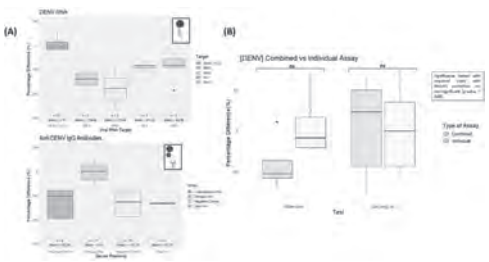

Fig2: (A) Individual and (B) combined testing.

QPA-17. Analysis of Fe element and interferon gamma in serum and spleen homogenates after injection of silica coated magnetic nanoparticles (SiO_2-Fe_3O_4). *M. Hasan*[1,2], J. Choi[1], H. Akter[1] and S. Lee[1] *1. Department of Digital Healthcare Engineering, Sangji University, Wonju, The Republic of Korea; 2. Department of Biochemistry and Molecular Biology, Bangabandhu Sheikh Mujibur Rahman Science and Tech. University, Gopalganj, Bangladesh*

Currently, the treatment of suppression of cytokine storm in severe COVID-19 patients includes cytokine receptor suppression and depletion of specific immune cells in addition to steroid treatment. Monoclonal antibody therapy is also one of the methods for depleting specific immune cells. It is a monoclonal antibody therapy against CD3, one of the important signaling molecules for T-cell receptor activation. Among others, T cells secrete interferon gamma (IFN-γ), a pro-inflammatory cytokine responsible for inducing inflammation. Therefore, monoclonal antibody therapy againstis a therapy that specifically depletes IFN-γ-secreting T cells. However, intravenous injection of an anti-CD3 monoclonal antibody targeting all T cells induces significant immunosuppression and has side effects such as high fever and chills. The purpose of this study is to prepare an optimized liquid phase as a CD3 antibody-magnetic nanoparticle (Ab-MNP) conjugate to inhibit the overactivation of T cells. In current study, we aimed to check distribution of Fe after acute admistration of silica-conjugated amine nanoparticles delivered by intravenous injection. Besides, the IFN- γ levels in serum and spleen homogenates will be analyzed. Finally, we will develop film-type microneedle patch using pulse-type magnetic stimulation to control the amount of liquid passing through the skin. The reason for choosing the spleen from the mouse organ is that it stores MNPs with a particle size of 50 nm administered in vivo. Therefore, the result is a difference in the concentration of Fe elements, which was 1.89×10^3 mg/kg in the spleen of a control mouse not administered with MNPs, whereas increases significantly to 1.93×10^3 mg/kg in that of a mouse administered with MNPs as shown in Fig. 1(a) and 1(b). IFN-γ level in spleen tissue and serum is increased after 10 days. Further, time kinetic analysis of biochemical and immunological parameters are required to confirm its suitability in bio-administration.

[1] N. S. Remya, S. Syama, A. Sabareeswaran, and P. V. Mohanan, Toxicity, toxicokinetics and biodistribution of dextran stabilized Iron oxide Nanoparticles for biomedical applications, International Journal of Pharmaceutics 511, 586-598 (2016). [2] F. Gao, An Overview of Surface-Functionalized Magnetic Nanoparticles: Preparation and Application for Wastewater Treatment, Chemistry Select 4, 6805-6811 (2019). [3] R. Q. Cron, R. Caricchio, and W. W. Chatham, Calming the cytokine storm in COVID-19, Nature Medicine 27, 1674–1675 (2021). [4] C. Kuhn and H. L. Weiner, Therapeutic anti-CD3 monoclonal antibodies: from bench to bedside, Immunotherapy 8, 889–906 (2016).

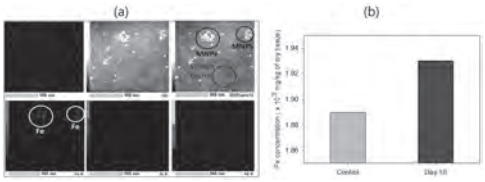

Fig. 1. (a) Images of transmission electron microscope and atomic intensities of Fe element and (b) Fe concentration by drainage of MNP in spleen tissues after a mouse administered with MNPs.

QPA-18. Easy synthesis of monodisperse Co/Zn-based ferrite nanoparticles and their antifungal activities on *Botrytis cinerea*. *S. Michea*[1,3], R.M. Freire[2,3], C. Robles-Kelly[4], C. Infante[4] and E. Silva[2,4] *1. Applied Chemical Science Institute, Universidad Autónoma de Chile, Santiago, Chile; 2. Instituto de Investigaciones Agropecuarias, Santiago, Chile; 3. Center for Development of Nanoscience and Nanotecnology, Santiago, Chile; 4. Instituto de Ciencias Biomedicas. Universidad Autonoma de Chile, Santiago, Chile*

In this work, we have displayed an easy way to produce monodisperse spinel nanoparticles (NPs), as well as the antifungal activity of $CoFe_2O_4$, $Co_{0.5}Zn_{0.5}Fe_2O_4$ and $ZnFe_2O_4$ nanostructures. Firstly, the structural, morphological and magnetic properties of each NP were fully investigated through x-ray diffraction (XRD), Transmission Electron Microscopy (TEM) and Vibrating Sample Magnetometer (VSM). The XRD data showed diffraction peaks related to the crystalline spinel phase. No additional phase was observed, which evidences the purity of the nanostructure synthesized. The TEM micrographs displayed monodisperse NPs with spherical morphology. The average sizes of $CoFe_2O_4$, $Co_{0.5}Zn_{0.5}Fe_2O_4$ and $ZnFe_2O_4$ NPs were found to be 6.87 ± 0.05 nm, 5.18 ± 0.01 nm and 11.52 ± 0.09 nm, respectively. The VSM data indicated the nanostructures are superparamagnetic at room temperature. Afterwards, the antifungal properties of the Co/Zn-based ferrite NPs against *Botrytis cinerea* were tested. So, the inhibition of mycelial growth by different concentrations (45 – 360 ppm) of NPs was measured. The most effective nanostructure was found to be $CoFe_2O_4$ with an EC_{50} value of 265 ppm. To go further and elucidate how the NPs are affecting *B. cinerea*, reactive oxygen species (ROS) production was measured. The results indicated that the $CoFe_2O_4$ monodisperse NPs are able to induce a burst of ROS in *B. cinerea,* promoting damage cellular.

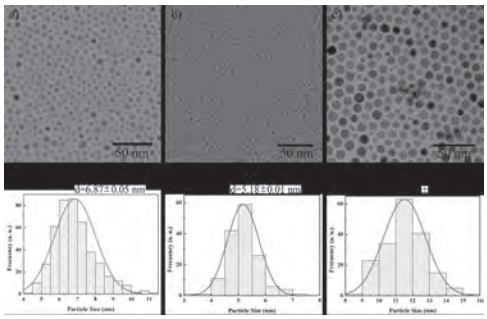

Fig. 1 TEM images and histograms size distribution of the particle size for a) $CoFe_2O_4$ b) $Co_{0.5}Zn_{0.5}Fe_2O_4$ and c) $ZnFe_2O_4$ respectively.

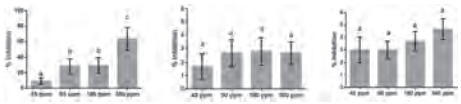

Fig. 2 Effect of nanoparticles on mycelial growth of *Botrytis cinerea* in solid media. The percentage of growth inhibition determined after 48 h of incubation at different concentrations of $CoFe_2O_4$, $Co_{0.5}Zn_{0.5}Fe_2O_4$ and $ZnFe_2O_4$. The nanoparticles tested were 45, 90, 180 and 360 ppm. Each bar represents the average of at least three independent experiments ± standard deviation. Letters indicate significant differences between each $CoFe_2O_4$ concentration, evaluated by Tukey's test; $p < 0.05$.

Session QPB
MANIPULATION OF MAGNETIC FLUIDS (Poster Session)

Norman M Wereley, Chair
University of Maryland, College Park, MD, United States

QPB-01. Simple Synthesis of Magnetic Nanomaterials by Microfluidics Process. *V. Singh*[1] and R. Singh[2] *1. School of Engineering Science and Technology, University of Hyderabad, Hyderabad, India; 2. School of Physics, University of Hyderabad, Hyderabad, India*

Magnetic nanomaterials such as magnetite (Fe_3O_4) are sought after for their promising applications in sensing, drug delivery, tissue engineering and are also used as contrast agents in magnetic resonance imaging [1] .Synthesis of these nanomaterials with good uniformity in size and shape is imperative for their use in different applications. Microfluidic-based synthesis in designed reactors is a new technology which controls the mixing of fluids within a fixed channel dimension (ranging from 10-100 μm), offers efficient mass transport in channels and also reduces reaction time.[2,3] Herein, we present a new synthesis strategy which utilizes 3D-printing technique to develop a microfluidic device for synthesis of Fe3O4 nanoparticles by droplet-based method.[4] The droplet-based method uses oil as a continuous medium which confines the reactants in a droplet, and each droplet functions as an individual reactor thereby providing high level of control on synthesis conditions. This strategy overcomes the limitations of conventional glassware-based synthesis such as polydispersity and batch-to-batch variability in nanoparticles. Enhanced magnetism and monodispersity in Fe3O4 nanoparticles were controlled by application of AC voltage across the electrodes placed beneath the reaction chamber of the device. The present device can be used for synthesing metal nanoparticles.

References: 1. A. H. Lu, E. Salabas, F. Schüth (2007) Magnetic nanoparticles: synthesis, protection, functionalization, and application. Angew. Chem. 119:1242-1266; Angew. Chem. Int. Ed. 46: 1222-1244 2. G. M. Whitesides (2006) The origins and the future of microfluidics. Nature 442:368–373 3. K. Ren, J. Zhou, H. Wu (2013) Materials for Microfluidic Chip Fabrication. Acc. Chem. Res. 46:2396–2406 4. V. Singh, R. Singh (2022) Voltage-Driven Microfluidic Synthesis of Magnetite and Gold Nanomaterials. J Flow Chem. *DOI: 10.1007/s41981-022-00231-3*.

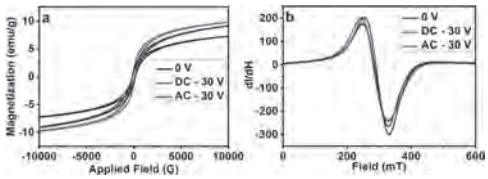

Fig. 1. (a) Magnetization vs Applied field (MH plots) and (b) electron spin resonance (ESR) spectra for various Fe3O4 NPs.

QPB-02. Dynamics of magnetic fluids and bidisperse magnetic systems undergoing oscillatory shear. E. Shel'deshova[1], *E. Sokolov*[1] and P. Ryapolov[1] *1. Southwest State University, Kursk, Russian Federation*

Magnetic fluids have a unique combination of magnetic properties, fluidity and colloidal stability, which has allowed them to find applications in a variety of technical devices, such as shock absorbers and sensors. One of the features of this smart material is the ability to control its physical properties using various combinations of magnetic influences. In this work, the dynamics of a magnetic fluid volume levitating in an uniform magnetic field of an electromagnet undergoing oscillatory shear is investigated. The samples with different physical parameters were considered, the dependence of magnetoviscous effect was investigated. It is shown that the microstructure of the sample and the presence of large magnetic particles have the greatest influence on the dynamics of the magnetic fluid undergoing oscillatory shear and magnetoviscous effect. The results of the work can be used to develop a method for express testing of magnetic fluid samples, as well as to develop acceleration and vibration sensors based on magnetic fluids [1]. The dependences of the viscosity for samples MF-1 – MF-4 are plotted, shown in Figure 1. The obtained dependences of the viscosity show an increase in its value by a factor of 5 for the MF-1 sample, with an increase in the field to 1000 kA/m, which can be explained by interparticle interactions and the formation of weakly bound aggregates in the near-wall layer in a more concentrated initial MF-1 sample. In a more diluted sample MF-2, such an increase in viscosity is not observed. The images MF-3, MF-4 are characterized by the presence of an excess free surfactant, which negatively affects the magnetoviscous effect. The work was carried out the part of the implementation of the program of strategic academic leadership "Priority-2030" (Agreements No. 075-15-2021-1155 and No. 075 -15-2021-1213) and as part of the implementation of the state task (No 0851-2020-0035).

1. Ryapolov P. A., Polunin V. M., Shel'deshova E. V, *JMMM* 496, 165924 (2020).

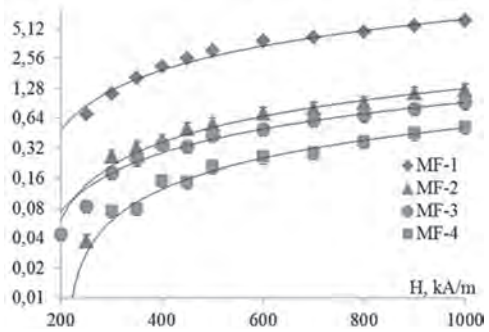

Fig. 1. Dependences of viscosity for samples MF-1 – MF-4

QPB-03. Wireless Manipulation of a Self-Assembled Magnetic Millirobot with a Multi-Modular Ring Structure Using an External Magnetic Field. *Y. Lee*[1], D. Lee[1] and S. Jeon[1] *1. Mechanical and Automotive Engineering, Kongju National University, Cheonan, The Republic of Korea*

Various biomedical magnetic robots have been widely investigated as a possible means to replace conventional invasive regimens [1-3]. In our previous research, we proposed a self-assembled magnetic millirobot with a multi-modular ring-like chain structure (SAMR) that can change its equilibrium formations under different conditions [4]. The SAMR is composed of several arc-shaped modules serially connected by a pin joint, and a magnet is inserted into each module (Fig. 1). Due to the interactive magnetic forces and torques within the modules, the SAMR can be self-assembled into a ring formation without a magnetic field or disassembled into a straight formation under an applied magnetic field. In this research, we further investigated the wireless manipulation abilities of the SAMR's mechanical motions. Based on the mechanical conditions of the SAMR shown in Fig. 1, we established a method that can generate and maneuver the SAMR's various mechanical movements, including self-assembly, disassembly, tumbling, crawling,

and cargo trapping motions simply via the control of an external magnetic field. Since such motions allow the low-invasive manipulation of the SAMR during the access to a target area and the performance of functions in the area, as shown in Fig. 1, these motion abilities can significantly improve the SAMR's usefulness as a minimally invasive device. In an experiment to verify the effectiveness of the proposed motion control method, the SAMR initially disassembled and loaded inside the medical syringe successfully self-assembled into a ring formation. The SAMR then sequentially showed tumbling, crawling, and cargo trapping and delivery motions actuated by different magnetic fields. This research can contribute to developing minimally invasive biomedical magnetic robots.

[1] M. Sitti, H. Ceylan, W. Hu, J. Giltinan, M. Turan, S. Yim, and E. Diller, "Biomedical Applications of Untethered Mobile Milli/Microrobots," *Proc. IEEE*, vol. 103, no. 2, pp. 205-224, 2015. [2] S. Yim and M. Sitti, "Soft-Cubes: Stretchable and self-assembling three-dimensional soft modular matter," *Int. J. Rob. Res.*, vol. 33, no. 8, pp. 1083–1097, 2014. [3] H. Lee and S. Jeon, "A Study on the Self-Assembly and Disassembly Abilities of a Multi- Modular Magnetic Millirobot," *J. Inst. Cont., Rob. Sys.*," vol. 25, no. 3, pp. 235-240, 2019. [4] H. Lee and S. Jeon, "An intravascular helical magnetic millirobot with a gripper mechanism performing object delivery and collecting motions actuated by precession rotating magnetic fields," *AIP Adv.*, vol. 11, pp. 025236, 2021.

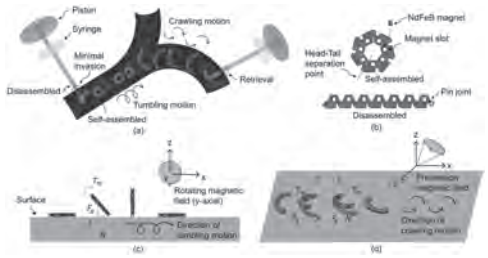

Fig. 1. Schematic view of the proposed SAMR in a human blood vessel. (b) Self-assembled and disassembled formations of the SAMR. (c) Tumbling motion of the SAMR actuated by a rotating magnetic field. (d) Crawling motion of the SAMR actuated by a precession magnetic field.

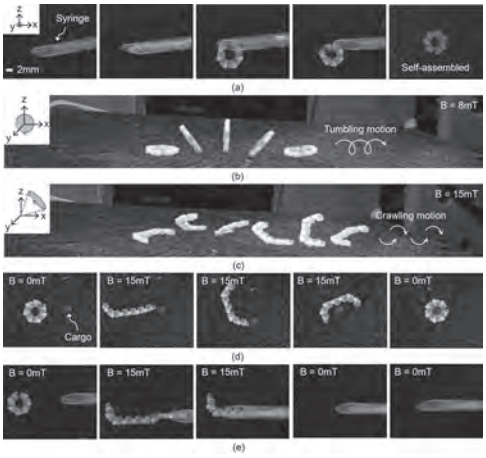

Fig. 2. (a) Self-assembly, (b) tumbling, (c) crawling, (d) cargo trapping, and (e) retrieval motions of the prototype SAMR actuated by different magnetic fields.

QPB-04. Design and Performance of A 3D-Printed Magnetorheological Fluid-Based Adaptive Vibration Isolator. *Y. Choi*[1], B. Yoo[1], J. Park[1] and N.M. Wereley[1] *1. Department of Aerospace Engineering, University of Maryland, College Park, MD, United States*

An effective vibration isolator (VI) strategy isolates payloads from vibration sources by introducing compliance. Passive isolators are low cost and easy to install but are tuned to a specific vibration spectrum, and rapidly lose effectiveness if the design point shifts. In contrast, adaptive vibration isolators using magnetorheological fluids (MRFs) continuously adapt to changing vibration spectra by adjusting a magnetic field using an appropriate control algorithm. Traditional fabrication methods using injection molding are economical only when large numbers are produced, which precludes customizing VIs for a specific available jitter space, natural frequency, or static displacement. 3D printing is advantageous for a magnetorheological vibration isolator (MRVI) because designs can be customized: the shape of the hydraulic rubber reservoir can be economically customized to meet the requirements of a specific application by tuning such properties as axial stiffness, bulge stiffness, diameter, height, and Shore hardness of the membrane wall. The MRVI, which is a squeeze-mode device, consists of a reservoir or rubber bellow with customizable stiffnesses, a plastic lid which houses an electromagnetic coil, and an MRF (Figure 1). The rubber bellow and plastic lid were fabricated using a Masked Stereolithography (MSLA) 3D printer. The electromagnet was mounted onto the lid, the reservoir was filled with an MRF, and the lid was twisted onto the reservoir using a large thread. Using a testing machine, the damper forces of the 3D-printed MRVI were measured under constant velocity conditions for different magnetic fields. From these tests, the magnetic field-controllable performances such as the dissipated energy and the dynamic force range of the MRVI were obtained (Figure 2). The feasibility of the 3D-printed MRVI was experimentally confirmed. In addition, using 3D printing, and by selecting Shore hardness of the material, wall thickness, bellow shape, and MRF Fe particle volume fraction, a broad range of VI applications can be addressed with this design methodology.

1. S. Kaul, "Modeling and Analysis of Passive Vibration Isolation Systems," Elsevier, 1st Ed., 2021, DOI: 10.1016/C2019-0-00013-1. 2. M. Brigley, Y. T. Choi and N. M. Wereley, "Experimental and Theoretical Development of Multiple Fluid Mode Magnetorheological Isolators," Journal of Guidance, Control, and Dynamics, Vol. 31, No. 3, pp. 449-459, 2008, DOI: 10.2514/1.32969.

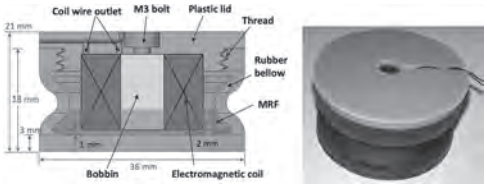

Fig.1: 3D-printed MRF-based vibration isolator

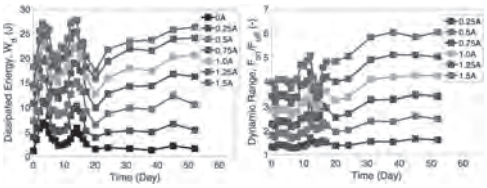

Fig.2: Magnetic field-controllable performances of the 3D-printed MRF-based vibration isolator

QPB-05. Magnetoactive Properties of Biocompatible Magnetic Hydrogel Composites: Effects of Magnetic Particulate Type and Magnetic Annealing. *J. Schewe*[1], J.M. Ennis[1], J. Lu[1], W.M. Howell[1], D.P. Fagan[1], T. Höft[2] and B. Nelson-Cheeseman[1] *1. Mechanical Enginneering, University of St. Thomas, St. Paul, MN, United States; 2. Mathematics, University of St. Thomas, St. Paul, MN, United States*

Magnetic hydrogels, or ferrogels, are smart materials that can mechanically deform in response to an applied magnetic field. Ferrogels possess potential applications in soft robotics, tissue engineering, artificial muscles, and controlled drug release due to their soft tissue-like state and biocompatibility potential. Hydrogels are a 3D hydrophilic polymer network linked by physical or chemical crosslinking, whereas ferrogels are a composite material that possess magnetic responsiveness due to the incorporation of a magnetic additive. Polyvinyl Alcohol (PVA) is unique among hydrogels due to the formation of physical crosslinks when subjected to cycles of freezing and thawing, enhancing mechanical properties without the use of a crosslinker that could compromise biocompatibility. The first aim of this work is to understand the differing effects of magnetically soft and hard additives on the magnetic, mechanical, and magnetoactive properties of PVA ferrogels by investigating PVA hydrogels impregnated with soft and hard magnetic particulate (magnetite (Fe_3O_4) and strontium ferrite ($SrFe_{12}O_{19}$), respectively). While magnetically hard polymer composites allow for more complex motion and actuation, soft magnetic additives often allow for greater response due to particle realignment when under a magnetic field. The next aim of this work studies the effects of magnetic annealing these ferrogels during crosslinking by comparing their resulting magnetic, mechanical, and magnetoactive properties with analogous control samples. Magnetoactive properties are determined by quantifying the angle of sample deflection in an applied transverse magnetic field, via a custom digital image overlay program. Scanning Electron Microscopy (SEM) is used to analyze the structural features of the hydrogel matrix and magnetic particulate. Results yield highly magnetoactive hydrogel samples with tunable responsiveness based upon magnetic particulate type, content, and presence of magnetic annealing. Figure 1 shows the magnetic responsiveness of ferrogels at varying magnetite contents.

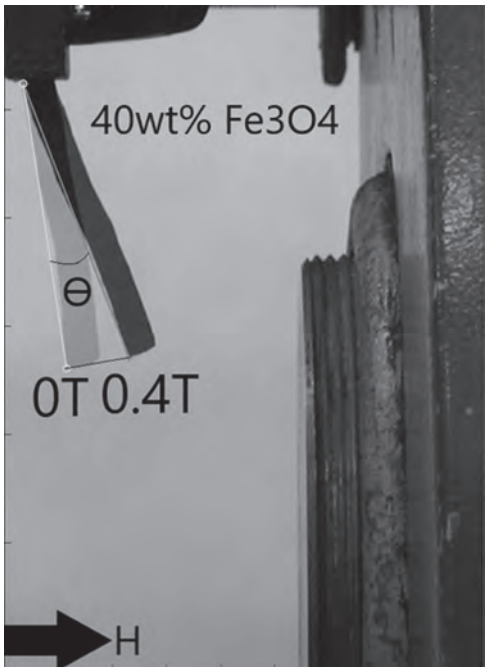

Fig. 1 Deflection of 40wt% magnetite-PVA Ferrogel under an increasing magnetic field(H)

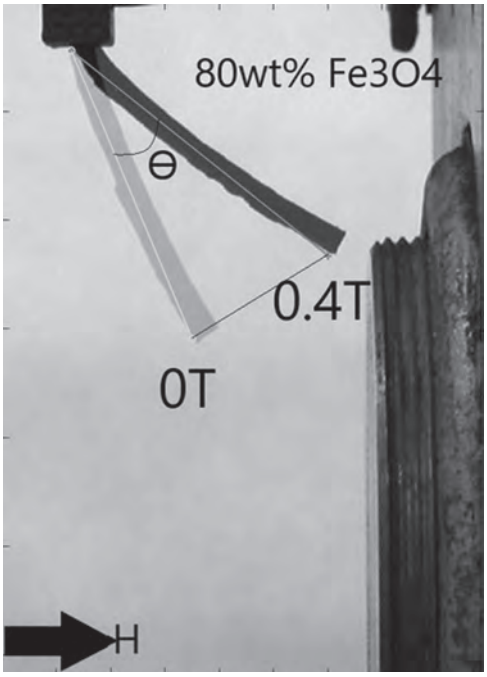

Fig. 2 Deflection of 80wt% magnetite-PVA Ferrogel under an increasing magnetic field(H)

QPB-06. Magnetic MOF composite material for decontamination of direct red 81 from polluted water. *M.E. Ossman*[1] *1. Environment and Natural Materials Research Institute, SRTA City, Alexandria, Egypt*

Herewith, magnetic MOF composite material was utilized as an efficient adsorbent for direct red 81 (DR81) dye from wastewater. The synthesized magnetic MOF was characterized using X-ray diffraction (XRD), scanning electron microscopy (SEM), field emission transmission electron microscopy (FETEM), Fourier-transform infrared spectroscopy (FTIR), thermal gravimetrical analysis (TGA), and Brunauer-Emmett-Teller (BET) surface area analysis. The adsorption profile of DR81 anionic dye onto the prepared magnetic MOF was investigated with various processing parameters such as pH, contact time, and dosage. The optimum dosage from the fabricated magnetic MOF for decontamination of DR81 was 2.0 g L-1 at pH=7 after 30 min. The maximum Langmuir monolayer adsorption capacity of the DR81 decontamination via the synthesized magnetic MOF was recorded 67.35 mg/g. These promising data confirmed the availability of the synthesized magnetic MOF composite as an excellent adsorbent material for the adsorption of DR81 from aqueous media. Acknowledgment: This paper is based upon work supported by Science, Technology & Innovation Funding Authority (STDF) under grant (43565).

Mona Ossman,1,* Eslam Salama, 1 Ali Hamdy,1 Hassan Shokry Hassan,2 Marwa F. Elkady2 1City of Scientific Research and Technological Applications (SRTA-City), New Borg El-Arab City, Alexandria 21934, Egypt 2Egypt-Japan University of Science and Technology, New Borg El-Arab City, Alexandria 21934, Egypt Correspondence should be addressed to Mona Ossman; mhr1410@hotmail.com

QPB-07. Withdrawn

QPB-08. High-precision 3D Reconstruction of Multiple Magnetic Targets Based on Center Weighting Method. *T. Lan*[1], J. Qiu[1], Y. Li[1], H. Sun[1] and S. Huang[1] *1. Key Laboratory of Optoelectronic Technology and System of Ministry of Education, College of Optoelectronic Engineering, Chongqing University, Chongqing, China*

High-precision 3D reconstruction of multiple magnetic targets aims to reconstruct the three-dimensional shape, position and magnetic susceptibility of magnetic targets based on discrete and noisy magnetic anomaly measurement data. It is widely used in anti-submarine, unexploded ordnance detection, subway magnetic pipeline detection and so on [1]. Currently, the research on three-dimensional reconstruction of multiple magnetic targets is still in the primary stage. Similar magnetic inversion technology is mainly studied in geological exploration, including morphological inversion and physical inversion. For morphological inversion, it needs to know the magnetic susceptibility in advance, which leads to some limitations in the reconstruction of unknown magnetic targets. For the physical inversion, because of the error of magnetic data and the lack of prior information, the effect of traditional physical inversion method is not satisfactory [2]. In order to solve this problem, this paper proposes a center weighting 3D imaging method based on normalized cross-correlation coefficient. The method selects magnetic gradient tensor data as observation data, calculates its cross-correlation coefficient with each cuboid cells. This can reduce the interference caused by magnetic measurement noise and errors of magnetic measurement parameters [3]. And visualize the results to obtain the preliminary distribution of magnetic target (Figure 1). Then, the spatial distribution and center position of the magnetic target are used as prior information to constrain the inversion equation. This can reduce the degree of freedom of the inversion equation and get the optimal solution of the reconstruction result. Our simulation and experimental results show that the proposed method can realize 3D reconstruction of several simple magnetic targets with a higher degree of fidelity (Figure 2).

[1] Y. Wang, I. I. Kolotov, D. V. Lukyanenko et al, Computational Mathematics and Mathematical Physics, Vol. 60, p. 1000–1007 (2020) [2] G. Yin, L. Zhang, Journal of Magnetism and Magnetic Materials, Vol. 482, p. 229–238 (2019) [3] Y. Li, J. Song, H. Xia et al, Journal of Applied Physics, Vol. 127,104701 (2020)

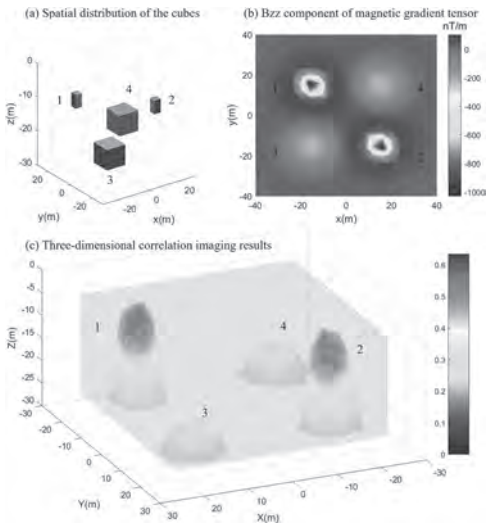

Fig. 1 Magnetic combined cubes at different depths

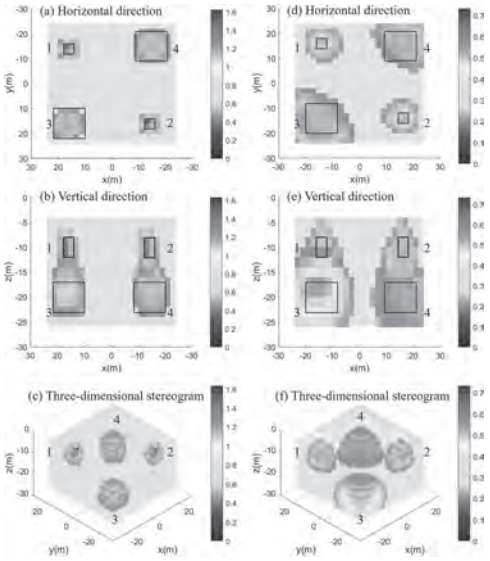

Fig. 2 The inversion results (magnetic susceptibility) : (a-c) the inversion results with optimization using the center weighting method, (d-f) the inversion results without optimization method. The black boxes outline the true shape

QPB-09. Adaptive Cascade Detection of Weak Magnetic Anomalies Based on Marine Predators Algorithm-Stochastic Resonance. *H. Sun*[1], Z. Wang[1], T. Lan[1], S. Zhang[1] and J. Qiu[1] *1. Key Laboratory of Optoelectronic Technology and System of Ministry of Education, College of Optoelectronic Engineering, Chongqing University, Chongqing, China*

Magnetic anomaly detection is a new detection technology that shows remarkable superiority in reliability and stealth performance[1]. However, it is quite challenging to effectively detect weak magnetic anomaly signals in the complex underwater environment[2]. Therefore, we proposed an adaptive cascade weak magnetic anomaly detection method based on Marine Predators Algorithm-Stochastic Resonance. Firstly, the main underwater background noise components such as geomagnetic noise, ocean current magnetic noise and wave magnetic noise were analyzed to simulate a more realistic underwater magnetic environment and enhanced the practical usability of the method. Then, according to the characteristics of magnetic anomaly signals, a cascade detection method of low-pass filtering, stochastic resonance, and threshold detection was designed to improve the detection probability of magnetic anomaly signals. In addition, in order to enable the proposed method to adaptively deal with the detection of weak magnetic anomalies in more applications, the marine predator optimization algorithm with better global and local search capabilities was used to improve the stochastic resonance system. Meanwhile, in order to improve the convergence speed and accuracy of the algorithm, the proposed method precalculated a certain number of typical scene solutions as the initial value of the optimization algorithm iteration, so that the system can detect anomaly signals more efficiently in the underwater environment with low signal-to-noise ratio. Simulation results show that the proposed method can improve the SNR by 6.03dB compared with EMD method[3] and 14.65dB compared with OBF method[4]. Therefore, in the low signal-to-noise ratio environment, the proposed method can effectively suppress environmental noise interference, improved the detection efficiency of magnetic anomaly signals, and had better accuracy, stability and detection efficiency than traditional methods. The method can provide theoretical basis and empirical reference for further application of magnetic anomaly data such as identification, location and tracking of underwater magnetic targets.

[1]Y. Xu, Z. Wang and S. Liu, IEEE Geoscience and Remote Sensing Letters, Vol. 19, p.1-5 (2022) [2]Y. Shen, J. Wang and J. Gao, IEEE Geoscience and Remote Sensing Letters, vol. 19, p. 1-4 (2022) [3]H. Zhou, Z. Pan and Z. Zhang, Ieice Transactions on Fundamentals of Electronics

Communications and Computer Sciences, vol. E100A, p. 2503-2506 (2017)
[4]B. Ginzburg, L. Frumkis, and B.-Z. Kaplan, Sensors and Actuators A: Physical. vol.102, p. 67-75(2002)

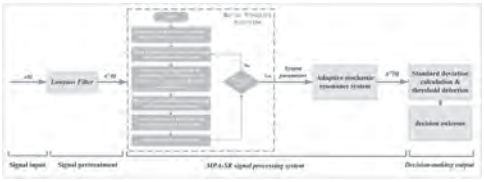

Fig.1 MPA-SR algorithm flowchart

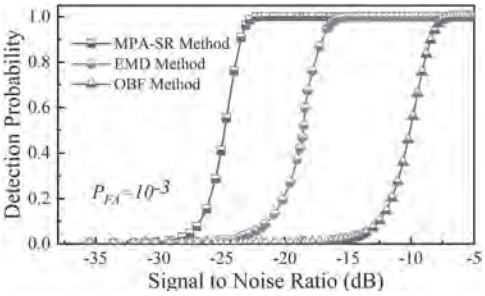

Fig.2 The detection probabilities of three methods

Session ROA
MAGNETIC CHARACTERIZATION FROM NANO TO MACRO

Peter Fischer, Co-Chair
Lawrence Berkeley National Laboratory, Berkeley, CA, United States
Alpha N'Diaye, Co-Chair
Lawrence Berkeley National Laboratory, Berkeley, CA, United States

CONTRIBUTED PAPERS

ROA-01. Development of a variable frequency, low current, low volume hysteresis loop tracer. D.M. Clarke[1] and *G. Vallejo-Fernandez*[1]
1. Physics, University of York, York, United Kingdom

A variable frequency, low current, low cost, high sensitivity magnetometer has been developed [1]. The system uses three MnZn ferrite rods to enhance the maximum field achievable by up to a factor 6 compared to the case where no ferrites are used. The system was tested using a suspension of magnetite nanoparticles in water. The magnetic response of the particles was investigated as a function of the maximum applied field and the frequency of operation. Volumes as low as 7 μl are required to obtain a signal to noise ratio of 8(47 kHz)/3(111 kHz) for a fluid with a saturation magnetisation of 1.07 emu/cm^3. Fields as high as 420 Oe can be applied by passing a current as low as 2.5 A through the primary coil at all operating frequencies. A resonant circuit is used to create an alternating current at a series of defined frequencies. The primary coil is 140 mm long, inner diameter of 10 mm, and 280 turns over three layers built on a PEEK former. Litz wire (200 strands, 0.071 mm width/strand) was used to reduce the effective impedance and negate the skin-depth effect. By itself, the primary coil generates a field of (27.5 ± 0.1) Oe/A with a field uniformity better than 2% over a 120 mm region. Two secondary coils wound in opposition were used to measure the sample signal as well as the field amplitude. Each coil consists of 18 turns of 0.2 mm copper wire. The high field (160 Oe/A), low current requirement is achieved through the use of three 40 mm long, 6 mm wide MnZn ferrite rods (Fair Rite, Material 78) [2]. This material provides a flux density of 4800 G at 5 Oe and 25°C measured at 10 kHz. A schematic of the primary and secondary coils is shown in Figure 1(a) while some of the measured hysteresis loops at 47 kHz are shown in Figure 1(b). The full description of the apparatus and the obtained data will be presented in the full paper.

[1] D. M. Clarke, and G. Valllejo-Fernandez, J. Magn. Magn. Mater. 552, 169249 (2022). [2] http://www.fair-rite.com/78-material-data-sheet/

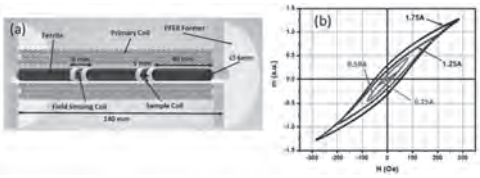

Figure 1. (a) Schematic diagram of the sensing setup and (b) Typical hysteresis loops measured at 47 kHz.

ROA-02. Development of a compact magnet for applying a highly uniform magnetic field to a diamond magnetic sensor by inverse problem analysis. *H. Tanaka*[1], Y. Murata[2], S. Yabukami[2] and A. Kuwahata[1] *1. Graduate School of Engineering, Tohoku University, Aobaku,Sendai, Japan; 2. Graduate School of Biomedical Engineering, Tohoku University, Aobaku,Sendai, Japan*

Magnetometer with diamond nitrogen-vacancy (NV) centers [1] is a highly-sensitive magnetic sensor under the application of a highly uniform (99.9%) bias magnetic field [2]. The integration of magnetometer with diamond NV magnetic sensors is required for various applications. However, there is a problem about the design of small magnet generating uniform magnetic field in the conventional methods. Therefore, in the study, we propose innovative method based on inverse problem approach for optimizing the shape of magnet. To optimize the shape of magnet, we estimate the shape of the magnet from the perfectly uniform magnetic field we set up. The magnet is groups of magnetic moment *m* as shown in Fig. 1(a). Figure 1(b) shows the optimized shape of magnet from the model of vertical rectangle. In Figure 1(c), we depicted cross-section of each z-stage of optimized the magnet vertical rectangle. Figure 1(d) shows the magnetic field *Bz* on the diamond surface. The uniformity was 98.5% before optimization and improved to 99.9% after optimization on the diamond surface. However, the uniformity on the entire diamond was low at 89.0%. To achieve the target magnetic field uniformity, we changed the thickness of the diamond NV center from 2mm to 0.1 mm and model from vertical rectangle to horizontal rectangle. Figure 2(a)(b) show the model of horizontal rectangle and the optimized shape of magnet. In Fig. 2(c), we depicted cross-section of each z-stage of optimized the magnet of horizontal rectangle. The magnetic field on the diamond surface was 99.6% and the uniformity of the entire diamond improved to 97.5%. We developed a method to determine the shape of a magnet from a highly uniform magnetic field. As the next step, we fabricate the optimized small magnet for diamond NV center and evaluate the improvement in magnetic sensitivity. Acknowledgement: This work was supported by the Uehara Memorial Foundation and Hitachi Global Foundation.

[1] A. Kuwahata *et al.*, *Scientific Reports* 10 (1), 1-9,(2020). [2] Alexander P. Nizovtsev *et al., nanomaterials* 11 (5), 1-13 (2021).

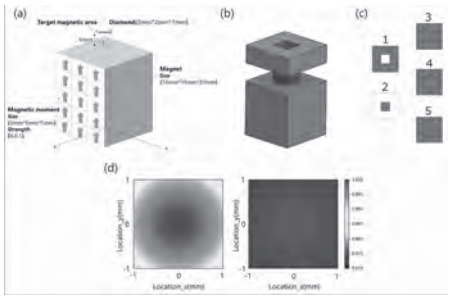

Figure 1. (a) The model of vertical rectangle before analysis. (b) Optimized the shape of magnet. (c) Cross-section of each z-stage of Fig. 1(b). (d) Magnetic field on diamond surface before and after analysis.

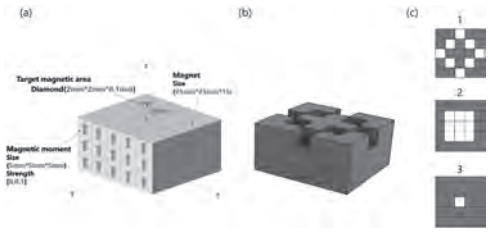

Figure 2. (a) The model of horizontal rectangle before analysis. (b) Optimized the shape of magnet. (c) Cross-section of each z-stage of Fig. 2(b).

ROA-03. Withdrawn

ROA-04. The Detection Limit of an Open-Source Magnetic Particle Spectrometer. *E. Mattingly*[1,2], A. Barksdale[3,2], E.E. Mason[2] and L. Wald[4,2] *1. Health Sciences and Technology, Massachusetts Institute of technology, Cambridge, MA, United States; 2. Martinos Center for Biomedical Imaging, Massachusetts General Hospital, Charlestown, MA, United States; 3. Electrical Engineering, Massachusetts Institute of Technology, Cambridge, MA, United States; 4. Radiology, Harvard Medical School, Boston, MA, United States*

Magnetic particle imaging (MPI) utilizes the nonlinear magnetic response of superparamagnetic iron oxide nanoparticles (SPIONs) for applications such as cell tracking, neuroimaging, and targeted hyperthermia. As SPIONs are central to MPI, understanding their properties is critical. A magnetic particle spectrometer (MPS) is often used to asses the SPIONs' magnetic properties. Despite MPS's utility in facilitating MPI research and nanoparticle chemistry, among other uses, there are limited commercial MPS devices and few comprehensive open-source resources on their construction and use. Here, we report the detection limit of an open-source MPS device [1]. Methods: Sensitivity limits were determined from an 11 phantom dilution series, each 4 μL of Synomag-D 70nm (Lot:16321104-02, Micromod Partikeltechnologie GmbH, Germany). Samples were placed in the apex of a microcentrifuge tube, ranging from undiluted (6 mg Fe/mL) to 0.98 μg Fe/mL. For each, we acquired three data-sets with 40 acquisitions (sinusoidal drive field, 10 mT, 23.8 kHz, 29 ms) with the sample in and 40 with the sample out. The mean of sample-in minus sample-out signal was plotted against SPION mass and fit using a linear regression. The detection limit was defined as the Fe mass at which the regression intercepted the standard deviation of the sample out acquisitions. We repeated this analysis for the 3rd, 5th, and 7th harmonic component of the signal. Results: The measured detection limit is 1.3 ng (fit R2=0.999) for the 3rd harmonic component of the signal, 4 ng for the 5th harmonic, and 7 ng for the 7th. Discussion: This open-source MPS device is relatively cheap and simple and has a sensitivity comprable or higher than other similar systems [2, 3, 4]. Iron laden cells carry roughly 50 pg per cell [4], thus we anticipate this detection limit to correspond to about 26 cells for those studies. Further, as the acquisition is only 29 ms per sample, and minimal sample preparation, it is well-suited for synthesis process validation.

[1] E. Mattingly, E. E. Mason, K. Herb, M. Sliwiak, K. Brandt, C. Z. Cooley, and L. L. Wald. OS-MPI: An open-source magnetic particle imaging project. International Journal on Magnetic Particle Imaging, 6(2):1–3, 2020. [2] M. Graeser, A. Von Gladiss, M. Weber, and T. M. Buzug. Two dimensional magnetic particle spectrometry. Physics in Medicine and Biology, 62(9):3378–3391, 2017. [3] N. Garraud, R. Dhavalikar, M. Unni, S. Savliwala, C. Rinaldi, and D. P. Arnold. Benchtop magnetic particle relaxometer for detection, characterization and analysis of magnetic nanoparticles. Physics in Medicine and Biology, 63(17), 2018. [4] N. Loewa, F. Wiekhorst, I. Gemeinhardt, M. Ebert, J. Schnorr, S. Wagner, M. Taupitz, and L. Trahms. Cellular uptake of magnetic nanoparticles quantified by magnetic particle spectroscopy. IEEE Transactions on Magnetics, 49(1):275–278, 2013.

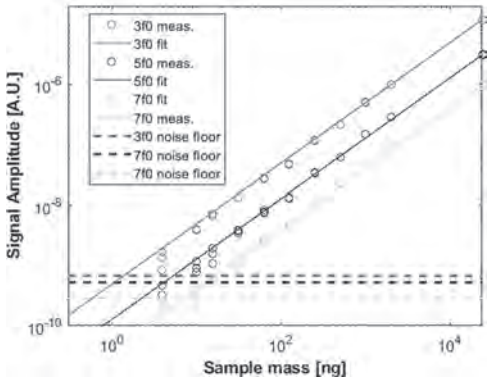

Fig. 1 Signal plotted as a function of SPION mass. Each circle is the mean measured signal of 40x 29 ms acquisitions, solid lines are the best fit, and dashed line is the noise floor for each harmonic.

INVITED PAPER

ROA-05. Scanning thermoelectric microscopy: applied to topological soliton systems. *C.W. Barton*[1], R. Puttock[1], E. Saugar[2], P. Klapetek[3], A. Fernandez-Scarioni[4], P. Frietas[5], K. Zeissler[1,6], A. Sola[7], V. Basso[7], M. Pasquale[7], H. Schumacher[4], T.A. Ostler[8], O. Chubykalo-Fesenko[2], C. Marrows[6] and O. Kazakova[1] *1. National Physical Laboratory, Teddington, United Kingdom; 2. Instituto de Ciencia de Materiales de Madrid (ICMM-CSIC), Madrid, Spain; 3. Czech Metrology Institute, Brno, Czechia; 4. Physikalisch-Technische Bundesanstalt, Braunschweig, Germany; 5. Instituto de Engenharia de Sistemas e Computadores (INESC-MN), Lisbon, Portugal; 6. University of Leeds, Leeds, United Kingdom; 7. Istituto Nazionale di Ricerca Metrologica, Turin, Italy; 8. Sheffield Hallam University, Sheffield, United Kingdom*

The interplay between thermal gradients and magnetic topological soliton systems represents an exciting frontier in the understanding of novel thermo-magnetic interactions at the nanoscale [1,2]. Thermally driven non-equilibrium spin polarised charge currents and their interaction with the non-trivial topology of skyrmions is central in understanding phenomena such as the topological Nernst effect in chiral magnetic systems within the context of spin caloritronics [3]. In this talk we will address aspects of scanning thermoelectric microscopy (SThEM), Fig 1 (a), where, we will present a novel thermal scanning probe technique that allows us to locally investigate the thermoelectric response from the magnetic domain structure in YIG [4] to nanomagnetic topological solitons: domain-walls and skyrmions. By building up a localised picture of the resulting spatially resolved electric field we can build an understanding of the underlying spin configuration. We will discuss experimental and modelling results which elucidate to the local response from a pinned domain wall system in an ultra-thin magnetic layer, Fig 1(b). We demonstrate that the domain-wall introduces an additional contribution to the total measured signal, Fig 1(c), which can only arise if we assume a Néel type domain-wall. We will also report on local thermoelectric measurements of skyrmionic systems where we have investigated a set of device structures based on chiral magnetic multilayers, Fig 1(d). Image Caption: Fig. 1. (a) Schematic representation of the sThEM measurement setup used in this work showing the heated AFM probe used to apply the local thermal gradient. The electric field is probed along the device and the integrated response is mapped pixelwise. (b-c) sThEM micrographs for saturated and domain wall pinned configurations, respectively. (d) sThEM micrograph of a skyrmion nucleated in a chiral magnetic multilayer.

[1] Jakub Zázvorka, et al, Thermal skyrmion diffusion used in a reshuffler device Nature Nanotechnology, 14, 658–661 (2019). [2] Zidong Wang et al, Thermal generation, manipulation and thermoelectric detection of skyrmions, Nature Electronics, 3, 672–679 (2020). [3] Alexander Fernández Scarioni, Craig Barton, et al, Thermoelectric Signature of Individual

Skyrmions, Phys. Rev. Lett. 126, 077202, (2021). [4] Alessandro Sola, Craig Barton, et al, Phys. Rev. Applied 14, 034056, (2020).

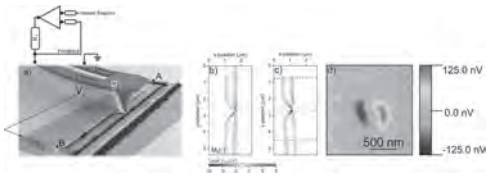

Fig. 1

CONTRIBUTED PAPERS

ROA-06. Automated Acquisition of Switching Dynamics in Reflexion Mode of MRAM Magnetic Tunnel Junctions. *S. Lequeux*[1], M. Mansueto[1], Q. Stainer[1], A. Bussiere[1], G. Zahnd[1], A. Chavent[1] and S. Salimy[1] *1. Hprobe, Grenoble, France*

Switch timings of MRAM technologies, such as Spin Transfer Torque (STT) and Spin Orbit Torque (SOT), are critical in the context of SRAM replacement for last level cache applications [1]. The operating conditions of Magnetic tunnel junction (MTJ) result from the compromise between writing current level, retention and stability during read operation. To optimize the operating conditions for a given application and tune the physical parameters of the MTJs, we propose a new system able to extract the incubation and switching times under writing pulses application. The proposed system operates by acquiring and analyzing the reflected signal of the writing pulse applied on the MTJ, which could be a 2 or 3 terminal (STT[2] or SOT[3]) MRAM. The test system includes a pulse generator, a set of RF circuits and a high-resolution scope. The test sequence operates in a fully automated manner, in a 2 steps process. Firstly, an average signal in both P (red line) and AP (blue line) states are acquired as reference measurements. Secondly, single shots or averaged measurements of the switching events are acquired and the reference data is subtracted, as shown in Fig.1 on STT-MRAM devices. The probability of switching and average switching time versus pulse amplitude and width can be extracted. The validity of fast macrospin switching, without any domain wall formation can be verified. With single shot measurements, switching time of single events can be acquired, as well as the incubation time before the switching occurs [2]. The full test flow is executed in a few seconds, enabling the possibility to test population of devices using automated probing stations. Using the system and our 3D magnetic generator, the test protocol can also be executed under application of an external magnetic field to study the field immunity of the device and the corresponding influence on the switching dynamics.

[1] P. Barla, V. K. Joshi, and S. Bhat, J. Comput. Electron. 20, 805–837 (2021). [2] J. Sampaio, S. Lequeux, P. Metaxas, *et al.*, APL 103, 242415 (2013). [3] E. Grimaldi, V. Krizakova, G. Sala, *et al*., Nature Nanotechnology 15, pages111–117 (2020).

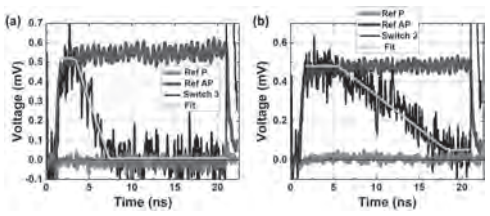

Fig. 1 Switching events measured in real-time with Hmap 2 software, pulse of 0.4V and 25 ns duration. The P and AP signals (red and blue lines) are both substracted to the P one. The signal of the switching event (black line) is averaged over 10 measurements. The orange line shows a linear fit of the switching.

ROA-07. Exploring antiferromagnetic resonances of NiO with frequency-domain THz spectroscopy. *T. Jeffrey*[1], W. Wu[2], J. Avenoso[2], L. Gundlach[2], J. Xiao[2], M. Jungfleisch[2] and J. Sklenar[1] *1. Physics and Astronomy, Wayne State University, Detroit, MI, United States; 2. Physics and Astronomy, University of Delaware, Newark, DE, United States*

The characterization and analysis of magnetization dynamics and magnetic damping of antiferromagnetic magnons is important in the field of antiferromagnetic spintronics. This is primarily because antiferromagnets have magnetic resonances in the THz range as compared to ferromagnetic resonance which tends to occur in the GHz range. In this work, we employ frequency-domain THz spectroscopy to explore the antiferromagnetic resonance frequency associated with monocrystalline NiO [1]. Specifically, a continuous-wave THz spectroscopy system is used to measure the antiferromagnetic resonance of three NiO cuts (111), (110), and (100). To find the absorption peak, a reference measurement is taken in addition to the NiO measurement. Raw data from the reference and NiO can be visually compared to see two effects: the THz system instrument response and Fabry-Perot interference pattern. During analysis, the instrument response and Fabry-Perot pattern are subtracted so that a clear absorption peak at the resonant frequency of NiO can be observed. An antiferromagnetic resonance, near 1 THz, is seen in each cut of NiO. Our results demonstrate the utility of working in the frequency domain to characterize antiferromagnetic materials that will be used eventually for ultrafast antiferromagnetic spintronic device technologies.

[1] Moriyama, Takahiro, et al., *Physical Review Materials* 3.5, 051402 (2019)

ROA-08. A Ferris-wheel ferromagnetic resonance technique for measurement of spin currents at the wafer level. *A. Rothschild*[1], N. Am-Shalom[1], N. Bernstein[1], M. Meron[1], T. David[1], E. Frohlich[1], B. Assouline[1] and A. Capua[1] *1. The Hebrew University of Jerusalem, Jerusalem, Israel*

We present a new ferromagnetic resonance (FMR) method that we term the "Ferris" FMR. In contrast to conventional FMR techniques where the sensitivity is achieved by a small signal modulation of the external magnetic field, here we apply a large amplitude modulation. This results in an FMR technique that is wideband, has significantly higher sensitivity as compared to conventional FMR systems, and measures the absorption lineshape rather than its derivative. Most importantly, the large-amplitude modulation turns out to expand the measured linewidth by ~ 3 times. Consequently, the spin Hall angle can be reliably resolved at lower current density and the measurement of Θ_{SH} becomes possible even at the wafer scale without patterning devices.

ROA-09. Neural Networks for Pattern Detection in Noisy signals for Eddy-current-based Non-Destructive Testing. *D.M. Caetano*[1,2] and S. Cardoso[3,2] *1. Advanced Sensor Interfaces and Circuits, INESC MN, Lisbon, Portugal; 2. Instituto Superior Técnico, Lisbon, Portugal; 3. SPINTRONICS AND MAGNETIC BIOSENSORS, INESC MN, Lisbon, Portugal*

Detecting of hole-like defects in materials is extremely important for production quality assurance, and safety applications; particularly when a single failure can result in catastrophic consequences, including injury or even loss of life. Non-destructive tests assess these characteristics without compromising the materials' integrity. One method for such evaluations uses perturbances in induced eddy currents to determine the existence of buried or surface defects. In [1] we proposed a probe and signal acquisition system based magnetoresistive sensors capable of acquiring the eddy currents' weak field. This work showed unprecedented spatial resolution (160 μm minimum defect distance) and the capacity for the detection of micrometric surface defects (50 μm smallest defect). In this work, we use our patented artificial neural networks (ANN) approach [2] that analyzes our probes' 2D scans and

accurately pinpoint hole-like defects even in very noisy signals (SNR below 6 dB). Figure 1 shows the full system and test setup comprising a probe, an acquisition system, a PC, and an XY table. The material under test is an aluminum mockup with drilled holes tested on the non-drilled side of the mockup. Figure 2 a) and b) shows the results of the test before and after the ANNs. The ANNs are designed and trained to detect the gaussian monocycle pattern that can be seen in Figure 2 c)-e). Their input is a 1D selection of N samples of the probe's 2D output. The number of samples is customizable (100 in this case). The algorithm is run, vertically, as a sliding window from top to bottom for every column. With this method, it is possible to detect a 100 μm defect even at 500 μm of depth.

[1] D. M. Caetano, T. Rabuske, J. Fernandes, M. Pelkner, C. Fermon, S. Cardoso, B. Ribes, F. Franco, J. Paul, M. Piedade e P. P. Freitas, "High-Resolution Nondestructive Test Probes Based on Magnetoresistive Sensors,," *IEEE Transactions on Industrial Electronics, vol. 66, no. 9, pp. 7326-7337,* September 2019. [2] D. M. Caetano, T. Rabuske, J. Silva, J. Fernandes e G. Tavares, "METHOD OF DETECTION AND CLASSIFICATION OF NON-PERIODIC SIGNALS AND THE RESPECTIVE SYSTEM THAT IMPLEMENTS IT,". Portugal Patente WO/2021/125987, 16 12 2020. [3] G. Almeida, J. Gonzalez, L. Rosado, P. Vilaça e T. G. Santos, "Advances in ndt and materials characterization by eddy currents," em *Proceedings CIRP, vol. 7, pp. 359–364 Sixth CIRP Conference on Manufacturing Systems 2013*, 2013.

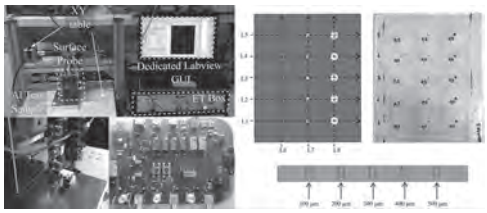

Figure 1: NDT system, probe, and Aluminum mock-up described in [3] with boreholes with diameters from 1 mm to 100 μm and distances to the opposing surface between 100 and 500 μm.

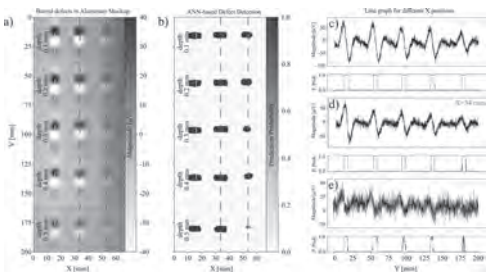

Figure 2: Scan of the mockup in Figure 1. The measurement is taken from the opposite side of the drilled openings. a) direct output from the probe, b) ANN's output, c-e) line plot for different X positions and ANN's output.

ROA-10. Trapped Flux Induced Artifacts in Magnetization Measurements of Thin Films Grown on Large Paramagnetic Substrates. *M. Roos*[1] and B. Zink[1] *1. Physics and Astronomy, University of Denver, Denver, CO, United States*

Materials used in spintronics and spin caloritronics, such as thin film ferrimagnetic yttrium iron garnet (YIG), are often grown on bulk substrates, such as gadolinium gallium garnet (GGG), due to their exceptional lattice matching and disordered magnetism.[1] Magnetometry measurements can resolve YIG thin films down to a few nanometers, but assuming a linear paramagnetic background when accounting for the GGG substrate can contribute significant artifacts in the resulting signal.[2] Superconducting magnet coils are susceptible to trapped flux, leading to measurements performed in the their fields to require precise calibration of the resulting magnetic field, particularly on films with small coercivites or grown on substrates with large paramagnetic susceptibilities. Using a 20nm YIG thin film grown on GGG as an example, we show that performing a simple linear paramagnetic background subtraction can produce artifacts, including negative remanence, vertical exchange bias, and shifts along the field axis. We demonstrate that direct measurements of standalone substrates in carefully reproduced field conditions and field correcting with a standard reference are two ways to minimize the inclusion of these magnetic artifacts in quantitative magnetometry measurements.

[1] H. Chang, P. Li, W. Zhang, T. Liu, A. Hoffmann, L. Deng, and M. Wu, Nanometer-thick yttrium iron garnet films with extremely low damping. IEEE Magn. Lett. 5, 1 (2014) [2] Roos, M. J., Quarterman, P., Ding, J., Wu, M., Kirby, B. J., & Zink, B. L.. Magnetization and antiferromagnetic coupling of the interface between a 20 nm $Y_3Fe_5O_{12}$ film and $Gd_3Ga_5O_{12}$ substrate. Physical Review Materials, 6(3), 034401 (2022)

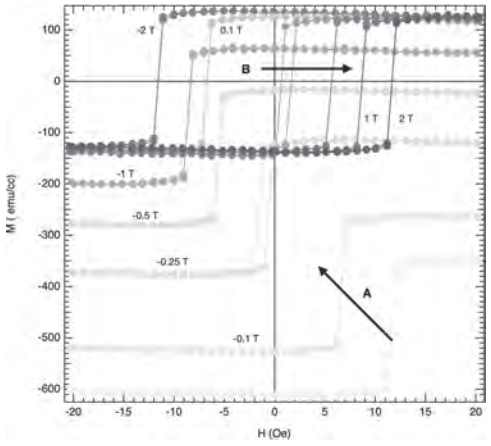

Fig. 1 Hysteresis loops of YIG with changing magnetic field histories and induced trapped flux for it and the directly subtracted GGG background. A) Direct subtraction of GGG taken with a different field history as the YIG causes vertical shifts. A 2 T field was initially applied to the YIG, then the trapped flux was shifted by applying the labeled field before each loop. B) Direct subtract of GGG with an identical field history shows the horizontal shift due to the trapped flux. Coercivities at this temperature are much less than 1 Oe.

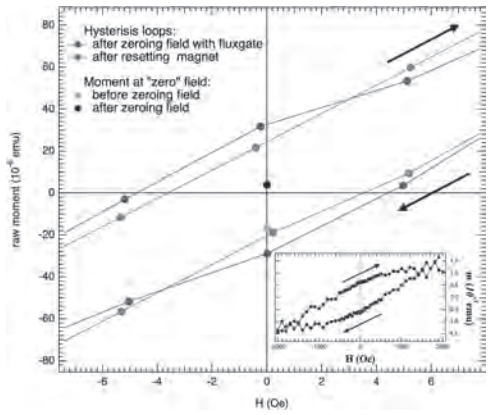

Fig. 2 Performing magnetometry on a GGG substrate in a superconducting magnet. Trapped flux induced during a 2000 Oe field hysteresis loop causes an apparent negative remanence, and can not be removed by resetting the magnet or zeroing the field with a fluxgate. The negative remanent disappears in a true zero field. Any appreciable field must be corrected for by a reference standard. Inset: the full field hysteresis loop.

ROA-11. Angular Dependence of Spin Polarization in Negatively Charged NV Defects in Diamond under Laser Illumination. *A. Patel*[1], Z. Chowdhry[2] and P. Bhallamudi[2,1] *1. Electrical Engineering, Indian Institute of Technology, Madras, Chennai, India; 2. Physics, Indian Institute of Technology, Madras, Chennai, India*

Nitrogen-Vacancy spins in diamonds are currently of great interest due to applications in nanoscale imaging and spectroscopy, masing and quantum technologies. The enhancement of spin polarization due to laser illumination is a key property that enables these applications [1] (ref Fig. 1). Understanding the dependance of NV spin-polarization on the angle between NV-axis and the magnetic field that is typically applied for these applications is important. Here I will present the results of our detailed measurements of the spin polarization of NV centers using an X-Band electron paramagnetic resonance spectrometer, both as a function of angle between the NV axis and the static magnetic field and the laser illumination power. We measured the signal for all three NV ground-state spin transitions, both single and double quantum transitions, with high resolution. We then compare these experimental results with a commonly used 7-level model [3], while accounting for spin mixing between the levels due to the large off axis component of the static field. While the overall trend broadly matches what is expected from the models, we surprisingly see the spin-polarization does not quench as quickly with NV-magnetic field angle as predicted by the model and is typically assumed. While similar observation has been reported [4] but not carefully studied, having both power and angular dependance allows us to rule out many spurious effects. We will discuss possible explanations for our data. This result has implications for future masing and other applications based on NV-diamonds.

[1] R. Schirhagl, K. Chang, et al., Annual review of physical chemistry, Vol. 65, p.83-105 (2014) [2] A. Patel, Z. Chowdhry, et al., 2021 IEEE Research and Applications of Photonics in Defense Conference (RAPID). IEEE, p.1-3 (2021) [3] J.P. Tetienne, L. Rondin, et al., New Journal of Physics Vol. 14.10, p.103033. (2012) [4] A. Sherman, L. Buchbinder, et al., Journal of Applied Physics, Vol. 129.14, p.144503 (2021)

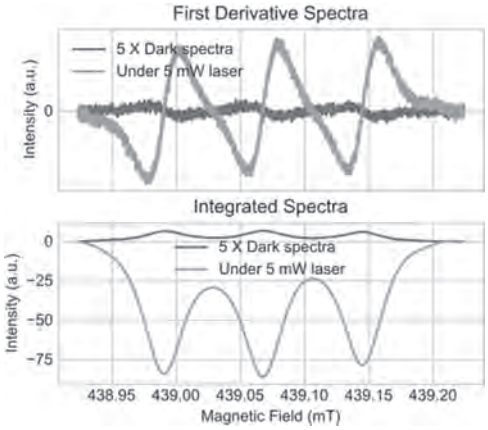

Fig. 1: X-Band EPR spectra of the masing transition. The inverting of the peak signifies population inversion and the significant increase in intensity is due to spin polarizaion under laser illumination. [2].

Session ROB
RECENT ADVANCES IN MAGNETIC IMAGING

Roopali Kukreja, Co-Chair
University of California, Davis, Davis, CA, United States
Nanna Zhou Hagström, Co-Chair
Stockholm University, Stockholm, Sweden

CONTRIBUTED PAPERS

ROB-01. Magnetization Reversal and Domain Structures in Perpendicular Synthetic Antiferromagnets Prepared on Rigid and Flexible Substrates. *S. Mohanty*[1], M. Sharma[1], A.K. Moharana[1], B. Ojha[1], E. Pandey[1], B.B. Singh[1] and S. Bedanta[1] *1. Physics, National Institute of Science Education and Research, Bhubaneswar, Jatni, India*

Synthetic antiferromagnets (SAF) are basically two ferromagnetic (FM) layers separated by a nonmagnetic spacer layer where both the FM layers are coupled antiferromagnetically. With metallic spacer, the coupling is dominated by Ruderman-Kittel-Kasuya-Yosida (RKKY) interaction [1, 2]. Here, we have studied magnetization reversal by varying the number of bilayer stacks [Pt/Co] as well as thicknesses of Ir space layer t_{Ir} on rigid Si (100) and flexible polyimide substrates. The sample with t_{Ir} = 1.0 nm shows a FM coupling, whereas sample with t_{Ir} = 1.5 nm shows an antiferromagnetic (AFM) coupling between the FM layers. The hysteresis loop measured by SQUID-VSM for two of our samples with t_{Ir}=1.5nm have been shown in fig1. At t_{Ir} = 2.0 nm, a bow-tie shaped hysteresis loop is observed indicating a canting of magnetization at the reversal. Higher anisotropy energy compared to the interlayer exchange coupling (IEC) energy is an indication of the smaller relative angle between the magnetization of lower and upper FM layers. We have also demonstrated the strain-induced modification of IEC as well as magnetization reversal phenomena. The IEC shows a slight decrease upon application of compressive strain and increase upon application of tensile strain, which indicates the potential of SAFs in flexible spintronics [3].

[1] R. Duine et al., "Synthetic antiferromagnetic Spintronics" Nat. Phys. 14(3), 217 (2018). [2] P. Bruno et al., "Oscillatory coupling between ferromagnetic layers separated by a nonmagnetic metal spacer", Phys. Rev. Lett. 67(12), 1602 (1991) [3] S. Mohanty et al., "Magnetization Reversal and Domain Structures in Perpendicular Synthetic Antiferromagnets Prepared on Rigid and Flexible Substrates", JOM, Vol. 74, No. 6, (2022).

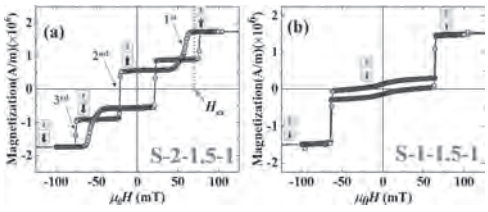

Fig. 1 Hysteresis loop measured by SQUID-VSM for samples (a) S-2-1.5-1 and (b) S-1-1.5-1 where the magnetic field was applied perpendicular to the film plane. S-2-1.5-1 is the sample with two layers of [Pt/Co] below and one layer of [Pt/Co] above the Ir spacer layer and S-1-1.5-1 is the sample with one layers of [Pt/Co] below and one layer of [Pt/Co] above the Ir spacer layer. In bothe the sample shown above, the Ir layer thickness is 1.5nm.

ROB-02. Phase Coexistence and Transitions between Anti- and Ferromagnetic States in a Synthetic Antiferromagnet. *C.E. Barker*[1], C.W. Barton[2], E. Haltz[1], F. Maccherozzi[3], B. Sarpi[3], S. Dhesi[3], O. Kazakova[2], T.A. Moore[1] and C. Marrows[1] *1. School of Physics and Astronomy, University of Leeds, Leeds, United Kingdom; 2. Quantum Technologies, National Physical Laboratory, Teddington, United Kingdom; 3. Diamond Light Sourice ltd, Harwell, United Kingdom*

Skyrmions—topologically protected vortex-like spin structures—have been proposed as the new information carriers in racetrack memory devices [1]. In order to realise such devices a small size, high speed of propagation, and minimal deflection angle are required. Modelling has shown that synthetic antiferromagnets (SAFs) present the ideal materials system to realise these aims [2]. However, their magnetic compensation makes observation of skyrmions difficult and indeed this was only recently achieved [3]. There is thus significantly more to understand about the behaviour of synthetic antiferromagnets and the skyrmions therein. Here we present a comprehensive magnetic force microscopy (MFM) and XMCD-PEEM study of a SAF multilayer composed of 20 magnetic layers alternating between CoB and CoFeB each coupled antiferromagnetically with a Ru spacer layer to the one above and below. PEEM results show that in the SAF phase the sample is spontaneously single-domain, and when exposed to a complicated field protocol, large defect-pinned domains can be stabilized. As shown in the hysteresis loop presented in Fig. 1 the SAF undergoes a phase transition between the compensated antiferromagnetic state and its field-polarised ferromagnetic state as a field is applied. MFM shows that in our samples this is as a result of defect-driven bubble nucleation where FM ordered regions nucleate and then expand to cover the entire film. Once the FM regions exceed a critical size they collapse into a skyrmion/stripe domain pattern and so retain a net zero magnetisation. At a narrow range of fields, e.g. as shown in Fig. 2 we observe a phase coexistence between the compensated AF state and the net-zero magnetisation FM state. As the magnetic field is increased we go on to observe isolated skyrmions at fields below saturation as expected in a FM system. These results give perspective on the ferromagnetic nature of skyrmions observed in systems at fields just below saturation and can help to inform the observation of true antiferromagnetic skyrmions.

[1] S. P. Parkin et al., Science 320, 190 (2008) [2] X. Zhang et al., Nature Communications 7, 10293 (2016) [3] W. Legrand *et al.*, Nature Materials 19, 34 (2020)

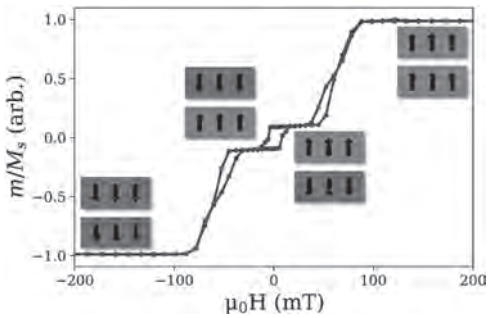

Fig. 1 M-H loop of our SAF along with a depiction of the magnetic order at each step.

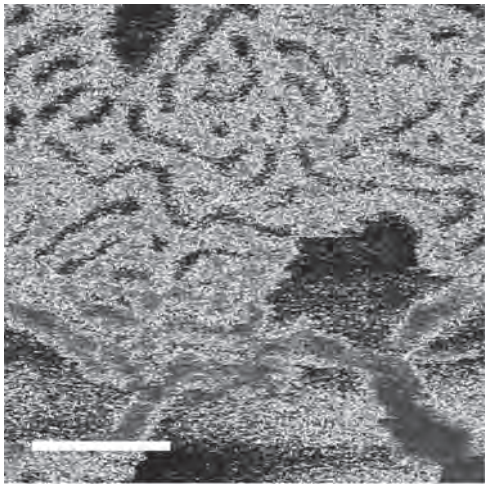

Fig. 2 Mixed phase state of our sample showing FM ordered chiral domains alongside SAF ordered single domains

ROB-03. Investigation of Ferro- and Antiferromagnetic Memory Structures using Scanning NV Magnetometry. *P.S. Rickhaus*[1], U. Celano[2], L. Zaper[1], A. Stark[1], M. Munsch[1], H. Zhong[1], C. Adelmann[2], P. van der Heide[2], A. Finco[4], V. Jacques[4], V. Garcia[5] and P. Maletinsky[3]
1. Qnami AG, Basel, Switzerland; 2. IMEC, Loewen, Belgium; 3. Departement of Physics, University of Basel, Basel, Switzerland; 4. Université de Montpellier, Montpellier, France; 5. CNRS Thales, Paris-Saclay, France

To improve magnetic memories, significant efforts are made to reduce the size and spacing of magnetic bits. This implies that failures and defects can only be discovered with a non-invasive technique that can resolve small magnetic fields with high spatial resolution. Scanning NV magnetometry (SNVM) is the emerging quantum sensing technique that offers the required sensitivity. We will demonstrate magnetic images of a few hot candidate materials for future magnetic memory devices. We will look at memory bits in antiferromagnetic chromia, antiferromagnetic cycloids in BiFeO3 [1], cobalt nanomagnets and ultra-scaled CoFeB nanowires [2]. We will reveal magnetic textures that are undetectable with standard characterization techniques. In this context, we will more broadly discuss the potential of SNVM as a powerful magnetic characterization tool.

[1] Phys. Rev. Applied 17, 044051 (2022) [2] Nano Lett. 21, 24, 10409–10415 (2021)

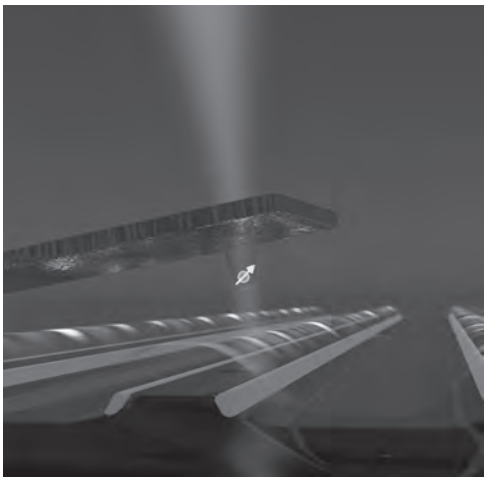

Fig. 1 Scanning NV microscopy is used to investigate nanowires for racetrack memory

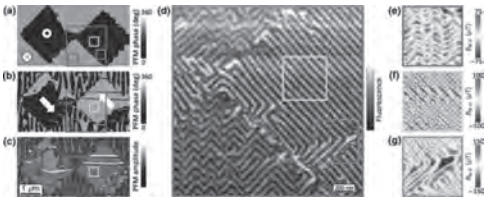

Fig. 2 Spin cycloids in BFO imaged with Scanning NV microscopy

INVITED PAPER

ROB-04. Magnetization Reconstruction Of Skyrmionic Textures From Lorentz TEM With Convolutional Neural Network. Y. Ren[1,2], X. Chen[1], *J. Kong*[3], H. Tan[1], H. Tan[1] and A. Soumyanarayanan[1,2] *1. Institute of Materials Research and Engineering, A*STAR, Singapore; 2. Department of Physics, National University of Singapore, Singapore; 3. Institute of High Performance Computing, A*STAR, Singapore*

Lorentz transmission electron microscopy (LTEM) is a high-resolution imaging technique used extensively to study complex magnetic configurations in chiral magnetic nanomaterials. However, the inference of the underlying magnetic configuration from the imaged domain wall contrast is not a straightforward task. Here we present a fully convolutional neural network (CNN) model that accepts an input LTEM image and predicts the corresponding magnetic domain configuration. A schematic of the workflow is shown in Fig. 1. Equilibrium magnetic domain configurations were generated with MuMax3 [1] using realistic magnetic parameters of chiral multilayers, and the corresponding LTEM images were obtained using MALTS [2] to train the CNN. A physics-inspired loss function mimicking the micromagnetic energy was used in the model training. We performed hyperparameters tuning and the best model was selected based on the validation outcomes. Representative examples of the model predictions are shown in Fig. 2. The trained model performs remarkably well when tested with fresh simulated LTEM images and gives reasonable predictions when applied to LTEM images from experiments. In addition, the model is capable of reliably predicting both the location and shape of the domains, as well as the Néel character of the domain walls. The success of the model is partially attributed to its custom loss function which penalizes physically unrealistic predictions. We thus demonstrate that deep learning can be an effective tool in the interpretation of LTEM images, paving the way towards more efficient material characterization and device developments.

1. A. Vansteenkiste, J. Leliaert, M. Dvornik, et al., AIP Advances 4, 107133 (2014). 2. S. Walton, K. Zeissler, W. Branford, et al., IEEE Transactions on Magnetics 49, 4795-4800 (2013).

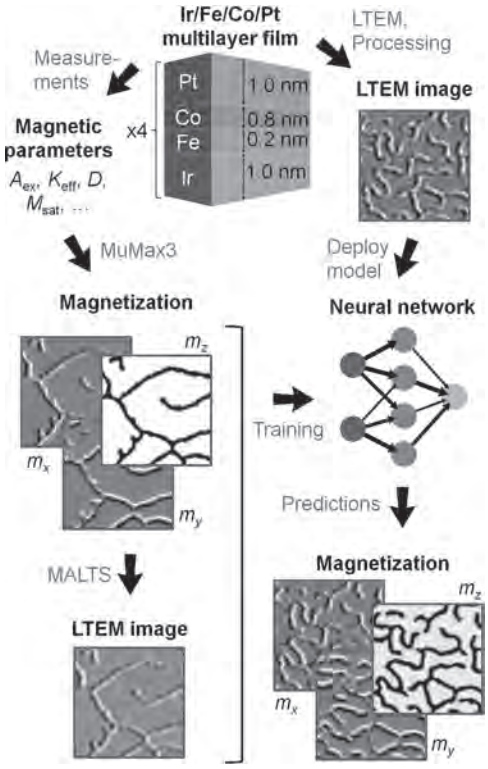

Fig. 1. Schematic of the workflow. Magnetic parameters based on experimental measurements were used to generate simulated LTEM training data. Trained CNN model was then used to infer the magnetization configurations from experimental LTEM images.

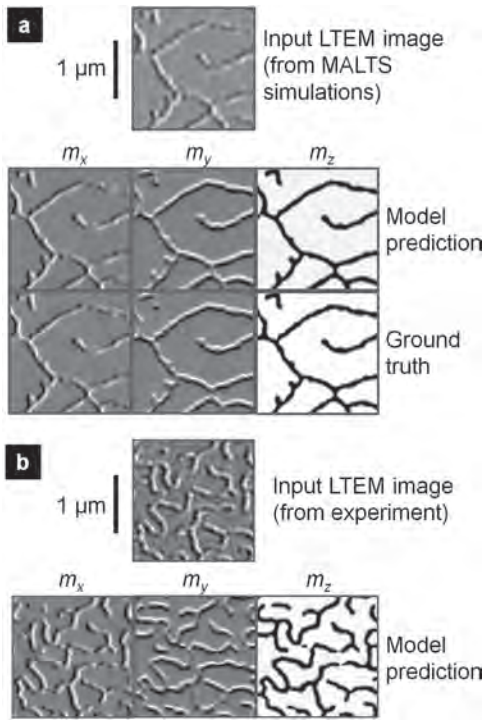

Fig. 2. Representative output of the trained model when given (a) a simulated LTEM image, and (b) an experimental LTEM image. In (a) we also show the actual magnetization configuration used to generate the simulated LTEM image for comparison to the predictions. In both (a) and (b), the model was able to infer realistic magnetization configurations.

CONTRIBUTED PAPERS

ROB-05. Phase Coexistence in a Chiral Synthetic Antiferromagnet Observed Using Lorentz Transmission Electron Microscopy.

K. Fallon[1], C.E. Barker[2], C. Kirkbride[1], S. Villa[1], D. McGrouther[1], T.A. Moore[2], G. Burnell[2], C. Marrows[2] and S. McVitie[1] *1. University of Glasgow, Glasgow, United Kingdom; 2. University of Leeds, Leeds, United Kingdom*

Chiral magnetic textures in perpendicularly magnetised synthetic antiferromagnets (SAFs) hold a lot of promise for device applications. Domain wall velocities up to 750 ms^{-1} have been demonstrated in [1] and attractive modifications to skyrmion properties are expected [2]. Through magnetic compensation, skyrmions in synthetic antiferromagnets (SAFs) are predicted to be smaller than their ferromagnetic (FM) counterparts and have a suppressed skyrmion Hall angle [3] (in FM systems this results in skyrmion motion at an angle to the driving force [4]). Here we study the field-driven transition between AF and FM interlayer alignment via Lorentz TEM. This transition is not widely studied and full characterisation is an important prerequisite for SAF-based devices. The sputter-deposited sample has structure $[Pt(3.5)/CoFeB(5)/Ru(5)/Pt(3.5)/CoB(8)/Ru(5)]_{x10}$ (thicknesses in Å). The hysteresis loop, measured with SQUID-VSM, typical of SAFs, is shown in Fig. 1. Fresnel imaging was performed in an external magnetic field to drive magnetisation reversal from positive to negative saturation. In this sample, the zero-field AF-aligned state appears to be uniform (corroborated by PEEM imaging). However, rich textures are observed during the AF to FM transition (over the pink region in Fig. 1) with two distinct types of contrast. Coexistence of these is illustrated in the Fresnel image in Fig. 2 where the contrast in the LHS of the image is both lower intensity and wider periodicity than the RHS. The transition begins via formation of the wide period texture (LHS Fig. 2) which first nucleates at -66 mT. The narrow period texture

first appears at -69 mT and by -80 mT covers the field of view. As the latter texture dominates at high fields we deduce it to be FM-aligned spin-spirals typical of chiral FM multilayers. The AF to FM transition takes place via the formation of an intermediate phase, which coexists with the multidomain FM state, which we are quantifying using LTEM.

[1] S.-H. Yang, K.-S. Ryu, and S. Parkin, Nature Nanotechnology, 10, 221–226 (2015) [2] W. Legrand, D. Maccariello, and F. Ajejas, Nature Materials, 19, 34–42 (2020) [3] T. Dohi, S. DuttaGupta, and S. Fukami, Nature Communications, 10, 5153 (2019) [4] W. Jiang, X. Zhang, and G. Yu, Nature Physics, 13, 162–169 (2017)

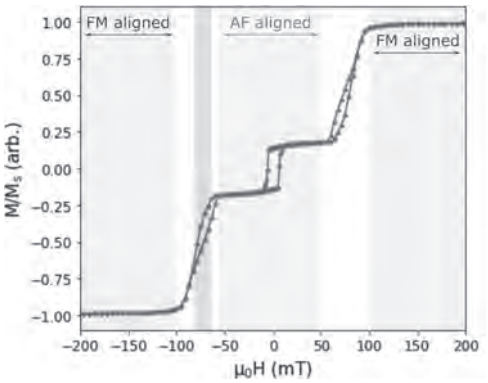

Fig. 1 Hysteresis loop of sample. The pink band between -66 mT and -80 mT highlights the field range where phase coexistence is observed.

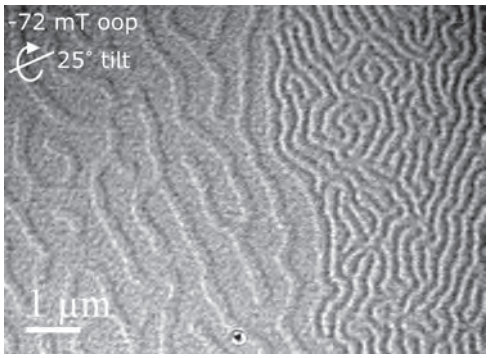

Fig. 2 Fresnel image taken during magnetisation reversal with two distinct types of contrast visible.

ROB-06. Ultrafast Lorentz Microscopy with Magnetic Field Excitation at Microwave Frequencies. *J.T. Weber*[1], N. Porwal[1], A. Wendeln[1], M. Winklhofer[1] and S. Schäfer[1] *1. University of Oldenburg, Oldenburg, Germany*

With the recent progress in pulsed high-brightness photocathodes, Lorentz imaging approaches in ultrafast transmission electron microscopy (UTEM) now offer a pathway for the investigation of magnetization dynamics with nanometer spatial and femtosecond temporal resolution [1,2]. Extending the available frequencies in field-driven ultrafast Lorentz microscopy to the GHz range, we developed an in-situ radiofrequency (RF) excitation sample holder for transmission electron microscopy based on a two-dimensional microwave cavity (Fig. 1a,b). As a first test case, we investigated ferromagnetic resonances in permalloy stripe arrays (Fig. 1f) which support localized magnonic modes identified by the back-reflected RF power (Fig. 1d,g). For ultrafast Lorentz microscopy, the RF excitation is phase-locked to the nanolocalized photoemission of ultrashort electron pulses from a Schottky field emitter, using high harmonics of an amplified laser system as a master clock for their synthetization [3]. Phase-resolved ultrafast Lorentz micrographs are expected to yield high-contrast FMR mode mapping. A simulated micrograph is shown in Fig. 1c. With these developments, we aim to establish ultrafast Lorentz microscopy as a versatile lab-scale imaging tool for femtosecond and picosecond transient states in ultrafast magnetism and magnonics.

[1] N. Rubiano da Silva et al., Phys. Rev. X 8, 031052 (2018). [2] M. Möller et al., Commun. Phys. 3, 36 (2020). [3] M.R. Otto et al., Struct. Dyn. 4, 051101 (2017).

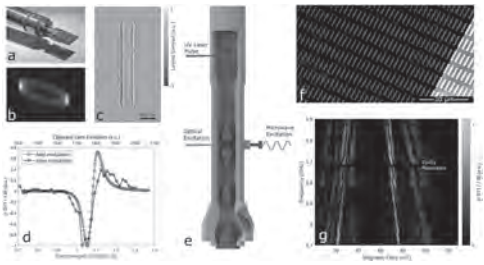

Fig. 1: Ultrafast Lorentz microscopy with (a) Self-build TEM sample holder with planar microresonator. (b) Time-averaged electron trajectories deflected by resonator microwave fields. (c) Simulated Lorentz contrast of a permalloy (Py) stripe excited at a ferromagnetic resonance. (d) Microwave absorption spectrum of a 25 nm Py film measured by lock-in amplification with field modulation (red circles) and by pulsed laser induced temperature modulation inside the electron microscope (black circles). (e) Overview of the Oldenburg UTEM instrument with microwave sample excitation. (f) Scanning electron micrograph of a Py stripe array on a silicon nitride membrane. (g) FMR frequency vs magnetic field map of the Py stripe array exhibiting avoided crossings at the resonance frequency of the planar microcavity.

ROB-07. Mapping In-situ Morphological Phase Transitions of Magnetic Domains in $[Co/Pt]_N$ under applied magnetic field. *M.M. Vaka*[1], J. Ray[1], C. Richards[1], O. Hellwig[2] and K. Chesnel[1] *1. Physics and Astronomy, Brigham Young University, Provo, UT, United States; 2. Chemnitz University of Technology, Chemnitz, Germany*

Ferromagnetic thin films with perpendicular magnetic anisotropy (PMA) provide an excellent support to develop media for high-density magnetic recording. To optimize the density of magnetic domains and control the magnetic response of the magnetic film to an applied magnetic field, further understanding of the domain pattern formation and evolution throughout the magnetization process is necessary. Here we study the in-situ morphology of magnetic domains in $[Co/Pt]_N$ multilayered thin films with PMA via magnetic force microscopy (MFM). We found that the domain pattern evolves between three distinct topologies: bubble pattern, short stripe pattern, and maze pattern. Previous studies[1-4] have demonstrated that the morphology of these patterns at remanence depends on the number of bilayer repeats, layer thickness, and maximum of the previously applied field. Here we extend the remanence study to explore the evolution of the domain patterns under in-situ magnetic field. Domain density and interdomain distance are key metrics for quantifying morphological changes in the domain patterns, as illustrated in Figure 1. Using MFM, we mapped the domain density and interdomain distance in response to the in-situ and maximum applied magnetic field up to 7.2 kOe. We completed these studies for layer repeats of N from 20 down to 10 and Co thicknesses from 30 Å down to 10 Å. We found three main types of in-situ phase transitions, which result in the previously observed remanent phase transitions Additionally, we found that the domain density is maximized with in-situ applied field when $N = 20$ with Co thicknesses of 30 Å.

1. A. S. Westover, K. Chesnel, K. Hatch, P. Salter and O. Hellwig, Journal of Magnetism and Magnetic Materials 399, 164-169 (2016). 2. K. Chesnel, A. S. Westover, C. Richards, B. Newbold, M. Healey, L. Hindman, B. Dodson, K. Cardon, D. Montealegre, J. Metzner, T. Schneider, B. Böhm, F. Samad, L. Fallarino and O. Hellwig, Physical Review B 98 (22), 224404 (2018). 3. Fallarino, A. Oelschlägel, J. A. Arregi, A. Bashkatov, F. Samad, B. Böhm, K. Chesnel and O. Hellwig, Physical Review B 99 (2), 024431 (2019). 4. A.

Gentillon, C. Richards, L. A. Ortiz-Flores, J. Metzner, D. Montealegre, M. Healey, K. Cardon, A. Westover, O. Hellwig and K. Chesnel, AIP Advances 11 (1), 015339 (2021).

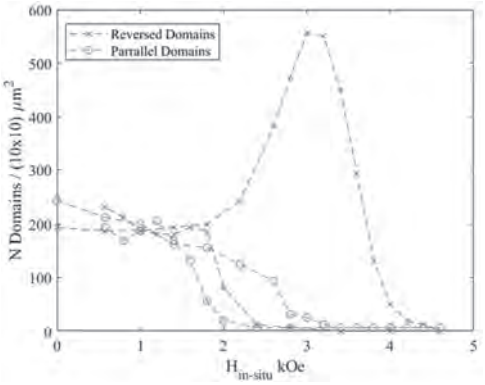

Fig. 1 Domain density plot for [Co(10 Å)/Pt(7 Å)]$_{20}$ as a response to the in-situ applied magnetic field, $H_{in\text{-}situ}$, and for a maximum applied magnetic field of 6.4 kOe. "Reversed domains" refers to domains where the magnetization is anti-aligned with the applied field while "parallel domains" refers to domains where the magnetization is aligned with the applied field.

ROB-08. Skyrmion detection with U-Net. *T.B. Winkler*[1], I. Labrie-Boulay[1], A. Romanova[1], D. Franzen[2], H. Fangohr[3,4] and M. Kläui[1]
1. Institut für Physik, Johannes Gutenberg University, Mainz, Germany; 2. Institut für Informatik, Johannes Gutenberg Universität, Mainz, Germany; 3. Scientific Support Unit for Computational Science, Max Planck Institute for the Structure and Dynamics of Matter, Hamburg, Germany; 4. Computational Modelling Group, Faculty of Engineering and Physical Sciences, University of Southampton, Southampton, United Kingdom

Magnetic skyrmions [1] are topologically stabilized, magnetic quasi-particles, which exhibit interesting physical phenomena and are also potential candidates for efficient neuromorphic computation schemes. On the micro-meter scale, they are detectable with Kerr-microscopy, using the magneto-optical Kerr-effect. However, depending on the material stack, temperature, the growth procedure and other influences, those measurement might suffer from noise, low-contrast, intensity gradients or defects, therefore manual data treatment is normally necessary to generate data that can be evaluated easily. Our approach is to use a convolutional neural network, based on the U-Net [2], to detect the position and shape of the skyrmions in our measurement data. This work was motivated by reports that machine learning has been successfully applied to (micro-) magnetic problems [3]. We are tuning the U-Net with various techniques to optimize the predictions and identify skyrmions and defects fast and with high reliability. A well-trained neural network is shown to minimize manual treatment of data. The approach is also easily extendable to other magnetic structures.

[1] Everschor-Sitte et al., *Journal of Applied Physics* 124, 240901 (2018) [2] Ronneberger et al., *MICCAI 2015. Lecture Notes in Computer Science*, vol 9351. Springer, Cham. (2015) [3] Alexander Kovacs et al., *Journal of Magnetism and Magnetic Materials* 491, 165548 (2019)

ROB-09. Revealing 3D Magnetic Textures in [Pt/Co/Cu]$_{15}$ Multilayers by Coherent X-ray Imaging with 5 nm Resolution. *R. Battistelli*[1*], S. Zayko[2], K. Bagschik[3], C.M. Günther[4], J. Fuchs[5], K. Gerlinger[5], L. Kern[5], D. Metternich[1], M. Schneider[5], D. Engel[5], S. Eisebitt[5], B. Pfau[5] and F. Büttner[1] *1. QM-NMAX, Helmholtz-Zentrum Berlin, Berlin, Germany; 2. Georg-August-Universität Göttingen, Göttingen, Germany; 3. Deutsches Elektronen-Synchrotron, Hamburg, Germany; 4. Technische Universität Berlin, Berlin, Germany; 5. Max Born Institute, Berlin, Germany*

In the fields of magnetism and spintronics, magnetic multilayers continue to thrive as pivotal structures to functionalize magnetic interactions, including the interfacial Dzyaloshinskii-Moriya interaction (DMI), and to engineer complex non-trivial spin textures [1-3]. However, previous research has focused almost exclusively on 2D structures. The challenge in studying 3D textures is in obtaining the necessary spatial resolution and sensitivity to resolve them. Here we show that this challenge can be met by reference-aided coherent diffractive x-ray imaging combining the robust Fourier Transform Holography with phase retrieval algorithms [4,5]. Based on this amplified wide-angle scattering, we achieve 5 nm spatial resolution for spin textures in Pt/Co/Cu magnetic multilayers, which allows us to clearly resolve fine domain walls (Fig.1c). Surprisingly, while conventional low-resolution images only show the well-known stripe domain state characteristic of such multilayers, our high-resolution images additionally reveal several small, mostly circular features of much weaker contrast (Fig. 1a,b), indicating a reduced net magnetization in the out-of-plane direction. Interestingly, while these features are clearly magnetic in nature and interact with the domain walls, they do not annihilate at the largest fields available in our system (220 mT). We associate the features to a localized increased surface roughness, leading to a local loss of perpendicular magnetic anisotropy promoting in-plane spin alignment and of 3D magnetic textures.

[1] F. Büttner et al., Nat. Phys. Vol. 11, p. 225-228 (2015) [2] F. Büttner et al., Nat. Nano Vol. 12, p. 1040-1044 (2017) [3] F. Büttner et al., Nat. Mater. Vol. 20, p. 30–37 (2021). [4] O. Kfir et al., Sci. Adv. Vol. 3, p. eaao4641 (2017) [5] S. Zayko et al., Nat. Commun. Vol. 12, p. 6337 (2021)

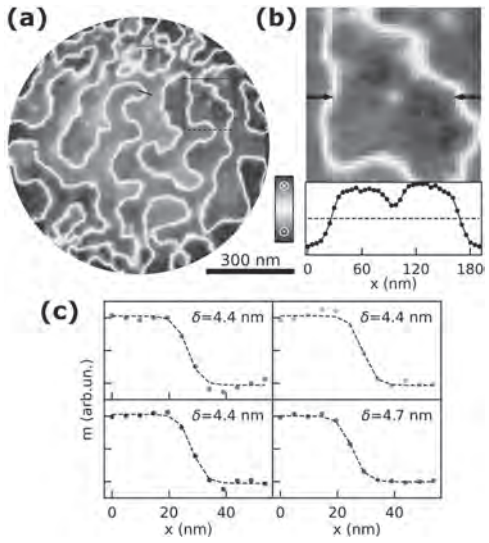

Fig. 1: High resolution imaging of pinning-induced 3D textures in Pt/Co/Cu. (a) ~5 nm resolution image. (b) Zoom-in on the dashed square in (a). (c) Domain wall profiles from (a), supporting the resolution claim.

ROB-10. X-ray vector magnetic tomography of Bloch points in magnetic microstructures and multilayers. J. Hermosa[1,2], A. Hierro-Rodríguez[1,2], A. Sorrentino[3], C. Quiros[1,2], J. Martin[1,2], L. Alvarez Prado[1,2], L. Aballe[3], E. Pereiro[3], *M. Velez*[1,2] and S. Ferrer[3] *1. Physics Dept., Universidad de Oviedo, OVIEDO, Spain; 2. CINN (CSIC-Univ. Oviedo), El Entrego, Spain; 3. Alba Synchrotron, Cerdanyola del Vallès, Spain*

The recent development of magnetic tomography [1] and laminography [2] techniques has allowed the quantitative characterization of 3D magnetization vector maps in thin films and nanostructures. Thus, vector analysis methods can be used to understand the experimental magnetization configurations and obtain a unified description of the different types of 3D domain walls and magnetic singularities. In this work we have studied by X-ray vector magnetic tomography (XVMT) the 3D magnetization configuration of a 140 nm thick permalloy microstructure [3] and a ferrimagnetic GdCo/NdCo/GdCo' trilayer [4]. In the Py microstructure, we observe a domain wall with non-trivial 3D configuration decorated by Bloch points such as the one in Fig. 1: composed of a linear tail-to-tail wall and a circulating vortex across the sample thickness. The corresponding emergent field B^e (calculated in the right part of Fig. 1) reveals the underlying topological singularity with charge -1, that acts as a sink of B^e lines. Changes in domain wall chirality are mediated by topological dipoles and triplets linked by horizontal bundles of emergent field lines. In addition, surface magnetic textures and helical vortices are found at the cross sections of vertical bundles of B^e lines [3]. In the GdCo/NdCo/GdCo' trilayer, the competition between anisotropy, exchange and magnetostatic interactions creates a peculiar stripe domain pattern with an exchange spring wall across the thickness at the top GdCo/NdCo interface [4]. The role of this boundary as a preferred site for nucleation of singularities will be discussed in detail (see e.g. the emergent field dipole in Fig. 2, composed of two Bloch points at different sample depths and opposite topological charges). Work supported by Spanish MICIN and Asturias FICYT.

[1] A. Hierro-Rodríguez, C. Quirós, A. Sorrentino, et al., *Nat. Comm., vol. 11, 6382, (2020).* [2] C. Donnelly, S. Finizio, S. Gliga et al., *Nat. Nanotechnol., vol. 15, 356-360, (2020).* [3] J. Hermosa, A. Hierro-Rodríguez, C. Quirós, et al. arXiv:2206.02499 [4] J. Hermosa-Muñoz, A. Hierro-Rodríguez, A. Sorrentino, et al., *Comm. Phys.* vol. 5, 26 (2022)

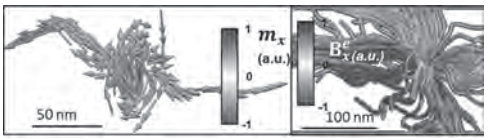

Figure 1: Magnetization and emergent field around a Bloch point in a 140 nm thick Py structure obtained from a XVMT experiment.

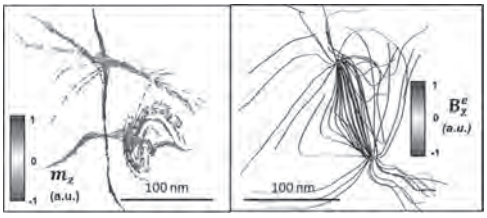

Figure 2: Magnetization around a Bloch point dipole linked by emergent field lines in the ferrimagnetic GdCo/NdCo/GdCo' trilayer: Note the magnetization divergence across the thickness for the Bloch point sitting at the top GdCo/NdCo interface with competing exchange and magnetostatic interactions.

ROB-11. Self-Assembly as a Tool to Study Strain-Dependent Magnetic Properties. *B. Singh*[1], J.A. Otalora Arias[2], T.H. Kang[1], I. Soldatov[1], D.D. Karnaushenko[3], C. Becker[3], R. Schäfer[1], D. Karnaushenko[3], V. Neu[1] and O.G. Schmidt[3,4] *1. Leibniz IFW Dresden, Dresden, Germany; 2. Universidad Católica del Norte, Antofagasta, Chile; 3. Center for Materials Architectures and Integration of Nanomembranes (MAIN), Chemnitz, Germany; 4. TU Chemnitz, Chemnitz, Germany*

Geometrical transformations, such as rolling a 2D ferromagnetic film into a 3D cylinder provide means to tune its magnetic properties generating different magnetic ground states [1]. Rolled-up magnetic membranes with azimuthal magnetic anisotropy are very attractive due to expected much higher domain wall velocity (compare to their planar counterparts) [2] and for applications as impedance-based field sensors [1]. However, a clear recipe for acquiring highly mobile azimuthal domains in a soft ferromagnetic tubular geometry is unclear. State of the art studies report the rolling of an extended ferromagnetic film (of hundreds of micro-meters), which after rolling converts into tubular geometry with 2-3 windings [1]. Changes in the magnetic domain configuration in such tubular geometries may arise from modifications of the shape anisotropy in addition to stress-induced anisotropy due to rolling. In our work, we report on rolling-induced azimuthal anisotropy in $Ni_{78}Fe_{22}$ stripes (as shown in figure 1a) purely due to strain, considering that curvature induced changes in shape anisotropy can be neglected due to reduced dimensions of our magnetic stripe in the azimuthal direction. For that, we employed a self-assembly rolling technology based on a polymeric platform, which allows choosing the shape and size of the magnetic structure willingly. Magnetic structures patterned on the polymeric platform can be bent controllably and hence the sign and magnitude of strain on the magnetic structure can be adjusted. We quantify the induced azimuthal magnetic anisotropy (figure 1c) by electrical measurements (figure 1b) capable of providing magnetic properties of magnetic structures hidden under the 3D polymer architecture.

[1] R. Streubel, O. G. Schmidt and D. Makarov, *J. Phys. D. Appl. Phys. 49*, 363001 (2016) [2] J. Hurst, O. Fruchart and D. Gusakova, *Phys. Rev. B 103*, 1 (2021)

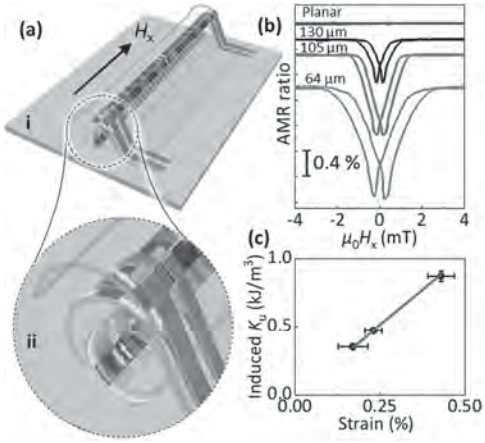

Figure 1: (a) Schematic illustration of self-assembly (a-i) roll-down approach for adjusting the size of curvature and strain in a functional magnetic layer on top of the polymeric platform (a-ii) magnified view of rolled-down structures, indicating tensile strain (yellow arrows) in the magnetic layer. (b) AMR hysteresis measured for planar and rolled-down stripes of different diameters (Ø) (c) Rolling induced azimuthal magnetic anisotropy (K_u) in magnetic stripes extracted from AMR hysteresis.

ROB-12. Three-Dimensional Nucleation Kinetics Through the First-Order Metamagnetic Phase Transition in B2-Ordered FeRh.

J. Massey[1,2], S. Treves[1,2], A. Apseros[1,2], S. Finizio[3], M.T. Grimes[1,2], J. Reuteler[4], C. Donnelly[5,6], T. Thomson[7], L. Heyderman[1,2] and V. Scagnoli[1,2] *1. Laboratory for Mesoscopic Systems, ETH Zurich, Zurich, Switzerland; 2. Laboratory for Multiscale Materials Experiments, Paul Scherrer Institut, Villigen, Switzerland; 3. Photon Science Department, Paul Scherrer Institut, Villigen, Switzerland; 4. ScopeM, ETH Zurich, Zurich, Switzerland; 5. Cavendish Laboratory, University of Cambridge, Cambridge, United Kingdom; 6. Max Planck Institute for Chemical Physics of Solids, Dresden, Germany; 7. NEST Research Group, The University of Manchester, Manchester, United Kingdom*

B2-ordered FeRh undergoes a thermally activated first-order phase transition between antiferromagnetic (AF) and ferromagnetic (FM) order upon heating, with a transition temperature between 350 - 380 K [1], making it an ideal candidate for use in a wide range of magnetic storage architectures [2]. The evolution of magnetic domains through the transition has been well-characterized [1-5]. However, behaviours such as the domain nucleation mechanism and subsequent evolution of the magnetic domains along the sample thickness through the phase transition remain unclear [1,3-5]. Here, we present three-dimensional (3D) reconstructions of the magnetic structure through the sample volume at various temperatures through the phase transition, achieved using magnetic laminography [6-7]. Imaging cross-sections through the sample thickness reveal that domains for both types of magnetic order nucleate at the surface and travel into the bulk of the sample with changing temperature. Creating a complex 3D magnetic structure, in which the evolution of the magnetic state along the sample thickness with temperature is non-uniform. We also observe quasi-uniform FM domains at 310 K when heating, in contrast to the expected flux-closed state [1], as well as AF regions where FM domain walls are expected. Both observations can be attributed to the exchange coupling between adjacent AF and FM regions, which plays a key role determining the FM configuration in this material.

[1] T. P. Almeida et al., Phys. Rev. Materials 4, 034410 (2020). [2] R. C. Temple et al., Phys. Rev. Materials 2, 104406 (2018). [3] C. Gatel et al., Nat. Comms. 8, 15703 (2017). [4] V. Uhlir et al., Nat. Comms. 7, 13113 (2016). [5] M. A. de Vries et al., Appl. Phys. Lett. 104, 232407 (2014). [6] C. Donnelly et al., Nature Nanotech. 15, 356 (2020) [7] K. Witte et al., Nano Lett. 20, 1305 (2020).

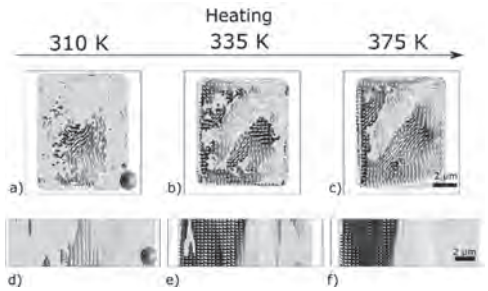

Fig 1. Reconstructed magnetic state when heating. (a)-(c) show the magnetic state for the top surface of the lamella. The sample area is shown in colour, which depicts the magnetization direction shown in the colour wheel in panel (a). The pink areas are those within the sample that are AF. At 310 K the sample shows a quasi-uniform FM domain, which develops into multi-striped domain at 375 K. The region between two adjacent, oppositely magnetized domains is the last to transition to being FM. (d)-(f) show the same information for a slice through the centre of the sample that encompasses the film thickness. FM domains nucleate at the surface and proceed into the bulk of the material with increasing temperature.

Session RPA
MAGNETIC CHARACTERIZATION AND IMAGING
(Poster Session)

Hendrik Ohldag, Co-Chair
Lawrence Berkeley National Laboratory, Berkeley, CA, United States
Thomas Feggeler, Co-Chair
Lawrence Berkeley National Laboratory, Berkeley, CA, United States

RPA-01. Influence of stress on the magnetic properties of ultra-thin silicon steel in high frequency range. Y. Li[1], *S. Song*[1], Y. Dou[1] and T. Chen[1]
1. School of Electrical Engineering, Hebei University of Technology, Tian-Jin, China

Ultra-thin silicon steel with thickness less than 0.1 mm can be used to make the iron core of high-frequency transformers and high-speed motor. The design of these electrical equipment often relies on the data of alternating magnetic characteristics measured under standard excitation, ignoring the influence of working conditions such as stress and temperature, etc.. Under stress conditions, the magnetic properties of the magnetic material are quite different from those under standard sinusoidal excitation. Therefore, it is very important to accurately measure the magnetic properties of ultra-thin silicon steel under stress conditions. Previously, many scholars have studied the influence of mechanical stress on the magnetic properties of conventional electrical steels [1-5]. However, there are few reports on the properties of high frequency materials under stress. When testing the properties of high frequency materials under stress, we can refer to the traditional testing methods of silicon steel. Compared with the other methods of stress application, such as motor or oil pressure, piezoelectric material has good flexibility and control accuracy, and it will not produce stray magnetic field to interference the measurement. The most important thing is that piezoelectric materials have good applicability to the magnetizer. In other words, it is not necessary to reconstruct the magnetic circuit structure and stress actuator, and the relevant experiments can be carried out directly by pasting piezoelectric materials in the sample. This paper uses the magnetizer proposed in paper [6], which has good test accuracy. The sample is ultra-thin silicon steel with 0.1 mm thickness (GT100). The size of the sample is 50 mm×50 mm. Two Macro Fiber Composite (MFC) [7] are symmetrically pasted on the upper and lower surfaces of the sample center. A maximum tensile or compressive stress of about 150 N or 107 MPa can be obtained in the sample along one direction. The distribution of stress is calculated by the FEM and shown in Fig. 1. It can be seen that the stress is uniform in the measuring region. Fig. 2 gives the hysteresis loops under different stress along rolling direction.

[1] Permiakov, V., et al. "Loss separation and parameters for hysteresis modelling under compressive and tensile stresses." *Journal of Magnetism & Magnetic Materials* 272.supp-S(2004):E553-E554. [2] Singh, D., et al. "Effect of stress on excess loss of electrical steel sheets." *IEEE* (2015):1-1. [3]Hameyer, et al. "Effect of mechanical stress on different iron loss components up to high frequencies and magnetic flux densities." COMPEL: The international journal for computation and mathematics in electrical and electronic engineering 36.3(2017):580-592. [4]Ali, K., Atallah, K. and Howe, D.. "Prediction of mechanical stress effects on the iron loss in electrical machines." Journal of Applied Physics 81.8(1997). [5]Naumoski, H., Maucher, A. and Herr, U. "Investigation of the influence of global stresses and strains on the magnetic properties of electrical steels with varying alloying content and grain size." Electric Drives Production Conference IEEE, 2015. [6]Yue, S., et al. "Comprehensive Investigation of Magnetic Properties for Fe–Si Steel Under Alternating and Rotational Magnetizations Up to Kilohertz Range." IEEE Transactions on Magnetics 55.7(2019):1-5. [7]Wilkie, W. K., et al. "Low-cost piezocomposite actuator for structural control applications." Proceedings of Spie the International Society for Optical Engineering (2000).

Fig 1

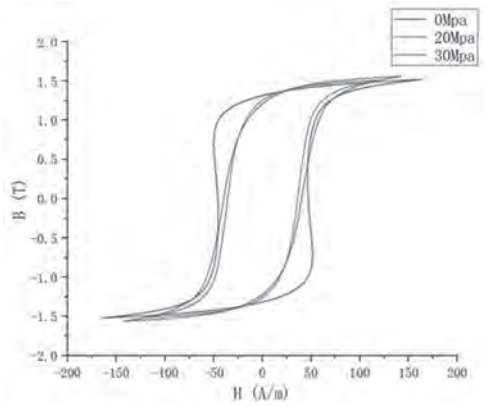

Fig 2

RPA-02. A Novel Method for Measuring Residual Flux Density of the Single-Phase Transformer Based on Phase Difference. Y. Wang[1], *Y. Ren*[1] and C. Liu[1] *1. Hebei University of Technology, Tianjin, China*

I Introduction The residual flux density (B_r) in the core is one of the reasons that cause the inrush current when the transformer is re-energized [1]. To effectively weaken the inrush current, it is necessary to measure the B_r. The Frequency Response Analysis (FRA) test and the voltage integration method are widely used in B_r detection [2], [3]. Considering the limitations of existing methods, results could be considered unreliable in some applications. The main purpose of this paper is to study the most effective method for measuring the B_r of transformers. II Theoretical analysis of the proposed method As shown in Fig. 1, the magnetic domain structure is different under B_r, resulting in changes in magnetic permeability, so the magnetizing inductance is different. When AC voltage with a small amplitude is applied to the primary winding, the impact on the transformer is almost negligible. The transient magnetic flux generated will be established based on the initial B_r. Combined with the field-circuit coupling analysis, the different B_r is the main factor causing the difference in the current waveform, manifested as a phase shift in the AC component of the response current. The relationship between the phase difference of the measurable parameters and the B_r is

established, which can realize the quantitative detection of the B_r in the transformer core with a closed magnetic circuit structure. III Conclusion The transformer core is modelled and analyzed using the finite element method, and the empirical formula between phase difference and B_r is obtained. It can be seen from Fig. 2 that the phase difference decreases with the increase of B_r, which means that the equivalent impedance tends to be more resistive. If the B_r is not taken into consideration when the transformer is re-energized, the inrush current will be easily generated. The measurement platform is built, and the maximum measurement error is less than 6.12%, proving that the method has high accuracy. The proposed method can measure B_r without any requirement on the transformer, which provides a reliable reference to weaken the inrush current.

[1] S. Zhang, C. G. Yao, X. Z. Zhao, et al. "Improved flux-controlled VFCV strategy for eliminating and measuring the residual flux of three-phase transformers," *IEEE Trans. Power. Deli*., pp. 1-1, Aug. 2019. [2] F. de León, A. Farazmand, S. Jazebi, et al, "Elimination of Residual Flux in Transformers by the Application of an Alternating Polarity DC Voltage Source," IEEE Trans. Power Del, vol. 30, no. 4, pp. 1727-1734, Aug. 2015. [3] W. Wei, Y. Liu, S. W. Mei, et al. "Study on residual flux evaluation method based on variable-regional integral during the voltage attenuation process," IEEE Innovative Smart Grid Technologies-Asia (ISGT Asia)., Oct. 2019.

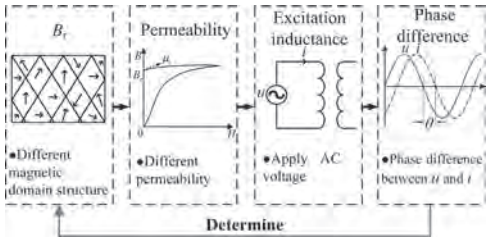

Fig. 1

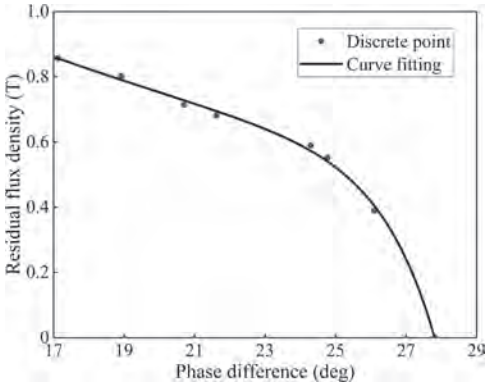

Fig. 2

RPA-03. A New Inductor Power Loss Model for Boost Converter during the Voltage Conversion Based on the Jiles-Atherton Model. J. Lee[3], K. Nidhi[1], *C. Li*[2,3], T. Liao[1] and K. Chen[2] *1. ESD Department, Richtek Technology Corp., ChuPei, Taiwan; 2. Department of Electrical and Computer Engineering, National Yang Ming Chiao Tung University, Hinschu, Taiwan; 3. Device Engineering, Vanguard international semiconductor Cop., Hinschu, Taiwan*

Abstract—The Jiles-Atherton (J-A) model [1] predicts that an inductor has different inductances at the current ramp-up time (t_{on}) and ramp-down time (t_{off}). For the first time, this phenomenon is observed at the boost converter (Fig. 1) during the voltage converter (Fig. 2) and a simple equation to depict it is derived. Moreover, the methodology to calculate the inductor power loss from the voltage conversion data directly for a boost converter is presented. I. Model and Experiment Result From Fraday law, the inductance is L=NdBA/(dt(dI/dt))=uNA d(H+M)/dI= L_o(1+dM/dH) (1) From the J-A model, the differential of total magnetization M is dM/dH=(M_{an}-M)/((dk/m)-a(M_{an}-M)) (2) where d=1 if dH/dt>0 and d=-1 if dH/dt < 0. From the experiment result in Figs. 3-5, M_{an}-M can be approximated to a constant M_D since the voltage almost keeps constant at each t_{on} or t_{off} based on L=V/(dI/dt). So, the inductance at t_{on} is given by L= L_o(1+mM_D/(k-aM_D)=L1 (3) The inductance at t_{off} is given by L= L_o(1-mM_D/(k+aM_D)=L2 (4) Figs. 3-5 show the voltage and current waveforms of the boost converter during the voltage conversion for the output currents (I_{OUT} in Fig. 1) 0A, 0.2A and 0.4A. However, the three different I_{OUT} waveforms have different t_{on} and t_{off} due to different slops by aligning their base current level with the current waveform for I_{OUT}=0A as shown in Fig. 6. It proves that an inductor has the different inductances at t_{on} and t_{off} and L1 at t_{on} is larger than L_o and L2 at t_{off} is smaller than L_o. This is caused by the hysteresis effect as shown in Fig. 7 since it follows the initial hysteresis loop, minor hysteresis curves i and ii for L_o, L1 and L2. Integrating the powers at t_{on} and t_{off} and divided by the period T, the inductor power loss for boost converter during the voltage conversion is P_{loss}=(L1-L2)dI_L(dI_L+2I_{MIN})/2T (5) where dI_L is the peak-to-peak inductor current, I_{MIN} is the minimum inductor current in Fig. 2. Table-I shows the input power, measured inductor power loss based on Figs. 3-5 and calculated inductor power loss based on Eq. (5). The calculated power loss is very close to the measured power loss, verifying Eq. (5) valid to calculate the inductor power loss from the electrical voltage conversion data directly.

[1] D. C. Jiles and D. L. Atheron, "Theory of Ferromagnetic Hysteresis," J. of Magnetism and Magnetic Materials, pp. 48-60, 1986.

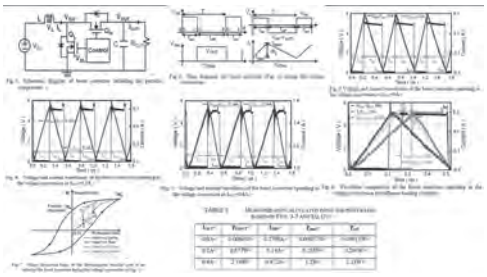

Figure 1

RPA-04. Origins of potential observational errors in field sweeping DC measurements for unidirectional magnetoresistance. *Y. Fan*[1], R. Saha[1], Y. Yang[1] and J. Wang[1] *1. Electrical Engineering, University of Minnesota, Minneapolis, MN, United States*

Different contributions and mechanisms of the unidirectional magnetoresistance (UMR) have become a recent research hotspot in spintronics. Field sweeping DC measurements are used to measure the value of UMR instead of second harmonic measurements. [1,2] In this paper, potential measurement errors in conventional DC measurements are studied. Oersted field and field-like torque usually do not influence the measurement, but a large field-like torque can result in anisotropic magnetoresistance (AMR) difference when the sample is not perfectly aligned. The existence of ordinary magnetoresistance (OMR) can also contribute to a large background. An alternative measurement method is demonstrated to address this issue. This work broadens the understanding of the error sources and provides a standard measurement method for UMR DC measurements.

[1] Duy Khang, Nguyen Huynh, and Pham Nam Hai. "Giant unidirectional spin Hall magnetoresistance in topological insulator–ferromagnetic semiconductor heterostructures." Journal of Applied Physics 126.23 (2019): 233903. [2] Chang, Ting-Yu, et al. "Large unidirectional magnetoresistance in metallic heterostructures in the spin transfer torque regime." Physical Review B 104.2 (2021): 024432.

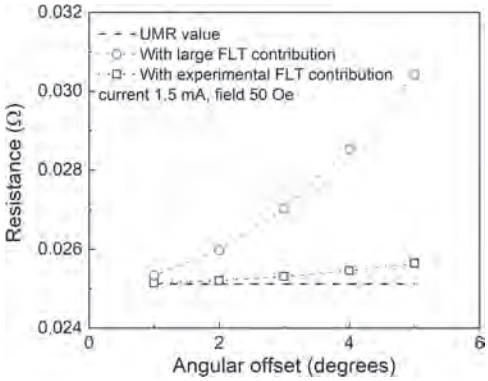

Figure 1. Spin-orbit torque contribution to the total measured signals with an angular measurement offset.

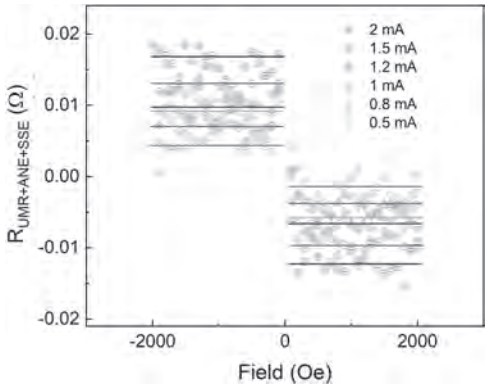

Figure 2. The field and current dependence of UMR signal for Ta/CFB bilayer with the angular-dependent DC measurement method.

RPA-05. Analysis of Nuclear Magnetic Resonance Metabolomics data for the detection of unborn baby health problems using deep learning. *P. Kumar*[1], S. Amara[1], D. Khan[1] and Y. Massoud[1] *1. Computer, Electrical and Mathematical Sciences and Engineering, King Abdullah University of Science and Technology, Thuwal, Saudi Arabia*

Amniotic fluid is a clear and pale yellowish liquid that surrounds and protects the fetus (unborn baby) throughout pregnancy [1]. The amniotic fluid analysis can diagnose certain health disorders in the unborn baby such as Down syndrome, Cystic fibrosis, Sickle cell disease, Tay-Sachs disease, and Neural tube defects [2]. Fig. 1 shows a 10-week-old human fetus surrounded by amniotic fluid within the amniotic sac [3]. This abstract presents a deep learning/machine learning pipeline that can be used for the prediction of health problems in an unborn baby by using deep learning or machine learning algorithm. The work is divided into two parts; (1) data collection, and (2) data processing and analysis. Fig. 2(a) shows data collection workflow. In the data collection, 20 samples of amniotic fluid are collected from a healthy and an unhealthy woman during 15~20 weeks of pregnancy [4]. After collecting the samples, the nuclear magnetic resonance (NMR) is performed for data acquisition [5]. Fig. 2(b) depicts workflow of data processing and analysis. In this part, metabolites data is normalized and a data reduction method like PCA is applied. After getting the preprocessed data, feature selection algorithms are performed to remove the irrelevant data. Three variable selection algorithms such as (i) Correlation-based feature selection (CFS), (ii) Partial least squares regression (PLS), and (iii) Learning Vector Quantization (LVQ) [4] are used. For each selected set of metabolites, support vector machine (SVM) models are generated using 10-fold cross-validation. To evaluate the performance and significance of the optimized model, we perform a permutation test. In the 10-fold cross-validation, the permutation test shuffles the class labels while using the same set of metabolites. For data analysis, we calculate true/false positives and true/false negatives for each round of our 10-fold cross-validation to report average sensitivity (TP/P) and specificity (TN/N) values along with the average of the area under the curve (AUC) [4].

[1]. C. M. Broek, J. Bots, I. V. Lasheras, M. Bugiani, F. Galis, S. V. Dongen, "Amniotic fluid deficiency and congenital abnormalities both influence fluctuating asymmetry in developing limbs of human deceased fetuses," PLoS One, vol. 8, no. 11, 2013. [2]. MedlinePlus [Internet], National Library of Medicine (US), "Amniocentesis (amniotic fluid test)," Available from: https://medlineplus.gov/lab-tests/amniocentesis-amniotic-fluid-test/ [3]. https://en.wikipedia.org/wiki/Amniotic_fluid. [4]. R. O. B. Singh, A. Yilmaz, H. Bisgin, O. Turkoglu, P. Kumar, E. Sherman, A. Mrazik, A. Odibo, and S. F. Graham, "Artificial intelligence and the analysis of multi-platform metabolomics data for the detection of intrauterine growth restriction," PLoS One vol. 14, no. 4, 2019. [5]. https://www.jeol.co.jp/en/products/nmr/basics.html.

Fig. 1. 10-week-old human fetus surrounded by amniotic fluid within the amniotic sac.

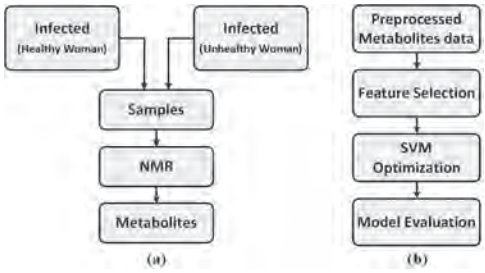

Fig. 2. (a) Overall data collection workflow. (b) Data processing and analysis workflow.

RPA-06. Role of Aggregation Dynamics in Magneto-Optical Scattering by Superparamagnetic Nanoparticles. N. Fried[2], W.J. Li[3] and *M. Syed*[1] *1. Physics, Rose-Hulman Institute of Technology, Terre Haute, IN, United States; 2. Institute of Physical Science & Technology, University of Maryland, College Park, MD, United States; 3. Physics, University of Maryland, College Park, MD, United States*

Superparamagnetic nanoparticles (SNPs) are widely used in biomedical applications like imaging, magnetic hyperthermia, drug delivery, etc. [1-2]. We present a continuation of our study of the scattering of dilute aqueous suspensions of single-domain magnetite nanoparticles using an AC Faraday rotation setup [3-5]. The setup employs a stabilized He-Ne laser (633 nm) along with an AC magnetic field (130-1120 Hz) that enables lock-in detection. We have measured the scattering response of magnetite nanoparticles that vary in diameter from 15 to 25 nm. Our previous results analysed the scattering of light by SNPs subjected to an AC magnetic field, utilizing the even harmonics of the intensity signal. In this study, we continue to investigate the leading even harmonic (2f) signal to analyse scattering, but with added emphasis on the initial polarization angle of the incident light (linearly polarized) and its relationship to the orientation of the applied magnetic field. This approach allows us to investigate how the direction of the applied

magnetic field results in a shape anisotropy for the SNP aggregates, and the effect that this anisotropy has on the scattering of light with varying angles of incident polarization. Differences in scattering are then related to the structural details of the aggregates as well as the time dynamics of the formation of these structures. The two orthogonal cases (transverse and longitudinal) that form the basis of this analysis are where incident polarization is perpendicular and parallel to the applied field (also the presumed long axis of aggregates), respectively. The scattering is also measured for various other angles between a parallel and perpendicular orientation. The model allows us to predict an angle for which the scattering is not affected by the application of the magnetic field. We show that the presence of this angle is confirmed by our data. Our results provide important insight into the role of nanoparticle size (core and hydrodynamic), particle concentration, and magnetic field profile (intensity and frequency) in the formation dynamics of clusters.

1. R. Hergt, S. Dutz, and M. Zeisberger, *Nanotechnology*, 21, (2010). 2. Y. Xiao and J. Du, *J. Mater. Chem. B*, 8, 3, 354–367, (2020). 3. S. Vandendriessche, W. Brullot, D. Slavov, V. Valev, and T. Verbiest, *Appl. Phys. Lett*., 102, (2013). 4. C. Patterson, M. Syed, Y. Takemaura, *Journal of Magnetism and Magnetic Materials*, 451, 248-253 (2018). 5. M. Syed, W. Li, N. Fried, and C. Patterson, *AIP Advances*, 11, 015328 (2021).

RPA-07. Evaluation of detection technique of magnetic nanoparticles using pulsed magnetic field. *M. Nishida*[1], S. Tanaka[1], M. Futagawa[1], Y. Takemura[2] and S. Ota[1] *1. Shizuoka University, Hamamatsu, Japan; 2. Yokohama National University, Yokohama, Japan*

Magnetic particle imaging (MPI) using magnetic nanoparticles (MNPs) as tracers can be used as an early diagnosis technique for cancer [1]. In a conventional MPI, two different magnetic fields, such as sinusoidal alternating current (AC) and direct current (DC) magnetic fields are continuously applied to detect particle-specific harmonics. In this study, we propose an imaging technique using a pulsed magnetic field. Applying a pulsed magnetic field with a small duty ratio reduces power consumption. In addition, the fast response of magnetization owing to the response of the pulsed magnetic field with a short rise time increases the detection sensitivity. Iron oxide nanoparticles of M-300 (Sigma High Chemical Co., Ltd., Kanagawa, Japan) were used as the measurement sample, and they were enclosed in a rectangular container with a base of 3 mm × 3 mm and a height of 1 mm. The square excitation coil for applying the pulsed magnetic field had two layers of 12 turns, each having a size of 7.5 mm. The detection coil for detecting the signal had one layer of 10 turns, each having a diameter of 2 mm and a distance of 2 mm between the detection coils. The amplitude of the applied pulse magnetic field was 3.0 mT. Figure 1 shows the two-dimensional (2D) measurement of the detected signal intensity of the MNPs. The white dotted line indicates the location of the sample. The center of the sample was set at 0 mm, and the signal was measured by moving the coil set. The peak signal intensity was obtained where the sample was located. When the diameter of the detection coil was increased, the signal intensity obtained from the sample increased. However, the signal distribution became coarse because of the external noise signal. Conversely, when the diameter was reduced, the noise signal decreased. When the distance between the detection coils was increased, the resolution decreased. In conclusion, the signals of MNPs were detected by the application of a pulsed magnetic field, and the sensitivity and resolution were improved by appropriately adjusting the diameter and spacing of the detection coils.

[1] B. Gleich and J. Weizenecker, Tomographic imaging using the nonlinear response of magnetic particles, Nature 435, 1214 (2005).

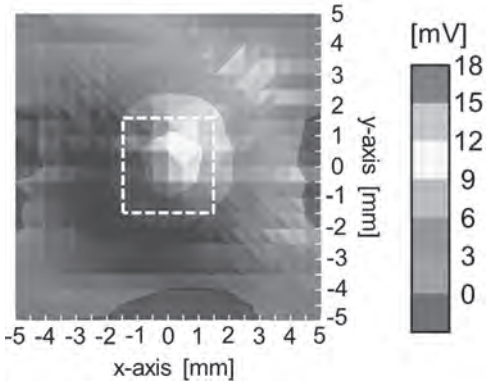

Fig. 1 2D imaging of phantom containing magnetic nanoparticle dispersed in water

RPA-08. Syntheses and Characterization of Core-Shell Iron-Based Magnetic Nanoparticles Dispersed in Carbon Matrix. *F.M. Iglesias*[1], H. Gyulasaryan[2], G. Chilingaryan[2], C. Alvarado[1], J. Gray[3], A. Manukyan[2], O. Bernal[1] and A.N. Kocharian[1] *1. Physics and Astronomy, California State University, Los Angeles, CA, United States; 2. Institute for Physical Research of NAS of Armenia, Ashtarak, Armenia; 3. Materials Characterization Lab, Pennsylvania State University, University Park, PA 16802, PA, United States*

In recent years there is a growing interest in synthesizes of novel iron-based nanoparticles and nanocomposites with high efficiency of thermal energy transfer suitable for use in magnetic fluid hyperthermia. The development of novel biocompatible magnetic nanoparticles (MNPs) for biomedical applications has been the subject of extensive exploration over the past two decades. Here we study the characteristics of carbon-coated ferromagnetic (Fe-Fe_3O_4)@C "core-shell" nanoparticles in samples with different concentration of iron synthesized by a solid-phase pyrolysis (SPP) of iron phthalocyanine ($FeC_{32}H_{16}N_8$) molecules. The sample with higher iron concentration additionally annealed at 250°C under the oxygen media produces (Fe_3O_4) shell on Fe nanoparticles. The structural and magnetic properties of these nanomaterials were conducted using Scanning Electron Microscope (SEM), High-angle annular dark-field scanning transmission electron microscopy (HAADF-STEM) images with elemental mapping data, Raman spectroscopy, X-ray diffraction (XRD), magnetometry, electron paramagnetic and ferromagnetic resonances (EPR, FMR). The STEM image in Fig. 1 demonstrates a presence of Fe-Fe_3O_4 "core-shell" nanoparticles of order ~ 50 nm with oxide shells in carbon matrix. The ferromagnetic hysteresis loops with residual magnetizations and coercive forces is shown in Fig. 2 at two different temperatures. The characteristics of magnetic heating of water-based solution with different concentrations of synthesized nanocomposites under the influence of an external magnetic field have been studied. The magnetic characteristics such as saturation magnetization and coercivity as well as the specific absorption rate (SAR) make these materials attractive for magnetic hyperthermia applications. This work was supported by European Union's Horizon 2020 research and innovation programme under grant agreement No 857502 (MaNaCa). The work at CSULA supported by the NSF CREST Grant #HRD-1547723.

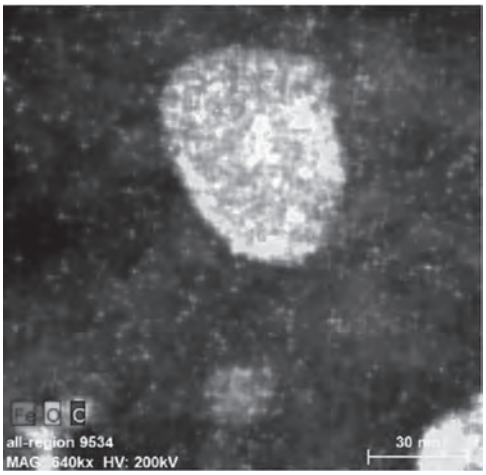

Fig. 1 High-resolution transmission electron microscopy images of iron/iron-oxide nanoparticles with core-shell architecture embedded in carbon matrix

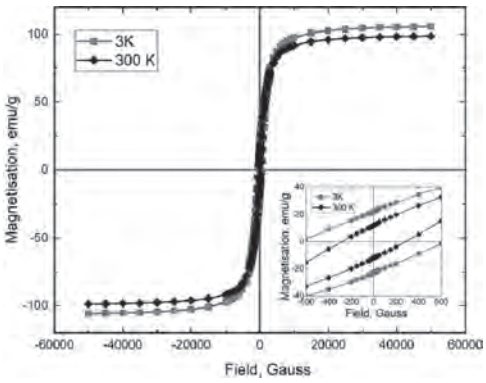

Fig. 2 Magnetization versus magnetic field shown for Fe-Fe_3O_4 nanoparticles at 3K and 300K

RPA-09. Preparation of probes for high-resolution magnetic force microscopy by orientation control of FePt layer. *S. Watanabe*[1], S. Nemoto[1], M. Doi[1] and T. Shima[1] *1. Tohoku Gakuin University, Tagajo, Japan*

Magnetic force microscope (MFM) is a type of scanning probe microscope (SPM) that detects and images the gradient of the stray magnetic field of the observed sample. Therefore, the magnetic domain image is greatly affected by the surface morphology of the probe and the magnetic properties of the coated magnetic thin film. If the strong stray magnetic field for the permanent magnet material disturbs the magnetization of the magnetic probe, accurate observation of the magnetic domain structure is difficult. $L1_0$ ordered FePt alloy with high uniaxial magnetocrystalline anisotropyis thought to be an candidate probe material because of its high corrosion resistance and high coercivity[1]. It has also reported that the orientation of the FePt layer can be controlled by introducing MgO layer[2]. However, there are only a few reports of magnetic domain images observed by MFM probes using FePt film. In this study, the orientation of the FePt layer was controlled by using a MgO under layer with varying film thickness and element additions in order to observe high-resolution magnetic domain images. The FePt coated probes were prepared using an ultra-high vacuum magnetron sputtering system. A MgO buffer layer was deposited on Si cantilever and Si substrate at room temperature (R.T.). Then, FePt was deposited at a substrate temperature T_s of 873 K and they were annealed at 973 K. The surface morphology of the probes was observed by scanning electron microscope (SEM). The crystal structure was evaluated by X-ray diffraction (XRD), and the magnetic properties weremeasured usinga superconducting quantum interference device (SQUID) magnetometer. From XRD patterns, the fundamental (002) and the superlattice (001) peaks from $L1_0$ ordered FePt phase have been clearly observed atthe FePt probe by the introduction of MgO buffer layer, and a clear magnetic domain image was observed. However, when a Cu-doped MgO layer was used, the peak intensity from the $L1_0$ ordered FePt phase increased and a magnetic domain image with even higher resolution was obtained. High-resolution mechanism will be discussed at the conference.

[1] T. Yamaoka, H. Tsujikawa, S. Hanamura, K. Andou, M. Shigeno, A. Ito, and H. Kawamura, *Microscopy Today*, 22 (2014) 12-17. [2] B. C. Lim, J. S. Chen, J. F. Hu, Y. K. Lim, B. Liu, G. M. Chow, and G. Ju, *J. Appl. Phys*. 103, 07E143 (2008).

- A -

*Best student presentation award finalist

- B -

*Best student presentation award finalist

- C -

*Best student presentation award finalist

*Best student presentation award finalist

- D -

*Best student presentation award finalist

- E -

*Best student presentation award finalist

- F -

*Best student presentation award finalist

- G -

*Best student presentation award finalist

- H -

*Best student presentation award finalist

*Best student presentation award finalist

- I -

- J -

*Best student presentation award finalist

- K -

*Best student presentation award finalist

*Best student presentation award finalist

- L -

*Best student presentation award finalist

*Best student presentation award finalist

*Best student presentation award finalist

- M -

*Best student presentation award finalist

*Best student presentation award finalist

- N -

*Best student presentation award finalist

- O -

*Best student presentation award finalist

- P -

*Best student presentation award finalist

- Q -

- R -

*Best student presentation award finalist

- S -

*Best student presentation award finalist

*Best student presentation award finalist

*Best student presentation award finalist

- T -

*Best student presentation award finalist

*Best student presentation award finalist

- U -

- V -

- W -

*Best student presentation award finalist

*Best student presentation award finalist

- X -

- Y -

*Best student presentation award finalist

- Z -

*Best student presentation award finalist

*Best student presentation award finalist